Giorgio Lollino
Daniele Giordan
Kurosch Thuro
Carlos Carranza-Torres
Faquan Wu
Paul Marinos
Carlos Delgado   *Editors*

Engineering Geology for Society and Territory – Volume 6

Applied Geology for Major Engineering Projects

ENG GEOL
IAEG
AIGI GEOL

Springer

Engineering Geology for Society
and Territory – Volume 6

Giorgio Lollino • Daniele Giordan
Kurosch Thuro • Carlos Carranza-Torres
Faquan Wu • Paul Marinos
Carlos Delgado

Editors

Engineering Geology for Society and Territory – Volume 6

Applied Geology for Major Engineering Projects

Editors

Giorgio Lollino
Daniele Giordan
Institute for Geo-Hydrological Protection
National Research Council (CNR)
Turin
Italy

Kurosch Thuro
Department of Engineering Geology
Technical University of Munich
Munich
Germany

Carlos Carranza-Torres
Department of Civil Engineering
University of Minnesota Duluth
Duluth, MN
USA

Faquan Wu
Institute of Geology and Geophysics
Chinese Academy of Sciences
Beijing
China

Paul Marinos
Geotechnical Engineering Department
National Technical University of Athens
Athens
Greece

Carlos Delgado
Escuela Universitaria de Ingeniería Técnica
   de Obras Públicas
Universidad Politécnica de Madrid
Madrid
Spain

Cover Illustration: Pont Ventoux, Val di Susa, north western Italy. Tunnel Boring Machine(TBM) used during the construction of the gallery used as deviation channel for a hydroelectric power plant. The TBM was used to drill a gallery of 4.3 km long and with circular diameter of 4.05 meters. *Photo*: Giorgio Lollino.

Printed on acid-free paper

Foreword

It is our pleasure to present this volume as part of the book series on the Proceedings of the XII International IAEG Congress, Torino 2014.

For the 50th anniversary, the Congress collected contributions relevant to all themes where the IAEG members were involved, both in the research field and in professional activities.

Each volume is related to a specific topic, including:

1. Climate Change and Engineering Geology;
2. Landslide Processes;
3. River Basins, Reservoir Sedimentation and Water Resources;
4. Marine and Coastal Processes;
5. Urban Geology, Sustainable Planning and Landscape Exploitation;
6. Applied Geology for Major Engineering Projects;
7. Education, Professional Ethics and Public Recognition of Engineering Geology;
8. Preservation of Cultural Heritage.

The book series aims at constituting a milestone for our association, and a bridge for the development and challenges of Engineering Geology towards the future.

This ambition stimulated numerous conveners, who committed themselves to collect a large number of contributions from all parts of the world, and to select the best papers through two review stages. To highlight the work done by the conveners, the table of contents of the volumes maintains the structure of the sessions of the Congress.

The lectures delivered by prominent scientists, as well as the contributions of authors, have explored several questions ranging from scientific to economic aspects, from professional applications to ethical issues, which all have a possible impact on society and territory.

This volume testifies the evolution of engineering geology during the last 50 years, and summarizes the recent results. We hope that you will be able to find stimulating contributions, which will support your research or professional activities.

Giorgio Lollino   Carlos Delgado

Preface

Engineering geology, a relatively young field, emerged through recognition of the need for geologic input into engineering projects. Today, this primary field has expanded as the statutes of its learned society, the IAEG, define: "Engineering geology is the science devoted to the investigation, study and solution of the engineering and environmental problems which may arise as the result of the interaction between geology and the works and activities of man as well as to the development of measures for prevention or remediation of geological hazards."

The role of engineering geology for major engineering projects and infrastructure construction is well represented in the papers included in this volume of the proceeding of the 12th IAEG congress, devoted to major engineering projects. The geologic input is not only confined to the initial stage of such projects but the contribution of engineering geology includes all stages for their completion, reflecting the present standing of engineering geology in geotechnical engineering.

A retrospective review of the development of engineering geology shows that in the early days, up to the 1950s or even the 1960s, what was understood as engineering geology was restricted to assessments, with general and qualitative engineering descriptions. Then this is followed by a second period of development until about the 1980s. The demands of the development of society required more knowledge for the behaviour of the ground. Now meaningful geological models could be provided. However, the quantitative component was weak, and contributions to the design of structures were limited. Although improved, the understanding of geology in the engineering milieu is not satisfactory. A third period starts from the 1980s but mainly from the 1990s. Engineering geology, keeping the core values so far developed, is now evolving towards geoengineering.

Indeed, today engineering geology not only offers services but is also a substantial and an integral component of geotechnical engineering in construction. It is present in all phases of investigation, design and construction:

1. Engineering geology defines the geological conditions, provides the geological model (formations, tectonics and structure), and translates it into engineering terms, providing suitable ground profiles at the appropriate scale. Its role is decisive for detecting the presence of geological hazards, in the selection of the site or the alignment of the engineering structure and for the basic principles of the construction method. It makes no sense to proceed without a sound knowledge of the geological model. Let us be a little dogmatic here: in the absence or misinterpretation of the geological model the construction or operation will almost certainly be associated with problems either small or large, as accidents, delays, cost over-runs or even failures may occur. On the contrary, if this model is known from the very beginning of the design, half the game has already been won ... *if at the very start the geological structure of the site is misinterpreted, then any subsequent ... calculation may be so much labour in vain.* (Glossop 1968, 8th Rankine Lecture). Therefore: start from the forest and then look at the trees.

2. After having understood the behaviour of the ground, engineering geology contributes to the definition of the properties of the geometrical, the selection of suitable design parametres and of the appropriate criteria. This a stage with a close synergy with engineering. An understanding of in situ stresses and groundwater conditions complete this stage.

3. Engineering geology is and should also be present at the design phase to ensure that calculations and simulations do not misinterpret the geological reality. John Knill in his first Hans Cloos lecture, in 2002, expressed strong concern that the *effectiveness of the integration of engineering geology within the geotechnical engineering remains to be improved*. This integration is a field of development in today's engineering geology, and papers in this volume contribute towards such advance.

4. Engineering geology is involved in construction in order to validate the assumptions of the design, to contribute in the application of measures in unforeseen or unforeseeable circumstances and to secure the implementation of the contract.

And, undoubtedly, geological and engineering judgement should never be neglected in this whole process of creating an engineering project. Next to knowledge, experience is needed for this judgment. Mark Twain said *Good judgment comes from experience. But where does experience come from? Experience comes from bad judgment*. However, the correct application of geological and engineering principles means that experience can also come from good judgement.

It is very satisfactory that this volume of proceedings of the 12th congress of IAEG embraces all the above mentioned, and a large variety of cases of engineering works is presented. Dams and tunnels are the majority of these cases but also foundations, offshore structures, roads, railroads, slope design, construction material, tailings, repositories are dealt with. Papers on engineering properties and geotechnical classifications, site investigation issues and influence of groundwater are present together with contributions on the behaviour of soft rocks and weak rock masses. Active tectonics also attract special attention.

The volume is expected to constitute a valuable and lasting source of reference in the field of engineering geology, in particular, and in geotechnical engineering, in general.

Contents

Part X   Geological Model in Major Engineering Projects

Part XVII   Sustainable Water Management in Tunnels

**Consiglio Nazionale delle Ricerche
Istituto di Ricerca per la
Protezione Idrogeologica**

The Istituto di Ricerca per la Protezione Idrogeologica (IRPI), of the Italian Consiglio Nazionale delle Ricerche (CNR), designs and executes research, technical and development activities in the vast and variegated field of natural hazards, vulnerability assessment and geo-risk mitigation. We study all geo-hydrological hazards, including floods, landslides, erosion processes, subsidence, droughts, and hazards in coastal and mountain areas. We investigate the availability and quality of water, the exploitation of geo-resources, and the disposal of wastes. We research the expected impact of climatic and environmental changes on geo-hazards and geo-resources, and we contribute to the design of sustainable adaptation strategies. Our outreach activities contribute to educate and inform on geo-hazards and their consequences in Italy.

We conduct our research and technical activities at various geographical and temporal scales, and in different physiographic and climatic regions, in Italy, in Europe, and in the World. Our scientific objective is the production of new knowledge about potentially dangerous natural phenomena, and their interactions with the natural and the human environment. We develop products, services, technologies and tools for the advanced, timely and accurate detection and monitoring of geo-hazards, for the assessment of geo-risks, and for the design and the implementation of sustainable strategies for risk reduction and adaptation. We are 100 dedicated scientists, technicians and administrative staff operating in five centres located in Perugia (headquarter), Bari, Cosenza, Padova and Torino. Our network of labs and expertizes is a recognized Centre of Competence on geo-hydrological hazards and risks for the Italian Civil Protection Department, an Office of the Prime Minister.

Problems in Buildings and Public Works Derived from Soils with Unesteable Structure and Soils with Large Volume Instability

Carlos Delgado Alonso-Martirena

1.1 Introduction

It is customary to analyze the behavior of foundations under the implicit assumption that the ground will suffer deformations and settle as a result of the increasing load transmitted by a construction in progress. Usually an estimation has to be made of the final movements to be expected in the construction (whether a building or a public work) in the short or in the long term.

Unfortunately, certain soils may exhibit large volume changes upon variations in moisture content, even while under constant external load. Since this affects completed structures under service (closed structures) and the resulting foundation movements progress rapidly, noticeable cracking occurs. If no remedial action is adopted, the pathology is prone to increase because the changes in moisture content occur seasonally.

The initial purpose of this communication is to identify two main groups of soils largely affected by moisture contents:

- Soils with metastable structure, more usually known as "collapsible" or "collapsing" soils.
- Soils with large volume instability. They are usually referred to as "swelling soils". However, this terminology may lead to error. In fact, swelling may be reduced to unharmful values by adequate contact pressures in foundations, that is to say, by adequately dimensioning the foundations. In arid regions, though during large periods of drought, the moisture content of high plasticity clays decrease to depths, below the round surface, that may reach 6 m and even more. The resulting "shrinkage" settlements are large and of rapid progress, as pointed out for collapsing soils, although their source is different. Collapse occurs though moisture increase, shrinkage is produced by moisture decrease. Engineering geology

must be well aware of those problems with moisture contact changes, and has to evaluate them properly through laboratory testing in order to come to adequate recommendations in the project geotechnical report, as it will be synthetically referred to subsequently. A final purpose of the communication will be to draw attention to the possibilities offered by the technique of reinforced grouting/through hydraulic fracturing of ground, using stable mixes of cement-bentonite) to stabilize those problematic soils, under foundations defectively designed and constructed.

1.2 Laboratory Identification of "Collapsing" and "Swelling" Soils

Figure 1.1, reproduced from Peck et al. (1974), shows the behaviors, in a double oedometer (or paired confined compression) test, characterizing those two types of peculiar soils.

As it is usual, the oedometric curves are represented in a semi logarithmic plot, where pressures are figured in log scale, as abscissae, and void ratios in arithmetic scale, as ordinates.

Curve **a** corresponds to a test started at the natural water content, and to which no water is allowed to access.

Curves **b** and **c** correspond to tests on samples to which water is added from the start, as it is normal practice in oedometer tests.

If curves **a** and **b** represent the behavior of the same soil (curve **b** lies entirely below curve **a**) the soil is said to have collapsed. Under field conditions, at effective presume p, the soil would exhibit void ratio e_0 being unsaturated (positive suction). The increase of water content until saturation would cause de void ratio, at pressure p1, to decrease to e1, with corresponding unit settlement of —— occurring suddenly, under the form of a collapse.

On the other hand, if the soil shows a behavior represented by curves **a** and **c** lying entirely above curve **a**) the soil is said to swell. The addition of water, under pressure p_1

C. Delgado Alonso-Martirena (✉)
Civil Engineering School, Technical University of Madrid
(U.P.M.), Alfonso XII 3 y 5, 28014, Madrid, Spain
e-mail: carlos.delgado@upm.es
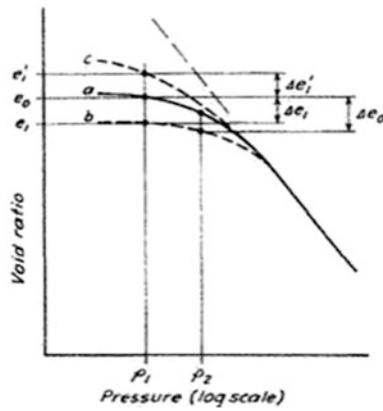
Fig. 1.1 Diagrams obtained in double oedometer tests

Fig. 1.2 Capillary produced contact pressure

would increase void ratio e_0 to e'_1, corresponding to a unit swelling of ——.

1.3 Essential Features and Locations of Collapsing Soils

Dudley (1970) published a valuable "Review of Collapsing Soils", which includes an extensive bibliography.

For collapse to occur the soil must have a structure that leads itself to this phenomenon. All cases reported by Dudley have a honeycomb structure of bulky shaped grains, with the grains held in place by some material or force.

In many cases the temporary strength is due to capillary tension. As the soil dries below the shrinkage limit, the water withdraws into narrow spaces close to the junction of the soil grains as shown in Fig. 1.2. In the expression for effective stress $\sigma = \sigma - u$, the excess pore water pressure **u** become negative. The actual effective stress becomes longer than the total stress applied by the load. For unsaturated silts, like the constituting loess materials (particles ranging in diameter from 0.02 to 0.002 mm), the effective stresses may be in the range of 0.35–3.5 kg/cm^2. For fine sands (beach sands) the maximum effective intergranular stress due to moisture films is in the order of 0.14 kg/cm^2.

The collapsing material may consist of sand with some silt binder. In this case the capillary forces apply around the silt to silt contacts and the silt to sand contacts as shown in Fig. 1.3.

When the bulky grains are bound by clay, the history of the soil formation is important, since a variety of arrangements are possible. The clay may be either formed in place or transported.

Clays may form in place by water acting on feldspars. One of the arrangements that would be produced is shown in Fig. 1.4. The figure shows a close-packed parallel arrangement of clay particles. Under desiccated conditions the
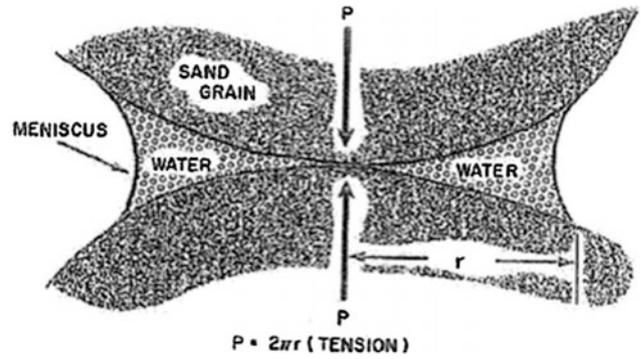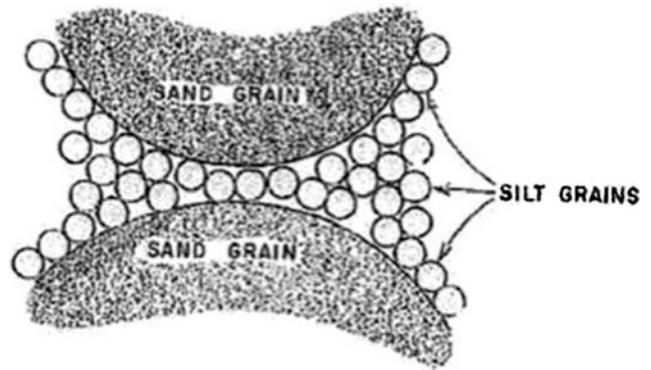
Fig. 1.3 Schematic arrangement of silt grains between two sand grains

strength may be considerable. The addition of water would cause the clay particles to separate to some extent, thereby producing a loss of strength.

Fig. 1.4 Schematic arrangement of sand grains, with aggregated clay particles

In areas of high rainfall much of the clay formed in place could be leached out, but when the rainfall is small, if the clay particles were dispersed in the pore fluid, the situation shown in Fig. 1.5 could develop. The resulting buttresses support and hold together the bulky grains large capillary tensions can also be present. When water is added the capillary tensions would be relieved and the ion concentration in the fluid would be reduced. This would increase the repulsive force existing between particles, as shown in Fig. 1.6.

However Warkentin and Yong (1900) found that, al constant void ratios, both kaolinite and montmorillonite had higher strength at lesser salt concentrations. It may occur that the void ratios and the temperature change when the salt concentration changes in situ the resistance to consolidation caused by the presence of the clay buttresses is a function of salt concentration, void ratio within the clay structure, and probably temperature. Many clays, a a matter of fact, expand as they cool in the vicinity of room temperature.

In the case of mudflows where the initial water content is not much more than required to attain a fluid condition, the ion concentration is probably high, and even the constant shearing action while in movement cannot maintain a dispersed arrangement. The clay particles would tend to cluster around the bulky grains in a flocculated structure. As drying progresses, some of the clay may be caught between the bulky grains, and other portions of the clay could be drawn into the narrow wedges adjacent to the bulky grains, as shown in Fig. 1.7.

Due to the variety of soil arrangement prone to collapse shown in Figs. 1.2, 1.3, 1.4, 1.5 and 1.7, those soils are present in extensive areas of the world. They have been associated with regions of moisture deficiency in any continent. Soils exhibiting this behavior must have an open structure, like those of aeolian origin, but as it has been shown, their origin may be also alluvial or even residual. Brink and Kantey (1961) described residual decomposed

Fig. 1.6 Repulsive and attractive energy al high and low ion concentrations
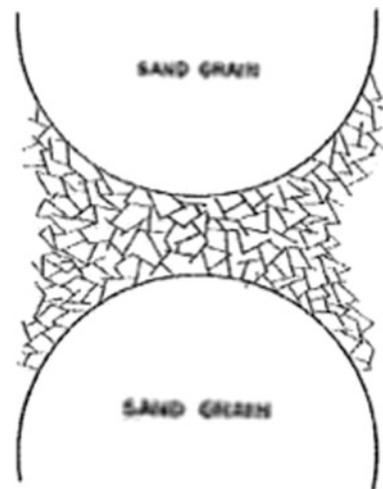
Fig. 1.7 Mud flow type of flocculated clay between two sand grains

granites near Cape Town, in Swaziland, in Northern Rhodesia and in Northern Transvaal that were found to collapse.

1.4 Essential Features and Locations of Swelling Soils

The potential capacity of a clayey soil to swell, as a result of water content increase, under moderate and constant unit load, is usually related to its plasticity index.

Fig. 1.5 Schematic arrangement of two sand grains with ring aggregation of clay

Peck et al. (1974) propose the following table:

Swelling potential	Plasticity index
Low	0–15
Medium	10–35
High	20–55
Very high	>35

However, the possibility, for a soil with a high swelling potential, to develop effectively this potential depends upon several conditions:

- The main condition is the difference existing between the soil moisture at the beginning of the construction, and the equilibrium moisture content of the soil, after the construction has been completed. Should this difference be high, that is to say, if the water content of the soil increases noticeably after construction, an important expansion of the unloaded or lightly loaded soil will occur. On the other hand, if the expansion is completely restricted, high and destructive swelling pressures would develop.

  Conversely, if the equilibrium water content were less than the initial water content, the soil would shrink instead of expanding.

- A second condition is the degree of compaction of the soil. The presence of a soil is placed at a high degree of compaction, or on a natural soil highly over consolidated, favor the expansion of a potentially high swelling soil if its water content is increased.

- A third condition is the unit load transmitted by the foundation once the construction has been completed. The higher the unit load, the lesser the swelling.

According to Peck et al. (1974) useful quantitative information may be obtained from the variation of swelling pressure obtained in an oedometer test in which example, with the water content corresponding to the start of the construction process, is subjected to a selected vertical pressure, and previously to let free access to water, is allowed to reach the equilibrium under that vertical pressure.

The selected vertical pressure is taking to be approximately twice the effective stress acting on the sample in the ground, before extraction. If a high swelling potential is expected, the selected vertical pressure may be taken even higher. Once the oedometer has been saturated the swelling is measured until equilibrium is reached. The vertical pressure is then reduced to half its initial value and, again, the equilibrium deformation is obtained. A new reduction to half is introduced in the vertical pressure, and the equilibrium deformation is registered. The process ends for a vertical pressure reduced to zero.

The results obtained are represented by a graph similar to that shown in Fig. 1.8.
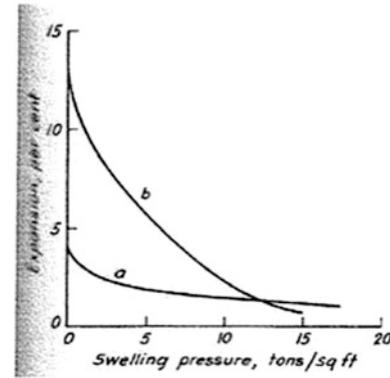
Fig. 1.8 Typical results obtained in swelling tests

- Curve **a** shows the behavior of a soil exhibiting a high swelling pressure for a reduced volume increase, but developing only a reduced swelling pressure after a moderate expansion is allowed. This type of behavior is typical of the swelling tertiary clays of the southern of Madrid (Spain).

- Curve **b** shows a more dangerous swelling behavior. Although the swelling pressure is moderate after a moderate expansion is allowed to occur, after the pressure is reduced to zero, the swelling is high.

A swelling test of this type just described is useful not only to determine the pressure necessary to avoid swelling of soil at certain depth, or to limit this swelling to an allowable value, but also to estimate the expected movements at the bottom of a basement excavation.

It is necessary to remark that, due to the disturbance of soil samples in the field and in laboratory activities, the test results are to be considered with care.

Swelling pathologies develop especially in light constructions with shallow foundations, as shown in Fig. 1.9 taken from Parcher and Means (1968).

Peck et al. (1974), in Fig. 1.10 show schematically the pathologic trends associated with a pier-supported structure in which grade beams would be in contact with a highly swelling soil.

Fig. 1.9 Pathology of brick wall with shallow foundation in swelling clay
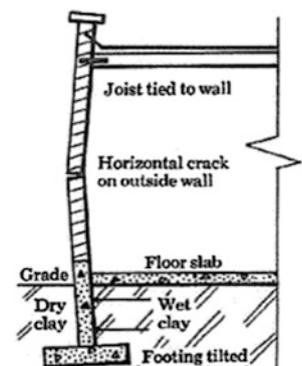
Fig. 1.10 Pathology of grade beam resting on swelling soil
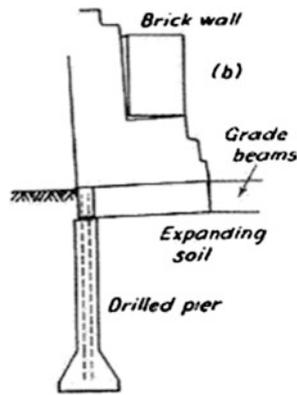
When the zone of seasonal variations in moisture extends to a depth greater than that below which drilled piers have been designed, attempts to form the bells of such piers may be unsuccessful because the clay in the zone of moisture changes likely to be highly slicken sided and successive caving of the blocks between slickensides might occur.

Even if the grade beams and floors of a structure, on piers of adequate depth, are not subjected to uplift forces (a clearance has been designed between the grade beams and the soil surface), the swelling soil tends to grip the shafts of the piers and lift them.

On the other hand, if the construction is located on a loping ground, it has to be taken into account that drilled piers have only a reduced resistance against lateral displacement and should not be expected to restrain down brill movements associated with creep.

Swelling soils are widespread all over the world. In fact they are montmorillonitic clays that might develop from the decomposition of volcanic glasses.

However although the expansion of those soils may be remediated in almost any case of construction (building or public work) by proper design measures (adequate contact pressure and depth of foundations, or soil substitution in the zone of more critical moisture changes in subsoil), in arid climates successive and important drought periods may cause the reduction of soil moisture and consequent shrinkage of soil down to important depths (6–7 in Sevilla, Spain).
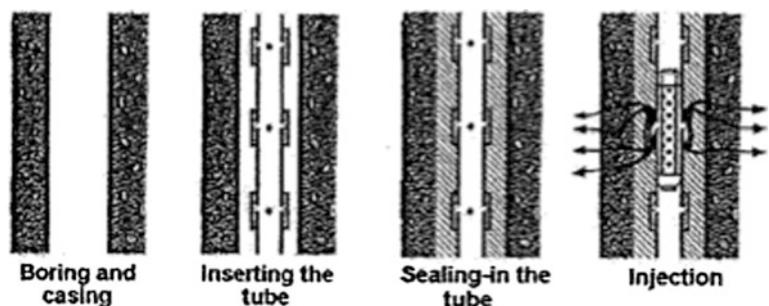
An important parameter to ascertain the problem of shrinkage of soils is the shrinkage limit, very low (10–11 %) in montmorillonitic clays. If the equilibrium moisture content below a construction is considerably higher than the final moisture content after "a chain of brought periods" considerable settlements may affect the construction independently of the load it transmits to the ground.

On the other hand, the settlement distribution may not be uniform since the water content reduction may be different at the outside limits of the foundation than under the central part of the building plan extension.

As it will be established in the next sections, a very effective means of solving the problem in all types of existing constructions (new constructions with structures and foundations made of reinforced concrete or old palaces and monuments of historic or architectonic high value) is the application of the technique of soil improvement by reinforced grouting.

1.5 Grouting by Hydraulic Fracture Through Sleeve Pipes

Although grouting has been, for a long time, considered as a procedure of ground impregnation (filling the voids of the soil with grout mixes, without disturbing the preexisting particle arrangement), very soon after the technique of sleeve pipes (Fig. 1.11) was introduced, the interest of hydraulically fracturing the ground was recognized in applications for alluvial soils sealing off. The initial permeability of the ground was lowered by creating inclusions of cement-bentonite that, after setting, would cause water to divert from straight paths, with a rapid increase of head loss.

If this hydraulic fracturing is systematically introduced in the ground, through successive injection steps (Fig. 1.12), the inclusions of hardened mix produced in the ground by neighboring sleeve-pipes may interfere with one another o, creating a "skeleton" within the ground mass to be improved (Fig. 1.13).

This will promote the improvement of the ground mechanical characteristics, namely increasing strength and stiffness. Figure 1.14, initially taken from Morgenstern and Vaughan (1963), would show maximum injection pressure

Fig. 1.11 Sleeve pipes grouting

Boring and casing Inserting the tube Sealing-in the tube Injection
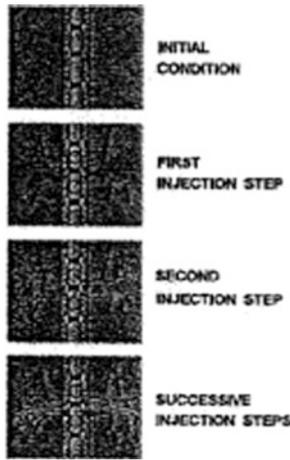
Fig. 1.12 Hydraulic fracture injection (successive steps)
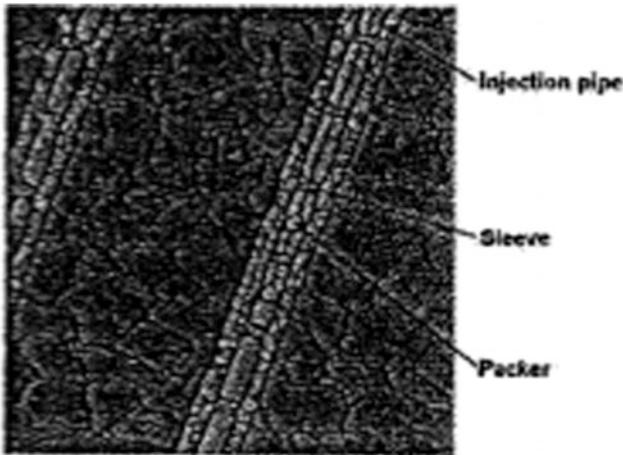
Fig. 1.13 Skeleton of hardened inclusions

$$\frac{\sigma_1' + \sigma_3'}{2} \operatorname{sen} \phi' = \frac{\sigma_1' - \sigma_3'}{2} - c \cos \phi'$$

$$P = P_e + \gamma_\omega h_\omega$$

$$\frac{P}{\gamma h} = 1 + \frac{c'}{\gamma h} \cot \phi'$$

Fig. 1.14 Assumed mechanism for hydraulic fracture

1.6 Use of Hydraulic Fracture Grouting to Solve Foundation Problems in Collapsing and Swelling Soils

1.6.1 Negative Effects of Collapse, Swelling and Shrinking of Soils on Shallow and Deep Foundations

P, for a saturated ground, to be reached without shear fracture, c and $\varnothing'$ representing the effective shear strength parameters of the ground. However, the ground, under hydraulic pressure, cracks (rupture in tension) before reaching plastic shear, as Vaughan himself established later for cores in the earth dams.

Santos et al. (2000) and Santos and Cuellar (2000) established that in case where P would represent the final "shut-in pressure" which would be sustained in the vicinity of an open "manchette" without any further mix take variation, the final relationship shown in Fig. 1.14 would link P with the c' and $\varnothing$ parameters of the treated ground. *Therefore, a ground which could not be permeated by cement— bentonite mix, could be improved, to a predesired condition, by hydraulic fracture grouting with prefixed shut-in-pressures.*

In relation to foundations on collapsible soils, Peck et al. (1974) established that if the possibility of wetting could not be ruled out and if the ensuing settlements were excessive, the foundation had to be established below the soil of potential collapse. Although they mentioned the possibility of inducing the collapse before building the structure, the real fact is that this procedure has been used successfully only to treat the foundations of earth dams or dikes that load completely the soil during construction and can usually tolerate settlements of more than 1 m. In connection with foundations for buildings or bridges it has not been successful.

In the case of piles or piers established in the collapsible soils, they need to be embedded adequate lengths below the bottom of the unstable foundation, and it has to be additionally taken into account that the subsequent wetting and collapse of the unstable soil are likely to induce negative skin friction on the foundation units, not to speak of the possibility of parasitic flexures on the shafts to occur, if the bottom of the collapsible foundation is sloping.

As it has been established in foregoing paragraphs, the term swelling soils imply not only the tendency to increase

in volume when water is available, but also to decrease in volume, or shrink, if water is removed.

Although adequately determined permanent contact pressures on swelling soils and the design of the floor structures with proper clearance from the surface of the expansive soil may cope with volume increase, only the location of the foundation below the critical depth of soil seasonal shrinkage could face the potential volume decrease. In the arid regions, in the presence of highly plastic clays or marls (as it occurs, for instance in southern Spain) this depth may be in excess of 6–7 m.

Deep foundations, in those highly swelling soils, are subject to parasitic tensions and flexures, and their construction is complicated because those materials, of high resistance for water contents below the plastic limit, may dramatically lose strength by water addition, because their extremely high suction potential (values of nearly 100 kg/cm^2 at 98 % degree of saturation have been measured at the Centro de Estudios y Experimentacion de Obras Publicas, CEDEX, in marls of southeastern Spain with 250 kg/cm^2 unconfined compressive strength).

1.6.2 Stabilization of Collapsing and Swelling Soils and Soft Rocks Means of Hydraulic Fracture Grouting and Bolting Through Sleeve Pipes

Santos et al. (2000) presented, in the book "Geotecnia en el año 2000" (Geothechnics in the year 2000), an in-depth analysis of the basic principles, execution and control of the hydraulic fracture grouting through a sleeve pipes, along with a number of outstanding applications of this technique. Their chapter in the book was entitled "Procedure for a predetermined ground improvement compatible with milimetric movements of the surroundings".

In fact, three main aspects of the technique of fracture grouting need to be pointed out:

- It is possible to pre-establish the volume of ground to be improved the cometrical "solid" to be treated) along with its final mechanical properties, insuring, during the process, only mill metric movements (2–3 mm) of structures above or in the vicinity of the treated ground.
- Both the control of movements of the structures and the resulting mechanical conditions of the improved ground can readily and quickly be controlled.
  As matter of fact, as it was verified by Santos and Cuellar (2000), testing of the ground by cross-hole geophysical technique, or by pressure meter tests show perfectly correspondent results. The comparison between the mechanical conditions of argillaceous marl, before and after the grouting could be achieved by the authors through load testing of two shallow footings (2 × 2 m and

1.50 m deep) on treated and untreated ground. The combined effects of grouting and bolting through sleeve-pipes resulted in multiplying by a factor of 10 the initial, already high, modulus of deformation of the marl.

- As long as the sleeve-pipes are properly distributed within the geometrical volume to be treated, their orientation may vary, that is to say, it is possible to achieve the drilling and grouting from any working area around the zone to be improved. This allows, for instance, in combination with the much reduced movements generated during the treatment, to reinforce the foundation of a construction without disturbing its normal operation.
  Successful stabilization of collapsing soils has been achieved below and behind existing constructions in the eastern zone of Spain (collapsible silts in the provinces of Alicante and Castellon). A special case of treating very loose salty sands was affected (and controlled by CEDEX) behind so-called "muro de cipres" (cypress wall) at the Generalife and below several foundations of the Alhambra de Granada (Spain).

In the southern Spain, light constructions (some of them family houses and schools) have been protected, from the pathologies created by high plasticity clayey subsoil in arid climate, by means of grouting of the soil down to a safe depth (around 7 m.) without disturbing the normal life in those constructions.

The southern wing of the Parador in Carmona (Sevilla, Spain) was about to be torn down because of its continuing movements, even after having been under primed with micro piles, and anchored, because having been built in a cliff supported by both collapsible formation (Albero) and swelling marls (Mayos del Guadalquivir) underneath. In 2005 the problems was completely solved by grouting through sleeve- pipes of both formation, and the Parador remains in perfect housing condition.

Delgado (2011) has shown that this technique is implacable to allow buildings construction on slopes in swelling soils, subject to seasonal creep. This is due to the fact that the treated ground may be dimensioned as high inertia counterforts that allow to stabilize the slope without any need for anchors or ties.

It has to be mentioned that the so-called MPSP technique (multiple packers sleeve pipes) allows the use of grouting through sleeve pipes even in fractured or fissured rock materials.

1.7 Conclusions

Many books in Soil Mechanics, an even a number of standards in Geotechnics, fail to point out that the foundations may suffer deformations and settle after the construction

operations have ended of the subsoil, below the contact level of those foundations, suffer changes in water content.

This is especially important in soils with metastable structure, that may collapse under soaking, and are therefore referred to as "collapsible soils", and in soils prone to severe changes of volume with changes in water content, termed "swelling soils" although their shrinkage when water content diminishes is even more serious.

The paper presents a summary of conditions leading to collapse or swelling/shrinkage, and shows that those problematic foundations are present in many countries of the world, although generally associated to arid climates.

Finally, reference is made to the technique of hydraulic fracture grouting that may solve the problems derived from those soils under existing constructions, and even in the present of slopes or cliffs, because the geometrical volume, to be achieved, and their final mechanical conditions may be designed in advance, executed with only mill metric movements of the ground below existing foundations, and the working surfaces may be selected with large flexibility. It is possible to check the differences between the ground conditions, before and after the treatment by the geophysical "cross-hole" technique, very easy to effect.

References

Brink ABA, Kantey BA (1961) Collapsible grain structure in residual granite soils in southern Africa. In: Proceedings fifth international conference on soil mechanics and foundation engineering, pp 611–614

Delgado C (2011)

Dudley JH (1970) Review of collapsing soils. J Soil Mech Found Div. In: Proceedings of American Society of Civil Engineers, SM3, May, pp 925–947

Parcher JV, Means RE (1968) Soil mechanics and foundations. Charles E. Merrill Publishing Co, Columbus

Peck RB, Hanson WE, Thornburn TH (1974) Foundation engineering, 2nd edn. Wiley, New York

Santos A, Martinez JM, Garcia JL, Garrido C (2000) Sistema de mejora prefijada del terreno compatible con movimientos milimetricos del entorno, Libro homenaje a Jose Antonio Jimenez Salas, Geotecnia en el ano 2000, Sociedad Espanola de Mecanica del Suelo y CEDEX, Madrid, pp 217–223

Santos A, Cuellar V (2000) Mechanical improvement of argillaceous marl through cement—based reinforced grouting. In: Rathmayer EH (ed) Proceedings of the 4th international conference on grouting, soil improvement, geosystems including reinforcement, Finnish Geotechnical Society, Building Information Ltd, Helsinki

Warkentin BP, Yong RN (1900) Shear strength of montmorillonite and kaolinite related to interparticle forces. Clay sand clay minerals, (NAS-NCR), Macmillan Co., London, pp. 210–218 (vol 11 of Earth Science, C.R)

Translating Geotechnical Risk in Financial Terms

2

Alessandro Palmieri

Abstract

Practitioners know that geotechnical uncertainty never ends until a tunnel is completed. In some cases, uncertainty extends into operation. The present note summarizes relevant project financing elements such as viability, risk allocation, and bankability. Main financial instruments for different project structures are outlined, highlighting their likely ranges of application. Two key instruments for managing project risks, the Geotechnical Baseline Report, and the Project Risk Register, are presented and their joint use illustrated. The importance of carrying over uncertainty along the entire project cycle (planning, construction, and operation) is elaborated by using a concept borrowed from the hydropower sector.

2.1 Project Sustainability

Achieving project sustainability is a pre-requisite for financing, together with project's technical and economical viability. A recurrent message is that "the project cannot be implemented because of lack of financing". While that is true in several cases, it is equally true that, in many instances, financing could be available with good project preparation and a robust financial architecture.

So what does it take to prepare a "good project"? Over the years, the threshold of environmental and social acceptability for large projects has significantly raised, and it would be very unwise to get financially involved in any operation where these aspects have not been fully addressed.

A group of international financing institutions have set out minimum requirements for a project to be financed. These principles, referred to as the "Equator Principles," were first designed in 2003 in conjunction with the International Finance Corporation (IFC—the private sector arm of the World Bank); the most recent version is dated June 2013 (for details see www.equator-principles.com).

2.2 Financial Viability

Government decision-making is based on the economic value of a project to a nation, but the financing of that project depends on its financial viability. Financial viability is the measure of the commercial strength of a project, generally assessed over a period of 15–20 years. It determines whether the project is robust enough to repay loans at commercial rates of interest even under a downside scenario, and whether it is likely to provide a sufficiently high return on equity to attract private investors.

Water infrastructure projects often fall in the gap between economic and financial viability. A project can be economically attractive and represent the preferred option when seen from a long-term national perspective, but when considered as a commercial investment it may be unable to generate adequate financial returns. Xiaolangdi Multipurpose Project represents a relevant example (Table 2.1).

The content of this paper reflects the experience of the author and, as such, does not necessarily represent policies or practices of the Salini-Impregilo Group.

A. Palmieri (✉)
Salini-Impregilo SpA, Milan, Italy

Table 2.1 Xiaolangdi multipurpose project on the yellow river (China)

Total costs US$3.5 billion, US$1 billion for resettlement. Completed 1 year ahead of schedule; cst savings 300 MUS$
Multipurpose reservoir: flood control, sedimentation management, maintaining adequate in stream flows, water supply, irrigation, hydropower replacing old, coal fuelled power plants
Economic rate of return unchanged from project appraisal (17.5–17.9 %,) but financial rate of return unsatisfactory because only energy sales accounted for. All other benefits accounted as public goods and not reflected in the financial analysis

Closing the gap between economic and financial viability requires consideration of project financing partnership.

2.3 Risk

A risk is anything that can have a negative effect on the project outcome. All risks ultimately translate into financial terms, and an investor will tend to judge her risk exposure by the amount she could lose compared with the amount she expects to gain at any particular stage in the lifecycle of the project. There are three main types of risks; mitigation measures are different for each of them.

Project specific risks, as related to contracting risks (delay and cost overruns), are very difficult to insure. Physical catastrophes like collapses and fires may, in some cases, be insurable. Insurance will generally only cover single events rather than systemic problems. Even then it may not cover the full losses; for example it might cover the cost of reinstatement but not necessarily the consequential losses resulting from the delay—and the latter can often be the larger element (Table 2.2).

In all cases, risk has a cost and risk cost depends on how risk is allocated among stakeholders. Combination of financial viability and risk assessment results in project

bankability, i.e. how attractive the project is for financial institutions.
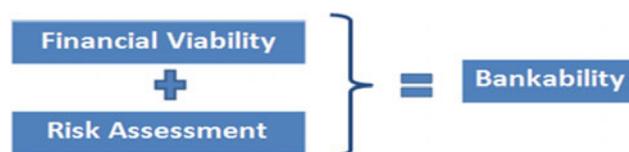
The most attractive projects rate AAA (triple A). BBB + is generally considered the minimum level for a project to generate investment interest. Bankability determines the interest rate and the tenure (duration) of the loan.

2.4 Main Financial Instruments and Project Structure

Several financial instruments, from private equity to concessionary finance, have been used for financing infrastructure projects; their choice is strongly dependent upon project structure and ownership. There is a wide spectrum of financing instruments, ranging from publicly sourced grants and soft loans through to financing on strictly commercial terms. With some generalisation it is possible to group these

Table 2.2 Project specific risks

Type of risk	Examples	Mitigation
Political (country)	Risk of nationalization	Guarantees
	Changes in law affecting status or financial position of project company	
Commercial	Market	Partially insurable
	Risk to revenue such as change in regulation or difficulties in enforcing payment	
	Defaulting off-taker	
Project	Site-specific risks such as cost and time overruns during construction	Usually not insurable
	Difficulties in obtaining necessary environmental permits and clearances	
	Uncertainty of addressing social issues which may arise	
	Hydrological risk	
	Transmission interconnection	

Table 2.3 Main financing instruments

Financing instrument	Source
Concessionary finance	Grants or soft loans (low interest or long tenure), usually from bilateral or multilateral aid agencies
Public equity	Public investment with the support of the government, often indirectly funded from bilateral and multilateral development banks (MDB) sources
Public debt	Project-specific loans from the government or from bilateral and multilateral development banks
Export credit agencies and guarantees	Finance direct from the export credit agencies, or from private commercial banks using guarantees from public MDBs
Private "commercial" debt	Loans from private banks, and from the commercial arms of the public MDBs. Also occasionally bond issues
Private equity	Direct investments made by private sponsors and other private investors, and by the public MDBs

disparate sources of finance into six broad categories of instruments (Table 2.3).

In general, the wider the gap between economic and financial viability in a project, the more that project will require concessionary and/or public finance. A financially strong project can be fully sustained by private financing.

The financial architecture of a project will depend on its viability and on the extent to which project risks can be mitigated. Project will not be attractive to the private sector if risks are not likely to be substantially mitigated. In that case, if economic value is large and the project is a national priority, financing will have to be public. A project can still attract private sector participation if one or more financially viable components can be "sliced" from the project, e.g. public financing for the dam and private for the powerhouse. The following diagram (Head 2005) exemplifies the decision-making process for assessing the appropriate project structure.

2.5 Geotechnical Risk and Project Risk Management

Geotechnical risks, in the form of unexpected geological conditions, are a serious factor in cost and schedule control on all major civil engineering projects. The amounts of money, involved in claims arising from geotechnical problems, are enormous and are taken very seriously by financing agencies. In spite of numerous attempts to deal with these situations by the incorporation of various clauses in contract documents, the problems persist. The best course of action is to define the geological conditions as early and as accurately as possible so that surprises are minimised. Unfortunately, that is not possible, or not considered possible, in most of the cases. At the same time, sharing risks associated with unpredictable events can substantially improve the success of a contract both in terms of cost and schedule control.
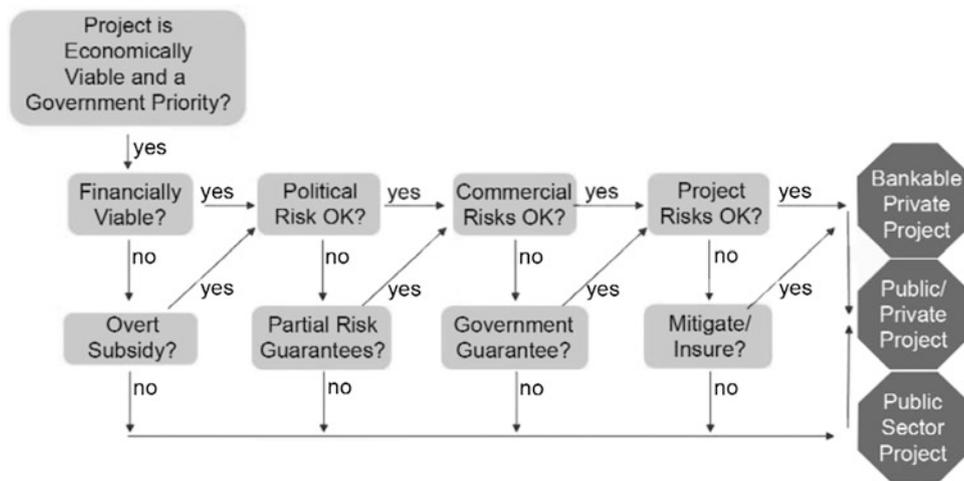
Table 2.4 Rock mass classification system

Rock class	Rock mass rating (RMR)	Percentage of excavation volume
I and II	61–80	80
III	41–60	10
IV	21–40	10

Table 2.5 Baseline statements regarding groundwater-associated trouble areas

Geotechnical feature	Baseline conditions
Peak groundwater inflows	Peak of 500 l/s with sustained inflows up to 125 l/s over a 100 m length of tunnel
Steady state groundwater inflows	100 l/s over 1,000 m
Hot water springs	At three locations during underground excavation with temperatures up to 70 °C and flow rates of 20 l/s
Groundwater pressure	About 250 m head of water at localized areas such as *creek X* and *creek Y* where there are perennial streams

Where the overall financial and contractual arrangements permit, it may be possible for the parties to agree on some form of risk sharing package; two key tools for that purpose are:

- Geotechnical Baseline Report (GBR), and
- Project Risk Register (PRR)

The GBR (ASCE 2007) aims to establish a contractual understanding of the site conditions, referred to as the geotechnical/geological baseline. Risks associated with conditions consistent with or less adverse than the baseline are allocated to the contractor and the owner accepts conditions significantly more adverse than the baseline. The more clearly defined the anticipated conditions, the more easily the encountered conditions can be evaluated. Therefore, the baseline statements shall be described using quantitative terms that can be measured and verified during construction. How the baseline has been set determines risk allocation and has a great influence on risk acceptance, bid prices, quantity of change orders and the final cost of the project.

Typical baseline conditions are those pertaining to distribution of rock types along tunnel route; they are generally expressed in terms of a rock mass classification system which has to be clearly defined in the tender documents, e.g. (Table 2.4).

The following are examples of baseline statements regarding groundwater-associated trouble areas, which are expected during construction of a tunnel (Table 2.5).

The Geotechnical Baseline Report (GBR) is a key element for the preparation of the Project Risk Register (PRR). The latter covers also risk elements such as design, technical/technological, labor, health and safety, etc. Several risk scenarios are identified in each category. For each scenario, the following elements are assessed:

- Frequency or probability of occurrence (as appropriate),
- Preventive measures,
- Potential consequences, before remedial measures,
- Remedial measures along with associated resources and costs,
- Schedule and cost consequences after remedial measures.
 Jointly, GBR and PRR allow to:
- inform decision making on the most appropriate project technology and procurement strategy,
- inform contract documents preparation, and allocate contingency funds,
- prepare Health and Safety Management Plans to be implemented during construction,
- manage design variations and associated claims during construction.

Not all project developers/owners have the same attitude towards such a transparent approach. Many still believe in the possibility of loading all the risks on the contractor, possibly with a turn-key, fixed cost, contractual arrangement. Experience has repeatedly proven that such expectation is, at best, very optimistic and, in reality, almost impossible to achieve. Unreasonable risk allocation strategies will keep good bidders away and attract entities who are ready to take advantage of the situations with pre-defined claims at the bid preparation stage. A review (The World Bank 1996) of water infrastructure projects, featuring important underground works, revealed significant schedule and cost overruns. It is the author belief that a large part of those overruns can be attributed to the contractual practices in use at the time of those projects (late 70' and 80'); recent practices, increasingly incorporating GBR and PRR elements, have proved to be conducive to better results.
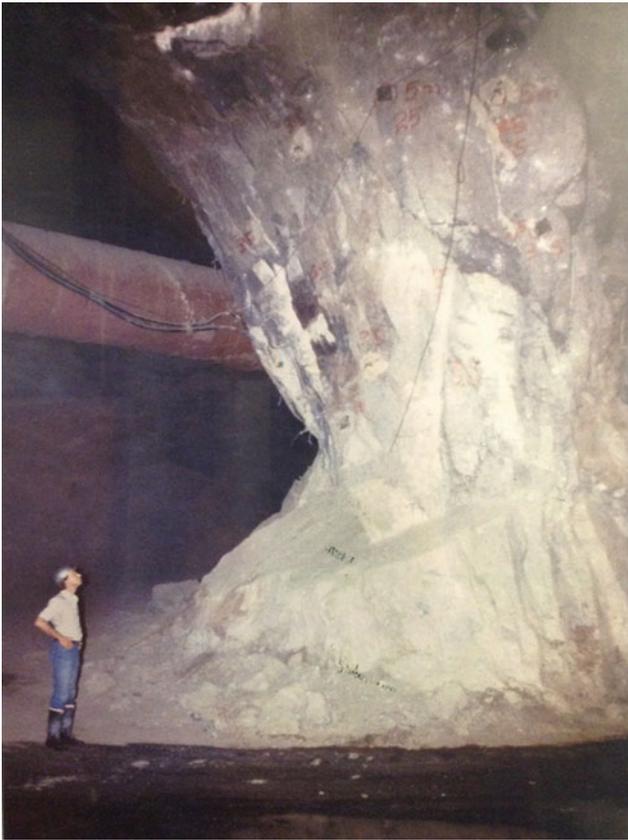
2.6 Uncertainty Management

Large civil engineering projects like dams, hydropower schemes, tunnels, underground caverns, etc. inevitably involve significant uncertainties that translate into financial and other types of risks. As much as risks cannot be totally removed, so uncertainties cannot be cancelled regardless of the amount of studies, investigations, contractual arrangements, financial engineering, etc.

The best way to manage uncertainties is to the carry them over along the planning process by periodically re-assessing the relative implications on safety, engineering, and financial aspects. At the pre-feasibility level of a project, uncertainties should be used to carefully plan studies and investigations for feasibility purposes.

Once feasibility is confirmed, residual uncertainties, including those that, meanwhile, have added to the list, should guide definition of contingency measures, including financial ones, for tender design purposes. Construction contracts, whatever their form (traditional, turn key, concessions, etc.), should incorporate measures to address residual uncertainties. The remaining ones, after construction and commissioning, should guide the preparation of operation and maintenance plans.

In a paper on hydro plant rehabilitation, Gummer and Obermoser (2008), refer to the concept of "unknown unknowns" (uK-uKs), which the US politician Donald Rumsfeld used in one summary of progress in Iraq (2002). They argue that the "uK-uKs" concept makes a lot of sense in apportioning contractual risk in hydro plant rehabilitation works. The concept is equally suitable in tunneling projects. The following plate exemplifies the "uK-uKs" concept in a tunneling context (Table 2.6).

"Known knowns" should be dealt with by a good design based on an adequate site investigation (Hoek and Palmieri 1998).

"Known unknowns" should be mitigated by appropriate contractual architecture; to that end it is advantageous to build sufficient flexibility into the contract so that design can be adapted during construction according to rock mass properties actually encountered. Such refinements can be based on back-analysis of measurements of excavation deformation and observations of excavation behavior. The following plate outlines an example of such approach, referring to tunneling in squeezing rock.

Convergence-based rock mass reinforcement

- GBR will specify expected baseline deformations δ values for different rock mass conditions.
- If δ values, as measured 2D away from the face, exceed the baseline value, additional support, pre-established in GBR, is installed.

Table 2.6 "uK-uKs" concept in a tunneling context

"uK-uKs"	Tunneling context	What to do
"Known knowns"	General geology, overburden, expected rock types, groundwater, etc	The problems lie in the detail, i.e. adequate site investigations at the planning stage
"Known unknowns"	Actual distribution of rock types along tunnel alignment, extent of fault areas, sudden water inflows, etc	Make adequate resources available, and provide for contractual flexibility
"Unknown unknowns"	Un-anticipated extensive fault area, large karst cavity with water and debris filling, mud-like soil within hard rock, etc	Make provision for investigations during construction (probe drilling, gas detection, etc.)

- Should excessive deformation be attributable to excavation (e.g. poor blasting), or excessive time lag in installing supports by the Contractor, the latter will bear the cost of additional support.
- In areas where baseline δ exceeds 1/3 of final lining's thickness, excavation diameter will be increased by δ.

A contract that imposes rigid designs and inflexible construction methods will almost certainly result in an inefficient and costly tunneling project.

"Unknown unknowns" can be minimised if investigation is embedded in the construction stage. A very important element in this respect is the stipulation, in contract documents, of mandatory probe drilling ahead of the tunnel face, at least in the stretches where the most problematic conditions are expected to occur. Comprehensive plotting of forecasting data and preparation of performance and geological forecasting report are also recommended.

Finally, residual uncertainties, after construction completion, should be incorporated in the Operation and Maintenance Plan of the Project.

References

ASCE (2007) Geotechnical baseline report for construction—suggested guidelines. American Society of Civil Engineers, Reston, VA

Head C (2005) The financing of water infrastructure—a review of case studies. World Bank, Washington DC

Hoek E, Palmieri A (1998) Geotechnical risks on large civil engineering projects IAEG congress. Vancouver, Canada

Gummer JH, Obermoser H (2008) A new approach to defining risk in rehabilitation works. Int J Hydropower Dams (5)

The World Bank (1996) Estimating construction costs and schedules—experience with power generation projects in developing countries. World Bank technical paper number 325

Large Deformation of Tunnel in Slate-Schistose Rock

A Case Study on Muzhailing Tunnel, Lan-Yu Railway, China

Faquan Wu, Jinli Miao, Han Bao, and Jie Wu

Abstract

Large deformation of soft rock tunnel has been one of significant problems in the railway construction in Northwestern China. The main causes led to the problem are large depth with high crustal stresses, soft rock with strong anisotropy and quick excavation. The paper is to introduce the large deformation of the slate-schistose rock tunnel in Lan-Yu railway construction, the essential factors affecting the deformation of carbonaceous slate tunnel including geological stress, special properties of the rock and its soften mechanism caused by excavation, rock pressure and its strengthening effect; some lessons from the geological investigation and design of tunnels.

3.1 Background

Large deformation of soft rock tunnels has been a difficult problem in the railway construction in mountain area of Northwestern China. Lan (Lanzhou)-Yu (Chongqing) railway is one of the typical cases. Large amount of tunnels of the railway line has to slow down or stop the excavation because of the lining systems has been broken by strong deformation. A big proportion of designed supporting system of tunnels has been changed because the class of rock quality has to be reduced from the original classification. And consequently a remarkable amount of investment has to be input for the change.

As well known, pararock formed from the clastic rocks of Paleozoic and Mesozoic eras are widely distributed in Northwestern China, particularly in the Qilian-Qinling area as shown in Fig. 3.1. Most of the rock shows laminar and schistose feature with significant anisotropy because slight or strong metamorphism.

On the other hand, the depth of railway tunnels going across Qilian-Qinling mountain area usually reaches several hundreds of meters. And meanwhile there is generally a certain amount of crustal stress because it is in a tectonic active belt. Geological stress along the railway line have been measure by hydraulic fracture method as Fig. 3.2 which indicates that the maximal horizontal stress varies among 10.47–33.82 MPa. Strong rock pressure is one of the driving forces for the large deformation.

The common procedure for tunnel design in China is in the following steps: engineering geological survey, classification of rock and modification based on the condition of geo-stress and groundwater in different sections of the tunnel; according to the current technical standards, design of the supporting system based on class of rock in each section. However, for lots of tunnels, it may be difficult to accurately classify the rock quality in the stage of geological survey because of the insufficient data. This will actually leads to

F. Wu · H. Bao
Institute of Geology and Geophysics, Chinese Academy of Sciences, Beijing 100029, China

J. Miao
China Railway Sixth Group Co. Ltd, Beijing 100036, China

J. Wu (✉)
Universidad Politecnica de Madrid, 28014 Madrid, Spain
e-mail: wj86716@hotmail.com
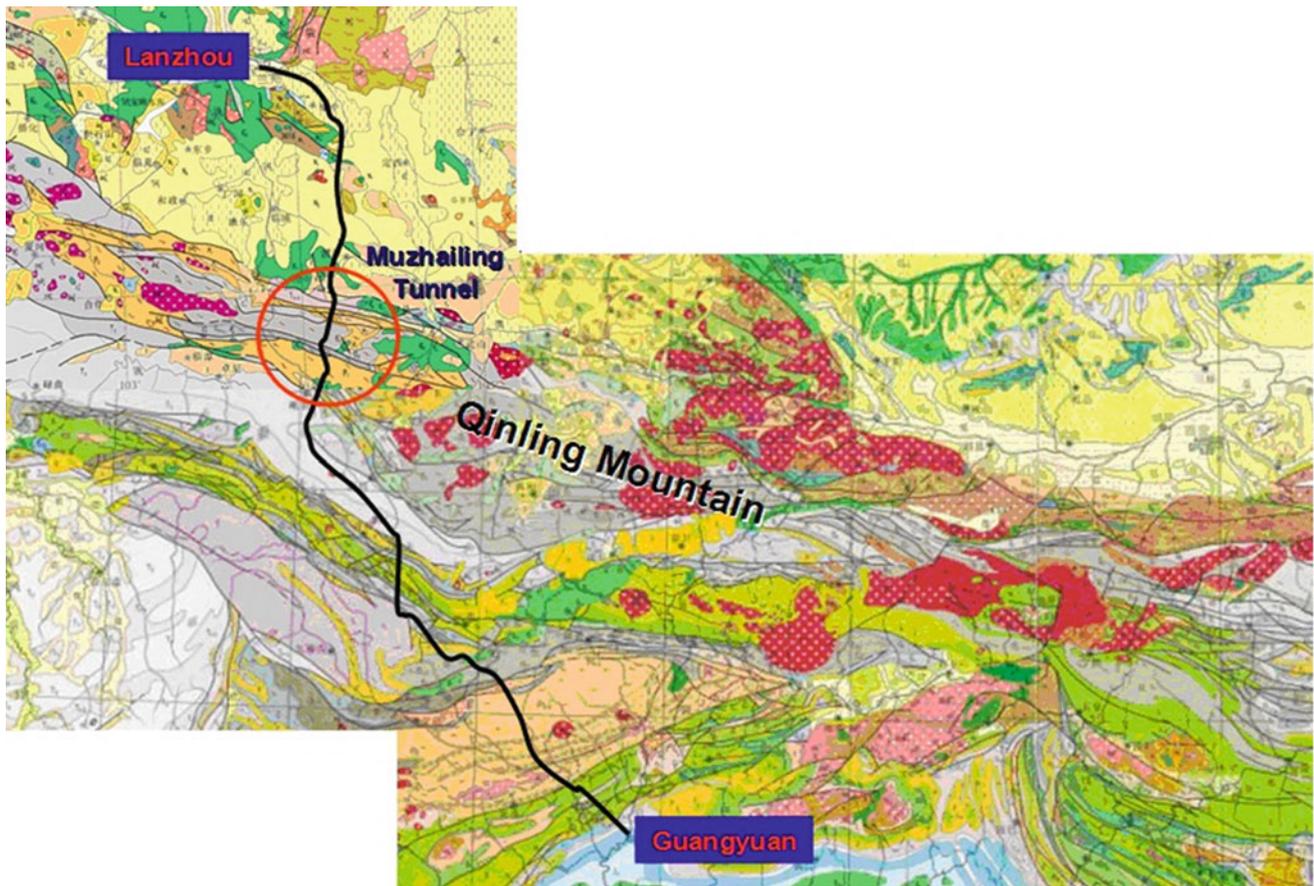
Fig. 3.1 Distribution of pararock along Lan-Yu railway line

Fig. 3.2 Geological stresses measured along the railway line from China Railway First Survey and Design Inst

the inappropriate design for the lining system, for the case of Lan-Yu railway it may be weaker than required for the problematic sections of the tunnels.

Tunnels are mainly distributed in the northern part of Lan-Yu line from Lanzhou to Guangyuan as shown in Fig. 3.2. Sixty-six tunnels with length of 343 km take 70 %

of the total length of the section, i.e. 493 km. Nine extremely long tunnels are the most difficult ones in the construction.

As some examples, Table 3.1 lists the data of 6 double-line tunnels in the Triassic slate which have changed the designed lining due to the reduction of rock class during the

construction. Around 72.0 % of the excavated length of tunnels has strengthened their supporting system.

A series of research work has been conducted to find the causes of large deformation and explanation for the change of design and rock classes. The paper is to introduce the large deformation of slate tunnels, taking Muzhailing tunnel as an example, the phenomena, causes of deformation and lessons learnt from it.

3.2 A Case of Large Deformation at Muzhailing Tunnel

Muzhailing tunnel is located at the section from Zhang County to Min County, which is designed mainly as two single line tunnels, but partly merged as a double lines tunnel. The length of left tunnel is 19,020 m and right 19,080 m respectively. The largest depth of tunnel reaches 715 m. For speeding the excavation process, 8 inclined shafts have been opened to increase work faces. However, the excavation of the tunnel still not finished after 5 years since started in March of 2009.

The strata in the area are mainly carbonaceous slate and sand stone from Devonian to Triassic systems. The thickness of a single layer of the rock varies around 2–10 cm and connected with carbonaceous films. This makes the rock very deformable while excavated (Fig. 3.3). The quality of the rock has been classified into III to IV grade based on the
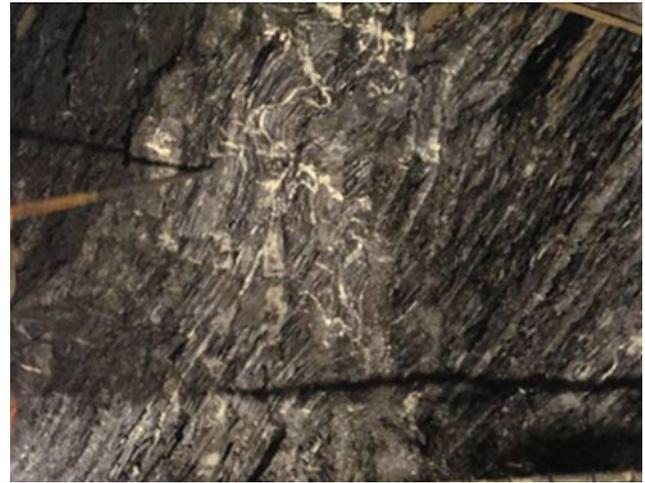
Fig. 3.3 Structure of the carbonaceous slate at Muzhailing tunnel

drilling and geophysical exploration at the geological survey stage.

Geological stress has been measured as shown in Fig. 3.2 near the tunnel and the maximal horizontal stress $\sigma_H = 27.16$ MPa at the direction of NE29 ~ 68°, a small inter-angle with the axis of the tunnel. The value of the measured stress indicates that it is in a horizontal stress state, i.e. $\sigma_1 = \sigma_H$.

The lining system of tunnel has been designed in a safer consideration comparing to the current technical standard. Table 3.2 lists the design parameters for the double-line

Table 3.1 Part of tunnels with lining changed[a]

Name of tunnel	Excavated (m)	Length of lining changed according to modification of rock class (m)							
		III to III+	III to IV	III to V	IV to IV+	IV to V	V to V+	Sum	Proportion (%)
Majiashan	3,910	40	3,049	25	558	60	0	3,732	95.4
Tongzhai	3,618	85	1,743	15	330	0	20	2,193	60.6
Qinggang	3,050	49	1,628	0	0	0	0	1,677	55.0
Xinchengzi	2,823	0	943	0	180	20	36	1,179	41.8
Maoyushan	2,863	0	2,193	50	447	10	8	2,708	94.6
Tianchiping	5,091	10	3,162	71	322	321	0	3,876	76.1
Sum	21,355	184	12,718	161	1,837	411	64	15,365	72.0

[a] From China Railway First Survey and Design Inst

Table 3.2 Parameters for the lining of double-line tunnel in IV–V class rock[a]

Class of rock	Reserved deformation space (cm)	Primary supporting system						Second lining, C35 reinforced concrete (cm)
		C30 Jet concrete (cm)	φ 22 Bolts		φ 8 Steel mesh (cm)	H150 Steel frame, spacing (m)		
			Length (m)	Spacing (m)				
IV	30	25	6.0	1.0 × 0.8	20 × 20	1.0		55 ~ 65
V	35	30	6.0–8.0	1.0 × 0.8	20 × 20	0.5		60 ~ 70

[a] From China Railway First Survey and Design Inst
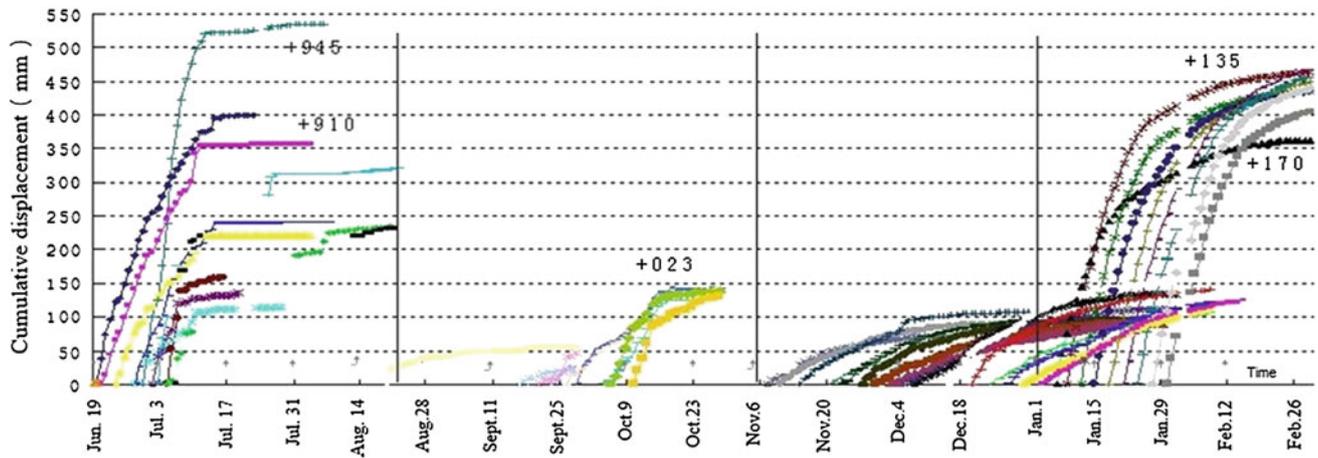
Fig. 3.4 Convergence deformation of the tunnel near Dazhangou shaft from China Railway First Survey and Design Inst

Table 3.3 Change of supporting grade[a]

	Excavated	III to III+	III to IV	IV to IV+	IV to V	V to V+	Sum	Proportion (%)
Left line (m)	7,687	125	855	3,275	5	480	4,739	61.6
Right line (m)	8,999	192	573	2,987	8	540	4,350	48.3

[a] From China Railway First Survey and Design Inst

tunnel in the IV and V class rock with high geo-stress condition. However, the deformation of tunnel still could not be controlled. Figure 3.4 shows the convergent deformation along with the excavation of the tunnel. The largest deformation could reach 530 mm in around 10 days.

Some experiences from the references (Mao and Yang 2005; Du 2011) indicate that to increase the stiffness of the lining system maybe one of the effective way for the control of the deformation of the tunnel. Four stages of tests have been conducted for different supporting measures. According to the results of the tests, 48.3–61.6 % in length of the tunnels have changed their design of linings (Table 3.3), mainly changed from grade IV to IV+ for strengthen their support systems.

3.3 Analysis on the Causes of the Deformation

Besides lots of field monitoring and tests, theoretical analysis has been done to find the reasons of the deformation of the tunnels. Two factors have been recognized as the main causes for the abnormal deformation, i.e., softening and anisotropisation of the carbonaceous slate by failure of inter-slice connection; increase effect of the rock pressure caused by softening of the rock. These two factors have not been taken into account in any of the current technical standards for tunneling, though there has been some modification for the classification of rock quality.

1. Softening and anisotropisation of carbonaceous slate

The slate is a kind of pararock composed of slices of sandstone cohered by carbonaceous films. The feature of the rock may be remarkably weakened due to the excavation of the tunnel. This is one of the reasons led to the softening of deformability and strength of the rock (Gao et al. 2011; Zhang 2010; Zhao et al. 2011; Zhao 2011).

The mechanism of the process could be explained by the diagrammatic sketch as Fig. 3.5. The slate rock is made of a series of hard slices and cemented by flaky minerals. It is hard
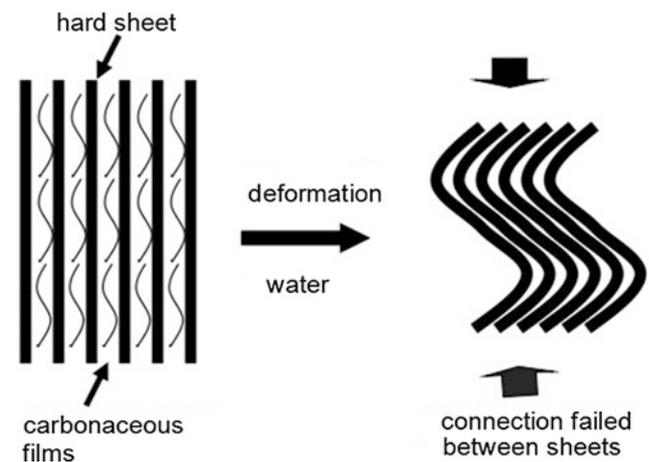
Fig. 3.5 Sketch showing the mechanism of softening and anisotropisation of slate
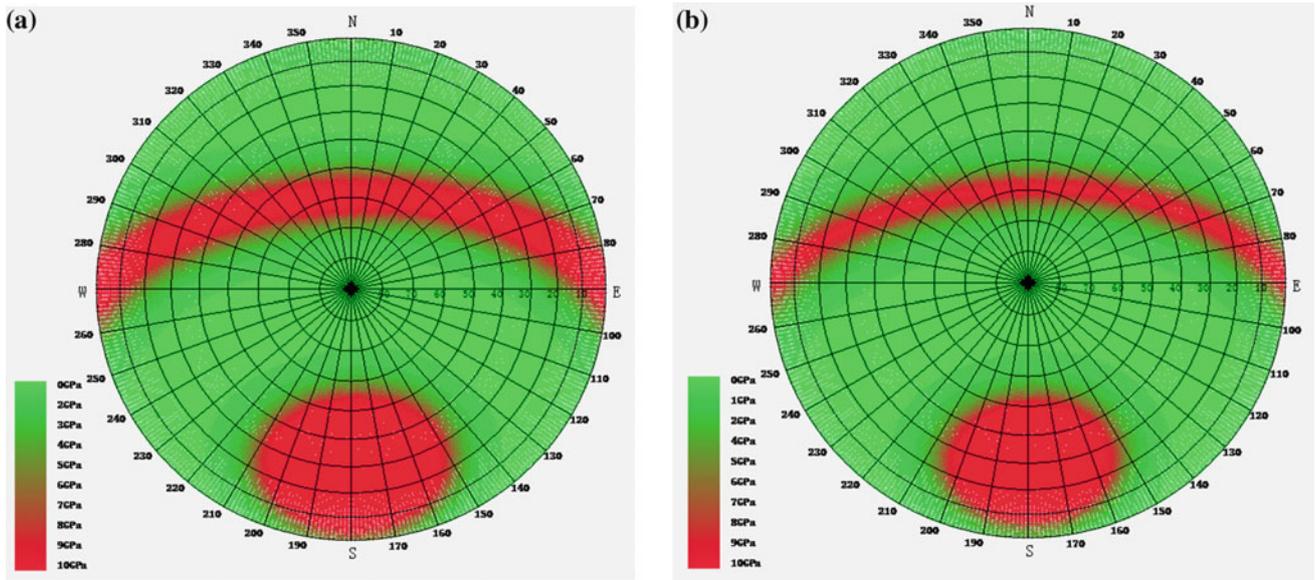
Fig. 3.6 Variation of modulus between original and disturbed state of the slate. **a** $E = 10$ GPa, $v = 0.4$, $a = 1$ m, $\varphi = 20°$, $c = 1$ MPa; **b** $E = 10$ GPa, $v = 0.4$, $a = 1$ m, $\varphi = 20°$, $c = 0$ MPa

originally like a brick, however, after excavation of tunnel, the deformation will easily break the connection between the slices. Thus the "brick" will be changed into "a stack of paper" with weaker mechanical property and notable anisotropy.

This can also be illustrated by the calculation of Yang's modulus of rock. The modulus of rock, E_m, can be calculated by the following formula Wu (1993):

$$E_m = \frac{E}{1 + \frac{32(1-v^2)}{\pi(2-v)} \lambda a h^2 \sin^2 \delta}$$

where E, v are the Yang's modulus and Poison's ratio of rock block, λ, a and δ are the density, average radius of a set of discontinuities and the inter-angle between the normal of the planes and acting stress, $h = \frac{\tau - (c + \sigma \tan \phi)}{\tau}$ is the ratio of residual shear stress on a discontinuity.

Figure 3.6 shows the calculated modulus of slate for the original state (relatively high pressure and well cohered) and after disturbed (pressure unloaded and cohesion between slices lost), where taking the parameters of rock block as $E = 10$ GPa, $v = 0.4$, the average radius and the cohesion of the discontinuities as $a = 1$ m and $c = 1$ MPa. The frictional angle of the planes has been measured in the field as $\varphi = 20°$, and after failure of the planes, the cohesion will be totally lost, i.e. $c = 0$ MPa.

The calculation has shown that the average modulus of rock before failure is 3.32 GPa, and it is reduced to 2.52 GPa after excavation, a 24.1–31.7 % reduction comparing with the average values.

2. Increase of the rock pressure

It is a common knowledge that the rock pressure to the lining system will increase while the mechanical property was weakened. It could be affirmed from the classic Kastner formula (Kastner 1951; Cai 2002)

$$p = (p_0 + c \, \cot \varphi)(1 - \sin \varphi) \left(\frac{a}{R_p} \right)^{\frac{2 \sin \varphi}{1 - \sin \varphi}} - c \, \cot \varphi$$

which infers that the rock pressure will definitely increase with the reduction of the strength of rock, i.e., c and φ. Where p_0, a and R_p are remote stress, radii of tunnel and plastic region of the surrounding rock respectively.

Numerical calculation has also shown that the rock pressure acting on the rigid lining of tunnel will significantly increase while the rock weakened. Taking a tunnel at a depth of 500 m, supported with 30 cm thick reinforced concrete lining, and the mechanical parameters are considered as $E_m = 20$ GPa, $v = 0.25$, $\varphi = 40°$, c = 12 MPa, $\sigma_t = 6$ MPa for hard rock and $E_m = 5$ GPa, $v = 0.4$, $\varphi = 30°$, c = 1 MPa, $\sigma_t = 0.5$ MPa for soft rock, Fig. 3.7 indicates that, the rock pressure for soft rock will be about two times of the hard rock.

On the other hand, the rock pressure will not only increase in quantity but also show unsymmetrical distribution due to the anisotropisation of the rock. A calculation by 3DEC has shown that the surrounding rock will move and bend inwards to the tunnel in the normal direction of beddings (Fig. 3.8a), which has been widely illustrated in practical phenomena.
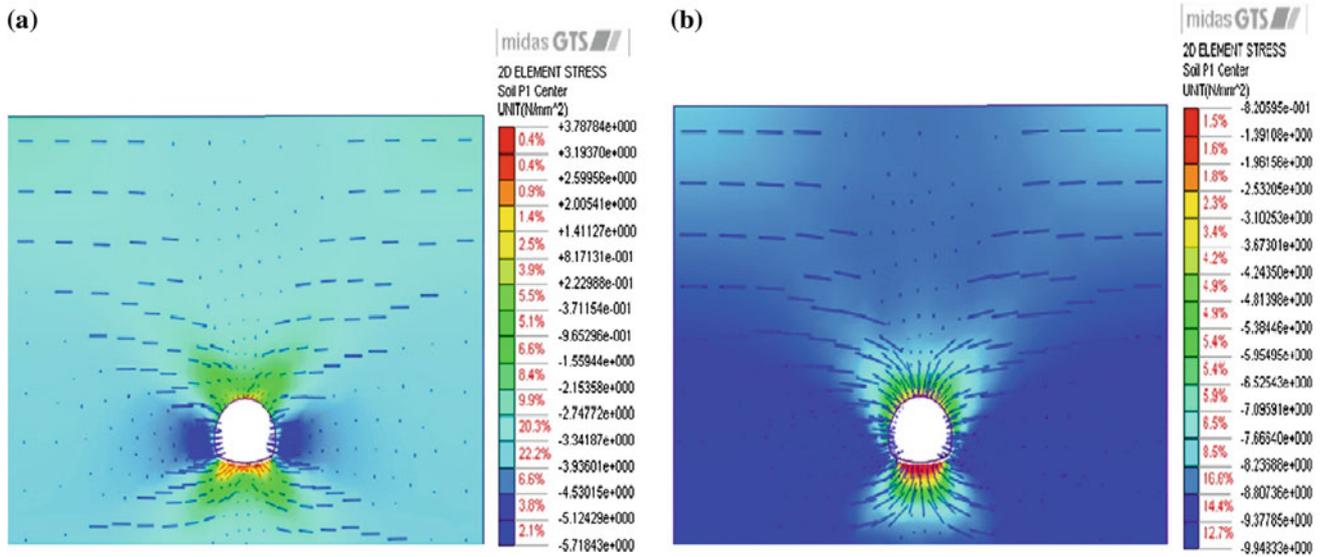
Fig. 3.7 The differences in rock pressure between hard rock and soft rock. **a** E_m = 20 GPa, v = 0.25, φ = 40°, c = 12 MPa, σ_t = 6 MPa; **b** E_m = 5 GPa, v = 0.4, φ = 30°, c = 1 MPa, σ_t = 0.5 MPa
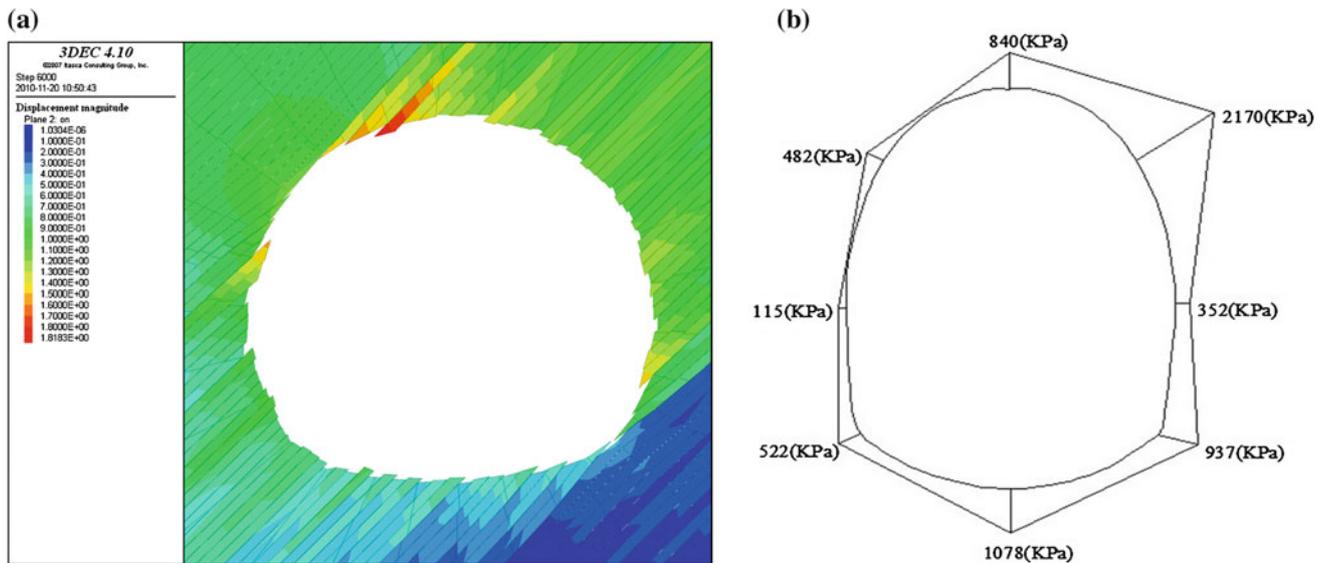
Fig. 3.8 Deformation Rock pressure of tunnel in layered rock. **a** Deformation of layered rock tunnel simulated by 3DEC; **b** Rock pressure measured at a tunnel of Lan-Yu railway

Rationally, there will be stronger rock pressure to the lining of tunnel as the deformation is restricted. A monitoring of rock pressure in Lan-Yu railway tunnel has affirmed that the contacting pressure has reached 2.17 MPa (Fig. 3.8b) which is much higher than our experiences, and the point with highest pressure located just at the place we discussed above.

No doubt, the higher the rock pressure, the stronger the deformation at the case without rigid lining.

3.4 Lessons Learnt from the Case

Some lessons have to be learnt from the practice of tunneling in Lan-Yu railway construction, mainly regarding to the current technical standards.

1. The special property of slate and schistose rock with weak cement should be taken into account of the classification of rock.

The current classification takes the rock as isotropic and with invariable mechanical property without considering any change by engineering disturbance. However, the schistose rock with weak cement by flaky minerals like carbonaceous films is much easy to be broken into anisotropic and soft medium when excavated. There should be some rules to reflect the softening and anisotropisation of rock due to the change of condition.

2. The deformation pressure should be considered in the rock pressure calculation for deep buried and soft rock tunnel.

The current standards for tunnel design mainly considers the broken-rock pressure, q, by the following formula

$$q \approx \gamma h, \quad h = 0.41 \times 1.79^s$$

where γ, h, and s are the unit weight, height of broken rock and the grade of rock. Because of the worst grade of rock is $s = 6$ in China, thus $h = 0.739 \sim 13.5$ m, and $q = 18.5 \sim 337.5$ kPa.

However, we have already known that the rock pressure for deep buried and soft rock tunnel will be much higher than the upper limit mentioned above. This indicates that a big element from deformation has not been involved into the rock pressure calculation. And it is just the crucial reason why we could not predict the large deformation and failure of surrounding rock of tunnels.

3. Asymmetric supporting system should be carried out in design of tunnel lining system

Obviously, evenly distributed bolts and symmetrical supporting system are not appropriate to the deformation control for schistose rock tunnel not only because they could not match the distribution of deformation, but also they could not work efficiently. For instance, a bolt parallel to the schistose plane could never strengthen the connection of the slices, but when goes across the planes will be much more effective. This is definitely a matter need to be taken into account in the current standards.

References

Cai M (2002) Rock mechanics and engineering, Science Press, 2002 (in Chinese)

Du Y (2011) Study on large deformation mechanics and controlling technique of soft-slate rock tunnel. Central South University

Gao C, Xu J, Li Z et al (2011) Experimental study of anisotropically mechanical characteristics of sandy slate in Xuefeng mountain tunnel. Rock Soil Mech 32(5):1360–1364

Mao H, Yang C (2005) Study on effects of discontinuities on mechanical characters of slate. Chin J Rock Mech Eng 24 (20):3651–3656 (in Chinese)

Wu F (1993) Principles of statistical mechanics of rock mass. Press of China University of Geosciences, 1993 (in Chinese)

Zhang X (2010) Study on large deformation cause analysis and engineering practice of carbonaceous slate tunnel. Chang'an University, Xi'an

Zhao Z (2011) Large excavation deformation analysis and controlling technical of carbonaceous slate in Tongzhai tunnel. West-China Explor Eng 12:184–186

Zhao S, Lin A, Yan X (2011) Large deformation analysis and controlling construction technical of vertical slate rock in Hadapu tunnel. Mod Tunn Technol 48(2):46–49

Addressing Geological Uncertainties in Major Engineering Projects

Convener Dr. Clark Fenton—*Co-convener* Pedro Refinetti Martins

Large civil engineering projects, including dams, lifelines and offshore energy developments are often situated in regions of spatially complex geology. Regardless of how detailed the site investigation is, such projects will always face a degree of uncertainty as to the exact nature of the ground conditions. Engineering geology has a central role in addressing these uncertainties. Using a thorough understanding of the geological history of a site, the materials present and of the current geological processes, in addition to those which operated in the recent past and those that may affect the site during the project lifetime and even during decommissioning, Engineering Geology provides the tools to identify, quantify and manage uncertainties in ground behaviour, engineering performance and environmental impacts. This session will highlight both current and emerging approaches for addressing geological uncertainties, including conventional deterministic and more novel probabilistic methods.

Effect of Petrogenesis on the Suitability of Some Pelitic Rocks as Construction Aggregates in the Tropics

Tochukwu A.S. Ugwoke and Celestine O. Okogbue

Abstract

Ten rock samples collected from five rock quarry units of Albian Asu-River Group (southeastern Nigeria) were studied megascopically and subjected to XRD to assess their petrography. The samples were subjected to degradability test to simulate their resistance to repeated wetting and drying common in tropical regions while nine of them, pelitic in composition, were further subjected to abrasion test to determine their abrasion value (LAAV) and impact test to determine their impact value (AIV). The field and petrographic studies showed that rocks of varying petrogenetic origins notably; hydrothermally altered pelitic rocks and volcanic bombs, pyroclastic rock, pelitic argillites and hornfels occur in the quarry units. XRD revealed that none of the rock types has significant amount of siliceous minerals implying that none is susceptible to alkali-aggregate reaction. Results of degradability test showed that the two pelitic argillites and one of the four hydrothermally altered pelitic rocks, having percentage mass loss ranging from 1.28 to 26.76 %, showed significant deterioration implying that the three rocks are not suitable for construction of structures like embankment and unpaved roads in tropical regions because of their petrogenesis and mineralogy. Results of the LAAV and AIV tests ranged from 9.40 to 14.00 and 19.00 to 24.00 respectively indicating that all the rocks are suitable for construction of all pavements sections. In general, all these results show that mechanical degradation of rocks is not only dependent on petrography but also on petrogenesis.

4.1 Introduction

Aggregates are non-renewable solid geologic materials used for construction purposes. Aggregates are either loose materials (e.g. sand and clay) or rock (e.g. igneous and metamorphic rocks). Works by Hudec (1980), George et al. (1990) and Bell (2007) had shown that suitability of rock as construction aggregate has most often being assessed based on the physical and mechanical properties of the rock with little or no attention paid on the possible influence of the rock's petrogenesis.

This work assesses the influence of petrogenesis on the suitability of some pelitic rocks as aggregate in tropical regions.

4.2 Regional Geology

The pelitic rocks studied in this work belong to the Albian Asu-River Group (southeastern Nigeria), which is the oldest lithostratigraphic unit of southern Benue Trough. Grant (1971) and Burke et al. (1971) reconstructed that the Benue Trough evolved as the third failed arm of a triple rift system

T.A.S. Ugwoke (✉) · C.O. Okogbue
Department of Geology, University of Nigeria, Nsukka, Nigeria
e-mail: tcugwoke@yahoo.com

C.O. Okogbue
e-mail: celeokogbue@yahoo.com

due to separation of South American and African plate, which was associated with faulting and subsidence of the major crustal blocks. According to Olade (1975), Ofoegbu (1983) and Ojoh (1990), the southern part of Benue Trough experienced three tectonic upheavals, which were characterized by volcanic eruptions, in Aptian/Pre-Albian, Turonian and Santonian Stages. The eruptions intruded the Asu-River Group that is mostly composed of low-grade regionally metamorphosed calcareous/silty shales (Obiora and Umeji 2004; Obiora and Charan 2010).

4.3   Field Studies and Laboratory Analyses

Ten rock samples collected from five mapped rock quarry units were studied megascopically and subjected to X-ray diffraction and degradability tests. The samples were code-named following the locations from they were collected.

About 3 g each of dry pulverized sample passing through sieve 150 μm was analyzed from $0° − 70°$ $2θ$ scan range using Shimadzu X-ray diffractometer (XRD-6000) to generate diffractogram. Prominent peaks of the diffractogram were matched and labeled by the mineral data card software of the diffractometer from which the dominant minerals contained in the sample were identified. Degradability test involved soaking dry lumps of rock samples each weighing between 120 and 180 g (W_{dry}), in potable water of about 24 °C contained in non-corrodible can for 48 h. Each sample was removed from water, washed with fresh water and finger pressure to detect particle(s) that might have lost cohesion. Particle(s) that got detached during soaking or washing was (were) carefully picked and air-dried to constant weight (W_p) to achieve complete dryness while the intact rock was air-dried for 24 h to achieve partial drying and thereafter subjected to another cycle. The experiment was repeated for 15 cycles and the cumulative percentage of mass lost (M_{lost}) at the 15th cycle was calculated using the equation:

$$M_{lost} = \left[\frac{\sum_{n=15}^{i} W_p}{W_{dry}} \right] \times 100 \%$$

Nine samples that were pelitic in composition were subjected to Los Angeles Abrasion (LAAV) and Impact value (AIV) tests following the grade A of IS: 383 and IS: 2386 (1963) standards respectively.

4.4   Results and Discussion

Table 4.1 shows the field observations, megascopic description, mineralogy, M_{lost}, LAAV and AIV of the analyzed samples. Although AGU1 and AGU2 occur at the

same location (Agu-Akpu) they are different rocks implying that there is an unconformity at that location, which was correlated with one observed at Okposi (OKP1, OKP2). From field and megascopic studies, AGU1, OKP1, ENY1 and ENY2 are the same rock type while AGU2 and EZZ are the same rock type. Hypabyssal features and co-occurrence of ONY1, ONY2 and ONY3 at Onyikwa rock units reveal that they are of same volcanic/igneous origin but their actual field occurrence had been distorted by a post Santonian tectonic event. The reconstructed petrogenesis, from field observations and petrography, is that ONY1 is a porphyroblastic hornfel that occurred between the pyroclastic rock (ONY2) and baked margin (ONY3). The implication of the above observations, when regional geology of the area is taken into consideration, is that AGU1, OKP1, ENY1 and ENY2 are hydrothermally altered pelitic rocks; AGU2, and EZZ are low-grade regionally metamorphosed pelites (argillite); OKP2 is hydrothermally altered volcanic bomb; ONY1 and ONY3 are pelitic hornfels while ONY2 is pyroclastic rock.

Table 4.1 reveals that the pelitic argillites (EZZ and AGU2), which show highest degree of deterioration (highest M_{lost}), are neither richer in water absorbent/soluble minerals nor more porous than other samples while the igneous rocks (ONY2 and OKP2) that show lowest degree of deterioration are neither more deficient in water absorbent/soluble minerals nor least in effective porosity. The pelitic hornfels (ONY1 and ONY3) contain more water absorbent/soluble minerals than the pelitic argillites (EZZ and AGU2) but do not show significant (≥1 %) deterioration.

Also, out of the four hydrothermally altered pelitic rocks (AGU1, OKP1, ENY1 and ENY2), OKP1 that is rich in water-absorbent/soluble minerals shows significant deterioration. It follows that deterioration (durability) of rocks due to repeated wetting and drying, characteristic of tropical regions, is dependent not only on the petrography but also on the petrogenesis of the rock. The implication of the degradability test results is that the three rocks, EZZ, AGU2 and OKP1, that show significant deterioration due to their petrogenesis and/or petrography, will obviously not resist repeated wetting and drying that occurs in tropical regions and are therefore not suitable aggregates for construction of structures like unpaved roads, embankment and facade in tropical regions.

Based on IRC (1970) standard, the LAAV and AIV indicate that all the rocks analyzed are suitable for constructing all sections of concrete and bituminous pavements. Contrary to general belief that all coarse-grained rocks are more prone to mechanical degradation than fine-grained ones, ONY1, which is coarse-grained, does not have higher LAAV and AIV relative to other samples that are much finer in grain size. This characteristic is attributed to the fact that ONY1, which is a pelitic hornfel, has attained significant

Table 4.1 Field occurrence, megascopic descriptions, mineralogy, cumulative percentage of mass lost, LAAV and AIV of the analyzed samples

S/n	Location/ rock unit	Sample	Field occurrence	Megascopic description	Dominant minerals and group	M_{lost} (%)	LAAV (%)	AIV (%)
1.	Enyigba	ENY1	Massive and non-fractured	Grey coloured, fine-grained and smooth surface. Spits into flaky portions when hammered	Paragonite (mica), Halloysite (kaolinite-serpentine), Pyrophyllite (talc), Chlorite-vermiculite-montmorillonite (mixed clay)	0.21	14.00	23.00
2.	Enyigba	ENY2	Massive and non-fractured	Very similar to ENY1 but less flaky	Antigorite (serpentine), Tremolite (amphibole), Lizardite (serpentine), Illite (clay), Osumillite (milarite), Hopeite (Phosphate)	0.12	13.60	24.00
3.	Okposi	OKP1	Unconformable surface, hypabyssal	Grey coloured and micaceous, silty and sub-rough surfaced.	Truscottite, Faujasite (zeolite), paragonite (mica), Sepiolite, Illite (clay)	1.28	9.80	19.00
4.	Okposi	OKP2	Randomly enveloped in OKP1	Sub-spherical in shape, grey coloured, silty sand-grained and micaceous. Resistant to hammering.	Lizzardite (serpentine), Chrysotile (serpentine), Ferropargasite (amphibole), Muscovite (mica)	0.00	9.40	20.00
5.	Agu-Akpu	AGU1	Massive	Similar to OKP1 but not micaceous	Truscottite, Faujasite (zeolite), Talc	0.12	9.70	22.95
6.	Agu-Akpu	AGU2	No visible bedding surface	Grayish ash coloured and fine-grained (silty)	Parahopeite (oxide), Muscovite (mica), Tremolite (amphibole), Riebeckite (amphibole), Osumillite (milarite), Chrysotile (serpentine)	11.63	12.00	22.95
7.	Onyikwa	ONY1	Fractured and hypabyssal features	Porphyroblastic/ poikiloblastic and very rough surfaced	Muscovite (mica), Riebeckite (amphibole), Kaolinite (clay), Anthophyllite (amphibole), Phlogopite (mica), Dickite (kaolinite-serpentine), Illite (clay), Ferropargasite (amphibole)	0.59	11.30	21.21
8.	Onyikwa	ONY2	The same as ONY1	Pyroclastic texture and rough surfaced.	Grunerite (amphibole), Osumillite (milarite), Montmorillonite (clay), Tremolite (amphibole), Ferropargasite (amphibole), Antigorite (serpentine), Riebeckite (amphibole)	0.03	NA	NA
9.	Onyikwa	ONY3	The same as ONY1	Ash-coloured, massive, smooth surfaced and angular edges.	Osumillite (milarite), Muscovite (mica), Tremolite (amphibole), Ferropargasite (amphibole), Phlogopite (mica)	0.06	11.00	22.00
10.	Ezzamgbo	EZZ	Tilt bedded	Grayish ash coloured and fine-grained (silty)	Anthophyllite (amphibole), Tremolite (amphibole), Sepiolite, Antigorite (Serpentine), Grunerite (amphibole)	26.76	10.00	20.99

NA Not analyzed

hardening due to thermal baking and is therefore more resistant to mechanical degradation than expected. The finding implies that resistance of rock to abrasion and impact may not be solely controlled by petrography (texture) but also by the petrogenesis.

All the rocks are deficient of siliceous mineral(s) and so none of them is susceptible to alkali-silicate reaction. However, two of the four hydrothermally altered pelitic rocks (ENY1 and ENY2) will be unsuitable for structural concrete in the tropics as they are likely to be prone to

stripping/popout due to their smooth surface and flaky nature. In general, only the hydrotheramally altered volcanic bombs (OKP2), pelitic hornfels (ONY1 and ONY3) and one of the hydrothermally altered pelites (AGU1) can be said to be suitable for construction of all types of civil engineering structures in the tropics.

4.5   Conclusion

This work has shown that suitability of rock as construction aggregate is not only dependent on its physical and mechanical properties but also on the petrogenesis of the rock particularly in the tropics where rocks are exposed to repeated rainfall and high temperature.

References

Bell FG (2007) Engineering geology (2nd edn). Butterworth-Heinemann, Elsevier. Linacre House, Jordan Hill, Oxford. 581 p

Burke K, Dessauvagie TFJ, Whiteman AJ (1971) Opening of the gulf of Guinea and geological history of the Benue depression and Niger Delta. Nature (Physical Science) 233:51–55

George SA, James MB, Edward WS (1990) Building with stone in Northern New Mexico. New Mexico geological survey guidebook. In: 41st field conference, Southern Sangre de-Cristo mountains, New Mexico, pp 405–416

Grant NK (1971) The South Atlantic, Benue trough and gulf of Guinea cretaceous triple junction. Bull Geol Soc Am 82:2295–2298

Hudec PP (1980) Durability of carbonate rocks as function of their thermal expansion, water sorption and mineralogy. ASTM Tech Pub 691:497–508

IRC:15 (1970) Indian Roads Congress. Tentative specification (for various types of construction methods)

IS: 2386 part IV (1963) Indian standard institution. Indian standard methods of test for aggregate for concrete

Obiora SC, Charan SN (2010) Geochemical constraints on the origin of some intrusive igneous rocks from the Lower Benue rift, Southeastern Nigeria. J Afr Earth Sci 58:197–210

Obiora SC, Umeji AC (2004) Petrographic evidence for regional burial metamorphism of sedimentary rocks in the Lower Benue rift. J Afr Earth Sci 38:269–277

Ofoegbu CO (1983) A model for the tectonic evolution of Benue Trough of Nigeria. Geol Rundschau 73:1007–1018

Ojoh K (1990) Cretaceous geodynamics evolution of the southern part of the Benue Trough (Nigeria) in the equatorial domain of the South Atlantic: stratigraphy, basin analysis and paleogeography. Bull Centers Resh Explor—Prod EIF—Aquitaine 14:419–442

Olade MA (1975) Evolution of Nigeria's Benue trough (Aulacogen). A Tectonic Model. Geol Mag 112:575–583

IS: 383, Indian standards Institution. Indian standard specification for coarse and fine aggregates from natural sources

Geological Society of London Engineering Group Working Party on Periglacial and Glacial Engineering Geology

David Giles, Martin Culshaw, Laurance Donnelly, David Evans, Mike de Freitas, James Griffiths, Sven Lukas, Christopher Martin, Anna Morley, Julian Murton, David Norbury, and Mike Winter

Abstract

In 2012 the Engineering Group of the Geological Society of London established a Working Party to undertake a state-of-the-art review on the ground conditions associated with former Quaternary periglacial and glacial environments and their materials, from an engineering geological viewpoint. The final report was not intended to define the geographic extent of former periglacial and glacial environments around the world but to concentrate on ground models that would be applicable to support the engineering geological practitioner. Key aspects of ground condition uncertainty would be addressed and developed within these ground models. The Working Party considered the following topics with respect to engineering geology: Quaternary Setting, Geomorphological Framework, Glacial Conceptual Ground Models, Periglacial Conceptual Ground Models, Engineering Materials and Hazards, Engineering Investigation and Assessment along with Design and Construction Considerations.

Keywords

Glacial • Periglacial • Ground model • Quaternary

5.1 Introduction

In 2012 the Engineering Group of the Geological Society of London established a Working Party to undertake a state-of-the-art review of ground conditions associated with former Quaternary periglacial and glacial environments and their materials, from an engineering geological viewpoint. The final report will concentrate on the development of new ground models that would be applicable to support the engineering geological practitioner, enhancing current knowledge, whilst focusing on their applicability to the engineering geologist. The ground models will be developed to communicate the complex and variable ground conditions that could be expected in these former periglaciated and glaciated terrains. The Working Party considered the following topics with respect to engineering geology: Quaternary Setting, Geomorphological Framework, Glacial Conceptual Ground Models, Periglacial Conceptual Ground Models, Engineering Materials and Hazards, Engineering Investigation and Assessment along with Design and Construction Considerations. Former glacial and periglacial settings present the engineering geologist with a complexity of vertically and laterally varying ground conditions with a high degree of uncertainty which require the use of conceptual ground models to fully understand and interpret, for example the complexities of the ice-marginal environment as conceptualized in Fig. 5.1. Such complexity can also be seen in Fig. 5.2, an example of the varying ground conditions associated with superficial valley disturbances in a former clay pit in Devon, UK.

D. Giles (✉) · M. Culshaw · L. Donnelly · D. Evans · M. de Freitas · J. Griffiths · S. Lukas · C. Martin · A. Morley · J. Murton · D. Norbury · M. Winter
Geological Society of London, Burlington House, Piccadilly, London, W1J 0BG, UK
e-mail: dave.giles@port.ac.uk
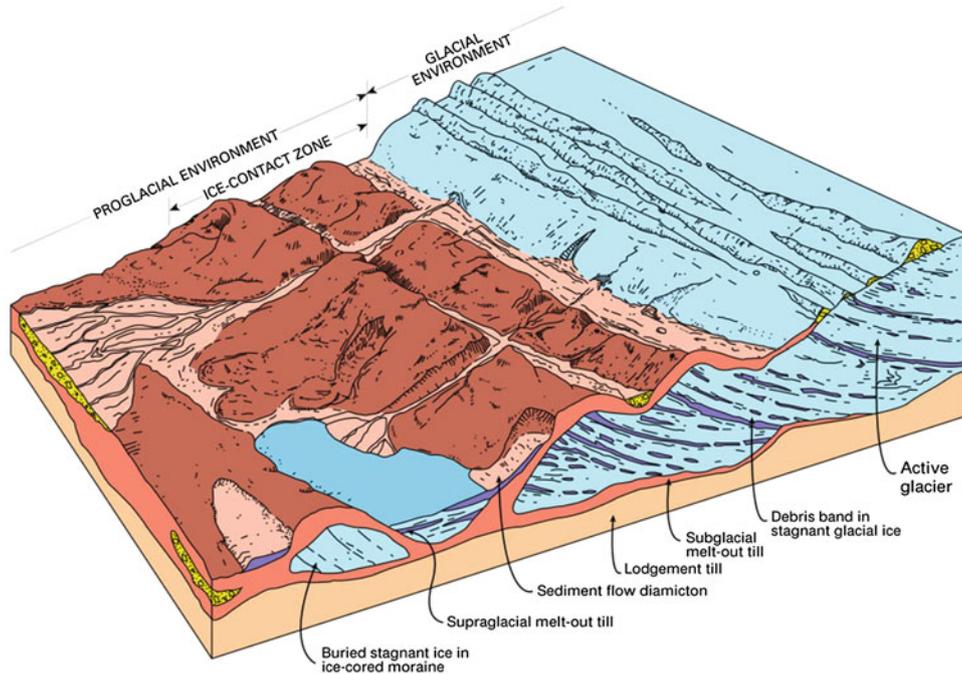
Fig. 5.1 Current supraglacial and ice-contact ground model (McMillan and Powell 1999)

Fig. 5.2 Periglacial environment: Superficial valley disturbances, Newbridge Ball Clay Quarry, Devon, UK. (Dump trucks in *bottom right* corner for scale)

5.2 Terms of Reference

The Periglacial & Glacial Engineering Geology Working Party (PGEGWP) has been established by the Engineering Group of the Geological Society and comprises officers and specialist participating members who will act as lead authors. The PGEGWP will produce a report, in book format, to complement the previous report on Tropical Residual Soils produced by an earlier Working Party of the Engineering Group, first published in 1990 and republished in book format in 1997 (Fookes 1997). A similar format was adopted by the Hot Deserts Working Party, which published their final report in 2012 (Walker 2012). It is intended that the report will be a state-of-the-art review on the ground conditions associated with former Quaternary periglacial and glacial environments and their materials, from an engineering geological viewpoint. There necessarily will be appropriate coverage of the modern processes and environments that formed these materials. A key aspect of the report will be to integrate soil description methodologies utilized by Quaternary scientists, engineering geologists and geotechnical engineers. Field workshops have been organized (Figs. 5.3 and 5.4) to consider various glaciogenic classification schemes specifically with their regard to their applicability to engineering geology.

It is not intended to define the geographic extent of former periglacial and glacial environments around the world, but to concentrate on ground models that would be applicable to support the engineering geological practitioner. The aim of the PGEGWP is to produce a report that will act as an essential reference handbook as well as a valuable textbook

Table 5.1 Example of a Terrain Unit definition table from the geomorphological setting chapter

Terrain unit	Relict frost mounds /relict ramparted ground-ice depressions: pingos
Image	 Small pingo remnant (approx. 30 m diameter) near to Thompson, Norfolk
Form/topography	Pingos are ice-cored mounds or hills developed in permafrost. Relict pingos and other ground ice mounds formed during Quaternary cold stages may be indicated by circular or ovate depressions, often surrounded by raised rampart-like rims with a peat or soft ground core. Two forms are identified, closed system (or hydrostatic) pingos and open system (or hydraulic) pingos. The former occur in lowland settings within the continuous permafrost zone, and the latter are more common in valley bottom and footslope localities in both discontinuous and continuous permafrost. Pingos can reach up to 70 m in height and up to 600 m in diameter
Landsystem	Lowland Periglacial Terrain
Process of formation	Formed by injection of water into near surface permafrost to form an ice core. Water under sufficient pressure to overcome overburden stress. Pressure can develop in two ways; Closed System where water is expelled from saturated coarse grained sediments during the refreezing of a talik (a zone of unfrozen sediment within a continuous permafrost) or Open System where artesian water pressures within a sub permafrost aquifer cause upward injection and freezing of water
Modern analogue	 Active Pingo, Innerhytte, Svalbard
Associated features	Related smaller ground ice phenomena associated with permafrost regions are lithalsas, mineral palsas, and seasonal ground ice mounds
Engineering significance	Compressible soils; differential settlement
References	Harris and Ross (2007), Hutchinson (1980, 1991, 1992)

for practicing professionals and students. The style will be concise and digestible by the non-specialist, yet be authoritative, up-to-date and extensively supported by data and collations of technical information. The use of jargon will be minimized and necessary specialist terms will be defined in an extensive glossary. There will be copious illustrations, many of which will be original, and many good quality photographs. The content of the report will embrace a full

Fig. 5.3 Working Party field discussion of glaciogenic soil classification and description methodologies at Barmston, East Yorkshire, UK. Section shows Skipsea Till overlain by subglacial canal fills
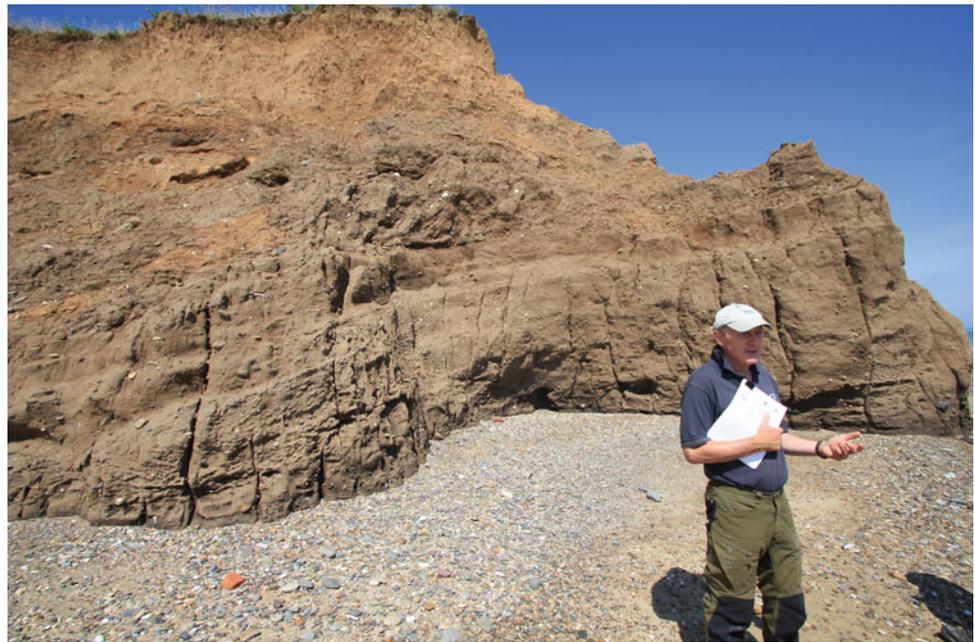
Fig. 5.4 Working Party field visit to North East England to discuss potential glacial sediment nomenclatures and ground models to be included in the final publication. Field description and assessment methodologies have been a core discussion point of the Working Party (Table 5.1)

range of topics, from the latest research findings to practical applications of existing information. Likely directions of research and predictions of future developments will be highlighted where appropriate. The report will be based on world-wide experience in periglacial and glacial terrain and will draw upon the experience of its members and publications on periglacial and glacial conditions.

The Working Party members will be collectively responsible for the whole report. Although each participating member will be the named author or co-author of one or more chapters, all members will be expected to review and

contribute to the chapters drafted by other members and would be acknowledged as such. Individual book chapters will be included in the Thomson Book Citation Index.

5.3 Chapter Listing with Lead Authors

The Working Party is chaired by Chris Martin, (BP) who will also draw together the diverse inputs that will be required for the introductory first chapter. Anna Morley

(Arup) is the Secretary of the Working Party while Professor Jim Griffiths (University of Plymouth) is the current Editor in Chief for the Engineering Geology Special Publications series. The chapter titles and lead authors of the remaining chapters are as follows:

- Quaternary Setting
  - Dr Sven Lukas, Queen Mary University of London
- Geomorphological Framework
  - David Giles, University of Portsmouth
- Glacial Conceptual Ground Models
  - Professor David Evans, Durham University
- Periglacial Conceptual Ground Models
  - Professor Julian Murton, University of Sussex
- Engineering Behaviour & Properties
  - Professor Martin Culshaw, University of Birmingham
- Engineering Investigation and Assessment
  - Dr Mike de Freitas, Imperial College
- Design & Construction Considerations
  - Dr Mike Winter, Transport Research Laboratory
- Geohazards and Problematic Ground
  - Dr Laurance Donnelly, Wardell Armstrong

References

Fookes PG (ed) (1997) Tropical Residual Soils: A Geological Society Engineering Group Working Party Revised Report. Geological Society, London

Harris C, Ross N (2007) Pingos and pingo scars. In: Elias SA (ed) Encyclopedia of Quaternary Science, Vol 2. Elsevier, Amsterdam, pp 2200–2207

Hutchinson JN (1980) Possible late Quaternary pingo remnants in central London. Nature 284:253–255. doi:10.1038/284253a0

Hutchinson JN (1991) Periglacial and slope processes. In: Forster A, Culshaw MG, Cripps JC, Moon CF (Eds) Quaternary Engineering Geology, Geological Society Engineering Geology Special Publication No. 7, 283–331. doi:10.1144/GSL.ENG.1991.007.01.27

Hutchinson JN (1992) Engineering in relict periglacial and extraglacial areas in Britain. In: Gray JM (Ed) Applications of Quaternary Research, Quaternary Proceedings No. 2. Quaternary Research Association, Cambridge, 49–65

McMillan A, Powell J (1999) BGS rock classification scheme. Volume 4, classification of artificial (man-made) ground and natural superficial deposits: applications to geological maps and datasets in the UK. British Geological Survey Research Report, RR 99–04, Keyworth

Walker MJ (ed) (2012) Hot Deserts: Engineering, Geology and Geomorphology: Engineering Group Working Party Report (No. 25). Geological Society, London

New Methods of Determining Rock Properties for Geothermal Reservoir Characterization

6

Mathias Nehler, Philipp Mielke, Greg Bignall, and Ingo Sass

Abstract

The influence of hydrothermal alteration on permeability, thermal conductivity and thermal diffusivity was investigated for more than 300 drill cores from the wells THM18, TH18 and THM19 of the Tauhara Geothermal Field (Wairakei, New Zealand). The measurements were performed with newly developed, portable laboratory devices. The anisotropic, intrinsic permeability was measured with a gas pressure Columnar-Permeameter, while the thermal conductivity and thermal diffusivity were measured with a device based on the optical scanning method. The hydrothermal alteration rank (argillic or propylitic) was determined semi-quantitative by methylene blue dye adsorption tests in combination with thin section analyses. Samples from the Huka Fall Formation and the Waiora Formation, composed of layered mud-, silt- and sandstones as well as pumice-rich tuffs deposited in a limnic environment as well as associated rhyolitic and andesitic intrusive rocks were examined. A prograde alteration with depth is indicated by an increasing amount of illite and the corresponding decrease of smectite. Generally lithologies of higher primary permeabilities are more affected by hydrothermal alteration. With an increase of secondary clay minerals the permeability decreases.

Keywords

Hydrothermal alteration • Thermal conductivity • Permeability

6.1 Introduction

The Tauhara Geothermal Field is part of the Taupo Volcanic Zone (TVZ). This zone is an active volcanic arc and back arc basin on the central North Island of New Zealand of Pliocene to Quaternary age (Wilson et al. 1995). Numerous wells were already drilled and field conditions are geologically as well as chemically and physically well defined. The epithermal system is characterized by 300 °C hot water, which rises from a depth of 5–8 km. Samples have been taken from well TH18, located at the resistivity boundary outside of the active geothermal area and from wells THM18 and THM19, which are situated within the center of the Tauhara Field, close to subsidence bowls. The samples were taken at intervals between 5 and 15 m depending on the heterogeneity of the respective stratigraphy.

Petrophysical measurements and petrographic characterizations of the samples were used to evaluate the effects of lithology and hydrothermal alteration on permeability, thermal conductivity and thermal diffusivity. In order to explain the measurement results more accurately, the samples were classified by lithological criteria. Nine distinct lithologies can be identified: silty mudstones, silty sandstones, pumice-rich crystal tuffs, sedimentary breccias, andesitic lavas, hydrothermal andesite breccias, rhyolitic lavas, rhyolitic breccias and igneous breccias.

M. Nehler (✉) · P. Mielke · I. Sass
Chair of Geothermal Science and Technology, Technische Universität Darmstadt, Schnittspahnstraße 9, 64287 Darmstadt, Germany
e-mail: M_Nehler@gmx.de

G. Bignall
GNS Science, 114 Karetoto Road, 3377 Wairakei, New Zealand
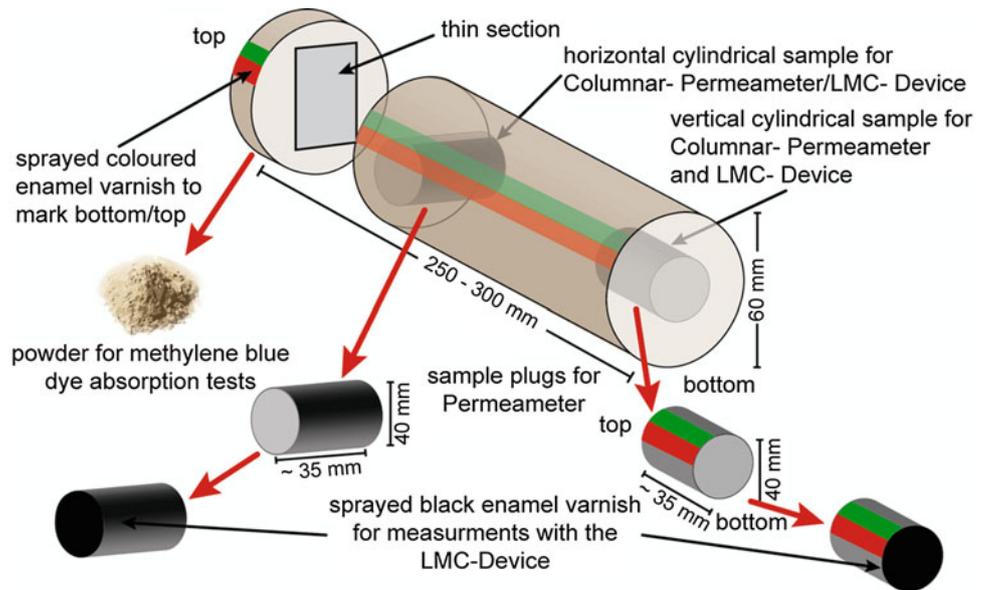
6.2   Sample Preparation

Oriented plugs (vertical and horizontal) were drilled out of existing drill cores with a diameter of 60 mm (Fig. 6.1). The cylindrical plugs must have a diameter of 40 mm and lengths between 30 and 45 mm for the measurements. Oriented thin sections were also prepared. Approximately 4 g of powder was pulverized for the semi-quantitative methylene blue dye adsorption tests (MEB) to identify the clay minerals. Plugs were dried at 40 °C for 48 h. After measuring the samples with the Columnar-Permeameter, they were prepared for the measurements with the Lambda Measuring Center (LMC). Therefore, the planar surface of the samples was sprayed with acrylic matt black enamel to achieve identical initial conditions.

6.3   Permeability Measurements

The intrinsic permeability (k_i) was determined according to Klinkenberg (1941) with a pressurized air driven, portable Columnar-Permeameter, which was invented by Hornung and Aigner (2002) and is described in detail by Arndt and Bär (2011). The specified measuring range is between 0.001 and 1,000 mD.

The gas permeability is measured at five different pressure stages (1,050, 1,250, 1,500, 2,000, 3,000 and 5,000 mbar) for each sample and is extrapolated to calculate the effective gas permeability for air under infinitely high air pressure. The pressure difference for all five stages remains identical and lies between 50 mbar for porous and up to a maximum of 1,000 mbar for slightly porous samples. The apparent permeability k_a [m²] is calculated for every single measurement by the means of Darcy´s law for compressible fluids and is plotted against the reciprocal mean pressure [1/p*] in the corresponding pressure stage (Klinkenberg plot). The apparent permeability k_a is associated with the intrinsic permeability k_i by the means of the Klinkenberg-factor b. The approach is used for permeabilities $<5 \times 10^{-14}$ m² and Klinkenberg-factors > 0.24 bar.

6.4   Thermal Measurements

The portable Lambda Measuring Center (LMC) was used to determine thermal conductivity (λ) and thermal diffusivity (a). It is a contactless method for measuring solid materials based on the optical scanning method with a fixed point heat source (Popov et al. 1999). The measuring range is between 0.5 W/(m K) and 5.0 W/(m K). To calculate λ of a sample it is necessary to use a standard of known thermal properties. Sample and standard are linked by Eq. (1):

$$\lambda_{sample} = \lambda_{standard} \cdot \frac{\Delta T_{standard}}{\Delta T_{sample}} \cdot K \qquad (6.1)$$

If steady state conditions are confirmed the sample surface is heated up for 2 s with 15 % power of the 150 W$_e$ Osram lamp. The temperature of the sample will then decrease at a rate depending on λ. The temperature difference ΔT is measured and the software determines λ by Eq. 6.1. To calculate a the sample is heated up again and the temperature is measured at a distance x to the heating point. The temperature maximum at a time t is determined by the software. With t and x the thermal diffusivity a can be calculated by

Fig. 6.2 Stratigraphic logs show the measurement results of the wells THM18, TH18 and THM19
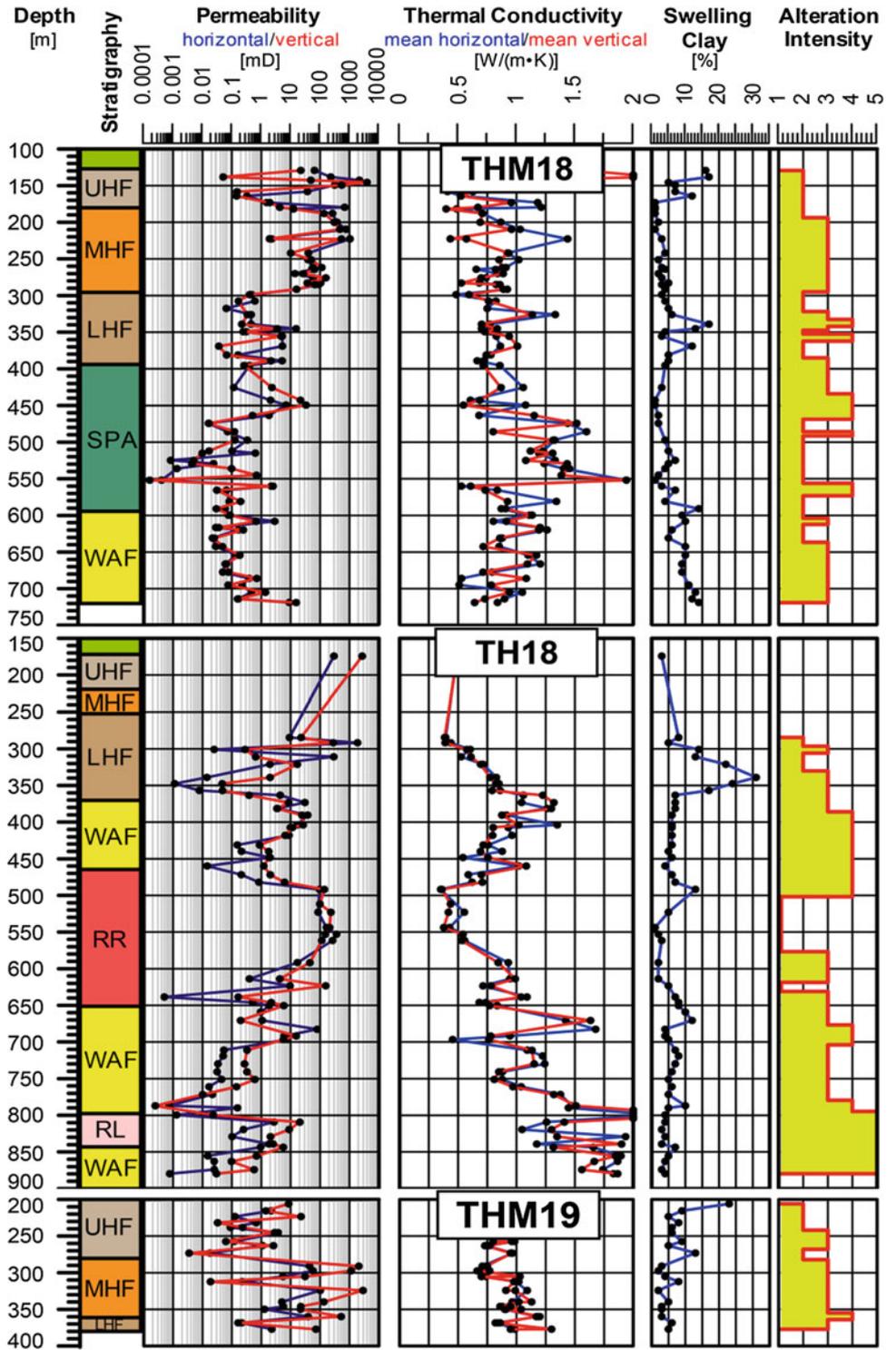
Eq. (6.2) (Hamm and Theusner 2010). The thermal diffusivity can be calculated with an analogues relation to the thermal conductivity including the time t instead of ΔT.

$$t = \frac{x^2}{a \cdot 6}$$ (6.2)

6.5 Methylene Blue Dye Adsorption Test (MEB)

The MEB is a semi-quantitative method to determine the amount of swelling clay (mainly smectite) in rocks and soil materials (Gunderson et al. 2000). The test is a common

method for determining the swelling clay content in water based drilling fluids, but can also be used to estimate the smectite/smectite-illite clay content in hydrothermal systems. These clays represent the predominant rock alteration products in the 50–200 °C zone above many high temperature, pH neutral, geothermal systems (Browne 1978). The methylene blue is an organic dye that shows a high selectivity for adsorption by reactive clay minerals as smectite, but is unaffected for adsorption by common clay minerals. This standardized (API 1988) technique uses a concentration of 3.74 g/l of methylene blue for the testing procedure. At this concentration the addition of 1 ml methylene blue dye solution is equivalent to an exchange capacity of 1 milliequivalent (1 meq) per 100 g cation. Based on the fact that smectites have an average cation exchange capacity of 100 meq/100 g, 1 ml of methylene blue is equivalent to 1 % of swelling clay content. The method is called semi-quantitative because of the actual cation exchange capacity of the swelling clays, which may vary from 80 to 150 meq/100 g.

6.6 Results

The results are characterized by a great variability depending on the source rocks (educts), the rank and intensity of the hydrothermal alteration, depth, primary permeability etc. (compare to Fig. 6.2).

The permeability is highly variable, but generally decreases with depth, while the thermal conductivity increases with depth. The pumice-rich crystal tuffs of the Middle Huka Fall Formation (MHF) and Waiora Formation (WAF) are characterized by relatively constant values of around 10 mD. Lithologies of greater permeabilities such as the tuffs are more affected by hydrothermal alteration and therefore show significant changes in their properties. With an increase of the fine fraction the permeability decreases.

The thermal conductivity varies between 0.35 and 2.50 W/(mK) showing a negative correlation with the permeability. Mud- and siltstones are characterized by a small range of measured values between 0.5 and 1.4 W/(m K). Silt- and sandstones show increased thermal conductivities with increasing alteration intensities. Pumice-rich crystal tuffs also have very high thermal conductivities when intensively altered. Compact lava units and the igneous breccia's show the highest thermal conductivities with maxima greater than 2.0 W/(m K). As might be expected, with increasing rock strength the thermal conductivity also increases.

A decreased amount of swelling clay (smectite) indicates a higher alteration rank. Peak concentrations occur at the UHF and LHF. A high amount of clay in highly altered sedimentary lithologies leads to low permeabilities, typically for caprocks. Smaller maxima occur within the WAF, indicating a general decrease of smectite with depth due to its natural stability range (70–160 °C).

With increasing depth the temperature, intensity and rank of the hydrothermal alteration also increases. The alteration type changes from argillic in the shallower parts to propylitic at greater depths (below 600 m). The primary mineral assemblage is predominantly replaced by clay minerals, calcite and secondary quartz. Therefore, hydrothermal alteration is generally prograde. Intensively altered rocks occur only in the deeper parts of the system, influenced by the propylitic alteration including silification processes. Greater permeabilities, such as fractures seem to facilitate this process. However, the hydrothermal alteration also depends on many other factors like mineralogy, texture, primary permeability and fluids.

References

API (1988) Recommended practice standard procedure for field testing drilling fluids. 12th edition 54 S., Washington, DC (American Petroleum Institute)

Arndt D, Bär K (2011) Forschungs- und Entwicklungsprojekt. 3D-Modell der geothermischen Tiefenpotenziale von Hessen. Abschlussbericht.—218 S., Darmstadt

Browne P (1978) Hydrothermal alteration in active geothermal fields-Annu. Rev Earth Planet Sci 6(1):229–250

Gunderson R, Cumming W, Astra D, Harvey C (2000) Analysis of smectite clays in geothermal drill cuttings by the methylene blue method for well site geothermometry and resistivity sounding correlation: WGC. Kyushu—Tohoku, Japan

Hamm K, Theusner M (2010) Lambda-Mess-Center LMC1. Installation und Bedienung. Manual—HTM Hamm & Theusner GbR. Erzhausen, Germany

Hornung J, Aigner T (2002) Reservoir architecture in a terminal alluvial plain: An outcrop analogue study (Upper Triassic, Southern Germany) part 1: Sedimentology and petrophysics. J Petroleum Geol 25(1):3–30

Klinkenberg LJ (1941) The permeability of porous media to liquids and gases. Drilling and production practice - Shell Development Co., pp 200–213 (American Petroleum Institute)

Popov YA, Pribnow DFC, Sass JH, Williams CF, Burkhardt H (1999) Characterization of rock thermal conductivity by high-resolution optical scanning. Geothermics 28(2):253–276

Rosenberg MD, Bignall G, Rae AJ (2009) The geological framework of the Wairakei–Tauhara Geothermal System, New Zealand. Special issue on the Wairakei Geothermal Field, New Zealand. 50 Years Generating Electricity 38(1):72–84

Wilson CJN, Houghton BF, McWilliams MO, Lanphere MA, Weaver SD, Briggs RM (1995) Volcanic and structural evolution of Taupo Volcanic Zone, New Zealand: a review. Taupo Volcanic Zone, New Zealand 68(1–3):1–28

Application of Reliability Methods to Tunnel Lining Design in Weak Heterogeneous Rockmasses

John C. Langford, N. Vlachopoulos, M.S. Diederichs, and D.J. Hutchinson

Abstract

Tunnel design in weak, heterogeneous materials such as flysch poses a variety of engineering challenges. The complex depositional and tectonic history of these materials leads to significant in situ variability in rockmass behaviour. Additionally, the alterations of sandstone and pelitic layers make rockmass characterization using traditional methods difficult. As a result, significant uncertainty exists in the ground response for a tunnel through such materials. Reliability-based methods can be used to better understand the impact this uncertainty has on convergence and tunnel lining performance. By assessing the impact of input uncertainty on ground response, the probability of failure can be evaluated for a given limit state. A quantitative risk approach can then be used to select the optimum design option on the basis of both safety and cost. This paper explores this issue further and presents a reliability-based, quantitative risk approach for the design of the Driskos tunnel along the Egnatia Odos highway in northern Greece.

7.1 Introduction

Weak, heterogeneous rockmasses such as flysch pose a serious design challenge for geological engineers. Due to the complex depositional environment and tectonic history, such materials exhibit generally low rockmass strength and a high degree of variability. As a result, a range of possible squeezing conditions can be encountered when excavating within a single unit. Given the safety and cost implications associated with squeezing in flysch, much work has been done to properly characterize these materials. To obtain reliable estimates of rockmass strength, a firm understanding of the relative presence of competent and incompetent layers is required. As these percentages will vary over the tunnel alignment, a conservative estimate is typically used to ensure a robust lining design is selected that is capable of withstanding the "worst" anticipated loading conditions. Such an approach leads to over-conservatism, which can have a substantial negative impact on both the project schedule and cost.

Reliability-based design (RBD) methods, when used in conjunction with more traditional design methods, can provide a more rational approach to quantify design risk in such highly variable rockmasses. By assessing the impact of input uncertainty on ground response, the probability of failure can be assessed for a given failure mechanism. This allows for a greater understanding of support performance and the application of a quantitative risk approach for design.

J.C. Langford
Hatch Mott MacDonald, Vancouver, Canada
e-mail: connor.langford@gmail.com

N. Vlachopoulos (✉) · M.S. Diederichs · D.J. Hutchinson
GeoEngineering Centre, Queen's University-Royal Military College, Kingston, Canada
e-mail: vlachopoulos-n@rmc.ca

M.S. Diederichs
e-mail: diederim@queensu.ca

D.J. Hutchinson
e-mail: hutchinj@queensu.ca
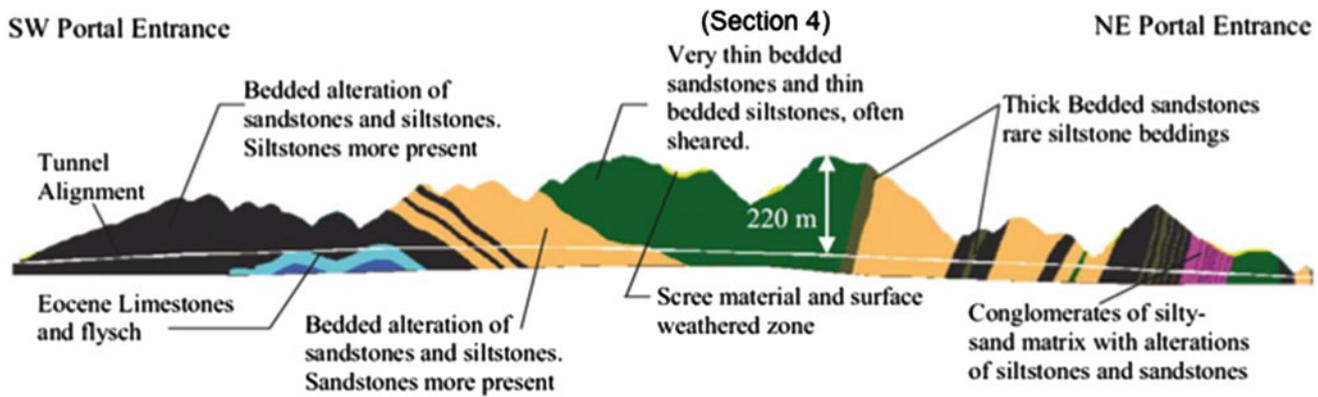
Fig. 7.1 Longitudinal topographic profile and idealized cross section for the Driskos tunnel (modified after Egnatia Odos S.A. 2003, Hoek and Marinos 2000)

This paper applies the reliability approach outlined in Langford et al. (2013) to perform a quantitative risk assessment for a number of support options at the Driskos twin tunnel along the Egantia Odos highway in northern Greece. This tunnel was excavated in a complex sequence of sandstone and siltstone layers (flysch) that experienced compressional deformations. Given the challenging geological conditions, excessive deformations and overstressing of the temporary support systems were experienced during excavation. The difficulties experienced and the scale of the project make the Driskos tunnel an excellent case study to illustrate the validity and benefits of a comprehensive risk-based design approach.

7.2 Case Study Area: Driskos Twin Tunnel, Egnatia Odos Highway

The Driskos twin tunnel is located within the Epirus region in the northwest corner of Greece. It was constructed as part of the Egantia Odos highway, which is a 670 km long construction project that consists of 76 twin tunnels raging in length from 800 m to 4,600 m and over 1,600 bridges. Each tunnel is horseshoe shaped with an internal diameter of 11 m internal diameter and a separation distance of approximately 13 m. The tunnels are approximately 4.6 km long and cross the NE Greek Pindos mountain chain under a maximum overburden of 220 m. The tunnel was constructed using a conventional drill and blast sequential excavation based on an observational design approach. A series of support categories were used based on the rockmass quality encountered.

7.2.1 Local Geology

The Driskos tunnel is situated in a series of varying lithological features of the Ionian tectonic unit adjacent to the Pindos isopic unit. The material is less tectonically disturbed than the Pindos Flysch meaning there is an absence of extensive chaotic zones within the Ionian Flysch. Based on the site investigation, a longitudinal section was prepared that details the major rock units and topography along the tunnel length (Fig. 7.1). The alignment was subsequently divided into 14 sections in Vlachopoulos et al. (2013) on the basis of geology, rockmass quality and in situ stress conditions. Of specific interest to this analysis is the area identified as Sect. 4, which extends from chainage 8 + 385 to 9 + 035, as significant squeezing issues were encountered.

7.2.2 Rockmass Characterization

In order to predict tunnelling problems in flysch, reliable estimates of the rockmass strength and stiffness must be obtained. Unfortunately, the heterogeneity and variability within flysch makes the determination of intact parameters extremely challenging. The classification system developed by Marinos and Hoek (2001) addresses this concern and allows an appropriate flysch category to be selected based on a Geological Strength Index (GSI). The GSI value considers the structure present and the relative composition of the rockmass with respect to sandstone and siltstone layers. After determining the flysch category, a weighted average approach can be used to estimate the uniaxial compressive strength (UCS), Hoek-Brown material constant (m_i) and the Modulus Ratio (MR) based on intact strength parameters for sandstone and siltstone.

The advantage of this approach is that it allows standardized inputs for the generalized Hoek-Brown method to be obtained. As such, an appropriate failure criterion can be developed for the flysch rockmass based on its intact strength and rockmass quality (GSI) over the tensile and compressive regions. The estimate of rockmass strength is based on the assumption that the rock behaves in an isotropic fashion at the

Fig. 7.2 Detailed geological section showing division of Sect. 4 into Sects. 4.1–4.5 (modified after Egnatia Odos S.A. 1998)
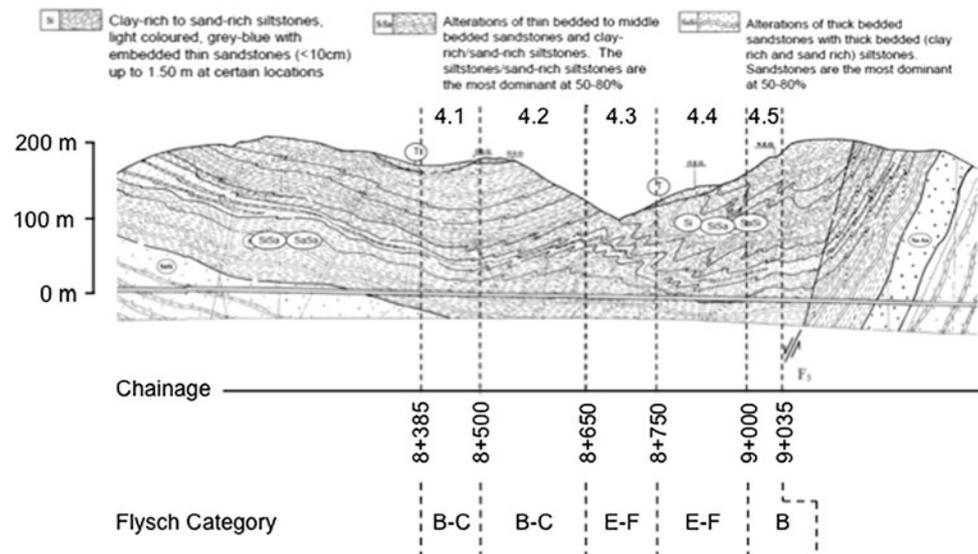
scale of the excavation due to the presence of several closely spaced discontinuities, which is appropriate in this case.

7.2.3 Support Categories and Excavation Approach

A series of five (I to V) support categories were developed on the basis of the expected rockmass quality conditions and initial estimates of support requirements were determined during the design phase. Categories III (15 cm unreinforced shotcrete), IV (20 cm shotcrete, HEB140 steel sets with 2 m centres) and V (25 cm shotcrete, HEB 160 steel sets with 2 m centres) are of particular interest for this analysis. Support was typically installed 2 m back from the face and a sequential, heading and bench excavation was used.

7.2.4 Uncertainty in Ground Conditions

Uncertainty in geological systems is typically divided into two categories: variability caused by random processes (aleatory) and knowledge-based uncertainty (epistemic). The natural variability in rockmass and in situ stress parameters is typically considered to be aleatory as the process of formation results in a real variation in properties from one spatial location to another. As this variability is inherent in the material, continued testing will not eliminate the uncertainty, but will provide a more complete understanding of it. Conversely, epistemic uncertainty exists as a consequence of limited information as well as measurement, statistical estimation, transformation and modelling uncertainty. As these components are a result of imperfect techniques, they should be reduced as much as possible.

In order to quantify uncertainty in the ground conditions, a series of homogeneous domains were established along Sect. 4 (Fig. 7.2). These Sects. (4.1–4.5) were developed on the basis of lithology, rockmass quality, presence of rockmass alteration and in situ stress conditions. The classification system by Marinos and Hoek (2001) was used to provide an indirect means of quantifying uncertainty for the intact strength and stiffness parameters for each of these domains. Based on the GSI values obtained for each domain, an appropriate flysch category was assigned and the corresponding weighted average was selected. A mean and standard deviation were then calculated for the UCS, m_i and MR for each domain based on the design values as well as acceptable ranges for sandstone and siltstone parameters. For this analysis, the in situ stress conditions in each domain were considered deterministically and calculated based on the overburden depth for each section. Hydrostatic stress conditions were assumed.

7.2.5 Analysis Method

For this study a two-dimensional, plane strain model was developed in the finite element modelling program 'Phase 2' by Rocscience Incorporated (http://www.rocscience.com). The full-face excavation of a single tunnel was considered for simplicity. Three-dimensional advance of the tunnel was simulated in a multi-staged two-dimensional model. The convergence-confinement method was used to describe the reduction in radial resistance at a particular point along a tunnel as the face advances. The approach by Vlachopoulos and Diederichs (2009) was also used to determine the timing for stiff support installation based on the longitudinal displacement profile (LDP) for the unsupported tunnel.
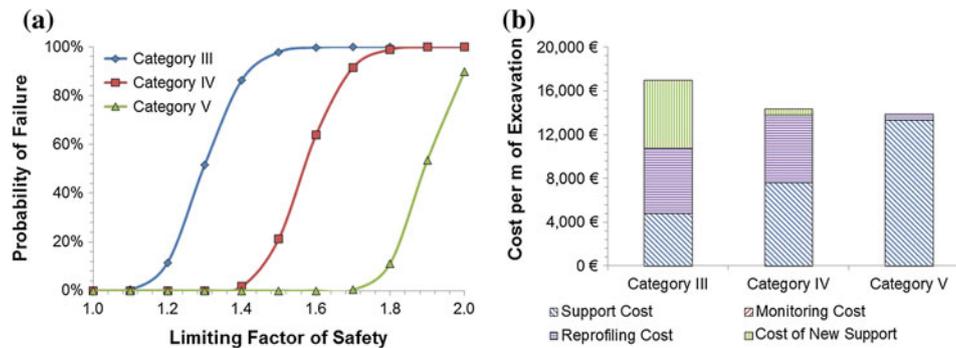
Fig. 7.3 For Sect. 4.3, **a** liner performance for the shotcrete in the wall based on different limiting factor of safety values and **b** breakdown of support costs and expected costs of failure (monitoring, reprofiling, installation of new support) for each liner category (costs are per metre of tunnel)

The structural stability of the lining systems was calculated using bending moment and thrust-shear force support capacity diagrams based on limiting factor of safety (FS) values developed according to Carranza-Torres and Diederichs (2009). The envelope of failure shown in these capacity diagrams is a graphical representation of the critical failure surface, separating the combinations of loads that are acceptable and those that exceed allowable limits. For this study, a limiting FS value of 1.3 was selected to ensure an appropriate level of safety for the tunnel.

7.2.6 Reliability Analysis

To assess the performance of each support category, reliability methods were used to determine the variability in ground response and liner loads. Unlike deterministic analyses, reliability methods directly incorporate the natural variability of the inputs into the design process. From this, a probability failure (p_f) can be established with respect to a specific failure mode, with "failure" defined as either the complete collapse of the structure (ultimate limit state, or ULS) or a loss of functionality (serviceability limit state, or SLS).

For this study, the modified point estimate method (PEM) proposed by Langford and Diederichs (2013) was used to determine the variability in liner loads and the probability of failure with respect to a limiting capacity curve (FS = 1.3). A quantitative risk assessment was used that considered both the probability and consequence of lining failure. With respect to the consequence of failure, two conditions were considered: (a) moderate damage, which would require monitoring and assessment by an engineer (failure of shotcrete in Category IV or V), and (b) complete failure of the lining, which would require re-excavation and the application of a higher class of support (failure of shotcrete in Category III or steel reinforcement in Category IV or V). For this analysis, support and failure costs were developed based on records from the Driskos tunnel project.

7.2.7 Results and Analysis

Each support category was modeled and uncertainty in thrust, bending moment and shear forces were calculated at each liner node based on the modified PEM approach. Based on the calculated liner load distributions, probabilities of failure were calculated based on different limiting capacity curves. In the interests of space, only the results from the shotcrete analysis in Sect. 4.3 are presented in Fig. 7.3a. The results illustrate the expected trend; a more robust support category will be able to sustain a greater rock load and therefore has a lower p_f.

To select the most appropriate support class for this section, a risk assessment was performed using the limiting p_f value (Fig. 7.3b). In this case, while Category III has the lowest support cost, the high probability of shotcrete failure leads to the highest reprofiling and risk costs. When Category IV and V are compared, it is clear that the expected reprofiling cost is significantly greater for the HEB140 steel sets than the HEB160. As such, Category V is considered to be the optimum support for Sect. 4.3 on the basis of economic risk.

As can be seen, this approach allows the improvement in safety for a given support category to be quantified, providing additional information to the Contractor and Owner with which to make design decisions.

References

Carranza-Torres C, Diederichs MS (2009) Mechanical analysis of circular liners with particular reference to composite supports. Tunn Undergr Space Technol 24(5):506–532

Langford JC, Diederichs MS (2013) Reliability-based approach to tunnel lining design using a modified point estimate method. Int J Rock Mech Min Sci 60:263–276

Marinos P, Hoek E (2001) Estimating the geotechnical properties of heterogeneous rock masses such as flysch. Bull Eng Geol Environ 60(2):85–92

Vlachopoulos N, Diederichs MS (2009) Improved longitudinal displacement profiles for convergence confinement analysis of deep tunnels. Rock Mech Rock Eng 42(2):131–146

Vlachopoulos N, Diederichs MS, Marinos V, Marinos P (2013) Tunnel behaviour associated with the weak Alpine rock masses of the Driskos Twin Tunnel, Egnatia Odos highway. Can Geotech J 50(1):91–120

Geological and Geotechnical Difference on Both Sides of the Same Tunnel

8

Pedro Olivença and Vítor Santos

Abstract

The excavation of Marão tunnel, located in the Northeast of Portugal, started simultaneously from both portals (East and West). The same method of excavation (Drill and Blasting—D and B), similar procedures for blasting and the primary support applied was the same and equivalent equipment used on both sides. Considering the same period of excavation, on the East side were excavated 2,300 m, while on the West side the excavation just 1,350 m were excavated. This differential on excavation between both sides of the tunnel, make it necessary to evaluate the causes that could justify this abnormal difference in excavation rates. To determine the cause of this difference in productivity, it was analyzed the geological features, the result of rock mass classifications and the geotechnical characteristics of the rock masses, which could influence the behavior of the excavation. Using descriptive statistics and multivariate analysis of data, applied to rock mass characteristics in each side of the tunnel, was possible to verify the existing differences, as well as the characteristics of the rock mass with greater relevance in the description of the geotechnical zoning for each side of the tunnel.

8.1 Introduction

The Marão tunnel excavation was advanced from both ends with the Drill and Blast (D and B) method. However, after the same time period, the east side advanced 2,300 m, while the west side only 1,350 m. At this point, the excavation was stopped due to contractual litigation between the Portuguese government and the concession company.

Marão tunnel is part of the A4 motorway that will link the cities of Amarante and Vila Real, in the Northeast of Portugal. This future infrastructure will have two parallel tunnels, each with a length of 5,600 m, a horseshoe cross-section with an invert arch and approximately 100 m^2 of section.

This tunnel will cross Marão mountain which reaches at its highest point around 1,200 m, in the alignment of the tunnel, with the maximum overburden of approximately 500 m.

Although the construction methodologies used on both ends of the tunnel were identical, two different construction teams were involved in the excavation, each one working on a different side of the tunnel, the productivity was quite different. It was important to find causes for this differences in productivity.

P. Olivença (✉) · V. Santos
Consultores Para Estudos de Geologia E Engenharia, CEGE, Algés, Portugal
e-mail: pedro.olivenca@cege.pt

V. Santos
CICEGe—Centro de Investigação Em Ciência E Engenharia Geológica, Faculdade de Ciências E Tecnologia Da Universidade Nova de Lisboa, Lisbon, Portugal
e-mail: vitor.santos@cege.com.pt

P. Olivença
GeoFCUL—Departamento de Geologia Da Faculdade de Ciências Da, Universidade de Lisboa, Lisbon, Portugal

Table 8.1 Rock mass zoning (CJC 2009)

Zone	RMR	Support	Excavation	Progress
ZG4	<20	Steel ribs and 30 cm of shotcrete	Partial excavation—top heading and invert excavation. Temporary invert on the top heading	0.6 m a 1.0 m
ZG3	20–35	15 cm of shotcrete reinforced with metalic fibres and 5 m Swellex rockbolts	Partial excavation—top heading and invert excavation	1.4 m a 2.0 m
ZG2	35–50	10 cm of shotcrete reinforced with metalic fibres and 5 m Swellex rockbolts	Full-face excavation	1.8 m a 3.0 m
ZG1	>50	5–10 cm of shotcrete reinforced with metalic fibres and 5 m Swellex rockbolts	Full-face excavation	2.6 m a 4.0 m

Although causes could be various, this article addresses the differences in geology and geotechnical parameters observed on each side of the tunnel, highlighting the regional geological context and geotechnical characteristics of the rock mass.

The project includes four geotechnical zones, with the characteristics shown in Table 8.1.

8.2 Methodology

Given these objectives, the geotechnical conditions encountered along the tunnel alignment were examined as one of the main factors influencing the productivity of any tunnel excavation (Costa-Pereira 1985).

RMR (Bieniawski 1989) was calculated along the tunnel alignment with the objective to determine the quality of the rock mass for tunneling and classify each excavation cycle in the respective geotechnical zone, as defined in the design.

By applying descriptive statistics to RMR values, it is possible to determine the quality of the rock mass occurring at each end of the tunnel.

The geotechnical zoning of the tunnel results from the RMR value, and was calculated systematically along the excavation, so for each side of the tunnel, it is important to calculate the percentage of occurrence of each zone.

As shown in Table 8.1, the better the quality of the rock mass, the less support needed to be applied, to ensure its stability and bigger lengths of excavation are possible.

As defined by Bieniawski, RMR results from the arithmetic sum of weights, assigned to a set of parameters. The multi correspondences analysis (MCA), widely applied for dimensionality reduction of variables (Davis 2002; Hill and Lewicki 2007) aims to determine the characteristics of the rock mass that have the greatest influence on geotechnical zoning.

8.3 Geology

The Marão mountain is composed of autochthonous formations of Cambrian to Lower Devonian age (Pereira 1987).

The major geological structure is an anticline formed during the Variscan Orogeny. Geological mapping of the region is shown in Fig. 8.1. The following units are present (Sá et al. 2005):

- Desejosa formation (Cambrian): interbedded shales and metasiltstone, present in all 2,300 m excavated from the east portal.
- Vale de Bojas formation (middle and lower Floian): characterized by polymictic conglomerates and thinner layers of psamitic metatuff. The tunnel excavations have not encountered this formation.
- Marão formation (middle Floian): consists of quartzites alternating with phyllites or psamitic rocks. The upper member of this formation has been encountered in west side of tunnel excavation.
- Moncorvo formation: a monotonous sequence of gray shale and is present in the west portal of the tunnel.

A Hercynian granitic intrusion is located at the western area of the tunnel. This caused regional metamorphism of the Moncorvo formation (west side), giving it greater resistance, which led to a brittle deformation behavior, developing open discontinuities, with blocks of substantial size (Coke and Santos 2012).

The Cambrian shales (east side), away from the granitic intrusion, were not affected by contact metamorphism.

8.4 Characterization of Rock Mass

The distribution of RMR values calculated systematically during excavation allowed us to evaluate the rock mass quality at each end of the tunnel. RMR values are higher on
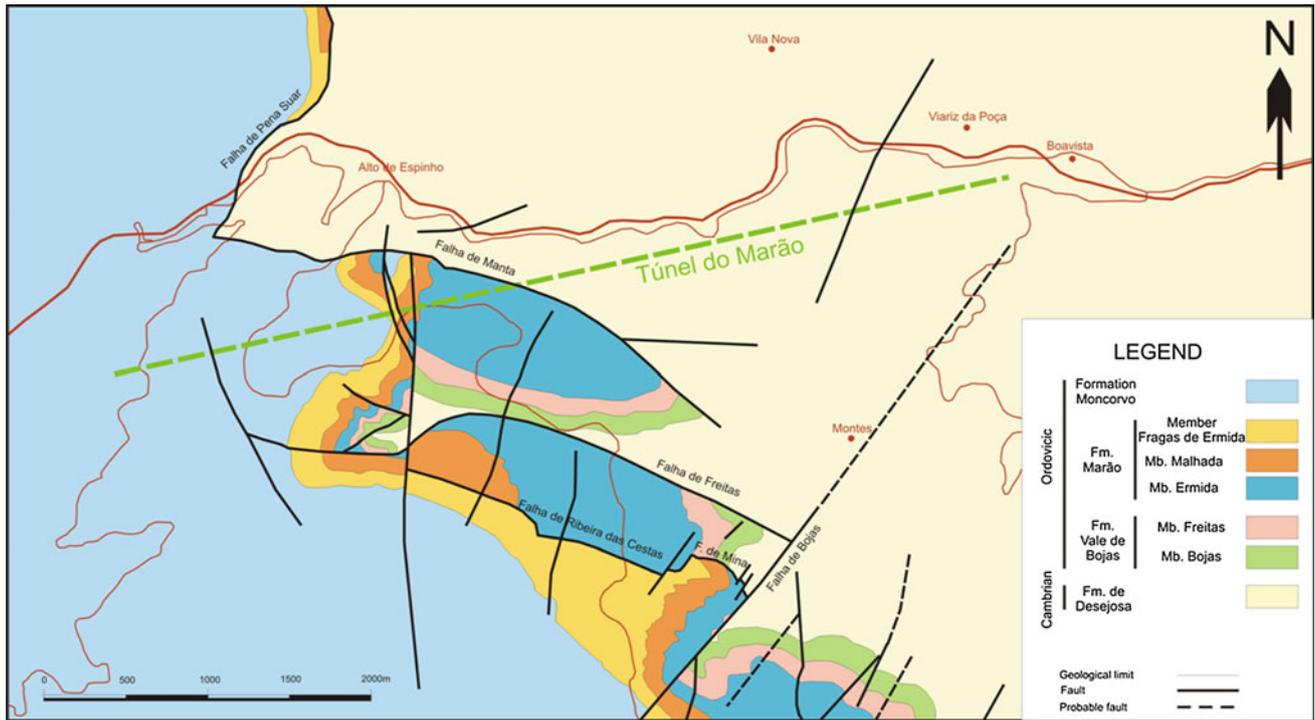
Fig. 8.1 Geological map of the tunnel area (Coke 2000)
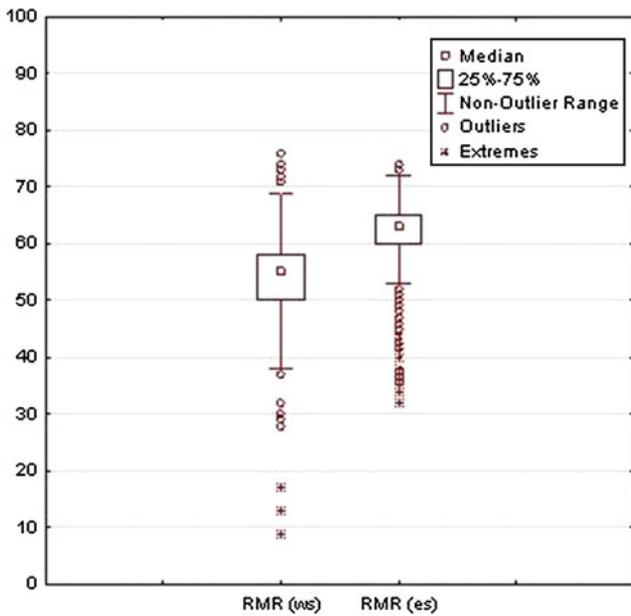
Fig. 8.2 Statistics RMR observed for the west side and east side of the tunnel

the east side, but show minor dispersion at the west end, which indicates greater heterogeneity of the rock mass in west side (Fig. 8.2).

RMR was used to divide the rock mass into various geotechnical zones, as defined in the design. The relative length of witch zone is present in Fig. 8.3.

Applying the MCA is possible to see that in the west side of the tunnel (Fig. 8.4a left), the ZG1(better geotechnical zone) is defined "equally" by all parameters of Bieniawski classification. The major factors in the definition of ZG2 were the discontinuities spacing—F2 and RQD values in the interval of 50–75 %. The ZG3 is defined by UCS results between 25 and 50 MPa and ZG4 (weaker geotechnical zone) is characterized by UCS results of 5–25 MPa and RQD values <25 %.

At the east side (Fig. 8.4b), the MCA shows that ZG1 all parameters of Bieniawski classification have influenced the RMR values obtained. The ZG2 is mainly conditioned by the characteristics of the weak discontinuities and ZG3 is defined by characteristics of the very weak discontinuities. The ZG4 (weaker geotechnical zone) was not found in the east side of the tunnel.

As known, different parameters are involved in RMR value, but some are more important to define each geotechnical zone and they are different for each side of the tunnel. While at the west end the characteristics associated with weaker geotechnical zones (ZG2, ZG3 and ZG4) are the UCS and RQD, at the east end the characteristics related with the discontinuities prevail (east side has no ZG4). On

Fig. 8.3 Frequency of geotechnical zone

Fig. 8.4 MCA of rock mass characteristics. West side (*left*). East side (*right*)

the better geotechnical zone (ZG1) all the parameters are important and present more or less in the same way on both sides of the tunnel.

8.5 Conclusions

Along Marão tunnel, the regional geological environment plays an important role in the characteristics of the rock mass encountered. The presence of contact metamorphism at the west end of the tunnel, affected the behavior of the rock mass. The effects of contact metamorphism, are not present at the east end of the tunnel.

The rock mass on the west side is more heterogeneous when compared with the east side, which resulted in a different distribution of the values of RMR observed, with generating lower values on the west side.

Among the parameters used to calculate RMR, some are particularly associated with a geotechnical zone and are different on each end of the tunnel. With identical lithologies at both ends of the tunnel, this fact reinforces that the importance of regional geological environment, is controlling the geotechnical characteristics present in the rock mass.

The lower quality of the rock mass observed on the west side of the tunnel, implies a distribution of rock mass classification in all geotechnical zones defined on design, the

presence of ZG4 and higher percentages of occurrence of ZG2 and ZG3, when compared with the east side of the tunnel.

The presence of more weaker zones in the west side of the tunnel, involved the need to apply larger quantities of support, lower excavation lengths and sometimes half-section excavation. All these factors significantly influence the productivity of excavation.

Bibliography

Bieniawski Z (1989) Rock mass classifications. Wiley, New York, p 251

CJC (2009) Memória descritiva e justificativa do projecto de execução do Túnel do Marão (p 154)

Coke C (2000) Evolução geodinâmica do ramo sul da Serra do Marão um caso de deformação progressiva em orógenos transpressivos. Universidade de Trás-os-Montes e Alto Douro (in Portuguese)

Coke C, Santos V (2012) Geologia estrutural na caracterização do comportamento geotécnico da escavação do Túnel do Marão. *Congresso Nacional de Geotecnia* (p. CD–ROM). Lisboa: Sociedade Portuguesa de Geotecnia (in Portuguese)

Costa-Pereira (1985) A geologia de engenharia no planeamento e projecto de túneis em maciços rochosos. Faculdade de Ciências e Tecnologia da Universidade Nova de Lisboa (in Portuguese)

Davis JC (2002) Statistics and data analysis in geology, 3rd edn. Wiley, New York, p 638

Hill T, Lewicki P (2007) Statistics: methods and applications. StatSoft, Tulsa, p 800

Pereira E (1987) Estudo geológico estrutural da região de Celorico de Bastos e sua interpretação geodinâmica. Faculdade de Ciencias da Universidade de Lisboa (*in Portuguese*)

Sá A, Meireles C, Coke C, Gutiérrez-Marco J (2005) Unidades litoestratigráficas do Ordovícico da região de Trás-os-Montes (Zona Centro-Ibérica, Portugal) (in Portuguese)

Development of Probabilistic Geotechnical Ground Models for Offshore Engineering

9

Konstantinos Symeonidis and Clark Fenton

Abstract

Traditional offshore site investigation (SI) practice focuses on characterising ground conditions around a single asset and its spatially-limited foundations. Applying a conventional approach to both widely distributed and deep water sites often limits the scope of geotechnical data gathering to principally remote geo-physical sensing combined with sparse sampling of questionable representative-ness. SI design can be improved to cope with distributed assets and multiple geo-hazards, while better SI sequencing and recent advances in geophysical techniques have improved the SI process considerably. However, the time and cost implications of applying these advances are potentially unacceptable when dealing with multiple facility footprints distributed over broad areas of seabed with complex, heterogeneous ground conditions, *e.g.*, wind farm developments on the UK continental shelf. A cost-effective alternative that integrates the inter-disciplinary SI functions better and embraces probabilistic ground models is required. Applying techniques developed for seismic hazard assessment with limited data sets, probability distribution functions can be derived allowing rational, fact-based 'forecasts'. This approach permits limited datasets to be evaluated for both epistemic uncertainty (data paucity) and aleatory (natural) variability, allowing the selection of representative geotechnical parameters. Probabilistic methods and spatial analysis techniques are applied to synthetic models of the seabed for the purpose of testing the effect of sampling, size and pattern, in accurately determining soil parameters, such as the undrained shear strength and friction angle or engineering parameters like pile penetration depth. A number of different sampling patterns are examined. The results suggest that there is a relation between pattern efficiency in describing the uncertainty and the existence of spatial trends in soil parameters or the existence of features like buried channels. These approaches have the potential to increase the efficiency of offshore SI, leading to more cost effective foundation design.

9.1 Introduction

The increasing development of multi-asset offshore projects has resulted into the need for better understanding of the complexities involved in their foundation design. It is important to understand how representative are the collected and tested samples in terms of geotechnical strength parameters and seafloor conditions. It is important to

K. Symeonidis · C. Fenton (✉)
Department of Civil and Environmental Engineering,
Imperial College, London, UK
e-mail: c.fenton@imperial.ac.uk

K. Symeonidis
Mott MacDonald, Glasgow, UK

understand how the chosen sampling patterns may affect the efficiency of the investigation. Natural phenomena commonly exhibit variability in their characteristics, which means that they cannot be predicted with absolute certainty. Deterministic geotechnical analysis can be more easily applied when parameter uncertainties are low and materials and their geometries are known with a degree of accuracy. However, in geotechnics most parameters used in analysis are uncertain, often because of a limited sampling programme. Engineers typically deal with this uncertainty by choosing conservative values for these parameters (Nadim 2007). In the offshore environment uncertainties include design loads and the structure's resistance (Baecher and Christian 2003).

Probabilistic techniques can complement traditional deterministic analysis, by quantifying the degree of uncertainty, evaluating the data acquisition strategies and assessing hazards (Fenton 1997).

9.2   Sampling Strategies

Sampling strategies are considered during the site investigation phase of a project and decisions should be made on sample size, pattern and density. Typical sampling schemes include: random; gridded; uniform; clustered; and traversed. The selection of sampling pattern depends on the geological setting and the expected variations within the sampled population. The sampling scheme must avoid under-sampling or even over-sampling a sub-population, for example stratification, thereby introducing data bias. Spatial

functions can be used to describe the variation of geological and geotechnical parameters. Spatial functions are continuous and typically observations closely spaced are auto-correlated. Dealing with spatial functions using classical statistics may not be adequate, thus regionalised variables may be required (Symeonidis 2012). This considers the properties of the spatial function and disregards the nature of the physical phenomenon (Olea 1984). Using probabilistic modelling and spatial analysis it is possible to evaluate the effect of the sampling parameters and to measure the influence in site investigation design.

9.3   Model Development and Statistical Evaluation

Symeonidis (2012) developed an approach to evaluate the efficiency of differing sampling strategies in obtaining representative geotechnical data. Synthetic data are created for two ground models Scenario 1 and Scenario 2 (Fig. 9.1). Each model describes a relatively simple setting consisting of an upper clay layer and a lower sand layer. For each model a number of parameters are provided along with their coordinates. These parameters are later considered as random variables in our analysis. These model parameters are:

- Mudline undrained shear strength (kPa)
- Variation in undrained shear strength for clay with depth (kPa/m)
- Angle of friction (°) for the lower sand layer
- Clay layer thickness (m)
- Pile penetration depth (m) calculated using API-RP2A.
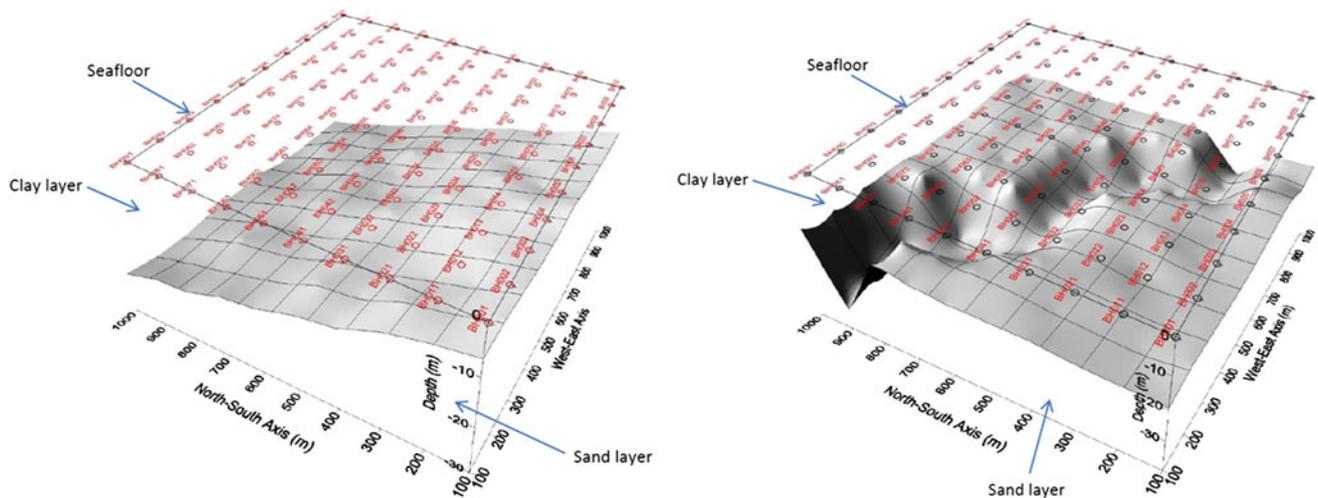
Fig. 9.1 *Scenario 1* a seabed defined by a clay layer and an underlying sand layer. The surface between the two layers is inclined towards the North. For this scenario 100 boreholes are given arranged in an equally spaced grid with separation distance 100 m, aligned to the North–South and East–West directions. *Scenario 2* a seabed defined by a clay layer

and an underlying sand layer. The sand layer forms a trough that it is roughly directed from NW to SE. Also, for this scenario 100 boreholes are given arranged in an equally spaced grid with separation distance 100 m, aligned to the North–South and East–West directions. The *grey* surface marks the boundary between the two layers

The data are provided in the form of a 10 by 10 rectangular grid of synthetic boreholes (BH) at 100 m intervals. Each BH contains the geotechnical parameters described above. The area of data coverage for each model is 1 km^2.

Different sampling patterns are the defined (Fig. 9.2). Then the completeness of these samples is statistically compared to the global population (herein called the Representative Sample [RS]) for each model. The analytical procedure involves the following approaches for each model

parameter: A: Descriptive statistics (histograms and frequency unit area diagrams). B: Inferential statistics (normal and lognormal distributions). C: Spatial analysis (contour maps with kriging and trend analysis with plane surface fit using polynomial regression). D: Sampling comparison. For each sampling pattern and sampling effort the sample is compared to the corresponding RS. The measures used for the comparisons are: (1) percentage difference between the mean values of the samples and the RS and (2) the maximum

Fig. 9.2 Typical sampling patters. **a** Random, **b** grid, **c** traverse 1, **d** traverse 2, **e** regular clustered, and **f** intersecting traverse
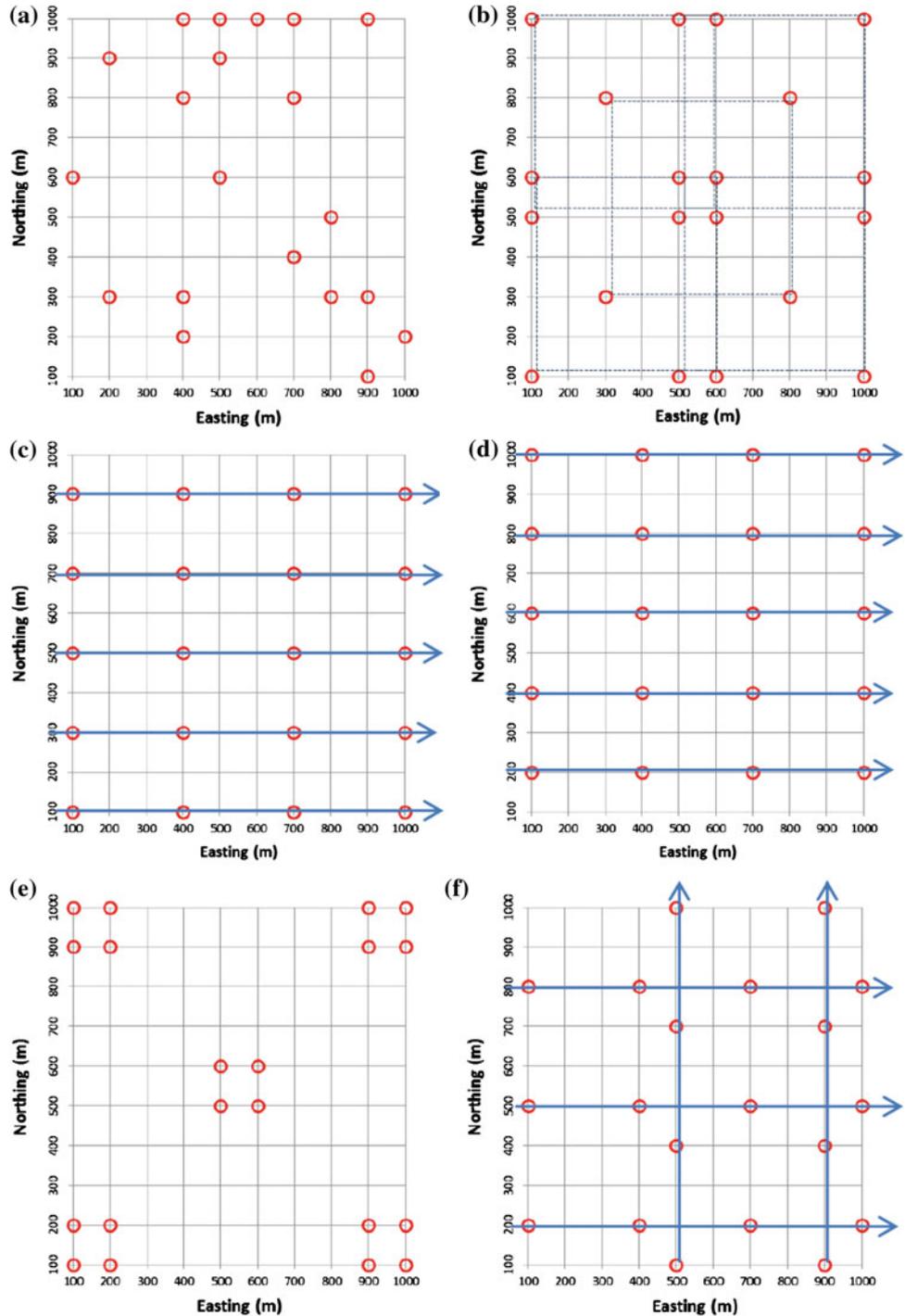
absolute difference of the theoretical distributions (normal and lognormal) defined by the sample and the RS, based on the K–S test formulation. From these comparisons the sampling patterns are ranked according to their efficiency. E: Kriging comparison: using the depth to the layer interface (derived from the model parameter z). Contour surfaces are created for each sampling pattern at the 3rd sampling effort (12 BHs) for Scenario 1 and for 3rd (12 BHs) and 5th (20 BHs) sampling efforts for Scenario 2. These contour surfaces are compared to the contour surfaces of the representative samples.

Sampling patterns (Fig. 9.2) are defined and tested on each models. The same maximum number 20 out 100 of sampling points for each pattern is applied. For each pattern, five (5) increments of four (4) new sampling points are added at each test iteration. Each of these increments is referred to as a sampling effort. For each pattern a custom Visual Basic (VBA) routine is created that applies the sampling procedure consisting of five sampling efforts (Fig. 9.2).

The first step in setting up the probabilistic modeling analysis is defining the procedures applied. For each parameter the workflow is applied for its Representative Sample (RS) and then for each sampling effort of the different sampling patterns. The formulation of the probabilistic model for each model parameter is performed in two parts (Fig. 9.3). Initially calculation of the descriptors of randomness is performed. Secondly the statistical distribution that best fits the empirical distribution derived in the initial stage is defined. Following selection of the distribution describing data variability, parameters that uniquely define this distribution are derived, along with tests that quantify the degree of fitness. Furthermore, based on the above analysis probabilities can be calculated from the proposed model distributions.

The spatial variability of the model parameters is displayed using contour maps that utilize point kriging. Trend analysis is then applied for each model parameter. This is modelled by a linear equation in the more simplistic approach along certain traverses at each model, using the least squares method. Trend analysis using the polynomial regression is also used to define large-scale trends and patterns in the data. Finally residual analysis is conducted for traverses along the model where the autocorrelation function is modelled for each RS for all model parameters.

Comparisons are performed in order to evaluate the efficiency of each sampling pattern in representing as accurate as possible each model parameter. Also, the performance of each sampling pattern is evaluated as the sampling efforts increase the sample size. The measures used are:

- Percentage difference between the mean values of the RS and each sample.
- Maximum absolute difference of the theoretical distributions (normal and lognormal) defined from the RS and each sample.
- The kriging technique for the parameter.

Contour surfaces are created for each sampling pattern. The difference between each sampling effort and the RS are mapped using kriging technique in order to evaluate the degree of difference. Sampling patterns with the smallest differences spatially are more efficient.

9.4 Results

Based on the statistical differences between the mean values for the parameters in the sampling efforts and the RS for each scenario the following observations are made:

Fig. 9.3 Schematic of the probabilistic modelling workflow
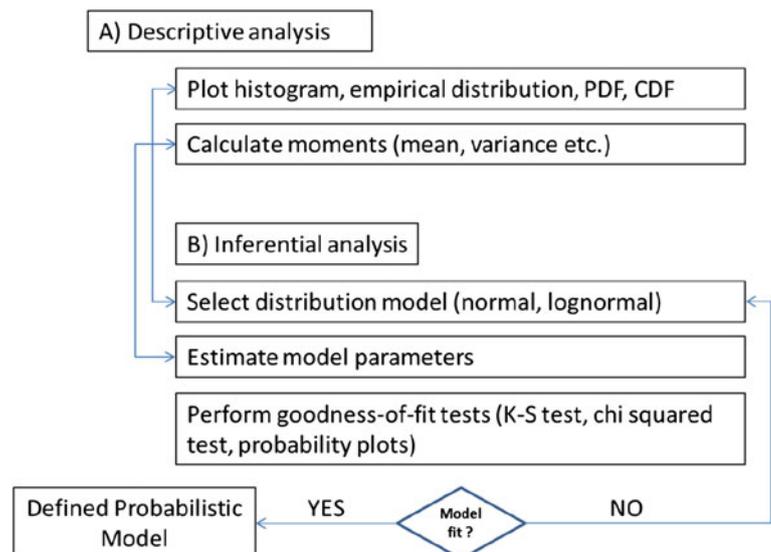
- Grid type sampling patterns (grid, traverse, and intersecting traverses) perform better when there is a distinct spatial trend in the parameter variability
- When the RS shows no spatial trend or when the range of variability is limited grid sampling shows limited advantage over random or clustered sampling patterns
- Sampling perpendicular to spatial trends has a poorer than expected efficiency. Intersecting traverse lines are more efficient than parallel traverses in this case.

These results are similar to those obtained by Olea (1984) using a universal kriging technique. In terms of efficiency of capturing the variability of the RS, regular sampling followed by stratified, then random and finally clustered sampling patterns, are most efficient.

When investigating depth parameters (the location of the clay-sand interface in the scenario models) inclined planar surfaces are best approximated using regular grid sampling. Elongated topography (the buried channel in Scenario 2) is best approximated using traverse sampling perpendicular to the trend of the feature. With increasing sampling points a uniform grid pattern becomes more efficient.

References

Baecher GB, Christian JT (2003) Reliability and statistics in geotechnical engineering. Wiley, Hoboken

Fenton GA (1997) Probabilistic methods in geotechnical engineering. Workshop presented at ASCE GeoLogan

Nadim, F. (2007) Tools and strategies for dealing with uncertainty in geotechnics. In: Probabilistic methods in geotechnical engineering, pp 71–95

Olea RA (1984) Sampling design optimization for spatial functions. Math Geol 16(4):369–392

Symeonidis K (2012) Development of probabilistic geotechnical ground models for offshore engineering, Unpublished M.Sc. thesis, Imperial College London, p 115

Baixo Sabor (Portugal) Upstream Dam Foundation: From Design Geological Predictions to Construction Geological Facts and Geotechnical Solutions

Jorge Neves, Celso Lima, Fernando Ferreira, and João Machado

Abstract

The upstream scheme of Baixo Sabor Hydroelectric Development includes a 123 m high dam with a crest length of 505 m. Two important geological faults that could affect the foundation of the dam were identified and characterized during the exploration works executed in the design phases. The foundation mapping performed during the construction phase allowed a detailed knowledge of these geological structures and complemented the existing data used by EDP for the detailed design of the engineering foundation treatment solutions.

Keywords

Sabor • Dam • Foundation • Fault • Treatment

10.1 Introduction

The Baixo Sabor Hydroelectric Development that EDP—Energias de Portugal, S.A. has under construction at the north of Portugal, at the Sabor River, a right bank tributary of the Douro River, includes two schemes located 12.6 and 3 km upstream of Sabor river mouth.

The upstream scheme (Fig. 10.1) is the largest and includes a concrete arch dam 123 m high with a crest length of 505 m and a total concrete volume of 670,000 m³. A controlled surface spillway is located in the central part of the dam, having four 16 m wide spans controlled by radial gates with a discharge capacity of 5,000 m³/s into a downstream plunge pool basin. At the right bank, the powerhouse is equipped with two reversible units, located in independent 79 m high and 11.5 m diameter shafts, topped by an unloading and erection building. Two independent and approximately parallel 5.7 m diameter headrace tunnels intersect the rock mass under the dam, connecting the reservoir with the powerhouse, with a 94 m head. The tailrace includes 2 tunnels and an outlet structure to operate the sluice gate.

The upstream dam is placed in a 1 km long NE–SW valley segment, with a deep, narrow and slightly asymmetrical transversal profile, 25 m wide at the base and 440 m at the crest level. The dam foundation consists in a medium to coarse grained, two mica, porphyritic granite, frequently showing mica orientation.

During the design phases, from mid-1990s to 2006, the performed geological and geotechnical investigations and characterization studies included detailed mapping of 13 trenches (2,300 m) and 6 galleries (180 m), 15 seismic refraction profiles and 3 electrical apparent resistivity profiles, 38 diamond drill holes (2,186 m), 388 Lugeon tests, 14 seismic refraction cross-hole sections, 41 borehole dilatometer (BHD) and 4 large flat jacks (LFJ) tests for in situ rock mass deformability evaluation, 3 stress tensor tube tests (STT) for in situ stress assessment, 31 joint shear tests and 18 sound velocity and 18 unconfined compressive strength tests.

J. Neves (✉) · C. Lima
EDP—Energias de Portugal, SA, Porto, Portugal
e-mail: jorgepacheco.neves@edp.pt

C. Lima
e-mail: celso.lima@edp.pt

F. Ferreira · J. Machado
Geoárea—Consultores de Geotecnia e Ambiente, Alfragide, Amadora, Portugal
e-mail: fernando.ferreira@geoarea.pt

J. Machado
e-mail: joao.machado@geoarea.pt

These exploration works and geotechnical characterization tests allowed the foundation to be subdivided into 3 zones. From the shallowest to the deepest, these zones are characterized, in average, by the following parameters:

- ZG3: W3–W5, F3–F5, RQD < 50 %, RMR < 40, $E_m \leq 5$ GPa, $\sigma_c < 35$ MPa
- ZG2: W2–W3, F2–F4, 50 % < RQD < 90 %, 37 < RMR < 64, $E_m = 7.5$ GPa, $\sigma_c = 53$ MPa
- ZG1: W1–W2, F1–F3, RQD > 90 %, 54 < RMR < 72, $E_m = 17.5$ GPa, $\sigma_c = 126$ MPa.

10.2 Design Geological Predictions

The geological investigations performed at the upstream Baixo Sabor dam site, particularly the trenches and galleries mapping complemented by drill hole data, allowed the identification and characterization of two important bedrock faults that influenced the foundation design and the slope excavations of adjacent slopes.

The first (fault nº 24) was identified at the left bank trenches, striking N10ºE and dipping 65ºE, filled with a 10–15 m thick quartz vein at the hanging wall and 3–4 m thick of sheared kaolinitized granitic mylonite (Fig. 10.2) at the footwall, predictably affecting the upstream slope excavation and the dam left abutment foundation. This clayey mylonitic zone was of particular concern to EDP designers due to its significant thickness, high deformability and unfavorable location that could cause slope stability and foundation deformability and permeability difficulties.

The second important geological structure was fault nº 11, a 10–15 m thick fault zone at the bottom of the valley, inferred by geomorphological interpretation and detected by rotary core drilling (core recovery losses, gouge fragments, intense rock mass fracturing and weathering) and later on, by seismic refraction cross hole sections performed inside exploration drill holes.

This geological structure was interpreted as a sub vertical fault zone that consisted in a few approximately parallel, N30ºE, sub vertical minor faults (Fig. 10.3) with decimetre- to metre-scale thick gouge filling, separated by intensely sheared ZG3 granite with low deformability modulus. The fault zone low to moderate permeability (2–8 Lugeon units) was attributed to fault gouge washing and fracture filling.

10.3 Construction Geological Facts

The rock mass geotechnical zoning analysis confirmed that the dam foundation was mostly composed of fresh to moderately weathered (W1–W3) granite with moderate to completely weathered (W3–W5) zones associated with faults (Fig. 10.4). Joints, wide to closely spaced (F2–F4), were assigned to 6 major sets. Tectonic structures such as quartz and pegmatite veins less than 0.5 m thick occur throughout the surface. Faults, assigned to 3 sets, are generally filled with clayey gouge and rock particles up to 0.5 m thick, bordered by irregular zones of highly weathered (W4–W5) rock mass with closely spaced discontinuities.
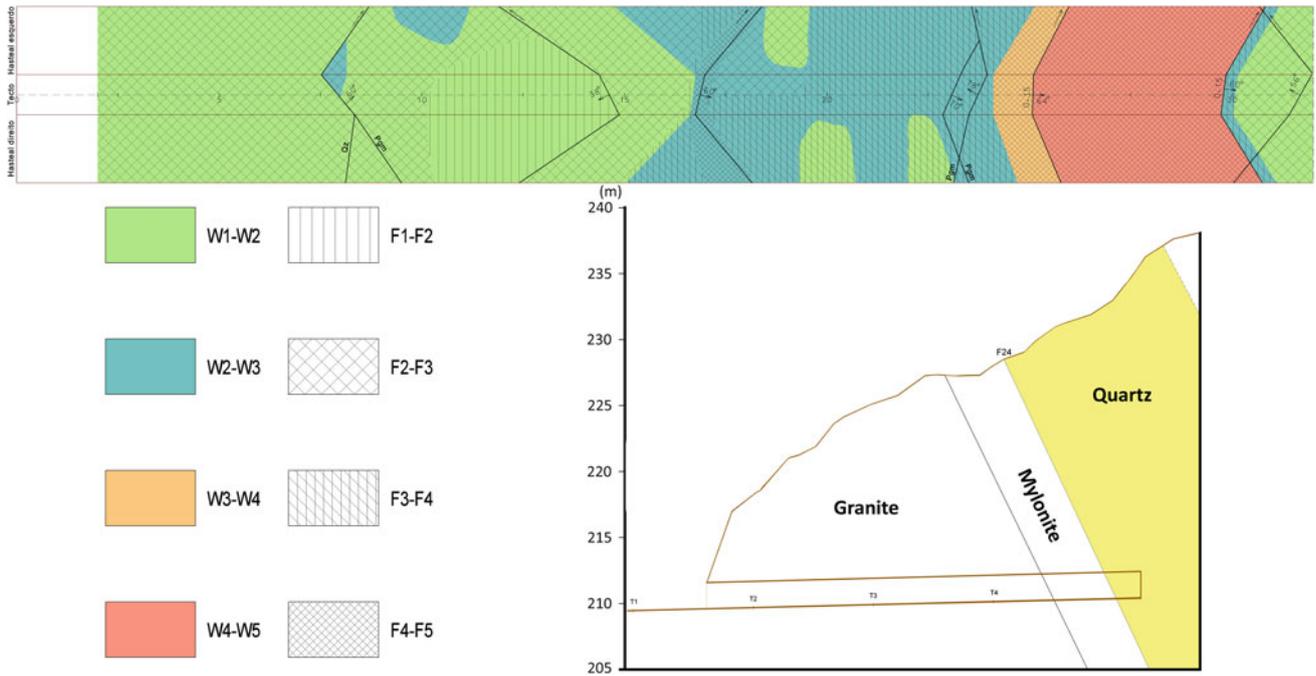
Fig. 10.2 Ceiling and wall mapping of GE1 gallery (walls folded to horizontal). W4–W5 zone corresponds to fault's mylonitic footwall, below quartz vein
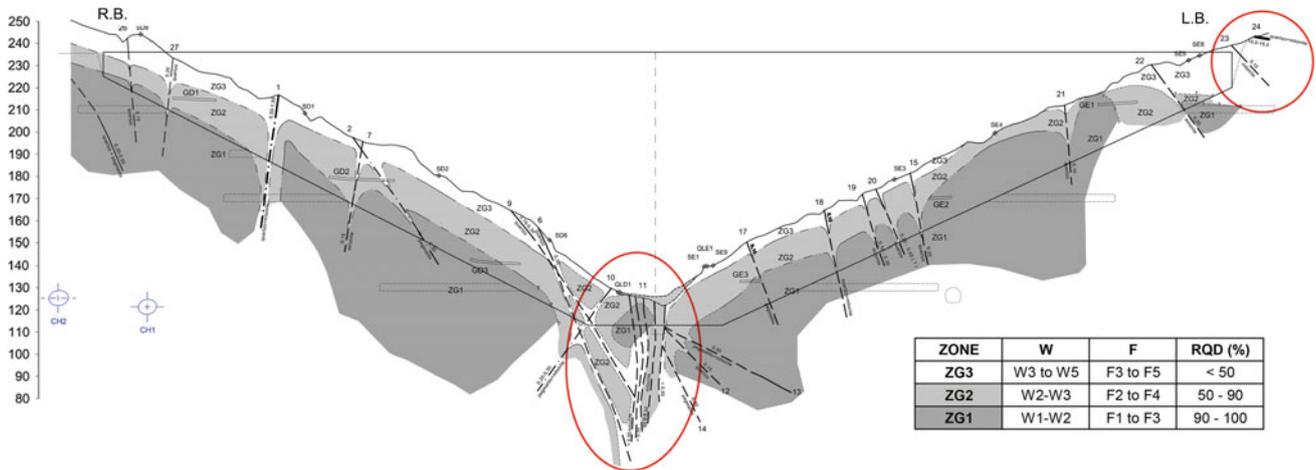
Fig. 10.3 EDP's design phase geological and geotechnical zoning—section through dam reference surface. Fault zones referred in text are inside *red ellipses*

Fault nº 24, at the left abutment, N8ºW-0º-26ºE, dipping 50º–70ºESE, has a 2–5 m thick footwall mylonitic zone with sandy clay fill, gouge fragments and intensely weathered and fractured granite and quartz. At the hanging wall occurs a quartz vein of 8.5–14 m thick mixed with hydrothermally altered granite (Figs. 10.4 and 10.5).

A large fault zone occurs at the bottom of the valley, bordered by 2 sub parallel major alignments (A and C), N10º-40ºE, dipping 60ºNW-90º (Figs. 10.4 and 10.6). They are filled with 0.05–0.5 m of clayey gouge at the hanging wall and have a 2–3 m thick weathered and highly fractured

rock mass zone at the footwall. These faults are linked by a dip-slip fault (B), N55ºE, dipping 70ºSE-90º-80ºNW with a 0.1–0.2 m thick mylonitic sandy clay fill and a 1.5 m thick associated weathered and highly fractured rock mass zone. A and B faults were included in fault zone nº 11, identified during the design phase and fault C corresponds to fault nº 10.

Fault E (Fig. 10.4) is a N20ºE sub vertical fault that occurs at the right bank of the Sabor river. Its fill includes a1–2 m thick quartz mass and a clayey mylonite with rock particles. Several other discontinuities occur throughout the
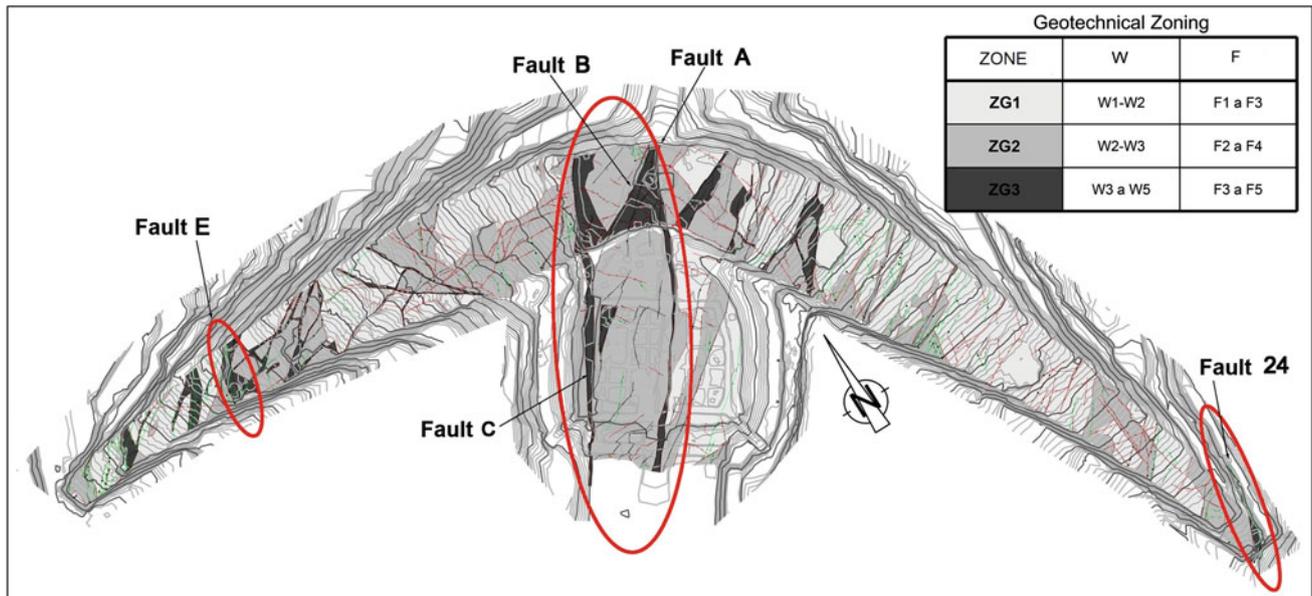
Fig. 10.4 Geoárea's simplified geological map and dam foundation geotechnical zoning. Fault zones referred in text are inside *red ellipses*
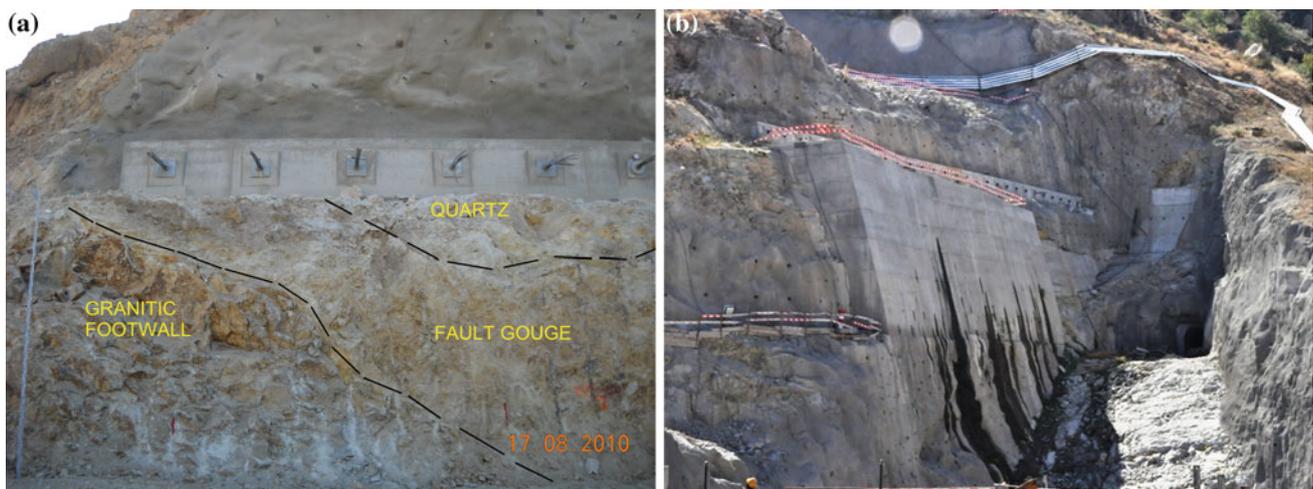
Fig. 10.5 **a** Fault nº 24. **b** Support wall and pre-stressed anchor beam

dam foundation but they weren't considered a geotechnical problem due to the reduced thickness of their fills and associated alteration zones.

10.4 Geotechnical Solutions

Dam foundation excavation depths were designed by EDP in order to guarantee an adequate embedding, mostly on good quality granitic rock (ZG1-dark grey zone in Fig. 10.3). The total excavation volume reached 560,000 m^3 and some foundation reconstitutions had to be made in lower quality

fault related sectors, such as nº 10/11 (A, B, C) and nº 24, but also in smaller ones like fault E.

The treatment solution executed on fault nº 24 near the left abutment, consisted of a support wall 8.5 m high and 30 m long, concreted against the upstream slope of the dam foundation excavation, below an anchored beam built as shown in Fig. 10.5, with the main objective of stabilizing that slope and the rock mass above it.

At the river bed, fault material was replaced by reinforced concrete several meters deep, on faults A, B and C (Figs. 10.4 and 10.6). Between the contraction joints 19 and 20, an additional gallery parallel to fault C was left inside the
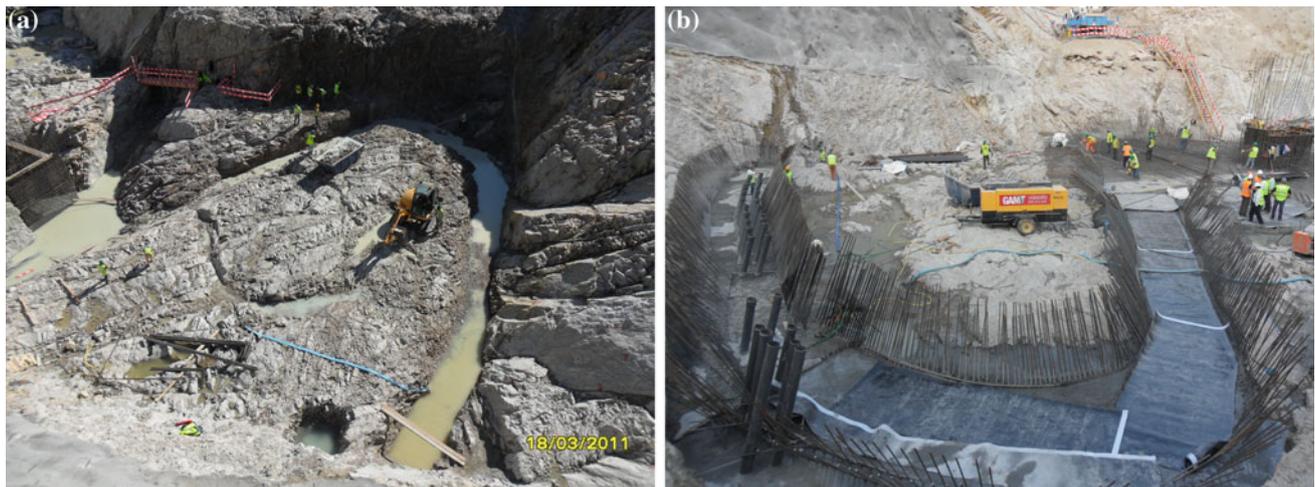
Fig. 10.6 **a** River bed faults excavations (*facing downstream*). **b** Placed reinforced concrete and PVC molds for posterior cement grout injection (*facing upstream*)

Fig. 10.7 Plan showing grout treatment holes configuration for faults A, B and C
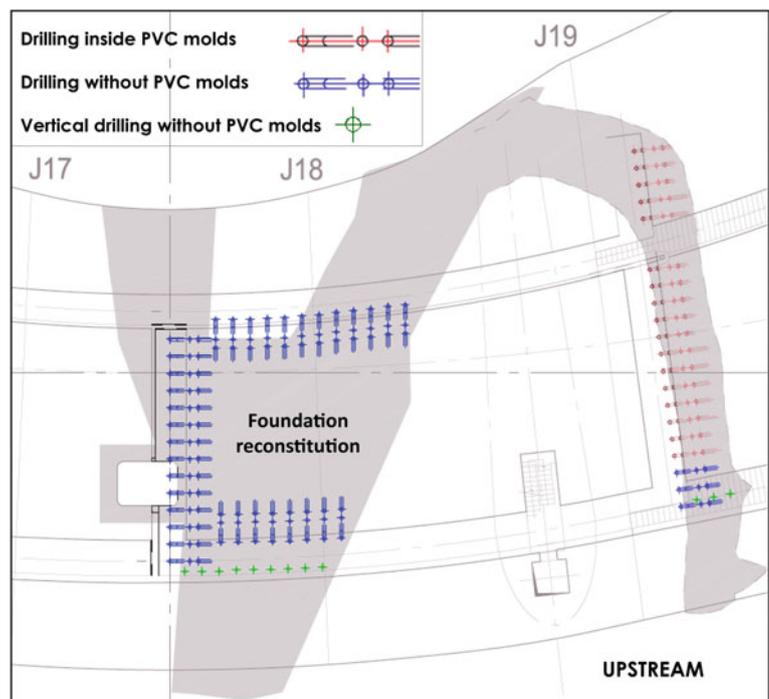
dam, in order to enable an adequate foundation treatment that consisted in fault gouge substitution by cement grout injection along these faults dip direction (Figs. 10.6 and 10.7). When dam concrete reached enough height, these localized treatments were followed by generalized cement grout injection (still ongoing) for foundation rock mass consolidation and waterproofing.

10.5   Final Remarks

The design phase predictions concerning geotechnical zoning and the main tectonic accidents intersecting Baixo Sabor upstream dam foundation were generally confirmed by the detailed geological mapping performed during the

construction phase. These data and those gathered during the design phases allowed the design of dam foundation treatment by generalized cement grout injection and fault zones treatment design solutions, to further improve foundation geotechnical characteristics, i.e. deformability, shear strength and permeability.

The Foundations of Constructions in Dobrogea—Romania, on Water Sensitive Soils, Loess

11

Gabriela Brîndusa Cazacu, Nicolae Botu, and Daniela Grigore

Abstract

This article presents the geotechnical characteristics of loess, wetting sensitive soil in Dobrogea. These lands are of Quaternary age, are found just below the topsoil and most buildings are founded on it. Problems can arise when the foundation on these lands is due to any softening of foundation soil with water from different sources, permanent or casual. It will present the parameters of geotechnical solutions for improvement when appropriate.

Keywords

Loess • Foundation • Dobrogea • Sensitive soil

11.1 Introduction

The loess is a category featured among continental, Quaternary, sedimentary formations.

The name loess was introduced in 1834 by C. Lyell, coming from the German *lose* or *loss,* used in Rhineland, with the meaning of loose, porous, brittle. Loess lands occupy about 10 % of the entire surface of the continents, a spread of loess in the world is shown in Fig. 11.1a, b, North America and China, and in Fig. 11.2 in Europe.

Loess deposits in Romania occupies an area representing 17 % of the entire country. In Dobrogea there are areas where loess thickness is up to 60 m.

11.2 Properties of Loess

Most buildings in Dobrogea are founded on loess and loess soils, hence the need to understand the behavior of these soils and changes in terms of land and loads on which the construction transmits it.

The minimum and maximum values of geotechnical parameters of loess, in the natural state, in the Dobrogea area are listed in Table 11.1.

11.3 The Collapse Risk of the Loess

Problems can arise when the foundation on these regions is due to any softening of foundation soil with water from different sources, permanent or casual.

Because of the extra moisture, the loess can become collapsible.

Depending on the behavior of the loess, increasing of moisture content it has been classified in two categories:

(A) lands which not settles under the geological load, but of deformation under the influence of the loads transmitted by the construction, are not in risk of collapsing.

(B) lands which settles in geological load, they may be in risk of collapsing.

G.B. Cazacu (✉)
S.C. Geotech Dobrogea SRL, 900532, Constanta, Romania
e-mail: brandusacazacu@yahoo.com

N. Botu · D. Grigore
Faculty of Civil Engineering and Building Services, Technical University "Gheorghe Asachi" Iasi, 700050, Iasi, Romania
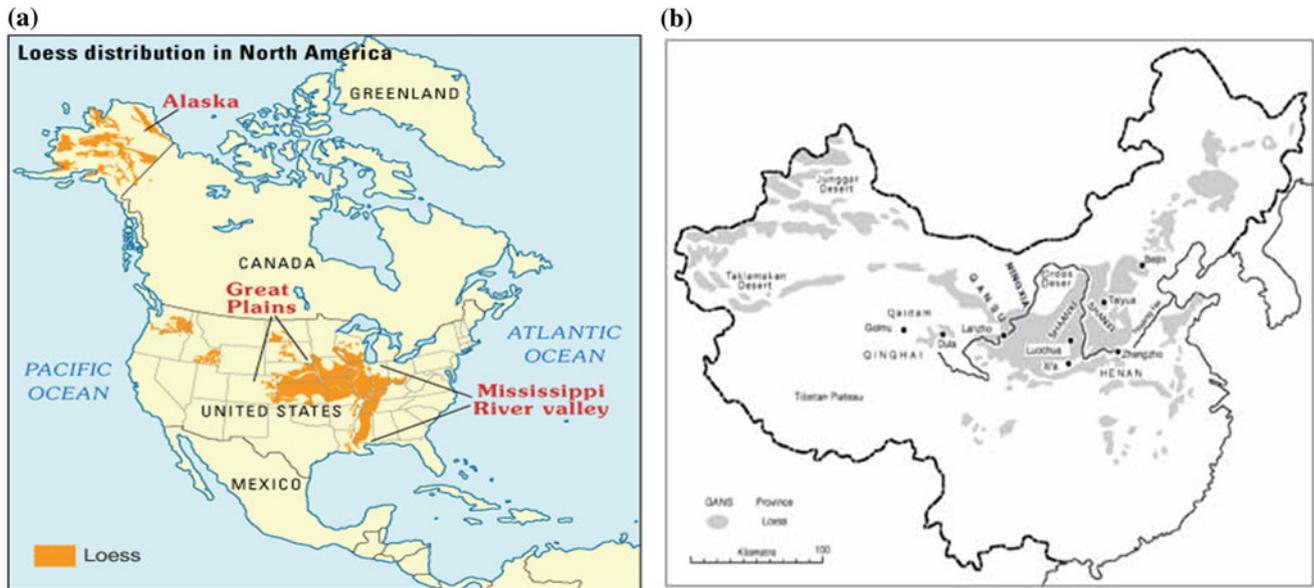
Fig. 11.1 Loess distribution. **a** In America de Nord. **b** China (*source* http://gec.cr.usgs.gov)
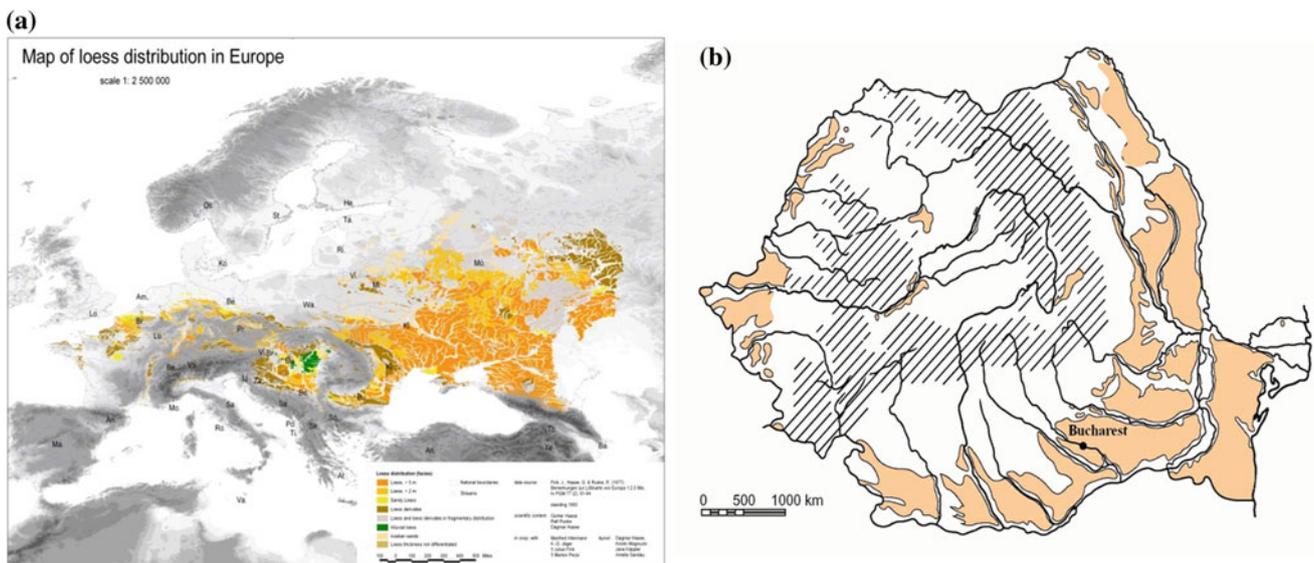
Fig. 11.2 Loess distribution (*source* Dagmar Haase/UFZ). **a** Europe. **b** Romania

Table 11.1 The minimum and maximum values of geotechnical parameters

Param	Clay (%)	Silt (%)	Sand (%)	w_L (%)	w_P (%)	w (%)	n (%)	Sr (%)	M2-3 (daN/cmp)	im3 (cm/m)	ϕ (grade)	c (kPa)
Min	14	50	3	32	12	7.8	46	0.4	18.7	0.6	5	5
Max	29	80	18	40	17	28.5	54	1	107	15	30	48

In order to make a correct classification of a soil, a comprehensive analysis of all the following parameters are required:

- parameters defining its composition and physical properties (granulometry, porosity);

- mechanical parameters: values of the index of the specific subsidence by wetting below the mark of 300 kPa and the structural strength obtained from endometrium testing;
- the thickness of loess, found in the history of the works from the area.

Fig. 11.3 Diagrams of compression subsidence

Load deformation curve
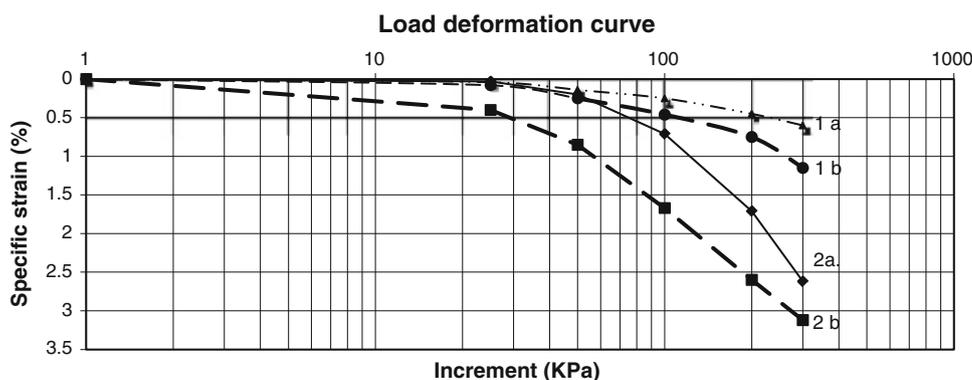
In the Dobrogea region loess of both categories occur, and their structural strength is based on the category they fall into: for 25–60 kPa is loess of category B and for 80–100 kPa is loess of category A.

In Fig. 11.3 are presented the diagrams of compression subsidence for the loesses with a low porosity, soil denoted by 1 and loesses with a high porosity, denoted by 2; (a) samples with natural moisture and (b) samples that were previously flooded.

11.4 Foundation Solutions

To ensure the normal behavior of buildings founded on land susceptible to wetting, there is a need for rational foundation systems and appropriate measures to avoid flooding of the foundation soil, both during and after construction. The humidity action on soils susceptible to wetting must be viewed from two perspectives, namely: the reduction in the bearing capacity and the growth of settlements under construction load transmitted (additional subsidence due to moisture). The foundation solutions are adopted according to the nature of the soil foundation, the hydrostatic level and construction characteristics:

- direct foundation on loess;
- foundation reinforced trough layers of cohesive soils (loess, loess lined with various waterproofing solutions, loess mixed with cement or lime);
- loess consolidation by intensive compaction (hard mallet and super hard) or with different injection solutions, heat treatment;
- adopting a foundation system that exceed sensitive soil layer wetting (deep foundations, piles, columns, etc.) and that are embedded in the insensitive wetting layer.

11.5 Conclusions

The infrastructure and construction on land susceptible to collapse under wetting have created problems. Their stability is not problematic under natural field conditions, but problems can arise if there are additional moistening that can cause deformations of buildings located on these moisted lands.

The special character of these lands is reflected in the fact that for them has been developed a normative—NP 125:2010 "Normative for foundation of construction on land susceptible to wetting". This legislation provides elements for identification, classification, conditions that have to be taken into account in designing, the recommended constructive and operation measures, maintenance and monitoring of buildings and facilities located on such lands.

References

Andrei S et al. La systematisation, le stockage et la reutilisation de informations geotechniques. Principe d' organisation d'une banque des donnees geotechniq

Andrei S et al (2006) The systematization and storing methods of information concerning the geotechnical parameters. XIII Danube European conference on geotechnical engineering, Ljubljana

Cazacu GB Contributions concerning the methods of establishing of geotechnical parameters of soils moisture sensitivity, Ph.D. thesis

Dianu VD (1982) Loess deposits as founding soils. Editura Tehnica

Ferreira RC, Monteiro LB (1985) Identification and evaluation of collapsibility of colluvial soils that occur in the Sao Paulo State. First international conference on geomechanics in tropical lateritic and saprolitic soils, vol I, Brazilia, pp 269–280

Muhs DR (2006) Late quaternary loess in northeastern Colorado: part I-age and paleoclimatic significance. Geol Soc Am Bull 111:1861–1875

Andrei S, Cazacu GB, Zarojanu D The systematization and storing methods of information concerning the geotechnical parameters. XIII Danube European conference on geotechnical engineering, Ljubljana

Influence of Micro-texture on the Geo-engineering Properties of Low Porosity Volcanic Rocks

Ündül Ömer and Amann Florian

Abstract

The geo-engineering properties of rocks often depend on their petrographic, mineralogical and micro-structural features, and the interaction of micro-texture and physico-mechanical properties is often relevant. A series of petro-physical and mechanical tests on low porosity volcanic rocks suggest that small changes in porosity or unit weight can cause strength variations. Petro-physical and quantitative mineralogical analysis were utilized to understand these variations. In addition, quantitative petrographic studies focusing on distribution of minerals and mineral dimensions were conducted. Microstructural studies were carried out on thin sections before and after mechanical loading to analyse the distribution of micro- and macro-cracks which formed during unconfined compression tests. The results of petro-physical, petrographic, micro-structural, and mineralogical analysis suggest, that both, the peak strength and crack initiation threshold are strongly influenced by the distribution of phenocrystals (e.g. biotite, plagioclase) and the ratio between the total content of phenocrystals to the fine-grained groundmass. On the other hand it was found that variations in petro-physical properties (e.g. unit weight) and Young's Modulus are associated with the mass fraction of minerals.

Keywords

Crack initiation • Elastic properties • Unconfined compressive strength • Quantitative petrography • Volcanic rocks

12.1 Introduction

Variations in geo-engineering properties associated with textural variations have been examined by many researchers (Prikryl 2006). Most of these studies investigated changes in petro-physical and mechanical properties based on qualitative and/or semi quantitative petrographical and mineralogical analysis. More recent studies were focused on variations in crack initiation (CI), peak strength (i.e. UCS), and crack propagation associated with micro-textural properties (Eberhardt et al. 1999; Nicksiar and Martin 2013). In this study the effect of micro-texture and mineral constituents on petro-physical (i.e. ultrasonic p-wave velocity V_p) and mechanical properties [i.e. UCS, CI, Young's modulus (E)] were investigated utilizing quantitative mineralogical and petrographic studies.

12.2 Methods

Mineralogy of the samples was determined with X-ray powder diffraction analysis (XRD). The quantitative mineral composition of the samples was determined with the Rietveld program AutoQuan (GE SEIFERT). Petrographic studies were used to trace the boundaries of individual minerals (e.g. plagioclase, amphibole, biotite) to quantify

Ü. Ömer (✉)
Geological Engineering Department, Istanbul University, 34320 Istanbul, Turkey
e-mail: oundul@istanbul.edu.tr; omer.undul@erdw.ethz.ch

Ü. Ömer · A. Florian
Engineering Geology, Swiss Federal Institute of Technology, 8092 Zurich, Switzerland

their area and distribution. Each mineral grain with a major axis >200 μm was traced. Mineral grains with a major axis <200 μm were considered as groundmass.

Unconfined compression tests were accomplished on a servo-hydraulic rock testing device with a digital feedback control. Axial load was applied in such a way as to maintain a constant radial displacement rate of 0.03 mm/min). Two strain based methods were used to determine the stress at CI: (1) according to Brace et al. (1966) and (2) according to Lajtai (1974).

12.3 Results and Interpretation

12.3.1 Mineralogical, Petrographic and Microstructural Properties

Macroscopically, the samples are composed of varying amounts of plagioclase, amphibole and biotite as phenocrysts and fine grained groundmass (Table 12.1). The areas of phenocrystals in respect to the investigated areas are given in Table 12.2. It should be noted that quartz and orthoclase were very rarely observed as phenocrystals, but the mass proportion of these minerals were considerably high (Table 12.1). These findings suggest that almost all of the orthoclase and most of the quartz exist within the groundmass. Thin sections taken after mechanical loading revealed that cracks initiate along boundaries between different minerals, and along the mineral—groundmass boundary. Cracks penetrating groundmass and Biotite phenocrystal are interpreted to form at higher axial stress (Ündül et al. 2013).

12.3.2 Physical and Mechanical Properties

With increasing orthoclase content the unit weight tend to decrease. Increasing content of quartz and plagioclase increase the unit weight (Fig. 12.1). This is most probably related to the higher density of quartz (2.63–2.65) and plagioclase (2.62–2.76) relative to orthoclase (2.55–2.63). An increasing mass fraction in plagioclase was also associated with an increase in V_p. On the other hand, the normalized area of basic microstructural components (Tables 12.2 and 12.3) did not provide any relations between unit weight and V_p.

Table 12.2 Normalized area of basic microstructural components obtained from thin section studies

SG	Groundmass (%)	Amphibole (%)	Biotite (%)	Feldspars (%)
1	51–59	2–16	2–9	13–34
2	54–56	5–21	4–13	18–24
3	47–63	11–26	0–13	12–34
4	53–61	4–20	1–9	16–40

SG sample group, *Feldspars* plagioclase felds + alkali felds

The study also suggests that with increasing mass fractions of quartz and plagioclase the Young's modulus increases (Fig. 12.2). An opposing effect on E was found for an increasing mass fraction of orthoclase. These tendencies might be associated with the different Young's modulus of these minerals [e.g. Quartz: 91–105 GPa; Orthoclase: 73–74 GPa; Plagioclase: 81–106 GPa, (Data provided from Prodaivoda et al. 2004)] and their net contribution to the bulk Young's modulus. Changes in Poisson's ratio were only dependent on changes in the normalized area of the ground mass. The Poisson's ratio decreases as the normalized area of the groundmass increases.

Unconfined compressive strength tests revealed UCS values ranging from 103–289 MPa. Only some specimen showed macroscopic cracks at failure. The crack initiation level was found to be 0.45–0.46 × UCS (Fig. 12.3).

It was observed that with an increasing normalized area of plagioclase and amphibole phenocrysts (i.e. normalized area of the groundmass decreases), CI and UCS increase (Fig. 12.4). Furthermore the data suggest that the UCS decreases with an increase in the normalized area of Biotite phenocrystal.

Ündül et al. (2013) showed on UCS test on Andesite specimens that cracks emanate from the boundaries of larger grains and penetrate the groundmass which primarily consists of orthoclase and quartz (Table 12.1). For larger normalized area of the groundmass, cracks, which formed under unconfined compression, were composed of cracks parallel to the maximum applied load and oblique cracks. With increasing phenocrystal area axial cracks dominate. This change in failure mechanism was associated with an increase in the radial strain in respect to the axial strain for axial stresses in excess of CI.

Table 12.1 Variations in mass fractions of dominant mineralogical components obtained with XRD studies

SG	Amph (%)	Biotite (%)	CM (%)	Orth. (%)	Plag. (%)	Quartz (%)
1	3.1–4.9	2.1–2.5	1.1–2.0	22.8–23.5	45.6–47.8	13.0–13.5
2	17.6–19.4	0.5–1.8	1.2–1.6	24.0–25.1	25.0–28.9	10.2–12.1
3	15.2–17.1	0.5–1.3	1.2–1.5	21.2–21.9	35.9–39.4	14.0–14.6
4	5.7–6.9	1.6–1.9	3.6–5.4	21.0–22.1	40.9–42.7	11.8–12.4

SG sample group, *Amph* amphibole, *CM* clay minerals, *Orth* orthoclase, *Plag* plagioclase
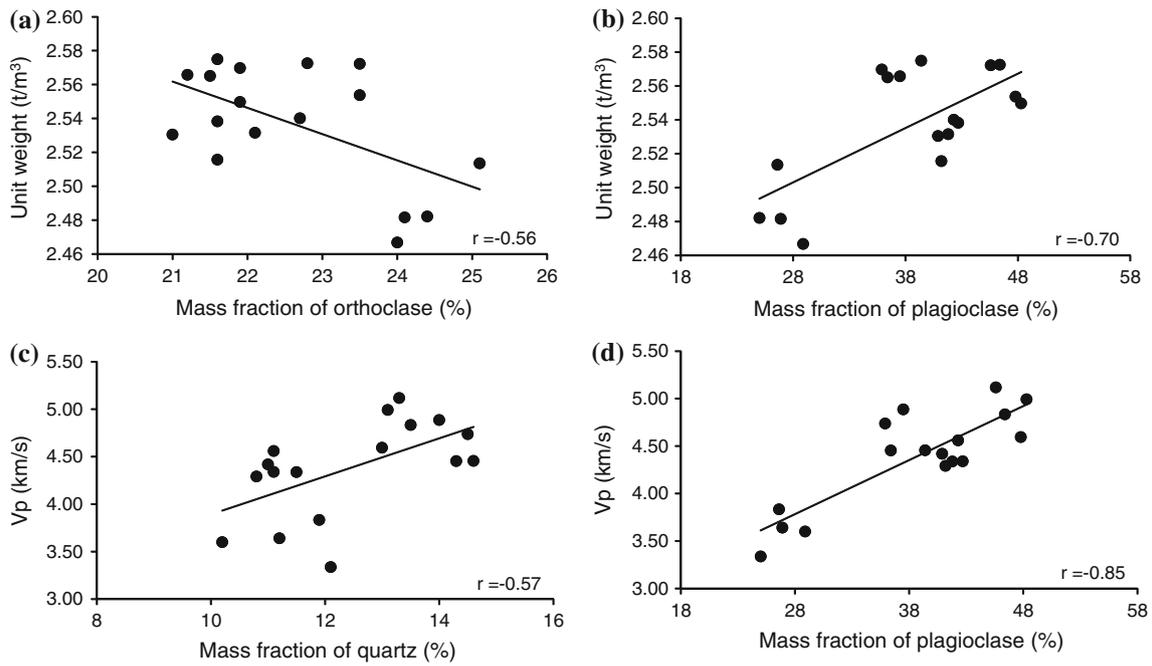
Fig. 12.1 The change of basic physical properties with mass fractions of different minerals. **a** Unit weight versus mass fraction of orthoclase. **b** Unit weight versus mass fraction of plagioclase. **c** V_p versus mass fraction of quartz. **d** V_p versus mass fraction of plagioclase

Table 12.3 Minimum and maximum values of some mechanical properties

SG	UCS (MPa)	σ_{ci} (MPa)[a]	σ_{ci} (MPa)[b]	Young's modulus (GPa)
1	108–271	107–126	101–127	55.3
2	103–199	47–78	46–79	30.2
3	148–289	62–130	63–129	52.4
4	144–163	69–74	65–73	39.3

SG sample group
[a] According to Brace et al. (1966)
[b] According to Lajtai (1974)
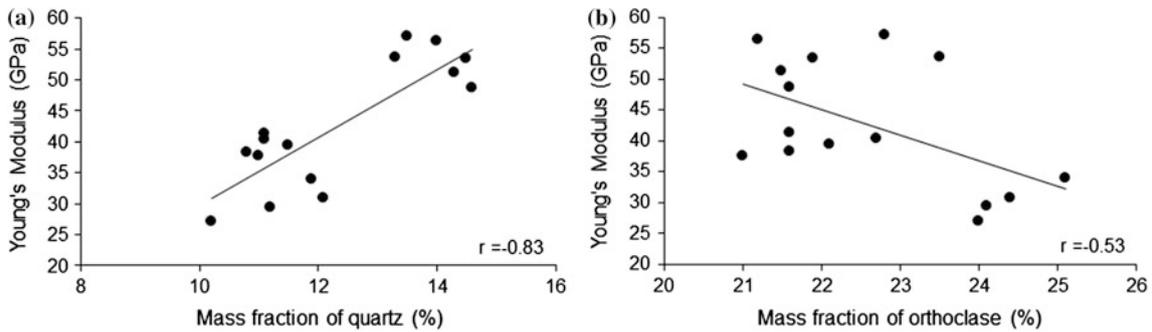
Fig. 12.2 The relation of Young's modulus with (**a**) the mass fraction quartz (**b**) the mass fraction orthoclase
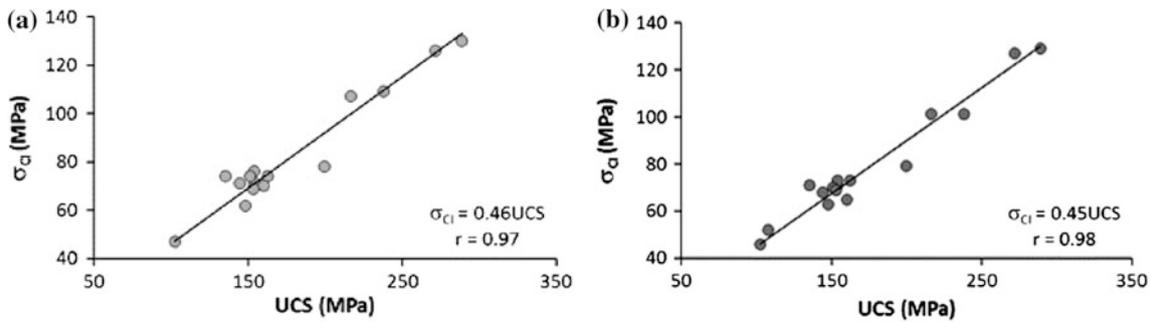
Fig. 12.3 The relation of crack initiation with UCS (**a**) crack initiation values obtained according to Brace et al. (1966) (**b**) crack initiation values obtained according to Lajtai (1974)
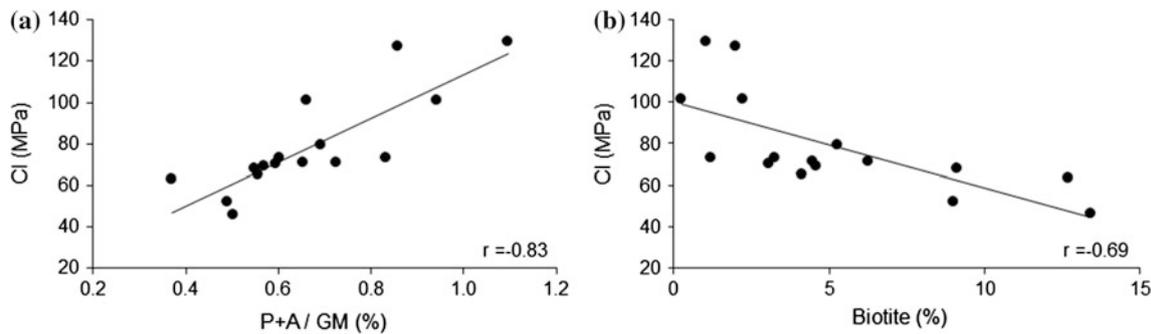
Fig. 12.4 The influence of the ratio of selected phenocrystals to groundmass on CI. P + A, represents the sum of the normalized areas of plagioclase and amphibole. GM represents the groundmass area (Ündül et al. 2013)

12.4   Conclusion

In this study quantitative petrographic and mineralogical data were utilized to quantify variations in micro-textural characteristics of andesitic rocks and their effect on crack initiation, UCS, Young's modulus and petro-physical properties. The synthesis of results showed that:

- The unit weight of the utilized rocks increases with increasing mass fractions of quartz and plagioclase, but decreases with increasing orthoclase content.
- No relation between the spatial distribution of minerals and petro-physical properties can be found. Petro-physical properties are dependent on the mass fractions of orthoclase, plagioclase and quartz.
- The crack initiation threshold was 0.45–0.46 × UCS.
- With increasing normalized area of plagioclase and amphibole phenocrystals the UCS increased. An increase in the normalized area of biotite phenocrysts caused a decrease in CI and UCS.
- With increasing mass fraction of orthoclase the Young's modulus decreased.
- Poisson ratio increases with decreasing normalized area of the groundmass.

- With increasing phenocrystal area the failure mode changes and was associated with an increased number of axial cracks.

References

Brace WF, Paulding BR, Scholz C (1966) Dilatancy in fracture of crystalline rocks. J Geophys Res 71(16):3939–3953

Eberhardt E, Stimpson B, Stead D (1999) Effect of grain size on the initiation and propagation threshold of stress-induced brittle fracture. Rock Mech Rock Eng 32(2):81–99

Lajtai EZ (1974) Brittle fracture in compression. Int J Fract 10(4):525–536

Nicksiar M, Martin CD (2013) Crack initiation stress in low porosity crystalline and sedimentary rocks. Eng Geol 154:64–76

Prikryl R (2006) Assessment of rock geomechanical quality by quantitative rock fabric coefficients: limitations and possible source of misinterpretations. Eng Geol 87:149–162

Prodaivoda GT, Maslov BP, Prodaivoda TG (2004) Estimation of thermoelastic properties of rock-forming minerals. Russ Geol Geophys 45(3):389–404

Ündül Ö, Amann F, Aysal N, Plötze M (2013) Micro-textural controlled variations of the geomechanical properties of andesites. In: Kwasniewski M, Lydzba D (eds) Eurock 2013 rock mechanics for resources, energy and environment. CRC Press, Boca Raton, pp 357–361

Conceptual Geological Models, Its Importance in Interpreting Vadose Zone Hydrology and the Implications of Being Excluded

13

Matthys A. Dippenaar and J. Louis van Rooy

Abstract

Vadose zone conditions are becoming increasingly important in site investigation, including, for instance, (1) the protection of the phreatic zone from surficial contaminants (aquifer vulnerability), (2) surface water–groundwater interaction and biodiversity, (3) water influencing infrastructure development and (4) problem soil behaviour resulting in surface expressions of subsurface volume change. This multidisciplinary paradigm involves a wide range of specialists, but at the root of issues pertaining to the vadose zone is the geological regime in which it occurs. A conceptual model should include all fundamental branches of geology, viz. stratigraphy, mineralogy and petrology, structural geology and physical geology. The importance of a proper geological model is addressed at the hand of selected case studies in urban and peri-urban South Africa. In all instances, the sites were developed with subsequent issues arising due to inadequate vadose zone investigation. To evaluate, geological models were compiled based on available geological and geomorphological information. Physical properties such as detailed soil profiles and grading analyses were inferred to address vertical and spatial material variability. Mineralogy of the various soil horizons was used in conjunction with bulk dry densities to determine porosity and to address pedogenetic and eluviation processes. Hydrological data include percolation tests and Atterberg limits and were inferred onto the model to clarify anticipated hydrological behaviour. The additional geological data improve the understanding of the case studies incorporating ephemeral hillslope wetlands, constructed fill and water addition through leaking pipelines and irrigation, through the addition of knowledge overlooked by hydraulic testing exclusively and accentuate the importance of proper geological understanding prior to hydrological interpretation. The major issues arising, apart from damage to infrastructure and contamination of water resources, are excessive rehabilitation costs, decrease in aesthetic value and general discontent of land owners and proximate residents. The geological model is imperative and should not be excluded or overlooked due to increasingly popular alternative methods of investigation.

13.1 Introduction

Urban development induces changes to the vadose zone, which is readily overlooked in compilation of a conceptual model prior to development. Made ground is of different grading and compaction than in situ materials, saturation is increased by irrigation or leaking pipelines, and surfaces are

M.A. Dippenaar (✉) · J.L. van Rooy
Engineering Geology and Hydrogeology, Department of Geology, University of Pretoria, Private Bag X20, Hatfield, Pretoria, 0028, South Africa
e-mail: madip@up.ac.za; matthys.dippenaar@up.ac.za; madippenaar@gmail.com
URL: www.up.ac.za/geology

Fig. 13.1 Perspectives on the vertical succession of earth materials [adapted from (**a**) Foster (1984, 2012), (**b**) Koita et al. (2013), (**c**) Hillel (2003), (**d**) Weinert (1980), Brink (1985); combined from Dippenaar and Van Rooy (2014)]
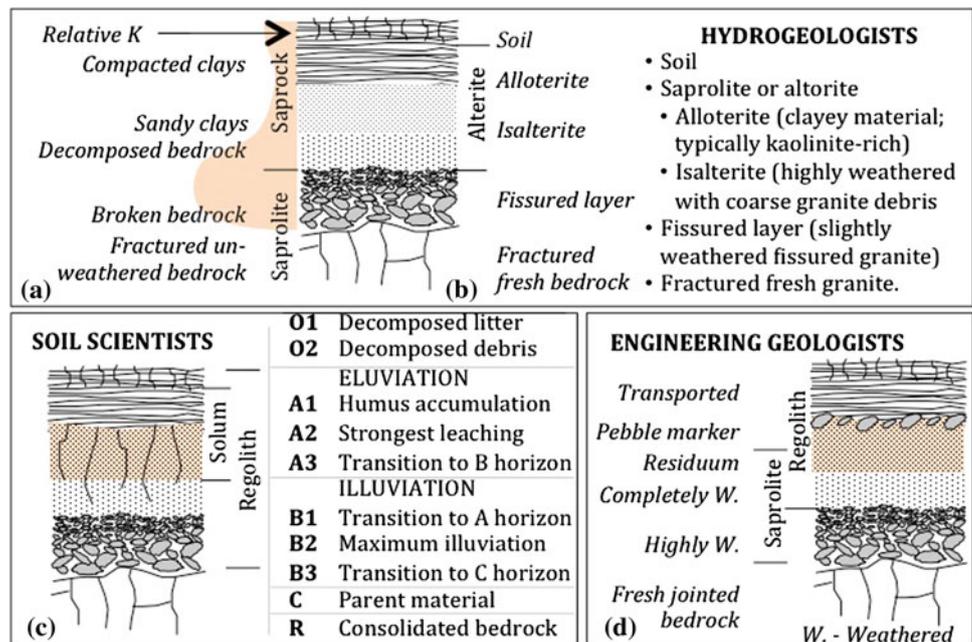
sealed as land is being developed. These are just come factors contributing to the already complex vadose zone.

The importance of proper vadose zone conceptualization, notably in urban settings, is explained at the hand of five case studies underlain by Lanseria tonalite gneiss of the Johannesburg Dome. Granites in South Africa are—given its age—highly variable due to an intricate tectonic and geomorphological history. These case studies illustrate the importance of conceptual vadose zone models, as well as the implications of exclusion.

13.2 Conceptual Models

Perspectives regarding the vertical succession of earth materials and the classification of soils vary between disciplines. Albeit based on different intentions, an all-encompassing multi-disciplinary approach may significantly improve information gained from soil profile descriptions (e.g. Dippenaar 2012). Various approaches to the classification of weathered earth materials are shown in Fig. 13.1.

Additional to the vertical variation, the spatial variation and subsurface hydrology can best be simplified by the catena concept, which has been well-documented (e.g. Schaetzl and Anderson 2005).

The importance of conceptual models is also well documented, e.g.:

- The importance thereof in groundwater models (Izady et al. 2013)
- The lack of proper understanding in conceptual hydrological models on land (Lahoz and de Lannoy 2013)

- The special circumstances in karst settings (Bakalowicz 2005)
- Incorporation of multidisciplinary data and different scales of observation (Dewandel et al. 2005)
- Considerations of different potential conceptual models in assessment of aquifer vulnerability (Seifert et al. 2007)
- Inclusion of subsurface flow in shallow saprolite and deep bedrock (Banks et al. 2009)
- Challenges and trends in geological visualisation and modelling (Turner 2006)
- The inclusion of historical data to potentially replace the conceptual model (Royse et al. 2009)
- The influence of alternative conceptual models on predicting beyond calibration base of the flow model (Troldborg et al. 2007)
- The concept of hydrostratigraphy contributing to proper conceptual modelling (Allen et al. 2007; Angelone et al. 2009; Heinz and Aigner 2003)
- The incorporation of geology, engineering geology, hydrogeology and geomorphology in advancing conceptual model quality Dippenaar and Van Rooy (2014).

Essentially the principles of the triangle of geomechanics and the triangle of engineering geology apply as shown in Fig. 13.2 (Bock 2006) after which actual data can be inferred to model scenarios.

The hydrological cycle is an intricate interaction between the lithosphere, atmosphere and biosphere and represents the movement of water in different phases. With respect to the vadose zone, more attention is generally given to the soil or plant root zone and the processes of surface water–groundwater interaction and evapotranspiration, often with the

Fig. 13.2 Triangle of geomechanics (*left*) and of engineering geology (*right*) (Bock 2006)
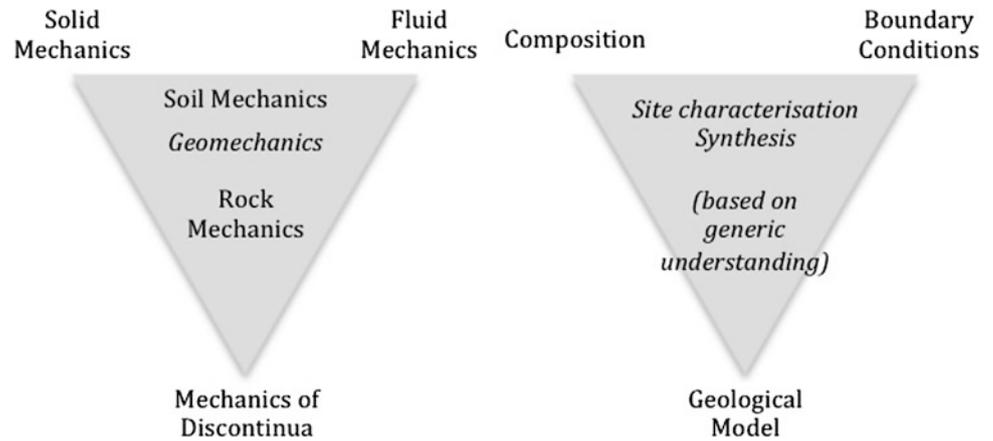
Fig. 13.3 Movement of water as depicted through the hydrological cycle (adapted from Todd and Mays 2005)
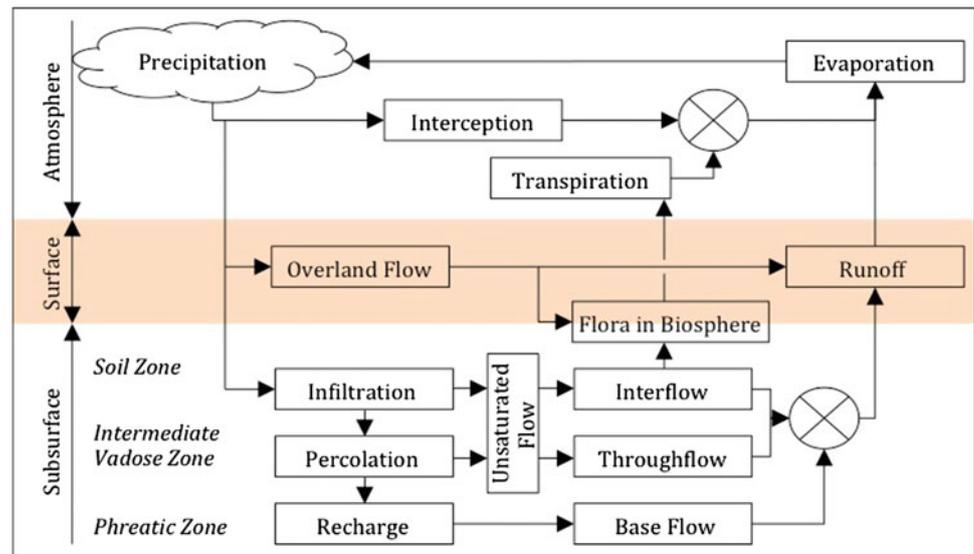
distinct exclusion of the deeper intermediate vadose zone (Fig. 13.3). Numerous aspects have to be considered when compiling a comprehensive vadose zone model. Some of these are illustrated in Fig. 13.4 and indicate the vast range of input in such conceptual models (Dippenaar et al. 2014):

1. **Atmosphere–Biosphere**
   1.1. Climate–precipitation, evaporation
   1.2. Plant water availability and transpiration
   1.3. Surface water–groundwater interaction
   1.4. Sensitive ecosystems
   1.5. Land use and land cover
2. **Soil Zone**
   2.1. Infiltration
   2.2. Perched water tables
   2.3. Interflow, throughflow
   2.4. Translocation and pedogenesis
3. **Intermediate Vadose Zone**
   3.1. Percolation to eventual recharge
   3.2. Soil vadose zone

3.3. Fractured rock vadose zone
3.4. Variable saturation.

13.3 Case Studies

For the purposes of explanation, geology and climate are kept as constant parameters and all case studies presented as situated on tonalite gneiss (Lanseria Gneiss, Johannesburg) within the Midrand and Johannesburg areas of South Africa.

13.3.1 Pedogenesis and Ephemeral Hillslope Wetlands

Randjesfontein, situated on tonalite gneiss of the Archaean basement complex in Midrand (RSA), was investigated during two subsequent stages. During the first, vegetation was absent due to veldt fire in the dry winter months. During

Fig. 13.4 Considerations in the compilation of a vadose zone model
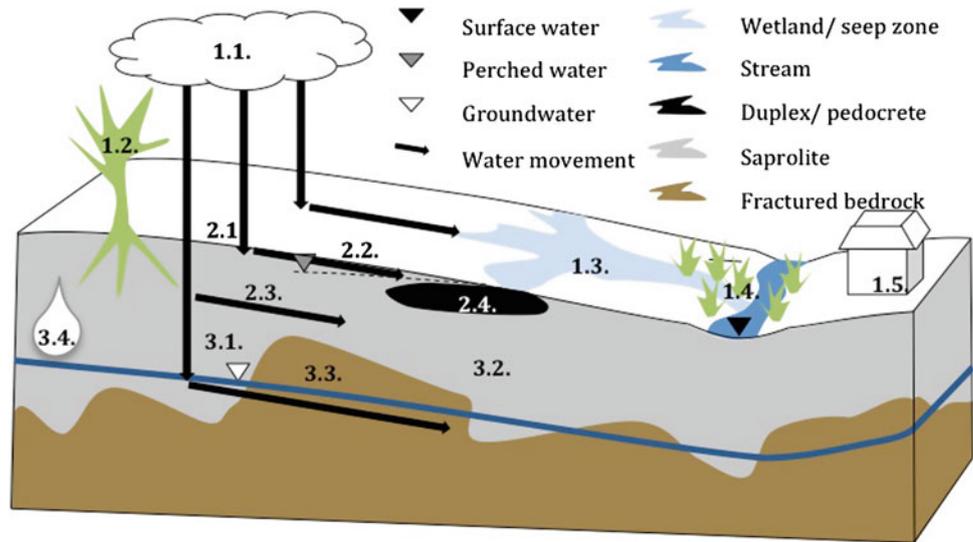
Fig. 13.5 Shallow interflow through glaubular to honeycomb ferricrete resulting in the formation of an ephemeral hillslope wetland on Archaean tonalite gneiss (Midrand, RSA) (adapted from Dippenaar et al. 2014)
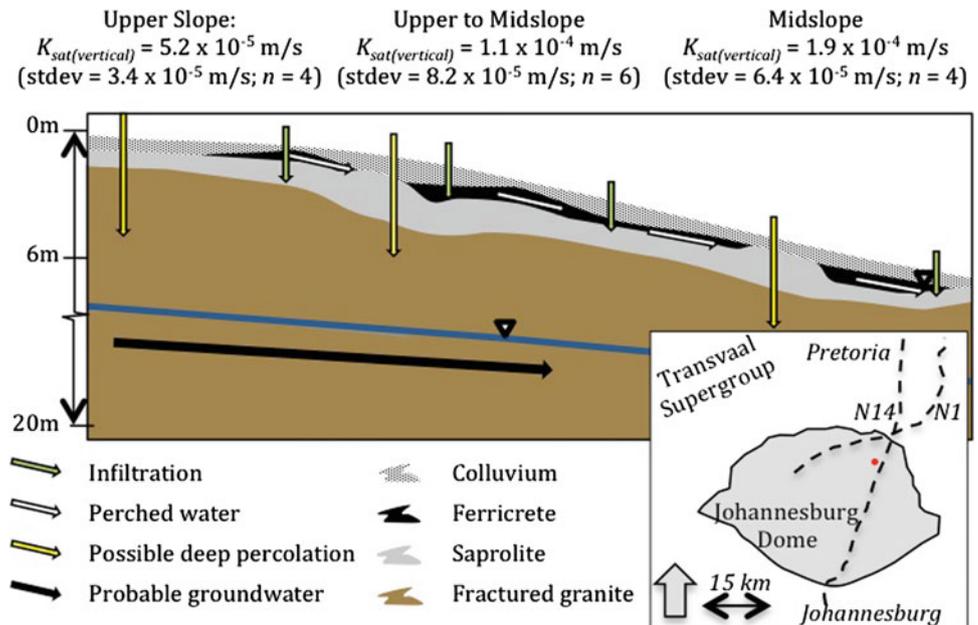
the second, the geotechnical investigation noted marshy areas at the site and deduced that the ferricrete in the profiles represents a periodically perched water table system. These markers were overlooked and, using only the absence of wetland vegetation indicators as proof, the site was excavated for construction. With changing seasons, the wetland wetted up again and water influx into the excavation resulted in cessation of construction as water collected at the excavation floor and wetland conditions regenerated on barren bedrock.

Of interest in the conceptual understanding of this study area are the following (Fig. 13.5):

- Ferricrete appears much more heterogeneously and anisotropically as anticipated. Given the $150 \times 50 \times 10$ m excavation, the varying thickness, as well as the localized absence, of ferricrete can clearly be seen. Important for the conceptual model is to properly infer the vertical and spatial extent of the pedocretes.
- In the instance of this study site, the ferricrete changed its role in the subsurface hydrology. With initial perching probably on low permeability bedrock, the process of pedogenesis progressively resulted in varying stages of ferruginization in residuum and the pebble marker. In the stages before nodular/glaebular and in the hardpan stage,

the ferricrete is of low permeability and porosity with water perched above. However, in the honeycomb phase, the porosity is low due to the cementation, but the calculated porosity of 0.15 as opposed to the overlying 0.21 exists as large connected pore spaces where parent soil has been washed out. The perching, therefore, occurs localized within the ferricrete, and not above.

13.3.2 Made Ground and Variably Compacted Fill

Urban hydrogeology has an increased variable: that of anthropogenic materials. These include a wide variety of materials of variable compaction and grading (e.g. uncompacted imported fill), as well as variable composition (e.g. contaminated land). In two separate studies in the suburbs of Alexandra and Linbro Park respectively, the following was found:

- Cut-and-fill operations have to be included as significant impacts on shallow interflow. This is notable in all three studies and the excavation through illuviation zones result in water being subjected to other lateral pathways and not necessarily deeper percolation. Compaction of imported materials may have higher porosity and/or permeability, fill for drainage systems may interrupt flow paths in unsaturated materials and induce imbibition rather than drainage, and retaining wall systems may become unstable and exhibit seepage through faces.
- Non-uniform building rubble and fill material may influence downslope properties and may create periodical waterlogged conditions in poorly compacted fill materials. This is notable in the central urban portions where old buildings are demolished for the construction of high rises, requiring deeper foundations and basements.

13.3.3 Increased Infiltration and Interflow

Increased water addition can be explained at a case study in Fourways (residential golf course). Significant additional volumes of water was released, resulting in the following:

- The natural systems were in hydrological equilibrium where water infiltrated and sporadic small wetlands occurred in Fourways. These areas were developed as the golf course and the residential areas on the perimeters and downslope.
- Increased golf course irrigation resulted in the formation of a perched water system where the high saturation of surface soils induced interflow on the bedrock interface.
- The main damage is with water imbibing into porous plaster and mortar, resulting in extensive damage to buildings.

13.4 Discussion

The geological model should include the vadose zone and all variability, whether natural or induced, in material properties and moisture contents. Urban development notably exacerbates the uncertainty in the vadose zone due to, for instance, surface sealing, disruption of natural structure and compaction, inducing increased flow, and diverting flow paths.

The variation in properties between the soil zone and intermediate vadose zone, and between the soils, saprolite and bedrock should be understood properly to ensure optimal construction. Damage to infrastructure on-site and off-site, drainage of wetlands, generation of waterlogged conditions, and weakening of retaining structures are just some of the significant results of proper understanding of the vadose zone.

The importance of the vadose zone exceeds vulnerability assessments and optimizing irrigation practices. It should be seen as a fundamental component of all hydrological and geotechnical assessments and should be included as a detailed component of any conceptual model.

References

Allen DM, Schuurman N, Deshpande A, Scibek J (2007) Data integration and standardization in cross-border hydrogeological studies: a novel approach to hydrostratigraphic model development. Environ Geol 53:1441–1453

Angelone M, Cremisini C, Piscopo V, Proposito M, Spaziani F (2009) Influence of hydrostratigraphy and structural setting on the arsenic occurrence in groundwater of the Cimino-Vico volcanic area (central Italy). Hydrogeol J 17:901–914

Bakalowicz M (2005) Karst groundwater: a challenge for new resources. Hydrogeol J 13:148–160

Banks EQ, Simmons CT, Love AJ, Cranswick R, Werner AD, Bestland EA, Wood M, Wilson T (2009) Fractured bedrock and saprolite hydrogeologic controls on groundwater/surface–water interaction: a conceptual model (Australia). Hydrogeol J 17:1969–1989

Bock H (2006) Common ground in engineering geology, soil mechanics and rock mechanics: past, present and future. Bull Eng Geol Environ 65:209–216

Brink ABA (1985) Engineering geology of southern Africa, vol 4. Post-Gondwana deposits. Building Publications, Pretoria

Dewandel B, Lachassagne P, Boudier F, Al-Hattali S, Ladouche B, Pinault J-L, Al-Suleimani Z (2005) A conceptual hydrogeological model of ophiolite hard-rock aquifers in Oman based on a multiscale and a multidisciplinary approach. Hydrogeol J 13:708–726

Dippenaar MA (2012) How we lose ground when earth scientists become territorial: defining "soil". Nat Resour Res 21(1):137–142

Dippenaar MA, Van Rooy JL (2014) Review of engineering, hydrogeological and vadose zone hydrological aspects of the Lanseria Gneiss, Goudplaats-Hout River Gneiss and Nelspruit Suite Granite (South Africa). J Afr Earth Sc 91:12–31

Dippenaar MA, Van Rooy JL, Breedt N, Huisamen A, Muravha SE, Mahlangu S, Mulders JA (2014) Vadose zone hydrology: concepts

and techniques. WRC report TT 584/13. Water Research Commission, Pretoria

Foster S (1984) African groundwater development: the challenges for hydrological science. IAHS. Wallingford UK. 3–12

Foster S (2012) Hard-rock aquifers in tropical regions: using science to inform development and management policy. Hydrogeol J 20:659–672

Heinz J, Aigner T (2003) Hierarchical dynamic stratigraphy in various quaternary gravel deposits, Rhine glacier area (SW Germany): implications for hydrostratigraphy. Int J Earth Sci (Geol Rundsch) 92:923–938

Hillel D (2003) Introduction to environmental soil physics. Academic Press, Waltham, p 494 (eBook)

Izady A, Davary K, Alizadeh A, Ziaei AN, Alipoor A, Joodavi A, Brusseau ML (2013) A framework toward developing a groundwater conceptual model. Arab J Geosci. doi:10.1007/s12517-013-0971-9

Koita M, Jourde H, Koffi KJP, Da Silveira KS, Biaou A (2013) Characterization of weathering profile in granite and volcanosedimentary rocks in West Africa under humid tropical climate conditions. Case of the Dimbokro Catchment (Ivory Coast). J Earth Syst Sci 122(3):841–854

Lahoz WA, De Lannoy GJM (2013) Closing the gaps in our knowledge of the hydrological cycle over land; conceptual problems. Surv Geophys. doi:10.1007/s10712-013-9221-7

Royse KR, Rutter HK, Entwisle DC (2009) Property attribution of 3D geological models in the Thames Gateway, London: new ways of visualising geoscientific information. Bull Eng Geol Environ 68:1–16

Schaetzl RJ, Anderson S (2005) Soils: genesis and geomorphology. Cambridge University Press, New York

Seifert D, Sonnenborg TO, Scharling P, Hinsby K (2007) Use of alternative conceptual models to assess the impact of a buried valley on groundwater vulnerability. Hydrogeol J 16:659–674

Todd DK, Mays LW (2005) Groundwater hydrology, 3rd edn. Wiley, New Jersey

Troldborg L, Refsgaard JC, Jensen KH, Engesgaard P (2007) The importance of alternative conceptual models for simulation of concentrations in a multi-aquifer system. Hydrogeol J 15:843–860

Turner KA (2006) Challenges and trends for geological modelling and visualisation. Bull Eng Geol Environ 65:109–127

Weinert HH (1980) The natural road construction materials of South Africa. Academica, Cape Town

Treatment of Fossil Valley in Dam Area: A Case Study

14

A.K. Singh and Bhatnagar Sharad

Abstract

Himalaya occupies a unique position internationally providing ample opportunities for hydro power development through its fast flowing rivers. The total potential of three major river system of Himalaya i.e. Indus, Ganga & Brahmaputra is estimated to be 65,623 MW (at 60 % Load factor). However, only about 25 % of this potential has been tapped so far. In recent times, when ideal locations for dam in Himalayan region have almost exhausted, many dams of variable dimensions are being constructed in adverse geological settings, taking into consideration various ground improvement techniques. These dam structures are often faced with the problems of sheared and fractured rock at the foundation grade, deep overburden, slope instability of the abutments, presence of solution cavities etc. Occasionally, in glaciated valleys, fossil valleys are formed due to change in river course by sudden blockade of river in geological past. These geomorphic features are easily picked up on the ground but to establish their extent at depth requires detailed subsurface investigations. Suitable remedial measures are formulated if these features are located in close vicinity of any engineering structures. The present paper deals with the fossil valley treatment carried out on the right abutment of Parbati Dam, Stage-II under construction by NHPC Ltd in Himachal Pradesh where extensive grouting using TAM technology was carried out in phased manner utilizing various grout mix, ultrafine cement, admixtures etc. Grouting pattern was evolved so that the whole fluvioglacial material lying in the vicinity of dam area could be grouted. Post grouting check holes and permeability tests showed marked reduction in permeability values before & after the grouting, ascertaining successful treatment of the fossil valley.

14.1 Introduction

Parbati H.E. Project-St-II (800 MW) is one of the largest hydroelectric projects in Himachal Pradesh, under construction by NHPC Ltd, a premier organization in India for

A.K. Singh · B. Sharad (✉)
Parbati H.E.Project, Stage-II, NHPC Ltd, Faridabad, Himachal Pradesh, India
e-mail: bhatnagarsharad2008@gmail.com

A.K. Singh
e-mail: aksighnhpc@gmail.com

hydropower development. The project is located on river Parbati, a tributary of Beas river in Distt Kullu of Himachal Pradesh. The project envisages construction of an 85 m high concrete gravity dam near village Barsheni/Pulga to divert River Parbati into the main water conductor system. The project is an μinter basin transfer scheme. The proposed 31.5 km long, 6 m finished dia HRT shall conduct water from Pulga via Garsa/Sheelagarh valley which shall ultimately be discharged into river Sainj, a downstream tributary of river Beas at Suind village where a surface power house is under construction for generating 800 MW of power. In order to augment the power generation it is planned to divert the discharge of Jigrai nala located downstream of Pulga

Dam into the reservoir. The discharge of other intermediate nalas i.e. Hurla nala and its tributaries (Manihar and Pancha nala) and flow of Jiwa nala shall also be diverted to HRT through small diversion structures i.e. trench weirs, feeder tunnels and drop shafts. The layout of the project is shown as Fig. 14.1.

14.2 Brief Regional Geology and Geo-Morphology of Project Area

The project is located in lesser Himalaya. The site is characterized by elevation ranging between El ± 1,200 m to El ± 2,200 m above MSL. The great difference in elevation is suggestive of a very young and immature topography conforming to the late orogenic uplift of the Himalayas marked by high mountains, narrow & glaciated valley, fossil valleys with steep slopes and escarpments.

In project area a variety of rock formations are exposed which have undergone extensive structural deformations due to tectonic activity associated with Himalayan orogeny. The deformations are exhibited in the form of folds, faults and thrusts. The main rock types in this region belong to Jutogh Banjar and Larji formations ranging in age from Precambrian to Permian and are separated by thrusted margins.

14.3 Geo-Technical Assessment of Dam Area

The dam site is located on Parbati river, near Pulga/Barseni village, in a narrow 'U' shape gorge, about 150 m downstream of its confluence with Tosh nala. At dam site the left right abutment rises steeply from the river bed with an average slope of 80°. Schistose quartzites with thin intercalated bands of contorted mica schist bands belonging to Kullu member of Jutogh Formation are exposed on both the abutments.

The rockmass is dissected by 3 sets of joints with foliation joints (040-060°/35–45°) favourably dipping in upstream direction. The other two sets having attitudes 180–210°/45°—and 250–310°/50–60° are also distinct.

The right bank is extensively covered with thick fluvioglacial material up to El ± 2,270 m (Ref: Photo 14.1) whereas on the left bank rock is exposed up to El ± 2,230 m with thin cover of slope wash material, however, beyond El ± 2,240 m the entire slope on left bank is also covered with thick fluvioglacial material.

The dam foundation has been laid in sound rock comprising of schistose quartzite rock, after removing 9–18 m of river borne material. Presently the intake structures & spillway blocks are under construction.

14.3.1 Fossil Valley

In close vicinity of dam axis, on right bank, the signature of the old course of Parbati river exists in the form of fossil valley. The depth of this valley is about 101 m and is filled with glacial moraines comprising of large boulders, pebbles & cobbles in silty matrix. This has also been established by the geological investigations carried out by Geological Survey of India & NHPC. Large accumulation of fluvioglacial material observed on the right bank of Parbati river is indicative of concealment of its original course which got buried under a thick pile of moraine deposits. It is believed that after the recession of glaciers in Pleistocene period, river

Fig. 14.1 Layout of Parbati stage-II project
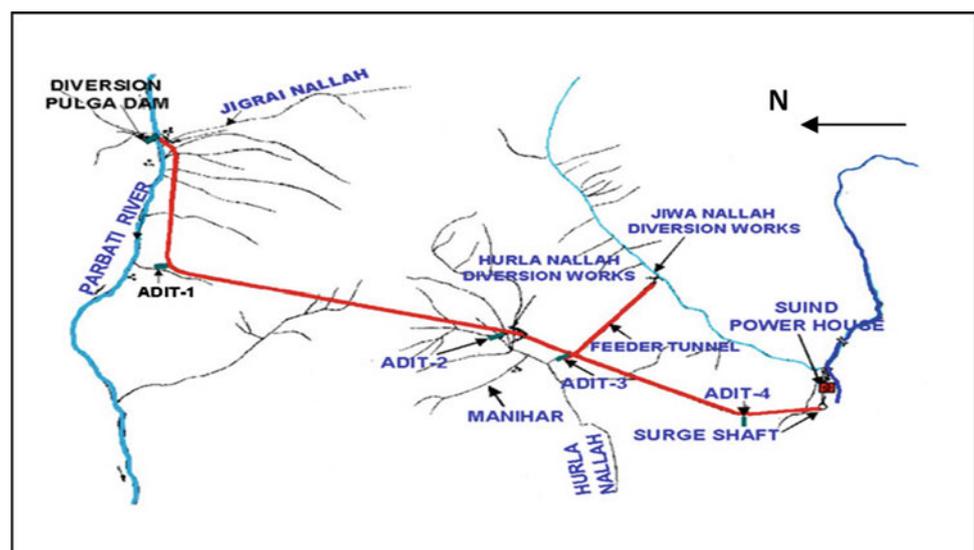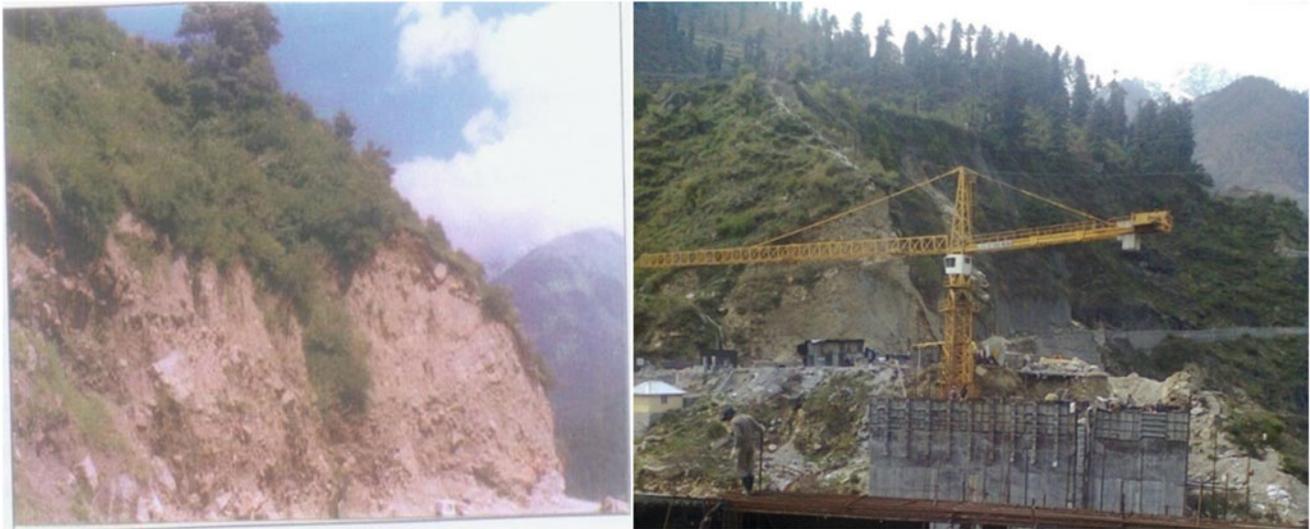
Photo 1 Exposures of fluvioglacial material on right bank

Parbati would have started flowing through the valley earlier occupied by glaciers. The valley seems to be occupied by moraines deposited by receding glaciers, leaving very limited space for river to flow, thereby reducing its transportation and eroding capacity which resulted in impoundment of a lake. The river then over toppled the barrier and followed a new course .The old river channel got filled with moraines and resulted in 'fossil valley'.

14.3.1.1 Geotechnical Investigations for Fossil Valley

Besides detailed geological mapping on 1:500 scale, the dam area in general and the fossil valley in particular was extensively investigated to establish the shape and extent of fossil valley. Following subsurface explorations were carried out:

14.3.1.2 Geophysical Surveys

Four seismic profiles namely P11-P14, aggregating to 800 m length was laid on the right bank in the fossil valley area. These profiles have established overburden depth of 80–90 m in the fossil valley area. A seismic velocity of 2,200 m/s was recorded indicating loose to semi compacted riverborne/fluvioglacial material.

14.3.1.3 Exploratory Drilling

The fossil valley area was explored by eight drill holes aggregating to 473 m depth. The deepest hole was 124 m. Permeability tests were also carried out in these holes. A brief account of drill holes is as under: (Table 14.1).

In general these holes established that fossil valley is mainly composed of four distinct type of material:

0-25 m-Yellowish brown to grey sand with boulders of granitic gneiss, quartzite & mica schist. Percentage of fine is more in comparison to coarse material.

25–30 m-Fine silt without pebble or boulders

30–60 m-Angular to sub angular boulders & pebbles of quartzite and schist

60–100 m-Silty sand with large boulders of gneiss, granitic gneiss.

14.3.1.4 Permeability and Groutability Tests

Variable overburden permeability ranging from 1×10^{-3} to 6×10^{-5} was noticed in fossil valley. Similarly the grout intake pattern indicated irregular & anisotropic condition of overburden. No effect of grouting (with normal cement) on reduction in permeability values were observed down to 22.6 m depth beyond which marginal decrease in permeability value were observed.

14.3.1.5 Exploratory Drift

A 220 m long drift was excavated on the right bank at El ± 2,166 m to explore the extent of the fossil valley. The drift started in rock comprising of schistose quartzites with band of biotite schist up to 130 m length. Between RD 130–210 m fluvioglacial material in silty matrix was observed. Beyond RD 210–220 m again schistose quartzite with thin bands of biotite schist were observed (Ref. Fig. 14.2). The above explorations established an 80 m wide and about 100 m deep fossil valley extending from u/s of dam to d/s of dam, near the diversion tunnel outlet portal.

14.4 Treatment of Fossil Valley

Leakage is apprehended through fossil valley, at the time of filling of the reservoir. Hence, it has been planned to create a cut off grout curtain by permeation grouting using TAM (*Tube a Manchhettes*) technique. This cut-off is proposed to

Table 14.1 Exploratory drill holes in fossil valley

Drill Hole no.	Location	Collar El (M)	Total depth (m)	Bedrock depth	Overburden/Bedrock characteristics
DH-2	Centre of fossil valley	2,204	116 m	101 m(El 2,103)	Quartz mica gneiss with schist bands
DH-3	u/s of DH-2	2,158	64	53 m (El 2,105)	Gneiss
DT-3	40 m u/s of dam axis extreme end of fossil valley)	2,175	45	21 m(El 2,154)	Quartzite with schistose quartzite bands
DT-5	D/s of dam axis(extreme end of fossil valley)	2,270	56	Bedrock not encountered	Riverborne/fluvioglacial material up to excavated depth
DDH/II/01	Fossil valley	2,201	60	Bedrock not encountered	Riverborne/fluvioglacial material up to excavated depth
DDH/II/03	Fossil valley	2,201	60	Bedrock not encountered	Riverborne/fluvioglacial material up to excavated depth
DDH/II/04	Fossil valley	2,197	61.5	Bedrock not encountered	Riverborne/fluvioglacial material up to excavated depth
DDH/II/05	Centre of fossil valley	2,200	124	101(EL2099)	Quartzite with mica schist bands
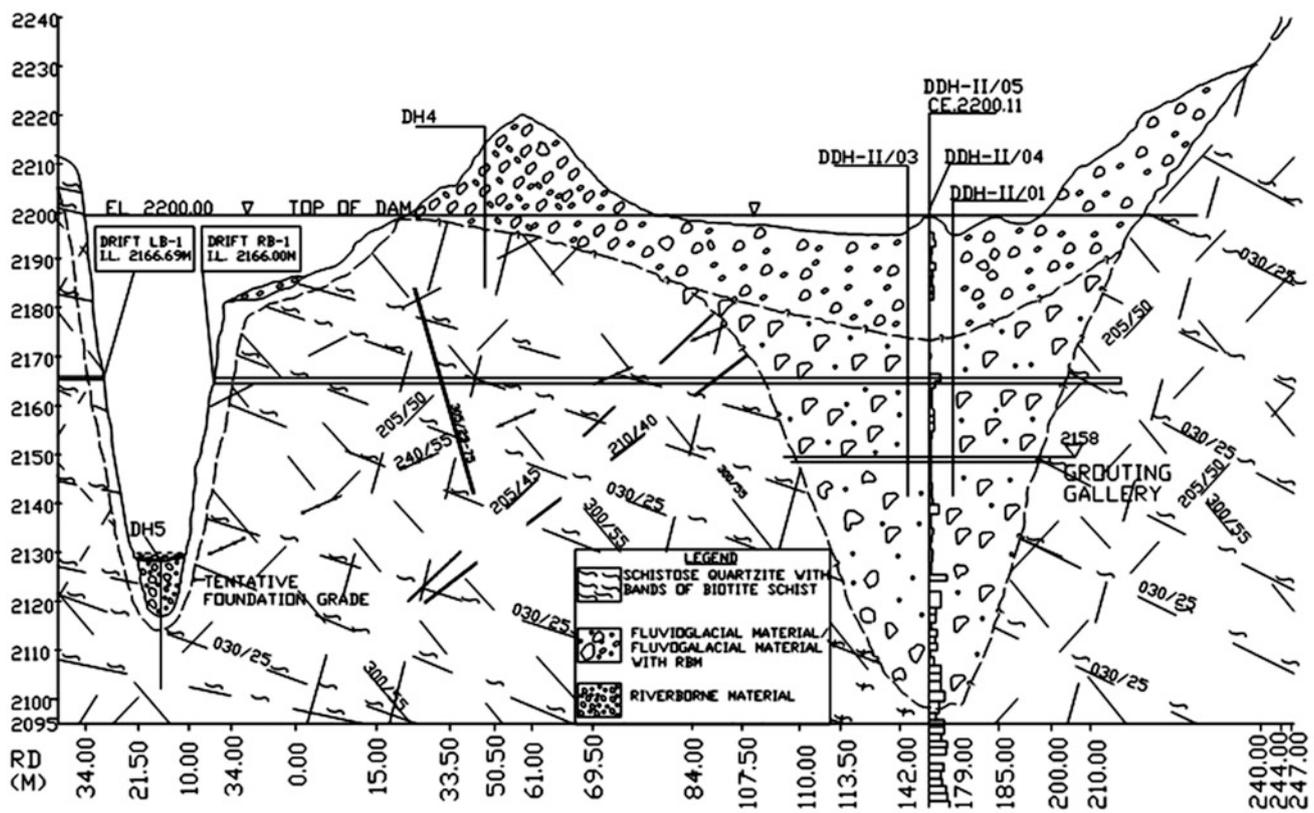
Fig. 14.2 Geological L-section of fossil valley

extend from the surface to alluvial/bedrock contact and up to 10 m into the bedrock. A 3.5 m × 3.8 m grouting gallery with portal at El ± 2,148 m was constructed to facilitate grouting. The grouting was carried out in two stages: In the first stage grouting was performed from surface at El ± 2,200 m to grouting gallery. This was designated as upper grout curtain. The length of upper grout curtain was 215 m. Drill hole ranging in depth from few meters to 50–55 m were drilled from the surface up to the level of grouting gallery at El ± 2,150 m. In the second stage the media between the grouting gallery & bedrock was grouted. This was designated as lower grout curtain. The length of the

Parbati Fossil Valley
Sketch of grout curtain pattern arrangement
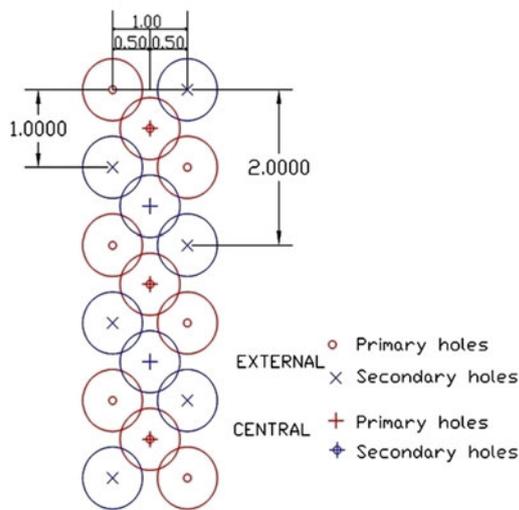
Fig. 14.3 Grouting pattern

lower grout curtain was 65–70 m. Overlapping between the upper grout curtain and lower grout curtain was ensured to have continuity.

14.4.1   Drilling/Grouting Equipment

Drilling was performed using three drilling rigs (Rodio SR52). One of the rig was electrically operated to be accommodated in grouting gallery. The holes were provided with a sleeve pipe (*tube a manchettes*) after retrieving the drill rods and before withdrawal of the casing. The borehole trajectory was measured utilizing the surveying instrument 'BORETRACK MKII'. The grouting was carried out by double acting piston pump type CIRO 10, operating at a maximum discharge pressure of 7.5 MPa. The plant had a computerized control & record unit to record the flow rate, grouting pressure and total grouted volume.

14.4.2   Grouting Pattern

Preliminary trials for selection of grouting components and composition were carried out in laboratory at Mumbai. Grouting was carried out in three rows i.e. upstream, downstream and central row. The distance between u/s & d/s hole was kept as 1 m from centre to centre. Holes of each row were also separated by a distance of 1 m. (Ref. Fig. 14.3). Grouting was achieved in two phases:

In the first phase u/s and d/s holes were grouted using fine cement (Blaine-4,500),while the second phase of grouting was carried out in the central hole using ultra fine cement (Blaine 10,000),after completing grouting of the external rows. Grouting was controlled by Pmax/Vmax (Pressure/ volume Ratio). P max varied from 5bars to a max. 35 bars, whereas V max for external holes was set at 180 liters while for central it was set at 350 liters.

14.4.3   Grouting Materials

Following grouting materials were used for treatment:
1. **Cement**: Cement of blaine >4,500 cm^2/g was used for permeation grouting.
2. **Ultrafine cement**: Ultrafine cement of 8,000 cm^2/g blaine was used to fill the voids between very fine particles.
3. **Admixtures**: Bentonite, silica gel (Sodium silicate), admixtures were also used.

For first phase of grouting following grout mixes were used:

Cement/water ratio = 0.5, Bentonite/water ratio = 2 %, Additive/water ratio = 0.5 %

For second phase of grouting carried out in central hole for upper curtain:

Cement/water ratio = 0.225, Bentonite/water ratio = 2.5 % & Additive/water ratio = 0.3 % were used.

Similar ratio was used for carrying out grouting in the lower curtain. In order to seal the hollow space between the grout hole and Tam sleeve pipe, a cement/water ratio of 0.5 and bentonite/water ratio of 5 % were used (Fig. 14.4).

In all 536 nos of boreholes of variable depth were done in a stretch of 175 m in the Upper Curtain including 179 holes in upstream, 181 in downstream and 176 in central row, whereas in lower curtain 232 nos of holes were done including 77 holes each in upstream and downstream row respectively and 78 holes in centre row. Six no of check holes were also done to a certain the efficacy of the grout curtain. Permeability test carried out in check holes have given a value of 1.54–5.3×10^{-5} against the targeted value of 1×10^{-4}. Similarly, for lower grout curtain 3 check holes have indicated permeability value between 2.6×10^{-5}–2.12×10^{-6} against the targeted 10^{-4} value. In addition, peizometers have been installed downstream of the curtain to monitor the variation in water level before and after impounding, to verify the grout efficacy. Overall, the test results showed marked improvement in ground condition after grouting.
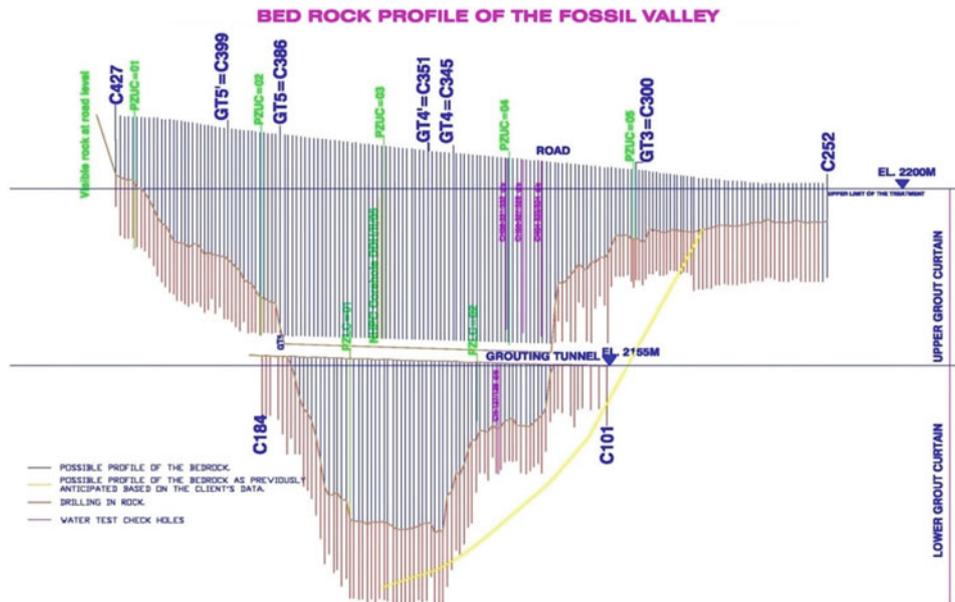
Fig. 14.4 Bed rock profile in fossil valley

14.5 Conclusion

The presence of an old fossil valley on the right bank of Parbati river was the main constraint in dam construction in Parbati H.E.Project (800 MW).Due to topographical condition it was not possible to shift the dam location elsewhere. Effective grouting techniques using TAM technology were carried out to consolidate the huge pile of fluvioglacial material. The grouting carried out in phased manner have shown considerable reduction in the permeability of the glacial material, however, it will be interesting to observe the efficacy of grouting during impoundment of the reservoir.

References

A report on reconnaissance geological investigations of Parbati Hydroelectric scheme, Kulu Distt, H.P, G.Pant & S.E.Hasan, Unpublished field season report by, GSI (March, 1970)

Cutoff/Grout curtain for fossil valley treatment, Parbati Hydroelectric Project-Stage-II, 800(4 × 200 MW)-Himachal Pradesh, India by RODIO, Trevi (March, 2005)

Detailed Project Report (Revised) on Parbati H.E. Project, Vol-IV Site Investigations & Geology, NHPC Ltd, Faridabad (September, 2000)

Applied and Active Tectonics

Convener Prof. Deffontaines Benoit—*Co-convener* Gerardo Fortunato

Tectonics (active or not) play a major role in engineering geology all over the world not only in crustal plate boundaries but also in intraplate areas. Urban geology, buildings and all anthropic constructions face major problems that we need to better take into consideration from the scientific as well as engineering point of view. Coseismic deformations due to earthquakes, as well as intersismic creep have to be better characterized and constrained from both new efficient methods and from all the past experiences we have had on active tectonic areas. This "Applied and Active Tectonics" session will focus on better localized, characterized, quantified, and modelized tectonic processes and their associated phenomena enriched by the numerous past experiences and by proposing new efficient methodologies and technologies. We hope also in this session to reinforce the links between scientists and engineering geologists in order to face seismic hazards and their disastrous implications.

A Case Study of Three-dimensional Determination of Stress Orientation to Crystalline Rock Samples in Wenchuan Earthquake Fault Scientific Drilling Project Hole-2

15

Weiren Lin, Lianjie Wang, Junwen Cui, Dongsheng Sun, and Manabu Takahashi

Abstract

Stress state around an earthquake fault is a key parameter to understand mechanisms of the fault rupturing. We tried to determine three-dimensional in-site stress orientations by anelastic strain recovery (ASR) measurements. As a case study, we applied this core based ASR method to two drill core samples retrieved from Wenchuan Earthquake Fault Scientific Drilling Project Hole-2. The core samples used for ASR experiments are chloritized diorite classified as a crystalline rock and retrieved from depths of 1,444 and 1,469 m in the hole-2, respectively. Anelastic strains of a core sample in nine directions, including six independent directions, were measured after its in situ stress was released by drilling. We obtained anelastic strain variation with time due to relaxation after its stress release. Then, the three-dimensional principal orientations of the in situ stress tensor at the two depths were successfully determined by determining the three dimensional principal orientations of the anelastic strain tensor. Our preliminary results showed both the stress regimes at the two depths are nearly strike slip faulting stress regime, and the maximum horizontal stress orientations are northwest–southeast or north-northwest–south-southeast. In addition, the results also suggested that the ASR method is applicable and useful for such in situ stress measurements in deep drilling projects.

Keywords

In situ stress • Stress orientation • Anelastic strain • Crystalline rock • Scientific drilling

15.1 Introduction

Determination of in situ stress state is very important both in geoscience and geoengineering fields. A great and destructive earthquake (Ms 8.0; Mw 7.9), the Wunchuan earthquake struck on the Longmenshan foreland trust zone in Sichuan province, China on 12 May 2008. Two almost parallel surface ruptures were observed, the main coseismic rupture developed along the Yingxiu-Beichuan-Qinchuan fault over a length of 275 km; and the other rupture was along Guanxian-Anxian fault over a length of 100 km approximately. In November 2008 about a half of year after the main shock of the Wunchuan earthquake, a very rapid scientific deep drilling project (Wunchuan Earthquake Fault Scientific Drilling, WFSD) started at Hongkou, Dujianyan,

W. Lin (✉)
Japan Agency for Marine-Earth Science and Technology (JAMSTEC), Nankoku, 783-8502, Japan
e-mail: lin@jamstec.go.jp

L. Wang · D. Sun
Institute of Geomechanics, Chinese Academy of Geological Sciences, Beijing, 100081, China

J. Cui
Institute of Geology, Chinese Academy of Geological Sciences, Beijing, 100037, China

M. Takahashi
National Institute of Advanced Industrial Science and Technology (AIST), Tsukuba, 305-8567, Japan

Sichuan to investigate physical and chemical properties of the active faults that slipped during the Wenchuan earthquake (Li et al. 2013). This drilling project consists of total five drilling holes which were or will be drilled to maximum depths of 0.5–3 km to penetrate in different faults at different sites. Following the first shallower pilot hole WFSD-1, the deeper main hole WFSD-2 was drilled to a total depth (TD) 2,284 m. WFSD-2 which completed in 2012 penetrated through the main fault zone which ruptured during the 2008 Mw7.9 Wenchuan earthquake.

To determine the in situ stress state after the Wenchuan earthquake in WFSD holes, we applied a core-based method called anelastic strain recovery (ASR) method into this drilling project. Following the first results carried out in WFSD-1 (Cui et al. 2013), we report our preliminary results on stress orientations determined from two chloritized diorite core samples of WFSD-2.

15.2 Methods

The principle idea behind the ASR method is that stress-induced elastic strain is released first instantaneously (i.e., as time-independent elastic strain), followed by a more gradual or time-dependent recovery of anelastic strain. The ASR method takes advantage of the time-dependent strain. Voight (1968) first proposed that anelastic strain could provide constraints on in situ stress; and then Teufel (1983) applied this in petroleum industry as a two-dimensional method. Matsuki (1991) showed that the method could be extended to three-dimensional stress and that it could constrain stress magnitudes. Recently, this three-dimensional method were successfully applied in various deep drilling projects (Lin

et al. 2006 etc.). In principle, the anelastic strain is induced by stress release of the core sample accompanying drilling. Therefore, the stress constrains obtained by ASR measurement are of the present-day stress state.

Matsuki (1991) showed that the orientations of the three principal in situ stresses coincide with the orientations of the three principal anelastic strains for isotropic viscoelastic materials. Thus, the orientations of the principal in situ stresses can be determined by calculating the orientations of principal strains based on anelastic strain data measured in at least six independent directions. In this study, we conducted the ASR experiments based on the basic principle suggested by Matsuki (1991) and employed the same test procedures and apparatuses as Cui et al. (2013). We carried the ASR measurements out at onsite laboratory of WFSD.

A local coordinate system in which the Z axis was parallel to the borehole axis and the X and Y axes were properly defined by referring to core surface situation (Fig. 15.1a). It means to allow selection of homogenous, crack-free and smooth locations for gluing strain gauges on the cylindrical surface of ASR sample. Six cross-type wire strain gauges and six single strain gauges were mounted on each ASR sample for measuring anelastic normal strain. Thus, the nine directions of the strain measurements were X (direction cosines: 1, 0, 0), Y (0, 1, 0), Z (0, 0, 1), XY (0.707, 0.707, 0), $-XY$ (−0.707, 0.707, 0), YZ (0, 0.707, 0.707), $-YZ$ (0, −0.707, 0.707), ZX (0.707, 0, 0.707), and $-ZX$ (0.707, 0, −0.707). In addition, two strain gauges were used for each of the nine directions (Fig. 15.1a, b).

The ASR measurement system used in this study consists of a data logger with a scanning box for recording strain and temperature data, a water bath (Constant Temperature Chamber) and a circulator for keeping the water temperature
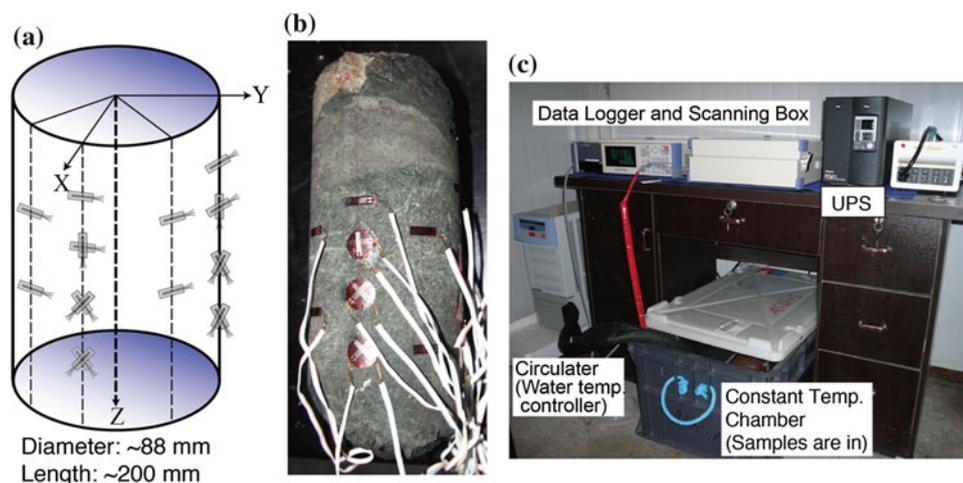
Fig. 15.1 **a** A schematic illustration of an ASR sample shows the X, Y, Z axes of a local coordinate system and the layout of the strain gauges glued on the surface of the cylindrical core sample. **b** A photograph of the ASR core sample taken from 1,469 m in WFSD-2. **c** A photograph of ASR measurement system set in the WFSD drilling onsite laboratory. *UPS* uninterruptible power supply
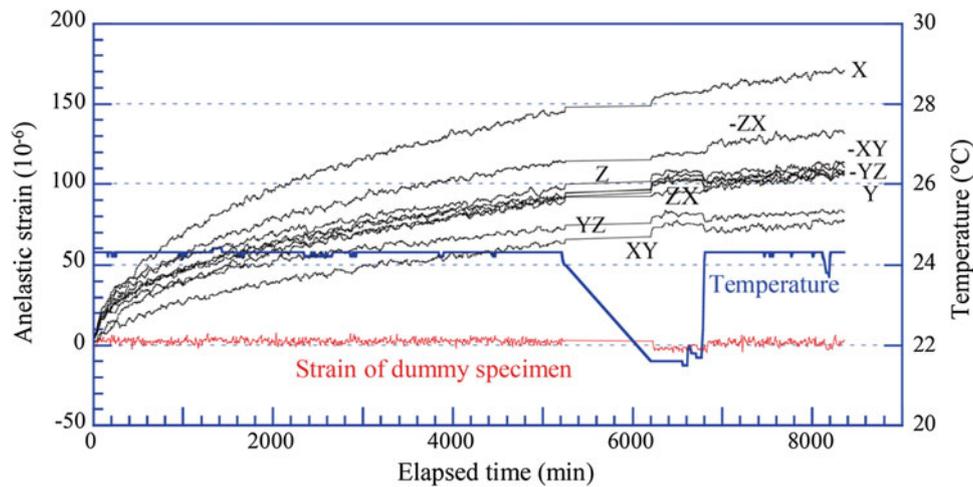
Fig. 15.2 Anelastic strain curves (labels of X, Y, Z etc. showing its measurement direction) were measured in nine directions during approximate 1 week of a core sample taken from 1,469 m in WFSD-2 as an example of anelastic normal strain recovery raw data

constant, and an uninterruptible power supply (UPS) to prevent measurement problems arising from electric power failures (Fig. 15.1c). Measurements of the ASR core sample (s) and a dummy rock sample, which did not undergo any deformation except thermal expansion, were acquired simultaneously. Purpose of the measurement of the dummy sample is to monitor the drift of the system and to correct the measured strain data if necessary. The strain gauges and two high-resolution thermistor thermometers were connected directly to the data logger, and the digital data were recorded every 10 min.

15.3   Preliminary Results

As an example of anelastic strain curves obtained from the WFSD-2 hole, raw data of anelastic strain in nine directions of a core sample taken from 1,469 m is shown in Fig. 15.2. The duration of the measurement period was approximate 6 days. During the experiment, a trouble made the electric power supply to shut down for about 16 h (from 5,200 to 6,200 min in Fig. 15.2) which is too long for capability of the UPS, thus the data was lack and the temperature in the chamber decreased. Except the no power supply duration, the constant temperature controller and chamber worked correctly, so the temperature change was less than ± 0.1 °C. As a result, the anelastic strains in all directions were extensional; all of the curves varied smoothly and similarly with increasing time. The values of the strain in the various directions, continuously measured for about 6 days depended on the orientation, the largest one (X direction) reached

more than 150 microstrains (0.015 %). The dummy sample showed that the drift of the measurement system was very small relative to the anelastic strain of the ASR sample. It indicates the strain of ASR samples were anelastic strain induced by the stress release accompanying drilling. Thus, these data could be used for the three-dimensional analysis to determine the orientations of principal strains.

From the measured anelastic normal strains in the nine directions, which included six independent directions, the anelastic strain tensor was calculated by least-squares analysis. By using a data set of the anelastic strain tensor for an arbitrary elapsed time, a data set of orientations of the three principal strains corresponding to that time can be determined. The determined orientations of and their variations as elapsed time increases are depicted as the curves from the beginning (open diamond symbols) to the end (solid diamond symbols) in Fig. 15.3 for core samples from 1,444 m and 1,469 m in WFSD-2, respectively. Then, the average (solid circles) of each principal orientation can be calculated by using the data from the beginning to the end. The orientations of the three principal anelastic strains must be the same as the orientations of the three principal in situ stresses. The three-dimensional stress orientations show a very good consistency with each other between the two samples. Our preliminary results show that both the stress regimes at the two depths are nearly strike slip faulting stress regime, and the maximum horizontal stress orientations are northwest–southeast or north-northwest–south-southeast which is coherence with the present known regional stress pattern. In general, the results can be considered reasonable and may suggest that the ASR method is well suited for the applications in directly
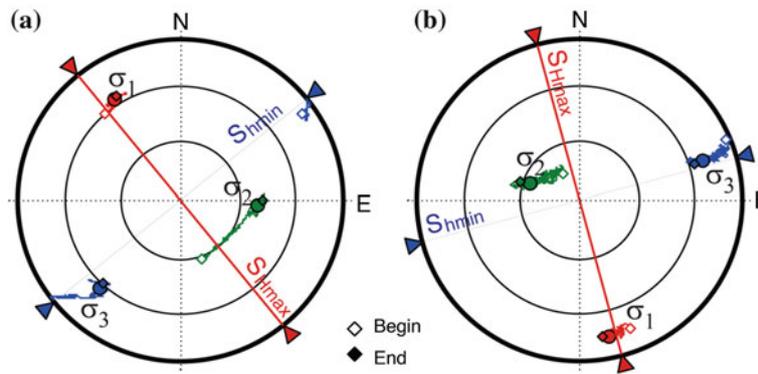
Fig. 15.3 Stereo projections (lower hemisphere) of orientations of three-dimensional principal stresses which are same as those of the principal anelastic strains from ASR measurements with respect to the true north coordinate system. The stress orientations were calculated from anelastic strain values at a certain range of elapsed times, thus the orientations vary with time increases. Open diamond symbol shows the beginning point and solid symbol shows the final point respectively; and the larger solid circles shows the average of the stress orientation from the beginning to the final point. **a** WFSD-2, 1,444 m, **b** WFSD-2, 1,469 m

determining the directions of principal in situ stresses in three dimensions in scientific deep drillings.

15.4 Summary

To determine three-dimensional principal stress orientations, we applied ASR (anelastic strain recovery) measurements using drill core samples taken from Wenchuan Earthquake Fault Scientific Drilling Project Hole-2. Here, we reported preliminary stress orientation results of the two chloritized diorite samples. We glued strain gauges on their cylindrical surface, and successfully obtained high quality anelastic strain data in at least six directions. And then, we determined the three-dimensional stress orientations by the strain–time curves. At the depths around 1,444 m and 1,469 m, the in situ stress regime about 3 years after the earthquake were nearly strike slip faulting stress regime, and the maximum horizontal stress orientations are northwest–southeast or north-northwest–south-southeast which is approximately perpendicular to the coseismic surface rupture.

References

Cui J et al (2013) Determination of three-dimensional in situ stress by anelastic strain recovery in Wenchuan earthquake fault Scientific Drilling Project Hole-1 (WFSD-1). Tectonophys, in-press, doi:10.1016/j.tecto.2013.09.013

Li H et al (2013) Characteristics of the fault-related rocks, fault zones and the principal slip zone in the Wenchuan earthquake fault Scientific Drilling Project Hole-1 (WFSD-1). Tectonophysics 584:23–42. doi:10.1016/j.tecto.2012.08.021

Lin W, Kwasniewski M, Imamura T, Matsuki K (2006) Determination of three-dimensional in situ stresses from anelastic strain recovery measurement of cores at great depth. Tectonophysics 426:221–238

Matsuki K (1991) Three-dimensional in situ stress measurement with anelastic strain recovery of a rock core. In: Wittke W (ed) Proceedings of 7th international congress rock mech., Aachen, 1, 557–560

Teufel LW (1983) Determination of in situ stress from anelastic strain recovery measurements of oriented core. In: SPE paper 11649, SPE/DOE symposium on low permeability. Denver, CO, 421–430

Voight B (1968) Determination of the virgin state of stress in the vicinity of a borehole from measurements of a partial anelastic strain tensor in drill cores. Felsmech Ingenieurgeol 6:201–215

Mathematical-Numerical Modeling of Tectonic Fault Zone (Tadzhikistan)

16

Ernest V. Kalinin, Olga S. Barykina, and Leili L. Panasyan

Abstract

The following paper formulates the criteria of fractured zone size assessment. This article is based on the thesis that the fault zone has to be regarded as a special engineering geologic massif, which is characterized by the stretched form, zonal structure and unfavorable engineering geological conditions. The authors suggest to pay principle attention to the detailed study of the fault structure, composition, sizes and other fault peculiarities. The site of Rogun Hydroelectric Station was reiterated as the object of study. It is situated in the highly complicated rock massif. The site region is characterized by the high activity of modern tectonic movements, and it provides for high strain state of the massif. With the help of boundary element method the questions of the conformity of observable changes in massif—to real width of faults' dynamic zone, its configuration, the location of stress concentration areas, free surface moving and variation of this parameters during the changes of different conditions were considered. A simulation shows that the zone of stress-strain state changing, received in calculation, is twice a large than it is fixed in nature.

16.1 Introduction

The study of tectonic faults is one of the most complex and actual problems of engineering geologic theory and practice. Fault tectonics plays a special role among the factors influencing the engineering geologic conditions. At the same time, there are a limited number of papers which consider the main elements of fault zones, their sizes, composition, properties and their influence on the hydroelectric facilities as well. The estimation of fractured zones influence is rather difficult and insufficiently explored problem in engineering geological investigations. Faults' dynamic areas (*fdz*) as

fractured zones, determined by S.I.Sherman, are not distinctly fixed in nature during investigations (Sherman et al. 1983). The zone which is determining by the formation character and its subsequent life is understood as this area. Within this zone the rock massif is undergoes by mechanical, structural and petrographic changes. So such zones play the negative role during the construction and operation of the facilities. During the construction the adverse phenomena are possible in this zone (such as: busting, inrushes, displacements of rocks and others), which are accompanied by the changes of stress-strain intensity near the faults.

The following paper formulates the criteria of fractured zone sizes assessment. With the help of boundary element method the questions of the conformity of observable changes in massif—to real width of faults' dynamic zone, its configuration, the location of stress concentration areas, free surface moving and variation of this parameters during the changes of different conditions.

E.V. Kalinin · O.S. Barykina (✉) · L.L. Panasyan
Moscow Lomonosov State University, Leninskie Gory 1, GSP-1, 119991 Moscow, Russia
e-mail: barykina@geol.mail.ru

16.2 Methodology of Mathematical-Numerical Modeling

Calculations were done by boundary element method. This method is not deserved rarely used for the solving those engineering geological problems, when the need of strain-stress state research of rock massif and its changing under natural and man-triggered factors is arisen. With the help of the boundary element method (*BEM*) the significant semi-infinite areas, which are often the subject of study in geology and engineering geology, are simply explored. *BEM* lets to solve complicated contact problems, associated with registration not only elastic interaction on the contiguous boundaries, but with irreversible deforming on the contacts, that is important in behavior of creviced environment studying (Crouch and Starfield 1987). Moreover, due to reduction on the geometric unit dimension, the problems of *BEM* use reduce the spending of the information preparation, memory and time of computation. So during the solution of number of engineering geological problems the *BEM* using is highly progressive.

16.3 The Geological Description of the Rogun Hydroelectric Station Site

The site of Rogun Hydroelectric Station, broken by numerous faults of different width, was selected as the investigation object. The Rogun Hydroelectric Station, at the Vakhsh River (Tadzhikistan), is situated in the complex geological media massif of cretaceous sand-stones and silt-stones. The site region is characterized by the high activity of the present tectonic movements, and it provides for high strain state of the massif. All the complex of station constructions is situated within the limits of an invisible tectonic block, limited by sub parallel Ionakhsh and Gulizindan Faults. The tunnel crossing the fault zone through has "flexible" construction. Complex tilt metric and deformational investigations (Starkov 1987) registered vertical movement in 1–3 mm/year of Ionakhsh Fault sides.

16.4 Schematization of Geological Conditions

The aim of mathematical-numerical modeling was the size estimation of near-fault changes (and so width *fdz* definition), the detection of stress spreading features within this zone and the move of free surface in main units. It was studied for this: firstly: stress-strain state of fault zone under gravitation; secondly: under gravitation and tectonic force; and thirdly: the direction and the value of the free surface move under gravitation and tectonic force. The rock massif considered as isotropic linear-elastic medium. The influence of the following factors was taken into account: topographic inequality; fracturing dislocation by the fault; force of gravity; horizontal contractive force, simulated tectonic force.

The width of Ionakhsh Fault together with crushing zone was taken as 20 m at the surface. The rocks are characterized by closed values of density and lateral deformation rate, so in modeling scheme it was taken: module of deformation—30 MPa; Poisson's ratio—0,3; density—2,6 g/sm3, horizontal contractive force—12 MPa.

Fig. 16.1 The scheme of mathematical-numerical modeling of tectonic fault zone for stress and move studying (*1* sand-stones, *2* aleurolites, *3* argillites, *4* fault, *5* depth, where stress is determined, *6* points of surface and their move direction; *7* the scale, *8* isolines of horizontal stress field, MPa)

16.5   Analysis of the Mathematical-Numerical Modeling Results

The modeling scheme and the results of stress-strain and movement studying are presented on the Fig. 16.1. The calculations show that the zone of faults' dynamic influence is limited 200 m at the lying side and 70 m at hanging side; and stress concentration zones are at the fault creek and at average part of the fault at the lying side and between hanging side of the fault and valley floor. Analysis of free surface movement shows that its direction is observed in massif and has uplift direction.

According to engineering geological investigations the width of Ionakhsh Fault is 80 m and with the crushing zone it is about 120 m. But according to the mathematical-numerical modeling its summary width is about 270 m. So a simulation shows that the zone of stress-strain state changing, received in calculation, is double the number of field investigations.

16.6   Conclusion

The mathematical-numerical modeling of fractured zones allows to predict currently unknown regularities, to work out the rational methods of the study of tectonic faults being in various engineering geological conditions, especially in the active tectonic areas, taking into consideration the construction experience and attracting the analogous method for the prediction of engineering geological processes influencing the stability of engineering construction.

References

Crouch Sl, Starfield A (1987) Boundary element method in solid mechanics. Mir, Moscow (in Russian)

Sherman SI et al (1983) The zones of faults' dynamic influence. Nauka, Novosibirsk (in Russian)

Starkov VI (1987) Tectonical deformations of the earth surface at the Rogun hydroelectric station site according to the results of instrumental meterages. Donisch, Dushanbe (in Russian)

Neotectonic and Mass Movements on the New Fez-Taza Highway (Northern Morocco)

17

Tabyaoui Hassan, Deffontaines Benoît, Chaouni Abdel-Ali, El Hammichi Fatima, Lahsaini Meriem, Mounadel Ahlam, Magalhaes Samuel, and Fortunato Gérardo

Abstract

The reflection initiated here, is in connection with an area poorly known from the geological point of view as it is composed of clayey, silty turbiditic sediments and structurally characterized by different geological domains (Saiss basin, Middle Atlas Mountain and Prerif ridges). Furthermore it is also characterized by the frequent mass movements of different nature and volume and a variety of erosion processes (such as rockfalls and rockslides, subsidence and collapse of roads, landslides, gully erosion and rain). We face here a unique chance to have a better geological and geomorphological control due to the construction of the new Fez-Taza highway in northern Morocco. Consequently, this study shows that mass movements are quite important especially in the Prerif ridge, where clayey rocks (clay-stones, marls, shales, muds, flyschs) newly outcrop on both side of this new highway. The factors that affect their occurrence are especially geology and soils, neotectonic movements and climate. The combination of satellite data interpretation, detailed mapping surveys, geophysical investigation, Digital Topographic Model, morphological and finally precise fieldwork campaigns, integrated within a Geographic Information System (GIS) helped to create geo-mapping documents for multi-source developer's in order them to pay attention to the potentially dangerous areas and to optimize safety works along such roads in some sections of the highway. At least such works lead us to differentiate Neotectonics and landslides (*s.l.*) and therefore simplify the passed and recent neotectonic history of the studied area.

T. Hassan (✉) · C. Abdel-Ali · E.H. Fatima · L. Meriem · M. Ahlam
Faculté Polydisciplinaire de Taza, Université Sidi Mohamed Ben Abdellah, B.P. 1223, Taza-Gare, Taza 35000, Morocco
e-mail: hassan.tabyaoui@usmba.ac.ma

C. Abdel-Ali
e-mail: alichaouni@yahoo.fr

E.H. Fatima
e-mail: fatima.elhammichi@usmba.ac.ma

D. Benoît
Laboratoire de Géomatique Appliquée (ENSG-IGN), Université de Paris-Est Marne-La-Vallée, UPEM, Marne-La-Vallée Cedex 2 77450, France
e-mail: benoit.deffontaines@univ-mlv.fr

D. Benoît
Laboratoire International Associé ADEPT CNRS-NSC France-Taiwan, 5 Bd Descartes, Marne-La-Vallée Cedex 2 77450, France

M. Samuel · F. Gérardo
AlphaGéOmega, 62 rue du Cardinal Lemoine, 75005 Paris, France
e-mail: magalhaes_samuel@yahoo.fr

F. Gérardo
e-mail: gerardo.fortunato@hotmail.com

17.1 Introduction

Important part of the Moroccan highway system¸ the Fez-Oujda highway connection extends the highway Rabat—Fez to form eventually a large structuring West–East axis that integrates with the existing network and major roads projects as Taza—Al Hoceima connection and Oujda—Nador. It is also an important section of the Maghreb highway which originates in Nouakchott, capital of Mauritania, and serves the major cities of North Africa to reach Tobruk in Libya.

The drawing of the highway connects the two cities of Fez and Taza over a distance of 127 km through a difficult and mountainous area. The axis of the tracing was chosen to follow the crests of hills encountered, to avoid as much as possible crossing wadis and to ensure the presence of hydraulic works for the drainage of rainwater. However, even after as much as possible the natural terrain, this track involves great heights of cuts and fills exposing beautiful outcrops and exposures in this geologically poorly known area. The trace crosses many wadis, the main ones being: Oued Sebou, Hamri, Bou Zemlane, Matmata, Bou Hellou, Zireg, Inaouène (3 crossings).

The Fez-Taza highway is situated in a continental climate relatively temperate with an average annual rainfall varying from 390 mm to 740 mm. Rainfall events are generally brutal and the greatest rainfall are concentrated in few days of the wet season. The close succession of exceptional rainfall events, are sources of risks to such kind of environments.

The new Fez-Taza highway cross three geological domains: the Saïss basin, the Middle Atlas Mountain and the Prerif ridge. In the Prerif, landslides are mainly mudslides and flows landslides (flowslides) (Tribak et al. 2012). Their genesis is the combination of several factors: geometric (related to the inclination of the topographic surface), lithological (related to marly land beneath the superimposed hard rocks), and structural (complexity of the structure and their deformation). However, in the Middle Atlas, these movements are instead represented by rockfalls of Liassic sandstones, limestones and dolomites. In the Saïss basin, the extension of marl land is an obstacle to carriers and structure determination. The highway route offers a unique chance to have better geological and geomorphological control. The trenches show rich outcrops teaching since they permit to better constrain the differences between landslide and neotectonic.

The studies of mass movement and neotectonic in the Fez-Taza highway are considered through a successive process. Visual interpretation of satellite data (Landsat, as well as High resolution data 60 cm ground resolution such as GeoEye) allowed delineating the various types of mass movements (landslides, rock and debris falls, earth flows). The differentiation of rock and debris falls was done with the aid of ancillary data (geology and Digital Topographic Model). Draping all the images on the DTM surface has clarified zones of detachment from zones of accumulation. Also, by superimposing, in a Geographic Information System (GIS), the available geological maps (Taza, Tahala and Sefrou at 1/50.000 scale), on the processed images, discrimination between features and facies that undergo rock and debris falls was possible. Field truthing campaigns were raised to detect and delineate earth creep. The resulting study, comprising mass movements that were known before our study, plus those newly discovered, are presented herein. Their studies will be considered through the analysis of the processes and factors governing the instability.

In this paper, we present a general geology review and a detailed description of the different types of mass movement across the new Fez-Taza highway, and the factors that affect their occurrence.

17.2 Geological Framework

The Fez-Taza highway crosses from west to east, three important domains: (1) the Saïss basin, (2) the northern side of the Middle Atlas Mountain and (3) the Prerif ridges south of the Rif mountain front.

- The Saïss basin constitutes with the Gharb basins a large depression that extends eastward from the Atlantic to the Taza Strait. The Saïss basin opened in Late Miocene after the collapse of the northern edges of the Western Meseta and the Middle Atlas (Bargach et al. 2003). It behaved as a subsiding marine basin during the Late Miocene, and then was lacustrine during Late Pliocene and Quaternary (Taltasse 1953; Feinberg 1986). The Prerif thrust sheets are interfingered with Upper Miocene rocks in the eastern part of the basin, and with Pliocene rocks in its western part (Moratti and Chalouan 2006).

- In the northern extremity of the tabular Middle Atlas, sub-horizontal Lower Liassic dolostones and limestones are covered by unconformable Plio-Quaternary conglomerates and the lacustrine limestones formations of the Saiss Basin or by the Quaternary fluvial or travertine formations (Charrière 1990; Gourari 2001; Ahmamou 2002; Hinaje 2004).

- The Prerif thrust sheets form the frontal part of the Rif Cordillera. They are a tectonic-sedimentary complex, thrust over the South-Rif corridor (former foreland basin) or the Middle Atlas. The Prerif Ridges comprise elongated hills, formed mainly by Jurassic to Miocene rocks. The ridges are interpreted as part of the Meseta-Atlas cover of the foreland, involved in thrusts of the External Rif—due to the contraction of the African margin during compression from Late Miocene extending to Middle Pliocene (Faugères 1978; Zizi 1996; Moratti and Chalouan 2006).
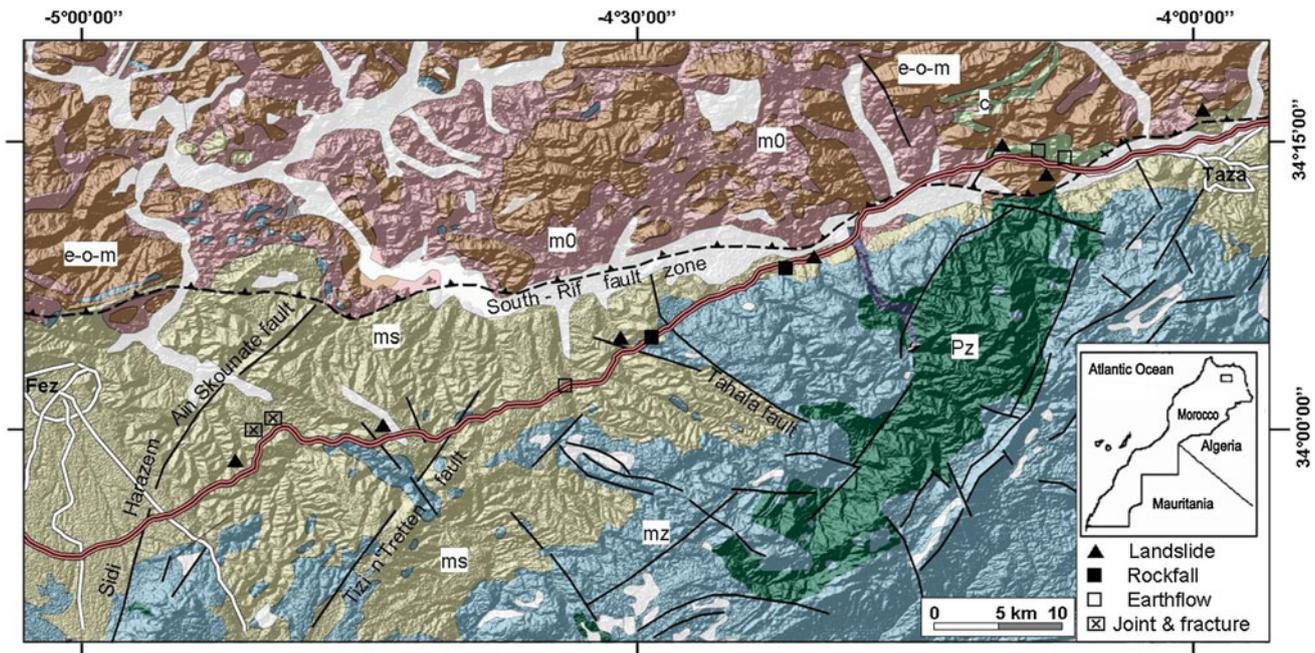
Fig. 17.1 Position of mass movements on the Fez-Taza highway on a geological and geomorphological background. *Pz* Palaeozoic, *mz* Mesozoic, *c* Cretaceous, *e-o-m* Eocene-Oligocene and Miocene, *m0* Middle Miocene, *ms* Upper Miocene

The structures recognized result of the effect of the overlapping tectonic layers recognized in the Rif area with folding-axis oriented WSW-ENE spilled southward and a brittle tectonic oriented NE-SW typical of Middle Atlas and associated with vertical synsedimentary movements, promoting subsidence and uplift of blocks (Sabaoui 1987). The major discontinuities correspond to (Fig. 17.1): (1) the south-Rif accident is an ENE-WSW-trending narrow elongated Prerif ridge, (2) the Tizi n'Tretten fault zone oriented NE-SW, (3) the Sidi Harazem—Ain Skounate fault zone is a set of parallel faults trending NE-SW (4) the Tahala fault oriented NW-SE confronts the liassic formation in the north to the upper Miocene marl cover in the south (Fassi Fihri and Feskaoui 1998).

17.3   Mass Movements Across the New Fez-Taza Highway

Landslides are complex phenomena that we attempt to explain by a number of relatively simple mechanisms resulting from topographic, geological, hydrological and climate condition. Some of these conditions may change over time. The analysis of these mechanisms in the Fez-Taza highway has led us to distinguish different types of slides. Figure 17.1 includes most mass-movement observed in the field. Some older, highlighted in the literature or by surveys conducted during construction are not included on this map.

In general, the Prerif nappes are the site of frequent mass movements. The factors that affect their occurrence are especially geology and soils, neotectonic movements and climate. Mass movements are quite important where clayey rocks (clay-stones, marls, shales, muds, flyschs) crops out. These rocks are potential shear planes as they retain water. The presence of these rocks types along the route of the Fez-Taza highway promotes various types of mass movements (Fig. 17.1).

17.3.1   Landslide

- The rotational slides (slumping) are very common in the Prerif and the Saiss sections of the highway (Fig. 17.1). The surface of these slides has a concavity upwardly facing with the possible presence of concentric cracks in plan and concave in the direction of sliding. This type of landslide concerns slopes with high steeply sloping (15–45°), consisting in particular of clay or marl materials. The instability is fostered by water infiltration in the most permeable layers or by the presence of swelling clays. This slide is quite common and attests to the renewal of marl and clay reliefs by artificial erosion (highway construction and canals).

- Translational slides are characterized by a shallow surface of rupture. This type of sliding interest slope formation in where predominant clay of Miocene or their

associated alteration coverage. Its mechanism is a translational movement of the field mass, more or less coherent, along a slightly inclined surface. The thicknesses of land set in motion are plurimetric and the debris spread to the base of the slope. These slides are very active and have been recognized in the Prerif at the western entrance of the city of Taza (Koudiate Zar Ramrama, 731 m). Their location is strongly influenced by water infiltration. An inventory of this type occurred during the rains period of February 2013 that showed that the distance could reach an horizontal length equal to two times the height of the slope where the break began.

- The clay flows dominate the reliefs of Koudiet Toumiyat located at the western entry of the city of Taza. These movements are the result of the evolution of deep rotational slides and originate in the downstream parts. This mass movement is recognized easily within the GeoEye images of Google Earth®. The clay flow is sometimes large and constitutes a risk due to the spread of debris on the northern side of the highway. The geological nature of the terrain represented by clays and gray marl late Miocene in age combined to steep slopes and to their water saturation, are the main factors triggering these movements and lead to a loss of structures slope stability on the side of the road. Field observations made on two field works (October 2012, February 2013), on the eastern part of Koudiet Toumiyat allowed us to see the growth and expansion of cracks running through the silty gravel formations based on the collapsed parts.

- The subsidence: corresponds to topographic depressions that are bowl-shaped due to the slow and gradual decline of soil without apparent breaks. They are manifested, by occasional vertical displacements of the ground surface in two different places in the Prerif and the Saiss basin. They are usually governed by the nature of clay and marl substrate (increase of the clays plasticity) during heavy rains.

17.3.2 Other Slope Movements

- Joints have been surveyed in the silt of Messinian in two sites in the South of Saiss basin (Region of Bled Cherada). The joints are predominantly oblique to the horizontal bedding and show preferred directions of N 130° E. They range in thickness from a few centimeters and in lengths up to 10 m. The average thickness of joints and the number per unit volume increases from west to east in the direction of digging of the Sebou River valley, suggesting that stress release of tension and alteration play an important role in fissure and joints genesis. However, the great majority of fissures and joints exhibit a matte surface texture without particles reorientation, with indications of brittle fractures rather than shearing.

- Gravitational displacement: the Jurassic formations of the Middle Atlas (limestones and dolomites rocks, and fractured joints), show traces of gravity moving rocks by translational motion without significant dissociation from the original material. These mountain slides are fossilized by post-Jurassic deposits.

17.4 Conclusions

The new Fez-Taza highway is characterized by frequent mass movements of different nature and volume. This section offers a unique chance to have better geological and geomorphological control. The trenches show rich outcrops teaching since they permit to better constrain the differences between landslide and neotectonic.

The combination of satellite data interpretation, detailed mapping surveys, geophysical investigation, DTM, morphological and finally precise fieldwork campaigns, integrated within a Geographic Information System (GIS) helped to create geo-mapping documents for multi-source developers. This instability corresponds in general to mass movement and dominates in the Prerif area. They are the result of geology and soils, recent and ongoing tectonic activity and climate.

Considering the risks of ground movement on some part of the Fez-Taza highway, the continuation and development of these researches is needed by actions such as the monitoring of movement, stability calculation, establishment of mechanical rupture models, modelling the motion path, research on protection techniques, development of files for each landslide. These actions will improve the understanding of these mass movements and attract the attention of developers on risk areas and potential or actual danger, and also the recommendation of stabilization works.

References

Ahmamou M (2002) Evolution et dynamique sédimentaires des carbonates fluvio-lacustres Plio-quaternaires dans le Saïss de Fès (Maroc). Thèse de Doctorat d'Etat, Université Mohamed V, Rabat, 230 p

Bargach K, Chalouan A, Galindo-Zaldivar J, Ruano P, Ahmamou M, Jabaloy A, Akil M, Sanz De Galdeano C, Chabli A, Benmakhlouf M (2003) Détermination de paléocontraintes à partir des galets striés des formations conglomératiques plio-quaternaires au front de la chaîne du Rif (Maroc) : la Ride de Trhat. Notes et Mémoires du Service Géologique, Maroc, 452, 99–108

Charrière A (1990) Héritage hercynien et évolution géodynamique alpine d'une chaîne intracontinentale : Le Moyen Atlas au sud-est de Fès (Maroc). Thèse d'Etat, Université Pau Sabatier, Toulouse III, France, 589 p

Fassi Fihri O, Feskaoui M (1998) Etude hydrogéologique de l'aquifère liasique du couloir Fès-Taza (Maroc). Karst Hydrology, IAHS Publ. no. 247, pp. 99–116

Faugères JC (1978) Les Rides sud-rifaines. Evolution sédimentaire et structurale d'un bassin atlantico-mésogéen de la marge africaine. Thèse Doct Etat. Univ. Bordeaux 1, n° 290, vol., 510 p., 11 tab., 119 fig., 42 pl

Feinberg H (1986) Les séries tertiaires des Zones Externes du Rif (Maroc). Biostratigraphie, paléoécologies et aperçu tectonique, Notes et Mém. Serv. Géol. Maroc 315, pp 192

Gourari L (2001) Etude hydrochimique, morphologique, lithostratigraphique, sédimentologique et pétrographique des dépôts travertino-détritiques actuels et plio-quaternaire du bassin karstique de l'oued Aggaï (Causse de Sefrou Moyen Atlas, Maroc). Thèse d'Etat, Univ. Sidi Mohammed Ben Abdallah, Fès, 476 p

Hinaje S (2004) Tectonique cassante et paléochamps de contraintes dans le Moyen et le haut Atlas (Midelt-Errachidia) depuis le Trias à l'Actuel. Thèse d'Etat Es-Sciences, Rabat 425 p

Moratti G, Chalouan A (2006) Tectonics of the Western Mediterranean and North Africa. J Afr Earth Sci (and the Middle East) 48(1):1

Sabaoui A (1987) Structure et évolution alpine de Moyen Atlas septentrional sur la transversale Tleta du Zerarda-Merhraoua. Thèse de 3ième cycle

Taltasse P (1953) Recherche géologiques et hydrogéologiques dans le bassin lacustre de Fès-Meknès. Notes et Mémoire, n° 115, 300 p. Service de géologie. Rabat, Maroc

Tribak A, El Garouani A, Abahrour M (2012) L'érosion hydrique dans les séries marneuses tertiaires du prérif oriental: agents, processus et évaluation quantitative. Rev Mar Sci Agron Vét (2012) 1:47–52

Zizi M (1996) Triasic-jurassic extentional systems and their Neogene reactivation in northern Morocco (the rides prérifaines and basin Guercif). Ph. D. thesis, Rice University, Houston

Importance of Geological Map Updates in Engineering Geology, Application to the Rif-Chain and Its Foreland (Northern Morocco)

18

Deffontaines Benoît, Tabyaoui Hassan, El Hammichi Fatima, Chaouni Abdel-Ali, Mounadel Ahlam, Lahsaini Meriam, Magalhaes Samuel, and Fortunato Gérardo

Abstract

This study focus on the importance of geological map updates in engineering geology. Presently we face such a huge quantity of data (1) acquisition of the earth surface (*s.l.*) such as multi-date remote sensing images, aerial photographs and Digital Terrain Model at various ground resolutions, High Resolution Data (HRD), and (2) lots of thematic data such as geological and geomorphological detailed works, thesis, report, mapping, etc… that it is needed and of major importance to gather and synthesize all these data in an up-dated numerical geological mapping. Therefore, we conducted a new multidisciplinary methodological approach; focus on Earth Sciences especially on the study of lithology, and structure. We use the contribution of all existing and available data such as digital terrain models (DTM), integrated of remote sensing space and airborne images. Recognition detailed geological materials and structures as well as the analysis and modeling of the physical processes controlling the deformation help also for the main focus of this research. The research is oriented in a first step towards the development of a Digital Terrain Model (DTM); the use of satellite images with multi-source, multi-resolution and multi-date (Radar-ERS, Landsat ETM 30 m, Aster 15 m and Quickbird 2.4 m up to Geo-Eye 60 cm) and aerial photographs; and Geological and geomechanical analysis of land facing the numerical simulation of tectonic deformation process, building on GIS software in order to update the geological map.

D. Benoît (✉)
Laboratoire de Géomatique Appliquée (ENSG-IGN), Université de Paris-Est Marne-La-Vallée (UPEM), 5 Bd Descartes, 77450, Marne-la-Vallée Cedex 2, France
e-mail: benoit.deffontaines@univ-mlv.fr

D. Benoît
Laboratoire International Associé ADEPT 539 CNRS-NSC France-Taiwan, 5 Bd Descartes, 77450, Marne-la-Vallée Cedex 2, France

T. Hassan · E.H. Fatima · C. Abdel-Ali · M. Ahlam · L. Meriam
Polydisciplinary Faculty of Taza, Sidi Mohamed Ben Abdellah University, B.P. 1223Taza-Gare, Taza 35000, Morocco
e-mail: hassan.tabyaoui@usmba.ac.ma

M. Ahlam
e-mail: ahlammounadelfst@gmail.com

M. Samuel · F. Gérardo
AlphaGéOmega, 62 Rue Du Cardinal Lemoine, 75005, Paris, France

18.1 Introduction

A geologic map displays the placement, distribution, characteristics, and age relationships of rock units and formation, along with structural features, on a two-dimensional base map. Everyone benefits directly or indirectly from ongoing geologic mapping such as local governments, industry, educators, and public depend on the information provided by geological maps to carry out their missions.

In morocco, Geological Survey of Morocco publishes the first geological map in 1927. Since then, the publications have continued, and to this day, it is not less than 1,600 articles (270 geosciences maps), are available to the public. Geological maps were made at scales from 1/500.000, 1/200.000, 1/100.000 and 1/50.000. Geological maps on paper format constitute three-quarters of the production of the Geological Survey, covering primarily the Northern Provinces.

Update of old geological maps is a good project involved in Morocco. Today, with the fast development of sensor techniques and computer methods, many kind of raster and vector based models for describing, modelling, and visualizing 3D spatial data are available. This development associated to the growth of engineering projects (construction of highways, urban development projects, etc.), the update of old geological maps in 2D and 3D become more and more important.

In this study, a multidisciplinary methodological approach is developed, in which the contribution of Earth Sciences is emphasized, as well as the contribution of digital elevation models (DEM) and integrated of remote sensing space and airborne images. Many works illustrate the importance of DEM and remote sensing in recognition of geological materials and structures as well as the analysis and modelling of the physical processes controlling the deformation (Douglas 1986; Klingebiel et al. 1988; Pryet et al. 2011). DEM are one of the most suitable tools for such kind of analysis. Although DEMs are currently being used for describing geological features related to geomorphology, hydrology and tectonics (Deffontaines 1990; 2000; Onorati et al. 1992; Seber et al. 1996; Spark and Williams 1996), they still have not become a common tool in geological mapping projects.

Modelling terrain relief via DTM is a powerful tool in GIS (Geographic Information System) analysis and visualization. In a GIS environment, three-dimensional images can be easily performed. The relief can be exaggerated and any type of 2D maps (Geological, Geophysical, etc.) can be draped over. With that, we can visualize the draped map of an area from any vantage-point.

The aim of this contribution is to illustrate the importance of the re-interpretation in the light of the new geological concepts and knowledge the DEM and remote sensing data combined with previous bibliographic works in providing valuable geological information that can be used as a guide in updating old geological map of Northern Morocco as a first step of a more regional project.

18.2 Methodology

Updating the geological map is the general purpose of this research. Several steps were undertaken.

1. First, available literature review was done for extracting information concerning the general geology and geomorphology of the study area. As a first application, the Prerif ridges, in northern Morocco have been chosen to illustrate the result of geological update. We look also forward to any drills, wells, seismic lines that may help to understand the 3D geometry.

2. In the second step, geological maps was scanned at 300 dpi using an A0 scanner, georeferenced in WGS84 projection in ERDAS Imagine 9.2, using a combination of latitude/longitude information and others references points on the map. Georeferencing was performed using a first order transformation with RMS-errors less than 0.3 m. The georeferenced map was then stored in Geotiff format at a scale of 1:50.000. The structural objects such as recognized fold axes, faults dip… are collected.

3. ASTER (Advanced Spaceborne Thermal Emission and Reflection Radiometer; METI/NASA 2009) Global Digital Elevation Model (GDEM) elevation data sets been used to perform the topographic analysis. The DEM data from this space mission cover most of the regions of the world and are publicly available (at no cost) at spatial resolutions of 1 arc second. The ASTER GDEM was resampled from 30 m (1 arc second) horizontal resolution to 15 m to minimize the terrain effect. The required study areas were, then extracted from DEM using there base map shape file in a WGS84 coordinate system. For this process, we used the software GLOBAL MAPPER 10v to crop the DEM with only required region's terrain data. Then, we used ArcGIS 10.2 software package to perform the spectral analysis over the DEM.

4. Correlation between DEM derived surfaces and geological maps: DEMs look at the surface from a strictly topographic point of view. Only the geological features reflected in the topography can be visible in DEM images. This fact allows DEMs to recognize geological structures, rock softness, and boundaries and drainage patterns (Ben Hassen et al. 2012; Duperet et al. 2003). The shaded topographic relief or hill-shadow of the DEM depicts relief by simulating the effect of the sun's illumination on the terrain. This technique was used for controlling and interpreting structural boundaries (Deffontaines 1990). These images are useful to display

Fig. 18.1 Geological setting and location of the studied area in northern Morocco. *1* Neogene and quaternary rocks, *2* Prerif ridges, *3* External prerif, *4* Internal prerif, *5* Mesorif, *6* Intrarif, *7* thrust nappes of intrarif origin, *8* Internal zones, *9* Flysch, *10* Middle atlas, *11* Meseta, *12* Location of the studied area
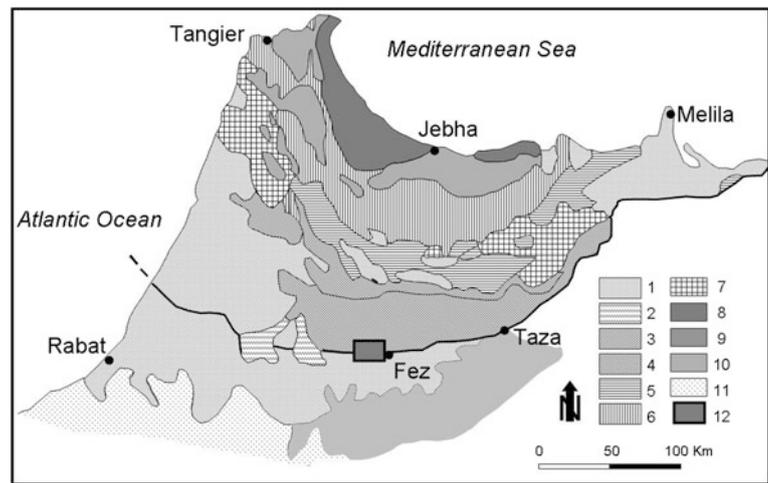
geological data related to landforms in terrains that show a close correlation between geology and topography. This initial exploration permits to further enhance lithological boundaries and to delineate areas where additional exploration is needed (satellites image analysis, field survey, etc.).

5. Data preparation and pre-processing of optical and microwave remotely sensed images, such as Landsat ETM + , ASTER 15/30 m and Quickbird 2.4 m were conducted using ERDAS software. Various image enhancement techniques were used to clearly visualize the images. Radiometric and geometric corrections were applied in order to remove the influence of the atmosphere and to get surface reflectance. Main values digital numbers (DN) of lithological units in individual Landsat and Aster bands were calculated and the values were plotted to see which band best discriminate the different lithologies. Based on the selected individual bands, image classifications were carried out using maximum likelihood classification. All the resulted images were subset into one projection system.

6. The geological map had then been redrawn and complete taking into account the previous items, our field experience, our field of competence (sedimentology as well as structural geology and engineering geology… and so on). For instance the legend and the existing lithologies had been revisited by field works and re-interpretation of the data.

18.3 Study Area

The Geological map of Fès-Ouest at 1:50.000 (Bruderer et al. 1950), communicates vast amounts of geological information. This map is edited by the Cherifienne Company of Oil for the Geological Survey of Morocco on 1950. It

shows the central part of the Prerif ridges. The Prerif thrust sheets form the frontal part of the Rif Cordillera. It corresponds to a tectonic-sedimentary complex, thrust over the South-Rif Corridor (Fig. 18.1).

To the south of this sheet, the Jbel Trhat area is chosen due to its complexity of folding and tectonic structure and history. This Prerifain ridge is a mountain area and corresponds to a fold with an E-W oriented axis, fewly deformed by faults. The estimate terrain elevation level is about 837 metres.

In this region, geological structures and rock unit boundaries show a strong correlation with relief. DEM and satellites images analysis show that geological boundaries may be mapped with detailed topographic analysis. Literature reviews (Bargach et al. 2004; Cherai et al. 2008; Lakhdar et al. 2004; Wernli 1978) and field works permitted to better understand the rock types, stratigraphy, structures and deformation history and then to update the geological map of this area Fig. 18.2.

This analysis show that Jbel Trhat is a complex anticlinal, with a kilometric length and periclinal ends, affected by thrusts of the Prerif nappe sheets. The fold is tighter toward the west, where layers of the southern side become overturned and a periclinal end can be observed. The fold asymmetry clearly indicates southward tectonic transport. This fold is probably active as it develops after Pliocene because conglomerates of this age are also overturned (Fig. 18.3).

In this portion of the map, the Prerif ridge shows a sedimentary sequence starting with a thick Jurassic sequence (J), with cancellophycus limestones of Aalenian and thick gray marls of Bajocian. The Neogene discordant on the Dogger starts with a calcareous and sandstone formation (60 m) of Lower Miocene (Burdigalian) (m1), surmounted by white marl (200–300 m) of Middle Miocene (m2). Unlike the geological map, our study confirms that the Middle

Fig. 18.2 Old and updated map of Jbel Trhat at 1/50,000 scale (work in progress). *J* Jurassic, *m1* Lower Miocene, *m2* Middle Miocene, *m3-1* Lower Tortonian, *m3a* Middle Tortonian, *m3 blue* and *gray* marls of Upper Tortonian—Messinian, *3-2* sandstone of Upper Messinian, *cl1* Pliocene, (cl3, qe & q1a) Quaternary

Fig. 18.3 Old and updated map of Jbel Trhat at 1/50,000 scale (work in progress). *J* Jurassic, *m1* Lower Miocene, *m2* Middle Miocene, *m3-1* Lower Tortonian, *m3a* Middle Tortonian, *m3 blue* and *gray* marls of Upper Tortonian—Messinian, (3-2) sandstone of Upper Messinian, (cl1) Pliocene, *cl3, qe & q1a* Quaternary
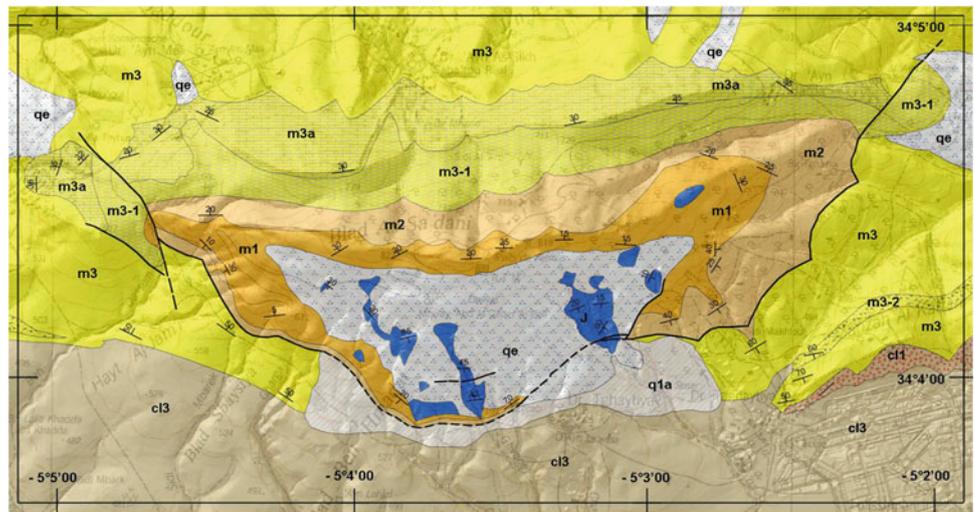
Miocene outcrops south of the Jbel Trhat. The Tortonian starts with bleu-gray marls (m3-1) and a cavernous yellow limestone (m3a). The Upper Tortonian—Messinian (m3) are represented by monotonous blue and gray marls series (800–900 m thick), intercalated by three sandy ferruginous beds, in turbidite character named "Grès I" and "Grès II" (Wernli 1978) (m3-2). The Pliocene correspond to polygenic conglomerates that crop out very locally (cl3). The quaternary is represented by variegated clays and silts (cl3). Alluvial fans and talus (qe) and mass rocks (q1a) are particularly abundant. They correspond to the accumulation of large blocks of calcareous or loam deposits supplied by clay.

The uses of satellites images and DEM permit to understand some typical scenarios of triggering or reactivation of mass movements and landslides (qe). The updated map shows some of theses phenomena (rockslide—landslide) that are the subject of detailed field investigations and geomechanical analyzes.

18.4 Results and Conclusion

DEM images have the ability to visualize structures and lithological boundaries reflected in the topography, especially those related to recent geological evolution. With DEM and satellites images, up-date of geological map become a dynamic process of gathering, evaluating, revising and up-dating geologic data and their implications and applications, both to the structure and to further exploration. Trend-topographic analysis in the Prerif ridge provides useful data about the role of doming processes and folding and faulting structures in the construction of the relief.

The results of this study support and come at a reference for any engineering further studies in this area. We are developing different types of maps of different scales (a) regional to local geological maps at a scale of 1:100.000 to 1/10.000 and (b) Engineering geological plan at even larger

scale such as 1:5.000 scale. These documents are of great use to Individuals, consulting and civil engineering offices, and of course to Government administrations.

References

Bargach K, Ruano P, Chabli A, Galindo-Zaldí´Var J, Chalouan A, Jabaloy A, Akil M, Ahmamou M Sanz De Galdeano C, Benmakhlouf M (2004) Recent tectonic deformations and stresses in the frontal part of the Rif Cordillera and the Saïs Basin (Fes and Rabat regions, Morocco): Pure appl Geophys 161 (2004) 521–540

Ben Hassen M, Deffontaines B, Rebai N, Turki MM (2012) Contribution of drainage network and LANDSAT ETM + photo-interpretation for homogenization of the geological mapping coverage: Application to some examples in Southern Tunisia. Photo-Interpretation Euro J Appl Remote Sens 2012(3):31p

Bruderer W, Gouskov N, Gubler J, Jacquemont P, Levy R, Tilloy R (1950) Carte géologique régulière du Maroc au 1:100.000 : Fès Ouest. Soc. Cherif. Petroles, Notes et Mémoires Services Géologique Maroc, N°109

Cherai B, Charroud M, Lahrach A, Babault J (2008) Influence de la tectonique compressive et des mouvements verticaux d'origine mantellique sur l'évolution quaternaire du Saïs entre le Rif et le Moyen Atlas (Maroc). Actes RQM4. Oujda 2008:171–181

Deffontaines B (1990) Développement d'une méthodologie morphonéotectonique et morphostructurale; analyse des surfaces enveloppes, du réseau hydrographique et des modèles numériques de terrains; Application au Nord- Est de la France. Thèse, Univ. Paris VI, France, 230 p

Deffontaines B (2000) Formes et déformations de la surface terrestre: approche morphométrique et application. Thèse d'habilitation à diriger la recherche, Université Pierre et Marie Curie, Paris, 65 p

Douglas DH (1986) Experiments to locate ridges and channels to create a new type of digital elevation model. Cartographica 23(4):29–61

Duperet A, Deffontaines B, Passalacqua O (2003) Critères géomorphométriques issus des modèles numériques de terrain au service des applications hydrologiques. Bulletin Société française de photogrammétrie et de télédétection. ISSN-0244-6014. 172, pp 107–121

Klingebiel AA, Horvath EH, Reybold WU, Moore DG, Fosnight EA, Loveland TR (1988) A guide for the use of digital elevation model data for making soil surveys: U.S. geological survey open-file report 88–102, 18 p

Lakhdar A, Ntarmouchant A, Ben Abbou M, Ribeiro M L, El Hamzaoui 0, El Ouadeihe K, Hessane MA (2004) Minéralisations sulfurées et activité hydrothermale post miocène: impact sur la signature géochimique des eaux thermales de Moulay Yacoub (Bordure septentrionale du Sillon Sud Rifain Occidental, Maroc Septentrional). 4eme Coll 3MA, p 7 Agadir (Maroc)

METI/NASA (2009) ASTER global digital elevation model by Ministry of Economy, trade and industry of Japan (METI) and the National Aeronautics and Space Administration (NASA). Available at: http://asterweb.jpl.nasa.gov/gdem.asp and http://www.gdem.aster.ersdac.or.jp

Onorati O, Poscolieri M, Ventura R, Chiarini V, Crucillà U (1992) The digital elevation model of Italy for geomorphology and structural geology. Catena 19:147–178

Pryet A, Ramm J, Chilès JP, Auken E, Deffontaines B, Violette S (2011) 3D resistivity gridding of large AEM datasets: a step toward enhanced geological interpretation. J Appl Geophys 75(2011):277–283

Seber D, Vallvé M, Sandvol E, Steel D, Barazangi M (1996) Middle east tectonics: applications of geographic information systems. CGS Today, 7.2.1–6

Spark RN, Williams PF (1996) Digital terrain models and the visualization of structural geology. In: De Paor DG (ed) Structural geology and personal computers. Computer methods in the geosciences, v 15. Elsevier Science Ltd, pp 421–446

Wernli R (1978) Micropaléontologie du Néogène post-nappes du Maroc septentrional et description systématique des Foraminifères planctoniques. Notes et Mémoires du Service Géologique N° 331 207p

Disaster Awareness Education for Children in Schools Around Geological Hazard Prone Areas in Indonesia

19

Muslim Dicky, Evi Haerani, Motohiko Shibayama, Masaaki Ueshima, Naoko Kagawa, and Febri Hirnawan

Abstract

Geological disaster awareness has been increasing recently in Indonesia, especially since the great Aceh's Tsunami & Earthquake. It is important that all stakeholders have reasonable understanding on disaster response. School communities generally have limited disaster education opportunities and knowledge. This could imply a low level of disaster awareness. This paper aimed to examine the knowledge on disaster response and to highlight the needs to introduce earth science for school communities by exploring three areas: (i) disaster education, (ii) respond to disaster event, (iii) knowledge of earth science. The study had been started since 2006, targeted on schools located on the areas that experienced and/or potential to earthquake and tsunami in the future. Several schools around the coastline of Indian Ocean of Sumatera, Java, Bali & Lombok islands had been visited. In each school, we examined the curriculum, preparedness to face disaster, and activity of mitigation. Our posters and pamphlets were also distributed. Presentation and short drama were performed in the classroom to measure understanding of the contents. Result showed that disaster awareness were generally out of curriculum, due to limited knowledge of the curriculum development. For the respond to disaster event, most of participants are unaware what to do when disaster happens. Our visit had increased the curiosity of school communities to learn more about these disasters. These results suggest that dissemination of entry level of earth science is deeply needed, since there is no such subject (especially geology) in primary to secondary level schools in Indonesia.

Keywords

Disaster awareness • Earthquake • Tsunami • School children • Indonesia

19.1 Introduction

Since the aftermath of great Aceh's Tsunami & Earthquake in December 2004, geological disaster awareness has been increasing recently in Indonesia. It is important that all stakeholders including school communities have reasonable understanding on disaster response. School communities generally have limited disaster education opportunities and knowledge. This could imply a low level of disaster awareness.

M. Dicky (✉) · F. Hirnawan
University of Padjadjaran, Bandung 40115, Indonesia
e-mail: dicky.muslim@unpad.ac.id

E. Haerani
Faculty of Geology, University of Padjadjaran,
Jatinangor 45363, Indonesia

M. Shibayama · M. Ueshima · N. Kagawa
Natural Environmental Research Institute, Osaka 543-0045, Japan
e-mail: shibayama@themis.ocn.ne.jp

This paper aimed to examine the knowledge on disaster response and to highlight the needs to introduce earth science for school communities by exploring three areas: (i) disaster education, (ii) respond to disaster event, (iii) knowledge of earth science.

19.2 Methodology

The activities had been started since 2006 and had targeted on elementary to senior high schools in several places, which located as the earthquake hazard and tsunami prone areas that experienced as well as potential areas of geological disaster in the future. Several schools around the coastline of Indian Ocean of Sumatera, Java, Bali & Lombok islands had been visited. In total, within 6 years there were more than 50.000 pamphlets and posters of earthquake and tsunami (Fig. 19.1) had been distributed in several schools and districts so far.

Participants in this study were stakeholders of education sectors in a remote area. For the purpose of this paper, the students & teachers were the focus of the study. The survey was piloted on a group of students & teachers from highest grade of each school.

Students & teachers involved in this research occupied public schools in the study area. The highest grade of each school was chosen as they have ability to read and write their opinion though in simple form. Teacher participants were chosen as they were the guardian of each classroom. We involved also the participation of the school principals as well as local government officers.

Pamphlets and posters for the tsunami and earthquake disaster prevention education are distributed directly as teaching materials. Pamphlets were prepared and printed in Osaka-Japan by several group of volunteers (Fig. 19.2), which then brought to Indonesia for this study. The posters are then posted in announcement board of each school, and the pamphlets are distributed to students and teachers in their classroom. Discussion session and short drama were performed in the classroom to measure understanding of the contents. The aim of discussion was to explore students & teachers' perceptions and knowledge of disaster education & response through a series of questions and answers (Shibayama et al. 2006).

A mixed method of descriptive and exploratory research design underpins this research. Descriptive & exploratory research designs are appropriate when little is known about the topic being investigated. Integration of quantitative and qualitative data which was generated from the survey, lends itself to the mixed method approach. According to Polit and Beck (2008) the greatest advantage of survey research for disaster issue is its flexibility and broadness of scope. Due to the limited amount of knowledge in the study area, the authors thought that a survey research would be more appropriate as it would generate a basic understanding of the phenomenon as well as reach a larger proportion of the population.

19.3 Result and Discussions

The word 'disaster' encompasses a myriad of occurrences and the meaning of the word is relative to each and every person experiencing the disaster. Generally speaking, a disaster or a major incident will overwhelm existing resources. However, in the context of this study it may be suggestive of a limited understanding as to what constitutes

Fig. 19.1 Pamphlets of earthquake (*left*) and tsunami (*right*) education for children in Bahasa Indonesia
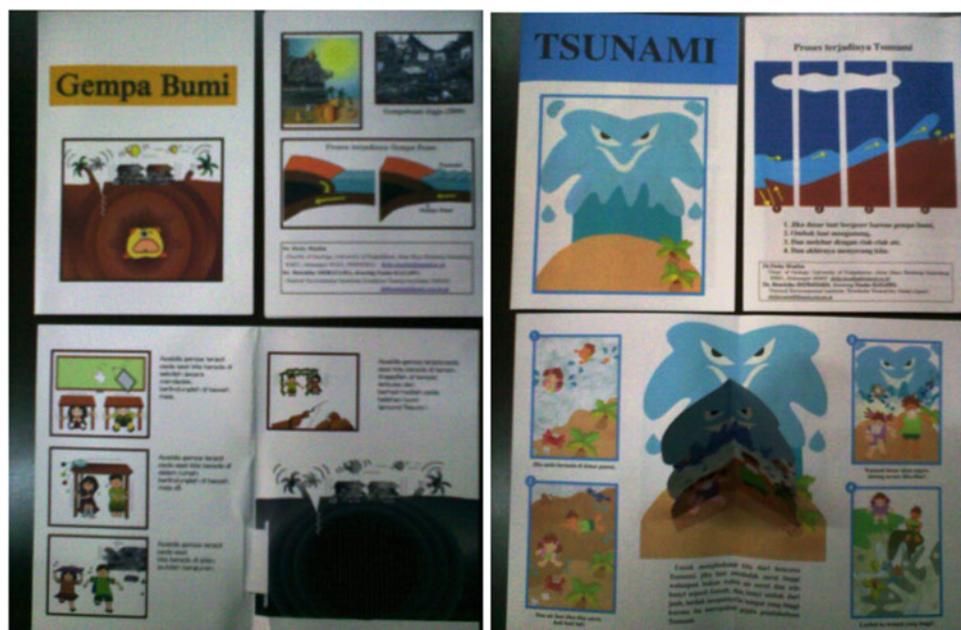
Fig. 19.2 Activities to prepare the pamphlets of tsunami and earthquake by volunteers in Osaka, Japan

a disaster or major incident especially related with geological event or hazard such as earthquake & tsunami as they are major disaster in Indonesia (Anonymous 2006).

19.3.1 Disaster Education

When we came to each school, first we introduced ourselves and discussed with the school principal and teachers about disaster education in their school, especially related with disaster curriculum development and teaching materials for earth science. After introduction session in front of the classroom, participants were asked to identify their perceptions of their own level of disaster knowledge and experience of earthquake or tsunami in simple form. Although most of all participants stated they know about earthquake or tsunami events but many stated they have no ideas about kinds of natural disaster in their area. It is possible that the majority of participants answered since they have read newspaper or watch TV about the recent disaster events in Indonesia and elsewhere but unfortunately they don't have idea for their own area.

For the purpose of this study the term 'education' refers to any didactic formal education included in curriculum, where 'training' refers to practical hands on approach to disaster knowledge. Both of terms constitute activities such as lectures, desk top exercises, real-time exercises, etc. Many of participants had never attended specific disaster training or education outside their schools. Only a small amount of participants stated they had attended minor disaster specific courses in an extra-curricular activity such as "boy scout".

For the purpose of this study 'disaster specific courses' were considered as those that have been created specifically with the purpose of training common people in any aspects of disaster preparedness and response.

It was interesting to note that many of participants reported that they have experienced a disaster or major incident in their life. Some examples provided by the participants included examples such as house fire, flood, landslide, etc. The terms 'disaster' and 'major incident' were not qualified in the survey, however participant responses are suggestive of limited understanding of what constitutes a disaster or a major incident. Questions regarding the disaster event did not differentiate between -to some extent- predictable (i.e. house fire, flood, drought, etc.) and unpredictable (i.e. earthquake, tsunami, etc.).

Coastal area of Indian Ocean had experienced natural disasters with mass casualties due to earthquake & tsunami events. But it seemed from our study that there were no particular developments on the school's curriculum to include disaster education so far in the study area.

19.3.2 Respond to Disaster Event

Using our teaching materials in the classroom, we discussed with participants to rate their knowledge in their own level about disaster preparedness, especially about respond when an earthquake or tsunami happen. Majority of participants stated they do not know about what to do when a disaster occurs in their area. When participants were asked to rate their level of knowledge about how preparedness had been

constructed in their school and surrounding area, many of them do not know about school preparation to prepare for a disaster event.

Majority of the participants did not know about simple form of disaster preparedness for earthquake and tsunami events such as evacuation route, safety area, survival kit, communication tools, etc. This result is parallel to the above data regarding students & teachers' own level of education for disaster. In both instances more than half the sample had less than optimal confidence in their own disaster awareness. This suggests a feeling among students & teachers of limited preparedness to respond to a disaster event.

After a series of discussion, we then performed drama and/or story telling with our teaching materials to emphasize the need for understanding the subject of tsunami and earthquake hazard to all participants in the classroom (Fig. 19.3). Especially to stress out the need to be calm in panic situation to escape from disastrous event in time of earthquake or tsunami occur. It is worthy to note that pamphlets adopted from Japanese comic created and produced in Japan along with the appearance of foreign researcher in the classroom seemed had increased psychologically the enthusiastic attention from students and teachers in each school.

19.3.3 Knowledge of Earth Science

Based on the discussions with school principal, teachers & students as well as local education section office, it is interesting to note that based on national curriculum, earth science is included in the subject of Geography instead of Geology course in all level of elementary to high school. Even in a region where previous geological disaster had occurred, local content of curriculum for disaster is not developed yet so far. This might be due to limited knowledge and understanding of teachers in each school we visited.

An overwhelming of participants in the classroom stated that earth science education for students & teachers is very important. The form of earth science education and/or disaster training that most respondents believed would be beneficial for students & teachers were real-time exercises. Lectures provided by other competent institution (i.e. university, company) is the most stated by participants.

Education and training opportunities for participants in this study appear to be difficult to access due to their location and availability. While literature highlights the importance of disaster education and training for students & teachers but little appears to be understood about what type of education and training would be the most appropriate for a particular attendees (Duong 2009).

19.4 Conclusion

Previous disaster response experience and appropriate disaster or earth science education appear to be essential ingredients in providing a prepared and safe school. In a community where previous disaster response experience is limited, appropriate disaster education and training for students & teachers may increase the level of disaster awareness and help to make school community feel less vulnerable when having to face the unexpected (Aguilar and Retamal 2009).

Standardizing disaster and earth science education and making it more available may create a more cohesive and self-assured workforce. Further research needs to be conducted in order to close the gap in knowledge that exists in this area and to determine appropriate strategies for increasing disaster awareness among stakeholders.

References

Aguilar P, Retamal G (2009) Protective environments and quality education in humanitarian contexts. Int J Educ Dev 29:3–16

Anonymous (2006) National Action Plan of Disaster Risk Reduction 2006–2009, Indonesian Gov. Printing Office (in Bahasa Indonesia), p 196

Duong K (2009) Disaster education and training of emergency nurses in South Australia. Australas Emerg Nurs J 12:86–92

Polit DF, Beck CT (2008) Nursing research: generating and assessing evidence for nursing practice, 8th edn. Lippincott, Williams & Williams, Philadelphia

Shibayama M, Muslim D, Kagawa N, Shibakawa A, Hiraoka Y, Ueshima M, Kawamura D, Ota K (2006) Making of tsunami pamphlet for school children in Indonesia and Japan, and disaster prevention education. IGEO Poster Session Abstracts, GeoSciEd V (Bayreuth, Germany), p 8

Analysis of Recent Deformation in the Southern Atlas of Tunisia Using Geomorphometry

20

Mehdi Ben Hassen, Benoît Deffontaines, and Mohamed Moncef Turki

Abstract

In this work, we propose to locate, characterize and quantify some topographic deformations linked to the seismotectonic context, and anthropogenic actions in the southern Atlas of Tunisia. The analysis of morphometric parameters (Residual Topography, Hypsometric Integral, Drainage anomalies, Maximum curvatures and Roughness) has revealed that three structures in the study area, J. Ben Younes, J. Bou Ramli and J. El Abiod, are distinguished by a specific morphometric and anomalous response which may reflect an important morpho-dynamic activity caused principally by the numerous reactivation of the Gafsa fault.

20.1 Introduction

Tunisia is submitted to a long time convergence of both African and Eurasian crustal plates. The latter collision creates the northern Atlas orogene and the N–S present stress field creates many small topographic displacements on the major

M. Ben Hassen (✉) · B. Deffontaines
Bât IFG, Laboratoire de Géomatique Appliquée (ENSG, IGN), Télédétection et Modélisation des Connaissances, Université Paris-Est Marne-la-Vallée, 5 Bd Descartes, Marne-la-Vallée, Cedex 2, 77454, France
e-mail: mahdigeo2002@yahoo.fr

B. Deffontaines
e-mail: benoit.deffontaines@univ-mlv.fr

M. Ben Hassen · M.M. Turki
Faculté des Sciences de Tunis, Département de Géologie, Université de Tunis El Manar, Campus Universitaire 2092, El Manar Tunis, Tunisie
e-mail: mohamedmoncef.turki@fst.rnu.tn

B. Deffontaines
Laboratoire de Géomatique Appliquée, Ecole Nationale des Sciences Géographiques, Institut Géographique National, Et Laboratoire International Associé ADEPT France-Taiwan CNRS-NSC, 6-8 avenue Blaise Pascal, Marne-la-Vallée, Cedex 2, 77455, France

faulted structure. The seismotectonic database that we settle for the Tunisia has shown that the southern Atlas of Tunisia is strongly influenced by this geodynamic context and manifested by a relatively high seismic potential (Fig. 20.1).

Several methods may be used to describe active tectonic zones, among which "geomorphometry" is useful. For instance, this method may help describing, analysing and measuring the morphology of land surface (Deffontaines 1990; Pike and Dikau 1995; Pike 2002; Dehn et al. 2001; Bolongaro-Crevenna et al. 2005).

20.2 Identification of Recent Deformations

In this section, we will try to establish the relationship between morphometric parameters and the structural context of the study area.

Five major morphometric parameters were analyzed: the residual topography, hypsometric analysis, analysis of drainage anomaly, maximum vertical curvature and roughness of terrain.

The interpretation of specific signatures of morphometric indices allowed us to distinguish three structures of Gafsa chain: J. Ben Younes and J. Bou Ramli (showed in Fig. 20.2) and J El Abiod (showed in Fig. 20.3).

Fig. 20.1 Location, morphological and seismotectonic contexts of the studied area (superimposed on altitudinal hill shaded SRTM data : Azimuth = N315°E, Elevation = 45°): fault (modified from Hfaiedh et al. 1991); instrumental seismological data (for the 1975–2013 period) were provided by the National Meteorological Institute (Tunis)
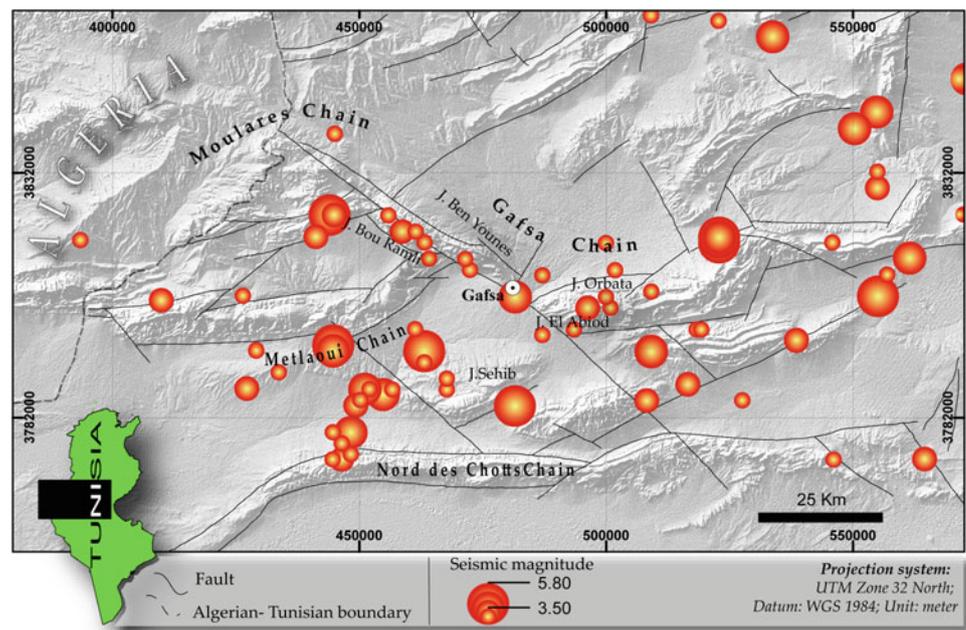
20.2.1 J. Ben Younes and J. Bou Ramli

Indeed, morphometric study shows that these reliefs are distinguished by many footprints of recent tectonic activity (Fig. 20.2):

- According to the catalog of the I.N.M., seven seismic events are occurred in this sector between 1977 and 2005 with a medium magnitude equal to 4. This reflects a relatively high seismic activity. The epicenters of these earthquakes are aligned along a NW-SE direction (Fig. 2.1).
- A high residual topography that can reach 470 m on the southern flank of J. Bou Ramli (Fig. 2.2).
- The Hypsometric Analysis in the Southern Atlas of Tunisia shows that the watersheds, located on the southwest flank of Ben Younes and Bou Ramli, have a higher hypsometric integral value (HI> 0.6) and a convex shape of the hypsometric curves. Their addition allows to delimit an area with immature landforms. The correlation with tectonic coverage of southern Atlas of Tunisia can be deduced that these high values of HI are located on the west of the Gafsa fault. Thus, the recent activity of this fault may explain the "youthfulness" of the landform in this area and the weakness of the climatic erosion compared to the active tectonic deformation (Fig. 2.3).
- The analysis of the hydrographic network of this sector shows a high frequency of drainage anomalies that may arise after the reactivation of one or more branch(s) of the Gafsa fault, inducing the deformation of the relief and setting up of these anomalies (Fig. 2.4).

- The ridges of these two structures show a very high maximum vertical curvature, while the NE flank varies from very low to medium (Fig. 2.5).
- The south-western flanks of these two structures have a significant surface rugosity expressed by a high roughness index. This roughness may reflect a strong present erosive potential (Fig. 2.6).

20.2.2 J. El Abiod

The area, located in the center of J. El Abiod (Gafsa chain) and whose height can reach 1,150 m, differs from other compartments of the landscape and it has special footprints of several morphometric parameters (Fig. 20.3):

- A relatively high concentration of earthquake epicenters reflecting a relatively high seismic activity (Fig. 3.1);
- A high residual topography (Fig. 3.2);
- South of J. Abiod, we clearly observed a "folding" of geological layers with a high roughness index, indicating a phase elastic compressive deformation that led to this structural configuration (Fig. 3.3);
- Disorder (multi-direction) of maximum curvature, thus defining a "disturbed area" in the center of the anticline (Fig. 3.4);
- A relatively high density of drainage (Fig. 3.5);
- A remarkable concentration of the drainage anomalies (Fig. 3.6).

On the other hand, the convex shape of the hypsometric curves and hypsometric integral value, relatively high

Fig. 20.2 Morphometric and seismic particularities of J. Ben Younes and J. Bou Ramli: **a** Epicenters of earthquakes, **b** Residual Topography, **c** Hypsometric Integral, **d** Drainage anomalies (*black*), **e** Maximum curvatures, **f** Roughness
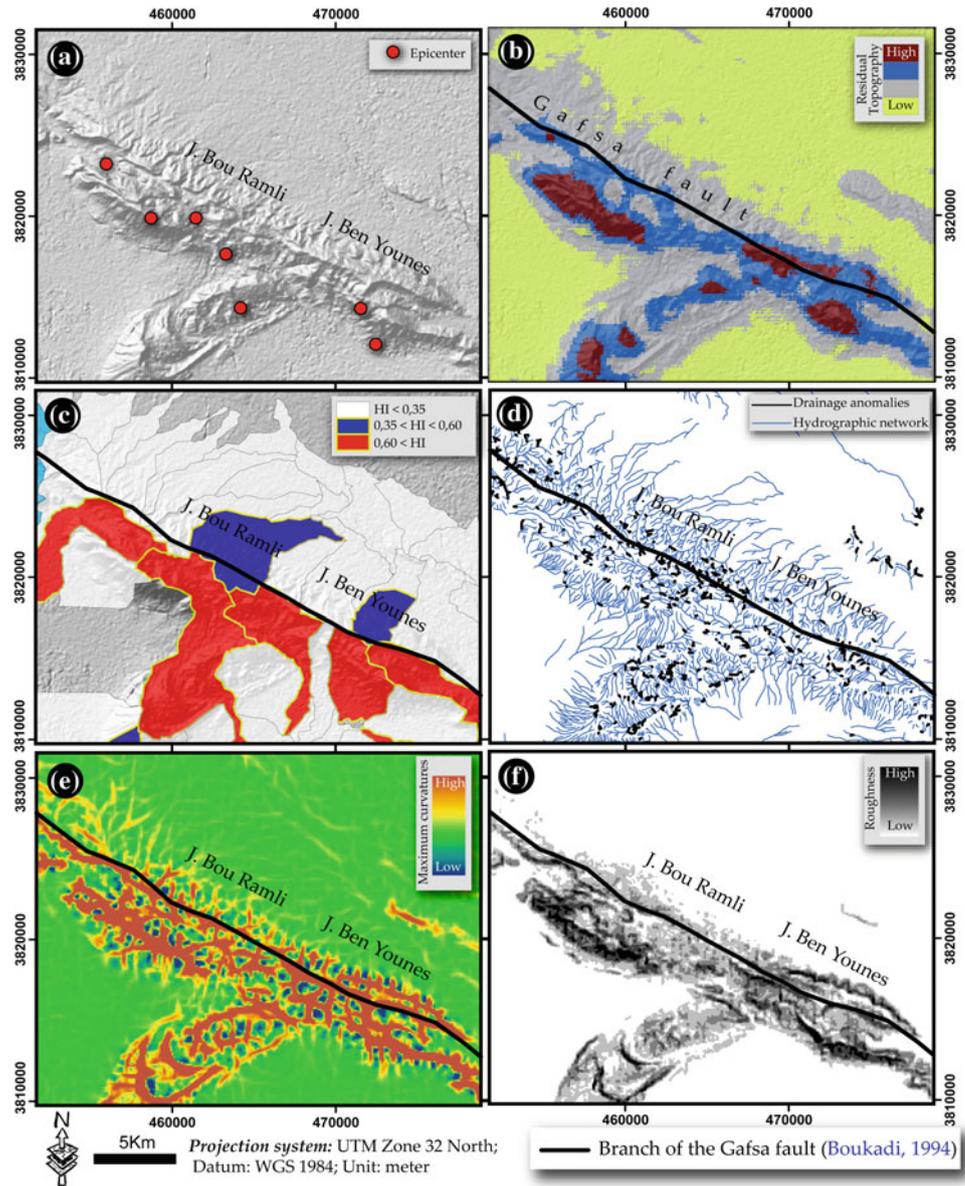
(IH> 0.5), watersheds located in this area reflect the immaturity terrain where erosion is still intense, reflecting the recent tectonic activity and/or low climate erosion.

20.3 Interpretation of Morphometric Indices

In this section, we will try to establish the relationship between morphometric parameters and the structural context of the study area.

The correlation of these indicators with the tectonic cover of the southern Atlas of Tunisia, can confirm the neotectonic reactivation of the Gafsa Fault as a major transpressive dextral strike-slip zone, under the influence of the N–S

present stress fields. It should be noted that the Gafsa fault is a deep accident probably dating from late Mesozoic that has been reactivated, several times, during the Cenozoic (Zouari et al. 1990) creating the Gafsa elongated chain above the fault zone. Thus, during the Jurassic and lower Cretaceous, the Gafsa fault has acted as a normal fault with a strong normal component. Also, this earlier distensive tectonics caused the movement of salt material along this accident (Bedir et al. 1992; Boukadi 1994; Zouari 1995). At the end of the Cretaceous, the tectonic inversion in the tethyan region took place. The Gafsa fault appears as a N120°E tranpressive dextral strike-slip fault under the influence of the displacement to the north of the African continent due to the opening of the Atlantic Ocean and the Tethyan sea closure.
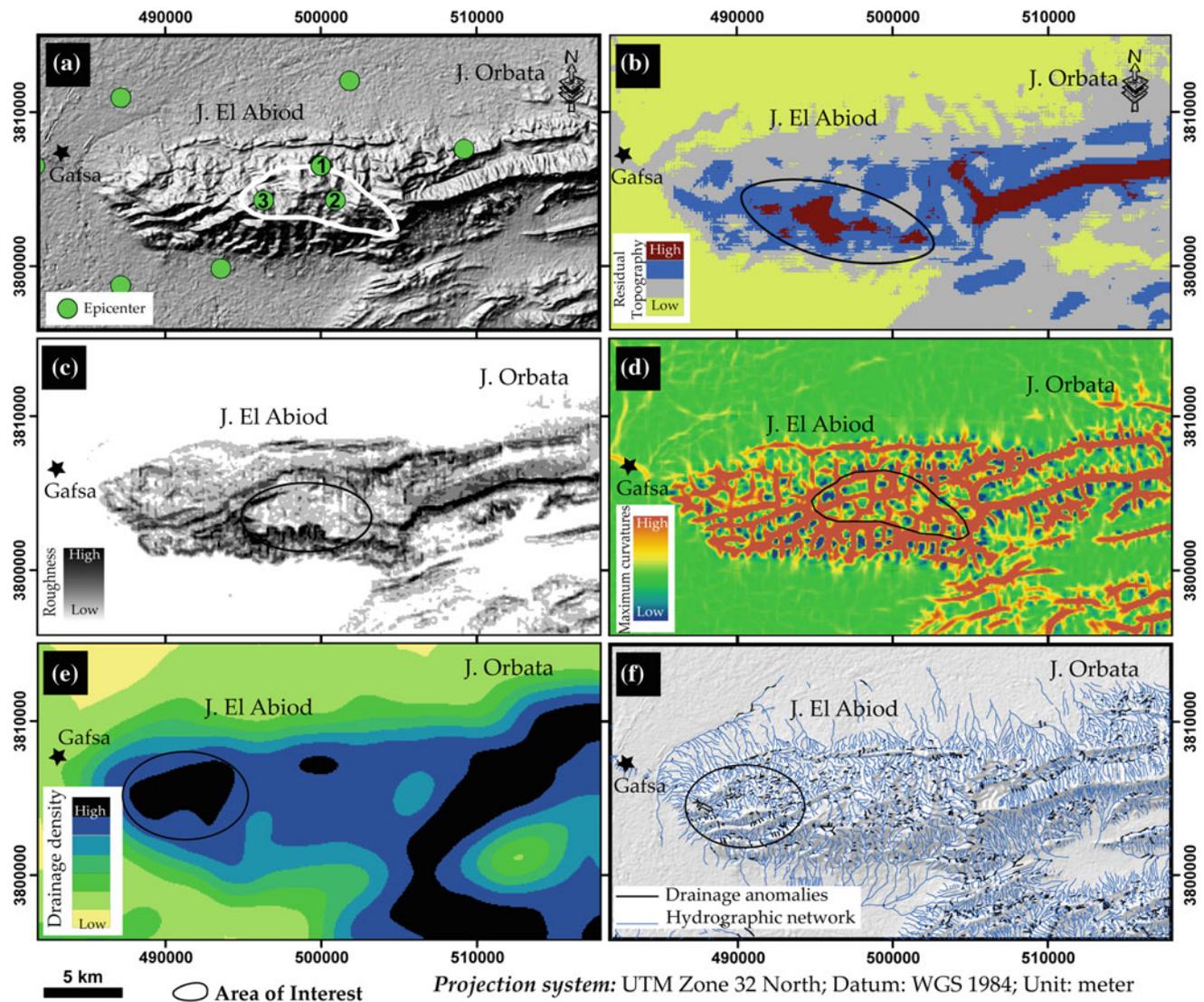
Fig. 20.3 Morphometric and seismic particularities of J. El Abiod: **a** Epicenters of earthquakes, **b** Residual Topography, **c** Roughness, **d** Maximum curvatures, **e** Drainage density, **e** Drainage anomalies (*black*)

But, it is difficult to distinguish between the tectonic and the halokinetic activities with only the morphometric methods. Thus, the tectonic activity of this fault can also be associated with the migration of the Triassic evaporitic material.

Indeed, the geological maps at 1/100 000 scale (produce by the ONM) and other studies, such as those of Zouari (1995), have indicated many local outcrops of Triassic materials in this region. Furthermore, the interpretations of seismic profiles have enabled Bedir (1995) and Hlaiem (1999) to show the presence of many Triassic salt bodies elongated several faults.

Thus, these two mechanisms (halokinesis and tectonics) have probable responsibility in the relief activity in this area and may explain their specific signature of the morphometric indices.

20.4 Conclusion

The identification of recent activity of faults (neotectonic) was performed in the Gafsa region (southern Atlas of Tunisia) based on the analysis of five geomorphometric parameters: the residual topography, hypsometric analysis, drainage anomaly, maximum vertical curvature and roughness of terrain.

The results of the morphometric analysis allowed us to confirm a probable recent activity of the Gafsa fault. Indeed, the kinematics of the Gafsa fault is clearly highlighted through the morphometric parameters by leaving its footprints on three highly immature landforms (J. Ben Younes, J. Bou Ramli and J. El Abiod) contrasting with the rest of the study area, located near the structural of Gafsa fault. On the

contrary, it is difficult to distinguish and differentiate between the tectonic and the halokinetic activities.

Indeed, we particularly insist on the relationship between the movement of salt and changes in morphometric parameters, confirming the strong relationship that exists between the morphological structure of the surface and deep structures.

The correlation between morphometric indices and geological coverage has shown that some morphometric anomalies are related to the lithological variations in the study area. In the plains, the absence of apparent neotectonic activity is related to the soft and detritic nature of the rocks that can quickly fill the synclinal depressions and hide the traces of faults. However, these traces are easier to identify in the higher areas.

Thus, the morphometric analysis of the DEM and the drainage network has to provide a more accurate insight into the morphodynamics of the study area. This is explained by their sensitivity towards the perturbations caused by recent tectonic activity or the effect of the lithological cover of the terrain.

References

Bedir M, Ben Youssef M, Boukadi N, Slimane F, Zargouni F (1992) Les événements séquentiels méso-cénozoïques associés au système de coulissements de l'Atlas méridional de Gafsa. 3ème Journée de l'Exploration Pétrolière (ETAP). Tunis

Bedir M (1995) Mécanisme des bassins associés aux couloirs de coulissements de la marge atlasique de la Tunisie : simo-stratigraphie, seismo-téctonique et implications pétrolières. Thèse de doctorat en Sciences géologiques. Thèse de doctorat Doctorat es-Sciences, Université Tunis II, p 412

Bolongaro-Crevenna A, Torres-Rodriguez V, Sorani V, Frame D, Ortiz AM (2005) Geomorphometric analysis for characterizing landforms in Morelos State. Mexico, Geomorphol 67:407–422

Boukadi N (1994) Structuration de l'atlas de Tunisie : signification géométrique et cinématique des nœuds et des zones d'interférences structurales au contact de grands couloirs tectoniques. Thèse de doctorat en Sciences Géologiques, Univ. Tunis II, Faculté des Sciences de Tunis, 249p

Deffontaines B (1990) Développement d'une méthodologie morphonéotectonique et morphostructurale; analyse des surfaces enveloppes, du réseau hydrographique et des modèles numériques de terrains; Application au Nord-Est de la France. Thèse, Univ. Paris VI, France, 230 p

Dehn M, Gärtner H, Dikau R (2001) Principles of semantic modeling of landform structures. Comput Geosci 27(8):1005–1010

Hfaiedh M, Attafi K, Arsovski M, Jancevski J, Domurdzanov N, Turki MM (1991) Carte sismotectonique de la Tunisie. Editée par l'Institut National de la Météorologie

Hlaiem A (1999) Halokinesis and structural evolution of the major features in eastern and southern Tunisian Atlas. Tectonophysics 306 (1):79–95

Pike RJ, Dikau R (1995) Advances in geomorphometry. Z Geomorphol N.F. Suppl Bd 101, 238 p

Pike RJ (2002) A bibliography of terrain modeling (Geomorphometry), the Quantitative Representation of Topography-Supplement 4.0. Open-File Report 02-465, U.S. Geological Survey

Zouari H (1995) Evolution géodynamique de l'Atlas centro-méridional de la Tunisie : stratigraphie, analyse géométrique, cinématique et tectono-sédimentaire. Thèse de doctorat d'état en sciences géologiques, 277p

Zouari H, Turki MM, Delteil J (1990) Nouvelles données sur l'évolution tectonique de la chaîne de Gafsa Bull Soc Géol Fr 8 VI, 621–629

Spatial Analysis of Remote Sensing Data in Early Stage of a Seismo-tectonic Research

Novakova Lucie

Abstract

In 1901, M4.7 earthquake hit the area of NE Bohemia, Czech Republic. The Hronov-Poříčí Fault (HPF) was found responsible for the event. Ongoing seismic monitoring proves the Hronov-Poříčí Fault Zone (HPFZ) is, in fact, the second most active area in the Bohemian Massif. Despite importance of the area, the HPFZ has not been described reasonably. Up to the moment, neither length of the HPFZ nor exact locations of its south branch are clear. Vagueness in length of the HPFZ causes large uncertainty in seismic risk assessment of the area. Integrated approach based on geographic information systems and remote sensing was employed to delineate lineaments in the wider HPFZ area. NASA provided Advanced Spaceborne Thermal Emission and Reflection Radiometer (ASTER) data was evaluated. ASTER digital elevation model provided basic topographic characteristics (surface curvature, slope and drainage systems). Edge detecting process was employed to define lineaments. Recent seismic activity and GPS monitored movements in the area were also assessed. The digital elevation model, extracted lineament, recent seismic activity, recent movements pointed out by GPS monitoring, were integrated and analysed in a geographic information system. Fault pattern suggested previously by various authors were compared with the GIS layers, and the extracted lineaments especially. Cross examination showed there are at least three possible variants of the south termination of the HPFZ. The spatial analysis also pointed out field tectonic mapping is necessary to describe the fault in detail and where to focus the survey.

Keywords

Active tectonics • Spatial analysis • Lineaments • Czech Republic

21.1 Introduction and Motivation

The knowledge of the range and continuation of a fault zone is very important for understanding the tectonic development and paleostress conditions of the study area, or for the estimation of earthquake hazard and risk. Previous works pointed out the magnitude of an earthquake is closely related to prolongation of the responsible fault (Wells and Coppersmith 1994).

Most studies focussed the Hronov–Poříčí Fault Zone (HPFZ) between the towns of Hronov and Trutnov. Despite the seismological importance of the HPFZ only the northern termination of the zone was described consistently so far. Assuming the southern termination of HPFZ is located in Poland or in Orlické hory Mts., the precise structural geological mapping of the brittle tectonic features has never been done within the whole range of the HPFZ area. Moreover, the tectonic conditions, its development and stress field remains poorly understand. The strongest earthquake was documented in 1901 with magnitude M4.7. Nowadays, it is supposed the HPFZ is about 30 km long.

N. Lucie (✉)
Department of Seismotectonics, Institute of Rock Structure and Mechanics AS CR, v.v.i, V Holesovickach 41, 18209 Prague, Czech Republic
e-mail: lucie.novakova@irsm.cas.cz

The maximum moment magnitude for such long fault might be M6.8. However, supposing the length three times higher, the maximum possible moment magnitude might be M7.4 (Wells and Coppersmith 1994). For this reason, it is highly important to specify length and range of the HPFZ precisely. The true length of the HPFZ should be considered when planning power plants, highways, tunnels and other engineering constructions in the broader area.

21.2 Geological and Tectonic Settings

The Hronov–Poříčí Fault Zone (HPFZ) is located in the easternmost part of the Trutnov–Náchod Depression. It is approximately 30–40 km long and up to 500 m wide system of parallel fractures, dividing two important structural units —the Intra Sudetic Basin and the Krkonoše Piedmont Basin. The NW-SE striking structure was formed due to the post-Cretaceous flexural folding and is filled with the Upper Cretaceous sediments and the Permo-Carboniferous volcano-sedimentary complex. The HPFZ had a complicated tectonic evolution, started in the late Paleozoic. Since then, several tectonic phases have taken place (Nováková 2014). The fault zone has been successively developed from an asymmetric anticline, whose steeply inclined SW part was axially disrupted due to the regional compression by a reverse fault. The main reverse fault (thrust) is accompanied by parallel or oblique normal or reverse faults. The reactivation of the HPFZ is recorded after the Upper Cretaceous sedimentation during the Late Saxonian tecto-genesis.

21.3 DEM Analysis

21.3.1 Method

Digital elevation model (DEM) was employed to assess major lineaments in the area in addition to thorough tectonics-focused review of previous mapping works. The Aster GDEM (LPDAAC 2013) of the HPFZ area and its surroundings was represented graphically as a shaded relief (Fig. 21.1a). Two orthogonal sunshine directions were utilized to avoid bias during later image processing. The Canny algorithm (Canny 1986) and Hough transformation (Duda and Hart 1972) were adopted. Image processing was carried out using the open-source image processor ImageJ (Schindelin 2012) implementing the Canny Edge Detector (Gibara 2011, Fig. 21.1b) and Hough Linear Transformation (Burger and Burge 2013) plugins respectively. We applied the Hough linear transformation to both whole (Fig. 21.1c) and partitioned images (Fig. 21.1d). The shaded relief images were divided into 20 (4 × 5) uniform square areas each. Directions of the linear structures identified in individual

partitions were displayed into rose diagrams. Finally, we confronted the automatic lineament identifications outputs to the tectonic mapping review.

21.3.2 Results and Discussion

Figure 21.1 shows ongoing results of the automatic lineament identification process. In the HPFZ area two major directions were found—NW–SE and WNW-ESE. These fault orientations are typical in the Bohemian Massif. The NW–SE direction is dominant (Fig. 21.2, left). In general, we found the lineament distribution provided by automatic processing similar to tectonic lines mapped during previous geological surveys (Fig. 21.2, right). Automatic lineament identification applied in individual partitions added two lineament orientations—W–E and WSW–ENE. Apparently, these two orientations are of local importance. It is obvious not all lineaments represent actual faults. Nevertheless the agreement between direction of the lineament and previously mapped fault direction (Nováková 2014) points out there is a link between terrain morphology and faults in the HPZF area. Moreover some of the lineaments identified in the square areas in actuality correspond to major faults including the HPFZ.

Four different parts can be distinguished due to spatial distribution of the lineament orientation (Fig. 21.1d and Fig. 21.3). These are stripes of the NW–SE orientation. Flat land on NE of the area represents the Sudetic Foreland. Lineaments here are ESE–WNW mainly. Morphologically significant stripe in the centre of the studied area is a Variscan relict mountain range. The NW–SE orientation dominates in this stripe. Strait line dividing these two parts is a clear demonstration of tectonic border of the Bohemian Massif in the area—250 km long the Sudetic Marginal Fault. SW end of the stripe corresponds to the HPFZ occurrence. W–E lineaments prevail in the SW part of the studied area. This terrain represents Permian-Carboniferous and Cretaceous basins. Fourth part could be identified in the SW corner where NW–SE orientation dominates again.

21.4 Lessons Learned

Spatial analysis of DEM data pointed out terrain lineaments in the HPFZ area and its vicinity. The identified lineament orientations correspond to geologically mapped tectonics. Moreover division due to local terrain lineament orientation matches main geological units in the area. Clearly, tectonics is responsible for many terrain lineaments in the HPFZ area. In addition, we showed open-source image processor ImageJ can be successfully utilized in spatial analysis of remote sensing data.
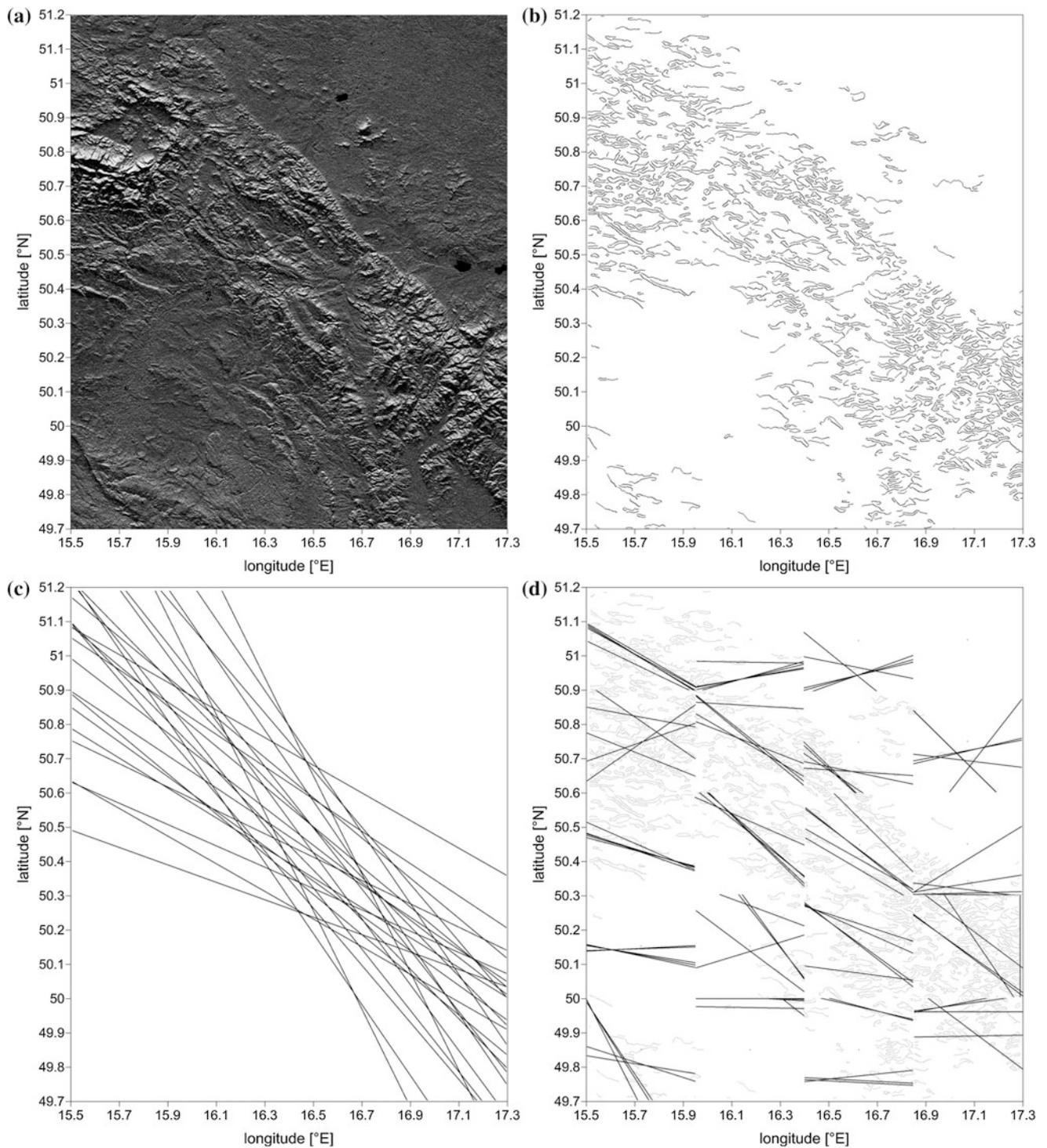
Fig. 21.1 Image processing. **a** Shaded relief of the HPFZ area. **b** Edge enhancement using the Canny algorithm. **c** Major lines identified using Hough algorithm in the whole area. **d** Major lines identified in partitions using Hough algorithm

Fig. 21.2 Dominant lineament orientations according to the automatic image processing (*left*) and fault orientations provided by geological mapping (*right*, Nováková 2014)
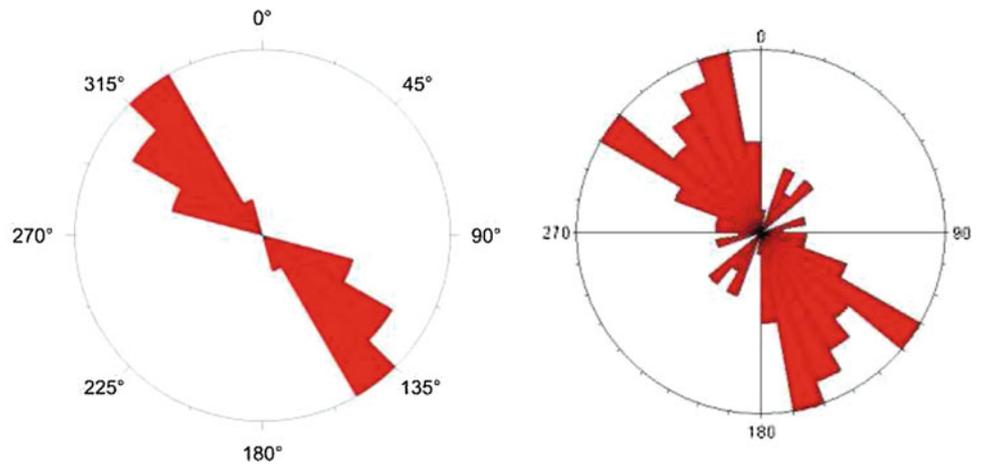
Fig. 21.3 Spatial distribution of the major lineament orientations in the HPFZ area
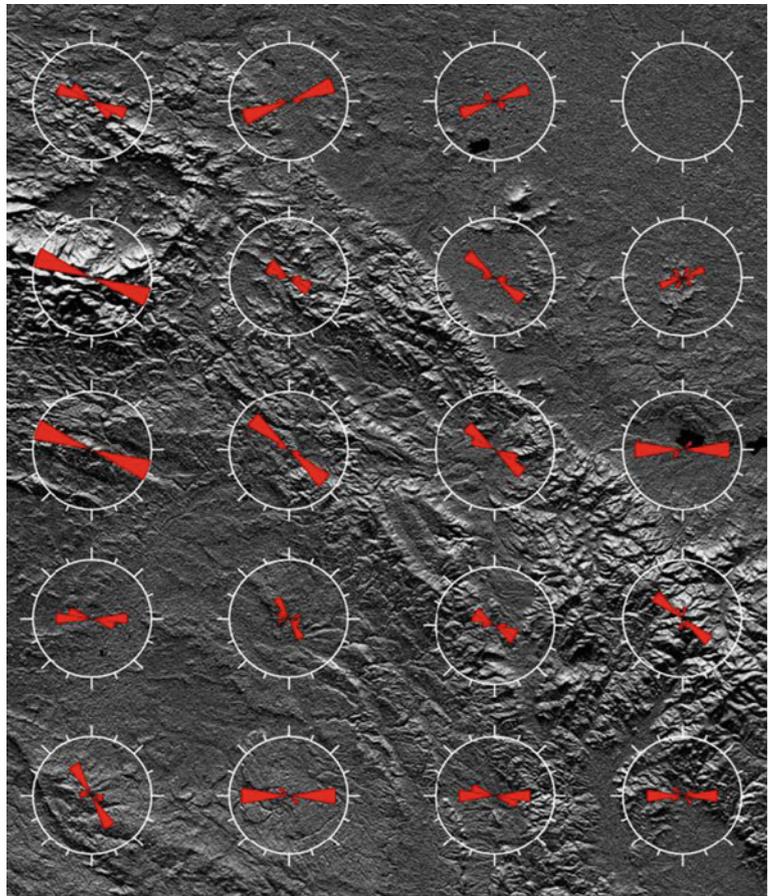
References

Burger W, Burge MJ (2013) Hough linear transformation plugin for ImageJ image processor, http://imagingbook.com/source

Canny JF (1986) A computational approach to edge detection. IEEE Trans Pattern Anal Mach Intell 8:679–714

Duda RO, Hart PE (1972) Use of the hough transformation to detect lines and curves in pictures. Commun ACM 15(1):11–15

Gibara T (2011) Canny Edge Detector plugin for ImageJ image processor. http://rsbweb.nih.gov/ij/plugins/canny/index.html

LPDAAC (2013) Global Data Explorer on-line application, http://gdex.cr.usgs.gov/gdex

Nováková L (2014) Evolution of paleostress fields and brittle deformation in Hronov-Porici Fault Zone, Bohemian Massif. Stud Geophys Geod 58:269–288. doi: 10.1007/sl1200-013-1167-1

Schindelin J, Arganda-Carreras I, Frise E, Kaynig V, Longair M, Pietzsch T, Preibisch S, Rueden C, Saalfeld S, Schmid B, Tinevez JY, White DJ, Hartenstein V, Eliceiri K, Tomancak P, Cardona A (2012) Fiji: an open-source platform for biological-image analysis. Nat Methods 9(7):676–682

Wells DL, Coppersmith KJ (1994) New empirical relationships among magnitude, rupture length, rupture width, rupture area, and surface displacement. B Seismol Soc Am 84(4):974–1002

Geomorphic Evidence of Active Tectonics: The Case of Djemila Fault (Eastern Algeria)

22

Youcef Bouhadad

Abstract

The Djemila active fault is a NE–SW trending and NW-dipping reverse fault. Historical seismicity around this fault is weak to moderate. However, field observations allowed us to observe differential uplifts of quaternary alluvial terraces on the hanging and foot walls. We interpret this as a strong evidence of recent tectonic activity. The uplifted terraces suggests an uplift rate of 0.14 mm/years. Therefore, the seismic potential of this fault may be greater than may be suggested by the historical seismicity of the region.

Keywords

Active reverse fault • Alluvial terraces • Uplift • Algeria

22.1 Introduction

At the outcrop scale field observations may provide useful information on the evidence of fault activity. Present-days landscapes result from the combined action of two factors the climate and tectonics (Molnar and England 1990; Burbank and Pinter 1999). Impact of tectonic in relief building has been suggested early and morphotectonics is now a widely recognized discipline for the study of morphological features related to tectonics (Scheidegger 2004). Active tectonics zones, mainly compressive context, exhibit several geomorphic features which may be used to understand the active faults history. Indeed, growth of faulted folds generates a response of the drainage system represented mainly by uplift/incision of alluvial fans and shift/diversion of drainage pattern (Mayer 1986; Shumn 1986; Merritts and Bulls 1989; Jackson et al. 1996; Pavlis et al. 1997; Bouhadad 2001; Lavé and Avouac 2001). Furthermore, trace of paleoearthquakes may be found in geomorphic records and then quantitative geomorphology provides rates of coseismic vertical and/or horizontal displacements that can be used as valuable tool for seismic hazard assessment (Merrits and Bull 1989; Keller et al. 1999; Martinez-Diaz et al. 2003). In this work we aim to discuss the geomorphic features related the Djemila active fault in northern Algeria (Harbi et al. 1999) (Fig. 22.1). In terms of geology, the studied area belongs to the Babor thrust sheet area formed by Jurassic-Cretaceous calcareous and marl. The known active faults of the region are: (i) the Kherrata fault which produced the February, 17, 1949 (Io = VII, MSK scale) earthquake and the youcef fault to the south and the Djemila fault studied herein.

22.2 Seismotectonics Setting

Northern Algeria belongs to the Africa-Eurasia plate boundary where tectonic plates are converging in the NW–SE direction (Anderson and Jackson 1988). The amount of shortening is about 4–6 mm/yr (De Mets et al. 1990). Consequently, the seismicity is relatively high and several majors earthquakes have been occurred in the past, particularly the Orleanville, September 9, 1954 (Ms = 6.5), the El-Asnam October 10, 1980 (Ms = 7.3) and the Zemmouri may 21st, 2003 (Mw = 6.9) (CRAAG 1994). Northern Algeria is NE–SW trending hills and mountains which forms the Tellean chain.

Y. Bouhadad (✉)
National Earthquake Engineering Center (CGS), B.P.252, Algiers, Algeria
e-mail: bouhadad_y@yahoo.com

Fig. 22.1 Seismicity and active faults of the Setif (eastern Algeria) region. (*1* (6.0 ≥ Ms ≥ 5.0), *2* (5.0 ≥ Ms ≥ 4.0), *3* (4.0 ≥ Ms ≥ 3.0), *4* (Ms < 3.0)
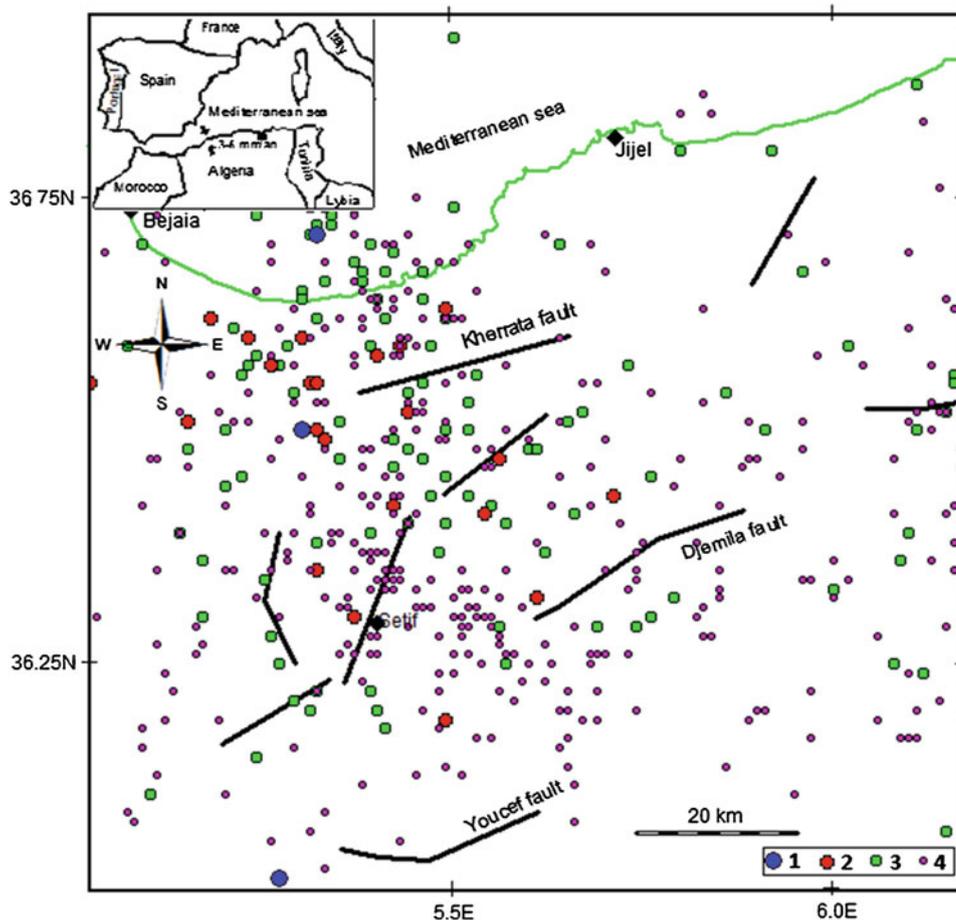
22.3 The Djemila Fault

The Djemila active fault shows a reverse mechanism and is trending NE-SW. It dips 50° toward the northwest. It constitutes a major geological structure of about 49 km of length (Vila 1980). The historical seismicity around this fault is weak to moderate. Nevertheless, field observations allowed us to identify a differential uplifts of quaternary alluvial terraces on the hanging and the foot walls. We interpret this as a strong evidence of recent tectonic activity. The uplifted terraces suggests an uplift rate of 0.14 mm/years for the hanging wall. Also, if we consider the length and the rate of terraces uplift, the seismic potential of the fault may be greater than may be suggested by the historical seismicity which extends back about two hundred years.

22.4 Conclusion

Geomorphic features may help to recognize evidence of active tectonics at an outcrop scale. Field work undertaken in the Djemila active fault allowed us to observe differential uplift of alluvial terraces on the hanging and the foot walls.

We interpret this as a geomorphic marker of the activity of the fault. The uplifted terraces suggests an uplift rate of 0.14 mm/years. Therefore, the seismic potential of this fault may be greater than may be suggested by the historical seismicity of the region. Hence, it is necessary to look in details to the seismic hazard implications of this fault.

References

Anderson H, Jackson J (1988) Active tectonics of the Adriatic region. Geophys JR Astr Soc 91:937–983

Burbank DW, Pinter N (1999) Landscape evolution: the interaction of tectonics and surface processes. Basin res 11:1–6

Bouhadad Y (2001) The Murdjadjo, western Algeria, fault-related fold: implications for seismic hazard. J Seismolog 4(5):541–558

CRAAG (1994) Les séismes en Algérie de 1365 à 1992. Publication du Centre de Recherche en Astronomie, Astrophysique et Géophysique, Département: Etudes et Surveillance Sismique, ESS, C.R.A.A.G, Alger-Bouzaréah

De Mets C, Gordon RC, Argus DF, Stein S (1990) Current plate motion. Geophys J Int 101:425–478

Harbi A, Maouche S, Ayadi A (1999) Neotectonics and associated seismicity in Eastern Tellian Atlas of Algeria. J Seismolog 3:95–104

Jackson J, Norris R, Yougson J (1996) The structural evolution of active fault and fold systems in central Otago, New Zealand: evidence revealed by drainage patterns. J Struct Geol 18:217–234

Keller EA, Gurroba L, Tierney TE (1999) Geomorphic criteria to determine direction of lateral propagation of reverse faulting and folding. Geology 27:515–518

Lavé J, Avouac JP (2001) Fluvial incision and tectonic uplift across the Himalayas of central Nepal. J Geophys Res 106 (11):26561–26591

Martinez-Diaz JJ, Masana E, Hernandez-Enrile JL, Santanach P (2003) Effects of repeated paleoearthquakes on the Alhama de Murcia Fault (Betic Cordillera, Spain) on the quaternary evolution of an alluvial fan system. Ann Geopysics 46 (5):775–791

Mayer I (1986) Tectonic geomorphology of escarpments and mountains fronts, In: Active tectonics, National academy press, Washington, DC, pp 125–135

Meritts D, Bull WB (1989) Interpreting quaternary uplift rates at the Mendocino triple junction Northern California, from uplifted Marine. Terraces—Geol 17:1020–1024

Molnar P, England P (1990) Late cenozoic uplift of mountain ranges and global mountain changes: chicken or egg? Nature 346:29–34

Pavlis TL, Hamburger MW, Pavlis GL (1997) Erosional processes as a control on the structural evolution of an actively deforming fold and thrust belt: an example from the Pamir-Tien Shan region, central Asia. Tectonics 16:810–822

Scheidegger AE (2004) Morphotectonics. 197 p, Edit. Springer, Berlin

Schumm S (1986) Alluvial river response to active tectonics: in Active tectonics. National academy press, Washington, pp 80–94

Vila J.M., 1980. La chaîne alpine d'Algérie orientale et des confins algéro-tunisiens. Thèse Sci. Univ. Paris, 665 p

Seismic Cycle of the Southern Apennine Deformation Front: The Taranto Gulf Marine Terraces Inputs and Implications

23

Benoît Deffontaines, Gérardo Fortunato, and Samuel Magalhaes

Abstract

Detailed tectonic analyses and geological mapping in muddy fold-belt front is a hard target. Using both fieldwork and GIS software associated to new soil datations (Sauer et al. in Soil development on marine terraces near Metaponto. Gulf of Taranto, Southern Italy, pp. 1–16, 2009) of the different marine terraces of the Taranto Gulf (Southern Italy), we were able to precise the location of the Metaponto-Pisticci staircase which appear to be situated above the first thrusting unit of the southern Apennine orogen corresponding to the deformation front. Consequently we can locate, characterize and quantify from an active tectonic point of view the deformation front of southern Apenines. By combining our data with (1) the AGIP seismic profile offshore the Taranto gulf that gives the precise geometry of the overthrusting sheet, (2) the known eustatic curve of the mediterranean sea along the southern Italian shore, and (3) the soil datations of the different terracic levels, we are now able to differentiate the signal of both active tectonic and eustatic processes and their related geomorphic features on the Taranto Gulf marine terraces. Therefore the observed seismic cycle of the Southern Apennine deformation front is revealed and characterized by a return period of about 261 ka, a vertical uplift of about 113 m and a shortening rate of 2.1 km by return period. Its deformation is not uniform and appear to be coherent with both a regular interseismic linear creep period (time = 251 ka/uplift = 71 m) and a rapid inferred cosismic uplift (time: lOKa/uplift = 42 m) that we interpret as a sismogenic period with probably numerous major earthquakes. Finally thanks to the marine terraces of the Metaponto-Pisticci staircase that lead us to better understand the deformation front of Southern Apenine and its associated landscape and to separate erosion and tectonic processes.

23.1 Introduction and Aim of This Study

How to locate, characterize and quantify the deformation front of an orogen especially in muddy and silty areas? Classical structural geological and geomorphological methods are then at there boundaries as the absence of hard geological layers increase the difficulty to get dips and therefore to reveal faulted and folded structures. As a case example, we focus herein on the NNW–SSE trending southern Apennine deformation front in Basilicate (Southern

B. Deffontaines (✉)
Laboratoire International Associé N°536 ADEPT France-Taiwan CNRS-NSC, and Laboratoire de Géomatique Appliquée ENSG/ IGN and UPEM, Paris, France
e-mail: benoit.deffontaines@univ-mlv.fr

G. Fortunato · S. Magalhaes
« AlphaGeOmega », 62, rue du Cardinal Lemoine, 75005, Paris, France

Italy) where it is noteworthy the approximative inferred location of the orogenic deformation front (Ferranti et al. 2009), and we use herein the well preserved marine terraces NE–SW trending of the Taranto Gulf in order to precise both the geometry and its recent structural history.

The recent development of geomatic tools (e.g. Geographic Information System—GIS associated with photo-interpretation) validated with new numerous available data, as offshore AGIP seismic profiles, combined with terrace marine soil datations (Sauer et al. 2009) and the abundance of scientific studies of the place (Gignout 1913; Gigout 1960; Hearty and DaiPra 1992; Caputo 2007; Westaway and Bridgland 2007, 2009, among others), lead us to (1) re-interpret the structural geometry of this deformation front, and therefore to (2) precise both (1) the seismic cycle and the uplift and shortening rates of this southern Apennine deformation front. At least, we are now able to propose new assumptions on the origin of the formation of the marine terracic levels and on the passed geological and geomorphological history of the place.

23.2 Geographic, Geologic and Geomorphologic Presentation

The Pisticci-Metaponto pleistocene, holocene staircase area is situated in the central part of the Taranto gulf (southern Italy) and consist of well preserved and clearly expressed marine terracic levels that runs from Taranto (Apulia) to the NE up to Rocca Imperiale (Calabria) to the SW on more than 65 km long and a width of about 25 km (Fig. 23.1).

From the geological point of view the marrine terraces lithology above the erosional surface is filled up with gravel deltaic deposits (bottomsets, and foresets) and above windy loemy and loessy deposits silts, and sands.

From the structural point of view, the geometry of the Pisticci-Metaponto area is difficult to know as the soft muddy area is lacking bedding dips and due to the impossibility to preserve through time any fault plane. From the bibliography and the existing geological maps (scale 1/100,000), the southern Apennine deformation front is inferred west of the Pisticci-Metaponto staircase (20 km) which is not affected by cartographic faults. Nonetheless Bentivenga et al. (2004) describe the existence of one NE–SW normal fault seen and situated north of the Pisticci-Metaponto staircase. From this observation, Bentivenga et al. (2004) propose that the Pisticci-Metaponto staircase is made of a only one unique marine terrace offsetted by several normal faults, parallel to the shoreline, that explains the observed scarps. Contrasting to that assumption, (Caputo 2007; Westaway and Bridgland 2007) and others, demonstrate the exact prolongation of the buried sediments on both sides of the marine terrasses scarps, proving that these scarps

are not fault scarps. Unfortunately we were not able to find the Bentivenga stuctural observation during our field work. The tectonic regime of the studied area is controversy Westaway and Bridgland (2007, 2009) described an isostatic normal global extension, contrasting with Caputo and Bianca (2009) that describe a more classical compressional one.

From the geodynamic point of view, the roll-back of the Calabria off Sardinia (10–12 Ma) and the resulting opening of the Tyrrhenian sea, the northern part of the arc progressively collided with Adria to create the Apennine (while in the same time the southern part collided to Africa that forms the Maghrebides). The Lucanian Apennine of southern Italy is a fold-and-thrust belt that developed following the closure of the Mesozoic Tethys Ocean by the subduction of the Adriatic microplate (continental lithosphere) beneath the Southern Apennine. The belt is composed of various tectonic units derived from alternating basins and platforms that were located onto the western edge of the Apulian passive continental margin (D'Argenio and Alvarez 1980). Since Oligocene time these paleogeographic domains, namely the Apenninic Platform, the Lagonegro Basin and the Apulian Platform (Scandone 1972), experienced orogenic contraction and were stacked north-eastwards along low-angle thrust faults to produce a complex accretionary wedge (Roure et al. 1991; Monaco et al. 1998). The outer, eastern parts of the wedge correspond to a thin-skinned fold-and-thrust belt; its allochtonous units mainly consist of a detached Miocene flysch and a tectonic "melange", the so-called Varicoloured Clays (Casero et al. 1988), whose paleogeographic provenance has been debated in the literature (Lentini 1979; Pescatore et al. 1988; Monaco et al. 1998). The internal deformation of this melange has been referred to a generic post-Early Miocene time.

From the bibliography it appears that the outer province of the southern Apennine belt was structured in Quaternary time, i.e. up to Middle Pleistocene times (Pieri et al. 1996; Patacca and Scandone 2001), and there is no direct evidence for ongoing contractional deformation at the thrust front. It has been suggested that at around 650–700 ka active convergence turned into a regime of tectonic quiescence and generalised post-orogenic uplift (Ambrosetti et al. 1982; Westaway 1993; Patacca and Scandone 2001). Neogene contractional deformation was accompanied by deposition of syn-orogenic sediments, that occurred extensively within satellite basins located on top of the evolving fold-and-thrust belt, and within foredeep basins located ahead of the advancing thrust fronts (Hippolyte et al. 1994). It seems that the present thrust front is now buried below the foredeep deposits of the Bradanic Trough, that separate the outermost province of the belt from the relatively undeformed Apulian foreland, and has been inferred from subsurface data (Sella et al. 1988). The thrust front crosses the present coastline

Fig. 23.1 Location of the
Taranto Gulf southeastern Italy,
known geological features,
quadrangle the studied area in
Italy. One may note the obliquity
of the NE–SW trending marine
terraces toward the inferred NW–
SE trending deformation front
(*dashed black line*)
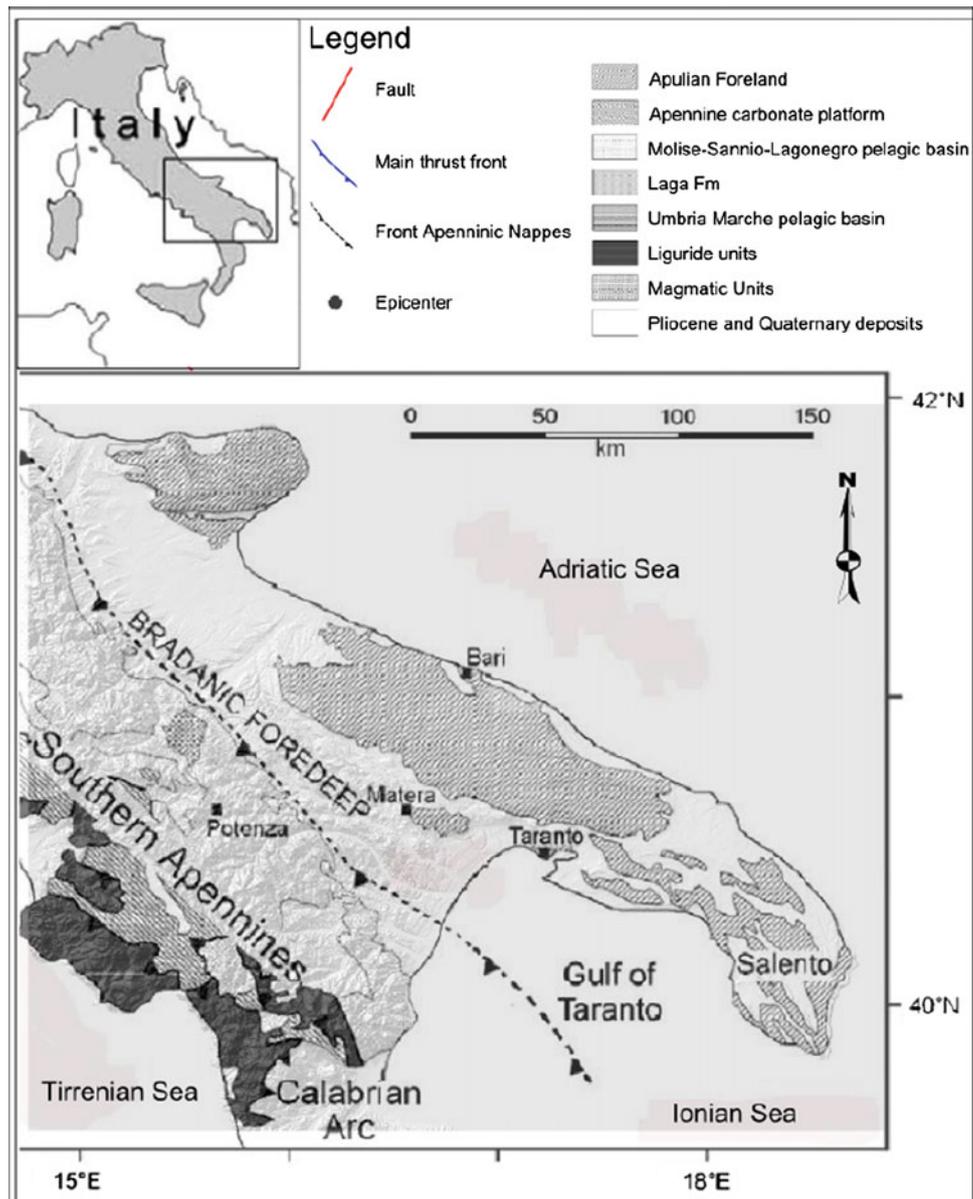
within the Taranto Gulf. In this area the bottom of the Ionian
Sea is relatively steep and reaches a depth of more than
2,000 m below the sea level at around 150 km from coast
line.

From the geomorphological point of view, many authors
had been working on this area differentiating from 1 marine
terracic level (Bentivenga et al. 2004), 6 (e.g. Mostardini
et al. 1966; Vezzani 1967), 7 (Cotecchia and Magri 1967), to
11 (Bruckner 1980 PhD thesis and 1982). So great scientific
divergence in the numbers despite the general agreement that
the marine terraces are the results of both interaction of
quaternary tectonics and glacio-eustatic sea level variations.

We distinguish by comparing the precise Digital Terrain
Model (a mixed of SRTM, GRDEM-ASTER, and a 8 m
ground resolution DTM) that we settled on the geological

maps (Geological Map of Italy 1:100,000—extract sheets
201-202-212) of the studied area on the Pisticci-Metaponto
staircase from the Ionian Sea shoreline (east to west) 11
different terrassic levels separated by scarps or bluffs fol-
lowing the assumption of Bruckner (1980, 1982); Sauer
et al. (2009).

In this paper, we will first have a closer look to the marine
terraces sedimentology and their datations by a discussion
about their validity, this will give us a curve: Altitude toward
Time. Then in a second stage we will update the structural
geology of the place by revealing the exact place of the
Apennine deformation front situated 40 km east of what was
inferred validated by numerous AGIP seismic lines and we
will then deduce by comparison the seismic cycle differen-
tiating the discontinuous uplift and shortening rates. At least,

finally we will discuss some of those implications on the geomorphology and the recent history of these Pisticci-Metaponto marine terraces.

23.3 Datations of the Metaponto/Pisticci Marine Terraces

The sedimentology of the Pisticci/Metaponto marine terraces, Bruckner (1980), Sauer et al. (2009), present a characteristic vertical sediment sequence and may be resume as follow and described below from bottom to top: (1) marine sediments such as clays and silts deposited in deeper shelf; (2) intermittent layers of loam, gravels and sands that compose the terrace base sediments deposited in a middle shelf, sublittoral or lagoonal environment; (3) A main gravel sediment body deposited in a beach environment; (4) a fine continental textured cover sediments that is from lagoonal, alluvial, colluvial or aerian origins (e.g.: loess or loehm). The evolution of the sedimentation correspond generally to the uplift of the place starting from a marine to a continental environment.

To get a datation of a marine terracic level is a hard task (Sauer et al. 2009) on the technical and methodological as well as the geomorphic point of views. From the technical and methodological point of view, numerous methods and techniques are used each one with its own error bars well explained in Sauer et al. (2009). From the geomorphological–geological point of view, it is needed to know what geomorphic or sedimentological feature to date due to the great diachronism of the different deposits that compose a marine terraces. For instance tides and glacio-eustatic fluctuations of the sea level create and modify the geometry and datations of the marine terraces that lead to several different ages depending on the depth of the dated material.

First at depth it is possible to date (1) the erosionnal base surface that correspond to the angular unconformity in between the bedrock and the surficial geology. That corresponds to the first transgression or Rising Sea Level (RSL). It is also possible to date (2) the surficial geology corresponding to the marine deposits linked to the transgression highstand, maximum stillstand and beginning of the regression (that correspond to the age of the marine gravel body). Then third possibility (3) is to date the lagoonal environment and the continental deposits such as the fluvial, alluvial, swampy colluvional deposits which act as agradation processe or the glacio-eustatic regression. Then (4) it is also possible to date during the lowstand sea level, the associated loamy or loessic aerian deposits, and finally to date (5) any reactivation of the glacio-eustatic sea level fluctuations that changes this theoretical general terrace

marine sedimentological succession. The Marine Terrace 1 (Petrulla site) of the Metaponto-Pisticci staircase (Table 23.1) illustrate such discrepancies.

Due to the diachronism of the different sediments that compose the marine terrace, the question is then what geological/geomorphic object do we need to date for a marine terrace in order to get the neotectonic informations ? For our point of view, taking into account the existing bibliography (Sauer et al. 2009), it is needed to date the last maximum sea level. Terrassic bluffs appear then as the only geomorphic isochrone feature on the Pisticci-Metaponto staircase as it is the result of the erosion of a unique paleoshoreline. That is why it is needed to carefully date the terrace immediately up and down of each scarps/bluffs. One may note that even for the soils datation it is possible to get different ages due to glacio-eustatic fluctuations as it is possible to stack and superimposed different paleosoils. To date loess will give you indications of the more recent loess/loamy sediments deposits that settled during each maximum glaciar periods (or minimum sea level).

Table 23.2 resume and gather all available location (cf. black dots of Fig. 23.2a), altitude and ages of the selected terracic levels as well as the facies and the associated soils. It is then possible to draw the curve age versus altitude (Fig. 23.3) which is not a continuous linear feature. The resulting curve evidence colinear and equivalent time long oblique flats and steep ramps that is highly comparable to the general geometry of the creep/asismic corresponding to the red curve/oblique flat and earthquake return period corresponding to the orange curve (steep ramps) of the repeated sismic cycle…

Table 23.3 above resume the main characteristics of the sismic cycle revealed through the soil datations of the Pisticci-Metaponto marine terraces. It distinguish both component of the uplift rate and the shortening one. In the following paragraph we will focus on which cycle this could be.

23.4 Location of the Apennine Deformation Front in Basilicate and Taranto Gulf (SE Italy)

Field geologists know that where the muddy rather flat bedding dip had been preserved that usually correspond to the not deformed zone contrasting with those without bedding that appear to be highly deformed but without any trace of fault planes. That is why it is uneasy to get the structure in the fields of such areas without (or so few) bedding dips and fault plane due to the muddy lithology. Fortunately it exists indirect methods of structural geomorphology in order to decipher the structures based for instance in the drainage

Table. 23.1 Example of the diachronism of datations of the T1 Marine Terraces (Petrulla area), depending on the *surficial* geologic and geomorphic objects and the used datation technique (modify from Sauer et al. 2009; all *OSL ages from* Zander et al. 2003, 2006 in Sauer et al. 2009; 230Thl234U ages from Bruckner 1980)

Marine Terrace 1 (Petrulla site—modified from Sauer et al. 2009)		
Technique	Depth (cm)	Age
OSL of loess	60 cm	16 ka BP
OSL of loess	90 cm	20.3 ka BP
OSL of loess	170 cm	24.9 ka BP
OSL of upper main gravel Body	nc	55.4 ka BP
OSL of terrace base	30 cm below surface	50.7 ka BP
U/Th of molluscs in upper mai gravel body	?	63 ± 3 ka BP
OSL of terrace base	90 cm below surface	73.8 ka BP
U/Th of molluscs in terrasse base	?	75 ± 7 ka BP
U/Th of molluscs in the lowest layer the main gravel body	?	110 ± 10 ka BP

Table. 23.2 Synthetic soil datations of the marine terraces of the staircase Pisticci-Metaponto. Til later than Brunhes/Matuyama boundary (780 ka) according to Bruckner (1980) (modified from Sauer et al. 2009)

Terrassic level Pisticci-Metaponto staircase	Coordinates (lat./long.) WGS84 Lat/lon	Altitude (m)	Age (ka)	MIS (mar. and fluvial sed.)	Sediments
TO (Lido di Metaponto)	40°21.05′ N–16° 49,91′ E	2	0,19	1	Aeolxan sand Beach sand
TO (Basentol/ Metaponto)	40°21.80′ N–16° 47,56′ E	5	7	1	Alluvial sed.
T1 (Petrulla)	40°21.58′ N–16° 46,40′ E	22	80	5.1	Loess Marine gravel
T2 (San Teodoro I)	40°21.32′ N–16° 44,68′ E	43	100	5.3	Young Alluv. Fine sed. Older All. Fine sed Fluvial Grav Sed Marine Gravel body
T3 (San Teodoro II)	40°22.11′ N–16° 44,75′ E	61	120	5.5	Alluvial Fine Sed
T4 (Marconia)	40°21.02/20,99′ N– 16°41,09/10′ E	96	195	7	Alluvial fine sed. Fluvial Grav. Sed. Marine Gravel Body
T5 (SE)	40°21.37′ N–16° 40,56′ E	120	310	9	Alluvial fine sed. Marine Gravel Body
T5 (NW)	40°21.73′ N–16° 37,94′ E	160	330	9	Alluvial fine sed. Fluvial Grav. Sed.
T6 (Tinchi I)	40°21.68′ N–16° 37,11′ E	196	405	11	Alluvial fine sed. Marine Gravel Body Marine Sand
T7 (Tinchi II)	40°21.87′ N–16° 36,25′ E	224	500	13	Alluvial fine sed. Marine gravel Marine sand
T8 (Pisticci)	40°22.14′ N–16° 35,25′ E	245	575	15	Colluvium Fluvial sediment + Tephra Layer
T9 (Rinne)	40°26.72′ N–16° 36,38′ E	320	670	17	Fluvial Sediment
T10 (Porcellini Brückner 1980)	40°26,844′ N ?–16° 35,962′ E ?	333 ?	730	19	?
T11 (?, Brückner 1980)	40°28'388′ N ?–16° 33,891′ E ?	427?	>780?	?	?
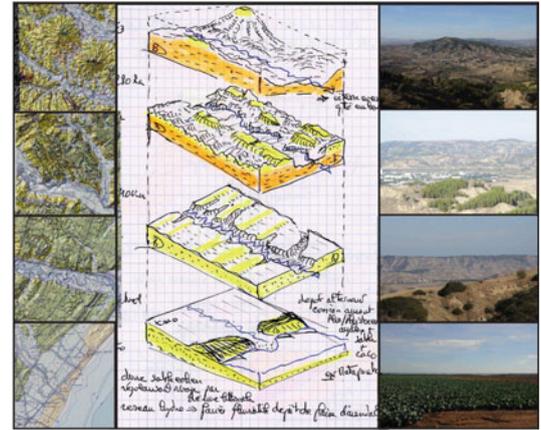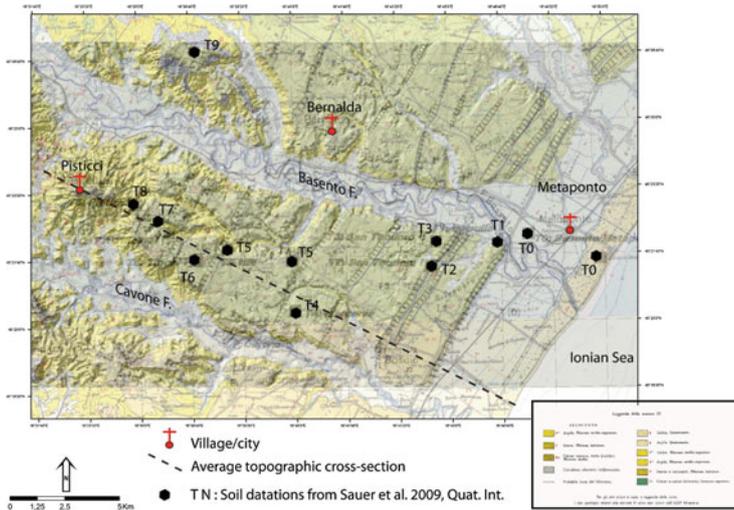
Fig. 23.2 Geomorphology of the Pisticci-Metaponto marine terraces. **a** Geological map superimposed above the hillshade DTM. *Black* large dots correspond to the location of the dated soils on the Metaponto-Pisticci marine terraces (modified from Sauer et al. 2009). Bluffs or scarps from Bruckner (1980) MNT SRTM, GRDEM-ASTER, MNT

208 m +intp of DTM (2,018 m). **b** Key examples of photographs, associated 3D sketch map and extract of geological map showing the increasing erosion of the older marine terracic levels (*bottom* to and *top* T9–11 respectively)

Fig. 23.3 Diagramm Age/Altitude of the Pisticci-Metaponto marine terraces (*green cross*); one may note the discontinuous uplift where we optimize in *red* (oblique flats) and in *orange* (steep ramps). The eustatic curve of the sea level during the last 450 ky (Holocene and Pleistocene time) is highlighted in *blue* below (Waelbroeck et al. 2002)
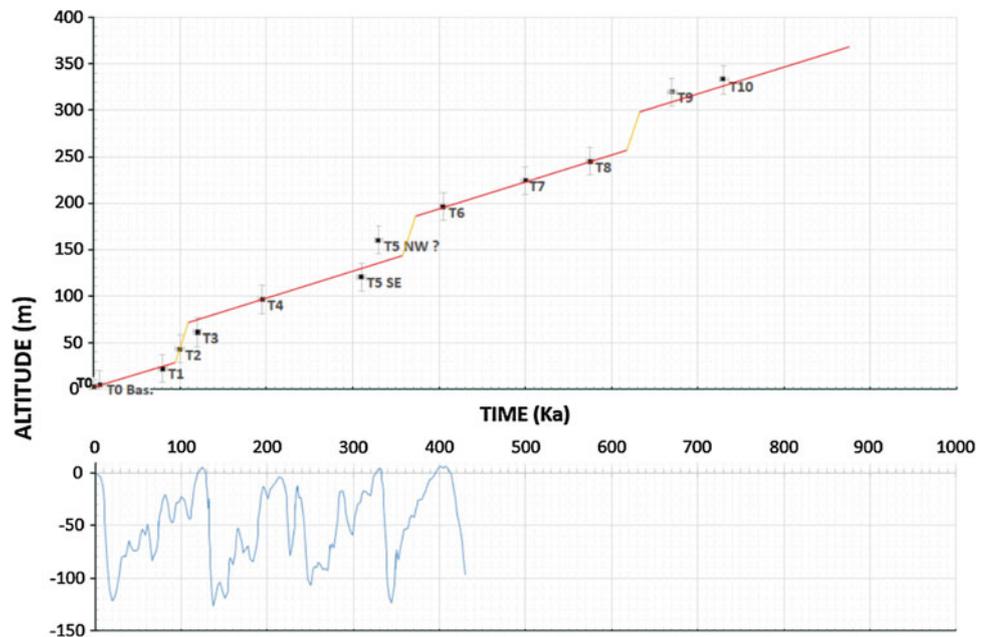
network geometry and its anomalies (Howard 1967; Deffontaines and Chorowicz 1991; Deffontaines et al. 1994, 2000). The circular and annular drainage NE of the Pisticci-Metaponto area contrast with the sub parallel one further north and lead us to trace the precise geometry of the deformation front which is situated close to the Matera city.
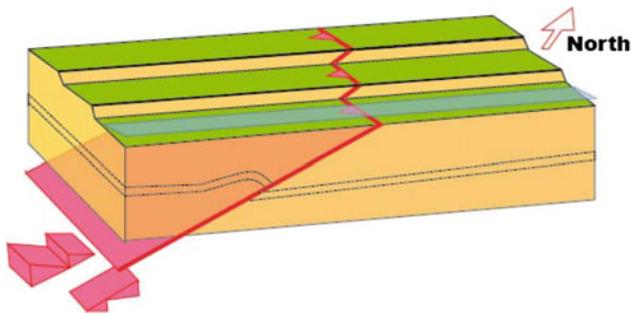
Fig. 23.4 3D view of the deformation of the Tarento gulf marine terraces (*Red plane*: Deformation front and thrusting Fault; in *green*: marine terraces and *brown* at the surface and terrassic scarps)

Numerous public parallel to the shoreline AGIP/ENI reflection seismic lines offshore Taranto Gulf are now public and available (http://unmig.sviluppoeconomico.gov.it/videpi/geografica.htm). The AGIP reflection seimic lines D484, F75_091, F75_089, F75_087 provide for instance the offshore Metaponto geometry of the rather flat ramp thrusting (6°TWT so real 3° "angle verging NNE dipping SSW) over the Adriatic continental lithosphere and validate the onshore geological interpretation above.

On the available AGIP offshore sismic reflection profile, one may note the presence of flat parallel reflection sismic layers of the bradanic trough ending to the south-west against a vertical misty zone which to our point of view characterize transpressive thick-skin strike slip faults. No thrust component is visible on the reflection profile and the vertical geometry is a clear tectonic feature. Therefore, we believe the present geometry of the deformation front is composed of both compression and transpressive faults revealing in the southern Apennine typical partitioning (external thrusting and internal strike-slip and normal faulting for the reajustement). Lentini et al. (2002) for instance highlighted numerous major NW–SE transpressive left lateral strike slip faults in the Lucanian area. Therefore contrasting the pure thin-skin model rootless nappes of the Apulian platform detached from basement (Mazotti et al. 2000), and contrasting also to the pure thick-skin model with basement involved thrusting (Menardi Noguera and Rea 2000), we believed that the southern Apennine face a mixed

in between both: thick (basement transpression) versus thin skin (decollement of the first thrusting units) tectonics which may better fit with the Steckler et al. (2008) teleseismic receiver data. The prevailing extension (Maggi et al. 2009) correspond to the western tectonic deformation and readjustment on the back of the thrusting and strike slip units.

The combination of both the seismic cycle with the offshore structural geometry lead us to propose the uplift and shortening rates situated in Table 23.3.

23.5   Discussion and Conclusions

Detailed soil datations of the different Pisticci-Metaponto marine terraces (Basilicata, Southern Italy) and the new geometry of the deformation front lead us to determine both its discontinuous uplift behaviour and therefore quantify the seismic cycle of the first unit situated above the deformation front of the southern Apennine orogenic belt following the tectonic model of Fig. 23.4. The sismic cycle correspond then to an alternance of asismic creep (246 ka, 71 m uplift, 5.5 mm/y shortening) and earthquake (15 ka, 42 m uplift and 53.5 mm/y shortening). They have strong implications in terms of oil exploration, maturation of the organic matter and on the tectonic history of the place (see for instance Jasvre et Pedley 2012).

Comparing the glacio-eustatic curve and the seismic cycle deduce above to the geological-geomorphological map, we may then be able to differentiate the glacio-eustatic or earthquake period origins of the scarps/bluffs situated above the Pisticci-Metaponto staircase. This give us the possibility to much better understand the passed and present evolution of Basilicate and related area.

If our reasoning is confirmed by further works and complementary datation (work in progress with Sauer et al.), one should assume that next rapid uplift very probably associated with major compressive and/or transtensive earthquakes will take place in 140 ka in Basilicata.

To our knowledge, it is the first time that scientists are able to determine interrelation in between both seismic and eustatic cycles and their related geomorphic features from a mapping point of view with this amount of confidence in

Table. 23.3 Characteristics of the seismic cycle: Marine terrace dotation versus altitude and seismic cycle, b, c, d = coordinate at the origin on the Y axis for the different straight lines with b = N.39; c = N.(−239); d = 0, with N = number of seismic cycle number. The shortening is deduced from the geometry of the thin skin decollement thrust (from the available offshore AGIP seismic section—see below)

Seismic cycle	Ages = X (ky)	Altitudes = Y (m)	Shortening (m)	Uplift rate (mm/y)	Shortening rate (mm/y)	Formulae
Oblique ramp = interseismic or creep	246	71	1354,76	0.28	5,507	Y = 0.2889X + b
Steep ramp = Cosismic Earthquakes return period	15	42	801,408	2.8	53,427	Y = 2.8193X + c
Average Seismic cycle	261	113	2156,168	0.43	8,261	Y = 0.4127X + d

such an active tectonic area. We hope this study will participate to better know the behaviour of the Apennine orogenic belt in Italy that will help to decrease the aggressivity against the civil protection commission after the recent Aquila earthquake episode.

References

Ambrosetti P, Carraro F, Deiana G, Dramis F (1982) Il sollevamento dell'Italia centrale tra il Pleistocene inferiore ed il Pleistocene medio. Contributi conclusivi alia realizzazione della Carta Neotettonica d'ltalia, Parte II, Pubbl. P.F. Geodinamica, vol 513. CNR, Rome, pp 219–223

Bentivenga M, Coltorti M, Prosser G, Tavarnelli E (2004) A new interpretation of terraces in the Taranto Gulf: the role of extensionnal faulting. Geomorphology 60:383–402

Bruckner H (1980) Marine Terrassen in Süditalien. Eine quartärmorphologische studie über das kiistentifland von Metapont. Düsseldorfer Geographische Schriften, 14, 235p

Bruckner H (1982) NF Suppl-Bd 43. Ausmab von erosion und akkumulation im verlauf des quartars in der Basilicata (Süditalien). Zeistchrift für Geomorphologie. Berlin, Stuttgart, pp 121–137

Caputo R (2007) Sea-level curves: perplexities of an end-user in morphotectonic applications. Glob Planet Change 57:417–423

Caputo R, Bianca M (2009) Comment on «late cenozoic uplift of southern Italy deduced from fluvial and marine sediments: coupling between surface processes and lower-crustal flow » by Westaway R. and Bridgland D. (Quaternary international 175:86–124), 204:98–102

Casero P, Roure F, Edignoux L, Moretti I, Muller C, Sage L, Vially R (1988) Neogene geodynamic evolution of the Southern Apennines. Boll Della Soc Geologia Ital 41:109–120

Cotecchia V, Magri G (1967) Gli spostamenti delle linee di costa quaternarie del mare ionico fra Capo Spulico e Taranto. Geologia Applicata e Idrogeologia 2:3–28

D'Argenio B, Alvarez W (1980) Stratigraphic evidence for crustal thickness changes on the southern Tethyan margin during the Alpine cycle. Geol Soc Am Bull 91:681–689

Deffontaines B, Chorowicz J (1991) Principle of drainage basin analysis from multisource data application to the structural analysis of the Zaire Basin. Tectonophysics 194:237–263

Deffontaines B, Lee JC, Angelier J, Carvalho J, Rudant JP (1994) New geomorphic data on Taiwan active orogen: a multisource approach, J Geophys Res, 99, B8: 20,243–20,266

Deffontaines B (2000) Formes et déformations de la surface terrestre: approches morphométriques et applications, Habilitation à Diriger des Recherches, Université Pierre et Marie Curie, P6,60p. + Annexes

Ferranti L, Santoro E, Mazzella ME, Monaco C, Morelli D (2009) Active transpression in the northern Calabria Apennines Southern Italy. Tectonophysics 476:226–251

Gignout M (1913) Les formations Marines pliocènes et Quaternaires de l'ltalie du sud et de la Sicile, Annales de l'université de Lyon, NSI, 36, 693p. (in French)

Gigout M (1960) Sur le quaternaire marin de Tarente (Italie), Comptes rendus de l'Académie des Sciences, 250, 1094–1096, Lyon, (in French)

Hearty PJ, Dai Pra G (1992) The age and stratigraphy of Middle Pleistocene and younger deposits along the Gulf of Taranto (Southeast Italy). J Coast Res 8(4):882–905

Hippolyte JC, Angelier J, Roure F, Casero P (1994) Piggyback basin development and thrust belt evolution: structural and paleostress analyses of Plio-Quaternary basin in the southern Apennines. J Struct Geol 12:159–173

Howard AD (1967) Drainage analysis in geologic interpretation: a summation. Bull Am Ass Petr Geol Tulsa 51(11):2246–3428

Jarsvre EM, Pedley A (2012) Petroleum potential in the Gulf of Tarento, AAPG Annual Convention and Exhibition, Long Beach, California, 22–25 Apr 2012

Kaveh HF, Deffontaines B (2008) La limite slikke/schorre dans la baie du Mont Saint Michel (Golfe Normand Breton NO France), Photo-Interpretation, 3–4, pp 28–44 and 81–86

Lentini F, Carbone S, Di Stefano A, Guarnieri P (2002) Stratigraphical and structural constraints in the Lucanian Apennines (southern Italy): tools for reconstructing the geological evolution. J Geodyn, pp 141–158

Monaco C, Tortorici L, Paltrinieri W (1998) Structural evolution of the Lucanian Apennines. J Struct Geol 20:617–638

Mostardini F, Pieri M, Pirini C (1966) Stratigrafia del Foglio 212, Montalbano Ionico. Bolletino del Serv Geol d'Italia 87:57–143

Patacca E, Scandone P (2001) Late thrust propagation and sedimentary response in the thrust-belt—foredeep system of the southern Apennines (Pliocene-Pleistocene). In: Vai GB, Martini IP (eds) Anatomy of an Annali di Geofisica, Istituto Nazionale di Geofisica, Balogna, Orogen: The Apennines and Adjacent Mediterranean Basins. Annali di Geofisica, Istituto Nazionale di Geofisica, Bologna, pp 401–440

Pescatore, T, Renda P, Tramutoli M (1988) Rapporti tra le unita` lagonegresi e le unita` sicilidi nella media Valle del Basento, Lucania (Appennino Meridionale). Memorie Delia Soc Geologica Ital 41:353–361

Pieri P, Sabato L, Tropeano M (1996) Significato geodinamico dei caratteri deposizionali e strutturali della Fossa bradanica del Pleistocene. Memorie Della Soc Geologica Ital 51:501–515

Roure F, Casero P, Vially R (1991) Growth processes and melange formation in the southern Apennines accretionary wedge. Earth Planetary Sci Lett 102:395–412

Sauer D, Wagner S, Bruckner H, Scarciglia F, Mastronuzzi G, Stahr K (2009) Soil development on marine terraces near Metaponto (Gulf of Taranto, Southern Italy). Quaternary International, Gulf of Taranto, pp 1–16

Scandone P (1972) Studi di geologia lucana: carta dei terreni della serie calcareo-silico-marnosa e note illustrative. Bollettino della Societe´ dei Naturalisti in Napoli 81:225–300

Sella M, Turci C, Riva A (1988) Sintesi geopetrolifera della Fossa Bradanica (avanfossa della catena appenninica meridionale). Mem della Soc Geologica Ital 41:87–107

Vezzani L (1967) Depositi Plio-Pleistocenici del litorale Ionico della Lucania. Atti della Accad. Gioenia di Sci Naturale in Catania 6 (18):159–180

Waelbroeck C, Labeyrie L, Michel E, Duplessy JC, McManus JF, Lambeck K, Balbon E, Labracherie M (2002) Sea level and deep water temperature changes derived from benthic foraminifera isotopic records. Quat Sci Rev 21:295–305

Westaway R (1993) Quaternary uplift of southern Italy. J Geophys Res 98:21741–21772

Westaway R, Bridgland David (2007) improved uplift modeling of the gulf of Taranto marine terraces. Quat Int 210:102–109

Westaway R, Bridgland D (2009) Reply to comment by Caputo R, Bianca M., on «Late cenozoic uplift of sothern Italy deduced from fluvial and marine sediments: coupling between surface processes and lower-crustal flow» by Rob Westaway and David Bridgland

2007 improved uplift modeling of the gulf of Taranto marine terraces. Quaternary international 210: 102–109

Zander AM, Fulling A, Bruckner H, Mastronuzzi G (2003) Lumineszneszdatierungen an litoralen sedimenten der terrassentreppe von Metapont, Süditalien. Essener Geogr Arbeiten 35:77–94 (in german)

Zander AM, Fulling A, Brückner H, Mastronuzzi G (2006) OSL dating of upper Pleistocene littoral sediments: a contribution to the chronostratigraphy of raised marine terraces bordering the gulf of Tarento South Italy. Geographfia Fisica e Dinamica Quaternaria 29:33–50

Rim Ghedhoui, Benoît Deffontaines, and Mohamed Chedly Rabia

Abstract

Thanks to its geographical position in the western Mediterranean domain, Tunisia faces, since mid-Cretaceous (Aptian/Albian time period), to the inversion of the Tethys due to the northward African plate motion toward Eurasia. The coastal Jeffara is a part of the southern zone of deformation witness of the eastward migration of Tunisia to the Mediterranean Sea. We focus herein following Perthuisot (Cartes géologiques au 1/50.000 et notices explicatives des feuilles de Houmet Essouk, Midoun, Jorf, Sidi Chamakh, 1985) and others on the neotectonic of the coastal Jeffara (southern Tunisia) and its engineering implications. Based on the results of previous studies and new evidences developed herein, we propose a new structural and geodynamic coastal Jeffara model, influenced by the continuous post lower cretaceous northward migration of northern African toward the Eurasian plates. We herein study the Digital Elevation Model (issued from SRTM), which was checked with field surveys and 2D numerous seismic profiles at depth both onshore and offshore. All data were, then, integrated within a GIS Geodatabase, which showed the coastal Jeffara, as a part of a simple N–S pull-apart model within a NW-SE right lateral transtensive major fault zone (Medenine Fault zone). Our structural, geological and geomorphological analyses prove the presence of NNW-SSE right lateral en-echelon tension gashes, off shore NW-SE aligned salt diapirs, numerous folds offsets, en-echelon folds, and so-on… that are associated with this major right lateral NW-SE transtensive major coastal Jeffara fault zone that affect the Holocene and the Villafrachian deposits. These evidences confirm the fact that the active NW-SE Jeffara faults correspond to the tectonic accident, located in the south of the Tunisian extrusion, which is active, since mid-cretaceous, as the southern branch of the eastward Sahel block Tunisian extrusion toward the free Mediterranean sea boundary. Therefore this geodynamical

R. Ghedhoui (✉) · B. Deffontaines (✉)
Laboratoire de Géomatique Appliquée, Université Paris-Est
Marne-La-Vallée (ENSG-IGN and UPEM), 5 Bd Descartes,
77450, Marne-la-Vallée Cedex 2, France
e-mail: rimaigs@yahoo.fr

B. Deffontaines
e-mail: benoit.deffontaines@univ-mlv.fr

R. Ghedhoui · B. Deffontaines
Laboratoire International Associé ADEPT 536 Taiwan–France,
CNRS-NSC, Université Paris-Est Marne-La-Vallée, 5 Bd
Descartes, 77450, Marne-la-Vallée Cedex 2, France

R. Ghedhoui · M.C. Rabia
U.R. "Géomatique et Géosystèmes" (02/UR/10-01), Université de
la Mannouba, BP 95, 2010, Mannouba, Tunisia
e-mail: rabiamch@gmail.com

movement explains the presence, offshore, of small elongated NW-SE, N-S and NE-SW transtensive basins and grabens, which are interesting for petroleum exploration.

24.1 Introduction

Despite the presence of various studies (Perthuisot 1977, 1985; Bouaziz 1986, 1995; Bouaziz et al. 2002; Rabia 1998; Touati and Rodgers 1998; Jedoui 2000; Deffontaines et al. 2008; Gabtni et al. 2009, 2011, 2012; Bodin et al. 2010), the structure of the Jeffara is still subject of conflict. Besides, the authors do not all agree about the history of the deformation of the region, as the neotectonic context seems complex and multi-phase since the Lower Paleozoic (Burrolet and Desforges 1982; Ben Ayed 1986; Bouaziz 1995; Bouaziz et al. 1999, 2002; Gabtni et al. 2012).

The aim of this study is, therefore, to better constrain the structural geometry and the neotectonic history of the coastal Jeffara using geomatics, remote sensing data, structural geology, detailed field investigation and numerous transverse onshore and off shore petroleum seismic profiles in order to propose a new structural model confirming the existence of a NW-SE major dextral fault zone allowing the eastern extrusion of the Sahel block, due to the migration of the African plate towards Eurasia (Deffontaines et al. 2008).

24.1.1 Geographical Location

The Tunisian Jeffara basin has a sub-tabular, flat and low topography (Ben Ayed and Kessibi 1981), bounded to the north and to the east by the Gabes Gulf and the Mediterranean sea; to the west by the morphological boundary of the Dahar domain, the layers of which disappear under the Oriental Grand Erg (Ben Ayed and Kessibi 1981; Bodin et al. 2010), and in the south east by the "administrative Tunisian–Lybian border". The Jeffara is subdivided into two distinct and structural units: (1) to the SW, the continental Jeffara, which constitutes the transition zone of Mesozoic and Cenozoic outcrops of Dahar, and (2) the coastal Jeffara that parallel the shoreline consisting of the island of Jerba and the two peninsulas of Jorf and Zarzis (Perthuisot 1977) (Fig. 24.1a, b).

24.1.2 Structural Overview

From the bibliography, it seems that the deformation of the coastal Jeffara is complex. Perthuisot (1977, 1985), for example, showed the presence of two quaternary, tectonic phases which are responsible for the present morphology of Jerba island and the Jorf and Zarzis peninsulas: (1) an extensional Eo-thyrrhenian phase (slightly post-villafranchian) and (2) a compressive Tyrrhenian phase. The latter (1) reactivated the faults N045°E and N165°E in sliding movements at the level of the base and (2) led to the formation, on the cover, of layers of a large radius of curvature. Both tectonic phases affect the Villafranchian "crust" deposits which lead him to date these two tectonic episodes.

In contrast, Bouaziz (1995), suggests in his excellent "These d'état" a structure organized in "half-graben", with the presence of faults in a scale of a principal direction of N120°E to N160°E. At least, we should take also, into careful consideration the work of Touati and Rodgers (1998) who advocates the presence of: (1) a Mio-Pliocene extension of NE-SW direction, having reactivated the faults that are inherited from the E–W dextral sliding of Santonian age, of the NE-SW extension of the upper Jurassic—lower Cretaceous (syn-rift phase), and (2) a post-Villafranchian compression directed NNW-SSE responsible for the shaping of the present topography.

Therefore previous authors proposed contrasting structural history for the Jeffara deformations, which seems complex and poly-phase, since the cretaceous (Burrolet and Desforges 1982; Ben Ayed 1986; Bouaziz 1995; Bouaziz et al. (1999, 2002); Rabia 1998; Touati and Rodgers 1998; Gabtni et al. 2009, 2011, 2012).

24.2 SRTM Data Analysis

From the Digital Terrain Model SRTM (Shuttle Radar Topographic Mission 2000) altimeter data, characterized by a matrix spacing of 3″ (0.0008333°), hill-shading maps of azimuths N000°E, N045°E, N090°E, and N135°E, having fixed elevation of the light source (30°) and the vertical exaggeration (20x) were calculated (Fig. 24.2b, c).

The structural field analyses and the Digital Terrain Model and aerial photographs photo-interpretation, done using the methodology developed in Deffontaines (1990, 2000), Deffontaines and Chorowicz (1991), of the different hill-shading maps and of their associated roses directions confirm the presence, in the study area, of alignments of
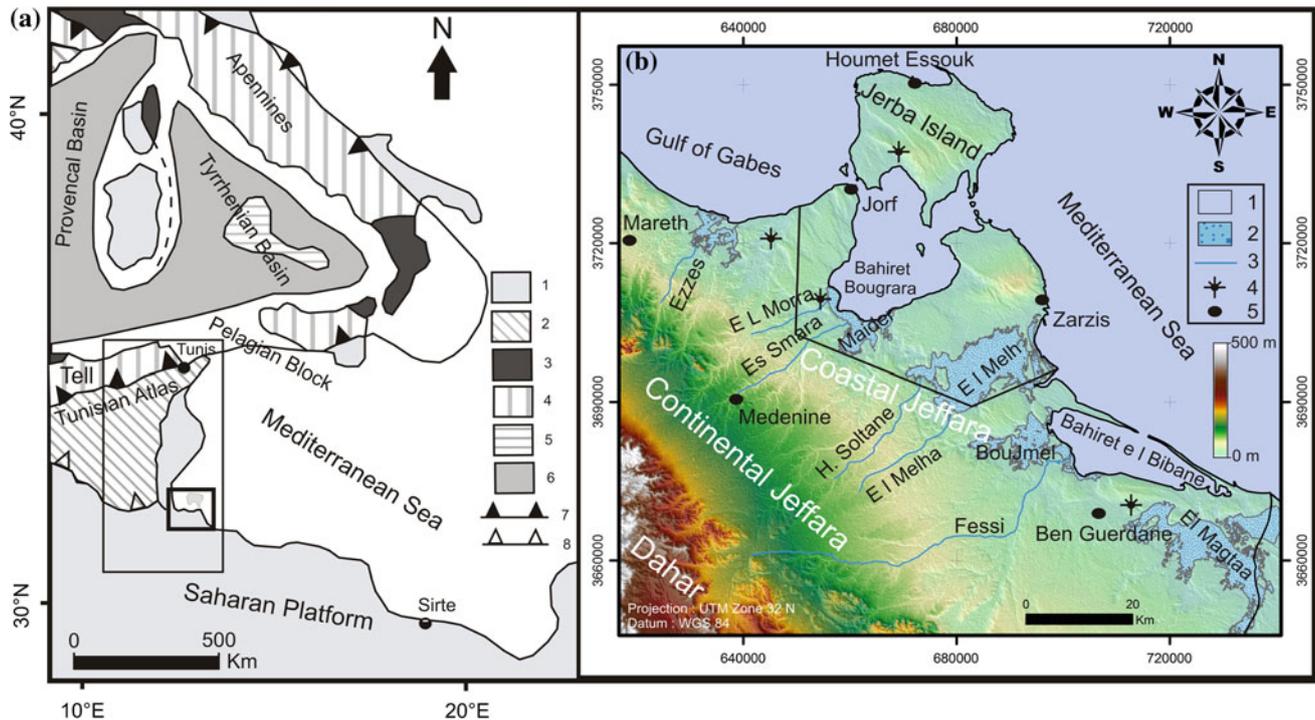
Fig. 24.1 **a** Geodynamic context of the western mediterranean domain (modified from Doglioni et al. 1999), Heavy black quadrangle in (**a**) correspond to the area (**b**) *1* continental platforms, *2* intracontinental fold belts, *3* crystalline massifs, *4* alpine chains, *5* neogene oceanic crust, *6* neogene thinned continental crust, *7* thrust fronts, *8* South Atlassic front; (**b**) geography of the studied area (*1* studied area, *2* sebkhas, *3* Oued/Talweg, *4* well, *5* town)

major faults NW-SE and WNW-ESE trending (Fig. 24.2a, d), as well asymmetric folds at the level of Jorf, Zarzis, and Jerba confirmed by the detail geological maps e.g. Perthuisot (1985) (see below).

24.3 Reinterpretation of the 1/50,000 Geological Maps and Contributions of Detailed Structural Field Work

The re-interpretation of the 1/50,000 geological maps in scale realized by Perthuisot (1985): Houmet Essouk (n°148), Midoun (n°149), Jorf (n°159), Sidi Chamakh (n°160) and Zarzis (n°160), associated with the hill shaded topography and fields observations show the presence of several examples of pedagogic structural cases which advocate the presence of an active NW-SE transtensive dextral strike-slip fault.

Though diachronic, the carbonated "Villafranchian crust" is an excellent indicator and marker of the current deformation highlighted by its vertical movements. Thus, the Villafranchian and Mio-Pliocene deposits are here re-interpreted in tectonic structures with the help of the detailed Perthuisot (1985) geological mapping: the depressions within the Villafranchian crust are interpreted as tension joints and normal faults associated with a major dextral movement (Fig. 24.3). The first example shows that the Villafranchian deposits appear on both sides of the Mio-Pliocene clays and sands depression, with a conservation of the altitudes of the Villafranchian on both sides. The absence of the vertical component and the rectilinearity of the small valley suggest that is marked by a structural tension gashes directed N130°E (NNW–SSE), perpendicular to the axis of the principal minimum constraint $\sigma3$ (NNE–SSW) (Fig. 24.3d). The second example concerns the cartographic asymmetry of the Villafranchian crust. Field observations and the study of the DEM-SRTM, confirm the presence of a variation in altitude on both sides of the elongated narrow valley and therefore, of a vertical component of the deformation, characterized by a higher altitude in its western side. The cartographic asymmetry and the difference of altitude are the proof of a subsidence of the NE compartment, which

Fig. 24.2 (**a**) Coastal Jeffara structural scheme compiled from different D.E.M. hill-shading maps (*1* city, *2* fault, *3* fold, *4* Azimuth N315°E); (**b**) SRTM DEM hill-shading of the studied area map (*1* Azimuth N225°E, Elevation: 30°, Vertical exaggeration: 20x); (**c**) rose diagram of the major photo-interpreted alignments
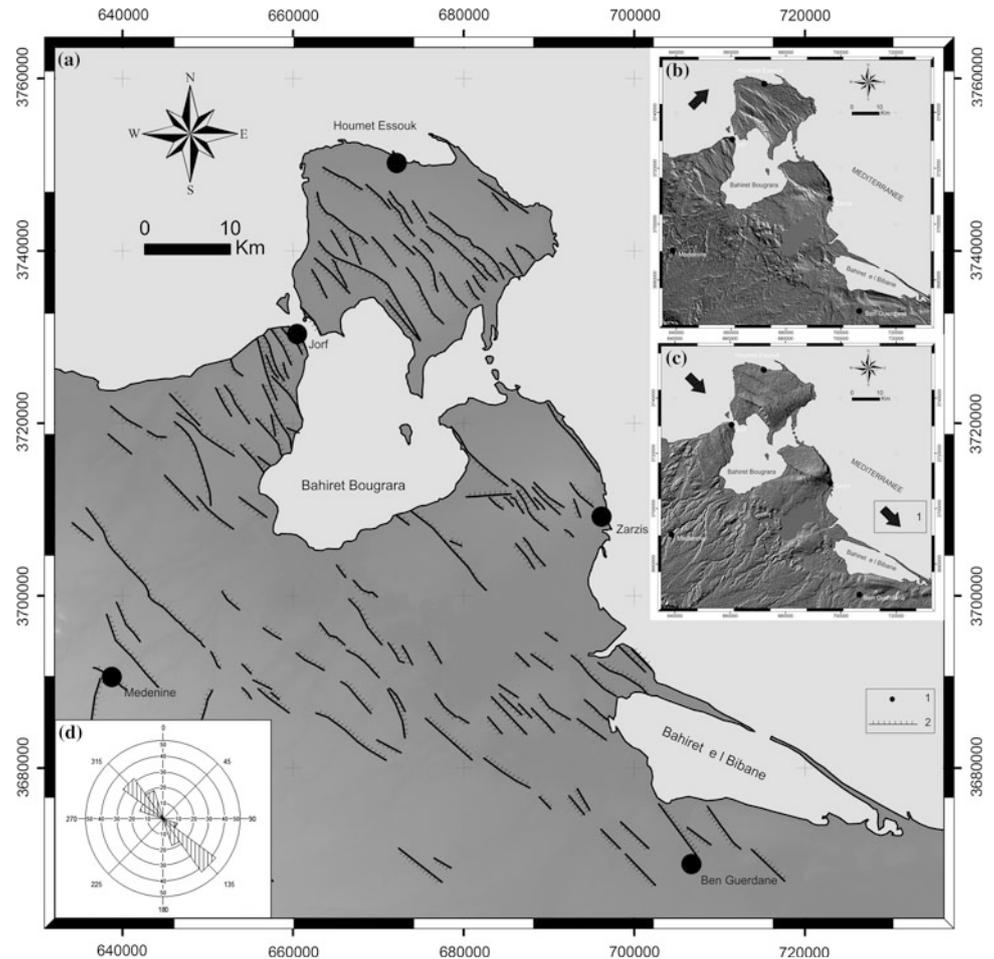
reveal therefore the presence of a normal fault (Fig. 24.3b). The sigmoid tectonic structures (in S), reveal a dextral strike slip going N120°E and N130°E, and are interpreted as "S" tension faults, associated with a dextral strike slip movement (Fig. 24.3b). Different cases correspond to structures in horst and graben, found between two normal faults with an opposite asymmetry on both sides (Fig. 24.3c).

continuity of seismic reflectors dipping towards the NE. It also shows the presence of a transparent and consequently a highly fractured zone in depth, characterized by NW-SE vertical faults. This geometry allows us to interpret them as strike-slip faults, supposed dextral, with a normal component toward the NE (Gabes gulf) and that are concentrated into several fault splays or slip corridors (Fig. 24.4).

24.4   2D Seismic Reflection Profiles

On shore 2D seismic reflection line (acquired by ETAP), NE-SW trending and perpendicular to the structures of the Jeffara is re-interpreted below: the profile P40 (NE on the right) is showing high fractured zones (reflector's dipping to the NE). It reveals an upper zone characterized by a big

24.5   Discussions and Conclusions

The analysis of the Digital Terrain Model (SRTM data) confirms the presence of: (1) alignments of major direction NW–SE, often mentioned in the bibliography (Perthuisot 1985; Ben Fergeni et al. 1990; Bouaziz 1995; Rabia 1998; Touati and Rodgers 1998; Gabtni et al. 2012), (2) directions
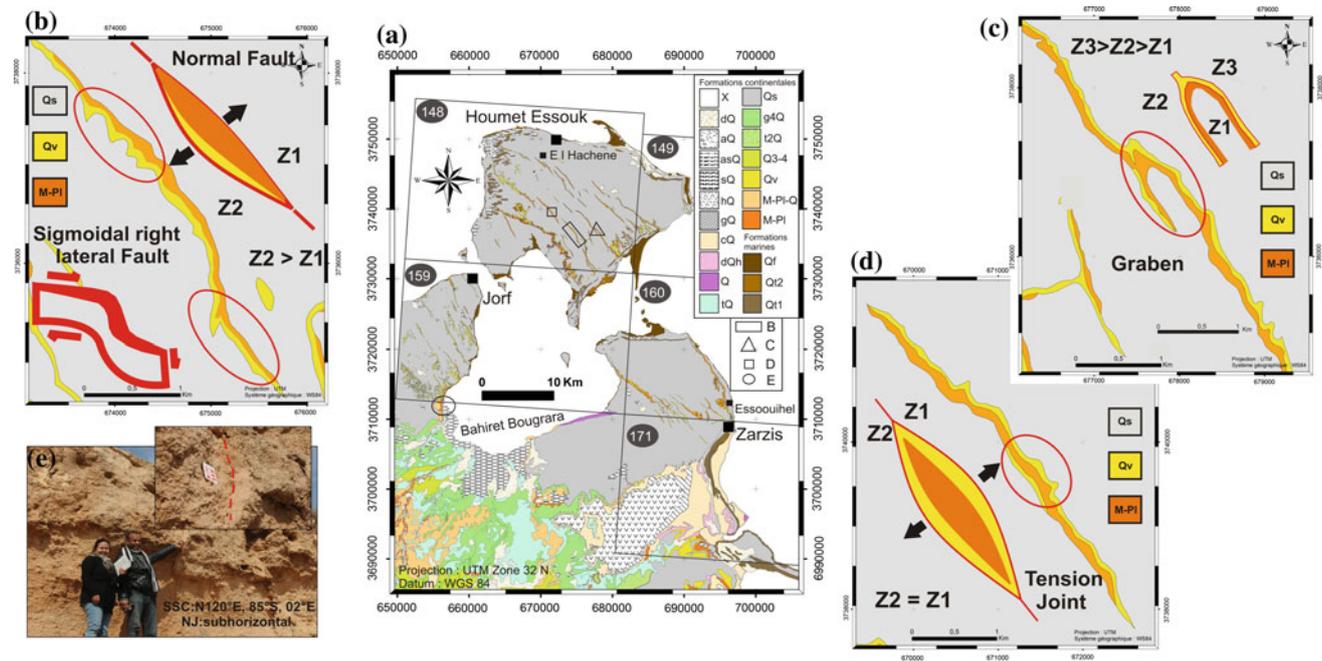
Fig. 24.3 (**a**) Mosaic of the detailed geological maps at 1/50,000 scale of Jerba island, Jorf and Zarzis (Southern Tunisia) (*148* Houmet Essouk, *149* Midoun, 159, Jorf: 160, Sidi Chamakh et 160: Zarzis); (**b**) Normal fault: (1) cartographical and lithological asymmetry, (2) difference in altitude; (**c**) graben structure bounded by two normal faults; (**d**) Tension joint: (1) cartographical and lithological symmetry, (2) altitude conservation on both sides of the tension joint; (**e**) Field photo showing a dextral strike slip fault on Pleistocene deposits (Boughara port, Bougrara, March 2102) affecting the Villafranchian carbonated crust; Lithology: continental formations (*dQ* actual dunes, *aQ* actual alluviums, *sQ* filling of continental sebkhas, *tQ* historic terrace, *Qs* red silts, *Qv* villafranchian: sauman coloured crust, *M-Pl* Mio-pliocene: claystones and sandstones with conglomeratic thin layers); marine and costal formations (*Qf* Flandrian beach sandstones, *Qt1* Neo-tyrrhénian sand dune or marine deposits, *Qt2* Eu-tyrrhenian sand dune or marine deposits) (modified from the geological maps at 1/50,000 scale)

NNW-SSE to WNW-ESE not as clear than the previous one, as well as folds in dextral offset on Zarzis Peninsula. The reinterpretation of geological maps at 1/50,000 reveals that the tectonic structures present in the island of Jerba and the Jorf and Zarzis peninsulas, may be interpreted in terms of (1) normal faults directed N120°E; (2) an-echelon dextral tension gashes, aligned along the N120°E azimuth, (3) tension gashes N130°E trending, (4) "Sigmoidal" tension gashes and (5) horsts and grabens located along large faulted corridor, surrounded by major, N120°E to N130°E transtensive dextral strike-slip faults (Fig. 24.5b).

The interpretation of numerous parallel 2D seismic lines reveals the presence of a dense number of vertical strike-slip faults with normal component, interpreted as "strike-slip corridors". Jerba, Jorf and Zarzis are, thus, located above a major dextral transtensive strike slip accident which is oriented N120°E to N130°E and which appears totally affected by highly frequent, vertical accidents. Those completely cut the costal Jeffara by corridors of many vertical faults oriented N120°E–N130°E with a small normal component.

In addition to the major NW-SE Gafsa-Tozeur fault, which stretches to the Jeffara and the NE-SW faults (Rabiaa 1998), evidence of dextral strike-slip movement was highlighted. These prove that the Jeffara fault corresponds to the major accident, bounding to the south, the Tunisian extrusion (Fig. 24.5a; see Deffontaines et al. (2008) this issue), helping the migration of the Sahel block towards the vacant border of the Mediterranean Sea. This also explains the presence, offshore, of NW-SE and NE-SW small oil basins, lying according to the opening of such fractures.

(a)

(b)

(c) P-40

(d) P-40

(e) P-40
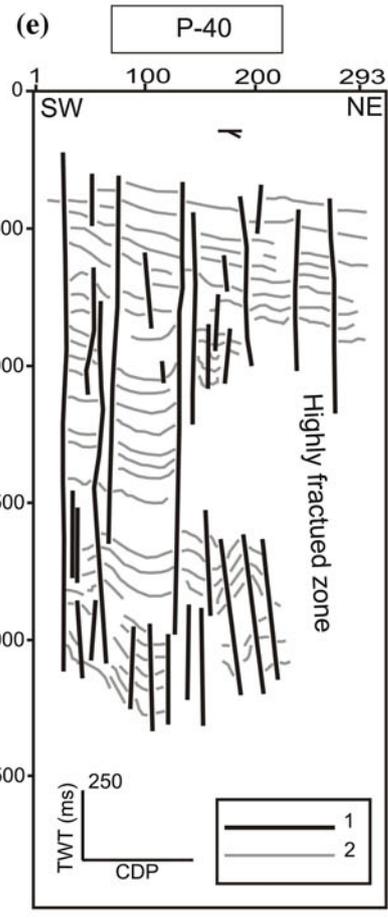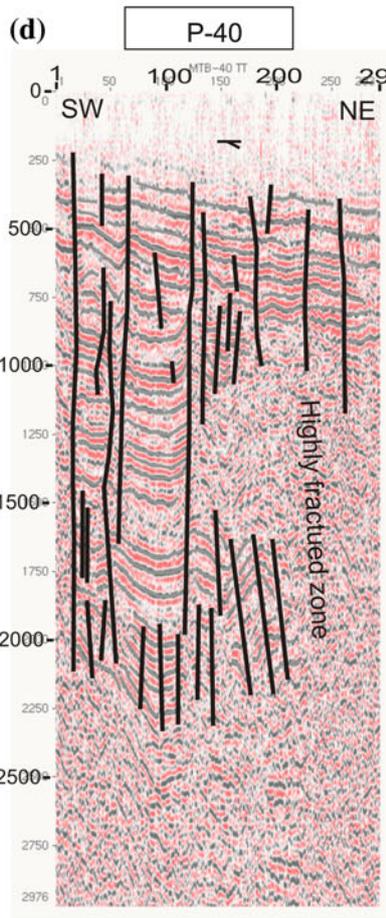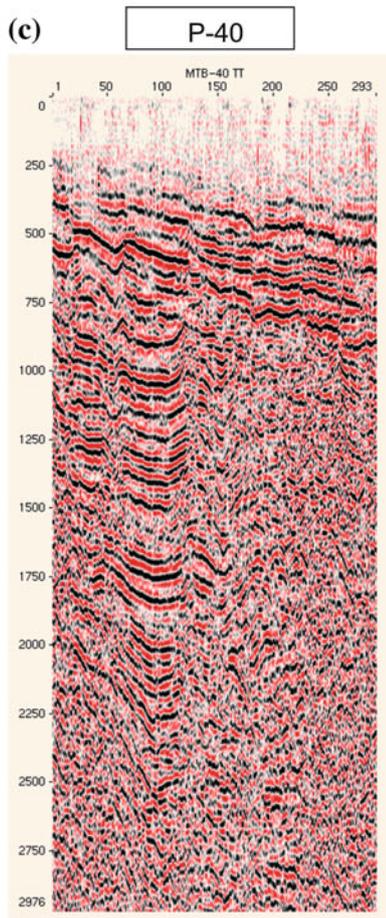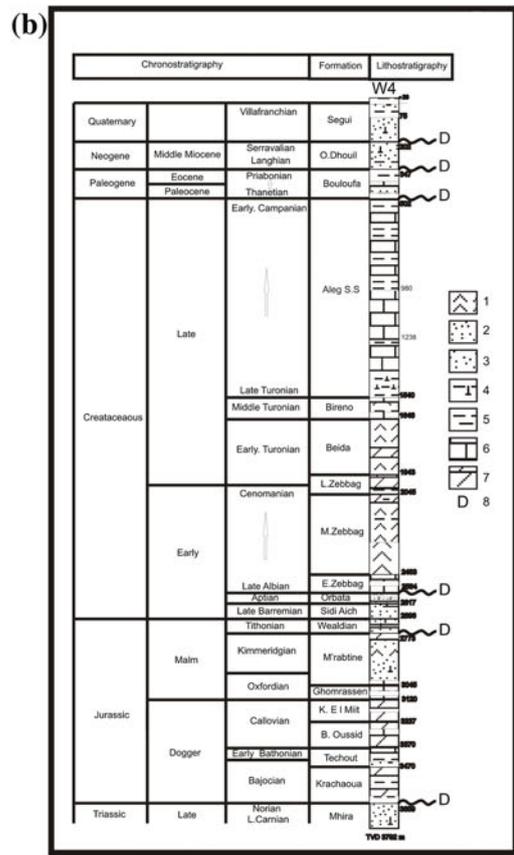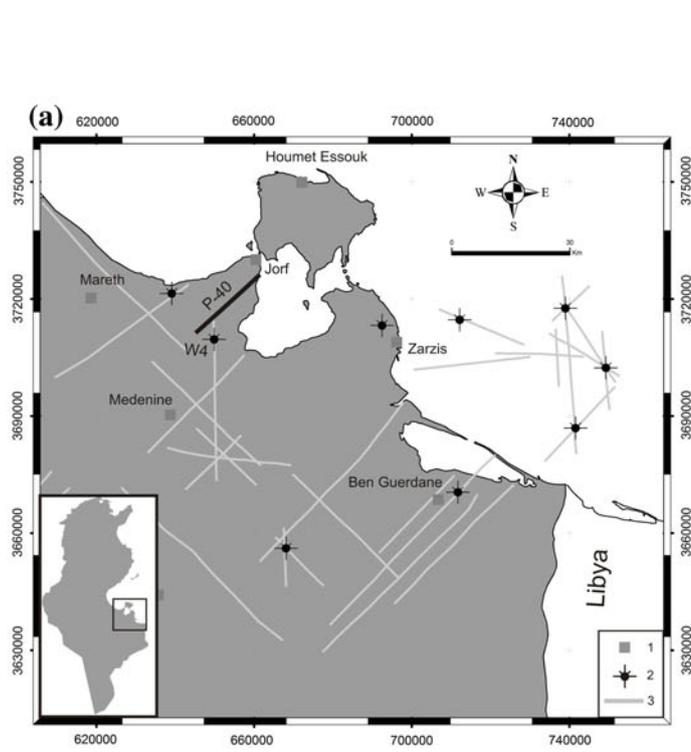
◄ **Fig. 24.4** (**a**) Block selected seismic lines (*1* town, *2* well, *3* seismic line; (**b**) lithostratigraphical units within W4 well (W4 geological report (ETAP), *1* gypsum and/or anhydrite, *2* sands, *3* sandstone, *4* marls, *5* claystone, *6* limestone, *7* dolomite, *D* unconformity); (**c**) seismic reflection profile (P40, ETAP); (**d**) transparency faires; (**e**) Interpretation of the line drawing (*1* fault, *2* reflector)
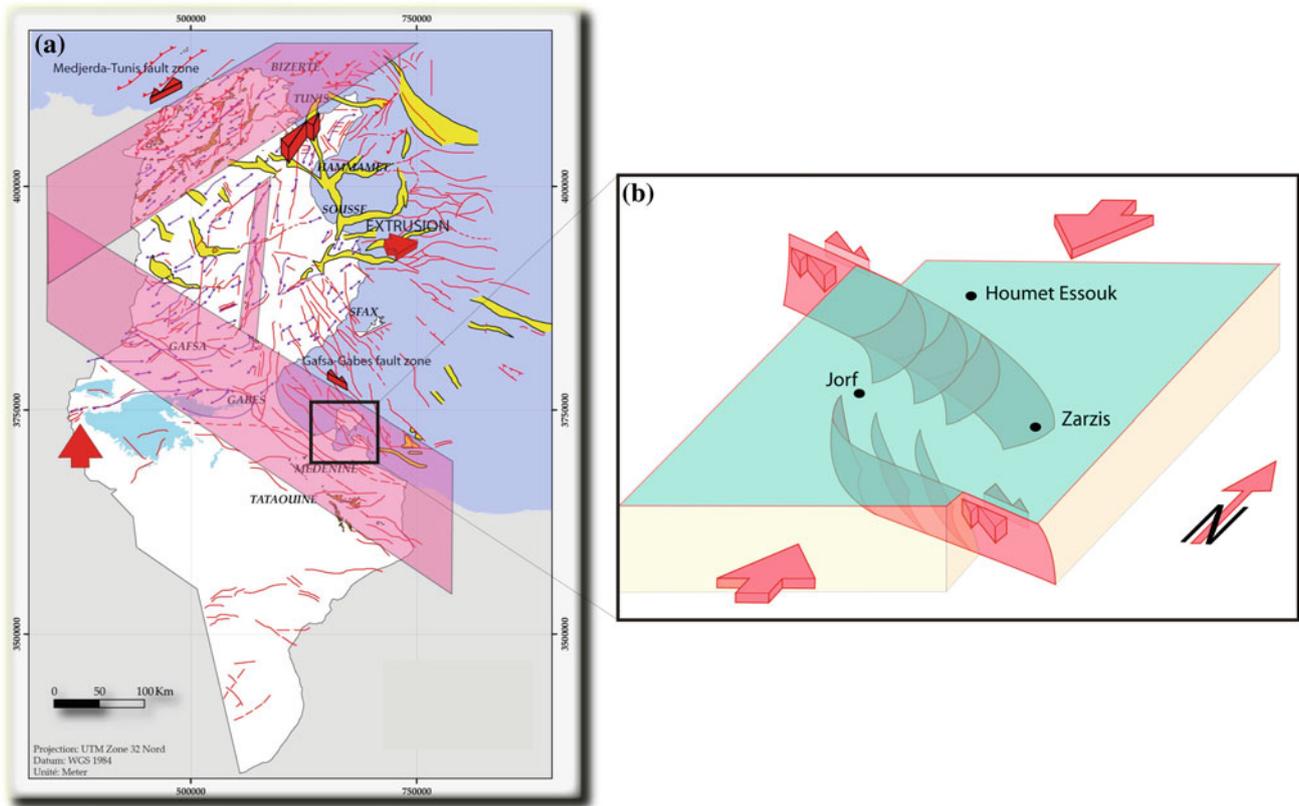
Fig. 24.5 (**a**) Geodynamic extrusion of Tunisia (Deffontaines et al. 2008, Potsdam); (**b**) 3 D synthetic block showing the geodynamic context of coastal Jeffara

References

Ben Ayed N (1986) Evolution tectonique de l'avant pays de la chaine alpine de Tunisie du début du Mésozoique à l'actuel. Thèse Doctorat d'Etat, Université Paris-Sud, Centre d'Orsay, p 328

Ben Ayed N, Kessibi M (1981) Mise en evidence de deux couloirs de décrochement E-W dextre en bordure de la plateforme saharienne (Tunisie méridionale), Actes du 1er Congrés National des Sciences de la Terre, Tunis, Sept 1981, pp 291–301

Ben Ferjani A, Burollet PF, Mejri F (1990) Petroleum geology of Tunisia, Mem ETAP, vol 1. Tunisia, Tunis, p 194

Bodin S, Petitpierre L, Wood J, Elkanouni I, Redfern J (2010) Timing of early to mid-cretaceous tectonic phases along North Africa: new insights from the Jeffara escarpment (Libya—Tunisia). J Afr Earth Sci 489–506

Bouaziz S (1986) La déformation dans la plateforme du Sud tunisien (Dahar et Jeffara): Approche multiscalaire et pluridisciplinaire. Thèse 3ième cycle, Université de Tunis, 180 p

Bouaziz S (1995) Etude de la tectonique cassante dans la plateforme et l'Atlas sahariens (Tunisie méridionale): Evolution des paléochamps de contraintes et implications géodynamiques. Thèse de Doctorat, Université de Tunis II, p 486

Bouaziz S, Barrier E, Turki MM, Tricart P (1999) La tectonique permo-mésozoique (anté-vraconienne) dans la marge sud téthysienne en Tunisie méridionale. Bull Soc Geol France 45–56

Bouaziz S, Barrier E, Soussi M, Turki MM, Zouari H (2002) Tectonic evolution of the northern african margin in Tunisia from paleostress data and sedimentary record. Tectonophysics 227–253

Burrolet PF, Desforges G (1982) Dynamique des bassins néocrétacés en Tunisie. Mémoire Géologique, vol 7. Université de Dijon, pp 381–389

Deffontaines B (1990) Digital Terrain Model and Morpho-neotectonics, application in the Strasbourg area, Rhinegraben, France. Bull INQUA NC 13:58–59

Deffontaines B (2000) Formes et déformations de la surface terrestre: Approches morphométriques et applications, Habilitation à Diriger

des Recherches (HDR). Université Pierre et Marie Curie, P6, p 60 +Annexes

Deffontaines B, Chorowicz J (1991) Principle of drainage basin analysis from multisource data, application to the structural analysis of the Zaire Basin. Tectonophysics 237–263

Deffontaines B, Slama T, Rebai N, Turki MM (2008) Tunisia structural extrusion revealed by numerical geomorphometry. Geol Soc Am spec workshop, Potsdam

Doglioni C, Fernandez M, Gueguen E, Sabat F (1999) On the interference between the early Apennines-Maghrebides back arc extension and the Alps-betics orogen in the Neogene geodynamics of the Western Mediterranean. Bol Soc Geol Ital 118:75–89

Gabtni H, Jallouli C, Mickus KL, Zouari H, Turki MM (2009) Deep structure and crustal configuration of the Jeffara basin (Southern Tunisia) based on regional gravity, seismic reflection and borehole data: how to explain a gravity maximum within a large sedimentary basin ? J Geodyn 142–152

Gabtni H, Jallouli C, Mickus KL, Turki MM (2011) Geodynamics of the Southern Tethysian Margin in Tunisia and Maghrebian domain: new constraints from integrated geophysical study. Arab J Geosci

Gabtni H, Alyahyaoui S, Jallouli C, Hasni W, Mickus KL (2012) Gravity and seismic reflection imaging of a deep aquifer in an arid region : case history from the Jeffara basin, southeastern Tunisia. J Afr Earth Sci 85–97

Jedoui Y (2000) Sédimentologie et géochronologie des dépots littoraux quaternaires: reconstitution des variations des paléoclimats et du niveau marin dans le Sud-Est tunisien. Thèse de Doctorat, Université Tunis II, p 338

Perthuisot JP (1977) Le Lambeau de Tlet et la structure néotectonique de l'ile de Jerba (Tunisie). Comptes Rendus des Seances de l'Academie des Sciences, Paris

Perthuisot JP (1985) Cartes géologiques au 1/50,000 et notices explicatives des feuilles de Houmet Essouk, Midoun, Jorf, Sidi Chamakh. Publications, Serv Geol Nat, Tunisie

Rabia MC (1998) Système d'Informations Géo-scientifique et Télédétection multi-capteurs: application à une étude mult-thèmes de la Jeffara orientale. Thèse de Docotrat, Université Tunis II, p 320

Touati MA, Rodgers MR (1998) Tectono-stratigraphic history of the Southern Gulf of Gabes and the hydrocarbon habitats. In: Proceedings of the 6th Tunisian petroleum exploration production conference, Tunis, Mai 1998, pp 343–370

Tunisia: A Mature Case Example of Structural Extrusion

25

Benoît Deffontaines, Mehdi Ben Hassen, and Rim Ghedhoui

Abstract

Neotectonics is revealed by numerous approaches such as a new re-interpretation and homogeneisation of the geological data set, earthquakes, field work studies and detailed numerical geomorphic analyses of the topography. Tunisia appear to be a case example for this kind of studies as it is affected by both active tectonics highlighted by few minor earthquakes and present numerous associated faults and folds. We develop first herein basic key geomorphic processing deduced from the bibliography and new indicators developed throughout this study, processed numerically through home made geodatabase, that lead us to propose a new structural scheme of extrusion revisiting the Tunisian neotectonic setting (Deffontaines et al. 2008, Postdam GFZ). We then update the Tunisian geological mapping by improving it with the high resolution existing Digital Terrain Model and remote sensing images. Fieldwork studies lead us to better solve mapping anomalies. At least we used numerous published existing seismic profiles that validate our model. We then propose herein an eastern extrusion model of Central Tunisia due to the northward migration of African plate toward Eurasia since mid cretaceous due to the Tethys inversion.

B. Deffontaines (✉) · M.B. Hassen · R. Ghedhoui
Laboratoire de Géomatique Appliquée, Université Paris-Est Marne-La-Vallée (UPEM), 5, Boulevard Descartes, Marne-La-Vallee, 77454, France
e-mail: benoit.deffontaines@univ-mlv.fr

M.B. Hassen
e-mail: mbenhass@ucalgary.ca

R. Ghedhoui
e-mail: rimaigs@yahoo.fr

B. Deffontaines · M.B. Hassen · R. Ghedhoui
Laboratoire International Associé ADEPT 536 CNRS-NSC, Aix-En-Provence, France

B. Deffontaines · M.B. Hassen · R. Ghedhoui
Laboratoire International Associé ADEPT 536 CNRS-NSC, Taipei, Taiwan

25.1 Introduction: State of the Art

Lateral extrusion along a collision zone has been proposed first in Tibet and Himalaya (Molnar and Tapponnier 1978; Tapponnier et al. 1983) and later extended to other mountain belts such as the Alps (Ratschbacher and Merle 1991) or in Taiwan (Angelier et al. 2009). Tectonic extrusion describes the lateral motion of structural units that move toward a weaker domain with respect to the mountain belt, in response to collision-induced shortening. The weak domain is often represented by a «free boundary» such as in analogue or numerical models. Such a mechanical exaggeration aims at producing clearer results. In the fields, the velocity and amplitude of extrusion are functions of (1) the shortening across the mountain belt, (2) the contrast in mechanical strength between the structural units within the belt and the adjacent weaker domains and (3) the existence of a

detachment level at depth that lead to the sliding of the overlying formations.

We aim at showing that despite the small size of the Tunisian Atlas mountain belt compared to Himalaya or the Alps, significant extrusion occurs at the eastern tips of the Tunisian collision zone since mid-cretaceous.

We focus herein on Tunisia as few recent structural studies prevail Fig. 25.1a, b) despite its tectonic activity (Boukadi 1994; Bouaziz et al. 2002; Hfaiedh et al. 1991). Furthermore Tunisia present a high quality of outcrops, as well as the huge quantity of remote sensing data and digital topographic data quite interesting to have a precise photo-interpretation (Deffontaines 1990, 2000 Deffontaines and Chorowicz 1991). Finally a quite good geological mapping (Perthuisot 1977, 1985 and so on.), microtectonic analzes (Bouaziz 1986, 1995, Bouaziz et al. 1999) as well as numerous available sismic reflection profiles and wells (e.g., and so on) that may be re-interprete and homogenize from North to South (Deffontaines et al. 2008; Ben Hassen et al. 2012).

We will first have a closer look to the extrusion southern branch so called Gafsa-Medenine (which are much more described in Ben Hassen et al. (2012 and this issue) of the

transpressive context close to the Gafsa city and by Ghedhoui et al. (this issue) for the transtensive context. The Gafsa-Medenine fault zone is then inferred as a major right lateral strike-slip fault. At least we will propose following the work of Deffontaines et al. (2008) a global geodynamic model for the Tunisian extrusion that govern the present deformation since mid cretaceous time.

25.2 The Gafsa: Medenine Fault Zone—A NW–SE Transpression to Transtension Right Lateral Strike-Slip Major Fault Zone

25.2.1 The Gafsa-Medenine NW–SE Right Lateral Strike-Slip Fault Zone

Numerous studies had been done on that specific area of the Tunisian Atlas (Ben Ayed 1986; Zouari et al. 1990; Bedir et al. 1992; Bedir 1995; Zouari 1995; Touati et Rodgers 1998; Ghabtni et al. 2009, 2011; Bodin et al. 2010). A detail Tunisian geomorphometric approach detailed in Ben Hassen et al. (2012 and this issue) show (1) the different topography
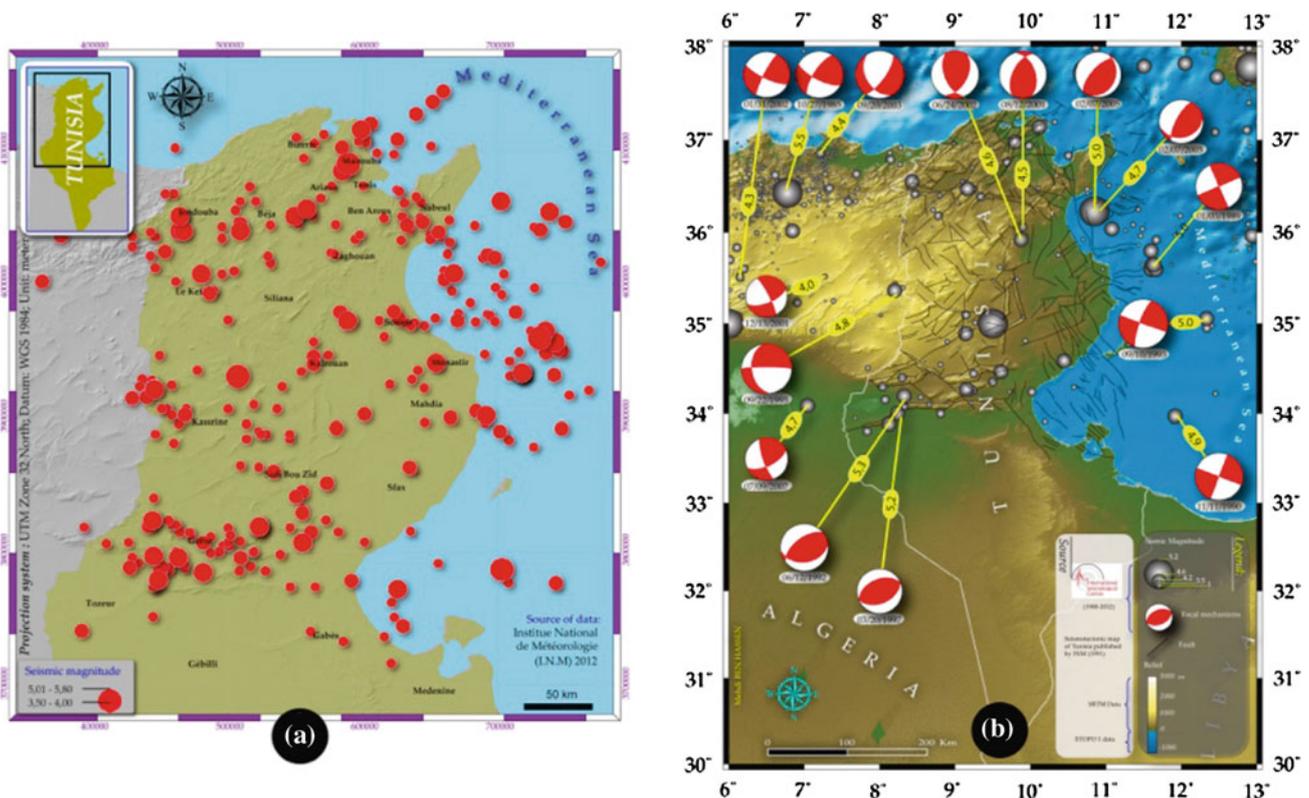
Fig. 25.1 **a** Earthquakes in Tunisia (M > 3.5) since 1970 (From INM data, in M.Ben Hassen, these UPEM, 2012); **b** Sismo-tectonic map of Tunisia (Sismic Magnitude and focal mechanisms parameters from the «Centre Seismologique International»; Topographic data from SRTM; bathymetric data from GTOPO30; faults from the sismo-tectonic map of Tunisia published by INM in 1991) from M. Ben Hassen these UPEM, 2012
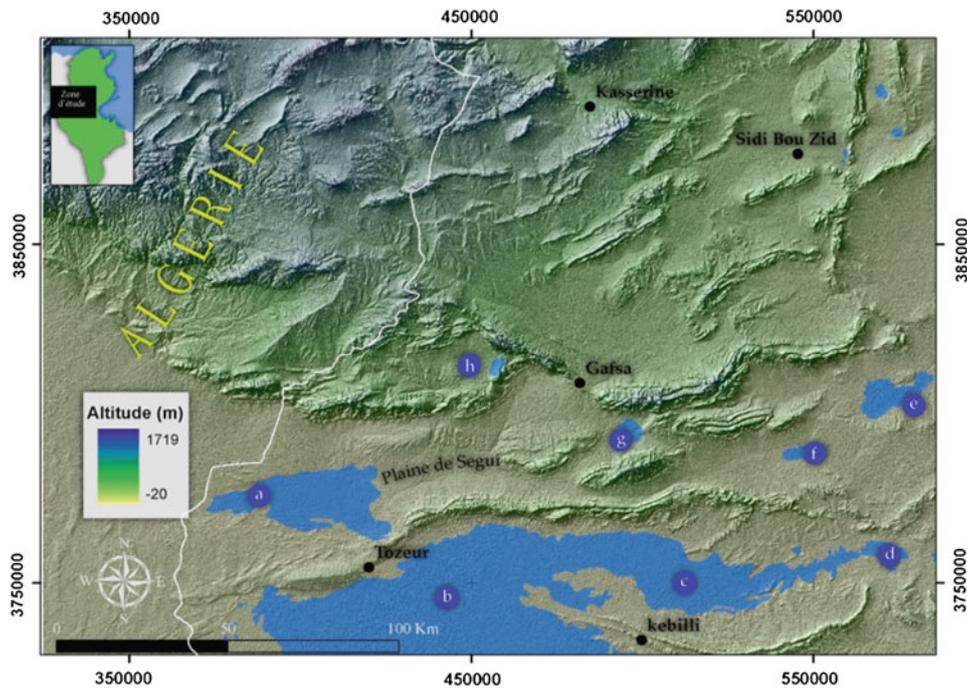
Fig. 25.2 Plains and depressions of the Southern Tunisian Atlas Tunisie: **a** Chott El Gharsa; **b** Chott El Jerid; **c** Chott El Fejaj; **d** Sebkhet El Hamma; **e** Sebkhet En Nouer; **f** Sebkhet Sidi Mansourr; **g** Sebkhet Guettar; **h** Garaat Ed-Douza
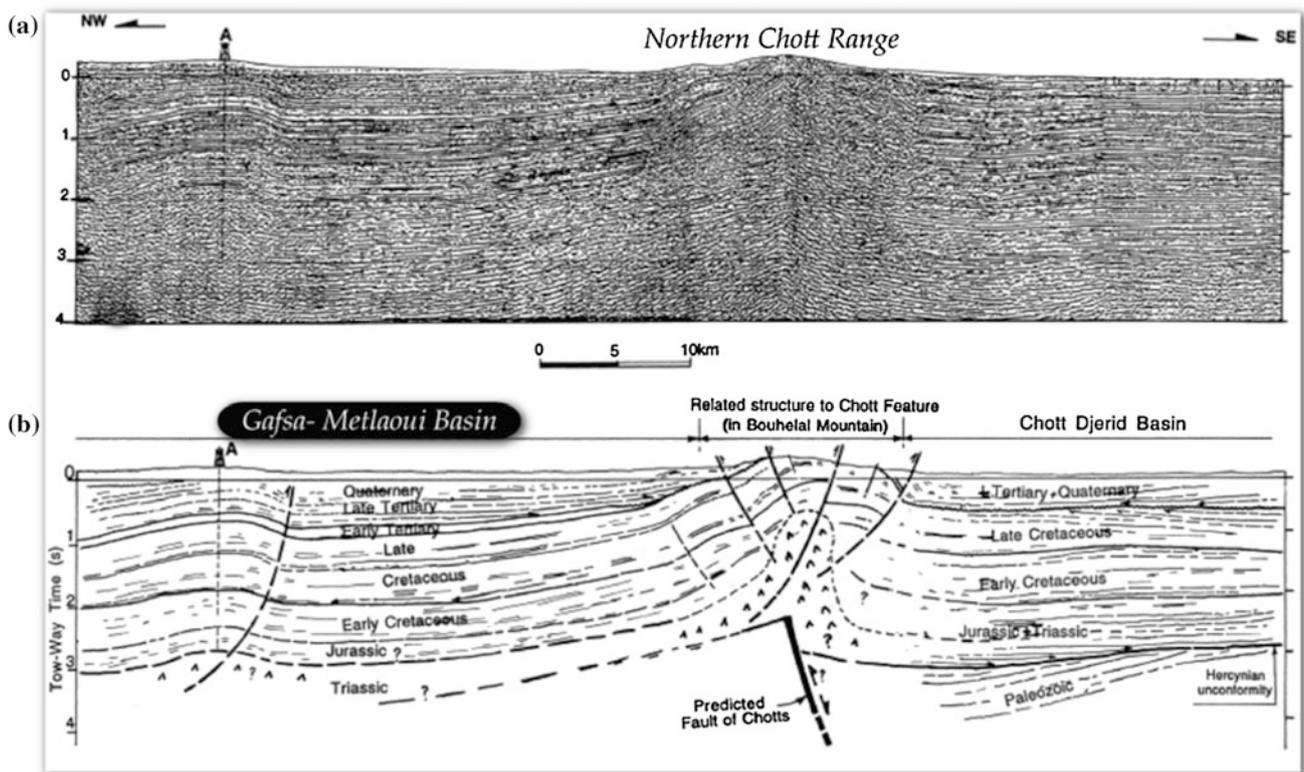
Fig. 25.3 Sismic reflexion profile highlighting the diapiric salty Jurassic to triassic formations (Mestaoua?) situated above a paleonormal Tethyan inverted normal fault on the Gafsa-Metlaoui basin (from Hlaiem 1999 in M. Ben Hassen PhD thesis UPEM, 2012)
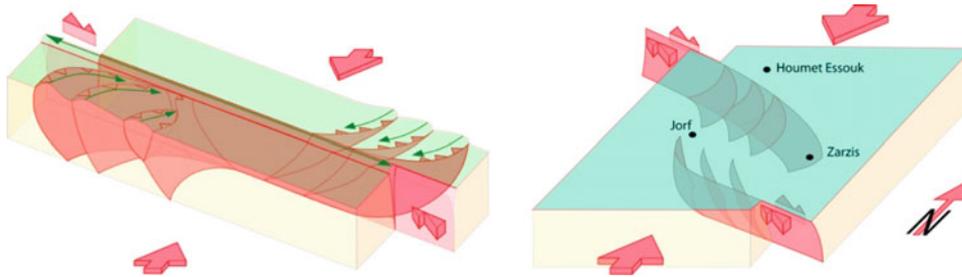
Fig. 25.4 4A: 3D structural model of the Gafsa Medenine fault zone: a transpressive NW-SE right lateral strike-slip fault zone close to Gafsa (West of the Gabes gulf—on the *left*) contrasting with the transtensive component close to Medenine (South of the Gabes gulf—on the *right*) see M.Ben Hassen et al. and R.Ghedhoui et al. (this issue)

(Fig. 25.2), the structures and their right lateral offsets, a quite simple N–S published seismic profile Fig. 25.3 (from Hlaiem 1999), and the interpretation of the area in terms of re-activation of a major NW–SE right lateral strike-slip transpressive fault zone (see the strike-slip Gafsa fault model on Fig. 25.3a). Whereas further SE on the coastal Jeffara area, south of the Gabes gulf, and close to the Medenine city, this Gafsa-Medenine fault zone taking into account the bibliography (Bouaziz 1986; Rabia 1998) is newly described by Rim Ghedhoui et al. this issue. The Medenine fault zone act as a transtensive right lateral strike-slip fault where pull apart prevail that create the Boughrara depression as illustrated by the Fig. 25.4b. The Boughrara may be filled locally by salt diapir(s) (see description of the origin of such below and in Ghedhoui et al. this issue).

25.2.2 The N–S Axis

The well known N–S axis acts therefore as a graben situated in between a transpressive and a transtensive tectonic domains. Therefore the N–S axis appear to be a N–S neutral elongated area» in between two distinct tectonic and topographic domains. If the western one corresponds to a transpressive high plateau (see Fig. 25.5) that contrasts to the transtensive eastern part of the N–S axis that correspond to the Sahel block or plain. The very thick buried Mestaoua formation Jurassic in age (upper Lias to Aalenian) composed of salt and evaporites, then fills in the faults zone and the gaps and creates different kind of diapirs.

- (1) some diapirs west of the N–S axis are situated in a N–S compressive environment above the former E–W Tethysian normal fault that are then inversed due to the African/Europe convergence;
- in other place the diapirs act as (2) transcurrent along the major fault zones that correspond to the left lateral Diapir fault zone zone NE-SW trending (Tunis Medjerda) and the NW-SE trending Gafsa-Medenine right lateral fault zone;

- and at least (3) diapirs may fill in N–S and oblique grabens at sea/offshore in a normal transtensive environment. These therefore have great oil implications especially on the reactivation of the diapirs and on the very particularly geometry of the different offshore oil traps that are situated close to the diapir itself.

We then may summarize the deformation in Tunisia as follow.

25.3 Discussion and Conclusions

On this Tunisian extrusion model deduced from structural drainage analyses and anomalies, drainage network classifications, specific and optimized analyses of the Digital Terrain Model (DTM-SRTM), summit level surface analyses. integrated within a GIS (Deffontaines 1990; Deffontaines et al. 1994; Deffontaines 2000; Ben Hassen et al. 2012, Ghedhoui et al. this issue.), and that take into consideration previous works (Bouaziz et al. 2002), we propose that the well known diapir fault zone (Medjerda-Tunis fault zone) correspond to a major left lateral transpressive to transtensive (from west to east respectively) trending northeastward acting as the northern major boundary of the Central Tunisia extrusion. It appears in the fields as a compressive structure linked to the behaviour of the continuous uplifting of the elongated NE-SW salt diapirs that parallel this major transcurrent extrusion tectonic zone. It is associated with the NW-SE trending well known Gafsa-Gabes fault zone (Ben Hassen 2012; Ben Hassen et al. 2012 and this issue, and Ghedhoui et al. (2013) and this issue) which is characterized by numerous en-echelon folds acting as a major right lateral fault zone that bounds the southern part of the central Tunisia extrusion (Deffontaines et al. 2008). Within the extruded central Tunisia, the North–South axis also known as Al Abiod N–S fault zone appear to be a reactivated graben closely associated with the eastern extrusion of central Tunisia and differentiating high Atlasic and low eastern tunisian Domain (Bouaziz et al. 2002). The N–S axis acts as

Fig. 25.5 Geodynamic extrusion of Tunisia (modified from Deffontaines and et al. Potsdam, 2008): The Tunis-Medjerda fault zone act as a transpressive to transtensive *left* lateral fault zone wheras the Gafsa-Medenine fautl act as a Transpressive to transtensive fault zone. The neutral area is highlighted by the N–S axis which behaves as a major graben infilled by the elongated diapir made of the *thick* salty Mestaoua serie (400–800 m thick)
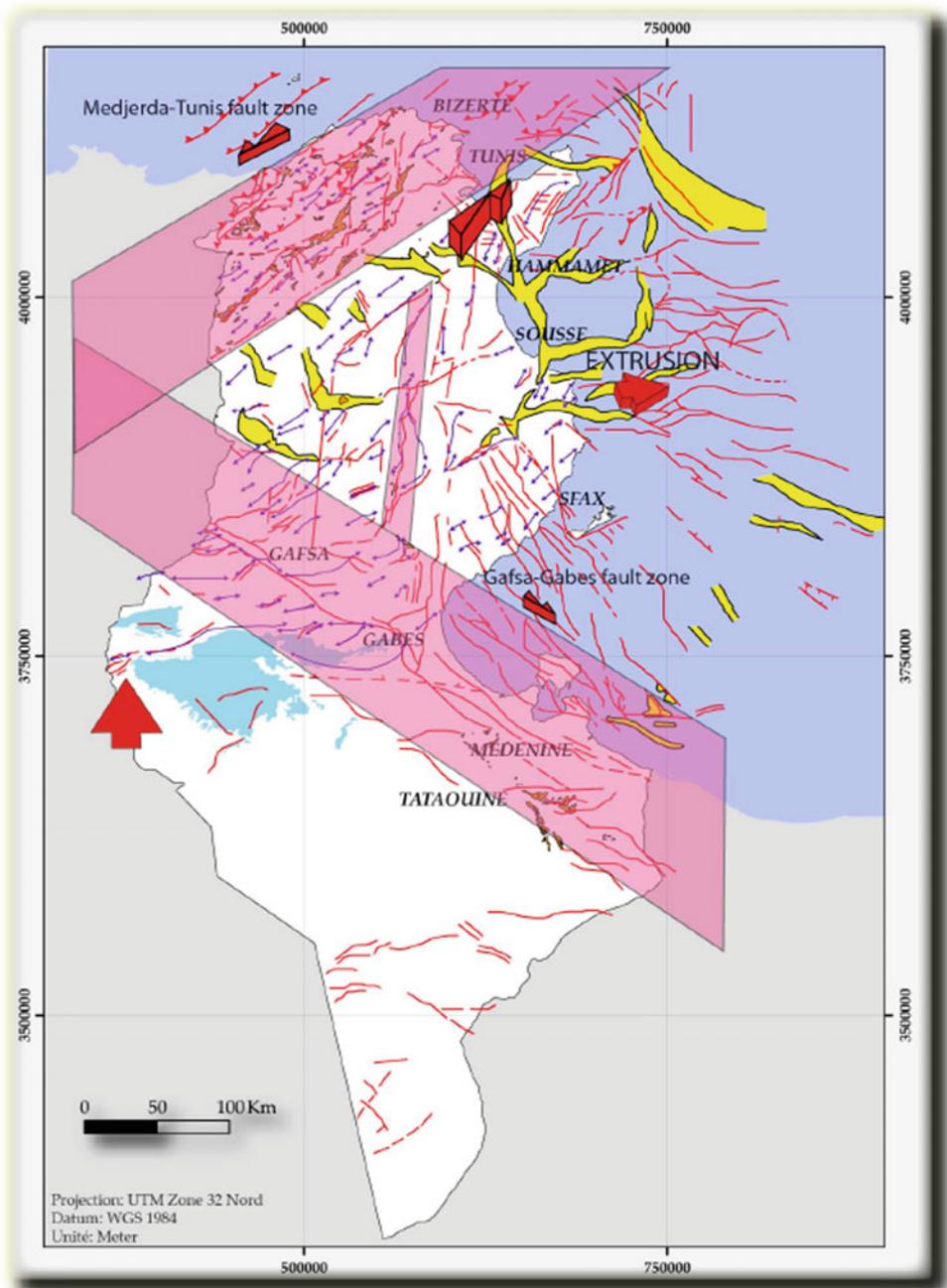
the neutral zone in bounding the transpressive domain on the West and the transtensive domain on the East. Therefore the N–S axis act as a normal fault/graben fills in by halocinetic processes which highlight outcropping compressive structures. We interpret this Tunisian extrusion active as a mature feature as it has been developing all along the Tethysian closure since mid-cretaceous (Bouaziz 1986). Our study therfore highlights that the different tectonic regimes that prevail since the inversion of the Tethys (mid-Creataceous Aptian-Albian?) is a mixed of both compression and strike slip tectonic regime affected by halocinesis local phenomenons. We therefore may reinterprete completely differently the passed history of Tunisia and this gives several major indications for engineering geology such as oil indications, sismic hazards and so on.

References

Angelier J, Chang TY, Hu JC, Chang CP, Siame L, Lee JC, Deffontaines B, Chu HT, Lu CY (2009) Does extrusion occur at both tips of the Taiwan collision belt? Insights from active deformation studies in the Ilan Plain and Pingtung Plain regions. Tectonophysics 466:356–376

Bedir M (1995) Mecanisme des bassins associes aux couloirs de coulissements de la marge atlasique de la Tunisie: simo-stratigraphie, seismo-tectonique et implications petrolieres. These de doctorat en Sciences geologiques. These de doctorat Doctorat es-Sciences, Universite Tunis II, 412 p

Bedir M, Ben Youssef M, Boukadi N, Slimane F, Zargouni F (1992) Les evenements sequentiels meso-cenozoiques associes au systeme de coulissements de l'Atlas meridional de Gafsa. 3eme Journee de l'Exploration Petroliere (ETAP). Tunis

Ben Ayed N (1986) Evolution tectonique de l'avant pays de la chaine alpine de Tunisie du debut du Mesozoique a l'actuel. These Doctorat d'Etat, Universite Paris-Sud, Centre d'Orsay, p 328

Ben Hassen M (2012) Analyse de la deformation recente dans l'Atlas meridional de la Tunisie par geomorphometrie et Interferometrie Radar (DInSAR). These de doctorat en Sciences de l'Information Geographique, Universite: Paris-Est Marne-la-Vallee/ France; et en geologie, Universite: Tunis El Manar/Tunisie. 341p

Ben Hassen M, Deffontaines B, Turki MM (2012) Contribution de la Geomatique (SIG et teledetection) pour la mise a jour de la couverture geologique a l'echelle du 1/ 100 000eme du sud de la Tunisie, Photo-Interpretation European Journal of Applied Remote Sensing, N° 2012/3, 31 p

Bodin S, Petitpierre L, Wood J, Elkanouni I, Redfern J (2010) Timing of early to mid-cretaceous tectonic phases along North Africa: New insights from the Jeffara escarpment (Libya—Tunisia). J Afr Earth Sci 58:489–506

Bouaziz S (1986) La deformation dans la plateforme du Sud tunisien (Dahar et Jeffara): Approche multiscalaire et pluridisciplinaire. These 3ieme cycle, Universite de Tunis, 180 p

Bouaziz S (1995) Etude de la tectonique cassante dans la plateforme et l'Atlas sahariens (Tunisie meridionale): Evolution des paleochamps de contraintes et implications geodynamiques. These de Doctorat, Universite de Tunis II, p 486

Bouaziz S, Barrier E, Turki MM, Tricart P (1999) La tectonique permo-mesozoique (ante-vraconienne) dans la marge sud tethysienne en Tunisie meridionale. Bull Soc Geol France 45–56

Bouaziz S, Barrier E, Soussi M, Turki MM, Zouari H (2002) Tectonic evolution of the northern african margin in Tunisia from paleostress data and sedimentary record. Tectonophysics 357:227–253

Boukadi N (1994) Structuration de l'atlas de Tunisie: signification geometrique et cinematique des nreuds et des zones d'interferences structurales au contact de grands couloirs tectoniques. These de doctorat en Sciences Geologiques, Univ. Tunis II, Faculte des Sciences de Tunis, 249 p

Deffontaines B (1990) Developpement d'une methodologie morphoneotectonique et morphostructurale; analyse des surfaces enveloppes, du reseau hydrographique et des modeles numeriques de terrains; Application au Nord-Est de la France. These, Univ. Paris VI, France, 230 p

Deffontaines B (2000) Formes et deformations de la surface terrestre: Approches morphometriques et applications, Habilitation a Diriger des Recherches (HDR), Universite Pierre et Marie Curie, P6, p. 60 + Annexes

Deffontaines B, Chorowicz J (1991) Principle of drainage basin analysis from multisource data, Application to the structural analysis of the Zaire Basin. Tectonophysics 194:237–263

Deffontaines B, Slama T, Ben Hassen M, Rebai N, Turki MM (2008) Tunisia structural extrusion revealed by numerical geomorphometry. Geol Soc Am spec workshop, Potsdam, June 2008

Gabtni H, Jallouli C, Mickus KL, Zouari H, Turki MM (2009) Deep structure and crustal configuration of the Jeffara basin (Southern Tunisia) based on regional gravity, seismic reflection and borehole data: How to explain a gravity maximum within a large sedimentary basin? J Geodyn 47:142–152

Gabtni H, Jallouli C, Mickus KL, Turki MM (2011) Geodynamics of the Southern Tethysian Margin in Tunisia and Maghrebian domain: new constraints from integrated geophysical study. Arab J Geosci 6:271–286

Hfaiedh M, Attafi K, Arsovski M, Jancevski J, Domurdzanov N, Turki MM (1991) Carte sismotectonique de la Tunisie. Editee par l' Institut National de la Meteorologie

Hlaiem A (1999) Halokinesis and structural evolution of the major features in eastern and southern Tunisian Atlas. Tectonophysics 306 (1):79–95

Molnar P, Tapponnier P (1978) Active Tectonics of Tibet. J Geophys Res 83:5361–5375

Perthuisot JP (1977) Le Lambeau de Tlet et la structure neotectonique de l'ile de Jerba (Tunisie). C. R. Acad Sci, Paris

Perthuisot JP (1985) Cartes geologiques au 1/50.000 et notices explicatives des feuilles de Houmet Essouk, Midoun, Jorf, Sidi Chamakh, Publications, Serv. Geol. Nat. Tunisie

Rabia MC (1998) Systeme d'Informations Geo-scientifique et Teledetection multi-capteurs: Application a une etude mult-themes de la Jeffara orientale. These de Docotrat, Universite Tunis II, p. 320

Ratschbacher L, Merle O (1991) Lateral extrusion in the Eastern Alps, part 2: structural analysis. Tectonics 2:245–256

Tapponnier P, Peltzer A, Le Dain Y, Armijo R, Cobbold P (1983) Propagation extrusion tectonics in Asia: new insights from simple exper-iments with plasticine. Geology 10:611–616

Touati MA, Rodgers MR (1998) Tectono-stratigraphic history of the Southern Gulf of Gabes and the hydrocarbon habitats. Proceedings of the 6th Tunisian petroleum exploration production conference, Tunis, Mai, pp 343–370

Zouari H (1995) Evolution geodynamique de l'Atlas centro-meridional de la Tunisie: stratigraphie, analyse geometrique, cinematique et tectono-sedimentaire. These de doctorat d'etat en sciences geologiques, 277 p

Zouari H, Turki MM, Delteil J (1990) Nouvelles donnees sur revolution tectonique de la chaine de Gafsa. Bull Soc Geol Fr 8(4):621–629

The Extrusion of South-West Taiwan: An Offshore-Onshore Synthesis

26

Benoît Deffontaines, Liu Char-Shine, and Chen Rou-Fei

Abstract

Neotectonic Interpretation of the different marine surveys (ACT, …) swath bathymetry and different onshore-offshore sismic profiles combined to classical structural fieldwork, geodetic, seismological and interferometric studies lead us to propose a global structural scheme and confirm the regional escape tectonics affecting both onshore-offshore of SW Taiwan. First, it is highlighted here the difficulty to only interprete the swath bathymetry even in the northern tip of the Manila accretionnary prism which is a rather simple geological context but affected by both (1) a strong amount of sedimentation due to the Taiwan mountain belt erosion, and (2) to the submarine erosion of the giant Penghu canyon. Second point, is the importance of the seismic interpretation in order to get the offshore bedding and structural data combined with the swath bathymetry and to the photointerpretation of the digital Terrain Model combined to the accurate geological maps to precisely delineate the blocks that is inferred to be submitted to a classical escape tectonic. Third, the precise study of the two new major structural boundaries Fangliao and Young-An structures which guides the SW Taiwan extrusion. Combined with onshore studies (e.g. interferometry (DINSAR), geodetic, seismology and field work) which gives (1) locations, characterization and quantification on the interseismic displacements and (2) lead us to modify our view of the global tectonic structures of the SW Taiwan. To conclude, it is highly recommended to combine both approach on and offshore geology in order to better understand geology and active structures in that part of the world.

B. Deffontaines (✉)
Laboratoire de Geomatique Appliquee (LGA),
Université Paris-Est Marne-La-Vallee (UPEM), 5 Bd Descartes,
77454, Marne-La-Vallee Cedex 2, France
e-mail: benoit.deffontaines@univ-mlv.fr

B. Deffontaines
Ecole Nationale des Sciences Geographiques (ENSG),
6, et 8 Avenue Blaise Pascal Cité Descartes—Champs-sur-Marne,
77455, Marne la Vallée Cedex 2, France

L. Char-Shine
National Taiwan University, Taipei, Taiwan ROC

C. Rou-Fei
Academia Sinica, Taipei, Taiwan ROC

26.1 Introduction

South of Taiwan, the Philippine plate, bounded by the Luzon volcanic arc, overrides towards the West the South China Sea oceanic crust into the Manila trench. This subduction is transformed northward and onshore into a continent subduction (Lallemand and Tsien 1997) or what is commonly called collision between the Philippine and Eurasian plates. In other words, Taiwan appears to be a large onshore accretionary prism. The convergence between the two plates provides a unique example in the world of the subduction of a continent under an oceanic crust. Thus, it is interesting to analyse in detail the ongoing processes related to plate

convergence in Taiwan, as a key example for geological studies of mountain building in the world (e.g., Suppe 1984; Suppe et al. 1985). Within this context, the transition in space and time between subduction and collision deserves particular attention. For this reason, the aim of this paper is to describe the structural and displacement pattern in SW Taiwan, where the transition from the offshore northernmost segment of the Manila Trench to the southernmost segment of the fold-and-thrust Taiwan belt occurs. Such a study implies the combined use of offshore and onshore sources of information.

The obliquity between the Chinese continental margin (Eurasian Plate) and the convergence of the Luzon volcanic arc (Philippine Sea Plate) involves progressive migration towards the South of the active collision (e.g. Biq 1972; Bowin et al. 1978; Wu 1978; Suppe 1984; Suppe et al. 1985; Ho 1986). In the Taiwan area, a present 82 mm/yr towards azimuth N310°E according to GPS measurements (Yu et al. 1995, 1997) reveal the high tectonic activity and the natural hazard importance of this study.

As indicated by Mouthereau et al. (1996) and confirmed by Yu et al. (1997) based on geodetic (GPS) studies, SW Taiwan is the region where maximum deformation occurs. However, few geologists have studied the detailed geometry and mechanisms of structures in SW Taiwan, mainly because of the scarcity of outcrops of suitable rock nature as mudstones prevail, abundance of flat lowlands and absence of differentiate reliefs, as well as the luxuriant vegetation. Sun (1964) published an interesting detailed photogeologic interpretation of the whole area using Howard's (1967) photointerpretation methodology, which takes into careful account the vertical offsets suggested by the topography and the detailed drainage network patterns (see also Deffontaines and Chorowicz 1991). In the coastal plain area of SW Taiwan, Sun (1964) therefore recognised numerous large, flat domes, which he interpreted as horsts and grabens. Later, Deffontaines et al. (1993) proposed the presence of oblique vertical transfer zones that affect the Foothills of Taiwan, probably inherited from the Eurasian passive margin and reactivated by the Plio-Quaternary Penglai orogeny. Deffontaines et al. (1997, 2000) moreover revealed the location of the deformation front of the orogen in the SW Taiwan, as well as the geometry of the pop-up structure for the Tainan anticline. Mouthereau et al. (2002), based on balanced geological cross-sections, confirmed the tectonic styles all along the western foothills of the orogenic belt of Taiwan, from North to South Taiwan confirming both the location of the deformation front in the SW Taiwan and oblique structures to the belt.

In this paper, we compile the structural information provided by recent offshore and onshore surveys to provide a spatially continuous reconstruction of the deformation and structure in SW Taiwan, from sea to land. We then propose a structural scheme of the onshore-offshore SW Taiwan. And using both GPS and DinSAR we propose to locate characterize and quantify the active structures. We use therefore a variety of tools, among which the major ones are the seismic reflection profiling at sea, the field work and mapping on land, and the morphological analysis both on land and at sea, as well as interferometric results of ALOS (JAXA) (DINSAR).

26.2 Tectonic Escape

If the theory of tectonic escape or extrusion has been documented close to collision zone since the 80s (Molnar and Tapponnier 1978; Tapponnier et al. 1983, see also Deffontaines et al. this issue), its application to SW Taiwan is uneasy mainly due to the small extension of the area, the lack of fields outcrop and the few geophysic evidences (no relief, few outcrops, lack of seismicity). Nevertheless Lu (1994, 1996) suggest to apply the phenomena to both side of the Taiwan orogen. More recently (Angelier et al. 1999; Lacombe et al. 2001) suggest a rigid blocks model where four blocks escape to the southwest along major structural discontinuities.

26.3 The Extrusion of SW Taiwan

Onshore seismic profiles have been shot in onshore SW Taiwan in the 50s and 60s. Few remain, apparently because of the difficult paper storage conditions under humid tropical climate. More recently, Suppe et al. (1985) and Yang et al. (2003) interpreted the Nanliao and Kuantzulin structures as underlain by stacking antiform and duplexes. Huang et al. (2005) also proposed a new structural interpretation of SW Taiwan, proposing a "triangle or thrusting wedge model" for the geometry of this complex area. Comparing two NW-SE offshore seismic sections and a single onshore seismic section and the corresponding line drawing interpretations, they suggested the presence of a "propagating intercutaneous nappe".

Despite the interest of such 2D structural approaches, due to the obliquity of the belt, major lateral component of the displacement exist so 3D representation was missing. This component is however clearly evidenced by both the GPS measurements (Yu et al. 1997), and the DinSAR results (Deffontaines 2000, 2004, 2005; Fruneau et al. 2001; Pathier et al. 2003; Mouthereau et al. 2003) and confirmed by "microtectonic" analyses in the field (Angelier et al. 2009). The work by Huang et al. (2005) thus provides a good example of the intrinsic limitations of the 2-D seismic interpretations when the deformation is 3-D in nature. Is worth noting that in a context where strike-slip and oblique

components of deformation play an important role geometrical pitfalls affect, and biased structural constraints may result from, balanced geological cross-sections. To summarise, except where structures and motion vectors have a common vertical plane of symmetry, structural reconstruction is a typical 3-D task and can hardly be resolved using 2-D means. This is the case in SW Taiwan. The aim of this contribution is therefore to use marine data with a variety of seismic profiles trends, onshore field data and full consideration of the morphological features of structural significance on both sides of the shoreline.

From the geographic point of view, the onshore SW costal plain of Taiwan appears to be an alternance of NNE-SSW trending elongated topographic ridges and trough (clearly seen on the hypsometric image of the 40 m ground resolution DTEM (Deffontaines et al. 1997), interpreted as the erosional remnance of both harder and softer rocks toward the strong erosion that affect this muddy area. Therefore it is difficult from classical photo-interpretation to decipher the exact places of anticlines and synclines axes even looking at drainage anomalies following the Deffontaines and Chorowicz (1991) methodology. Studies in the fields were confirmed by existing accurate geological mapping done by CPC and the Geological survey of Taiwan (MOEA) which were of great help.

From the lithological point of view, the foreland sequence of SW Taiwan is composed of a more than 5 km very thick, massive and monotonous undercompacted mudstone (e.g. Chou 1991; Hsieh 1972; Lacombe et al. 2001; Brusset et al. 2003; Huang et al. 2005). etc. As shown for instance by the TN-1 wells, drilled in the northern part of the Tainan structure in 1968 and described by Hsieh (1972). Above the thick mudstones was recognized the "Tainan formation" composed of yellowish gray, very thin fine grained sands containing few fossils. Its lower part contains light gray fine grained sands with gray clay rich in mollusks. Then A formation which is composed of bluish gray mudstone intercalated with light gray, very fine grained calcareous siltstone which may be related to Erchunghi formation of northern Taiwan. Then develops the *Upper Gutingkeng* (gray sandy mudstone or sandy siltstone intercalated with gray muddy sandstone 700 m thick is equivalent of the upper part of the Cholan formation) and the *Lower Gutingkeng* formations (bluish gray massive mudstone, more than 3,800 m thick and corresponding to the Cholan formation in northern Taiwan), and ends the wells due to technical problems by the Niaotsui formation which is more than 300 m thick and consist of dark gray massive mudstone.

From the structural point of view, several major domains onshore and offshore (see Liu et al. 2005) were distinguished and highlighted by faults, whatever there activity, which are coarsely described below: The Tainan Basin (TB) is situated on the southern edge of the Eurasian continental plateau showing extensional features far from SW Taiwan and reactivated in a compressionnal environment close to the deformation front (Deffontaines et al. 1997; Lacombe et al. 1999, 2001; Mouthereau et al. 1996, 1999, 2001). His formation is due to the N–S stretching of the Eurasian margin in Middle Eocene to Oligocene time and to the NW-SE stretching due to the opening of the South China Sea. (2) The Pingtung Plain (PP) is situated in between the eastern low metamorphic Central Range bounded by the Chaochou fault (CCF) and the SW Foothills where the Kaoping river flows guided by a N–S elongated diapiric ridge (Huang et al. 2005), and at least the accretionnary prism Lundberg et al. (1991), and Reed et al. (1991) first described from seriated seismic profile (R/V Mona-Wave) the structure of the wide Manila accretionary prism close to Taiwan. *The deformation front (DF)* onshore Deffontaines et al. (1997) and offshore (Liu et al. 1997) is situated west of the Tainan ridge.

So after a global presentation of the analysed and interpreted data used first offshore, where we will focus on the two major structures that bounds the potential escape zone in order to retrace the arguments second we will look for onshore arguments using fieldwork, geodetic measurements and simologic approach, before the discussion, conclusion and perspectives (Figs. 26.1 and 26.2).

Difficulties occurred to interpret the geology at some places where submarine large erosion occur (the Penghu Canyon) and where steep slopes make structural interpretation difficult. However, these studies revealeds two major discontinuities: the Fangliao Fault Zone and the Young-An Fault Zone, shortly described below.

1. **The Fangliao fault zone and associated submarine landslides** Numerous marine surveys had been done close to the Hengchun peninsula and the topographic and geomorphic description of have already been done (You et al.). We herein interpret these data in terms of structural geology, proposing that a major left lateral strike-slip fault characterises the Fangliao canyon, as shown by the structural interpretation of the parallel seismic profiles illustrated below.

The detailed analysis of the bathymetry (data from Liu Char-Shine ad co-workers) provides evidence of two major landslides on the western flank of the Hengchun peninsula. These sliding masses fill in the Fangliao canyon, inducing a typical "horse foot" trace in the bathymetry. They correspond to the sliding of the missing western flank of the anticline located west of Hengchun (see Fig. 26.3).

2. **The Yung-An Fault Zone and the Penghu canyon** Numerous seismic sections acquired during the Taiwan-France ACT survey crosscut the complex Penghu canyon. The seismic, 3,5 Khertz interpretation of this domain was difficult because of the presence of deep slopes and intense erosion of the complex Penghu
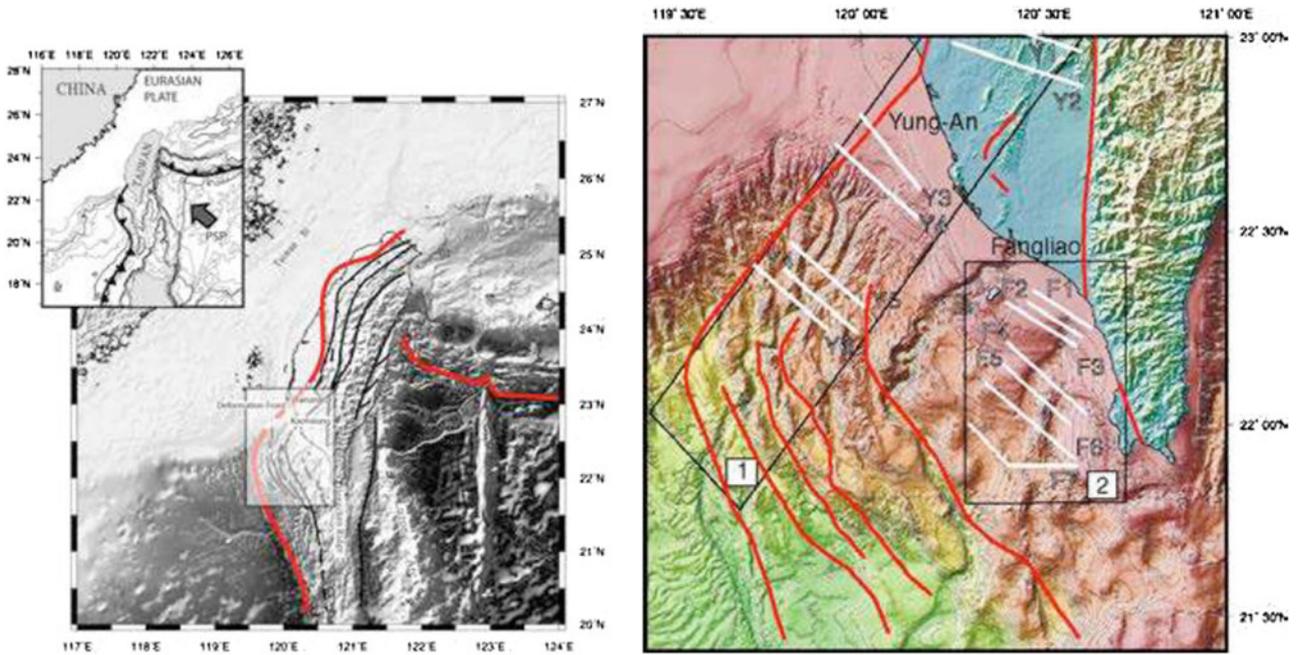
Fig. 26.1 Geodynamics of Taiwan and quadrangle location of studied area. **a** *Left* one may note the onshore-offshore situation of the studied area situated in the incipient collision zone (Lallemand et al. 1995) in between Manila subduction zone to the south and the collision zone onshore Taiwan. **b** *Right* location of the offshore seismic (sismic reflection profiles Fangliao fault zone (F1 to F7) from north to south respectively, Young-An fault zone: Y1 to Y5 from North to South also
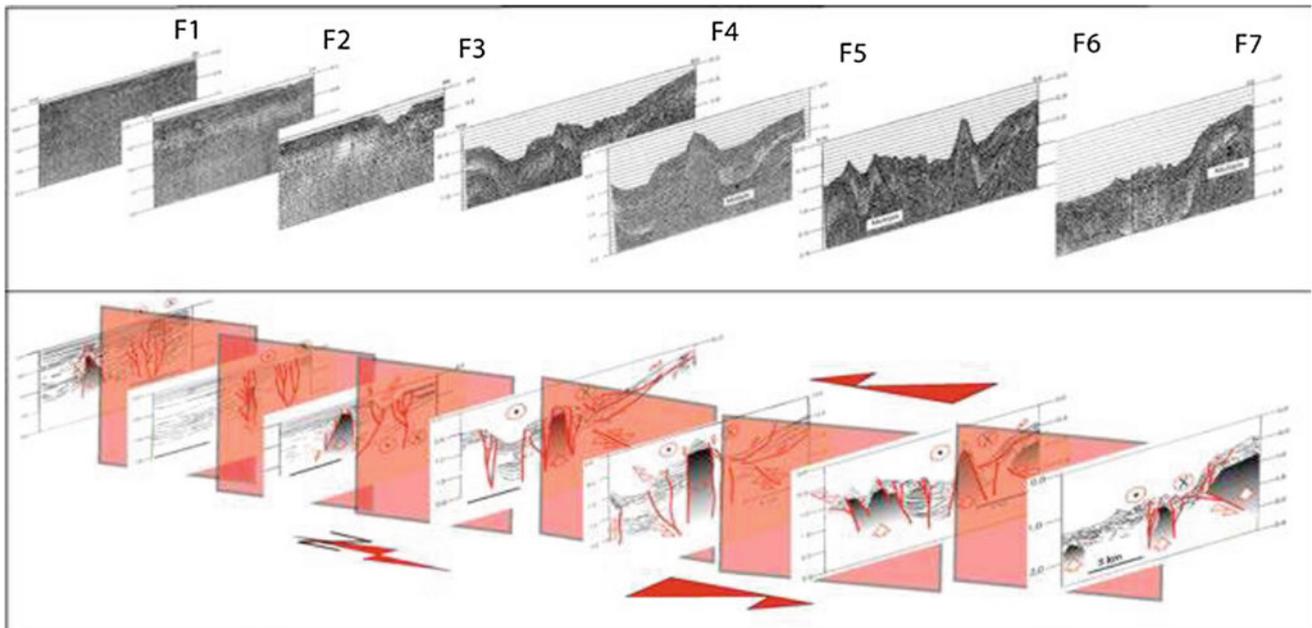
Fig. 26.2 The Fangliao left lateral fault zone SE boundary of the SW Taiwan extrusion. One may note the left lateral transtensive strike-slip fault zone which is injected by an elongated mud diaper south of the neutral zone (North to the *left*, *red lines* correspond to faults)

canyon system. Whereas a classical hill shading (see method described in Deffontaines et al. 1993) highlights NE-SW morphological discontinuities within the Manila accretionnary prism, the demonstration of the existence of a major structural discontinuity is given by the detailed seismic profile analysis and interpretation (especially location of faults, folds and dip of layers). Therefore, the Young-An fault zone appears to be a positive flower
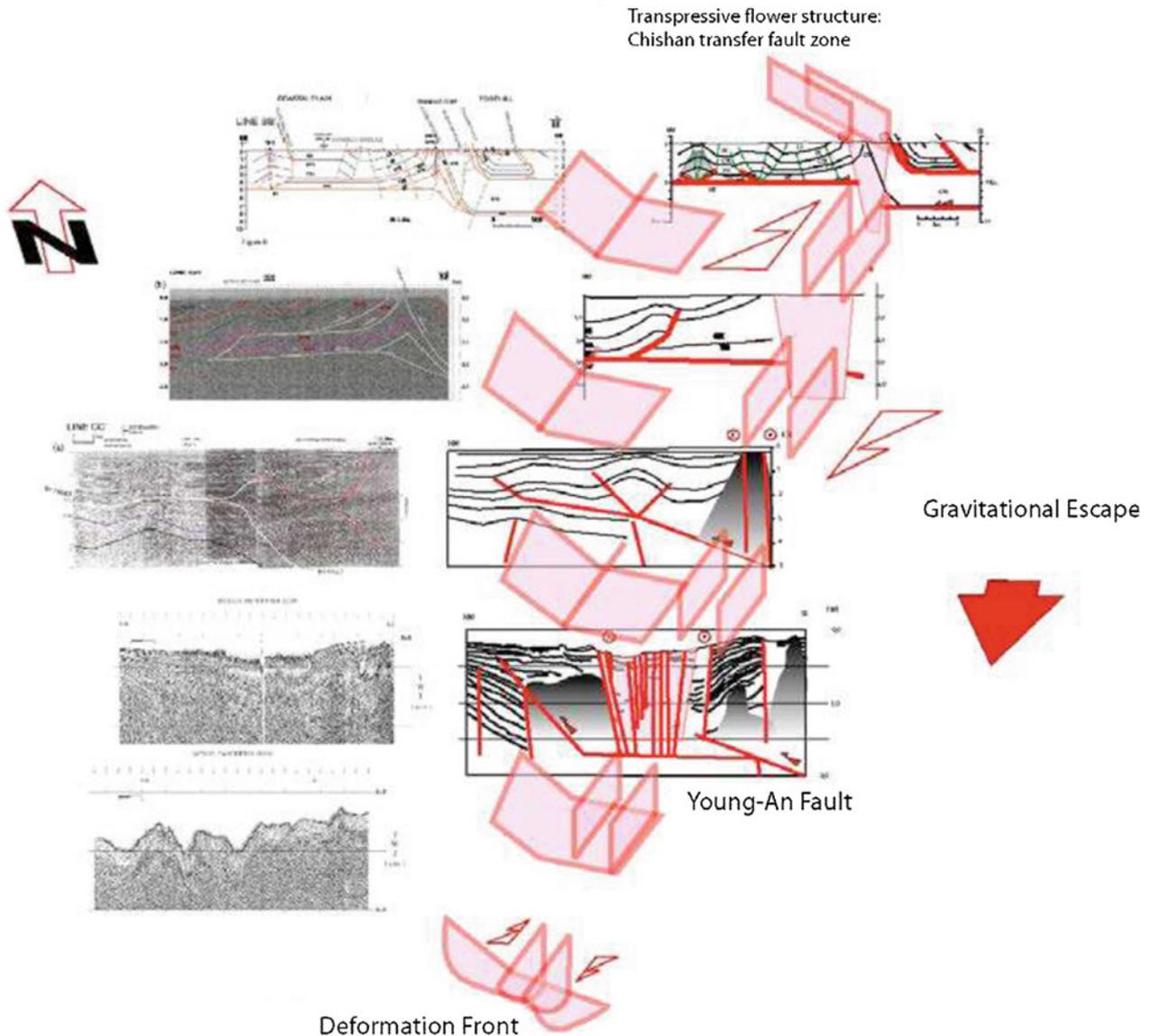
Fig. 26.3 The western boundary of the SW Taiwan extrusion: the Yung-An alignment (Transfer, vs. strike-slip, and role of the erosion) that correspond to tectonic partitioning

structure marked locally by an elongated pressure ridge above the fracture zone. This major fault zone is right-lateral, as shown by the numerous offset of folds on both sides of it. Also note that its displacement at depth, close to the deformation front, is less important than the displacement close to the shoreline, because of reactivation during the geological evolution (Figs. 26.4 and 26.5).

From the GPS point of view, In the first approximation, rather than involving heterogeneous displacement, the interseismic deformation of the Pintung basin mainly consists of a relatively continuous deformation, as shown by the surprisingly regular pattern of displacement data recorded at numerous GPS stations. The offshore boundaries of the basin however corresponds to two major structural discontinuities, the Fangliao canyon that we interpret as a major left-lateral fault zone (associated with submarine landslides affecting the western flank of Hengchun anticline, west of the peninsula) and the Young-An fault zone that we interpret as the major right-lateral fault zone facilitating the offshore extrusion of the Pintung basin. We suspect the existence of another right-lateral fault zone northwest of the YAFZ, which would affect the Penghu canyon as marked by submarine drainage anomalies. These major offshore fault zones are not well-preserved onshore, which is not surprising in light of the active erosion of SW Taiwan and of the soft lithology in the studied area. Numerous hazards are related

Fig. 26.4 Thrusting component in the concrete dyke close to the Tsenwenghsi (river), the shortening is clearly seen by the pipe completely squeezed within the thrust fault plane (B. Deffontaines slide)

Fig. 26.5 General deformation model of the SW Taiwan
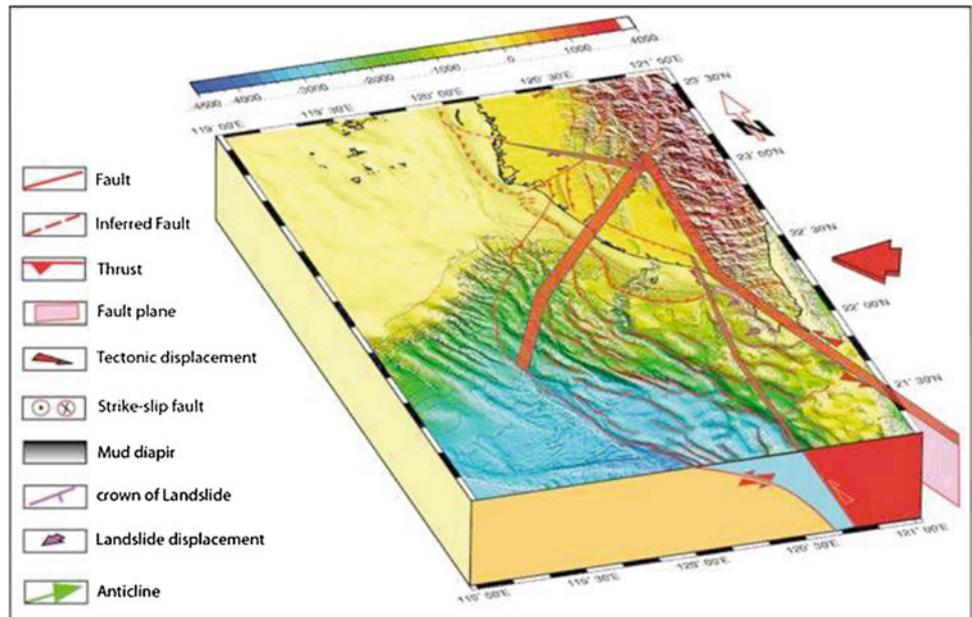
to these major structural fault zones, including possible earthquakes (despite the seismic gap or lack of present earthquake activity) and tsunamis that could be triggeres by submarine landslides such as those evidenced close to the Hengchun peninsula or above the deformation front (Deffontaines et al. 1999).

26.4 Discussion and Conclusion : The Model of Extrusion of SW Taiwan

Several structural key points arises resulting of our study in the SW Taiwan: The backstop (eastern boundary correspond to the Chaochou fault the indentor is the Peikang high and the western boundary that correspond to the continental slope of the eurasian plate and the Tainan basin. Highlighted by the shelf break before the erosion by the Penghu canyon. The relative sismic gap is linked to the soft marly gutingken formation that gives a rather continuous deformation at the surface revealed by both the interferometric wok as well as the GPS data.

The two lateral boundaries of this SW Taiwan extrusion are to the west the Young-An fault zone ending in the city of Chishang onshore which act as a triple junction. The Fangliao/chaochou onshore split offshore into two distinct major fracture zones the fangliao canyon and the Hengchun fault.

The mud diapirs offshore (Liuchyu island act as grabens that parallel to the extrusion displacement which highlight the transtensive component of the deformation. The neutral zone correspond to the Fengshan transfer fault zone already described by Deffontaines et al. 1993 and 1999. This fault correspond to a graben like structure which differenciate two distinct tectonic domain a transpressive one on the NE and a transtensive one in the SW. Many perspectives arise in terms of gas hydrates as soon as the structural geometry is much better know in that place.

References

Angelier J, Barrier E, Chu HT (1986) Plate collision and paleostress trajectories in a fold-thrust belt: the Foothills of Taiwan. Tectonophysics 125:161–178

Angelier J, Chu HT, Lee JC (1997) Shear concentration in a collision zone: kinematics of the Chihshang Fault as revealed by outcropscale quantification of active faulting, Longitudinal Valley, eastern Taiwan. Tectonophysics 274:117–143

Angelier J, Yu SB, Lee JC, Hu JC, Chu HT (1999) Active deformation of Taiwan collision zone: discontinuities in GPS displacement field. In: Proceedings of the international symposium on Subduction et collision active dans le SE asiatique, Fourth colloquium on sino-French cooperation program in Earth sciences, Montpellier, France

Biq C (1976) Western Taiwan earthquake-faults as miniature transform faults. Bull Geol Surv Taiwan 25:1–8

Biq C (1989) The Yushan-Hsuehshan megashear zone in Taiwan. Proc Geol Soc China 32:17–20

Bonilla MG (1975) A review of recently active faults in Taiwan. USGS Open-report, pp 1–55 (75-41)

Bonilla MG (1977) Summary of quaternary faulting and elevation changes in Taiwan. Mem Geol Soc China 2:43–56

Byrne T, Crespi J, Pulver M, Spiker E (1999) Deformation of the Taiwan hinterland: strike-slip faulting, extrusion or both? In: Proceedings of the international symposium on subduction et collision active dans le SE asiatique, Fourth colloquium on sino-French cooperation program in Earth sciences, Montpellier, 9–12 May 1999

Chen H (1984) Crustal uplift and subsidence in Taiwan: an account based upon retriangulation results. Spec Publ Central Geol Surv 3:127–140 (in chinese)

Davis D, Suppe J, Dahlen FA (1983) Mechanisms of fold-and-thrust belts and accretionary wedges. J Geophys Res 88(B2):1153–1172

Deffontaines B, Lee JC, Angelier J, Carvalho J, Rudant JP (1994) New geomorphic data on Taiwan active orogen: a multisource approach. J Geophys Res 99(B8):20243–20266

Deffontaines B, Lacombe O, Angelier J, Chu H-T, Mouthereau F, Lee C-T, Deramond J, Lee J-F, Yu M-S, Liew P-M (1997) Quaternary transfer faulting in Taiwan Foothills: evidence from a multisource approach. Tectonophysics 274:61–82

Deffontaines B, Liu C-S, Angelier J, Mouthereau F, Lacombe O (1999a) Quaternary tectonic evolution of offshore SW Taiwan. In: Proceedings of the international symposium on Subduction et collision active dans le SE asiatique Fourth colloquium on sino-French cooperation program in Earth sciences, Montpellier, 9 ± 12 May 1999

Deffontaines B, Chu H-T, Angelier J, Lee C-T, Mouthereau F, Li F-C, Brusset S, Chang C-P, Sibuet J-C, Chang T-Y, Lacombe O, Liu C-S, Deramond J, Lee J-C, Lu C-Y, Hu J-C, Yu M-S, Lee J-F, Bureau D (1999b) Onshore ± offshore Taiwan earth science data base within a geographical information system. In: Proceedings of the international symposium on Subduction et collision active dans le SE asiatique, Fourth colloquium on sino-french cooperation program in Earth sciences, Montpellier, 9–12 May 1999

Fruneau B, Pathier E, Raymond D, Deffontaines B, Lee CT, Wang HT, Angelier J, Rudant JP, Chang CP (2001) Uplift of Tainan foreland (SW Taiwan) revealed by SAR interferometry. Geophys Res Lett 28:3071–3074

Fuh S-C, Liu C-S, Wu M-S (1997a) Migration of the Canyon systems from Pliocene to Pleistocene in area between Hsyning structure and Kaoping slope and its application for hydrocarbon exploration. Pet Geol Taiwan 31:43–60

Fuh S-C, Liu C-S, Lundberg N, Reed D (1997b) Strike-slip faults offshore southern Taiwan: implications for the oblique arc-continent collision processes. Tectonophysics 274:25–39

Ho CS (1986) A synthesis of the geologic evolution of Taiwan. Tectonophysics 125:1–16

Hu JC, Angelier J, Yu SB (1997) An interpretation of the active deformation of southern Taiwan based on numerical simulation and GPS studies. Tectonophysics 274(1–3):145–169

Huang C-Y, Wu W-Y, Chang C-P, Tsao S, Yuan P-B, Lin C-W, Kuan-Yuan X (1997) Tectonic evolution of accretionary prism in the arc-continent collision terrane of Taiwan. Tectonophysics 281:31–51

Hung J-H, Wiltschko DV, Lin H-C, Hickman J-B, Fang P, Bock Y (1999) Structure and motion of the southwestern Taiwan fold-and-thrust belt. TAO 10(3):543–568

Hsu T-L, Chang HC (1979) Quaternary faulting in Taiwan. Mem Geol Soc China 3:155–165

Lacombe O, Mouthereau F, Deffontaines B, Angelier J, Chu H-T, Lee CT (1999) Geometry and quaternary kinematics of fold-and-thrust units of SW Taiwan. Tectonics 18(6):1198–1223

Lacombe O, Mouthereau F, Angelier J, Deffontaines B (2001a) Structural, geodetic and seismological evidence for tectonic escape in SW Taiwan. Tectonophysics 333:323–345

Lallemand SE, Tsien H-H (1997) An introduction to active collision in Taiwan. Tectonophysics 274:1–4

Lee TQ, Angelier J (1995) Analysis of magnetic susceptibility anisotropy of the sedimentary sequences in southwestern foothills of Taiwan and its tectonic implications. In: Proceedings of the International conference and Third sino-French symposium on Active Collision in Taiwan, Abstracts volume, 22–23 March 1995, Taipei, Taiwan, pp 213–218

Liu CS, Huang IL, Teng LS (1997) Structural features off southwestern Taiwan. Mar Geol 305–319

Lu CY (1994) Neotectonics in the foreland thrust belt of Taiwan. Petrol Geol Taiwan 29:15–35

Lu CY, Malavieille J (1994) Oblique convergence, indentation and rotation tectonics in the Taiwan Mountain belt: insights from experimental modelling. Earth Plan Sci Lett 121:477–494

Lu CY, Angelier J, Chu H-T, Lee J-C (1995) Contractional, transcurrent, rotational and extensional tectonics: examples from northern Taiwan. Tectonophysics 246:129–146

Lacombe O et al (2001b) Tectonophysics 333:323–345

Lu CY, Jeng FS, Chang KJ, Jian WT (1998) Impact of basement high on the structure and kinematics of the western Taiwan thrust wedge: insights from sandbox models. TAO 9(3):533–550

Lundberg N, Reed D, Liu C-S, Lieske J (1997) Forearc-basin closure and arc accretion in the submarine suture zone south of Taiwan. Tectonophysics 274:5–23

Mouthereau F, Angelier J, Deffontaines B, Lacombe O, Chu HT, Colletta B, Deramond J, Yu MS, Lee JF (1996) Cinematique actuelle et recente du front de chame de Taiwan. CR Acad Sci, t. 323, II, Paris, pp 713–719

Mouthereau F, Angelier J, Deffontaines B, Brusset S, Lacombe O, Chu H-T, Deramond J (1998) Folds and fault kinematics and tectonic evolution of the southwestern thrust belt of onshore Taiwan. In: Annual meeting of geological society of China, Chungli, 20–21 March 1998, p 140

Mouthereau F, Lacombe O, Deffontaines B, Angelier J, Brusset S (2001) Deformation history of the southwestern Taiwan foreland thrust belt: insights from tectono-sedimentary analysis and balanced cross-sections. Tectonophysics 333:293–322

Ratschbacher L, Merle O (1991) Lateral extrusion in the Eastern Alps, part 2: structural analysis. Tectonics 2:245–256

Rau RJ, Wu FT (1998) Active tectonics of Taiwan orogeny from focal mechanisms of small-to-moderate earthquakes. TAO 9:755–778

Reed D, Lundberg N, Liu C-S, Kuo B-Y (1992) Structural relations along the margins of the offshore Taiwan accretionary wedge: implications for accretion and crustal kinematics. Acta Geol Taiwan 30:105–122 (Science reports of the National Taiwan University)

Rocher M, Lacombe O, Angelier J, Chen H-W (1996) Mechanical twin sets in calcite as markers of recent collisional events in a fold-and-thrust belt: evidence from the reefal lime-stones of southwestern Taiwan. Tectonics 15(5):984–996

Sengor AMC, Gorur N, Saroglu F (1985) Strike-slip faulting and related basin formation in zones of tectonic escape: Turkey as a case study, vol 37. SEPM Special Publications, pp 227–264

Seno T, Stein S, Gripp AE (1993) A model for the motion of Philippine Sea Plate consistent with NUVEL-1 and geological data. J Geophys Res 98:17941–17948

Sun SC, Liu CS (1993) Mud diapirs and submarine channel deposits in offshore Kaohsiung-Hengchun, southwest Taiwan. Petrol Geol Taiwan 28:1–14

Suppe J (1984) Kinematics of arc-continent collision, dipping of subduction, and back-arc spreading near Taiwan. Mem Geol Soc China 4:67–90

Suppe J, Hu CT, Chen Y-J (1985) Present-day stress directions in western Taiwan inferred from borehole elongation. Petrol Geol Taiwan 21:1–12

Tapponnier P, Peltzer A, Le Dain Y, Armijo R, Cobbold P (1983) Propagating extrusion tectonics in Asia: new insights from simple experiments with plasticine. Geology 10:611–616

Teng LS (1990) Geotectonic evolution of late Cenozoic arc-continent collision in Taiwan. Tectonophysics 183:57–76

Tsai Y-B (1986) Seismotectonics of Taiwan. Tectonophysics 125: 17–37

Wu F, Rau R-J, Salzberg D (1997) Taiwan orogeny: thin-skinned or lithospheric collision? Tectonophysics 274:191–200

Yeh YH, Barrier E, Angelier J (1991) Stress tensor analysis in the Taiwan area from focal mechanisms of earthquakes. Tectonophysics 200:267–280

Yu SB, Chen HY (1996) Spatial variation of crustal strain in the Taiwan area, Sixth Taiwanese geophysical meeting, Chiayi, November 1996, abstract volume, pp 659–668

Yu SB, Chen HY (1998) Strain accumulation is Southwestern Taiwan. TAO 9(1):31–50

Yu S-B, Chen H-Y, Kuo L-C (1997) Velocity field of GPS stations in the Taiwan area. Tectonophysics 274:41–59

Yu S-B, Kuo L-C, Punongbayan RS, Ramos EG (1999) GPS observation of crustal deformation in the Taiwan-Luzon region. Geophys Res Lett 26(7):923–926

Active Tectonic Risk Assessment—Problems with Soil and Soft Sediment Deformation Structures

Philip E.F. Collins

Abstract

Many sites feature soils and sediments that have undergone syn- or post-depositional deformation. Typical forms of deformation include load casts, wedges, involutions and diapirs. In studies on geologically-young (Quaternary) soils and sediments in much of northwest Europe and some other areas, such forms are frequently attributed to the former action of non-glacial freezing and thawing during past cold periods. Similar features are found in arctic and high altitude areas. They are used to help reconstruct past climate and associated ground thermal regimes, including the extent of permafrost. The identification of the features as being relict with a low likelihood of such intense freeze-thaw processes being replicated has implications for site risk assessment and, consequently, design. Features that reflect syn- or post-depositional deformation elsewhere in the world, or in pre-Quaternary rocks, are frequently attributed to strong ground motion, and are used to help reconstructed past earthquake histories, both for regions and for individual potentially-active tectonic structures. There are direct implications for risk assessment and design. In theory, since the processes related to ice growth/decay and cyclic ground motion might be expected to be different, it should be possible to differentiate between them using diagnostic criteria. Unfortunately, either because different researchers are unconsciously biased by their training (perhaps causing the difference in interpretation depending on geographical region and the age of the features), or because the criteria are inadequately defined and are equally applicable to different processes, problems remain for fully understanding site risk. This paper compares the current state of diagnostic features used for interpreting deformations and uses these to explore possible interpretations and implications of a range of features found in apparently 'cryogenic' and 'palaeoseismic' settings. It ends with a call for a renewed focus on developing a robust and testable diagnostic toolkit for site investigation of soil and soft sediment deformation structures so that the features can be understood in terms of either "fossil" ice processes or active tectonic risk.

P.E.F. Collins (✉)
Brunel University, Kingston Lane, Uxbridge, London,
UB8 3PH, UK
e-mail: philip.collins@brunel.ac.uk

27.1 Introduction

Unexpected ground conditions are a major area of risk for construction and infrastructure management. Frequently, carefully executed site investigation can successfully identify difficult ground and provide a framework for mitigation. A limitation can, however occur, where subsurface features are unclear, ambiguous, or where the investigator has limited experience of differentiating apparently similar features. Soft sediment and soil deformation structures are a good example of this as they may be missed in typical borehole and trial pit sampling. The deformation mechanism can also be difficult to determine. Finally, the investigator may interpret deformation features based on prior experience, and education.

A better understanding of soft sediment deformation structures is needed as this will permit both a better understanding of long term risk (e.g. do the structures represent potentially active or relict soil processes), and current ground conditions (e.g. different processes may create different three dimensional structures that may affect macro-scale shear, consolidation and drainage).

27.2 Potential Causes of Soft Sediment and Soil Deformation Structures

A wide range of processes are known to create deformation structures. These include sub-marine slumps, glacial action, burrowing by animals, roots, freeze-thaw and earthquakes. The last two will be considered here as they can both potentially affect large areas and, as discussed below, can produce similar features. Interestingly, the they also link to two groups of investigators—those educated principally in the impact of climate change (particularly former periglacial conditions), and those educated in seismic impacts.

As soil temperatures pass below 0 °C, the soil water progressively freezes, resulting in compression and heave. Localised variability is caused by soil materials with different thermal properties, and varying amounts of water. Very low temperatures can cause a reversal of the ice expansion, inducing tension, and sometime cracking. As soil thaws, localized settling may occur, associated with plastic creep. High porewater pressure may be induced by the downwards migration of a freezing front, or by rapid thaw. This can induce liquefaction.

During a seismic event, horizontal and vertical pressure waves can result in oscillations between compression and tension. Dry soil may crack, buckle or disintegrate. Wet soil may plastically deform, shear or liquefy. This is particularly the case during larger magnitude events, and where a cohesive surface layer prevents the rapid vertical release of porewater.

27.3 Comparison of Selected Soft Sediment and Soil Deformation Features Attributed to Periglacial and Seismic Action

One of the most commonly-cited criteria to differentiate periglacial and seismic deformations is geographical extent. If cold climate conditions were responsible, then similar forms should, in principle, be found across a broad region. In reality, the formation of deformations by frost action is dependent upon the type of soil/sediment, water availability and local variations in geothermal flux. Theoretically, at least, deformations with a seismic origin should be focused around the responsible faults, with a change in deformation style away from the epicenter. Again, exactly what deformation occurs is determined by factors such as event magnitude/depth, plasticity, liquefaction potential and depth of burial. Ambreysis (19xx) found evidence for liquefaction many tens of kilometres from fault ruptures.

As a result, it is sensible to consider whether the detailed form of deformation structures can be used to differentiate causal mechanisms. In theory, different rates and directions of deformation should be associated with freeze-thaw and shaking. Unfortunately, a comparison of deformation features described in the scientific literature indicates a significant amount of overlap. Some examples of these are given in Table 27.1.

27.4 A Quaternary Case Study from South-Central England

Mid-Quaternary fluvial sands and gravels, unconformably resting on moderately permeable Eocene sands underlie an almost flat river terrace at Eversley Common, Hampshire, UK. The site occurs beyond the maximum glacial limits and will have experienced repeated cold-warm climate shifts

Table 27.1 Selected deformation structures attributed to periglacial and seismic processes

Periglacial		Seismic	
Form	Process and key features	Form	Process and key features
Vertically oriented clasts	Differential freeze-thaw heave between a clast and the soil/sediment matrix leading to vertical movement and alignment. May occur at a uniform depth across a unit/site	Aligned clasts	Clasts aligned to flow of liquefied material. Localised
Fissure fill/ Sediment wedge	Gravity driven (i.e. downwards) infilling of thermal contraction or mass movement-induced fissure. Typically wider at top. May show stratification	Dyke—Neptunian (formed under water)/Fissure fill (sub-aerial)	Gravity driven (i.e. downwards) infilling of seismically-induced fissure. Typically wider at top. May show stratification
		Dyke—injection	Pore fluid pressure driven infilling of fissure (principally upwards). Typically narrower at top. Particles may be graded (fining up)
		Sill—injection	Pore fluid pressure driven infilling of fissure (principally lateral)
Flame structures	Plastic upwards deformation under cyclic freeze-thaw stress	Diapiric structures	Plastic upward deformation under seismic load stress. Grades into injection dykes if soil/sediment becomes fully liquefied. Reflects deeper unit having a lower dynamic viscosity than overlying soil/sediment. Margins may feature micro-faults, with upwards displacement. Adjacent areas may show evidence of subsidence
Load cast, pillow structures	Isolated mass of sediment that has sunk into an underlying unit that has experienced freeze-thaw induced plastic deformation, liquefaction and/or localised consolidation producing density changes. Range of sizes (<cm to >m)	Load cast, pillow structures	Isolated mass of sediment that has sunk into an underlying unit that has experienced hydro-plastic deformation, liquefaction and/or localised consolidation due to cyclic shear density changes. Range of sizes (<cm to >m).
Involutions	Plastic deformations resulting from ice growth and decay. May also result from rapid thaw settlement and liquefaction	Sismoslump/ Involutions	Convoluted sedimentary structures reflecting in situ deformation due to cyclic lateral seismic loading. Under and overlying strata may be intact or show grading (increasing deformation towards surface). Structures may show no sign of compression due to subsequent burial

over ∼0.5–0.6 Ma. It is also close to the Variscan Front, a major East-West fault zone that runs approximately parallel to the former ice maximum limit (Fig. 27.1). Only one nearby small historical earthquake is known (Musson 1994).

Soft-sediment deformation structures at the site, including load casts, flames/diapirs, possible dykes, homogenites, oriented clasts and 'kink' structures. A boudinage-like structure indicative of high pore-water pressure and lateral migration was observed in one exposure (Fig. 27.1). In some exposures, there is evidence for an initial significant deformation event or phase, with later modification by slowly acting processes, including limited vertical realignment of stones.

If periglacial action was responsible for the larger structures, their large size suggests a deep seasonal thaw layer. Regional permafrost has been hypothesized (Hutchinson and Thomas-Betts 1990), though there is no unambiguous local evidence for its presence. If it was present, this might explain features that would require a reduction in the permeability of the underlying Tertiary sands.
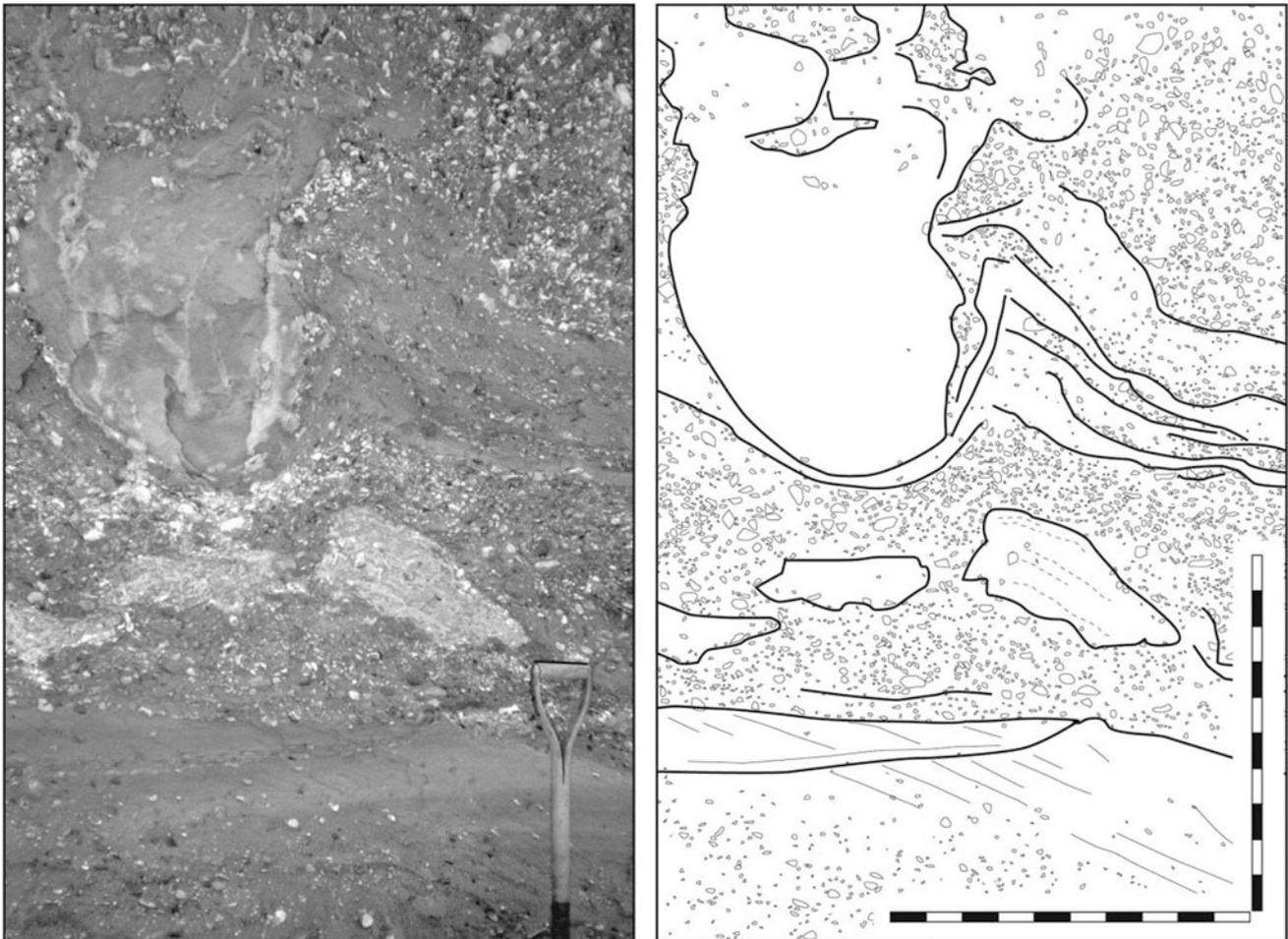
Deformed ground from a Quaternary fluvial site in south-central England

Fig. 27.1 Soft sediment deformation structures, Eversley Common, UK. Note load cast, 'boudinage-like' structure and angular 'kink'

The absence of significant historical seismicity might suggest an earthquake origin is unlikely. However, the deformations are large and, if they are seismically-formed, would represent a large and perhaps infrequent event. In addition, the 'kink' structure shown in Fig. 27.1 may indicate abrupt compression occurring above a partially liquefied layer. This raises the probability of a large seismic event affecting the site at some point in the past, though does not necessarily disprove a periglacial hypothesis.

27.5 Conclusions

The apparent similarity of soft sediment and soil deformation structures presents a significant challenge for site (and indeed regional) risk assessment. Careful examination may allow causes to be determined, but site investigators need to be aware of the bias introduced by their own training. Significant problems exist if the evidence is in the form of

narrow borehole records and samples, especially if the samples are disturbed.

Further work is needed on deformation structures. In particular, robust criteria for differentiating rapid and slow deformation in different types of material need to be developed.

References

Hutchinson JN, Thomas-Betts A (1990) Extent of permafrost in southern Britain in relation to geothermal flux. Q J Eng GeolHydrogeol 23:387–390

Musson R (1994) A catalogue of British earthquakes. BGS technical report no. WL/94/04

Formation of Earthquake Faults by the Fukushima Hamadori Earthquake and an Estimation of Displacement Distribution Around the Faults Using Airborne LiDAR Data

28

Shunsuke Shinagawa, Shuji Anan, Yasuhito Sasaki, Sakae Mukoyama, Shin-ichi Homma, and Yoko Kobayashi

Abstract

A series of earthquake faults was produced by the 2011 Fukushima Hamadori Earthquake (Mw 7.1), which broke out one month after the Great East Japan Earthquake. Two lines of earthquake faults appeared extending 30 km in length. They were inferred to be located partly on the active faults and partly on its extended line. The purpose of this presentation is to analyze these faults. We made use of a new method of airborne LiDAR data in the investigation of the displacement distribution by the earthquake. The results obtained fit generally well with the distribution data of net fault displacement produced by field investigation. Furthermore, the results suggest that the earthquake caused block tilting and land subsidence. Our new method makes available information difficult to obtain by the conventional method of field research of displacement distribution and it is useful for investigation immediately after the earthquake.

28.1 Introduction

The Fukushima Hamadori Earthquake occurred on April 11, 2013, one month after the Great East Japan Earthquake of March 11. It formed earthquake faults near the Itozawa Fault (14.7 km in length) and Yunodake Fault (15.8 km in length). At the Itozawa Earthquake Fault, which is situated near the hypocenter, the maximum vertical displacement is 220 cm, while at the Yunodake Earthquake Fault which is farther from the hypocenter, it is 80 cm (e.g. Toda and Tsutsumi 2013).

The earthquake faults actually appeared not where they were assumed to be by the past topographical interpretations. Thus improving the accuracy of active fault survey methods is now an imminent task for the applied geological research. It is necessary to confirm the location of emerged earthquake faults to compare with the results of various other survey methods.

In order to estimate the locations where earthquake faults would emerge, and the magnitude of displacement which they would cause, investigation is generally done in situ, but this method is extremely time-consuming and costly. In recent years, however, airborne LiDAR surveying has pervaded rapidly. It is now possible to make use of this technology for our purpose doing the measurements before and after an earthquake. In this research, first, DEM differential analysis was conducted making use of LiDAR surveys performed at two different times, before and after the earthquake, and the earthquake fault displacement distribution was assumed. Then the data were compared with the in situ survey results; the effectiveness of the new method was verified.

S. Shinagawa (✉) · S. Anan · Y. Sasaki
Public Works Research Institute, Tsukuba, Japan
e-mail: sinagawa@pwri.go.jp

S. Mukoyama · S.-i. Homma · Y. Kobayashi
Kokusai Kogyo Company Limited, Tokyo, Japan

28.2 Differential Analysis of Results of the Two Airborne LiDAR Surveys

28.2.1 Principle and Method of the Differential Analysis

The value of difference of elevation can be easily calculated from bi-temporal DEM pair. However, in order to get the accurate distance and direction of the ground movement, it is necessary to obtain the three-dimensional locus of the point.

In this study, we applied the technique of image matching analysis to the measurements of the ground displacement (Japan Patent No. 4545219). Since the visual image is two-dimensional planar surface, and the directly measured distance is a horizontal element, the elevation value corresponding to each planar coordinate point has to be calculated by the three dimensional vector. However, because the image made from DEM has the elevation value at each grid point, the vertical component is available by interpolation of the DEM elevation value around the endpoint of the calculated vector. A remarkable advantage of this technique is that it does not require neither the measurement for mapping nor selection of specific characteristic for tracking. Moreover, random point cloud data provide with areal and spatial quantitative movement.

High resolution DEM that can be made of the airborne LiDAR survey is useful as it enables us to produce measurable image from a terrain model. In case there is a wide area crustal movement caused by an earthquake etc., to get more accurate ground displacement rate, it is necessary to obtain measurement data for correction. For a good image matching analysis, it is preferable that the image should show geomorphic quantity without the azimuthal anisotropy. The PIV method was selected for the image matching analysis in this study. The movement was identified by the image correlation, and the movement vectors were calculated by the average of several movement parts in the search area.

28.2.2 Measurement Precision and Precautions

For the images used in this study, 1 pixel is the single grid size of 2 m × 2 m DEM. And the search window size is 64 pixels × 64 pixels (128 m × 128 m). In image matching, sub-pixel interpolation was employed, so it is normally possible to calculate displacement of about 1/10 pixel size. Since 2 m

grid of topographical data was set to be 1 pixel, it is assumed that the reliable displacement is ±20 cm.

28.2.3 DEM Used for the Analysis

The research site covers the area where earthquake faults were formed by the Fukushima Hamadori Earthquake. The DEM used was 2 m grid data based on the airborne LiDAR data of before and after the Fukushima Hamadori Earthquake (Table 28.1).

28.2.4 The Impact of Wide Area Crustal Movement on DEM and Its Cancellation

In the study area, crustal movement caused by the Great East Japan Earthquake and the Fukushima Hamadori Earthquake overlaps. Therefore it is necessary to cancel the displacement caused by other than our target earthquake. No displacement data are available of the Great East Japan Earthquake of March 11, nor of the after slip from March 11 to April 11 when Fukushima Hamadori Earthquake occurred. Therefore a planar distribution model of displacement based on a primary polynomial approximation was prepared making use of the daily values at April 9, produced by three GNSS-based Control Stations around the survey region. The values of each grid provided by the model were assumed to be as the sums of the displacement caused by the earthquake of March 11 and the after slip during the period from March 11 to April 11.

28.2.5 Analysis Procedure

(1) Displacement distribution before and after the earthquake

First, shaded slope maps before and after the earthquake were prepared making use of DEM. Then horizontal displacement was obtained for each 128 m^2 area by image matching analysis, and the difference of average elevations of matched area was taken as the vertical displacement. The centers of the search windows were shifted in the south-north and east-west direction by 64 m each to draw the vectors of displacement (Fig. 28.1).

(2) Displacement distribution along the earthquake faults

In order to clarify the details of the displacement distribution across the earthquake faults, the differences between

Table 28.1 DEM used for the analysis

	Date of surveying	Grid size (m)	Note
Before the earthquake	Sep., 2006 to Feb., 2007	2	Taken by Kokusai Kogyo Co. Ltd
After the earthquake	May 11 to June 10, 2011	2	Provided by geospatial information authority of Japan[a]

[a] High precision elevation data for restoration and disaster prevention measurement
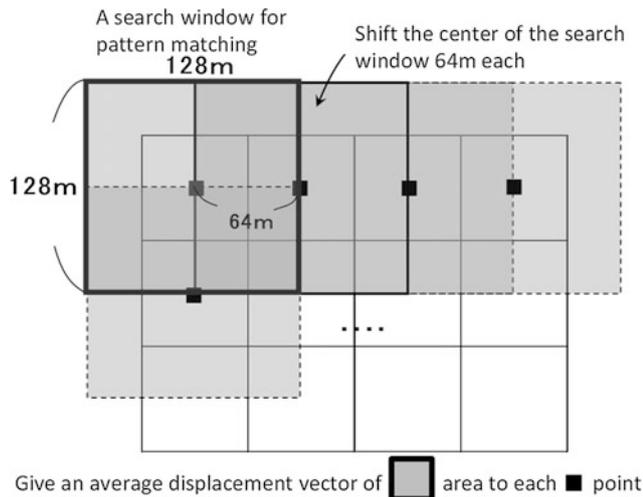
Fig. 28.1 The procedure to obtain the vectors of displacement (Shinagawa et al. 2013)

Fig. 28.2 The procedure to obtain the displacement values along the earthquake fault (modification of Shinagawa et al. 2013)

the two grids were sought, each covers the upheaved and subsided points with an earthquake fault in between. Given the displacement values of the measured point of 64 m mesh explained above as well as positional information of the measurement points, the displacement value of meshes including measuring points were given to each measurement point. The differential of the set of points 120 m apart straddling the fault line was presumed to be the earthquake displacement which was estimated by differential analysis (Fig. 28.2). Regarding the vertical displacements, the relative rise on the northeast side was given a positive value. As to the horizontal displacements at right angles with the strike of the faults (N55°W for the Yunodake Earthquake Fault and N20°W for the Itozawa Earthquake Fault), displacements were estimated by calculation. Positive values were given to the right lateral displacements and negative values to the left lateral displacements respectively.

28.3 Comparison of Results of Differential Analysis with Those of In Situ Survey

Figure 28.3 shows the vertical displacement distribution and horizontal displacement vector of the entire area covered by differential analysis.

28.3.1 Vertical Displacement

The comparison between the results of our study and those of in situ survey indicates that the area where vertical displacement was confirmed to have occurred conforms with the distribution of ground surface earthquake fault almost

exactly. By and large our estimates of vertical displacement give somewhat larger values than those of the in situ survey data.

Although our study site does not adequately encompass the earthquake affected area, our results suggest the land block enclosed by the Itozawa Earthquake Fault and the Yunodake Earthquake Fault has inclined to north-east. It also indicates that the land block has subsided remarkably on the west side of the Itozawa Earthquake. These observations are in harmony with those of the crustal movement study based on the interference SAR (Geospatial Information Authority of Japan 2011).

We see in Fig. 28.3 that subsidence has occurred in the distribution area of the valley bottom plain. Since alluvial deposits cover the valley bottom plains, it is possible that earthquake motion caused consolidation subsidence. The estimated subsidence varies from point to point as indicated in Fig. 28.3, but any subsidence greater than 20 cm was detected in this study.

28.3.2 Horizontal Displacement

In our study site, displacement from north-east to east-northeast is dominant. Estimated displacement near the electronic reference point conforms almost perfectly with the magnitude and direction of displacement that the Geospatial Information Authority of Japan measured immediately after the earthquake.

The horizontal displacement near Itozawa Earthquake Fault generally runs in the direction of east-northeast at right angle with the earthquake fault, but the direction and magnitude of land surface displacement change beyond the fault.

Fig. 28.3 Vertical and horizontal displacement distribution estimated by geomorphic image matching analysis using airborne LiDAR data before and after the 2011 Fukushima Hamadori Earthquake (modification of Shinagawa et al. 2013)
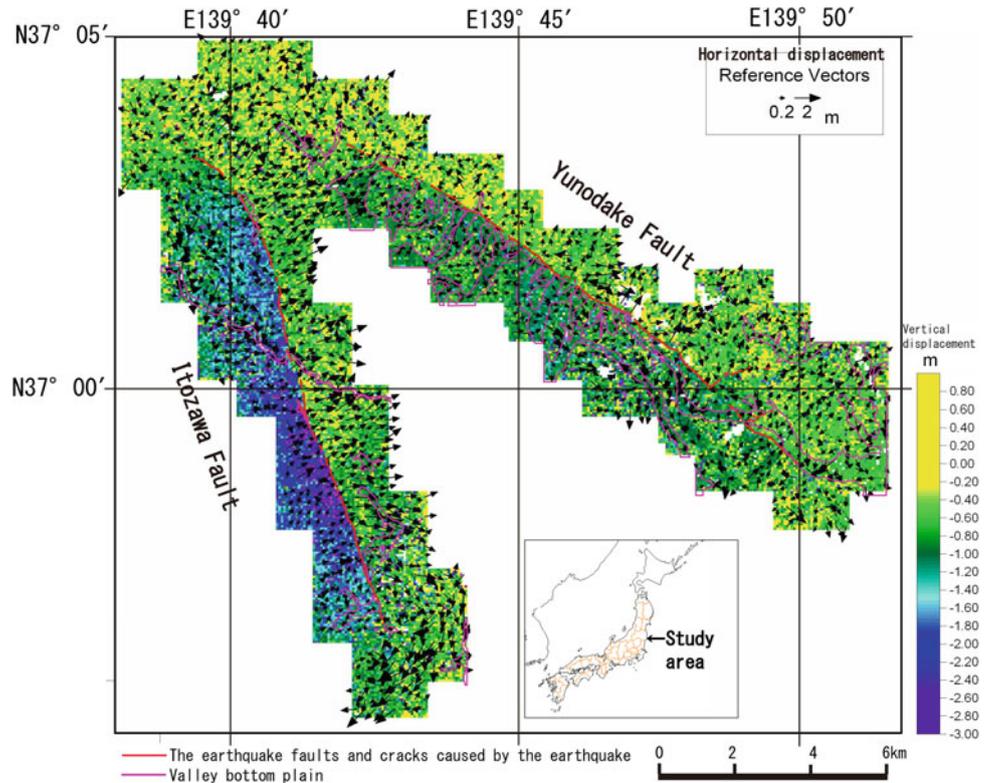
Near the south end of the Itozawa Earthquake Fault, there is a relatively large displacement band with a fixed width which runs in the direction of south–west. This band of displacement corresponds with the course of aircraft that performed the measurement before the earthquake. The fact that airborne LiDAR were performed at different times with this vicinity as the boundary of two surveys may suggest this unique trend was caused by an error in the process of amalgamating two different sets of data taken at different times.

28.3.3 Verification of the Results of Displacement Analysis of the Earthquake Faults

Figure 28.4 is an example (the vertical displacement of Idosawa Fault) of the results of differential analysis in comparison with those of in situ survey. The direction and magnitude of displacement in vertical as well as horizontal component vary greatly by the measured point. The moving average of the 1,000 m sections along the line of the fault

Fig. 28.4 The vertical displacement of the Itozawa Fault (Shinagawa et al. 2013)
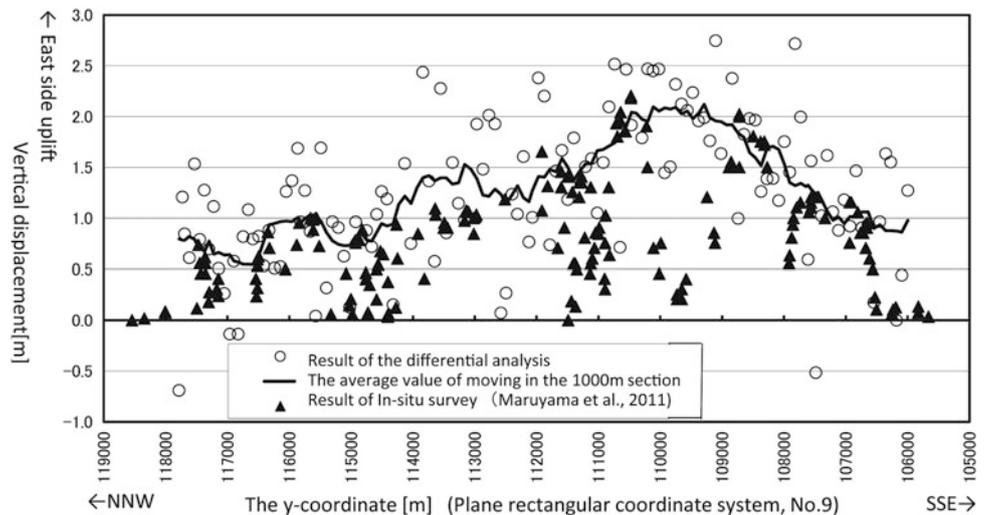
generally encompasses the values of the larger side of in situ survey data. In in situ surveys the measured value of displacement at the fault is taken as "displacement". However, since displacement of land near the fault often accompanies flexural deformation of land, in situ data tend to be underestimated. Take this into account the moving average of the 1,000 m sections would produce correction effect. There are cases where the data of in situ and differential analysis differ greatly. There are three possible factors that cause such large differences; first, the deformation occurred which did not accompany a clear earthquake fault. Second, the earthquake motion has caused ground settlement hence subsidence around the fault. Third, a matching error may have been caused by an incorrect identification in similar topographical sites.

28.4   Conclusion

The method of DEM differential analysis employed to investigate the earthquake faults caused by the 2011 Fukushima Hamadori Earthquake clearly indicates ground surface displacement distribution around the earthquake faults. However we need to cautiously exclude extreme values in the data. The specific causes of such extreme values are unknown.

The ground surface displacement data produced by the DEM differential analysis overlaps with the upper side of in situ measurement data. One advantage of the differential analysis is that it produces information with respect to a ground settlement phenomenon which accompanies not only fault displacement, but tilt motion and earthquake motion over the area. This is not available through the conventional in situ survey.

References

Geospatial Information Authority of Japan (2011) http://www.gsi.go.jp/cais/topic110425-index-e.html

Maruyama T et al (2011) http://unit.aist.go.jp/actfault-eq/Tohoku/report/idosawa/idosawa.pdf

Shinagawa S et al (2013) J Jpn Soc Eng Geol 53:271–281

Toda S, Tsutsumi H (2013) Bull Seis Soc Am 103:1584–1602

Applied Geology for Infrastructure Projects

Convener Eng Svetozar Milenkovic—*Co-convener* Zoran Berisavljevic

This session aims to enlighten and emphasize the importance of applied geology as the one of the key factors in rational designing and construction of large-scale infrastructure projects such as motorways and railways. Contributions should range over a wide spectrum of the applied geology involvement through development of site investigations and characterization, empirical and numerical modelling, presenting illustrative and innovative case studies of infrastructure projects, and to underline needs and benefits of cooperation between geologists and civil engineers, which seems to be the weakest link in the designing process. Whether it is needed to perform bearing capacity and settlement calculations, slope stability or some other analysis, particular emphasis is placed on determining appropriate soil and rock parameters as they are the basis of every geotechnical design. The experiences and lessons learnt from past projects are highly appreciated and warmly welcome in the session.

Field Monitoring of the Behavior of Pile-Net Composite Foundation in Oversize-Deep-Soft Soil

Yu-feng Wang, Qian-gong Cheng, and Jiu-jiang Wu

Abstract

For the observation of the behavior of the pile-net composite foundation in oversize-deep-soft soil, some cross sections in the Chaoshan railway station were selected for field monitoring. According to the recorded data, an analysis on the behavior of this structure was conducted with the following conclusions reached: (1) At the beginning of filling, the values of the earth pressure on pile tops and in the soil between piles both increased abruptly. And the growth rate of the earth pressure on pile tops is higher than that of soil between piles. When the depth of fill hits a certain value, the pile-soil stress ratio will reach its maximum value with an arching effect appeared. (2) As the increase of filling depth, pore water pressure increased with excess pore water pressure generated. After the filling, the distribution of excess pore water pressure disappeared gradually. (3) The axial force and the skin resistance of tube pile present a close relationship with the properties of each stratum. (4) The settlement value of each layer is also relevant to its depth and properties with its settlement ratio directly proportional to the increase of filling depth. (5) As the increase of filling depth, the tensile displacement of geogrid presents an increasing trend. The increase of the tensile displacement of geogrid in soil between piles presents a lag effect with its lag time about 50 days. (6) The generation of lateral displacement is accompanied with the filling of embankment. Nearer the surface, the value of lateral displacement was higher. And as the increase of depth, it decreased gradually. For different layers, the value of lateral displacement also varies.

Keywords

Oversize-deep-soft soil • Pile-net composite foundation • Field monitoring • Bearing capacity • Settlement characteristics

29.1 Introduction

Recent years, pile-net composite structure, as a new treatment technology, has been widely used in construction for its advantages. This technique emerged in the world since 1970s. However, the first theoretical study was just appeared in 1990,

Y. Wang (✉) · Q. Cheng (✉) · J. Wu
Department of Geological Engineering, Southwest Jiaotong University, Chengdu 610031, Sichuan, China
e-mail: wangyufeng1987118@126.com

Q. Cheng
e-mail: chengqiangong@home.swjtu.edu.cn

which is the present of the empirical formula of pile-soil stress ratio proposed by Jones et al. After then, Low et al. studied the arching effect of soil between piles and the effect of geogrid in theory and experiment (Low et al. 1994). The real sign for the worldwide usage of this structure should be the appearance of British Standard 8006 presented by the U.K. in 1995, which fills up the blank in the design of pile-net composite foundation. So far, the research of pile-net composite structure has achieved fruitful results (Helwany et al. 2003; Graeme et al. 2005; Huang et al. 2005; Abusharar et al. 2009). But, there is still no uniform cognition for the complex of this structure, especially in the usage of soft soil subgrade (Bergado et al. 2000; Han and Gabr 2002; Chen et al. 2008; Kousik 2010; Borges and Oliveira 2011).

Here, in order to learn the behavior of pile-net composite foundation in soft soil further, authors take the oversize-deep-soft soil (its area reaches 2.5×10^5 m^2) in the Chaoshan railway station as a case study to observe the deformation of foundation strengthened with pile-net composite structure. During the research, the field monitoring of the surface settlement, lateral displacement, pile-soil stress ratio, pore water pressure, axial load and skin resistance of tube pile, and stretching of the geogrid was conducted. And then, based on the analysis of these data, the bearing capacity and settlement mechanism of the pile-net composite foundation in oversize-deep-soft soil is discussed to provide insight into fundamental understanding of such cases.

29.2 Experiment Setup

29.2.1 Geological Background

The studied area locates at the Chaoshan railway station in Chaoan County, Guangdong Province. In this area, the strata are mainly composed of muck, muddy silty clay, and silty sand deposited in the alluvial-lacustrine (Q_4^{al}) and marine-continental (Q_4^{mc}) environment of the Quaternary, with high water content, high liquid limit, high compressibility, high porosity, underconsolidated, low strength, etc. So, the bearing capacity of this area is very poor. The detailed geological profile of the testing section and the CPT data are illustrated in Fig. 29.1.

29.2.2 Instrument Setup

According to the field condition, the section located at the mileage of DK207+373 was chosen for field monitoring. In this section, the soft soil foundation was strengthened with

tube piles (type: PHC 500 A 100-12; diameter: 0.50 m; thickness: 0.1 m; concrete grade: C60), pile caps, ground beams (adopted C35 concrete and were cast-in-place), cushions, and geogrids, as shown in Fig. 29.2. After the construction process of tube piles and ground beams, a ballast mattress layer with both geogrid layers interbedded was paved on the top. And the total thickness of this layer is 0.6 m. The relevant design value of bidirectional tensile strength of geogrides is 80 kN/m.

The filling process of this section was conducted from March 29 to April 27, 2010 with its final depth of fill reached 2.2 m. And the installation of the monitoring instruments, including earth pressure cells, wire stress gauges, displacement transducers, settlement gauges, inclinometers, and pore pressure gauges, is finished during the filling process. Figures 29.3 and 29.4 show the layout of each instrument. The information of the instruments is listed in Table 29.1.

29.3 Results and Discussion

29.3.1 Pile-Soil Stress Ratio

According to the monitoring data, the variations of the average earth pressures on the pile top and in the soil between piles were obtained (Fig. 29.5) with their ratio shown in Fig. 29.6. The monitoring began on March 15, 2010, and ended on October 9, 2010, lasting more than 6 months. From Figs. 29.5 and 29.6, the following trends were observed:

1. The distributions of earth pressure and pile-soil stress ratio can be divided into three stages as the variation of filling height.

The first stage is the construction period from March 15, 2010 to April 26, 2010. In this process, the earth pressure on pile top presents a gently linear increasing trend with its

Fig. 29.1 Geological profile of the testing section and the CPT data
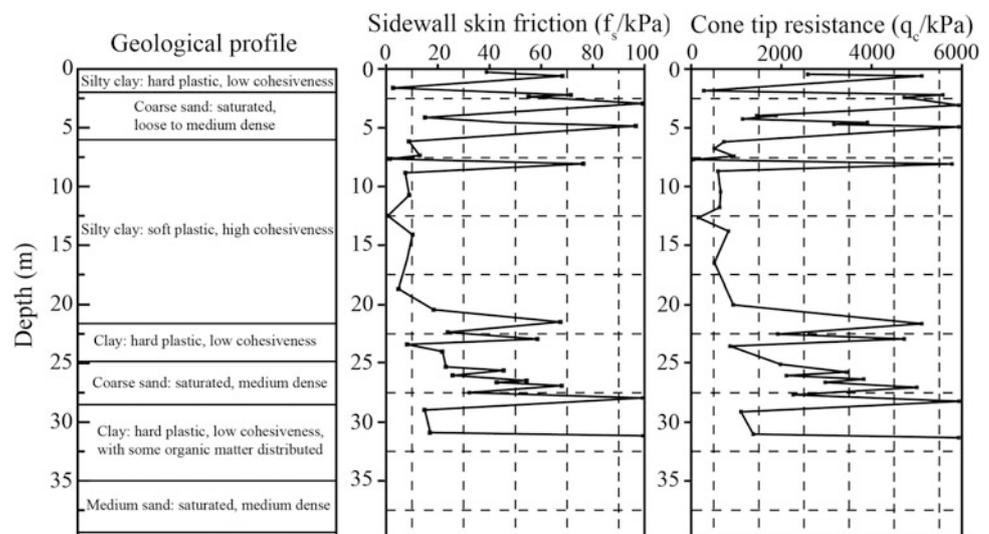
Fig. 29.2 Cross-sectional view
of the strengthening scheme (unit:
m)
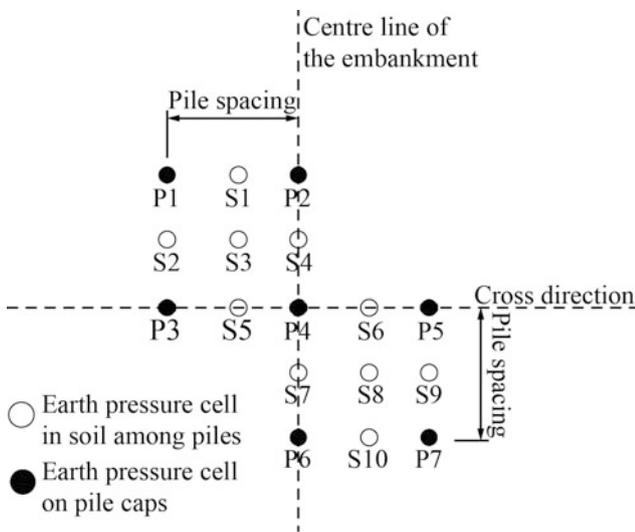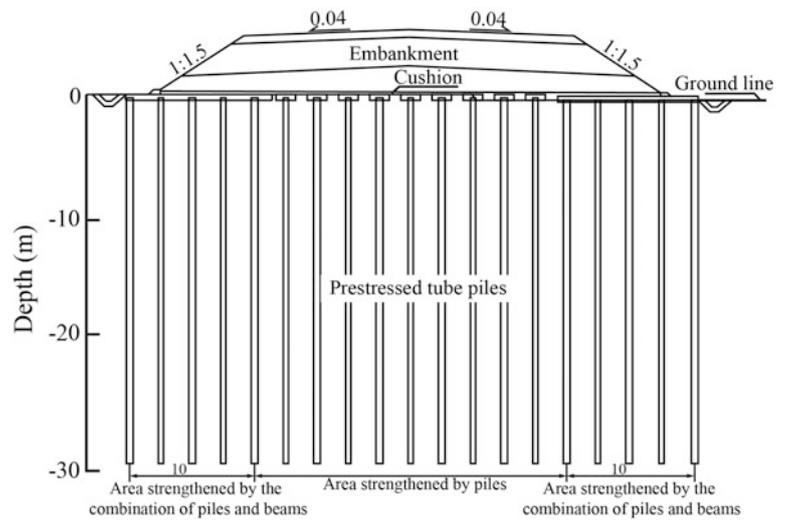
Fig. 29.3 Layout of the earth pressure cells

growth rate at 0.97 kPa/d during the first 15 days. From the
16th to the 42nd day, its growth rate increased to 1.75 kPa/d.
For the earth pressure in soil, it also presents an increasing
trend from the 1st to 37th days with its average growth rate
at 0.45 kPa/d. However, from the 38th to the 42nd days, the
earth pressure in soil presents a decreasing trend as the
increase of filling height, which may be induced by the
generation of soil arching effect. The pile-soil stress ratio
displays an increasing trend with its changing rate reached
0.09/d.

The second stage is the stabilization phase in the post
construction period, which lasts for 136 days. During this
stage, the earth pressure on pile top continued to increase
with its growth rate decreased to 0.197 kPa/d. The pressure
acting on the soil between piles continued to decrease at a
changing rate of 0.024 kPa/d. The pile-soil stress ratio still

shows an increasing trend with its increasing rate only being
0.017/d which is much smaller than that in the first stage.

The final stage lasted from July 19 to October 9, 2010,
which is the unloading process of construction. As the
excavation of the filled layer, the earth pressure and pile-soil
stress ratio both show a downward trend. However, during
the 194th to 203rd days, the pile-soil stress ratio increased
slightly due to the continuous adjustment of the cushions on
the load borne by piles and the soil between piles.

2. The earth pressure in soil between piles is much smaller
   than that on piles. After the filling, the pile-soil ratio was
   always larger than 1. At the end of the monitoring, it even
   reached 7.6, which indicates that soil between piles barely
   supports the load and the main load is borne by piles.
3. From Fig. 29.5, around on the 35th day of filling, the
   earth pressure in soil between piles reached its maximum
   value 0.1747 MPa, which indicates the generation of soil
   arching effect after this point. At the same time, the load
   borne by the soil between piles began to transfer to piles.
   The specific filling height is approximately 1.85 m, i.e.,
   the height of the soil arch is 1.85 m, a little larger than the
   theoretical value.

29.3.2 Pore Water Pressure

The monitoring of pore water pressure is from April 10 to
October 6, 2010. For comparison, data measured by PPG02–
PPG05 were plotted in Fig. 29.7a, and that from PPG9 and
PPG10 were plotted in Fig. 29.7b. Others were damaged
during the construction without data obtained.

As shown in Fig. 29.7, the followings can be obtained:

1. During the first 9 days from March 29, 2010, there is no
   obvious increase for pore water pressure as the increase
   of filling height.

(a)

(b)
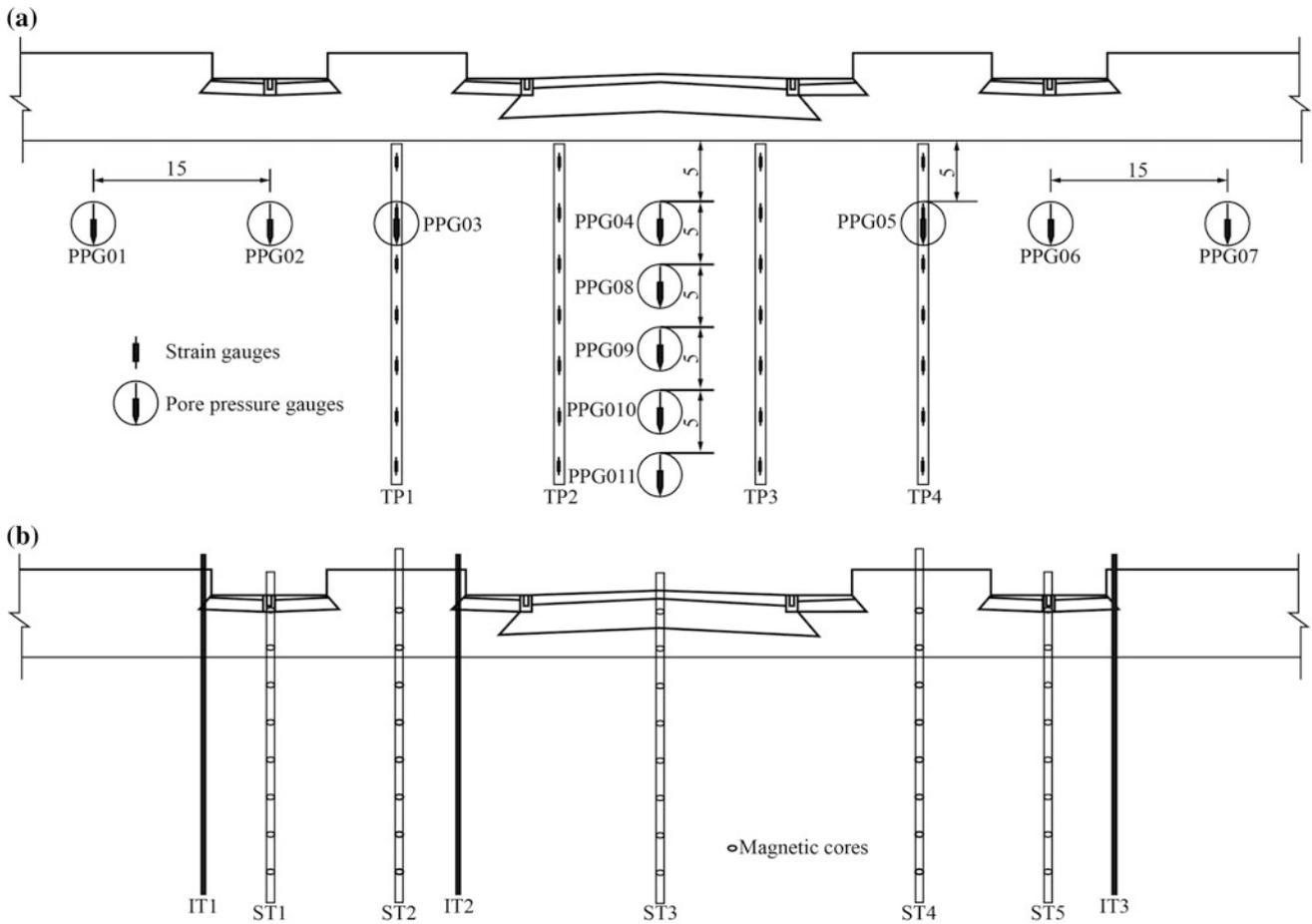
Fig. 29.4 Layout of the substructure instruments (unit: m). **a** Layout of the pore pressure gauges and the wire stress gauges, **b** Layout of the settlement tubes *ST* and the inclinometer tubes *IT*
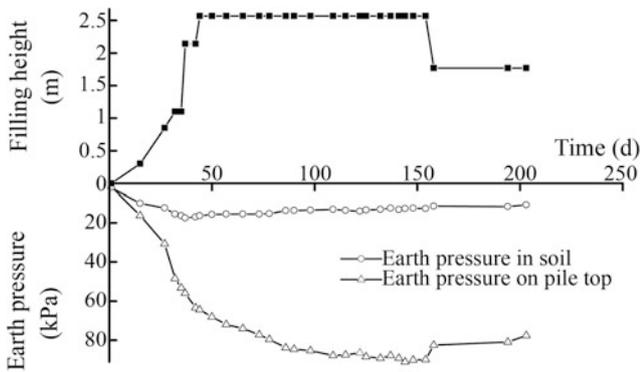
Fig. 29.5 Variations of the earth pressure
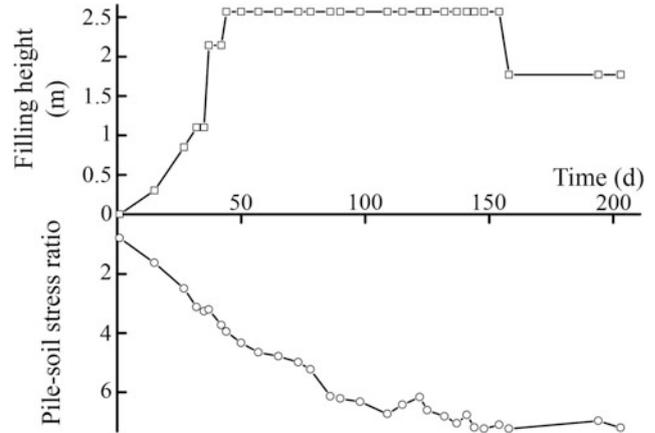
Fig. 29.6 Variations of the pile-soil stress ratio

2. The pore water pressure increases with excess pore water pressure generated during the filling stage and decreases with excess pore water pressure dissipated during the interruptions in construction. For example, during the period from the 5th to the 6th day, the pore water pressure measured by PPG04 increases from 0.0421 to 0.0502 MPa as the filling height increases from 0.85 to 1.1 m. However, the pore water pressure decreases from 0.0502 to 0.0463 MPa during the intermission from the 7th to the 9th day.

Fig. 29.7 Pore water pressure with filling height and time
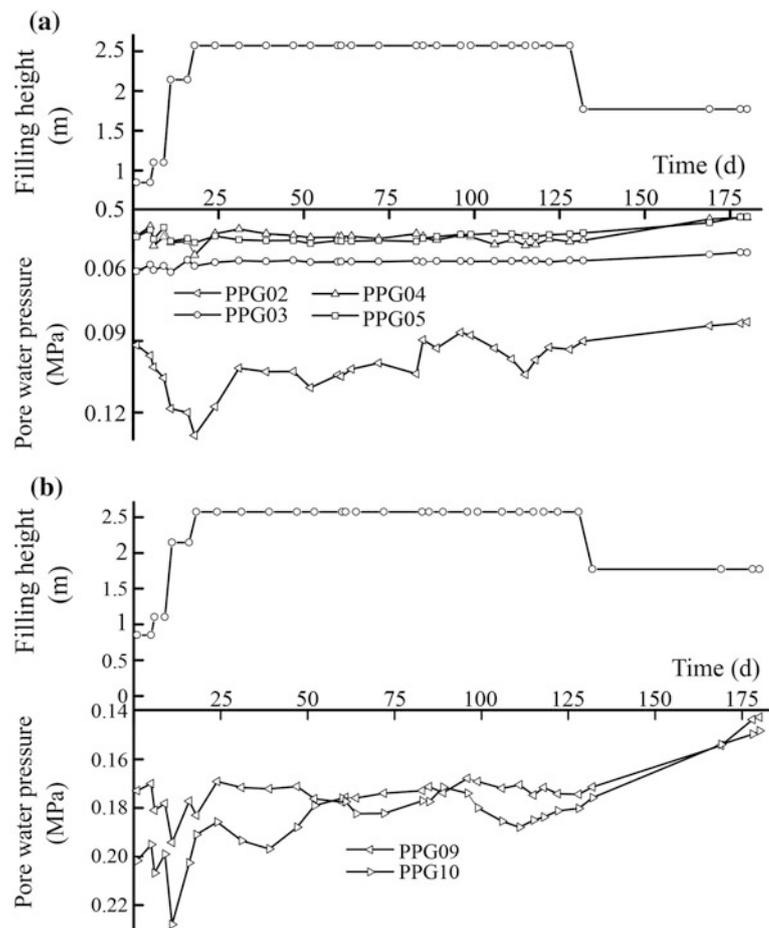
3. As the finish of filling, the value of pore water pressure goes into stable with slight fluctuations observed, such as, the value measured by PPG03 which fluctuated between 0.0563 and 0.0587 MPa. Besides the PPG02, the others also display similar trend. Different from others, the value measured by PPG02 presents a wide fluctuation due to the influence of construction machine with its value fluctuated from 0.09 to 0.13 MPa.

4. On the 132nd day, due to the need for construction, the filled layer was excavated 0.8 m depth. And during the excavation, the water pressure decreased correspondingly. For example, the value measured by PPG03 decreased from 0.0563 to 0.0531 MPa, and that of PPG04 reduced from 0.176 to 0.149 MPa. This indicates that the variation of pore water pressure is closely related to the overlying load.

29.3.3 Axial Force of Piles

During construction, some wire stress gauges installed on TP1 were destroyed. So, the data monitored by the rest on other piles (TP2, TP3, and TP4) were used for analysis as shown in Fig. 29.8. From Fig. 29.8, some observations are obtained as follows.

1. As the variation of depth, the axial force displays in nonlinear with its maximum value appeared at 21 m depth. That is to say, the axial force increases with depth at the range of 3–21 m, and decreases with depth at the range of 21–36 m.

2. The load transfer of the axial force is closely related to the properties of layers where the tube pile distributed. Take the TP4 as example, it can be observed that, at the depths of 3–6 and 21–36 m where the coarse sand, medium sand, and silt layers distributed, the axial force increases faster than that at the depth of 6–21 m where the clay and soft clay layers distributed.

3. With increasing time and overlying load, the axial force of piles all increased with different fluctuations. At the depths of 3–9 and 30–36 m, the growth rate of the axial force is slower than that at the middle part.

4. The distribution of the axial force on each pile reveals that the layers composed of clay and coarse sand shared most of the overlying load. And the axial force at the bottom of pile is small but not zero. All these indicate that the tube piles in this section appear to be an end-bearing friction pile.
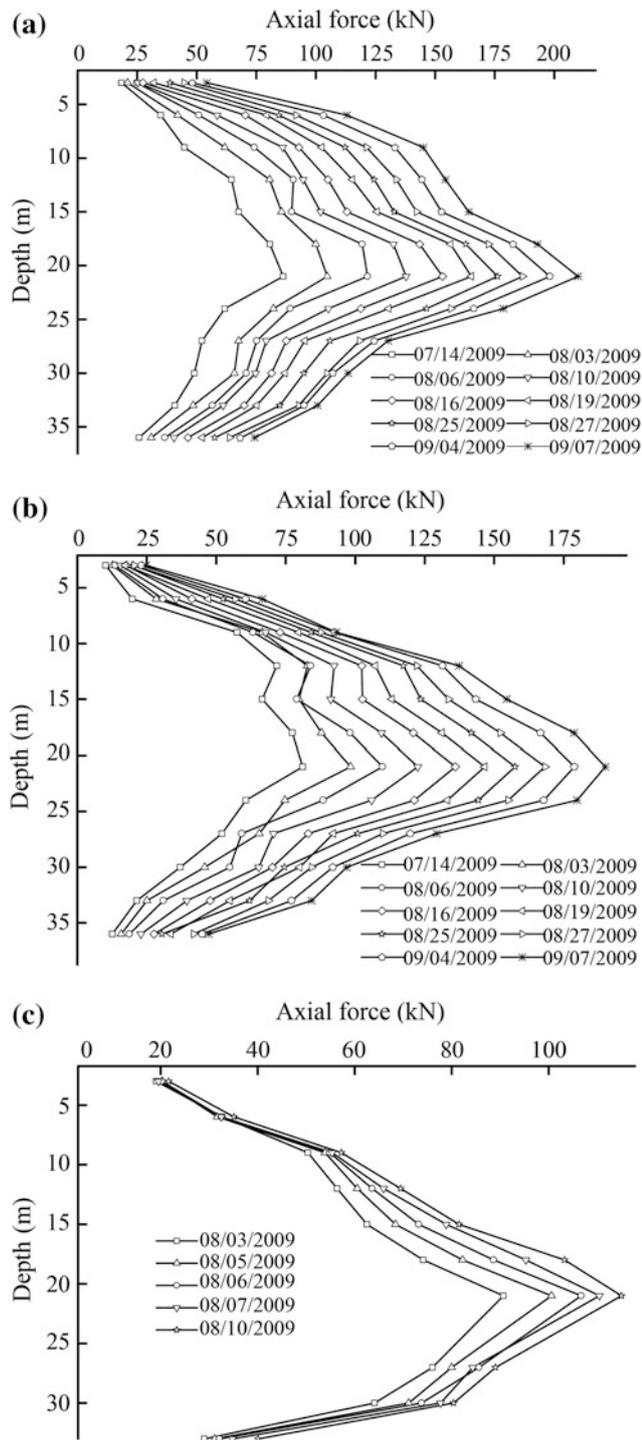
Fig. 29.8 Curves for the axial force as a function of depth. **a** Measured by TP2. **b** Measured by TP3. **c** Measured by TP4

29.3.4 Layered Settlement

The ST4 was destroyed during construction, so the data recorded by the magnetic cores installed on ST1, ST2, ST3, and ST5 were analyzed in this paper. The variations of layered settlement with filling height and time are plotted in Fig. 29.9. From these figures, the following trends are obtained.

1. As the variations of time and filling height, the settlements at different depths all present obvious increases. And in the cross-sectional direction of the subgrade, the settlements also differ, i.e., the nearer the settlement tube away from the center line of the subgrade, the larger the settlement.

2. When the filling speed is relatively fast, the growth rates of the layered settlements at different depths also increase. Take the example of ST2, during the 77th–104th days, as the filling height of the monitoring section changed from 0.85 to 2.75 m rapid, the data measured by magnetic cores on ST2 present a relatively high rate of increase with a steep decrease in the settlement curves, as shown in Fig. 29.9b.

3. After the rapid increase of settlement in each layer due to the fast increase of filling height, the settlement then decreases at different rates during the following 10 days, which can observed in each subfigure. For example, on the 104th day of construction, the settlement measured by the magnetic core at the depth of 0.82 m on ST5 was 111 m, however, it fell to 101 mm on the 125th day with 10 mm decreased.

4. The settlements in the layers composed of soft soil are relatively larger than others. And after the filling, the layered settlements at different depths almost tend to steady with little fluctuations. During whole monitoring process, the growth rate of the settlement is almost directly proportional to the filling speed.

29.3.5 Behavior of Geogrid

During construction, a total of five displacement transducers were installed on the bottom of the first layer of geogrid in the testing section with their labels as FDT1, FDT2, FDT3, FDT4, and FDT5, respectively. Among them, FDT1, FDT3, and FDT5 were installed at the center of pile caps in plane, and the rest were at the center of the soil between piles. After installation, just FDT2, FDT3, and FDT5 worked normally with their data shown in Fig. 29.11. From Fig. 29.11, the followings can be observed (Fig. 29.10).

1. As the increase of filling height, the elongation of the geogrid also increased, especially for FDT2 located in the soil between piles. And the elongation of the geogrid overlays on the soil between piles is larger than that on the pile tops. When the monitoring is finished, the elongations measured by FDT3 and FDT5 on the pile tops are 0.36 and 0.53 mm, respectively; however, that measured by FDT2 overlays on the soil between piles reaches 1.17 mm, which is 2–3 times larger than the

Fig. 29.9 Settlement variations
with filling height and time.
a Measured by the magnetic cores
on ST1. **b** Measured by the
magnetic cores on ST2.
c Measured by the magnetic cores
on ST3. **d** Measured by the
magnetic cores on ST5
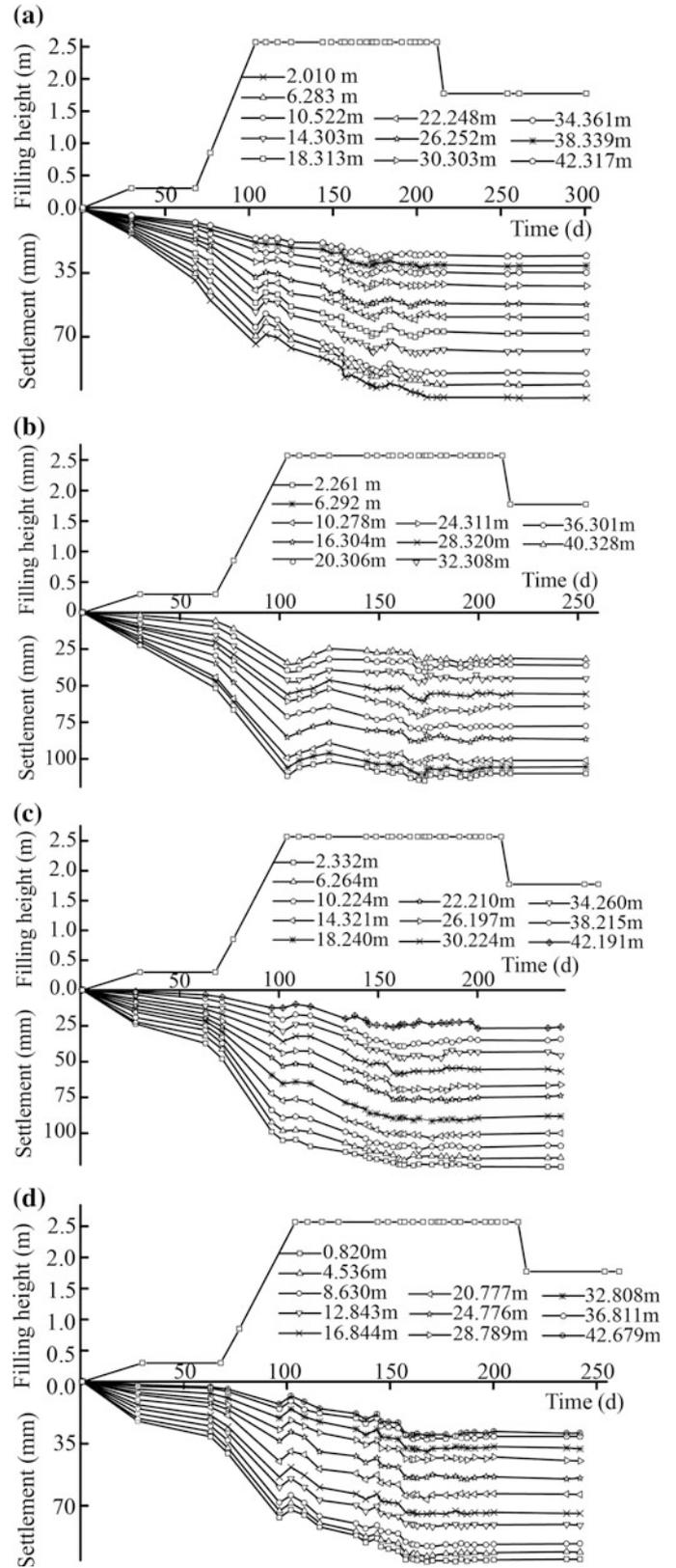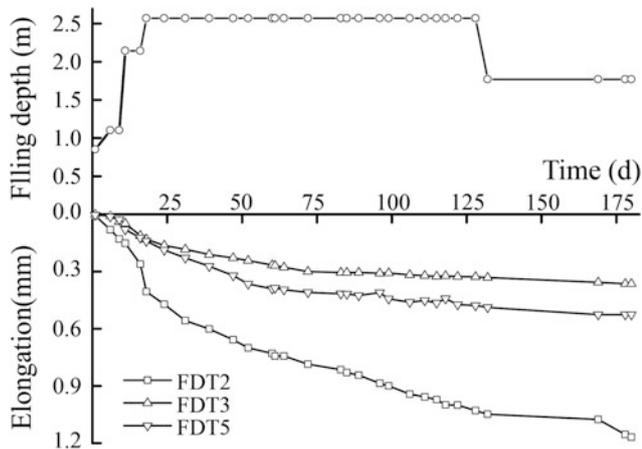
Fig. 29.10 Elongation variations with time and filling height

former. It can be inferred that the elongation rate and the tension of the geogrid overlaid on soil between piles are both larger than those on pile top, but the overall elongation and tension of the geogrid are not necessarily large.

2. The curve recorded by FDT2 reveals that the elongation variation of the geogrid overlaid on the soil between plies presents a lag effect as the increase of filling height. The delay time is about 50 days. In the first 11 days of filling, the average changing rate of elongation is 0.014 mm/d. However, in the following 8 days from the 16th to 24th of filling, the average changing rate of elongation increased to 0.026 mm/d. The reason for the display of this phenomenon is that, as the filling develops, the settlement difference between soil and pile increased gradually. So, the geogrid overlaid on soil between piles began to play its role with elongation increased.

29.3.6 Lateral Displacement

After the layout of inclinometer tubes, the IT3 was destroyed. And the IT1 was also abandoned some days later due to the need of construction. Hence, only part of the data recorded by IT1 and the whole recorded by IT2 were used for analysis with their variations shown in Figs. 29.11 and 29.12. From these figures, the following observations can be obtained.

1. The lateral displacement emerged as soon as the filling process began and shows a decreasing trend as the increase of depth. The lateral displacements at the bottom of both piles are both near zero and fluctuated slightly with time and over loading. The maximum values of both piles at different days all emerged at the depth of 0–10 m.
2. As the filling and the consolidation of soil proceeding, the lateral displacement of the embankment increases accordingly. In Fig. 29.12, it can be observed that, during
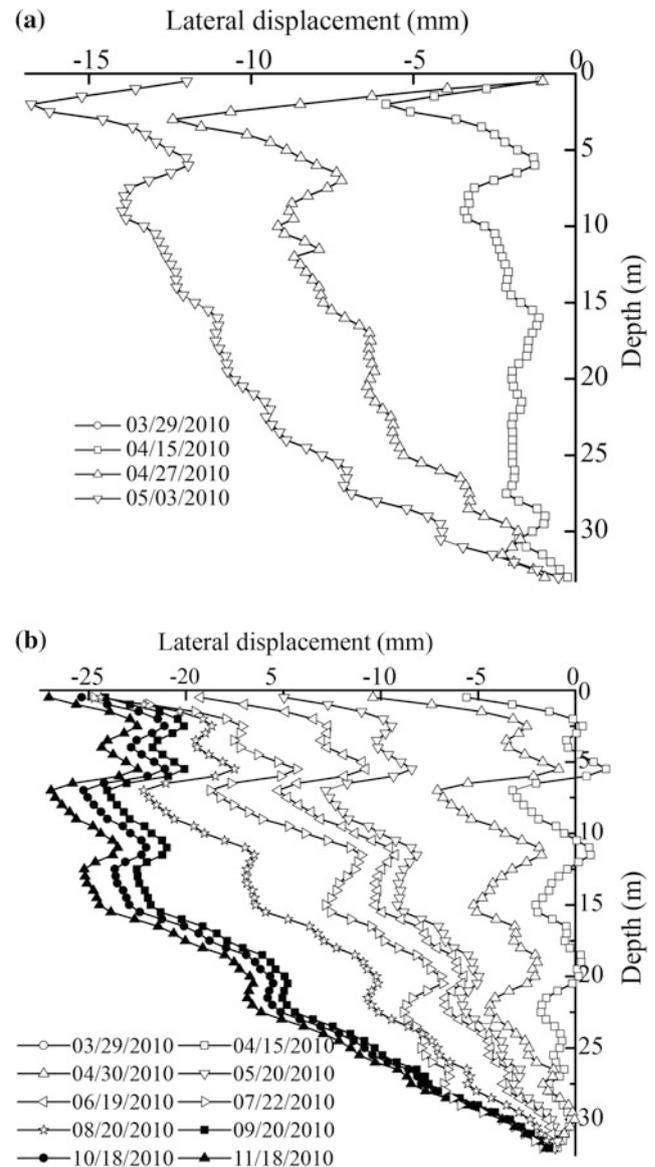
Fig. 29.11 Lateral displacement with time and depth. a Recorded by IT3. b Recorded by IT2

the filling, the growth rate of the lateral displacement is obviously higher than that during the post filling period. For example, during the fill period from March 29, to April 27, 2010, the maximum growth rate of the lateral displacement measured by IT2 reaches 0.247 mm/d. However, during the post filling period from April 27 to November 18, 2010, the maximum growth rate of the lateral displacement measured by IT2 is only 0.075 m.

3. The lateral displacement of the embankments under loading also varies in different soil layers. Generally, the lateral displacement of the embankment in soft soil layers, such as the silty clay layers or clay layers, is relatively larger than that in other layers. Furthermore, the

Fig. 29.12 Maximum lateral
displacement with time and depth
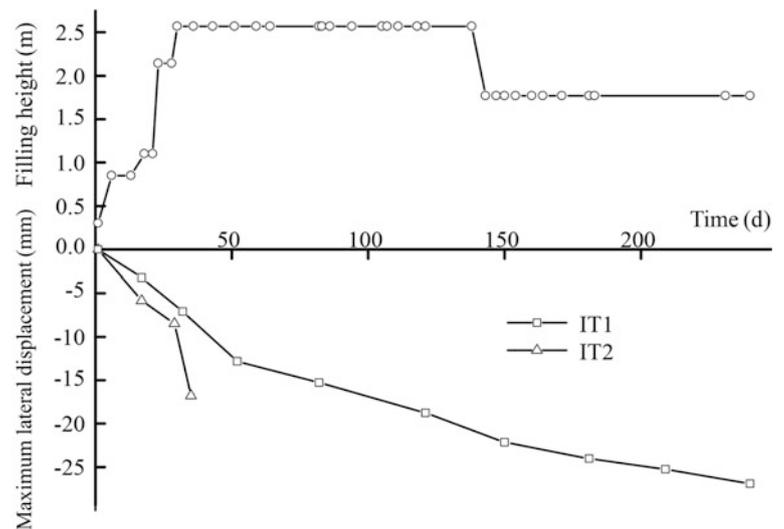
Table 29.1 Types and quantities of instruments in the testing section

Category	Earth pressure cells	Pore pressure gauges	Wire stress gauges	Magnetic cores	Displacement transducers	Inclinometer tubes
Amount	17	11	52	110	5	3
Embedded time	03/13/10	11/08/09–11/17/09	08/03/09	11/08/09–11/17/09	03/20/10	11/08/09–11/17/09
Measuring range	0.4 MPa	0.4 MPa	Tension range: 20 kN Pressure range: 10 kN	Accuracy: 1 mm Maximum: 50 m	30 mm	Accuracy: 0.1 mm Maximum: 40 m
Working principle	Vibrating string	Vibrating string	Vibrating string	Magnetic type	Vibrating string	Resistive
Locations	7 on pile caps, 10 in soil between piles	1 hole with 1 gauge	13 in each testing piles	22 in each settlement tube	2 on pile caps, 3 in soil between piles	3 in near the slope of the embankments

lateral displacement around the dividing line of both soil layers is also relatively larger.

4. The maximum values of the lateral displacements recorded by both inclinometer tubes are all smaller than 30 mm, which indicates that, the layout of the pile-net composite structure strengthens the stability of the subgrade effectively.

29.4   Conclusions

The objective of this paper is to gain insight into the behavior of pile-net composite foundation in oversize-deep-soft soil. From the study, the following conclusions can be drawn.

1. As the variation of filling height, the distributions of earth pressure and pile-soil stress ratio can be divided into three stages. The earth pressure in soil between piles is much smaller than that on pile tops. After the filling, the pile-soil stress ratio is always larger than 1 with its maximum reached 7.6, which indicates that the tube piles play a good role with most of the load shared.

2. Due to most of the load is borne by tube piles, there is no obvious increase for pore water pressure as the increase of filling height. In the coarse sand layer and the medium sand layers, the release of the excess pore water pressure is faster than that in the silt layer and the silty soil layer.

3. As the variation of depth, the axial force displays in nonlinear with its maximum value appeared at 21 m depth. And the load transfer property of the axial force is closely related to the properties of layers where the tube pile distributed. At the depth where the coarse sand, medium sand, and silt layers distributed, the axial force

increases faster than that at the depth where the clay and soft clay layers distributed.

4. During whole monitoring process, the growth rate of the layered settlement is almost directly proportional to the filling speed. When the filling is rapid, the growth of settlement will increase fast with a decrease phase occurred after the fast filling. The variation of settlement is also related to depth and the properties of the soil layers. Besides, differential settlement also occurs at different locations along the cross-sectional direction of the subgrade.

5. The elongation of the geogrid increases with filling, and the elongation rate and the tension of the geogrid overlaid on the soil between piles are both larger than those on the pile tops. Besides, there is a lag effect on the elongation variation of the geogrid overlaid on the soil between plies as the increase of filling height. And the delay time is about 50 days.

6. The lateral displacement emerged as soon as the filling process began and shows a decreasing trend as the increase of depth. Similar to the display of axial force, the lateral displacement also varies in different soil layers.

References

Abusharar SW, Zheng J-J, Chen B-G et al (2009) A simplified method for analysis of a piled embankment reinforced with geosynthetics. Geotext Geomembr 27(1):39–52

Bergado DT, Teerawattanasuk C, Youwai S et al (2000) Finite element modeling of hexagonal wire reinforced embankment on soft clay. Can Geotech J 37(6):1209–1226

Borges JL, Oliveira MD (2011) Geosynthetic-reinforced and jet grout column-supported embankments on soft soils: numerical analysis and parametric study. Comput Geotech 38(7):883–896

British Standard 8006 (1995) Code of practice for strengthened/reinforced clays and other fills. British Standards Institute

Chen RP, Chen YM, Xu ZZ (2008) A theoretical solution for pile-supported embankments on soft soils under one-dimensional compression. Can Geotech J 45(5):611–623

Graeme D, Skinnera R, Kerry R (2005) Design and behaviour of a geosynthetic reinforced retaining wall and bridge abutment on a yielding foundation. Geotext Geomembr 23(3):234–260

Han J, Gabr MA (2002) Numerical analysis of geosynthetic-reinforced and pile-supported earth platforms over soft soil. J Geotech Geoenvironmental Eng 128(1):44–53

Helwany SMB, Wu JTH, Froessl B (2003) GRS bridge abutments—an effective means to alleviate bridge approach settlement. Geotext Geomembr 21(3):177–196

Huang J, Han J, Collin JG (2005) Geogrid-reinforced pile-supported railway embankments—A three-dimensional numerical analysis. Transp Res Rec 1936:211–229

Kousik D (2010) A mathematical model to study the soil arching effect in stone column-supported embankment resting on soft foundation soil. Appl Math Model 34(12):3871–3883

Low BK, Tang SK, Choa V (1994) Arching in piled embankment. J Geotech Eng 120(11):1917–1938

Qian-gong Cheng, Yu-feng Wang, and Jiu-jiang Wu

Abstract

For the research of the deformation behavior of excavated high loess slope reinforced with the combination system of soil nails and pre-reinforced-stabilizing piles. An open cut slope is chosen as an example for field monitoring with the following results obtained: (1) As the excavation depth increasing, the pre-reinforced-stabilizing piles all moved toward outside due to the existence of earth pressure behind piles. (2) As the increase of excavated depth, the value of earth pressure before piles presents a nonlinear variation with one maximum point appeared along depth. Differing from that before piles, the fluctuation of the earth pressure behind piles obviously increased with both maxima points distributed along depth. (3) Similar to the display of earth pressure, the distribution of the reinforcement stress along piles also fluctuated as the increase of excavation. (4) The axial nail load presents an obvious increase during excavation, which indicates that the layout of soil nails played an effective role for the stabilization of excavated slope. (5) Based on the distribution of axial nail load during excavation, it is inferred that the potential sliding surface of slope soil above piles displays in an arc-shape with its toe of slip surface located at the top of pile.

Keywords

High loess slope • Soil nails • Pre-reinforced-stabilizing piles • Field monitoring • Deformation

30.1 Introduction

The technique of soil nailing has been used worldwide in recent years for its simple usability and economic efficiency in stabilizing slope and supporting excavation (Schlosser 1991; Chen 2000; Li et al. 2008; Da Costa and Sagaseta 2010; Gong et al. 2011). Based on this technique, some other supporting measures, such as, composite soil-nailing walls, composite structure with piles and soil nails, composite structure with scattered row piles and soil nails, etc., have also been widely applied in construction (Yang et al. 2005; Liu et al. 2010; Zhang et al. 2011). However, the application of these composite structures in loess slope is still scare, especially in high loess slope (>30 m) (Hu et al. 2010).

Here, in order to learn the deformation behavior of excavated high loess slope reinforced with the combination system of soil nails and pre-reinforced-stabilizing piles further, an open cut slope, located at the entrance of Guanyintang tunnel in Shan County, is chosen as an example for field monitoring, which is meaningful in improving the design level of high loess slope along railway to guide practices in the future. During the research, the field monitoring of the lateral displacement, earth pressure, reinforcement stress, and axial nail load, etc., was conducted. And then, based on the analysis of these data, the supporting mechanism of the combination system of soil nails and pre-reinforced-stabilizing piles in high loess slope is discussed to provide insight into fundamental understanding of such cases.

Q.-g. Cheng (✉) · Y.-f. Wang · J.-j. Wu
Department of Geological Engineering, Southwest Jiaotong University, Chengdu, 610031 Sichuan, China
e-mail: chengqiangong@home.swjtu.edu.cn

30.2   Field Monitoring Setup

30.2.1   Excavation

The studied area locates at the entrance of Guan Yintang Tunnel in Shan County, Henan Province, with its open cut slope composed of loess. The excavation of the slope was divided into seven stages. And the detailed information of stages 1–6 is shown in Fig. 30.1. The last stage is the refilling of soil after the finish of the open cut tunnel construction, which is not exhibited in this figure.

30.2.2   Instrument Setup

According to the field condition, the piles, numbered $8^{\#}$ and $10^{\#}$, were chosen for monitoring. Along the vertical reinforcing steel bars distributed near the front and back sides of both piles, four inclinometers were installed with their numbers $8^{\#}A$, $8^{\#}B$, $10^{\#}A$, and $10^{\#}B$. In addition, 32 earth pressure cells and wire stress gauges were also installed with 2 m spacing in vertical. Take the example of pile $8^{\#}$, the detailed locations of these instruments are presented in Fig. 30.2.

Fig. 30.1 Excavation profile

Fig. 30.2 Layout of monitoring instruments along pile $8^{\#}$ (unit: cm)

Fig. 30.3 Layout of soil nails used for monitoring
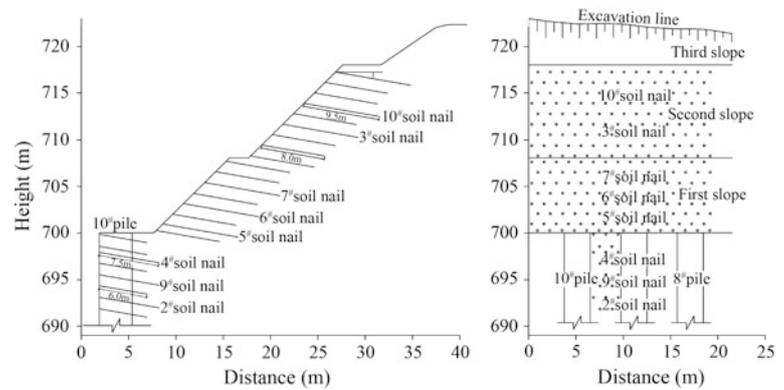
Besides the monitoring of the behavior of piles, some instruments were also installed along soil nails to record the interaction between soil and nails. Figure 30.3 shows the layout of the soil nails used for monitoring. All of the soil nails were installed at 10° from horizontal with different lengths. Along each of the nails, numbered $2^\#$, $3^\#$, $4^\#$, $5^\#$, $6^\#$, $7^\#$, $9^\#$, and $10^\#$, wire stress gauges were instrumented with 1.5 m spacing. The diameter of each nail is 25 mm. In Fig. 30.3, the $1^\#$ and $8^\#$ nails were not presented, which are 3 m long.

30.3   Results and Discussion

30.3.1   Deformation Behavior of Piles

30.3.1.1   Horizontal Displacements of Piles

The horizontal displacements of piles are recorded by in-clinometers. Based on the readings, the deflection-depth curve of pile and the horizontal displacement-time curve of pile top were obtained, respectively. For the displays of these curves of piles $8^\#$ and $10^\#$ are similar, just the data of pile $8^\#$ are presented in this paper as shown in Figs. 30.4 and 30.5. Here, the negative value indicates the displacement is outward of the slope.

From Figs. 30.4 and 30.5, we may see the followings.

(1) During excavation, the pre-reinforced-stabilizing piles moved toward outside due to the existence of earth pressure behind piles with their maximum horizontal displacements appeared at the top surfaces. For the A-side of pile $8^\#$, the maximum horizontal displacement reaches 91.8 mm.

(2) Along piles, the shapes of the deflection-depth curve of the A-sides are parabolic type with regular variations.

(3) Before the excavation reaching 4 m, the variation of pile top horizontal displacement is great, which indicate that, at the beginning of excavation, the slope moved outward rapid. When the excavated depth reaches 9.5 m, the variation of pile top horizontal displacement becomes gently with the corresponding value of $8^{\#A}$ fluctuated between −86 and −92 mm. This indicates that, when the excavated depth reaches certain value, the earth pressure behind piles tends to steady with a gentle variation of pile top displacement occurred.

(4) During the unloading stage, the horizontal displacement of pile displays a decrease tendency, which exhibits that unloading can promote the stability of slope.

All these natures indicate that the horizontal displacement of pile can be divided into instantaneous displacement and secondary displacement. The former occurs in a short time after excavation or unloading. And then, the later occurs due to the variation of earth pressure induced by soil rheology.

30.3.1.2   Earth Pressure Distribution Along Piles

According to the data recorded by the earth pressure cells along pile $8^\#$, the variations of earth pressures with time and depth are showed in Figs. 30.6 and 30.7, from which we may see the followings.

(1) For the A-side of pile $8^\#$, the earth pressure increases with depth ranging from 0 to 16 m and turns into decrease when depth exceeds 16 m. That is to say, the maximum value of earth pressure distributed at the depth of 16 m with its value reached 388.27 kPa.

(2) The variation of earth pressure along the B-side of pile $8^\#$ also displays in nonlinear as the variation of depth with both maxima points distributed. The values at both maxima points are 235 and 334 kPa, respectively.

(3) As the variation of time and excavation depth, the earth pressure along the A-side of pile $8^\#$ decreases gradually. That is because, with excavation, the pile began to deform with the earth pressure gradually transformed into active soil pressure from earth pressure at rest.

(4) Along both sides of pile $8^\#$, the decrease of earth pressure during the stages 1 and 2 is obviously faster than that of other stages, which indicates that the earth pressure tends to stable with time.
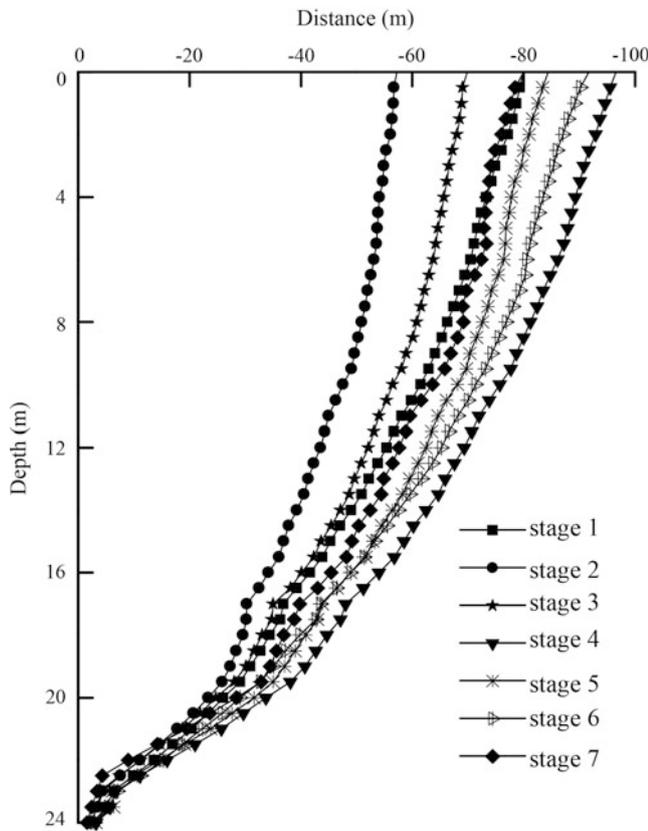
Fig. 30.4 Deflection of the pile

30.3.1.3 Reinforcement Stress Along Piles

For the monitoring of the internal stress of piles, some wire stress gauges were installed on the concrete reinforcing bars distributed at the both sides of piles 8[#] and 10[#]. Here, the data monitored by the wire stress gauges on pile 8[#] were used for analysis as shown in Figs. 30.8 and 30.9. From both figures, some observations are obtained as follows. Here, positive value indicates the tensile stress.

(1) In stages 1 and 2, the reinforcement stress along the A-side of pile 8[#] is negative indicating the existence of compressive stress. However, in the following stages, the value turns into positive gradually, which indicates the appearance of tensile stress. Differing from the A-side, the reinforcement stress along the B-side of pile 8[#] is always in negative.

(2) During the first stage, the variation of the reinforcement stresses along both sides of pile 8[#] is obviously greater than that in other stages, especially at the very beginning of stage 1. That is because, at the beginning of excavation, the concrete of piles was just poured several days with very low strength. The earth pressure loaded on the piles was mainly shared by the concrete reinforcing bars distributed in piles. So, the growth rate of reinforcement stress in the first stage is fast. In the following stages, the strength of the poured concrete of piles increased greatly with more earth pressure borne. Hence, the growth rate of reinforcement stress in the following stages reduced rapidly.
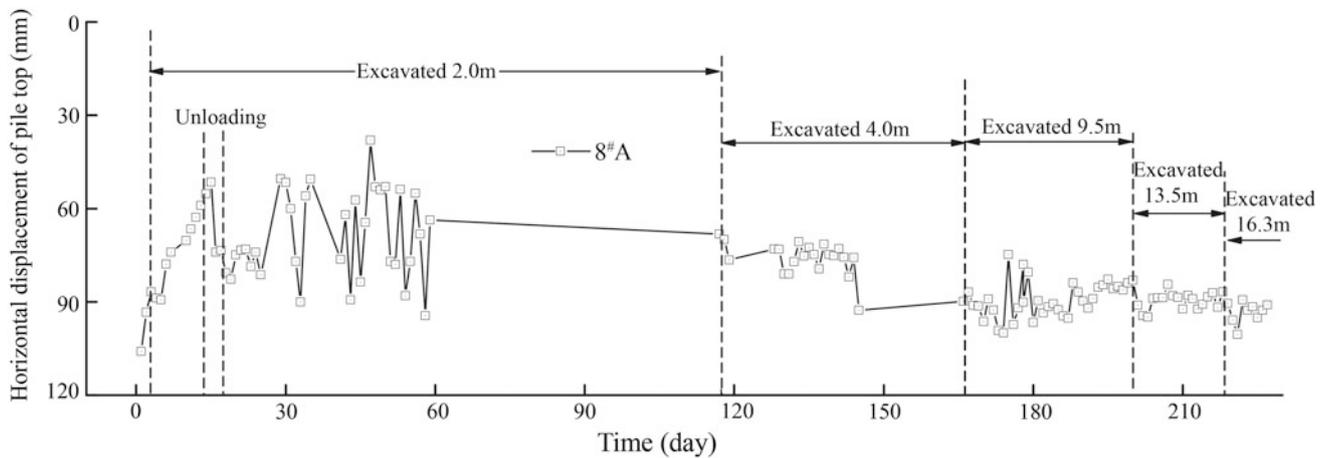
Fig. 30.5 Horizontal displacement-time curve of pile top with excavation and time
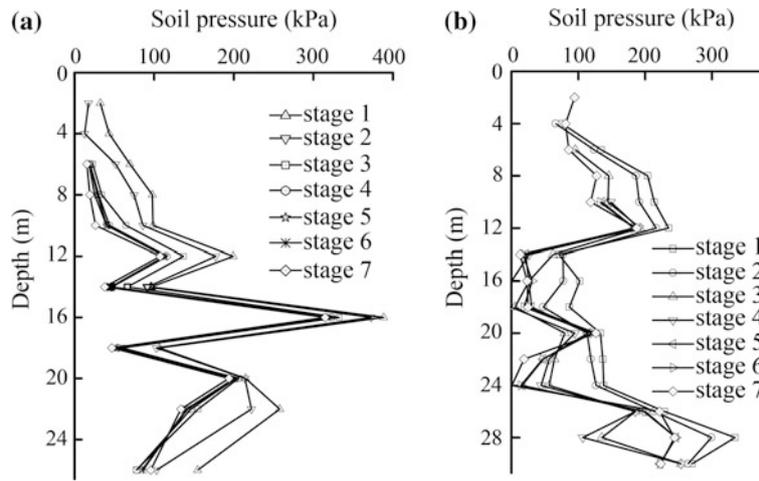
Fig. 30.6 Earth pressure variations with depth and excavation
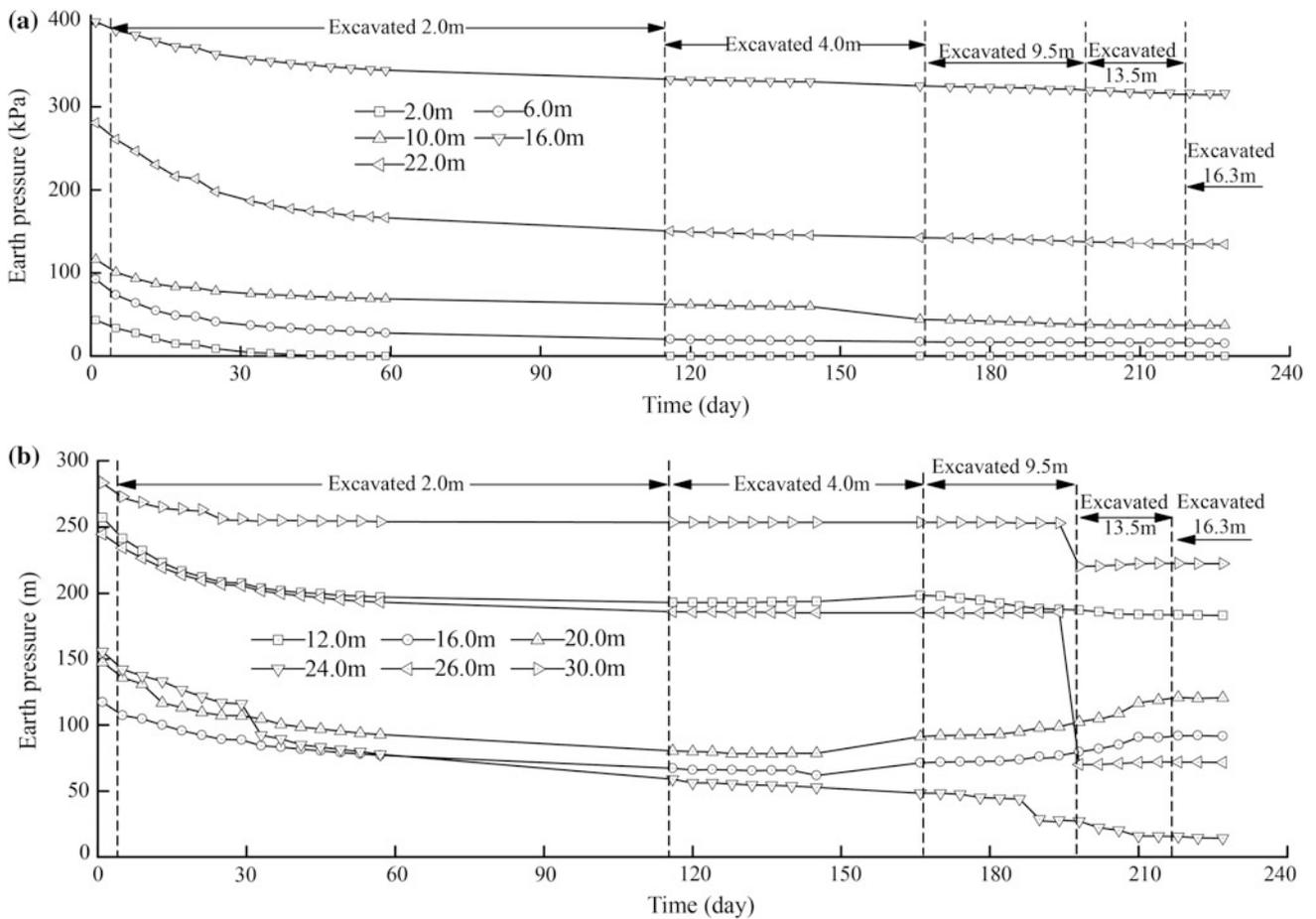
Fig. 30.7 Earth pressure variations with excavation and time
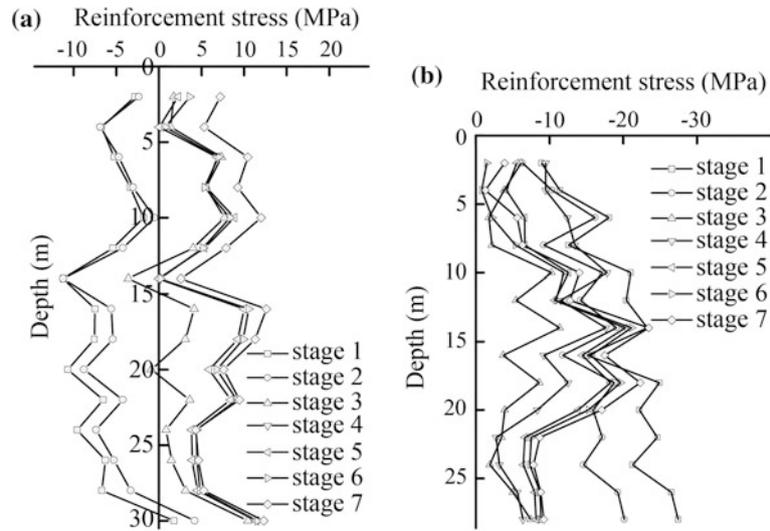
Fig. 30.8 Reinforcement stress variations with depth
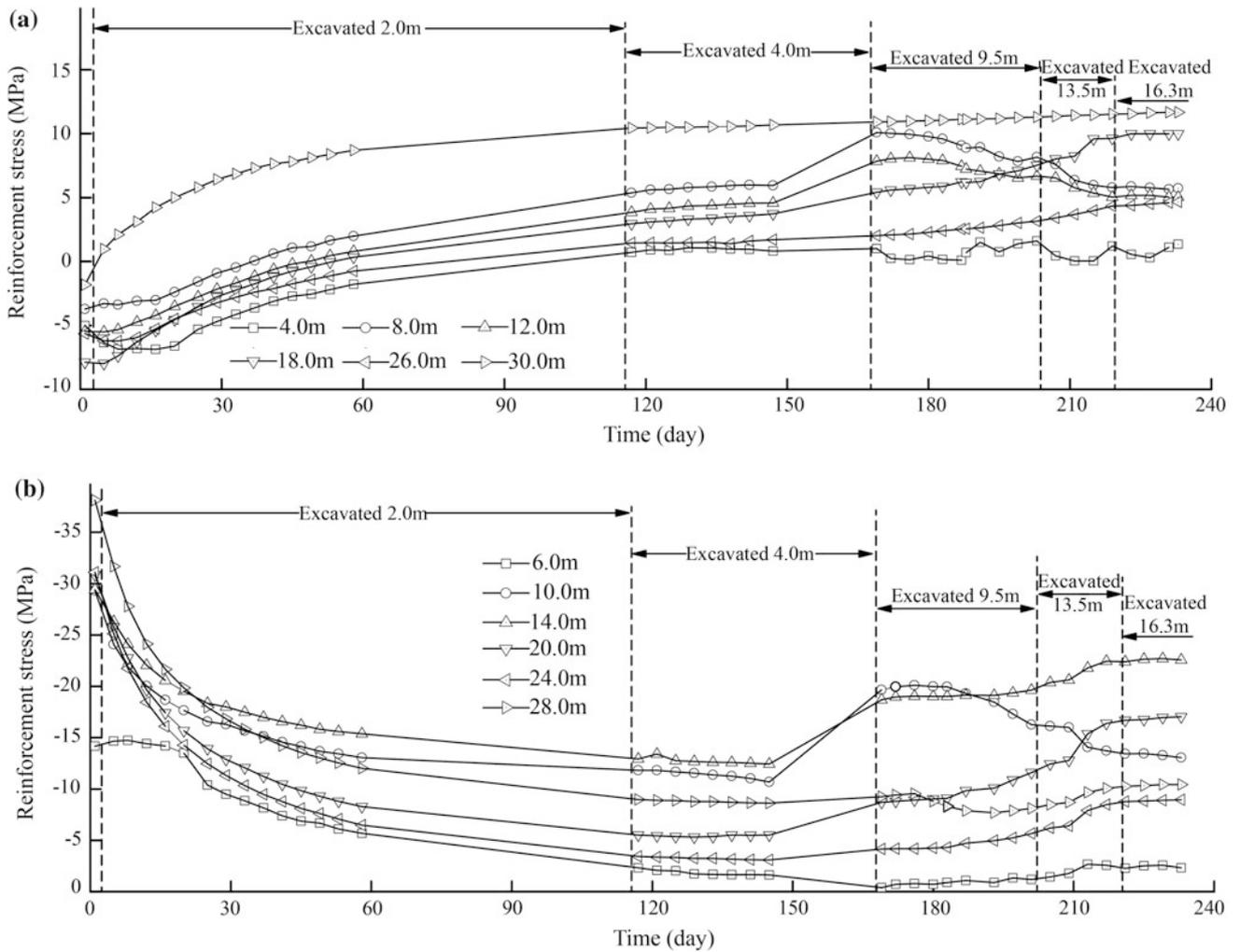
Fig. 30.9 Reinforcement stress variations with excavation and time

Fig. 30.10 Stress-time-nail length curves of soil nails installed in the soil above piles. **a** 3# soil nail. **b** 5# soil nail. **c** 6# soil nail. **d** 7# soil nail. **e** 10# soil nail
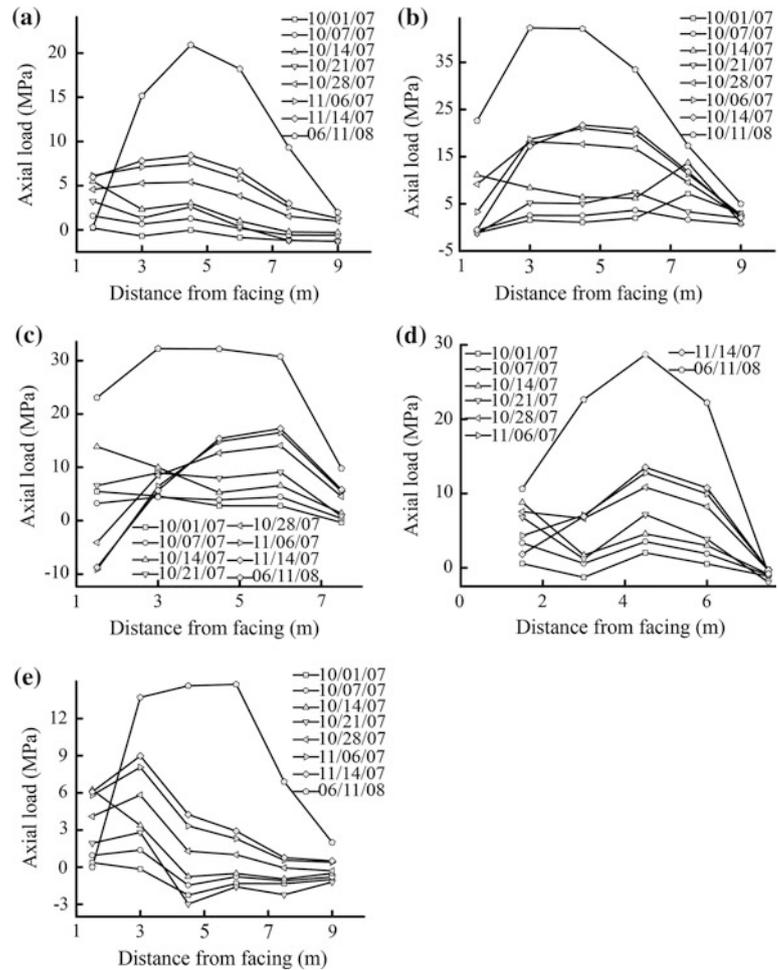
(3) For the variation of the reinforcement stress along the A-side of pile 8#, an obvious fluctuation can be observed during the stage 4 with following characteristics presented.

- At the depth of 0 to 4 m, the A-side of pile 8# is vacant, the value of reinforcement stress is nearly zero.
- At the depth of 6–12 m, the reinforcement stress firstly presents a rapid increase as excavation, and then decreases gradually as the adjustment of earth pressure loaded on piles.
- At the depth of 14–26 m, the reinforcement stress increases continuously as the increase of bending moment suffered by piles.
- At the depth of 28–31 m, the piles inserted into bedrock with minor displacement occurred. The reinforcement stress in this part tends to stable.

(4) For the variation of the reinforcement stress along the B-side of pile 8#, it also displays obvious fluctuation in the stage 4 with some characteristics similar to that of the A-side presented.

30.3.2 Behavior of Soil Nails

Besides the monitoring of pre-reinforced-stabilizing piles, the axial load in each instrumented soil nail was also obtained from wire stress gauge readings. Based on the monitored data, the behaviors of soil nails installed in different sections of the slope are obtained as shown in Figs. 30.10 and 30.11.

From these figures, it can be concluded as follows.

(1) For the nails installed in the soil above piles, the nearer the nails away from the toe of the slope, the larger the axial load. Hence, the maximum value among these soil nails appears on the 5# soil nail which reaches 42 MPa.

(2) At the very beginning of the installation of soil nails, the interaction between the cement paste around nails and soil is incomplete, so the axial loads along soil nails display irregular variations with their maximum distributed near the facing. As the improve of the interaction between nails and soil, the distribution of

Fig. 30.11 Stress-time-nail length curves of soil nails installed in the soil between piles. **a** 2$^\#$ soil nail. **b** 4$^\#$ soil nail. **c** 9$^\#$ soil nail
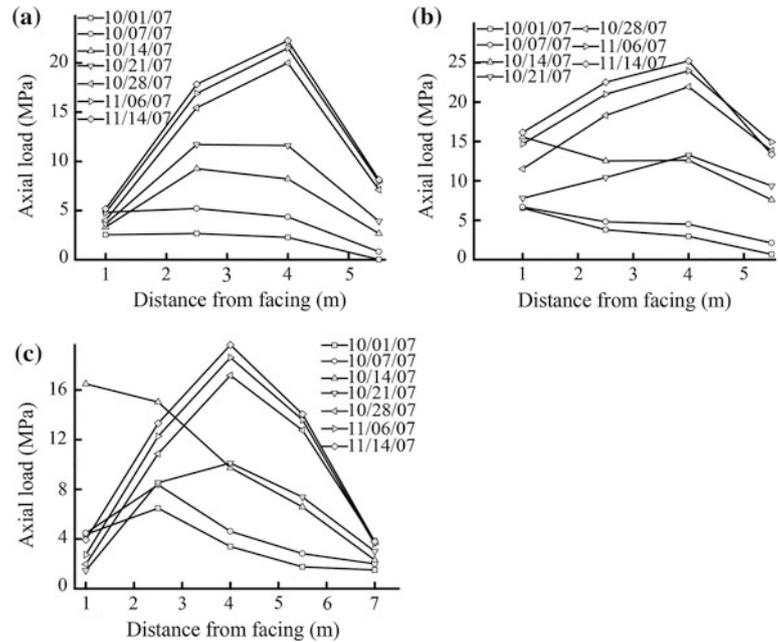
axial load along each nail shows in an parabola form with its maximum registered at the mid of nails.

(3) For the nails installed in the soil between piles, the positions of their maximum values are similar, which are distributed 4 m away from the facing.

(4) As the excavation work processed, the axial loads along nails increases continuously with its growth rate decreasing, which indicates that the soil nails play an effective role in the control of slope deformation. There is no obvious failure occurred in slope during excavation.

(5) Rainfall plays an important role in the deformation of slope, especially for the part near the facing. Due to the slope facing where the soil nails distributed was not reinforced with guniting, the axial loads near the facing increase obviously during rainfall.

Based on the display of the stress-time-nail length curves, the potential slip plane in slope above piles can be inferred as shown in Fig. 30.12.
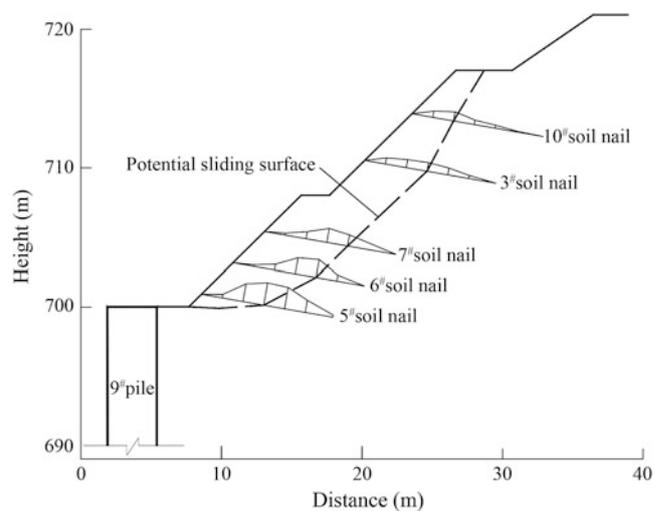
Fig. 30.12 Location of the potential sliding surface in the slope above piles

30.4 Conclusions

The objective of this paper is to gain insight into the deformation behavior of excavated high loess slope reinforced with the combination system of soil nails and pre-reinforced-stabilizing piles. From the study, the following conclusions can be drawn.

(1) During excavation, the pre-reinforced-stabilizing piles all moved toward outside due to the existence of earth

pressure behind piles. The maximum horizontal displacement of the A-side of the pile 8$^\#$ reaches 91.8 mm.

(2) As the increase of excavated depth, the value of earth pressure before piles presents a nonlinear variation with its maximum appeared at the depth of 16 m. Differing from that before piles, the fluctuation of the earth pressure behind piles obviously increased with both maxima points distributed at the depths of 12 and 28 m, respectively.

(3) Similar to the display of earth pressure, the distribution of the reinforcement stress along piles also fluctuated as

the increase of excavation. During the first stage, the variation of the reinforcement stresses along both sides of pile $8^{\#}$ is obviously greater than that in other stages, especially at the very beginning of stage 1.

(4) According to the recorded data of axial nail load, it is revealed that the axial nail load presented an obvious increase during excavation, which indicates that the layout of soil nails played an effective role for the stabilization of excavated slope.

(5) Based on the distribution of axial nail load during excavation, it is inferred that the potential sliding surface of slope soil above pre-reinforced-stabilizing piles displays in an arc-shape with its toe of slip surface located at the top of pile. Instead, the potential sliding surface of soil between piles is present in an polyline type.

References

Bin L, Min Y, Zhiyin Y et al (2010) Design and practice of composite structure with scattered row piles and soil nailing for pit-protection. China Civil Eng J 106–114

Chen Z (2000) Soil nailing application in foundation engineering. China Building Industry Press, Beijing (in Chinese)

Da Costa A, Sagaseta C (2010) Analysis of shallow instabilities in soil slopes reinforced with nailed steel wire meshes. Eng Geol 113:53–61

Gong C, Cheng Q, Yang L, Yuan GB, Wang YF (2011) Case study of deformation behaviour of high loess slope in excavation. J China Railway Soc 32:120–124

Hu J, Xie Y, Wang W (2010) Study of stability characteristics of multi-stair high cut slope in loess highway. Chin J Rock Mech Eng 3093–3100

Li J, Tham LG, Junaideen SM et al (20080 Loose fill slope stabilization with soil nails: full-scale test. J Geotech Geoenvironmental Eng 134:277–288

Schlosser F (1991) Soil nailing recommendations. Presses de l′ENPC, French

Yang ZY, Zhang J,Wang K (2005) Development of composite soil-nailing walls. Chin J Geotech Eng 27:153–156

Zhang LL, Zhang QX, Ma QX (2011) Soil nail's axis force of pile-anchor composite soil-nailed wall. J Beijing Univ Technol 1338–1342

Effects of Alkali Silica/Aggregate Reaction on Concrete Structures in Bundelkhand Region, Central India

31

Suresh Chandra Bhatt and Bhuwan Chandra Joshi

Abstract

The Bundelkhand massif covering 26,000 km^2 area forms the northern segment of Indian shield. It mainly consists of Bundelkhand gneissic complex (3.1 Ga) and granitic complex (2.5 Ga). These gneisses and granitoids are mainly traversed by E–W and NE–SW trending shear zones. Betwa a tributary of Yamuna is marked by number of concrete dams which are major resources of water in this region. The rock fragments of granites, gneisses, migmatites, basic, ultrabasics and metasedimentaries have been used as coarse aggregate for construction of dams. The main constituents of these rocks are strained quartz, altered feldspar and elastic (mica) minerals. The progressive development of reaction rims of alkali-aggregate and silica reactions were observed in three concrete dams; Sukuwa Dukuwa, Kamala Sagar and Saprar dams. The petrological studies of coarse aggregates (deformed gneisses, schist and granites) reveal that the higher percentage of strained quartz (50–60 %), altered feldspar (25–35 %) and elastic (micaceous) minerals with clayey matrix were found most deleterious reactive agents to cause alkali aggregate/silica reactions. It also indicates that the low-alkali cement and supplementary cementing materials have not been used with reactive aggregates to prevent AAR and ASR reactions.

31.1 Introduction

Numerous concrete structures such as dams and bridges have been suffering from alkali silica (ASR) and alkali aggregate reactions (AAR) since long time. The ASR and AAR has been considered deleterious reactions between alkalis in cement and certain variety of silica and altered feldspar present in aggregate. The ASR and AAR reactions commonly produce expansion by exerting pressure on surrounding matrix and cause extensive distress and cracking in concrete structures (Pan et al. 2012). Normally the higher the alkali content of the cement and the higher the cement content of the concrete, the greater the rate of expansion and cracking. The cracking of the concrete creates channels for water movement in the concrete, which may lead to an increase in saturation. It is universally accepted that the strength of concrete will directly depend on strength and engineering properties of aggregates (Popovics 1979). The low degree of weathering and good strength would be strong quality of an aggregate to resist abrasion and degrading in mixture of Portland cement, which effectively withstand the forces applied by traffic, reservoir and running water during service life of pavements, dams, bridges and other concrete structures (Balbaki et al. 1992; PCCM Manual 1989). Since the identification of AAR (1940), the petrological and mineralogical studies of AAR susceptible aggregates along with their chemistry and laboratory tests to predict swelling and cracking in concrete, have been considered important tools to cope up with this problem.

S.C. Bhatt (✉) · B.C. Joshi
Department of Geology, Institute of Earth Sciences, Bundelkhand University, Jhansi, India
e-mail: geoscb@yahoo.com
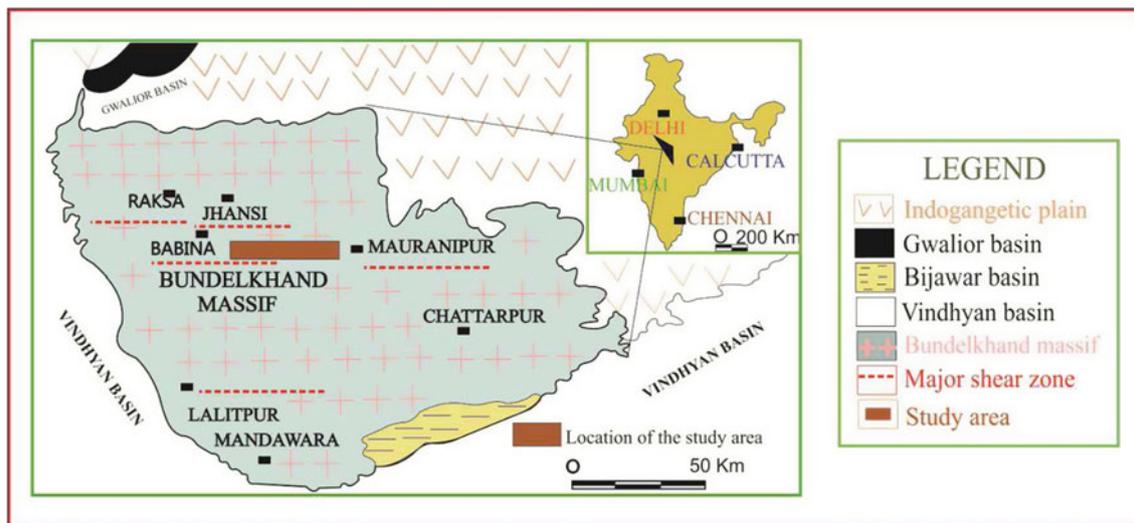
Fig. 31.1 Geological map of Bundelkhand region showing location of the study area

Betwa a major tributary of Yamuna is marked by number of concrete dams in Bundelkhand region of Central India (Figs. 31.1 and 31.2). In this paper the observations on petrographic examinations of aggregate and progressive development of reaction rims have been observed in Sukuwa Dukuwa, Kamala Sagar and Saprar dams (Fig. 31.3). The Saprar, Jamini and Dhasan are major tributaries of Betwa, across which these dams have been built up (Fig. 31.2). Rajghat, Matatila, Sukuwa-Dukuwa, Paricha, Kamla sagar etc. are other major dams in this terrain. Most of them are constructed on the river Betwa. Present paper mainly focuses on the identification of optical and mineralogical characters of reactive strained quartz, altered feldspar and other reactive micaceous minerals present in most of coarse aggregates used in these concrete structures.

31.2 Geomorphological and Geological Set Up

The study area occupying the northern territory of Bundelkhand massif is represented by rugged and undulating topography (Fig. 31.2). The low to moderate hills ranging 200–300 m height mainly constitute different types of granites and linear quartz reefs. The rivers of the area characterized by meandering (curved) and straight courses are assumed to be flowing through fractures/faults (Fig. 31.2). These rivers originating from high ranges of Vindhyans, are flowing SW–NE in this granitic country.

Geologically three major groups of rocks are recognised in the study area (Fig. 31.1). The TTG gneisses (3.3 Ga), gneisses (3.2 Ga) with inclusions of amphibolites and migmatites and mylonitised gneisses constitute gneissic

complex. The metasedimentary and metavolcanics (2.56 Ga) forms the metasedimentary complex while the porphyritic hornblende and grey granite (2.5 Ga), pink granite, mylonitised granite, quartz reefs and mafic dykes belong to the granitic complex (Basu 1986, 2007; Roday et al. 1995; Bhatt and Hussain 2008; Bhatt and Gupta 2009; Bhatt and Mahmood 2012). The E–W to ENE–WSW and NE–SW trending major brittle ductile crustal shear zones are also traced in the investigated area (Fig. 31.1).

The banded light to dark grey and fine to medium grained multiply folded (F_1–F_3) mafic gneisses are exposed in and surroundings of Ghisauli, Badera, Jaunpur and Chaurara villages located in the south of Babina town (Fig. 31.1). Thes rocks (3297+83 Ma; Mondal et al. 2002) associated with mica schists, migmatites, quartzites, amphibolites, ultramafics and mafics are also exposed near Kuraicha and Baragaon to the south of Mauranipur (Fig. 31.1). They also show sheared contact with pink granites in southeast of Kuraicha and south of Chituad in Mauranipur sector. The northern margins of the massif, compact granitoids are demarcated by the pink granitic gneisses. The fine grained, greyish to dark green mafic and ultramafic lensoidal bodies associated to gneissic complex are also traced (3249+ Ma). The fine grained and sheared fuchsite quartzite occurring as isolated patches within the older mafic gneissic terrain, are noticed near Sukwan Dukwan reservoir in the south of Babina (Fig. 31.1).

Based on field setting and petrogical characters five types of granites are reported in Bundelkhand region. (1) The greyish green hornblende granite and (2) light to dark grey coarse grained leucogranite constituting large porphyries of quartz and feldspar (mainly orthoclase) are occurring in the form of small hillocks and in lensoidal bodies of this massif

Fig. 31.2 Physical relief map and location of dams
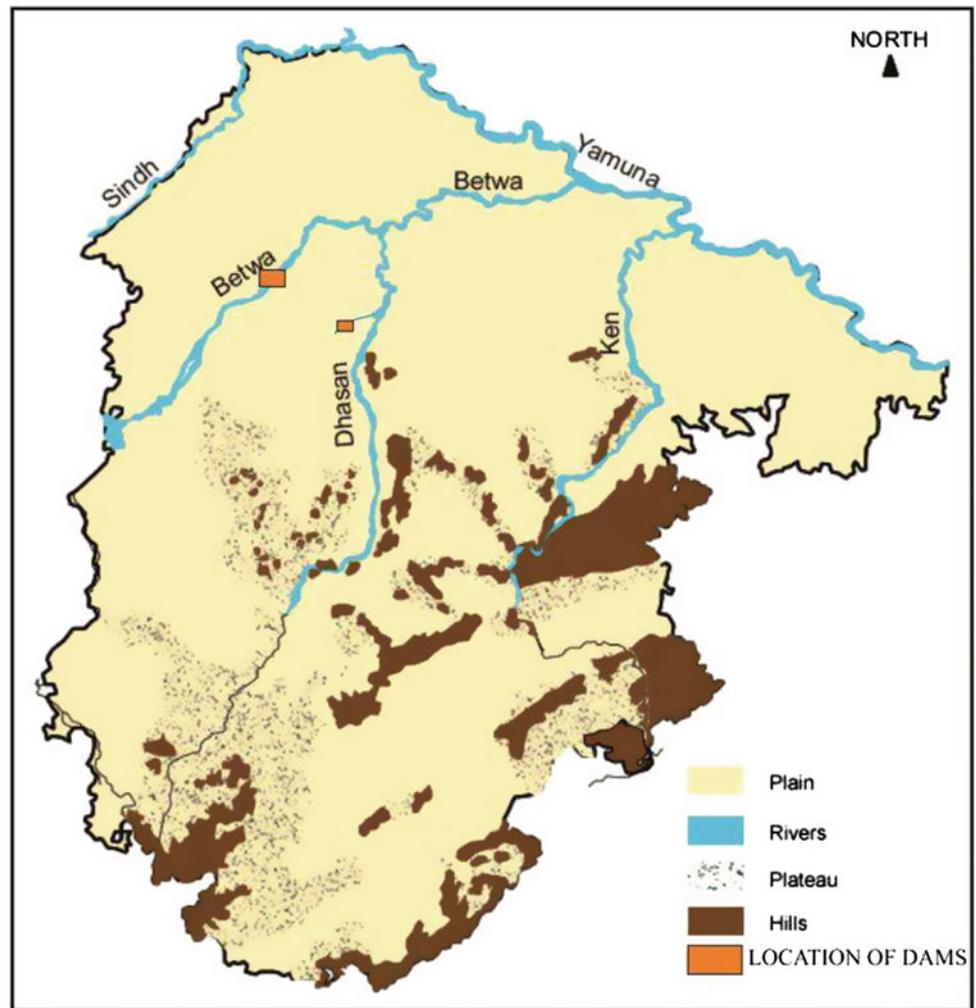
(Fig. 31.1). (3) The large tracts of massive, compact, pinkish to dark red and coarse grained pink granites are widely distributed in the northern and southern parts of the massif (Fig. 31.1). (4)The huge outcrops of fine to medium grained, light to dark pink granitoids and (5) fine to medium grained grey granites are appeared as dome shaped hillocks in this massif (Fig. 31.1). The sheared contact between gneisses and granites is also marked in the south of Mauranipur (Fig. 31.1).

The major quartz reefs exhumed parallel to NE–SW trending shear zones are recorded as spectacular tectonic features. These reefs are offsetting older gneissic complex, iron formation and granitites at several places. The white to milky white recrystallised quartz are found as main constituents of these reefs. The dark grey, fine to medium grained and NW–SE trending dolerite dykes (Rao 2000–2150 Ma) are considered last magmatic phase in this massif.

Petrographic and Microstructural study of coarse Aggregates: The petrographic analysis rocks used as coarse aggregates in concrete were carried out under polarising microscope and discussed below.

Gneisses: The fine to medium grained mafic gneisses constitutes subhedral to anhedral phenocrysts of quartz, feldspar (mainly orthoclase and plagioclase) and muscovite with accessories of biotite and chlorite (Fig. 31.4b). The earlier formed host quartz grains are tabular to elongate and about 50–60 % are strained. The foliation (gneissosity) is defined by preferred orientation of elongated and ribbon quartz and feldspar grains along with flakes of muscovite and biotite. The quartz grains exhibit strong undulose extinction, deformation lamellae and fractures (Fig. 31.4b, d, e). The eqigranular recrystallised quartz grains formed due to granular effects are found on the margins of host grains. The medium grained and cleaved orthoclase are sometimes seems to altered microcline. The plagioclases are twinned and exhibit kinking effects. At places brown flakes of biotite appeared as altered green chlorite. Magnetite occurs as inclusions.

The streaky and granite gneisses are sheared and predominantly constitute rotated phenocrysts of quartz and k-feldspar (Fig. 31.4d). The asymmetrical and rotated porphyroclasts of quartz and feldspar are dominantly displaying sinistral sense of shear movement.

Fig. 31.3 a Kamla Sagar Dam
showing effects of alkali silicate
and alkali aggregate reactions.
b Saprar Dam showing signatures
of alkali silicate and alkali
aggregate reactions. **c** Sukuwa-
Dukuwa Dam showing signatures
of alkali silicate and alkali
aggregate reactions
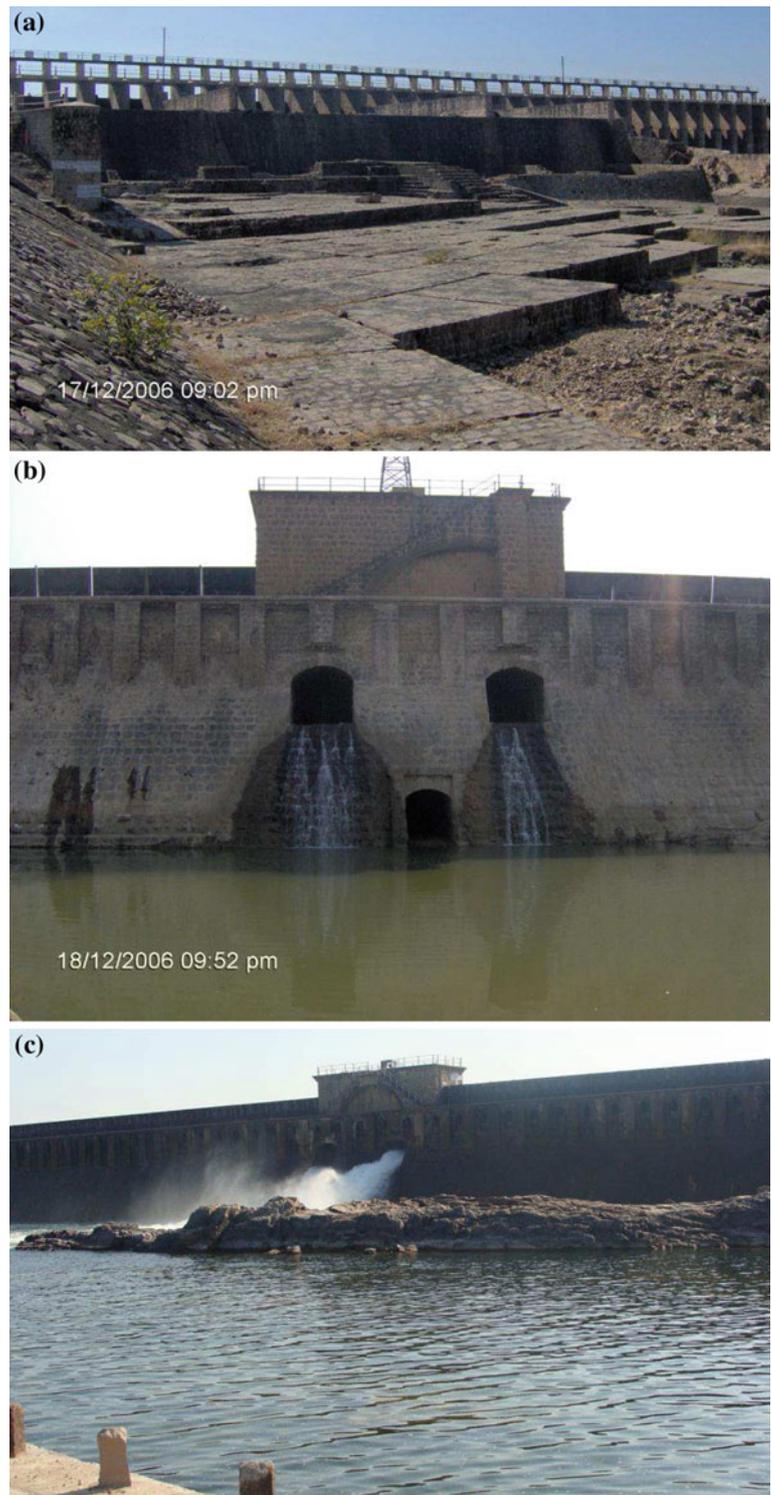
Mylonitised Gneisses: Three types of mylonite (proto-mylonite, mylonite and ultramylonite) zones have been distinctly identified. The protomylonite mainly constituting large phenocrysts (0.2–04 mm) of quartz and K-feldspar (50–90 %), are characterized by strong undulose extinction and deformational lamellae (Fig. 31.4d). The recrystallised quartz grains are widely occurring in margins of host quartz. The progressive growth of mylonitic foliation is represented by preferrely oriented fabrics of elongated and ribbon of quartz (strained) and feldspar grains (Fig. 31.4e). Due to excessive reduction in grain size and dynamic recrystallisation, the proto, blasto and S–C mylonites were progressively
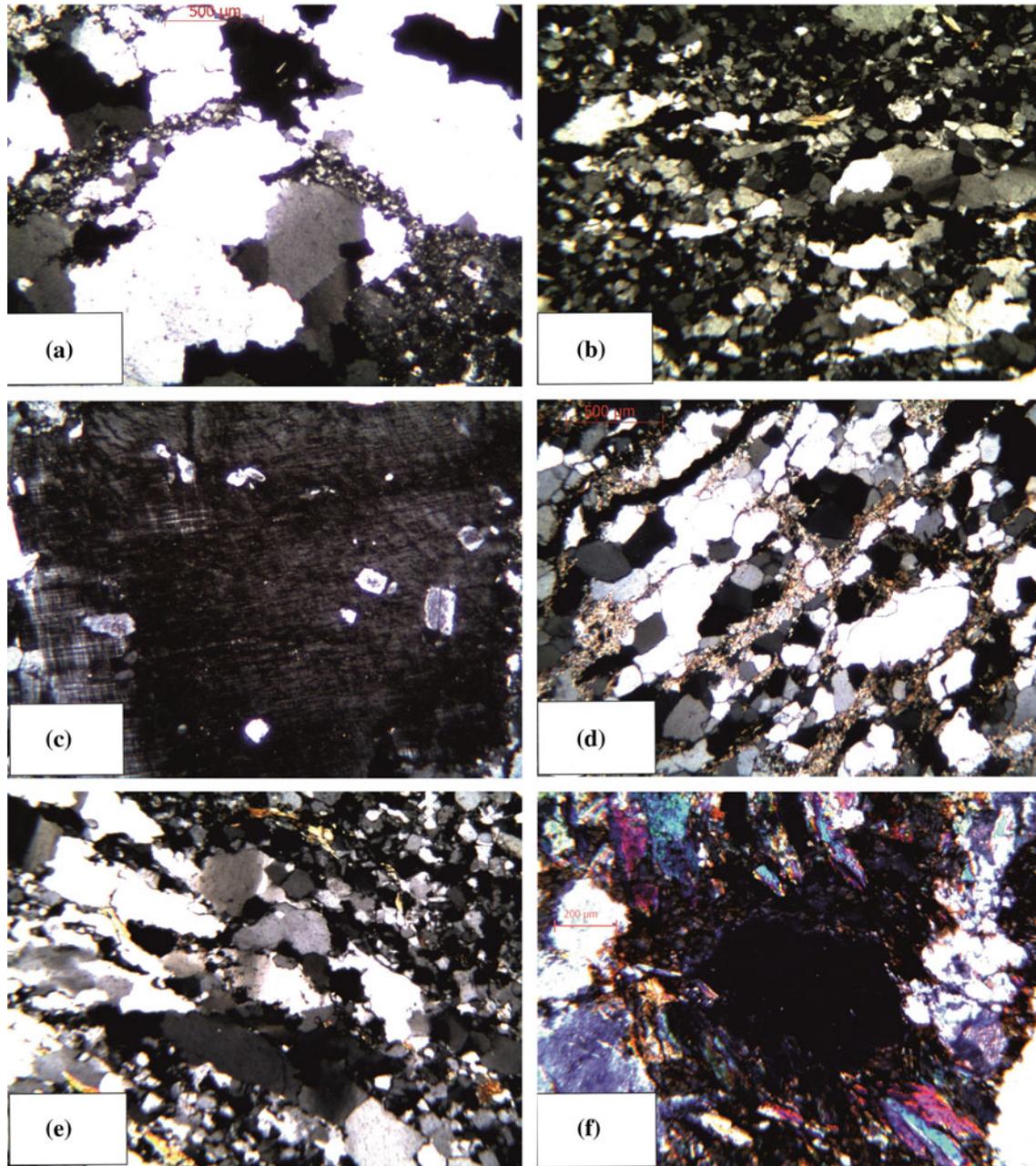
Fig. 31.4 **a** Photomicograph showing polygonal host quartz grains with rare recrystallised (strained) quartz grains in grey granite. **b** Photomicrograph showing elongated strained quartz grains displaying unulose extinction and recrystallisation in gneisses. **c** Orthoclase showing alteration effects with inclusion of recrystallised quartz in granite gneiss. **d** Mylonitic foliation represented by preferred orientation of elongated quartz and feldspar grains in mylonitised gneisses. **e** Photomicrograph showing hornblende, pyroxenes and flakes of flaky minerals. **f** Photomicrograph showing S–C planes in sheared gneisses.

evolved (Fig. 31.4d, e). The alteration effects (microclinisation) and kink bands are also seen in few phenocrysts of orthoclase (Fig. 31.4c) and plagioclase respectively.

Schist: The interclations of mica-schist are also noticed within these mafic gneisses near Kamla Sagar dam. The schistosity is represented by alternating quartz and micaceous bands. Quartz, feldspar, muscovite found as important minerals. Few shreds of mica, zircon, biotite and magnetite are also reported as accessories.

Mafic/Ultramafics: The peridotite and pyroxenite mainly constitute olivine, plagioclase, pyroxenes, amphiboles (mainly hornblende), talc and chlorite as main mineral

constituents. The colourless faint green and anhedral grains of olivine contain inclusion of iron. Orthopyroxenes dominantly consisting of enstatite, occasionally enclose olivine to form poikilitic texture. Among amphiboles green to greenish brown hornblende are dominantly found whereas tremolite and chromite are rarely occurred.

Migmatites: The grey to dark green well folded lensoidal bodies of migmatites are found in the downstream of Kamla Sagar dam. The leucocratic (quartz and feldspar) and dark bands (mafic minerals) are characteristic features of these rocks. Quartz, feldspar (orthoclase, microcline and plagioclase) biotite, muscovite, chlorite are observed as chief mineral constituents.

Quartzite: Few outcrops of quartzites are occurred as small lenses within the sheared gneissic complex to the north of Mauranipur. Quartz, sericite, chlorite, rutile and tourmaline were examined as main minerals constituents. The medium to coarse grained quartz grains (angular to subhedral) appeared as lenses. The small streaks of biotite with rare plagioclase and magnetite occur in quartz laminae. The fine grained fuchsite quartzite mainly constitutes alternating bands of quartz (0.5–l cm) and fuchsite (1.5–3 cm). The fuchsite mainly appears as dark green shreds with bands of quartz.

Grey Granite: Quartz, K-feldspar, plagioclase and mica are found as main mineral constituents. Plagioclase appeared with altered core, is followed by outward and a relatively free zone. The tabular to polygonal quartz grains (subhedral to euhedral) constitute 20–30 % of total composition of rock. The secondary recrystallised quartz grains found in the margins of host grains. Anhedral to euhedral phenocrysts of orthoclase constitute 40–50 % of total composition. Microcline showing perthetic growth and perfect cleavage is also observed in few thin sections. Magnetite and recrystallised quartz grains are seen as inclusions. Brown to greyish brown laths of biotite are also seen.

Pink Granite: Pink granite displaying porphyritic texture contains large phenocrysts of quartz, orthoclase, microcline and plagioclase. Magnetite, zircon, chlorite and rutile occurred as accessories. Subhedral to euhedral quartz grains embedded within recrystallised matrix and plagioclase showing twining and perfect cleavage are also observed. The medium to coarse grained and well cleaved orthoclase forms 70–75 % of total rock composition. The perthetic growth in microcline with inclusion of quartz is also noticed. Magnetite and recrystallised quartz occur as inclusions. Biotite is found in small shreds.

31.3   Discussion

The petrographic observations done on coarse aggregates reveal that the mylonitised (sheared) gneisses, granites, quartzite and schist containing higher percentage of strain

quartz (60–80 %), altered feldspar (30–35 %) and micaceous minerals may be considered more susceptible to alkali silicate and alkali aggregate reactions. It was also observed that the size of quartz may have adverse influence on deterioration of concrete. However, the average grain size do not show any discernible effect on expansion of concrete. It is also inferred that the microstructural features like cleavage, fractures, kinks, deformation lamellae, undulose extinction, dynamic recrystallisastion and twining examined in quartz, feldspar and micaceous minerals may have serious effects on strength of rock aggregate and corresponding concrete. Apart from this, the crystalline forms of silica (chert, chalcedony and cryptocrystalline quartz) found in various rock aggregates may also be responsible to cause alkali silica or alkali silicate reactions. The feldspar, mica and clayey minerals may cause kaolisation, oxidation and other carbonic reactions and eventually accelerate the alkali silicate reaction. Therefore, the shape, size and microstructural characters of rock aggregate along with the percentage alkali present in cement paste may be considered important parameters for determination of strength of concrete.

The most of the dams in the study area particularly Sukuwa Dukuwa and Saprar dams are more than 50 years old. The reaction rims and minor cracks observed in these concrete dams indicate that the ASR and AAR reactions have become more progressive since last few years and may further cause extensive cracks and great damage to these structures. Since, there are no proper preventive measures to stop deleterious ASR and AAR reactions in these dams. Therefore, it is suggested that such dams may be abandoned. It is also advisable that the low alkali content cement should be used and potentially reactive aggregates have to be identified before construction.

References

Balbaki W, Balbaki M, Benmokrane B, Aitcin PC (1992) Influence of specimen size on compressive strength and elastic of high performance concrete. American Society of Testing Materials, p 113–118

Basu AK (1986) Geology of parts of the Bundelkhand granite massif. Central India: Rec Geol Survey India 17(2):61–124

Basu AK (2007) Role of the Bundelkhand Granite Massif and the Son Narmada mega fault in Precambrian crustal evolution and tectonism in Central and Western India. J Geol Soc India 70:745–770

Bhatt SC, Hussain A (2008) Structural history and fold analysis of Basement Rocks around Kuraicha and adjoining area Bundelkhand massif, Central India. Geol Soc India 72:331–347

Bhatt SC, Mahmood K (2012) Deformation pattern and microstructural analysis of sheared gneissic complex and mylonitic metavolcanics of Babina-Prithipur Sector, Bundelkhand Massif, Central India. Indian J Geosci 66(1):79–90

Bhatt SC, Gupta MK (2009) Tectonic significance of shear indicators in the evolution of Dinara Garhmau shear zone, Bundelkhand Massif, Central India. In: Kumar S (ed) Magmatism tectonism and

mineralization. Macmillan Publishers India Ltd., New Delhi, pp 122–132

Mondal MEA, Goswami JN, Deomurari MP, Sharma KK (2002) Ion microprobe Pb^{207}/Pb^{206} age of Zircon from the Bundelkhand massif, northern India for crustal evolution of Bundelkhand Aravalli protocontinent. Precambr Res 117:85–100

Pan JW, Feng YT, Wang JT, Sun QC, Zang CH, Owen DRJ (2012) Modelling of alkali-silica reaction in concrete: a review. Front Struct Civ Eng 6(1):1–18

Popovics S (1979) Concrete-making materials. McGraw Hill Book Company, New York, p 370

Rao JM, Rao GVSP, Widdowson M, Kelly SP (2005) Evolution of proterozoic mafic dyke swarms of the Bundelkhand Granite Massif, Central India. Curr Sci 88(3)

Roday PP, Diwan P, Singh S (1995) A kinematic model of emplacement of quartz reef and Indian subsequent deformation patterns in central Bundelkhand batholith. Proc Ind Acad Sci (Earth-Planet Sci) 104(3):465–488

Applied Engineering Geology Methods for Exemplar Infrastructure Projects in Malopolskie and Podkarpackie Provinces

32

Zbigniew Bednarczyk and Adam Szynkiewicz

Abstract

More than 90 % of landslides in Poland in number of 35,000 is located in the Malopolskie and Podkarpackie provinces. They are causing serious economic loses every year. In 2010, these reached 2.9 bln EUR during the flood in southern Poland. The research was connected with EU financed projects for road reconstructions. The mass movements size of 0.4–2.2 mln m^3 had low rates of displacement from few mm to over 5 cm a year. Colluviums built from saturated flysch soil–rock mixtures required usage of specific multidisciplinary engineering geology methods. Ground conditions were difficult for in situ and laboratory test. The investigation methods included high quality core sampling, GPR scanning, laboratory index, IL oedometer, triaxial and direct shear tests. Mapping by GPS-RTK method was employed for actualization of landslide morphology. Inclinometer and piezometer monitoring measurements were performed by the period of over 6 years. The new real-time early warning system the first of its kind in Poland was installed in 2010 in Beskid Niski Mountains. Obtained data provided parameters for LEM and FEM slope stability analysis. It allowed control of landslide behavior before, during and after stabilization works. The research proved that chosen investigation methods helped in remediation works. The results of the study reveal that large flysch landslides were difficult for counteraction and remediation methods should be considered very carefully. Comprehensive monitoring and modelling before the counteraction stage could lead to a better recognition of landslide remediation possibilities and early warning.

Keywords

Engineering geology site investigations • Landslide monitoring

32.1 Localization and Landslide Geology

The research was performed on the area of southern Poland, where damages to infrastructure, transportation networks or private properties caused by the landslides are the most common in the country. Investigations were conducted on 23 landslides with serious threats to the public roads or other important infrastructure. Mass movements localization and instrumentation in Beskid Niski is presented on Fig. 32.1. Landslides were formed in marine flysch deposits folded during Alpine Orogenesis. Intensive erosion in river valleys and high groundwater level, during the Holocene era, characterized by thick weathering zones activated huge numbers of landslides (Gil et al. 1974; Raczkowski and Mrozek 2002). The main reason for landslides occurrence were high slope inclination combined with flysch type geology. Heterogeneous mixture of soils and rocks were involved in creep processes. Mass movements were reactivated in wet periods many times. Saturated claystones had mechanical parameters as weak cohesive soils. Sandstones usually occurred as thin layers with different degree of digenesis. It allowed water infiltration together with seepage due to many

Z. Bednarczyk (✉)
Poltegor-Institute, Parkowa 25, 51-616, Wrocław, Poland
e-mail: zbigniew.bednarczyk@igo.wroc.pl

A. Szynkiewicz
Kart-Geo, Bacciarellego 39/1, 51-649, Wrocław, Poland
e-mail: adam.szynkiewicz@gmail.com

crack and joints. Movements were usually localized on slopes of inclination varied from 15° to 35° with shallow groundwater levels from 0.5 to 2.0 m. Colluviums depths were changing from few to dozens of meters. Intensive rainfalls together with floods, erosion in river valleys, snow melting and variations of the pore pressure inside soil layers were enhancing the sliding activity (Bednarczyk 2008, 2010, 2012). The problem has intensified in May/June 2010, after intensive rainfalls and flood in southern Poland (Fig. 32.2).

32.2   Field Investigations

Landslides built from rock-soil flysch type deposits required site-specific investigations. These needs site inspection, engineering geology investigations, actual water balance as well as measurements of various specific trigger parameters. Presented investigations included over 600 m of core drillings diameter of 132 mm, depths of 9–30 m together with NNS sampling. Ground Penetration Radar scanning length of 10 km were carefully scaled by boreholes. GPS-RTK method supplemented by conventional geodesy methods was found an effective way of landslide mapping. Over 500 m of inclinometer casings and piezometers were installed for slopes instrumentation. Landslides sizes, depths, failure mechanisms, lithology and engineering geology parameters and groundwater conditions were recognized this way. Implementation of different types of ground movement, groundwater level and pore pressure monitoring allowed

identification of landslide triggers. A new on-line instrumentation was built at Szymbark landslides. Obtained data was applied for modeling of slope stability and design of landslide stabilization works (Fig. 32.3).

32.3   Laboratory Tests

Laboratory tests included index tests (grain size, moisture content, Attenberg limits, bulk density, density of soil particles, content of organic/bitum. material), direct shear, oedometer and triaxial CID tests. Soils represented silty loams, silty clays to claystones, had high moisture content of 18–37 %, liquidity index of 0.1–0.8, eff. cohesion of 6.5–10 kPa, eff. angle of shearing resistance of 11–15° and a very high compressibility. The highest moisture content of ≈30 % and plasticity index of 30–40 % were observed in samples taken near the sliding surface (Fig. 32.4). The slip surface depths of 2–16 m were in good agreement with index test results.

32.4   Landslide Monitoring

Identification of landslide triggers were performed using standard and real-time monitoring methods. Validation of the monitoring results for 23 sites in the network was possible due to continuous site inspection program. Groundwater table depths and pore pressures were measured in
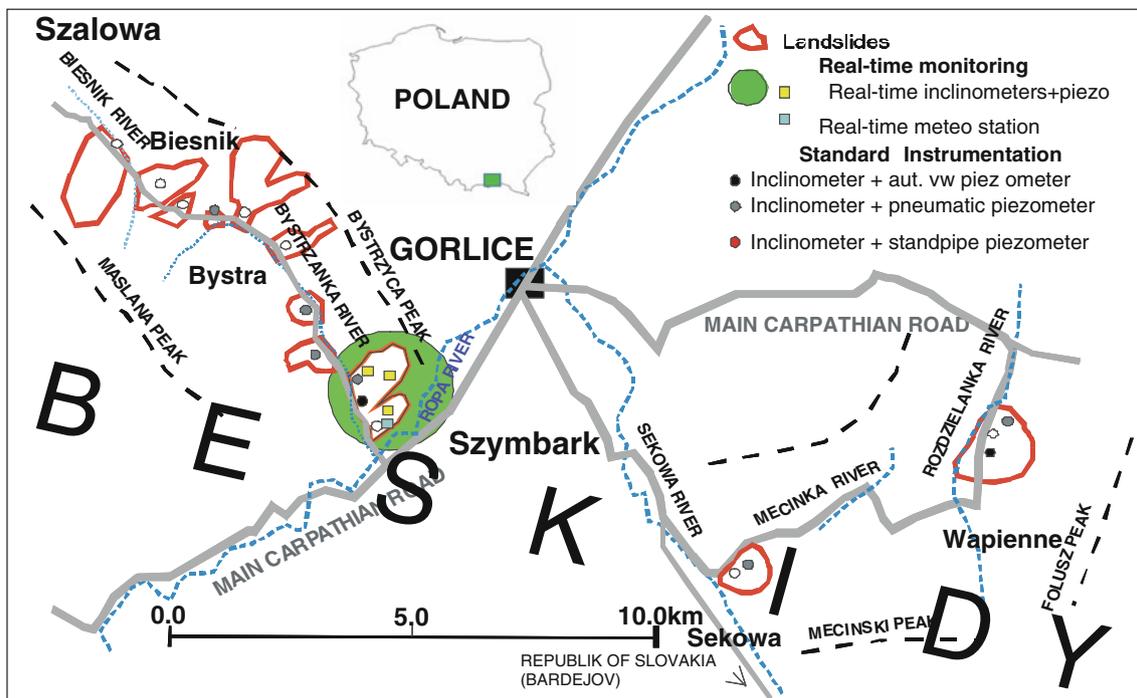
Fig. 32.1 Landslide localization
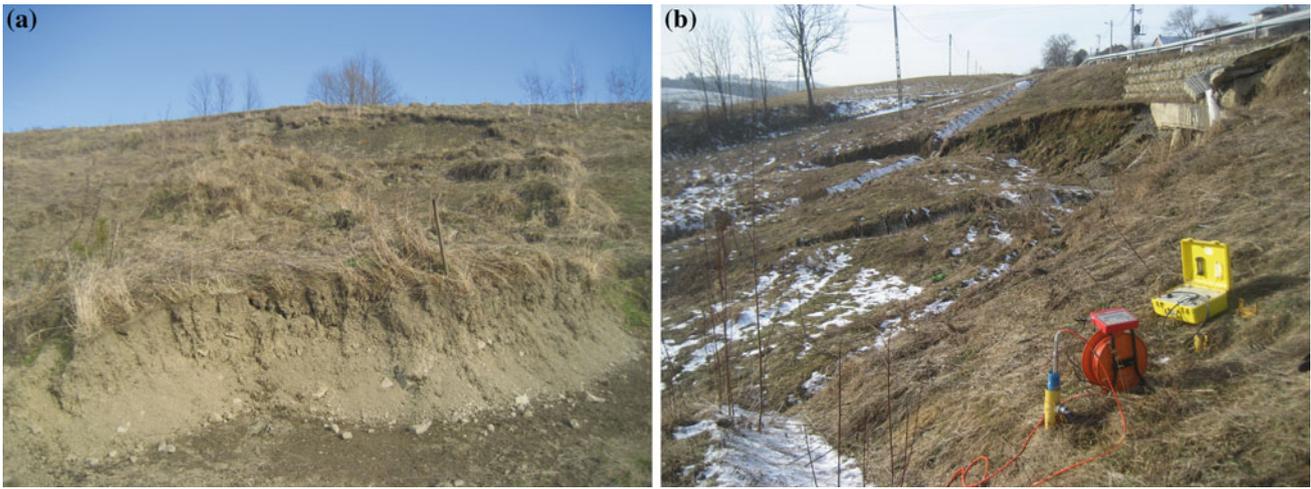
Fig. 32.2 Landslide activation. **a** Szymbark. **b** Strzeszyn—monitoring measurements
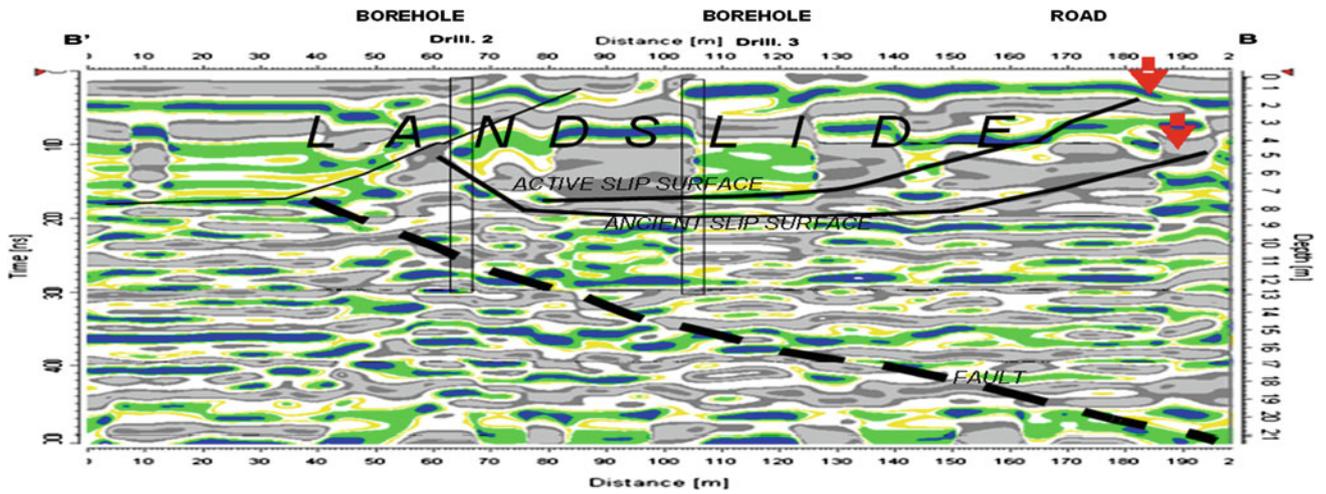
Fig. 32.3 GPR profile Sekowa landslide

Fig. 32.4 Index laboratory tests, Szymbark landslide
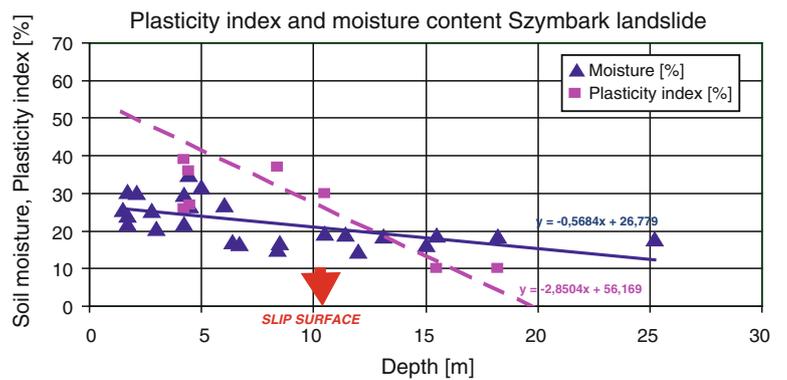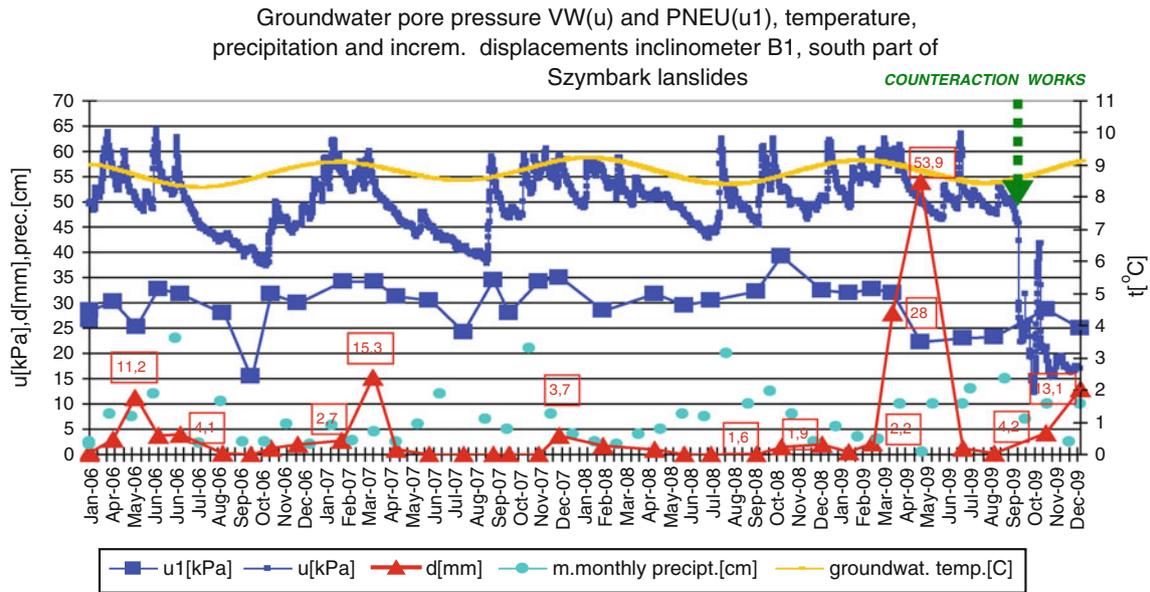
Fig. 32.5 Monitoring measurements Szymbark landslide

order to estimate effective stresses using standpipe, pneumatic and automatic vibrating wire piezometers. Subsequent monitoring surveys performed by the period of over 6 years, every 30–45 days determined the magnitudes, depths, directions and rates of displacements. The displacements varied from several up to 400 mm (after damage of inclinom. casing).

The movements usually occurred after the pore pressure reached 50–100 kPa on the slip surface. Comparison of displacements, pore pressure, groundwater level depth, temperature and precipitation data shows, that the largest displacements at Szymbark landslides occurred when the pore pressure decreased after high value periods in May–June 2006 (9.6–11 mm), during stabilization works in Dec. 2006 (49 mm) and May–June 2010 (Fig. 32.5). The first in Poland, real-time monitoring system was installed in May 2010 in Szymbark. Installation was realized just before record high precipitations of 100 mm/m^2 in 3 h time. Four on-line stations installed over the public road included two 3D inclinometers (12 and 16 m, totally 56 tilt sensors), one in-place inclinometer (14 m, 3 IP uniaxial sensors), automatic pore pressure transducers and automatic weather station. Total deformation sqrt (x^2 + y^2) reached 34–50 mm during 34 months time (Fig. 32.6).

32.5 Numerical Modeling

The slope stability analyses based on assumption of rotational failure were realized using LEM Janbu, Bishop methods and FEM methods (Figs. 32.7, 32.8). The applied

approach allowed analyzing influence of high pore water pressure on the shear strength reduction. Proposed counteraction methods were tested using classical LEM methods. At Sekowa landslide, values of relative factor of safety Fs, calculated by Bishop method, were slightly above Fs = 1.13 before stabilization and Fs = 1.58 after it. Expected displacements were calculated by FEM methods, SoilVision codes and linear elastic models. Monitoring data were included in boundary conditions definitions. The expected displacements on Sekowa landslide are presented on Fig. 32.8. The final FEM mesh indicated that landslide was active and dangerous for the public road.

32.6 Design and Control of Stabilization Works

The results of exemplar counteraction works together with chosen investigation, monitoring and stabilization methods are presented in are presented in Table 32.1. The basic landslide remediation questions were addressed to the effective mitigations needed to maintain stability. At Sekowa remediation included gabion wall built on micropiles foundation along the river (Fig. 32.9). Second retaining wall on micropiles foundation was installed above the road. Drainage system lead down groundwater to the river and to a new culvert under the road. At Szymbark landslide partial stabilization at the front landslide part was decided. It included gabion walls along the river, surface and internal drainage system, two new culverts under the road, horizontal drainage boreholes with filters, anchors 20 m long to the bedrock, and
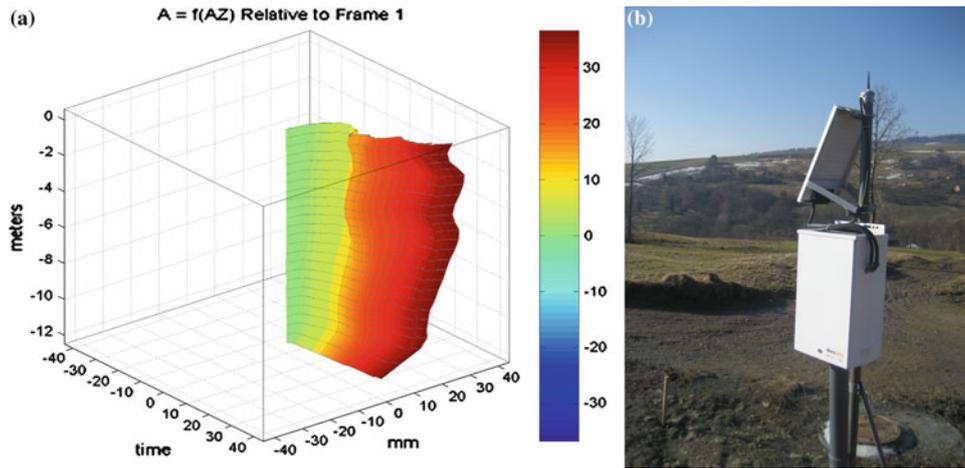
Fig. 32.6 On-line monitoring. **a** 3D displacements plot. **b** Field Station
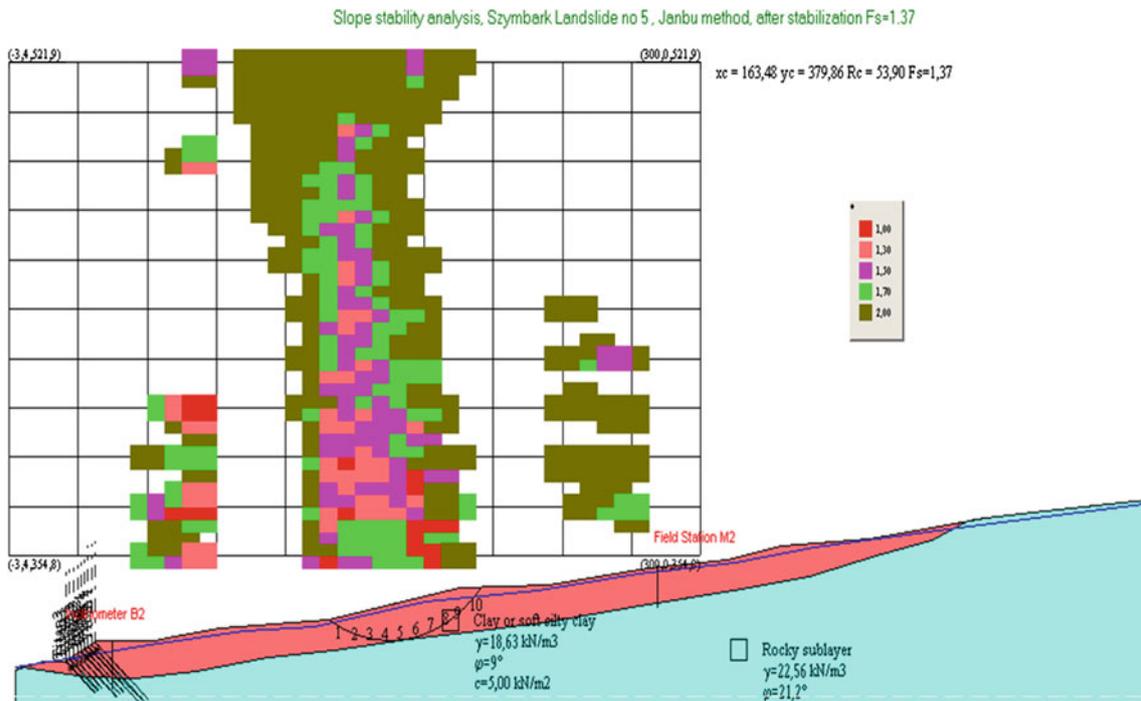
Fig. 32.7 LEM numerical modelling, Szymbark

Geobrugg high tensile wire mesh. The pore pressure values after counteraction dropped in both areas (from 45 to 30 kPa at Sekowa and from 70 to 15–50 kPa at Szymbark). Groundwater level depths were lowered from 0.5–1.3 to 2.2–3.0 m. The movements before counteraction works varied from 26 to 138 mm. In some cases they increased to over 60 mm during remediation, but after usually were lowered to ± few mm (Fig. 32.10). However, on Szymbark landslide, displacements up to 10 mm were recorded after remediation works. In May-June 2010 they increased after intensive rainfalls up to 18 mm, what was detected by early warning system.

Fig. 32.8 FEM numerical modelling, Sekowa
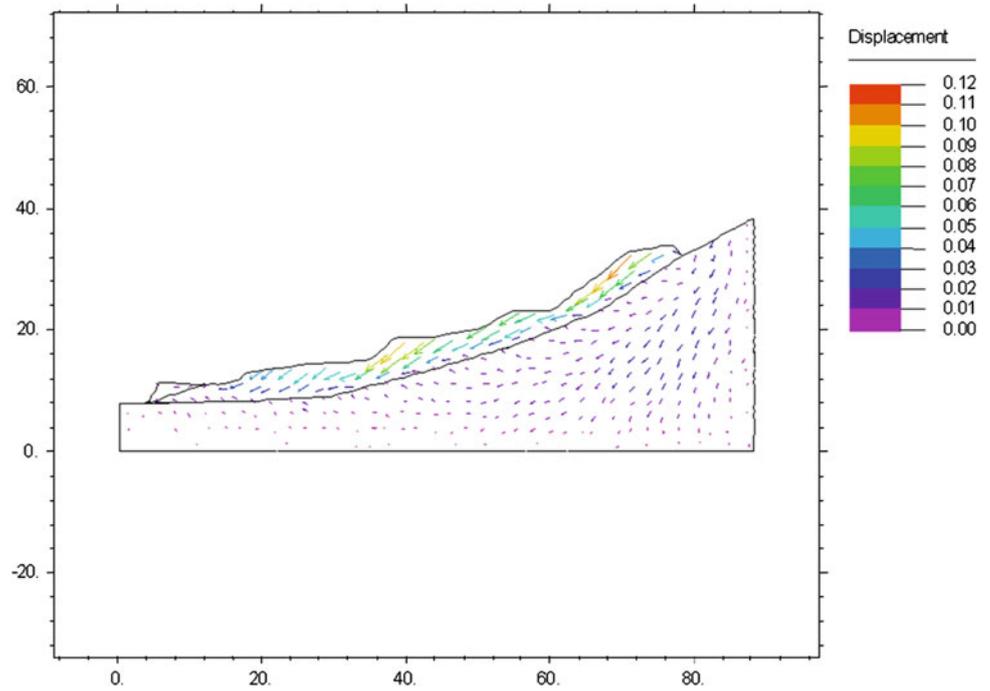
Table 32.1 Control of mitigation measures

Landslide	Vol. (m³)	Depth (m)	Displacements, (mm) before during after stabilization			Investigation methods	Counteraction methods
Sekowa	0.4	2.7–5.1	26	61	4–5	Boreholes, lab. tests, GPR, GPS-RTK, inclinometers, pore pressure transducers piezometers	Retaining gabion wall on pile foundation, micropiles, surface drainage system
Szymbark	2.2	1.3–5.0	138	19	8–13	Boreholes, lab. tests, GPR, GPS-RTK, inclinometers, pore press. stand + on-line	Gabion walls, anchors, high tensile wire mesh, internal and surface drainage

Fig. 32.9 Stabilization of
Sekowa landslide

Fig. 32.10 Control of
stabilization works, Sekowa
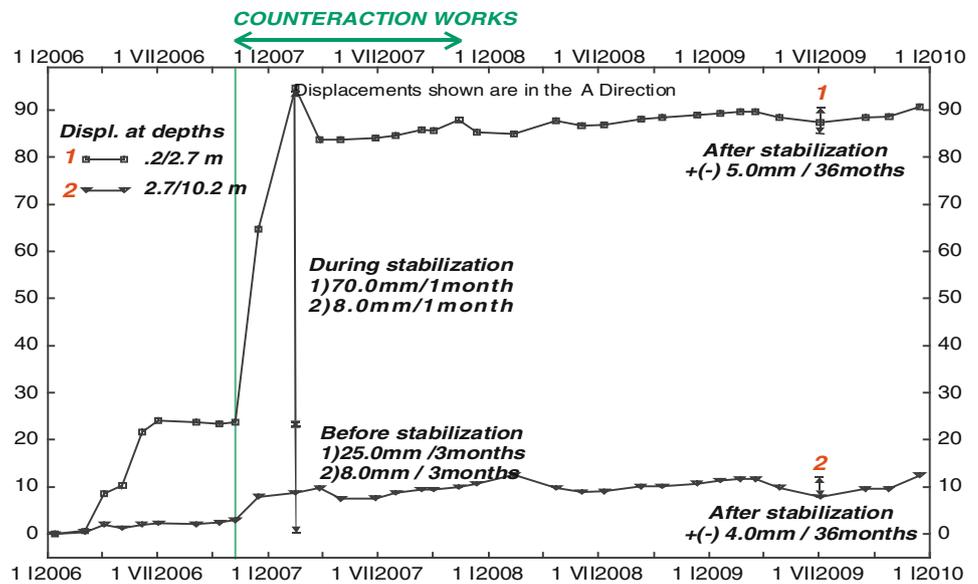
32.7 Conclusions

The research proved that chosen investigation, monitoring and modelling methods were useful for infrastructure projects. The continuous site inspection programme detected displacements from few mm to 40 cm to the depths of 1.3–18.0 m. The main triggering factors were connected with precipitations and changes of pore pressure. Proposed stabilization methods were fully effective at Sekowa landslide and four other landslides. In Szymbark the remediation limited displacement ranges. The results of the study reveal that large flysch landslides were difficult for counteraction and remediation should be considered very carefully. Comprehensive monitoring and modelling methods before the counteraction stage could lead to a better recognition of remediation possibilities and early warning. Implementation of a new real-time monitoring techniques enabled continuous observation of landslide behavior to apply appropriate management to the sites of highest risk to the road network.

References

Bednarczyk Z (2012) Geotechnical modelling and monitoring as a basis for stabilization works at two landslide areas in Polish Carpathians. In: Proceedings of 11th International & 2nd North American Symposium on Landslides. Canadian Geotechnical Society, Banff, Canada, Balkema, Taylor and Francis, pp 1419–1425

Bednarczyk Z (2010) Soil-structure interaction on three stabilized flysch landslides in polish carpathians. In: *The Proceedings of the First International Conference on Advances in Multiscale Mechanics AIMM'10*. KAIST, South Korea, Techno-Press, pp 1389–1397

Bednarczyk Z (2008) Landslide geotechnical monitoring network for mitigation measures in chosen locations inside the SOPO Landslide Counteraction Framework Project Carpathian Mountains, Poland The First World Landsl. Forum, Tokyo, ICL, UN, pp 71–75

Gil E, Gilot E, Kotarba A, Starkel L (1974) An early Holocene landslide in the Niski Beskid and its significance for paleogeographical reconstructions. St Geom Carpat-Balc 8:69–83

Raczkowski W, Mrozek T (2002) Activating of landsliding in the Polish Flysch Carpathians by the end of 20th century. Studia Geom Carpatho Balcanica 36:91–111

A Brief Overview of the Typical Engineering Characteristics of Tropical Red Soils

George Brink

Abstract

Tropical soils in many ways have unique characteristics that can mainly be ascribed to the compositions and micro-structures of a material developed under hot, wet soil-forming conditions. For the purpose of this article, the term "tropical soil" will loosely refer to soils formed under such conditions, predominantly through chemical weathering processes. Most of these soils contain abundant iron and aluminium oxides due to the rapid breakdown of feldspars and ferromagnesian minerals, the removal of silica and bases and the concentration of iron and aluminium oxides or sesquioxides (sesquioxide = three atoms of oxygen to two atoms of another element i.e. Al_2O_3 or Fe_2O_3). Due to the high iron content, these soils are more often than not red in colour. The unique processes and conditions of soil formation in a tropical environment directly result in material compositions and structures that influence the engineering properties of tropical soils and the determination of these properties. Tropical soils do not behave in a similar fashion to temperate zone soils and consequently do not behave as expected when using conventional laboratory testing methods. This includes the susceptibility of the material to physical and mechanical breakdown, as well as a change in material properties due to cementing of the available sesquioxides. It is the aim of this paper to summarise and discuss the established unique engineering properties associated with soils formed in a tropical environment as summarised in the existing literature.

33.1 Introduction

The title of this article implies that tropical soils are sufficiently distinctive to be evaluated separate from conventional soils from more temperate climatic regions. Tropical soils in many ways have unique characteristics that can mainly be ascribed to the compositions and micro-structures of a material developed under hot, wet soil-forming conditions. For the purpose of this article the term "tropical soil" will loosely refer to soils formed under such conditions, predominantly through chemical weathering processes and separate from those soils formed in areas subject to more temperate climates with distinct seasonal variations. Throughout the available literature, tropical soils can broadly be subdivided into (i) tropical red

soils and (ii) tropical black soils. Due to the significant differences in material properties and engineering behaviour of the two identified general tropical profiles, emphasis will predominantly be placed on the discussion and investigation of tropical red soils in this paper.

Tropical red soils are often erroneously referred to either as 'laterites', 'laterite soils', 'latosols' or 'lateritic soils'. The existing chemical, geological and geotechnical data concerning laterites confirm that a universal, standardised terminology used to describe these materials has not been established and numerous inconsistencies have developed in the identification, classification and nomenclature between tropical red soils and laterites. For the purpose of this article, the term "laterite" refers solely to those materials or soil horizons which either represent laterite formation in the form of hardened pedogenic horizons or contain distinct evidence of laterization in the form of nodules, concretions or distinct discolouration, and is excluded from the tropical red soils category discussed here.

G. Brink (✉)
Exxaro Resources, PO Box 9229, Pretoria 0001, South Africa
e-mail: george.brink@exxaro.com

33.2 Unique Engineering Characteristics of Tropical Red Soils

The usefulness of conventional index and strength tests for the identification and engineering classification of tropical soils has been questioned in the past, primarily due to the dependence of such tests on the sample preparation process and the variation of the natural soil structure.

33.2.1 Index and Physical Properties

The well-known global classification systems, such as the Unified Soil Classification System (USCS), are all based on the grain size distribution and Atterberg Limits for soils from temperate climatic environments. The clay minerals in these soils are generally stable, allowing for the relatively accurate determination of the index properties and allowing the development of numerous relationships between index properties and engineering behaviour. Due to the instability of clay minerals in tropical soils and the susceptibility of changes in material properties on drying, the relationships between the results of classification tests and the engineering behaviour are not as easy to obtain for tropical red soils (Mitchell and Sitar 1982). Further, it should also be kept in mind that drying not only occurs during sampling and testing, but also depends on the local climatic conditions, drainage and profile position. This may result in significant heterogeneity in the established regional soil characteristics (Fig. 33.1).

Northmore et al. (1992) established that index property values of tropical red soils are extremely sensitive to pretreatment of the samples prior to testing, particularly to pre-drying and, for plasticity and shrinkage tests, to the degree of manipulation or mixing of the test sample. Drying of tropical red soils typically result in irreversible changes in the physical properties of the material. This initiates aggregate

Fig. 33.1 Established variability in Atterberg limits tropical and lateritic soils from Ghana (Gidigasu 1974)

formation and cementation by sesquioxides and the irreversible loss of water from the structures of hydrated clay minerals (Table 33.1).

The unique features of weathering and pedogenesis in tropical environments result in compositions and structural development that directly influences the engineering properties of these soils and their determination. Cementation of particles by the sesquioxides, together with the hydrated states of some minerals, lead to high void ratios, low compressibility and potentially high permeabilities compared to the high plasticity values and clay contents.

It is generally assumed that the permeabilities of in-situ tropical red soils are high (up to 10^{-2} cm/s), but as was the case with characterizing the strength of these materials the available data on the permeabilities of undisturbed tropical soils are very limited. Northmore et al. (1992) recorded values of 1.1×10^{-3}–5.8×10^{-6} cm/s for the Kenya specimens and 5.6×10^{-4}–2.2×10^{-6} cm/s for the specimens from Indonesia. This roughly equals the established permeabilities of silty materials or very fine sands from more temperate environments. As the permeability of a material is highly dependent on its structure, there is a significant variation in the available permeability results of undisturbed specimens and those permeabilities determined on remoulded specimens. The permeability of remoulded and compacted tropical red soils was found to vary between 1×10^{-6} and 1×10^{-8} cm/s (Saunders and Fookes 1970), with Northmore et al. (1992) reporting a "hundred to three hundred fold" decrease in the permeability of remoulded specimens compared to the values established for undisturbed specimens.

The effect of sub-surface biotic activity on the overall permeability of tropical red soils should not be neglected. Blight (1991) has highlighted the influence of termite activity on the overall permeability of the soil, as well as that of open channels from plant roots and other organisms. The presence of these cavities may increase the overall permeability by up to several orders of magnitude.
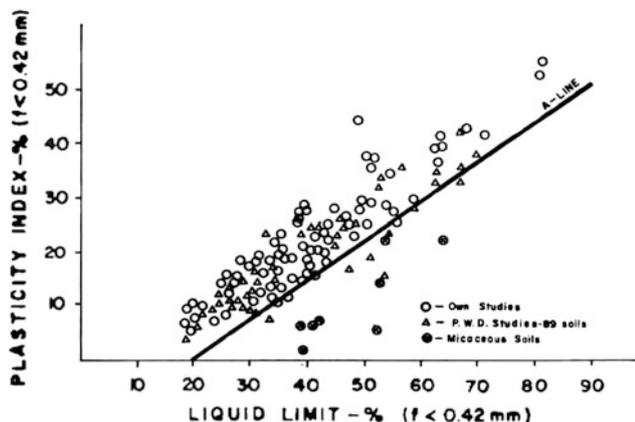
33.2.2 Mechanical Properties

The available published data on the strength testing of undisturbed samples of tropical red soils is limited, with the majority of available test results reflecting the shear strength parameters obtained from remoulded specimens. During their study, Northmore et al. (1992) determined the shear strength characteristics for a number of undisturbed and remoulded samples of tropical red soil from Kenya and Indonesia. Values of effective cohesion (c′) were found to be highly variable, ranging from 0 to 97 kPa and values of effective angle of internal friction (ϕ′) in the range of 11° and 44° for those tests completed on undisturbed samples. These represent a big variation in values and are generally higher

Table 33.1 Effect of drying on index properties of hydrated clay from Hawaiian Islands (Gidigasu 1974)

Property	Natural moisture content	Partially air dried	Completely air dried
Sand (%)	30	42	86
Silt (%)	34	17	11
Clay (%)	36	41	3
Liquid limit (%)	245	217	NP
Plastic limit (%)	135	146	NP
Plasticity index (%)	110	71	NP

NP = Non plastic

Table 33.2 Summary of available shear strength characteristics of undisturbed samples of tropical red soils

Reference	Average dry unit weight (kg/m^3)	Friction angle (°)		Cohesion (kPa)	
		Range	Average	Range	Average
Vargas (1974)	–	23–33	28	0–59	24
Tuncer and Lohnes (1977)	1,300	27–57	42	48–345	163
Fos (1973)	1,150	36–38	37	22–28	25
Northmore et al. (1992) (Indonesia)	836	11–36	22	2–97	32
Northmore et al. (1992) (Kenya)	1,112	12–44	25	0–55	24

than those soils similar plasticity or clay fraction but formed in temperate environments. Wesley (1988) comments that test results of allophane-rich soils generally reflect soils of higher shear strength values than those of halloysite-rich soils (Table 33.2).

The residual friction angles of remoulded or destructured materials were found to vary between 18° and 41° (mostly 28°–38°), with effective cohesion values ranging between 0 and >50 kPa (De Graft-Johnson et al. 1969; Gidigasu 1974; Saunders and Fookes 1970). In an effort to establish the effect of remoulding on the engineering behaviour of the soil, Northmore et al. (1992) also determined the shear strength characteristics of two sets of destructured and compacted samples to compare with the results obtained from the testing of the undisturbed samples. The test results revealed largely similar stress-path and strength behaviour despite the large structural differences of disturbed and destructured materials. In both cases the compacted specimen revealed higher effective friction angles than the undisturbed samples.

Northmore et al. (1992) concluded from their testing of tropical red soils from Indonesia and Kenya that there appears to be a positive relationship between the effective shear strength of tropical soils and its plasticity index and moisture content. This is the opposite of the established relationship in clayey soils from temperate climatic regions. A general positive relationship further exists between the increases in the effective strength of the material with an increase in depth below natural ground level, most likely due to either the development of material structure.

Consolidation test data from the literature indicates highly variable initial void ratios, typically varying between 0.92 up to 5.36. It has generally been assumed that the tropical red soils are fairly incompressible compared to clays from temperate climates, but the available consolidation test results on undisturbed samples reflect very high rates of primary consolidation (indicating high rates of short term settlement), making the calculation of the consolidation coefficient (C_v) very difficult. When evaluating the rate of consolidation according to the percentage of consolidation in the first minute of testing, it is evident that allophone-rich materials generally experience a reduction in the consolidation rate with increasing stress, whereas halloysite-rich samples tend to maintain a high rate of consolidation throughout. C_v values typically range between 6.3×10^{-6} and 2.5×10^{-2} cm^2/s. The consolidation coefficients of compacted or remoulded tropical red soils were found to typically range between 1×10^{-1} and 1×10^{-3} cm^2/s (Saunders and Fookes 1970). The compressibility results (M_v) ranges from high to very low, with an overall decrease in compressibility with an increase in the applied stress. Secondary consolidation (C_a), used as an indication of the long term consolidation behaviour of the soil, was also found to generally increase with an overall increase in the applied stress (Northmore et al. 1992).

33.3 Conclusions

The unique processes and conditions of soil formation in a tropical environment directly result in material compositions and structures that influence the engineering properties of tropical soils and the determination of these properties. The available undisturbed and remoulded results discussed here reflect a significant variation in the values in the shear strength characteristics of tropical red soils and, as was found to be the case with the index properties, the heterogeneity of the material characteristics, degree of weathering and cementation are the most likely all reasons for the variations. It is therefore recommend that the data from index tests alone should not be used to distinguish between soils formed in different climatic regimes and from different parent rock types. However, it may be possible to make use of the classification tests, gradings and Atterberg Limits to establish a correlation with the expected engineering behaviour for specific application and based on local experience.

Test results of undisturbed and remoulded soil specimens confirm that tropical red soils are highly sensitive to structural breakdown and manipulation. Manipulation of the material using heavy equipment may result in marked changes in characteristics and the ease with which it is handled on site. Further, the sensitivity of tropical red soils to drying was found to result in changes (frequently irreversible) in the physical characteristics of the material, mainly due to aggregate formation and cementation by sesquioxides and the irreversible loss of water from the structures of hydrated clay minerals.

References

Blight GE (1991) Tropical processes causing rapid geological change. In: Forster A, Culshaw MG, Cripps JC, Little JA, Moon CF (eds) Quaternary engineering geology, Engineering geology special publication, vol 7. Geological Society, London, pp 485–490

Buchanan F (1807) A journey from Madras through the Countries of Mysore, Canara and Malabar, vol 2. East Indian Company, London, pp 436–460

Fermor LL (1911) What is laterite? Geol Mag 5(8):453–462

De Graft-Johnson JWS, Bhatia HS, Gidigasu MD (1969) The engineering characteristics of the lateritic gravels of Ghana. In: Proceedings of special session engineering properties of lateritic soils, 7th international conference soil mechanics foundation engineering, Mexico, vol 1, pp 117–128

Gidigasu MD (1974) Degree of weathering in the identification of laterite materials for engineering purposes—a review. Eng Geol 8:213–266

Joachin AWR, Kandiah S (1941) The composition of some local soil concretions and clays. Trop Agric 96:67–75

Lacroix A (1913) Laterites of Guinea and alteration products associated with them. Nouveau Arc Mus Hist Nat 5:255–356

Marques JJ, Schulze DG, Curi N, Mertzman SA (2004) Major element geochemistry and geomorphic relationships in Brazilian Cerrado soils. Geoderma 119:179–195

Martin FJ, Doyne HC (1930) Laterite and lateritic soils in Sierra Leone. J Agric Sci 20:135–143

Millard RS (1962) Road building in the tropics. J Appl Chem 12: 342–357

Mitchell JK, Sitar N (1982) Engineering properties of tropical residual soils. Engineering and construction in tropical and residual soils. In: Proceedings of the ASCE geotechnical engineering division speciality conference, Honolulu, Hawaii, pp 30–58

Northmore KJ, Culshaw MG, Hobbs PRN, Hallam JR, Entwisle DC (1992) Engineering geology of tropical red clay soils: summary findings and their application for engineering purposes. British geological survey technical report WN/93/15

Pendelton RL (1936) On the use of the term laterite. Am Soil Surv Bull 17:102–108

Saunders MK, Fookes PG (1970) A review of the relationship of rock weathering and climate and its significance to foundation engineering. Eng Geol 4:289–325

Uehar G (1982) Soil science for the tropics. Engineering and construction in tropical and residual soils. In: Proceedings of the ASCE geotechnical engineering division speciality conference, Honolulu, Hawaii, pp 13–27

Wesley LD (1988) Engineering classification of residual soils. In: Proceedings of the 2nd lnternational conference on geomechanics in tropical soils, Singapore, vol 1, pp 77–84

Remote Analysis of Rock Slopes with Terrestrial Laser Scanning for Engineering Geological Tasks in Reservoir Planning

Hieu Trung Nguyen, Tomás M. Fernandez-Steeger, Hans-Joachim Köhler, and Rafig Azzam

Abstract

Building the lower basin of a pumped-storage hydropower plant in an active limestone quarry without any sealing is a challenging project. A proper site investigation is crucial to increase the overall efficiency of planning as well as realisation by anticipating potential problems and sticking points. The local geology comprises a complex system of reef structures and bedded sequences that is intersected by faults. Sets of faults can be identified on different scales and the fracturing patterns vary vertically and horizontally. Both the ongoing quarrying as well the sheer size and steepness of the outcrop prevent any extensive data acquisition using traditional methods. Therefore, terrestrial laser scanning (TLS) was used to map the quarry and to create a high resolution digital elevation model (HRDEM). The HRDEM allows to perform spatial analysis with respect to the distribution of geohydraulic and geotechnical properties of the rock mass in the quarry. The major advantages of this approach are the increased level of detail, a substantial improvement of documentation and synergetic effects that arise from the multiple different applications of scan data e.g. for analysis, interpretation, planning and solving geohydraulic and geotechnical issues. It has shown in practice that this multi-facetted usage of the collected data outweighs the initial efforts of data collection and processing by far.

Keywords

Pumped-storage hydropower • Rock mass characterization • Terrestrial laser scanning • Blautal

34.1 Introduction

For the planning approval of the pumped-storage hydropower plant (PSH) Blautal, commissioned by the municipal utilities Ulm (SWU) and EDUARD MERKLE GMBH & CO. KG, extensive geohydraulic and geotechnical site investigations are mandatory. Located about 4 km of the spring Blautopf in the karst landscape of the Swabian Jura's southern edge in Southern Germany, the PSH shall have an installed capacity of 60 MW by a built-in reservoir of 1.1 million m³ and a height difference of 170 m. Initial planning has stipulated an unsealed lower basin situated on a mountainside inside the quarry as the preferred option of construction. The absence of any sealing means that the basin will be incorporated within the natural groundwater. Due to the subsequent use, the mine plan provides that the limestone will be quarried to 10 m below the groundwater table, creating a steep, 95 m high rock slope next to the eastern bank of the basin. As there are environmentally sensitive biotopes nearby, the anticipated impact on natural groundwater conditions must be limited in space. Therefore, two major aims have been defined for the site-investigation: To specify the potential influence on the groundwater during excavation, PSH construction and operation time on the one hand. On the other hand first estimations of the expected dynamic

H.T. Nguyen (✉) · H.-J. Köhler
Dr. Köhler & Dr. Pommerening GmbH, Am Katzenbach 2, 31177 Harsum, Germany
e-mail: hieu.nguyen@koehler-pommerening.de

T.M. Fernandez-Steeger · R. Azzam
Department of Engineering Geology and Hydrogeology, RWTH Aachen University, Lochnerstraße 4-20, 52064 Aachen, Germany

Fig. 34.1 Tripod mounted instrument, scanning a 65 m height slope. *Light-colored lime* —and marlstone, complex geological features and different rock face conditions due to ongoing quarrying complicate the rock classification

stress changes within the rock are to be given, since pore water pressure can significantly reduce slope stability (Köhler et al. 2013). To meet these goals, a detailed geohydraulic and geotechnical rock mass description is essential. The obtained information serves as input data for a detailed geohydraulic rock mass model with special emphasis on the location and spatial distribution of discontinuities as well as their degree of karstification. This will allow a hydraulic characterization of the rock mass and the identification of potential failure mechanisms due to increased buoyancy or sliding wedge formation. The local geology comprises a complex system of reef structures and bedded sequences that is intersected by faults. Sets of faults can be identified on different scales and the fracturing patterns vary vertically and horizontally. Both the ongoing quarrying as well the sheer size and steepness of the outcrop prevent any extensive data acquisition using traditional methods (Fig. 34.1). In the presented study area, traditional manual recording would be very laborious and time-consuming and therefore economically not feasible, as outlined above. Thus, remote sensing by terrestrial laser scanning (TLS) was used to map the quarry and subsequently used to create a high resolution digital elevation model (HRDEM).

34.2   Methodology

Terrestrial laser scanning utilizes reflected laser pulses emitted from a tripod-mounted scanning instrument (Fig. 34.1) to determine distances to targets of interest. The scanned surfaces are recorded as point data with accuracy ranging from 4 to 3 cm. Thus, TLS data provide the possibility to measure and visualize topographic relief down to centimeter resolution for close-up digital inspection.

Provided that the exact scanner position is known, each point can be georeferenced and used to compute a digital elevation model (DEM). The newly generated DEM in turn can be registered with color photographs and serve as the basis for engineering geological rock mapping. The entire quarry has been time-efficiently scanned from different positions by a terrestrial laser scanner with average point spacing from 10 to 15 cm, including additional scans of selected slopes with 2 cm point spacing. Each scanner position has been determined by the use of Real Time Kinematic (RTK) satellite navigation. In addition, a photographic mapping has been applied to assist data analysis and interpretation. Applying the data preparation and processing after (Nguyen et al. 2011), a DEM of the quarry in 1 m resolution and HRDEMs of different slope exposures in 2 cm are used to create up to date topographic maps, cross-sections and virtual outcrop models. Thus, different— otherwise laborious—tasks can be completed in a `virtual lab', even for inaccessible areas.

34.3   Applications: A Spatial Analysis Approach

The following descriptions focuses on how to transform structural information from a HRDEM of a jointed rock mass into an organized discontinuity-network. For this purpose, the characterization of a rock mass has been exemplarily executed on a virtual outcrop model of the steep eastern slope of the investigation site. Due to low coloring diversity and the complex geological structure with its multiple reef formations and interconnected bedding, an interactive data interpretation is required for the rock mass characterization. In the beginning, an orthogonal projection of the HRDEM allows to precisely visualize the morphology

Fig. 34.2 Manual rock map by using the HRDEM. It forms the basis to locate geological features and to determine their attitude
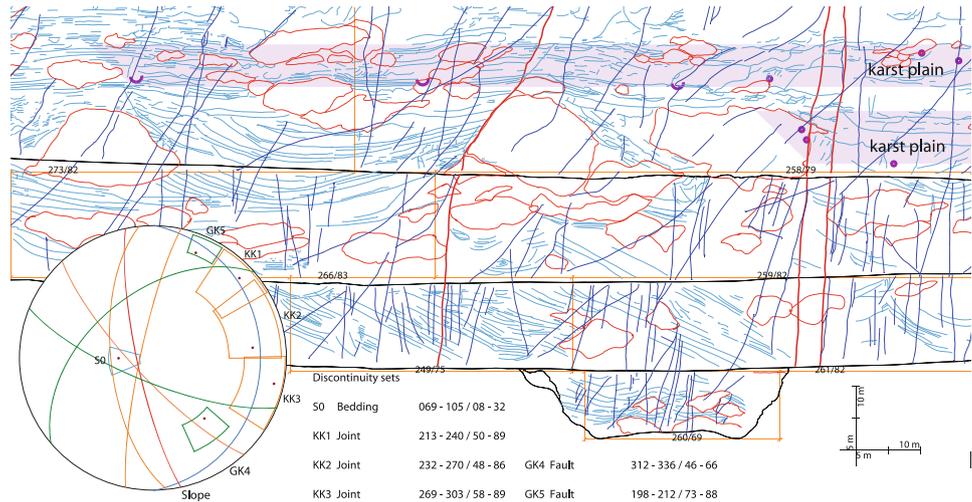
of vertical and overhanging rock faces with an adaptable map scale for an adequate display. This enables different applications, e.g. the traditional mapping by simply tracing geological structures, the measuring of geometric features and the estimated localization of karst plains and shafts (Fig. 34.2). Identified features are from top to bottom: thin calcareous marlstone layers with underlying massive and clustered biohermal limestone interlocked with reworked framework elements and stratified limestone in the intermediate basins. All these structures are bound together by secondary encrustation or cementation. Apart from the bedding-planes, the fracture network consists of two conjugate sets of steep closely spaced joints and two conjugate sets of widely spaced faults with normal down-dip displacement. At different levels of elevation, karst features are exposed. However, it was difficult to clearly separate different lithological units during manual pre-allocation: As the joint patterns of the examined outcrop are complex and intersecting, tracing certain discontinuities often became unclear and ambiguous. Thus, analyzing the HRDEM in a virtual lab has to be repeated under different display conditions (angle of view, angle of light, color shade, photographic overlays). In a later stage, an adjustment by secondary data, e.g. calculated or estimated discontinuity frequency, has proved to be very helpful. To this extent, the framework of a discontinuity-network has been established by a heuristic description, encompassing the discontinuities in a rock mass. For the next step, using the orientation of each computed vertex or face of the HRDEM, a TLS data set can be automatically compiled into local dip and strike direction. This enables the researcher to map the populations of structural slope facets, to carry out a stereographic analysis and then ultimately identify discontinuity sets. For a time-efficient approach, the HRDEM has been divided into several partitions prior to structural analysis in order to decrease the noise generated from the spatial variability of

identical fracture patterns over the entire outcrop. In order to identify individual sets, overpopulated steep west inclined facets resulting from manmade slope expositions have to be removed before transforming the orientation data into density patterns. By using the frequency distribution of spatial orientations, several present discontinuities can be characterized from the density pattern by successively decimating dominant sets to emphasize subdominant orientations (Köhler 2013). With the possibility to color and visualize identified sets within the HRDEM, it shows that the analyzed orientation data can be related to flat-angled east dipping bedding surfaces, to steep NNW-SSE and WSW-ENE striking conjugate joints and to subdominant steep WNW-ESE striking faults and a few NE-SW striking faults (Fig. 34.2).

Application continued with extracting traces of geological features by using an algorithm which sets closely spaced scanlines onto the partitions of the HRDEM and utilizes a moving search window for corner detection. By computing the intersection points between the scanlines and traces, resulting discontinuity frequency and their spatial pattern can be visualized into a grid, suitable for designating homogeneous areas (Fig. 34.3a). Here, discontinuity spacing showed distinguishable areas of closely to widely spaced joints. Again, a cross validation with manual pre-allocation is necessary, as scan resolution and rock faces determine the quality of traceable features and spacing data (Fig. 34.3b). However, as the HRDEM depicts the in situ condition of the slope, blasting of ongoing mining operations significantly increases the joint density, creating a disordered network that strongly differs from the original, tectonically induced, system of fractures. These areas were treated separately for evaluating the discontinuity connectivity in the rock mass (Fig. 34.3b). By displaying those features with other surface characteristics in engineering geological plans and other visual methods of displaying field data like cross-sections or

Fig. 34.3 a Narrow spaced scanlines shows spatially different joint density, separating massive reef bodies and thinly bedded marlstone layers. At the time of the recording, different blasting techniques altered traceable joint densities. **b** Translated into density classes for a practical use. As low resolution areas, fresh blasting works and anthropogenic features influence the classification, the results has to be field-validated
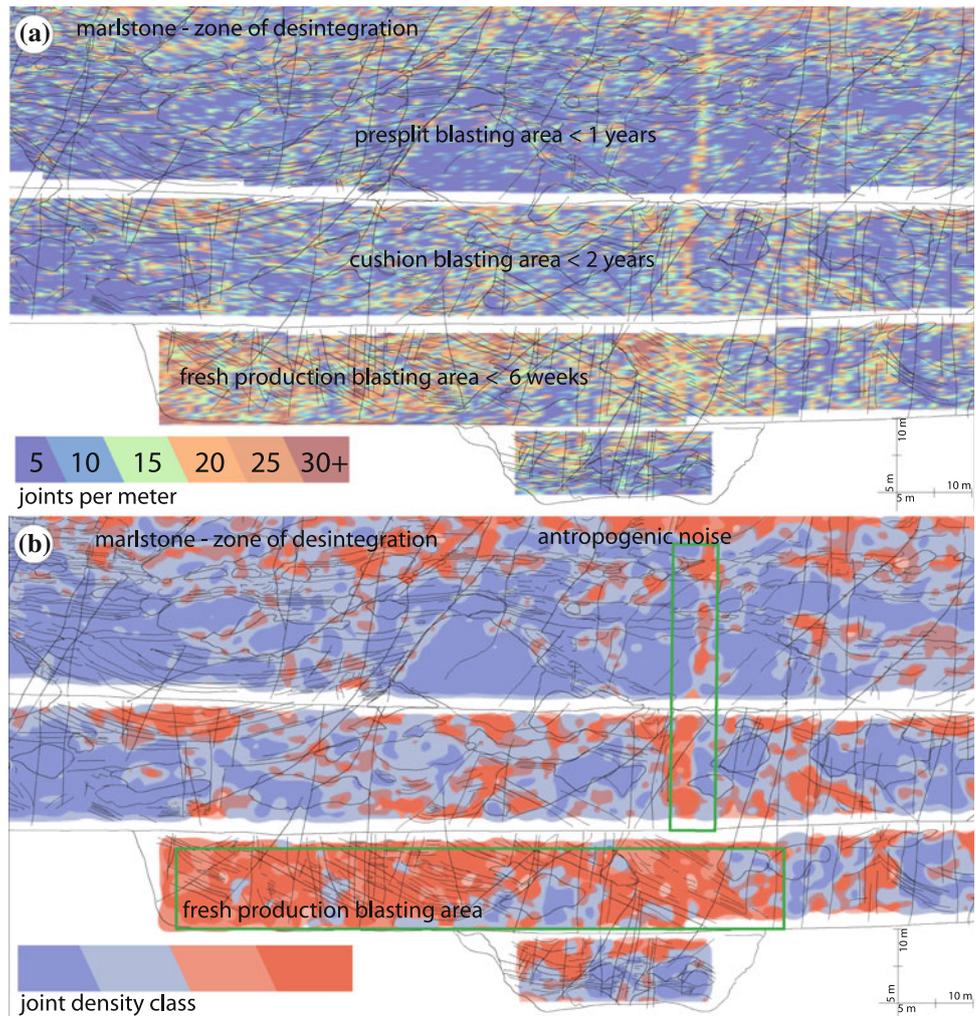
3D models, a high horizontal and vertical precision of the different information locations was secured. Based on this data and in combination with the results from prior applications, a discontinuity network can finally be organized as sets of discontinuities with identified spacing, persistence and attitudes. The major advantage of this procedure is the generation of detailed multiple-layered thematic 3D maps which provided a substantial improvement of data, knowledge representation and documentation, which in turn can be used as a template for ongoing applications as rock slope stability analysis.

34.4 Conclusion

The use of remote sensing with TLS shows that maps and cross sections generated from TLS data serve as a record of the spatial location of actual data and are suitable tools for characterizing discontinuities in a rock mass in detail over a large area. Operational experiences prove that primer higher efforts for data collection and processing will be compensated by far due to multi-use of data and flexibility in data supply, in terms of quantity and quality. The key advantage is that according to the investigation process and demand, data can be extracted and aggregated at varying levels of detail to respond quickly and economically to changing project requirements.

References

Köhler H-J, Hennings S, Nguyen HT, Fernández-Steeger TM (2013) Structural analysis for permeability and stability assessment by use of TLS for the pumped storage hydropower plant Blautal.—19. Tagung für Ingenieurgeologie, München, 13–15 März 2013, pp 395–400

Nguyen HT, Fernández-Steeger TM, Wiatr T, Rodrigues D, Azzam R (2011) Use of terrestrial laser scanning for engineering geological applications on volcanic rock slopes an example from Madeira Island (Portugal). Nat Hazards Earth Syst Sci 11:807–817

Dynamically Loaded Anchorages

35

Santoro Federica, Monia Calista, Antonio Pasculli and Nicola Sciarra

Abstract

The present work regards the study of soil-structure interaction, in particular during pull-out tests on anchorages. Due to the complexity of the system, numerical analyses carried out by a commercial code, based on the Finite Difference Method (FDM), were performed. In order to calibrate the overall selected approach, first of all, a simple two-dimensional model of the system was firstly study. The preliminary results and suggestions for incoming 3D modeling improvements are discussed. Furthermore attention has been focused on the nature of the impulsive impacting force due to a virtual debris flow or avalanches striking on the structure, including the anchorages, in order to correctly simulate the test of pull out. Accordingly, a simplified, preliminary model of the anchorages-net system, including the effect of the mass deposition, is proposed and discussed.

35.1 Introduction

Currently the anchoring techniques are undergoing major development; in many cases these may offer a solution to the problems of stability at different depths (Hobst and Zajic 1983; Mashimo and Kamata 2002). At the same time the use of numerical modeling codes, performed on well defined geological and geotechnical model, becomes important in the design phase and the prevention of geological risks, as for example phenomena of collapse. In the case of numerical modeling which provide for the study of the interaction between soil and structures, the problem becomes more complex. For this reason it is necessary to start with simplified models, in order to control and manage data better, and then proceed with gradually more complex models that can provide results as close as possible to reality. In this context also criteria, which are used for the evaluation of the forces transmitted by debris flow or avalanche impact against structures, become important. As regard, it must be said that in most cases these criteria neglect the actions that occur in the initial phase of the phenomenon; also the results of experiments reported in the literature do not provide useful information for the design of structures for protection, because measured pressures at the impact have larger dispersion. Typically to estimate the actions exerted by the fluid flows, a modified value of the hydrodynamic pressure exerted by a fluid in permanent motion is considered, or a multiple of the hydrostatic pressure. Actually, the pressures that arise at the impact can reach extremely high values, although the duration of the actions of maximum intensity is very short. So the impulsive nature of the phenomenon is evident (Federico and Amoruso 2005, 2008). Actually the anchorages object of this study are part of a barrier system in which they are connected through break devices to a frame and a net. Furthermore in this work we explore the feasibility to develop a semi-analytical model of the system based on the elasticity of the net. In addition, the elastic and dissipative behavior of bolts and wire-rope dissipation are also

S. Federica (✉) · M. Calista · A. Pasculli · N. Sciarra
INGEO Department, University of Chieti—Pescara, Via dei Vestini 31, 66100, Chieti, Italy
e-mail: f.santoro@unich.it
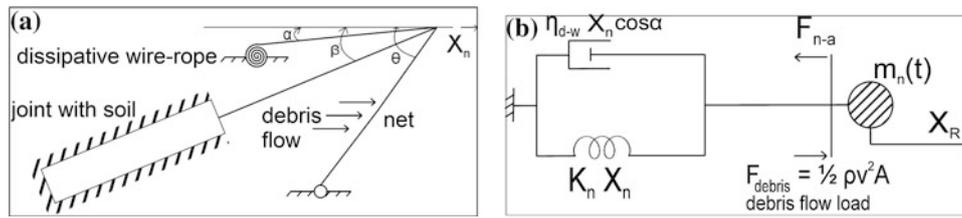
Fig. 35.1 **a** Simplified conceptual 2D system. **b** Scheme of the mechanical model

included. Moreover, as the consequence of the debris or avalanche interaction with the net is a mass deposition, during the time transitory, the mass of the system increases at a rate proportional to the debris flux and to the solid fraction. In order to study the overall response, as first step, a collection of point like (zero-dimensional), interacting elements, is assumed to be suitable in catching the mean dynamical features of the phenomena. Accordingly, the related mechanical model is based on concentrated masses, interacting to each other by elastic rings and dash-pots. The mass of the net is variable and increasing with time. The 'air bag' effect that smoothes the impulsive load due to debris impact may be observed. Actually the momentum transferred during the impact between the debris and the net frame system is delayed. As a consequence the intensity of the transmitted forces to the bolts is reduced. This semi-analytical model to calculate the impulsive force that is necessary to simulate pull out tests is currently under study by our research team. We are focusing our attention on the behavior of the anchorages and their interaction with surrounding soil. The achieved results will be discussed in a forthcoming, more detailed paper. As well as for other studies (Pasculli et al. 2006; Sciarra et al. 2011) conducted by our research group, also this study was performed by a commercial computer code, FLAC2D 6.0, based on FDM approach (Finite Differences Method). The selected code is commonly used to analyze static and dynamic problems, including dry and wet conditions. Moreover the simulations of structural elements, for example piles, anchorages, etc. are allowed as options (Itasca Consulting Group Inc 2008). Anchorage-net system: first modeling attempt.

In this paper only a preliminary description of the mathematical model of the anchorage-net system we are performing is given. Thus, to investigate how the anchorages work and to study the dynamical loads to which they are subject, we assumed that the simplified two-dimensional system, sketched in Fig. 35.1a, is a reasonable representation of the actual barrier system. As first approach, we considered the net as a point mass affected by elasticity (elastic spring) linked to the dissipative wire rope (dash pot) by a 'parallel' connection (same displacements), as reported in Fig. 35.1b. The mass of the net is assumed to increase with time because of the deposition of the solid fraction of the debris. The tensile force due to the anchorage and the load of the debris

flow are assumed to be the external forces acting on the net-system. In order to study the dynamics of the system, as first step, we applied the balance of the forces only along the direction parallel to the slope topography, where the selected anchorage is located. Balance of force momentums were not considered, as the net is assumed to be only hinged. Thus through a simple inspection of the 'conceptual' model of the sub-system shown in Figs. 35.1 and 35.2, the following scalar equation follows:

$$\frac{d}{dt}\left[m_n(t)\frac{dx_n}{dt}\right] = -F_{n-a}\cos\beta - \eta_{d\text{-}w}\frac{dx_n}{dt}\cos\alpha - k_nx_n + F_{debris}.$$

This can be arranged in the following expression:

$$m_n(t)\frac{d^2x_n}{dt^2} = -F_{n-a}\cos\beta - \left[\eta_{d-w}\cos\alpha + \frac{dm_n(t)}{dt}\right]\frac{dx_n}{dt} - k_nx_n + F_{debris}$$

(35.1)

where 'n' stands for net; 'a' anchorage; 'd' dissipation; 'w' wire-rope; $m_n(t)$ is the increasing mass associated to the net, x_n the displacement coordinate of the net along the slope topography (see Fig. 35.1); $F_{n-a}\cos\beta$ and $\eta_{d-w}\frac{dx_n}{dt}\cos\alpha$ are respectively, the projection along the $\hat{x}_n$ direction (see also Fig. 35.1) of the tensile force exerted by the anchorage on the net and the dissipative force of the wire rope for which a linear law was assumed; η_{d-w} is the 'equivalent' dissipation coefficient; k_nx_n includes the elasticity of the net and F_{debris} is the load exerted by the solid fraction of the debris. It is worth to note that the debris mass deposition on the net affects the dynamics of the system like a further viscous force.

As a simple assumption we set $\frac{d}{dt}m_n(t) = \rho \cdot v$ where ρ and v are, respectively, the density of the solid fraction and the velocity of the debris. Assuming, for the sake of simplicity, ρ and v constant in time, it follows: $m_n(t) = m_n + \rho vt$. The debris flow load is introduced considering the dynamical pressure exerted against the net, thus according to the kinetic term of the Bernoulli law, the following expression yields: $F_{debris} = 1/2(\rho v^2 \cdot A \cdot sen\theta)$ where $A \cdot sen\theta$ is the projection of the area A of the net on a plane perpendicular

Fig. 35.2 a Distribution of
displacement vectors after the
application of load and before
failure; **b** geometrical model of
interfaces; **c** shear stress
increment after failure;
d exaggerated grid after failure
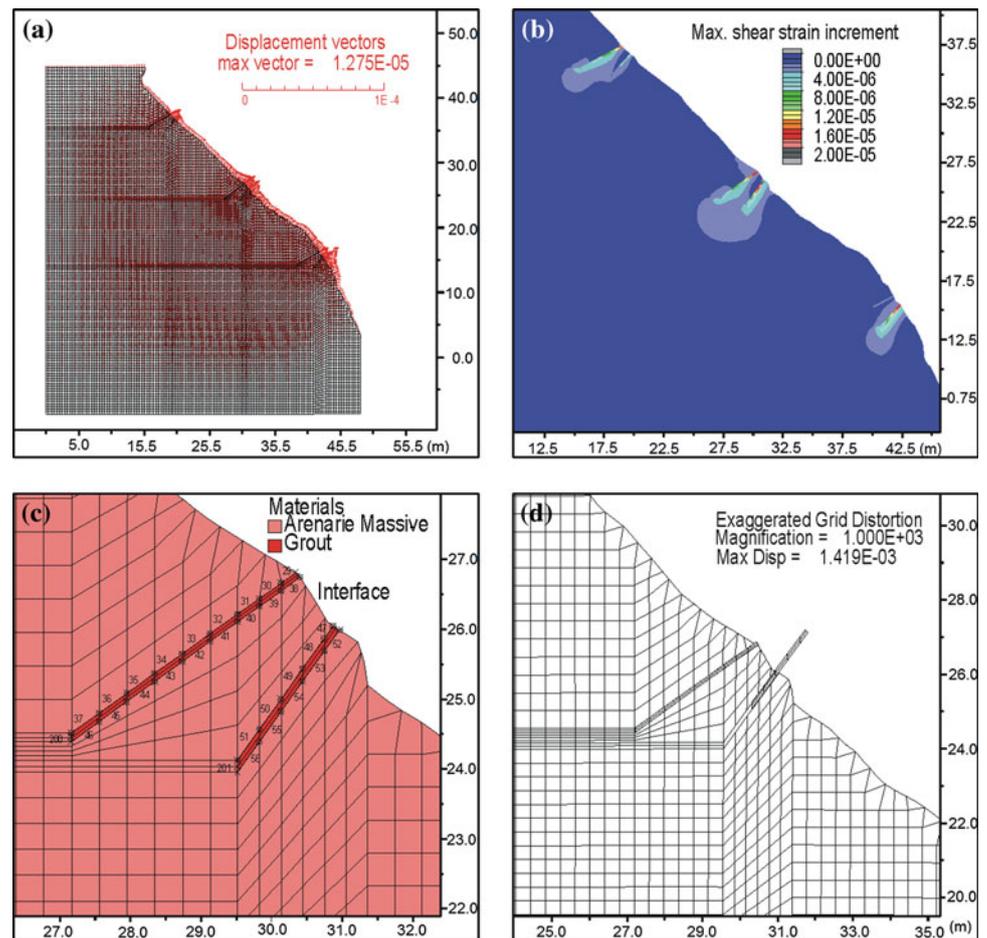
to the debris flow direction. More details about the model
will be given in further works. In particular the term F_{n-a}
will be computed including also the dynamical response of
the soil-anchorage system.

35.2 Test Case

The study area is located in the central part of Italy, in the
western area of the Abruzzo Region, along the A24
highway. The two sections of interest are located next to
the left side of Varri valley (Rome direction) and to the
right side of a near valley that belongs to a tributary of
Turano river (L'Aquila direction); They are included
between 800 and 900 m above sea level. The two artificial
slopes, that have been modeled, are very steep, and at
places vertical.

A detailed geological and geomechanical survey allowed
to define the geological setting and the geotechnical features
of the area, that is part of the margin of Monti Carseolani,
belonging to the carbonatic Laziale-Abruzzese platform

(Parotto and Praturlon 1975; Mariotti 1992), which is con-
nected to the fore deep of the Salto-Tagliacozzo basin.

In particular, in the two studied slopes we can see the
following deposits:

- Massive Sandstones (Messinian): coarse particle size,
  interbedded with decimetric strata with fine particle size
  (thickness 30 m).
- Detritic-sandstone deposit: thickness 0.5–2 m (Slope-
  L'Aquila direction (highway progressive km 63 + 350–
  65 + 600).
- Stratified sandstone (Messinian): thinly stratified,
  associated with sandstones with coarse particle-size in
  decimetric strata (thickness 30 m).

Physical and mechanical parameters that were used to
develop geotechnical model employed in the subsequent
steps of numerical modeling are shown in Table 35.1. The
two sections were modeled using Mohr Coulomb constitu-
tive model, in order to focus the attention on the yielding and
the successive failure of soil surrounding the anchorages.
We chose to simulate soil and structure with grid and
interface elements that connect soil and anchorages.

Table 35.1 Geotechnical parameters of deposits outcropping in the two slopes and geotechincal parameters of interfaces and physical—mechanical parameters of anchorage

Geotechnical slopes features		Geotechnical features—interfaces	
Massive sandstones		Normal stiffness	1E7–1E6 kN/m³
Density	22 kN/m³	Shear Stiffness	1E7–1E6 kN/m³
Friction angle	35–40°	Cohesion	50 kN/m²
Effective Cohesion	150/200 kN/m²	Physical-mechanical parameters—anchorage	
		Density	2.4 kN/m³
Debris		Bulk modulus	6.833E7 kN/m²
Density	20 kN/m³	Shear modulus	6.4E6 kN/m²
Friction angle	32°	Diameter	0.1 m
Stratified sandstones		Length	3–4 m
Density	20.8 kN/m³		
Friction angle	30–35°		
Effective Cohesion	100–150 kN/m²		

In the first phase it was necessary to work on a two-dimensional simplified model, in order to understand how to manage and control steps and results. So a square mesh was used, assuming a simple vertical structure (also simulated by square mesh) inserted near the symmetry axis of the soil grid. Between the soil grid and the structure some interface elements were inserted, depending on the mesh size, and they were monitored in terms of shear force and shear displacements. Starting from the simplified model we continued using a progressively more complex model, up to the sections described previously.

The two sections were represented by a grid with square mesh (about 0.35 m for side). In order to simulate pull out tests over the structure (also simulated with grid elements) variable loads, ranging from 10^3 N up to 10^5N were assumed. The instability of the system, by a numerical computational point of view, occurred when the load of 10^5N was applied. Both anchorages slipped and the max displacement vector measured was 2.07×10^{-4} m. Also it was possible to monitor and correlate shear stress and shear displacements of different point located on the interface (Fig. 35.2).

35.3 Conclusions

In this article the analysis set up and the initial phase of the work in which a static variable force is applied to a simple two-dimensional model in order to calibrate and verify first results were discussed. These first results are encouraged, accordingly a 3D analyses are under developing, taking into account not only the application of the static variable force, but also the dynamic time history load, derived from the considerations explained in this article about the impulsive

phenomena. The simple mathematical-mechanical modeling describing anchorage system, preliminarily proposed in this paper, will be furthermore developed.

References

Federico F, Amoruso A (2005) Numerical analysis of the dynamic impact of debris flows on structures. Proceedings of ISEC-0-3rd International structural engineering and construction conference, Shunan, Japan

Federico F, Amoruso A (2008) Simulations of mechanical effects due to the impact of fluid—like debris flows on structures. Italian J Eng Geol Environ 1:5–24

Hobst L, Zajic J (1983) Anchoring in rock and soil. Publisher Elsevier, Amsterdam, pp 311–320

Itasca Consulting Group Inc. (2008) Dynamic analysis, FISH in FLAC, getting started, structures, users guide, example application, verification problem—FLAC Version 6.0. Minneapolis, Minnesota USA

Mariotti G (1992) Note introduttive alla geologia dell'Appennino centrale. AA. VV. (Eds.) VSimposio Paleoecologia Delle Comunità Bentoniche - Guida all'escursione, pp 30–45

Mashimo H, Kamata H (2002) Experimental investigation the effect of rock bolts on tunnel stability in sandy ground. Physical modelling in geotechnics ICPMG '02, Rotterdam, Balkema, pp 797–801

Parotto M, Praturlon A (1975) Geological summary of the central appennins. Quad. de La Ricerca Scientifica, 90:257–311, CNR, Roma

Pasculli A, Calista M, Mangifesta M (2006) The effects of spatial variability of mechanical parameters on a 3D landslide study. Proceedings of the 4th international FLAC symposium on numerical modeling in geomechanics, Madrid, Spain, May 29–31 2006. Paper: 01–05 (ISBN 0-9767577-0-2)

Sciarra N, Calista M, Marchetti D, D'amato Avanzi G, Pochini A, Puccinelli A (2011) Geomechanical characterization and 3d numerical modeling of complex rock masses: a slope stability analysis in Italy. Proceedings of the 2nd International FLAC/DEM symposium, February 14–16 2011, Melbourne, Australia

Matthieu Sturzenegger, Tim Keegan, Ann Wen, David Willms, Doug Stead, and Tom Edwards

Abstract

On November 25, 2012, a rockslide occurred along the Canadian National Railway tracks, approximately 150 km northeast of Vancouver, Canada. The volume of the slide was approximately 53,000 m^3. It caused four days of service disruption and the collapse of a rock shed protecting the tracks. This paper studies the triggering factors and the failure mechanism based on a combination of airborne and terrestrial LiDAR data, site investigation and discrete fracture network (DFN) modeling. This work provided input parameters for subsequent run-out analysis and design of a railway protection structure (rock shed).

36.1 Introduction

On November 25, 2012, Canadian National Railway (CN) had a major rock and debris slide cover the track along the Fraser Canyon, approximately 25 km north of Boston Bar, British Columbia, Canada (Fig. 36.1). The slide was approximately 70 m wide, with 9 m of debris covering the

M. Sturzenegger (✉) · A. Wen · D. Willms
Klohn Crippen Berger Ltd., Vancouver, BC, Canada
e-mail: mSturzenegger@klohn.com

A. Wen
e-mail: awen@klohn.com

D. Willms
e-mail: dwillms@klohn.com

T. Keegan
Klohn Crippen Berger Ltd., Edmonton, AB, Canada
e-mail: Tkeegan@klohn.com

D. Stead
Department of Earth Sciences, Simon Fraser University, Burnaby, BC, Canada
e-mail: dstead@sfu.ca

T. Edwards
Canada National Railway, Edmonton, AB, Canada
e-mail: tom.edwards@cn.ca

track, resulting in a service disruption of more than four days. The rock slide resulted in the collapse of a rock shed, protecting the track from this historically unstable rock slope (Fig. 36.2).

Keegan (2007) shows that ground hazards are CN's third most costly type of railway hazard and that amongst ground hazards, "rock" landslides contribute to 4.3 % of the annual cost related to train accidents; rock landslide may also transform into "debris" landslides, which constitute 5.8 % of the annual accident cost.

This paper presents a rockslide investigation, which incorporates both remote sensing techniques and discrete fracture network (DFN) modeling in order to optimize the characterization and back-analysis of the rock instability. The paper describes the triggering mechanism, geometry, and failure mechanism of the rockslide. This study formed the first phase of a combined rockslide hazard assessment and protection structure design project.

36.2 Site Conditions and Geological Setting

36.2.1 Climate and Seismicity

In the area, the daily average temperature ranges between −2 and 21 °C, in January and July, respectively. The annual
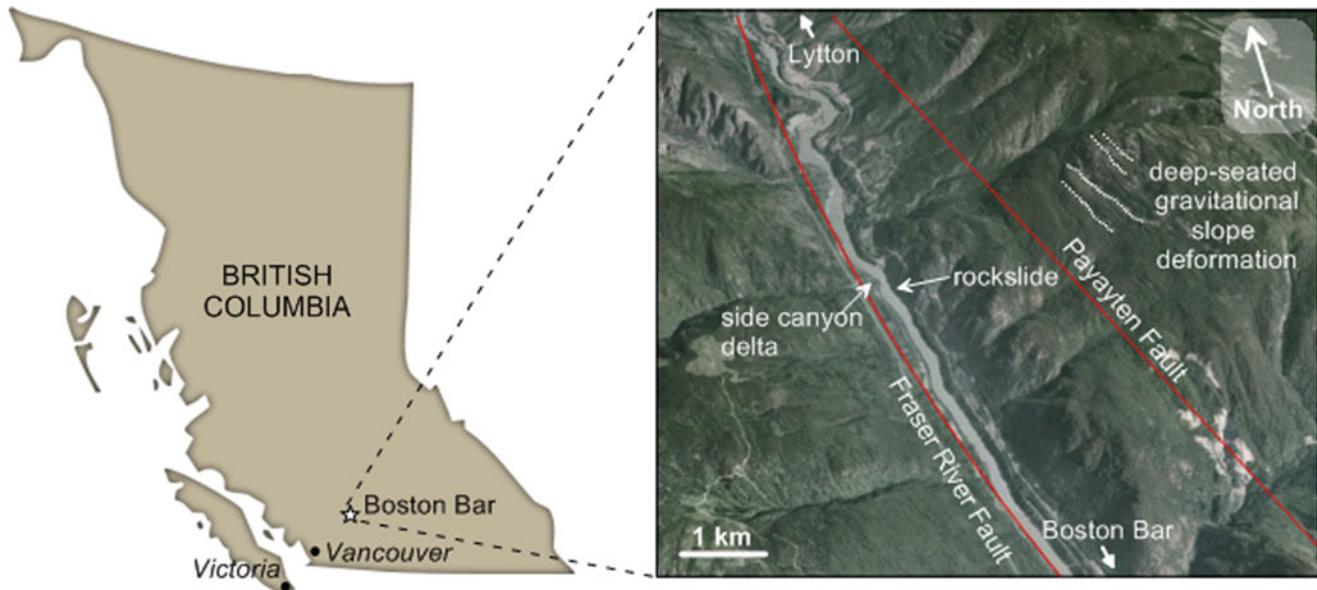
Fig. 36.1 Rockslide area location, geomorphology and regional faults
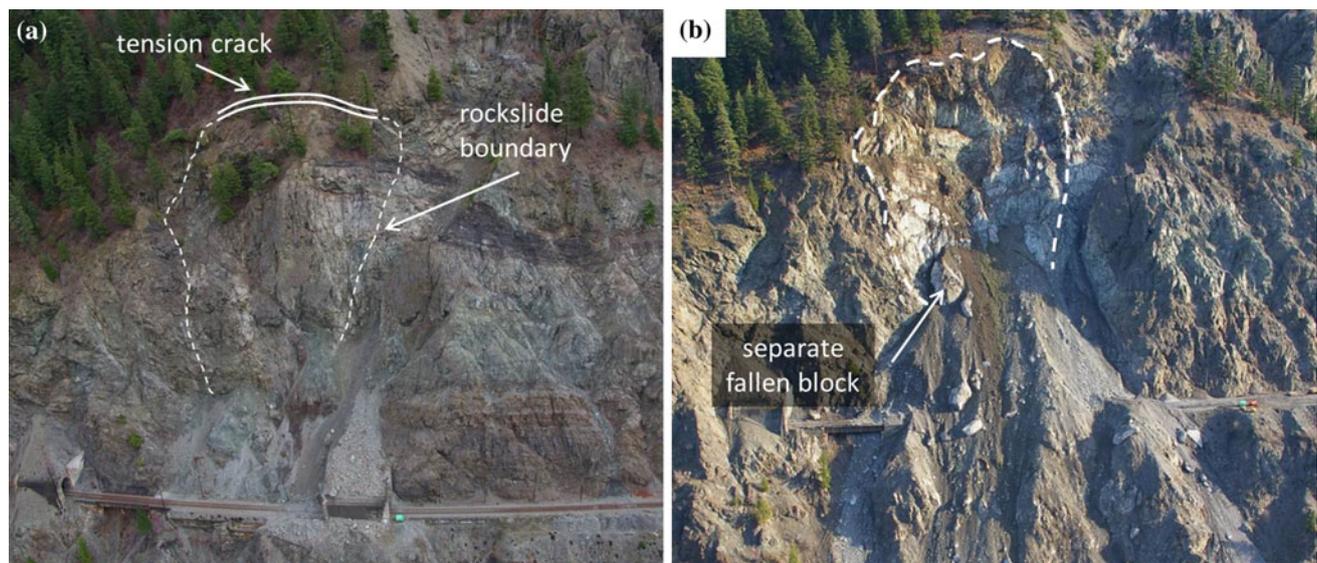
Fig. 36.2 Rockslide. Pre-slide (**a**), and post-slide (**b**), topography

precipitation is 432 mm. From November to March, half of precipitation is snowfall (Environment Canada 2013). The Jackass Mountain weather station located near the rockslide indicated a first series of freeze–thaw cycles preceded by three rainfall periods of 2 to 5 days at the end of October and beginning of November 2012. During mid-November, three days of high-intensity rainfall were recorded, with an average and maximum daily precipitation of 13.1 and 21.5 mm, respectively; these three days of precipitation represent more than the 90th percentile of the long-term November record, and can be defined as an "extreme weather event" (IPCC 2007). The night of November 24 2012 marked the onset of a second series of freeze–thaw cycles.

A review of seismic data indicated that earthquakes are unlikely to have destabilized the rock slope, and consequently, it appears that the likely trigger factor was the succession of freeze–thaw cycles, accompanied by heavy precipitation.

36.2.2 Geological Setting

The rockslide area is located on the steep eastern bank of the Fraser River between Lytton and Boston Bar, approximately 300 m above the river level and 120 m above the railway tracks (Figs. 36.1 and 36.2). The river parallels the right lateral Fraser River Fault, which forms the boundary between the Coastal Belt and the Intermontane Belt of the Canadian Cordillera. The Pasayten Fault is located upslope, on the east side of the valley.

Post-glacial river erosion has resulted in the formation of terraces in many places along the river bank. However, terraces are absent near the rockslide, and a small side-canyon delta on the west side of the Fraser Canyon, upstream of the site, deflects the river flow against the east side of the canyon, accelerating erosion at the base of the slope (Piteau 1977). There is evidence for mountain-scale deep-seated gravitational slope deformation on the east flank of the Fraser River valley, including ponds, talus, and antislope scarps (Fig. 36.1b). The recent rockslide occurred within the boundary of a paleo-landslide (Fig. 36.3a).

The bedrock consists of the Jackass Mountain Group, a thick succession of Cretaceous shallow-water deltaic sedimentary rocks (MacLaurin et al. 2011). Rocks exposed along the track comprise greyish brown and highly fractured argillite, with locally well developed, steeply dipping cleavage. The rock overlying the argillite and exposed mid-slope above the track is a sandstone or sandy siltstone. At the top of the slope, a massive, thick-bedded pebble conglomerate forms a line of prominent cliffs (Fig. 36.3a). The bedding dips moderately into the slope.

Three seismic refraction lines done on the slope directly above the rockslide back scarp indicated that competent bedrock lies 20–22 m below the surface, progressively decreasing to 12 m upslope. Competent bedrock is overlain by a layer of fractured and weathered bedrock; this layer is approximately 15 m thick directly above the failure surface, progressively decreasing to 7 m upslope. Approximately 5 m of overburden overlies the fractured bedrock.

Two local faults were observed at the rockslide location (Fig. 36.3). Fault 1 (F1) is sub-vertical and strikes NW–SE, slightly oblique to the rock slope. It appears below the tunnel at Mile 109.4 and its trace extends along the base of the rockslide through a gully, where it can be recognized as a surface with calcite coating. A black shale layer shows a 20 m offset along the gully suggesting an apparent normal displacement (Fig. 36.3). Fault 2 (F2), which is characterized by very smooth surfaces and calcite coating, can be observed along the north side of the failure surface where the black shale layer is folded. It is an apparent reverse fault with an apparent offset of a few meters.

36.3 Rockslide Characterization and Analysis

The rockslide occurred on November 25, 2012. Prior to the event, tension cracks (Fig. 36.2a) were observed, which would eventually form the back scarp of the failure surface. A rockslide volume of 53,000 m^3 was estimated based on the comparison of pre- and post-slide digital elevation models (DEMs).

Rock slope characterization (Table 36.1) was undertaken using a combination of aerial imagery, terrestrial and airborne LiDAR, field mapping and seismic refraction. Terrestrial and airborne LiDAR data proved to complement each other to capture both the steep rock faces and moderately dipping talus zone of the terrain.

It was observed that the failure surface (Domain 2 in Fig. 36.3a) consists of three sectors. In Sector A (to the north), the failure surface mostly follows the fault F2. In
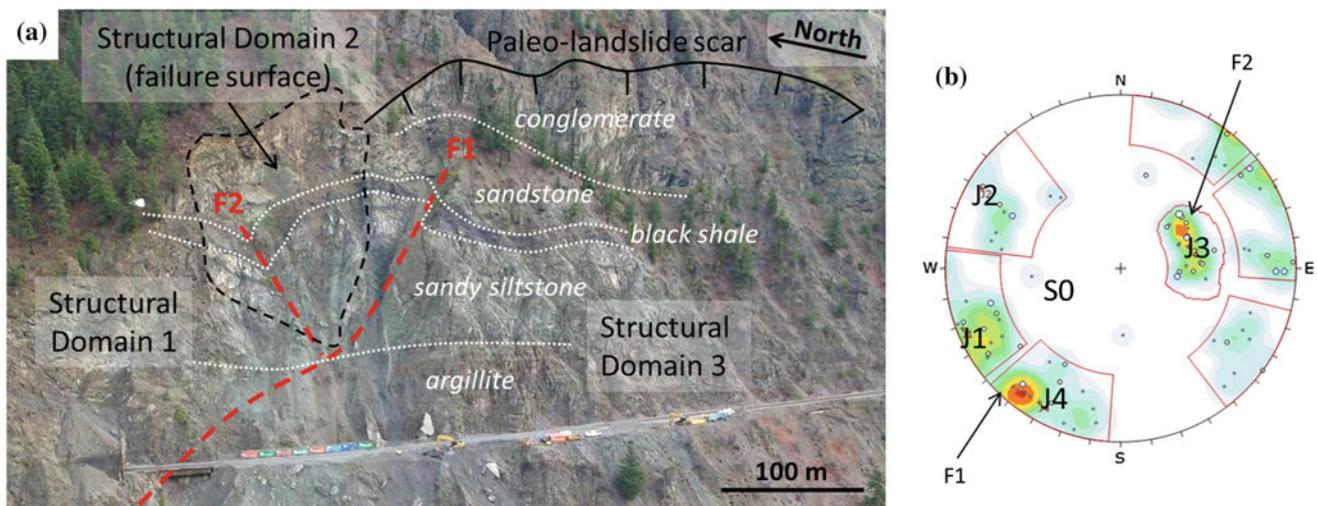
Fig. 36.3 Rockslide area. **a** Local geology and structure. **b** Stereonet (lower hemisphere) for Structural Domain 2 (S0 represents the bedding)

Table 36.1 Domain 2 (failure surface) discontinuity parameters

Set	No. of joints	Dip (°)	Dip direction (°)	Joint length (m)			Joint spacing (m)		
				Min	Mean	Max	Min	Mean	Max
J1	22	88	69	3.0	12.1	22.0	0.3	2.5	6.6
J2	17	85	120	3.0	9.9	28.0	2.4	7.2	12.1
J3	20	44	252	5.0	11.5	25.0	1.4	5.6	9.0
J4	19	84	31	3.0	8.0	26.0	0.9	3.3	9.0
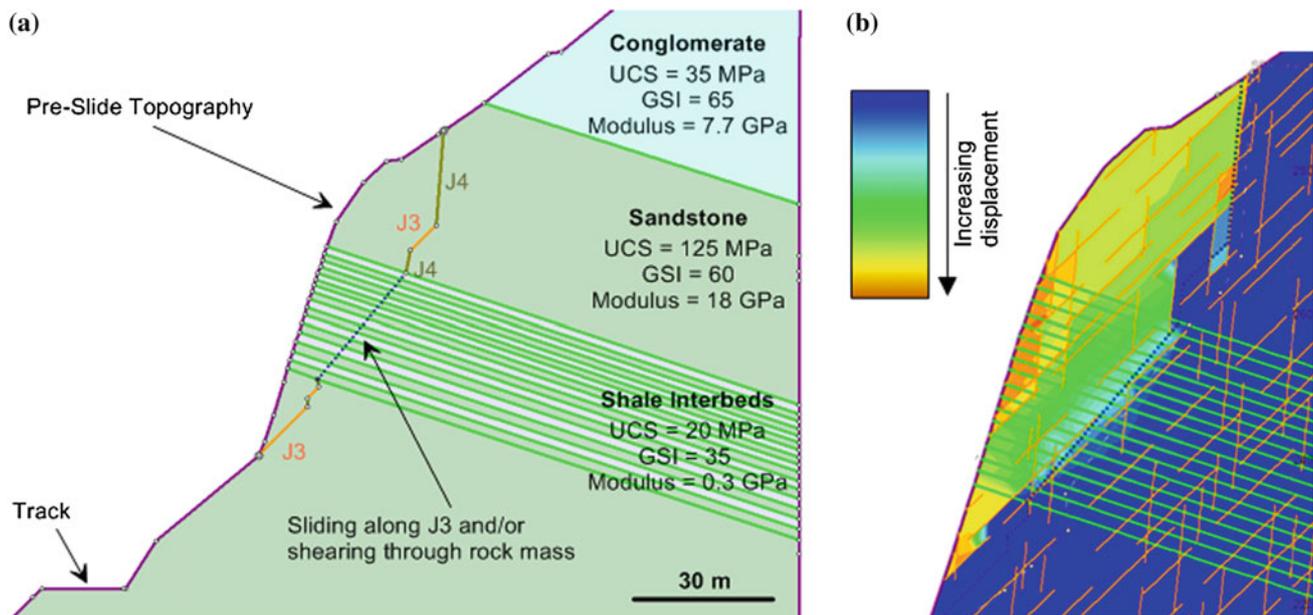
Fig. 36.4 Rockslide back-analysis. **a** Cross section. **b** Relative displacement obtained with *Phase2* with DFN model

Sector B (along the center), the failure surface follows a combination of joint sets J3, J4, and likely some component of intact rock bridges. In Sector C (to the south), the failure surface appears to be quite irregular and composed of a combination of joint sets J2, J3, J4 and intact rock bridges. The failure mechanism is complex, with a major component of two-dimensional sliding in Sectors A and B, and lateral release in Sector C. At the top of the three sectors, a combination of J1, J2 and J4 provided upper release through open sub-vertical joints.

A separate block failed along the northern part of the main failure surface (Fig. 36.2b), probably by sliding along joint set J3 and/or fault F2. This generated a massive block of sandstone having a volume of approximately 400 m³.

Based on rock slope characterization, a cross section was selected for finite element (FE) modeling using the software *Phase2* (RocScience) (Fig. 36.4). The Hoek-Brown rock mass criterion and a Mohr-Coulomb constitutive model for the discontinuity shear strength were assumed. Several back-analysis scenarios, with varying persistence, friction angle, and cohesion along a stepped failure surface were modeled.

Only the most realistic case, which incorporates a DFN model to reproduce the failure surface, is illustrated in this paper.

DFN generation in *Phase2* requires input and calibration of joint persistence and spacing (joint sets J3 and J4, see Table 36.1) so that the DFN matches the post slide profile (Fig. 36.4). A back analysis showed that in order to achieve a critical strength reduction factor (SRF) of 1.0, a 44° friction angle was required.

36.4 Discussion and Conclusion

The rockslide location coincides with the presence of two local faults, small-scale folds of the sedimentary layers, and a paleo-landslide scar (Fig. 36.3a). A daylighting joint set also played a major role in destabilizing the slope (Fig. 36.3b). Other major rockslides have been reported to coincide with structural features (e.g., Brideau et al. 2009; Pedrazzini et al. 2011; Sartori et al. 2003) and/or the location of a paleo-landslide (e.g., Mathews and McTaggart 1978).

These structural and morphological characteristics should be used as criteria for the identification of future potential rockslides along infrastructures, such as railway tracks.

The results of the finite element analysis suggest that the incorporation of a DFN model can realistically reproduce the step-path geometry of the failure surface. Consequently, DFN models may become increasingly valuable in the modeling of similar cases (Gischig et al. 2011; Oppikofer et al. 2011; Sturzenegger and Stead 2012). However, it should be noted that finite elements modeling may not always be appropriate to simulate absolute displacement along a discrete surface. In this study, the reliability of the results was constrained using an initial limit equilibrium analysis, which is more commonly used in the industry.

References

Brideau M-A, Yan M, Stead D (2009) The role of tectonic damage and brittle rock fracture in the development of large rock slope failures. Geomorphology 103:30–49

Environment Canada (2013) Canadian climate normals 1971–2000 (Lytton). http://climate.weatheroffice.gc.ca/climate_normals/index_e.html

Gischig V, Amann F, Moore JR, Loew S, Eisenbeiss H, Stempfhuber W (2011) Composite rock slope kinematics at the current Randa instability, Switzerland, based on remote sensing and numerical modeling. Eng Geol 118:37–53

Intergovernmental Panel on Climate Change (IPCC) (2007) 4th report, climate change 2007

Keegan T (2007) Methodology for risk analysis of railway ground hazards. Ph.D. thesis, Department of Civil and Environmental Engineering, Edmonton, Alberta

MacLaurin C, Mahoney J, Haggart J, Goodin J, Mustard P (2011) The Jackass Mountain Group of south-central British Columbia: depositional setting and evolution of an early Cretaceous deltaic complex. Can J Earth Sci 48:930–951

Mathews W, McTaggart K (1978) Hope rockslides, British Columbia, Canada. In: Voight B (ed) Rockslides and avalanches. Elsevier, Amsterdam, pp 259–275

Oppikofer T, Jaboyedoff M, Pedrazzini A, Derron M-H, Blikra LS (2011) Detailed DEM analysis of a rockslide scar to improve the basal failure surface model of active rockslides. J Geophys Res 116 (F2):22 pp

Pedrazzini A, Jaboyedoff M, Froese C, Langenberg W, Moreno F (2011) Structural analysis of Turtle Mountain: origin and influence of fractures in the development of rock slope failures. In: Jaboyedoff M (ed) Slope tectonics. Geol Soc London, Spec Publ 351:163–183

Piteau D (1977) Regional slope-stability controls and engineering geology of the Fraser Canyon. Geol Soc Am Rev Eng Geol 3:85–111

Sartori M, Baillifard F, Jaboyedoff M, Rouiller JD (2003) Kinematics of the 1991 Randa rockslides (Valais, Switzerland). Nat Hazards Earth Syst Sci 3:423–433

Sturzenegger M, Stead D (2012) The Palliser rockslide, Canadian Rocky Mountains: characterization and modeling of a stepped failure surface

Experimental Study on Water Sensitivity of the Red Sand Foundation in Angola

Wei Zhang, Zhenghong Liu, Jianguo Zheng, Sumin Zhang, and Yongtang Yu

Abstract

In Angola's capital Luanda and its surrounding areas, there distributing abundant brownish red sand called Quelo, which possesses the characteristics of softening and collapsibility when immersed with water. So how to improve the red-sand foundation reasonably and economically is of vital importance and urgency for the infrastructure construction of the area. Based on certain housing project in a typical red sand site in Luanda, a large in-situ water immersion experiment on the site was performed, which simulate the foundation treatment of replacement cushion, foundation dimension and load value of actual buildings. This paper records this experimental study and aims to investigate into the effectiveness of foundation treatment method, this paper records and studies the water-immersion deformation of the foundation after treatment and the rules of water permeation. The results show that: (1) the special formation structure of the red sand site determined a wider impacted area after water immersion; (2) the mudstone distributed under the red sand layer may expand slightly after water immersion; (3) the indoor test tends to exaggerate the hazard of red-sand collapsibility; (4) the bearing capacity of red-sand after softening with water-immersion should be adopted in the foundation design of multi-storied residential buildings on the red-sand site, and (5) the foundation treatment of replacement cushion is effective and reasonable.

Keywords

Quelo sand • Collapsible soil • Softening with water immersion • Foundation treatment • Permeability

37.1 Introduction

In Luanda, the capital city of western African country Angola, and its surrounding areas, there is wide distribution of a brownish red silty sand soil called Quelo (or Muceque), which possesses collapsibility and deteriorated mechanical properties after immersed with water. This unique physical and mechanical feature of the soil often poses much jeopardy to local construction projects.

According to existing literature, Quelo sand is thought to be Pleistocene marine sediments which were initially composed of fine sand and medium sand particles, but later, were remodeled and laterized under the terrestrial environment, producing clay mineral compositions of kaolinite, illite and iron oxide (hematite and goethite). The iron oxide contained in the soil is the main reason of its being red in color.

The collapsibility of Quelo sand has been discovered and proved by Novais-Ferreira and Silva (1961) adopting the method of plate loading test (PLT), and by Silva (1970) using consolidation test method. The results of these tests show that with low moisture content, the subsoil was able to withstand high load (up to 800 kPa) with small settlement; but once saturated, the bearing capacity will decrease due to the bonding failure of particles.

W. Zhang · Z. Liu (✉) · J. Zheng · S. Zhang · Y. Yu
China JK Institute of Engineering Investigation and Design, Xi'an, China
e-mail: 22232508@qq.com

Currently, as a number of infrastructure projects are under construction in the Quelo sand distributed areas in Luanda, how to design the foundation of the buildings has become focal attention. Usually the design follows two schemes: one is to follow the foundation design for collapsible soil, which requires either manual replacement of part or all of the collapse soil with non-collapsible soil by way of certain measures, or using piles that penetrate the whole collapsible soil layer; the other is to design according to the bearing capacity of the subsoil after its softening with water-immersion, which, in this case, can meet the bearing capacity with simply replacement of the compacted cushion. The former scheme can ensure the safety of the buildings but require relatively high cost, while the latter one, though with low cost, needs further research on its safety. Based on one of the house construction projects in Luanda, this study probes into the rationality of designing foundations on Quelo sand site where the soil possesses property of softening and collapsibility after water-immersion. For this purpose, water immersion experiment was carried out aiming to investigate the prototype foundation of five-storied buildings to obtain data revealing rules of water permeation in the foundation soil and the additional deformation of the foundation when soaked with water.

37.2 Engineering Geological Conditions of the Test Site

Located in southern part of Luanda city, about 14 km to the Atlantic on the west and about 15 km to the Kwanza River on the south, the testing site possesses the stratum structure shown in Table 37.1 and Fig. 37.4, which resembles the typical structure of Quelo sand distribution. The brownish red silty sand② layer is the typical Quelo sand layer and contains low moisture in tree-covered district. Both the in-situ testing index in the borehole (SPT and dynamic penetration test) and the collapsibility coefficient in the indoor test are impacted greatly by water content within the soil. The silty sand③$_2$ layer, which takes on mixed-color, is mainly made up with white, yellow and red soil blocks. The silty sand③$_1$ layer, serving as the transitional layer between the layers of silty sand② and silty sand ③$_2$. Both the sandstone④$_1$ layer and the mudstone④$_2$ layer are of weak diagenesis, and some of the mudstone samples have shown swelling during the indoor test.

Soil samples are taken from the borehole to conduct indoor test, and the physical and mechanical property indexes (average) of each layer of the foundation soil have been obtained and is shown in Table 37.1. The collapsibility coefficient is obtained from confined compression test, and

the test pressure, for the depth within 10 m underground the pressure being 200 kPa, and for the layer below 10 meters underground the pressure being the saturated deadweight of the overlying soil layer. As shown in Table 37.1, the silty sand layers of ②, ③$_1$ and ③$_2$ are found with high collapsibility coefficients according to the indoor test results, and the self-weight collapse settlement under the self-weight stress below the compacted cushion in Fig. 37.4 is calculated at 173 mm according to formula 1.

$$\Delta_{zs} = \sum_{i=1}^{n} \delta_{zsi} h_i \qquad (37.1)$$

Where δ_{zsi} means the self-weight collapsibility coefficient of layer i, while h_i refers to the thickness of the ith layer in mm.

And no ground water of any kind has been found within 30 m underground at the testing site.

37.3 Scheme of the In-Situ Test

37.3.1 Design of the Building Foundation

The construction project supporting the in-situ test includes 424 five-storied residential buildings with the height of 15 m. Main body of the buildings adopts brickwork structure, and the foundations are built in area where the Quelo sand is the main bearing stratum. According to the PLT, the characteristic value of bearing capacity of the Quelo sand is between 100 and170 kPa, averaging at 120 kPa when softened with water immersion. If the basic design of the foundation adopts this bearing capacity, the follow scheme can be generated: (1) adopting the reinforced concrete strip foundation base, with the bottom width of 1.0–1.6 m, and the buried depth being 1.0 meter; the average additional stress being 120 kPa; (2) replace the soil within 1.0 meter depth under the reinforced concrete base with refilling compacted cushion of brownish red Quelo sand material.

37.3.2 Arrangement of the Test Pit

The purpose of the full-scale foundation immersion test is to prove the validity of the above foundation design scheme in terms of safety, so the foundation treatment, the buried depth and the form of the foundation base, as well as the apron are all simulations of the real construction engineering arrangement. As shown in Figs. 37.1 and 37.4, the plane of the water immersion test pit is a rectangular, two foundation

Table 37.1 Physical and mechanical property index of the foundation soil

Layer no.	Soil type	t/m	w/%	ρ_d /g·cm^{-3}	d_s	$E_{s1\text{-}2}$ /MPa	δ_s	δ_{zs}	Soil color
②	Silty sand	7.3	5.9	1.66	2.67	13.4	0.020	0.014	Brownish red
③₁	Silty sand	2.3	6.1	1.72	2.68	16.6	0.021	0.021	Variegated, mainly red
③₂	Silty sand	2.9	8.6	1.80	2.68	17.2	0.014	0.013	Variegated (white, yellow and red)
④₁	Sandstone	3.0	10.2	1.70	2.68	16.1	0.009	0.009	Variegated, mainly off-white
④₂	Mudstone		15.2	1.71	2.73	18.9			Grayish green

t layer thickness, w water content, ρ_d dry density, d_s specific weight of soil particle, $E_{s1\text{-}2}$ compression modulus under pressure of 100–200 kPa, δ_s coefficient of collapsibility, δ_{zs} self-weight coefficient of collapsibility
Soil classification is based on China's *Code for Investigation of Geotechnical Engineering* (GB 50021–2001, 2009 Edition)
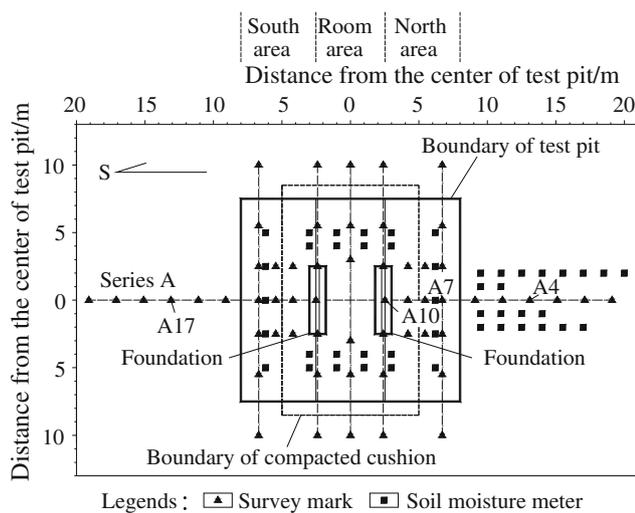
Fig. 37.1 Layout of the test pit

strips with 5 m long and 1.2 m wide are placed in the center of the test pit, and the basic axis distance is 4.8 m. Below the foundation is a whole sheet of compaction replacement cushion, 1.0 m thick. From north to south, the test pit can be divided into three areas: "the north area", "the room area" and "the south area".

To monitor the deformation of the foundation and subsoil in the process of testing, 58 deformation observation marks have been arranged in and around the test pit (Fig. 37.1). To monitor the rule of water permeation in the process of testing, 46 (Fig. 37.1) soil moisture meters have been buried in and outside of the testing pit with buried depth being 2–10 m below the bottom (lowest point) of the testing pit.

37.3.3 Testing Process

The test includes the following steps: (1) Apply load of 147 t (the first loading) on the foundation before the immersion test, with the corresponding additional contact stress of the concrete base being 123 kPa, close to 120 kPa, the average additional stress of the building foundation; (2) immerge exclusively the north area of the test pit with water, see Fig. 37.2a, to stimulate and test the immersion range and the deformation feature of the foundation when the outside of the building were fully immerged with water; (3) immerge the whole pit with water, see Fig. 37.2b; (4) increase the load to 191 t (the second loading), with the corresponding additional contact stress of the base increasing to 159 kPa; (5) Again immerge the whole pit with water.

37.4 Field Test Results

37.4.1 Volume of Immersion

The test injected a total of 5,530 m^3 of water into the pit with the duration of 111 days, which was divided into the three periods of a, b, and c as shown in Fig. 37.3. The three periods include the period of immersing the northern area of the site exclusively, the period of full immersion of the construction site after the first load and the period of full immersion of the site after the second load, with immersion volumes of 948, 3,570 and 1,012 m^3 respectively. Due to limitation of the outside conditions, water-break appeared in the process of immersion (see Fig. 37.3).
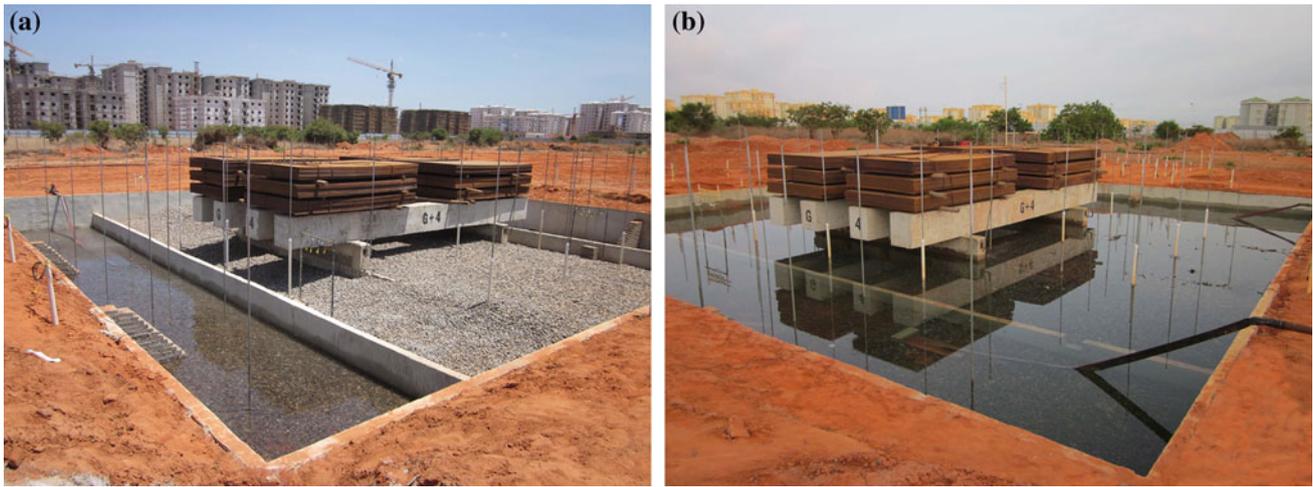
Fig. 37.2 Scene of immersion testing site. **a** Test pit with only the north area immersed. **b** Test pit with full water immersion
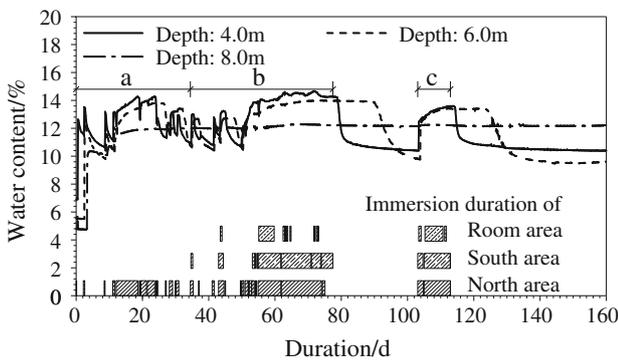
Fig. 37.3 Water content changing with time in north area

37.4.2 Rule of Water Permeation

By way of calibration and through the readings of the moisture meters buried in the subsoil, the real-time moisture content of the soil can be obtained. Figure 37.3 shows the moisture content (mass fraction) curve changing with time of the north area (outside the compaction cushion) monitored at the respective depth of 4.0, 6.0 and 8.0 m of the test pit. It can be seen from Fig. 37.3 that when water reached the place where the moisture meters were buried, water saturation of the soil increased obviously, and correspondingly, the readings of the meters also changed. By analyzing the changes of the readings of all the 46 moisture meters, the real-time
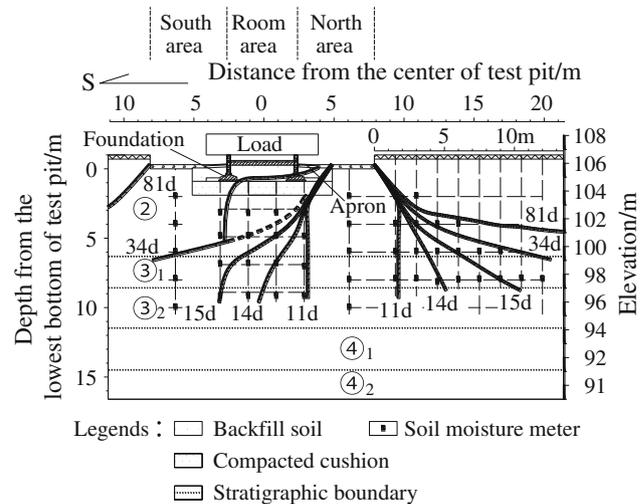
Fig. 37.4 Soaking range at different duration days

immersion range of water in the process of the test can be acquired. Figure 37.4 shows the immersion range curve at different times after the test beginning.

As can be seen from Fig. 37.4, the immersion test has made the all natural Quelo sand in the pit soaked by water (the 81st d curve of Fig. 37.4). Figures 37.3 and 37.4 also reveal the following phenomena:

(1) When soaked with water, moisture content of the silty sand② layer experienced a sharp increase at first, and then gradual increase; But when the water was stopped,

the moisture content experience of the layer was a sharp decrease first, which was then followed by gradual decrease (Fig. 37.3).

(2) Moisture content of the subsoil of the silty sand② layer is closely related with water supply. As shown in figure 37.3, water content at the depth of 4.0 and 6.0 m both experienced a process of first increasing and then decreasing each time when the subsoil was immerged in water and when the water was cut off.

(3) For the mixed-colored silty sand ③₂ layer and the subsoil of lower part of ③₁ layer, their moisture content remained constant for a long time once it was increased (Fig. 37.3).

(4) During the early stage of immersion, the direction of water penetration was mainly vertical, with the lateral infiltration distance less than 2 m; but as the soaking continues till the water infiltrating surface reached the silty sand③₂ layer, water invasion range gradually expanded to the lateral side; Approaching the ending period of the immersion, the minimum angle between the saturation line and the horizontal plane was about 8° (the 81st d curve of Fig. 37.4).

The above phenomena indicate that, the silty sand② layer possesses good water permeability (with larger permeability coefficient), and the silty sand③₂ layer and the underlying sandstone and mudstone possess poor permeability (with smaller permeability coefficient). So in the process of immersion, water can penetrate very far in the lateral direction. Therefore, when the thickness of the Quelo sand was poor, the ground water can easily increase the moisture content in the Quelo sand layer under the foundation, and form upper perched water that submerges the Quelo sand layer.

37.4.3 Deformation of the Foundation

During the process of the test, precision leveling instrument was used to monitor the pre-set deformation observation marks regularly every day to acquire the additional deformation data of the foundation after water immersion. The curves of the deformation changing with time are shown in Fig. 37.5, recorded by the most representative A4, A7, A10 and A17 observations marks (plane position shown in Fig. 37.1). Figure 37.6 shows the settlement section connected by the deformation marks of the above A series at different times (i.e. along the north and south axis of shown in Fig. 37.1) after the test started with first immersion.
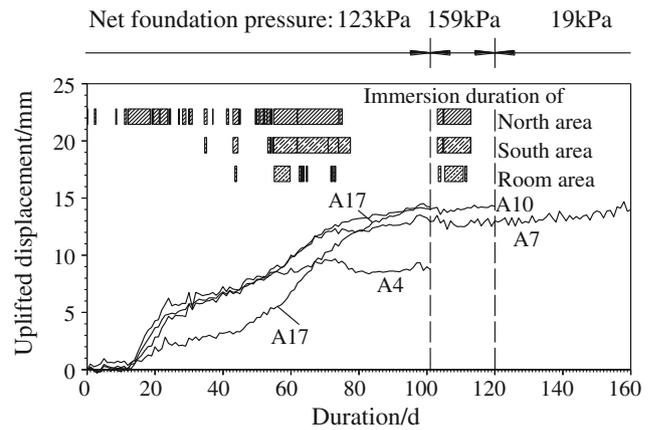
Fig. 37.5 Deformation curve of the most representation marks changing with time
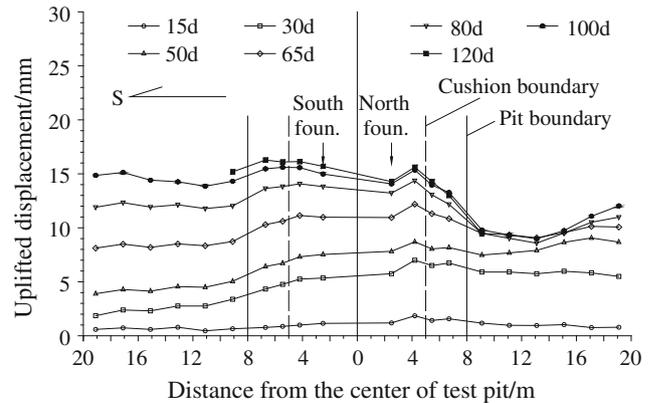
Fig. 37.6 Settlement section connected by A series of deformation marks at different times

Analyses on the monitoring results show that certain amount of uplift rather than obvious settlement occurred after water immersion on each of the deformation observation marks. Other marks (for example, A7, A10 and A17 in Fig. 37.5), except the marks set to the north of the test pit, have lifted continuously in the test. While the marks to the north of the test pit was also witnessed with continuous uplift at the starting period of the test, slight settlement appeared during the ending period of the first loaded water immersion (the 74th d after the test started). Comparing

Figs. 37.5 and 37.4, it is clear that within 11d after the test started, though layers of silty sand②, ③₁ and ③₂ were all wetted with water, no obvious deformation appeared on any of the observation marks; but with the on-going of the immersion, uplifting gradually appeared on all the marks. This phenomenon indicates that the deformation is mainly caused by the weak expansion of the mudstone④₂ layer after being wetted with water. During the late period of the first loading (100d after the test started), the uplift deformation readings of the marks were between 9.0 and 17.0 mm, with the average of 14.3 mm. Figure 37.6 reflects the deformation of the foundation from another perspective. As can be seen from Fig. 37.6, that (1) the deformation of the foundation has no obvious difference with its surrounding foundation soil after immersion though the base has been loaded with 123 and 159 kPa; (2) a "deformation groove" can be seen in the ground north of the pit, and the reason may be that it is located in area covered by trees, where the moisture content of Quelo sand is low and where the collapse intensity is bigger, so certain collapse settlement formed when the place was immersed with water. If the depth of the groove were regarded as the collapsible settlement of the Quelo sand after immersion, the collapsibility volume is relatively small (less than 6.3 mm).

Analyzed comprehensively, the overall deformation value after water-immersion is small, and no significant collapse settlement appeared in the Quelo sand. This means that water-immersion is not enough to cause inhomogeneous deformation that may affect the safety of the building. This also indicates, therefore, that for multi-storied civil buildings, it is feasible to design the foundation on the basis of the bearing capacity of the Quelo sand after being softened with water immersion, given its unique engineering properties.

37.4.4 Discussion

According to the indoor test results, the collapse settlement of the subsoil of the test site could be 173 mm under self-weight pressure alone after water immersion when calculated with formula 1. Its settlement value would be much larger if additional stress was taken into account. However, the actual collapse settlement measured in the in-situ test was very small. So this indicates that evaluation of the foundation soil engineering property generated from indoor tests exaggerates the risks of the foundation soil, and the designs based on data thus obtained tends to be too conservative.

Similar deviation in the volume of collapse settlement obtained through the in-door calculated value with formula 1 and through the in-situ measured value was also found existing in construction projects in China's loess distribution area, the typical collapse site in the world. It is believed that the contradiction is mainly caused by the differences of soil structures and stress conditions existing between the indoor test soil samples and the actual construction site. Therefore, the current *Code for building construction in collapse loess regions* practiced in China has stipulated that in evaluating the collapsibility, loess with collapse coefficient smaller than 0.015 is regarded as non-collapse loess, and shall not taken into account when calculating the collapse settlement. Besides, the calculation of self-weight collapse settlement value is also based on formula 1, but with a correction coefficient between 0.5 and 1.5 (the lowest one used for the southeast region; and the largest one for northwest region). For the Quelo sand, similar effect may also exists in the calculation of collapse settlement, where exaggerated settlement value may be resulted if calculated through indoor test by way of formula 1.

37.5   Conclusions

On the basis of an actual house construction engineering project and simulating the cushion replacement method, foundation dimensions and loading value adopted in actual project, this paper reported an in-situ water immersion test conducted on full-scale foundation in typical Quelo sand areas, and the comprehensive research on the foundation reaction after water immersion and on the rule of its water permeation. The following findings have been reached:

(1) Typical Quelo sand site consists of a top layer of Quelo sand of high permeability, and a lower layer of mixed-colored sand, sandstone and mudstone with low permeability. This unique stratum makes water permeate far laterally when the ground keeps being soaked in water, leading wider plane of immersion range.

(2) The mudstone under the test site expands slightly after immersion, which causes the upward deformation of the foundation but with limited value.

(3) Though indoor tests show that the Quelo sand is with collapsibility, the in-situ test results have shown collapse settlement value much smaller than that obtained through the indoor test. So the indoor test has exaggerated the risks of the Quelo sand. This phenomenon is in line what has been discovered in some of China's loess (typical collapsible soil) site.

(4) In the in-situ immersion test, there is no obvious difference in the deformation between the soaked foundation and those in other districts. Therefore, in designing the foundation of multi-storied house-buildings, the bearing capacity of the red sand can adopt that after the soil being soaked and softened, and it is feasible to improve the Quelo sand foundation soil with cushion replacement.

Reference

Novais-Ferreira H, e Silva CAF (1961) Soil Failure in the Luanda Region. Geotechnique Study of These Soils. Proc. 5th Int. Conf. Soil Mech. Found. Eng, Paris

Silva JAH (1970) Engineering geology and geotechnical behaviour of expansive and collapsing soils of Angola. Tese do Estágio Realizado no Imperial College of Science and Technology, Londres

Geological Characterization and Stability Conditions of the Motorway Tunnels of Arrangement Project of the NR43, Melbou (W. Béjaïa)

Nassim Hallal and Rachid Bougdal

Abstract

The oriental coastal region of Béjaïa city is situated in the mountainous chain of the Babors. The relief is steep as well as slopes which are very abrupt. In the North, the Babors coastal massif dominates the Mediterranean Sea forming the Cap of Aokas and Djebel Djamaa N' sia in the city of Melbou. The recent realized tunnels (T1, T2) cross the limestone massif of Djebel Djamaa N' sia dated of the Jurassic era, which shows an intensive deformation due to the fracturing as well as to the karstification. Several instabilities have been observed at the time of their realization. Both tunnels (T1, T2) are excavated by mining in two sections; Skullcap and stross. Basing on the geologic survey, the geotechnical interpretation and the geomechanical classification of Bieniawski are the basis for what the retaining type were stopped (Flies, anchoring bolts or the special processes for particular cases).

Keywords

Babors • Tunnels • Instability • Support systems • Geomechanic classification

38.1 Introduction

In the framework of the extension of NR43 (Béjaïa), two tunnels (T1, T2) were executed for the aim of crossing the limestone massif of Djebel Djemaa N' sia. The total length of the both tunnels is about 1,497 m (Fig. 38.1).

The thickness of the skullcap cover is approximately 170 m for T2 and 135 m for T1. These two tunnels were excavated by mining in two sections, skullcap and stross.

38.2 Presentation of the Work

The arrangement project of the NR43 consists in the realization of two tunnels, which are monotube with two ways, of a width of 11.10 m, to 7.23 m of height and a 2 × 4 m road. A quoted pavement of 80 cm in Width on the both sides (sea and mountain) in every tunnel is also planned.

38.3 Geological Setting

The tunnels T1 and T2 on the NR43 which cross the massif of Djebel Djamaa N' sia are situated in the Melbou municipality. The geological formations observed in both tunnels have the same nature of the Jurassic limestone (Coutelle 1979).

38.4 Geology of the Studied Area

The massif of Djebel Djemaa N' sia is featured by hard limestone rocks (Figs. 38.5 and 38.6), grey color and brown patina (Leikine 1971). Most of the outcrops show an intense deformation due to the paroxysmal phase of the Miocene (kirèche 1993), that is expressed by fractures more or less closed papered with calcite and iron oxides deposits. The stratification plans are observed in several points on the extreme of the massif; they are characterized by directions

N. Hallal (✉) · R. Bougdal
Scientific University of Algiers USTHB, Algiers, Algeria
e-mail: geoaokas@yahoo.fr

R. Bougdal
e-mail: bougdalr@yahoo.fr

Fig. 38.1 Situation map of both tunnels (T1, T2)
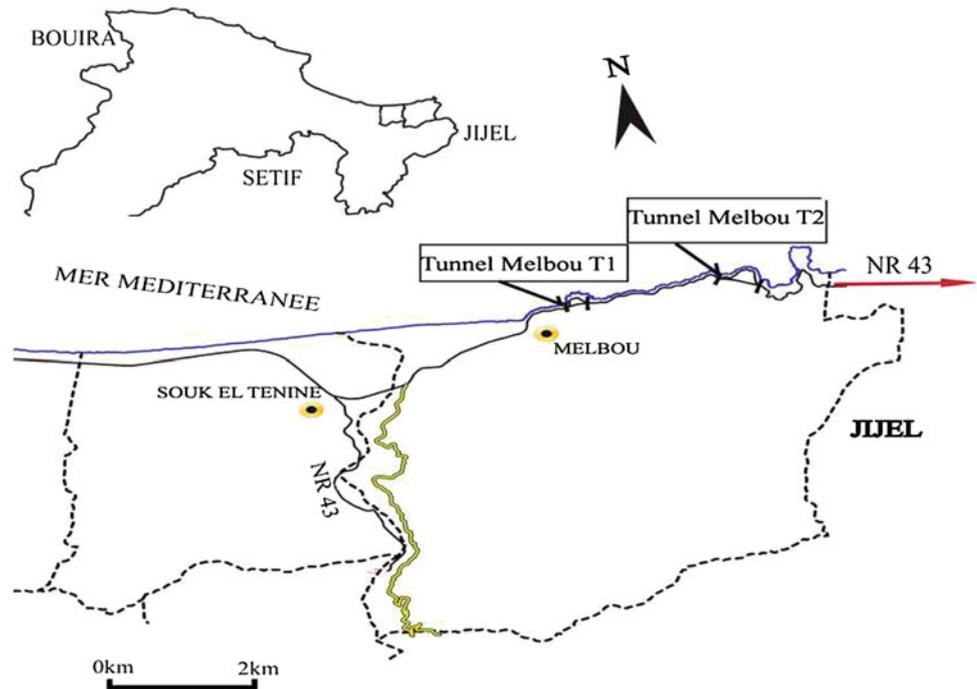
Fig. 38.2 Karstic cavity in the tunnel T1

Fig. 38.3 Karstic cavity in the tunnel T2

going from N040° to N070° and dips from 40° to 75° southward.

A big vertical fault (N070°) is observed on the Djebel Djemaa N'sia upstream side. Secondary faults, which break off in the contact of the major fault, are observed along the NR43.

Along the borders of this massif, limestone breaches few to well concreted and masses landslides with reddish clay matrix are observed, they mask the limestone feet of cliffs at around depressions from the East tunnel portal T02 (PK 0 +900) until the Melbou exit of (PK 1+700), where we find

strengthened sand beds which are surmounted by a layer of reddish clays.

From the tunnel T02 (PK 0+900) to the slope of the ravine, schist formations (crossed by the engineering work) appear, the first one is of marly nature and yellowish to brunette color which is in unconformity on a gray to black clay formation, crossed by calcite veins of very variable thicknesses (Obert 1981).

Fig. 38.4 **a** Stereographic diagrams of the measures inside tunnel T1. Lower hemisphere. **b** Stereographic diagrams of the measures inside tunnel T2. Lower hemisphere
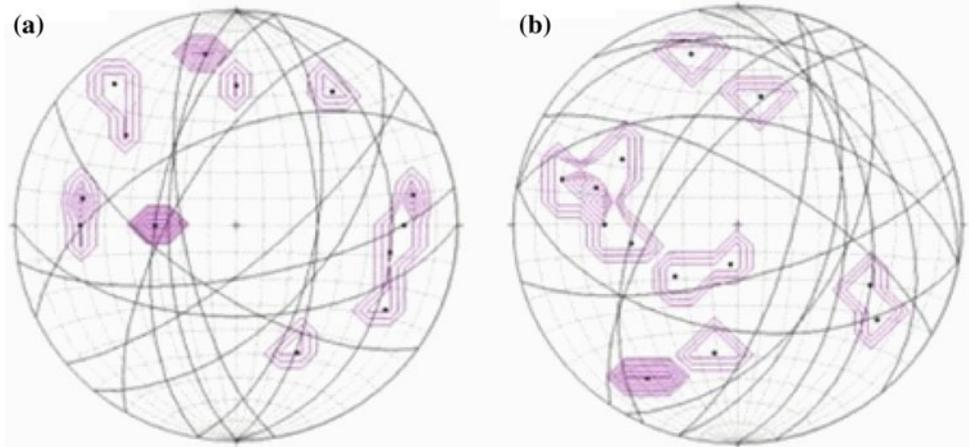
38.5 Main Causes of Instability

38.5.1 The Fracturing

The limestone massif is crossed by a big vertical fault (N070°), Observed on the upstream side of Djebel Djemaa N' sia. The continuation of this fault toward the southeast controls the geomorphology of limestone massif bounds. Secondary fault systems, which break off in the contact of the major fault, are observed along the NR43. Three sets of faults were registered along these tunnels during the digging works. The first one presents a direction of N025° to N040°, the second presents a direction of N050° to N075° and the third is characterized by a N090° direction.

A systematic measurement of the fracturing was effectuated during the progress in both tunnels (Fig. 38.4). As a consequence, data have been collected and statistically treated by a stereographic projection. These analyses confirm the existence of three fractures families.

Fractures observed at both tunnels are the result of the fracturing engendered by the tectonic movements of compression undergone by the rocks' formations during geologic history (Kirèche 1993). Three families of discontinuities are observed. They present, generally, the same orientation as the families observed in the Tunnel of Cap Aokas (Hallal and Bensafia 2011; Bougdal 2009). The spacing and the thickness of the discontinuities are very variable, they contain mostly brunette to yellowish clays, with sometimes alternations of thin layers blackish. These zones are mostly the seat of detachment of dihedral due to the bad holding of the rock.

38.6 Karstification

The limestone massifs of the Babors Lias are known by the existence of numerous dissolution and subterranean canal cavities which can develop on several kilometers.

In the calcareous massif of Djebel Djamaa N' sia, the karstic cavities were met throughout the drilling of both tunnels T1 and T2. They are characterized of a simple clayey filling of in the typical open karstic canal, passing by a karstic levels or sealed cavities. The majority of these phenomena develop on fracturing plans.

For the tunnel T1, several karstic spaces and caves were met, The most important were met in PK 0+121 (Fig. 38.2) and in PK 0+223 (Fig. 38.3), where the first one requires 49 m^3 of the concrete for its filling and the second space presents a total volume of 2,199.92 m^3 situated on highly-rated upstream of the tunnel axis. Besides, several karstic space were also been met, they are characterized by clayey fillings and intense fracturing associated with breaches. Between the Pk 0+760.90 and 0+780.80 a karstic system developed. Indeed, this part of the tunnel is characterized by fillings furniture established by pebbles and blocks of limestone wrapped in a brown and yellowish clayey matrix. This training presents a very precarious stability. None of the recut karstic space is really active from the point of view of in-rushes of water. For the tunnel T2, a karstic zone was met during the digging between Pk 0+169 and Pk 0+114. It is established by blocks centimeter in metrics wrapped in a reddish clayey matrix. The most important were met at the level of Pk 0+100, Pk 0+157 and in Pk 0+177 underlined by the presence of stalactites and stalagmites. The cave met at the level of Pk 0+177 presents a stream of low debit and an alluvial deposits testifying of a former strong flow.

38.7 Hydrogeology

38.7.1 General Framework

The fracturing and the karstification confers to the calcareous massif of Djebel Djemaa N' sia (massif of Babors) a sufficient permeability for the infiltration and the accumulation of subterranean waters (Obert 1981). The

hydrogeologic situation of both tunnels is identical; it is represented in both cases by the Jurassic permeable limestone formations. The flows of groundwater met are those of karstic type through a discontinuity network and karstic channels.

The tunnel T2 is different from the tunnel T1 in this case by the presence of a small ravine of an important debit during the rainy periods, So it emerges from this hydrogeologic situation that more or less important water in-rushes could arise during the drilling of the tunnel and infiltrations of water can be expected in the tunnel T2 during the drilling.

38.7.2 In-Rushes of Water in Tunnels

38.7.2. Tunnel T1
- No coming water occurred during the works of excavation;
- A water seepage resulting from fractures in direct contact with karstic space;
- A water seepage is especially observed in skullcap, they appeared near the karstic space and to the contact of the faults;
- Numerous seepages are observed in tectonic zones, with very low debit.

38.7.2. Tunnel T2
- The temporary nature of the comings waters shows that it is mainly percolations waters till the surface of the rock massif in rainy period;
- Seepage and coming of water were more frequent near the karstic cavity, they appeared skullcap to the right of fractures. In the karstic space, met at the level of Pk 0 +177, a stream of weak debit was met and sediment trainings witness of a high debit of water.

In both tunnels, during heavy rain, the coming of water were systematically listed and gauged when their debit allowed it.

38.8 Behavior of the Rock Massif in the Progress

During the digging works, the observations made during the progress to estimate the holding of the rock after mining and to recover extra profiles in the unstable zones are proved true difficult because of the works of marinating and bleeding, Which followed directly mine blasting, and fast pose of a protection coat of concrete thrown in skullcap and partially in facings.

38.8.1 Skullcap

The unsticking of the dihedrals is inexistent in skullcap during the progress of both tunnels, a little lesser in tunnel T2, situated in the faults zones.

The holding of the rock in skullcap has been proved globally good to very good, rarely bad or very bad in intensely broken or karstified zones.

38.8.2 Facings

For both tunnels, the holding of the rock in facing has been proved globally good to very good, with some noticed instabilities. A bad to very bad holding in intensely broken zones, in the zones of weaknesses as well as in the karstic spaces.

38.8.3 Attack Front

Faces presented a good behavior, with some limited cases of bad holding due to the fracturing and to the karstification of the rock and to the nature of filling.

38.9 Geotechnics

38.9.1 Geomechanical Characteristics of Rocks

- According to the standard IN ISO 14689-1, the calcareous massif of DJ Djemaa N' sia presents a resistance to compression with a rocky matrix estimated as high to very high.
- The results of mechanical tests made on the calcareous massif within the framework of the study of each constraint met in the progress (fractured and karstic zones) revealed low resistance in the compression with a rocky matrix globally less resistant.

38.10 Application of the Method of BIENIAWSKI in the Crossed Massif

The method applied for the classification of the rock massif of DJ Djemaa N' sia is the method of BIENIAWSKI (Bieniawski 1968; Barton et al. 1974), in order to arrive at a global evaluation of its quality.

The Figs. 38.5 and 38.6 summarize the evolution of the variation of the RMR and the retaining structure set up according to the digging in both tunnels.
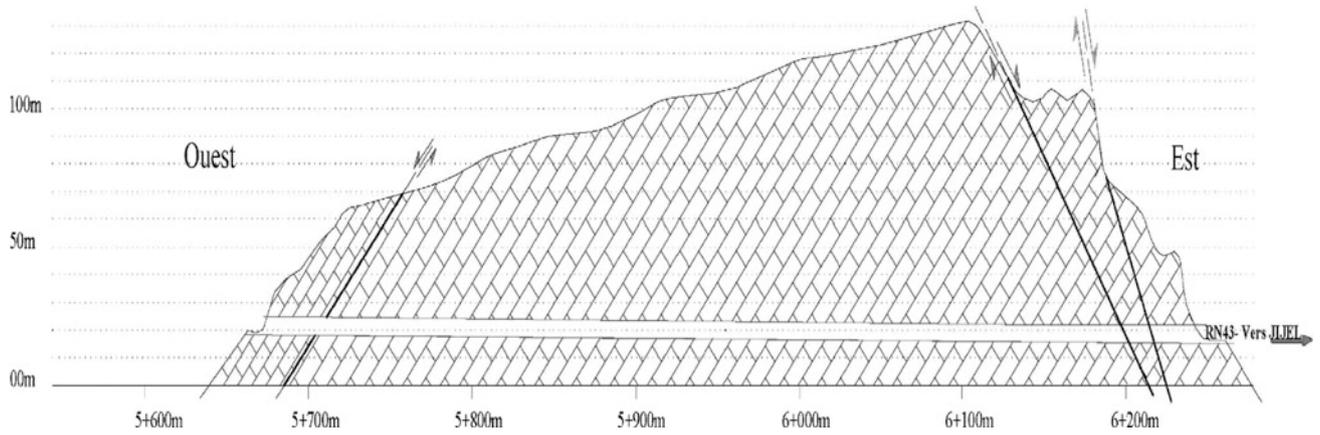
Fig. 38.5 Geological and geotechnical cup of the tunnel T2
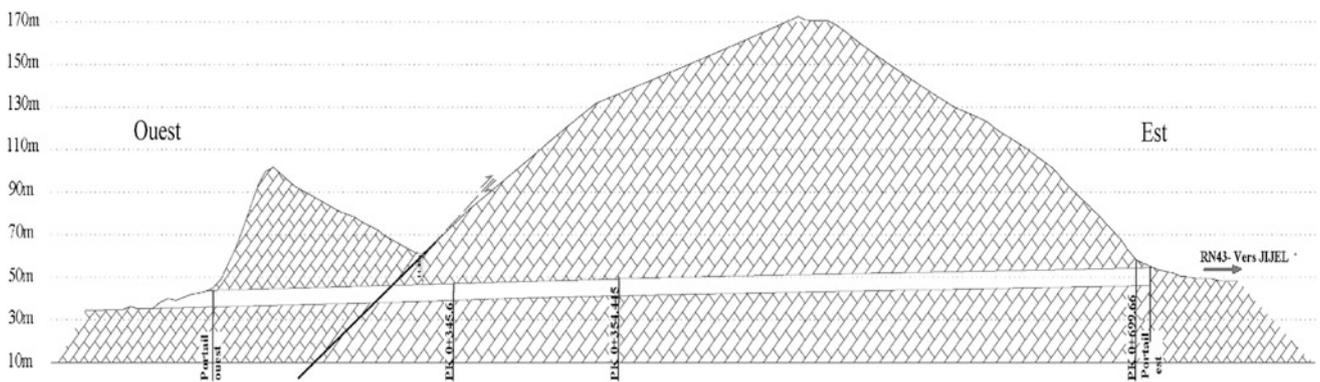
Fig. 38.6 Geotechnical and geological cup of the tunnel T1

Fig. 38.7 Variation of RMR and type of retaining structure realized along T2

Fig. 38.8 Variation of RMR and type of retaining structure realized along T1

These figures show that the geotechnical characteristics of the met rock formations are variable. The bad characteristics were met in the zones of strong fracturing and the karstic zones which coincide with the zones of faults. The variation of the RMR along tunnels T1 and T2 is given in the following Figs. 38.7 and 38.8.

38.11 Conclusion

The study and the follow-up geologic works made along both tunnels (T1, T2), allowed us to collect a significant number of data which found the following utilities:

From a geologic point of view, the massif crossed by tunnels is essentially represented by limestones dolomitic massifs of the lower Jurassic.

From a hydrogeologic point of view, no ground-water was revealed in the massif and no coming of water was observed in the tunnel T1, except for the inside of the tunnel T2 in Pk 0+177, a stream of weak debit was met.

The analysis of the in situ tests results and those in laboratory, realized within the framework of the study of each met constraint and according to the standard IN ISO 14689-1 used for the classification of calcareous massif of DJ. Djemaa N' sia, the geomechanical characteristics of the crossed massif are summarized as follows:

- A compression resistance with a rocky matrix estimated as high to very high for the calcareous massif of Djebel Djemaa N' sia.
- The geomechanical application of the classification of Bieniawski shows that the geological and geotechnical characteristics of the crossed massif vary along traces, It shows a succession of zones classified in the categories II (good), III (average), IV (bad) and V (very bad).

By basing itself on the Bieniawski classification, the retaining structures adopted for every classification in every tunnel are the following ones:

In the category II (C)
- A coat of concrete thrown by thickness 50 mm;
- Bolts of anchorings of 4 m length with a stitch of 1.5 m × 1.5 m.

In the category III (B10)
- A coat of welded fatigues dress;
- A coat of concrete thrown by thickness 10 cm;

- Bolts of anchorings of 4 m length with a stitch of 1 m × 1.5 m.

In the category IV (A)
- A coat of concrete thrown by thickness 150 mm;
- A coat of welded fatigues dress;
- Arch reticule (H = 94 mm), spaced of 1 m;
- A coat of welded fatigues dress;
- Bolts of anchorings of 4 m length with a stitch of 1 m × 1 m.

In the category V
- Bend umbrella;
- A coat of welded fatigues dress;
- Arch reticule (H = 162 mm), spaced of 1 m;
- A coat of welded fatigues dress;
- A coat of concrete thrown by thickness 200 mm;
- Bolts of anchorings of 4 m length with a stitch of 1 m × 1 m.

References

Barton N, Lien R, Lunde J (1974) Engineering classification of rock masses for the design of tunnel support. Rock Mech 189–239

Bougdal R (2009) Doublement du tunnel de Cap Aokas, synthèse des données géologiques et géotechniques. Rapport géologique (Document interne)

Coutelle A (1979) Géologie du Sud-Est de la grande Kabylie et des Babors d'Akbou. Thèse doctorat sciences, Paris

Hallal N, Bensafia W (2011) Dédoublement du tunnel d'Aokas: Géologie et caractérisation géotechnique du massif traversé. Stabilité de l'ouvrage. Mémoire MASTER. USTHB. Alger

Kirèche O (1993) Evolution géodynamique de la marge tellienne des Maghrébides d'après l'étude du domaine parautochtone schistosé. Thèse doctorat sciences, Université d'Alger (USTHB)

Leikine M (1971) Etude géologique des Babors occidentaux (Algérie). Thèse de doctorat, Université de Paris

Obert D (1981) Etude géologique des Babors orientaux (Domaine tellien, Algérie). Thèse de Doctorat, Université Pierre et Marie Curie, France

A Modified Freeze-Thaw Laboratory Test for Pavement Sub Soils Affected by De-icing Chemicals

39

Assel Sarsembayeva and Philip Collins

Abstract

De-icing chemicals are the most effective and cheap method to prevent winter slipperiness on pavement surfaces in urban settings. Analysis of existing experimental studies and theoretical methods shows that solutions of de-icing chemicals run off surfaces and are deposited in adjacent soils. However, there is a lack of knowledge about the effect of de-icing chemicals on the engineering properties of pavement sub soils, where the de-icing agents may penetrate beneath the pavement surface. This is a particular issue as pavement surfaces typically cool and warm at a faster rate than surrounding areas. In particular, during seasonal freeze-thaw cycles, the lower freezing point of the chemical solution may induce moisture migration toward a freezing front within the sub soil, leading to increased heave potential, and subsequent thaw collapse. The paper describes an experimental study that simulates the movement of water and de-icing solution from the deposition area upward to the highway's sub base. The chemical effect of de-icing solutions on the strength characteristic, water and chemical content of each 10 cm layer of tested soil column will be assessed by in situ measurement and post-experiment analysis. In the long run the impact of the de-icing chemicals precipitation on the bearing capacity and deformation of sub base soils of roads will be evaluated.

Keywords

Roadside soil • De-icing chemicals • Engineering properties • Moisture migration

39.1 Introduction

Since the 1950s de-icing chemicals have been the most popular and effective method to keep highways surfaces clean and safe from winter slipperiness as the freezing temperatures of de-icing chemicals are much lower than pure water (Bing and Ma 2011). This freezing point can be determined from the eutectic diagram of each type of de-icing chemical.

De-icing chemicals are the cheapest way to prevent ice formation and usually guarantee its quick removal from the pavement surfaces. There are various types of inorganic de-icing agents, the freezing temperature of which can be determined from the eutectic diagram (Dreving 1954; West 1982). Widely used agents include chlorides, which are cheap but corrosive, and organic compounds like acetates, formats and urea, which are not so aggressive to crops and metals, but more expensive and may case an unpleasant smell of vinegar during use.

De-icing salts can be delivered to soil near roads by runoff and spray and cause the secondary salinization of the roadside area. There are numerous reports on simulation works and field observations of the deposition and redistribution of de-icing chemicals in the roadside environment (e.g. Norrström and Jacks 1998; Blomqvist and Johansson 1999; Lundmark and Olofsson 2007; Lundmark and Jansson 2008).

A. Sarsembayeva (✉) · P. Collins
Brunel University, Kingston Lane, Uxbridge, Middlesex, UB8 3PH, London, UK
e-mail: assel.sarsembayeva@brunel.ac.uk

Fig. 39.1 The moisture migration in the highway basement reviewed without the usage of de-icing chemicals
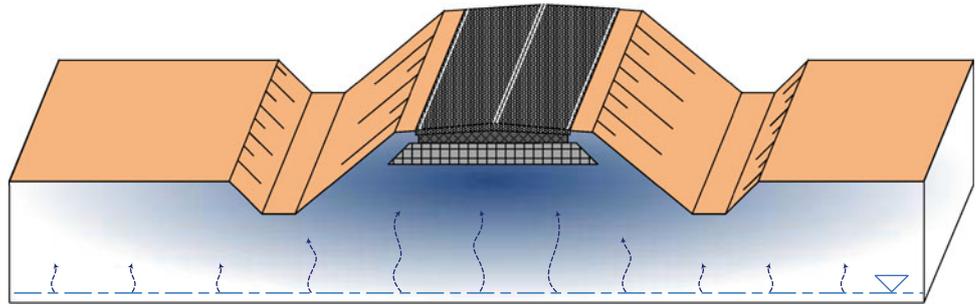
Deposition of de-icing salts in the roadside inevitably changes the chemical content and moisture regime of the subsoil. This may have a great effect on its bearing capacity, especially during seasonal freeze-thaw cycles. Furthermore, it keeps the moisture of the nearby soil in a liquid state (Kane et al. 2001).

As the thermal conductivity of pavement materials is far and away higher than the adjacent soils the thermal gradient causes significant migration of moisture upward the freezing front that is where pavement layers (O'Neill 1983; Othman and Benson 1993; Giakoumakis 1994; Kane et al. 2001; Vidyapin and Cheverev 2008). Figures 39.1 and 39.2 describe the moisture migration toward the freezing front in winter period.

In the spring, when the swelled mass of sub soils starts to thaw and drain, a loss of bearing capacity occurs, as shown in Fig. 39.3 (Othman and Benson 1993; Simonsen and Isacsson 1999; Qi et al. 2006; Vidyapin and Cheverev 2008).

We hypothesis that the ability of de-icing chemicals to keep moisture in a liquid state at low temperature may enhance moisture migration toward the highway subsoil in cold periods. Progressive, but slow freezing to below the eutectic point, such as occurs in areas like Central Asia and Siberia, is likely to induce cryosuction of the unfrozen soil moisture, inducing frost heave (Hoekstra 1966; O'Neill 1983; Othman and Benson 1993; Qi et al. 2006; Bronfenbrener and Bronfenbrener 2010a, b; Matsumura and Yamazaki 2012). This will enhance thaw-related loss of bearing capacity of highways in the spring.

In situ measurement of the migration, and cyclic freezing and thawing of de-icing agents is problematic. Instead, a modified frost heave test methodology has been developed.

39.2 Development of a Laboratory Model

The laboratory method for frost heave and thaw weakening susceptibility observations of soils is based on ASTM D5918-06 Standard, (2007). The installation scheme of this test simulates the movement of water and de-icing solution from the deposition area upward to the highway's sub base. A series of identical insulated soil columns within a

Fig. 39.2 Migration of salt-water solution in the highway basement during the freezing
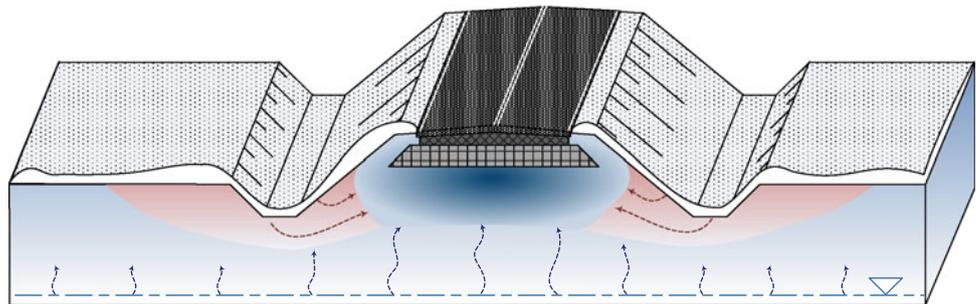
Fig. 39.3 The thawing process in the highway basement during the spring
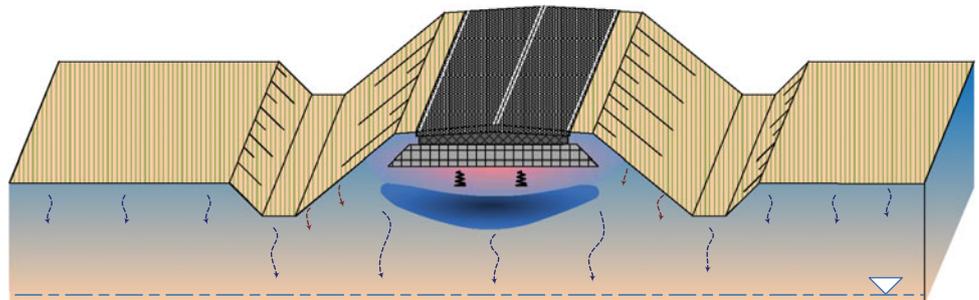
Fig. 39.4 Laboratory model for frost heave and thaw weakening susceptibility
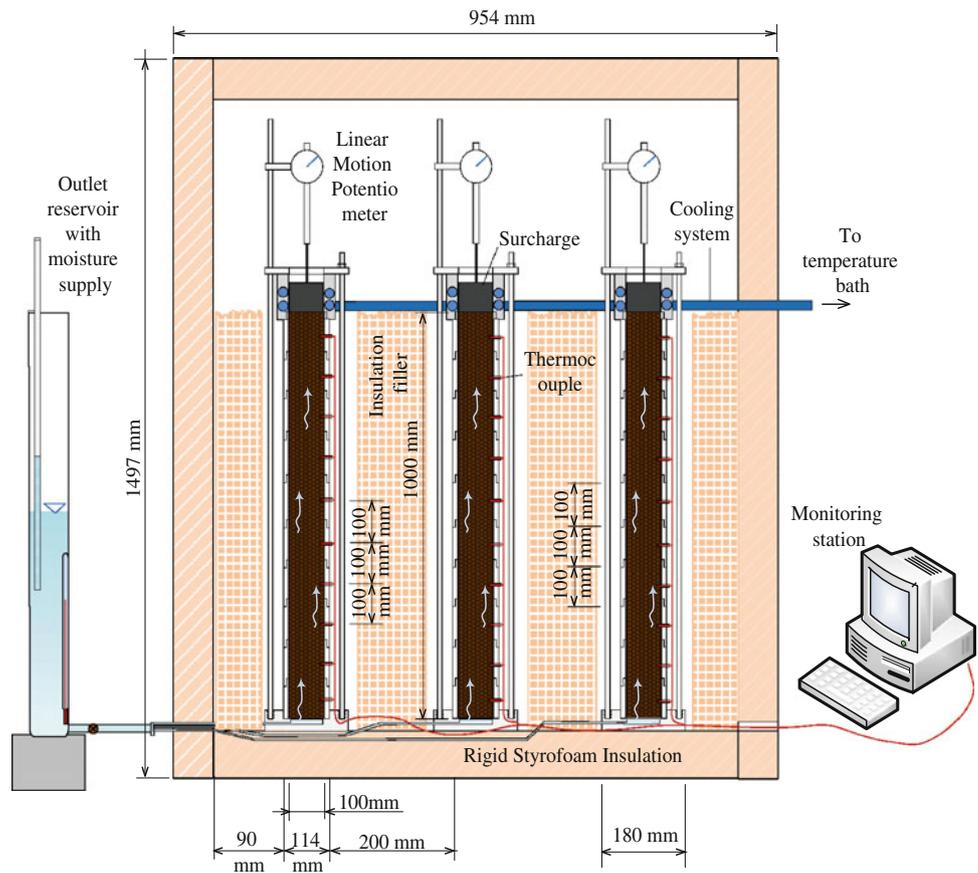
temperature controlled cabinet are connected to a constant head (Mariotte) supply reservoir, and chilled from the top. A schematic representation of the test equipment is presented on Fig. 39.4.

Unlike the ASTM Standard, the height of the soil columns was increased from 15 cm to 1 m, which allows testing the thermal gradient after each 10 cm in detail. Nine soil columns can be tested simultaneously, which permits triplicate tests.

The plastic mould for the soil column consists of 10 identical acrylic sectional rings which allow easy assembly and dismantling of the soil column. Each acrylic ring has an inside diameter of 100 mm, outside diameter of 110 mm, and height of 100 mm. The soil is separated from the acrylic rings by a long rubber sleeve.

Each acrylic ring has a mid-height drilled hole for a thermocouple sensor which takes temperature readings at regular intervals, with up to 90 thermocouple readings at a time, collated using a data logger.

The constant head of supplied moisture is provided by a Marriotte water supply reservoir, which has a vacuum tight fitting glass tube in the top of the reservoir to provide the equal water pressure. The reservoir also allows control of the elevation of the reservoir liquid. The bottom of the reservoir
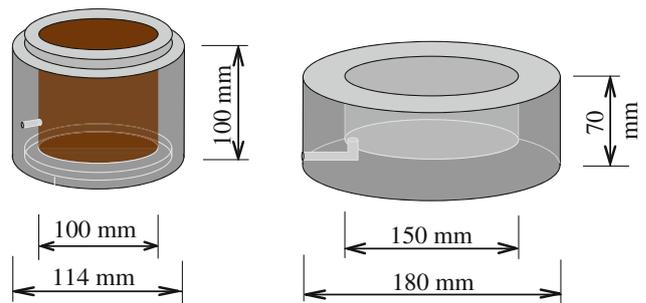
Fig. 39.5 Plastic mould section and base plate for testing a soil sample

is connected to the sample by a flexible plastic tube joined to the specimen base plate (Fig. 39.5).

Freezing from the top is implemented by chilling collars and metal surcharges which have good heat conductivity and cause isotropic chilling on the sample surface. The surcharge weight by a circular disk with a 2.72 kg of mass is placed on the top of the soil specimen to simulate natural overloads from the upward layers of pavement. This cooling construction allows the vertical sliding of the surcharge inside the chilling collar and at the same time provides the equal effective vertical stress during the heave frost.

Fig. 39.6 Freezing-thawing cycle tests procedure
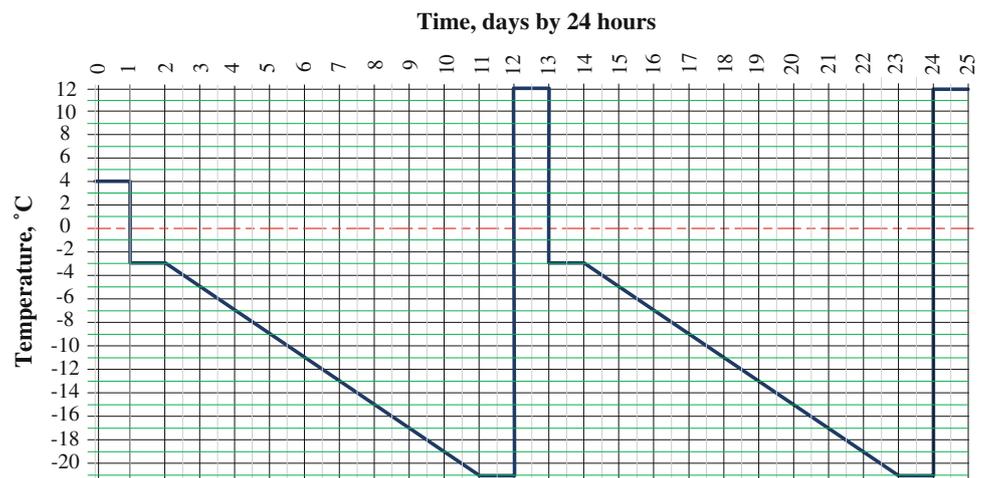
The testing process consists of two freezing-thawing cycles. The bottom temperature remains stable at 4 °C, while the top of the soil column is gradually cooled by 2 °C per day until it reaches −20 °C. After each cycle stage, 3 columns of soil are collected for further tests. The experiment is run using different de-icing agents and with deionized water, to permit a comparison.

The temperature control chamber is to be made from rigid Styrofoam insulation material and adapted to have the capacity to hold 9 samples.

The testing process consists of two freezing-thawing cycles and represented in the Fig. 39.6. The first 24 h is a conditioning period when both the top and bottom are held in 4 °C. In the first freezing period the temperature of the cooling collars is lowered to −3 °C and is held at this grade for 24 h. After this period the cooling temperature decreases steadily at a rate of −2 °C per day. At the same time, the bottom moisture supply temperature remains stable at 4 °C during the all test. When the cooling temperature reaches −21 °C it is again be kept for 24 h. Afterward 3 soil columns are removed for checking moisture and chemical content while the chilling equipment is to be switched off for 24 h to allow the thawing and drain of the remaining soil columns. After this thawing period another 3 soil columns samples are extracted and checked for engineering properties as well as chemical content tests.

The second freezing cycle is identical to the first, with the last 3 soil columns removed and tested at the end.

Testing for mechanical properties in the current research includes: particle size distribution, plasticity limits, index and activity of clays, moisture content after each test stage of testing, dry density and bulk density after each test stage of testing, cohesion C and angle of internal friction φ, CBR charts at each stage after each stage of testing, coefficient of permeability and coefficient of consolidation.

39.3 Expected Outcomes

- Improved understanding of the migration of de-icing solutions in highway sub soils.
- Development of a reliable methodology for the experimental study of the thermal and humidity regime of highway sub soils, including the use of de-icing chemicals.
- Evaluation of the impact of de-icing chemicals' precipitation on the bearing capacity and deformation of sub base soils of roads

39.4 Conclusions

The laboratory investigation will examine the significance of the secondary salinization process and freeze-thaw in highway sub soils. The degree to which the de-icing chemicals migrate upwards towards a freezing front under pavement layers will be assessed. Any change to the soils' mechanical properties due to the presence and behavior of de-icing agents will be evaluated.

References

ASTM D5918-06 Standard (2007) The laboratory method for frost heave and thaw weakening susceptibility. Annual book of ASTM standards, vol 04.08, pp 401–412

Bing H, Ma W (2011) Laboratory investigation of the freezing point of saline soil. Cold Reg Sci Technol 67(1–2):79–88

Blomqvist G, Johansson E (1999) Airborne spreading and deposition of de-icing salt—a case study. Sci Total Environ 235(1–3):161–168

Bronfenbrener L, Bronfenbrener R (2010a) Frost heave and phase front instability in freezing soils. Cold Reg Sci Technol 64(1):19–38

Bronfenbrener L, Bronfenbrener R (2010b) Modeling frost heave in freezing soils. Cold Reg Sci Technol 61(1):43–64

Dreving VP (1954) The phase rule. Moscow State University, Moscow

Giakoumakis SG (1994) A model for predicting coupled heat and mass transfers in unsaturated partially frozen soil. Int J Heat Fluid Flow 15(2):163–171

Hoekstra P (1966) Moisture movement in soils under temperature gradients with the cold-side temperature below freezing. Water Resour Res 2(2):241–250

Kane DL, Hinkel KM, Goering DJ, Hinzman LD, Outcalt SI (2001) Non-conductive heat transfer associated with frozen soils. Glob Planet Change 29(3–4):275–292

Loch JPG (1981) State-of-the-art report—frost action in soils. Eng Geol 18(1–4):213–224

Lundmark A, Jansson P (2008) Estimating the fate of de-icing salt in a roadside environment by combining modelling and field observations. Water Air Soil Pollut 195(1–4):215–232

Lundmark A, Olofsson B (2007) Chloride deposition and distribution in soils along a deiced highway—assessment using different methods of measurement. Water Air Soil Pollut 182(1–4):173–185

Matsumura Shinji, Yamazaki Koji (2012) A longer climate memory carried by soil freeze–thaw processes in Siberia. Environ Res Lett 7(4):045402

Norrström AC, Jacks G (1998) Concentration and fractionation of heavy metals in roadside soils receiving de-icing salts. Sci Total Environ 218(2–3):161–174

O'Neill K (1983) The physics of mathematical frost heave models: A review. Cold Reg Sci Technol 6(3):275–291

Othman MA, Benson CH (1993) Effect of freeze-thaw on the hydraulic conductivity and morphology of compacted clay. Can Geotech J 30(2):236–246

Qi J, Ma W, Song C (2008) Influence of freeze–thaw on engineering properties of a silty soil. Cold Reg Sci Technol 53(3):397–404

Qi J, Vermeer PA, Cheng G (2006) A review of the influence of freeze-thaw cycles on soil geotechnical properties. Permafrost Periglac Process 17(3):245–252

Simonsen E, Isacsson U (1999) Thaw weakening of pavement structures in cold regions. Cold Reg Sci Technol 29(2):135–151

Vidyapin IY, Cheverev VG (2008) The hydraulic of freezing saline soils. Earth Cryosphere 12(4):43–45

West DRF (1982) Ternary equilibrium diagrams. Chapman and Hall, London New York

A Geotechnical and Geochemical Characterisation of Oil Fire Contaminated Soils in Kuwait

Humoud Al-Dahanii, Paul Watson, and David Giles

Abstract

As a consequence of the Saddam Hussein 1991 Iraqi led invasion of Kuwait more than 600 oil wells were set fire to as part of a scorched earth policy while retreating from the country. This action created a series of "oil lakes" and hydrocarbon contamination within the desert causing serious environmental damage. Some 23 years later after the fires were extinguished the ground affects of these actions can still be detected. This paper will present the results of a detailed geotechnical and geochemical investigation into the current ground conditions now present in the Burgan Oil Field some 35 km south of Kuwait City. Detailed geotechnical testing together with hydrocarbon analysis using a Gas Chromatograph—Mass Spectrometer (GCMS) have been carried out on samples from varying depths within the Greater Burgan Oil Field. A detailed geological, geotechnical and geochemical ground model has been developed to present the findings of these investigations. The area under study has major development plans for both housing and infrastructure. Subsequent Quantitative Human Health Risk Assessments have been undertaken to determine the potential levels of risk posed to any future urban developments within these affected areas. The paper will report on this assessment detailing the hazards posed and the tools used to assess them. Potential risks will be discussed and mitigation and management scenarios will be highlighted.

40.1 Introduction

The state of Kuwait has experienced serious environmental damage as a consequence of the formation of multiple oil lakes and hydrocarbon contamination resulting from the destruction caused in the Gulf War of 1991. Of the 810 active oils wells operating in Kuwait in 1991, 730 were damaged or set ablaze during the conflict (Fig. 40.1). This research set out to assess the hydrocarbon contamination and geotechnical effects of the oil fires still being encountered some 20 years plus after the war.

40.2 Site Description

The area under study was located in the Greater Burgan oilfield (Fig. 40.2) which lies in the Arabian Basin. The Greater Burgan field is the largest clastic oil field in the world covering an area of 838 km^2, located in south eastern Kuwait. The oil field is subdivided into the Burgan, Magwa and Ahmadi sectors based on the underlying geological structure (Kaufman et al. 2000). At the height of the destruction smoke plumes from the Greater Burgan oil fires extended over 50 km from the well sites up to an altitude of 2.5 km. Spillages from ruptured pipelines resulted in

H. Al-Dahanii · P. Watson
School of Civil Engineering and Surveying, Portsmouth, UK

D. Giles (✉)
School of Earth and Environmental Sciences, University of Portsmouth, Portsmouth, UK
e-mail: dave.giles@port.ac.uk

Fig. 40.1 Burning oilfield during Operation Desert Storm, Kuwait (USACE)

Fig. 40.2 Oil fields in Kuwait (Kuwait Oil Company KOC)
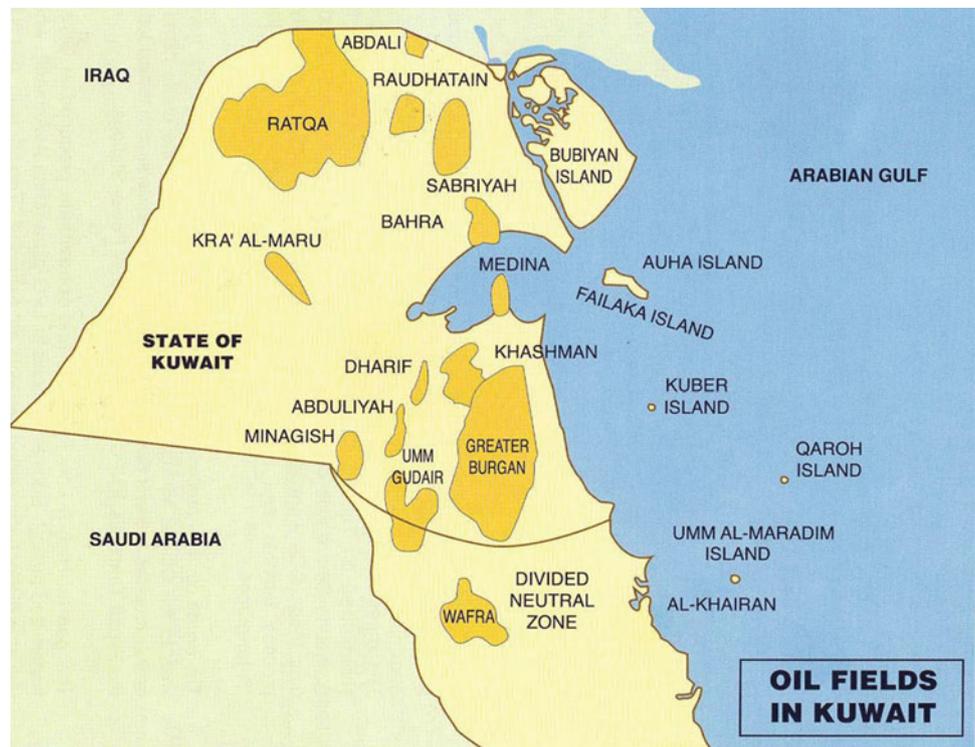
numerous oil lakes which caused extensive contamination and environmental damage.

40.3 Site Geology

Kuwait is dominated by rocks of Tertiary age dating from the Palaeocene to the Eocene (Al-Sulaimi and Mukhopadhyay 2000). Limestones, dolomites and evaporitic sequences (anhydrites) from the Umm Er Radhuma, Rus and Dammam Formations are unconformably overlain by sandstones of the Kuwait Group which include the Fars and Ghar Formations, again overlain by the Dibdibba Formation. The solid geology of the Greater Burgan site is located within the Fars and Ghar Formations with interbedded sands and clays, some sandstones and weak white nodular limestones (Hunting Geology and Geophysics 1981). Superficial deposits are predominantly Aeolian sands, with occasional gravels with sands, muds and calcareous sandstones in the coastal areas. (Table 40.1).

Table 40.1 Generalised stratigraphy of the study area

GENERALISED STRATIGRAPHY				HYDRO GEOLOGICAL UNITS
QUATERNARY SEDIMENTS (< 30m)		Unconsolidated sands and gravels, gypsiferous and calcareous silts and clays		Localised Aquifers
KUWAIT GROUP	DIBDIBBA FORMATION (200 - 200m)	Gravelly sand, sandy gravel, calcareous and gypsiferous sand, calcareous silty sandstone, sandy limestone, marl and shale, locally cherty		Aquifer
	FARS & GHAR FORMATIONS *Unconformity*	Localised shale, clay and calcareous silty sandstone		Aquitard
HASA GROUP	DAMMAM FORMATION (60 - 200m)	Chalky, marly, Dolomitic and calcarenitic limestone		Aquifer
		Nummulitic limestone with lignites and shales		Aquitard locally
	RUS FORMATION (20 - 200m)	Anhydrite and limestone		Aquiclude
	UMM ER RADHUMA FORMATION (300 - 600m)	Limestone and dolomite (calcarenitic in the middle) with localised anhydrite layers		Aquifer
	Disconformity	Shales and marls		Aquitard
ARUMA GROUP		Limestone and shaly limestone		Aquifer

The Greater Burgan oil fields main producing reservoirs are within the Cretaceous Burgan, Mauddud and Wara Formations, all sandstones (Fig. 40.3).

40.4 Investigation and Testing

A significant number of ground investigation boreholes were commissioned to determine the site specific geology and to collect samples for both geotechnical and geochemical characterization. The Burgan and Magwa sectors were chosen for this more detailed investigation. Both near surface (ground level), shallow (up to 2 m) and deep (up to 6 m) samples were taken to determine the critical zones for hosting potential contamination or problematic ground conditions. Standard in situ and laboratory geotechnical tests were undertaken including Standard Penetration Tests,

Fig. 40.3 Typical site profile showing degraded hydrocarbon contamination

Table 40.2 Example chemical results from Greater Burgan Field Al-Magwa

S.I	T.P. No.	Depth of sample (m)	Water soluble chloride (Cl⁻)		Water soluble sulfate			pH	
			%	PPM	as SO$_3$ %	PPM	as SO$_4$ %	PPM	
1		0.00	0.0425	425	0.1240	1240	0.1488	1,488	7.84
2	(0,100 m)	0.25	0.0283	283	0.0919	919	0.1103	1,103	8.94
3		0.50	0.0567	567	0.0746	746	0.0895	895	8.61
4		1.00	0.1645	1645	0.0304	304	0.0365	365	7.83
5		1.50	0.0822	822	0.0902	902	0.1082	1,082	8.29
6		2.00	0.0567	567	0.0554	554	0.0665	665	8.36

Fig. 40.4 Gas chromatogram of hydrocarbon contaminated soil from Abdally sector
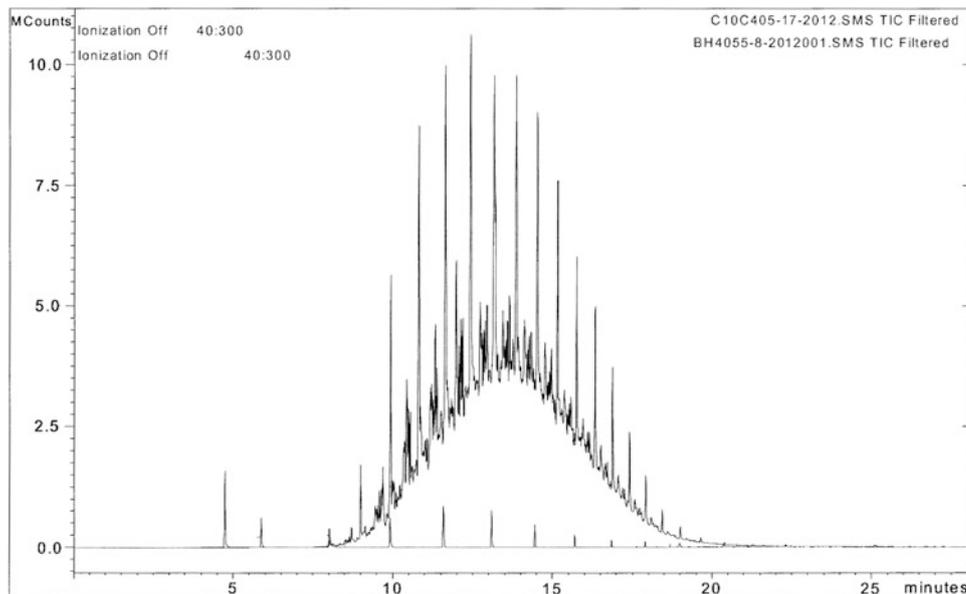
particle size distribution analysis, Atterberg Limits and Direct Shear tests where applicable. Chemical testing was primarily performed using Gas Chromatograph Mass Spectrometry (GCMS) to ascertain the nature of the residue hydrocarbons present together with elemental analysis. Water soluble chlorides and water soluble sulphates were also tested for (Table 40.2). The GCMS enabled the speciation of the hydrocarbons present in order to determine the degradation that had taken place since the original spillages in 1991 (Fig. 40.4).

40.5 Contamination Modeling

Currently a human health exposure assessment utilizing the ground investigation and laboratory test results is being undertaken using the RISC (Risk Integrated Software for Cleanups) software tool for performing human health risk assessments for hydrocarbon contaminated sites using fate and transport models to estimate receptor point concentrations in indoor and outdoor air and groundwater (ESI n.d.). The sites being assessed are potential future housing developments associated with the expansion of the city of Al Ahmadi. Both airborne and ingestions pathways are being assessed for a variety of receptors.

40.6 Summary

The legacy of the Saddam Hussein 1991 invasion of Kuwait and the subsequent destruction of the oil producing facilities is still detectable in the geotechnical and geochemical soil profile. Human Health Risk Assessments are being undertaken and contamination remediation strategies designed to enable future developments on or near these sites. Elevated Total Petroleum Hydrocarbons (TPH) levels have been detected as expected and their potential impact is currently being evaluated.

References

Al-Sulaimi J, Mukhopadhyay A (2000) An overview of the surface and near-surface geology, geomorphology and natural resources of Kuwait. Earth Sci Rev 50(3):227–267. doi:10.1016/S0012-8252(00)00005-2

ESI (n.d.) RISC—integrated software for cleanups. Retrieved from http://esinternational.com/risc/

Hunting Geology and Geophysics (1981) Photographic survey of the State of Kuwait. Submitted to the Kuwait Oil Company, Kuwait

Kaufman RL, Kabir CS, Abdul-Rahman B, Quttainah R, Dashti H, Pederson JM, Moon MS (2000) Characterizing the Greater Burgan field with geochemical and other field data. SPE Reservoir Eval Eng 3(2):118–126. doi:10.2118/62516-PA

**Comparison Between Neural Network
and Finite Element Models for the Prediction
of Groundwater Temperatures in Heat Pump
(GWHP) Systems**

41

Glenda Taddia, Stefano Lo Russo, and Vittorio Verda

Abstract

A fundamental aspect in groundwater heat pump (GWHP) plant design is the correct evaluation of the Thermally Affected Zone (TAZ) that develops around the injection well. This is particularly important to avoid interference with previously existing groundwater uses (wells) and underground structures. Temperature anomalies are detected through numerical methods. Computational fluid dynamic (CFD) models are widely used in this field because they offer the opportunity to calculate the time evolution of the thermal plume produced by a heat pump. The drawback of these models is the computational time. This paper aims to propose the use of neural networks to determine the time evolution of the groundwater temperature downstream of an installation as a function of the possible utilization profiles of the heat pump. The main advantage of neural network modeling is the possibility of evaluating a large number of scenarios in a very short time, which is very useful for the preliminary analysis of future multiple installations and optimal planning of urban energy systems. The neural network is trained using the results from a CFD model (FEFLOW) under several operating conditions. The final results appeared to be reliable and the temperature anomalies around the injection well appeared to be predicted well.

Keywords

Groundwater heat pump • Thermally affected zone • FEFLOW • Neural networks • Italy

41.1   Introduction

The market for geothermal heat pumps has grown considerably in the last decade (Lund et al. 2011; Bayer et al. 2012) and is one of the fastest-growing renewable energy technologies. A typical groundwater-based well-doublet scheme for heating or cooling (Banks 2009) typically comprises three elements:

1. An abstraction well, from which water is abstracted at a rate Q and a temperature Te
2. A heat-transfer system (a heat exchanger or a heat pump), which either extracts heat from, or rejects heat to, the groundwater flux;
3. One (or more) re-injection well(s), at a distance L from the abstraction well, where water is reinjected at a rate Q and temperature Tr. For space-cooling schemes, $\Delta T = (Tr - Te) > 0$ and for heating schemes $\Delta T < 0$. Thus, in the case of open-loop heat pumps, the water re-injected into the aquifer has a different temperature from the water of an undisturbed aquifer ($\Delta T \neq 0$). This thermal disturbance (Thermally Affected Zone, TAZ) propagates through the groundwater and may affect the temperature of water withdrawal operated by downstream installations

G. Taddia (✉) · S.L. Russo

Department of Environment, Land, and Infrastructure Engineering (DIATI), Politecnico di Torino, Corso Duca degli Abruzzi 24, 10129 Turin, Italy
e-mail: glenda.taddia@polito.it

S.L. Russo
e-mail: stefano.lorusso@polito.it

V. Verda
Department of Energy (DENERG), Politecnico di Torino, Corso Duca degli Abruzzi 24, 10129 Turin, Italy
e-mail: vittorio.verda@polito.it

(Lund et al. 2011; Chung and Choi 2012). Moreover a thermal plume may pose an internal risk to the sustainability of the well doublet due to the phenomenon of thermal feedback. In fact, if the well separation is insufficient there could be a risk that a proportion of the discharged warm water will flow back to the abstraction well. Computational fluid dynamic (CFD) models are widely used in this field because they offer the opportunity to calculate the time evolution of the thermal plume produced by a heat pump, depending on the characteristics of the subsurface and the heat pump (Yang et al. 2011; Nam and Ooka 2010; Zhou and Zhou 2009). In this case we using the finite element FEFLOW package. Neural networks could represent an alternative to CFD for assessing the TAZ under different scenarios referring to a specific site.

The development of artificial neural networks (ANNs) began approximately 70 years ago (McCulloch and Pitts 1943). This paper aims to propose the use of neural networks to determine the time evolution of the groundwater temperature downstream of an installation, as the function of possible utilization profiles of the heat pump. Due to the large variety of scenarios that can take place, these profiles need to be approximated in order to be easily expressed with a limited number of parameters and simple time functions. Various different simulations covering a wide variability range of the main characteristics of an installation have been conducted on the test case of Politecnico di Torino. These results are used to train the neural network.

41.2 Test Site Hydrogeology and FEFLOW Numerical Modeling

The test site is the Politecnico di Torino and is located in the urban area of Turin, the capital of the Piemonte Region in northwest Italy (geographical coordinates 45°03′45″N, 7°39′43″E, elevation 250 m asl).

The urban area of Turin is mainly situated on the outwash plain of several glaciofluvial coalescing fans connected to the Pleistocene-Holocene expansion phases of the Susa glacier. The plain extends between the external Rivoli-Avigliana Morainic Amphitheatre (RAMA, Susa Glacier) on the west side and Torino Hill on the east (see Fig. 41.1). The site is located in the central part of the urban area between the Dora Riparia River to the north, the Sangone River to the south, and the main draining Po River to the east, which flows northeast along the western border of Torino Hill. Two 47 m-deep wells having the same technical characteristics are present at the site. One is used for groundwater extraction (named P2), the other for injection (named P4). Injection well P4 is located 78 m from extraction well P2, almost directly downflow with respect to the local unperturbed potentiometric gradient. A piezometer (named S2) 47 m deep.

The potentiometric surface 17 m below ground level displays a W-to-E gradient of 0.269 % toward the Po river. The saturated thickness of the unconfined aquifer at the site is approximately 30 m. The buildings connected to the existing GWHP plant, are used for university offices and laboratories. The groundwater levels and temperature are measured in the extraction and injection wells and in the piezometer using through specific monitoring probes submerged 2 m below the groundwater level. The measured average undisturbed groundwater temperature is 15.0 °C along the saturated zone as experimentally determined from multi-temporal temperature logs in the wells and piezometer. This temperature is practically constant throughout the year. The average mesh spacing in the modelling domain is 15 m, and this was refined to 3 m in the area close to the wells to provide enhanced estimation of thermal plumes.

In particular, the time delay required for the thermal plume to reach three points located 20, 30, and 60 m downstream of the injection well has been calculated as a function of the mesh size. Several control points were included downgradient with respect to the injection well in order to check the evolution of the thermal plumes over the space. Control points 19, 21, 24, and 26 are placed along the line that connects the injection well with the piezometer, while control points 20, 22, 23, 25, and 27 are projections of previous control points along the groundwater flow direction. The horizontal angle between the two lines is almost 30°. Control points 19–23, 25, and 27 are located 10 m from the injection well while control points 24 and 26 are 20 m from it (see Fig. 41.2). Rainfall infiltration was not included in the calculations, owing also due to a lack of measured infiltration data. Appropriate FeFlow time-varying functions (TVFs) for Q and ΔT were defined by means of a post-processing phase of the monitoring data obtained from the heat pump plant monitoring system. The TVFs have been discretized considering a time step of one day, while the automatic computational time-step has been used for FeFlow simulations.

41.3 Simulation Results and Neural Network Model Applied to the Test Site

As multiple simulations are performed to train the neural network model, a parameterization of the scenarios is required.

Two additional parameters are associated with the groundwater: the first parameter is the maximum temperature change between water re-injection and withdrawal (from 0 to 12 °C), while the second parameter is associated with the partial load operation. Intermediate values correspond to a combination of these limiting cases. In order to show the main effects of the previous parameters, have been analyzed
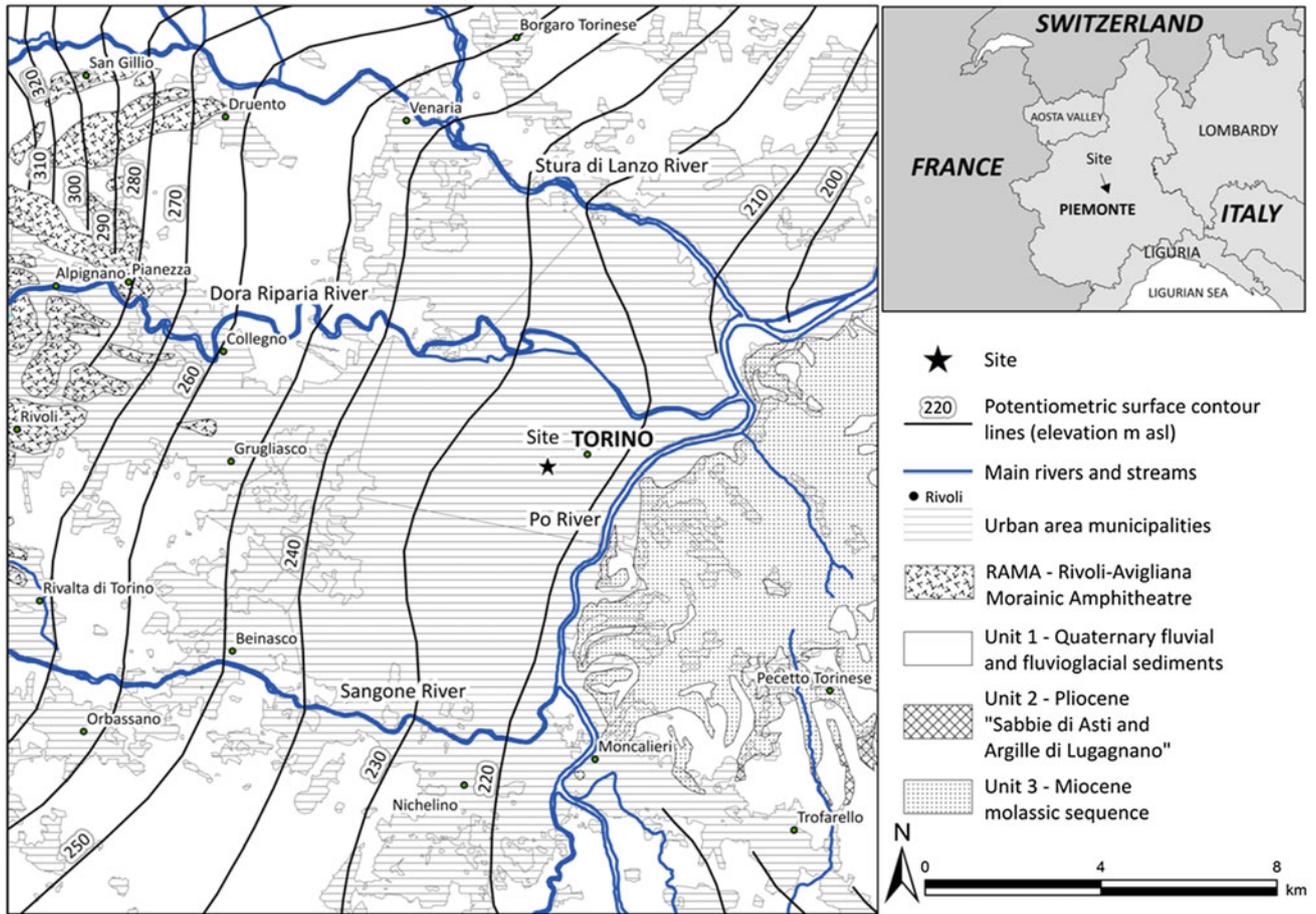
Fig. 41.1 Hydrogeological map of the Turin area and location of the site under investigation
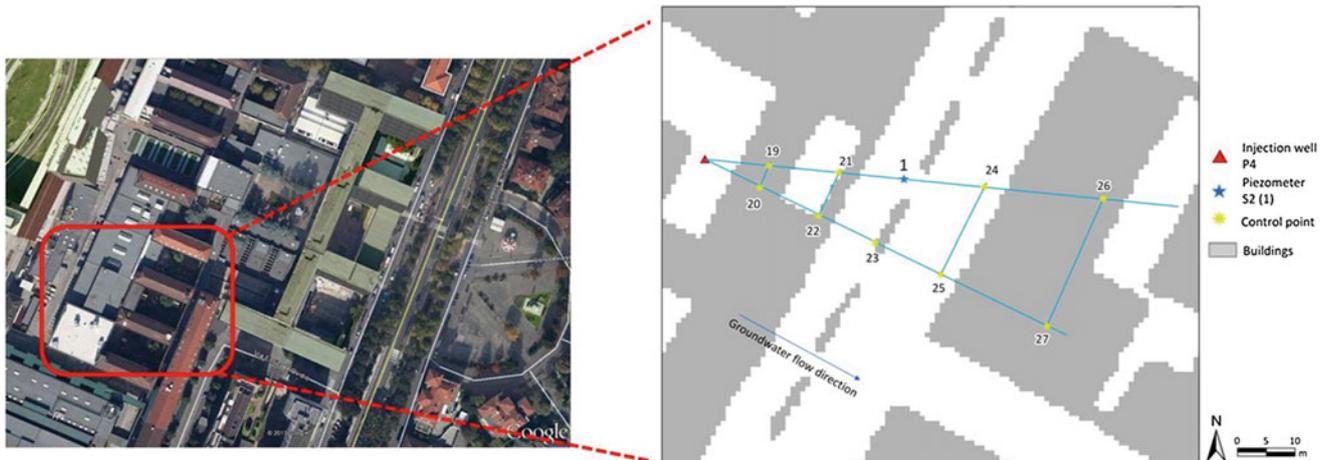
Fig. 41.2 Plan view of the control points on the topographical map

three principal scenarios and it were modelled using FEFLOW and appropriate FEFLOW time-varying functions (TVFs) for Q and ΔT. The first two scenarios are different because of a different maximum value of the re-injection temperature (3.3 °C in the first scenario and 11 °C in the second scenario). The third scenario is similar to the first one but a small value of the reduction in mass flow rate is considered, which means that when the heating/cooling load decreases, the heat pump is primarily operating by reducing the re-injection temperature change with respect to the

extraction temperature. The results obtained by modelling these scenarios are compared by checking the groundwater temperatures at two control points downstream of the injection well: point 27, located 60 m downstream in the groundwater flow direction, and point 26, located 63 m downstream and at 30° with respect to the groundwater flow direction. The maximum temperature in scenario 2 is about 20.5 °C, which is about 5.5 °C less than the injection temperature in this scenario. Temperature reduction is due to mixing effects and heat conduction. In scenarios 1 and 3, the maximum temperature is about 17 °C, which is about 1 °C lower than the injection temperature. This different behaviour is explained by the reduced driving force (smaller temperature gradient) with respect to scenario 2. This also means that groundwater temperatures in the three scenarios tend to converge at longer distances, where temperature gradients are small.

The network is characterized by five inputs: time, maximum heating load (0–600 kW), maximum cooling load (0–600 kW), maximum temperature variation between water re-injection and water withdrawal (0–12 °C), and water mass flow rate withdrawal reduction at partial load (0–1).

Figure 41.3 shows a comparison between the temperature profile at the piezometer calculated using the neural network and the values simulated using FEFLOW. The two curves show similar trends and very close values, which means that the ANN model is quite reliable even in the case of a utilization profile of the heat pump very different from that used for the parameterization. The temperature difference between the peak temperatures obtained with the two models is 0.34 ° C, while the root mean square error in a period of 200 days is 0.46 °C. The largest temperature deviation is about 1 °C. This result is considered satisfactory, considering that the simulation with the ANN has been performed treating the case as if the load profile were not known, that is as if the installation of the heat pump were only planned.
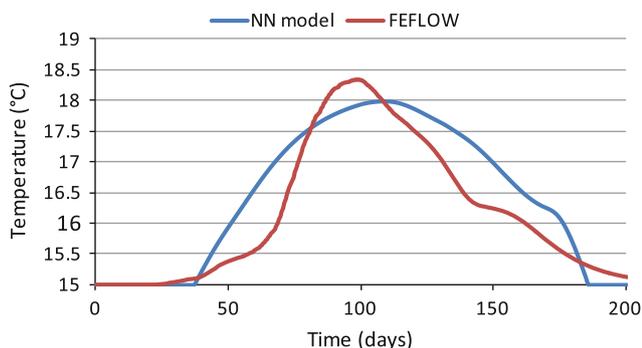
41.4 Conclusions

In this paper, the use of a neural network model to predict groundwater temperature profiles at a specific site is proposed. The network is trained using simulations performed using FEFLOW. In the case of a simulation performed using real profiles of water withdrawal and variable re-injection temperature, the neural network model is still able to predict the groundwater temperature profile as a function of time. The results are quite satisfactory since the average temperature deviation is about 0.46 °C and further improvements are possible, by increasing the number of simulations that are used for the training process. There may not be significant computational advantage in this approach, since the training process requires various simulations, nevertheless the ANN model can be easily implemented into optimization procedures and used by people that is not expert on CFD modelling. Once the model has been trained, it is possible to evaluate a large number of scenarios in a very short time, which is very useful while performing the optimization of operating strategies in order to minimize the overall energy used and environmental impact or for the preliminary analysis of future multiple installations, when the temperature of extracted temperature may be different than the unperturbed value. This is possible provided that the application of the neural network is performed on the same aquifer that has been considered for the model training. If the characteristics of the aquifer changes (in particular, the unperturbed velocity of groundwater), the model must be retrained.

References

Banks D (2009) Thermogeological assessment of open-loop well-doublet schemes: a review and synthesis of analytical approaches. Hydrogeol J 17(5):1149–1155. doi:http://dx.doi.org/10.1007/s10040-008-0427-6

Bayer P, Saner D, Bolay S, Rybach L, Blum P (2012) Greenhouse gas emission savings of ground source heat pump systems in Europe: a review. Renew Sustain Energy Rev 16(2):1256–1267. doi:10.1016/j.rser.2011.09.027

Chung JT, Choi JM (2012) Design and performance study of the ground-coupled heat pump system with an operating parameter. Renew Energy 42:1–2. doi:10.1016/j.renene.2011.08.054

Lund JW, Freeston DH, Boyd TL (2011) Direct utilization of geothermal energy 2010 worldwide review. Geothermics 40 (3):159–180. doi:10.1016/j.geothermics.2011.07.004

McCulloch WS, Pitts W (1943) A logic calculus of the ideas immanent in nervous activity. Bull Math Biophys 5:115–133

Nam Y, Ooka R (2010) Numerical simulation of ground heat and water transfer for groundwater heat pump system based on real-scale experiment. Energy Build (42):69–75. doi:http://dx.doi.org/10.1016/j.enbuild.2009.07.012

Yang QC, Liang J, Liu LC (2011) Numerical model for the capacity evaluation of shallow groundwater heat pumps in Beijing plain, China. Procedia Environ Sci 10:881–889

Zhou Y, Zhou Z (2009) Simulation of thermal transport in aquifer: a GWHP system in Chengdu, China. J Hydrodyn 21:647–657

Fig. 41.3 Comparison between temperatures simulated with FEFLOW and calculated with the ANN model

Ground Stiffness Evaluation Using the Soil Stiffness Gauge (SSG)

42

Mário Quinta-Ferreira

Abstract

The stiffness of a ground mass is a useful parameter to understand its mechanical behaviour under service. Despite the advantage provided by the knowledge of the ground stiffness, this parameter was seldom determined in the past, because it required elaborated in situ tests. At present, the stiffness can be easily determined with a soil stiffness gauge (SSG) that is a light and user-friendly equipment. The fast measurement and the good usability of the SSG are great advantages, together with the ability to compute the stiffness modulus of the ground assuming a Poisson's ratio. Based on a case study of a deteriorated pavement of a bus park the contribution of the SSG to the characterization of embankments and pavement layers is presented. The field and laboratory data demonstrated that the low stiffness modulus resulted from low quality embankment materials, reduced pavement thickness and deficient drainage of the pavement foundation.

42.1 Introduction to the SSG

The Soil Stiffness Gauge (SSG) allow to easily determine the stiffness of a soil layer and thus to compute the stiffness modulus of the ground, assuming a Poisson's ratio. This equipment can be very useful in quality control of unbound materials, in the determination of the stiffness or deformation modulus related to the relative compaction, in the identification of structural abnormalities, also allowing to quantify the strength increase with time of stabilized materials (Abu-Farsakh et al. 2004; Alshibli et al. 2005; Nazzal 2003; Seyman 2003; Batista 2007; Quinta-Ferreira et al. 2012). The SSG also allows on time corrective action during the construction process, which results in gains in efficiency and cost savings, avoiding subsequent corrective work.

The SSG technology was originally developed by the United States defence industry for the detection of landmines, having evolved to provide the design of a light equipment with only 10 kg (Fiedler et al. 1998 reported by Nazzal 2003). The stiffness is obtained causing very small vibrations on 25 different frequencies between 100 and 196 Hz, and measuring the resulting deformation ($<1.27 \times 10^{-6}$ m at 125 Hz). The apparatus used is the GeoGauge (Humboldt 2007), that records the stiffness value for each of the 25 frequencies and presents the average value. The soil deforms an amount δ proportional to the outside radius of the base ring (R), the Young's modulus (E), the shear modulus (G) and the Poisson's ratio (υ). The stiffness (K) is obtained dividing the force (P) by the deflection (δ) it produces (K = P/δ). According to Poulos and Davis (1974) the stiffness for a ring load in an elastic half-space is given by: K = (P/δ) = (3.54 GR)/(1 − υ), being K the stiffness, G the shear modulus, R the radius of the load ring and υ the Poisson's ratio. Knowing the Poisson's ratio the stiffness modulus is computed using the relation: Eg = K $(1 - \upsilon^2)/1.77R$.

M. Quinta-Ferreira (✉)
Department of Ciências da Terra, Geosciencies Center, University of Coimbra, Largo Marquês de Pombal, 3000-272, Coimbra, Portugal
e-mail: mqf@dct.uc.pt

The depth of measurement with the GeoGauge is between the surface and approximately 31 cm. The range of functionality is between 3 and 70 MN/m for stiffness, and between 26.2 and 610 MPa for the stiffness modulus. The Poisson's ratio may vary between 0.20 and 0.70 in increments of 0.05 (Humboldt 2007).

The tests with the GeoGauge were performed using an internal procedure described by Quinta-Ferreira et al. (2008) based on the recommendation of the GeoGauge Guide (Humboldt 2007) and on the ASTM D6758 (2008).

42.2   Some Applications of the SSG

In the control of embankments using the SSG a reference value of deformability must be used, which should be related to the relative compaction, and the results should be carefully evaluated based on experience. Abu-Farsakh et al. (2004) found that the maximum values of the stiffness modulus and the dry unit weight of two soils, clayey silt and sandy clay, do not occur simultaneously, tending to occur on the dry side of the compaction curves. As the construction procedures tend to require a moisture content within ±2 % of the optimal, they concluded that the SSG modules can vary about 40 % in this range, while the dry unit weight varies only 2.5 %. As a result of this observation, Abu-Farsakh et al. (2004) argue that the change in stiffness in this range is much larger than the dry unit weight, so that the use of stiffness as a criteria for acceptance is difficult to implement due to their sensitivity to the variation of water content.

As indicated by Alshibli et al. (2005) both the SSG and the impact deflectometer (FWD) apply a dynamic force to estimate the elastic modulus of the material, however with FWD the energy applied is much greater than the one applied by the SSG. Both tests assume that it is an elastic half-space in which a load is applied and the measurement of the surface deflection is used to calculate the elastic modulus of the layer.

A comparative evaluation of the in-place stiffness modulus using a van-integrated falling weight deflectometer (FWD) and the GeoGauge on a limestone all-in-aggregate (AIA), used in the base course of a highway pavement (Quinta-Ferreira et al. 2008, 2012) allowed to conclude that the dry unit weight is related with the stiffness modulus obtained with the SSG. The deflections measured in the centre of the FWD plate are related with the modulus obtained with the SSG. Considering as reference the equivalent modulus obtained with the FWD the moduli computed for the 85th percentile with both the FWD and the SSG, show a difference lower than 20 %. The deflections obtained with the FWD and the modulus obtained with the SSG show a similar pattern of dispersion. The results allowed a good coherence between both tests, indicating that the SSG can be used for in-place modulus evaluation, structural uniformity and pavement design validation.

42.3   Evaluation of Deteriorated Pavements

Shortly after the start of operation of a bus park, huge pavement deterioration were observed, that required to clarify the causes. Based on the visual assessment of the deteriorations four grades were considered (Fig. 42.1): Grade 1—No visible signs of deterioration; Grade 2—Deteriorated Pavement, without loss of functionality; Grade 3—Pavement very Deteriorated, eventually presenting open cracks and losses of bitumen in small areas; Grade 4—Pavement destroyed with complete loss of functionality or even non-existent, occurring in a small areas.

To clarify the causes of bad pavement performance the following works were done: (a) surface geological reconnaissance of the site and surrounding area, (b) measurement of the stiffness of the pavement and foundation ground using the SSG, (c) opening of three test pits in locations presenting the worst behaviour, SSG measurements and collection of samples for laboratory tests; (d) completing laboratory tests (Table 42.1), (e) interpretation of the results of field and laboratory.

Mainly based in the observation of the three test pits, the following units were defined:—Asphalt layer;—aggregate;—fill soil. The thickness of the layers measured in the test pits did not represented the average in the bus park because the prospection was carried out in the more deteriorated locations were the asphalt or aggregates were depleted and mixed with the foundation materials, as in test pit P1. The bedrock of the bus park consists of medium to coarse grained porphyroid biotite granite, having feldspar crystals reaching ten centimetres in length, and presenting a large range of weathering, since slightly weathered to decomposed. The bus park platform was constructed mainly on an embankment of decomposed granite, and in a very small part over an excavated area, at east.

The study with the SSG was done in 18 test locations, evenly distributed through the bus park (Fig. 42.1). Three readings in each location were made, considering the average result. In each one of the test pits two measurements with the GeoGauge were done: one in the pavement and the other in the soil underneath. The value used for the Poisson's ratio was 0.35. The average values obtained for the deformability modulus are shown in Fig. 42.1. From the analysis of Fig. 42.1 it can be stated that the lowest Eg values are located in the worst areas classified as grade 4 and grade 3. In areas without pavement deteriorated (grade 1) the deformability values were higher, which is consistent with the best material performance.

Fig. 42.1 Zoning of the pavement degradation in the bus park and test locations
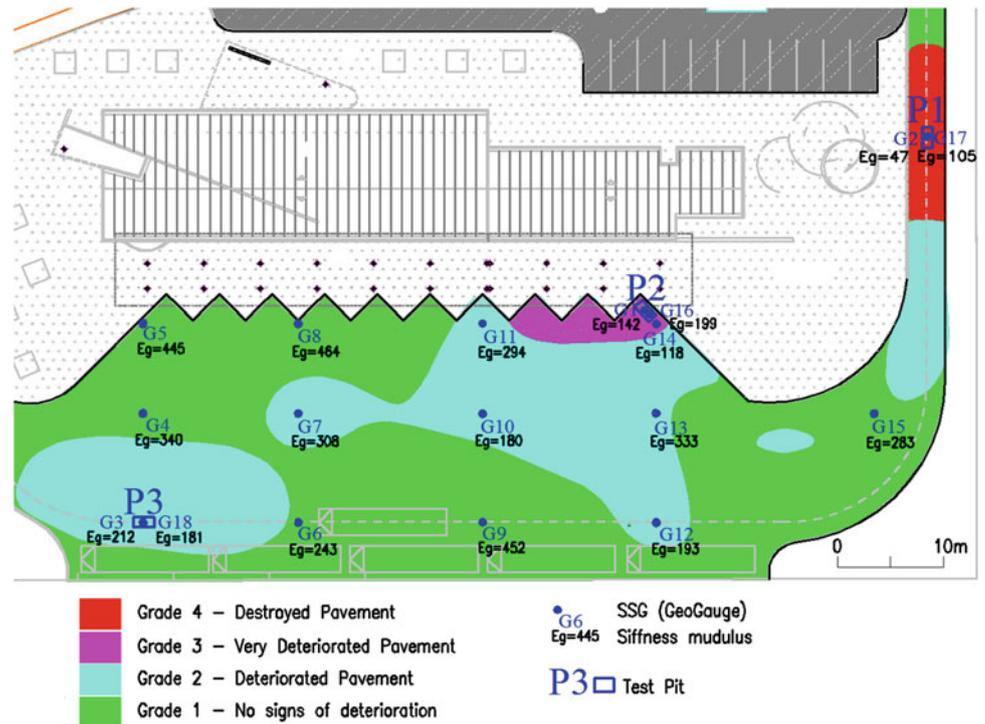
Table 42.1 Properties of soils tested

Location	P1	P2	P3
Depth (m)	0.1–1.3	0.1–0.6	0.15–1.0
Stiffness (MN/m)	4.9–11.1	15.0–30.0	19.1–22.3
Stiffness modulus (MPa)	46.7–105.0	142.1–198.7	181.1–211.8
LL (%)	36	33	33
IP (%)	11	5	6
<0.074 (%)	24.3	21.3	18.7
Sand equivalent	17	16	23
$\gamma_{dmáx}$ (kN/m^3)	18.0	19.0	–
W_{opt} (%)	13.5	11.2	–
CBR (%)	3	5	–
ASTM	A-2-6	A-1-B	A-1-B
USCS	SM	SM	SM

Based on the tests performed it is possible to conclude that soils P1 and P2 have worse characteristics than soil P3 (Table 42.1). These poor results are in accordance with the higher grade of degradation of the pavement observed around test pit P1 (Fig. 42.1) with a total loss of asphalt and even aggregate that was pushed by the passage of the buses.

In test pit P2 it was observed that the pavement waved during the passage of the buses, due to the saturation of the soils in the foundation. It was also observed that the deteriorated asphalt was pushed by the wells of the buses, overriding the sidewalk.

The observation of the pavement and the laboratory tests allowed to identify, characterize and understand that the pavement structure presented low stiffness modulus in significant areas, which was aggravated by the reduced foundation drainage. The soils in the pavement foundation had too much fines, high liquid limits and plasticity index as well as low CBR values. The pavement rehabilitation was based on an appropriate redesign, together with an efficient drainage, both at surface and in deep.

42.4 Final Remarks

Both our results and the ones that it was possible to find in the bibliography, showed that the SSG (the GeoGauge) is a device with great practical applicability, that is possible to relate with other geotechnical tests. The ease of use is a great advantage of the SSG. In the case study presented the field and laboratory data demonstrated that the low stiffness modulus resulted from low quality embankment materials, reduced pavement thickness and deficient drainage of the pavement foundation.

References

Abu-Farsakh MY, Alshibli K, Nazzal M, Seyman E (2004) Assessment of in situ test technology for construction control of base courses and embankments. Technical report nº FHWA/LA.04/385. Louisiana Transportation Research Center, Baton Rouge, LA, USA, p 126

Alshibli KA, Abu-Farsakh M, Seyman E (2005) Laboratory evaluation of the geogauge and light falling weight deflectometer as construction control tools. J Mater Civil Eng 17(5):560–569

ASTM D6758 (2008) Standard test method for measuring stiffness and apparent modulus of soil and soil aggregate in-place by an electromechanical method. American Society for Testing and Materials, ASTM International, West Conshohocken, PA

Batista LCM (2007) Determinação de parâmetros de deformabilidade de camadas de um pavimento a partir de ensaios de campo. Dissertação de Mestrado, G.DM-159/07, Dep. Engenharia Civil e Ambiental, Universidade de Brasília, Brasília, DF, p 182 (in Portuguese)

Fiedler S, Nelson C, Berkman F, DiMillio A (1998) Soil stiffness gauge for soil compaction control. Public Road, FHWA 61(5):5–11

Humboldt (2007) GeoGaugeTM user guide. Model H-4140. Soil stiffness/modulus gauge. Version 4.0. Humboldt Mfg. Co. Norridge, Illinois, USA

Nazzal MD (2003) Field evaluation of in situ test technology for Qc/Qa during construction of pavement layers and embankments. Louisiana State University, Master of Science thesis in civil engineering

Poulos HG, Davis EH (1974) Elastic solutions for soil and rock mechanics. Wiley, Hoboken, pp 167–168

Quinta-Ferreira M, Santarém Andrade P, Castelo Branco F (2008) Alguns resultados do GeoGauge e do deflectómetro de impacto (FWD) na caracterização de pavimentos. XI Cong. Nacional de Geotecnia/IV Cong. Luso Brasileiro de Geotecnia, Coimbra, p 8 (in Portuguese)

Quinta-Ferreira M, Fung E, Andrade PS, Branco FC (2012) In-place evaluation of a limestone base course modulus, using a van integrated falling weight deflectometer (FWD) and the GeoGauge (SSG). Road Mater Pavement Design, p 15. doi:10.1080/14680629.2012.735794

Seyman E (2003) Laboratory evaluation of in situ tests as potential quality control/quality assurance tools. Louisiana State University, Master of Science thesis in Civil Engineering

Influence of Fracture Systems and Weathering on the Sustainability of Rock Excavation Made for the Purpose of Infrastructure Construction

43

Radoslav Varbanov, Miroslav Krastanov, and Rosen Nankin

Abstract

The problems related to rock slope stability of excavations realized in differing in genesis rock complexes are the object of the present paper. The stability of these slopes depends on the natural fracture system in the massif, the additional fracture systems occurring in the rock masses during the excavation works as well as on the resistance against weathering of the rock massif. The investigation of the above problems was carried out in the excavations of the Sofia-Mezdra railway line, which crosses the Stara Planina Mountain chain. The mountain ridges are built of rock complexes with various composition and genesis. The railway construction was started in the middle of the 19th century. The commissioning of the line was on November 8, 1899. Rock slopes with different height and inclination were formed during the railway construction. In the course of a period exceeding 110 years the rock slopes have been subjected to weathering processes that have inevitably exerted effect on their stability too. The modern safety requirements for the railway line operation impose the performance of different stabilization activities. The design of the safety measures is connected with the assessment of the rock slope stability as of the present moment. The diverse geotechnical characteristics and geological conditions of rock massifs, built of sedimentary rocks (argillites and sandstones), metamorphic rocks (gneisses and quartzites) and volcanic rocks (various diabase types), have been considered.

43.1 Introduction

A spatial model of the fracture systems is composed on the base of field measurements. Qualitative assessment (rock mass rating) of the massifs is made on the base of this model. The results show that in some zones of the rock massifs "rock wedges" have been formed, which are unfavorably inclined towards the excavation slope. The origin of slope deformations has been already observed along some of these weak zones. Shear strength assessment is made along the fractures of the "rock wedges", formed both in the natural terrain and in the railway line excavations. Data are presented for the quantitative assessment of the risk of rock massif slope destruction in the natural state, as well as in the zone of the artificial rock slopes.

43.2 Location and Geomorphology

The studied region is situated in West Bulgaria in the Iskar River valley, at a distance of 40 km to the north of the capital Sofia (Fig. 43.1). The relief in the region is mountainous, with an average altitude above 700 m. The lowest parts of

R. Varbanov · R. Nankin
University of Architecture, Civil Engineering and Geodesy, Sofia, Bulgaria

M. Кrastanov (✉)
Geological Institute "Strashimir Dimitrov", Bulgarian Academy of Sciences, Sofia, Bulgaria
e-mail: miroivanov@mail.bg
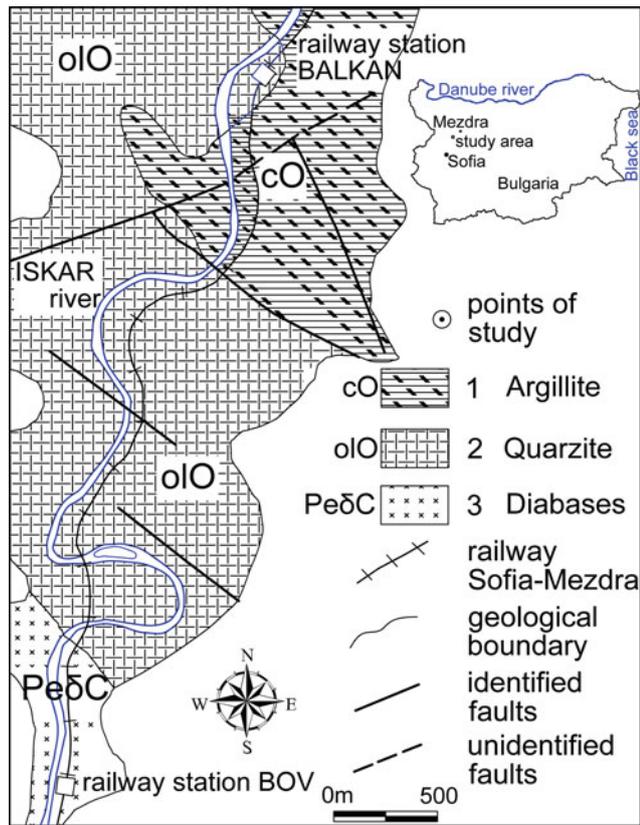
Fig. 43.1 Geological map and location on study area

the relief are in the Iskar River bed—about 450 m. In geomorphologic respect the region is a part of the Stara Planina Mountain chain system. Its contemporary relief was formed under the influence of diverse geological and erosion denudation processes.

43.3 Geological-Tectonic Structure

In geological respect, rocks of Carboniferous and Ordovician age are outcropped in the direction from north to south. The Carboniferous rocks are built of the diabases (PeδC2) of the Petrohan pluton, occupying a narrow strip in the initial zones of the studied railway section. The rest part of the railway alignment is built almost entirely of the Olistostrome unit (olO), represented by quartzites, aleurites and phylitized argillites. These rocks are formed as stacks, separating several olistostromes with relatively large sizes. The thickness of the olistostrome unit exceeds 800 m. The end zones fall within a region built mainly of the argillites and aleurites of the Clayey Metagroup (cO), which are metamorphized in a green schist facies. The lower boundary represents an abrupt lithological contact with the underlying aleurite-quartzite metagroup. It is discordantly covered on top by the rocks of

the Petrohan Terrigenic Group. The thickness of the metagroup exceeds 300 m. The considered region falls within the Berkovitsa tectonic unit, building the southern most highly uplifted segment of the West Balkan zone. Numerous longitudinal, transverse and oblique fault disturbances are established in this region. Some of them are with proved older embedding and repeated tectonic activation. The oblique faults, affecting the investigated railway section, are grouped in two systems with directions 140–170° and 65–80°. The great diversity of the tectonic structures influencing the explored region determines the intense tectonic activity, shaping the relief as well as providing prerequisites for the development of hazardous and risk phenomena and processes.

43.4 Methods of Investigation

Rock massif assessment (Rock Mass Rating—RMR) has been performed for the purposes of the design of stabilization activities in three of the most widespread rock complexes along the railway alignment. The two most widely utilized classifications of rock masses are applied—of Bieniawski (1976, 1989) and Barton et al. (1974). The following six criteria are used in the RMR evaluation: (1) Uniaxial compressive strength of the natural massif in its natural state and after about 100 years of weathering; (2) Determination of rock massif quality (Rock Quality Designation—RQD); (3) Measurement of the distances between the fracture systems for "a natural rock massif and a fractured rock massif due to construction activities and weathering processes"; (4) State of the fracture systems; (5) Hydrogeological conditions in the zone of the fracture systems; (6) Spatial orientation of the fractures and type of fracture surface.

43.5 Engineering Geological Characteristics

The engineering geological conditions are characterized on the base of the mapping and in situ investigations carried out. Most generally, one qualitative assessment is made for the present state of the rock varieties, subjected to the influence of the weathering processes in the course of 113 years, which build the slopes of the studied section (Bov station and Balkan stop) of the Sofia-Mezdra railway line. Rocks of the three genetic groups are outcropped in this section of the railway, from south to north, as follows: magmatic (diabases), metamorphic (quartzites) and sedimentary (argillites), as shown in Fig. 43.1. The qualitative assessment is made on the base of the field investigations mainly by means of two parameters: RMR (Rock Mass Rating—Bieniawski) and GSI (Geologycal Strength Index—Hoek and Marinos), as well as on one probabilistic
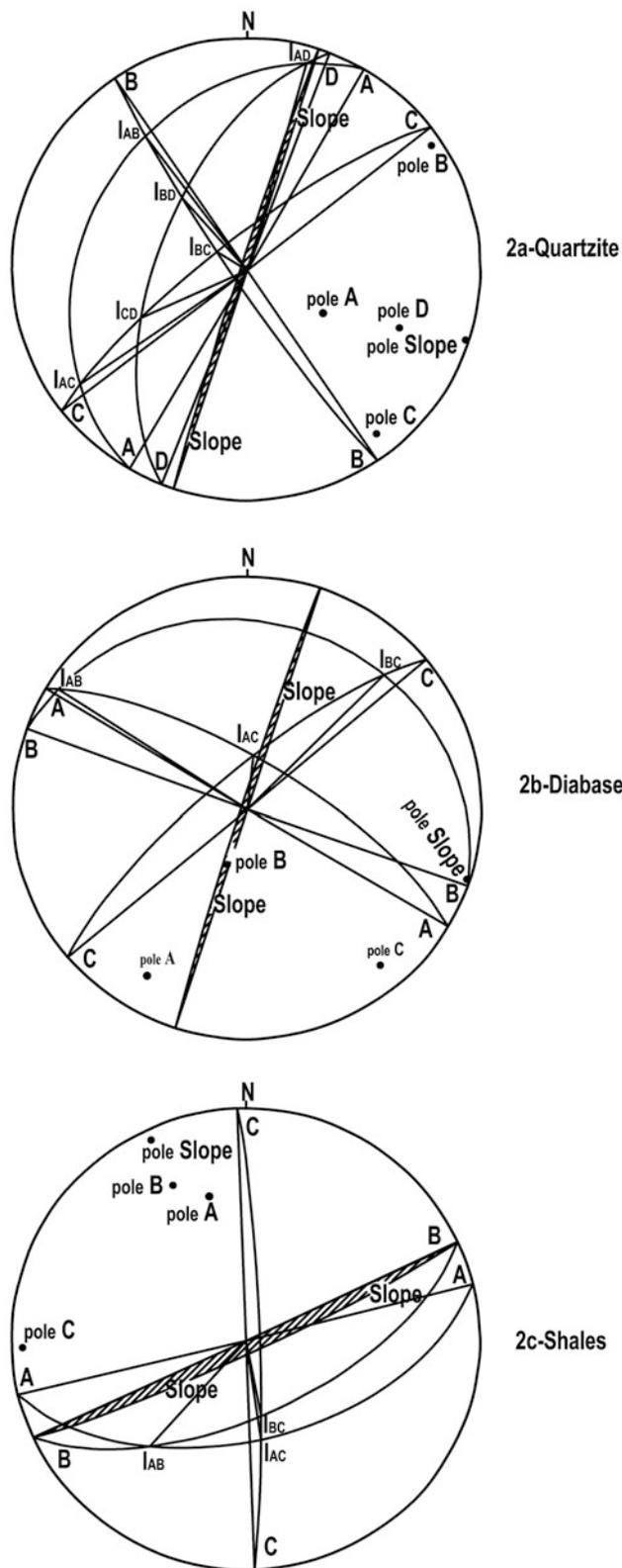
Fig. 43.2 Stereographic projections on system cracks and slope. *A–A*—projection of the system cracks *A*; pole *A*—pole cracks of the system *A*; *I_AB*—projection of the intersection of the systems cracks *A* and *B*

Table 43.1 Values of the elements of the fracture systems and the slope

Rock masses	System of cracks/ slope	Elements of occurrence crack systems and slopes	
		Dip direction $\alpha(\ldots^\circ)$	Dip $\psi(\ldots^\circ)$
Quartzite	System A	300	31
	System B	236	85
	System C	322	79
	System D	291	59
	Slope	288	88
Diabases	System A	31	73
	System B	20	21
	System C	320	77
	Slope	288	88
Argillite	System A	166	54
	System B	155	63
	System C	88	85
	Slope	155	85

assessment concerning the possibility of wedge formation, along which there is a hazard of rock mass caving. The probabilistic assessment was realized by field measurements of the elements of embedding of the basic fracture systems and the slope, exerting impact on the rock massif stability. The investigations were realized by means of stereographic projections of the fracture systems and the slope (Fig. 43.2) of the excavation. The studied elements of embedding of the fracture systems and the slope are given in Table 43.1. The rest part of the investigated section is almost entirely built of quartzite metamorphic rock, for which it is obvious (Fig. 43.2a) that the projections of the intersection lines (I_{AB} and I_{AC}) of the fracture systems lie and cross the slope projection, which provides the possibility of caving wedge formation in the rock massif, while the projection of the intersection line I_{BC} does not lie on the slope projection and hence there is no hazard of rock massif caving. The zone around the Bov station is built of diabase magmatic rock and it is seen in Fig. 43.2b that the projections of the intersection lines (I_{AB}; I_{AC}; I_{AD}; I_{BC}; I_{BD} and I_{CD}) of the fracture systems lie on and cross the slope projection, providing the possibility of caving wedge formation in the rock massif. The slopes in the end zones of the considered section are built by argillite sedimentary rock and it is seen in Fig. 43.2c that the projections of the intersection lines (I_{AB}; I_{AC} and I_{BC}) of the fracture systems lie on and cross the slope projection, which gives the possibility of forming hazardous caving wedges in the rock massif. The assessment of the state and the classification of the different types of rock massifs according to RMR and GSI are shown in Table 43.2.

Table 43.2 Values of RMR and GSI for different rocks, revealing along the study route

Classification parameter	Exploration of various geological rock masses		
	Diabases	Quartzite	Argillite
Uniaxial compressive strength (MPa)	39	48	24
Rating	4	4	2
Rock quality designation (%)	87.5	87	72.5
Rating	17	17	13
Spacing of discontinuities (m)	0.19	0.25	0.14
Rating	8	10	8
Condition of discontinuities	Slightly rough surface, separation <1 mm, slightly weathered walls	Rough surface, separation <1 mm, slightly weathered walls	Slickenside surfaces or gouge <5 mm thick or separation 1–5 mm continuous
Rating	25	25	10
Ground water conditions	Completely dry	Completely dry	Dripping
Rating	15	15	4
Orientation of discontinuities	Fair	Fair	Favorable
Rating (slopes)	−25	−25	−5
Rock mass rating (RMR)	44	46	32
Rock mass classes determined from total ratings			
Class number	III	III	IV
Description	Fair rock	Fair rock	Poor rock
Geological strength index (GSI)	39	41	27
Structure of rock masses	Blocky/disturbed	Blocky/disturbed	Disintegrated
Surface conditions	Good	Good	Poor

43.6   Conclusion

The rock massifs built of diabases and quartzites, which occupy definite zones of the considered alignment, are classified according to RMR as class III, with geotechnical state of medium strong rock massif. While these built of argillites are classified as class IV, with geotechnical state of weak rock massif. In accordance with the GSI classification of rock massifs, the diabases and quartzites have a small-block structure with disintegrated zones and good state of the fractures, while the argillites are with fragmentary structure and poor state of the fractures. The argilites are with the lowest value of RMR, which explains the problems that occured during exploitation of the railway line in the zones, where there are some.

The above mentioned characteristics of the rock massifs, established as a result of the researches done, are a sign of weathering processes that create conditions for formation of fracture systems. The latter, in turn, lead to the formation of rock wedges of different sizes in the massif. To protect the railway line are fulfilled protective measures, such as caving of rocks, removal of vegetation on the slopes, construction of retaining walls and safety nets, anchored in the bedrock.

References

Angelov V et al (2008) Explanatory note to map sheet K-34-35-G (Lakatnik), Sofia

Barton NR, Lien R, Lunde J (1974) Engineering classification of rock masses for the design of tunnel support. Rock Mech 6(4):189–239

Bieniawski ZT (1973) Engineering classification of jointed rock masses. Trans S Afr Inst Civ Eng 15:335–344

Hoek E (2006) Practical rock engineering

Hoek E, Dieberichs M (2006) Empirical estimation of rock mass modulus. Int J Rock Mech Min Sci Geomech Abstr 43:203–215

Ilov G (2009) Applied mechanics rocks: rocks and building foundations in rock

Weihua Zhao, Nengpan Ju, and Jianjun Zhao

Abstract

Characterized by high seismic intensity and high geological disaster risk, the geological condition of Longmenshan is complex and unique. How to carry out route alignment in such complicated geological background and avoid geohazards is one of key issues. Based on the geological background, including landform, lithology, Geological tectonic, geohazards distribution, acquired by remote sensing and field investigation, this paper firstly compared route schemes of the Chengdu-Lanzhou railway in Longmenshan mountain area, and regarded the Jushui river basin as recommendation for relatively less geohazards and no gobs. Then this paper secondly evaluated route schemes related to geohazards distribution and geohazards features in Jushui river basin, and regarded the D2K scheme as preferred option, which avoid large-scale and typical geohazards in the form of "early into tunnel and later out of tunnels" by longer tunnels.

Keywords

Geological condition • Geohazards • Route alignment • Route optimization

44.1 Introduction

The Chengdu-Lanzhou railway is a key infrastructure of The Western Development Strategy of China. The general trend of the project determined the railway must across the Longmenshan faults zone (Zhu et al. 2009). The geological condition in this zone is complex and unique with the feather called "four extremely, three high". The "four extremely" are extremely strong topological incision, extremely complex and active tectonic, extremely weak rock mass and extremely significant Wenchuan earthquake effect. The "three high" are high crustal stress, high seismic intensity and high risk of geohazards (Huang 2011; Du et al. 2012). How to carry out route alignment in such complicated geological background and maximally avoid geohazards is one of key issues (Wu et al. 2010; Yang et al. 2010; Huang et al. 2013).

44.2 Geological Conditions of Study Area

The geomorphology of the study area is characterized by high mountains and deep valleys. The gradient of slopes along river is generally larger than 35°. Lithologies of stratums expose completely, comprising limestone, dolomite, sandy conglomerate, shale and magmatic rock. The proposed schemes in Longmenshan zone are located between the Front Fracture of Longmenshan and the Central Fracture of Longmenshan. Suffered by the Wenchuan earthquake, a large number of slopes failed and developed abundant geohazards with high density (Huang and Li 2009). These geohazards distribution is controlled by river system and fault lines (Huang and Li 2009).

44.3 Route Comparison and Selection Based on Geological Conditions

The geohazards are acquired by RS interpretation and checked by investigation. By comparing the landform, geological tectonic, hydrology, gobs and related aspects, this paper analyzed advantage and disadvantage of each scheme

W. Zhao (✉) · N. Ju · J. Zhao
State Key Laboratory of Geohazard Prevention and
Geoenvironment Protection, Chengdu University of Technology,
Chengdu 610059, Sichuan, China
e-mail: weihuageo@gmai.com

Table 44.1 Comparison of route schemes in three river basin in Longmenshan region

Schemes	Shitingjiang	Mianyuanhe	Jushuihe
Route	A6K et al.	A16K, C2K et al.	CK, C1K, DK, D1K, D2K et al.
Landform	Steep mountains; narrow and deep valley	Narrow valley except Qingping; steep mountains	Open terrain, wide valley along the lines in Jushui town and Erlangmiao et al.
Lithology	Magmatic rock; diorite; limestone; dolomite	Limestone; dolomite; siliceous rock	Thick-layer limestone; dolomite; sandy slate
Geological tectonic	• Route perpendicular to the Longmenshan faults	• Route perpendicular to the Longmenshan faults	• Route perpendicular to the Longmenshan faults
	• The front Longmenshan fracture has no obvious movement	• The surface ruptured by front Longmenshan fracture	• The front Longmenshan fracture has no obvious movement
	• The central fracture dislocated the Guanghan-Yuejiashan railway	• The ground surface at the central fracture has severe motion and lifted to 1.3 m	• The ground surface at the central fracture has small rupture
Geohazards (landslides, rock falls and debris flow)	• Large density of geohazards, the maximal value up to 12/km^2	• Large density of geohazards, the maximal value up to 11/km^2	• The maximal value of density of geohazards is 7/km^2
	• More large-scale landslides, such as Ganhekou landslide	• More large-scale landslides, such as Tianchixiang landslide, yibadao landslide and Xiaogangjian dam lake	• Less large-scale landslides, the large-scale landslides such as Daguangbao, Laoyingyan and Dazhuping far away from railway
	• Landslides and rockfalls provided abundant resources for debris flow	• Landslides and rockfalls provided abundant resources for debris flow, such as the outbreak of the Qingping debris flow in 2010, against construction of tunnels	• Abundant resources for debris flow in Jinxigou valley
Gobs	More gobs along the route within 1 km with large range, such as Jinhe phosphorite, Songlin coal mine et al., have obvious deformation	There are more gobs along the route within 2 km with three surface subsidence, and Tianchi first well, Qingping phosphorite et al. are nearby the route	There are no gobs along the route within 1 km. The straight-line distance from closest coal mine is 1.3 km. There's no deformation

in the three river basins and suggested the best one. The comparison listed in Table 44.1. Compared with Shitingjian river basin and Mianyuanhe river basin, the Jushui river basin has relatively open terrain, the Longmenshan faults in this basin has no obvious movement and rupture, density of geohazards relatively small, resources and scale of debris flow relatively less and small. Taking all geological conditions in account, the Jushui river basin was recommended as the best region.

44.4   Route Optimization in Jushui River Basin Based on Geohazards

The Jushui river basin was recommended as best region, but specific to this basin, development degree of geohazards in different parts is inhomogeneous. Based on investigation and according to the principle that as far as possible to avoid geohazards, this paper next compare and optimize routes in the Jushui river basin listed in Table 44.2. Route Schemes and Geohazards' Distribution that Infecting Route Alignment are shown in Fig. 44.1. The proposed schemes in Longmenshan are located between the Front Fracture of Longmenshan (F2 faults system) and the Central Fracture of Longmenshan (F3 faults system). With F2 and F3, the region was divided to Jushui, Jushui to Gaochuan and Gaochuan to Maoxian three parts. In Table 44.2, compared with other schemes, the D2K scheme pass through this basin by adopting long tunnels, and successfully avoid typical large-scale geohazards triggered by Wenchuan earthquake, such as the Guantan landslide (Fig. 44.1) (Zhao et al. 2010), Yongjiashan unstable slope, Shiziyuan rockfall, Ganmofang landslide (Fig. 44.1). Slopes of tunnel entrances and exits have lesser hazards with small-scale. Thus, the D2K scheme has some advantages and was recommended as optimization.

Table 44.2 Comparison of route schemes in Jushui river basin

Segment	Route Scheme	Tunnels		Number of geohazards near exits and entrances of tunnels		Geologic instruction
				Entrance	Exit	
Jushui (Piedmont of Longmenshan)	CK	Kuzhuan tunnel		8	35	The Guantan landslide is a large-scale anti-inclined landslide induced by strong earthquake and follow-up rain, which slid from top to toe and formed dammed lake. The route scheme C1K go through Yudongshan–Guanxian–Lianghekou, and infected by this landslide, and the route DK, D1K and D2K exit at Yongjiashan and avoid the Guantan landslide
	C1K	Number one tunnel		0	1	
	DK	Dapingshan tunnel		1	10	
	D1K	Yudongshan tunnel		0	8	
	D2K	Anxian tunnel		0	8	
Jushui to Gaochuan (between the front fracture and the central fracture)	CK	Yongjiashan	Shibanlou	59/57	50/24	• The Yongjiashan unstable slope is close to the front fracture of Longmenshan, which has many dangerous rocks that threaten CK
	C1K	Number 2	Number 3	3/14	22/5	• Slopes along Yuejinqiao–Shiziyuan–Dengjiaping are steep and not suitable to build railway bed or bridge. The D2K avoid the hazards
	DK	Shiziyuan	Dengjiaping	10/3	7/1	• The Shibanlou tunnel was located on unstable slope with landslides and rockfalls. The geohazards developed in groups against entrance and exit of tunnels and should be avoided
	D1K	Shiziyuan tunnel		0	7	• Exit of Shiziyuan tunnel is located at Erlangmiao, which slope has low altitude difference and gentle slope. The river valley is broad and low hazard density
	D2K	Shiziyuan tunnel		0	4	
Gaochuan to Maoxian (behind the central fracture)	CK	Longmenshan tunnel		44	37	• The exit of Longmenshan tunnel of CK and C1 K is located at upper reaches of Lengjingou valley. Abundant loose accumulation triggered by earthquake is located in the valley and easily form debris flow under storm
	C1K	Longmenshan tunnel		3	1	
	DK	Longmenshan tunnel		2	1	
	D1K	Longmenshan tunnel		0	1	
	D2K	Longmenshan tunnel		0	1	• The geological conditions of D1K and D2K in Gaochuan are better
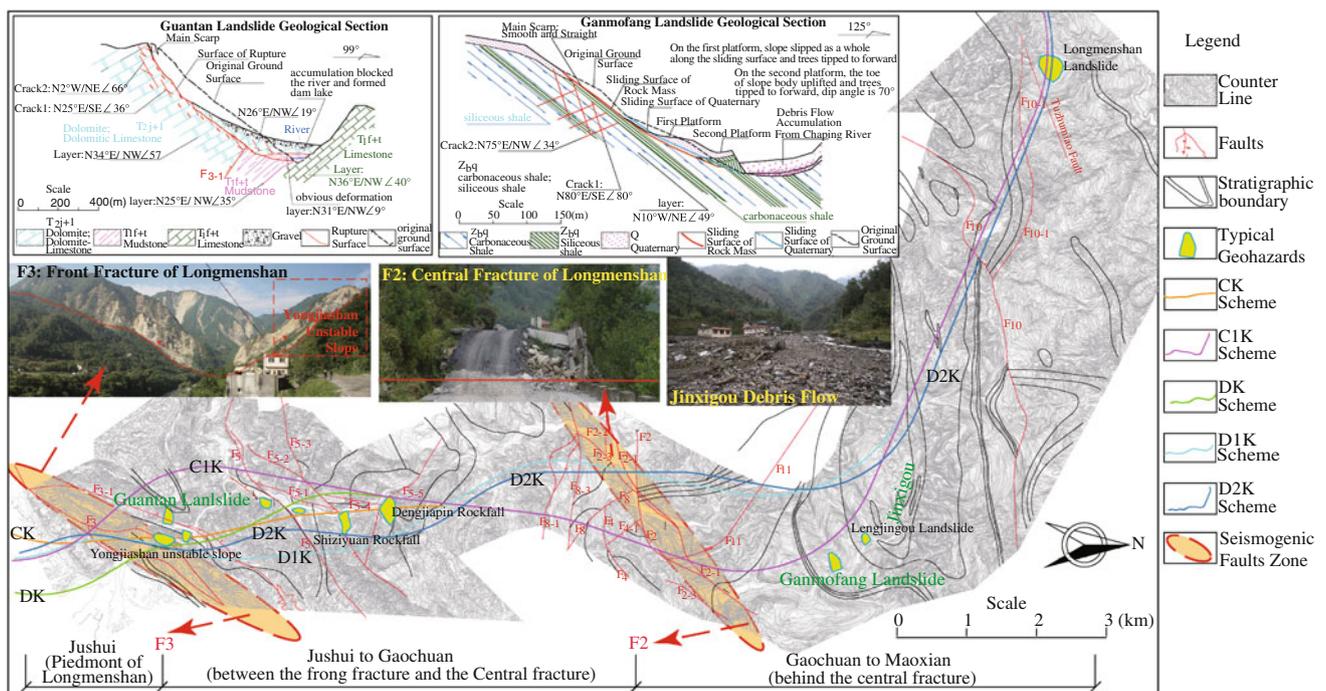
Fig. 44.1 Route schemes and Geohazards' distribution that infecting route alignment

44.5 Conclusion

Based on geological background acquired by RS and field investigation, this paper firstly compared routes schemes of the Chengdu-Lanzhou railway in Longmenshan mountain area, and regarded the Jushui river basin as recommendation with relatively less geohazards and no gobs. Then this paper secondly compared routes schemes in Jushui river basin, and regarded the D2K scheme adopting long tunnels, as preferred option, which avoid large-scale and typical geohazards. The work of this paper provided geological basis for the Chengdu-Lanzhou railway alignment.

References

Du YB, Yuan CB, Wang YD, Tao Y (2012) Major geological hazard and geological alignment of Chengdu-Lanzhou railway. J Railway Eng Soc 8:11–15 (in Chinese)

Huang R, Li W (2008) Research on development and distribution rules of geohazards induced by Wenchuan earthquake on 12th May, 2008. Chin J Rock Mech Eng 27(12):2585–2592

Huang R, Li W (2009) Analysis on the number and density of landslides triggered by the 2008 Wenchuan earthquake. China. J Geol Hazards Environ Preserv 20(3):1–7 (in Chines)

Huang R, Li Y, Qu K, Wang K (2013) Engineering geological assessment for route selection of railway line in geologically active area: a case study in China. J Mt Sci 10(4):495–508

Wu G, Xiao D, Jiang L et al (2010) Problems about engineering geology of high-grade railway route selection in complicated mountainous areas. J Southwest Jiaotong Univ 45(4):527–532 (in Chinese)

Yang C (2012) Analysis of the controlling factors of Chengdu-Lanzhou railway location in 5.12 Wenchuan earthquake-stricken areas. In: Proceedings of the 1st international workshop on high-speed and intercity railways, vol 147. Lecture notes in electrical engineering, pp 385–394

Zhao J, Ju N, Li G, Huang R (2010) Failure mechanism analysis of Guantan landslide induced by Wenchuan earthquake. J Geol Hazards Environ Preserv 21(2):92–96

Zhu Y, Wei Y, Zhong X (2009) Route selection and overall design of railway in high seismic intensity mountain area: a case study of the Chengdu-Lanzhou railway. Analysis and investigation on seismic damages of projects subjected to Wenchuan earthquake, pp 808–816 (in Chinese)

John Johnston, Stephen Fityus, Olivier Buzzi, Chris Rodgers,
and Robert Kingsland

Abstract

The economic Permian coal deposits of the Newcastle Coal Measures of Eastern Australia are characterized by frequent tuffs and tonsteins, of predominantly clay character. Compared with their associated sedimentary rocks, these have undesirable engineering properties. This paper describes the results from a series of studies undertaken to characterize these materials in their context as engineering materials. The large number of tuff units throughout the coal measures are found to vary greatly in their composition and texture, with many being dominated by high plasticity, expansive clays. This makes them difficult to compact, with low dry densities and high optimum water contents. Their treatment as earthworks materials is reviewed and data is presented which quantifies variability in their engineering properties, as determined from a major earthworks project. Methods of successfully incorporating them into earthworks designs are discussed.

Keywords

Tuff • Clay tuff • Tuffaceous clay • Swelling clay

45.1 Introduction

The Newcastle coal measures (NCM) are a late Permian aged geological sequence, located in the north east corner of the Sydney Basin. This sequence is well known for its economic coal deposits and unique geology, and for the large proportion of tuff and tuffaceous strata found within it, when compared to other geological sequences of the Sydney Basin (Ives 1995).

Tuffs are sedimentary rocks of volcaniclastic origin. They may be crystalline or vitric in nature. Tuffs derived from thin ashfalls, that have undergone devitrification to form kaolinitic or bentonitic claystones, are described as tonsteins (Diessel 1985). Air-fall from volcanic eruptions often deposit over large areas, and so tuff units display high lateral continuity. In the NCM they are commonly associated with coal and carbonaceous rocks, as shown in Fig. 45.1, making them useful as stratigraphic markers (Kramer et al. 2001). Estimates on the amount of tuffaceous material within the Newcastle coal measures vary from 19 and 20 % (Ives 1995 and Diessel 1985, respectively) to 25 % (Brakel 1989).

Tuffs in the NCM are highly variable in chemical composition and mineralogical makeup, and this makes their engineering properties highly variable. Different ash sources, together with varying depositional environments, have resulted in different clay mineral assemblages being

J. Johnston
RCA Australia, 92 Hill Street, Carrington, 2294, Australia
e-mail: johnj@rca.com.au

J. Johnston · S. Fityus (✉) · O. Buzzi
The University of Newcastle, University Drive, Callaghan, 2308, Australia
e-mail: stephen.fityus@newcastle.edu.au

C. Rodgers
Roads and Maritime Services, Sydney, NSW, Australia

C. Rodgers · R. Kingsland
Hunter Expressway Alliance, Sydney, NSW, Australia

R. Kingsland
Parsons Brinckerhoff, Sydney, NSW, Australia
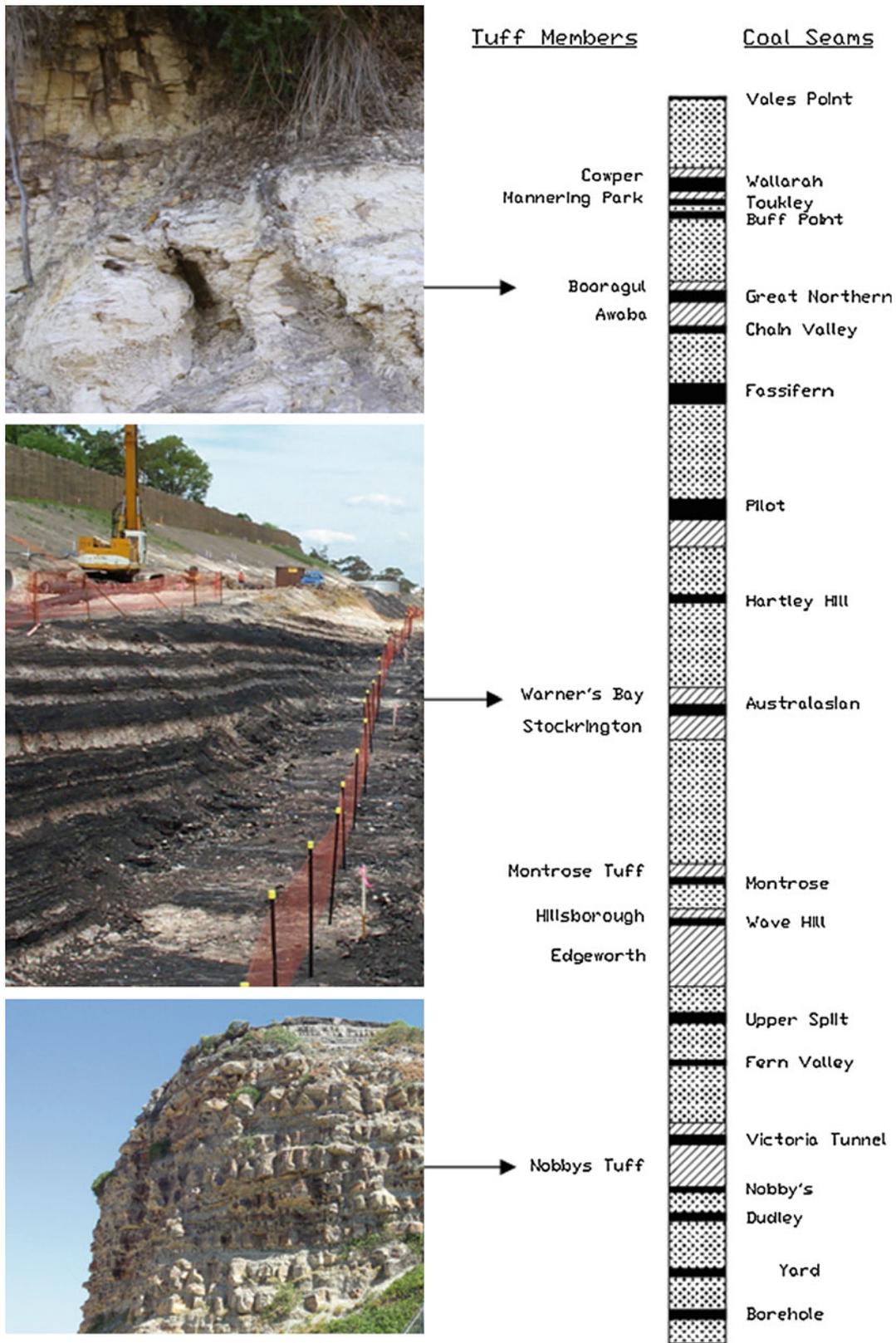
Fig. 45.1 Stratigraphic column of the Newcastle coal measures showing named and unnamed tuff units, with photographs of some well-known units
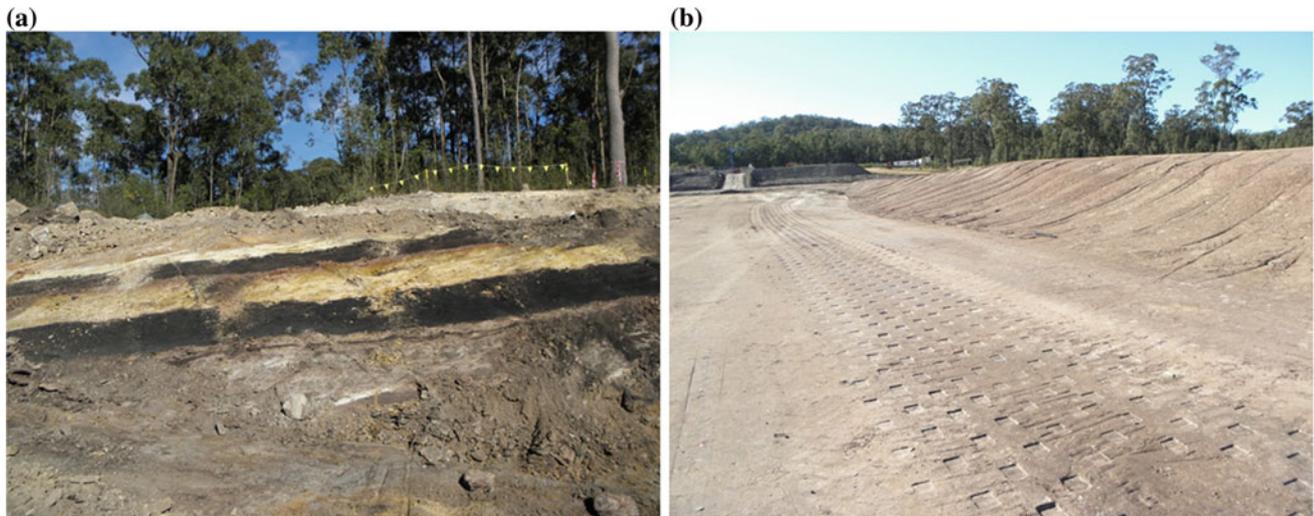
Fig. 45.2 Tuffs encountered while constructing the Hunter expressway. **a** Several tuff bands in a cutting. **b** Reworked material in compacted fill

produced, with the wet, humid swamps forming highly montmorillonitic clays, and locally acidic environments forming kaolinite clay minerals (Seedsman 1989).

The high proportion of clay minerals in the Permian tuffs and tonsteins makes them problematic when used in engineering works. Problems relate primarily to their typically low strength and their tendency for significant volume change upon water absorption. This makes them prone to slake when exposed and to heave when unloaded (Seedsman 1989). When disturbed and remolded, they readily form highly plastic clays with low dry densities and high optimum water contents which are undesirable for earthworks applications (Fityus et al. 2005).

Due to the large amount of tuffaceous materials contained within the NCM, these materials are frequently encountered in earthworks and excavations. This was particularly so for the Hunter Expressway Project, where numerous tuffaceous strata were encountered. In its 13 km long eastern part through the NCM, the 2 million cubic metres of earthworks included around 70 % of intermixed tuffaceous and carbonaceous materials. Examples are shown in Fig. 45.2. Under normal circumstances, these materials would be spoiled or relegated to non-structural uses. However, this was not an option for this project, and instead, they were utilized in encapsulated fill in several large embankments. Use of these materials in structural embankments, however, has afforded an excellent opportunity to comprehensively characterize their earthworks properties. This paper provides a summary of this.

45.2 Engineering Properties of Tuffs on the Hunter Expressway Project

45.2.1 Compaction Properties

When remolded and compacted, the tuffs used in this project display highly variable standard Proctor compaction behaviour, as shown the 3 curves in Fig. 45.3a, for tuffs coming from adjacent geological sequences. Figure 45.3b shows that across the entire project, there is a general trend of lower OMC values correlating to higher MDD values, reflecting the variability in clay content and its systematic effect on engineering properties. Figure 45.3c shows that the MDD values span the range from very low values of 1.3 t/m^3 to more normal values of 2.0 t/m^3, but that the distribution is skewed toward lower values with a mean of around 1.6 t/m^3.

Figure 45.3d shows that the optimum water contents are generally normally distributed, with all samples falling between 10 % and the relatively high value of 40 %, with a mean of around 22 %.

45.2.2 Plasticity and Swelling Properties

Figure 45.4a shows that more than half of the CBR values were found to be between 0 and 5 %, with 80 % of all values between 0 and 20 %. Values as low as 1 % were measured. Figure 45.4b shows the values found for plasticity index
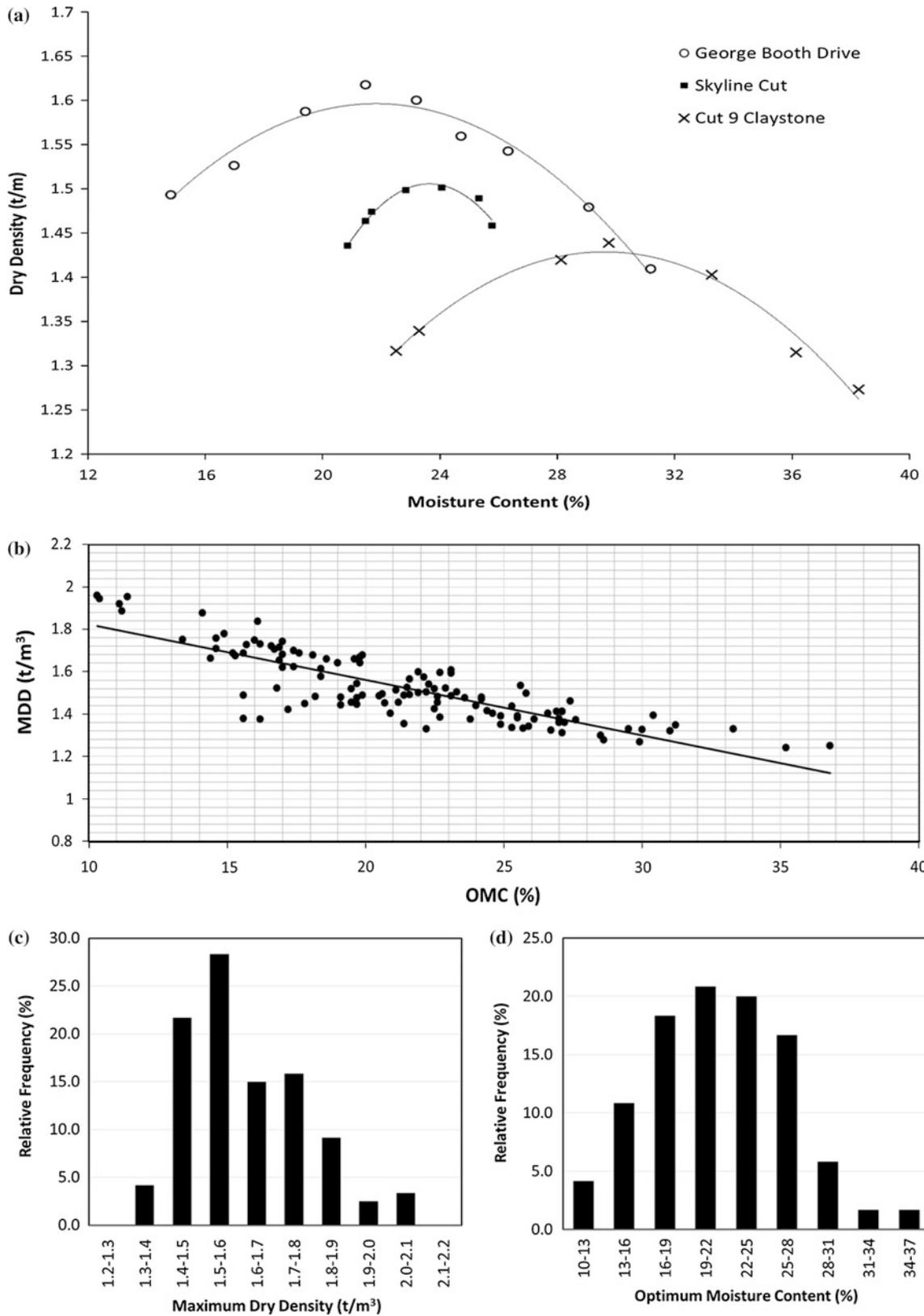
Fig. 45.3 Compaction data for NCM tuffs. **a** Standard proctor compaction curves for three typical NCM tuffs. **b** Maximum dry density versus optimum moisture content for 120 samples. **c** Relative frequency of MDD. **d** Relative frequency of OMC
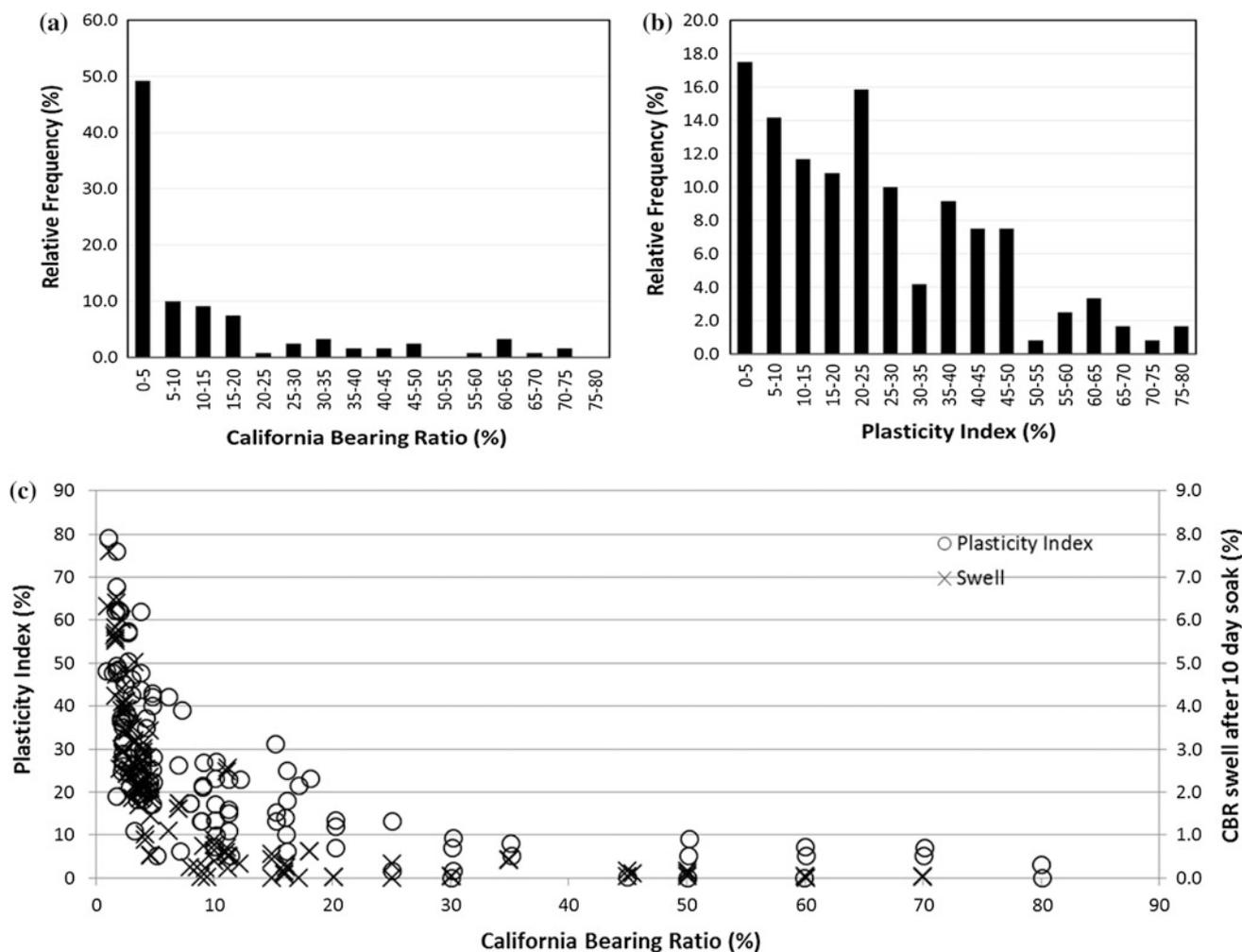
Fig. 45.4 California bearing ratio and plasticity index data. **a** Relative frequency of CBR. **b** Relative frequency of PI. **c** Correlation between 10 day soaked CBR and plasticity index and swell

were far more variable, with 90 % of values falling between 0 and 50 %, but with some extreme values as great as 80 %. Figure 45.4c shows that for samples with lower CBR values, the swell after 10 days of soaking was as great as 8 %, with all materials with CBR values less than 10 % recording some swell, and the many samples with CBR less than 5 % swelling from 3 to 8 %.

45.3 Conclusion

The results presented show that the engineering properties of tuffs and tuffaceous claystones from the Newcastle Coal measures are highly variable and generally unfavorable. Swell is a major issue for dimensional control of earthworks. On this project, surcharged encapsulation was used to control swelling of remolded tuffs in embankments up to 13 m high. Swelling is a complicated problem, influenced by compacted dry density, initial water content, confinement

and moisture change (Buzzi et al. 2011). In designing embankments from compacted remolded tuffs, it is necessary to place them at a water content and dry density, such that under their confining stress, they will neither expand nor collapse as their water content changes. This was a key aspect in the design phase of the Hunter Expressway.

References

Brakel AT (1989) Correlation of the Permian coal measure sequences of eastern Australia. Bur Min Res Bull 231:193–203

Buzzi O, Giacomini A, Fityus S (2011) Towards a dimensionless description of soil swelling behaviour. Geotechnique 61:271–277

Diessel CFK (1985) Tuffs and tonsteins in the coal measures of New South Wales, Australia. Dixieme Congres International de Stratigraphie et de Geologie du Carbonifere, Madrid, 1983, pp 197–210

Fityus S, Hawkins G, Delaney M, Morton S (2005) An overview of engineering geology and geotechnical challenges in the Newcastle region. Aust Geomech 40(1):5–28

Ives MJ (1995) Stratigraphy and engineering properties of the Newcastle and Tomago coal measures. Engineering geology of the Newcastle-Gosford region. Sydney, Australian Geomechanics Society, pp 223–240

Kramer W, Weatherall G, Offler R (2001) Origin and correlation of tuffs in the Permian Newcastle and Wollombi coal measures, Australia, using chemical fingerprinting. Int J Coal Geol 47:115–135

Seedsman RW (1989) Claystones of the Newcastle coal measures, NERDDC project C0902, report number 749. ISSN: 0811-9570

Vertical Harbour Quay Rehabilitation Using Ground Anchors

46

Liliana Ribeiro and Alexandre Santos-Ferreira

Abstract

Issues related to structure design are a danger to future user's safety, as well as leading to higher economic costs, resulting in overruns of the initial budget. Sometimes, during works, unexpected situations could arise, requiring constant monitoring and verification. In recent years, ground anchors usage in soil and rock, has been increasing. It's efficiency makes them widely applied. Regarding harbour constructions, the use of permanent ground anchors is restricted, due to constraints related to surroundings and corrosion, being usually reserved to special cases where other solutions are unavailable or inappropriate. This paper describes the problems derived from ground anchors rupture, used in a vertical quay wall, located in Pinhão (Portugal) fluvial harbour, and the necessary studies for a remedial project, including a new design for the ground anchors, performed as rehabilitation and strengthening of the quay structure. Finally, some comparisons and conclusions are made between the pre-design, which supported construction and lead to its collapse, and the results reached during rehabilitation process.

Keywords

Ground anchors • Rehabilitation • Quay • Harbour

46.1 Introduction

In order to improve docking conditions in Pinhão fluvial harbour (Portugal), a vertical quay wall with 81 m length was built, with enough capacity for tourism boats (hotel boats) to use. Those boats usually require 80 m long docking posts.

Pinhão vertical quay wall was developed in upstream junction of Douro and Pinhão rivers.

L. Ribeiro (✉) · A. Santos-Ferreira
IPTM, I. P, Edf. Vasco da Gama, Rua General Gomes Araújo, 1399-005, Lisbon, Portugal
e-mail: liliananinhosribeiro@gmail.com

A. Santos-Ferreira
e-mail: asf1954@netcabo.pt

A. Santos-Ferreira
CICEGe—Faculty of Sciences and Technology (FCT), University Nova of Lisbon, Quinta da Torre, 2829-516, Caparica, Portugal

The location of this quay wall, on the right bank of Douro River, is shown in Fig. 46.1.

The structural solution adopted consists in an anchored Larssen sheet pile wall.

46.2 Pre-design

The pre design considerations, for both the initial and rehabilitation design, will be briefly described.

46.2.1 Local Geology

In order to access local geology a set of Dynamic Probing Light (DPL) tests, along the alignment of the future structure, were performed. The results showed formations of weathered shale, presented in Fig. 46.2.

When those formations were not emerged, a soil layer overtops them with usually less then 2 m thickness. The

Fig. 46.1 Location of Pinhão quay harbour

Fig. 46.2 Pinhão geological profile
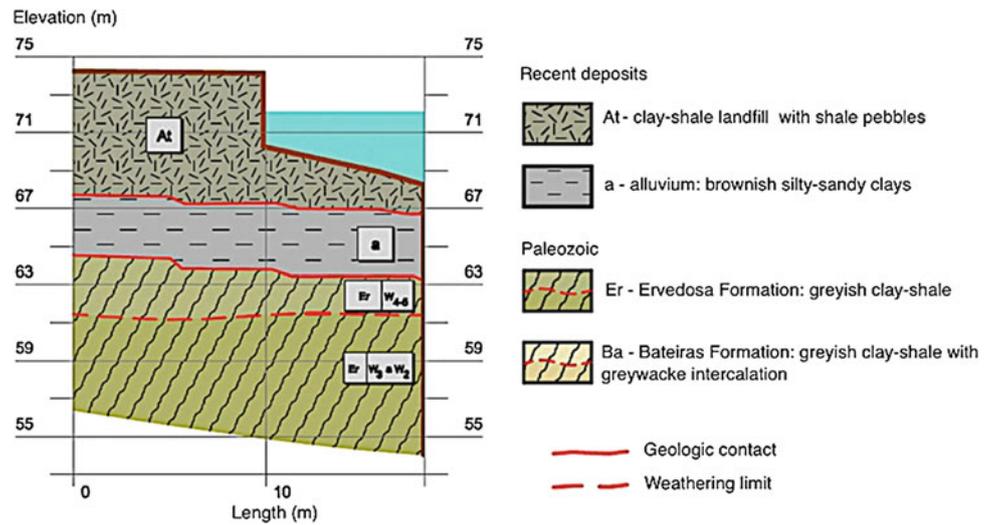
geotechnical characteristics obtained through the DPL test are presented on Table 46.1.

46.2.2 Pre-design Considerations

The ship type considered in the design is a passenger ship intended for river tourism with 1,500 deadweight tonnage (dwt), 80 m overall length, 10 m breadth and 3.6 m draught.

Table 46.1 Geotechnical characteristics of site material

Material specific weight (kN/m³)	Emerged landfill $\gamma = 18$ Submerged landfill $\gamma' = 10$ $\gamma = 20$ Emerged rock fill $\gamma = 18$ Submerged rock fill $\gamma' = 10$ $\gamma = 20$ Water $\gamma = 10$	Material geotechnical characteristics	Landfill material $\phi' = 30^\circ$ $c' = 0{,}0$ Rock fill material $\phi' = 45^\circ$ $c' = 0{,}0$ Weathered shale $\phi' = 25^\circ$ $c' = 0{,}0$ Shale $\phi' = 40^\circ$ $c' = 60$ kN/m²

Table 46.2 Obtained results in pre design

Service phase					Ground anchors
Considered water levels	Embeddedness (m)	Sheet pile (m)	Momentum (kN · m/m)	Reaction on tendon (kN/m)	Total length 16 m
No water	4.05	9.40	339.5	158.9	
Minimum level	4.25	9.65	286.1	154.9	Bond length 4 m
Maximum level	3.89	9.29	199.7	116.9	
Full	3.73	9.13	169.4	87.7	Inclination 25°

Table 46.3 Active pressures over the structure, in pre-design phase

Active pressures	
Pre-design (first project) (kN)	Pre-design (rehabilitation project) (kN)
134.7	159.83

Table 46.5 Results obtained to ground anchors free length

Ground anchors free length	
Pre-design (first project) (m)	Pre-design (rehabilitation project) (m)
12.0	15.0

Table 46.6 Results obtained to stability of potential slip surfaces analysis

Stability of potential slip surfaces analysis			
Pre-design (rehabilitation project)			Pre-design (first project)
Safety factor	Static analysis	Pseudo-static analysis	
	7.562	2.604	3.02

Table 46.4 Results obtained to ground anchors bond length

Ground anchors bond length		Effectively used (m)
Pre-design (first project) (m)	Pre-design (rehabilitation project) (m)	
4.0	3.0	6.0

Fig. 46.3 Global safety analysis and shear stress analysis
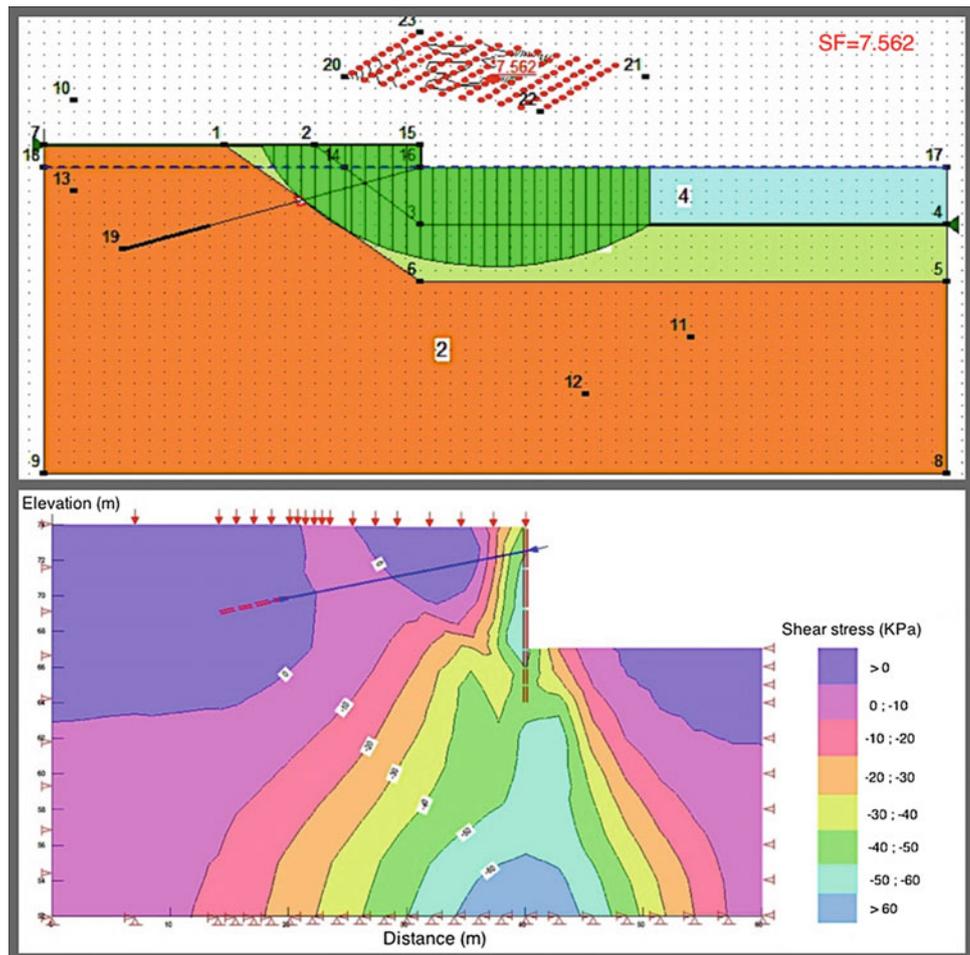
The active static impulses acting on the structure were defined by the Coulomb theory. Seismic impulses were calculated by Mononobe-Okabe method.

For the first pre-design phase Larix Cubus software was used and the results are presented in Table 46.2.

Short after finishing the vertical quay harbour construction, the ground anchors tendons suffered rupture.

In this paper a review is presented to access the collapse causes. For this attempt, a comparison of obtained results in the initial project, and those obtained in the rehabilitation work phase, will be made.

46.3 Rehabilitation Phase

Although the quay wall was not subject to normal use, some ground anchors have broken. The sheet pile wall, and overtopping beam did present neither deformations, nor excess stresses.

To rehabilitate the structure two options were available:

- First option was demolish the entire quay wall. This option was step aside due to timing and economic constrains;
- Second option was, re-design new ground anchors. Those new ground anchors would be placed at the mid point between the first stage anchors.

46.3.1 New Ground Anchors Pre-design

In the rehabilitation phase pre-design, the empirical diagrams of Terzaghi and Peck (1948) were used to assess the active impulses over the sheet pile wall, and the (Bustamante and Doix 1985) method was used to ground anchors design (Ribeiro 2012).

A 2D stress-strain analysis, as well as a limit equilibrium analysis was also performed to assess the overall stability.

The results are presented in Tables 46.3, 46.4, 46.5 and 46.6 and Fig. 46.3.

46.4   Final Remarks

The obtained results of rehabilitation phase pre-design allows us to state that:

- In the initial design (pre-collapse), the ground active pressures over the structure were underestimated. This may be a fact to justify the ground anchors bad behavior (rupture), however this is may not be the only reason;
- In the initial design (pre-collapse), the ground anchors free-length was too short. So, it's possible that fixed anchor zone lies within a ground mass prone to failure.

The study of global stability can be said that:

- The global security coefficients, evaluated in the study compared with those obtained by the designer, both are within required values for this type of work. So, apparently this is not the reason for the disruption of anchors of the initial project.

The stress-strain analysis developed in rehabilitation pre-design phase show that the rehabilitated structure should present a good behavior; as the rehabilitated quay is in service since November 2011, the observation of its behavior shows a good fit within pre-design phase.

References

Bustamante M, Doix B (1985) Une méthode pour le calcul des tirants et des micropieux injectés. Bull. Liaison Ponts et Chaussées. Paris, Laboratoire Central des Ponts et Chaussées. 140:75–91

Ribeiro L (2012) Ancoragens em estruturas portuárias. Análise de um caso de obra. Master's thesis, FCT-UNL, Quinta da Torre, Almada

Terzaghi K, Peck R (1948) Soil mechanics in engineering practice, 1st edn. Wiley, New York

The Importance of the Existing Engineering Geological Conditions During the Building Construction on the Terrain Affected by Sliding

47

Dragoslav Rakić, Zoran Berisavljević, Irena Basarić, and Uroš Đurić

Abstract

Performing of the deep excavations leads to an imbalance in the terrain and consequences are frequent occurrences of local sliding, collapse, settlement and even destruction of the adjacent facilities. Therefore, knowledge of the existing engineering geological data is very important, because in urban areas problems of interaction of the new facility and geological environment are not the only ones that need to be solved, but also the influences of the other structures located in vicinity. Aggravating circumstances are terrains with complex engineering geological conditions affected by active, dormant but also stabilized landslides. In this paper the importance of knowing engineering geological conditions and history of landslide processes is highlighted with the example of the construction of a shopping mall in a densely populated area of the Serbian capital-Belgrade. The results of engineering geological and geotechnical researches are chronologically presented starting from the first landslide activation in 1970 and its reactivations in 1981 and 1992. By the latest research results, the existence of "fossil" landslide is registered for the first time in this part of the terrain. Based on that, the project for the protection of surrounding terrain was done due to the deep foundation pit excavation.

Keywords

Engineering geological conditions • Fossil landslide • Residual strength

47.1 Introduction

In developed urban areas, the lack of available space on the surface is a problem and it is solved by the use of underground space. This often includes the performance of deep excavations with the protection of existing facilities. However, the choice of inadequate protection measures often leads to negative consequences with significant material costs and in some cases human lives are endangered. Due to the specific conditions of performing a deep excavation such as: variation in different soil types, limited space, difficult and demanding work conditions, excavation speed etc., conditions of the natural geological environment are especially important. Therefore, the base for the deep excavations performances is the engineering geological maps which should be practical, concise, clear and with adequate graphical and numerical representation of the terrain.

47.2 Geological Terrain Composition and Characteristics of the Sliding Process

The terrain where the shopping mall was built is a densely populated, hilly area of the capital of Serbia—Belgrade. The terrain basis, within the exploration area, consists of marine basin sediments which are the oldest sediment layers of Paratetis near Belgrade. They are presented with marls (Lg),

D. Rakić (✉) · I. Basarić · U. Đurić
Faculty of Mining and Geology, University of Belgrade, Djušina 7, 11000 Belgrade, Serbia
e-mail: rgfraka@rgf.bg.ac.rs

Z. Berisavljević
Koridori Srbije d.o.o., Kralja Petra 21, 11000 Belgrade, Serbia

which are intensively modified in the surface layer, and they formed a surface weathering zone of degraded marl clays (Lg*). Quaternary cover is formed over this complex and it is made of different lithogenetic sediments in which diluvial sediments dominate on the slope ground part and alluvial-proluvial sediments on the flat part of the terrain next to a stream. Loess diluvium (dl-l) and a thin layer of diluvial clays (dl-gl) are separated within the diluvial sediments. Alluvial-proluvial sediments are characterized by polycyclic sedimentation with material gradation in vertical direction, so that within these sediments three areas are distinguished: clays (al-gl), clayed sands (al-gp) and clayed gravels (al-gš). Greater part of the terrain is covered by uncontrolled fill mainly made of construction waste, and it is divided into two parts: the so-called old fill (n_s) which was formed before 1970 and the fill which was formed after that (n). The wider zone of the terrain belongs to the region that includes an area of active, dormant and stabilized landslides (Fig. 47.1). The shopping mall is located on the landslide that was activated for the first time in 1970. Its activation started due to the trench excavation for the installation of sewer pipes along local streets. Then the first engineering geological terrain explorations were performed and based on these results its remediation was carried out by the system of drainage

trenches filled with sand and gravel. This drainage system was not sufficient to perform a permanent repair, because the landslide was reactivated in 1981. The researches that were performed in 1981, had an aim to protect the street that propagates through the frontal area of the landslide scar, but the remediation of the entire slope towards the local stream was not considered. For those reasons, in the frontal part of the landslide the retaining structure of reinforced concrete piles was built, with the average length of 12 m. Afterwards, the terrain surface affected by sliding was arranged. The slope got a natural layout that did not indicate the existence of the active sliding process. However, in 1992, the sliding process was reactivated and expanded to the southwest of the site, and the landslide re-affected central parts of the slope below the retaining structure. For these reasons, the retaining structure was extended along the street, and the gravel embankment (n_k) was built out in the central part, at the bottom of the slope which beside the function of ballast provided mitigation of the slope inclination (Fig. 47.2). It can be concluded that the sliding process on this site was periodically active and with uneven temporal frequency. It is exactly due to these frequent sliding processes, that the terrain was avoided for construction even though the site is in the narrow city core.
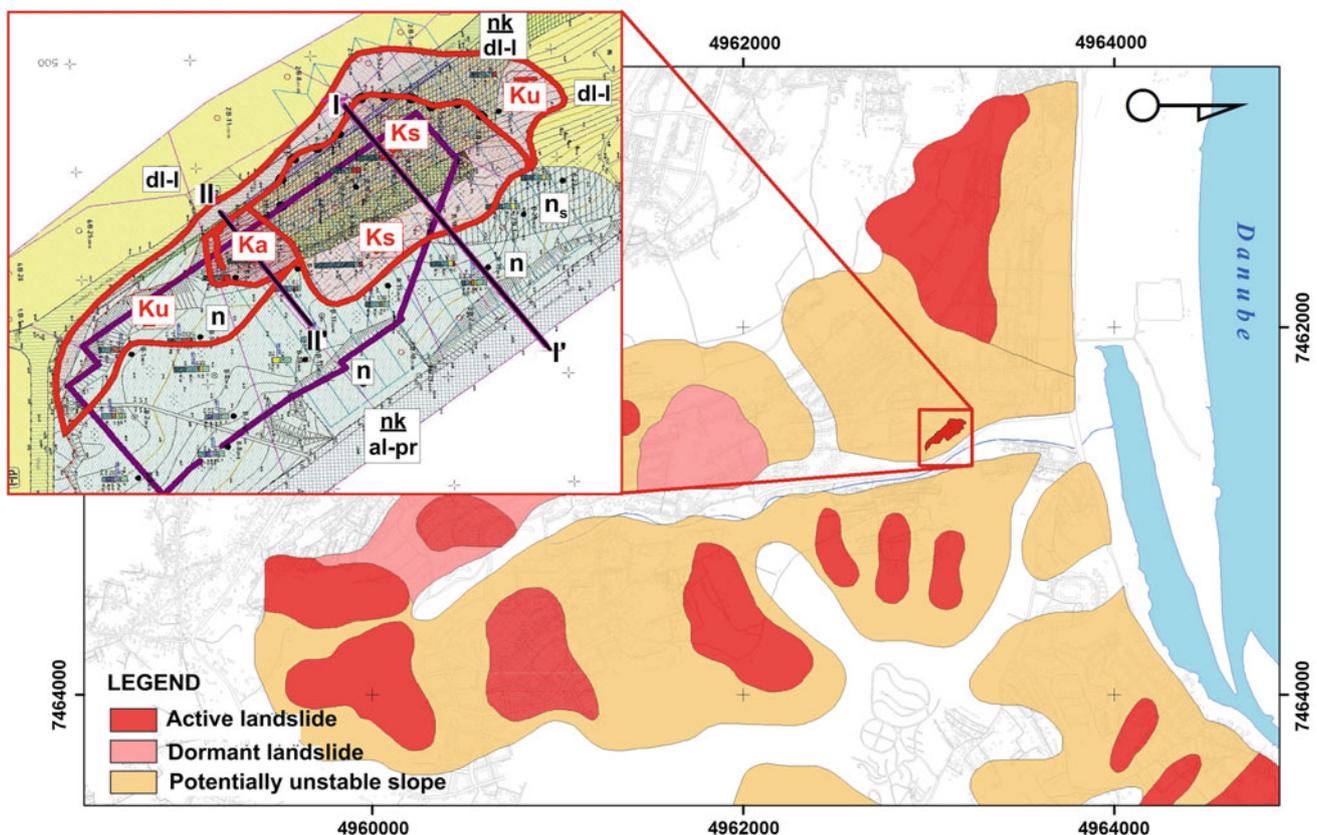
Fig. 47.1 Map of registered landslides along the local stream with engineering geological map of microlocation
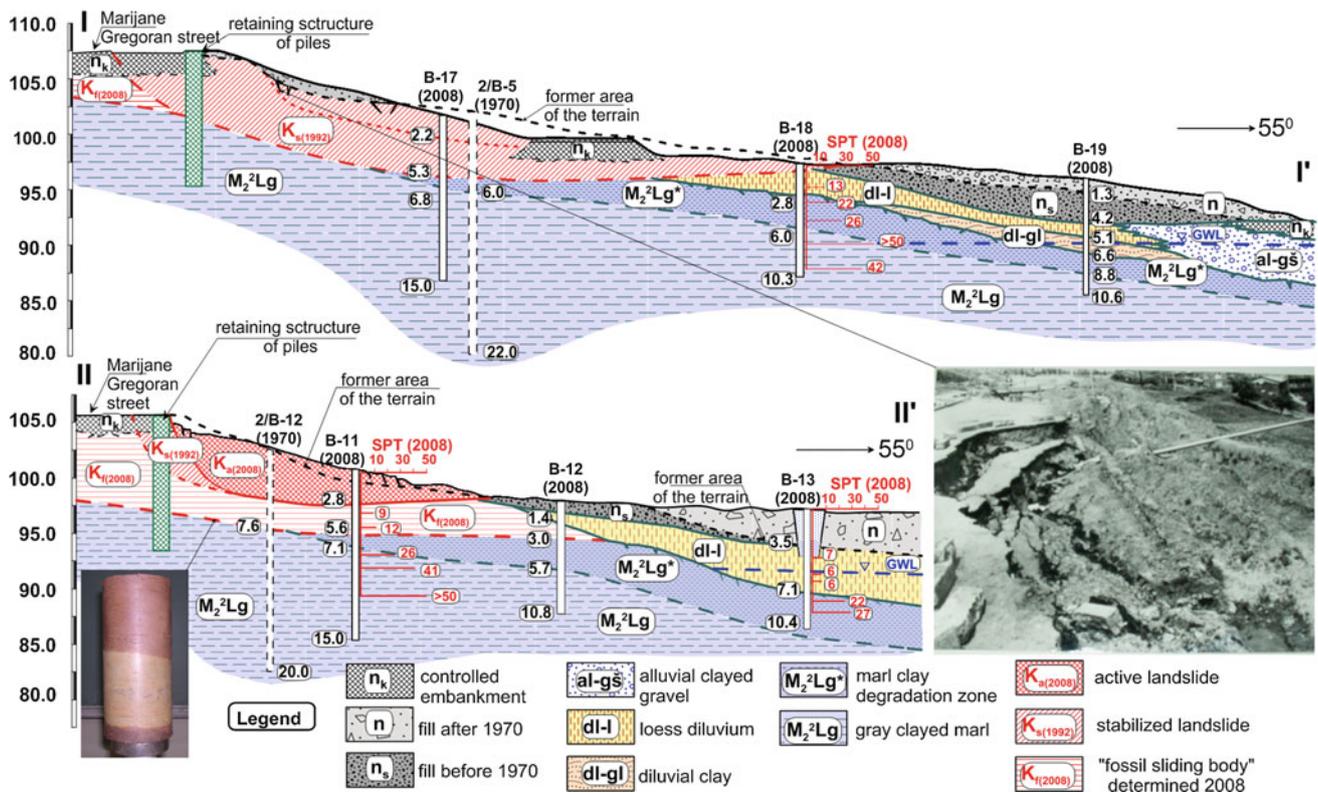
Fig. 47.2 Characteristic engineering geological cross sections of the terrain

47.3 Defining Engineering Geological Models

The latest engineering geological explorations at this site were performed for the construction of the shopping mall "Merkur", which was built in the meantime. For this occasion, the terrain zoning according to degree of stability was performed (Fig. 47.1), where the terrain was separated into: terrain affected by an active sliding (Ka), terrain on which the remediation measures were carried out (Ks) and terrain on which the landslide was dormant (Ku). Based on these researches, the active slip surface at a depth of 5.0 m (Fig. 47.2) was determined. In the repaired part of the sliding body, the groundwater table was determined at a depth of 3.5 m up to 8.0 m, while in the landslide foot part in the active zone of the sliding body, the groundwater table was measured at a depth of 1.6 m. Apart from the fact that the causes of relatively recent slides formation were determined, the latest engineering geological researches, helped discover for the first time the existence of "fossil landslide" in this part of Belgrade's terrain (Fig. 47.2).

This confirms the known fact that in the wider Belgrade area along the right bank of the Danube, the sliding processes occurred in the past and in most cases were stopped

by the formation of the loess cover (Rakić et al. 2009). This periodic activity of terrain sliding had caused a chaotic mixture of several lithological members within the colluvial mass where degraded marl clays (gL*) and diluvial clays (dl-gl) dominate. Lithological heterogeneity also affected the parameter values of shear strength that varied in a wide range. Due to the prevailing primary brittle, crystallizing and cementation bonds, cohesion of immovable degraded marl clays was $c' = 42–60$ kPa, while in the predominantly saturated, cracked and softened weathering zone it is minimized to the so-called apparent i.e. temporary cohesion of the weak and unstable hydrocolloid relations and equalled $c' = 5–22$ kPa (Rakić et al. 2000). In 1970 and later in 1981 laboratory tests were performed and gave the results of the residual internal friction angle of saturated colluvial soil samples. Also, the back-analyses were performed giving the mobilized shear strength parameters at failure along the slip surface. The latest laboratory tests have mostly yielded lower residual values for the internal friction angle $\varphi'_r = 11–12°$ (Fig. 47.3).

In the process of the stability analysis, several engineering geological cross sections of the terrain were considered taking into account the groundwater level. Considering that the newly formed sliding body affected surface parts of "fossil
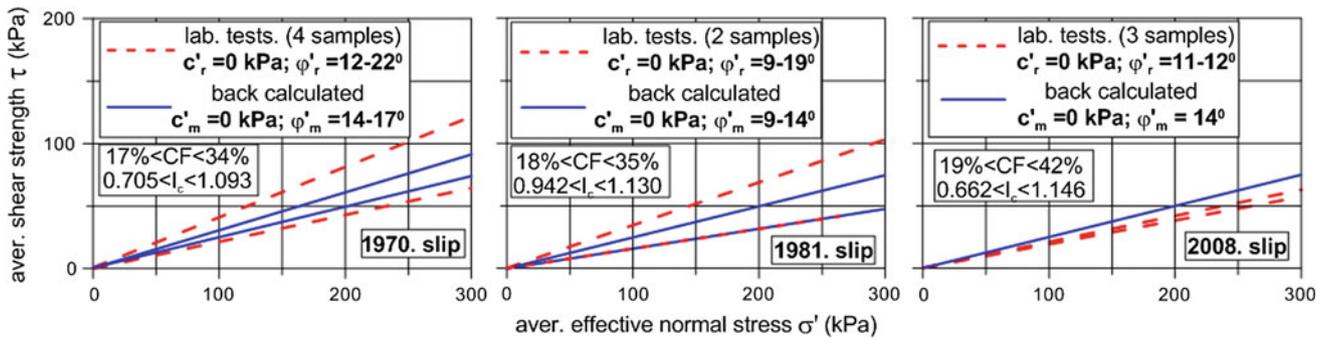
Fig. 47.3 Residual shear strength depending on the time activity of the landslide
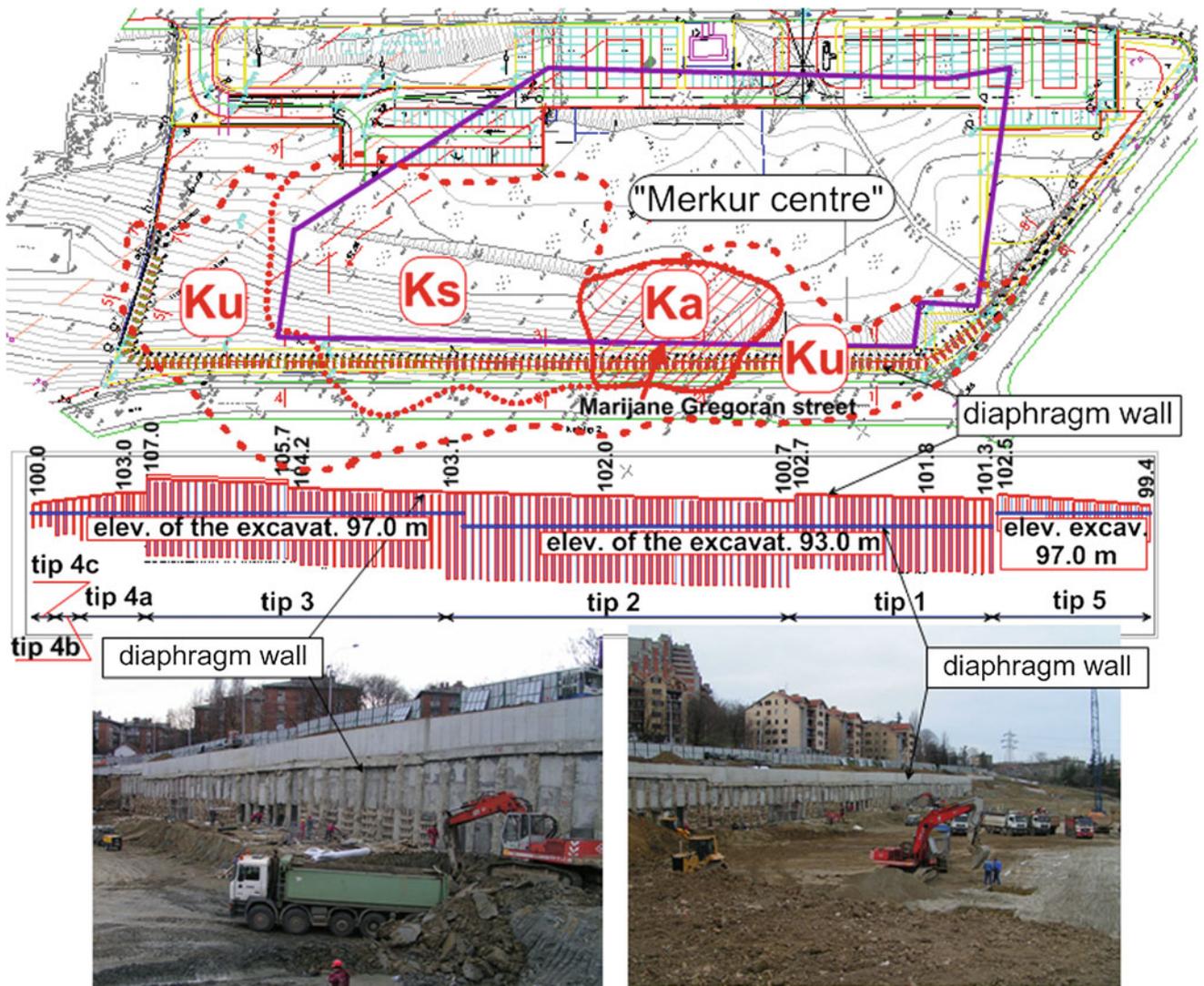
Fig. 47.4 Protection of foundation excavation

landslide" in one part of the terrain, as a corresponding slip surface for the securing of the foundation pit, a contact of the zone of degraded marl clays and grey marls was proposed. Conditional internal friction angle was determined from the limit equilibrium condition by back-analysis i.e. for the adopted safety factor $F_s = 1.0$, and assuming that along the slip surface $c'_r = 0$ kPa (Popescu 2002). The value of the conditional internal friction angle $\varphi'_m = 14°$ (Fig. 47.3) was obtained by the back-analysis method, which was later used to determine the force of a potential sliding body on the retaining structure.

47.4 Remediation Measures

Depending on the morphology of the terrain, the depth of the foundation pit excavation ranged from 8.3 to 14.0 m. This implied removing the entire colluvial part in the facility domain, whether it is the active, stabilized, dormant or "fossil" part. It also required taking into account the possibility of cutting the existing drainage trenches which were built after sliding in 1970.

Thus formed excavation had a lower elevation related to the pile base elevation of the existing retaining structure along the street, questioning its stability and the stability of the major road i.e. the slope above it on which there are residential buildings (Fig. 47.4). As the basic remediation measure and the foundation pit protection measure, the reinforced concrete diaphragms were designed. Along the street of Marijana Gregoran they were placed in the so-called "comb arrangement" perpendicularly to the reinforced concrete structure of piles, and connected with the overhead slab at a certain depth (Anagnosti and Stambolić 2008). Groundwaters from the slope are collected by the drainage curtain, which was placed between the diaphragms, and transferred in a controlled process through drainage pipes and shafts system to the city sewage. The reinforced concrete diaphragms were designed according to deepest determined

slip surfaces ("fossil" or dormant), which were defined in the contact of degraded marl clay zone and grey marl zone.

47.5 Conclusion

Due to the inaccessibility of locations, as well as the economic factors and scarce resources for research purposes, we are not always able to perform the necessary amount of exploration works which are objectively necessary to obtain reliable data. This especially refers to urban areas, where not only the problems of interaction between the new structure and geological environment need to be solved but also the influence of other structures located in the vicinity. In this regard, systematization and reinterpretation of the existing engineering geological and geotechnical data are very useful, because in these areas the unfavourable engineering geological conditions are not the only problem, but also insufficient knowledge of them. Therefore, we should not forget that the absence of sliding traces on a surface does not always prove its past stability.

References

Anagnosti P, Stambolić S (2008) The main project for securing the foundation pit of the "Merkur" shopping mall. Karaburma, Belgrade

Popescu ME (2002) Landslide causal factors and landslide remedial options. In: Proceedings of 3rd international conference on landslides, slope stability and safety of infra-structures. Keynote Lecture, Singapore, pp 61–81

Rakić D, Čaki L, Dragaš J (2000) Progressive softening of the belgrade clayey deposits owing to underground construction. In: An international conference on geotechnical and geological engineering. GeoEng2000, Melbourne, Australia

Rakić D, Nikolić A, Kostić S, Berisavljević Z (2009) Geotechnical investigations terrain for building the trade center "Merkur". In: Karaburma, 3th conference geotechnics in civil engineering, Association of Civil Engineers of Serbia (ACES), Zlatibor, pp 123–128

GIS Based, Heuristic Approach for Pipeline Route Corridor Selection

48

Ludwig Schwarz, Klaus Robl, Walter Wakolbinger, Harry Mühling, and Pawel Zaradkiewicz

Abstract

Large diameter pipeline systems play an increasingly important role in the supply of population and economy with natural resources like oil, gas and water all over the world. Due to the fact that the sources are often located far off from the consumer, pipeline systems consequently have to cross large distances, facing various social, environmental and geological constraints along their route. Therefore pipeline route selection is a constraint based corridor selection and narrowing process. With the first definition of the project corridor and the successive narrowing of this corridor down to the corridor of interest decisive milestones of the final pipeline alignment are set, which, if at all possible, can only be modified with extensive timely and economic effort during later project stages. On the other hand pipeline routing teams are increasingly confronted with an extensive amount of data and ever tighter project schedules specified by the pipeline owner. In order to cope with the enormous amount of data in short time and to define a safe and economic route corridor in a transparent and traceable way, not only for the client but also for lenders, authorities, stakeholders, NGOs, etc. a GIS based, heuristic pipeline corridor selection approach was developed for the Trans Anatolian Natural Gas Pipeline Project (in the following referred to as TANAP) in close cooperation of engineering geologists, routing engineers and GIS experts. The process is a desktop based procedure including data collection, classification and above all their spatial evaluation utilizing GIS technology.

L. Schwarz (✉) · K. Robl
ILF Beratende Ingenieure ZT GmbH, Feldkreuzstraße 3, 6063, Rum, Austria
e-mail: ludwig.schwarz@ilf.com

W. Wakolbinger
LandMark GmbH&Co.KG, Peilsteinstraße 3a, 83435, Bad Reichenhall, Germany

H. Mühling
ILF Beratende Ingenieure GmbH, Werner-Eckert-Straße 7, 81829, Munich, Germany

P. Zaradkiewicz
ILF Consulting Engineers Polska SP.zo.o., Osmanska 12, 02-823, Warsaw, Poland

48.1 Introduction

The TANAP project is an approx. 1,800 km long, 56 in. pipeline system that intends to transport natural gas to be produced in Caspian region via Turkey to Europe. It traverses the whole of Turkey in east-west direction between the Turkish-Georgian border and the Turkish-Greek, respectively the Turkish-Bulgarian border. These three border crossings constituted the benchmarks for pipeline route selection. Additionally it has to be mentioned that an offshore route via the Black Sea was excluded by the client. However in the western Turkey a short offshore section had

Fig. 48.1 Overview of the project area (framed area)
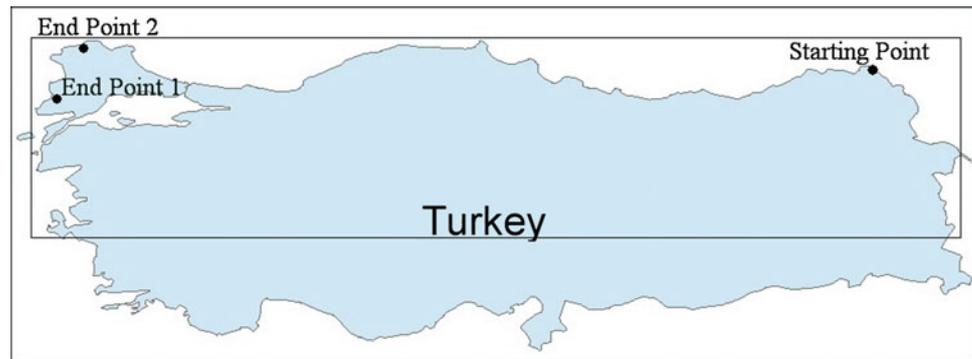
to be considered some place along the Bosporus, Marmara Sea or Dardanelles (Fig. 48.1).

The basic principal of pipeline route selection is to find the shortest connection between the start and the end point. The degree of deviation from this principal is governed by the constraints encountered within the corridor.

Along the TANAP project area various constraints are encountered that cover aspects of social and environmental impact, public safety, constructability, structural integrity of the pipeline and land use. Therefore pipeline route selection is a constraint based corridor selection and narrowing process. The following corridors are typically established during the narrowing process:

1. Project Corridor (width typically 20–40 % of the pipeline length)
2. Corridor of Interest (width typically 2–4 % of the pipeline length)
3. Preferred Corridor (typically 1–2 km wide)
4. Specified Corridor (typically 200–500 m wide)
5. Pipeline Centerline and Construction Corridor

The constraints utilized in each narrowing step depend on the size of the constraint with respect to the respective corridor width. Thus small sized constraints that can easily be bypassed within the corridor of concern are not considered in the respective narrowing step (e.g. landslide prone areas are considered in the definition of the corridor of interest rather than individual landslides, archeological sites are typically not considered before defining the preferred corridor). Consequently the investigation detail and the route accuracy increase inversely proportional to the width of the corridor under investigation in the course of the narrowing process. Early stages of corridor narrowing are purely based on desktop work while field work and ground truthing become increasingly important with the reduction of the corridor width. The subject paper describes the first two steps of the narrowing process from the definition of the project corridor to the selection of the corridor of interest.

48.2 Methodology

Modern information society provides extensive amount of data in electronically processible form available on short term including geological and terrain data (lithology, landslides, karst, seismicity, active fault lines, mining areas, digital terrain model, etc.), environmental data (protected areas, land use, etc.) and social data (population density, settlement areas, development areas, existing and planned infrastructure, military areas, etc.). Handling the enormous amount of data in short time has turned into a major challenge especially for large infrastructure projects. Therefore GIS based data management has become state of the art for several decades now (e.g. Avtar et al. 2011; Blais-Stevens et al. 2012; Sydelko and Wilkey 1994). GIS software also provides sophisticated tools for data processing, evaluation and presentation.

For the TANAP Route corridor selection a process was adopted utilizing GIS Cost Distance analysis tools. After the various datasets are fed into the system and organized in different layers, the individual datasets are further classified with each class assigned a cost factor (please note that costs in GIS language is a synonym for a function of time, distance, or any other factor that incurs difficulty or an outlay of resources). Within the described procedure the assignment of the cost factor is the most critical process with respect to the final result. For constraints related directly to construction cost factors are fairly easy to estimate since they are based on actual costs and thus can be derived from previous projects (e.g. influence of terrain on pipeline construction). For constraints not directly related to construction (e.g. protected areas, land use etc.) cost factors are much more difficult to quantify since they depend on "soft" factors like the political situation, social acceptance, etc. The process of cost factor selection is further complicated by the fact that not only the cost factors within one dataset have to match each other but also the cost factors between all datasets. Over or under prediction of the cost factor of one dataset can have a

significant impact on the result. Thus the selection of cost factors is to a large extent a heuristic process that considers experience from previous projects but is also based on assumptions to account for missing information and uncertainties. The selection process is furthermore an iterative process where the individual cost factors have to be calibrated comparing the outcome of the evaluation in specific route sections to experience from previous projects.

GIS cost analysis tools are usually raster based. Therefore the area of concern is split into a raster of cells where the size of the individual cells is selected based on the size of the area of concern and the level of detail of the considered constraints. In a next step the total cost factor of each cell is determined as a cumulative cost factor of the individual constraints encountered within one cell. For this purpose the software also offers the possibility to weight the different constraint raster that make up the cost raster. Thereby the "Weighted Sum" tool overlays several raster, multiplying each by their given weight and summing them together.

The result of this calculation already provides first clues about suitability of the area for pipeline construction (see Fig. 48.2).

The informative value of these cumulative cost factors is still limited as they provide spot data only and not data over length. This means that considering the entire pipeline length it may be more reasonable to cross critical areas exhibiting high costs if a reduction of pipeline length can be achieved. To overcome this limitation a Cost Distance raster is calculated for the entire project corridor. The cost distance tools determine the shortest weighted distance (or accumulated travel cost) from each cell to the nearest source location. When moving from a cell to one of its four directly connected neighbors (vertical or horizontal movement), the costs to move across the links to the neighboring node is 1 times the cost factor of cell 1, plus the cost factor of cell 2, divided by 2. If the movement is diagonal, the costs to travel over the link is 1.41 (or the square root of 2) times the cost factor of cell 1 plus the cost factor of cell 2, divided by 2 (ESRI 2012) (Fig. 48.3).

The graphical output of the result shows a raster map with increasing costs from the start point to the end point (see Fig. 48.4).
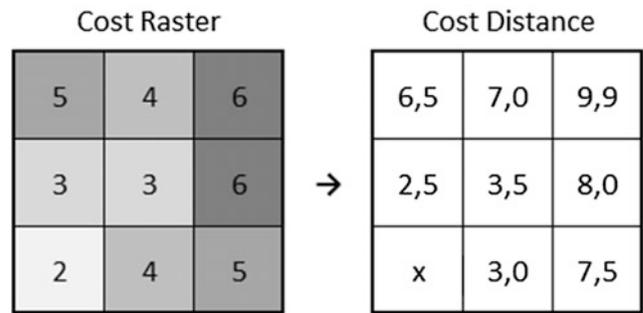
Fig. 48.3 Example for "cost distance" calculation: lowest accumulated cost distance to move from start point x to upper-right cell = (3 + 6) *SQRT(2)/2 + 3,5 = 9,9

To receive a corridor map the calculation is run twice, (1) from the start point and (2) from the end point. Finally the results of both calculations are summarized. Classifying the result from low to high values enabled us to determine the project corridor (see Fig. 48.5).

48.3 Results and Discussion

The Cost Corridor map shown in Fig. 48.5 provides a very distinct picture of the project corridor. The dashed area was thus selected for the next assessment step the definition of the corridor of interest. For this step additional and more detailed constraints were added and the classification of the constraints used in the previous assessment partly refined. As expected the result of the project corridor assessment enabled further narrowing of the corridor. But the result also showed a braided net of possible corridors rather than just one distinct corridor. This outcome is only an apparent limitation of the procedure since it actually accommodates the requirement of the authorities to investigate route alternative during environmental impact assessment. So based on the cost corridor map of the corridor of interest three alternative route corridors, each approx. 2 km wide, were defined and investigated in detail, both on desktop but also by extensive field works. These works concluded in the definition of the 2 km wide preferred route corridor which was then subject to more detailed investigation works including

Fig. 48.2 Combined constraint map, costs increase from white to black, *dashed line* indicates derived project corridor
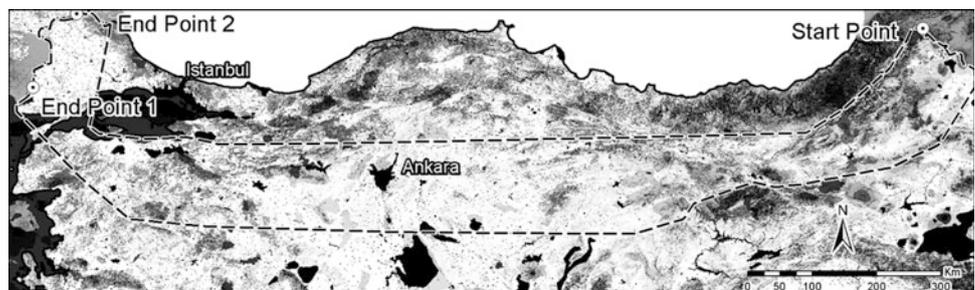
Fig. 48.4 Cost distance map, calculated from start point, costs increase from white to black, *dashed line* indicates derived project corridor
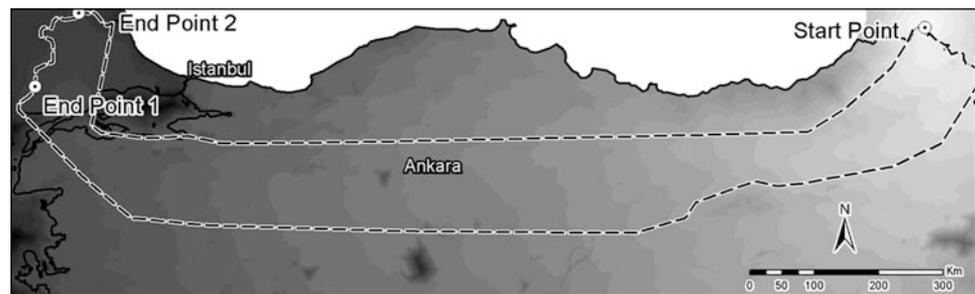
Fig. 48.5 Cost corridor map, costs increase from white to black, *dashed line* indicates derived project corridor
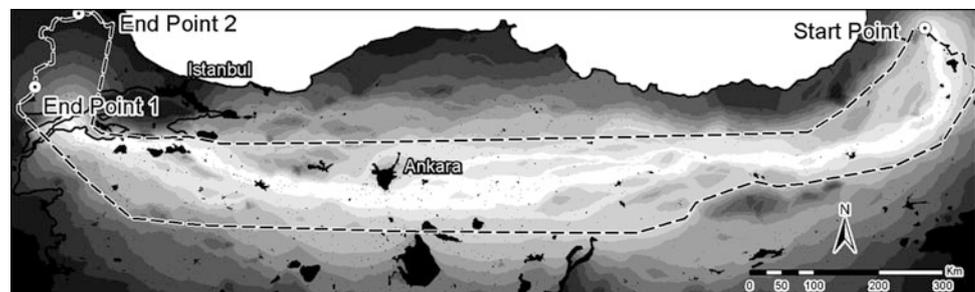
remote sensing techniques, geohazard mapping, environmental and social impact assessment, etc.

The assignment of cost factors proofed to be the most sensitive part of the entire procedure and thus has to be conducted with care. For this certain sections have to be identified within the corridor which allows an empirical calibration of the cost factors. Furthermore it has to be considered that cost factors are dependent on numerous project specific factors. Therefore there is no general set of cost factors to be utilized on similar projects. In fact the selection has to be carried out individually for each project in form of an iterative process considering experience, both of the involved geologists/engineers and from existing projects in the region, as well as local and project specific conditions.

One big advantage of GIS based corridor assessment is that changes like reclassification of the constraints or adjustment of the cost factors can be conducted within a small time frame, allowing covering large areas within short time.

48.4 Conclusions

Due to the fact that constraint classification and cost factor allocation requires experience of the involved disciplines (route engineers, engineering geologists) the described

methodology is not suitable for novices in the field of infrastructure corridor selection. Despite this limitation GIS based pipeline corridor assessment proved to be a powerful tool for fast and reproducible early corridor selection phases. Its use is not confined to pipeline projects but can equally be utilized for different types of above- and underground infrastructure projects whereat the classification of the constraints and quantification of the allocating cost factors has to take the type of infrastructure into account.

References

Avtar R et al (2011) Landslide susceptibility zonation study using remote sensing and GIS technology in the Ken-Betwa River Link area, India. Bull Eng Geol Environ 70:595–606

Blais-Stevens A et al (2012) Landslide susceptibility mapping of the sea to sky transportation corridor, British Columbia, Canada: comparison of two methods. Bull Eng Geol Environ 71:447–466

Esri (2012) ArcGIS 10.1

Sydelko PJ, Wilkey PL (1994) GIS least-cost analysis approach for sitting gas pipeline ROWs. Technical Information Center, Oak Ridge, Tennessee

A Study of Ground Natural Temperature Along Tabriz Metro Line 2, Iran

49

Ebrahim Asghari-Kaljahi, Karim Yousefi-bavil, and Mahyar Babazadeh

Abstract

The cities extension, request for developing and increasing underground transportation system. One of this ways in big cities is urban tunnels or metro. Tabriz often located on alluvial deposits, so these tunnels repose in these deposits. In this study we investigate engineering geology aspects of Tabriz Metro line 2, approximately 22 km long. Then it is described about natural temperature measuring of ground layers, and effect of this temperature in metro construction and using. Ground natural temperature is depended on atmosphere temperature and mineralogy of soil and groundwater condition. Some of clayey minerals are radioactive and increase ground temperature. Also, groundwater flowing may affect the ground natural temperature. In metro construction for tunnel boring machine (TBM) and exploitation of tunnel, knowing nature temperature is necessary. In this study, ground natural temperature is measured between 15 and 25 m depth. These measuring shown that the ground natural temperature is between 13 and 18 °C.

49.1 Introduction

Today, heavy traffic and city transportation are the big cities problems which can be reduce by subway transportation. Tabriz, one of the Iran's crowded metropolitan, faced the traffic problem, can be managed by subway/Metro construction. In line with Tabriz Metro extension, Tabriz Metro Line 2 (TML2) construction is carrying out along E-W with approximate length of 22 km. More than 120 boreholes with

E. Asghari-Kaljahi (✉)
Department of Geology, University of Tabriz, Tabriz, Iran
e-mail: e-asghari@tabrizu.ac.ir

K. Yousefi-bavil
Department of Geological Engineering, Middle East Technical University, Ankara, Turkey
e-mail: yousefibavil.karim@metu.edu.tr

M. Babazadeh
Young Researcher Club, Science and Research Branch, Islamic Azad University, Tabriz, Iran

depth of 25–45 m were drilled for Geotechnical study of the project (P.O. Rahvar 2008). To study ground strata and their strength, Standard Penetration Tests (SPT), Pressure meter and Permeability tests were accomplished. During boreholes drilling desired disturbed and undisturbed samples were obtained and necessary physical, mechanical and chemical tests were fulfilled.

Knowing natural ground temperature in tunneling is essential especially for its ventilation in utilization phase (Department of Justice and Attorney-General 2012). In order to earth layers thermometry, thermometer installed in some boreholes and natural ground temperature in tunnel (depth of 15–25 m) was measured.

49.2 Tabriz Geology

Tabriz is surrounded by Oun-Ebne Ali Mountains with trend of E-W in north and Sahand volcanic with low heights in south. Tabriz plain stretch out E-W due to mentioned

mountains. General slope of plain is due to the west and result in general drainage of surface and sub-ground water toward west. Plain mostly covered with alluvial sediments (Geological Survey of Iran 1993). TML2 route from Qaramalek in west to Baghmisheh has rather smoother slope and toward east they become hills and associated with numerous domes. Along the TML2, elevation difference between lowest and highest point reaches almost 280 m. In east part of the TML2 between Baghmisheh and Marzdaran it can be seen small folds and faults that result in layers rotation, fracturing and displacements (Hooshmand et al. 2012).

49.3 Engineering Geology

TML2 route from Garamalek area in west to Baghmisheh area is covered by alluvial sediments, and in continue to east Marlstone and Claystone and Siltstone layers have outcrops and/or with a thin cover of sediment in ground surface. Under this alluvium sediments near Abbasi Street toward east, layers of Marl, Sandstone and Conglomerate located in depth of less than 10 m. According to investigations, length of TML2 can be categorized into 5 general zones:

Zone 1: distance between Sanat Square in Garamalek to Jahad Square Conjunction. In this zone, west of Tabriz, up to studied depth (almost 30 m) alluvial deposits consist of fine grain and sand alternation. Groundwater table varies between 5 and 18 m.

Zone 2: distance between Jahad Square Conjunction to Selab-Aghzi in Abbasi Street. In this zone, subsurface layers mainly consist of coarse grain alluvial sediments (Gravel and Sand) whit rock fragments (Boulder and cobble) floated in them. Also, interlayer fine grain alluvial exist among this coarse grain sediments, however tunnel routes in this area mainly passes through coarse grain deposits.

Zone 3: distance between Selab-Aghzi in Abbasi Street to Shahid-Fahmideh Square. In this zone along Abbasi Street, week rock layers of claystone, mudstone, sandstone and marlstone underlain with surface alluvial layer with thickness of 5–15 m. In this part metro tunnel settles inside rock layers. Surface alluvial layers constitute of fine and coarse grain alluvial deposits that mainly were classified as SM, ML and CL. Groundwater table reached between 5 and 25 m in this part and inside rock layers occasionally gaseous artesian water exist.

Zone 4: distance between Shahid-Fahmideh Square to Eastern of Baghmisheh.

In this zone, subsurface layers mainly formed from coarse grain (Sand-Gravel) and fine grain (Clay-Silt) alluvial. Tunnel routes in this segment passes through the fine and coarse grain sediments. This zone groundwater depth varies between 5 and 20 m and gaseous artesian water has been observed.

Zone 5: distance between Baghmisheh to Tabriz International Exhibition. Mostly, this zone constitute of weak rock layers of marl, claystone, mudstone and sandstone.

49.4 Groundwater Condition

Groundwater table varies greatly along TML2. Although, groundwater flows out as artesian in Fahmideh square's boreholes, in some boreholes groundwater did not reach to the great depth. Overly, groundwater depth varies between 2 up to over 30 m. Water table levels decline from east to west which representative of groundwater flows from east to west, and this condition somehow coincides with Tabriz Plain slopes.

During drilling in BH-2, West of Fahmideh Square, groundwater reached approximately in 5 m but after end of drilling groundwater table raised and overflowed with slight flow. The noticeable point regarding groundwater in this borehole exists of CO_2 solution in the water. The amount of gas inside the groundwater is remarkable and based on conducted tests it is approximately 1 %.

Studies have shown that aquifer within alluvial sediments is separated from aquifer within rock bed in east part. In other words, within impermeable rock layers, fossil water and occasionally gaseous under-pressure water exist as lenses with no extension. The reason of existence of under-pressure water within rock strata is alternation of impermeable layers (Claystone and Marlstone) and permeable layers (weak Conglomerate) which water was constrained within permeable layers.

49.5 Ground Natural Temperature

Ground natural temperature has been studied in located depth of tunnel. To do so, along TML2 route with distance of 2–2.5 km from each other, electrical thermometers were installed in depth of 15–25 m and were read in different times. Figure 49.1 shows the location of boreholes where thermometers were installed. In installing of thermometers it should be ensured that there is a complete contact between instrument and surrounding layers. After installation in subjected depth, inside boreholes completely filled with site soil. This process depends on the accuracy required in testing. Main aim in filling the boreholes is minimizing the impact on thermal regime of the earth which is not possible without free groundwater flow prevention. After installation of thermometers, borehole will be filled with bored soil of boreholes through two ways:

(a) Layers of material to be dumped and compacted
(b) Appropriate ratio of material mixed with water and dumped inside borehole by teremi pipe.
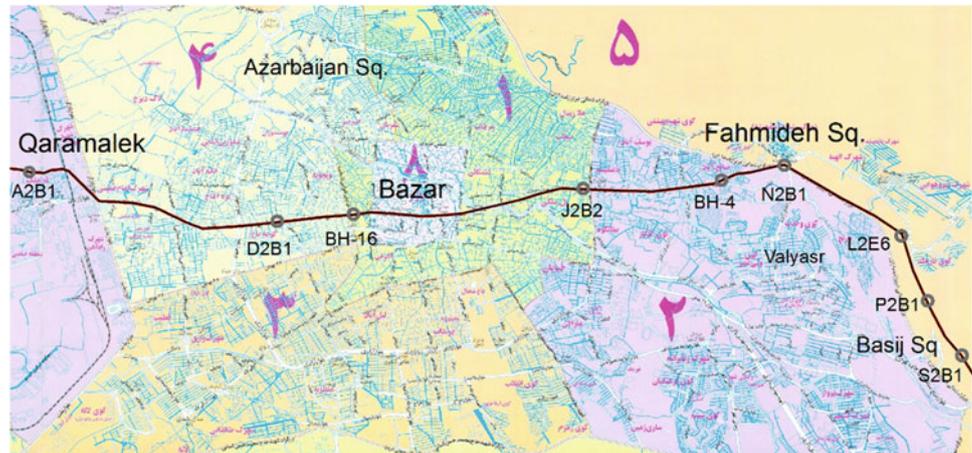
Fig. 49.2 Electrical thermometer tool

Fig. 49.3 Natural ground temperature measurements

Also, where installed thermometers levels were below the groundwater level, borehole can be filled with bentonite-cement slurry, the bentonite pellets and/or any similar waterproof material which satisfies the complete filling of the borehole.

A picture of thermometer tool and reading set has shown in Fig. 49.2 and a picture of thermometer and measuring devise has shown in Fig. 49.3.

Boreholes Location which thermometers installed and their special position has shown in Table 49.1. In all boreholes, thermometry instrument set below the water table.

Immediately after installation of tools, thermometer readings carried out in different times, and their results have shown in Fig. 49.4. Several days after installation, temperature values stabled and natural thermal of earth gained. It is between 13 and 18 °C. Great primary temperature (immediately after installation) is due to

dehydration of bentonite-cement grout that poured for sealing the borehole. It was observed relatively lower temperature in east part boreholes than the west part, which had high values. Of course ground type affects the results that constitute of soft rocks in east part rather than centre and west, consist of alluvial, for its low temperature. The temperature changes diagram in different boreholes were illustrated in Fig. 49.4.

49.6 Conclusion

Ground natural temperature of TML2 Tunnel route (depth of 15–25 m) studied by installation of some electrical thermometers. Studies show that ground natural temperature varies between 12.8 and 18.1 °C. Almost higher temperature observed in fine alluvial deposits, medium in coarse grain

Table 49.1 The location of thermometers measured temperatures

Borehole	Borehole location	Borehole location coordinates			Temperature (°C) after 120 days	Ins. depth (m)	GWD (m)
		X	Y	Z (m)			
A_2B_1	Khane Sazi	46º 14′ 00.0″	38º 05′ 20.1″	1,372	17.1	18	15.9
D_2B_1	Qare Aghaj St.	46º 15′ 53.2″	38º 04′ 52.6″	1,392	17.6	20	8.2
BH-16	Qajil area	46º 16′ 59.1″	38º 04′ 48.3″	1,404	17.1	24	8.8
J_2B_2	Abbasi Sq.	46º 19′ 33.9″	38º 04′ 41.4″	1,458	15.3	21	9.0
BH-4	Mikhak Park	46º 21′ 02.6″	38º 04′ 31.5″	1,485	14.8	19.5	6.1
N_2B_1	Fahmideh Sq.	46º 21′ 50.1″	38º 04′ 36.2″	1,508	15.2	23	16.1
L_2E_6	Baghmishe town	46º 22′ 43.4″	38º 04′ 19.0″	1,533	15.3	16	15.1
P_2B_1	Marzdaran town	46º 23′ 22.9″	38º 03′ 26.2″	1,565	14.1	20	10.3
S_2B_1	Tabriz int. exh.	46º 24′ 02.6″	38º 02′ 10.4″	1,614	12.9	23.3	10.6

Fig. 49.4 Temperature variations with elapsing time in various boreholes
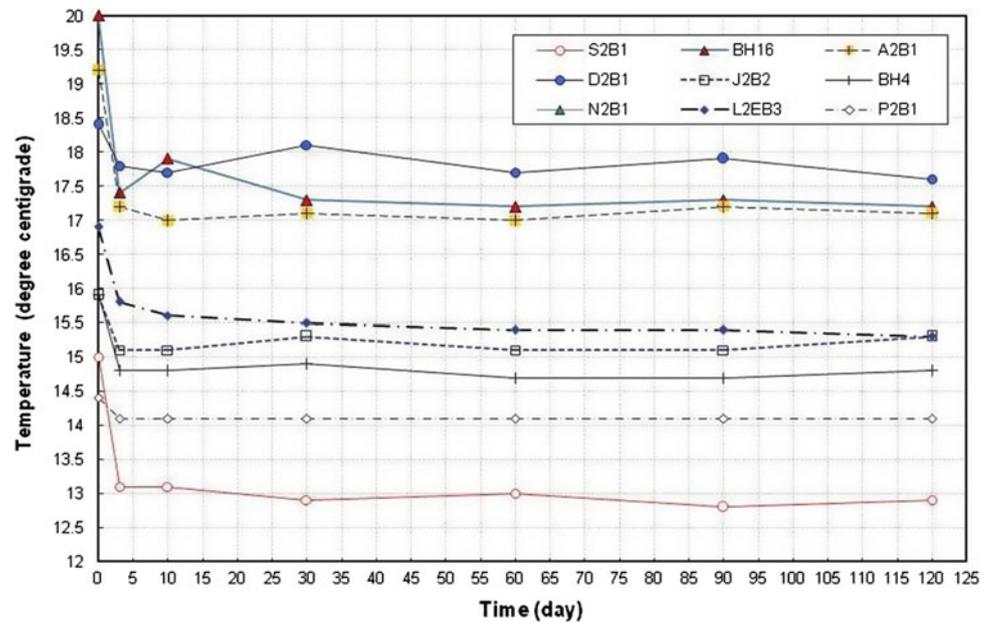
alluvial sediments and lower temperature in Marly layers. Where groundwater table is in shallow depth, relatively higher temperature and where it is deeper, the lowest temperature observed.

References

Department of Justice and Attorney-General (2012) Tunneling code of practice 2007, Workplace Health and Safety Queensland

Geological Survey of Iran (1993) Tabriz geology map, scale 1/100,000

Hooshmand A, Aminfar M, Asghari E, Ahmadi H (2012) Mechanical and physical characterization of Tabriz marls, Iran. J Geotech Geol Eng 30(1):219–232

P. O Rahvar Consulting Engineers (2008) Geotechnical investigation report of TML2 project

The Challenges of Site Investigations, Dredging, and Land Reclamation: A Port Hedland (Western Australia) Project Perspective

50

P. Baker, J. Woods, M. Page, and F. Schlack

Abstract

Port Hedland, Western Australia is the largest bulk commodities export port in the world. The construction of wharves and stockyards requires significant dredging and land reclamation. Significant planning, logistical and technical challenges must be overcome for nearshore geotechnical site investigations to be successful. The sub-surface geology of Port Hedland harbour is often considered relatively straightforward, yet geotechnical investigations have not always provided sufficient or appropriate data, with some projects culminating in spectacular disputes between contractors and developers. The dredged materials are deposited in offshore spoil dumps, as well as onshore in dredge material management areas (DMMAs). Successful land-reclamation is achieved by separating the fines fraction leaving a sand-gravel soil (known as grits). The fines are typically pumped to designated fines settlement areas.

Keywords

Port hedland • Nearshore • Investigations • Dredging • Reclamation

50.1 Introduction

Port Hedland, Western Australia is the largest bulk commodities export port in the world. In the year ending 30 June 2013, 286 Mt (million tonnes) of cargo left Port Hedland, 280 Mt of which was iron ore bound for Asian steel mills, the remainder consisting mostly of salt, manganese, chromite, and copper.

Prior to the first major development of the port in the 1960s, the maximum natural depth of the harbour was about 9 m. With ongoing development and decreasing availability of deep water parts of the port, recent expansions and proposed facilities are increasingly situated in shallower areas. Hence the significance of dredging and land reclamation components of port expansion projects continues to increase, as does the onus on engineering geologists to provide timely, accurate and appropriate input of data from nearshore site investigations into large multidisciplinary project engineering teams. The current extent of dredged areas is clearly visible at low tide (Fig. 50.1).

50.2 Preparation, Logistical and Technical Challenges

50.2.1 Health Safety and Environmental Management

Prior to any site investigation a hazard identification workshop (HAZID) is conducted with all relevant parties involved in the investigation, including the engineering

P. Baker · M. Page
WorleyParsons, Perth, 6000, Australia
e-mail: paul.baker@worleyparsons.com

M. Page
e-mail: michael.page@worleyparsons.com

J. Woods (✉)
WorleyParsons, Calgary, SP09-19, Canada
e-mail: jonathan.woods@worleyparsons.com

F. Schlack
Port Hedland Port Authority, Port Hedland, 6721, Australia
e-mail: frans.schlack@phpa.com.au
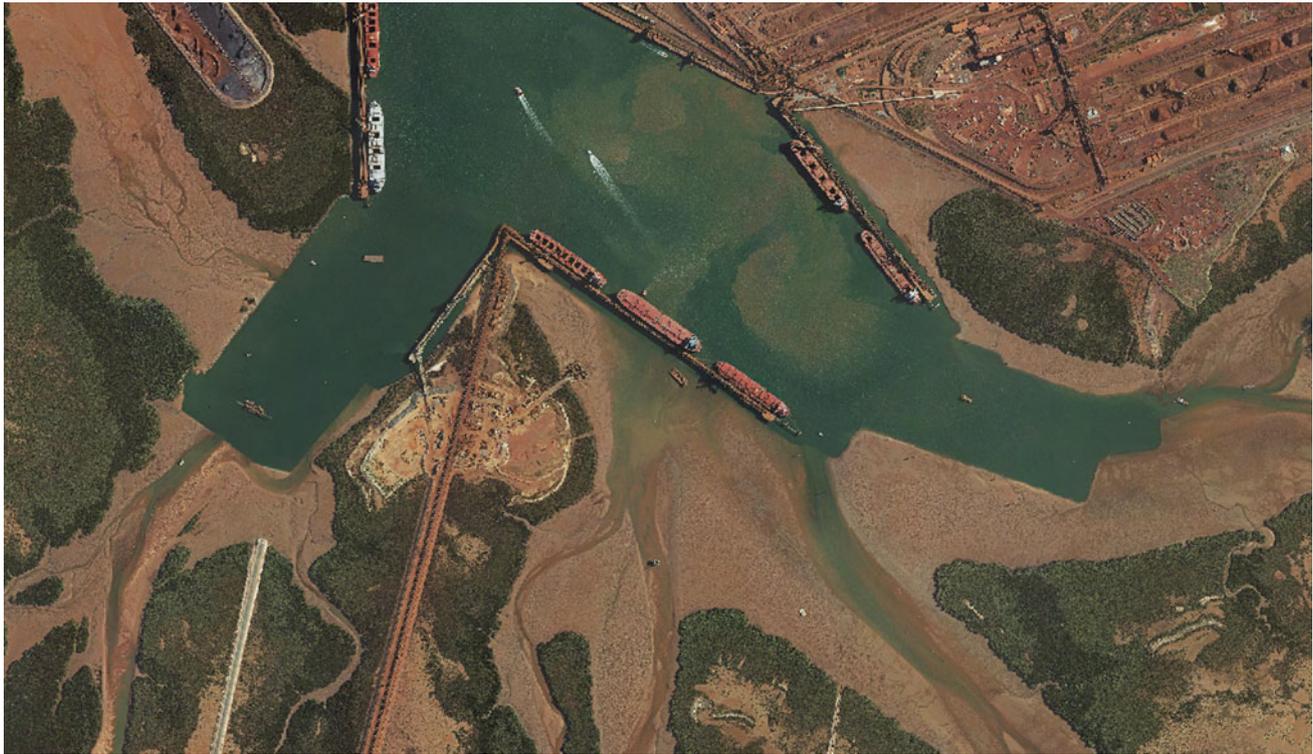
Fig. 50.1 Aerial photograph of Port Hedland Harbour at low tide (courtesy of Port Hedland Port Authority 2013)

geologists. The purpose of the HAZID is to identify potential hazards from activities that are conducted on site, assign a risk (hazard and consequence) to these activities, and identify ways to mitigate risk.

All environmental issues for the nearshore investigation are assessed and these range from oil spills from hydraulic equipment through to the risk of a cyclone.

A key health and safety focus for nearshore investigations during the Australian summer is the need for detailed cyclone management plans. An average of about five tropical cyclones form off the Pilbara coast each year, with generally one or two systems resulting in the port being placed on alert or ultimately evacuated and closed. The systematic and efficient approach to cyclone management is essential for any work conducted in the port.

50.2.2 Operational and Logistical Challenges

The initial challenge is in securing a window of time where there is a berth and suitably-sized crane available for assembly of the jack-up on which the drilling rig and auxiliary equipment are placed.

Prior to any borehole moves or tows the port authority has to be contacted and permission granted. The towing of a fully loaded jack-up barge occurs at a slow pace (3–4 knots) and the amount of time required for towing has to allow for

sea state, shipping movements, mechanical failure, and potential for grounding.

Port Hedland experiences a large tidal range, with a maximum astronomical variation of 7.5 m above Chart Datum (CD) and a maximum flood tide rate of 1.5 knots. The large tidal range and powerful currents typically dictate when operations such as barge movements are viable and when shallow areas of the port can be accessed. The large tidal range necessitates the need for flexibility in timing of work shifts and durations, placing unusual demands on personnel as well as equipment. At times, the low tide restricts access to the jack-up or prevents the support/emergency evacuation vessel from standing nearby.

50.3 Geology and Dredging

50.3.1 Nearshore Geology

Basement geology comprises Archaean granitic rocks of the Pilbara Craton. Overlying the basement rocks is an accumulation of mostly Pleistocene sediments with a relatively thin surficial cover of Holocene sediment (Fig. 50.2).

Surficial Holocene deposits include shallow marine, beach and dune sediments comprised of calcareous shells, reworked alluvium and calcareous rock fragments, which accumulate along the coastline, and fine grained deposits
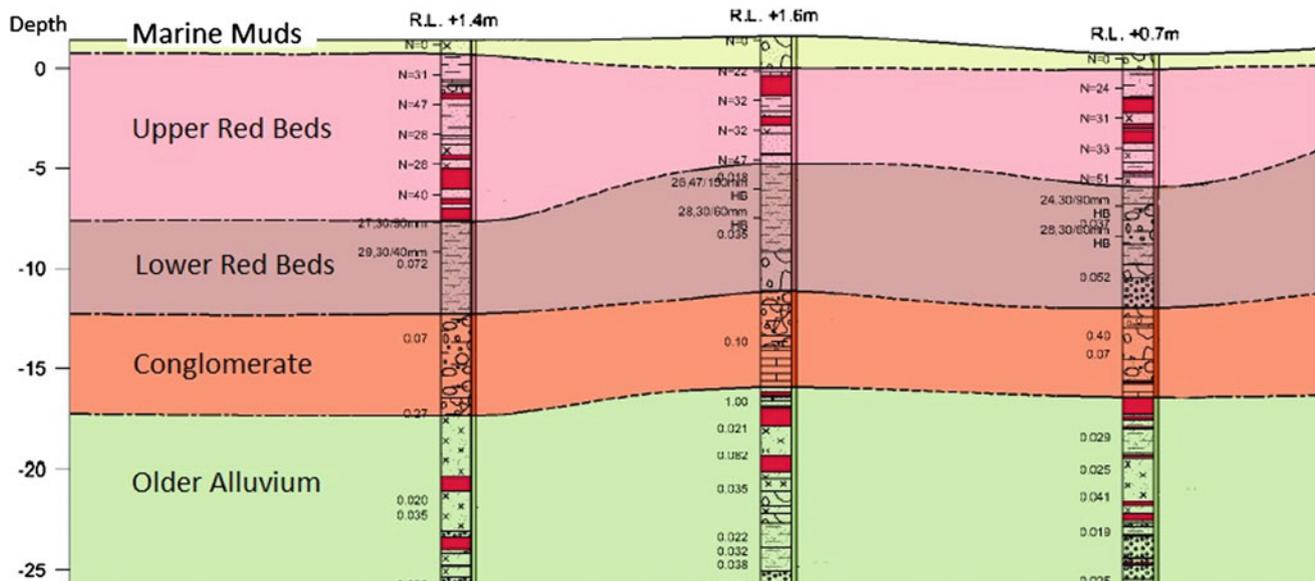
Fig. 50.2 Typical geological profile in Port Hedland Harbour

comprising estuarine muds which accumulate in tidal creeks and flats. The majority of the underlying Pleistocene deposits comprise siliciclastic terrigenous sediment, including quartz, feldspar, lithic fragments and clays, eroded from basement rocks in the hinterland and transported to the coastal plain. Characteristically, much of the alluvium is 'red' due to grain coating and staining of the clayey matrix by iron oxides and is known locally as the 'Red Beds'.

Changes in sea level during the Quaternary have resulted in periodic exposure and submergence of the coastal plain sediments, as well as influencing the elevation of the groundwater table. This has contributed to post-depositional alteration/diagenesis of sediments in the Port Hedland area. Dissolution and precipitation has resulted in the induration of sediments into weakly to well-cemented rock. The presence of calcrete cementation in the Lower Red Beds differentiates it from the Upper Red Beds (Fig. 50.2). The underlying Conglomerate is variably cemented and is high strength rock in parts. Induration may also be imparted by the in situ alteration of clays (e.g. kaolin clays) into cementing forms such as palygorskite.

50.3.2 Implication of Geology on Dredging

The purpose of a nearshore geotechnical investigation is to determine the nature of the material to be dredged, used and disposed of (Bray et al. 2001). Geotechnical aspects that are fundamental to the understanding of the dredging process and the evaluation of dredging projects include the in situ characteristics of the material to be dredged, the change in strength and volume of the material during the dredging and

relocation process, and the potential for change in material grading and the behaviour of the material during and after placement in the reclamation area.

The sub-surface geology of Port Hedland harbour is often considered relatively straightforward, yet the geological interpretation has not always accurately assessed or adequately communicated the geological risks for dredging and reclamation to project teams or contractors. Consequently, expensive claims have arisen as a consequence of extreme abrasion and excessive cutter, pump and pipeline wear caused by the combination of angular quartz and plastic fines forming armoured clay balls, with associated lost time and schedule delays.

The characteristics of the material within Port Hedland harbour have an effect on the suitable dredging plant to be used for a dredging campaign. The Marine Muds can be dredged by small suction dredges or backacter dredges. This material is often deposited in offshore spoil grounds as opposed to on land because the Marine Muds are a known acid sulfate soil. The dredging of berth pockets and turning circles penetrates the Red Beds and Conglomerate layer. These units contain quartz and lithic fragments; the hardness, shape, size and angularity of which has a significant effect on the abrasiveness, particularly in pumping operations from a cutter suction dredge. Of particular effect in Port Hedland is the formation of clay balls which contain abrasive quartz gravel; the quartz tends to protrude from the clay balls, making them highly abrasive.

The amount of fines being dredged will also have to be monitored in terms of the extent of sediment plumes (environmental impact) and its management in land reclamation, as discussed below.

50.4 Materials—Land Reclamation and Fines Management

Once dredged, some materials are deposited in offshore spoil dumps, as well as onshore in dredge material management areas (DMMAs). Reclamation management during the construction phase has to be tightly controlled. Selection of pipeline routes has to be executed according to a predetermined Reclamation Management Plan. The point at which dredge spoil is discharged into the reclamation area may change during the course of reclamation and survey control is required to monitor the rapidly advancing reclamation. Excess water and suspended silt also has to be guided towards a distal pond where pumps extract it from the reclamation area, to name just a few aspects that have to be strictly enforced.

Understanding how particle size distribution changes as a consequence of the action of cutter-suction dredging, proves invaluable in developing strategies for land reclamation. Successful land-reclamation is achieved by separating the fines fraction leaving a gravelly sand soil (known as grits). Dozers working the dredge spoil as it is discharged into the reclamation area contour and traffic compact the material. As the dozers work the dredge spoil, excess water carries the fines across the carefully contoured surface to a holding pond, from which the fines are typically pumped to designated fines settlement areas. With good management, spoil from dredging the Red Beds and Conglomerate (discussed in Sect. 3) becomes gravelly well-graded sand with a fines content between 5 and 10 %. This material is an excellent construction material for use in civil construction of roads, stacker and reclaimer embankments and general industrial land. When compacted to 98 % maximum modified dry density, the material can have an internal angle of friction (phi′) of 40–44° (derived from direct shear tests) and a unit weight around 20.5 kN/m^2.

To size a fines settlement pond, a bulking factor of 5 is applied to the fines content of the Red Beds.

References

Bray RN, Bates AD, Land JM (2001) Dredging, a handbook for engineers, 2nd edn. Butterworth-Heineman, Oxford

Bureau of Meteorology (2013) Climatology of Tropical Cyclones in Western Australia. Available from http://www.bom.gov.au/cyclone/climatology/wa.shtml. 19 Aug 2013

Fire & Emergency Service Authority of Western Australia (2013) Prepare cyclone smart. Government of Western Australia. Available from http://www.dfes.wa.gov.au/safetyinformation/cyclone/Pages/publications.aspx. 19 Aug 2013

Port Hedland Port Authority (2013) Cargo statistics and port information leaflet

The Role of Geological Analysis in the Design of Interventions for the Safety of the Road Asset. Some Examples

51

Serena Scarano, Roberto Laureti, and Stefano Serangeli

Abstract

The Design Management—Geotechnical Unit of ANAS (National Public Road Company) is often involved in study and monitoring activities regarding some instability events affecting the road asset; generally, those events tend to compromise the functionality of the infrastructure. These circumstances are generally caused by geomorphological, hydrogeological or stratigraphic arrangements, and triggered by specific rainfall conditions that tends to modify the whole stability of the road body and the slope complex as a whole. In particular, as examples of ANAS experiences, two case histories are illustrated. Both situations concern reinforced embankments that, following rainy periods, have shown strong evidence of instability. In order to size the stabilization measures, necessary for the road restoration, a thorough study of the phenomenon, in both cases, was developed. It was realized by different stages of investigation and monitoring of roadway displacement. In addition to a thorough geological and geomorphological survey, useful in the identification of particular instability surface forms, specific site-investigation campaigns were prepared and completed by the installation of topographic, geotechnical and interferometric monitoring instruments. At the same time, the geometry of the instability and the evolution mechanisms of the movements were quantified, determining the relationships between the movements and the external conditions, especially the meteorological and hydraulic ones. This analysis is aimed to obtain all the information useful to define the lines of action that ensure the final safety of the road asset.

Keywords

Road embankment • Instability • Strains • Stabilization

51.1 Introduction

Road infrastructures are designed keeping into account the stresses deriving from the modifications of the environmental context that includes them, in order to guarantee their functionality during their whole life. In recent times there have been examples where stretches of road embankments, built in geomorphological contexts and hydrogeological conditions of particular sensitivity, have shown over time, as a result of particular climatic conditions, internal deformations greater with respect of those provided by the project and tolerable from the structure.

The case-histories illustrated as follows relate to earth-reinforced embankments that, following rainy periods, have shown strong evidence of instability, which have partially compromised their functionality, leading to the temporary closure to traffic of the road sections. The Geotechnical Unit of the Design Management of ANAS S.p.A., frequently interested in the study of this kind of events, has been involved in the study, monitoring, site-investigation activities, in order to identify the causes and the mechanisms of instability evolution in act and, finally, to propose and design the stabilization solutions.

S. Scarano (✉) · R. Laureti · S. Serangeli
Design Management, Anas S.p.A., Rome, Italy
e-mail: se.scarano@stradeanas.it

Subsequently, in order to acquire all the knowledge necessary to understand the geological and geotechnical reference context, as well as to establish the project interventions of final consolidation of the embankments, specific site investigation campaigns have been prepared, completed by instrumental and monitoring survey. These campaigns consisted of the realization of boreholes pushed deep inside the laying surface of the embankment, with the aim to reconstruct the geological reference model and the thickness of the embankment involved in the movement. The monitoring consisting, however, in the implementation of several independent topographical, instrumental and interferometric systems of reading, as well as instrumented sections such as inclinometers, assestimeter, piezometers, mechanical fessurimeter, optical targets, in order to evaluate the areal extent of the instability phenomenon and to record the different rates and trends of the displacement.

51.2 Case Histories

Two examples of damages occurred inside hearth-reinforced embankments, part of the italian road network, are after described. In that cases it was necessary to analyze the events and, therefore, to design the consolidation works and safety settings, in order to restore the circulation of traffic. Despite the two cases are concerning two different environmental and climate context, in both the events the main factor was represented by the rainfall seepage inside the slope of the road body. In fact, the main instability happened after long rainy periods. The consequent growth of the pore pressure, with the exceeding of the shear resistance of the embankment-slope system, therefore, triggered the strain events.

51.2.1 Rome Hinterland

In December 2010, along an important road, following a prolonged rainy period, there has been a deformation phenomenon with significant proportions, that affected a stretch of the reinforced embankment, causing the partial closure to traffic of the road (Fig. 51.1).

In the first emergency phase a provisional safety intervention was prepared by means of a drainage system and installation of metal gabions, in order to lower the pore pressure and, at same time, to create an overload to the foot of the slope, with a stabilizing function. A campaign of site-investigation, instrumental and topographical monitoring was subsequently implemented. It included the execution of 13 boreholes, the use of three piezometers, one inclinometer and one assestimeter, with cadenced readings.

The acquired data have allowed to define a very detailed geological reference model, centred on the instability area. It is represented by geological formations belonging to the prevulcanic sedimentary sequence of the Roman area (De Rita et al. 1995), consisting, for the most part, by sands and gravels, with clay and silty levels, oxidized horizons and peaty levels, referred to beach and infralittoral and, furthermore, to fluvial and brackish depositional environments

Fig. 51.1 Damages and tension cracks along the roadway

(Faccenna et al. 1995). These deposits are followed by pyroclastic materials, belonging to the Sabatini Mounts volcano, with cineritic matrix with pumice. They contains, sometimes, slag and lithic lava and volcaniclastic reworked levels (Fig. 51.2) (Ventriglia 2002).

The geological and hydrogeological models, so defined, showed that the sand deposits underlying the road embankment contain an appreciable water circulation that influenced the equilibrium conditions of the roadway. This aquifer is of semiconfined kind, because it's enclosed between the pliocenic clayey substrate (to the bottom) and a layer of silty clay (to the top). Because of a prolonged infiltration due to the rainfall, the sandy aquifer has developed a growth of the pore pressure and the rising of the piezometric surface. It caused filtration phenomena within the body of the overlying embankment, and the creation of a sliding circular surface, placed immediately behind the reinforced-heart body.

The definitive safety interventions consisted of the realization of a bulkhead of large diameter piles, interventions of consolidation of the soil and, furthermore, of civil works of water gathering (Fig. 51.3) (Facchini and Nart 2006).

51.2.2 Liguria (Northern Italy)

In the Imperia province (Liguria—Northern Italy) a section of road interchange, consisting of a series of ramps located along a slope and supported by reinforced embankments (Comendini and Rimoldi 2013), suffered the first signs of instability in early 2011, as a result of high rainfall intensity events, that have affected the whole Region.

Following the deformational events, preliminary works were made. They were represented by draining trenches above the road and, later, by local consolidation works of the enbamkment.

Between the months of October and November 2012, because of the repetition of high intensity and long-term rainy events, a recovery of deformation was recorded, causing the appearance of large tension cracks along the road surface, which led ANAS to define a complete consolidation design of the body of the embankment (Fig. 51.4).

At this point, another intervention has been made, represented by the realization of sub-horizontal drains in the body of the embankment. A monitoring plan has also set up, in parallel with a deep geotechnical site-investigations campaign, represented by 69 topographic control points, 10 inclinometers, 4 assestimeters, 10 piezometers, 7 mechanics fessurimeter and the implementation of an interferometrical monitoring, after described.

The complex of the acquired data have allowed to identify a reference geological model (Lanteaume 1968), represented by a calcareous-marly substrate, belonging to the "Borghetto d'Arroscia-Alassio" and "Moglio-Testico" Units, which with "S. Remo-M. Saccarello" Units constitutes the "Flysch with Elminthoides" Formation of Ligurian-Piedmont Domain (Boni and Vanossi 1960). The substrate is covered, in surface, by a layer of eluvial-colluvial deposits, with significant clay content. The site-investigations have also shown the presence of a main sliding surface inside the cohesive materials that covers the bedrock, immediately below the reinforced embankment affected by the deformation, together with evidence of waterflow inside the fractured part of the rock mass.

So, works of definitive stabilization were realized. They consist of two lines of bulkheads with large diameter piles, with the aim to support the actions of pushing from upstream and to anchor the embankment to the rock substrate. The
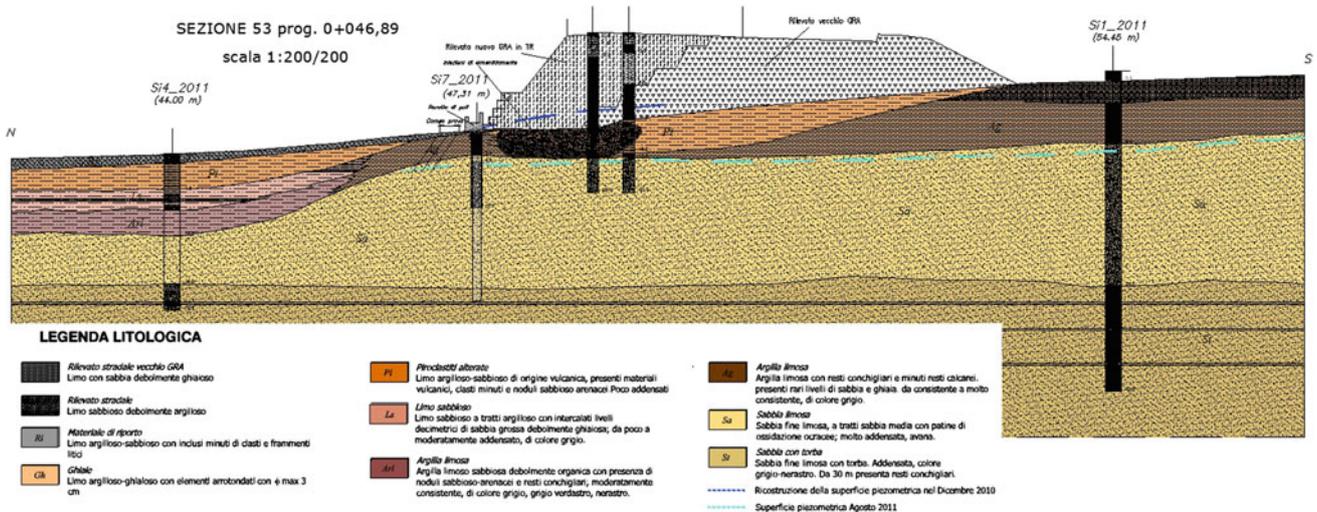
Fig. 51.2 Cross geological section in the damaged site
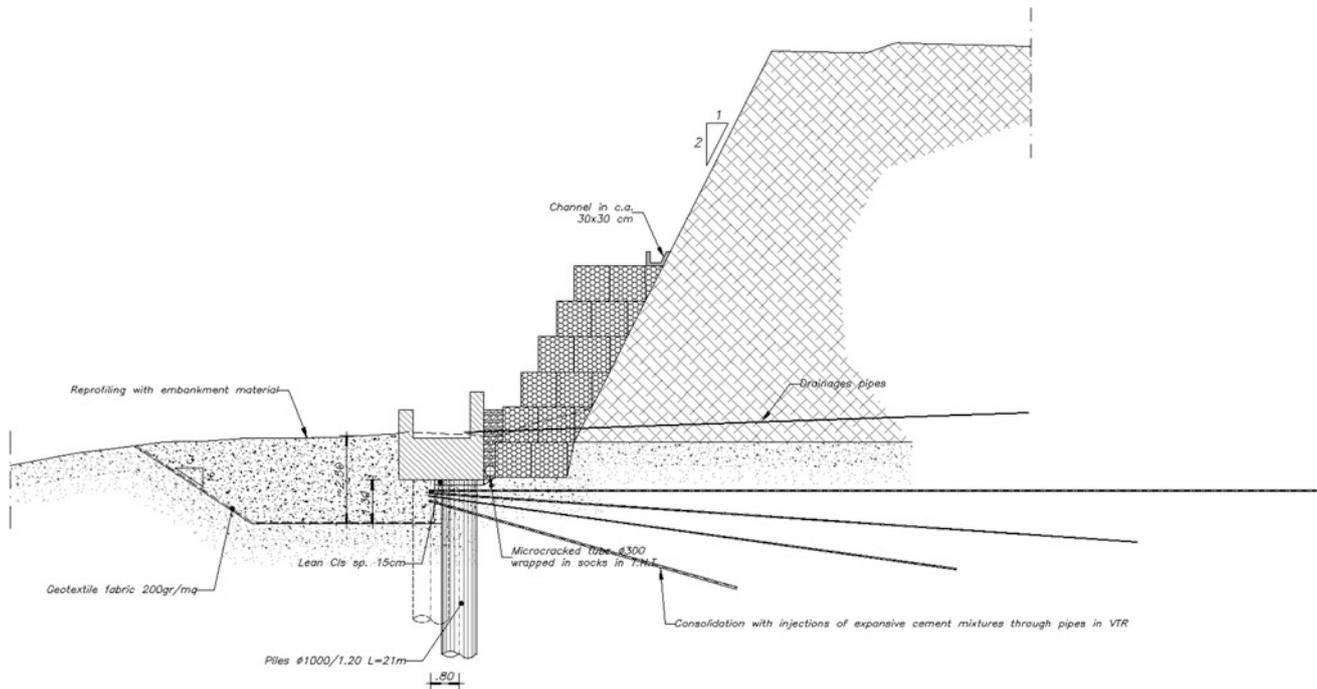
Fig. 51.3 Cross section showing the stabilization works

second bulkhead has been placed on the foot of the embankment and it also reach the bedrock. The works are completed with drainage works along the slope upstream of the embankment (Fig. 51.5) (Bianco 2001).

51.2.2.1 Interferometric Monitoring (Nhazca Data): Comparison Before and After the Interventions

For the evaluation of the areal extension of the instability phenomenon and for a determination of the rates and trends

Fig. 51.4 Overview, from the opposite slope, of the road interchange
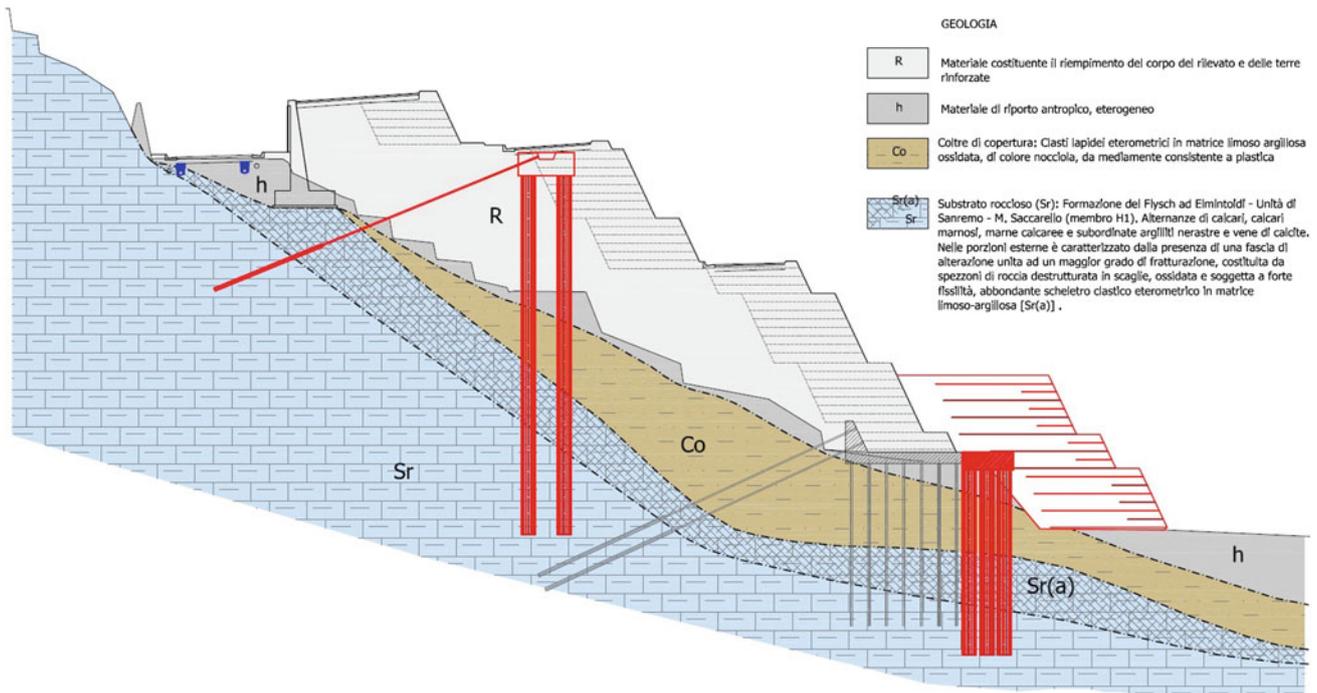
Fig. 51.5 Cross geological section, completed with the designed stabilization works

of the displacements, a monitoring station with SAR interferometry Terrestrial (TInSAR) has been installed, by Nhazca (spin-off of La Sapienza University) on the opposite slope. Through this technique, chromatic maps of the survey area were obtained, calculated by comparing the phase value of each pixel of images acquired at different times, that represent the bidirectional movements along the line of sight of the instrument (line of sight) (Fig. 51.6).

The magnitude of displacement in the following time, from the monitoring network installation, were between −1.5 and −3 mm/day, on approach to the sensor along the line of sight. The embankment has undergone major shifts at the base and in the most western part, while further upstream and eastern portions the movements were more contained. The terrains beyond the foot of the embankment, retaining walls at the entrances of tunnels and the wall on the side of
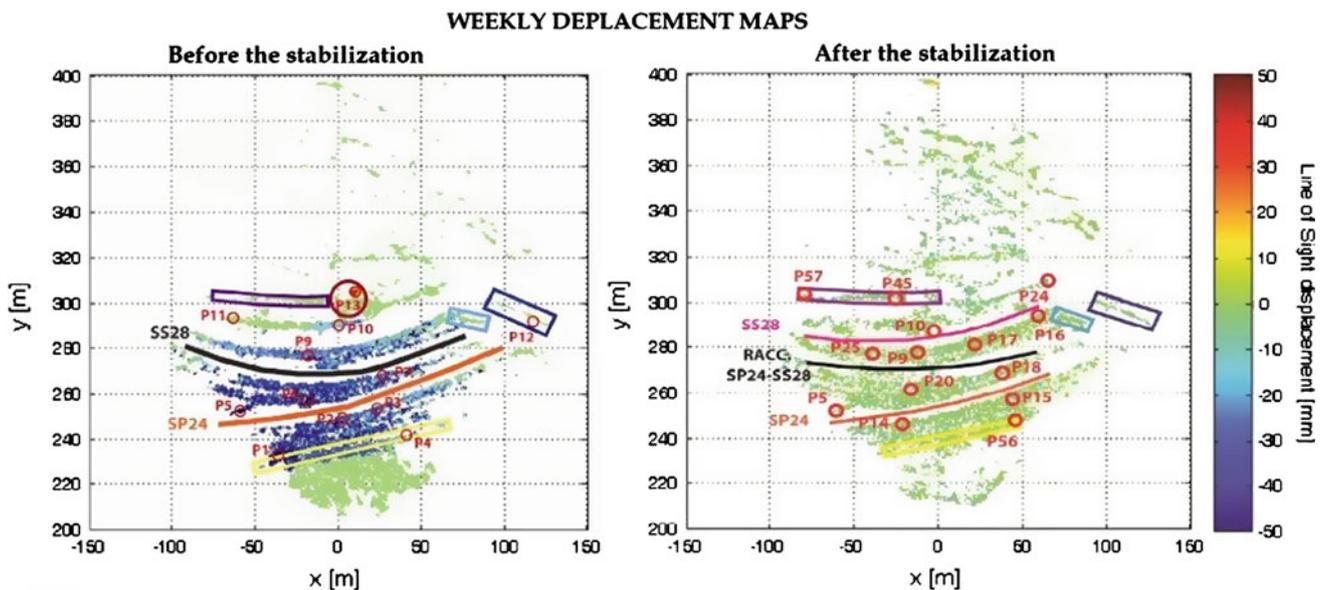
Fig. 51.6 Shift TInSAR map before and after the stabilization works

the embankment, however, have undergone no appreciable movement. The rates recorded over the entire displacement have undergone a gradual deceleration in subsequent periods from the initial movement. Just after the completion of the first measures stabilization (anchored bulkheads) the movements were reduced abruptly to zero.

51.3 Conclusions

In the field of road engineering, as well as the design of new road, the occurrence of damages or slides affecting the road body, causes to acting in the maintenance and safety of existing works that, over time, have been damaged.

In the first emergency, usually, preliminary work are carried out in order to temporary safe the road asset and to assure the traffic along it. In a second phase it is essential to operate with definitivesolutions.

To achieve this, the most information about the soils on which the road will be located and surrounding area are essential. Such information can help to formulate hypotheses about kinematics and mechanism of landslides, in order to propose appropiate design solutions for the last safety.

For this reason it is important to have an adequate campaign of geological site investigations and instrumental and topographic monitoring of the area. So the knowledge of the geological reference model is fundamental in the choice of design solutions to be adopted in the road planning.

The case histories show the fundamental role, as a cause of the damages, played by the response of the road body related to the particular hydrogeological features.

References

Bianco PM (2001) Strutture in terra rinforzata contro il dissesto idrogeologico. Maggioli Editore

Boni A, Vanossi M (1960) Ricerche e considerazioni sul Flysch della Liguria occidentale. Atti Istituto Geol Univ Pavia, vol XI

Comendini M, Rimoldi P (2013) Terre rinforzate. Flaccovio Editore, Palermo

De Rita D, Faccenna C, Funiciello R, Rosa C (1995) Stratigraphy and volcano-tectonics. In: Trigilla (ed) The Volcano of the Alban Hills, Tipografia SGS Roma, 33–71

Faccenna C, Funiciello R, Marra F (1995) Inquadramento geologico strutturale dell'area romana. Mem Descr Carta Geol D'It L:31–47

Lanteaume M (1968) Contribution à l'étude géologique del Alpes Maritimes franco—italiennes. Mèm Carte Géol Fr:405

Facchini Massimo, Nart Massimiliano (2006). Ripristino di sedi stradali con tecniche a basso impatto ambientale. Le strade, vol 6

Ventriglia U. (2002). Geologia del territorio del comune di Roma, Amministrazione provinciale di Roma, Roma

Groundwater Level Variation and Deformation in Clays Characteristic to the Helsinki Metropolitan Area

52

Tiina-Liisa Toivanen and Jussi Leveinen

Abstract

The aim of this study was to use various modelling approaches to examine the groundwater level changes and other factors influencing subsidence and soil compaction in clay deposits characteristic to the Helsinki metropolitan area in Finland. The research area is Perkkaa in Espoo, located in the Helsinki metropolitan area in the coastal area of Southern Finland. The surface of the studied area is mostly covered by clay, with a thickness varying between 5 and 15 m. The urban development of the Perkkaa area began in the beginning of the 1970s. The hydrogeological environment in the area has been considerably altered by construction, and it has also led to lowering of the groundwater levels. As a result, there are large deformations, especially on the streets and the yards. Using an available laser scan data, GPS-measurements of the levels of ditches and minor streams, and drilling and geological maps provided by the city of Espoo and Finnish Geological Survey of Finland, it has been possible to create a 3d model of the geological main units in the research area and estimate the depth of the clay deposits. The 3d model was used further to model the changes in the groundwater flow in the research area. On the basis of this study, significant reduction in the groundwater levels are induced by the drainage systems and particularly the underground pipeline systems rather than changes in the recharge in the area due to construction.

52.1 Introduction

The factors influencing deformation and subsidence in clay deposits include manmade loadings and variation of groundwater level. In addition to natural seasonal variation, groundwater levels are influenced by changes in land use, underground construction, changes in climate, and geological uplift. The aim of this study was to use various modelling approaches to examine the groundwater level changes and other factors influencing subsidence and soil compaction in clay deposits characteristic to the Helsinki metropolitan area in Finland.

The index properties and stress deformation characteristics of Finnish clay deposits have been the subject of a number of studies since the 1960s and geotechnical investigation results are documented in databases particularly in the Helsinki metropolitan area. Therefore, somewhat surprisingly, geotechnical designs rely typically at most on few site specific measurements of index properties. A part of the study was to examine how reliably the existing data could be used in determining the risks of excessive consolidation and soil deformation by estimating the deformation characteristics based on the available statistical data.

T.-L. Toivanen (✉) · J. Leveinen
Department of Civil and Environmental Engineering, Aalto University, Espoo, Finland
e-mail: tiina-liisa.toivanen@aalto.fi

J. Leveinen
e-mail: jussi.leveinen@aalto.fi

52.2   Engineering Geological Setting

The research area is Perkkaa in Espoo, Finland, located in the Helsinki metropolitan area in the coastal area of Southern Finland. The size of the research area is approximately 2.7 km^2. The development of the Perkkaa area began in the beginning of the 1970s. Since then, the hydrogeological environment has been considerably altered by construction, and it has also led to lowering of the groundwater levels. As a result, there are large vertical deformations, especially on the streets and yards. The city of Espoo has been observing the deformations on the two main streets in the area. According to the measurements, the maximum soil subsidence on the two streets is roughly 0.5 m compared to the original surface levels. Considering the constant re-paving and repair works on the streets, it is likely that the actual maximum subsidence is on the order of 0.7–0.8 m.

In general, the geology and topography of the area is characteristic to Southern Finland. The surface of the studied area is mostly covered by clay, with a thickness varying between 5 and 15 m. In the southern and middle parts of the area, the soft soil layer can be over 20 m thick. The water content of the clay varies considerably, mostly being between 70 and 140 %. A silt and sand layer a couple of meters thick can be commonly found beneath the clay deposits, on top of a 1- to 5-m-thick layer of till that overlies the bedrock. The studied area is bordered by a fill area to the east, a silt/sand moraine area to the west, and a moraine/bedrock area to the north and south. Most of the area is elevated less than 2 m above the Baltic Sea level. In the northern part of the area, at the moraine and exposed bedrock areas, the elevation varies, being 10 m at its highest (Ojala 2011). The research area is a part of well-defined catchment area, which provides good boundaries for modelling the flow of the groundwater and the changes in its level.

The investigations carried out by State Technical Research Centre 40–50 years ago provide still the most comprehensive assessment of soil engineering geological properties in Finland. The results summarized in Gardemeister (1975) involved 48 drill cores of fine grained soil samples collected from different parts of the country. The data published by Gardemeister include estimates of water content, and void ratio, which can be used to assess consolidation deformation of fine sediments, based on the method introduced by Helenelund (1951). Since this approach relies on relatively easily obtainable index properties, the method is widely utilized in prediction of soil deformations in Finland. Therefore, in the following, the distributions of the relevant index properties for the method are used to assess stochastically the soil consolidation and subsidence due to changes in water table and man-made loadings.

52.3   Land Use of the Research Area

52.3.1 The Urban Development of the Area

The development of the Perkkaa area started in the 1970s, which was a period of rapid urbanization in the Helsinki metropolitan area. The first buildings in Perkkaa were residential high-rise apartment buildings, and a bit later, first few office blocks were constructed. After the 70s the area remained mostly static, until the 90s, which was the period of gradual built up with mostly residential projects. Today, the Perkkaa area is home to about 4,000 inhabitants. During the past few years some office blocks has been built in the east side of the area. The development of the area will continue within next few years.

52.3.2 Foundations and Drainage

In the southern and central parts of the area the depth of the soft soil can be up to 20 m and the buildings have been built on piles. The western parts of the area have less or no soft soil layers on them, and the buildings have been constructed on shallow foundations. In most of the buildings the subgrade surface reaches the depth of a few meters below the ground level. In each property groundwater is drained a couple of meters below the original ground surface.

All urban infrastructure e.g. plumbing and drinking water systems, heating pipelines that are susceptible to frost damage are buried subsurface to a sufficient depth. If no insulation is used this depth typically exceeds 1.8 m.

The yards and alleys have not had originally any specific foundations, and no ground improvement methods have been used.

52.4   Data and Modeling Approaches

Using an available laser scan data, GPS-measurements of the levels of ditches and minor streams, and geotechnical soil investigations and geological maps provided by the city of Espoo and Finnish Geological Survey of Finland, it has been possible to create a 3d model of the geological main units in the research area and estimate the depth of the clay deposits. The geological 3d-model and available groundwater level estimates made in the geotechnical investigations were used to compile a groundwater flow model using USGS Modflow in GMS—software utilities. The objective of the flow modeling was not to estimate actual elevation of the groundwater level but assess the drawdown induced by the drainage systems and pipeline trenches (Astm 1999).

Subsequently, soil subsidence/consolidation was estimated stochastically after the following assumptions:

- The water content method (Helenelund 1951) can be estimated to assess the soil deformation (due to consolidation).
- The unsaturated part of the fine sediments, "the dry crust", is 1.0 m thick and remains undeformed.
- The input soil properties are water content and dry specific weight for the dry crust and the saturated zone and are assumed to follow distributions obtained by Gardemaister (1975) for Litorina sediments.
- Groundwater drawdown that has been resulting mainly from draining associated with various subsurface infrastructures, is local and within the range of 0–2 m.
- Aggregate material layers applied in building sites and road construction are 1–1.5 and consequently induce a load of 26–39 kPa.

52.5   Results and Discussion

The results of the stochastic calculations indicate that similar construction practices as applied in the study area will likely yield substantial consolidation or subsidence in Southern Finland. The thicker the clay-formation, the more substantial the subsidence is. Based on the sensitivity analysis, the water content appears as the key parameter. Even if the site specific water contents would be close the minimum end of the distribution obtained by Gardemaister (1975), the subsidence will exceed 0.1 m with 95 % probability if the soil thickness reaches 3.0–5.0 m. Both the predictions of subsidence and the uncertainties involved will increase with the thickness of the clay deposits. For over 5 m thick clay deposits obtaining a 0.2 m subsidence or less appears a mission impossible.

In the study area rain and snow-melt is collected from the roofs of the flat roofed buildings to the municipal waste water system. Also at the yards of the buildings the surface run-off is directed to the drainage systems. Also substantial part of the area is today asphalt paved areas, which could also be expected to reduce the overall recharge. However, in quite opposite way, the optimized i.e. automatically calibrated recharges in outcrop slope areas suggest about 10 % higher recharge when calibration is done to the groundwater observations taken during the late 80s and the 90s compared to observations taken in the late 60s. The observations represent sporadic measurements of the "undisturbed" groundwater levels related to the geotechnical investigation activities during preceding construction, not systematic monitoring and reliable time series. Taking into account the uncertainty of the groundwater data, results suggest at most that not significant changes in the catchment scale recharge appear to have happened. Since significant part of the development has taken place in the areas of fine sediments, which originally low to insignificant recharge, the overall
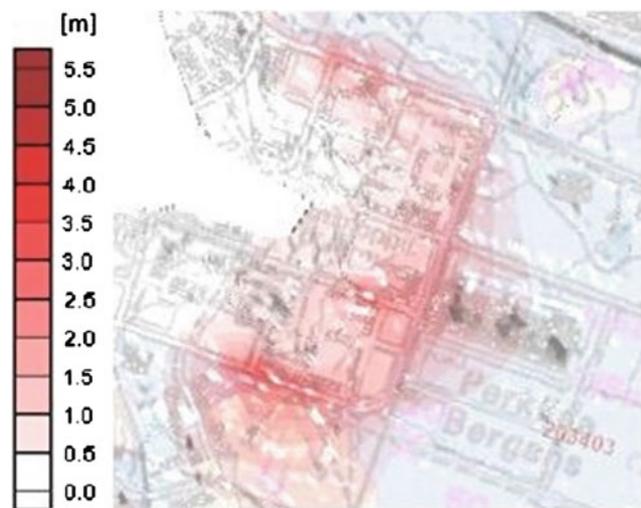
Fig. 52.1 Drawdown in groundwater levels in the Perkkaa area based on the numerical groundwater flow model

impacts of the recharge have been small. As suggested by the numerical groundwater flow model, significant reduction in the groundwater levels are induced by the drainage systems and particularly the underground pipeline systems rather than changes in the recharge. Results based on the numerical groundwater flow model are shown in Fig. 52.1.

52.6   Conclusions

Based on this study, lowering of the ground water levels due to construction can have a significant effect on subsidence in clay deposits even just a few meters deep. Lowering of the ground water levels cause deformations and in that way major costs of repairs. In addition to the direct costs it can also have an effect on the prestige of the area and the values of apartments in the district. The condition of the street and yards has an obvious influence on the satisfaction of the area residents, and thereby on their experience of personal safety (Kyttä et al. 2013).

In contrast with the current planning practices, the effects of possible lowered ground water levels should thus be taken into account proactively in the zoning and planning processes, to avoid structural damage and expensive recurring repair works on the streets and yards.

References

Astm (1999) Standard guide for subsurface flow and transport modelling, D5880–95

Gardemaister R (1975) On engineering-geological properties of fine-grained sediments in Finland. Dissertation, Technical Research Centre of Finland, Building Technology and Community Development, Publication, vol 9, 91 p

Helenelund KV (1951) Om konsolidering och sättning av belastade marklager (On consolidation and settlement of loaded soil layers). Dissertation, Finland Technical Institute, Helsinki

Kyttä M, Broberg A, Tzoulas T, Snabb K (2013) Towards contextually sensitive urban densification: location-based softGIS knowledge revealing perceived residential environmental quality. Landscape Urban Plan 113:30–46

Ojala AEK (2011) Construction suitability and 3D architecture of the fine-grained deposits in Southern Finland—examples from Espoo. Geol Surv Finland Spec Pap 49:126–136

Determine of Tunnel Face Stability Pressure in EPB Machine with Use Analytical Methods (Case Study: Mashhad Metro Line2)

53

Mehdi Abbasi and Mohsen Abbasi

Abstract

This article discusses the face stability of the soil in front of the TBM cutterhead and includes calculations of face stability for 27 cross sections for Mashhad Urban Railway Line 2 with use analytical methods. In the case of the MURL2 Project a TBM will be applied with an Earth Pressure Balance shield. The objective of this study is to advise on a support pressure which has to be applied during the different phases of the tunnel boring process of MURL2. The 27 cross sections have been selected for their spreading over the sections between the stations and the locally present soil overburden. During the shield tunnelling process, subsoil is cut loose by the cutting wheel. The main failure mechanism, which may occur, is inward collapse or cave in. To prevent the cutting face from collapsing, a supporting pressure can be applied by the TBM.

Keywords

Face stability • Analytical methods • EPB machine • MURL2

53.1 Introduction

MURL2 with total length of about 14 km is extended from North-East of Mashhad, to South-East and contain 12 stations along the route. The line 2 shall be able to prepare services for about 10,000 passengers per hour per direction. The tunnel was bored by two earth pressure balance (EPB) shield. The characters of this EPB machine presented in Table 53.1.

The stability of the face is one of the most important factors in selecting the adequate method of excavation of a tunnel. This is particularly true for mechanized tunneling and specific boring machines (TBM).

53.2 Local Properties

Calculations for the face stability have been performed for 27 cross sections of the MURL 2. This part discusses the soil properties at the relevant cross sections. The 27 cross sections have been selected for their spreading over the sections between the stations and the locally present soil overburden.

53.2.1 Geotechnical Soil Parameters

The geotechnical soil parameters which have been derived from the geotechnical reports (IMN consultant engineers Co. 2010) and are used for the calculations of the face stability, are summarized in the following Table 53.2.

53.3 Face Stability Theory

In the case of the MURL2, a TBM will be applied with an EPB shield. In the case of an EPB shield, the soil that is excavated is collected in the chamber directly behind the

M. Abbasi (✉)
IMN Consulting Engineers Co., Tehran, Iran
e-mail: Mehdi_abbasi1980@yahoo.com

M. Abbasi
IMN Consulting Engineers Co., Mashhad, Iran
e-mail: Abbasi.mohsen1982@gmail.com

Table 53.1 TBM's technical parameters

Parameter	Value	Unity
Diameter of cutterhead	9.43	m
Diameter of front shield	9.38	m
Diameter of rear shield	9.35	m
Length of TBM shield	10	m
Weight of TBM	7,000	kN
External diameter of tunnel lining	9.1	m

cutting wheel. The excavation chamber needs to be completely filled for the support pressure that is delivered by the hydraulic jacks to be conveyed to the cutting face. The supporting pressure on the cutting face can be regulated by varying the pressure delivered by the hydraulic jacks. A second way of regulating the supporting pressure can be achieved by varying the speed at which the soil that has been excavated is transported from the excavation chamber by the auger.

53.3.1 Analytical Calculation Models

A first conservative estimation of the upper and lower bound of the required supporting pressure can be found relatively easy by assuming the soil mass acts according to Mohr-Coulomb's failure criterion and by applying Rankine's theory of earth pressure (Eq. 53.1). At inward collapse, horizontal effective stresses will be in the active state (Rankine) and thus a lower bound for the required supporting pressure can be found.

$$q_{min} = \sigma'_h + p_w = K_a \cdot \sigma_v'' - 2 \cdot c \cdot \sqrt{(K_a)} + p_w \quad (53.1)$$

$$K_a = (1 - \sin\emptyset)/(1 + \sin\emptyset) \quad \text{and} \quad p_w = \gamma_w \cdot h$$

The formula mentioned above is a relatively simple approach to the problem and is only applicable for 2D situations. In practice, the occurring failure mechanisms in shield tunnelling will be 3D. It can be expected that the minimum support pressure in a 3D situation will be lower than in a 2D situation due to the higher strength of the soil, caused by cohesion and friction forces along the sliding planes of a 3D failure mechanism (e.g. arching effects). A number of analytical face stability models are available from literature, which take into account both the 2D situations as

well as the 3D situations. Three method use in this paper consist: Anagnostou and Kovári (1994), Jancsecz and Steiner (1994) and Leca and Dormieux (1990).

53.3.2 Comparison of Calculation Models for MURL2

Each model for the analysis of face stability as described in Sect. 53.3.1 has its own strengths and weaknesses. To assess which model is the most suitable for the MURL2 project, a comparison has been made for two cross sections, 2a and 9b (Table 53.4). Cross section 2a is representative for the clayey soils of the first part of the trajectory and section 9b for the more sandy and gravelly soils of the latter part. The results of the calculations of the minimum required face support pressures, applying the methods described in Sect. 53.3.1, are given (Table 53.3). The crown of the tunnel has been taken as a reference level for comparison purposes.

53.4 Calculation of Face Stability

53.4.1 Calculation Method Minimum Soil Pressure

The minimum soil pressure is the pressure in the lower boundary of the soil pressure at which no instability occurs of the soil in front and above the excavation face. The minimum support pressures are calculated according to the Jancsecz and Steiner method. Jancsecz and Steiner have designed a 3D face stability model based on a soil wedge in front of the excavation face. This method considers the forces on a possible and probable failure mechanism, with the use of limit equilibrium analysis to determine the limit earth pressure acting on the tunnel face. The model is designed to calculate minimum support pressures only. The maximum support pressure is discussed in Sect. 53.3.2. The Jancsecz and Steiner failure model consists of two parts:

- soil wedge in front of the face (lower part);
- soil silo above the wedge (upper part)

The method is based on the analysis of the force equilibrium on a soil wedge in front of the tunnel face. With the different values of overburden and angle of internal friction, as present in the cross sections, the three dimensional earth pressure coefficient KA3 is found. With this parameter and

Table 53.2 Averages of geotechnical parameters all sections

Geotech. unit no.	Geotechnical unit description	Unit bulk weight dry (kN/m³)	Unit dry weight γ dry (kN/m³)	Ø°	c' (kPa)
I	Silty clays	18	16.5	30	14.5
II	Clayey sands	18.5	17	32.2	4.9
III	Clayey gravel (with sand)	20.5	18.5	37.5	0

Table 53.3 Face support pressures calculated applying different methods

	Section 9b-gravelly soil	Section 2a-clayey soil
Ka	60	62
Jancsecz and Steiner	62	67
Anagnostou and Kovari	65	54
Leca and Dormieiux-lower bound	12	5
Leca and Dormieiux-upper bound	110	107

Fig. 53.1 Min and max support pressures at tunnel axis

the vertical earth pressure, the horizontal soil pressures at different TBM levels can be found. The minimum earth pressures at the relevant soil pressures are assessed at the crown, the axis and the heel of the tunnel. The model of Jancsecz and Steiner takes the ratio of C/D into account. If this C/D ratio is smaller than 2, the model assumes that no arching in the soil above the excavation face will occur. For the calculation of the minimum soil face pressure, the surface loads are taken into account. For those situations where the tunnel is below a road, traffic loads (20 kN/m^2) are

Table 53.4 Min and max support pressures at the tunnel crown, axis and heel

Cross section (km)		Overburden height (m)	Geo-techn. unit at tunnel axis	Crown (kN/m^2)		Axis (kN/m^2)		Heel (kN/m^2)	
				max.	min.	max.	min.	max.	min.
−1a	−0.35	8.7	I	137	59	219	77	301	95
−1b	−0.05	9.8	I	156	63	238	81	320	99
−1c	0.3	10.3	I	165	65	246	83	328	101
−1d	0.65	9.8	I	157	63	239	81	321	99
−1e	1.2	9.2	I	145	61	227	79	335	123
−1f	1.48	9.8	I	155	63	239	81	354	130
0a	1.58	10.3	I	188	70	273	89	388	138
0b	1.8	9.2	I	144	61	228	79	325	111
0c	2.2	9.2	I	145	61	227	79	309	97
1a	2.4	8.9	I	144	61	226	79	307	97
1b	2.55	13.6	I	226	72	308	89	390	105
1c	2.95	11.6	I	190	70	272	88	354	106
2a	3.6	10.4	I	168	66	250	84	332	102
2b	3.95	10.6	I	172	67	254	85	336	103
3a	4.6	10.5	I	168	66	250	84	332	102
3b	5.05	8.6	I	134	59	216	77	298	95
3c	5.95	7.9	I	123	56	205	75	287	93
4a	6.45	12.3	I	201	73	282	91	364	109
5a	7.9	18	II	309	88	393	105	477	121
6a	9.15	11.1	I	185	69	267	88	349	106
7a	9.69	12.9	I	212	75	293	93	375	111
7b	10.3	10	I	174	67	256	85	338	103
8a	10.91	10.1	III	165	52	258	67	352	82
8b	11.57	11.1	II	183	64	267	81	351	98
9a	11.87	16.8	I	284	90	366	108	448	126
9b	12.6	12.1	III	225	62	318	77	411	91
10a	13.35	25.4	III	449	95	542	109	635	123

applied. If the cross section is below a building, the building loads are applied in the model.

53.4.2 Calculation Method Maximum Soil Pressure

The maximum soil pressure is the pressure at which the soil in front of the excavation face does not exceed the vertical pressure. The maximum soil pressure is determined at the different levels of the TBM. Surface loads are not taken into account for this upper pressure boundary, because they are not permanently present.

53.4.3 Minimum and Maximum Support Pressure

In tunneling by TBM, it is good practice to ascertain a safety buffer between the minimum and maximum soil pressure, usually with a value of 20 kN/m^2. This pressure buffer will also be applied for the MURL2 tunnel. Applying the theory of Jancsecz and Steiner as described in Sect. 53.3.1 and the method of determination of the maximum soil pressure of Sect. 53.3.2, the lower and upper boundaries for the minimum and maximum soil pressure are found. To these values the buffer pressure of 20 KN/m^2 is added to come to the minimum and maximum support pressures. In the Fig. 53.1 a schematization of the upper and lower boundary of the support pressures are given. The support pressure of the TBM should remain in the hatched area. The calculations

have been performed for the supporting pressure at the tunnel crown, axis and heel (Table 53.4).

53.5 Conclusions

The evaluation of the tunnel face-support pressure is a critical component in both the design and construction phases of TBM. In this article, lower bound minimum support pressures and upper bound maximum support pressures have been determined for 27 cross sections. It is tried to assess the lower and upper bound at critical locations of the tunnel route. In between the cross sections, the support pressures of the TBM should be maintained near the most feasible levels of the support pressures, based on the local conditions and geology. It is strongly recommended to obey the limits of the lower and upper support pressures, in order to avoid problems with the stability of the excavation face.

References

Anagnostou G, Kovari K (1994) The face stability of slurry-shield-driven tunnels. Tunn Undergr Space Technol 9(2):165–174

IMN consultant engineers Co (2010) Geotechnical reports of MURL2

Jancsecz S, Steiner W (1994) Face support for a large mix-shield in heterogeneous ground condition. In: Tunneling '94, Institution of Mining and Metallurgy, London

Leca E, Dormieux L (1990) Upper and lower bound solutions for the face stability of shallow circular tunnels in frictional material. Geotechnique 40(4):581–606

Numerical Modeling of Interrelationships Between Linear Transportation Infrastructures and Hydro-geological Hazard in Floodplains

54

Rosamaria Trizzino

Abstract

The development and efficiency of transportation infrastructures has always been a central element in the planning and management of territory, not only with regard to the social and economic aspects but also for the management of environmental emergencies, in particular those of Civil Protection. In the valleys most usual design solution is the road embankment. In the presence of a surface water table the realization of a road embankment causes more or less marked alterations of the piezometric levels, with serious problems to vehicular traffic. Typically in such situations to avoid the risk of flooding of the roadway engineers tend to increase the height of the embankment, thus increasing the overload in the foundation soil and thereby creating new risk situations. In this paper it is proposed a modeling study aimed at determining the interactions between the geometric and geomechanical properties of foundation—road body—roadway and surface and deep water table levels, in order to identify risk scenarios. The numerical analysis has been carried out by a finite element calculation code taking into account different combinations of water level depth and embankment height for different lithological and geotechnical properties of the foundation soils. The obtained results show that there are some critical combinations of the above parameters that can cause the rise of the water level well above the ground surface not only at the road embankment but also in the surrounding areas up to tens of meters from the road.

Keywords

Hydro-geological hazard • Embankments • Roads • Soil stresses • Flooding

54.1 Introduction

The development and efficiency of transportation infrastructure has always been a central element in the planning and management of territory, not only with regard to the social and economic aspects but also for the management of environmental emergencies, in particular those of Civil Protection. In this context, the efficiency of road and railroad infrastructures appears to be a fundamental issue or even a discriminating element to the effectiveness of specific interventions in the presence of natural and human made environmental "disasters".

It is well understood then the importance of properly assessing the interactions between transportation infrastructure and the natural and built environment and in particular the influence of the hydrogeological, geological and geomorphologic conditions on the serviceability of the roads and railroads. But it is only in recent years, with the beginning of the great highway construction, that it has been highlighted the complexity of the territory—road—vehicle relationship and thus the need for extensive research in the design of the geometry of the road both in relation to the physical characteristics of the territory (in particular geomorphologic and hydro-geological) and the conditions of vehicular traffic.

R. Trizzino (✉)
CNR, IRPI, via Amendola, 122/i, 70125, Bari, Italy
e-mail: r.trizzino@ba.irpi.cnr.it

As a matter of fact, water levels play a fundamental role both in relation to the triggering and evolution of landslides (Cotecchia et al. 1996; Polemio and Trizzino 1999; Spilotro et al. 2000) and for interference with the operation of transportation infrastructure (see for example the case of the landslide of Montaguto, Irpinia, Southern Italy, where the earthflow covered the SS90 road and the railway line) (Giordan et al. 2013) (Fig. 54.1). Many of the issues relating to the roads in floodplains are in fact due to the presence of surface water table and/or runoff of meteoric water. In valley floor areas most usual design solution is the road embankment. In the presence of a surface water table the realization of a road embankment can cause more or less marked alterations of the piezometric levels, which can create serious problems to vehicular traffic. Typically, in such situations, to avoid the risk of flooding of the roadway engineers tend to increase the height of the embankment, thus increasing the overload in the foundation soil and thereby creating new risk situations.

In this regard, Eurocode 7 (Geotechnical design of Civil Engineering works) establishes that the design shall ensure that the deformation of the embankment will not cause a serviceability limit state in the embankment or in structures, roads or services sited on, in or near the embankment. Actions in which ground- and free-water forces predominate shall be identified and the possibility of deformations due to changes in the ground-water conditions should be taken into account.

When deriving the actions that embankments impose on adjacent infrastructures or any reinforced parts of the ground, the differences in the stiffnesses should be considered (EN 1997-1:2004, Sect. 12.3). In the same way, in deriving design distributions of pore-water pressure, account shall be taken of the possible range of anisotropy and heterogeneity of the soil.
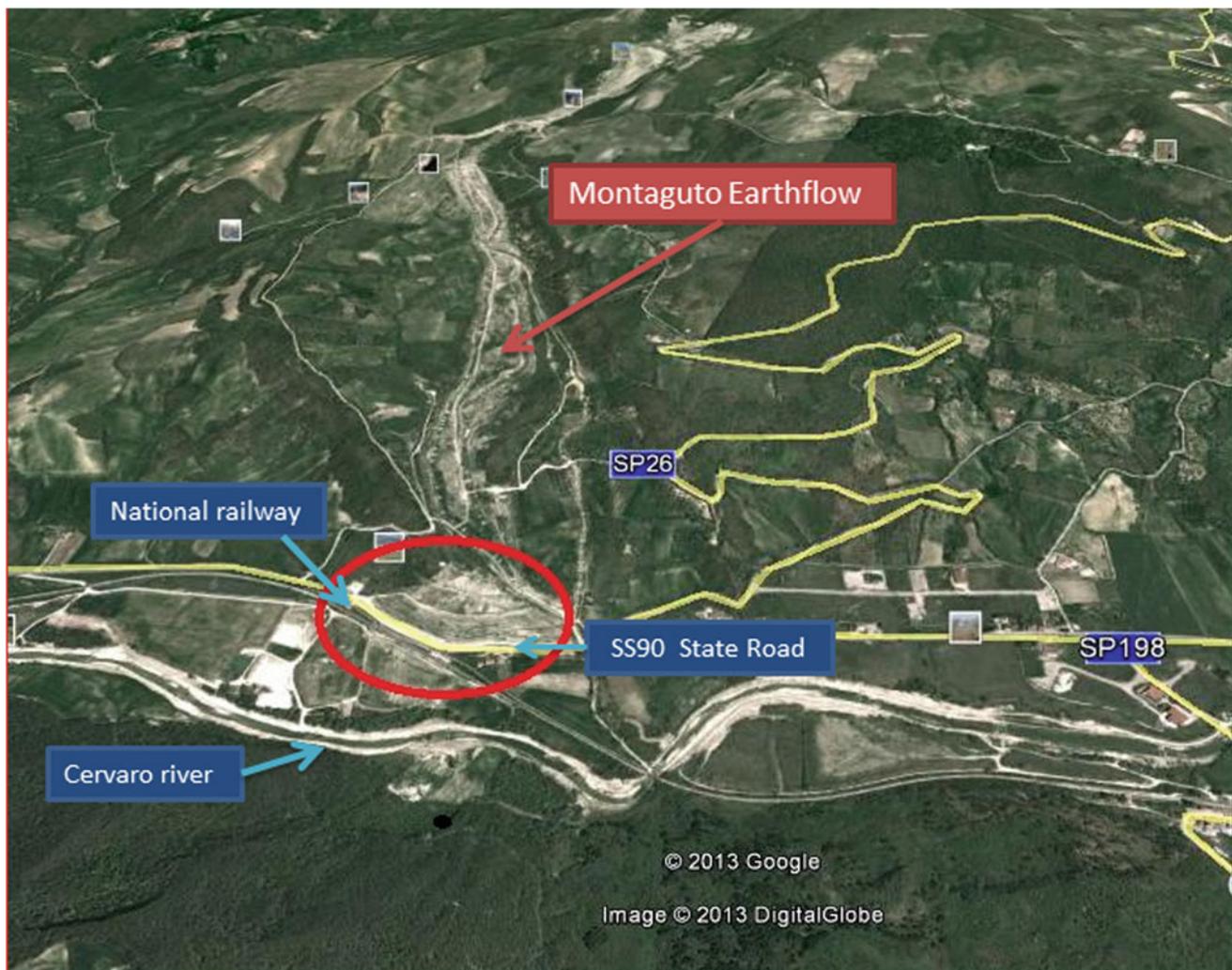
Fig. 54.1 Montaguto earthflow (Irpinia, Southern Italy). Note the State Road SS90 and the national railroad in the Cervaro river valley which were covered by the landslide debris

Starting from these issues, in this paper it is proposed a modeling study aimed at determining the interactions between the geometric and geomechanical properties of the foundation soil- road body—roadway system and surface and deep water table levels. The analysis has been carried out in a parametric form by a finite element calculation code taking into account different combinations of water level depth and embankment height for different lithological and geotechnical properties of the foundation soils.

54.2 Principles of the Method

As stated in the Eurocode 7 (Cap. 12.7) the stability of an embankment acting as a dam to a large degree depends on the pore-water pressure distribution in and beneath the embankment.

As well known, the construction of an embankment generates an increase of the soil stresses beneath the infrastructure; this causes the modification of the void ratio and then of the hydraulic conductivity of the subgrade soil. In the presence of a surface water table the fulfilment of a man made embankment can create an excess of pore-water pressure that leads to the rise of the piezometric surface up to the ground level. When the water table reaches the ground level downstream we can have the flooding of more or less large areas even to several meters (15–20 m and more) from the transportation infrastructure (Maltinti et al. 2000).

Moreover, the rise of the piezometric level upstream can cause the instability of the up-slope scarp of the road embankment creating failure surfaces and more or less large soil slips that lead to the global instability of the infrastructure with the loss of serviceability of the road (Serviceability Limit State).

To determine the stress-strain behavior of the soil beneath the embankment and to compute the consequent excess pore-water pressures a Finite Element Model has been developed together with a coupled consolidation analysis. The first step has been to select a particular constitutive model that was consistent with the soil conditions and the objective of the analysis. It has been assumed an effective stress elastic-plastic model with pore-water pressure changes.

In the presence of a road embankment it is fundamental to take into account the capillarity phenomena that can lead to plasticize the foundation levels. In this analysis unsaturated flow conditions have been considered by defining a hydraulic conductivity function $k = k(s)$, where s is the negative pore-water pressure (suction) of the sub-soil (Cafaro et al. 2008). As well known, this function will show a different trend for different material properties, so the response of the foundation soil to the construction of an embankment will depend on the sub-soil strata succession (Hoffman and Tarantino 2008; Kawai et al. 2000; IGWMC 1999; Schnellmann et al. 2010).

To take into account the decrease of the hydraulic conductivity when the soil grain structure becomes more compact, a K-modifier function has been defined modifying the Ksat by a factor depending on the vertical effective stress state. It has been assumed that K diminishes by a factor of 10 as the effective stress increases from 10 to 100 kPa.

Finally, the soil consolidation problems have been solved using a coupled stress/pore-pressure analysis to determine the excess pore-water pressures dissipation with time by solving simultaneously both equilibrium and flow equations.

54.3 Results and Conclusions

The conceptual model has been applied to a hypothetic road embankment made of gravelly-sandy soil classified as A1 in the Italian CNR-UNI 1006/63 Code for the road body materials. Different embankment heights have been considered from 2 to 20 m. The analysis has been carried out in a parametric form considering different properties of the subsoil strata and various depths of the water table. The stress-strain modifications beneath the embankment and the Pore-Water Pressures have been calculated by means of the Finite Element Computation Code GEOSTUDIO 2007, SIGMA/W and SEEP modules. Main results are shown in Figs. 54.2, 54.3 and 54.4. In Fig. 54.2 are reported the vertical stress modifications and the piezometric level rise after the placement of an embankment of 4 m for an initial water table depth of 5 m beneath the ground level. The piezometric height increase resulting in these conditions is of 1.50 m, whereas for an embankment of 10 m and a water table depth of 5 m the Δhw is equal to 2.60 m (Fig. 54.3), dangerously closer to the road foundation. The situation is ever more dangerous for an embankment of 10 m and an initial water table depth of 1 m (Fig. 54.4): in this case, as shown in the figure by the shadows areas, the piezometric level rises up to and above the ground level. But the unexpected result is that this water rising takes place at a distance of about 15 m from the road and involves an area up to 100 m up and down stream that is, in particular hydro-geological conditions, flooding risk.

In conclusion, the results obtained from this preliminary study showed that there is a significant relationship between the geo-mechanical soil properties and the road safety and serviceability that induce to carry out further investigations and computations on this topic.
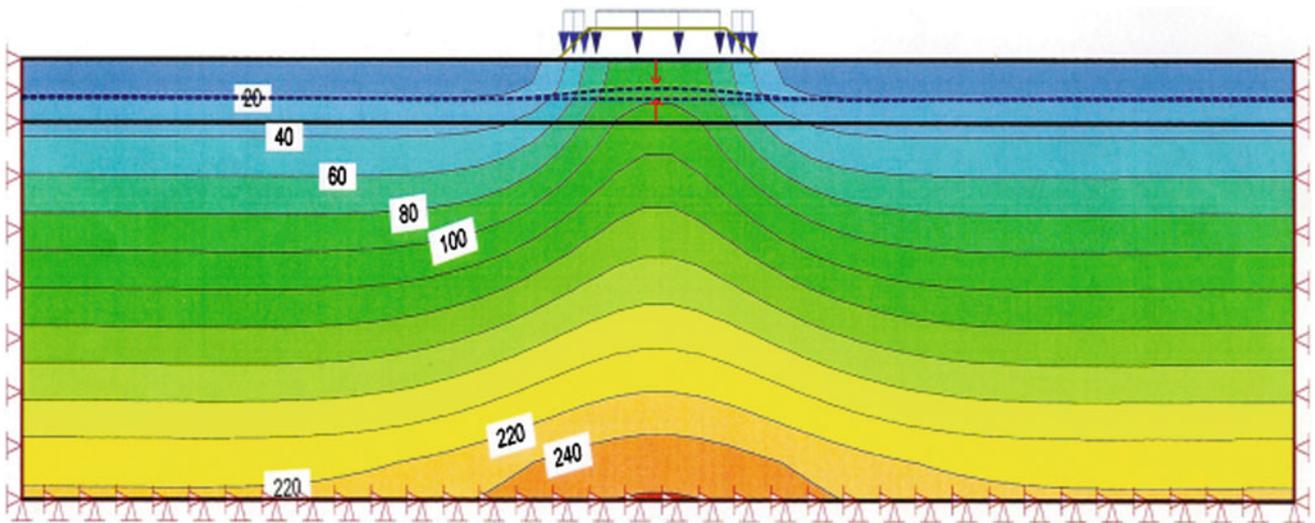
Fig. 54.2 SIGMA/W solve analysis results with isolines of vertical stresses distribution (kPa) for an hypothetical embankment. Height $H = 4$ m; water table depth $h_w = -5$ m; thickness of compressible stratum $S1 = 8$ m; piezometric level rise (*red arrows*) $\Delta h_w = 1.50$ m
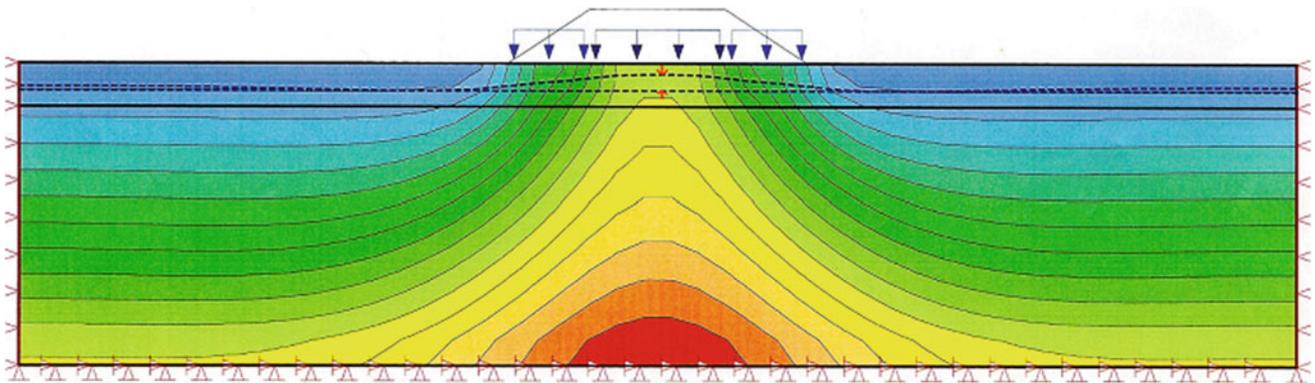
Fig. 54.3 SIGMA/W solve analysis results with isolines of vertical stresses distribution (kPa) for an hypothetical embankment. Height $H = 10$ m; water table depth: $h_w = -5$ m; thickness of compressible stratum: $S1 = 8$ m; piezometric level rise (*red arrows*) $\Delta h_w = 2.60$ m
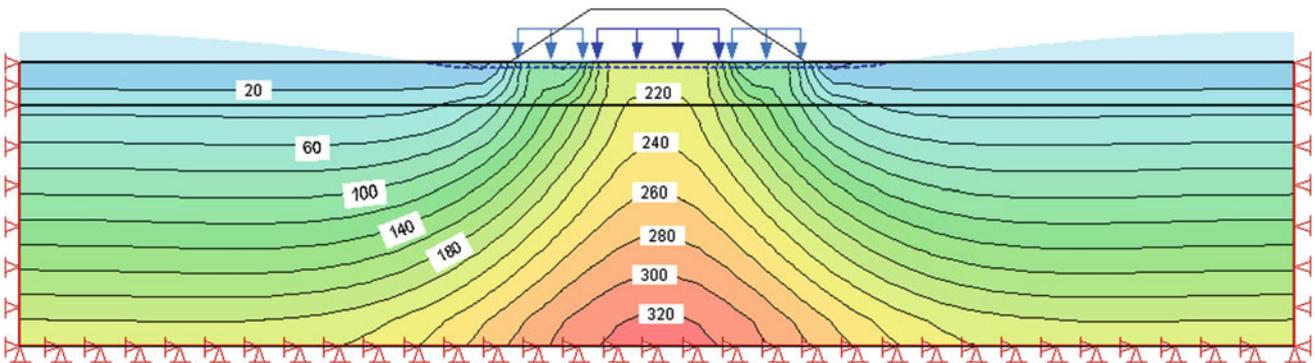
Fig. 54.4 SIGMA/W solve analysis results with isolines of vertical stresses distribution (kPa) for an hypothetical embankment. Height $H = 10$ m; water table depth: $h_w = -1$ m; thickness of compressible stratum: $S1 = 8$ m. Note the shadow light blue areas (water surface) above the ground level

References

Cafaro F, Hoffman C, Cotecchia F, Buscemi A, Bottiglieri O, Tarantino A (2008) Modellazione del comportamento idraulico di terreni parzialmente saturi a grana media e grossa. Rivista Italiana di Geotecnica, no. 3/2008, pp 54–72

Cotecchia V, Parise M, Polemio M, Trizzino R, Wasowski J (1996) Primi risultati della ricerca sulla frana di Acquara-Vadoncello (Senerchia,AV) eseguita nell'ambito del progetto CEE –Environment Landslide evolution controlled by climatic factors in seismic areas—Prediction methods and warning criteria. Accademia Nazionale dei Lincei, Conv. "La stabilità del suolo in Italia: zonazione della sismicità-frane", Roma

Giordan D, Allasia P, Manconi A, Baldo M, Santangelo M, Cardinali M, Corazza A, Albanese V, Lollino G, Guzzetti F (2013) Morphological and kinematic evolution of a large earthflow: the montaguto landslide, southern Italy. Geomorphology, 187, pp 61–79

Hoffman C, Tarantino A (2008) Effect of grain size distribution on water retention behaviour of well graded coarse material. In: 1st European conference on unsaturated soils, 2–4th July 2008, Durham, UK

Kawai K, Kato S, Karube D (2000): The model of water retention curve considering effects of void ratio. In: Rahardjo H, Toll DG, Leong EC (eds) Unsaturated soil for Asia, pp 329–334

IGWMC (1999) Hydrus 2D: simulating water flow, heat and solute transport in variably saturated media .In: U. S. Salinity Lab. Agriculture. Research Service and U. S. Dept of Agriculture Riverside California

Maltinti F, Portas S, Annunziata F (2000) Soluzioni progettuali per il ripristino delle condizioni idrogeologiche preesistenti alla costruzione di un rilevato stradale. X Convegno S.I.I.V, Catania, pp 1–11

Polemio M, Trizzino R (1999) Hydrogeological, kinematic and stability characterization of the 1993 Senerchia landslide(Southern Italy). Landslide News, no. 12:12–16

Schnellmann R, Busslinger M, Schneider HR, Rahardjo H (2010) Effect of rising water table in an unsaturated slope. Eng Geol 114:71–83

Spilotro G, Coviello L, Trizzino R (2000) Post failure behaviour of landslide bodies. In: Proceedings of 8th ISL, Cardiff, Wales, pp 26–30

Convergence Predictions and Primary Support Optimization of the Tunnel Progon

55

Zoran Berisavljevic, Svetozar Milenkovic, Dusan Berisavljevic, and Nenad Susic

Abstract

The tunnel Progon is being constructed as a part of Corridor 10 highway project about 5 km north from the border crossing with Bulgaria in southern Serbia. During the design process 2D finite element analysis was utilized with the objective to investigate an influence of different support systems on the convergence across an excavation. Two models were used in calculations. The first model is elastic perfectly-plastic with constant stiffness independent of the stress level. The second model assumes hyperbolic relationship between the deviatoric stress and axial strain and stress dependent stiffness. This model also accounts for small strain stiffness of soil. In order to allow for a certain convergence across an excavation the load reduction method was utilized. Convergence monitoring is currently ongoing for the excavated portion of approx. 700 m of the tunnel exit portal. The measurements show cumulative displacements in the range of 1–3 cm. Results obtained by the analyses prior to the tunnel construction are in good agreement with the measurements. Convergence is approx. 5 cm when MC model is used and around 1 cm in the case of HS-small model, thus limiting the measurement results from the lower and upper bound.

Keywords

Mohr-Coulomb • HS-small • Plastic points • Convergence • β-method

55.1 General Settings

The tunnel "Progon" is located in the southern part of the Republic of Serbia on the highway E-80 (Dimitrovgrad bypass). According to design (Highway Institute 2012) two paralel tunnel tubes are to be constructed on the axial distance of 27.5–30.0 m. Length of the left and right tubes are L = 1,084.44 m and L = 1,065.74 m, respectively.

Z. Berisavljevic (✉)
Koridori Srbije Ltd, 21 Kralja Petra St, 11000 Belgrade, Serbia
e-mail: berisavljevic_zoran@yahoo.com

S. Milenkovic
Highway Institute, 257 Kumodraska St, 11000 Belgrade, Serbia

D. Berisavljevic · N. Susic
Institute for Material Testing, Blvd. vojvode Stepe 43, 11000 Belgrade, Serbia

Approximately 100 m of tunnel entrance portal and 60 m of tunel exit portal will be constructed in an open excavation (cut and cover method). The tunnel will be excavated by means of Sprayed Concrete Lining (SCL) method. The tunnel structure shall be closed and arched with an equivalent diameter of D ≈ 12 m.

Results of geotechnical field investigations showed that the tunnel tubes will be excavated in sediments of quaternary age consisting of clay with gravel and cobbels interbedded with parts consisting predominantly of clay. Height of overburden varies and an average height of 20 m is adopted for the analyses.

The objective of this paper is to present results of the primary support optimization done during the preparation of the main design. Support types are a combination of different structural elements: shotcrete, anchors, micropiles, forepole umbrella, etc. Support consisting of shotcrete and forepoles will be more closely examined, Fig. 55.1.

Fig. 55.1 View on borehole core samples, tunnel tubes and forepoles as a face protection

55.2 Model Assumptions and Analysis of Results

All analyses are performed by assuming plane strain conditions in software packadge Plaxis that is based on the finite element method (FEM). The model consists of 2,476 15-noded triangular finite elements (average size of 1.782 m). The mesh is refined in the zone of tunnel excavations. It is assumed that material cannot sustain tensile stresses. Influence of pore water pressure is not considered as the groundwater level was not observed during the site investigations.

Firstly, the analysis is performed with an assumption of unsupported excavation of tunnel tubes. The material is described with an elastic perfectly-plastic model assuming linear Coulomb-Mohr failure criterion. The model consists of six parameters, namely: γ, E, c, φ, υ i ψ, i.e. unit weight of soil, modulus of elasticity, cohesion, angle of shearing resistance, Poisson's ratio and angle of dilatancy,

respectively. Adopted parameters correspond to the B category of the main design with values of: $\gamma = 20$ kN/m^3, $E = 70$ MPa, $c = 0.04$ MPa, $\varphi = 24°$, $\upsilon = 0.3$ i $\psi = 0°$.

In the first calculation phase the initial stress state is generated based on the K_0 procedure. This assumption is valid due to tunnel construction in relatively young, normally consolidated and tectonically undamaged sediments. After the initial stress generation the excavation phase is performed.

Results showed that without an adequate support system excavations would collapse (chimney type failure).

This can be seen on a plot of plastic points, Fig. 55.2. Abovementioned indicates that support of excavations is needed.

Subsequent analyses are performed with an assumption of immediate installation of tunnel lining. The case considered is lining made of shotcrete and previously installed forepoles. Shotecrete lining is modeled as a plate element (Brienkgreve and Broere 2011), described with two parameters, namely axial (EA) and flexural (EI) rigidity. According to
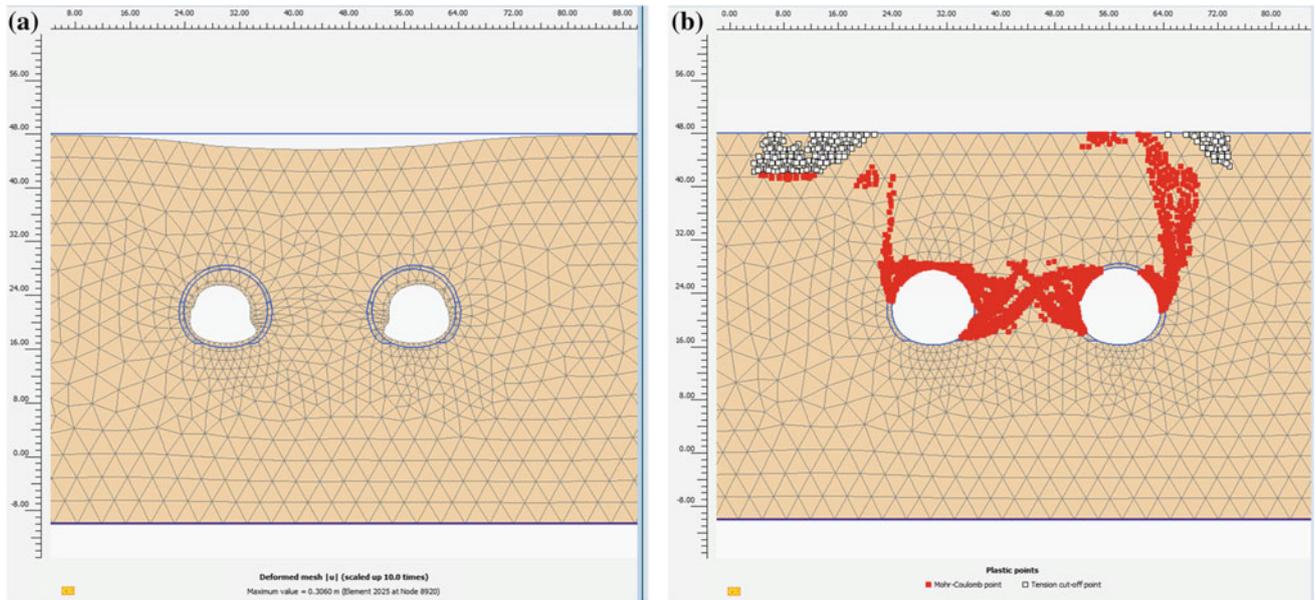
Fig. 55.2 **a** Deformed mesh showing ground surface settlement and deformations of tunnel contours, **b** development of plastic tension and shear zones

design the thickness of shotcrete is d = 35 cm. Elastic modulus of shotcrete is reasonably assumed to be E = 20,000 MPa (Hoek and Bawden 1993). It is worth mentioning that elastic modulus of shotcrete is time dependent, but this property is not included in the analyses.

Forepoles are modeled as proposed by Hoek (2004), where the zone of influence is taken to have properties obtained in a process of weighted averages of properties of

steel, grout and surrounding soil. This material with predefined thickness of ≈0.60 m has following values of parameters: E = 1,200 MPa, c = 0.15 MPa (other parameters are the same as for surrounding soil).

Figure 55.3a shows analysis results with an immediate installation of tunnel lining. The heave of an invert and ground surface can be observed. The heave is a consequence of applied Coulomb-Mohr elastic perfectly-plastic model.
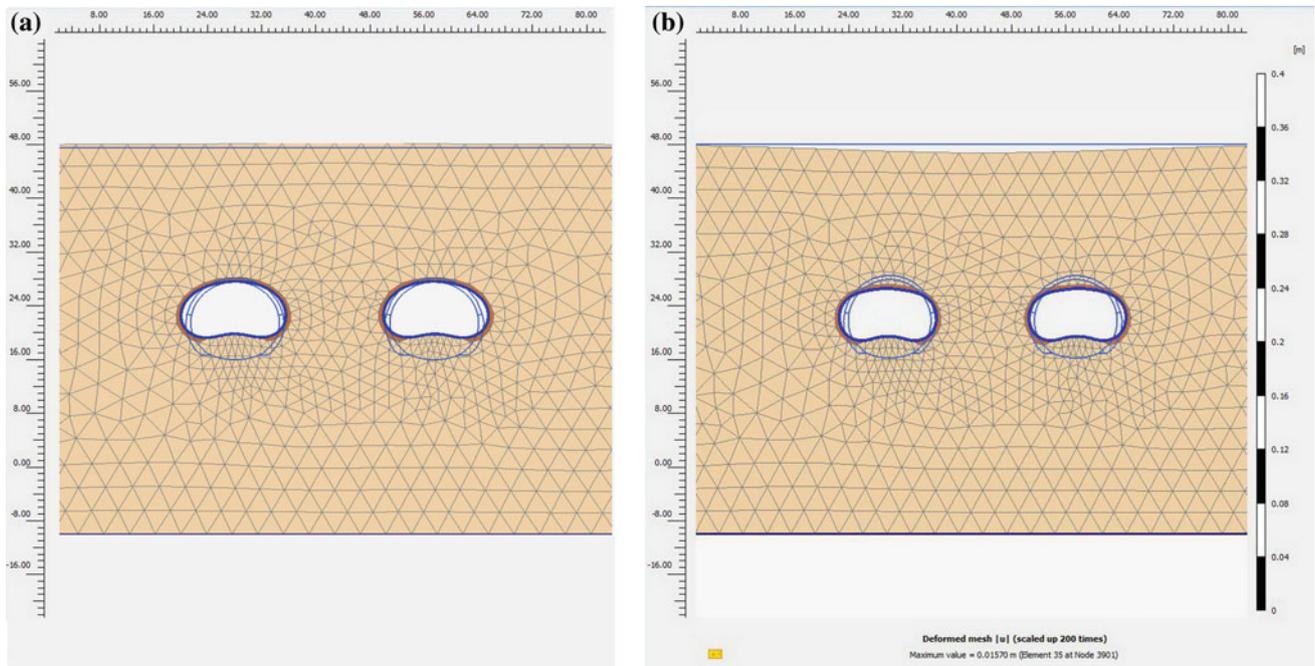
Fig. 55.3 Ground displacements in case of **a** MC model, **b** HSsmall model

Table 55.1 Parameters of the HSsmall model

γ kN/m^3	E_{oed}^{ref} MPa	E_{50}^{ref} MPa	E_{ur}^{ref} MPa	c MPa	$\varphi°$	$\psi°$	G_0^{ref} MPa	$\gamma_{0.7}$ −	m −	R_f −
20	10.90	21.40	85.60	0.04	24	0	120	0.0001	0.5	0.9

where: E_{oed}^{ref}—tangent stiffness for primary oedometer loading at the reference level of normal stress of 0.1 MPa, E_{50}^{ref}—secant stiffness for 50 % of ultimate load in standard drained triaxial test, where $\sigma_{3 =} 0.1$ MPa, E_{ur}^{ref}—unloading/reloading stiffness in standard drained triaxial test, where $\sigma_{3 =} 0.1$ MPa, G_0^{ref}—reference shear modulus at very small strains, $\gamma_{0.7}$—shear strain at which $G_s = 0.722 G_0$, m—power for stress-level dependency of stiffness, R_f—failure ratio

The convergence of an invert, with shotcrete support, is 3.87 cm and if considering both shotcrete and forepoles convergences are insignificantly smaller, i.e. 3.78 cm.

In order to show an influence of the higher order model on convergence predictions, analysis is repeated by applying HSsmall model. This model assumes stress dependent stiffness taking into account stiffness at small strains. Parameters used to describe the model are presented in Table 55.1.

Certain parameters are derived from laboratory tests, and others are adopted as proposed in Brienkgreve and Broere (2011). Advantage of this model compared to others is his relative insensitivity to chosen domain size.

Figure 55.3b shows results of a n analysis with HSsmall model. Convergence of invert is 1.60 cm without forepoles and 1.57 cm with forepoles. Ground surface settlements are 0.79 and 0.64 cm, respectively. The differences between the two models are obvious if Fig. 55.3a, b are compared.

Above mentioned analyses are not realistic due to some time needed for support to be installed, thus it is necessary to allow for an initial convergence of the excavation prior to support installation. This is achieved by applying β-method. In this way it is possible to consider 3D arching effect and deformations of the tunnel face. The idea is that the initial stresses acting around the location where the tunnel is to be constructed are divided into a part $(1-\beta)p_k$ that is applied to the unsupported excavation and a part βp_k that is applied to the supported excavation. The β coefficient $(0 < \beta < 1)$ is an experience parameter depending on the tunnel round length and equivalent diameter. Some proposals for its determination could be found in literature (Moller 2006; Moller and Vermeer 2004). Baudendistel (1979) proposed values for parameter β after considering vertical crown displacements of tunnels from 3D linear-elastic analysis. Table 55.2 shows values of parameter β for a tunnel with a horse shoe profile.

The design proposed that the round length d, of the tunnel, is to be not more than 1 m (Milenković et al. 2009). If this length is compared to equivalent diameter of D ≈ 12 m, the β coefficient is found to be 0.5.

Results of analyses performed by using MC model are presented in Fig. 55.4. In Fig. 55.4a contours of unsupported excavations (for β = 0.83) are deformed over 30 cm which would eventually lead to a collapse as shown in Fig. 55.2.

Table 55.2 β coefficient for different ratios of round length d, and excavation diameter D (after Baudendistel 1979, reproduced in Moller 2006)

d	1.5 D	D	0.5 D	0.25 D	0.125 D	0
β	0.0	0.02	0.11	0.23	0.41	0.72

The mode of deformation indicates that the largest displacements are in the tunnel crown, so this zone needs to be strengthened. Second analysis, Fig. 55.4b, is performed assuming excavation under forepoles (according to design), for β = 0.5. In this case the displacements are largest in the tunnel crown and heave of an invert is observed. If forepoles are extended around an excavation the largest displacements are found in the zone of invert, Fig. 55.4c.

The following analyses include the installation of lining by allowing it to accept the rest of the stresses acting around the tunnel excavation. Figure 55.4d shows the displacements of the tunnel excavations after applying shotcrete support. Fig. 55.4e shows the displacements of combined shotcrete support and forepoles installed according to design. The displacements induced by installation of shotcrete lining can be found as a difference between the displacements shown in Fig. 55.4e, b. Similar conclusions can be made if Fig. 55.4d, f are compared, when forepoles are extended around excavation contours. Results show that the differences in displacements are largest in the zone of an invert. The reason for this is installation of forepoles which transferred the displacements from the tunnel crown towards the invert, causing its heave. Performed analyses imply that besides the shotcrete support with forepoles, prevention from invert heave needs special consideration.

55.3 Comments and Conclusions

Convergence monitoring is currently ongoing for the excavated portion of approx. 700 m of the tunnel exit portal (reaching steady state plane strain conditions). The measurements show cumulative displacements in the range of 1–3 cm, Fig. 55.5.
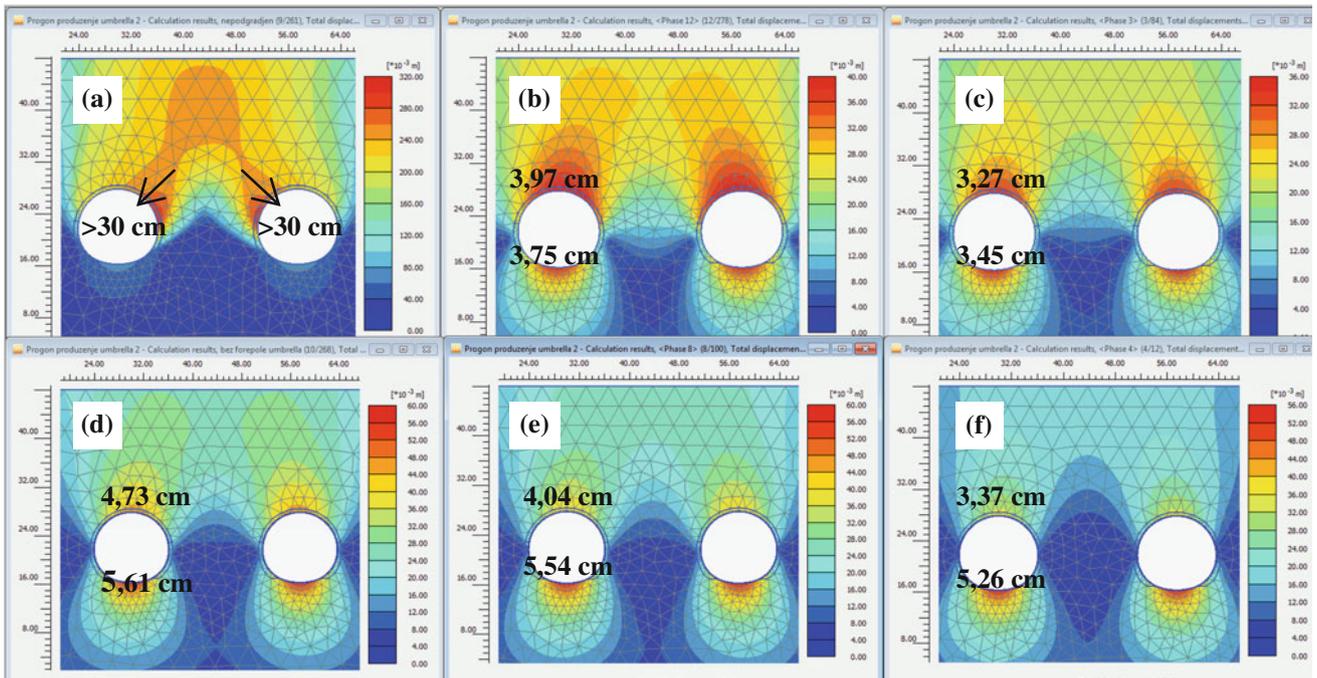
Fig. 55.4 Shadings of total displacements around tunnel excavations **a** Unsupported tunnel excavations, β = 0.83, **b** Tunnel excavation with forepoles according to design, β = 0.5, **c** Forepoles extended towards the invert, β = 0.5, **d** Supported excavation with the shotcrete lining, β = 1, **e** Shotcrete and forepoles according to design, β = 1, **f** Shotcrete and forepoles extended towards the invert, β = 1

Fig. 55.5 Typical convergence profile of one cross-section in plane strain conditions
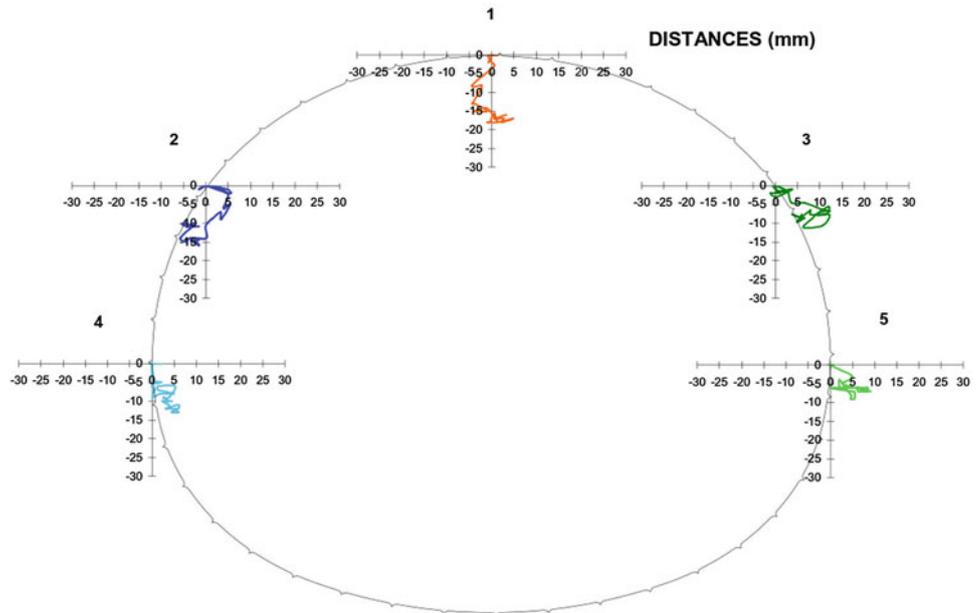
If HSsmall model is used for convergence predictions (accounting for arching effect and deformations of the tunnel face) values of approx. 1 cm are obtained.

In this way convergence is approx. 5 cm when MC model is used and around 1 cm in the case of HSsmall model, thus limiting the measurement results from the lower and upper bound.

Obtained results are highly dependent on the constitutive model used to represent material behavior and the value of β parameter.

References

Baudendistel M (1979) Zum Entwurf von Tunneln mit großen Ausbruchsquerschnitt. In: Berechnung, Erkundung und Entwurf von Tunneln und Felsbauwerken / Computation, Exploration and Design of Tunnels and Rock Structures. Rock Mechanics / Felsmechanik / Mécanique des Roches, vol 8. pp 75–100. doi:10.1007/978-3-7091-8564-3_6

Brienkgreve RBJ, Broere W (2011) Plaxis 2DV10: finite element code for soil and rock analyses. Delft University of Technology & Plaxis b.v. Delft

Hoek E (2004) Numerical modelling for shallow tunnels in weak rock. http://geotecnica.dicea.unifi.it/hoek_shallow.pdf

Hoek E, Kaiser PK, Bawden WF (1993) Support of underground excavations in hard rock. Mining Research Directorate and Universities Research Incentive Fund, Ontario, p 225

Milenković S et al (2011) In geotechnics of hard soils—weak rocks: geotechnical conditions for the construction of tunnel "progon" on the dimitrovgrad bypass in Serbia. In: Anagnostopoulos A, Pachakis M, Tsatsanifos Ch. (eds) 15th European conference on soil mechanics and geotechnical engineering, Athens, September 2011. IOS Press BV, Amsterdam, p 2064

Moller SC (2006) Tunnel induced settlements and structural forces in linings (Dissertation). Institute of Geotechnical Engineering, Stuttgart

Moller SC, Vermeer PA (2004) In underground space use. Analysis of the past and lessons for the future: on design analyses of natm-tunnels. In: Solak E (ed) Proceedings of the international world tunnel Congress and the 31st ITA general assembly, Istanbul, May 2005. Taylor and Francis Group, London, p 1384

Quarry Site Selection and Geotechnical Characterization of Ballast Aggregate for Ambo-Ijaji Railway Project in Central Ethiopia: An Integrated GIS and Geotechnical Approach

Regessa Bayisa, Raghuvanshi Tarun Kumar, and Kebede Seifu

Abstract

The main objective of the present study was to select potential quarry sites and to characterize the rock for ballast aggregate for proposed Ambo-Ijaji railway project in central Ethiopia. The study area is located in the Oromia Regional state which is around 120 km from Addis Ababa on way to Ambo town. The quarry site selection criteria was formulated and applied in GIS environment by incorporating factors such as; slope of the quarry rock face, distance of the quarry site, land use/land cover, accessibility, overburden thickness, rock type and degree of weathering. Thus, six quarry sites were evaluated for their suitability. Further, representative rock samples from quarry sites were collected and tested for physical, mechanical and chemical properties to ensure that the source rock is suitable for ballast aggregate. In addition, petrographic analysis was also made to understand the correlation of engineering properties with petrographic parameters. The results revealed that all six quarry sites satisfies the selection criteria and are suitable to provide ballast aggregate. The engineering laboratory tests indicates that the test values for unit weight, Los Angeles Abrasion value, soundness test by sodium sulfate, specific gravity, and unconfined compressive strength are within the specified limits except for three quarry sites which have water absorption values higher than the standard specifications. From the correlation of petrographic test with different engineering test results it has been found that the petrographic parameters has an important role in controlling engineering properties of rocks.

56.1 Introduction

For railway, ballast is the most important sub-structure. The selection of suitable quarry site for ballast is based on pre-defined criteria such as; type of rock and its weathering grade, distance from the proposed rail alignment, thickness of overburden at proposed quarry site, landuse and land-cover, accessibility to proposed quarry site etc. After the selection of suitable quarry site the next component of evaluation is to determine the quality of ballast rock based on different physical and mechanical properties of the source ballast rock (Raisanen et al. 2006).

R. Bayisa (✉) · R.T. Kumar · K. Seifu
School of Earth Sciences, College of Natural Sciences, Addis Ababa University, Po Box 1176, Addis Ababa, Ethiopia
e-mail: bayyee.2001@gmail.com

R.T. Kumar
e-mail: tkraghuvanshi@gmail.com

K. Seifu
e-mail: seifukebede@yahoo.com
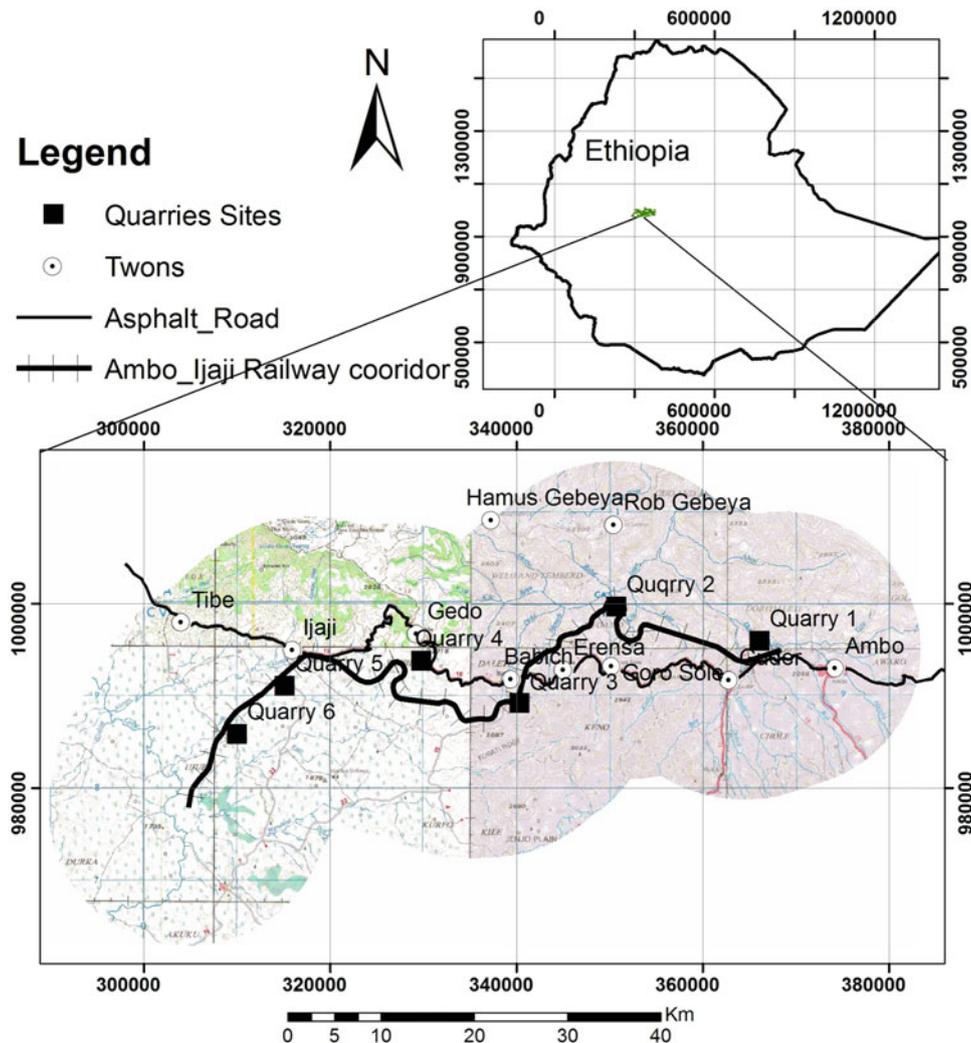
Fig. 56.1 The location map of the study area

The present study was conducted for Ambo-Ijaji Railway Project in Central Ethiopia. The corridor of the study area has the total length of 94 km which starts from Ambo and extend upto Ijaji. Geographically, the area is bounded by the UTM coordinates of 304809-368349E and 977872-994953N (Fig. 56.1). The regional geology of the present study area is characterized by three main geological formations; (i) The Precambrian basement rocks, biotite gneiss with minor intercalation of fine to medium grained undifferentiated schist are exposed in the North of the study area (Abebe et al. 1998; Kidane 2010). (ii) The Mesozoic sedimentary rocks; sandstone, Limestone, gypsum and shales, mainly exposed around northwest of the study area. (iii) The Cenozoic volcanic rock covers large parts of the study area and mainly consists of lower and upper volcanic sequences. In addition, the western part of Ijaji and Tibe area is covered by Quaternary Sediments (Fig. 56.2). The main objective of the present study was to identify the suitable quarry sites for

the proposed Ambo-Ijaji railway project and to assess the geotechnical characteristics of the ballast material.

56.2 Suitability Evaluation of Quarry Sites as per the Selection Criteria

During the present study the selection criteria was formulated by considering parameters such as; slope, distance of the site, overburden soil thickness, landuse/landcover, general accessibility and rock type with its degree of weathering. In total six quarry sites were initially identified by considering the suitable rock type and optimum distance from the proposed rail line alignment (Fig. 56.1). Later, the general selection criterion was formulated (Table 56.1) and was applied in GIS environment to identify the suitable quarry sites. The evaluated suitability based on selection criteria is presented in Table 56.2.
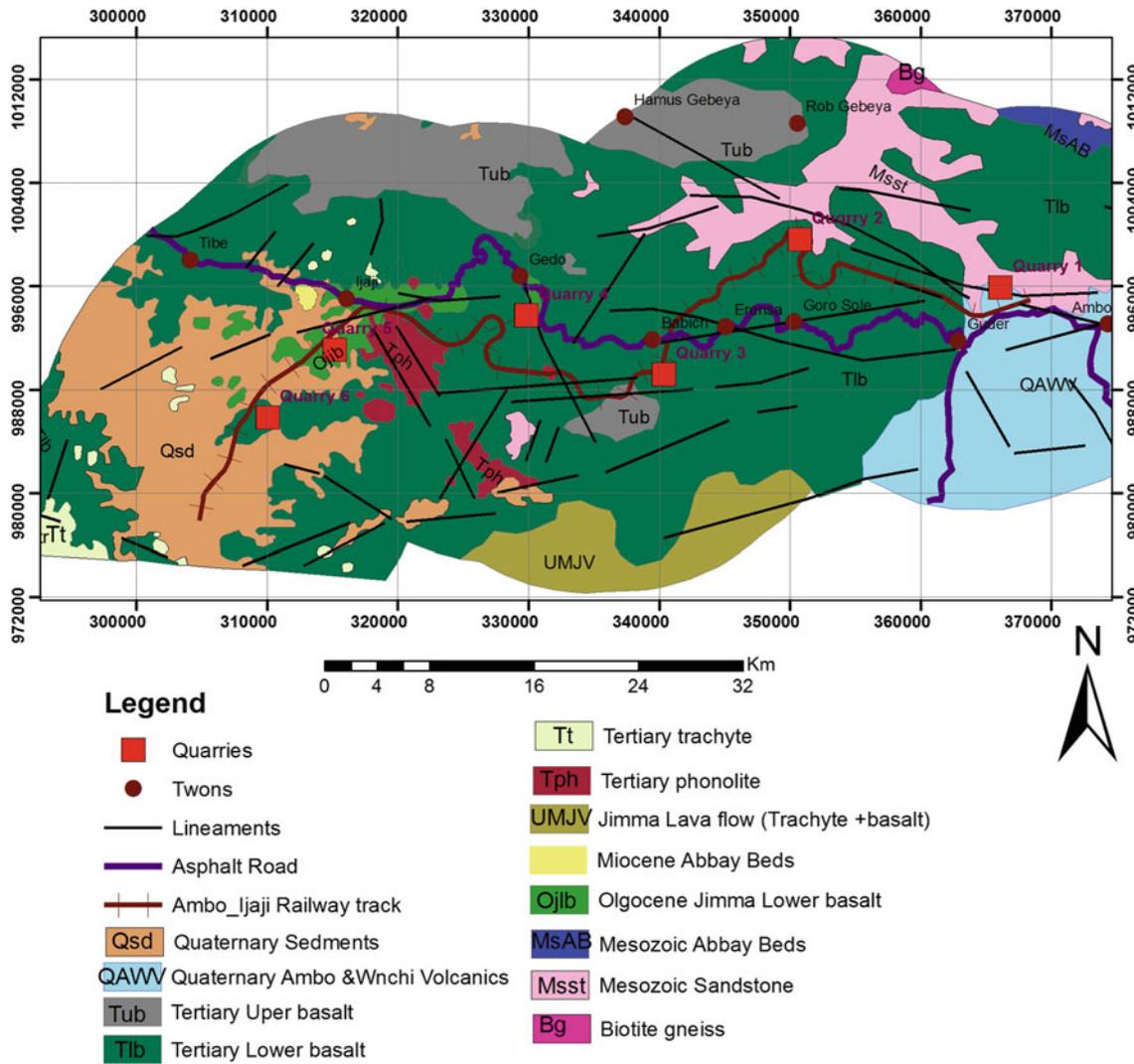
Fig. 56.2 Geological map of the study area

Slope factor was considered and evaluated in terms of quarry's hazard. It is imperative to mention that more steeper the slope more instability problems may be encountered. Thus, the surrounding environment will be degraded due to such slope instability problems.

Quarry site distance and their accessibility condition may affect the economy, increase in transportation time and may result into environmental pollution. Transporting the rock aggregate to a long distance can consume more fuel and much time which can ultimately affect the economy of the project.

Overburden soil thickness is also an important parameter. Removal of thick soil cover impart additional cost to the quarrying activity, thus directly affects the project economy.

The *land use/land cover* is important parameter in evaluating the impact of quarry on the surrounding environment. Thus, during the selection of suitable quarry site, type of land use/land cover that has less susceptibility to the impact of quarrying activity has been considered.

Rock quality is an important parameter as different rock types with varied weathering grades can demonstrate different engineering properties.

In general, to determine the overall suitability of each quarry site based on the six evaluated parameter, equal weights were given to the parameters and later their average value was calculated. According to the average evaluation results (Table 56.2) all quarries are identified as suitable except quarry 1 which is identified as highly suitable.

56.3 Ballast Rock Characterization

To ensure the suitability of the source rock from the selected quarry sites sampling and laboratory analyses were performed. To assess the suitability of ballast material, sodium sulfate soundness test, compressive strength test, specific gravity test, Los Angeles Abrasion value test, Water

Table 56.1 Formulated potential quarry site selection criteria

Types of parameters	Conditions of parameter	Suitability condition	Value
Quarry site slope angle parameter in degree	>45	Unsuitable	1
	30–45	Slightly suitable	2
	15–30	Suitable	3
	0–15	Highly suitable	4
Quarry site distance from each other along the corridor	<10 and >50 km	Unsuitable	1
	10–15 and 40–50 km	Slightly suitable	2
	15–20 and 30–40 km	Suitable	3
	20–30 km	Highly suitable	4
Quarry site distance from the proposed track corridor (offset)	<30 m and >5 km	Unsuitable	1
	30–50 m and 4–5 km	Slightly suitable	2
	50–100 m and 3–4 km	Suitable	3
	100 m to 3 km	Highly suitable	4
Estimated overburden soil thickness of the quarry sites	>4 m	Unsuitable	1
	2.5–4 m	Slightly suitable	2
	1.5–2.5 m	Suitable	3
	0–1.5 m	Highly suitable	4
Landuse/Landcover of the quarry sites	Dense settlement and cultural heritage area	Unsuitable	1
	Moderately Settlement and forested area	Slightly suitable	2
	Rarely populated, agricultural land and less vegetated grass land	Suitable	3
	Bare land and grass land	Highly suitable	4
Type of rock in the proposed quarry sites (if it is not weathered)	Shale, slate and pumice	Unsuitable	1
	Limestone, Sandstone and Siltstone	Slightly suitable	2
	Granite, Diorite, Gabbro, quartzite and hard mineral and well-cemented sedimentary rock	Suitable	3
	Basalt, rhyolite, andesite	Highly suitable	4
Weathering degree of the proposed quarry material	Highly weathered	Unsuitable	1
	Moderately weathered	Slightly suitable	2
	Slightly weathered	Suitable	3
	No weathering	Highly suitable	4

absorption test, unit weight test and petrographic thin section analysis were performed. These laboratory tests were conducted following "American Railway Engineering Maintenance-of-way Association Manual" (AREMA 2009). The laboratory test results with recommended specifications for representative samples from six quarry sites are presented in Table 56.3.

Sodium sulfate soundness test is used to estimate the aggregate soundness when they are subjected to the weathering action. The test conducted on representative samples

Table 56.2 General suitability conditions of the proposed quarry sites as per formulated selection criteria

Quarry sites	Selection criteria parameters	Condition of quarry sites as per given parameter	Suitability conditions	Value
Quarry 1	Slope angle	Slopes fall within 0°–15° class	Highly suitable	4
	Distance and accessibility	Distance from the corridor 1.4 km and distance from the existing road is 1.8 km	Highly suitable	4
	Overburden thickness	Overburden soil thickness ranges from 0.5 to 1 m	Highly suitable	4
	Land use/Land cover	It is located partly on the small grass land and partly on the farm land	Suitable	3
	Rock type and weathering degree	It is the slightly weathered porphyritic olivine basaltic material	Suitable	3
Quarry 2	Slope angle	The dominant slope class is 30°–45°	Suitable	3
	Distance and accessibility	It is 0.6 km from the corridor and 21 km from the quarry 1	Highly suitable	4
	Overburden thickness	Overburden soil thickness range from 0.5 to 1 m	Highly suitable	4
	Land use/Land cover	It is located on less vegetated land and surrounded by small farm lands	Suitable	3
	Rock type and weathering degree	It is moderately weathered porphyritic basaltic material	Slightly suitable	2
Quarry 3	Slope angle	In general slope is within 15°–30° slope class	Suitable	3
	Distance and accessibility	It has 0.5 km offset and 17.5 km distance from quarry 2. Earth road exists	Suitable	3
	Overburden thickness	Overburden soil thickness ranges from 0.5 to 1.5 m	Highly suitable	4
	Land use/Land cover	Mainly it is covered by less vegetated land.	Suitable	3
	Rock type and weathering degree	Slightly weathered trachy-basalt is present	Suitable	3
Quarry 4	Slope angle	Majority of the slopes fall into 30°–45°	Slightly suitable	2
	Distance and accessibility	Its distance from quarry 3 is 19.3 km and it needs 1.8 km access road	Suitable	3
	Overburden thickness	Overburden soil thickness range from 0.5 to 1 m	Highly suitable	4
	Land use/Land cover	It is covered by less vegetated land	Suitable	3
	Rock type and weathering degree	It is a slightly weathered porphritic olive basalt	Suitable	3
Quarry 5	Slope angle	Almost entire slopes fall within 15°–30° slope class.	Suitable	3
	Distance and accessibility	Earth road exists and its distance from preceding quarry 4 is 16.5 km	Suitable	3
	Overburden thickness	Overburden soil thickness range from 0.5 to 1.5 m	Highly suitable	4
	Land use/Land cover	It is mainly covered by less vegetated grass land and is surrounded by farm land	Suitable	3
	Rock type and weathering degree	It is the slightly weathered aphinitic basalt	Suitable	3
Quarry 6	Slope angle	Almost entire slopes fall within 0°–15° slope class	Highly suitable	4
	Distance and accessibility	It is 8.2 km from quarry 5	Slightly suitable	2
	Overburden thickness	Overburden soil thickness ranges from 0.5 to 1.5 m	Highly suitable	4
	Land use/Land cover	It is covered by less vegetated grass land and surrounded by farm land	Suitable	3
	Rock type and weathering degree	Slightly weathered trachy basalt rock is present	Suitable	3

demonstrated values within the range of 0.9–1.4 % which is well within the permissible limits (≤5.0 %).

Uniaxial Compressive strength (*UCS*) *test* is performed to determine the strength of the intact rock. According to Instruction manual on concrete test hammer, as cited in Tawake (2007), the rock with UCS value > 20 MPa can be accepted as suitable aggregate source rock. The test results showed that the UCS values for all samples falls in the range of 34–45 MPa which are well within the permissible limits (Table 56.3).

Table 56.3 Geotechnical laboratory test results

Test types		Quarry 1	Quarry 2	Quarry 3	Quarry 4	Quarry 5	Quarry 6	Permissible Limit*
Soundness loss % by sodium sulfate		1.3	1.4	1.1	0.98	0.90	0.92	≤5.0 %
Compressive strength (Mpa)		36	34	38	42	45	44	>20 Mpa
Specific gravity	Apparent (Bulk) specific gravity	2.938	2.918	2.958	2.988	2.999	2.990	≥2.60
	Saturated surface dry (SSD) specific gravity	2.804	2.801	2.814	2.913	2.926	2.916	
	Oven dry (OD) specific gravity	2.801	2.799	2.806	2.899	2.906	2.900	
Unit weight	Unit weight in dry condition (kg/m^3)	2,238	2,218	2,298	2,301	2,305	2,303	≥1,400 (kg/m^3)
	Unit weight in SSD condition (kg/m^3)	2269.3	2249.5	2329.7	2322.9	2325.8	2324.2	
Percentage of void content (%)		19.94	20.60	17.94	20.47	20.36	20.43	
Los Angeles abrasion value (%)		14.8	14.9	14.5	14.3	14.0	14.1	≤25 %
Water absorption test values in %		1.4	1.42	1.38	0.95	0.90	0.92	≤1 %

*AREMA (2009)

Specific gravity is related to the density of the rock and can control both vertical and horizontal holding capacity of ballast aggregate. According to Indraratna et al. (2006), the higher specific gravity of parent rock ensures greater holding capacity and lower degradation of the ballast aggregate. The bulk specific gravity for all representative samples satisfies the standard specification (Table 56.3), as all the values are above 2.60.

The *Bulk density* (unit weight) of an aggregate is the weight (mass) of an aggregate per its unit volume. The results showed that the Unit weight for all representative rock samples satisfies the standard specification (Table 56.3), as all values are above 1,400 (kg/m^3).

The *Los Angeles Abrasion test* is to measure the load resistance of ballast material. This test measure the toughness of ballast aggregate and is used to determine the ability of ballast aggregate to survive the contact force (Raymond and Bathurst 1994). The results shows that all the values for representative rock samples satisfies the standard specification (Table 56.3), as the values are less than 25 %.

Water absorption test is conducted to measure the ability of an aggregate rock to absorb water and to know the sensitivity to degradation. The results shows that the rocks from quarry 1, 2 and 3 have water absorption values higher than the specification while for quarry 4, 5 and 6 the values are within the specification (Table 56.3). However, even if the water absorption value of samples from quarry 1, 2 and 3 is more, it is expected that more fresh suitable rock would be available during the quarrying operation, as the samples during the present study were collected near to the surface.

56.4 Correlation of the Engineering Properties with Petrography

The engineering properties of ballast aggregate source rock mainly depends on its mineralogical composition, the size and shape of its minerals, presence or absence of micro cracks in it and the degree of weathering. During the present study the thin sections were prepared for the representative rock samples from each quarry site and later these were analyzed under petrographic microscopy.

In the present study the rock sample from *quarry* 5 is the 1st most suitable in comparison to samples from other quarry sites in terms of its engineering test results. The better engineering quality of the rock from quarry 5 has resulted from abundance of compacted opaque minerals that were surrounded with very fine grained ground mass. Both fine grained texture of ground mass and the abundance of highly compacted opaque minerals in this rock has played a significant role in providing better engineering quality to the ballast aggregate material. However the opaque minerals have high potential for alteration, therefore if the ballast aggregate has more opaque minerals such as; iron oxide it will readily be affected by weathering.

The rock sample from *quarry* 3 is acidic and has high silica content in comparison to samples from other quarry sites. However, laboratory test results revealed that the quality of this rock falls into 4th order in its suitability. Further, the rock sample from quarry 3 has more than 70 % feldspar minerals that are elongated and lath shaped with

trachitic texture. This lath shape and trachitic texture may affect grain to grain interlocking capacity of the minerals in the rock, thus resulting into poor engineering quality of the rock.

Further, existence of micro cracks in the rock material can affect its engineering properties. Particularly, when the compressive stress is applied on the rock aggregate, the preexisting inter-granular micro cracks and the grain boundary micro cracks extends and transform into the trans-granular micro cracks. These micro cracks were observed in the rock samples from *quarry* 1, *quarry* 2 *and quarry* 6.

The rock sample from *quarry* 1 has more volcanic glass in comparison to other samples. Besides, presence of calcite phenocrysts was also observed. Based on the laboratory test result quarry 1 was classified as 5th order in its suitability, as compared to other quarry sites. Relatively low suitability of quarry 1 has resulted probably from the presence of abundant volcanic glass, existence of micro cracks and from the presence of soft secondary mineral calcite. Based on laboratory test results the rock sample from *quarry* 2 is placed into 6th order of suitability as ballast source material. From the hand spacemen observation it has been observed that the rock sample from quarry 6 was highly weathered as compared to other samples. Thus, presence of micro cracks and high degree of alteration (weathering) has resulted into reduction of engineering quality of this rock.

56.5 Conclusion

The present study was conducted for Ambo-Ijaji Railway Project in Central Ethiopia. The main objective of the study was to identify the suitable quarry sites for the proposed project and to assess the geotechnical characteristics of the ballast material. To meet out the objective of the study, selection criteria was formulated by considering parameters such as; slope, distance of the site, overburden soil thickness, landuse/landcover, general accessibility and rock type with its degree of weathering. The general selection criterion was applied in GIS environment to identify the suitable quarry sites. The results revealed that all quarries are suitable as per the selection criteria. Further, to assess the suitability of ballast material, sodium sulfate soundness test, compressive test, specific gravity test, Los Angeles Abrasion value test, Water absorption test, unit weight test and petrographic thin

section analysis were carried out on the representative samples. The test results revealed that all the samples possess values within the specified limits, except rocks from quarry 1, 2 and 3 which have water absorption values higher than the standard specifications. However, it is expected that more suitable rock would be available during the quarrying operation, as the samples during the present study were collected near to the surface. Further, based on the petrographic examination results it is deduced that the high engineering quality rock from quarry 5 has probably resulted from the abundance of opaque minerals and its fine grained texture, whereas low quality rock from quarry 2 was from its high degree of alteration and existence of micro cracks in it. Similarly, based on the laboratory test result relative low suitability of quarry 1 has resulted probably from presence of abundance volcanic glass, existence of micro cracks and presence of soft secondary mineral calcite. In general, from the correlation of petrography with different engineering test results it may be conclude that the petrographic parameters (mineralogical composition, grain texture, micro crack and secondary minerals) play an important role in controlling engineering properties of ballast aggregate rocks.

References

Abebe T, Mazzarini F, Innocenti F, Manetti P (1998) Yerer-Tullu Wellel volcanotectonic lineament: a transtensional structure in central Ethiopia and the associated magmatic activity. J Afr Earth Sci 26(1):135–150

American Railway Engineering and Maintenance of Way Association (AREMA) (2009) Manual for railway engineering, vol. 1, Roadway and Ballast, USA, 1292 pp

Indraratna B, Khabbaz H, Salim W, Christie D (2006) Geotechnical properties of ballast and the role of geosynthetics in rail track stabilization. Univ Wollongong Res Online 3:91–101

Kidane T (2010) Final Report on Structural and Geological Mapping for the Wolkite Ambo Ground Water Potential Assessment Project. Water Works Design and Supervision Enterprise (unpublished), Addis Ababa Ethiopia

Raisanen M, Mertamo M, Stenlid L, Viitanen J (2006) Laboratory crushing of rock aggregates. Paper number 411, Geological Survey of Finland

Raymond GP, Bathurst RJ (1994) Repeated load response of aggregates in relation to track quality index, vol. 31. Queen University, Canada, pp 547–554

Tawake AK (2007) Assessment of potential terrestrial aggregate sources on Ghizo Island, Solomon Islands. EU EDF8-SOPAC project Report No 107

Radon Emanation Techniques as an Added Dimension in Site Investigation of Water Storage Facilities

57

Gary Neil Davis and Mannie Levin

Abstract

For dams and reservoirs, the assessment of the basin watertightness relies on identification of structural weaknesses. Conventional site investigations can readily be complimented by carrying out radon emanation studies, relying on unique properties of this radioactive noble gas, and easier transmission via fractured, faulted and porous rock zones. Recent studies for an abstraction weir supplemented the conventional ground investigations with radon emanation studies to confirm the locality of a suspected fault zone which traverses the founding bedrock. The successful location of the structural weakness, hidden beneath 20–30 m of alluvium, allowed optimal location of monitoring boreholes; proving the value of this technique in such studies.

Keywords

Site investigation • Radon emanation • Structural weaknesses

57.1 Introduction

Dam and reservoir studies must include assessment of the basin watertightness. Conventional studies would typically comprise investigation of the regional and structural geology, and would include engineering geological mapping, as well as utilising satellite imagery; with follow-up studies potentially including drilling and test pitting, as well as laboratory testing.

Although well known in groundwater studies (Levin 2000), radon emanation techniques are finding increasing application in other areas, such as for the investigation of dams and reservoirs.

The radon emanation technique enables identification of structural weaknesses, particularly when obscured by the drift geology, and allows the subsequent investigations to be more focused.

The technique rests on the emission of the α-particle by the radioactive isotope Radium (Ra226) which produces the gas Radon (Ra222). The radium in turn is naturally produced during the decay of Uranium (U238); where uranium is present in most rock types, in minerals such as zircon, mica, apatite etc.

Radon, being a noble gas, has the ability to migrate from its source without chemical interference, and emanates from the mineral surfaces into the rock pores or dissolves in the water phase where present. Radon (Ra222) is radioactive with a half-life of 3.8 days. Due to its half-life it is present in groundwater for up to 15 days. This unique combination of features underlies the interest in radon gas as a geophysical tracer.

Various researchers have shown that radon is released mainly through rapid diffusion along imperfections to the particle surface and that crystal imperfections therefore play a vital role. This means that the fraction of the radon released to ground water and soil air will depend largely on the physical nature of the rock and associated fluid phases, rather than on the uranium concentration in the rock. It therefore follows that increased concentration can be expected from fractured, faulted and porous rock zones, as illustrated in (Fig. 57.1).

G.N. Davis (✉) · M. Levin
Aurecon South Africa (Pty) Ltd, Pretoria, South Africa
e-mail: gary.davis@aurecongroup.com
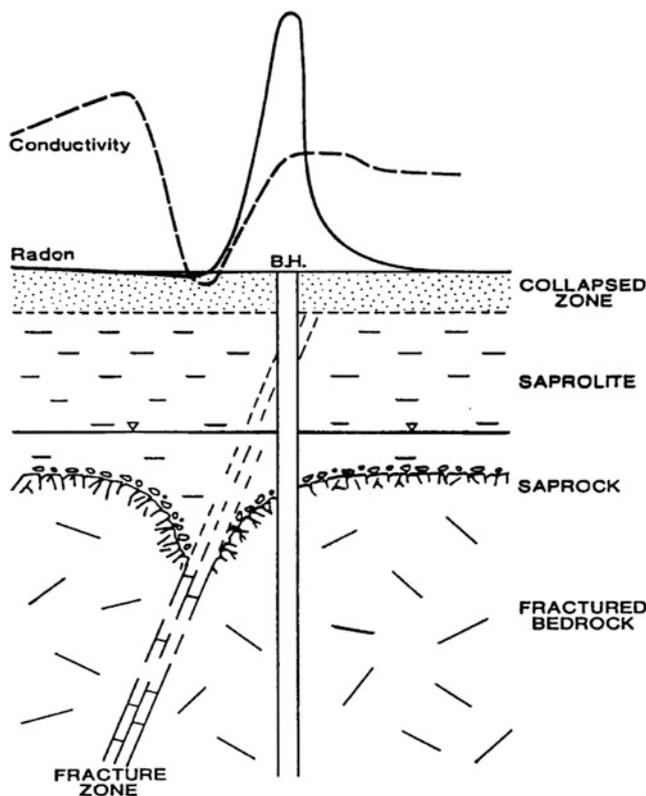
Fig. 57.1 Radon technique illustrated, after Wright (1992)

57.2 Methodology

The radioactivity makes radon easy to measure in small concentrations. The most widely used method of detection in aerial surface radon surveys is the nuclear tracks ("track etch") method, due to its simplicity. The method is applied mainly in soils covering the rock formations from which the radon is assumed to migrate. The distribution (diffusion) pattern depends on the structures in the underlying rock and therefore the areas of higher radon concentration correspond with fractures, faults or other more permeable zones. Knowledge of the underlying geology is essential for interpretation of results.

The radon emanation technique can therefore be employed to confirm the presence of discontinuities such as mentioned, at a particular site. This knowledge is crucial to ensure appropriate measures are not considered in the design and construction phases; otherwise these features could be key in later problems linked to uncontrolled seepage or leakage.

This method has been employed with some success in South Africa; a case in point being an abstraction weir planned as an integral part of a water transfer scheme.

57.3 Case History—Vlieëpoort Abstraction Weir

The abstraction weir is a key component in an interbasin water transfer scheme. The envisaged structure will be roughly 350 m in length. The structure will only be up to 15 m above river level, but the substantial alluvial deposits will see innovative founding solutions. The need for a detailed understanding of the foundation seepage potential gave impetus to utilizing these radon emanation studies to supplement the site investigations.

57.3.1 Geological Setting and Investigation History

The weir site is located at a narrowing of a valley where the Crocodile River cuts through the Vlieëpoort Mountains, and is characterised by a substantial thickness of alluvial material, overlying bedrock comprising Banded Ironstone Formation (BIF). Initial concerns that the site might have been underlain by dolomitic rocks—which would have added a further dimension to the study—proved unfounded.

The alluvium thickness generally varies between 20 and 30 m, but is shallower towards the flanks where alluvium thicknesses between 11 and 13 m were recorded. A maximum alluvium thickness of 39.5 m was recorded.

Limited exploratory drilling was conducted at the weir site during initial feasibility-level investigations (DWA 2008). The follow-up design investigations (TCTA 2010) commenced with geophysical surveys, comprising gravimetric and resistivity surveys, with the aim of identifying any linear features which might be present, as well as defining variations in bedrock elevation. These anomalies were then targeted for further exploratory drilling of rotary core boreholes as well as percussion boreholes.

The gravity and resistivity surveys revealed the presence of possible fault zones, and extrapolation between these geophysical anomalies indicated possible alignments of these geological features, which were subsequently targeted for follow-up drilling.

57.3.2 Radon Emanation Studies

The significant thickness of the alluvium, coupled with indications of possible fault zones, contributed to concerns relating to potential seepage via the founding horizons. At the same time the downstream farming community also had concerns regarding the potential foundation cut-off, and the possible effects on the aquifer represented by the
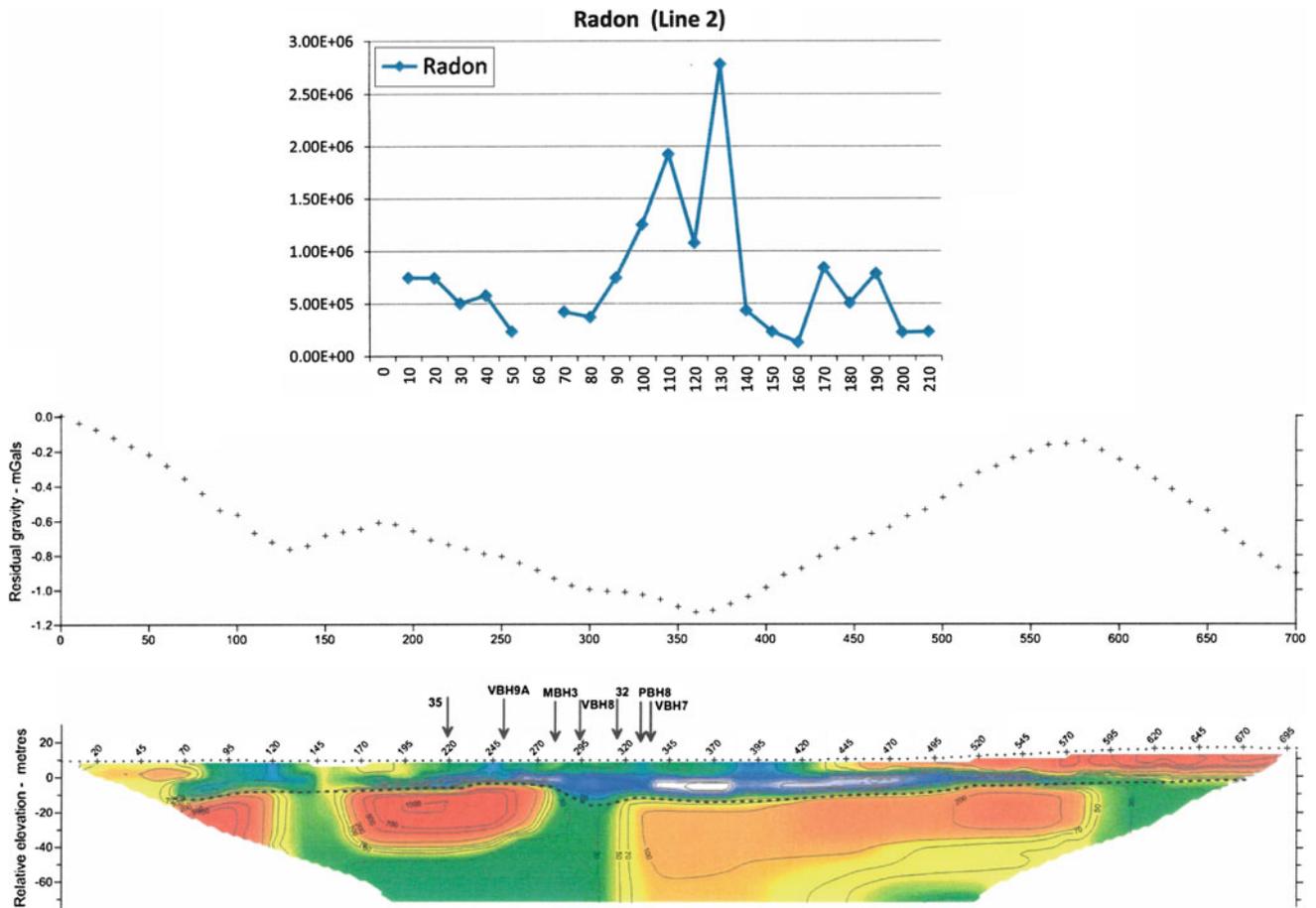
Fig. 57.2 Radon concentration profile (*right bank*)

downstream alluvium. It was subsequently decided to conduct a radon survey; both to confirm the presence and orientation of the potential fault traversing the site and further to use these results to optimally locate a series of monitoring boreholes.

Two radon profile lines were selected; one each on the opposite banks, running parallel to the river, centered on the anomalies recognized in the geophysical survey and the drilling results. The passive Radon Gas Monitors (RGMs) were placed in shallow auger holes about 500 mm deep and 10 m apart. The RGMs were left for 2 weeks and were then removed for processing and recording. The analysed radon values were plotted against the traverse distance for each profile (Fig 57.2).

57.3.3 Study Findings

The anomalous peak radon values were considered to indicate vents in the geological structure, with high radon emanating at these points. Furthermore, these localities were found to correspond to the geophysical resistivity anomalies (Fig. 57.2).

The corresponding anomalous radon survey results from the respective traverses were considered to indicate the location of the fault immediately downstream of the planned weir structure, and slightly oblique to the river. This information was used to determine optimal positions of a number of monitoring boreholes; these boreholes were subsequently drilled and continue to be monitored.

57.4 Conclusions

The radon emanation studies proved invaluable in confirming the position of a structural weakness, i.e. the presumed fault, located downstream of the abstraction weir. This was particularly notable when considering the thickness of the alluvium; typically between 20 and 30 m.

In this example the locality of the presumed fault was not the primary concern in terms of founding conditions, as the substantial alluvium thickness presents its own unique challenge in terms of a founding solution. In any event it had been assumed that faults would intersect the founding bedrock.

In terms of a quick and reliable method of locating structural weaknesses within the founding bedrock, however, the radon studies were invaluable; and allowed optimal locations for groundwater monitoring boreholes to be determined.

References

Department of Water Affairs, South Africa (2008) Mokolo crocodile (West) water augmentation project (MCWAP) feasibility study. Report 8, detail geotechnical investigations, phase 2. Prepared by Africon in association with Kwezi V3 Engineers, Vela VKE, WRP Consulting Engineers and specialists

Levin M (2000) The Radon emanation technique as a tool in ground water exploration. Borehole Water J 46:22–25

TCTA (2010) Mokolo crocodile water augmentation project (MCWAP). Contract No TCTA 07-041. Consulting services for MCWAP. Phase 1: geotechnical investigations, vol 3. Geotechnical interpretive report, July 2010. Prepared by Mokolo Crocodile Consultants

Wright EP (1992) The hydrogeology of crystalline basement aquifers in Africa. In: Wright EP, Burgess WG (eds) The hydrogeology of crystalline basement aquifers. The Geological Society, London

Capturing and Communicating Geologic Variability and Uncertainty

Convener Dr. Jeffrey Keaton—*Co-conveners* Helen Reeves, William Haneberg, Steve Parry, Rosario Basurto

Geologists tend to talk to each other using jargon that is not useful to non-geologists who could benefit from the geologic information. Dashed and queried lines geologists use to represent variability and uncertainty are not adequately documented or quantified for communication with non-geologists. Engineers need good site characterization for risk assessment and reliability-based design projects which require rigorous expression of uncertainty. Geologists need to participate in this process or be marginalized by engineers treating geology as a completely random variable or expressed only in terms of quantitative geotechnical data. This session will focus on capturing variability and uncertainty in geology and communicating it for broad use.

Improving Geotechnical Uncertainty Evaluation in Reliability-Based Design

58

Fred H. Kulhawy

Abstract

Modern geotechnical engineering often embraces uncertainty directly. For foundations, load-and-resistance-factor-design (LRFD) and multiple-load-and-resistance-factor-design (MRFD) formats are used. For "basic LRFD", the ground is simply treated as another structural component. In the more advanced design formats, the resistance factors attempt to capture some key geologic and geotechnical issues. These factors are a function of the general soil/ground strength or stiffness, as well as the quality of the key design data (strength, modulus, etc.) as obtained from different methods of site investigation, expressed as a coefficient of variation (COV) of the parameter related to the mean or trend line in-situ. These issues are addressed herein, and it is shown that the advanced formats deal with actual ground conditions more realistically. As ground professionals, we need to push code developments to reflect the reality that ground conditions need to be addressed explicitly. Recommendations are made for foundations in both soil and rock.

58.1 Background

The basic principles of reliability-based design (RBD) were introduced into civil engineering well over 60 years ago, and their origin and basic development, for all practical purposes, were driven by the structural engineering community. As would be expected, the design equations were set up to reflect structural practice and convenience. For simplified RBD, the basic design equation is:

$$\eta\, F_n \leq \psi\, Q_n \qquad (58.1)$$

in which F_n = nominal (unfactored) load, Q_n = nominal capacity, η = load factor (≥ 1), and ψ = resistance factor (≤ 1),

resulting in the name "load-and-resistance-factor-design" (LRFD). Much effort was placed on refining the loading, and it is common to see ηF_n combinations for dead and live loads and, in advanced design scenarios, additional terms for other load combinations or mechanisms. By contrast, there was relatively little effort made in resistance evaluation, because the properties of structural materials, such as steel or concrete, do not vary greatly. In fact, the structural designer specifies the desired material and its properties. In this development, the load and resistance factors are specified in increments of 0.05, with no finer "grading". These apparently are sufficient for structural design.

The geotechnical engineering community did not embrace RBD as readily, likely because of the quantification of the capacity and the resistance factor. In fact, when the early structural RBD codes were being developed, Lumb and others (Kulhawy 2010) were just in the early phases of developing the basic statistics of geotechnical properties. To illustrate, the First International Conference on Applications of Statistics and Probability to Soil and Structural

F.H. Kulhawy (✉)
School of Civil and Environmental Engineering, Cornell University, Hollister Hall, Ithaca, NY 14853-3501, USA
e-mail: fhk1@cornell.edu

Engineering was held in Hong Kong in 1971. There were 33 papers in the proceedings (15 structural), and 11 of them focused on soil statistical properties. There were 26 attendees (soil and structural). Clearly, although there were some pioneers working on some aspects of geotechnical RBD 40–50 years ago, they certainly were the exception.

Only during the past 20–30 years has geotechnical RBD been embraced more widely, although there remains a segment of the community that still questions its merits. The geotechnical research has shown that the resistance factor must be examined more carefully, because it can be highly variable. Also studies have shown that it is more efficient and accurate to formulate the basic design equation as:

$$\eta\, F_n \leq \psi_s Q_{sn} + \psi_t Q_{tn} + \psi_w W \qquad (58.2)$$

in which the ψ values are calibrated for each distinctive term in the geotechnical capacity equation (side resistance, tip resistance, weight). This format is known as multiple-load-and-resistance-factor-design (MRFD). And the protocol of 0.05 increments for the resistance factor should be dropped.

58.2 Foundations in Soil

There has been much research done for RBD of foundations in soil. Some has been rather simplified, while others have been sophisticated to varying degrees. Clearly, the status to date is varied. An overview is given by Kulhawy et al. (2012).

In its most simplified form, there is "basic LRFD", which employs Eq. 58.1 and makes numerous simplifying assumptions. For example, consider the case given in Table 58.1 by the AASHTO code, which basically governs the design of transportation structures (bridges) in the U.S. In this code, Eq. 58.1 is used, a recommendation is given for use of a design equation to calculate Q_n (but is not mandatory), there is no guidance on how to use this design equation, and there are no requirements for the specific site investigation and testing to be done to characterize the site and evaluate the soil properties to be used to calculate Q_n. To be fair, there are general guidelines for site investigation and testing in the code. But once the site soil type has been broadly characterized, a table would be entered for a particular foundation type, loading mode, and ground response.

For illustration, Table 58.1 would be used for drilled shafts in clay during undrained uplift loading. The calibration used to assess the resistance factor for this code is simplified, based on simple distributions, judgment, and fitting. As noted in the table, it is a "nominal" value that is to cover a range of target reliability index values.

This approach implicitly assumes that a good quality site investigation and appropriate soil testing is to be done. The reality is that approaches differ between states, designers, and certainly between bridge types. Clearly, a major long-span crossing will require more attention than a small rural crossing.

Geotechnical engineers who understand reliability well are fully aware of the shortcomings of this "basic LRFD" approach and have developed and promoted more rigorous and accurate alternatives. Perhaps the first "complete" study of this type was done by Phoon et al. (1995). This work focused on the need for proper and thorough site characterization that will be sufficient to delineate clearly the site stratigraphy. Once the stratigraphy is defined, the pertinent design properties must be evaluated. This process requires quality site investigation and testing that can establish the property mean or trend line, by layer with depth. The testing should be sufficient to quantify, at least simply, the property variability via its standard deviation (SD). The coefficient of variation (COV) is then the SD/mean.

Detailed studies have shown that the COV varies greatly as a function of field or laboratory test (e.g., Phoon et al. 1995; Phoon and Kulhawy 1999a, b). The precise COV would only be used directly in RBD if detailed numerical simulations were to be employed. For most designs, only a good approximation is necessary to select meaningful resistance factors. Table 58.2 shows the nominal ranges of

Table 58.1 Undrained ultimate uplift resistance factor for drilled shafts designed using AASHTO (2010)

Soil	Ψ_u
Clay	0.35[a]

Note Target reliability index (β_T) = 2.5–3.5 (nominal 3.0)
[a] reduce by 20 % if a single shaft (equivalent to β_T = 3.5)

Table 58.2 Ranges of soil property variability for reliability calibration (Phoon et al. 1995, updated Phoon and Kulhawy 2008)

Geotechnical parameter	Property variability	COV (%)
Undrained shear strength, s_u	Low[a]	10–30
	Medium[b]	30–50
	High[c]	50–70
Effective stress friction angle, ϕ'	Low[a]	5–10
	Medium[b]	10–15
	High[c]	15–20
Horizontal stress coefficient, K_o	Low[a]	30–50
	Medium[b]	50–70
	High[c]	70–90

[a] typical of good quality direct lab or field measurements
[b] typical of indirect correlations with good field data, except for the standard penetration test (SPT)
[c] typical of indirect correlations with SPT field data and with strictly empirical correlations

Table 58.3 Undrained ultimate uplift resistance factors for drilled shafts designed by $F_{50} = \Psi_u Q_{un}$ or $F_{50} = \Psi_{su} Q_{sun} + \Psi_{tu} Q_{tun} + \Psi_w W$ (Phoon et al. 1995)

Clay	COV of s_u (%)	Ψ_u	Ψ_{su}	Ψ_{tu}	Ψ_w
Medium	10–30	0.44	0.44	0.28	0.50
(mean $s_u = 25-50$ kN/m^2)	30–50	0.43	0.41	0.31	0.52
	50–70	0.42	0.38	0.33	0.53
Stiff	10–30	0.43	0.40	0.35	0.56
(mean $s_u = 50-100$ kN/m^2)	30–50	0.41	0.36	0.37	0.59
	50–70	0.39	0.32	0.40	0.62
Very stiff	10–30	0.40	0.35	0.42	0.66
(mean $s_u = 100-200$ kN/m^2)	30–50	0.37	0.31	0.48	0.68
	50–70	0.34	0.26	0.51	0.72

Note Target reliability index = 3.2

property variability based on the results of extensive studies. As shown, the COV groupings are minimal and represent ranges that are easily implemented in practice. Note that the deformation modulus would have similar values as K_o. Akbas and Kulhawy (2010) illustrate well how site-specific data can improve the variability estimates.

Based on the actual or nominal COV for the soils at the site, more realistic resistance factors can be selected that are representative of the actual site conditions. Table 58.3 illustrates resistance factors for the same class of undrained problem as Table 58.1, but taking into account ground conditions more realistically. The first column defines the overall clay stiffness/strength, the second defines the property variability as a function of exploration and testing general quality, and the third is the rigorously calibrated resistance factor for the defined conditions. Note that better quality investigation/testing allows for a higher resistance factor. This approach can be defined as "extended LRFD". Columns 4–6 present the resistance factors for the MRFD approach given by Eq. 58.2, in which each capacity term has its own calibrated resistance factor. MRFD allows for the most rigorous and accurate design matching the calculated and target reliability indices. The calibration for MRFD is a bit more complicated, and different terms dominate nonlinearly in the process, but its application in practice is straightforward. Note that all factors change gradually, without the 0.05 abruptness.

58.3 Foundations in Rock

There has been relatively less research done for RBD of foundations in rock. Some of this work is summarized in Kulhawy and Prakoso (2007). Most codes have adopted the "basic LRFD" approach described previously, with all of its limitations and with correlations to the intact rock uniaxial compression strength (q_u). Prakoso and Kulhawy (2011) describe a better "extended LRFD" approach, in which there is no needed differentiation for general rock stiffness/strength as in soil, but there are still three categories of COV for the strength (q_u), with correlated resistance factors. The same range of COV variability (10–30, 30–50, 50–70) is appropriate for q_u. Low corresponds to good quality drilling, sampling, and testing; medium corresponds to lower grade field efforts or indirect correlations such as the point load test; and high corresponds to minimal efforts, index correlations such as the Schmidt hammer, or field estimates with geologic hammer and such.

Although RBD evaluations for foundations in rock have been correlated with the intact rock q_u, there will be inevitable misuses of this work. While doing a project review this past year, I encountered a foundation RBD based on the rock mass q_u computed from the geological strength index (GSI), with settlements computed from the GSI as well. This RBD is simply wrong.

The GSI has become an important tool for various rock engineering problems, but it must be remembered that it is based upon a careful engineering geologic description of the rock mass. It is a qualitative index and empirical and, as Evert Hoek has stated numerous times in his papers on the GSI, "do not try to be too precise" and "quoting a range is more realistic than citing a single value". Before using the GSI, be sure to read the following papers that provide solid guidance on its proper use (Marinos and Hoek 2000; Marinos et al. 2005).

It should also be noted that, being a qualitative index, the GSI does not have any quantitative statistics. Assigning any means or COVs to the GSI are purely ad-hoc and may be

misleading. However, the deformation modulus correlations with GSI are somewhat more quantitative, but they still are strictly empirical. If they are to be used, a high variability should be expected, with COV = 70–90%, based on Table 58.2.

58.4 Concluding Comments

Modern geotechnical engineering has been moving toward embracing uncertainty directly. Design equations for foundations can be expressed in basic LRFD, extended LRFD, or MRFD formats. In basic LRFD, the ground is simply treated as another structural engineering entity that is characterized by a single resistance factor defined solely by broad material type. Hopefully, proper ground investigation and testing issues are addressed in the analysis/design evaluation, but design codes are particularly deficient and lax in this regard.

The other, more advanced, formats used in soil attempt to capture some key geologic and geotechnical issues. The resistance factors are a function of the general soil/ground strength or stiffness, as well as the quality of the key design data (strength, modulus, etc.) as obtained from different methods of site investigation, expressed as a coefficient of variation (COV) of the parameter related to the mean or trend line in-situ. Generic guidelines are suggested to assist in this overall evaluation of ground condition and its variability. MRFD formats provide the most accurate assessments. Thorough local site evaluations can improve on these generic guidelines.

For foundations in rock, the basic LRFD format is comparable to that for soil. The extended LRFD format again attempts to capture some key geologic and geotechnical issues, but this format is still relatively simple. MRFD is not available. Cautions must be exercised in rock property evaluations, especially if the GSI is used. It is qualitative and empirical, and it must be used as it was intended.

To advance our geo-profession and capture geologic and geotechnical issues properly, we need to move away from "basic LRFD" and into at least "extended LRFD" or preferably MRFD.

References

AASHTO (2010) LRFD bridge design specifications, 5th edn. American Association of State Highway and Transportation Officials, Washington, DC

Akbas SO, Kulhawy FH (2010) Characterization of geotechnical Variability in Ankara clay: a case history. Geotech Geol Eng 28 (5):619–631

Kulhawy FH (2010) Uncertainty, reliability and foundation engineering: the 5th Peter Lumb lecture. Trans Hong Kong Inst Eng 17 (3):19–24

Kulhawy FH, Phoon K-K, Wang Y (2012) RBD of foundations—a modern view. Geotechnical state of art and practice (GSP 226). ASCE, Reston, pp 102–121

Kulhawy FH, Prakoso WA (2007) Issues in evaluating capacity of rock sockets. In: Proceedings of the 16th SE Asian geotechnical conference, Kuala Lumpur, pp 51–61

Marinos P, Hoek E (2000) GSI: a geologically friendly tool for rock mass strength estimation. In: Proceedings of the GeoEng2000, Melbourne, pp 1422–1442

Marinos V, Marinos P, Hoek E (2005) The geological strength index: applications and limitations. Bull Eng Geol Environ 64:55–65

Phoon K-K, Kulhawy FH (1999a) Characterization of geotechnical reliability. Can Geotech J 36(4):612–639

Phoon K-K, Kulhawy FH (1999b) Evaluation of property variability. Can Geotech J 36(4):625−639

Phoon K-K, Kulhawy FH (2008) Serviceability limit state RBD. Chapter 9 in RBD in geotechnical Engineering. Taylor & Francis, London, pp 344–384

Phoon K-K, Kulhawy FH, Grigoriu MD (1995) RBD of foundations for transmission line structures. Report TR-105000. Electric Power Research Institute, Palo Alto

Prakoso WA, Kulhawy FH (2011) Some observations on RBD of rock footings, GeoRisk 2011(GSP 224). ASCE, Reston, VA, pp 600–607

Communicating Geological Uncertainty: The Use of the Conceptual Engineering Geological Model

59

Christopher Jack and Steve Parry

Abstract

Rock engineering requires an in-depth understanding of the rock mass. However, geological data is often superficially evaluated and interpreted in isolation, without reference to an overall model. Given geological variability and complexity, the lack of an interpretative framework can result in misleading or incorrect interpretations. The existence of a conceptual engineering geological model is particularly useful at the feasibility stage of a project. This paper illustrates a simple conceptual engineering geological model for a proposed cavern site in Hong Kong. The model allows the identification and evaluation of geological uncertainty and has applications including the optimisation of the site investigation, facilitating early risk assessment and decision making and allowing cost estimates to be made.

Keywords

Conceptual model • Caverns • Hong Kong

59.1 Introduction

This paper presents a conceptual engineering geological model for the rock engineering aspects of a proposed cavern site at Sha Tin, Hong Kong. The purpose of the caverns will be to allow the relocation of a nearby sewage treatment works underground. The model was developed for tender evaluation purposes. Key uncertainties and risks identified by the model are also discussed, along with some initial findings and applications. It has been assumed that the caverns will be situated at >30 m depth and will be of similar dimensions to some existing caverns in Hong Kong (120 m long, 17 m high, 15 m span).

59.2 Conceptual Engineering Geological Model

The conceptual model approach follows the recommendations of IAEG commission C25 (Parry et al. in press) in that it is '*based on understanding the hypothetical relationships between engineering geological units, their likely geometry, and anticipated distribution. This approach, and the models formed, are based on concepts formulated from knowledge and experience and are not necessarily related to real three-dimensional space or time*'. The models in this paper are based on the published geological maps and memoirs and an interpretation of a 1:5,000-scale digital elevation model (DEM). The focus is on the evidence for structural geological control and the models incorporate the authors' experience and knowledge. No site specific ground investigation was available.

Figure 59.1 is a conceptual model of the faults and lineaments in the region of the cavern interpreted from these data sets. The main trends, in decreasing order of magnitude, are NE-SW, NW-SE, ENE-WSW and WNW-ESE. Regional dyke swarms also follow these trends, with NE being the dominant trend. As a result of the tectonic and igneous

C. Jack (✉)
Christopher Jack Rock Engineering Limited, 20/8 Bruntsfield Avenue, Edinburgh, EH10 4EW, UK
e-mail: chris.jack@cjrockeng.com

S. Parry
Parry Engineering Geological Services, 12a Riverside Court, Calver Mill, Calver, Derbyshire, UK

Fig. 59.1 Proposed cavern site—location and regional structural geological model (image © 2011 Google, © GeoEye, ©2011 DigitalGlobe)
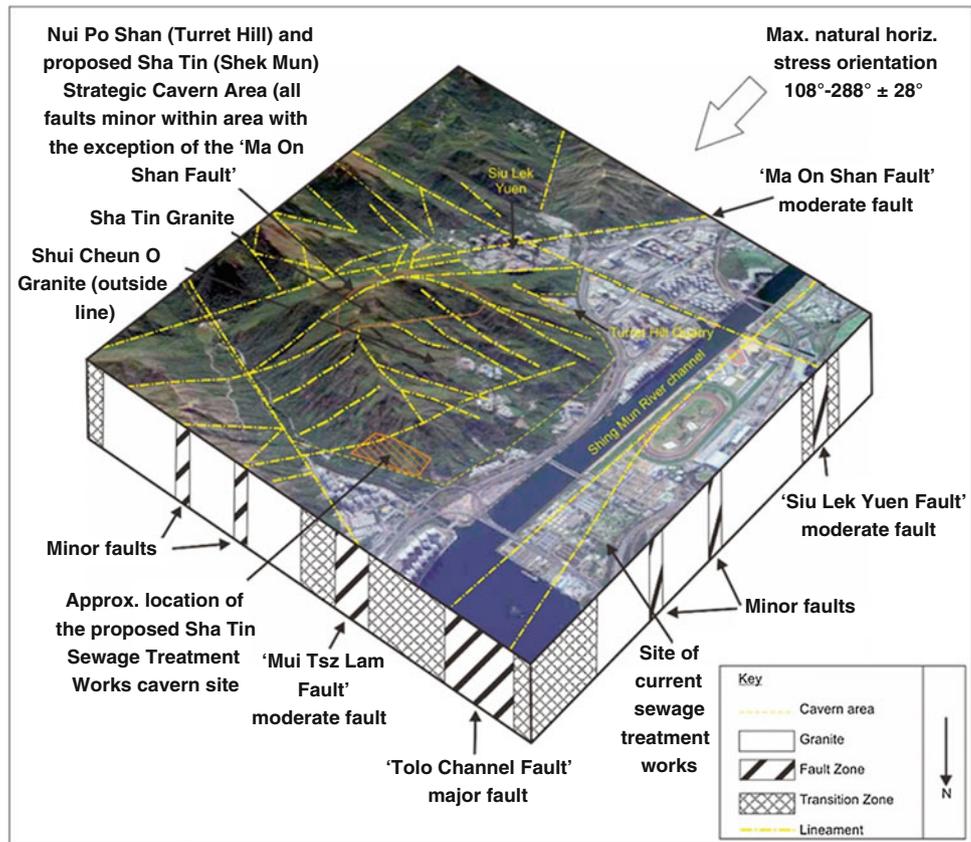
history, it is considered that structures with similar orientations are likely to exist at all scales from microstructures, through shear fractures and joints, to faults. The geology of the cavern site comprises the Shui Chuen O Granite of Cretaceous age. This intrusion was strongly controlled by the dominant NE structural trend and is elongated in this direction. Tectonic activity continued after the granite intrusion, with subsequent faulting and intrusion by dykes, again mainly following the NE orientation. Whilst some of the data shown is observational (i.e. from the published geological map), this has significant uncertainties associated with it, with most faults denoted as 'uncertain'. In addition, the lineaments extracted from the DEM have no ground control.

Once the geological history of the cavern area was established, an evaluation of likely discontinuity types and their potential engineering implications was undertaken and synthesized (Jack et al. 2012). The discontinuities are discussed below and are shown schematically in Fig. 59.2. Note that while the model in Fig. 59.2 shows spatial relationships, these are only indicative. The discontinuity data is extrapolated from the regional conceptual model and combined with published data; the depth of weathering and weathering grades are based on local experience.
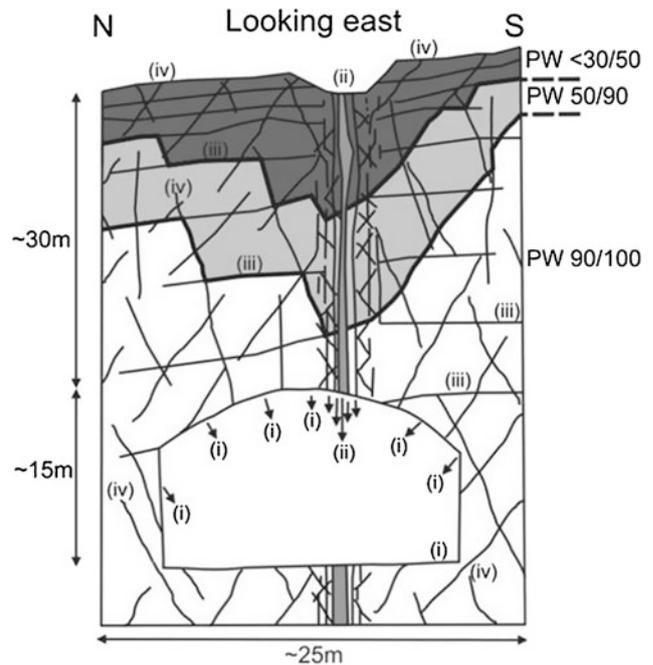
Fig. 59.2 Conceptual engineering geological cross section of the cavern site, notation: (i) potential block fall, (ii) minor fault with potential for cave-in, (iii) sheeting joints, (iv) subvertical discontinuities, PW—partial weathering (GEO 1988)

Faults. No major or moderate faults appear to cross the cavern site, although some possible minor faults do, particularly at the southern end of the site. Possible materials along the minor faults include breccia and fault gouge. Adjacent to the faults, the frequency of shear fractures may increase markedly and the rock may be shattered. The faults may also be partially or fully silicified and/or intruded by dykes. Unless unweathered or re-cemented by high strength secondary mineralisation, the fault material will be "weak". The minor faults may result in increased overbreak, block falls, cave-in and high groundwater inflow in the caverns which can be difficult to control. Assessed feasibility parameters: GSI 10–30 (20). Q, RMR and RMi have not been assessed as it is better to assess faults individually and in detail.

Sheeting joints: Such joints are commonly developed in Hong Kong in coarse grained granites and coarse ash tuff. Orientations will likely vary with slope aspect at the cavern site, possibly towards the NE and E. Sheeting joints are unlikely to be encountered in the caverns as they are rarely developed at depths >30 m. If present, they are likely to be widely spaced and weakly developed (Hencher et al. 2011) and they may form surfaces from which blocks could fall, or release planes for sidewall blocks. For feasibility purposes the sheeting joints are considered to have an effective friction angle of 42° (Hencher and Richards 1982). However, the angle of friction could be much less if some of the sheeting joints are dilated, weathered and/or have significant kaolin or other infill. Joint Roughness Coefficient (JRC, Barton 1973) values might range between JRC 10 and 20.

Steeply dipping discontinuities: It is assumed that the principal discontinuity sets will have broadly the same orientation as the faults. This assumption is reasonable for feasibility purposes, as the main discontinuity sets in Hong Kong granites are typically found to follow the main fault trends. These will typically control the stability in the proposed caverns. In the absence of other information, the discontinuities are assumed to be rough planar with an angle of friction of 40° (Hencher and Richards 1982), although this could be much less where discontinuities are slickensided or weathered. JRC values between 5 and 10 have been assumed.

Rock mass: The cavern site is assumed to be situated in slightly decomposed Shui Chuen O Granite. Based on Palmstrom and Stille (2010), the granite is classed as '*jointed rocks or blocky materials—Class B—rocks intersected by joints and partings—jointed homogenous rocks*' and '*jointed rocks or block materials—Class C—jointed rocks intersected by seams or weak layers—prominent weathering along joints*'. Consequently, it is assessed that the main issues associated with the typical rock mass will be block falls and areas of water inflow. The following ranges of parameters are considered to be appropriate for feasibility purposes (averages in brackets). Strength: 100–200 MPa (150 MPa); block volume: 0.01–15 m^3 (0.5 m^3); GSI: 50–80 (70); Q: 0.7 [RQD 75, J_n 9, J_r 1, J_a 3, J_w 0.66, SRF 2.5] to 38 [RQD 100, J_n 4, J_r 1.5, J_a 1, J_w 1, SRF 1] (11 [RQD 90, J_n 6, J_r 1.5, J_a 2, J_w 1, SRF 1]); RMR: 40–90 (70).

In situ *stress*: The maximum horizontal component of the natural stress field is assumed to be orientated at $108° - 288° \pm 28°$ (Free et al. 2000) as site-specific data was not available for incorporation into the model.

59.3 Key Uncertainties and Risks

The following key uncertainties have been identified based on the model:
- The possible presence, nature and engineering properties of any faults.
- The nature and properties of the shear fractures and joints.
- The groundwater regime.
- The state of in situ stress.

The nature and properties of the rock material, including weathering, are of secondary importance providing that the cavern can be located in good quality rock with one diameter or more of rock above the crown. In this case it is the discontinuities that will control the overall stability of the cavern. The key risks highlighted by the model are associated with large uncertainties because of the current lack of site-specific engineering geological data and include block fall, cave-in and excessive groundwater inflow.

These uncertainties and risks should be managed through the use of an uncertainty register and a risk register. The uncertainty register will recommend actions to be taken to address the uncertainties and the risk register will recommend actions to mitigate the risks. Key uncertainties that cannot be satisfactorily resolved during later stages of the project will become risks and will be added to the risk register. However, such registers are of little use if their contents are not communicated effectively to the project team and this must be one of the engineering geologist's key priorities throughout the project.

Where possible uncertainties should be quantified. This makes it easier to communicate the importance of the uncertainties to other specialists including planners and engineers. It also makes uncertainties more tractable to analysis and incorporation within economic, risk, reliability and probabilistic analyses. Examples of how uncertainties can be quantified include assigning monetary values to uncertainties or probabilities of occurrence. However, some uncertainties cannot be sensibly quantified and judgment will always rule in geological considerations.

59.4 Findings and Applications

The paper demonstrates the usefulness of the conceptual model approach in allowing the visualisation of the engineering geological setting and the derivation of potential uncertainties and risks. Despite its simplicity and the significant uncertainties, it is possible to derive the following from the model.

- It appears that the geology of the site is suitable for cavern development.
- Future site investigations should focus on the discontinuities (at all scales), the groundwater regime and the in situ stress.
- The key risks are block fall, cave-in and excessive groundwater inflow.
- The depth of the caverns should be greater than 30 m, eliminating most or all of the concern for sheeting joints, highly weathered rock and undesirable effects of low in situ vertical stress.
- For feasibility stage considerations of a cavern at shallow or intermediate depth, the longitudinal axis should ideally be orientated along the bisection line of the largest intersection angle of the strikes of the two dominant sets of discontinuities. This should reduce instability and overbreak. With reference to Fig. 59.1, the ideal direction is N–S.
- In addition, at the feasibility stage, it is a common consideration that the major in situ horizontal stress should be parallel to the longitudinal axis of the cavern to reduce instability, which is approximately E–W.
- Therefore on balance the model suggests the best orientation is E–W.

- The assessment of the ground conditions, together with the rock mass classifications, allows for an initial estimation of construction costs.

References

Barton N (1973) Review of a new shear strength criterion for rock joints. Eng Geol 7:287–322

Barton N, Lien R, Lunde J (1974) Engineering classification of rock masses for the design of tunnel support. Rock Mech 6(4):189–236

Free MW, Haley J, Klee G, Rummel F (2000) Determination of in situ stress in jointed rock in Hong Kong using hydraulic fracturing and over-coring methods. In: Proceedings of the conference on engineering geology HK 2000, Institution of Mining and Metallurgy, Hong Kong Branch, pp 31–45

GEO (1988) Geoguide 3, Guide to soil and rock description. Geotechnical Engineering Office, Civil Engineering Department, Hong Kong

Hencher SR, Richards LR (1982) The basic frictional resistance of sheeting joints in Hong Kong granite. Hong Kong Eng 11(2):21–25

Hencher SR, Lee SG, Carter TG, Richards LR (2011) Sheeting joints: characterisation, shear strength and engineering. Rock Mech Rock Eng 44(1):1–22

Jack CD, Parry S, Hart JR (2012) Structural geological input for a potential cavern project in Hong Kong. In: Proceedings of the 32nd annual seminar, geotechnical division, the Hong Kong Institution of Engineers

Marinos P, Hoek E (2000) GSI—a geologically friendly tool for roc mass strength estimation. In: Proceedings of GeoEng 2000 conference, Melbourne, pp 1422–1442

Palmstrom A, Stille H (2010) Rock engineering. Thomas Telford, London

Parry S, Baynes FG, Culshaw MG, Eggers M, Keaton JF, Lentfer K, Novotny J, Paul D (in press) Engineering geological models—an introduction: IAEG Commission 25. Bull Eng Geol Environ

Evaluating the Effects of Input Cost Surface Uncertainty on Deep-Water Petroleum Pipeline Route Optimization

60

William C. Haneberg

Abstract

A resampling-based stochastic simulation approach was used to evaluate the uncertainty that may be associated with geologically constrained least-cost path pipeline route optimization. A smoothed version of a composite geocost surface from a deep-water pipeline routing project was resampled and the results used to generate a series of equally probable cost surface realizations, which were in turn used as the basis for the same number of route optimizations. Eighty percent of the simulated routes followed a 500–2,000 m wide corridor nearly parallel to the baseline route (based upon complete information) between two hypothetical pipeline termini located about 25 km apart. Twenty percent followed an alternate corridor of approximately the same width. These results suggest that, while the general method of geologically constrained pipeline route optimization is a relatively robust one, uncertainties in geological input will at the least create a least-cost route corridor rather than a single least-cost route and may suggest realistic alternatives that must be critically evaluated in light of the available geological information.

60.1 Introduction

Proper assessment of geologic hazards for deep-water oil and gas developments in which billions of dollars of capital may be at risk requires both a reproducible logical framework and an understanding of the uncertainty and natural variability inherent in geological information. In pipeline route selection, the overriding objective is to find the shortest route that satisfies both primary requirements such as terminus locations and secondary constraints such as areas of geological, biological, or cultural concern (Tootill et al. 2004).

One logical framework that has proven useful on a number of pipeline route evaluations, including deep-water petroleum pipeline routes crossing tens of kilometers of potentially hazardous seafloor, is geologically constrained least-cost path optimization (e.g., Feldman et al. 1995; Haneberg et al. 2013; Price 2010; Yildrim et al. 2007; Luettinger and Clark 2005). In least-cost path optimization, a composite cost surface is developed from a variety of qualitative and quantitative geologic and bathymetric information. Each hazard or attribute is mapped separately, weighted, normalized, and then added to the others to create the composite cost map. Then, steepest path algorithms are used to determine the least expensive route in terms of the spatially variable cost integrated over the length of the route. Implicit in the analysis is the assumption that the composite cost used in the optimization is proportional to the actual cost of pipeline route characterization, design, construction, maintenance, operation, and, if appropriate, decommissioning.

W.C. Haneberg (✉)
Fugro GeoConsulting Inc., 6100 Hillcroft, Houston, TX 77081, USA
e-mail: whaneberg@fugro.com
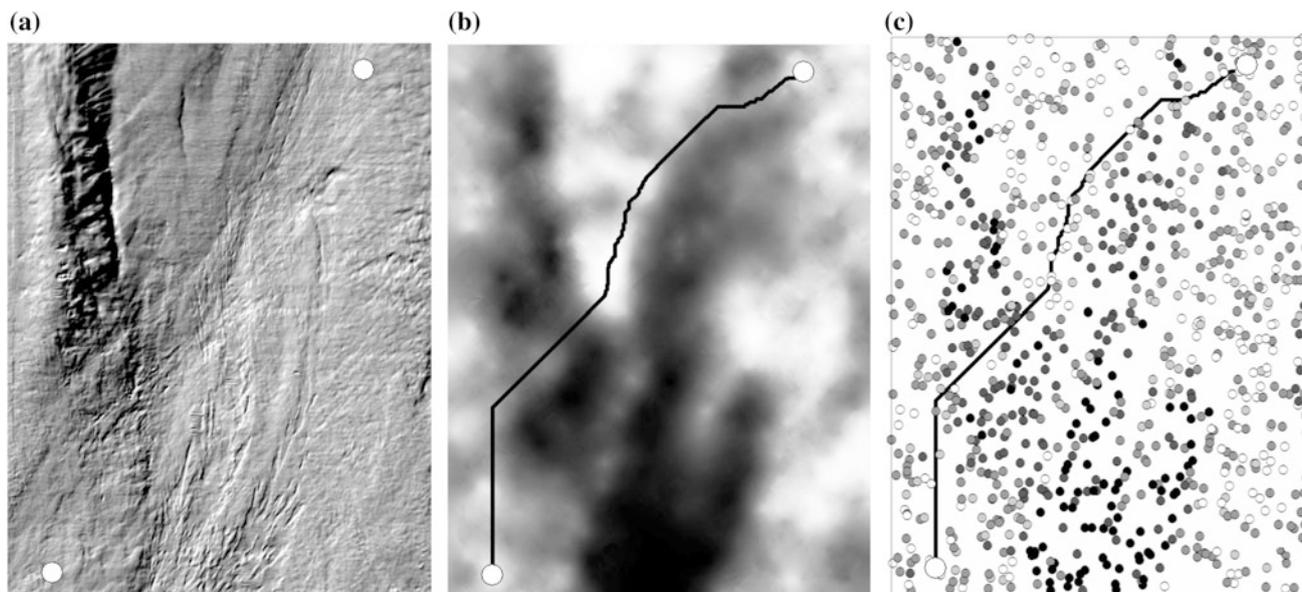
Fig. 60.1 a Shaded relief seafloor rendering of the study area showing the two hypothetical pipeline termini used in this paper. Illumination is from the northwest. **b** Smoothed representation of the cost surface used in the real pipeline route selection along with the baseline least-cost optimized route. Dark areas are high cost and light areas are low cost. **c** Locations and relative costs of 1,000 randomly sampled points based on the kriged cost surface. Images cover an area of approximately 18 km by 24 km

One of the complications of least cost path optimization is that considerable professional discretion is required to select and evaluate the relative importance of the variables used to construct the composite cost map. Moreover, the variables may differ from project to project and region to region, making a completely standardized or codified approach unrealistic.

Some kinds of information used to guide pipeline route selection, for example the mapped extents of past slope failures, can be uncertain because they are inherently subjective. That is to say, different geologists are almost certain to produce slightly different maps from the same data (Haneberg and Keaton 2012; Keaton and Haneberg 2013). Other kinds of information, for example the results of regional process-based slope stability simulations, are uncertain because they incorporate model uncertainty, parameter uncertainty, and spatial variability of geotechnical properties. The latter can be partially accommodated using probabilistic formulations that treat input values as random variables with distributions that may differ among soil units or engineering geologic facies (Haneberg et al. 2009, 2013; Haneberg 2012). Similarly, some kinds of information, for example the location of a past slope failure, are categorical (either it exists at a point or it does not, although the exact extent may be subjective, as discussed above, and if only two states are possible then the variable becomes binary) whereas others, for example, slope angle or seafloor radius of curvature, are continuous and can take on a range of values.

As a consequence of these complexities, the composite geocost surface will itself be continuously variable and uncertain to a degree that is difficult to analyze because each of its components will have its own kind and degree of uncertainty. One practical approach to begin understanding the effect of composite cost surface uncertainties, which is described in this paper, is to sample a sufficient number of random points from a cost surface, which is known in statistics as bootstrapping (Efron 1979), and then use those points to seed conditional simulations of equally probable alternative cost surfaces (known as realizations). Haneberg (2006) used a similar approach to generate realizations of digital elevation model error fields and evaluate their effects on subsequent slope stability calculations.

60.2 Method

In this work, the effects of cost surface uncertainty were evaluated using a resampling-based (bootstrap) geostatistical conditional simulation approach. The cost surface map for an actual deep-water pipeline routing project was first sampled at 1,000 randomly located points. Composite cost values from the sampled points were then kriged and used to generate 10 equally probable realizations of the cost surface using conditional Gaussian simulation with normal score transformation as implemented in the Geostatistical Analyst

Fig. 60.2 Four of the ten equally probable cost surface realizations and associated least-cost optimized pipeline routes. Each realization is generally similar but different in detail from the others, simulating the effects of input uncertainty on the routing algorithm
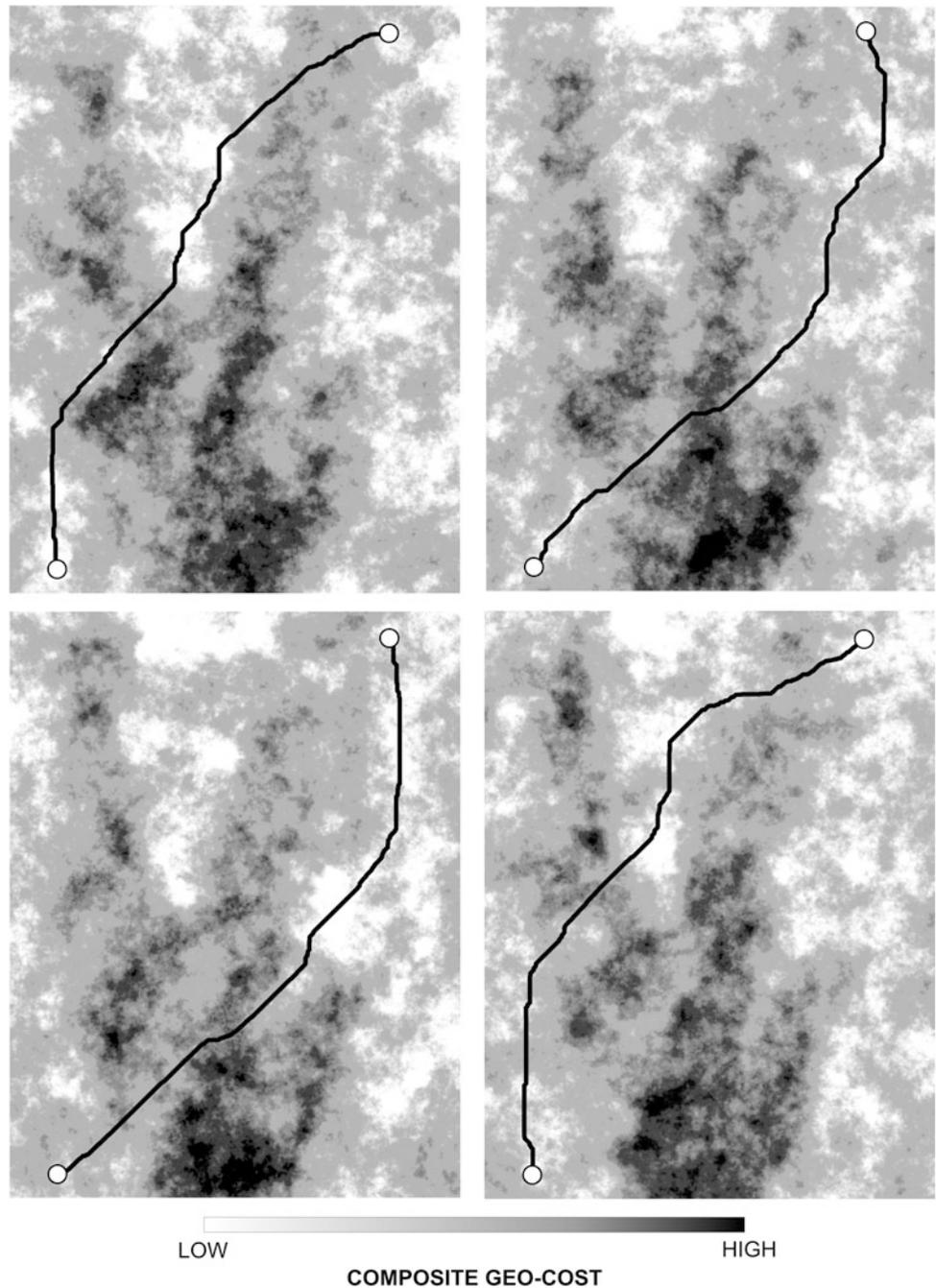
extension to ArcMap 10.1. The term "conditional" means that values were fixed at the 1,000 randomly chosen points, in essence to anchor the results to the real map upon which they are based, and simulated at all other points. The process is easily automated, and in a real project one would typically generate many more equally probable realizations, perhaps 100 or more, for consideration. The much smaller number of 10 used in this paper was chosen to simplify the illustrations while still demonstrating the principles of the method.

Two hypothetical pipeline termini about 25 km apart and separated by a variety of seafloor conditions were selected. Then, a least-cost route between the two termini was calculated for each of the 10 cost surface realizations. Neither the actual pipeline termini nor the specific geohazard layers used to create the actual cost surface, which are confidential, are described here. Only a smoothed version of the actual cost surface is shown and then in terms of relative, not absolute, values.
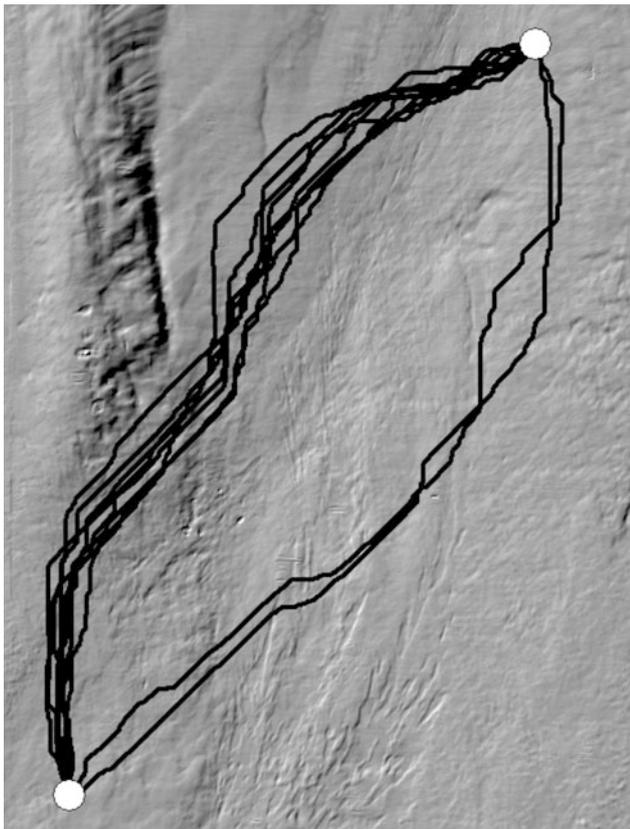
Fig. 60.3 All 10 simulated routes superimposed on a shaded seafloor rendering. Actual pipeline routing projects use many realizations, perhaps 100 or more, to generate a stochastic cloud of equally probable pipeline routes and highlight areas most sensitive to input uncertainty

60.3 Results

The example area for this study covers an area of approximately 18 km by 24 km as illustrated in Fig. 60.1a, which is a shaded relief rendering generated from the seafloor return in a 3-D seismic data volume. It was created by digitally picking the seafloor return using seismic interpretation software and then converting it from two-way travel time to depth using a standard polynomial equation (Advocate and Hood 1993). Water depths range from about 200 m in the south to more than 2,000 m in north. The white circles in the SW and NE corners of the image are the two hypothetical pipeline termini used in this analysis.

Figure 60.1b shows a smoothed representation of the actual composite cost surface used for a pipeline routing project in this area (the actual project used different pipeline termini than those shown in Fig. 60.1a). Dark shades represent areas of high cost whereas light shades represent areas of low cost. No scale is shown because the costs are relative and normalized to each other; hence, their absolute magnitudes are inconsequential. The black line in Fig. 60.1b is the least-cost route obtained using the kriged cost surface and

considered the baseline case. Note how the route follows a path of relatively light shaded (i.e., low cost) areas between the two termini.

Figure 60.1c shows the 1,000 randomly sampled points, as above shaded according to their relative cost (dark for high and light for low) along with the baseline route for reference.

A total of 10 cost surface realizations were generated for this study and 4 of those are shown in Fig. 60.2. Note that while the general distribution of high and low costs is similar in each of the 4 realizations, details such as the continuity of low-cost corridors differ slightly from realization to realization. As in Fig. 60.1, dark shades represent high costs and light shades represent low costs. Each of the 4 cost surface images in Fig. 60.2 also shows the least-cost path route calculated for that surface.

Figure 60.3 shows all 10 route realizations superimposed upon a seafloor rendering to illustrate the range of variability. Out of the 10 realizations, 8 follow a fairly well defined corridor ranging in width from about 500–2,000 m. Two of the simulated routes, as were shown in Fig. 60.2, depart from that corridor and follow a second corridor of similar width. Comparison of the 4 cost surfaces in Fig. 60.2 shows that in those two realizations the simulated routes departed significantly from the baseline case because of the existence of a relatively low cost alternative pathway.

References

Advocate DM, Hood KC (1993) An empirical time-depth model for calculating water depth, northwest Gulf of Mexico. Geo-Mar Lett 13:207–211

Efron G (1979) Bootstrap methods: another look at the jackknife. Ann Stat 7:1–26

Feldman SC, Pelletier RE, Walser E, Smoot JC, Ahl D (1995) A prototype for pipeline routing using remotely sensed data and geographic information system analysis. Remote Sens Environ 53:123–131

Haneberg WC (2012) Spatially distributed probabilistic assessment of submarine slope stability. In: Offshore site investigation and geotechnics: proceedings of 7th international conference, London, 12–14 Sept 2012, pp 551–556

Haneberg WC (2006) Effects of digital elevation model errors on spatially distributed seismic slope stability calculations: an example from Seattle, Washington. Environ Eng Geosci 12:247–260

Haneberg WC, Bruce B, Drazba MC (2013) Using qualitative slope hazard maps and probabilistic slope stability models to constrain least-cost pipeline route optimization. In: Proceedings of offshore technology conference, 5–9 May 2013, Houston, Texas, Paper OTC 23980

Haneberg WC, Keaton JR (2012) Ground truth: an obstacle to landslide hazard assessment? Geol Soc Am Abst Programs 44(7):345

Haneberg WC, Cole WF, Kasali G (2009) High-resolution LiDAR-based landslide hazard mapping and modeling. Bul Eng Geol Environ 68:273–286

Keaton JR, Haneberg WC (2013) Landslide inventories and uncertainty associated with ground truth. In: Wu F, Qi S (eds) Global view of

engineering geology and the environment. Taylor & Francis, London, pp 105–110

Luettinger J, Clark T (2005) Geographic information system-based pipeline route selection process. J Water Resour Plan Manage 131:193–200

Price G (2010) Geographic information systems pipeline route optimization (GISPRO). In: Proceedings of 10th ESRI petroleum user group conference, Houston, 22–24 Feb 2010, paper 1237

Tootill NP, Vandenbossche MP, Morrison ML (2004) Advances in deepwater pipeline route selection—a Gulf of Mexico case study. In: 2004 offshore technology conference, Paper OTC 16633

Yildrim V, Aydinoglu AC, Yomralioglu T (2007) GIS based pipeline route selection by ArcGIS in Turkey. In: Proceedings of ESRI international user conference, 18–22 June 2007. http://proceedings. esri.com/library/userconf/proc07/papers/papers/pap_2015.pdf (accessed 6 Jan 2013)

Scanline Sampling Techniques for Rock Engineering Surveys: Insights from Intrinsic Geologic Variability and Uncertainty

61

Helder I. Chaminé, Maria José Afonso, Luís Ramos, and Rogério Pinheiro

Abstract

Discontinuity surveys are based on collecting rock data from fieldwork and are an essential component of rock-mass quality estimation in rock engineering. Strength, deformability and permeability characteristics of a rock-mass are strongly influenced by its discontinuities. Scanline surveys are a reliably technique in which a line is drawn over an outcropped rock surface and all the discontinuities intersecting it are measured and described. The discontinuity geometry for a rock-mass is characterised by the number of discontinuity sets, mean density and the distributions for location, orientation, size and spacing/fracture intercept. Rock site investigation deals with several key elements that need to be addressed, namely the information required to characterise the rock system and the intrinsic uncertainty associated with this information. This way, quantifying the information content of the on-site measurements and creation a database is vital to be used for decision making processes and risk assessment on rock engineering design projects. In addition, a clear geology framework plays a key-role to support the investigation of all rock engineering projects. Nevertheless, the intrinsic variability of geological, petrophysical and geotechnical properties must be quantified for reliability-based design and to decrease the geological uncertainty. All geologists and engineers' practitioners must have the aim to contribute to the correct study of the ground behaviour of soil and rock, their applications in sustainable design with nature and environment and to satisfy the society's needs.

61.1 Introduction

Barton (2012) argues the *"Discontinuous behaviour provides rich experiences for those who value reality, even when reality has to be simplified by some empiricism"*. This impressive quotation describes the general framework of the complexity of the heterogeneous rock-mass behaviour. The lessons learned on several geoengineering projects stress the importance of the accuracy of the basic geological and geotechnical data information related to the rock masses characterization and assessment.

Linear or circular sampling or sampling within windows along a scanline are accurate approaches to the systematic record of discontinuities (joints, fractures, faults, veins, etc.).

H.I. Chaminé (✉) · M.J. Afonso · L. Ramos · R. Pinheiro
Laboratory of Cartography and Applied Geology (Labcarga),
Department of Geotechnical Engineering, School of Engineering
(ISEP), Polytechnic of Porto, Porto, Portugal
e-mail: hic@isep.ipp.pt

M.J. Afonso
e-mail: mja@isep.ipp.pt

L. Ramos
e-mail: lcr@isep.ipp.pt

R. Pinheiro
e-mail: rfsp@isep.ipp.pt

H.I. Chaminé · M.J. Afonso
Centre GeoBioTec, University of Aveiro, Aveiro, Portugal

In several geologic and geotechnical frameworks this is, moreover, the easiest and fastest way to collect discontinuities data (e.g., Priest and Hudson 1981; Hudson and Priest 1983; Priest 1993; Mauldon et al. 2001; Rohrbaugh et al. 2002; Priest 2004; Peacock 2006; Chaminé et al. 2010, 2013; Pinheiro et al. 2014). Scanline surveys will provide an amount of reliable information concerning structural geology, petrophysical and geotechnical features of rock masses, either in boreholes or exposed rock surfaces (Fig. 61.1). However, some procedures must be fulfilled to avoid systematic or random errors (Terzaghi 1965; ISRM 1981; CFCFF 1996; Hudson and Cosgrove 1997). Collecting data for the basic geotechnical description of rock masses is of considerable importance for the prediction of scale effects in rock mechanical behaviour (Cunha and Muralha 1990).

The characteristics of discontinuities can be estimated using scanline sampling techniques (Fig. 61.2), but the accuracy is subject to bias (e.g., Priest and Hudson 1981; Priest 1993; Park and West 2002; Rohrbaugh et al. 2002). According to Mauldon et al. (2001) the circular sampling tools and estimators (such as fracture trace intensity, trace density and mean trace length) eliminate most sampling biases, due to orientation and also correct many errors owing to censoring and length bias. Conversely, Wu et al. (2011) argue the predictions based on the rectangular window methods were found to be more accurate than that based on the circular window methods.

In this work, we highlight the importance of an integrative approach for geoengineering purposes of field surveys performed with scanline techniques on free rock-mass faces in diverse contexts, such as quarrying, underground excavations and hard-rock hydrogeotechnical studies. All studies should be developed in a GIS platform by using the following tools: field mapping, morphotectonic analysis, structural geology, rock geotechnics and hydrogeomechanics. This approach led us to a better understanding of the relevance of rock masses heterogeneity for geoengineering purposes at different scales and to reduce the intrinsic variability and uncertainty in collecting geologic and geotechnical data.

61.2 Rock Scanline Surveys: A Reliable Tool to Unbiased Sampling

Discontinuity features play a major role in controlling the mechanical behaviour of a rock-mass (Priest and Hudson 1981). Discontinuities are generally characterised in terms of the following properties (e.g., ISRM 1981; Priest 1993, 2004): orientation, frequency or spacing, size and shape, aperture, conductivity, surface geometry, strength and stiffness. Describing only the discontinuities which seem to be important can be considered as a subjective method of fracturing surveying. From a statistical perspective, it is important to set up a rigorous unbiased sampling regime at the rock face such as (Priest 2004): sampling all traces of discontinuities within a defined area (window sampling), all that intersect a circle (circle sampling) or all that intersect a straight line (scanline sampling). ISRM (1981) stated that a scanline survey is an objective method for recording and describing rock fracturing on a rock-mass exposure (Fig. 61.3).

Fig. 61.1 The main scientific and technical fields of applications of scanline sampling technique surveys related to engineering geosciences, rock engineering and geotechnical engineering
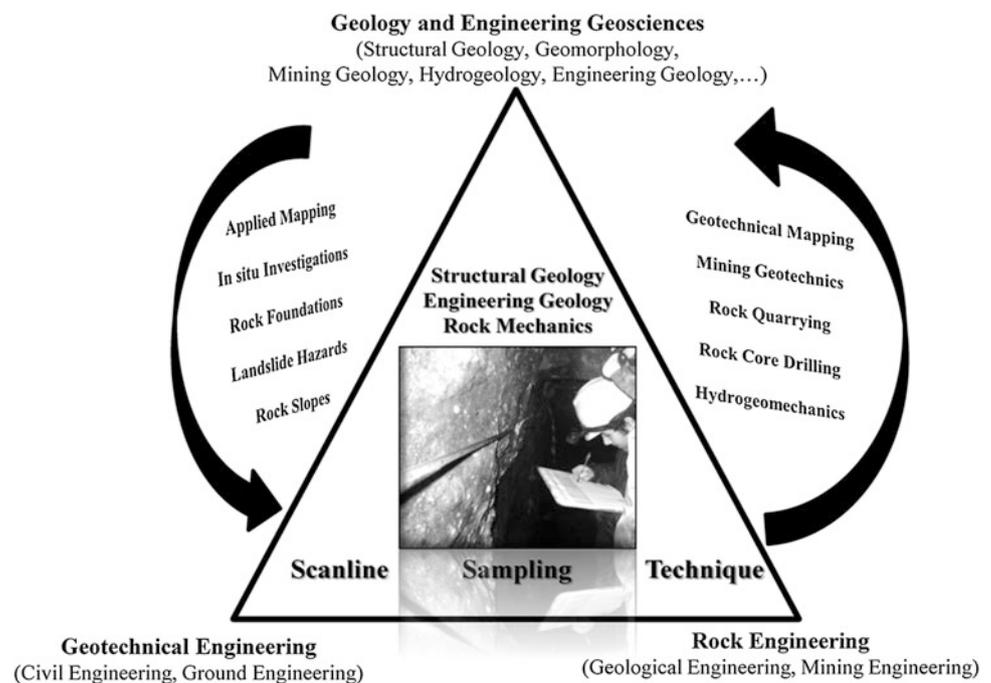
Fig. 61.2 Rock scanline surveys framework to rock design (slope, tunnel, quarry and cavern): a reliable tool to reduce the intrinsic geologic variability and uncertainty
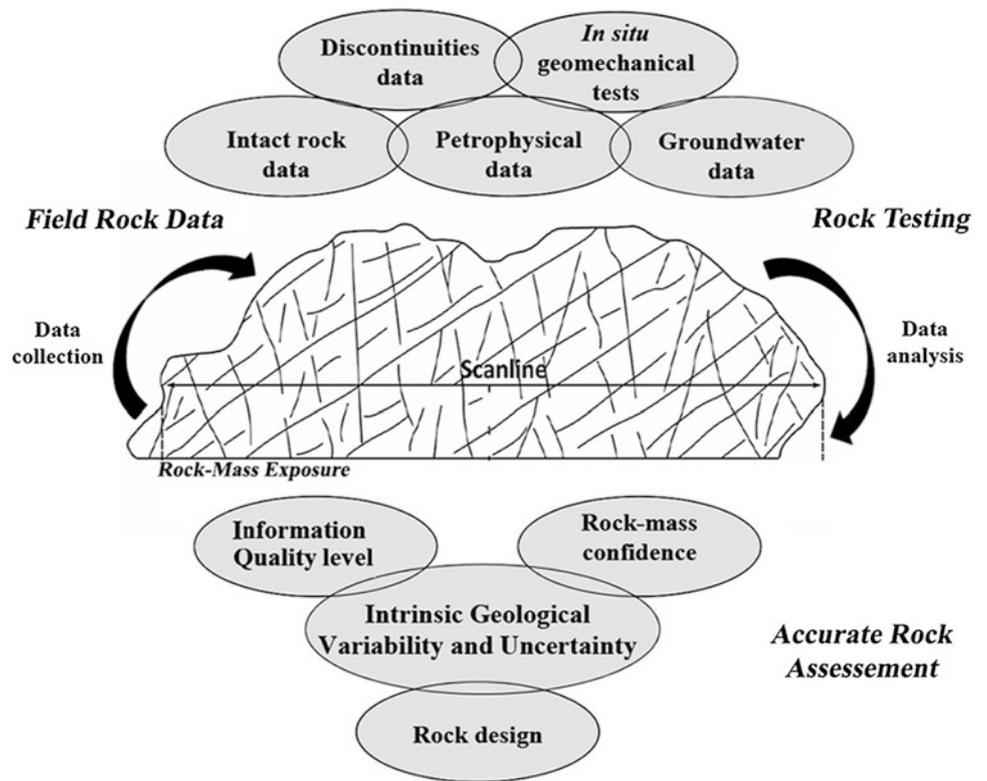
Fig. 61.3 The description/classification/behaviour *versus* assessment/design/modelling of heterogeneous and fractured rock masses
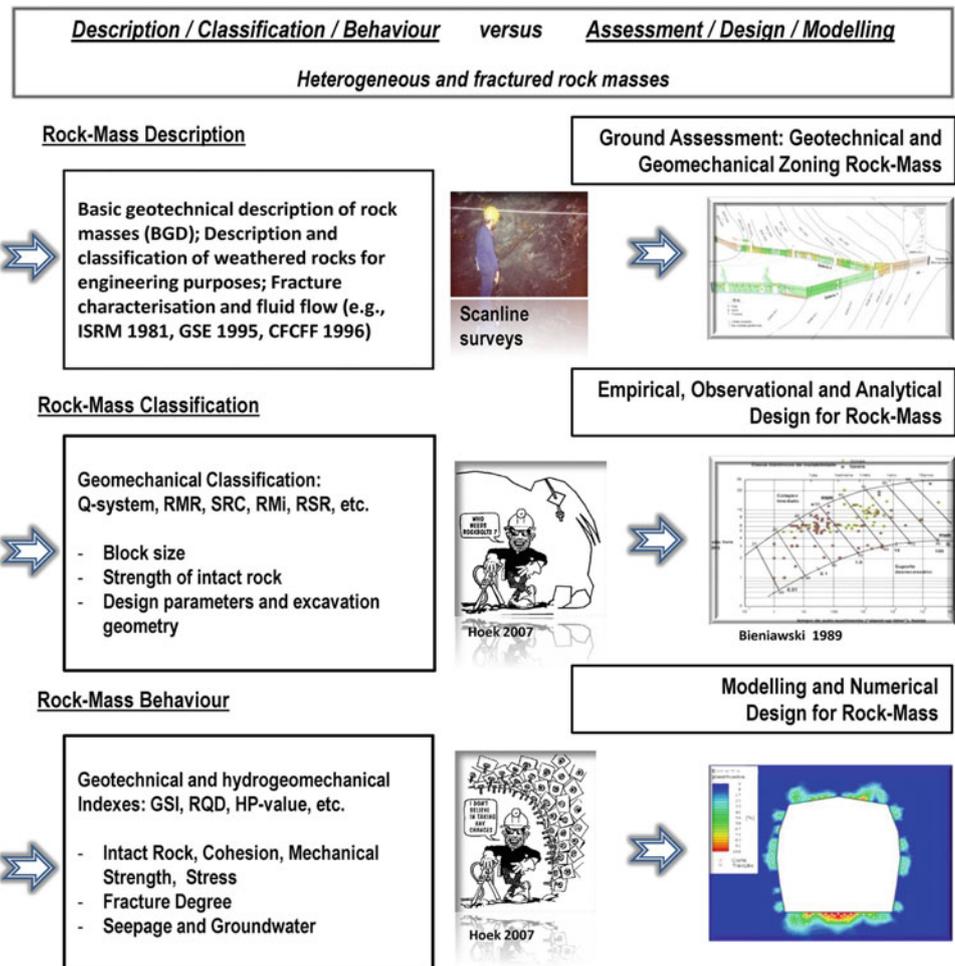
61.3 Concluding Remarks

A clear geology and structural geology framework plays a key-role to support the investigation of all rock engineering projects (Hudson and Cosgrove 1997; Hoek 2007; De Freitas 2009; Chaminé et al. 2013; Shipley et al. 2013). The heterogeneity of the geological properties of rock masses is very significant in geoengineering issues (Hudson and Cosgrove 1997). Particularly, the assessment of in situ block size plays a key-role in rock engineering design projects, such as mining, quarrying and highway cutting operations (e.g., Lu and Latham 1999; Haneberg 2009; Chaminé et al. 2013). In addition, the evaluation based on engineering geosciences, geohydraulic and geotechnical features of rock masses involve combining parameters to derive quantitative geomechanical classifications for geoengineering design (e.g., Bieniawski 1989; Gates 1997; Smith 2004; Barton 2006, 2012; Hoek et al. 2013). In short, good rock engineering must be based in good engineering geosciences, and the big issue raised by Pells (2008), "*what happened to the mechanics in rock mechanics and the geology in engineering geology*", is still valid. However, the intrinsic variability of geological, petrophysical and geotechnical properties must be quantified for reliability-based design and to decrease the uncertainty (e.g., Mazzoccola et al. 1997; Hoek 1999; Keaton 2013). In addition, Mazzoccola et al. (1997) stated an important issue: "*Is there enough information available for design?*".

References

Barton N (2006) Rock quality, seismic velocity, attenuation and anisotropy. Taylor & Francis, London, 729 p

Barton N (2012) From empiricism, through theory, to problem solving in rock engineering: a shortened version of the 6th Müller Lecture. ISRM News J 14:60–66

Bieniawski ZT (1989) Engineering rock mass classifications: a complete manual for engineers and geologists in mining, civil, and petroleum engineering. Interscience, Wiley, New York, 272 p

CFCFF [Committee on Fracture Characterization and Fluid Flow] (1996). Rock fractures and fluid flow: contemporary understanding and applications. National Research Council, National Academy Press, Washington DC, 568 p

Chaminé HI, Afonso MJ, Silva RS, Moreira PF, Teixeira J, Trigo JF, Monteiro R, Fernandes P, Pizarro S (2010) Geotechnical factors affecting rock slope stability in Gaia riverside (NW Portugal). In: Williams A et al (eds) Proceedings 11th Congress, IAEG. CRC Press, Auckland, pp 2729–2736

Chaminé HI, Afonso MJ, Teixeira J, Ramos L, Fonseca L, Pinheiro R, Galiza AC (2013) Using engineering geosciences mapping and GIS-based tools on georesources management: lessons learned from rock quarrying. Eur Geol Mag J Eur Fed Geol 36:27–33

Cunha AP, Muralha J (1990) Scale effects in the mechanical behaviour of joints and rock masses. Memória 763. LNEC, Lisbon 44 p

De Freitas MH (2009) Geology: its principles, practice and potential for geotechnics. Q J Eng Geol Hydrogeol 42:397–441

Gates W (1997) The hydro-potential (HP) value: a rock classification technique for evaluation of the groundwater potential in bedrock. Environ Eng Geosci 3(2):251–267

Haneberg WC (2009) Improved optimization and visualization of drilling directions for rock mass discontinuity characterization. Environ Eng Geosci 15(2):107–113

Hoek E (1999) Putting numbers to geology: an engineer's viewpoint. Q J Eng Geol Hydrogeol 32(1):1–19

Hoek E (2007) Practical rock engineering. Hoek's Corner, RocScience, p 342

Hoek E, Carter TG, Diederichs MS (2013) Quantification of the geological strength index chart. In: Proceedings geomechanics symposium 47th US rock mechanics, San Francisco, CA, ARMA 13-672, pp 1–8

Hudson JA, Cosgrove JW (1997) Integrated structural geology and engineering rock mechanics approach to site characterization. Int J Rock Mech Min Sci Geomech Abs 34(3/4):136.1–136.15

Hudson JA, Priest SD (1983) Discontinuity frequency in rock masses. Int J Rock Mech Min Sci Geomech Abs 20:73–89

ISRM [International Society for Rock Mechanics] (1981) Basic geotechnical description of rock masses. Int J Rock Mech Min Sci Geomech Abs 18:85–110

Keaton J (2013) Engineering geology: fundamental input or random variable? In: Withiam JL, Phoon K-K Hussein M (eds) Foundation Engineering in the face of uncertainty: honoring Fred H. Kulhawy. ASCE. GSP 229. pp 232–253

Lu P, Latham JP (1999) Developments in the assessment of in situ block size distributions of rock masses. Rock Mech Rock Eng 32(1):29–49

Mauldon M, Dunne WM, Rohrbaugh MB Jr (2001) Circular scanlines and circular windows: new tools for characterizing the geometry of fracture traces. J Struct Geol 23(2–3):247–258

Mazzoccola DF, Millar DL, Hudson JA (1997) Information, uncertainty and decision making in site investigation for rock engineering. Geotech Geol Eng 15:145–180

Park HJ, West TR (2002) Sampling bias of discontinuity orientation caused by linear sampling technique. Eng Geol 66(1–2):99–110

Peacock DC (2006) Predicting variability in joint frequencies from boreholes. J Struct Geol 28(2):353–361

Pells PJN (2008) What happened to the mechanics in rock mechanics and the geology in engineering geology. J South Afr Inst Min Metall 108:309–323

Pinheiro R, Ramos L, Teixeira J, Afonso MJ, Chaminé HI (2014) MGC–RocDesign|CALC: a geomechanical calculator tool for rock design. In: Alejano LR, Perucho A, Olalla C, Jiménez R. (eds) Proceedings of Eurock2014, Rock Engineering and Rock Mechanics: Structures in and on Rock Masses (ISRM European Regional Symposium, Vigo, Spain). CRC Press/Balkema, Taylor & Francis Group, London. pp. 655−660. (on pen-drive insert, ISRM Paper CH100)

Priest SD (1993) Discontinuity analysis for rock engineering. Chapman and Hall, London 473 p

Priest SD (2004) Determination of discontinuity size distributions from scanline data. Rock Mech Rock Eng 37(5):347–368

Priest SD, Hudson JA (1981) Estimation of discontinuity spacing and trace length using scanline surveys. Int J Rock Mech Min Sci Geomech Abs 18(3):183–197

Rohrbaugh MB Jr, Dunne WM, Mauldon M (2002) Estimating fracture trace intensity, density, and mean length using circular scan lines and windows. AAPG Bull 86(12):2089–2104

Shipley TF, Tikoff B, Ormand C, Manduca C (2013) Structural geology practice and learning, from the perspective of cognitive science. J Struct Geol 54:72–84

Smith JV (2004) Determining the size and shape of blocks from linear sampling for geotechnical rock mass classification and assessment. J Struct Geol 26(6–7):1317–1339

Terzaghi RD (1965) Sources of errors in joint surveys. Géotechnique 15:287–304

Wu Q, Kulatilake PHSW, Tang H-M (2011) Comparison of rock discontinuity mean trace length and density estimation methods using discontinuity data from an outcrop in Wenchuan area, China. Comput Geotech 38(2):258–268

A Suggested Geologic Model Complexity Rating System

Jeffrey R. Keaton

Abstract

A geologic model captures selected geologic qualities in a region and at a site. An engineering geologic model is relevant to a project and includes specific project aspects. Geology expressed quantitatively, describing variability and uncertainty, is needed in projects employing reliability-based design. Geologists use line style to convey confidence in interpretation of location and nature of lithologic contacts and faults. Mapped lines have error related to scale, terrain, and methods, and uncertainty related to interpretation and allotted field time. A geologic model complexity rating system suggested herein has nine components, four of which are related to regional-scale geologic complexity and five of which pertain to site-scale complexity, terrain characteristics, information quality, geologist competency, and time allotted to prepare the model. Rating criteria and scores are organized into four levels. Simple, uniform, predictable conditions are assigned scores of 3, whereas complex, unpredictable conditions have scores of 81; intermediate conditions have scores of 9 or 27. Possible cumulative scores range from 27 to 729. Cumulative scores can be converted into a form suitable for reliability-based design by defining the highest possible score as the mean value for the geologic model and the actual score as the model standard deviation. Conditions with a maximum score would have coefficient of variations COV = 1.0. The lowest possible COV would be 0.037 (=27/729). Geologic model COVs could be added to geotechnical COVs. This paper seeks to encourage geologists to translate their interpretive understanding into geotechnical parameters needed by engineers for use in Ground Models.

62.1 Introduction

A geologic map or section is a type of geologic model. It is an artistic representation of one interpretation of geologic features and relationships inferred from limited observations of the distribution of rock types, surficial deposits, and geologic structures often with little or no subsurface data or laboratory test results (Keaton 2013). An engineering geologic model is a geologic model relevant to a proposed project that includes pertinent engineering aspects. Geology must be expressed in quantitative terms that describe complexity and uncertainty explicitly to have value in engineering projects, particularly those that employ reliability-based design (RBD). Geologists convey confidence in interpretation with solid, dashed, dotted, and queried lines on geologic maps and sections. The mapped lines have location

J.R. Keaton (✉)
AMEC Americas, Inc, 6001 Rickenbacker Road, Los Angeles 90040, USA
e-mail: jeff.keaton@amec.com

error related to map scale, terrain, vegetation, and field methods, and uncertainty related to the competency level of the geologist and the time allotted for field mapping (FGDC 2006). The FGDC does not specify target values for zones of confidence for digital geologic maps because they are made to satisfy widely varied purposes and needs.

Geologic complexity refers to the qualities and details that are the focus of geologists seeking to understand the history of geologic processes that have occurred to produce the formations as they appear in the field today (Morgenstern and Cruden 1977). Geotechnical complexity relates to variability in strength, stiffness, and hydraulic conductivity of soil and rock masses as these properties might affect the performance of engineered works. Morgenstern and Cruden (1977) state "The most important contribution to increased reliability of site characterization of complex conditions comes from an extra effort associated with geological mapping with the interpretation of the nature of the geotechnical complexity."

Hoek (1999), in the introduction to the second Glossop Lecture, recognizes that geologists tend to be uncomfortable in putting numbers to qualitative observations. He discusses aspects of rock mass rating systems and then comments on the rockfall hazard rating system by Pierson and van Vickle (1993). Hoek (1999) comments that this rating system is based on a set of simple observations that can be made from a slow-moving vehicle and that it contains all the components required for an engineering evaluation of public risks. Hoek (1999) also comments that no direct instructions are given as to how the rating score should be used.

Reliability-based design in geotechnical engineering is challenged by a need for improved calibration of factors used in the process and specifically for layered soil profiles (Kulhawy et al. 2012). Quantitative tools for subsurface investigation, particularly the cone penetration test (CPT), have been used in geotechnical engineering for many years as a means for developing site soil profiles. The quantitative nature of CPT results and the need for geotechnical parameters make geologic methods of interpreting site stratigraphy undesirable, particularly if the geologist is unable to express uncertainty and variability in useable terms.

Burland's Soil Mechanics Triangle (Burland 1987; Keaton 2013) has Geologic Model, Ground Model, and Geotechnical Model in the corners (Fig. 62.1). The Geologic Model represents the site geologic conditions relevant to the proposed project, whereas the Ground Model is the Geologic Model expressed in terms of engineering parameters. The Geotechnical Model is predictive based on project loads and performance requirements. It is the goal of this paper to aid in taking one step towards translating the geologists' interpretive understanding into geotechnical parameters needed by engineers for the Ground Model.

62.2 Geologic Model Complexity Rating System

A geologic model complexity rating system proposed herein has nine components (Fig. 62.2), four of which are related to the regional-scale complexity of the geology (genetic

Fig. 62.1 Burland's (1987) soil mechanics triangle as modified by Keaton (2013)

Category		Rating Criteria and Score			
Component	Points	3	9	27	81
Regional-scale geologic complexity	Genetic - deposition or emplacement	Simple, uniform conditions	Generally simple, predictable conditions	Somewhat complex, generally predictable conditions	Highly complex and variable conditions
	Epigenetic - structural or deformational	No faulting or folding observed or expected	One episode of limited faulting and folding expected	Two episodes of limited faulting and folding expected	Multiple episodes of major faulting and folding expected
	Epigenetic - alteration or dissolution	Unlikely because of geologic setting	Possible because of geologic setting	Likely because of geologic setting	Known to exist
	Epigenetic - weathering and erosion	Uniform weathering profile; minor erosion	Generally regular weathering profile; some erosion	Irregular weathering profile; moderate erosion	Highly irregular weathering; extensive erosion, buried valleys
	Site-scale geologic complexity	Vertically and laterally uniform over project site	Generally regular over project site	Irregular over project site	Highly irregular over project site
	Terrain features	Some relief; many good exposures	Some relief; some good exposures	Strong relief; poor exposures	Heavy vegetation; few or very poor exposures
	Information quality	Extensive data from multiple sources	Limited data from few sources	Reconnaissance level information only	Existing information only; desktop study
	Geologist competency level	Professional Geologist with local field experience	Professional Geologist with field experience in non-similar geology	Geology degree or training with some field experience	No geology training or field experience
	Alotted time or level of effort	Ample time; well-developed interpretation	Adequate time; thoughtful interpretation	Brief time; thoughtful interpretation	Brief time; rushed interpretation

Fig. 62.2 Geologic model complexity rating system, rating criteria, and scores

deposition or emplacement, epigenetic deformation, epigenetic alteration, and epigenetic weathering and erosion). The other five components pertain to site-scale complexity of the geology, terrain characteristics, information quality, geologist competency, and time allotted to prepare the model. These components were mentioned in Morgenstern and Cruden (1977; geologic and geotechnical complexity), FGDC (2006; geologic complexity, terrain, information quality, geologist competency, allotted field time), FHWA (2011; information quality levels), NRCS (2002; outcrop confidence), and Pierson and van Vickle (1993; rating levels and scoring system).

Rating criteria and scores are organized into four levels (Fig. 62.2) similar to rockfall hazard rating systems (Pierson and van Vickle 1993). Simple and uniform conditions can be predicted with confidence and are assigned scores of 3, whereas complex and nonuniform conditions cannot be predicted and are assigned scores of 81; intermediate conditions have scores of 9 or 27. Actual scores will have values associated with multiple conditions for different components.

Thus, possible cumulative scores for the nine categories range from 27 to 729. A possible way to convert cumulative scores into a form suitable for reliability-based design would be to define the coefficient of variation (COV, ratio of standard deviation to the mean value) of the highest possible score as 1.0 and use 729 as the designated mean value for the geologic model. The actual score for the conditions of the site being evaluated would be accepted as the standard deviation since COV is an expression of variability. The COV of the lowest possible score would be 0.037 (=27/729). The COV of the interpreted geologic model should not be used alone in geotechnical analyses; instead, it should be applied to the geotechnical parameters that are used to convert the geologic model into a ground model. For example, if the CPT data and laboratory test results produced strength parameters that the geotechnical engineer believed have $COV_{geotech} = 0.2$ and the geology were simple, predictable, and well documented (i.e., $COV_{geology} = 0.037$), then the combined $COV_{ground} = 0.2 + 0.037 = 0.237$. The engineer may choose to round the COV_{ground} to 0.2, but at least the geology would be considered explicitly and have its own score.

Consider a site condition with tectonic activity, deformation, alteration, complicated surficial deposits (landslides), heavy vegetation, poor topographic maps, and an entry-level geologist who is given less than a week to develop an interpretation. The score might be $COV_{geology} = 1.0$. If the engineer's CPT data and laboratory test results were taken to have $COV_{geotech} = 0.25$, then the combined $COV_{ground} = 1.25$, which would attract the attention of the design team members in their application of reliability-based design methods. In reality, the COV can greatly exceed 1.0; therefore, quantifying geologic complexity is an important topic that deserves further consideration and discussion.

62.3 Conclusions

The geologic model complexity rating system proposed in this paper seems to cover a spectrum of components that contribute to complexity and variability in geologic conditions. It appears to be simple and scoring for a project should be straightforward. The project management aspects could be brought into focus as a source of risk (Baynes 2010) if inadequate time had been allocated for the site geologic characterization task. At a minimum, application of the geologic model complexity rating system would provide a reason for meaningful dialog between engineers and geologists and for geologists to begin to work harder at "putting numbers to geology" (Hoek 1999). Hopefully, this process will help geologists better understand what is needed from a geotechnical perspective for engineers to deliver reliability-based design projects.

This paper is part of the broad range of considerations under the "actuarial" initiative being given by Commission No. 1 (Engineering Geological Characterisation and Visualisation) of the International Association for Engineering Geology and the Environment (IAEG).

References

Baynes FJ (2010) Sources of geotechnical risk. Q J Eng GeolHydrogeol 43:321–331

Burland JB (1987) Nash lecture: the teaching of soil mechanics—a personal view. In: Groundwater effects in geotechnical engineering, vol 3. Proceedings of 9th European conference on soil mechanics and foundation engineering, Balkema, Rotterdam/Boston, pp 1427–1441

FGDC (2006) FGDC digital cartographic standard for geologic map symbolization. US Geological Survey Geologic Data Subcommittee, Federal Geographic Data Committee Document Number FGDC-STD-013-2006, 33 (plus 250 pages of appendices)

FHWA (2011) Subsurface utility engineering. Federal Highway Administration, US Department of Transportation, http://www.fhwa.dot.gov/programadmin/sueindex.cfm (13 Jun 2012)

Hoek E (1999) Putting numbers to geology—an engineer's viewpoint (second glossop lecture). Q J Eng Geol 32:1–19

Keaton JR (2013) Engineering geology: fundamental input or random variable? In: Withiam JL, Phoon KK, Hussein MH (eds) Foundation engineering in the face of uncertainty. ASCE, Reston, pp 232–253 (Geotechnical Special Publication 229)

Kulhawy FH, Phoon KK, Wang Y (2012) Reliability-based design of foundations—a modern view. Geotechnical Engineering State of the Art & Practice: Keynote Lectures from GeoCongress 2012 Geotechnical Special Publication 226. ASCE, Reston, pp 102–121

Morgenstern NR, Cruden DM (1977) Description and classification of geotechnical complexities. In: International symposium on the geotechnics of structurally complex formations, vol 2, Italian Geotechnical Society, pp 195–204

NRCS (2002) Rock material field classification system. US Department of Agriculture Natural Resources Conservation Service, National Engineering Handbook Part 631 Geology, Chapter 12, http://directives.sc.egov.usda.gov/viewerFS.aspx?hid=21423 (13 Jun 2012)

Pierson LA, van Vickle R (1993) Rockfall hazard rating system—participants' manual. Federal Highway Administration Publication No. FHWA-SA-93-057, Washington, DC

Managing Uncertainty in Geological Engineering Models for Open-Pit Feasibility

63

Rosalind Munro and Jeffrey R. Keaton

Abstract

Open-pit mines rely on geology for economic feasibility based on mineral value and geotechnical parameters. Pit slope angles may control economics; therefore, open-pit mine design utilizes a reliability approach that specifies confidence interval, precision index, and practical strength values. The geological model for economic evaluation is developed before pit slope stability analyses are undertaken and is based on lithology and mineralization, both of which are essential for the geological engineering model. The preliminary mine plan includes a shell for the ultimate pit based on assumed pit slope configuration that includes haul-road benches. Geological engineering characterization utilizes the geological model to identify locations for geotechnical bore holes and detailed mapping of rock structure to document aspects critical for slope stability. Uncertainty is common; rock structure variability is represented from direct observation of selected outcrops and from detailed logging of rock core. Lithologies that form the ultimate pit walls are sampled for unconfined compression testing. Samples of a single lithology from different bore holes reflect formation variability. Typically, a few (3–15) samples of each lithology are tested. The desired precision index and reliability may not be met for a specified confidence interval with a limited program; these parameters cannot be determined until test-result variability is known. Geological uncertainty may be managed for open-pit mines by using practical strength values, drilling a few additional bore holes, and performing additional unconfined compression tests.

Keywords

Confidence interval • Precision index • Reliability • Practical strength value

63.1 Introduction

Open-pit mine feasibility involves geology in two different but related ways. The initial use of geology is for general economic feasibility based on mineral value, concentration, and distribution. The preliminary mine layout provides access to the ore using realistic overall pit slope angles and haul-road grades based on assumed geotechnical parameters. Subsequent use of geology is for evaluating the assumed geotechnical parameters to define the steepest stable pit slope angles needed to access the ore body. Small slope angle changes have immense effect on economics of an open-pit mine that is hundreds of meters deep because of the volume of rock and overburden that must be excavated, hauled, and stored during mine development.

The mining industry is accustomed to performing statistical analyses of mineral values that start with relatively few assay tests and are supplemented incrementally with additional assay results. It stands to reason that the mining industry would use a reliability-based approach for selecting strength parameters for designing open-pit mine slopes

R. Munro (✉) · J.R. Keaton
AMEC Americas, Inc, 6001 Rickenbacker Road,
Los Angeles, 90040 USA
e-mail: rosalind.munro@amec.com

initially based on few data points that are supplemented over time. Even the "final" geological model of a mine is tested continuously with blast-hole samples assayed for ore control. A reliability-based approach specifies confidence interval (typically 95 %) and precision index (initially 1.5 for general use), as well as a reliability factor (i.e., non-failure likelihood) appropriate for the project or component being analyzed. The reliability-based approach supports selection of practical strength values for use in engineering stability analyses.

The geological model for economic evaluation of mineral resources usually is developed before the geological engineering for pit slope stability is undertaken. The geological model of the mine is based on lithology, mineralization, and alteration (Fig. 63.1a), all of which also are essential for the geological engineering model. Mine geologists put much effort into developing an accurate three-dimensional (3D) geological model which tends to be accepted in total as the basis for the engineering geological model. The preliminary mine plan will include a shell for the ultimate pit based on assumed pit slope configuration that includes haul road ramps and inter-ramp benches (Fig. 63.1b). The geological engineering characterization program utilizes the geological model of the mine to identify a few locations, often no more than 10, for geotechnical bore holes and locations based on exposed lithology for detailed mapping of rock structure to document aspects that are critical for slope stability. Uncertainty is common in geological engineering characterization. A scale dependency for pit slope stability also exists with bench face angles being steeper than inter-ramp angles, and inter-ramp angles being steeper than the overall pit slope angle (Fig. 63.1b). Rock structure variability is based on direct observation of selected outcrops and from detailed logging of rock core and treated statistically separate from rock strength.

Samples of rock core selected from lithologies in which the pit will be excavated are tested for unconfined compression. Samples of the same lithology obtained from different bore holes are considered collectively in an attempt to represent the variability of the lithologic unit. Typically, a small number (3–15) of unconfined compression tests will be performed for each lithology. Drawing defensible conclusions from analyses of small sets of data requires a statistical approach described by Gill et al. (2005).

63.2 Statistics of Small Data Sets

Statistical analyses of data such as unconfined compression test results utilize the degrees of freedom associated with the number of tests performed, the t-distribution related to the degrees of freedom, the calculated confidence interval based on test results, the probability associated with the t-distribution, and the Chi squared distribution based on the t-distribution probability (Gill et al. 2005). Therefore, the desired confidence interval, precision index, and reliability may not be met with a limited geological engineering characterization program and the parameters cannot be determined until the variability in test results is calculated. The results of the initial characterization lead to a practical value of rock strength for use in stability analyses and a recommendation for managing uncertainty with a minimum number of additional bore holes and unconfined compression tests intended to attain the desired confidence interval, precision index, and reliability factor for the open-pit mine.

Laboratory test results are a subset of the possible tests that could be performed on the rock controlling the stability of open-pit mine slopes (Gill et al. 2005). The reliability of the statistics calculated from small data sets (e.g., mean and standard deviation) depends on the number of samples tested. The number of tests needed to attain a desired confidence interval is calculated with Eq. 63.1 (Appendix A). Gill et al. (2005) recommend that values of precision index Pi be based on project importance; $Pi \leq 1.5$ is suggested for routine mining projects, $Pi \leq 1.35$ is suggested for mining
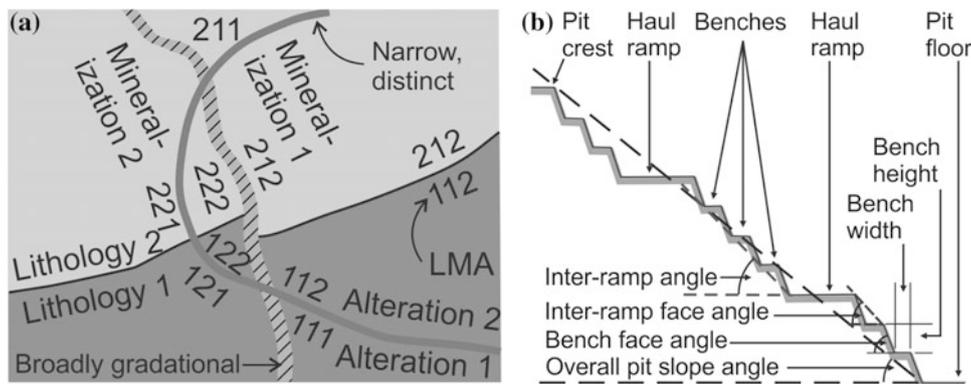
Fig. 63.1 **a** Simple geological model; two lithologies, two levels of mineralization, and two degrees of alteration. Three-number sequences denotes lithology-mineralization-alteration (*LMA*). **b** Pit slope geometry and terms. Both parts are modified from Read and Stacey (2012)

facilities with higher importance, such as shafts, and for routine civil engineering projects, whereas $Pi \leq 1.2$ is suggested for projects in which public safety may be an issue. Gill et al. (2005) also recommend that 95 % be used for Ic for all projects. They note that $Pi = 1.0$ cannot be reached because doing so would require that an infinite number of specimens be tested. Furthermore, the mean and standard deviation of test results would have to equal the true mean and standard deviation of the rock formation, and Ic would be 100 %.

If Ic is designated to be 95 %, then $\beta = 0.975$ from Eq. 63.2 (Appendix A) and t_β can be determined based on the number of samples tested and the appropriate degrees of freedom for the specific analysis. The ratio of true mean of the rock formation and the mean of the laboratory tests is given by Eq. 63.3 (Appendix A). At this point, all parameters in Eq. 63.1 (Appendix A) are known, with Pi having been specified for the project importance. Therefore, Eq. 63.1 can be solved for Pi (Eq. 63.4, Appendix A) so that its actual value can be determined. Equation 63.1 also can be solved for t_β (Eq. 63.5, Appendix A) using Pi calculated from Eq. 63.4, which will enable calculation of β and Ic for the actual test results. t_β can be obtained by interpolating from tables in statistics textbooks or using utilities in electronic spreadsheets or mathematics applications. The ratio of true standard deviation of the rock formation and the standard deviation of the laboratory tests is given by Eq. 63.6 (Appendix A).

A practical strength value associated with a desired or target stability probability (i.e., non-failure probability) is given in Eq. 63.7 (Appendix A) as the lower bound of the true value of mean strength minus the upper bound of the true standard deviation of strength. Target values of Ic, Pi, and Ps not being met is an indication that additional testing is needed to increase the degrees of freedom. Additional testing may or may not result in a smaller coefficient of variation (COV, the ratio of standard deviation to mean), but it will improve the t-distribution parameters.

A feasibility assessment of an open-pit mine pit shell used samples from five borings in two rock types; the unconfined compressive strength (UCS) data are from a real project, but no details are needed for this discussion. Twelve UCS tests were performed on samples of Rock Type 1, whereas Rock Type 2 had four tests (Table 63.1). Initial values used in the feasibility-level statistical analysis were $Ic = 95$ % and $Pi = 1.5$. Selected parameters for the two rock types are summarized in Table 63.2 and Fig. 63.2. Target values of Ic and Pi were exceeded for Rock Type 1, but were not met for

Table 63.1 Unconfined compressive strength (UCS) test results for two rock types

Rock type	UCS (MPa)	Ns	$\bar{X}$	sd	COV
1	60, 65, 66, 77, 80, 89, 90, 93, 106, 113, 122, 141	12	91.83	24.77	0.270
2	27, 41, 53, 68	4	47.25	17.44	0.369

Table 63.2 Statistical values for UCS data in Table 63.1

Rock type	Ic (%)	Pi	Lower μ (MPa)	Upper σ (MPa)	Ps (%)	PSV(Ps) (MPa)
1	96.83	1.44	75.39	46.47	85	21.29
					92	0.03
2	58.26	5.22	37.80	34.19	39	0.02

Target $Pi \leq 1.5$, $Ic \geq 95$ %

Fig. 63.2 Summary of unconfined compression strength of two rock types
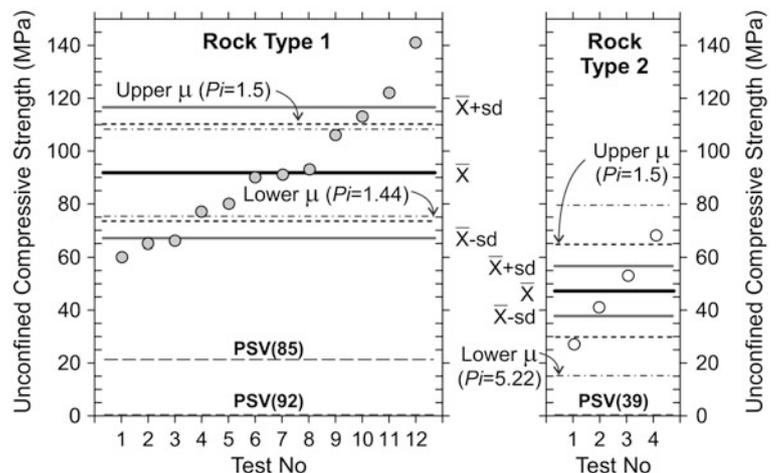
Rock Type 2, indicating that additional tests are needed to attain target Ic and Pi values. Gill et al. (2005) show that $Ps = 85\%$ results in a true stability probability of approximately 99 % for $Ic = 95\%$, whereas the stability probability is approximately 90 % for $Ps = 65\%$. The highest Ps value for Rock Type 2 that produces $\text{PSV}(Ps) \approx 0$ is 39 % for $Ic = 58\%$. Rock Type 1 tests support $Ic = 97\%$ so the PSV (85) strength would be appropriate for stability analyses, and a higher PSV might be justified by using a lower Ps value because $Ic > 95\%$.

63.3 Conclusions

Uncertainty in geological engineering models at the mine feasibility level can be managed by relying on geological models of lithology, mineralization, and alteration, along with UCS tests on a small number of samples of the rock that will support the pit slopes. Statistical analyses of UCS test results are essential to select strength values that have suitable stability probabilities and are consistent with desired confidence limits and precision indexes. The geological engineering model at the mine feasibility level provides the foundation for model refinements and improved precision in later phases of mine development.

Appendix A: Statistics Equations for Sect. 63.2

Equations for Sect. 63.2 are in this appendix (modified from Gill et al. 2005).

$$Ns = \left[\left(\frac{Pi+1}{Pi-1} \right) t_\beta \frac{sd}{\bar{X}} \right]^2 + 1 \tag{63.1}$$

$$Ic = 100(2\beta - 1); \text{ consequently, } \beta = 0.5(1.0 + Ic/100) \tag{63.2}$$

$$1 - \left(\frac{Pi-1}{Pi+1} \right) = 1 - \varepsilon_m \le \frac{\mu}{\bar{X}} \le 1 + \left(\frac{Pi-1}{Pi+1} \right) = 1 + \varepsilon_m \tag{63.3}$$

$$Pi = \frac{\bar{X}\sqrt{Ns-1} + sd\, t_\beta}{\bar{X}\sqrt{Ns-1} - sd\, t_\beta} \tag{63.4}$$

$$t_\beta = \frac{\bar{X}}{sd} \sqrt{Ns-1} \frac{Pi-1}{Pi+1} \tag{63.5}$$

$$\sqrt{\frac{Ns}{\chi^2_\beta}} \le \frac{\sigma}{sd} \le \sqrt{\frac{Ns}{\chi^2_{(1-\beta)}}} \tag{63.6}$$

$$\text{PSV}(Ps) = \frac{2}{Pi+1}\bar{X} - n_\alpha \sqrt{\frac{Ns}{\chi^2_{(1-\beta)}}} sd \tag{63.7}$$

Ns = the number of test results, Pi = precision index, t_β = the t-distribution, β = parameter related to the desired confidence interval, Ic, $\bar{X}$ = mean of the test results, sd = standard deviation of the test results, μ, = true mean of rock formation, σ = true standard deviation of rock formation, ε_m = maximum relative error, χ^2 = Chi squared distribution, $\text{PSV}(Ps)$ = practical strength value associated with a designated or target stability probability (i.e., non-failure probability), n_α = probability coefficient obtained from the normal density function, and $\alpha = Ps/Ic$ with the restriction that $Ps \ll Ic$ for conditions with small mean and large standard deviation to avoid PSV $(Ps) < 0$. The t-distribution requires $Ns - 1$ degrees of freedom.

References

Gill DE, Corthesy R, Leite MH (2005) A statistical approach for determining practical rock strength and deformability values from laboratory tests. Eng Geol 78:53–67

Read J, Stacey P (2012) Guidelines for open pit slope design. CRC Press, Balkema, 496 p

Construction in Complex Geological Settings – The Problematic of Predicting the Nature of the Ground

Convener Prof. Ana Paula F. da Silva—*Co-conveners* Lazaro Zuquette, Ricardo Oliveira, Joaquim Pombo

Nowadays, development has been pushing the occupation of brownfields or any other type of ground previously set aside due to its poor geotechnical characteristics. Additionally, civil engineering projects have been growing in complexity and therefore require higher geotechnical knowledge. In this scope, the role played by the specialist in engineering geology during design has gained even more relevance, since its expertise is fundamental for maximizing the data gathered from site investigation and, afterwards, for building an approximate geological model of the ground and defining its geotechnical properties. The aim of this session is the presentation and discussion of case studies that illustrate the way engineering geology deals with geological complexity and their modelling, since no matter how sophisticated tools the design team might use, basic knowledge of the ground sis still the cornerstone of everything.

Engineering Geological and Geotechnical Cartographic Modeling as a Methodological Basis for Engineering Surveys and Design in Complex Geological Environment

64

Felix Rivkin, I. Kuznetsova, A. Popova, I. Parmuzin, and I. Chehina

Abstract

The methodological principles and methods of the creation of new geotechnical cartographic models are considered on the basis of engineering-geological and permafrost cartographic models. Creation of the geotechnical cartographic models is considered as a method of optimizing the interaction between project designers and geologists working in complex natural environment and presenting the results of research in the form adapted for the design. The results of application of the geotechnical models are examined for the implementation of the pipeline projects in complex environment.

Keywords

Engineering geocryological cartographic model • Geotechnical cartographic model • Complex geoenvironment

64.1 Introduction

The main purpose of the investigations of pipeline routes is to obtain information for the design and construction. The more complex the natural conditions of the study area are the greater demands are placed on the results of investigations.

The engineering-geological and permafrost conditions predetermine the choice of technical design solutions at a large extent. There is a feedback on the other hand, i.e., the pre-selected design solutions greatly affect the scope and methods of the natural environment studies. Therefore, the establishment of functional connections between the engineering-geological conditions and design solutions allows optimizing of both site investigations and the design itself. It provides the opportunity to focus the study of natural conditions and ground properties at the most challenging areas. Further studies, therefore, are directed towards detailing of engineering-geological conditions and the specific technical solutions.

GIS-based research is one of the methods of site investigations, design and construction optimization in complex natural environment. Development of the multi-scale GIS cartographic models as an information support method for engineering research and design is often used in Russia. Normally, these methodological solutions are applied for the challenging projects, for example, during the development of oil and gas fields in the Arctic, the construction of trans-regional systems of main pipelines, etc. (Rivkin et al. 2004, 2006).

It should be noted that the creation of multi-scale and multi-purpose (Rivkin et al. 2010; Rivkin 2012) cartographic models (with their further consistent detailing) is most effective at the early stages of the project, prior to the major investments in the field engineering investigation and design.

64.2 Methods

Contemporary engineering-geological and geocryological conditions in the permafrost area result from a complex interaction of various environmental factors. Therefore, for

F. Rivkin (✉) · I. Kuznetsova · A. Popova · I. Parmuzin · I. Chehina
Fundamentproject OJSC, Moscow, Russia
e-mail: f-rivkin@narod.ru

the development of engineering and geocryological cartographic models it is pertinent to analyze the interaction of the main factors that determine geotechnical conditions that, in turn, specify permafrost conditions. It means that it is necessary to combine two disparate groups of factors—the engineering-geological (mainly regional) and the permafrost (mainly zonal) data in a general analytic scheme. This analysis is performed in a synthetic matrix form, since it is virtually impossible to construct a hierarchical system to analyze groups of heterogeneous factors.

Geostructural and tectonic conditions, geomorphology and lithology are traditionally regarded as the regional factors for engineering-geological and permafrost conditions assessment. At first, geostructural and major tectonic elements of the study area are singled out, than the main geomorphic features such as watersheds, slopes, valleys, rivers, sea, river and glacial terraces are distinguished.

At the end, differentiation of regional factors is completed by identifying the main types of lithological or cryo-lithological sections.

The zonal factors depend on the latitudinal location of the study area: the climate, vegetation, landscape, the depth of seasonal freezing and thawing—that is, the factors that determine the current permafrost conditions in upper part of the ground cross-section.

These two groups of factors are grouped in a hierarchical manner and are arranged along the axes of the matrix. Thus, the matrix of the regional and zonal factors multivariate analysis presents not only a form for the analysis of the interaction of environmental factors, but, in fact, the legend to the GIS-based cartographic models of engineering-geocryological conditions (GIS-EG). In such a methodological statement GIS-EG illustrates a variety of engineering and permafrost conditions and identifies most complicated areas.

Fig. 64.1 Geotechnical cartographic models. **a** The schematic map of the pipeline route with complex natural conditions. **b** The schematic geotechnical cartographic model of the pipeline main design solutions
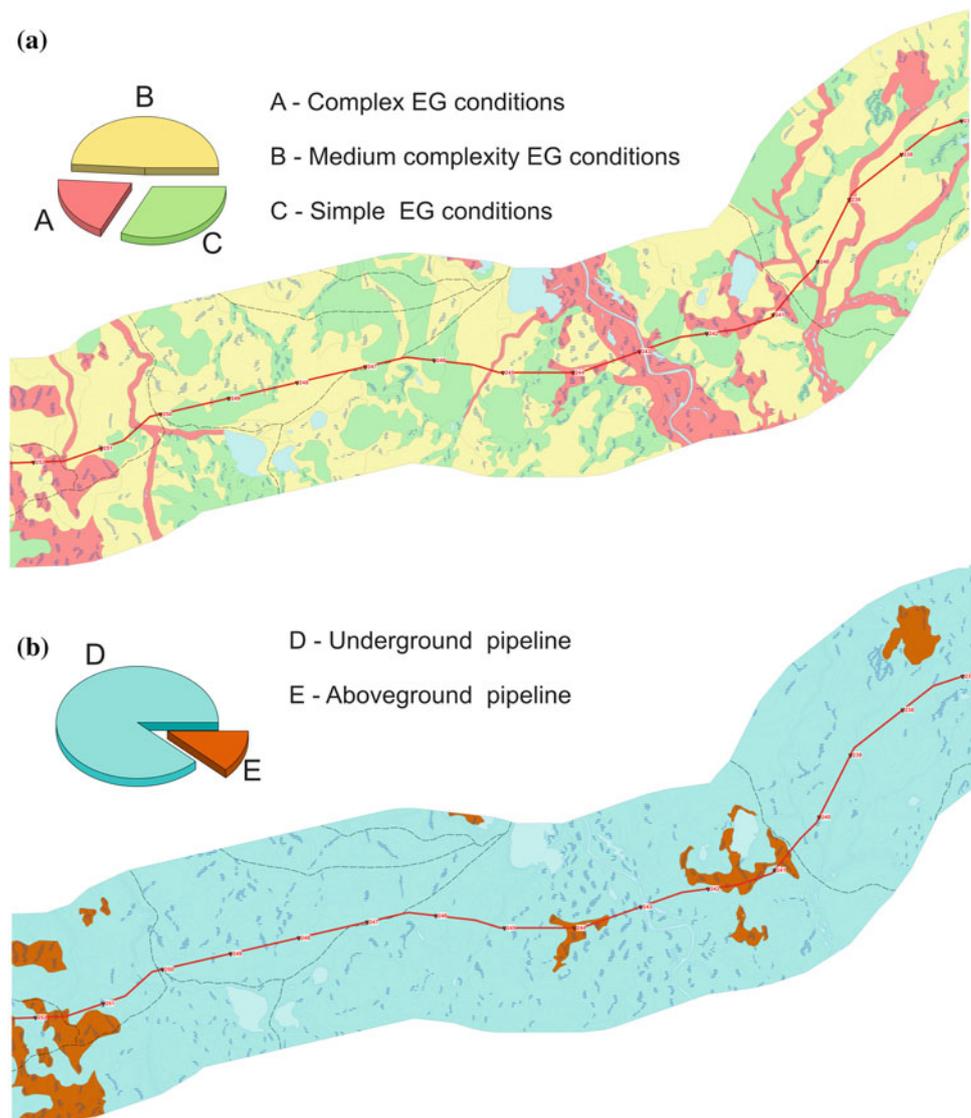
So, the first important step of the pipeline route investigations is the development of the GIS-based cartographic models of engineering geological conditions in the permafrost areas and consistent specification of those models and their characteristics.

A large number of standard technical solutions for foundation structures is used in the Arctic. Each of them was designed for certain engineering-geological and permafrost conditions. Good practice has been developed for application of standard technical solutions in well-defined natural conditions. In other words, the correspondence between the natural environment and the types of appropriate foundations has been formed.

The applicable range of technical solutions includes only those of them which were justified for technical, engineering-geological, environmental, and economic characteristics. Thus, the second step involves the methodical development of a set of possible technical solutions in the areas with complex engineering-geological environment. These areas have been identified at the first step, and their spatial position was presented at GIS-based cartographic model of the engineering-geocryological conditions (GIS-EG). So, the second step is the development of a wide range of geotechnical solutions for foundation structures for the different types of the geocryological conditions.

The third step involves the methodical integration of the results of the first and second phases—the cartographic expression of the location of various technical solutions along the pipeline route in the form of a spatial geotechnical model. It starts from the transformation of a synthetic matrix legend for map of engineering-geological conditions into the matrix legend for the geotechnical cartographic model. On the basis of the transformed matrix that comprises the legend for the map, geotechnical cartographic model (GIS-GCM) is developed. All selected engineering-geological plan units are shown on the geotechnical models as the areas where the recommended technical solutions or construction methods should be applied.
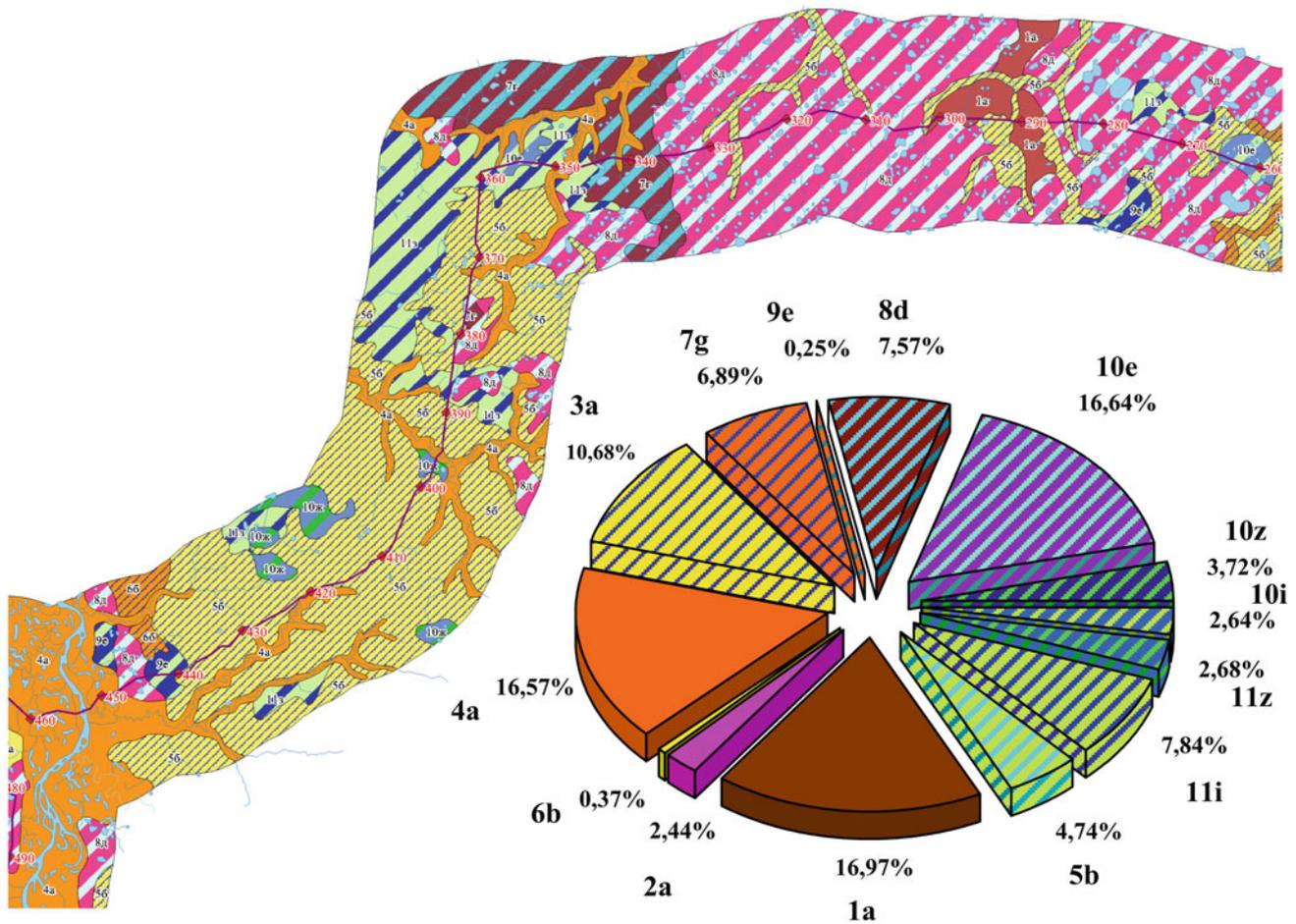
Fig. 64.2 The schematic geotechnical cartographic model (fragment of the design solutions map of pipeline route). Diagram presents percentage of the total length of all selected areas with different design solutions. Indexes (1a, 2a, ..., 11z) show types of engineering-geocryological areas with various pipeline foundation solutions are recommended (e.g. 1a—10 m long pile foundation without thermal stabilization of soils; 11z—12 m long pile foundation for the pre-thawing of frozen grounds, with a thermal shield)

64.3 Results and Discussion

Geotechnical cartographic model is actually a methodological bridge between the results of engineering-geological investigations and design. This model explicitly shows the connection between the design and the geotechnical and geocryological conditions. Such methodological solutions come out from the necessity to optimize the site/route investigations and design according to the particular natural environment. They are usually applied for large-scale transregional pipeline projects laid in complicated geological conditions. They are also used for the infrastructure development, oil and gas fields in the permafrost area (Arctic and sub-Arctic).

Analysis of this information provided recommendations for certain design solutions. The above-ground laying was recommended at the geologically-complex sites, whether at the other sites the simpler and less expensive underground laying was applied. The GIS-based cartographic model allows interpreting this information in a quantitative way. Figure 64.1 shows the quantitative ratio of above and underground pipeline laying and exemplifies the geotechnical cartographic model developed at the preliminary stage of the investigation.

The complex areas on the Fig. 64.1 are highlighted by red: propagation of icy ground and hazardous geological processes. This information allowed to recommend certain design solutions. Within the complex areas above-ground pipeline was recommended, whereas at other sites—underground installations, which are simpler and less expensive.

Further development of this method is associated with a detailed GIS-EG and GIS-GCM. It allows not only to differentiate areas with above-ground and underground laying, but also highlights areas with various pipeline-supporting piles design (Fig. 64.2). Analysis of the pipeline design solutions map allows to perform a quantitative analysis of the results of route investigations for geotechnical conditions assessment and design. The diagram on Fig. 64.2 shows the percentage of sites with complex conditions, and a performed quantitative assessment of the application of certain technical solutions that forms the ground for the construction cost estimate.

Therefore, the informational support of the site investigations and design can justify the choice of design solutions based not only on the complexity of natural conditions and the length of such sites, but also taking into account the cost estimate of construction.

64.4 Conclusion

The establishment of specialized GIS-EM & GCM is a modern methodological interconnection basis between geotechnical and permafrost studies and construction design. It allows optimizing both the engineering-geological investigations and design in complex environment, and creating of an information base to justify the selection of design solutions and construction methods. On the other hand, this method makes it possible to concentrate investigations at the most challenging areas, increasing their information value, and therefore their efficiency.

References

Rivkin FM (2012) Geotechnical maps in the structure of information support for geotechnical investigations. In: Proceedings of tenth international conference on permafrost. Extended Abstracts, The Northern Publisher, Salekhard, pp 471–472

Rivkin FM, Ivanova NV, Kuznetsova IV (2006) Geoinformation modeling of engineering geocryological conditions for risk assessment during survey of the Yamal-Western Europe Pipeline (Yamal Segment). In: Proceedings of XIth international congress for mathematical geology, Liège, Belgium, 3–8 Sept, S09-23, p 4

Rivkin FM, Kuznetsova IL, Ivanova NV, Popova AA, Parmuzin IS (2010) Multi-purpose engineering geological cartographic for information support for engineering surveys, designing, and monitoring. In: Proceedings of 11th congress of the IAEG, Auckland, 5–10 Sept 2010, pp 2415–2419

Rivkin FM, Kuznetsova IL, Ivanova NV, Suhodolsky SE (2004) Engineering-geocryological cartographic for construction purposes in permafrost regions. In: Engineering Geology for Infrastructure Planning in Europe. Springer, Berlin, pp 172–178

Experiences Learned from Engineering Geological Investigation of Headrace Tunnel on Sedimentary Rock—Xekaman3 Hydropower Project—Lao PDR

65

Nguyen Song Thanh and Dao Dang Minh

Abstract

Xekaman3 hydropower project is located in Sekong province, Southern of Lao PDR. Site investigation for the project was carried out from January 2003 to May 2010 at damsite, water intake, headrace tunnel (7,400 m) and powerhouse area. Unfortunately, for the tunnel section from vertical well No 1 (GD1) to vertical well No 2 (GD2) with the length of 710 m, many complex geological phenomena happened and it influences significantly the whole construction scheduled and total investment of the project. This paper presents the causes of those phenomena, ways to solve problems and methods of improvement for the tunnel section mentioned above. The authors also mentioned some experiences learned through geological investigation process for headrace tunnel of Xekaman3 hydropower project and possibility of applying these experiences for the projects with similar geological conditions.

65.1 Introduction

The headrace tunnel of Xekaman3 hydropower project with total length of 7,400 m runs through some different formations such as: Long Dai formation (O_3-S_1 ld), Song Bung formation ($T_{1-2}sb$) and Quaternary system. In the tunnel section from vertical well No 1 (GD1) to vertical well No 2 (GD2—Km6 + 830) with the length of 710 m (see Fig. 65.1), the whole section belongs to Song Bung formation with main composition as follows :

- Upper member: Grey–reddish grey thick bedded siltstone, sandstone with fine grain; sandstone, gritstone with coarse grain in upper part.
- Middle Member: Mainly reddish brown thick bedded siltstone; intercalated with lenses of blackish grey sandstone, siltstone, shale.

- Bottom Member: Mainly red thick bedded sandstone with fine-medium grain intercalated with lenses of red siltstone.

Two alternatives of tunnel in this section were considered. Initially, this tunnel section was designed on the ground with the depth of pillar is about 30–40 m from the ground. And then, due to complex geology, it is changed to underground alternative and the depth of tunnel is about 145 m below ground surface.

This paper presents some experiences learned during investigation and construction of this tunnel section, especially for changing of alternative from On the ground to Underground and treatment experiences for tunneling section in complex geology.

65.2 Site Investigation Phases and Results

In the pre-Feasibility Stage (FS) stage, in the section from surge tank to the powerhouse, the tunnel was initially designed on the ground. So, base on this design, boreholes

N.S. Thanh (✉) · D.D. Minh
FECON Foundation Engineering and Underground Construction Company, 15th Floor CEO Building, Pham Hung St, Hanoi, Vietnam
e-mail: thanhns@fecon.com.vn
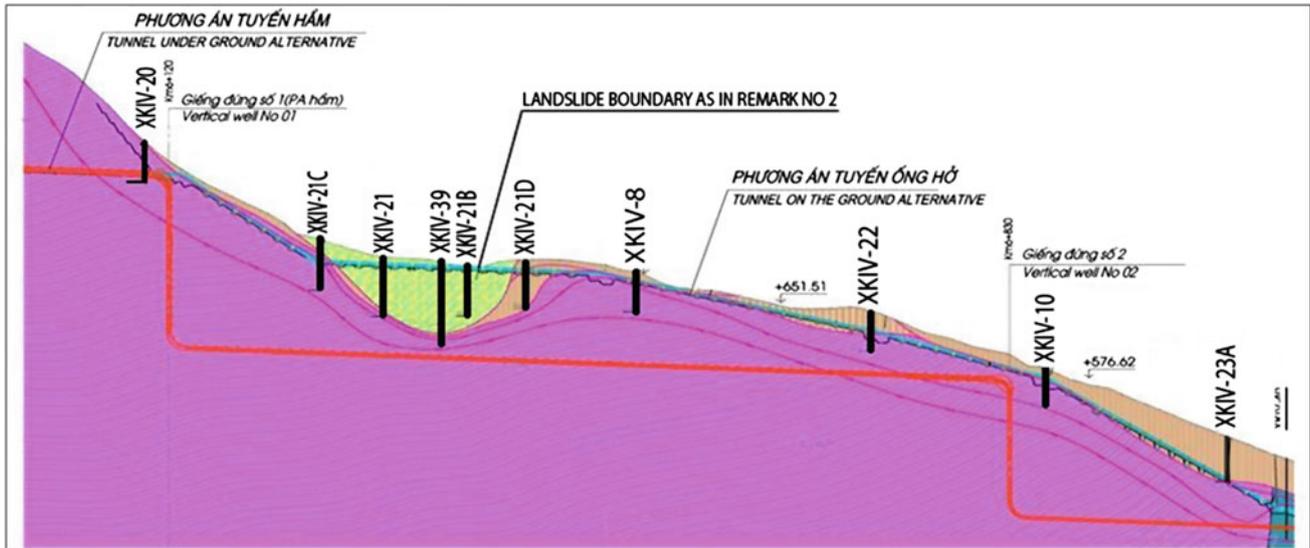
Fig. 65.1 Landslide boundary at penstock based on Remarks No 1 and No 2

XKIV-08, XKIV-09, XKIV-10, XKIV-20, XKIV21, XKIV-22, XKIV-23, XKIV-28 were located at pillars with the depth ranges from 30 to 40 m (see Fig. 65.1). During FS stage, many kinds of geotechnical investigation were implemented. As the result of investigation, geotechnical engineers had delimitated the complex geology area for this tunnel section (Fig. 65.1) and figured out the engineering geological parameters for designers, as mentioned hereafter.

65.2.1 Remark No 1

- Engineering geological map, large scale for the studied area and the distribution of different soils and rocks, thickness of weathering layers in the studied area to the depth of 40 m was established.
- Preliminary definition of the boundary of old landslide along the axis of On the ground tunnel section surrounding borehole XKIV-21 to the depth of about 50 m and confirmed that the section from XKIV-09 to XKIV-22 on the engineering geological profile does not belong to the old landslide.
- In the borehole logs of XKIV-09, XKIV-22, from depth of 16.4 m (XKIV-09), 23.7 m (XKIV-22) and deeper, rock belongs to IIA zone (fractured rock zone) or IIB zone (fresh rock zone).
- Determination of the physico-mechanical properties of weathering rock zones.
- Determination of the hydrogeological conditions of study area.

As listed above and concerning complex geology, designers decided that additional site investigation must be carried out in FS stage to:

- Determine exactly the boundary of old landslide on the ground and underground along the tunnel axis.
- Determine exactly depth of weathered rock zones IB, IIA and IIB.

Then, the final decision to change this tunnel section from On the ground to Underground was made by the designers and approved by the Investor—Viet Lao Power Company Ltd. As requested, on August 2004, 6 additional boreholes, XKIV-21A, XKIV-21B, XKIV-21C, XKIV-21D, XKIV-23A, XKIV-23B, were located around borehole XKIV-21 with depths of 30–50 m (Fig. 65.1). The results of these boreholes lead to Remark No 2.

65.2.2 Remark No 2

- The boundaries of old landslide was redefined: 209 m long, starts from left of XKIV-21C to XKIV-21D borehole along the axis of tunnel; its deepest point rest 74 m below the surface (Fig. 65.1).

Base on Remark No 2, designers decided to change this tunnel section from on the ground to underground and this design will be applied for investigation of technical design (TD) stage. The main purposes of the investigation for this stage were:

- Assess the exact boundaries of old landslide underground. It is noted that their limits up to this stage is not a concern anymore!
- Determined the exact engineering geological conditions from surface to a depth below the tunnel.

For those purposes above, in TD, only one borehole XKIV-39, 90 m deep, was carried out. The results of XKIV-39 lead to the Remark No 3.

65.2.3 Remark No 3

The maximum depth for the bottom of old landslide was 70 m.

Based on this finding, designers decided that the depth of tunnel's bottom of the new design section will be located at elevation of +590 m, 20–25 m lower the bottom of the old landslide and, with this elevation, the tunnel section would run completely in fractured rock zone IIA or fresh rock zone IIB. With this design and since March 2009, the tunneling from GD2 towards the GD1 was undertaken. Unfortunately, during construction of this tunnel section, many complex geological phenomena happened.

Confronted with situation of very poor and complicated geological conditions as mentioned, the Investors requests designers and geological engineers to verify and assess again the geological conditions of tunnel section from vertical No 1 (GD1) to vertical No 2 (GD2), based on the detected geological conditions, geological data records of constructed tunnel sections and recommends to carry out additional geotechnical drilling for the remaining unconstructed tunnel section.

65.3   Changes During Tunneling

65.3.1 Reassessment of Results of Previous Stage and Data Records During Tunneling

Based on the detected very poor and complicated geological conditions of the tunnel section as mentioned above, engineering geological engineers had carefully reassessed the results of geological investigation of FS and TD stages and analyzed the geological description report for constructed tunnel section. Unfortunately, some mistakes were found, namely:

- As in Remark No 1, in borehole logs of XKIV-09 and XKIV-22, the estimation of bedrock zone encountered is not correct.
- The extension of old landslide is not 209 m as assessed in Remark No 2. In fact, along the axis of tunnel, the landslide is 530 m (Fig. 65.2).
- Bottom of old landslide as indicated in Remark No 3 with the depth of 70 m is not correct. It leads that the selection of depth of tunnel 90 m is not enough to avoid the landslide. One of other mistake is that, during drilling additional borehole XKIV-39, the required depth is 90 m, but the final depth of this borehole is only 81 m, not reaching the bottom of tunnel! In TD stage, this is unacceptable.
- The geological description document during tunneling is too sketchy.

As analyzed and due to some incorrections mentioned above, according to the requirement of Investor, a survey unit carried out 3 additional boreholes, XKIV-BS1, XNKIV-BS2 and XKIV-BS3, for the remaining unconstructed tunnel section (Locations in the Fig. 65.2). Main purpose of these additional drilling is to determine exactly the extension and depth of old landslide and evaluate the geological conditions in the unconstructed tunnel section from GD2 to GD1.

In case of whole tunnel section locates on the body of old landslide, then possibility of adjustment for this section from underground to on ground would be considered. The result of these additional boreholes lead to the Remark No 4.
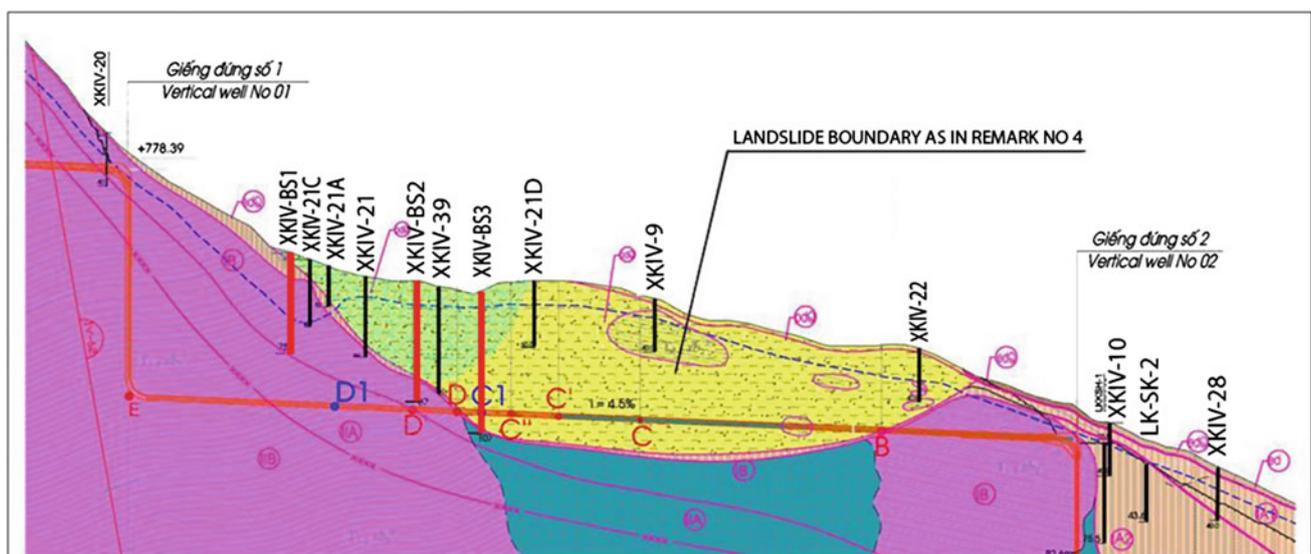
Fig. 65.2 Landslide along the axis of tunnel section after adjustments according to Remark No 4

65.3.2 Remark No 4

- The maximum depth of old landslide is 125 m, not 70 m as stated in Remark No 3 (Fig. 65.2)
- The remaining old landslide body along the axis of tunnel from current tunnel face (Km6 + 392) to the original bedrock boundary is 20 m and there is no need to adjust the tunnel from underground to on the ground. To ensure safety for tunneling in this 20 m remaining, reinforcement solutions must be applied.

As mentioned above, reinforcement grouting for the 20 m remaining old landslide body is selected by the Investor to be performed.

65.3.3 Reinforcement Grouting for Remaining Tunnel Sections

Base on the existing and actual geological conditions, the reinforcement grouting while drilling parallel with the axis at the tunnel face is impossible because it is not safe for workers and equipments; therefore, reinforcement grouting using vertical drilling along the axis of tunnel was selected. To ensure the flows of liquid cement mortar would not go into tunnel, the section near the final tunnel face (km6 + 392) must be blocked by concrete during grouting.

At present, the whole tunnel section construction from tunnel face km6 + 392 to the vertical well GD1 has finished successfully.

65.4 Conclusion and Recommendations

1. In this particular project, at the beginning of FS-stage investigation, by studying topography-geomorphology, the existing old landslide is confirmed and then, it could have been recommended adjusting the location of tunnel to avoid running through it.
2. After an engineering geological object which could be harmful to the safety of project is defined (as the old landslide mentioned above), it is necessary to perform some additional investigation methods and, for each method, specific criterion should be listed in advanced. For any reasons, if any one of specific criterion is not defined clearly then additional site investigation must be implemented. In this case, some investigation experiences should be noted :

   - The main purpose of borehole XKIV-39 is to define the depth of old landslide but it is stopped at 81 m while design depth is 90 m. This is not acceptable because the depth of borehole did not underpass the depth of tunnel. In this case, the borehole XKIV-39 should have been redrilled.
   - The geological description of tunnel while tunneling should be detailed enough so that reinforcement solution for specific tunnel section could be applied successfully. In dealing with geological problems, the collaboration between designers and constructor is very important.

References

SDCC Song Da Consulting JS Company (2005) Report on engineering geological investigation of main works of Xekaman3 hydropower project—FS (Dec-2003) and technical design stage (Mar 2005)

SDCC Song Da Consulting JS Company (2010) Additional report on engineering geological investigation of tunnel (section from vertical well No1-GD1 to vertical well No2-GD2) of Xekaman3 hydropower project, detailed design stage—Lao PDR

Engineering Properties of Badlands in the Canadian Prairies

66

Khan Fawad and Azam Shahid

Abstract

The main objective of this paper was to investigate the engineering properties of badlands in the Canadian Prairies. Under the prevalent semi-arid climate, soils in the area undergo extensive variations due to alternate wet-dry cycles. The soil profile has three distinct sediments: fissured sandstone with a steep slope of 60°; popcorn-textured mudrock with a mild slope of 30° and; eroded pediment with a flat slope of 3°. The fines content increased from dry to wet state with 17–33 % for sandstone, 4–98 % for mudrock, and 21–42 % for pediment. The consistency limits indicated that the water adsorption capacity is highest for mudrock followed by sandstone and then by pediment. The water retention curve of sandstone showed bimodal distribution with a low air entry value (6 kPa) pertaining to drainage through cracks and a high air entry value (150 kPa) associated with flow through the soil matrix. The mudrock and pediment followed a unimodal water retention curve with a single matrix air entry value of 5 kPa. These results explain the observed surface erosion and internal piping through the sandstone and the genetic relationship between the sandstone and the pediment.

66.1 Introduction

Badlands are rugged landscapes comprising of loose materials and are commonly found in arid and semi-arid regions of the globe. The engineering properties of such sediments are derived from geologic history and climatic conditions. This is particularly true for the Canadian Prairies where badlands originated from Cretaceous rocks, comprise of sands through clays, and undergo cyclic saturation and desaturation due to seasonal variations in meteorological parameters. The surface lithology continuously evolves due to alternate fluvial erosion (rain splash, sheet wash, overland flow, concentrated flow, and pipe flow) and water deficiency (evaporation, transpiration, cracking, sapping, and mass movement). The effect of these processes is experienced differently by the various badland sediments at a given site.

A typical example of an incessantly transforming terrain is the Avonlea badland (latitude 50.0367 and longitude 105.0667) in southern Saskatchewan, as given in Fig. 66.1. The region has experienced eight glacial advances and retreats during the Quaternary (Christiansen 1979). The last glacier, the Laurentide ice sheet, reached its maximum extent about 18,000 years B.P. This 1,000 m thick ice gradually retreated in the north-eastward direction and eventually disappeared around 8,000 years B.P. The emerging surface rocks were extensively eroded by the preceding scouring actions of the advancing glaciers. The melting ice cut the exposed materials and created steep-sided channels and deeply incised rills. With increasing floods, the less resistant Cretaceous rocks of the Eastend Formation were washed

K. Fawad · A. Shahid (✉)
University of Regina, 3737 Wascana Parkway, Regina S4S 0A2, Canada
e-mail: shahid.azam@uregina.ca

Fig. 66.1 Map of southern Saskatchewan showing the investigated area
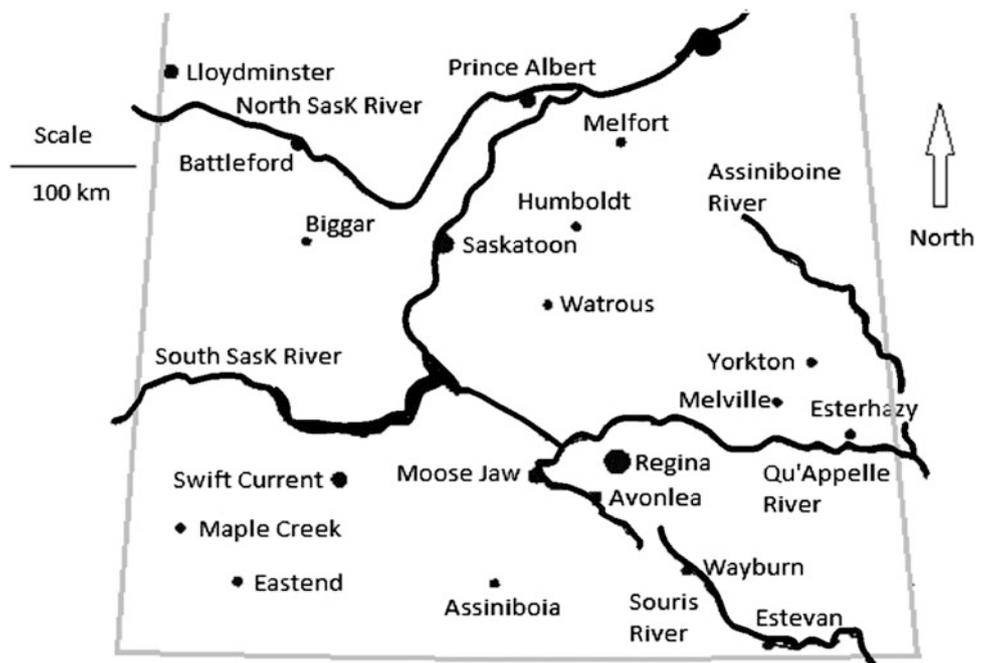
away and deposited on the plains (Byers 1959). The present-day sandstone and mudrock originated from the Maastrichtian age (66–72 Ma).

The prevalent seasonal weather variations dictate the engineering properties of the deposited materials. Overall, the area falls under a semi-arid (BSk) climate according to the Köppen climate classification system. The average monthly temperature varies between −15 °C in January to 19.6 °C in July with an annual mean of 3.2 °C. Likewise, the average annual precipitation is 366 mm with a minimum of 10 mm in June and a maximum of 64 mm in February. Precipitation occurs as winter snowfall (November to March) that freezes the soil and as summer rainfall (April to October) that results in high surface runoff. Further, temperature variations between day and night or successive rainfall events during the summer result in cyclic saturation-desaturation of the exposed materials. A clear understanding of the water movement through these surface sediments is required from an engineering perspective.

The main objective of this paper was to determine the engineering properties of Avonlea badlands. Based on site investigations, three representative soils (sandstone, mudrock, and pediment) were selected for laboratory characterization. Index properties were determined for preliminary soil assessment. The water retention curve was determined to understand the water holding behavior of the three sediments and their interaction through erosion.

66.2 Materials and Methods

Field investigations were carried out through several 1-day visits during periods of no rainfall. Representative soil samples of the three distinct sediments (sandstone, mudrock, and pediment) were collected from the top 300 mm layer for detailed material characterization. The samples were obtained in 20 L containers, sealed to conserve the field water content, transported to the Advanced Geotechnical Engineering laboratory at the University of Regina, and stored at 24 °C.

The geotechnical index properties were determined for preliminary soil assessment according to the following ASTM test methods: specific gravity (Gs) by the Standard Test Method for Specific Gravity of Soil Solids by Water Pycnometer (D854-06); grain size distribution (GSD) under both dry and wet conditions using the Standard Test Methods for Particle-Size Distribution (Gradation) of Soils Using Sieve Analysis (D6913-04(2009)); and consistency limits by the Standard Test Methods for Liquid Limit, Plastic Limit, and Plasticity Index of Soils (D4318-10).

The water retention curve was determined in accordance with the ASTM Standard Test Methods for Determination of the Soil Water Characteristic Curve for Desorption Using a Hanging Column, Pressure Extractor, Chilled Mirror Hygrometer, and/or Centrifuge (D6836-02(2008)e2). To

Table 66.1 Summary of index properties

Soil property	Sandstone	Mudrock	Pediment
Specific gravity, G_S	2.7	2.8	2.7
<0.075 mm (%)	33 (17)	98 (4)	42 (21)
<0.002 mm (%)[3]	15	67	17
Liquid limit, w_l (%)	39	96	31
Plastic limit, w_p (%)	31	47	23
USCS symbol	SM	CH	SC

Note Numbers in parentheses pertain to dry condition

develop a clear understanding of the entire curve, data over a wide range were generated using a pressure extractor for high water content samples and a dew point potentiometer (WP4-T) for low water content samples.

66.3 Index Properties

Table 66.1 summarizes the geotechnical index properties of the investigated sediments. The measured G_s correlated well with material type, namely; 2.7 for sandstone containing iron-based constituents, 2.8 for mudrock possessing clay minerals, and 2.7 for pediment receiving washed materials from the above (Imumorin and Azam 2011). The fines content (<0.075 mm) increased from dry to wet states for all materials: sandstone, from 17 to 33 %; mudrock, from 4 to 98 %; and pediment, from 21 to 42 %. This is attributed to the removal of particle coating from the larger grains due to physical detachment of ultrafine particles, chemical dissolution of soluble materials, and breakdown of larger aggregates. Further, the corresponding clay size fraction (<0.002 mm)

due to wetting measured 15 % for sandstone, 67 % for mudrock, and 17 % for pediment. These data suggest that grain size thinning in sandstone (classified as silty sand, SM) and pediment (classified as clayey sand, SC) was due to coating removal from sand size grains thereby resulting in erosion whereas the phenomenon was related to breakdown of clay aggregates in mudrock (classified as a fat clay, CH).

66.4 Water Retention Curve

Figure 66.2 gives the water retention curves in the form of volumetric water content (θ) versus suction for the investigated materials. The measured data for the sandstone fitted well to a bimodal distribution with two air entry values (AEV): a lower value (6 kPa at $\theta = 65$ %) corresponding to drainage through cracks followed by a higher value (150 kPa at $\theta = 40$ %) associated with flow through soil matrix. When the field samples were progressively desaturated, air first entered into the discontinuities at low suction (Fredlund et al. 2010). The fissures originate from geologic overburden

Fig. 66.2 Water retention *curves* for the investigated sediments
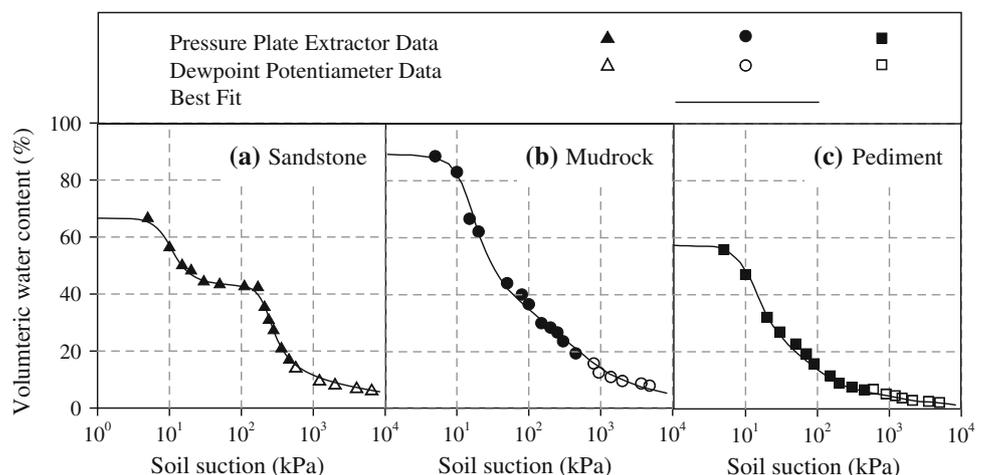
removal and grow over time due to material erosion and dissolution during water flow. According to Azam and Khan (2014), seasonal variations in water availability (snow melt in spring and rainfall in summer) and water deficiency (low rainfall and freezing in fall and winter) result in physical and chemical weathering at Avonlea. Because of the associated increase in fines, these particles got trapped in the relatively bigger pore spaces around the coarser particles. Water flow through the recently developed smaller pores resulted in the observed matrix AEV that, in turn, correlated well with the dense nature of the material. Finally, the residual suction was found to be 500 kPa (at $\theta = 15$ %) and is attributed to the low clay content of the sandstone.

The water retention curve of the mudrock exhibited a unimodal trend with an AEV of 5 kPa (at $\theta = 83$ %) due to drainage through large pores. Such a low AEV for a fat clay is attributed to desiccation cracks in the material from an initially saturated condition. Despite some healing due to expansive clay minerals, numerous swell-shrink cycles over geologic time render these discontinuities to have much lower tensile strengths than the soil aggregates thereby leading to a quick drainage through these paths of least resistance. Subsequent application of suction affected the aggregated soil structure and eventually forced air to enter into the pore system of the popcorn-like motif. Further desaturation resulted in driving water through the individual aggregates and eventually resulted in a residual suction of 1,500 kPa (at $\theta = 12$ %). Overall, the water retention curve correlated well with the high clay content and the high water adsorption capacity of the mudrock.

A unimodal water retention curve was obtained for the pediment. The AEV for this material was found to be 5 kPa (at $\theta = 53$ %) and the residual suction was 80 kPa (at $\theta = 15$ %). These values corroborated well with the granular and loose nature of the pediment, as observed in the field and measured in index properties.

The volumetric water content values at saturation indicated that water storage was highest for mudrock ($\theta = 83$ %) followed by sandstone ($\theta = 65$ %) and then by pediment ($\theta = 53$ %). These saturated conditions during a rainfall together with the water retention curve (unsaturated conditions during dry weather) mean that the eroded and dissolved materials from the sandstone are washed away and get deposited in the pediment because pores in the intermediate mudrock are sealed due to clay swelling. This

confirms the genetic relationship between the sandstone and the pediment, as postulated by Raghunandan and Azam (2012).

66.5 Conclusions

Knowledge of the engineering properties of soils is vital for civil infrastructure construction in surface sediments that are directly affected by seasonal weather variations. Three distinct sediments (fissured sandstone with a steep slope of 60°; popcorn-textured mudrock with a mild slope of 30° and; eroded pediment with a flat slope of 3°) found at the Avonlea badland site were characterized. Based on laboratory investigations, the main conclusions of this work can be summarized as follows. The fines content increased from dry to wet state with 17–33 % for sandstone, 4–98 % for mudrock, and 21–42 % for pediment. The consistency limits indicated that the water adsorption capacity is highest for mudrock followed by sandstone and then by pediment. The water retention curve of sandstone showed bimodal distribution with a low AEV of 6 kPa pertaining to drainage through cracks and a high AEV of 150 kPa associated with flow through the soil matrix. The mudrock and pediment followed a unimodal curve with a single AEV of 5 kPa. These results mean that the eroded and dissolved materials from the sandstone are washed away and get deposited in the pediment because pores in the intermediate mudrock are sealed due to clay swelling. This confirms the genetic relationship between the sandstone and the pediment.

References

Azam S, Khan F (2014) Geohydrological properties of selected badland sediments in Saskatchewan, Canada. Bull Eng Geol Environ 73:389–399

Byers AR (1959) Deformation of the Whitemud and Eastend Formations near Clay bank, Saskatchewan. Trans R Soc Can 53:1–11

Christiansen EA (1979) The Wisconsinan deglaciation of Southern Saskatchewan and adjacent areas. Can J Earth Sci 116:913–938

Fredlund DG, Houston SL, Nguyen Q, Fredlund MD (2010) Moisture movement through cracked clay soil profiles. Geotech Geol Eng 28:865–888

Imumorin P, Azam S (2011) Effect of precipitation on the geological development of badlands in arid regions. Bull Eng Geol Environ 70:223–229

Raghunandan ME, Azam S (2012) Effect of dry-wet cycles on material composition of badlands. In: Proceedings, 65th Canadian geotechnical conference, vol 338. Winnipeg, Canada, pp 1–6

Case Studies of Post Investigation Geological Assessments: Hunter Expressway

67

David J. Och, Robert Kingsland, Sudar Aryal, Henry Zhang, and Geoff Russell

Abstract

This paper presents two case studies where detailed site specific engineering geological assessment during construction justified major changes to the approved design of road infrastructure elements to suit actual site conditions which resulted in a better engineering outcome and substantial cost savings. The road project was the Hunter Expressway, located in the Hunter Valley, some 120 km north of Sydney, which is a 40 km long four-lane dual carriageway motorway currently at the final stage of construction. Two locations (Bridge Viaduct 3 and Retaining Wall—RW18) were selected as case studies because the detailed construction-phase mapping work provided a refinement to the geological models that enabled the design of key elements to be changed or modified. This paper will present the detail of these two case studies and demonstrate the value of detailed site specific engineering geological assessment during construction in achieving better engineering outcomes.

67.1 Introduction

This paper presents two engineering geological mapping case studies for the eastern 13 km section of the Hunter Expressway, which was recently delivered as an alliance contract under the project name Hunter Expressway Alliance (HEA).

The Hunter Expressway provides a long-awaited relief of congestion and improvement of passenger and freight traffic movement in the region along the route between Sydney and Brisbane, the busiest road transport corridor in Australia.

This paper demonstrates the value of detailed construction-phase geological and geotechnical assessments that provided refinement, which enabled the design of key elements to be changed or modified during construction to deliver more robust and cost effective design solution for the project.

67.2 Project Geology

The project is underlain by the upper part of the Newcastle Coal Measures comprising a relatively thick unit of coarse-grained sandstone interbedded with beds of conglomerate, laminated fine-grained sandstone, siltstone, coal and tuff. Colluvium is present on the slopes and alluvium is deposited in the valley floor. The tuffaceous sedimentary rocks comprise tuffaceous sandstone, tuffaceous siltstone and tuffaceous claystone. The tuffaceous claystones are low-strength rocks that are particularly susceptible to weathering and are highly reactive (Aryal et al. 2013).

D.J. Och (✉) · R. Kingsland · S. Aryal · H. Zhang
Parsons Brinckerhoff, 680 George St, Sydney, 2001, Australia
e-mail: doch@pb.com.au

D.J. Och
School of Biological, Earth and Environmental Sciences, University of New South Wales, Kensington, Australia

G. Russell
NSW Transport, Roads and Maritime Services, Newcastle, Australia

Structurally these rocks are cut by a dominant high-angled joint set trending NNE to NE with a subordinate joint set trending to the west. Also associated with the dominant joint set are some low to moderately angled joints, usually clay lined. This formation also forms prominent escarpments alongside with deep valleys which have exploited prominent tectonic joint sets. Valley cutting and associated horizontal stress relief of these thicker rigid sandstone units has resulted in irregular inter-bed fractures. Colluvial debris of variable thickness masks the frontal slope of these escarpments. Large areas of the project alignment, including the case study locations, are underlain by former underground coal mine workings predominantly in the Borehole Seam which was mined in various collieries during the early 1900s at typical depths of 70–100 m (Kingsland et al. 2012).

67.3 Geotechnical Investigation Phases

The project had four phases of geotechnical site investigation that formed the basis of the design of the expressway. Phase 1 was the geotechnical investigation for the conceptual design and planning approval. Phases 2 and 3 were completed for the concept design, project costing and detailed design. In some areas of the project alignment, factors such as time constraints, access limitations, environmental and cultural issues controlled the level of field investigations that could be completed at targeted locations for detailed design of specific earthworks or concrete structures. In these areas the detailed design was developed based on the geotechnical data available at the time. Phase 4 was completed during the construction period. It is this forth phase of investigation, predominantly geological mapping, that will be elaborated in the project case studies discussed.

67.4 Project Case Studies

The two case studies are presented herein. In both cases, a major review of the detailed design was required due to the reason that the actual site conditions differed from the design assumptions. Detailed geological assessment of the actual ground conditions exposed during construction together with further geotechnical modelling to suit the observed conditions formed the basis for the redesign of the structures. Regular site geotechnical inspections were carried out to validate the new design during construction.

67.4.1 Case Study 1: Viaduct 3 Abutment

Viaduct 3 comprises twin continuous, three span, single cell box girder bridge superstructures, approximately 199 m in length, carrying the eastbound and westbound carriageways of the expressway across a deep valley with steep side slopes within a densely forested rugged terrain—the Sugarloaf Range.

The detailed design of the substructures supporting the bridge was based on the subsurface investigation data available at the time of design and included bored piled foundations under the abutments (Fig. 67.1a). After the site was cleared for construction of the abutments, the area became accessible and surficial features including rock outcrops exposed. Detailed geological mapping of the abutment and the slope areas beneath the proposed piled foundation was undertaken, which revealed that the foundation geology below the western abutment (Abutment B) comprised sound rock with no adverse rockmass structures and was assessed to be much more competent from the surface. These actual conditions encountered were considered to be equally suitable for pad foundations (Fig. 67.1b).

Subsequent checks on bearing, sliding, eccentricity and overturning in accordance with AS5100 indicated that pad footings were adequate. Allowance for potential mine subsidence was also made from structural design perspective.

The design of Abutment B was therefore changed to pad foundation on the basis of detailed engineering geological mapping (Fig. 67.1c, d), the adequacy of the geotechnical capacity and stability and accommodation of mine subsidence.

67.4.2 Case Study 2: Cut10a Extension

The Expressway cut through a steep side hill (slope 2H:1 V or steeper locally) and formed a side cut on the north side of the alignment. A piled retaining wall RW18, 60 m long and 5 m maximum height, was selected as the design solution to retain the side slope in this section taking into consideration the alignment corridor constraints, clearing limit restrictions, cutting depth and geology. The geotechnical model for the design was based on all test data available from the area including borehole BH1056 (Fig. 67.2a–c), which was the only borehole completed at the detailed design closest to the wall. This borehole was located downstream of the proposed RW18 location as access to the upstream area for geological mapping or drilling was not possible during the design stages due to steep pre-existing topography and dense forestation. Geotechnical data available at the time of detailed design indicated that, at the highest section of the wall, the slope materials that would need to be retained would comprise about 2 m thick alluvium/residual clay over 5 m of extremely low to very low strength rockmass overlying high strength rock (Fig. 67.2a, b) and this profile was adopted as the geotechnical model for the retaining wall design.

The slope above proposed RW18 became more accessible only following corridor clearing at the start of the
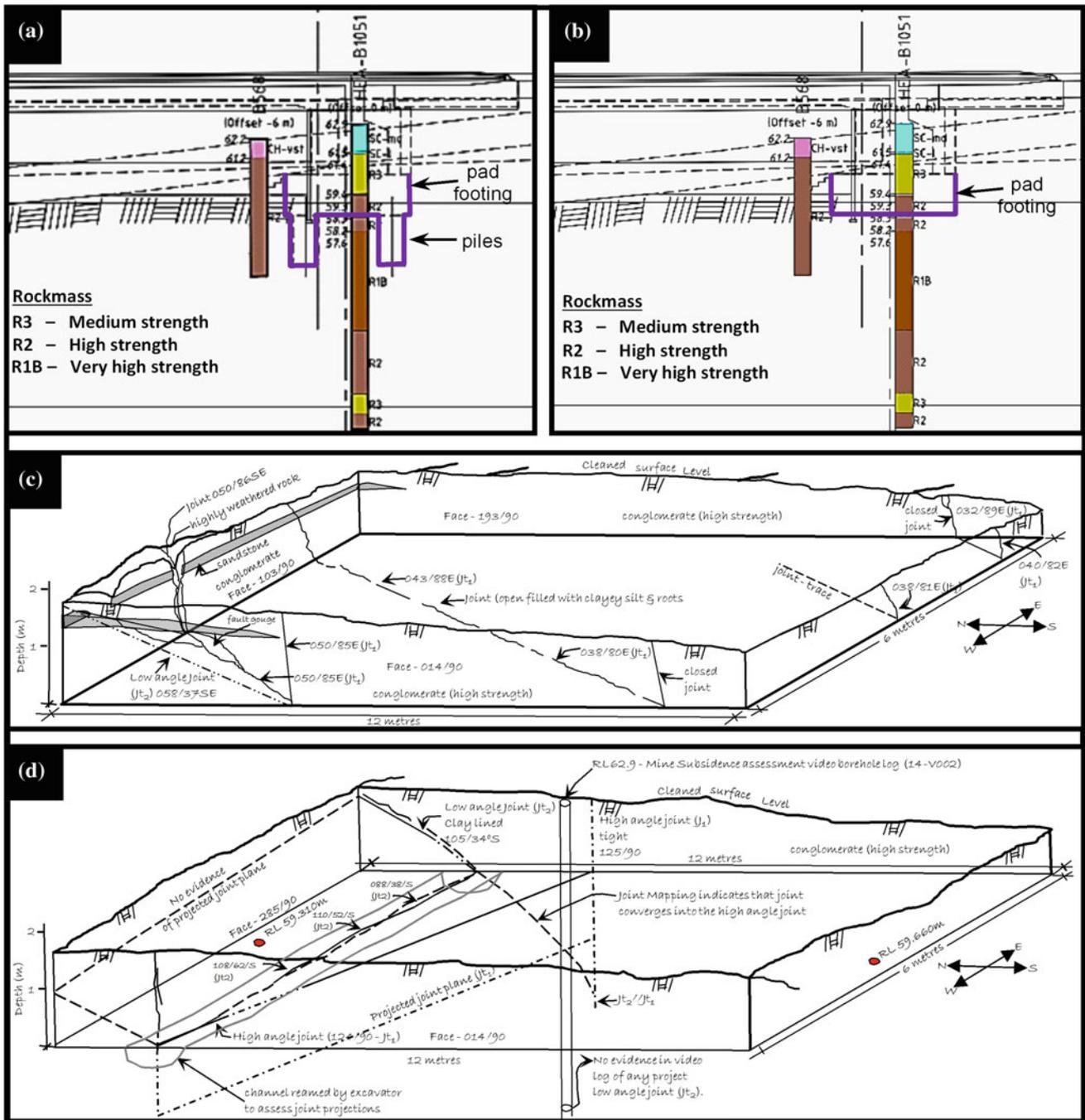
Fig. 67.1 **a** Original bored piled foundation design for BW11. **b** Revised pad footing design,.**c** Detailed geological mapping of excavated foundation pad—eastbound. **d** Detailed geological mapping of excavated foundation pad—westbound

construction phase. However, temporary excavation into the slope for site access road at the start of construction activities triggered localised slumping of superficial layers of in situ and colluvial materials on the upper batter section (section above the proposed wall) (Fig. 67.2d, e). The slope was stabilised by removal of slumped, dislodged and loosened materials which inadvertently resulted in further steepening of the pre-existing steep natural slope forming the upper batter.

Subsequently, a detailed geological mapping (Fig. 67.2e) was carried out that followed further subsurface investigations including one borehole upstream of the slope and two
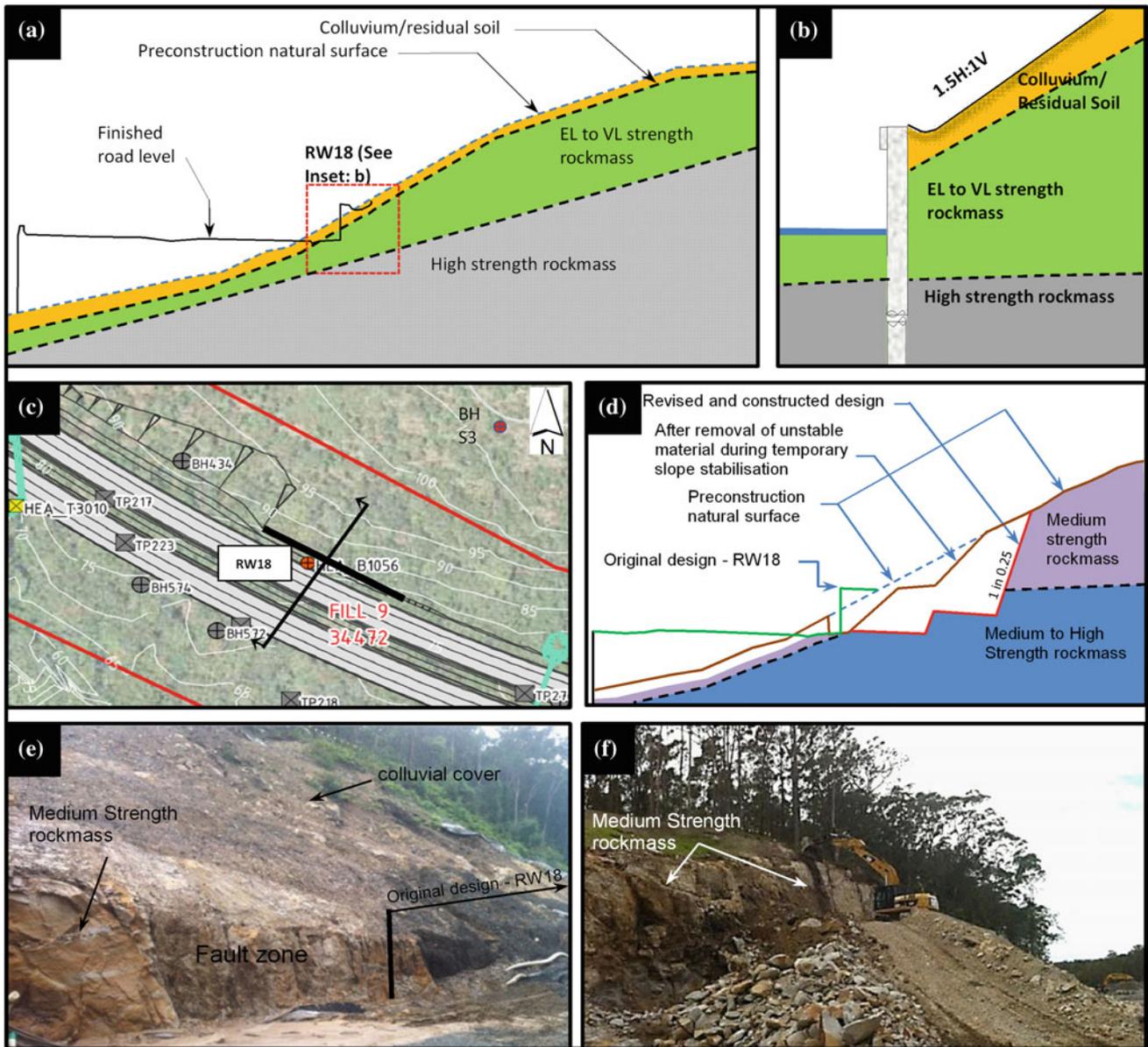
Fig. 67.2 a Original and revised design detail for RW18 and assumed geotechnical model. **b** Inset, with details of geotechnical model used for design at highest section of the wall **c** Location of geotechnical investigations used for original design. **d** Section detailing original design and the revised and constructed design. **e** Slope assessed during initial corridor clearing at the start of the construction phase. **f** Slope assessment which included geological mapping and test pitting

adjacent to the wall location in conjunction with progressive geotechnical inspection of the excavation and test pitting (Fig. 67.2f). The results of these investigations showed that the slope to the design road level and beyond composed of undisturbed rockmass with generally high strength sandstones and siltstones below a thin cover of residual soil and weak rock (1–2 m) at the natural surface. The outcome of investigations provided new opportunities to review the

geological models adopted to develop the retaining wall solution and revise if an alternative, more cost effective design would be possible to replace the retaining wall solution

The geological data collected during the initial investigations and during construction were reviewed to compare the actual geological conditions against design assumptions. The in situ materials forming the slope were assessed to be much more competent than the earlier design interpretation

and based on these results, it was determined that the proposed retaining wall could be deleted and replaced by a steep rock batter with support/protection treatment where required (Fig. 67.2d, f).

67.5 Conclusion

The case studies presented from the Hunter Expressway (Bridge Viaduct 3 and Retaining Wall—RW18) illustrates the benefit of thorough construction phase geological mapping. The mapping executed when large areas of rock mass were exposed during construction enabled the geological models to be refined and in places considerably modified. As a result, approved geotechnical designs were able to be optimised deliver the best for the project solution with a considerable cost savings. These case studies demonstrate the critical importance of adequate engagement of engineering geologists during the construction phase to validate,

challenge and modify design assumptions; ultimately achieving better engineering outcomes.

References

Aryal S, Kingsland R, Rees P, Russell G, Stahlhut O, Wheatley D (2013) Hunter Expressway, Australia: dealing with poor ground and subsidence. In: Proceedings of the institution of civil engineers, civil engineering special issue 166. ICE Publishing, London, Issue CE5, pp 22–27

Kingsland RI, Mills KW, Stahlhut O, Huang Y (2012) Mine subsidence treatment and validation strategies on Minmi to Buchanan section of the Hunter Expressway. In: Proceedings of the 11th Australia–New Zealand conference on geomechanics—ground engineering in a changing world, 15–18 July 2012, Crown Conference Centre, Melbourne, Australia

Contribution to the Behavior Study and Collapse Risk of Underground Cavities in Highly Saline Geological Formations

68

Mohamed Chikhaoui, Ammar Nechnech, Dashnor Hoxha, and Kacem Moussa

Abstract

The problem of saline soils reserved from occupation at Oran, North Algeria remained relatively unexplored or little known until recent years. Consequently, some studies were conducted, especially to characterize the real impact of an airport on these soils. The characterization of the real problems of saline soils, as well as the study of the behavior of their collapse under the coupled effect of thermal, mechanical and hydraulic, remains poorly known specially under an airport, where the instabilities and the risks of sudden collapses is an unknown problem for the authorities and citizens and the impact on the environment is not mastered. Under the action of water charged with carbon dioxide which dissolves the limestone, chalk or gypsum, many natural cavities are created. There are also pockets of dissolution filled with silt in the chalk, due to the irregularity of the contact chalk/silt. The flow of water can also enlarge the fractures at depth causing the silt that fills them and thus creating a surface subsidence due to infiltration. This phenomenon is found mainly in the dry valleys. To account for the effect of the hydro-thermomechanical coupling in predicting the collapse of saline soils, solutions were proposed for improvement of saline soil with a geosynthetic reinforcement, drainage, etc. These solutions are necessary for the proper design of airfield runways to avoid a disaster.

Keywords

Saline soils • Sebkha • Runways • Coupling • Disaster

M. Chikhaoui (✉) · A. Nechnech
Faculty of Civil Engineering, USTHB, 16111 Bab Ezzouar, Algeria
e-mail: mch_gcg16@yahoo.ca

A. Nechnech
e-mail: nechnech_a@yahoo.fr

M. Chikhaoui · A. Nechnech
Laboratory of Environment, Water, Geomechanics and Works LEEGO-USTHB, Bab Ezzouar, Algeria

D. Hoxha
Laboratory of PRISME—Faculty of Civil Engineering, Polytech'Orleans, Orleans, France
e-mail: dashnor.hoxha@univ-orleans.fr

K. Moussa
Department of Earth Sciences, FSTGAT, Oran University, Oran, Algeria
e-mail: moussakacem@yahoo.fr

68.1 Introduction

In the plain, about 6 km in the south of the town of Oran and Northern of the great Sebkha of Oran, Es-Senia airfield is located (Fig. 68.1). While the Es-Senia Oran airport is located near the large of Sebkha (western Algeria). Its extension has required the completion of a second runway. The presence of the Sebkha (salty lake) induces a rather complex geotechnical environment. This complexity is duo to the presence of dissolution cavities, of different sizes, in gypsum and the flat topography, promoting water stagnation.

Fig. 68.1 Aerial view of the great Sebkha and view of the airfield of Oran, Chikhaoui et al. (2011)

68.2 Geological Factors and the Water Chemistry on Sebkha

Two important factors have governed the development of depression tectonics and climates conditioning subsequently the hydrographic network and vegetation fixation. Sedimentological analysis revealed that the climate of the sebkha, switches from sub humid to a semi-arid climate. The dynamics of Sebkha was reconstructed from the elements and geomorphological structures, Moussa (2007).

The active tectonics in Algeria is located in the northern part of the country. This region is located at the Africa-Eurasia boundary; the tectonic activity expresses the ongoing convergence between these two tectonic plates. Offshore, deformation affects the abyssal plain located close to the continent, by folding the Plio-Quaternary sediments cover. Along the slope and the continental platform, active structures with a continental extension crosscut this region. The coastal tectonics generates the coastal uplift with an average uplift of 0.50 m, Yelles-Chaouche et al. (2006). The climate of the Sebkha is Mediterranean in terms of daily and seasonal variations of precipitation, but steppe character in terms of the average temperature, annual rainfall and its seasonal distribution; it is the result of a coastal Mediterranean climate and a desert climate shelter, Moussa (2007).

Indeed, the region has a semi-arid climate characterized by an irregular rainfall, with dominance of brutal rain showers and prolonged dry season during which the heat causes intense evaporation. In winter, rain dissolves deposits of evaporites seconding materials salt solids. In summer, evaporation and capillary action causes a rise of salt resulting in the formation of efflorescence at surface.

Hydrogeology shows the superposition of two bodies of water, one deep freshwater (110 m) and located at the Messinian limestone, the other shallow salt water (82 m) located at the Pliocene formations. All around the Sebkha, several marshes are made per capillary of salt water back to the surface of the lake, Moussa (2007). The human activities have a significant influence on the physico-chemical quality of groundwater. This interaction affects the content of major elements (Ca^{+2}, Mg^{+2}, Na^+, K^+, Cl^-, SO_4^{2-}, HCO_3^-...etc.).

The Sebkha is represented by a recent alluvial deposit with the composition: sodium chloride 20 %, calcium sulfate 5 %, silica (SiO_2) 50 %, alumina and iron 20 %, carbonate of lime and magnesia 5 %, sodium chloride 1/5 % of salt Sebkha. The lake basin is supplied by sodium chloride brines down ravines of Tessala and especially by a Triassic layer that would contain per liter about 1.78 g of sodium chloride, 11 g of calcium chloride and 4 g of potassium chloride a rate of 193 g of salt, Boualla et al. (2011, 2013).

The northern side of the basin receives fresh water, located at the average depth of 4 m; the Triassic water is six times saltier than the Mediterranean water. This indeed gives 30 g/l of salt, while the one of the great Sebkha closes 180 g/l of chlorides, so it's a real salt mine; the Triassic water rises to the surface by capillary action and distributes its salts throughout the thickness of alluvium it crosses.

The decrease of the dry residue of floodwaters, cause increased levels of Ca^{++}, HCO_3^- and a subsequent decrease of the Na^+ and Cl^-. Sodium chloride (NaCl) salt is the most dominant in the water and soil of the Sebkha. The waters of the Sebkha are sodium chlorides and sulphates, Moussa (2007).

68.3 Geotechnical Problems and Soil Improvement

Under the action of water charged with carbon dioxide which dissolves the limestone, chalk or gypsum, many natural cavities are created (Fig. 68.2). One may observe dissolution pockets filled with silt in the chalk, due to the irregularity of the contact chalk/silt, Chikhaoui et al. (2011, 2013). The presence of underground cavities beneath a airfield pavement can be very dangerous, as collapse or subsidence occurs very likely.

Fig. 68.2 Photos of various cavities at Es-Senia airport, Chikhaoui et al. (2011)

The method that has been advocated for the detection of its cavities is the forced compaction along the track. This is followed by an excavation to a depth of 1.35 to 1.5 m to eliminate the surface cavities, then high energy compaction using a 50-t compactor at the bottom, to obtain good density at the base but also to identify cavities.

To avoid risk of collapse at the long term, the use of geosynthetics (geogrid 30/30 and geotextile 400/50) has become indispensable. The out of balance occurs when the subgrade can no longer exert an equal reaction to the applied load, the upper layers in turn unleash. There will be punching of the ground seat. Figure 68.3a, b show that for a given load, there is a relationship between the bearing capacity of the soil and the thickness of the pavement, Chikhaoui et al. (2011).

The principle is based on the assumption that the introduction of geotextile and geogrid may contain a cavity of 1 m in diameter with an overload of 345 kN/m². After treatment of the pavement foundation layer the thickness will be circa 69 cm, a reduction of 50 % of the total thickness, Chikhaoui et al. (2011, 2013). The aim is to divide all surchanges over a larger area and reduce pressure on the foundation soil to increase the bearing capacity. The incorporation of biaxial geogrids allows a lateral confinement of the foundation and reduction in the amount of aggregates in the range of 40–60 %, while offering the same capacity and the same functionality.

Geotextiles are often used in road and airport works as a tool for separation and filtration. Their performance as reinforcement depends on the geotextile-soil interaction. The study of geotextile-soil interaction under cyclical load (wheel), carried out by Bhandari and Han (2010), shows that the geotextile placed at a depth of 25.0 mm led to the registration of smaller displacement (Fig. 68.4a), than the unarmed case (Fig. 68.4b).

68.4 Dissolution Mechanism

It is known that the bicarbonate ion is the basis of the formation of calcium carbonate ($CaCO_3$) which is poorly soluble in water, and it is the main component of limestone:

$$Ca^{2+} + 2HCO_3^- \rightarrow CaCO_3 + H_2CO_3$$
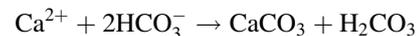
where H_2CO_3 is carbonic acid.
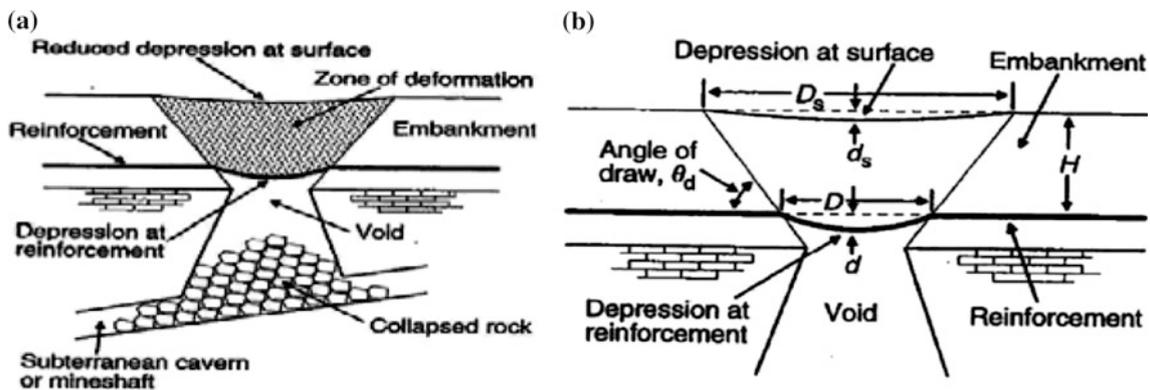
Fig. 68.3 **a** Conceptual role of reinforcement in limiting surface deformations due to subsidence, BS-2006. **b** Parameters used to determine reinforcement, BS-2006
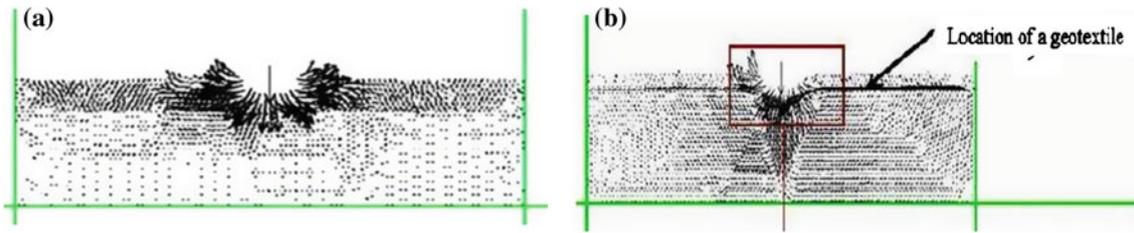
Fig. 68.4 a Field of displacement vectors of particles with no reinforcement geotextiles (the maximum displacement % 13.26 mm. **b** With geotextile reinforcement at a depth of 25 mm (max % 11.9 mm), Bhandari and Han (2010)

Fig. 68.5 Diagram for underground genesis of cavities in great Sebkha
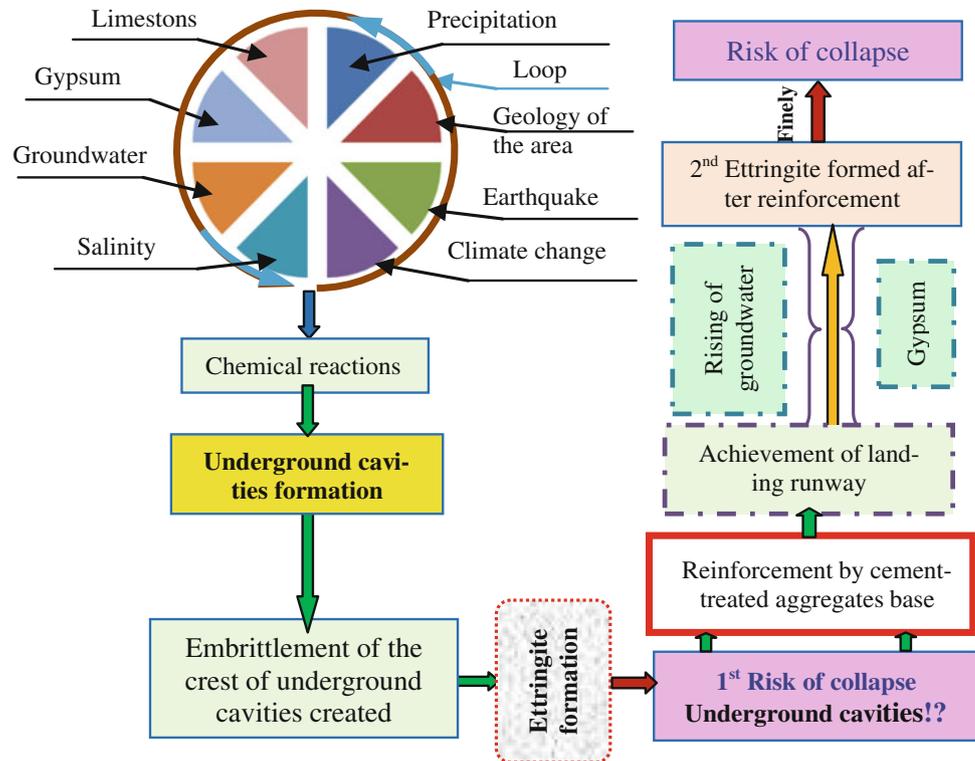
In an acidic medium, the calcium carbonate is converted to a calcium bicarbonate $(Ca^{2+}, 2HCO_3^-)$, which is very soluble in water, it is definitely a salt of a weak base $(Ca(OH)_3^-, pKa \approx 12)$ and a weak acid $(2HCO_3^-, pKa \approx 6)$, Boualla et al. (2011). The $Ca(OH)_3^-$ at atmospheric pressure and ambient temperature, gaseous and volatile is able to react with a strong acid to obtain calcium salts, water and carbon dioxide.

$$CaCO_3 + 2HCl \rightarrow CO_2 + CaCl_2$$
$$CaCO_3 + 2RCOOH \rightarrow CO_2 + CO_2 + Ca(RCOOH)_2$$
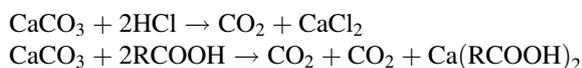
Under the simultaneous actions of groundwater leading the dissolution of gypsum and natural successive effects of earthquakes and dryness periods in Sebkha cause the creation of ettringite around weak areas of limestone. In

geological times, this dislocation resulted in underground cavities which might collapse at any time under different dynamic actions (landing of airplanes) refer to Fig. 68.5.

68.5 Conclusion

The chemical nature of water depends on the path it has followed from the ground surface to the aquifer system. At first, it undergoes a surface modification due to the evaporation and then it evolves in the unsaturated zone and finally acquires the mineralization on the level of the water due to its contact more or less along the reservoir rock. All chemical analysis of samples basin Sebkha, have revealed an understanding of some parameters describing the physico-chemical water quality. The dominance of bicarbonate

indicates that they constitute the bulk of the mineralization of the water, Boualla et al. (2011, 2013). In addition, the seismic activity is amplified all around the Sebkha Moussa (2007). This explains the accelerating of underground cavities formations. Subject to understand the mechanism of formation of cavities, it requires studying the exchanges matter in CO_2 at the water—atmosphere interface and those in Ca^{2+} and CO_3^{2-} ions in water interface—rock, Chikhaoui et al. (2011, 2013).

References

Bhandari A, Han J (2010) Investigation of geotextile-soil interaction under a cyclic vertical load using the discrete element method. J Geotextiles Geomembranes 28:33–43

Boualla N, Benziane A, Derrich Z (2011) Reflection of investigations physicochemical watershed Sebkha Oran. ScienceLib, Editions Mersenne: Environnement, vol 3, N°:111104

Boualla N, Moussa K, Benziane A (2013) Spatialisation des parametres physico-chimique pour la reconnaissance de l'etat des ressources en eau du bassin Sekha d'Oran. ScienceLib, Editions Mersenne: Geologie, vol 5, N°:130910

Chikhaoui M, Nechnech A, Moussa K (2013) Contribution to the study of coupling hydro-thermo mechanical for the prediction of collapses of airfield runways built on saline soils. In: 14th REAAA conference, P02A. Kuala Lumpur, Malaysia, pp 638–648, 26–28 Mar 2013

Chikhaoui M, Nechnech A, Haddadi S, Ait-Mokhtar K (2011) Contribution a la prediction des effondrements des pistes d'aerodromes construites sur des sols salins. XXIVe Congres mondial de la Route. Mexico, Ref. 0671, 26–30 Sep 2011

Moussa K (2007) Etude d'une Sebkha; la Sebkha d'Oran (Ouest algerien). Doctorat thesis Es-Sciences, Oran University, Algeria

Yelles-Chaouche A, Boudiaf A, Djellit H, Bracene R (2006) La tectonique active de la region nord-algerienne. CRAAG. Algeria. Elsevier, C.R. Geo- science, vol 338, pp 126–139

Seabed Properties for Anchoring Floating Structures in the Portuguese Offshore

69

Joaquim Pombo, Aurora Rodrigues, and A. Paula F. da Silva

Abstract

Anchoring structures in marine environments requires a good knowledge of seabed properties, based on laboratory tests and geophysical data acquisition. This work is addressed to the analysis of one anchor site located off the Portuguese coast, combining laboratory tests and high resolution seismic profiling. Seven different classes of sediments were individualised (according to United Soil Classification System), and coherent with the sedimentary layer architecture identified in the geophysical profiles; data provided awareness about the thickness of the unconsolidated sedimentary layer to the bedrock.

69.1 Introduction

The recent implementation of policies for a sustainable development in the energy sector has led some countries, including Portugal, to seek new energy resources, with particular focus in renewable ones, namely those associated with the Ocean: tides, waves and offshore wind.

Due to the inaccessibility and constant site modifications, marine environments present extra difficulties for engineering geology modelling. Such complexity is expressed not only on the extremely high energy of environmental agents, both meteo and oceanographic, but also on the natural vertical and lateral variability of the marine sedimentary cover. In this context, the adequate offshore geological and geotechnical studies are due to support the implementation of those projects (Randolph and Gourvenec 2011), otherwise it can increase the cost of project or compromise its economic viability altogether.

Marine geotechnical studies are still innovative in Portugal, especially in the offshore, where the marine resources have the major potential. The first phase is underway, with the preliminary characterization of a small area of 13 km^2 and 30–60 m of depth in the Northern Portuguese shelf of S. Pedro de Muel. The purpose is to perform a multidisciplinary characterization of the upper layer of the continental shelf, considering not only the geologic parameters (bedrock topography and sedimentary layers thickness, internal stratigraphy and lateral facies variability), but also the geotechnical properties of the sediments.

This study will present the first marine geotechnical characterization of the Portuguese offshore, supported by the geologic description of the studied area.

69.2 Methods

The site investigation carried out in the study area, encompassed the following: acoustic and geophysical surveys (multibeam echo sounders, sub-bottom profiler and boomer); followed by two sediment sampling surveys with vibrocorer and grab sampler. Data and sample locations are displayed in

J. Pombo (✉) · A. Rodrigues
Instituto Hidrográfico, Lisbon, Portugal
e-mail: joaquim.pombo@hidrografico.pt

A. Rodrigues
e-mail: aurora.bizarro@hidrografico.pt

A.P.F. da Silva
CICEGe and Dept. Ciências Da Terra, Faculty of Sciences and Technology (FCT), Univ. NOVA of Lisbon, Lisbon, Portugal
e-mail: apfs@fct.unl.pt
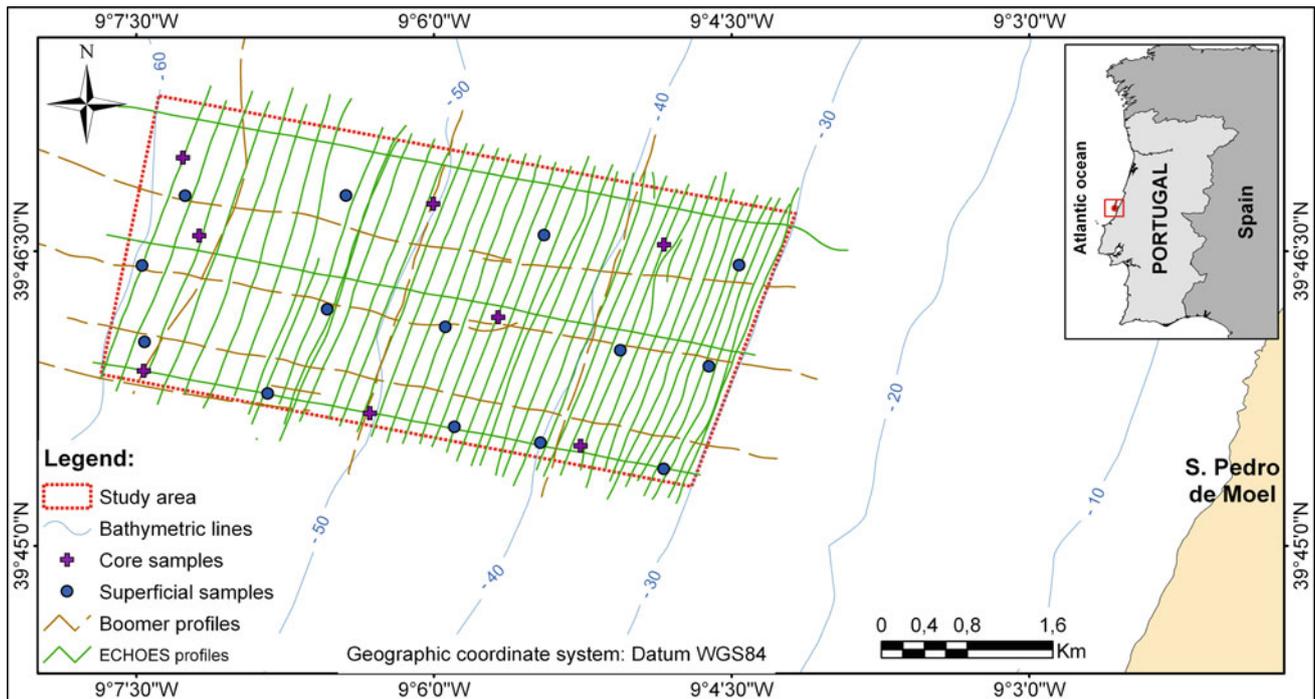
Fig. 69.1 The study area and location of seismic profiles, superficial and vertical sediments sampling

Fig. 69.1. Multibeam and sub-bottom profiling data (50 profiles) was acquired simultaneously with a Kongsberg EM710 and IXSEA Echoes 3500 chirp. Additional boomer profiles (9 profiles) were acquired with an Applied Acoustics Engineering AA200 system.

Two sampling surveys were performed using electrical vibrocorer Rossfelder P5 (8 vertical samples) and a Smith McIntyre grab (14 superficial samples).

Once in the laboratory, the corers were submitted to several tests, namely magnetic susceptibility, P-wave determination and X-ray radiography.

After extraction (2–2 cm) with a metallic ring, samples were analyzed using international normalized methods: the grain size distribution; determination of particle density; specific weight; determination of water content; carbonate content; organic matter content; Atterberg limits; and triaxial tests (CK_0D).

69.3 Preliminary Results

69.3.1 Morphology and Bottom Sediments Characterization

Multibeam data allowed the construction of a MDT surface (Fig. 69.2a), which showed that the area has a very smooth morphology with no major outcrops.

Despite the general gentle slope (about 0.3 %), a morphologic structure is recognized at 55 m of depth, consisting in a 1 m vertical displacement of the sea bottom. This feature marks the transition of a fine sedimentary deposit (between 30 and 55 m of depth) to a coarser one (between 55 and 60 m of depth), the latter also being characterized by wave ripples (NE-SE) about 3 m wavelength and 19 cm height according to Nichols (2009). In the rest of the studied area no morphological features were recognized.

The backscatter energy of the multibeam survey was analysed and processed with the GEOCODER engine (University New Hampshire), allowing the remote classification of the sea floor (Fig. 69.2b). Comparing the backscatter mosaic with the MDT surface, there is a good match between both surfaces, with the less intensity of the backscatter corresponding to the finer sediments and the higher intensity (lighter areas) corresponding to the coarser sediments.

The classification of the superficial samples and the uppermost 15 cm of the vertical samples according to Unified Soil Classification System (ASTM D2487-06), allowed the identification of three distinct sedimentary units (Fig. 69.3):

- Sand deposits poorly calibrated (SP), between 30 and 45 m of depth, characterized by fine sand in the order of 97 % and fine sediments less than 3 %; $C_u = 1.95$ and $C_c = 1.02$;
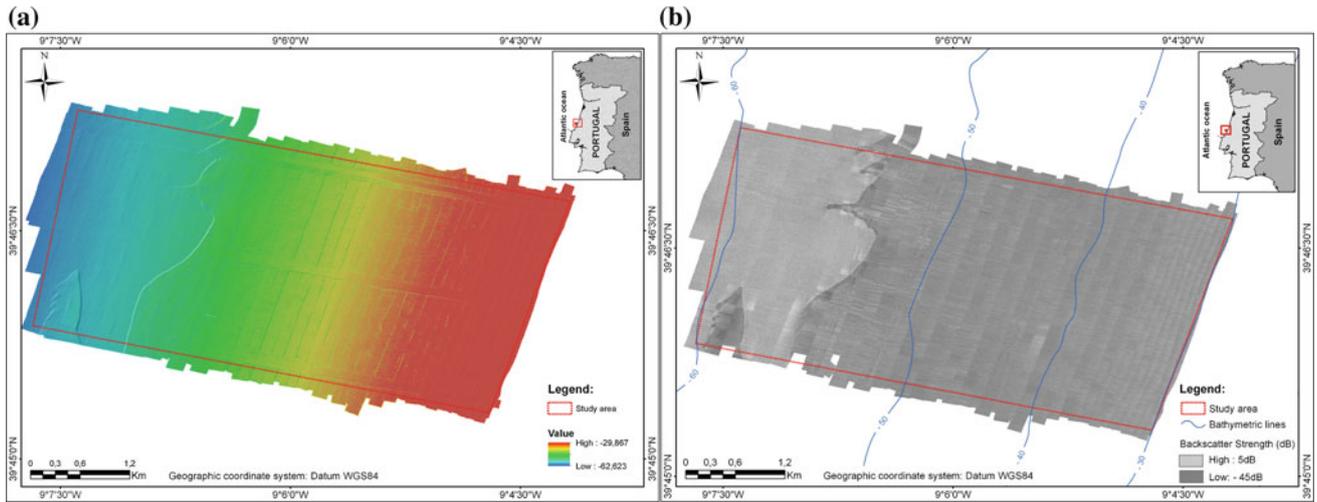
Fig. 69.2 Multibeam processed data: **a** MDT surface and **b** backscatter mosaic

Fig. 69.3 Mapping of the identified superficial sedimentary deposits (USCS): isopach of the unconsolidated sedimentary layer and location of the boomer seismic profile
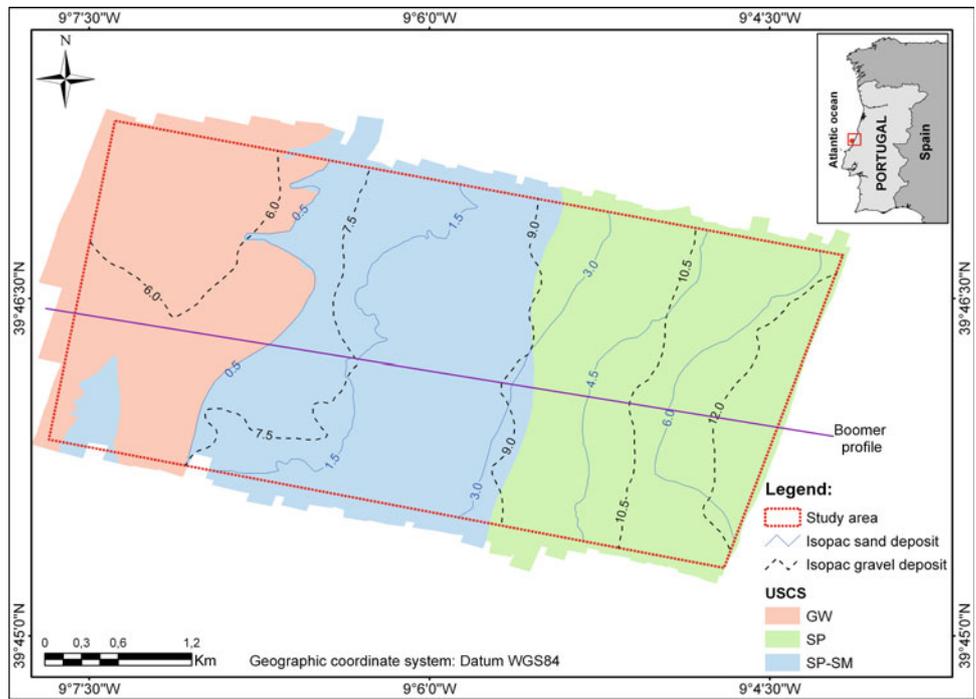
- Silty sand deposit (SP-SM) between 45 and 55 m of depth, characterized by poorly calibrated fine sands (91 %) and about 9 % of fine sediments; $C_u = 3.89$ and $C_c = 1.68$;
- Sandy gravel deposit (GW), between 55 and 60 m of depth, characterized by 78 % of well graded gravel, 19 % of sand and 3 % of fine sediments; $C_c = 2.31$ and $C_u = 5.62$.

69.3.2 Geological Structure

Geophysical profiles indicate that superficial units (identified in the backscatter) correspond to the major sequences identified in the geologic structure of the area. The basal sedimentary unit, a coarser deposit (sandy gravel sediments), covers the bedrock and is exposed in the deeper area, below
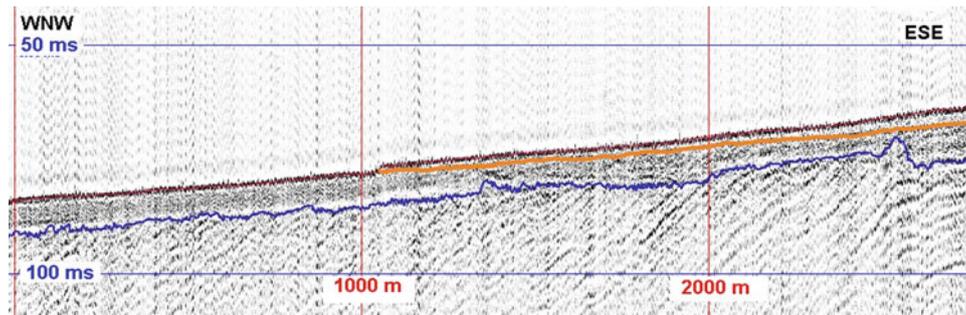
Fig. 69.4 Extract of a representative boomer seismic profile. *Blue line* corresponds to the top of bedrock and *orange line* to the top of the coarser unit and base of the finer deposit; brown reflector is the sea bed
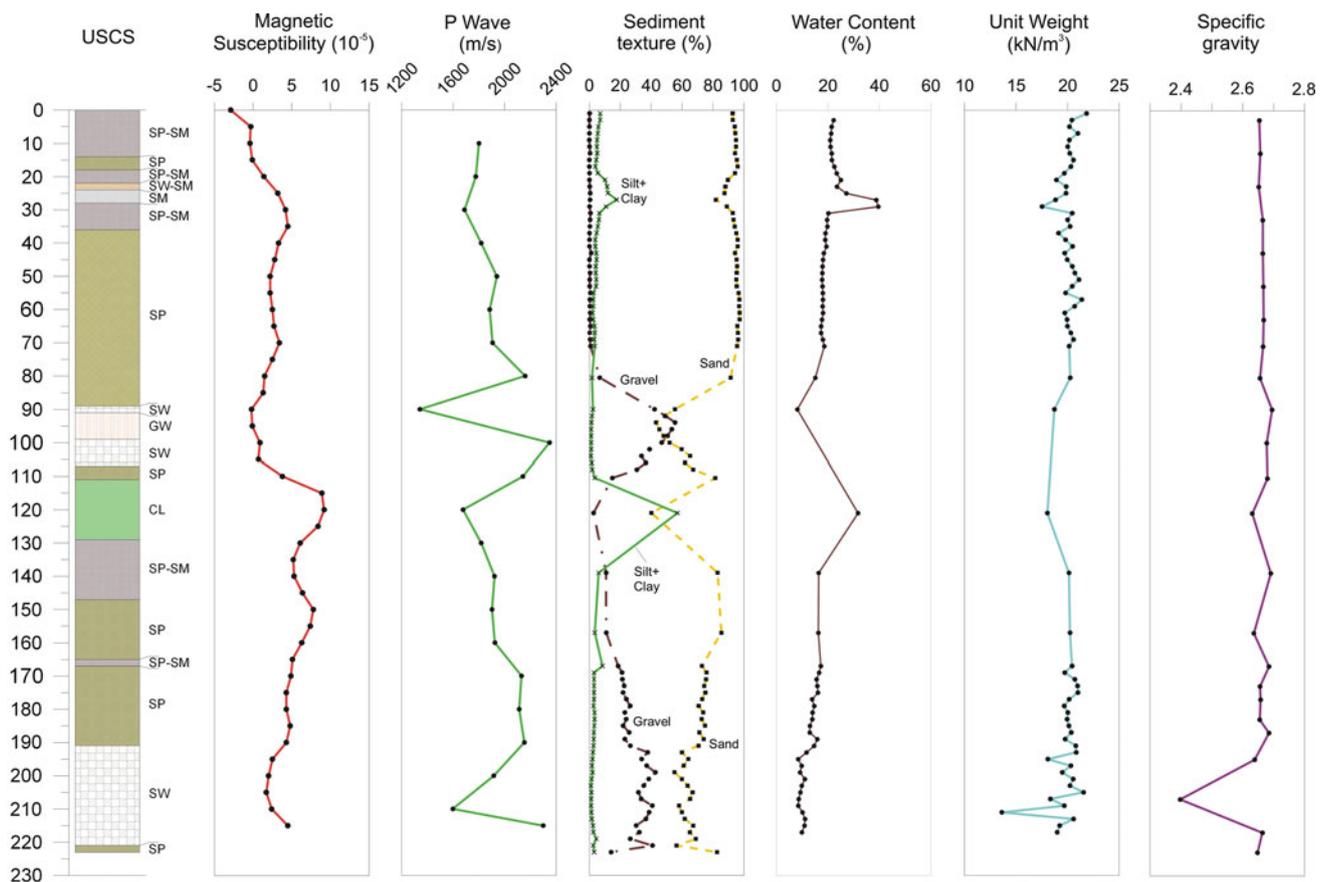
Fig. 69.5 Geotechnical proprieties of the marine deposits versus depth

55 m of depth. The more recent unit, covering the coarser deposit, is identified in the shallow area, and is composed by sandy sediments (Fig. 69.4).

According to the isopach distribution (Fig. 69.3), the sandy deposit increases its thickness towards the coast line, from 0.5 to 7 m, while the sandy-gravelly deposit, despite the difficulty in the basal delimitation, seems to be a thicker unit (5–13 m, also increasing westward).

69.3.3 Sedimentary Layer and Geotechnical Characterization

The first 15 cm of the sedimentary cover (Fig. 69.5) are characterized by negative or null susceptibilities, probably because of high pore fluid contents; this susceptibility also increase with the increasing silt-clay fraction in the sediments. The higher values (9×10^{-5} SI) are measured at

110 cm coinciding with the presence of a sandy silt level (55 % of silt-clay fraction). Deeper levels have lower susceptibility values due to the increase in the grain-size and biogenic particles.

The grain size also interferes with the compressional waves velocity (vp), as it was shown by Buckingham (2005). The lower value (1,260 m/s) was registered at 90 cm in the transition between the sandy gravel layers and finer ones. On the sandy silt level (between 110 and 128 cm), the wave velocity is 1,600 m/s, in agreement with the values observed by Hamilton (1980) for this type of sediment, while at the gravelly sand level a maximum value of 2,400 m/s was registered.

The water content along the profile is highly variable with the vertical variation of textural parameters: a content of about 20 % is typical of the sandy sediments, 17 % of the sandy gravel sediments and values between 30 and 40 % in the muddy sediments. The highest values are inversely correlated with the volume weight of the sediments as expected, due to the presence of muddy sediments.

The Atterberg Limits, determined for the sandy silt layer (between 110 and 128 cm), indicate a liquidity limit (LL) of 39 % and plasticity index (PI) of 16 %, which, according to USCS (ASTM D 2487-06), corresponds to the CL group. This type is characteristic of a sandy lean clay inorganic with medium plasticity (Burmister 1949 *in* Das 2006) and with active clays (A = 1.4) (Skempton 1953).

The density of the particles varies between the 2.40 and 2.69, with no apparent trend with depth. The minimum value of 2.40 is registered at the 207 cm, probably correlating with the biogenic particles.

The mechanic characterization of the sediments is currently ongoing and is performed by triaxial tests, which will allow defining the resistant parameters of the sediments.

69.4 Conclusions

The depositional architecture, recognized in the seismic profiles, was confirmed with an integrated analysis of sedimentologic and geotechnical parameters, resulting in a more accurate identification of internal interfaces and heterogeneities.

Although the data interpretation is still in a preliminary stage it was possible to identify 7 types of different sediments that reflect the source variability and equilibrium with different meteorological and oceanographic conditions, along the depositional cycle.

The use of two non-destructive methods, magnetic susceptibility and compression waves, revealed itself to be quite satisfactory for the identification of the different interfaces, although the compression waves should be made in lower intervals.

References

Buckingham MJ (2005) Compressional and shear wave properties of marine sediments: comparisons between theory and data. J Acoust Soc Am 117(1):137–152

Das MB (2006) Principles of geotechnical engineering. Toronto. ISBN:0-534-55144-0

Hamilton El (1980) Geoacoustic modeling of the sea floor. J Acoust Soc Am 68(5):1313–1340

Nichols G (2009) Sedimentology and stratigraphy, 2nd edn. Wiley-Blackwell, Hoboken. ISBN 978-1-4051-9379-5

Randolph M, Gourvenec S (2011) Offshore geotechnical engineering. Spon Press. ISBN13:978-0-415-47744-4 (hbk)

Skempton A (1953) The colloidal activity of clays. In: Proceedings of 3rd international conference on soil mechanics and foundations engineering, vol 1, pp 57–61

Model of Permafrost Thaw Halo Formation Around a Pipeline

Pavel Novikov, Elizaveta Makarycheva, and Valery Larionov

Abstract

Permafrost thawing around buried pipelines transporting warm hydrocarbons can result in dangerous bending of the pipeline and it's possible damage. Prediction of the permafrost-pipeline thermal interactions reflected in the thawing halo dimensions is an important problem both for design and operation of the pipeline. The aim of this work was to develop a predictive model of thawing halo formation with high ratio of the accuracy in estimating thawing halo dimensions to the quality of input data. A theoretical model that considered factors possibly influencing permafrost-pipeline thermal interaction was developed. Oil pipeline field experiments were performed in Eastern Siberia, Russia. Thaw halo extent and other local factors were measured. Then calculated thawing halo dimensions were compared with the measurements obtained in the field experiment. In addition evaluation of the individual influence of each factor considered in the model was performed in numerical studies. The developed and tested predictive model of permafrost thaw halo formation demonstrated a reasonable ratio of accuracy in estimating thawing halo dimensions to the quality of input data. The dimensions of the thawing halo were most sensitive to the temperature of the transported hydrocarbons, thermal conductivity of frozen soil and the initial temperature field of permafrost within the region of the pipeline's thermal influence.

Keywords

Permafrost • Pipeline • Thaw halo • Thermal interaction • Soil properties

70.1 Introduction

Heat released from buried pipelines transporting warm hydrocarbons progressively thaws surrounding permafrost forming a permafrost thaw halo around the pipeline. Due to the non-uniform distribution of soil properties and massive ice deposits in the permafrost, differential settling of soil under the pipeline is likely to occur. This differential settlement results in bending strain in the pipe's wall which could lead to overstress and possible damage to the pipeline.

P. Novikov (✉) · V. Larionov
Bauman Moscow State Technical University, Moscow, Russia
e-mail: novikov-p-a@yandex.ru

E. Makarycheva · V. Larionov
Emergency Situations Research Center Ltd., Moscow, Russia

70.2 Aim

This work was dedicated to the prediction of permafrost thaw halo formation around a pipeline. A reasonably accurate predictive model of pipeline thermal interaction with permafrost is difficult but realizable if detailed data on all of the relevant factors influencing this interaction are available (Jianfeng et al. 2009). But today obtaining full and precise information about these factors is quite difficult.

The aim of this work was to develop a predictive model that provides high ratio of the accuracy in estimating thawing halo dimensions to the quality of input data.

Table 70.1 Input data list

Group name	Parameters
Pipeline parameters	Pipe wall temperature (t_{oil}); pipe outside diameter; pipe wall thickness; thermal insulation coating thickness (h_{ins}); thermal conductivity coefficient of thermal insulation coating; trench geometry
Ground and backfill properties	Layer thickness; thermal conductivity coefficient of thawing ground (S_t); thermal conductivity coefficient of frozen ground (S_f); heat capacity of thawing ground (C); moisture content; density; porosity; melting temperature; thawing factor; compressibility factor of thawing ground; density
Permafrost parameters	Depth; average annual temperature near the daylight surface (t_{perm})
Climate data	Average monthly temperatures; average monthly wind speed; average monthly snow depth; power density of solar radiation; air-ground heat transfer coefficient; daylight surface albedo

Fig. 70.1 Permafrost thaw halo measurement (*1* a daylight surface; *2* a pipeline; *3* a seasonally thawing layer; *4* a measured border of the thawing halo; the size of cells is 1 × 1 m)
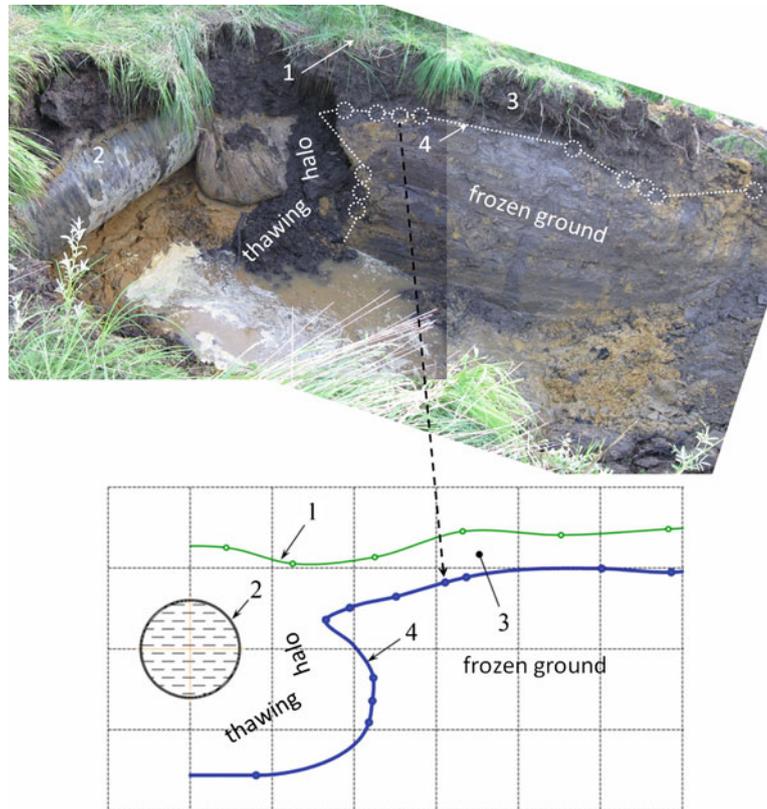
70.3 Model

A list of factors (temperature of the transported hydrocarbons, soil properties, geometry of the trench, etc.) possibly influencing permafrost-pipeline thermal interaction was constructed (Table 70.1) and from this list a model predicting this interaction was created.

70.4 Oil Pipeline Field Experiment

Permafrost thaw halo was measured around the oil pipeline located in Eastern Siberia, Russia. Measurements of thaw halo extent were taken for two sections of the pipeline after

3 years from the start of its operation (Makarycheva et al. 2013). In addition, all information about local conditions that affect permafrost-pipeline thermal interaction was collected as accurately as possible.

Measurements of thaw halo for the first section in June are shown on Fig. 70.1.

70.5 Validation

The thawing halo formation around the pipeline was calculated via the developed theoretical model using conditions recorded at the pipeline as input data. Then calculated halo dimensions were compared with the measurements of the thawing halo for each of two sections during June and

Fig. 70.2 Comparison of the measured and calculated permafrost thaw haloes (*1* a daylight surface; *2* an initial position of the pipeline; *3* a current position of the pipeline (by taking into account ground subsidence); *4* a border of the trench; *5* a measured border of the thawing halo; *6* a seasonally thawing layer; *7* a seasonally frozen layer; *8* a measured border of the seasonally frozen layer; *9* a calculated border of the thawing halo; *10* a calculated depth of the thawing halo under the pipeline; the size of cells is 1 × 1 m)
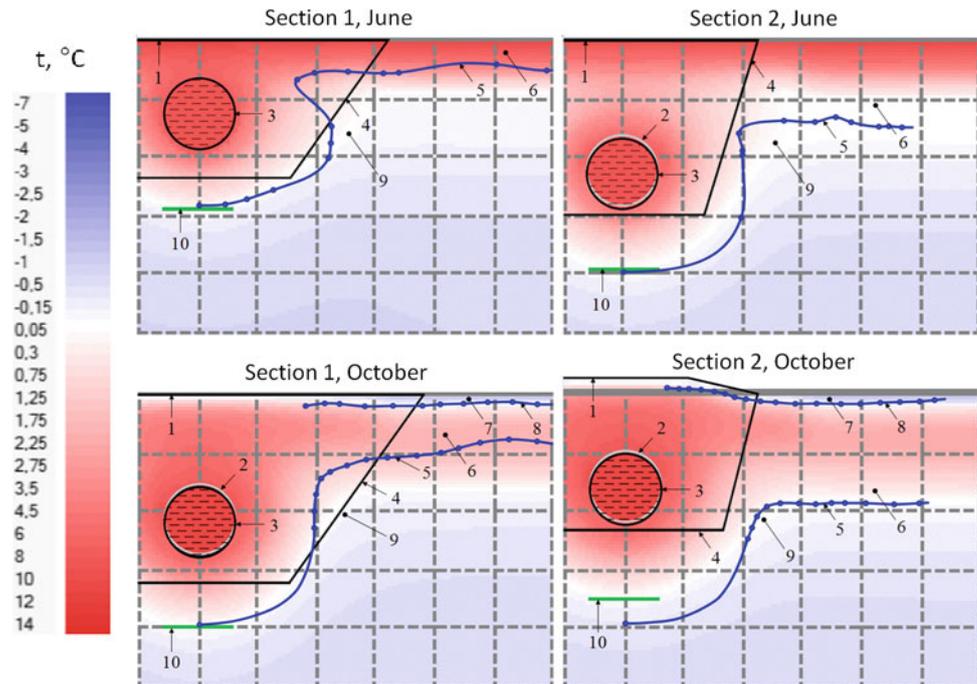
October in the third year of the pipeline's operation. Figure 70.2 demonstrates the agreement between calculated and measured results.

70.6 Demands on Initial Data Accuracy

Factors that could be managed during the pipeline design or operation were chosen among all the factors influencing the thawing halo formation. A series of numerical studies was conducted to evaluate the impact of each of these factors on permafrost thaw halo dimensions. The most influential six manageable factors are presented in the Table 70.2.

70.7 Conclusions

In conclusion, the predictive model of permafrost thaw halo formation that makes reasonable demands on initial data quality and provides sufficient accuracy of calculated thawing halo dimensions was developed and tested. According to the results of the numerical studies, the dimensions of the thawing halo are most sensitive to the temperature of the transported hydrocarbons, thermal conductivity of frozen soil and the initial temperature field of permafrost within the region of the pipeline's thermal influence. The developed model can be used as a basis for further investigations of the stress state of a pipeline in the conditions of soil subsidence.

Table 70.2 Influence of each factor on permafrost thaw halo formation

Factor[a]	−				Nominal input				+			
	Thawing halo dimensions, m				Thawing halo dimensions, m				Thawing halo dimensions, m			
	Depth under a pipe	Half-width	STL, m	SFL, m	Depth under a pipe	Half-width	STL, m	SFL, m	Depth under a pipe	Half-width	STL, m	SFL, m
Section 1, June												
C (∓ 30 %)	2.90	2.81	0.91	–	2.90	2.84	0.91	–	2.90	2.97	0.91	–
t_{oil} (∓ 30 %)	2.78	2.56	0.91	–					3.10	3.03	0.91	–
S_f (∓ 30 %)	3.10	2.69	0.91	–					2.85	2.97	0.91	–
S_t (∓ 30 %)	2.90	2.34	0.84	–					2.90	3.09	0.91	–
h_{ins} (on/off/-)	2.55	2.66	0.91	–					–	–	–	–
t_{perm}(∓ 30 %)	2.85	2.50	0.91	–					3.10	3.25	0.91	–
Section 2, June												
C (∓ 30 %)	3.93	2.13	1.41	–	3.93	2.13	1.41	–	3.93	2.13	1.41	–
t_{oil} (∓ 30 %)	3.73	1.88	1.72	–					4.10	2.38	1.84	–
S_f (∓ 30 %)	4.13	2.31	0.94	–					3.80	1.97	1.41	–
S_t (∓ 30 %)	3.88	2.00	0.97	–					3.98	2.25	1.91	–
h_{ins} (on/off/-)	3.43	1.91	1.41	–					–	–	–	–
t_{perm}(∓ 30 %)	3.78	1.94	1.09	–					4.09	2.31	1.53	–
Section 1, October												
C (∓ 30 %)	3.98	2.75	1.91	0.19	3.98	2.15	1.60	0.18	3.95	2.16	1.69	0.19
t_{oil} (∓ 30 %)	3.75	1.97	1.69	0.19					4.15	2.38	1.69	0.19
S_f (∓ 30 %)	4.20	2.25	1.63	0.13					3.80	2.06	1.69	0.19
S_t (∓ 30 %)	3.93	2.00	1.44	0.28					3.98	2.06	1.69	0.19
h_{ins} (on/off/-)	3.38	1.94	1.63	0.19					–	–	–	–
t_{perm}(∓ 30 %)	3.80	2.00	1.56	0.19					4.20	2.41	1.91	0.19
Section 2, October												
C (∓ 30 %)	3.50	2.70	1.91	0.19	3.48	2.20	1.87	0.18	3.48	2.70	1.91	0.19
t_{oil} (∓ 30 %)	3.30	2.50	1.88	0.19					3.65	3.05	1.88	0.19
S_f (∓ 30 %)	3.68	3.00	1.88	0.13					3.35	2.65	1.94	0.22
S_t (∓ 30 %)	3.43	2.28	1.66	0.28					3.50	2.90	1.91	0.09
h_{ins} (on/off/-)	3.00	2.60	1.88	0.19					–	–	–	–
t_{perm}(∓ 30 %)	3.35	2.65	1.72	0.19					3.56	2.85	2.16	0.19

STL Seasonally thawing layer, *SFL* Seasonally frozen layer

[a] see Table 70.1

References

Jianfeng X, Basel A, Ayman E, Paul J (2009) Permafrost thawing-pipeline interaction advanced finite element model. In: Proceedings of the ASME 28th international conference on ocean, Offshore and arctic engineering OMAE 2009, Honolulu, Hawaii, pp 97–102, 31 May–5 June 2009

Makarycheva EM, Larionov VI, Novikov PA (2013) Experimental studies of thawing halo for verification and calibration of forecasting mathematical models. Herald Bauman Moscow State Tech Univ 1 (48):109–116

Assessing Rock Mass Properties for Tunnelling in a Challenging Environment. The Case of Pefka Tunnel in Northern Greece

Vassilis Marinos, George Prountzopoulos, Petros Fortsakis, Fragkiskos Chrysochoidis, Konstantinos Seferoglou, Vassilis Perleros, and Dimitrios Sarigiannis

Abstract

The investigation of alternative solutions for the Thesaloniki Ring Road has been one of the major project design challenges in the recent years in Greece. Pefka tunnel was included in one of the alternatives that have been proposed and thoroughly examined. The total length of the tunnel was ~ 1450 m and it had two branches, with three lanes per branch. According to the geological design, the tunnel was to be excavated through a great variety of formations, such as travertine, shales and graphitic shales, alternations of meta-siltstones and graphitic shales, schistosed and intensively folded meta-siltstones, limestones, gabbros and peridotites. The large number of in situ and laboratory tests allowed (a) the reliable estimation of the intact rock properties and (b) the development of new relationships between the uniaxial compressive strength (σ_{ci}) and the point load test index (I_{s50}). These values were used for the estimation of the rock mass properties employing different methodologies. Finally, based on all available data, the anticipated rock mass behaviour in tunnel excavation is described. The key issues of this procedure are illustrated in the present paper.

Keywords

Weak rocks • Tunnel behaviour • Rock properties • Geotechnical classifications • I_{s50} correlations

71.1 Introduction

The aim of the alternative solutions for the Thessaloniki Ring Road was to decongest the traffic volume on the existing ring road and improve the access to the airport around the city. Pefka tunnel (~ 1450 m) was included in one of the alternatives that have been proposed and thoroughly examined. It had two branches, with three lanes per branch. The maximum inner width of the section is ~ 14.50 m, the maximum inner section height ~ 10.50 m and the maximum overburden height ~ 60.0 m.

Since the tunnel was to be excavated in the vicinity of the town of Pefka through a great variety of formations with different geotechnical parameters, a detailed geotechnical investigation program was carried out. The paper describes the key issues of the geological and geotechnical design focusing on the geological model, the estimation of the rock mass parameters and the anticipated ground behaviour during the excavation.

V. Marinos (✉)
Faculty of Sciences, School of Geology, Division of Geology, Aristotle University of Thessaloniki, 541 24, Thessaloniki, Greece
e-mail: marinosv@geo.auth.gr

G. Prountzopoulos · P. Fortsakis · F. Chrysochoidis · K. Seferoglou
Odotechniki Ltd, 59 3rd September Street, 10433, Athens, Greece

V. Perleros
56 Dionysou Street, 152 34, Halandri, Greece

D. Sarigiannis
Egnatia Odos S.A., 6th km Thessaloniki—Thermi, 60030570 01, Thessaloniki, Greece

71.2 Geological Setting

The outer ring road of the city of Thessaloniki is mainly situated in the foothills of Hortiatis Mountain. The Pefka Tunnel is located at the NE foothills of the Asvestochori valley along the tectonic trench of SE-NW direction.

The tunnel was planned to be driven in the Aspri Vrysi—Hortiatis unit formations of the Perirodopic zone (graphitic schists, meta-siltstones and limestones) and also in ophiolitic ones (peridotites, gabbros). The unit of Aspri Vrysi—Hortiati consists of metamorphosed old flysch series that have been transformed to clayey schists, black graphitic and light green schists, siliceous schists and metasiltstones. These formations may alternate in places. Limestones are interjected inside the schists and conclude this unit. Peridotites and gabbros are also met in separate places. Finally, in the wider area of exit portal deposits of travertine are found, originating from older karstic springs discharges of. These formations are assigned with certain codes (G1–G7) and presented in detail in the following paragraphs. The geological longitudinal section of the tunnel is illustrated in Fig. 71.1.

The graphitic schists (G2b) have clayey-silty composition and intense schistosity. Their main characteristics are the frequent shears along the schistosity and occasional clay-fillings. While the formation generally has a seamy-disturbed structure, it is sometimes found foliated with clayey zones. However, it gradually alternates with more compact and less schistosed metasiltstones (G3b). Green schists (G2a) are limited in the tunnel overburden zone. They are chlorite schists, which are disturbed with slickensided to clayey surfaces. In depth the formation becomes more compact with well-defined schistosed structure. Siliceous schists (G2c) are particularly strong and have a more compact structure. Another formation met along the tunnel is the metasiltstones (G3a). They are highly schistosed and folded, but retain compact structure. The schistosity does not separate the overall rock mass, but is contained within the blocky structure. However there are some fractured zones found along faults, where the rock mass is disturbed or even disintegrated.

Limestones (G4) are also found in the tunnel area, but their connection to other formations is not well defined. They are white, recrystallized and compact with minimum fracturing and it is believed that are found as tectonic "lenses" within the schists. The basic and ultrabasic rocks are met in the central part of the tunnel, building a compact and blocky rock mass. The formation of gabbros (G5) extends near the exit portal while the peridotites (G6) at the centre of the tunnel. In depth, they have generally compact (blocky) structure without exhibiting any schistosity or serpentinisation, while on the surface they are found more disturbed and loosened due to weathering. Finally, travertine (G1), eluvia and scree (G7) deposits are also found in the area, but they are not affecting the tunnel construction significantly.

71.3 Engineering Geological—Geotechnical Model

The geotechnical investigation for the Pefka tunnel comprised 23 sampling boreholes, one for a pressuremeter test and one for a dilatometer test, totally adding up to 1290 m. Thirteen piezometers were installed for the monitoring of the groundwater table as well as two inclinometers for the monitoring of ground movements in an area that was susceptible for a potential landslide. The geotechnical evaluation procedure included the following steps:

- Description of the geological formations in the project area (e.g. G1, G2). Different rock mass qualities could be found under the same geological formation.
- Rock mass characterization applying the GSI system on borehole cores.
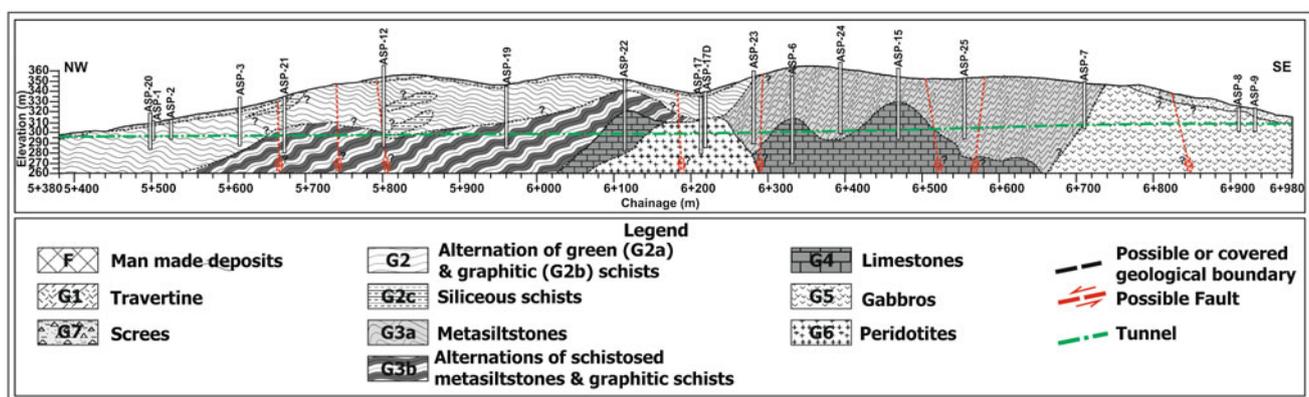
Fig. 71.1 Geological section of Pefka tunnel

- Evaluating the borehole data, five rock mass categories were defined (A, B, C, D, E) corresponding to different rock mass structure and quality of the discontinuities (Fig. 71.2).
- Statistical assessment of intact rock properties for all formations (e.g. G1, G2)
- Estimation of the rock mass parameters for every combination of geological formation and rock mass category (e.g. G2-D, G3-A).
- Description of the anticipated ground behaviour during tunnel excavation.

The rock mass quality was evaluated using the GSI rock mass characterization system (Marinos and Hoek 2000; Marinos et al. 2005) (Fig. 71.2) and the rock mass behaviour was categorized using the Tunnel Behaviour Chart (TBC) proposed by Marinos (2012). Based on this evaluation the rock mass types were:

- Rock Mass Type A: Blocky to intact rock masses with good interlocking and fair to good quality of the surfaces of discontinuities. These rock masses are expected to be stable and only local gravity failures may be observed (Geological formations: G3a, G4, G6).
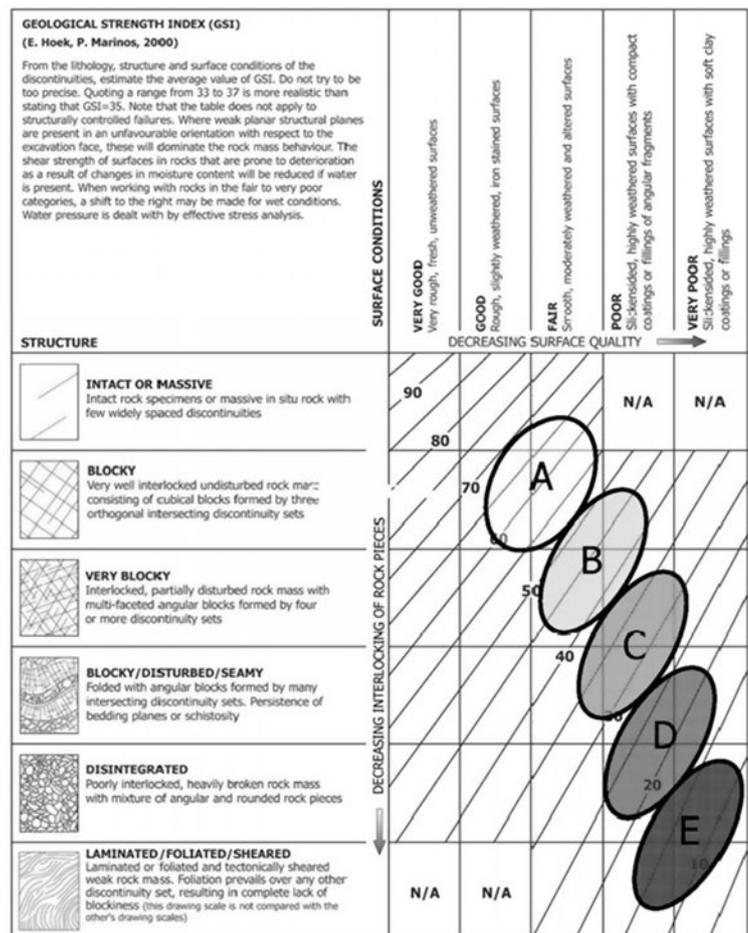
Fig. 71.2 GSI projections for every rock mass category (A–E)

Table 71.1 Engineering geological—geotechnical parameters for a number of combinations of geological formation (e.g. G1, G2) and rock mass category (e.g. A, D)

Geotechnical unit	GSI	σ_{ci} (MPa)	m_i	E_i (MPa)	γ (MN/m^3)	E_m (Mpa)
G2-B	40	15	6	5,000	0.027	1,200
G2-E	15	6	6	2,500	0.025	140
G3a-A	60	18	7	9,000	0.027	4,500
G3a-E	15	12	7	6,000	0.025	250
G3b-E	15	10	7	5,000	0.025	220
G4-A	65	28	12	24,000	0.027	12,000
G5-B	45	14	27	15,000	0.027	3,000
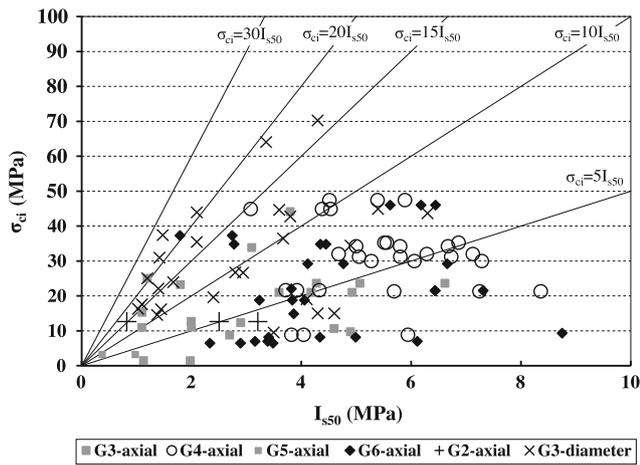
Fig. 71.3 Correlation between the results $I_{s(50)}$ and σ_{ci} values for the rocks: (i) G2: Schists, (ii) G3: Metasiltstones, (iii) G4: Limestones, (iv) G5: Gabbro, (v) G6: Peridotite

- Rock Mass Type B: Blocky to very blocky rock masses with fair to poor quality of the surfaces of discontinuities. Wedge fall or slide is the most probable failure mechanism (Geological formations: G2, G3a, G3b, G5).
- Rock Mass Type C: Blocky to seamy /disturbed rock masses with fair to poor quality of the surfaces of discontinuities. The potential failure mechanism in these rock masses would be small wedge failures or chimney type failures. (Geological formations: G2, G3b, G6).
- Rock Mass Type D: Disturbed to disintegrated rock masses with fair to poor quality of the surfaces of discontinuities. The potential failure mechanism would be chimney failure, due to the disturbance that decreases the overall cohesion, which could propagate to more extensive ravelling. In the tunnel section of high overburden, depending on the intact rock strength, small deformation could be developed. (Geological formations: G2, G3b).
- Rock Mass Type E: Sheared and laminated rock masses with poor to very poor quality of the surfaces of discontinuities. Significant deformation and face instabilities

may be developed in the area of high overburden or slope instabilities near the portals due to low rock mass strength. (Geological formations: G2, G3a, G3b).

The representative values of the engineering geological and geotechnical parameters for a number of Geotechnical Units are summarized in Table 71.1. Among a significant number of the numerous laboratory and in situ tests that were carried out, the indirect estimation of the intact rock uniaxial compressive strength (σ_{ci}) via the results of the Point Load test (Is_{50}) are presented here. Since there is a large scatter in the equations correlating Is with σ_{ci}, (e.g. Kahramman 2001; Tsiambaos and Sabatakakis 2004), a case specific correlation was established. Based on the results that are presented in the Fig. 71.3 the average value of the $\sigma_{ci}/I_{s(50)}$ ratio varied for the different formations from 5.25 to 9.90.

71.4 Conclusions

The paper is addressing a methodology developed for assessing rock mass properties in view of tunnel excavation in a challenging environment, using the case of Pefka Tunnel in northern Greece. The tunnel alignment was designed to cross eight distinct geological formations, each demonstrating different rock qualities. The methodology used consisted a four step assessment plan that evaluated the separate parameters (geological formations, intact rock properties, rock mass type, rock mass properties and rock mass behaviour) and achieved to designate the tunnel sections with similar anticipated rock mass behaviour and potential failure mechanisms, allowing the simplification and the optimization of the temporary support design.

References

Kahraman S (2001) Evaluation of simple methods for assessing the uniaxial compressive strength of rock. Int J Rock Mech Min Sci 38:981–994

Marinos P, Hoek E (2000) GSI—a geologically friendly tool for rock mass strength estimation. In: Proceedings of the GeoEng2000 at the

international conference on geotechnical and geological engineering, Melbourne, Technomic publishers, Lancaster, pp 1422–1446

Marinos V (2012) Assessing rock mass behavior for tunnelling. J Environ Eng Geosci 18(4):327–341

Marinos V, Marinos P, Hoek E (2005) The geological strength index: applications and limitations. Bull Eng Geol Env 64:55–65

Tsiambaos G, Sabatakakis N (2004) Considerations on strength of intact sedimentary rocks. Eng Geol 72:261–273

Vítor Santos, A. Paula F. da Silva, and M. Graça Brito

Abstract

As known, geological conditions are a complex challenge in any civil engineering work, however this is not as relevant as in tunnelling where ground knowledge usually has many uncertainties at the beginning of the construction phase. The prediction of the ground quality of advancing tunnel face represents, itself, a key step during tunnelling, allowing to prepare and mobilize the most appropriate means to proceed with the works, with an adequate level of safety, quality and efficiency. The authors tested a quantitative methodology for prediction of rock mass quality during drill and blast excavation. The paper is based on the application of three mathematical prediction methods for the estimation of rock mass quality: linear regression, geostatistical kriging and neural networks algorithms. Additionally, a fourth empirical method was also applied, based on engineering geologist's expertise, aiming to assess the deviation of the quality prediction. The methodology was tested using RMR information of several tunnels, dug in a granitic rock mass, integrating the power generation reinforcement of Picote dam, located in the northeast of Portugal. The obtained results revealed, for all cases, a significant correlation between the estimated RMR and the observed value, thus raising good expectations for the progress of the ongoing research works.

Keywords

RMR prediction • Mathematical modelling • Advance tunnel face

72.1 Introduction

Rock mass characterization for tunnel excavation results from geological and geotechnical surface mapping, complemented by indirect and direct prospecting methods. At the beginning of the construction phase, usually there is still a high level of uncertainty in the geological (including hydrogeological and tectonic) model, leading to unpredictable hazardous situations. To mitigate such lack of information, the authors tested a quantitative methodology for prediction of rock mass quality during drill and blast (D&B) excavation, aiming to select an adequate quantitative methodology for predicting rock mass rating (RMR) values and to anticipate the rock mass quality of the advancing tunnel face, providing considerations on the geotechnical behaviour of the ground. The earlier determination of the rock mass quality of the ground to be dug allows for the timely mobilization of necessary resources to ensure the stability of the tunnel, safeguarding quality, safety and effectiveness of construction.

The selected methodology should anticipate the behaviour and natural heterogeneity of the rock mass during the tunnel construction phase and must, also, be easy to

V. Santos (✉) · A.P.F. da Silva · M.G. Brito
CICEGe, Faculdade de Ciências e Tecnologia (FCT), Univ. NOVA de Lisboa, Lisbon, Portugal
e-mail: silva.santos@gmail.com

A.P.F. da Silva
e-mail: apfs@fct.unl.pt

M.G. Brito
e-mail: mgb@fct.unl.pt

A.P.F. da Silva · M.G. Brito
Dept. Ciências da Terra, Faculdade de Ciências e Tecnologia (FCT), Univ. NOVA de Lisboa, Lisbon, Portugal

implement and to produce immediate results, in order to respond to the dynamics of the D&B excavation. Hereafter, the results of the application of three mathematical prediction methods and of one empirical method are presented and their validity is discussed.

72.2 Case Study Presentation

The Picote II Repowering Scheme is located in the northeast of Portugal, near the Spanish border, in International Douro River, around 25 km south of Miranda do Douro (Fig. 72.1). Table 72.1 presents the tunnels that integrate the scheme works and summarizes their geometric characteristics.

In the study area, there are porphyritic two-mica granites, classified during the construction with the geomechanical classification (Bieniawski 1989). The RMR was registered at each section from the main tunnels integrating the hydraulic circuit.

72.3 Methodology

Usually, D&B excavation methods use daily dynamic excavation cycles allowing the prediction of rock mass quality and reducing the need for complex methods of treatment to improve rock mass quality.

This paper presents the results of the application and test of the benefits of using a set of mathematical models (geostatistics and neural network models) to assess the quality of rock mass and predicting the geotechnical behaviour of the advancing tunnel face during D&B. Geostatistical models have been widely used in the fields of geosciences, namely in the geotechnical domain (Brito et al. 1997), as well as neural network models have in geological (Leu and Adi 2011) and geotechnical (Miranda et al. 2007) studies.

The methodology adopted is described by the two following steps:

1. Estimation of the RMR of the advancing tunnel face by using (i) linear regression correlation, (ii) ordinary kriging geostatistical method, and (iii) neural networks method;
2. Comparison of the RMR values estimated by the mathematical models and the RMR obtained by the empirical knowledge of an engineering geology expert.

The progress of the excavation is simulated by repeating the procedure successively for each of the tunnels previously excavated sections, corresponding to an average length of about 3 m; this means that the prediction of ground quality corresponds to a distance of approximately 3 m beyond the excavation face (Fig. 72.2). This process is repeated for each of the tunnels of the case study, allowing the simulation of the RMR value of the advancing tunnel face.

The linear regression method was applied by considering the data concerning the last excavated sections: 3 (n, $n - 1$, $n - 2$), 5 (n, $n - 1$, ..., $n - 4$) and 10 (n, $n - 1$, ..., $n - 9$),

Fig. 72.1 Components of Picote II (Portugal) repowering scheme (EDP 2006, modified)
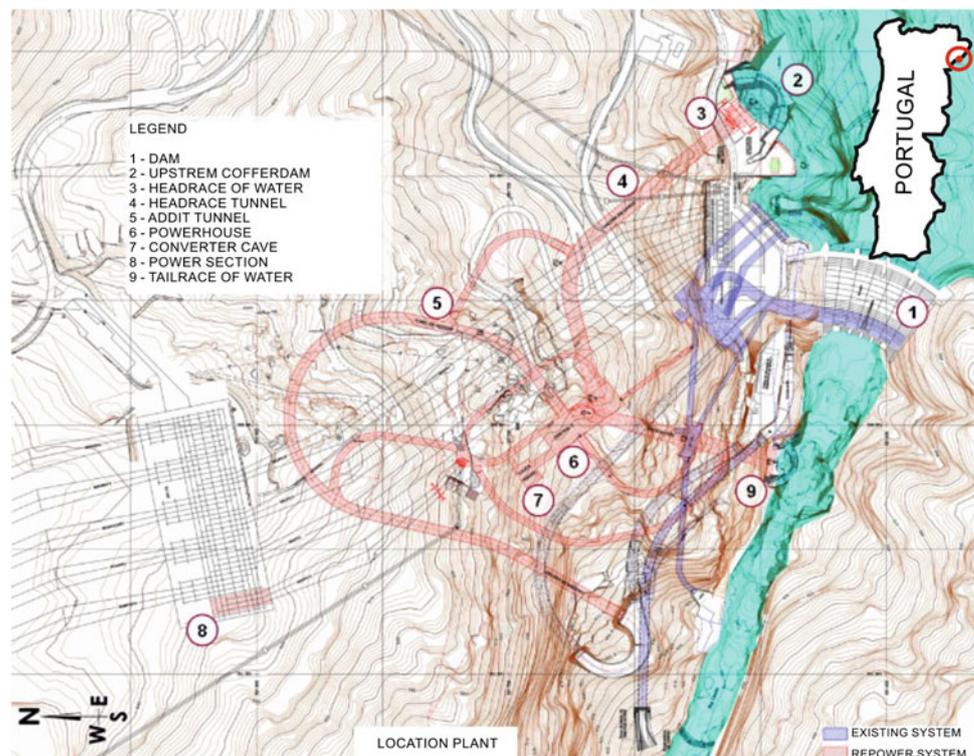
Table 72.1 Geometry of the underground main structures (adapted from EDP 2006)

Tunnel	Code	Length (m)	Diameter (m)	Height (m)	Section area (m^2)
Headrace	GC	300	12	12	113
Tailrace	GR	150	12	12	113
Powerhouse addit	TAC	625	8.5	8.1	62
Headrace addit	GAGC	141	5	5.5	26
Top powerhouse addit	GAAC	204	5	5.5	26
Tailrace addit	GAR	252	5	5.5	26
Gates chamber addit	GACC	121	5.5	5.8	29
Ventilation and safety	GVS	155	3.7	4	14.5

Fig. 72.2 Scheme for data collection of rock mass quality
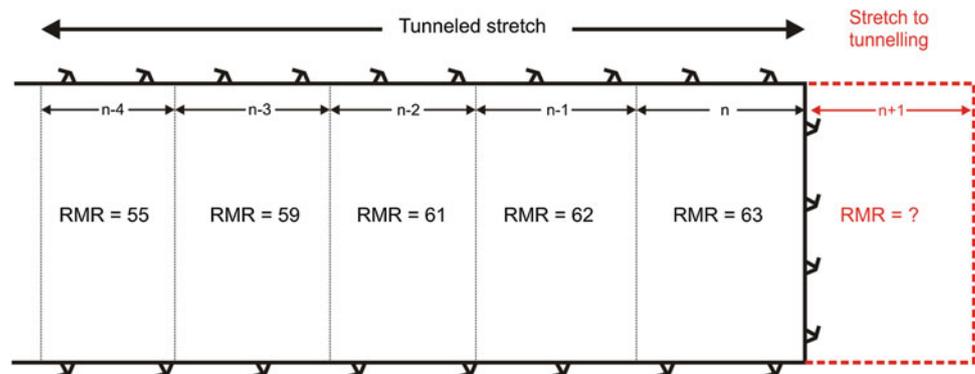
where section n corresponds to the last excavated tunnel face. Prediction of RMR values are obtained from the linear regression between observed—obs, and estimated RMR values, for a 3 m extension for the next $n + 1$ tunnel face.

Geostatistical kriging modelling started with the structural analysis of RMR behaviour along the sequential excavated tunnel sections ($n; n - 1; n - 2; ...; 1$). The obtained variogram was adjusted with a spherical model for an amplitude a, corresponding to the distance at which RMR values are no longer correlated. Ordinary kriging is used to estimate RMR values for a face at distance of $n + 1$.

For the application of neural networks methodology (neu), five independent columns containing the RMR value of the last five excavated tunnel sections ($n, n - 1, ..., n - 4$) and one dependent column that corresponds to the RMR estimated for the next ($n + 1$) section were considered. For each advancing face of the tunnel, new neural networks are generated, based in regression-based automated network search algorithms. The type of the neural networks used was the multi parallel layer (MPL) type, with $2 - 20$ hidden units. The active functions to develop the hidden neurons in MPL were the identity, logistic and the exponential, using a decay weight in a range between 0.0001 and 0.001. The number of neural networks generated was 20; of these, the one that showed less error in test is selected.

The empirical (exp) methodology is based on the analysis of RMR values along the excavated length. This methodology was applied to the case study using an experienced geological and geotechnical monitoring operator. All RMR values observed until section n were considered and arranged in a graphic presentation of RMR *versus* the extension excavated.

For evaluation of results, the correlation between the estimated RMR values *versus* in situ RMR_{obs} was determined and the respective relative and absolute estimation errors were analyzed. The signal of this errors was also discriminated as, in this context, it represents an over or underestimation of rock mass quality and, consequently, of its stability/safety. To understand the influence of the tunnels geometry (length and cross sections area) in the RMR errors, the trending of errors along the tunnels sections was also analyzed.

72.4 Results and Considerations

The RMR estimated values obtained were subjected to statistical analysis as summarized in Fig. 72.3, where it is possible to refer that: (i) the values estimated by empirical method (RMR_{exp}) are the most similar to the RMR observed values (RMR_{obs}); (ii) the regression method applied to the last 3, 5 and 10 excavation sections (RMRregr3, RMRregr5
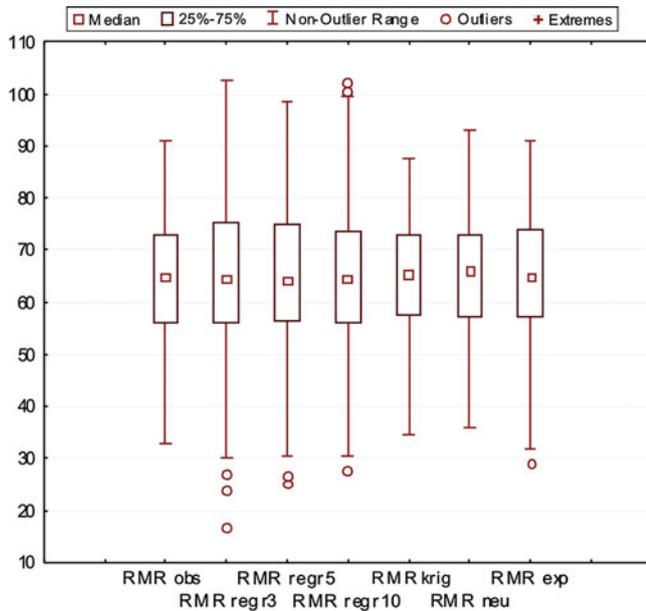
Fig. 72.3 Box-plot for estimated RMR values

and RMRregr10) presents extreme values in addition to the observed ones; and (iii) the RMR values estimated by ordinary kriging (RMR_{krig}) and neural networks (RMR_{neu}) methods do not represent the maximum and lowest values of real RMR (RMR_{obs}).

Regarding the average values, all methodologies revealed values close to those observed and, additionally, 50 % of the estimated values showed identical values to RMR_{obs}.

The methodologies that showed the highest correlation (88 %) between the estimated and the observed RMR were the empirical (*exp*) and ordinary kriging (*krig*). Nonetheless, other approaches have also presented satisfactory results (correlations above 79 % for the remaining ones).

The interpretation of the estimation errors was performed for each of the methodologies, and Figs. 72.4 and 72.5 show, as an example, the analysis applied to the estimated errors obtained by the regression method in the last three sections (*regr3*). Comparing the graphs obtained for all methods it can be stated that: (i) the average errors obtained with the different estimation methods are very similar and show a normal distribution; (ii) kriging method (*krig*) presents the smallest error amplitude; (iii) neural network method (*neu*) presents the highest RMR error values; (iv) in general, the dispersion of the error is broadly identical throughout the range of RMR with some exceptions for RMR values ranging between 40 and 60; and (v) there is not a clear correlation between the errors and the length /cross section of the excavated tunnels.

The empirical method (*exp*) reveals, itself, as the most effective, showing the relevance of an expert in the monitoring of tunnel construction. However, the use of mathematical tools represents also a good helper for less experienced operators.

Fig. 72.4 Distribution of average errors (regr3 method)

Histogram of exp error abs
exp error abs = 488*5*normal(x; 0.0615; 5.7262)
Kolmogorov-Smirnov test exp error abs: D = 0.1129; p < 0.0100; Lilliefors-p < 0.01
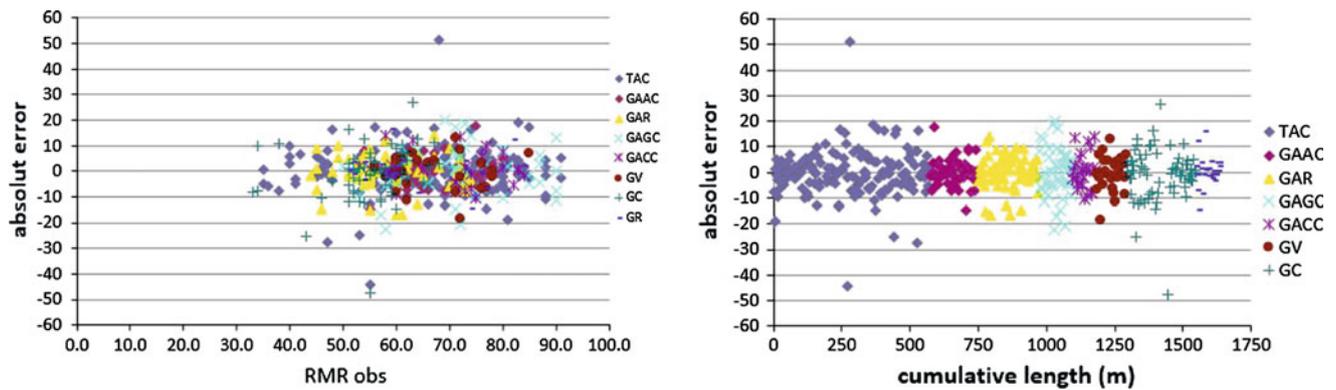
Fig. 72.5 Behaviour of absolute error of RMR: observed by expert, *left*, and by extension of different types of tunnels, *right* (regr 3 method)

72.5 Conclusions

The mathematical methodologies used for predicting the quality of a granitic rock mass by estimating the values of advancing tunnel face during D&B excavation works presented very good results, with high correlation between the estimated and the observed RMR values. Nonetheless, the skills and knowledge of an engineering geologist expert is still the most efficient and accurate method for monitoring geotechnical behaviour of rock mass excavation and avoid potential unexpected situations that may occur during tunnelling.

References

Bieniawski Z (1989) Rock Mass Classifications. Wiley, Hoboken, p 251

Brito MG, Durão F, Pereira HG, Rogado JQ (1997) Classification of heterogeneous industrial rocks: Three different approaches. In: Pawlowsky Glahn V (ed) IAMG'97–3rd annual conference international association mathematical geology. Barcelona, pp 875–879

EDP (2006) Aproveitamento hidroeléctrico do Douro Internacional - Reforço de Potência de Picote - Estudo Geológico Geotécnico, p 63

Leu S, Adi T (2011) Probabilistic prediction of tunnel geology using a Hybrid Neural-HMM. Eng Appl Artif Intell 24:658–665

Miranda T, Correia G, Sousa LR (2007) Use of AI techniques and updating in geomechanical characterisation. In 11th congress of the international society for rock mechanics: courses. ISRM, Lisboa, p 31

The Medium- to Long-Term Effects of Soil Liquefaction in the Po Plain (Italy)

73

Elio Bianchi, Lisa Borgatti, and Luca Vittuari

Abstract

The 2012 Emilia seismic sequence has shed light on some unusual geomorphological processes and related landforms observed in the Po Plain between the provinces of Modena and Bologna, namely small-scale sinkhole formation, in a non-karstic setting. In some of the areas previously affected by sinkholes, during the Emilia earthquakes, widespread coseismic effects were observed, as soil liquefaction, sand venting and ground cracks. Before 2012, these effects have been seldom observed in the Po Plain, mainly because of moderate seismicity. Known historical earthquakes, or eventually older events, could have been the original triggering factor of liquefaction of susceptible soils at shallow depth and formation of dikes and sills, as precursors of future sinkholes. To test this model, data collection on boundary conditions and a number of further field experiments is ongoing. In particular, the research is focused on three main issues: the setup of a geological model of the area, taking into account structural a tectonic features; the analysis of surface displacements horizontal (geodynamic) and vertical displacements (natural and/or artificial subsidence) and their relationships with the development of sinkholes. This is performed through the exploitation of SAR interferometric data and GPS data; geological and geotechnical characterization of soils, through a number of continuous boreholes, trenches and CPT tests for building cross sections and 3D models of areas prone to sinkhole development. These pieces of information are used for set up a numerical model and simulating the process of sinkhole triggering ad evolution in the River Po alluvial plain.

Keywords

Liquefaction • Sinkholes • GPS • InSAR • Po plain

73.1 Introduction and Methods

In Italy, natural sinkhole phenomena which are not directly connected to fluvial or karst processes are relatively uncommon Caramanna et al. (2008). On the basis of previous works, as well as available geological, geomorphological and geotechnical data (Bonori et al. 2000, 2010; Castellarin et al. 2006), the possible triggering factors and the evolution of these phenomena are described. An inventory carried out some years ago accounted for 28 areas affected by this type of sinkholes (Fig. 73.1).

To unravel the long- and short-term evolution of these landforms, a geological model of the area is built, taking into account structural a tectonic features; the analysis of surface displacements horizontal (geodynamic) and vertical displacements (natural and/or artificial subsidence) and their relationships with the development of sinkholes. This is performed through the exploitation of SAR interferometric data and GPS data; geological and geotechnical characterization of soils, through a number of

E. Bianchi (✉) · L. Borgatti · L. Vittuari
Dipartimento di Ingegneria Civile, Chimica, Ambientale e dei Materiali DICAM, Università di Bologna, Viale Risorgimento 2, 40136, Bologna, Italy
e-mail: elio.bianchi2@unibo.it
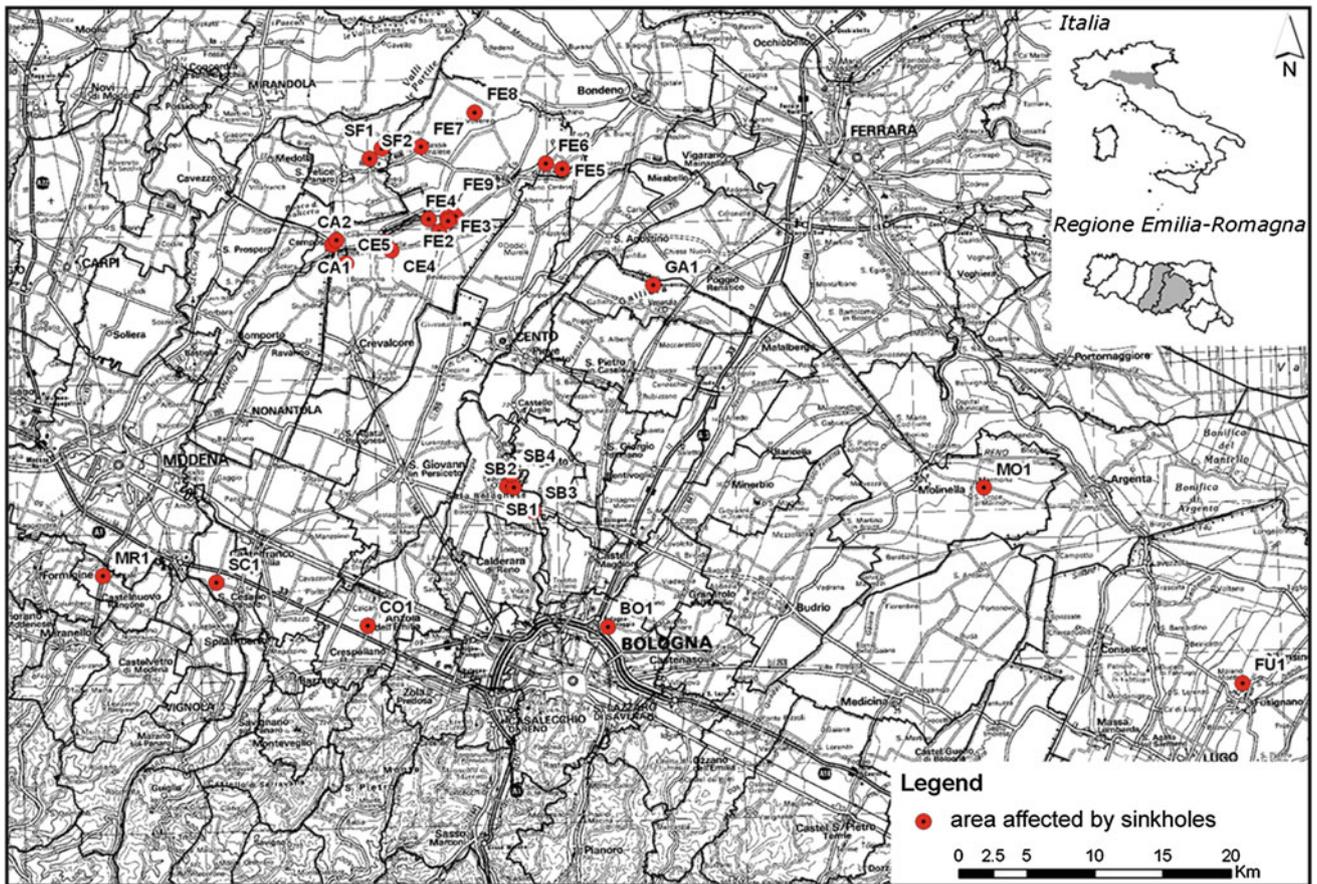
Fig. 73.1 Areas affected by sinkhole phenomena. Most of the areas are located in the Provinces of Modena and Bologna

Fig. 73.2 *Top* Cretaceous 3D structural model built in Rms (by ROXAR)
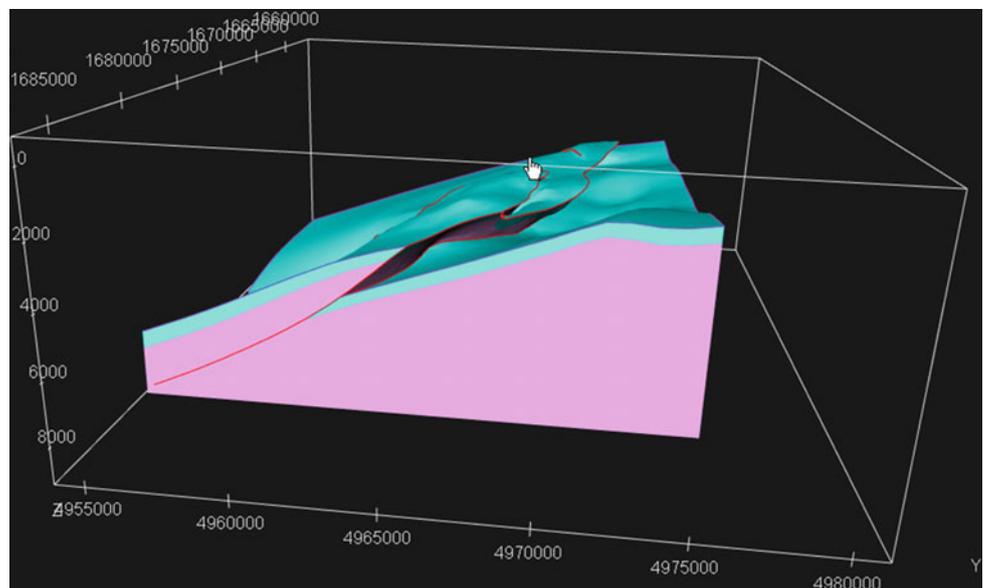
continuous boreholes, trenches and CPT tests for building cross sections and 3D models of areas prone to sinkhole development. These pieces of information are to be used to set up a numerical model and simulate the process of sinkhole triggering ad evolution in the River Po alluvial plain.

73.2 Structural Model

In this work we created a three-dimensional geometrical model of a sector of the Ferrara-Romagna fold and thrust system buried under the Plio-Pleistocene sediments of the Po Plain in order to model numerically the active stress field of the region (namely, the Mirandola fold). The input data derived from interpretation of seismic lines and geological sections reported in the literature (Boccaletti et al. 2003; Fantoni and Franciosi 2009; Pieri and Groppi 1981). A quality control was made using deep wells for oil exploration. The main tectonic elements in the model consist of a set of ramps that converge downward to the main detachment likely located within the Upper Triassic units (Fig. 73.2). A 3D model of deep geological units is needed to understand which are the structures which have generated ancient and recent earthquakes and their level of activity. This is an important issue to understand whether there is a correlation between the geomorphological phenomena observed before and after the earthquakes of May 2012.

73.3 PSInSAR Data Over the Study Area

Through monitoring 2003–2010 period, two datasets of satellite images (ascending and descending) were analyzed. The presence of the two datasets acquired with different geometry on the same area made it possible to carry out the decomposition of the motion, that is to calculate for each measuring point, the vertical component (up-down) and horizontal (E–W) of the movement starting from the original measurements carried out along the Line of Sight to the satellite (LoS). For each acquisition geometry (ascending and descending), the velocity of the movement is referred to

a point located on the vertical projection of the buried thrust above the surface, that is, where the thickness of the alluvial deposits is lower and therefore the Mesozoic substratum is more superficial. The spatial distribution of the velocity of surface displacement (horizontal and vertical) indicates a gradual increase moving away from the peak of the buried thrust in the direction of N–N—and S–SW (Fig. 73.3a, b). This technique allows us to measure and distinguish the phenomena of compaction induced by human activities (i.e., water pumping), and natural subsidence, and measure instantaneous effects, which depend on the movement of deep structures and which occur with earthquakes that may cause raising and lowering of the surface and locally soil liquefaction. The rate field has highlighted the presence of the effects of subsidence of the order of a few mm/y. The cause of such behaviour was not analyzed in detail, however, by analogy with other cases examined, it is possible to relate this increase in speed with the thickness variation of the compressible alluvial deposits. The decomposition of the motions (2003–2010 period), showed that the area of study is concerned essentially of vertical movements, with speeds generally lower than 5 mm/yr, while the horizontal component of the E–W is practically negligible.

Permanent deformation in the Po Valley from GPS data resulted in shortening with limited rates of a few mm/y Devoti et al. (2011). After the two earthquakes of May 2012, the maximum horizontal offset was observed at MO05, the site nearest to the epicenter of the main shock (30 mm horizontal and 73 mm vertical movement. Devoti (2012). This information, combined with the interferometric data, can help us to distinguish deep geodynamic effects from superficial and more local effects due to geomorphological processes and geotechnical characteristics of the soils.
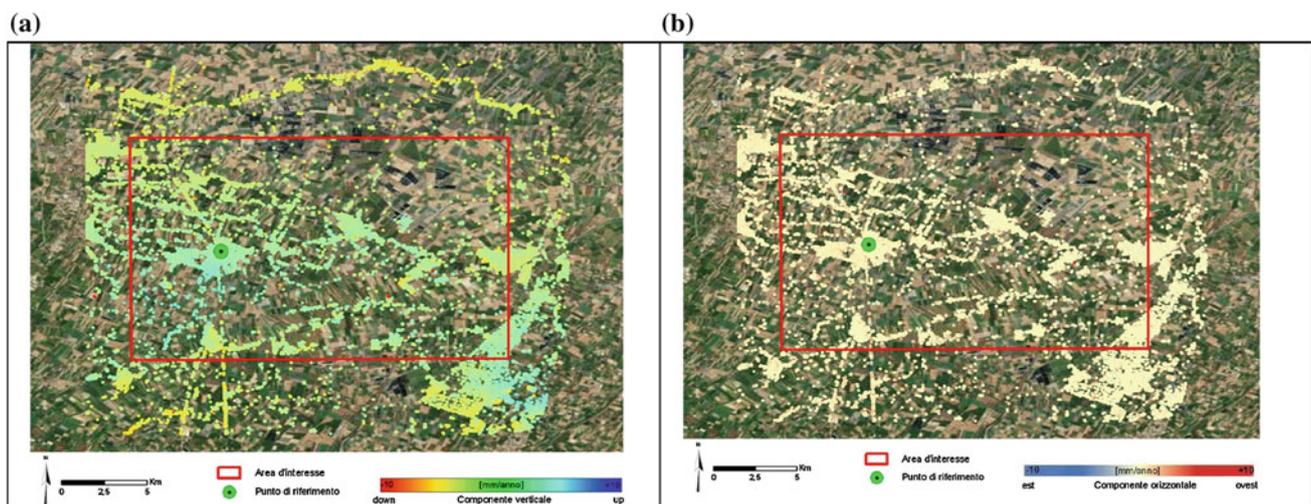
Fig. 73.3 **a** Vertical component of the velocity field. **b** Horizontal component E–W direction of the velocity field

73.4 Geological and Geotechnical Characterization of Sinkoles

These phenomena tend to develop in different geological settings. From the geomorphological point of view, some sinkhole occur near the apex of apenninic large alluvial fans, as well as in the lower alluvial plain (elevation from 64 to 6 m a.s.l.); generally, the areas fall within relatively short distances from streams, rivers and artificial channels. In most cases, the affected soils have silty-sandy texture related to alluvial ridges. The sinkholes appear both on arable land (61 %) and in orchards (25 %). Some of the sinkholes have formed in areas characterized both by low and by high rates of subsidence (from 5 to 50 mm/yr in the period 1992–2006, ARPA Ingegneria Ambientale 2007). On the basis of Cone Penetration Tests interpretation based of Schmertmann (1978) (Fig. 73.4), some of the affected areas have been characterized with reference to lithology, stratigraphy and relevant geotechnical parameters (Borgatti et al. 2010). The top unit is an overconsolidated cohesive soil, with sufficient clay fraction to form and retain shrinkage cracks in the so-called active zone (that locally can reach 5 m in depth). At a depth in the order of 6–10 m, a loose sandy unit can be typically found. The formation of seismically-induced liquefaction features is favored by: presence of liquefiable sediments (preferably a clean sand with a thickness of 1 m or more), an overlying low-permeability cap of silt and clay at least 1 or 2 m and less than 10 m in thickness, and a shallow water table (see Obermeier and Pond 1999). As these areas appeared to be prone to liquefaction, the evolution of sinkholes may be eventually related to liquefaction events.

The predisposing factors of modern sinkhole phenomena, thus, appear to depend on the stratigraphy and grain size distribution of recent loose alluvial sediments at shallow depth, and on specific hydraulic conditions of shallow semi-confined aquifers in the distal sectors of alluvial ridges. Ground shaking can cause liquefaction of susceptible soils and subsequent upsurge and eventual ejection of sands along pre-existing or newly formed ground cracks, eventually due to shrinkage in the active zone and/or coseismic fracturing in the overconsolidated cap. With time, at shallow depths, in clastic planar dikes and sub- horizontal sills, resedimentation and packing occur and small-scale proto-chambers may evolve, by successive collapses and enlargement, also accelerated by the erosion of infiltrated water in permeable materials. The ultimate triggering factor for the formation of the sinkhole, also after a relatively long time-lag from the original liquefaction event, may be related to local accidents that cause the final collapse of roofs (new seismic shaking, water table sudden drawdown, heavy vehicles transit etc.).

73.5 Conclusions

The 2012 Emilia seismic sequence has shed light on some peculiar processes and landforms. Previously, liquefaction phenomena have been seldom observed in this area, mainly because of moderate seismicity. During the Emilia earthquakes widespread coseismic effects were observed, as soil liquefaction and ground cracks. On the basis of the data gathered so far, a sinkhole evolution model is proposed: these landforms may be considered as secondary medium-term

Fig. 73.4 Geotechnical model of one of the case studies. *1* arable land, with clay, silt and sand, overconsolidated at places (qt = 0.6÷6.0 MPa); *2* low to medium consistency clay and silt (qt = 0.5÷1.5 MPa); *3* consistent clay and silt (qt > 1.5 MPa); *4* low consistency to soft clay and silt (qt ≤ 0.5 MPa); *5* sand and sandy silt with varying relative density (1.0 < qt < 10.0 MPa). In *red* the curve of the CPT; in *blue* the groundwater level, as measured in superficial wells

effects of earthquake-induced liquefaction. Known historical earthquakes, or eventually older events, could have been the original triggering factor of liquefaction of susceptible soils at shallow depth and formation of dikes and sills, as precursors of future sinkholes. In order to confirm this conceptual and geotechnical model, field and lab work is ongoing, also in order to set up a numerical model to simulate the process.

References

ARPA Ingegneria Ambientale (2007) La subsidenza in Emilia-Romagna. Il monitoraggio tramite interferometria satellitare. Esperienze a confronto. Arpa rivista **1**/2008

Boccaletti M, Bonini M, Corti G, Gasperini P, Martelli L, Piccardi L, Tanini C, Vannucci G (2003) Carta sismotettonica della regione Emilia-Romagna. Scala 1:250.000. Regione Emilia-Romagna

Bonori O, Ciabatti M, Cremonini S, Di Giovanbattista R, Martinelli G, Maurizzi S, Quadri G, Rabbi E, Righi PV, Tinti S, Zantedeschi E (2000) Geochemical and geophysical monitoring in tectonically active areas of the Po Valley (Northern Italy). Case histories linked to gas emission structures. Geogr Fis Dinam Quat 23:3–20

Borgatti L, Bianchi E, Bonaga G, Gottardi G, Landuzzi A, Marchi G, Mastrangelo A, Rodorigo S, Vico G, Vittuari L (2010) Fenomeni di sprofondamento del piano di campagna in pianura padana: il ruolo del contesto geologico, geomorfologico e geotecnico. In: Nisio S (ed) 2° Workshop internazionale I Sinkholes, Roma, 2009, pp 181–201

Caramanna G, Ciotoli G, Nisio S (2008) A review of natural sinkhole phenomena in Italian plain areas. Nat Hazards 45(2):145–172

Castaldini D (1987) F° 75 Mirandola: un esempio di cartografia geomorfologica. Atti della Riunione dei Ricercatori di Geologia, Milano

Castellarin A, Rabbi E, Cremonini S, Martelli L, Piattoni F (2006) New insights into the underground hydrology of the eastern Po Plain (northern Italy). Boll Geof Teor ed Appl 47:271–298

Devoti R, Esposito A, Pietrantonio G, Pisani AR, Riguzzi F (2011) Evidence of large-scale deformation patterns from GPS data in the Italian subduction boundary, Earth Planet. Sci Lett 311:1–12. doi:10.1016/j.epsl.2011.09.034

Devoti R. (2012) - Combination of coseismic displacement fields: a geodetic perspective, Annals of Geophysics, 55 (4); doi:10.4401/ag-6119

Fantoni R, Franciosi R (2008) Geological framework of Po Plain and Adriatic foreland system. In: Proceedings of the 70th EAGE conference and exhibition, Rome

Fantoni R, Franciosi R (2009) Mesozoic extension and Cenozoic compression in Po Plain and Adriatic foreland. Rendiconti online Soc Geol It 9:28–31

Obermeier SF, Pond EC (1999) Issues in using liquefaction features for paleoseismic analysis. Seismolog Res Lett 70(1):34–58

Pieri M, Groppi G (1981) Subsurface geological structure of the Po Plain, Italy. Progetto finalizzato Geodinamica- Sottoprogetto 5, Modello strutturale, C.N.R., Pubbl. 414, Roma

Schmertmann JH (1978) Guidelines for CPT: performance and design. Report FHWA-TS-78-209, Federal Highway Administration, Washington DC

Engineering Geological Problems in Deep Seated Tunnels

Convener Prof. Kurosch Thuro—*Co-convener* Heiko Käsling

Deep seated tunnels suffer both from high stress conditions and adverse rock conditions. In this session, contributions are welcome which address such problems during tunnel works using conventional as well as mechanical excavation. Focus may be on general engineering geological conditions, rock mechanical problems, stress-induced problems such as rock bursting and spalling, excavation problems or modelling of such conditions. Another focus may be on the TBM performance under high stress conditions, generating penetration problems or facing instability during TBM or conventional tunnelling, as well as connected problems including tool wear or machinery demolition. Contributions may include case studies, comprehensive views or methodical approaches.

Leaching Characteristics of Heavy Metals from Mineralized Rocks Located Along Tunnel Construction Sites

74

Nohara Yokobori, Toshifumi Igarashi, and Tetsuro Yoneda

Abstract

Soil and groundwater pollution caused by acid rock drainage (ARD) containing heavy metals leached from mineralized rocks is a serious environmental problem. Mineralized rocks are widespread throughout Hokkaido, Japan, and several tunnels for the Hokkaido Bullet Train Line are planned to be constructed through these mineralized areas. In this study, batch and column leaching experiments were conducted to investigate the leaching characteristics of heavy metals from the mineralized rock samples collected in these areas. The results showed that the mineralized samples contained substantial amounts of sulfide minerals (e.g., sphalerite (ZnS)), and that cadmium (Cd) was incorporated in some of these sulfide minerals. Moreover, the leaching concentrations of lead (Pb), Cd and arsenic (As) were higher than the Japanese environmental standards. The results of the column leaching experiment showed that these mineralized rocks could continuously release high concentrations of heavy metals for a long time. Therefore, such rocks should be disposed of properly to prevent the contamination of the surrounding environment.

Keywords

Heavy metals • Mineralized rocks • Sulfide minerals • Leaching

74.1 Introduction

Acidic leachate loaded with heavy metals and toxic metalloids is a very serious environmental problem because of the rapid deterioration of the surrounding soil and groundwater. This problem is usually limited to mining sites and mine tailings dams, but recent tunnel projects in Japan have excavated rocks that generated similarly acidic and heavy metals/metalloids loaded leachates when exposed to the environment (Tabelin and Igarashi 2009; Tatsuhara et al. 2012). The problem associated with these tunnel excavated rocks is similar to those of pyrite-rich mine wastes because the rocks are excavated along mineralized areas rich in sulfide minerals (Salinas Villafane et al. 2012a, b). When exposed to surface oxidizing conditions, these sulfide minerals, especially pyrite, are destabilized releasing acidity and high concentrations of heavy metals and metalloids (Younger et al. 2002). These phenomena are expected in the construction of the Hokkaido Bullet Train Line because tunnels will be excavated through mineralized areas of the island. Hazardous elements leached from excavated rocks have potential for soil and groundwater contamination without proper treatment. Therefore, it is important to understand the leaching characteristics of heavy metals from these rocks for the proper waste management of the tunnel excavated rocks. In this study, we evaluated the relationships between the mineral compositions and leaching characteristics of heavy metals from mineralized rocks.

N. Yokobori (✉)
Graduate School of Engineering, Hokkaido University, Sapporo, 060-8628, Japan
e-mail: yokobori@trans-er.eng.hokudai.ac.jp

T. Igarashi · T. Yoneda
Faculty of Engineering, Hokkaido University, Sapporo, 060-8628, Japan

74.2 Materials and Methods

74.2.1 Site Description

Nine rock samples were collected near the planned tunnel construction sites. Figure 74.1 shows the sampling locations and the planned Hokkaido Bullet Train Line.

74.2.2 Chemical and Mineralogical Analyses

Chemical composition of the rock samples was quantified using X-ray fluorescence spectrometer (XRF) while the mineralogical composition of rock samples was determined using X-ray diffractometer (XRD). Surface observation and analysis was conducted using optical microscopes and electron probe microanalyser (EPMA).

74.2.3 Batch Leaching Experiments

Leaching characteristics of heavy metals from the samples were evaluated by conducting batch reactor-type experiments. The leaching experiments were done by mixing 15 g of crushed rock (<2 mm) and 150 ml of deionized water at 120 rpm for 6, 24 and 168 h using a reciprocal shaker. After shaking, the pH, electrical conductivity (EC), redox potential (ORP) and temperature of the suspensions were measured. The suspensions were then filtered through 0.45 μm membrane filters. The concentrations of heavy metals and coexisting ions in the filtrates were measured using an inductively coupled plasma atomic emission spectrometer (ICP-AES) and ion chromatographs, respectively.

74.3 Results and Discussion

74.3.1 Chemical and Mineralogical Properties of the Rocks

Chemical and mineralogical compositions of the rocks are summarized in Tables 74.1 and 74.2, respectively. Sulfur and Zn contents of samples K1-1, K1-3 and K1-4 were greater than 10 wt%, consistent with the detection of sphalerite (ZnS) in these samples. The Cd contents of K1-1, K1-3 and K1-4 were also substantial at 1,120, 919 and 3,510 mg/kg, respectively. The Pb contents of samples containing galena were also substantial reaching wt% levels

Fig. 74.1 Sampling locations and the planned Hokkaido Bullet Train Line
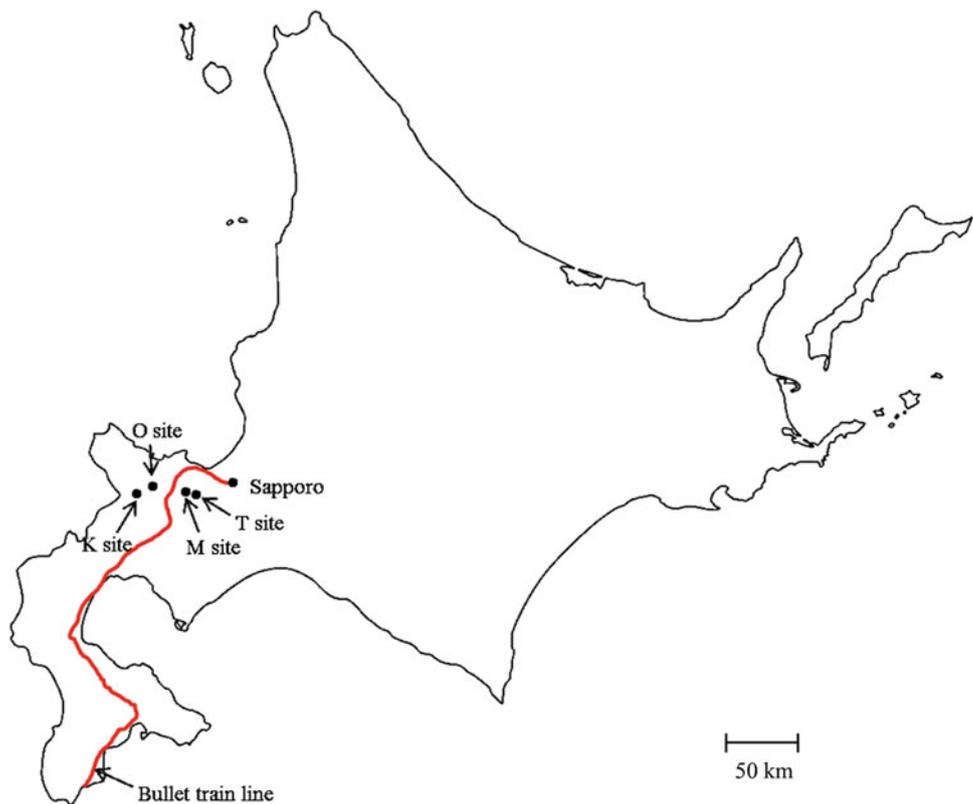
Table 74.1 Chemical compositions of mineralized rocks

Sample	SiO$_2$ (wt%)	Al$_2$O$_3$ (wt%)	Fe$_2$O$_3$ (wt%)	MnO (wt%)	S (wt%)	Zn (wt%)	Pb (mg/kg)	Cd (mg/kg)	As (mg/kg)
K1-1	–	0.4	0.52	0.107	33.5	25.4	287,000	1,120	1
K1-2	71.2	12.9	2.42	0.009	0.93	0.069	124	5.3	7.2
K1-3	37.1	3.3	2.18	0.186	13.5	26.9	456	919	438
K1-4	4	0.7	1.7	0.365	22.2	41.8	42,600	3,510	1,580
K3-1	76.2	4.5	1.34	0.094	1.15	0.46	2,890	33.8	16.8
O-1	32.2	–	8.2	33.7	1.34	1.46	4,720	44.4	32
T-1	41.2	0.037	0.69	0.493	0.109	0.052	309	5.68	5.14
M-1	46.1	0.089	5.21	0.005	2.82	0.005	22	6.2	32
M-2	46.2	2.27	0.649	0.004	0.171	0.001	113	7.43	4.82

Table 74.2 Mineralogical composition of the rocks

Sample	Identified minerals
K1-1	Sphalerite, galena, anglesite, susannite
K1-2	Quartz, pyrite, muscovite
K1-3	Quartz, sphalerite, barite
K1-4	Sphalerite, galena, cerussite, barite
K3-1	Quartz
O-1	Quartz, muscovite
T-1	Quartz
M-1	Quartz, pyrite
M-2	Quartz

(e.g., K1-1 and K1-4). Very high As contents were measured in samples K1-3 and K1-4, which were ca. two and three orders of magnitude higher than background levels, respectively. Although Cd and As contents of some of the rocks were relatively high, mineral phases containing these elements were not detected by XRD, indicating that they are present in the rocks as impurities in the other mineral phases.

Figure 74.2 shows the results of the optical microscopic observations of sphalerite. Numerous small pyrite grains are found around sphalerite. The sphalerite grain is also not homogenous as illustrated by the different hues under polarized light. Another sphalerite grain was analyzed using EPMA, and the results are shown in Fig. 74.3. The elemental maps of Zn and S were coincident with each other, indicating that this mineral is indeed sphalerite. Cadmium was also found inside this sphalerite grain, suggesting that it exists in the rock as an impurity of sphalerite. Moreover, Cd is not the only impurity found in sphalerite. As illustrated in Fig. 74.3d, As is also preferentially distributed in the core of the sphalerite grain. These results suggest that Cd and As could be released from the rock during the destabilization of sphalerite.

74.3.2 Leaching Characteristics of Arsenic, Cadmium and Lead

Table 74.3 shows the leachate pH and the leaching concentrations of heavy metals (As, Fe, Cd, Pb and Zn) after 24 h shaking. Among the rock samples, M1-1 had the lowest pH at 3.94, which could be attributed to its substantial pyrite content. In contrast, the other samples had slightly acidic to neutral pH values. The concentrations of As in the leachated were all lower than the environmental standard of Japan (10 µg/L) except for K3-1. These very low As leaching concentrations could be attributed to its immobilization via adsorption/co-precipitation with Fe-oxyhydroxides that precipate at pH > 4. The leaching concentrations of Cd exceeded the environmental standard (10 µg/L) from five of the samples evaluated. Likewise, seven samples had

Fig. 74.2 Photomicrographs of sphalerite taken with reflected (**a**) and polarized light microscopy (**b**)
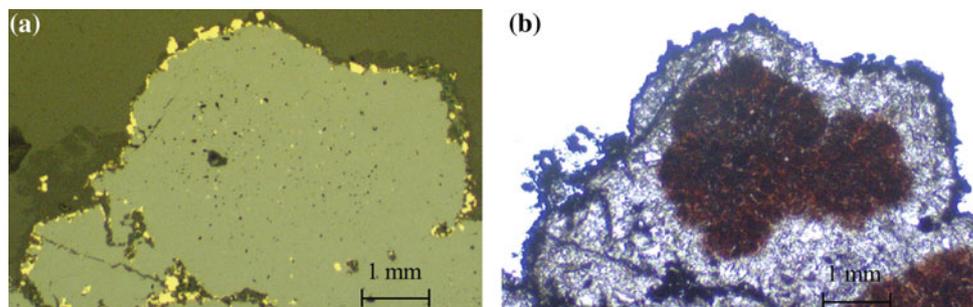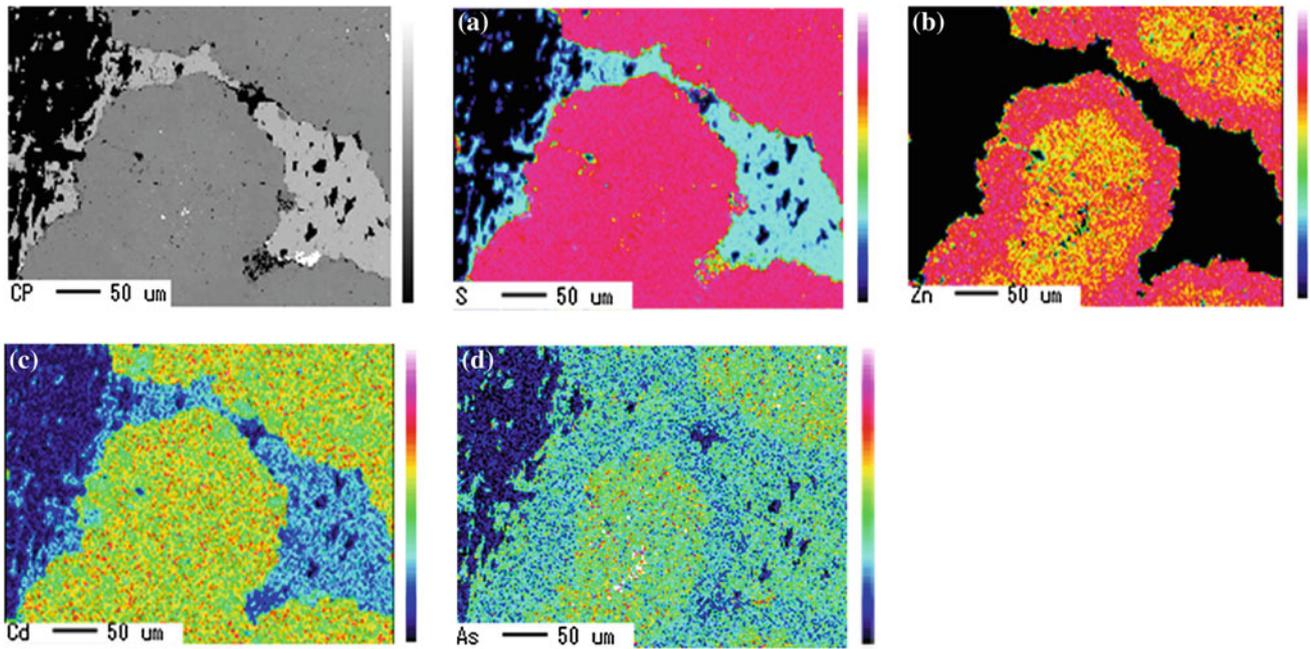
Fig. 74.3 The elemental maps of S (**a**), Zn (**b**), Cd (**c**), and As (**d**) at a magnification of 50 μm. The color intensity shows the relative abundance of the elements in the regions with black and white colors representing 0 and 100 %, respectively

Table 74.3 The pH and leaching concentrations of heavy metals after 24 h shaking

Sample	pH	As (μg/L)	Fe (mg/L)	Cd (mg/L)	Pb (mg/L)	Zn (mg/L)
K1-1	5.18	2.04	2.04	0.243	7.78	60.6
K1-2	4.15	1.98	9.75	0.028	0.255	5.18
K1-3	6	2.32	ND	0.019	0.126	27.9
K1-4	6.06	1.68	ND	0.436	7.53	51.7
K3-1	5.29	32.5	0.183	0.025	4.42	4.6
O-1	7.21	1.8	ND	ND	0.119	0.16
T-1	7.62	ND	ND	ND	ND	ND
M-1	3.94	ND	39.2	ND	1.06	1.47
M-2	4.75	ND	1.98	ND	ND	0.001

ND Not detected

Fig. 74.4 Comparison of the leaching concentrations of Pb and Cd from sample K1-4 (high sphalerite content) and K3-1 (no sphalerite content); **a** shaking time of 24 h, **b** shaking time of 168 h
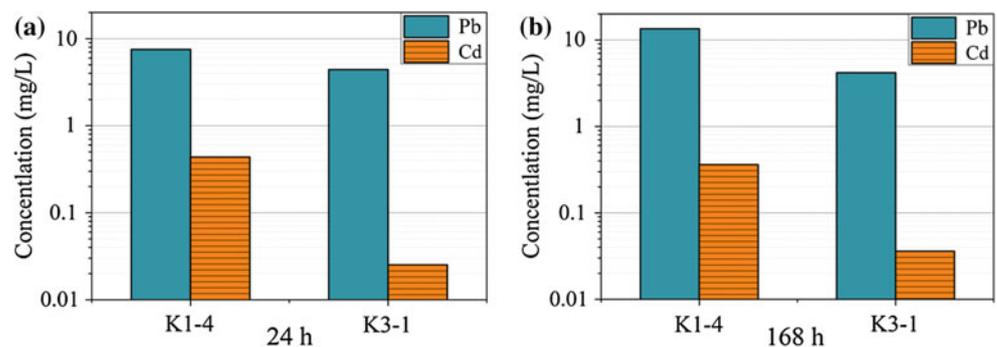
leaching concentrations of Pb higher than the environmental standard (10 μg/L). Figure 74.4 shows that the leaching concentration of Cd from K1-4 (high sphalerite content) was ca. ten-times higher than that of K3-1 (no sphalerite content),

regardless of the shaking time. There is also a strong positive correlation between Cd and Zn as illustrated in Fig. 74.5. These results indicate that the leaching of Cd is caused primarily by the weathering of sphalerite. The study shows
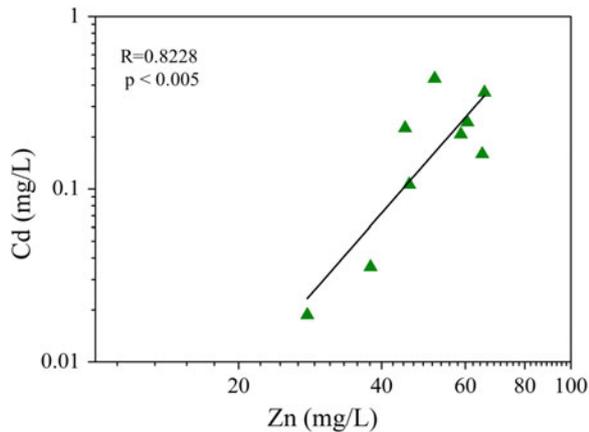
Fig. 74.5 Correlations of the leaching concentrations of the Cd and Zn

that sphalerite could be used as an index of the risks of Cd leaching for the tunnel construction of the Hokkaido Bullet Train Line.

74.4 Conclusions

Tunnel excavated rocks from mineralized areas contain substantial sulfide minerals that could release acidic leachates loaded with heavy metals and toxic metalloids when exposed to the environment. This study found that the leaching of these heavy metals and toxic metalloids was closely related to the mineral composition of the rocks.

Although pyrite was not detected in most of the samples, substantial Cd and As were still measured because they existed in the rocks as impurities of sphalerite. The leaching concentrations of As were insignificant in most of the samples because of the weakly acidic to neutral pH values of the leachates. However, Cd and Pb concentrations were substantial and exceeded the environmental standard of Japan. In particular, the release of Cd is closely related to the weathering of sphalerite. Thus, sphalerite could be used as an index of the risks of Cd leaching potential of the rocks excavated from the tunnels of the Hokkaido Bullet Train Line.

References

Tabelin CB, Igarashi T (2009) Mechanism of arsenic and lead release from hydrothermally altered rock. J Hazard Mater 169:980–990

Tatsuhara T, Arima T, Igarashi T, Tabelin CB (2012) Combined neutralization–adsorption system for the disposal of hydrothermally altered excavated rock producing acidic leachate with hazardous elements. Eng Geol 139–140:76–84

Salinas Villafane OR, Igarashi T, Kurosawa M, Takase T (2012a) Comparison of potentially toxic metals leaching from weathered rocks at a closed mine site between laboratory columns and field observation. Appl Geochem 27:2271–2279

Salinas Villafane OR, Igarashi T, Harada S, Kurosawa M, Takase T (2012b) Effect of different soil layers on porewater to remediate acidic surface environment at a closed mine site. Environ Monit Assess 184:7665–7675

Younger PL, Banwart SA, Hedin RS (2002) Mine water: hydrology, pollution, remediation. Kluwer Academic, London

Christoph Butscher

Abstract

The swelling of clay-sulfate rocks often poses a severe threat to tunnels. It causes serious damage and produces high additional costs during construction and operation. The swelling of clay-sulfate rocks is triggered by water access to anhydrite-bearing layers. Therefore, we propose that groundwater flow is a key factor controlling the swelling process. A case study from the Jura Mountains in Switzerland is presented that uses numerical groundwater models to calculate flow rates at the anhydrite level in different tunnel sections. The approach assumes that an increase of groundwater flow rates into anhydrite-bearing layers after tunnel excavation corresponds to an increase in swelling. A sensitivity study analyzes the impact of hydraulic parameters on calculated flow rates. Analyzed parameters include the hydraulic conductivity of geological units, properties of the excavation-damaged zone and the hydraulic potential in aquifers near the tunnel. Implications for site investigation and potential measures to counteract the swelling problem are suggested.

Keywords

Swelling • Clay-sulfate rocks • Groundwater flow • Tunnel engineering

75.1 Introduction

Tunneling in clay-sulfate rocks often leads to engineering problems because of swelling of such rock (Einstein 1996). Swelling results in heave of the tunnel invert and damage of the lining. The clay-sulfate rocks of the Triassic Gipskeuper ("Gypsum Keuper") formation are very often impacted by swelling. Examples are known from the Swiss and French Jura Mountains and the Stuttgart metropolitan area in Germany (Steiner 1993). Swelling problems in clay-sulfate rocks are also reported from other countries, including Spain (Alonso et al. 2013), Saudi Arabia, Poland, Italy and Texas/USA (Yilmaz 2001, and references therein).

C. Butscher (✉)
Division of Engineering Geology, Karlsruhe Institute of Technology (KIT), Institute for Applied Geosciences, Karlsruhe, Germany
e-mail: christoph.butscher@kit.edu

Different mechanisms are interacting in the swelling of clay-sulfate rocks, including osmotic water uptake and hydration of clay minerals and the transformation of anhydrite into gypsum (e.g., Madsen and Nüesch 1991). These swelling mechanisms require water inflow. Because water inflow into clay-sulfate rocks is a prerequisite for swelling, it is likely that groundwater flow is an important controlling factor for the swelling process, albeit groundwater flow rates in clay-sulfate rocks are often small and may not be realized during tunnel construction.

The present study is based on the work of Butscher et al. (2011). They investigated the effects of tunneling on groundwater flow at the Chienberg tunnel in the Swiss Jura Mountains. In two tunnel sections built in the Gipskeuper, heavy swelling occurred after tunnel excavation, while in two other sections with similar geological configuration observable swelling was absent (Fig. 75.1). The study used finite element groundwater models (code FEFLOW (Diersch 2009)), and showed that groundwater flow was strongly increased after tunneling in the tunnel sections with swelling, but not in the sections without swelling. High flow rates

in anhydrite-bearing layers were therefore considered to indicate high swelling risk.

The present study adds a parametric study to the previous study. It aims at determining the sensitivity of model parameters. "Sensitive" model parameters are those strongly affecting calculated flow rates in the anhydrite-bearing layers near the tunnel. Sensitive parameters are therefore considered to have strong impact on the swelling risk. Knowledge of the sensitive parameters provides indications for exploration and planning of the tunnel and points at measures that are most promising to reduce the swelling risk.

75.2 Methods

75.2.1 Numerical Groundwater Models

Four transverse cross-sections (A to D) perpendicular to the axis of the Chienberg tunnel and one longitudinal cross-section (E) parallel to the tunnel axis were constructed (Butscher et al. 2011). Cross-sections A and C represent the geological situation of the two swelling zones in the tunnel (c.f., Fig. 75.1). Cross-sections B and D represent the geological situation of the zones with similar geological configuration as in the swelling zones, but without observable swelling. The geological cross-sections were taken as a basis for steady-state, two-dimensional, finite element groundwater models. Figure 75.2 schematically shows the setup of the groundwater model of the transverse cross-section A. Model setup, boundary conditions and hydraulic properties of the models as well as model calibration are described in detail by Butscher et al. (2011).

75.2.2 Parametric Study

The parametric study is specifically aimed at answering two questions: (1) What parameters should be determined by experiments in order to receive accurate model results? (2)

Fig. 75.2 Model setup for cross-section A. *Q* Quaternary, *GKw* weathered Gipskeuper, *GK* Gipskeuper, *LK* Lettenkeuper, *MKAqf*, Muschelkalk Aquifer, *MKaqt* Muschelkalk Aquitard

Which measures during tunnel construction or remediation have most impact on groundwater flow and are therefore expected to be most effective in reducing the swelling risk?

Typical values of hydraulic properties were assumed in a reference model. These values were varied in different scenarios. Six different parameter sets with five different parameter values (scenarios) each were used (Table 75.1). The sensitivity of the parameters, i.e., the impact of the parameters on model results, was determined by calculating flow rates at the anhydrite level in the analyzed cross-sections for the different scenarios and comparing the results of the scenarios.

75.3 Results

Table 75.2 indicates the sensitivity of investigated parameters. Most important parameters, having strong impact on flow rates into anhydrite-bearing layers, are the hydraulic conductivity of the upper aquifer and of the excavation-damaged zone (EDZ), as well as the hydraulic head in the upper aquifer.

Figure 75.3 exemplarily illustrates how the sensitivity (Table 75.2) has been estimated, using the head in the upper and in the lower aquifer as an example. Variation of the hydraulic head in the upper aquifer strongly changes flow rates at the anhydrite level, indicating a high sensitivity of this parameter (Fig. 75.3 top). For example, the flow rate in transverse cross-section A doubles if the hydraulic head in

Fig. 75.1 Analyzed cross-sections and swelling zones of the Chienberg tunnel

Table 75.1 Scenarios and corresponding parameters

	Scenario 1	Scenario 2	Scenario 3	Scenario 4	Scenario 5
K upper aquifer (m/s)	1e−4	1e−5	**1e−6**	1e−7	1e−8
K Gipskeuper (m/s)	1e−10	1e−11	**1e−12**	1e−13	1e−14
K EDZ (m/s)	**1e−6**	1e−7	1e−8	1e−9	1e−10
Thickness EDZ (m)	0	1	**2**	4	6
Head upper aquifer (m)	RM −20	RM −10	**RM**	RM +10	RM +20
Head lower aquifers (m)	RM −20	RM −10	**RM**	RM +10	RM +20

Bold reference scenario. *K* hydraulic conductivity, *EDZ* excavation-damaged zone, *RM* reference model

Table 75.2 Summary of sensitivity of model parameters

Model parameter:	K upper aquifer	K Gipskeuper	K EDZ	Thickness EDZ	Head upper aquifer	Head lower aquifers
Sensitivity:	+	−	++	−	+	−

K hydraulic conductivity, *EDZ* excavation-damaged zone, ++ very high sensitivity, + high sensitivity, - moderate sensitivity, − no sensitivity

the upper aquifer is assumed 20 m higher than in the reference model. By trend, such an observation can be made in all transverse cross-sections (A to D) and in the corresponding sectors of the longitudinal cross-section. In contrast, variation of the hydraulic head in the lower aquifers (Fig. 75.3 bottom) does not influence calculated flow rates (i.e., flow rates in each section are equal in all scenarios), indicating that flow rates are not sensitive to this parameter.

75.4 Discussion and Implications for Tunneling in Clay-Sulfate Rocks

This study assumes that high flow rates in anhydrite-bearing layers indicate a high swelling risk. In order to quantify flow rates adequately using numerical groundwater models, it is important to determine sensitive model parameters at the study site by field experiments. Sensitive parameters found in this study include the hydraulic conductivity of the aquifer above the tunnel, which can be determined by pumping and/or Lugeon tests, as well as the hydraulic head in this aquifer, which can be measured by pore water pressure or water level measurements.

Some of the sensitive parameters found in this study can be influenced by engineering measures. For example, the hydraulic head in the upper aquifer strongly influences flow rates into anhydrite-bearing layers. If the hydraulic head would be lowered by adequate drainage systems or by active pumping, flow rates and accordingly the swelling potential could possibly be reduced. In this study, also the properties of the EDZ strongly influence flow rates into anhydrite-bearing layers. Excavation techniques that reduce the formation of an EDZ, for example using a tunnel boring machine or a road header instead of blasting, could therefore be advantageous with respect to the swelling problem.
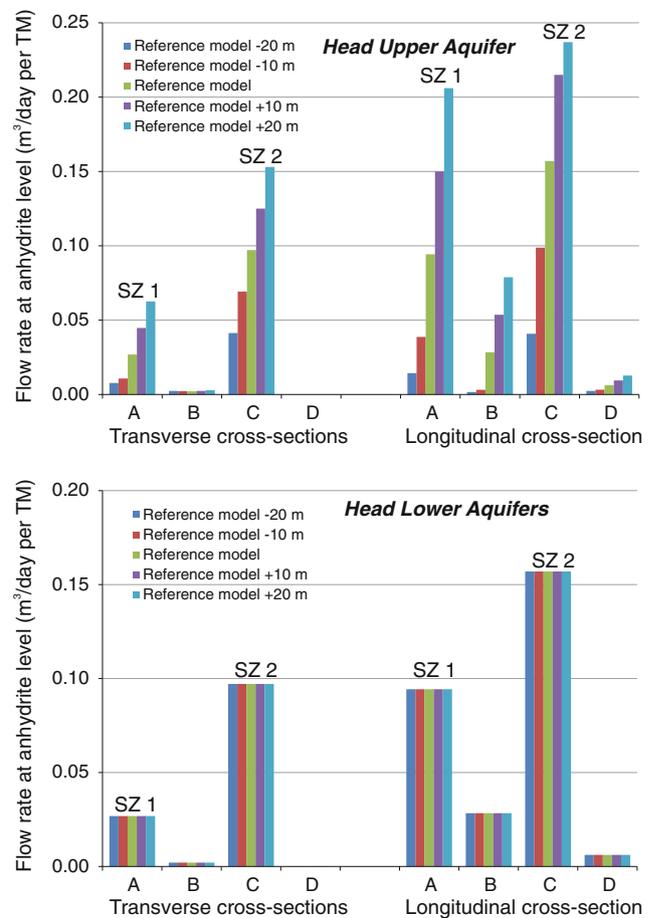
Fig. 75.3 Results of parametric study for the parameters "hydraulic head of upper aquifer" (*top*) and "hydraulic head of lower aquifers" (*bottom*). The graphs show flow rates after tunneling at the anhydrite level for different scenarios (parameter values). The parameter "hydraulic head of upper aquifer" shows high sensitivity (flow rates within a section vary strongly between scenarios). The parameter "hydraulic head of lower aquifers" is not sensitive (same flow rate within a section for all scenarios). *TM* tunnel meter, *SZ* swelling zone

References

Alonso EE, Berdugo IR, Ramon A (2013) Extreme expansive phenomena in anhydritic-gypsiferous claystone: the case of Lilla tunnel. Geotechnique 63(7):584–612

Butscher C, Huggenberger P, Zechner E, Einstein HH (2011) Relation between hydrogeological setting and swelling potential of clay-sulfate rocks in tunneling. Eng Geol 122:204–214

Diersch H-JG (2009) FEFLOW—Finite element subsurface flow and transport simulation system, Reference manual. DHI-WASY, Berlin

Einstein HH (1996) Tunnelling in difficult ground—swelling behaviour and identification of swelling rocks. Rock Mech Rock Eng 29 (3):113–124

Madsen FT, Nüesch R (1991) The swelling behaviour of clay-sulfate rocks. In: ISRM 7th international congress on rock mechanics, vol 1, Aachen, pp 285–288

Steiner W (1993) Swelling rock in tunnels: Characterization, effect of horizontal stresses and construction procedures. Int J Rock Mech Min Sci 30(4):361–380

Yilmaz I (2001) Gypsum/anhydrite: some engineering problems. Bull Eng Geol Environ 59:227–230

Marlène C. Villeneuve

Abstract

The disc cutting process for TBM excavation is dependent on the ability of the discs to initiate and propagate fractures into the tunnel face. At any depth, the geomechanical characteristics of the rock will determine how efficiently the fracture initiation and propagation processes occur. In deep tunnels the stresses induced at the tunnel boundary can lead to stress-induced failure mechanisms such as spalling and bursting. This paper examines the impact of geomechanical characteristics in combination with induced stresses at the tunnel face on the disc cutting process. TBM performance data and tunnel face maps were combined with mineralogy, grain size and fabric for deep tunnels in granitic and foliated massive rocks to determine how induced stresses enhance or hinder the fracture initiation and propagation processes. The impact of the induced stress varies with different geomechanical characteristics depending on the orientation and relative magnitudes of the stresses. In addition, stress rotation and relaxation ahead of the face can lead to stress-induced fracture creation at the face, which acts to precondition the rock prior to the cutters excavating. These results show that the sensitivity of different rock types to stress-related enhancement or hindrance of disc cutting must be taken into account for deep tunneling projects and are used to propose a geomechanical characterisation approach to identify potential for increased or reduced disc cutting efficiency in deep tunnels.

76.1 Introduction

The excavation process for a hard rock TBM involves fragmentation occurring between disc cutters, which apply cyclical pressure on concentric rings, or kerfs, in the tunnel face (Roxborough and Phillips 1975). This fragmentation can comprise the creation of chips or fines, the former being the more efficient fragmentation process. The chipping process is the generation of chips when tensile fractures are induced into the rock, and then propagate parallel to the tunnel face. Grinding is the generation of fines when

fractures do not propagate through the rock and only comminution occurs at the cutter-rock interface.

Numerical modelling of the chipping process (Villeneuve et al. 2012) has shown that geomechanical characteristics, which enhance fracture initiation and propagation will favour chipping over grinding. In particular, the results showed that increased mica content and decreased quartz to feldspar ratio will promote fracture initiation and propagation, and that fractures will propagate easiest along fabric.

Observations in deep TBM tunnels show that spalling can affect the tunnel face, however, this does not necessarily correspond to spalling at the tunnel wall. The two photos in Fig. 76.1 show two examples of tunnel faces in deep Alpine tunnels. While both tunnels have smooth walls without spalling, the tunnel on the right has spalling in the face. The stress-rock interaction at the tunnel face is different than at the walls, leading to this difference in behaviour. TBM

M.C. Villeneuve (✉)
Department of Geological Sciences, University of Canterbury,
Christchurch, New Zealand
e-mail: marlene.villeneuve@canterbury.ac.nz

Fig. 76.1 Photos of tunnel face in massive rock in deep Alpine tunnels excavated by TBM. (*left*) stable face, where kerfs are distinctly visible; (*right*) unstable face affected by stress-induced spalling (note the smooth, stable walls)

performance in areas of face spalling can be improved or reduced depending on the severity of spalling (Kaiser 2005), irrespective of the impact of spalling at the walls. Consideration must, therefore, be taken for spalling at the face, even if spalling at the walls is not anticipated. This paper shows how stress and geomechanical characteristics affect excavation and presents a characterisation scheme to identify conditions where advance rates can be impacted by spalling at the tunnel face.

76.2 TBM Performance in Deep, Highly Stressed Tunnels

TBM performance data (penetration rate, thrust, torque and rpm) were analysed to assess TBM performance in zones with recorded face instability. To account for the loss of time arising from the need to clear the TBM head of rock blocks (not to be confused with utilisation: maintenance, support, cutter change, etc.) the TBM data were examined for stopped thrust with continued head rotation: Thrust = 0, RPM ≠ 0. The active driving time is defined as the time during which the TBM head was turning, regardless of whether or not there was thrust. The net advance rate (NAR) is a measure of the distance travelled by the TBM in one stroke divided by the amount of time the TBM was actively driving. Ease of chipping is represented by the drillability index (DI), which is the penetration rate divided by the thrust. A higher DI value represents rock that is easier to excavate, either due to a more efficient chipping process or preconditioning of the face by induced stresses.

NAR is non-unique, where low NAR can either arise from low penetration rate or face instability. To identify face instability NAR is compared to DI to differentiate between low NAR values arising from tough excavation conditions (correspondingly low DI) and arising from face instability (correspondingly high DI). This was validated with depth of failure maps from deep TBM Alpine tunnels (Fig. 76.2).
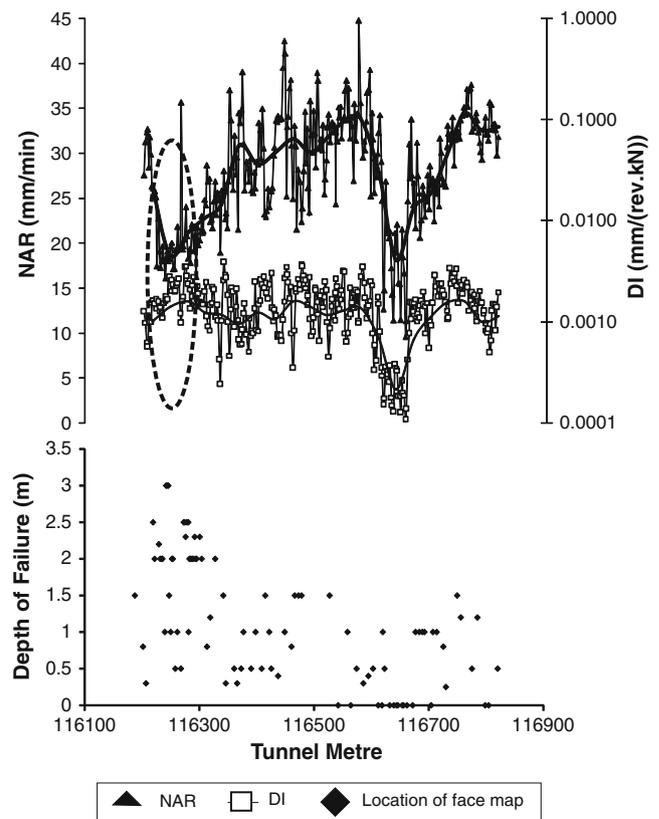
Fig. 76.2 Comparison between TBM NAR and DI (*above*) and depth of face failure (*below*) along a section of deep tunnel. High depth of failure occurs at low NAR and high DI locations (*dashed ellipse*), and no face failure occurs at low NAR and low DI

76.3 Investigation of Stress Impacts on Face Instability and Chipping

Geomechanical characteristics were recorded in a deep Alpine tunnel in massive rock over a continuous length of nearly 400 m, of which 10 % experienced face instability leading to decreased TBM performance. The characteristics were grouped into domains according to dominant
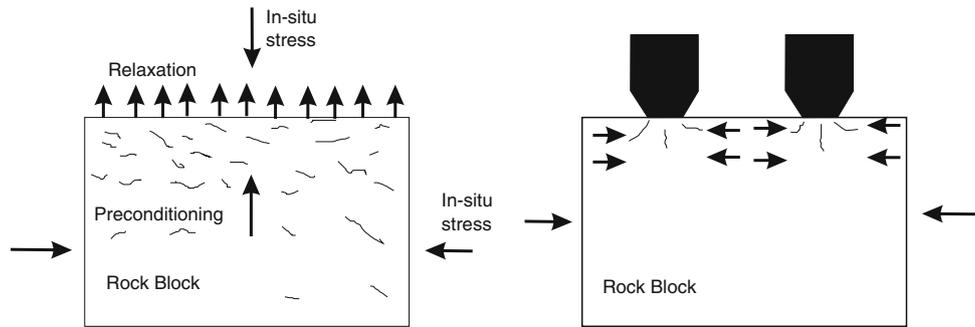
Fig. 76.3 Schematic of numerical models used to investigate the effect of stress on: (*left*) preconditioning at face; (*right*) fracture initiation and propagation at cutter-rock interface; face is at *top*
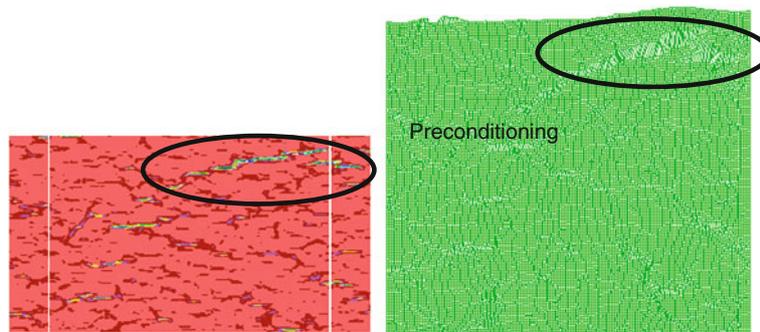
Fig. 76.4 Numerical model outputs of strain (*left*) and deformed grid (*right*, 5x vertical magnification) after 'excavation' showing potential face instability; model is 100 mm wide, face is at *top*

mineralogy, grain size, fabric, metre scale variability and stability of the tunnel walls (Villeneuve et al. 2007). The geological domains most associated with face instability have high mica content (typically 10–20 %), bimodal grain size distributions defined by clasts and matrix, fabric defined by schistosity or cleavage oriented between 0–21° to the tunnel face, greater than 10 m scale variability, and 5–30 % spalling of the tunnel walls.

Numerical modeling of the cutting process (using FLAC, as in Villeneuve et al. 2012) was used to refine the field observations. The models simulated the stress changes at the face arising from the excavation process, and leading to preconditioning (Fig. 76.3, left). The models then simulated the action of the cutters on different rock types (Fig. 76.3, right), with and without preconditioning.

76.4 Geomechanical and Stress State Impact on TBM Performance

The modeling shows that relaxation of sufficiently high in-situ stresses at the face leads to an outward deformation, which can initiate tunnel face-parallel fractures (Fig. 76.4). This "preconditioning" of the face by newly initiated fractures can improve the chipping process, but can also lead to
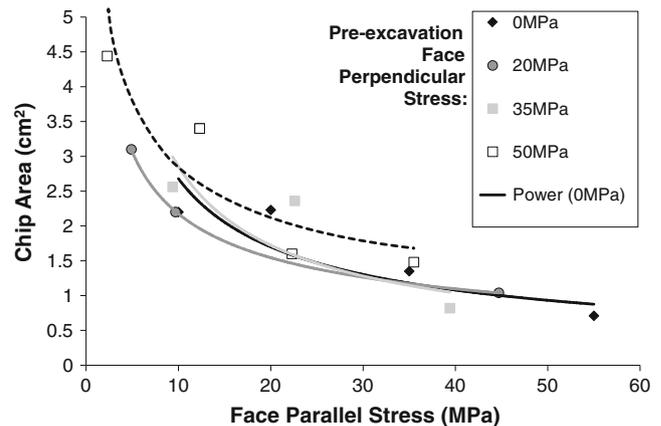
Fig. 76.5 Chip area compared to face parallel stress for samples with different magnitudes of preconditioning stress and fabric oriented and 0° to the tunnel face; UCS ≈ 100 MPa

spalling and face instability. Preconditioning improves chipping most where the in-situ stress perpendicular to the tunnel face is >50 % of UCS, and depends less on the in-situ stress parallel to the tunnel face (Fig. 76.5 white squares). Stress parallel to the tunnel face greater than 20 % of UCS can hinder fracture propagation from the cutter-rock interface, particularly for fabric sub parallel to the tunnel face (Fig. 76.5).

Table 76.1 Characterisation scheme for stress-induced impact on TBM performance

Characteristics	Preconditioning	Chipping performance
Face perpendicular stress (>50 % UCS)	Possible; face instability possible at high stress/strength ratio	Improved if preconditioning occurs
Face-parallel stress (>20 % UCS)	No impact	Reduced if fracture propagation is hindered
Fabric	More likely in rocks with fabric oriented sub-parallel (0–30°) from tunnel face	Improved; reduced by face-parallel stress, notably if fabric is sub parallel (0–30°) to face
Mica content	More likely if >10 %	Improved if >12 %

Rocks with fabric have greater preconditioning than isotropic rocks, especially where the fabric is sub parallel to the face, with less impact where it is oblique ($\sim 30°$), and limited impact where it is at high angle (>60°) to the face. Preconditioning is low to moderate in isotropic rock, is concentrated in mica grains, and increases slightly with mica content, but does not vary greatly with grain size (Villeneuve 2008). Rocks with fabric and higher mica content tend to improve chipping performance (Villeneuve et al. 2012). When stress is taken into consideration preconditioning leads to even greater chipping performance.

Table 76.1 can be used to identify the risk of poor TBM performance due to stress-induced face instability or poor fracture propagation. TBM projects at risk of this behaviour should consider the time required to clear blocks, additional wear on the TBM, and the disconnect from wall spalling. TBM performance prediction should also account for the potential for face-parallel stresses to reduce penetration rate.

76.5 Conclusions

Field and numerical modelling investigations show that TBM performance can be reduced by certain geomechanical characteristics and in-situ stresses. Stress relaxation at the tunnel face can lead to preconditioning the rock or, if sufficiently severe, spalling and face instability. Preconditioning will improve TBM performance by creating new fractures for chip generation, but face instability will decrease TBM performance due to the need to clear blocks. Rocks with mica content >10 % and fabric at low angle to the face are at greatest risk. The proposed characterisation scheme can be used to identify projects at risk so that investigations, design and project planning can address this behaviour.

References

Kaiser PK (2005) Tunnel stability in highly stressed, brittle ground–rock mechanics considerations for Alpine tunnelling. In: Löw S (ed) Geologie und Geotechnik der Basistunnels am Gotthard und am Lötschberg. vdf Hochschulverlag AG and der ETH Zürich, pp 183–201

Roxborough FF, Phillips HR (1975) Rock excavation by disc cutter. Int J Rock Mech Min Sci Geomech Abstr 12:361–366

Villeneuve MC (2008) Examination of geological influence on machine excavation of highly stressed tunnels in massice hard rock. PhD thesis, Queen's University, Kingston, Canada

Villeneuve MC, Diederichs MS, Kaiser PK, Frenzel C (2007) Geomechanical characterisation of massive rock for deep TBM tunnelling. In: Proceedings of rock mechanics: meeting society's challenges and demands, Vancouver, BC, Canada

Villeneuve MC, Diederichs MS, Kaiser PK (2012) Effects of grain scale heterogeneity on rock strength and the chipping process. Int J Geomech 12:632–647 (special issue)

Geotechnical Design of an Underground Mine Dam in Gyöngyösoroszi, Hungary

77

Vendel Józsa, Zoltán Czap, and Balázs Vásárhelyi

Abstract

The investigated copper mine is located in the north of Hungary at the Mátra mountain range. There are several mines in this volcanic mountain, which have been quarried since the early medieval ages. This abandoned heavy and non-ferrous metal mine is about 340-m deep. Mine closure had become necessary due to environmental reasons, because the stored water was highly acidic. The goal of this paper is to present a complex rock engineering design for infilling the drift ways. First of all, a rock mass characterization was necessary for determining the different rock-mass parameters, along with the hydrogeological conditions. Secondly, the stability of the dam was verified by different lengths, applying a geotechnical software using the finite element method. The filling material (ash) originated from a nearby power plant. The dam was designed with a corresponding drainage system and drainage capacity. The filling ash was retained with geogrid-reinforced gabion walls.

77.1 Introduction

Gyöngyösoroszi is located in North Hungary, at the southern slopes of the Mátra mountains, which is the highest mountain in Hungary. The copper mining started as far back as in 1767–1769. At the beginning of 1980, parallel with the mine operation, a special mine inflow operating system was developed against the acidic water. In 2012 the mine definitively closed and it was decided to be infilled because of some environmental problems, such as acidic water among others. A drainage system was also necessary to be developed along with the dam construction. The goal of the dam design was to (a) hold the infill material and (b) to allow the mine water to flow away (i.e. working like a filtering). The global factor of safety applied for the static calculations was $\gamma_R = 2$.

The designed cross section area with the shaft of the mine is presented in Fig. 77.1. The subsurface is around 762 m above sea level. There are 7 floors in different depths: 1st floor at 424 m down to the 7th floor at 708 m above sea level (see Fig. 77.1).

In the first case, the 1st floor was infilled and the dam design was focused on this level. The rock mass properties were determined by in situ measurements and laboratory tests. These parameters with the slurry and the dam materials are summarized in Table 77.1. The rock mass parameters were calculated by using the rock mass classification, according to Hoek et al. (2000) and the suggestion of Rowe (2001).

77.2 Design of the Underground Mine Dam

During the design of the underground mine dam, the following steps were calculated and taken into consideration:
- the phase of infilling

V. Józsa (✉) · Z. Czap
Department of Geotechnics, Budapest University of Technology and Economics, Budapest, Hungary
e-mail: jozsavendel@gmail.com

B. Vásárhelyi
Department of Structural Engineering, University of Pécs, Pécs, Hungary

Fig. 77.1 Shaft and mine system in Mátraszentimre (surface ∼760 m above sea level)
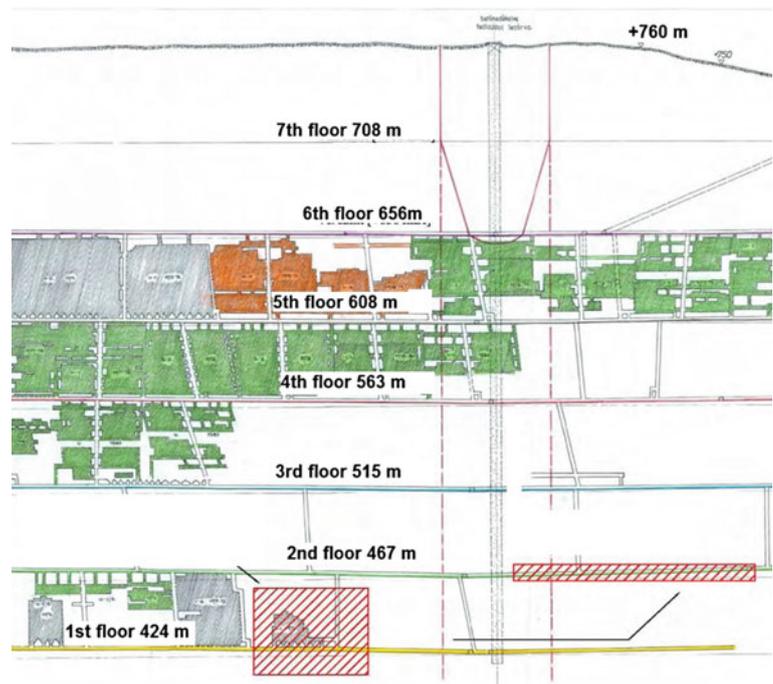
Table 77.1 Mechanical parameters

		Rock mass	Liquid slurry	Solid slurry	Aggregated rock
Inner friction angle (ϕ)	Degree	25		25	40
Cohesion (c)	kPa	1,100			
Deformation modulus (E)	MPa	1,000		20	100
Poisson ratio (ν)	–	0.37	0.5	0.49	0.25
Sat. density (γ)	kN/m^3	24	14.2	14.2	20

- end of the infilling,
- permanent state.

Plaxis 3 D Tunneling finite element method (3-dimensional) was used for these calculations as the classical 2-dimensional geotechnical calculations cannot be used here because of the complexity of the geometry and stress states. It was important to model the evolving vault system and the changing stress field in the rock mass. It was also important to analyze the different stress states, such as when the dam is in a hydrostatic condition, or when the water pressure is continuously changing due to the drainage system.

It was not possible to calculate with the solidified slurry due to the maximum volume of the infill material, the capacity of the transportation, the possibility of the sectionalizing and the optimal infilling technology (Blight 2010).

Figure 77.2 presents the finite element model of the investigated mine dam (for the cases of using L = 5, 10 and 15-m long dam).

The material of the slurry consists of sand and crushed rock mixture without silt and clay. The mechanical parameters of this mixture are better than the parameters of natural aggregate systems. It was assumed that the interface ratio between the slurry and the rock mass was 2/3.

At the first step of the calculation, 8 MPa environmental pressure was used on the studied area in the primary stress state. At the second step the secondary stress state was modeled with calculating the stress field after the mine construction. This is the initial state for further calculations.

Firstly, the 5-m long dam was implemented in the finite element model (see Fig. 77.2). Due to this, the stress field had changed. The inner pressure of the dam was increased up to 284 kPa connecting to the safety level. The axial deformation with displacement is presented in Fig. 77.2. This calculation was repeated with dam lengths of $L = 10$ m (1.25 MPa) and $L = 15$ m (4.41 MPa). Figure 77.3 shows the capacity of the dam plotted after the different calculation steps.
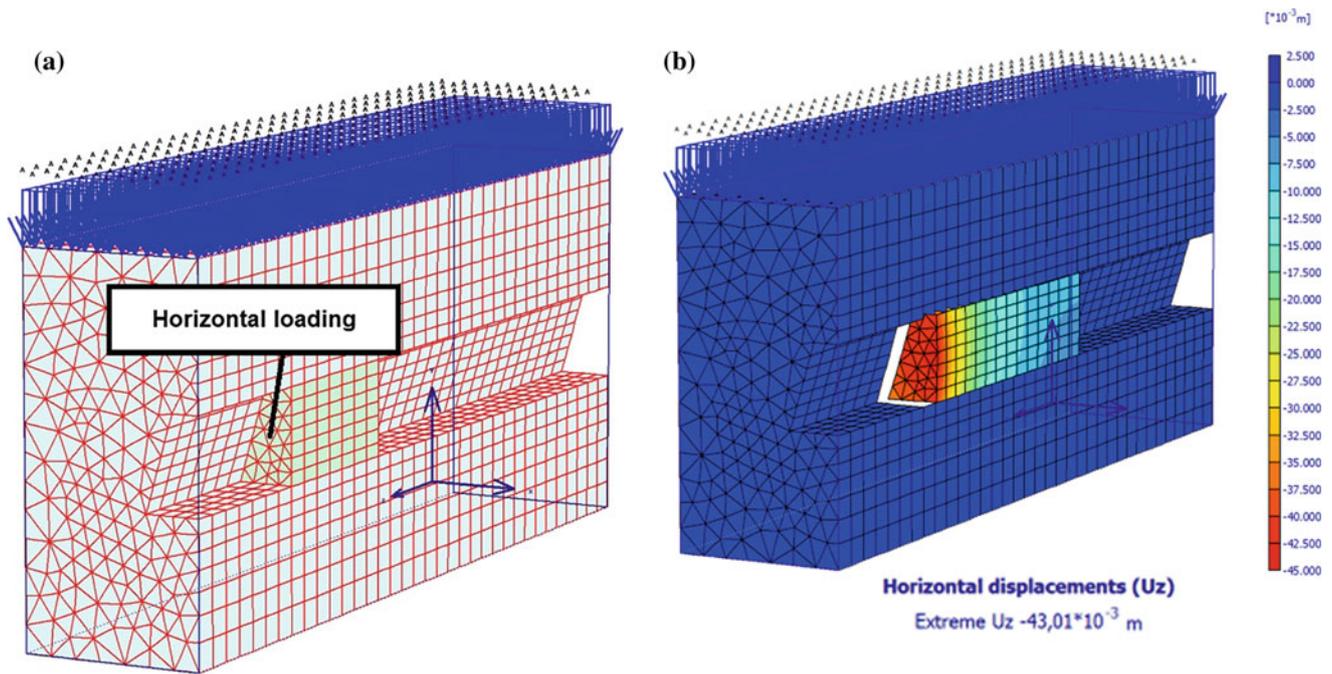
Fig. 77.2 **a** The modeled dam and **b** the deformation in axial direction

Fig. 77.3 Capacity of the different dam lengths after the calculation steps and the relationship between the capacity and the length of the dam
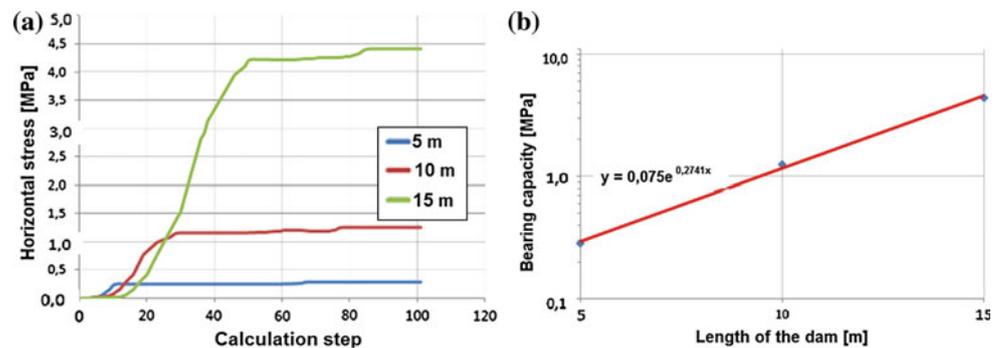
It can be seen that the capacity of the dam (CA) increased significantly with its length (*L*). Based on the calculation, the following exponential equation represents the correlation between the dam length and capacity:

$$CA = 0.075 \exp(0.2741\, L) \qquad (77.1)$$

Using this equation, the minimum length of the dam was 5.8 m. Drainage is possible during the operation of the dam, so only an effective stress can develop. This effective stress was calculated from the different depths of the first and second mine levels (H).

The next calculation process was defined to solidify the slurry. It had to be taken into account that some part of the mine had become sealed. The water pressure increases to the surface level of the model. The model was expanded with a vertical shaft for investigating the influence of vertical stresses. Due to the extremely high pressure, a soil-hardening model could be used. In Fig. 77.4 deformation, compaction and stress change were plotted due to this pressure change.

The locations of the dams were changed and their shape was also modified because the tunnel becomes smaller towards the saved area. Both the roof and the side of the
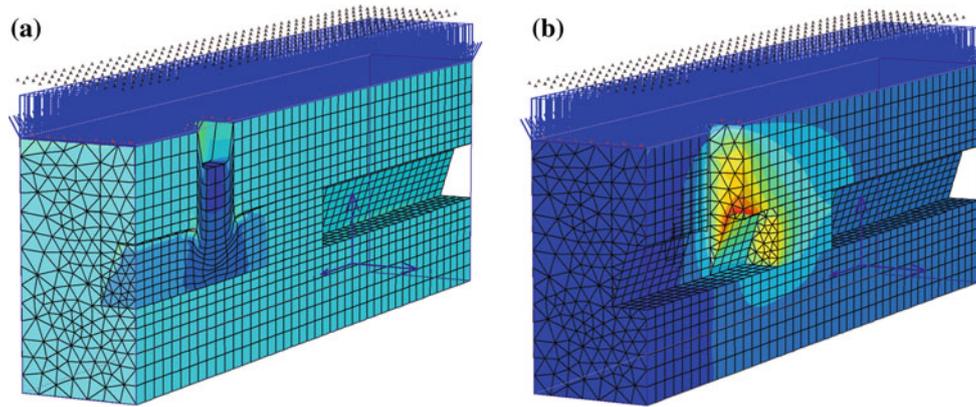
Fig. 77.4 L = 5 m long dam after infilling. **a** Compaction due to 8 MPa pressure and **b** the axial deformation and displacement (the slurry material is not presented)
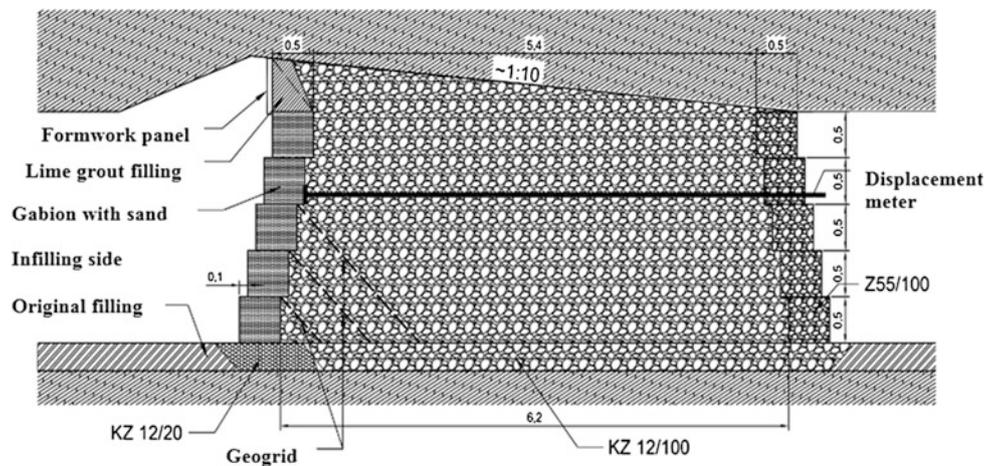
Fig. 77.5 Cross section of the dam

Fig. 77.6 Front view of the dam (June 2012)

tunnel decrease by approximately 1:10. The cross section of the design mine dam is presented in Fig. 77.5.

The construction of the dam in its almost finished stage is presented in Fig. 77.6. The stability of the retaining structure was not decreased, the drainage system of the dam is still working. The pressures of the dam, arising out of the slurry, have decreased after the solidification of the slurry (Wolkersdorfer 2008).

77.3 Summary

The solution we proposed has proven to be good both theoretically and practically.

By using the finite-element test method, it has been demonstrated that the retaining capacity of the dam depends on its length not linearly but exponentially (Fig. 77.3, Eq. 77.1). Its behaviour is analogous with the Terzaghi

method used when the tunnel face stability is checked and when the loads to the lining are determined (silo pressure). We have managed to design a well-cleanable drainage system, where the risk of clogging is almost zero. The mine-water cannot bypass the dam, which is an existing threat in the event of watertight concrete/reinforced-concrete structures. The rock material used for the construction of the dam is more corrosion-proof than concrete, which renders any loss of strength impossible in the course of time.

The feasibility of building and operating a system like this has been established; it can be used for the closure of other floors too, and it can be put into action in other cases as well. As regards costs, it is very advantageous too.

References

Blight G (2010) Geotechnical engineering for mine waste storage facilities. Taylor & Francis, London

Hoek E, Kaiser PK, Bawden EF (2000) Support of underground excavations in hard rock. Balkema, Amsterdam

Rowe RK (2001) Geotechnical and geoenvironmental engineering handbook. Kluwer, Dordrecht

Wolkersdorfer Ch (2008) Water, management at abandoned flooded underground mines: fundamentals tracer tests, modelling, water treatment (mining and the environment). Springer, Berlin, p 465

An Approach on the Types and Mechanisms of Water Inrush in Traffic Tunnel Constructions in China

Li Tianbin, Zuo Qiankun, Meng Lubo, and Xue Demin

Abstract

Water inrush is a kind of most common geologstical hazards during tunnel constructions. Based on a lot of water inrush cases, this paper discusses the types and mechanisms of water inrush during traffic tunnel constructions in China. According to the groundwater source and geological structures of aquifers, tunnel water inrush can be classified into five types, namely, gushing by cutting through surface water, gushing by cutting through an aquifer, water inrush from fault zones, water inrush from Karst pipes, water inrush from other structural fracture zones. Based on case studies and mechanical analyses, the mechanisms of tunnel water inrush are revealed as cutting through and gushing free, hydraulic splitting of fissures, hydraulic fracturing of impermeable rock wall, and static-dynamic disturbance of the discontinuities of rockmasses.

78.1 Introduction

Water inrush is a kind of most common geological hazards during tunnel construction, which greatly endangers tunnel construction from safety, time and economic aspects (Wang et al. 2001; Shamma et al. 2003). In recent years, based on the theoretical study and practical application, types and mechanism analysis of water inrush had been obtained some achievements and experiences. Wang et al. (2001) proposed several types of water inrush, that is, water inflow, water inrush from Karst pipes, water inrush from fault zones, water inrush for hydraulic fracturing, water inrush for bulging fracturing. Jiang et al. (2006) discussed the mechanism of water inrush from the aquifer parallel to the tunnel. Zhang et al. (2008) presented water inrush can be caused by tension failure of impermeable layer, shear failure of fissures, hydraulic expansion of fissures, failure of key block of rocks. A lot of engineering practices show that a correct understanding of the mechanism of water inrush is much important for its mitigation. Therefore, based on collecting and analyzing a lot of water burst cases, this paper summarizes and presents systematically the main types of water inrush and its mechanisms during traffic tunnel construction in China.

78.2 Tunnel Water Inrush Types

78.2.1 Gushing by Cutting Through Surface Water or Groundwater

If the hydrostatic pressure exceeds the strength of rock between the working face of tunnel and surface water or groundwater, or excavation and blasting build hydraulic connections between them, water inrush will happen, as

L. Tianbin (✉) · Z. Qiankun · M. Lubo · X. Demin
State Key Laboratory of Geohazard Prevention and Geoenvironment Protection, Chengdu University of Technology, Chengdu, 610059, Sichuan, China
e-mail: ltbsklgp@qq.com

Z. Qiankun
Sichuan Provincial Transport Department Highway Planning Survey, Design and Research Institute, 1#, Wuhou Hen Jie St, Chengdu, 610041, China

water inrush occurred at K328 + 567.2 ∼ +575.4 in Jin-yunshan Tunnel and at K348 + 262 ∼ +250 in Zhongli-angshan Tunnel.

78.2.2 Gushing by Cutting Through an Aquifer

Groundwater is gushing directly or along water-conducting fissures when tunnels cut through aquifers. For instance, water inrush at K42 + 786 ∼ K42 + 796 in Shizizhai Tunnel of Dashan expressway was caused by cutting through an aquifer in sandstone layers.

78.2.3 Water Inrush from Fault Zones

Extensional faults developed in thick aquifers have large cavity with loose fragments and store abundant groundwater from both hanging wall and heading wall. Once they are revealed, water inrush will happen just like the one at K12 + 200 in Dabashan Railway Tunnel.

Water inrush often occurs in water-conducting faults under the condition of highly permeable stratum interbedded with slightly permeable stratum, in which hydraulic connection is established by fault zones. For example, water inrush occurred in Bieyancao Tunnel of the Yichang-Wanzhou road was caused by the pressures of groundwater from a fault zone.

In addition, water inrush can happen in the hanging wall of impermeable compressional fault zone nearby, where groundwater is rich correspondingly due to the high crushing of hanging wall and the water stop of fault zone. Water inrush occurred in the hanging wall of a regional fault is a typical case in Dayaoshan Tunnel of the Beijing-Guangzhou railway.

78.2.4 Water Inrush from Karst Pipes

It has been indicated by a lot of cases that tunnel water inrush is highly risky in the growth area of Karst. Once excavation cuts through the water-rich Karst pipes in tunnels, water inrush will occur, e.g., the one at ZK32 + 927 of Huayingshan Highway Tunnel in 1997 and 1998.

78.2.5 Water Inrush from Other Structural Fracture Zones

The fracture zones in the axis parts of anticline and syncline are often rich in water, where once excavation cuts through, water inrush is easy to happen. The water inrushes at K297 + 100 ∼ K297 + 800 in Maoba 1# Tunnel (Ma 2010)

and at DK354 + 235 ∼ DK361 + 764 in Yuanliangshan Tunnel (Liu 2004) are typical cases of anticline and syncline fracture zones, respectively.

When water-rich interstratified fracture zones in sedimentary rocks are cut through by tunnel constructions, water inrush will occur. For example, the work face blasting at K42 + 375 in Shizizhai Expressway Tunnel triggered water inrush of 8950 m^3/d from interstratified fracture zone between quartz sandstone layer and silty mudstone layer.

78.3 Tunnel Water Inrush Mechanisms

78.3.1 "Cutting Through and Gushing Free" Mechanism

This kind of water inrush mechanism often occurs in the condition of cutting through the water-rich pipes or fissures in surrounding rocks. When excavation reveals water-rich Karst pipes or water-bearing fissures with good connectivity around the surrounding rocks, groundwater is gushing free. In general, initial water inrush flows along many discontinuities during non-exposed fully pipes or fissures; water flows along one or two orifices after exposed fully pipes or fissures and increase rapidly in short time.

78.3.2 "Hydraulic Splitting of Fissures" Mechanism

As the impermeable rockmass become thinner due to excavation, and water-bearing fissures are constantly expanding under high water pressures, the impermeable rockmass is split, thus leading to water inrush. Joints or fissures in stratum can open, slide and be spilt under high water pressures. Mechanical sketch of hydraulic splitting of fissures is shown in Fig. 78.1.

According to the theory of fracture mechanics, there are three fissure types during fissure evolution process. Type I is "open type" caused by tensile stresses perpendicular to the fissure surface. Type II is "slide type" caused by shear stresses parallel to the fissure surface. Type III is "spilt type" caused by shear stresses perpendicular to the fissure surface. I-II compound type appears when the normal stresses on the fissure surface are tensile stresses. Fissure failure criterion can be expressed by: $K = K_\xi$. Where K and K_ξ are strength factor and limit strength of fissure, respectively. K is given by:

$$k_I = \sigma_n \sqrt{\pi a} \qquad (78.1)$$

$$k_{II} = \tau \sqrt{\pi a} \qquad (78.2)$$
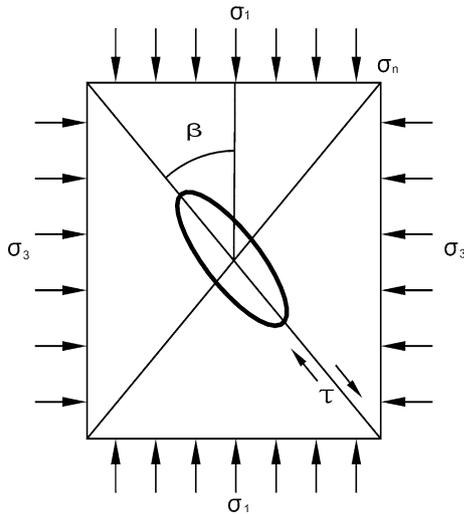
Fig. 78.1 Mechanical mechanism of hydraulic splitting of fissures

where σ_n is the normal stresses on the fissure surface, τ is the shear stresses on it, a stands for 1/2 fissure length.

78.3.3 "Hydraulic Fracturing of Impermeable Rock Wall" Mechanism

According to the different space combinations of impermeable rock wall and tunnel, hydraulic fracturing of the rock wall can be described as rockmass bending failure or shearing failure.

It is observed from Fig. 78.2 that the impermeable rock wall with high strength and adequate thicknesses can initially bear the water pressures, whereas it becomes thinner during excavation process, it cannot, thus leading to bending failure and water inrush. The failure criterion of the impermeable rock wall is given by:

$$\sigma \geq [\sigma] \tag{78.3}$$

where σ is the largest tensile stress of rock wall, $[\sigma]$ is the allowable tensile stress of rock wall.

The impermeable rock wall with lower strength or unfavorable discontinuities under water pressures fractures generally with plastic shear feature, leading to water inrush, as shown in Fig. 78.3. The shear failure criterion of the impermeable rock wall is given by:

$$\tau \geq \tau_f \tag{78.4}$$

$$\tau_f = \sigma \tan(\phi) + c \tag{78.5}$$

where τ is the shear stresses on the most unfavorable surface of rock wall, τ_f is the shear strength of rock wall, σ is the normal stress on the shear surface, c and φ are the cohesion and internal friction angle of rock wall, respectively.

78.3.4 "Static-Dynamic Disturbance of the Discontinuities of Rockmasses" Mechanism

Dynamic disturbance caused by blasting and surrounding rock stress redistribution can lead to fracture expansion, relaxation and opening of compressive fault zone and instability of surrounding rocks. Once these unfavorable geological structures connect with aquifers, water inrush will occur in tunnels.

As shown in Fig. 78.4, the hard surrounding rocks have different space geometry due to joints and fractures in them. After excavation, the key block of rockmass initially become instability due to blasting disturbance and stress releases, and then other blocks are deformed or collapse, consequently, aquifers are connected with tunnels and then water inrush appears.

With the influences of blasting and excavation, larger additional tangential stress and confining pressure changes within a certain range of compressive fault result in fault relaxation and opening. When this action makes tunnel to connect with aquifer or water-rich hanging wall, then water inrush appears (Fig. 78.5).

Fig. 78.2 Water inrush due to bending failure of impermeable rock wall
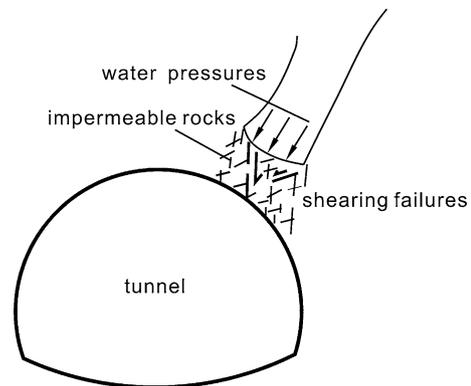
Fig. 78.3 Water inrush due to shearing failure of impermeable rock wall
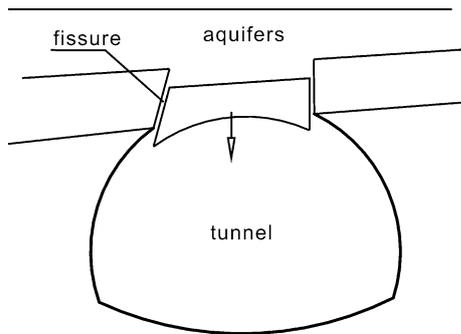
Fig. 78.4 Water inrush due to the instability of key block of rockmass

78.4 Conclusions

(1) According to the groundwater source and geological structures of aquifers, tunnel water inrush can be classified into five types, namely, gushing by cutting through surface water, gushing by cutting through an aquifer, water inrush from fault zones, water inrush from Karst pipes, water inrush from other structural fracture zones.
(2) Complex geological conditions and rockmass structures and variable interaction between tunnel and aquifer structure lead to complicated mechanism of water inrush in tunnels. Based on collecting and analyzing a lot of water burst cases, the mechanisms of tunnel water inrush are revealed as cutting through and gushing free, hydraulic splitting of fissures, hydraulic fracturing of impermeable rock wall and static-dynamic disturbance of the discontinuities of rockmasses.
(3) Analyses of the types and mechanisms of water inrush provide theoretical basis for water inrush prediction and mitigation in tunnels and play an important role in the effective control of water inrush.
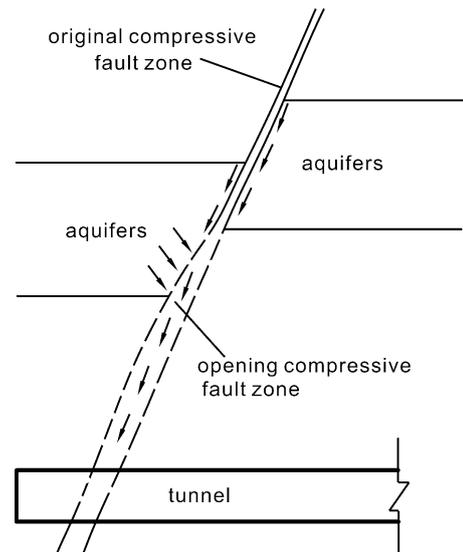
Fig. 78.5 Water inrush due to opening of compressive fault zone (Jiang et al. 2006)

References

Jiang JP, Gao GY, Li XZ (2006) Mechanism and mitigation of water inrush in railroad tunnels. China Railway Sci 27(5):76–82
Liu ZW (2004) Water inrush mechanism and mitigation in Karst Yuanliangshan tunnel Ph.D. thesis. China University of Geosciences, Beijing
Ma XH (2010) Geological hydrology analysis of water inrush mechanism and mitigation in Maoba 1# Tunnel. Sichuan Build Mater 36(4):139–141
Shamma Duke D, Fordham S, Freeman E, Tempelis J (2003) Tom arrowhead tunnels: assessing groundwater control measures in a fractured hard rock medium. In: Proceedings-rapid excavation and tunneling conference, New Orleans, pp 296–305
Wang JX, He J, Yang LZ (2001) Hydrogeological analysis for karst water inrush in large-scale underground engineering. Hydrol Eng Geol 4:49–52
Zhang W, Li ZG, Wang QS (2008) Causes and mitigation of water inrush in Karst tunnels. Tunnel Constr 28(3):257–262

Numerical Analysis of the Influence of Tunnel Dimensions on Stress and Deformation Around Tunnels in Rocks

G.E. Ene, C.T. Davie, and C.O. Okogbue

Abstract

Numerical studies of a generic arched-roof profile tunnel was carried out in order to investigate the influence of geometric size on stress distribution and deformation in rockmass surrounding tunnels which can be optimized in design and construction of underground works. Results show that increasing the aspect ratio of the arched-roof tunnel will cause corresponding increase in the magnitude and size of zone of adverse compressive stress concentration at the tunnel sidewall while the extent of de-stressing zone at the invert/crown decreased. The converse is true for increasing span to height ratio. Similarly, the horizontal displacement of rock mass in the vicinity of the tunnel sidewall shows an increasing trend with increasing aspect ratio of the tunnel. In contrast, the tunnel seems not to experience significant variation in vertical displacement of the floor and roof at increasing aspect ratio. These observed trends in variations of the phenomena of stress re-distribution and deformation in rocks surrounding tunnels with tunnel dimensions demonstrate that stress induced instabilities can be effectively regulated by adopting appropriate dimensions relative to rockmass properties and engineering objective.

Keywords

Dimensions • Tunnels • Stress-distribution • Deformation

79.1 Introduction

In most civil engineering structures such as highways, power generation and distribution facilities, mainline haulage in mines (stopes and shafts), hazardous waste repositories and aqueducts that integrate tunnels or caverns, the horse-shoe tunnel cross-sectional profile are often preferred due to ease of construction and engineering objectives (Hoek and Brown 1980; Brady and Johnson 1989; Hoek 2000; Zhu and Zhao 2004; Cai et al. 2007; Lunardi 2008). However, the arched-roof cross-section which usually consists of crown with

circular outline resting on a rectangular base is prone to instabilities at the crown, foot and shoulders of the ribs and failures in associated civil and mining structures often result from invert heave, even when supported (Hoek 2001; Hsu et al. 2004). The ground on support suffers from loading and bending moments from unstable slabs caused by delayed failures. In all situations, failures are linked to induced stress effects and the response of rockmass in terms of stress re-distribution and deformation (Brady and Brown 1993; Jeager et al. 2008). The key issues in design and construction of the tunnels and caverns in rocks, therefore, is the prediction of the pattern of stress re-distribution and amount of deformation that may result during and after construction. Such prediction is important for selection of appropriate excavation technique and advance rate and effective support system in order to reduce project cost, avoid inadequate or excessive support situation and prevent unstable excavation (Yeung and Leong 1997; Hoek 2001; Hsu et al. 2004; Lunardi 2008). Unfortunately, precise prediction of the two

G.E. Ene (✉) · C.O. Okogbue
Department of Geology, University of Nigeria, Nsukka, Nigeria
e-mail: ezekwesiliene@yahoo.com

C.T. Davie
School of Civil Engineering and Geosciences, University of Newcastle, Newcastle upon Tyne, UK

parameters is often difficult and constitutes a complex geo-mechanic problem exacerbated by highly variable and indeterminate rockmass properties, transient in situ stress and fluctuating groundwater conditions (Hoek and Brown 1980; Whittaker and Frith 1990; Chen and Zhao 2002; Pariseau 2007; Lunardi 2008). This paper reports a numerical investigation of the effect of tunnel dimensions on stress re-distribution and deformation processes in surrounding rockmass which can enable tunnel dimensions to be optimized in design to modify and regulate the stress-induced failures.

79.2 Methodology

The tunnel shape for the generic model is an arched-roof rectangular cross-section which consists of an arch (5 m radius) profile roof with 7 m high sidewalls and 10 m span. The probable effect of tunnel dimension on deformation and stress re-distribution mechanism in rocks around the tunnel is studied using the height (H) to width (W) ratio. To implement this, the generic tunnel shape (Fig. 79.1) H/W ratio, 1.2 (12 m/10 m), is to be varied to 0.5, 0.6, 0.75, 1, 1.2, 1.4, and 2.0 in each simulation. It is important to point out that the tunnel shape effect could be duplicated in such simulation and can result in spurious results. To curtail such effect, the arch profile geometry is maintained and adjustments to simulate for size influence are effected by increasing or reducing the arch radius and/or the sidewall.

The problem domain is defined by Ubiquitous Joint constitutive model and massively jointed shale characteristics from FLAC Rock Data bank with the following rock properties: density = 2,700 Kg m^{-3}, shear modulus = 8.81E9 Pa, bulk modulus = 4.3E9 Pa, cohesion = 3.84E7 Pa, friction = 14.4°, tensile strength = 14.5 MPa, dilation = 0.0 and rockmass properties: joint angle = 30°, cohesion = 0.5E6 Pa, friction = 36°, tensile strength = 0.0 and dilation = 0.0. The tunnel is a relatively deep one, located at 500 m below the surface. The tunnel was excavated by unloading process. The stress state of rockmass and displacements at the mid-point of the roof, floor and sidewall were studied. Model solution validation (Fig. 79.2) compares numerical results of a circular profile tunnel with values of calculated tangential stresses using closed form analytical solution (Hoek and Brown 1980). Both solutions show good agreement at some locations and the deviations at the other locations are attributed to some yielding numerical solution in contrast to elastic analytical equation. Since the results of the numerical solutions and, for the purpose of possible extrapolation to other domain which may be characterized with rockmass properties that can vary considerably, a sensitivity analysis of the model input strength parameters was carried out. The possible variations
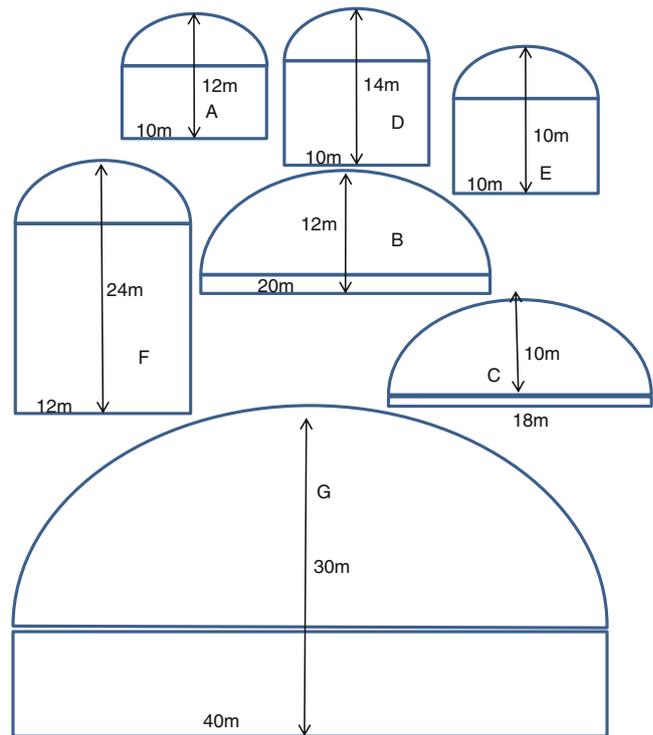
Fig. 79.1 Arched-roof profile tunnel of different height to width (aspect) ratio investigated in this study. Aspect ratio of *A* 1.2; *B* 0.6; *C* 0.5; *D* 1.4; *E* 1.0; *F* 2.0; and *G* 0.75 (*Scale* 1 cm: 3 m)

in the value of the material properties were scaled from measured and reported values based on Goodman (1989) and AASHTO 1989. The stability of the tunnel is judged by the maximum value of horizontal displacement of the right sidewall. In all the simulations, it is only the parameter under investigation that is allowed to vary within in each case, others parameters and the model set-up are caused to remain constant (Bardsley et al. 1990; Wu et al. 2001). The sensitivity of the following parameters: bulk modulus, shear modulus, cohesion, tensile strength and angle of internal friction were considered. In order to compare the sensitivity of the various parameters, the sensitivity factor, S$_k$, (Bedford and Cooke 2001; Zhu and Zhao 2004) was employed. The sensitivity factor expresses the ratio of the relative change in a system property P (ðp = |dp|/p) to the change in certain parameter k (ðk = |dk|/k) thus, $S_k = \frac{(|dp|/p)}{(|dk|/k)}$.

79.3 Results and Discussion

79.3.1 Influence of Tunnel Size and Dimensions

The influence of the ratio of tunnel height to width (aspect ratio) on the stress patterns is shown graphically in Fig. 79.3. From the figure, it is highlighted that the loading of
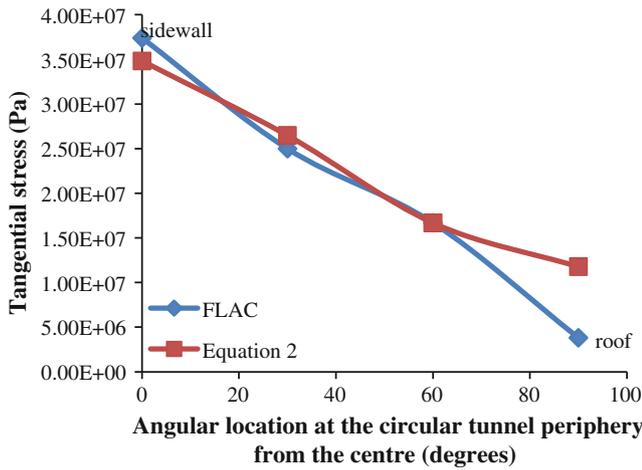
Fig. 79.2 Tangential stress at the periphery of a circular tunnel in biaxial stress field (k = 0.63) from similar locations solved using closed form equation and FLAC

Fig. 79.3 Variation of maximum principal stress with aspect ratio of the arched-roof tunnel

compressive stress at the sidewall increases with increasing aspect ratio of the excavation. On the other hand, the tensile stress at the floor and the arched roof show decreasing trends with increasing height to width aspect ratio. In contrast, a reversed trend of decreasing compressive stress magnitude at ribs and increasing tensile region at the invert/crown is observed for width to height aspect ratio. At the same aspect ratio, similar trends in variation of stress re-distribution and type can be demonstrated by increasing the cross-sectional area of the excavation (increased excavation volume). A typical example is presented in Fig. 79.4a, b for aspect ratio of 1.2.

The aspect ratio of the underground excavation seems to have little or no effect on the vertical displacement of rock mass around the excavation perimeter under the present biaxial stress state and material model as illustrated in Fig. 79.5a. However, a remarkable sharp deviation from the general insignificant variation trend at an aspect ratio of 0.75 is worthy of note. For instance, a closer check of the model aspect ratio relative to its dimensions shows that the tunnel which exhibits the anomalous maximum displacement has dimensions of 40 m span and 30 m height. Despite the relatively low value of the aspect ratio (0.75), greater displacements were recorded due to the larger size of the excavation. The implication of this observation is that the displacement of rock mass under the given stress field is probably less dependent of the aspect ratio but rather on the volume of the excavation. This suggestion is investigated further and confirmed using the aspect ratio of 1.2 and increasing only the size of the tunnel. The results show reasonable changes in maximum vertical displacement that will result from enlarging the tunnel size at the same aspect ratio (Fig. 79.6). Indeed, at the tunnel floor, the maximum vertical displacement tends to increase with increasing size
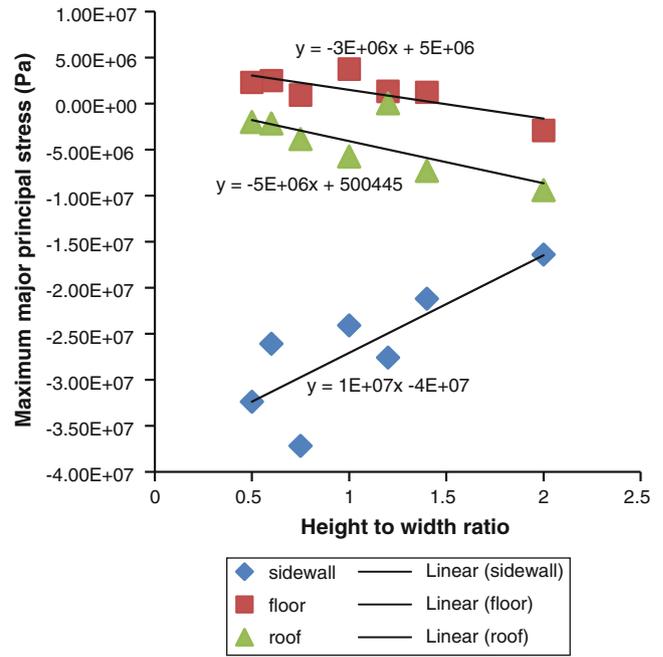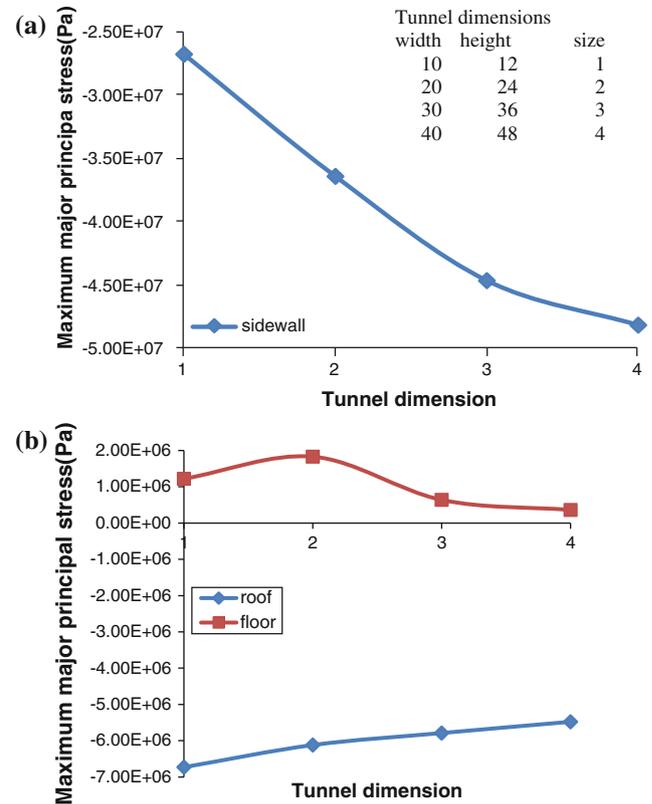
Fig. 79.4 **a** Variation of maximum principal stress with excavation volume of the arched-roof tunnel. **b** Variation of maximum principal stress magnitude and type with varied height to width ratios

of the excavation while the roof will experience decreasing values as the tunnel dimension is increased (see Fig. 79.6a). Contrary to these observed trends in vertical displacements, the horizontal displacement can vary considerably with variation in opening dimensions at constant aspect ratio. Figures 79.5a and 79.6b exemplify that horizontal displacement at the tunnel sidewall exhibit significant increase in maximum value with increasing aspect ratio and increasing size at the same aspect ratio respectively.

79.3.2 Parametric Analysis

The parametric analysis of input parameters for index of rockmass geomechanical properties reveals two categories of sensitivity relative to maximum horizontal deformation of the unsupported tunnel rib. The first group is made up of rockmass cohesion and friction and joint cohesion that show insignificant variation in sidewall deformation at varied values and therefore considered insensitive to the tunnel stability. The second group includes bulk and shear moduli of rockmass and orientation and friction of joints that show significant sensitivity to tunnel deformation at varied amounts. Figures 79.7 and 79.8 show the sensitivity function plots for the second group of parameters. The function plots
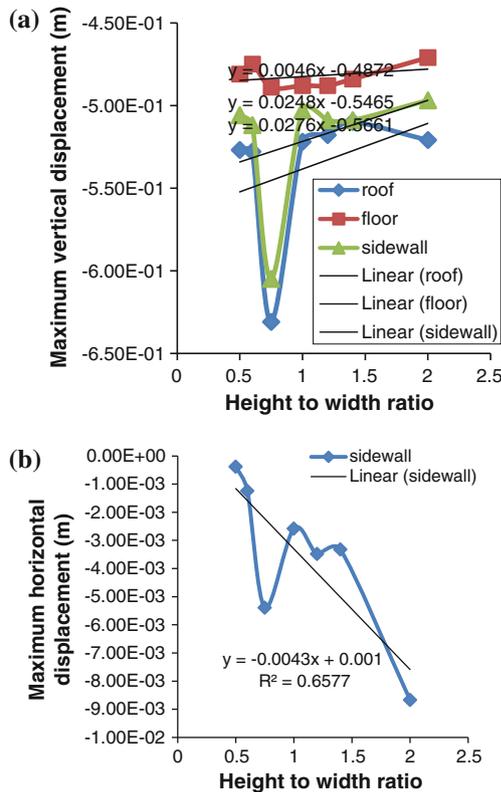
Fig. 79.5 **a** Variation of maximum vertical displacement with varied tunnel aspect ratio. **b** Variation of maximum horizontal displacement with varied tunnel aspect ratio
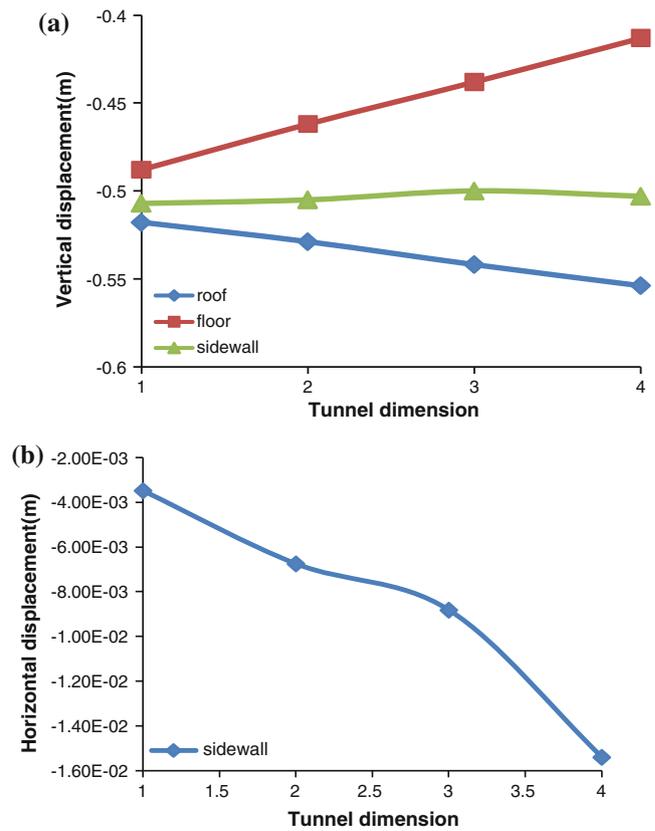
Fig. 79.6 **a** Variation of maximum vertical displacement with excavation volume of the arched-roof tunnel for aspect ratio of 1.2. **b** Variation of maximum vertical displacement with excavati volume of the arched-roof tunnel for aspect ratio of 1.2 (sidewall)

are adopted for the purpose of interpreting, statistically, the relative variability in the sensitivity of material properties which is of important concern in assessing the stability of the tunnel and optimization of testing schemes (Wu et al. 1991).

Figure 79.7 illustrates the sensitivity function plots for shear and bulk modulus. As presented in the figure, the sensitivity curves of both parameters show remarkable disparity. The sensitivity of the bulk modulus to maximum displacement of the tunnel sidewall increases sharply with increasing
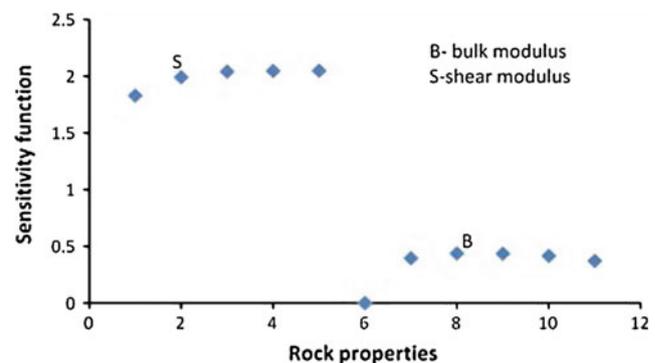
Fig. 79.7 Variation of sensitivity factor with bulk and shear modulus
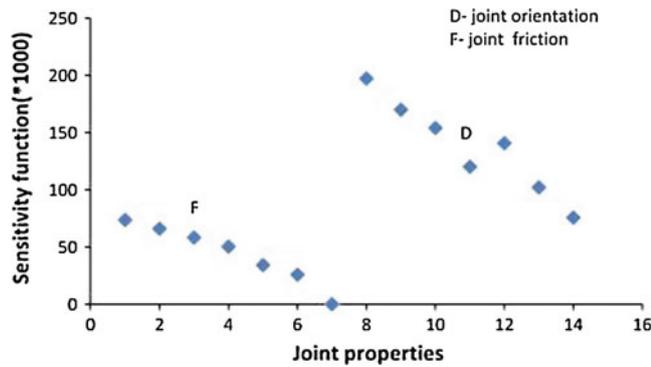
Fig. 79.8 Variation of sensitivity factor with joint dip angle and friction

79.4 Conclusion

The numerical studies of a generic arched-roof profile tunnel using finite difference code and constitutive model of Ubiquitous Joint have allowed for the evaluation of the effect of tunnel dimensions design parameters on stress distribution and deformation in surrounding rockmass as well as parametric analysis of rockmass properties. Increasing the tunnel aspect ratio (height to width) caused corresponding increase in adverse stress compressive stress magnitude and extent on the ribs and decreasing trend for tensile region at invert/crown. The converse is true for increasing width to height ratio. The horizontal displacement of rock mass in the vicinity of the tunnel sidewall increases with increasing aspect ratio of the tunnel. Also, at increasing aspect ratio, the tunnel seems not to experience significant variation in vertical displacement of the floor and roof, except for increased tunnel size which will show both increasing stress concentration and deformation.

bulk modulus values at lower values but appears to stabilize at higher values. The sensitivity factor of the shear modulus increases with increasing values of shear modulus up to an optimal value. Beyond this value, the sensitivity of shear modulus decreased with increasing shear modulus values. However, for the basic parameter values of 8.81 GPa for bulk modulus and 4.3 GPa for shear modulus, the corresponding calculated sensitivity factors are 2.04 and 0.43 respectively. It follows, therefore, that if the assessment of the stability of the generic tunnel should be based on the maximum horizontal displacement of the tunnel sidewall, then the most sensitive rock strength parameter will be bulk modulus because of its high sensitivity value compared to the other parameters. The implication of the results of the sensitivity evaluation of rock parameters is manifest on the effect of under or over-estimation of such parameter on the stability of the tunnel (Wu et al. 1999). For example, whereas a 30 % relative errors in measurement of cohesion and angle of internal friction values of the rock mass will result in insignificant error in the predicted maximum horizontal displacement of the right tunnel sidewall, similar relative error in the bulk modulus and shear modulus will lead to 61.2 % (2.04 × 30 %) and 12.9 % (30 % × 0.43) relative error in the predicted maximum horizontal sidewall displacement (Zhu and Zhao 2004).

The result of the sensitivity analysis of joint strength parameters is illustrated graphically in Fig. 79.8. From the figure, it is evident that both the joint dip angle and joint friction angle display increasing sensitivity with increasing parameter values. However, for the basic parameter set, 36° for joint friction and 30° for joint dip angle, the corresponding sensitivity factors are 0.14 and 0.05 respectively. This means that a 50 % error in the measurement of both parameters will result in 7 and 2.5 % error respectively in the predicted maximum deformation of the tunnel sidewall. In that case, the stability of the generic tunnel under the present model is more sensitive to the friction angle of the dip compared to the angle of dip of the joint.

References

Bardsley WE, Major TJ, Selby MJ (1990) Note on a Weibull property for joint spacing analysis. Int J Rock Mech Min Sci Geomech 27:133–134

Bedford T, Cooke R (2001) Probabilistic risk analysis: foundations and methods. Cambridge University Press, Cambridge

Brady BHG, Brown ET (1993) Rock mechanics for underground mining, 2nd edn. Chapman & Hall, London, pp 23–48

Brady TM, Johnson JC (1989) Comparison of finite difference code and finite element code in modelling an excavation in an underground shaft pillar. In: Pietruszczak S, Pande GN (eds) Proceedings of 3rd international symposium on numerical modelling in geomechanics (NUMOG III), Niagara Falls, pp 608–619

Cai M, Morioka H, Kaiser PK, Minami M, Maejima T, Tasaka Y, Kurose H (2007) FLAC/PFC Coupled numerical simulation of a large-scale underground excavations. Int J Rock Mech 44(4):550–564

Chen SG, Zhao J (2002) Modelling of tunnel excavation using a hybrid DEM/BEM method. Comput Aided Civi Infrastruct Eng 17:381–386

Cundall PA (2001) A discontinuous future for numerical modelling in geomechanics? Proceedings of Institution of Civil Engineers. Geotech Eng 149:41–47

Goodman RE (1989) Introduction to Rock mechanics. Wiley, New York, pp 23–67

Hoek E (2001) Big tunnels in bad rocks 2000 Terzaghi Lecture. J Geotech Geoenviron Eng ASCE 127(9):726–740

Hoek E, Brown ET (1980) Underground excavations in Rock. Institution of Mining and Metallurgy, London, pp 1–68

Hsu SC, Chang SS, Cai JR (2004) Failure mechanisms of tunnels in weak rock interbedded with structures. Int J Rock Mech Min Sci 41 (3):01–06

Jeagar JC, Cook NGW, Zimmerman RW (2007) Fundamentals of Rock mechanics. Blackwell Publishing, London, pp 345–380

Lunardi P (2008) Design and construction of tunnels: analysis of controlled deformation in Rocks and soils (ADECO-RS). Sprnger-Verlag, Berlin, pp 2–78

Pariseau WG (2007) Design analysis in Rock mechanics. Taylor & Francis/Balkema, Leiden, pp 34–98

Whittaker BN, Frith RC (1990) Tunnelling design stability and construction. Institution of Mining and Metallurgy, London, pp 4–38

Wu C, Hao H, Zhao J, Zhou XX (2001) Statistical analysis of anisotropic damage of the Bukit Timah granite. Rock Mech Rock Eng 34:23–28

Yeung MR, Leong LL (1997) Effects of joint attributes on tunnel stability. Int J Rock Mech Min Sci 34:3–4

Zhu W, Zhao J (2004) Stability analysis and modelling of underground excavations in fractured rocks Elsevier, Amsterdam, pp 289

Analysis of Stress Conditions at Deep Seated Tunnels—A Case Study at Brenner Base Tunnel

80

Johanna Patzelt and Kurosch Thuro

Abstract

Deep seated tunnels like the Brenner Base Tunnel suffer from high in situ or primary stress conditions. This has significant effects on the deformation pattern and failure mode and therefore on the construction of the tunnel. High in situ stress conditions are a result of the rock cover which reaches approximately 1,700 m at the Brenner Base Tunnel. In collaboration with the Brenner Base Tunnel Society BBT SE, in situ stress conditions were modeled in a multitube tunnel system in different rock conditions. A rather ductile rock type, the Innsbruck quartzphyllite, and a rather brittle rock type, the Tux Central Gneiss, were used to calculate several models with the 2D-finite element code Phase2 and the 3D-finite element code RS3 (rocscience). Due to residual tectonic stresses caused by the collision of the African and Eurasian plates horizontal stresses are often increased. For the Innsbruck quartzphyllite section a 70° dip angle was used, within the section of the Tux Central Gneiss no deviation from the vertical was assumed due to geological and geophysical results. Apart from the rock cover and the direction of the main principle stress, further parameters were needed for modeling: young's modulus, uniaxial compressive strength, poisson ratio, friction angle and cohesion of the rock types have been used from site investigation reports. The performed numerical modeling showed that the secondary stresses have the same orientation as the primary stresses, hence the maximum stress appeared in the tunnel walls and minimum stress is concentrated in invert and crown.

80.1 Introduction

In the course of a scientific cooperation of the TU Munich Department of Engineering Geology with the Brenner Base Tunnel BBT SE modeling were done at eight different cross sections in the region of the Innsbruck quartzphyllite and the Tux central gneiss. Modeling of the secondary stresses and

the associated deformation were done by using the 2D finite element program phase2 and RS3 (rocscience).

80.2 Location and Characteristics of the Cross Sections

Five different cross sections were modeled in the region of Innsbruck quartzphyllite and three cross sections are located in the region of the Tux central gneiss. The cross sections in the Innsbruck quartzphyllite were distinguished by their different tube arrangements with connecting tunnels and various expansions in the range of the multifunction station Innsbruck Ahrental.

J. Patzelt (✉)
Pöyry Infra GmbH, Salzburg, Austria
e-mail: johanna.patzelt@poyry.com

K. Thuro
Technische Universität München, Munich, Germany
e-mail: thuro@tum.de

80.3 Parameters

For the modeling parameters were given by Brenner Base Tunnel (BBT/Geoteam 2008) as well as from the Inn Valley tunnel (Thuro 1996). In a case study different rock parameters were varied (Patzelt 2010).

Following input parameters were used for modeling of rock:

- Unconfined compressive strength
- Poisson's ratio
- m_i (Hoek-Brown failure criterion, Hoek et al. 2002)
  Following parameters were used to characterize the rock mass:
- young's modulus
- Disturbance factor D as a function of the exploration method (blasting, TBM)
- Geological Strength Index GSI (Hoek et al. 2002).

80.4 Modeling

The specified cross sections were digitized and the geological prognosis from preliminary studies was added in form of layers with constant widths (Fig. 80.1). Because of the geometry some rock thicknesses had to be shown exaggerated, otherwise it would come to elements notional artifacts due to the network used for the calculation of 2D and 3D finite element code.

For the competent rocks the Hoek-Brown failure criterion was used. The Hoek Brown failure criterion characterized at the best the rock mass parameters for the rocks given in this range. In none of the different failure criterions any anisotropy factors could be added. A range of 10 points of GSI

value was given by BBT/Geoteam (2008). They characterized the block sizes and this controls the rock mass quality. For the "weak" material of the Inn Valley fault zone none rock parameters were given, so only characteristic values for friction angle and cohesion are specified, that it can be characterized by the Mohr-Coulomb failure criterion.

In deep seated tunnels joints play a dominant role in the stress states and the solvability. Closed fractures or joints have only a minor role, since they are usually not mechanically effective. The results show that the tangential discontinuities have an influence on the stress transfer and deformations and lead to higher amounts of deformation. Nevertheless, only deformation amounts in the range of maximum 10 cm were determined.

80.4.1 Rock and Rock Mass Parameters

In summary, the used parameters for the modeling are listed in Tables 80.1 and 80.2. They are all based on the documents of BBT/Geoteam (2008). The complete list of parameters is in Patzelt (2010: 73 ff) for further details.

80.4.2 Primary Stress Conditions

The primary stresses are composed of the superposition of stresses and the induced stresses of the tectonic plate collision. The tectonically induced stresses lead mainly to an inclination of the resulting principal stress. The angle of inclination with the most realistic results is 70° in Innsbruck quartzphyllite region. In Fig. 80.2, the primary stress conditions for cross sections B are shown. From hydrofracturing
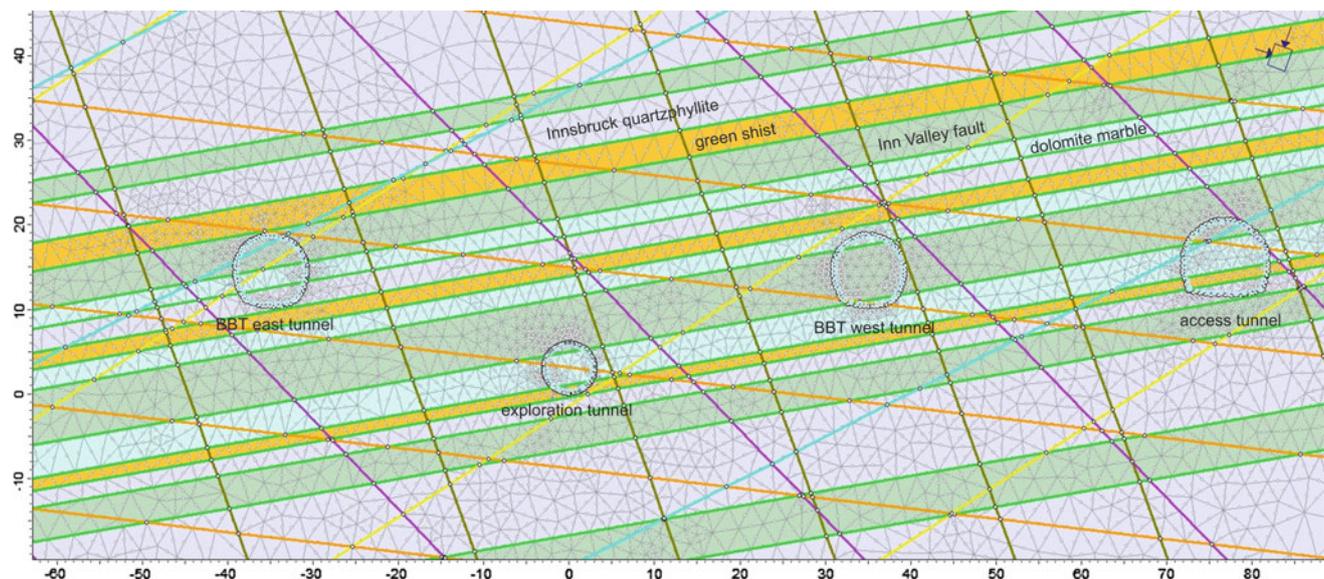
Fig. 80.1 Cross section B (part of multifunction station Innsbruck Ahrental)

Table 80.1 Summary of the used rock properties

Rock	UCS [MPa]	E-Modul [MPa]	m_i	ν	GSI
Innsbruck quarzphyllite	40	5,087	12	0.19	50
Dolomite marble	30	7,662	10	0.20	65
Green shist	55	6,187	15	0.15	45

Table 80.2 Summary of the used properties in the Inn Valley fault zone

Rock	E-Modul [MPa]	c [MPa]	φ [°]	ν
Inn Valley fault	1,000	0.5	28	0.19

tests it is known, that the ratio of σ1 and σ3 varies in the Wipptal between 0.3 and 1.2.

80.4.3 Stress Redistribution When Opening the Face into Sub-Areas

Further modeling should take into account the stress redistribution during successive advance of the various tunnels. In conventional propulsion of the advance in top heading, bench and invert was divided and implemented in the modeling to represent the stress redistribution (Fig. 80.3).

80.4.4 Secondary Stress Conditions

In the modeling can be seen that the secondary stresses extend in about the same direction as the primary stresses (Fig. 80.4). The maximum secondary stresses pass through the dip angle shifted slightly in the region of eastern invert on the west elm as well as the transition to the invert. While the minimum σ1 stresses preferably spread in the layer of Inn Valley fault, the minimum σ3 stresses propagate especially in the layers of dolomite marble, which has the lowest rock mass compressive strength. The maximum σ3 stresses are arranged accordingly 90° to σ1 stresses. The minimum stresses sweep in the range between 0 and 4.5 MPa.

80.4.5 Deformation

The determined total deformation amounts—without e.g. anchor, reinforced concrete—scatter in the range of 10 cm to a maximum of 2 m, which was determined from a full-surface opening of a large face at an overburden of 890 m.

The largest deformation amounts occur in the region of Innsbruck quartzphyllite. By an overburden of 870 m is clearly seen that the rounded profile of the exploratory tunnel is the cheapest variant advance (Fig. 80.5). For the given geometry of the main tunnel tubes is seen especially at the junction of elm that increased deformations are generated.
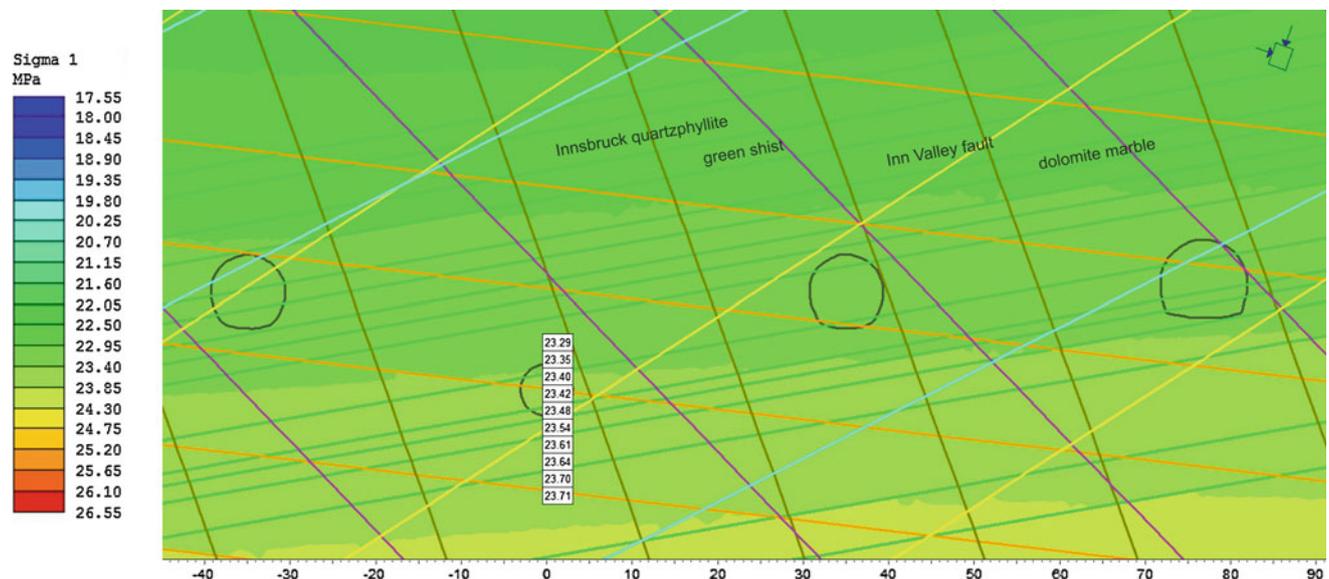
Fig. 80.2 In-situ stress conditions at cross section B
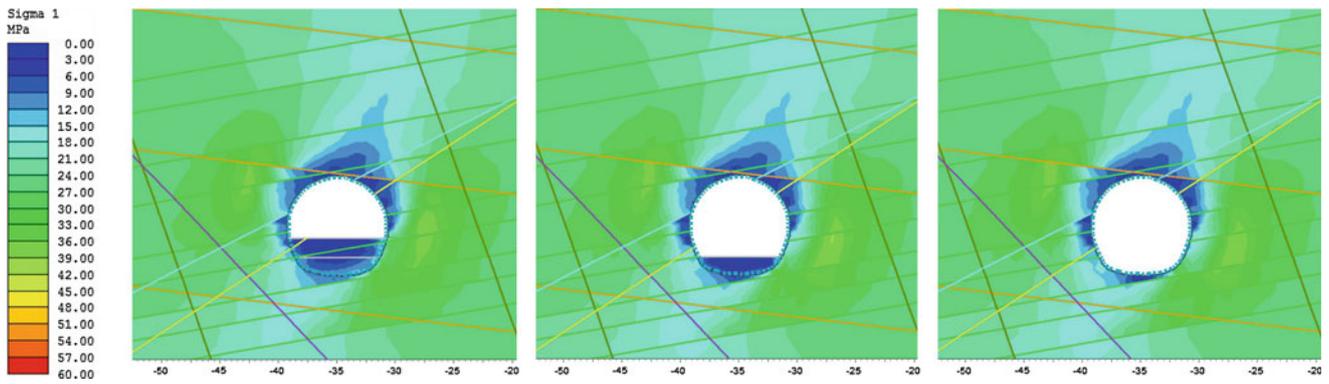
Fig. 80.3 Stress redistribution due to excavation of crown, side wall and invert applying conventional propulsion
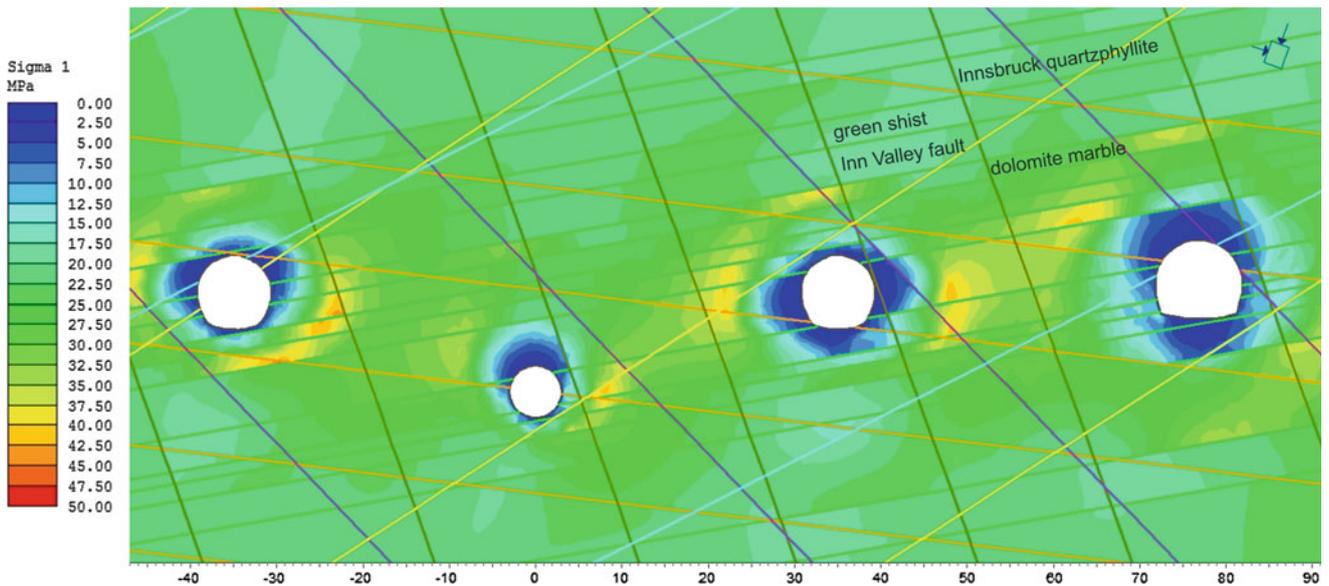
Fig. 80.4 Illustration of σ1 stresses. Minimum stresses are plotted in *dark colors*; maximum stresses are shown in *light colors*
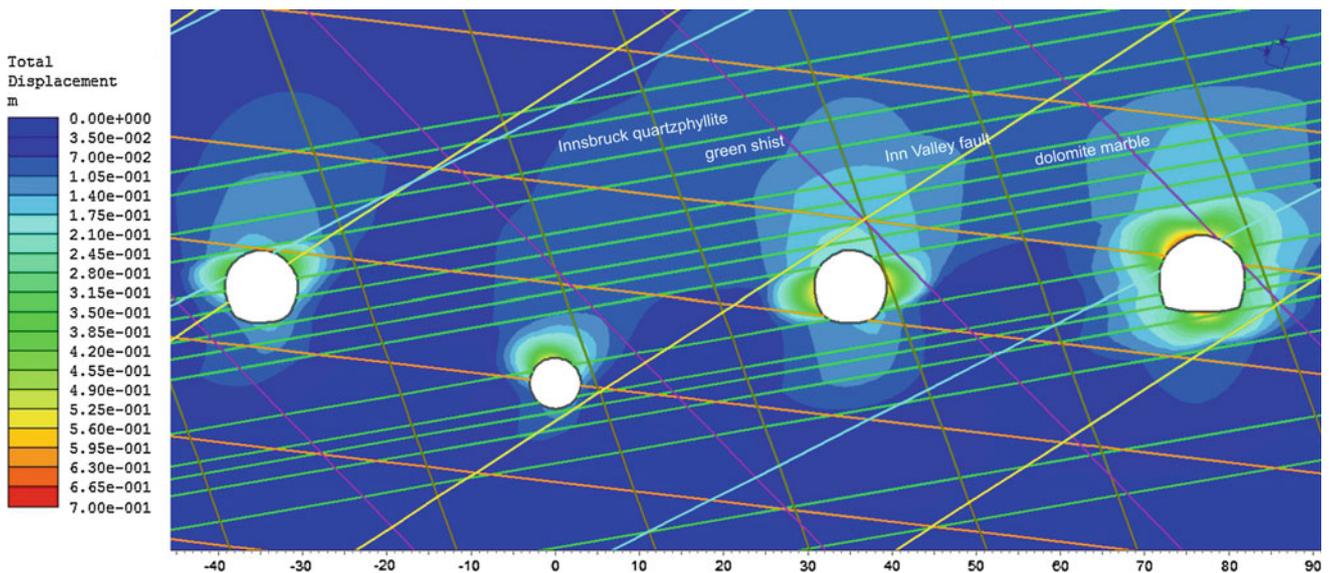
Fig. 80.5 Illustration of the deformation pattern (overburden 890 m). Maximum deformations add up to 7–10 cm at crown and tunnel sides

80.5   Conclusions

The influence of the primary stresses was examined on the stress distribution at high overburden in the Brenner base tunnel, taking account of:

- Complex geometric conditions (in particular the positions of the tunnels in a multifunction station),
- given rock and rock mass characteristics from the reports of preliminary studies,
- the orientation and training of the separation surface structure and fault zones,
- loosening of the factor D (blasting/TBM),
- and the orientation of the primary and secondary stresses.

  The parameters were varied so that uncertainties in the determination or natural variations could be mapped.

References

BBT/Geoteam (2008) Ausbau Eisenbahnachse München—Verona. Brenner Basistunnel. UVE. Technische Projekt-aufbereitung. Geologie, Geotechnik, Hydrogeologie. Haupttunnel. Gebirgsarten, Gebirgsverhaltenstypen, Störzone—Haupttunnel—137 S, Technischer Bericht und Längenschnitt G1.2i-01—1 Plan 1: 25 000

Hoek E, Carranza-Torres C, Corkum B (2002): Hoek-Brown Failure Criterion—2002 Edition. In: Proceedings NARMS-TAC conference, Toronto, 1: 267—273

Patzelt J (2010) Modellierung des sekundären Spannungs-zustandes tiefliegender Tunnelbauwerke am Beispiel des Brenner-Basistunnels—Unveröffentl. Masterarbeit, Lehrstuhl für Ingenieurgeologie, Technische Universität München, 84 S, München

Rocscience (2010) Phase2 Version 7. Manual (digital)

Thuro K (1996) Bohrbarkeit beim konventionellen Sprengvortrieb. Geologisch felsmechanische Untersuchungen anhand sieben ausgewählter Tunnelprojekte—149 S, Münchner Geol. Hefte, B1, München (Technische Universität München)

Acoustic Emission Technique to Detect Micro Cracking During Uniaxial Compression of Brittle Rocks

81

Carola Wieser, Heiko Käsling, Manuel Raith, Ronald Richter, Dorothee Moser, Franziska Gemander, Christian Grosse, and Kurosch Thuro

Abstract

Excavation of deep underground openings causes redistribution of primary stresses and induces initiation and propagation of micro cracks. Changes in rock properties ahead of an advancing tunnel face may influence stability and penetration rates in TBM tunneling. This study is part of a PhD project where the focus is on stress-induced micro cracking and its influence on rock strength reduction. We demonstrate results from acoustic emission (AE) measurements on two homogeneous diorite samples tested under uniaxial compression. The aim was to gain information about the influence of experimental setup and settings on AE events in brittle rock. From the stress strain curve and the number of acoustic signals, main deformation stages could be determined. A three-dimensional localization of acoustic events showed a typical conjugate shear system. Future work will include tests on different rock types after inducing controlled damage by uniaxial loading. Lateral strain measurements combined with AE analysis will be applied in order to quantify rock damage and its influence on rock strength.

81.1 Introduction

Any excavation of deep underground openings influences the in situ stress state in the surrounding rock mass. According to that, rock samples retrieved from highly stressed rock masses are subjected to stress changes resulting from the unloading process (e.g. Teufel 1989; Meglis 1991). As uniaxial compressive strength is usually determined several days or weeks after sampling, the relaxation process may still be in progress when the tests are performed. Deformation and strength parameters determined in the laboratory cannot be transferred to in situ stress conditions without further considerations. The detection and quantification of stress-induced damage, the time-dependence of the relaxation process as well as the influences on rock strength and deformation properties are of key interest for determining the rock strength at the time of excavation.

Acoustic emissions (AE) are elastic sound waves generated during crack formation or growth. It is well known, that loaded rock specimen emit acoustic signals which can be detected and analyzed with regard to rock damage. The waves are converted into electric signals by piezoelectric transducers which are connected to an amplification and data acquisition system. An overview of acoustic emission testing and its application is given in Grosse and Ohtsu (2010).

This paper presents the results of preliminary AE measurements on brittle rock during unconfined compression. A 3-dimensional localization of AE events was performed and deformation stages as well as stress levels in the stress–strain curve could be assessed according to the methods of Bieniawski (1967) and Martin (1997). These tests represent

C. Wieser (✉) · H. Käsling · K. Thuro
Chair for Engineering Geology, Technische Universität München, Arcisstr. 21, 80333 Munich, Germany
e-mail: carola.wieser@tum.de

M. Raith · R. Richter · D. Moser · F. Gemander · C. Grosse
Chair of Non-Destructive Testing, Technische Universität München, Baumbachstr. 7, 81245, Munich, Germany

the first stage of an investigation to examine and quantify the influence of fracture damage on unconfined compressive strength and deformation characteristics of brittle rocks.

81.2 Experimental Setup

We tested two specimens of homogeneous, porphyritic, fine- to medium-grained diorite from Nittenau, south-east Germany (Bavarian Forest), containing mainly feldspar, biotite and quartz (Fig. 81.1). Samples were prepared for testing with a diameter of 8 cm and a length to diameter ratio of 2:1 (Mutschler 2004). Uniaxial loading was applied under servo-control at a constant velocity rate of 0.1 mm/min. During the tests, axial strain was measured by position sensors installed between the load plates.

14 piezoelectric transducers attached to the sample surface and another two guard sensors glued to the load plates recorded background noises deriving from the hydraulic device (experimental setup shown in Fig. 81.2). The pre-amplifier included a bandpass filter with a frequency range of 10 kHz–1 MHz. Low frequencies, originating from the hydraulic pump of the loading frame were eliminated by a high-pass filter with a cutoff frequency of 10 kHz. Depending on the type of sensor, a pre-amplification of 27–33 dB was applied. AE were recorded by an automatic data acquisition system (TranAX by Elsys) using a slew rate trigger and a sampling frequency of 5 MHz.

81.3 Data Analysis

Data analysis was carried out using the software SquirrelAE which was developed at the Chair of Non-destructive Testing at Technische Universität München. Using a signal-based AE method, recorded waveforms were analyzed, although we focus on results from 3D source localization in this study. The software includes an automated picking algorithm based on the Akaike Information Criterion (AIC). The accuracy of the onset detection process is critical for a reliable localization of AE events. Localization was analyzed using the Bancroft (1985) algorithm which was developed to solve global positioning system (GPS) equations. Furthermore, the iterative algorithm of Geiger (1910) was applied which was originally established for the localization of earthquakes. Kurz (2006) gives an overview of several algorithms and their scope of application. Thus, the algorithm providing the best results depends on boundary conditions and sensor covering.

81.4 Experimental Results

In a first test, the influence of Teflon (PTFE) as a means for minimizing end effects was tested during unconfined compression. Two Teflon sheets of 2.8 mm thickness were inserted between rock specimen and load plates to reduce acoustic signals resulting from friction at the end surfaces.
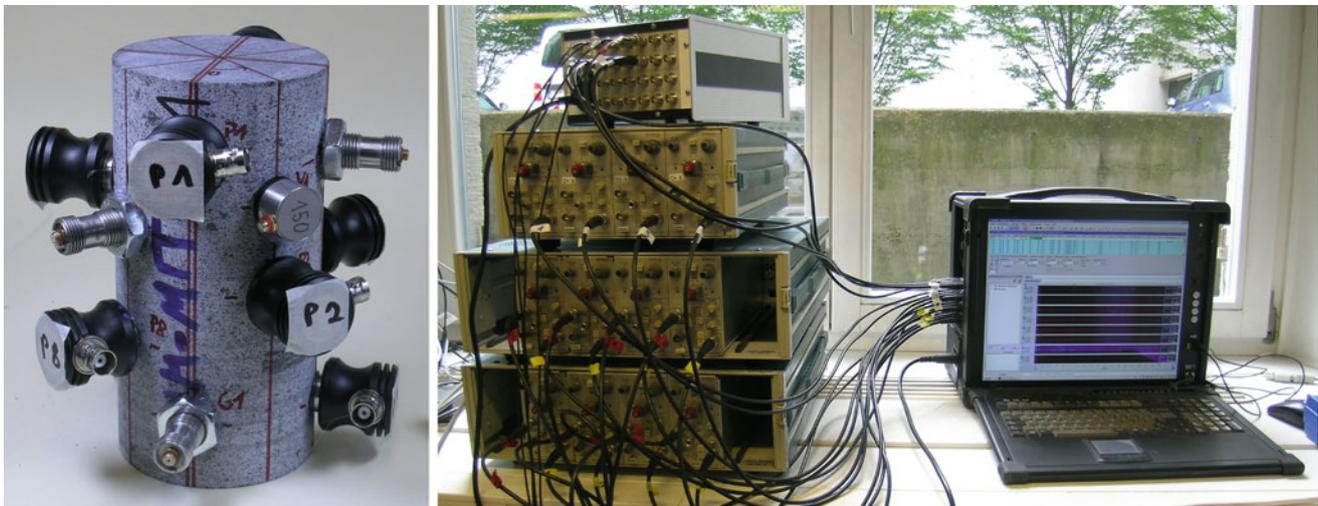
Fig. 81.1 *Left* 14 piezoelectric transducers attached to diorite sample from Nittenau (Bavarian Forest), *Right* pre-amplification and data acquisition system connected to the sample
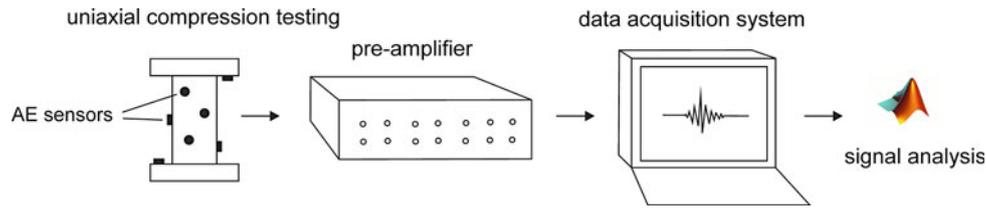
Fig. 81.2 Experimental setup of AE instrumentation and data acquisition system. Axial strain was measured by position sensors between the load plates

The rock sample was loaded uniaxially with and without Teflon. The influence of the material was visible as a decrease in the gradient of the recorded stress-strain-curve, resulting in a deformation modulus 40 % lower when PTFE was applied. As a proper determination of rock parameters was not possible with the attenuating effect, subsequent tests were carried out without Teflon. The effects and the usability of PTFE foils and plates for a reduction of end effects will be investigated more thoroughly in future tests.

A second uniaxial compression test was performed according to Mutschler (2004) with constant loading until failure without PTFE plates. From the number of AE events different stages of crack development could be determined (Fig. 81.3). According to Eberhardt et al. (1999), the first deformation stage is characterized by the closure of existing cracks aligned at an angle to the load whereas parallel cracks may open. The stress–strain curve is non-linear during this deformation stage. In our test, the crack closure threshold σ_{cc} can be set at about 31 % the peak strength (σ_c), which is 218 MPa.

The second stage is marked by the linear section of the stress–strain curve where linear elastic deformation occurs and only a few acoustic emissions were released. Event numbers increase again at a stress level of about 0.64 σ_c which represents the crack initiation threshold σ_{ci} where stable crack growth takes place (Bieniawski 1967). According to Cai et al. (2004), the crack initiation threshold

of most rocks usually ranges from 0.3 to 0.5 σ_c which is clearly lower than what our test revealed. A significant increase in events and an overall high AE activity indicates the onset of unstable crack growth and crack coalescence. This phase begins at a crack damage threshold σ_{cd} of 0.85 σ_c and thus, it is more consistent with existing studies, which state a crack damage stress level between 0.7 and 1.0 σ_c (Cai et al. 2004). With a combined analysis of the volumetric strain curve, a more precise determination of this threshold could be achieved. Thus, in the next test series, lateral strain measurements will be implemented in the experiments.

In the following, results from localization are presented. Figure 81.4 (left) shows a 3D plot of localized AE events. A typical conjugate shear pattern is representative of the typical fracture pattern observed after unconfined compression. A concentration of events occurred in the bottom and top and may be contributed to friction between end surfaces and load plates or stress concentrations on the edges of the sample. In the lower right part of the specimen a distinct accumulation of events is visible where also high energy signals are localized.

Compared to the results from localization, the tested specimen shows a different failure pattern. As shown in Fig. 81.4 (right) a rock fragment split off the sample due to a fracture sub-parallel to the stress direction. As the test was stopped shortly after failure, further major cracks were restricted which may have developed under continuing

Fig. 81.3 *Left* stress–strain curve from uniaxial compression test. Deformation stages in crack development were determined from the stress–strain curve and AE events per 15 s, *Right* final fracture pattern showing one crack aligned parallel to the loading direction
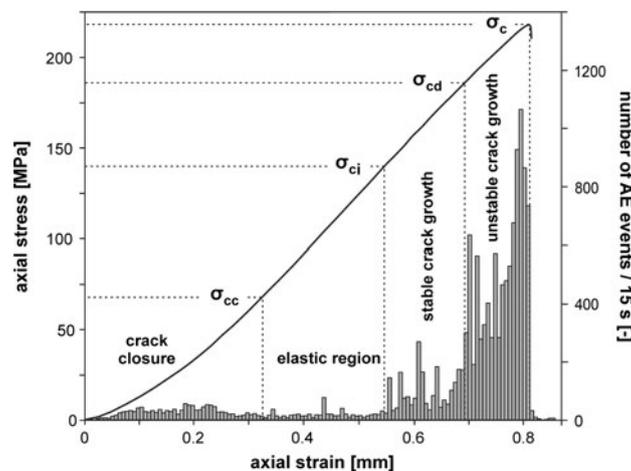
Fig. 81.4 *Left* AE event localization shows a typical conjugate shear system. Larger markers represent better correlation coefficients, red markers show higher event energies. *Right* view in z-direction with an accumulation of events on the right side where final fracture occurred
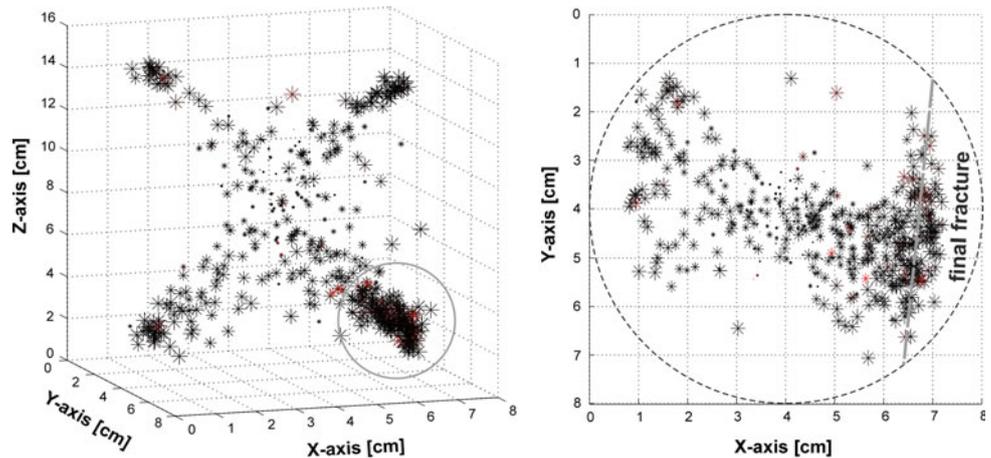
loading. Illustrated in Fig. 81.4 (left) and the sectional view in Fig. 81.4 (right), the final macroscopic fracture can also be reproduced in AE as an accumulation of events is visible in the right side of the cylinder.

volumetric strain measurements will be carried out combined with elastic wave velocity measurements and petrographic investigations.

81.5 Conclusion

This paper presents results of two uniaxial compression tests on homogeneous diorite (Nittenau) samples which were combined with AE measurements in order to confirm the applicability and accuracy of the experimental setup. In a preliminary test, the influence of Teflon sheets as a means for minimizing end effects was investigated. The results showed that although acoustic emission events were minimized at the end surfaces, the stress–strain curve was clearly altered due to attenuation effects. In a second uniaxial compression test, no PTFE plates were applied although friction effects were clearly visible at the end surfaces. From the stress–strain curve and AE distinct deformation stages in crack development could be defined. A 3D plot of AE events displays a typical conjugate shear system which developed during unconfined compression testing. In contrast, the final fracture pattern shows a thin rock fragment which split off the rock but did not reveal the expected conjugate shear planes. Yet, a significant accumulation of AE events on the edge of the specimen indicates the subsequent fracture pattern prior to failure.

This study demonstrates that AE analysis represents a practical non-destructive testing technique to show fracture processes inside a homogeneous rock specimen. Further research will focus on stress-induced damage, time-dependent relaxation and their influence on rock strength and deformation properties. For this purpose, AE as well as

References

Bancroft S (1985) An algebraic solution of the GPS equations. IEEE Trans Aerosp Electron Syst AES-21 7:56–59

Bieniawski ZT (1967) Mechanism of brittle fracture of rock. Int J Rock Mech Min Sci 4:395–406

Cai M, Kaiser P, Tasaka Y, Maejima T, Morioka H, Minami M (2004) Generalized crack initiation and crack damage stress thresholds of brittle rock masses near underground excavations. Int J Rock Mech Min Sci 41(5):833–847

Eberhardt E, Stead D, Stimpson B (1999) Quantifying progressive pre-peak brittle fracture damage in rock during uniaxial compression. Int J Rock Mech Min Sci 36:361–380

Geiger L (1910) Herdbestimmung bei Erdbeben aus den Ankunftszeiten. Kgl Ges d Wiss Nachrichten Math-Phys Klasse 4:231–349

Grosse C, Ohtsu M (2010) Acoustic emission testing. Basics for research—applications in civil engineering. Springer, Berlin, 396 p

Kurz JH (2006) Verifikation von Bruchprozessen bei gleichzeitiger Automatisierung der Schallemissionsanalyse an Stahl- und Stahlfaserbeton. Diss., Institut für Werkstoffe im Bauwesen, Universität Stuttgart, Stuttgart, 197 p

Martin CD, Read RS, Martino JB (1997) Observation of brittle failure around a circular test tunnel. – Int J Rock Mech Min Sci 34 (7):1065–1073

Meglis IL, Engelder T, Graham EK (1991) The effect of stress-relief on ambient microcrack porosity in core samples from the Kent Cliffs (New York) and Moodus (Connecticut) scientific research boreholes. Tectonophysics 186:163–173

Mutschler T (2004) Neufassung der Empfehlung Nr. 1 des Arbeitskreises "Versuchstechnik Fels" der Deutschen Gesellschaft für Geotechnik e. V.: Einaxiale Druckversuche an zylindrischen Gesteinsprüfkörpern. Bautechnik 81(10):825–834

Teufel LW (1989) Acoustic emissions during anelastic strain recovery of cores from deep boreholes. In: Khair (ed) Rock mechanics as a guide for efficient utilization of natural resources. Balkema, Rotterdam, pp 269–276

Towards a Uniform Definition of Rock Toughness for Penetration Prediction in TBM Tunneling

82

Lisa Wilfing, Heiko Käsling, and Kurosch Thuro

Abstract

In TBM tunneling, performance prediction is a major issue since calculated excavation costs and construction time of a tunnel project are mainly based on it. Prediction is dependent on the accuracy of geological and geotechnical input parameters. Besides rock strength, toughness of the excavated rock has a significant influence on penetration and cutting efficiency as increasing toughness requires greater energy to induce complete failure. Yet, existing definitions of rock toughness are not adequate or suitable for incorporation in a performance prediction model for TBM tunneling. To develop a common definition and classification system, we used standard laboratory tests (Uniaxial Compression Test, Brazilian Tensile Test). Based on this test data we analyzed several factors that can characterize rock toughness like the ratio of compressive to tensile strength (Z-coefficient), ratio of plastic to elastoplastic strain, specific failure energy and destruction work. We expect future analysis to focus on Z-coefficient but we aim to revise the classification system of Schimazek and Knatz as results showed no good correlation. Also the ratio of plastic to elastoplastic strain is a promising tool for future research. Obviously, destruction work characterized rock toughness but the determination of this parameter depends a lot on machine stiffness and settings.

Keywords

Rock toughness • TBM tunneling • Penetration prediction • Uniaxial compression

82.1 Introduction

The prediction of TBM-performance is an essential tool to estimate costs and construction time of tunnel projects. Therefore the research group ABROCK (collaboration between universities, clients and contractors) deals with the improvement of existing prediction models as well as with the development of a new, adapted model (Schneider et al. 2012).

Apart from uniaxial compressive strength (UCS), rock toughness significantly affects performance respectively penetration of a TBM (Becker and Lemmes 1984; Gehring 1995). The tougher a rock behaves, the slower cracks propagate and the more energy is needed to cause chipping and effective rock excavation. But the implementation of rock toughness in a prediction model is problematic as no suitable definition exists. Therefore, the aim of this work is the development of a common and suitable method for rock toughness characterization to gain better results in TBM performance prediction.

82.2 State of the Art

Schimazek and Knatz (1976) as well as Becker and Lemmes (1984) described in their research the first definition of toughness by the ratio Z of UCS to BTS (Brazilian tensile strength). Since then, the coefficient Z is commonly used. On the basis of their results they set the threshold of brittle ($Z > 10$) to tough ($Z < 10$) rocks at $Z = 10$. Additionally,

L. Wilfing (✉) · H. Käsling · K. Thuro
Technische Universität München, Chair of Engineering Geology,
Arcisstr. 21, 80333, Munich, Germany
e-mail: lisa.wilfing@tum.de

Thuro (1996) added the ranges of very brittle ($Z > 20$) and very tough ($Z < 5$) to this classification.

Hughes (1972) characterizes the stiffness of rocks with the *specific energy* e_s that is required to bring a rock sample to failure (Fig. 82.1). Gehring (1995) seized this idea under the term of *specific failure energy* w_f and implemented it in his prediction model for TBM performance as he observed good correlation between w_f and penetration rate at different tunnel projects. Thuro (1996) extended this method of energy-requirement to the important range beyond failure of the specimen, so called post-failure-range. Tough rocks do have a distinct post-failure-range whereas brittle rocks nearly have none. *Destruction work* W_z is calculated by the entire area (pre- & post-failure-range) beneath the stress-strain-curve and therefore shows a significant difference between brittle and tough rock. This post-failure-range has already been described by Wawersik and Fairhurst (1970). During their laboratory research program they determined two different post-failure behaviors but did not apply this observation to brittle, respectively tough rocks. The *post-failure-modulus* P_f that is determined with a regression line in the post-failure-range (Fig. 82.1), is one possibility to describe this part of the stress-strain curve (Thuro 1996).

Tough rocks show furthermore a distinct *plastic strain* ε_{pl} right before failure (Fig. 82.1). In contrast, brittle rocks demonstrate a high *elastoplastic strain* ε_{el} with minor *plastic strain* ε_{pl} before failure. The transition point where elastoplastic behavior passes over into plastic behavior is called σ_{cd} (point of irreversible crack damage, Eberhardt 1998) and is determined subjectively or by volumetric strain measurements during uniaxial compression.
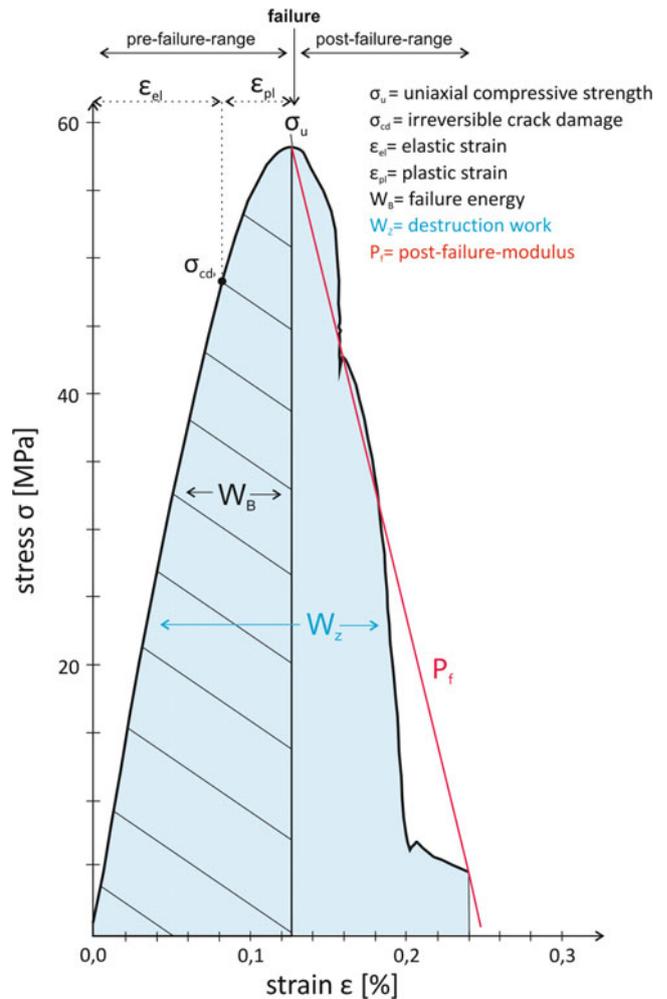
Fig. 82.1 Schematic stress–strain curve of a uniaxial compression test with the toughness defining parameters

82.3 Methodology

Basic research is done with standard laboratory tests like Uniaxial Compression Test (DGGT Testing Recommendation No.1) and Brazilian Tensile Test (DGGT Testing Recommendation No.10). To validate the toughness characterizations, following parameters are analyzed (Fig. 82.1):

• Ratio UCS to BTS (σ_u / σ_t)	• Failure energy W_B
• Post-failure-modulus P_f	• Destruction work W_Z
• Ratio plastic to elastoplastic strain ($\varepsilon_{pl} / \varepsilon_{el}$)	

Furthermore, Acoustic Emission measurements (AE) during Uniaxial Compression Test are planned to determine σ_{cd} and to investigate whether brittle or tough rocks show different fracture propagation as well as velocities. These parameters were already analyzed by Eberhardt (1998) but only on the basis of brittle rocks.

We also expect a distinct increase of acoustic signals at the transition σ_{cd} of elastoplastic to plastic strain as from there on crack propagation is irreversible (Eberhardt 1998). Therefore AE helps to reveal the transition point with a higher accuracy and to provide a precise calculation of the ratio plastic ε_{pl} to elastoplastic ε_{el} strain for the characterization of toughness. To develop a basic definition for rock toughness, tests have been primarily made with homogenous rocks like basalt, anhydrite, diorite and granite. In the next step, also inhomogenous rocks like gneiss, amphibolite and

greenschist have been analyzed. Samples have been chosen under the aspect of a wide range, so that rocks commonly known as tough/brittle have been picked out.

82.4 Results and Discussion

First results of UCS-tests verify the assumption that basalt has a brittle and anhydrite tough failure behavior. Figure 82.2 (left) shows the stress-strain curve of basalt from a quarry in Bavaria. According to ISRM (1978) the UCS of the rock is classified 'extremely high' (470 MPa) and shows by definition of Thuro (1996) an 'extremely high destruction work' (939 kJ/m^3). In contrast, the anhydrite specimen from the Haselgebirge in Austria (Fig. 82.2 right) has a UCS of 60 MPa and consequently only a moderate destruction work of 100 kJ/m^3.

Having a closer look at the stress-strain curves reveals that anhydrite with a far lesser destruction work ($\Delta = 839$ kJ/m^3) shows a much more developed post-failure-range and therefore a tougher failure behavior then basalt. Basalt as typical brittle rock has almost no post-failure-range. Hence, the characteristic of brittle rocks is that destruction work W_z is almost equivalent to failure energy W_B (Fig. 82.2 left). This comparison illustrates that destruction work as single parameter is not sufficient for toughness characterization so that more factors have to be included. Determination of destruction work also depends on stiffness and settings of the used testing machine and can at worst vary a lot between different testing laboratories.

Ratio of plastic to elastoplastic strain ($\varepsilon_{pl}/\varepsilon_{el}$) is suitable for a first, vague characterization of toughness as they can be detected visually by stress-strain curves. The tested specimens show results for $\varepsilon_{pl}/\varepsilon_{el}$ from 0.05 (basalt) to 0.71 (anhydrite). As described in Chap. 2, these values are just an approximation because of subjective determination of the transition point σ_{cd} but show promising correlation results and have to be verified with volumetric strain measurements. Planned Acoustic Emission Tests can also define this point in a more detailed way so that an implementation in a prediction model is reasonable.

Figure 82.3 illustrates the results of 7 tested rock types with the UCS values and corresponding BTS as well as 110 test results from the rock data base of the Chair of Engineering Geology, TUM (Menschik et al. 2013). With a colored background, the classification of Schimazek and Knatz (1976) extended after Thuro (1996) is marked. Additionally the mean values of Basalt, Amphibolite and Anhydrite have been highlighted.

Tested **Basalt** samples show Z values of up to 28 and are classified as very brittle. This correlates to the failure behavior of Uniaxial Compression Test and analysis of the stress-strain curve in Fig. 82.2 left.

Amphibolite is commonly assumed to behave tough. To validate this assumption three different varieties of Amphibolite have been tested. Variety 2 and 3 show very high mean UCS values between 190 and 290 MPa. These samples derive from quarries and are used as ashlar. Amphibolite-1 is taken from a tunnel project and has lower quality (85–150 MPa). Contrary to the expectations, all amphibolite samples (except one) are not classifiable as 'tough'.

Anhydrite has Z values around 13, so according to the classification, it is called 'brittle'. Stress-strain curves (Fig. 82.2 right) in contrast show a distinct post-failure-range and a tough failure. Furthermore, all results in Fig. 82.3 (220

Fig. 82.2 Stress σ–strain ε curve of basalt (*left*) and anhydrite (*right*) as typical examples of brittle (basalt) respectively tough (anhydrite) rock failure behavior
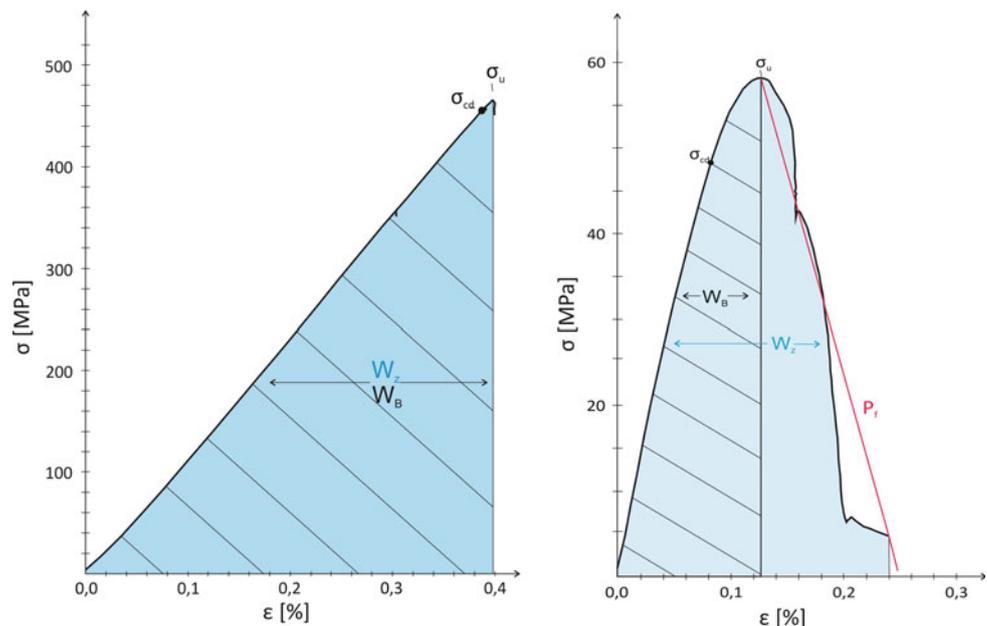
Fig. 82.3 Ratio Z (UCS/BTS) of analyzed rock types and results from TUM rock data base. Highlighted are Anhydrite/Basalt (typical example for tough/brittle) and Amphibolite. Results are plotted with the existing classification system of Schimazek and Knatz (1976), extended after Thuro (1996)
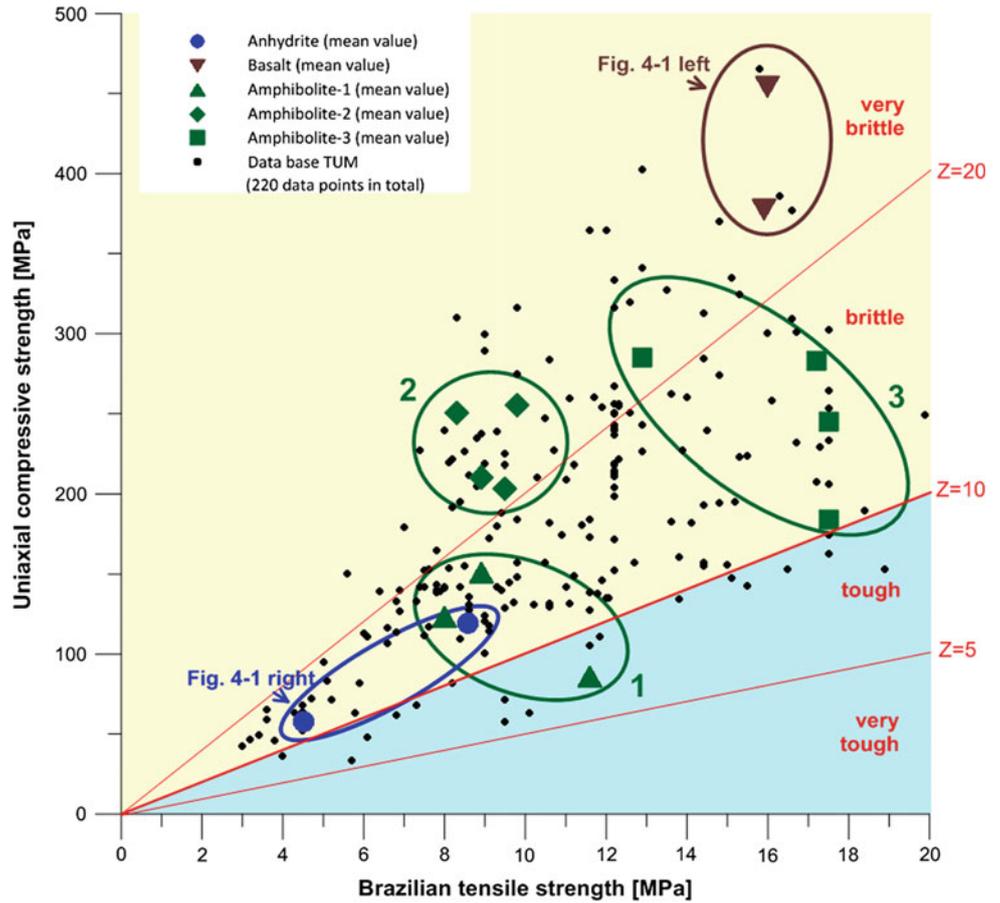
Fig. 82.4 Mean Z coefficient of analyzed rock types plotted against the ratio of destruction work to failure energy. Colored background describes post failure behavior at uniaxial compression test
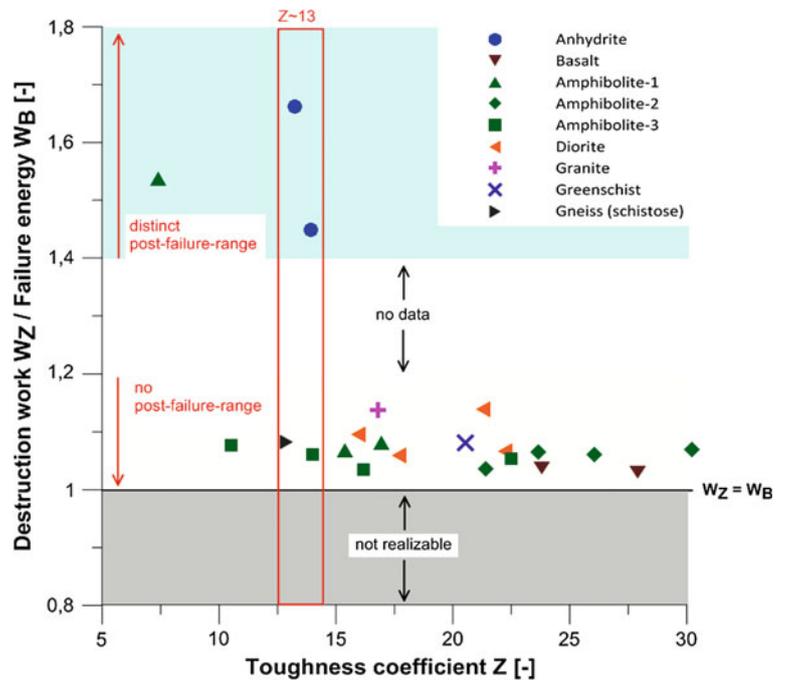
data points in total) reveal that only very few points are plotted in the classification field 'tough' or 'very tough'. These data points belong mainly to limestone with a high percentage of marl.

As the existence of a post-failure-range is one of the main characteristic of tough rocks, the ratio of destruction work W_z to failure energy W_B is illustrated in Fig. 82.4. Brittle rocks should have W_Z/W_B values of about 1 as W_Z is almost equal to W_B (Fig. 82.2 left). In contrast, values notably higher than 1 should define tough rocks as they have a significant post-failure-range ($W_Z \gg W_B$). The diagram demonstrates that 3 data points of rocks with a tough post-failure behavior do have a high W_Z/W_B value from 1.4 to 1.7. Mean Z values from all other rock samples range between 1.03 and 1.14. However, there is yet no significant trend visible that correlates low Z coefficients with high W_Z/W_B ratios. Z values around 13 show W_Z/W_B values from 1.1 to 1.7 depending on rock type (Fig. 82.4, red rectangle).

82.5   Conclusion

Most of the tested rocks had Z values higher than 10 and are classified as 'brittle' or 'very brittle' even if the stress-strain curve shows tough failure behavior. This demonstrates that the existing classification system of Schimazek and Knatz (1976) has to be revised and updated to get a better correlation with stress-strain curves. Moreover the Z values of one rock type (e.g. Amphibolite-1,-2,-3) vary a lot so that an implementation of the existing Z-coefficient into a prediction model seems unsuitable.

Additionally the investigations showed that the post-failure-range is a main characteristic of tough rocks. For a common classification, this part should be clearly described with values like the ratio of W_Z/W_B. However, these parameters have to be analyzed in detail with more rock types. Furthermore, an extended laboratory program with acoustic emission testing is planned to gain a better understanding of fracture propagation in rocks and therefore, a distinct determination of the transition point from elasto-plastic to plastic behavior.

The topic of rock toughness has not only significance for prediction models in tunneling but also for the industry. In the future, the laboratory results should also be transferred to breakability of rocks in quarry companies. Moreover, toughness defines fracture propagation in rocks. This is an important issue for understanding the mechanism of rock falls.

References

Becker H, Lemmes F (1984) Gesteinsphysikalische Untersuchungen im Streckenvortrieb. Tunnel 2:71–76

Eberhardt E (1998) Brittle rock fracture and progressive damage in uniaxial compression. PhD thesis, Department of Geological Sciences, University of Sasketchewan, Saskatchewan, 334 S

Gehring K (1995) Leistungs- und Verschleißprognosen im maschinellen Tunnelbau. Felsbau 13–6:439–448

Hughes HM (1972) Some aspects of machining. Int J Rock Mech Min Sci 9:205–211

ISRM (1978) Suggested methods for the quantitative description of discontinuities in rock masses. Commission on standardization of laboratory and field tests, Document No. 4, Int J Rock Mech Min Sci 15:319–368

Menschik F, Thuro K, Käsling H, Bayerl M (2013) Vorstellung einer Datenbank zur Dokumentation und Analyse von Labordaten sowie im Feld gewonnen Kennwerten. 19 Tagung für Ingenieurgeologie (Munich)

Schimazek J, Knatz H (1976) Die Beurteilungen der Bearbitbarkeit von Gesteinen durch Schneid- und Rollenbohrwerkzeuge. Erzmetall 29:113–119

Schneider E, Thuro K, Galler R (2012) Forecasting penetration and wear for TBM drives in hard rock—Results from the ABROCK research project. Geomech Tunn 5:537–546

Thuro K (1996) Bohrbarkeit beim konventionellen Sprengvortrieb. Münchner Geologische Hefte, München, 145 S

Wawersik WR, Fairhurst C (1970) A study of brittle rock fracture in laboratory compression experiments. Int J Rock Mech Min Sci 7:561–575

Stability Analysis of Accidental Blocks in the Surrounding Rockmass of Tunnels in Zipingpu Hydroelectric Project

Yanna Yang, Mo Xu, Shuqiang Lu, and Hong Liu

Abstract

Instable rock masses formed by structural plane boundaries can take great threaten to the underground tunnel excavation and the supporting structural stability. The boundary effect of structural planes in the rock mass should be considered during the underground tunnel excavation. The stability of the support system and rocks were determined by the preferred structural plane. Zipingpu key hydraulic project is located at Shajinba reach, upriver of Minjiang River, being built for agricultural irrigation and civil water supply. It also has integrative benefits such as preventing flood, generating electricity, environmental protection and tourism. Taking aim of stability analysis and assessment of surrounding rock mass of underground seepage tunnels in the right bank of Zipingpu hydraulic key project, and based on the survey and statistical analysis of structural planes of the diversion tunnels, structural rock mass discontinuity and the strength of fractured rock mass were studied in-depth, and three dominant directions of the structural planes included in the rock masses were divided through statistical analysis. Preferred structural planes were not long, randomly distributed distribution and extremely disadvantageous if they were connected as cutting or sliding block boundaries. The accidental rock masses were searched through the theory and method of slope rock block stability analysis system, and morphological property, stability and sensitive affected factors of them were analyzed. Rock masses which were prone to be damaged were identified and the length of the anchor bolt of the support system was designed.

Keywords

Structural planes • Accidental blocks • Stability analysis • Zipingpu hydroelectric project

Y. Yang (✉) · M. Xu (✉)
State Key Laboratory of Geohazard Prevention and Geoenvironment Protection, Chengdu University of Technology, Chengdu, Sichuan 610059, China
e-mail: yangyanna@cdut.cn

M. Xu
e-mail: xm@cdut.edu.cn

S. Lu
Hubei Engineering Research Center of Geological Hazards Prevention, China Three Gorges University, Yichang, Hubei 443002, China
e-mail: 381055335@qq.com

H. Liu
Chengdu Institute of Survey and Investigation, Chengdu, Sichuan 610081, China
e-mail: 123676858@qq.com

83.1 Introduction

One of the most important problems in tunnel excavation is to take the accidental falling of rock blocks that are formed by faults and discontinuities in the rock mass into consideration (Lee and Song 1998). Removability analysis of for falling of blocks falling should be conducted on the rock blocks based on a precise characterization of discontinuities in the rock masses around the tunnel. Analysis methods with more information about the block stability have been introduced since the block theory was suggested by Goodman and Shi (1985), which makes it possible to analyze the stability of rock blocks on slopes or around underground openings. This theory enabled us to test the combination of joint and to

Fig. 83.1 The site of Zipingpu water control project
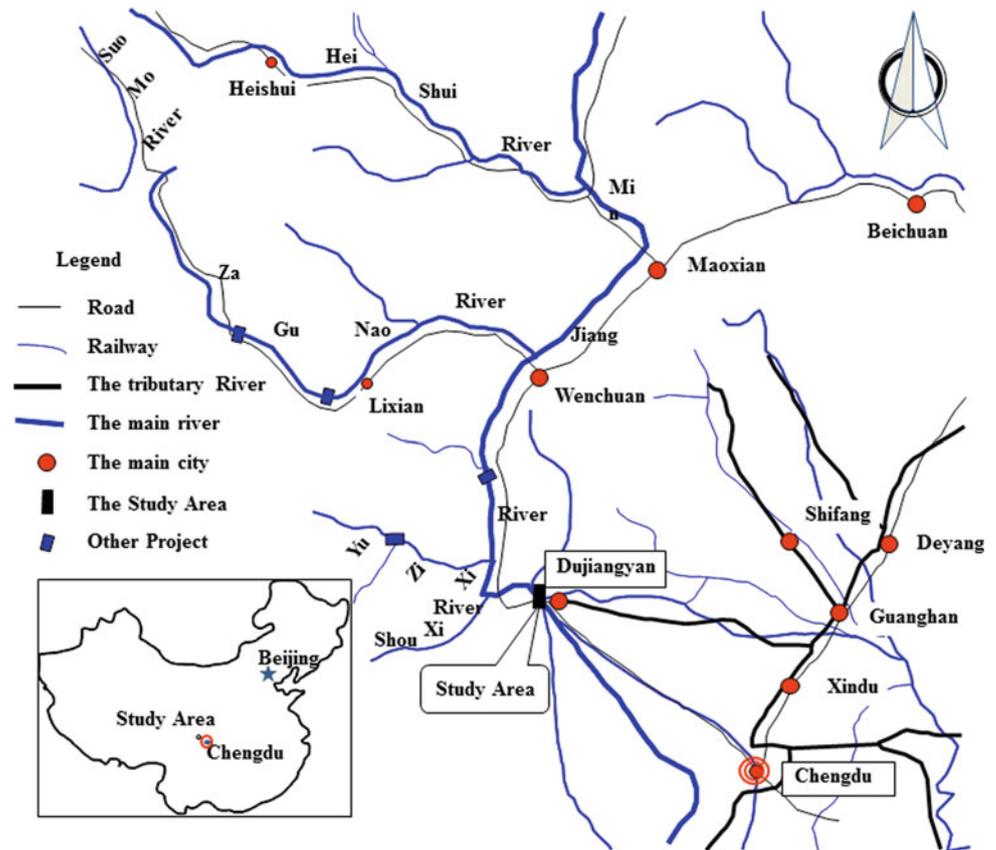
determine the safety factors of removable blocks with relatively simple and fast method because it uses only the orientation and friction angle of each joint set as the main input parameters. A three-dimensional statistical joint modeling technique was used to analyze the stability of rock blocks which were generated from the joints and the tunnels were analyzed for their volume, height, perimeter, safety factor, and probability of occurrence (Jae-Joon Song et al. 2001).

The natural stress field of the surrounding rock around the underground opening has changed during or after the excavation of the underground opening, and such a change brings instabilities or potential instable blocks to the original stable underground rock mass. The random blocks formed entirely by the mutual combination of random structural planes formed unknown relationship with position, scale and the underground project. The shape, number and scale of the random blocks in the surrounding rock were controlled by the layout of the underground project and the structural features of the rocks, while the stability of the random blocks was determined by the project characteristics of the rock, the stress state of the surrounding rock and the mechanical property of the structural plane. At present, the deterministic model and the generalized model of the surrounding rock structure and the research findings of the rock mechanical parameters, together with the openings (openings group) layout condition were mainly used to analyze the stability of

the blocks formed by mutual surrounding limitation of each level of structural planes. The evaluation for random block stability in the opening surrounding rock was based on geological investigation and exploration. For the surrounding rocks that generate special structural planes, block analysis method was used to find out the disadvantageous combination with other structural planes, and to determine the sliding direction, the sliding plane, the incision plane and the area of the incision plane, the possible volume and weight of the instable block (Ju 2005). Further, under gravity and the stress of surrounding rock, block ultimate balance theory was used to calculate the partial stability of the block assembled by structural planes, which provided proofs for the consolidating procedure. The evaluation method mainly included stereographic projection based on block theory, entity proportion projection, vector calculation method, etc.

Zipingpu water control project was located in Shajinba which was a section from the upstream of Minjiang River to Dujiangwan Weir river, 60 km from the northwest of Chengdu, Sichuan, China, and the downstream of this project was 9 km from Dujiangyan City (as Fig. 83.1 shown). This project was mainly for agricultural irrigation and civil water supply, as well as for integrative benefits such as preventing flood, generating electricity, environmental protection and tourism, and further, and it was a water adjusting project between the irrigation area of Dujiangyan and
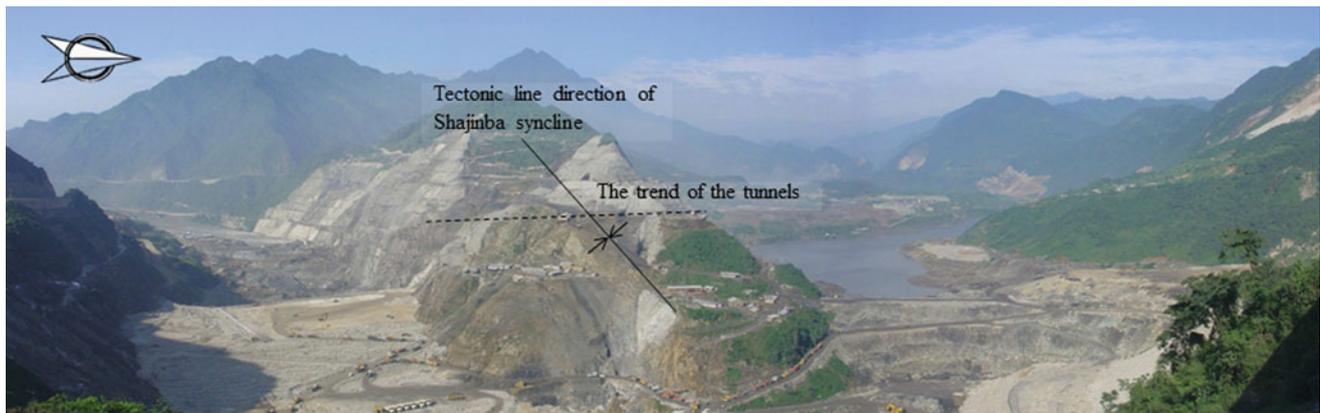
Fig. 83.2 The direction of the tunnels is intersected with the tectonic *line* of Shajinba syncline

Chengdu City. Zipingpu water control project was one of the key projects of infrastructure construction during China's Tenth Five Year Plan Period and also the landmark project in China's Development of the West Regions. After the reservoir was completed, it could play the role of adjustment in the period of high water flow and low water flow. Therefore it greatly relieved the water supply conflict between the irrigation area of Dujiangyan City and Chengdu City. This project had a 156 m-high dam, 877 m normal impounded level, 11.12×10^8 m³ total reservoir capacity and 760,000 KW installed capacity. The strip-like mountain ridge on the right bank of the project area took on north and east arc-strip shapes in the plane before the construction, with a length of more than 1,000 m, the width of the bottom being (with the waterside as the boundary) 400–650 m and the width of the top being (according to normal high water level) 50–250 m.

The strip-like mountain ridge on the right bank of the project area was a complete north-oriented and east-oriented pitched syncline—Shajinba syncline (as Fig. 83.2 shown). The sequences of the rock layers are normal, with no large fault going through. The bedrock was a typical flysch construction of are nacreous shale with coal of Xujiahe Group of upper Triassic Period. Still, the inside of the bed rock was mostly thick layered and hard fine packsand, with a small proportion of shale. The hydraulic structures in the project junction area were arranged within the strip-like mountain ridge on the right bank, including the ground factory buildings (four installations) behind the dam, open spillways adjacent to the right end of the dam, four underground openings that generate power by diverting water, one sand-washing underground opening and two flood-discharging and sediment-releasing underground openings transformed from two flow-guiding underground openings. Among these projects, the four underground openings that generate power by diverting water were respectively 1#, 2#, 3#, 4#, and they were sequentially arranged from the mountain to the outside of the mountain. The thickness of the rock wall between the two underground openings that generate power by diverting water was 12–12.5 m. The maximum thickness of the two adjacent underground openings was increased to about 40 m after vertical three-dimensional intersection evacuation. The direction of the opening axis was intersected with the angle of the rock layer direction, and the geological conditions passed through by them are quite similar. The stability analysis of the random block masses was very important for the integral and partial stability researches of the surrounding rock of the opening under the highly intensive project layout and the special surrounding stress field.

83.2 Methodology

In the design period of the Zipingpu water control project, it had started from the angle that the intensity of the redistributed surrounding stress of the underground opening project being the lowest and the number of the blocks being the fewest, and it was best for the integral stability of the opening groups, and the best trending direction of the underground opening groups axis was integrally analyzed and optimally determined as NE25°. After the project layout and the opening scale were fixed, "window technique" (or network measuring method, usually 2×2 m²) to track were used to investigate and measure different types of structural planes shown in the construction field surrounding rock, and make fisher cluster analysis to determine the level of the advantageous structural planes and the main development direction in the surrounding rock of the openings. Next, according to the development scale, intensity, shape and the project property of the openings in the practically measured structural planes, equatorial horizon projection and entity proportion projection methods were adopted to search all the possible structural planes one by one in the underground opening areas, and then all the random blocks, their shapes and scales were obtained. Further, mobility theory was used to determine the formed and potential mobile blocks.

Underground-opening sidewall block stability analysis program USASW (Ju 2005) worked out by State Key Laboratory of Geohazard Prevention and Geoenvironment Protection (Chengdu University of Technology) was used to make a fast evaluation about the stability of the surrounding rock blocks of the openings to effectively improve the safety of construction and optimize the design for system roof bolt.

As the excavation face height of the underground opening of the project was only 8–9 m, and the width is 12 m, the possibility that the top of the opening forms large-scaled mobile blocks was very little. The formed small-scaled blocks had a little effect on the stability of the openings, and such an effect could be omitted in analyzing the blocks on the top arch of the opening.

83.3 Results

83.3.1 Development Characteristics of Structural Planes of Dominant Group and the Shear Resistance Index Value

According to the project geology grading in the structure investigation, there was no type I fault-zone structural plane developed in the investigated openings. Type II and type III structural planes were mainly fault zones and interlayer compressive zones made of some shuttered zones or soft materials. Generally, the direction was clear and could be regarded as deterministic structural plane. Types IV and V fissure structural planes developed in the surrounding wall were the main boundaries to cut surrounding rock to form random blocks, and the IV and V fissure structural planes including the structural planes developed along the sandstone level, the long and big cut-layer structural planes developed in the vertical level and a number of matrix fissures developed randomly. The IV and V fissure structural planes were used as the main objects for measuring in the use of statistical method. The structural planes shown in the surrounding rock of the four underground openings that conduct water were precisely measured, and 1,400 pieces of detailed information about the fissure were gained. The results of the fisher cluster analysis displayed that there were four dominant groups of structural planes developed in the surrounding rock of the underground opening groups of the Shajinba syncline, and the properties of the structural planes were shown in Table 83.1. Referring to existed rock physical mechanics testing result, shear resistance index value of the structural plane was gained. From the perspective of safety, the cohesive strength value C of the shear resistance index in the structural plane was 0, because the structural planes in the inlet and outlet of the openings had many argillized interlayers and low cohesive force.

83.3.2 Stability Evaluation of Random Blocks

The structural planes developed in each opening gained in the investigation of practical field geology were combined with each other. Corresponding occurrences and parameters of possible sliding plane, cutting planes of the top surfaces and sliding boundary planes were put into the analysis program of the underground opening block stability. Through calculation, the geometrical shape, volume and stability coefficient of the blocks were gained. The axis orientation of the underground opening group was 132º. The side walls of the upstream and downstream were nearly vertical when the block was determined and the block stability was calculated. The occurrence of the sidewall on the right wall was $N48ºW/NE\angle90º$ and on the left wall was $N48ºW/SW\angle90°$. Image theory was used to determine the development and distribution of the sidewall blocks on the left and right walls.

The calculation and analysis results showed that the left wall of the underground opening group inlet at the syncline NW side did not form blocks easily, and the right wall possibly formed instable blocks, with most of the blocks being sliding planes with low stability which was only 0.283. Instable blocks were possibly formed on the left and right walls of the underground opening group inlet at the syncline SE side. The left wall of the opening was mostly intersected with the opening-oriented at small angles. The structural plane trending towards the exposure surface was the sliding surface whose stability coefficient was only 0.233. For the right wall of the opening, the dual sliding surface was formed by the orthogonal intersection between the bedding layers whose stability coefficient was 1.065. The volumes of the instable blocks were not too large to form serious hazards to the construction and support designs of the underground. The geometric shape of the block didn't vary greatly with the gap changing of the structural plane, and its stability was irrelevant to the gap of the structural plane.

The distribution and stability of blocks in different parts of the underground openings were shown in the Table 83.2. As it could be seen, the instable blocks distribution density gradually reduced from the inside of the ridge to the outside. The proportion of the number of the instable blocks of each opening in the total number was approximate. The volumes of the instable blocks were not large. The maximum thickness of the instable block was 9.03 m, and the minimal was about 1.5 m.

For the blocks formed randomly by types IV and V structural planes, the method of combining system anchor rod with reinforced anchor rod was preferable. The maximum thickness of the instable block was 9.03 m. The random blocks could be anchored by 8–12 m system anchor rod.

Table 83.1 The dominant groups of structural planes developed in the surrounding rock of the underground tunnels of Shajinba syncline and their shear resistance index value

Serial number	Occurrence	Position in the project	Property of the structural plane	Index of shear resistance for structural surface		
				Friction coefficient (f)	Internal friction angle φ(°)	Cohesive force C (MPa)
IV bedding fissure	N7°E/SE∠54°	The inlet section of underground opening at syncline NW	The bedding fissures mainly develop in the inlet and outlet of the underground opening groups and the two edges of the syncline. The maximum occurrence inclination angle in the NW side reach about 70° and the largest occurrence inclination angle in the SE side is 85°.	0.40 ∼ 0.45	18 ∼ 22	0
IV bedding fissure	N76°E/NW∠45°	The outlet section of underground opening at syncline SE	The clearer the fissure is to the core, the even the inclination angle is. The angle is only 25° in the core of the syncline. The extending length is more than 10 m, going through the three walls of the opening, flat and smooth. The openness degree is varying from 50 to 100 mm, and parts of the fissures are filled with some secondary interlined soil and some calcites. The fissures are distributed with some argillite interlayers. The gap in the medium and fine sand of the fissures is 0.3–06 m, with the largest gap being 2 m	0.40 ∼ 0.45	18 ∼ 22	0
IV bedding fissure	N30°E/NW∠34°	The inlet section of underground opening at syncline NW	The variation of the occurance is large. The extension length is more than 10 m, going through the three walls of the opening, flat and smooth. There is no filling in the structural plane, with most of the planes being closed. The gap among the fissures is 0.4-0.6 m. The gap is only about 0.15 m when the development is intensive	0.50 ∼ 0.55	22 ∼ 24	0
	N32°E/SE∠70°	The outlet section of underground opening at syncline SE		0.50 ∼ 0.55	22 ∼ 24	0
V matrix (randomly) structural plane	N60° ∼ 85°W/ SW∠54° ∼ 70°	The inlet and outlet of the underground opening groups and the two edges of the syncline	They develop randomly, with great variation in occurance and property. The trace length on the opening wall is 3–8 m around, with a small number being more than 20 m. The plane is flat and a little rough. Some of the planes have secondary soil, sandstone detris, shed coal, etc. The cohesive degree is low, and the openness is 2–5 mm. The gap among the fissures varies largely, with 0.2–0.6 m averagedly among the medium and fine sandstone, and part of the powder sandstone being more than 1 m. As the direction of the structural planes are approximately parallel to to axis of the opening, the effect on the partial stability of the opening is large	0.55	24	0

Table 83.2 Distribution and stability analysis of the accidental rock masses of the tunnels in Zipingpu hydroelectric project

Tunnel NO.	Length of the opening investigated (m)	Number of the blocks		Volume of the instable block (m^3)		The minimum value of the stability	The maximum thickness of the instable block (m)
		Total number	Instable number	Maximum value	Minimum value		
Tunnel 1$^{\#}$	271	8	4	7.26	0.09	0.222	9.03
Tunnel 2$^{\#}$	305	7	3	4.79	1.22	0.249	7.9
Tunnel 3$^{\#}$	236	6	3	0.19	0.4	0.188	1.44
Tunnel 4$^{\#}$	262	1	1	13.1	13.1	0.327	7.57

83.4 Discussion

In the design of underground opening group of the strip-shaped ridge on the right bank of Zipingpu water control project, although the instability of blocks in construction had been taken into consideration, it was still possible that there were unknown control large-scaled blocks formed by types IV and V random structural planes with types II and III deterministic structural planes due to the condition limitations in the geological investigation.

References

Goodman RE, Shi G (1985) Block theory and its application to rock engineering. Prentice-Hall, Englewood Cliffs, p 338

Ju N (2005) Systematical engineering geological study on the stability of surrounding rock mass with large span high side-wall underground caverns and their support proposals. PhD thesis of Chengdu University of Technology(in Chinese)

Lee C-I, Song J-J (1998) Stability analysis of rock blocks around a tunnel. In: Proceedings of 3rd international conference mechanical jointed faulted rock (MJFR3), pp 443–448

Mc Cullagh P, Lang P (1984) Stochastic models for rock instability in tunnels. J R Stat Soc B 46 Ž2 pp 344–352

Song JJ, Lee CI (2001) Estimation of joint length distribution using window sampling. Int J Rock Mech Min Sci 38:519–528

Engineering Geological Problems Related to Geological Disposal of High-level Nuclear Waste

Convener Prof. Weimin Ye—*Co-conveners* Yujun Cui, S. Tripathy, Xu Yongfu, Tang Chaosheng, Yonggui Chen

The ultimate disposal of high-level nuclear waste (HLW) requires their isolation from the environment for a long time. The most favoured method is burial in stable geological formations more than 500 metres deep. In order to ensure the safety of such a disposal system for a long time (generally recognized as 10 000 years), issues related to the engineering geological properties of host geological formations and buffer/backfill materials have been widely investigated in the world. This session will offer a multidisciplinary platform for researchers to exchange current achievements made in their investigations on host geological formations, groundwater, buffer/backfill materials, etc., of the geological repository.

Feasible Study of the Siting of China's High-Level Radioactive Waste Repository in an Area of Northwest China

84

Yuan Gexin, Zhao Zhenhua, Chen Jianjie, Jia Mingyan, Han Jimin, and Gao Weichao

Abstract

With the fast development of national nuclear industry, it is extremely urgent to disposal the high-level radioactive waste (HLW) properly. Aqishan area lies to the south of Turpan in Xinjiang Province. As one of the important candidate sites for China's HLW repository, it has many potential advantages, such as arid climate, water poverty, sparse population, large-scale granite body, and high crustal stability. The preliminary work proves that: (1) Granite batholith is widely distributed over the Aqishan area, which had formed in Late Hercynian—Early Indosinian period, with a thickness of over one thousand meters; (2) The Aqishan area is in a state of peneplain, with the latest fault activity in Middle Pleistocene and the seismic intensity of VI degree; (3) The total dissolved solids (TDS) of groundwater is up to 100 g/L because of high evaporation intensity, and the isotope data indicate that the groundwater is mainly recharged from atmosphere precipitation. Through an overall evaluation of the Aqishan area, it is found to be the feasible site for China's HLW disposal.

84.1 Introduction

Disposal of high-level radioactive waste (HLW) is generally implemented by deep geological disposal (Min 1998). Geological disposal stores long-lived radioactive materials in a stable geological repository, a geological unit which is required to remain stable for tens of thousand years. In this way, the risk of accidental waste exposure caused by human or natural disturbance can be reduced to a significantly low level. The principles for siting of an HLW repository mainly include sparse population; stable geological condition with no mineral resources; and host rocks with sufficient thickness and area, simple hydrogeological environment, low porosity, high thermal conductivity, great mechanical strength, and high thermal and radiation stability. According to the *Guideline of Site Preselection for HLW Repository* issued by the Commission of Science, Technology and Industry for National Defense and in view of the favorable factors such as non-permanent residents, arid climate, and large granite pluton in a northwest region, the granite zone in Aqishan area of northwest China is presently thought to have potential advantages for building a geological HLW repository in terms of climatic condition, geographical environment, granite pluton distribution, water resource distribution, crustal stability, and HLW safety management.

In this study, comprehensive geological studies have been focused on the large intact Xianshuigou granite pluton in this region. Surface geological mapping, seismic method, and transient electromagnetic exploration, combined with rock fracture statistics and engineering property testing, are used to study the distribution of granite pluton and the characteristics of rock minerals, as well as the lithology of surrounding strata; structural characteristics and integrity of granite pluton; and the morphology and type of deep granite

Y. Gexin · Z. Zhenhua (✉) · C. Jianjie · J. Mingyan · H. Jimin · G. Weichao
Northwest Institute of Nuclear Technology, 710024 Xi'an, China
e-mail: starzzh@gmail.com

Z. Zhenhua
Nanjing University, 210093 Nanjing, China

pluton. Associated hydrogeological characteristics are analyzed with relevant topographical and surface-water chemical data and groundwater isotope values; regional crustal stability is evaluated according to the characteristics of tectonic movement combined with those of seismic activity and geophysical field within and surrounding the northwestern region; the Quaternary geology and climate—environment change trend are evaluated by surveying the periods of regional tectonic activity and the characteristics of paleo-environmental evolution.

84.2 Traffic, Physical Geography, and Society

The northwest region is located in southeast Turpan, Xinjiang Uygur Autonomous Region. This region is approximately 160 km distant from Turpan City. The West-East Natural Gas Transmission Pipeline crosses the north part (Fig. 84.1) and connects to Dikaner County via a Class III highway. The terrain is relatively flat and most areas are reachable with vehicles.

Topographically, there are mainly denuded hills and plains in the northeastern region. The altitude of the flat terrain is 1050–1150 m above sea level. The climate is arid and water sources are lacking. The drainage system is poorly developed with no permanent runoff. Annual precipitation is 20–60 mm and the total precipitation time is less than 20 days. Annual average evaporation capacity is up to 2250–2900 mm. There are no permanent residents. To solve water shortage problems, domestic water is generally supplied from other regions.

84.3 Geological Characteristics of Xianshuigou Granite Pluton

There are mainly five granite zones surrounding the Aqishan area, which are generally composed of Middle—Late Variscan and Indosinian intrusive rocks with a total area of approximately 1200 km^2. The present survey focuses on Xianshuigou granite pluton, a regular oval-shaped pluton with an area of approximately 300 km^2. Few dykes are developed in the granite zone, which exert less impact on the integrity of pluton.

In the Late Carboniferous—Permian period, Tarim and Junggar plates collided; associated independent intrusions and regional dykes from different sources were widely distributed. In the Permian period, regional curst was uplifted due to NS extrusion; ductile crust below the uplift belt underwent selective melting due to the reduction of pressure (caused by the uplift of brittle crust) and the increase in heat energy (transformed from kinetic energy of tectonic movement); then, molten magma was uplifted and localized in the NE-SW-trending fracture zone after differentiation, leading to the formation of Xianshuigou granite pluton (Xinjiang Bureau of Geology and Mineral Resources 1997).

According to the results of remote sensing, aeromagnetic interpretation, and field geological survey, Xianshuigou granite zone mainly consists of four intrusions (Fig. 84.1). The outcropped sedimentary strata consist of hornfels and skarns of the Lower Carboniferous Gandun Formation and alluvial gravel and alluvial aeolian deposits of the Quaternary Holocene strata. Flesh red medium-grained syenogranite
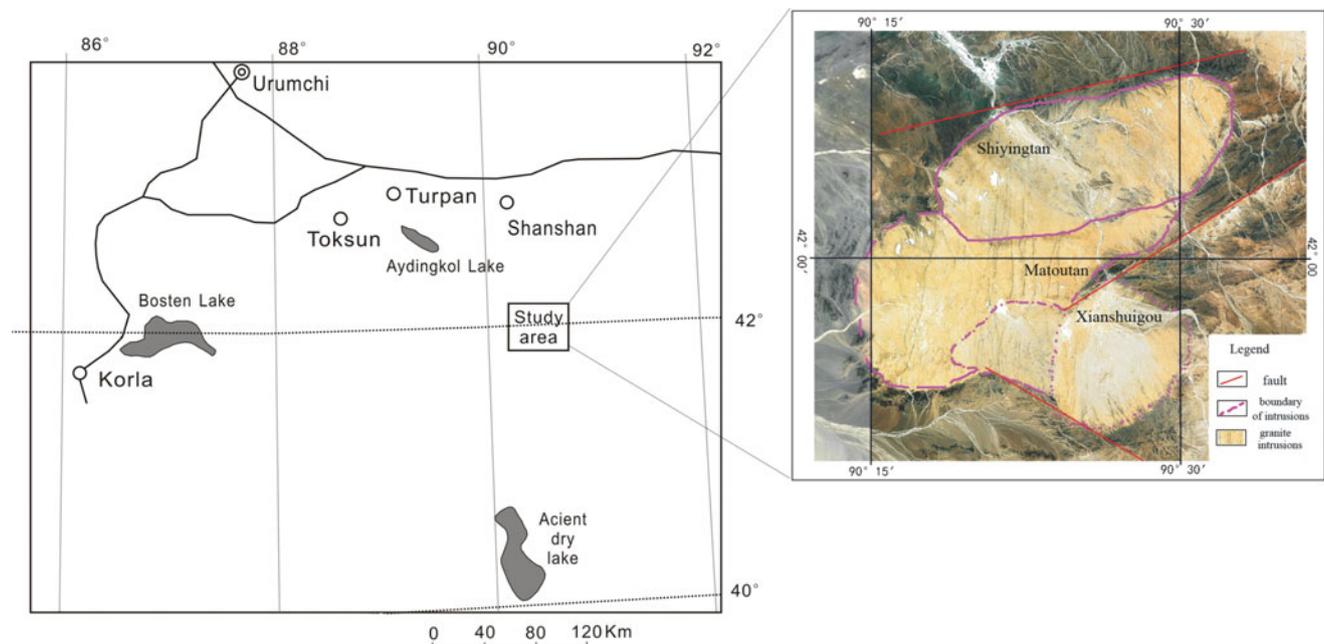
Fig. 84.1 Sketch map of the location of granite pluton in the area

Fig. 84.2 Resistivity profile of Xianshuigou granite pluton determined by transient electromagnetic method
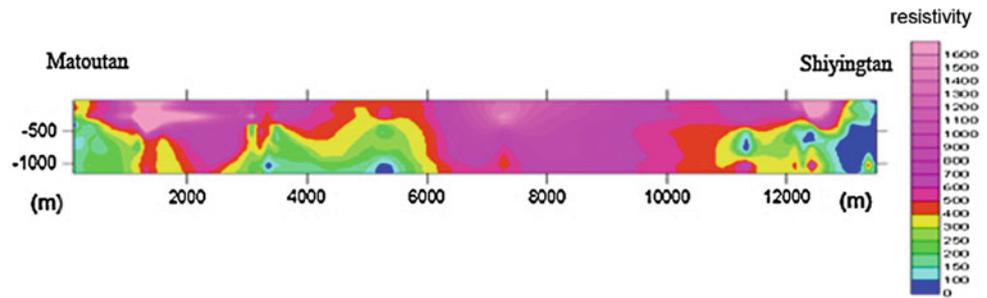
forms the pluton with strongest γ-ray spectrum field in the whole zone. In the granite rock outcrops near Xianshuigou, the latest strata intruded are Lower Permian strata with the zircon U-Pb isotopic age of 200.1 Ma (Xinjiang Bureau of Geology and Mineral Resources 1997). Together the characteristics of geophysical field reflected by the pluton, we preliminarily identify Xianshuigou granite pluton as Early Indosinian intrusive rocks (according to *prospecting report of Xianshuigou granite zone*, 2004).

The development of internal fault in Xianshuigou granite pluton is explored with an ATEM Transient Electromagnetic System. The exploration profile is 600 m long and nearly EW trending, with depth inversion at 200 m. The resistivity is high in the upper part of the profile, which decreases with increasing depth. Within the depth of 150 m, the resistivity is greater than 1000 Ωm and shows even electrical distribution. The electric property is evenly distributed with no substantial changes in the horizontal direction. There are no abnormal segments with abrupt vertical changes. No anomalies of fault structure are found in the profile.

The morphology of granite pluton on the plane is investigated by remote sensing-based geological interpretation and site exploration; the vertical morphology of deep pluton is explored mainly using transient electromagnetic technique and shallow high-resolution seismic reflection wave method.

Through the exploration with transient electromagnetic (Fig. 84.2) and seismic methods and comparative interpretation of geological profile, we propose that the pluton may belong to large-scale granite batholith; there may exist underlying strata at 400–900 m depth of the granite pluton at 4–5 km north of Matoutan; there are no large fractures within the granite pluton; and the thickness of the granite pluton is greater than 1000 m.

84.4 Hydrogeological Conditions of Xianshuigou Granite Zone

Xianshuigou granite pluton is located in an area with a typical continental climate, dry weather and less rain, windy spring and autumn, and large temperature difference between day and night. There is no perennial water; all valleys are seasonal ravines which only have temporal floods flowing after rainstorms; the evaporation is rapid.

The major type of groundwater within the pluton is bedrock fissure water. Due to insufficient supply, granite fissure water is lacking. According to the *1:500000 regional hydrogeological survey report of Shanshan—Aqishan region* (1978), groundwater has been drilled in the north at the depth less than ten and a few meters; the unit water inflow is 19 m³/d, and groundwater salinity is 33.31–125.27 g/l, i.e., saline–brine water.

Topographically, the study area is high in south and low in north, with surface runoff flowing toward a northwest lowland, Aydingkol Lake (Fig. 84.3). There is no perennial surface runoff. Groundwater recharge completely depends on the infiltration of atmospheric precipitation, i.e., non-continuous supply. This area is arid with less rain; average annual rainfall is 20–60 mm only, mostly concentrated in summer; temporary surface floods are commonly formed after occasional storms.

In the arid and hot climate, annual evaporation is a hundred times more than precipitation. Thus, groundwater discharge is dominated by evaporation in this region.

Stable hydrogen (δD) and oxygen (δ¹⁸O) isotope data of groundwater indicate that the source of groundwater recharge is infiltration of atmospheric precipitation. The δD-δ¹⁸O relationships of groundwater samples from different areas are compared. As compared to those from the central area, water samples from the south and north margin of Kuruketage Mountains have small δD/δ¹⁸O slope, indicating that groundwater migrates from the center area to two sides.

84.5 Crustal Stability

Regional crustal stability is evaluated by analyzing the data of regional geophysical field, deep fault zone, seismic activity, and neotectonic unit division, combined with the results of field geological survey.

An average Bouguer gravity anomaly map compiled by the Geophysical Exploration Team of Xinjiang Bureau of Geology (1983) shows that there is a nearly EW-trending gravity anomaly in the south of the study area whose

Fig. 84.3 3D terrain map of study area
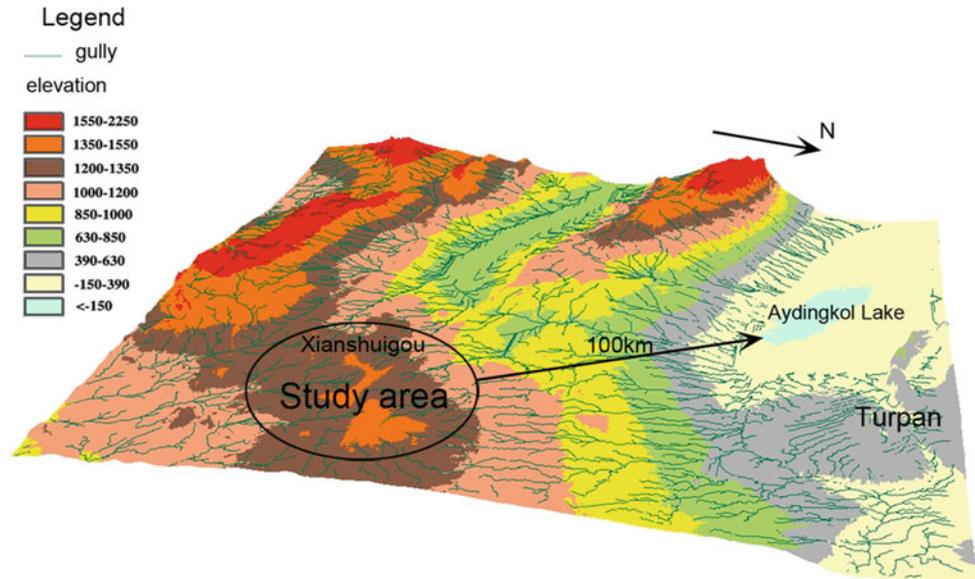
amplitude is $(-110 \text{ to } -170) \times 10^{-5}$ m/s^2. The study area is situated in a nearly EW-trending gravity gradient wide—gentle zone with the amplitude of $(-120 \text{ to } -130) \times 10^{-5}$ m/s^2; this indicates that there is no large faults crossing this area. According to the 1:50,000 regional aeromagnetic ΔT plane anomaly map of Xinjiang (1989), the aeromagnetic anomaly is wide and flat, indicating that the geological body is homogeneous in the granite zone. According to the Moho depth contour map (1997) in *Xinjiang Geological and Mineral Chronicles*, the study area is located on the margin of an EW-trending gradient zone; the crust thickness is 46 km which changes smoothly.

As shown in the regional epicenter distribution map (Fig. 84.4), Xianshuigou granite pluton lies in the north of Aqikekuduke fault (Fig. 84.4, No.1) where seismic events are relatively rare and the earthquakes are generally less than magnitude 5.0. As shown in the seismic intensity map of Xinjiang, the seismic intensity of the study area is magnitude VI. Overall, the study area is associated with weak seismic activity.

There are mainly two regional deep faults developed around the study area (Fig. 84.4), mostly thrusting strike-slip or reverse faults. Ophiolite, mictite, and acidic granite are distributed along the faults.

Aqikekuduke fault (Fig. 84.4, No.1) is approximately 30 km south to the study area. This fault is NW-EW-NE trending and more than 1400 km in full length. It is overall south-dipping at 50°–80°, as classified as a dextral strike-slip and reverse fault. In the south of the study area, the profile of the fault shows that a gravel layer overlies the fault zone. Thermoluminescence dating samples collected from the find sand lens of sand—gravel layer are estimated to be (143.70 ± 12.21) ka BP (according to *regional crustal stability report of northeast of Korla*, 2010). According to the profile, Bolokenu—Aqikekuduke fault has never been active since the Late Pleistocene period, thus belonging to Early—Middle Pleistocene fault.

Yamansu fault (Fig. 84.4, No.2) is approximately 40 km north of the study area, part of which is associated with pluton emplacement. Regionally, this fault is nearly EW

Fig. 84.4 Regional network distribution of earthquake epicenters (January 1970–2005, M ≥ 2.5)
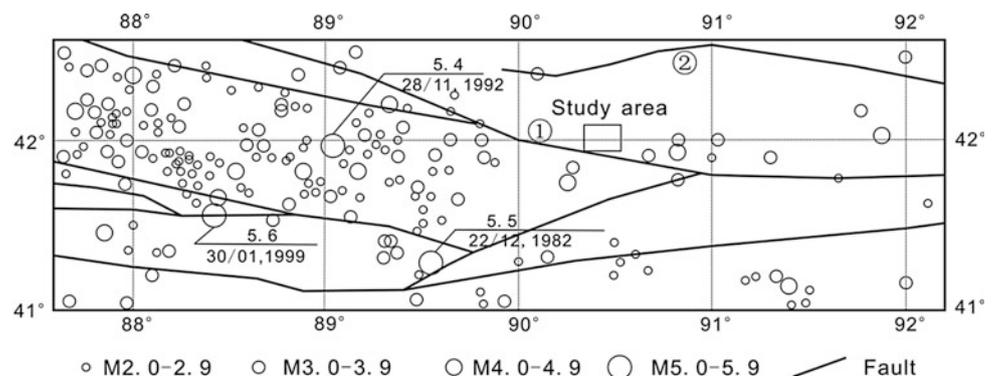
trending and extends in a soothing wavy pattern. It is generally north-dipping at 60°–70° and belongs to high-angle thrust fault, i.e., brittle—ductile fault. This fault does not dislocate the Middle—Late Pleistocene strata. Therefore, Yamansu fault is identified as an Early Pleistocene fault.

Together the above results indicate that the study area is located in a granite zone with less aeromagnetic anomalies, no abnormal abrupt changes in the EW distribution, and wide—gentle gravity gradient. This area is located in a crustal structure on the margin of an EW-trending gradient belt, which has relatively simple structure with no large faults. The study area lies in a slight uplift zone with weak seismic activity and low seismic intensity (<VI). That is, the neotectonic activity is weak and regional crust is relative stable in the study area.

84.6 Preliminary Assessment

In the northeastern region, Xianshuigou granite pluton belongs to early Indosinian intrusive rock; this pluton is affected by post-tectonic movement to a relatively low degree; there are no large faults in the pluton, with few faults and dykes developed only; the geological repository has complete surrounding rock mass, high engineering strength, and uniform stable engineering performance. Xianshuigou granite pluton is of batholith type, whose thickness is generally greater than 1000 m. The granite pluton has an area of more than 300 km^2, providing enough space for engineering disposal. Regional structure has little impacts on the pluton. The geophysical field is relatively stable and the seismic activity is weak, with seismic intensity of magnitude VI. Therefore, the preselected site is a relatively stable area conducive to long-term storage of HLW. The northeastern region is a water-poor area where the arid climate and pluton characteristics prevent the infiltration of surface precipitation. Therefore, the water system has little impact on the repository. The groundwater flow path is quite long, approximately 100 km to Aydingkol Lake in the northwest direction.

Overall, the northeastern region has good prospects as a preselected area of geological repository for HLW disposal.

Future feasibility study of the northwestern region as a preselected area of geological repository for HLW disposal needs to investigate the lithological evolution and distribution patterns of deep granite pluton; combined with geophysical data, more deep drillings should be carried out.

References

Min M (1998) Principles of the disposal of the radioactive waste [M]. Atomic Energy Press, Beijing

Xinjiang Bureau of Geology and Mineral Resources (1997) Regional geology of Xinjiang Province [M]. Geology Publishing House, Beijing

A New Apparatus for the Measurement of Swelling Pressure Under Constant Volume Condition

85

C.S. Tang, A.M. Tang, Y.J. Cui, P. Delage, and E. De Laure

Abstract

A new constant volume cell was developed, allowing the measurement of swelling pressure without any strain adjustment and any effect of the stiffness of the testing device. By employing this new cell, the swelling behavior of compacted soil specimen under different suctions (57, 38, 9 and 0 MPa) was investigated. The results show good repeatability, indicating the reliability of the new cell and validating the test procedures adopted. Moreover, the developed cell is quite convenient to study the long-term swelling behavior of soil since no load adjustment is necessary. The obtained results show that, during the progressive wetting by applying successively the suctions of 57, 39, 9 and 0 MPa, the swelling pressure increases to 0.17, 0.31, 0.46 and 0.89 MPa, respectively. The swelling pressure and the time required to reach equilibrium are function of suction. Vapour-wetting and water-wetting show different hydration mechanisms and result in different swelling behavior: the swelling pressure develops slowly and gradually to finally reach stabilization upon vapour-wetting, while it increases quickly to a peak value and followed by a small decrease upon water-wetting.

85.1 Introduction

Expansive soil is a "problematic" soil, and widely distributes in many regions in the world. Generally, the parameter of swelling pressure is commonly employed to characterize the swelling properties of expansive soils (Shi et al. 2002). In the past decades, swelling pressure was defined in many ways and the measured value depends significantly on the test procedures adopted (Bilir et al. 2008).

The constant-volume swell test is one of the popular methods for measuring the soil swelling pressure. It is usually performed through strain-controlled technique in the laboratory (Tripathy et al. 2004). There are two common strain-controlled techniques: (1) applying small incremental load to compress the specimen to bring its height to the initial value as the specimen begins to swell upon wetting. Once the swelling pressure reaches equilibrium, the final applied total load is regarded as the swelling pressure (Al-Shamrani and Dhowian 2003); (2) restraining the specimen

C.S. Tang (✉)
School of Earth Sciences and Engineering, Nanjing University, Hankou Road 22, Nanjing, China
e-mail: tangchaosheng@nju.edu.cn

C.S. Tang · A.M. Tang · Y.J. Cui · P. Delage · E. De Laure
Ecole des ponts—ParisTech, U.R. Navier/CERMES, 6-8 av. Blaise Pascal, Cité Descartes, 77455, Marne-la-Vallee, France
e-mail: anhminh.tang@enpc.fr

Y.J. Cui
e-mail: yujun.cui@enpc.fr

P. Delage
e-mail: delage@cermes.enpc.fr

E. De Laure
e-mail: delaure@cermes.enpc.fr

vertical movement by a rigid reaction frame. The rigid frame reacts against the sample through a high capacity load cell, which was used to measure the swelling pressure of soil sample (Aiban 2006). However, in practice, to obtain or ensure a strict constant-volume condition is not of easy task. For the former technique, each incremental load corresponds actually to a compression on the specimen, and may result in the specimen's structure changes in each cycles of swelling-compression. Moreover, in order to compress to the initial volume, the applied load should overcome the friction between specimen and oedometer/ring wall, resulting in higher measured swelling pressure. For the later one, Tang et al. (2011) found that the "constant-volume" was significantly dependent on the stiffness of the load cell and test equipment, and the measured swelling pressure error can reach 1–2 MPa.

For the purpose of improving the measurement accuracy of constant-volume swell test, a new apparatus was developed. The details of the apparatus and test procedure in controlling the constant-volume condition are presented in this paper. Using this apparatus, swelling tests over a wide range of suction were performed and the obtained results were discussed.

85.2 Development of New Constant Volume Cell

For better controlling the constant-volume condition in swelling tests, a new constant volume cell was developed and illustrated in Fig. 85.1. This cell mainly consists of three stainless steel parts: top, middle and bottom parts. The pressure sensor used to measure the swelling pressure was fixed inside the top part and directly in contact with the top surface of the soil specimen. The cylindrical soil specimen (70 mm in diameter and 10 mm in height) was placed inside the middle part. A porous stone was placed on the bottom part and in contact with the bottom surface of the soil specimen. Two inlets in the bottom part ensured the circulation of water (liquid or vapor) for the suction control. In

addition, two outlets of the middle part ensured the water/vapor evacuation from the top surface of soil specimen.

85.3 Material Used

The soils used were taken from Bure (North-eastern France). It contains 40–45 % clay minerals (illite–smectite interstratified minerals being the dominant clay minerals), 30 % carbonates and 25–30 % quartz and feldspar. The specific gravity of this material is 2.70. The obtain soil was air-dried (w = 2.8%) and crushed to powder. The aggregate size distribution after crushing determined by dry sieving is presented in Fig. 85.2.

85.4 Experimental Method

The air-dried soil powder was statically compacted in the middle part of the constant-volume cell to the target dry density of 2.0 Mg/m^3. The specimen size is 70 mm in diameter and 10 mm in height. A total of three identical soil specimens, T1, T2 and T3, were prepared. The initial suction of the specimen was at about 100 MPa (air-dried). After compaction, the three parts of the cell were fixed together by screws (Fig. 85.1a).

In the present work, swell tests were performed at different suctions (e.g. 57, 38 and 9 MPa). The experimental setup is shown in Fig. 85.3. During the test, suction was controlled by the vapor equilibrium technique using various saturated salt solutions. An air pump was used to ensure the vapor circulation in the system. The swelling pressure was recorded automatically using a personal computer. Considering that the relative humidity imposed by given salt solution is highly dependent on temperature, the room temperature was maintained at 20 ± 0.5 °C. For specimen T1, a suction of 57 MPa was initially applied. After the equilibrium was reached, a subsequent wetting was applied by a suction of 38 MPa. For specimen T2, the same procedure as that of T1 was applied to investigate the repeatability of the test. For specimen T3, a suction of 9 MPa was
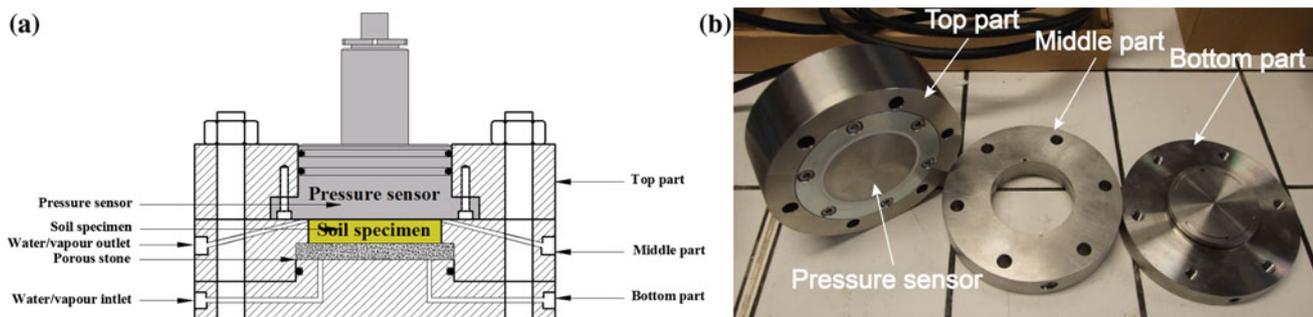
Fig. 85.1 **a** Schematic diagram of the constant-volume cell; **b** picture of the three parts of the constant volume cell
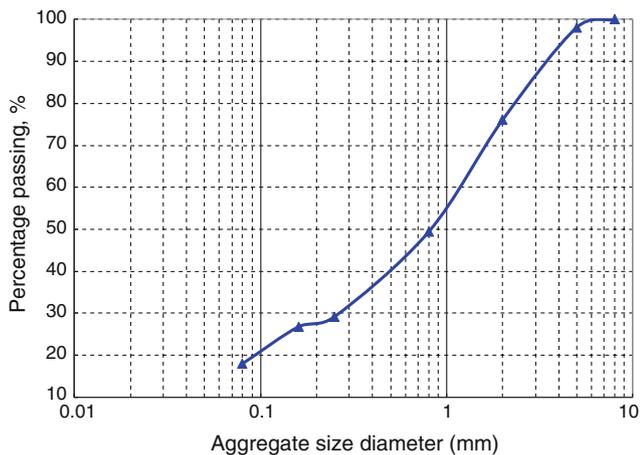
Fig. 85.2 Aggregate size distribution of the crushed soil
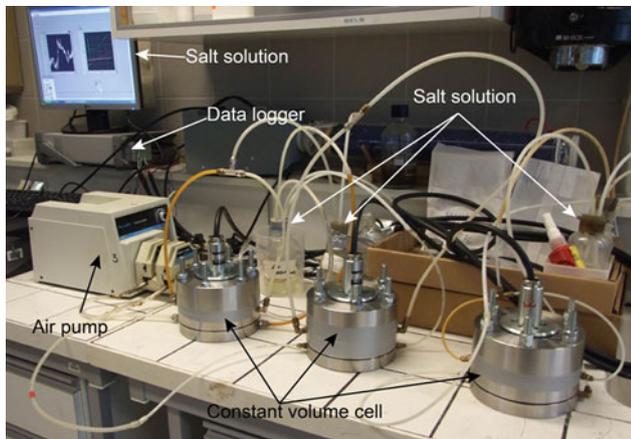
Fig. 85.3 Schematic diagram of the test setup adopted in the investigation

firstly applied. After the equilibrium was reached, distilled water was injected at a constant pressure of 15 kPa from the bottom inlet of the cell to saturate the specimen.

85.5 Results and Discussion

The results of the swelling tests are presented in terms of swelling pressure versus elapsed time (Fig. 85.4). As expected, at each suction level, the measured swelling pressure increases quickly in the beginning and then gradually reaches equilibrium upon further wetting. In Fig. 85.4a, the swelling curves of T1 and T2 are similar, indicating that the employed test procedures have good repeatability and the developed cell is reliable. For sspecimens T1 and T2, about 10 days are needed to reach equilibrium at suction of 57 MPa, and the final swelling pressure is about 0.17 MPa. The subsequent wetting path (suction controlled at 38 MPa) increases the final swelling pressure to

about 0.31 MPa and the time needed to reach the equilibrium is about 20 days. For test T3 (Fig. 85.4b), a suction of 9 MPa was applied initially. That induced a final swelling pressure of about 0.46 MPa and the time needed to reach the equilibrium is about 30 days. After that, distilled water was injected into the cell to saturate the specimen (zero suction). It can be observed that once the distilled water was injected, the swelling pressure increased suddenly to 0.92 MPa as a peak value followed by a small decrease to a stabilized value of 0.89 MPa.

The obtained results indicate that the time required to reach equilibrium depends on the suctions applied. When the specimens were gradually wetted by increasing the relative humidity (RH), water vapor was absorbed and moved towards the inside of the specimen under the effect of the suction gradient (Push 1982). But with the wetting that continues, the corresponding suction gradient gradually decreases and finally reaches equilibrium as well as the rate of vapor migration. The required equilibrium time therefore depends on two factors: the rate of vapor migration and the initial suction gradient. At a higher initial suction gradient, although the initial vapor migration rate inside the specimen is higher, more time would be required to reach suction equilibrium because more water was needed. This explains the observed behavior shown in Fig. 85.4: only about 10 days was required to obtain a stabilized swelling pressure at the applied suction value of 57 MPa but 30 days at 9 MPa.

Figure 85.4 also shows that the swelling pressure is function of suction. This phenomenon is associated with the hydration mechanisms in the level of swelling clay minerals. As presented in the previous studies, the swelling behavior of soil is the results of two combined processes: (1) the progressive absorption of successive layers of molecules in the interlayer spaces inside the clay particles results in an enlargement of interlayer distance; (2) the subdivision of particles into thinner ones that are made up of a smaller number of stacked layers, and leads to larger inter-particles pores (Delage 2007). However, the adsorption of water molecules between the layers inside the clay particles is function of suction; a decrease of suction gives rise to an increase of absorbed water layers. In the present work, the applied suction changes from 57 to 9 MPa, the corresponding RH increases from 66 to 93.7% at 20 °C. According to the results of Chipera et al. (1997), the maximum absorbed water layer in clay particles may be up to 2 layers.

In Fig. 85.4b, the development of swelling pressure curve during water-wetting stage is much sharper than that during vapor-wetting stage. Moreover, a slight decrease of swelling pressure after the peak value is observed. It may be attributed to the different hydration mechanisms between the vapor-wetting and the water-wetting. The hydration mechanism of vapor-wetting has been described above. The water

Fig. 85.4 Evolution of swelling pressure with elapsed time at different suction levels **a** specimens T1 and T2 and **b** specimen T3
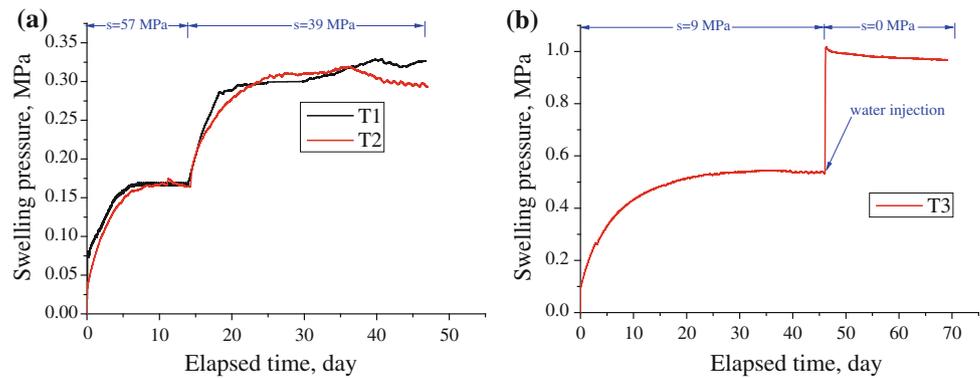
vapor is initially absorbed in small intra-aggregate pores with relative low mitigation rate. However, during water-wetting, water enters the inter-aggregate pores quickly. On one side, the aggregates begin to expand due to hydration, giving rise to a sudden increase of swelling pressure; on the other side, the continued hydration process simultaneously weakens the bonds between aggregates and soil skeleton loses its stiffness. Consequently, structure collapse occurs and causes a drop after the peak swelling pressure (Fig. 85.4b). This observation is consistent with the results presented in the previous researches (Push 1982; Komine and Ogata 1994; Cui et al. 2002).

85.6 Conclusions

1. An apparatus was developed for better performing constant swell test. The pressure sensor instead of traditional load cell was used to measure the swelling pressure of specimen during wetting, which can effectively minimize the measurement errors from the deformation of the system.
2. By applying the developed apparatus, the swelling pressure of compacted soil specimens under suction-controlled condition was measured. The results show good repeatability, indicating the reliability of the new apparatus and validating the test procedures adopted.
3. The final swelling pressure of specimen increased with decreasing suction, while the equilibrium time increased with decreasing suction.
4. Vapour-wetting and water-wetting show different hydration mechanisms and resulted in different swelling behavior.

References

Aiban SA (2006) Compressibility and swelling characteristics of Al-Khobar Palygorskite, eastern Saudi Arabia. Eng Geol 87:205–219

Al-Shamrani MA, Dhowian AW (2003) Experimental study of lateral restraint effects on the potential heave of expansive soils. Eng Geol 69:63–81

Bilir ME, Sari D, Muftuoglu YV (2008) A computer-controlled triaxial test apparatus for measuring swelling characteristics of reconstituted clay-bearing rock. Geotech test J 31:1–6

Chipera SJ, Carey JW, Bish DL (1997) Controlled-humidity XRD analyses: application to the study of smectite expansion/contraction. In: Gilfrich JV et al (eds) Advances in X-ray analysis, vol 39, pp 713–721

Cui YJ, Loiseau C, Delage P (2002) Microstructure changes of a confined swelling soil due to suction controlled hydration. Unsaturated soils. In: Proceedings of the 3rd international conference on unsaturated soils (UNSAT 2002), Recife, Brazil (ed. Jucá, J.F.T., de Campos, T.M.P. and Marinho, F.A.M.), Lisse: Swets and Zeitlinger, vol 2, pp 593–598

Delage P (2007) Microstructure features in the behaviour of engineered barriers for nuclear waste disposal. In: Schanz T (ed) Experimental unsaturated soils mechanics, proceedings of international conference on mechanics of unsaturated soils. Springer, Weimar, Germany, pp 11–32

Komine H, Ogata N (1994) Experimental study on swelling characteristics of compacted bentonite. Can Geotech J 31:478–490

Push P (1982) Mineral-water interactions and their influence on the physical behaviour of highly compacted Na bentonite. Can Geotech J 19:381–387

Shi B, Jiang H, Liu Z, Fang HY (2002) Engineering geological characteristics of expansive soils in China. Eng Geol 78:89–94

Tang CS, Tang AM, Cui YJ, Delage P, Barnichon JD, Shi B (2011) Study of the hydro-mechanical behaviour of compacted crushed argillite. Eng Geol 118(3–4):93–103

Tripathy S, Sridharan A, Schanz T (2004) Swelling pressures of compacted bentonites from diffuse double layer theory. Can Geotech J 41:437–450

2D and 3D Thermo-Hydraulic-Mechanical Analysis of Deep Geologic Disposal in Soft Sedimentary Rock

86

Feng Zhang and Yonglin Xiong

Abstract

In deep geological disposal for high level radioactive waste (HLW), one of the most important factors is to study the thermo-hydraulic-mechanical (THM) behavior of the natural barrier, usually a host rock during heat process and hydraulic environment change. In this paper, based on a thermo-elasto-viscoplastic model for soft rock proposed by Zhang and Zhang (2009), a finite element method (FEM) has been developed to simulate the THM behavior of geological disposal. Considering the different cooling period before the disposal of HLW, two cases of 2D and 3D analyses are conducted to estimate long-term stability of the host rock. From the simulated results, the cooling period before the disposal of HLW is very important to the safety of the waste sealing construction.

86.1 Introduction

In deep geological disposal for high level radioactive waste, one of the most important factors is to study the thermo-hydraulic-mechanical (THM) behavior of the natural barrier, usually a host rock during heat process and hydraulic environment change. The high level radioactive materials might permeate with underground water through the barrier systems to biosphere. The temperature effect on soft sedimentary rock due to the heat emitting from the nuclear waste canisters also needs to be investigated. The water absorption may induce a swelling of geo-materials that might lead to a damage of the nuclear waste containers. All these THM behaviors of the natural barrier need to be well understood in order to guarantee the safety and the efficiency of the waste sealing construction in long time. In this paper, Based on a

thermo-elasto-viscoplastic model proposed by Zhang and Zhang (2009), a program called as 'SOFT', using FEM for spatial discretization and the finite difference method (FDM) for time domain in soil-water-heat coupling problem, has been developed to simulate the THM behavior of the host rock.

86.2 2D and 3D THM Simulations

Due to the symmetric geometry and loading conditions, only a half area is considered in the numerical simulation. 2D FEM mesh is showed in Fig. 86.1, in which the area is a rectangle of 210 m × 520 m, the right and left side are fixed in x direction, while the bottom side is restricted in vertical direction. The initial stress is calculated by gravitational analysis. For thermal condition, the initial temperature of whole considered area is 20 °C. The ground surface is always kept 20 °C all time and the heat insulation is assumed for other three sides. The initial total water head is given as 520 m. All the boundaries except the surface are undrained condition. The nuclear waste repository is a circle with 20 m in diameter and its center lies at the place 300 m below the surface.

F. Zhang (✉) · Y. Xiong (✉)
Department of Civil Engineering, Nagoya Institute of Technology, Showa-Ku, Gokiso-Cho, Nagoya, 466-8555, Japan
e-mail: cho.ho@nitech.ac.jp

Y. Xiong
e-mail: ylxiong1986@hotmail.com
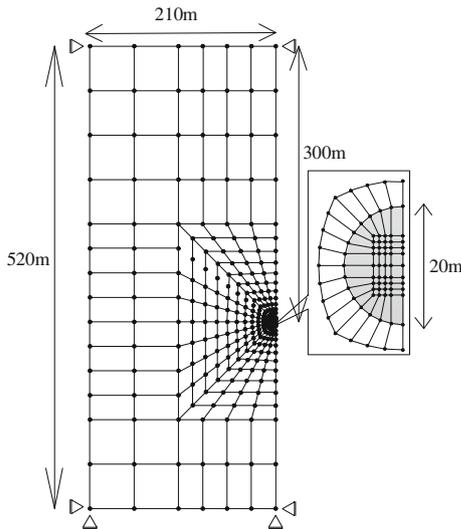
Fig. 86.1 2D FEM mesh
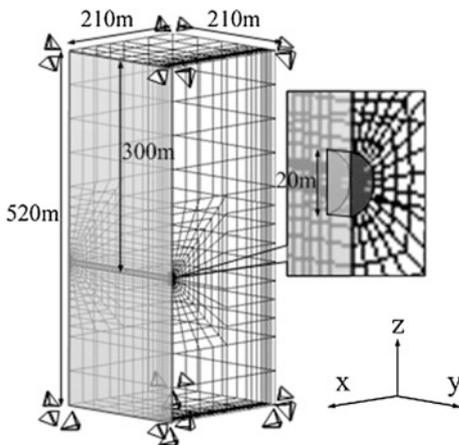
Fig. 86.2 3D FEM mesh

Figure 86.2 shows 3D FEM mesh that consists of 3,380 eight-node hexahedrons whose vertical section is the same as the 2D mesh. The initial and boundary conditions of the stress, the temperature and water head are also the same as those in 2D analysis. The thickness of the repository is the half of the diameter, that is, 10 m.

In the FE-FD analysis, a durative time of 300 years is simulated. In reality, the repository ratio of HLW is only about 1.6 % (Thunvik and Braester 1991). In present simulation, therefore, 1.6 % of heat emission is given and is showed in Fig. 86.3. In the THM analysis with FE-FD scheme, the influence of the convection of water flow is negligible because the maximum velocity of pore water is less than 10^{-8} (m/s) within the soft rock. The soft rock is
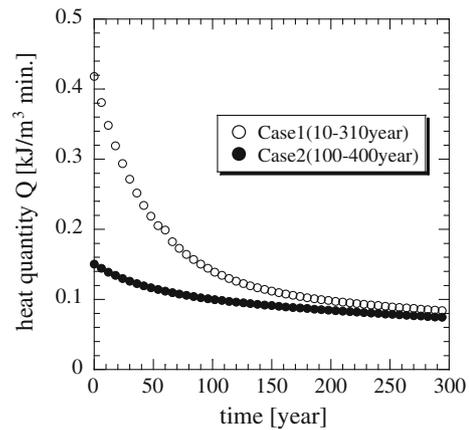
Fig. 86.3 Heat emission of HLW as the input in FEM

considered to be saturated. The technological and engineering barriers are assumed to be elastic in the THM simulation and the parameters of the materials used are listed in Table 86.1.

First of all, the 2D analysis will be discussed. Figure 86.4 shows the distribution of temperature at specified times. From the figure, it is known that the temperature is increasing initially due to the emission of the heat. In Case 1, the temperature begins to decrease during 75–150 years, and then cools down to a certain value. There is no clear further decrease of temperature within the calculated time. In addition, the generated temperature in Case 1 is much higher than that in Case 2.

Figure 86.5 shows the distribution of total water head at specified times. With the increase of temperature, the water head in two cases is also increasing with time, because the thermal expansion coefficient of water is much higher than that of the rock. And later, as the migration of the pore water, the excessive water is allowed to dissipate and consequentially turns to hydrostatic pressure.

Figure 86.6 shows the distribution of the plastic shear strain $\sqrt{2I_2^p}$ at specified times, where I_2^p is the second invariant of deviatoric plastic strain tensor. It is known from the figure that the maximum shear strain occurs in the area of 45° with horizontal direction.

By comparing the results from the two cases, it is found out that the magnitude of the increase of total water head and the plastic shear strain in Case 1 is much larger than that in Case 2 due to the difference of the generated temperature.

3D analysis is then discussed in the following section. Figures 86.7, 86.8 and 86.9 show the distribution of temperature, water head and the plastic shear strain at specified times respectively. It is found out from these figures that the same tendency observed in 2D analysis is confirmed in 3D analysis, except that the magnitude in 3D analysis is much smaller than that in 2D analysis.

Table 86.1 Physical properties and material parameters of soft sedimentary rock

Parameters			Physical properties		
Young's modulus E (MPa)	1,000.0		Pre-consolidated yield stress p_c (MPa)		0.30
Poisson's ratio v	0.120		Thermal expansion coefficient α_T (1/K)		8.0×10^{-6}
Stress ratio at critical $R_{CS}(=\sigma_1/\sigma_3)$	5.5		Permeability k (m/s)		10^{-9}
Plastic stiffness E_p	0.015		Thermal conductivity K_t (kJ m^{-1} K^{-1} Min^{-1})		0.2
Potential shape parameter β	1.1		Specific heat C (kJ Mg^{-1} K^{-1})		840
Time dependent parameter α	0.5		Heat transfer coefficient of air boundary α_c ((kJ m^{-2} K^{-1} Min^{-1})		230
Time dependent parameter C_n	0.025				
Over consolidation parameter $\mathbf{a}$	3,000		*Specific heat of water C_w (kJ Mg^{-1} K^{-1})*		4,184
Reference void ratio N (e_0 at σ_{m0} = 98 kPa)	0.50				

Fig. 86.4 Distribution of temperature (°C) at specified times (2D)
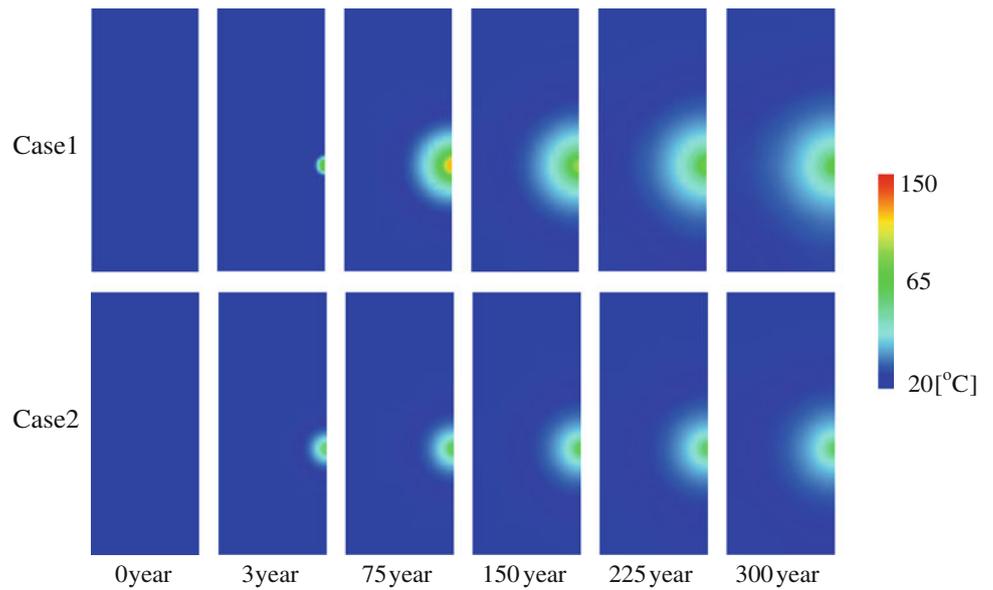
Fig. 86.5 Distribution of water head at specified times (2D)
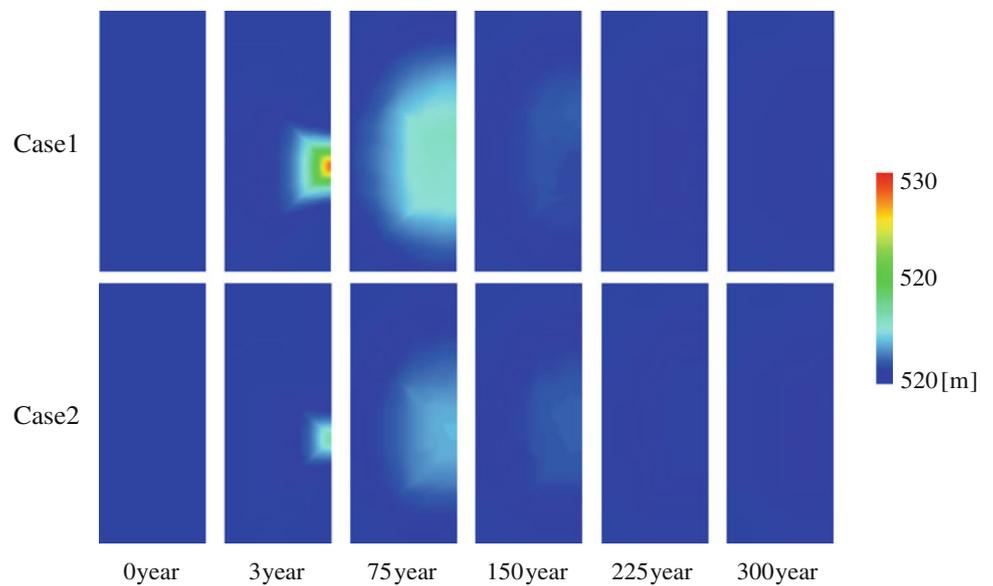
Fig. 86.6 Distribution of $\sqrt{2I_2^p}$ at specified times (2D)
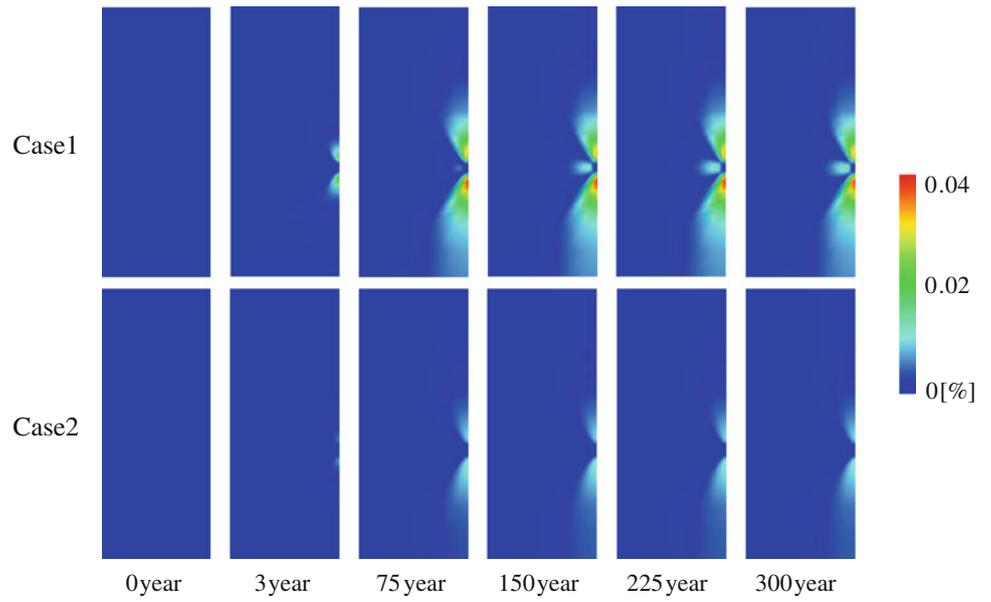
Fig. 86.7 Distribution of temperature (°C) at specified times (3D)
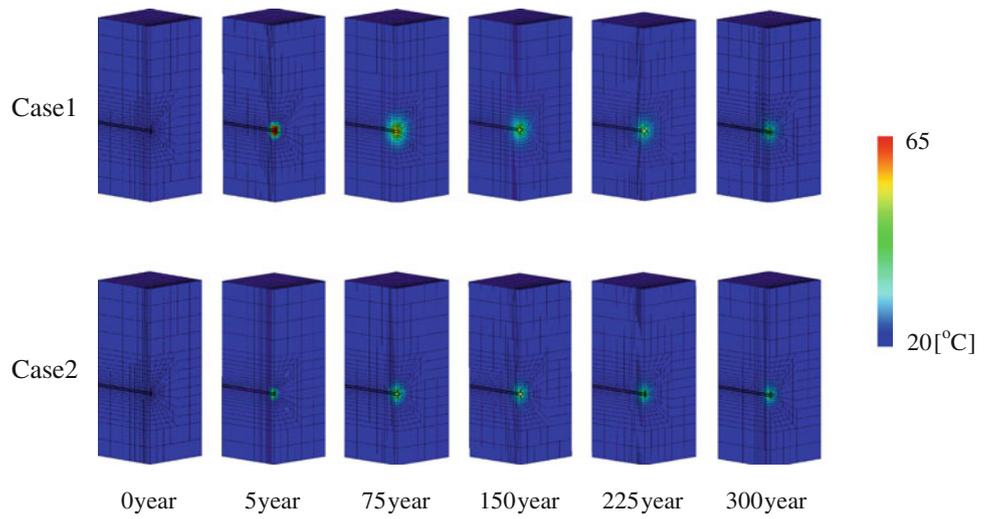
Fig. 86.8 Distribution of water head at specified times (3D)
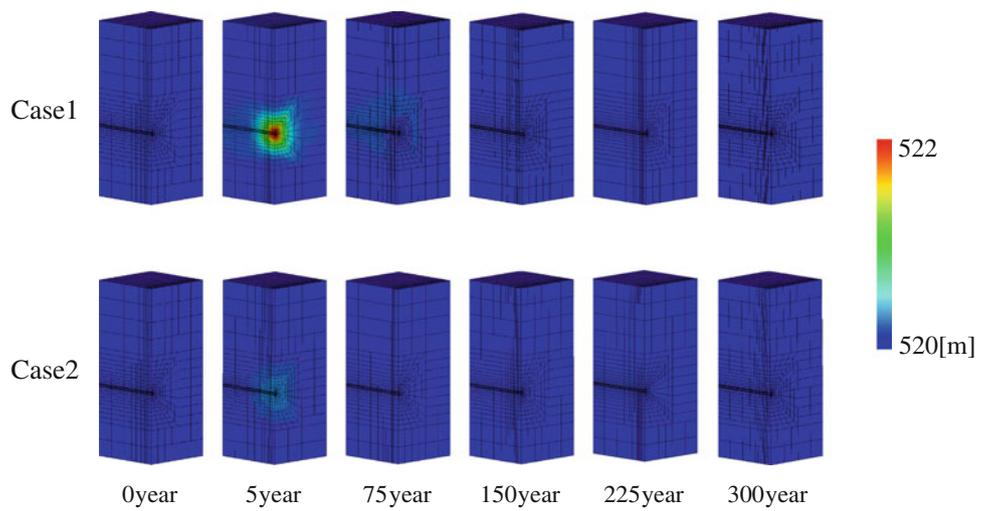
Fig. 86.9 Distribution of $\sqrt{2I_2^p}$ at specified times (3D)
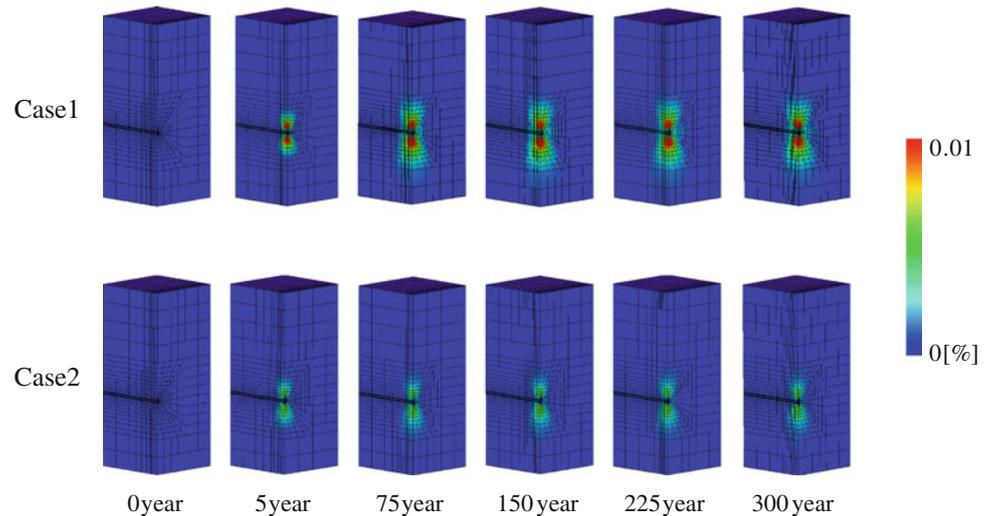
86.3 Conclusions

In this paper, 2D and 3D THM analyses on deep geological disposal of HLW with FE-FD scheme have been carried out the following conclusions can be given:

In 2D analysis, two cases are considered for different cooling period in the air before the geological disposal. It is revealed that the calculated physical quantities, such as the temperature, that total water head, the plastic shear strain in Case 1, are much larger than those in Case 2. In other words, the cooling period is very important factor for the long-term stability of the waste sealing construction.

In 3D analysis, the same tendency is observed. But the THM quantities are much smaller than those in 2D analysis. The reason is quite clear because in 3D analysis, the heat source is a point source, and the heat emission/transferring are conducted in spatial domain, resulting in a relative small concentration of heating.

References

Thunvik R, Braester C (1991) Heat propagation from a radioactive waste repository (SKB 91 reference canister). Technical report, pp 91–26

Zhang S, Zhang F (2009) A thermo-elasto-viscoplastic model for soft sedimentary rock. Soils Found 49(4):583–595

Anisotropy in Oedometer Test on Natural Boom Clay

Linh-Quyen Dao, Yu-Jun Cui, Anh-Minh Tang, Pierre Delage, Xiang-Ling Li, and Xavier Sillen

Abstract

The mechanical behaviour of Boom Clay has been studied for many years in the context of geological disposal of radioactive waste in Belgium. The aim of this study is to investigate the anisotropic behaviour of Boom Clay in terms of compressibility and hydraulic conductivity. Oedometer tests (with effective vertical stress (σ'_v) up to 32 MPa) were carried out on samples of various orientations: parallel, perpendicular and inclined 45° to the bedding plane. The compressibility index (C_c) and swelling index (C_s) were compared. Only a slight difference between these parameters was observed, suggesting that the anisotropic behaviour of Boom Clay cannot be revealed under the test conditions adopted. The hydraulic conductivity (k) was also determined by the Casagrande's method for different values of vertical effective stress (σ'_v). Unlike compressibility, the hydraulic conductivity, however, showed a clear anisotropic behaviour with $k_{ver} < k_{inc} < k_{hor}$.

Keywords

Boom clay • Anisotropy • Compressibility • Hydraulic conductivity • Oedometer test

87.1 Introduction

In Belgium, Boom Clay is considered as a potential host formation for the geological disposal of high level radioactive waste. The Boom Clay formation was deposited 30 million years ago (Oligocene Epoch). At the location of the Belgian Underground Research Laboratory (URL) HADES, close to the city of Mol, its thickness is about 100 m. Understanding the thermo-hydro-mechanical (THM) behaviour of the host formation is an important part of the feasibility and safety case for the geological disposal of high-level, heat-emitting radioactive waste. Indeed HM properties will condition the excavation techniques to be used for repository construction while THM properties will determine the long-term evolution of stresses, pore pressures and temperatures in the surrounding host rock after the emplacement of the waste.

The behaviour of Boom Clay is considered as cross-anisotropic due to the bedding resulting from deposition (Delage et al. 2007; Lima 2011). It is hence important to take into account the effects of inherent anisotropy in the design and development of structures in Boom clay such as the HADES URL, situated at a depth of about 225 m.

Most oedometer tests carried out till now on Boom clay have been made in a standard fashion with the loading/unloading direction perpendicular to bedding. In this paper, the compressibility and swelling properties of Boom Clay are investigated through high pressure oedometer tests carried out on samples oriented differently with respect to the bedding plane. The hydraulic conductivity was also determined based on Casagrande's method.

L.-Q. Dao · Y.-J. Cui (✉) · A.-M. Tang · P. Delage
Ecole des Ponts ParisTech, Navier/CERMES, Marne la Vallée, France
e-mail: yujun.cui@enpc.fr

X.-L. Li
EURIDICE, Mol, Belgium

X. Sillen
ONDRAF, Brussels, Belgium

87.2 Materials and Methods

Boom Clay specimens of 50 mm in diameter and 20 mm in height were hand-trimmed from two "horizontal" cylindrical cores (cylinder axis is parallel to bedding) obtained from drillings executed from the HADES URL: core 1b 2006-5 (70 mm diameter and bored in 2006) and core 19C 49–75 (100 mm diameter and bored in 2007). Three samples with various bedding orientations were extracted from these cores: vertical sample ($\alpha = 0°$), inclined sample ($\alpha = 45°$) and horizontal sample ($\alpha = 90°$) (Fig. 87.1). The characteristics of these specimens are shown in Table 87.1. Note that the initial properties (including dry density, water content and void ratio) of the three samples are comparable. The vertical and inclined samples (in Test 1 and Test 3) were saturated (S_r is around 100 %) while the horizontal sample was partially desaturated ($S_r = 91$ %).

In order to study the anisotropy of compressibility, oedometer tests with loading/unloading/reloading were performed on three samples as shown in Fig. 87.2. The effective vertical stress (σ'_v) was stepwise increased up to 32 MPa. This stress is much larger than those experienced by the clay around the URL but this allowed a better determination of the compression index Cc. After being hand-trimmed from cores, specimens were installed in the oedometer cell and loaded up to the in situ vertical effective stress ($\sigma'_v = 2.4$ MPa) prior to being put in contact with water so as to avoid swelling and corresponding changes in the initial intact microstructure (Delage et al. 2007). The sample was saturated at 2.4 MPa with a synthetic water having a similar chemical composition to the field pore water. The composition of this solution is described in Le (2008). Afterwards, step unloading to 0.125 MPa, reloading up to 16 MPa, unloading again to 0.125 MPa, reloading up to 32 MPa and finally unloading to 0.125 MPa were performed. At the end of each step of loading or unloading, the axial strain of sample was verified so as to be consistent with the French standard: $\Delta H/H_0 < 5 \times 10^{-4}$ for a period of 8 h (AFNOR 1995).

The hydraulic conductivity was determined following Casagrande's method. For this purpose, the results were plotted in a semi-logarithmic scale [Nova 2010, see Eq.

(87.1)]. The relationship between the hydraulic conductivity and the coefficient of consolidation is recalled in Eq. (87.2).

$$c_v = 0.197 \frac{H^2}{t_{50}} \tag{87.1}$$

$$c_v = \frac{k}{\gamma_w m_v} = \frac{kE_{oed}}{\gamma_w} \tag{87.2}$$

where H is the drainage length, equal to the half-height of the specimen, t_{50} is the time for 50 % consolidation, k is the hydraulic conductivity, γ_w is the unit weight of water ($\gamma_w = 9.81$ kN/m^3), m_v is the oedometric compressibility.

Based on Eqs. (87.1) and (87.2), the hydraulic conductivity k is determined as follows:

$$k = \frac{0.197 H^2 \gamma_w}{t_{50} E_{oed}} \tag{87.3}$$

87.3 Results and Discussions

87.3.1 Anisotropy of Compressibility and Swelling Index

The compression curves from the oedometer tests on three Boom Clay samples (vertical, inclined, horizontal) are shown in Fig. 87.2. Note that a slight swelling of about 0.5 % was observed during the saturation stage with synthetic solution under 2.4 MPa. In Fig. 87.2, only the results obtained after the saturation stage are presented, i.e. all curves start from the end of saturation under an effective vertical stress equal to 2.4 MPa that corresponds to in situ stress. A total of 90 days was needed for the oedometer test to be finished.

The unloading/reloading curves of the three samples exhibit a similar behaviour. Comparable loops were obtained along loading cycles. From the results of oedometer tests, the consolidation index (C_c) and the swelling index (C_s) were calculated for several loading/unloading steps: loading from 4 to 16 MPa (C_{c1}), unloading from 16 to 4 MPa (C_{s2}), then loading from 4 to 32 MPa (C_{c3}) and unloading from 32 to 4 MPa (C_{s4}). The results are presented in Table 87.2. It can
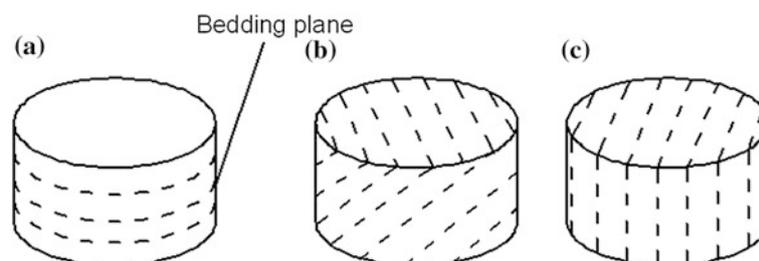
Fig. 87.1 Three types specimens used in oedometer test: **a** vertical sample ($\alpha = 0°$); **b** inclined sample ($\alpha = 45°$); **c** horizontal sample ($\alpha = 90°$). α: angle between the axis of specimen and the axis perpendicular to the bedding plane

Table 87.1 Properties of the three Boom Clay specimens: dry density ρ_d, water content w, void ratio e and degree of saturation S_r

Test	Core of origin	Distance from extrados (m)	Drilling date	Angle α (°)	ρ_d (Mg/m³)	w (%)	e	S_r (%)
1	19C 49-75	20.1–21.4	2007	0	1.648	23.8	0.625	100
2	1b 2006-5	4.77–5.97	2006	90	1.622	22.1	0.646	91
3	1b 2006-5	4.77–5.97	2006	45	1.631	23.6	0.637	99
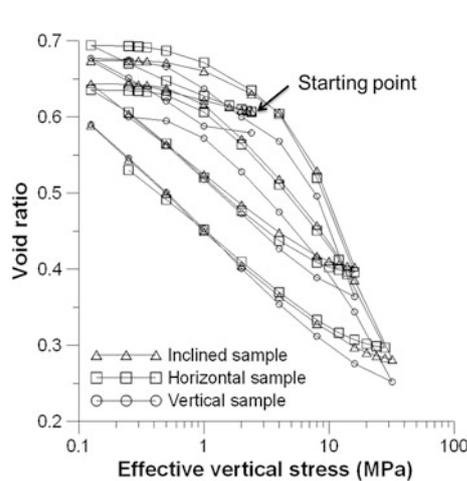
Fig. 87.2 Void ratio versus effective vertical stress for oedometer test on three Boom Clay samples (vertical, horizontal, inclined 45°)

Fig. 87.3 Anisotropy of hydraulic conductivity of Boom Clay

be observed that similar values of C_c and C_s are obtained regardless of the sample orientation. This may seem to be in contradiction with the expected anisotropic behaviour of Boom Clay. This may be due to the difficulty in graphically determining Cc and Cs, the perturbation of the clay around the URL (cores are taken at different distances of the gallery), the perturbation of the samples (of which the age is different) due to preparation and the difficulty of separating primary consolidation from secondary consolidation (see Cui et al. 2009). More tests with better control such as oedometer test on less perturbed samples (fresher, taken at

greater distance from the gallery under a more realistic range of loading), and triaxial test are needed to clarify this point.

87.3.2 Anisotropy of Hydraulic Conductivity

Based on Casagrande's method, the hydraulic conductivity of the samples were determined for the loading part started from 1 MPa up to 16 MPa ($\sigma'_v = 1$ MPa $\rightarrow$ 2.4 MPa $\rightarrow$ 4 MPa $\rightarrow$ 8 MPa $\rightarrow$ 16 MPa). As shown in Fig. 87.3, the values for the three samples show the same variation trend, i.e., they decrease when the effective vertical stress (σ'_v) increases. Also, the results showed an important anisotropy in terms of hydraulic conductivity: $k_{ver} < k_{inc} < k_{hor}$.

A summary can be found in Yu et al. (2011) of values for the hydraulic conductivity of (close to) undisturbed Boom Clay at Mol, determined from a large number of laboratory and in situ measurements. Comparison shows that the horizontal conductivity obtained from oedometer tests in this study (k_{hor} around 10^{-11} m/s) is higher than that measured in situ (5×10^{-12} m/s). For the vertical hydraulic conductivity, the values obtained here ($k_{ver} = 2 \times 10^{-12}$ m/s) is however similar to that measured in situ ($k_{ver} = 2.3 \times 10^{-12}$ m/s). This suggests that the perturbation of the sample used for the determination of vertical hydraulic conductivity is less than that used for the determination of the horizontal one.

Table 87.2 Compression index (C_c) and swelling index (C_s) of three Boom Clay samples

	Vertical sample $\alpha = 0°$	Inclined sample $\alpha = 45°$	Horizontal sample $\alpha = 90°$
$\varepsilon_{v\ max}$ (%)	22.95	21.72	22.88
C_{c1}	0.339	0.337	0.346
C_{s2}	0.105	0.075	0.07
C_{c3}	0.272	0.292	0.283
C_{s4}	0.113	0.091	0.086

87.4   Conclusions

A series of oedometer tests were carried out with loading/
unloading/reloading cycles on three Boom Clay samples
oriented differently. The anisotropy of compressibility and
swelling properties was analysed first. It was observed that
the compression and swelling index, C_c and C_s are similar
for different orientations. It should be noted, however, that
for better determining these indexes, a maximum vertical
stress as high as 32 MPa was applied, that is much higher
than the in situ stress estimated at 2.4 MPa. To assess the
anisotropic behaviour of Boom Clay for conditions that are
more representative of the construction, operation and post-
closure evolution of a repository for radioactive waste, tests
with better control and within a narrower stress range around
the in situ value are recommended. The anisotropy of
hydraulic conductivity of these three samples was also
examined. As opposed to the compressibility properties, a
significant anisotropy in terms of hydraulic properties was
found. However, comparison with the in situ measurement
shows that the vertical hydraulic conductivity is similar but
the horizontal one is much higher, suggesting a more sig-
nificant perturbation of the sample used for the determina-
tion of the horizontal conductivity. Furthermore, the age of

cores used and the creep phenomenon may also be factors
affecting the results obtained.

References

AFNOR (1995) Sols: reconnaissance et essai: essai de gonflement à
    l'oedomètre. Détermination des déformations par chargement de
    plusieurs éprouvettes. XP, pp 94–091
Cui YJ, Le TT, Tang AM, Delage P, Li XL (2009) Investigating the time-
    dependent behaviour of Boom Clay under thermomechanical load-
    ing. Géotechnique 59:319–329. doi:10.1680/geot.2009.59.4.319
Delage P, Le TT, Tang AM, Cui YJ, Li XL (2007) Suction effects in
    deep Boom Clay block samples. Géotechnique 57:239–244. doi:10.
    1680/geot.2007.57.2.239
Le TT (2008) Comportement thermo-hydro-mécanique de l'argile de
    Boom. PhD thesis, Ecole Nationale des Ponts et Chaussées
Lima A (2011) Thermo-hydro-mechanical behaviour of two deep
    Belgian clay formations: Boom and Ypersian Clays. PhD thesis,
    Universitat Politèchnica de Catalunya
Nova R (2010) Soil mechanics. Wiley, New York
Yu L, Gedeon M, Wemaere I, Marivoet J, De Craen M (2011) Boom
    Clay hydraulic conductivity. A synthesis of 30 years of research
    (External Report SCK-CEN, 2011). http://publications.sckcen.be/
    dspace/handle/10038/7504

The OECD/NEA Report on Self-sealing of Fractures in Argillaceous Formations in the Context of Geological Disposal of Radioactive Waste

88

Helmut Bock

Abstract

Self-sealing of fractured geologic media is of prime importance in the understanding of long-term radionuclide mobility and safety of deep geological repositories for long-lived radioactive waste and spent fuel. It is often cited as one of the decisive factors favouring the choice of argillaceous formations as host rocks for deep disposals. A report of the Nuclear Energy Agency (NEA) of the Organisation for Economic Co-operation and Development (OECD) provides an overview and synthesis of the current understanding of, and conceptual approaches to, the processes that lead to sealing of natural and induced fractures in argillaceous media at typical repository depths. Systematic evidence of self-sealing is collected with reference to laboratory tests, underground research laboratory (URL) field tests and geologic and geotechnical analogues, whereby the bulk of the information stems from the URLs at Bure (Callovo-Oxfordian formation), Mol (Boom Clay) and Mont Terri (Opalinus Clay). The physical, mechanical, geochemical and hydro-mechanical processes and mechanisms are reviewed and their respective contribution to sealing of fractures assessed. It is concluded that the scientific knowledge on self-sealing has progressed to a level which, for soft and slight to moderately indurated argillaceous formations, justifies the inclusion of sealing processes in the performance assessment (PA) of deep geological repositories.

88.1 Introduction

Deep geological repositories for high-level radioactive waste require the waste to be isolated from the bio- and hydro-sphere over a time span of about 1 million years. Various programmes in the assessment of potential repository sites have shown that argillaceous formations have a very low hydraulic conductivity and that transport is dominated by diffusion. Theoretically, fractures within these formations have the potential to act as preferential flow paths however, there are indications that fractures in argillaceous formations exhibit similar hydraulic properties as intact rock. Assuming that fracturing is a dilatational process calls for an explanation of why initially hydraulic active features become tight over time. The phenomenon of fractures becoming, with the passage of time, less conductive and finally hydraulically insignificant is commonly termed "*self-sealing*".

In this context, attention is drawn to a report of the Nuclear Energy Agency (NEA) of the Organisation for Economic Co-operation and Development (OECD) in Paris (Bock et al. 2010). The Report provides a comprehensive overview and synthesis of the current understanding of, and conceptual approaches to, the processes that lead to sealing of fractures in argillaceous media at typical repository depths. The structure of the OECD/NEA Report is shown in Fig. 88.1.

The paper at hand provides an overview of some of the key aspects of the Report, in particular on:

H. Bock (✉)
Q+S Consult, Bad Bentheim, Germany
e-mail: qs-consult@t-online.de

Fig. 88.1 Flow chart of the OECD/NEA Report on self-sealing (Bock et al. 2010)
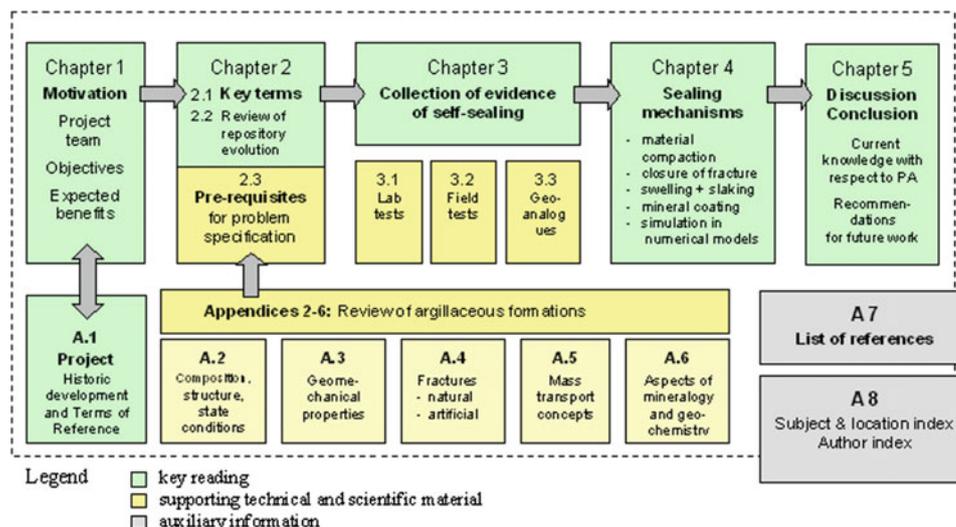
- evidence of self-sealing in argillaceous formations in laboratory tests, URL field tests and geologic and geotechnical analogues (Sect. 88.2 of this paper);
- mechanisms which contribute to sealing (Sect. 88.3 of this paper), and
- relevance of self-sealing for performance assessment (PA) in connection with the Safety Case (Sect. 88.4 of this paper).

88.2 Evidence of Self-Sealing

The Report compiles overwhelming evidence that self-sealing is a common phenomenon in a wide variety of argillaceous soils and rocks currently being considered in the context of deep geological repositories.

Self-sealing can be observed over a large spread of scales: At the millimetre to decimetre scale in laboratory test samples (see Sect. 88.2.1), at about repository scales (1–100 m range) in URL field tests (see Sect. 88.2.2) and at the kilometre scale in geologic and geotechnical analogues such as

old traffic tunnels and hydrocarbon reservoirs (see Sect. 88.2.3).

Self-sealing occurs at various rates which depend on the site-specific circumstances such as the type of clay minerals, degree of induration and chemistry of the porewater. At the tested sites there is a consistent permeability reduction trend, irrespectively of the type and dimension of the test. Typically, the reduction rate is in the order of about 10^{-1} to 10^{-2} per annum, meaning that, over a time span of 1 year, the permeability is reduced to 10^{-2} of its initial value.

88.2.1 Laboratory Tests

Figure 88.2 shows an example of fracture sealing as evidenced by inspection of the tested sample.

Beyond direct inspection of the tested samples, as in the example of Fig. 88.2, the following types of laboratory tests were considered in the Report:

1. combined isotropic loading ($\sigma_1 = \sigma_2 = \sigma_3$) and permeability tests;

Fig. 88.2 Visualisation of the sealing process of a Boom Clay sample by μCT technique— **a** before and **b** after saturation of a 38 mm ⌀ sample (Bernier et al. 2004)
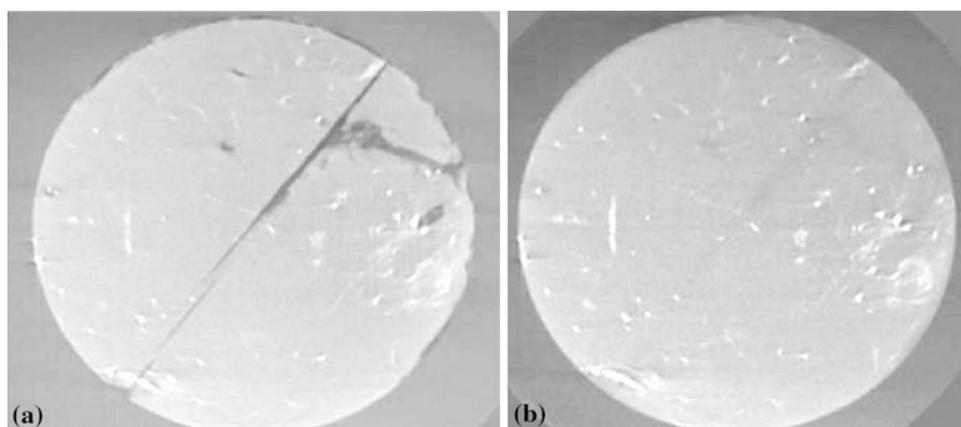
Table 88.1 Overview of URL field tests considered in the OECD/NEA Report URL /URF

URL/URF	Target formation overburden	In situ tests considered in context with self-sealing
Mont Terri, Switzerland	Opalinus Clay $\sim$ 240 m	EB Engineered barrier experiment
		EH EDZ self-sealing experiment
		EZ-A EDZ cut-off experiment
		SE SELFRAC-I and -II experiments
		HG-A gas path through host rock and along seal
		SE-H self-sealing with heat (Timodaz)
HADES Mol, Belgium	Boom Clay 230 m	Oxidation front in mine-by test (connecting gallery)
		Time-dependent hydromechanical response (SELFRAC-III)
		Collapsing borehole and instrumented core experiments (SELFRAC-IV)
Bure, France	Callovo-Oxfordian 490 m	KEY EDZ sealing barrier experiment

2. combined triaxial loading ($\sigma_1 > \sigma_2 = \sigma_3$) and permeability tests;
3. combined direct shear and permeability tests;
4. re-compaction and re-saturation in combined triaxial and permeability tests; and
5. experimental discrimination between mechanical closure of fractures by increased normal stress and swelling of the fracture wall material.

All of the above laboratory tests (sample sizes in mm- to dm-range) disclosed that self-sealing is a very common phenomenon in a wide variety of argillaceous soils and rocks which are currently considered in context with deep geological repositories.

88.2.2 Field Tests in URLs

URL field tests can be considered as a key to confidence building in the performance of argillaceous formations to host long-lived radioactive waste and spent fuel. Scientifically, many URL programmes constitute research right at the forefront of geomechanics and geo-engineering.

The structure of the Report reflects the particular importance of the Mont Terri URL in Switzerland, the HADES URF in Belgium and the Bure URL in France in considering the topic of self-sealing in argillaceous formations (see Table 88.1).

The in situ URL tests (samples in the 1–100 m range) disclosed that self-sealing is a very common phenomenon in a wide variety of argillaceous soils and rocks which are currently considered in context with deep geological repositories, from plastic clays (Boom Clay in the HADES URF) to indurated clays (Opalinus Clay at Mont Terri and Callovo-Oxfordian argillites at the Meuse-Haute Marne URL in Bure).

88.2.3 Geologic and Geotechnical Analogues

Field observations on self-sealing in argillaceous formations have been made in surface outcrops, shallow and deep boreholes and in geotechnical structures such as traffic tunnels. There is a large pool of technical and scientific methods which are employed (Table 88.2). For details and results, ref. to Bock et al. (2010).

Table 88.2 Overview of field observations on self-sealing effects in argillaceous formations

Method	Target formation	Overburden (m)	Study object
Mapping; core and borehole logging	Opalinus clay	$\leq$40	Surface outcrops; shallow boreholes
Tunnel mapping		$\leq$800	Traffic tunnels in Northern Switzerland
Core logging and permeability testing	Boda clay	$\sim$1,050	Structure of fault zones
Mapping and lab micro-porosity studies	Variscan claystone	Not applicable	Reconstruction of the permeability evolution of fault zone lithotypes
Mapping, core logging; modelling	Sandstone-claystone sequence	Not applicable	Specification of clay smear potential (CSP), shale gouge ratio (SGR), etc.
Borehole logging; chemical analysis	Argillaceous formations in general	100–500	Tracer concentration profiles
Mapping and joint formation theory		< $\sim$300	Surface outcrops and URLs

Table 88.3 Sealing mechanisms considered in the OECD/NEA Report and their sealing potential in argillaceous formations

Mechanism		Sealing potential	Remarks
Compaction of intact rock (pore space reduction)		Low	Limited importance as the formations considered have already been pre-compacted
Closure of fracture (subject to normal stress increase)		Moderate to high	Good theoretical knowledge
Contraction of fracture (subject to shear)		Moderate to very high	Dilatation/contraction mechanism, augmented by re-orientation of clay platelets
Creep		High to very high	Based on a bundle of micro-mechanisms
Swelling		Very high	Tends to be the most dominant factor in the sealing of fractures
Slaking	Body slaking	Low to moderate	Limited to non-existing knowledge on underlying mechanisms; poor data base, if any
	Surface slaking	Low, if any	
Mineral precipitation		Limited	Stability of precipitated material unclear

88.3 Sealing Mechanisms

It is scientific consensus that self-sealing in argillaceous media is attributable to a number of processes and mechanisms. For safety assessment and PA it is important to understand the sealing mechanisms and their possible interactions with each other. Guided by observations and evidence collected earlier, specific mechanisms were selected and considered in detail. These are listed in Column 1 of Table 88.3. The sealing potential, as disclosed in the Report, is indicated in Column 2 of that table.

88.4 Relevance of Self-Sealing for Performance Assessment (PA)

In a final step, all relevant self-sealing issues (conditions of the geological setting and mechanisms) were classified on their relevance for the performance assessment (PA) of the Safety Case. The classification scheme was in line with that developed by Mazurek et al. (2003) for the FEPCAT project of the OECD/NEA.

It turned out that there is not a single self-sealing issue left which would require "*substantially more work/thoughts, … at least in some cases*" (Bock et al. 2010, p. 163). Obviously, the general knowledge on self-sealing has progressed to a level at which critical deficiencies are absent. It is concluded that, at least for soft and slight to moderately indurated argillaceous formations, it is justified to include the process of self-sealing in the performance assessment (PA) of deep geological repositories.

References

Bernier F et al (2004) SELFRAC—fractures and self-healing within the excavation disturbed zone in clays. Final report. 5th EURATOM Framework Progr., Brussels (EU-Commission), p 64

Bock H, Dehandschutter B, Martin CD, Mazurek M, de Haller A, Skoczylas F, Davy C (2010) Self-sealing of fractures in argillaceous formations in the context of geological disposal of radioactive waste. NEA Report 6184:1–311, Paris (OECD/NEA)

Mazurek M, Pearson FJ, Volckaert G, Bock H (2003) Features, events and processes. Evaluation catalogue for argillaceous media. OECD/NEA 4437, ISM 92-64-02148-5

Permeability and Migration of Eu(III) in Compacted GMZ Bentonite-Sand Mixtures as HLW Buffer/Backfill Material

Zhang Huyuan, Yan Ming, Zhou Lang, and Chen Hang

Abstract

Compacted GMZ bentonite-sand mixtures are studied as a feasible buffer/backfill material for high-level radioactive waste (HLW) disposal in China. This paper is concentrated on the hydraulic conductivity and the migration of Eu(III) in the compacted mixtures of Gaomiaozi bentonite added with quartz sand with various ratio from 0 to 50 %. Permeability tests were conducted using a flexible wall permeameter with the influent of distilled water and 2.0×10^{-5} mol/l Eu(III) solution, respectively. Test results indicated that the hydraulic conductivities measured varied about 10^{-10} cm/s, and no significant change was found with sand ratio increasing from 0 to 50 %. The migration of Eu(III) through compacted specimen was studied by effluent monitoring and Eu(III) extraction from specimen sections after permeability test. The apparent diffusion coefficients of Eu(III) estimated by Eu(III) concentration profile in the specimens varied at the level 10^{-14} m^2/s, when the compacted mixtures had a sand ratio ranging from 0 to 50 %.

Keywords

HLW • Eu(III) solution • Hydraulic conductivity • Diffusion coefficient

89.1 Introduction

Compacted bentonite-sand mixtures have been proposed as a suitable buffer/backfill material in the HLW repository in China. The function of buffer/backfill material is to retard convective water and the migration of radionuclides through buffer by adsorption to the matrix. Therefore, the hydraulic conductivity and diffusion coefficient of radionuclides on compacted bentonite-sand mixtures play an important role in assessing the performance of buffer/backfill material.

Low permeability is the key factor to fulfill the barrier function for buffer/backfill material. Zhang et al. (2011) has studied the permeability of bentonite-sand mixtures with different sand ratio. Sivapullaiah et al. (2000) has studied the

effect of sand ratio, dry density and porosity on hydraulic conductivities.

The migration of radionuclides in compacted bentonite has been studied by many researchers. Most of the diffusion tests were mainly focused on the effect of sand ratio (Iida et al. 2011), and solution concentration (Wang et al. 2004), etc. on the diffusion coefficient. In this paper, permeability test and the solution migration test were conducted on the cylindrical specimens with flexible wall permeameter (US Hombolt). Hydraulic conductivities were measured and the effect of Eu(III) solution on permeability was discussed to provide a reference for the design of buffer/backfill material for HLW disposal in China.

89.2 Materials and Methods

89.2.1 Materials

The constituent of the mixtures evaluated in this test includes a processed GMZ bentonite, from Inner Mongolia, and the quartz sand from Yongdeng County in Gansu Province,

Z. Huyuan (✉) · Y. Ming · Z. Lang · C. Hang
School of Civil Engineering and Mechanics, Lanzhou University, Lanzhou 730000, China
e-mail: zhanghuyuan@lzu.edu.cn

Y. Ming
e-mail: yanm12@lzu.edu.cn

Table 89.1 Physical properties of GMZ bentonite

Physical properties						
Particle diameter	Montmorillonite content	Specific surface area	Air-dried water content	Plastic limit	Liquid limit	Specific gravity
<2 μm	74 %	570 m^2/g	10.53 %	32.43 %	228 %	2.71

China. The physical properties of the bentonite are summarized in Table 89.1. The particle density of quartz sand used in this research is 2.65 g/cm^3 and particle diameter ranges from 0.5 to 1.0 mm.

The sand ratio, R_s, is defined as the dry mass ratio of the quartz sand to bentonite-sand mixtures. Quartz sand is uniformly added into the bentonite with R_s = 0, 10, 20, 30, 40 and 50 %, respectively. And then a spray of water is performed to achieve even objective water content, followed by compaction of cylindrical specimens with the size of 100 mm in diameter for the tests.

89.2.2 Methods

Two separate tests were conducted, namely, permeability test and Eu(III) migration test, to measure the hydraulic conductivity of compacted bentonite-sand mixtures with various densities and sand ratio, and to understand the migration of radionuclide in the bentonite-sand mixtures barrier. The flexible wall permeameter was used in this test (Zhang et al. 2011). Table 89.2 lists the parameters of specimens used in permeability test and Eu(III) migration test.

89.2.2.1 Permeability Test

After the cylindrical specimen was positioned into the permeameter cell, distilled water was used to saturate the specimen with "back-pressure saturation" method: the back pressure and

confining pressure were applied step by step. After saturation, hydraulic conductivity was measured at the seepage stage.

The water head in the standpipe was monitored as a function of time, and the hydraulic conductivity of the specimen was calculated from the falling head method according to Darcy's laws.

89.2.2.2 Eu(III) Migration Test

The specimens were first saturated with distilled water for 23d as the same as that in permeability test by back-pressure method. After saturated, the distilled water was switched to solution containing 2.0×10^{-5} mol/l Eu(III) to start the Eu(III) migration test. Effluent was collected periodically, filtered through 0.45 μm pore size and chemically analyzed by ICP-MS. After 300d, experiment was terminated, followed by slicing the specimen into thin sections at about 0.50 mm in depth. The Eu(III) in each slice was extracted and measured with ICP-MS (Zhou et al. 2013).

89.3 Results and Discussions

89.3.1 Hydraulic Conductivities

Figure 89.1 shows hydraulic conductivities of bentonite-sand mixtures when distilled water was used as influent. Generally, hydraulic conductivities decrease with time and finally become stable. In the early permeation stage, hydraulic conductivities

Table 89.2 Parameters of specimens for permeability tests and Eu(III) migration tests

Test	Specimen	Sand ratio (%)	Diameter (cm)	Height (cm)	Dry density (g/cm^3)	Water content (%)
A	M0	0	10.20	3.28	1.61	16.40
	M10	10	10.16	3.26	1.72	16.30
	M20	20	10.02	3.48	1.79	19.20
	M30	30	10.31	3.93	1.64	9.80
	M40	40	10.15	3.66	1.91	13.50
	M50	50	10.22	3.91	1.97	11.00
B	N0	0	10.20	2.18	1.56	17.10
	N10	10	10.20	2.15	1.59	14.13
	N20	20	10.20	2.15	1.58	12.65
	N30	30	10.20	2.12	1.63	10.92
	N40	40	10.20	2.11	1.63	9.62
	N50	50	10.20	2.12	1.63	8.74
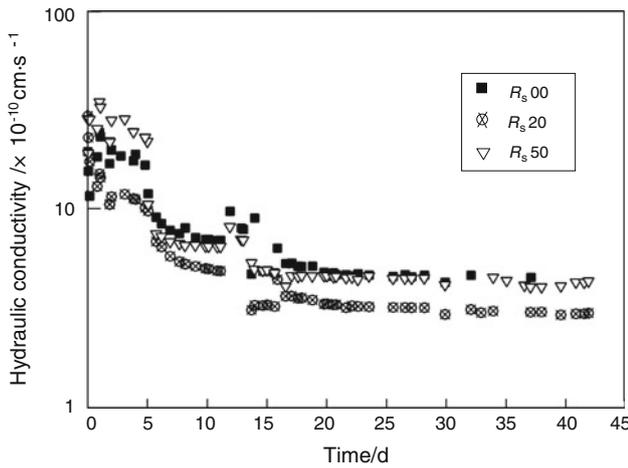
Fig. 89.1 Hydraulic conductivity with distilled water vs. time

Fig. 89.2 Hydraulic conductivity vs. sand ratio

decrease obviously. This is because that montmorillonite in bentonite swell with water continuously, leading to block mixtures' internal pore. In the later stage of permeation, hydraulic conductivities remain almost the same, regarded as final hydraulic conductivities of bentonite-sand mixtures. The measured data shows that hydraulic conductivities of mixtures are at the range of $3.34–8.85 \times 10^{-10}$ cm/s, which means that hydraulic conductivities are at the same order of magnitude, even so the sand ratio varies from 0 to 50 %. As a result, the original impermeability of pure bentonite can be kept while the sand ratio is less than 50 %. Similarly, hydraulic conductivities with Eu(III) solution are at the range of $2.07–5.23 \times 10^{-10}$ cm/s, at the same order of magnitude as permeated with water.

89.3.2 Effect of Sand Ratio on Hydraulic Conductivity

Sand ratio is a major factor influencing permeability of bentonite-sand mixtures. Figure 89.2 displays that the hydraulic conductivities of bentonite-sand mixtures have little change with the sand ratio increases when sand ratio is less than 85 %. In contrast, hydraulic conductivities of compacted bentonite-sand mixtures have a rapidly growing with sand ratio increases from 85 % (Zhang et al. 2011). This research indicates that the original low permeability of pure bentonite can be kept while the sand ratio is less than 50 % in case that both distilled water and Eu(III) solution permeated through the mixtures.

89.3.3 Eu(III) Concentration Profiles

The migration test was performed to investigate the migration characteristics of Eu(III) in compacted bentonite-sand mixtures. The equation of solution is (Zhou et al. 2013):
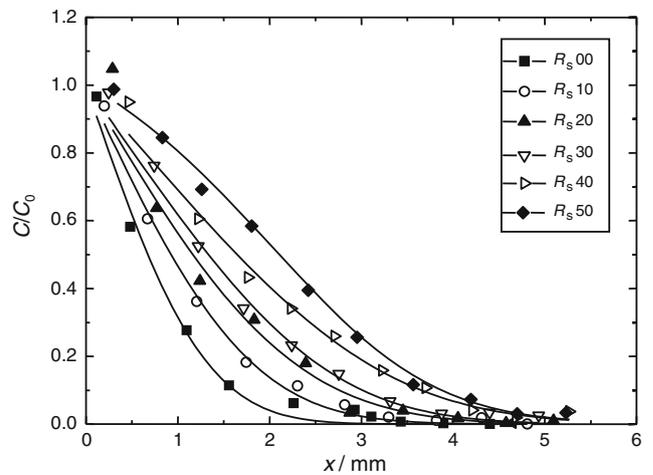
Fig. 89.3 Eu(III) concentration profiles and the fitting curves after 300d permeation

$$\frac{C}{C_0} = \frac{1}{2}\mathrm{erfc}\left[\frac{x - (v/R_d)t}{2\sqrt{D_a t}}\right] \qquad (89.1)$$

where C is the concentration (liquid phase) of Eu(III) at a distance x from the solution-bentonite interface at time t, and C_0 is the concentration of Eu(III) at the interface between the bentonite and the bulk solution, v is the seepage velocity, R_d is the retardation factor, D_a is the apparent diffusion coefficient.

Concentration profiles based on Eq. 89.1 for Eu(III) with different sand ratio were given in Fig. 89.3. Solid lines were the fitting curve from Eq. 89.1. For different sand ratio, it was observed that the fitting curves described well the experimental data.
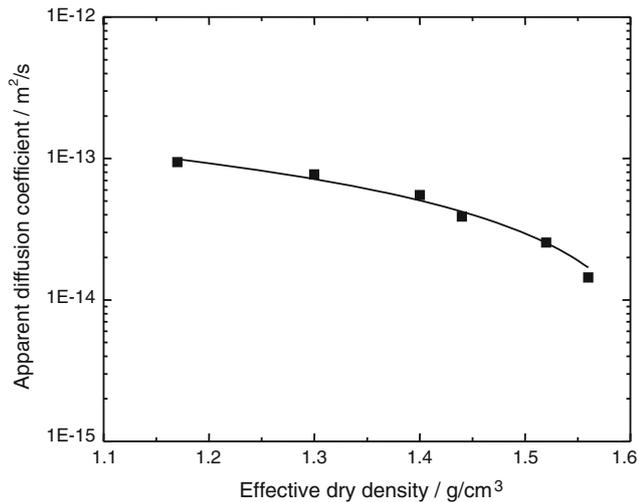
Fig. 89.4 Effect of effective dry density on the apparent diffusion

89.3.4 Effect of Effective Dry Density on Diffusion Coefficient

Figure 89.4 presents that the effect of effective dry density as described by Dixon et al. (1999) on apparent diffusion coefficient, D_a. An exponential reduction in apparent diffusion coefficient with the effective dry density was observed, which is similar to the conclusion of Sawatsky and Oscarson (1991). The reduction in D_a with increasing effective dry density was mainly attributed to an increase in the tortuosity as the effective dry density increased (Yu and Neretnieks 1997). Increasing clay content in per unit-volume of the mixtures tends to enhance the adsorption ability of bentonite-sand mixtures, and decline the diffusion coefficient. Moreover, the reduction in D_a with increasing in effective dry density was largely ascribed to an increase in the anion exclusion volume in the bentonite with increasing effective dry density, which likely decreases the effective size of the pores and so to influence the tortuosity or geometric factor (Sawatsky and Oscarson 1991).

89.4 Conclusions

1. The hydraulic conductivities of compacted bentonite-sand mixtures with sand ratio ranging from 0 to 50 % are $K = 3.34$–8.85×10^{-10} cm/s when permeated with distilled water, and $K = 2.07$–5.23×10^{-10} cm/s when permeated with Eu(III) solution. This means that pure bentonite can be mechanically improved by addition of quartz sand without increasing its impermeability.
2. The apparent diffusion coefficients of Eu(III) in compacted bentonite-sand mixtures are $D_a = 1.44$–9.41×10^{-14} m²/s. The decrease in D_a with increasing effective dry density is attributed to an increase in the tortuosity, anion exclusion volume and adsorption ability of bentonite-sand mixtures as bentonite content is increased.

References

Dixon DA, Graham J, Gray MN (1999) Hydraulic conductivity of clays in confined tests under low hydraulic gradients. Can Geotech J 36:815–825

Iida Y, Yamaguchi T, Tanaka T (2011) Experimental and modeling study on diffusion of selenium under variable bentonite content and porewater salinity. Nucl Sci Technol 48:1170–1183

Sawatsky NG, Oscarson DW (1991) Diffusion of technetium in dense bentonite. Water Air Soil Pollut 57–58:449–456

Sivapullaiah PV, Sridharan A, Stalin VK (2000) Hydraulic conductivity of bentonite-sand mixtures. Can Geotech J 37(2):406–413

Wang XK, Chen YX, Wu YC (2004) Diffusion of Eu(III) in compacted bentonite-effect of pH, solution concentration and humic acid. Appl Radiat Isot 60:963–969

Yu JW, Neretnieks I (1997) Diffusion and sorption properties of radionuclides in compacted bentonite. SKB, Stockholm, technical report TR97-12

Zhang HY, Zhao TY, Lu YT et al (2011) Permeability of bentonite-sand mixtures as backfill/buffer material in HLW disposal under swelling conditions. Chin J Rock Mech Eng 30:3149–3156 (in Chinese)

Zhou L, Zhang HY, Yan M et al (2013) Laboratory determination of migration of Eu(III) in compacted bentonite-sand mixtures as buffer/backfill material for high-level waste disposal. Appl Radiat Isot 82:139–144

Correlative Research on Permeability and Microstructure of Life Source Contaminated Clay

Liwen Cao, Yong Wang, Pan Huo, Zhao Sun, and Xuezhe Zhang

Abstract

Based on the test results deriving from laboratory simulation experiment device which consists of a waste layer, a drainage layer, a compacted clay layer, from the top down, as well as a contaminants recirculation system, and a few test instruments, falling head permeability test and scanning electron microscopy (SEM) are conducted to determine the permeability and microstructure of the contaminated clay at four pollution depths: 22.5, 45.0, 67.5 and 90.0 cm respectively. Consequently, quantitative relationship among such parameters as permeability coefficient k, total pore area A, area void ratio e, and mean pore size d_0 with pollution diffusion depths are explored. Finally, the evolution mechanism of the permeability and microstructure of contaminated clay related to life source is revealed. The researches show as follows: with the increase of pollution depth, permeability coefficient k, total pore area A, area void ratio e as well as mean pore size d_0 are increasing, and their relationship can be summarized as $k = 7\ln(A) - 200e^2 + 160e + 2d_0^2 - 12d_0 - 8$; Under such effects as ions exchange and adsorption, organic materials and suspended solids coagulation as well as complex chemical reactions between contaminants and clay, with pollution depth increasing, the clay permeability is improved due to the decreased influence of contaminants and their degradation products on clay, as well as the increased total pore area and void ratio.

Keywords

Life source contaminated clay • Permeability • Microstructure

The compressibility and shear strength of industry contaminated clay especially polluted by waste alkaline liquor, salt, acid and alkali, were studied by the predecessor researchers (Zhu et al. 2011), meanwhile the migration and recrystallization were touched (Negim et al. 2010).The microstructure of clay was detected by TEM and SEM combined with such computer image processing technologies as Photoshop and Mapinfo (Bogas et al. 2012; Shi and Jiang 2001; Al-Mukhtar et al. 2012). In this paper, such techniques as geotechnical test, scanning electron microscopy (SEM) and Matlab software are performed to determine correlation among the permeability coefficient and microstructure of contaminated clay by life source contaminants.

90.1 Samples of Contaminated Clay Related to Life Source

An experimental device constructed with domestic waste layer, gravel drainage layer and compacted clay from the top down is developed. The domestic waste layer principally consists of readily degradable kitchen waste, leaf, furnace cinder as well as waste paper and fruit. The gravel drainage layer filled by sand ranging from 2 to 10 mm in size is installed below the domestic waste layer. The clay is compacted in 100 cm thick for study.

L. Cao (✉) · Y. Wang · P. Huo · Z. Sun · X. Zhang
School of Resource and Earth Science, China University of Mining and Technology, Xuzhou 221116, China
e-mail: caoliwen@cumt.edu.cn

Through a series of physical, chemical and biological reactions, leachate is produced by domestic waste, and then, contaminated clay is formed by leachate seeping. After 2 years seeping, clay samples at four pollution depths: 22.5, 45.0, 67.5 and 90.0 cm are extracted from the experimental device. Thus, four groups contaminated clay samples, as well as one group of original clay sample are prepared.

90.2 Permeability and Microstructure of Contaminated Clay Related to Life Source

90.2.1 Permeability of Life Source Contaminated Clay

The permeability coefficient of contaminated clay related to life source at such four pollution depths as 22.5, 45.0, 67.5 and 90.0 cm, are indicated in Table 90.1. The experimental results show that the permeability coefficient of the contaminated clay declines by contaminants seeping.

90.2.2 Microstructure Parameters Extraction

The SEM microstructures of contaminated clay related to life source at the depths 22.5, 45.0, 67.5 and 90.0 cm see Fig. 90.1. We can conclude that the pore in the upper part of the clay is less than that of in the lower part one, and, the grain in upper part distributes more even. Then, based on optimal threshold values, the SEM images are quantified by Matlab software.

90.2.2.1 Basic Structure and Pore Size Extraction
Such basic structure parameters as total particle area, total pore area, mean particle area, mean pore area, area porosity and area void ratio are extracted by Bwlabel and Sum function. And then, such pore size parameters as maximum, minimum and mean pore size are extracted by Region props function, meanwhile, conversion coefficient is used so that the unit of binary image (pixel) can be converted to length unit. On the basis of conversion coefficient, the unit of the pore size parameters extracted is transformed to length unit. Maximum, minimum and mean pore sizes which are

transformed are increasing with the pollution depth deepening. Now, taking area void ratio as an example, it's changing in pore size distribution with the increase of pollution depth being showed in Table 90.2.

Combining with the precious experience of predecessors in respect of pore size distribution as well as Find and Ismember function, the pore size distribution in contaminated clay are classified into six categories: macro-pore, medium-pore, minor-pore and fine-pore, micro-pore, tiny-pore.

90.2.2.2 Microstructure Analysis
There exists a noteworthy growth in total pore area, area porosity and mean pore size with the pollution depth increasing in life source contaminated clay, which is identical with the intuitive analysis of SEM images. The feature of pore distribution is distinction at different pollution depth. Firstly, the contaminated clay at 22.5 and 45.0 cm depth mainly contain unimodal minor-pore, as well as bimodal fine/micro-pore without macro-pore. However, the contaminated clay at 90.0 cm depth mostly consists of unimodal macro-pore, as well as bimodal macro/medium-pore. Consequently, undergoing the life source contaminants, the clay displays transformation from macro-pore to micro-pore. Furthermore, there exhibit a structure evolution from minor-pore to macro-pore in contaminated clay with the pollution depth increasing. Although ostensibly changed slightly in quantity, the micro-pore universally exists in various pollution depths of clay, but there have actually experienced the progress from larger pore and to smaller pore since the contaminants seeping.

90.2.3 Correlation Between Microstructure and Permeability

According to the experimental date, such correlations as between permeability coefficient(k) and total pore area (A), area void ratio (e), mean pore size (d_0) are taken respectively. Then, $r = \ln(A)$, $s = (e - 0.4)^2$ and $t = (d_0 - 2.98)^2$ are ordered for the linear correlations between k and r, as well as s and t, then, formula (1) is obtained:

$$k = 7\ln(A) - 200e^2 + 160e + 2d_0^2 - 12d_0 - 8 \quad (1)$$

Available accuracy which is defined as $100\% - |\text{in situ value} - \text{predicted value}|/\text{in situ value}$, is used to compared in situ with the predicted value of k, and, the predicted value comes from the formula (1), then the available accuracy is 91.21, 96.26, 97.69 and 97.93 % at 22.5, 45.0, 67.5 and 90.0 cm pollution depth clay respectively.

Table 90.1 Permeability coefficient of contaminated clay related to life source

Pollution depth cm	22.5	45.0	67.5	90.0	0
Permeability coefficient k 10^{-7} cm/s	8.57	26.5	32.5	35.1	52.1

Fig. 90.1 Microstructure images of contaminated clay at the depths. **a** Microstructure image of clay at pollution depth 22.5 cm. **b** Microstructure image of clay at pollution depth 45.0 cm. **c** Microstructure image of clay at pollution depth 67.5 cm. **d** Microstructure image of clay at pollution depth 90.0 cm
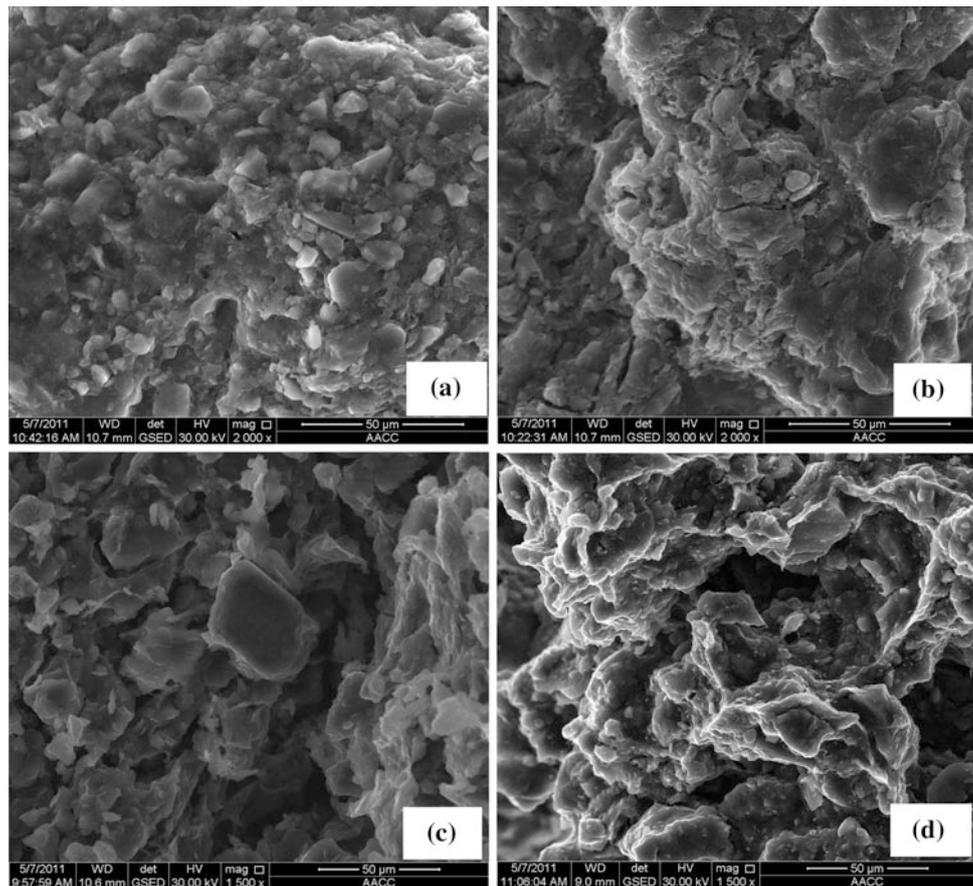
Table 90.2 Area void ratio and pore size distribution of contaminated clay at the depths

Pollution depth cm	Macro-pore ≥ 40 μm	Medium-pore 40 ∼ 20 μm	Minor-pore 20 ∼ 5 μm	Fine-pore 5 ∼ 2 μm	Micro-pore 2 ∼ 1 μm	Tiny-pore < 1 μm
22.5	0.0000	0.0000	0.0137	0.0109	0.0055	0.0053
45.0	0.0000	0.0000	0.0714	0.0306	0.0037	0.0072
67.5	0.1345	0.0578	0.1466	0.0096	0.0047	0.0038
90.0	0.2246	0.0836	0.0539	0.0080	0.0030	0.0019

90.3 Mechanism Analysis on the Permeability of Contaminated Clay Related to Life Source

The effect of chemical corrosion as well as biological degradation on clay will reveal during the clay saturated by contaminants seeping. Thus, it is necessary to interpret the modification mechanism of the contaminated clay permeability from three stages.

90.3.1 Primary Seepage Stage

Ion exchange plays a major role in the primary seepage stage. For example, such low ion with bigger crystal radius as Na^+, Ca^{2+} are exchanged by high valence ion as Fe^{3+} during the life source contaminants seeping, which will result to thin the electrical double layers on the clay surface, and lead to grow the attractive force between clay particles, then, cause clay particles flocculating, moreover, to increase the pore area, porosity and the clay permeability, accordingly.

90.3.2 Medium Seepage Stage

Adsorption reveals obviously with the development of life source contaminants seeping. The suspended solid and organic matter generated through anaerobic decomposition of microorganism can be constantly adsorbed on the surface of clay particles nevertheless. Furthermore, A great variety of metabolites can be readily adsorbed on the clay particles and suspended solids intercepted without decomposing, resulting in a notable decline in porosity and in permeability.

90.3.3 Saturated Seepage Stage

With life source contaminants seeping, the clay may interact with the contaminants by means of chemical bonds, promoting soluble salts to insoluble compounds (carbonates and phosphates) through chemical reactions under a certain oxidation-reduction potential and pH value. The precipitates filling the clay pores can prevent fluid from permeating. Additionally, large amounts of reproduction of microorganisms in clay may preclude seeping. Consequently, the permeability of clay will still decrease when undergoing the saturated seepage by contaminated fluid.

Clay undergoes from saturated seepage stage to medium seepage stage, and to primary seepage stage. First of all, the upper part of clay which is near to the waste layer will reach to saturated stage, where suspended solids, organic matters and insoluble carbonates from chemical reactions between clay and the life source contaminants are created, then, clay pore will be clogged, and the distribution of macro-pore and medium-pore will be lessened. In summary, specifically, such role as ion exchange, adsorption, the deposition of suspended solid and organic matter, the dissolution of soluble salts and insoluble salt precipitation by complex chemical reactions between the clay and life source contaminants take diverse influence on the clay permeability during the different seeping stage.

90.4 Conclusions

The clay suffered from the life source contaminants decrease in permeability because of a significant reduction in porosity and pore size. The clay presents a gradual enhancement in permeability for the transformation of well-to-poorly saturated effects with the pollution depth increasing. The correlation between microstructure and permeability coefficient is developed.

In the three seeping stage, such actions as ion exchange, adsorption, the deposition of suspended solid and organic matter, the dissolution of soluble salt and insoluble salt precipitation play a different role on the clay permeability.

References

Al-Mukhtar M, Khattab S, Alcover JF (2012) Microstructure and geotechnical properties of lime-treated expansive clayey soil. Eng Geol 139–140:17–27

Bogas JA, Gomes A, Gomes MG (2012) Estimation of water absorbed by expanding clay aggregates during structural lightweight concrete production. Mater Struct/Materiaux et Constructions 45(10):1565–1576

Negim O, Eloifi B, Mench M et al (2010) Effect of basic slag addition on soil properties, growth and leaf mineral composition of beans in a cu-contaminated soil. Soil Sediment Contam 19(2):174–187

Shi B, Jiang HT (2001) Research on the analysis techniques for clayey soil microstructure. Chin J Rock Mech Eng 20(6):864–870 (in Chinese)

Zhu CP, Liu HL, Shen Y (2011) Laboratory tests on shear strength properties of soil polluted by acid and alkali. Chin J Geotech Eng 33 (7):1146–1152 (in Chinese)

Diffusion of La^{3+} in Compacted GMZ Bentonite Used as Buffer Material in HLW Disposal

91

Yonggui Chen, Lihui Niu, Yong He, Weimin Ye, and Chunming Zhu

Abstract

It has been studied that the GMZ bentonite which has a chemical barrier property can play an important role in retarding the migration of radioactive nuclide. In order to understand the diffusion properties of nuclide in GMZ bentonite, a series of experiments were conducted to obtain the apparent diffusion coefficient of La^{3+} in GMZ bentonite under different dry density and pH value conditions using a autonomous ion diffusion instrument. The results show that the apparent diffusion coefficient of La^{3+} decreases significantly with the increasing dry density or pH value. The influence of dry density on the diffusion is very apparent for a low dry density, and the influence gradually slow down with the increase of dry density. At last the influence mechanism of the dry density and pH value on diffusion coefficient was also analyzed.

91.1 Introduction

The deep geological disposal which based on a multi-barrier system is the most appropriate means for safe disposal of high-level radioactive waste (HLW). Bentonite has been chosen as the buffer/backfill material for this disposal because of good mechanical buffer resistance, low permeability, better swelling property and adsorption property (Wen 2006).

The chemical barrier properties of bentonite are mainly manifested in retarding the migration of radioactive nuclide. Considering most of the nuclide uranium, thorium, plutonium in disposal repository are actinide elements, and lanthanide and actinide elements have similar electronic configuration inside and outside layer which determine their similar physical and chemical properties. Therefore the lanthanide ions are always selected instead of radionuclide in the study. In this work, effects of the dry density and pH value on the diffusion property of La^{3+} in GMZ bentonite were studied.

91.2 Experimental

91.2.1 Materials

The GMZ bentonite derived from inner mongolia China was used in this experiment. Its major mineral is (Wang and Su 2006): montmorillonite 75.4 %, quartz 11.7 %, crystaballite 7 %, feldspar 4.3 %, calcite 0.5 %, kaolinite 0.8 %. It has been studied that GMZ bentonite has strong cation exchange capacity, hydration ability and strong adsorption ability.

Y. Chen (✉) · L. Niu · Y. He · W. Ye · C. Zhu
Tongji University, 1239 Siping Road, Shanghai 200092,
People's Republic of China
e-mail: cyg@tongji.edu.cn

Y. Chen · Y. He
Changsha University of Science and Technology,
Changsha 410114, People's Republic of China

91.2.2 Experiment

The instrument used in this experiment is a self-designed ion diffusion instrument consists of an organic glass shell and two stainless steel rings. Before the diffusion, the soil was saturated and then the bottom of the instrument was controlled being impervious. During diffusing, the ion migrated along a single direction. Therefore the flow velocity of water in the soil is zero, which can be regarded as pure diffusion of ions.

The GMZ bentonite samples with the diameter of 20 mm and the thickness of 30 mm were prepared with different dry density. Each test would last about 90 days at a given dry density and pH value. After diffusion, the bentonite was cut into 2 mm thick slices and then dissolved in 30 ml 0.5 M HCl solution for 24 h. The amount of La^{3+} in the slice was measured by ICP. One-dimensional non-steady-state diffusion of La^{3+} in compacted GMZ bentonite can be described by Fick's second law:

$$\frac{\partial c}{\partial t} = D\frac{\partial^2 c}{\partial x^2} \tag{1}$$

where D is the diffusion coefficient in compacted bentonite (m^2/s), C is the La^{3+} concentration in diffusion solution (mol/l), t is the diffusion time (s) and x is the distance from the diffusion source (m).

91.3   Results and Discussion

The results are illustrated in Table 91.1. Table 91.1 shows that the apparent diffusion coefficient of La^{3+} for the soils with the dry density of 1.3, 1.5 and 1.7 g/cm^3 under different conditions.

91.3.1 Effect of Dry Density on the Diffusion

It can be seen from the Table 91.1 that the apparent diffusion coefficient of La^{3+} decreases notably with increasing dry density. It is obvious that the dry density paly an important role on the diffusion coefficient for the low dry density soils.

Table 91.1 The results of La^{3+} diffused in compacted GMZ bentonite

Test	Dry density (g/cm^3)	Solution concentration (mol/L)	pH	Diffusion time (s)	D_a ($\times 10^{-12}$ m^2/s)
(1)	1.3	5.2×10^{-3}	7.5	6.840×10^6	15.82
(2)	1.5	5.2×10^{-3}	7.5	5.849×10^6	3.018
(3)	1.7	5.2×10^{-3}	8.9	8.533×10^6	2.513
(4)	1.7	5.2×10^{-3}	7.5	7.236×10^6	2.708

With the increase of dry density, the influence gradually slows down. The mechanism of the influence of dry density on the ion diffusion basically can be explained as following: (1) Changes of dry density affects ion distribution coefficient which affect the ion diffusion coefficient. The soil with a high dry density has a large surface area, and it could adsorb more cationic relatively than that with a low dry density. This resulted in the ion distribution coefficient increased thus the diffusion coefficient decreased (Muurinen and Lehikoinen 1995). (2) Elevated dry density decreases the effective porosity of the bentonite which results in a decrease in diffusion coefficient (Sawatsky and Oscarson 1991). (3) Changes of dry density affects the layer spacing. With the increase of dry density, layer spacing of bentonite decreases, and lead to the ion diffusion coefficient decreases (Kozaki et al. 2005). (4) Changes of dry density cause the main diffusion process changed which lead to the changes of diffusion coefficient (Wang 2003).

91.3.2 Effect of PH on the Diffusion

Table 91.1 also showed that the apparent diffusion coefficient of La^{3+} decreases slightly with increasing pH value.

The influence mechanism of pH value on the ion diffusion coefficient can be explained that the change of pH value affects the absorption of ions in bentonite. Quite a few scholars have done some works on the effect of pH value on ions diffusion. Wang (2003), Wang and Chen (2004) and Wang and Liu (2004) studied the effects of pH value on the diffusion of Cs, Sr and Eu ions in compacted MX-80 bentonite and found the adsorption of ions increased with the increasing of pH, which lead to the diffusion coefficient of ions decrease. Giannakopoulou and Haidouti (2007) studied the diffusion of Cs ion under different pH and found the similar results. The adsorption of Cs is less under low pH value and, the adsorption is maximum when the pH increase to 8. Because of the competitive adsorption of H^+ and Cs^+ leading to the adsorption of Cs^+ decreases under low pH. With the increase of pH, the negative charge on the surface of the bentonite increased and then resulted in the Cs^+ adsorption increased sharply.

91.4   Conclusions

1. A self-designed apparatus was conducted to study the diffusion characteristics of rare earth ions in the compacted GMZ benotnite used as Chinese buffer/backfilling material in the HLW disposal.
2. The diffusion coefficient of La^{3+} in the compacted GMZ bentonite decreases notably with increasing dry density.

3. The diffusion coefficient of La^{3+} in the compacted GMZ bentonite decreases slightly with increasing pH value.

References

Giannakopoulou F, Haidouti C (2007) Sorption behavior of cesium on various soils under different pH levels. J Hazard Mater 149:553–556

Kozaki T, Fujishima A, Saito N et al (2005) Effects of dry density and exchangeable cations on the diffusion process of sodium ions in compacted montmorillonite. Eng Geol 81:246–254

Muurinen A, Lehikoinen J (1995) Evaluation of phenomena affecting diffusion of cations in compacted bentonite. Nuclear Waste Commission of Finnish Power Companies, YJT-95-05, p 70

Sawatsky NG, Oscarson DW (1991) Diffusion of technetium in dense bentonite. Water Air Soil Pollut 57–58:449–456

Wang J, Su R (2006) Deep geological disposal of high-level radioactive waste in China. Chin J Rock Mech Eng 25(4):649–658

Wang XK, Chen YX (2004) Diffusion of Eu(III) in compacted bentonite—effect of pH, solution concentration and humic acid. Appl Radiat Isot 60:963–969

Wang XK, Liu XP (2004) Effect of pH and concentration on the diffusion of radiostrontium in compacted bentonite—a capillary experimental study. Appl Radiat Isot 61:1413–1418

Wang XK (2003) Diffusion of ^{137}Cs in compacted bentonite: Effect of pH and concentration. J Radioanal Nucl Chem 258(2):315–319

Wen ZJ (2006) Physical property of China's buffer material for high-level radioactive waste repositories. Chin J Rock Mech Eng 25 (4):794–800

Yongfu Xu and Ling Cao

Abstract

The mechanical properties of unsaturated soils are a function of matric suction, and can be obtained based on currently available procedures. However, each procedure has its limitations and consequently cares should be taken in the selection of a proper procedure. Fractal approach seems to be a potentially useful tool to describe hierarchical systems and is suitable to model the pore structure of unsaturated soils. In this paper, the soil–water characteristics (SWC), unsaturated hydraulic conductivity function and unsaturated shear strength were derived from the fractal model for the pore-size distribution (PSD), and were expressed by only two independently physical parameters, the fractal dimension and air-entry value. The predictions of the proposed soil–water characteristics, unsaturated hydraulic conductivity and unsaturated shear strength were in good accord with the published experimental data.

92.1 Introduction

The matric suction is an important stress state variable to express the mechanical properties of unsaturated soils. The relationship between the matric suction (ψ) and the radius (r) of the incurvated surface between pore-air and pore-water is expressed by the Young-Laplace equation, here is written as $\psi = 2\sigma\cos\alpha/r$, here ψ is the matric suction, σ is the surface tension, α is the contact angle. The mechanical properties of unsaturated soils are correlated to the microstructures of soils through the Young-Laplace equation.

The pore-size distribution (PSD) can be described by a fractal model because pores are invariable at any characterized scale used to examine them (Xu and Sun 2002). Fractal dimensions can be defined in connection with real-world data, and they can be measured approximately by means of experiments (Mandelbrot 1982). In this paper, the pore-size distribution was studied using fractal theory, and soil–water characteristics (SWC), hydraulic conductivity and shear strength of unsaturated soils were deduced from the fractal model for the soil pore-size distribution.

92.2 Soil–Water Characteristics

For fractal pore-size distribution (PSD), a power-law existing between the scale of measurement (r) and the pore phase of Eq. (1).

$$N(A, r) = Cr^{-D} \qquad (1)$$

for some positive constant C. The total volume of the pores with the radius less than r is given by

$$V_p = \int_0^r N4\pi r\,dr = Ar^{3-D} \qquad (2)$$

Y. Xu (✉) · L. Cao
Shanghai Jiao Tong University, 800 Min Hang Road,
Shanghai 200240, China
e-mail: yongfuxu@sjtu.edu.cn

where $A = 4\pi CD/(3 - D)$. Fractal dimension spans a large range from 1.0 to 3.0.

The pore water within unsaturated soils can be divided into three forms (Wheeler and Karbue 1996) (Fig. 92.1): bulk water within those void spaces that are completely flooded, meniscus water surrounding all inter-particle contact points that are not covered by bulk water and absorbed water (which is tightly bounded to the soil particles and acts as parts of the soil skeleton). When the volumetric water content is less than its residual value, the pore-water is tightly absorbed by soil particle and cannot move freely and seen as a part of soil particles. The contribution of the filled pores with radius $r \rightarrow r+dr$ to the water content is given by

$$dA = N4\pi r^2 dr / V_T \quad (3)$$

where A is the relative volumetric water content, and $A = \theta - \theta_r$, θ and θ_r are the actual and residual volumetric water content, respectively. The residual volumetric water content is the volumetric water content at which the effectiveness of matric suction to cause further removal of water requires vapour migration. Combining Eqs. (1) and (3) with the Young-Laplace equation, the soil–water characteristic curve is obtained as follows

$$S_e = \left(\frac{\psi}{\psi_e}\right)^{D-3} \quad (4)$$

where S_e is the effective degree of saturation, and $S_e = A/A_s$, ψ_e is the air-entry value, $\psi_e = 2\sigma\cos\alpha/R$, R is the maximum radius of soil pores. The residual volumetric water content θ_r is not always made routinely, in which case it has to be estimated by extrapolating available soil–water characteristics data towards lower water content, such as shown in Fig. 92.1.

Figure 92.2 shows the soil pore-size distribution obtained from mercury intrusion porosimetry (Watabe et al. 2000). It is obtained that the fractal dimensions of the pore-size distribution of S-02, S-03 and S-04 are 2.66, 2.63 and 2.51, respectively. The maximum radius is the radius at which the pore volume reaches the maximum value, and is defined as the intersection between the fitting line and the line of $V_p/V_T = 100\%$, here V_T is the total volume of soil pores. The maximum radium of the soil pores of S-02, S-03 and S-04 are 0.125 mm, 0.06 mm and 0.006 mm, respectively. According to the Young-Laplace equation, the air-entry values of S-02, S-03 and S-04 are 12.5, 2.5 and 25 kPa, respectively.

The soil–water characteristic curves are predicted using Eq. (4) for the soils of S-02, S-03 and S-04. The air-entry value and fractal dimension of S-02, S-03 and S-04 are obtained from Fig. 92.2. Predictions of Eq. (4) show in good accord with the experimental data of the soil–water characteristic curve in Fig. 92.3.

92.3 Unsaturated Hydraulic Conductivity

The relatively hydraulic conductivity (k_r) is the ratio of the hydraulic conductivity at any degree of saturation (k_w) to the hydraulic conductivity at saturation (k_s). The relative hydraulic conductivity is related to the radius of the soil pores and the pore-size distribution (Mualem 1976). Using the fractal pore-size distribution and the Young-Laplace equation, Xu (2004a) gave the relative hydraulic conductivity

$$k_r = \left(\frac{\psi}{\psi_e}\right)^{3D-11} \quad (5a)$$

$$k_r = S_e^{(3D-11)/(D-3)} \quad (5b)$$

Fig. 92.1 Pore-water formation in soils
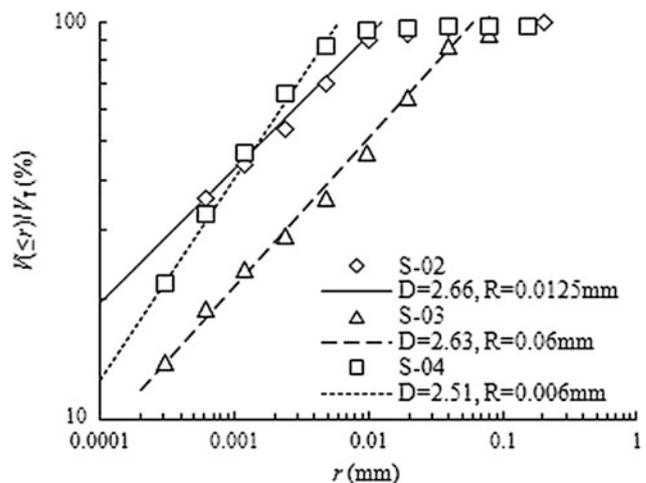
Fig. 92.2 Fractal model for PSD
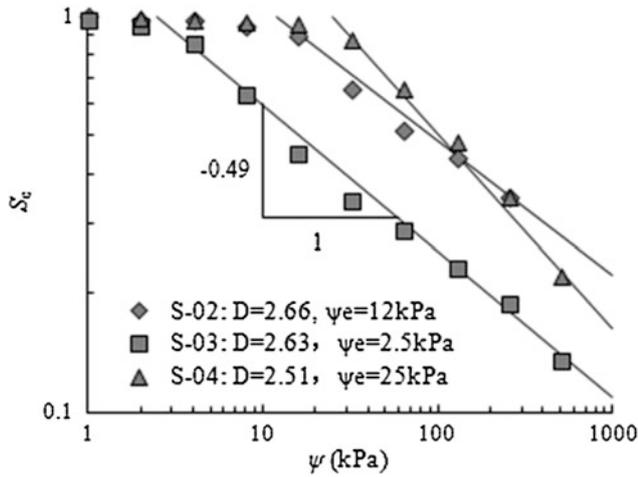
Fig. 92.3 Experiments versus prediction of SWC

Fig. 92.4 D and ψ_e obtained from SWC

The soil–water diffusivity (d) can be obtained from the unsaturated hydraulic conductivity and the soil–water characteristics, and is written as

$$d = k_s k_r |d\psi/d\theta| \tag{6}$$

Substituting Eqs. (5a) and (5b) into Eq. (6), it is obtained

$$d = k_s \psi_e \left(\frac{\psi}{\psi_e}\right)^{2D-7} \tag{7a}$$

$$d = k_s \psi_e S_e^{(2D-7)/(D-3)} \tag{7a}$$

Smettem and Kirkby (1990) gave the experimental data of the soil–water characteristics for haploxeroll loam, shown in Fig. 92.4. The fractal dimension is 2.63, and the air-entry value is 0.14 kPa obtained from Fig. 92.4. Using the fractal dimension and the air-entry value, the unsaturated hydraulic conductivity and the soil–water diffusivity can be predicted. The comparisons between the experimental data and the predictions of unsaturated hydraulic conductivity and the soil–water diffusivity are shown in Fig. 92.5.

92.4 Effective Stress and Unsaturated Shear Strength

The effective stress of unsaturated soils was given by Bishop and Blight (1963)

$$\sigma' = (\sigma_n - u_a) + \chi\psi \tag{8}$$

where ψ is matric suction, χ is a parameter related to the water content, and is written as (Xu 2004b)

$$\chi = \left(\frac{\psi}{\psi_e}\right)^{D-3} \tag{9}$$
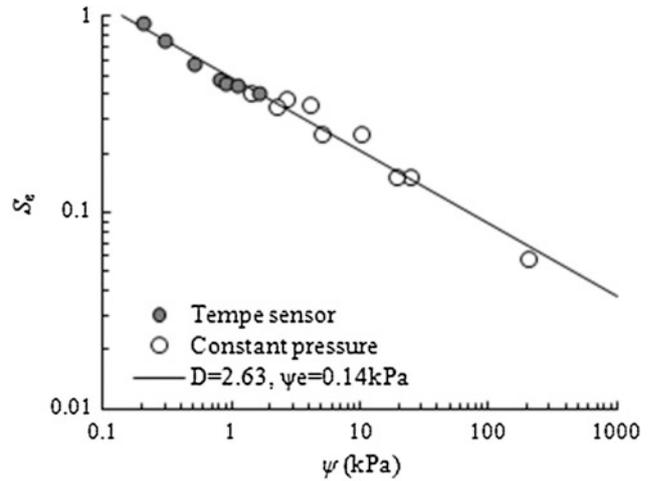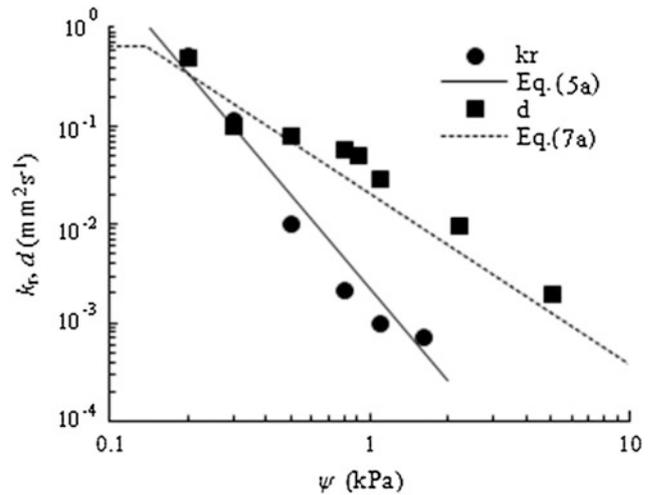
Fig. 92.5 Prediction of k_r and d

Substituting Eq. (9) into Eq. (8), effective stress of unsaturated soils is written as

$$\sigma' = (\sigma_n - u_a) + \psi_e^{3-D}\psi^{D-2} \tag{10}$$

According to the Mohr-Coulomb criteria and effective stress formula, the shear strength of unsaturated soils is given by

$$\tau_f = c' + (\sigma_n - u_a)\tan\phi' + \psi_e^{3-D}\psi^{D-2}\tan\phi' \tag{11}$$

Experimental data of the soil–water characteristics and shear strength with different matric suction and net stress of weathered granite soil were collected from Lee et al. (2005). The residual water content was nearly 10 % and increased with the net confining stress. The air-entry values were 2.3, 3.7, 5.1 and 6.5 kPa under net confining stress of 0, 100, 200
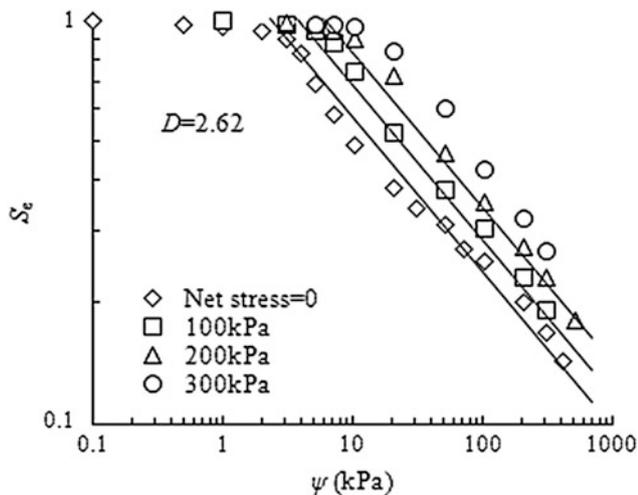
Fig. 92.6 D and ψ_e obtained from SWC

and 300 kPa, respectively given by Lee et al. (2005). Using the residual water content and the air-entry value, the fractal dimension of weathered granite soil can be evaluated from the soil–water characteristics. The fractal dimension of weathered granite soil was 2.60 obtained from Fig. 92.6. The effective shear strength parameters of weathered granite soil were also given by Lee et al. (2005). The effective cohesion (c') and internal friction angle (φ') were 20 kPa and 41.4°, respectively for weathered granite soil.

Using fractal dimension and the air-entry value, effective stress can be calculated from Eq. (10). The relationship between shear strength and effective stress was predicted and shown in Fig. 92.7. Experimental data of shear strength with
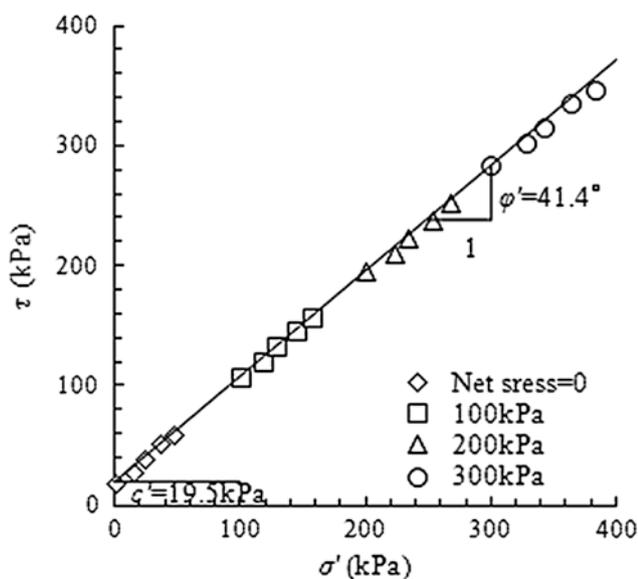
Fig. 92.7 Verification of shear strength

different matric suction and net normal stress were nearly located at the same line in the plane of τ–σ'. It is implied that effective stress expressed in Eq. (10) can well express the relationship between shear strength and effective stress. The prediction of shear strength using Eq. (11) was conducted using the effective shear strength parameters, the air-entry values and fractal dimensions. The effective shear strength parameters and air-entry values were given by Lee et al. (2005), and fractal dimensions were obtained from Fig. 92.6.

92.5 Conclusion

A new theoretical method is given to predict the soil–water characteristics, unsaturated hydraulic conductivity, unsaturated soil–water diffusivity, effective stress and shear strength in this paper. According to the results of mercury intrusion porosimetry, the soil pore-size distribution can be described by fractal model. Under the assumption of absorbed water being a part of the soil particle, the fractal model for the pore-size distribution is equivalent to that for the soil–water characteristics. That is, the fractal dimension and the air-entry value have the same values obtained from the pore-size distribution and the soil–water characteristics. The fractal dimension and the air-entry value obtained from the soil–water characteristics were successfully used to prediction unsaturated hydraulic conductivity and the soil–water diffusivity.

A new theoretical formula for the effective stress of unsaturated soils is presented in this paper. Two parameters, the fractal dimension and the air-entry value, in the effective stress formula can be obtained from the pore-size distribution and the soil–water characteristics. The proposed effective stress was verified by the experiments of unsaturated shear strength.

References

Bishop AW, Blight GE (1963) Some aspects of effective stress in saturated and unsaturated soils. Geotechnique 13:177–197

Lee IM, Sung SG, Cho GC (2005) Effect of stress state on the unsaturated shear strength of a weathered granite. Can Geotech J 42:624–631

Mandelbrot BB (1982) The fractal geometry of nature. W.H. Freeman, New York

Mualem Y (1976) A new model for predicting the hydraulic conductivity of unsaturated porous media. Water Res Res 12:513–522

Smettem KRJ, Kirkby C (1990) Measuring the hydraulic properties of a stable aggregate soil. J Hydrol 117:1–13

Watabe Y, Leroueil S, Le Bihan J-P (2000) Influence of compacted conditions on pore-size distribution and saturated hydraulic conductivity of a glacial till. Can Geotech J 37:1184–1192

Wheeler SJ, Karbue D (1996) Constitutive modeling. In: Alonso EE, Delage P, Proceedings of the 1st International Conference Unsat Soils AA. Balkema, Rotterdam

Xu YF, Sun DA (2002) A fractal model for soil pores and its application to determination of water permeability. Physica A 316:56–64

Xu YF (2004a) Calculation of unsaturated hydraulic conductivity using a fractal model for the pore-size distribution. Comput Geotech 31:549–557

Xu YF (2004b) Fractal approach to unsaturated shear strength. J Geotech Geoenviron Eng, ASCE 3:264–274

Thermal Effects on Chemical Diffusion in Multicomponent Ionic Systems

Hywel R. Thomas and Majid Sedighi

Abstract

A theoretical formulation for diffusion of multiple ions is presented in this paper which considers the effects of electrochemical and thermal diffusion potentials. The work presented is of relevance to applications such as the geological disposal of high level radioactive waste, where limited experimental information is available on ionic transfer in compacted clay buffer under non-isothermal conditions. The proposed approach incorporates the overall charge conservation in the formulation of multicomponent chemical diffusion. Thermal diffusion, i.e. Soret effect is studied in more detail by considering an explicit approach to include this process in the formulation. A detailed description of the theoretical developments is provided. A series of simulations using the proposed formulation is presented which involves pure diffusion of multiple ions under thermal gradients. The results are compared with experimental data reported in literature.

Keywords

Multicomponent chemicals • Thermal diffusion • Clay barrier • Theoretical modeling

93.1 Introduction

Understanding of chemical processes in clay buffer under thermal or thermo-hydraulic conditions is of key importance for safety assessment and design of engineered barrier systems proposed for geological disposal of high level radioactive waste. The transport of chemical ions in low permeability clays and more specifically in expansive clays is dominated by the diffusion mechanism. This in fact, is highly affected by the specific microstructure evolution and surface electrostatic forces of the clay minerals (Pusch and Yong 2006). As the result, the diffusion rate of an ionic species varies with the type of moving ion in the system. This requires the modelling of the process under different effective diffusion coefficients for different ions and under electrochemical potential effects (e.g. Appelo and Wersin 2007).

Under non-isothermal conditions, further developments and investigations of the diffusive behaviour of multicomponent chemicals, due to the effects of combined electrochemical and thermal diffusion potentials is desirable, in order to obtain a better understanding of the chemical processes under coupled THCM behaviour. This paper presents advances to the theoretical formulation of multicomponent chemical diffusion. In particular, a framework for coupling thermal diffusion with diffusion due to electrochemical potential is presented. This latter potential arises from the transport of ions with different rates of diffusion. A general equation for diffusion of multicomponent chemicals has been developed which considers coupled electrochemical and thermal diffusion potentials in multi-ionic systems. An approach has been incorporated for estimating the thermal diffusion coefficient or the Soret coefficient in the absence of sufficient experimental data in clays.

A comprehensive description of the new formulation developed and model application has been provided by Thomas et al. (2012). This paper aims to revisit the latter

H.R. Thomas (✉) · M. Sedighi
Geoenvironmental Research Centre, Cardiff University, Queen's Buildings, Newport Road, CF24 3AA, Cardiff, UK
e-mail: ThomasHR@cf.ac.uk

M. Sedighi
e-mail: SedighiM@cf.ac.uk

development with further focus on theoretical approach, governing equations and testing the model developed. A series of validation tests on the developments against experimental results reported in the literature are presented and a comparison between developed theoretical formulation and experimental data is provided.

93.2 Theoretical Model Development

It is well established that under non-isothermal conditions, a temperature gradient can also induce mass flow due to thermal diffusion, i.e. Soret-Ludwig effect or Soret effect. Therefore, electrochemical diffusion has to be coupled with thermal diffusion in order to obtain an overall understanding of the combined effects. Modelling the diffusion of multi-component chemicals considering solely the electrochemical effects (i.e. under isothermal conditions) has been well developed and applied for aqueous solutions, porous media and clays (e.g. Lasaga 1979; Appelo and Wersin 2007). Further development of the modelling of the combined diffusion process due to electrochemical and thermal diffusion potentials (i.e. under non-isothermal conditions) in multiple ionic systems is proposed here.

Thomas et al. (2012) showed that the diffusion flux presented in Eq. (1) can be presented in an expanded form, following Lasaga (1979) and Balluffi et al. (2005) as:

$$J_i^{\text{Diff}} = -\frac{D_i^0 c_i}{RT} \frac{\partial \mu_i}{\partial c_i} \nabla c_i - \frac{D_i^0 c_i}{RT} F z_i \nabla \Phi - \frac{D_i^0 c_i}{RT} \frac{Q_i^*}{T} \nabla T \quad (1)$$

where, the first term of the equation represents the diffusion flux due to the chemical potential, the second term denotes diffusion due to electrical potentials and the third term represents the thermal diffusion. D_i^0 and c_i is the tracer diffusion coefficient and concentration of the subscripted component. R denotes the gas constant. μ_i represents the chemical potential and z_i is the charge of the ion of the ith chemical component. F denotes the Faraday's constant, Φ refers to the electrical potential of the solution and T is the absolute temperature. Q_i^* represents the "heat of transport" of the ith chemical component which corresponds to the energy state of the diffusing ions in the regions with different temperatures which directly corresponds to the entropy of transport (Agar et al. 1989; Balluffi et al. 2005).

Substituting the electrical potential calculated and the derivative of chemical potential with respect to chemical concentration, the expanded form of diffusion flux equation is obtained, given as:

$$J_i^{\text{Diff}} = -D_i^0 \left(1 + \frac{\partial \ln \gamma_i}{\partial \ln c_i} \right) \nabla c_i + \frac{z_i D_i^0 c_i}{\sum_{k=1}^{nc} z_k^2 D_k^0 c_k} \sum_{j=1}^{nc} z_j D_j^0 \left(1 + \frac{\partial \ln \gamma_j}{\partial \ln c_j} \right)$$
$$- \frac{D_i^0 c_i}{RT} \frac{Q_i^*}{T} \nabla T + \frac{z_i D_i^0 c_i}{\sum_{k=1}^{nc} z_k^2 D_k^0 c_k} \sum_{j=1}^{nc} \frac{z_j D_j^0 c_j}{RT} \frac{Q_j^*}{T} \nabla T$$

$$(2)$$

where, γ_i is the activity coefficient of the ith chemical component. nc represents the number of chemical components in the solution.

The above equation represents the diffusion process comprising two main compartments of chemical (molecular) diffusion (the first two terms on the right hand side of the equation) and thermally induced mass diffusion (the second two terms on the right hand side of the equation) incorporated the effects related to the electrical potential sourcing from different diffusion coefficients.

Limited experimental information on thermal diffusion effects and the coefficients is available for mixed electrolyte systems and clays. In the absence of sufficient experimental data, a theoretical approach is adopted here to study the overall effects of thermal diffusion. In aqueous solutions, the heat of transport for single chemical in a dilute solution can be related to the thermal diffusion coefficient or the Soret coefficient (Agar et al. 1989). Accordingly, the heat of transport of the ith component in solution can be obtained as a function of ion tracer diffusion and its valence, given as (Agar et al. 1989):

$$Q_j^* = A z_i^2 D_i^0 \left(1 + \frac{\partial \ln \gamma_i}{\partial \ln c_i} \right) \quad (3)$$

where, A is a constant value, i.e. 2.20×10^{12} and 2.20×10^{12} depending on the hydrodynamic boundary conditions (Agar et al. 1989).

In a general form, the diffusive transport of the ith chemical component in pore water of the clay, considering the diffusion flux comprising chemical and thermal components can be presented:

$$\frac{\partial \theta_l c_i}{\partial t} + \frac{\partial \theta_l s_i}{\partial t} = -\nabla \cdot \sum_{j=1}^{nc} \tau_i \theta_l D_{ij}^0 \nabla c_j - \nabla \cdot \sum_{j=1}^{nc} \tau_i \theta_l D_{ij}^T \nabla T$$

$$(4)$$

where θ_l stands for the volumetric liquid content and s_i stands for the sink/source term related to the geochemical reactions at which the ith component is produced or depleted by the reactions. τ_i is the tortuosity factor of the porous

medium which can be different for anions and cations in clays. The molecular diffusion coefficient, i.e. D_{ij}^0 and thermal diffusion coefficient, i.e. D_{ij}^T, can be presented according to the theoretical developments presented above as:

$$D_{ij}^0 = -\delta_{ij} D_i^0 \left(1 + \frac{\partial \ln \gamma_i}{\partial \ln c_i} \right) + \frac{z_i D_i^0 c_i}{\sum_{k=1}^{nc} z_k^2 D_k^0 c_k} z_j D_j^0 \left(1 + \frac{\partial \ln \gamma_j}{\partial \ln c_j} \right) \quad (5)$$

$$D_{ij}^T = -\delta_{ij} D_i^0 c_i \left(\frac{A z_i^2 D_i^0}{RT^2} \right) \left(1 + \frac{\partial \ln \gamma_i}{\partial \ln c_i} \right) + \frac{z_i D_i^0 c_i}{\sum_{k=1}^{nc} z_k^2 D_k^0 c_k} z_j D_j^0 c_i \left(\frac{A z_i^2 D_i^0}{RT^2} \right) \left(1 + \frac{\partial \ln \gamma_j}{\partial \ln c_j} \right) \quad (6)$$

where, δ_{ij} is the Kronecker's delta function which is equal to 1 when $i = j$ and equal to 0 when $i \neq j$. It is noted that the term $\left(\frac{A z_i^2 D_i^0}{RT^2} \right)$ represents the "Soret" coefficient, i.e. S_i^T, which is theoretically described here. This value can also be replaced by experimentally determined values.

The described formulation described was implemented in the chemical module of a coupled thermal, hydraulic, chemical and mechanical model (THCM), developed at the Geoenvironmental Research Centre (e.g. Thomas and He 1995; Thomas et al. 2012). Further details of formulation development and implementation have been provided by Sedighi (2011) and Thomas et al. (2012).

93.3 Theory Application and Validation

Theoretical formulation developed is examined via a series of thermal diffusion simulations developed based on similar experimental tests carried out by Leaist and Hui (1990). Two series of simulations are presented including (i) thermal diffusion of NaOH in water (binary solution) at four different concentrations and (ii) thermal diffusion of a mixed NaCl–NaOH solution in water (ternary solution). The simulations were performed once using the theoretical equation for the Soret coefficient using Eq. (3) and once using the Soret coefficients reported from results of experiments carried out by Leaist and Hui (1990). The results are compared and discussed.

The simulation exercises consisted of a cell in which the solution was subjected to a constant temperature gradient across the cell by fixing the temperature at 30 and 20 °C at the boundaries similar to the condition described in experimental research by Leaist and Hui (1990). Four initial concentrations of NaOH solutions were considered, i.e. 0.001, 0.005, 0.015 and 0.02 mol/l. The composition considered for simulations of the ternary solution of NaCl–NaOH was 0.005–0.015 (mol/l), i.e. [NaCl]/[NaOH] = 0.005/0.01g (mol/l).

The studied domain is 1 cm long which was discretised into 100 equally sized 4-noded quadrilateral elements for numerical analysis. The temperature was considered to be fixed at 20 and 30 °C at the boundaries. The initial temperature of the solution is 25 °C. Different diffusion coefficients have been considered for the involved chemical components. The tracer diffusion coefficients of Na$^+$, Cl$^-$ and OH$^-$ions in the simulations are 13.3×10^{-10}, 20.3×10^{-10} and 52.7×10^{-10} m^2/s, respectively (Lasaga 1979).

Figure 93.1 presents the results of simulations in terms of concentration variation with distance from cold boundary at steady state for NaOH solution (Case I) and NaCl–NaOH solution (Case II) analysed, respectively. The results presented by "lines" are related to simulations in which the theoretical approach for the Soret coefficient in Eq. (3) whilst the results presented by "symbols are those achieved based on the experimentally determined Soret values reported by Leaist and Hui (1990). The values of the Soret coefficient associated with each concentration in the graphs represent the average value of the Soret coefficients reported by Leaist and Hui (1990).

Fig. 93.1 Results of simulations depicting the concentration profiles at steady state of the NaOH-water binary solutions at different concentrations (Case I) and NaOH–NaCl-water ternary solution (Case II)
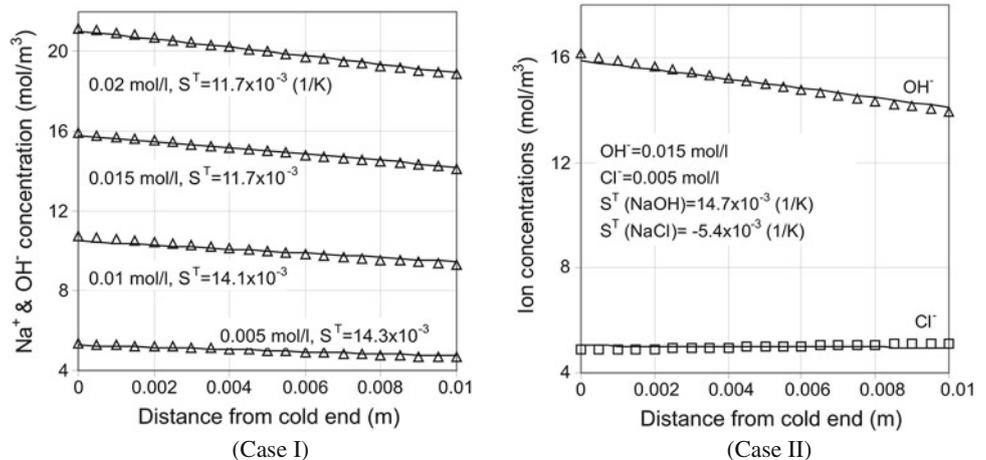
The simulation results show a close agreement between the theoretical approach adopted for thermal diffusion and the experimental values reported by Leaist and Hui (1990). The results show a good correlation between simulations based on the adopted approach and on the experimentally determined values for the Soret coefficient in the case of OH$^-$ ions.

In the case of the ternary solution, Leaist and Hui (1990) reported negative values for the Soret coefficient for NaCl. This implies that in the ternary solutions, chloride ions tend to move toward hot side in contrast with the general trend observed in binary solutions. The trend observed in this case using the theoretical approach does not represent a reverse process; however the mode generated very close correlation with the results using the experimentally reported values for the Soret coefficient.

Comparison between the results of the simulations on ternary and binary solutions indicates that: (i) coupling the chemical and electrical effects has increased the rate of chloride diffusion away from heat source and (ii) the rate of diffusion towards the colder side for OH$^-$ ions has shown an increase in compassion with the binary solution. The behaviour observed is related to the application of the electro-neutrality conditions in the formulation developed.

Since different diffusion coefficients are used in the simulation, the overall charge must be conserved during the analysis according to the formulation of diffusion developed. The model results for all simulations conserve the overall charge during the analysis and at steady state, verifying the transport equation for multicomponent chemicals under coupled electrochemical and thermal diffusion potentials.

93.4 Conclusions

Application of the theoretical approach proposed is of interested in problems such as chemical behaviour of compacted bentonite under high level radioactive waste repository conditions. Further insight into the diffusion of ions in multicomponent system of compacted clays can be achieved using presented model.

The approach proposed considers the effects of electro-chemical and thermal potentials on the diffusion of multi-component chemicals under coupled conditions. The model incorporates the overall charge conservation in the formulation of multicomponent chemical transport both on molecular and thermal diffusion. The theoretically determined the Soret coefficients provide values close to the experimentally reported values for ionic species based on the validation example provided in this paper. The approach proposed can be used and extended to study the behaviour of multiple ions present in clay-water system under thermal effects.

References

Agar JN, Mou CY, Lin J (1989) Single-ion heat of transport in electrolyte solutions: a hydrodyamic theory. J Phys Chem 93:2079–2082

Appelo CAJ, Wersin P (2007) Multicomponent diffusion modeling in clay systems with application to the diffusion of tritium, iodide and sodium in Opalinus clay. Environ Sci Technol 41:5002–5007

Balluffi RW, Allen SM, Carter WC (2005) Kinetics of materials. Wiley Interscience, Wiley

Lasaga AC (1979) The treatment of multicomponent diffusion and ion pairs in diagenetic fluxes. Am J Sci 279:324–346

Leaist DG, Hui L (1990) Conductometric determination of the Soret coefficients of a ternary mixed electrolyte, Reversed thermal diffusion of sodium chloride in aqueous sodium hydroxide solutions. J Phys Chem 94:45–447

Pusch R, Yong RN (2006) Microstructure of smectite clays and engineering performance. Taylor and Francis, London

Sedighi, M (2011) An investigation of hydro-geochemical processes in coupled thermal, hydraulic, chemical and mechanical behaviour of unsaturated soils. Ph.D. Thesis, Cardiff University, UK

Thomas HR, He Y (1995) Analysis of coupled heat, moisture, and air transfer in a deformable unsaturated soil. Géotechnique 45:677–689

Thomas HR, Sedighi M, Vardon PJ (2012) Diffusive reactive transport of multicomponent chemicals under coupled thermal, hydraulic, chemical and mechanical conditions. Geotech Geol Eng 30 (4):841–857

W.M. Ye, Wei Su, Miao Shen, Y.G. Chen, and Y.J. Cui

Abstract

Highly compacted sand-bentonite mixtures are commonly recognized as potential buffer/backfill materials using in deep geological repository for high-level radioactive waste disposals. After water retention curve was determined, instantaneous profile method was employed in this paper for measuring unsaturated hydraulic conductivity of highly compacted GMZ01 bentonite and quartz sand mixture (7:3), with a dry density of 1.90 g/cm^3, under confined conditions. Results show that, as suction decreased from 60 MPa to zero, the measured unsaturated hydraulic conductivity firstly decreased and then turned to increase. This phenomenon can be explained in terms of microstructure changes during hydration under constant-volume conditions.

Keywords

GMZ01 bentonite • Sand-bentonite mixture • Unsaturated hydraulic conductivity • Suction • Constant volume

94.1 Introduction

As one of the key properties of buffer/backfill materials, the hydraulic property of the compacted bentonite has drawn much attention. Dixon et al. (1987) tested the hydraulic conductivity of saturated compacted bentonites and analyzed the related influencing factors; Komine (2004) predicted the saturated permeability of bentonite based on porosity changes. For the unsaturated bentonite, Cui et al. (2008) found that with suction decreases, the unsaturated permeability decreases to a certain value and then turns to increase under both confined and unconfined conditions. Ye and Qian (2009), Ye et al. (2010) obtained the similar conclusion by testing on GMZ01 bentonite.

GMZ bentonite is a preferable buffer/backfill material for Chinese deep geological disposal program. Under confined conditions, the unsaturated hydraulic conductivity of the highly compacted GMZ bentonite (1.70 g/cm^3) changes from 1.13×10^{-13} to 8.41×10^{-15} m/s (Ye and Qian 2009). While under unconfined conditions, it is about 1.0×10^{-12}–1.0×10^{-15} m/s (Ye et al. 2010). Based on Kozeny-Carmen semi-empirical function, Niu et al. (2009) proposed a semi-empirical equation for the calculation of unsaturated hydraulic conductivity of GMZ01 bentonite with consideration of micro-structural changes.

In this paper, water retention curves of compacted quartz sand-GMZ01 bentonite (3:7) mixture are determined under confined conditions. Humidity controlled hydration test was conducted to measure the evolutions of relative humidity at different locations along axial direction of the cylindrical specimen. The instantaneous profile method was employed

W.M. Ye · W. Su (✉) · M. Shen · Y.G. Chen · Y.J. Cui
Key Laboratory of Geotechnical and Underground Engineering of Ministry of Education, Tongji University, Shanghai, 200092, China
e-mail: suweiown@163.com

W.M. Ye
e-mail: ye_tju@tongji.edu.cn

W.M. Ye
United Research Center for Urban Environment and Sustainable Development, The Ministry of Education, Beijing, China

Y.J. Cui
Laboratoire Navier, Ecole des Ponts ParisTech, Paris, France

for obtaining the unsaturated hydraulic conductivity. Mechanism was analyzed from the microstructure aspect.

94.2 Materials

A mixture of quartz sand and GMZ01 bentonite (3:7) was used. A dry density of 1.90 g/cm^3 for compacted specimen was chosen in order to obtain an equivalent dry density of 1.70 g/cm^3 for bentonite in the mixture.

GMZ01 bentonite contains chemical compositions of SiO_2, Al_2O_3 and H_2O. It has specific gravity of 2.66, Liquid limit and plastic limit are 276 and 37 %, respectively. Total specific surface area is 570 m^2/g. Cation exchange capacity is 77.30 mmol/100 g. Dominant exchange cations are Na$^+$ (43.36 mmol/100 g), Ca^{2+} (29.14 mmol/100 g), Mg^{2+} (12.33 mmol/100 g) and K$^+$ (2.51 mmol/100 g). Main mineral compositions: 75.4 % montmorillonite, 11.7 % quartz, 4.3 % feldspar and 7.3 % cristobalite.

Quartz sand used originates from Fengyang, Anhui province, China. Chemical compositions of the sand are SiO_2 (99.20 %), Al_2O_3, Fe_2O_3 and CaO. particle size is 0.075–0.1 mm, specific gravity is 2.65.

94.3 Experiments

94.3.1 Determination of Water Retention Curves

For determination of water retention curves of specimens under constant volume conditions, the osmotic technique and vapor equilibrium technique were employed. Suctions of 309, 110, 82, 21, 9 and 4 MPa (vapor equilibrium technique), as well as 0.1 and 0.01 MPa (osmotic technique) were conducted.

94.3.2 Unsaturated Infiltration Test

Specimen preparation. Quartz sand and GMZ01 bentonite were carefully mixed (3:7) and fully stirred to a uniform state. Initial water content of the mixture was equilibrated to 9 %. Then, the mixture was compacted to 150 mm in height, 50 mm in diameter and dry density of 1.90 g/cm^3 using a custom-designed compaction mold. The cylindrical specimen was compacted in three layers in order to ensure the whole homogeneity.

Apparatus and unsaturated hydraulic conductivity test. The apparatus used by Ye and Qian (2009) was employed in this study. After removing from compaction model, compacted specimen was pushed into the cell immediately and sealed in the cell, kept for days until the homogeneity was reached. Then infiltration test was started with water being injected into the specimen through the inlet at the bottom of the cell under 1 m waterhead, i.e., 10 kPa. The volume of infiltrated water was recorded using the pressure-volume controller. Variations of humidity were recorded by five sensors, among which four were fixed (equal-spaced) on the sidewall and one in the upper plate of the cell. When the humidity near water inlet approached to saturation, the test was finished.

94.4 Results and Analyses

Water retention characteristics. Figure 94.1 shows the measured water retention curve of the specimen. It is obvious that the water content of the mixture increases at a declining rate as suction decreasing, which is consistent with reports of Chen et al. (2006) about compacted GMZ bentonite.

Unsaturated hydraulic conductivity. Evolutions of humidity with time of the specimen (Fig. 94.2) shows that the relative humidity at 30 mm from the inlet reaches 90 % after 300 h hydration, 1,200 h for the same value at 60 mm. While much more time needs for other locations.

With results in Figs. 94.1 and 94.2, suction profile and hydraulic head profile can be determined. Then hydraulic gradient and water flux can be calculated. Based on Darcy's law, the variation of hydraulic conductivity with suction (Fig. 94.3) was calculated by the following equation:

$$k_w = -\frac{1}{A} \cdot \frac{q}{\frac{1}{2}[i_t + i_{t+\Delta t}]} \tag{94.1}$$

where A is cross-section area of specimen; q is water flux; i_t is hydraulic gradient at time t.
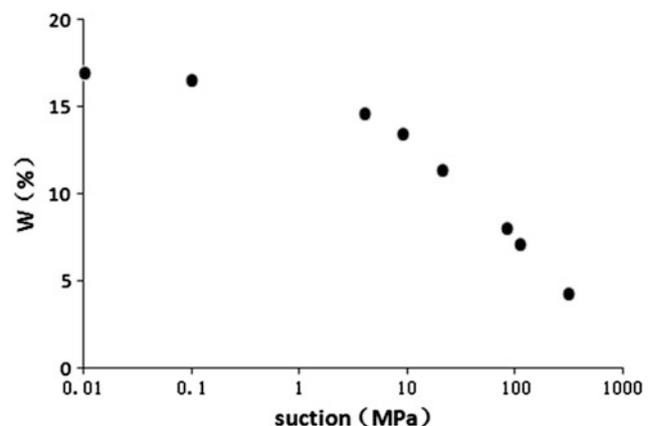
Fig. 94.1 SWRC of confined compacted sand-GMZ01 bentonite mixture
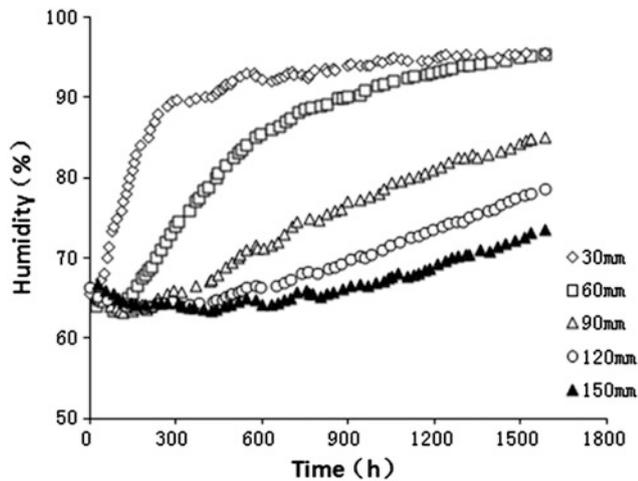
Fig. 94.2 Evolutions of humidity with time of the sand-GMZ01 bentonite mixture
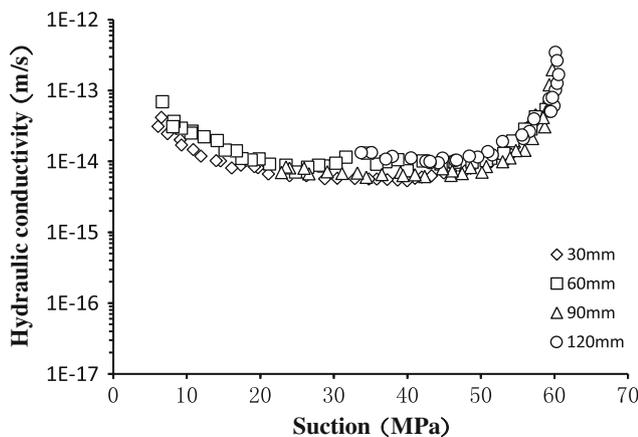
Fig. 94.3 Unsaturated hydraulic conductivity evolves with suction

94.5 Discussion

Figure 94.3 indicates that the unsaturated hydraulic conductivity of the confined specimen firstly decreases (30–60 MPa) and then turns to increase (6–30 MPa) with decreasing suction. Literatures point out that two contrasting processes and their interactions are responsible for this phenomenon. During hydration, bentonite particles expand into macro-pores during wetting under confined conditions, leading to a decrease of the macro-pore volume, thus the unsaturated hydraulic conductivity decreases (Cui et al. 2002). Meanwhile, the flowing area in the compacted mixture increases with decreasing suction, resulting in an increase of the unsaturated hydraulic conductivity (Benson and Gribb 1997).

At the beginning of hydration, the effective flow is largely dependent on the cross-sectional area of existing porous channels. As the hydration continues, on the one hand, clay expands, occupying the effective flow channels; on the other hand, gels of clay particles exfoliated from larger aggregates or grains fill the channels, especially the wider ones, and reorganize there, resulting in the clogging of water path. This phenomenon can lead to hydraulic conductivity decrease (Pusch et al. 2012). With suction sequentially reducing, the effect of bentonite expansion is getting weaker, the increasing of effective flow cross-sectional area due to the diffusional character of water makes hydraulic conductivity increase (Pusch and Yong 2003).

94.6 Conclusion

The hydraulic conductivity of sand-GMZ01 bentonite mixture under confined conditions firstly decreases and then turns to increase with the suction decreasing. This variation law is similar to the hydraulic conductivity of pure bentonite under confined conditions.

References

Benson CH, Gribb MM (1997) Measuring unsaturated hydraulic conductivity in the laboratory and field. In: Unsaturated soil engineering practice, New York, ASCE, 0-7844-0259-0. Geotechnical Special Publication No. 68, pp 113–168, 344

Chen B, Qian LX, Ye WM, Cui YJ, Wang J (2006) Soil-water characteristic curves of Gaomiaozi bentonite. Chin J Rock Mech Eng 25:788–793

Cui YJ, Loiseau C, Delage P (2002) Microstructure changes of a confined swelling soil due to suction controlled hydration. In: Jucá JFT, de Campos TMP, Marinho FAM (eds) Unsaturated soils. Proceedings of the 3rd international conference on unsaturated soils (UNSAT 2002), Recife, Brazil, vol 2. Swets & Zeitlinger, Lisse, pp 593–598

Cui YJ, Tang AM, Loiseay C, Delage P (2008) Determining the unsaturated hydraulic conductivity of a compacted sand—bentonite mixture under constant-volume and free-swell conditions. Phys Chem Earth 33:s462–s471

Dixon DA, Cheung SCH, Gray MN, Davidson BC (1987) The hydraulic conductivity of dense clay soils. In: Proceedings of 40th Canadian geotechnical conference, Regina, Saskatchewan—Canada, pp 389–396

Komine H (2004) Simplified evaluation on hydraulic conductivities of sand–bentonite mixture backfill. Appl Clay Sci 26(1–4):13–19

Niu WJ, Ye WM, Chen B, Qian LX (2009) SWCC and permeability of unsaturated gaomiaozi bentonite in free swelling condition. Chin J Undergr Space Eng 5:952–955

Pusch R, Yong R (2003) Water saturation and retention of hydrophilic clay buffer—microstructural aspects. Appl Clay Sci 23:61–68

Pusch R, Richard P, Zuzana W, Liu X, Sven K (2012) Role of clay microstructure in expandable buffer clay. J Purity Util React Environ 1(6):297–322

Ye W, Qian L (2009) Laboratory test on unsaturated hydraulic conductivity of densely compacted Gaomiaozi Bentonite under confined conditions. Chin J Geotech Eng 31:105–108

Ye W, Niu W, Chen B, Chen Y (2010) Unsaturated hydraulic conductivity of densely compacted Gaomiaozi bentonite under unconfined conditions. J Tongji Univ (Nat Sci) 38(10):1439–1443

Adsorption, Desorption and Competitive Adsorption of Heavy Metal Ions from Aqueous Solution onto GMZ01 Bentonite

95

W.M. Ye, Yong He, Y.G. Chen, Bao Chen, and Y.J. Cui

Abstract

The geochemical processes of adsorption, desorption and competitive adsorption on bentonite are important for the long-term safety assessment of high-level nuclear waste (HLW) repositories. In this paper, batch adsorption, desorption experiments of Cr(III) and the competitive adsorption experiment with Cu(II) were performed in aqueous solutions on Gao-miao-zi (GMZ) bentonite. Results show that the pH value significantly affect the Cr(III) adsorption/desorption on GMZ bentonite. Both adsorption and desorption isotherms are consistent with the Freundlich equation. The distribution coefficients (K_d) were calculated from the competitive adsorption test; Higher K_d values of Cr(III) were obtained than that of Cu(II), indicating the stronger retention capacity of Cr(III) on GMZ bentonite in a binary metal system.

Keywords

GMZ01 bentonite • Adsorption • Desorption • Competitive adsorption • Heavy metal ions

95.1 Introduction

Bentonite has excellent adsorption properties and possesses adsorption sites available within its interlayer space as well as on the outer surface and edges (Tabak et al. 2007). Because of the retardation for the transport of radionuclides from the repository to the environment, bentonite has attracted great interest in nuclear waste management.

In recent years, many studies have focused on the adsorption of heavy metals on bentonite and under different experimental conditions (Bhattacharyya and Gupta 2008; Chen et al. 2012). These works showed that soil pH, temperature, time, and ionic strength were reported to be important factors that influence the adsorption of heavy metals on bentonite. Adsorption/desorption is a major process responsible for the fate of heavy metals in soils, since the mobility of heavy metals is directly related to their partitioning between soil and soil solution (Sparks 2001).Thus, the study of desorption is conducive to elucidate adsorption process on soil, to recover heavy metal ions from adsorbent, and to multiple regenerate adsorbent (Chen et al. 2013). Most soil-metal bonding information has been derived from studies conducted using single-metal system (Gomes et al. 2001). However, the presence of only one heavy metal ion is a rare situation in reality. Thus, it is important to study the affinity of bentonite toward the adsorption of specific metal ions to investigate their removal from multi-component solutions. Though application of bentonite in the field of waste water treatments has proliferated in recent years, efforts in analyzing desorption and competitive adsorption properties on bentonite, especially on GMZ bentonite in China, is still lacking. Where, the GMZ bentonite has been considered as a possible

W.M. Ye (✉) · Y. He · Y.G. Chen · B. Chen · Y.J. Cui
Key Laboratory of Geotechnical and Underground Engineering of Ministry of Education, Tongji University, Shanghai, 200092, China
e-mail: ye_tju@tongji.edu.cn

Y.G. Chen
e-mail: 12heyong@tongji.edu.cn

W.M. Ye
United Research Center for Urban Environment and Sustainable Development, The Ministry of Education, Beijing, China

Y.J. Cui
Laboratoire Navier, Ecole des Ponts ParisTech, Paris, France

material for construction of engineering barrier in deep geological repository for high-level radioactive waste disposal in China (Ye et al. 2010).

The aim of this work is to review the adsorption/desorption properties of Cr(III) on GMZ bentonite, to analyze the affinity of bentonite toward the adsorption of specific metal ions.

95.2 Experimental

95.2.1 Materials

The raw GMZ01 bentonite used in this work was extracted from the northern Chinese Inner Mongolia autonomous region, 300 km northwest from Beijing. The mineralogical composition was quantitatively analyzed by using the X-ray diffraction method. The bulk composition (mass fraction) was determined as follows: 75.4 % montmorillonite, 11.7 % quartz, 7.3 % cristobalite, 4.3 % feldspar, 0.8 % kaolinite, 0.5 % calcite. This shows that the proportion of montmorillonite is dominant in the GMZ01 bentonite. The cation exchange capacity (CEC) of GMZ01 bentonite is 0.773 mmol/g and the specific surface area (SSA) is 570 m^2/g (Ye et al. 2010). Stock solutions of Cr(III) and Cu(II) with the concentration of 1.923×10^{-3} mol/L were prepared from its nitrate and sulfate, respectively.

95.2.2 Batch Adsorption Studies

The adsorption capacity of Cr(III) on GMZ bentonite was investigated by using batch technique in polyethylene centrifuge tubes sealed with a screw cap under ambient conditions. When adsorption equilibrium reached, the suspension was centrifuged and most of the supernatant was exchanged with the same volume of the background electrolyte solution of NaCl. The competitive adsorption was carried out under a varying temperature from 293 to 323 K. The concentrations of Cr(III) solution before and after adsorption were measured by using an ultraviolet–visible (UV–VIS) spectrophotometer, WFJ2100, at a wave length of 540 nm. The concentrations of Cu(II) solution before and after adsorption were measured by using an atomic absorption spectrophotometer, WFX-1F2B2.

The adsorbed amount of heavy metal ions on GMZ bentonite was calculated from the difference between the initial concentration and the equilibrium one:

$$q_e = \frac{(C_o - C_e)V}{m} \quad or \quad \%removal = \left(\frac{C_o - C_e}{C_o}\right) \times 100 \tag{95.1}$$

where q_e (mg/g) is the amount of heavy metal ions adsorbed on bentonite, C_0 (mg/L) is the initial concentration of heavy metal ions in suspension, C_e (mg/L) is the aqueous concentration of heavy metal ions in equilibrium solution, V (L) is the volume of heavy metal ions solution, and m (g) is the mass of the adsorbent.

Equilibrium distribution coefficient (K_d, L/mg) used extensively for charactering various heavy metal ions adsorption and desorption, was calculated as:

$$K_d = \frac{q_e}{C_e} \tag{95.2}$$

95.3 Results and Discussion

95.3.1 Effect of pH on Adsorption and Desorption

Figure 95.1 shows that the adsorption capacity increases as pH increases from 1.0 to 7.0. Above pH 7.0, its effect on the adsorption become significant and reaches a plateau (Chen et al. 2012). However, the desorption rate decreases gradually at pH 1–9 and maintains a high level around pH = 1 (Chen et al. 2013).

The adsorption and desorption mechanism of Cr(III) on GMZ bentonite can be explained as follows: (i) in acidic region both the adsorbent and adsorbate are positively charged and the net interaction is that of electrostatic repulsion and (ii) the positively charged metal ions face a good competition with the higher concentration of H^+ ions present in the acidic reaction mixture. It has been found that at low pH solution most heavy metals become mobile and adsorption onto clay particles becomes less effective.
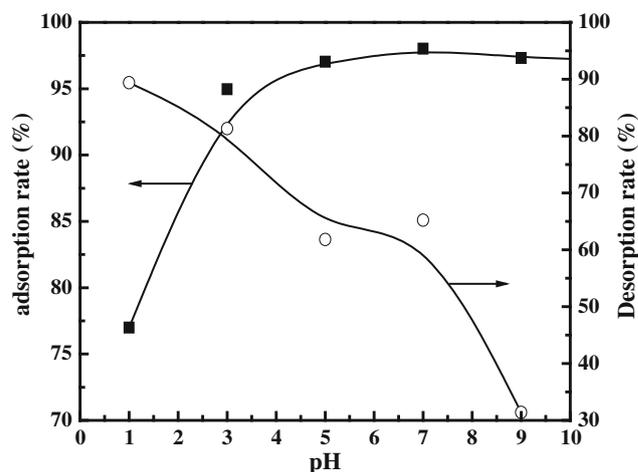
Fig. 95.1 Effect of pH on Cr(III) adsorption and desorption (Chen et al. 2012, 2013)

95.3.2 Adsorption and Desorption Isotherms

Figure 95.2 shows the adsorption and desorption isotherms of Cr(III) on GMZ bentonite (Chen et al. 2013). The equilibrium data were correlated with the Freundlich isotherm. The Freundlich equation [Eq.(95.3)] was used:

$$q_e = k_F C_e^{1/n} \text{ or, in linear form} : \lg q_e = \lg k_F + 1/n \lg C_e \tag{95.3}$$

where k_F is the constant indicative of the relative adsorption or desorption capacity of the adsorbent ($mg^{1-1/n} \cdot L^{1/n} \cdot g^{-1}$) and $1/n$ is the constant indicative of the intensity of the adsorption or desorption. A plot of $\lg q_e$ against $\lg C_e$ gives a straight line, the slope and the intercept of which correspond to $1/n$ and $\lg k_F$, respectively.

The results show that the data obtained for Cr(III) adsorption and desorption fit well to the Freundlich model. Similar results have been reported by Turin and Bowman (1997), Shirvani et al. (2006) for herbicide and cadmium desorption from Casa Grande and Palygorskite soil, respectively.

95.3.3 Competitive Adsorption of Cu(II)/Cr(III) in Binary Metal Ions Solution System

Figure 95.3 shows that the K_d value for each metal in the studied samples was used to compare the adsorption capacities of bentonite for the metals. A high K_d medium value indicates a high metal retention by the solid phase through adsorption and chemical reactions.

The sequence of adsorption affinity of metals according to the distribution coefficient (K_d) toward bentonite was found
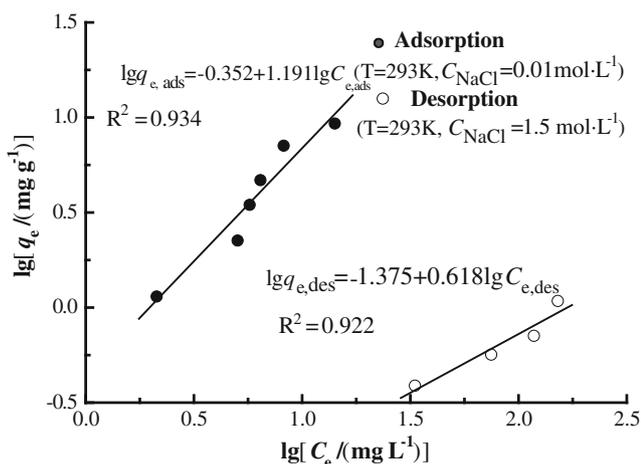
Fig. 95.2 Freundlich adsorption and desorption isotherms on GMZ bentonite (Chen et al. 2013)
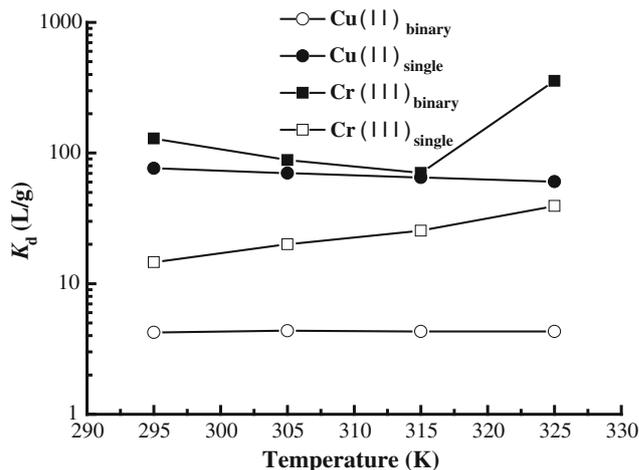
Fig. 95.3 K_d values in single or binary system

to be the following: $K_{d \text{ binary}}$ (Cr)>$K_{d \text{ single}}$ (Cu)>$K_{d \text{ single}}$ (Cr)>$K_{d \text{ binary}}$ (Cu), indicating that Cr(III) was stronger adsorbed by bentonite than Cu(II) in binary metal system. Similar results that the Cr(III) had the higher affinity to kaolinite than Cu(II) have been reported by Covelo et al. (2007).

95.4 Conclusions

In this study, the adsorption/desorption properties of Cr(III) on GMZ bentonite were reviewed and the competitive adsorption was also analyzed. The following conclusions can be drawn:

The pH value is an important factor in the Cr(III) adsorption/desorption on GMZ bentonite.

Both adsorption and desorption isotherms are consistent with the Freundlich model.

The GMZ bentonite has stronger retention capacity of Cr (III) than that of Cu(II) in a binary metal system.

References

Bhattacharyya KG, Gupta SS (2008) Adsorption of a few heavy metals on natural and modified kaolinite and montmorillonite: a review. Adv Colloid Interface Sci 140:114–131

Chen YG, He Y, Ye WM, Lin CH, Zhang XF, Ye B (2012) Removal of chromium (III) from aqueous solutions by adsorption on bentonite from Gaomiaozi, China. Environ Earth Sci 67(5):1261–1268

Chen YG, He Y, Ye WM, Sui WH, Xiao MM (2013) Desorption of Cr (III) adsorbed onto GMZ01 bentonite: effect of shaking time, ionic strength, temperature and pH. Trans Nonferrous Met Soc China

Covelo EF, Vega FA, Andrade ML (2007) Competitive sorption and desorption of heavy metals by individual soil components. J Hazard Mater 140:308–315

Gomes PC, Fontes MPF, da Silva AG, Mendonca ED, Netto AR (2001) Selectivity sequence and competitive adsorption of heavy metals by Brazilian soils. Soil Sci Soc Am J 65:1115–1121

Shirvani M, Kalbasi M, Shariatmadari H, Nourbakhsh F, Najafi B (2006) Sorption–desorption of cadmium in aqueous palygorskite, sepiolite, and calcite suspensions: isotherm hysteresis. Chemosphere 65:2178–2184

Sparks DL (2001) Elucidating the fundamental chemistry of soils: past and recent achievements and future frontiers. Geoderma 100:303–319

Tabak A, Afsin B, Aygun SF, Koksal E (2007) Structural characteristics of organo-modified bentonites of different origin. J Therm Anal Calorim 87:375–381

Turin HJ, Bowman RS (1997) Sorption behavior and competition of bromacil, napropamide, and prometryn. J Environ Qual 26 (5):1282–1287

Ye WM, Chen YG, Chen B, Wang Q, Wang J (2010) Advances on the knowledge of the buffer/backfill properties of heavily-compacted GMZ01 bentonite. Eng Geol 116:12–20

Snehasis Tripathy, Ramakrishna Bag, and Hywel R. Thomas

Abstract

Laboratory isothermal swelling pressure tests were carried out on compacted MX80 bentonite at 25 and 70 °C with distilled water as the hydrating fluid. Assessment of the swelling pressure was carried out using the electrical triple-layer theory for interacting clay platelets. An increase in the temperature reduced the swelling pressure of the bentonite on account of decrease in the Gouy-layer charge, mid-plane potential and distance functions. Agreements between the calculated swelling pressures from the triple-layer theory and the experimental results were found to be reasonable for compaction dry densities of less than 1.45 Mg/m^3.

Keywords

Laboratory test • Bentonite • Swelling pressure • Temperature • Triple-layer theory

96.1 Introduction

Compacted bentonites have been proposed to be used as buffer around the waste canisters in the deep underground storage of high-level waste. The insitu boundary conditions in this case dictate exposure of compacted bentonites to elevated temperature and hydration upon fluid uptake from host rock. Therefore, research works in this context have been carried out by several researchers in the past (Pusch 1980; Pusch et al. 1990; Villar and Lloret 2004; Lloret et al. 2004; Romero et al. 2003, 2005; Jacinto et al. 2009; Ye et al. 2009, to name few).

An increase in the temperature has been shown to decrease the swelling pressure of compacted bentonites. Similarly, water retention capacities of bentonites and other swelling clays have been shown to decrease with an increase in the temperature. Pusch (1980) stated that the reduction of swelling pressure is due to the presence of less stable interlayer and inter-particle water at higher temperature. An increase in the temperature increases the kinetic energy of

the water molecules and tends to reduce the hydration of the clay particles. The thermal properties of water have been considered to explain the reductions in the water retention capacities of bentonites. For example, the surface tension of water decreases with an increase in the temperature causing a reduction in the matric suction. Romero et al. (2003) stated that the changes in water retention induced by temperature are associated mainly with temperature dependence of the interfacial tension and wetting coefficient, and with thermal expansion of entrapped air.

Mitchell and Soga (2005) stated that, an increase in the temperature has two effects, such as that the dielectric constant of the pore fluid decreases and the Debye length (i.e., the maximum possible diffuse double layer thickness) increases. Electrical double-layer calculations (Tripathy et al. 2004; Schanz and Tripathy 2009) would clearly indicate that, independent effects of various parameters should not be considered while drawing conclusions on the salient features of the electrical double layer associated with interacting clay platelets systems. An increase in the temperature and a decrease in dielectric constant of the pore fluid tend to reduce the Debye length for a given clay-water system.

Laboratory tests were carried out in order to study the influence of temperature on the swelling pressure of compacted bentonite. The electrical triple-layer (i.e., the clay surface, the Stern-layer, and the diffuse double layer)

S. Tripathy (✉) · H.R. Thomas
Cardiff University, Cardiff, UK
e-mail: Tripathys@cf.ac.uk

R. Bag
National Institute of Technology, Rourkela, India

theory or the Stern theory as applicable to interacting clay platelets and for constant surface potential case (Verwey and Overbeek 1948; Tripathy et al. 2013) was used to assess swelling pressures for a range of swollen dry densities.

96.2   Material and Method

Commercially available MX80 bentonite containing 84 % montmorillonite was used in this study. The specific gravity of the bentonite was found to be 2.76. The liquid limit, plastic limit and shrinkage limit of the bentonite were found to be 385, 43 and 15.8 %, respectively (Bag 2011).

The swelling pressure tests were carried out in an oedometer cell designed and developed at Cardiff University (see Fig. 96.1). Specimens were prepared by compacting MX80 bentonite at a water content of about 10 % for a range of dry densities between 1.25 and 1.8 Mg/m^3. In an attempt to eliminate the influence of post-compaction residual lateral stresses on swelling pressures, after the compaction process, the compacted specimens were extruded and inserted back into the specimen rings prior to testing them for swelling pressures. Distilled water was used as the hydrating fluid. The tests were terminated once the measured swelling pressures were equilibrated. In total, seventeen tests were carried out (twelve tests at an ambient temperature of 25 °C and five tests at 70 °C). Based on the final water contents and the mass of the specimens, the swollen dry densities of the specimens were calculated. The calculated swollen dry densities were found to be smaller than the compacted dry densities of the specimens prior to testing. Reductions of dry densities of the specimens are attributed due primarily to the expansion of the measuring system.

96.3   Results and Discussion

The experimental dry density versus swelling pressure results are shown in Fig. 96.2. The swelling pressure decreased with an increase in the temperature. A reduction in the swelling pressure due to an increase in the temperature was found to be about 15–20 % for the range of dry density considered in this study.

From the triple-layer theory dealt with in this study (Tripathy et al. 2013), it was noted that an increase in the temperature increases the electric potentials at the Stern plane and in the mid-plane, and decreases the Stern-layer charge, the Gouy-layer charge, the Debye length, and non-dimensional mid-plane and distance functions. Therefore, a reduction in the swelling pressure of bentonites due to an increase in the temperature is well supported from theoretical considerations (Fig. 96.2).

Reasonably good agreements can be noted between the calculated results from the theory and experimental results for dry densities less than or equal to about 1.45 Mg/m^3. At a dry density of 1.45 Mg/m^3, overlapping of the Stern-layers

Fig. 96.1 Schematic of the swelling pressure device used in this study
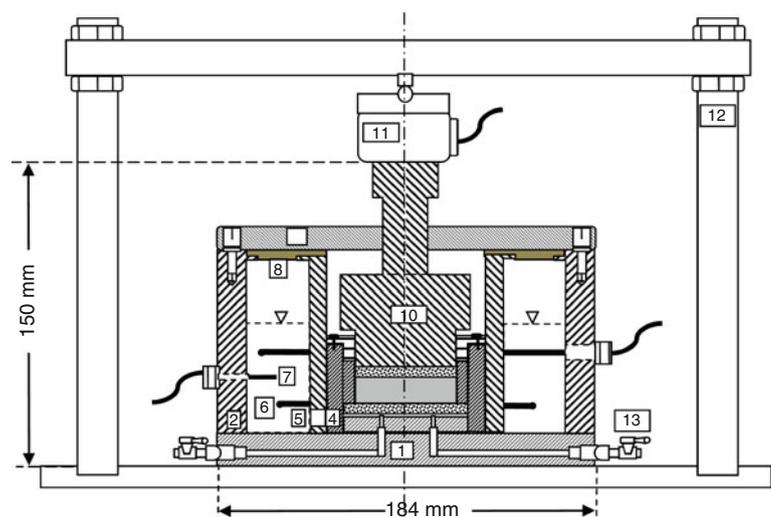
1. Device base
2. Outer casing
3. Inner separator ring
4. Inner housing unit
   Specimen ring
   Top porous disc
   Bottom porous disc
   Compacted specimen
   Locking collar
   Locking key
5. Oil chamber for elevated
   iso-thermal test
6. Electric coil
7. Thermocouple
8. Oil chamber cover
9. Top lid
10. Pressure pad
11. Load cell
12. Loading frame
13. Fluid supply
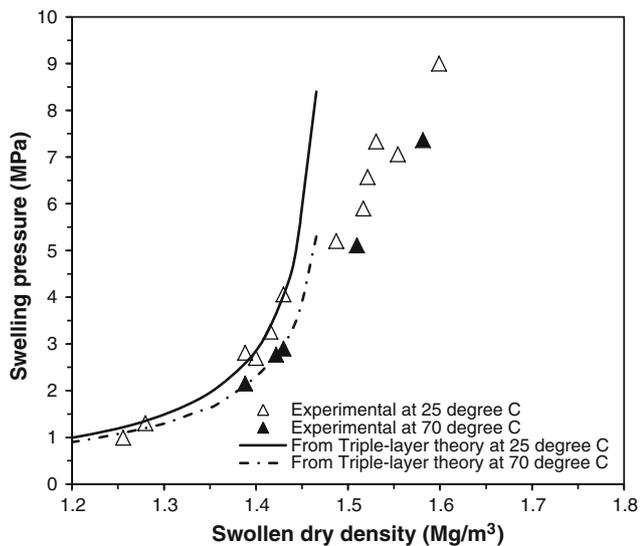
Fig. 96.2 Dry density versus experimental and theoretical swelling pressure plot

among the clay platelets occurs (i.e., the distance between two parallel clay platelets is equal to 1.0 nm). Swelling pressures at swollen dry densities greater than about 1.45 Mg/m^3 stem from forces associated with hydration of surfaces of clay platelets and the exchangeable cations.

96.4 Conclusions

Laboratory swelling pressure tests were conducted on compacted MX80 bentonite in order to study the influence of elevated temperature on the swelling pressure. The electrical triple-layer theory was used to explore various parameters responsible for a variation of the swelling pressure due to an increase in the temperature.

The study showed that an increase in the temperature reduced the swelling pressure of compacted specimens as has been noted by several researchers in the past. Electrical triple-layer calculations showed that a decrease in the swelling pressure due to an increase in the temperature is the combined influence of increase in the electric potentials at the Stern plane and in the mid-plane, and decrease in the Stern-layer

charge, the Gouy-layer charge, the Debye length, and non-dimensional mid-plane and distance functions. Agreements between the calculated and the experiment swelling pressures of compacted MX80 bentonite were very good for swollen dry density less than or equal to 1.45 Mg/m^3.

References

Bag R (2011) Coupled thermo-hydro-mechanical-chemical behavior of MX80 bentonite in geotechnical applications. PhD thesis, Cardiff University

Jacinto AC, Villar MV, Gomez-Espina R, Ledesma A (2009) Adaptation of the van Genuchten expression to the effects of temperature and density for compacted bentonites. Appl Clay Sci 42:575–582

Lloret A, Romero E, Villar MV (2004) FEBEX II project final report on thermo-hydro-mechanical laboratory tests. Publicación Técnica ENRESA 10/04, Madrid, 180 pp

Mitchell JK, Soga K (2005) Fundamentals of soil behaviour. Wiley, New York

Pusch R (1980) Swelling pressure of highly compacted bentonite. SKB Technical report, TR-80-13

Pusch R, Karlnland O, Hokmark H (1990) GMM-a general microstructural model for qualitative and quantitative studies of smectite clays. SKB technical report 90-43, Stockholm, Sweden

Romero E, Gens A, Lloret A (2003) Suction effects on a compacted clay under nonisothermal conditions. Géotechnique 53(1):65–81

Romero E, Villar MV, Lloret A (2005) Thermo-hydro-mechanical behaviour of two heavily overconsolidated clays. Eng Geol 81:255–268

Schanz T, Tripathy S (2009) Swelling pressure of a divalent-rich bentonite: Diffuse double-layer theory revisited. Water Resour Res 45, W00C12. doi:10.1029/2007WR006495

Tripathy S, Bag R, Thomas HR (2013) Effect of stern-layer on the compressibility behaviour of bentonites. Acta Geotech. doi:10.1007/s11440-013-0222-y

Tripathy S, Sridharan A, Schanz T (2004) Swelling pressures of compacted bentonites from diffuse double layer theory. Can Geotech J 41:437–450

Verwey EJW, Overbeek JThG (1948) Theory of the stability of lyophobic colloids. Elsevier, Amsterdam

Villar MV, Lloret A (2004) Influence of temperature on the hydro-mechanical behaviour of a compacted bentonite. Appl Clay Sci 26:337–350

Ye WM, Cui YJ, Qian LX, Chen B (2009) An experimental study of the water transfer through confined compacted GMZ bentonite. Eng Geol 108(3–4):169–176

Effects of Stress and Suction on the Volume Change Behaviour of GMZ Bentonite During Heating

Wei-Min Ye, Qiong Wang, Ya-Wei Zhang, Bao Chen, and Yong-Gui Chen

Abstract

Unsaturated compacted bentonite is considered by several countries as sealing/backfill material in the deep geological repository for high-level radioactive waste (HLW). In the field conditions, where bentonite is subjected to coupled thermo-hydro-mechanical actions, its thermo-mechanical behavior may change with suction and stress variations. This work focuses on the compacted Gaomiaozi (GMZ) bentonite, which has been chosen as potential sealing/backfill material in the Chinese repository concept. The effects of vertical stress and suction on the volume change behaviour during thermal loading (heating) were experimentally investigated. A high pressure oedometer frame permitting simultaneous control of temperature, suction and pressure was used for testing. Compacted samples were heated from the original temperature of 20 to 80 °C at total suctions ranging from 4.2 to 110 MPa, and vertical stress of 0.1 or 5 MPa. Results show that heating at constant suction and vertical stress induces either swelling or contraction. At a constant vertical stress, samples with higher suctions swell during heating, and the lower the suction the lower the swelling strain; on the contrary heating resulted in a thermal contraction with lower suctions. At a constant higher suction (110 MPa), sample swells during heating; however, for a relative lower suction, a contraction was induced by heating for a higher vertical stress of 5 MPa. In short, at high pressure and low suction, heating tends to induce contraction, while at low pressure and high suction, heating induced expansion.

97.1 Introduction

Thermo-mechanical behavior of expansive clays used as sealing/backfill materials for high-level radioactive wastes (HLW) disposal has attracted large attentions. As it is subjected to coupled thermo-hydro-mechanical (T-H-M) actions, induced by the water infiltration from the geological barrier, stresses generated by the swelling, and heat dissipation from the nuclear waste packages, changes of water content (suction) and stress change may have great impacts.

This work focuses on the Gaomiaozi (GMZ) bentonite, which has been chosen as potential sealing/backfill material in the Chinese repository concept. A series of heating test

W.-M. Ye · Y.-W. Zhang · B. Chen · Y.-G. Chen
Key Laboratory of Geotechnical and Underground Engineering of Ministry of Education, Tongji University, Shanghai 200092, China

W.-M. Ye
United Research Center for Urban Environment and Sustainable Development, The Ministry of Education, Shanghai 200092, China

Q. Wang (✉)
Centre of Excellence for Geotechnical Science and Engineering, The University of Newcastle, Callaghan NSW 2308, Australia
e-mail: wangqiong139@hotmail.com

were performed on compacted samples with vertical stress and suction control. The results obtained allowed the analyzing of the vertical stress and suction effect on the volume change behavior during heating.

97.2 Materials and Method

97.2.1 Materials

The Gaomiazi GMZ bentonite from Inner Mongolia Autonomous Region, China, was used. With a high content of montmorillonite (74.5 %), it has an average specific gravity of 2.66, a liquid limit of 313 %, and a plastic limit of 38 %. The cation exchange capacity (CEC) is 62.59–82.06/100 g, and the total specific surface is 570 m^2/g.

All tests were performed on compacted samples. The GMZ01 bentonite powder with an initial water content of 8.6 % was used for the samples preparation. Samples were statically compacted in a thick-walled compaction cell (50 mm in internal diameter) at a controlled rate of 0.375 kN/min to the desired dry density of 1.70 Mg/m^3.

97.2.2 Experimental Methods

An oedometer frame with simultaneous control of temperature and suction was used. It consists four main parts: (1) oedometer cell (50 mm in inner diameter); (2) loading system; (3) suction controlled system and (4) temperature control system. The soil specimen, sandwiched by two porous disks, was put in the oedometer cell with two valves both at the top and bottom of the cell for water or air circulation. A suction control system by vapour equilibrium method was connected to these valves for suction imposition (4.2–110 MPa). Suctions of Saturated saline solutions at different temperatures calibrated by Tang and Cui (2005) were employed. The vertical stress was applied through a loading piston on the top, by a double arms lever system (Marcial et al. 2002); the axial displacement was monitored by a micrometer dial gauge (with a precision of 0.001 mm) fixed on the piston. A water bath with a thermostat was used for temperature control (with a precision of ±0.1 °C).

In order to study the effect of vertical stress and suction on the volume change behaviour during heating, five samples listed in Table 97.1 were tested. From the as-compacted state (with an initial water content of 8.6 %), different suctions were first imposed by vapour phase technique (4.2, 38 and 110 MPa by saturated solutions of K_2SO_4, NaCl, K_2CO_3, respectively). Once the suction equilibrium was reached, a vertical stress of 0.1 or 5 MPa was applied up to the stabilisation, i.e. a volumetric strain rate of less than 0.01 % within 8 h. Specimens were then heated at a speed of

Table 97.1 Test programme

Test No.	Suction (MPa)	Vertical stress (MPa)
T-01	4.2	0.1
T-02	38	0.1
T-03	110	0.1
T-04	38	5
T-05	110	5

10 °C/2 h to 80 °C, during which constant suction and vertical stress were maintained, and the vertical strain of specimens were measured.

97.3 Results and Discussion

Figure 97.1 presents the volumetric change of compacted GMZ01 bentonite during heating at different suctions under a constant vertical stress. It presents a significant effect of suction on the heating induced volume changes. At a constant vertical stress of 0.1 MPa (Fig. 97.1a), samples with higher suctions (110 and 39 MPa) swell during heating from 20 to 80 °C. On the contrary heating resulted in a thermal contraction with a relative lower suction (4.2 MPa). For the vertical stress of 5 MPa (Fig. 97.1b), similar phenomena were obtained: at high suction of 110 MPa, swelling was observed during heating; while, at a relative lower suction of 39 MPa, heated induced a few expansion, and then a tendency toward contraction. All results evidence the significant effect of suction on the heating induced volumetric stain: at a constant vertical stress, heating induces expansion under higher suction and a contraction under lower suction. This is consistent with the conclusion of Tang et al. (2008) from MX80 bentonite, where the suction effect was explained by the softening of the swelling clay aggregates due to suction decrease (Tang et al. 2008; Tang and Cui 2009).

From the results shown in Fig. 97.1, it can be also observed that the shift suction between dilation and contraction are different for different vertical stress: under a lower vertical stress of 0.1 MPa, heating led to swelling at 38 MPa suction; however, contraction was induced under a higher vertical stress of 5 MPa at the same suction level (i.e. 38 MPa). To further analyze the effect of vertical stress on heating induced volumetric changes, experimental results (shown in Fig. 97.1) at the same suction was re-plotted versus vertical stress in Fig. 97.2. It presents that under a higher suction of 110 MPa, heating resulted in expansion under both 0.1 and 5 MPa vertical stresses. However, it is not the case at 38 MPa suction, where a contraction was obtained for a higher vertical stress of 5 MPa. This implies that heating tends to induce a contraction at high pressure and low suction. This phenomena is in agreement with the

Fig. 97.1 Volume changes during heating at different suction **a** $p = 0.1$ MPa, **b** $p = 5$ MPa
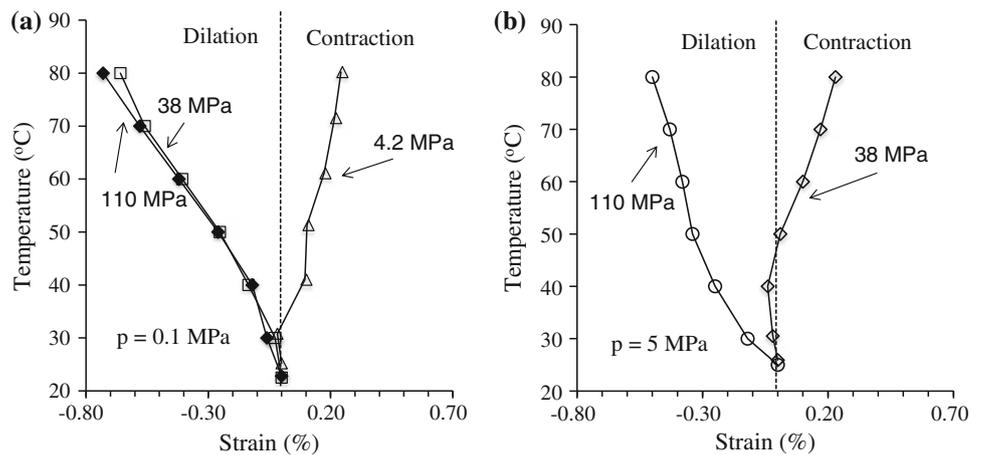
Fig. 97.2 Volume changes during heating under different vertical stress **a** $s = 110$ MPa, **b** $s = 38$ MPa
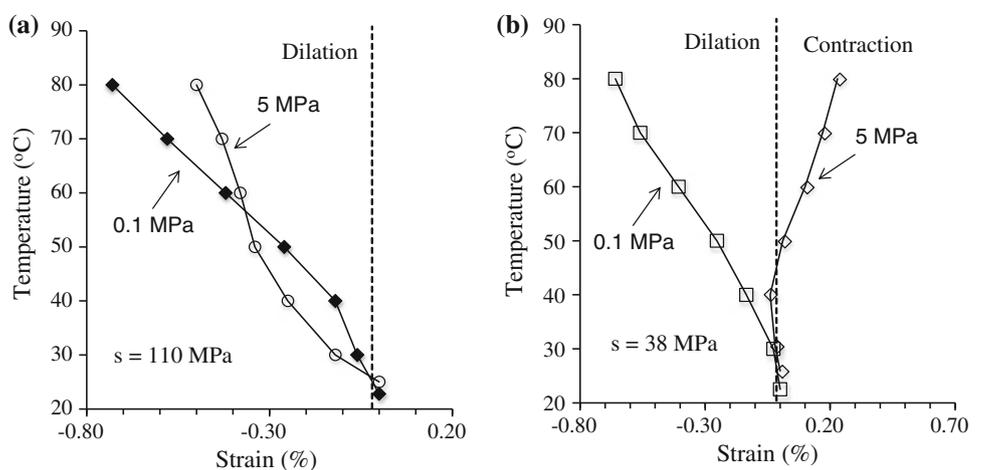
observations of Romero et al. (2005) and Tang et al. (2008) from FEBEX bentonite and MX80 bentonite, respectively.

97.4 Conclusion

The effects of vertical stress and suction on the volume change behavior of GMZ01 bentonite during thermal loading (heating) were experimentally investigated in this study. It was observed that heating at constant suction and vertical stress induces either swelling or contraction. At a constant vertical stress, samples swell at higher suction and contract at lower suction during heating. Regarding the constant suction, samples at both higher and lower vertical stress swell upon heating at a high suction; however, for a relative lower suction, contraction was induced by heating at a higher vertical stress compared to the expansive at a lower vertical stress.

In a word, heating induces expansion under low pressure and high suction; while at high pressure and low suction, heating tends to induce a contraction.

References

Marcial D, Delage P, Cui YJ (2002) On the high stress compression of bentonites. Can Geotech J 39:812–820

Romero E, Villar MV, Lloret A (2005) Thermo-hydro-mechanical behaviour of heavily overconsolidated clays. Eng Geol 81:255–268

Tang AM, Cui YJ (2005) Controlling suction by the vapour equilibrium technique at different temperatures and its application in determining the water retention properties of MX80 clay. Can Geotech J 42:287–296

Tang AM, Cui YJ (2009) Modelling the thermomechanical volume change behaviour of compacted expansive clays. Géotechnique 59:185–195

Tang AM, Cui YJ, Barnel N (2008) Thermo-mechanical behaviour of compacted swelling clay. Geotechnique 58(1):45–54

Preliminary Assessment of Tunnel Stability for a Radioactive Waste Repository in Boom Clay

P. Arnold, P.J. Vardon, and M.A. Hicks

Abstract

This paper investigates the stability of tunnel galleries of a radioactive waste repository in Boom Clay, with specific reference to the current Dutch disposal concept. In this preliminary study an isotropic analytical solution has been implemented within a reliability based framework to assess the mechanical response of the Boom Clay, accounting for the aleatory uncertainty in soil property values. The performance, that is, the extent of the plastic zone with respect to a set limit state, is then quantified in terms of exceedance probability rather than using a single deterministic value. This allows for input into a quantifiable and more transparent decision making process. The effect of defining material parameter correlation within the statistical description of soil property values is illustrated via correlated and uncorrelated analyses. The results of this preliminary analytical investigation present a vital input for later two- and three-dimensional numerical modelling of the current disposal concept for a generic Dutch radioactive waste repository in Boom Clay, for both the pre- and post-closure analyses.

Keywords

Analytical methods • Boom clay • HLW • Radioactive waste • Tunnelling

98.1 Introduction

In many countries around the world, it is proposed to manage radioactive waste in the long-term via geological disposal in hard rock (e.g. granite), salt rock or clay rock. The Dutch national programme is currently investigating the use of clay rock, i.e. Boom Clay, with a proposed repository situated at over 500 m depth and with a stratum thickness of about 100 m (Verhoef et al. 2011). The Boom Clay formation exists under most of the Netherlands and the location of the repository is at present unknown, although the inherent properties of Boom Clay are known to vary with both depth and location (e.g. Barnichon et al. 2000). The geomechanical

and consequential financial feasibility of such a repository need to be investigated. Moreover, with approximately 10 km of shafts, galleries and tunnels (Verhoef et al. 2011), the cost increase associated with an increase in concrete lining thickness or increase in gallery spacing is significant. For example, the cost of the lining has been estimated to be approximately 80 % of the cost of the tunnel construction (Barnichon et al. 2000).

This paper investigates tunnel stability in Boom Clay at approximately 500 m depth. An analytical model incorporating elasto-plastic material behaviour has been developed and utilised to account for, in a simplified manner, the strain-softening behaviour which typically is encountered for Boom Clay under low confining stresses (e.g. Horseman et al. 1987; Barnichon et al. 2000). The uncertainty of material parameters has been considered by using the Monte Carlo Method (MCM), with the objective to identify the most important parameters. Analyses with both uncorrelated

P. Arnold · P.J. Vardon (✉) · M.A. Hicks
Geo-Engineering Section, Delft University of Technology,
PO Box 50482600 GA, Delft, The Netherlands
e-mail: p.j.vardon@tudelft.nl

and correlated material parameters have been undertaken to investigate the effects of parameter uncertainty on predictions of tunnel response.

98.2 Theoretical Formulation

The analytical framework has been formulated with a series of simplifying assumptions. In the main, these are to enable a closed-form solution, so that probabilistic analyses can be more efficiently undertaken. For this model they are: (i) the tunnel cross section is circular; (ii) plane strain conditions are considered; (iii) the liner is impermeable; (iv) the tunnel is excavated horizontally and deep, i.e. depth $\gg$ radius; (v) the soil exhibits elasto-plastic behaviour with linear strain softening; (vi) the soil is over-consolidated; (vii) the soil is homogeneous and fully saturated; (viii) the in situ stress state and material response is isotropic; (ix) a single tunnel is considered; (x) the loading is axisymmetric to the tunnel centreline; and (xi) the analysis considers the steady state long term conditions.

Given the assumptions above, the equilibrium of total stresses around a radial symmetric cavity as outlined in Fig. 98.1 can be expressed as

$$\frac{\partial \sigma'_{rr}}{\partial r} + \frac{\sigma'_{rr} - \sigma'_{\theta\theta}}{r} + \frac{\partial u_w}{\partial r} = 0 \qquad (98.1)$$

where r is the radial polar coordinate, σ'_{rr} is the effective radial stress, $\sigma'_{\theta\theta}$ is the effective tangential (hoop) stress, u_w is the pore water pressure and the total stress is $\sigma = \sigma' + u_w$. The long term and impermeable liner assumptions imply that $\partial u_w / \partial r = 0$ in this example. The associated radial, tangential and axial strains are

$$\varepsilon_{rr} = \frac{\partial u_r}{\partial r}; \quad \varepsilon_{\theta\theta} = \frac{u_r}{r} \quad \text{and} \quad \varepsilon_{zz} = 0 \qquad (98.2)$$

where u_r is the radial displacement. The isotropic elastic response is given by Hooke's law and a Drucker-Prager (DP) yield function, f, is employed accounting for linear strain softening as defined in Chen et al. (2012):

$$f\left(\sigma'_{rr}, \sigma'_{\theta\theta}, \varepsilon^p\right) = q - p' \tan \varphi' - c'(\varepsilon^p) \qquad (98.3)$$

where p' is the mean effective stress, q is the deviatoric stress, φ' is the effective friction angle and $c'(\varepsilon^p)$ is the effective cohesion as a function of the accumulated plastic strain, which, when calibrated via uniaxial compression tests, i.e. $p' = \sigma'_a/3$ and $q = \sigma'_a$, is defined as

$$c'(\varepsilon^p) = \left(1 - \frac{\tan \varphi'}{3}\right)\left(a\varepsilon^p + \sigma'_{y,0}\right) \qquad (98.4)$$

where a is a scalar, σ'_a is the axial stress and $\sigma'_{y,0}$ is the initial yield stress. The plastic strain is approximated using the Von Misses equivalent plastic strain rate, i.e. $\varepsilon^p \cong 2/3\left(\varepsilon^p_{\theta\theta} - \varepsilon^p_{rr}\right)$, for which the incremental components are

$$d\varepsilon^p_{rr} = d\lambda \frac{\partial g}{\partial \sigma'_{rr}} \quad \text{and} \quad d\varepsilon^p_{\theta\theta} = d\lambda \frac{\partial g}{\partial \sigma'_{\theta\theta}} \qquad (98.5)$$

where the plastic potential $g \equiv f$, i.e. assuming associated flow, and $d\lambda$ is a scalar multiplier. For isotropic initial conditions the isotropic elastic response is

$$\sigma'^e_{rr} = \sigma'_0 + \left(\bar{\sigma}'_{rr} - \sigma'_0\right)\frac{r^2_{pl}}{r^2} \quad \text{and} \quad \sigma'^e_{\theta\theta} = \sigma'_0 - \left(\bar{\sigma}'_{rr} - \sigma'_0\right)\frac{r^2_{pl}}{r^2} \qquad (98.6)$$

where the effective vertical and horizontal in situ stresses are $\sigma'_{h,0} = \sigma'_{v,0} = \sigma'_0$, $\bar{\sigma}'_{rr}$ is the radial effective stress at the elasto-plastic (EP) interface and r_{pl} is the EP radius, i.e. the radius at which the material first yields.

From Eq. (98.6) it follows that $\bar{\sigma}'_{rr} + \bar{\sigma}'_{\theta\theta} = 2\sigma'_0$, from which, by substitution into the yield condition [Eq. (98.3)] at the initial state ($\varepsilon^p = 0$), the radial and tangential stresses at the EP interface can be computed:

$$\bar{\sigma}'_{rr} = \left(1 - \frac{\tan \varphi'}{2}\right)\sigma'_0 - \left(\frac{1}{2} - \frac{\tan \varphi'}{6}\right)\sigma'_{y,0}$$
$$\bar{\sigma}'_{\theta\theta} = \left(1 + \frac{\tan \varphi'}{2}\right)\sigma'_0 + \left(\frac{1}{2} - \frac{\tan \varphi'}{6}\right)\sigma'_{y,0} \qquad (98.7)$$

The radial and tangential stresses in the plastic zone are

$$\sigma'^p_{rr}(r) = \bar{\sigma}'_{rr} + D_{11}\left[\varepsilon^p_{rr}(r) - \bar{\varepsilon}_{rr}\right] + D_{12}\left[\varepsilon^p_{\theta\theta}(r) - \bar{\varepsilon}_{\theta\theta}\right]$$
$$\sigma'^p_{\theta\theta}(r) = \bar{\sigma}'_{\theta\theta} + D_{21}\left[\varepsilon^p_{rr}(r) - \bar{\varepsilon}_{rr}\right] + D_{22}\left[\varepsilon^p_{\theta\theta}(r) - \bar{\varepsilon}_{\theta\theta}\right] \qquad (98.8)$$

where $\bar{\varepsilon}_{rr}$ and $\bar{\varepsilon}_{\theta\theta}$ are the radial and tangential strains at the EP interface and D_{ij} are the components of the stiffness matrix with $D_{ij} = D_{ji}$ (Graziani and Ribacchi 1993). The cavity pressure, i.e. the maximum stress at the soil-lining interface, is $p_c = \sigma_{rr}(r_c)$. The stresses in the residual plastic (RP) zone are computed from the yield function at the ultimate state and the equilibrium condition (Eq. 98.1).

98.3 Analysis, Results and Discussion

Following the initial design specifications of the Dutch radioactive waste repository (Verhoef et al. 2011), the High Level Waste (HLW) is to be disposed of in cells with a cavity excavation radius of $r_c = 1.6$ m, spaced $b_c = 50$ m apart. An isotropic in situ stress state of $\sigma_0 = 10$ MPa and a
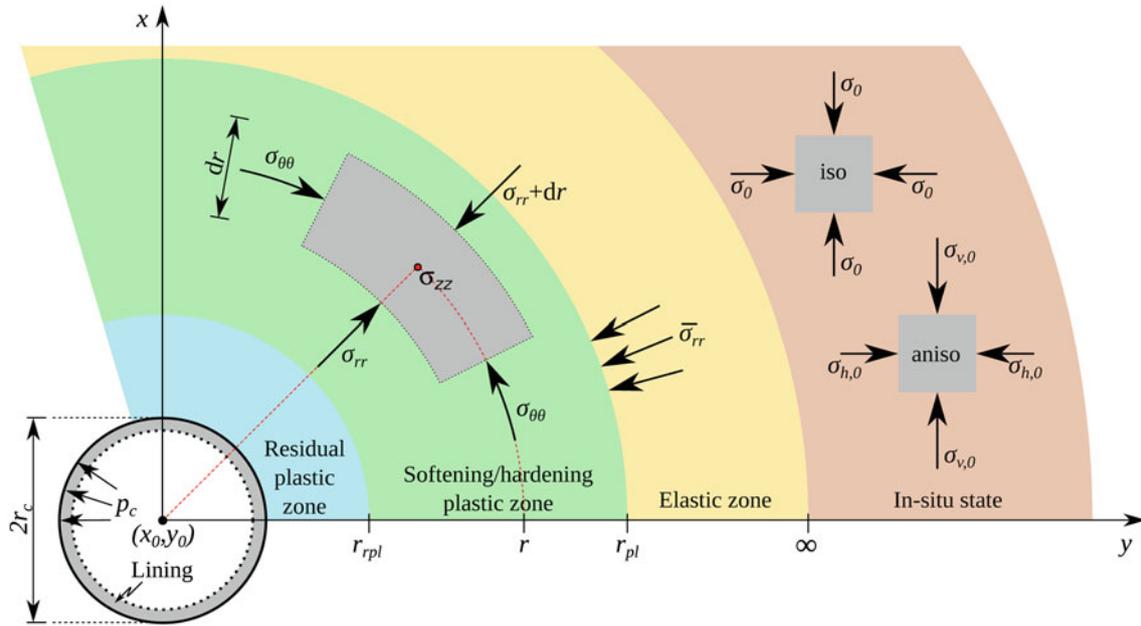
Fig. 98.1 Schematic description of stresses around a cavity opening where r_c is the excavated cavity radius, p_c is the cavity pressure (i.e. acting on the liner), r_{pl} is the plastic radius, r_{rpl} is the residual plastic radius, σ_{rr}, $\sigma_{\theta\theta}$ and σ_{zz} are the total radial, tangential and axial stresses, $\bar{\sigma}_{rr}$ is the total radial stress at the EP interface, $\sigma_{h,0}$ and $\sigma_{v,0}$ are the total *horizontal* and *vertical* in situ stresses

pore water pressure of $u_{w,0} = 5.0$ MPa is assumed, based upon an approximate 500 m depth. Three hypothetical cavity pressures, $p_c = \{5.5, 6.5, 7.5\}$ MPa, were considered for the example in this paper.

Information on the Boom Clay property values, especially their variance and covariance, are very scarce and primarily exist up to a depth of about 250 m. Moreover, even from the extensively investigated Boom Clay at the HADES test site in Mol (Belgium), with samples obtained at a depth of 223 m, still only a limited amount of good quality data are available for a statistical interpretation. Table 98.1 summarises the values of the mean μ_{X_i} and standard deviation σ_{X_i} of the six material properties of the multivariate random vector $X \sim \mathcal{N}(\mu_X, \sigma_X, R_U)$, required by the analytical solution, which have been collected from data at depths of 200–550 m

based on investigations in the Netherlands (Barnichon et al. 2000; Wildenborg et al. 2000) and in Belgium (e.g. Bernier et al. 2007; Deng et al. 2011; Bésuelle et al. 2013). There are significantly less data available for describing the correlation between individual parameters and therefore reasonable estimates have been made where appropriate. Two cases are investigated, i.e. the uncorrelated case for which all $\rho_{X_i,X_j} = 0$ and the correlated case, with R_U being the cross-correlation matrix in Standard Normal space as defined in Table 98.1. Through selecting the correlation estimates, the intention of this analysis is to serve as an illustration of the potential effect of correlation on the system response. A total number of $N_r = 150{,}000$ MC realisations are performed for each cavity pressure within each case. Figure 98.2 shows the set of deterministic stress distributions based on the mean

Table 98.1 Point statistics describing Boom Clay property values

Variable X		Unit	μ_X	σ_X/μ_X			R_U			
Initial cohesion	c_o'	MPa	0.5	0.20	1.0	0.75	−0.5	0.5	0.25	0.5
Residual cohesion	c_r'	MPa	0.25	0.10	$\rho_{c_r',c_0'}$	1.0	−0.5	0.5	0.25	0.5
Friction angle	φ'		11.0	0.20	$\rho_{\varphi',c_0'}$	$\rho_{\varphi',c_r'}$	1.0	0.25	0.25	−0.5
Young's modulus	E	MPa	500	0.15	$\rho_{E,c_0'}$	$\rho_{E,c_r'}$	$\rho_{E,\varphi'}$	1.0	0.5	−0.25
Tangent modulus	E_t	MPa	200	0.15	$\rho_{E_t,c_0'}$	$\rho_{E_t,c_r'}$	$\rho_{E_t,\varphi'}$	$\rho_{E_t,E}$	1.0	−0.25
Poisson's ratio	v	–	0.2	0.05	$\rho_{v,c_0'}$	$\rho_{v,c_r'}$	$\rho_{v,\varphi'}$	$\rho_{v,E}$	ρ_{v,E_t}	1.0

Where μ_X are the means, σ_X are the standard deviations and ρ_{X_i,X_j} are the symmetric cross-correlation coefficients of R_U

Fig. 98.2 Stresses around excavated cavity with impermeable concrete liner. The stresses $\bar{\sigma}$ correspond to the EP interface (r_{pl}/r_c) and $\hat{\sigma}$ to the RP interface (r_{rpl}/r_c)
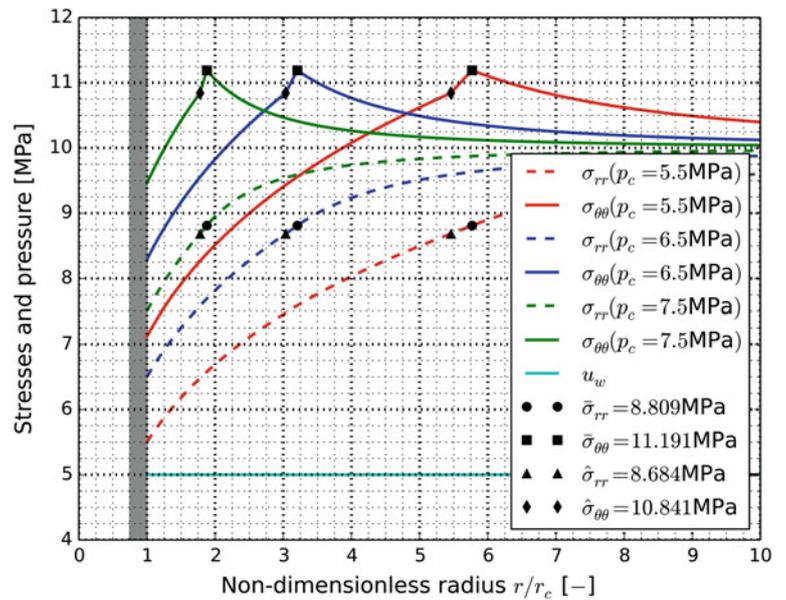
Fig. 98.3 Probability of failure, i.e. $P_f = P[r_{pl} > r_{pl,lim}]$. The *solid line* corresponds to the uncorrelated case and the *dashed line* to the correlated case
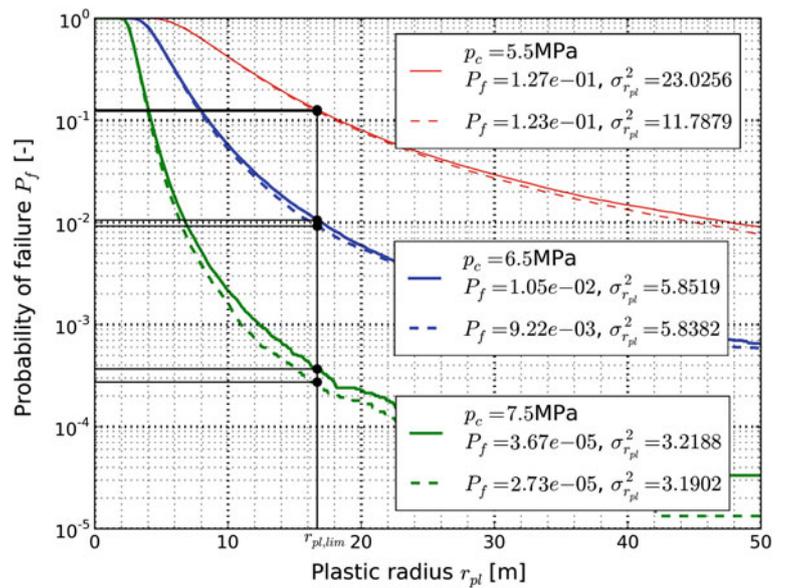
soil property values μ_X. The three zones highlighted in Fig. 98.1 are evident, with the EP and RP interfaces extending non-linearly with the linear decrease in cavity pressure.

The exceedance probability for a MC analysis can be computed by $P[G(X) > 0] = N_f/N_r$, for which the number of failed realisations is $N_f(G(X) > 0)$ with respect to the performance function $G(X)$. Given the design exceedance criterion for the extent of the plastic zone, $G(X) = r_{pl} - r_{pl,lim}$, with $r_{pl,lim} = b_c/3 = 16.7$ m corresponding to a hypothetical limiting plastic radius. Figure 98.3 summarises the associated exceedance (failure) probabilities, which, as expected, increase with decreasing

liner support. It is evident that for the correlated case the variance of the response decreases, which thus leads potentially to lower failure probabilities, e.g. 0.0274 % over 0.0367 % for $p_c = 7.5$ MPa. Hence, a knowledge of the material parameter correlations reduces uncertainty for this performance assessment.

98.4 Conclusions

A preliminary study of the mechanical response of Boom Clay, around disposal galleries of a radioactive waste repository, has been carried out. An elasto-plastic, strain

softening analytical solution has been implemented, within a reliability based framework and initial results have been presented. Three zones can be clearly identified; the elastic zone, the strain softening zone and the residual zone. The effect of the aleatory uncertainty on the probability of failure is illustrated, along with the impact of correlating material parameters, which, in this investigation, leads to a reduction of the exceedance probability.

References

Barnichon JD, Neerdael B, Grupa J, Vervoort A (2000) CORA 18: Project TRUCKII. Waste and Disposal Department, SCK·CEN, Mol, Belgium

Bernier F, Li X-L, Bastiaens W (2007) Twenty-five years geotechnical observation and testing in the tertiary Boom Clay formation. Géotechnique 57(2):229–237

Bésuelle P, Viggiani G, Desrues J, Coll C, Charrier P (2013) A laboratory experimental study of the hydromechanical behavior of Boom Clay, rock mechanics and rock engineering (online). doi:10.1007/s00603-013-0421-8

Chen SL, Abousleiman YN, Muraleetharan KK (2012) Closed-form elastoplastic solution for the wellbore problem in strain hardening/softening rock formations. Int J Geomech 12(4):494–507

Deng YF, Tang AM, Cui YJ, Nguyen XP, Li X-L, Wouters L (2011) Laboratory hydro-mechanical characterisation of Boom Clay at essen and mol. Phys Chem Earth, Parts A/B/C 36(17–18):1878–1890 (Clays in natural & engineered barriers for radioactive waste confinement)

Graziani A, Ribacchi R (1993) Critical conditions for a tunnel in a strain softening rock. In: Proceedings of the international symposium on assessment and prevention of failure phenomena in rock engineering, Istanbul, Turkey, pp 199–204

Horseman ST, Winter MG, Entwistle DC (1987) Geotechnical characterization of Boom Clay in relation to the disposal of radioactive waste. Nuclear Science and Technology, EUR 10987, Commission of the European Communities

Verhoef E, Neeft E, Grupa J, Poley A (2011) Outline of a disposal concept in clay. OPERA-PG-COV008, COVRA, NL

Wildenborg A, Orlic B, de Lange G, de Leeuw CS, van Weert F, Veling EJM, de Cock S, Thimus JF, Lehnen-de Rooij C, den Haan EJ (2000) CORA 19: transport of radionuclides disposed of in clay of tertiary origin (TRACTOR)—Final report, Utrecht, The Netherlands

Measurements of Acoustic Emission and Deformation in a Repository of Nuclear Waste in Salt Rock

99

Jürgen Hesser, Diethelm Kaiser, Heinz Schmitz, and Thomas Spies

Abstract

Measurements of acoustic emission have been performed since 1994 in a repository of nuclear waste (a former salt mine) in combination with deformation measurements in order to monitor the mine structure regarding stability and the integrity of the rock mass. Measuring acoustic emissions, the generation of micro- and macrocracks in the rock mass can be detected. Therefore this method provides the identification and observation of high levels of load and of load changes in large-scale. Generally, an analysis in detail requires the inclusion of additional measurements and numerical calculations. The generation of microcracks and macrocracks leads to a volume increase, which can be quantified by deformation measurements. The results show that areas of high acoustic emission activity are in good accordance with zones of larger deformations.

99.1 Introduction

The anthropogenic invasion by the construction of underground openings (e.g. boreholes, drifts, chambers, caverns) and the utilization of these openings (e.g. heat production, exploitation of raw minerals, energy storage, waste disposal) lead to changes of the state of stress combined with rock mass deformations. If the load of the rock mass exceeds a rock mass specific limit, microcracks and macrocracks will be generated, which can cause a loosening up with the result of changes in bearing behaviour and permeability. Regarding the stability of underground bearing systems and the integrity of geological barriers, such areas with ongoing generation of microcracks and macrocracks have to be detected at an early stage and the damage development has to be predicted (Heusermann 2001).

On the one hand, microcrack generation involves the emission of seismic energy, which is transmitted through the rock mass in form of seismic waves. This acoustic emission (AE) can be detected using piezoelectric sensors. Networks of sensors enable the localization of AE. On the other hand, microcracks induce a small but irreversible volume increase (dilatancy), which can be observed by deformation measurements. The combination of both monitoring methods, AE and deformation measurements, together with other investigation methods, like numerical calculations (e.g. Fahland et al. 2005) and laboratory tests enable a detailed analysis of the geomechanical behaviour of the rock mass with regard to the evaluation of stability and integrity.

J. Hesser (✉) · D. Kaiser · H. Schmitz · T. Spies
Federal Institute for Geosciences and Natural Resources (BGR),
Hanover, Germany
e-mail: juergen.hesser@bgr.de

D. Kaiser
e-mail: diethelm.kaiser@bgr.de

99.2 Measuring Methods

99.2.1 Acoustic Emission Measurements

With acoustic emmission (AE) measurements, seismic energy of high frequencies is recorded, due to generation or expansion of cracks with small dimensions in the scale of millimetres to centimetres. Elastic seismic waves propagate from these cracks into the solid rock and are recorded at frequencies of 1–100 kHz. Three networks of up to 32 sensors were installed in boreholes in the mine, in total 90 sensors. The principle of AE measurements is sketched in Fig. 99.1. The signals are digitized, analysed and stored automatically. Automatic processing includes localization and determination of the strength (magnitude) of the microcrack events (Spies and Eisenblätter 2001). Currently approximately 2,000 events are localized per hour allowing detailed monitoring of temporal and spatial variations of microcrack processes (Köhler et al. 2009; Becker et al. 2010).

AE measurements are a suitable monitoring method for highly excavated rock mass areas, because microcrack generation and therefore areas of dilatancy can be detected reliably.

99.2.2 Deformation Measurements

From the mechanical point of view, the volume increase induced by microcrack generation as well as displacements caused by macrocracks or fractures can be observed by deformation measurements. Deformations close to the openings can be determined by convergence measurements. Deformations at a greater distance to the openings can be monitored by borehole measurements, using extensometers
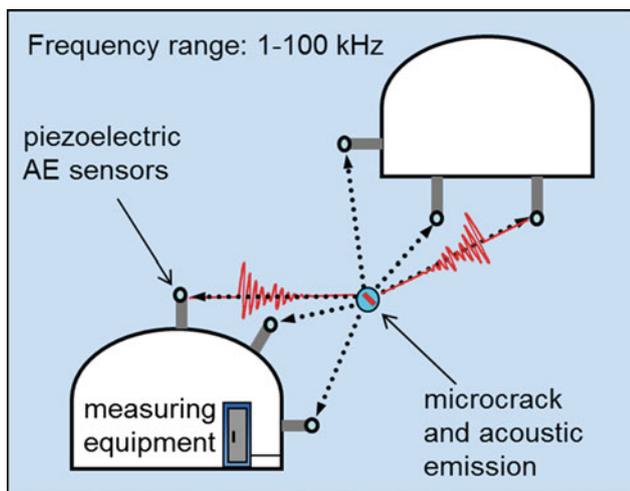
Fig. 99.1 Principle of acoustic emission measurements in mines

or inclinometers. The observation of discrete joint faces can be performed with fissurometers.

Convergence measurements are carried out to determine the deformation of openings by measuring the distance of points on the cavity perimeter. The rock mass deformation along the axis of a borehole is gathered by extensometers, repeatedly measuring the distance of anchor points in the borehole to a reference point near the cavity contour. Displacements perpendicular to the axis of a borehole in the rock mass are measured with inclinometers, determining the change of inclination of borehole segments. With fissurometers, the relative displacements of joint faces on the cavity perimeter are observed. Details on these measuring methods are described in Dunnicliff (1993).

99.3 Measuring Results

The measurements described above were performed in the central mine segment whose chambers were backfilled using salt concrete. The results of the measurements show the effects of backfilling on the rock mass behaviour. The monitored mine area is characterized by a high density of excavation and therefore by high loads of the pillars between the large chambers, which are arranged one above the others. As the preservation of the underground stability and the rock mass integrity in this mine area were the main objective, the selected chambers were backfilled in succession with salt concrete from the second half of 2003 up to the beginning of 2011. Apart from the AE sensors many geotechnical sensors were installed in the central mine region to monitor the temporal development of temperature, stress and deformation.

With the backfilling, the humidity in the salt mine increased and the hydration of the salt concrete led to a temperature increase in the rock mass. Also a strong increase of the AE activity with characteristic concentrations was observed in the vicinity of the backfilled chambers. Mostly the microcrack generation was concentrated in the roof of the chambers as well as in the pillars. Generally, high microcrack activity continued for several years. Figure 99.2 shows locations of AE events in the central mine area in a vertical cross section.

In Fahland et al. (2005) the temperature increase was identified as the cause of the microcrack generation in this area, induced by the exothermic hydration. Hesser and Spies (2007) showed with a laboratory experiment, that the increase of humidity also leads to increased microcrack activity, at least in the vicinity of the backfilled openings.

Two extensometers were installed in the roof of chamber 2n at the second level in the southern part of the chamber. The determined section deformations of the extensometers are shown in Fig. 99.3. During the whole measuring time, a vertical extension of the pillar was observed. First, in the
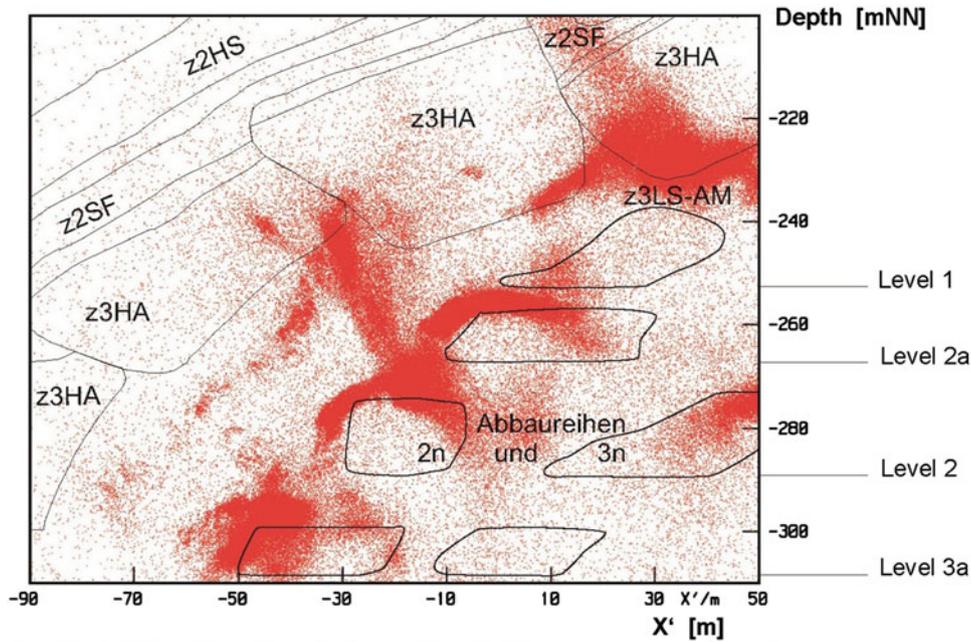
Fig. 99.2 Locations of AE events in the year 2010 in a vertical cross section in the central area of the salt mine with a sketch of the excavation chambers and the geological units
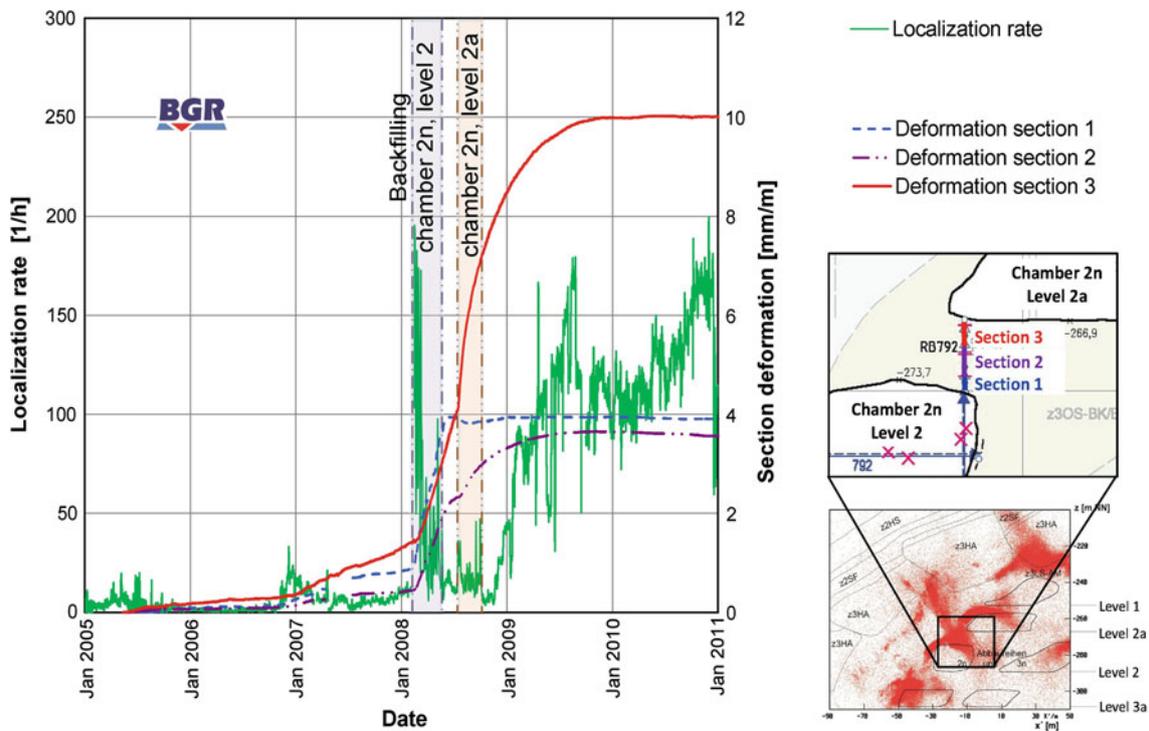
Fig. 99.3 Results of AE and deformation measurements before, during and after backfilling of chambers 2a on level 2 and level 2a

years 2005 and 2006, this extension was very small. The backfilling of chambers below the chamber 2n on the second level led to a deformation increase in 2007.

In 2008 the chambers 2n on the levels 2 and 2a were backfilled (see Fig. 99.3). This backfilling activity led to a significant increase of the vertical pillar deformation right at

its beginning. In the roof of chamber 2n at the second level and in the centre of the pillar the deformation reached a value about 4 mm/m in 2009. In the floor of chamber 2n on level 2a (section 3) the vertical pillar extension of 10 mm/m at the end of 2009 was much higher than other ones.

Figure 99.3 also shows a strong rise of the AE activity in the roof of the chamber with the beginning of the backfill activity in 2008. Later on, the activity decreased up to the second half of 2008. Backfilling the chamber on level 2a led only to small changes of the AE activity but to an obvious increase of deformation in the floor of chamber 2n on level 2a. After both chambers were backfilled, the AE activity increased again to a relatively high level since the end of 2008.

If there had been only dilatant processes in the pillar, a quite symmetric deformation distribution would have been observed by the extensometer measurements, with decreasing deformation from the pillar centre to the openings. Indeed, maximum pillar extension was found in the floor of chamber 2n at level 2a. Thus the opening of a joint face or concordant relative displacements in this area can be assumed.

A detailed evaluation shows that the AE activity increase started earlier than the increase of deformation. In this case, the microcrack generation could be detected by AE measurements before measurable deformations occurred.

Nevertheless, the comparison of the AE localization rate with the deformation development in Fig. 99.3 shows that an increase of AE activity is not strongly linked to an increase of vertical deformation in the roof of the chamber. In the years 2009 and 2010 the AE activity in the pillar increased while the section deformations reached constant values.

99.4 Conclusions

For more than 18 years AE activity has been monitored in a former salt mine resulting in a large dataset of more than 90 million localized microcrack events. These measurements are an important contribution to the monitoring of the mine to assess the stability of the mine and the integrity of the rock mass. Spatial and temporal changes of the rock mass load can be identified and observed in large-scale using this method. But for a detailed analysis of the observed events and their processes the results of other geotechnical measurement methods have to be included.

With backfilling of the excavation chambers in the central area of the salt mine, the temperature in the rock mass increased. The backfilling with salt concrete also resulted in a strong and long lasting increase of AE activity, especially in the roof of the chambers. The increased microcrack activity was associated with larger deformations. This is often the case as also in other parts of the mine the AE activity and the deformations are correlated. In one pillar the temperature increase caused the activation of a joint face. With extensometer measurements the opening of the joint face respectively relative displacements in the joint face was verified.

References

Becker D, Cailleau B, Dahm T, Shapiro S, Kaiser D (2010) Stress triggering and stress memory observed from acoustic emission records in a salt mine. Geophys J Int 182:933–948. doi:10.1111/j.1365-246X.2010.04642.x

Dunnicliff J (1993) Geotechnical instrumentation for monitoring field performance. Wiley, New York, 577 p. ISBN 0-471-00546-0

Fahland S, Eickemeier R, Spies T (2005) Bewertung von Gebirgsbeanspruchungen bei Verfüllmaßnahmen im ERAM. 5. Altbergbaukolloquium vom 3. bis 5. November 2005. Verlag Glückauf GmbH; TU Clausthal

Hesser J, Spies T (2007) The influence of humidity on microcrack processes in rock salt. In: Wallner M, Lux K-H, Minkley W, Hardy Jr R (eds) Proceedings of SaltMech6—6th conference on the mechanical behaviour of rock salt, pp 45–52. Taylor and Francis, London

Heusermann S (2001) Beurteilung der geomechanischen Stabilität und Integrität von Endlagerbergwerken im Salzgebirge auf der Grundlage geologischer und ingenieurgeologischer Untersuchungen. Geologische Beiträge Hannover 2:159–174

Köhler N, Spies T, Dahm T (2009) Seismicity patterns and variation of the frequency-magnitude distribution of microcracks in salt. Geophys J Int 179:489–499. doi:10.1111/j.1365-246X.2010.04642.x

Spies T, Eisenblätter J (2001) Acoustic emission monitoring of closely spaced excavations in an underground repository. J Acoust Emission 19:153–161

Engineering Geology and Design of Hydroelectric Power Plants

Convener Luca Soldo—*Co-convener* Eng Massimo Cadenelli

The inherent technical, economical and environmental benefits of hydroelectric power make it an important contributor to the future world energy mix, particularly in developing countries. Engineering Geology represents a wealth of expertise which can ensure that future projects will be planned, constructed and operated with full respect for the environment. Engineering geologists support the design of hydroelectric power plants from the very begin-ning phases of planning and interpretation of the investigations, understanding the design geotechnical parameters. In the following, they must recognize the geological, hydrogeological and geotechnical hazard factors that may arise as a result of the interaction between geology and the planned works studying the necessary measures for their prevention and mitigation. This session aims to be a round table for an open analysis of the engineering geology "best practices" along the design protocol of hydropower plants.

Reinhold Steinacher and Gyeltshen Kuenga

Abstract

A large-span underground Powerhouse cavern and a medium-size Transformer cavern with an average overburden of 280 m have been excavated following the New Austrian Tunnelling Method (NATM). The two caverns are separated in between by 35 m rock ledge. The encountered rock mass of crystalline assemblages are meta-sediments consisting of an intercalation of Mica Schists, Quartzites and Gneisses. This intercalation of brittle and ductile acting rock mass with very close to close spacing of schistosity planes did not pose major problems during excavation. The support system designed has proved to be adequate during construction and was verified by geotechnical monitoring. For western means sparse site investigation was compensated by sound engineering geological mapping and strict site supervision.

100.1 Introduction

The Dagachhu Hydropower Project (DHPP) is a run-of-river scheme being developed on the Dagachhu River in the south-western Dzongkhag (district) of Dagana in Bhutan. The major components of the project consist of a diversion dam, intake structures, surface desilting chambers, a mainly underground water conductor system of 9,100 m lengths, a surge tank, a vertical pressure shaft (270 m) and penstocks. Electricity is produced in an underground Powerhouse (PH). The water is finally diverted back to the main river course through the 680 m long tailrace tunnel (TRT). With an installed capacity of 126 MW, the Powerhouse owns two vertical axis Pelton turbines of 63 MW each. The project is expected to generate around 515 GWh of clean energy annually and to contribute to the reduction of greenhouse gas emissions in the region.

Situated in the heart of the eastern part of the 2,500 km long Himalayan range, Bhutan has a complicated topography and geomorphology due to the geo-historical processes. Harnessing the potential hydropower resource of estimated 30,000 MW is a major challenge due to the complex Himalayan geological set-up, logistics and accessibility and seasonal severe weather conditions. Due to heavy vegetation, high overburden and rugged nature of the terrain, geological investigations are difficult to perform. Therefore answering questions about rock mass quality within the planning phase of the project becomes a major issue. This led to severe cost and time overrun in several earlier hydropower projects in Bhutan.

The Powerhouse Complex of Dagachhu Hydropower Project consists of two main caverns: the Powerhouse (PH), 62.5 m × 23.88 m × 37 m (l × b × h) and the Transformer Cavern (TF), 52 m × 14.5 m × 16 m (l × b × h). The two are separated in between by 35 m rock column connected by two short bus-duct tunnels. A Main Access Tunnel (ACT), two Penstock tunnels and an Emergency Exit tunnel (EET)

R. Steinacher (✉)
Engineering Geologist, Bernard Consulting Engineers SE, Hall, Austria
e-mail: reinhold.steinacher@bernard-ing.com

G. Kuenga
Dagachhu Hydro Power Corporation Limited, Dagana District, Kingdom of Bhutan

at the eastern side of PH as well as other auxiliary tunnels for construction access had to be excavated. It is located in spur projection at the left bank of the river as shown in the layout Fig. 100.1. Both caverns are aligned in North-South direction. For a more detailed (geological) description of the project see Holzleitner et al. (2008), Holzleitner and Fish (2012), Steinacher (2013), Gyeltshen and Steinacher (2013) and Gyeltshen et al. (2013).

This paper presents engineering geological aspects of the rock mass as encountered during investigation and construction and the support systems implemented to ensure immediate stability and safety as well as long term service performance. Further, instrumentation for the geotechnical monitoring and its interpretation used for design verification are presented.

100.2 Site Investigation

During the feasibility level study, several geological missions by the consultant had taken place with the aim to gain understanding and to be able to adjust the project to the existing geological settings. Engineering geological mapping of the project area in the Scale 1:10,000 was executed. Based on these results the layout for a detailed subsurface investigation program was developed. A detailed geological mapping of selected areas such as adits and portals in the Scale 1:5,000 followed. Three core drillings >200 m depth were executed at the Powerhouse area to detect fault zones and probable slope instabilities, investigate rock type, get information on the groundwater conditions and to gain rock samples for laboratory testing. The in situ stress conditions at the Powerhouse site were measured by conducting hydrofracturing tests.

Following the detailed investigation program, geotechnical interpretation and assessment of the rock mass behaviour were prepared. Some direct consequences arose of the site investigations:

- The Powerhouse cavern was rotated to gain a north-south direction to reach a sub perpendicular position to the strike of schistosity.
- It was decided to go for full face excavation of top heading rather than execute subdivided excavation.

100.3 Encountered Geological Conditions

The encountered rocks are dominated by an alternation of phyllitic Biotite–Muscovite–Garnet–Schist (Micaceous Schist), micaceous Quartzite and Gneiss in layers reaching from centimetres to several metres. At some places a very narrow intercalation is present, where a distinction is barely possible (see Fig. 100.2).

Rock mass encountered was of fair to poor quality in the top heading and of fair to good quality in the benches.

Distribution of Rock Quality Designation values (RQD) and Q-value ranges are shown in Fig. 100.3. Shear zones were encountered only very subordinate, mostly as 5–10 m long 1–5 cm gouge filled foliation parallel shear zones. One major weakness zone with about 1–3 m thickness was encountered parallel foliation from top heading down to the 3rd bench.

The whole Powerhouse Complex lies below the groundwater table. During excavation of the top heading and benching about 1.5 l/s of dripping to slightly flowing water was observed. Two litres per second are present as slightly dripping seepage from top heading and anchors on side walls after full excavation.

Fig. 100.1 Layout of the Powerhouse Complex at Dagachhu Project
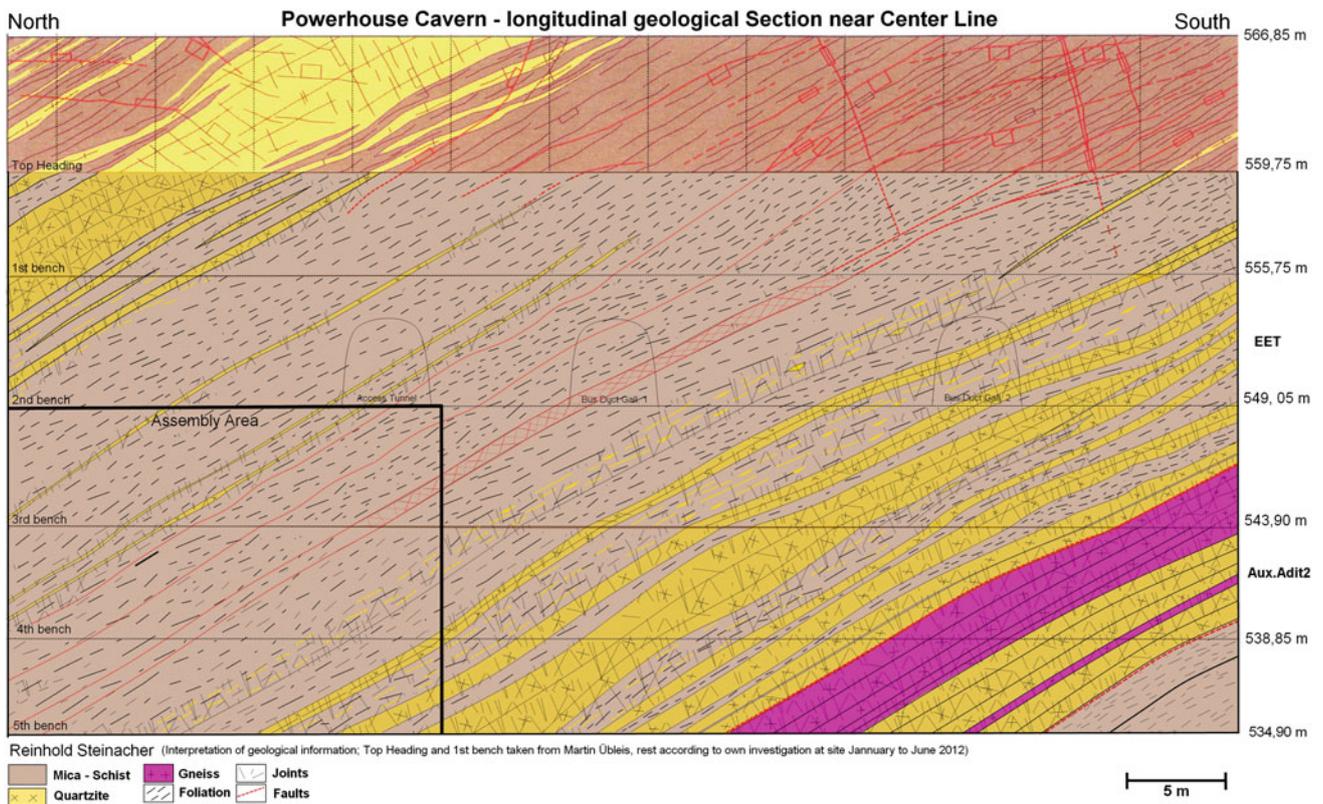
Fig. 100.2 Longitudinal section at *center line* of Powerhouse Cavern (*brown* Mica-Schist; *yellow* Quartzite; *magenta* Gneiss; *red* faults)
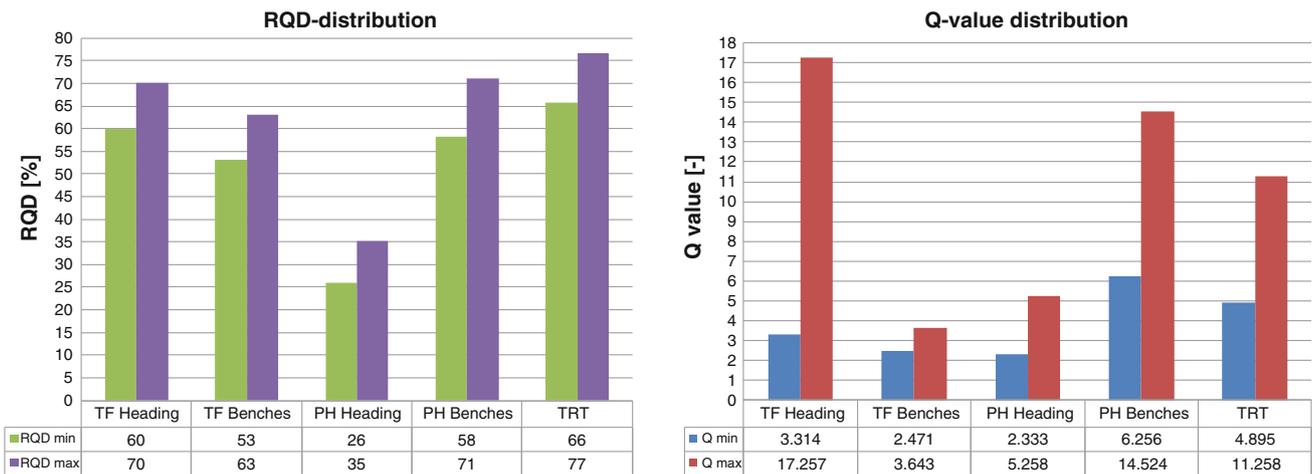
Fig. 100.3 Arithmetic mean of minimum and maximum values for RQD (*left*) and Q-values (*right*) for Transformer Cavern (*TF*), Powerhouse (*PH*) and Tailrace Tunnel (*TRT*)

100.4 Evaluation of Site Investigation

The drill cores were of bad quality and showed an unnaturally high degree of fracturing and core loss. The fracturing was assigned to the drilling process rather than the natural rock mass quality. An RQD could not been gained from the drill cores and had to be estimated from the field. Documentation of TCR (Total Core Recovery) brought at least some hints on rock mass quality but as well was not satisfactory. Performed laboratory tests (f.i. UCS) showed a high variety in results. Nevertheless, the performed site investigation proved sufficient to plan and construct the Powerhouse and Transformer Caverns. No unforeseen geological

conditions were encountered. The rock mass at top heading was stable enough to be excavated full face and the chosen support measures were adequate. Geological mapping proved to be an efficient tool to gain information on rock mass conditions and general rock mass behaviour. This is especially true for this remote area in southern Bhutan where performance of core drilling as well as in situ and laboratory testing are not comparable with western standards. Rock mass characterization in the field hereby plays a crucial role to get at least approximate values for rock mass strength and an assessment of rock mass behaviour.

100.5   Support, Instrumentation and Monitoring

The concurrent support systems provided consisted of 32 mm diameter, 6 m long rock bolts at spacing of 3 m centre to centre (c/c) staggered both ways, lattice girder at spacing of 1.5 m c/c and three layers of welded wire mesh embedded in shotcrete having characteristic strength of 35 MPa. The minimum overall built-up thickness of shotcrete was 450 mm applied in four layers in the crown and 400 mm thick in three layers in the walls.

After completion of the heading excavation, installation of the primary support was started. Permanent Bar Anchor (PBA), 36 mm diameter, 15 m long ground anchor system with pre-stressing were installed. This was the main (primary) support system designed to support the rock mass deformation expected to occur during the subsequent bench excavation. The 1st bench excavation was started only after the complete installation and application of pre-stressing force to all PBAs in the top heading. Each bench excavation was performed with bench height of 4–5 m with provision of immediate support and installation of PBAs. The excavation of the entire Powerhouse cavern was completed on 21st June 2012.

As one of the fundamental principles of NATM bireflex targets (70), load cells (19) and multipoint borehole extensometers (19 MPBX) have been installed to observe rock mass behaviour during construction to ensure safety and adequacy of the support systems (construction control) and for monitoring of the long-term performance of the support system and the overall structure.

Against contractual agreements zero readings of the bireflex-targets were taken 1–2 days after excavation and support. Therefore monitored displacements do not represent absolute values. Due to the relative moderate excavation advance in Top Heading the magnitude of the "pre-displacement" may be of a magnitude of 30–50 mm. This would bring the total displacements into the expected and estimated range of about 60–80 mm. The crown targets showed settlements while the side wall targets tended to

show a combination of settlement and movement into the excavated cavity. This might also be correlated with encountered geological features where a foliation parallel weakness zone could be identified during excavation dipping approximately with 30°–40° towards North-East. Many targets showing deformation greater than 5 mm lie near or above this weakness zone. Also load cells showed the influence of this zone. Both MPBX and Load Cells indicated maximum levels below 2D numerical modelling results of 60 mm and 780 kN respectively. The support system designed has proven to be adequate during construction.

100.6   Challenges and Conclusions

A close interaction between the *Dagachhu Hydropower Corporation*, *Bernard Engineers* as consultant and the contractor (*Hindustan Construction Company*) were crucial for the project success. NATM has proven an efficient and safe way to construct the Powerhouse Complex at Dagachhu, even though the Indian contractor had little experience with this kind of tunnelling concept. An independent and strict consultant was very efficient for all parties to ensure an up-to-date excavation and support methodology.

Geological field mapping was crucial for the assessment of engineering geological parameters in this remote area where in situ and laboratory testing does not reach western standards. The use of rock mass classification schemes though, should only be performed by an experienced geologist. These schemes are suitable to recognise trends in rock mass quality changes and to have a base of discussion with non-geologists. Q-values from different processors taken at the same outcrops rather show disillusioning results (Steinacher 2013).

Challenges encountered during construction should be mitigated beforehand by strict contract agreements and their enforcement on site. On the Indian subcontinent typical challenges may be:

- Seepage water management generally is not taken serious during construction stage. Soaked working areas lead to problems with accessibility and therefore time delay during mucking and supply with equipment. Strict guidance and enforcement of contractual agreements must prevent bad water management.
- Sub-contractors of the main contractor are employed for works like installation of Permanent Bar Anchors or Geotechnical measurement of bireflex targets. If conflicts arise or payment delays occur the sub-contractor stops work, which in most cases also hampers main construction works.
- Indian contractors are quite inflexible to changes in methodology. Financial stimulations in contract may help to change this attitude.

References

Gyeltshen K, Steinacher R (2013) Engineering geological aspects of the underground powerhouse at Dagachhu Hydropower Project, Bhutan. In: Druk Green Power Corporation Limited (eds) 25 years of learning, Proceedings of the 1st Druk Green technical conference, Chuckha, Dec 2013, Bhutan, pp 337–355

Gyeltshen K, Wangdi S, Dorji T (2013) Application of Permanent Bar Anchors (PBA) support system in underground powerhouse of Dagachhu Hydropower Project in Bhutan. In: Druk Green Power Corporation Limited (eds) 25 years of learning, Proceedings of the 1st Druk Green technical conference, Chuckha, Dec 2013, Bhutan, pp 1–19

Holzleitner W, Aichinger J, Fish M (2008) The Dagachhu Hydropower Project, Bhutan. Jahrbuch Tunnelbau 2008:1–3

Holzleitner W, Fish M (2012) NATM underground structures of the Dagachhu HPP. In: Stipek W, Galler R, Bauer M (eds) 50 years NATM—Experience reports. ITA Austria, Wien, pp 163–168

Steinacher R (2013) Engineering geological aspects of the 126 MW Hydropower Plant Dagachhu in Bhutan. In: Proceedings of the 19 conference for engineering geology, Technical University of Munich, pp 75–81

N.G. Maksimovich and V.T. Khmurchik

Abstract

Microbes are ubiquitous on the Earth and take an active part in the transformation of the geological environment. Their activity can change the geochemical parameters of ground and groundwater and lead to undesirable consequences after the building of hydrotechnical facilities, especially pressure ones. The geological and chemical survey of one of the ground dams of Kama–Volga rivers cascade (The Ural, Russian Federation) revealed the unusual deviations in chemical content of drain water and the presumable suffusion process at the dam basement. The aim of our study was investigation of the dam's ground and water to reveal another deviations in their characteristics, which in turn could help to assess the stability of the dam. We investigated the composition of water-dissolved organic matter (gas chromatography–mass spectrometry analysis), the composition of subsoil gases of the dam (gas analysis), and performed mineralogical analysis of sediments settled at the bottom of the dam's drain system (X-ray diffraction analysis); chemical analysis of water of various aquifers under the dam basement was performed too; also, the microbiological investigations of the dam's ground and water samples were made. We suppose, the results of investigation demonstrate the presence of an active microbiota in dam's ground and water, and microbiota metabolism could lead to hazardous changes in physical-mechanical properties of dam's ground and, eventually, the unstable state of the dam itself.

101.1 Introduction

Microbes are ubiquitous on the Earth and take an active part in the transformation of the geological environment, including the impact on ground and groundwater (Bolotina and Sergeev 1987; Kuznetsov et al. 1962; Maksimovich and Hmurchik 2012; Radina 1973). Microbial processes can change the geochemical parameters of ground and groundwater and lead to undesirable consequences after the building of hydrotechnical facilities, especially pressure ones (Koff and Kozhevina 1981; Maksimovich et al. 2001).

The geological and chemical survey of one of the ground dams of Kama–Volga rivers cascade (The Ural, Russian Federation) revealed the unusual deviations in chemical content of drain water and the presumable suffusion process at the dam basement. We supposed, the main cause of deviations observed was the existence of microbiological processes in the dam's ground and water, and tried to explain the detected phenomena from this point of view.

The aim of our study was more proper investigation of the dam's ground and water to reveal another deviations in their characteristics, which in turn could help to assess the stability of the dam.

N.G. Maksimovich · V.T. Khmurchik (✉)
Natural Science Institute, Perm State National Research University, Perm, Russian Federation
e-mail: khmurchik.vadim@mail.ru

N.G. Maksimovich
e-mail: nmax54@gmail.com

101.2 The Description of the Dam's Ground and Water

The studied dam is the part of Kama–Volga rivers cascade dams (The Ural, Russian Federation). The basement of the dam is presented of alluvial sediments up to 18 m in thickness. The sediments are consisted of clays, loams, sandy loams, and, in the upper part of geological column, of fine sands. Sand bands are observed in clays and loams. Sand and gravel deposits are in the lower part of geological column. The distribution and the composition of gravel-pebble strata are not uniform. Lenses of fine sand and interlayers of clays are observed in the gravel-pebble strata, peat is presented in the strata too (Mamenko 1967).

101.2.1 Hydrological and Hydrochemical Conditions Before the Dam Construction

Groundwater was widespread in alluvial deposits and located in sands and gravel-pebble rocks before the dam construction. Water table was 3–9 m below ground surface and had slope gradient to riverbed in 0.006–0.012 grad m^{-1}. Average filtration coefficient of alluvial horizon was 14, and 26–82 m day^{-1} in it gravel-pebble layer. Alluvial groundwater was weakly mineralized and HCO_3–Ca in chemical content.

101.2.2 Hydrological and Hydrochemical Conditions After the Dam Construction

Significant changes in hydrodynamical and hydrochemical conditions, which were caused by a number of factors, such as change in hydrostatic heads of groundwater, filtration of fresh water from the reservoir etc., have occurred since the dam construction. Alluvial aquifer became confined and has a local hydrostatic head at present. It water table is located at the depth of 1 m below the dam surface under it basement. Total salinity of alluvial aquifer's water is 100–200 mg dm^{-3} (up to 400 mg dm^{-3} sometimes) and it increases downstream in general; water of alluvial aquifer is HCO_3–Cl–Na–Ca in chemical content at present. The alluvial aquifer has a close hydraulic connection with the waters of the Kama River. Moreover, it seems to exist the local hydrogeological windows between alluvial aquifer and underlying aquifers, which could cause the increased content of chloride ions (up to 168 mg dm^{-3}), which was observed in individual observational wells of alluvial aquifer.

Geological and chemical survey of the dam revealed the elevated concentration of Fe^{2+} ions in drain water and the settlement of Fe–(hydr)oxides at the bottom of the dam's drain system. As well as this features resembled suffusion process, more proper investigation was done to assess the stability of the dam.

101.3 Methods

We investigated the composition of water-dissolved organic matter (gas chromatography–mass spectrometry analysis on "Agilent 6890/5973N"), the composition of subsoil gases of the dam (gas analysis on "Ecoprobe-5"), and performed mineralogical analysis of sediments settled at the bottom of the dam drain system (X-ray diffraction analysis on "D2 Phaser"). Chemical analysis of water of various aquifers under the dam basement was performed too. Also, the microbiological investigations of the dam's ground and water samples were made.

101.4 Results of Investigation

The chemical analysis of alluvial horizon's water under the dam basement revealed the presence of zone with elevated contents of Fe^{2+}, HCO_3^- and NH_4^+ ions. This water contains the high amount of water-dissolved organic matter—108–122 mg dm^{-3} (whereas it content did not exceeds 30–40 mg dm^{-3} in groundwater of the Ural region). The main features of water-dissolved organic matter were non-hydrocarbon character and technogenic origin. The content of chloroform-extracted bitumen was 1.1–1.6 mg dm^{-3} in range, and the oil-product content was less than 0.07 mg dm^{-3}. The hexane fraction of water-dissolved organic matter consisted of oxygen-containing compounds mainly, the presence of sulfide sulfur (up to 6 %) was found in the hexane fraction too.

The analysis of subsoil gases of the dam revealed the occurrence of regions with elevated contents of CH_4, C_2–C_5 hydrocarbons and volatile organic compounds.

The studies of the mineralogical composition of the sediments settled at the bottom of dam's drain system revealed a predominance of authigenic minerals' complex (calcite, amorphous iron hydroxides, goethite, hydrogoethite, and pyrite) over allotigenic one (quartz minerals). The newly-formed minerals—slices of calcite and pyrite—were detected.

Microbiological investigations of the dam's ground and water revealed the presence of an active metabolizing microbiota in them. Bacteria, isolated from the core and water samples, consumed organic matter, SO_4^{2-} and NO_3^- ions, produced gases and leached Fe ions from the dam's ground samples.

101.5   Conclusions

We suppose that the results of investigation, which were described in Sect. 101.4, demonstrate the presence of an active microbiota in dam's ground and water. Microbial activity could lead to the mobilization and removal of substances (for example, in the form of chemical elements' atoms) from the body and the basement of the dam due to the following processes and factors: bacterial formation of gases could increase tense state of the ground and cause the unconsolidation process; the removal of individual chemical elements from the ground could lead to destruction of it mineral skeleton and reduction of the mechanical firmness of ground; microbiological processes could change microaggregate and chemical composition of ground, dispergate clay minerals, increase ground's wetting ability, and decrease it filtration capacity; exometabolites, formed by microorganisms, could exhibit surface-active properties and reduce the strength of the structural bounds in the ground. So, the intensification of bacterial processes, which could be caused by supply of elevated concentrations of organic matter from anywhere, could lead to hazardous changes in physical-mechanical properties of dam's ground and, eventually, the unstable state of the dam itself.

References

Bolotina IN, Sergeev EM (1987) Microbiological studies in engineering geology. Eng Geol 5:3–17 (in Russian)

Koff GL, Kozhevina LS (1981) The role of microorganisms in the change of geological environment. Eng Geol 6:63–74 (in Russian)

Kuznetsov SI, Ivanov MV, Lyalikova NN (1962) The introduction to geological microbiology. The USSR Academy of Sciences, Moscow, 239 p (in Russian)

Maksimovich NG, Hmurchik VT (2012) The influence of microorganisms on the mineral composition and properties of grounds. Perm State Univ Bull, Ser Geol 3(16):47–54 (in Russian)

Maksimovich NG, Menshikova EA, Kazakevich SV (2001) Possibility of increasing the aggressiveness of groundwater during construction on pyrite-containing clay soils. In: Proceedings of the international symposium on "Engineering-geological problems of urban areas", vol 2. Aqua–Press, Ekaterinburg, pp 545–551

Mamenko GK (1967) The dam on the Kama river. In: Geology and dams, vol 5. Energiya, Moscow (in Russian)

Radina VV (1973) The role of microorganisms in the formation of ground properties and their tense state. Hydrotech Eng 9:22–24 (in Russian)

Factors Controlling the Occurrence of Reservoir-Induced Seismicity

Xin Qiu and Clark Fenton

Abstract

Reservoir-induced seismicity (RIS) is defined as the failure of a pre-existing fault due to reservoir impoundment or water level fluctuations. 127 RIS cases have been recorded around the world, with four events of M > 6. RIS is triggered by a complex interaction between a number of factors including reservoir size, stress regime, hydrogeological condition and reservoir-filling history. Using statistical evaluation of worldwide data the relationships among these factors are investigated. The occurrence of RIS shows a strong correlation with reservoir size, faulting regimes, rock types and background seismicity. However these factors alone are certainly not necessary or sufficient conditions for the triggering of RIS. As the interactions between water movement and geology can be significantly complex, a detailed study on the Xinfengjiang reservoir is presented. Examination of fault location, orientation and permeability structure indicate that the NNW Shijiao-Xingang-Baitian fault is responsible for the majority of seismic events, including the $M_s6.1$ mainshock. The hydrogeological conditions causing RIS are discussed.

Keywords

RIS • Hydrogeological regime

102.1 Introduction

Reservoir-induced seismicity (RIS) is defined as the failure of a pre-existing fault due to the presence of a reservoir impoundment or water level fluctuations. Of the 127 RIS cases reported around the world 4 cases triggered earthquakes $M \geq 6$, 15 cases involved earthquakes $5.9 \geq M \geq 5$ and 32 were $4.9 \geq M \geq 4$ (Qiu 2012). Through the examination of the observations recorded at different RIS sites around the world as well as the detail case study on Xinfengjiang reservoir, correlation between the occurrence of RIS and different inducing factors is assessed.

Although RIS occurs in reservoirs with varying dam heights, the likelihood of occurrence increases with increasing dam height; 17 % of the deep reservoirs with dam heights >150 m have triggered seismicity. A similar relationship is observed with reservoir capacity. Although there is a positive correlation between reservoir size (dam height and capacity) and the probability of RIS occurrence, reservoir size is neither a necessary nor a sufficient condition for RIS to occur since many RIS cases occur in small reservoirs and many large reservoirs do not trigger seismicity.

Examining tectonic setting it is noted that 79 % of the RIS reservoirs are located in normal or strike-slip faulting environments, while only 21 % are in reverse faulting environments (Qiu 2012). Simple Mohr-coulomb failure models show that the addition of vertical loading from reservoir impoundment will act to promote fault stability in a reverse faulting regime, hence the lack of RIS (Qiu 2012).

X. Qiu · C. Fenton (✉)
Department of Civil and Environmental Engineering, Imperial College London, London, UK
e-mail: c.fenton@imperial.ac.uk

102.2 Xinfengjiang Reservoir, China

Xinfengjiang reservoir in southeast China has a capacity of 1.4×10^{10} m^3 and a dam height of 105 m. It is situated above a large E-W trending Late Mesozoic granite body. Soon after impoundment in October 1959, an increase in earthquake frequency was observed. On 19 March 1962, a M_s6.1 earthquake occurred 5 months after the first peak reservoir level was reached. Focal mechanisms indicated that the main shock was on a steep, NNW-striking left-lateral strike-slip fault. Seismic activity started to decrease after 1965 (Ding 1989).

Most of the earthquakes $M_s \geq 3$ are located within three regions: A, B and C (Fig. 102.1). Region A is characterised by the intersection several faults. Regions B and C are associated with the NE- to NNE-striking faults.

The location of a fault relative to the reservoir determines whether the oscillating reservoir loads have a stabilising or destabilising effect (Roeloffs 1988). The Heyuan fault (1, Fig. 102.1) is a shallow-dipping thrust fault inclined towards the SE with the reservoir located on its footwall. The oscillating reservoir load should not induce seismicity on the fault. Few earthquakes have occurred on the Heyuan fault, except for the middle segment where it is intersected by Shijiao-Xingang-Baitian fault (4, Fig. 102.1). The Renzishi fault (2, Fig. 102.1) is a steeply-dipping reverse fault; the northern segment of the fault dips SE while the southern segment dips towards the NW. The reservoir is located on the footwall of the northern segment, and on the hanging wall of the southern segment. Most RIS events are located along the northern segment of Renzishi fault in the reservoir

Fig. 102.1 Distribution of epicentres of $M_s \geq 3$ earthquakes (July 1961–June 2008)

and the middle segment is directly beneath the reservoir (Fig. 102.1). Earthquake focal mechanisms indicate that Shijiao-Xingang-Baitian fault (4) is the fault that is responsible for the M_s6.1 mainshock (Ding 1989). The Roeloffs (1988) fault location model explains the spatial distributions of epicentres around the reservoir.

Most RIS cases are caused by the reactivation of existing faults rather than the development of new ruptures (Morris et al. 1996). The possibility of reactivation for major faults in the Xinfengjiang area can be evaluated based on their orientations with respect to the regional stress field. This slip-tendency analysis is carried out using a MATLAB plug-in application (Neves et al. 2009). The results of this analysis indicate that the faults striking NNW have the highest slip tendency while faults striking NE/NNE direction are less likely to move (Qiu 2012).

Faults are structurally anisotropic and lithologically heterogeneous. In terms of permeability, they can either assist or impede water flow depending on their permeability structures (Caine et al. 1996). NE/NNE-striking faults around Xinfengjiang reservoir are reverse faults, usually ductile in nature. As there are no circulating paths for water to diffuse in this type of fault, RIS is unlikely to be triggered. The NNW-striking faults are strike-slip with distributed conduit type of permeability, leading to a greater possibility of RIS.

Fracture permeability around the reservoir is estimated to see if it lies within the seismogenic permeability range proposed by Talwani et al. (2007). Fractures within the seismogenic permeability range allow pore water to diffuse as Darcian flow, thus making it easier to induce seismicity. The estimated hydraulic diffusivity values (1–5 m^2/s) correspond to a permeability value range of 5×10^{-15}–2.5×10^{-14} m^2. This is within the seismogenic permeability range, indicating that RIS is likely to occur.

Analysis of fault location, slip tendency and permeability structure indicate that the NNW Shijiao-Xingang-Baitian fault (4, Fig. 102.1) is the structure responsible for the majority of earthquakes, including the M_s6.1 mainshock.

Although there is a reasonably good correlation between reservoir level and seismicity a period of delayed response is observed, when earthquakes occur sometime after peak reservoir level is attained (Qiu 2012). The M_s5.1 and M_s5.3 earthquakes occurred immediately after the exceedance of previous peak water level. This may be due to the Kaiser effect; if a material is experiencing cyclic loading with increasing stress, there is an increase in microseismicity (in the form of acoustic emission) if the highest stress level of the previous loading cycle (maximum water level) is exceeded (Lavarov 2003). It is notable that the M_s6.1 mainshock did not occur immediately after the first peak water level, but occurred when the water level was decreasing. One possible explanation could be although the
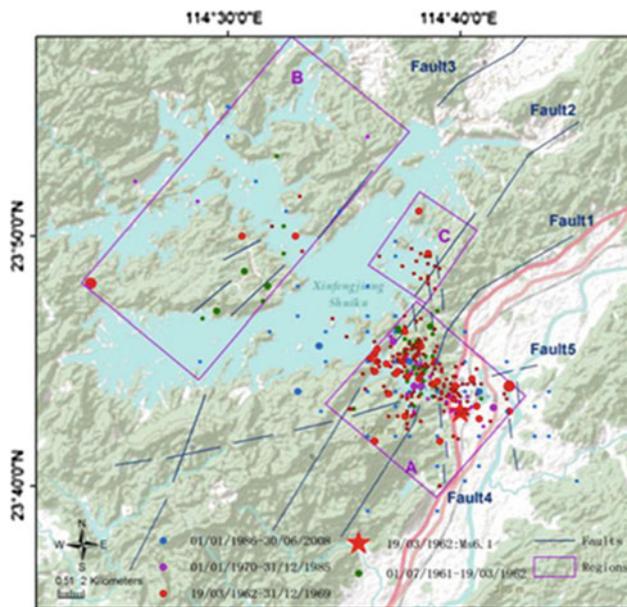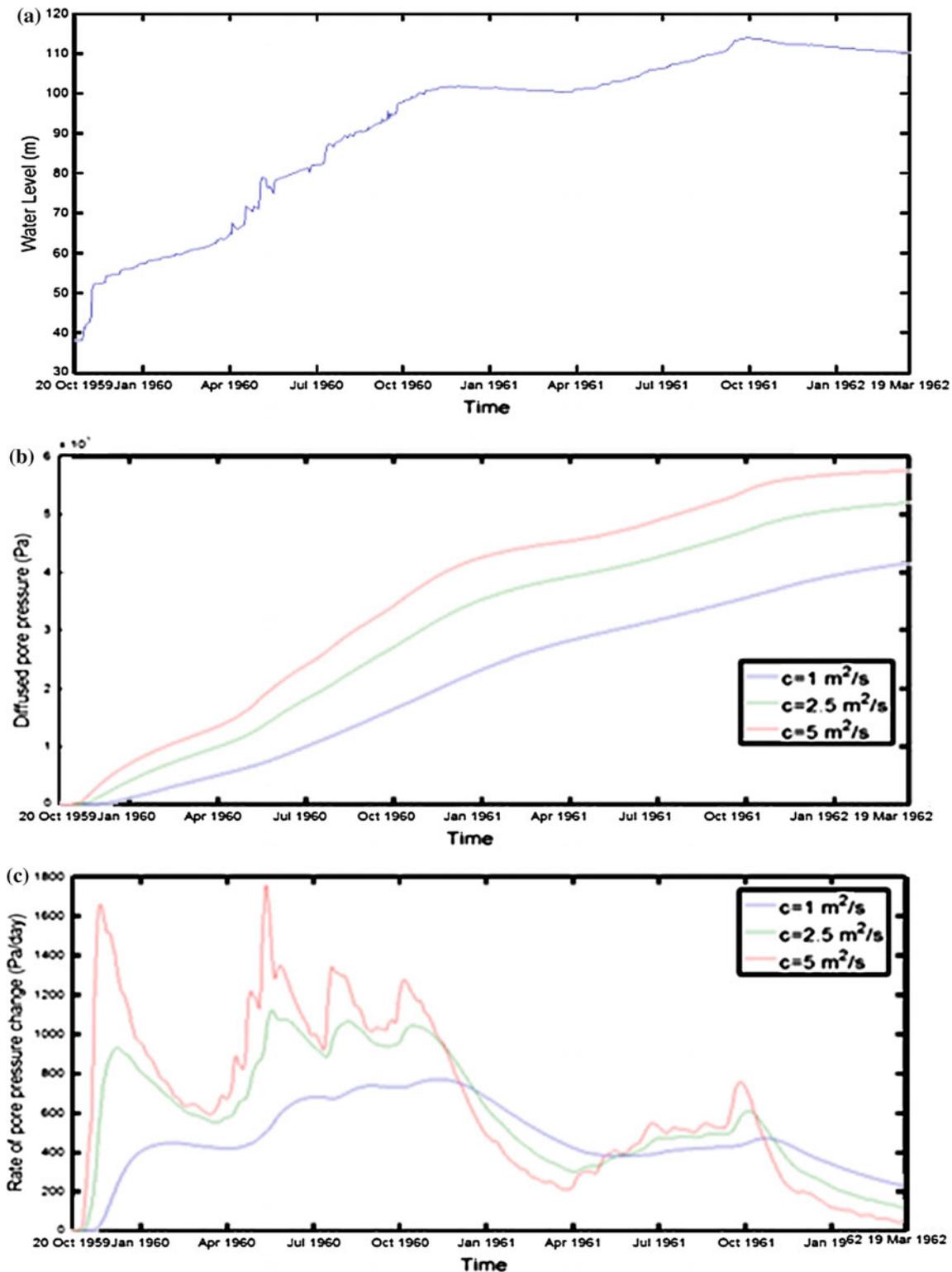
Fig. 102.2 Water level fluctuation (**a**), pore pressure diffusion history (**b**) and rate of pore pressure change (**c**), at the hypocentre of 19th Mar 1962 M_s6.1 main shock

reservoir level is decreasing, the pore pressure at the hypo-central location is still increasing. This hypothesis is only true if pore pressure diffusion is the dominant mechanism, since both the vertical elastic stress increase and undrained pore pressure increase due to compression are short term effects. The Mohr-Coulomb failure model used to calculate

the stress field during the reservoir filling history indicates that the increase in vertical stress has negligible effect on triggering seismicity since the reservoir is located in a strike-slip faulting regime (Qiu 2012). This implies that RIS is only triggered by either the instantaneous undrained pore pressure increase due to elastic compression or pore pressure diffusion. To evaluate the relative importance of each of these effects the magnitudes of each are estimated. The maximum undrained pore pressure increase at the hypocentre of the main shock is estimated to be around 70 kPa using the Skempton effect (Talwani and Acree 1984). The diffused pore pressure is estimated using the approach of Talwani et al. (2007). The calculated pore pressures for 50 $M_s \geq 4$ earthquakes in the reservoir area during the period of 1961–2008 vary from 281 to 680 kPa, much larger than the undrained pore pressure increase, implying pore pressure diffusion should be the dominant mechanism in increasing pore pressure and reducing the effective stress. As the effect of undrained pore pressure increase due to elastic compression is instantaneous, by the time pore pressure front diffuses to the hypocentral location, this undrained effect may have already disappeared. Thus, the threshold of the diffused pore pressure can be interpreted as the threshold pore pressure for inducing seismic events. However, the threshold pore pressure values only indicate the pore pressure required to trigger an earthquake at a particular location, such as the epicentre of the M_s6.1 mainshock. It does not effectively explain why this mainshock occurred during a period of decreasing water level. To explain this phenomenon, a MATLAB routine is built to model the pore pressure diffusion history (Fig. 102.2) at the hypocentre of the M_s6.1 mainshock (Qiu 2012). Several important observations can be made. Firstly, the shape of pore pressure diffusion and water level fluctuations appear to be very similar, indicating a direct correlation. Secondly, the variations of the diffused pore pressure at hypocentral locations are dependent on the value of hydraulic diffusivity. When the hydraulic diffusivity is higher (c = 5 m/s^2), the diffused pore pressure will rise or diminish faster after experiencing a water level change, compared to low values of diffusivity. In addition, for the lower diffusivity case (c = 1 m/s^2), there is a delay between the reservoir impoundment and the onset of pore pressure increase. The initial increase in pore pressure for the lower diffusivity case is negligible. This delay of pore pressure could be due to the fact it takes longer for pore pressure front to arrive at the hypocentral locations for such low diffusivity values. Prior the M_s6.1 mainshock, although the water level was decreasing, the diffused pore pressure at the hypocentre was stilling increasing. A similar trend is observed for the M_s4.1 earthquake on 20th Feb 1962 foreshock. The rate of pore pressure increase is higher during the foreshock period than during the mainshock, indicating that in the long term, if the water fluctuations are small compared to the initial

filling stage, the diffused pore pressure at a particular location may slowly diminish through time. However for the aftershock event of M_s4.3 on 6th December 1963, both the water level and the diffused pore pressure at the hypocentre were decreasing. This implies that failure of a fault does not always occur when the effective stress is at a minimum. Future approaches to explain this phenomenon should focus on earthquake-induced hydrological changes and deviatory effects of pore pressure drop (Qiu 2012).

102.3 Conclusions

Induced earthquakes are possible but not an inevitable consequence of the impoundment of a reservoir. Because of the complexity and variety of factors, any strategy for the limitation of RIS hazards should consider the overall complexity of the phenomenon. Analysis of global data shows that only when a combination of factors are present, can seismicity can be triggered. It is important therefore to maintain focus on the interrelation of diverse concurrent factors rather than to isolate any single one.

The evolution of the hydrogeological regime of the reservoir area plays the most important role in triggering and timing RIS. Concurrently, the stress regimes and the filling history can also be seen to contribute significantly, as highlighted by the case of Xinfengjiang reservoir. In order to develop a more comprehensive understanding of the triggering mechanisms, a series of RIS case histories should be subject to similar analysis. The modelling of pore pressure diffusion history is a particularly promising approach as it allows investigation of RIS sensitivity in relation to the hydrological conditions at hypocentral depths.

References

Caine JS, Evans JP, Forster CB (1996) Fault zone architecture and permeability structure. Geology 24:1025–1028

Ding YZ (1989) Reservoir-induced Seismicity. Seismological Press, Beijing (in Chinese)

Lavarov A (2003) The Kaiser effect in rocks: principles and stress estimation technique. Intl J Rock Mech Min Sci 40:151–171

Morris A, Ferril D, Henderson D (1996) Slip-tendency analysis and fault reactivation. Geology 24:275–278

Neves M, Paiva L, Luis J (2009) Software for slip-tendency analysis in 3D: a plug-in for Coulomb. Comput Geosci 35:2345–2352

Qiu X (2012) Reservoir-induced seismicity. Unpublished ME dissertation, Imperial College, London, 139 p

Roeloffs E (1988) Fault stability changes induced beneath a reservoir with cyclic variations in water level. J Geophys Res 93(B3): 2107–2124

Talwani P, Acree S (1984) Pore pressure diffusion and the mechanism of reservoir induced seismicity. PAGEOPH 122:947–964

Talwani P, Chen L, Gahalaut K (2007) Seismogenic permeability, ks. J Geophys Res 112:B07309. doi:10.1029/2006JB004665

Condition of Boguchany Concrete Dam Foundation According to Instrumenal Observations

103

E.S. Kalustyan and V.K. Vavilova

Abstract

Construction of 76 m high Boguchany concrete gravity dam on the Angara River in Siberia was finished in 2012 and reservoir filling started. The dam foundation is composed of trap intrusion presented by dolerites, heterogeneous by composition and properties. Since the start of construction in 1983 there have been conducted observations over the state of the rock foundation, which is subject to impacts of severe climatic conditions with annual temperature fluctuations up to 100 °C. During the period from 1998 to 2006 actually there was no construction work at the dam, however, instrumental observations continued. In the article the analysis is given of 30-year instrumental observations over the rock foundation deformations at various depths and over the temperature of rocks; relation was revealed between the foundation deformations with loads from the dam concrete, the water level of reservoir and temperature of ambient air.

Keywords

Dolerites • Concrete gravity dam • Monitoring deformations

103.1 Introduce

The Angara River originates from Lake Baikal. Due to this fact the river runoff under natural conditions is well regulated and in the high-water season it is only two times as much as that in the low-water season. The length of Angara is 1,850 km, the annual river runoff is 145 km³. Taking into account its favorable hydrological conditions the Angara River was an ideal site for construction of hydro power plants already since the twenties of the XX-th century. The Angara water resources development in the interest of power generation was started only after the World War II with construction of the Irkutsk Hydro Power Plant (HPP). In 1955–1967 the second stage of the cascade—Bratsk HPP—was built. The Bratsk HPP reservoir with a full storage of 179.1 km³ is one of the largest in the world. In 1980 the third stage of the Angara cascade was created on the Angara River —the Ust-Ilim HPP. At present the next stage of the cascade —the Boguchany HPP has been put into commercial operation the energy of which will make it possible to start developing the natural resources of the Angara region.

103.2 Monitoring Deformation of the Boguchany Concrete Dam

The Boguchany concrete gravity dam site is located in the wide Angara river valley. From the total length of the water retaining structures of 2,670.6 m and a height of 76 m the concrete gravity dam occupies 809.3 m in the left-bank part which are divided into 34 sections (Fig. 103.1).

The concrete structures fully rest on the trappean intrusion represented by dolerites varying in composition and properties. The peculiarity of the concrete dam foundation was determined by the composition and extent of the

E.S. Kalustyan · V.K. Vavilova (✉)
Branch of Institute Hydroproject, Geodynamic Research Center,
Volokolamskoe Shosse 2, 125993, Moscow, Russia
e-mail: vergor@pochta.ru

E.S. Kalustyan
e-mail: office@geodyn.ru

Fig. 103.1 General view of the Boguchany concrete gravity dam

mineralogical alteration of the dolerites. Excavation operations in these rocks caused significant de-stressing of the rock mass up to formation of dolerite detritus. Core logs of the boreholes arranged in the instrumentation installation areas before placing the concrete into the dam showed that more jointed rock with swelling minerals amounted to 1–5 %—of the total volume in sections 6–19 of the left-bank abutment; 6–30 %—in river channel sections 20–24, 30–31, 33–34 and 30–70 %—in sections 25–29. It was considered that this fact should have an effect on properties of the rock mass in the concrete dam foundation, on its deformation indices and deformation uniformity as well as on the behavior during the construction and at the initial stage of operation—during the reservoir filling. Taking this into account the concrete placement into the concrete dam body was started from section 24 in 1983 year.

During construction of the Boguchany concrete dam the assessment of the foundation condition based on the results of in situ tests along with check measurements of deformations in the near-contact and active zones and temperature included special studies of the foundation. The data obtained during these special studies made it possible to assess the deformation irregularity of the foundation before the reservoir filling and to obtain the input data for determining deformation indices for different areas of the dam foundation (Smulskiy 1992).

The peculiarity of the Boguchany dam foundation consists in significant length of the water-retaining structures where measurements of deformations had to be conducted in the near-surface and active foundation zones. Heterogeneity of rocks was complemented here by harsh external conditions such as climatic effects with considerable variations of external air temperature which became the most important load in conditions of long-term development. In the 1990s of

the last century the construction progress was impeded by the absence of financing.

Considerable temperature variations together with other factors defined the expediency of conducting special studies. Annual temperature variations during the whole period of observations at the Boguchany HPP site attained 100° (Fig. 103.2). In 2012 year the reservoir filling commenced under conditions of positive water temperatures in the Angara River introduced significant changes in distribution of foundation temperatures in the near-surface zone from the upstream side of the concrete dam.

Project of the Boguchany HPP concrete structures started in 1982 with laying the concrete in section 24 is practically completed at present. At that, stresses in the foundation of the first sections of the concrete dam due to concrete placement vary on the whole from 1.40 to 2.41 MPa. The crucial point is that stresses achieved by the time of reservoir
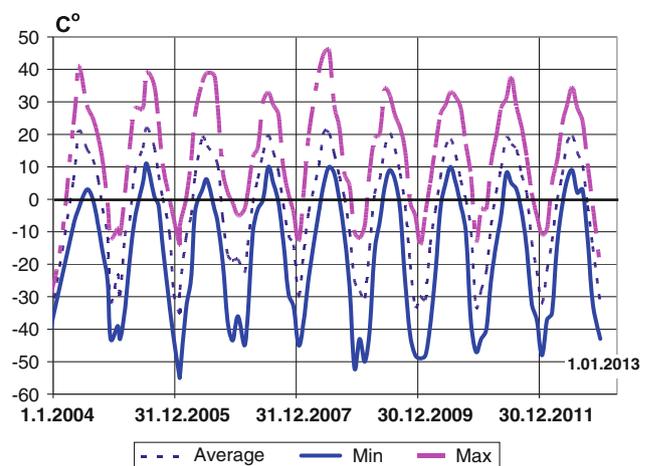
Fig. 103.2 Temperature of ambient air

filling at the foot of the concrete dam in all sections considerably exceeded the extent of de-stressing of the foundation as a result of rock excavation in the dam excavation pit (Kalustian et al. 2000).

Consolidation measures in the foundation of the concrete dam sections started in 1987 have been completed. The contact grouting, the 45 m deep single row grout curtain, and drainage measures have been perform.

For measure deformations in the surface zone of the concrete dam foundation to a depth of 2–5 m vibrating wire transducers of linear deformations LDT-10 with extension rods, 2,000 and 5,000 mm long, were used. Rock strain gauges were installed in the foundation of the majority of sections (from 6 to 34 sections) since commencement of concrete placement in 1983. Practically in all sections the instruments were installed by the beginning of the concrete placement into the foundation of the respective section. Due to this fact it was considered that the vibrating wire transducers measured relative deformations of the surface layer of the rock foundation from the moment of concrete placement into the concrete dam body of the Boguchany HPP. Based on the results of field observations it was possible to determine actual deformations of the surface and active areas of the dam foundation during all periods of the construction and at the initial stage of reservoir filling and the unique material was obtained for the analysis of foundation deformations in the severe climatic conditions of the building site. In the process of the field observations relative deformations in the surface zone of foundation were measured by the vibrating wire transducers on a monthly basis. The interval of taking readings at the initial stage was determined by concrete placement rate in the dam sections.

Out of 34 sections of the Boguchany HPP concrete dam, four sections—Nos. 12, 21, 28, 31 are measuring sections. These sections are most fully equipped with instruments for measuring relative deformations and temperature both in the body and in the foundation of the dam to depths of 2–7.5 m from the upstream and downstream faces side. The remaining 30 sections of the concrete dam are equipped with instruments for assessing deformations and temperature of the foundation from the concrete dam upstream face side.

The analysis of the results of the long-term field observations showed that vibrating wire instruments of domestic production—jointmeters LDT-10 with special extension rods continue to record deformations in the foundation surface part under the concrete dam sections both to depths of 2–16 m.

The civil work at the construction of the Boguchany concrete dam was conducted in the severe climatic conditions of Siberia with considerable drop of temperatures (Fig. 103.2). Therefore, along with recorded deformations it was essential to assess the values and distribution pattern of outer temperatures and the temperatures in the foundation both in the "rock—dam concrete" near-contact zone and in
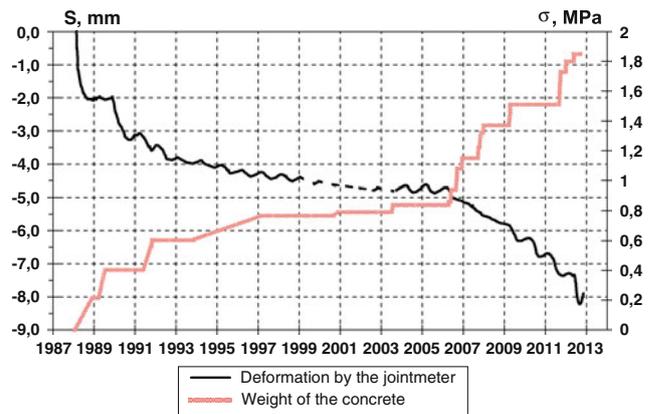
Fig. 103.3 Deformations near-contact 2 m zones foundation in the section 18 during the construction of the dam

depth within the active rock mass zone as well as water temperatures.

For the Boguchany HPP concrete dam foundation thermal actions represented additional loads causing de-stressing in the areas of uncovered rock mass especially in the hazardous HPP excavation pit area. In these conditions one of the possible scenarios of unfavourable condition development could form, i.e. cracks formation in the open areas of the foundation from the dam upstream face side. According to this scenario cracks could form from the upstream face side long before the onset of the reservoir filling, even at the building stage. The field observations showed that such developments had been avoided.

Special investigations included the assessment of stresses acting on the toe of the dam due to the weight of the concrete being placed (Fig. 103.3).

This made it possible to obtain data required for assessment of deformation indices for the foundation of different sections and to assess the deformation nonuniformity of the near-contact and active zones of the concrete dam foundation.

103.3   Results of Special Studies of the Modulus of Deformation of the Concrete Dam Foundation

The analysis of operation of damaged concrete dams showed that with different correlations of deformation indices of the foundation and dam the conditions of failure risk realization tended to develop. For estimation of the modulus of deformation value in separate sections of the Boguchany concrete dam and deformation non-uniformity of its foundation it was required to assess the stresses at the toe of the concrete dam foundation and respective settlements of the surfaces and active zones on the basis of the monitoring data.

Fig. 103.4 Graphic of the reservoir filling
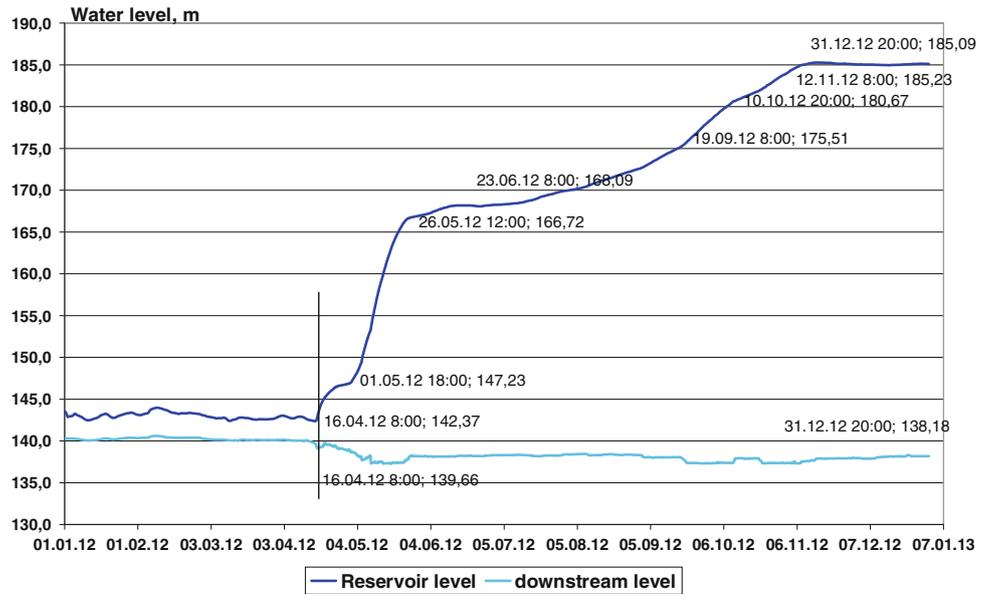
The deformation of the compressed foundation under the weight of the placed concrete is taken into account when calculating the values of the modulus of deformation. Characteristic of dolerite composing the Boguchany concrete dam foundation is a long time period when the rock mass comes to its natural condition that can be explained by the impact of environmental conditions and temperature variation in particular (Kalustian and Vavilova 2011).

The monitoring data on the foundation deformations for the entire period since 1983 as well as the results of special studies for determining the stresses at the base of dam concrete during concrete placement have been used as initial data for determination of the modulus of deformation of dolerites in the foundation of different sections of the Boguchany dam. Based on the obtained data a preliminary conclusion was drawn that the modulus of deformation in the foundation of sections No. 12–17 was higher ranging from 1,4984 to 11,166 Mpa than in sections No. 18–32. The modulus of deformation in sections No. 18–32 ranged from 6,013 to 10,644 Mpa with stresses in sections No. 18–24 ranging within 0.83–1.70 Mpa and in the foundation of sections No. 24–32 ranging within 1.48–1.76 Mpa. Generally the modulus of deformation of the concrete dam foundation may be considered lower than the modulus of deformation of the dam concrete.

The computations show that modulus of deformation in the near-contact and active zones of the foundation are different. In particular, a more deformable interlayer has formed in the concrete dam-rock foundation near-contact zone featuring the modulus of deformation equal to 1.6–3.3 GPa. The presence of this interlayer must be advantageous for stress distribution in the "dam-foundation" contact zone

In consideration of commencement of the Boguchany reservoir filling since 16.04.2012, new stage began in the dam operation (Fig. 103.4). Instrumental monitoring of the foundation in this case acquires a special importance as it allows for the areas of possible most unfavorable condition in the foundation to be identified even before the full supply level is attained and engineering protection measures to be taken. At the same time with water level rise in the reservoir there appeared new factors determining the deformations and temperature of the near-contact and active zones as well as general conditions of the foundation (Kalustian 2013).

Several typical features of deformations in the surface zone of the concrete dam foundation taking place with commencement of the reservoir filling are shown in Fig. 103.5.
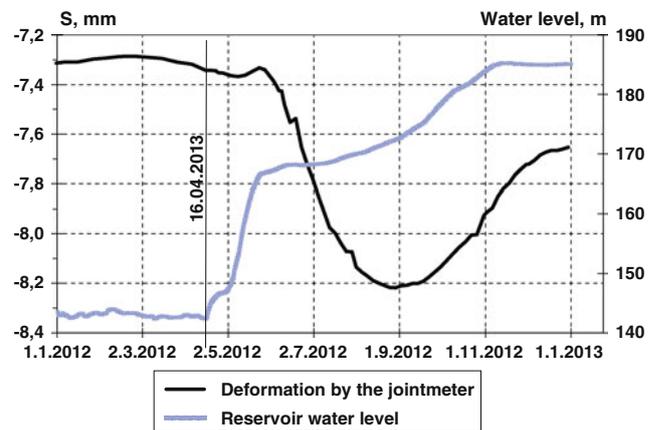
Fig. 103.5 Deformations near-contact 2 m zones foundation in the section 18 during of the reservoir filling

103.4   Conclusion

With start of reservoir filling the deformations of concrete dam foundation at Boguchany HPP both in the active and contact zones are depend by the reservoir water pressure. At that, foundation vertical deformations induced by the weight of water in the reservoir considerably exceeded horizontal displacements. On the whole, at reservoir filling to the intermediate elevation 185 m the condition of the structure is in the project state; the joint «rock—concrete» from the upstream side of the concrete dam is in the compressed state.

References

Kalustian E (2013) Dam construction and geomechanics. Moscow, Rads-RRL, 120 p

Kalustian ES, Gorbushina VK, Koryabin IA (2000) Condition of the foundation bed for the concrete dam of the Boguchany hydroelectric power plant as determined from field observations. Hydrotech Construct 34(4):163–167

Kalustian ES, Vavilova VK (2011) Boguchany HPP monitoring. Hydrotech Construct 12:36–37 (in Russian)

Smulskiy PY (1992) The Boguchany dam on the Angar River, vol 12. Geology and Dams, Moscow (in Russian)

Study on Reservoir and Water Inrush Characteristic in Nibashan Tunnel, Sichuan Province, China

104

Sixiang Ling, Yong Ren, Xiyong Wu, Siyuan Zhao, and Limao Qin

Abstract

The Nibashan tunnel is a major project mountain tunnel on Ya'an to Lugu lake expressway in Sichuan province. The tunnel relative elevation of about 2,100 m and the maximum depth of 1,701 m, belongs to the deep buried and extra-long tunnel. The tunnel's strata are mainly igneous rock of Suxiong Formation, Lower Sinian. The rock type belongs to rhyolite (69 %), andesite (21 %) and a small amount of pyroclastic rocks, dykes and terrigenous clastic rocks. Based on the field investigation and drilling data of Nibashan tunnel, analysis of igneous rock reservoir space and performance factor by the lithology, lithofacies, fractures, structure and diagenesis of igneous rock. It considered that the igneous rock reservoir water storability was mainly affected by tectonism, and the reservoir site is located in the tectonic fracture zone. Finally, through the high pressure water pressure test and pumping test of drilling on Nibashan tunnel, obtaining the water reservoir and water inrush characteristic of igneous rock and geological flaws in tunnel, and providing a theoretical basis to construct safely and smoothly the tunnel.

104.1 Introduction

The hydrodynamic system and dynamic equilibrium of surrounding rocks undergo drastic changes due to the excavation of underground projects, which causes instant release of the energy stored in underground water gush to the tunnel face (Lin and Song 2012). Water inrush in tunnels is characterized by suddenness, high speed, and high pressure, and it is highly destructive, which can do tremendous damage to construction and operation of tunnels and damage the environment, even serious safety accident (Wang et al. 2004; Li et al. 2011; Li and Li 2014). Therefore, the water inrush scourge was a very serious problem for the deep tunnel. In recent years, more than 100 cases of water inrush have been observed in China, causing serious losses of economics and deterioration of construction conditions (Zhao et al. 2013). The previous researchers have studied water critical pressure, water inrush prediction method, water inrush risk assessment, and treatment measures in the mining roadway, expressway tunnel and railway tunnel (Zhang and Peng 2005; Meng et al. 2012; Li et al. 2013; Zhao et al. 2013).

The Nibashan tunnel is located in the edge of Longmeshan fault, and has the igneous rocks. The maximum depth of the tunnel is 1,701 m, and about 5 km length tunnel deeper than 1,600 m. As a result, a large number of underground water is stored in the igneous rock fissures and joints in mountain. The formation of water inrush passages is mostly the geological

S. Ling · Y. Ren · X. Wu (✉) · S. Zhao · L. Qin
Department of Geological Engineering, Southwest Jiaotong University, Chengdu, Sichuan 610031, People's Republic of China
e-mail: wuxiyong@126.com

X. Wu
Key Laboratory of High-Speed Railway Engineering, Ministry of Education, Chengdu, Sichuan 610031, People's Republic of China

flaws, including fault, fracture, joints and unfavorable section in the surrounding rock over a tunnel (Shi and Singh 2001). Some scholars have researched the microscopic pore characteristics in acidic volcanic reservoir from the oil and gas exploration (Pang et al. 2007). The water reservoir space has characteristics of complexity, instability and heterogeneity, because of the igneous compositions are uneven, the condensation environmental differences and the uneven degree of porosity and fissures. The water inrush is likely to occur in the fault zone and joint fissures developing zone. Generally, the water inrush accident occurs unexpectedly, especially cause the serious accident at fault zones. Therefore, it is essential to accurately understand the reservoir characteristic of the igneous rocks and the water inrush features in Nibashan tunnel, and it can provide some effective technical countermeasures to assure the safety of tunnel construction.

104.2 Geological and Engineering Setting

The overall length of the Nibashan tunnel is about 10 km (Fig. 104.1). The tunnel is located on an anticlinal fold and the geological structure is controlled by geofracture, eg. Baohuang and Caodaping fault (Fig. 104.1a). From field investigation, the tunnel is covered with igneous rock and carbonates in Sinian Age (Fig. 104.1b). And also, we designed five drills to do the injection test and pumping test

in the geological prospecting (Fig. 104.1b). The tunnel construction method is a drilling and blasting method. The tunnel will be established a twin tunnel, and each tunnel is designed two-lane single-way and the design speed is estimated to be 80 km/h. The lithology of tunnel is mainly composed of rhyolite, andesite and carbonatite, and few of granite porphyry, pyroclastic rock and dike. The Nibashan mountain ridge is the watershed of surface water, the mean annual rainfall is 742 mm in the north of watershed, and 1,300 mm in the south of watershed. Therefore, the atmospheric precipitation can recharge amply groundwater at the location of tunnel.

104.3 The Characteristic of Water Reservoir Space

104.3.1 The Features of Lithology and Petrography

The lithology of tunnel is mainly belongs to igneous rock, including rhyolite (69 %), andesite (21 %) and some other clastic rock. From the field investigation and drilling data, the numbers of fissures in rock is granite porphyry > rhyolite > andesite > diabasic dike. From the perspective of rock lithofacies, the flowing facies, erupting facies and volcanic sedimentary facies is equal to 59, 37 and 3 %, respectively,

Fig. 104.1 The anticline profile and geological structure diagram of tunnel in Nibashan region
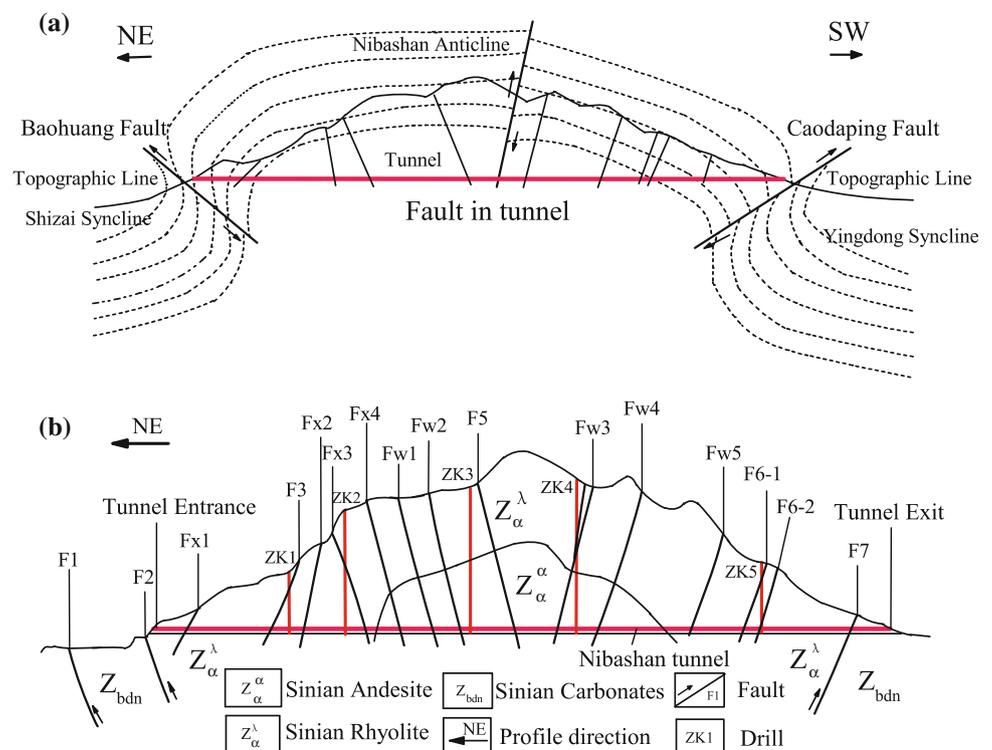
Table 104.1 Different type of pore in different rock at Nibashan tunnel

Petrography	Lithology	Pore type
Flowing facies	Stomatal and striated rhyolite	Stomata, almond stomata, dissolved pore
Erupting facies	Rhyolitic and crystal tuff, volcanic breccia	Stomata, intergranular pore, matrix pore
Volcanic sedimentary facies	Tuff, tuffaceous sandstone/breccia	Interparticle pore
Volcanic channel facies	Granite porphyry, diabasic dike	Columnar joints, contact zone fissures

from the drilling data. The porosity and permeability of rock, belongs to flowing facies and erupting facies, has a higher level, while the volcanic sedimentary facies rock has a lower level because of the sedimentary environment and diagenesis. The water storage performance statistics are shown in Table 104.1. From the combination of lithology and petrography, the most beneficial part for water reservoir is volcanic breccia and tufflava. However, the rhyolite proportion is 69 % in tunnel and the rhyolite is the main storage space at rock part.

104.3.2 The Effect of Fissures

From the field investigation, the joints and fissures of rock on tunnel surface are divided into four directions: N10°–50°W, N50°–80°E, N10°–20°E and N70°–90°W, respectively (Fig. 104.2). The dip of fissures and joints can be divided into three types: 0°–10° (horizontal fissure), 10°–60° (oblique or reticular fissure) and 60°–90° (high angle fissure), respectively. The proportion of high angle fissures, oblique fissures and horizontal fissures are 56, 42 and 2 %, respectively. The joints and fissures are one of types to water storage spaces. On the other hand, the fissures and joints are the seepage channel, which make the isolated primary pore connected with each other and promote significantly the development of secondary pores. Therefore, the joints and fissures can improve the water reservoir performance of igneous rock in Nibashan tunnel. From the drilling data, we found the deep fissures can reach up 1,000 m depth by the
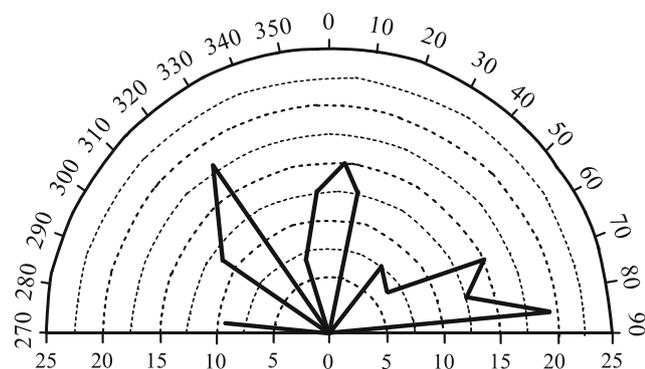
data of water color (incrustation), indicating that provide the water reservoir and seepage channel arrive to tunnel.

104.3.3 Reservoir of Structure and Dyke

The geological structure of Nibashan Mountain belongs to anticlinal fold and it displays the "Ω" shape (Fig. 104.1). The reverse fault (F2 and F7) located in the sides of the anticline, making the anticline into a symmetrical shape. The surface water flow to the anticlinal flanks, and then infiltrate into the underground affected by the terrain, fault and secondary folds. The faults of tunnel are mainly the compressor-shear fault, and this fault and the tensile fissures nearby the fault are the important part of water reservoir. Affected by the Nibashan anticline, the fault enriched the water at axis of anticline, such as F5 and Fw3 fault.

104.4 The Features of Water Inrush

In order to understand the extent of fissures and rock permeability, it should be tested by high-pressure water injection test. In the field, we choose the ZK1, ZK2 and ZK4 drill to do this test and the maximum pressure can reach up 4.5 MPa. Test objects including the complete bedrock and faults. The test diagrams (P–Q curves) are listed in Fig. 104.3 and the analytical results are shown as follows:

(1) In the ZK1 drilling, the location range of 128–136 m and 139–149 m is the fracture zone of fault F3, namely that the test results represent the water inrush model of fault F3. The curve of Fig. 104.3a, b belong to the "washout type" (D type) in the Water Resources and Hydropower Engineering borehole water pressure test procedures (SL 31-2003) (Ministry of Water Resources, P. R. China 2003), because the curve has obvious inflection point at 2 MPa in the Fig. 104.3a, b, and the seepage flux abruptly increases with decreasing the slope of line when the pressure is greater than 2 MPa. It shows that the fracture zone of fault F3 contains large number of broken rocks and the permeability is range of 0.012–0.0775 m/d from test in fault F3. Therefore, the blocking materials, such as clay materials, will be washed away when the pressure is greater than 2 MPa,

Fig. 104.2 The strike of joints rose diagram in tunnel overlay surfaces area
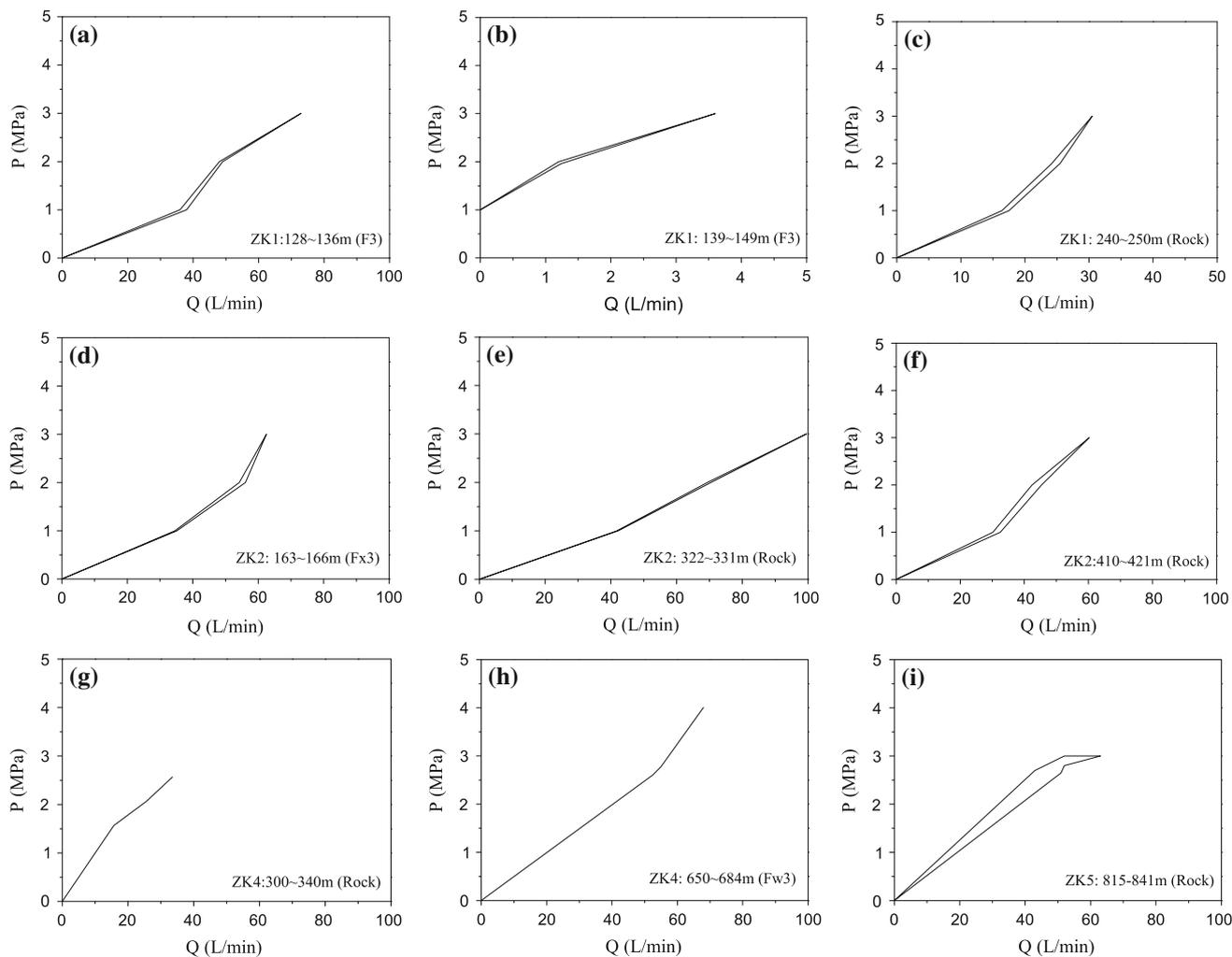
Fig. 104.3 The P–Q curves of high-pressure water injection test in tunnel site area

namely that the point of F3 in tunnel will be threatened under this pressure.

(2) The location range of 163–166 m represent the fault of Fx3 in the ZK2 drill. The P–Q curve belongs to the "turbulence model type" (B type) in the Water Resources and Hydropower Engineering borehole water pressure test procedures (SL 31-2003). From this curve (Fig. 104.3d) (Ministry of Water Resources, P. R. China 2003), the rock permeability and the flux are in higher level and the flux gradually decreases with increasing the pressure. Through test, the permeability of fault Fx3 is equal to 0.0768 m/d. Compared with F3, the blocking materials (e.g. clay) of fault F3 is washed easily from the fissures at the high pressure.

(3) The part of 300–340 m in ZK4 drill represent the complete rock-mass. The P–Q curve has obvious inflection point at 1.6 MPa, and then the seepage flux increases with the decreasing the slope of line when the

pressure is greater than 1.6 MPa (Fig. 104.3g) (Ministry of Water Resources, P. R. China 2003). This curve belongs to the "expanding type"(C type) in the Water Resources and Hydropower Engineering borehole water pressure test procedures (SL 31-2003) (Ministry of Water Resources, P. R. China 2003). From the drilling data, most of the drill core RQD value is less than 30. Therefore, the fissure fillings are occurred the displacement and deformation when the water pressure greater than 1.6 MPa.

(4) The part of 650–684 m in ZK4 drill represent the fault Fw3. The P–Q curve belongs to "washout type" (D type) in the Water Resources and Hydropower Engineering borehole water pressure test procedures (SL 31-2003) (Ministry of Water Resources, P. R. China 2003), because this section has a higher seepage flux under the lower pressure and the curve has obvious inflection point at 2.5 MPa in the Fig. 104.3h and the seepage flux

abruptly increases above 2.5 MPa. It indicates that the rock of fault Fw3 has lots of fractures or joints and the permeability is in higher level under low pressure. However, the blocking materials are washed out at 2.5 MPa pressure, and the water channel is opened and lead to the seepage flux abruptly increase above 2.5 MPa. The P–Q curve convex to the P line as increasing pressure, it maybe consist with the rock hasn't reach up the saturation state. The seepage flux hasn't increase abruptly when the pressure is greater than 3 MPa (Fig. 104.3h). Therefore, the critical pressure of hydraulic fracturing fissure should be greater than 3 MPa as increasing depth under 684 m in ZK4 drill.

(5) In the ZK5 drill, the location range of 815–841 m represent the complete rock-mass. The P–Q curve belongs to the "laminar flow model type" (A type) from the specification of SL 31-2003 (Fig. 104.3i). The permeability is less than 10^{-3} m/d, consisting with the ROD is greater than 65 % from the drilling data.

(6) The part of 240–250 m in ZK1, 322–331 m and 410–421 m in ZK2 drill represent the complete rock-mass. The P–Q curves belong to the "turbulence model type" (B type) from the specification of SL 31-2003, indicating that the rock-mass has good permeability when the pressure is in lower condition (Fig. 104.3c, e, f, h).

From the high-pressure water injection test data, showing that the rock-mass are developed lots of fissures in tunnel site area. The rock permeability is in higher state when pressure in lower condition, while the flux gradually decreases with increasing pressure. The fillings of fissure and fault are washed away to make the fissure form the flow channel when the pressure is in 1.6–2.0 MPa, and lead to the flux gradually increase under this state. That is to say, the fissure and fault occurs the "washout type" water inrush when the piezometric head reach about 1.6 MPa. Expect for the location 815–841 m of ZK5 drill, we have choose the section of 820–825 m of ZK4 drill to do the high-pressure water injection test, while pressure gage was broken abruptly when the water pressure reached up 4 MPa. According to the test found that the deep rock fissure occurred hydraulic fracturing when the critical pressure is greater than 4 MPa when depth reach up 800 m, and this pressure increase with increasing depth. And also, we choose the 1,388 m point of ZK4 drill to do the pumping test, and the permeability is equal to 7×10^{-4} m/d. The rock core is the rhyolite, and the rock has lots of joints and fissures. The black iron manganese disseminated body and chloritization was found on the surface of joints and fissures. Therefore, the water reservoir mainly stored in rhyolite, and the water can arrive to deeper tunnel location.

Affected by water reservoir, the water inrush type in the tunnel can be categorized into two. One is the water flux decreases rapidly and short duration, and the other is the water flux keeps the stable state and longer duration. The former one is reasons for the water reservoir is debunked, but lack of the recharge into tunnel and lead to the flux decreases rapidly. The latter one is closely linked with the groundwater and water reservoir, the water pressure keep in higher level state in a certain period to make the water inrush last longer time. From the field and tunnel excavation monitor, the volcanic rock undoubtedly has a good water storage space, and the maximum water flux can reach 25,000 m³/d.

104.5 Conclusion

We studied the features of water reservoir and water inrush in Nibashan tunnel. Some conclusions can be drawn from the above discussion:

(1) The main water reservoir is the pores and fissures of rhyolite and andesite in tunnel, and some groundwater can be as deep as 1,000 m. The fault fracture zone and dike are often contain large number of groundwater and closely contact with the movement of groundwater, where is the most possibility to occur the serious water inrush accident in tunnel.

(2) The shallow of entrance are enriched phreatic water, and the part near the anticlinal axis enriched the groundwater as increasing depth. The deep water reservoir affected by the oblique and reticular fissure.

References

Li S, Zhou Z, Li L et al (2013) Risk assessment of water inrush in karst tunnels based on attribute synthetic evaluation system. Tunn Undergr Space Technol 38:50–58

Li X, Li Y, Zhou S (2011) Study and application of forecasting system for water inrush under high pressure in Xiamen Submarine Tunnel construction based on GIS. Procedia Environ Sci 10:999–1005

Li X, Li Y (2014) Research on risk assessment system for water inrush in the karst tunnel construction based on GIS: case study on the diversion tunnel groups of the Jinping II Hydropower Station. Tunn Undergr Space Technol 40:182–191

Lin G, Song R (2012) Research on the mechanism and treatment technology of mud gushing in karst tunnel. Tunnel Construct 32 (2):169–174 (in Chinese)

Meng Z, Li G, Xie X (2012) A geological assessment method of floor water inrush risk and its application. Eng Geol 143–144:51–60

Ministry of Water Resources, P. R. China (2003) Water Resources and hydropower engineering borehole water pressure test procedures (SL 31-2003), pp 7–21

Pang Y, Zhang F, Qiu H et al (2007) Characteristics of microscopic pore structure and physical property parameter in acidic volcanic reservoir. Acta Petrolei Sinica 28(6):72–77 (in Chinese)

Shi LQ, Singh RN (2001) Study of mine water inrush from floor strata through faults. Mine Water Environ 20(3):140–147

Wang TT, Wang WL, Lin ML (2004) Harnessing the catastrophic inrush of water into new Yungchuen Tunnel in Taiwan. Tunn Undergr Space Technol 19:418

Zhang J, Peng S (2005) Water inrush and environmental impact of shallow seam mining. Environ Geol 48(8):1068–1076

Zhao Y, Li P, Tian S (2013) Prevention and treatment technologies of railway tunnel water and mud gushing in China. J Rock Mech Geotech Eng 5:468–477

Differential Settlement Control Technologies of the Long Submarine Tunnel Covered by Municipal Road

105

Cuiying Zhou and Zhen Liu

Abstract

Differential settlement control technologies for the long submarine tunnel covered by municipal road under complex geological condition are studied by depending upon a typical composite tunnel called the Western Corridor Connecting Project from Shenzhen to Hong Kong. Based on the analysis and generalization of the geological conditions of the research area, the computation sections and their corresponding parameters are selected, the differential settlement of all the selected sections in the tunnel area are calculated by the specification method and the nonlinear finite element method, the differential settlement isoline map of the tunnel box and the overlaying municipal road are obtained, the secondary consolidation settlements after construction are predicted. The optimization design and control schemes to the key control bids are proposed. And the results provide useful references for the design, construction and decision making of the project.

105.1 Introduction

Differential settlement of soft soil is one of the most difficult problems in geotechnical engineering. Differential settlement control for the long submarine tunnel covered by municipal road under complex geological condition is not only a complicated problem of differential settlement, but also a

difficult problem needed to be solved both in engineering practice and theoretical research.

Currently, domestic and international researches on differential settlement mainly focus on the following aspects as (Wu Sheng-fa and Sun Zuo-yu 2005) forecast of the process of structure settlement, calculation of final settlement and specific measures to control differential settlement etc. Major methods to study and analyze consolidation settlement of foundation can be divided into the following three categories: empirical formula method (Li Guangxin 2004), model test method (Li Guangxin 2004), and numerical analysis method (Zhe Xueshen 1998). As a traditional method for calculation of consolidation settlement, empirical formula method includes: layer-wise summation, Skempton—Bjerrum three-dimensional stress effect, Huang Wenxi three-dimensional deformation and compression method, the Cambridge model, simulation curve method (Du and Zhang 2005; Lin and Cao 2006), Janbu tangent modulus method, Lambe stress path method etc. Empirical formula method is

C. Zhou (✉)
School of Engineering, Sun Yat-sen University, Guangzhou, 510275, China
e-mail: ueit@mail.sysu.edu.cn

C. Zhou · Z. Liu
Research Center for Geotechnical Engineering and Information Technology, Sun Yat-sen University, Guangzhou, 510275, China

Z. Liu
School of Marine Sciences, Sun Yat-sen University, Guangzhou, 510275, China

aimed at simplifying engineering practice, with similar assumptions, and poor adaptability. It is usually used to solve simple structures. For complex structure, it has complicated calculation steps. Often as a result of geological and complexity of engineering factors involved, it is difficult to calculate the process of a more comprehensive reflection of the actual situation. There are often results of the error, and it is often difficult to find a reasonable solution. When the structure has a unique pattern, and loads as well as materials are very complex, model tests are needed to determine the mechanical behavior. Model test is divided into field test and lab test. Field test includes standard penetration test and pressuremeter test. Lab test includes seepage force model test and centrifugal model test (Han 2005, Zheng Yonglai et al. 2005, Zhan 2006), etc. However, model tests are often subjected to restrictions on site and equipment and only for small- scale tests. It is difficult to fully reflect the actual structure, also, the labor and material costs are expensive. Therefore, the calculation of a more comprehensive project to reflect the actual geological conditions has become the key to solve this problem. Numerical analysis (Xiong Chunbao et al. 2006; Hu et al. 2005; Du and Zhu 2005) represented by finite element method, is the product of research on modern soil mechanics. Since the 1970s, with the development of computer and application of finite element technology, complicated calculation of geotechnical problems have been compiled into finite element programs, and more accurate results have been obtained. Numerical simulation, as a "numerical experiments", can replace the expensive model test to some extent. What is more, if it is combined with the test results, more technical and economical benefits can be achieved. The use of numerical analysis can reach a comprehensive, more rigorous consideration on deformation properties of soil and boundary conditions.

Based on a typical composite tunnel called the Western Corridor Connecting Project from Shenzhen to Hong Kong, as well as in considering the unique compound road structures or various geotechnical structures which attach to the complexity of geological conditions, the causes of differential settlement have been analyzed. Furthermore, through calculation and analysis, this research has brought up the rule of differential settlement of the tunnel structure and its control measures, proposed the optimized proposals and specific control measures, and predicted post-construction settlement of the project, providing a significant reference for the project design, construction, and the owners in their decision-making. At the same time, this reference is also valuable to the study of differential settlement under complicated geological conditions and control measures for the differential settlement.

105.2   General Project Information

105.2.1   Brief Project Introduction

Shenzhen-Hong Kong western corridor connecting project is an important component of the Shenzhen-Hong Kong western corridor. This connecting project is a dedicated two-way six-lane passageway for the Shenzhen-Hong Kong transit vehicles, with designed driving speed of 80 km/h. It starts at YueLiangWan Road, passes through northern foot of Nan-Shan Mountain, Dongbin Road and Houhai Bay, intersects with Industrial Road, Houhai Road, the planning Houhaibin Road and Keyuan Avenue, finally finishes at the export of Shenzhen-Hong Kong Port. The main line (ramps not included) is approximately 4.5 km (with underground structure 3.08 km and elevated structure 0.735 km). Blocks along the connecting project can be divided into three categories: Nanshan Mountain scenic spot, urban construction area and planning district. The general layout of the main line uses a combination scheme of whole-buried and sinking road structures.

105.2.2   General Information of Foundation Treatment

East from K2+837 (Contract section IV to contract section VII) was the section full of thick silt. Southeast from K3+820 was the region of large stone reclamation embankment, and northeast from K3+820 was the region of blasting toe-shooting reclamation. Due to the buried weak layer existed along the construction areas, a variety of foundation treatment options have been taken as followed: a major program of grouting reinforcement for contract section IV to V, particularly sleeve valve grouting reinforcement of mud and silt-based soil for the junction of the planning Metro line 2 and the connecting project. A diameter of 400 PHC (prestressed pipe pile) was applied to the thick mud layer in the tunnel area at reclamation section W-M. For the beach in the north of the reclamation area, foundation treatments such as stone pier replacement, riprap blasting toe-shooting method were applied. At the same time, dynamic compaction was used to the original seawall, as well as the stone pier replacement was taken to deal with the mud in the south. The excavation and support at section IV to W have taken a variety of treatment options: section IV to V mainly use vertical excavation, with secant piles applied to both sides of the pit. Step-slope was adopted to the north of section IV, when slope rate method and row piles were used as the support method. Section VII, that is, the ramps, took the method of step-slope in excavation, and the support method

in this section was basically the same as section W. Among them, because of the step-slope used in the north of section VI, large slope in the north side led to a wide range of high-filling.

105.3 Analysis of Differential Settlement

105.3.1 Cause of Differential Settlement

According to the general information of the project, engineering geological conditions in section IV to VII, which are the key parts of the whole connecting project, are complex and changeable. Intricate and ever-changing foundation conditions as well as the wide range of high-filling caused by the large slope in the north side would lead to differential settlement of the cabinet. After the completion of the backfill in excavation, road fill and paving were carried out above the cabinet and within the width of the municipal road. Foundation treatment has been carried out in most of the cabinet coverage area, particularly in the reclamation area pre-stressed pipe piles applied, however, no foundation treatment has been applied to some parts of the municipal road which are beyond the cabinet area (Note: blasting toe-shooting or dynamic compacted stone pier was used only for the mud within the scope of the pit). As a result, when municipal road paving was completed, damages such as cracking or fluctuation would emerge as the result of large transverse differential settlement of the road. In summary, the causes of differential settlement can be attributed as: (1) Differential foundation condition caused differential settlement of the case structure. (2) Since different foundation treatments options were applied, longitudinal differential settlement of the case structure occurred as a result. (3) Negative friction, which was caused by single sided backfill load at the pit (8–11 m) and filling load over the cabinet (3 m), led to differential settlement of the case structure. (4) After the municipal road was constructed over the cabinet, transverse differential settlement occurred at the areas on either side beyond the scope of the cabinet. (5) Different foundation treatments brought about longitudinal differential settlement of the municipal road.

105.3.2 Section Selection

Considering many factors comprehensively, section selection should follow the principles as below: (1) In underlying stratum, which has great change, particularly weak strata (such as muddy loam) or relatively thick gravelly mild clay. (2) Both sides of conjoin in two different foundation treatment scheme in longitudinal direction (axis of tunnel). (3) In the excavation and backfilling area. (4) The area of different arrangement form of box. (5) The area of different distribution form of municipal road. (6) The section should be near to investigation drillings in order to keep aboriginality and authenticity of the parameters. If there is no investigation drillings nearby, or investigation drilling is so shallow that information of lower strata can't be obtained, the section should be selected in the principle of using investigation near it. (7) Select the section at a distance of 100 m in the other areas in order to ensure the data foundation of calculation analysis.

According to the principles above, based on *Working Drawings of Western Corridor Connecting Project from Shenzhen to Hong Kong* (bid IV-bid VIII) and *Geologic Survey Report of Western Corridor Connecting Project from Shenzhen to Hong Kong,* 26 sections are selected to calculate from bid IV to bid VII. There are four different types in overlying representative structure and distribution form as: (1) vertical excavation bid of the pit (shown in Fig. 105.1), (2) large-scale excavation bid of the pit (shown in Fig. 105.2), (3) single-box bid of ramps (shown in Fig. 105.3), (4) multi-box bid of ramps (shown in Fig. 105.4).

105.3.3 Calculation Parameters Selection

1. Determination of underlying soil layer parameters

   This underlying soil layer in the site usually includes silt, gravel sand, clay, coarse (gravel) sand containing cohesive soil, coarse (gravel) sand containing organic matter, muddy loam, gravelly mild clay, loam containing gravel, gravelly clay, completely decomposed granite and so on. Analyzing the geological investigation data of connecting engineering comprehensively, the calculation of parameters is mainly obtained by *Geologic Survey Report of Western Corridor Connecting Project from Shenzhen to Hong Kong* (Hereinafter referred to *survey report*).

2. Backfill parameters selection

   According to Road *Engineering Overall Arrangement Drawing of Western Corridor Connecting Project from Shenzhen to Hong Kong* and the design scheme provided by the owner, roadbed filling is designed to be sandy cohesive soil and gravel cohesive soil, which should be compacted by layered backfill. Referred to *Highway Roadbed Design Specification (JTGD30-2004),* the soil mechanics parameters are selected as calculation parameters of backfill and put into the model to calculate.

3. Parameters selection of dynamic compaction stone pier replacement area

   Referred to *Composite Foundation Design and Construction Guide* edited by Gong Xiaonan, the enhanced body and the matrix are regarded as composite soil. Compressibility of composite soil is evaluated by composite compression modulus, also, referred to foundation treatment

Fig. 105.1 Foundation vertical excavation section
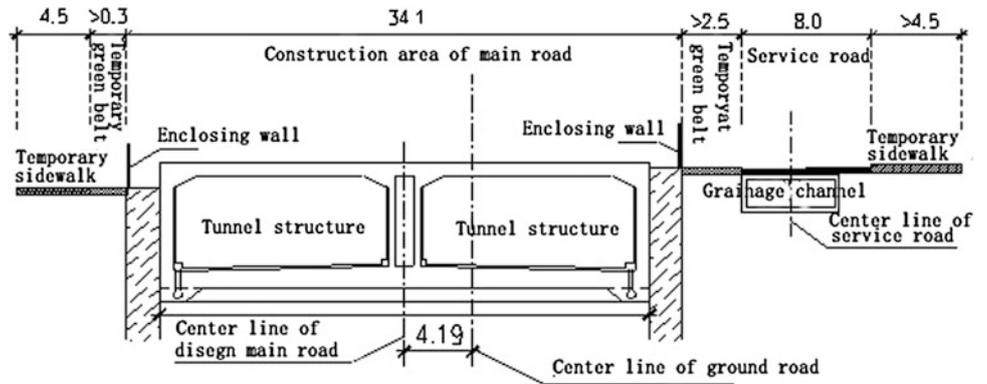
Fig. 105.2 Large-scale excavation bid to the north of reclamation area
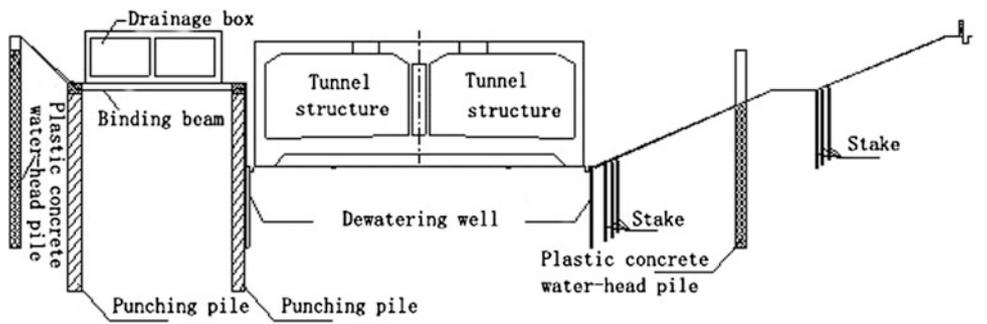
Fig. 105.3 Foundation pit section of single-box bid in the ramp
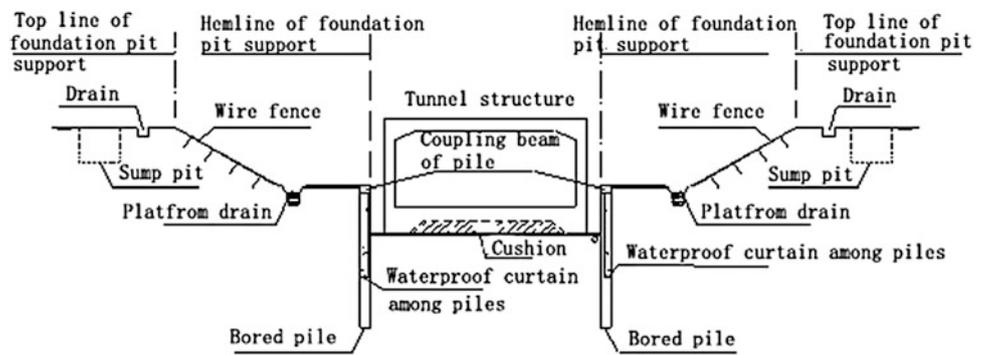
Fig. 105.4 Foundation pit section of multi-box bid in the ramp
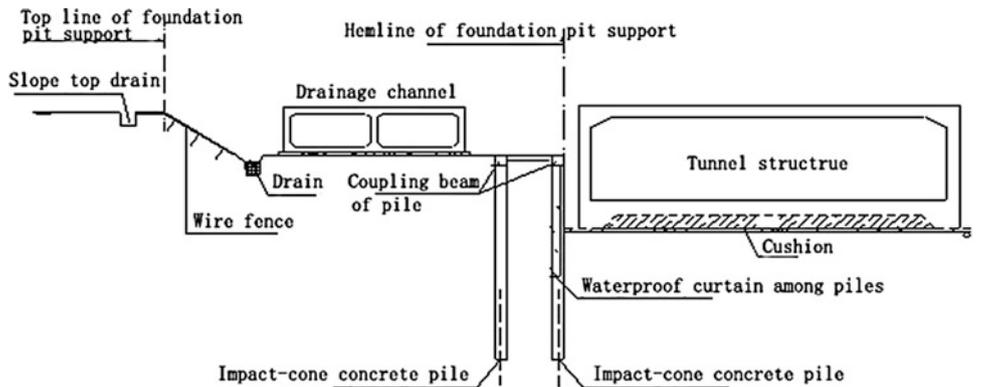
requirements in *Road Foundation Treatment Construction Description in Reclamation Area of Western Corridor Connecting Project from Shenzhen to Hong Kong* (Hereinafter referred to *construction description*): deformation modulus of stone pier composite foundation should be more than 18 Mpa, the deformation modulus of Dynamic compaction stone pier replacement area is determined to be 19 Mpa.

4. Groundwater level determination

Referring to survey report, groundwater condition and the suggested values of design water lever to the east of K2+837 milepost, in order to fully reflect the impact of settlement on the road, the paper adopts the lowest anti-floating design water level. after pit backfill.

105.4 Results Analysis and Discussion

105.4.1 Analysis Methods and Calculation Results

Using the standard method to simplify the mathematical model and non-linear finite element model, combined with the section selected before and calculation parameters related, settlement values of 26 sections are calculated (shown in Figs. 105.5, 105.6, 105.7, 105.8)

105.4.2 Results Analysis and Discussion

105.4.2.1 The Differential Settlement of Box Structure Due to Differential Ground Conditions

By the compare of Figs. 105.5 and 105.6, the differential settlement exists in the structure apparently. Base on the geological data of section selected, foundation conditions is a principal factor, e.g. the differences of north and south thickness of gravelly mild clay layer under foundation of section ZXK2+750, ZXK3+280, ZXK3+365, ZXK3+730 are all 6 m exceeded. This obvious horizontal thickness maldistribution of the subjacent bed, in the additional stress (box structure load, municipal road embankment load, etc.), caused the transverse differential settlement of the box structure.

105.4.2.2 Box Structure Longitudinal Differential Settlement Caused by Different Foundation Treatment Plan

In Figs. 105.5 and 105.6, obvious differential settlement exists in the longitudinal of the box structure. It is due to the different foundation treatment plan. Sections of large settlement mainly distribute in the areas where the foundation treatment is natural foundation and gravelly mild clay layer is thick. E.g. where section ZXK3+550, ZXK3+640, ZXK3+730 are all use the natural foundation treatment, and the thickness of gravelly mild clay layer are 16–22 m, In where 1AK0+100 is, although the prestressed pipe pile processing was taken, the thickness of gravelly mild clay layer under the pile. And small settlement section mainly located in ZXK82+750, ZXK2+865, ZXK2+965, ZXK3+115 and ZXK3+215 of bid N, where its natural geological condition is good or it take the grouting strengthening foundation treatment.

Fig. 105.5 Result of settlement standard method and FEM to south side of box
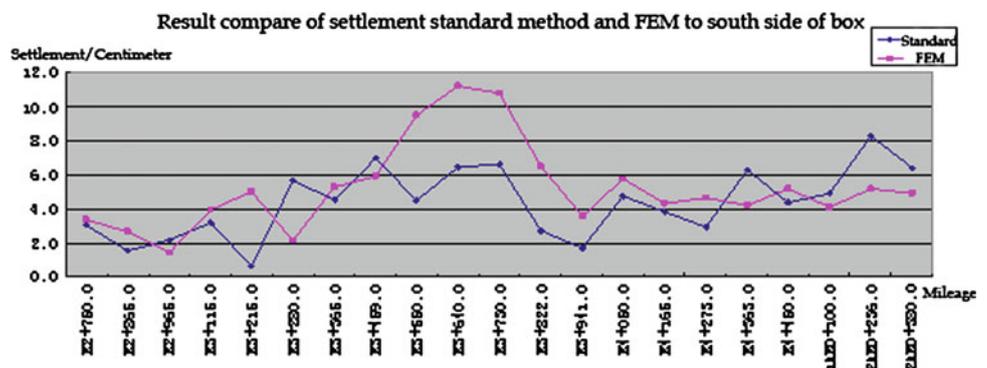
Fig. 105.6 Result of settlement standard method and FEM to north side of box
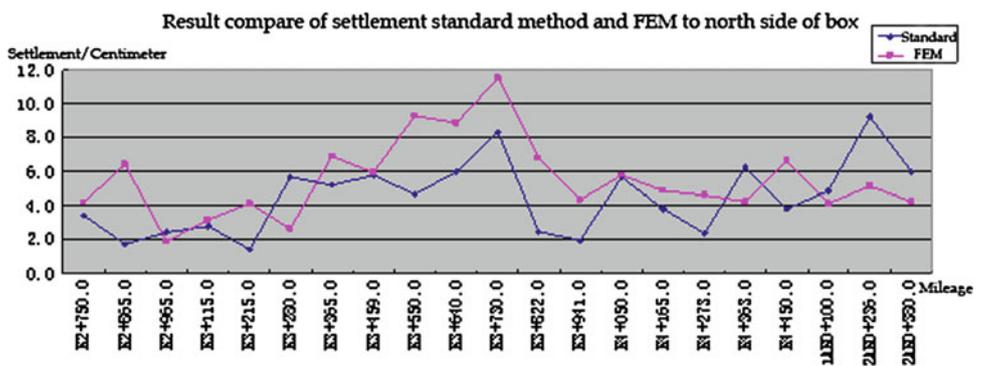
Fig. 105.7 (Road longitudinal settlement of south side of municipal road) Result compare of standard method and FEM
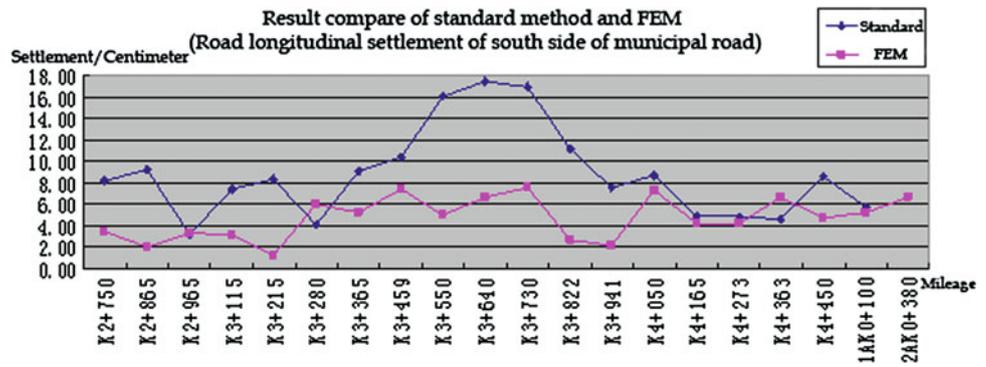
Fig. 105.8 (Road longitudinal settlement of north side of municipal road) Result compare of standard method and FEM
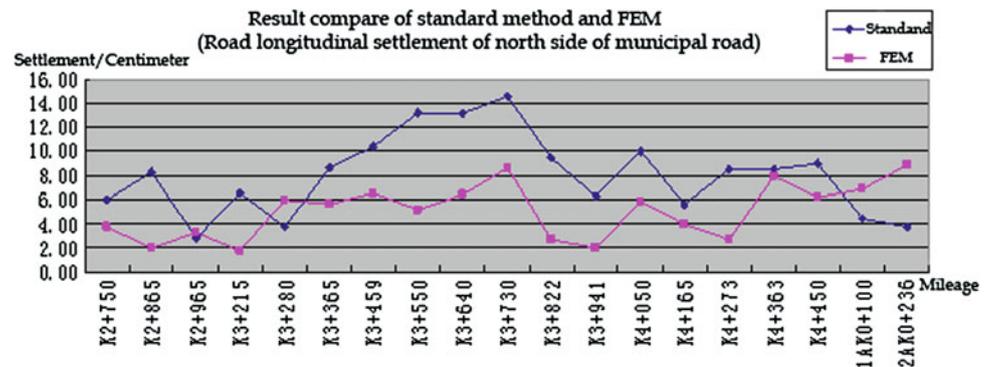
105.4.2.3 The Differential Settlement of the Box Structure is Caused by the Negative Friction, Which is Produced by the Pit Unilateral Backfill Soil Load (8–11 m) and Box Overlying Soil Load (3 m)

Based on the calculation results comparing analysis of the section in reclamation area from Figs. 105.5 and 105.6, lateral differential settlement is outstanding in the large slope. After the large slope construction completion, the north of the box will have 9–10 m high backfill soil, in addition, 3 m high municipal road embankment in the upper. The compression deformation of the north of box cuneiform new soil itself will produce large negative friction to the box, causing differential settlement, the north of box cuneiform new soil produce large additional stress in the bottom of the box. The differential distribution of the stress in both sides of the box causes the differential settlement.

105.4.2.4 The Municipal Road Across the Box, the Differential Settlement Beyond the Scope of the Both Sides of the Box

Form the comparing analysis of Figs. 105.7 and 105.8, the horizontal settlement difference of the municipal road is generally 1.1–2.2 cm, maximum 4.14 cm. But due to the

difference occurs between the edge of the box and the municipal road boundary(part of municipal road beyond the scope of the box), plane distance is very small (most around 3.5 m), so that the difference is most around 3–6 ‰, some times arrives 10–14 ‰, maximum to 17 ‰. Besides related to the thickness of subjacent bed, the reason of lateral differential settlement is also related to the change of natural foundation condition.

105.4.2.5 The Municipal Road Longitudinal Differential Settlement Caused by Different Plans of Foundation Treatment

As Figs. 105.7 and 105.8 shown, the difference of longitudinal settlement of adjacent area from bid 4–7 is about 2–3 cm. The main reasons to longitudinal differential settlement are two: (1) Different foundation treatment of adjacent area, i.e. the juncture of natural foundation and grouting reinforcement, (2) Stratum are complicated and the thickness change greatly, i.e. the thickness of gravelly mild clay under ZXK3+730, ZXK3+640, 1AK0+100 is 16–22 m. The isoline map of the municipal road settlement is drawn by MapGis (Fig. 105.9), which clearly shows the differential settlement situation of the whole.
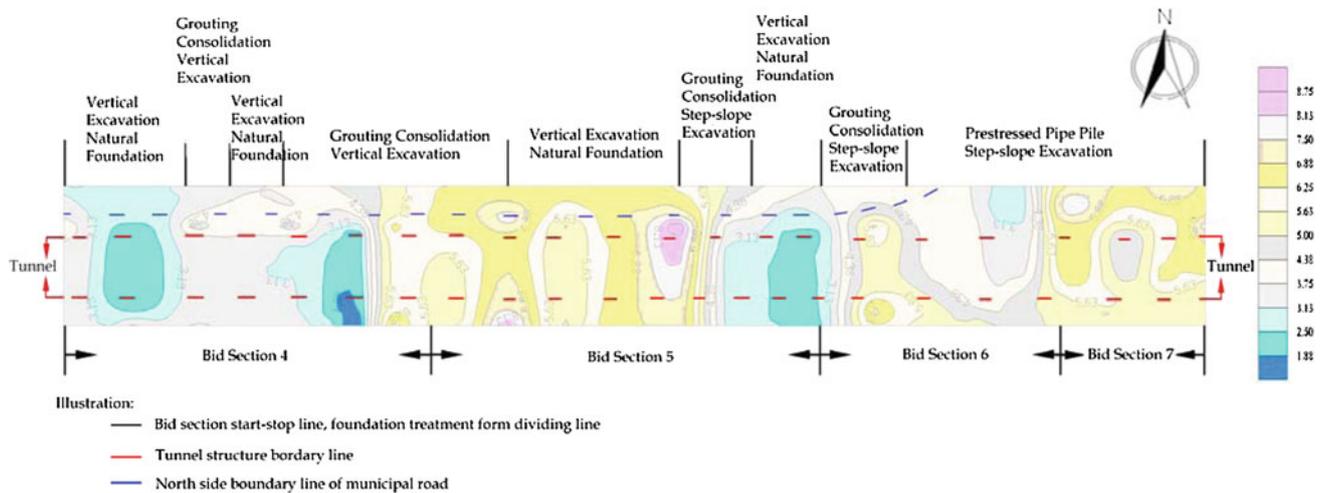
Fig. 105.9 Municipal road pavement longitudinal settlement isoline

Fig. 105.10 Foundation pit of reclamation area follow-up treatment plan
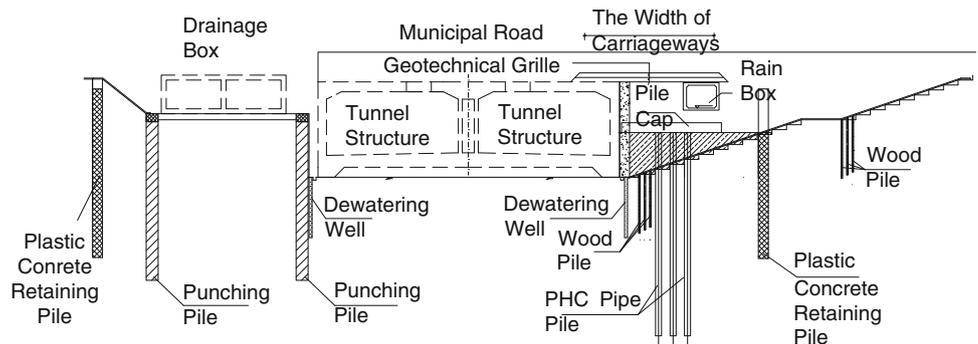
105.5 Control Scheme

Base on the analysis, one main reason for differential settlement is the excavation and backfilling asymmetry (Fig. 105.2). Shanghai Municipal Design Institute bring up bearing the weight of high backfill soil by three rows PHC and flat bedplate in the slope of north reclamation area, in order to reduce the adverse effects of north highfill to tunnel structure stability and differential settlement. The design (shown in Fig. 105.10) laid down 20 cm thick plain concrete access board on the reinforced cushion, making road

settlement even comparatively. This research was based on the *Standards in Guangdong Province—Building Foundation Design Specifications (DBJ15-31-2003)* and the *Technology Norms of Pile Foundation Construction (JGJ94-94),* puts forward optimum idea, which under the requirements in bearing, through expanding the pile spacing and shorten the pile length, achieve the effect of economic security (Fig. 105.11).

Through the comparing analysis we know, comparing with without special treatment of backfill scheme, after control measures, the absolute settlement of the box is reduced and the settlement difference of both sides of box

Fig. 105.11 Settling image of section ZXK4+165 after control measures
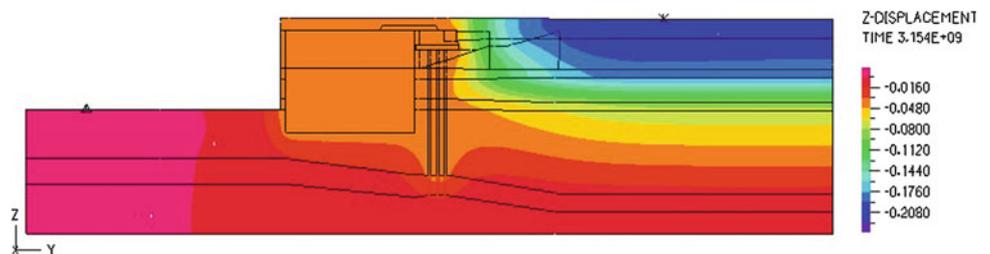
and the road decreased significantly. As the figure shows, pile and flat bedplate is used to bear the weight of high backfill in the northern slope. It plays an obvious role to improve the differential settlement of enclosure structure, making the settlement difference of box sides and road control effectively.

105.6 Conclusions

1. Through the comparative analysis, the overall trends of municipal road horizontal settlement by two methods are the same, but the settlement value of FEM are commonly less than standard method. And the analysis results of the two method both show that: the differential settlement of box are caused by uneven foundation conditions, difference of foundation treatment schemes, the asymmetry of foundation pit and excavation backfill, and the differential settlement of municipal road is caused by the different treatment schemes of road across the box and differential settlement of municipal road is mainly caused by the reasons of the road crossing over the cabinet and different proposals of foundation treatments. It should be pointed out that: the influences of the stress history, which the layers under the box went through, to the layers' physical and mechanical properties are not considered in the settlement calculation. If consider, the differential settlement will be larger.

2. Because the calculating parameters are selected according to the engineering geology survey report before construction, while the layer under the place had gone through complex stress historical process such as filling, excavation, structure and foundation backfill, the use of the parameters may cause certain effect to the results. The absolute calculation value may be too large while the differential settlement may be smaller. But according to the supplementary experimental results of later sampling of Shenzhen engineering institute (considered stress history comprehensively), the parameter values such as deformation modulus is far less than those of exploration stage. Considering comprehensively the statistical significance of the parameters of exploration stage, the parameters selection and calculation analysis are only based on the survey report. Some scenes in situ tests are suggested. Strengthening the field observation, obtaining

reasonable calculating parameters and actual settlement situation to analyze and control.

3. In the future, the road will exist many other factors which can not be estimated very well, i.e. in the rain the filled soil moisture and subsidence may be caused, at the same time, unpredictable factors such as overloaded vehicles, impact load, vibration, etc. still can be existed. But these factors are not considered in this calculation, which makes the results tends to safety.

References

Du H, Zhang J (2005) The exponential curve fitting of the calculation of the subsoil settlement method and its application. Soil Eng Found 19(1):54–56

Du S, Zhu J (2005) Numerical analysis of interaction between underpass and soil across the railway. Undergr Space 1(2):242–246

Brand EW, Brenner RP (1981) Soft clay engineering. Elserier Scientific Publishing Company, Amsterdam

Fu H (2006) Optimizing back-analysis parameters for settlement prediction based on sensitivity analysis. J Changsha Univ Sci Technol (Nat Sci) 3(2):24–28

Han L (2005) Centrifuge model test and analysis on foundation settlement of metro river-crossing tunnel. Undergr Eng Tunn, 13–15

Hu Qi et al (2005) Three-dimensional numerical simulation analysis of settlements of buildings on soft soil. Rock Soil Mech (12):2015–2018

Li X (2005) Numerical analysis of the settlement of high fill embankment. Soil Eng Found 19(3):56–58

Lin Q, Cao X (2006) Discussion of soft soil foundation post-construction settlement prediction method. Subgrade Eng 2:78–80

Liu Y (2005) Application of improved genetic algorithm to predict the settlement of soft soil roadbed. Site Inv Sci Technol 1:29–31

Peng T et al (2005) Prediction of soft ground settlement based on BP neural network-grey system united model. Rock Soil Mech 26 (11):1810–1814

Shangai Municipal Engineering Design Institute (2005) Chongqing communications research and design institute etc. Construction Description of Road Foundation Treatments for the Reclamation in the Western Corridor Connecting Project from Shenzhen to Hong Kong

Xu F et al (2005) Research on the Final settlement prediction based on the first-hand observed data. West-China Explor Eng 1:1–3

Zhan X (2006) How to do the geotechnical engineering forecast and calculation. Guangdong Sci Technol 152:74–76

Zhang C et al (2005) Prediction of the Settlement of highway soft foundation by BP-NN model. Geol Sci Technol Inf (24):115–117

Zhang W, Li L (2005) The application of grey system theory in the rockfill subgrade settlement calculation. Jilin Sci Technol Commun 4:3–5

Zhou Y (2005) Embankment settlement deformation forecast based on the grey theory. West-China Explor Eng 1:52–53

Chontal HPP, Geological Features on Site Location and Dam Type

106

Cristina Accotto, Giuseppe Favata, Enrico Fornari, Nikolaos Kazilis, Marco Rolando, and Attilio Eusebio

Abstract

The Chontal Hydropower Plant is located along the Guayllabamba River, in the North-West of Ecuador, 100 km from Quito, in the districts of Pichincha and Imbabura. The geology of the dam area has strongly influenced the dam site location and the dam design: due to the geological characteristic of the area, not satisfactorily determined during a previous feasibility study, the layout of the plant has been entirely changed. During the review of the feasibility study, which foresaw two hydropower plants in cascade, new geological investigations have been carried out, acquiring more detailed information on the geology of the Guayllabamba River along the stretch of interest. In particular, a deep pervious old buried river channel has been detected and extensively investigated. Further to the new geological information, the inadequacy of the feasibility design, due to a deficiency of geological data, has been assessed, in particular with reference to the both reservoirs and dams site. Several design alternatives have been developed, changing both dams' location, type and number (1 or 2). A multi-criteria analysis and risk analysis have been carried out to identify, according to the Client, the design arrangement. Chontal Hydropower Plant is an example of the influence of geological features on the choice of dam site and dam design. The paper is focused on the dam design, and its relationship with the geology.

106.1 Introduction

The Chontal Hydropower Plant is located along the Guayllabamba River, in the North-West of Ecuador, 100 km from Quito, in the districts of Pichincha and Imbabura. The plant incorporates a 142 m high RCC dam, a 870 m long headrace tunnel on the left bank of the river, a 14 m-diameter surge shaft, a 88 m high penstock shaft, a 200 m high pressure tunnel, an outdoor powerhouse equipped with 2 Francis turbines, and a tailrace channel. The plant has a total installed capacity of 194 MW, exploiting a hydraulic gross head of about 130 m.

The final arrangement of the Chontal HPP, and in particular the dam design, is completely different from the one foreseen in the feasibility design, because of strongly influence of the geology in the site area.

The paper is focused on the main geological features and its relationships with the design development, from the formulation of alternatives up to the final design.

106.2 The Feasibility Design Layout (1979–1980)

To understand the development of Chontal HPP, it is suitable an analysis of the layout selected during the feasibility design study, carried out in 1979–1980 by the former INE-CEL (Instituto Ecuatoriano de Electrificación).

C. Accotto · G. Favata (✉) · E. Fornari · N. Kazilis · M. Rolando · A. Eusebio
Geodata Engineering S.p.A., Turin, Italy
e-mail: gfa@geodata.it
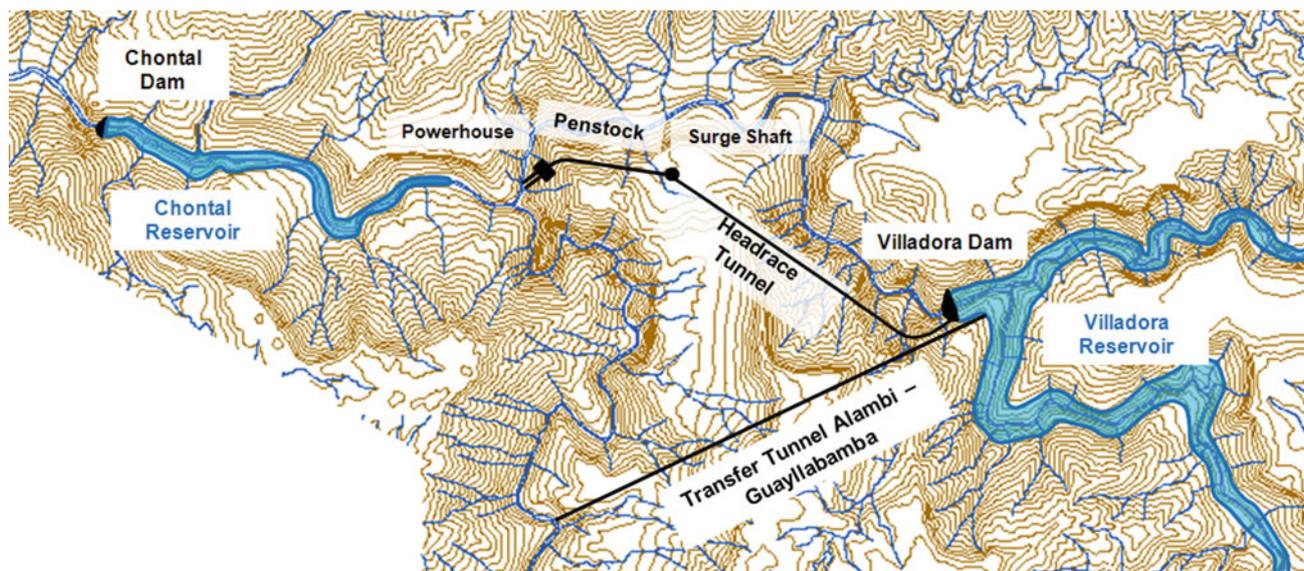
Fig. 106.1 Feasibility study layout

The feasibility design, carried out in 1979–1980, foresaw two plants, Villadora and Chontal, each one with a dam located on the Guayllabamba River. The upstream plant, Villadora, foresaw an arch dam 165 m high; the downstream one, Chontal, foresaw an arch gravity dam 68 m high with powerhouse at its toe. To increase the energy production, a hydraulic tunnel was foreseen to convey water from the Alambi River, a downstream tributary of Guayllabamba River, to Villadora reservoir. The general layout of the two plants is shown in Fig. 106.1.

In the dam area of Chontal only few site investigations, and in particular no boreholes, were carried out. However, in the feasibility study, it was foreseen the possible existence of an old buried channel (paleo-channel) along the right bank, identified by two seismic profiles. These two profiles show a bedrock with waves velocities of about 4,800 m/s. In correspondence of the buried channel, the waves velocities decrease up to 560 m/s. No more investigations were carried out during the feasibility design study, and therefore the conclusions of the feasibility study was the needed of more investigations, in particular boreholes and seismic profiles, to define the geometry of the old buried channel.

106.3 Geological Investigations

106.3.1 Investigation Plan

During the review of the feasibility design it has been recorded that the geophysical investigations carried out indicate the presence, along the right bank, of a depression filled with material through which seismic waves move at very slow velocities. The depth and extent of this depression, however, had not been clarified, since the geophysical surveys were not accompanied by verification through boreholes. The geological information therefore wasn't enough to develop a final design on the basis of the feasibility study, since characteristics, permeability and resistance parameters of the material in the depression were not available.

For the above reasons, it was suggested to carry out, and afterwards was carried out, a detailed geological survey in the project area, as well as field and laboratory investigations.

The following geological studies have been carried out:

- Geological survey at the dam site
- Geological survey of the old buried channel along the right bank
- Geological survey of the reservoir
- Detailed analysis of the joint sets at the dam site

Moreover, several geological investigations have been carried out to investigate the buried channel, such as geophysical profiles, boreholes and permeability tests.

106.3.2 Results of Geological Investigations

The detailed geological mapping and the field investigations allowed to identify the old buried channel, as well as the characteristics of its composing materials.

106.3.2.1 General Geological Features of the Area

The area considered for the development of hydroelectric projects is along Rivers Guayllabamba, Intag and Alambi. The river valleys are narrow, with high and steep slopes that would seem ideal for the construction of dams.

In the area of interest the rock formations are granodioritic rocks. In the outcrops that appear on the riverbed the rock appears sound and fresh, with relatively high resistance, close to the values of intact rock. Therefore it could be concluded that the rock mass in the studied area generally could be considered suitable for dam foundation.

106.3.2.2 The Old Buried Channel

The presence of the old buried channel has been identified through the detailed geological survey and field investigations, allowing the preparation of the map shown in Fig. 106.2.

The paleo-channel, as well as the actual riverbed, have been developed along zones of weakness of the rock mass. Occasionally, the old channel and the actual river bed coincide.

The paleo-channel materials are constituted by old alluvial deposits, lagoon deposits and laharitics deposits, with different values of permeability depending on the content of fine material. The overall permeability of the paleo-channel is difficult to estimate through conventional tests, due to the diversity of involved materials. Moreover, it is difficult to predict the long-term behavior of that materials under a high hydraulic gradient such the one that occurs in presence of high-head dams. The possible occurrence of internal erosion, with consequent increase of permeability and therefore serious risks related to plant functionality and stability, could not be discarded.

This critical situation has been considered and duly analyzed in all places where the paleo-channel is located within a possible reservoir area, since it could have direct or indirect communication with areas located downstream of the dam, with consequent water leakage from the reservoir. It should be considered that the leakage of water could have serious consequences on plant functionality, and therefore significant investments could be required to avoid it.

106.4 The Selection of Final Layout

106.4.1 The Study of Alternatives

On the basis of the geological features of the site and, in particular, taking into account the presence of the paleo-channel, it was necessary to select possible dam sites where the paleo-channel is coincident with the actual river bed and their axes are coincident or at least slightly sub-parallel, in order to avoid the risk of severe leakage from the reservoir. The study of alternatives, therefore, has been carried out following this principle.

Twelve alternatives (including the feasibility study layout) have been analyzed. Eleven of these alternatives foresaw two plants in cascade, as in the feasibility study layout, with different dam sites, while the last alternative foresaw only one high-head dam in the Chontal sector.

To facilitate the screening of the alternatives qualitative criteria were established, based on safety and risk analysis which allows to select or eliminate those alternatives that don't have adequate conditions, and to minimize future risks
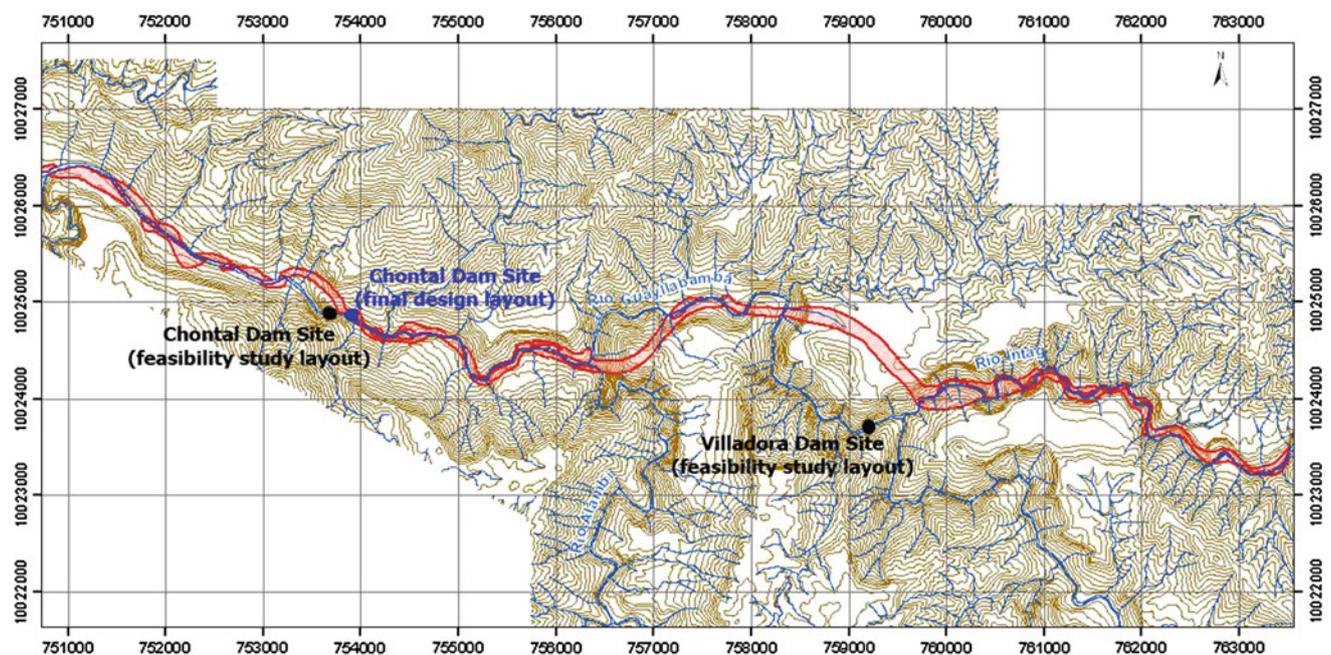
Fig. 106.2 Location of the old buried channel, after geological survey and field investigations
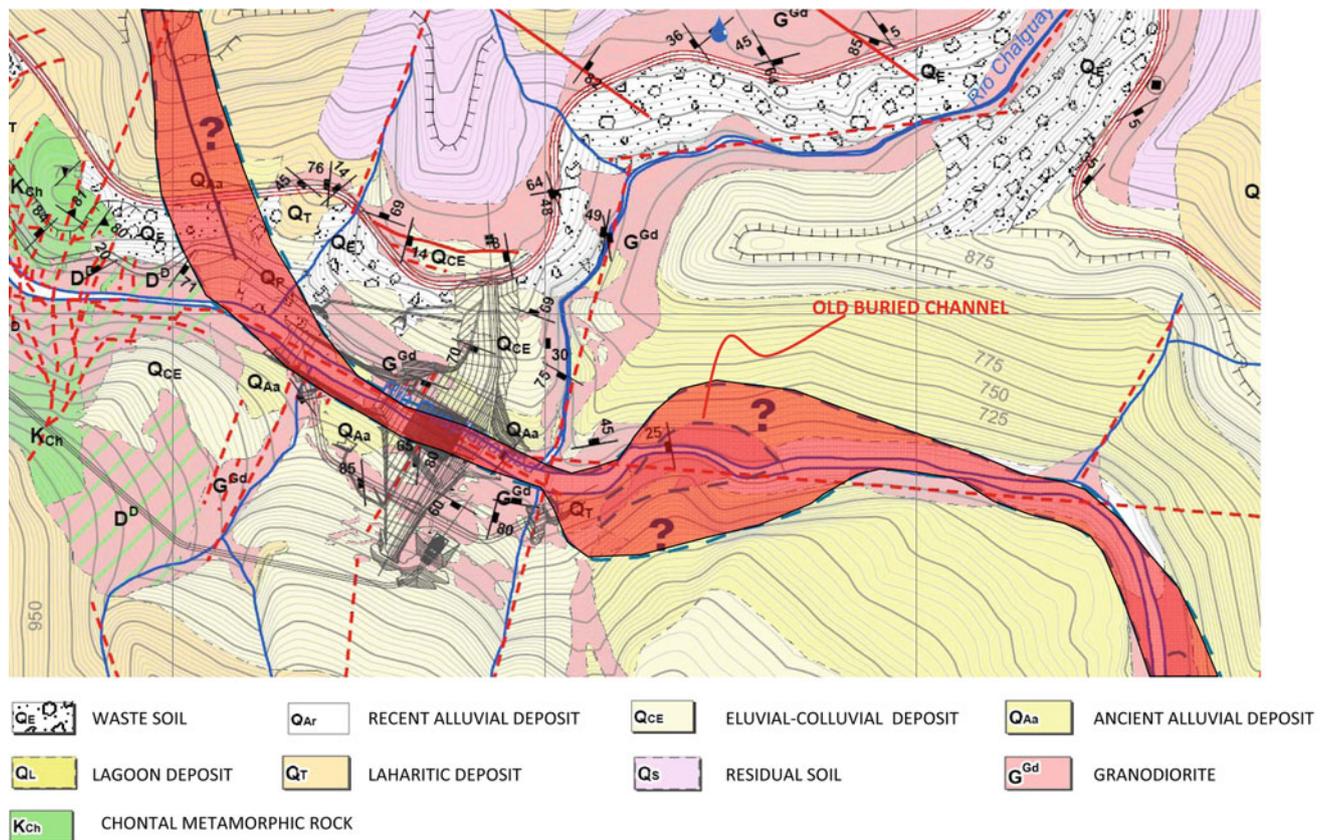
Fig. 106.3 Final layout, dam site with relevant geological characteristics

that will require additional repair works with subsequent related costs. For the screening of the alternatives six criteria have been used: (i) topographical and morphological; (ii) hydrological and sedimentological, (iii) geological and geotechnical, (iv) environmental, (v) economic, (vi) technical criteria related to civil works (e.g., dam stability).

As result of the preliminary screening, five viable alternatives have been selected. Afterward, a cost estimate for each viable alternative has been carried out, taking into account the prices for the civil works, as well as for electromechanical and hydromechanical equipment. Furthermore, the multicriteria analysis has been used to select the final layout. The identification of these criteria is organized in hierarchical levels, as follows:

- Feasibility criteria, focus on the issues relevant to general feasibility of the project
- Economical criteria, focus the attention on total cost and back discounted cost of the works
- Environmental criteria, focus the attention on environmental aspects during works execution as well as during plant operation

The technical feasibility considers geological criteria (seismic risk, rock mechanics, presence of faults, risk of landslides), complexity of the civil works, complex underground works, access availability, construction phases, expropriations, environmental authorizations.

The economic feasibility considers costs and benefits by energy production.

Finally, the environmental feasibility considers the impacts during construction, and impacts during plant operation.

For each alternative, the list of evaluation criteria was completed by assigning a rating to each criterion, ranging from "inadequate", "unacceptable", "acceptable" and "optimal" evaluation. The rating assignment was made according to expert judgment and quantitative criteria.

106.4.2 The New Layout: Feasibility Study and Final Design

106.4.2.1 The New Feasibility Study (2010)

At the end of the multi-criteria analysis, a new layout has been selected. The geological criterion allows to discard one of the five viable alternatives, for the risk of stability problems of the right bank near the dam site, related to the presence of the paleo-channel.

The selected alternative foresee a high-head dam (142 m) and an outdoor powerhouse, with a total installed capacity of

194 MW. The dam site is located about 120 m downstream of the Chalguayacu river confluence with the Guayllabamba river. At the dam site the paleo-channel is coincident with the actual river bed, as it is shown in Fig. 106.3. The selected dam site remove the risk of severe leakage from the reservoir, and the subsequent risk of internal erosion of the paleo-channel.

A new feasibility study has been realized for the selected layout. During this study, new geological investigations have been carried out. The geological investigations carried out on both banks of the dam site consist in geophysical seismic refraction (11 profiles on the right bank and 9 on the left bank, with a total length of 1,550.0 m), boreholes (7 on the right abutment, 8 on the left abutment and 3 along the river bed), with a total length of 963 m, geological surveys and geostructural surveys. The investigations confirm that the selected site has excellent characteristics for the dam foundation. The rock mass is a granodiorite, slightly fractured or sound, with permeability ranging from 10^{-5} to 10^{-7} cm/s, and local values of about 10^{-4} cm/s. The compressive strength of the rock is in the range 50.0–100.0 MPa,

the elastic modulus is 64.1 GPa, and the equivalent friction angle, is ranging between 46° and 57°.

In some areas the rock is covered by alluvial and/or laharitic sediments, in particular along the right bank. In Figs. 106.4 and 106.5 there are shown respectively the geological profile along the dam axis, and a geological section in correspondence of the dam spillway.

The dam type has been selected considering geological morphological, hydrological and geotechnical aspects, as well as materials availability and economical aspects. The selected dam type is the RCC (roller compacted concrete) gravity dam.

106.4.2.2   The Final Design

The geological studies allowed to accurately determine the depth of alluvial materials, and therefore to determine the planimetric position of the dam and the excavations needed to reach the sound rock mass.

A curtain grouting is foreseen to reduce leakage through the dam foundation and to reduce the uplift pressures (in conjunctions with drain holes). A perimetrical plinth is foreseen to realize the grouting curtain, which will be
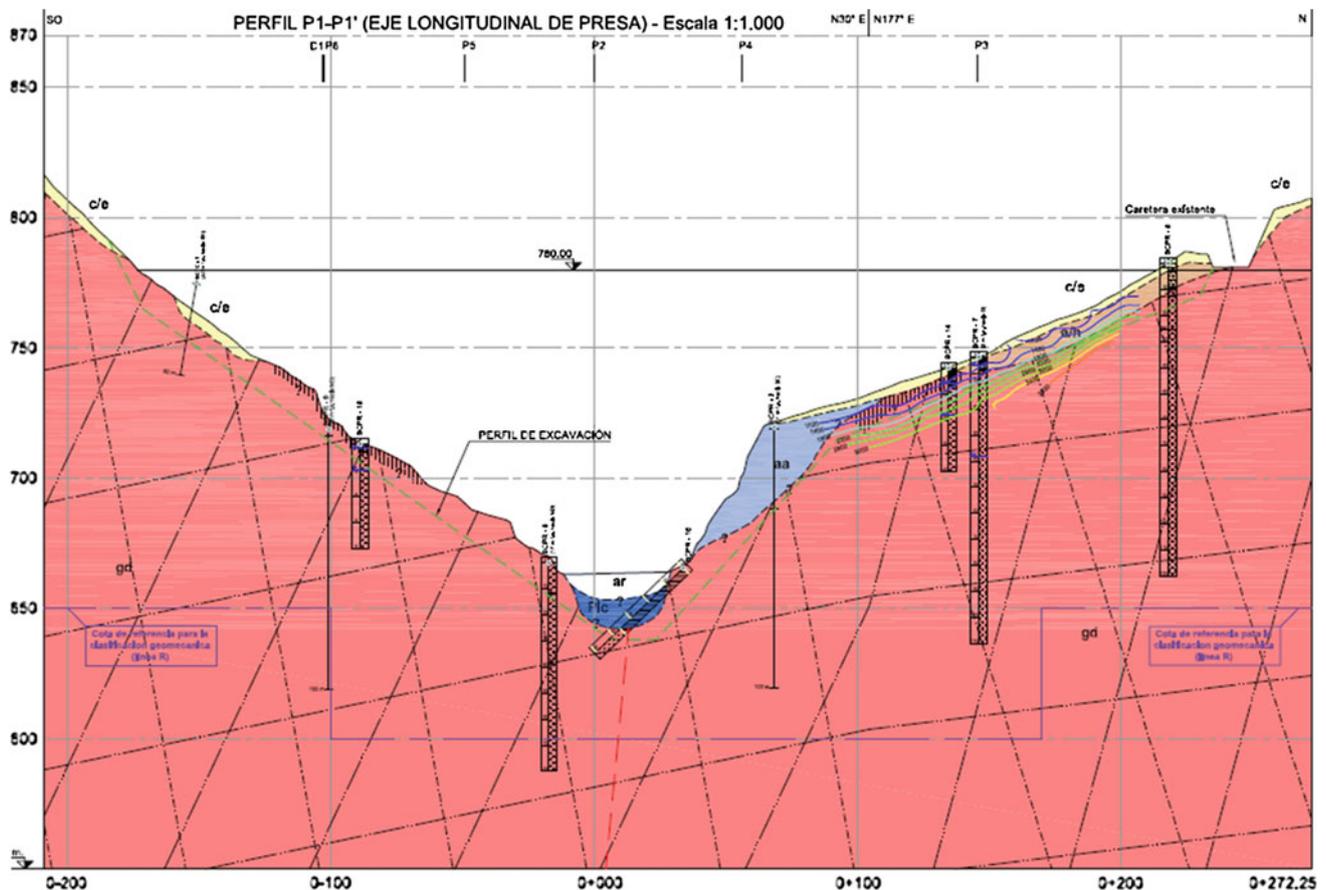
Fig. 106.4 Geological profile along the dam axis
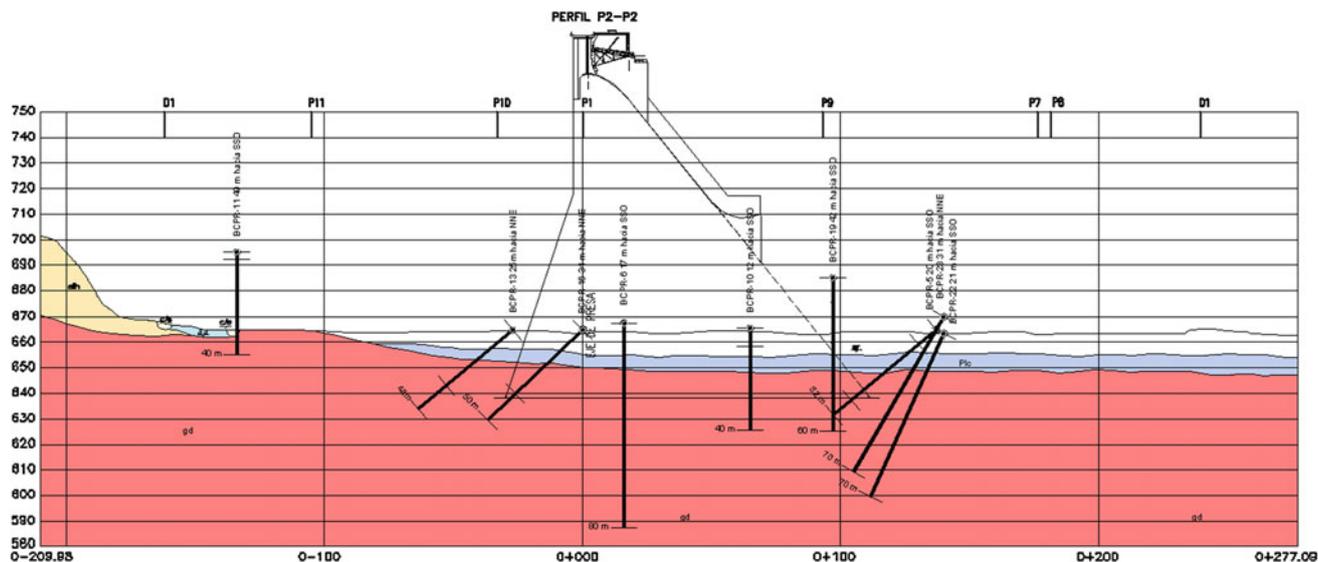
Fig. 106.5 Geological section along the dam spillway (river bed)

realized sequentially: the primary grout holes will be spaced 12 m, the secondary 6 m and the tertiary holes, if required, will be spaced every 3 m. According to the results of the Lugeon tests (51 tests on the left bank, 81 tests on the right bank and 29 tests along the river bed), the depth of the grouting curtain reaches values of 80 m in correspondence of the river bed.

106.5 Conclusions

The dam design is strongly influenced by the geology of the area, from the feasibility study to the final design. Adequate geological investigations and expert interpretation of the data are required in order to reach a good knowledge of the geological characteristics which could affect the design choices.

In the example of Chontal Hydropower Plant, reported in the present paper, the geological features of the project area have shown, during the review phase of the previous feasibility study, the inadequacy of the previous layout, and the need of more detailed studies. The acceptable dam sites have been controlled by the presence of an old buried channel, identified through a detailed geological survey. During the screening of the alternatives, the geological criterion, in conjunction with other technical, economical and environmental criteria, has guided the selection of the best alternative. Finally, during the new feasibility study and the final design of the selected alternative, the geological

characteristics of the dam site determined some design choices, such as the exact planimetric position, the required foundation excavations, and the curtain grouting extension.

References

ASCE (1989) Civil engineering guidelines for planning and designing hydroelectric developments, vol 1

Barton N (2007) Rock quality, seismic velocity, attenuation and anisotropy. Taylor & Francis, UK

Bell FG (2007), Engineering geology. Elsevier, Amsterdam

Fell R, MacGregor P, Stapledon D, Bell G (2005) Geotechnical engineering of dams. Balkema Publishers, Boca Raton

Fetter CW (2001) Applied hydrogeology. Prentice Hall, US

Golzé AR (1977) Handbook of dam engineering. Van Nostrand Reinhold Co., New York

Hoek H, Palmieri A (1998), Geotechnical risks on large civil engineering projects, keynote address for theme I. International Association of Engineering Geologists Congress, Vancouver, Canada, 21–25 Sept 1998

Jansen RB (ed) (1988) Advanced dam engineering for design, construction and rehabilitation. Springer, Berlin

Londe P, Sabarly F (1967) Écoulements de percolation dans les massifs rocheux servant d'appui aux barrages. La Houille Blanche 1:37–46

Plata Bedmar A, Araguás Araguás L (2002) Detection and prevention of leaks from dams. Balkema Publishers, Boca Raton

USBR (1987) Design of small dams, 3rd edn

Verzani L, Soldo L, Uttini A, Vendramini M, Accotto C, Principi S, Ricci G, Eusebio A (2012) Lo studio geologico e geomeccanico applicato a progetti idroelettrici nelle Ande ecuadoriane. Geoingegneria Ambientale e Mineraria, XLIX 1:39–48

Volpe RL, Kelly WE (eds) (1985) Seepage and leakage from dams and impoundments. ASCE

Geological Model in Major Engineering Projects

Convener Mr. Erik Wunder—*Co-convener* Nicole Borchardt

Society is looking for a balance between quality of life and environmental protection. In this search, the wide spectrum of possibilities goes through discussions on renewable sources of energy and the use of underground space. The adequacy of infrastructure occurs through major engineering projects, where the geology applied to engineering plays a key role, from the conceptual design until its construction. In this context, the development of a realistic Geological Model is essential to describe the natural rock mass surroundings that should be worked to host the project in such a way that it gives subsidies to quality of design, feasibility of the project and for formatting contractual clauses regarding the assumption, contingency and sharing geological risk. The purpose of this session is to emphasize the role of the geologist in drafting the Geological Model and characterize the Geological Model as one of the main contributions of engineering geology for major engineering projects.

Evaluation of Geological Model in Construction Process of Sabzkuh Tunnel (Case Study in Iran)

107

Majid Taromi, Abbas Eftekhari and Jafar Khademi Hamidi

Abstract

Geological and geotechnical surveys, in general, should precede the tunnel excavation to ensure its safety. Also they should be continued during the tunnel excavation, because the geological condition can be changed unexpectedly while the tunnel is under construction. Tunnel face stability is one of the main issues in tunnel excavation in soft and alluvial grounds in order to keep the construction process stable and prevent localized face collapse. Choosing of an appropriate excavation method is influenced by geological and geotechnical studies and comprehensive and appropriate use of these data in tunnel designing. The Sabzkuh tunnel was excavated mainly in fault zones, alluvial, shale and limestones using the conventional and shielded tunnel boring machine (TBM) Methods. An advance length of 1.5 m without any support system caused many difficulties during the excavation of Sabzkuh tunnel. So, to overcome the complicated ground conditions and tunnel collapse, the excavation method were shifted from full face to sequential excavation in addition to decreasing the excavation step. This paper discusses some of the key geotechnical challenges faced in the tunnel design, including characterization of ground conditions, selection of appropriate design parameters, and evaluation of excavation and support installation sequence based on monitoring and analyzing ground behavior during construction.

107.1 Introduction

The stability of underground structures is a key issue during design and construction. Depending on the geotechnical conditions and influencing factors, different failure modes can be expected. Also, depending on the potential failure modes, project specific requirements and boundary conditions, specific construction measures to ensure stability have to be chosen.

Submitting of a geological model, design parameters estimation, excavation and support system choosing with minimum risk, safety providing and cost reduction are major challenges for tunnel construction process in complicated ground conditions. Therefore, sufficient prior studies, interpretation, analysis, and process of data in an updatable model in order to planning for construction process are important in a tunnelling project. One of the most significant stages in tunnel construction is the displacement estimation of surrounding rock masses and support type regarding ground conditions and excavation method. The amount of tunnel wall displacement and required support is dependent upon the size of tunnel, available initial stresses, rock mass

M. Taromi (✉)
Department of Civil Engineering, Islamic Azad University, South Tehran Branch, Tehran, Iran
e-mail: majidtarami@ymail.com

A. Eftekhari
Department of Geology, Tarbiat Modares University, Tehran, Iran
e-mail: msc.eftekhari@yahoo.com

J. Khademi Hamidi
Department of Mining Engineering, Tarbiat Modares University, Tehran, Iran
e-mail: jafarkhademi@modares.ac.ir

properties, and tunnel excavation method Hence, the selected tunnel excavation method plays an important role in tunnel stability.

Sabzkuh–Choghakhor water conveyance tunnel with 10,617 m in length and 0.01 % in gradient is under construction in south-western Iran (Fig. 107.1). The tunnel is going to be excavated by a double shield tunnel boring machine (DS TBM). The information obtained from the site, including field reconnaissance, geotechnical and geophysical studies revealed that the tunnel from the beginning to chainage 0+390 km (T1) is located in the alluvium. So, taking into consideration the application range of DS TBM and its limitation for working in alluvial soils, this part of the tunnel is being excavated by conventional methods (Eftekhari et al. 2013a, b; Saeidi et al. 2012).

The results obtained from the numerical and sensitivity analysis on the soil geotechnical parameters demonstrated that a small part of tunnel face would provide a safe and stable excavation at the beginning of the tunnel drive. After full face excavation of 35 m and confronting unexpected ground conditions, a face collapse started and developed rapidly. This problem caused a failure in the tunnel portal area. In order to overcome this situation, Arch Support Technique (Eftekhari et al. 2013b) was employed. Various excavation methods such as open cut, DSM, freezing, jet grouting and sequential excavation method was used to excavate remaining part of tunnel.

Data obtained from previous studies usually are not sufficient for constructing process. In this situation, observation methods together with experience have an important role in tunnel construction. In Sabzkuh tunnel, after failure occurance in full face excavation, different applicable methods within similar geological conditions were chosen. Taking the strengths and weaknesses of each method as well as cost and time management into account, the sequential excavation method (SEM) due to its flexibility and compatibility with tunnel condition was selected.

A series of 3-D simulations using the finite different and finite element methods were performed in order to investigate the influence of the following aspects: (a) unsupported distance between the excavation face and the installation of support lining; (b) partial-face excavation.

Therefore, in this paper, the importance of geological studies in order to reduce the likelihood of unforeseen conditions, and monitor the design and construction with regard to geotechnical and geological interpretations are emphasized.
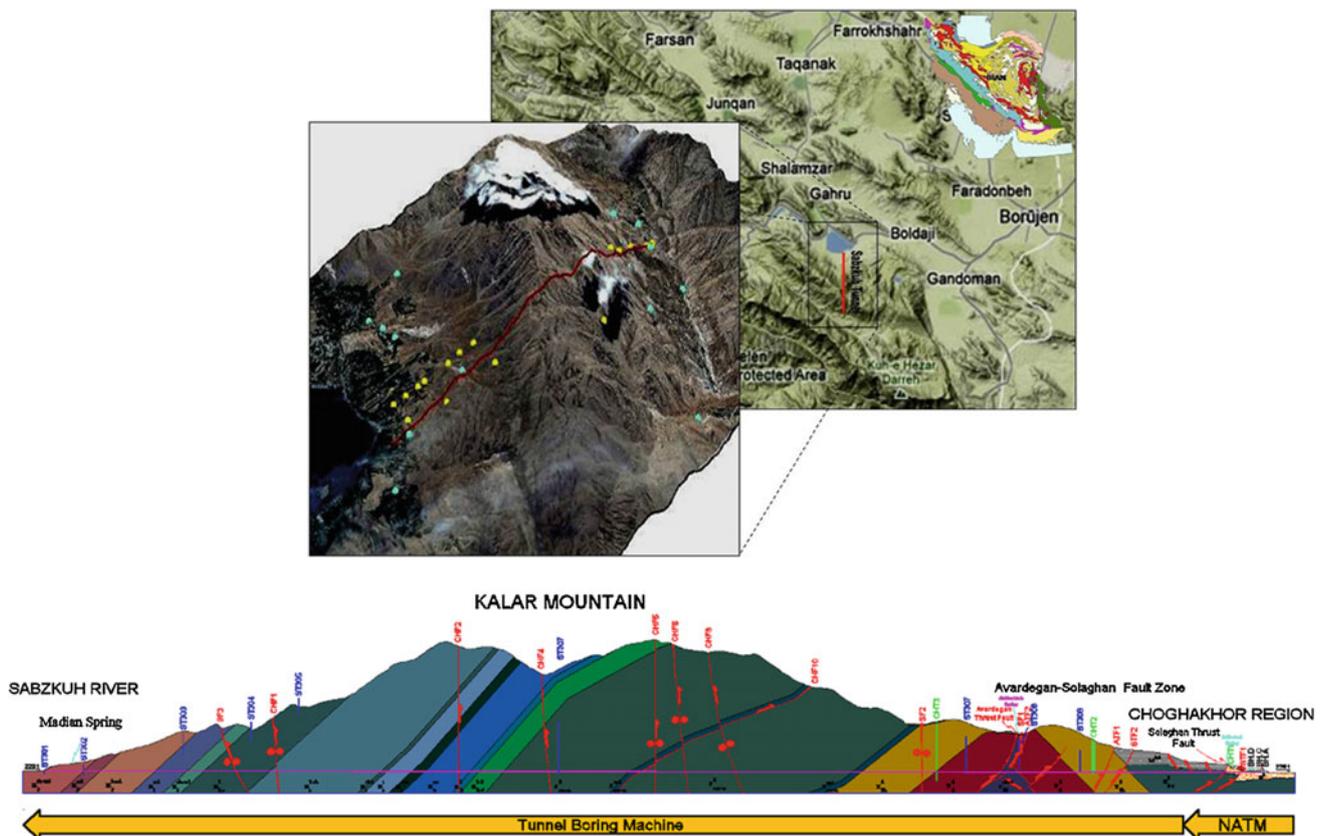
Fig. 107.1 Sabzkuh tunnel location (*above*) and longitudinal geological profile (*below*) (Taromi et al. 2013)
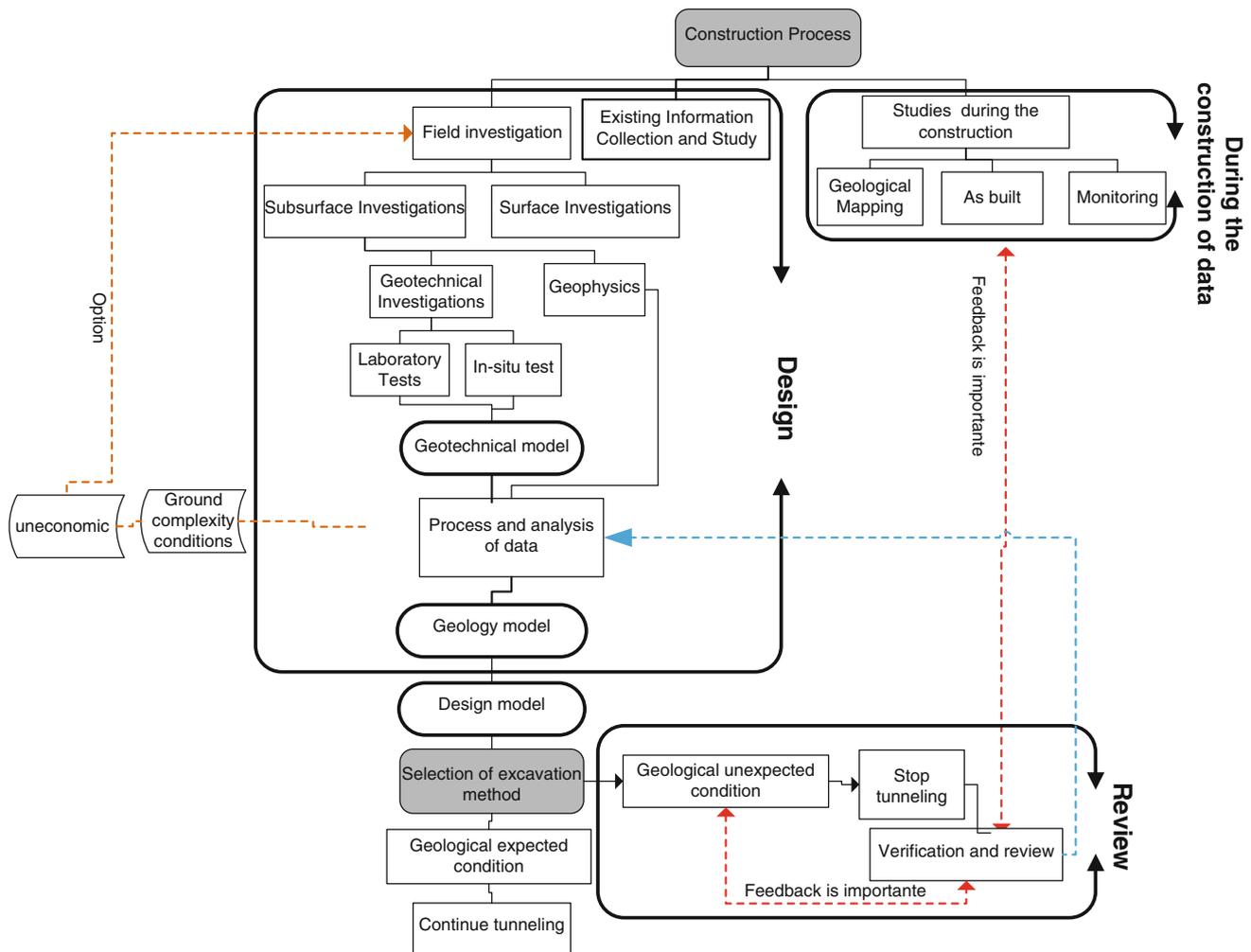
Fig. 107.2 Construction process algorithm (Taromi et al. 2013)

107.2 Construction Process

Due to the variation in the geotechnical conditions (the static system and the capacity of ground and supports), the design of an underground structure cannot be compared to a structural design of other buildings where the loads, the system, and the characteristics of the materials used are known.

In a tunnel constructing method, preparation of geological and geotechnical models and its design is very important (Fig. 107.2). This process contains analysing the data outcome from geological engineering, determination of ground design parameters, preparation of basic scheme for excavating and maintenance, evaluation of hazards, revising and correction of studies and risk management. These models may be changed or modified after reaching more accurate data during excavation. Respecting to complication of ground behaviour and uncertainty of available models, these models should be updatable and changeable in confront with unpredicted situation. Therefore, these models will be reliable if they can be simultaneously updated with new obtained data. Geological model proposing construction site with suitable engineering judgment has significant role in construction process.

107.2.1 Geological Model

Geological model is a basic prerequisite in tunnelling in order to improve safety and reduce costs. In tunnel excavation, field investigation cost is just about 3 % of total cost, which is considered unimportant by employer; however, it is very important due to probability, and uncertainty which exist in assumptions of modelling. Available experiences in United States shows that more than 55 % of contractor claims in tunnelling is about the ground condition that could reduce by more rigorous studies (Robinson et al. 2001). Regarding to experiences available in Iran, exploration cost is about 1–2 % of the total construction costs. Accordingly, appropriate data is not provided for designers.

In addition to site investigation studies at the feasibility and preliminary design phases, the geological studies carried out during construction have an important role in tunnelling process (Kolymbas 2005; Eftekhari et al. 2013a, b).

In Sabzkuh tunnel project, because of complicated ground conditions, geological reports does not cover all the ground parameters. So, geological models have been revised since the beginning of tunnel excavation. Face mapping and on-site modelling are followed at frequent intervals as the tunnel advances. This is done for the selection of the required support systems and optimum excavation pattern in different ground conditions.

107.2.2 Geotechnical Modelling

Increasing demand on geotechnical model in primary stages of a project in order to gather exploration operation information is felt more than ago. This model provides some initial information of ground properties and possibility of tunnel excavation for engineers and designers. These concepts can be updated and corrected in varied ground condition during excavation by additional studies.

Noticeable part in geotechnical studies is the correlation of these studies with geological ones, which is usually ignored in most projects. Subsequently, geotechnical studies are planned, performed and analyzed independently, regardless of the results of the geological studies. In other words, lack of engineering geology in correlation with geotechnical engineering can be felt clearly. In such this situation, complete expected studies about natural ground conditions are not done and lots of problem in interpolation of surface and subsurface data will be occurred. This process according to physical governing condition without regard to the nature of composition of soil in geological history is not only sufficient, but also causes great mistakes somehow. Hence, a geotechnical model can be expected to provide accurate results just when it is based on right knowledge of geological condition.

107.2.3 Design Model

In underground structure engineering there are two major aspects that must be addressed during the design phase. The first and most important is developing a realistic estimate of the expected ground conditions and their potential behaviours as a result of the excavation. The second is to design an economic and safe excavation and support system for the specified ground behaviours. The design process begins with the feasibility study and continues through the preliminary design, the detailed design, the tender design, and also the construction. The design is constantly updated during each stage, as more information is available. This requires the involvement of geological and geotechnical experts in all phases of a project.

During the design phases the inherent complexity and variability in many geological settings prohibits a complete picture of the ground structure and quality to be excavated. The geotechnical design is targeted to a continuous refinement of the models and decision criteria. Besides a high professional standard, a systematic and consistent, well documented evaluation and decision process is of paramount importance. Uncertainties in the ground model shall be considered in the design.

The variability of the geological architecture including the local ground structure, ground parameters, in-situ stress and ground water conditions requires employing a consistent and specific procedure during the design process. The key influences governing the geotechnical design are the ground conditions and behaviour.

Based on the ground characteristics and the expected ground behaviour, a feasible construction concept, consisting of excavation method, sequence of excavation, support and auxiliary methods, is chosen.

For stability analysis and reaching an appropriate tunnel model three analytical, observational and empirical methods are used. In recent decades, some numerical approaches such as FEM, BEM, DEM and FDM have been considerably spread. By using these methods, modelling of complicated geometry and different loading and employing of appropriate constitutive model is possible. Furthermore performance method can be modelled by this model.

A number of numerical methods have been developed in civil engineering practice. This methods are used extensively for analysis of underground excavation design problems.

For the analysis of tunnelling in soil, continuum analysis is generally accepted, where the domain can reasonably be assumed to be a homogeneous media. The continuum analysis includes Finite Element Method (FEM), Finite Difference Method (FDM), and Boundary Element Method (BEM).

Finite element or finite difference analysis has been used for a wide range of engineering practices for last several decades. Complex, multi-stage models can be easily created and quickly analyzed. The analyses provide complex material modelling options and a wide variety of support types can be modelled. Linear element, usually modelled as beam elements, can be applied in the modelling of shotcrete, concrete layers, and steel sets. Almost every project today requires numerical modelling to predict behaviour of structures and the ground.

107.3 Design and Construction of Tunnelling Work—Sabzkuh Tunnel

107.3.1 Loading

Unlike the rock tunnel in which the rock mass characteristics are used in estimated pressure imposed on support system (e. g. confinement-convergence analytical method, Ground Reaction Curve (GRC) and rock mass classification systems), in shallow tunnels and in particular in soil or soft ground tunnels, soil shear strength based analytical methods are used for estimation of support load. The support load estimated from various methods in Section T1 along the Sabzkuh tunnel is summarized in Table 107.1. The width and height of the tunnel are 4.9 and 5.4 m, respectively.

The vertical and horizontal loads on the support system estimated from various methods are given in Table 107.1. Terzaghi calculation model considers the soil cohesion and friction angle simultaneously, and consequently provides more accurate and more reasonable results compared to other methods. Meanwhile, for safety reasons, the lining horizontal and vertical pressures were selected 0.09 and 0.2 MPa, respectively.

107.3.2 Analysis of a Composite Liner with the 'Equivalent Section' Approach

Use of sprayed concrete or shotcrete as primary support is a standard practice in tunnel design and construction (see, for example, Hoek and Brown 1980; American Society of Civil Engineering 1984; Eisenstein et al. 1991; Franzen 1992). Steel arches can also be used with or without additional support or reinforcement to stabilize blocky or deformable ground. If the magnitude of loads transmitted by the ground to the support is large enough to preclude shotcrete alone or if squeezing or raveling behavior requires complete surface coverage, steel sets are commonly used in combination with shotcrete. This combination can be in the form of a complete composite annulus or may be a semi-circular or partial arch configuration (Table 107.2).

107.3.3 Stability Analyses

In Sabzkuh tunnel, designers used FEM as the stability analysis method in the design model with input data given in Table 107.3 (Itasca Consulting Group 1997). The obtained results are seen in Fig. 107.3. It can be revealed that the tunnel is stable with 1.5 m excavation step and 5.5 cm vertical displacement. Accordingly, full face excavation of

tunnel section was chosen referring to the results of design model (Fig. 107.4).

After 35 m advance of the tunnel in full face excavation, a critical zone appeared and tunnel collapsed due to the redistribution of in-situ stresses around the excavation and formation of wide plastic zone as well as excessive axial displacements (Fig. 107.5).

The incident of tunnel collapse showed that the reliability of analytical methods in prediction of engineering behaviour in soil mechanic is largely dependent on the certainty of input data. Accurate measurement of in situ soil geotechnical parameters is difficult and sometimes impossible. In other hand, due to anisotropicity, the results of in situ soil tests cannot be used directly as design input data. In order to overcome these troubles, regarding to appropriate application of support system in collapses, excavation method should be optimized by considering available condition, outcome data and data which is gained during construction. Therefore, in a tunnel design model many uncertainties have geological and geotechnical source (Anagnostou and Kovari 1992).

107.4 Sequential Excavation Method

The Sequential Excavation Method (SEM), also commonly referred to as the New Austrian Tunnelling Method (NATM), is a concept that is based on the understanding of the behaviour of the ground as it reacts to the creation of an underground opening. This method needs minimum ground deflection and avoiding of softening and strength reduction. In this method, dividing tunnel section into smaller headings and their sequence excavation control the stress-strain condition and prevent it from collapse.

To be able to determine the encountered ground type, the geological documentation during construction has to be targeted to collect and record the relevant parameters specified in the design. Additional observations, like indications of overstressing, deformation and failure mechanisms, as well as results from probing ahead and the evaluation of the

Table 107.1 Estimation of support load in Sabzkuh tunnel, section T1

Load	Ref.	Equation	Value (MPa)
Vertical	Terzaghi	$\frac{B_1\left(\gamma - \frac{2c}{B_1}\right)}{k\tan\varphi}\left[1 - e^{\frac{KD\tan\varphi}{B_1}}\right]$	0.136
	S.F.		0.20
Horizontal	Terzaghi (1)	$0.3\gamma(0.5m + h_p)$	0.046
	Terzaghi (1)	$\frac{B_1\left(\gamma - \frac{2c}{B_1}\right)}{k\tan\varphi}\left[1 - e^{\frac{KD\tan\varphi}{B_1}}\right]$	0.059
	S.F.		0.09

Table 107.2 Input data for the analysis of a semi-circular liner comprised of shotcrete and steel sets according to the 'equivalent section' approach (Carranza-Torres and Diederichs 2000)

Geometry data	Shotcrete properties
$R = 2.60$ m (arch radius) $b = 0.75$ m (with of composite section) $s = 0.75$ m (spacing between steel set) $n = 1$ (number of steel sets along width)	
IPB140 Steel Set Properties	(1) Steel set, (2) Shotcrete
$t_s = 0.133$ m (height of the section) $A_s = 3.14 \times 10^{-3}$ m^2 (area of the section) $I_s = 1.030 \times 10^{-5}$ (moment of interia of the section) $E_s = 200000$ MPa (Young s Modulus) $\upsilon_s = 0.2$ (Poisson s ratio) $t_c = 0.2$ m $E_c = 22,900$ MPa (Young s Modulus) $\upsilon_c = 0.15$ (Poisson s ratio) $\sigma_c^c = 21$ MPa (tensile strength) $\sigma_t^s = -240$ MPa (tensile strength)	 Equivalent section
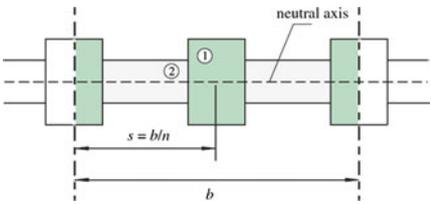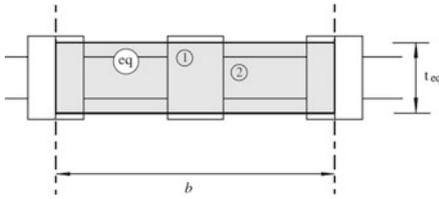
$D_{eq} = 3612.38$ MN	$K_{eq} = 12.076$ MNm^2	$t_{eq} = 20$ cm	$E_{eq} = 24.05$ GPa

Table 107.3 The soil properties as input data in FEM

Parameter	Value	Unit
Type of material behaviour	Drained	-
Total unit weight (γ)	18.5	KN/m^3
Young's modulus (E_s)	40	MPa
Poisson's ratio (ν)	0.25	-
Cohesion (c)	35	KN/m^2
Friction angle (ϕ)	25	degree

geotechnical monitoring are used to update the ground model and predict the conditions ahead of the face.

Based on the predicted ground conditions, the system behaviour in the section ahead has to be assessed under consideration of the influencing factors, and compared to the framework plan. Particular attention has to be paid on potential failure modes.

Hence, as a solution regarding to geological mapping and by using monitoring reports and revising the geological model, behaviour and classification of ground was investigated again in order to assess the excavation method (Terzaghi 1950; Heuer 1974). A prediction of the distribution of the excavation classes based on the results of the exploration and of stability analyses and on experience. The excavation sequence, round lengths and support measures for excavation classes B are given in Fig. 107.6 and Table 107.4.

FEM analyses in conjunction with empirical methods were used to evaluate potential ground behaviour upon tunnel excavation and to determine the required excavation sequence and support measures.

Fig. 107.3 Displacement vectors at the tunnel face
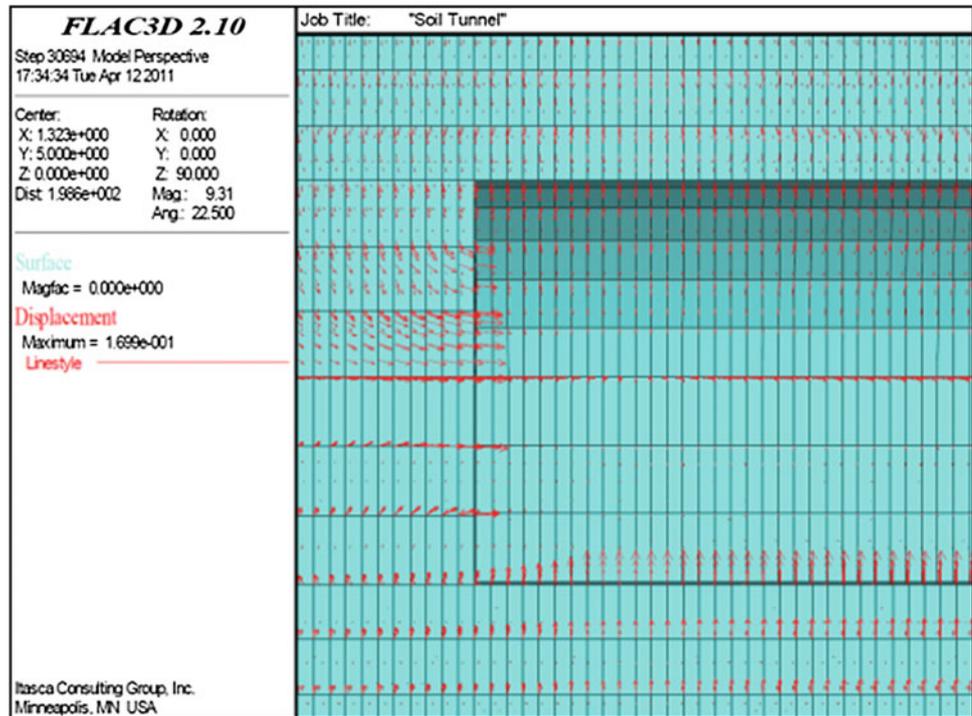
Excavation and Support Class (ESC)	Class A	
	Top, Bench Heading	**Invert**
Excavation Method	Mechanical Excavation (Backhoe)	
Unsupported Round Length (m)	1.5	15
Lining — Shotcrete (C25)	t=30cm	-
Lining — Reinforcement	Steel set+WWF	
Lining — Concrete (C21)	-	t=40cm
Tunnel Face Support	None	
Advance Support	None	
Trailing Distance	Continuous	

Fig. 107.4 Excavation and Support Class "A" for the tunnel

107.4.1 Stability Analysis for the Stages of Construction

Application of the NATM is based on empirical knowledge and local experience and may be adjusted according to observation. The use of numerical analyses with techniques such as the finite element method (FEM), could be of great value for this type of design. The use of numerical analyses to help tunnel design is becoming more popular both in industry and academic environments. In order to analyse the deformations and stability of the tunnel face excavated by NATM/SEM, the Plaxis 3D Tunnel software was used (Fig. 107.7) (Brinkgreve and Vermeer 2001).

The tunnelling construction process is simulated sequentially in several stages. Each construction stage may involve soil excavation and/or support lining construction.

– **Geometry**

In this study, the tunnel geometry and construction stages were simulated. The tunnel diameter and depth are 5 and 30 m, respectively. With regard to the symmetric geometry

Fig. 107.5 Collapse in initial part of Sabzkuh tunnel (T1) (Eftekhari et al. 2013b)
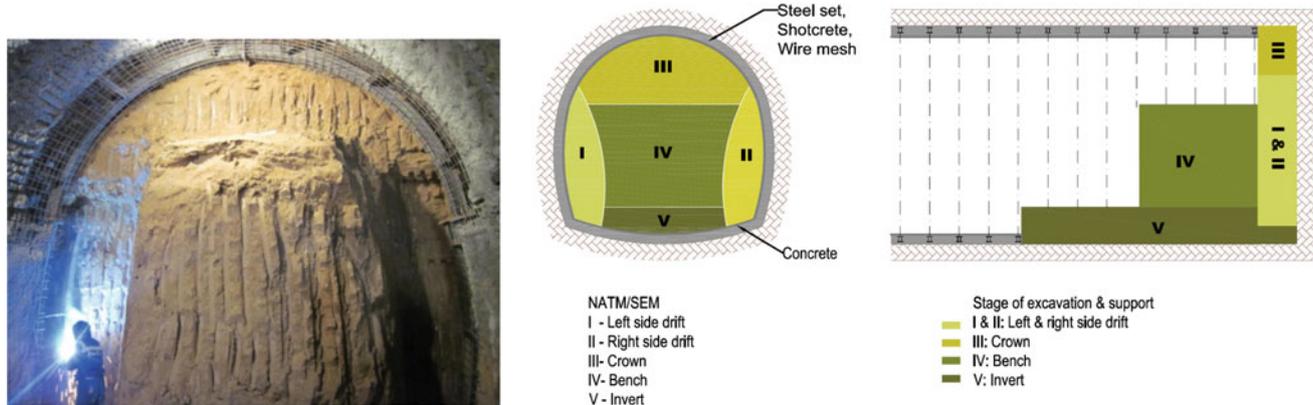
Fig. 107.6 Sequence of construction work

Table 107.4 Excavation and support class B for tunnel (after collapse)

Excavation and support class (ESC)		Class B				
		Side drift (I)	Side drift (II)	Crown (III)	Bench (IV)	Invert (V)
Excavation method		Mechanical Excavation (Backhoe)		Workman	Mechanical excavation (Backhoe)	
Unsupported round length (m)		0.75–0.85			3	7.5
Lining	Shotcrete (C25)	t = 25 cm			-	
	Reinforcement	Steel Set+WWF				
	Concrete (C21)	-			t = 40 cm	
Tunnel face support		A layer of flashcrete may be required			None	
Advance support		Typically none; Locally pre-spilling or grouted pipe arch canopy (L = 4–6 m, D = 7.5 cm); alternatively ground improvement				
Trailing distance		Depending on the monitoring results, the encountered geotechnical conditions and result of stability analyses				

Fig. 107.7 Staged construction preview of SEM method
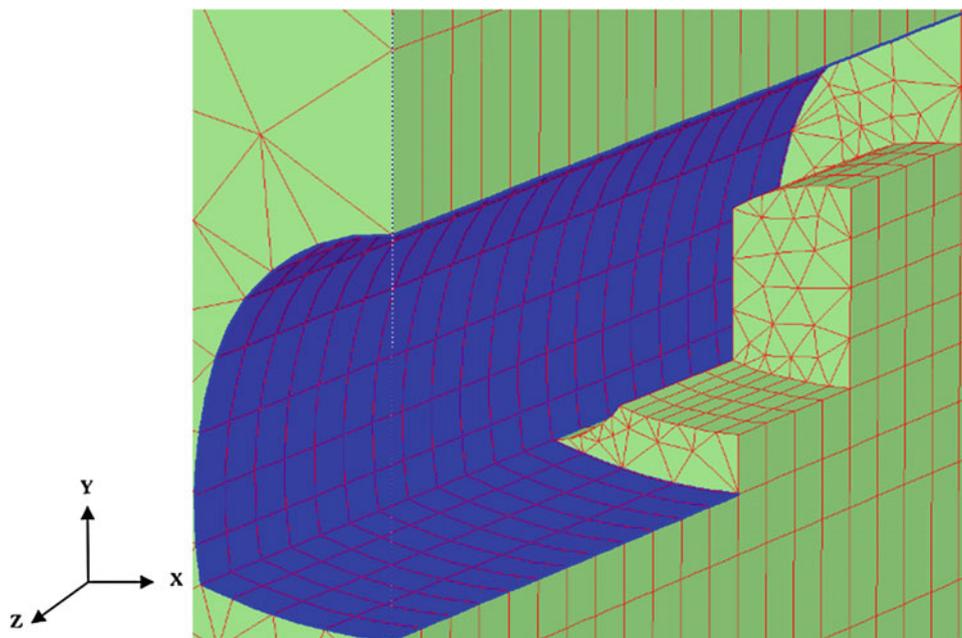
Table 107.5 Material properties of the soil

Parameter	Name	Sandy clay	Unit
Material model	Model	Mohr-Coulomb	-
Type of material behaviour	Type	Drained	-
Soil weight above phr. level	γ_{unsat}	15	KN/m^3
Soil weight below phr. level	γ_{sat}	18.5	KN/m^3
Young's modulus (constant)	E_{ref}	5×10^4	KN/m^2
Poisson's ratio	ν	0.3	-
Cohesion (constant)	c_{ref}	17	KN/m^2
Friction angle	ϕ	28	°
Dilatancy angle	Ψ	0	°

of the tunnel, on either side or one half of the tunnel can be modelled. In this study, left half of the tunnel was selected. The model has dimensions of $25 \times 50 \times 50$ m in X, Y and Z directions, respectively.

– **Material properties**

In modelling material behaviour, the constitutive model of Mohr-Coulomb was used. The elastic-plastic Mohr-Coulomb model involves five input parameters, i.e. E and v for soil elasticity; φ and c for soil plasticity (Table 107.5). This model represents a 'first-order' approximation of soil or rock behavior. It is recommended to use this model for a first analysis of the problem considered.

– **Deformations**

The results of the analyses indicate that the tunnel is quite stable and initiated deformations are relatively low and can be controlled in an acceptable range (Fig. 107.8).

107.5   Monitoring

Ground deformation monitoring in tunnelling is a common means for selecting and controlling the excavation and support methods among those predicted in design, ensuring safety during tunnel excavation (including personnel safety
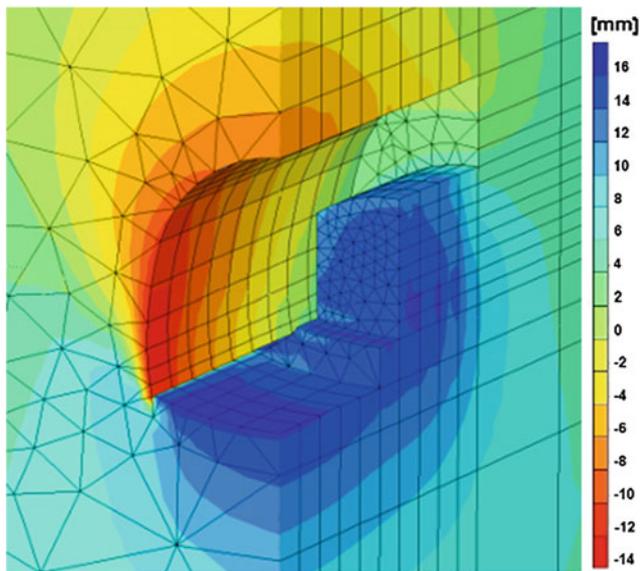
Fig. 107.8 Extreme displacements in tunnel face, Vertical displacements (Uy), Extreme Uy 13 mm (Crown)

inside the tunnel and safety of structures located at ground surface) and construction quality (Kavvadas 2005).

Ground deformation monitoring and its application in tunnel design and construction is illustrated using examples from the Jubilee Line Extension of London Underground (Burland et al. 2001; Mair 2001), from Lines 2 and 3 of the Athens Metro (Kavvadas 1997, 1999), from Resalat (Fakhimi et al. 2012) and Niayesh road tunnel project in Iran (Ghorbani et al. 2012), and from Dranaz tunnel, Sinop,

Turkey (Aydin et al. 2004). An overview of the application of the observational method in tunnelling projects is given by Powderham (1994). Tsatsanifos et al. (1999) and Kontogianni et al. (2004) present interesting case studies of excessive deformations causing failure of mountain tunnels in Greece.

Ground deformation monitoring has different objectives in mountain and urban tunnels. In mountain tunnels, the main objective of deformation measurements during construction is to ensure that ground pressures on the temporary support system are adequately controlled, i.e., there exists an adequate margin of safety against roof collapse, bottom heave, failure of the excavation face, yielding of the support system, etc. Control of ground pressures ensures a safe and economical tunnel structure, well adapted to the inherent heterogeneity of ground conditions.

Typically, the majority of ground deformation takes place ahead and close to the tunnel face, from about one tunnel diameter ahead of the face up to about 1.5 diameters behind the face (e.g., Chern et al. 1998; Kavvadas 1999; Hoek 1999, 2001; Kontogianni and Stiros 2002). Thus, instruments placed on the tunnel wall (e.g., 3D optical reflector targets) or installed in the ground from the tunnel wall (e.g., rod extensometers) should be put in place as early as possible.

In Sabzkuh tunnel, a continuous geodetic monitoring began using two targets mounted on the tunnel wall and one target in tunnel crown at about 20 m intervals. The targets were mounted at least one meter behind the tunnel face. Recordings were followed in a regular and predetermined time intervals (Fig. 107.9).

Fig. 107.9 Tunnel convergence at chainage 0+040
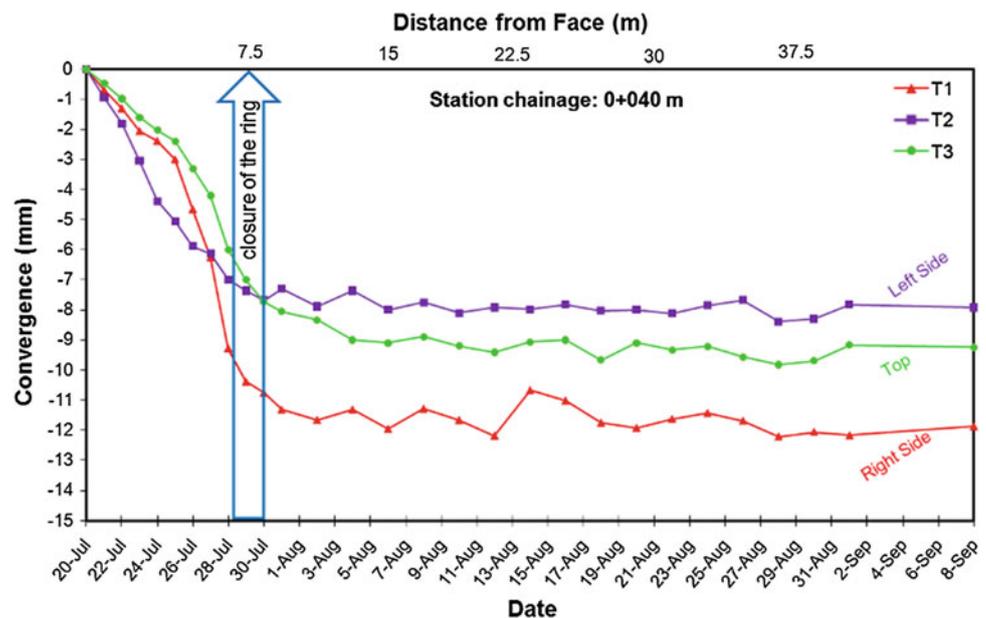
107.6 Conclusion and Summary

In construction process of Sabzkuh tunnel, a geotechnical model independently and without respect to geological model was planned, performed and analyzed. Lack of correlation between these two models and ground complicated situation and uncertainties provided some inappropriate information for designers and affected the analytical model as well as excavation method. After unworkability of full face excavation, a data server established in order to gather data of field studies and as built finding, regarding to previous experiences. This server helped to enhance prior construction method. The main specification of this server was its updatable in confront with new data.

Obtained results showed a complicated geological model, which needed frequent exploration, analysis and behaviour checking of surrounding soil moss in order to find the most economical and stable excavation model and support in face with different conditions. So, NATM/SEM method was selected due to its workability and flexibility in confront with tunnel site condition.

This case study demonstrates once again the importance of early detection or prediction of potentially problematic zones (via probe drilling and monitoring) in tunnelling, especially through mixed or difficult ground conditions characterized by alternating layers, faulting and localized zones of high water pressure. Because mechanical detection methods cannot be fully relied upon, availability of experienced personnel to predict and deal with such instability problems effectively and promptly is the best insurance for successful completion of tunnelling contracts.

References

American Society of Civil Engineering (1984) Guidelines for tunnel lining design. In: O'Rourke TD (ed) ASCE Technical Council on Research. Technical Committee on Tunnel Lining Design

Anagnostou G, Kovari K (1992) Ein beitrag zur static der ortsbrust beim hydroschidvortrieb.-in: Probleme bei maschinellen tunnivortrieben? Geratehersteller und anwender berichten. Beitrage zum symposium vom 22./23. Oktober 1992, TU Munchen

Aydin A, Ozbek A, Cobanoglu I (2004) Tunnelling in difficult ground: a case study from Dranaz tunnel, Sinop, Turkey. Eng Geol 74:293–301

Brinkgreve RBJ, Vermeer PA (2001) Manual of Plaxis 3D tunnel. A.A. Balkema, Rotterdam

Burland JB, Standing JR, Jardine FM (2001) " Building response to tunneling" case studies from construction of the Jubilee Line Extension. Thomas Telford Publishers, London

Carranza-Torres C, Diederichs M (2000) Mechanical analysis of circular liners with particular reference to composite supports. For example, liners consisting of shotcrete and steel sets. Tunn Undergr Space Technol 24(2009):506–532

Chern JC, Yu CW, Shiao FY (1998) Tunnelling in squeezing ground and support estimation. In: Proceedings of regional symposium on sedimentary rock engineering, Taipei, pp 192–220

Eftekhari A, Taromi M, Saeidi M (2013) Complexity of the ground conditions and non compliance with basic assumptions in the trench stability analysis: a Case Study in Iran. In: 7th SASTech 2013, Iran, Bandar-Abbas, 14–15 Mar 2013

Eftekhari A, Taromi M, Saeidi M (2013) Collapse zone passing through with IPE arc support technique (IAST): (a case study in Iran), 10th Iranian tunneling conference, "Underground space and the 3rd millennium development goals" Iran, Tehran

Eisenstein Z, Kuwajima FM, Heinz HK (1991) Behaviour of shotcrete tunnel linings. In: Proceedings of rapid excavation and tunnelling conference, Seattle, pp 47–57

Fakhimi A, Salehi D, Mojtabai N (2012) Numerical back analysis for estimation of soil parameters in the Resalat tunnel project. Tunn Undergr Space Technol 19:57–67

Franzen T (1992) Shotcrete for underground support: a state-of-the-art report with focus on steel-fibre reinforcement. Tunn Undergr Space Technol 7(4):383–391

Ghorbani M, Sharifzadeh M, Yasrobi S, Daiyan M (2012) Geotechnical, structural and geodetic measurements for conventional tunnelling hazards in urban areas—The case of Niayesh road tunnel project. Tunn Undergr Space Technol 31:1–8

Heuer RE (1974) Important ground parameters in soft ground tunneling. In: Proceeding of specialty conference on subsurface exploration for underground excavation and heavy construction, ASCE, New York

Hoek E, Brown ET (1980) Underground excavations in rock. The Institute of Mining and Metallurgy, London

Hoek E (1999) Putting numbers to geology—an engineer's viewpoint. Q J Eng Geol 32:1–19

Hoek E (2001) Big tunnels in bad rock. J Geotech Geoenviron Eng 127 (9):726–740

Itasca Consulting Group (1997) FLAC3D, fast Lagrangian analysis of Continua in 3 Dimensions. Version 2.1. Minneapolis

Kavvadas M (1997) Analysis and performance of the NATM excavation of an underground station for the Athens Metro. In: Proceedings of 4th international conference on case histories in geotechnical engineering, St. Louis, Missouri USA, March 1998 (paper No 6.11)

Kavvadas M (1999) Experiences from the construction of the Athens Metro project. Proceedings of 12th European conference of soil mechanics and geotechnical engineering, Amsterdam, June 1999. Invited Lect 3:1665–1676

Kavvadas M (2005) Monitoring ground deformation in tunnelling: current practice in transportation tunnels. Eng Geol 79(2005):93–113

Kontogianni V, Stiros S (2002) Shallow tunnel convergence: predictions and observations. Eng Geol 63(304):333–345

Kontogianni V, Tzortzis A, Stiros S (2004) Deformation and failure of the Tymfristos tunnel, Greece. J Geotechn Geoenviron Eng, ASCE 130(10):1004–1013

Kolymbas D (2005) Tunnelling and tunnel mechanics, a rational approach to tunnelling. Springer, Berlin. ISBN-13 978-3-540-25196-5

Mair RJ (2001) Research on tunneling-induced ground movements and their effects on buildings—lessons from the Jubilee Line Extension. In: Proceedings of international conference on response of buildings to excavation-induced ground movements, Imperial College, London, 17–18 July, CIRIA Special Publication, vol 199. CIRIA Publications, London, UK, pp 3–26. http://www.ciria.org.uk/index.html

Powderham AJ (1994) An overview of the observational method: development in cut and cover and bored tunnelling projects. Geotechnique 44(4):619–636

Robinson RA, Kucker MA, Gildner JP (2001) Levels of geotechnical input for design—build contracts. In: Proceedings of rapid

excavation and tunnelling conference, Society for Mining, Metallurgy, and Exploration, Inc., Littleton, Colorado, pp 829–839

Saeidi M, Eftekhari A, Taromi M (2012) Evaluation of rock burst potential in Sabzkuh water conveyance tunnel, IRAN: a case study. In: 7th Asian rock mechanics symposium, ARMS 2012, Seoul, Korea, 15–19 Oct 2012

Taromi M, Eftekhari A, Saeidi M (2013) Adoption of an appropriate excavation method in construction process (case study: Sabzkuh

tunnel, Iran). In: International conference on civil engineering, architecture and urban sustainable development, Tabriz, Iran

Terzaghi K (1950) Geologic aspects of soft ground tunneling. Chapter 11 in applied sedimentation. In: Task R, Parker D (eds) Wiley, New York

Tsatsanifos CP, Mantziaras PM, Georgiou D (1999) Squeezing rock response to NATM tunnelling. A case study. In: Proceedings of the international symposium on geotechnical aspects of underground construction in soft rock, Tokyo, Japan, pp 167–172

Geological Design for Complex Geological-Structural Contest: The Example of SS 125 "Nuova Orientale Sarda"

108

Serena Scarano, Roberto Laureti and Stefano Serangeli

Abstract

The following work is an example of road design in geologically complex environments, which requires a particular accuracy in the definition of the Geological Reference Model. In the studied area the rock masses involved in the plan are strongly deformed by tectonic activity that occurred over time. For this reason, the analysis of geological formations has been addressed, above all, to the study of geomechanical features, such as strength resistance and elastic properties of the rock mass. The integrated analysis of the data coming from geo-structural and geomechanical surveys carried out on rocky outcrops in the area, and of the data obtained from site investigation and laboratory test on rock samples, has allowed to improve the characterization of rock masses and the definition of Rock Quality Indexes. The study provided the values of GSI for both formations, used to obtain the geotechnical parameters, adopted for the design of project interventions. The project included the study on the reuse of soil and rocks coming from the excavations, ahead of the ascertainment of their environmental characteristics by means of chemical analysis. Abnormalities in the chemistry of some samples are interpreted as due to the nature and evolution of the geological formations, and not to environmental pollution.

Keywords

Rock masses • Geological reference model • Geostructural relief • Reuse of soil • Chemical analysis

108.1 Introduction

A fundamental role in order to define the geotechnical characterization of soils and the geomechanical characterization of rock mass, is played by the identification of the geostructural and geomechanical features, and the Geological Reference Model, of the geological units outcropping in the area where the road plan is located. All this factors affects the resulting choice of design solutions.

An example is represented by the design of the new SS 125 "Nuova Orientale Sarda" Tronco Tertenia—San Priamo 1° Lotto—1° e 2° Stralcio.

The track of the whole parcel, developed in the south-east part of the island, 100 km far from Cagliari, along the Torrente Quirra Valley, is long more or less 13 km and is composed by 11 viaducts for a whole length of 750 m, and 3 tunnels (1 artificial and 2 natural).

108.2 Geological and Structural Framework

The road plan is located along the lower part of the right slope of the Rio Quirra Valley, in a complex geological contest, that outcrops along it. This valley follows the development of a transtensive tectonic element with regional importance, of which the path follows the development. The

S. Scarano (✉) · R. Laureti · S. Serangeli
Direzione Centrale Progettazione, Anas S.p.A, Rome, Italy
e-mail: se.scarano@stradeanas.it

Fig. 108.1 Schematic
geostructural diagram of the
Paleozoic basement in the south-
eastern Sardinia
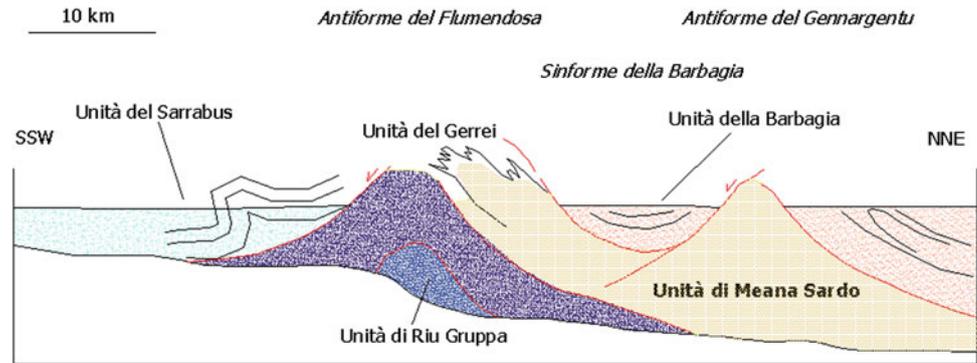
valley is bordered by mountains composed by the Paleozoic basement units, represented by an alternations of meta-sandstones, metapelites, metavulcanites, metaepiclastites, metaconglomerates and greenish-gray shales, affected by polyphasic deformation, schistosity and by a medium-low degree of metamorphism. The terrains interested by the construction of the road belong to the Meana Sardo tectonic Unit, overlapped on Gerrei Unit; the Meana Sardo Unit is overlapped by the Genn'Argiolas unit (Fig. 108.1) (Calvino F. 1959).

108.2.1 Local Stratigraphic Succession

The units, that are directly involved by the project, have been identified in the literature, in the formational strati-graphic nomenclature, with the terms of S. Vito Sandstones and Monte Santa Vittoria Formation.

108.2.1.1 S. Vito Sandstones

This formation is placed at the base of the Meana Sardo Unit and is composed by an association of metarenites and quartz-mica metapelites, with shiny appearance, and, rarely, by metasandstones and thin levels of gray and greenish-gray metaquarzoarenites, with intercalations of gray or black metapelites and metasiltstones. In the middle part of the formation there are often metaconglomerates with elements of metasiltstones and metasandstones. In the section covered by the plan of the new SS 125, the outcrop formation is affected by schistosity, levels and lists of quartz, reflecting phenomena of *boudinage* or elongation in the stresses direction.

The basis of this lithostratigraphic unit does not outcrop; it rests with tectonic contact on the Gerrei Unit and is cov-ered, in unconformity, by metaconglomerates of Muravera or, directly, from the Monte Santa Vittoria Formation.

The unit is referred to the Cambrian—middle/lower Ordovician (Calvino F. 1963, 1972).

108.2.1.2 Monte Santa Vittoria Formation

This formation is composed by two different lithofacies, represented by: metaepiclastites (cfr. Manixeddu and Monte Corte Cerbos Formations of Bosellini and Ogniben, 1968) to prevailing volcanic matrix, of various granulometry, with intercalations of metagraywackes, metasandstones and met-aconglomerates with quartz pebbles, identified with the acronym MSVa; metagraywakes and metandesites (cfr. Serra Tonnai Formation of Bosellini and Ogniben, 1968), known as MSVb and represented by volcanic greenish metagraywakes, with intercalation of greenish-gray meta-vulcanites with composition from basaltic to andesitic. The formation is related to an effusive activity from intermediate to basic composition and deposition of graywakes resulting from the rearrangement of the volcanic deposits. The unit is referred to the Middle Ordovician (Pertusati et al. 2001a, 2001b).

These two formations have been involved in a series of plicative structures, which lead the San Vito sandstones to

Fig. 108.2 S. Vito sandstones. Small fold deformations in the micaceous metapelites

Fig. 108.3 Monte Santa Vittoria formation. Metagraywakes and compact metandesites

outcrop into the antiform cores, and the Monte Santa Vittoria Formation in the sinform cores.

In addition to these two formations, the tectonic unit includes the Muravera Metaconglomerates Formation, made up polygenic, heterometric, often coarse metaconglomerates, in quarzoarenitics matrix, not outcropping in the study area.

The bedrock just described is, at times, covered by ancient conoid deposits, including blocks and heterometric pebbles of metamorphic substrate, mixed with sandy-silty matrix reddened and well thickened; eluvio-colluvial blankets, consisting of angular blocks in silty matrix, without sorting; recent alluvional deposits, stabilized and thickened, and current alluvional deposits, formed by blocks and

pebbles with poor matrix (Figs. 108.2 and 108.3) Carmignani et al. (2001a, 2001b).

108.3   Geostructural and Geomechanical Characterization

The road design in such rock masses has required a study of the geomechanic quality features Bieniawski (1974, 1976), that lead to the definition of their strength and of the elastic parameters of the rock masses (Clerici et al. 1986).

The site investigation data come from different campaigns, subsequently held in trust by ANAS, and include 71 boreholes, 10 geomechanical survey points, 38 geognostic trenches and 11 refraction seismic bases.

Therefore, the classification of rock masses has been made starting by data obtained during the geostructural and geomechanical survey of the rock outcrops (ISRM 1974, 1978, 1981), obtaining the GSI index (Hoek and Brown, 1997). Then a comparison between the results coming from survey and those obtained from site-investigation and laboratory tests (RQD, Point Load Test, uniaxial compression of rock samples) was made (Fig. 108.4).

This comparison led to the attribution of geotechnical parameters on the basis of which the project interventions have been designed.

Based on the obtained values of the index GSI, the two studied formations have been included in the "Geological Strength Index for Jointed Rocks" (Marinos and Hoek 2000) (Fig. 108.5) diagram. In this diagram the GSI values, obtained from survey data (oval empty areas) are drawn

Fig. 108.4 Example of schmidt diagram

GEOLOGICAL STRENGTH INDEX FOR JOINTED ROCKS (Hoek and Marinos, 2000)

From the lithology, structure and surface conditions of the discontinuities, estimate the average value of GSI. Do not try to be too precise. QUoting a range from 33 to 37 is more realistic than stating that GSI = 35. Note that the table does not apply to structurally controlled failures. Where weak planar structural planes are present in an unfavourable orientation with respect to the excavation face, these will dominate the rock mass behaviour. The shear strength of surfaces in rocks that are prone to deterioration as a result of changes in moisture content will be reduced is water is present. When working with rocks in the fair to very poor categories, a shift to the right may be made for wet conditions. Water pressure is dealt with by effective stress analysis.

SURFACE CONDITIONS

VERY GOOD - Very rough, fresh unweathered surfaces
GOOD - Rough, slightly weathered, iron stained surfaces
FAIR - Smooth, moderately weathered and altered surfaces
POOR - Slickensided, highly weathered surfaces with compact coatings or fillings or angular fragments
VERY POOR - Slickensided, highly weathered surfaces with soft clay coatings or fillings

STRUCTURE — DECREASING SURFACE QUALITY ⟹

DECREASING INTERLOCKING OF ROCK PIECES

INTACT OR MASSIVE - intact rock specimens or massive in situ rock with few widely spaced discontinuities — 90, 80, N/A, N/A

BLOCKY - well interlocked undisturbed rock mass consisting of cubical blocks formed by three intersecting discontinuity sets — 70, 60

MSV

VERY BLOCKY - interlocked, partially disturbed mass with multi-faceted angular blocks formed by 4 or more joint sets — 50, 40

SVI

BLOCKY/DISTURBED/SEAMY - folded with angular blocks formed by many intersecting discontinuity sets. Persistence of bedding planes or schistosity — 30

DISINTEGRATED - poorly interlocked, heavily broken rock mass with mixture of angular and rounded rock pieces — 20

LAMINATED/SHEARED - Lack of blockiness due to close spacing of weak schistosity or shear planes — N/A, N/A, 10

LEGENDA

— Valori GSI per MSV da rilievi geostrutturali
— Valori GSI per SVI da rilievi geostrutturali

▨ Valori GSI per MSV ricavati da dati di sondaggio e di laboratorio
▨ Valori GSI per SVI ricavati da dati di sondaggio e di laboratorio

together with the ones obtained from site investigation and laboratory tests (oval hatched areas).

In general, it shows a good correspondence between the two sets of data, with an appreciable overlap between the areolas, which represents the index variability fields for the two units.

108.4   Environmental Study

The project, in addition to the precise definition of MGR, with a high degree of reliability, includes the study on the reuse of soil and rocks coming from the excavation, preceded by their environmental characterization works.

Through chemical analysis of environmental characters, in fact, anomalies in the soil samples chemical parameters coming from the layers of surface alteration of the substrate, and from alluvial deposits, found along the path, have been found.

In some samples, the values of arsenic, zinc, mercury and cobalt are higher than Contamination Threshold Concentration. This situation, in an area characterized by the presence of a mining site (Baccu Locci), at the foot of Mount Cardiga, can be refers, however, to the so-called "natural background". In fact, during the mining activity, metal sulfides (zinc and lead overall) and arsenopyrite were extracted, so it confirms the presence of those chemical elements inside the minerals founded into the rock mass.

The lithologies forming the bedrock, by which dismantling/alteration alluvial deposits and eluvio-colluvial accumulations originated, contain mineralization. Thus, there is a correlation between the mineralogical and petrographic composition of the sediments accumulated and the nature of the geological formations outcropping in the area of immediate concern, in which widespread circulation of hydrothermal fluids led, locally, to the formation of appreciable concentrations of metal-bearing metal sulphides.

108.5   Conclusions

The road design, especially in presence of infrastructure of considerable extent, presupposes a thorough knowledge of the geological and geotechnical characteristics of the soils outcropping in the area of roadway location and interacting with the planning civil works.

This is possible to obtain through direct studies of the area, through surface surveys, integrated with the data coming from geological site investigations planned on the basis of the design elements.

In the present case, in particular, the geological units belong to the ancient metamorphic substrate, whose behavior is difficult to achieve only following the laboratory

characterization. Therefore we proceeded through the geo-structural and geomechanical characterization of rock masses, by which we have obtained the geotechnical design parameters. In particular, the work involved the evaluation of geomechanical characters from both the examination of the direct geological analysis of the outcrops present, and the systematic analysis of data obtained by site investigations (boreholes), integrated with laboratory testing on rocks. The results, obtained through two different ways, indicate a significant convergence.

Another aspect that is often necessary to consider, is the environmental one, mainly if the design choices allow the recycling of materials resulting from excavations. The environmental characteristics of these soils are determined by chemical analysis regulated by national legislation.

References

Bieniawski ZT (1974) Estimating the strength of rock materials. J S Afr Inst Min Metall 74:312–320

Bieniaswski ZT (1976) The geomechanics classification in rock engineering applications. In: Proceedings of 4th international congress on rock mechanics, vol 2, pp 51–58

Calvino F (1959) Lineamenti strutturali del Sarrabus-Gerrei (Sardegna sud-orientale). Boll. Servizio Geologico d'Italia, Roma 81:489–556

Calvino F (1963) Carta Geologica d'Italia alla scala 1:100.000, "Foglio 227 Muravera". Servizio Geologico d'Italia, Roma

Calvino F (1972) Note illustrative della Carta Geologica d'Italia, "Foglio 227 Muravera", 1–58

Carmignani L, Conti P, Pertusati PC, Barca S, Cerbai N, Eltrudis A, Funedda A, Oggiano G, Patta ED (2001) Carta Geologica d'Italia alla scala 1:50.000, "Foglio 549 Muravera". Servizio Geologico d'Italia, Roma

Carmignani L, Conti P, Pertusati PC, Barca S, Cerbai N, Eltrudis A, Funedda A, Oggiano G, Patta ED, Ulzega A, Orrù P (2001) Note illustrative della Carta Geologica d'Italia alla scala 1:50.000, "Foglio 549 Muravera". Servizio Geologico d'Italia, Roma, 140 pp

Clerici A, Griffini L, Pozzi R (1986) Procedura per l'esecuzione di rilievi strutturali geomeccanici di dettaglio su ammassi rocciosi a comportamento rigido. Geologia Tecnica 3(88):21–31

Hoek E, Brown ET (1997) Practical estimates of rock mass strength. Int J Rock Mech Mining Sci Geomech Abstr 34:1165–1186

ISRM—International Society of Rock Mechanics—Commission on Standardization of Laboratory and Field Tests (1974) Suggested methods for determining shear strength. Committee on field tests, Doc. n.1

ISRM—International Society of Rock Mechanics—Commission on Standardization of Laboratory and Field Tests (1978) Suggested methods for the quantitative description of discontinuities.in rock masses. Inte J Rock Mech Mining Sci Geomech Abstr 15 (6):319–368

ISRM—International Society of Rock Mechanics—Commission on Standardization of Laboratory and Field Tests (1981) Rock characterization testing and monitoring. Suggested methods. In: Brown ET (ed). Pergamon Press, Oxford

Marinos P, Hoek E (2000) GSI: a geologically friendly tool for rock mass strength estimation. In: Proceedings of the GeoEng2000 at the international conference on geotechnical and geological engineering, Melbourne, Technomic publishers, Lancaster, pp 1422–1446

Marinos P, Hoek E (2001) Estimating the geotechnical properties of heterogeneous rock masses such as flysch. Bull Eng Geol Environ 60:82–92

Pertusati PC, Sarria E, Cherchi GP, Carmignani L, Barca S, Benedetti M, Chighine G, Cincotti F, Oggiano G, Ulzega A, Orrù P, Pintus C (2001)a Carta Geologica d'Italia alla scala 1:50.000, "Foglio 5419 Jerzu". Servizio Geologico d'Italia, Roma

Pertusati PC, Sarria E, Cherchi GP, Carmignani L, Barca S, Benedetti M, Chighine G, Cincotti F, Oggiano G, Ulzega A, Orrù P, Pintus C (2001)b Note illustrative della Carta Geologica d'Italia alla scala 1:50.000, "Foglio 5419 Jerzu". Servizio Geologico d'Italia, Roma, 168 pp

The "A12—Tor dè Cenci" Motorway: Geological Reference Model and Design Solutions in Presence of Soft Soils

109

Stefano Serangeli, Roberto Laureti, and Serena Scarano

Abstract

The link that connects the A12 "Roma-Civitavecchia" with the "Roma (Tor de 'Cenci)—Latina" motorway (today designed but not built) is a road infrastructure of considerable size and importance. It needs a very detailed Geological Reference Model, defined in each design phase through the analysis of numerous geological surveys and site investigation data. In the preliminary phase of the plan we found very useful to keep account of the considerable amount of data concerning the area surrounding the designed motorway. At a later stage we realized a very detailed geological survey and site investigation activity, especially referred to the scale of the main viaducts. This study has allowed us to define the sequence of the different lithofacies and their geometric relationships. The presence, in the subsoil, of highly deformable organic soils, with peat layers, characterized also by a low shear strength, has influenced the design solutions. In fact, throughout the development of the road axis, different interventions were used with the aim to reduce the settlements of the road body. So, the study of the plan was marked by the reduction of the applied load, keeping as low as possible the project level and the height of the embankments. At the same time it was necessary to design some embankments providing the use of very light materials (expanded clay, Polystyrene) and particular solutions for the foundations design of the main bridges and viaducts.

109.1 Introduction

The design of the new connection between the A12 "Roma-Civitavecchia" and the "Roma (Tor de 'Cenci)—Latina" motorways (the last one still in project) was developed, on behalf of "ADL—Autostrade del Lazio SpA", by "Direzione Centrale Progettazione" of ANAS SpA (National Public Roads Company). It represents an example of a particularly detailed definition of the Geological Reference Model, as a prerequisite to the accomplished identification of geological problems and, finally, of consequent adoption of appropriate design measures.

This aspect is fundamental in order to build this kind of infrastructure, characterized by very important civil works (especially bridges and viaducts). The deepening of the MGR, achieved through the different stages of the project, has allowed us to define the sequence of the different lithofacies and their evolution, and their geometrical relationships. Starting from this modeling, the Geotechnical Reference Model, necessary for a correct evaluation of related design issue, was completely defined.

The road project extends for about 16 km, through the Roman countryside (Fiumicino Plain) and the hinterland. It is composed by 4 viaducts with considerable development, of which the longest exceeds 2.7 km and another one crosses the Tevere River, and one artificial tunnel.

S. Serangeli (✉) · R. Laureti · S. Scarano
Direzione Centrale Progettazione, Anas S.p.A., Rome, Italy
e-mail: s.serangeli@stradeanas.it

109.2 Studies and Geological Surveys

The project corridor and the surrounding areas were already covered by existing infrastructure (Fiumicino Airport and Motorway, "Rome Trade Fair District", Roma-Pisa Railway). For this reason, it was interested by several site-investigation activities; so that its subsoil appears, therefore, well-known from the geological and geotechnical point of view. Particularly, the bad features of the recent organic soils are just well-known.

During the preliminary design, the geological reference model was, therefore, essentially defined by using a massive amount of available data (65 boreholes; 27 static penetration tests (CPT and CPTU); 2 trenches and other 31 boreholes coming from preexisting investigations).

During the later stage of the design, it was realized a very detailed geological survey, together with a specific site-investigation campaign, especially referred to the scale of the main viaducts and bridges, in order to improve both the geological and geotechnical models.

This site investigation, carried out in 2012, consists of:

- 12 boreholes, including undisturbed sampling for laboratory testing;
- 11 static penetration tests with piezocone for interstitial pressure measurements (CPTU);
- 5 geophysical tests (Down Hole).

During the execution of borehole, a total of 75 dynamic penetration tests SPT and 38 undisturbed samples were carried out.

109.3 Local Stratigraphic Succession

The studies described above, together with bibliographic data, ISPRA EX APAT gave the opportunity to focus on the geological context of the project, in which various depositional and erosional stages in different genetic environments overlap each other, so that the sedimentary prevulcanic substrate consists first of marine units, then transitional ones and, finally, continental formations.(Faccenna et al. 1995; Ventriglia U 1971, 1990, 2002)

The oldest geological formation, as identified in the studied region, is represented by "*Monte delle Piche Formation*" (*MDP*), a marine-clayey deposit over which recent pyroclastic and alluvial sediments have been settled. These units are represented by "*Ponte Galeria Formation*": in particular, in the area, there are the "*Membro della Pisana*", characterized by three lithofacies (1. conglomeratic-sandy lithofacies, PGL3a; 2. clayey-sandy lithofacies, PGL3b; 3. sandy lithofacies, PGL3c). These elder units have been splitted by a system of small faults with Apenninic directions, which have lowered the substrate according to a system of steps, with other antiapenninic system and north-south direction (Funiciello R and Parotto 1978).

Along Tiber'plan, with an unconformity, there are more recent soils of alluvial and marsh and lacustrine environment ("*Sintema del fiume Tevere*"), with high organic content, divided into different lithofacies: SFTa, sandy gravel and gravelly coarse sand; SFTb, sands, silty sands and sandy silts; SFTc, organic cohesive deposits and peats (Conato 1980).

In correspondence of the hills, other unconformities separate the succession MDP/PGL from subsequent pyroclastic soils, of the Colli Albani volcanic apparatus ("*Tor dè Cenci Unit*", *TDC*, "*Pozzolane Rosse*", *RED*, "*Villa Senni Formation/Pozzolanelle*", VSN_2). Alternating with these terms there are continental and fluvial soils, called: "*Valle Giulia Formation*" (*VGU*), "*Fosso del Torrino Formation*" (*FTR*), "*Castelporziano Unit*" (*CLZ*) (De Rita D et al. 1988, 1989, 1995).

The upper fluvial-lacustrine deposits, with an high content of organic matter, have features of high deformability and low resistance (Molin et al. 1995; Servizio Geologico d'Italia 1967; Società Geologica Italiana 1990).

109.4 The Major Viaducts ("Tevere Viaduct" and "Interconnessione Viaduct")

The "Tevere Viaduct" is 1,424.86 m long; it is placed above the alluvial deposits belonging to Tiber River System, covered by recent alluvial soils. Here the substrate is characterized by a "steps" conformation, due to the presence of a series of faults, aligned NNE-SSW, that have displaced it, causing its deepening from a depth of about 25–30 m ad the edge of the main valley, near to the confluence of Fosso del Torrino, towards west, where it lies regularly at more than 65–70 m.

The viaduct is divided into two parts, a first composed by 13 spans variable from 30 to 150 m, while the second one is composed by 11 spans from 30 m (for the spans of the shore) to 40 m (for intermediate spans).

For the first part of the bridge, the foundations are direct compensated or indirect with driven piles, outside the embankment of the river; they are indirect, with diaphragms, inside the levees.

For the last part all foundations are indirect with large diameter bored piles (D = 1,500 mm); piles are circular for hydrodynamic problems, related to the presence of a River Tiber tributary (Fig. 109.1) (Calu).

The "Interconnessione Viaduct" stretches for about 2,250 m. The geological units under the viaduct are almost entirely represented by the alluvial deposits that extend in a uniform manner, for the whole extension of the viaduct. Here the substrate is regular and it's located below, at depths greater than 70 m.

This viaduct is composed by 62 spans on the northbound carriageway and 65 spans on the southbound carriageway, with variable ports from 26 to 126 m.
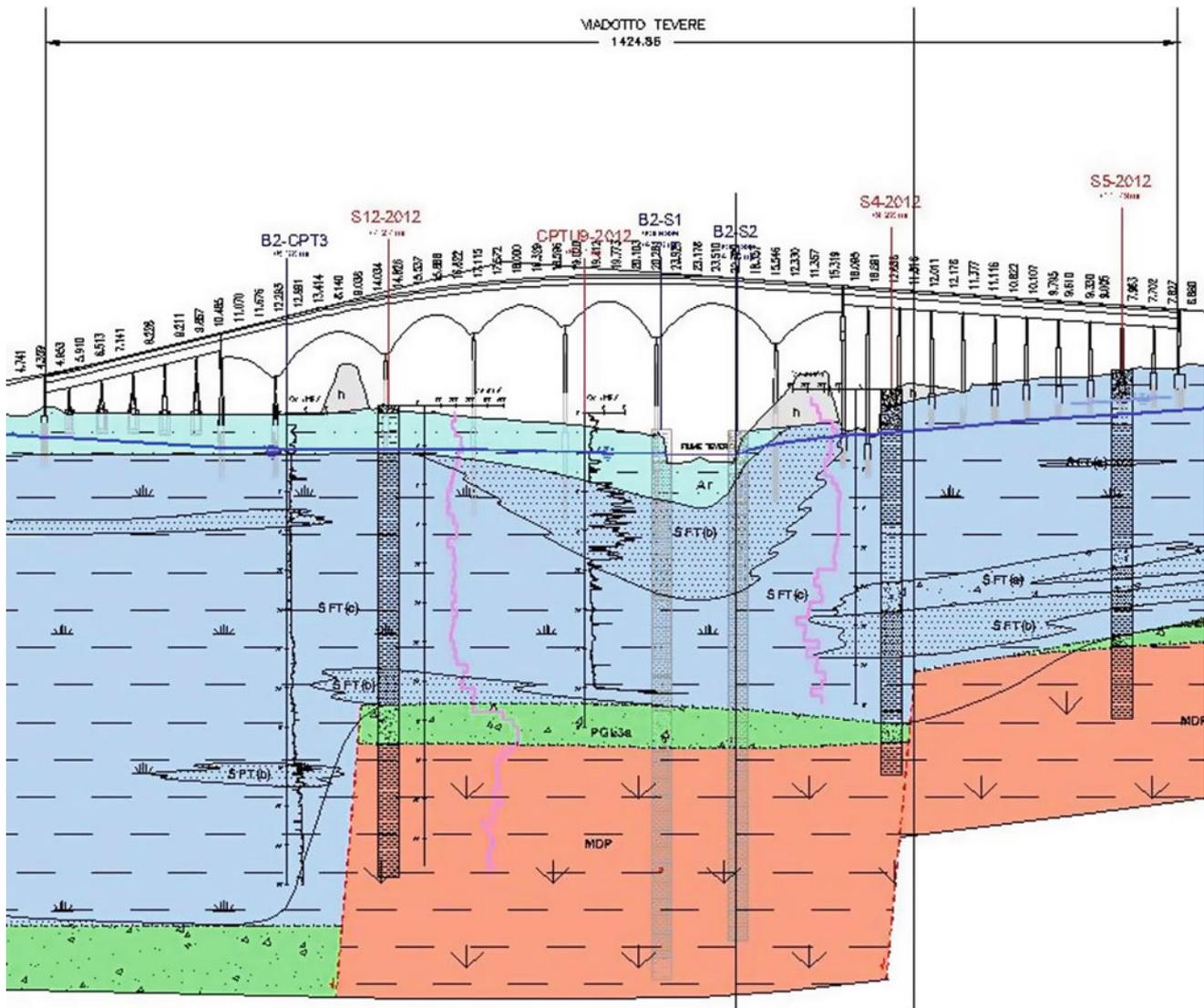
Fig. 109.1 Tevere Viaduct

In general, the foundations are direct, compensated, with protruding plinth on the terrain surface; in correspondence of spans more than 40/45 m wide, the foundations are not compensated, but deep, with piles of 70 m, for obvious load problems (Fig. 109.2).

109.5   Design Solutions

The high deformability and low resistance features of the upper deposits have influenced the design solutions developed along the axis road.

Therefore, different types of intervention, aimed at reducing the probable subsidence of the road body, also delayed in time, have been used. So, the study of geometry road body was marked by the reduction of overload transmitted, lowering the project level and the height of the embankments. At the same time some of the hightest embankment have been made of lightened material, in different ways for different traits: (1) insertion of metal pipes ARMCO type; (2) adoption of sintered expanded polystyrene (EPS) in preformed blocks; (3) use of expanded clay for the construction of the embankment. The application of a geogrid reinforcement has been envisaged to improve the resistance of the laying surface, below the remediation layer.

The foundational solutions, adopted for the principal viaducts, are also differentiated, related to the local context: compensated direct foundations, deep foundations of diaphragms, deep foundations of large diameter piles, deep foundations on beaten precast piles (Fig. 109.3).
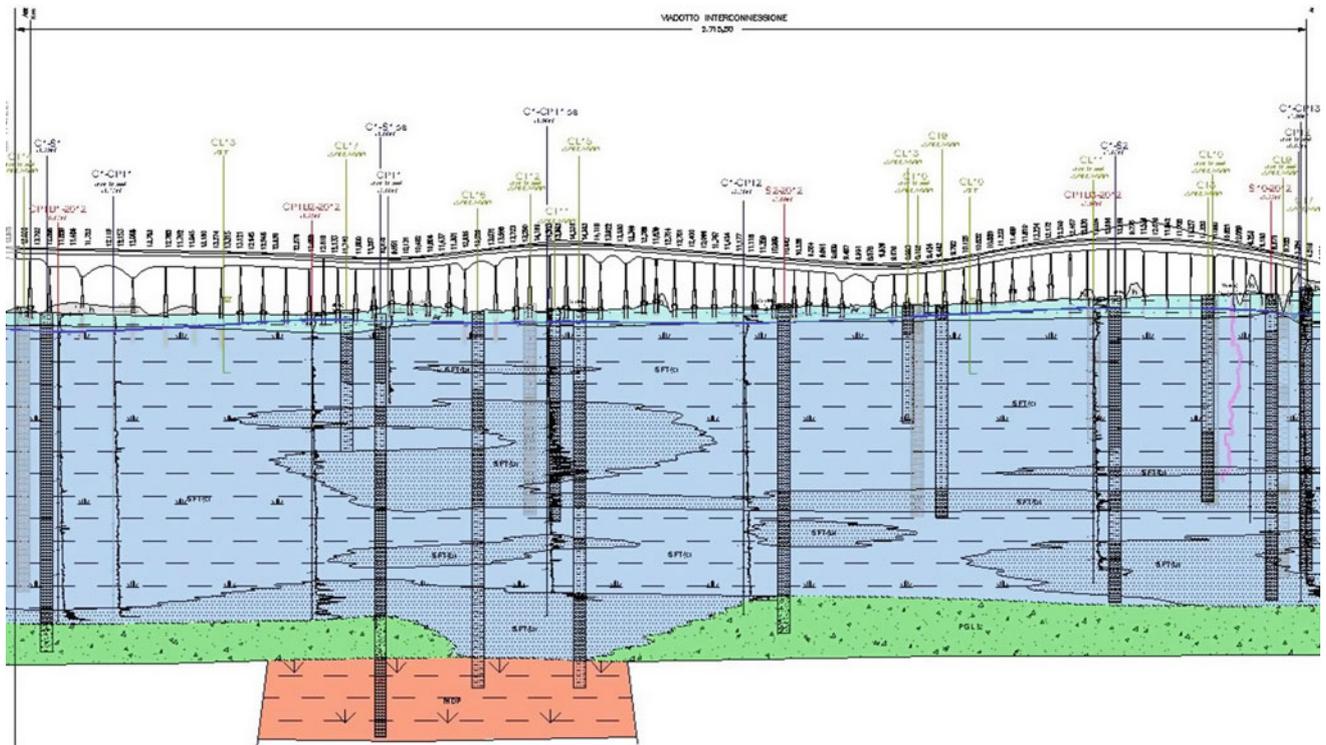
Fig. 109.2 Interconnessione Viaduct

Fig. 109.3 Example of section used
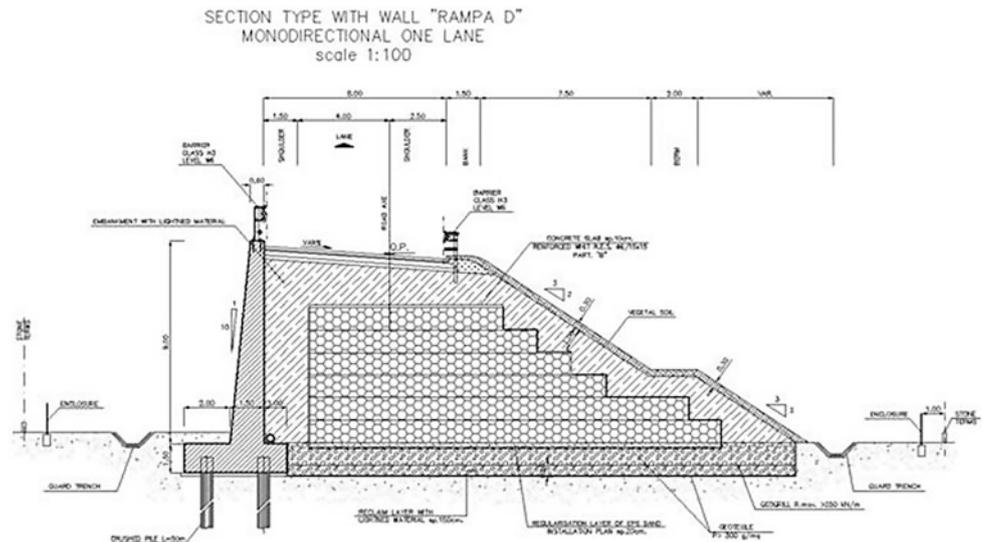
109.6 Conclusions

As is known, the evaluation of the characteristics of the soils on which a road infrastructure will be located has a fundamental importance. This is because, very often, there are geological complex situations and geotechnical soils with specific responses to stress.

The characterization of these soils derived from progressive cognitive insights and careful site investigation and testing on site and on laboratory on samples taken during the execution of different boreholes.

The study shows that, in the development of the various phases of the project, we have reached to a progressive deepening of the Reference Geological Model, based on the implementation of the knowledge framework. The modeling

thus defined, according to the evolutionary context in terms of the gestructural and stratigraphic structure, has allowed to define in detail the particular aspects of the subsoil involved by the road project and its relationship with the marine units of the substrate. The subsoil, in fact, is characterized, mainly, by significant thicknesses of recent soils with poor geotechnical characteristics (low strength and high deformability). It has finally allowed to transfer to the geotechnical design all the necessary elements for the proper engineering design of interventions.

References

Conato V, Esu D, Malatesta A, Zarlenga F (1980) New data on the Pleistocene of Rome. Quaternaria 22:131–176

De Rita D, Faccenna C, Funiciello R, Rosa C (1995) The volcano of the Alban hills: stratigraphy and volcano-tectonics. In: Trigila R (ed) The volcano of the Alban hills

De Rita D, Funiciello R, Parotto M (1989) Carta geologica del complesso vulcanico dei Colli Albani ("Vulcano Laziale"). Progetto Finalizzato "Geodimamica"—Gruppo Naz. Vulcanologia, SELCA, Firenze, CNR Roma

De Rita D, Funiciello R, Rosa C (1988) Caratteristiche deposizionali della II colata piroclastica del Tuscolano-Artemisio (Complesso vulcanico dei Colli Albani, Roma), Bollettino GNV, IV, 278–297

Faccenna C, Funiciello R, Marra F (1995) Inquadramento geologico strutturale dell'area romana. Mem. Descr. Carta Geol. d'It., vol 50, La Geologia di Roma—Il centro storico, a cura di R. Funiciello

Funiciello R, Parotto M (1978) Il substrato sedimentario nell'area dei Colli Albani: considerazioni geodinamiche e paleogeografiche sul margine tirrenico dell'Appennino centrale. Geologica Romana, vol 17, pp. 233–287

ISPRA ex APAT—Università Roma Tre. Servizio Geologico d'Italia. Carta Geologica d'Italia in scala 1:50.000. Foglio 374 Roma

ISPRA ex APAT—Università Roma Tre. Servizio Geologico d'Italia. Carta Geologica d'Italia in scala 1:50.000. Foglio 387 Albano Laziale

Molin D, Castenetto S, Di Loreto E, Guidoboni E, Liberi L, Narcisi B, Paciello A, Riguzzi E, Rossi A, Tertulliani A, Traina G (1995) Sismicità di Roma. Mem. Descr. Carta Geol. d'It., vol 50, La Geologia di Roma—Il centro storico, a cura di R. Funiciello

Servizio Geologico d'Italia (1967) Carta Geologica d'Italia 1:100.000. Foglio 150—Roma

Società Geologica Italiana (1990) Guide Geologiche regionali, Volume V, Lazio. BE—MA Editrice

Ventriglia U (1971) La Geologia della città di Roma. Amministrazione Provinciale di Roma

Ventriglia U (1990) Idrogeologia della Provincia di Roma, Volume IV, Regione orientale. Amministrazione Provinciale di Roma

Ventriglia U (2002) Geologia del territorio del comune di Roma. Amministrazione Provinciale di Roma

The Geological Reference Model for the Feasibility Study of the Corredor Bioceanico Aconcagua Base Tunnel (Argentina-Chile Trans-Andean Railway)

Mattia Marini, Giuseppe Mancari, Antonio Damiano, Marta Alzate, and Michel Stra

Abstract

The Corredor Bioceanico Aconcagua base tunnel (CBA-BT) is a planned 53 km-long double pipe railway tunnel which will cross the Principal Cordillera of the Andean Thrust System under a maximum topographic cover of 2,000 m. The structural framework of the tunnel corridor is represented by a domino-style array of thrusts with ramp-flat geometry which detach along weak gypsum levels and stack diverse volcano-sedimentary terranes tectonically. As part of the CBA-BT feasibility study, the terranes crossed by the tunnel were mapped in detail and their component units were framed in a stratigraphic and palaeogeographic perspective overlooked by the earlier Geological Reference Model (GRM). Main results are: (i) the recognition of three different stratigraphic successions originally deposited in contiguous palaeo-domains of the Mesozoic Aconcagua Basin and (ii) the understanding of their mutual relationships; (iii) the description of thickness and lithofacies changes of the alluvial deposits of the Tordillo Formation; (iv) the re-interpretation of some gypsum levels, formerly referred to the Auquilco Formation, as part of the Mulichinco Formation (Mendoza Group). The implications of such advances on the GRM for a deep underground infrastructure are vast as they can help improve prediction of geological, structural and geomechanical data to excavation level, thereby contributing to implementation of future subsoil investigation, economic risk assessment and design optimization.

Keywords

Corredor Bioceanico Aconcagua • Base tunnel • Geological reference model • Andean Principal Cordillera • Volcano-sedimentary succession

110.1   Introduction

In feasibility-preliminary design of deep underground infrastructure the Geological Reference Model (GRM) is mostly intended to: (i) give a comprehensive picture of the infrastructure geology; (ii) share geological uncertainties with other professionals of the design team; (iii) contribute to decision making upon nature and location of integrative geognostic investigation aimed at tackling uncertainties. Although the reliability of the GRM of this early planning phases is generally low due to scarcity of direct geognostic investigations, the model consistency mainly resides in good understanding of surface geology and its successful extrapolation to excavation level.

Especially in sedimentary terranes with brittle tectonics, the unravelling of subsoil geology greatly benefit from detailed field mapping and correlation of terranes across thrusts with significant shortening. This is mainly because correlating consists in crudely restoring original spatial-temporal relationships between type-successions, thereby providing useful constraints for structural geology reconstructions and prediction of spatial heterogeneities in rock masses to be excavated.

M. Marini (✉) · G. Mancari · A. Damiano · M. Alzate · M. Stra
SEA Consulting s.r.l., Corso Bolzano, 14, 10121, Turin, Italy
e-mail: mattia.marini@uniroma1.it

The case study of the Corredor Bioceanico Aconcagua base tunnel (CBA-BT hereafter; Argentina-Chile Trans-Andean railway) is an example of a deep-underground infrastructure crossing a thrust-belt which involves a complex and understudied volcano-sedimentary succession. This paper presents the results of geological-structural surface mapping conducted in the frame of the feasibility study of the CBA-BT along with implications for project implementation.

110.1.1 Project Description and Framework Geology

The CBA-BT is a 53 km-long double-pipe tunnel (presently under feasibility study) which will cross the Andean Thrust System along a East-West transect between the Santiago del Chile and Mendoza districts (Fig. 110.1).

The structural framework of the CBA-BT is related to the Andean orogenesis which started during the early Cretaceous in response to subduction of the oceanic crust of the Nazca Plate (eastern Pacific Ocean) underneath the South American Plate. Convergence of these plates caused tectonic inversion of pre-existing extensional faults related to rifting of the proto-Atlantic ocean which during the Mesozoic delimited a number of sedimentary basins, among which the Aconcagua-Neuquen Basin (Vincente 2006).

The study corridor of the CBA-BT is located in the central segment of the Andean Thrust System which from west to east can be subdivided into three main sectors, the thin-skinned Aconcagua Belt of the Principal Cordillera and the thick-skinned Frontal Cordillera and Precordillera (Ramos et al. 2004). The CBA-BT remains entirely within the Aconcagua belt, which consists of a domino structure of thrusts with ramp-flat geometry detaching the Mesozoic succession from its basement along weak levels of gypsum.

110.1.2 Methods and Materials

A geological-structural field survey was carried out during Spring 2009–Summer 2010 over a 4 km-wide corridor straddling the tunnel axis and the Rio del Las Cuevas Valley (Fig. 110.1). All the field data were collated in a geographic information system repository which allowed spatial queries and accurate drawing of geo-structural maps and cross-sections.

The study corridor was first divided into four homogeneous geological-structural domains (Fig. 110.1) according to surface geology and then characterized acquiring a number of geomechanical stations, thereby providing a comprehensive picture of the full range of rock mass types at excavation level.

The GRM was then improved thanks to the 3D visualization of the project geology achieved building a fence-diagram (Fig. 110.2) from longitudinal and serial transverse cross-sections.
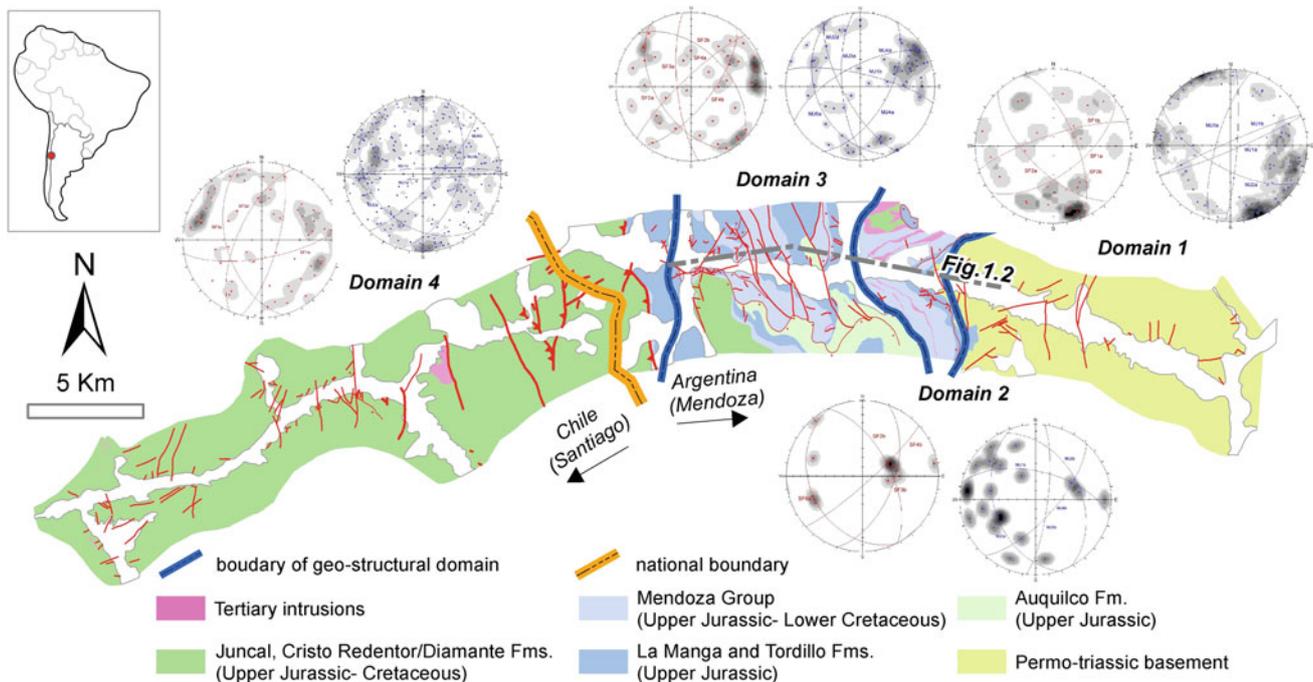
Fig. 110.1 Simplified geological map of the study area and stereographical projections of main faults (*left*) and master joints (*right*) for each geo-structural domain
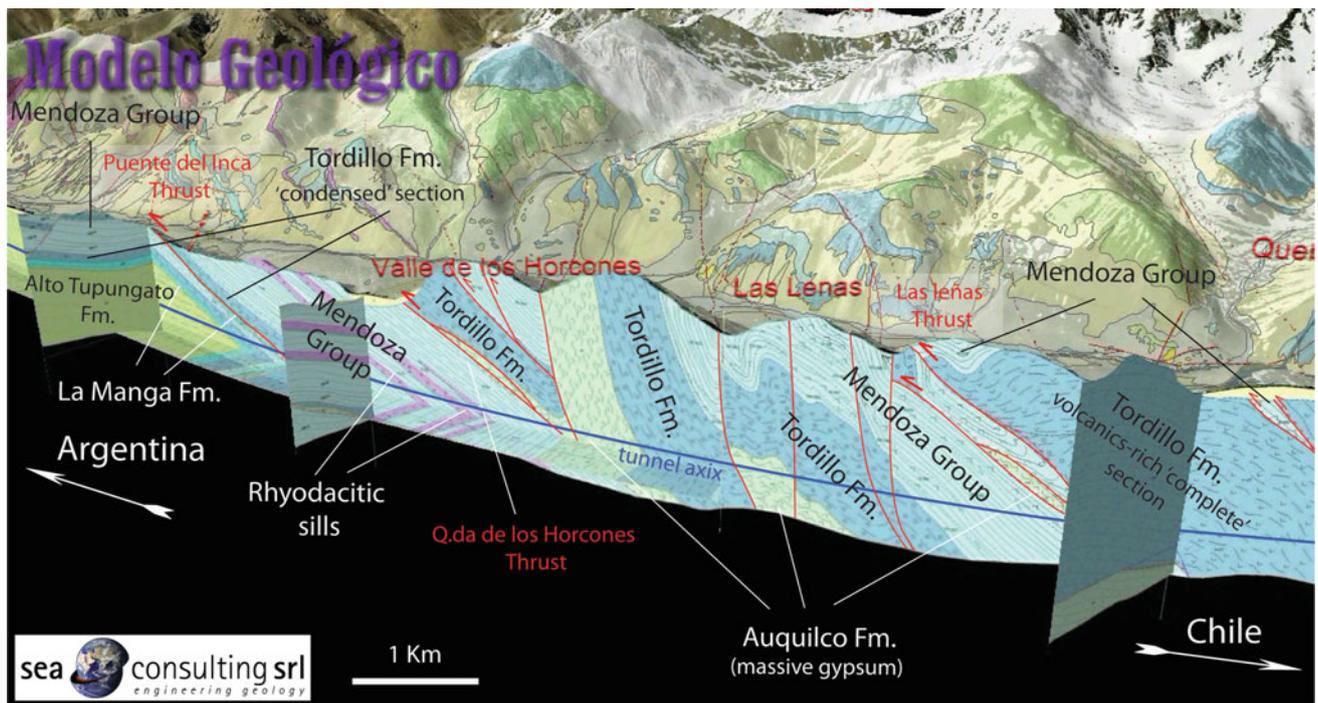
Fig. 110.2 Geo-structural fence diagram of the Argentinean stretch of CBA-BT. Note the thickness and lithofacies changes of the Tordillo Fm. across thrusts and the structural position of the Auquilco Fm

To assess the potential for water inflow in the tunnel, the geology was typified into hydrogeological complexes (i.e. fractured or porous media with homogeneous permeability characteristics) and elements (permeability fairways/boundaries, infiltration/recharge areas etc.) based on literature data from analogue scenarios (Dematteis et al. 2006; Perello et al. 2007). In addition, the reconstruction of deep flow paths was conditioned to the geochemistry of selected springs, including S_{34} and ^{18}O isotopic analysis on samples from the highly-mineralized waters of Puente del Inca and Agua Salada springs.

110.2 Results

Three different sedimentary successions deposited in as many palaeo-domains of the Aconcagua Basin were recognised in the study area making an advancement on the earlier GRM. These are, from east to west and from lower to upper in the thrust belt edifice: (i) a 'condensed', autochthonous succession (Puente del Inca Thrust sheet, domain 2 in Fig. 110.1) sitting on its Permo-Triassic basement (domain 2) and comprising, from bottom to top, marls and marly limestones (30 m; La Manga Fm., Oxfordian), alluvial conglomerates and sandstones (50–70 m; Tordillo Fm., Kimmeridgian) and a thick package (800 m; Mendoza Group, Tithonian-Neocomian) composed of shelfal

limestones (Quintuco Fm.) alluvial conglomerates and marginal-marine limestones (Mulichinco Fm.) and thin-bedded marls, silts and sandstones (Agrio Fm); (ii) an allocthonous succession (Quebrada des Horcones and Las Leñas Thrust sheets, domain 3 in Fig. 110.1) detached along the massive gypsum of the Auquilco Fm. (Kimmeridgian) and comprising a thicker, volcanic clasts-rich Tordillo Fm. (300–500 m), which passes upward to restricted-marine organic-rich marls and shales intercalated in their uppermost part by gypsum and andesitic lavas; (iii) a clastic-volcanic succession (Quebrada Navarro and Las Quevas Thrust sheets, domain 4 in Fig. 110.1) composed of alluvial to marginal marine sandstones and volcanic clast-rich conglomerates with frequent lava intercalations (Tordillo, Quintuco and Mulicinco Fms.), shelfal limestones (Agrio Fm.), andesitic volcanics (Juncal Fm. Upper Jurassic-Cretaceous) and continental clastics (Cristo Redentor/Diamante Fm., Upper Cretaceous). In the Chilean side of the study corridor the Mendoza Group is not present as it passes laterally to the Juncal Fm.

By a structural standing point, the lowermost thrust in the structural edifice is the Puente del Inca Thrust (left-hand side of Fig. 110.2) which doubles the La Manga Fm.-Tordillo Fm. section and shows no evidence of gypsum at surface. Moving upward in the edifice, evidences of the Auquilco Fm. gypsum as detachment level are found in the Quebrada des Horcones and Las Leñas Thrusts (central part of

Fig. 110.2). Between these two thrusts, the geological structure is further complicated by NW-SE sinistral transpressive faults. Further up in the edifice, the tectonic shortening due to the Quebrada Navarro Thrust and Las Cuevas Thrust is relatively small and encompasses for the tectonic thickening of the Tordillo Fm. and its overthrusting by the Juncal Fm., respectively (right-hand side of Fig. 110.2). In the Chilean side of the project, due to the rheology of the Juncal Fm. the total shortening is even smaller and mainly accommodated by conjugated systems of NE-SW and NW-SE transpressive faults. At surface, the rock mass around these faults generally show evidences of hydrothermal alteration, which suggests they may potentially have a major role in underground water circulation. Also, these faults are locally intruded by trachi-dacitic and tonalitic lavas of Miocene age. Intrusive bodies are present on the Argentinian side as well in form of a granitoid dome at Los Penitentes and gently discordant rhyodacitic sills crosscutting the Puente del Inca Thrust sheet.

Lastly, geochemistry of water samples from Puente del Inca and La Salada springs confirm the model of Ramos (1993) which entails circulation of meteoric waters along relatively deep flow paths within gypsum and anidrithe masses associated to thrusts and resurgence along faults.

110.3   Discussion and Conclusions

Mapping of the lithofacies and thickness changes within the Mesozoic sedimentary succession of the Aconcagua Basin was undertaken as part of a detailed geological-structural field survey of the CBA-BT project corridor. The results are consistent with stratigraphic and palaeogeographic data from previous literature. In particular, two different sections within the Tordillo Fm. were recognized along the tunnel trace consisting of: (i) a easterly, 'condensed' section dominated by reddish conglomerates and sandstones (Puente del Inca Thrust sheet) and (ii) a westerly 'complete' section, previously attributed to the Juncal Fm., which thickens and is enriched in volcanic clasts toward the west. Moreover, the uppermost conglomerates of the Puente del Inca Thrust sheet

were reinterpreted as part of the Mulichinco Fm. and correlated to the gypsum-bearing deposits of the Quebrada des Horcones Thrust sheet. These amendments to the earlier GRM allowed revaluating some tectonic features (e.g. inverse faults vs. thrusts) as well as the extrapolation of geology to excavation level (e.g. the occurrence of massive gypsum of the Auquilco Fm. and conglomeratic facies of the Tordillo Fm.) and deep flow paths.

The case study of the CBA-BT presented in this paper shows how a structural-geological survey can help improve prediction of the along-tunnel distribution of rock mass quality, deformation styles and water inflow. Geological-structural field studies can therefore provide a key contribution to the implementation of future subsoil investigation, economic risk assessment and design optimisation in deep underground infrastructure.

References

Aguirre-Urreta MB, Lo Forte GL (1996) Los depósitos tithoneocomianos. Geología de laregión del Aconcagua, provincias de San Juan y Mendoza, República Argentina. Dirección Nacional del Servicio Geológico, Anales 24:179–229, Buenos Aires

Dematteis A, Perello P, Torri R, Marini M, Venturini G (2006) Characterisation of permeability distribution for deep tunnel projects: examples from the Brenner and Lyon-Turin basis tunnels. In: Abstract volume, PANGEO AUSTRIA 2006, Innsbruck, Sept 2006

Perello P, Burger U, Torri R, Marini M (2007) Hydrogeological characterisation and water inflows forecasts for the Brenner Basistunnel. In: Abstract volume. Brenner Basistunnel und Zulaufstrecken, Innsbruck 1–2 Mar 2007

Ramos VA (1993) Geología y estructura de Puente del Inca y el control tectónico de sus aguas termales. Simposio sobre Puente del Inca. 12° Congreso Geológico Argentino and 2° Congreso de Exploración de Hidrocarburos (Mendoza), Actas, vol 5, pp 8–19

Ramos VA, Zapata T, Cristallini E, Introcaso A (2004) The Andean thrust system—latitudinal variations in structural styles and orogenic shortening. In: McClay KR (ed) Thrust tectonics and hydrocarbon systems, vol 82. AAPG Memoir, pp 30–50

Vincente JC (2006) Dynamic paleogeography of the Jurassic Andean basin: pattern of regression and general considerations on main features. Revista de la Asociación Geológica Argentina 61 (3):408–437

UHE Belo Monte: Geological and Geomechanical Model of Intake Foundation of Belo Monte Site

Jose Henrique Pereira and Nicole Borchardt

Abstract

The hydroelectric plant of Belo Monte, on the Xingu River, is located in northern part of Brazil, in the state of Pará and is characterized by a complex of dams, canals, dikes and reservoirs. The main set Intake /Power House will be deployed on site called Belo Monte. This paper presents the geological and geomechanical model developed for the foundation of the Intake in the Belo Monte Site. These studies have been developed within the consortium Intertechne-Engevix-PCE. For the development of the Project of Belo Monte was necessary to improve the geological and geomechanical model preliminarily designed in the previous steps of design to the structure of Intake in Belo Monte Site. The conception and development of this model was fundamental in the development of the stability studies for Intake, with reference to the presence of discontinuities that form the main systems of joints that cut the rock mass in that location. In developing this model were considered the data obtained from drill holes executed at various stages of design, geological and geotechnical mapping of the exposed foundations and field observations of excavation of provisional and definitive slopes. That information was the reference for the determination of the main systems of discontinuities that cut the rock mass in the region of the Intake structure. Subsequent analyzes have defined the main parameters that characterize such systems, particularly with regard to their spatial distribution geomechanical characteristics, persistence and spacing. It should be emphasized that the model presented in this work aims to define in general terms the behavior of the rock mass that serves as the foundation for Intake. However, the stability analysis of the structure was conducted block by block, as the foundations are exposed, and based on surface mappings and identifying the main features potentially conditioners of the stability of these blocks.

Keywords

Geological model • Geomechanical model • UHE Belo Monte • Intake

111.1 Geological Characterization of the Intake Foundation

According to the design criteria established, the Intake of Belo Monte Site must be founded on sound migmatite to moderately altered (A1/A2) belonging to stratigraphic unit Complexo Xingu. Thus, the occurrence of sedimentary rocks

J.H. Pereira (✉) · N. Borchardt (✉)
Intertechne Consultores S.A, Av. Iguaçu, 100, Curitiba, Brazil
e-mail: jhp.box@hotmail.com

N. Borchardt
e-mail: nb@intertechne.com.br

(rhythmites) deposited over the crystalline basement and the migmatitic rocks with higher levels of alteration must necessarily be removed for the deployment of the structure.

111.1.1 Partitioning of the Rock Mass

The main systems of discontinuities occurring in the Intake region consists, mainly, of geological discontinuities with high dip associated with sub-horizontal discontinuities, which were characterized at various previous stages of project.

In these previous studies were identified three sets of joints potentially influential on the stability of the Intake, denoted by S1, S1′, and S6, for which were established, respectively, the following preferential attitudes: horizontal to 20°; EW/20–40°N and NW–EW/65–90°NE–SW.

On the final design with the exposure of bedrock of the crystalline basement, resulting from the excavations required for implementation of the project, preliminary and definitive mappings contemplating structural surveys and new boreholes were conducted to characterize and confirm the major systems of discontinuities and their preferential directions.

Based on these last data was prepared a stereogram of poles frequency for the discontinuities identified, and is presented in Fig. 111.1.

The analysis of the stereogram indicates that four major sets of joints occur in the region being called by S1, S2, S3, and S5. Addition to these main sets was identified other, less expressive, called by S1′. The spacial distribution of such sets, obtained from surveys carried out, can be summarized as shown in Table 111.1 below.

Table 111.1 Summary of the directions of the main sets of discontinuities

Sets of joints	Attitude
S1	Horizontal to 20°
S1′	NW/20°–45° NE
S2	NW/60°–90° NE or SW
S3	ENE/60°–90° NW or SE
S5	~NS/70°–90° E or W

111.1.2 Characterization of the Main Sets of Joints

111.1.2.1 Subhorizontal Set of Joints: S1

This set of joints is characterized by features of low angle (horizontal to 20°) with dips preferentially toward NE. The features mapped on surface generally consist of discontinuities with millimeter openings to sealed, sometimes with the presence of altered material in thicknesses typically ranging from millimeter to centimeter. The walls of these features usually show up sound to slightly altered (oxidized), especially in the lower elevations, as can be seen on the discontinuities exposed in the ramp of penstocks, excavated between units 1 and 8. The joints of this system, identified in surface mapping and borehole analysis, shows walls usually rough with roughness index (JRC) usually around 10.

At the foundation of the Intake "steps" are likely formed in the rock mass for these discontinuities, most often as a result of the constructive process of excavation to obtain the dimensions of the project.

Generally, the discontinuities associated with this system have persistence of the order of 10–15 m, average spacing of

Fig. 111.1 Intake of Belo Monte site—overall stereogram of poles frequency
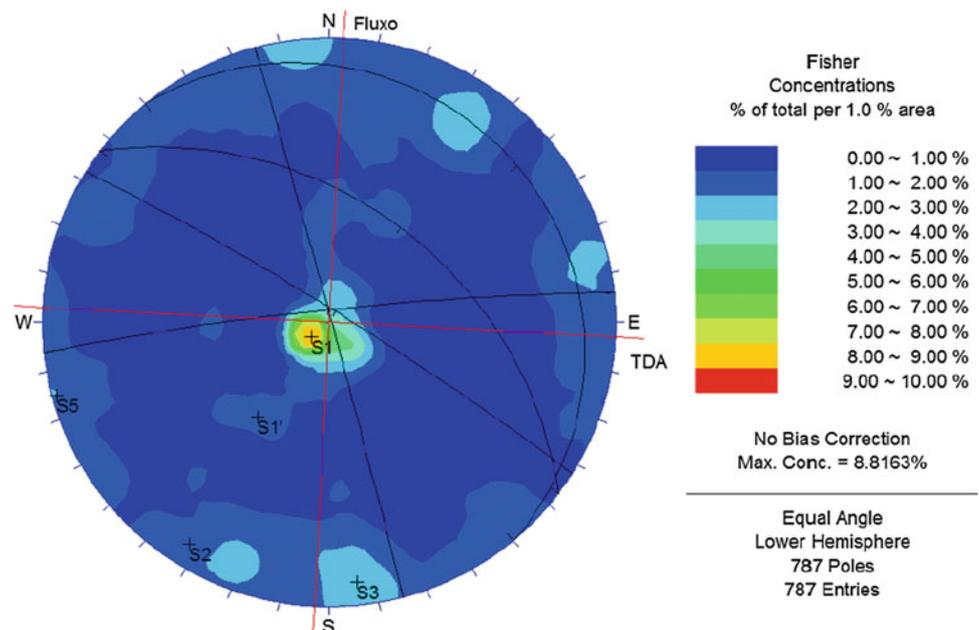
about 2 m, with local variations to lower numbers, especially near the top of excavated rock.

111.1.2.2 Vertical Set of Joints: S2 E S3

These sets have dips between 60° and 90° with ranging directions between NE–SW (S2) and NNW–SSE (S3). Are characterized by discontinuities generally planar to slightly undulating, with walls usually sound to slightly altered, rock to rock contact and roughness index (JRC) ranging between 8 and 12. The surveys performed in boreholes and surface mappings on the Intake foundation indicate that the features associated with this system have persistence between 8 and 10 m, with average spacing between the planes of discontinuities around 3.5 and 4.0 m.

The mappings performed in the Intake region have also identified some transcurrent faults with direction equivalent to set of joints S3 (ENE), but with persistence more expressive and high upstream dip (above 60°), present in the founding Intake and Power House region.

111.2 Geological and Geomechanical Model

The main sets of joints that influenced the model definition to Intake of Belo Monte Site are denoted by S1, S2 and S3, whose main features have been detailed in previous sections.

In Fig. 111.2, below, a isometric model of Intake excavation is presented, which are schematically represented the three main sets of joints that cut the rock mass. This guidance model indicates the spatial position of these sets and does not reproduce the persistence observed in the surveys carried out.

In this figure is observed that the discontinuities system S1 are arranged with main dips to northeast, which results in an attenuation of these angles in the flow direction. Whereas that the most frequent dips directions for this system vary between azimuths 40–60° (see Fig. 111.1), the apparent dips in the flow direction for this system range from 0 to 16°, taking as reference the true dips between 0 and 20°.

Fig. 111.2 Isometric model of intake excavation—spatial arrangement of the major sets of joints
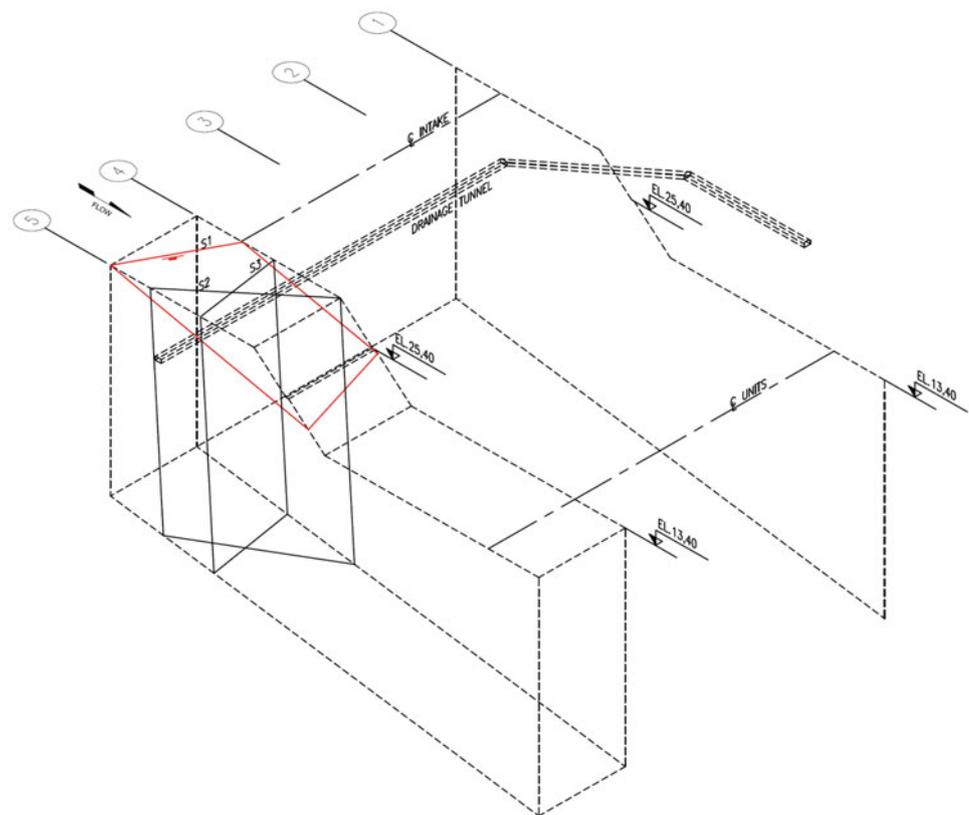
Fig. 111.3 Typical geological
section of the founding of Intake
showing the massive migmatitic
cut by discontinuities systems S1
(subhorizontal) and subvertical
sets S2/S3

Still based on surveys carried out, it was possible to establish the persistence and spacing of the main systems of discontinuities occurring in the Intake, as already detailed above.

The analysis of this information leads to the development of a geological model for the foundation of Intake where the rock mass is compartmented for vertical and subhorizontal discontinuities with persistence between 8 and 15 m and spacing ranging from about 2 m, for system S1, and about 4 m for the verticals (S2 and S3).

The spacing and the relative small persistence of discontinuities that cut the rock mass development a model as shown in Fig. 111.2, where the joints are interrupted and discontinuous along the projection of the structure of Intake, occurring that way significant "bridges" of sound rock interspersing the joint plans, giving to the rock mass a high strength envelope (Fig. 111.3).

Based on information currently available, from the mappings, and knowledge of the rock mass behavior, was definitely a strength envelope for the rock mass with reference to the failure criterion proposed by Hoek-Brown (2002). Based on that criteria, and using the computer program developed by Hoek (RocLab) was adopted the following parameters:

σ_{ci} = Uniaxial compressive strength of intact rock = 150 MPa (*)

GSI = Geological Strength Index = 70

mi = constant of the material (migmatito) = 29

D = disturbance factor in the face of the massive detonation process = 0, 7

Ei = modulus of deformation of the intact rock = 80 GPa (*)

(*)—average values obtained in tests on migmatite samples

Based on these parameters was obtained following strength envelope for the rock mass:
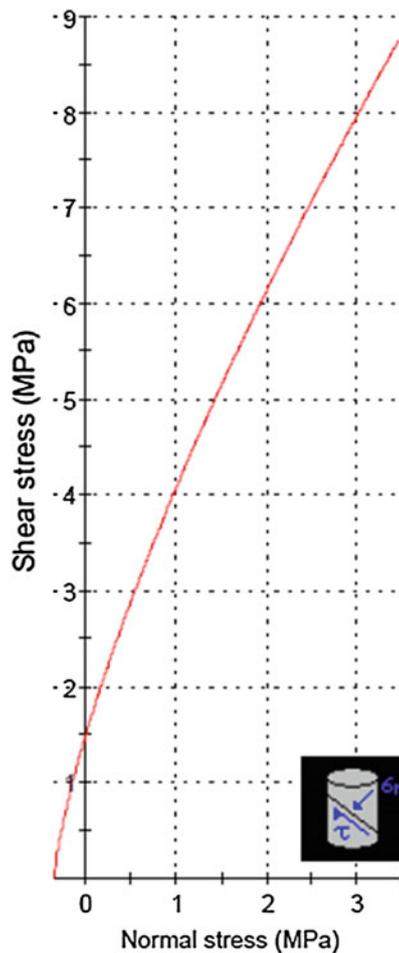
Hoek-Brown Classification
    intact uniaxial comp. strength (sigci) = 150 MPa
    GSI = 70   mi = 29   Disturbance factor (D) = 0.7
    intact modulus (Ei) = 80000 MPa
Hoek-Brown Criterion
    mb = 5.579   s = 0.0129   a = 0.501
Mohr-Coulomb Fit
    cohesion = 1.751 MPa   friction angle = 65.07 deg
Rock Mass Parameters
    tensile strength = -0.348 MPa
    uniaxial compressive strength = 16.960 MPa
    global strength = 48.592 MPa
    deformation modulus = 27009.19 MPa

Based on this analysis the strength envelope for the rock mass is represented by the following equation:

$$\tau = 1,7 \text{ MPa} + \sigma_n . \text{tg } 65°$$

For the evaluation of influence of the most persistent discontinuities identified by the mappings on Intake stability, should be considered specific parameters for the materials that constituting these features. In these analyzes should also consider the geological the Intake stability model and the results of evaluations of persistence and spacing defined for each system individually.

111.3 Conclusions

The conception of geomechanical model of the Intake of Belo Monte was of great value for characterization of the main systems of discontinuities present in the foundation of the intake and the definition of the main cinematic possibilities of rupture.

The subhorizontal systems were identified since the beginning of these studies as potentially destabilizing for the structure of intake and were object of special attention during the whole process of excavation and exposure of the foundation.

In order to ensure the safety factors adopt by the Project for the structure of the Intake, stability analyzes through the rock mass were conducted block by block, having as reference the discontinuities identified and characterized by geological mapping performed after exposure of the end surfaces of excavation.

The geomechanical characteristics of discontinuities that comprise those systems had variations with respect to the filler, opening, rock walls conditions and persistence, defining thereby changing parameters of cohesion and friction angle for each particular feature.

To estimate these parameters along the plane of the mapped features, was considered the formulation presented by Hoek (2007) for determining the instantaneous friction angle and cohesion, which were defined based on the estimates of the residual friction angle, joint coefficient

roughness (JRC), joint compressive strength (JCS) and the normal stress applied in the plane of discontinuity.

Such analyzes have shown that the features of low angle, although potentially unstable, presented parameters and geomechanical characteristics appropriate to ensure the safety factors required by the project, even when considering their association with the vertical set of joints S2 and S3.

References

Barton N (1976) The shear strength of rock joints. Int J Rock Mech Min Sci Geomech. Abstr 19:255–279

Barton N, Choubey V (1977) The shear strength of rock joints in theory and practice. Rock Mech 1(2):1–54

Hoek E (1994) Strength of rock and rock masses. Int Soc Rock Mech News J 2(2):4–16

Hoek E, Carranza-Torres C, Corkum B (2007) Hoek-Brown failure criterion, 2002 edn. In: Proceedings of NARMS-TAC conference, Toronto, 1, 267–273

Hoek E (2007) In: Practical rock engineering. Shear strength of discontinuites, Chap. 4, 60–72

Roberto Laureti, Serena Scarano, and Stefano Serangeli

Abstract

In road design, the Geological Reference Model plays an important role, especially in presence of complex geological conditions. In these areas, especially where is evident the role played by tectonics in the determination of geological-stratigraphic framework, the Geological Reference Model can be completed during various phases of the project, together with the improvement of the knowledge context. This case-history represents an example of application of this process. The first reconstruction of the model has been developed through the analysis of the available literature, especially referred to the geological, geomorphological and site-investigation data. After, a first survey phase has been completed. It represented the conceptual base to plan specific site-investigation, geophysical and laboratory survey, especially referred to the most geological and design critical situations. So that the Geological Reference Model has been gradually improved, highlighting particular tectonic structures, hardly detectable only by field geological and geomorphological survey. Finally, the design solutions, adopted for the civil works situated along the path, have been determined according to the identified geological conditions.

Keywords

Geological reference model • Geostructural reconstruction • Site-investigation • Serre chain

112.1 Introduction

As part of the upgrading of southern Italy road infrastructures, ANAS started the project to build the new S.S.182 "Trasversale delle Serre", located in the central-southern Calabria. The aim is to connect, from west to east, the two great coastal roads: the A3 Salerno—Reggio Calabria motorway, which runs along the tyrrenian coast, and the S.S. 106 "Jonica", along the Ionian sea.

The project road shown in this work is composed by two lots, 4 and 5, with a total length of 7.5 km, connecting the towns of Gagliato and Soverato.

R. Laureti (✉) · S. Scarano · S. Serangeli
Anas S.p.A., Design Management, Geological and Geotechnical Unit, Rome, Italy
e-mail: r.laureti@stradeanas.it

The land orography is, mainly, characterized by a series of mountain, which constitute the "Serre Chain". The geological and geomorphological characterization of the soils influences, considerably, the development of the civil works along the road and the design solutions used. These are represented by: 12 viaducts, 3 bridges, 3 artificial and 1 natural tunnels.

112.2 Reconstruction of the Geological Reference Model

During the design of the road the Geological Reference Model has been developed, and it has been continuously improved through several phases of deepening of the knowledge framework of the area, from the geological point of view (geological, geostructural, geomorphological, hydrogeological survey, and site-investigation). At the beginning of the road design activity, a first survey phase has

been completed. It represented the conceptual base to plan specific site-investigation, geophysical and laboratory surveys, especially referred to the most geological and design critical situation

112.2.1   Site-Investigation Program

The site-investigation campaign consisted of 31 boreholes, 17 trenches, 13 Down-Hole tests and 2 Cross-Hole tests for seismic characterization of soils. On undisturbed and reworked samples, geotechnical laboratory and chemical tests, for the purpose of environmental characterization according to the new DM 161/12,[1] were carried out. In addition, in order to optimize the management of the soils coming from the excavation, with undeniable environmental advantages, the design has provided the reuse, in the construction of embankments, not only of the sandy-gravel formations, but also of the silty-clay soils, after lime-treatment. So that, in an experimental way, we conducted a study on the suitability of that soils, determining the performance characteristics of the mixtures studied.

112.2.2   Local Stratigraphic Sequence

The geological-structural model, as defined, is characterized by the presence of a Paleozoic granitic substrate, on which Plio—Pleistocenic continental and marine formations lie with unconformity.

The upper part of the road crosses a mountain ridge, elongated in east-west direction. It is composed by conglomeratic deposits, generated from the dismantling of the crystalline substrate and deeply affected by extensional tectonics, which has faulted the structure, causing a framework made by blocks lowered towards the Ionian sea. The conglomeratic deposits (Cg) consist of large and eterometric granitic and tonalitic blocks, with dimensions of 2–3 m, generally well rounded, embedded in a dark/brown sandy and sandy-coarse matrix of arkose nature. The conglomerates are moderately cemented and have interbedded by coarse sands.

Above, in stratigraphic continuity with them, there are the hold sands and sandstones (Ps) consisted of quartz—feldspathic/quartz-mica sands, from fine to coarse, with color varying from yellowish to brown, plane-parallel stratified, as well thickened to variously cemented.

At the top, the Plio-pleistocenic sequence ends with blue-gray hard clays, sometimes marly (Pa), which, mainly,

outcrop in the lower part of the road, characterized by small hills, which often shows, above their slopes, landslides of various proportions (Fig. 112.1).

112.2.3   Particular Tectonic Situations

Situations of particular interest have emerged by the detailed geological analysis of the road design. Of course they affected, consequently, the design solutions. Along the fluvial incision of the Fosso Turriti, for instance, in correspondence of the confluence with the River Ancinale, the crystalline bedrock turns out stepped by a complex fault system, that created a series of buried structural blocks, elongated in WNW-ESE direction. The main buried horst consists of granite and it is covered by the pliocenic clay and sandy formations, laying under a thick alluvial deposit. In this stretch of the road design, there is a viaduct with a wide curve of about 120°, intersecting the tectonic structure along multiple directions.

The central piles of the viaduct are placed above the buried horst, made by the crystalline substrate (granite), whose roof, highlighted by the survey, is positioned at a depth of about 20 meters. Along an hypothetical section that cuts transversally the valley, it is evident that this block represents a tectonic "step", structurally lowered in comparison with the SW ridge, but raised compared to the NE sector, which forms the basis of the graben, where the river has set its course. Above the granite, the marine series is represented by the gray-blue clays (Pa) and, under that, by the sandy formation (Ps) with a maximum thickness of 6 m. Obviously the series appears here condensed and reduced, because of the control practiced by the morphology substrate on the sedimentation. The bedrock and the marine formations are covered by a thick alluvial deposit (above all sands and gravels) (Fig. 112.2).

112.3   Design Solutions

The critical situations derived from different local geological settings, highlighted by a detailed geological analysis, have suggested the adoption of different design solutions for the civil works along the road in project.

The most important viaducts, such as the "Turriti Viaduct" and the "Ancinale Viaduct", set to the tectonic structure analyzed before, have been provided with deep foundations in relation to the not exactly optimal geotechnical characteristics of the outcropping deposits.

For this purpose, the use of foundational wells, instead of large diameter piles, turns out to be more efficient also from the operational point of view. In fact, the strong heterogeneity of soils, especially of the alluvial and conglomeratic deposits, is a severe limit to executive technology of the "classics"

---

[1] Decreto del Ministero dell'Ambiente e della tutela del Territorio e del Mare 10 agosto 2012, n. 161 - Regolamento recante la disciplina dell'utilizzazione delle terre e rocce da scavo (G.U. n. 221 del 21 settembre 2012).

Fig. 112.1 Outcrop of the hold sands and sandstones
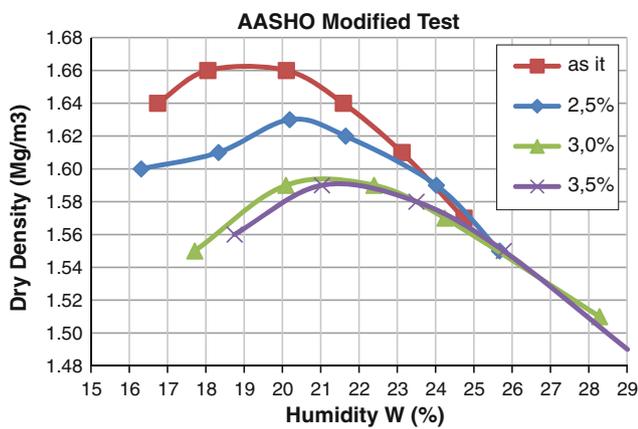
Fig. 112.3 Curve compaction of the AASHO mod. test performed on mixtures

structural foundational elements, without forgetting that the movement of machinery on the slopes requires the prior construction of site roads and non-trivial size temporary civil works. The geometric conditions of use of supporting structures, which are mostly set on strong transversal escarpment, require the use of flexible structures such as reinforced soil. Furthermore the achievement of the global stability conditions requires the realization of overseeing works on the foot, composed by "light" and resistant elements as the micropiles.

112.4 Lime Treatment of Clay Coming from Excavations

Clay materials, coming from the trenches excavations, will be reused in embankment, after their stabilization with lime, based on the studies specifically realized.

This study, in addition to determining the suitability to the treatment of the excavation soils, has compared the performance of different blends, comparing the variability fields of the most significant geotechnical parameters with the variation of lime percentage and the ripeness degree. The percentage of lime to be included was assessed from initial consumption of lime (ICL) +0.5 % up, forming 3 different mixtures with different lime content: 2.5–3.0–3.5 %. Each mixture was also tested for two different maturation states (after 1 day and after 14 days). In particular, from the AASHO mod. test performed on mixtures, we can observe a significant flattening of the compaction curve with the increase of the content in lime. It constitutes one of the main benefits for machinability of the treated material. The same test has shown how the intermediate mixture with 3.0 % of lime is those that provides the best performance benefit in relation to the amount of binder added, because the transition to the richer mixture does not provide an appreciable improvement of quality performance (Fig. 112.3).
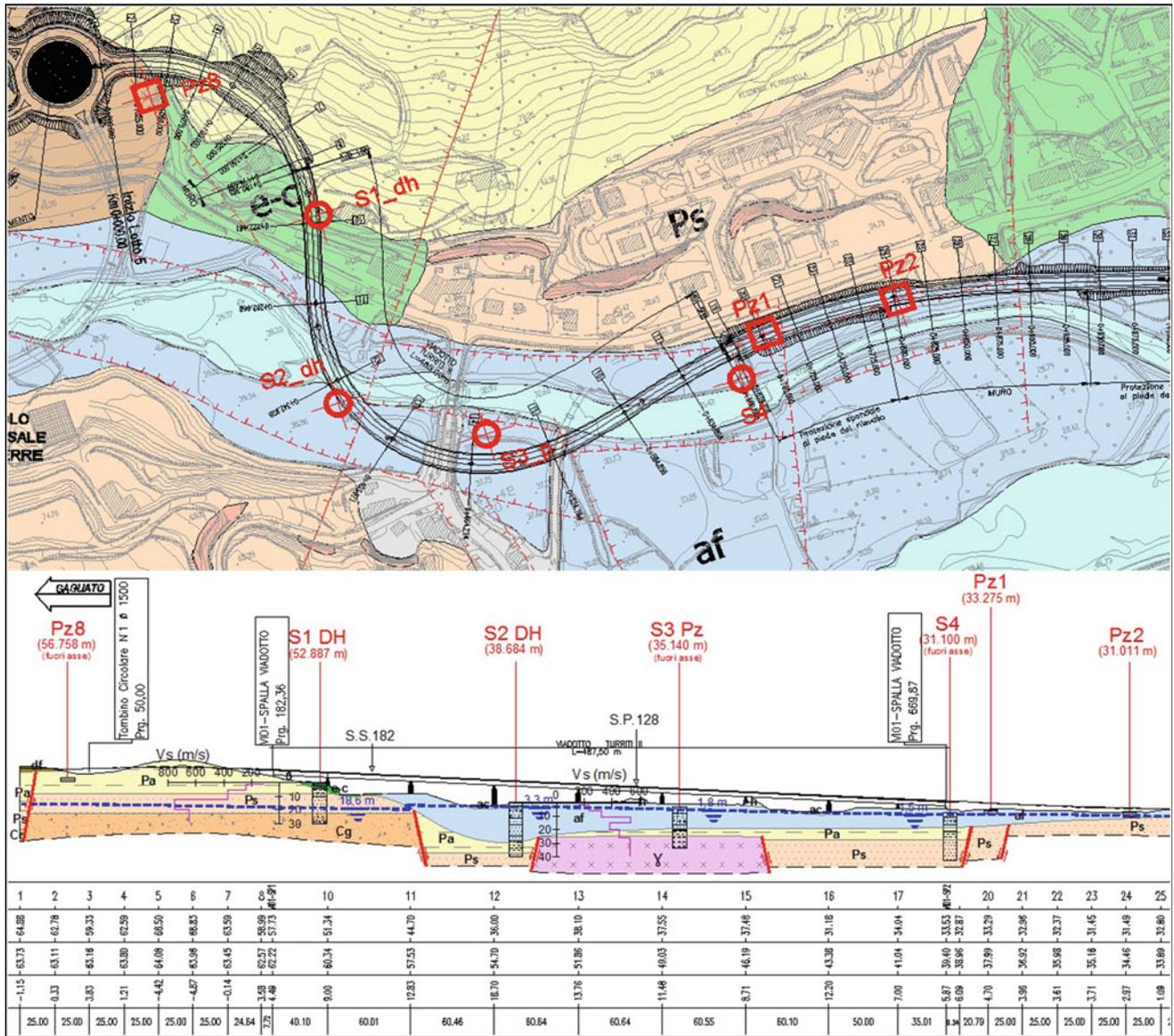
Fig. 112.2 Geological section along the tectonic structure of the Turriti Viaduct

112.5 Conclusions

Of course the design of a road infrastructure, of whatever extent, needs, from the early stages of study, a careful reconstruction of the reference geological model.

It allows, starting from the general geologic framework of the wide area, to have a detailed framework that permits to get the geotechnical characteristics of the soils involved by the road project and to make appropriate choices about the design elements to be introduced.

The definition of the geological reference model is obtained from the analysis of data provided by the geological surveys in the area or those suitably programmed. Particular situations, such as the geostructural setting through the Ancinale river, have been described by the deepening of the model, due to the site investigation data.

As described in this paper, sometimes, on the basis of specific design choices, specific studies are very important, such as the study of lime treatment, useful for the evaluation of reuse in embankment of clayey materials from excavations in the trenches.

References

AA.VV Capitolato speciale d'appalto parte II: Norme Tecniche—ANAS

Amodio Morelli L, Bonardi G, Colonna V, Dietrich D, Giunta G, Ippolito F, Liguori V, Lorenzoni S, Paglionico A, Perrone V, Piccaretta G, Russo M, Scandone P, Zanettin Lorenzoni E, Zuppetta A (1976) L'arco Calabro-Peloritano nell'orogene appenninico-maghrebide. Memorie della Società Geologica Italiana 17:1–60

APAT (2007) Rapporto sulle frane in Italia: il Progetto IFFI. Metodologia, risultati e rapporti regionali. Rapporti APAT, 78

Barbano M, Casentino M, Lombardo G (1980) Isoseismal maps of Calabria and Sicily earthquake. Work no. 341, CNR—Progetto Finalizzato Geodinamica, Catania

Cariboni Luigi (1996) L'impiego della calce nelle infrastrutture viarie —Le Strade, 9/1996

Cotecchia V, Guerricchio A, Melidoro G (1986) The geomorphic crisis triggered by the 1783 earthquake in Calabria (southern Italy). Atti del congresso "Engineering geology problems in seismic areas", Potenza, Napoli, 13–19 aprile 1986, 6, 245–304

Galadini F, Meletti C, Vittori E (2001) Stato delle conoscenze sulle faglie attive in Italia: elementi geologici di superficie. Risultati del progetto 5.1.2. "Inventario delle faglie attive e dei terremoti ad esse associabili", Gruppo Nazionale per la Difesa dai Terremoti (G.N.D. T.)

Ghisetti F, Vezzani L (1981) Contribution of structural analysis to understanding the geodynamic evolution of the Calabria arc (Southern Italy). J Struct Geol 3:371–381

Ghisetti F (1981) L'evoluzione strutturale del bacino plio-pleistocenico di Reggio Calabria nel quadro geodinamico dell'arco calabro. Bollettini della Società Geologica Italiana 100:433–466

Miyauchi T, Dai Pra G, Sylos Labini S (1994) Geochronology of pleistocene marine terraces and regional tectonics in the Tyrrhenian coast of south Calabria, Italy. Il Quaternario 7:17–34

Ogniben L (1973) Schema geologico della Calabria, in base ai dati odierni. Geol Romana 12:243–585

Scandone P, Giunta G, Liguori V (1974) The connection between the Apulia and Sahara continental margins in the Southern Apennines and in Sicily. Memorie della Società Geologica Italiana 13:317–323

Tortorici L, Monaco C, Tansi C, Cocina O (1995) Recent and active tectonics in the Calabrian arc (Southern Italy). Tectono-physics 243:37–55

Valensise G, Pantosti D (1999) The database of potential sources for earthquakes larger than magnitude 5.5 in Italy. EUG 10, volume degli abstract, pp 542–543

Impacts of Environmental Hazards to Critical Infrastructures

Convener Dr. Paolo Frattini—*Co-conveners* Kyriazis Pitilakis, Carmelo Dimauro, Matteo M. Montini, Giovanni B. Crosta, Serena Lari

Territorial economic and social integration requires secure accessibility of people and goods through safe infrastructures, such as roads, railways and oil-gas pipelines. These are affected by a high number of hazards (earthquakes, floods, landslides, industrial explosion and transportation of dangerous goods) that can damage existing and planned infrastructures. Damage to infrastructures has also a clear transnational dimension, since the consequences of transportation disruptions in one region can propagate to other regions. However, this dimension is poorly accounted for in risk assessment and emergency response during disasters, due to the absence of a comprehensive and integrated resilience methodology and the lack of a joint strategy for risk management. The general objective of this session is to present contributions related to the assessment, prevention and efficient management of geological and geotechnical risks along the main existing and future critical infrastructures.

M.G. Winter

Abstract

Even in the absence of serious injuries and fatalities, rainfall-induced debris flow events can have significant socio-economic impacts when roads are affected. These include the cost of clean-up and repair, and of diversion. Costs also include those associated with the severance of access to/from remote communities for services and markets for goods; employment, health and educational opportunities; and social activities. The extent of such impacts depends upon the vulnerability shadow cast, which can be extensive and its geographical extent may be determined by the road network rather than the small footprint of the event itself. Indeed, such small events may (at most) directly affect a few tens of metres of road but cast a vulnerability shadow amounting to thousands of square kilometres.

Keywords

Landslides • Debris flow • Vulnerability • Area • Socio-economic impacts

113.1 Introduction

The risks associated with landslide hazards affect many parts of the world and many different cultures. The elements at risk may include infrastructure, public service buildings, commercial property and residential property as well as the occupants and users of such facilities. The type of element at risk and the vulnerability of those elements determine what might be described as a reasonable and proportionate response to a given risk profile.

In Scotland, rainfall-induced debris flow events often affect the strategic road network. Even in the absence of serious injuries and fatalities, such events have significant socio-economic impacts. These include the severance of access to and from relatively remote communities for services and markets for goods; employment, health and educational opportunities; and social activities in addition to clean-up, repair and delay costs. The types of economic

impacts were summarized by Winter and Bromhead (2012) who also pointed out that the vulnerability shadow cast can be extensive and that its geographical extent can be determined by the transport network rather than the relatively small footprint of the event itself. The vulnerability shadow is presented here as a means of articulating the geographically dispersed impacts of landslide events.

113.2 Debris Flow in Scotland

Rainfall-induced debris flows affect the Scottish strategic road network on a regular basis (Winter et al. 2005, 2006, 2009). Figure 113.1 shows the 2007 event at the A83 route. The photograph is taken from the opposite side of the valley and even in this small area evidence of numerous past events can be clearly seen.

The mass movement comprised two discrete but related parts. First, the flow above the road commenced with a relatively small slide (or slides) into an existing drainage channel. This then triggered the movement of a large amount of marginally stable material in and around the stream channel of which an estimated 400 tonnes was deposited at road level. Second, this material blocked the open drain

M.G. Winter (✉)
Transport Research Laboratory (TRL), 13/109 Swanston Road,
Edinburgh EH10 7DS, UK
e-mail: mwinter@trl.co.uk
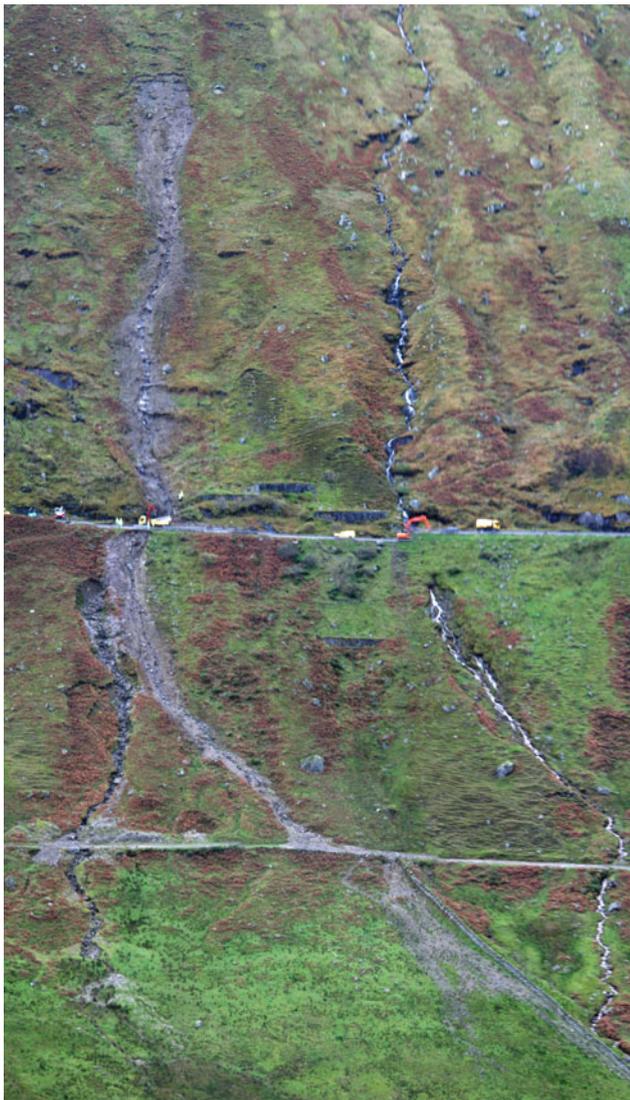
Fig. 113.1 Debris flow of 03:00 h on Sunday 28 October 2007 at the A83 rest and be thankful. The head scar is at 370 m, A83 at 240 m and the old road at 180 m. Both recent (*lighter area*) and older (*darker*) erosion is visible below the main road and to the left of the recent scar

which carries water along the road to a series of culverts beneath. While the material from above the road had limited impact upon the slopes below the road, water diverted from the drain was channelled across and over the edge of the road causing some significant undercutting of the slope below and associated deposition further down the hill as can be seen in Fig. 113.1.

The culvert at this location was around 400 mm diameter and thus marginal for water flows let alone for debris. It is also clear that the culvert does not follow a straight path, which would reduce its capacity and increase the potential for blocking. Additionally, water flowed from the culvert at an angle to the hillside of considerably less than ninety degrees and caused the older erosion visible in Fig. 113.1.

The A83 site has long been very active and debris flow events and associated closures in 2007, 2008, 2009, 2011 and 2012 had an adverse effect on the travelling public. The area has become the focus of extensive landslide management and mitigation activity (Anon 2013; Winter and Corby 2012).

Major injuries have not resulted from rainfall-induced debris flow events that have affected the Scottish strategic road network for some years. The impacts of such events are socio-economic, particularly the severance of access to/from remote communities. Substantial disruption is experienced by local and tourist traffic, and goods vehicles as a result of such events. The maximum (July/August) daily traffic levels at the A83 Rest and be Thankful are 5 to 6,000 vehicles (AADT). The minimum traffic levels in January and February are roughly half the maxima.

The major contribution that tourism and related seasonal industries make to Scotland's economy means that the impacts of summer events are particularly serious, but the impacts of winter events should not be underestimated.

113.3   Economic Impacts

The economic impacts of landslide events as they relate to roads or other forms of transport infrastructure were summarized by Winter and Bromhead (2012) in three categories as follows.

Direct economic impacts include the direct costs of clean-up and repair/replacement of lost/damaged infrastructure in the broadest sense and the costs of search and rescue. These are relatively straightforward to estimate for any given event.

Direct consequential economic impacts relate to disruption to infrastructure and are really about loss of utility. For example, the costs of closing a road (or implementing single-lane working with traffic lights) for a given period with a given diversion, are relatively simple to estimate using well-established models. The costs of fatal/non-fatal injuries may also be included here and may be taken (on a societal basis) directly from published figures. While these are set out for the costs of road traffic accidents, or indeed rail accidents, there seems to be no particular reason why they should be radically different to those related to a landslide as both are likely to include the recovery of casualties from vehicles. Indeed, for events in which large numbers of casualties may be expected to occur data relating to railway accidents may be more appropriate.

Indirect consequential economic impacts relate to the loss of opportunity and potential loss of confidence. The economies of remote rural areas can be particularly dependent upon transport and if a route is closed for a long period then confidence in local business can be affected. Manufacturing and agriculture are a concern as access to markets is constrained, the costs of access are increased, and business

profits and viability are affected. There may also be impacts on tourist (and other service economy) businesses. It is important to understand how the reluctance of visitors to travel to and within landslide areas is affected after an event that has received publicity and/or caused casualties and how a period of inaccessibility (reduced or complete) affects short- and long-term travel patterns to an area for tourist services. Such costs are a fundamental element of the overall economic impact on society and are thus important to governments as they should affect the case for the assignation of budgets to landslide risk mitigation and remediation activities. However, these are also the most difficult costs to determine as they are generally widely dispersed both geographically and socially.

113.4 Vulnerability Shadow

The vulnerability shadow (Winter and Bromhead 2012) is closely linked to economic impacts and determines their extent and magnitude. The shadow cast can be extensive and its geographical extent can be determined by the transport network rather than the relatively small footprint of the event itself.

In the case of the A83 the event itself was of the order of around 400 m^3 with a footprint that closed a few tens of metres of the road. The vulnerability shadow has been evaluated using knowledge of the local transport networks and the socio-economic activity associated with the network that has been built up over a period of 25 years. This includes an
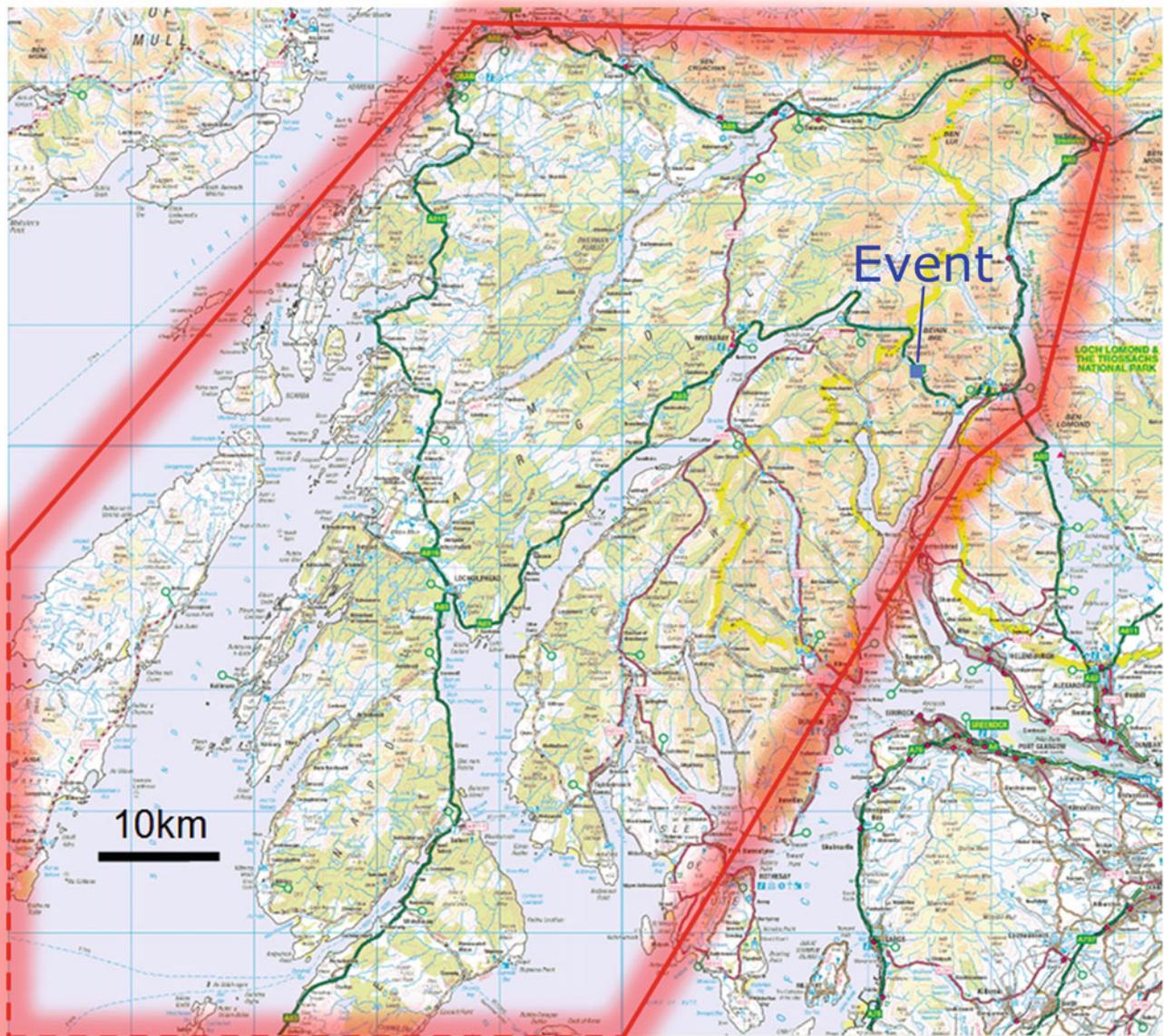
Fig. 113.2 A relatively small debris flow event (*blue square*) closed the A83 at the rest and be thankful in October 2007; the vulnerability shadow cast (bounded in red) was extensive (Winter et al. 2013; Winter 2013)

holistic evaluation of major nodes, origins and destinations and includes both experience and knowledge gleaned from formal surveys (e.g. Winter et al. 2013). The vulnerability shadow was thus estimated (Fig. 113.2) to be of the order of 2,800 km^2 (allowing 20 % for areas of sea). The area has a population density of approximately 13/km^2 (www.argyll-bute.gov.uk). Tentatively, the event may have had an economic impact upon approximately 36,400 people in Argyll and Bute, plus any transient (e.g. tourist) population.

Hong Kong SAR has an average population density of around 6,500/km^2 (www.gov.hk) which dictates a much greater transport network density. Thus, and for the sake of comparison, in order to have an economic impact on the same number of people the vulnerability shadow cast need only be approximately 5.6 km^2 (2 km by 2.8 km). It is not suggested that the economic impacts would be similar for events with vulnerability shadows of these diverse sizes in Argyll and Bute and Hong Kong. However, it is clear that the low density/dispersed network in Argyll & Bute dictates a large vulnerability shadow while the much more dense/less dispersed network in Hong Kong means that vulnerability shadows will be small, with the exception of events that affect critical infrastructure corridors, as more alternatives routes will exist and will be more proximal to the event.

A landslide on the B1 route in the Blue Mountains of Jamaica effectively severed the local coffee production industry from the most direct route to the international market for this high value product. As such a single landslide event placed severe constraints on the economy of the Blue Mountains. Again, while the footprint of the actual event was relatively small, the vulnerability shadow was projected over a much greater area creating tangible economic and social losses.

113.5　Conclusions

Linear infrastructure such as services, communications and transport networks presents significant risk factors including the near-continuous temporal occupation of the hazard zone, high vulnerability to damage, adverse orientation (as often

the design demands limited gradients). The construction of the infrastructure itself may also increase landslide susceptibility (e.g. cuts, fills, interruption of groundwater flow, concentration of water).

The vulnerability shadow for socio-economic factors may be projected over a much greater area (orders of magnitude) than the event footprint. It is largely the nature, extent and density of the transport network that determines the extent of the vulnerability shadow cast. This, in turn, determines the magnitude of the consequential economic impacts. In a sparsely populated area such as western Scotland the transport network is dispersed and the vulnerability shadow is likely to be large, while in an area with a dense network, such as Hong Kong, a similarly sized event is likely to produce a vulnerability shadow orders of magnitude smaller.

The vulnerability shadow is presented here as a means of articulating the geographically dispersed impacts of landslide events.

References

Anon (2013) A83 Trunk road route study: part A—A83 rest and be thankful. Final report. Report prepared by Jacobs for Transport Scotland, 212 p. http://www.transportscotland.gov.uk/road/maintenance/landslides. Accessed Mar 2013

Winter MG (2013) A classification scheme for landslide management and mitigation. Int J Landslide and Environ 1(1):123–124

Winter MG, Bromhead EN (2012) Landslide risk—some issues that determine societal acceptance. Nat Hazards 62:169–187

Winter MG, Corby A (2012) A83 rest and be thankful: ecological and related landslide mitigation options. Published Project Report PPR 636. Transport Research Laboratory, Wokingham

Winter MG, Macgregor F, Shackman L (eds) (2005) Scottish road network landslides study, 119p. The Scottish Executive, Edinburgh

Winter MG, Heald A, Parsons J, Shackman L, Macgregor F (2006) Scottish debris flow events of August 2004. Q J Eng Geol Hydrogeol 39(1):73–78

Winter MG, Macgregor F, Shackman L (eds) (2009) Scottish road network landslides study: implementation. Transport Scotland, Edinburgh 278 p

Winter MG, Kinnear N, Shearer B, Lloyd L, Helman S (2013) A technical and perceptual evaluation of wig-wag signs at the A83 rest and be thankful. Published Project Report PPR 664. Transport Research Laboratory, Wokingham

Active Faults at Critical Infrastructure Sites: Definition, Hazard Assessment and Mitigation Measures

114

Alexander Strom

Abstract

A definition of active faults crossing critical lifelines that uses both time interval during which movements have occurred and the threshold displacement/rate value that require special technical measures to ensure construction safety, is proposed. Accuracy of active faults delineation and criteria used for their identification depends on type of hazard—while active faults considered as causative tectonic structures can be derived based on indirect evidence, faults passing directly across construction site or lifeline route must be proved by direct evidence of past offsets. Ability of different types of engineering structures to sustain fault displacements should be considered both for site investigations and mitigation measures planning. The proposed approach requires better interconnection of earth scientists and design engineers al all stages of project implementation.

114.1 Introduction

One of the strict requirements when selecting engineering structures' placements or routes is to avoid sites that can be crossed by active faults. While buildings, dams, or factories can be shifted to safer site if such fault would be identified, routes of critically important lifelines such as trunk pipelines, roads, railroads often can not bypass active faults and special measures should be anticipated to ensure structures' safety and/or operating capacity. Effectiveness of such measures was proved at the Trans-Alaska oil pipeline crossed by the active Denali fault. Special studies provided reliable input data allowing proper design of fault crossing that sustained ∼6-m lateral offset during large (M 7.9) 2002 Denali earthquake (Haeussler et al. 2004).

From the engineering point of view, an active fault is a boundary between more or less rigid blocks moving against each other. Motion could be either continuous with constant or variable rate, or episodic, associated with earthquakes and have dual effects on engineering constructions and lifelines. First, active faults are the main type of causative tectonic structures responsible for large earthquakes which strong motion affects vast areas and must be considered for hazard assessment even if they pass distant from the construction site. On the other hand, they can affect engineering utilities directly. In both cases definition of what should be considered as an "active fault" is critical, since delineation of such feature at or close to the construction site or lifeline route implies expensive protection measures. Inadequate attribution of faults to the "active" category could complicate construction significantly or even make it economically inefficient. Though methods of active faults' identification and study are well developed, nevertheless, in actual practice their definitions are still inconsistent. It results in different approaches to their identification, quantification, and hazard assessment, which, in turn, are interconnected with engineering protection measures.

A. Strom (✉)
Geodynamics Research Centre, Branch of JSC "Hydroproject Institute", Moscow, Russia
e-mail: strom.alexandr@yandex.ru

114.2   Definition

A generally applied definition for active fault in "active tectonics" literature is: "*A fault that has been ruptured at least once during given period of time must be considered as active*" (Allen 1975; Trifonov 1985; Hancock et al. 1991; Nikonov 1995). The duration of this "reference period of time" ranges, most often, from ∼10,000 years up to ∼1,000,000 years. In some "extreme" definitions time interval decreases up to decades (period of instrumental geodetic observations) (Kuzmin 2004) or increases up to 2,000,000 years (Lunina et al. 2012). Considering typical recurrence intervals between large earthquakes accompanied by surface faulting that range from several hundreds years to several tens thousands years, the most reasonable time interval for hazard assessment of lifelines is from 50,000 to 100,000 years. Besides formal probabilistic reasoning this interval is best supported by commonly used dating methods (^{14}C, OSL).

However, from engineering point of view such definition is incomplete, since it does not determine the threshold displacement value. Faulting recurrence estimates are necessary for risk assessment mainly, which is the economic issue, while engineering itself requires single-event or cumulative offset value and fault kinematics that predetermine design of the protection measures. Besides, discrimination of the potentially dangerous active faults at the structures' foundation depends at a large extent on the type of the designed structure. While some rigid (e.g. concrete) structures could be sensitive even to minimal displacement, flexible steel structures such as pipeline could accommodate much larger offset. Moreover, as for pipelines, pipe thermal or hydrodynamic deformations considered for the design could be large enough (SNiP 1996; American Lifelines Alliance 2005) to provide additional constraints of the threshold value. With due regard to the above considerations we proposed following definition of active fault for the new version of Russian Guidelines on seismic design of hydraulic facilities: "*A fault must be considered as active one if there is evidence of permanent or periodical displacements in Late Pleistocene—Holocene (during last 100,000 years), with such single-event offset value or displacement rate that pose a threat to the construction and require special engineering or placement measures to ensure its safety*". Such approach requires close co-operation between earth scientists studying hazardous natural phenomena and design engineers. Designers should provide basic characteristics of the proposed construction and its ability to resist deformations, which threshold value must be considered by earth scientists.

The following reasoning relates to trunk pipelines mainly. Here the main goal is to prevent pipeline leakage and environmental pollution, rather then maintain its working capacity. For such infrastructure elements as roads and railroads it seems that it is much more efficient to monitor them regularly and to repair in case of rupturing event rather than to protect from unacceptable deformations.

114.3   Hazard Assessment

If a hazard (in the probabilistic meaning of this term) of rupturing and corresponding risks are high enough, the following parameters must be provided to design a fault crossing: possible rupture location and its accuracy; expected single-event displacement (for seismic ruptures) or displacement rate (for creeping faults); fault kinematics. Additional input data includes width of secondary deformations zone, style and values of these deformations.

While for causative faults kilometres-scale accuracy of their location can be acceptable, active faults that can affect structures directly must be localised much more precisely (Besstrashnov and Strom 2011). Accuracy predetermines usage of direct and indirect evidence of activity. Delineation of causative faults is often based on a set of indirect evidence of fault activity, but only direct evidence allows tracing of active faults that cross a construction site or critical lifeline route. Only direct evidence of past surface rupture allows estimating of future offset value and direction with an accuracy acceptable for engineering purpose. Indirect evidence of fault activity, indicating high permeability for fluids, does not provide information on the mechanical mobility of fault sides. Hazard predetermined by permeability might require different protection measures than those against mechanical displacements provided by active faults.

Probabilistic seismic hazard assessment (PSHA) that is widely used in engineering practice implies that shorter the considered time interval is, lower strong motion parameters (intensity, acceleration, velocity) should be. It follows from the fact that strong motion at a particular construction site can be caused by seismic waves from multiple earthquake sources, both local and distant. Recently, the probabilistic approach was applied for fault displacement analysis (PFDHA) (Youngs et al. 2003). However, its applicability for particular fault crossing seems to be problematic. First, unlike PSHA, it deals with a unique feature—a particular active fault (or active fault segment) for which it is difficult if not impossible to collect statistically representative data. Second, according to pipeline construction codes (Honegger and Nyman 2004), seismic design is performed for two levels of seismic loading—Strength-Level Earthquakes (SLE) with recurrence of 200 year and Ductility-Level Earthquakes (DLE) that can occur once in 1000 years. But a similar approach for surface faulting assessment is not applicable, since usually surface faulting occurs once in more than 1000 years (such offset could be equalised to the DLE), while no rupture at all along the same fault occur

more often. If a rupturing event would occur during pipeline lifetime, displacement would be most likely equal to a characteristic value (Schwartz and Coppersmith 1984).

114.4   Mitigation Measures

Safety measures for critical infrastructures, which cross active faults, strongly depend on the lifeline type. For pipelines aim of these measures is to exclude leakage which can be provided by special engineering efforts. Crossing of the Trans-Alaska ground-surface oil pipeline with the Denali that sustained fault rupturing during the 2002 Denali fault includes special compensator placed on rails with Teflon coating to facilitate its slipping against the ground in case of earthquake. This construction proved its efficiency during the 2002 Denali earthquake (Haeussler et al. 2004).

Significant efforts were undertaken to ensure safety of the Sakhalin-1 and 2 Projects in Russia. Their additional complexity was conditioned by the strict requirement to have buried pipelines that reduce the degree of pipe freedom at a large extent in comparison with ground-surface pipelines. Nevertheless, special "dog leg" tracing of pipeline close to its crossings with active faults, use of trapezoid-shape trenches with drainage aimed to avoid freezing of trench fill during winter period, and other technical measures allowed construction of fault crossings that could accommodate offsets half as much as the design displacement values— $1.5 \times D_{des}$ (Mattiozzi and Strom 2008; Strom et al. 2009).

As mentioned above, railways and highways safety can be achieved, mainly, by regular monitoring and obligatory run-time inspections after large earthquakes, before traffic reopening. Any engineering solutions aimed to retain operational integrity of railroads and highways crossed by active faults after large earthquakes seem to be too complex and economically inefficient.

114.5   Conclusions

The proposed definition of active faults that cross critical lifelines routes includes assessment of the displacement value and/or rate of permanent fault movements (tectonic creep)—parameters really used as an input data for engineering design of fault crossings. The traditionally determined parameter—i.e. recurrence of displacements and/or mean rate calculated for the entire earthquake cycle can be used for risk assessment mainly.

Ability of different types of engineering structures to sustain fault displacements should be considered both for site investigations and mitigation measures planning to avoid exceptional selection of sites that, in fact, do not require special technical measures to ensure structures' safety. Such

approach need better interconnection of earth scientists and design engineers at all stages of project implementation. Special analysis of cases studies is needed to investigate if similar approach could be applied for other geological processes associated with mechanical displacements, such as block slides, in particular (Hungr et al. 2013).

References

Allen CR (1975) Geological criteria for evaluating seismicity. Bull Geol Soc Am 86:1041–1057

American Lifelines Alliance (2005) Guidelines for assessing the performance of oil and natural gas pipeline systems in natural hazard and human threat events

Besstrashnov VM, Strom AL (2011) Active faults crossing trunk pipeline routes: some important steps to avoid disaster. Nat Hazards Earth Syst Sci 11:1433–1436

Hancock PL, Yeats RS, Sanderson DJ (eds.) (1991) Characteristics of active faults. J Struct Geol 13:1−240

Haeussler PJ, Schwartz DP, Dawson TE, Stenner HD, Lienkaemper JJ, Sherrod B, Cinti FR, Montone P, Craw PA, Crone AJ, Personius SF (2004) Surface rupture and slip distribution of the Denali and Totschunda faults in the 3 November 2002 M 7.9 Earthquake, Alaska, BSSA, 94, 1 No. 6B, pp 23–52 (2004)

Honegger DG, Nyman DJ (2004) Guidelines for the seismic design and assessment of natural gas and liquid hydrocarbon pipelines

Hungr O, Leroueil S, Picarelli L (2013) The Varnes classification of landslide types, an update. Landslides. doi:10.1007/s10346-013-0436-y

Kuzmin YO (2004) Modern geodynamics of fault zones. Phys Earth 10:95–111 (in Russian)

Lunina OV, Gladkov AS, Gladkov AA (2012) Systematization of active faults for seismic hazard assessment. Pac Geol 31:49–60 (in Russian)

Mattiozzi P, Strom A (2008) Crossing active faults on the Sakhalin II onshore pipeline route: pipeline design and risk analysis. In: Santini A, Moracittie N (eds) 2008 seismic engineering conference commemorating 1908 Messina and Reggio Calabria earthquake, pp 1004–1013

Nikonov AA (1995) Active faults, definition and problems of their identification. Geoecology 4:16–27 (in Russian)

Schwartz DP, Coppersmith KJ (1984) Fault behavior and characteristic earthquakes—examples from the Wasatch and San Andreas fault zones. J Geophys Res 89:5681–5698

SNiP 2.05.06.85* (1996) Russian State construction code "trunk pipelines" (in Russian)

Strom A, Ivaschenko A, Kozhurin A (2009) Assessment of the design displacement values at seismic fault crossings and of their excess probability. In: Huang R, Rengers N, Li Z, Tang C (eds) Geological engineering problems in major construction projects. Proceedings of 7th Asian regional conference of IAEG, 9–11 Sept 2009, Chengdu, China

Trifonov VG (1985) Peculiarities of active faults evolution. Geotectonics 2:16–26 (in Russian)

Youngs RR, Arabasz WJ, Anderson RE, Ramelli AR, Ake JP, Slemmons DB, McCalpin JP, Doser DI, Fridrich CJ, Swan FH III, Rogers A, Yount JC, Anderson LW, Smith KD, Bruhn RL, Knuepfer PLK, Smith RB, dePolo CM, O'Leary DW, Coppersmith KJ, Pezzopane SK, Schwartz DP, Whitney JW, Olig SS, Toro GR (2003) A methodology for probabilistic fault displacement hazard analysis (PFDHA). Earthq Spectra 19:191–219

Foundation Damage Responses of Concrete Infrastructure in Railway Tunnels Under Fatigue Load

115

L.C. Huang and G. Li

Abstract

The concrete foundation in railway tunnel settles gradually following long-term exposure to repeated loads by trains on the track. We established two foundation numerical models of a railway tunnel and their structure responses under the loads by trains and verified the methodology by field testing. With these models, we examined the relationship between the train velocity and the vertical dynamic coefficient, demonstrated that the damages in the concrete foundation resulted from fatigue damage accumulation due to repeated loads. In concrete foundations with rebar, the attenuation rate of stress was higher than those without rebar, thus having better structure responses. In conclusion, we advise to increase the reinforcement ratio of the concrete foundation of tunnel railways to improve its structure responses.

Keywords

Concrete foundation • Railway tunnel • Structure response • Simulation model

115.1 Introduction

The concrete foundation of a railway tunnel settles gradually following long-term exposure to repeated loads by running trains on the track, which is more obvious in the west of China with the soft soil foundation. So there are many engineering problems in the foundation of railway tunnel, but it is pity that some engineers do not pay much attention in the design and construction, and the design codes are often times outdated. Because of the difficulty to simulate the foundation structure under railway live load, the calculation results can not reflect the real stress state. Jin et al. (2005) used the Newmark method to solute the dynamic

L.C. Huang · G. Li (✉)
School of Engineering, Sun Yat-sen University, Guangzhou, China
e-mail: badboy955@163.com

L.C. Huang
e-mail: hlinch@mail.sysu.edu.cn

equilibrium equation, and then calculated the vibration load history. Jones et al. (2003) simulated the vibration propagation on tunnels. Moghimi and Tonagh (2008) performed a parametric study to identify the effects of road surface roughness on various parameters, such as vehicle speed, aspect ratio of steel girders, stiffness of neoprene, type of vehicle, vehicle lane eccentricity and initial bounce of the vehicle, on dynamic load allowance using non-linear dynamic simulation. Jiang et al. (2010) analyzed the seismic response of underground utility tunnels through shaking table testing and finite element method (FEM) analysis. It showed that the numerical results matched the experimental measurements very well. A theoretical study of the stability of a two-mass oscillator moving along a beam on a visco-elastic half-space was analyzed by Metrikine et al. (2005), who, using Laplace and Fourier integral transforms and expressions for the dynamic stiffness of the beam derived the point of contact with the oscillator. The propagation of vibration generated by a harmonic or a constant load moving along a layered beam which was resting on the layered half-space was investigated theoretically by Sheng et al. (1999).

The aim of our study is to find out the reason of tunnel foundation cracks, to descript the damaging effects of the loads by trains on the concrete foundation of railway tunnels, and to explore a better modality of building concrete foundation in railway tunnels.

115.2 Computational Model

A railway tunnel in the west of China is chosen as the research model in this paper, with the three-dimensional simulation analysis, shown in Fig. 115.1.

In the computation, the surrounding rock is classified as IV by the design standard of railway tunnel in China. Table 115.1 shows the corresponding parameters for these materials.

In order to find out the reason of tunnel foundation cracks by trains live loads on the concrete foundation of railway tunnels, two computational models have been implemented here:

Model I—the concrete (C20) foundation is the plain concrete structure, and the depth is 30 cm;
Model II—the concrete (C20) foundation is the reinforced concrete structure, and the depth is 20 cm.

115.3 Field Testing Model

In order to verify the actual stress responses with the numerical simulation results, a field testing of the foundation base was implemented in this tunnel.

In both models, five inbuilt pressure cells were embedded at the top of the concrete foundation that is exactly located under the sleeper, as shown in Fig. 115.2. Seven
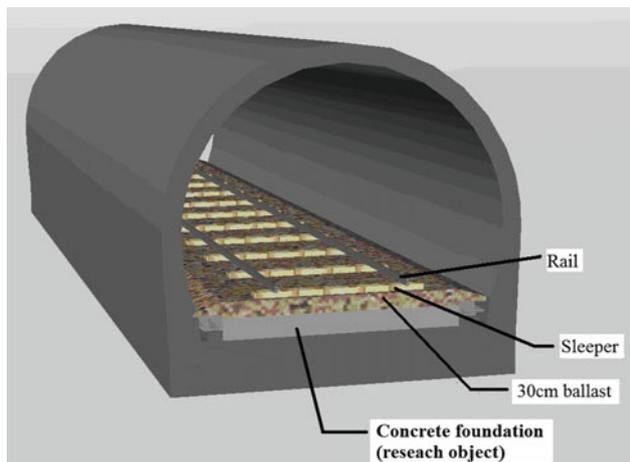
Fig. 115.1 Sketch map of the cross section of the tunnel structure under the rails (*unit* cm)

accelerometers embedded at the top of the concrete foundation, which are located under the sleepers and exactly located in between them; the specific dimensions are shown in Fig. 115.2.

Being identical with the simulation conditions, the load used in the field test was Shaoshan III locomotive. It was stopped only at specific locations in order to measure the static stresses. In the dynamic tests, the data pertaining to the load of the running train, the Shaoshan III locomotive, were recorded as the effective measured results.

As the speeds of the train in the field testing varied from 15 to 28 km/h, we took an average speed of 22 km/h in the calculation. The average stress ($\bar{\sigma}$), mean-variance (δ_σ), and statistical maximum values (σ_{maximum}) are shown in Tables 115.2 and 115.3.

These results showed that the maximum dynamic pressure stress in the top of foundation base was only 0.293 MPa under the live load of the train, which is also considerably less than the compression strength of the concrete material of the tunnel concrete foundation. In other words, the concrete foundation base of the tunnel cannot be damaged under the vertical pressure stress of the running train.

Tables 115.2 and 115.3 suggests that the average dynamic stresses are approximately 1.2–1.4 times of the static stresses in the foundation base, which implies that the live load of the train clearly affects the foundation base.

115.4 Comparison Results

The structure responses and the vertical dynamic coefficient at an average speed of 22 km/h are compared between the measuring results from field testing and the theoretical results from numerical simulation (Table 115.4). The distribution of the stresses at the top of the foundation base is shown in Fig. 115.3.

It shows that the numerical simulation results are in good agreement with the results of the field testing. In the entire concrete foundation base, the maximum stress is located exactly under the two rails and the minimum stress at the middle of the sleeper. It can be concluded that the damage in the concrete is likely to occur not from attaining an elastic limit under the static loads but more likely from the damage accumulation in fatigue due to repeated loadings. At this point, we conclude that the disrepair and damage in the concrete foundation are usually detected in the longitudinal direction, immediately below the two rails, and thus, the concrete foundation surface should be reinforced in the transverse direction. At the same time, in order to enhance the tensile capability and to decrease the formation of cracks in the concrete foundation, it is reasonable to adopt the compact reinforce bar.

Table 115.1 Material parameters

No.	Material	E (GPa)	γ (kN/m^3)	Φ (°)	μ	C (kPa)
1	Surrounding rock	6	21	50	0.30	25
2	Lining (C20 concrete)	26	23	N	0.20	N
3	Bedding (C20)	26	23	N	0.20	N
4	Ballast	0.15	24	30	0.27	5
5	Sleeper (C40)	36.0	28	N	0.15	N
6	Rail	210.0	77	N	0.28	N

Note E is the Young's modulus, γ is the bulk density, φ is the inter friction angle, μ is the Poisson's ratio, and C is the cohesion force

Fig. 115.2 Arrangement plan of the testing locations at the upper of the concrete foundation (*unit* cm)
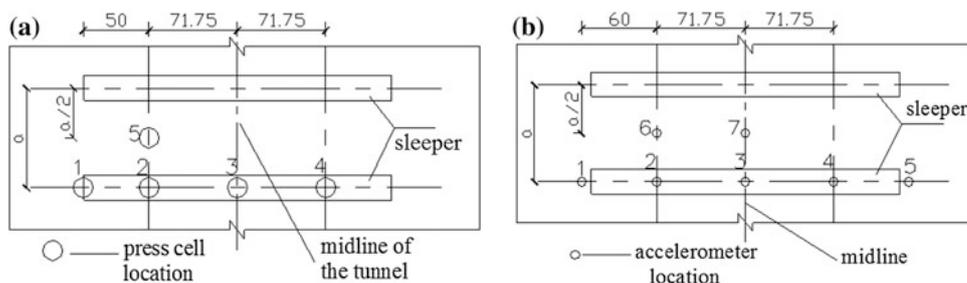
Table 115.2 Statistic values of the dynamic stresses in Model I (MPa)

Stress item	1	2	3	4	5
$\bar{\sigma}$	0.087	0.232	0.052	0.161	0.123
δ_σ	0.017	0.047	0.010	0.022	0.010
$\sigma_{maximum}$	0.112	0.293	0.072	0.198	0.137

Table 115.3 Statistic values of the dynamic stresses in Model II (MPa)

Stress item	1	2	3	4	5
$\bar{\sigma}$	0.097	0.200	0.038	0.236	0.107
δ_σ	0.006	0.030	0.006	0.029	0.014
$\sigma_{maximum}$	0.112	0.293	0.048	0.284	0.131

Table 115.4 Comparison between testing values and the computational values

Locations			1		2		3	
			Stress (MPa)	Dynamic coefficient	Stress (MPa)	Dynamic coefficient	Stress (MPa)	Dynamic coefficient
Model I	Testing	Static	0.063	1.381	0.171	1.889	0.040	1.300
		Dynamic	0.087		0.232		0.052	
	Computation	Static	0.070	1.086	0.075	1.080	0.060	1.083
		Dynamic	0.076		0.081		0.065	
Model II	Testing	Static	0.075	1.293	0.168	1.190	0.030	1.267
		Dynamic	0.097		0.200		0.038	
	Computation	Static	0.070	1.086	0.074	1.081	0.059	1.085
		Dynamic	0.076		0.080		0.064	

Fig. 115.3 Stresses distribution on the top of the of the concrete foundation
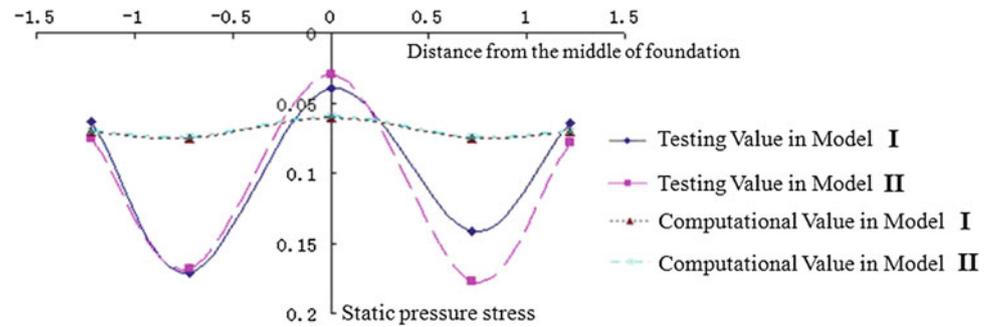
115.5 Main Conclusions

(1) The thicker the foundation base, the greater the stresses are. However, it is not advisable to improve the tunnel foundation base by simply increasing the thickness of the concrete foundation; it is more advisable to improve the structure responses of the tunnel foundation base by adopting the compact reinforced concrete structure.

(2) Lateral tensile stress is the main factor that causes damages to the foundation base.

(3) The damages in the concrete foundation occur more likely from fatigue damage accumulation due to repeated loadings rather than from attaining an elastic limit under static loads.

References

Fiala P, Degrande G, Augusztinovicz F (2007) Numerical modeling of ground-borne noise and vibration in buildings due to surface rail traffic. J Sound Vib 301(3):718–738

Huang LC, Xu ZS, Zhou CY (2009) Modeling and monitoring in a soft argillaceous shale tunnel. Acta Geotechnics 4(4):273–282

Jones CJC, Thompson DJ, Petyt M (2003) A model for ground vibration from railway tunnels. Transport 153(2):121–129

Jiang LZ, Chen J, Li J (2010) Seismic response of underground utility tunnels: shaking table testing and FEM analysis. Earthquake Eng Eng Vibr 9(4):555–567

Jin LX, Zhang JS, Nie ZH (2005) Dynamic inverse analysis for vibration-load history of high-speed railway. Chin J Traffic Transport Eng 5:27–32

Moghimi H, Tonagh HR (2008) Impact factors for a composite steel bridge using non-linear dynamic simulation. Int J Impact Eng 35:1228–1243

Madshus C, Kaynia AM (2000) High-speed railway lines on soft ground: dynamic behavior at critical train speed. J Sound Vibr 231 (3–5):689–701

Metrikine AV, Verichew SN, Blaauwendraad J (2005) Stability of a two-mass oscillator moving on a beam supported by a visco-elastic half-space. Int J Solids Struct 42(3–4):1187–1207

Sheng X, Jones CJC, Petyr M (1999) Ground vibration generated by a load moving along a railway track. J Sound Vibr 228(1):129–156

Assessment and Risk Management for Integrated Water Services

Loretta Gnavi, Glenda Taddia, and Stefano Lo Russo

Abstract

Drinking water supply and waste water networks and treatment systems provide essential services to the community. These infrastructures are vulnerable and subject to a wide range of risks; damage and operation interruptions that require immediate restoration and management of the emergency, may occur. The vulnerability of water supply systems is nowadays the focus of attention of everyone responsible for their security and good performance. Direct effects caused by disasters involve the physical damage to the infrastructure while indirect damage is linked to the additional expenses that the water companies need to incur in order to respond to the emergency, as well as the loss of revenue due to the interruption of their services. The analysis and risk assessment for the Integrated Water Services relating to natural hazards and/or human origin threats is based upon the equation that correlates the risk to the probability of occurrence of an adverse event, the vulnerability and the consequences. The paper presents an overview of the general framework and the risk tools useful for the risk management for Integrated Water Services.

116.1 Introduction

Drinking water supply and waste water networks and treatment systems are vulnerable and subject to a wide range of risks. In the third edition of the Guidelines for Drinking-water Quality, the World Health Organisation (WHO 2008) has emphasized that a comprehensive risk management approach represents the best way to ensure safe drinking water supply, considering the entire supply system, from source to tap. As part of risk management, WHO recommends preparation of Water Safety Plans (WSPs), including system assessment, operational monitoring and management plans.

The knowledge of the different sources of risk and the interrelationships between them have not yet been systematized. The final objective of this study will be to define some guidelines applicable to the national context and useful for the development of an integrated methodology that allows the evaluation, quantification and management of natural and human origin hazards for the Integrated Water Services. Models in this sense have been developed for national contexts in Australia (NHMRC/NRMMC 2004), New Zealand (Ministry of Health 2005a, b), Sweden (SNFA 2007), Denmark (DWWA 2006) and Norway (NFSA 2006).

L. Gnavi (✉) · G. Taddia (✉) · S.L. Russo (✉)
Department of Environment, Land, and Infrastructure Engineering (DIATI), Politecnico di Torino, Corso Duca degli Abruzzi 24, 10129 Turin, Italy
e-mail: loretta.gnavi@polito.it

G. Taddia
e-mail: glenda.taddia@polito.it

S.L. Russo
e-mail: stefano.lorusso@polito.it

116.2　Risk Assessment for the Integrated Water Services

The analysis and risk assessment for the Integrated Water Services relating to natural hazards and/or human origin threats is based upon the equation that correlates the risk to the probability of occurrence of an adverse event, the vulnerability and the consequences. This analysis must include:

- a procedure to identify all possible hazardous events (floods, landslides, earthquakes, terrorist attacks, intrusions and sabotage to critical components, etc.). Among the natural hazards, earthquakes, floods and droughts are the three most significant hazards that can cause water utilities damage;
- a methodology for the analysis of response mode and the vulnerability of the system and its components (Fig. 116.1), in case the adverse event occur;
- a procedure for the evaluation of the consequences in case the occurrence of an adverse event should compromise, for example, the continuity of drinking water supply. The consequences should be evaluated from the environmental, social, economic and legal point of view.
- a procedure for the assessment and risk management, which, once identified and quantified, place to confirm whether this is tolerable and if the control and prevention measures are adequate, and to identify appropriate strategies for mitigating risk.

The vulnerability assessment is essentially a four-step procedure (AWWA 2001):

1. identify and describe the separate components of the water supply total system;
2. estimate the potential effects of probable disaster hazards on each component of the system;
3. establish performance goals and acceptable levels of service for the system;
4. if the system fails to operate at desired levels under potential disaster conditions, identify key or critical system components responsible for the condition.
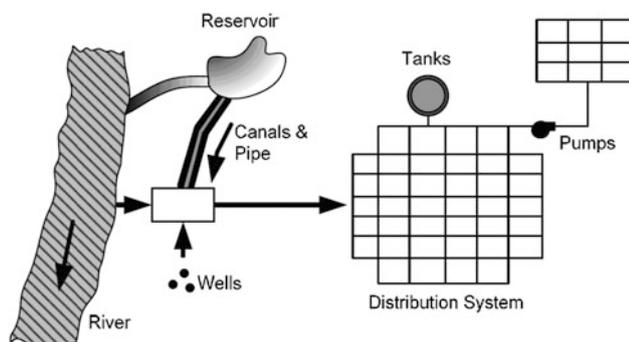
Fig. 116.1 Elements and vulnerable points in a general water supply system (*source* Haestad et al. 2003)

The risk assessment can be conducted by splitting the system into sub-systems in turn subdivided into components that, in the case in which they reach a given limit state that produces breakage or malfunction, the crisis of the entire system may occur. The division of the system into components should take into account, as much as possible, the interactions between the different components and the sub-systems.

Nowadays the methods of risk analysis (Table 116.1) can be more or less detailed, qualitative and/or quantitative, based on the use of standard indicators and implemented with inductive and deductive logical processes.

The identification of hazards can be based on experiences from the past, checklists and structured methods such as Failure Modes and Effects analysis (FMEA).

The qualitative methods generally requires less input data; the most common qualitative risk assessment is risk ranking. Risk estimation with risk matrices is a useful and efficient tool and it is easy to understand and present data.

The aim of quantitative methods is to provide an estimation of the risk level in absolute terms. A wide range of quantitative methods exists.

Among the methods that can be both qualitative and quantitative, the Event tree analysis (ETA) and the Fault tree analysis (FTA) should be mentioned. A fault tree is a logic diagram modelling failure events that may occur in a system and the interactions between these events. The top event may represents a failure in delivering the required quantity and/or quality of drinking water.

The availability of a system that, through the mapping of the global and local fragility of the networks system, might provide indications on the most likely "break" points, represents a useful tool for the planner that can ensure effectiveness and efficiency in the processes of network implementation and management.

116.3　Example on Risk Assessment for Water Utilities

In order to provide some examples on risk assessment practice the integrated water production and management services of Società Metropolitana Acque Torino (SMAT) S. p.A. can be taken into account. SMAT S.p.A. manages some of the largest, most advanced drinking water supply and waste water networks and treatment systems in Europe. It produces every year more than 260 millions cubic metres of quality drinking water. About 70 % of the supplied water comes from wells which are fed by one or more from 40 to over 100 m deep groundwater tables and 14 % is taken from Pian della Mussa, Sangano and other spring sources. The water taken from the Po river totals 16 % of the water introduced into the network. Through an approximately

Table 116.1 Overview of possible risk analysis methods for use in water safety plans (*source* Rosèn et al. 2007)

Risk analysis method	Stage in the risk analysis process	Qualitative/ quantitative	Part of water supply system	Water quality/ water quantity	Data requirements	Need of training
Hazard and operability analysis techniques (HAZID)	Hazard identification	Qualitative	All	Both	Low	Novice
Hazard and operability analysis (HAZOP)	Hazard identification	Qualitative	Treatment distribution	Both	Medium	Specialist
Preliminary hazard analysis (PHA)/ risk and vulnerability analysis (RVA)	Hazard identification risk estimation	Qualitative	All	Both	Medium	Novice
Failure modes, effects, and criticality analysis (FMECA)	Hazard identification Risk estimation	Qualitative	Treatment Distribution	Both	High	Specialist
Fault tree analysis	Risk estimation (causes)	Qualitative/ quantitative	All	Both	High	Expert
Reliability block diagram	Risk estimation (causes)	Qualitative/ quantitative	All	Both	High	Expert
Event tree analysis	Risk estimation (consequences)	Qualitative/ quantitative	All	Both	High	Specialist
Human reliability assessment (HRA)	Risk estimation (causes)	Qualitative/ quantitative	Treatment Distribution	Both	High	Expert
Physical models	Risk estimation (consequences)	Quantitative	All	Both	High	Expert
Quantitative microbiological risk assessment (QMRA)	Risk estimation (consequences)	Quantitative	All	High	Quality	Expert
Barriers and bow-tie diagram	Risk estimation	Qualitative/ quantitative	All	Both	Low	Specialist

12,000 km long network, SMAT S.p.A. distributes drinking water to about 2.2 million people, and collects urban waste water through 8,000 km of sewers. 412 small-, medium- and large-sized sanitation systems constantly run and sanitise about 350 million cubic metres of waste water every year.

Currently the SMAT crisis plan for water supply plants provides an assessment based on the Failure Modes and Effects analysis. For each event (flood, earthquake, snow or ice, wind, contamination, electricity supply failure, vandalism, terrorism, electrical fault, mechanical/hydraulic failure, human error, etc.) the following parameters are evaluated: (1) the probability of the event (from 1 remote to 10 very high); (2) the areas of the facility involved; (3) the potential failure modes; (4) the potential failure effects; (5) the severity of the failure effects (from 1 barely perceptible to 10 extremely severe; (6) control measures and containment activities; (7) evaluation of the effectiveness of control measures and containment activities (from 1 high to 10 unlikely).

On the basis of the previous evaluations a Priority Risk Index (PRI) is defined and should be compared with the severity of the failure effects. If the effect of the failure is more serious, then the intervention threshold is lower, in order to contain the effect itself. For example, situations with high severity (grade 9–10) require the implementation of measures already with PRI > 40, while situations with low gravity (1) require interventions with PRI > 150.

A further step forward could concern the analysis through quantitative methods; the main advantage of a quantitatively estimated risk is that it facilitates comparison with other risks and acceptable levels of risk in absolute terms.

A logical approach could be to first perform a qualitative risk assessment, covering the entire system, and later to apply a quantitative method for a more detailed assessment.

To fulfil this objective, it may be necessary to carry out risk analysis at various levels: (1) Integrated analysis of the total water supply system, (2) Specific analysis of the raw water source, the treatment system, the distribution network and/or the plumbing system, (3) Specific analysis of technical systems/operational activities and (4) Analysis of subfunctions within the system.

Fault tree analysis can be identified as a suitable method to quantitatively estimate risk; it makes possible to model failures as chains of events and thus consider interactions between components and events.

To analyse the entire drinking water system, it can be divided into three sub-systems: raw water, treatment and distribution. The main reason for this division is to make it possible to calculate which part of the system contributes most to the total risk. Another reason is that it shows more easily how different parts of the system may compensate for failure in other parts.

The overall failure event is the supply failure and may arise due to: (1) quantity failure, i.e. no water is delivered to the consumer; or (2) quality failure, i.e. water is delivered but is unfit for human consumption.

The fault tree analysis cannot include health effects of drinking water not fulfilling the quality standards. To also include health effects (assessing the risk of human infection) the fault tree method may be combined with a Quantitative Microbial Risk Assessment (QMRA).

The fault tree analysis furthermore provides a detailed system description that can be used to identify options to reduce the risk.

116.4   Conclusions

To facilitate risk management of water utilities, including preparation of Water Safety Plans, suitable methods and tools for analysing systems and comparing risk-reduction measures are necessary. Since water utilities are very diverse and exhibit different types of risks, one single method cannot be used in all cases; both qualitative and quantitative methods can provide useful information.

An effective risk analysis requires basic knowledge about possible risks, characteristics of potential hazards, and comprehensive understanding of the associated cause-effect relationships within the water system.

The generic framework described aims at providing support and structure for risk management in preparation of Water Safety Plans. The analysis of some examples on risk assessment for water utilities will form the basis for the choices and decisions on control measures to increase the security of the Integrated Water Services. The continuation of the study aims to provide useful results in order to draw the attention of the managers of Integrated Water Services on the priorities and possible alternatives to be considered in the organization and in the choice of maintenance or updating of the system which they are responsible.

References

AWWA (2001) emergency planning for water utility management. American Water Works Association, Manual of water supply practices-M19, 4th edn

DWWA (2006) Guidelines for safe drinking water quality (in Danish), Danish Water and Wastewater Association, Skanderborg

Haestad M, Walski TM, Chase DV, Savic DA, Grayman W, Backwith S, Koelle E (2003) Advanced water distribution modeling and management. Haestad Press, Waterbury

Ministry of Health (2005a) Drinking-water standards for New Zealand 2005, New Zealand Ministry of Health, Wellington

Ministry of Health (2005b) A framework on how to prepare and develop public health risk management plans for drinking-water supplies, New Zealand Ministry of Health, Wellington

NFSA (2006) Improved safety and emergency preparedness in water supply: Guidance (in Norwegian), Norwegian Food Safety Authority, Oslo

NHRMC/NRMCC (2004) National water quality management strategy: Australian drinking water guidelines. National Health and Medical Research Council and Nature Resource Management Ministerial Council, Australian Government

Rosèn L, Hokstad P, Lindhe A, Sklet S, Røstum J. (2007) Generic framework and methods for integrated risk management in water safety plans, TECHNEAU report. Deliverable no. D 4.1.3, D 4.2.1, D 4.2.2, D 4.2.3

SNFA (2007) Risk and vulnerability analysis for drinking water supply (in Swedish), Swedish National Food Administration, Uppsala

WHO (2008) Guidelines for drinking-water quality [Electronic Resource]: Incorporating first and second addenda, vol 1, Recommendations, 3rd edn. World Health Organization, Geneva

Murgese Davide, Giraudo Giorgio, Testa Daniela, Airoldi Giulia,
Cagna Roberto, Bugnano Mauro, and Castagna Sara

Abstract

Natural risk assessment for urban areas and infrastructures is important for the definition of management and prevention plans against consequences of natural events. In this paper we present the results of a multi-risk assessment for the Cuneo Province road network. The study defined specific risk levels with regard to landslides, floods, torrential floods, debris-flows, snow-avalanches, earthquakes and forest fires. Consequences for infrastructures were assessed by quantifying exposed elements value and vulnerability. All acquired data are then combined in order to produce specific hazard and risk maps. Specific risk levels were then processed to produce a multi-risk map for the Cuneo province road network. Landslide runout was numerically simulated in a GIS environment, for a comparison with hazard assessment results obtained following the methodology here proposed. Multi-risk assessment represents a valuable tool for enhancing scheduling activities related to the implementation of mitigation structure/measures and for supporting the coordination of risk management procedures at a cross border level.

Keywords

Multi-risk • Natural hazard • GIS • Roads • Vulnerability

117.1 Introduction

Road networks represent a key factor in the emergency phase, for they are the most effective way for reaching and providing assistance to affected areas. Also, they are exposed elements and it is important to provide a reliable and updated risk assessment for these infrastructures. Road networks often extend over areas with variable morphological conditions and, for this reason, different risk scenarios have to be considered. In order to perform a reliable risk evaluation it is important to collect all data that allow the accurate assessment of all risk components: hazard, vulnerability and value of exposed elements. These parameters are often expressed following different approaches (e.g. qualitative, quantitative) and by using different measurement systems. Risk assessment requires specific procedures for the homogenization of processed data. Hazard and risk maps are a powerful tool for providing risk information to the population and all authorities involved in risk management and civil protection activities. Reliable risk assessment results allow the audit of risk management procedures, the implementation/correction of existing approaches/structures/organizations, the revision of maintenance programs and the improvement in funds allocation for strategic interventions. Natural risk assessment is a complex activity and the

M. Davide (✉) · T. Daniela · A. Giulia
SEA Consulting srl, 4e-arth (for environment, for ecology, for education for earth our planet), Turin, Italy
e-mail: murgese@4e-arth.eu

G. Giorgio
Cuneo Province, Public Works Sector Civil Protection Services, Cuneo, Italy

C. Roberto · B. Mauro · C. Sara
Polithema Società di Ingegneria srl, Turin, Italy

adopted methods have to be clearly described to allow a correct implementation of risk management procedures. This is particularly relevant when risk management is performed at a cross-border level by authorities from different regions and countries, as in the area of Cuneo and Imperia Provinces (Italy) and the Provence-Alpes-Côte d'Azur region (France). This paper illustrates the results of natural risk assessment for the Cuneo Province road network, based on the methodology defined by the technicians of Cuneo and Imperia Provinces (Giraudo et al. 2012) the project was part of the Strategic Program **Risknat** a cross-border project in the framework of the program Alcotra France-Italy (2007–2013), developed between 2009 and 2012, focusing on natural hazards in mountain areas.

117.2 Methods

The multi-risk assessment of Cuneo Province road network was referred to the following processes: landslides, floods, debris-flows, torrential floods, snow avalanches, forest fires and earthquakes. Risk assessment was performed according to the methodology defined by Cuneo and Imperia Provinces (Giraudo et al. 2012). Considered infrastructures extend over areas with different morphological conditions (flood-plains, hills, mountain areas), with a total length of 862 km. Each road was divided into segments; each segment was defined by nodes corresponding to road intersections or other critical points (e.g. towns crossed by the examined road). Risk level was calculated for each segment. The study was divided into three main phases:

Phase (1)—hazard elements (features to be stored as shape files) were acquired from (i) existing databases (e.g. IFFI, SIFRAP, PAI, SIVA, Forest territorial Plans) owned by public authorities, such as Piedmont Region, Piedmont Environmental Protection Agency (ARPA Piemonte), Cuneo Province and Po Basin Authority, and (ii) public reports on past events (e.g. ARPA and or Piedmont Region event reports). Acquired data were used to produce inventory maps for each natural hazard. Road network data were provided by Cuneo Province and ANAS (Italian National Road Agency). Road segments were identified along each considered infrastructure, based on the presence of intersections with other roads and the distribution of urban centres and public services. The study area (1,277 km^2 wide) was defined according to the distribution and dynamics of hazard phenomena and the distribution of exposed elements.

Phase (2)—collected information were validated by means of aerial photographs interpretation and field survey. Data related to hazard-mitigation structures and other structures along the roads (bridges, embankments, tunnels) were also collected in the field and stored into a specifically designed database.

Phases (3)—**(3a)** data on hazard phenomena were stored as shape files in a GIS geo-database, each file corresponding to a specific hazard type. Each feature of the shape files was then characterised in terms of hazard level. Hazard levels are expressed as numbers ranging from 1 (low hazard level) to 4 (very high hazard level). Parameters used for hazard calculation were those derived from features geometry and other hazard characteristics, according to the method proposed by Giraudo et al. (2012). **(3b)** Each road segment was characterised in terms of specific vulnerability and exposed value, both expressed as numbers ranging from 0 to 1 (Giraudo et al. 2012). Specific vulnerability was calculated as the combination of the efficacy level assigned to hazard-mitigation structures and damage proneness in case of e specific natural event. The value of exposed elements was determined according to the following parameters: road network hierarchy, existence of alternative paths to the considered segment and segments representing the unique access to relevant territorial elements stored into the database of Civil Protection Department of Cuneo Province (e.g. strategic factories, small urban centres, etc.). **(3c)** Specific and multi-risk levels were calculated for each segment, on the basis of the relationships with hazard features, which were established by means of specific algorithms in the GIS environment. According to the distribution of risk numeric results (natural breaks of series values defined in a GIS environment), four risk classes were defined (low, moderate, high, and very high). Specific risk and multi-risk maps were produced for the analysed road network of Cuneo Province. Also, numerical modelling of runout for 20 critical landslides (shallow, rotational and complex) was performed (Fig. 117.1). This activity provided a detailed risk scenario in case of propagation of mobilised materials towards the examined roads. Modelling was made by using the software RASH (Pirulli 2005). The model calculates the runout based on 10 × 10 m grid size DTM according to Voellmy (1955) equation.

117.3 Results and Discussion

Hazard assessment results were organized in form of specific hazard maps, where each process was represented according to its hazard level. Studied phenomena are generally characterised by "high" to "very high" hazard levels, exception made for earthquakes, whose hazard levels range from "moderate" to "high". Forest fires are usually characterised by "low" hazard level (Table 117.1).

Landslide hazard: shallow landslides and rock falls are characterised by the highest number of feature with "very high" hazard level. This result is mainly related to the expected velocity of the phenomena. Hazard levels recorded for the other types of landslide (Table 117.1) generally range

Fig. 117.1 Example of landslide runout modelling results (landslide type: shallow landslide; location: Viandio Municipality, Stura Valley). Landslide specific risk for the road segment is also indicated
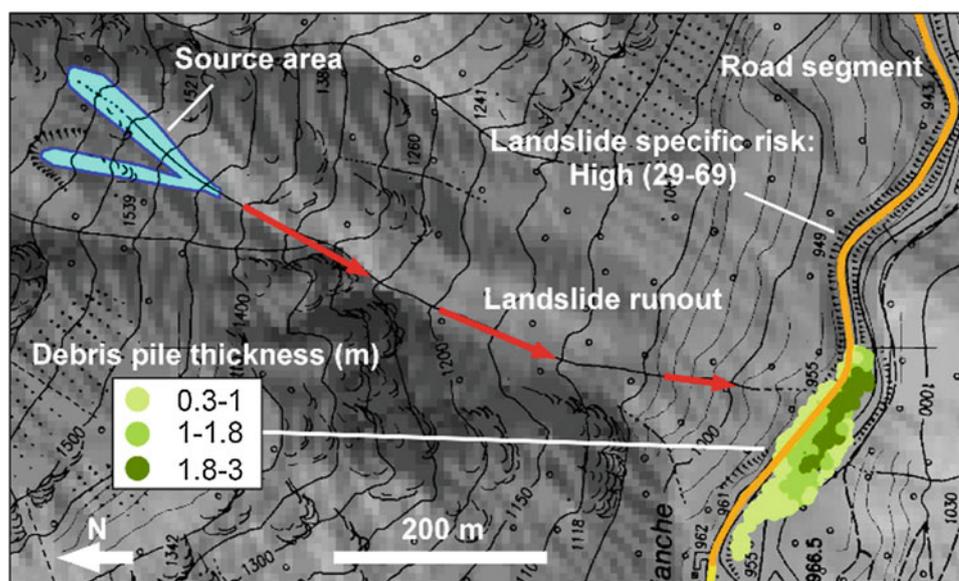
Table 117.1 Hazard levels calculated for each phenomenon

Natural Hazards		Low (%)	Moderate (%)	High (%)	Very high (%)
Landslide	AC/CR	0.04	0.07	0.48	5.59
	AS	0.15	0.07	1.75	29.39
	CL	7.27	1.38	4.14	12.46
	CM	0.56	1.04	2.42	0.60
	DG	0.71	0.86	0.00	0.00
	SR	0.34	9.44	9.14	0.30
	ST	0.04	1.53	8.17	1.75
	X	0.30	0.00	0.00	0.00
Floods		31.00	1.00	23.00	45.00
Torrential floods		25.00	10.00	31.00	34.00
Debris flows		7.00	11.00	32.00	50.00
Snow avalanches		0.40	9.80	29.80	60.00
Forest fire		90.86	9.09	0.04	–
Earthquakes		19.00	50.00	31.00	–

Landslide codes *AC/CR*—rock fall (*AC* punctual r.f.; *CR* areal r.f.); *AS* shallow landslide; *CL* creeping; *CM* complex movement; *SR* rotational slide; *ST* translational slide; *DG* deep seated gravitational slope deformation; *X* sinkhole. Percentages are referred to the number of features considered for the representation of each studied process

from moderate to high. *Flood hazard*: sectors with "very high" hazard levels are those characterised by processes with high energy levels (Fluvial zones A and high hazard level areas according to the Po Basin Hydrogeological management Plan—PAI) and average recurrence intervals between 20 and 50 years. *Torrential flood hazard*: "very high" or "high" hazard levels are principally related to: (1) more than 5 critical events in 100 years; (2) large volume of sediment that can be mobilised in case of intense precipitations. *Debris-flow hazard* is referred to alluvial-fan sectors. In this case the assessment takes into account the hazard level of

torrential floods combined with the channel conditions along the alluvial fan. Debris-flow hazard ranges from "high" to "very high" and is associated to: (1) critical flow conditions for water and/or solid load, mainly due the presence of obstacles on the path along the alluvial fan; (2) streams characterised by "very high" hazard level. *Snow avalanches* with "very high" or "high" hazard levels are those characterised by an extension greater than 50,000 m², with short average recurrence interval (less than 1 year). Value of exposed elements was calculated for each one of the 361 considered road segments (Table 117.2a). Nearly 90 % of

Table 117.2 **a** Road segments falling in the different exposed value classes. **b** Number of road segments potentially affected by studied natural hazards and average vulnerability level to each considered natural process

A) Number of road segments	Exposed value (E)			
	Low	Moderate	High	Very high
361	**0**	**42**		**143**
			176	

B) Natural hazards	Number of hazard features affecting road segments	Average specific vulnerability (V)
Landslides	677	
		0.77
Floods	616	
		0.32
Torrential floods	140	
		0.34
Debris flows	149	
		0.77
Snow avalanches	119	
		0.96
Forest fires	6,631	
		0.60
Earthquakes	361	
		0.50
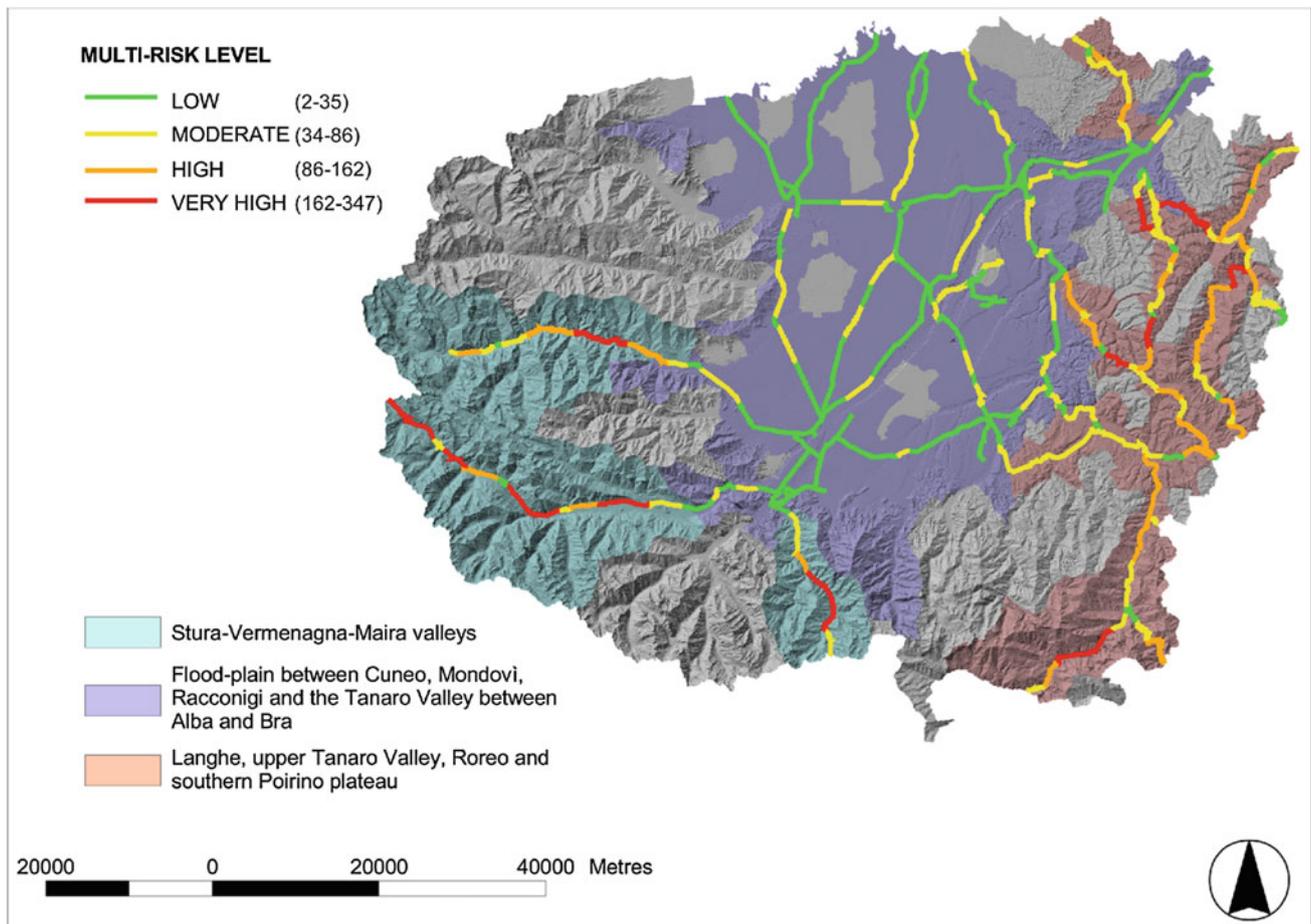
Fig. 117.2 Multi-risk map for the Cuneo Province road network. Numbers in brackets indicate the limits of the four multi-risk levels

road segments has a value belonging to the classes "high" or "very high". Segments characterised by "very high" exposed value commonly belong to the primary network system, for which no alternative connections are present. "High" exposed values mainly relate to secondary road-network segments. Vulnerability was assessed for road segments potentially affected by the inventoried processes: a specific vulnerability level was calculated for each studied natural phenomena (Table 117.2b). Highest values are related to the occurrence of landslides, debris-flows and snow avalanches, providing useful support for scheduling the implementation of mitigation measures.

The combination of hazard levels, exposed values and vulnerability resulted in specific risk and multi-risk maps (Fig. 117.2). Based on multi-risk levels, three homogenous sectors were identified:

(a) Stura-Vermenagna-Maira valleys: risk-level ranges from high to very-high; this sector is characterised by the potential occurrence of all considered natural phenomena.

(b) Flood-plain between Cuneo, Mondovì, Racconigi and the Tanaro Valley between Alba and Bra: risk level ranges from low to moderate; it is related to the potential occurrence of floods, forest fires and earthquakes;

(c) Langhe, upper Tanaro Valley, Roero and southern Poirino plateau: roads in this sector are characterised by risk levels mainly ranging from moderate to high, because of the potential hazard related to landslides, torrential and alluvial-fan activity, floods, earthquakes and bushfires.

Twenty landslides were selected for runout modelling to assess the reliability of landslide hazard assessment method adopted in this study. Numerical simulation reproduced the expected conditions in case of landslide activation. Obtained hazard scenarios following the two approaches indicated that the procedure proposed in this project provides a reliable hazard classification (Fig. 117.1).

117.4 Conclusions

This study provided the assessment of specific natural hazard and natural risk for the Cuneo Province road network. Specific risk were combined in order to produce a multi-risk map to provide the technician of Cuneo Province a reference document during the risk management process. The quantitative assessment of all risk elements (hazard, value and vulnerability of exposed elements) allows the enhancement of scheduling procedures for the implementation of mitigation measures to be adopted.

References

Giraudo G, Faletto C, Grosso GF, Galli M, Spano M, Isoardi P, Pozzani R (2012) Metodologie di analisi del multi-rischio. http://www.provincia.cuneo.it/protezione-civile/progetti/progetto-risknat

Pirulli M (2005) Numerical modelling of landslide runout, a continuum mechanics approach, PhD Thesis Geotechnical engineering, Politecnico di Torino, Italy

Voellmy A (1955) Über die Zerstörungskraft von Lawinen. Schweiz. Bauzeitung 73:159–165, 212–217, 246–249, 280–285

Superficial Hollows and Rockhead Anomalies in the London Basin, UK: Origins, Distribution and Risk Implications for Subsurface Infrastructure and Water Resources

118

Philip E.F. Collins, Vanessa J. Banks, Katherine R. Royse, and Stephanie H. Bricker

Abstract

Recent findings in London show that the subsurface is much more complex than expected, with a number of apparently anomalous features that present a direct hazard to infrastructure development and a risk to ground water management. Of these features, one of the least understood are the large superficial hollows which occur in the rockhead—in much of the London Basin, this is the top of the London Clay Formation—and which are infilled by a range of Quaternary deposits, principally alluvial sands and gravels deposited by the River Thames and its tributaries. The hollows range in size and shape. Several are a few hundred metres across and can be up to 40–50 m deep, though determining their exact form is problematic. The soil and sediment infill of the hollows differs substantially from the surrounding ground in terms of strength and drainage, as well as some differences in chemistry. This presents a real hazard to infrastructure as there is a potential for vertical and horizontal movement, flooding, as well as increasing the risk of contamination of the deeper aquifer. In the paper, the locations and characteristics of known hollows and deformed strata are reviewed and evidence for how they formed is reassessed, systematically considering different hypotheses (scour, ground ice, karst subsidence, seismo-tectonic). From this we consider the implications for continued development of subsurface infrastructure development, and for water resources.

118.1   Introduction

Increasingly, infrastructure development in large cities is exploiting the subsurface for key resources and space. Unexpected ground conditions present key risks to projects during construction and operation e.g. due to subsidence and groundwater contamination.

In the London area of south east England, a major source of risk is unexpectedly deep sequences of permeable, often unconsolidated Quaternary sediments and soils (sand, gravel, clay, silt, fractured/puttied chalk and peat). Typically, these occur beneath the floodplain and low terraces of the River Thames and some of its tributaries. Interest in these infilled hollows has increased because of major infrastructure projects e.g. CrossRail and the Olympic Park. There is also new interest in the hydrogeology of the London Basin as groundwater flow is both a resource and area of risk. In addition, evaluation of existing and new borehole and exposure data suggests a much greater degree of structural complexity in the geology of the London Basin. Several of the known hollows occur at historic water sources and near to newly-identified geological faults.

P.E.F. Collins (✉)
Brunel University, Kingston Lane, Uxbridge,
London, UB8 3PH, UK
e-mail: philip.collins@brunel.ac.uk

V.J. Banks · K.R. Royse · S.H. Bricker
British Geological Survey, Keyworth, Nottingham,
NG12 5GG, UK

While the general location of many of the hollows is known, their full geometry is uncertain. A large number of borehole records exist for the London Basin, but these are geographically clustered, often shallow, and often of low quality. As a result, it is probable that several, perhaps many undiscovered hollows remain. There is a clear need to be able to predict the probability of encountering these hollows, or the deformed ground associated with them. It is also important to determine the cause of the hollows, both in terms of helping to predict their occurrence, but also to assess if they are potentially active features.

118.2 Locating Superficial Hollows in the London Basin

Numerous hollows have been encountered in the London Basin over the past 150 years. These were examined in the 1970s (Berry 1979; Hutchinson 1980), and this catalogue has been updated and digitized by the British Geological Survey,

linked to the development of the Joint London Basin Model (BGS 2013 http://www.bgs.ac.uk/londonBasinForum/JLBM. html) (Fig. 118.1). Work is ongoing, linked to the activities of the London Basin Forum.

The digitization of the dataset has enabled the distribution of the hollows to be considered in their geological and geographical contexts (Banks et al. in prep). GIS analysis has identified key geographical contexts that, in combination, are associated with known hollows: proximity to present-day river channels, artesian ground water conditions, thickness of London Clay, proximity to known geological structures. Based on this analysis, a provisional risk evaluation has been produced. This is a major step forward, but still needs to be refined, not least because knowledge of the location of the known hollows is influenced by a spatially skewed borehole data set. Despite this limitation, this GIS analysis has helped define some of the major contexts which will have controlled the formation of the hollows. These include availability of water, confining layers, geological structures and geomorphological position.
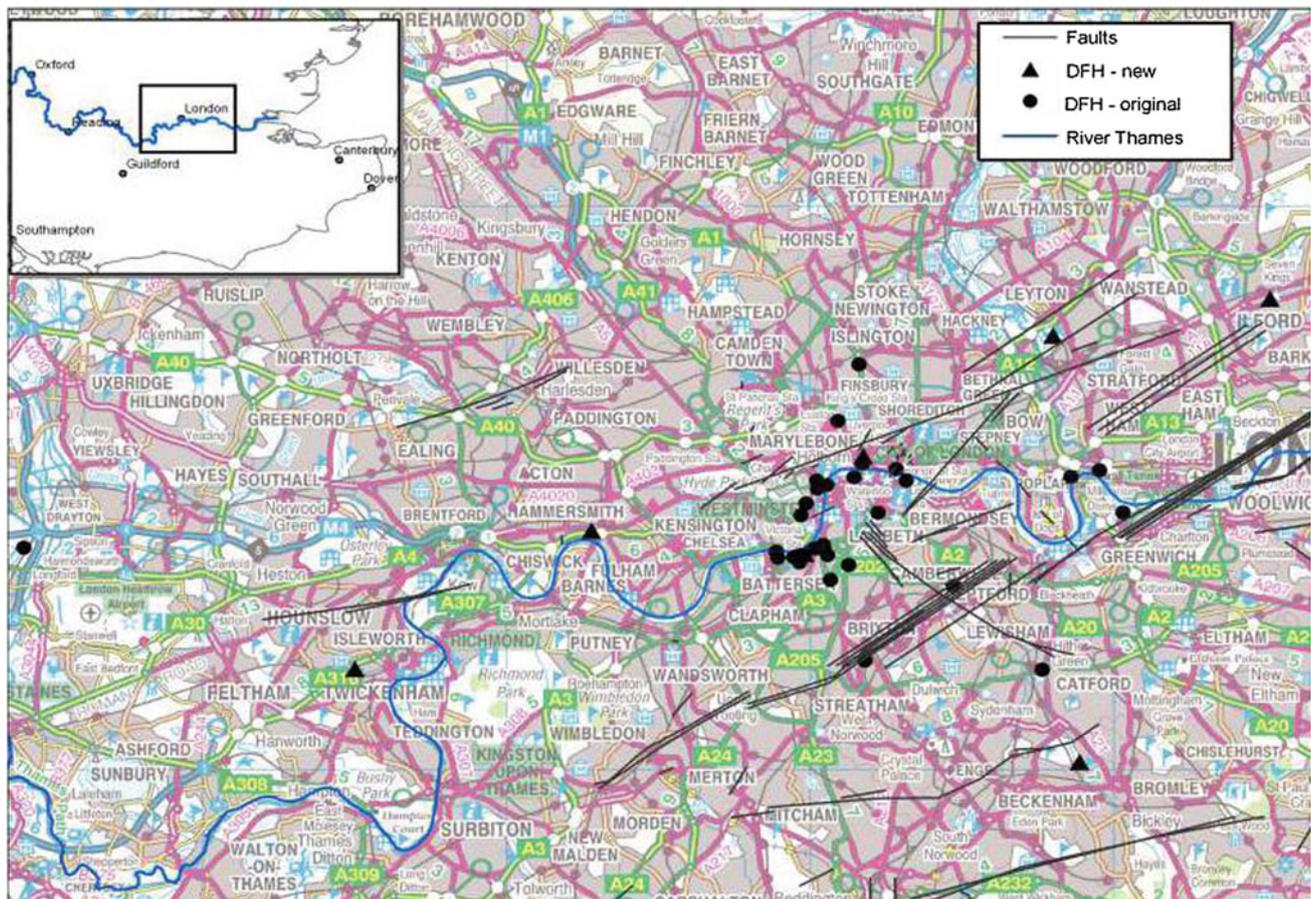
Fig. 118.1 Location of known superficial hollows in London. Point data British Geological Survey ©NERC. Contains Ordnance Survey data ©Crown Copyright and database rights 2014

118.3   Characteristics of Superficial Hollows in the London Basin

The full characteristics of the superficial hollows and the surrounding strata are generally unknown. Those that have a reasonable number of high quality borehole records, including some encountered during the CrossRail project, appear closed with no obvious inlet/outlet. Several are a few hundred metres across and can be up to 40–50 m deep. Most appear to have elongate forms.

The majority in central London are inaccessible for re-examination as they are located beneath buildings, roads and other infrastructure. Similar features, however, occur else-where in the London Basin, most notably in the valley of the River Kennet, a major tributary of the Thames. In this area, several hollows and their surroundings have been studied, both in quarry exposures and using boreholes. These include sites at Woolhampton, Brimpton and Ashford Hill (Fig. 118.2).

A detailed reconstruction of the London Clay rockhead at Woolhampton reveals a deep closed hollow with steep margins (Collins et al. 1996). Infilling strata showed evidence of post-depositional tilting towards the centre of the hollow that occurred between ∼15 and ∼11 ka BP. At nearby Brimpton, a similar hollow was infilled between ∼100 and ∼74 ka BP (Bryant et al. 1983; Worsley and Collins 1995), though no evidence of tilting was reported. No data are available for the strata below the rockhead at Woolhampton or Brimpton.

A feature at Ashford Hill has been described (Hawkins 1953; Hill 1985), based on boreholes, many of which extend below the base of the hollow. These permit a provisional 3 dimensional reconstruction of the subsurface stratigraphy (Fig. 4). The hollow is closed, but extends along the valley floor. Sediments in the hollow, indicate local lacustrine, marsh and fluvial conditions as the hollow formed, followed by subsidence of the hollow's centre and mass movements from the over-steepened margins. Deeper boreholes indicate that a mass of brecciated and puttied Cretaceous Chalk, has penetrated upwards through up to 60 m of Tertiary strata (Fig. 118.3).

118.4   Possible Origins

Several hypotheses have been proposed to explain the presence of superficial hollows and associated features in the London Basin. These vary from simple to complex, and most rely on assumptions of former conditions and limited data. Based on the features from the Kennet valley, hypotheses for the origin of the hollows can be assessed.

a. 'Pingo' (or related ground-ice form). Regional palaeoclimatic reconstructions suggest that permafrost is likely to have existed at various times, though the local evidence for it is ambiguous. The available data show no evidence of the ramparts that surround many relict and active pingos. Work on active pingos (Mackay 1998) suggest a ± planar base associated with the maximum depth reached by the massive segregated ground ice—this would not be likely to leave a deep hollow on melting. The infilling sediments suggest ongoing subsidence after hollow formation—at Ashford Hill, this may be continuing to present.

b. River scour. Some hollows may be due to locally deep erosion in the past. The Kennet hollows do not occur at confluence points, where scour is potentially at a maximum. Several of the hollows are also very deep, penetrating beyond the likely maximum depth of scour.

c. Localised consolidation settlement. The depth of the hollows is too great and the underlying strata are already over-consolidated.

d. Karst subsidence. Dissolution-prone puttied Chalk is present beneath the hollow at Ashford Hill. Boreholes penetrating solid Chalk nearby show the presence of cavities at depth. Both may have contributed as micro-faults, tilting and breccias in the hollow infill suggest that both slow and rapid collapse occurred.

Fig. 118.2 Digital elevation model of the Kennet valley region, western London Basin (*dark blue* low elevation; *white* high elevation) showing location of known superficial hollows
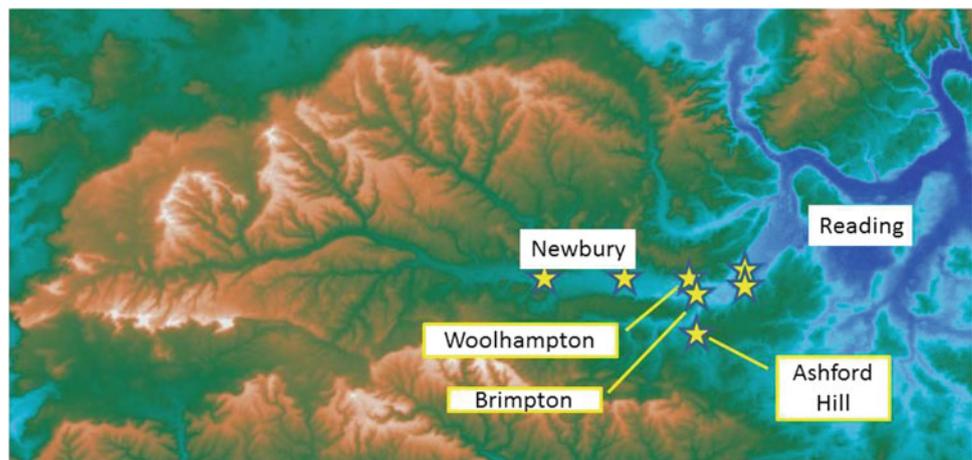
Fig. 118.3 Conceptual ground model for Ashford Hill, showing the superficial hollow and associated deformed strata
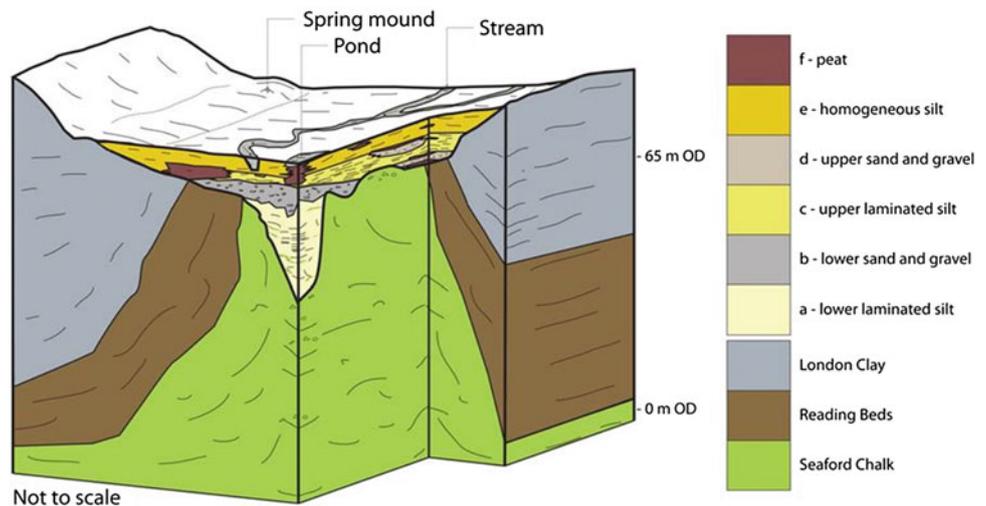
Derived from data and drawings in Hawkins 1953 and Hill 1985, and field observations 1991-2013

The origin of the Ashford Hill Chalk intrusion (similar features are known in central London), is uncertain. Freeze-thaw associated with the development and decay of permafrost may have been involved, though permafrost depth in former cold stages is uncertain. There is also a lack of experimental studies of how freeze-thaw affects heavily loaded Chalk.

However the Chalk was broken up, it was then mobilized. Loading was almost certainly involved as movement was towards the valley centre—this may have been through creep as the horizontal gradients are shallow. Upwards movement may have been driven by high groundwater pressures (Hutchinson 1980). A confining permafrost layer might have enhanced this, though cold stage regional groundwater tables may have been lower than present. The Ashford Hill valley appears structurally controlled and upwards movement of the Chalk may have exploited a pre-existing fault or joint. Additional loading to drive this might have come through a seismic event, though this is speculative. Flow structures were found in Chalk samples collected in the 1930s and 1980s, but these might have been due to sampling.

118.5 Conclusions

The superficial hollows and associated deformations remain problematic. The 'pingo' hypothesis, as a single causal mechanism at least, seems unsupported by the available evidence. Hollow formation can be explained by a simple hypothesis involving dissolution-driven subsidence, though uncertainty remains over the extent of areas affected by this, and whether it remains a significant hazard. A more complete understanding of the risk will only come when the nature and extent of Chalk intrusion is better understood.

References

Berry FG (1979) Late quaternary scour-hollows and related features in central London. Q J Eng Geol 12:9–29

BGS (2013) Joint London basin model. British Geological Survey. http://www.bgs.ac.uk/londonBasinForum/JLBM.html. Accessed 21 Oct 2013

Bryant ID, Holyoak DT, Moseley KA (1983) Late Pleistocene deposits at Brimpton, England. Proc Geol Assoc 94:321–343

Collins et al (1996)

Hawkins HL (1953) A pinnacle of chalk penetrating the Eocene on the floor of a buried river-channel at Ashford Hill, near Newbury, Berkshire. Q J Geol Soc Lond 108:233–260

Hill DT (1985) Quaternary geology of large-scale superficial features at Ashford Hill, Hampshire, England. Unpubl. PhD thesis, University of Reading

Hutchinson JN (1980) Possible late quaternary pingo remnants in central London. Nature 284:253–255

Mackay JR (1998) Pingo growth and collapse, Tuktoyaktuk Peninsula Area, Western Arctic Coast, Canada: a long-term field study. Geographie Physique et Quaternaire 52:271–323

Worsley P, Collins PEF (1995) The geomorphological context of the Brimpton late pleistocene succession (south central England). Proc Geol Assoc 106:39–45

Analysis of the Interaction Between Buried Pipelines and Slope Instability Phenomena

Lisa Borgatti, Alessandro Marzani, Cecilia Spreafico Margherita, Gilberto Bonaga, Luca Vittuari, and Francesco Ubertini

Abstract

Economic and social integration across Europe requires secure lifelines, such as roads, railways and pipelines. Existing and planned lifelines may come across a large number of different natural and anthropic hazards. For instance, past catastrophic events have dramatically shown that steel pipelines may be highly vulnerable to permanent ground deformation due to earthquakes and landslides. Therefore, their behaviour when exposed to processes that can generate large displacement and strain (co-seismic deformation and faulting, liquefaction, earth and rock slides and flows, rock falls) needs to be assessed. In fact, and in particular if toxic and/or flammable materials are transported, structural damage with eventual leakage might result in a severe risks for both human life and the environment, with associated relevant economic costs. To such purpose, in this work, a methodology for the assessment, prevention and efficient management of geological risks, mainly landslides, in steel buried pipelines will be presented. The proposed procedure aims at reducing the risk of environmental disasters and the subsequent huge financial and environmental losses.

Keywords

Landslide • Steel buried pipelines • Permanent ground deformation

119.1 Introduction

Industrialized countries have widespread and intricate networks of infrastructures that support and ensure the effectiveness of many crucial services for our society. Among the different lifelines, important pipeline networks for transportation of oil, gas and water are generally buried below ground surface for technical, aesthetic, safety, economic and environmental respect reasons. As pipeline systems are spread over large areas, they may come across a variety of possible natural hazards. In mountainous areas, for example, past catastrophic events have shown that pipelines are highly vulnerable to permanent ground deformation due to landslides. Therefore, the behaviour of these infrastructures when exposed to slope movements has to be assessed, in particular if toxic and/or flammable materials are transported. In fact, in case of structural damage, with eventual leakage, the risk for human life, for the environment and for the economy could be severe.

The assessment of these problems, the modelling and the mitigation measures have been tackled with in different studies (among others: Liu et al. 2010; Magura and Brodniansky 2012; Rajeev and Kodikara 2011; Zheng et al. 2012). In this context, the main purpose of this study is to determine the stress state induced by slope movements on buried steel pipelines, in order to develop tools and strategies for the monitoring and the prediction of residual life of the pipeline, together with new design solutions for their protection.

L. Borgatti (✉) · A. Marzani · C. Spreafico Margherita · G. Bonaga · L. Vittuari · F. Ubertini
Department of Civil, Chemical, Environmental and Materials Engineering DICAM, Alma Mater Studiorum, Università di Bologna, Viale del Risorgimento 2, 40136, Bologna, Italy
e-mail: lisa.borgatti@unibo.it

119.2 Methodology

The method proposed by the Indian Institute of Technology Kanpur (2007) "Guidelines for seismic design of buried pipelines", was adopted to compute the maximum deformations in pipes due to ground deformation. Such methodology was selected among the available ones being very flexible with respect to possible different scenarios (longitudinal and transversal pipe crossing, liquefaction, faults, seismic action), as well as because simple and straightforward to be applied. The main idea is that the limit deformations in tension and compression caused by ground movements, namely Permanent Ground Deformation (PGD), should be lower than the allowable ones. Such limit deformations can be computed by proper formulae for two limit cases, i.e. the pipeline crossing longitudinally and transversally the PGD zone, and as a weighted sum of the two limit cases for pipelines crossing the PDG and an arbitrary angle. To such scope (i) the geometrical and mechanical data of pipeline, (ii) the geotechnical parameters of the soil, (iii) and the extension and magnitude of the PGD zone, must be known.

At this purpose, a georeferenced database was created (in UTM-ED50), elaborating data of different layers, within a GIS environment. In particular, the considered layers are: the database of the elements of the pipelines network (location, geometrical, physical and operational data) provided by the company operating the gas distribution service; the landslides inventory provided by Regione Emilia-Romagna geological survey; the geotechnical parameters of the soils inferred from lab data on typical landslide material in this geological context (clayey-silty soil: cohesion c = 10,000 Pa; specific weight γ = 20,000 N/m^3; friction angle ϕ = 18°).

At first the landslides were classified on the basis of the state of activity (dormant landslides and active landslides) and on the type of movement. In the investigated area, the landslides are about 800; 520 of them classified as dormant, while the others 280 defined as active (or suspended); they are generally characterized by slow movements (mm/year—cm/year). The majority of these movements are rockslide or earth slides and flows, which are also the most common types of landslides in the northern Apennines. In this geomorphological context, pipeline damage caused by landslides is mainly due to the intermittent reactivation of existing landslides generally due to intense and/or prolonged rainfall.

Next, superimposing the data of the different layers, the pipelines involved in instability phenomena were identified. In particular, 57 out of 103 pipeline elements of the so-called fourth type (i.e., with pressure in the interval 1.5–5 bar) were found in zones of prominent slope instability. For such pipes, the direction and magnitude of the ground movement with respect to the pipe direction was analysed, to distinguish among the two cases of longitudinal and transversal crossing, and so to allow a proper selection of the formula provided in the guidelines.

119.2.1 PGD Estimation

The PGD was estimated by means of two different approaches. The first one estimated the PGD occurred since the pose of the pipeline on the basis of geomorphological evidence and expert knowledge by assigning to each type of landslide a range of velocity (with minimum, average and maximum values, e.g. for very slow landslides, 0.005, 0.010 and 0.015 m/year respectively), determined according to the classification of Cruden and Varnes (1996), and considered to act at the depth of the pipe. The area and the length of the landslide bodies were obtained from the landslide inventory.

Available data from in situ geotechnical monitoring systems (e.g., inclinometers) have been used for the estimation of slope movements on the ground surface and at depth in the vicinity of pipelines. Inclinometer data were analysed to calculate the actual displacements. In general, the data appeared to be scarce, the instruments often placed far away from the pipeline and the monitored period not appropriate.

The second method to define the PGD used velocity data from satellite interferometry; the analysis procedures described in PST-A Guidelines (MATTM 2009) were followed. Ascending and descending ENVISAT images were collected between 2003 and 2008 in the frame of PST-A (Extraordinary Plan of Environmental Remote Sensing) project; they were processed by the companies T.R.E. S.r.l. and e-GEOS with the PS InSAR techniques. These datasets were resampled on a square grid mesh in order to make them comparable: the average velocity value of the Permanent Scatterers (PS) located inside each grid cell was assigned to the centroid of the cell. The velocity values recorded along the ascending and descending orbits were geometrically combined to obtain the velocities along the vertical and E-W horizontal direction; it must be assumed that the N-S horizontal velocity of deformation is negligible (one of the main limitations of the PS technique is, in fact, the difficulties in recording horizontal movements along the N-S direction). These velocities were combined obtaining an averaged value to be used in the formulas.

119.3 The Case Study

The municipality of Santa Sofia (Forlì-Cesena, Emilia-Romagna, Italy) was chosen as case study. One-sixth of the area of this municipality is affected by landslides of various types and state of activity and it can be considered as representative of the geological and geomorphological setting

of the northern Italian Apennines. The considered steel pipe network for gas distribution has an overall length of 42 km and about a quarter of the pipelines of the network are exposed, in different ways, to landslides. The pipelines are of the so-called continuous type, i.e. the various segments are welded together, in steel, and are classified, according to the operative pressure, in pipes of the fourth type (i.e., pressure 1.5–5 bar) and of the sixth type (i.e., pressure 0.004–0.5 bar). In this work, pipelines of the fourth type, characterized by a larger diameter, as they generally imply a greater danger in case of catastrophic events, were considered. The most common causes of failure for these pipes are related to the high tensile stresses in correspondence of the welded joints (yielding and ruptures) as well as to the relevant axial compression on the walls of the pipeline (local instabilities). An examples is presented, describing a fourth type pipeline crossing transversely a dormant landside (Fig. 119.1). Velocity data available from 2003 to 2008 from four PS positioned inside the landslide area and rather close to the pipelines were analysed. Results show a very good correspondence with the estimated range of expected velocities from Cruden and Varnes (1996). In fact, the PS results provided an average velocity of about 5 mm/year along E-W direction, toward east, and about 2 mm/year in the vertical direction, whereas Cruden and Varnes assume 6 mm/year for slow landslides. An average velocity of 5.84 mm/year was assumed for the computation of the PGD.

For the transversal crossing the maximum axial strain in the pipe due to the PGD was calculated as the minimum resulting from two pipe-soil models: the first refers to a large width of PGD zone and pipeline is assumed to be flexible; whereas the second refers to narrow width of PGD zone and pipeline is assumed to be stiff. In both models the initial stresses in the pipelines due to internal pressure and temperature change, were added to the value of maximum axial strain due to PGD and then compared to the allowable strains for continuous pipelines according to the guidelines proposed by ASCE (1984), ALA (2005) and JSCE (2000).

119.4 Discussion

In Fig. 119.2 the results for the considered steel pipeline are shown. In particular, the PGD at year 1998 was considered null and only strains due to operative pressure and temperature were considered. From 1998 to 2080 the maximum pipe strain was computed according to the "Guidelines for seismic design of buried pipelines" (2007) by adding to the initial value the strain due to the PGD. This last term was computed by assuming an average velocity of 5.84 mm/year, as the one computed from ENVISAT data in the period 2003–2008. By doing so, the estimated residual life of the pipelines can be assessed by comparing the maximum strain with the allowable strain that in this case is related to a
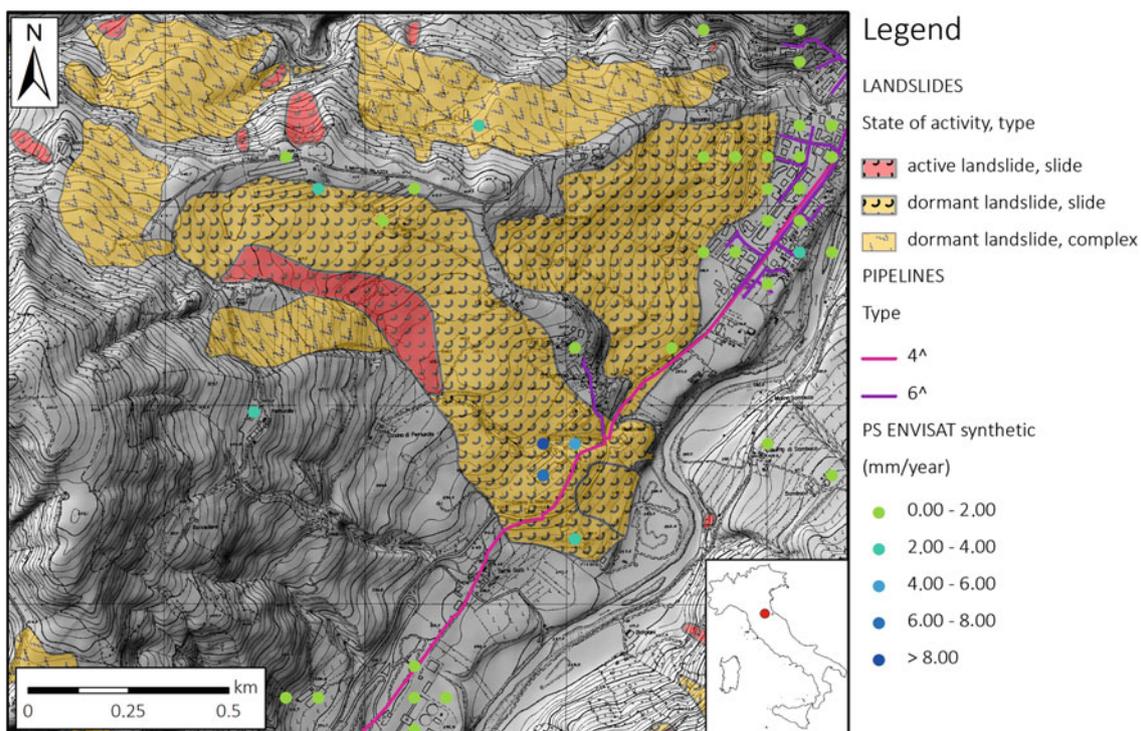
Fig. 119.1 Geographical location and sketch of landslide 35101, in Santa Sofia municipality (Forlì Province, northern Apennines, Italy) and pipelines affected by slope instability processes
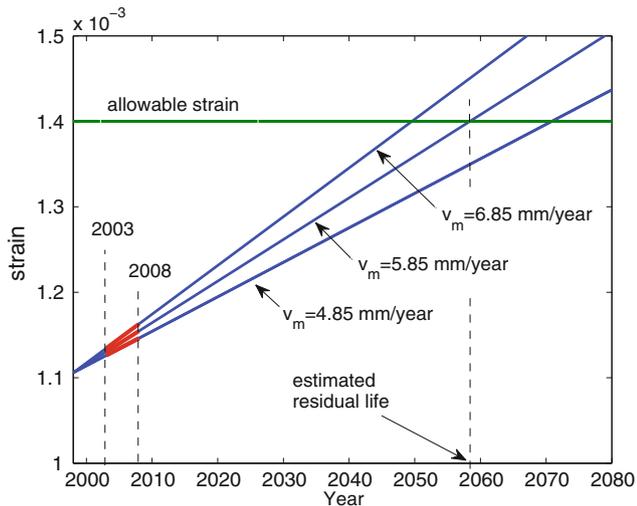
Fig. 119.2 Maximum pipe strain due to temperature and pressure (year of pose 1998) along with strain due to PGD (velocities extrapolated from ENVISAT data measured in the period 2003–2008)

compressive strain that can yield pipe wrinkling. Of course, this estimation strongly depends on the assumption of an active landslide body displaying steady-state displacements during the considered period. Further calculations could consider actual velocity and acceleration (i.e., rapid dynamic actions), as well as depth of movements, based on in situ geotechnical instruments. Moreover, differential velocities could be accounted for inside the landslide body.

119.5 Conclusions

The results show that, on the basis of technical data on the pipeline and of the available data on slope instability phenomena, it is possible to calculate the tensions that have acted and that are acting on the pipeline, due to PGD. This computation can be performed easily and eventually updated in near-real-time. In addition, the projection of the PGD in time allows for an estimation of the pipelines residual life. The outlined procedure is a suitable tool in a proper strategy

for assessing and managing the risk under both ordinary and emergency conditions in mountainous areas prone to slope instability phenomena. Moreover, the procedure, by assigning to the various sections and components of the network a value of relative vulnerability, allows targeted strategies of network maintenance to be programmed.

References

ALA (2005) Seismic guidelines for water pipelines. A report by public-private partnership between Federal Emergency Management Agency (FEMA) and National Institute of Building Sciences (NIBS), American Lifelines Alliance (ALA)

ASCE (1984) Guidelines for the seismic design of oil and gas pipeline systems. Committee on gas and liquid fuel lifelines, American Society of Civil Engineers (ASCE), US, Nyman DJ (Committee chairman)

Cruden DM, Varnes DJ (1996) In: Turner AK, Schuster RL (eds) Landslides: investigation and mitigation. Transportation Research Board Special Report 247. National Academy Press, WA, p 36

Indian Institute of Technology Kanpur (2007) IITK-GSDMA Guidelines for seismic design of buried pipelines (Indian Institute of Technology Kanpur, Gujarat State Disaster Management Authority National Information Center of Earthquake Engineering—NICEE Publication)

JSCE (2000) Recommended practices for earthquake resistant design of gas pipelines. Earthquake resistant codes in Japan. Japan Society of Civil Engineering (JSCE), Japan Gas Association

Liu PF, Zheng JY, Zhang BJ, Shi P (2010) Failure analysis of natural gas buried X65 steel pipeline under deflection load using finite element method. Mater Des 31(3):1384

Magura M, Brodniansky J (2012) Experimental Research of Buried Pipelines. Proc Eng 40:50

MATTM (2009) Direzione Generale per la Difesa del Suolo del Ministero dell'Ambiente e della Tutela del Territorio e del Mare. Linee guida per l'analisi di dati interferometrici satellitari in aree soggette a dissesti idrogeologici. http://www.pcn.minambiente.it/GN/leggi/LINEE%20GUIDA%20PER%20ANALISI%20DI%20DATI.pdf. Accessed 5 May 2014

Rajeev P, Kodikara J (2011) analysis of an experimental pipe buried in swelling soil. Comput Geotech 38(7):897

Zheng JY, Zhang BJ, Liu PF, Wu LL (2012) Failure analysis and safety evaluation of buried pipeline due to deflection of landslide process. Eng Fail Anal 25:156

The Importance of Rockfall and Landslide Risks on Swiss National Roads

120

Philippe Arnold and Luuk Dorren

Abstract

To obtain standardized information on the type, frequency, intensity and location of natural hazards that threaten national roads, the federal roads office FEDRO initiate a Swiss-wide project in 2008. This paper presents the methodology used in this project and presents a summary of the monetarised risks of the evaluated road sections. The natural hazards that need to be assessed are snow avalanches, rock- and icefall, flooding, debris flows, landslides (permanent, spontaneous and slope type debris flows) and collapse dolines. Risk hot spots mainly occur due to road closure related to rockfall or bank erosion. Damage to infrastructure represents generally only up to 20 % of the total calculated risk; person risks (casualties) add up to 8 % of the total risk. Rockfall is responsible for 35 % of the total calculated risk, rock avalanches for 8 %, permanent landslides for 5 %, spontaneous landslides for 3 % and slope-type debris flows for 1 %.

120.1 Introduction

Natural hazards such as avalanches, rockfall, landslides and flooding persistently threaten Alpine regions (e.g., BUWAL 1999; Rudolf-Miklau et al. 2006; Bezzola and Hegg 2007). The rockfall event of June 2006 on the Gotthard highway, the road destructing flooding and landsliding events in August 2005 or the numerous snow avalanches in the winter of 1999 show that road infrastructure, its users and its availability are vulnerable to the impact of natural hazards. Since January 2008, the federal roads office (FEDRO) is responsible for the Swiss national road network (highways and the main alpine passes). Before then, the national roads were managed by Cantonal road services. As a result, Swiss-wide, standardized information on the type, frequency, intensity and location of natural hazards that threaten national roads, as well as the costs of required protective measures, was not available. The FEDRO therefore decided to initiate a swiss wide project, called "national hazards on national roads—NHNR" with the technical support of the Federal Office for the Environment (FOEN), aiming at quantifying and mapping all risks due to natural hazards threatening Swiss national road network (total length = 1892 km) comparable to the work of Roberds (2005). At the moment of writing, almost all alpine national roads have been analysed, which allows to analyse the importance of rockfall and landslide related risks on national roads. This paper will present the methodology used in the project and presents a summary of the monetarised risks of the evaluated road sections.

P. Arnold (✉)
Federal roads office FEDRO, Bern, Switzerland
e-mail: philippe.arnold@astra.admin.ch

L. Dorren (✉)
Bern University of Applied Sciences, Zollikofen, Switzerland
e-mail: luuk.dorren@bfh.ch

L. Dorren
Federal office for the environment FOEN, Bern, Switzerland

120.1.1 Project Organisation

The FEDRO is in charge of the project coordination; technical support and expertise on hazard and risk analysis is provided by the division of hazard prevention of the Federal Office for the Environment (FOEN). The field and modeling studies needed for the hazard and risk analysis are being done by consortiums of collaborating geotechnical firms. They work on sections of the Swiss national road network with a length of 30–70 km. In general, each consortium consists of an interdisciplinary project leader with experience in natural hazards, an avalanche expert, one or two geological experts, a hydraulic engineering/flooding expert and a risk analysis expert. Approximately one and a half year is available to complete the natural hazard assessment in a given highway section and subsequently, the risk analysis is finalised within the following 3–4 months.

The developed project methodology, which will be described in the subsequent section, allows for a very detailed risk analysis. The key challenge is to ensure a similar level of detail in the hazard assessments of the different geotechnical bureaus. Our approach therefore obliges a discussion on the hazard scenarios for the different hazard sources with the experts in the terrain in the first half year of each subproject per highway section. The results of the hazard assessment proved that this is essential and effective. Also, a thorough proof of the hazard assessment results and the underlying, transparently presented, calculations and assumptions has shown to be of key importance. In total, 45 subprojects for different highway sections are defined; 20 of these are finished.

120.2 Project Methodology

The detailed project methodology is published in FEDRO (2012). This methodology describes in detail the following 4 main parts: (1) hazard assessment, (2) risk analysis, (3) risk evaluation and (4) planning of protective measures. As such the methodology defines the natural hazards to be studied, the study perimeter, the standards to be used, the risk equations, and parameter values to be used, as well as the products to be delivered. The methodology does not prescribe models for simulating the different natural hazards to be assessed; it only prescribes the required products in detail, as well as a maximum transparency and traceability of the methods, models and assumptions used.

The natural hazards that need to be assessed are:

- snow avalanches
- rock- and icefall, rock avalanches
- flooding and debris flows
- landslides (permanent, spontaneous and slope type debris flows)
- collapse dolines

To aim for a Swiss-wide homogeneous and comparable dataset, 4 event-size scenarios (return period 0–10 yrs, 10–30 yrs, 30–100 yrs, 100–300 yrs and intensity classes low, medium and high) should be defined for each the potential hazard source area. The so called damage potential perimeter that is to be taken into account is the area covered by the highway with a 10 m buffer, as well as surrounding facilities (e.g., parking places, technical tunnel installations, …). The risk analysis is carried out on one or two lines that represent the road axes and on surrounding facilities.

To standardise the risk analysis, we developed an internet based risk calculation tool called RoadRisk (http://www.roadrisk.admin.ch/). This tool is WebGIS-based and intersects the intensity maps of all studied natural hazards for the defined return periods with the damage potential. It calculates the total risk (cf. Fig. 120.1) based on the following "damage" types:

- Direct impact (R_{direct}),
- Collision with deposits on the road or with cars that are impacted by natural hazards ($R_{collision}$),
- Damage to infrastructure (R_{damage}),
- Precautionary road closure ($R_{preclos}$),
- Road closure after an event ($R_{postclos}$).

Casualties are also expressed in costs and is based on a value of 5 million CHF per human life. Therefore, variables required are the maximum speed defined at the highway section, the average number of cars passing daily, the probability of having a traffic jam, the daily costs for road closure (varying between 150,000 and 4,000,000 CHF/day), the lethality of the people in a car being hit or colliding with deposits, etc. To calculate the daily costs due to road closure, we use a model developed by IVT-ETH (Erath 2011). This model allows quantifying the costs caused by the closure of a road section in the national road network taking into account:

- time loss due to detours for passenger cars and lorries
- increase of costs due to an increase in the number of accidents
- cancelled professional and leisure trips

Both a summer and winter scenario for road closure have been calculated for all section in the national road network. The winter scenario accounts for the closure of alpine passes due to snow in wintertime. The final step in the Swiss-wide national hazards on national roads project is the risk evaluation. For that purpose, three evaluation criteria have been defined to identify risk hot-spots.

Criterion (1) is the individual probability of death. For this FEDRO defined a threshold of $1 * 10{-5}$ per year. The value applies to road users who regularly drive on a national road section. If this threshold is exceeded due to natural hazards, all possible protective measures for the problematic hazard source have to be evaluated. The limit value of the
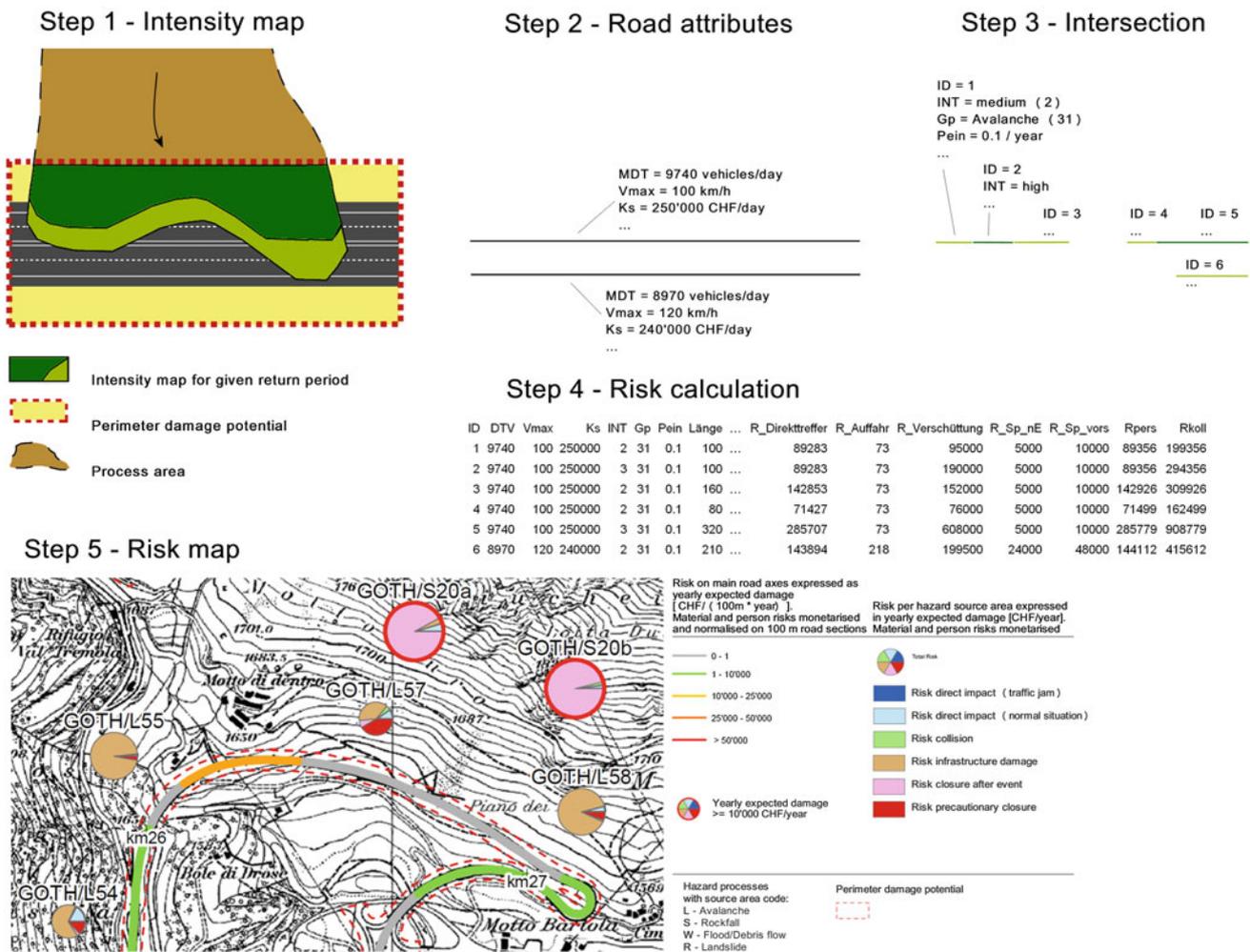
Fig. 120.1 Explanation of the major steps in the risk calculation tool. *1* Import of the intensity map for a given process and return period; *2* Importation of the road axis lines and accompanying attributes; *3* Intersection of the road axes and the intensity map; *4* Creation of a joined attribute table and risk calculation per damage type; *5* Display of the risk values in a map

probability of death of $1 * 10{-5}$ per year is derived from the average probability of fatalities of all 15-year-olds in Switzerland. Here, a risk of death 10–100 times lower is assumed to be acceptable by society for deaths caused by natural hazards. The higher value ($1 * 10^{-5}$) is selected based on PLANAT (2009). The other two evaluation criteria are (2) total risk per road section >10,000 CHF/100 m * year and (3) total risk per hazard source or per secondary facility >10,000 CHF/year.

No protection goals with absolute limit values are defined for the collective or person risks. At locations where one of these three criteria is exceeded, possible risk reduction measures will be studied. These measures will subsequently be implemented only if those measures prove to be cost-effective. This means that the yearly risk reduction should be equal or larger than the yearly expected damage.

120.3 Results

The results of the 20 completed subprojects (approx. 30–70 km highway sections) show that potential damages per 100 m highway section due to gravitational natural hazards can add up to several 100,000 CHF/year, summing up to several millions CHF/year for entire road sections. Figure 120.2 shows the risk hot spots on the completed highway sections.

In most cases risk hot spots occur due to road closure in areas that are strongly affected by rockfall or bank erosion. Details (as shown in Fig. 120.3) show that direct damage to infrastructure represents generally only up to 20 % of the total potential damages, but can reach up to 40 % for some hazard sources. Person risks (victims) are mostly to be expected due to falling rocks, rock avalanches, debris flows
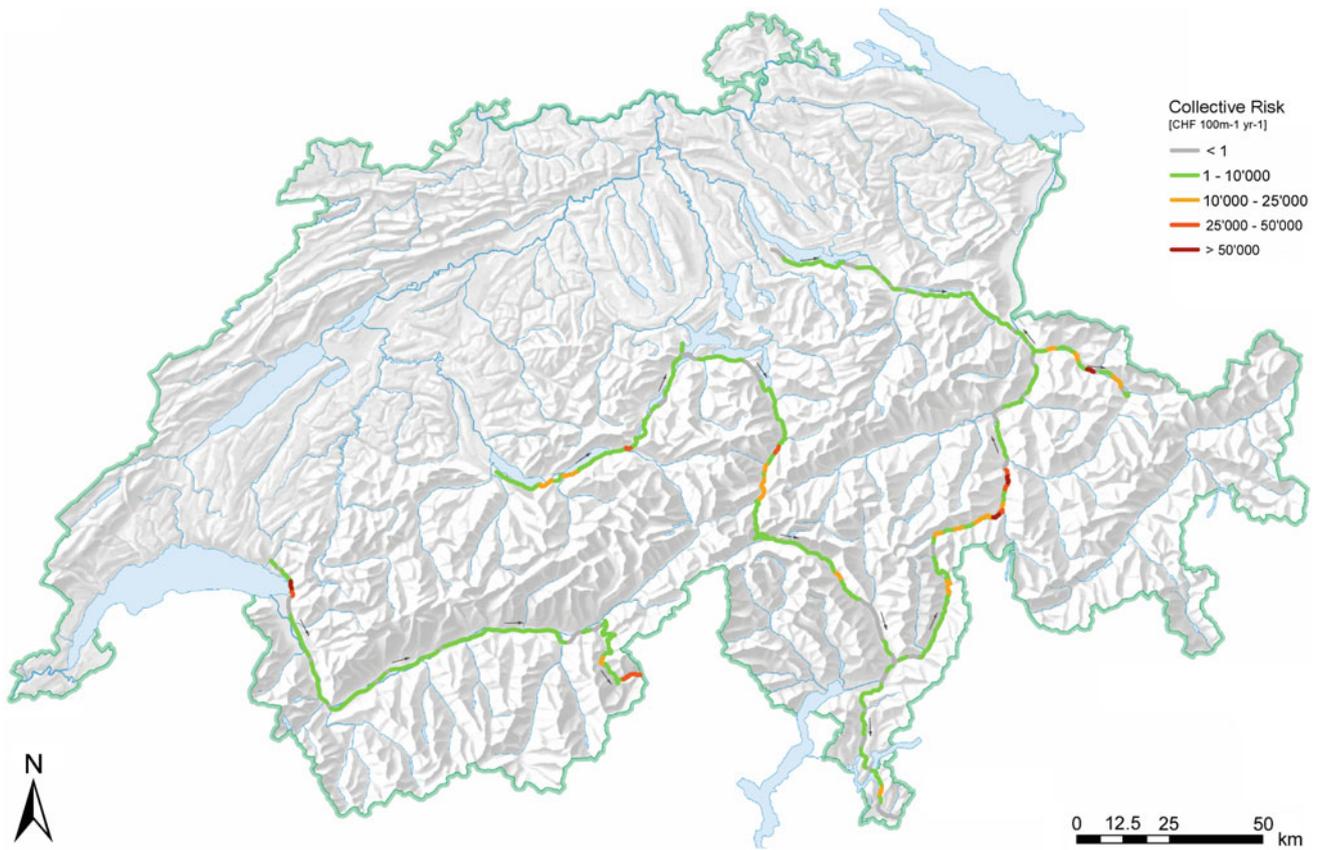
Fig. 120.2 Overview of the risk hot spots (total risk > 10,000 CHF/100m ∗ year) on the Swiss national road sections that have been analysed between 2008 and 2014

Fig. 120.3 Risk details per hazard and damage type for all analysed road sections
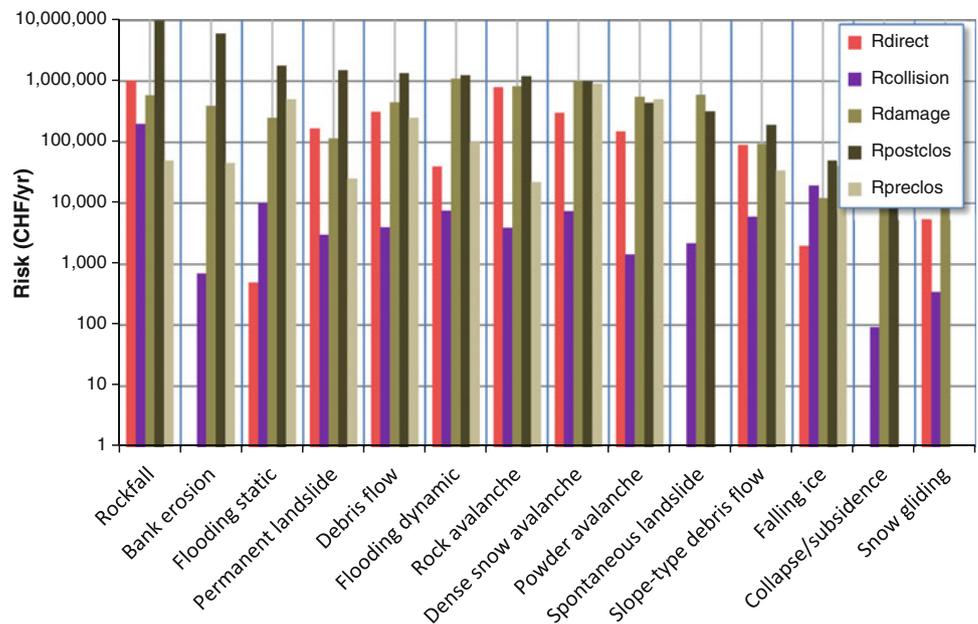
and dense snow avalanches, which add up to 8 % of the total risk. Road closure is responsible for 75 % of the total calculated risk on the national roads that have been assessed so far. Regarding geological mass movements, the results show that rockfall is responsible for 35 % of the total calculated risk, rock avalanches for 8 %, permanent landslides for 5 %,

spontaneous landslides for 3 % and slope-type debris flows for 1 %. Finally subsidence processes due to doline collapse account for 0.1 %.

References

Bezzola G-R, Hegg C (2007) Ereignisanalyse Hochwasser 2005. Teil 1 – Prozesse, Schäden und erste Einordnung. Bundesamt für Umwelt BAFU, Bern und der Eidgenössischen Forschungsanstalt für Wald, Schnee und Landschaft WSL, Birmensdorf

BUWAL (1999) Leben mit dem Lawinenrisiko - Die Lehren aus dem Lawinenwinter 1999. Bundeamt für Umwelt, Wald und Landschaft (BUWAL), Bern

Erath A (2011) Vulnerability of road transport infrastructure. Ph.D. Thesis, ETH Zürich, Zürich

FEDRO (2012) Natural hazards on national roads: risk concept. Methodology for risk-based assessment, prevention and response to gravitative natural hazards on national roads. ASTRA Documentation 89001. Federal Roads Office, Bern. http://www.astra.admin.ch/dienstleistungen/00129/00183/01156/index.html?lang=en

PLANAT (2009) Risk concept for natural hazards, strategy natural hazards Switzerland (in German, www.planat.ch)

Roberds W (2005) Estimating temporal and spatial variability and vulnerability. In: Hungr O, Fell R, Couture R, Eberhardt E (eds) Landslide risk management. Taylor and Francis Group, London, pp 129–158

Rudolf-Miklau F, Ellmer A, Gruber H, Hübl J, Kleemayr K, Lang E, Markart G, Scheuringer E, Schmid F, Schnetzer I, Weber C, Wöhrer-Alge M (2006) Hochwasser 2005 - Ereignisdokumentation. Bundesministerium für Land- und Forstwirtschaft, Umwelt und Wasserwirtschaft, Sektion Forst, Abteilung Wildbach- und Lawinenverbauung, Wien

Innovative Methods in Characterization and Monitoring of Geotechnical Structures

Convener Prof. Anna Maria Ferrero—*Co-conveners* Marco Barla, Andrea Segalini, Gessica Umili

Technological and scientific developments have contributed to improve geological-geotechnical characterization and monitoring of geotechnical structures. This is due to the use of miniaturized sensors, new materials, data acquisition, transmission and analysis by web-oriented platforms. Although the measured quantities remain the same (displacements, rotations, strains, stresses, water pressures, temperatures, etc.) monitoring and data acquisition systems are dramatically changed. The quality and quantity of the data made available "real-time" contribute to the assessment of the actual behaviour. According to Eurocode7 the observational method in which the design is reviewed during construction is a consolidated practice in geotechnical engineering. This is strictly connected to measurement to ascertain that the actual behaviour is within the acceptable limits. Since the nature of the acquired data is fundamental, the innovations will significantly improve the design approach.

Th. Mutschler, D. Groeger, and E. Richter

Abstract

One of the major tasks in quantitative description of discontinuities in rock masses is the determination of their spatial orientation. In recent years, Terrestrial Laser Scanning (TLS) allows a three-dimensional point mapping of surface points with high accuracy. By thinning and meshing the mapped points with a specific software tool, the natural surface can be modeled by planar elements and analyzed in standard CAD software. If the surface represents discontinuity planes and if it is not heavily distorted by natural processes such as erosion, a simple algorithm can be used that allows to identify discontinuities and to determine their spatial orientation. The paper describes the application of this method in a karst cave. TLS measurements were carried out under very harsh conditions. The results of the procedure are presented and their validity is proven on a chosen surface area by comparing the results to in-situ measurements with a stratum compass.

Keywords

Discontinuity systems • Dip and strike • TLS • Karst cave

121.1 Introduction

The behavior of rock mass is dominated by its discontinuities; hence the information about their spatial orientation is an important issue (ISRM 1978). Usually, the spatial orientations are measured with a stratum compass. If several sets of discontinuities exist and the area of interest is large, such measurements are highly time-consuming. Several authors have applied different remote sensing methods, such as stereophotography and digital image processing (Gaich et al. 1999) and later the processing of point clouds generated by Light Detection And Ranging (LiDAR, Kemeny 2005) or TLS, to determine the spatial orientation of discontinuities. Most of the applications of remote sensing methods were related to above-ground problems. Subsequently, the usage of remote sensing methods in a karst cave in Indonesia is presented.

121.2 Location, TLS Hardware and Scanning Technique

The cave "Gua Seropan" is located in the south of Middle Java, Indonesia. The lime rocks in this region are intensively karstified and hold huge caves systems. Ongoing solution and erosion processes mainly caused by a cave river have created canyon-like karst structures with varying morphology. The area of highest interest is located around a waterfall, where the three most dominating sets of discontinuities are clearly visible (Fig. 121.1).

In this part of the cave the canyon-like cross section changes to a hall-like shape. The walls of the cave consist of joint faces and the roof is formed by stratification faces.

Th. Mutschler (✉)
Institute of Applied Geosciences, Karlsruhe Institute of Technology, Karlsruhe, Germany
e-mail: thomas.mutschler@kit.edu

D. Groeger
Institute of Geotechnical Engineering and Mine Surveying, Clausthal University of Technology, Clausthal, Germany

E. Richter
COS Systemhaus, Ettlingen, Germany

Fig. 121.1 Dominating sets of discontinuities (*left*); eroded discontinuity faces (*right*)

However, not all parts of the faces around the waterfall are suitable for the analysis presented in this paper. At the lower sections of the walls the solution and erosion processes resulted in wash-outs of the joint faces (Fig. 121.1) and the detection as flat planes is not possible anymore.

Within the scope of the IWRM-project—Indonesia (http://www.iwrm-indonesien.de), the surface of the karst cave was mapped by TLS in 2009 (Schmitt 2010). The TLS system deployed in Gua Seropan was a Leica HDS 6000, which works with the phase-shift-method. In contrary to the time-of-flight-method (TOF), the phase-shift method works much faster. Consequently it enables higher resolution on the object surface in the same time. Moreover, it provides higher short-range accuracy. The distance accuracy of a single measurement is 5 mm at 25 m at a surface reflecting

of only 18 % of the incident light. Its main disadvantage of a shorter adjustment distance was of no significance. The high resolution scans with lateral point distances of <10 mm covered even small details and discontinuities. Compared with photogrammetric systems the presence of heavy spin-drift and poor light conditions were no problem for TLS.

The high, narrow and stretched geometry of the cave demanded closely neighbored scanner positions to catch all details. The lateral orientation of the scans was determined with the help of targets (spheres and black and white targets) (Fig. 121.2). Whenever possible, the targets were placed on survey points with known coordinates. Despite a maximum range of 79 m, the mean distance between two scanner positions was chosen to be about 15 m. Thus, the cave was mapped from 19 different scanner positions.
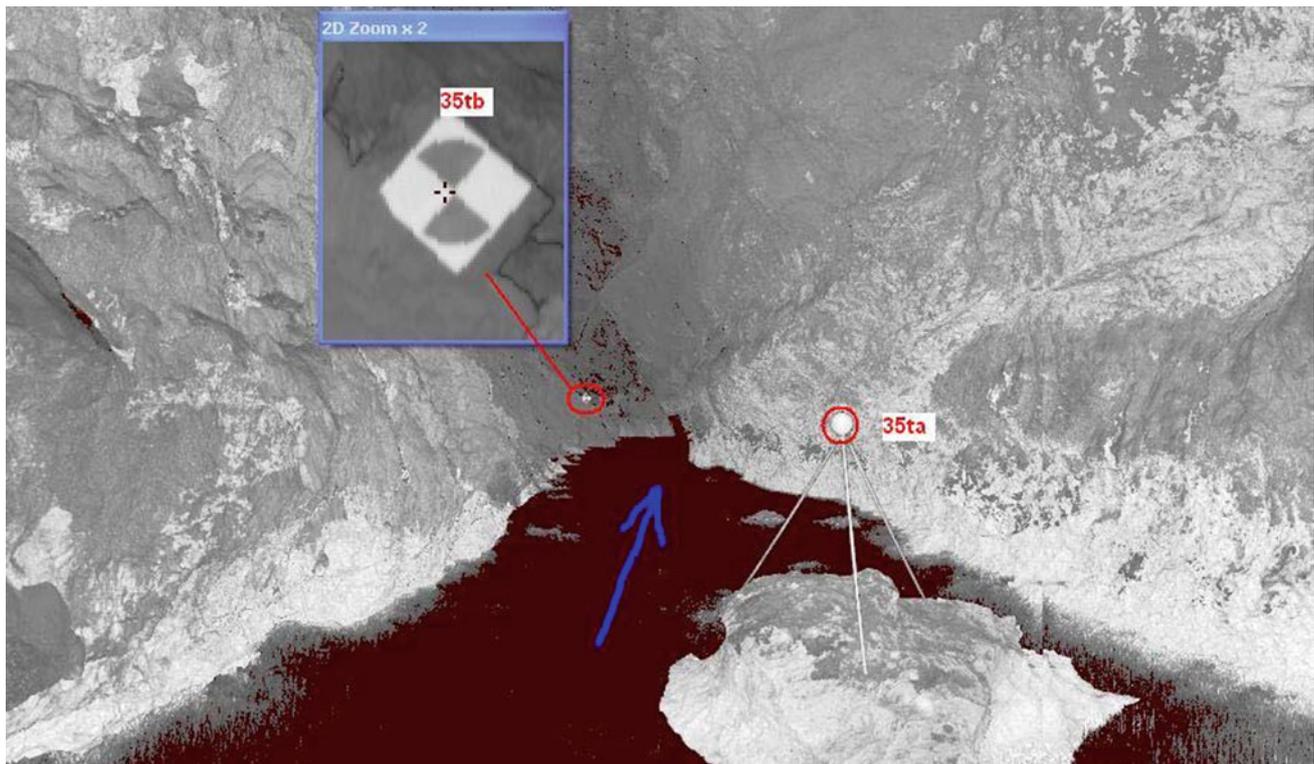
Fig. 121.2 Intensity image of a point cloud with a *flat black* and *white* target as well as a *sphere* on a *tripod*
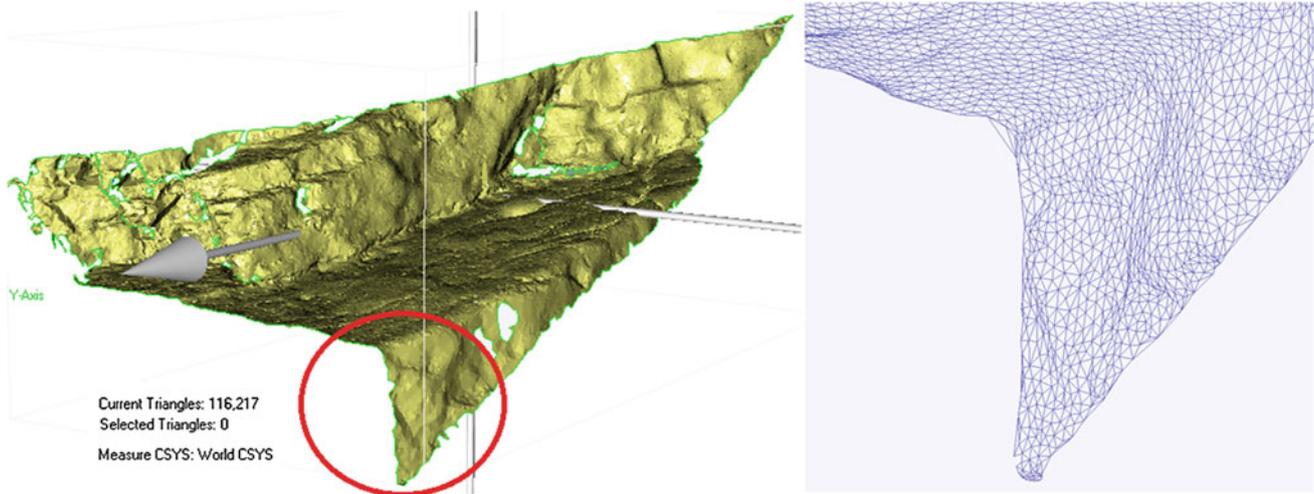
Fig. 121.3 Section of the meshed point cloud, 8 m long (*left*); view of the area inside the *red circle*, *triangle* with 2 cm edge length (*right*)

121.3 Processing of Point Clouds and CAD Models

Pre-processing of TLS measurements was done in several steps, beginning with the removal of erroneous and surplus measurements in each point cloud, followed by the positioning of the point clouds relatively to each other. The point clouds were oriented by both matching of overlapping parts and artificial targets (Fig. 121.3) that are part of the point cloud. After the relative orientation and the merging of the point clouds, the absolute orientation of all scans inside a superior coordinate system was calculated.

The modeling of the natural cave surface was done by calculating a mesh of triangles or polygons. For further data processing, the point clouds were converted to a CAD data format. The focus, hereby, lay in the thinning of the data sets without changing or losing the orientation of the natural surface of the cave.

There are different kinds of algorithms to reduce the number of the triangles of the mesh. The simplest approach, the uniform sampling, is re-calculating the point cloud or mesh, so that the points are equidistant to each other. This does not necessarily preserve all discontinuities and results in a huge amount of data. Yet, if smooth surfaces are given this approach is better suited. Here the requirement of smooth surfaces was only granted for some parts of the cave walls and the roof. Therefore, the so called curvature-based filter was used. It allows the preservation of the discontinuities by reducing the number of points for meshing the surfaces with triangular elements. As a result, the generated meshes possessed a low density inside flat areas and became higher near and across edges.

For the whole cave 15 CAD section models were generated of which 4 were used for the most interesting area around the waterfall. Figure 121.4 shows one model which is divided in three parts: the roof (blue), the sidewalls (silver) and the area which was not investigated because of coverage with rock fall material (black). In addition to the analysis of a whole model, specific areas, which are mainly dominated by discontinuity faces, were chosen to validate the results of the whole model.

The coordinates of each triangular element were extracted from the CAD models to a spreadsheet. By applying a simple algorithm, the dip angle and the dip direction were calculated. The fact, that the curvature-based filter led to different areas area sizes of the triangles, was handled by a weighting factor that incorporated the area of a single triangular element to the over-all area of the model. If the area of the discontinuity faces dominates the over-all area of the cave surface, an analysis of the spatial orientation of the discontinuities can be carried out.

121.4 Results

In order to validate the procedure, the algorithm was applied to a surface area with dominant discontinuity faces and the results were compared to field measurements with a stratum compass. Figure 121.5 shows the results of both the field measurements and the analysis of the CAD the Lambert azimuthal equal-area projection.

It can be seen, that a good match between the field measurements (263°/72°) and the analysis of the CAD model (250°/78°) is achieved. Besides the spatial orientation of the joint face, the spatial orientation of the bedding can be seen from the analysis of the CAD model.

Fig. 121.4 CAD model around
the water fall
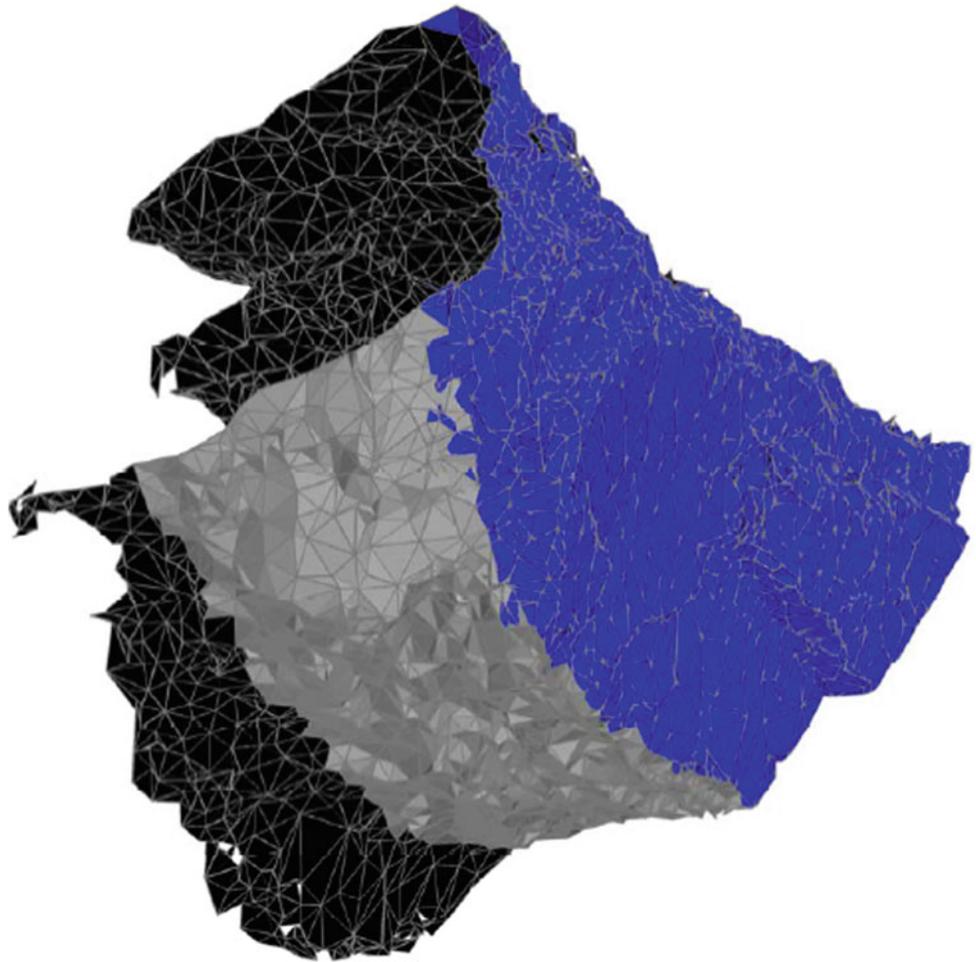
By splitting the 4 models into roof and wall, the joint sets and the bedding set could be considered separately (Fig. 121.6). The spatial orientation of the bedding has a dip direction of 20° and a dip angle of 10° approximately. In addition, the right figure indicates two joint sets. One has a dip angle of nearly 90° and a dip direction of around 250° and the other dips with 60° in a direction of 130°.

From the analysis it can be seen that if the discontinuity faces dominate the surface of the cave, a further revision of the models by excluding wash-outs or other phenomena changing the natural discontinuity faces must not be considered. As a result of the genesis of a karst cave this requirement is usually satisfied, so that the analysis introduced is supposed to hold in general.
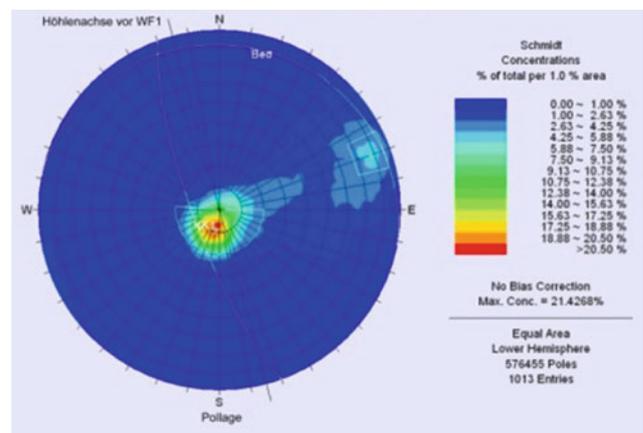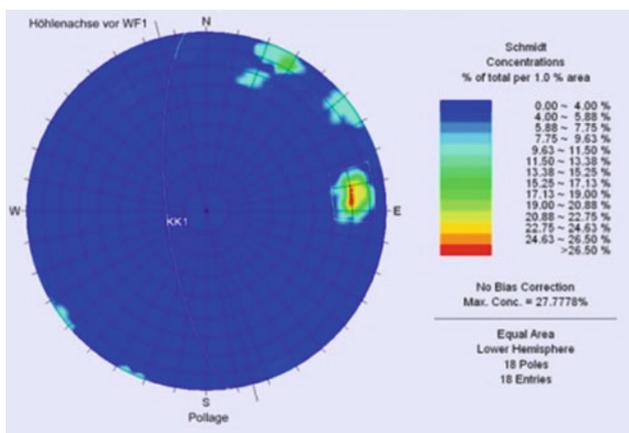
Fig. 121.5 Field measurement (*left*), CAD model (*right*)
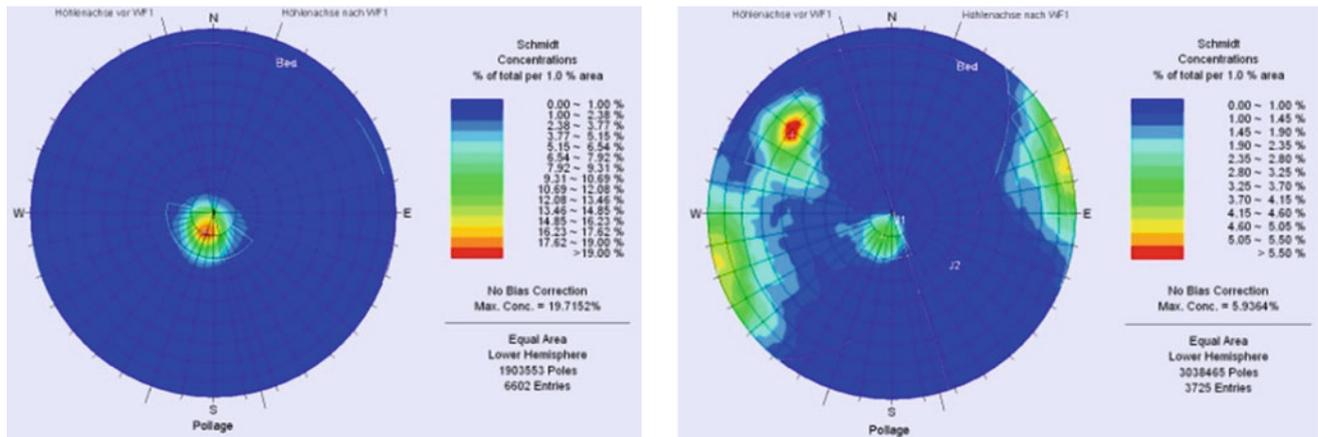
Fig. 121.6 Cave roof (*left*), cave walls (*right*)

121.5   Conclusions

The following conclusions can be drawn:

- TLS is suited to provide the data for the determination of the spatial orientation of discontinuities even under harsh conditions in a karst cave.
- Areas which are almost inaccessible can be fully covered.
- Curvature-based filtering is able to reduce the data amount significantly without losing detailedness.
- The validation on a specific area shows good agreement.
- Due to the area-weighted evaluations, an exclusion of eroded and altered areas can be neglected if the surface is dominated by discontinuity faces.

References

Gaich A, Fasching A, Gruber M (1999) Stereoscopic imaging and geological evaluation for geotechnical modelling at the tunnel site. Felsbau 17 Nr 1:15–21

ISRM Commission on Testing Methods (1978) Suggested methods for the quantitative description of discontinuities in rock masses. Int J Rock Mech Min Sci 15:319–368

Kemeny J, Turner K, Norton B (2005) LIDAR for rock mass characterization: hardware, software, accuracy and best-practices. In: Tonon F, Kottenstette J (eds) Workshop laser and photogrammetric methods for rock face characterization, ARMA

Schmitt G (2010) Geodetic contributions to IWRM-projects in middle Java. Indonesia J Appl Geodesy 4:167–175, de Gruyter 2010

A. Veiga and M. Quinta-Ferreira

Abstract

The Hetangian Dagorda claystone Formation occupies the core of a diapir outcropping in part of the city of Leiria, exhibiting a complex geological structure. The geological and geotechnical characterization is presented based in field observation and laboratory tests allowing to conclude that the Dagorda clay soils exhibit an unfavourable behaviour for urban occupation, due to the presence of expansive clay minerals. When partially saturated these soils can lead to cracking of walls and floors, or even to endanger the stability of buildings, if they have not been strengthened to resist to expansive soil. The presence of soluble minerals, mainly gypsum and seldom halite, can allow the formation of voids and eventually the deformation or collapse of the ground. Suitable safety procedures, in order to prevent hazards should be used.

Keywords

Dagorda formation • Claystone • Laboratory tests • Leiria diapir • Land occupation

122.1 Introduction

The Dagorda claystone Formation occupies the core of a diapir, outcropping partially in the city of Leiria, exhibiting a complex geological structure (Fig. 122.1). This Formation is dated from the Hettangian and is constituted by clay, silt, occasionally with gypsum or even halite, and intercalations of limestone and marls. The presence of gypsum and halite, both soluble minerals, must be taken in account during the engineering works. Saline water can also be aggressive to concrete and iron components of the structures.

Laboratory tests performed on more than 30 samples collected in outcrops and shallow excavations, corresponding to decompressed soils, allowed to determine their geotechnical parameters and to characterize the materials variability. Identification tests (grain size analysis, Atterberg limits, specific gravity, methylene blue value), characterization tests (Proctor compaction and CBR) together with mechanical tests (direct shear tests and oedometric tests) were done. In order to identify the types of clay present in these materials, X-ray diffraction tests were performed.

122.2 Lithological Characterization

According to Teixeira et al. (1968) the nucleus of the diapir is constituted by red or grey marls and clays with gypsum, and by dolomite and marly limestone. Based on the field observations in outcrops, it was possible to identify red and grey clays, silty or marly clays and claystone, and thin layers of marly limestone. This lithological diversity was influenced by the diapiric tectonics that affected the area in the Mesozoic, generating quite heterogeneous terrains.

A. Veiga (✉)
Geosciences Center, Polytechnic Institute of Leiria, Campus 2, Morro do Lena—Alto Vieiro, 2411-901, Leiria, Portugal
e-mail: anabela.veiga@ipleiria.pt

M. Quinta-Ferreira
Department of Ciências da Terra, Geosciences Center, University of Coimbra, Largo Marquês de Pombal, 3000-272, Coimbra, Portugal
e-mail: mqf@dct.uc.pt

Fig. 122.1 Geological map of Leiria (in Teixeira et al. 1968)
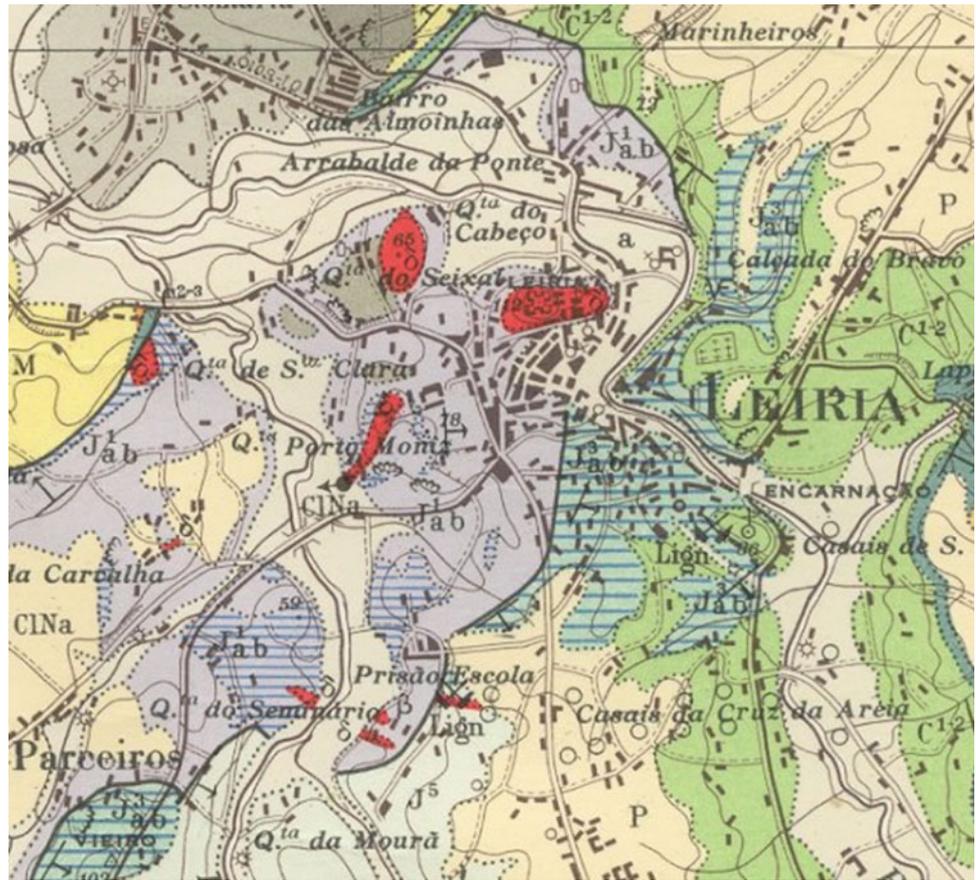
122.3   Laboratorial Characterization

122.3.1   Tests for Classification, Identification and Description

The laboratory tests were done using samples collected in outcrops or in small excavations corresponding to decompressed soils. In order to classify the soil samples, a few laboratory tests were done: grain-size distribution using dry sieving and sedimentation, consistency limits, specific gravity and methylene blue test.

Figure 122.2 presents the grading curves of the samples, showing that fine grained soils are predominant. Table 122.1 presents a summary of the samples characteristics.

The average value of G_s is characteristic of fine soils. The I_p values correspond to soils of low to medium plasticity and the Ic values classify these soils from soft to stiff,

Fig. 122.2 Grain size distribution *curves* (Veiga 2012)
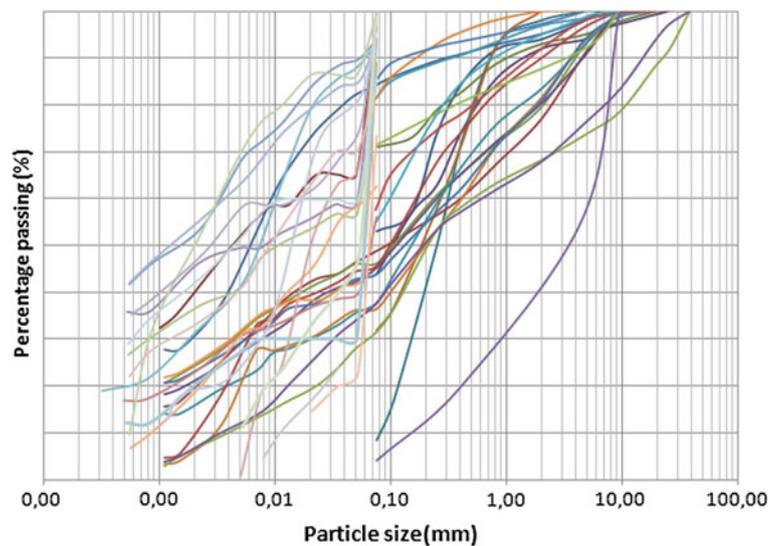
Table 122.1 Summary of the samples characteristics (Veiga 2012)

	Max	Min	Av	Med	Mo	S	n
sWater content (%)		3.0	11.3	10.9	14.5	6.64	24
G_s	2.95	2.46	2.68	2.65	2.6	0.12	28
Liquid limit (W_L) (%)	49	17	32	30	30	7.68	42
I_P	30	4	13.7	14	16	5.5	41
Consistency index (I_c)	4.24	0.28	1.9	1.9	2.36	0.87	38
Ac	0.87	0.21	0.5	0.5	–	0.17	23
MBV (g/100 g)	5.6	0.70	2.6	2.7	2.8	1.12	32

Ac—Activity, G_s—specific gravity, I_p—plasticity index, MBV—methylene blue value, Max—maximum, Min—minimum, Av—average, Med—median, Mo—mode, S—standard deviation, n—number of samples

predominantly hard. A_c values correspond to inactive normal clay. The average of MBV corresponds to water sensitive soils.

122.3.2   X-Ray Diffraction Tests

To identify the types of clay present in these materials, X-ray diffraction tests were performed in 6 samples. Two techniques were used: the proposed by Biscay (1965) and the proposed by Thorez (1976). Three of the samples are grey, showing predominantly illite, but also kaolinite and chlorite. These clays are characterized by low to very low ion exchange capacity, and therefore no expansibility, corresponding to soils presenting a stable behaviour. The two red samples have a high content of smectite (54 and 29 %), and a significant content of interstratified clays and illite. The smectite has a high adsorption capacity for water molecules, leading to higher volumetric variation. Although the number of samples is small, the results showed a relationship between colour and their clay composition, with predominance of illite in the grey clay, and the predominance of smectite in the red clay.

Amado et al. (2003) studied the chemical and mineralogical composition of these soils concluding that they have a quite variable chemical composition, ranging from highly carbonated with low Fe content soils, to silicate-aluminium with significant Fe content. The Mg content presents a large variation related with the presence of dolomite limestone and

clay minerals. Clay minerals (smectite, montmorillonite, illite and kaolinite), calcite, dolomite, quartz and gypsum minerals were also identified, using X-ray diffractometry.

122.3.3   Geotechnical Classification

The laboratory tests, allowed to do the geotechnical classification of the samples. The obtained soil classification is presented in Fig. 122.3.

According to the unified soil classification, these soils are mostly classified as low plasticity clay (CL—62 %), while according to the AASHTO soil classification, they belong mainly to group A-6. Concerning the behaviour, the predominance is for materials that are impermeable to semipermeable when compacted, presenting fair shear strength and fair compressibility when compressed and saturated, and reasonable to good workability as building material. Most of the clay materials present a very bad behaviour in layers under pavements.

122.3.4   Compressibility Testing

Oedometer tests were conducted on intact and remoulded samples. The tests were performed with induced stresses from 25 to 800 kN/m^2. After determining the parameters defining the stress-strain relationships, it was possible to obtain the preconsolidation stress (σ_p'), overconsolidation

Fig. 122.3 Unified soil classification (**a**) and AASHTO soil classification (**b**)
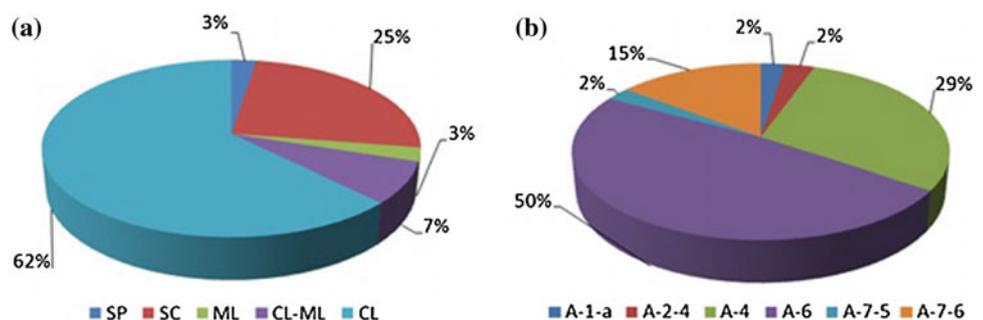
Table 122.2 Statistical results from oedometer tests (Veiga 2012)

	Max	Min	Av	Med	s	n
σ'_p (kpa)	250.0	22.0	60.0	103.2	83.8	13
OCR	97.0	1.4	24.2	36.0	32.9	13
C_c	0.278	0.029	0.171	0.166	0.077	16
c_v (cm^2/min)	4.6	0.1	1.9	1.8	0.009	16

ratio (OCR), compression index (C_c) and coefficient of consolidation (c_v) (Table 122.2). The oedometer tests revealed overconsolidated soils, medium compressibility index and average vertical c_v of 1.9 cm^2/min. These tests were used to estimate permeability, revealing soils with very low permeability (between 8.2×10^{-10} and 7.5×10^{-9} cm/s).

122.3.5 Strength and Compaction

Direct shear tests were performed on remoulded samples. The results showed a wide scatter of the peak shear strength, with 65 % of the results between 29° and 36°, with a median of 30.4°.

The uniaxial compressive strength tests were done during the construction of the Leiria municipal stadium. The samples were obtained during drilling at depths between 14.5 and 19.5 m. The uniaxial compressive strength values range between 0.7 and 21.4 MPa (Tecnasol 2001), corresponding from stiff soils to moderate strength rocks. The median value is 2.72 MPa corresponding to very soft rocks, being unattractive as foundation materials.

From nine Proctor compaction tests it was possible to obtain γ_{dmax} and $w_{ópt}$ values. The upper $w_{ópt}$ is very high (19 %) conferring high deformability to these materials when used as embankment. The CBR index and expandability were obtained from eight CBR tests at 95 % compaction grade. The very low values of the CBR index (between 0 and 7) and the fine character of these materials give them a poor ability for use as backfill material, and the low strength makes them unattractive as foundation material.

122.4 Conclusions

The results allow to conclude that the Dagorda clay soils exhibit an unfavourable behaviour for urban occupation due to the presence of expansive clay minerals. When partially saturated these soils can lead to cracking of walls and floors,

or even to endanger the stability of buildings, if they have not been dimensioned to resist to expansive soil. The presence of soluble minerals, mainly gypsum and seldom halite, can allow the development of voids and eventually the deformation or even the collapse of the ground. These cavities are difficult to identify, requiring special prospection techniques.

Despite the bad geotechnical behaviour of the Dagorda claytstone, the city of Leiria is expanding to this area because of its high economic value. The geological and geotechnical characterization allowed to foreseen the unfavourable geotechnical behaviour upon occupation, requiring suitable safety procedures, in order to prevent engineering hazards.

References

Amado C, Veiga A, Quinta-Ferreira M, Velho J (2003) Análise de problemas de Geologia de Engenharia em zonas diapíricas: os casos de Belo Horizonte, Santa Clara e Morro do Lena (Leiria). [M. P. Ferreia]. A geologia de engenharia e os recursos geologicos. s.l.: Imprensa da U C, Coimbra, 2003 (in Portuguese)

Biscaye PE (1965) Mineralogy and sedimentation of recent deep-sea clay in the Atlantic Ocean in the adjacent seas and oceans. Geol Soc Am Bull 76:803–832

Tecnasol FGE (2001). Estádio Dr. Magalhães Pessoa. Projecto de execução. Relatório geológico-geotécnico do maciço de fundação. Câmara Municipal de Leiria. Setembro 2001 (in Portuguese)

Teixeira C, Zbyszewski G, Torre de Assunção C, Manuppella G (1968) Carta Geológica de Portugal, na escala 1/50 000. Notícia explicativa da folha 23-C (Leiria). (S. G. Portugal, Ed.) Lisboa (in Portuguese)

Thorez J (1976) Practical identification of clay minerals. In: Lelotte G (ed) vol 1. Belgium, p. 90

Veiga AQV (2012) Caracterização geotécnica dos terrenos do vale tifónico Parceiros-Leiria. Coimbra. www: http://hdl.handle.net/10316/19906. PhD thesis (in Portuguese)

Cristina Occhiena, Charles-Edouard Nadim, Arianna Astolfi,
Giuseppina Emma Puglisi, Louena Shtrepi, Christian Bouffier,
Marina Pirulli, Julien de Rosny, Pascal Bigarré, and Claudio Scavia

Abstract

The presence of abandoned and unstable underground cavities can give rise to a potential risk of surface collapse, particularly alarming when the presence of buildings is attested on the surface. The INERIS (Institut National de l'Environnement Industriel et des Risques, France) has carried out many studies, in recent years, investigating the effectiveness of several methodologies, devoted to monitor the evolution of the damaging mechanisms, reducing the risks of surface instability. Among the investigated methodologies, the acoustic monitoring has appeared as a suitable technique to detect damaging processes. During 2012 the Brasserie quarry, an old limestone mine located in the South-East of Paris (France) was instrumented with microphones to detect the acoustic waves generated by the collapse of blocks from the roof and the walls of the cavity. A series of tests were carried out with the aim of determining the propagation characteristics of sound and the attenuation of the acoustic waves inside the complex geometry of the quarry. Preliminary data processing concerned the classification of the recorded signals: the analysis of the signal-to-noise ratio (SNR) evidenced that the quarry can be subdivided into three main areas on the base of different attenuation attitude. The presence of critical areas and paths influencing the wave propagation also emerged. The research is still in progress. Specific analyses will be carried out to deepen the aspects related to the source localisation, simulating the acoustic behaviour of the quarry to obtain maps of sound attenuation and reverberation times.

123.1 Introduction

Many anthropogenic (mines, quarries, storage facilities, etc.) or natural (as karsts) underground cavities are responsible for surface instabilities caused by different mechanisms. These mechanisms depend on the cavity and can be global like the subsidence or the collapse of the overburden, or more local like the sinkholes (Didier 2008).

In France, especially in the northern regions, the closure and abandonment of many mines, largely exploited in the XIX and XX centuries, has evidenced the necessity of the management of these phenomena: monitoring the evolution of the triggering mechanisms plays a major role in the risk

C. Occhiena (✉) · M. Pirulli · C. Scavia
Department of Structural, Geotechnical and Building Engineering,
Politecnico di Torino, Torino, Italy
e-mail: cristina.occhiena@polito.it

C.-E. Nadim · C. Bouffier · P. Bigarré
Institut National de lEnvironnement Industriel et des Risques
(INERIS), Verneuil-en-Halatte, France

A. Astolfi · G.E. Puglisi · L. Shtrepi
Department of Energy, Politecnico di Torino, Torino, Italy

J. de Rosny
Laboratorie Ondes et Acoustique, Institut Langevin, Grenoble,
Italy

reduction, which is especially important when the presence of stakes is attested on the surface (Nadim 2009).

Local phenomena as sinkholes cannot be easily monitored neither by the classical geotechnical or geophysical methods. Therefore, the INERIS (Institut National de l'Environnement Industriel et des Risques, France) carried out several studies in recent years to identify the correct methodologies aiming at detecting any damaging process that could lead to consequences at the surface.

Recent studies evidenced that, among other possible methodologies, the acoustic monitoring can be adopted as a useful technique to detect and record rock falls, thus to monitor the evolution of sinkholes and/or localised collapses inside quiet cavities.

The acoustic technique has been applied to some case studies in order to define a suitable methodology to collect and analyse data, with the objective of locating the most active areas and identifying the critical periods characterised by an intense activity.

The Brasserie quarry was instrumented with 5 microphones on January 2012.

Later, on November 2012, a campaign of measurements was planned to better understand the propagation of sound inside of the quarry. The main objective of the experiments was twofold. On the one hand it was the determination of the attenuation of the acoustic waves due to the action of the existing surfaces of the quarry, like pillars and boundaries. On the other hand it was the investigation on the source localisation process.

To this aims, the data collected during the measurement campaign were classified on the base of the signal-to-noise ratio (SNR) and preliminarily analysed for the acoustic characterisation in this phase of study.

In the present paper, the preliminary results and the description of the upcoming works and expectations will be outlined after the description of the tests carried out in the quarry.

123.2 Site Description

The site under study is the Brasserie quarry, an old limestone mine located in the South-East of Paris (France) (Fig. 123.1). The quarry has been mainly exploited using the room and pillar technique, over approximately 4.5 Ha. The depth of the quarry does not exceed 25 m and several starts of sinkholes and extended roof falls have been observed. The quarry is open to visitors and administrative buildings lie above the quarry surface, so the quarries inspection office (Inspection Générale des Carrières de Paris) decided to set up a monitoring system within the quarry to reduce the risk for both surface and underground instabilities.
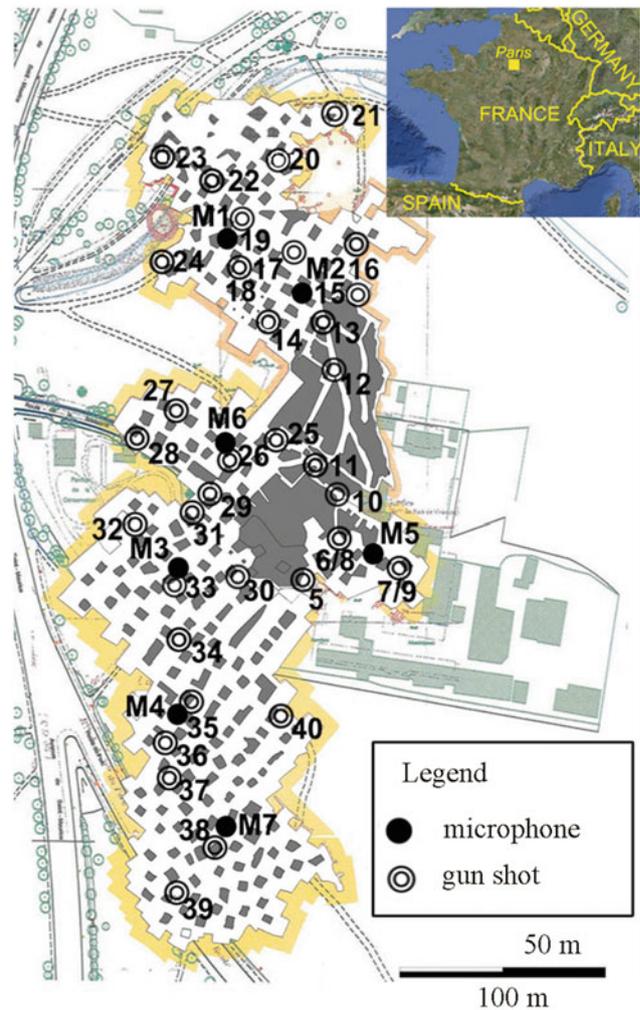
Fig. 123.1 The microphone array and the gun shot spatial distribution inside the quarry

On January 2012 the site was instrumented by the INERIS through the installation of an acoustic monitoring network which consisted of 5 microphones and 2 geophones, spread all over the quarry.

On November 2012 a campaign of measurements was carried out in order to provide a dataset for the determination of the acoustic energy attenuation inside the quarry. For that matter, the geophones were temporarily removed and 3 more microphones were installed, and one of them could be easily moved. Three types of acoustic sources were emitted, referring to the emission of artificial sounds simulating the block falls and the firing of 40 gunshots in different positions in the quarry (Fig. 123.1).

The final purpose of the experiment was the characterisation of the source event: to this aim the different types of sources used in the measurements campaign helped in localising, dimensioning and evaluating the attenuation effect.

In order to investigate the wave propagation and the attenuation attitude inside the quarry, the impulse responses generated by the gun shots were first analysed and classified.

123.3 Analysis of the Gun Shot Recordings

The recorded signals were processed with a Matlab®-based code for the computation of the SNR, defined as the ratio between a signal level and the corresponding background noise level. Theoretically, the background noise should be detected by recordings of some seconds for each microphone of the array. These recordings should be used to assess the ratio between the event sound level and the background noise in each sector of the quarry. Since this was not possible, a method to elude the lack of the background noise recordings at each microphone was used: a procedure based on the short-term average/long-term average (STA/LTA) method was implemented. The difference stands in computing the ratio of two average amplitudes between a short-term window and a long-term window on the same recording, instead of calculating the ratio between two tracks of equal time duration.

The main function of the code to the SNR computation is to perform a loop that scans the signal isolating a portion of the track within a floating window. The selected portion is sent to a secondary function, which subdivides the signal portion into 2 sections and computes the SNR as:

$$SNR = 20 \log_{10} \left(\frac{A_{s2}}{A_{s1}} \right) \qquad (123.1)$$

where A_{s2} and A_{s1} are the root mean square amplitudes of the two sections of the signal, respectively.

A SNR value is computed at each step while the floating window scrolls the signal. The trend of the SNR exhibits a maximum in correspondence to the first time arrival of sound; in fact, before the sound arrival there should be only noise while after the arrival time the components due to the recording of the acoustic wave should be prevailing.

The SNR is a good indicator of the acoustic attenuation and of the quality of the audio recordings. The attenuation is a complex phenomenon that generally increases with the distance from the source, i.e. loss of the intensity of the sound energy. Moreover, it is sensitive to other environmental physical properties such as absorption and diffusion. SNR was chosen in alternative to the signal sound pressure level only since it is a relative measure, and therefore enables the comparison of the acoustic condition between different measuring positions that may be affected by various background noise levels.

In Fig. 123.2 is shown the SNR versus the source-microphone distance, first considering all the microphone positions (Fig. 123.2a) and then for each microphone positions (Fig. 123.2b–h). From this evaluation it is possible to
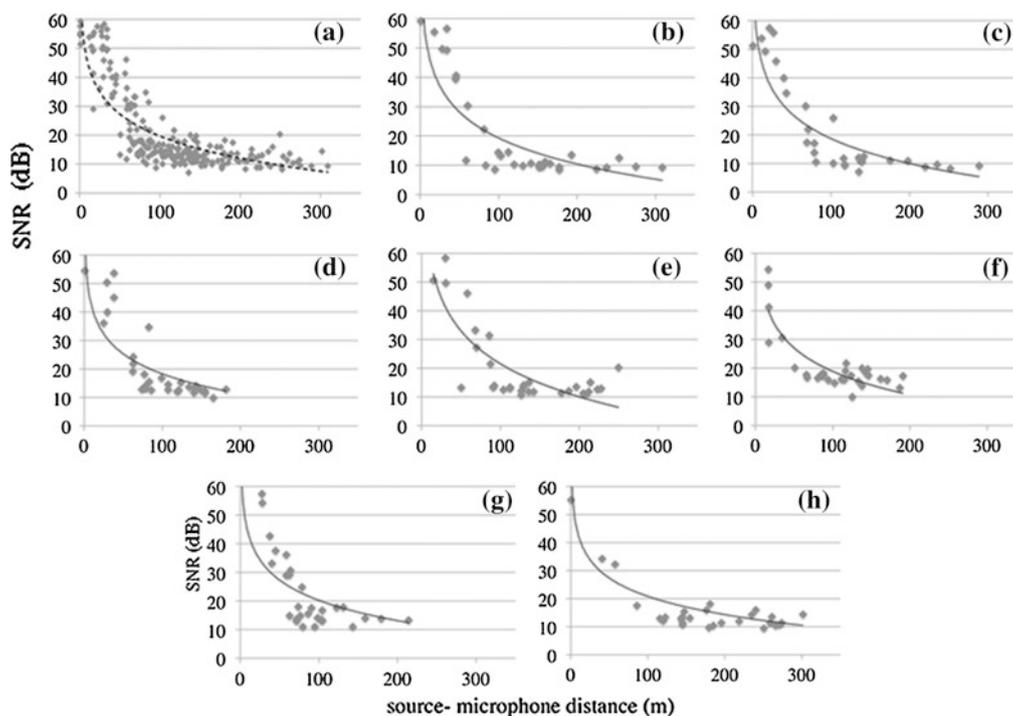
Fig. 123.2 SNR, in dB, as a function of the source-microphone distance for: **a** all the microphones; **b** microphone 1; **c** microphone 2; **d** microphone 3; **e** microphone 4; **f** microphone 5; **g** microphone 6; **h** microphone 7
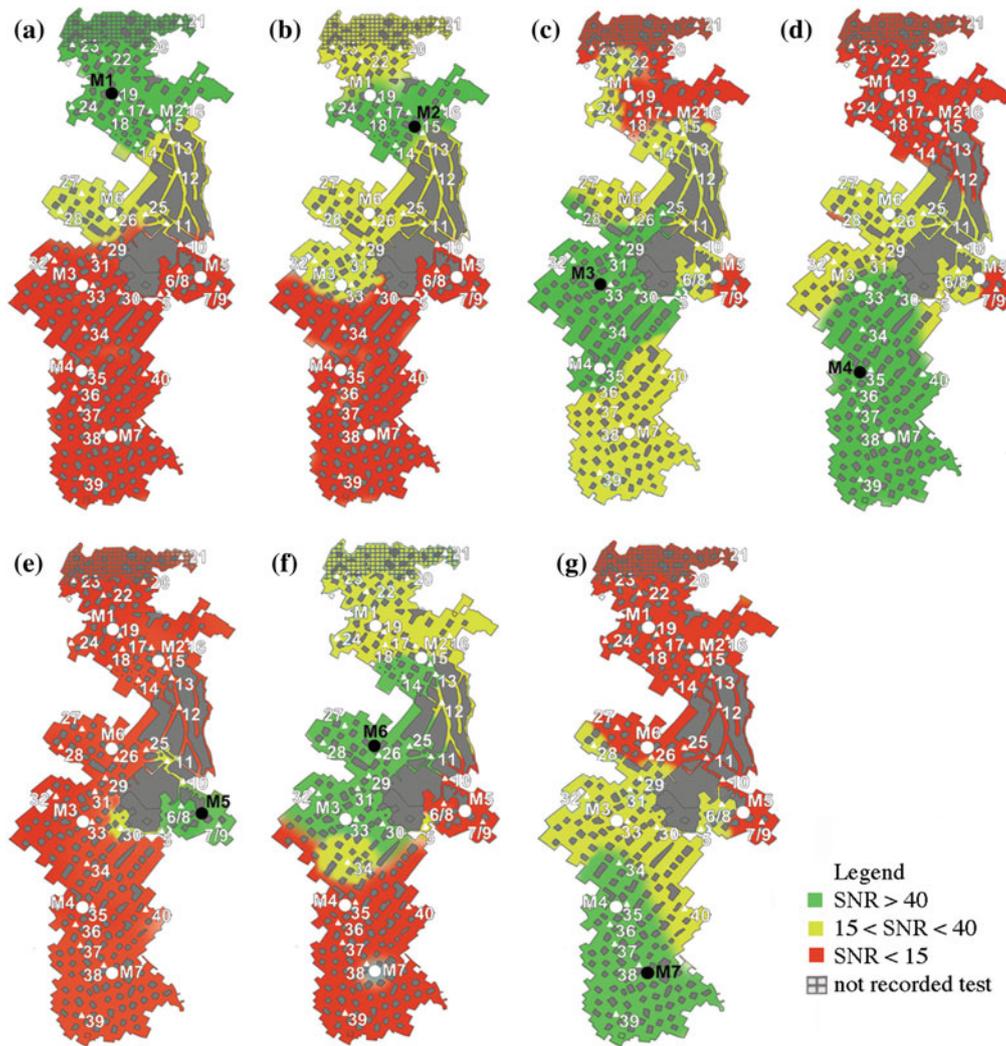
Fig. 123.3 Sensitivity map for: **a** microphone 1; **b** microphone 2; **c** microphone 3; **d** microphone 4; **e** microphone 5; **f** microphone 6; **g** microphone 7

consider that the source signal is fairly repeatable. The graphs of Fig. 123.2 are an attempt to obtain a relationship between the measured acoustic pressure level and the source-microphone distance. A more deep slope in SNR decreasing up to about 100 m is shown for all the microphones, and afterward a constant behaviour with an increase in the distance from the source.

The analyses described above have led to the creation of a 'sensitivity' map for each microphone position: the different areas of the Brasserie quarry have been coloured according to the SNR computation (Fig. 123.3). The green areas identify the zones where signals with SNRs higher than 40 dB were registered; the yellow areas identify the origin zones of signals with SNR between 15 dB and 40 dB, and the red areas the zones where the signals produced from the gunshots could not be recorded by the microphone under analysis (SNR < 15 dB).

A detailed analysis of the colour distributions evidenced that there are critical corridors (dotted line in Fig. 123.4a) and a zone characterised by a complex geometry (orange area in Fig. 123.4a), which are responsible for the low communicability between the northern and the southern portions of the quarry, and for the total isolation of the sector surrounding microphone 5 (blue area in Fig. 123.4a). In fact, all the sources fired in the area close to microphone 5 (blue area in Fig. 123.4b) were recorded with a high SNR and a good signal quality only by microphone 5.

On the base of the above mentioned observations, the quarry volume could be divided into four main areas (areas 1, 2 and 3 and 4 in Fig. 123.4b), characterised by different acoustic behaviour within each area. Moreover the propagation between the identified areas is difficult and affected by high attenuations.
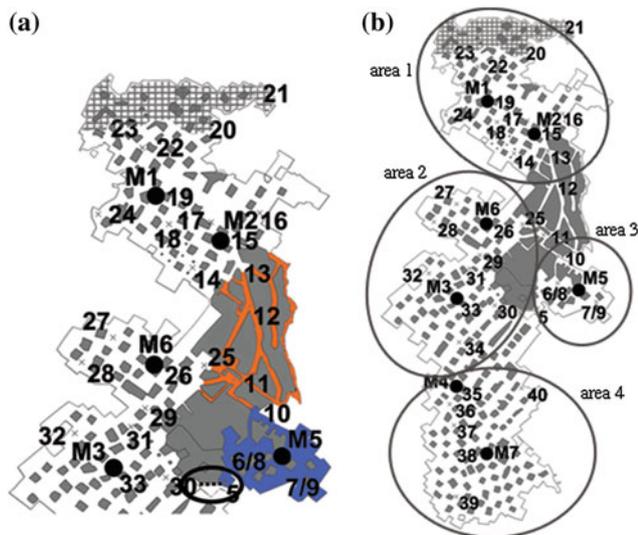
Fig. 123.4 a Identification of the critical corridor and areas; **b** identification of the four main areas characterized by specific attenuation attitudes

123.4   Conclusions and Further Developments

The present paper describes the preliminary results obtained from the processing of the data collected by an acoustic monitoring system during a measurement campaign inside an old limestone quarry.

The simple observation of the quarry map evidenced the presence of four isolated areas characterised by different geometries and volumes. This observation was confirmed and deepened by the analysis of the SNR computed for the signals recorded during a set of tests with gunshots. The classification of the tracks on the base of the SNR has led to the drawing of 'sensitivity' maps indicating each microphone's response to the acoustic stimuli of gunshots (i.e. for

each sensor the quarry volume was subdivided in areas where the gunshots resulted to be with high, medium or very low SNR). The maps allowed to conduct a primary evaluation of the acoustic attenuation for the firings and could be a useful support to the assessment of the array implantation and to plan possible modifications to the sensor distribution. Moreover it emerged that critical corridors and a complex geometry area delimit four sectors, isolating the northern, the middle, the southern and the eastern portions of the quarry.

Further developments of the research are considered: specific analyses will be carried out in cooperation with the Department of Energy of the Politecnico di Torino through the use of the commercial acoustic software ODEON®. This will allow to deepen the aspects related to the source localisation (i.e. natural block fall), simulating the acoustic behaviour of closed spaces to obtain maps of sound attenuation and reverberation. To this aim the gunshot recordings will be used for the evaluation of the impulse response and the computation of the reverberation time. The data collected will be employed to calibrate the prediction model of the quarry.

The use of a code developed by the Institute Langevin of the CNR of Paris (France) for the simulation of the acoustic wave propagation is also planned. A comparison between the obtained results could allow a more accurate determination of the sound propagation characteristics in a site with complex geometries and heavy uncertainties.

References

Didier C (2008) The French experience of post mining management, Post Mining 2008, Nancy, 6–8 Feb 2008

Nadim CE (2009) Surveillance en grand de cavités souterraines complexes par méthode acoustique. Analyse préliminaire de données de référence: rapport d'étape, Internal Report, DRS-09-99345-10707A, INERIS, Paris, France

Investigative Procedures for Assessing Subsidence and Earth Fissure Risk for Dams and Levees

Kenneth C. Fergason, Michael L. Rucker, Bibhuti B. Panda, and Michael D. Greenslade

Abstract

Investigative procedures for assessing land subsidence and earth fissure risk for dams and levees have been developed for projects in arid regions of the USA. The overall assessment includes evaluation of the overall subsidence experienced in the vicinity of a subsidence-impacted structure, detailed investigation to search for earth fissures, prediction/modeling of future subsidence and related earth fissure development, delineation of risk, and recommendations for moving forward, such as engineered solutions and monitoring. Utilizing the findings of subsidence investigation, additional investigative methods for earth fissure search include photogeologic (lineament) analysis, assessment of the capability of near-surface soils to develop an earth fissure, assessment of the degree of ground disturbance, detailed site inspection, seismic refraction profiling for concealed earth fissures, and excavation of trenches. Such an investigation must include investigative techniques capable of detecting earth fissures that lack significant surficial expression. Satellite-based interferometry by repeat pass synthetic aperture radar (InSAR) provides unique information about active land subsidence over large areas. The subsidence or deformation image known as an interferogram can also, with proper interpretation, reveal some preliminary subsurface information about alluvial basin geometry, lithology and hydrology where active land subsidence is interpreted. Effective subsidence risk assessment and mitigation requires understanding and quantifying historic subsidence, and estimating potential future subsidence that could impact the dams and levee infrastructure. Basin alluvium and bedrock interface geometry, and basin alluvium lithology changes and interfaces, profoundly influence patterns and degree of subsidence. Characterization includes collection and synthesis of historic survey and well data, surface geophysical methods for basin and bedrock characterization, and when available, InSAR to document recent or current subsidence patterns. Utilizing a synthesis of this information, subsidence modeling matching

K.C. Fergason (✉) · M.L. Rucker · B.B. Panda
AMEC Environment and Infrastructure, Inc., 4600 East
Washington Street, Suite 600, Phoenix, AZ 85034, USA
e-mail: ken.fergason@amec.com

M.L. Rucker
e-mail: michael.rucker@amec.com

B.B. Panda
e-mail: bibhuti.panda@amec.com

M.D. Greenslade
Flood Control District of Maricopa County, 2801 West Durango
Street, Phoenix, AZ 85009, USA
e-mail: mdg@mail.maricopa.gov

documented historic subsidence and estimating potential future subsidence can be developed to assess potential impacts on dam and levee infrastructure. Utilizing the results of site characterization and subsidence modeling, a finite-element stress-strain model can be developed to estimate past and future ground strain. Estimated tensional strain values can be utilized to predict where earth fissures are likely to initiate with future subsidence and reduce the risk of failure.

Keywords

Subsidence • Earth fissure • Dam • Levee • Guidelines

124.1 Introduction

Depletion of groundwater resources in many deep alluvial basin aquifers in the Western USA is causing ground subsidence. Ground subsidence can severely and adversely impact infrastructure by changing the ground elevation, ground slope (grade) and through the development of ground cracks known as earth fissures, develop into large gullies. Earth fissures have the potential to undermine the foundations of dams, levees, and other pertinent structures and cause system failure.

Earth fissures that have been exposed to flowing water will most likely have observable surficial expressions such as ground cracking, piping holes, vegetative and tonal lineaments, and similar features. However, uneroded earth fissures often do not have surficial expression.

Earth fissures are presumed to have caused the failure of Picacho Dam in South-Central Arizona in 1955. In addition, earth fissures have been identified in close proximity to or underlying the foundations of McMicken Dam and Powerline Flood Retarding Structure (FRS) in Central Arizona (AMEC 2003, 2008). Both structures are earthfill embankments with maximum height of 25–35 feet that are founded on alluvial fill. A segment of McMicken Dam was rehabilitated in 2006 and construction of an interim dam safety measure at Powerline FRS was completed in 2013.

124.2 Investigative/Procedural Methods

Existing literature providing recommendations for and/or descriptions of investigative techniques and procedures for land subsidence and earth fissure investigations for dams and levees is sparse. The Arizona Land Subsidence Group, through the Arizona Geological Survey published a document titled Suggested Guidelines for Investigating Land-Subsidence and Earth Fissure Hazards in Arizona (Arizona Land Subsidence Interest Group 2011). A similar publication from the Utah Geological Survey is currently in publication limbo as stake-holders work out issues associated with the publication. The Flood Control District of Maricopa County (District) contracted AMEC Environment & Infrastructure, Inc. (AMEC) to develop procedural guidelines for investigating land subsidence and earth fissuring with input from an independent consultant (GeoSouthwest LLC) and the regulatory agency, Arizona Department of Water Resources (ADWR) Dam Safety (AMEC 2011). The investigative/ procedural methods summarized in this paper are adapted from these procedural documents. More detailed publications that discuss these methods include Fergason et al. (2013), Rucker et al. (2013), and Panda et al. (2013).

Subsequent to performance of an evaluation of overall subsidence experienced in the vicinity of a subsidence-impacted structure, a detailed investigation to search for

• Repeat-Pass Synthetic Aperture Radar Interferometry (InSAR)	• Deep refraction microtremor (ReMi)
	• Shallow ReMi
• Photogeological lineament analysis	• Fissure detection by seismic refraction signal trace analysis
• Geological reconnaissance of photolineaments and terrestrial search for earth fissures	• Subsurface characterization by seismic refraction
	• Trench investigation
• Deep resistivity soundings	• Future subsidence prediction
	• Stress–strain modeling

earth fissures must be performed. Such an investigation must include investigative techniques capable of detecting earth fissures that do not have significant surficial expression. Procedural documents have been developed for the following geohazard investigation and analysis techniques to perform such an investigation (AMEC 2011):

Each procedural document includes detailed descriptions of each geohazard investigative/assessment method inclusive of supporting documentation; qualifies the level of uncertainty associated with each method; allows for the transfer of methods to future similar projects; and establishes procedures with which all interested agencies and stakeholders will concur.

These procedures are modified and updated from those developed by AMEC with input from GeoSouthwest, LLC and the ADWR Dam Safety Division for use by the District (AMEC 2011). These guidelines have not been developed as a prescriptive recipe for planning. The approach, its associated protocols and recommended methods are presented with the intent of providing a generic basis for independently developing site-specific strategies. A project-specific plan should provide sufficient flexibility to allow interim adjustments to the analysis as the process evolves.

124.3   Overview of InSAR

InSAR data can detect relative terrain elevation changes to a possible 0.2–0.4 inch (5–10 mm) resolution under favorable radiometric conditions, where the ground surface is divided into individual 'pixels' with a size of about 100 feet (30 m) across. InSAR can be utilized for general subsidence geometry, detailed deformation data, input data for modeling and other applications, and monitoring. Additionally, interpreted subsidence patterns aid in determining the subsurface geology in areas where active subsidence is observed.

124.4   Subsidence Estimation

A primary subsidence mechanism is increasing effective stress due to groundwater level decline within saturated compressible basin alluvium. Ultimate subsidence magnitude at a given location is a function of change in effective stress, compressible alluvium thickness and material modulus. Modulus is typically a function of depth and effective stress. Subsidence rates are assumed to largely be a function of rate of groundwater level decline, alluvium permeability (or hydraulic conductivity) and distance from groundwater level stress points (i.e. pumping wells). Basin alluvium and bedrock interface geometry, and changes and interfaces in basin alluvium lithology, profoundly influence patterns and magnitude of subsidence. Characterization includes collection

and synthesis of historic survey and well data, surface geophysical methods for basin and bedrock characterization, and when available, InSAR to document recent or current subsidence patterns. Utilizing a synthesis of this information, subsidence modeling matching documented historic subsidence and estimating potential future subsidence can be developed to assess potential impacts on dam and levee infrastructure.

As in other geotechnical applications addressing ground settlement, several approaches may be applied to the problem of estimating subsidence due to groundwater withdrawal. Empirical approaches such as presented by Bell (1981) provide a 'rule-of-thumb' based on a ratio of subsidence for a given amount of groundwater decline; for the Las Vegas area, this ratio is reported to be about 20:1 (water level decline to subsidence) for fine-grained alluvium and about 40:1–60:1 for coarse-grained alluvium. Subsidence estimation based on traditional soil mechanics principles and soil parameters suffer from the general inability to obtain relevant, and relatively undisturbed, alluvium material samples for laboratory consolidation or triaxial testing. Such undisturbed sampling would have to be successful at depths of several hundred feet to in excess of 1,000 feet. Even if such sampling were to be successful, a relatively very few data points would have to suffice to characterize huge volumes of heterogeneous basin alluvium.

The approach to subsidence estimation summarized in this paper is, at a given location, to estimate modulus through the column of compressible alluvium, apply the increase in effective stress through that column from a given groundwater level decline, and calculate the vertical displacement (subsidence) from the resulting strain. Initial and final groundwater levels, or beginning and ending water levels for a distinct time period, are needed to calculate change in effective stress. Compressible alluvium thickness or depth is needed to which to apply change in effective stress. A compressible alluvium modulus profile, with modulus increasing with depth, must be estimated. Alluvium modulus is also a function of the alluvium lithology; surface geophysics provides means to assess alluvium thickness and lithology when useful well data is not available. Finally, to estimate time-dependent lateral propagation of subsidence from pumping centers, alluvium mass permeabilities or hydraulic conductivities must be estimated and distance to pumping centers assessed.

124.5   Stress-Strain Model

The relationship between pore fluid pressure changes and aquifer system compression is based on the principle of effective stress proposed by Terzaghi (1925), where effective stress is the difference between the total stress and the pore

fluid pressure. The total stress represents the geostatic load. Under this principle, when the total stress remains constant, a change in pore fluid pressure causes an equivalent change in effective stress within the aquifer system. This results in a small change in volume in an aquifer system that is governed by the compressibility of the aquifer system skeleton. Conceptually, the change in pore pressure with time is related to the change in porosity. Subsidence is estimated by multiplying the change in porosity by the vertical thickness of the medium.

The amount of compaction and fissure location are closely related to the thickness and skeletal compressibility of fine-grained sediments within the aquifer system. In a region having thick compressible aquitards (fine sediments) of low vertical conductivity, the pore fluid pressure does not simultaneously equilibrate with the head in the surrounding aquifer. Instead, a pore fluid pressure gradient develops across the aquitards, driving the slow drainage of water from the aquitards into the aquifer. Because the compaction of an aquitard results from head change in the aquitard itself, the subsidence of the land surface lags behind the head decline measured in wells tapping more permeable sediments within the aquifer. This time delay leads to continuing subsidence despite static or recovering hydraulic heads observed in the field (Hoffmann et al. 2003). Modeling subsidence and deformation of the alluvium in response to changes in groundwater levels in the aquifer system requires addressing displacements and pore water pressure changes simultaneously in a coupled manner. A fully coupled analysis requires that both the stress-deformation and seepage dissipation equations be solved simultaneously. This coupling is typically achieved by using finite element-based computer programs that link seepage modeling with stress–strain deformation modeling.

References

AMEC Earth and Environmental, Inc. (AMEC) (2003) Earth Fissure Investigation Report, McMicken Dam, Maricopa County, Arizona. Prepared for the Flood Control District of Maricopa County, Contract FCD 2000C006—Work Assignment Nos. 4 and 5, April 11

AMEC Earth and Environmental, Inc. (AMEC) (2008) Supplemental Earth Fissure/Ground Subsidence Investigation Report, Powerline Flood Retarding Structure, Pinal County, Arizona. Prepared for the Flood Control District of Maricopa County. Contract FCD 2006C020, Work Assignment No. 2. AMEC Job No. 7-117-001082. June 4

AMEC Earth and Environmental, Inc. (AMEC) (2011) Procedural Documents for Land Subsidence and Earth Fissure Appraisals. Prepared for the Flood Control District of Maricopa County, Contract FCD2008C016—Work Assignment No. 13. May

Arizona Land Subsidence Interest Group (2011) Suggested Guidelines for Investigating Land-Subsidence and Earth Fissure Hazards in Arizona. Arizona Geological Survey Contributed Report CR-11-D. August

Bell JW (1981) Bulletin 95, Subsidence in the Las Vegas Valley, Nevada Bureau of Mines and Geology, Mackay School of Mines, University of Nevada, Reno

Fergason KC, Rucker ML, Greenslade MD (2013) Investigative procedures for assessing earth fissure risk for dams and levees, United States Society on Dams, 33rd annual meeting and conference, Phoenix, AZ, 11–15 Feb 2013

Hoffmann J, Galloway DL, Zebker HA (2003) Inverse modeling of interbed storage parameters using land subsidence observations, Antelope Valley California. Water Resour Res 39(2):1−13

Panda BB, Rucker ML, Fergason KC (2013) InSAR as a subsidence characterization tool for flood control dam studies, United States Society on Dams, 33rd annual meeting and conference, Phoenix, AZ, 11–15 Feb 2013

Rucker ML, Fergason KC, Greenslade MD, Hansen LA (2013) Characterization of subsidence impacting flood control dams and levees, United States Society on Dams, 33rd annual meeting and conference, Phoenix, AZ, 11–15 Feb 2013

Terzaghi K (1925) Principles of soil mechanics, IV, settlement and consolidation of clay. Eng News Rec 95(3):874–878

Chiara Colombero, Cesare Comina, Anna Maria Ferrero,
Giuseppe Mandrone, Gessica Umili, and Sergio Vinciguerra

Abstract

Rock slope monitoring is a major aim in territorial risk assessment and mitigation. The high velocity that usually characterizes the failure phase of rock instabilities makes the traditional instruments based on slope deformation measurements not applicable for early warning systems. On the other hand the use of acoustic emission records has been often a good tool in underground mining for slope monitoring. In this paper the design and installation of a monitoring system based on acoustic emission aimed at interpret and forecast a large rock instability phenomenon is reported together with some preliminary geophysical and geomechanical studies performed.

Keywords

Rock slope instability • Slope monitoring • Acoustic emission • Cross hole seismic tomography

125.1 Introduction

Rock slope instabilities are usually preceded by slow small entity deformations that can precede a dynamic fast failure. Small deformations, which can be recorded with standard devices (e.g. extensometer, etc.) and new remote sensing technologies (e.g. Lidar, GBInSAR, etc.), can be very significant to forecast instability development. Prior to the ultimate fracture, the rock also releases energy and it determines the generation of microtremors. The record and monitoring of acoustic emission can be therefore an alternative strategy for forecasting dynamic ruptures and is widely applied in mine monitoring (Kwiatek and Ben-Zion 2013).

For these reasons we propose to monitor and detect small signals of impending failures and mitigate natural hazards, by:

1. quantification of critical damage thresholds triggering dynamic failure, throughout the 'in situ' identification of characteristic slow deformation signals and accelerating patterns before impending 'large scale' failure events;
2. setting up of early warning models for forecasting the time of rupture with application to natural hazards;
3. transferring knowledge between multi-scale signs of slow deformation before dynamic failure from the laboratory to field.

To do this, the installation of a series of devices based on acoustic emission/microseismic approaches is planned in a test site where standard monitoring systems have been installed several years ago and, consequently, a set of data is already available. The installation of the monitoring network will be accompanied by a detailed geophysical and geomechanical characterization of the test site, in order to establish the best nodes position; to define the seismic velocity field of the rock mass, which is a fundamental parameter for the following monitoring step; to define the internal characteristics of

C. Colombero · C. Comina (✉) · A.M. Ferrero · G. Mandrone · S. Vinciguerra
Department of Earth Sciences, University of Turin, Turin, Italy
e-mail: cesare.comina@unito.it

A.M. Ferrero
e-mail: margheritaferrero@yahoo.it

G. Umili
Department of Civil, Environmental and Territory Engineering, University of Parma, Parma, Italy

the monitored landslide and to image the fracturing state and the relative variation in seismic velocities between altered and intact rock to be related with geological observations (both sounding results and overall fracturing state).

Moreover rock physical and mechanical characterization will be carried out in laboratory on the main lithologies, throughout measurements of basic parameters such as elastic constants, fracture strength, density, porosity and elastic wave velocities. This will allow a direct comparison with the same parameters registered in the field.

In this paper the preliminary results of both geophysical tests and geological characterization are presented together with plans for the installation of the acoustic emission/ microseismic network.

125.2 Geological Framework

The site that has been chosen for the study is the rock slope of the Madonna del Sasso, that is affected by a rock instability phenomenon, highlighted by neat and long lasting episodes of slow deformation recorded by standard measurement devices such as inclinometers, topographic measurements and fissurometers.

The cliff of Madonna del Sasso is located along the western shore of Orta Lake and takes its name from the eighteenth-century sanctuary located at about 650 m a.s.l. In this area a granitic rock mass, called Granito di Alzo, outcrops; this is part of Lower Permian granitoid masses and, in the past, it was subjected to mining activity. It is late-Hercynian magmatic intrusion, not metamorphosed and generally little deformed (Boriani et al. 1992; Giobbi Origoni et al. 1988) that occurs along the contact between the "Serie dei Laghi" and the Ivrea-Verbano Zone. These granites, commonly known as "Graniti dei laghi", constitute a large batholith elongated in NE–SW direction that intrudes both the "Scisti dei laghi" and the Stron Ceneri zone. This batholith includes five plutons among which, that of study area, the Alzo-Roccapietra Pluton, of granite-granodiorite composition, outcropping between the lower Sesia Valley and the Orta Lake.

A preliminary geomechanical characterization (based on previous data and brief surveys) leads to define the rock mass on which the Sanctuary is built as intact or massive, with widely spaced discontinuities (GSI > 70) characterized by good surface quality. The rock mass characterization has been carried out by means of a conventional survey (Lancellotta et al. 1991) that has identified (Fig. 125.1) four main joint sets (K1 (110/75), K2 (0/80), K3 (150/15) and K4 (50/75)). Particularly along the K4 discontinuity there is a clear evidence of movement: a decimetric step is visible on the yard and on the small walls in front of the sanctuary.

125.3 Geophysical Site Investigation

A cross-hole seismic tomography has been performed between the two available inclinometric boreholes S1 and S2 in the area in front of the Sanctuary (Fig. 125.1). In cross-hole seismic tomography, seismic sources are located both in well and on the surface and are shot into receivers located in a nearby well or on the same surface. The travel times of the first arrivals are then used to produce a tomographic velocity cross-section of the subsurface between the two wells (Bregman et al. 1989; Calnan and Schuster 1989; Lines and LaFehr 1989; McMechan et al. 1987). Crosshole tomography is expected to provide better resolution than surface based seismic methods, since most of the energy does not travel through the highly attenuating near surface and the travel distances are shorter. In addition, the resolution of cross-hole tomography is not depth-limited since most of the energy travels between the wells and a trans-illumination of the imaged medium is achieved. This is even more important in a fractured medium, as the one object of the study, where waves can have complicated travel paths, not easily interpreted by the surface alone.

To perform the tests, a Borehole Impacter Source by Geotomographie GmbH has been used as in-hole source in the S2 borehole in three different locations till a depth of about 6 m (after this depth an obstruction of the hole casing didn't allow further penetration) while an hammer, impinging both vertically and horizontally, has been used as surface source in three different locations along the line connecting the two holes. A prototype borehole string equipped with 8 three component geophones (10 Hz) stiffly connected by a bar, that allows to control geophone orientation, has been progressively lowered (with a 2 geophone superposition each subsequent positioning) in the S1 sounding at different depths till the maximum available depth of 27 m. On the surface 4 three component geophones (2 Hz) have been moreover used. First break picking has been performed on the acquired seismic traces to allow for both P and S wave velocities imaging. Data have been inverted to obtain a tomographic image by the use of GeoTom® software.

The P wave velocity seismic image depicted by cross-hole tomography is reported in Fig. 125.2 together with the acquisition scheme, traced rays after the inversion and ray coverage. The seismic image correlates well both with the evidence of the soundings logs and with the expected fracture state. An high velocity of the intact granite formation is revealed and two main fractures are also evidenced showing a velocity reduction and a major localization of seismic rays. These fractures compare well with the K4 system which, between the two boreholes, shows also a surface manifestation (Fig. 125.1).
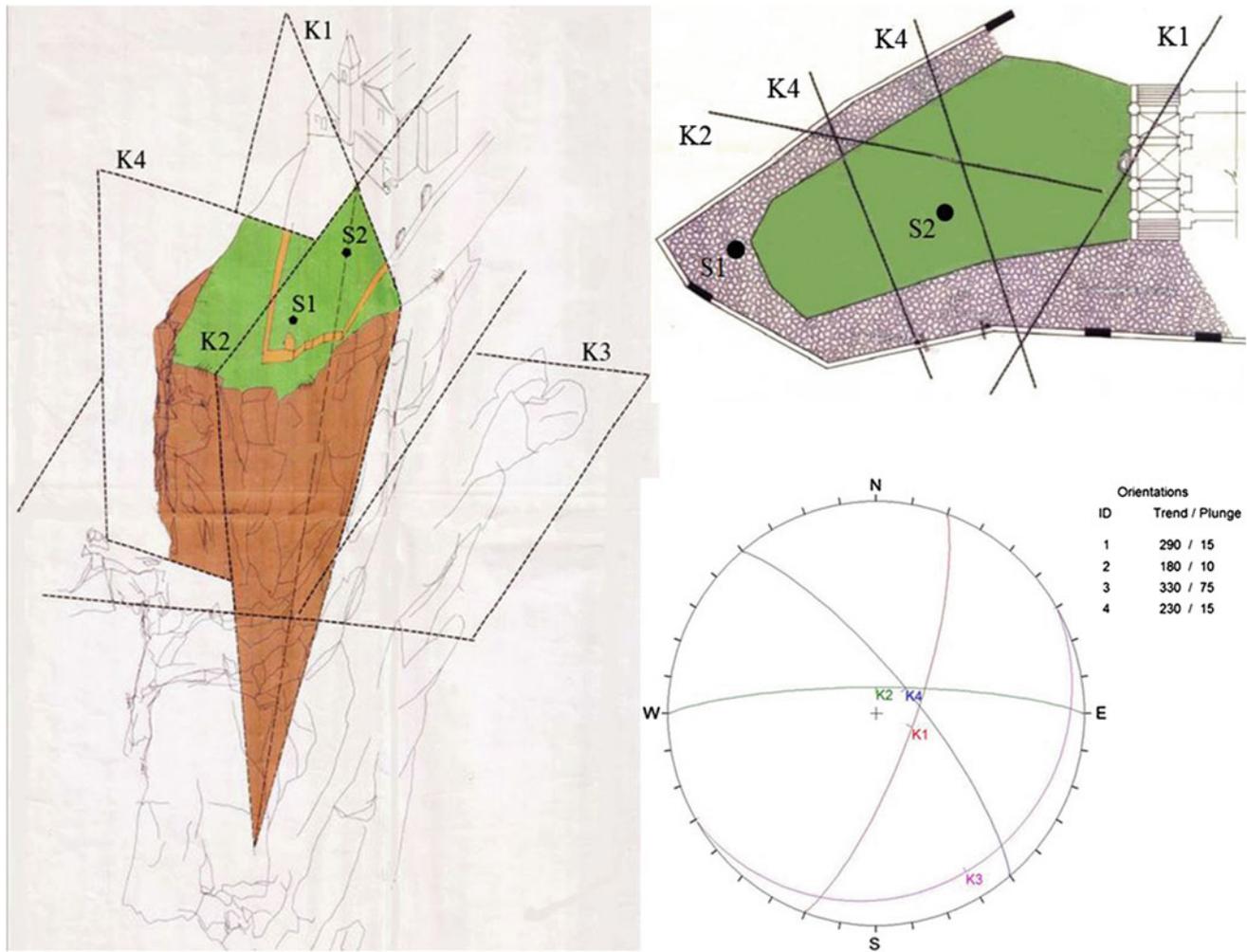
Fig. 125.1 Slope schematic structure: **a** assonometric and **b** plan views together with **c** surveyed joint sets after Lancellotta et al. 1991

125.4 Evaluation of the Slope Stability

On the basis of the geological and geophysical characterization, a preliminary kinematic analysis of the slope has been performed, by means of a software implemented by the authors, to better understand the possible instability phenomena that are occurring in the rock mass. Input parameters were the granite density (2.6 g/cm^3), the rock mass height (about 200 m) and the orientation of the main joints sets (see Figs. 125.1 and 125.2). This analysis has outlined 2 different kinds of sliding phenomena and a toppling phenomenon that could be compatible with rock mass structure: planar sliding along K4, wedge sliding along the intersection between K1 and K2 and toppling on K4. In order to identify the stability conditions of the slope some parametrical analysis have been carried out with the limit equilibrium approach. Both discontinuity persistence and the friction angle have been varied between realistic values determined by in situ observations and bibliographic data. Different water contents

in the discontinuity have also been considered. In Fig. 125.3 the slope factor of safety for planar sliding for different discontinuity persistence is shown.

For all the considered failure mechanisms the factor of safety can go below one even if the presence of a small amount of rock bridges can guarantee a global stability. Water can play a major role in all the examined cases, however for toppling it can be the triggering effect even for a discontinuity partial saturation (around the 50 %). Rock bridges failure is consequently a very strategic phenomenon that needs to be surveyed.

125.5 Concluding Remarks and Future Works

The paper shows an ongoing work concerning the study of the possible application of innovative monitoring systems based on acoustic emissions to rock slope instability. The characterization studies based on geomechanical and
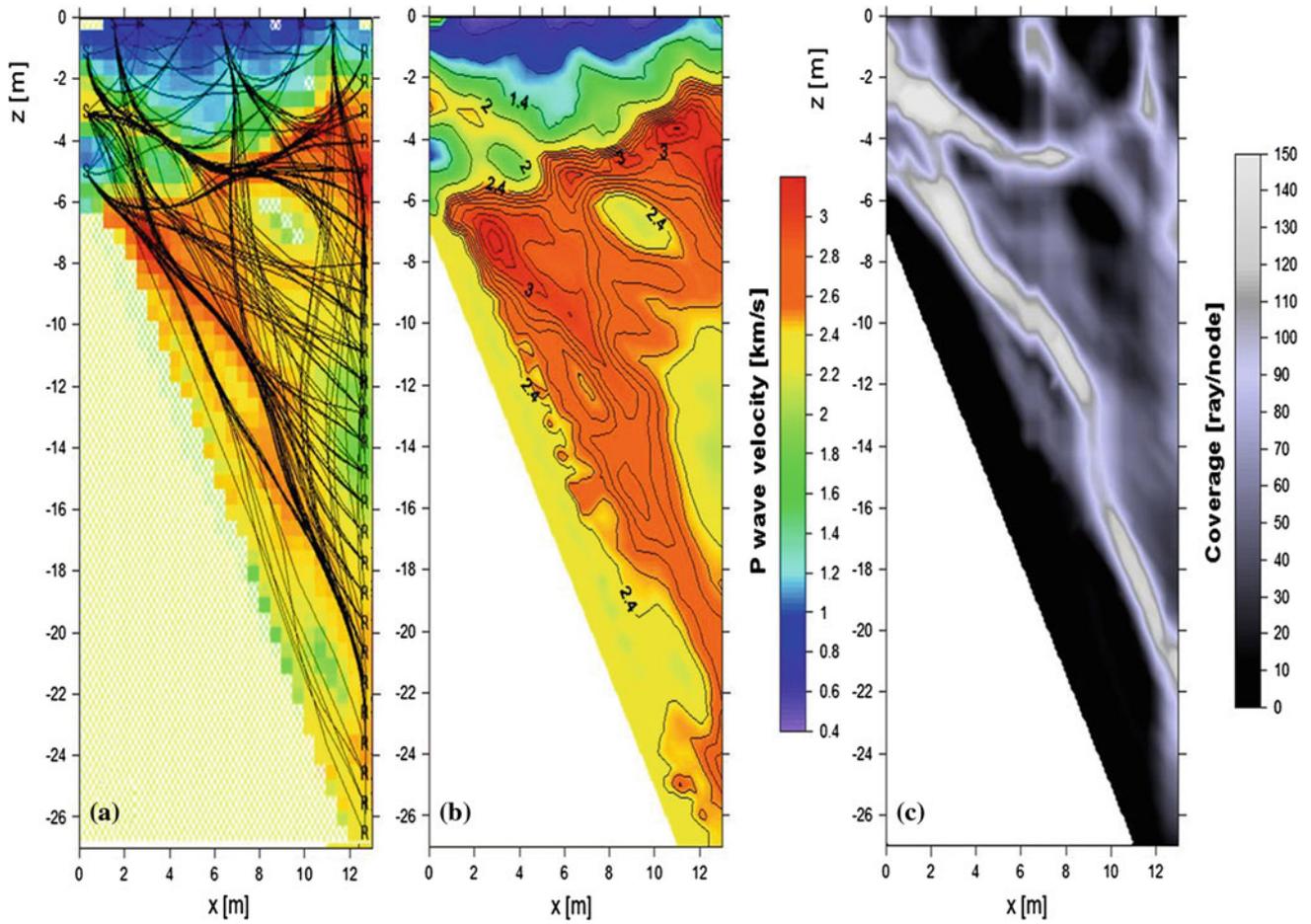
Fig. 125.2 Result of the cross-hole seismic tomography: **a** acquisition scheme (S are seismic sources and R receivers) and traced rays after the inversion; **b** P wave seismic imaging and **c** ray coverage

Fig. 125.3 Factor of safety versus persistence for **a** planar sliding and factor of safety versus water content for **b** toppling
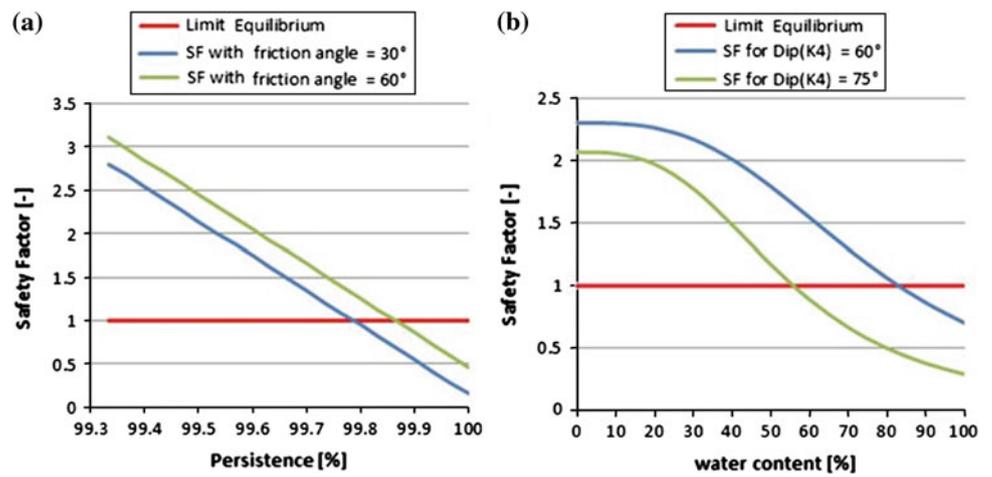
Fig. 125.4 Instrument location in relation to the fracture
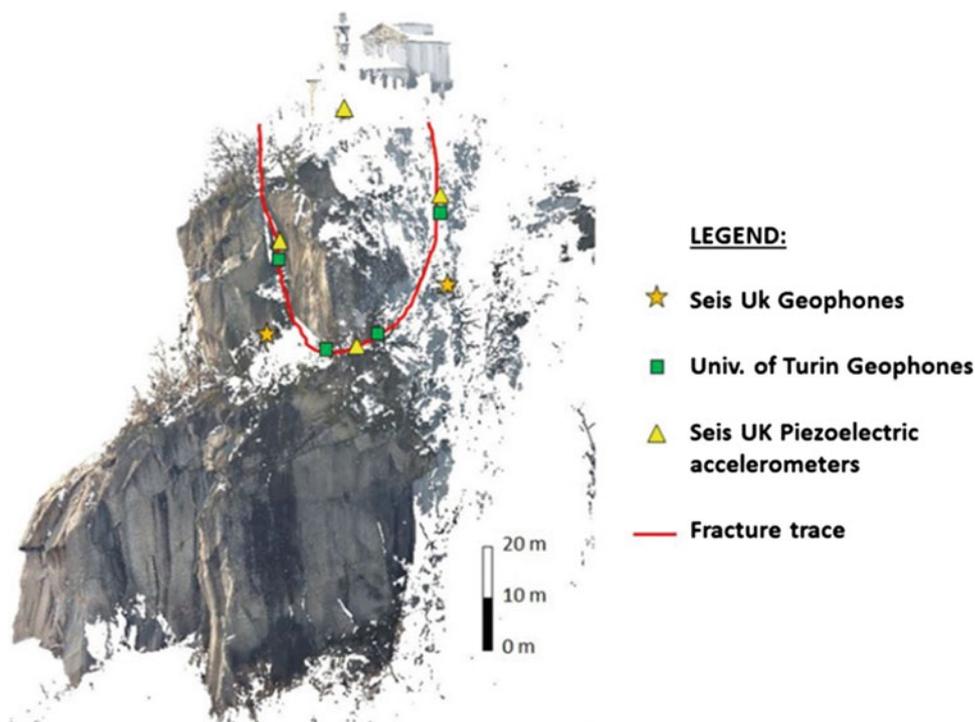
geophysical tests allowed to carry on simple parametrical analysis to preliminary better understand the instability mechanism and to design the monitoring systems that will be placed and verified in the next future. Stability analysis showed that the stability of the slope is due to rock bridges. Their failure progress can results in a global slope failure. Consequently we propose to install a monitoring system to record the energy realised by the rock bridges dynamic ruptures. The devices layout is reported in Fig. 125.4. We aim to identify the characteristic signs of impending failure, by deploying an array of instruments designed to monitor subtle changes of the mechanical properties of the medium and installed as close as possible to the source region. A "site specific" micro-seismic monitoring system to detect micro-seismic events which reflect the subtle changes of the mechanical properties of the medium, made of 4 triaxial piezoelectric accelerometers operating at frequencies up to 23 kHz with a conventional monitoring for seismic detection (4.5 Hz seismometers) and ground deformation (strainmeters), provided by the University of Turin and SEIS-UK is proposed. The high-frequency equipment will allow us to develop a network capable of recording events with Mw < 0.5 and frequencies between 4.5 and 20 kHz. Sensors will be installed within short boreholes (2–4 m) adjacent to the probable slip surface, in order to maximize the coupling

and improve the transmissivity. Waveforms will be stored for detailed analyses.

References

Boriani A, Caironi V, Giobbi Origoni E, Vannucci R (1992) The Permian intrusive rocks of Serie dei Laghi (Western Southern Alps). Acta Vulcanol 2:73–86

Bregman ND, Bailey RC, Chapman CH (1989) Crosshole seismic tomography. Geophysics 54:200–215

Calnan C, Schuster GT (1989) Reflection and transmission cross-well tomography: Presented at the 59th annual international meeting, society exploration geophysicists, expanded abstracts, pp 908–911

Giobbi Origoni E, Bocchio E, Boriani A, Carmine R, De Capitani L (1988) Late-Hercynian mafic and intermediate intrusives of Serie dei Laghi (N-Italy). Rend Soc It Mineral Petrol 43:395–410

Kwiatek G, Ben-Zion Y (2013) Assessment of P and S wave energy radiated from very small shear-tensile seismic events in a deep South African mine. J Geoph Res: Solid Earth 118:3630–3641. doi:10.1002/Jgrb.50274

Lancellotta R, Gigli P, Pepe C (1991) Relazione tecnica riguardante la caratterizzazione geologico-strutturale dell'ammasso roccioso e le condizioni di stabilità della rupe. Private comunication

Lines LR, LaFehr ED (1989) Tomographic modeling of a cross-borehole data set. Geophysics 54:1249–1257

McMechan GA, Harris JM, Andesron LM (1987) Cross-hole tomography for strongly variable media with applications to scale model data. Bull Seismol Soc Am 77:1945–1960

Combining Finite-Discrete Numerical Modelling and Radar Interferometry for Rock Landslide Early Warning Systems

Francesco Antolini and Marco Barla

Abstract

A new methodology for rock landslides Early Warning Systems is presented in this paper. The methodology is based on the integration between monitoring, thanks to the Ground-Based Interferometric Synthetic Aperture Radar technique, and advanced numerical modelling, with the combined Finite-Discrete Element Method. The integration procedure converges to a final decisional algorithm that represents the continuous and real time verification protocol for the monitored landslide.

Keywords

Numerical modelling • Radar interferometry • Landslide • Early warning

126.1 Introduction

The assessment of the evolution scenarios of rock landslides, as well as the associated hazard and risk, is, in general, a complex task. When it is not possible to reduce the hazard with cost-effective slope stabilization works or decrease the vulnerability of the exposed elements, real time monitoring associated to well defined Early Warning Systems (EWS) can be used for the mitigation of the risks (Di Biagio and Kjekstad 2007). In these situations the monitoring systems should be able to measure continuously over time physical quantities that can be used to predict the landslide short-term behaviour. EWS are then adopted to allow elements exposed to risk (e.g. the population) to evacuate the hazardous areas as a consequence of an alarm. For large rock landslides, the physical quantities that have proved to be most interesting for EWS are displacements and velocities.

The Ground-Based Interferometric Synthetic Aperture Radar (GBInSAR) and the combined Finite-Discrete Element Method (FDEM) were respectively selected to be part of an EWS for landslides. This EWS is based on the integration between the real-time monitoring of landslides surface displacements and velocities and on the realistic numerical prediction of their behaviour. An extensive description of the two techniques can be found respectively in Atzeni et al. (2014); Barla and Antolini (2012), Barla and Beer (2012), Barla et al. (2010, 2012), Luzi (2010), Mahabadi et al. (2012).

126.2 The Proposed Integration Methodology

The integration methodology is constituted of four main components, here called "modules", as shown in Fig. 126.1:
- radar monitoring module;
- conventional monitoring module;
- characterization and modelling module;
- verification module.

The first three modules are the source of input data for the verification module (or the decisional algorithm) of the process. The algorithm allows for the continuous assessment of the alert levels and determines the respective actions to be undertaken in order to keep an adequate level of safety for the elements exposed to risk. The integration methodology proposed can be hence considered as an EWS. The surface displacements, velocities and accelerations have been selected as the main quantities to be taken into account and measured. Modules 1, 2 and 3 (radar monitoring,

F. Antolini (✉) · M. Barla
Politecnico di Torino, Corso Duca degli Abruzzi 24, 10129 Turin, Italy
e-mail: francesco.antolini@polito.it

Fig. 126.1 Flow chart of the proposed integration methodology
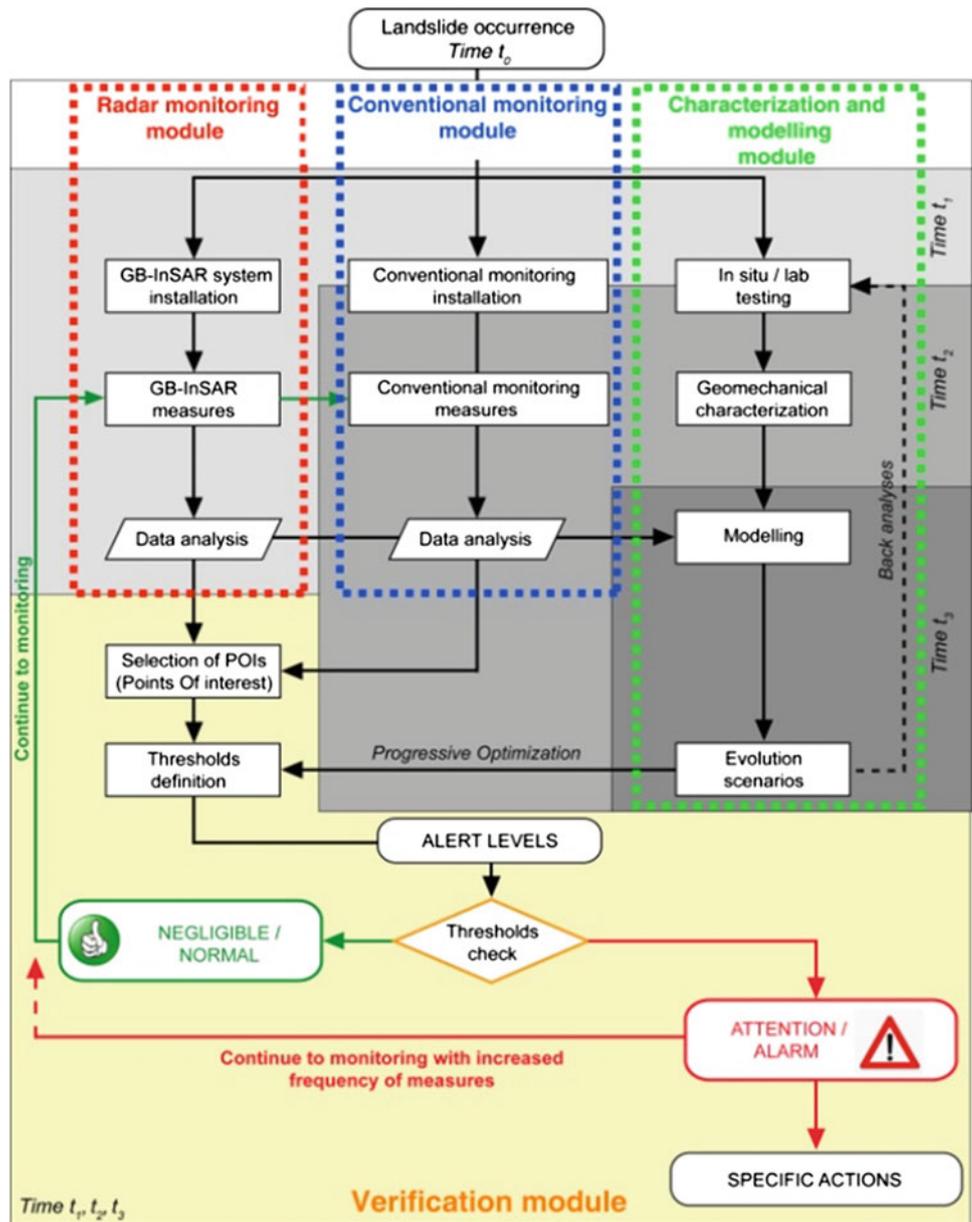
conventional monitoring and characterization and numerical modelling) act in parallel with some of their phases related each other by transversal connections. The modules are also characterized by specific temporal constraints which indicate the time needed to perform all the listed activities.

The temporal constraints are intended as follows:

- t_0: is the initial reference time; for a first time failure, this is the time of landslide occurrence while for a dormant or potential landslide this represents the time of reactivation;
- t_1: from the time immediately next to t_0 to the following 3 days;
- t_2: from 3 to 20 days following t_0;
- t_3: more than 20 days from t_0.

126.2.1 Radar and Conventional Monitoring Modules

The first step to adopt in the proposed methodology, in emergency and just after a landslide occurrence or reactivation, is the installation of a GBInSAR system. The capability of the radar to measure very quickly (near real time) and continuously, over large areas, displacements and velocities with a sub-millimetric accuracy and in almost all weather conditions without the need to install targets on the slope, makes this tool unique among the slope monitoring systems. These features allow for obtaining displacement and velocity maps of the monitored scenario just few hours after the system installation (t_1). Other monitoring systems,
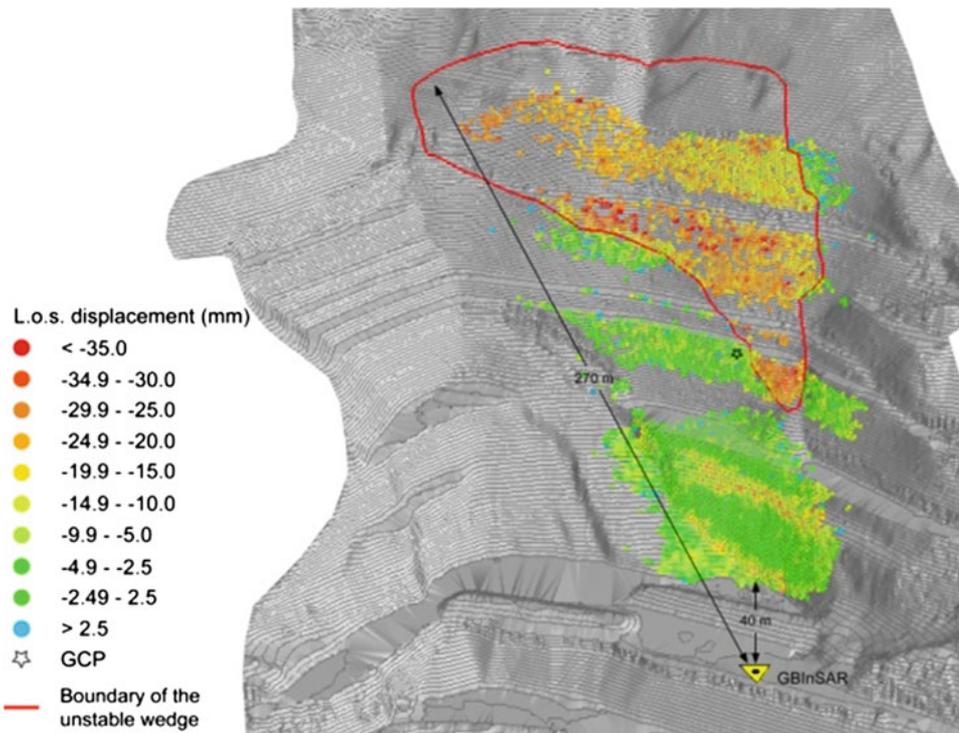
Fig. 126.2 GBInSAR displacement map projected over a digital elevation model
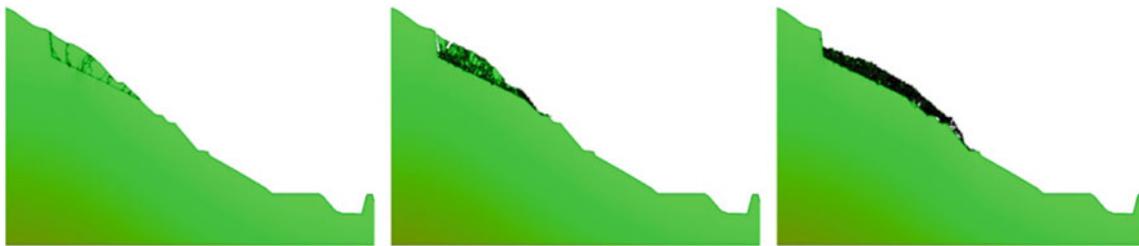
Fig. 126.3 Results of a FDEM numerical analysis

which for the sake of simplicity have been here indicated as conventional, even remote-sensing based, very often require days or weeks to became fully operative. Consequently they have been considered in a different temporal frame (t_2).

After the installation of a GBInSAR system it is possible to obtain a nearly continuous displacement and velocity field of the observed area. Figure 126.2 shows an example of displacement map obtained with the GBInSAR projected over a Digital Elevation Model of the monitored area.

Another important aspect that should be emphasized concerns the data acquisition frequency (sampling rate) of a radar system. The possibility to obtain a displacement map updated every 10 min or less, fully satisfies the requirements for a real time monitoring system and, especially in emergency conditions, represents an important added value for EWSs.

126.2.2 Characterization and Modelling Module

This module includes in situ investigations, field surveys (geological, geomorphological, structural, geophysical), laboratory tests for the geomechanical characterization of intact rock and discontinuities and the numerical modelling of the instability phenomenon. Here, a combined finite-discrete element method (FDEM) is used to model triggering and run out of a landslide. This method allows one to investigate brittle failures of slopes from initiation through transportation and deposition as shown in the example of Fig. 126.3. Moreover the back analysis of already occurred failures, along with a continuous calibration process over monitoring data, as they become available, allows for the results of the numerical models to be used in scenario-based analysis.

All the listed activities are typically time demanding and should be considered in a reference time spanning from few days to few weeks (t_2–t_3) after the landslide occurrence.

126.2.3 Verification Module

The last section of the proposed algorithm is the verification module which is the core of the integration methodology. It represents the set of operations needed to determine continuously and in near real time the alert levels related to a particular instability phenomenon, using the data provided from at least one of the modules previously described. The decisional module does not present any particular time constraint as it can be reached in a time which is variable from t_1 (few hours after the landslide occurrence) to t_3 (few weeks) depending on the particular combination of the modules chosen.

The decisional module is composed of three different phases:

- selection of Regions of Interests (ROIs);
- definition of thresholds and alert levels;
- verification.

The ROIs are portions of a landslide characterized by an homogenous kinematic behaviour (i.e. type of motion, direction, trend of displacement, degree of activity). The adoption of ROIs allows to take into account the heterogeneities in the geomechanic behaviour of complex and compound landslides.

When the decisional module is reached directly through the radar module (t_1), the thresholds can be only determined on the basis of the direct observation of the time series of the radar displacements maps, due to the lack of other information. As a consequence, the thresholds thus defined will be markedly conservative. From the results of the FDEM modelling, by means of a progressive optimization procedure, the initial conservative thresholds will be eventually modified to be used for the medium and long term monitoring of the landslide.

A typical set of 3 alert levels and 2 thresholds (attention and alarm) are adopted. Each alert level is then associated to a state of activity of the landslide (normal or seasonal activity, increased activity, possible collapse) and to a list of actions to be engaged for the mitigation of the risk. Alert levels are triggered by exceeding the relative threshold for one, or a combination, of the monitored parameters. In the proposed scheme the responses associated to each alert level imply also a feedback loop to the frequency of measurements in the radar and conventional monitoring modules. Finally, once the alert levels and the respective thresholds have been selected, the verification phase of the algorithm simply concerns the continuous and real time monitoring of the selected parameters over the ROIs and the comparison with the pre-defined thresholds values.

126.3 Conclusions

In this paper a novel contribution to the set-up of a cost-effective EWS for rock landslides was illustrated. This was obtained through the combination of innovative remote sensing techniques (i.e. GBInSAR) with advanced numerical modelling (i.e. FDEM).

References

Atzeni C, Pieraccini M, Barla M, Antolini F (2014) Early warning monitoring of natural and engineered slopes with Ground-Based Synthetic Aperture Radar. Rock Mechanics and Rock Engineering, doi:10.1007/s00603-014-0554-4

Barla M, Antolini F (2012) Integrazione tra monitoraggio e modellazione delle grandi frane in roccia nell'ottica dell'allertamento rapido. In: Barla G, Barla M, Ferrero A, Rotonda T (eds) MIR 2012 - Nuovi metodi di indagine e modellazione degli ammassi rocciosi. CELID, Torino

Barla M, Beer G (2012) Editorial: special issue on advances in modelling rock engineering problems. Int J Geomech 12(6):617

Barla G, Antolini F, Barla M, Mensi E, Piovano G (2010) Monitoring of the Beauregard landslide (Aosta Valley, Italy) using advanced and conventional techniques. Eng Geol 116:218–235

Barla M, Piovano G, Grasselli G (2012) Rock slide simulation with the combined finite discrete element method. Int J Geomech 12(6):711–721

Di Biagio E, Kjekstad O (2007) Early warning, instrumentation and monitoring landslides. In: 2nd regional training course, RECLAIM II, 29 Jan–3 Feb 2007

Luzi G (2010) Ground based SAR interferometry: a novel tool for geoscience. Geosci Rem Sens New Achievements, p 26

Mahabadi O, Lisjak A, Munjiza A, Grasselli G (2012) Y-Geo: a new combined finite-discrete element numerical code for geomechanical applications. Int J Geomech 12(6):676–688

A Tool for Semi-automatic Geostructural Survey Based on DTM

Sabrina Bonetto, Anna Facello, Anna Maria Ferrero, and Gessica Umili

Abstract

Tectonic movement along faults is often reflected by characteristic geomorphological features such as linear valleys, ridgelines and slope-breaks, steep slopes of uniform aspect, regional anisotropy and tilt of terrain. In the last years, the remote sensing data has been used as a source of information for the detection of tectonic structures. In this paper, we present a new approach for semi-automatic extraction and characterization of geological lineaments. The overall positive aspects of this semi-automatic process were found to be the rapidity of preliminary assessment, the possibility to identify the most interesting portions to be investigated and to analyze zones that are not directly accessible. This method has been applied to a geologically well-known area (the Monferrato geological domain) in order to validate the results of the software processing with literature data. Results obtained are discussed and preliminary remarks are put forward.

127.1 Introduction: State of the Art

In geology the satellite remotely sensed data has been used as source of information for the detection of tectonic structures such as faults, large-scale fractures, and fracture zones (Wladis 1999; Morelli and Piana 2006; Hashim et al. 2013). Geological lineaments are parameters that can be used in assisting mineral prospecting, hydrogeology studies, tectonic studies for the delineation of major structural units, analysis of structural deformation patterns and identification of geological boundaries.

Generally, in literature, the extraction of geological lineaments can be grouped into three main approaches: (i) manual extraction (Jordan and Schott 2005), (ii) semi-automatic extraction (Lim et al. 2001; Jordan et al. 2005), and (iii) automatic extraction (Masoud and Koike 2011; Saadi et al. 2011). Manual and semi-automatic approaches are greatly influenced by the experience of the analyst, while automatic extraction depends on the algorithms efficiency and on the information content in the image (Hashim et al. 2013).

Normally, lineaments can be detected due to their geomorphological features, such as morphotectonic elements, drainage network offsets and stream segment alignments, and/or spectral criterion, such as tonal change, pattern and textures, using (stereo-) aerial photographs and other remotely sensed imagery.

S. Bonetto · A.M. Ferrero
Department of Earth Sciences, University of Turin, Valperga Caluso 35, 10125 Turin, Italy

A. Facello (✉)
CNR-IRPI, Strada delle Cacce, 73, 10135 Turin, Italy
e-mail: facelloanna@gmail.com

G. Umili
Department of Civil, Environmental and Territory Engineering, University of Parma, Parco Area delle Scienze 181/A, 43124 Parma, Italy

Regarding the Digital Terrain Model (DTM), this has been used as shaded relief model either alone or in combination with remotely sensed images on a regional scale. Moreover, three-dimensional view with image drape and digital cross sections have been used for morphotectonic investigations (Jordan et al. 2005).

In this paper, authors propose the use of an innovative method for the extraction of geological features using a semi-automatic approach. The method will be discussed and presented in the following sections. The overall positive aspects of this semi-automatic process were found to be the rapidity of preliminary assessment, the possibility to identify the most interesting portions to be investigated and to analyze zones that are not directly accessible.

127.2 Software

The method is based on the assumption that a geological lineament can be geometrically identified as a convex or concave edge of the surface of a DTM, particularly in presence of a structural control of the geomorphological evolution of the analyzed areas.

The code CurvaTool (Umili et al. 2013) was originally developed to automatically detect edges on Digital Surface Model (DSM) of natural rock mass outcrops, assuming that they represent the discontinuity traces. In this work the code CurvaTool has been applied to DTM of large portion of territory in order to automatically detect edges which represent potential geological lineaments. As natural outcrops, also the earth surface can have an infinite variety of shapes whit different dimensions, but a common characteristic is generally their non-planar surface. In fact, the surface has often edges that can be both asperities or depressions.

The code quantifies the non-planarity by means of principal curvature values associated to the DSM/DTM points; the user is asked for two thresholds on principal curvature: the first one to detect significant convex edges and the second one to detect significant concave edges. After the identification, edges are segmented in order to obtain the segments that better interpolate the obtained polyline.

Post-processing operations are required in order to filter and to classify segments representing items of interest among all the reconstructed edges: therefore specific algorithms, called Filter in the following, have been created to perform these operations. The user is asked for the minimum edge length and the orientations of the expected lineaments clusters (expressed by an angle respect to the North and the relative standard deviation). Filter code deletes edges shorter than the fixed length and classifies them attributing each edge to the correspondent input cluster. Non-classified edges are recorded as "others".

127.3 The Test Area: The Monferrato Geological Domain

The Monferrato has been selected as the area-test to verify the software application in the lineaments identification on a large scale.

The Monferrato is located in correspondence of the Alps-Apennines Junction Zone; it is an highly deformed geological domain, but is also rife with literature data which are very helpful for a suitable validation of the results in software applications. Most of the information about faults trending and their distribution result either from field evidences and small-scale kinematic observations or they have been verified by the geomorphological and spectral analysis with remote sensed imagery (Morelli and Piana 2006). In Monferrato, because of a rich vegetation and human activity, the substratum is poorly exposed and a small number of outcroppings is present. Therefore, direct evidences of the structural lineaments are not easily detectable on the field and, sometimes, their presence is just supposed for stratigrafical reasons.

In the Monferrato, geological succession is divided in a lower part of strongly deformed Apennine calcareous flysch (late Cretaceous to middle Eocene age) and an upper terrigenous succession (middle Eocene—Pliocene) resting unconformably on the previous one (Clari et al. 1995). In particular, the sedimentary sequence is mainly composed of marls, arenites, siltstone (with locally interbedded sandstone), evaporates, mudrocks and sandstones. The stratigraphic succession is characterized by lateral thickness variations and by the occurrence of local unconformities; it is poorly folded, but highly tilted and deformed in reason of a continuous uplift (also recent) which caused a structural control during geomorphological evolution. Steep slopes, well-organized drainage network, fractures and faults are the evident consequences of that interaction.

Tectonic boundaries divide the Monferrato geological domain in tectonostratigraphic units which are characterized by distinctive sedimentary evolution, stratigrafical sequence, geometries and amount of deformation. Despite the structural complexity and the presence of many deformation zones, four main systems faults have been recognised in Monferrato (Piana 2000; DeLa Pierre et al. 2003). They are oriented NW–SE, NE–SW, E–W and N–S respectively.

127.4 Data Discussion

A preliminary approach to the software application consisted in the lineaments identification in a geologically well-known area in order to validate the results of the software processing with literature data. Since the structural setting is
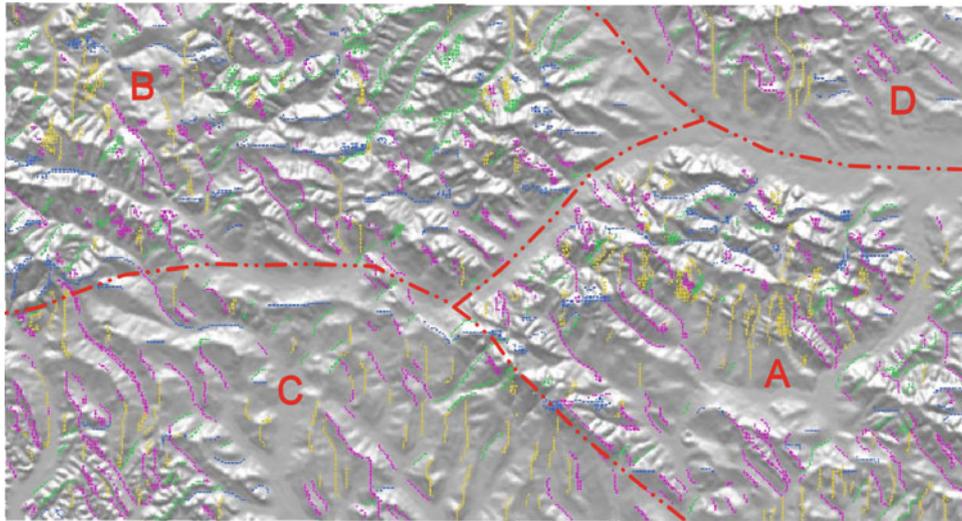
Fig. 127.1 Image of Monferrato DTM with lineaments extracted by CurvaTool and processed with Filter. Four sets are visible: L1 (fuchsia), L2 (*green*), L3 (*blue*) and L4 (*yellow*)
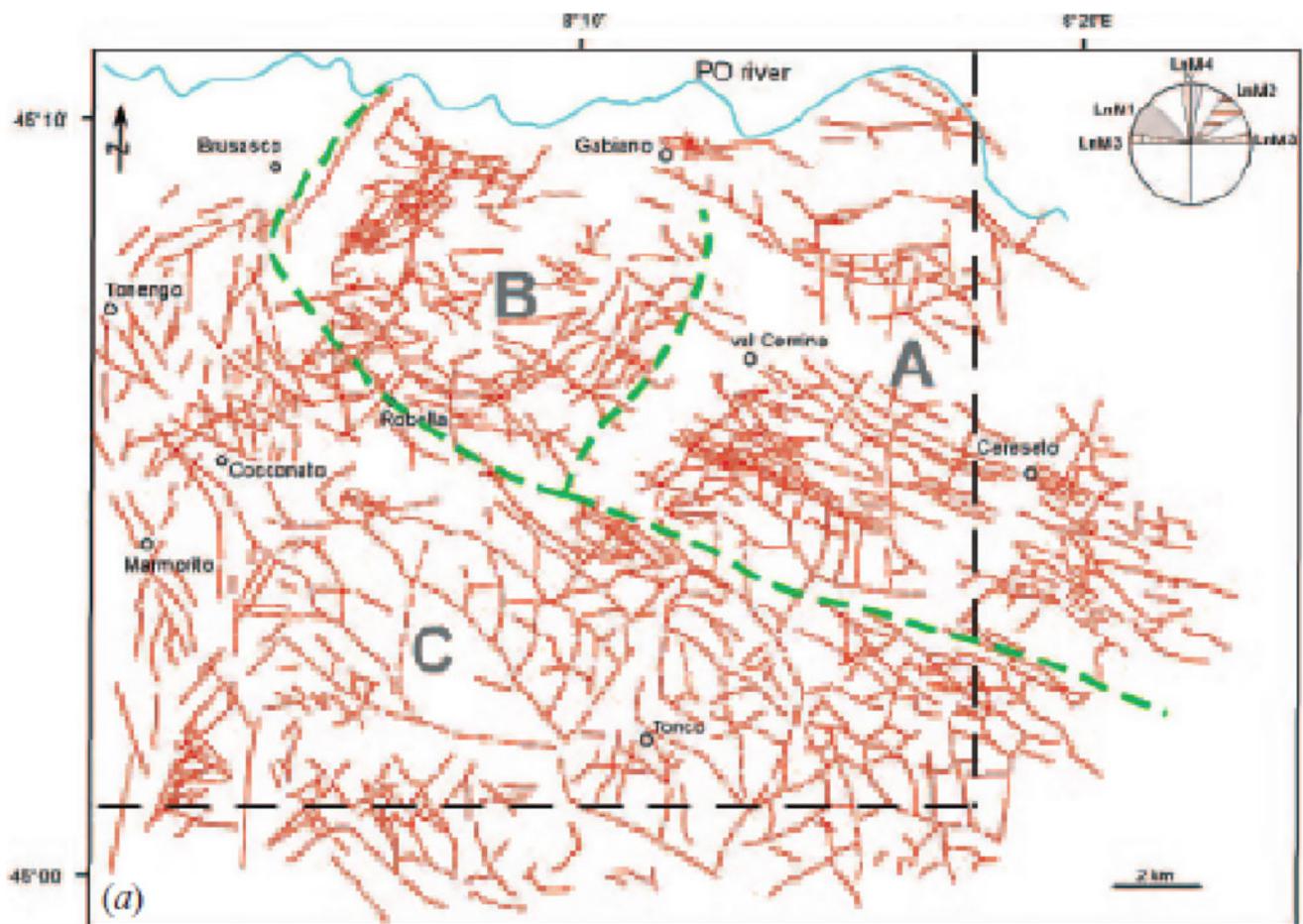
Fig. 127.2 Image of Monferrato DTM with lineaments extracted by Spot HVR data (*source* Morelli and Piana 2006)

well-known, a DTM of the Monferrato domain was processed by CurvaTool software, furnishing a preferential range of directions as a geometrical filter to simplify the lineaments identification. A large number of lineaments were found and different filters were tested to obtain a final simplified image.

Geological structures manually extracted through photo-interpretation, remote sensing and analysis of geological maps were compared with the semi-automatic outputs of CurvaTool and Filter. According to literature data (Piana 2000), the CurvaTool processing of the DTM of the Monferrato area identified several lineaments oriented coherently with the main four lineament systems.

The image representing the results (Fig. 127.1) displays a greatest lineaments length and frequency on NW–SE direction (L1), whereas short and intermediate lengths generally occur on the E–W (L3) and N–S (L4) average direction. The NE–SW lineaments (L2) are usually short, the longest ones are concentrated in the north-western part of the map.

In particular, the NW–SE striking system is uniformly distributed and shows a regular geometry and direction, generally with long or intermediate-length lineaments. The N–S striking system is present in the whole area with a different distribution and length and it is particularly frequent in the southern area of the map.

The distribution and length of the lineaments were compared with the geological structures collected at different scales, resulting by field work (DeLa Pierre et al. 2003) and Spot and SAR image analysis (Morelli and Piana 2006).

As for Morelli and Piana (2006), according to geometry and spatial distribution of the lineaments, different sectors should be recognized (Fig. 127.2).

From the centre to the north-western part of the map (sector B), all lineament systems were recognized. The NW–SE and the NE–SW striking systems are predominant; in particular, the sector B is the only one within the NE–SW striking system is particularly distributed and shows the longest lineaments. The L1 consists of long and intermediate-length lineaments; the L3 is well represented, particularly with intermediate length. The N–S lineaments are less frequent and their geometrical features are not so clear in that sector.

The south–eastern part of the map (sector A) is characterised by long and evident L1 lineaments and L3 lineaments of intermediate length (particularly distributed in the north and north–western part of the sector). The L2 system is poorly represented, whereas the L4 system has a wider distribution than in sector B, particularly in the centre of the sector.

The south western part of the image (sector C) is the poorest deformed area. It is characterised by the lowest frequency of the lineaments: L1 system is still present with a few intermediate-length lineaments, L2 and L3 systems are poorly represented and are concentrated principally on the northern and north–eastern border of the sector respectively. Unlike the other sectors, the L4 system is clearly represented and regularly distributed in the whole sector.

The north–eastern area (sector D) is too small to make statistical analysis, even if L1 and L4 systems seem to be predominant.

127.5 Conclusion

Through this work, the authors the authors propose and prove the use of an innovative method for the extraction of geological features using a semi-automatic approach. This method has applied in the identification of lineaments features in an area geologically known (Monferrato domain) in order to validate the results obtained with the data of literature.

By comparing, it is possible to note a good correspondence between literature data and the preliminary CurvaTool results, as regard to geometry and distribution of the main lineaments systems.

According to the final remarks, the first results of software application are good. Software should be improved, at any rate the correspondence between lineaments and geological structures are mainly not direct and a post-processing subjective interpretation by the user is anyway necessary.

References

Clari P, DeLa Pierre F, Novaretti A, Timpanelli M (1995) Late Oligocene-Miocene sedimentary evolution of the critical Alps/Apennines junction: the Monferrato area, Northwestern Italy. Terra Nova 7:144–152

DeLa Pierre F, Fioraso G, Piana F, Boano P (2003) Foglio 157 'Trino' della Carta Geologica d'Italia alla scala 1: 50,000. APAT, Dipartimento Difesa del Suolo, Roma

Hashim M, Ahmad S, Johari MAM, Pour AB (2013) Automatic lineament extraction in a heavily vegetated region using Landsat Enhanced Thematic Mapper (ETM+) imagery. Adv Space Res 51 (5):874–890

Jordan G, Schott B (2005) Application of wavelet analysis to the study of spatial pattern of morphotectonic lineaments in digital terrain models. A case study. Remote Sens Environ 94(1):31–38

Jordan G, Meijninger BML, Van Hinsbergen DJJ, Meulenkamp JE, Van Dijk PM (2005) Extraction of morphotectonic features from DEMs: development and applications for study areas in Hungary and NW Greece. Int J Appl Earth Obs Geoinf 7:163–182

Lim CS, Ibrahim K, Tjia HD (2001) Radiometric and geometric information content of TiungSat-l MSEIS data. In: TiungSAT-1: from inception to inauguration, pp 169–184

Masoud A, Koike K (2011) Auto-detection and integration of tectonically significant lineaments from SRTM DEM and remotely-sensed geophysical data. ISPRS J Photogr Remote Sens 66:818–832

Morelli M, Piana F (2006) Comparison between remote sensed lineaments and geological structures in intensively cultivated hills

(Monferrato and Langhe domains, NW Italy). Int J Remote Sens 27 (20):4471–4493

Piana F (2000) Structural setting of western Monferrato (Alps-Apennines junction zone, NW Italy). Tectonics 19:943–960

Saadi NM, Abdel Zaher M, El-Baz F, Watanabe K (2011) Integrated remote sensing data utilization for investigating structural and tectonic history of the Ghadames Basin, Libya. Int J Appl Earth Obs Geoinf 13:778–791

Umili G, Ferrero AM, Einstein HH (2013) A new method for automatic discontinuity traces sampling on rock mass 3D model. Comput Geosci 51:182–192

Wladis D (1999) Automatic lineament detection using digital elevation models with second derivative filters. In Photogrammetric Engineering & Remote Sensing 65(4):453–458

New Perspectives in Long Range Laser Scanner Survey Focus on Structural Data Treatment to Define Rockfall Susceptibility

Andrea Filipello, Leandro Bornaz, and Giuseppe Mandrone

Abstract

Laser scanning techniques are nowadays more and more used in engineering geology in order to describe slope instability assessment. In this study it is described an application of a new Terrestrial Laser Scanner that offers an extremely long measurement range and the procedure applied for geological data treatment. Point cloud, 3D models, "solid images" and DEM generated from Terrestrial Laser Scanner survey were managed with Ad Hoc, a software platform with specific tools for geological and geomechanic analysis.

Keywords

Laser scanner • Rockfall • Geomechanical classification • GIS tools

128.1   Introduction

The use of Terrestrial Laser scanners (TLS) are very useful where the starting point to evaluate stability properties is a morphological investigation. Laser scanners are nowadays successfully used also to study stability problems by measuring geomechanic parameters, such as distance measurements, angles, DIP and DIP direction of discontinuities, volumes. The introducing of new very long range laser scanner open a series of new very interesting perspectives.

In order to obtain a correct geometrical information, laser scanner technique requires special management during acquisition and data treatment. This is more important if very long range acquisition is carried out due to geodethic problems (Biasion et al. 2005; Bornaz and Dequal 2003; Fricout et al. 2007).

A. Filipello · G. Mandrone (✉)
Department of Earth Sciences, University of Torino, Via Valperga Caluso 35, 10125 Turin, Italy
e-mail: giuseppe.mandrone@unito.it

A. Filipello · G. Mandrone
AG3 S.r.l., Via Valperga Caluso 35, 10125 Turin, Italy

L. Bornaz
Ad Hoc 3D Solutions S.r.l., Fraz. La Roche 8, 11020 Gressan, AO, Italy

The study site is located in the lower Aosta Valley (NW Italy), near the village of Hone. The planimetric extension of the study area is approximately 63 ha, the slope has a vertical height of about 700 m, from the bottom valley (345 m a.s.l.), up to the ridge, located at about 1,060 m a.s.l.

128.2   Laser Scanner Data Acquisition

Acquisition should be correctly planned and executed in order to obtain a valuable final result and a real time data check is suggested. This operation depends on the characteristics of the laser scanner used too: in our case it is the new RIEGL VZ4000. This instrument is very innovative and offers a lot of new possibilities and a very long range measurement performance. It can acquire points at more than 4,000 m with high accuracy and a very small laser beam. Despite this, the data can be very noisy and they must be used and treated very carefully due to "distortions" introduced by the very long range measurements, the echo digitization and the online waveform processing techniques on which the laser is based.

When an object has a complex shape or when a single scan cannot record the whole object, a series of scans must be done. These series has to be correctly planned to avoid hidden areas. To plan the survey we have to pay attention not only to the shape of the object, but also to the instrument

characteristics (such as vertical and horizontal field of view, maximum range,…). In this test site we had the problem that the morphology of the study area is very steep and instrument, unlike other Riegl instruments, cannot be tilted and has a limited field of view along the vertical axes.

To measure at 4–6 km with a laser rangefinder it is necessary to digitally model and consider a lot of atmospheric parameters. If the very long range acquisition (4–6 km) is carried out from a airplane (ALS), these parameters are quite easy to be considered because the laser beam through all different atmospheric layers perpendicular each to the other. In TLS instead, the laser ray can have (depending on the laser range measurement, the laser emission angle, and the earth curvature) a very high and changeable incident angle with the atmospheric layers. So the laser ray can be strayed in a different way along its path.

In our case this aspect has greatly complicated the acquisitions. We had to carry out acquisitions only from the valley floor due to the impervious slopes on each side of the valley, not achievable by walking. The relationship between the height of the rock wall and the planar distance between laser position and the upper part of the cliff was not enough to acquire the whole site using the VZ4000 vertical FOV. So, we had to carried out 4 scans using the VZ4000 and a set of acquisition using the VZ400 (used in the lower part of the cliff). Moreover, a GPS and topographic surveys have to be carried out because the acquired data must be geo-referenced. In our case, 5 GPS GCP was acquired.

128.3 Data Processing

RIEGL's V-Line technology is based on echo digitization and online waveform processing. The VZ4000 in addition is equipped with multiple-time-around capability (MTA). This combination allows users to benefit from the high pulse rate also from very long range and thus to achieve high measurement densities on the object (Fig. 128.1). The elaboration (ambiguity resolution) of multiple-time-around capability (MTA) is accomplished using the algorithms and software developed by RIEGL in addition to classical data treatment. The result of this operation is a point cloud with more information in the remote part. The operation known as "preliminary data treatment" concerns data filtering, vegetation and artifacts removal, point cloud registration, multiple scan triangulation operations.

The noise reduction is one of the preliminary fundamental operations because laser scanner data always have noise that is lower than the tolerance of the used instruments. In order to obtain a "noise free" model of the object, it is necessary to use specific algorithms able to reduce or even eliminate the acquisition errors that can be found in the point clouds. Simply visualizing the data acquired with the VZ4000 after the MTA processing, it is possible to see a lot of noise in the 3D point cloud (Fig. 128.2). Sometimes it is also necessary to remove scattered points that do not belong to the object. In the particular case of rocky faces with irregularities that could produce rock falls, it is common practice to reinforce the stability of the walls using protection barriers. In environmental surveys the vegetation has to be considered too. Usually vegetation and scattered points removal operation is performed manually by the operator. In our case the data was elaborated using specific automatic algorithms developed by Ad Hoc 3D Solutions (Fig. 128.3). The used algorithms have been suitably modified to properly consider the new VZ4000 data. The result of these procedures is a complex, "noise free" point cloud (without any outliers, gross or systematic errors, vegetation and artifacts).

Usually, more than one scan is needed to completely describe a rock wall. In these cases each scan has its own reference system: the reconstruction of the 3D model of the surveyed object requires the registration of the scans in a single reference system. As Dip and Dip directions have to be measured and integration with regional DSM, the reference system has to be properly choose (X along East, Y along North and Z along the vertical direction).

If the 3D acquired data must be geo-referenced in a cartographic reference system some problems due to cartographic projection deformations have to be considered to correctly estimate the alignment and the real displacement.
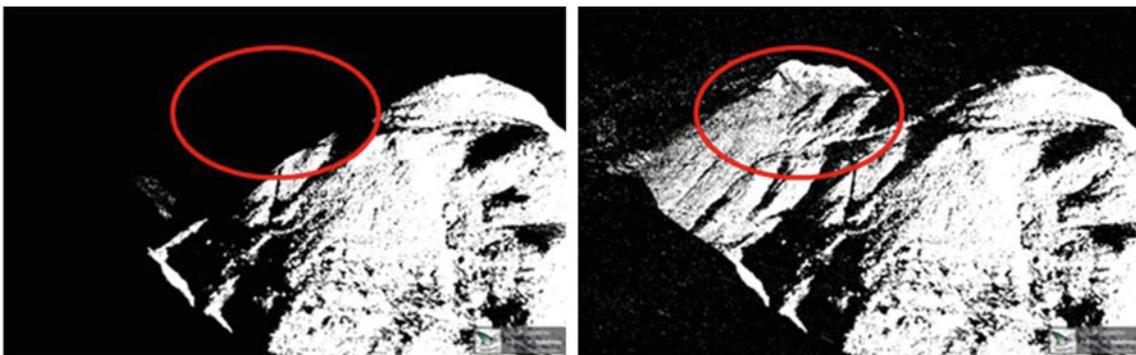
Fig. 128.1 Original data (*left*). Original data with MTA pre-processing (*right*)
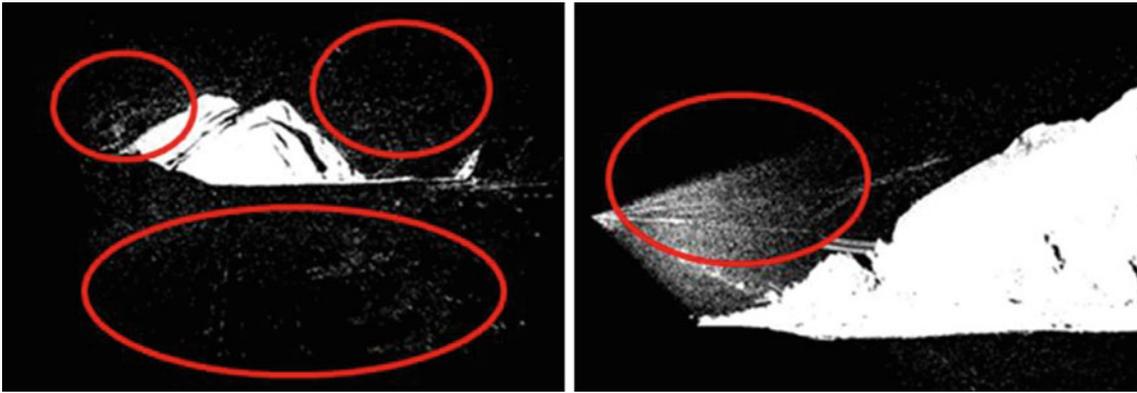
Fig. 128.2 Original VZ4000 data. Noise in the acquisition
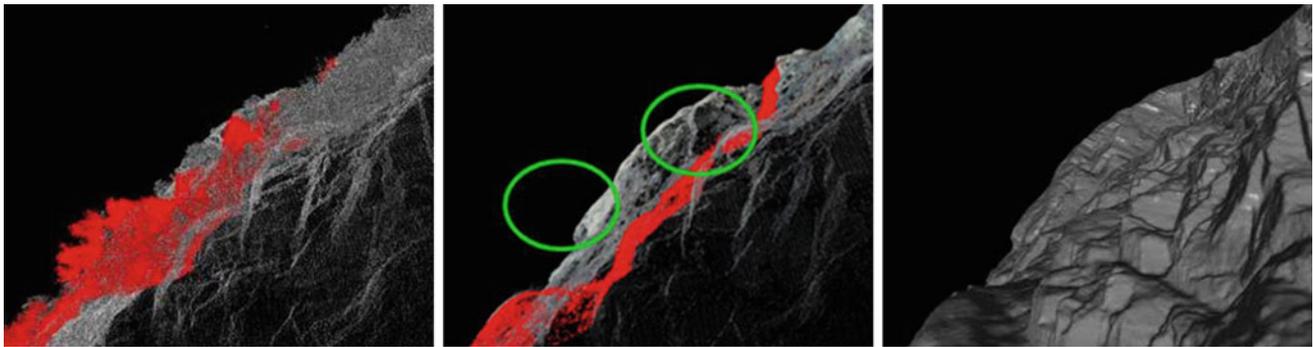
Fig. 128.3 Vegetation filter: original 3D point cloud (*left*), filtered point cloud (*center*) and 3D surface (*right*)
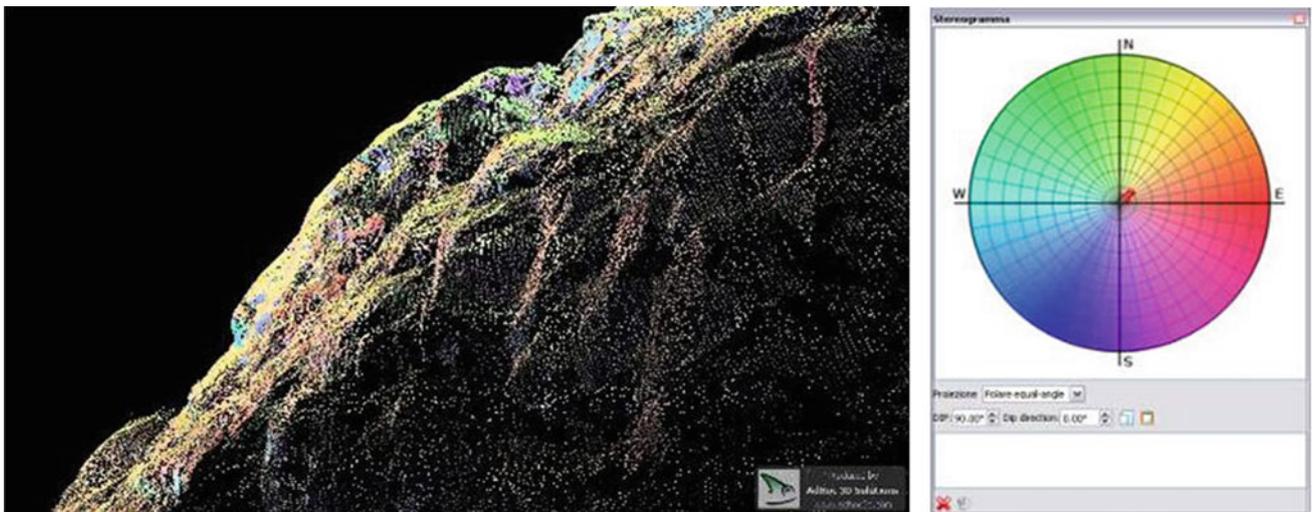
Fig. 128.4 Final noise free point cloud. DIP DIPDIR colored

The problems related to reference systems is generally underestimated or completely overlooked. Certainly it can be neglected if you are acquiring and georeferencing a very small site (considering the topographic field and the earth curvature).

If we try to align some scans in a cartographic system the result (errors on GCPs) can be poor due to the cartographic deformations, the earth curvature and the geoid undulation. In particular if the rock wall is in mountain as the deformations groove with the height. But rules are essential when

Fig. 128.5 Final noise free surface of the rock wall. 19.7M points—39.4M facets
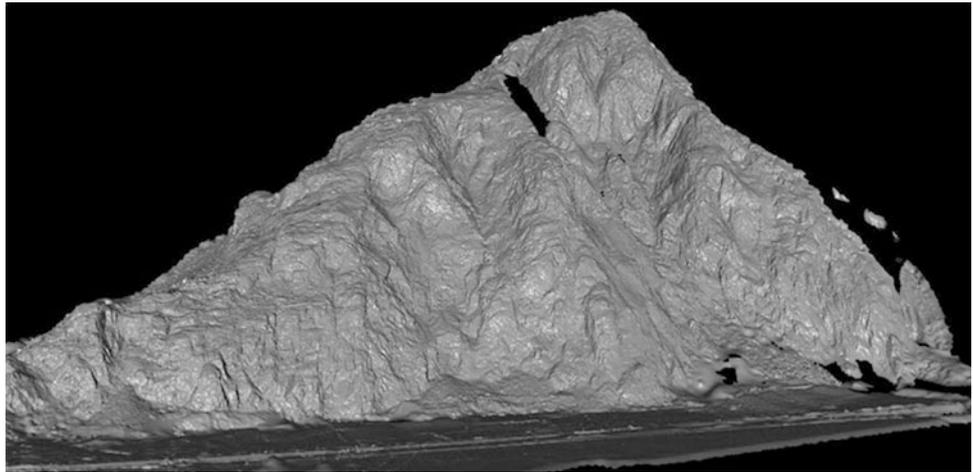
you want to integrate data acquired with different methodologies and techniques. In order to integrate TLS, aerial laser scanner, GPS, photogrammetry, geophysics data a.s.o, we have to consider the different reference systems. The troubles come when you try to merge the data coming from the two instruments (e.g. TLS and ALS), that are not suitable. This operation is generally carried out using ICP, thus minimizing alignment errors but forgetting completely the deformations induced by the reference systems and thus committing a serious error from a topographical point of view. Ad Hoc 3D Solutions developed a proprietary and patented technique able to solve the merging problem between TLS and cartography. Our technique uses a rigorous geodetic approach, that is the basis for monitoring of rock walls or glaciers.

The same technique allow us to acquire TLS data in a local reference system and extract every information from the point cloud without deformations, convert all in the 3D model and extract features in the cartographic reference system by rigorous transformations. The system allow to collect, merge and correctly manage laser scanner data coming from different sources, also in different epochs (very useful for monitoring). This approach was used to correctly georeference the VZ4000 3D data with a very high global accuracy (~ 5 cm). This accuracy is checked on site on a big set of control points. The georeferencing and alignment algorithm used as homologous and georeferencing points, to obtain the final point cloud, both GCP that natural points having particular geometric characteristics and consider all the geodetics rules in a correct way. The final result is a noise free, correctly aligned and georeferenced point cloud,

available in all reference systems, fully integrated with the regional UTMED50 DSM.

128.4 Conclusion

Detailed studies for rock fall hazard are necessarily based on knowledge of the morphological and mechanical characteristics of the cliff. When the morphology of the cliff makes difficult a direct access the use of climbing techniques for access to the wall is recommended, but not always possible for economic or safety reasons. The use of terrestrial laser scanner (TLS) in addition to the traditional techniques of investigation is becoming more widespread. The result of a terrestrial laser scanning is a points cloud that reproduces the morphology of the investigated target.

In this study a complete 3D survey of the area is carried out, using a methodology that integrates Terrestrial Laser Scanner, GPS and photogrammetry. In particular, a new long range laser scanner has been tested (Riegl VZ4000) in steep and large area along the right flank of the lower Aosta Valley. The 3D VZ-Line laser scanner offers very long range, up to 4000 m. In fact for this case, was developed a specific procedures and methodologies for the treatment and correct management of a terrestrial laser scanner survey of a site larger than 2 km. This kind of instruments open new perspectives on environment applications, but it is very important to balance real capabilities and real limits.

The data treatment carried out by Ad Hoc 3D Solutions allow to obtain not only a simple point cloud, but a 3D true colored 3d model (using an independent HDR

photogrammetric survey, Fig. 128.4) where each point have a series of additional information (e.g. dip, dip dir,…). Finally, using a specific surface reconstruction algorithm, the surface of the rock wall have been generated (Fig. 128.5). A set of solid images were generated too in order to allow experts to extract information not only from the 3D model but using a more simple interface to use the 3D.

Only at this point it is possible to start measuring geo-mechanic information focused to slope stability analysis.

References

Biasion A, Bornaz L, Rinaudo F (2005) Laser scanning applications on disaster management. First international symposium on geo-information for disaster management (Gi4DM), Jan 2005

Bornaz L, Dequal S (2003) A new concept: the solid image. Int Arch Photogram Remote Sens Spat Inform Sci 34:78–82

Fricout B, Villemin T, Bornaz L (2007) Remote analysis of cliff outcrops using laser DDSM and digital images. Geophys Res Abs 9 (08194):200

Andrea Filipello, Giuseppe Mandrone, and Leandro Bornaz

Abstract

Laser scanning techniques are nowadays more and more used in engineering geology in order to assess slope stability. In this study it is described an application of a new Terrestrial Laser Scanner that offers an extremely long measurement range and the procedure applied in geologic data treatment. Point cloud, 3D models, "solid images" and DEM generated from Terrestrial Laser Scanner survey were managed with Ad Hoc, a software platform with specific tools for geologic and geomechanic analysis. The assessment of rockfall prone area has been developed according to two approaches: deterministic and empirical. In the first case the detection of potentially unstable blocks, typically done with field surveys in case of outcrops of limited extension, were performed directly on the point cloud and on solid images. In the second case GIS tools were used allowing to apply the geomechanic classification SMR Romana for each pixel. Results obtained from both approaches is compared as a further data validation procedure.

Keywords

Laser scanner • Rockfall • Geomechanical classification • GIS tools

129.1 Introduction

Detailed studies for rock fall hazard are necessarily based on knowledge of morphologic and mechanic characteristics of rock masses. When morphology of slopes make difficult field surveys, the use of climbing techniques for access to the wall is needed but not always possible for economic or safety reasons. The use of Terrestrial Laser Scanner in addition to the traditional techniques of investigation is becoming more widespread. The result of a terrestrial laser scanning is a point clouds that reproduces the morphology of the investigated target.

In this study a complete 3D survey of the area was carried out, using a methodology that integrates Terrestrial Laser Scanner, GPS and photogrammetry (Fig. 129.1). In particular, a new long range laser scanner has been tested (Riegl VZ4000) in a large (about 2 km^2) and steep area along the right flank of the lower Aosta Valley. The 3D VZ-Line laser scanner offers very long range, up to 4,000 m. Specific procedures and methodologies for the treatment and correct management of the terrestrial laser scanner survey of the test site were developed. These kind of instruments open new perspectives in environmental applications but it is very important to balance real capabilities and technical limits.

In addition, a set of solid images were generated in order to allow experts to extract information not only from the 3D model but also using a more simple interface.

Both automatic data extraction procedure from point cloud and interpretation on solid images have been applied. The assessment of rock fall prone area has been developed according to deterministic and empirical approaches. In the

A. Filipello · G. Mandrone (✉)
Department of Earth Science, University of Torino, Via Valperga
Caluso 35, 10125 Turin, Italy
e-mail: giuseppe.mandrone@unito.it

A. Filipello · G. Mandrone
AG3 S.r.l., Via Valperga Caluso 35, 10125 Turin, Italy

L. Bornaz
Ad Hoc 3D Solutions S.r.l., Fraz. La Roche 8, 11020 Gressan,
AO, Italy

Fig. 129.1 Laser scanner survey: the study area is about 1,500 m in elevation and about 2,000 m in length
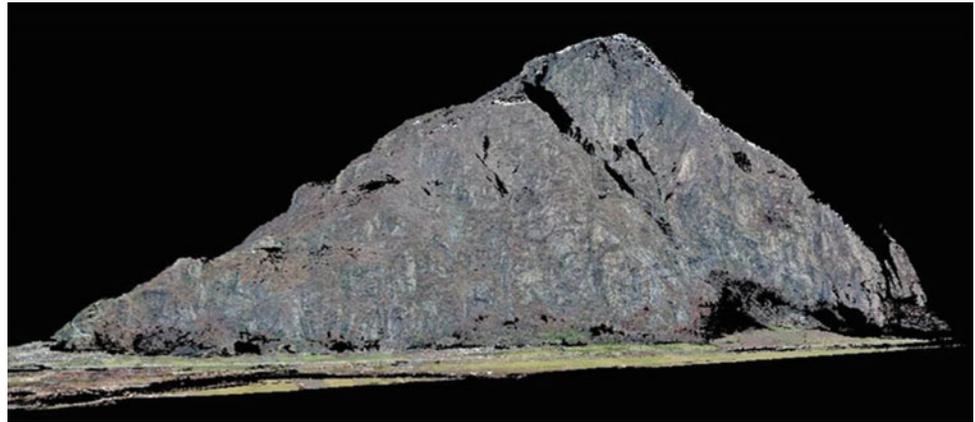
first case, the detection of potentially unstable blocks, typically done with direct surveys in case of outcrops of limited area, were evaluated also on the point cloud and on the solid images. In the second case, GIS tools that allow to apply the geomechanic classification SMR Romana for each pixel were used.

129.2 Study Area

The study site is located in the lower Aosta Valley (NW Italy), within the municipality of Hone. The planimetric extension of the studied area is approximately 63 ha (much less than the survived one), the slope has a vertical height of about 700 m, from the bottom valley (345 m a.s.l.), up to the ridge, located at about 1,060 m a.s.l.

Lithologies identified are mainly lithoids: in most of the study area soil covers are thin or non-existent. Tree and shrub vegetations are mainly located on alluvial fans or on terraces. The study area consists mainly of Gneiss Minuti of the Sesia Lanzo Zone and it is frequently affected by rock falls. During a recent collapse in the 20 Feb 2012, the municipal Waste Recycling Centre—located at the base of the slope—was involved in rock falling and it was closed as a precautionary measure.

129.3 Geomechanical Data Collection

The geomechanic and morphostructur characterization of discontinuities has been carried out by three different approaches (Fig. 129.2):

(a) standard geomechanical field survey of the rock masses;
(b) automatic extraction of dips and dip directions from laser point clouds;
(c) manual measurement of the discontinuities on "solid images" by selection of an area, computation of the

mean plane that best fit the selected points; from the plane equation, dip and dip direction can be extracted.

The field surveys were done following ISRM "Suggested Methods" (ISRM 1978). The rock mass characterizations fallow the Geological Strength Index (GSI) index (Hoek and Marinos 2007), that is based on the description of two factors, rock structure and block surface conditions. Physical access to higher parts of the slope was difficult and only 5 scan lines were measured, mainly located at the base of cliff. Discontinuities characteristics were investigated through the description of surface morphology, roughness, persistence, block size and rock fracturing degree.

An objective of traditional geomechanic surveys was also to demonstrate the capabilities of laser scanner in geometric measure. In fact, an automated extraction procedure was applied to obtain dip and dip direction of every point belong the cloud of laser scanning. The extraction of surfaces derives from a segmentation of the point cloud based on criteria of proximity and points similarity. A normal vector for every point is calculated and the corresponding plane equation is derived. The dip/dip direction data sample was very large (over 250.000 measures) and can not be used directly in a stereo net analysis program. For this reason the test site has been spitted into four slices, according to a vertical geometric pattern. The choice of dividing the area of study in vertical zones depends on the orientation of schistosity (next to verticality) that force to distinguish vertical morpho-structural domains.

It is not always easy to recognize structural features in a textured Dense Digital Surface Model (DDSM), especially if the study area is large, while the interpretation of morphostructural elements is easier when performed on high-resolution digital photos. The solid image approach (Bornaz and Dequal 2003) simplifies this task, it keeps the image in its original geometry and resolution, and reprojects point clouds obtained from laser scanning systems on the image itself (Fig. 129.3). In this way it's possible to select a discontinuity directly on the photo and obtain the
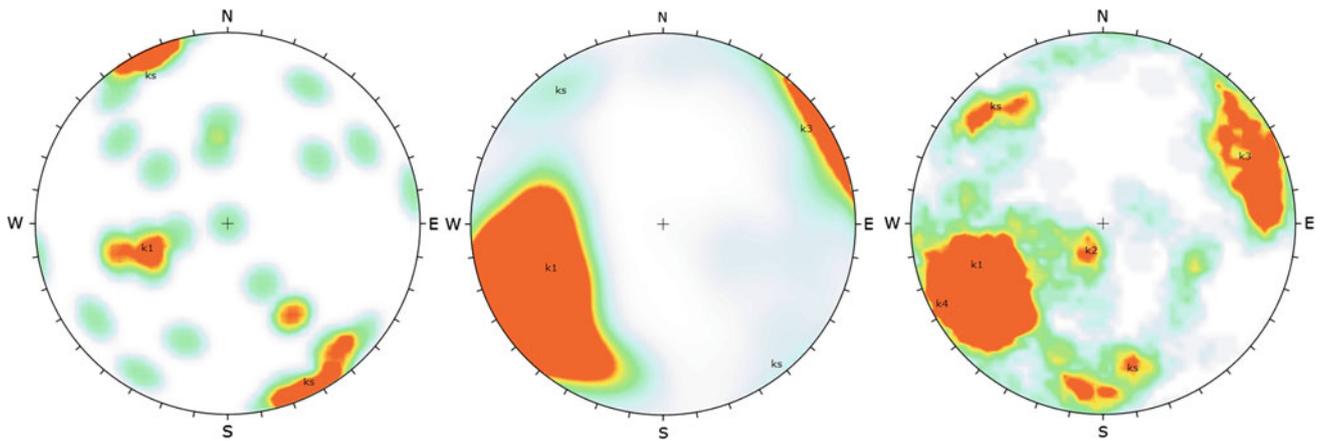
Fig. 129.2 Different approaches in geomechanic surveys: from *left* to *right*, example of the 3 approaches are shown

Fig. 129.3 Example of measurement on solid image of discontinuities surfaces

corresponding orientation that is derived computing the best fitting surface of the selected points. The high quality of solid images has allowed to interpret rock mass quality according to the GSI index also for impervious areas.

129.4 Rockfall Susceptibility

Every code for rock fall simulation requires a starting locations: it can be a single and well definite block or an area with diffuse sources. The identification of potential rock fall source areas requires susceptibility mapping. In this study, the susceptibility evaluation was obtained according to two different approaches: deterministic and empirical (Fig. 129.4).

Point cloud, 3D models and solid images have been used to identify rock fall sources. For each source area a monograph card was filled containing data on position

(coordinates x, y, z), volume, shape, an indication on more probable collapse mechanism and on a kinematic analysis based on discontinuity orientation that isolate the block. Overall 39 local rock fall sources have been identified in the area. About half of the blocks have an expected volume less than 25 cubic meters, but situations with potential volumes that can exceed hundreds of cubic meters were observed. The information about the block volume, very important for rock fall simulation, were computed as the difference between DDSM and the plans obtained from the projection in depth of discontinuities.

To identify areas with an high rock fall susceptibility and with an diffuse instability, the r.SMR GIS tool (Filipello et al. 2010) has been applied. The calculation procedures of r.SMR is implemented as raster modules of a Open-Source GIS. The r.SMR module is based on geomechanic classification and uses the continuous equations introduced by (Tomás Jover et al. 2007). The input data are: DEM, dip and
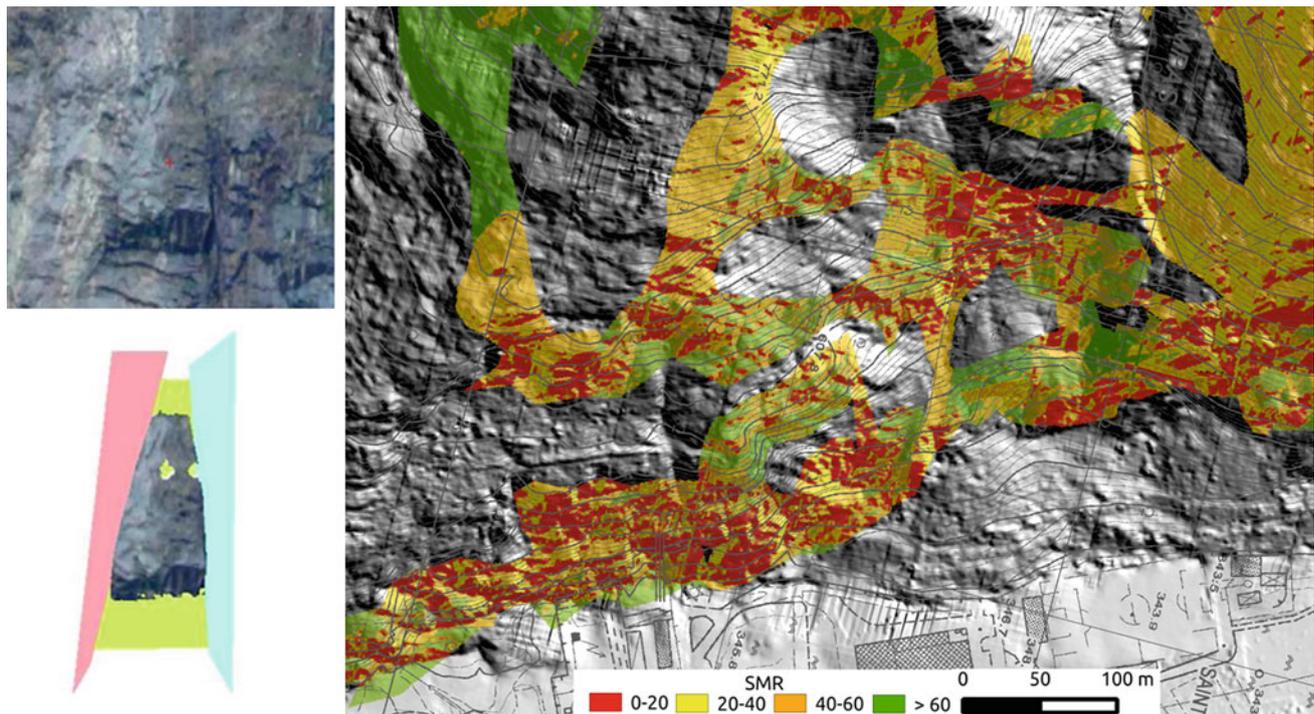
Fig. 129.4 Examples of deterministic (*left*) and statistic (*right*) approach for rock fall susceptibility evaluation

dip direction of discontinuity, the F4 index (Romana 1993) and the RMRb index (Bieniawski 1989).

The result is a raster map showing the distribution of the Slope Mass Rating (Romana 1993) for the analyzed system of discontinuity. For each discontinuity code returns two raster maps, one for planar sliding and the other for toppling.

129.5 Discussion and Conclusion

The test site is a challenging rock face in the lower Aosta valley periodically affected by collapses. The direct access to most of the cliff is virtually impossible and, therefore, we had to resort to alternative techniques, and in particular the laser scanner surveys, in order to measure some parameters essential for the assessment of the propensity to collapse.

In this article has been verified the reliability and consistency of measurements made directly on site and those made using remote sensing. This allowed to develop, with greater reliability over the input data, two different approaches for mitigation of landslide risk: the first deterministic (identifying the individual unstable blocks), the other statistic (testing the intersection between systems of discontinuity and rock wall). Both agree in identifying most critical areas and allow a operation plan aimed minimizing risk of rock falling on valley floor.

References

Bieniawski ZT (1989) Engineering rock mass classifications: a complete manual for engineers and geologists in mining, civil and petroleum engineering, 1st edn. Wiley, New York, p 251. ISBN 978-0-471-60172-2

Filipello A, Giuliani A, Mandrone G (2010) Rock slopes failure susceptibility analysis: from remote sensing measurements to geographic information system raster modules. Am J Environ Sci 6(6):489–494

Hoek E, Marinos P (2007) A brief history of the development of the Hoek-Brown failure criterion. Soils Rocks 2:1–8

ISRM (1978) Suggested methods for the quantitative description of discontinuities in rock masses. Int J Rock Mech Min Sci Geomech Abstr 15:319–368. doi:10.1016/0148-9062(78)91472-9

Neteler M, Bowman MH, Landa M, Metz M (2012) GRASS GIS: a multi-purpose open source GIS. Environ Model Softw 31:124–130

Romana MR (1993) A geomechanical classification for slopes: slope mass rating, vol III, Cap. 23. In: Hudson JA (ed) Comprehensive Rock Engineering. Imperial College-Pergamon Press, p 45. ISBN:0-08-042066-4

Tomás Jover R, Marchal JD, Serón Gáñez JB (2007) Modification of slope mass rating (SMR) by continuous functions. Int J Rock Mech Min Sci 44:1062–1069. doi:10.1016/j.ijrmms.2007.02.004

Artificial Neural Networks in Evaluating Piezometric Levels at the Foundation of Itaipu Dam

130

Bruno Medeiros, Lázaro Valentin Zuquette, and Josiele Patias

Abstract

Itaipu Dam is an engineering work of high importance. Located at the border between Brazil and Paraguay in the Paraná River and with approximated geographical coordinates 25°24′29″S, 54°35′21″W, it feeds these two countries with electrical energy and has to be constantly monitored in order to maintain its levels of quality and security. Over two thousand instruments, including more than 650 piezometers, have been installed for the monitoring of the dam and they provide continuous data about several characteristics of its foundation and structure. The evaluation of piezometric levels in dams is important for it reflects the values of the uplift pressure that acts on the structure of the dam. The utilization of new methods in such an analysis can provide agility to decisions-taking by the security team of the dam. Depending on the method applied, a better comprehension of the phenomenon in time and space may be achieved. This study employs Artificial Neural Networks (ANN) to simulate the behavior of the piezometers installed in a geological discontinuity in the foundation of Itaipu Dam. It considers different types of entry data in a Multilayer Neural Network and determines the best ANN architecture that is closest to the real situation. Some parameters have a higher weight in the variation of the piezometric levels, whereas some others do not affect it considerably. A geological geotechnical model of the foundation rock fractures would be helpful to improve the entry data and achieve better results.

130.1 Introduction

The study of the acting forces on dams has high importance in the evaluation of their security. New methods for that analysis are required in order to provide agility in decisions-taking by the security teams who are in charge of maintaining such structures.

Itaipu Binacional is the world's second largest dam, and first in generation of energy. It has a crucial paper in the economy of Brazil and Paraguay and even for its surrounding territories. By the time of its construction it was severely instrumented as to ensure great levels of quality and its stability.

B. Medeiros (✉) · L.V. Zuquette
São Carlos School of Engineering, University of São Paulo, São Paulo, Brazil
e-mail: brunomedeiros.eng@gmail.com

L.V. Zuquette
e-mail: lazarus1@sc.usp.br

J. Patias
Itaipu Binacional, Foz do Iguaçu, Brazil
e-mail: jpatias@itaipu.gov.br

In order to attend international codes and local laws, it was established a program of control of the instrumentation of Itaipu. Most instruments are read every month, while piezometers and flow meters are read every 15 days (Itaipu Binacional 1994). Such a work has created a database of about 30 years of continuous readings, which has to be handled and analyzed.

The use of Artificial Neural Networks (ANN) allows the insertion of such data into computational programs together with other characteristics of the dam, and provides new ways of obtaining and analyzing data.

In this context, this study proposes the utilization of ANN to evaluate the behavior of 48 piezometers situated at a discontinuity in Itaipu foundation.

130.2 Study Area

Itaipu is located at the border between Brazil and Paraguay with approximated coordinates 25°24'29"S, 54°35'21"W. It is compound of several types of structures as can be seen in Fig. 130.1.

This study focuses on the structure 3, which is above a discontinuity called Joint D that is intensely instrumented. 48 piezometers were installed on Joint D and measure its hydraulic pressure.

130.3 Data Preparation

For the use of ANN, it is necessary to provide the network data that represent the behavior wanted to be reproduced. Some characteristics of the Joint D were not directly available for this use.

By the time of Itaipu construction its foundation was vastly investigated and the Joint D was mapped. Using its contour map and the installation elevation of the piezometers, a digital elevation model (DEM) was generated in ArcGIS® software with *Topo to Raster* tool. From this model, were extracted values of elevation of the joint topography, slope and orientation for the exact location of each of the 48 piezometers. This data were used together with the piezometric readings as entry data of the ANNs.
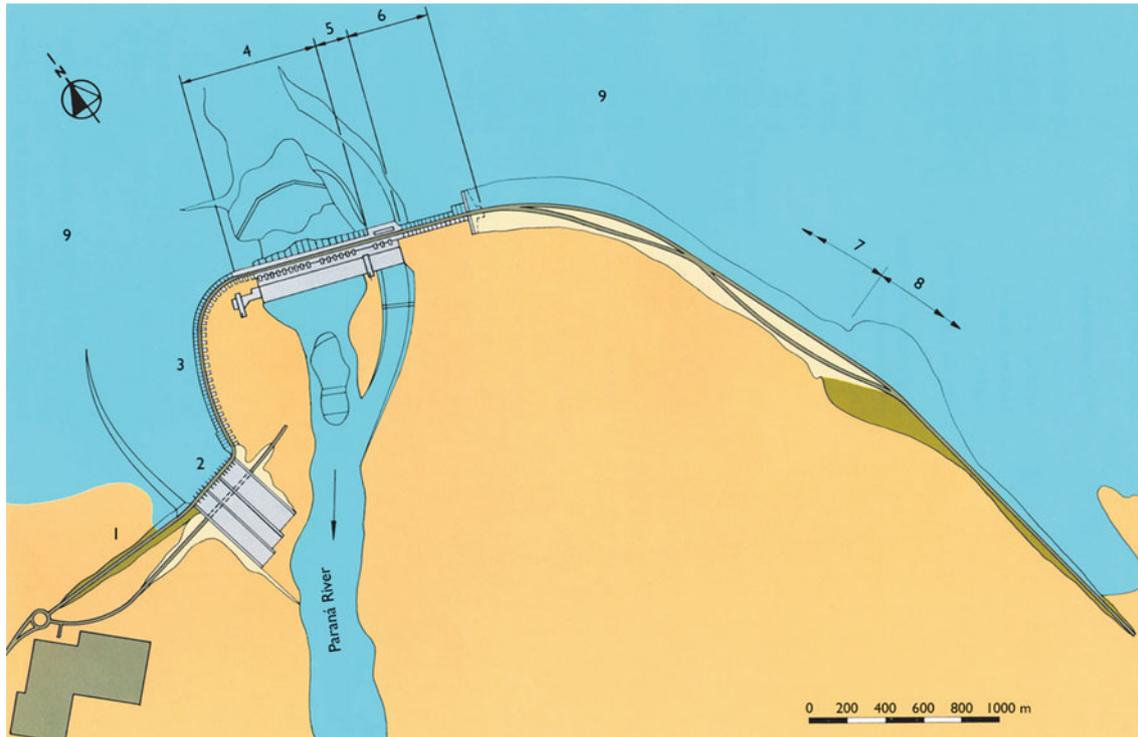
Fig. 130.1 Types of dams in Itaipu hydroelectrical complex. *1—right* earth dam; *2*—spillway; *3—left* side dam (buttresses); *4*—main dam (buttresses); *5*—diversion structure (concrete); *6—left* binding dam (buttresses); *7*—rock fill dam; *8—left* earth dam; *9*—reservoir. Modified from: Itaipu Binacional (1994)
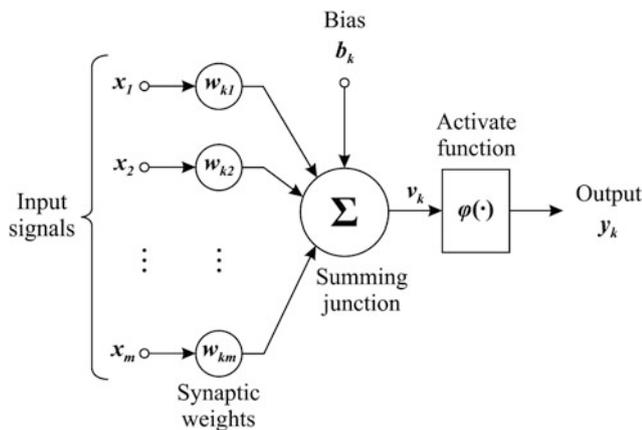
Fig. 130.2 Parts of an artificial neuron. Font: Haykin (1999)

Table 130.1 Groups of piezometric same behavior

Group	Code	Group	Code
Orientation north	ON	Elevation D	ED
Orientation east	OE	Elevation E1	EE1
Orientation south	OS	Elevation E2	EE2
Orientation west	OW	Slope 1	S1
Elevation A1	EA1	Slope 2	S2
Elevation A2	EA2	Slope 3	S3
Elevation B	EB	Slope 4	S4
Elevation C	EC	–	–

130.4 Artificial Neural Networks

The idea of creating an artificial system that would represent the concept of functioning of the human brain has been studied for many years, since late 19th and early 20th centuries (Hagan et al. 1996). Modern thought on this matter were developed by McCulloch and Pitts (1943), and since then it has been widely spread through the sciences, being used in engineering, medicine, stock market, and others.

The artificial neuron works like the human neuron receiving signals, weighting them and compiling into one or more answers. The Fig. 130.2 shows a concept of how it is organized.

130.4.1 Piezometric Readings Preparation

In order to organize all data available from the 30 years of readings of the instruments, electronic worksheets were elaborated. In this study, the 48 piezometers that monitor the Joint D were selected. The worksheets showed the identification of each instrument, its location in UTM coordinates, the installation elevation of the piezometer, the date of the reading, and the measured value of piezometric elevation.

Not all readings were executed on the same days for all 48 instruments. A work was performed to correct this on the worksheets and normalize the amount of data for each piezometer. It was only maintained the readings that were executed for all instruments on the same days. This resulted in an amount of 733 readings for each of the piezometers of Joint D, totalizing 35,184 values.

Each of the series of readings of the piezometers was put into graphics. Analyzing the behavior presented it was seen that some piezometers behaved similarly. From this observation it was possible to establish groups that could generate

different neural networks, and ease their process of learning. These groups received the nomenclature as seen on Table 130.1.

Some groups were seen to represent a most coherent and homogeneous behavior between the piezometers, as can be seen on Fig. 130.3. These groups were chosen to be used in ANN learning process. They are: EA1, EA2, EB, EC, ED, EE1, EE2, OE, OS, S1, S2 and S3.

130.4.2 Choice of the Best ANN Architecture

Some tests were performed in order to check the best architecture of ANN that would well represent the behavior expected. These input data were used: installation elevation of the piezometer, orientation, declivity, topographic elevation of the DEM, and the last two readings of each piezometer. The worksheets of each group was randomized and separated into two parts: 60 % for training and 40 % for validation.

On MatLab® software, the ANNs were programed to use 20 neurons in the input layer, and 1,000 epochs of training. For each of the groups analyzed several training sessions were performed. It was seen that it was necessary to increase the number of epochs, so it was adjusted for 2,000, and the sessions were run again. After the end of a session, the algorithm was adjusted to use 5 more neurons in the input layer. It was made until the number of neurons was 40.

130.5 Conclusions

The results were satisfactory for it showed an average percentage error of 0.132 % between the expected values and the obtained with the simulations. For each group the average, minimum and maximum percentage error can be seen on Table 130.2.

The Fig. 130.4 shows a comparison between the values expected for the group EB, and those obtained by the ANN simulation, and below the percentage error.

Fig. 130.3 Behavior of piezometers of group EB
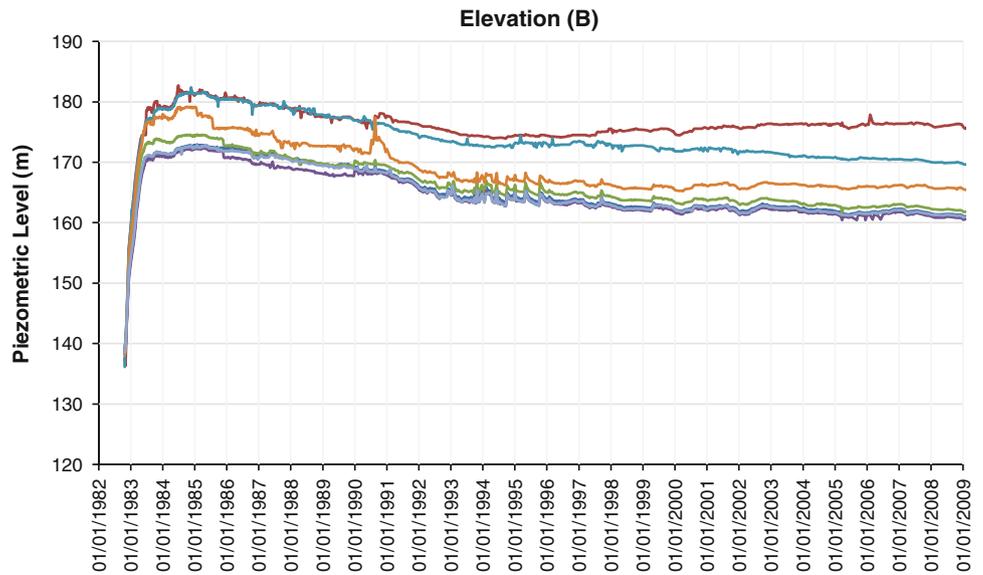
Table 130.2 Percentage error of the ANN simulation for each group

Group	Average percentage error	Minimum percentage error	Maximum percentage error
D1	0.174	0.000	12.561
D2	0.221	0.000	16.974
D3	0.139	0.001	13.672
EA1	0.143	0.000	6.971
EA2	0.057	0.000	1.285
EB	0.167	0.000	10.820
EC	0.159	0.001	3.658
ED	0.143	0.000	13.987
EE1	0.083	0.000	0.818
EE2	0.049	0.000	7.460
OE	0.191	0.000	13.944
OS	0.053	0.000	5.266
Average	**0.132**	**0.000**	**8.951**

Fig. 130.4 Values expected and obtained, and percentage error for the group EB
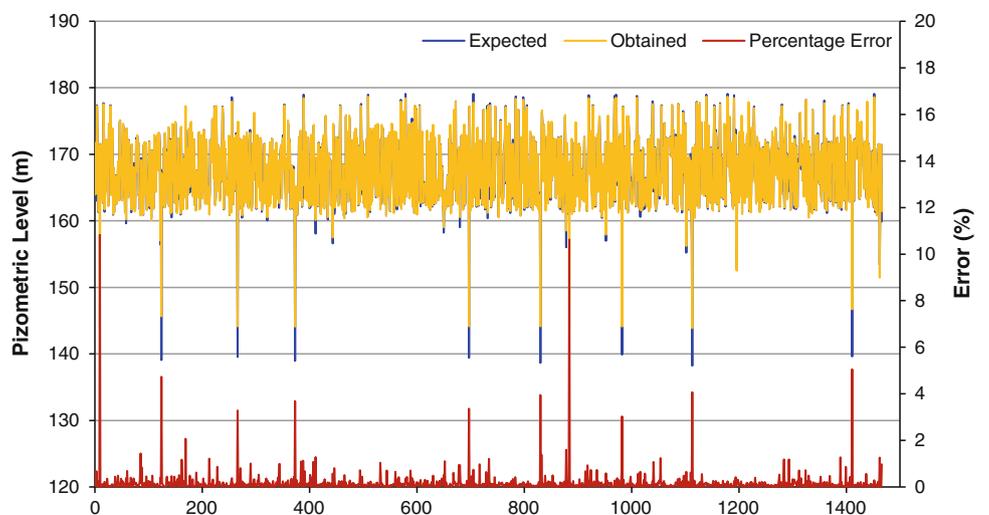
It is seen that Artificial Neural Networks was a useful tool for the comprehension of piezometric behavior in the foundation of Itaipu Dam. With the correct input data, it can be consistent in presenting a well-adapted model that corresponds reality. With the results of this study it is possible to apply these created ANNs for spots that are not instrumented and possibly receive good response of how would its behavior be in case there was an instrument installed there.

References

Hagan MT, Demuth HB, Beale M (1996) Neural network design. PWS Publishing Company, Boston

Haykin S (1999) Neural networks: a comprehensive foundation, 2nd edn. Pearson Prentice Hall, New Jersey

Itaipu Binacional (1994) Itaipu hydroelectric project: engineering features. Curitiba

McCulloch WS, Pitts WH (1943) A logical calculus of the ideas immanent in nervous activity. Bull Math Biophys 5:115–133

Giovanni Nico, Andrea Di Pasquale, Marco Corsetti, Giuseppe Di Nunzio, Alfredo Pitullo, and Piernicola Lollino

Abstract

The work mainly discusses the use of the Ground-Based Synthetic Aperture Radar (GBSAR) interferometry technique to observe and control the behavior of earthfill or rockfill embankments for dam impoundments. This non-invasive technique provides overall displacements patterns measured with a sub-millimeter accuracy. The need of reliable monitoring of old embankment dams is rapidly increasing since a large number of these structures are still equipped with old monitoring devices, usually installed some decades ago, which can give only information on localized areas of the embankment. A case study regarding the monitoring of an earthfill dam embankment in Southern Italy by means of GBSAR interferometry is presented.

131.1 Introduction

The present work mainly discusses the use of the Ground-Based Synthetic Aperture Radar (GBSAR) interferometry technique, as integrated with the available in situ traditional monitoring data as well as Finite Element analysis, to observe and control the behavior of earthfill or rockfill embankments for dam impoundments. The need of reliable monitoring of old embankment dams is nowadays rapidly increasing since a large number of these structures are still equipped with old monitoring devices, usually installed some decades ago, which are generally capable to provide only information on local areas of the embankment.

A Synthetic Aperture Radar (SAR) is an active microwave sensor used to produce 2D microwave images of the observed scene (Massonnet and Feigl 1998). The main advantage of microwave images is their capability to observe a scene without the need of solar illumination and in any weather condition. In the last decade, Ground-Based SAR (GBSAR) systems have gained an increasing interest in different applications such as monitoring of dams, landslides, buildings, bridges, or to extract information on terrain morphology (Guccione et al. 2013; Di Pasquale et al. 2013). The SAR interferometry (InSAR) technique relies on the processing of two SAR images of the same scene obtained by almost the same position. The phase difference φ between the corresponding pixels of two coherent complex-valued SAR images provides displacements measurements of structures and natural scenes with a sub-millimetre precision. The GBSAR system is installed at a distance from the observed object ranging from less than one hundred metres

G. Nico (✉) · P. Lollino
Consiglio Nazionale delle Ricerche, Istituto di Ricerca per la Protezione Idrogeologica, Via Amendola 122/I, 70126 Bari, Italy
e-mail: g.nico@ba.iac.cnr.it

A. Di Pasquale
DIAN srl, Z.I. La Martella, III Trav. G.B. Pirelli sn, 75100 Matera, Italy

M. Corsetti
D.I.C.E.A, Università la Sapienza, Via Eudossiana 18, 00184 Bari, Italy

G. Di Nunzio · A. Pitullo
Consorzio di Bonifica della Capitanata, Corso Roma 2, 71121 Foggia, Italy

up to four kilometres. The interferometric processing of two coherent SAR images results in a map of displacements occurred between the acquisitions of the two SAR images. Radar measurements give the projection along the radar line-of-sight of the 3D displacement vector. The main advantage of GBSAR interferometry with respect to traditional techniques is its capability to provide 2D information on the overall displacement field rather than measurements of displacements in only a few points.

131.2 Test-Site

The experiment described in this paper has been carried out at the Occhito's earth dam managed by the Consorzio di Bonifica di Capitanata (CBC). This 432 m-long and 60 m-high earth dam is one of the biggest ones in Europe. At present this dam is monitored with an array of piezometers, inclinometers and sensors of pressure. Furthermore, the position of a set of marks along the crest and the downstream surface is measured by topographic techniques (see Fig. 131.1).

131.3 GBSAR Results

In this section we present the results obtained by GBSAR technique. Two 2-h measurement campaign have carried out from two different positions. The two installation positions,

A and B, are reported in Fig. 131.1. The two measurement positions are located at the basis of the dam, on opposite sides, in order to reconstruct the true displacement vector. In fact, interferometric SAR measurements can only provide the line-of-sight (LOS) component of the displacement. The aim the campaign has been to set a "zero" measurement with respect to which to compare radar measurements to be acquired in future campaigns.

Figure 131.2 shows a picture taken from the installation position of GBSAR system denoted as A in Fig. 131.1. From this position the radar observed more than a half of the dam surface and the concrete structural elements represented on the right hand side of the picture. A 2-h measurement campaign has been done. The amplitude of one of the SAR images acquired on this dam is represented at the top of Fig. 131.4. Pixels with a higher value of dB correspond to patches on the dam surface with a higher scattering capability of radar signal. The comparison with the optical picture in Fig. 131.3 helps to easily recognize the different portions of the dam. The map of surface displacements measured by the radar during the 2-h campaign is displayed at the bottom of Fig. 131.4. As mentioned before, radar measurements can provide only the line-of-sight (LOS) component of the displacement vector, which that shown in Fig. 131.4. It is worth noting that this due this property of radar measurements, the GBSAR system should be properly installed in order to avoid a line-of-sight perpendicular to the expected displacement vectors. Figure 131.5 reports the
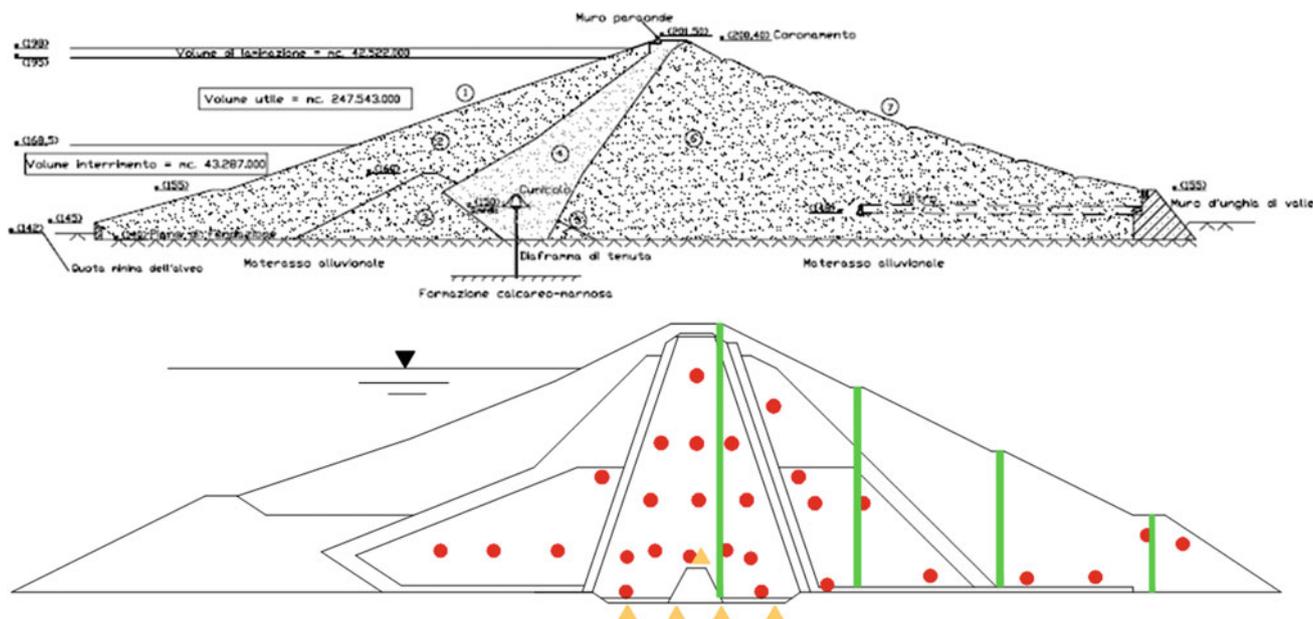
Fig. 131.1 Occhito's earth dam: (*top*) Geometry; (*bottom*) localization of sensors: piezometric cells (*circles*), pressure cells (*triangles*), inclinometers/assestimeters (*vertical columns*)

Fig. 131.2 The two installation positions of the GBSAR sensor
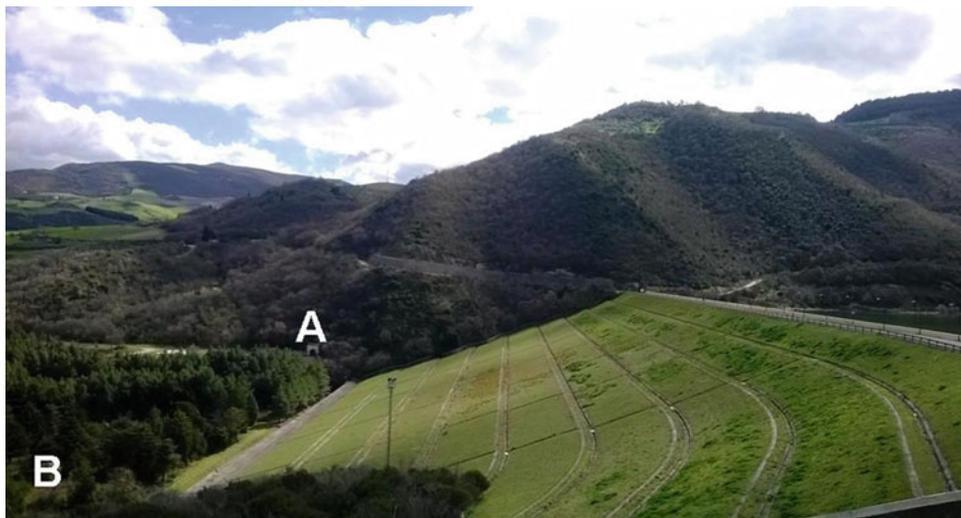
Fig. 131.3 Picture of the Occhito dam as seen by the installation position A of the GBSAR sensor

frequency distribution of displacement measurements. The mean and standard deviation values are, respectively, 0 and 0.3 mm. Due to the short time interval of monitoring this statistical figures provide the precision and accuracy of the interferometric GBSAR measurement. Further assessments of the GBSAR capability to provide unbiased sub-millimetre precision measurements of surface displacements can be found in (Di Pasquale et al. 2013).

Figure 131.6 shows a picture taken from the installation position of GBSAR system denoted as B in Fig. 131.1. From this position the radar observed the remaining part of the dam not observed form position A. The amplitude of one of the SAR images acquired on this dam is represented at the top of Fig. 131.7. The map of surface displacements measured by the radar during the 2-h campaign is displayed at the bottom of Fig. 131.7.

Fig. 131.4 (*Top*) amplitude of the radar image; (**b**) LOS displacement map in radar coordinates as measured from position A
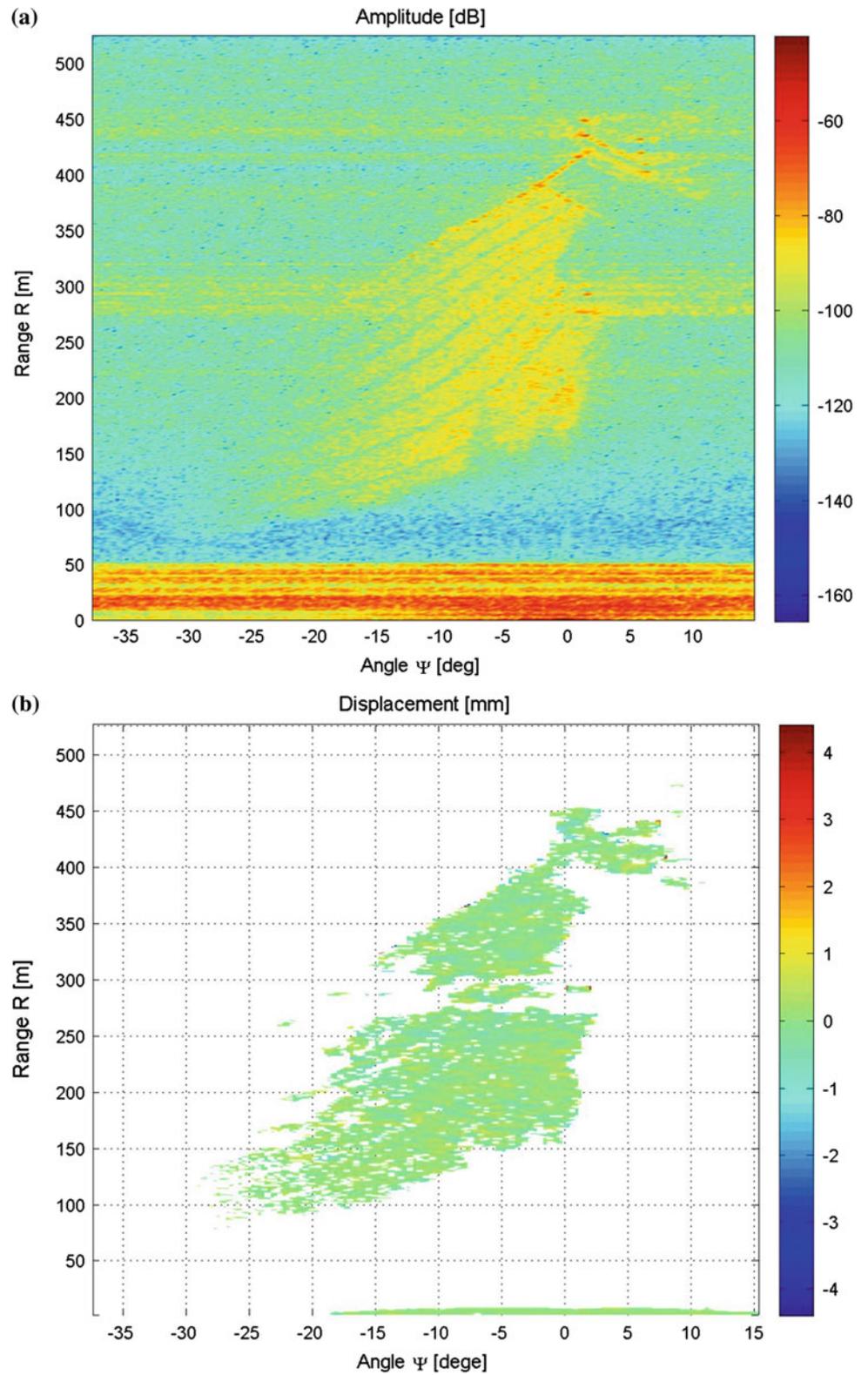
Fig. 131.5 Frequency
distribution of dam surface
displacement values
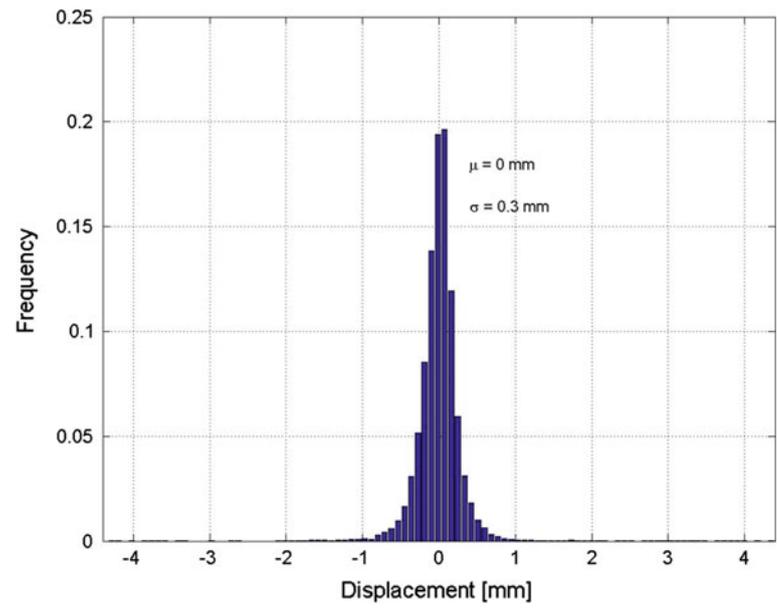
Fig. 131.6 Picture of the
Occhito dam as seen by the
installation position B of the
GBSAR sensor
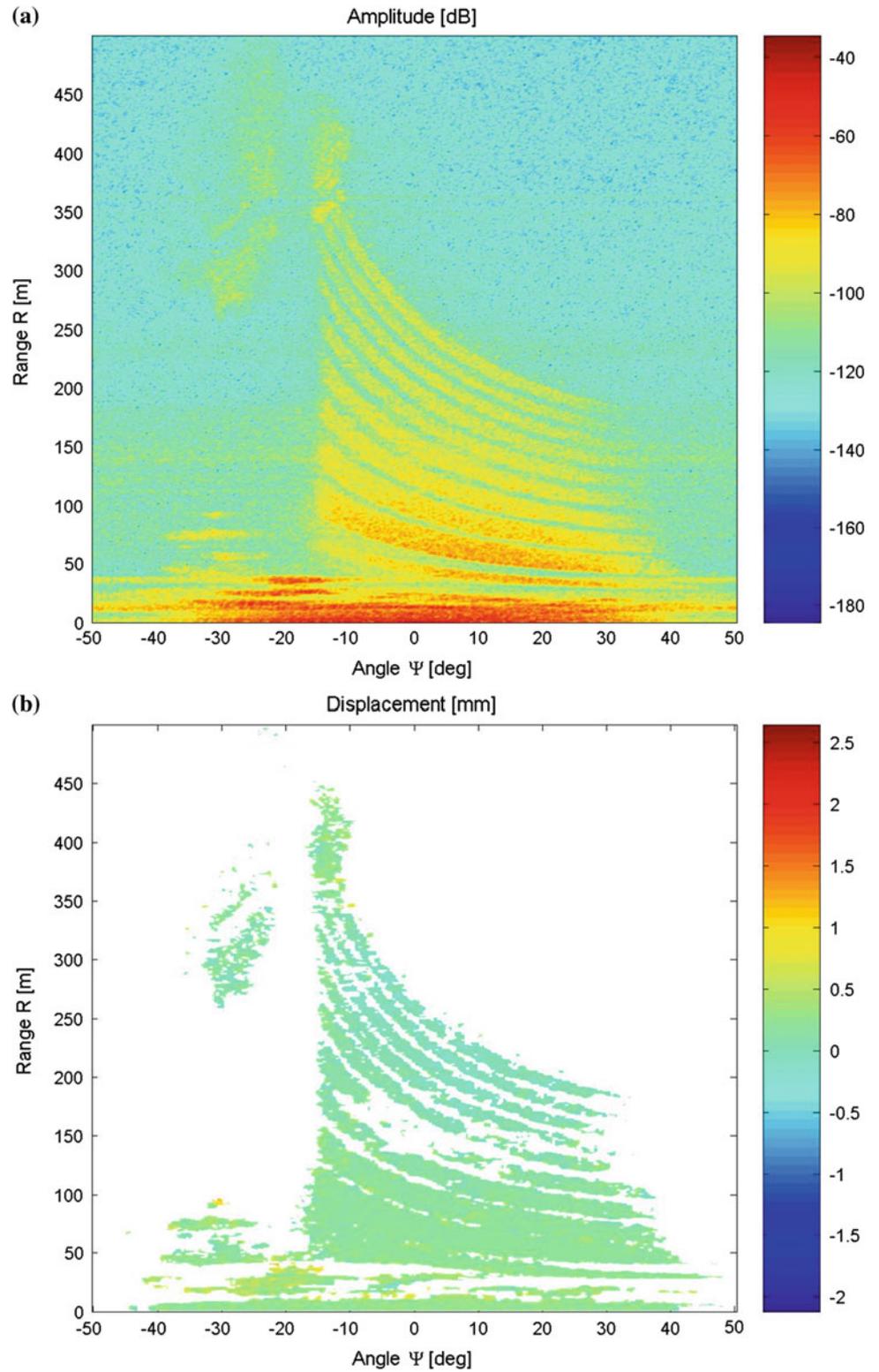
References

Massonnet D, Feigl KL (1998) Radar interferometry and its applications to changes in the Earth's surface. Rev Geophys 36:441–500

Guccione P, Zonno M, Mascolo L, Nico G (2013) Focusing algorithms analysis for ground-based SAR images. In: Proceedings of the international geoscience and remote sensing symposium, Melbourne, Australia, 21–26 July

Di Pasquale A, Corsetti M, Guccione P, Lugli A, Nicoletti M, Nico G, Zonno M (2013) Ground-based radar interferometry as a supporting tool I natural and man-made disasters. In: Proceedings of the 33rd annual EARSeL symposium, Matera, Italy, 3–6 June

Modelling and Optimization of the Biological Treatment in the Conception of Water-Treatment Plants Whith Activated Sludge

Moncef Chabi and Yahia Hammar

Abstract

The pond of aeration, or airy biological reactor, is the major element of a water-treatment plant with activated sludge. His functioning packages the quality of the treatment, the network mud and the energy expenditure. The good knowledge of the hydrodynamics of these reactors is an essential stake to improve their conception and thus to optimize their functioning. Our study is interested in the use of the code of calculation FLUENT for the simulation of the flows in ponds of aeration the case of the water-treatment plant of Souk-Ahras, where the functions of aeration and admixture are separated. This software uses the method of the volumes finished to solve the equations of Navier-Stockes in turbulent regime. The final goal lives in the definition of technical capacities to improve the functioning of the work. Finally, we highlight the influence of the aeration on the speeds of circulation and the phenomena of ascending convection of the water (spiral spring—flows), responsible for a decrease of the transfer of oxygen in the pond. The impact of a horizontal speed on certain types of spiralflows is studied. Big spiral spring - flows disappear totally from a speed of 0,3 m.s^{-1}. These simulations are led for various geometries of ponds

Keywords

Channel of oxidation • Flow • Hydrodynamics • Transfer of oxygen • Agitation

132.1 Introduction

The secondary treatment is essentially a biological oxidation of the dissolved materials. The agents of this oxidation are microorganisms, in particular aerobic bacteria, susceptible to feed on present organic matters in waste water. The secondary processing plants thus appear as ponds of culture where we put in touch a bacterial population and the effluent to be treated in the presence of oxygen.

These ponds called also ponds of oxidation operate a free bacterial biomass associated in plops. These flakes of muds include heterotrophic microorganisms and autotrophes nitrifiants when the residence time of the mud is self-important so that their multiplication produces an active biomass in the treatment.

This reproduction of microorganisms intervenes in favorable conditions, when their growth is important is that bacterium beginning dividing. The exo-polymers which they secrete allow them to gather together in plops settlings.

The chosen conditions of operation are the ones which favor the settling of these plops. In this case, the biomass can be separated by a second settling where the extracted mud is recirculate towards the pond of aerobic treatment.

The aeration can be assured on surface by turbines or at the bottom by processes of banister of distribution of air bubbles. The efficiency on transfer can be improved by the increase of the height of water.

M. Chabi (✉) · Y. Hammar
Badji Mokhtar University, Annaba Box 12, 23000 Annaba, Algeria
e-mail: moncef.chabi@univ-annaba.org

Y. Hammar
e-mail: yahia.hammar@univ-annaba.org

The process with activated sludges is at present the most valid process of biological purge of residual waters. His big advantages are:

- Security as regards the degree of purge of handled waters, because the most important factors of influence, for example contribution of residual water, and bacterial mass, are controllable,
- A bigger efficiency than with the bacterial beds, than this process is much less dependent on the temperature,
- A shorter phase of starting up (less than 2 weeks) with regard to compared with the bacterial beds (4 in 6 weeks),
- total Absence of smells and flies.

This process allows to handle residual waters from 100,000 to 200,000 living equivalents, and it calls on all the same to certain notions important for the exploitation…

132.2 Display of the Zone of Study

132.2.1 Presentation of the Wilaya de Souk Ahras

The wilaya of Souk-Ahras localized in the east of the country covers a total surface of 4 359,65 km². The map below represents the demarcations of the wilaya as follows:

- the wilaya of Tarf in the North-East,
- the wilaya of Guelma in the North-west,
- the wilaya of Tebessa in the South
- the wilaya of Oum el Bouaghi in the South-west

- and the border Algéro-Tunisienne in the East (Fig. 132.1).

The wilaya of Souk-Ahras is situated in the extremity is of the zone tellienne, crossed from east to west by the oued Medjerda which is a cross-border stream, its paying pond covers a surface of 7,870 km² only 1,411 km² are distributed on the Algerian territory.

The valley of the wilaya of Souk-Ahras and known by a very heterogeneous geology, represented by sedimentary trainings the oldest age of which is Sorted out it and, constituted generally by limestones, wills, marls, gravel and alluviums, it forms a pivotal zone between the Tell Atlas in the North and Saharan Atlas in the South.

132.2.2 Presentation of the Treatment Plant for Souk-Ahras

The water-treatment plant of the city of Souk-Ahras is intended to handle domestic waste water before their discharge in the oued of Medjerda of among which:

- The first stage allows to handle the pollution resulting from a population of 150,000 equivalents living.
- The second stage will carry its capacity in 225,000.

The station is designed to work in a low(weak) mass responsibility, thus according to the process of a prolonged aeration. By this process, we obtain a good efficiency of elimination of the DBO, the stabilization "mineralization" of secondary muds will be made within the pond of aeration (Fig. 132.2).

Fig. 132.1 Map of demarcation of the wilaya of Souk-Ahras

Fig. 132.2 View google—earth of the treatment plant for Souk-Ahras
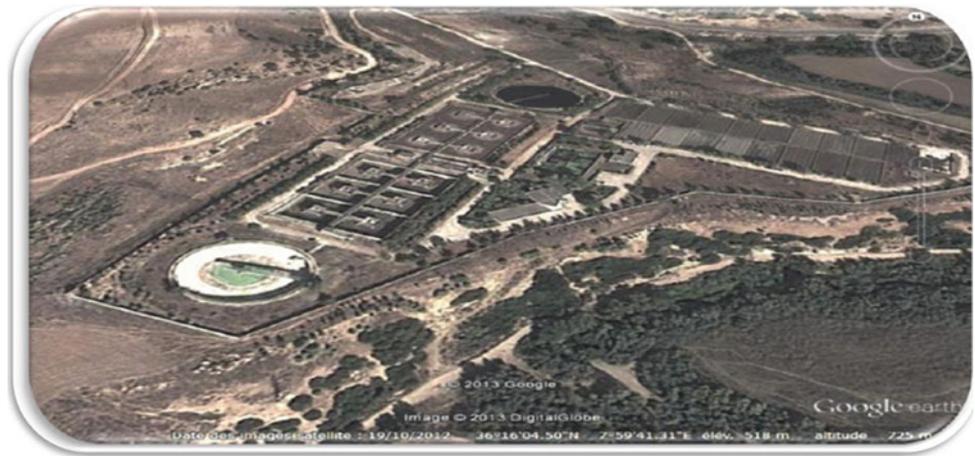
Table 132.1 Characteristics of the trial of the installation

Hydraulic residence time	21 h
Residence time of muds	20 days
Concentration in mud	5 g/l
Nominal flow	30 000 m^3/d

The characteristics of the treatment plant are defined in the Table 132.1:

132.2.3 Biological Reactor

There are two different and identical ponds of aeration having the following characteristics:

- Length: 66 m
- Width: 44 m
- Height of water: 4.5 m
- unitarian Volume: 13,068 m^3
- total Volume: 26 136 m^3

Waters arriving in these ponds are brewed with the mixed liqueur and the muds of recirculation from the secondary decanter.

This pond is equipped with 12 ventilators of surface. Their characteristics are the following ones: of chap AVL 3,750 (supplier TMI), power 75 kW, tension 380/660 V 50 Hz (Fig. 132.3).

132.3 Tool of Simulation Gambit and Flow

132.3.1 The Tool Gambit

GAMBIT is a software which allows to create meshings which can be used in particular under FLUENT.

The mailleur is a preprocessing in the simulation software. He allows to generate a meshing structured or not structured in Cartesian, polar, cylindrical address and phone coordinates or axisymétriques. He can realize complex meshings in two or three dimensions with stitches of chap rectangle or triangle.

To build a meshing, it is good to follow the following approach:

- define the geometry.
- realize the meshing.
- define the parameters of computation zones.

132.3.1.1 Define the Geometry

The geometry includes the physical positions of characteristic points define the zone which we have to mesh: spatial address and phone coordinates of four summits of a square; of the starting point (Fig. 132.4)

132.3.1.2 Realize the Meshing

For structured meshings, we can make the connection between the geometry and the meshing, also, before realizing the meshing, it is necessary to specify in writing on one hand the geometry adopted to define the zone to be meshed, on the other hand the numbers of stitches corresponding to the characteristic points of the geometry. A knot can then be spotted by these physical address and phone coordinates x and y.

Besides, he can be advantageous to define intermediate points which are not essential to the definition of the geometry but which allow to bound the zones in which stitches will be adapted to refine the meshing near walls for example either to marry at best the shape of the obstacles, the walls or others (Fig. 132.5).

132.3.1.3 Define the Parameters of Computation Zones

When the geometry was created, when the conditions in the limits were defined, it is necessary to export the meshing. msh (mesh = meshing in English) so that Flow is capable of reading it and of using it (Fig. 132.6).
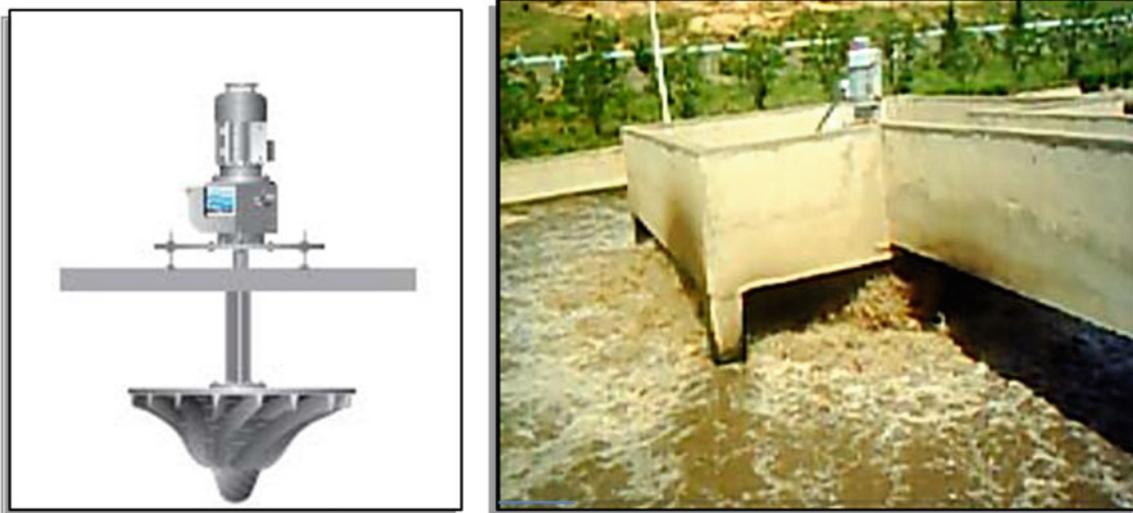
Fig. 132.3 The system of aeration of surface
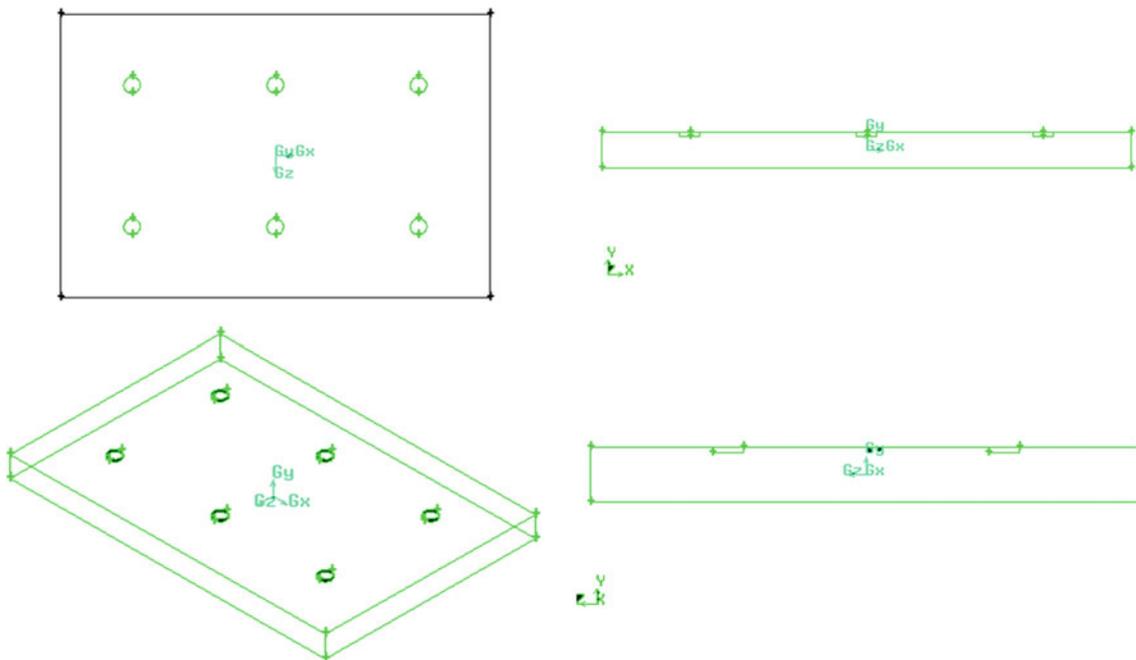
Fig. 132.4 The construction of the pond of aeration of the treatment plant for Souk Ahras

We can then close Gambit by protecting the session (if we wish to open it) and throw Fluent.

132.3.2   The Tool Fluent

Fluent is a commercial code CFD very used in the industry. He allows to solve the fluid sellings (fields of speeds, temperature), it is the reason why one it chosen to realize our simulation.

The simulation in Digital Fluid mechanics (Computational Fluid Dynamics: CFD), is used for the modelling, the visualization and the analysis of the fluid sellings and thermal transfers. She allows the users to optimize the performances of the new concepts, while reducing the cycle of marketing, the associated risks and the costs.
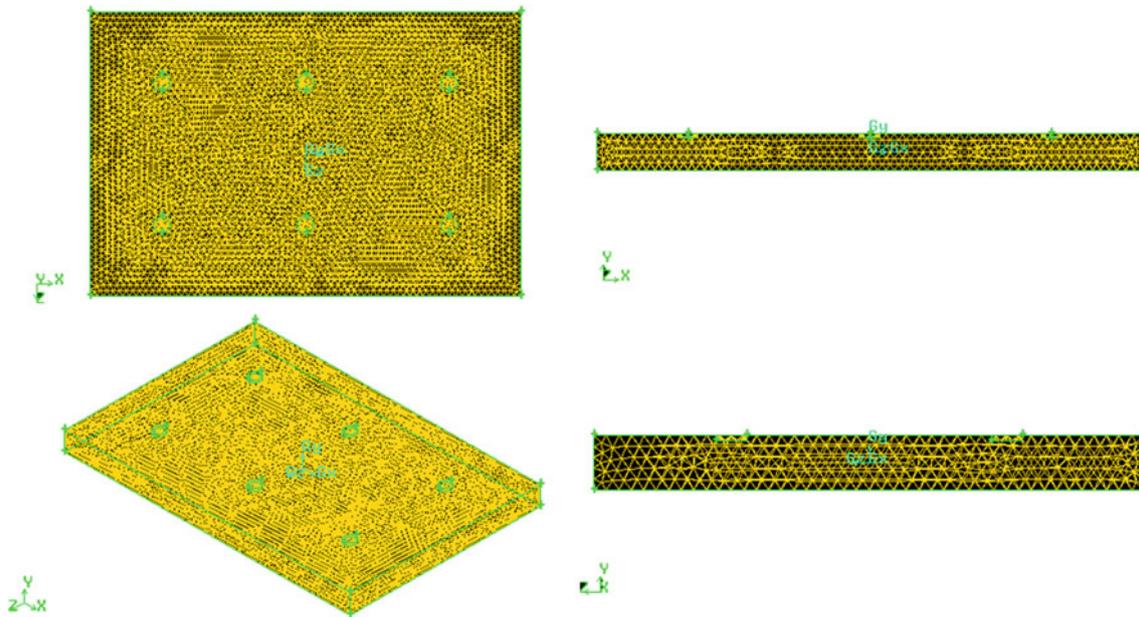
Fig. 132.5 The meshing of the pond of aeration of the treatment plant for Souk Ahras
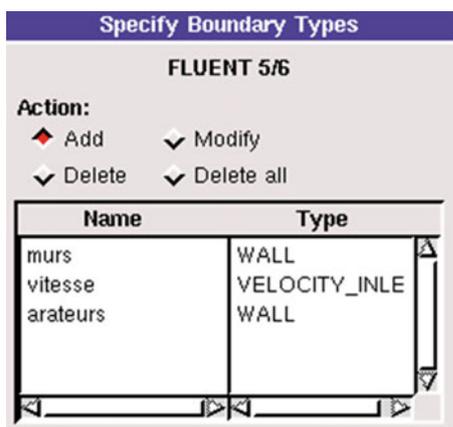
Fig. 132.6 The conditions on the verge of our treatment plant

For more than 10 years, Flow, world leader in digital Simulation of the Fluid software sellings and departments. The solution of the most adapted simulation strives to offer, whether it is for the whole industry, research or engineering education of tomorrow. This solution spends by services of technical audience, studies with way, and by personalized formations.

The siege of the group Fluent is situated to Lebanon, New Hampshire, the USA, and account of the subsidiaries in Belgium, England, France, Germany, India, Italy, Japan and Sweden. Its software are also sold worldwide thanks to joint-ventures, partnerships and distributors in Korea, Australia, Brazil, China, Taiwan, Czech Republic, the Middle East and in most of the European countries.

132.3.2.1 Choice of the Model of Turbulence

Because the geometry is in 3D, and because the geometry is a pond of aeration with 6 ventilators of surface of chap slog slow, compared with the rest of the domain of calculate the choice of 3D double precision seem the most suited to our simulation (Fig. 132.7).

Fluent proposes various modellings of the turbulent selling. Among which the not viscous, laminar, turbulent sellings etc. (Table 132.2).

The characteristics of materials are given in the following Table 132.3:

These properties are then loaded in signs materials of the software FLUENT.

132.4 Results

The method of the finished volumes is an approach very often used for the dynamic calculations in thermal because of its ease of implementation.

In the approach of the finished volumes, the value calculated in the center of the volume represents the approximation of the variable considered on all the volume. In the case of the use of a not structured meshing (triangulation of Delaunay), the "central" points of triangles and squares used to represent the approximation of the field of temperature do not belong inevitably to the orthogonal of the borders, but this does not prevent from having a correct evaluation of flows and temperatures

```
FLUENT [3d, dp, pbns, lam]
File  Grid  Define  Solve  Adapt  Surface  Display  Plot  Report  Parallel


      Welcome to Fluent 6.3.26

      Copyright 2006 Fluent Inc.
      All Rights Reserved

Loading "C:\Fluent.Inc\fluent6.3.26\lib\fl_s1119.dmp"
Done.


> Reading "C:\Users\Moncef\Desktop\arateurs.msh"...
   20784 nodes.
     144 mixed wall faces, zone   3.
     288 mixed velocity-inlet faces, zone   4.
   15926 mixed wall faces, zone   5.
  191013 mixed interior faces, zone   7.
   99596 tetrahedral cells, zone   2.

Building...
     grid,
     materials,
     interface,
     domains,
     zones,
         default-interior
         murs
         vitesse
         arateurs
         fluid
     shell conduction zones,
Done.
```

```
Grid Check

 Domain Extents:
   x-coordinate: min (m) = -3.300000e+001, max (m) = 3.300000e+001
   y-coordinate: min (m) = -2.250000e+000, max (m) = 2.250000e+000
   z-coordinate: min (m) = -2.200000e+001, max (m) = 2.200000e+001
 Volume statistics:
   minimum volume (m3): 9.015031e-003
   maximum volume (m3): 3.883456e-001
     total volume (m3): 1.305402e+004
 Face area statistics:
   minimum face area (m2): 7.656329e-002
   maximum face area (m2): 1.139717e+000
 Checking number of nodes per cell.
 Checking number of faces per cell.
 Checking thread pointers.
 Checking number of cells per face.
 Checking face cells.
 Checking bridge faces.
 Checking right-handed cells.
 Checking face handedness.
 Checking face node order.
 Checking element type consistency.
 Checking boundary types:
 Checking face pairs.
 Checking periodic boundaries.
 Checking node count.
 Checking nosolve cell count.
 Checking nosolve face count.
 Checking face children.
 Checking cell children.
 Checking storage.
 Done.
```

```
Number faces swapped: 5
Number faces visited: 660

Number faces swapped: 0
Number faces visited: 649
No nodes moved, smoothing complete.
Done.
```

Fig. 132.7 The data entry of meshings on Fluent

Table 132.2 Advantages and inconveniences of the various models of turbulences

Models	Advantages	Inconveniences
Spalart-Allumaras	Economic (1 equ). Well for the sellings averagely complex.	Is not widely tested.
STD k-ε	Strong, economic and relatively precise.	Results mediocre for complex sellings (strong gradient of pressure, rotation and swirl).
RNG k-ε	Well for sellings averagely complex (impact of jet, separation of sellings, secondary sellings)	Limited by the hypothesis of isotropic turbulent viscosity.
Realizable k-ε	Offer the same advantages as the RNG. Recommended in the case of turbomachines.	Limited by the hypothesis of isotropic turbulent viscosity.
Reynolds Stress Model (RSM)	The most complete model physically (transport and the anisotropie of the turbulence are kept account there)	Requires more weather CPU. The equations of momentum and turbulence are closely linked.
SST et standard k-ω	Model the most recommended for the problems connected to turbomachines, better than Realizable k-ε	Require a bigger resolution of the meshing on the borders (no laws in walls).

Table 132.3 Properties physical appearance of materials used in the simulation

Materials	Thermal conductivity (W/m.k)	Density (kg/m$^{3`1}$)	Mass thermal capacity (j/kg.k)	Viscosity (kg/m.s)
Water	0.6	998.2	4,182	0.001003

Residues are calculated from the corrections in variables; pressure, speed, temperature of the problem between the present iteration and the previous iteration.

In most of the cases, the convergence criterion by default in FLUENT, residual is self-important. The solution converges when residues affect 10^{-3}. However, in certain cases it is necessary to urge the calculations to 10^{-4} to see 10^{-6}. Thus There is no universal ruler.

To make sure of the convergence of the calculations, we use two visual criteria. The first one consists in observing the curves of residues defined by the equations, drawn by Flow, according to the iterations. When residues are weak (lower than 10^{-3} at least) and when curves become flat as illustrated below, we can consider that the solution is affected (Figs. 132.8, 132.9, and 132.10).
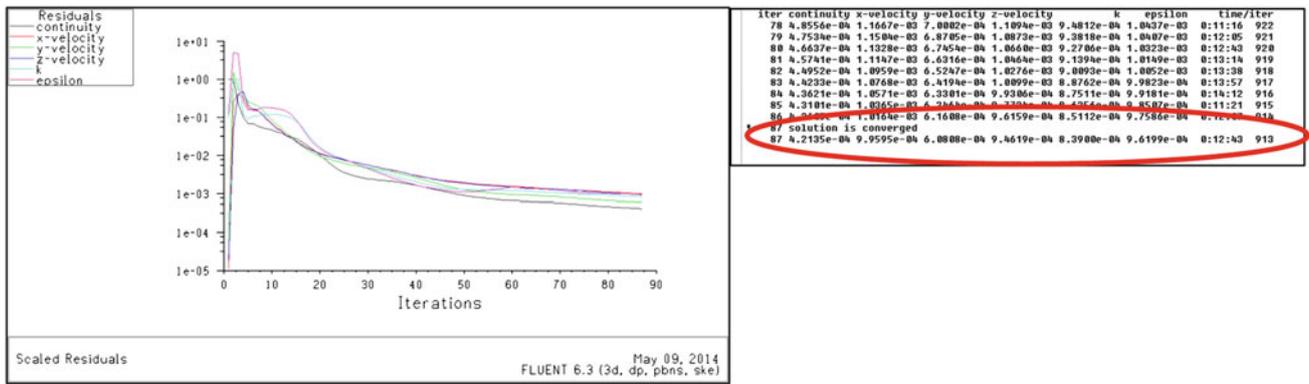
Fig. 132.8 Results of the convergence of the system of the treatment plant

Fig. 132.9 The distribution of the turbulence in the treatment plant
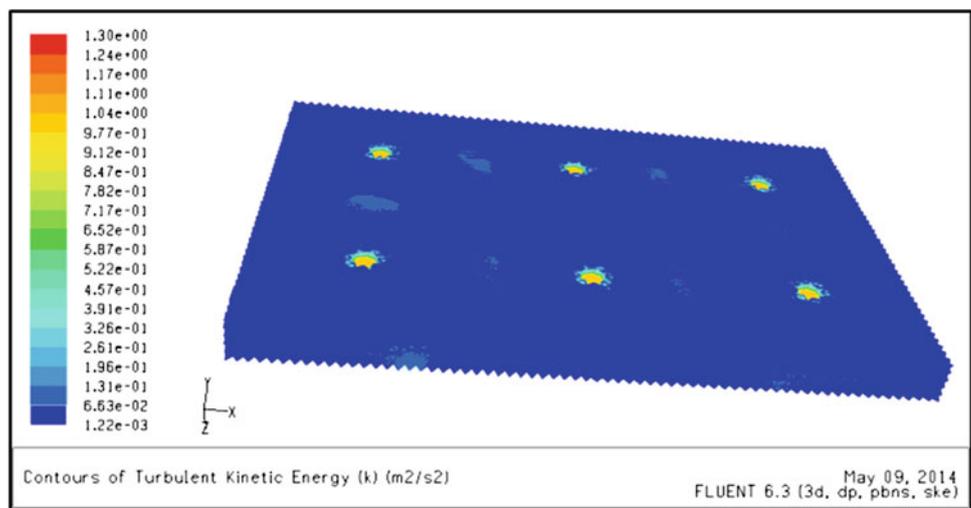
Fig. 132.10 The distribution of the speed in the treatment plant
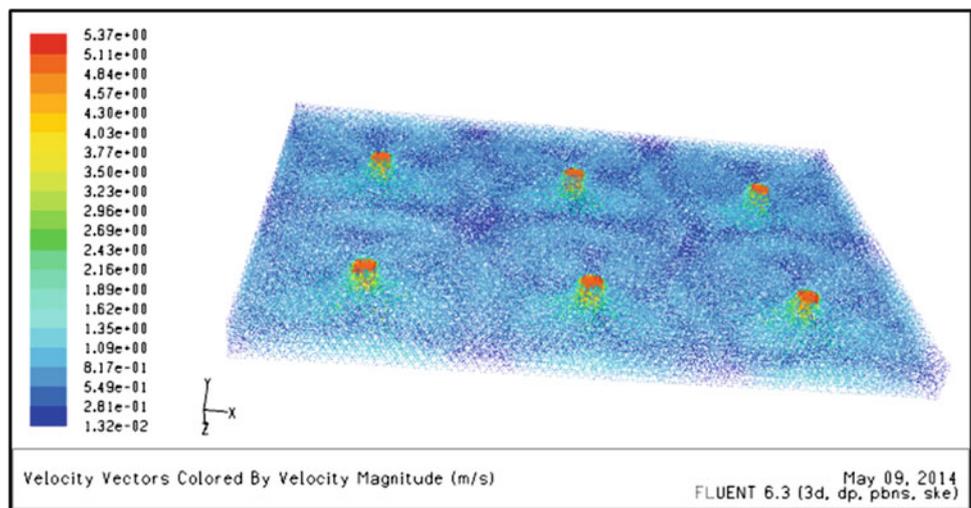
132.5 Conclusion

The distribution of it We used for it the code of calculation Flow. At first, it was necessary to validate this digital model by means of experimental measures made on the biological reactor of the water-treatment plant of Souk-Ahras. We compared the measures of momenta experimentally on the site with those feigned by means of Flow. It was shown that the model of the biological reactor could be validated. The sellings in a biological reactor filled with clear water flow reproduced correctly thus.

References

Abusam A, Keesman KJ, Meinema K, Van Straten G (2001) Oxygen transfer rate estimation in oxidation ditches from clean water measurements. Water Res 35(8):2058–2064

Boumansour BE, Ounaïes F, Roche N, Vasel JL (1999) Tracer gas method characterization of oxygen transfer in dense membrane reactors. In: 3ème Congrès International de recherche-L'eau et sa réutilisation, INSA Toulouse, p 77–82. 9–10 nov 1999

Chatelier P (1991) Simulation de l'hydrodynamique des chenaux d'oxydation par l'utilisation des équations de Navier-Stokes associées au modèle k-ε : évaluation de la vitesse de circulation, Thèse de doctorat, INSA Toulouse, p 220

Duchène Ph, et Héduit A (1990) Aération et brassage en stations d'épuration : efficacité des divers systèmes, Inf Tech du Cemagref 78(2):7

Duchène Ph, et Héduit A (2009) Expérience et interprétation de mesures de performances d'aération en boues activées. 23e Symposium sur les eaux usées. Réseau environnement, Laval (Québec), p 6. 28–29 Nov

Large Projects Impact Assessment, Mitigation and Compensation

Convener Prof. Giuseppe Spilotro—*Co-convener* Canora Filomena

Infrastructure development, both in fast-developing and in more developed countries, is supported by innovative technologies, which makes every large project feasible. We think of bridges, dams and reservoirs, high-speed railways, pipelines across land and seas, energy farms, drilling and tunnelling activities, etc. The impact produced by such types of works should be predictable on the basis of the experience gained on similar projects, but it can also be surprisingly different, either due to inherent complexities in the concerned environment, as to the true extension of the impact, or, even for a new social awareness, supported by measuring capabilities, previously unavailable.

The assessment of the impacts is the first necessary step: it needs not only a reasonable evaluation of interaction between project and environment elementary components, but also of their reciprocal interaction. The assessment should be directed to the mitigation, which is in the space and in the time and should represent the relevant part of the project, while the compensation is outside of the space and the time. The question is: Can they be sufficient to maintain the overall balance as sustainable?

Mining with Filling for Mitigating Overburden Failure and Water Inrush Due to Coalmining

Wanghua Sui, Gailing Zhang, Zhaoyang Wu, and Dingyang Zhang

Abstract

This paper investigates the heights of overburden failure with cut-and-fill mining method using empirical formula, scaled model tests and numerical simulations. An equivalent cutting height was proposed for calculating overburden failure with formulas and from measurement data. Scale model tests and numerical simulations show that the heights of caving zone and water flow fractured zone due to mining with filling decreased obviously compared to those due to caving mining. The results also indicate that mining with filling method has protective function for overlaid unconsolidated clay and sand layers.

Keywords

Mining with filling • Water and sand inrush • Mining under water body • Water flow fractured zone

133.1 Introduction

Mining under water bodies will suffer from groundwater and sand inrush if fractures reach the aquifers and form flowing pathways. To reduce the fracture heights is a useful method to avoid water inrush from overlying aquifers. Filling mining can realize this and create safety for mining under water-bearing strata.

The paste filling technology was first used in 1979 in the Grund lead-zinc ore mine. It was applied to the Walsum Colliery (Mez and Schauenburg 1998) to mitigate surface subsidence in 1991. The first Chinese paste filling system was constructed in the Jinchuan mining area in 1990s. In 2006, filling method was first used in the Taiping Coalmine, Shandong province, China. By now, researchers have studied the properties of paste materials, filling methods, overburden failure and subsidence due to filling mining (Zhou

et al. 2004). This paper presents the prediction, assessment, and practice using the paste backfilling method to mitigate overburden failure for preventing water and sand inrush through a case study in the Taiping Coalmine under unconsolidated aquifers.

133.2 Hydrogeological and Engineering Geological Conditions

The strata in the Taiping Coalmine include the Ordovician, the Carboniferous, the Permian, the Jurassic and Quaternary Systems. The sand aquifers at the bottom of the Quaternary System threaten coal mining safety. The specific capacity of the bottom aquifers ranges from 0.023 to 0.11 L/s·m. A clay layer with a thickness of 2–5 m distributes above Panel S02. The plastic index of this layer ranges from 12 to 24. During the first slice mining in Panel S02, the water inflow rate was less than 6 m^3/h. It indicates that mining the first slice weakly affects the integrity of this clay layer. It still plays an important role in preventing water inflow from the unconsolidated aquifers during backfilling mining the second slice.

W. Sui (✉) · G. Zhang · Z. Wu · D. Zhang
China University of Mining and Technology, 1 Daxuelu Rd, 221008 Xuzhou, China
e-mail: suiwanghua@cumt.edu.cn

Fig. 133.1 Cross section of
Panel S02 in the Taiping
Coalmine. *1*—Water flow
fractured zone due to mining the
first slices of Panel S04;
2—Water flow fractured zone due
to mining the first and second
slices of Panel S02
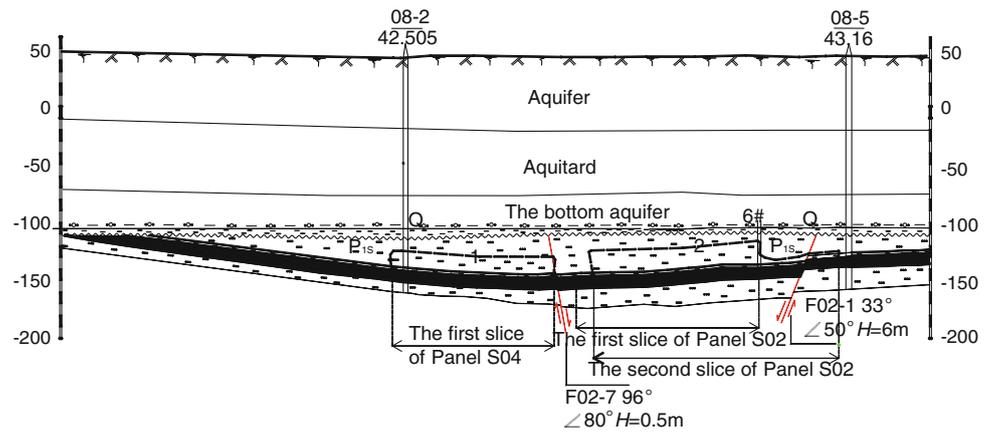
Table 133.1 Mechanical property of overburden and Seam 3

Types	RQD (%)	σ_c (MPa)	σ_s (MPa)	E (GPa)	λ
Fine sandstone	61	21.6–25.0	1.46–1.54	2.06–2.72	0.20–0.24
Mudstone	57	5.7	0.45	–	–
Seam 3	–	8.45	0.51	1.31	0.29

σ_c is the uniaxial compression strength, σ_s is the tensile strength, E is the modulus of deformation, λ is the Poisson's ratio

Table 133.2 Main influencing factors on safety mining of Panel S2

H_b (m)	H_o (m)	H_a (m)	K (m/d)	q (L/(s·m))
23.5–29.2	−116.5−−108.2	1.4–5.0	0.234–0.47	0.023–0.11

H_b = thickness of overburden; H_o = elevation of base rock surface
H_a = thickness of Quaternary bottom clay layer
K = hydraulic conductivity of the bottom aquifer; q = specific capacity

Figure 133.1 shows a cross section of Panel S02, which depicts the relationship between overburden and excavation. The Quaternary System is about 160 m. Table 133.1 lists the engineering geological types and characteristics of the bedrock above Panel S02 with a thickness ranging from 23.5 to 29.2 m. Table 133.2 lists the influencing factors on mining safety in Panel S02.

133.3 Heights of Overburden Failure

133.3.1 Empirical Method

The heights of the caving and the water flow fractured zones and the surface subsidence for the first slice with caving method have been studied through experiments and in situ detections. To calculate the heights of backfilling method, we proposed a concept of equivalent mining thickness, which equals to a uniform thickness of thin coal seam. This equivalent mining thickness can be estimated by $m_e = m - m_f$, where m_e is the equivalent cutting height, m is cutting height and m_f is thickness of filling body.

According to in situ measurements data during backfilling mining in the Taiping Coalmine, the convergence of roof and floor before backfilling is general 329 mm, non-backfilling account is 190 mm and the compression of backfilling body is estimated to be 63 mm for a cutting height of 2.2 m, therefore, the equivalent mining thickness is 0.58 m. Table 133.3 lists the heights of overburden failure for mining the first and second slices separately, which are calculated from empirical formulae proposed by Code (Coal Industry Bureau of PRC 2000).

133.3.2 Scale Model Test

The scaled model is designed according to the prototype of Panel S02 of the Taiping Coalmine. The length scale is selected as $b = 1/150$, the time constant $a = \sqrt{b} = 0.082$, the unit weight ratio $C_\gamma = 1.5/2.5 = 0.6$, and strength ratio $C_R = 1/250$. The model mining process, deformation and cracks were recorded by a high-speed digital camera and a fracture gauge.

Table 133.3 Results of heights of overburden failure by different methods

Slices and method	h (m)	Scaled model test		Empirical method		Numerical simulation	
		H_c (m)	H_f (m)	H_c (m)	H_f (m)	H_c (m)	H_f (m)
1#, caving	2	6.82	18.21	6.6	18.88	7.6	19.2
2#, filling	2	7.24	21.46	6.6	19.85	8.4	22.2
2#, caving	2	–	–	–	–	10.6	25.8

1# = the first slice; 2# = the second slice; h = cutting thickness; H_c = caving zone; H_f = water flow fractured zone
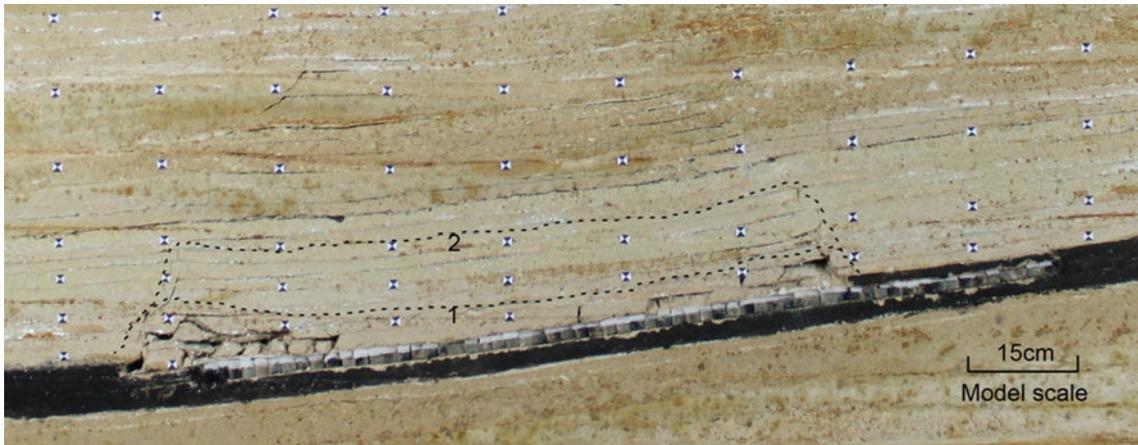
Fig. 133.2 After mining the second slice. *1*—caving zone; *2*—water flow fractured zone

Figure 133.2 shows the development of overburden failure and deformation due to mining the first slice of Seam 3 with caving mining and the second slice using the backfilling mining.

After the first slice mined out, the caving zone and fractured zone formed a shape of "the saddle", the height of caving zone is 6.8 m, and the water flow fractured zone is up to 18.2 m.

In the mining process of the second slice, the overburden in the expanded region without mining the first slice was deformed weakly, only produced a few micro fractures. After finishing mining, the heights of the caving and the water flow fractured zones grow to 7.24 m and 21.46 m, respectively. Compared to the height of overburden failure after mining the first slice, it increases much smaller when mining the second slice using backfilling method. In the expanded region the height of the water flow fractured zone is 3.82 m and did not form the caving zone (Fig. 133.3).

Table 133.3 lists the results of overburden failure using different methods. The numerical simulation was conducted using FLAC (Wu 2013). If the second slice is excavated by caving method, its caving zone and water flow fractured zone can reach 10.6 m and 25.8 m, higher than those induced by backfilling method. It was inferred that the paste backfill mining can control the growth of fractures, and it is significant for mining under thick unconsolidated aquifers and thin bedrock.
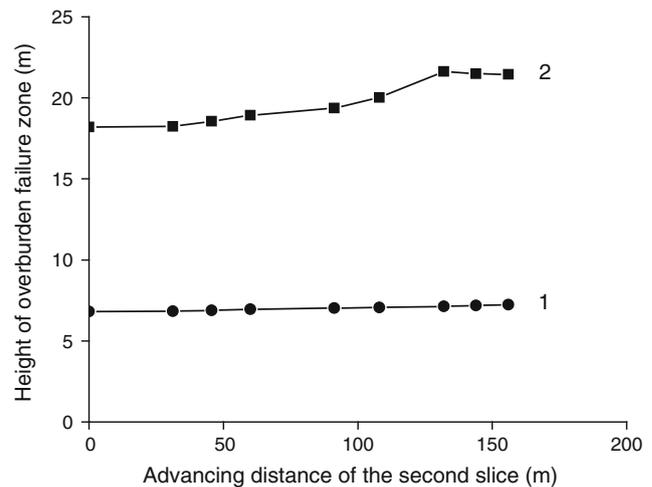
Fig. 133.3 The height of overburden failure after mining the second slice by backfilling method. *1*—caving zone; *2*—water flow fractured zone

133.4   Conclusions

This paper presents a concept of equivalent mining thickness for calculating the overburden failures of mining by paste backfilling. The overburden failure was studied using scaled and numerical simulations. The results show that the caving

and water flow fractured zones due to the mining of the second slice with paste backfilling increased relatively small. And there was only the water flow fractured zone formed in expanded area without mining the first slice. Comparing the overburden failure results in different mining methods, we found that the paste backfilling was useful in inhibiting obvious damage of the overburden failure. The heights of the water flow fractured zone with theoretical calculation were in good agreement with that of scale test and numerical simulations. The paste backfilling used in coalmining under thin bedrock and unconsolidated aquifers provides an effective method to mitigate the overburden failure, and prevent panels from groundwater and sand inrush hazards.

References

Coal Industry Bureau of the PRC (2000) Regulations for setting coal pillar and mining under buildings, water bodies, railways and main roadways. China Coal Industry Publishing House, Beijing (in Chinese)

Mez W, Schauenburg W (1998) Backfilling of caved-in goafs with pastes for disposal of residues. Australasian institute of mining and metallurgy publication series no. 1, In: Proceedings of the 1998 6th international symposium on mining with backfill, Minefill, p 245–248

Wu Zhaoyang (2013) Overburden failure and surface subsidence due to mining with paste backfilling under thick unconsolidated layers and thin bedrock. China University of Mining and Technology, Xuzhou

Zhou Huaqiang, Chaojiong Hou, Sun Xikui et al (2004) Solid waste paste filling for none-village-relocation coal mining. J China Univ Min Technol 33(2):154–158

Florian Köppl, Kurosch Thuro, and Markus Thewes

Abstract

The wear of cutting tools is a major issue in tunneling with Hydroshield TBM in soft ground, because it is a common reason for unplanned downtime. The replacement of cutting tools requires access to the excavation chamber, which is only possible with hyperbaric works or at fixed positions with prearranged grout blocks. In order to improve predictability of the maintenance stops, an empirical prognosis model for the required maintenance stops for changing of cutting tools and the amount of tools was developed. Based on the new Soil Abrasivity Index (SAI), the model helps to estimate distances between maintenance stops and the required amount of cutting tools to be changed. The authors validated the prognosis model based on the original reference projects. The validation lead to an adaption of the prognosis process and individual correction factors in the model itself. The article therefore describes the updated prognosis model.

Keywords

Hydroshield TBM • Soft ground • Excavation • Tool wear • Prognosis

134.1 Introduction

The replacement of cutting tools on Hydroshield TBMs is done with hyperbaric works in the excavation chamber or at fixed positions with grout blocks, in order to maintain face stability during the interventions. The position of the maintenance stops therefore and the obtainable length of the intervals between them are determined by the wear of the cutting tools. At the same time boundary conditions in the projects are often critical for hyperbaric works, particularly under buildings, at low overburden or very high water pressure. Köppl and Thuro (2013) developed an empirical prognosis model, to estimate the distances L_I in m between the maintenance stops I and the number of cutting tools $n_{c,I}$ to be replaced. The model enables foresighted planning, in order to avoid critical areas as described above. Validation of the prognosis model with reference to the original projects used in the data analysis allowed to introduce improvements to the prognosis process and to specify correction factors. The article summarizes the update model.

134.2 Empirical Wear Prognosis Model

134.2.1 Basic Data

The basic data for the prognosis model contain a complete geotechnical data set, as e.g. detailed by Scholz and Wendl (2010), the TBM design, e.g. the cutter head layout and expected values for TBM advance parameters.

F. Köppl (✉)
Herrenknecht AG, Schlehenweg 2, 77963 Schwanau, Allmansweier, Germany
e-mail: koeppl.florian@herrenknecht.de

K. Thuro
Technische Universität München, Arcisstr. 21, 80333 Munich, Germany

M. Thewes
Ruhr-Universität Bochum, Universitätsstr. 150, 44780 Bochum, Germany

For the prognosis process, homogeneous geotechnical sections are formed along the tunnel axis, using the criteria recommended by Köppl and Thuro (2013) and assigned with a whole-numbered index z beginning at the start of the tunnel:

- Constant share of different soil types in the excavation face in % (±10 %)
- Constant thickness of the cover above the tunnel axis in m (±5 m)
- Constant water table above the tunnel axis in m (±5 m).

134.2.2　Estimation of the Cutting Distance S_c

The expected value for the cutting distance $s_{c,e(z)}$ in km of each individual tool on the cutter head within a geotechnical section is estimated using the correlation with the Soil Abrasivity Index $SAI_{(z)}$ which is estimated for each section by Eq. 134.1:

$$SAI_{(z)} = \left(\frac{EQC_{(z)}}{100}\right) \cdot \tau_{c(z)} \cdot D_{60(z)} \qquad (134.1)$$

In Eq. 134.1 $EQC_{(z)}$ [%] is the Equivalent Quartz Content, $D_{60(z)}$ [mm] the grain size where 60 % of all grains are smaller than the given value and $\tau_{c(z)}$ [kN/m^2] the shear strength of the soil, estimated by the Mohr-Coulomb criterion, using the shear parameters of the soil and the vertical primary stress at the tunnel axis $\sigma_{n(z)}$ [kN/m^2]. In Eq. 134.2 h_i [m] is the thickness of the soil layers above the tunnel axis and γ_i [kN/m^3] unit weight, considering the actual dry or saturated conditions:

$$\sigma_{n(z)} = \sum_i h_i \cdot \gamma_i \qquad (134.2)$$

The basic value of the cutting distance $s_{c,b(z)}$ [km] is estimated with the $SAI_{(z)}$ as shown by Köppl and Thuro (2013) for disc cutters (Eq. 134.3) and scrapers (Eq. 134.4):

$$s_{c,b(z)} = 288 + \exp\left(-0.004 \cdot \left(SAI_{(z)} - 1.640\right)\right) \quad (134.3)$$

$$s_{c,b(z)} = 271 + \exp\left(-0.004 \cdot \left(SAI_{(z)} - 1.634\right)\right) \quad (134.4)$$

For disc cutters, $s_{c,b(z)}$ is corrected by the tip width b_{SR} [mm] of the cutter ring. With reference to the most common value for b_{SR} of 19 mm, the correction factor f_b is calculated by (Eq. 134.5):

$$f_b = \frac{b_{SR}}{19} \qquad (134.5)$$

For scrapers, $s_{c,b(z)}$ is corrected by the actual penetration rate $p_{a(z)}$ [mm/rot] of the individual scrapers. Köppl and

Thuro (2013) subdivide this step with two separate factors f_p and f_k, considering the expected penetration rate $p_{e(z)}$ [mm/rot] and the number of identical scrapers ksc per cutting track. Both factors indirectly cover the actual penetration rate $p_{a(z)}$ of the individual scrapers, since $p_{e(z)}$ is split between all identical scrapers on a cutting track (ksc) depending on their angular distance δ_a [°]. The verification of the model proved it to be more appropriate to directly consider $p_{a(z)}$ for correction in Eq. 134.7.

Assuming a symmetrical cutter head layout, the actual penetration rate $p_{a(z)}$ [mm/rot] of a scraper can be roughly estimated by Eq. 134.6:

$$p_{a(z)} = \frac{p_{e(z)}}{k_{sc}} \qquad (134.6)$$

$$f_p = \frac{1}{1.6^{\log_{0.5}\left(\frac{16}{p_{a(z)}}\right)}} \qquad (134.7)$$

The expected values for the cutting distance $s_{c,e(z)}$ for disc cutters and scrapers are calculated by multiplication of the basic value $s_{c,b(z)}$ with the respective factors f_b or f_p. The expected value for the cutting distance $s_{c,e(z)}$ is valid within a defined range of additional influencing factors on the wear of the cutting tools which were qualified, but not quantified in the data analysis. A description of these factors and the respective range is given by Köppl and Thuro (2013).

134.2.3　Estimation of the Maintenance Stops I

For the prognosis process the maintenance stops I are assigned with a whole-number index k in ascending order beginning at the start of the tunnel. The chainage $L_{I,act(k)}$ [m] of the stops $I_{(k)}$ for replacement of cutting tools over the tunnel axis depends on the advance distance $L_{I(k)}$, [m] achieved between the stops. The maximum value $L_{I,max(k)}$ [m] of $L_{I(k)}$ is defined by the wear limits of the tools.

Starting with unworn tools, the maximum achievable advance distance $L_{I,c(k)}$ [m] for each individual cutting tool is estimated by Eq. 134.8 using the expected value of the penetration rate $p_{e(z)}$ [mm/rot] and the track radius r_s [mm].

$$L_{I,c(k)} = \frac{s_{c,e(z)} \cdot p_{e(z)} \cdot 1.000}{2 \cdot \pi \cdot r_s} \qquad (134.8)$$

Considering all cutting tools on the cutter head, the maximum advance distance $L_{I,max(k)}$ of the TBM is given by the minimum value out of all values for $L_{I,c(k)}$:

$$L_{I,max(k)} = \min_c\left(L_{I,c(k)}\right) \qquad (134.9)$$

For the planning of the actual advance distance, $L_{I(k)}$ can be selected lower or equal to $L_{I,max(k)}$ without compromising the wear limits of the cutting tools:

$$L_{I(k)} \leq L_{I,max(k)} \qquad (134.10)$$

Within the section $L_{I(k)}$ each tool performs the partial cutting distance $s_{c(k)}$ [km], which is calculated using the actual penetration rate $p_{e(z)}$ [mm/rot] over $L_{I(k)}$:

$$s_{c(k)} = \frac{L_{I(k)} \cdot 2 \cdot \pi \cdot r_s}{p_{e(z)} \cdot 1.000} \qquad (134.11)$$

Considering the expected value for the cutting distance $s_{c,e(z)}$ [km], the partial utilization factor $e_{c(k)}$ of each cutting tool over $L_{I(k)}$ is calculated by:

$$e_{c(k)} = \frac{s_{c(k)}}{s_{c,e(z)}} \qquad (134.12)$$

The advance sections $L_{I(k)}$ are strung together consecutively from the start of the tunnel. The actual chainage $L_{I,act(k)}$ [m] of each maintenance stop $I_{(k)}$ is calculated by accumulation of all sections $L_{I(k)}$ excavated until $I_{(k)}$:

$$L_{I,act(k)} = \sum_{1}^{k} L_{I(k)} \qquad (134.13)$$

The cumulative utilization factor $e_{c,act(k)}$ of each tool at a stop $I_{(k)}$ is calculated by accumulation of the partial utilization factors $e_{c(k)}$ in the advance sections $L_{I(k)}$:

$$e_{c,act(k)} = \sum_{L_{a(k)}}^{L_{I,act(k)}} e_{c(k)} \qquad (134.14)$$

Cutting tools may go through more than one advance section $L_{I(k)}$, so the lower constraint of the sum in Eq. 134.14 is set at $L_{a(k)}$ which equals the chainage $L_{I,act(k)}$ of the stop $I_{(k)}$, where the individual tool was assembled on the cutter head.

The process in Eqs. 134.8–134.14 supposes, that the maintenance stops $I_{(k)}$ and $I_{(k+1)}$ are located in the same geotechnical section, represented by the expected values for $s_{c,e(z)}$ and $p_{e(z)}$ in Eqs. 134.8 and 134.12. In case $L_{I(k+1)}$ crosses a boundary between geotechnical sections, the process in Eqs. 134.8–134.14 needs to be subdivided, considering different values for $s_{c,e(z)}$ and $p_{e(z)}$ in the legs of the different geotechnical sections.

134.2.4 Estimation of the Tool Changes n_c

Starting at a given maintenance stop $I_{(k)}$ the process in Eqs. 134.8–134.10 allows to plan the advance distance $L_{I(k}$

$_{+1)}$ to the next stop $I_{(k+1)}$. The chainage $L_{I,act(k+1)}$ of $I_{(k+1)}$ and the cumulative utilization factor $e_{c,act(k+1)}$ result from Eqs. 134.11–134.14, using $L_{I(k+1)}$.

The calculation of the maximum achievable advance distance $L_{I,c(k)}$ [m] in Eq. 134.8 starting from the stop $I_{(k)}$ assumes unworn tools, independent of the actual cumulative utilization factor $e_{c,act(k)}$. Consequently Eq. 134.14 may produce values for $e_{c,act(k+1)}$ greater than 1 for individual tools. For these tools the wear limit would be exceeded during the planned advance distance $L_{I(k+1)}$, leading to potential damage due to excessive wear. Therefore they have to be changed at the actual stop $I_{(k)}$, in order to enable the selected advance distance $L_{I(k+1)}$. Accordingly the general criterion for tool changes during a maintenance stop $I_{(k)}$ can be formulated as:

$$e_{c,act(k+1)} > 1 \qquad (134.15)$$

Following the criterion in Eq. 134.15, the number of cutting tools $n_{c,I(k)}$ to be changed during each maintenance stop $I_{(k)}$ can be accumulated over all cutting tools c on the cutter head by:

$$n_{c,I(k)} = \sum_{c} e_{c,act(k+1)} > 1 \qquad (134.16)$$

The prognosis process focuses on planning of the advance distances $L_{I(k+1)}$. The criterion for replacement of cutting tools in Eq. 134.15 is designed to enable the selected value for $L_{I(k+1)}$. Consequently the criterion may also effect preventive tool changes at values of $e_{c,act(k)}$ lower than 1. This relation reflects the higher impact of the stops $I_{(k)}$ on TBM advance compared to $n_{c,I(k)}$. It also implies that any change in the advance distances $L_{I(k+1)}$ effects on $n_{c,I(k)}$ and vice versa.

134.2.5 Adaption Algorithm

The prognosis model as detailed in Eqs. 134.1–134.16 does not consider the given conditions of the project regarding accessibility of the excavation chamber. In order to ensure realistic results it is mandatory to check these conditions at each planned chainage $L_{I,act(k)}$ of the maintenance stops $I_{(k)}$. In case the chainage $L_{I,act(k)}$ of a stop $I_{(k)}$ is located in a critical section, the model allows for adaption by:

- Variation of the basic data (e.g. layout of the tools or penetration rate p_e).
- Selection of different values for $L_{I(k)}$ in Eq. 134.10.

The variation of theses parameters effects the chainage of all maintenance stops $I_{(k)}$. It is therefore recommended to do the adaption in small iterative steps. The same process may also be used to analyze the propagation of variances of the basic data in the model by developing different prognosis scenarios.

134.3 Conclusion

The prognosis model provides a comprehensive method to estimate the required maintenance stops $I_{(k)}$ for Hydroshield TBM in soft ground. This method can be effectively used to reduce the impact of unplanned demand for TBM maintenance, especially in projects with complex geotechnical conditions and in densely populated areas. Thus the overall impact of this tunneling method on the project environment may be reduced to a minimum already in the planning stage.

The prognosis elaborated in the planning stage of a project requires follow up during the advance phase. Primarily to validate the assumptions in the prognosis, but also for comprehensive documentation of additional data for development of the prognosis model, as for example demonstrated by Wendl et al. (2010), Düllmann et al. (2013) and Hollmann et al. (2013).

References

Düllmann J, Hollmann F, Thewes M, Alber M (2013) Analysis of soil-mechanic-interactions (Part 1): processing of TBM-machine-data and extraction of excavation-specific data. In: Proceedings of the EURO:TUN 2013. Aedificatio Publishers, Freiburg, pp 621–634

Hollmann F, Düllmann J, Thewes M, Alber M (2013) Analysis of soil-mechanic-interactions (Part 2): influences on the excavation-specific data of TBM-machine data. In: Proceedings of the EURO: TUN 2013. Aedificatio Publishers, Freiburg, pp 635–648

Köppl F, Thuro K (2013) Cutting tool wear prognosis and management of wear related risks for Hydroshield TBM in soft ground. In: Proceedings of the 18th ICSMGE. Presses du Ponts, Paris, pp 1739–1742

Scholz M, Wendl K (2010) Geological aspects of slurry shield drives. In: Proceedings of the 11th IAEG congress. CRC Press, London, pp 3507–3513

Wendl K, Scholz M, Thuro K (2010) A new approach to engineering geological documentation of slurry shield drives. In: Proceedings of the 11th IAEG congress. CRC Press, London, pp 3827–3834

Risk and Mitigation of the Large Landslide of Brindisi di Montagna

135

Giuseppe Spilotro, Filomena Canora, Roberta Pellicani, and Francesco Vitelli

Abstract

The *Brindisi di Montagna Scalo* landslide is located in Basilicata region (Italy), about 18 km south-east of Potenza. It consists on an active earth-flow with a longitudinal extension of about 700 m. The accumulation zone extends till the Basento's riverbed (on the left side), which is partially obstructed. This area is periodically fed with debris or mud moving along the flow channel, due to both the reactivations of the earthflow along the landslide channel caused by wintry rainfalls and the retrogression of the crown towards upstream and deconstruction of collapsed soil in different parts of the landslide body. The risk induced by this earth flow derives from the presence, on the right bank of Basento river, of a railway line and, a little further away, of the state road 407 "Basentana". The aim of this work is the analysis of the possible design solutions in order to mitigate the risk. The assessment of risk mitigation measures for the *Brindisi di Montagna Scalo* landslide was differentiated for the three main geomorphological zones of the landslide: alimentation area, landslide channel and accumulation zone.

Keywords

Landslide • Risk • Mitigation

135.1 Introduction

The *Brindisi di Montagna Scalo* landslide consists on an active earth-flow with can be classified as a "rotational slide-flow" (Cotecchia et al. 1986; Cruden and Varnes 1986; Bentivenga et al. 2006). Basically, it is a flow, deriving from the toe of an existing terrace of rotational landslide affecting Red Flysch formation, and it is located within a pre-existing watershed in Varicolored Clays formation.

G. Spilotro · R. Pellicani (✉)
Department of European and Mediterranean Cultures,
University of Basilicata, Matera, Italy
e-mail: pelliro@libero.it

F. Canora
School of Engineering, University of Basilicata, Potenza, Italy

F. Vitelli
Freelance Geologist, Potenza, Italy

The instability of the area is related to the morphology of the slope, which is steep where Red Flysch outcrops and becomes less steep where Varicolored Clays outcrop.

The risk induced by the *Brindisi di Montagna* earth flow derives from the presence, on the right bank of Basento river, of a railway line and, a little further away, of the state road 407 "Basentana" (Fig. 135.1). The erosion of the dam, created by the landslide toe into the riverbed, may cause the outflow of significant amount of water and debris downstream. Along the slope, the landslide has already damaged a provincial road.

In the past years, gabions and retaining walls on piles were realized, on the left bank of the river, in order to contain the landslide toe. Subsequently, part of the retaining wall was damaged due to a reactivation of the earth flow, causing the mobilization of debris towards the riverbed and the consequent restriction of the outflow section of Basento (Fig. 135.2). Because of this, a reservoir has been created immediately upstream of the landslide dam. At the section of

Fig. 135.1 Accumulation area of the landslide occluding Basento riverbed

Fig. 135.2 Basento River occluded by landslide debris and parts of existing retaining wall

Basento blocked by landslide debris, the river flow has a higher velocity and, therefore, its erosive capacity increases.

In order to reduce the risk induced by the landslide to the infrastructures, located near the toe, the evolutions of landslide toe in relation to the groundwater income from the rear crown area, to the rainfalls and to the river floods have been analyzed.

Some floods, in February and March of the last year, produced an increase of the river level up to 1.5 m above the crown of the gravity wall retaining the railway embankment,

removing the soil on the back of the wall and triggering instability processes at the toe of the same embankment.

135.2 Measures for Risk Mitigation

The aim of this work is the analysis of the possible design solutions in order to mitigate the risk. In general, the mitigation measures aim, on the one hand, to stabilizing the landslide phenomenon, in order to reduce the retrogression of the crown and the contribution of debris to the accumulation zone; on the other, to the protection of the infrastructures located near the landslide toe, on the right side of Basento river, by realizing engineering structures able to dispose safely the flood flows, in case of severe obstruction of Basento's riverbed.

The assessment of risk mitigation measures for the *Brindisi di Montagna Scalo* landslide was differentiated for the three main geomorphological zones of the landslide: alimentation area, landslide channel and accumulation zone.

The alimentation area develops in the "Red Flysch" formation and has a lobed-shape like a fan, with different minor scarps within the landslide body. The main scarp is located at 670 m a.s.l. and has a total width of about 500 m. In this area little landslide ponds and accumulations of saturated soil are present. The alimentation area is also characterized by the presence of groundwater which feeds the landslide basin. For this reason, in this area the main mitigation measure consists in avoiding the groundwater and surficial water feeding of the crown area by means of a drainage system, that intercepts the groundwater and is constituted by draining panels positioned transversely to the landslide crown and connected to a deep well with automatic pumping system. It is also needed to intercept the superficial waters with a hydraulic enclosure, realized in the stable area (upstream of the main scarp) through channels. Finally, in order to remodel and regularize the edge of the crown it is possible to use soil nailing, micropiles, gabions, etc. The main problem connected to this type of drainage system is the durability at long time within landslide body constituted by fine graded terrain.

In correspondence of the landslide cannel, the mitigation techniques are generally influenced by the thickness of the landslide debris. As in this case it is about 6–7 m, the suggested mitigation technique can consist of rows of large diameter piling, with piles not connected in head, and draining trenches for the drainage of surface and deep waters.

The stabilization of the accumulation zone of the landslide aims to make the riverbed of Basento stable, even in conditions of overflowing of the river. In this area, the protection of the railway embankment is a priority, as it is in complete erosion due to the periodic flooding of the river.

The proposal mitigation measures have been the following (Fig. 135.3):

- Removal of the landslide debris, which block the riverbed of Basento, from the accumulation zone.
- Realization of a diaphram, on the left side of the river, in order to reshape the stretch of the riverbed, upstream of the section blocked by the landslide toe.
- Realization of a diaphram, on the right side of the river and at a distance of about 10 m from the existing gravity wall, composed by piles of a diameter of 600 m and a length of 14 m, with a wall at the pile top of a height of about 3 m and longitudinal extension of 67 m.
- Filling with selected draining material between the existing wall and the diaphram.

Fig. 135.3 Cross section of the area near the landslide toe with the structural measures for mitigating risk
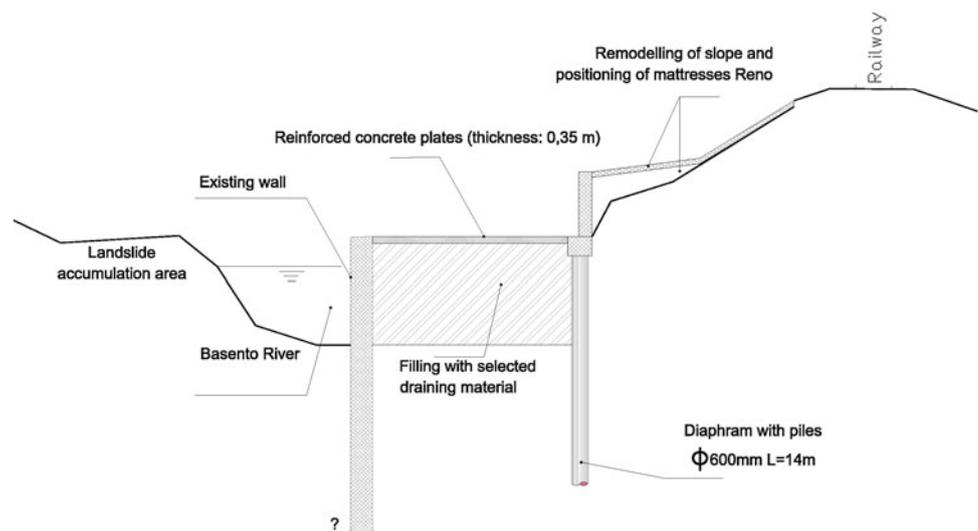
- Positioning of reinforced concrete plates, of a thickness of about 35 cm, connecting the top of the existing gravity wall and the top of the piles of the diaphram.
- Positioning of Reno mattresses from the top of the new wall to the railway line, for the erosion control of the embankment.

135.3 Conclusions

As risk controlling is the process of measuring or assessing risk and then developing strategies to manage the risk, in addition to the design of mitigation measures, the following monitoring program has been recommended:

- Monitoring of the hydraulic flow through the Basento's section blocked by the landslide.
- Monitoring of the landslide superficial displacements at the alimentation and accumulation zones by means of GPS localizators, specifically designed for this purpose.

- Monitoring of the landslide deep displacements by means of TDR measurements.
- Monitoring of groundwater by means of piezometers.

References

Bentivenga M, Grimaldi S, Palladino G (2006) Caratteri geomorfologici della instabilità del versante sinistro del fiume Basento interessato dalla grande frana di Brindisi di Montagna Scalo (Potenza, Basilicata). Giornale di Geologia Applicata 4:123–130

Cotecchia V, Del Prete M, Federico A, Fanelli GB, Pellegrino A, Picarelli L (1986) Studio di una colata in formazioni strutturalmente complesse presso Brindisi di Montagna Scalo (PZ). Associazione Geotecnica Italiana-Atti del XVI convegno Nazionale di Geotecnica, pp 14–16 maggio, Bologna

Cruden DM, Varnes DJ (1986) Landslide types and processes. In: Landslides: investigation and mitigation, Turner AR and Schuster RL (ed) Sp. Rep. 247, Transportation Research Board, National Research Council, National Academy Press, Washington D.C., pp 36–72

Environmental Impact of a Motorway Tunnel Project on an Important Karst Aquifer in Southern Latium Region: The Case of Mazzoccolo Spring (Formia, Italy)

Giuseppe Sappa, Flavia Ferranti, and Sibel Ergul

Abstract

Due to the heavy traffic problems in Formia downtown, a motorway project was designed to reduce traffic congestion in the fastly growing city. The proposed motorway passes over one regionally an important karst aquifer feeding Mazzoccolo spring, in the southeast part of Latium Region. This paper deals with the analysis of the most important environmental impacts on this vulnerable karst aquifer and, as a consequence, on groundwater coming out form the Mazzoccolo Spring, which feeds one of the most important drinking water supply network in South Latium Region. A multisystem approach has been applied for vulnerability analysis using SINTACS method. The climatic, topographic, geomorphological and hydrogeological data and field investigations of previous works has been employed. On the other hand, this approach was also evaluated by geochemical and isotope tracers techniques of groundwater samples for the identification of environmental impacts. According to the proposed project, the Motorway tunnel has a significant environmental impact, on the vulnerability of the karst aquifer and hence, on the water supply networks. Thus, based on these analyses the highway investment strategy adapted to Variant of the SS 7 (Appian Way) project should ensure the protection of groundwater resources designing a new variant route avoiding the construction of Mola Mountain tunnel.

Keywords

Karst aquifer • Vulnerability • Protection • Infrastructure project

136.1 Introduction

The preservation and protection of groundwater is a topic of increasing technical relevance, due to the widespread of infrastructure designs for human settlements and technological development, which makes today executable any kind of civil work, regardless of the environmental impacts. On the other hand, water demand is increasing all over the world, and also in the south part of Latium Region, Central Italy, groundwater is the most important resource of drinking

G. Sappa (✉) · F. Ferranti · S. Ergul
DICEA, Department of Civil, Building and Environmental Engineering—Sapienza, University of Rome, Via Eudossiana 18, 00186, Rome, Italy
e-mail: giuseppe.sappa@uniroma1.it

and agricultural purposes (Casa et al. 2008; Sappa et al. 2012). In this region, Mazzoccolo is the most important karst spring that feeds drinking water supply networks of Formia and other communities with a rate of 900 l/s (Ialongo 1983). For more than a decade, due to heavy traffic problems on the motorway SS 7—Appia, Formia (LT), a new design of a tunnel, passing thorough Mola Mountains, has been discussed. Besides, due to increasing urbanization, the downtown of Formia city has already moved to close to the catchment area of Mazzoccolo spring. Currently, because of the heavy traffic problems in SS 7 (Appia), close to the center of Formia town, a variant motorway project was proposed which has to be built far from the urban area. The performed designed works for the proposed variant will have several negative impacts on the groundwater systems both quantitatively and qualitatively. In the proposed project solutions, the possible interactions between motorway tunnel

and the karst aquifer that feeds the Mazzocolo spring seem to be not considered in details. The designed tunnel, whose total length is 4 km has the potential to have an adverse effect on the karst aquifer. Here we try to suggest appropriate methodological approaches in the aim of highlighting the adverse environmental impacts on Mazzoccolo spring and some preliminary indications for designing a different, less impacting, layout of the motorway. Thus, the application of a vulnerability mapping as a multitracing approach (Civita 1998) was considered for the protection of this important groundwater system suggesting more detailed development of the design to reduce negative impacts and save costs. In the present work, the appropriate methodological approaches were applied for the protection and preservation of Mazzoccolo spring where groundwater emerges from the karst aquifer. Based on previous studies, for the identification of environmental impacts on the groundwater, data from different locations and field observations were employed. The new design solutions for proposed variant should ensure the reduction of potential negative impacts on the groundwater systems in the area, considering the interactions between the Mola Mountain tunnel and fragile karst aquifer.

136.2 Geological and Hydrogeological Setting

Mazzoccolo spring take place on the base of Pliocene conglomerates, which is tectonically in contact with the limestones. This spring is located at an altitude of 11.5 m above sea level, where the area is more fractured due to the intersection of numerous faults (Ialongo 1983). Mazzoccolo spring is caught at an elevation of 7.50 m by a drainage tunnel, whose layout is generally parallel to the slope (Fig. 136.1). The morphological setting of the study area is characterized by conglomeratic limestone on the hills (Mola Mountain), surrounded by clayey-arenaceous and alluvial deposits of debris (Di Nocera 1983). The abundance of groundwater is due to the permeability of the limestone (high fractured and deep karst), which stores a significant quantity of rainwater feeding perennial springs. The Pliocene conglomerates are strongly cemented, while the contacts with different formations show highly fractured structures. The karstified limestones stored the water and discharge Mazzoccolo spring and also some smaller pools occur to the west part. The underground reservoir of Mazzoccolo spring was formed by high permeable limestones for karstic fractures outcropping to the N–W and N–NW of the spring (Di Nocera 1983), while the bottom is composed of impermeable dolomites underlying the West part of the limestones.

136.3 Project Description

The preliminary design of the variant of the SS 7-Appia provides, bypassing the town of Formia, the excavation of a motorway tunnel in Mola Mountain with 4,578 m length as represented in Fig. 136.2. According to the proposed design, tunnel layout has a convex trend with respect to the surface and presents the highest elevation at about 119 m a.s.l. in a central position between the two entrances. The lowest planimetric distance between the tunnel axis and the Mazzoccolo group (springs-wells) is of 1 km, while the minimum height difference between the base of the gallery and the springs is of 80 m (Manfredini 1984).

136.4 Results and Conclusions

The present work deals with the environmental impact assessment of the designed motorway tunnel on karst aquifer, feeding Mazzoccolo spring, employing SINTACS method (Civita 1998). The hydrogeochemical monitoring activities were carried out, from May 2006 to January 2007, in the framework of this study. The stable isotopes of ^{2}H and ^{18}O in groundwater samples provided some important information about aquifer active recharge areas, aquifer morphology, spring discharge areas and the origin of rainfalls (Fig. 136.3). The elevation of the recharge area ranges between 600 and 800 m a.s.l. The geochemical analysis showed that all the sampled waters belong to the Ca-HCO$_3$ facies, reflecting the characteristics of the carbonate karst aquifer of western Aurunci Mts. It was also observed that one sample, taken in August, show very low mineralization with low electrical conductivity and a high pH value (EC = 28 μS/cm and pH $\sim$ 9). For the evaluation of this phenomenon, the recharge elevation data was employed. Two different hypotheses have been developed and each based on a specific groundwater circuit. The pH value is related to scarce precipitations occurred in summer assuming that the source may return the "purging" of a previous meteoric recharge. However, considering the nature of karst basin, the low EC and the high value of pH in groundwater, taken in August, may be related to the presence of some sinkholes which are able to quickly convey the meteoric precipitation into the aquifer. In fact, between Ruazzo Mountain and the Mazzoccolo spring some dolines and ponors were found (Civita 1998).

The vulnerability analysis, carried out by SINTACS method (Fig. 136.4), shows that the karst aquifer feeding the Mazzoccolo spring has a high vulnerability, while presents very low capacity of groundwater protection.

Fig. 136.1 Drainage gallery of Mazzoccolo spring
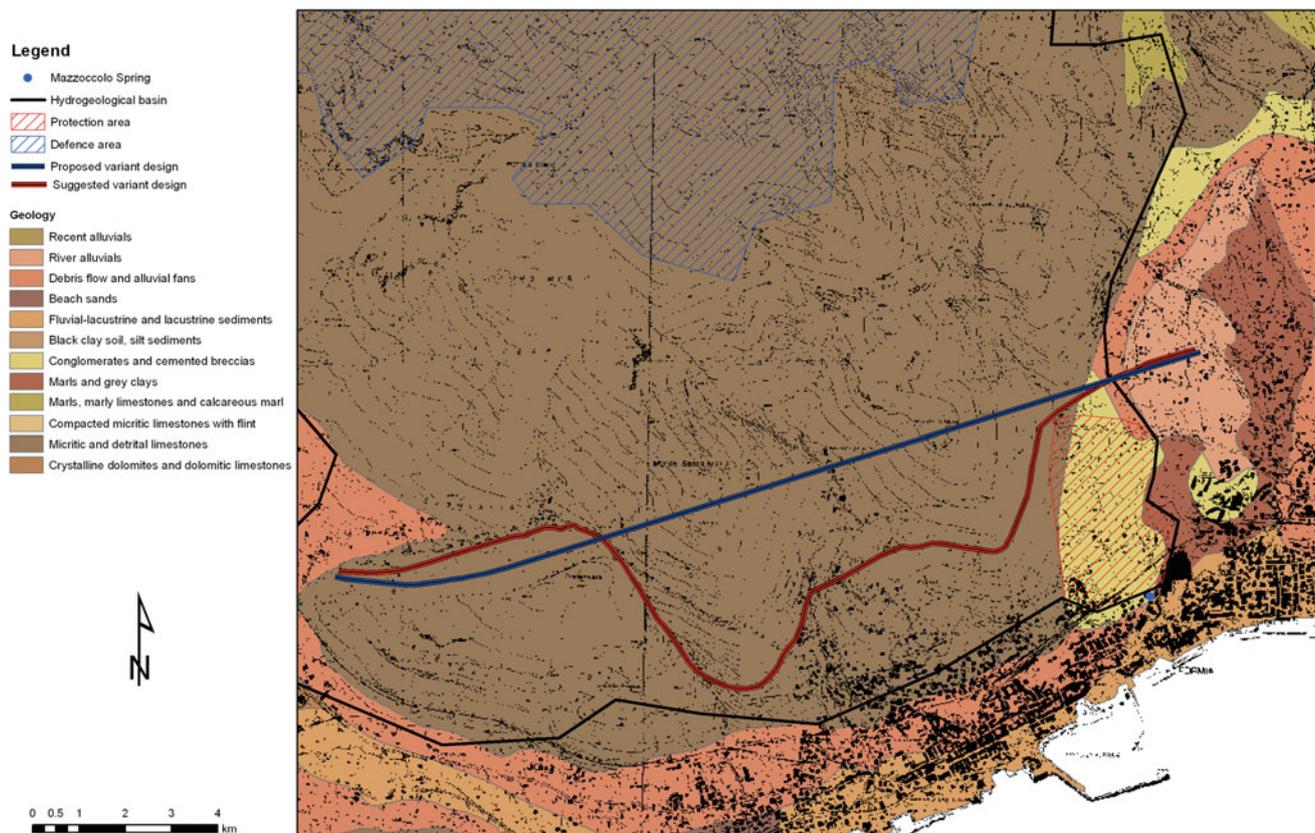
Fig. 136.2 Proposed variant design

According to the current knowledge, it is not possible to evaluate if the proposed design of Mola Mountain tunnel, located perpendicularly at the flow lines of the karst aquifer feeding the Mazzoccolo spring, will be held in the saturated or undersaturated zones of the aquifer. If the tunnel excavation passes through unsaturated zone of the aquifer, in any case it will meet tectonically fractured karstic zones draining the infiltrated water to the saturated zone. In the case of the saturated zone, the elevation difference between the base of the tunnel and Mazzoccolo spring may cause a simultaneous rise of the groundwater table of some dozen of meters during excavation (Civita 1998). These processes will have several negative impacts on the groundwater systems both quantitatively and qualitatively. Anyway previously studies, carried on in the late 70s (Civita 1998), have not clarify the hydrogeological system which was a useful tool for the evaluation of interactions between motorway tunnel

excavation and vulnerable aquifer. Thus, in this study the geochemical and isotopic characterization of groundwater give us an important information about the vulnerability of this karst aquifer and hydrogeological regime of the area which contributes the environmental assessment strategies. On the base of these results, Mazzoccolo spring is partially fed by short residence time groundwater, with a short self-purification of rainwater effect due to the interception of karst cavities. At the same time, the long residence times lead us to consider the high vulnerability of Mazzoccolo spring without giving information about the purging of previous recharge. In conclusion, before to start the realization of the proposed project, it is necessary to perform some artificial tracer tests and a careful geomorphological investigation to identify the existing karst cavities with a detailed geostructural modeling. Consequently, we suggest a different motorway design, involving a superficial route,

Fig. 136.3 Infiltration areas of
Mazzoccolo spring
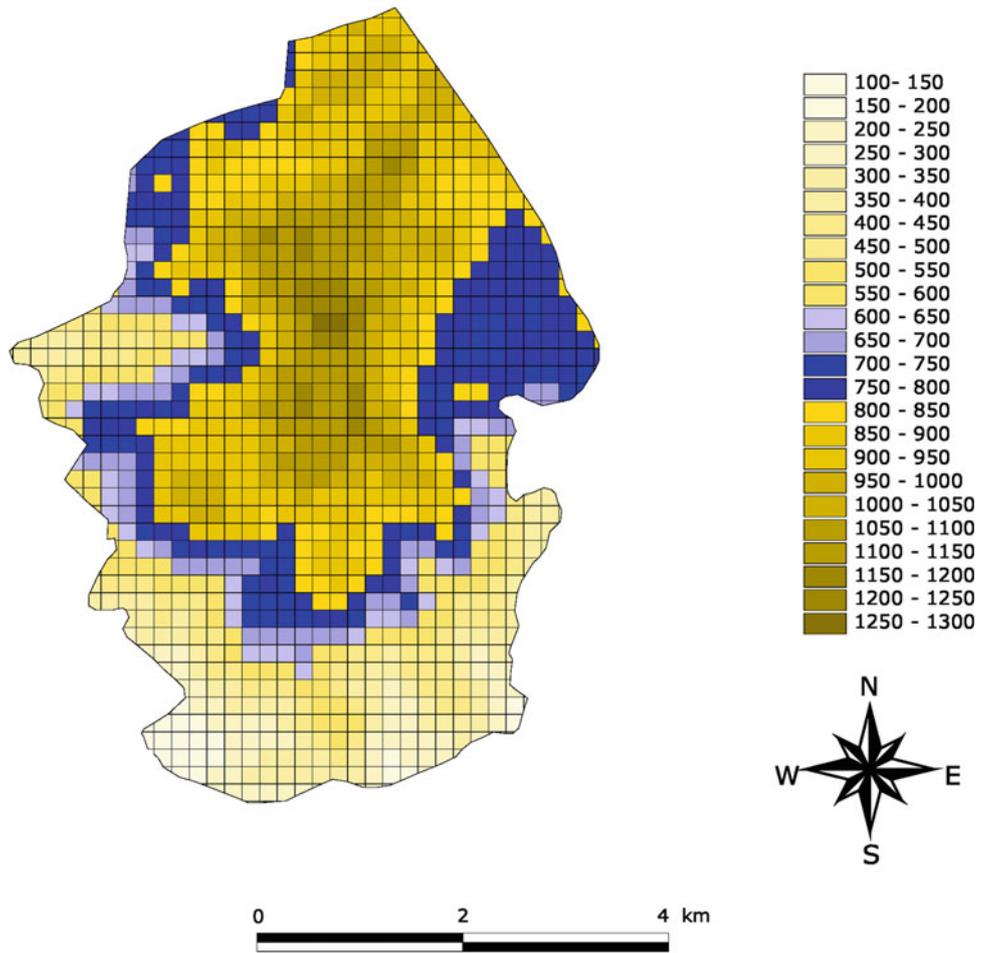
Fig. 136.4 Vulnerability map of the karst aquifer feeding the Mazzoccolo spring
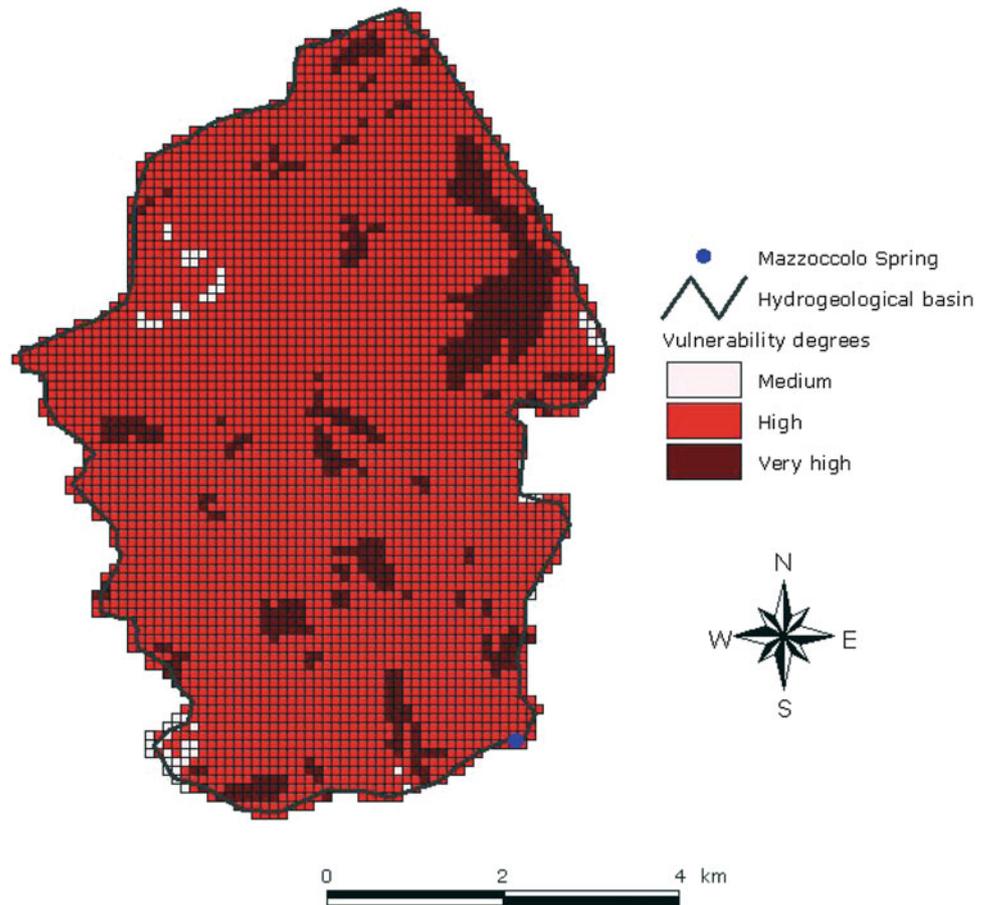
even longer than the previous one, avoiding the construction of Mola Maountain tunnel and involving high self-purification capacity soils.

References

Casa R, Rossi M, Sappa G, Trotta A (2008) Assessing CropWater demand by remote sensing and GIS for the Pontina Plain, Central Italy, water resources Management, September 2008

Civita M. (1998) Parere tecnico sui possibili impatti della variante pedemontana alla SS 7 (Appia) sull'acquifero che alimenta le sorgenti Mazzoccolo in Formia (Latina). Comune di Formia (Provincia di Latina)

Di Nocera S. (1983) Studio idrogeologico Sorgente Mazzoccolo. Relazione geologica. Amministrazione comunale di Formia

Ialongo N (1983) Studio idrogeologico Sorgente Mazzoccolo. Relazione idrogeologica. Amministrazione comunale di Formia

Manfredini M. (1984) Studio sulle caratteristiche idrogeologiche e sui problemi di protezione della Sorgente Mazzoccolo. Comune di Formia

Sappa G, Barbieri M, Ergul S, Ferranti F (2012) Hydrogeological conceptual model of groundwater from Carbonate aquifers using environmental isotopes (^{18}O, ^{2}H) and chemical tracers: A case study in Southern Latium Region Central Italy. J Water Res Prot 4:695–716

Properties and Behaviour of Weak and Complex Rock Masses in Major Engineering Projects

Convener Dr. Vassilis Marinos—*Co-conveners* George Stoumpos, Petros Fortsakis

Numerical analysis and computational methods in geotechnical engineering are fields where great progress has been achieved. However, in the case of weak and complex rock masses, the results still involve uncertainties due to the difficulties in the reliable estimation of intact rock properties and the realistic quantification of rock mass properties and behaviour. The special features of these rock masses regarding both their structure and lithology impose a more specialized research. The weak rock masses could be cases with very low intact rock properties, highly tectonized or/and weathered rock masses, rock masses with members of low strength and/or inherent heterogeneity. This session may contain papers on weak and complex rock masses, regarding in situ and laboratory testing, characterization, geotechnical classification, design properties, behaviour, support measures and performance of the construction method adopted in the design approach according to the engineering project.

Rock Mass Quality Rating (RMQR) System and Its Application to the Estimation of Geomechanical Characteristics of Rock Masses

Ömer Aydan, Resat Ulusay, and N. Tokashiki

Abstract

In this study, a new rock mass quality system designated as Rock Mass Quality Rating (RMQR) is explained and its application to the estimation of geomechanical properties of rock masses is described. First, a brief outline of the input parameters of RMQR and their ratings are given. Then the unified formula proposed by the first author is used for estimating the rock mass properties as a function of intrinsic properties of intact rock material and they are compared with the results of the in situ tests carried out in Japan and those estimated from some other empirical relationships developed by some researchers.

Keywords

RMQR • Rock mass • Intact rock • Geomechanical properties • Empirical relation

137.1 Introduction

The qualitative description of rock masses by means of classification systems and subsequent correlation to establish engineering quantities has become one of the most challenging topics in rock engineering. However, many available rock classification systems have some repetitions such as RQD and discontinuity spacing resulting in essence doubles the influence of the spacing of discontinuities on the final rating. In addition, although the effect of water particularly on water-sensitive rocks plays an important role in decrease of their geo-mechanical properties, this effect is not adequately considered in the existing rock mass classification systems. By considering the scale effect for rock masses, laboratory testing on rock masses is not always easy and is very cumbersome. For this reason, in situ tests are generally preferred. But in situ tests are directly time consuming, expensive and quite cumbersome to conduct. Therefore, the recent tendency is to obtain rock mass properties from the utilization of properties of intact rock and rock classification indexes, which have some drawbacks. In this study, a new rock mass rating system designated as Rock Mass Quality Rating (RMQR) proposed recently by the authors (Aydan et al. 2013) is explained. Geomechanical properties of rock masses are estimated from the utilization of properties of intact rock and RMQR as one of applications of this system.

137.2 Rock Mass Quality Rating (RMQR)

The parameters associated with discontinuities could be the discontinuity set number (DSN), discontinuity spacing (DS; spacing of dominant discontinuity set, mainly thoroughgoing discontinuity set) and discontinuity condition (DC). The weathering of rocks causes the weakening of bonds and decomposition of constituting minerals into clayey materials. The alteration process may act on rock mass in a positive or negative way. As the intact rock is one of the important

Ö. Aydan
Tokai University Shizuoka, Shizuoka, Japan
e-mail: aydan@scc.u-tokai.ac.jp

R. Ulusay (✉)
Department of Geological Engineering, Hacettepe University, Ankara, Turkey
e-mail: resat@hacettepe.edu.tr

N. Tokashiki
Department of Civil Engineering, Ryukyu University, Okinawa, Japan

elements influencing the mechanical response of rock masses, weathering and/or the negative action of hydrothermal alteration may be accounted as the degradation degree (DD) of intact rock. There are also cases, that some rocks may absorb groundwater electrically or chemically, resulting in the drastic reduction of material properties and/or swelling. In addition to seepage condition of groundwater (GWSC), the water absorption characteristics of rocks (GWAC) should also be taken into account.

RMQR has six basic parameters, which provides rating of each parameter, and ranges between 0 and 100 (Table 137.1). If detailed surveys on the conditions of discontinuities are carried out, a more detailed rating is necessary for characterization of rock discontinuities. For the evaluation of discontinuity condition from detailed surveys, Table 137.2 is recommended together with roughness concept of surface profiles by ISRM (2007). RMQR could be related to the well-known two rock mass rating systems, RMR (Bieniawski 1989) and Q-system (Barton et al. 1974), through some relations given in Fig. 137.1. It should be noted that the value of RMR is generally less than the value of RMQR. One reason may be such that the RMQR includes the effect of water absorption, which is not counted in RMR. The other reason may be the exclusion of intact rock strength in RMQR.

137.3 Relation Between Rock Mass Properties and RMQR

Aydan et al. (2013) provided relations for six different mechanical properties of rock mass using the proposed relation by Aydan and Kawamoto (2000) using RMQR as an independent parameter. It is given in the following form for any mechanical properties of rock mass in terms of those of the intact rock.

$$* R_{DC} = R_{DCA} + R_{DCI} + R_{DCR}$$

$$\alpha = \alpha_0 - (\alpha_0 - \alpha_{100}) \frac{RMQR}{RMQR + \beta(100 - RMQR)}$$

(137.1)

where α_0 and α_{100} are the values of the function at RMQR = 0 and RMQR = 100 of property α, β is a constant to be determined by using a minimization procedure for experimental values of given physical or mechanical properties. When a representative value of RMQR is determined for a given site, geomechanical properties of rock mass can be obtained using Eq. (137.1) together with the values of constants given in Table 137.3 and the values of intact rock for a desired property.

Table 137.1 Classification parameters and their ratings for rock mass quality rating (RMQR)[a]

Degradation degree (DD)	Fresh	Stained	Slight degradation	Moderate degradation	Heavy degradation	Decomposed
Rating (R_{DD})	15	12	9	6	3	1 − 0
Discontinuity set number (DSN)	None (solid or massive)	One set plus random	Two sets plus random	Three sets plus random	Four sets plus random	Crushed or shattered
Rating (R_{DSN})	20	16	12	8	4	1 − 0
Discontinuity spacing (DS) or RQD (%)	None or DS ≥ 24 m	24 > DS ≥ 6 m	6 > DS ≥ 1.2 m	1.2 > DS ≥ 0.3 m	0.3 > DS ≥ 0.07 m	0.07 m > DS
	100			100 > RQD ≥ 75	75 > RQD ≥ 35	35 > RQD
Rating (R_{DS})	20	16	12	8	4	1 − 0
Discontinuity condition (DC)	None	Healed or intermittent	Rough	Relatively smooth and tight	Slickensi-ded with thin infill or separation (t < 5 mm)	Thick fill or separation (t > 10 mm)
Rating (R_{DC})	30	26	22	15	7	1
Groundwater seepage condition (GWSC)	Dry	Damp	Wet	Dripping	Flowing	Gushing
Rating (R_{GWSC})	9	7	5	3	1	0
Groundwater absorption condition (GWAC)	Non-absorptive	Capillarity or electrically absorptive	Slightly absorptive	Moderately absorptive	Highly absorptive	Extremely absorptive
Rating (R_{GWAC})	6	5	4	3	2	1-0

[a] RMQR = R_{DD} + R_{DSN} + R_{DS} + R_{DC} + R_{GWSC} + R_{GWAC}

Table 137.2 Ratings for sub-parameters of discontinuity condition excluding "None" and "Healed or intermittent" classes

Aperture or separation		None or very tight, <0.1 mm	0.1–0.25 mm		0.25–0.5 mm	0.5–2.5 mm	2.5–10 mm	>10 mm
Rating (R_{DCA})*		6	5		4	3	2	1 − 0
Infilling		None	Surface staining only		Thin coating <1 mm	Thin filling 1 < t<10 mm	Thick filling 10 < t < 60 mm	Very thick filling or shear zones 60 mm < t
Rating (R_{DCI})*		6	5		4	3	2	1-0
Rough-ness	Descriptive	Very rough	Rough		Smooth undulat-ing	Smooth planar	Slicken-sided	Shear band/zone
	ISRM (2007) profile No.	10	9	8	7	6	5	4	3	2	1 − 0
Rating (R_{DCR})*		10	9	8	7	6	5	4	3	2	1 − 0

Fig. 137.1 The relations between **a** RMQR and RMR, and **b** RMQR and Q
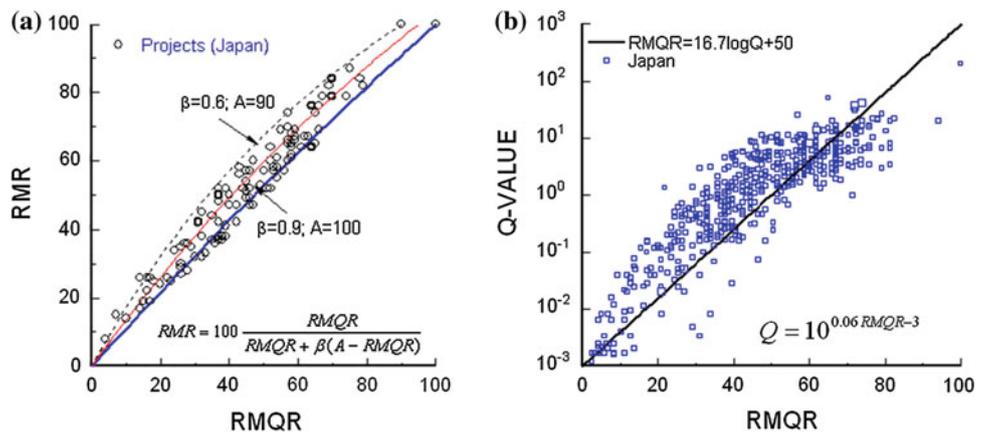
Table 137.3 Values of α_0, α_{100} and β for various properties of rock mass

Property (α)	α_0	α_{100}	β
Deformation modulus	0.0	1.0	6
Poisson's ratio	2.5	1.0	0.3
Uniaxial compressive strength	0.0	1.0	6
Tensile strength	0.0	1.0	6
Cohesion	0.0	1.0	6
Friction angle	0.3	1.0	1.0

The empirical relations for normalized properties presented in the previous section are compared with the experimental results from in situ tests carried out at various large projects in Japan (Fig. 137.2). The experimental results on normalized elastic modulus of rock mass are closely represented by Eq. (137.1) together the values given in Table 137.3 and they are clustered around the curve with the value of coefficient β as 6.

Figure 137.3 compares the experimental results on various rock masses ranging from igneous rocks to sedimentary rocks with empirical relations for normalized uniaxial compressive strength (UCS) and tensile strength of rock masses by those of intact rock. The UCS of rock masses plotted in this figure are mostly obtained using rock shear test together with Mohr-Coulomb failure criterion. The experimental results generally confirm the empirical relation given in Eq. (137.1).

In literature, there is almost no in situ experimental procedure or experimental results for the tensile strength of rock mass to the knowledge of the authors. The authors (Aydan et al 2013) utilized back-analysed data on the stable and unstable (failed) cliffs using a theory based on the cantilever theory and fitted the inferred tensile strength of the rock mass normalized by that of intact rock using Eq. (137.1).

Fig. 137.2 Comparison of experimental data for **a** deformation modulus and **b** Poisson's ratio of rock mass with Eq. 137.1 with the parameters given in Table 137.3
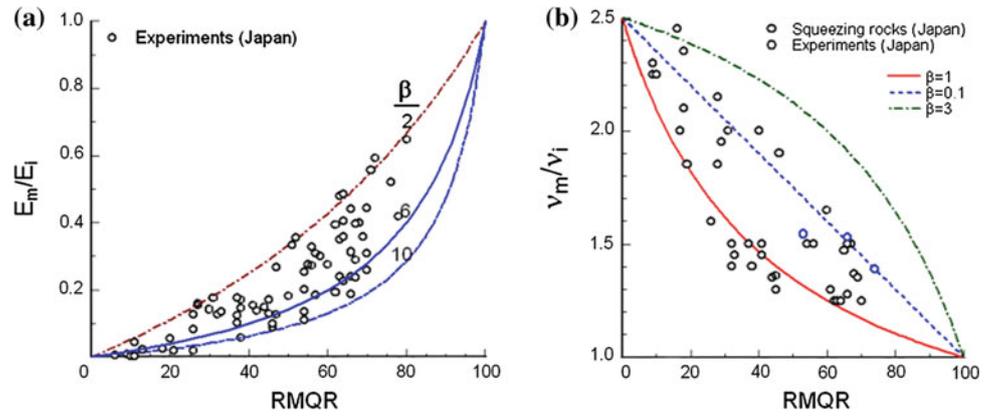
Fig. 137.3 Comparison of experimental data for **a** uniaxial compression and **b** tensile strengths of rock masses with Eq. (137.1) with the parameters in Table 137.3
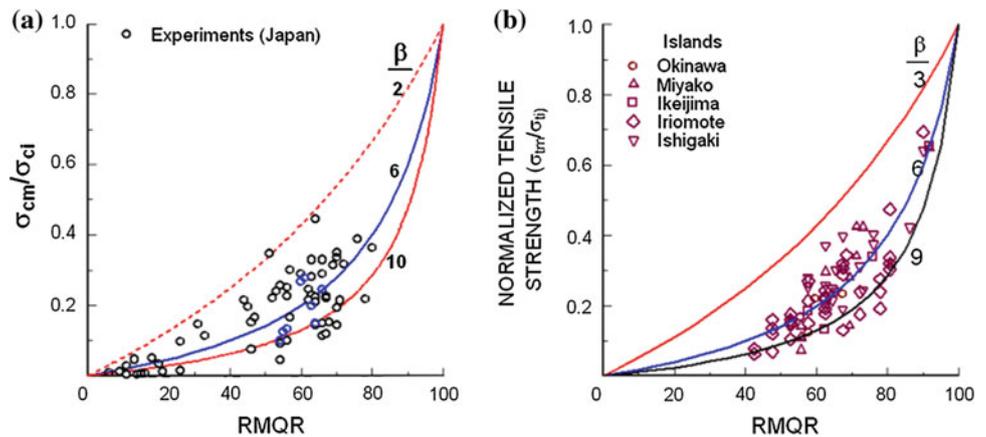
The results are plotted in Fig. 137.2b by varying the value of empirical constant β between 5 and 7. It is found that the value of empirical constant β could be designated as 6 in view of inferred tensile strength of rock mass.

related rock masses. Furthermore the authors strongly suggest that the relations for normalized properties should be used for evaluating properties of rock mass using properties of intact rock and its rock mass rating.

137.4 Conclusions

In this study, a new rock mass rating system (RMQR) is described to assess the physical state of rock mass and used for the evaluation of engineering properties of rock masses utilising the unified empirical relation proposed by Aydan and Kawamoto (2000) and compared with actual measurements on rock masses in various sites of Japan. The comparison of the empirical unified formula together with the values of constants was found to be quite consistent with in situ experimental results for data compiled from Japan. The comparisons between experimental results and estimations indicate that the presented relations are quite promising. Therefore, the empirical relations used in this study should be quite useful tool for engineers involved in projects

References

Aydan Ö, Kawamoto T (2000) Assessing mechanical properties of rock masses by RMR rock classification method. In: Proceedings of GeoEng 2000 symposium, Sydney, Paper No. OA0926 (on CD)

Aydan Ö, Ulusay R, Tokashiki N (2013) A new rock mass quality rating system: rock mass quality rating (RMQR) and its application to the estimation of geomechanical characteristics of rock masses. Rock Mechanics and Rock Engineering (doi 10.1007/s00603-013-0462-z)

Barton N, Lien R, Lunde I (1974) Engineering classification of rock masses for the design of tunnel supports. Rock Mech 6(4):189–239

Bieniawski ZT (1989) Engineering rock mass classifications. Wiley, New York

ISRM (2007) The complete ISRM suggested methods for rock characterization, testing and monitoring: 1974–2006. Ulusay R, Hudson JA, (eds.), Suggested methods prepared by the ISRM commission on testing methods, compilation arranged by the ISRM Turkish National Group, Kozan Ofset, Ankara

Investigation and Treatment of Problematic Foundations for Storage Dams: Some Experience

138

Wynfrith Riemer and rer nat

Abstract

Certain geological conditions require specific efforts in exploration, sampling and testing to obtain representative material parameters. Whereas in many geological environments already routine classification systems offer a practical approach to initial site characterization, other geological environments cannot be treated in a standardized way. The paper selects two geological regimes to illustrate potential pitfalls affecting the comprehensive identification and characterization of a dam site: sites with important development of residual soils, sites in possibly karstic environment. Case histories exemplify concerns related to these environments.

138.1 Introduction

Large dams count among the most impressive civil engineering structures but the success of their implementation and operation decisively depends on non-engineered elements: the rock or soil in the foundation of the dam and the materials forming the reservoir and its rims. Composition and properties of the respective geological materials are the product of a complex history. Clarifying the geological history allows to adjust the dam and its appurtenant structures to the foundation and to treat the foundation and basin so they will adequately respond to the stresses generated by the project. Proceeding from basic geological concepts as facies, lithology, tectonic history specific considerations and concerns can be formulated as guidance for the engineering geological, hydrogeological and geotechnical investigation and design of the project (cf. ICOLD 2009; Fookes et al. 2000). In the experience of the author, volcanic environments, residual soils and soluble, karstic formations required

particularly close attention. Because of the limited space, the paper will briefly mention residual soils and will deal more in detail with karstic conditions.

138.2 Residual Soils

Only two aspects are mentioned in relation to residual soils:

(1) Mechanical and hydrgcological properties are largely controlled by texture and are not reliably assessed by soil classification and tests on disturbed samples (Fookes 1997; ICOLD 2005). Testing is preferably done in situ and, for this purpose, the excavation of pits and shafts is particularly useful for geological and geotechnical investigation of residual soils.

(2) Lateral variation in soil profile and thickness can be very significant. The case of the Amaluza dam (Ecuador) is mentioned. Up to the crest level of the dam the granodiorite provided an excellent foundation but silty-sandy residual soils, locally with large core stones, caused serious stability problems for the cut above the crest and upstream of the dam near the power intake. Exploration had concentrated on the area of the footprint of the dam and the immediately adjacent problems were not anticipated.

W. Riemer (✉)
Technische Universität Berlin, Berlin, Germany
e-mail: wynriemer@t-online.de

r. nat
Consultant, Trier, Germany

138.3 Soluble Formations

138.3.1 General

Gorges formed in carbonate rocks offered morphologically attractive conditions for the construction of some of the highest existing dams: Vajont, Ingoury, Berke, Karun I and III, Bakhtyari, Cajon to name a few of them. The presence of karst was accepted and treated successfully.

Karst develops in soluble rocks like carbonates, sulfates and halites with engineering interest focusing on carbonates because of their wide distribution. The category also includes conglomerates with high carbonate content (e.g. the Tertiary conglomerates of Meteora and at the Kremasta dam site in Greece and along the Kopriicay in Turkey). Dolomite, in some regions acting as aquiclude (Milanovic 1981, 2000; Breznik 1998) displayed the most prominent karst development at the Ataturk site. Solution of dolomite tends to produce sandy, non- cohesive residue, easily eroded, potentially liquefiable and difficult to grout.

138.3.2 Specific Concerns

Notorious problems with these rocks are directly and indirectly associated with karst phenomena and cover a wide range:

- Loss of carbonate from the rock reduces shear strength and raises deformability (e.g. the marly limestones in the foundation of Khao Laem dam)
- Collapse of karstic voids under static and hydraulic loads. Prominent cases are the Keban dam in Turkey, the Lar dam in Iran. In Germany, the bottom of a tailings reservoir collapsed and all tailings, fortunately innocuous material, disappeared in the karstic voids of the Devonian limestone. The Perdikkas reservoir in Greece was abandoned when sinkholes formed in the valley floor and absorbed the run-off.
- Problems due to rapid dissolution. The effect becomes most critical where sulfates are present. At the Mosul dam in Irak the seepage water daily leached > 40 tons of gypsum from the foundation (Guzina et al. 1991). The headrace tunnel of Pueblo Viejo project in Guatemala failed following rapid dissolution of anhydrite.
- Erosion/suffusion of karst residues from dam foundations has in several cases rapidly increased seepage losses to unacceptable magnitudes. Remedial treatment became necessary at Mujib in Jordania and Aoulouz in Morocco (Mekboul et al. 1999). Progressive erosion of the karstic foundation eventually rendered the Henne dam in Germany useless and it was replaced by a new dam shifted upstream.

- Seepage losses from the reservoir can reach magnitudes affecting the viability of operation of the project. Before remedial treatment, the Keban reservoir lost up to 26 m^3/s and losses from the Lar reservoir (Iran) peak at about 16 m^3/s. Underseepage of about 12 m^3/s at the Ataturk dam was considered economically acceptable.
- Uplift resulting from underseepage and artesian conditions in karstic horizons endanger the stability of the foundation of the dam, of appurtenant structures and valley flanks downstream of the dam. Therefore, common practice provides extensive drainage systems at dam sites in karst. At Karun I in Iran, wells relieve the artesian head of a dolomite horizon at the toe of the dam and several galleries control the groundwater levels in the abutments downstream of the dam. At the Ataturk site, an internally drained tub assures the uplift stability at the powerhouse (Riemer and Andrey 1991) and when reservoir filling undesirably raised the pressure under the spillway chute, an additional drainage gallery was driven. At the Kremasta dam, drain galleries capture the seepage through karstic rock to keep the uplift in the right valley flank at a level which grants slope stability.

138.3.3 Investigations

The presence of karst conditions can be elusive and in many projects the importance of karst proved difficult to establish or was entirely overlooked. At the Perdikka site, the samples recovered from the boreholes had not given a distinction between clastic Neozoic sediments and karst residues of metamorphic limestone. At Ataturk, an exploratory adit eventually proved the karst development which a number of well performed core drillings had not clearly detected. At the Henne dam site, the karst hazard associated with the limestone layers alternating with calcareous keratophyr tuffs had not been recognized. Although the technology of geological exploration has improved with new developments in geophysics, in core sampling and borehole logging, the site investigations in formations with potentially karstic rocks always require additional efforts. Some aspects to be mentioned in this context are:

- Karst may have developed in past geological times in an environment significantly differing from the actual setting. Mantled or covered karst can be hidden from observation under more modern deposits. Paleokarst can exist in places where actual hydrogeological conditions would not imply solution effects.
- Karst groundwater gradients are flat (frequently on the order of %o) and levels can be very deep. At the Polifiton reservoir in Greece, piezometers had to be drilled to 800 m depth to reach the water table. At such depth,

accurate measurement of the water level becomes difficult and, with the flat gradients, readings can be misleading if deviation of the borehole is disregarded.

- Water level fluctuations in karst can be very rapid, propagating as waves in the permeable rock with low storage coefficient (cf. Yevyevich 1980). Thus, if readings are not taken at short intervals, hydrogeological transients are easily missed.
- Hydrogeological non-homogeneity of the karst aquifer can be misleading if insufficient data on the configuration of the water table are available.
- The permeability of karstic rocks is difficult to determine. Breznik (1998) recommends to apply high pressures in Lugeon tests to obtain more representative results. Even so, normal statistics of point permeability tests tend to be misleading. At Ataturk, some 1500 Lugeon tests in the initial series of grout holes gave a median of 7 and a mean of 14.5 Lugeon Units (Fig. 138.1a). This would normally correlate to a permeability on the order of 10^{-6} m/s. Permeability estimated from pumping tests fell into the order of 10^{-4} m/s. Model simulations, calibrated to seepage observed after reservoir filling, confirmed the high range of permeability.
- Hydrogeological techniques, involving environmental and artificial tracers, usefully complement the more conventional explorations in karst environment.

138.3.4 Engineering Geological Assessment of Karst Conditions

Whereas in other types of rock masses the estimates of parameters related to mechanical strength and deformation essentially provide the basis for design, and these can in a first step be approximated by classification systems and empirical correlations, a substantially wider range of parameters has to be handled in soluble rocks.

Hydrogeological considerations, chemical stability and resistance to erosion/suffusion may become decisive and have to be evaluated in conjunction with the mechanical properties of the rock.

Milanovic (1981) summarizes classification systems that have been proposed for karst formations. But these systems concentrate on morphological features and regional geological aspects, only indirectly related to engineering geology. As Milanovic points out, there are also restrictions to specific geological environments. The experience with many projects suggests that implications of the presence of soluble rocks for dams and reservoirs can be assessed considering mainly four parameters: (1) the mechanical strength of the rock mass, described e.g. by Ocm (Hoek 2005), (2) the size of voids created by solution which can range from mm to tens of m, (3) the large scale karst porosity, open or filled, typically on the order of a few percent, (4) the permeability, e.g. determined by Lugeon tests. Figure 138.2 illustrates the suggested approach. At project A, the rock mass has a significant proportion of large karstic voids, according to the permeability mainly open, and of a size where collapse is likely to occur. The caves will have to be stabilized by backfill. At project B, the hazard of collapse is marginal, the low permeability indicates filled voids, prone to complicate grouting. At projects C and D mechanical stability is adequate, medium permeability in conjunction with the low proportion of voids will facilitate grouting.

138.3.5 Design Considerations and Options for Treatment

- Separating karstic domain from Reservoir. A lateral valley with karstic limestone was separated from the Bigge reservoir (Heitfeld 1991).
- Blanketing. A bituminous facing seals a karst outcrop projecting into the Mornos reservoir (Heitfeld 1991) and

Fig. 138.1 Summary of Lugeon tests in primary holes of Ataturk grout curtain. **a** Histogram and fitted log-normal distribution. **b** Bar diagram Lugeon values against depth
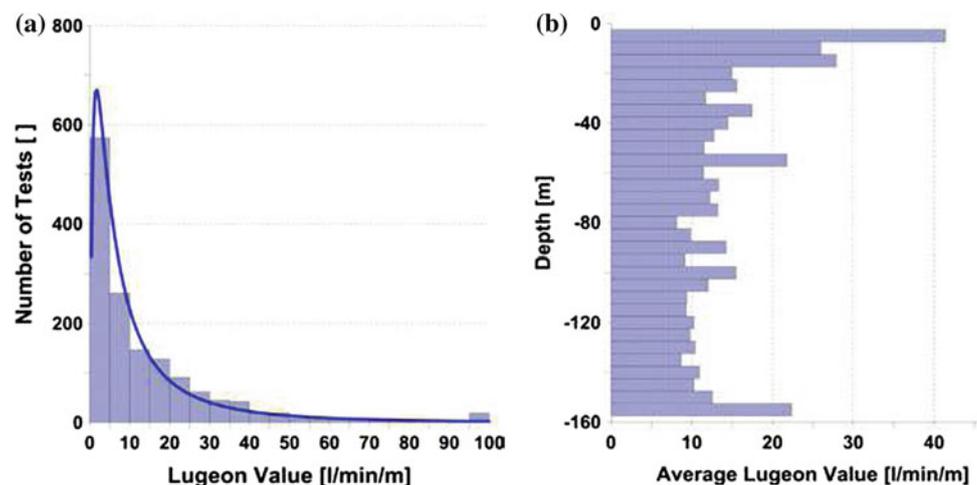
Fig. 138.2 Proposed scheme for classification of karst rocks for dam foundations. The size of the bubbles represent the dimensions of karst voids
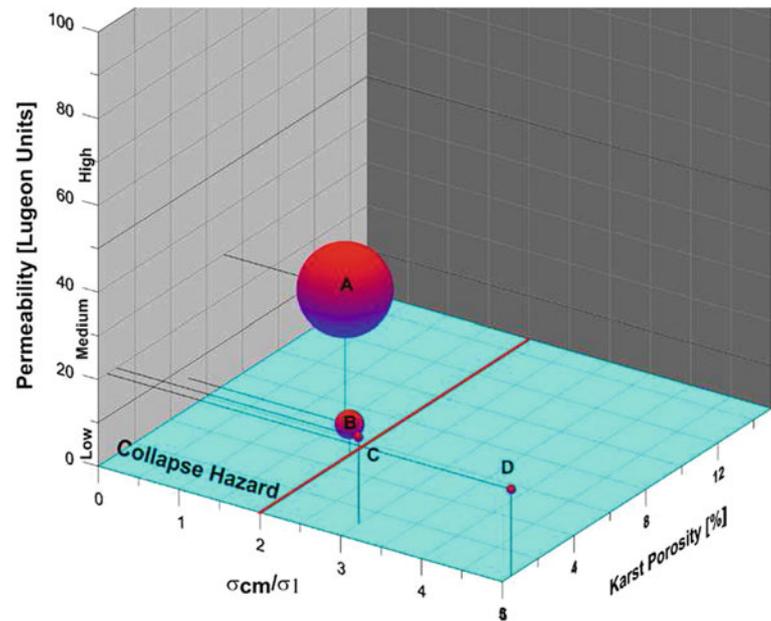
a concrete blanket covers karstic limestone at the Planinsko Polje (Breznik 1998). In other cases blanketing with membranes or low permeability soils has been applied.

- Grout curtains and diaphragms have been constructed on many projects. But, whereas in other rocks the vertical and lateral extension of the curtain rarely exceed the height of the dam, some curtains in karst reach a multiple of the height of the dam into the underground and stretch laterally far into the abutments and reservoir rims. In the Dinaric karst, active solution is frequently found to 200 m below valley floor and paleo-karst may reach more than 1,000 m into the rock (Milanovic 1981, 2000; Breznik 1998). At the Ataturk site, the permeability does not decrease significantly with depth (see Fig. 138.lb) and the curtain was locally taken to 300 m below valley

floor. Data collected for 30–40 dams on karst foundation show a typical depth of about 1.5 times the height of the dam, mean density of grout and test holes 0.6 m per square meter of the curtain and average grout absorption of 200 kg/m^2 (see Fig. 138.3).

Treatment of filled karst tends to be particularly demanding. At the Berke dam, compaction grouting at 60 bar pressure proved an economical alternative to construction of a diaphragm (Basar et al. 1999), whereas at many other dams diaphragms had to be constructed.

Even if initial treatment of karst foundations succeeded, the risk of deterioration remains (e.g. Aoulouz dam, Mekboul et al. 1999; Wolf Creek USSD 2013). Therefore, a comprehensive monitoring system and access for maintenance treatment should be provided (e.g. Riemer et al. 1995).
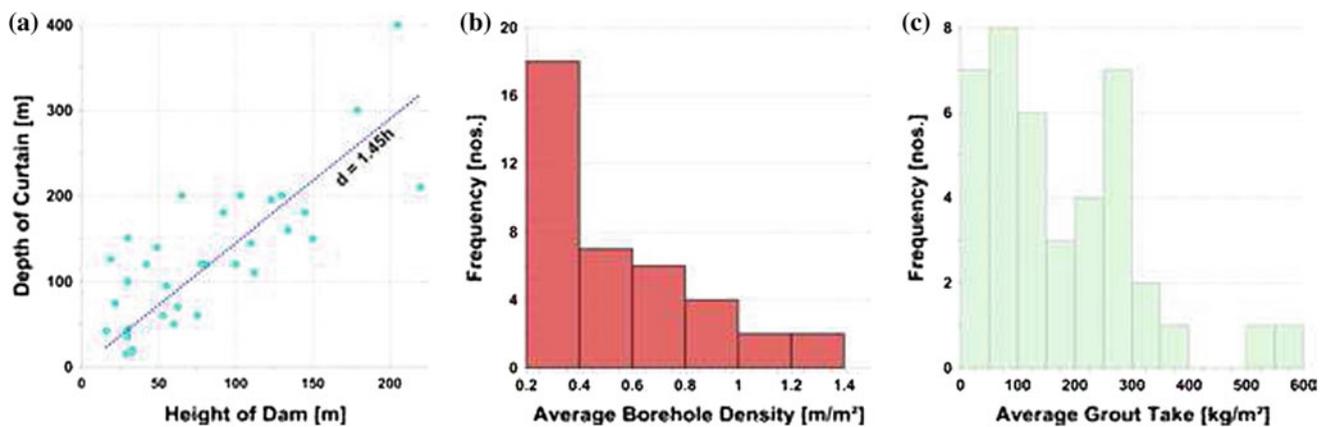
Fig. 138.3 Statistics of grout curtains in karst foundations of dams. **a** Depth of curtain versus height of dam. **b** Density of boreholes per square meter of curtain. **c** Grout absorption per square meter of curtain

138.3.6   Cost

Little information has been published on financial and economical aspects of karst treatment. But these aspects can attain decisive importance for the viability of a project. In this regard the Khao Laem project, Thailand, can be mentioned. The cost of treating dam foundation and reservoir rims was about three times higher than the construction cost of the 90 m high CFRD.

References

Basar M, Altug S, Vauloup L (1999) Berke arch dam and HEPP Turkey: foundation treatment of karstic limestone in suspended curtain. In: Turfan M (ed) ICOLD 67th Annual Meeting, Dam Foundations Problems and Solutions, pp 233–250

Breznik M (1998) Storage reservoirs and deep wells in karst regions. Balkema, 251 p

Fookes PG (1997) Tropical residual soils: a geological society engineering group working party revised report, 184 p

Fookes PG, Haynes FJ, Hutchinson JN (2000) Total geological history: a model approach to the anticipation, observation and understanding of site conditions. GeoEng 1:370–460

Guzina BJ, Saric M, Petrovic N (1991) Seepage and dissolution at foundations of a dam during the first impounding of a reservoir. In: Proceedings of 17th international congress of ICOLD, Q.66 R78

Heitfeld KH (1991) Talsperren. Lehrbuch der Hydrogeologie, Band 5. 468 p

Hoek E (2005) Uniaxial compressive strength versus Global strength in the Hoek-Brown criterion. RocScience web site

ICOLD (2005) Dam foundations, geologic considerations, investigation methods, treatment, monitoring. Bulletin 129

ICOLD (2009) Tropical residual soils as dam foundations and fill material. Bulletin 151

Mekboul M, Chraibi AF, Saidsallam M (1999) Aoulouz dam additional treatment in the grout curtain after reservoir filling. In: Turfan M (ed) ICOLD 67th annual meeting, Dam foundations problems and solutions, pp 117–132

Milanovic PT (1981) Karst hydrogeology. 434 p

Milanovic PT (2000) Geological engineering in karst. 347 p

Riemer W, Andrey JD (1991) Baugrundbehandlung am Ataturk Damm. Ber. 8. Nationale Tagung fur Ingenieurgeologie, Berlin, 1991, pp 167–174

Riemer W, Gavard M, Turfan M (1995) Ataturk dam—hydrogeological and hydrochemical monitoring of grout curtain in karstic rock. Verification of geotechnical grouting, ASCE geotechnical special publication no. 57, pp 116–126

USSD (2013) Dams of the United States. 205 p

Yevyevich V (1980) Investigation of karst hydrogeology, hydrology and water resources in southern Turkey. In: Proceedings of LRST international symposium on Karst hydrogeology, pp 55–117

Dissolution Influences on Gypsum Rock Under Short and Long-term Loading: Implications for Dams

Nihad B. Salih, Philip E.F. Collins, and Stephen Kershaw

Abstract

Dissolution of soluble substrates such as gypsum presents a major hazard to dams in many parts of the world. This research simulates hypothesised conditions beneath the Mosul Dam, northwest Iraq, where collapse of a karstic system associated with continuous fresh water supply from its reservoir is a recognised problem. Gypsum rocks from northern Iraq and similar rocks from Bantycock gypsum mine, UK, were analysed for short-term mechanical response following immersion (5–50 weeks) and long-term loading during immersion (maximum 50 weeks). New experimental devices were developed from a conventional oedometer. Cylinder samples provided a proxy for massive gypsum strata. Samples were permanently submerged at atmospheric water pressure, with groundwater recharge, flow and dissolution simulated by regular changes of water. Stress on each sample was progressively increased to a maximum of 2,688 kPa. Small increases in strain were recorded by the end of each test but no failures occurred within 60 days. However, notable failure due to atmospheric water pressure and axial stress occurred over long time periods. Visible physical changes included a decrease in sample mass and volume. Similar change was recorded in ultrasonic velocities. These indicate that gypsum collapse risk beneath dams requires prolonged exposure to dissolution. The modified device performed well and was robust, and demonstrates that such a modification can provide a simple low cost system for conducting laboratory creep tests on weak rocks.

139.1 Introduction

Gypsum rock underly more than 20 % of the earth surface (Johnson 2005) with seven million km² underlain by highly soluble gypsum ($CaSO_4.2H_2O$) bearing rocks in a large number of countries (Cooper 2006). Its solubility in pure water is 2.531 g/l at 20 °C, around 140 times lower than halite and 4 times larger than $CaCO_3$ (Johnson 2006).

Gypsum rock is common in Iraq, mainly in the Mid-Miocene Fatha (Lower Fars) Formation (Jassim and Goff 2006) and is associated with significant geotechnical problems. This is particularly the case in sites with high hydraulic gradients such as near dams (Salih 2013) e.g. the Mosul Dam, which is underlain by thick gypsum beds which are severely affected by dissolution and karstification, including general subsidence and sinkholes.

While cavity formation due to dissolution is known, mechanical change leading to creep and brittle failure has received little attention. This is significant as the formation of cavities will transfer load to surrounding, potentially weakened gypsum.

Gypsum resistance to compression is not high. Its average uniaxial compressive strength (UCS) is around 13.73 MPa, but it demonstrates considerable variability between 9.41 to

N.B. Salih (✉)
University of Sulaimani, Sulaimani, Iraq
e-mail: nihad_baban@yahoo.com

P.E.F. Collins · S. Kershaw
Brunel University, London, UK

15.99 MPa (Kenneth 2005). While, others found their UCS is medium/moderately strength, varied from 24.1 to 40.8 and 18 to 36 MPa generally (Bell 1981; Karacan and Yilmaz 1997).

Clearly, exposure to water is a key control on gypsum dissolution (Jassim and Goff 2006). The chemical composition of this water is important and cause significant variability in rates. As a result, to control this, distilled water has commonly been used in experimental studies on dissolution. The degree of saturation also affects gypsum strength as measured in mechanical tests (Ali 1979; Elizzi 1976; Ergun and Yilmaz 2000; Gao et al. 2011; Sconnenfeld 1984), as may the soaking period (Gao et al. 2011; Sconnenfeld 1984).

139.2 Materials and Methods

The collection of gypsum in Iraq was limited by security concerns, though some samples could be collected from Bazyan, North of Iraq. Similar gypsum occurs in the highest strata of the Triassic Norian Mercia Mudstone Group (Cropwell Bishop Formation) at Bantycock mine (Worley and Reeves 2007). Both of sites feature thick gypsum rock layer, similar to those beneath the Mosul Dam.

NX cylinder samples (54 mm diameter and L/D = 2.5) were prepared following common practice (ASTM 2010; Bieniawski et al. 1978; Dreybrodt et al. 2002). A suitable loading rate of 0.025 MPa/s was determined following ASTM and ISRM standards (ASTM 2010; Bieniawski et al. 1978). A circumferential extensometer was used in the mid height of cylinders to calculate the radial strain (Fig. 139.2c). Ultrasonic observations were recorded for each sample in air dry state and after each of the immersion periods.

Unloaded gypsum samples were slowly saturated by vacuum, then soaked at atmospheric pressure at 5, 10, 15, 30 and 50 weeks. Three samples were used at each time interval for short-term loading tests. Continuous loading (2,688 kPa) using a modified oedometer was also applied to samples for 50 weeks. During soaking, the water was changed every 7 days and conductivity measurements taken. A full account of the methodology can be found in Salih (2013).

139.3 Results

139.3.1 Short-Term Results

See Figs. 139.1, 139.2, 139.3, 139.4 and Table 139.1, 139.2.
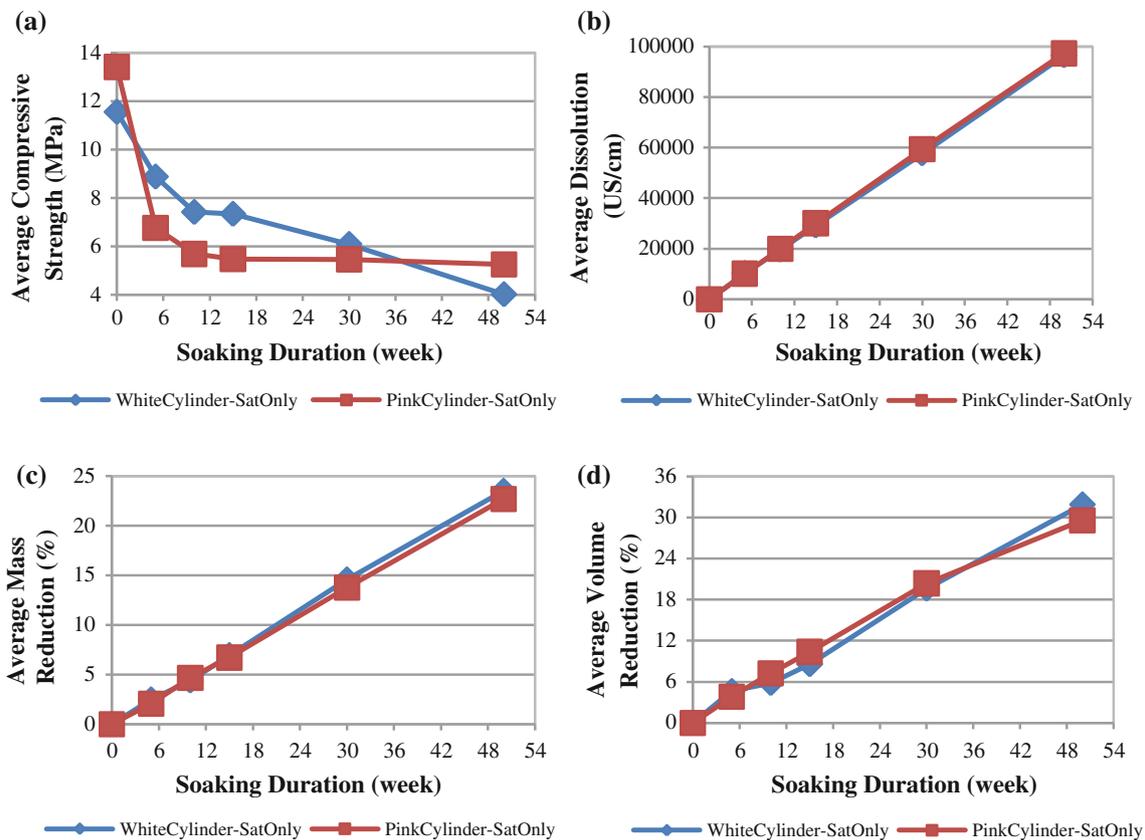
Fig. 139.1 Comparisons among short term loaded cylinders a is for compressive strength b is for dissolution c is for mass reduction and d is forvolume reduction. Each calculated values are the average of three tested cylinders

Fig. 139.2 **a** Gypsum outcrop, Bazyan/Iraq **b** Bantycock Mine/UK gypsum blocks **c** The extensometer in the mid-length of a cylinder

Fig. 139.3 The failed cylinders after short-term loading: **a** The white/Bantycock gypsum. **b** The pink/Bantycock gypsum. **c** The Iraqi gypsum
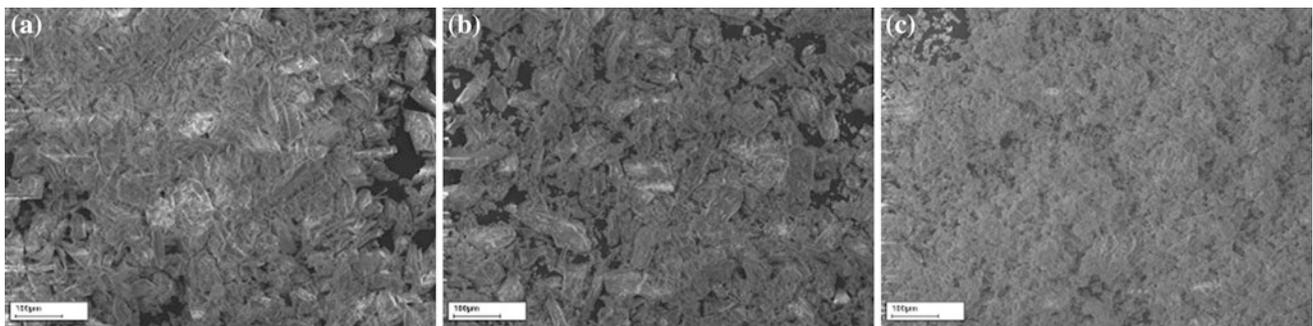
Fig. 139.4 Variations in gypsum crystal size, visualized using SEM: **a** The white/Bantycock gypsum. **b** The pink/Bantycock gypsum. **c** The Iraqi gypsum

139.3.2 Long-Term Results

See Fig. 139.5

139.4 Discussion

It is clear that saturation weakens gypsum rock, and this weakness progressively develops over time where there is a flow of water. This is relevant to the context of dams, and other large structures, where groundwater flow is enhanced, and where fresh water is constantly being introduced to the gypsum.

All the samples showed signs of dissolution, manifested as a change in shape over time. This change in shape does not, however, explain all the weakening that took place. There must also be a contribution from changes taking place within the samples.

Several characteristics of the gypsum influence the rate of dissolution weakening. Iraqi samples dissolved at a faster rate that the UK samples. This appears to be due to the size of the gypsum crystals, which were larger in the samples from Bantycock mine.

The larger dissolution values of Iraqi samples under atmospheric pressure than white/Bantycock samples in short-term datasets (Fig. 139.1) were correlated with the

Table 139.1 Description of the UK and Iraqi gypsum particles, the description based on Scanning Electronic Microscope (SEM) photos presents in Fig. 139.4

Gypsum sample type	Particle size (micron)	Particles gradation	Particles shape	Notes
White/Bantycock, UK (see Fig. 139.4a)	4–114	Poorly graded	Have three shapes randomly: longitudinal, semi-square and semi-circular/elliptical	Very sharp edges of particles, mostly medium size, some large and small sizes are found
Pink/Bantycock, UK (see Fig. 139.4b)	2–177	Not very well graded	Mostly semi-elliptical and longitudinal	Middle and large sizes are more than fine size
Iraqi (see Fig. 139.4c)	1–28	Looks well graded	Mostly semi-circular and semi-elliptical	Mostly fine particles, some concentration of fine particles with impurities/other minerals together make dense look for some places

Table 139.2 Ultrasonic observation of white/Bantycock gypsum cylinders

Cylinder state	Transit time (Useos)	Velocity (m/s)	Path length (mm)	Elastic modulus (GPa)
Air-dry	27.77	18,870.67	108.67	159.7
Saturated under atmospheric pressure				
5 week	27.03	18,821.7	108	100.2
10 week	26.3	18,821.67	104.66	82.97
15 week	26.17	18,498.33	104.33	68.27
10 week	19.833	15,974.33	79.33	63.47
15 week	10.633	14,588.67	42	61.2
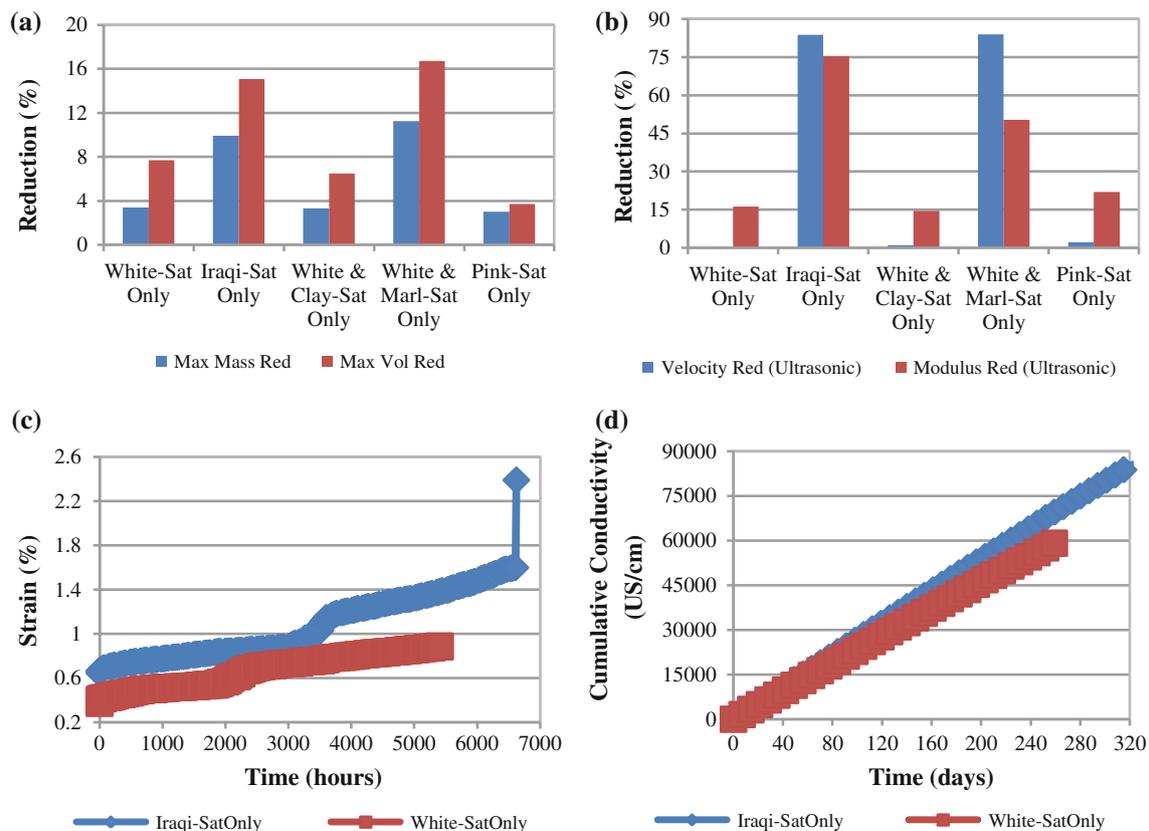
Fig. 139.5 Comparisons among long-term loaded cylinders. **a** Volume and mass reduction after 60 days. **b** Ultrasound velocity and modulus reduction after 60 days **c**, **d** are for 1 year loaded cylinders, Iraqi cylinder failed after 6,800 h as shown in part (**c**)

effects of gypsum crystal size and shape in characterizing the dissolution process i.e. larger crystals dissolve less quickly than smaller crystals. Slight differences in impurities within the gypsum, as reflected by the different colours of gypsum from Bantycock (white and pink) may also contribute to differences in response e.g. Fig. 139.1a where the strength of the pink gypsum declines much more quickly than the white gypsum. The shape of internal structures, determined by cracks and fissures, may also be a factor as these allow fresh water to penetrate the gypsum. In addition, many of the cracks contain impurities that have different mechanical and chemical properties to the gypsum. Samples that were soaked without loading showed more evidence of weakening through crack-enhanced dissolution than samples under constant load for 50 weeks. This may be because the high load caused the cracks to close through simple translational movement and through small amounts of creep. It should be noted that the water was under atmospheric pressure during these tests. Under pressure conditions similar to those found beneath large dams such as at Mosul, water may well be able to penetrate thin cracks.

The research has a number of implications for large structures than both load the ground and modify groundwater flow, such as large dams:

- The role of percolating fresh water in enhancing dissolution is confirmed. The significant head difference induced by a dam can be expected to increase the potential for groundwater flow and increase the likelihood of cavity formation. Similar effects could be induced by localized dewatering, or by wetter conditions caused by climate change.
- Importantly, the dissolution does not just generate macrocavities. There is also alteration of apparently intact gypsum which increases its potential for failure.
- Sometimes subtle differences in gypsum, such as impurities and crack frequency can have a significant impact on the timing of failure.

139.5 Conclusion

The research has shown that the evolving behavior of weak soluble rocks such as gypsum can be investigated in the laboratory over extended periods. It highlights that the hazard presented by such rocks is not just simply one of dissolution induced cavities. It is also a progressive weakening of the rock mass itself.

Clearly, the findings suggest that the risk of failure in large dams is a result of a more complex set of processes than may have been expected. This has implications for mitigation solutions. If the problem is perceived as just being caused by cavity formation, then a solution might be to simply fill the cavities with grout on an *ad hoc* basis. This ignores the weakening of the 'solid' gypsum—and may make the problem worse. Localized injections of grout are likely to deflect and focus groundwater flow on the intact gypsum. This creates a risk of enhanced generation of new cavities, and of forcing more water into the gypsum and so reducing its overall strength.

Other than removing dams such as that at Mosul and elsewhere—an unattractive option given the need for water and power—the only solution is a systematic approach to creating a deep impermeable barrier that will significantly slow, or even stop, the movement of fresh water through the gypsum rock. Such a solution will inevitably be expensive, and challenging to achieve, but the cost must be weighed up against the risk of losing an essential piece of infrastructure.

References

Ali SA (1979) PhD thesis, University of Sheffield, UK

Bell FG (1981) Geotechnical properties of some evaporitic rocks. Bull Int Assoc Eng Geol 24:137–144

Bieniawski ZT, Franklin JA, Bernede MJ, Duffaut P, Rummel F, Horibe T, Broch E, Rodrigues E, Van Heerden WL, Vogler UW, Hansagi I, Szlavin J, Brady BT, Deere DU, Haweks I, Milovanovic D (1978) Suggested methods for determining the uniaxial compressive strength and deformability of rock materials. Int J Rock Mech Min Sci Geomech Abstr 16(2):135–140

Cooper AH (2006) Gypsum dissolution Geohazards at Ripon, North Yorkshire, UK. Field Trip Guide Ripon, IAEG

Dreybrodt W, Romanov D, Gabrovsek F (2002) Karstification below dam sites: a model of increasing leakage from reservoirs. Environ Geol 42:518–524

Elizzi MAS (1976) PhD thesis, University of Sheffield, UK

Ergun K, Yilmaz I (2000) Geotechnical evaluation of Miocene gypsum from Sivas-Turkey. Geotech Geol Eng 18:79–90

Gao H, Liang W, Yang X, Zhang G, Yue G, Zhang P (2011) Experimental study of mechanical property of gypsum rock soaked in hot saturated brine. Chin J Rock Mech Eng 30(5):935–943

Jassim SZ, Goff CJ (2006) Geology of Iraq. Prague and Moravian Museum, Brno, Dolin

Johnson KS (2005) Subsidence hazards due to evaporite dissolution in the United States. Environ Geol 48:395–409

Johnson KS (2006) Gypsum-Karst problems in constructing dams in the USA. Environ Geol 53:945–950

Karacan E, Yilmaz I (1997) Collapse dolines in Miocene gypsum: an example from SW Sivas (Turkey). Environ Geol 29(3/4):263–266

Kenneth SJ (2005) Subsidence hazards due to evaporite dissolution in the United States. Environ Geol 48:395–409

Salih NB (2013) PhD thesis, Brunel University/London, UK

Sonnenfeld P (1984) Brines and evaporates. Academic Press, London

ASTM Standards (2010) ASTM D7012-10 (Approved 15/01/2010)

Worley N, Reeves H (2007) Application of engineering geology to surface mine design, British gypsum, Newark Nottinghamshire. (Field Guide, 2007). http://nora.nerc.ac.uk/3225/1/Keyworth_Field_Trip.pdf. Accessed 21 Nov 2012

Underground Works in Weak and Complex Rock Mass and Urban Area

140

Serratrice Jean François

Abstract

This paper concerns the constructions of twin tunnels in a weak and complex rock mass and an urban area below the city of Toulon (France). The project is presented at fist time, then geological context and hydrogeological context. Both tunnels are built in thrusted grounds and under sea level. These grounds possess a high degree of heterogeneity and a high degree of fracturation at all scales inherited from their tectonic history. On a large part of the linear, the layers are arranged in reverse order of their depositional age. The second part of the paper addresses some geotechnical properties of the grounds. Then, some features about monitoring and surface settlements are presented. It seems that in some places, unusual responses of the ground appear at the surface, that reveals the strong influence of the local structure of the rockmass and, maybe, initial stress state. But the latter is unknown in all cases.

140.1 Introduction

Tunneling at shallow depth causes deformations in the rockmass and then deformations at the surface. These deformations are mainly represented by settlements, which are not uniform but are concentrated vertically above the tunnel axis in the form of a trough. The problem is particularly acute in urban area where settlements affect all components of the urban fabric such as buildings, structures, roads and networks. At depth, deformations can affect other constructions, especially when twin tunnels are built and the second interacts with the first, but more generally underground structures or deep foundations, which have not necessarily been designed to withstand excavation of a tunnel in their neighborhood. So tunneling in urban area requires control of ground movements to prevent excessive déformations on surrounding structures.

This paper concerns the constructions of twin tunnels in a weak and complex rockmass and an urban area below the city of Toulon (France) (Durand 1991; Gilbert et al. 2008). The project is presented at fist time, then geological context and hydrogeological context for this works built in thrusted grounds and under see level. The second part of the paper addresses example of geotechnical properties of the grounds. Then, some features about monitoring and surface settlements are présented. In some places, unusual responses of the ground appear at the surface, that seems to reveal the strong influence of the local structure of the rockmass and, maybe, initial stress state.

140.2 Project and Geological Context

The Toulon Underground Crossing project includes two road tunnels designed to establish continuity between the A 50 motorway in the west of Toulon (to Marseille) and the A 57 motorway in the east (to Nice). Each of the works extend over about 3,000 m with a central part drilled over

S.J. François (✉)
CETE Méditerranée, 13593 Aix en Provence, France
e-mail: jean-francois.serratrice@developpement-durable.gouv.fr

1,800 m and then covered trenches at the ends. The works were carried out over several attacks from the ends and from intermediate shafts. The civil works of the north tunnel took place from the early 1990s until 2001, and between 2007 and 2011 fir the south tunnel. Both phases account for shutdown periods. The full-face excavation was carried out mechanically. The choice of type of pre-supports and supports to install was operated according to the nature and state of the ground encountered, underground deformations and surface deformations from monitoring and provisions of surface settlements.

Both tunnels are fit into old grounds very tectonised by origins of the Primary area and then Permian and Triassic grounds. The stratigraphic succession is as follows: Quaternary with colluvium, alluvium and fills; Keuper with clays, cargneules and clusters of gypsum; Muschelkalk with dolomitic limestones, marls and sandstones; Permian with sandstones and mudstones; Stephanian with sandstones and black shales (coal); Socle with strongly folded quartzophyllites. This stratigraphic sequence from Permian to Muschelkalk appears on the east side of the site. In contrast, grounds appear in reverse order of their age in the west and central part of the city of Toulon, which constitutes the singularity of the site (Rat and Serratrice 2004). At the regional level, this area is located at the northern edge of the thrust sheet of Cap Sicié. Thrusting in direction SW-NE dated Tertiary is responsible for the disruption of the stratigraphic sequence. The Triassic formations are overlain by Permian sandstones and mudstones and then topped themselves by Stephanian sandstones and coal shales in the form of shell structures. The ante-stephanian formations represented by quartzo-phyllites overlay this set under the Quaternary cover. It is likely that other tectonics movements have occurred later to achieve the mechanical initial state that prevails underground today. The site investigations showed three families of groundwater (Serratrice 2004).

Thus and for a large part, the diversity of the grounds encountered, their state and the complexity of their arrangement have prevented the geological and geotechnical knowledge of the site, which turned imperfect at every stage of the project, despite the geological and geotechnical site investigations during successive campaigns, the first of which began in 1971, and despite the investigations carried out with the progression of the works. Moreover, constraints imposed in urban areas are not in favor to site investigations.

140.3 Geotechnical Aspects

The data come primarily from core drilling and in situ testing. Shafts and exploratory tunnels were excavated too. Laboratory tests were carried out in large numbers, and pressuremeter tests, but also pump tests, plate tests, etc. Monitoring the digging of the north tunnel has been used to observe grounds under this scale, describe their state and fracturation, characterize water inflows, measure underground deformations, etc.

Before the beginning of work in south tunnel, new site investigation by drilling, analysis of test results and synthesis of all these new data led to identify 21 families of grounds. All the state characteristics and mechanical properties of these families are dispersed due to the geological history of the rockmass which was destructured by thrusting.

The geotechnical site investigations during the successive campaigns by in situ testing favored the use of the pressuremeter. Numerous holes were drilled at various depths (up to 60 m). To the total, more than 3,500 tests were carried out to cover the different formations throughout the site. Figure 140.1 shows the histograms of pressuremeter modulus measurements E_M for Triassic marls, One layer of the 21 grounds families. In the first case of an arithmetic scale, the modulus distribution takes an exponential shape. In the second case of a logarithmic scale, the distribution takes a log-normal shape. The averages of E_M calculated in logarithmic scale are smaller than those calculated with an arithmetic scale and dispersion is less in the logarithmic scale.

Fig. 140.1 Pressuremeter modulus in linear scale and logarithmic scale
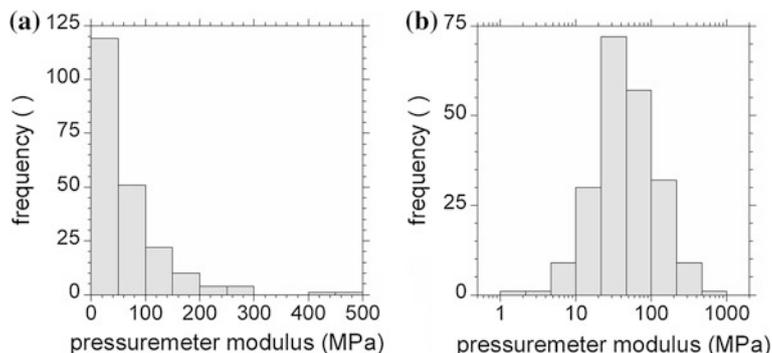
140.4 Behaviour of the Rockmass

The Toulon Underground Crossing project is imbedded in a complex rockmass and below an urban area, which made the construction a very difficult works. Given the issues due to the presence of surrounding building at the surface, special provisions have been considered at the design stage and during construction works.

The methods have also evolved based on the lessons learned from the construction of the north tunnel. Expertise of the state and performances of all the constructions at the surface was carried out previously in the perimeter of influence of the tunnels (50 m at least on either side of each of the axes of the two tunnels). The survey program was constituted by an important process of underground deformations monitoring with measurement of convergences between the walls and extrusion at the tunnel faces. But it is especially at the surface that an important survey program has been developed, initially manual, and then automated using motorized theodolites (Serratrice and Dubois 2004; Caro-Vargas and Beth 2012). This monitoring is based on the topographic survey of targets sealed on the buildings or points carried by the roads. Measurements were collected in databases and then exploited. This monitoring was supplemented by periodic visits of buildings and networks. The results of measurements at the surface and underground associated with systematic survey by exploratory drilling during tunneling and then the analysis of these data made possible to drive the works and choose the profiles best suited to the grounds encountered and the rate of deformations observed. Innovative methods of exploitation of the data have been developed, which were used to examine carefully the evolution of longitudinal profiles of settlements or settlements troughs at the surface (Serratrice and Magnan 2002; Serratrice and Dubois 2004). Still based on clues warning often tenuous, these methods based on monitoring have proven effective in most cases to guide the project.

Fig. 140.3 Settlements profile

For each of the two tunnels, the final settlements were represented on a map of iso-values for the whole site. The map clearly shows pits and lumps of the final settlements trough along the tunnels axis. The lateral extension of the trough was greater than 50 m in some places. Sometimes the shape of the trough fits well with the structures encountered in the ground. For example, the map on the Fig. 140.2 shows the final settlements in the west part of the north tunnel. The tunnel is drawn at steps of 25 m. Iso-settlement curves are represented every 10 mm and every 2 mm. The grid spacing is 50 m. A particular trough appears which adopts an oblique direction relative to the tunnel axis. It happens that the trough coincides perfectly with a fault structure encountered by the tunnel at depth. The trough is set in the same direction that the fault F (N100).

An other example shows that settlements troughs are sometimes decentered in a transverse profile as illustrated on Fig. 140.3. The dots represent the measurements when the tunnel face crosses the sections (hollow dots) and then the final settlements when the tunnel face is far from the profile 3 months later (solid dots). The curves represent the

Fig. 140.2 Part of the settlements trough at the surface

settlements profiles calculated for the centered Gaussian representations. In this example, the shift of the actual trough indicates a lateral heterogeneity of the rockmass. This heterogeneity is likely due to structural effects inherited from thrusting. But it is often difficult to establish a link between the nature, the structure, the mechanical properties of the ground observed during the excavation at the scale of the tunnels face and the final shape of the trough at the surface. It is even more difficult to detect these heterogeneities across a tunnel section during the site investigations and the design stage, at a time when it would be useful to provide reliable estimates of surface settlements.

140.5 Conclusion

The heterogeneity of the rockmass increases the difficulties for the construction of shallow tunnels in urban areas. To anticipate potential difficulties, the construction operations, which must remain based on a thorough knowledge of the ground behaviour and the techniques used, have only warning signs often tenuous. In this context, the deformation monitoring underground and at the surface plays an predominant role. On the surface, monitoring the dynamics of settlements in longitudinal profiles during the advance of the tunnel face, or better at three dimensions, gives a privileged means of observation. Overall, it seemed a fairly direct relationship between surface settlement and structure into the tectonized rockmass. But in some places along the works, it appeared a strong influence of the initial structural and mechanical states into the rockmass in the context of high tectonized media.

References

Caro-Vargas B, Beth M (2012) Observational method using real time surface settlement monitoring: The South Toulon Tunnel project. GeoCongress 2012, Oakland, California, pp 3109–3118

Durand JP (1991) Liaison A50/157, Traversée Souterraine de Toulon. Tunn Ouvrages Souterrains 106:177–179

Gilbert G, Serratrice JF, Thiebaut H, Marguet P, Le Bissonnais H, Vigouroux JP (2008) Deuxième tube de la traversée souterraine de Toulon. Congrès Internationnal AFTES, Monaco

Rat M, Serratrice JF (2004) Tunnel de Toulon. Contexte géologique, hydrogéologique et géotechnique. Rev Trav 806:25–30

Serratrice JF, Magnan JP (2002) Analyse des tassements de surface pendant le creusement du tunnel nors de la traversée souterraine de Toulon. Bull Lab 237:5–36 (P&C, Paris)

Serratrice JF (2004) Tunnel de Toulon. La piézométrie. Rev Trav 806:75

Serratrice JF, Dubois P (2004) Tunnel de Toulon. Interprétation des deformations en surface. Rev Trav 806:76–79

Vinod Kumar Kasliwal

Abstract

In Engg Geology, a weak rock is considered as one whose deformation modulus is 1/2 to 1/5 of the enclosing surrounding rock. Such rocks are treated by replacing them with concrete plugs of suitable strength to depths as recommended by USBR Formula (Shasta and Friant Dams) and/or as by Japanese Team (Fumio Ishii et al.). These methods have their limitations since in each of them, it is assumed that the weak rock zone/fracture is bounded on each side/abutment by rocks that are strong having competent deformation modulus and that such rocks exist for a sufficient width so as to act as abutments of beam/bridge. But when the shearing, fracturing and faulting is so frequent and close-spaced that this condition is not available, then the problem is how to construct a gravity dam. One such 81 m high straight gravity dam across Jakham river in Chittorgarh distt, Rajasthan, India has been constructed by providing doubly-reinforced cantilever rafts for the foundations. The Jakham Dam is a 81 m high straight gravity dam across the river of same name Jakham, a tributary of Mahi river. The dam is located in a 150 m deep gorge with near-vertical escarpment slopes at the neck of a wide open valley, thereby making it an ideal topographical site. The rocks exposed are ferruginous quartzite belonging to pre-Aravallis (Archean). They are hard, brittle and have undergone extensive fracturing, folding, faulting and shearing to the extent that up to 65 % of the foundation rocks are affected by them so much so that while one abutment and the river bed shows faulting the other abutment shows presence of a cave. Further, while the fractures and joints are occupied by red ocherous clays, the bedding planes are frequently occupied by talcose bands. The paper highlights the geological conditions in the foundations by detailed (1:100) mapping so as to identify competent rock areas to which the load/stresses of the dam have been successfully transferred by means of cantilever rafts.

141.1 Introduction

Construction of the 81 m high and 235 m long straight gravity masonry dam in Chittorgarh (now Pratapgarh) district, Rajasthan, India (Fig. 141.1a) was commenced in the year 1970 and its 1.5 M cum reservoir was first filled in 1988.

The dam site is located in the north-south band of a 150 m deep Z-shaped gorge. The foundations rocks of the dam are formed by pre-Aravalli (Archean) quartzites which are extensively folded, fractured and sheared. Due to difficulty in approaching the dam site and steepness of the walls of the gorge, very limited explorations were carried out. On the basis of these investigations, foundation grades for the various blocks were suggested and excavations commenced. However on reaching the suggested grades a great variance was observed. Even at this stage it was considered to abandon this site and look for an alternate, but after evaluating geological and engineering and socio-economic considerations it was decided to construct the dam at this site.

Director (Retd) from Geological Survey of India. Now working as a Engineering Geology Consultant.

V.K. Kasliwal (✉)
Engineering Geology, A6, Hospital Road, Ashok Nagar, Jaipur, India
e-mail: vkkasliwal@hotmail.com
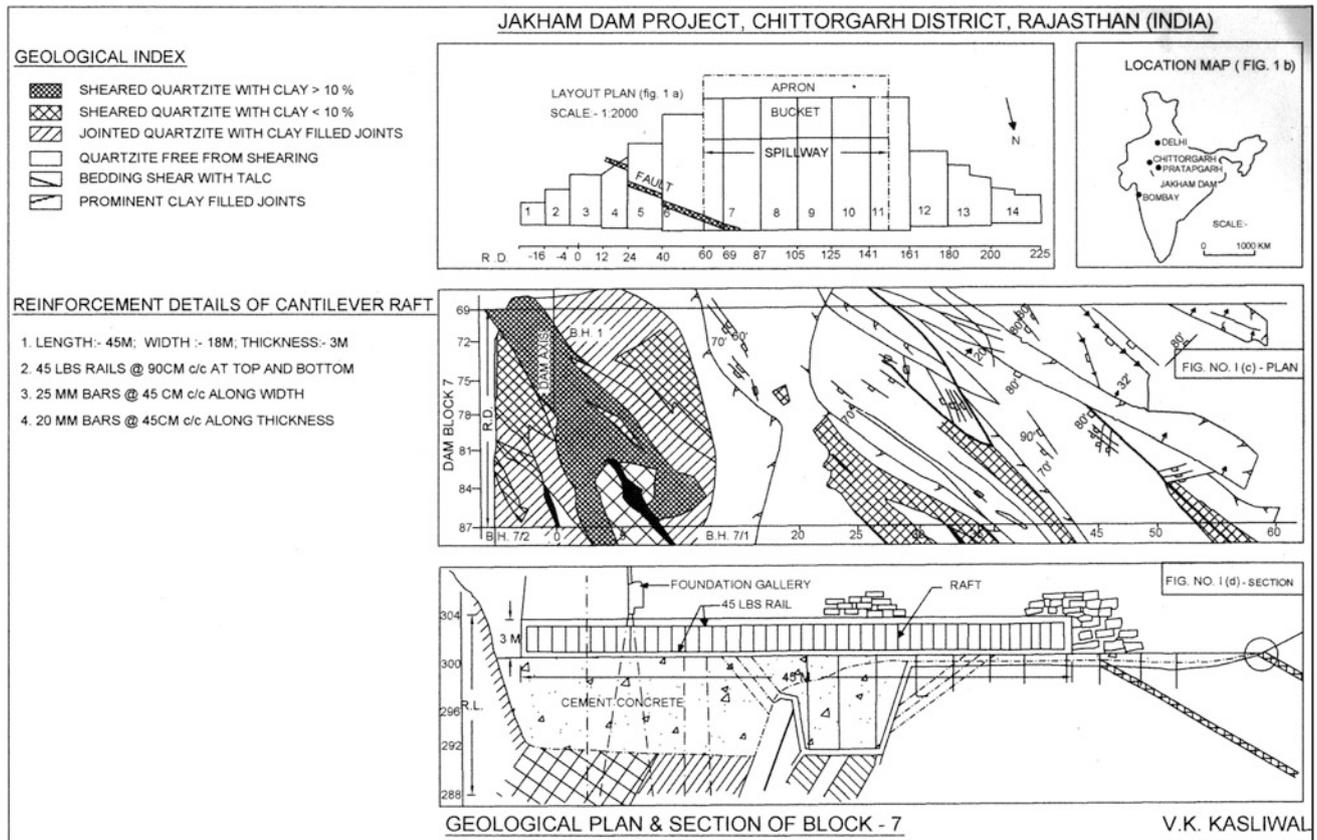
Fig. 141.1 Geological plan and section of block 7

To determine the competence of the various rock units, in situ testing by plate-bearing tests was carried out. These tests gave results which did not match the observed geological conditions (Kasliwal 1983). Hence a detailed geological appraisal of the foundation conditions distinguishing the fractured, faulted and sheared rock vis-a-vis sound rock capable of withstanding the stress conditions was undertaken for all the foundation blocks. This paper, as an example/illustration, brings out by detailed mapping (1:100) of the geology of the 81 m high spillway block no 7, to arrive at foundation treatment.

141.2 Geology

So as to understand the complex geological set up at the dam site, background information thereon shall be helpful in understanding of the foundation problems.

141.2.1 Geology at Dam Site

At the dam site foundation rocks are pre-Aravalli (Archean-II; >2550 m.y) ferruginous quartzites frequently traversed by talcose bands. These generally occur along bedding. They strike askew to the dam axis in a NNW-SSE to N–S direction and dip at 30*–40* in a WSW to West. These quartzites are extensively folded, faulted and sheared. Non-overflow blocks 4–6 on the left abutment and parts of Overflow (spillway) blocks 6 and 7 in the river section are traversed by a 0.5–1.75 m thick fault zone (Fig. 141.1b). The fault zone consists of pulverized quartzite, red ocherous clay and talcose bands. Striking parallel to the fault zone there are a number of shear bands so much so that at times up to 65 % of foundation rocks are affected by them. One such similar 3.5 m thick shear zone has affected the toe-region of blocks 9–12 on the right abutment due to which a large cave with a natural water-spring has been formed Further, the foundation rocks are open jointed and have a Equivalent Permeability of 41.14–54.11 Lugeons,. It is in this complex geological background that the dam has been successfully constructed.

141.2.2 Geology of Block 7

Block 7, lies between R.D. (Reduced Distance) 69 and R.D. 87 m in the deepest part (R.L. 300 m).of river bed. Initially, only one NX borehole was drilled to investigate the rock conditions On the basis of this borehole it was anticipated that suitable foundation rocks shall be available at a depth of

about 8.0 m (R.L. 292 m) but on actual excavations no substantial improvement in the rock conditions was observed. Four more shallow holes were put to find out the rock conditions at depth. These too showed no improvement even at 13 m depth (R.L. 287 m). Although the fault has not affected the foundations of this Block, yet at the Block-joint at R.D. 69 m the effect of the fault is manifested in the footwall of the fault. Here the rocks are broken up into highly sheared and broken bands/strips which are profusely filled with red ocherous clay (Fig. 141.1c). The thickness of this zone is about 7 m. Enclosing this zone were jointed quartzites with clay filled joints so much so that the entire heel region was occupied by them. They extended on the upstream and have an aggregate thickness of about 14 m (Kasliwal 1975). Hence it was not possible to provide a beam.

In situ plate bearing tests were carried out in the fault-affected abutment Block 5 and river bed Block 7 These showed that the values obtained for different rock conditions did not match the observed geology. The deformation modulus varied from $0.39 \times 10 \times 5$ kg/cm $\times 2$ for the fault zone material as compared to $0.28 \times 10 \times 5$ kg/cm $\times 2$ for the jointed rock. It was therefore decided to provide cantilever rafts, for which suitable rock conditions that could take the additional foundation stress needed to be identified.

Large scale (1:100) mapping undertaken to identify competent quartzites showed that between 10 m d/s (downstream) of dam axis to 40 m d/s, the quartzites are sound, free from shearing and contain few clay filled joints, whereas further on the downstream they are blocky jointed. Using this information, doubly acting cantilever raft was provided with the stresses of the heel region being transferred to the sound quartzites in the middle third area of the foundations.

141.3 Conclusions

The foundation rocks of the 81 m high Jakham Dam are quartzites, which contain talcose bands. These have undergone extensive shearing and faulting so much so that treatment for these zones could not be provided on the basis of the formula suggested by USBR or the Japanese Team. In situ tests carried out to determine the deformation modulus of the different rock members did not match the observed geology. Hence, a detailed mapping of the foundation rocks was carried out to delineate the extent of shearing vis-a-vis the sound rock. On the basis of this mapping, foundation area was identified which could be loaded. Hence doubly reinforced cantilever rafts were designed for load transfers using 45 lbs rails at 90 cm c/c with 25 mm distribution bars at 45 cm c/c covering the entire foundation area (Fig. 141.1d). This method has been adopted for all the Blocks 4–12. i.e. the Dam virtually floats on RCC raft foundation; A Dam with Floating Foundations. This solution to the complex and weak rock masses has been successful and the Dam has been operational for more than a decade now.

Reference

Kasliwal VK (1975) A note on the geology of block 7. Jakham Dam. Unpublished report of Geological Survey of India

Kasliwal VK (1983) A geotechnical appraisal of the in situ tests at Jakham Dam, Chittorgarh District, Rajasthan, India. International symposium on in situ testing, vol 2, pp 71–76, Paris

Classification of "Loosened Rock Mass" Based on Cases of Dam Construction

Takahiro Eguchi, Katsuhito Agui, and Yasuhito Sasaki

Abstract

In Japan, dams have been built in the mountainous area of many even now. However, sites that contain rock is not suitable as the basis of the dam is increasing recently. "Loosened rock mass" is one of the bedrock that is not suitable for the foundation of the dam. For this reason, if there is a "loosened rock mass" on the site, it is necessary to countermeasures. For example, excavation of loosened rock mass, modification of dam position, etc. In addition, the range and properties of looseness are different for each site by the terrain, the geology, the geological structure, the formation process of slope. Therefore, in the construction site of the dam, in order to understand exactly the properties and nature of looseness, it is necessary to careful survey. In this study, we tried to systematic classification of loosened rock mass in order to be able to compare the range and properties of the looseness of the site in dam construction in the future. When classifying systematically loosened rock mass, we focused on the following points as an element of the classification. "Slope movement pattern", "range regulation factor", "property regulating factor". We have set five slope movement pattern. And, combining "range regulation factor" and "property regulating factor", we have classified into 15 types and 9 pattern.

142.1 Background and Purpose

In Japan, dams have been built in the mountainous area of many even now. However, sites that contain rock is not suitable as the basis of the dam is increasing recently. Because, the site that dam construction can be is limited.

"Loosened rock mass" is one of the bedrock that is not suitable for the foundation of the dam.

This research defines the state of rock mass called looseness as "situation in which deformation, volume increase, or density reduction etc. Caused by stress release, action of gravity, or action of weathering, etc., Which is called "looseness", causes, occurrence, opening, slippage etc. of cracks, and while the state of the rock mass is retained, overall it has become easily deformed and its non-elastic property becomes large" (Sasaki et al. 2005).

Loosened rock mass is high permeability and low strength as the basis of the dam.

Further, the stability of the slope is low when excavation.

In addition, the nature of the looseness is confirmed in multiple in the loosened rock slope in general.

For this reason, if there is a loosened rock mass on the site, it is necessary to countermeasures. For example, excavation of loosened rock mass, modification of dam position, etc.

In addition, the range and properties of looseness are different for each site by the terrain, the geology, the geological structure, the formation process of slope.

Therefore, in the construction site of the dam, in order to understand exactly the properties and nature of looseness, it is necessary to careful survey.

T. Eguchi (✉) · K. Agui · Y. Sasaki
Public Works Research Institute, 1–6 Minamihara,
Tsukuba 305-8516, Japan
e-mail: eguchi@pwri.go.jp

As a result, at dam construction sites where the rock mass has loosened, the cost of the survey and of countermeasure works tends to be far higher than at an ordinary dam construction site.

Thus, the investigation of loosened rock mass, idea to reduce the cost of investigation has been required.

If the range and properties of looseness are understood early on, more effective ways of the survey methods, the survey positions and the countermeasures are selected. As a result, the costs of surveys and countermeasures are reduced.

If there is a case that the range and properties of looseness are similar, it is possible to develop a survey plan by reference in the case.

However, such a comparison has not been done much. Because, many cases of loosened rock mass have not been systematically organized.

Therefore, in this study, we tried to systematic classification of l loosened rock mass in order to be able to compare the range and properties of the looseness of the site in dam construction in the future.

142.2   Concept and Result of Classification

When classifying systematically loosened rock mass, we focused on the following points as an element of the classification.

Processes of looseness: In order to estimate the properties and range of looseness in three dimensions, it is necessary to estimate the processes of looseness. Therefore, we focused it as an element of the classification.

But, the processes of looseness, are different in each site. Therefore, they can not be used as an element directly.

Therefore, We have focused as a classification element the type of affect slope movement (in this paper, this is called "slope movement pattern") in looseness of the slope.

Geological structure that characterizes the range of looseness (in this paper, this is called "range restriction factor"): Results of the analysis of the case, We have confirmed plurality of site that the range of the looseness is limited by geological structure (for example, fault).

If this structure is found, the range of looseness easily can be estimated by checking the distribution. Therefore, we focused it as an element of the classification.

Geological property or structure that characterizes the properties of the loosened rock (in this paper, this is called "property classification factor"): Results of the analysis of the case, We have confirmed plurality of sight that geology is related to the property of loose, for example, distribution areas of specific geology and range of crack opening is roughly consistent.

If this geological property or structure is found, the property or distribution areas of looseing easily can be estimated by checking the distribution. Therefore, we focused it as an element of the classification.

How to combine elements is as follows. First, We have classified the cases of looseness using the "slope movement pattern". Next, we have subdivided there using the "range restricting factor" and "property regulating factor".

Dam site number of the subject of the current study was 39.

In the 39 cases, "slope movement pattern" was confirmed five cases.

"Range restriction factors" was confirmed eight cases (example: fault, low angle cracs, etc.). "Property classification factor" was confirmed four cases (example: milonitization, directly under weathered granite, etc.).

Combining them, we have classified into 15 types and 9 pattern. Classification results are shown in Table 142.1.

142.3   The Contents of the Classification

Slope movement pattern are classified into the following five.
(a) Toppling
(b) Dip slope deformation
(c) Gravity deformation
(d) Crack opening of the shallow part of stress release
(e) Landslide

Here, the definition of (c) Gravitational deformation is as follows. There is the opening cracks or small deformation of rock mass in deep point of the slope, but there isn't toppling or slip. The definition of (d) Crack opening of the shallow part by stress release is as follows. There is opening cracks in shallow part of the slope, but there isn't a small deformation of the rock mass.

Figure 142.1 shows an exemplary four cases of slope movement pattern excluding (e).
(A) of slope movement pattern is toppling. And range restriction factor is low angle cracks. In this slope, chart falls down, and the influx of clay and the opening of the crack is happening. Just above the black slate, low angle cracks are well developed. There isn't looseing under the low angle cracks.
(B) of slope movement pattern is dip slope deformation. And range restriction factor is deterioration appears along the low angle layer, but does not extend overall. A part of pumice tuff is deteriorated. And sandy tuff at the top of the pumice is formed structure of the blocks.
(C) of slope movement pattern is gravity deformation. And the property classification factor is the link of the weak layer classifying degree of looseness. The river side of

Table 142.1 Result of classification of loosened rock

Forms of variation	Toppling		Dip slope deformation		Gravity deformation	Crack opening of shallow part by stress release			Landslide
Pattern name	T-1	T-2	T-3	D-1	G-1	G-2	O-1	O-2	L-1
Existence of range restricting factors	O	×	×	O	×	×	×	×	O
Example of range restricting factors	•Fault •Low angle crack			•Intersection of 2 faults •Fault and that with low-angle layer deterioration intersecting •Fault •That with low angle layer strength reduction •Deterioration appears along the low angle layer, but does not extend overall					•Slip surface
Existence of property classification factor	×	O	×	×	O	×	O	×	×
Example of property classification factor		•Myloniteization			•Link of weak layer classifying degree of looseness		•Directly under weathered granite •Along bedding plane		
Number of cases	3	1	6	6	4	8	2	5	4
Number of types	2	1	1	5	1	1	2	1	1

Fig. 142.1 Representative examples. **a** Example of toppling. **b** Example of dip slope deformation. **c** Example of gravity deformation. **d** Example of crack opening of shallow part by stress release
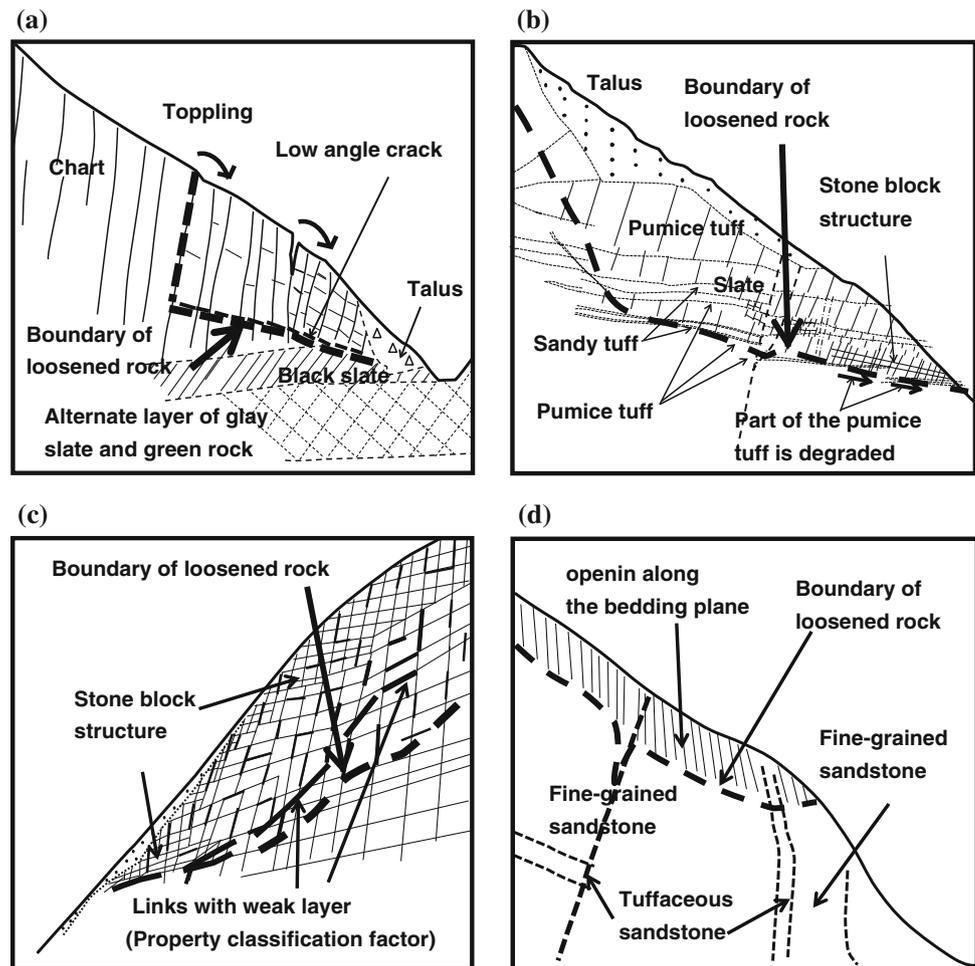
the weak layer, the phenomenon of opening cracks, the structure of the blocks, or the deformation of the rock mass occurs. The mountain side of the weak layer, the deformation degree of rock mass and the opening width of the crack is small.

(D) of slope movement pattern is gravity deformation. Range of looseness is limited to the surface layer portion. Crack is open to the bedding planes along the fine-grained sandstone.

142.4 Concept of Investigation by the Classification

It is summarized as follows the concept of loose rock survey based on the results of classification.

The toppling is subdivided into three types as shown below. In type 1, range restriction factor is present. In type 2, property classification factor is present. Both factors are not present in type 3. Therefore, the survey of the toppling, it is important to confirm the existence of "range restricting factor" and "property classification factor" firstly.

In all cases of dip slope deformation and landslide, range regulation factors were found. Therefore, in these slope movement patterns, it is advisable to look for a similar type by checking the contents of the range restriction factor.

In all cases of gravity deformation and crack opening of the shallow part of stress release, range regulation factor was not confirmed.

However, a few cases were found the property regulating factor. Therefore, in these slope movement patterns, it is advisable to look for a similar type by checking the contents of the property regulating factor.

142.5 Summary

In this study, we tried to systematic classification of loose rock in order to be able to compare the range and properties of the looseness of the site in dam construction in the future.

When classifying systematically loose rock, we focused on the following points as an element of the classification. "Slope movement pattern", "range regulation factor", "property regulating factor". We have set five slope

movement pattern. And, combining "range regulation factor"and "property regulating factor", we have classified into 15 types and 9 pattern.

By using this classification, when you survey a rock looseness the future, we can select the cases that are similar to the classification case. And we can select the appropriate methods of countermeasures and survey position. As a result, it is expected that the cost related to survey and countermeasure for loose rock is reduced.

And, We want to continue this research and increase the classification pattern of loose rock.

References

Eguchi T et al (2012) Pattern classification of loose rock in dam construction case. In: Proceedings of annual meeting of JSEG, pp 85–86 (in Japanese)

Sasaki Y et al (2005) Actual situation and tentative classification of loose rock at dam site. Eng Dams 228:10 (in Japanese)

Sasaki Y (1999) Survey methods of loosened rock. Civ Eng J 41(2):8–9 (in Japanese)

Watari M (2005) Original birth of active landslide and "sagging" by gravitational deformation on mountain slope. J Jpn Landslide Soc Landslides 41(5):503–512 (in Japanese)

Numerical Analysis of a Crossover Cavern Excavated in a Complex Rock Mass as Part of the Hong Kong Express Rail Link Project

D.K. Koungelis and R. Lyall

Abstract

Kier Kaden OSSA Joint Venture is currently constructing Express Rail Link Contract No 824—Ngau Tam Mei to Tai Kong Po Tunnels for the MTR Corporation Limited. A critical review of the available ground investigation data and the regional geology was carried out to investigate the geological characteristics of the area surrounding Ngau Tam Mei shaft and the Crossover Cavern. The following paper outlines the methodology for designing the temporary support necessary for the Crossover Cavern to support the excavation during the construction period and until the permanent lining has been cast. The design process outlined below includes an assessment of the required support using the 'Q' method and empirical design charts developed by the Norwegian Geotechnical Institute, followed by a series of numerical analysis using UDEC to verify the suitability of the temporary support design.

143.1 Introduction

Donaldson Associates Limited (DAL) was appointed by Kier Kaden OSSA Joint Venture (KKOJV) to design a section of tunnel to be constructed as part of the Guangzhou-Shenzhen-Hong Kong Express Rail Link (XRL). The contract (C824) involves design of the temporary and permanent linings for 2.6 km of running tunnel comprising twin bore single track SCL tunnels and a twin track Crossover Cavern (26.9 m wide by 16.6 m high by 115 m long). Permanent shafts (NTM and TKP) constructed at either end of the contract. DAL designed the temporary support for all tunnels and shafts and permanent lining for tunnels only. Preliminary ground investigation in the area of NTM shaft identified shearing features which meant that ground investigation data was limited due to difficult terrain resulted in a number of uncertainties about the ground conditions adjacent to the NTM shaft. DAL considered the overall rock quality in the area to be better than anticipated at tender stage and that shear zones recorded in the ground investigation could in fact be weathered hydrothermal zones which exhibit dramatically different characteristics to conventional shear zones. A number of locations for the Crossover Cavern were considered during a value engineering exercise and it was agreed to build the cavern 25 m south of the shaft, connected by a shortened length of tunnel to limit or negate any interaction between the Crossover Cavern and the NTM shaft from an engineering and technical point of view.

143.2 Geology and Ground Investigation

The geology at the location of the Crossover Cavern is Middle Jurassic Tai Mo Shan Formation of the Tsuen Wan Volcanic Group which comprises predominantly lapilli-lithic bearing coarse ash crystal tuff (GCO 1988). These are noted to be some of the oldest group of rocks within Hong Kong and were

D.K. Koungelis (✉)
Donaldson Associates Limited, Glasgow, Scotland
e-mail: d.koungelis@donaldsonassociates.com

R. Lyall
Donaldson Associates (Asia) Limited, Hong Kong, China
e-mail: r.lyall@donaldsonassociates.com

Fig. 143.1 Cores of Fe stained tuff adjacent to hydrothermal mineralized zones and zones of no recovery due to disturbance during drilling

formed prior to the most recent granitic intrusions which are dominant on Hong Kong Island and the Kowloon Peninsula; therefore the rock at NTM has been subjected to regional volcanic/hydrothermal activities. Additionally, the Geological memoir (GCO 1989) identifies some WSW-ENE striking bands of 'sandstone' (possibly volcaniclastic sedimentary units) along with a dyke of feldsparphyric rhyolite to the south of the proposed Cavern on the southern slope of Kai Keung Leng, the mountain which is being tunnelled through. The effect of hydrothermal activity in altering the geological conditions is highlighted by (Williams 1991). The majority of tunnels in Hong Kong have been built in granites and south of the Tai Mo Shan fault. Other than small water tunnels, no large diameter railway tunnels have been constructed within ground conditions similar to this site. Three phases of ground investigation were carried out at various points throughout the project design stage and prior to construction. These were: Preliminary Design Stage, Detailed Design Stage and Post Contract Award (AGI). The preliminary ground investigation identified zones of highly weathered tuff and no recovery which the borehole logs recorded as 'fault gouge'. Similar features were identified in the detailed design ground investigation which led to the interpretation of faulted or sheared ground adjacent to the NTM shaft. A number of quartz dykes

and mineralisation associated with hydrothermal fluids such as pyrite and galena were also recorded in the boreholes. The DAL geotechnical team identified this mineralisation to be both 'fresh' and 'weathered' therefore used this as a basis for re-evaluating the geological conditions in the areas by considering the regional geology. The review concluded that shearing of the rock mass occurred in the past however mineral rich hydrothermal fluids had infiltrated the rock mass predominantly along the open fissures created by shearing. Over time, these fissures were filled by quartz and sulphides rich minerals such as pyrite and galena effectively 'healing' the rock mass and improving the overall rock quality. However, where water is still able to flow along joints or along the quartz veins, oxidation of the pyrite occurred causing the rock mass to become deeply iron stained and to form localised discrete weathering features which have been disturbed during drilling and recorded as "no recovery" (Fig. 143.1).

143.3   Analysis

A review of all available data was carried out to assess the rock mass characteristics and derive 'Q' (Barton et al. 1974) ranges to be used for the design of the temporary support for

Table 143.1 Temporary support requirements for the crossover cavern

Temporary support class	Mapped 'Q' range	Dowel spacing (m)	Dowel length (m)	Sprayed concrete thickness (mm)
CC-3	1 ≤ 'Q' < 2.5	1.70	8.00	125
CC-4	0.1 ≤ 'Q' < 1	1.30	8.00	250

Table 143.2 Summary of joint set orientations

Joint set number	Dip (°)	Dip direction (°)	Apparent dip (°)
1	61	148	339
2	03	148	355
3	67	355	329

the rock mass within the Crossover Cavern. Dip and dip direction information, was input into DIPS software to allow pole plots and contour plots to be produced. These plots have been used to assess the number and orientation of joints within the rock mass. Numerical modelling, using the discrete element code UDEC was carried out to assess the stability of the Crossover Cavern during the various excavation stages. Details of each of these design elements are discussed in the following sections. The initial stage in the determination of the temporary support for the Crossover Cavern was carried out using the empirical 'Q'-method. 'Q' value ranges (between 0.1 ≤ 'Q' ≥ 6) for design were agreed with the main contractor.

Temporary support for all 'Q' ranges was determined for detailed design. This paper focuses only on the assessment of a combination of temporary support classes; i.e. CC-3 and CC-4 (Table 143.1), where a 5 m thick discrete zone (i.e. CC-4—Hydrothermal zone) exists above crown of the Crossover Cavern, within a rock mass of CC-3 (Fig. 143.2). Hence, numerical analysis predictions will be presented only for this case. For these analyses, discontinuity orientations (dip/dip direction) were collated and input into DIPS. Stereographical equal area, lower hemisphere projections were used to generate contour plots allowing the dominant joint sets and their relationships to be determined (Table 143.2).

Numerical modelling of the Crossover Cavern has been carried out using UDEC. The purpose of these calculations was to interrogate the structural forces imposed on the temporary support sprayed concrete and rock bolts, and

resulting deformations, following each stage of construction. The aim of the numerical modelling was also to verify that the temporary support determined (Table 143.1) using empirical methods (Barton et al. 1974) is adequate to stabilise the open excavation until such a time as the permanent lining is installed. Predicted loads imposed on the bolts have been used to select dowel diameter and steel grade and that the bolt length extends beyond the anticipated yield zone. A deformable block model using Mohr Coulomb criterion has been adopted, assigning strength and deformation parameters to the blocks. Immediately surrounding the Crossover Cavern, a joint pattern was superimposed on top of the deformable block model to determine the effect of the jointing, which will create an anisotropy of movement and stress (Fig. 143.2). These discontinuities were assigned shear strength parameters (Table 143.4). The rock mass parameters are presented in Table 143.3. Design parameters for the analysis were based on intact rock properties. The rock mass was assumed to be dry during construction with a coefficient of earth pressure at rest Ko = 1.2. The overburden depth of 140 m has been modelled using an equivalent 'block load'. 50 % of stress relaxation was assumed prior to any temporary support installation. The tunnel profile and excavation sequence has been modelled, including the sequence of support installation (bolts and sprayed concrete) following excavation. To allow bolt support to be installed immediately following excavation of the individual headings, 4.0 m long Swellex friction dowels will also be installed on a staggered pattern between the 8.0 m long bolts. Each phase of excavation is allowed to run to equilibrium before the next dig and support phase is modelled.

Fig. 143.2 UDEC block model
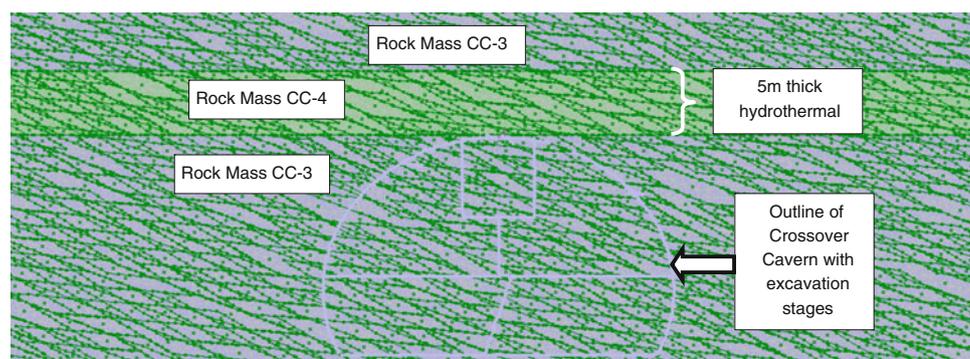
Table 143.3 Intact rock properties for UDEC model

Temp. Support class	Density (kg/m³)	Bulk modulus (GPa)	Shear modulus (GPa)	Friction angle (°)	Cohesion (MPa)	Tension (MPa)	Dilation (°)
CC-3	2600	13.8	10.4	35	8.337	0	10
CC-4	2600	5.5	1.85	30	0.525	0	0

Table 143.4 Joint properties for UDEC model

Temp. support class	Normal stiffness (GPa/m)	Shear stiffness (GPa/m)	Friction angle (°)	Dilation (°)	Tension (kPa)	Cohesion (kPa)
CC-3	12	1.2	37	7	0	50
CC-4	7	1.0	30	0	0	0

Fig. 143.3 Predicted rock dowel loads
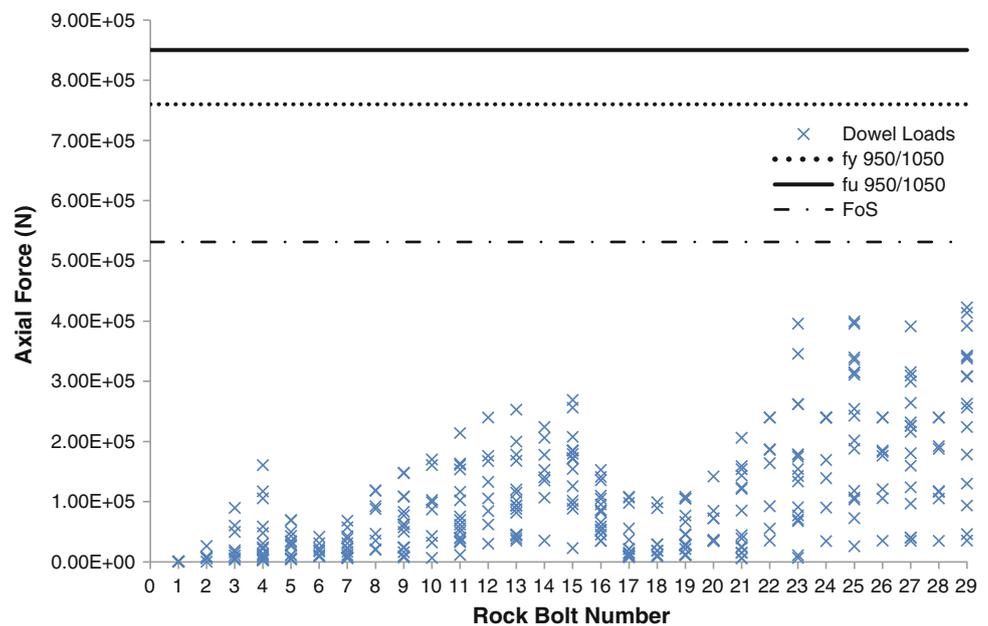
143.4 UDEC Predictions

The final deformations and forces developed in the rock bolts following excavation and installation of temporary support from the UDEC analysis is presented in Figs. 143.3 and 143.4. The predicted maximum vertical displacements (occurred at the crown) were limited to <50 mm (Fig. 143.4). The factor of safety achieved (broken line on Fig. 143.3) on the loads developed in the high yield steel bars (solid line on Fig. 143.3 indicates the ultimate load of

the rock bolts) was satisfactory (FoS ≥ 2.0 being achieved). Based on the UDEC output, the adoption of 26.5 and 32 mm diameter high yield grouted steel bar (Grade 950/1,050 N/mm²) is considered to be appropriate for the Crossover Cavern for temporary support class CC-3 and CC-4 respectively. The analysis indicate that the recommended temporary support for the particular ground conditions, will be satisfactory and the excavation will remain stable throughout construction. Figure 143.5 shows the Cavern excavation finished with the required temporary support installed.
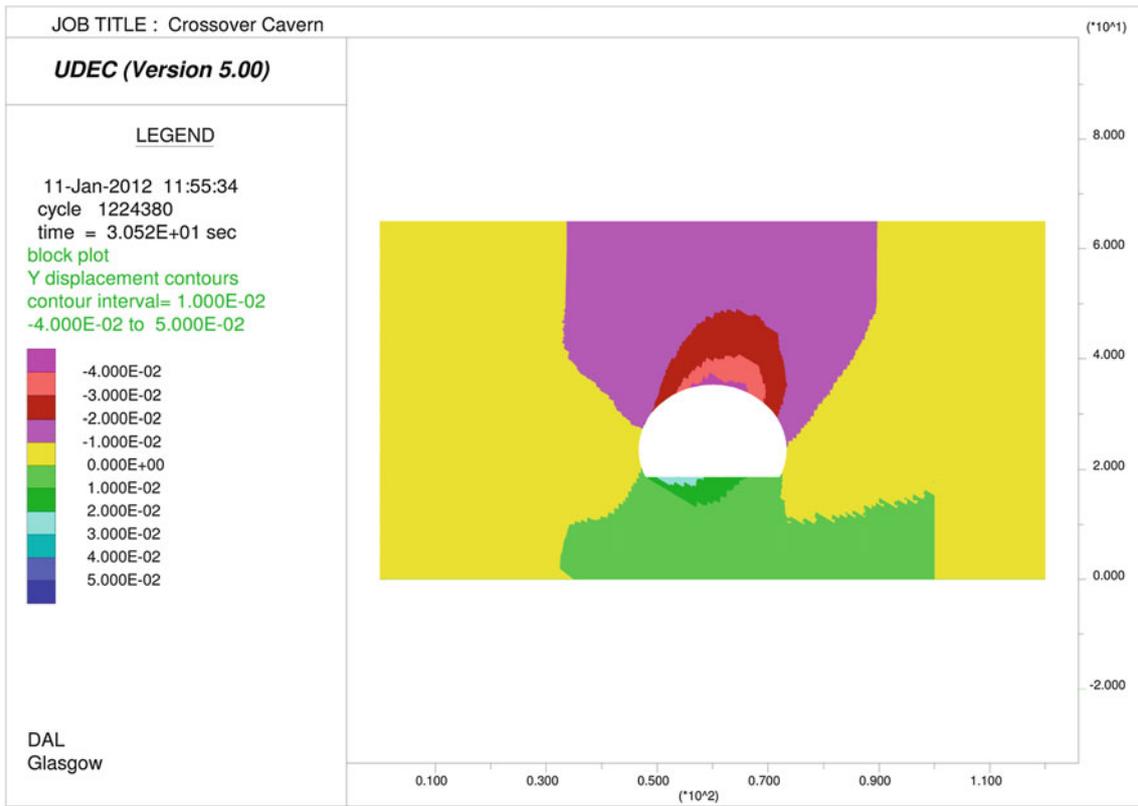
Fig. 143.4 Predicted vertical displacements

Fig. 143.5 Full face excavation of the Crossover Cavern

143.5   Discussion

A critical review of the available ground investigation data and the regional geology was carried out for C824 to investigate the geological characteristics of the Crossover Cavern. The ground conditions were found to be better than anticipated at tender stage due to hydrothermal minerailsation having a positive impact on the rock mass, confirming the 26.9 m span Crossover Cavern could be moved into an area previously thought to contain a number of shear zones.

References

GCO (1988) Hong Kong geological survey sheet 6 (1:20,000). Solid and superficial geology for Yuen Long. Geotechnical Control Office, Hong Kong

GCO (1989) Hong Kong geological survey memoir no. 3. Geology of the Western New Territories. Geotechnical Control Office, Hong Kong

Williams T (1991) The story of Lin Ma Lead Mine, 1915–1962. Geol Soc Hong Kong Newslett 9(4):3–27

Barton NR, Lien R, Lunde J (1974) Engineering classification of rock masses for the design of tunnel support. Rock Mech 6(4):189–236

The Influence of Geological History on Preferred Particle Orientation and the Observed Anisotropy of Over Consolidated UK Mudrocks

144

Stephen Wilkinson and Clark Fenton

Abstract

One of the major aspects of mudrocks which influences their engineering behaviour is anisotropy, especially that of strength and stiffness. Anisotropy is caused by an underlying preferential alignment in particle orientations. Many factors contribute to the production of enhanced preferred particle orientations including: sedimentation process; particle shapes; bioturbation; burial depth; tectonism; weathering; and aging; in short the material's entire geological history. Initial structure is formed by sedimentation processes during deposition. These are then modified by post-depositional events. With burial, the particles of sediments tend to rearrange to allow for a decrease in void ratio which is combined with an expulsion of water from the soil. Much of the southern UK is underlain by mudrocks of Mesozoic and Cenozoic age displaying some degree of preferred particle orientation and hence anisotropy in their engineering behaviour. The degree of particle orientation is quantified by analysis using environmental scanning electron microscope imagery. Anisotropy in engineering behaviour has been quantified by a range of laboratory and field, static and dynamic, methods that allow the anisotropic elastic behaviour of the mudrocks to be investigated at very small strains. Generally good agreement is observed between four fully independent methods for evaluating the elastic G_{VH} stiffness mode. The results of both the image analysis and the laboratory testing build up a picture of microstructure anisotropy that results from the total geological history of each of the mudrocks investigated.

144.1 Introduction

Microstructure is defined as the combination of the arrangement of particles which is known as "fabric" and the cementation between particles which is known as "bonding" (Gasparre and Coop 2008). Every element of the microstructure of mudrocks is formed as a result of events occurring during the mudrocks geological history. One of the most important aspects of soil fabric for engineers is anisotropy of properties such as strength and stiffness. Anisotropy is caused by the co-alignment of platy particles such as clay minerals. Although particle alignments can form during deposition (Barden and Sides 1971), alignments are often enhanced through an increase in the applied load i. e., burial. This process has been observed both experimentally in the laboratory (Vasseur et al. 1995), and through field observations (Ho et al. 1999). Other factors which influence the orientation of particles during burial are determined within the environment of deposition (Kim et al.

S. Wilkinson
Department of Civil Engineering, Xi'an Jiaotong-Liverpool University, Suzhou, China

C. Fenton (✉)
Department of Civil and Environmental Engineering, Imperial College London, London, UK
e-mail: c.fenton@imperial.ac.uk

2001), the chemistry of pore fluids (Meade 1964). Thus many aspects of the geological history of a soil can influence its final degree of anisotropy.

144.2 Measurement of Preferred Particle Orientation

High quality, undisturbed block or wireline cored samples were obtained from several sites (Fig. 144.1) in the southern part of the UK to allow comparisons with previously analysed samples of London Clay (e.g. Gasparre et al. 2007). Each site was selected to minimise the influence of post-depositional tectonism (Wilkinson 2011). All of the samples were imaged using an environmental scanning electron microscope (E-SEM). Vertically and horizontally orientated broken surfaces were imaged separately (Fig. 144.2). Three different techniques were used to make measurements of preferred particle orientation. The results presented here (Table 144.1) are the ratio of the maximum and minimum eigenvalues (λ_a) of the orientation matrix:

$$OM = \begin{bmatrix} \frac{1}{n}\sum_{i=1}^{n}\cos\theta_i\cos\theta_i & \frac{1}{n}\sum_{i=1}^{n}\cos\theta_i\sin\theta_i \\ \frac{1}{n}\sum_{i=1}^{n}\cos\theta_i\sin\theta_i & \frac{1}{n}\sum_{i=1}^{n}\sin\theta_i\sin\theta_i \end{bmatrix} = \begin{bmatrix} a & b \\ c & d \end{bmatrix}$$

$$\lambda e = \frac{\lambda_{\max}}{\lambda_{\min}} \quad \text{where} \quad \lambda = \frac{a+d}{2} \pm \left(4bc + (a-d)^2\right)^{1/2}$$

where θ is the maximum ellipse angle for an ellipse which has the same moment of inertia as particles identified using, in this case, the upper 25 % of grey levels (shades from a light grey to white) within the electron microscope images taken of broken surfaces in a vertical orientation. As anisotropy of strength and stiffness is derived from the comparison of vertically and horizontally orientated samples, preferred particle orientation should theoretically also require the comparison of vertically and horizontally orientated broken surfaces. However, samples with high measured preferred particle orientations on vertically orientated surfaces in some cases show increased preferred particle orientation on horizontally orientated surfaces, often caused by steps in the surface between the horizontally orientated planes. Thus a comparison between preferred particle orientations from vertically and horizontally orientated samples has a tendency to reduce the measured level of preferred particle orientation in strongly aligned samples. Therefore the best measurements are obtained using vertically orientated samples alone.
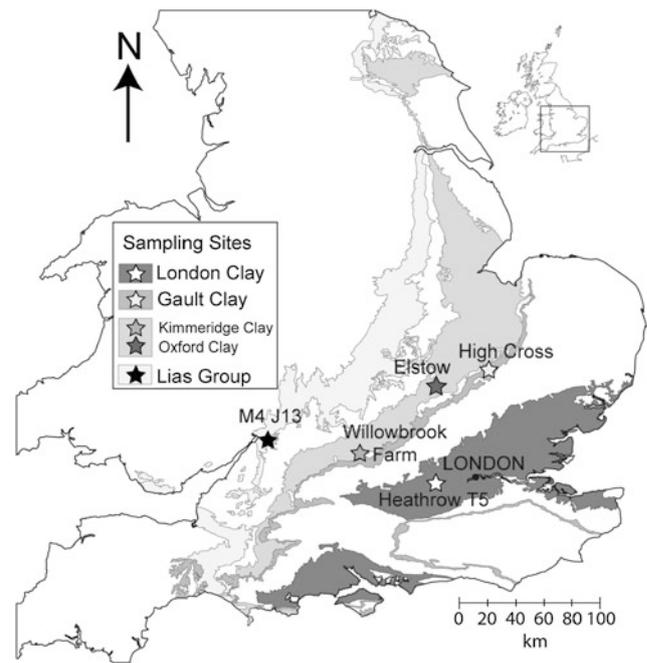
Fig. 144.1 Mudrock sampling locations

In addition to the method above, half circle addition and three-dimensional surface aspect analysis was also used to quantify anisotropy. All three methods produced similar results (Wilkinson 2011).

Comparison of the quantified measurements of preferred particle orientation and laboratory measurements of the anisotropy of elastic stiffness (Wilkinson et al. 2011), show a good correlation (Fig. 144.3).

144.3 Discussion

Since particle arrangements are a result of geological history, it is implied that geological observations may be used to predict/indicate the engineering behaviour of mudrocks. The preferred particle orientations in turn have a strong correlation with engineering behaviour. The depositional history of soils can be inferred through the field observations and classification of soils. Burial and uplift histories can be assessed by a combination of stratigraphic reasoning, measurement of the uplift of terraces and through apatite fission track analysis. By assuming constant geothermal gradients the maximum depths of burial can be assessed. High values of preferred particle alignment are obtained for the Gault, Oxford, and Lias Group Clays, spanning a broad range of burial depths. This shows that although burial depth is important for the development of individual mudrock

Fig. 144.2 Normalised rose diagrams of particle orientations for individual images for all sampled mudrocks. Note comparison of particle alignment between vertical and horizontal cut surfaces
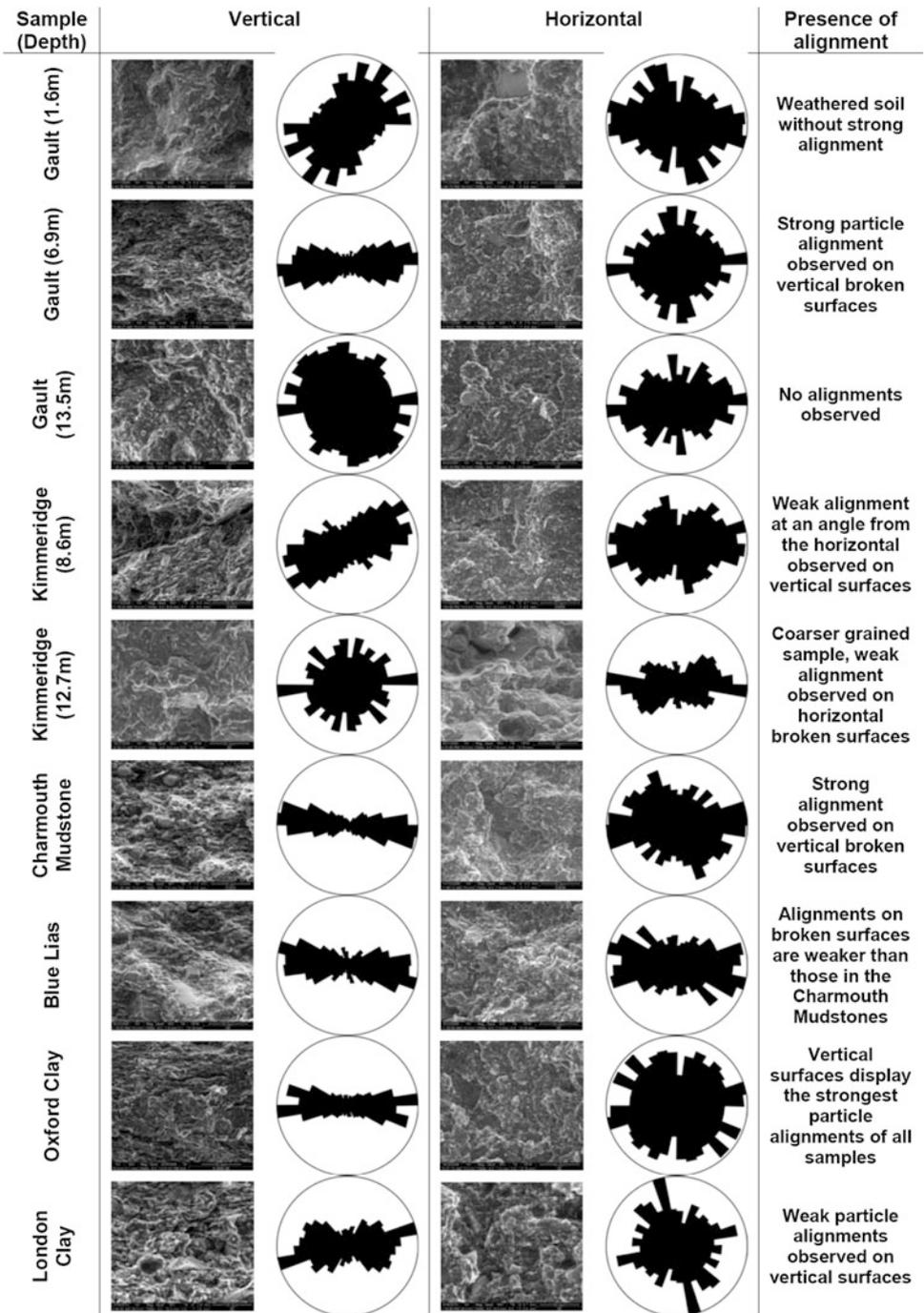
Table 144.1 The average value of preferred particle orientation based on all images take from a single sample surface using magnifications between X600 and X1500

	Gault			Kimmeridge		Charmouth mudstone	Blue lias	Oxford clay	London clay
Depth	1.6	6.9	13.5	8.6	12.7				
λa	1.54	3.28	1.61	2.05	1.44	3.64	2.72	3.97	2.13
SD	0.19	0.38	0.41	0.43	0.19	0.65	0.61	0.78	0.58

Standard deviations (SD) from image measurement tend to be higher where preferred particle orientation is higher
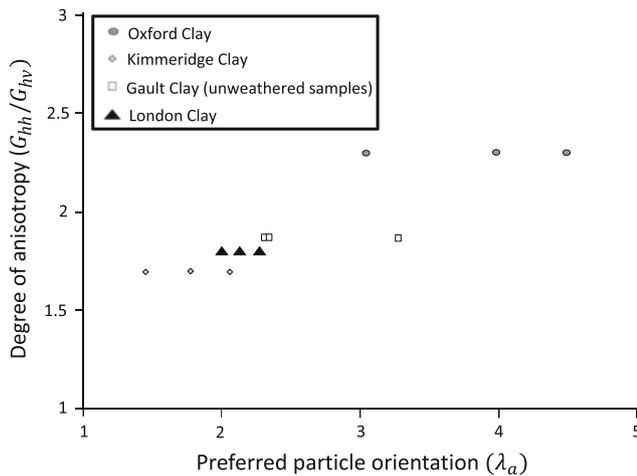
Fig. 144.3 Plot of the degree of anisotropy of stiffness and measurements of preferred particle orientation

structure, it cannot be used alone as an indicator of the preferred particle orientation. Arguably the depositional setting of each mudrock horizon is more important as it creates the initial conditions from which each mudrock evolves during its burial and uplift history. For example, the Kimmeridge Clay samples are from a shallow, coarse grained area of the depositional basin. These samples contain a large proportion of sand and silt grains. Some horizons have a relatively low measurement of preferred particle orientation, as the silt grains prevent the platy clay minerals from aligning (Barden and Sides 1971).

The final element for consideration in the geotechnical cycle is the weathering and erosion of soils. The evidence from the shallow samples of the Gault Clay is that weathering results in a reduction in preferred particle orientation. One out of five sample of the shallow Gault Clay samples displayed a much stronger preferred particle orientation. The enhanced weathering along joints, which as they are weaker zones are preferentially susceptible for forming the broken surfaces, completely replaces the orientations which are present in regions in the blocks between the joint surfaces. With continued weathering, depositional and burial structures may be completely removed.

144.4 Conclusions

Structural and strength anisotropy in mudrocks is determined by the geological history of the material. The full geological history of a sample can be defined by burial and uplift histories which can be well identified using apatite fission track analysis data. Although burial is important for the formation of preferential orientations in a single mudrock it cannot be used as a unique indicator to compare different mudrocks. Within an individual mudrock the burial history determines how structure evolves. The depositional variation within mudrocks is greater than that between any other sediment type and so most mudrock formations are not directly comparable. Within individual formations natural variations in the depositional environment can cause the structure and engineering properties of a mudrock to alter within the stratigraphic sequence. In deeply buried unweathered mudrocks, clay mineral and low silt content are good indicators of high levels of particle alignment. The most important factors which can reduce alignment in soils are the presence of silt/sand and weathering processes. The first is a result of the environment of deposition the second is a result of the present day environment.

References

Barden L, Sides G (1971) Sample disturbance in the investigation of clay structure. Géotechnique 21(3):211–222

Gasparre A, Coop MR (2008) Quantification of the effects of structure on the compression of a stiff clay. Can Geotech J 45:1324–1334

Gasparre A, Nishimura S, Coop MR, Jardine RJ (2007) The influence of structure on the behaviour of London clay. Géotechnique 57 (1):19–31

Ho N, Peacor DR, Pluijm BAVd (1999) Preferred orientation of phyllosilicates in Gulf Coast mudstones and relation to the smectite-illite transition. Clays Clay Miner 47(4):495–504

Kim JW, Lee YDE, Tieh TT (2001) Effects of laboratory consolidation on petrophysical properties of fine-grained marine sediments: electron microscope observations. Mar Georesour Geotechnol 18:347–360

Meade RH (1964) Removal of water and rearrangement of particles during the compaction of clayey sediments—review. US Geol Surv Prof Pap 479-B:23 p

Vasseur G, Djeran-Maigre I, Grunberger D, Rousset G, Tessier D, Velde B (1995) Evolution of structural and physical parameters of clays during experimental compaction. Mar Pet Geol 12(8):941–954

Wilkinson S (2011) The microstructure of UK mudrocks. PhD: unpublished PhD thesis, Imperial College London, 400 p

Wilkinson SA, Brosse CH, Fenton R, Kamal H, Jardine RJ, Coop MR (2011) An integrated geotechnical study of UK mudrocks. In: Anagnostopoulos et al (eds) Proceedings of the 15th European conference on soil mechanics and geotechnical engineering, part 1, pp 305–210

Mechanical Characterization of Weathered Schists

145

Thomas Le Cor, Damien Rangeard, Véronique Merrien-Soukatchoff, and Jérôme Simon

Abstract

Fractured and weathered rocks such as Brioverian schists are encountered in the West part of France. Their important variability, in terms of alteration and mechanical properties, is a problem regarding the geotechnical design of retaining structures and are foreseen when excavating the second subway line in the city of Rennes starting in 2014. Results of mechanical laboratory characterization carried out on schist samples extracted from various locations in Rennes are presented. Uniaxial compression test and direct shear test results show an important variability of the material and a great sensitivity to water.

145.1 Introduction

Previous studies on the Brioverian schist (Jégouzo 1973; Le Corre 1978) have focused on the geological context of its formation whereas its mechanical behaviour is less

T. Le Cor (✉) · D. Rangeard
Civil Engineering and Mechanical Engineering Laboratory, INSA/IUT Rennes, European University of Brittany, 20 Avenue Des Buttes de Coësmes, CS 14315, 35043 Rennes Cedex, France
e-mail: thomas.lecor@groupe-dacquin.fr

D. Rangeard
e-mail: damien.rangeard@insa-rennes.fr

T. Le Cor · J. Simon
Design department, Groupe Dacquin, Parc d'activités des Portes de Bretagne Servon-sur-Vilaine, 35530 Brittany, France
e-mail: jerome.simon@groupe-dacquin.fr

V. Merrien-Soukatchoff
Equipe Génie civil & Géotechnique, Département Ingénierie de la Construction et Energétique, CNAM, 2, Rue Conté, Case Courrier 341, 75141 Paris Cedex 03, France
e-mail: veronique.merrien_soukatchoff@cnam.fr

V. Merrien-Soukatchoff
Laboratoire de Géodésie et de Géomatique (L2G), Le Mans, France

acknowledged. The Brioverian massif is the occidental part of the European Variscan belt and is composed of sediments that formation age estimates between 750 and 520 Ma. These sediments were submitted to a greenschist type metamorphism. The numerous constructions in Brioverian formations in Rennes, including the excavation of the second subway line beginning in 2014, incites to improve the knowledge on the mechanical properties of this type of ground. The high variability in a matter of degree of fracturing, alteration, clay content (Le Cor et al. 2013) is an important problem when it comes to determining mechanical parameters used to design retaining structures. Considering the high density of fractures of the Brioverian schist, mechanical characterization requires to study the intact rock matrix and the discontinuities in order to have a global understanding of its behaviour.

To evaluate the mechanical strength of the rock matrix, uniaxial compression tests were carried out on plane-parallel samples extracted from different sites spread over Rennes (Fig. 145.1). The mechanical parameters of opened discontinuities, in the direction of the schistosity (cohesion and friction angle), corresponding to the weakest plane of the rock, were determined using direct shear tests on small samples (sheared surface of approximately 50 × 30 mm).
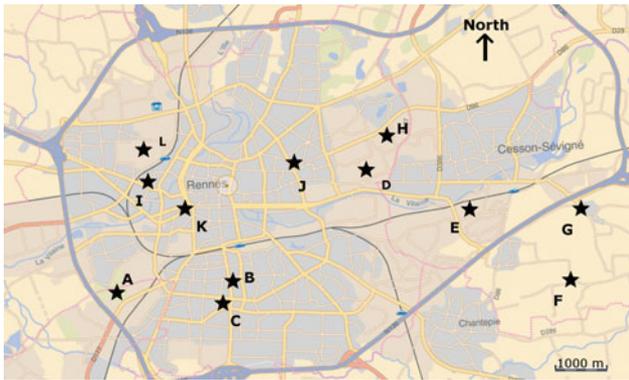
Fig. 145.1 Localization of the sampling sites (www.Géoportail.fr)

The results of these two types of tests are presented in the next sections of this paper.

145.2 Uniaxial Compression Tests

Uniaxial compression test is a simple method used to estimate the uniaxial compression strength (UCS) of a material (concrete, rock…) whether with isotropic or anisotropic mechanical properties (Nasseri 2003). Brioverian schists are foliated inducing a transverse isotropic behaviour. Due to the impossibility of drilling the rock without breaking it, the tested samples were plane-parallel and cut in an approximate size of 60 × 30 × 30 mm. Difficulties of sampling in weathered rocks is not unusual (Marques et al. 2010). Consequently, only specimens with a loading direction according to the schistosity have been tested to present. Samples with schistosity oriented perpendicularly to the loading could not be obtained because of losses during the cutting. In order to obtain a good planarity and parallelism of the loading faces of the samples, a plaster treatment was tested but gave the same results as the use of a ball joint between the loading plate and the loading axis which required much less preparation. Each site was tested using at least 6 samples stored in different conditions: 3 samples
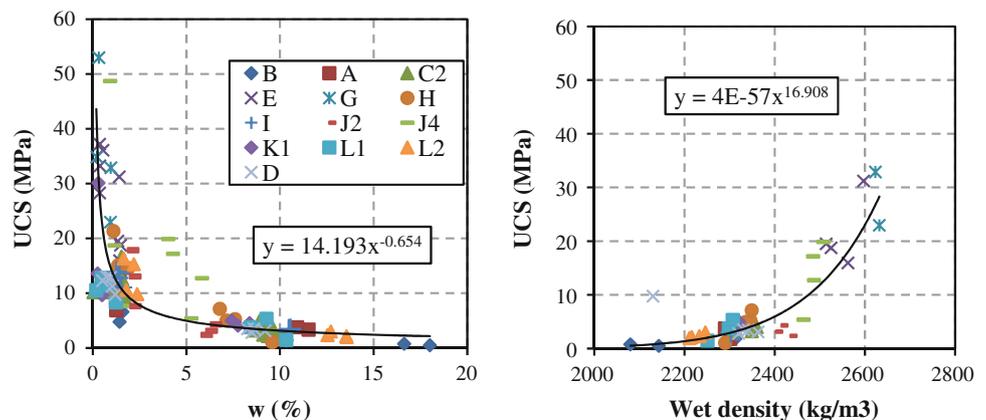
dried during a week at ambient temperature (water content lower than 1 %) and 3 samples immersed in water during a week (water content of the samples varied from 1 to 17 %). In all, 94 samples were tested: 48 "dry" samples and 46 "wet" samples. The results obtained are displayed on Figs. 145.2 and 145.3

An important influence of water condition is observed: the UCS decrease with the increase of the water content of the samples, when on the contrary, the UCS increase with the wet density. These variations are fitted to power laws which were observed by different authors on altered metamorphic rocks (Sousa et al. 2005; Marques et al. 2010; Vásárhelyi and Ván 2006). The variation of the water content after the same duration of immersion from a sampling site to an other can be explained mainly by the differences of clay content in the samples. Indeed, a clayey sample will have a greater sensibility to water than a sandstone type sample, particularly if the clays are of the swelling type.

As displayed on Fig. 145.3, a good correlation between water content and wet density was obtained, revealing that the samples with the lowest density are the ones reaching the highest water content and consequently the lowest UCS.

145.3 Direct Shear Test

Brioverian schists present, in situ, an important fracturing. These fractures constitute privileged plans of failure during excavation works. The characterization of these plans can be done using direct shear test on small samples of material presenting an opened joint. In order to perform these tests, we were able to use a direct shear test installation mainly used for soils (Fig. 145.4). Indeed, shearing opened joints require much less energy than necessary for a closed joint.

The experimental program consisted in testing samples from 11 different sites and in two different conditions: dry joint and joint immersed in water. Samples tested were of different sizes but the sheared surface was approximately about 60 × 30 mm. The preparation of the samples required

Fig. 145.2 Evolution of the UCS with the water content (*left*) and the density of the wet samples (*right*)

Fig. 145.3 Evolution of the water content with the wet density (*left*) and the tangent Young's modulus with the UCS (*right*)
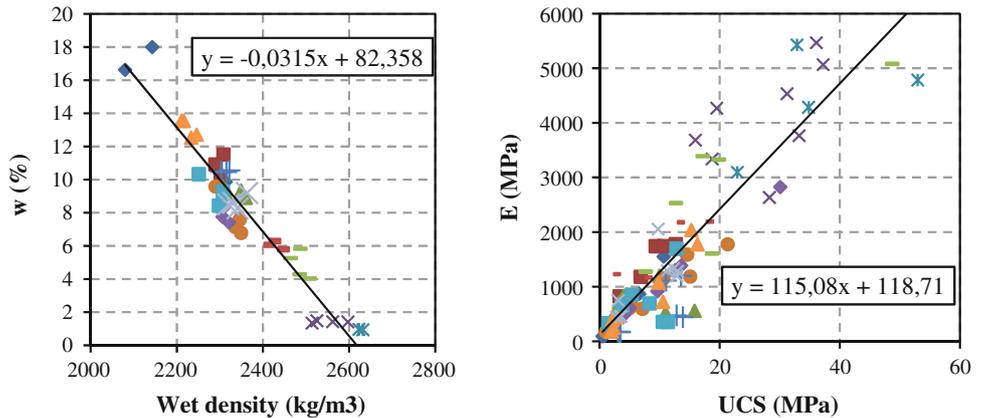
Fig. 145.4 Experimental shear test equipment

to seal both part of the samples in a mortar in order to maintain it during the test and also to facilitate the application of the vertical stress.

To compensate our limited stock of material, cyclic loadings were carried out on each sample (3–5 different normal loading were used) at a constant speed of 0.5 mm/min. Cyclic loading can lead to an important decrease of the mechanical characteristics of joints compared to joints

sheared only once (Jafari et al. 2003). In our study an average decrease of 13 % on the cohesion and 7.5 % on the friction angle was observed when using cycling loading. For each site at least 3 samples were tested in dry conditions and for 6 sites 3 "wet" samples with the joint immersed in water 10 min prior to the test and before application of the normal stress. In the majority of the tests carried out, there was no distinct shear peak but a plateau, so that the couple (σ, τ) was determined by averaging this plateau. The results of these tests are displayed on Figs. 145.5 and the values of the Mohr Coulomb parameters for each tested site are summarized on Table 145.1.

As it can be observed on Fig. 145.5, despite the fact that the sites tested were all issued from the same geological formation, there is an important variability in the shear strength measured. Furthermore, the results presented on Fig. 145.3 indicates that the presence of water during shearing have an important influence on the behaviour of the joint, leading, in all the sites tested (except site A), to a decrease of the friction angle whereas two clear tendencies can be identified for the cohesion (an increase can be observed for the sites E, B and J whereas it's a decrease for the sites A, L, C2 and C3). However, if we consider the average cohesions and friction angles in both dry and wet

Fig. 145.5 Shear stress versus Normal stress in dry conditions and with joint immersed in water. "d" stands for dry and "w" for wet
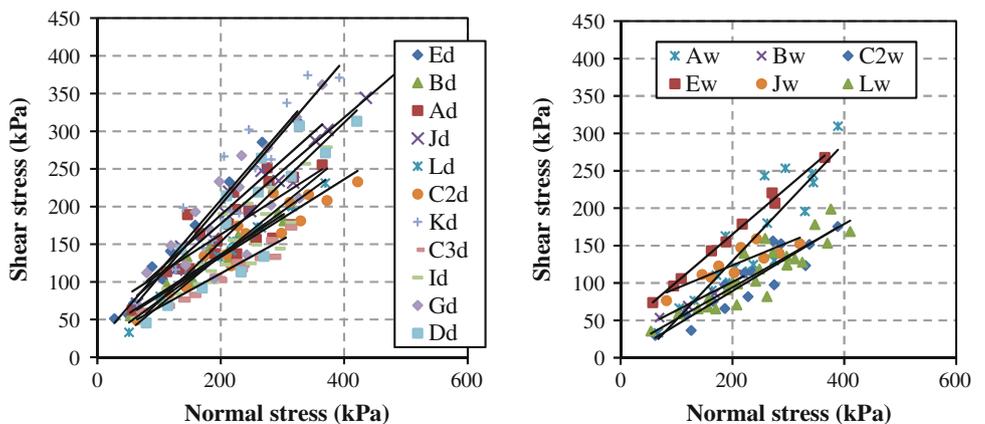
Table 145.1 Mohr Coulomb parameters of the different sites tested

Site	Mohr Coulomb parameters				Dry-wet/dry	
	C′(kPa)		φ′(°)		ΔC′(%)	Δφ(%)
	Dry state	Wet state	Dry state	Wet state		
E	18.7	42.5	41.1	34.8	−127.9	15.5
B	31.6	36.3	27.6	12.3	−15.0	55.6
A	57.3	−24.2	27.8	35.8	142.2	−28.7
J	36.5	62.2	35.2	17.1	−70.4	51.4
L	35.4	9.2	25.6	23.0	74.0	10.2
C2	29.9	−1.2	27.3	24.4	104.0	10.7
K	10.5	36.5	43.8	30.6	−247	30.2
C3	26.7	22.9	22.7	16.9	−59.2	26.2
I	0.9	/	33.9	/	/	/
G	32.5	/	39.0	/	/	/
D	−4.9	35.2	38.4	25.9	/	/
Average	**25**	**24.4**	**32.9**	**24.5**	**2.5**	**25.5**

conditions, a decrease of the two parameters is observed (2.5 % for the cohesion and 25.5 % for the friction angle) when tests occurred with the joint immersed. These observations have been made by other authors on clay rocks discontinuities (Pellet et al. 2013) but with a decrease of the mechanical parameters more important (about 50 %).

145.4   Conclusion

Brioverian schist, considering the low to medium mechanical strength obtained, can be classified as a HSSR type of ground (Hard Soil Soft Rock) if we refer to the classification proposed by Anon (1979a). The important impact of moisture on the mechanical strength of this material has been emphasized for each site tested.

UCS of the material tested varied in a large range from 5 to 50 MPa when the water content is lower than 5 %. However, for higher water content, the UCS ranges from 1 to 7 MPa. The results of the direct shear tests lead to the same results as the uniaxial compression tests: presence of water affected the shear strength of the opened joints tested. The decrease observed reached an average 3 % for the cohesion and 26 % for the friction angle.

To conclude, the sensitivity to water of this type of material should not be underestimated, especially when designing retaining structures such as planned for the second subway line of Rennes. Measuring water content is fast, affordable and gives good indications on the mechanical strength of the Brioverian schist.

References

Anon. (1979) Classification of rocks and soils for engineering geological mapping. Part 1—Rock and soil materials. Bull Int Assoc Geo 19:364–371

Jafari MK, Amini Hosseini K, Pellet F, Boulon M, Buzzi O (2003) Evaluation of shear strength of rock joints subjected to cyclic loading. Soil Dyn Earthq Eng 23(7):619–630

Jégouzo P (1973) Petrographical and structural study on lower Vilaine shales and granites. Phd thesis, Rennes University (in French)

Le Cor T, Rangeard D, Merrien-Soukatchoff V, Simon J (2013) Physical and mechanical characterization of weak schistose rocks. In: EUROCK 2013 symposium

Le Corre C (1978) Approche quantitative des processus synschisteux. L'exemple du segment Hercynien de Bretagne Centrale. Phd thesis, Rennes 1 University, Rennes, 382 pp (in French)

Marques EAG, Barroso E, Menezes Filho AP, Vargas EDA (2010) Weathering zones on metamorphic rocks from Rio de Janeiro-Physical, mineralogical and geomechanical characterization. Eng Geol 111:1–18

Nasseri M (2003) Anisotropic strength and deformational behavior of Himalayan schists. Int J Rock Mech Min Sci 40(1):3–23

Pellet FL, Keshavarz M, Boulon M (2013) Influence of humidity conditions on shear strength of clay rock discontinuities. Eng Geol 157:33–38

Sousa LMO, Del Rio LMS, Calleja L, Argandoña VGR, Rey AR (2005) Influence of micro-fractures and porosity on the physic-mechanical properties and weathering of ornamental granites. Eng Geol 77:154–168

Vásárhelyi B, Ván P (2006) Influence of water content on the strength of a rock. Eng Geol 84:70–74

Qinghong Dong, Fei Liu, and Qiang Zhang

Abstract

This study focuses on prevention and control of water issues when mining under the alluvium and thin bedrock in coalmines. At first a dual structure to describe the soil and rock transition belt in this situation is abstracted. Then a series of similar material simulations on considering the formation combination of hard/soft layers, fault and formation dip of certain degree are made to assess the affect caused by the dual structure to deformation and failure and each factor forms a specific deformation and failure characteristics. In addition, by obtaining cores from borehole and recording graphs of the wall of borehole, the deformation and failure characteristics and water blocking capability of the dual structure are verified. The research shows that the clay/rock structure has the coordination deformation characteristic, which is the deformation of the clay attaching to the ancient erosion surface of bedrock. If there appear no dramatic rock deformation and fracture, the clay layer will still has structural stability and continuity after mining.

Keywords

A dual structure • Clay • Thin bedrock • Coordination deformation • Continuity

146.1   Introduction

It has an important economic and social significance to mine the coal under water bearing layer and water body in China. The approach to keep mining safety is leaving coal or rock pillars above the coal seam in China like that in Britain, Japan, Australia and the former Soviet Union which have accumulated a lot of experiences for mining under water body (Liu 1982; Pertersion 1980; Zou 1998). The national regulation about underwater mining has been promulgated in 2000(State Bureau of Coal Industry 2000). Moreover, there are a lot of new understandings of the underwater mine have been gathered since 1950s (Liu 1998). When mining the coal seam under the water bearing layer of unconsolidated layers and shallow buried under the ancient erosion surface, the loose layer, bedrock composed of a dual structure which is a soft and hard contact or transition zone from up to down. This transition belt exhibits complex deformation and failure characteristics. Some works about the mechanical properties and deformation characteristics of deep clay has confirmed the continuity and impermeable stability of this bottom clay during mining (Sui et al. 2007; Huang 2009; Xu 2004; Ma et al. 2008; Li et al. 2000). The main work in the paper is to find the trends of the dual structural changing by model tests and in situ observations during or after coal mining.

146.2   A Dual Structure and Its Geological Conditions

In the eastern regions of China, the coal seams which lie under the unconsolidated layers of Quaternary or Neogene systems with water bearing layer in it, lake, river, and ocean water body and have a thin overlying rock pillars under extreme conditions are now being exploited because of the huge energy demand. As a result the upper boundary of mining area is rising accordingly.

Q. Dong (✉) · F. Liu · Q. Zhang
School of Resources and Geosciences, China University of Mining and Technology, Xuzhou, China
e-mail: dongqh@cumt.edu.cns

As mentioned above, almost the thickness of the overlying rock is not greater than the height of the fractured zone. This kind of situation can conduct water flow easily. So the overlying bedrock is called thin bedrock for its relative thickness (Tu et al. 2004; Zhang 2004; Hu et al. 2006; Guo et al. 2006; Xuan 2008). In this situation, the soil-rock structure is a dual structure for water resistance. And its deformation and continuity are the most noteworthy features of mining safety. When the mining damage forming the caving zone, fractured zone and sinking/bending zone that extend to the bottom clay, the induced water passage would appear and cause water gushing. Actually there are many factors which have important influences on the deformation and failure of the dual structure.

Considering the most general case, because of the overlaying bedrock is composed by weathered sandstone, limestone, shale and etc., the rock mass is a combination of multi-engineering geological types of different weathering degree, different hardness or weakness. Therefore, the structure of overlying rock mass can be divided into 3 main kinds. They are the full of soft, full of hard and soft to hard from top to bottom. According to the inclination of strata, the situations of gently inclined (<35°) and moderately dipping (35°–55°) have been considered in the next experiments and analysis.

146.3 Affect of Formation Combination to the Deformation of Dual Structure

In order to observe the impact of stratum transformation and combination to the deformation of dual structure, a model without faults cutting from Yanzhou diggings, China is selected as the basic prototype. The basic parameters of the dual structure proportionately meet the actual site.

The observation is completed aided by a series model tests. Previous model tests about mining deformation and failure is mainly to reveal the changing process of caving zone, fractured zone and surface movement. But the discuss about the weak part of the dual structure is inadequate (Zhang et al. 2003). Obeying the regulations of model test, the uniaxial compressive strength of rock is taken as the main control parameter. Each similar model is equipped with the material equal to the 3 kinds of combination mentioned in part 2. The models all have a thickness of 30 cm, length of 150 cm, while the height is adjust according to the geometric scale and the depth of upper load. Figure 146.1 illustrates the overall trend of the relations between the formation combination and the deformation of the dual structure of gently inclined coal measures. The weathering zone and the clay layer covering on are inhibitions to the growth of the height of water flowing fractured zone. But each specific structure of the overlying strata gives a different deformation and failure phenomenon.

For the structure in Fig. 146.1a is a soft-hard combination. The hard roof forms a structure named masonry beams structure above the caving zone during mining. Then the soft part which is the weathered zone or mudstone attached to the masonry beam structure. This may play a coordinating role in the process of deformation. The clay at the bottom of Quaternary system will move toward the settlement direction by the driver of the overburden loads and is restricted by the edge of rock surface. The clay can maintain good continuity after large deformation.

If the overburden rock is soft-soft combination (Fig. 146.1b), it is difficult to form a masonry beams structure. As a result there appear a large range of overburden collapse but in general it converges within the weathered zone. Since the low strength and large deformation, the overlying clay is driven to keeping cover on the rock surface. But if the weathered zone is too weak or loose, the overlaying rock collapse may lead to ionospheric phenomena under the clay layer.

While the overburden rock is hard-hard combination (Fig. 146.1c), the masonry beams were formed during caving steadily. Above this is the upper rock mass under a structural stability situation. The deformation is too smaller for the overburden loads to drive the clay to move. This deformation almost has no affect on clay continuity.

These deformation characteristics indicate that the movement of the clay is limited by the bedrock surface deformation. The deformation of the dual structure determines its ability to maintain continuity and impermeable ability.

Fig. 146.1 Affect of formation combination to the deformation of dual structure. **a** Soft-hard combination. **b** Soft-soft combination. **c** Hard-hard combination

146.4 Affect of Faults to the Deformation of Dual Structure

In the coal mine with large faults density, mining equipment often makes its way by cutting the rock mass on the side of fault In order to avoid moving and re installation especially in the case of the fall <0.5 m or even more the fall <2 m in small faults density areas. Take a coal mine under unconsolidated layers in Yongcheng diggings, China for example, there are 4 faults lies in the area that the overlaying rock is no more than 30 m thick. All the faults are perpendicular to the direction of workface. The falls are 0.5–2 m and the dips are 45–75°. Similar material models are installed to simulate the situation of no fault, fault with dip angle 45° and 75°. The simulation reproduced the process of the deformation characteristics of the dual structure as shown in Fig. 146.2.

It can be seen from Fig. 146.2 that the fault affect to the dual structure cannot be ignore especially about the continuity of clay layer. The no fault condition model reveal a Normal mining subsidence basin in the bedrock surface. The clay layer attaching to the bedrock surface is still extending smooth and continuous during the subsidence or deformation, without obvious break (Fig. 146.2a). In the one fault mode, the bedrock surface subsidence basin affected by the fault. The subsidence around the fault zone is a little larger and the largest settlement appears in end of the fault (Fig. 146.2b, c).

It is obviously that the Clay layer attached to the bedrock surface appears an uneven settlement. The fault rupture may cause clay dislocation or destruction can be seen from the above results. The dual structure also has the synergistic deformation characteristics, but the continuity of clay layer is closely related to the fault activity. The aquifuge faces the risk of deterioration and even more being cut off or collapse. As a result in mining engineering, ground water in flow or underground quicksand will happen.

146.5 Affect of Inclination to the Deformation of Dual Structure

The dip of coal seam and inclination of the Erosion surface also have significant effect on the deformation and failure of the dual structure. It was reported in the paper that mainly discussed the deformation of overlaying rock relate to its combination of dip of coal seam and inclination of the Erosion surface (Dong et al. 2013). The works was done through a similar material model and a numerical model basing on the geological condition of a mine in Xuchang diggings, China. The basic parameters of the Dual structure proportionately meet the actual site as part 2.

The studies show that increasing of coal seam dip causes the overburden deformation and destruction offset towards the uphill. And the inclination of the erosion surface also has the same affect on overburden deformation and failure. But the affect induced by this offset on the covering layer of Neogene or Quaternary was almost rarely reported. The results of the similar material simulation are shown in Fig. 146.3. It can be seen that maximum height of overburden failure does not end within the bedrock surface, but there is a part of the top extending into the clay layer at the bottom of the Neogene systems. From the view of deformation, the main cause of the destruction occurred in the clay layer during the simulation should be part of mining
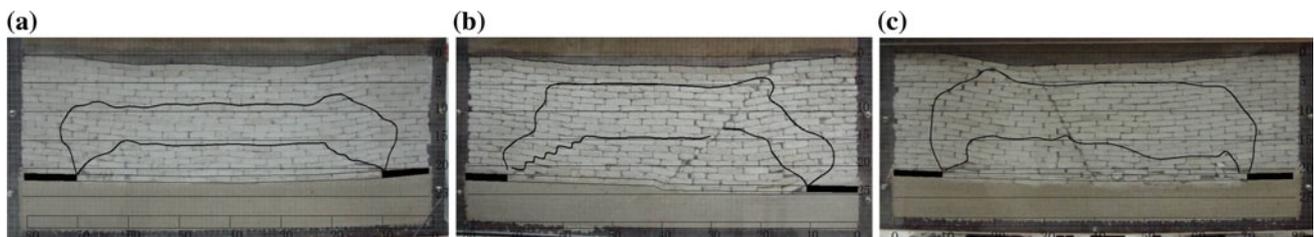

Fig. 146.2 Affect of faults to the deformation of dual structure. **a** No fault model. **b** One fault, dip = 45°, fall = 2 m. **c** One fault, dip = 75°, fall = 2 m
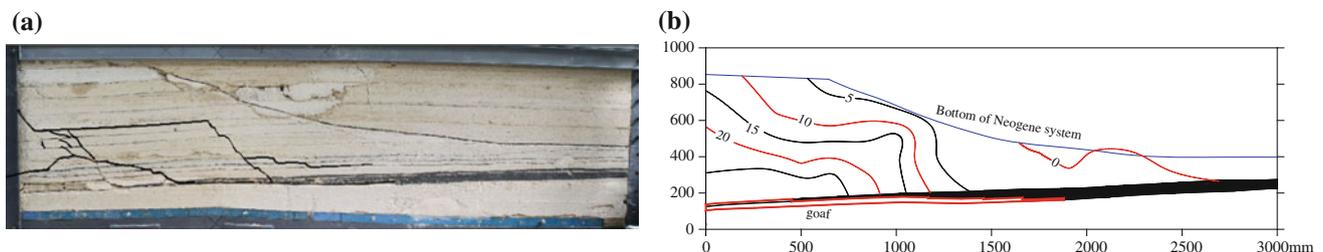

Fig. 146.3 Affect of inclination to the deformation of dual structure. **a** Deformation and failure. **b** Displacement offset of overlaying rock
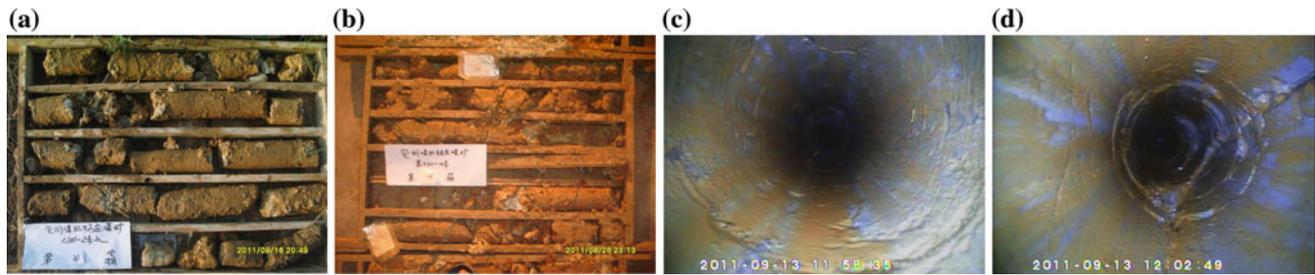
Fig. 146.4 Deformation and failure trends after mining. **a** Clay, **b** Sand, **c** overlaying rock (*top*) **d** overlaying rock (*middle*)

subsidence and horizontal movement. But the lack of confinement of the model is another reason that cannot be completely ruled out by now.

If the mining thickness is limited to a certain scale, the mining failure would do not cause dramatic damage and breakage to the clay at the bottom of Neogene system. And the impermeable role of the clay at the bottom of Neogene system can be controlled and protected.

146.6 Deformation and Failure Trends After Mining

In addition to the above regulations about the dual structure obtained by testing, An on-site observation was designed to evaluate the deformation and destruction of the dual structure after mining 14 years. The test site lies in a coal mine in Yanzhou diggings and the dual structure and the geological conditions are basically the same with the model shown in Fig. 146.1. This research area was recovered in 1997 and the first hierarchical is only 2.2 m in thickness at the bottom of coal seam which is 9 m in thickness. In the on-site observation, all the soil samples from the drill hole have been photographed and all the wall of drill hole of overlaying rock was recorded by television imaging technique. The situation of the soil samples and overburden rock fissures are shown in Fig. 146.4.

From the photos and images of television, the clay at the bottom of Quaternary system is basically completely (Fig. 146.4a). But the sand layer looks like the loose sand without bonding (Fig. 146.4b). This may be due to the disturbances of drilling. This phenomenon is well proving the continuity of the clay layer after the first cutting for a long period of time. In other words, the fissures in the clay layer were bridged well because of the overburden load and the role of water-physical properties. According the borehole imaging, the fractured zone or disturbance area of low levels in the upper part of the bedrock the fractures are still can be seen but in the closed state (Fig. 146.4c). In the lower part of the bedrock, larger and steeply dipping fractures occurred. The walls of the Fissure are basically contacting with each other and partially opening as a small gap (Fig. 146.4d). The

top of the hydraulic conductivity fractured zone after the first mining slice did not go through the weathered zone in the bed rock. The television imaging of four drill holes can explain the long time mining subsidence and consolidation of clay lead a series of changes to the dual structure. The fissures in the overlaying rock have been closing and the settlement is becoming to stabilize gradually. The clay layer keep covering on and attaching to the bedrock and its continuity did not change significantly after mining. It is suggested that, if the clay layer is thick enough, it was stable and impermeable. The resisting of this clay layer still has significance to further repeated exploration.

146.7 Conclusions

1. The dual structure is a typical geological model to analysis the deformation and failure of mining under unconsolidated layers and thin bedrock. The top edge of the cracking range is obviously reduced because of the thin bedrock and overlying clay. The synergistic deformation of the clay and overlying rock is of great significance to analysis the continuity and impermeable ability of the dual structure.
2. The combination of overlaying rock is a main factor that affect on the deformation and failure of the dual structure. Hard-hard combination, soft-hard combination may lead little change to the continuity of the clay layer while soft-soft combination may lead destruction to the clay layer. Because of the plastic of the clay and the weak rock mass, the dual structure always appears a process of plastic deformation and this will cause the uniform, continuous deformation of the clay.
3. The fault and inclination of strata are main reasons to the offset of settlement, abnormal deformation and destruction in local areas.
4. It was found that the rock fissures have the tendency of compaction but having not been filled after a long time since the first cutting. The fissures in the clay layer were bridged well because of the overburden load and the role of water-physical properties.

References

Dong QH, Chen K, Du ZJ, Sui WH (2013) A case study of overburden failure and deep quicksand prevention. In: The international symposium & 9th Asian regional conference of IAEG

Guo WJ, Chen SJ, Li FZ (2006) Study on strip mining size under thick alluvium and thin bed rock. J China Coal Soc 31(6):747–751

Huang QX (2009) Simulation of clay aquifuge stability of water conservation mining in shallow-buried coal seam. Chinese J Rock Mech Eng 28(5):988–992

Hu BN, Zhao YX, Zhang HX (2006) Surface movement parameters and practice effect of strip mining under thick alluvium and thin bedrock. Coal Min Technol 11(1):56–58

Liu TQ (1982) Experiences about mining under the sea in Australia. Mine Survey 3:48–51

Liu TQ (1998) The optimization design theory and technology about the pillar for the outcrop coal seam. Coal Industry Publishing House, Beijing

Li WP, Ye JG, Zhang L, Duan ZH, Zhai LJ (2000) Study on the engineering geological conditions of protected water resources during coal mining action in Yushenfu mine area in the North Shaanxi Province. J China Coal Soc 25(5):449–454

Ma JR, Qin Y, Zhou GQ (2008) Research on triaxial shear properties of clay under high pressures. J China Univ Min Technol 37(2):176–179

Bureau National Coal Industry (2000) Regulations of resorting coal mining and pillars leaving under buildings, water bodies, railroads and main mines and entries. Coal Industry Press, Beijing

Pertersion HF (1980) Northeast submarine of British. World Coal Technol 3:40–43

Sui WH, Cai GT, Dong QH (2007) Experimental research on critical percolation gradient of quicksand across overburden fissures due to coal mining near unconsolidated soil. Chinese J Rock Mech Eng 26(10):2084–2091

Tu M, Gui HR, Li MH, Li W (2004) Testing study on mining of waterproof coal pillars in thick loose bed and thick coal seam under ultrathin overlying strata. Chin J Rock Mech Eng 23(20):3494–3497

Xu YC (2004) Mechanic characteristics of deep saturated clay. J China Coal Soc 29(1):26–30

Xuan YQ (2008) Research on movement and evolution law of breaking of overlying strata in shallow coal seam with a thin bedrock. Rock and Soil Mech 29(2):512–516

Zou YS (1998) The practice and understanding of safety mining under water body in 20 years. Coal Sci Technol 1:53–55

Zhang GL, Cai R, Dong QH, Chen DJ, Zhao QJ, Liu ZX (2003) Engineering geologic mechanical model experimental study on the overburden failure induced by coal mining. Coal Geol China 15(5):34–36

Zhang SK (2004) The law of mining pressure in shallow seam. Ground Press Strata Control 21(4):32–34

Geomechanical Assessment on a Metasedimentary Rock Cut Slope (Trofa, NW Portugal): Geotechnical Stability Analysis

M.J. Afonso, R.S. Silva, P. Moreira, J. Teixeira, H. Almeida, J.F. Trigo, and H.I. Chaminé

Abstract

This work emphasises the importance of a detailed geomechanical study to a better geotechnical understanding of a weak rock mass. In addition, Geographic Information Systems (GIS) tools for spatial analysis and rock database overlay were applied. The stability of a metasedimentary rock cut slope in Trofa region (NW Portugal, Iberian Peninsula) was studied. The main geomorphological, geological, geotechnical and geomechanical constraints were characterised and integrated along a highly deformed phyllitic rock mass. The scanline sampling technique of discontinuities has been applied to the study of basic geotechnical description of free rock mass surfaces. In order to classify the quality of the phyllitic rock mass, basic Rock Mass Rating (RMR), Slope Mass Rating (SMR) and the Geological Strength Index (GSI) were applied. The structural and geotechnical solution for the stabilisation of the cut slope was outlined. This methodology turned out to be valuable to understand the behaviour of slope stability in weak rock mass and it can be useful to the accurate estimation of future unstable rock slope.

M.J. Afonso (✉) · R.S. Silva · P. Moreira · J. Teixeira · H. Almeida · J.F. Trigo · H.I. Chaminé
Laboratory of Cartography and Applied Geology (LABCARGA), DEG, DEC, School of Engineering (ISEP), Polytechnic of Porto, Porto, Portugal
e-mail: mja@isep.ipp.pt

R.S. Silva
e-mail: rui.m.santossilva@gmail.com

P. Moreira
e-mail: pfsm.82@gmail.com

J. Teixeira
e-mail: joaat@isep.ipp.pt

H. Almeida
e-mail: henriquemm.almeida@gmail.com

J.F. Trigo
e-mail: jct@isep.ipp.pt

H.I. Chaminé
e-mail: hic@isep.ipp.pt

M.J. Afonso · J. Teixeira · H.I. Chaminé
Centre GeoBioTec, University of Aveiro, Aveiro, Portugal

147.1 Introduction

The design of slopes in heterogeneous weak rock masses presents a major challenge to the engineering design. The complex structure of these materials, resulting from their tectonostratigraphic features, means that they cannot easily be classified in terms of widely used rock mass classification systems (Hoek et al. 1998; Marinos and Hoek 2001). Rock mass outcrops need a correct in situ geotechnical evaluation on slopes for engineering purposes. Basic geotechnical description of rock masses requires the characterisation of its geological and geomechanical features, particularly discontinuities behaviour and intact rock properties (e.g., Priest 1993; Zenóbio and Zuquette 2009; ISRM 2007; Chaminé et al. 2010). It has been recognised that discontinuities have a major influence on the mechanical properties of a rock-mass, namely on slopes. This perception has major consequences for the assessment of the engineering behaviour of a rock mass. This work presents the results of a combined geotechnical and geomechanical studies of Trofa phyllitic cut slope (NW Portugal), which was excavated in order to construct a road.

147.2 The Study Area

147.2.1 Regional Background: Trofa Region

The northwest portion of the Iberian Massif is crossed by major deep crustal faults. Trofa region is located in the vicinity of regional fault/shear zones. The regional tectonic framework comprises a Palaeozoic metasedimentary highly fractured and folded basement rock (Fig. 147.1). It defines some main tectonic lineaments orientation, trending N-S and NW-SE. The geological units that outcrop in the study area are darkish phyllites and metagraywackes interbedded with metasiltites (Teixeira et al. 1965).
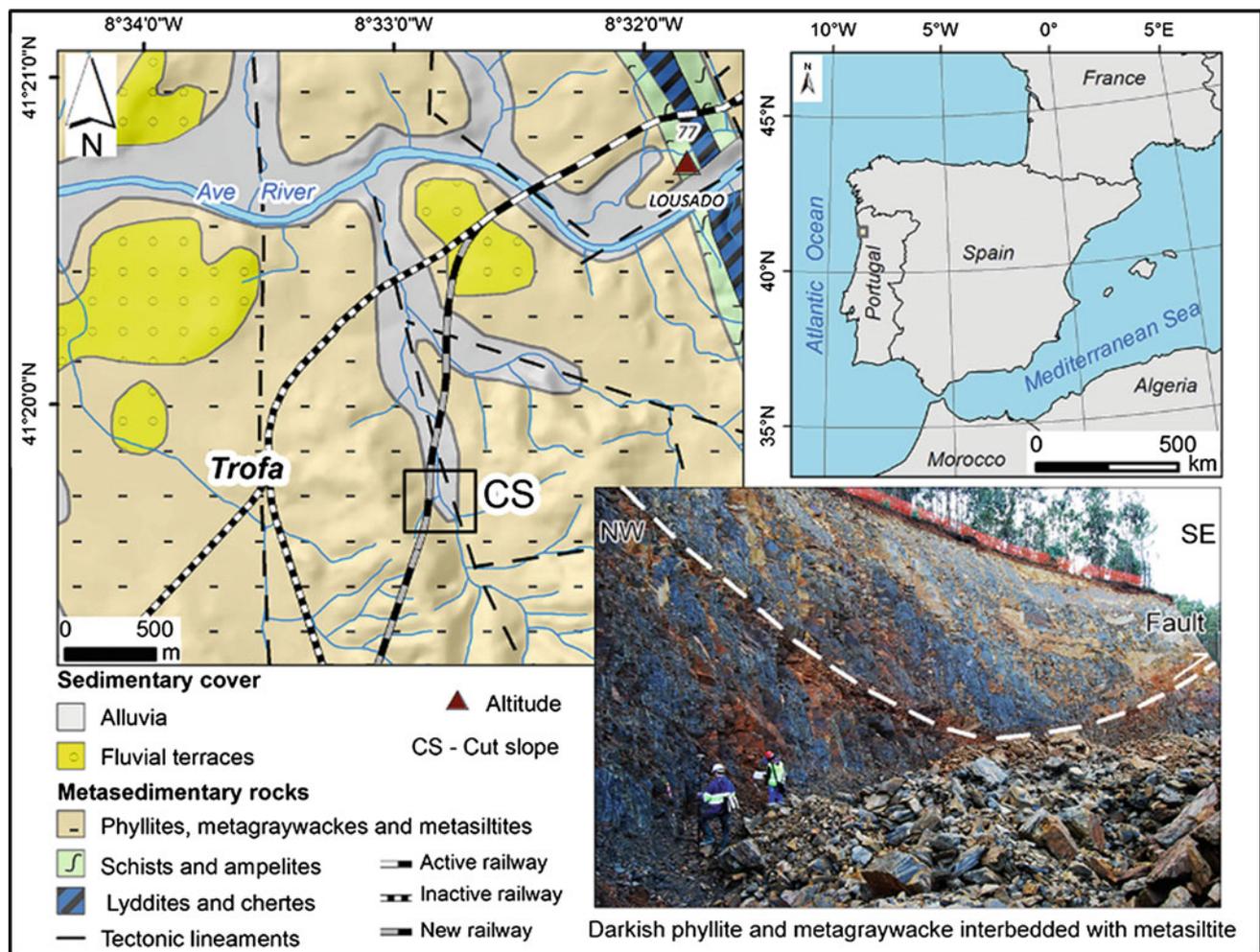
Fig. 147.1 Geological framework of Trofa area (NW Portugal, Iberian Peninsula), updated from Teixeira et al. (1965)

147.2.2   Methodology

This study involved, beforehand, a topographic, morpho-structural and geotectonical characterisation of the study area and, in a subsequent stage, a geotechnical and geomechanical assessment. The main features were compiled and integrated along the rock cut slope. A high-resolution GPS (Trimble GeoExplorer) was used for the fieldwork surveys. The scanline sampling technique was applied to the study of basic geotechnical description of free rock mass surfaces (ISRM 2007). To establish the main discontinuity sets, the structural geology data collected at the slope site were analysed with Dips 6.0 software (Rocscience). Weathering grade of rock material was used following the proposals by GSE (1995) and ISRM (2007). In addition, uniaxial compressive strength was assessed by Schmidt Rebound Hardness after the recommendations by ISRM (2007). In order to classify the quality of the tectonised phyllitic rock mass, the geomechanical classification systems and indexes, such as Rock Mass Rating (RMR; Bieniawski 1989) and Slope Mass Rating (SMR; Romana 1993) and Geological Strength Index (GSI; Hoek et al. 1998, 2013) were applied. Furthermore,

SMR, Markland Test (Wyllie and Mah 2004), Slide 5.0 and Swedge 5.0 software (Rocscience), and the European Standard Eurocode 7 were used to the stability analysis and to identify potential slope failure mechanisms. Geomechanical modelling and the design of the reinforcement elements were developed with Phase^2 6.0 software (Rocscience). A structural and geotechnical solution for the stabilisation of the cut slope was presented.

147.2.3   Results and Discussion

The slope has a curvilinear outline (Fig. 147.2), varying from WNW-ESE to NNW-SSE orientation, and a dip with a steep angle (70–85º). Trofa cut slope is constituted mainly by micaceous-clayish phyllites and metagraywackes, with fine-grained quartz veins, which outcrop fresh to slightly weathered and highly tectonised.

A detailed geological and geomechanical characterisation was performed. Concerning the basic geotechnical description of rock mass, 368 discontinuity (mainly joints) measurements were taken and 71 geomechanical stations were carried out for
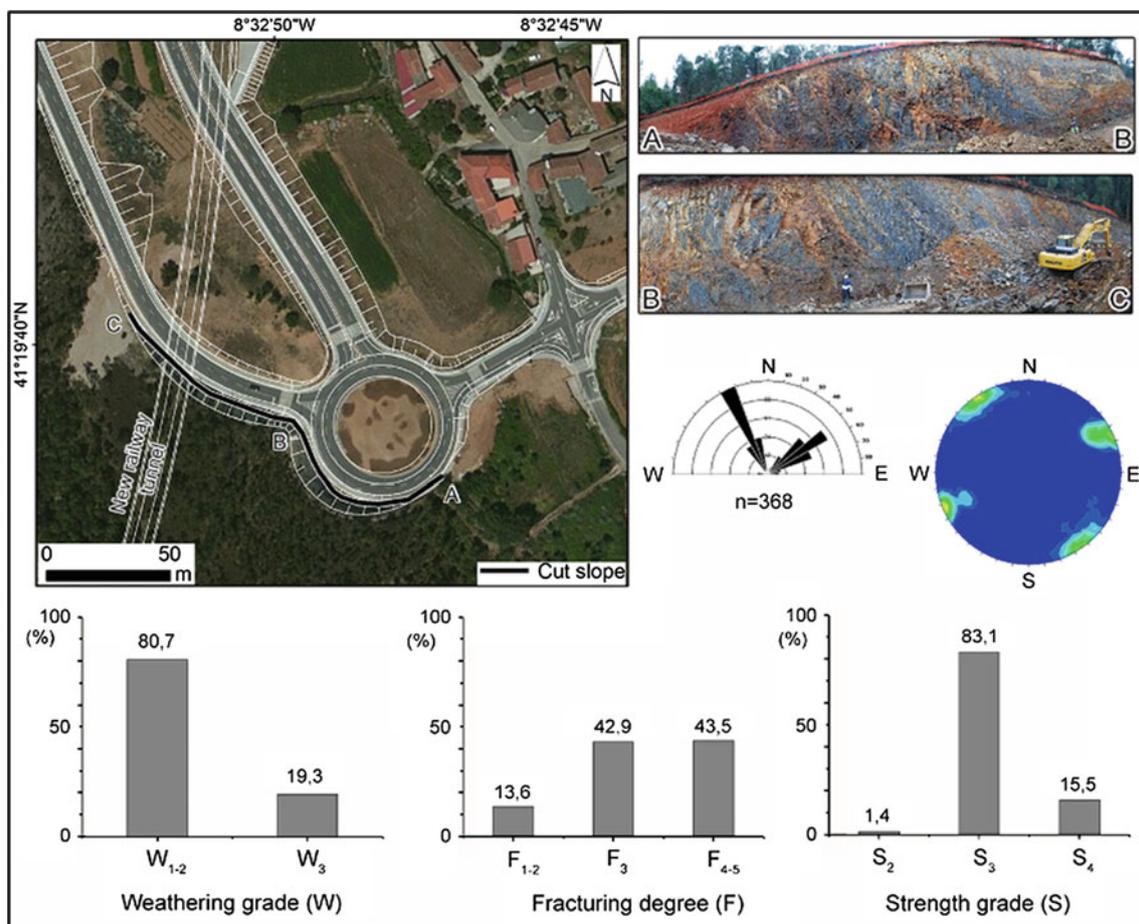
Fig. 147.2 Location and view of Trofa cut slope (ABC), (*upper part* of the figure); main discontinuity sets and other geotechnical parameters (*lower part* of the figure)

Table 147.1 Summary of the basic geotechnical parameters from the studied rock slope (Trofa)

Basic geotechnical description of rock mass parameters (after ISRM 2007)										
Slope (length/height, m)	Weathering grade (W)	Discontinuity type	Main discontinuity sets	Aperture (mm)	Fracture intercept / Spacing (F)	Persistence (m)	Roughness (R)	Filling	Seepage	Uniaxial Compressive Strength (σc)
165.3 / 15	Fresh to slightly weathered (W$_{1-2}$)	Predominantly joints, and faults	N155°E; 80° NE/SW N60°E; 75°NW/SE (n = 368)	Closed (< 0.5)	Very close to moderate spacing (F$_{4-5}$ to F$_3$) average value = 37 cm	Very low (< 1) to low (1–3)	Undulating, rough (R$_{1-2}$) to smooth (R$_3$)	None	Damp	Moderate to low (S$_3$ to S$_4$) 25–35 MPa

Table 147.2 Synthesis of the rock mass classifications and the geomechanical parameters

Slope features		Rock mass classification and index			Geomechanical parameters adopted		
Geological unit	Failure type	RMR$_{basic}$ Bieniawski (1989)	SMR Romana (1993)	GSI Marinos and Hoek (2001); Marinos et al. (2005)	Cohesion, c (kPa) Bieniawski (1989); Design value (Eurocode 7)	Friction angle, ϕ (°) Bieniawski (1989); Design value (Eurocode 7)	Intact rock parameter (m$_i$) Marinos et al. (2005)
Phyllites, metagraywackes with metasiltites	Mainly wedge, also toppling and planar failures	25–35 IV Poor rock	25–35 IVb to IVa Poor rock	20–30 Poor to fair rock	40	22.4	9
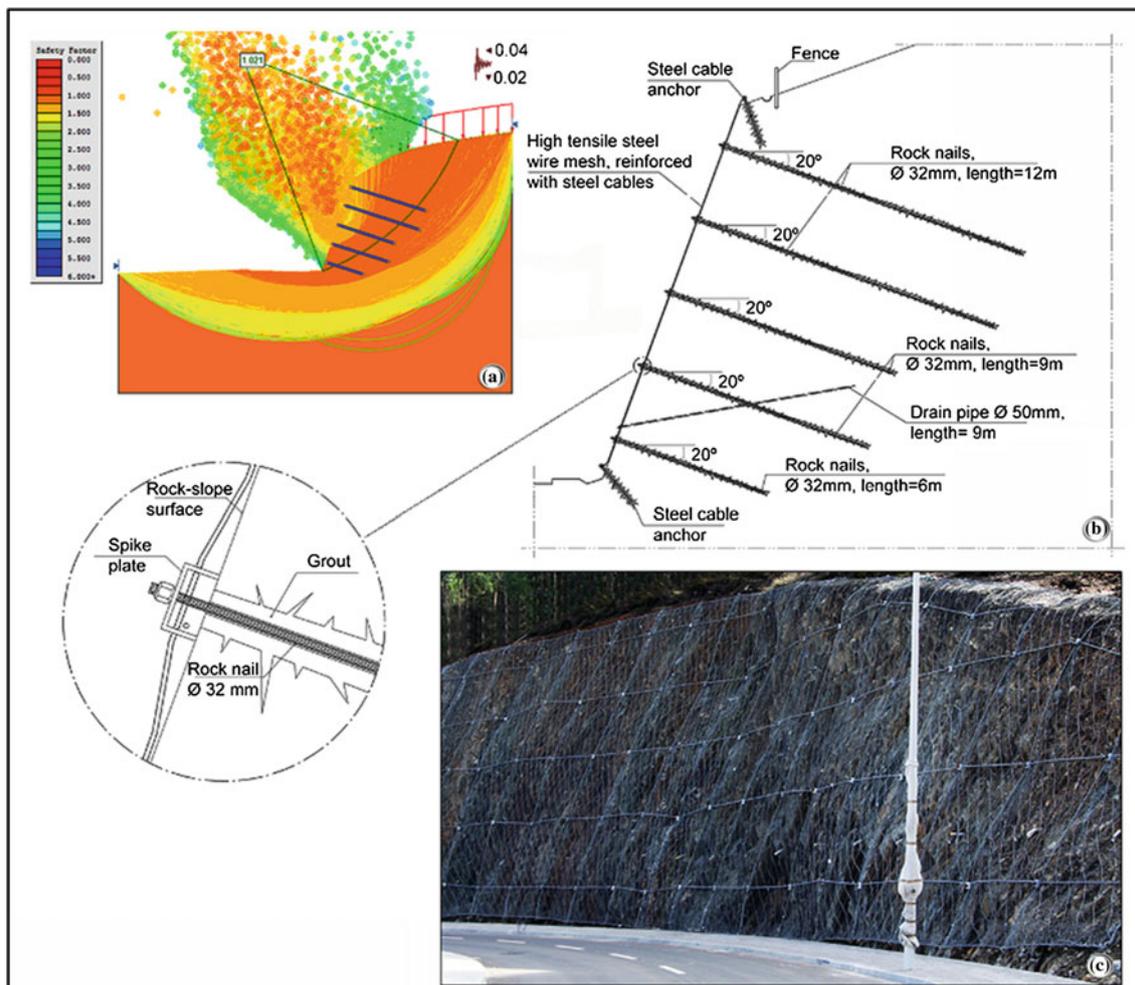
Fig. 147.3 Stabilisation solution design adopted for the studied rock slope. **a** example of slope stability analysis; **b** schematic cross-section with the main reinforcement features; **c** photo of the final stabilisation

the Schmidt Rebound Hardness technique. Table 147.1 summarises the most important geological and geotechnical parameters compiled and analysed in situ for the rock slope. Table 147.2 synthesises the adopted geomechanical parameters and rock mass classifications. The rock mass has dominantly a poor quality, seldom a fair quality. The GSI index appears, in general, to be more optimistic. The slope was classified as unstable and the potential failure types are mainly wedge slides, yet toppling and planar failures may occur.

A stabilisation program has been accomplished after the geological, geotechnical and geomechanical studies. A solution composed of high tensile wire mesh, reinforced with steel cables connected with rock nails and anchors, on the slope borders, was implemented. A level of drain pipes was installed near the base of the slope (Fig. 147.3).

147.3   Concluding Remarks

Geomechanical classification systems can be a way of evaluating the dynamic of rock cut slopes, based on the most important characteristic and structural parameters (Pantelidis 2010). Besides, these geomechanical indexes and classification systems are one of the techniques currently in use for slope stability analyses. The main advantage of using a rock mass classification scheme is that it is a simple and effective way of representing rock mass quality. The slope stability of rocks is an important issue in rock engineering. This holds for both the design and construction stages. Currently, a number of methods are being used for the assessment of slope stability (e.g., Goodman 1989; Romana 1993; Pettifer and Fookes 1994; Irigaray et al. 2003; Pantelidis 2010; Chaminé et al. 2010). Rock slope instabilities area major hazard for human activities often causing economic losses, property damages and maintenance costs, as well as for injuries or fatalities (Fernández et al. 2003; Pantelidis 2010). The combined geotechnical and geomechanical studies of Trofa metasedimentary rock cut slope based on several geomechanical classification systems and indexes proved to be a tool of great utility in the geotechnical slope stability assessment and also to the reinforcement design. This interdisciplinary methodology was vital to understand the geo-hazards in the weak rock mass of Trofa region and must be important to the accurate prediction of future slope instabilities.

References

Bieniawski ZT (1989) Engineering rock mass classifications: a complete manual for engineers and geologists in mining, civil, and petroleum engineering. Interscience, Wiley, NY, p 272

Chaminé HI, Afonso MJ, Silva RS, Moreira PF, Teixeira J, Trigo JF, Monteiro R, Fernandes P, Pizarro S (2010) Geotechnical factors affecting rock slope stability in Gaia riverside (NW Portugal). In: Williams A et al (eds) Proceedings 11th congress. Auckland, CRC Press, IAEG, pp 2729–2736

Fernández T, Irigaray C, El Hamdouni R, Chacón J (2003) Methodology for landslide susceptibility mapping by means of a GIS: application to the contraviesa area (Granada, Spain). Nat Hazards 30:297–308

Goodman RE (1989) Introduction to rock mechanics, 2nd edn. Wiley, NY 576 p

GSE [Geological Society Engineering Group Working Party Report] (1995) The description and classification of weathered rocks for engineering purposes. Q J Eng Geol Hydrogeol 28(3):207–242

Hoek E, Marinos P, Benissi M (1998) Applicability of the geological strength index (GSI) classification for very weak and sheared rock masses: the case of the Athens Schist formation. Bull Eng Geol Environ 57:151–160

Hoek E, Carter TG Diederichs MS (2013) Quantification of the geological strength index chart. In: Proceedings geomechanics symposium 47th US rock mechanics. San Francisco, CA, ARMA 13–672, pp 1–8

Irigaray C, Fernández T, Chacón J (2003) Preliminary rock-slope-susceptibility assessment using GIS and the SMR classification. Nat Hazards 30:309–324

ISRM [International Society for Rock Mechanics] (2007) The complete ISRM suggested methods for characterization, testing and monitoring. In: Ulusay R, Hudson JA (eds) Suggested methods prepared by the commission on testing methods. ISRM, Ankara, Turkey, pp 1974–2006

Marinos P, Hoek E (2001) Estimating the geotechnical properties of heterogeneous rock masses such as flysch. Bull Eng Geol Environ 60:85–92

Marinos V, Marinos P, Hoek E (2005) The geological strength index: applications and limitations. Bulletin of Engineering Geology and the Environment, 64(1):55–65

Pantelidis L (2010) Rock slope stability assessment through rock mass classification systems. Int J Rock Mech Min Sci 46(2):315–325

Pettifer GS, Fookes PG (1994) A revision of the graphical method for assessing the excavatability of rock. Q J Eng Geol Hydrogeol 27 (2):145–164

Priest SD (1993) Discontinuity analysis for rock engineering. Chapman and Hall, London 473 p

Romana M (1993) A geomechanical classification for slopes: slope mass rating. In: Hudson J (ed) Comprehensive rock engineering. Pergamon, Oxford, 3: pp 1–45

Teixeira C, Medeiros AC, Assunção CT (1965) Notícia explicativa da Carta Geológica de Portugal, escala 1/50000, Folha 9☐A (Póvoa de Varzim). Serviços Geológicos de Portugal, Lisboa

Wyllie DC, Mah CW (2004) Rock slope engineering: civil and mining, 4th edn. Spon Press, London 431 p

Zenóbio A, Zuquette L (2009) Geotechnical mapping of rock masses in natural slopes using geomechanical classifications. In: Culshaw MG et al (eds), Engineering geology for tomorrow's cities (IAEG'2006). Geological society, London, engineering geology special publications, 22 [on CD-ROM insert, Paper 173]

Geomechanical Characterization of a Weak Sedimentary Rock Mass in a Large Embankment Dam Design

148

Gian Luca Morelli and Ezio Baldovin

Abstract

The geomechanical characterization of a weak and tectonically undisturbed sedimentary rock mass ("molasse"), carried out for the design of a large embankment dam in the Kurdistan Region (Iraq), is presented. In view of the relevant dimensions of the dam and of its main ancillary works, the rock mass characterization has represented one of the basic focus of the geological and geotechnical investigations. However, various uncertainties have been considered to potentially affect the final estimate of the engineering properties of rock masses in the context of the present study. In particular, besides the natural variability of weak rocks characteristics and the well-known difficulties in their realistic estimation, uncertainties may also arise from the potential incompleteness of the basic data available, mainly due to time and budget limitations. In order to quantify such uncertainties and adequately incorporate their effects into the design process, a probabilistic approach based on Monte Carlo method has been adopted to determine the probability distribution functions describing the rock mass strength parameters. A practical example of application of the followed probabilistic approach to the design of large excavation rock slopes is briefly illustrated.

Keywords

Weak rocks • Geomechanical characterization • Probabilistic approach • Slope stability

148.1 Introduction

The Mandawa Dam is presently under construction for irrigation, hydropower production and drinking water supply, in the Kurdistan Region (Northern Iraq) along the main course of the Greater Zab River, a major left tributary of the Tigris River. The dam is a 65 m high embankment with gravel and sand shells and a central silty core. It extends straight for about 1,000 m from the two extreme abutments and includes, on the left side, a concrete structure composed of three blocks housing the main hydraulic structures for the temporary diversion, the bottom outlets and the inlets of the penstocks of the hydropower plant (Fig. 148.1). A very large spillway channel is located on the right side, separated from the dam. The subtended reservoir has a maximum storage capacity of about 520 million m^3.

The foundations of the left concrete part of the dam body and of the spillway channel have required the design of large excavations on both river banks, resulting in cut multi-bench rock slopes even more than 80 m high.

148.2 Site Geology and Geotechnical Investigations

The rock mass characterization was based on data gathered from an investigation geotechnical campaign carried out during the 2012, that has included a total of 1,700 m

G.L. Morelli (✉) · E. Baldovin
Geotecna Progetti S.r.l, Via Roncaglia, 14, 20146 Milan, Italy
e-mail: gianluca.morelli@geotecna.it; gl.morelli.geo@gmail.com
URL: http://www.geotecna.it

E. Baldovin
e-mail: ezio.baldovin@geotecna.it
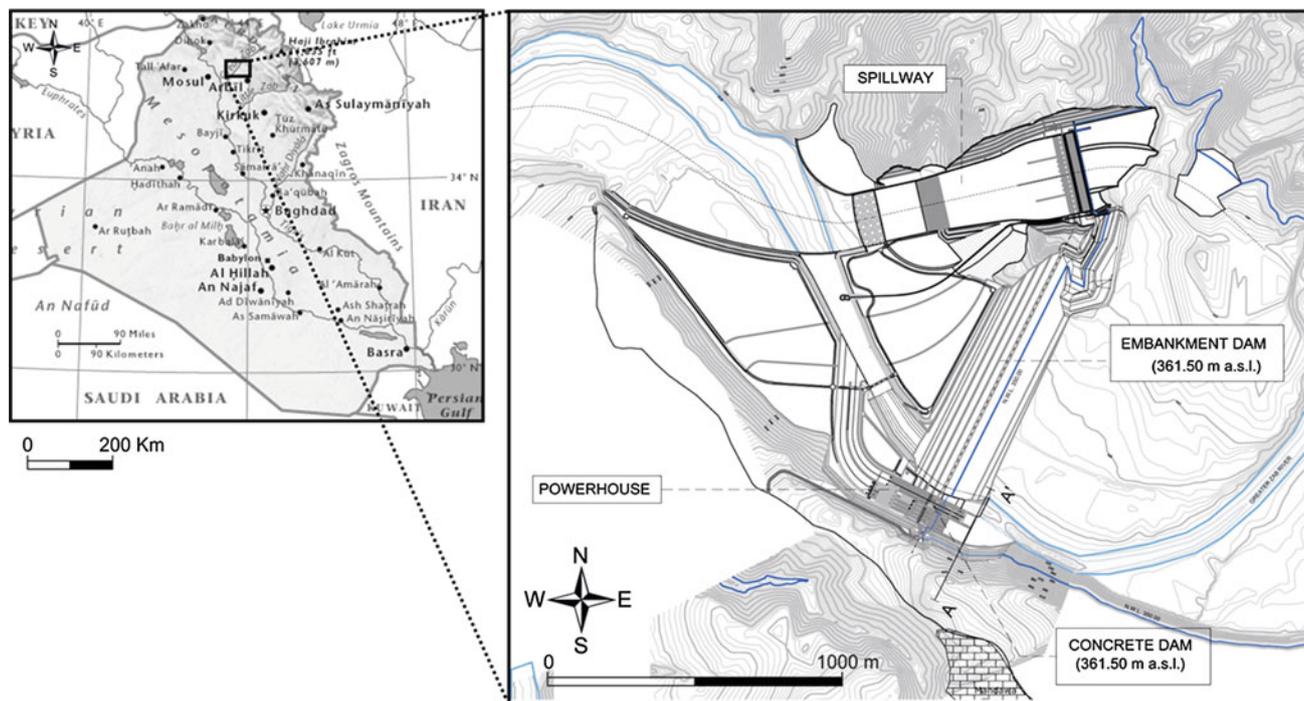
Fig. 148.1 Dam location map and general layout of works

borehole drillings, 60 geotechnical laboratory tests on selected rock cores (mainly uniaxial compression tests on specimens at natural water content and physical property determinations) and field geological mapping. In the dam area, the local bedrock consists of the Upper Miocene sedimentary Mukdadiyah Formation, composed of a clastic sequence of pluri-metric alternations of reddish siltstone and grayish silty sandstone members. It was formed in a mostly fluvial depositional environment in front of the Zagros Mountains belt and appears not significantly interested by orogenic deformations. Both sandstone and siltstone members are stratified and show grain size and induration degree rather variable among layers. Three discontinuity sets intersecting at right angles, one of which coincident with the sub-horizontal bedding and the others consisting of sub-vertical tensile joints striking sub-parallel and sub-orthogonal to the river course, were observed in the bedrock. Spacing and persistence of vertical joints result well correlated with the thickness of layers and usually varies in the range 0.5–3 m. Discontinuities in sandstone are mostly undulated, rough and free of infilling materials; those in siltstone (mainly the bedding surfaces) are frequently planar and moderately rough, sometimes with skinny silty coatings on the surfaces. Weathering effects are limited to the few superficial meters of the bedrock and disappear rapidly with depth.

148.3 Rock Mass Characterization

The rock mass has been characterized with reference to an equivalent-continuum model and the GSI classification system, combined with the strength properties of the intact rock, has been used to derive the Hoek-Brown strength parameters (Hoek et al. 2002). The uniaxial compressive strength (UCS) of the rock matrix has been evaluated through compressive tests on core specimens at varying natural water contents. The UCS values resulted sensitive to saturation degree (Sr, %) and correlated to the dry density (ρ_{dry}, Mg/m^3) of specimens. The average saturation degree of tested samples was about 30 %. Relationships linking UCS and the main index properties of intact rocks have been established by multiple linear regression analyses of the available laboratory test results, in the form

$$UCS_{sandstone}(MPa) = -66.61 - 0.107Sr(\%) \\ + 41.282\rho_{dry}(Mg/m^3)\left[R^2 = 0.69\right] \tag{148.1}$$

$$UCS_{siltstone}(MPa) = -45.27 - 0.116Sr(\%) \\ + 28.876\rho_{dry}(Mg/m^3)\left[R^2 = 0.64\right] \tag{148.2}$$

For studied rocks, established relationships allow to predict the UCS for specified values of dry density and degree of saturation expected in situ (e.g. saturated under reservoir water level and naturally wet above) and imply, for tested samples, an average reduction of the UCS between dry (Sr = 0 %) and fully saturated (Sr = 100 %) in the order of about 50 % for sandstone and 60 % for siltstone, rather in line with previous literature findings (e.g. Palmström 1995; Romana and Vásárhely 2007). Proposed relationships have, evidently, not general validity and should then be applied with extreme care for other rock types and in different geological contexts. The GSI index of the rock mass at the depths of the planned excavations has been assessed on the base of data collected from core logging and field mapping. The method reported by Hoek et al. (1995), based on traditional Q-System descriptor codes (Barton et al. 1974), has been used to quantitatively estimate the GSI through the relationship

$$GSI = 9 \ln(RQD/Jn \times Jr/Ja) + 44 \qquad (148.3)$$

where RQD = Rock Quality Designation (%); Jn = rating for number of joint sets; Jr = rating for joint roughness and Ja = rating for joint alteration and filling. The GSI obtained

for the unweathered bedrock with the described quantitative approach resulted in general accordance with the indicative range suggested by Hoek et al. (2005) for "blocky" molasses.

148.4 Probabilistic Approach in Rock Mass Characterization

To quantify the possible variability of rock mass properties and to incorporate its effects into the design process, a probabilistic approach based on the classical Monte Carlo (M-C) method has been used to derive the probability density functions (PDFs) of the Hoek-Brown (H-B) strength parameters. At this scope, probability distributions have been assessed for the input parameters used to calculate the UCS of intact rocks, i.e. ρ_{dry}, and the GSI of rock masses, i.e. the RQD and the Jr and Ja factors, by considering available field and laboratory data. On the base of such input distributions, the PDFs for UCS and GSI have been calculated by best fitting the results of M-C simulations conducted using Eqs. 148.1, 148.2 and 148.3 (Table 148.1 and Fig. 148.2). The input parameters considered for simulations have been implicitly assumed to be random and independent variables.

Table 148.1 Monte Carlo simulations inputs and outputs

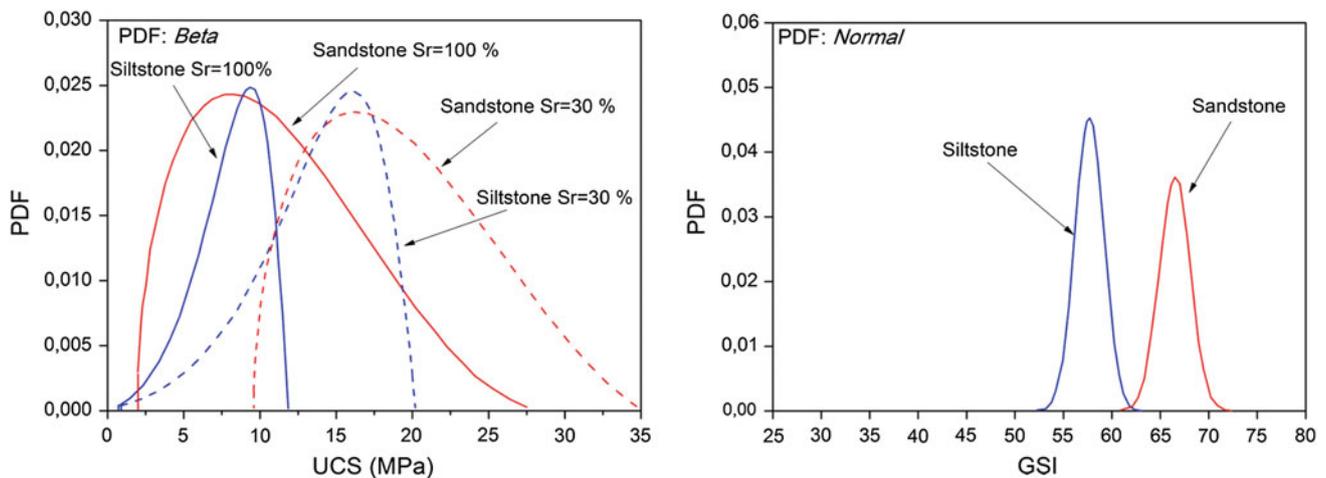|		Parameters and probability distributions input into Monte Carlo simulations	Output parameters and PDFs from M-C simulations	
Intact rock	ρ_{dry}	LogNormal (Trunc: min and max values of lab tests)	UCS	Beta
	Sr	Constant = 30 % (naturally wet) and 100 % (saturated)		
Rock mass	RQD	Weibull (Trunc: min = 0 to max = 100)	GSI	Normal
	Jn	Constant = 9 (n. 3 joint sets)		
	Jr, Ja	Normal		

Fig. 148.2 Plots of the PDFs obtained from Monte Carlo simulations for UCS (*left*) and GSI (*right*)

The mean values of the H-B constant m_i have been derived from literature, arbitrarily assuming normal distributions with coefficient of variation (COV) of 10 %. By using the probability distributions previously defined for GSI and m_i, the PDFs of the H-B strength parameters of the rock mass, s, m_b and a, have been determined using the Monte Carlo method. The disturbance factor D has been set to zero in calculations.

148.5 Example of Application in Rock Slope Design

An example of application of the described probabilistic characterization approach in the Mandawa Dam project mainly relates to global stability analyses performed for the rock slopes to be excavated in the reservoir nearby the left side of the dam, where the HPP headrace inlets and the bottom outlets intakes have been planned (analysis section A–A' in Fig. 148.1). Since the structural setting of the rock mass does not control the stability of such slopes, global analyses were performed assuming Bishop's circular failure surfaces and using the probabilistic analysis option available in the program SLIDE (Rocscience Inc.). The possible presence of tension cracks, coincident with the joints striking nearly parallel to the river course, has also been considered. The input probability functions of main geotechnical parameters and tension crack depth derived from Monte Carlo simulations and used in the analyses, are summarized in Table 148.2.

The typical slip surface considered in the analyses and the probability of failure obtained by varying the overall slope angle α, are shown in Fig. 148.3.

Analyses were performed considering the most severe condition of rapid drawdown of the reservoir, from the maximum to the minimum level without the drainage of the slope, coupled with the maximum seismic action (defined from a peak design earthquake acceleration of 0.2 g). The overall slope angle of 50° finally chosen for the design, resulting from a multi-bench shaped profile of interposed 3 m benches with vertical drops of 15 m and scarps inclined 3v:2 h (Fig. 148.3-left), allows to advantageously reduce to zero the risk of global failure of the analyzed slope (Fig. 148.3-right), ensuring, in the long term, the full operability of the dam outlets and the HPP production.

Table 148.2 Main input parameters used for the slope stability analyses

Property		PDF	Mean	Std. Dev.	Min	Max
Siltstone	UCS(sat)[Mpa]	Beta	15.79(7.89)	2.91(2.54)	0.63(0.5)	20.26(12.14)
	H-B "s"	LogNorm	0.0096	0.0019	0.0044	0.0202
	H-B "a"	LogNorm	0.503	0.0001	0.502	0.505
	H-B "m_b"	LogNorm	0.8939	0.1047	0.508	1.312
Sandstone	UCS(sat)[Mpa]	Beta	19.70(12.21)	5.77(5.77)	9.65(2.16)	35.04(27.54)
	H-B "s"	LogNorm	0.021	0.01	0.01	0.05
	H-B "a"	LogNorm	0.502	0.0001	0.501	0.503
	H-B "m_b"	LogNorm	5.149	0.624	3.166	7.762
T. Crack	Depth [m]	Uniform	20		10	30
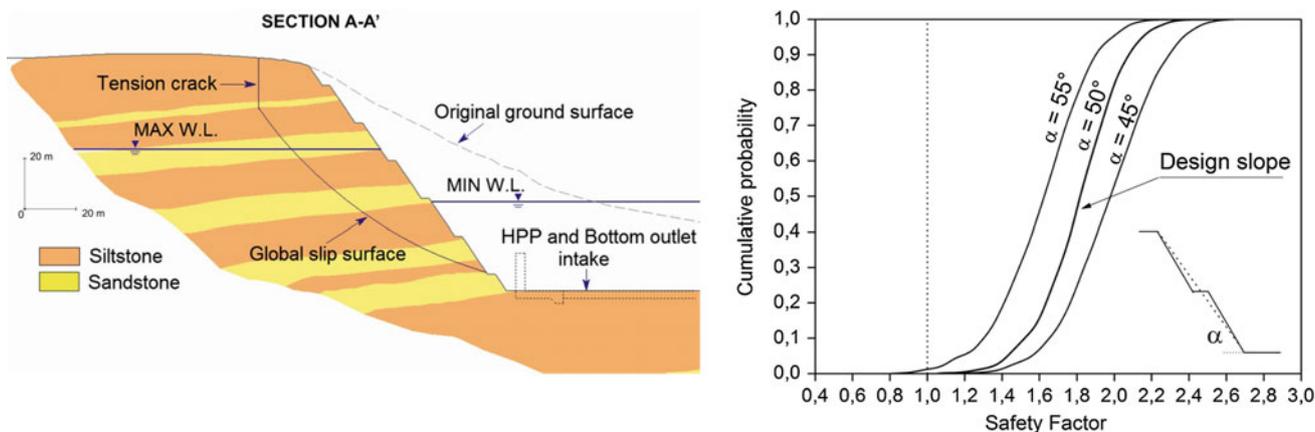
Fig. 148.3 *Left* Slope geology and typical slip surface analyzed; *Right* probability of failure obtained by varying the overall slope angles

148.6   Conclusions

A geomechanical rock mass characterization approach based on probabilistic analyses has been performed for a large embankment dam design, enabling to take into account and to quantify the possible variability of the engineering properties of the bedrock. A practical example showing how this approach has been applied to the design of cut rocky slopes has been presented. According to the wide literature available today on this subject, the adoption of a probabilistic design method proved to be suitable for managing uncertainties in rock properties assessment and can be particularly effective when, as in the presented case, the difficulties usually encountered in characterizing a weak rock mass have to be faced with time and budget limitations.

References

Barton NR, Lien R, Lunde J (1974) Engineering classification of rock masses for the design of tunnel support. Rock Mech 6(4):189–239

Hoek E, Kaiser PK, Bawden WF (1995) Support of underground excavations in hard rock. Rotterdam, Netherlands In: Balkema (eds)

Hoek E, Carranza-Torres CT, Corkum B (2002) Hoek-Brown Failure Criterion—2002 Edition. In: Proceedings of 5th North American rock mechanics symposium

Hoek E, Marinos PG, Marinos VP (2005) Characterisation and engineering properties of tectonically undisturbed but lithologically varied sedimentary rock masses. Int J Rock Mech Min Sci 42:277–285

Palmström A (1995) RMi—a rock mass characterization system for rock engineering purposes. PhD thesis, University of Oslo, Norway, p 400

Romana M, Vásárhely B (2007) A discussion on the decrease of unconfined compressive strength between saturated and dry rock samples. In: 11th Congress of the international society for rock mechanics—Ribeiro e Sousa, Olalla and Grossmann (eds), pp 139–142

Experimental Study of Anisotropically Mechanical Features of Phyllite and Its Engineering Effect

Meng Lubo and Li Tianbin

Abstract

Based on conventional triaxial compression tests for phyllite with various orientation angles, the relationships of mechanical features, confining pressure and anisotropy are discussed. The results indicate that the peak strength, residual strength, elastic modulus and Poisson's ratio increase with increasing confining pressure. The effect of confining pressure on the elastic modulus is relatively smaller than the peak strength and Poisson's ratio. The peak strength and Poisson's ratio decrease with orientation angle increases. The effect of anisotropy on the peak strength is larger than Poisson's ratio. The split and shear mechanisms are observed, their failures are brittle and ductile, respectively. The three modes of surrounding rock failure in deep tunnel are derived from the test results, which are split and buckling, split and shear, shear sliding.

149.1 Introduction

Deep underground engineering's environments typically have one important feature: high geostress level. Research on soft rock mechanical property under high confining pressure conditions are very important, which can help understand the surrounding rock stability for deep underground engineering.

Anisotropy is an important property of rock masses, and is one of the focus and hotspot of research for many experts and scholars. Lots of anisotropy behaviors of transversely isotropic rock have been investigated by tests and theoretical analysis (Jaeger 1960; Ramamurthy et al. 1993), the mechanical properties of layered rock mass have been discussed by uniaxial compression tests (Li 2008; Liu et al. 2012), the elastic parameters and strength for transversely isotropic rocks have been investigated by triaxial compression tests (Liu et al. 2013). However, the mechanical features and failure modes of phyllite for deep tunnel is relatively less. So a phyllite conventional triaxial compression tests with various orientation angles is studied. The results of this research will provide a reference for phyllite surrounding rock stability analysis for deep underground engineering under high geostress conditions.

149.2 Test Scheme

Phyllite samples, which are collected from a drill hole of the ChengLan railway tunnel under high geostress conditions, are cylindrical specimens with a diameter of 45 mm and a length of 100 mm. The testing is performed with the professional standard of People's Republic of China (SL264-2001).

Defining the planes of weakness making an angle β with the axis of the major principal stress, the angle β is designated as the "orientation angle". The tests are conducted at

M. Lubo (✉) · L. Tianbin
State Key Laboratory of Geohazard Prevention and
Geoenvironment Protection, Chengdu University of Technology,
Chengdu, 610059 China
e-mail: menglubo@163.com
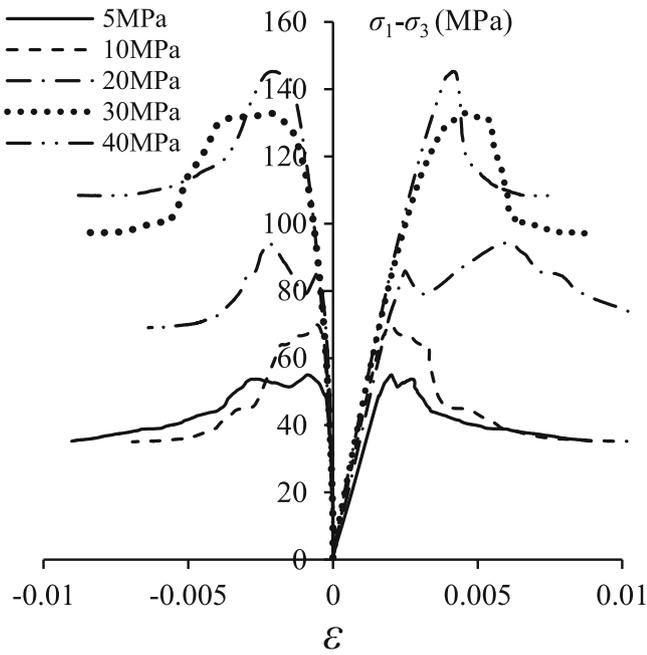
Fig. 149.1 Stress-strain curves of specimens ($\beta = 15°$)

specified orientation angles of 0, 15 and 30°. The MTS815, produced in the U.S.A., is used for testing. The confining pressure ($\sigma_2 = \sigma_3$) is controlled at 5, 10, 20, 30, and 40 MPa.

The testing sequence is presented as follows:

1. The specimen is installed according to the requirements of test machine.

2. The load control is adopted; the confining pressures are loaded with predetermined values at the rate of 5 MPa/min, the confining pressure is maintained at the predetermined pressure.

3. The axial deformation control is then adopted, and the rate is 0.1 mm/min, until the specimen is destroyed.

149.3 Results and Discussion

149.3.1 Mechanical Features and Confining Pressure

The stress-strain curves for typical samples are shown in Fig. 149.1. The rock deformation of samples can be divided into three phases: the elastic deformation, yield and failure phases. The peak strength increases with increasing confining pressure from 5 to 40 MPa. Contrast the peak strength at confining pressure of 5 MPa, the peak strength increased by 26.8 % ($\sigma_3 = 10$ MPa), 69.9 % ($\sigma_3 = 20$ MPa), 121.2 % ($\sigma_3 = 30$ MPa), 162.7 % ($\sigma_3 = 40$ MPa), respectively.

The elastic modulus (E_{50}) and Poisson's ratio (μ_{50}) can be determined with the following equations (Gao et al. 2005):

$$B = \varepsilon_3 / \varepsilon_1 \tag{149.1}$$

$$\mu_{50} = (B\sigma_1 - \sigma_3)/((2B - 1)\sigma_3 - \sigma_1) \tag{149.2}$$

$$E_{50} = (\sigma_1 - 2\mu_{50}\sigma_3)/\varepsilon_1 \tag{149.3}$$

Fig. 149.2 Relationship between the E_{50}, μ_{50} and confining pressure ($\beta = 15°$). **a** Elastic modulus. **b** Poisson's ratio

Fig. 149.3 Typical stress-strain curves of phyllite specimens with fixed confining pressure. **a** $\sigma_3 = 5$ MPa. **b** $\sigma_3 = 40$ MPa

Fig. 149.4 Relationship between the peak strength, Poisson's ratio and orientation angle. **a** Peak strength. **b** Poisson's ratio
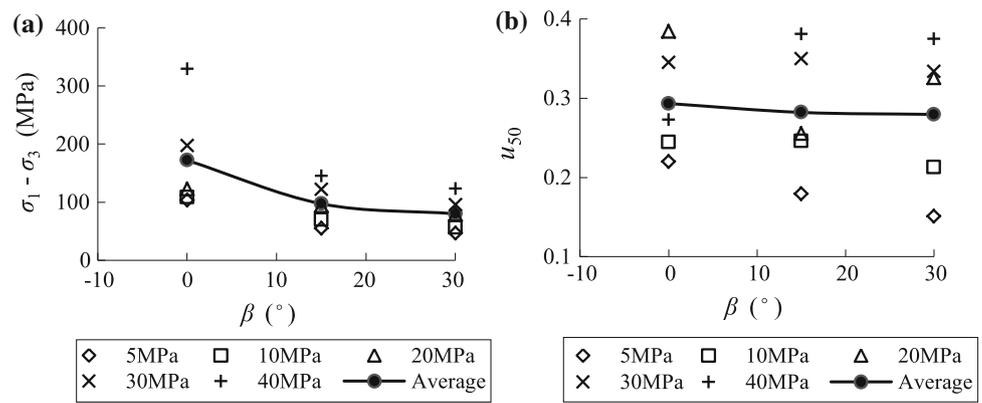
where μ_{50} is the Poisson's ratio, E_{50} is the secant modulus of elasticity at half of the peak strength, σ_1 is the axial stress, ε_1 is the axial strain, σ_3 is the confining pressure, and ε_3 is the lateral strain.

The relationships between the E_{50}, μ_{50} and confining pressure are shown in Fig. 149.2. The E_{50} and μ_{50} increase with increasing confining press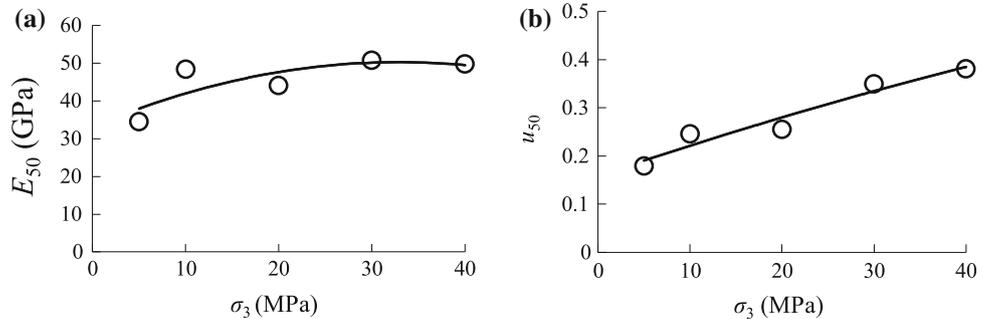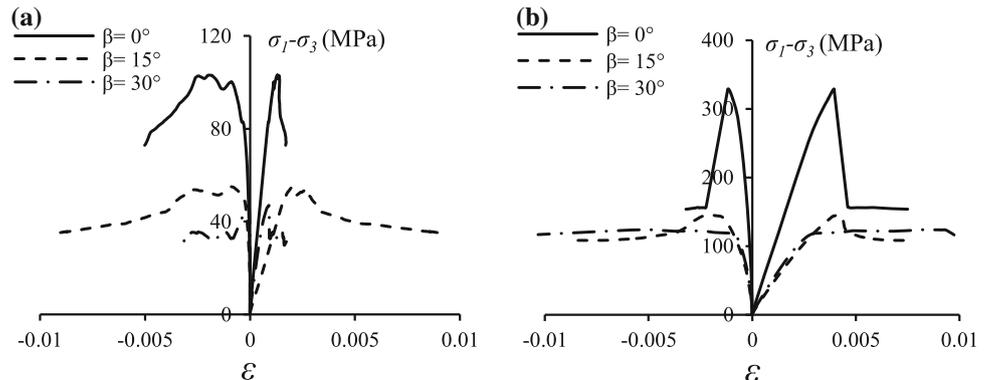ure at the same orientation angle. Contrast the E_{50} and μ_{50} at confining pressure of 5 MPa, the E_{50} increased by 40.3, 28, 47.3, 44.5 %, and the μ_{50} increased by 37.2, 42.5, 95.3, 112.8 %, respectively.

The deformation and damage of the specimens are closely related to the confining pressure. The high confining pressure can improve the mechanical properties of phyllite, the strength and stiffness of the phyllite increase with increasing confining pressure, and the residual strength also slightly increases with confining pressure increases. The effect of confining pressure on the elastic modulus is relatively smaller than the peak strength and Poisson's ratio.

149.3.2 Mechanical Features and Anisotropy

The typical stress-strain curves of phyllite specimens with fixed confining pressure are shown in Fig. 149.3. The stress-strain curves indicate that the failure mode of rock with various orientation angles is different. When $\beta = 0°$, rock generates brittle failure; when $\beta = 30°$, rock generates ductile failure.

The relationships between the peak strength, Poisson's ratio and orientation angle are shown in Fig. 149.4. The peak strength decreases with increasing orientation angle at the same confining pressure. The average peak strength of the specimens is 172.2, 97.4, and 80.1 MPa when $\beta = 0, 15, 30°$. The ratio of uniaxial strength perpendicular to strength at orientation of 30° is defined as the degree of anisotropy, the degree of anisotropy of average peak strength is 2.1 ($\beta = 0°$) and 1.2 ($\beta = 15°$).

Fig. 149.5 Typical failure patterns

The average Poisson's ratio decreases with increasing orientation angle at the same confining pressure. The average Poisson's ratio of the specimens is 0.293, 0.282, and 0.280 when $\beta = 0, 15, 30°$. The degree of anisotropy on Poisson's ratio is smaller than the peak strength.

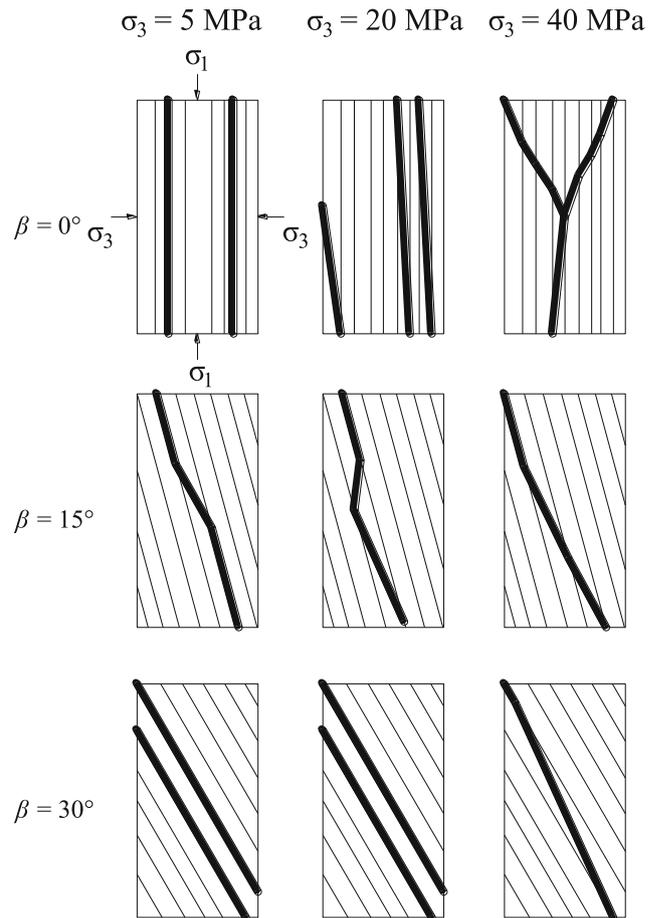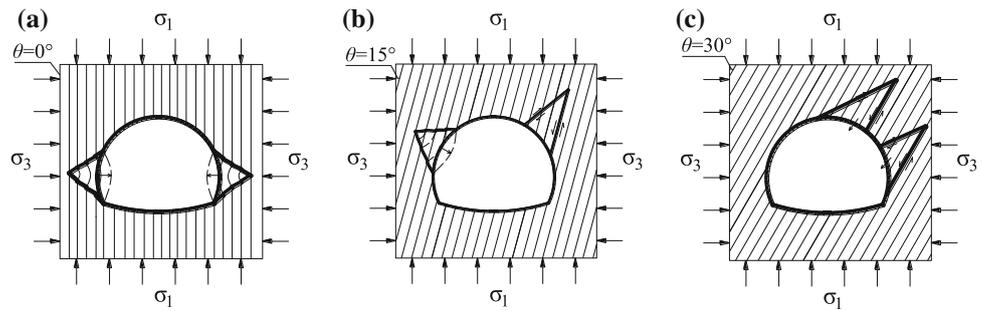**Fig. 149.6** Failure patterns of surrounding rock in deep tunnel. **a** Split and buckling. **b** Split and shear. **c** Shear sliding

149.3.3 Mechanism of Samples Failure

The typical failure patterns are shown in Fig. 149.5. At confining pressure of 5 and 20 MPa (low confining pressure condition), splitting along the foliation planes is common toward low value of β, specifically $\beta = 0°$. At $\beta = 15°$, shearing and splitting failure is observed. At $\beta = 30°$, the phyllites show a pure shear failure across the planes of the foliation.

Under high confining pressure of 40 MPa, at $\beta = 0°$, splitting along the foliation planes and shear failure along a plane oblique to the foliation planes is observed. At $\beta = 15°$ and $30°$, the specimens sheared along the weak planes with some development of "kinks", i.e., step-shaped sloping plane, the shearing mechanism controls the behavior of rocks.

The confining pressure of brittle-ductile diversion decreases along with the orientation angle increases; at $\beta = 0°$, the confining pressure of transition is about 30 MPa; at $\beta = 30°$, the confining pressure of transition decreases to 5 MPa.

149.3.4 Modes of Tunnel Surrounding Rock Failure

According to the above test results, the three failure modes of surrounding rock in deep tunnel are inferred, as shown in Fig. 149.6. The angle θ is designated as the angle of the major principal stress and the rock layer plane. when $\theta = 0°$, the thin layer is easily bent and split, the vertical rock layers in sidewalls tend to be bent under the major principal stress and buckles towards the tunnel, as shown in Fig. 149.6a.

When $\theta = 15°$, the thin rock layer in left arch is easily bent and split (Fig. 149.6b), and in right shoulder, the combination of joints leads easily to the development of potential wedges, the shear sliding mechanism controls the behavior of wedges.

When $\theta = 30°$, the shear mechanism controls the behavior of surrounding rocks (Fig. 149.6c), shear sliding of wedge is mainly controlled by discontinuities, shear sliding may

appear in the right arch, shoulders and sidewalls of the tunnel.

149.4 Conclusions

1. The peak strength, residual strength, elastic modulus and Poisson's ratio of the phyllite increase with increasing confining pressure. The effect of confining pressure on the elastic modulus is smaller than the peak strength and Poisson's ratio.
2. The peak strength and Poisson's ratio decrease with increasing orientation angle. The effect of anisotropy on the peak strength is larger than Poisson's ratio.
3. The split and shear mechanisms of samples are observed, their failures are brittle and ductile, respectively.
4. The three modes of surrounding rock failure in deep tunnel are derived from the test results, which are split and buckling, split and shear, shear sliding.

References

Gao CY, Xu J, He P et al (2005) Study on mechanical properties of marble under loading and unloading conditions. Chin J Rock Mech Eng 3:456–460

Jaeger JC (1960) Shear failure of anisotropic rock. Geol Mag 97(1):65–72

Li ZC (2008) Experimental study on the uniaxial compression of anisotropic rocks. J Railway Sci Eng 03:69–72

Liu SL, Chen SX, Yu F et al (2012) Anisotropic properties study of chlorite schist. Rock Soil Mech 12:3616–3623

Liu YS, Fu HL, Wu YM et al (2013) Experimental study of elastic parameters and compressive strength for transversely isotropic rocks. J Cent S Univ (Sci Technol) 08:3398–3404

Ramamurthy T, Venkatappa Rao G, Singh J (1993) Engineering behaviour of phyllites. Eng Geol 33:209–225

The Professional Standard Compilation Group of People's Republic of China. SL264-2001, Specifications for rock tests in water conservancy and hydroelectric engineering. China Water Power Press, Beijing

Maja Bitenc, D. Scott Kieffer, Kourosh Khoshelham, and Rok Vezočnik

Abstract

Rock joint roughness characterization is often an important aspect of rock engineering projects. Various methods have been developed to describe the topography of the joint surface, for example Joint Roughness Coefficient (JRC) correlation charts or disc-clinometer measurements. The goal of this research is to evaluate the accuracy, precision and limits of Terrestrial Laser Scanning (TLS) for making remote measurements of large-scale rock joints. In order to find the most appropriate roughness parameterization method for TLS data and to analyse the capability of TLS for roughness estimation, experiments were made with a 20 × 30 cm joint sample. The sample was scanned with TLS and compared to reference measurements made with the Advanced TOpometric Sensor (ATOS) system. Analysis of two roughness parameterization methods, virtual compass and disc-clinometer, and angular threshold method, showed that the latter is less sensitive to noise. Comparative studies of ATOS and TLS roughness parameters indicate that the TLS can adequately quantify surface irregularities with a wavelength greater than 5 mm from a distance of 10 m.

150.1 Introduction

Rock joint roughness is an important factor influencing the potential for shear displacement to occur along an unfilled discontinuity at low normal stress (Patton 1966). Several methods have been developed to measure and parameterize roughness amplitude, anisotropy and scale effects, and to utilize these results in a joint shear strength failure criterion, e.g. (Patton 1966; Barton and Choubey 1977; Grasselli and Egger 2003). Prior research has typically considered small joint samples (<1 m²) measured in the laboratory environment. Comparatively few studies have investigated larger scale measurements of roughness in the field using shadow profilometry, total station, TLS, photogrammetry and ATOS. Among these, TLS enables fast, accurate and detailed acquisition of distant, inaccessible, large-scale surfaces. TLS data can be used for the extraction of first-order roughness (Sturzenegger and Stead 2009), which is defined by Priest (1993) as "surface irregularities with a wavelength greater than about 10 cm", but the scale and range limitations of TLS measurements have yet to be investigated.

This contribution summarizes an experiment designed to investigate the intrinsic scale and range limitations of TLS. The influence of TLS data resolution and noise on roughness

M. Bitenc (✉)
Eleia iC d.o.o., Dunajska cesta 21, 1000 Ljubljana, Slovenia
e-mail: maja.bitenc@student.tugraz.at; bitenc.m@gmail.com

M. Bitenc · D.S. Kieffer
Institute of Applied Geosciences, Graz University of Technology, Rechbauerstraße 12/EG, Graz, 8010 Austria

K. Khoshelham
ITC Faculty of Geo-information Science and Earth Observation, University of Twente, Hengelosestraat 99, 7514 AE, Enschede, The Netherlands

R. Vezočnik
DFG Consulting, d.o.o., Pivovarniška 8, 1000 Ljubljana, Slovenia

measurements is studied with ATOS data serving as a reference. Two different roughness parameterization methods are tested to evaluate parameter sensitivity to noise.

150.2 Quality of TLS Point Cloud and Roughness

The quality of a TLS point cloud, namely point accuracy and precision, and resolution, define to what detail roughness amplitude and wavelength (scale) can be observed.

The accuracy and precision of laser point position depends on instrumental errors of laser scanner, environmental conditions (e.g. lightness) and surface features (e.g. reflectivity). If noise is not separated and eliminated from the data, the joint roughness will be overestimated (Khoshelham et al. 2011). In this research, only noise related to the TLS range is considered. Besides, it is assumed that the noise is randomly distributed and that no systematic errors are present. With such assumptions, noise can be reduced by averaging redundant data points. Roughness parameter sensitivity to noise is studied using ATOS data, to which different levels of noise were added. Differences of roughness parameters computed from the noiseless and noise-induced ATOS data indicate the parameter noise sensitivity.

The resolution of TLS points is governed by nominal point spacing set at acquisition and actual footprint size, which depends on scanning geometry and laser beam width. The effective resolution defines the level of detail that can be resolved from a scanned point cloud. Decreasing resolution (i.e. increasing the sampling interval), results in smoothing of the discontinuity surface, indicating that data resolution defines roughness scale. Ignoring the variation of measurement resolution leads to misleading roughness estimation (Tatone and Grasselli 2012). Thus, when comparing joint roughness parameters using different measurement techniques, data should first be resampled to the same resolution.

150.3 Parameterization Methods

In this research, two roughness parameterization methods are applied. To facilitate roughness computations, the coordinate system of the data was aligned with the mean joint plane, with the x- and y-axis coinciding with joint dip and strike, respectively, and the z-axis with roughness amplitude.

The compass and disc-clinometer technique is a traditional, contact-based method of joint roughness measurement (Fecker and Rengers 1971). Discs of different sizes are placed on the joint surface. Dip and dip direction of the disc is measured, which correlate to roughness amplitude and direction, respectively. Roughness scale-dependency can be evaluated using discs of different sizes. The compass and disc-clinometer method is applied to digital data by using orthogonal least squares (OLS) linear regression. For the TLS data having embedded noise, a plane is fitted to all laser points lying within the area covered by a virtual disc. Data redundancy reduces the noise effect on plane calculation. For the reference ATOS data (which are assumed to be free of error) iterative plane fitting is performed.

The angular threshold concept was initially developed to identify potential contact areas during direct shear testing of artificial rock joints (Grasselli 2001). Based on joint surface damage patterns, it was found that only portions of the joint surface that face the shear direction and are steeper than a threshold inclination θ^* provide shear resistance. A higher proportion of steeply inclined facets is indicative of a rougher surface, and is reflected by a larger area under the curve that expresses the potential contact area ratio as a function of θ^*. The area under the curve is taken as the roughness parameter (henceforth referred to as the Grasselli parameter, R). The parameter R depends on shearing direction and the 3D surface representation, but does not consider the scale effect.

150.4 Experiments and Results

Data acquisition. A joint sample of fossil rich limestone was fixed on a wooden plate equipped with eight reference targets (Fig. 150.1a). The smaller circular ATOS targets with radius 7 mm were placed precisely at the center of 10 cm square TLS targets (Fig. 150.1b). The sample and targets were scanned with the Riegl VZ400 laser scanner (Riegl 2013), and imaged with the ATOS I measurement system (Capture3D 2013). Multiple TLS measurements were taken with different nominal resolution in the perpendicular direction and at a distance of 10 m.

Data preparation. The target centers were extracted from corresponding point clouds. The ATOS target centers were processed simultaneously with data acquisition in the ATOS I software. TLS target centers were computed using an image matching algorithm (Kregar et al. 2013). Using target coordinates the TLS and ATOS datasets are co-registered and transformed into a new coordinate system aligned with the joint plane. To eliminate TLS range noise and to enable roughness parameter comparison, both ATOS and TLS point clouds were interpolated into 1 and 5 mm grids. Each grid center was assigned the median height of the points within the grid cell. The triangulated 1 mm ATOS grid is shown in Fig. 150.1c.
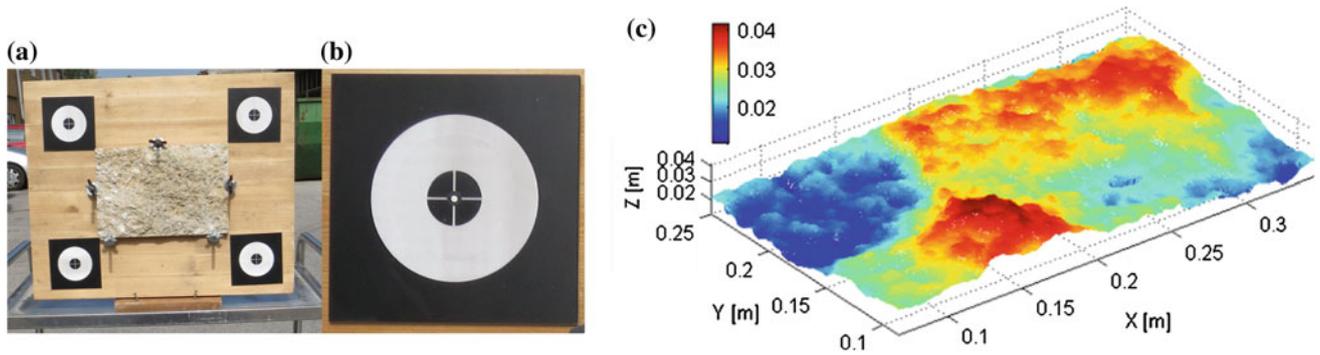
Fig. 150.1 **a** Experimental setup with joint sample and registration targets; **b** target zoom-in; and **c** triangulated surface from 1 mm ATOS grid (**c**)

150.4.1 Roughness Parameter Sensitivity to Noise

For the virtual disc-clinometer and Grasselli parameter algorithm, the dimension of the virtual disc and the grid size are chosen to be 5 mm, respectively. Reference ATOS parameters are then computed based on the described methodologies (Sect. 150.3). Five noise levels (1–5 mm) are added to the ATOS data and roughness parameters are recomputed. The median and 25th–75th percentiles of differences between reference and noisy parameters are shown in Fig. 150.2, where the dip differences are computed for the same disc positions (Fig. 150.2a) and Grasselli parameter differences for the same directions (Fig. 150.2b). Boxes 1–5 in Fig. 150.2 correspond to the five noise levels. Comparing the medians in Fig. 150.2, one can see that the dip is more sensitive to noise (i.e. has bigger median differences) than the Grasselli parameter. The reason might be that dip is computed directly from the data points and that orthogonal

least squares results in artificially steep planes, when the noise level is close to disc size.

Reference ATOS dip measurements were also compared to results computed from original TLS data and 1 mm gridded TLS data (Fig. 150.2a, 6th and 7th box, respectively). Comparison of the 6th box to 7th shows that noise reduction by averaging the height within 1 mm grid cells was successful. The reference ATOS Grasselli parameters are compared to parameters computed from 5 mm grid TLS data (Fig. 150.2b, 6th box). Comparison of the 6th box to 1st indicates that TLS data resampled in 5 mm grid contain less than 1 mm noise.

150.4.2 Roughness Parameter Comparison

Based on results summarized in Sect. 150.4.1, TLS roughness parameters are compared to the reference ATOS parameters. A TLS grid of 1 mm and 5 mm are taken as

Fig. 150.2 Median (*horizontal lines*) and 25th–75th percentiles (*boxes*) of parameter differences indicate: **a** dip magnitude; and **b** Grasselli parameter noise sensitivity at a scale of 5 mm. Boxes 1–5 correspond to 5 noise levels from 1 mm to 5 mm, boxes 6 and box 7 to TLS data of different noise level
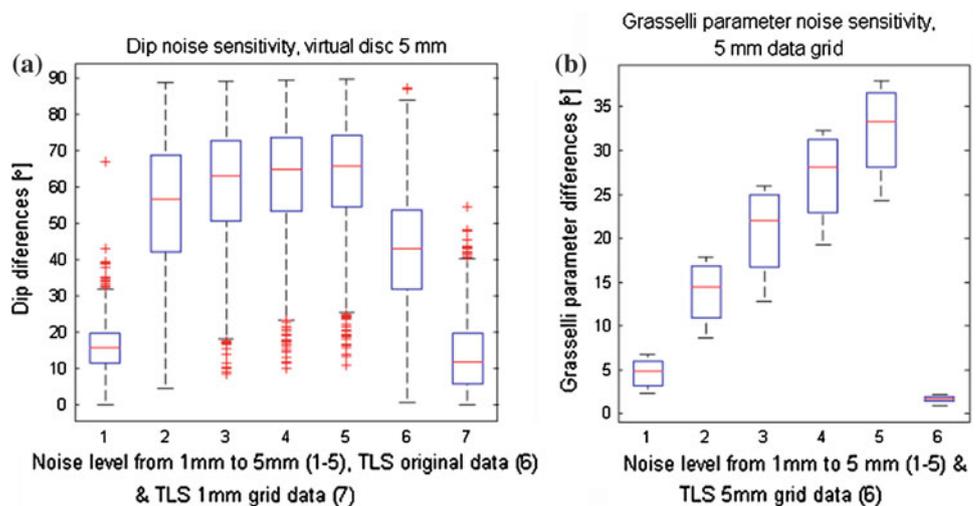
Fig. 150.3 Stereoplots comparing normalized ATOS and TLS roughness parameters computed with **a** virtual disc-clinometer method and **b** Grasselli method

input for the virtual disc-clinometer and Grasselli methods, respectively. Stereoplots in Fig. 150.3 show ATOS and TLS roughness parameters normalized to interval between zero (minimum) and one (maximum), which enables more detailed comparison. Direction 0° corresponds to y-axis (see Fig. 150.1c).

150.5 Conclusions

The use of TLS data for joint roughness computation has been investigated using two empirical roughness parameterization methods (virtual disc-clinometer method and Grasselli ang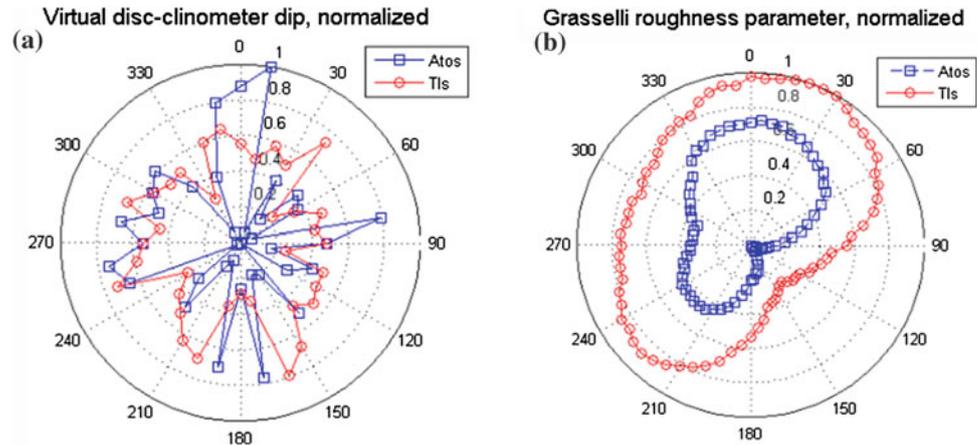ular threshold method). Both methods are capable of representing roughness amplitude and its direction dependency. The sensitivity of roughness parameter measurements to TLS noise indicates that the Grasselli parameter is least sensitive. Dips of discs and the Grasselli parameters computed from gridded TLS data (reduced noise) were compared to the same parameters computed from reference ATOS measurements. Plot of maximum virtual disc dips in all dip directions show relatively poor correlation between ATOS and TLS results. Grasselli parameter plot show a significantly higher correlation between the data sets; however, the TLS surface roughness is systematically overestimated.

References

Barton N, Choubey V (1977) The shear strength of rock joints in theory and practice. Rock Mech Rock Eng 10(1):1–54

Capture3D (2013) Atos I, configurations. Accessed Oct 2013, from http://www.capture3d.com/products-ATOSI-configuration.html

Fecker E, Rengers N (1971) Measurement of large scale roughness of rock planes by means of profilograph and geological compass. In: Proceedings symposium on rock fracture, Nancy, France

Grasselli G (2001) Shear strength of rock joints based on quantified surface description. École Polytechnique Fédérale de Lausanne. Lausanne, EPFL

Grasselli G, Egger P (2003) Constitutive law for the shear strength of rock joints based on three-dimensional surface parameters. Int J Rock Mech Min Sci 40(1):25–40

Khoshelham K, Altundag D et al (2011) Influence of range measurement noise on roughness characterization of rock surfaces using terrestrial laser scanning. Int J Rock Mech Min Sci 48(8): 1215–1223

Kregar K, Grigillo D, et al (2013) High precision target center determination from a point cloud. ISPRS workshop laser scanning 2013. Antalya, Turkey. ISPRS Annals of the Photogrammetry, Remote Sensing and Spatial Information Sciences, vol II-5/W2

Patton FD (1966) Multiple modes of shear failure in rock. 1st ISRM Congress. Lisbon, Portugal, International Society for Rock Mechanics, pp 509–513

Riegl (2013) Laser Scanner VZ-400, Datasheet. Accessed Oct 2013, from http://www.riegl.com/nc/products/terrestrial-scanning/produktdetail/product/scanner/5/

Sturzenegger M, Stead D (2009) Close-range terrestrial digital photogrammetry and terrestrial laser scanning for discontinuity characterization on rock cuts. Eng Geol 106(3–4):163–182

Tatone B, Grasselli G (2012) An investigation of discontinuity roughness scale dependency using high-resolution surface measurements. Rock Mech Rock Eng 1–25

Elaboration and Interpretation of Ground Investigation Data for the Heterogeneous 'Athens Schist' Formation; from the 'Lithological Type' to the 'Engineering Geological Formation'

Georgios Stoumpos and Konstantinos Boronkay

Abstract

Line 4A of the Athens Metro will encounter the Athens Schist, a heterogeneous rock mass comprising a variety of slightly metamorphosed lithological types. Due to the complexity of the rock mass, interpretation of ground investigation data poses a challenge since the direct attribution of laboratory and in situ data to geotechnical design profiles is not appropriate. The methodology that was applied for the evaluation of these data is based on the scheme lithological type—engineering geological unit—engineering geological formation—geological formation, each being a subgroup of the latter. The main aspect of this approach takes into consideration the scale of reference of each assigned category of geomaterials. This elaboration and interpretation methodology, in conjunction with the engineering geological profile, which is compiled in terms of engineering geological formations, provides a comprehensive background for all subsequent geotechnical design needs.

151.1 The Project

Line 4A of the Athens Metro is a new planned line comprising 9 stations and ∼8 km of a single ∼9.5 m diameter tunnel. The line will connect the central-north suburbs of Athens with the city centre, passing through some of the most densely populated neighbourhoods which, at this moment, are not served by a rapid transit system. This paper refers to the methodology that was adopted for the elaboration of ground investigation data in the framework of the production of the General Final Design of Line 4A.

151.2 The Geological Setting

The alignment, of Line 4A runs along the west slopes of Tourkovounia (or Lykovounia) hill range; the tallest and most extensive hill range within the Athens basin which divides it into eastern and western parts.

The geological setting of the project consists of alpine formations and local thin quaternary and man-made deposits. The alpine formations are (from top to bottom) the Crest Limestones, the Sandstone-Marl Sequence and the Athens Schist (Upper and Lower). The quaternary deposits include scree and alluvial deposits. Man-made deposits of small thickness are also locally encountered. Of these geological formations, the one that is being discussed in this paper is the Athens Schist, due to its heterogeneity and complexity.

G. Stoumpos (✉) · K. Boronkay (✉)
Attiko Metro S.A., Messoghion 191, 11525 Athens, Greece
e-mail: gstoumpos@ametro.gr

K. Boronkay
e-mail: kboronkay@ametro.gr

Fig. 151.1 Typical transition from the upper to the lower Athens Schist. The transition is marked by the presence of a shear zone between 17.9–19.3 m

151.2.1 Athens Schist

This formation is an upper Cretaceous heterogeneous rock mass that comprises a variety of slightly metamorphosed lithological types (Marinos et al. 1971) which can be distinguished into two sub-formations: the upper and the lower (Fig. 151.1).

The heterogeneity of the Athens Schist is evident in the frequent, yet often unsystematic, alternations of members with significant differences in terms of mineral composition, grain size and strength; differences that result from the stratigraphic and tectonic inherent intricacy of the rock mass.

The upper formation (commonly referred to as the upper unit, Koukis and Sabatakakis 2000) consists mainly of alternations of metasandstones and metasiltstones. Limestones, calcareous sandstones, calcareous siltstones, schists (chlorite quartzitic, chlorite epidote, calcareous chlorite) as well as phyllites and calcareous phyllites are also encountered. Limestones are often karstified. Sporadically, thin layers and lenses of quartz can be found. The alternations comprise beds which may reach several meters in thickness for the hard rock (metasandstones) but usually are of the order of some decimetres. Even where metasandstones prevail, thin interlayers of weaker material (metasiltstones) are present in most cases.

The lower formation (commonly referred to as the lower unit, Koukis and Sabatakakis 2000) comprises shales, metasiltstones and metasandstones. Thin layers of calcareous metasandstones, chlorite schists as well as intercalations and lenses of quartz are also encountered. The lower Athens Schist is considered the poorest rock mass when compared with the upper formation, since its constituents, and especially the prevailing shales, are of a weaker nature.

151.2.2 Tectonics

Athens Schist constitutes a tectonic nappe pile, formed during Upper Cretaceous (alpine) folding and thrusting. As a result, the rock mass usually exhibits intense fracturing even within its relatively competent members and shear zones are frequent in the form of cataclasites or clayey fault gauge. The formations are persistently folded and locally intensely folded with tight to isoclinal rootless folds.

It has to be noted that, due to its weaker nature, the lower formation was more vulnerable to tectonic deformation. As such, plastic deformation and shearing is more intense with shear zones of considerable thickness (of the order of some meters). In these shear zones the Athens Schist exhibits a chaotic structure with persistent metasandstone and quartz lenses "flowing" in a fissured clayey matrix. In many cases, due to the difference in brittleness between the upper and the lower unit, the transition is manifested by the presence of a shear (detachment) zone (Koukis and Sabatakakis 2000; Fig. 151.1).

151.3 The Challenge

Due to the complexity of the rock mass, interpretation of ground investigation data poses significant challenges. Since the rock mass is heterogeneous with alternations of weaker (e.g. metasiltstone) and stronger members (e.g. metasandstone) the direct attribution of laboratory and in situ tests' data to geotechnical profile strata is not appropriate.

Regarding the Attiko Metro projects, it is common practice to utilize the Hoek–Brown failure criterion to derive strength and deformability parameters for design needs. Hoek–Brown failure criterion emphasises on the lithology of the intact rock, through the intact rock strength σ_{ci} and the constant m_i and on the quality of the rock mass through the Geological Strength Index (GSI). GSI is a system that allows for a reduction in the intact rock parameters by evaluating the structure and the discontinuity surface condition. GSI was introduced because '*a system based more heavily on fundamental geological observations and less on "numbers" was needed*' (Hoek and Marinos 2007).

Indeed, this is the case with the Athens Schist. It is apparent that due to the heterogeneity (various alternating lithological types) and the tectonic history (intense shearing and/or fracturing) of the rock mass, the elaboration of given intact rock properties and the attribution of GSI values requires systematic and careful steps as well as geological and engineering geological awareness.
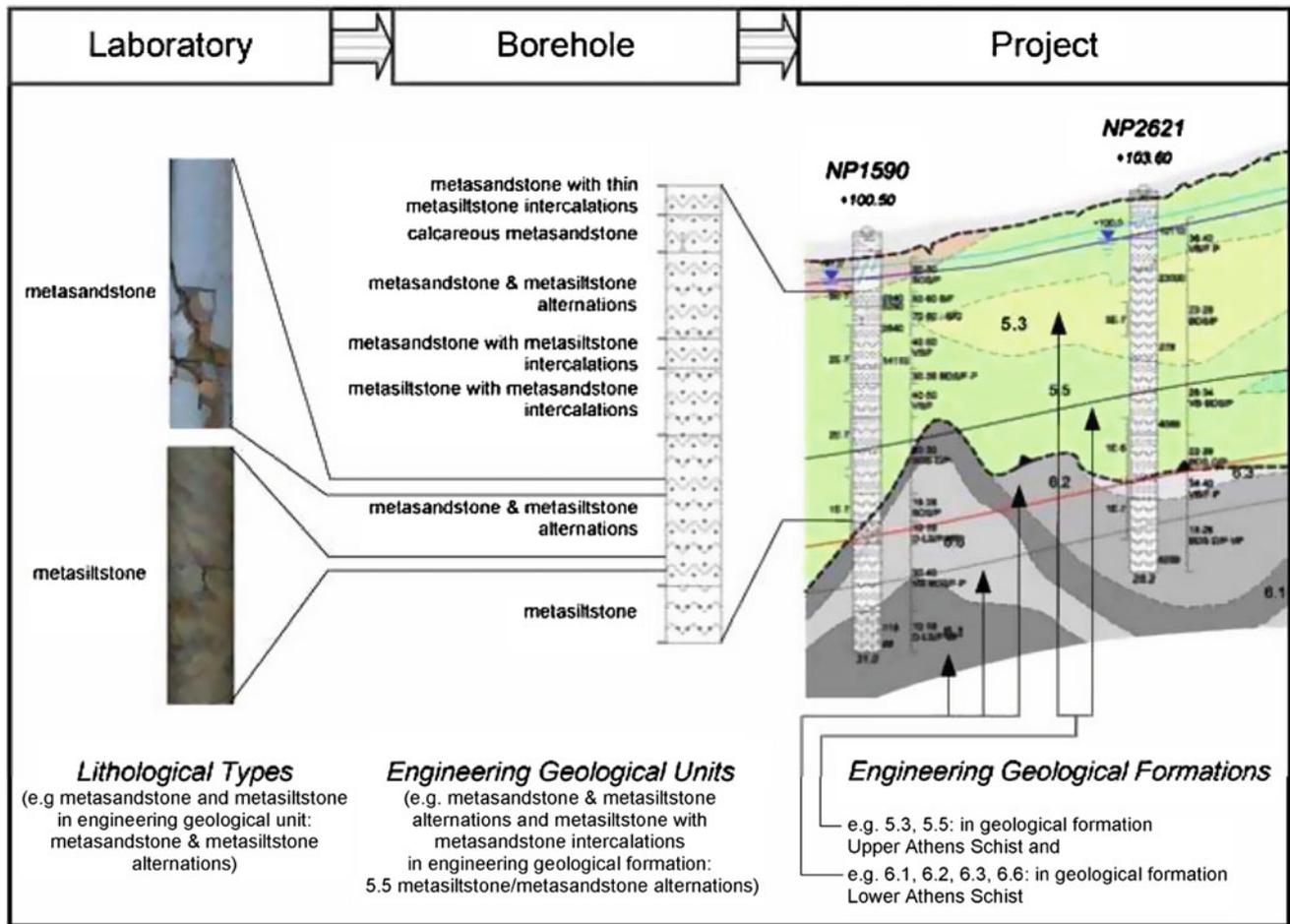
Fig. 151.2 Explanatory graph showing the "flow" of the approach from the laboratory sample scale to the project site scale, namely from the lithological type to the engineering geological formation. In reality, two processes that feed one another, are simultaneously undertaken; synthesis of data from the engineering geological units to the engineering geological formations and analysis of data from the engineering geological units to the lithological types

151.4 The Approach

The methodology that was applied is based on the scheme lithological type—engineering geological unit—engineering geological formation—geological formation, each being a subgroup of the latter (see Fig. 151.2). The main aspect of this approach takes into consideration the scale of reference of each assigned category of geomaterials. Namely, the lithological type refers to the laboratory samples, the engineering geological unit refers to the borehole samples, the engineering geological formation refers to the project site and the geological formation refers to the broader area. In other words, the behaviour of the rock mass during project construction is best described when referring to engineering geological formations. Thus, all available data had to be "translated" in terms of engineering geological formations and attributed to them.

During borehole logging, description and rock mass classification referred to engineering geological units. In this context, the engineering geological unit is the basis of the evaluation and the primary information that was recorded. Obviously, the engineering geological units often comprised more than one lithological type.

These lithological types that were distinguished within the engineering geological units were identified and categorized. Lithological types where the basis for the elaboration of all ground investigation data that refer to the intact rock, namely uniaxial compression tests and point load tests. Moreover, the engineering geological units were grouped
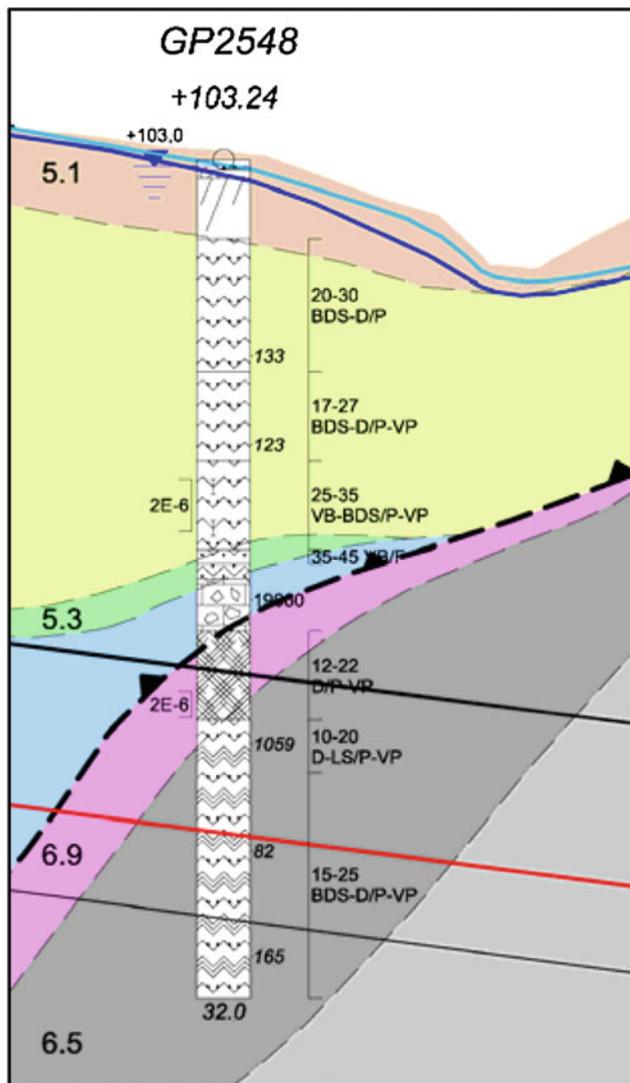
Fig. 151.3 Detail of the geological—hydrogeological—geotechnical longitudinal section. The primary information, namely borehole logging and GSI value as well as structure and surface conditions, are shown in and on the right of the borehole column respectively. q_u and σ_{ci} laboratory tests' results are shown adjacent to the right of the borehole column (in kPa) while in situ permeability tests' results are shown adjacent to the left of the borehole column (in m/s) with the length of the tested section of the borehole also being indicated. The background shows the engineering geological formations (5.1, 5.3, 6.9 etc.). The section is accompanied by a table with proposed σ_{ci}, m_i, GSI and MR values per engineering geological formation (this table is not presented in the present paper since the production of the GFD of the project is still in the pre-tender phase)

into engineering geological formations. These formations are the basis for the engineering geological longitudinal section and the cornerstone of the whole scheme. Rock mass

classification values that where assigned to engineering geological units where elaborated to refer to engineering geological formations. This procedure was based on reducing GSI values for the length of the core run on which they have been assigned.

Intact rock properties were elaborated in terms of lithological types per engineering geological formation. Alongside, for each lithological type the constant m_i was considered.

Based on the Marinos et al. (2011) work on heterogeneous rock masses, the percentage of participation of the various lithological types in each engineering geological formation was taken into account and as such, intact rock properties per engineering geological formation were derived.

151.5 The Outcome

This elaboration and interpretation methodology offers a full set of intact rock parameters and rock mass classification values, per engineering geological formation, that can be directly inputted into the Hoek–Brown failure criterion.

In conjunction with the engineering geological profile (geological-hydrogeological-geotechnical longitudinal section), which is compiled in terms of engineering geological formations (see Fig. 151.3), this approach provides a comprehensive background for all subsequent geotechnical design needs.

References

Hoek E, Marinos P (2007) A brief history of the development of the Hoek–Brown failure criterion. Soils and Rocks, vol. 2, Nov 2007

Koukis G, Sabatakakis N (2000) Engineering geological environment of Athens, Greece. Bull Eng Geol Environ 59(2):0127–0135

Marinos G, Katsikatsos G, Georgiadou-Dikeoulia E, Mirkou R (1971) The Athens' Schist formation, I. stratigraphy and structure. Annales Géologiques des Pays Helléniques, 1ere série, tome 23, 183–212 (in Greek)

Marinos V, Fortsakis P, Prountzopoulos G (2011) Estimation of geotechnical properties and classification of geotechnical behaviour in tunnelling for flysch rock masses. In: Anagnostopoulos A et al (eds) Proceedings of the 15th European conference on soil mechanics and geotechnical engineering. Part 1, Athens 2011, pp 435–440

Incorporating Variability and/or Uncertainty of Rock Mass Properties into GSI and RMi Systems Using Monte Carlo Method

152

Mehmet Sari

Abstract

This paper introduces a probability-based methodology that can be used to evaluate alternative approaches on account of the uncertainties associated with predicting the rock mass properties. The use of this methodology is illustrated through its application for two rock mass case studies. In this regard, the probabilistic spreadsheet models are developed for the strength estimation of Kizilkaya ignimbrite and New Zealand greywacke. The frequency histograms and/or the density functions that best describe the data distribution are used as inputs in GSI and RMi systems. This approach allows the variability and/or uncertainty of the available data to be adequately taken into account during simulations. The developed spreadsheet models are also used to quantify the influence of various material and discontinuity characteristics on the resultant strength properties of the studied rock masses. Sensitivity analysis explicitly shows that joint spacing and UCS of intact rock are the most effective parameters on the estimated rock mass strengths.

152.1 Introduction

A rock mass is a system composed of intact rock pieces separated by a network of discontinuities consisting one or more joint sets, where mechanical behavior and properties are highly variable. Intact rock refers to unfractured blocks between structural discontinuities. A discontinuity is described as "a plane of weakness that has zero or low tensile strength or tensile strength lower than stress levels generally applicable in engineering applications" (Anonymous 1977). Discontinuous rock masses are generally heterogeneous, anisotropic and there is unpredictable spatial variability in both the intact material and discontinuity properties. Due to the heterogeneous properties of the intact rock material and the discontinuity network these masses show a high degree of variability. The intact rock strength indicates the ability of the jointed rock mass to resist shearing failure through the intact pieces of rock. Each discontinuity has a different degree of strength along its length. Therefore, any acceptable solution to a jointed rock mass model should consider both variability of the intact rock and the discontinuities that govern the stability of the rock masses. However, a clear distinction should be made to clarify the difference between the variability of the GSI and σ_{ci} since the first one corresponds to a large volume of rock mass and the second one to a small specimen.

Due to the uncertainty of inherent characteristics that define rock masses, each will exhibit high degree of variability, and thus cannot be evaluated based on deterministic approaches. Empirical models developed for the estimation of rock mass properties are based on the rock mass classification systems such as Q, GSI, RMi. These systems involve a large number of input parameters, each subject to substantial uncertainty. As stated by Riedmuller and Schubert (1999) the complex properties of a rock mass could not sufficiently be described by a single number. Since there are

M. Sari (✉)
Department of Mining Engineering, Aksaray University, 68100
Aksaray, Turkey
e-mail: mehmetsari@aksaray.edu.tr

so many elements or factors that influence the engineering properties of rock masses and the inherent variability of the value is very large, it is important to describe and characterize rock masses in a way to find representative ratings and values for use in engineering design. An accurate assessment of rock mass strength must involve sensitivity analysis and must attempt to model the inherent variability and uncertainty in these parameter estimates.

The Monte Carlo method may be a useful tool for rock engineers and engineering geologists who study in complex rock mass conditions. This technique already takes into considerations such as anisotropy, heterogeneity and other factors which lead the rock to behave stochastically. Probabilistic sensitivity analysis is one method for performing a sensitivity analysis in which all parameters subject to uncertainty are varied simultaneously by Monte Carlo sampling from the distributions postulated for those parameters.

This study is aimed to develop a methodology for taking uncertainty and/or variability caused by natural phenomenon. For this purpose, intact rock and discontinuity properties of two different rock masses are defined as probability distributions in GSI and RMi systems. The developed stochastic models are used to estimate the probability distributions of rock mass strength and the most effective parameters on the estimated values.

152.2 Previous Studies

In the literature, there are a limited number of studies which considers only the stochastic estimation of strength and deformability characteristics and variations of rock masses. Kim and Gao (1995) presented a probabilistic method of estimating the mechanical characteristics of a rock mass, using the third type asymptotic distribution of the smallest values (extreme value statistics) and MC simulation. They used the chi-square goodness-of-fit test to prove that the distribution reflects the inherent variability of the properties of a basaltic rock. Hoek (1998) applied the same method to estimate variation in the Hoek–Brown properties of a hypothetical rock mass, and assuming that all three input parameters of the criterion can be represented by normal distributions. Sari (2009) and Sari et al. (2010) demonstrated the use of MC simulations to evaluate the strength and deformability of rock masses by including the uncertainties of the intact rock strength and discontinuity parameters. They concluded that the MC method provided a viable means for assessing the variability of rock mass properties.

152.3 Materials and Method

152.3.1 Kizilkaya Ignimbrite

The Kizilkaya ignimbrite well outcrops at Kizilkaya village and in the Ihlara Valley (Fig. 152.1). The study area covers the historical and touristic Ihlara Valley, which is about 14 km in length and covers 52 km^2. The rocks in the study area are basically classified as pyroclastic, called Selime tuffs, Kizilkaya ignimbrites, and Hasandag ashes. With the influence of both water and wind erosion, interesting rock shapes and morphological figures have been formed in the slopes of the valley. There are also joint systems developed on the rock mass as a result of cooling of material deposited during volcanic eruptions.

The engineering geological properties of the exposed Kizilkaya ignimbrite were determined on the basis of field observations/measurements and laboratory tests by the author. The main orientation, spacing, persistence, aperture, filling, weathering, and roughness of the discontinuities were described using the scan-line survey method following the ISRM (2007) description criteria. A total of 260 discontinuities were measured along a straight outcrop surface using a measuring tape and compass. A total of 18 rock blocks were collected from the field, then 112 cube specimens were
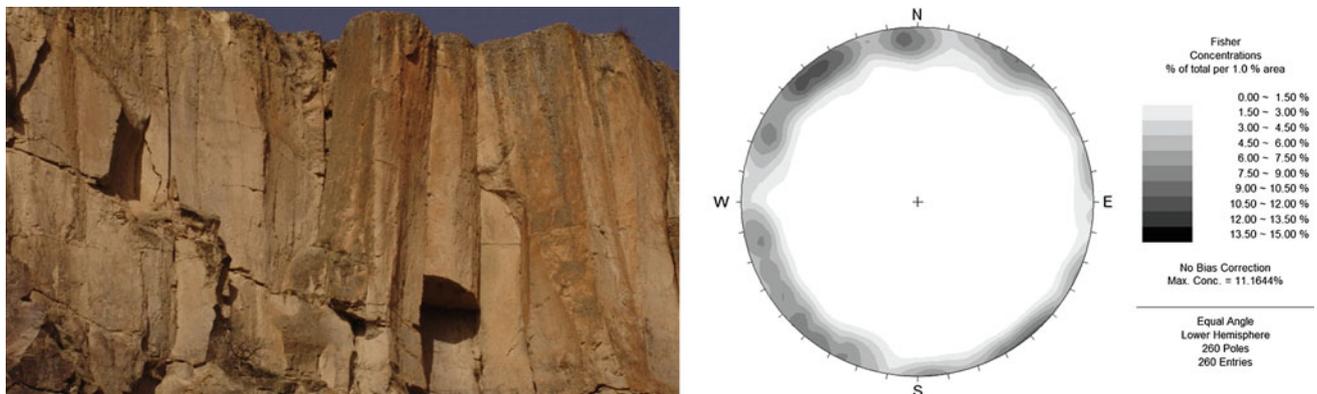

Fig. 152.1 A view of the Kizilkaya ignimbrite and discontinuity orientations

Table 152.1 Discontinuity and intact rock properties of Kizilkaya ignimbrite

Parameter	Distribution type (Mean ± Std. dev.)
UCS (MPa)	Normal (46.06 ± 8.63)
Joint spacing (m)	Lognormal (2.575 ± 1.195)
Joint persistence (m)	Normal (27.09 ± 6.79)
Joint aperture (cm)	N. exponential (3.31 ± 3.26)
Joint roughness	25 % Very rough, 50 % rough, 25 % smooth
Weathering	25 % Fresh, 50 % slightly, 25 % moderately
Infill	50 % Unfilled, 25% sand and gravel, 25 % soft fillings
Groundwater	Dry
m_i	Normal (13.0 ± 2.0)

Table 152.2 Discontinuity and intact rock properties of New Zealand greywacke

Parameter	Distribution type (Mean ± Std. dev.)
UCS (MPa)	Normal (244.7 ± 33.3)
Joint spacing (cm)	Exponential (5.1)
Joint persistence (m)	Lognormal (0.36 ± 0.58)
Joint aperture (mm)	15 % None, 30 % 0.1<, 40 % 0.1–1, 10 % 1–5, 5 % 5>
Joint roughness	5 % Very rough, 50 % rough, 10 % slightly rough, 30 % smooth, 5 % slickensided
Weathering	50 % Fresh, 25 % slightly, 25 % moderately
Infill	30 % Unfilled, 50 % hard filling, 15 % 5 mm< soft filling, 5 % 5 mm> soft filling
Groundwater	Dry
m_i	Normal (17.0 ± 1.5)

prepared from the blocks for laboratory testing. The uniaxial compressive strength (UCS) tests were conducted according to Turkish Standards of methods of testing for natural building stones (TS 699 1987). These values are given in Table 152.1.

152.3.2 New Zealand Greywacke

Closely jointed greywacke rock masses are widespread throughout New Zealand and much of New Zealand's infrastructure is constructed upon greywacke rock masses (Fig. 152.2). Cook (2001) aimed to find common physical properties of defects typical of NZ greywacke rock masses, use these data to identify parameters which have a greater effect on rock mass strength. Cook (2001) measured the following rock mass properties: joint orientation, defect spacing, persistence length, type of joint termination, defect aperture, type of infilling material, type of surface roughness,

waviness. A database of greywacke properties was also developed by Stewart (2007) based on previous studies upon un-weathered greywacke around New Zealand. The database included descriptions of greywacke defect properties and mechanical properties of the intact rock and joints. Greywacke in the study area is composed of hard sandstones, sandstones inter-bedded with mudstones, and mudstones. The summary information for this dataset is given in Table 152.2.

152.3.3 GSI and RMi Classification Systems

The Geological Strength Index (GSI) (Hoek et al. 1995) and the Jointing Parameter (JP) of the Rock Mass index (RMi) (Palmstrom 1995) are two of the most known and frequently used indexes. RMi has been developed by Palmstrom (1995)
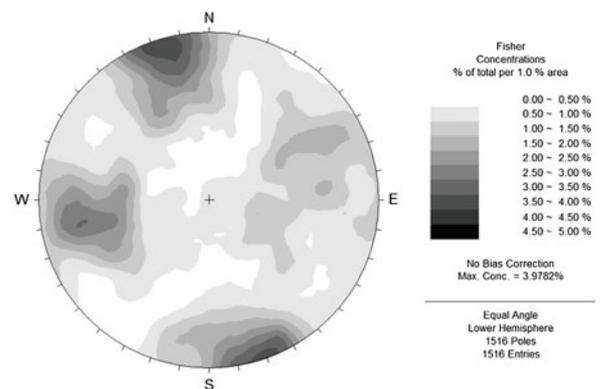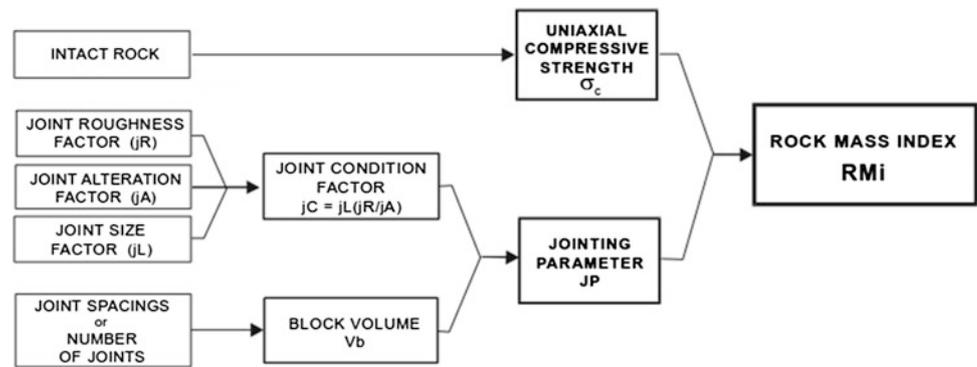

Fig. 152.2 A view of the New Zealand greywacke and discontinuity orientations

Fig. 152.3 The layout of the rock mass index, RMi (after Palmstrom 1995)

with input of the geological parameters that have the greatest influence on rock mass strength (Fig. 152.3).

RMi is based on the principle that the joints intersecting a rock mass tend to reduce its strength. Consequently, it is expressed as:

$$RMi = \sigma_c \times JP \qquad (152.1)$$

Here σ_c = the uniaxial compressive strength of intact rock (in MPa), measured on 50 mm samples. JP = the jointing parameter, expressing the reduction in strength of the intact rock caused by the joints. It incorporates the main joint features in the rock mass. The jointing parameter was found as

$$JP = 0.2 \times jC^{0.5} \times V_b^D \qquad (152.2)$$

where $D = 0.37 \times jC^{-0.2}$.

At failure, the generalized Hoek–Brown criterion relates the maximum effective stress, σ_1 to the minimum effective stress σ_3 through the functional relation:

$$\sigma_1 = \sigma_3 + \sigma_{ci}\left(m_b\frac{\sigma_3}{\sigma_{ci}} + s\right)^a \qquad (152.3)$$

where m_b extrapolates the intact rock constant m_i to the rock mass:

$$m_b = m_i \exp\left(\frac{GSI - 100}{28 - 14D}\right) \qquad (152.4)$$

σ_{ci} is the uniaxial compressive strength of the intact rock and s and a are constants that depend upon the rock mass's characteristics:

$$s = \exp\left(\frac{GSI - 100}{9 - 3D}\right) \qquad (152.5)$$

$$a = \frac{1}{2} + \frac{1}{6}\left(e^{-GSI/15} - e^{-20/3}\right) \qquad (152.6)$$

The uniaxial compressive strength of the jointed rock masses is calculated from the following equation suggested by Hoek et al. (2002)

$$\sigma_c = \sigma_{ci}s^a \qquad (152.7)$$

The concept of a global "rock mass strength" σ_{cm} is proposed by Hoek et al. (2002) and it could be estimated from the Mohr–Coulomb relationship as

$$\sigma_{cm} = \sigma_{ci}\frac{(m_b + 4s - a(m_b - 8s))(m_b/4 + s)^{a-1}}{2(1 + a)(2 + a)} \qquad (152.8)$$

The most recent version of the generalized Hoek–Brown failure criterion (Hoek et al. 2002) is employed to estimate the rock mass strengths of the Kizilkaya ignimbrite and New Zealand greywacke. In the Hoek–Brown criterion, the GSI is the most important scaling parameter for allocating the strength and deformation properties determined in the laboratory to the field scale rock mass (Hoek et al. 1995). In earlier versions of this criterion, Bieniawski's RMR was used for this scaling process. Due to the usage of different rating scales for each parameter, the RMR is more suitable for variability determination. It is possible to objectively obtain a frequency distribution of RMR for computing purposes in a probabilistic analysis. However, by using a GSI chart only a subjective estimate of variability to field scale rock mass can be possible. The following relation is suggested by Hoek (1998):

$$GSI = RMR_{89} - 5 \qquad (152.9)$$

Since GSI system is mostly descriptive in nature and prone to subjectivity, a linkage between descriptive

geological terms and measurable field parameters has been proposed by Sonmez and Ulusay (1999), Cai et al. (2004) and Russo (2009). Cai et al. (2004) proposed a quantitative approach, using block volume and joint condition factor, to utilize the GSI system. Once the block volume (V_b) and the joint condition factor (J_c) are known, the GSI value can be determined from the following equation presented by Cai and Kaiser (2006):

$$GSI = (26.5 + 8.79 InJ_c + 0.79 InV_b)/(1 + 0.0151 InJ_c - 0.0253 InV_b)$$

$$(152.10)$$

where J_c is a dimensionless factor and V_b is in cm^3.

On the basis of the conceptual similarity of the GSI with the Joint Parameter (JP) used in the RMi, Russo (2009) derived a relationship between the two indexes in order to obtain a reliable, quantitative assessment of the GSI by means of the basic input parameters for the determination of the RMi. On the basis of the above correlations, a quantitative estimation of the GSI is made, by defining the parameters concurrent to the evaluation of JP, i.e. the block volume (V_b) and the joint condition factor (jC) as follows:

$$GSI = 153 - 165/(1 + (JP/0.19))^{0.44} \qquad (152.11)$$

152.4 Monte Carlo Simulation and Sensitivity Analysis

The probabilistic spreadsheet models are developed for the estimation of rock mass strengths of Kizilkaya ignimbrite and New Zealand greywacke. The frequency histograms and/or the density functions that best describe the data distribution in Tables 152.1 and in 152.2 are used as inputs in GSI and RMi systems. Excel add-in ModelRisk (Vose Software 2012) program provides a simple and intuitive implementation of a MC simulation together with prepared spreadsheet models. In a MC simulation, a random value is selected for each of the inputs, based on the range of estimates. The model is calculated based on this random value. The result of the model is recorded, and the process is repeated many times. At the end, basic statistics (mean, standard deviation, range, min, max, etc.) for the output are computed from the collected data.

In this study, 5,000 iterations are performed for different rock mass properties using the Latin Hypercube sampling method. This method applies stratified sampling technique to closely resemble the input probability distribution with fewer realizations. Although there are some correlations expected between input parameters, they are assumed to be independent for the sake of simplicity of the problem at hand.

The frequency distributions of calculated GSI values are given in Fig. 152.4 for the Kizilkaya ignimbrite and New Zealand greywacke, respectively. It can be easily discerned that the GSI values estimated from the RMR system (Eq. 152.9) for both rock types illustrate more consistent and less scattered data compared to two equations suggested by Cai and Kaiser (2006) (Eq. 152.10) and Russo (2009) (Eq. 152.11). One of the fallows of Cai and Kaiser (2006) method is that it consistently produces GSI values greater than 100 which is meaningless. In spite of having closer mean values between Cai and Kaiser (2006) and RMR equations, three suggested methods predict dissimilar and highly variable values of GSI for the same rock masses.

Estimated strength values of rock masses are given in Fig. 152.5. Two equations suggested by Hoek et al. (2002) and the one calculated from RMi of Palmstrom (1995) predict completely different strength values. Necessary GSI values for the estimation of σ_c and σ_{cm} values in the Hoek–Brown failure criterion are the ones calculated from the RMR dependent equation (Eq. 152.9). For the Kizilkaya ignimbrite, the estimated rock mass strength of σ_{cm} and RMi are very close to each other, around to 12.5 MPa. For New Zealand greywacke, however, values of σ_c and σ_{cm} are closer than RMi value. It can be said that different rock mass properties of two completely dissimilar rocks are subjected to different rock mass behavior. This is mostly due to attaining various priorities to rock mass characteristics in their empirical equations by the founders.

Fig. 152.4 Simulated GSI frequency distributions of **a** Kizilkaya ignimbrite and **b** New Zealand greywacke using three quantitative approaches
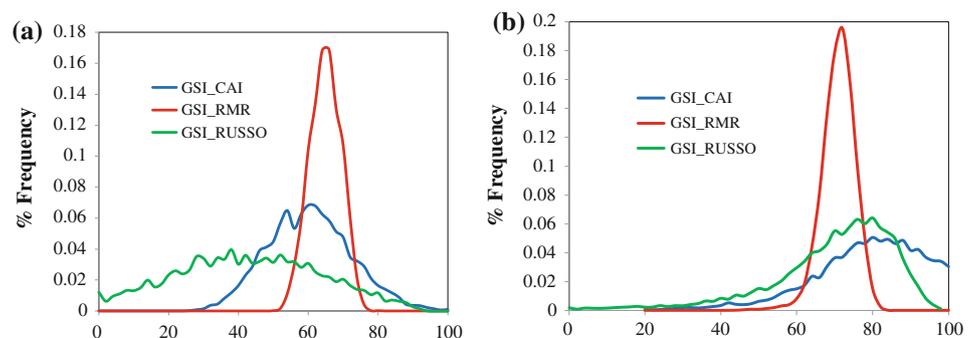
Fig. 152.5 Probabilistic estimates on the rock mass compressive strength (MPa) of **a** Kizilkaya ignimbrite and **b** New Zealand greywacke using GSI and RMi systems
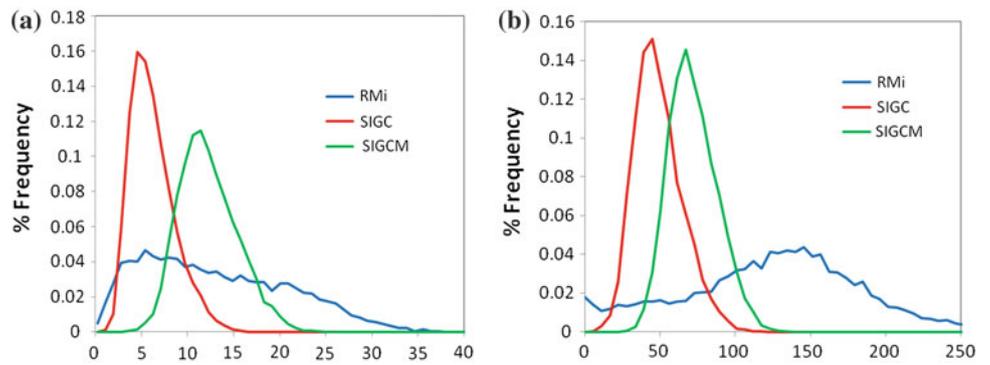
Fig. 152.6 Spider plots for **a** RMi and **b** σ_c of the Kizilkaya ignimbrite
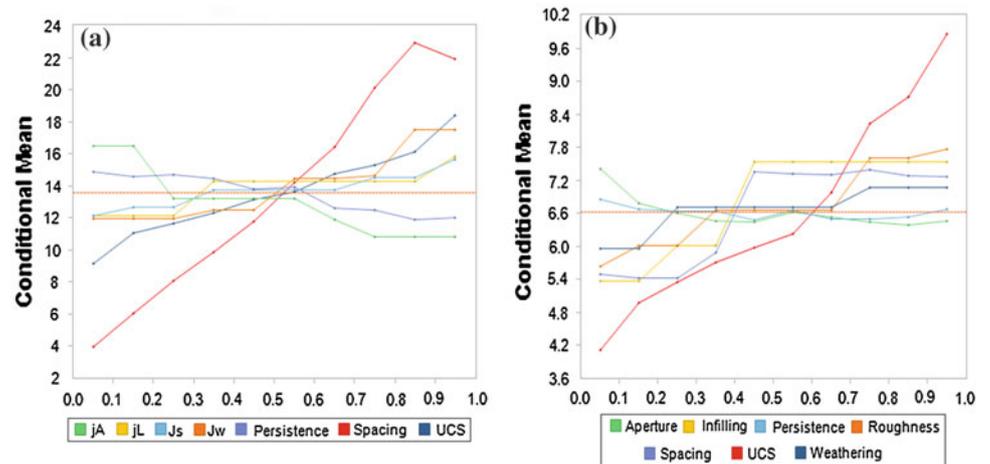
Fig. 152.7 Spider plots for **a** RMi and **b** σ_c of the New Zealand greywacke
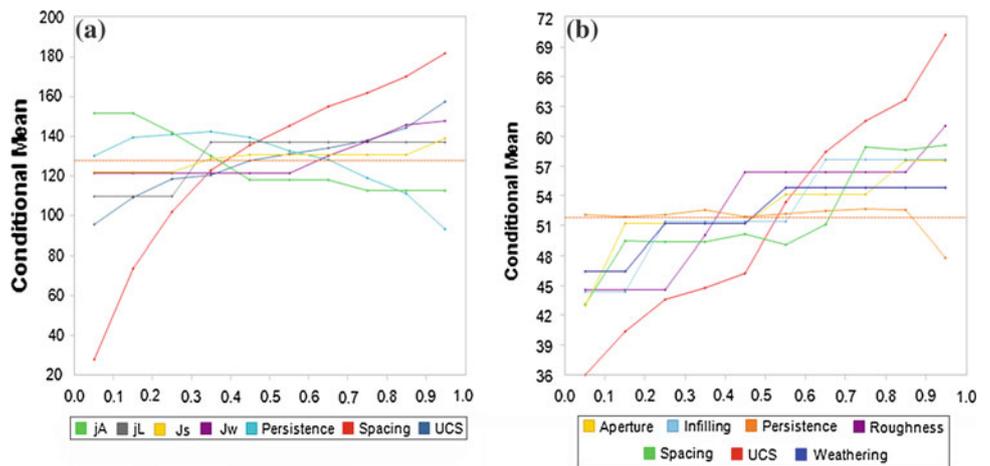
Sensitivity analysis is a method employed to find most influential input parameters on the output parameters. If an input parameter changes every time on its full range during simulation while other parameters are kept constant on their mean values, potential effects of each input parameter can be easily discerned on the output results. There are some methods for performing sensitivity analysis on the data,

namely, rank order correlations, contribution to variance and spider plots. Spider plots describe graphically how sensitive value of an output variable is to the input variables of a simulation model. The flatter the line for an input variable, the less sensitive it is.

In Figs. 152.6 and 152.7, an analysis has been performed on the sensitivity of the mean of the RMi and σ_c outputs. It has been performed by splitting up simulation data from input distributions into ten groups in terms of their cumulative probability. The simulation data are filtered by software for each of these groups to find the corresponding RMi and σ_c mean values that occurred when the input variable being analyzed lies within each percentile band. The statistic of interest (i.e. mean in this case) is then calculated for the filtered data. Repeating this analysis across each percentile range for each selected input variable produces the spider plots in Figs. 152.6 and 152.7.

In these plots, the horizontal dashed line shows the mean of the unfiltered RMi and σ_c values as a reference. The vertical range that an input line covers reflects the degree of sensitivity that output statistic has to this input value. So, for example, when spacing lies in its 0–10 % range in Fig. 152.6, the RMi mean is approaches to 4 MPa, and when spacing lies in its 90–100 % range, the RMi mean is closer to 22 MPa, a difference of 18 MPa. Reviewing all graphs, it can be easily discerned that while the mean values of RMi is most sensitive to spacing of Kizilkaya ignimbrite and New Zealand greywacke, the mean values of σ_c is most sensitive to UCS of the two rock masses.

152.5   Conclusions

A probability based analysis is performed in the study to account for uncertainty and/or variability reflected by most of the rock masses encountered in large construction projects. Three empirical equations proposed to calculate GSI value quantitatively are investigated for the estimation of strength of two rock masses subject to completely different geologic characteristics. First equation is the generic one proposed by Hoek and Brown (1997) for estimating GSI values from the RMR scores. Second and third ones are proposed by Cai and Kaiser (2006) and Russo (2009) to estimate GSI values quantitatively. It was found that three suggested equations generated completely different values of GSI. It was also found that the most influential parameters were depended on which equations were used in the estimation of rock mass strength. In case of calculated RMi, the most effective input parameter on the rock mass strength was the spacing of discontinuities. On the other hand, in case of σ_c and σ_{cm}, the most influential input parameter was the UCS of intact rocks.

Regarding the estimation of the GSI in the design stage, Cai (2011) is recommended to apply the point estimate method, which reflects rock mass property uncertainties in the numerical analysis of tunnel and cavern stability. Inclusion of more data in the design process may not only provide a more accurate estimation and allow for the recognition of dispersion, but can also alter the ultimate estimate that is made.

References

Anonymous (1977) The description of rock masses for engineering purposes. Report by the Geological Society Engineering Group working party. Quart J Eng Geol 29:67–81

Cai M, Kaiser PK, Uno H, Tasaka Y, Minami M (2004) Estimation of rock mass deformation modulus and strength of jointed hard rock masses using the GSI system. Int J Rock Mech Mining Sci 41:3–19

Cai M, Kaiser PK (2006) Visualization of rock mass classification systems. Geotechnol Geol Eng 24:1089–1102

Cai M (2011) Rock mass characterization and rock property variability considerations for tunnel and cavern design. Rock Mech Rock Eng 44:379–399

Cook GK (2001) Rock mass structure and intact rock strength of New Zealand greywackes. M.Sc thesis, University of Canterbury

Hoek E, Kaiser PK, Bawden WF (1995) Support of underground excavations in Hard Rock. Balkema, Rotterdam 215

Hoek E, Brown ET (1997) Practical estimates or rock mass strength. Int J Rock Mech Min Sci 34:1165–1186

Hoek E (1998) Reliability of the Hoek–Brown estimates of rock mass properties and their impact on design. Int J Rock Mech Min Sci 35:63–68

Hoek E, Carranza-Torres CT, Corkum B (2002) Hoek–Brown failure criterion-2002 edition. In: Proceedings of 5th North American Rock mechanics symposium, Toronto, Canada, pp 267–273

ISRM (2007) The complete ISRM suggested methods for rock characterization, testing and monitoring: 1974–2006 [Ulusay R, Hudson JA (eds)]. ISRM Turkish National Group, Ankara, 628 pp

Kim K, Gao H (1995) Probabilistic approaches to estimating variation in the mechanical properties of rock masses. Int J Rock Mech Min Sci 32:111–120

Palmstrom A (1995) RMi-a rock mass characterization system for rock engineering purposes. Ph.D. thesis, University of Oslo

Riedmuller G, Schubert W (1999). Rock mass modeling in tunneling versus rock mass classification using rating methods. In: Proceedings of the 37th US Rock mechanics symposium, Vail, Colorado

Russo G (2009) A new rational method for calculating the GSI. Tunn Undergr Space Technol 24:103–111

Sari M (2009) The stochastic assessment of strength and deformability characteristics for a pyroclastic rock mass. Int J Rock Mech Min Sci 46:613–626

Sari M, Karpuz C, Ayday C (2010) Estimating rock mass properties using Monte Carlo simulation: Ankara andesites. Comput Geosci 36:959–969

Sonmez H, Ulusay R (1999) Modifications to the geological strength index (GSI) and their applicability to stability of slopes. Int J Rock Mech Min Sci 36:743–760

Stewart SW (2007) Rock mass strength and deformability of unweathered closely jointed New Zealand greywacke. Ph.D. thesis, University of Canterbury, 455 pp

TS 699 (1987) Tabii Yapı Taşları-Muayene ve Deney Metotları. Türk Standartları Enstitüsü, Ankara (in Turkish)

Vose Software (2012) ModelRisk help, Vose Software. www.vosesoftware.com

Using of Multivariate Statistical Analysis in Engineering Geology at the Pest Side of the Metro Line 4 in Budapest, Hungary

153

Nikolett Bodnár, József Kovács, and Ákos Török

Abstract

The geological setting of a part of the new metro line in Budapest, Hungary is very complex and large amount of ambivalent historic data available on the physical properties of rocks. The Late Oligocene–Miocene sediments representing wide ranges of lithologies and mechanical properties. Core logs, drilling reports and records of laboratory analyses were studied for better understanding of the local geology, and to prepare a database on engineering geologic properties of the materials. Using this database, geologic sections were prepared and multivariate statistical analyses were used. Based on it four distinct groups were identified including swelling clays, non-swelling clays, medium clays, sands + silts. The results allowed a better correlation of the strata in the area, and a reconstruction of the geologic evolution. The obtained data sets can be used as input parameters for the design of the tunnel and stations.

153.1 Introduction

The construction of the new metro line (line no 4) of Budapest is nearly completed. The studied section is located in the central part of the line between Kelenföldi Railway Station and Keleti Railway Station (Fig. 153.1).

In the mid-60 to early 80s 500 exploration drillings for the construction of the metro line (Szlabóczky 1988). The physical parameters of these drillings and the later period exploration boreholes were used for the present study. The aims were to outline the engineering geological properties of a mixed sedimentary system including bentonitic clays, silts and sandy deposits. The tunnel system and the stations of the studied area are located in this heterogeneous system. By using multivariate statistical analyses it is possible to estimate the physical parameters of these lithotypes.

153.2 Geological Settings

Along the metro line Eocene, Oligocene and Miocene strata are covered with Quaternary sediments (Raincsákné 2000) (Figs. 153.2 and 153.3).

The metro line can be divided into three parts on the basis of geological-tectonical settings: Buda part (from the Kelenföld railway station to the Gellért square), the Danube crossing part (from the western part of the Gellért square to the Pest lower quay) and Pest part (from the Fővám square to the Keleti railway station, Dózsa György street).

On the studied area the sediments become younger from the SW to NE on the other riverside in Pest. The line cut through Upper Oligocene and Miocene strata. This part is lithologically more diverse. The Oligocene and Miocene beds are covered by river deposits of the Danube which contains groundwater (Juhász 2000) (Fig. 153.4).

N. Bodnár (✉) · Á. Török
Department of Construction Materials and Engineering Geology, University of Technology and Economics, Műegyetem rakpart 3, Budapest, 1111, Hungary
e-mail: bodnar.nikolett@gmail.com

J. Kovács
Department of Applied Geology, Eötvös Loránd University, Pázmány Péter sétány 1/C, Budapest, 1117, Hungary

Fig. 153.1 The studied area in Budapest marked by a *rectangle*
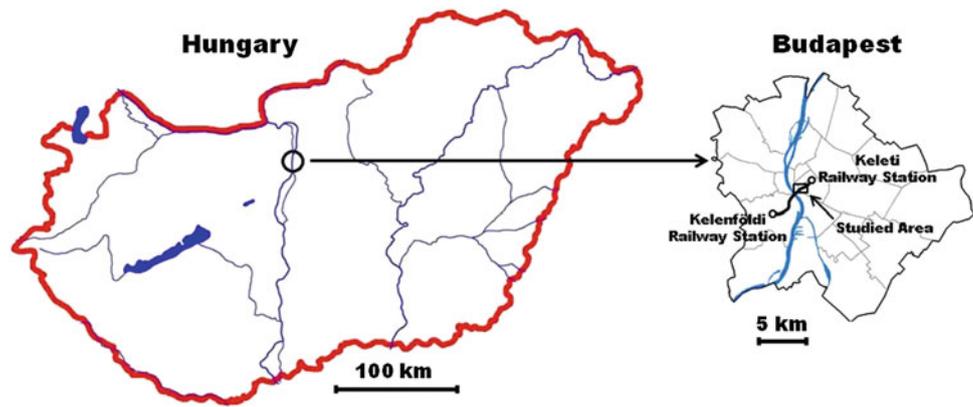
Fig. 153.2 Uncovered geological map
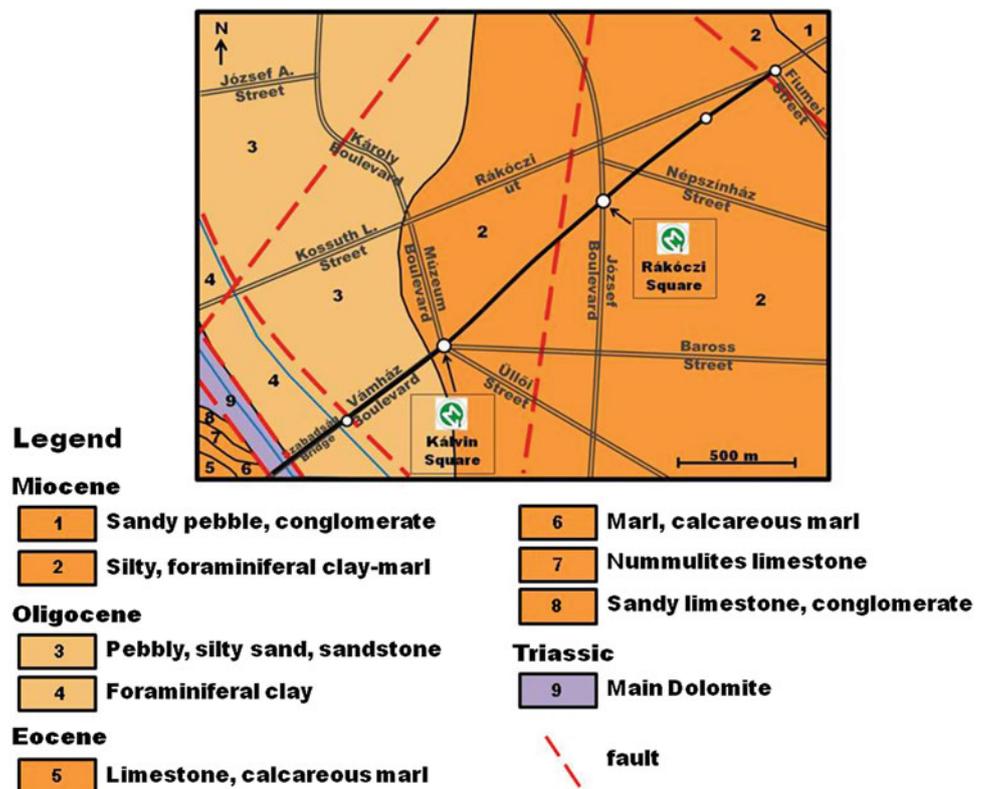
153.3 Methods

The data used in this study was obtained from borehole logs and core descriptions. Data set of the boreholes was used for the statistical analyses. Several of these parameters (e.g. index of plasticity) cannot be defined for such lithologies.

From the selected and gathered twelve parameters data filtration showed that there are very poor correlation between several properties, thus these values should not be taken into consideration in multivariate statistical method (Miller and Kahn 1962). After the filtration only five parameters remained including void ratio, dry bulk density, angle of friction, cohesion and compressive strength. 252 samples

Fig. 153.3 Covered geological map

Legend

Holocene

1	Anthropogenic fill
2	Sandy pebble, sand
3	Silty sand, silt, clay
4	Humus-rich flood deposits, loam
5	Sand, silty sand
6	Sand with rock debris and pebble

Eocene

8	Marl, calcareous marl
9	Nummulites-Lithotamnium limestone
10	Sandy limestone, conglomerate

Triassic

| 11 | Main dolomite |

Legend

Quarternary

Pebble, sand, silt

Miocene

Pebble, sand, silt

Clay

Bentonite

Discordance

Borehole

Fig. 153.4 Typical engineering geological borehole at the studied area

which contain 1,260 data were analysed by the means of mathematical statistics.

Cluster analysis was used to form groups from different samples according to their similarity. Additionally discriminant analysis was also performed according to the method listed in (IBM 2010).

153.4 Results

The cluster analysis of 252 samples of the five parameters provided four groups as results. The samples were not evenly assigned into the four groups. In some groups more, while in some other clusters fewer samples were found. The four groups are: swelling clays, non-swelling clays, medium clays, sands + silts. Interestingly, that the bentonites (which are usually among the swelling clays) do not belong to the group of swelling clays in this analysis (Fig. 153.5). Based on these results it has become clear, that these bentonites are more permeable than most bentonites. The average water conductivity of these samples was 10^{-7} m/s, although the mean values of water conductivity of bentonites is 10^{-10} m/s in general.

The groups created with the cluster analysis were verified with discriminant analysis, which proved that the groups were mathematically correct.

Fig. 153.5 Results of cluster
analysis: **a** bulk density, **b** void
ratio, **c** angle of friction,
d compressive strength,
e cohesion. Ranges are marked by
solid vertical lines, *boxes* indicate
the *upper* and *lower quartile* with
horizontal lines representing
median values. Extreme values
are indicated by *dots*
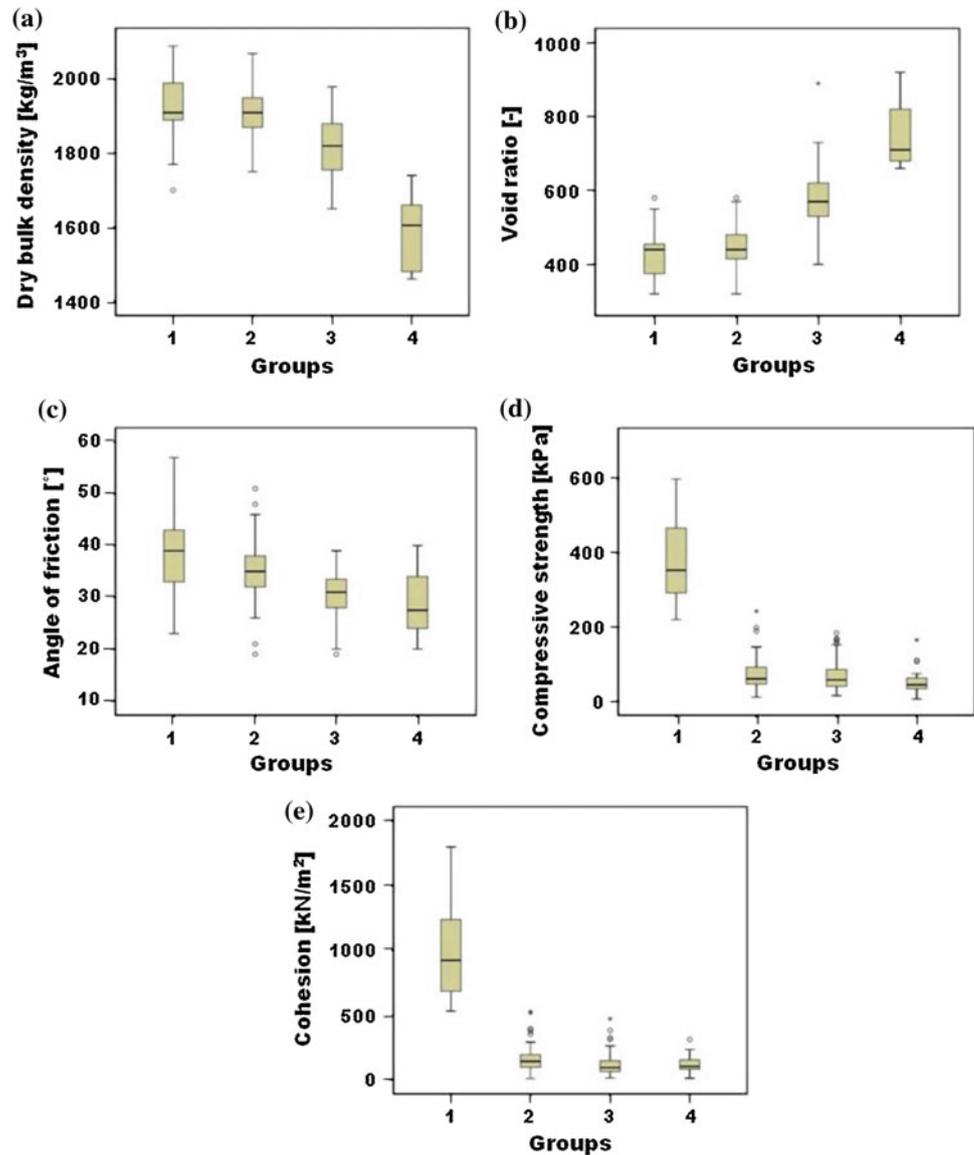
153.5   Conclusions

The studied area has a complex geological structure with
thin impermeable strata and lenticular aquifer bodies that
makes difficult to use simple engineering geological input
parameters for the design of the new metro line in Budapest.
This study has proved that the use geomathematical and
multivariate statistical methods allow the distinction of
poorly described and very mixed laboratory and lithological
data sets, that were made in the past. It was possible to
identify four groups including swelling clays, non-swelling
clays, medium clays, sands + silts. The multivariate statis-
tical analyses provided valuable information for under-
standing the geomechanical parameters of lithologies and
helped in outlining the input values for the design of the
structures.

References

IBM (2010) Introduction to statistical analysis with PASW Statistics.
    IBM Company, Chicago IL, USA, 274 p
Juhász J (2000) A 4. sz. metró kutatásának hidrogeológiai ereményei
    (Results of hydrogeological exploration of metro line)—Földtani
    Kutatás, 37/2, 25–35 pp (in Hungarian)
Miller RL, Kahn JS (1962) Statistical analysis is the geological
    sciences. Wiley, New York, 483 p
Raincsákné Gy (2000) A Budapest 4. sz. metróvonal és környezetének
    földtani viszonyai (Geological setting of metro line 4 and its
    environment)—Földtani Kutatás, 37/2, pp 4–19 (in Hungarian)
Szlabóczky P (1988) A metrós fúrások földtani eredményeinek átfogó
    ismertetése (Complex geological evaluation of core drillings of
    metro)—Földtani Közlöny, 118/1, 61–66 pp (in Hungarian)

R.F.C. Souza and O.J. Pejon

Abstract

Materials in which the change in moisture content leads to an increase in their volume are known as expansive soils, and may cause damages in engineering works. Due to lack of soil with better qualities, and the need to use these soils as construction materials, it is necessary to study this behavior. Tests were performed with the inundation of samples with distilled water by the constant volume method. In addition to the mineralogical and geotechnical tests (index properties), the samples were submitted to the methylene blue adsorption test and the scanning electron microscopy. Results of swelling tests showed higher swelling pressure for compacted air dried samples, with reached values about 200 kPa, while 133 kPa for undisturbed air dried samples. Low values of swelling pressures can be justified by the absence of minerals of smectites group. Finally, the results of swelling pressure tests were compared with the values obtained from relations proposed in the literature to predict swelling pressure of expansive soils.

Keywords

Swelling pressure • Swelling clays • Expansive soils

154.1 Introduction

The phenomenon of expansion in soils can intensely affect civil engineering, such as highways, runways, railroads, canals, and buildings, causing damages in their structures. Swelling soils presents volume changes when in contact with water and can mobilizing considerable swelling pressure. Many factors influence the mechanism of swelling, and this phenomenon can be affected by physical soil properties and also state stress (Nelson and Miller 1992).

Numerous studies have been published relating swelling pressure to index properties and predicting methods. The index properties are related such as dry unit weight, initial water content, consistence limits, clay content, and cation exchange capacity (Alonso et al. 1992). To predict and evaluate the swelling pressures it has been proposed laboratory tests. The most commonly used tests are the free swell, constant volume, zero swell and swell-consolidation tests that examining swelling behavior in one direction (Basma et al. 1995). In addition, empirical relations have been developed with the basic soil properties and swelling pressure (Raman 1967; Chen 1988; Pereira and Pejon 1999).

The objective of this paper is to present results of swelling pressure in clay materials through equipment designed to measure the expansion constant volume.

154.2 Materials and Experimental Methods

The studied materials are from Sao Paulo state, southeastern Brazil, they are sedimentary materials (claystones and silt-stone) from Corumbatai Formation (Permian) and exhibit geological and geotechnical characteristics leading to expansive behavior, as high clay. These materials do not

R.F.C. Souza (✉) · O.J. Pejon (✉)
University of Sao Paulo, Ave. Trabalhador Sancarlense, 400, Sao Carlos, 13.566-590, Brazil
e-mail: rafaela_faciola@yahoo.com.br

O.J. Pejon
e-mail: pejon@sc.usp.br
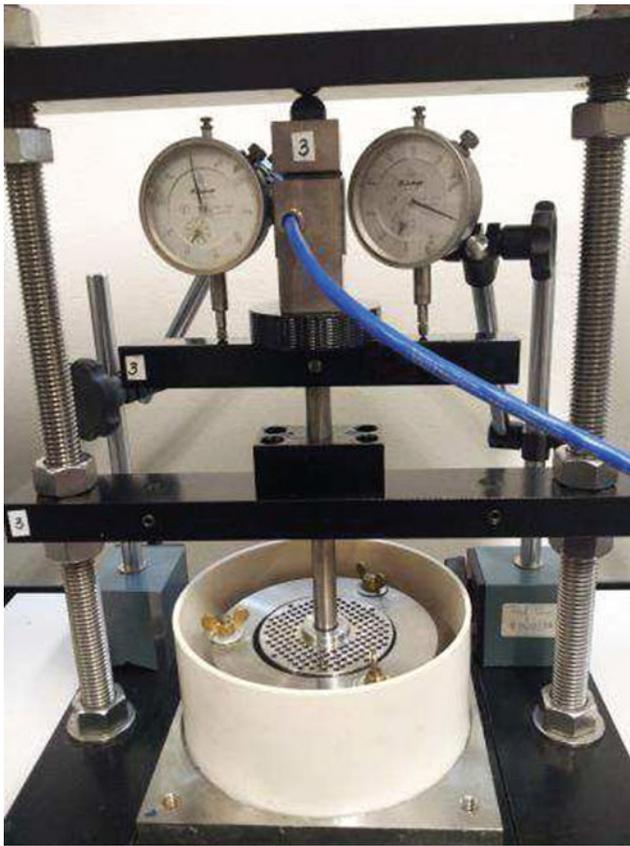
Fig. 154.1 Axial swelling stress in manual press

Table 154.1 Soil geotechnical and mineralogical properties

Soil characteristics	
Percentage of clay content	52
Bulk density (Mg/m^3)	1.81
Specific gravity (Mg/m^3)	2.69
Dry density (Mg/m^3)	1.46
Optimum moisture content (%)	23.7
Void ratio	0.84
Porosity (%)	45.65
Degree of saturation (%)	76.24
LL (%)	76
PL (%)	32
PI (%)	44
CEC (cmol$^+$/kg)	31.05
SS (m^2/g)	242.75

reserved to conduct the tests. The swelling tests are performed in undisturbed and compacted samples and air-dried in atmosphere conditions before testing.

The materials were characterized for their geotechnical properties and mineralogical composition. Samples were submitted in dry unit weight test, moisture content, consistence limits, grain-size distribution, X-ray diffraction of clay fraction, cation-exchange capacity, and methylene blue adsorption.

To determine the swelling pressure has been developed a device that consist a manual press similar to that proposed by ISRM (1989). This equipment allows measuring the expansion of the material at constant volume. Figure 154.1 shows the equipment that consist a set of manual press with an edometric cell and a load cell.

The volume constant method is a technique called the direct method because of its ability to provide the swelling force directly (Kayabali and Demir 2011). This test consists in soil

exhibit in their mineralogical constitution the expansive clay mineral montmorillonite, but have properties that indicate their potential to volume change, such as high water absorption capacity, and plasticity index (IP = 44). Natural soil samples were collected from the side of the highway where it is located the Corumbatai Formation, and were

Fig. 154.2 X-ray diffractometer of the Corumbatai Formation sample

Fig. 154.3 Swelling pressure:
a Undisturbed samples;
b Compacted samples; and
c Compacted at optimum
moisture content sample
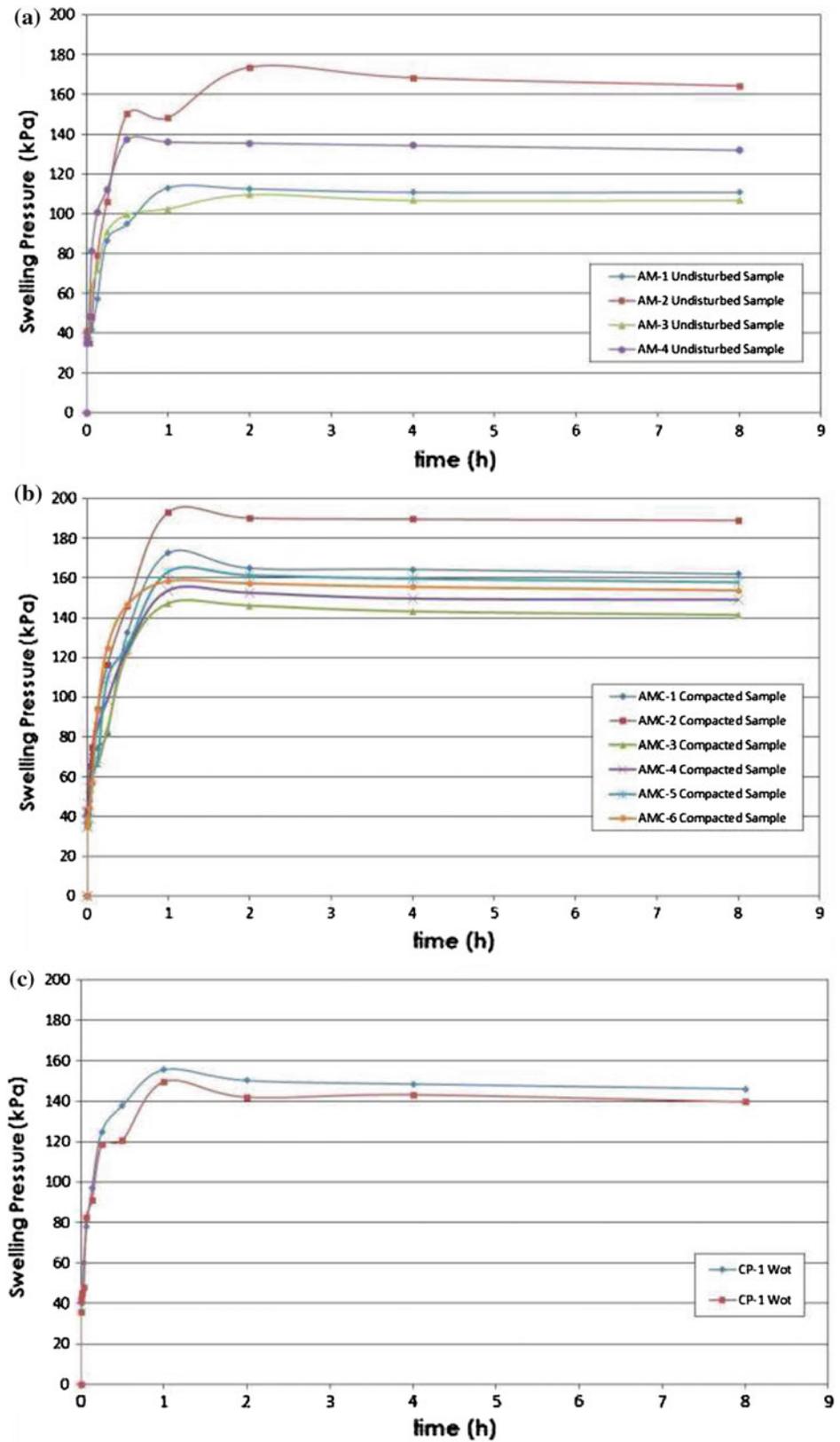
sample placed in oedometer cell. It is placed in the manual load device, and a seating of 25 kPa is applied, so there is no difference between piston connected to the load cell and the top plate on the sample. In a next step, the soil sample is inundated with water, and increments of vertical stress are applied to prevent swelling. At the time the specimen is

Table 154.2 Medium values of sample properties

Sample condition	Moisture content$_{medium}$ (%)	Density$_{medium}$ (Mg/m^3)
(a)	9.36	1.47
(b)	11.63	1.57
(c)	23.68	1.47

inundated, variations from the deformation are read, and it's preferably kept between 0.005 and 0.01 mm. The specimen remains under pressure and there is no tendency to swell. After 24 h, the vertical stress is recorded as the swelling pressure.

154.3 Results and Analyses

Three conditions of specimen were used to compare swelling pressure. The first series of test included determination of swell pressure using four undisturbed samples, and the second series using six compacted samples in optimum moisture content. In the first two conditions analyzed, the samples were molded and placed to dry in atmosphere air until the moisture content stabilization. Two compacted samples were tested at optimum moisture content in the third condition.

Table 154.1 shows the results of the characterization tests and mineralogical compositions performed with the Corumbatai Formation material. The sample presents fine particle in almost all its composition, varying from 52 % of clay and 44 % of silt. The high porosity and low density can also explain the expansive behavior. The consistence limits values were high which indicates a highly plastic material. The cationic exchange capacity (CEC) and specific surface are indicative of clay minerals with normal activity, and the probable minerals are illite and halloysite.

No smectite clay mineral group was exhibited by X-ray diffraction (Fig. 154.2). Illite and kaolinite were the dominant clay minerals detected. This result was confirmed in thermal differential analysis.

According to the correlations proposed by Raman (1967) and Chen (1988) about consistence limits, this material can be characterized as very expansible. However, about correlation proposed by Pereira and Pejon (1999) considering clay percentage and methylene blue volume, this material present low swell, due to the presence of kaolinite and absence of smectite.

Swelling pressure results are presented in Fig. 154.3 in (a) for the first, (b) second, and (c) to third condition analyzed. The undisturbed sample presented swelling pressure about 150 kPa, and it is clear by the result shown in Fig. 154.3b that compacted samples increased the swelling behavior. Undisturbed sample reached maximum axial swelling pressure in about 2 h with 173 kPa, while compacted sample reached it in about 1 h with 193 kPa of maximum value. The compacted air-dry sample reached maximum axial swelling pressure in about 1 h with 155 kPa. In general, the swelling

pressure showed similar values which were not very significant in terms of magnitude. The swelling pressure reached similar values to samples tested at optimum moisture content. Therefore, according to Table 154.2, the moisture content did not influence on the expansion, but only did so on the effect of compaction.

154.4 Conclusions

The Corumbatai Formation materials did not exhibit mineral of smectite group, but present an expansive behavior, showing values of swelling pressure. The geotechnical properties also indicated that the material presents a potential expansive behavior. Results showed that swelling pressure can be more expressive in compacted samples with higher densities. The device presented satisfactory performance and simple handling, and it can be applied to other types of expansion tests.

We conclude that sedimentary materials with high clay content, highly plastic and low percentage of expansive clay minerals also need attention before to deploying large or small buildings. Therefore, careful with this type of material should start from the design phase, extending to all stages of construction, even in the post use, since the expansion can cause damage to the building (cracks and breaks), which can shorten life, or derail in extreme situations.

References

Alonso EE, Gens A, Josa A (1992) A unified model for expansive soil behavior. In: Proceedings of the 7th international conference on expansive soils, Dallas, Tex., 3–5, Texas Tech University Press, Ludbbock, Tex., pp 24–29

Basma AA, Al-Homoud AS, Malkawi AH (1995) Laboratory assessment of swelling pressure of expansive soils. Appl Clay Sci 9 (5):355–368

Chen FH (1988) Foundation on expansive soils. American Elsevier Science Publication, New York

ISRM: International Society for Rock Mechanics (1989) Commission on swelling rock and working group on swelling rocks of the commission on testing methods. Suggested methods for laboratory testing of argillaceous swelling rocks. Int J Rock Mech Min Sci and Geomech Abstr 26(5):415–426

Kayabali K, Demir S (2011) Measurement of swelling pressure: direct method versus indirect method. Can Geotech J 48:354–364

Nelson JD, Miller DJ (1992) Expansive soils: problems and practice in foundation and pavement engineering. Wiley, 259 p

Pereira EM, Pejon OJ (1999) Estudo do potencial expansivo dos sedimentos ar- gilosos da Formação Guabirotuba na Região de Alto Iguaçú—PR. 9 Congresso Brasileiro de Geologia de Engenharia. ABGE, 16 p, São Pedro–São Paulo

Raman V (1967). Identification of expansive soils from the plasticity index and the shrinkage index data. Indian Eng Calcutta 11(1): 17–22

V. Marinos, P. Fortsakis, and G. Stoumpos

Abstract

The term weak rock mass is usually associated in design and construction with potential problems or even failures, although this is not always the case. Weak rock masses could be cases with very low intact rock properties, highly tectonized or/and weathered rock masses, rock masses with members of low strength and/or inherent heterogeneity. In this paper, the potential problematic behaviour of weak rock masses in tunnel excavation and dam foundation is discussed. A rock mass could be generally characterized as weak when its potential failure is driven by the inadequacy of its strength (σ_{cm}) as a system to bear the stresses that are imposed upon it and not by local failure of its components (intact rock and discontinuities). On the other hand, anisotropic failures like planar slides in dam abutments or wedge failures in tunnels do not constitute failure patterns that can be directly associated with weak rock masses. A general borderline could be that a weak rock mass: (i) in tunnelling can develop shear failures and deformations even under medium overburden and (ii) in dams can raise serious concerns for the foundation using any other dam type (e.g. arch dam, concrete gravity dam) than an earth/rock fill dam.

155.1 Introduction

Typically, the term weak rock mass, if not correctly assessed is associated in design and construction with potential problems or even failures. However, this term usually attempts to describe and quantify the quality of the rock mass via an absolute geotechnical approach, without implying the problematic rock mass behaviour, irrespective of the kind or characteristics of the project. Therefore a weak rock mass could be associated with severe squeezing in tunnelling under considerable overburden and the same weak rock mass could be stable for excavation in smaller depth. On the other side tunnelling through a very competent rock mass could be a stable project or associated with failures such as wedge slide under low overburden or rockburst.

Marinos (1993) described that the weak rock masses could be distinguished to the rock masses that were "born" weak (e.g. mudrocks, siltstones), the ones that became weaker through a retrogression from an original stronger material (weathering, alteration or tectonic deformation) and the rock masses that became weaker, although still strong, since they are associated by genesis with weak rocks at a scale affecting the engineering behaviour of the formation

V. Marinos (✉)

Faculty of Sciences, School of Geology, Laboratory of Engineering Geology and Hydrogeology, Aristotle University of Thessaloniki, 54124 Thessaloniki, Greece
e-mail: marinosv@geo.auth.gr

P. Fortsakis
School of Civil Engineering, Department of Geotechnical Engineering, National Technical University of Athens, Heroon Polytechniou 9, 15780 Zografou, Athens, Greece

G. Stoumpos
Attiko Metro S.A., 191–193 Messoghion Avenue, 11525 Athens, Greece

they belong (alternation of competent and incompetent rocks —heterogenous rock masses such as flysch). Thus, it is difficult to draw limits in order to stick the label "weak rock" since other intrinsic or secondary features may impose a weak rock mass behaviour (stress dependent and time dependent behaviour, as creep or swelling or dissolution, change of water content, slaking, inherent anisotropy).

Regarding the intact rock, many different definitions of the weak rock can be found in literature, usually associated with the Uniaxial Compressive Strength (UCS, σ_{ci}). Rocha (in Oliveira 1993) proposed $\sigma_{ci} = 2$ MPa as the limit between the soils and rocks. According to the definition of ISRM (1981) $\sigma_{ci} = 2–6$ MPa corresponds to very weak rocks whereas 6–20 MPa to weak rocks. Similar definitions could be set for the rock mass strength (e.g. σ_c, σ_{cm}).

The characterization of the rock mass as weak primarily depends on the lithology of the intact rock and the state of the rock mass. These can all be quantified by the use of e.g. the intact rock strength σ_{ci} and the Geological Strength Index (GSI) as for the case of the Hoek-Brown failure criterion. In that sense, to describe a rock mass as weak or strong should be a straightforward process regardless of a particular project. However, this is not always the case.

Indeed, it is easy to categorize a rock mass with, for example, $\sigma_{ci} < 5$ MPa and GSI < 20 as weak or a rock mass with, for example, $\sigma_{ci} > 100$ MPa and GSI > 70 as strong. Yet, the question that arises has to do with all the rock masses that lay amidst. This is why one has to consider the engineering project type, scale and geometry. After all, the attribution of the term weak or strong to a rock mass "as it stands" is only academically useful. It is the project-rock mass interaction that is important and in particular the types of failure that are associated with each given conditions.

The potential problematic behaviour of a category of weak rock masses in tunnel excavation and dam foundation is discussed in the paper. In general, anisotropic failures such as planar slides in dam abutments, wedge failures in tunnels do not constitute failure patterns that can be associated with weak rock masses. For example in the case of tunnelling the weak rock masses would be related with the tunnel face instability, large displacements or overstress of the support shell and not with gravity driven problems like ravelling ground or wedge failure.

Consequently, a rock mass could be characterized as weak when its potential failure is driven by the inadequacy of its strength (σ_{cm}) to bear the stresses that are imposed upon it; inadequacy that refers to the rock mass as a whole and not as individual constituents (only intact rock or only discontinuities). Moreover, the characterization of the rock mass in an engineering problem does not only depend on the rock mass properties but also to the potential failure pattern. A general borderline could be that a weak rock mass: (i) in tunnelling can develop shear failures and deformations even

under relatively low overburden and (ii) in dam foundation raise serious concerns for the foundation using any dam type (e.g. arch dam, concrete gravity dam) apart from an earth fill dam.

155.2 Weak Rock Masses and Tunnels

Conventional excavation of tunnels within weak rock masses can be better approached by identifying the failure modes that could potentially emerge. These failure modes are usually associated with stress-induced phenomena such as face instability and squeezing, manifested by tunnel face extrusion, tunnel closure or shell overstress.

A factor that could be adopted to identify a weak rock mass behaviour in tunnelling is the ratio of the rock mass strength divided by the geostatic stress at the tunnel level (σ_{cm}/p_o, Hoek and Marinos 2000). The low values of this ratio could be a result of high excavation depth or/and low σ_{cm} that is further analysed in low σ_{ci} and/or low GSI. The Tunnel Behaviour Chart (TBC, Marinos 2012) in Fig. 155.1 is a comprehensive tool to indicate combinations of rock mass structure, intact rock strength and overburden height that may develop stress-induced behaviour.

Typical examples of such behaviour include tectonized heterogeneous sedimentary sequences such as flysch, highly tectonized, altered and/or weathered ophiolites such as foliated serpentinites, heavily sheared homogeneous sedimentary rocks of low intact rock strength such as claystones, shales, molassic formations etc.

For example, molassic formations, when confined in depth, have not developed stress relaxation, and exhibit a compact structure and usually correspond to high GSI values (Marinos et al. 2013). Nevertheless, the intact rock strength, especially in the case of siltstones, is usually low, thus leading to a low rock mass strength and potentially to weak rock mass behaviour. On the other hand, there are cases where namely strong rock masses have developed a typical weak rock mass behaviour. One example would be the excavation of the new Gotthard Tunnel in the area of Faido where a yielding support was adopted for the excavation through a tectonically sheared and foliated gneiss formation under the overburden of 1100 m (Personal observation).

155.3 Weak Rock Masses and Dams

Dam foundation in weak rock masses often includes challenges like compressible rock masses, presence of incompetent members and fractured and sheared zones of low to very low strength, poorly to medium cemented rocks, diverse heterogeneity and presence of cavities. These conditions often lead to a single choice selection of the
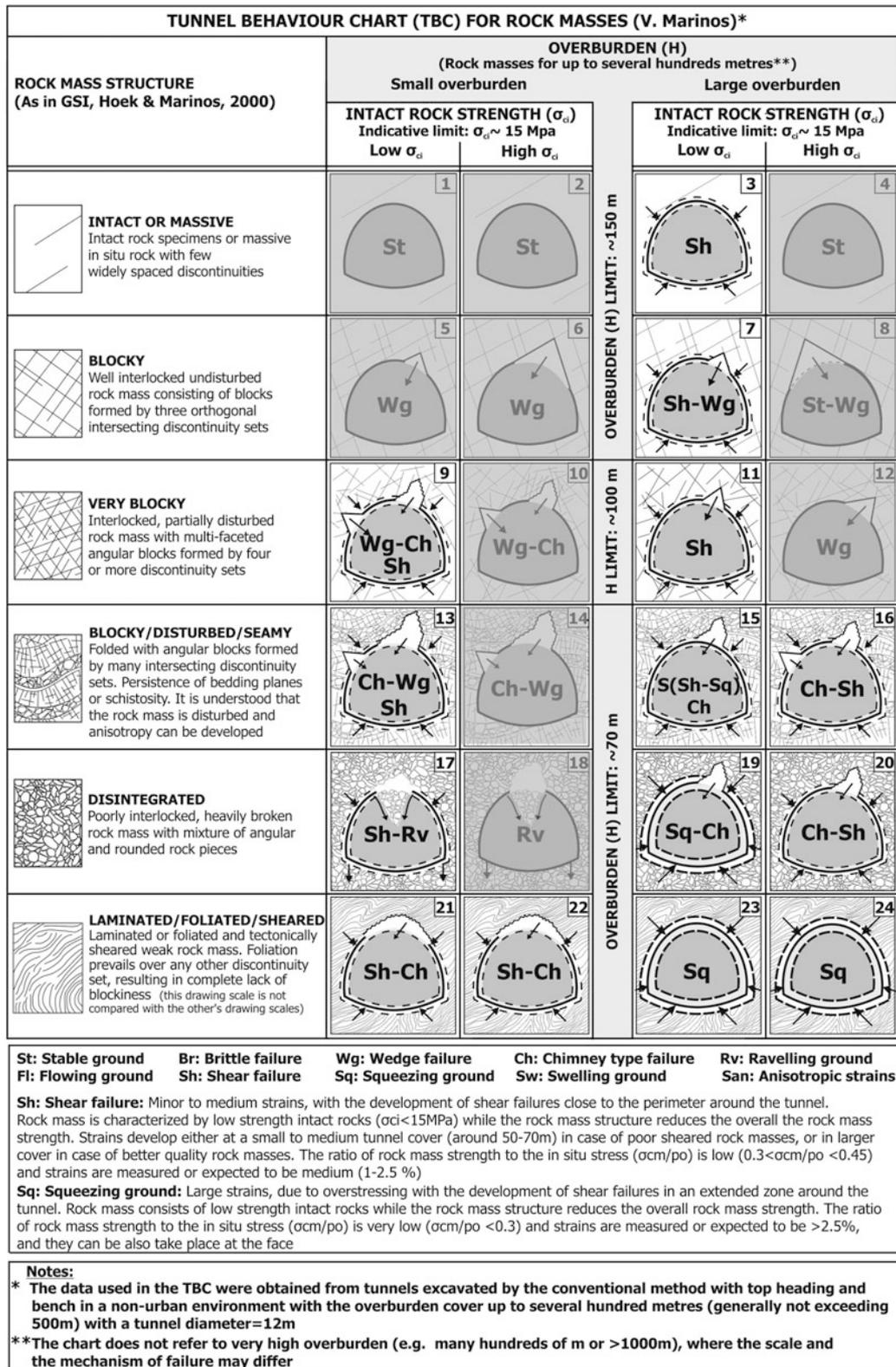
Fig. 155.1 Tunnel behaviour chart (TBC). Stress-controlled problematic behaviour that corresponds to weak rock masses is highlighted (Marinos 2012)

Table 155.1 Rock mass elements that can characterise a rock as "weak" in dams

Rock material	Engineering geological elements enabling, if present, to characterise the rock as "Weak rock mass" in dam foundation
Conglomerate, Sandstone	Poor cementation material (e.g. clayey), low diagenesis. Low strength and deformation modulus. Cases with frequent intercalations with pelitic interlayers
Marl, Siltstone Mudstone, Slate	Presence of clayey minerals, poor cementation. Possible laminated with diagenetic planes. When tectonically disturbed they form very weak rocks masses
Clayshale	Low rock mass strength (foliated structure, low intact rock strength) and deformation modulus -Sheared surfaces, slickensided surfaces. Swelling minerals. Slaking potential
Evaporites	Dissolution phenomena, presence of voids (gypsum, halite). Swelling (anhydrite)
Limestone, Marble	Internal karstic structure, voids empty or soil filled. Cases of intercalations of weak pelitic layers (phyllites in the case of marble)
Molasse	Alternations of sandstones with siltstones (most common). Diverse heterogeneity. Presence of members with low strength. Slaking potential when exposed
Flysch	Alternations of sandstones with siltstone the most common. Diverse heterogeneity. Presence of members with low strength. Unlike molasse tectonically disturbed structures (structural complexity in space due to folding and presence of sheared tectonic zones and layers). Persistence of discontinuities with low strength in depth
Volcanic rocks	Generally strong, but may alternate with pyroclastic compressible, swelling or erodible material. Heterogeneity in strength and deformation modulus. Weathering or alteration with presence of unstable minerals/high plasticity soils. Joints from cooling/lava tunnels
Pyroclastic rocks	Highly erodible, collapsible or swelling. Extreme variability within the fromation
Granite	Generally strong but possibility of extended weathering presence. Irregular weathering profile and bedrock interface (less weathered boulders within completely weathered material). Concealed sheet joints close to surface
Basic-Ultra basic/ Ophiolites	Generally strong but peridotites may present serpentinized zones of low strength in irregular geometry within the mass. Shear zones with altered compressible material
Graphitic-Chlorite schists. Phyllites	Dense schistosity with weak planes. Possible low strength and modulus. Weathered to other clay minerals
Gneiss	Generally strong. Weak in extended weathered/sheared brecciated zones only
Quartzite	Strong but often quartzitic layers alternate with incompetent phyllites
Metamorphic schists	Generally strong. Possible presence of weak zones due to tectonic shears and to slickensided schistosity planes

construction of an embankment, earth/rock fill dam and/or, seldom, the strengthening of the foundation zone or the selection of an alternate dam location. Cases where various rocks can be characterized as "weak" in dam foundation engineering are presented in Table 155.1.

155.4　Conclusions

The term weak rock mass attempts to describe and quantify the quality of the rock mass via an absolute geotechnical approach, irrespective of the kind or characteristics of the project. However, it is the authors' view that the type of engineering project is also important in order to predict the behaviour of the rock mass during construction.

Several definitions and a discussion about the limits of weak rock masses were presented in the paper and a classification of weak rock masses according to the engineering project type was directed. The authors assessed the problematic behaviour of weak rock masses in tunnel excavation and dam foundation in order to achieve this scope.

Characterisation of "weak rock masses" according to the engineering project type was performed based on different approaches. In tunnelling, the combinations of rock mass structure, intact rock strength and overburden height that may lead to the development of stress-induced behaviour were highlighted. In dam foundation the engineering geological elements enabling, if present, to characterise different kinds of rock as "weak rock" were presented.

References

Hoek E, Marinos P (2000) Predicting tunnel squeezing in weak heterogeneous masses. Tunnels and Tunnelling International, Part 1, November Issue, pp 45–51; Part 2, December Issue, pp 34–36

International Society for Rock Mechanics (ISRM) (1981) Commission on classification of rocks and rock masses. Int J Rock Mech Min Abstr. 18:85–110

Marinos P (1993) General report session 1: hard soils-Soft rocks: geological features with emphasis to soft rocks. geotechnical engineering of hard soils-soft rocks. In: Anagnostopoulos et al (eds) Balkema, Rotterdam, ISBN 9054103442, pp 1807–1818

Marinos V (2012) Assessing rock mass behavior for tunnelling. J Environ Eng Geosci XVIII(4):327–341

Marinos V, Fortsakis P, Prountzopoulos G (2013) Tunnel behaviour and support in molassic rocks. The experiences from 12 tunnels in Greece. In: Kwasniewski M, Lydzba D (eds) Rock mechanics for

resources, energy and environment (EUROCK2013). CRC Press, Boca Raton, pp 909–914

Oliveira R (1993) Weak rock materials. In: Proceedings of the 26th annual conference of the engineering group of the geological society, Leeds, UK, Sept 1990

Applicability of Weathering Classification to Quartzitic Materials and Relation Between Mechanical Properties and Assigned Weathering Grades: A Comparison with Investigations on Granitic Materials

A. Basu

Abstract

The ongoing process of weathering in nature produces progressive but intricate changes in rock microstructure. Evaluating mechanical behaviors of rock materials with reference to weathering grades is, therefore, important for an engineering work encountering weathered rocks. The common 6-fold weathering classification for uniform materials is meant to capture gradational change of rock materials depending on degree of decomposition. Research in this regard has been limited within polymineralic rocks (e.g. granite etc.) where degree of alteration of constituent minerals helps recognize such gradation. Quartz being the most resistant mineral to weathering is the chief mineral constituent of quartzite and therefore, capturing intricate gradational change of quartzite in response to weathering or categorization of weathering grades of quartzitic materials is a challenging task. In line with the author's involvement in three different research topics, this paper presents salient points in categorizing weathering grades of granitic rock materials from Hong Kong and southeastern Brazil that are subsequently compared with the issues in characterizing weathering grades of quartzitic rock materials from eastern India. An overall assessment of mechanical behaviors of these rocks with reference to assessed weathering grades is also outlined.

156.1 Introduction

The ongoing process of weathering in nature produces progressive but intricate changes in rock microstructure at shallow depths where most engineering works are confined, especially in tropical and sub-tropical areas. The most widely used weathering classification system such as ANON (1995) by and large resembles the 6-fold classification scheme developed by Moye (1955) in which Grades I–IV represent rocks whereas higher grades stand for soils. The weathering classification for engineering purposes has been formulated to address the need for a common but simple basis of communication with underlying messages mainly on the possible ranges of mechanical properties (e.g. Dearman and Irfan 1978; Hencher and Martin 1982). Research in this regard has been limited within polymineralic rocks (e.g. granite etc.) where degree of alteration of constituent minerals helps recognize such gradation. Quartz being the most resistant mineral to weathering is the chief mineral constituent of quartzite and therefore, capturing intricate gradational change of quartzite in response to weathering or categorization of weathering grades of quartzitic materials is a challenging task. Subsequently, research on mechanical characterization of quartzitic materials with reference to weathering grades does not seem have gained much attention where quartzite is considered as one of the competent/suitable rocks for various engineering purposes.

In this paper, the author first presents salient points in categorizing weathering grades of granitic rock materials from Hong Kong and southeastern Brazil that are

A. Basu (✉)
Department of Geology and Geophysics,
Indian Institute of Technology Kharagpur,
Kharagpur 721302, India
e-mail: abasu@gg.iitkgp.ernet.in

Table 156.1 Weathering classifications of granitic and quartzitic materials

Hong Kong granite (after Basu 2006)		Granite from southeastern Brazil (after Basu et al. 2009)		Quartzite from eastern India (after Basu et al. 2011)	
Characteristics	WG	Characteristics	WG	Characteristics	WG
No discoloration	I	No discoloration	I	No discoloration/ staining	I
Grains have vitreous luster		Grains have vitreous luster		Grains have vitreous luster	
Equigranular texture with intact grain boundaries		Equigranular texture with intact grain boundaries		Intact grain boundaries	
Slight to moderate staining	I–II				
Grains have vitreous to sub-vitreous lustre					
Intact grain boundaries					
High staining	II	Slight to moderate staining	II	Slight to moderate staining	II
Grains have sub-vitreous to dull luster		Grains have vitreous to sub-vitreous lustre		Grains have vitreous to sub-vitreous luster	
Intact grain boundaries		Intact grain boundaries		Intact grain boundaries	
		Grains have sub-vitreous to dull luster	II–III		
		White clay minerals are common			
		Intact grain boundaries			
Moderately decomposed	III	Moderately decomposed	III	Moderately stained	III
Soft white clay minerals can be scratched by nail		Abundant soft white clay minerals can be scratched by nail		Grain boundaries not very intact	
Grain boundaries not very intact		Intact grain boundaries		Can be broken easily by a geological hammer	
Can be broken easily by a geological hammer		Can be broken easily by a geological hammer			
Moderately to highly decomposed (more gritty and clayey appearance of feldspars)	III–IV				
Can be broken more easily by a geological hammer					
Highly decomposed (powdery feldspars) with loose grain boundaries	IV	Highly decomposed (powdery feldspars) with loose grain boundaries	IV	Highly stained with loose grain boundaries	IV
NX core can be broken by hand		Large pieces can be broken by hand		Large pieces can be broken by hand	
Does not slake in water		Does not slake in water		Does not slake in water	

Fig. 156.1 Photomicrographs depicting differences in intactness of quartz grain boundaries and in overall staining with respect to weathering grades of quartzites from eastern India (after Basu et al. 2011)
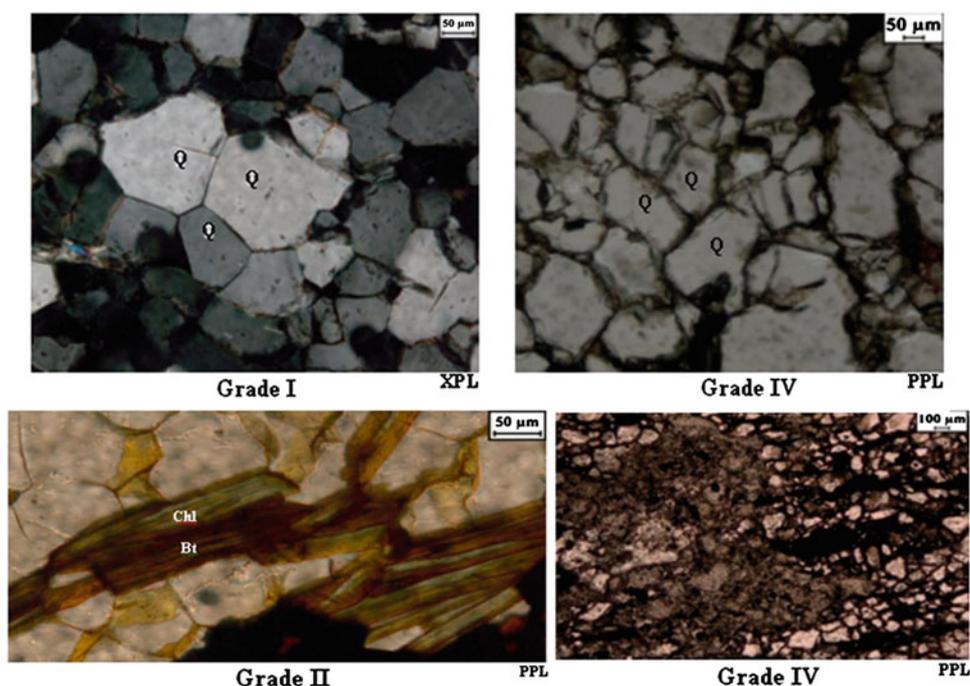
subsequently compared with the issues in characterizing weathering grades of quartzitic rock materials from eastern India. An overall assessment of mechanical behaviors of these rocks with reference to assessed weathering grades is also outlined.

156.2 Categorization of Weathering Grades of Granitic and Quartzitic Materials

Granitic rocks of various weathering grades from Hong Kong were investigated by Basu (2006). These rocks belong to the intrusive units of Kowloon Granite and Mount Butler Granite (Sewell et al. 2000). A set of six recognition factors (discoloration and staining, grain boundaries, relative strength, decomposition, microcracking, and disintegration) was identified and used by Basu (2006) to describe gradational changes of the granitic rocks over the weathering spectrum. It was proposed that a weathering classification system with intermediate grades (if possible to be recognized) as presented in Table 156.1 (broadly in compliance with the common 6-fold classification) is more efficient or detailed than the 6-fold classification in capturing the weathering induced changes of granitic rocks (up Grade IV). Microscopic observations like increase in chloritization of biotites, sericitization of feldspars and quartz intra-granular crack density with the enhancement of weathering intensity also substantiated this weathering classification (Table 156.1).

A weathering classification (broadly conformable with the common 6-fold material classification scheme) for granitic rocks that belong to the Itu Granitic Complex (IPT 1981) in southeastern Brazil was presented by Basu et al. (2009) (Table 156.1). However, an intermediate class 'Grade II–III' was assigned in this classification (Table 156.1) with its distinct differentiable decompositional characteristics compared to Grades II and III. Microscopic studies also substantiated this classification.

Basu et al. (2011) attempted to apply the 6-fold weathering classification scheme to quartzitic rock materials from Chaibasa Formation (Saha 1994) at Jaduguda in the state of Jharkhand, eastern India. Although individual quartz grains of investigated quartzitic materials do not portray any discoloration as a manifestation of degree of decomposition, macroscopic appearances of these rocks differ noticeably as weathering intensifies because of alteration of other minerals (e.g. biotite and other iron bearing minerals) that constitute less than 5 % of the entire rock volume and loosening of quartz grain boundaries. Consequently, the common 6-fold classification provides a solid guideline even in case of quartzitic materials to categorize weathering grades (Table 156.1 and Fig. 156.1).

156.3 Mechanical Behaviors of Granitic and Quartzitic Materials with Reference to Weathering Grades

Uniaxial compressive strength (UCS) and tangent Young's modulus at 50 % of the peak stress (E) were determined as per stipulations by ASTM (2001) in all three investigations carried out by Basu (2006), Basu et al. (2009, 2011).

Table 156.2 Ranges of mechanical parameters with respect to assessed weathering grades of granites and quartzites

Hong Kong granite (after Basu 2006)

WG	I	I–II	II	III	III–IV	IV
UCS (MPa)	196.45–116.30	106.34–83.13	68.21–31.14	26.83–13.61	25.14–7.64	6.32
E (GPa)	53.19–42.90	31.79–21.92	25.32–7.02	15.82–5.22	11.83–5.38	4.46
BTS (MPa)	11.36–8.48	7.76–4.73	5.24–3.80	2.07–1.20	1.85–1.68	0.97

Granite from southeastern Brazil (after Basu et al. 2009)

WG	I	II	II–III	III	IV
UCS (MPa)	214–153	161–134	137–107	88–73	Undetermined
E (GPa)	70.17–61.49	61.18–55.23	54.51–47.19	52.00–41.08	Undetermined

Quartzite from eastern India (after Basu et al. 2011)

WG	I	II	III	IV
UCS (MPa)	205.76	114.75–51.71	80.00–42.46	42.44
E (GPa)	45.56	15.88–6.07	5.22–3.45	1.08
BTS (MPa)	11.35–8.99	8.50–2.54	4.79–1.87	2.29–1.65

Brazilian tensile strength (BTS) was determined following ISRM (1978) and ASTM (2001) specifications by Basu (2006) and Basu et al. (2011). The ranges of these parameters with reference to assessed weathering grades (WG) of granites and quartzites are summarized in Table 156.2. Although deterioration of the rock materials is apparent from the decreasing trend of these parameters as weathering intensifies, overlapping of values over adjacent grades is often observed. In case of all three parameters (i.e. UCS, E and BTS) of granites and quartzites, the maximum absolute drop takes place in the early stage of weathering. This can be attributed to sudden augmentation of micro-cracks/flaws of both granitic and quartzitic materials with the onset of weathering. As weathering advances, weakening of the skeletal structure of these rocks also proceeds in a progressive manner. However, at elevated stages of weathering, absolute drops in these parameters due to change in weathering grade do not remain as sensitive to weakening of the skeletal structure or mechanical coherence of granites and quartzites due to induced heterogeneity and flaws as they do at the early weathering stage.

156.4 Conclusions

Based on the study presented in this article, the following conclusions are drawn:

- The conventional 6-fold weathering classification for uniform materials is as capable of capturing gradational weathering induced changes of quartzitic materials as it is for polymineralic crystalline rocks like granite.
- The highest degree of sensitivity of UCS, E and BTS of both granite and quartzite at the early stage of weathering can be attributed to sudden augmentation of micro-cracks/flaws of these materials with the onset of weathering.

References

Anon QJ (1995) Eng Geol 28 207–242

ASTM (2001) ASTM Standards on Disc, 04.08, West Conshohocken, PA

Basu A (2006) PhD thesis, The University of Hong Kong

Basu A, Celestino TB, Bortolucci AA (2009) Rock Mech Rock Eng 42 73–93

Basu A, Ghosh N, Das M (2011) J Eng Geol XXXVII 217–223

Dearman WR, Irfan TY (1978) In: Proceedings of the international symposium on deterioration and protection of stone monuments, UNESCO, Paris, 5–9 June 1978

Hencher SR, Martin RP (1982) In: McFeat-Smith I, Lumb P (eds) Proceedings of the seventh southeast Asian geotechnical conference, Hong Kong

IPT (Instituto de Pesquisas Tecnologicas) (1981) Mapa Geologico do Estado de Sao Paulo

ISRM (1978) Int J Rock Mech Min Sci Geomech Abstr 15:99–103

Moye DG (1955) J Inst Eng 27:287–298

Saha AK (1994) Crustal evolution of Singhbhum North Orissa, Eastern India. Geological Society of India Memoir 27

Sewell RJ, Campbell SDG, Fletcher CJN, Lai KW, Kirk PA (2000) The pre-quaternary geology of Hong Kong. Geotechnical Engineering Office, Hong Kong

J. Oke and N. Vlachopoulos

Abstract

The mechanics associated with forepoling structures explicitly, has never been fully investigated in order to determine the associated support mechanics when installed in isolation and/or in groups as an umbrella arch. Further, numerically, these support structures cannot be modelled using the commonly used, industry standard, two-dimensional (2D) numerical software packages. In numerical software using three-dimensional (3D) codes, these support elements are commonly standardized using pile or rockbolt simplified noded elements that do not truly describe their behaviour when subjected to the true 3D stress conditions that result at face or near the face due to the tunnel or mining excavation process. As such, a deficiency exists with regards to prediction of the interaction of umbrella arch support systems with forepoles element for tunnelling practices within weak rock masses. Methods have been developed in order to predict the behaviour of radial support systems to include temporary support elements such as rock bolts, steel sets, and liners such as the convergence-confinement method. However, these tools do not have the ability to capture the influence of support systems installed longitudinally at the face of tunnel such as forepole, and core reinforcement elements. In an attempt to improve tunnel design strategies, this paper will focus on the mechanical response of the application of the forepole element as part of the umbrella arch method installed in deep and shallow excavations; As well, other issues associated (influences) with the use of forepoles are also highlighted and discussed.

157.1 Introduction

This paper defines the concept of utilizing forepole temporary support elements in conjunction with the convergence-confinement method (Carranza-Torres and Fairhurst 2000) for design purposes. It also introduces concepts that are related to the forepole/support arch concept and the gaps which currently exist with their usage. The primary and specific purpose of this portion of the investigation was to capture the support-rock interaction/mechanics associated with the forepole temporary support elements (as seen in Fig. 157.1). The forepole umbrella creates a stable excavation environment. One postulated mechanism of support is the redirection of 3D stress flow around the tunnel (Gibbs et al. 2007). This concept has also been labeled the arch effect by (Lunardi 2000). In order to attempt to determine the true impact of a forepole umbrella on an excavation, an extensive 3D numerical model is required. Such 3D numerical models were developed within FLAC3D (Itasca

J. Oke · N. Vlachopoulos (✉)
GeoEngineering Centre, Queen's-Royal Military College of Canada, Kingston, ON K7K 7B4, Canada
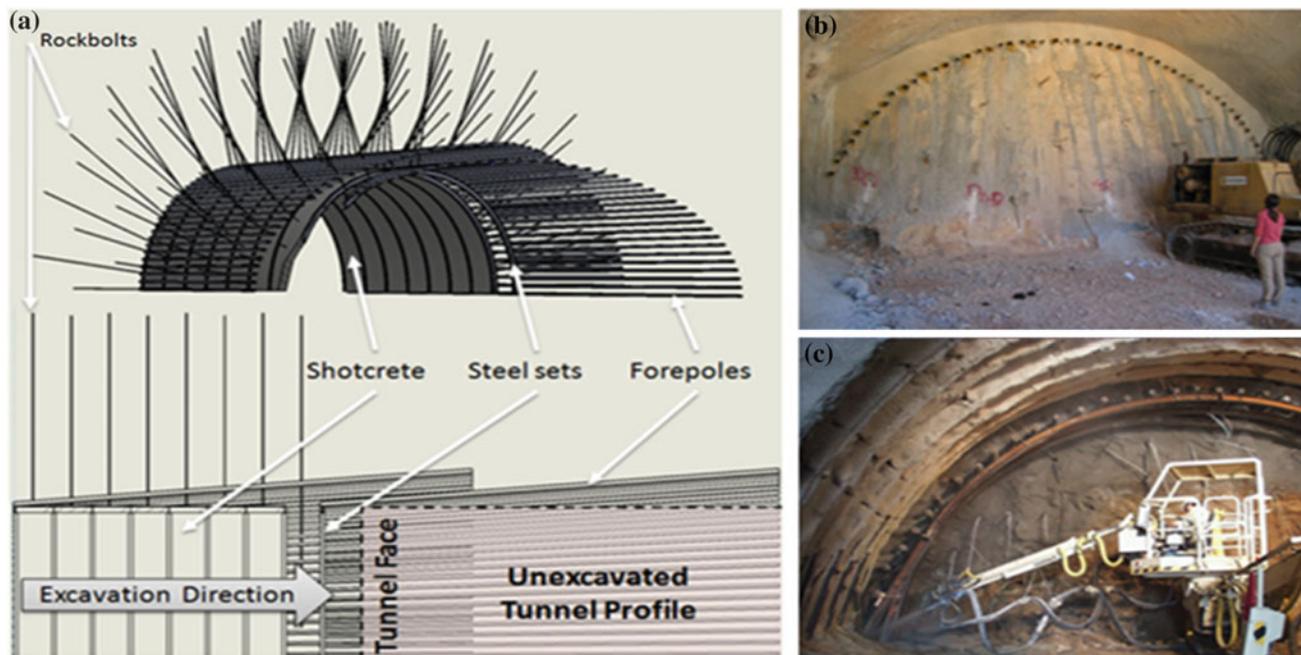e-mail: vlachopoulos-n@rmc.ca

Fig. 157.1 a Nominal temporary structural support system used as part of the observational method of support. Elements shown are: forepoles without niches; steel sets (i.e. H-piles); *shotcrete*; and *rockbolts*. Core face reinforcement is not depicted. **b** Forepole installed at the crown of a tunnel excavation. **c** Forepole installed resting on steel sets of a tunnel excavation

2009) for the analysis cited herein. Selected factors of consideration when designing with forepole elements are: spacing between forepoles, positioning, and the size of the forepoles. Other factors that contribute to (but not limited to) the influence and performance of forepole elements is the way that they are simulated numerically, their influence at the design stage (i.e. influence on analytical, unsupported solutions) and their use in the reduction of surface settlements in shallow tunnel environments. These factors affecting the performance of the forepole support element and overall tunnel behavior are highlighted and summarized below.

157.2 Forepole Temporary Support Elements: Nomenclature

Forepoles are temporary support elements employed most often in tunnelling projects associated with weak rock. They are used ahead of the face (in combination with other temporary support), and add stabilization the plastic zone created ahead of the face due to tunnelling effect. They are installed longitudinally to allow for stable excavation underneath the structural umbrella, formed by an arrangement of multiple forepoles (Fig. 157.1). The use of the name forepole as opposed to other support elements has been addressed recently by Oke et al. (2013). The authors proposed specific nomenclature associated with temporary

support systems for the design and construction of tunnels. By definition, forepoles have a larger diameter than spiles and their lengths are greater than the height of the tunnel excavation.

157.3 Factors Affecting the Performance of Forepole Support Elements and Tunnel Behaviour

157.3.1 Forepole Spacing, Positioning, and Size

The authors investigated the effects of forepole spacing, positioning and size with respect to tunnel performance (Oke et al. 2012a). A parametric analysis associated with the spacing design parameter was initiated as spacing was increased by 0.05 m until 0.20 m in order to observe the effects of the increased spacing, to cases of 30 cm and beyond. Further points were then investigated to capture the full range of spacing and to ensure the baseline run was capturing the minimal group (or forepole interaction) effect from the influence of adjacent forepoles The results of such an analysis are seen in Fig. 157.2 for a 6 m overhang of the umbrella arch consisting of overlapping forepole elements. The results indicate that when the forepole member is of small diameter (less than 60 cm), it is able to "pass through" the rock mass, allowing the rock mass to flow around it.

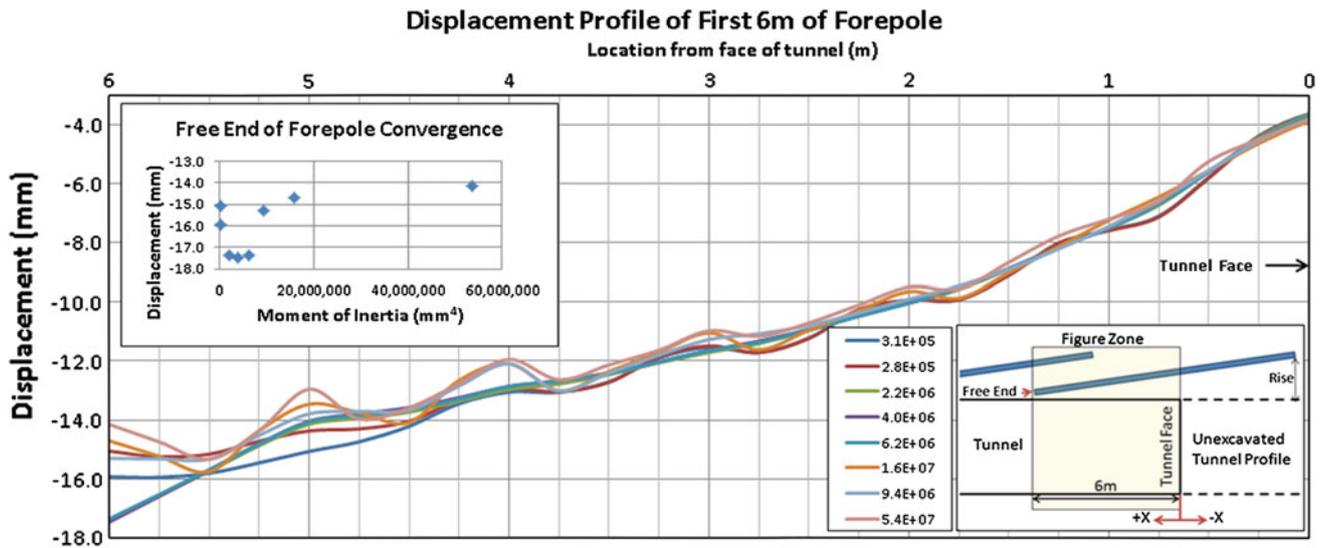## Displacement Profile of First 6m of Forepole

Fig. 157.2 Displacement profile of first 6 m of forepole from numerical analysis of varying size with 6 m of overhang. The plot illustrates the values of displacement of the free end of the forepole

However, if the forepole is too stiff, the rock mass will fail and flow around the structural support member. Having a diameter smaller than 60 cm or modulus of inertia greater than 1.6e7 mm^4 created less tunnel convergence. However, it is necessary to note that the 3D numerical analysis was conducted using a continuum model, and thus, failure modes of overbreak and spalling could not be simulated. It was determined that the optimal range of forepole sizes (within the respective rockmass) should have a modulus of inertia less than 6.2 mm^4, while also having a diameter no less than 101 mm. The reader is referend to the paper cited for further details concerning the findings of the this investigation; conclusions from the research are also summarized in the conclusion section of this paper herein.

157.3.2 Numerical Modelling of Forepole Elements

As with any numerical analysis, there are limitations associated with the use of an idealized element within a numerical software package. Within FLAC3D (Itasca 2009),

the forepole was modelled a pile element. The pile element is a straight segment of uniform, bisymmetrical cross-sectional properties lying between two nodal points with six degrees-of-freedom per node. Both a normal-directed (perpendicular to the pile axis) and shear-directed (parallel with the pile axis) frictional interaction occurs between the pile and the finite difference grid. This idealized frictional interaction is illustrated in Fig. 157.3. In addition to skin-friction effects, end-bearing effects can also be captured. Piles may be loaded by point or distributed loads. The element is defined by its geometric, material and coupling-spring properties. The only interaction the forepole has with the rock mass is through other structural members (i.e. forepole is connected to the liner, and the liner is connected to the rock mass), and interaction parameters (coupling-spring properties). These coupling-spring parameters are a function of the rock mass parameters (internal angle of friction for the rock mass φ_{rm}), annulus created during installation, and grout injected into and around the element (if used). These parameters are difficult to obtain without in situ testing (Volkmann and Schubert 2007). The interaction parameters were investigated in the paper by the authors
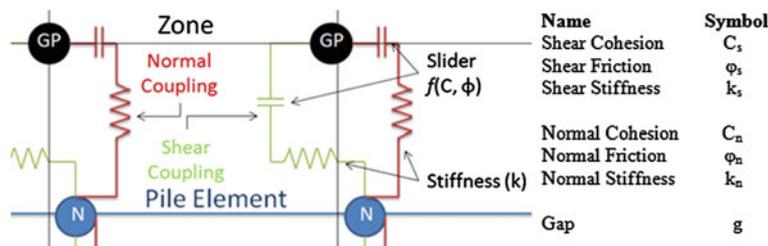

Fig. 157.3 Ideal illustration of normal and shear interaction of the pile element on the zone. Interface elements connecting the forepole (pile element) with the rock (zone)

(Oke et al. 2012b) and it was determined that the magnitude of these input parameters had a significant influence to the overall behaviour of the tunnel under varying conditions and values. As such, one must ensure the proper values or range of values are utilized as inputs to numerical models. Of note is that the influence of interaction stiffness and cohesion on the overall tunnel convergence as well as the longitudinal forepole displacement. For more details associated with this study, the reader is referred to Oke et al. (2012b).

157.3.3 Modified Longituninal Displacement Profile due to Forepole Support

The Convergence-Confinement method (Carranza-Torres and Fairhurst 2000) is a simple engineering design method which has aided tunnel designers with determining preliminary designs (through trial and error) of temporary support arrangements using crude approximations. A summary of the salient components of the method and supporting material can be found within RocSupport (2013). The Longitudinal Displacement Profile (LDP) as part of the Convergence-Confinement Method is an analytical approach which associates the tunnel wall deformations with the actual physical location along the tunnel axis. The LDP consists of Elastic Solutions and several empirical plasticity models of varying intensity (Vlachopoulos and Diederichs 2009). The elastic solutions are reasonable for plastic analysis provided that the plastic radius of the tunnel does not exceed twice the radius of the tunnel. Furthermore, when the plastic radius is greater than twice the radius of the tunnel, two equations are required to capture the profile transitioning at the tunnel face (i.e. one relationship to describe the

deformation past the face into the rock mass and another relationship to capture the displacement of the open tunnel cavity). This transitioning is in agreement with other authors such as Unlu and Gercek (2004). However, none of the referenced LDPs take into consideration the effect of temporary support. To improve upon this, the authors have built upon and modified the work of Vlachopoulos and Diederichs (2009). Conceptually, the unsupported and supported (i.e. supported with forepoles) LDP is seen in Fig. 157.4. The authors have determined a series of relationships that allow for the adjustment of the LDP based on the use of temporary support. The method can provide an improved approximation of the stress fields ahead of the tunnel face. This improved approximation can also be used for the simplification of stresses which are applied to pre-support measures (umbrella arches, core-reinforcement, etc.). Additionally, this work highlights the requirement for further modification/improvements to the LDP with respect to curvature when support is installed. This requirement is essential in order to ensure accurate installation of support.

157.3.4 Reduction of Surface Settlement due to Forepole Umbrella Arch Support

The authors have calibrated a three dimensional (3D) numerical model to the documented work of Yasitli (2012), in an effort to capture the reduction of surface settlement when a Forepole Grouted Umbrella Arch (FpGUA) is added to the pre-existing support system. However, the calibration of such support elements is a challenging endeavour due to the interaction parameters used in the numerical analysis. The authors' calibration has also enabled them to further
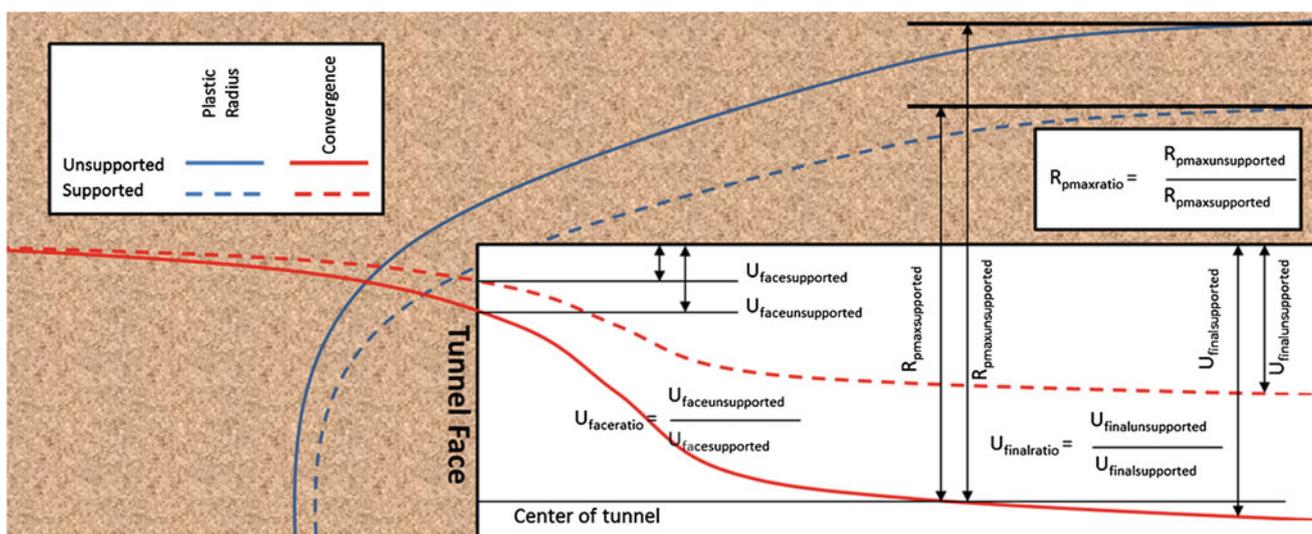

Fig. 157.4 Illustration of the change of the plastic radius, final convergence of the tunnel and displacement of the tunnel face due to support, where U displacement and R radius)

quantify the Umbrella Arch Selection Chart (UASC) (Oke et al. 2013), a design chart developed in order to aid tunnel engineers and designers in terms of the type of Umbrella Arch to use for certain tunneling conditions. The results of FLAC3D analysis were validated through a comparison of selected analytical solutions for surface settlements as well as cited examples in literature.

157.4   Summary and Conclusions

The authors have undertaken a series of research studies associated with the mechanistic behavior of forepole support elements as part of the overall Umbrella Arch temporary support scheme. Each of the factors investigated have contributed to a better understanding into the behavior and influences of the use of these systems as well as the associated limitations. A significant contribution to the tunnelling industry is the development of the Umbrella Arch Selection Chart (UASC). With more rigorous research in this regard, an optimized use of forepoles within the overall temporary tunnel support scheme can be realized.

References

Carranza-Torres C, Fairhurst C (2000) Application of the convergence-confinement method of tunnel design to rock masses that satisfy the Hoek-Borwn failure criterion. TUST 187–213

Gibbs P, Lowrie J, Keiffer S, McQueen L (2007) M5 East—design of a shallow soft ground shotcrete motorway tunnel. Australas Tunn Soc 1–6

Itasca (2009) FLAC3D v4. Fast lagrangian analysis of continua in 3 dimensions

Lunardi P (2000) The design and construction of tunnels using the approach based on the analysis of controlled deformation in rocks and soils. T&T int 3–30

Oke J, Vlachopoulos N, Marinos V (2013) The pre-support nomenclature and support selection methodology for temporary support systems within weak rock masses. Geotech Geol Eng J 31(5). doi 10.1007/s10706-013-9697-4

Oke J, Vlachopoulos N, Diederichs MS (2012a) Sensitivity analysis of orientations and sizes of forepoles for underground excavations in weak rock. In: American Rock Mechanics Association 46th US Rock Mechanics/Geomechanics Symposium, June 2012, Chicago, IL, USA

Oke J, Vlachopoulos N, Diederichs MS (2012b) Improved input parameters and numerical analysis techniques for temporary support of underground excavations in weak rock. In: Proceedings of the 21st Canadian Rock Mechanics Symposium RockEng12, May 2012. Edmonton, Alberta, Canada

Rocscience (2013 Jan 17) RocSupport v3.011

Unlu T, Gercek H (2004) Effect of Poisson's ratio on the normalized radial displacements occurring around the face of a circular tunnel. Tunn Undergr Space Technol 547–553

Volkmann G, Schubert W (2007) Geotechnical model for pipe roof supports in tunneling. In: Proceedings of the 33rd ITA-AITES World Tunneling Congress, underground space—the 4th dimension of metropolises. Taylor & Francis Group, Prague, ss 755–760

Vlachopoulos N, Diederichs MS (2009) Improved longitudinal displacement profiles for convergence confinement analysis of deep tunnels. Rock Mech Rock Eng 42(2):131–146. doi:10.1007/s00603-009-0176-4

Yasitli N (2012) Numerical modeling of surface settlements at the transition zone excavated by New Austrian Tunneling Method and Umbrella Arch Method in weak rock. Saudi Soc Geosci

Guang Ming Ren, Xin lei Ma, Bo Wen Ren, and Min Xia

Abstract

Along with the thorough development of underground engineering, people pay more attention on the long-term deformation stability of the tunnels. However, creep characteristic is an important factor to arouse surrounding rock deformation failures and control engineering designs. Phyllite is a common soft rock in engineering practice, when sample is saturated, water will not only impose the softening effect on phyllite, but also it will influence their creep mechanical properties under the long-term loads. In this paper, selecting samples from headrace tunnel GaoPingpu hydropower station in China, we carried out the shear creep test of saturated phyllite along the schistosity surface under different stress levels. Further, we systematically analyzed and compared the test results with the samples in air-dried conditions, and found that water has great effects on the strength of phyllite: the long-term strength and yield stress of saturated phyllite are only 70–78 and 75–89 % of the air-dried ones respectively. At the same time, based on the Burgers creep model, we discussed the impacts of water on the creep parameters' values of phyllite. This result can provide a theoretical basis to calculate the creep deformation of the tunnel surrounding rocks.

Keywords

Phyllite • Shear creep • Softening effect • Creep parameters

158.1 Introduction

Research on rheological test first began in 1901, and its main purpose was to explore the rock deformation and flow properties from a geologic perspective (Liu 1994). As time goes by, numerous rock engineering accidents have happened due to the rock creep, and the significance of rock creep and its aging strength in engineering have been gradually recognized. In recent years, rock rheology has

become a hot issue in the study field of rock mechanical properties, and one of the main methods is laboratory testing (Yang and Cheng 2011; Yang et al. 1999; Maranini and Brignoli 1999; Li et al. 2008; Li and Xia 2000; Boitnott 1997; Fabre and Pellet 2006; Tomanovic 2006; Pierre et al. 2005; Chen et al. 2008; Yang et al. 2005; Gao et al. 2010; Liu et al. 2009). The influence of water has been studied in details as the experimental variables for its significance in affecting the creep characteristics of rock and its strength of schistosity surface. Wawersik and Brown (2007) demonstrated experimentally that the creep deformation of granite and sandstone increases with increasing water content. In addition, dry and saturated specimens will differ significantly in their stabilization creep rates. For porous sandstones, Bernabk et al. (1994) found that the presence of water dramatically increased the creep rates near failure compared to dry samples. Based on the creep test of red sandstone, Sun et al. (1999) discovered that the long-term compressive strength of saturated brittle-viscous red sandstone was about

G.M. Ren (✉) · X.l. Ma · B.W. Ren · M. Xia
State Key Lab of Geological Hazard Prevention and Engineering
Geological Environment Protection, Chengdu University of
Technology, No. 1 Erxianqiao East Road, 610059,
Chengdu, China
e-mail: renguangming@cdut.cn

X.l. Ma
e-mail: maxinlei1990@163.com

46.3 % greater than the air-dried rock samples. Zhu and Ye (2002), through performing the creep test on tuff, have obtained the influence rule of water on the creep properties of rock. Guangting et al. (2004) also proved that the instantaneous deformation modulus of weak conglomerate significantly reduced after being soaked in water and its rheological properties became more obvious. Xie and Shao (2006) revealed that the creep deformation of porous chalks is much higher in water saturated sample than in oil saturated sample (the creep properties of oil saturated samples are similar with dry samples). Chen et al. (2009) used Burgers model to describe the creep properties of red-bed soft rock and also found that the effect of moisture content on creep properties of red-bed soft rock was extremely remarkable. Chen et al. (2010) perfected the influence rules of water on the creep properties of red-bed soft rock through more in-depth research. To sum up, recently, some international scholars have studied a lot about water influences on creep properties of the rock mass, such as granite, sandstone and tuff rocks etc. However, fewer articles have reported the effect of water on the shear creep characteristics of soft rock along the schistosity surface. Hence this paper focus on the study of shear creep characteristics of the soft phyllite under air-dried and saturated conditions. It provides the rheological parameters for the engineering designs, thus having an important practical and theoretical significance.

158.2 Sample Characteristics and the Test Method

Experimental samples are collected from the Gao Pingpu hydropower station diversion tunnel in FuJiang, SiChuan. And they belong to the Maoxian Group of Silurian Strata (Smx) .Through the indoor rock sliced identification, samples are determined to be the slightly weathered sericite-greisen phyllite. And the main minerals of the phyllite are quartz and sericite with a small amount of fine-grained carbonate and pyrite, which has a fine granular blastic texture and phyllitic structure. We have chosen four air-dried samples and four saturated specimens in our test, and divided them into four groups (A#$_{1,2}$–D#$_{1,2}$) correspondingly. Since phyllite rock is soft, contains schistosity plane, and is prone to be fragmentized, therefore, we used irregular cubes, sized approximately 70–80 mm × 70-80 mm × 80 mm (length by width by height). The average density of air-dried specimens is 2.78 g/cm^3; Its average water absorptivity is about 61 %; the saturated average water absorptivity is 77 %.And for the saturated simples, in order to maintain their saturated state during the entire test, the samples were placed in a specially

made test basin and submerged in the water .The water level was kept 1–2 cm above the vertical top of the specimen. Because the rocks mass are easy to be soften and slacken by water, the saturated specimens were made from air-dried specimens directly before the experiment. The test was performed under relatively constant temperature and humidity conditions on the special rock creep test device which belongs to the State Key Lab of the Chengdu University of Technology. It was conducted along the schistosity of the phyllite, and according to the Tjong-Kie Tan loading method (Tan and Kang 1980) to be applied pressure which is a step wise loading function whereby, in this manner, the creep deformation can be obtained as a function of stress and time on only one sample. In order to reduce the measuring error caused by the heterogeneity of the deformation of the samples, the shear rheometers were installed in different directions, and the mean values of their records were taken as the final values (He et al. 2002). According to quick shear tests, the normal stress was confined as 0.20, 0.40, 0.60, 0.80 MPa respectively. And the shear stress was divided into 6–14 levels with each level sustaining approximately 72 h (under every shear stress step, after 72 h, the shear creep displacement of the test in a day would be less than 0.001 mm, which had met the stability standard of the creep displacements) (Specifications for rock tests in water conservancy and hydroelectric engineering, SL264-2001, in Chinese). We have made sure that each specimen deformed along the schistosity during the last stage of the loading process. This integrated test revealed the shear deformation —time curves of phyllite under the same normal stress, but different shear stresses.

158.3 The Analysis of Creep Experimental Curves of Phyllite Under Air-Dried and Saturated Conditions

According to the above method, we got the typical shear creep curves of air-dried and saturated specimens under multi-level stress, as shown in Fig. 158.1. The shear creep curves of samples at all load levels were extremely similar and the samples did not show any obvious accelerated shear creep. As the test loaded, phyllite instantly showed elastic response followed by creep deformation which grew along with time and the rate of which gradually slowed down as the time getting longer. Finally, both samples went into the stable creep stage. Since then, the creep deformation increased continuously at a very small constant speed over the period of time. In the final loading phase of each specimen, a sudden shear failure appeared in a short time.
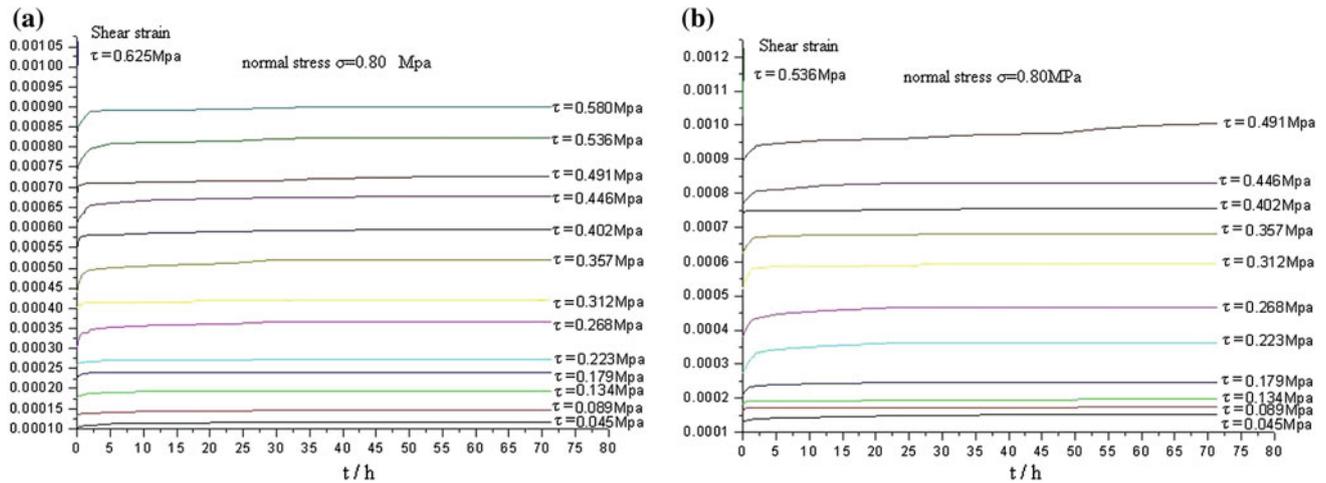
Fig. 158.1 Sheer creep curves under the normal stress of 0.800 Mpa **a** air-dried sample D#$_1$, **b** saturated sample D#$_2$

158.4 Analysis of the Effect of Water on Phyllite Rheological Parameters

158.4.1 The Rock Creep Model and Parameters Determination

Based on multiple domestic and foreign studies of rock creep characteristics and the shear creep curves of this test, in this paper, we selected Burgers mechanical creep model to describe the creep characteristics of phyllite. It is connected in series with Maxwell and Kelvin models which is applicable to viscoelastic rock. It can well express creep properties, such as instantaneous deformation, decelerating creep and steady creep etc. (Zhou 1990; Cai 2002; Xu 1997). According to the properties of series, Burgers constitutive equation (Zhou 1990) is:

$$\ddot{\tau} + \left(\frac{E_1}{\eta_2} + \frac{E_2}{\eta_2} + \frac{E_1}{\eta_1}\right)\dot{\tau} + \frac{E_1 E_2}{\eta_1 \eta_2}\tau = E_2 \ddot{\varepsilon} + \frac{E_1 E_2}{\eta_2}\dot{\varepsilon} \quad (158.1)$$

where τ is shear stress (MPa); E is the elastic deformation modulus (MPa) and η is viscous fluid viscosity (0.1 Pa·s). Based on the instantaneous superposition principle, the creep equation of Burges model is established as follows:

$$\varepsilon = \frac{\tau_0}{E_1} + \frac{\tau_0}{\eta_1}t + \frac{\tau_0}{E_2}\left(1 - \exp(-\frac{E_2 t}{\eta_2})\right) \quad (158.2)$$

Besides, Eq. (158.2) shows that: When t = 0, the model performs instantaneous elastic deformation. Then the strain gradually increases with the time going on. Finally, the creep deformation is increased by the viscous components creeping steadily.

By using the Burgers model and the least square method, we can obtain the creep curves. And then, the creep parameters for Burgers model, such as E_1, E_2, η_1, η_2, can be confirmed.

158.4.2 Analysis of the Effect of Water on Rheological Parameters of Phyllite

158.4.2.1 Analysis of the Effect of Elastic Modulus E_1 and E_2

The value of the instantaneous elastic modulus (E_1) of the air-dried and saturated specimen is similar and its average ratio is 1.280. This illustrates that water has a small impact on the instantaneous elastic modulus of phyllite. In addition, E_1 of each sample went up slightly along with the increase of shear stress, which means that the instantaneous elastic strain of phyllite made almost linearly elastic change with shear stress increase. The instantaneous elastic strain curves are shown in Fig. 158.2.

As shown in Fig. 158.2, under the same water condition, the instantaneous deformation of specimens was closely correlated to the normal stress and shear stress. Namely, when the shear stress was kept at a constant level, the normal stress and the instantaneous shear displacement of rock samples were negatively correlated; In contrast, when the normal stress was kept constant, the shear stress and the instantaneous shear displacement of rock samples showed the positive correlation. Furthermore, it also indicates that the instantaneous elastic strain of saturated specimen is greater than air-dried ones. And when the shear load increases, the increment of instantaneous elastic strain of the water-saturated specimens was greater than the air-dried samples as well. This may be caused by the ability of water
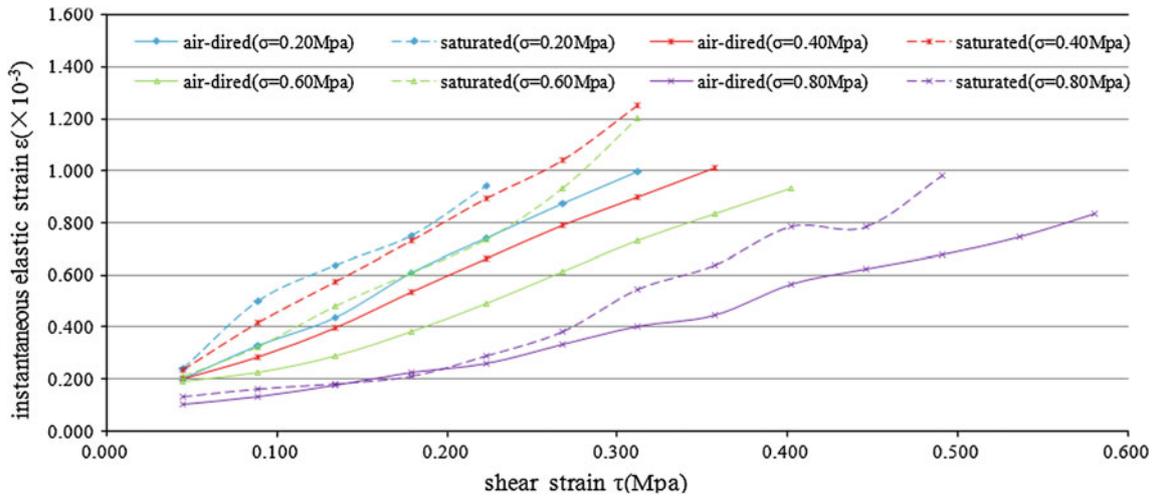
Fig. 158.2 The curves of shear stress—instantaneous strain

to dissolve and soften the rocks. Similarly, water has a comparable influence on E_1 and E_2, and the ratio of E_2 under air-dried condition to that under saturation is 1.326. In other words, the elastic modulus of phyllite E_1, E_2, under the influence of water, will reduce by about 21.9 and 24.6 %, respectively.

158.4.2.2 Coefficient of Viscosity η

The viscous coefficient η is a critical parameter to the viscous characteristics of rock. It varies with the stress level and water content of the test samples. The value of η_1, η_2 are relatively discrete. But in terms of the average, the value of η_1, η_2 under the air-dried condition are 1.275 and 1.724 times of those under water-saturated state, respectively. In other words, the viscous coefficient η_1, η_2 decrease by about 21.6 and 42.0 %, respectively.

158.4.3 Determining the Phyllite Shear Creep Constitutive Equation

As the stress of the test samples is small and little difference amongst them, and if the effect of stress on creep parameters is not considered, the average creep parameters of air-dried and water-saturated samples can be obtained, then the creep parameters were applied into Eq. (158.2), so we can get the phyllite creep constitutive equation:

$$\mathrm{Air-dried}$$
$$\varepsilon(\mathrm{t}) = \frac{\tau}{0.48} + \frac{\tau}{764.859}t + \frac{\tau}{6.580} \times \left(1 - e^{-0.185t}\right)$$

$$\mathrm{Saturated:}\ \varepsilon(\mathrm{t}) = \frac{\tau}{0.357} + \frac{\tau}{432.974}t + \frac{\tau}{4.961} \times \left(1 - e^{-0.240t}\right)$$

158.4.4 The Phyllite Shear Strength

The long-term strength is one of the important parameters reflecting the creep properties of rock. Through the isochronous curves, a most commonly method, we can get the value of strength (Sun 1999; Zhou 1990). And it is based on some related specification of rock mechanics test. Here, we joined the turning points by smooth curve, so the corresponding stress of the arc is the long-term strength of the sample. Then we listed every sample's long-term strength in Table 158.1. And through the tests, we presented the yield stress of each sample (τ_f) in Table 158.1 together.

Comparing the long-term strength and yield stress of the air-dried samples with the saturated ones (in Table 158.1.), these obvious conclusions are easy to be indicated: under the same normal stress, the long-term strength of saturated phyllites is only 0.70–0.78 times of the air-dried ones and the mean value is 0.747 times; to the yield stress of the saturated phyllite, it is 0.75–0.89 times of the air-dried samples and the average is 0.830. These results demonstrate

Table 158.1 The long-term strength and yield stress of phyllite under different conditions

Group NO.	A#$_1$	A#$_2$	B#$_1$	B#$_2$	C#$_1$	C#$_2$	D#$_1$	D#$_2$
Normal stress/Mpa	0.20		0.40		0.60		0.80	
Conditions	Air-dried	Saturated	Air-dried	Saturated	Air-dried	Saturated	Air-dried	Saturated
the long-term strength/Mpa	0.245	0.171	0.31	0.242	0.345	0.253	0.48	0.365
Yield stress/Mpa	0.357	0.268	0.402	0.357	0.446	0.357	0.625	0.536

Table 158.2 The long-term shear strength parameters of the phyllite under air-dired and saturated conditions

Parameters conditions	C_∞/Mpa	Φ_∞/°
Air-dried	0.175	19.34
Saturated	0.121	16.01

that phyllite is easy softened by water, resulting in the decrease of its strength. Based on the normal stress and the long-term strength listed in Table 158.1, we determined the parameters of the long-term shear strength and is presented in Table 158.2.

As shown in Table 158.2, the strength parameters of phyllite decrease because of the softening effect of water. And the reduction of C_∞ and Φ_∞ is 0.054 Mpa and 3.33°, respectively.

158.5   Conclusions

The experiment was conducted along the schistosity surfaces. The shear creep curves of phyllite, under the air-dried and saturated conditions, perform the similar form. All of the tested phyllite has the instantaneous and steady deformation behavior under the action of shear stress. And finally the shear failure happened suddenly. At the same time, the instantaneous deformation of specimen, if under the same water content, is closely correlated to the normal stress and shear stress. Namely, as the shear stress was constant, normal stress and the instantaneous shear deformation of rock samples were negatively correlated; and when the normal stress was steady, the shear stress showed a positive correlation with the instantaneous shear deformation of rock samples.

In accordance with Burgers model, comparing the creep property of air dried samples with water-saturated ones, the conclusion emerged with stark clarity: the average values of the elastic modulus E_1, E_2 and the viscous coefficient η_1, η_2 of phyllite, under the action of water, will reduce by about 21.9, 24.6, 21.6 and 42.0 %, respectively.

For the air dried and water saturated samples, the analysis of the test results about the long-term strength and yield stress demonstrate that: under the same normal stress, the long-term strength of saturated phyllite is 0.70–0.78 times of the air-dried ones (the average is 0.747); the ratio of the yield stress of the saturated samples is 0.75–0.89 times of the air-dried specimens (average value is 0.830); and the value of strength parameters (C_∞ and Φ_∞) of the saturated samples reduced 0.054 MPa and 3.33°, respectively. All of above properly proved that water can soften phyllite and decrease its strength. This result will be useful to determine the long-term strength of the similar rock-mass in other future engineering projects.

References

Liu X (1994) The conspectus of rock rheology. Geological Publishing House, Beijing (in Chinese)

Yang S-Q, Cheng L (2011) Non-stationary and nonlinear visco-elastic shear creep model for shale. Int J Rock Mech Min Sci 48(6):1011–1020

Yang C, Daemen JJK, Jian-hua YIN (1999) Experimental investigation of creep behavior of salt rock. Int J Rock Mech Min Sci 36(3):233–242

Maranini E, Brignoli M (1999) Creep behaviour of a weak rock: experimental characterization. Int J Rock Mech Min Sci 36(1):127–138

Li Y, Wang Z, Tang M et al (2008) Relations of complete creep processes and triaxial stress-strain curves of rock. J Cent South Univ Technol 15(s1):311–315

Li Y, Xia C (2000) Time-dependent tests on intact rocks in uniaxial compression. Int J Rock Mech Min Sci Geomech Abstr 37(3):467–475

Boitnott GN (1997) Experimental characterization of the nonlinear rheology of rock. Int J Rock Mech Min Sci 4

Fabre Géraldine, Pellet Frédéric (2006) Creep and time-dependent damage in argillaceous rocks. Int J Rock Mech Min Sci 43(6):950–960

Tomanovic Z (2006) Rheological model of soft rock creep based on the tests on marl. Mech Time-Depend Mater 10:135–154

Béresta P, Antoine Blumb P, Pierre Charpentiera P, Gharbia H, Valés F (2004) Very slow creep tests on rock samples. Int J Rock Mech Min Sci 42:569–576

Chen Y-j, Wu C, Fu Y-M (2008) Rheological characteristics of soft rock structural surface. J Cen S Univ Technol 15(s1):374–380

Yang S, Su C, Xu W (2005) Experimental investigation on strength and deformation properties of marble under conventional triaxial compression. Rock Soil Mech 26(3):475–478 (in Chinese)

Gao YN, Gao F, Zhang ZZ et al (2010) Visco-elastic-plastic model of deep underground rock affected by temperature and humidity. Min Sci Technol 20(2):183–187

Liu X, Su J, Wang X (2009) Experimental investigation on shear rheological properties of tuff lava with different grades. Chin J Rock Mech Eng 28(1):190–197 (in Chinese)

Sun J (2007) Rock rheological mechanics and its advance in engineering applications. Chin J Rock Mech Eng 26(6):1081–1106 (in Chinese)

Bernabk Y, Fryer DT, Shively RM (1994) Experimental observations of the elastic and inelastic behaviour of porous sandstones. Geophys J Int 117:403–418

Sun J (1999) Rheological behavior of geomaterials and its engineering applications. China Architecture & Building Press, Beijing (in Chinese)

Zhu H, Ye B (2002) Experimental study on mechanical properties of rock creep instauration. Chin J Rock Mech Eng 21(12):1791–1796 (in Chinese)

Guangting L, Hu Y, Fengqi C et al (2004) Rheological property of soft rock under multiaxial compression and its effect on design of arch dam. Chin J Rock Mech Eng 23(8):1237–1241 (in Chinese)

Xie SY, Shao JF (2006) Elastoplastic deformation of a porous rock and water interaction. Int J Plast 22(12):2195–2225

Chen W, Yuan P,Liu X (2009) Study on creep properties of red-bed soft rock under step load.Chin J Rock Mech Eng 28(s1):3076–3081 (in Chinese)

Chen C, Lu H, Yuan C et al (2010) Experimental research on deformation properties red-bed soft rock. Chin J Rock Mech Eng 29 (2):261–270 (in Chinese)

Tan TK, Kang WF (1980) Locked in stresses, creep and dilatancy of rocks, and constitutive equations. Rock Mech 13(1):5–22

He M, Jing H, Sun X (2002) Engineering mechanics of soft rock. Science Press, Beijing (in Chinese)

SL264-2001 (2001) Specifications for rock tests in water conservancy and hydroelectric engineering (in Chinese)

Zhou W (1990) Advanced rock mechanics. Hydraulic and Hydroelectricity Press, Beijing (in Chinese)

Cai M (2002) Rock mechanics and engineering. Science Press, Beijing (in Chinese)

Xu Z (1997) Rock mechanics. Hydraulic and Hydroelectricity Press, Beijing (in Chinese)

Radioactive Waste Disposal: An Engineering Geological and Rock Mechanical Approach

Convener Prof. Ákos Török—*Co-convener* Jian Zhao

Handling of radioactive waste represents a major environmental concern in modern society due to existing nuclear power plants and is also related to the management of contaminated land after major nuclear catastrophes. The rationale of this session is to provide a forum to papers dealing with various aspects of radioactive waste disposal on surface, near surface and in subsurface storage facilities. It covers aspects of engineering geology, rock mechanics, environmental geology and hydrogeology of site selection, site operation and post-closure periods. The results of in situ and laboratory analyses, including engineering geological and rock mechanical measurements at small and large scales are also included with special emphasis on the existing experimental sites, planned and operating depositories. Computer modelling of the geological environment (soft and hard rock) in combination with hydrogeological and heat transfer models will also form parts of the session.

Investigation of Mineral Deformation and Dissolution Problems Under Various Temperature Conditions

159

J.H. Choi, B.G. Chae, C.M. Jeon, and Y.S. Seo

Abstract

To understand the effects of temperature on the pressure dissolution of mineral, we conducted some experiments using monocrystalline quartz samples. The first of these was a flow thorough experiment to investigate temperature effects for dissolution mechanism. The samples were stressed mechanically by pressing one sample against the other. The flow through experiments was conducted at two different temperatures (35 and 70 °C) at the same pH (pH 11.7) level. The value of the applied stress was 7.32 and 25.27 MPa. During each of these dissolution tests, the solution was sampled regularly and analyzed by an Inductively Coupled Plasma-Atomic Emission Spectrometry (ICP-AES) technique to measure Si-concentration. With the measured Si-concentration, a dissolution rate constant was computed for variety of stress and temperature conditions. It is therefore shown that the rate constant is proportional to the temperature, as expected and as indicated in the literature. It should be noted that the rate constant for the highly stressed case (25.50 MPa) and highly temperature case were considerably greater than for the mildly stressed cases and lower temperature cases. Also, island-channel patterns characterized by micro-cracks a few nanometers in length were seen on the dissolved parts of the samples. The findings and the measured data in this research may be useful for the future development of theoretical models for pressure dissolution and its validation.

Keywords

Quartz dissolution • ICP-AES • CLSM • Dissolution rate

159.1 Dissolution Experiment

The samples for the dissolution experiments were taken from a block of monocrystalline quartz, which may have involved some crystalline lattice defects. The contact area of specimen for flow-through experiments, it was 7.068 mm^2.

A flow through setup was used for the second series of experiments to keep the pH level constant (11.7). Reagent grade NaOH was used to adjust pH of the solution. After the dissolution experiments, the contact areas of the quartz specimens were observed by the confocal laser scanning microscope (CLSM) to identify the type of the dissolution mode (Choi et al. 2008). For quantitative evaluations of the dissolution speed, the Si concentration was measured by Inductively Coupled Plasma Atomic Emission Spectomerty (ICP-AES) to obtain the dissolution rate.

J.H. Choi (✉) · B.G. Chae · C.M. Jeon
Korea Institute of Geoscience and Mineral Resources, 124 Gwahang-no, Yuseong-gu, Daejeon, 305-350, Korea
e-mail: jhchoi@kigam.re.kr

Y.S. Seo
Chungbook National University, 52 Naesudong-ro, Heungdeok-gu, Cheongju Chungbuk, 361-763, Korea

159.1.1 Flow-Through Experiment

A schematic diagram of the flow through experiment is shown in Fig. 159.1. The experimental setup consisted of two subsystems: a loading subsystem in a temperature-controlled oven and a CSLM observation subsystem.

The quartz sample was held in a liquid chamber filled with a NaOH solution. The pH level of the solution was 11.7, and the flow speed was 0.15 ± 0.05 ml/h. An iron weight was mounted on the liquid chamber to apply mechanical stress. The solution was sampled every three or four days to measure Si-concentration and to calculate the actual dissolution rate as a function of elapsed time.

159.1.2 Surface Observation and Analysis

After the dissolution test, the surface conditions of the samples were observed by CLSM. The CLSM was an Olympus OLS1100, which uses an Ar laser with a wavelength of 488 nm. The scanning method was light polarization using two resonant galvano mirrors, which enable high-speed, high resolution imaging of a wide area. The size of the image data (the number of pixels) given by the CLSM is usually chosen as $1,024 \times 1,024$. With a 100× lens, the resolution (length per pixel) is about 125 nm for an imaging area of 0.128×0.128 mm^2. A higher magnification may be achieved by digitally zooming from a factor of 1–6. To obtain the dissolution rates, the Si concentrations were measured using an ICP-AES (SPS1500R), which uses an Ar gas to create high-energy plasma. Following a standard procedure for the ICP-AES, the equipment first was calibrated with a standard solution of known Si-concentrations, and then liquid in the current experiments were tested. The overall and actual dissolution rates were calculated from the time variations of the measured Si-concentrations.

159.2 Results and Discussions

159.2.1 Surface deformation

In this study, the contact surfaces of the quartz samples were observed after the dissolution test by CLSM. In Fig. 159.2a–d, the CLSM photos show the elevation of the scanned area of the sample. The small photos in (a), (b) and (d) are the upper contact area. The whitish area indicates a lower elevation, therefore indicating dissolved parts. As seen in these images, the dissolved parts are found only on the contact area.

159.2.2 Temperature Effect

To observe the temperature effect on dissolution, experiments were carried out at three different temperatures (35 and 70 °C). The pH level was kept at 11.7 using the flow through setup. The applied stress for these series of tests was either 7.32 or 25.27 MPa. The levels of stress and pH were thus determined to emulate chemio-mechanical conditions that could be encountered in deep underground nuclear waste disposal facilities. The Si-concentration was measured with the ICP-AES by sampling the solution every three or four days to observe the temporal evolution.

The experimental results are shown in Table 159.1 as Si concentrations and as the dissolution rates at each sampling interval. Note that the overall dissolution rates are shown at the bottom row of this table. The data given in this table are plotted in Fig. 159.3 as a function of time. The plots show

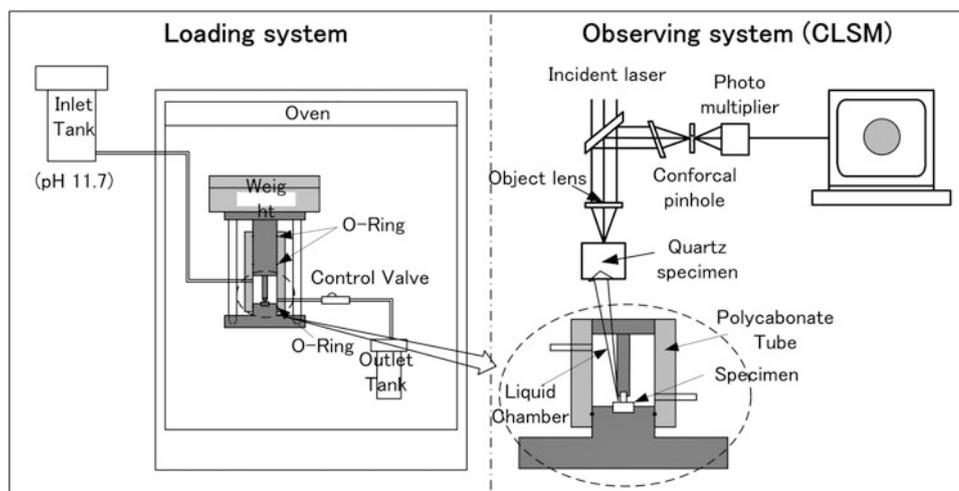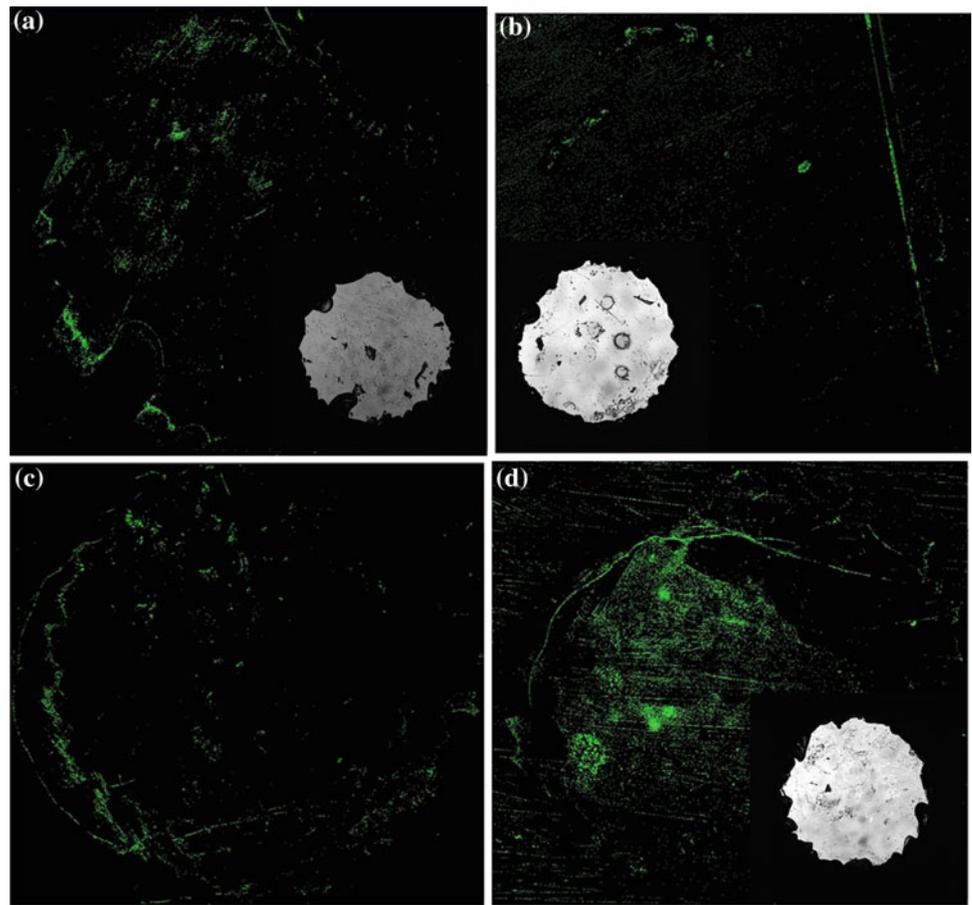**Fig. 159.1** Schematic diagram of the flow-through experimental setup

Fig. 159.2 CLSM photos of the dissolved surfaces of the samples

Table 159.1 Time variation of the actual dissolution rate and the overall dissolution rate (v)

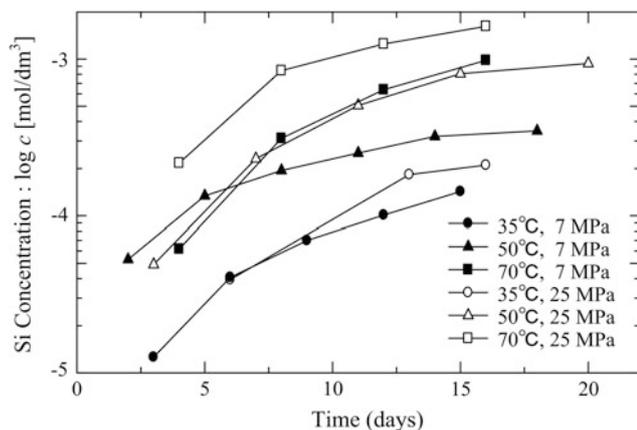| Days	7.32 MPa			25.27 MPa		
	35 °C	50 °C	70 °C	35 °C	50 °C	70 °C
2		5.64E−11				
3	8.95E−12			2.95E−10	3.49E−11	
4			3.28E−11			1.15E−10
5		3.44E−11				
6	9.98E−12			1.40E−11		
7					5.53E−11	
8		2.47E−11	6.65E−11			1.67E−10
9	1.02E−11					
10				4.61E−11		
11		2.22E−11			6.82E−11	
12	1.06E−11		7.99E−11			1.27E-10
13				1.25E−11		
14		2.33E−11				
15	1.23E−11				7.46E−11	
16			8.59E−11	1.15E−11		1.13E−10
17						
18		1.74E−11				
20					5.50E−11	
v	1.04E−11	2.76E−11	6.63E−11	1.27E−11	5.86E−11	1.31E−10

Fig. 159.3 Time variation of Si-concentration

that the dissolution rate is proportional to the temperature at every applied stress level.

The observed temperature dependence may be explained by the adsorption mechanism. According to a sodium sorption experiment Berger et al. (1994), the interaction between the cation and surface was dramatically changed by increasing the temperature from 25 to 150 °C. They explained that sodium has a weak interaction with the surface at a low temperature, but it undergoes specific adsorption at a higher temperature. Hence, the dissolution rate increases with increased temperature in this study. The isotherms for these results are as follows:

$$\upsilon = 1.62 \times 10^{-12}T - 4.87 \times 10^{-11} \quad \text{at 7.32 MPa} \tag{159.1}$$

$$\upsilon = 3.38 \times 10^{-12}T - 1.08 \times 10^{-10} \quad \text{at 25.27 MPa} \tag{159.2}$$

159.3 Conclusions

In this work, quartz dissolution rates were measured by flow through experiments using monocrystalline quartz specimens. The experiments were carried out at various temperature levels to develop dissolution rate isotherms. It was found that the dissolution rate increases with an increase in each of the experimental parameters, i.e., temperature, as reported in the literature. It should be noted, however, that our results show that the stress accelerates quartz dissolution so significantly that the rate constants for the samples with applied stress were four to five orders of magnitude greater than those for the samples with no stress. Because the effect of mechanical stress on the dissolution is of great importance, the activation energy E_a was calculated and presented as a function of stress to show that E_a is inversely proportional to the applied stress. With regard to the dissolution mechanism, CLSM observation revealed that the island-channel model best describes the condition of the dissolved surface of the specimens. This means that the dissolution may be viewed as a growth of surface breaking cracks. Hence, the significance of stress in quartz dissolution may be partly attributed to stress concentration at the crack tip, which could accelerate crack growth.

References

Berger G, Cadore E, Schott J, Dove PM (1994) Dissolution rate of quartz in lead and sodium electrolyte solutions between 25 and 300 °C : Effect of the nature of surface complexes and reaction affinity. Geochim et Cosmochim Acta 58(2):541–551

Choi JH, Anwar AHMF, Ichikawa Y (2008) Observation of time-dependent local deformation of crystalline rocks using a confocal laser scanning microscope. Int J Rock Mech Minig Sci 45:431–441

Analysis of Permeability Coefficient Along a Rough Fractures Using a Homogenization Method

160

Chae Byung-Gon, Choi Jung Hae, Seo Yong-Seok, and Woo Ik

Abstract

To compute a permeability coefficient along a rough fracture that takes into account the fracture geometries, this study performed detailed measurements of fracture roughness using a confocal laser scanning microscope, a quantitative analysis of roughness using a spectral analysis, and a homogenization analysis to calculate a permeability coefficient at the micro- and macro-scale. The homogenization analysis is a type of perturbation theory that characterizes the behavior of microscopically inhomogeneous material with a periodic boundary condition in microstructure. Therefore, it is possible to analyze accurate permeability characteristics that are represented by the local effect of the facture geometry. The C-permeability coefficients that are calculated using the homogenization analysis for each rough fracture model exhibit an irregular distribution and do not follow the relationship of the cubic law. This distribution suggests that the permeability characteristics strongly depend on the geometric conditions of fractures, such as the roughness and the aperture variation. The homogenization analysis may allow to produce more accurate results than the preexisting equations for calculating permeability.

Keywords

Permeability coefficient • Rough fracture • Confocal laser scanning microscope • Homogenization analysis • Multi scale

160.1 Introduction

It is important to evaluate a long-term safety of natural barrier for radioactive waste disposal in rock masses. Among the characteristics of natural barrier, fluid flow along the rock fractures is one of the most important factors to migrate the nuclide. Therefore, it is necessary to evaluate the permeability of rocks, especially permeability along rock fractures. Many researches that take the fracture geometries into consideration have contributed to the ability to characterize the fluid flow in a fractured rock mass. Initially, a parallel plate model with an impermeable matrix was used (Kranz et al. 1979; Renshaw 1986; Snow 1965). This model is based on a cubic law that implies that the flow rate is proportional to the cube of the fracture aperture. A model composed of a rough fracture's surfaces with an impermeable matrix has also been suggested (Renshaw 1986; Brown 1987; Cook et al. 1990; Neuzil and Tracy 1981; Pyrak-Nolte et al. 1988; Witherspoon et al. 1980; Zimmerman et al. 1992). This model takes into consideration the partial contact areas along the fracture walls that may result from roughness of the fracture. Recently, a realistic fracture model has been suggested that uses the real geometry of a fracture that simulates the

C. Byung-Gon (✉) · C.J. Hae
Korea Institute of Geoscience and Mineral Resources, 124, Gwahang-no, Yuseong-Gu, Daejeon, 305-350 Korea
e-mail: bgchae@kigam.re.kr

S. Yong-Seok
Chungbuk National University, 52, Naesudong-no, Heundeok-Gu, Cheongju, 361-763 Korea

W. Ik
Kunsan National University, 558, Daehangno, Kunsan, 573-701 Korea

permeability characteristics (Kranz et al. 1979; Cook et al. 1990; Olsson 1992; Raven and Gale 1985; Trimmer et al. 1980; Zimmerman and Bodvarsson 1996). The results of the previous studies that were mentioned above have shown that the permeability characteristics change irregularly because of the fracture geometries. Particularly in a rough rock fracture, the fluid flow occurs as a selective flow, such as a channel flow that is dependent on the fracture roughness. Therefore, a numerical analysis of the permeability characteristics should include the fracture geometry when possible.

The purpose of this study was to calculate the permeability of a single fracture while taking the true fracture geometry into consideration. The fracture roughness was measured using a confocal laser scanning microscope (CLSM). These data were used to reconstruct a fracture model for numerical analysis using a homogenization analysis (HA) method. The HA method is a perturbation theory that was developed to characterize the behavior of a microscopically inhomogeneous material that involves periodic microstructures. The HA permeability coefficient was calculated based on the local fracture geometry and the local material properties (the water viscosity).

160.2 Analysis of the Fracture Roughness

The specimens in the study were composed of Jurassic coarse-grained granite. These specimens were collected from the drilled cores in the Iksan area in the mid-western part of Korea. The six core specimens, which contained a single, fresh fracture that was parallel or subparallel to the long axis of the core, were studied in detail. They were referred to as GRA, GRB, GRC, GRD, GRE, and GRF and were 5.5×11.0 cm in size (Fig. 160.1).

Fig. 160.1 Core specimens used for the measurements of roughness

The fracture roughness was measured using a confocal laser scanning microscope (CLSM; Olympus OLS 1,100) to collect high resolution digital data on the surface roughness. The CLSM has a high level of resolution and contrast in the direction of the light axis because of its confocal optics. In this study, the sampling spacing was 2.5 μm for the x and y directions. To collect the 2-D roughness data, one scan line was placed on the fracture's surface along the long axis of the fracture. The resolution for the z-direction was 10 μm in the study because the difference in the roughness from the highest peak to the lowest peak was large.

After the Fourier spectral analysis and the noise reduction procedures were done for all of the data for each specimen, a reconstruction procedure of the roughness geometry was performed using the influential frequencies of all of the components of frequency. The reconstructed roughness was in agreement with the measured roughness data. The reconstructed roughness features were used to develop the fracture models for the analyses of the fluid flow along a fracture (Fig. 160.2).

160.3 Computation of the Permeability Coefficients of the Rough Fracture Models Using a Homogenization Analysis

For the calculation of the permeability coefficients with the consideration of the detailed fracture geometries, this study introduced the homogenization analysis (HA) method. The HA method is a perturbation theory that was developed to characterize the behavior of a microscopically inhomogeneous material that involves periodic microstructures (Ichikawa et al. 1999; Sanchez-Palencia 1980). The HA permeability coefficient was calculated based on the local fracture geometry and the local material properties (the water viscosity). HA method considers flow characteristics in both micro scale and macro scale by introducing the incompressible Navier-Stokes equation. The method calculates characteristic velocity and characteristic pressure in a unit cell using a micro scale equation, and then, calculates HA-permeability coefficient. It draws a macro scale equation, namely HA-flow equation, by averaged material velocity and HA-permeability coefficient.

The C-permeability coefficients were computed using several rough fracture models. The important objective of the homogenization analysis was to understand the changes of the permeability characteristics that are dependent on the roughness patterns. The fracture models were constructed with a consideration of the fracture roughness that was analyzed using the fast Fourier transform.
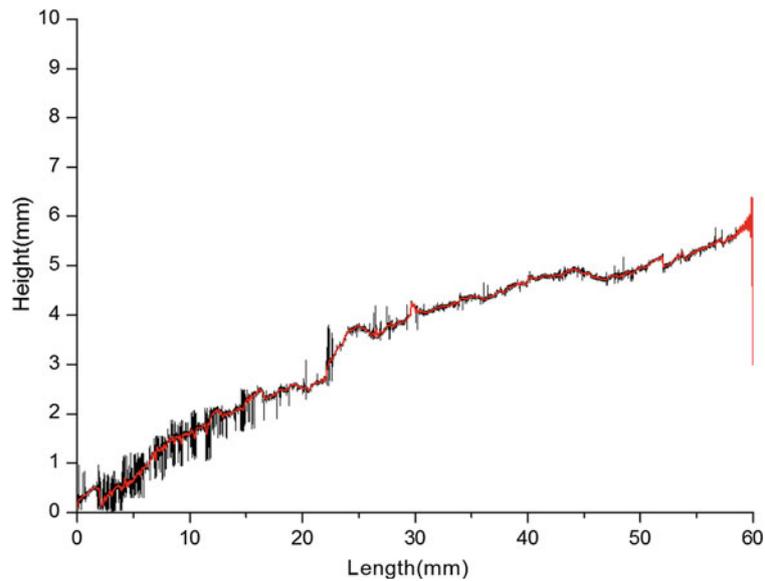
Fig. 160.2 Comparison of the measured roughness data of the *left* part of GRA (*black*) with the smoothed roughness data (*red*)
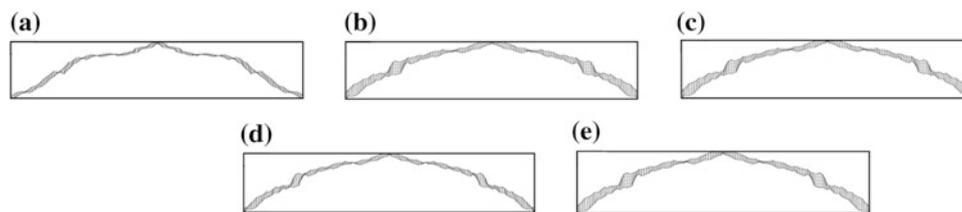

Fig. 160.3 Fracture models of GRA showing various roughness features and apertures at each stage. Exaggerated 100 times in the *vertical* direction. **a** 1st stage **b** 2nd stage, **c** 3rd stage, **d** 4th stage, and **e** 5th stage

The HA permeability characteristics were determined for various roughness conditions. For several types of roughness features that were measured using the CLSM, the upper fracture wall was displaced at intervals of 1 mm in the shearing direction. This shear displacement was introduced for five stages, which resulted in various aperture values along the fracture. The permeability coefficient was calculated at every stage of this displacement. The fracture models of each specimen are shown in Fig. 160.3.

The results of the C-permeability coefficients at each stage of the shear displacement are shown in Table 160.1. It was determined that the permeability coefficients were irregularly ranged from 10^{-4} to 10^{-1} cm/sec, whereas the coefficients of the previous parallel plate models were uniformly distributed within certain range. This difference of permeability between this study and the parallel plate models was due to the complicated change in the roughness and the aperture values, which increased the shear displacement in the current models.

Table 160.1 Permeability coefficients of the five stages of shear displacement for each specimen

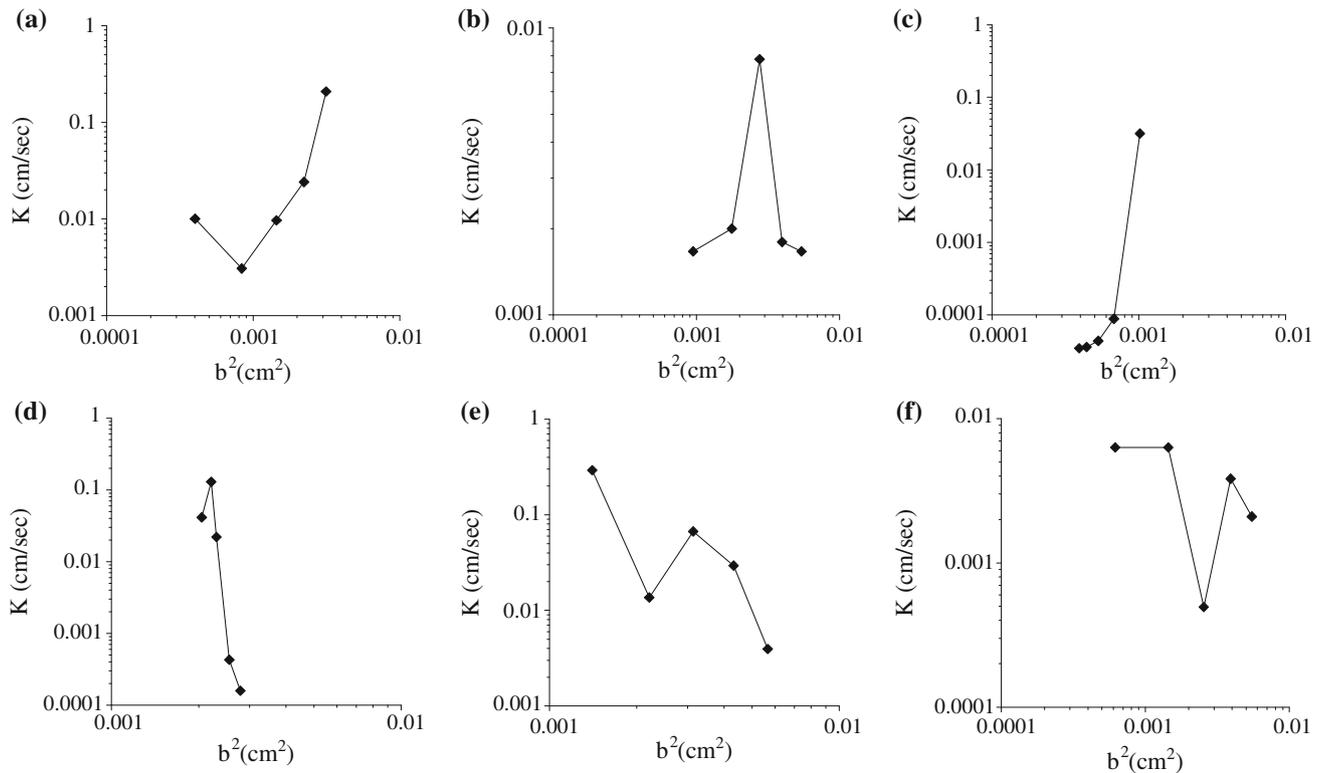| Shear disp	C-permeability coefficient (cm/sec)					
(mm)	GRA	GRB	GRC	GRD	GRE	GRF
1.0	7.46E-03	1.67E-03	1.68E-01	1.43E-01	5.05E-01	5.31E-03
2.0	2.28E-03	2.00E-03	4.67E-04	4.45E-01	2.35E-02	5.31E-03
3.0	7.18E-03	7.79E-03	2.32E-04	7.60E-02	1.16E-01	4.16E-04
4.0	1.79E-02	1.79E-03	1.91E-04	1.48E-03	5.09E-02	3.22E-03
5.0	1.55E-01	1.67E-03	1.83E-04	5.94E-04	6.83E-03	1.76E-03

Fig. 160.4 Relationship between the C-permeability coefficients and the aperture square. **a** GRA, **b** GRB, **c** GRC, **d** GRD, **e** GRE, and **f** GRF

The relationships between the square of the mean aperture, $b2$, and the calculated permeability are shown in Fig. 160.4. The nonlinear relationship indicates that the cubic law was not suitable for the rough fracture case.

160.4　Conclusion

The fracture roughness was measured in detail using the CLSM in this study. The measured data were analyzed to identify the effective geometrical characteristics using a Fourier spectral analysis and low pass filtering. To characterize the hydraulic conductivity, the permeability along a single fracture was computed using the HA method and the measured fracture geometry data. Taking into consideration the change of the roughness pattern along a fracture, the permeability coefficient was calculated using the rough fracture models. The calculation results revealed various changes in the permeability that depended on the roughness patterns and the aperture values. The irregular distribution of the roughness and the aperture along a fracture may introduce a negative proportional relationship between the aperture and the permeability coefficient, even though the mean aperture becomes larger. This relationship clearly demonstrates that the permeability characteristics are very sensitive to the geometry of the roughness and the aperture.

On the basis of the above results, the homogenization analysis method is suggested as an appropriate numerical method for the analysis of fracture permeability. Because the HA method considers the fracture geometries on the micro- and macro-scale, this method can be used to understand the permeability characteristics, such as the local effect and the overall influence, of a fracture. The understanding of the permeability characteristics of each rock fracture by the HA method can contribute to the evaluation of overall hydraulic conductivity of rock masses and fracture networks in deep disposal of radioactive wastes.

References

Brown S (1987) Fluid flow through rock joints; the effect of surface roughness. J Geophys Res 92:1337–1347

Cook A et al (1990) The effects of tortuosity on flow through a natural fracture. In: Proceedings of the 31st US symposium on Rock mechanics. pp 371–378

Ichikawa Y et al (1999) Unified molecular dynamics and homogenization analysis for bentonite behavior: current results and future possibilities. Eng Geol 54:21–31

Kranz R, Frankel A, Engelder T (1979) The permeability of whole and jointed Barre Granite. EOS Trans AGU 58:1229

Neuzil C, Tracy J (1981) Flow through fractures. Water Resour Res 17:191–199

Olsson W (1992) The effect of slip on the flow of fluid through a fracture. Geophys Res Lett 19:541–543

Pyrak-Nolte L, Cook N, Nolte D (1988) Fluid percolation through single fractures. Geophys Res Lett 15:1247–1250

Raven K, Gale J (1985) Water flow in a natural rock fracture as a function of stress and sample size. Int J Rock Mech Min Sci Geomech Abstr 22:251–261

Renshaw C (1986) On the relationship between mechanical and hydraulic apertures in rough-walled fractures. J Geophys Res 100:24629–24636

Sanchez-Palencia E (1980) Non-homogeneous media and vibration theory. Springer-Verlag, Berlin

Snow D (1965) A parallel plate model of fractured permeable media. PhD thesis, University of Califonia, Berkeley, USA

Trimmer D et al (1980) Effect of pressure and stress on water transport in intact and fractured gabbro and granite. J Geophys Res 85:7059–7071

Witherspoon P et al (1980) Validity of cubic law for fluid flow in a deformable rock fracture. Water Resour Res 16:1016–1024

Zimmerman R, Bodvarsson G (1996) Hydraulic conductivity of rock fractures. Transp Porous Media 23:1–30

Zimmerman R, Chen D, Cook N (1992) The effect of contact area on the permeability of fractures. J Hydrol 139:79–96

In Situ Quantification of Hydrocarbon in an Underground Facility in Tight Salt Rock

161

Benjamin Paul, Hua Shao, Jürgen Hesser, and Christian Lege

Abstract

Within the framework of hydraulic characterisation of deep geological formations for the disposal of high level radioactive waste, a long-term investigation program has been carried out to quantify local hydrocarbon occurrences (HCO) regarding the exploration of tight salt rock. In twenty boreholes, each with a length of 6 m and a diameter of 46 mm, the volume of the exposed hydrocarbons (HC) and the influenced area in the rock mass have been determined. These boreholes were plugged with mechanical single packers. For a few years the pressure development in these boreholes has been recorded automatically and the amount of HC flowed into the test-interval was measured. The pressure development within the twenty boreholes differs significantly in dependence on the borehole locations. In terms of pressure increase, four groups can be distinguished: almost no, low, intensive and very intensive. Based on the equation of state for ideal gas and considering the gas composition as determined by laboratory analysis, the calculated gas amount agrees very well with the measured data. The chemical analysis of exposed gas and fluid phase hasn't shown significantly changes of the chemical composition in time. The evaluation of long-term monitored pressure development and the chemical analysis provide a better understanding concerning the distribution of HC in tight sedimentary rock mass.

161.1 Introduction

A repository for high level radioactive waste has to encase the radioactive material for a long time to prevent contact with fluids and a release of any radioactive material. The prediction for a safe deposition of high level radioactive waste in an underground repository for about 1 million years requires detailed knowledge of chemical and physical properties of the host rock. One of the most significant issue is ascribed to the hydraulic integrity in dependence of mechanical, chemical and thermal influences. Another important issue, which may affect the safety and the assessment of the suitability, especially related to the disposal of heat producing radioactive waste, is the occurrence of HC. HC were counted to the natural components of salt rock (Bornemann et al. 2008; Gerling et al. 1991). If HC are detected, their distribution and possible interconnectivities have to be determined and the volume of these occurrences has to be estimated with regard to the long-term performance of the potential repository.

161.2 Investigation Layout and Instrumentation

A long-term investigation program concerning the volume of HCO and potential interconnectivities has been carried out in a salt dome in northern Germany in a depth of about

B. Paul (✉) · H. Shao · J. Hesser · C. Lege
Federel Institute for Geosciences and Natural Resources (BGR),
Stilleweg 2, 30655 Hannover, Germany
e-mail: benjamin.paul@bgr.de

840 m bsl. The HC appear in the "Staßfurt" series (z2) almost exclusively within the "Knäuelsalz" (z2HS1). To quantify the HCO in the near field of galleries 20 boreholes, each with a length of 6 m and a diameter of 46 mm, were drilled and afterwards plugged with mechanical single packers to measure the pressure development and the inflow volume of gaseous and liquid HC. The boreholes were drilled at locations where HC were visible either with common artificial light or with ultraviolet light. For reference purpose few additional boreholes were drilled and instrumented in areas were no HC were detected. The (detailed) localisation of the measuring boreholes in HC impregnated areas is based on the mapping results of Amelung and Schubert (2000) and an additional visual survey. Additional results from core analysis of adjacent boreholes were considered. The HCO were classified regarding the intensity of fluorescence (Amelung and Schubert 2000). The boreholes should engage an area with a high amount of HC but a leakage through the Excavation Damaged Zone (EDZ) should be avoided. To achieve this, the single packers were set in a borehole depth of about 3 m. Depending on inclination and orientation of the boreholes the minimal distance between packer and side wall is about 2–3 m. All boreholes were drilled upwards in order that gravitation could be used for sampling. Two pipes with an inner diameter of 4 mm enable the separate sampling of the liquid and the gaseous phase of the HC. The chemical composition of the liquid and gaseous phase has been determined in regular intervals.

161.2.1 Equipment

Due to the investigation of HC, the used equipment is explosion protected. The measuring system consists of a mechanical single packer system, pressure sensors, a measuring and control system (MCC) as well as pipes for sampling and cables (Fig. 161.1). The volume of each test interval has been reduced using a dummy made of high quality polytetraflourethylene (PTFE) in order to detect minor pressures.

161.2.2 Realisation of the Measurements

After drilling the packer system was installed immediately to reduce the primarily degassing of the HCO. In the first time after installation every 30 s pressure values were recorded automatically. Depending on the pressure development the frequency was adapted for the specific borehole conditions.

Due to safety reasons the maximum pressure build up has been restricted to 1 MPa by the local mining authority. The MCC has the possibility to send an alert if the pressure comes close to the maximum pressure. When the alert has been triggered, staff from the operating company got samples of liquid and gaseous HC and reduced the pressure in the test-interval. The amount of the sampled gases and liquids were measured and documented periodically. In some cases, especially shortly after the installation, some boreholes had to be opened during the weekend because of the rapid pressure increase and the lack of manpower. The loss of gas, however, was approximated based on the measured gas flow rate before and after opening.

161.3 Data

The 20 boreholes cover a wide range of different HCO. From clearly under common artificial light visible HC over slightly only under ultraviolet light visible HC to locations without HC (referential boreholes) all transitions are included in the investigation program. Due to pressure development and amount of HC, four main categories can be distinguished:

Category 1: almost no pressure build up (<0.03 MPa; no venting needed)

Category 2: low pressure build up (<1 MPa; no venting needed)

Category 3: intensive pressure build up (initially frequent pressure build up; venting needed)

Category 4: very intensive pressure build up (permanent pressure build up; venting needed)

Eleven boreholes, more than a half of all boreholes, belong to category 1, with almost no pressure build up. Four of these boreholes are reference boreholes, which were drilled in areas where no HC were suggested. Two boreholes show a low pressure build up and can be allocated to category 2. One of them was drilled to determine the pressure development of a HCO which is connected to a thin anhydrite layer. Four boreholes belong to category 3 with an intensive pressure build up. Only three boreholes have an extraordinary position because of their very intensive pressure build up and the amount of inflowing gaseous and liquid HC (Table 161.1).

The two boreholes 6 and 6a were drilled to investigate the extent of a visible HCO and the interconnectivity between these boreholes. The two boreholes cross each other with a minimal distance of about 0.6 m. Borehole 6 showed a very intensive and long lasting pressure build up with an amount of more than 2,000 l under standard conditions, while borehole 6a showed no evidence of HC occurrences at all.

Fig. 161.1 Schematic sketch of the measurement setup
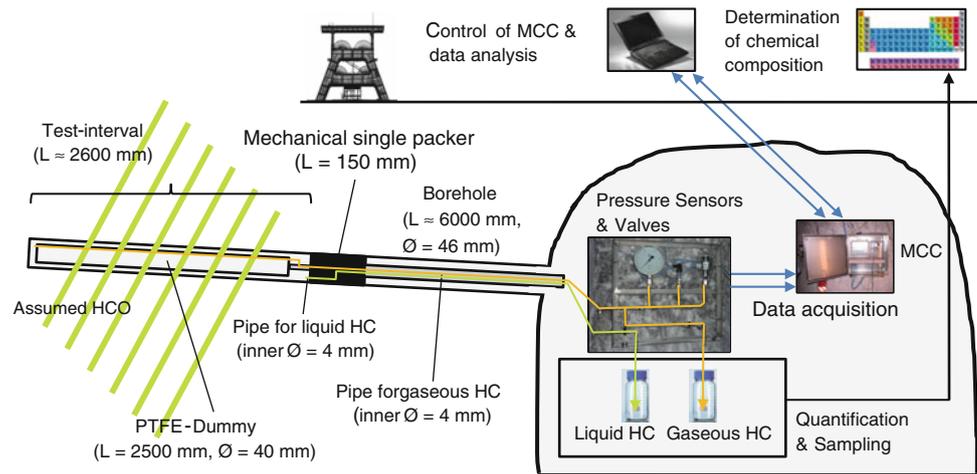
Table 161.1 Summary of boreholes without category 1, except borehole 6a as at December 2012

Borehole	Period (d)	Total sampled gas (stdl)	Total sampled liquids (ml)	Total samples gaseous/liquid	Pressure build up	Category
1	537	121.0	1,350	14/6	Intensive	3
2	514	1,331.7	1,883	99/69	Very intensive	4
3	517	287.3	1,443	19/15	Very intensive	3
4	516	80.4	93	9/5	Very intensive	3
5	515	3,271.6	16,015	176/159	Very intensive	4
6	511	2,383.3	1,664	150/112	Very intensive	4
6a	510	–	–	–	Almost no	1
7	252	148.2	575	9/4	Intensive	3
8	314	3.7	–	1/0	Low	2
9	70	–	–		Low	2

161.3.1 Data Analysis

Based on the measured pressure development the volume of the inflowing gas was approximated by using the mass balance equation. The inflowing gas is assumed to be an ideal gas so that the following state equation is valid:

$$m = P * \frac{V}{R_S * T} = P * \frac{V}{(\frac{R}{M} * T)} \qquad (161.1)$$

P   interval pressure (Pa)
R_s spec. gas constant (J/kg K)
M   molecular weight (kg/mol)
V   interval volume (m^3)
R   universal gas constant 8.314472 (J/kg K)
T   absolute temperature (K)

Under isothermal conditions the mass flow can be calculated with:

$$m = \frac{\partial m}{\partial t} = \frac{V}{R_S * T} * \frac{\partial P}{\partial t} \qquad (161.2)$$

The specific gas constant depends on the gas composition. A synthetic gas constant value was calculated according to a composition of about 40 % methane, 40 % nitrogen and 20 % other gases (carbon dioxide, propane and oxygen), given by the chemical analysis of samples. The measured and calculated gas volume correlates very well. Figure 161.2 shows exemplarily the correlation of the calculated and measured gas volume of borehole 2.

For calculation purposes the gas volume at the beginning was set to a constant volume between 1.4 and 2 l in dependence on the pipe length and the installation depth of the packer. This volume should be reduced by the inflow of liquid HC during measuring. The reduction has been considered in the calculation in the way that the inflowed volume of liquid HC is subtracted from the entire volume. The inflow of

Fig. 161.2 Correlation of calculated and measured gas volume on the basis of data of borehole 2
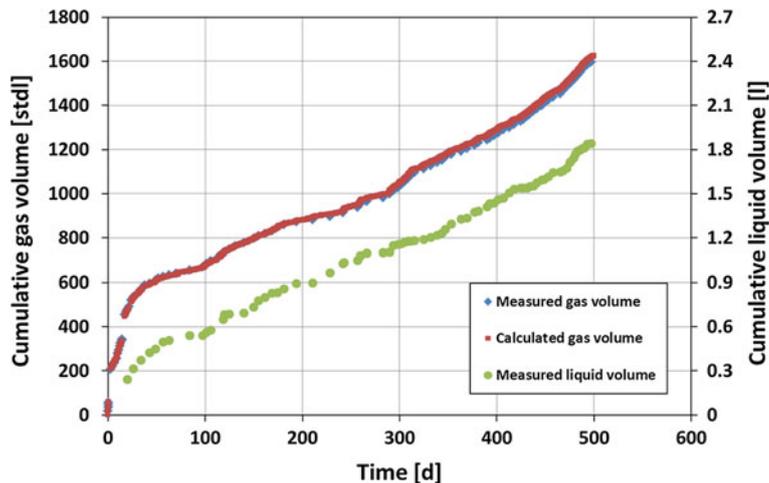
liquids is assumed to be nearly linear within a sampling interval. By a known mass flow the volume of gas under normal conditions can be calculated at a certain time with:

$$V_t = m * (t - t_1)/\rho_{syn} \qquad (161.3)$$

t   point of time of last pressure determination

ρ_{syn} synthetic density of gases

Hence the cumulative gas volume can be calculated by summarising V_t.

161.4   Conclusions

Generally, liquid and gaseous HC occurred simultaneously, based on the data measured up to now. If a drilling encounters a HCO, gaseous HC were released due to pressure decrease. To determine the amount of gaseous and liquid HC the inflowing HC were measured separately. These measured data were used to verify the calculations, which are based on the pressure data. The excellent accordance of calculated and measured results confirms the suitability of the presented calculation method for determination

of inflowing HC in relation to the measured pressure development. Because of the influence of the liquid phase on the entire volume, a measurement of the liquid phase is still necessary. The investigation showed that adjacent boreholes, even within a distance of less than 1 m to each other can behave completely different. Reason for that is the very low permeability in tight salt rock beyond the excavation disturbed zone, which prevents the mobilisation of HC. The estimation of a hydraulic relation between two boreholes depending on category 4 is not yet possible because of the continuing intensive pressure development.

References

Amelung P, Schubert J (2000) Dokumentation der Kondensatvorkommen im Hauptsalz der Staßfurt-Folge, unpubl. report, DBE, Gorleben/Peine

Bornemann O, Behlau J, Fischbeck R, Hammer J, Jaritz W, Keller S, Mingerzahn G, Schramm M (2008) Description of the Gorleben site Part 3: results of the geological surface and underground exploration of the salt formation structure. BGR, Hannover

Gerling P, Beer W, Bornemann O (1991) Gasförmige Kohlenwasserstoffe in Evaporiten des deutschen Zechsteins. Kali und Steinsalz 11:376–383

Relationship Between the Fractal Dimension
and the Rock Mass Classification Parameters
in the Bátaapáti Radioactive Waste Repository

162

Rita Kamera, Balázs Vásárhelyi, László Kovács, and Tivadar M. Tóth

Abstract

A fractured rock mass is divided by the fracture sets into mixed shapes of blocks and wedges. The geotechnical parameters of the rock mass are obviously dominated by the presence and the spatial distribution of fracture sets. In rock engineering, the determination of geotechnical parameters of rock masses is a key issue for the prediction of expected behaviour of the fractured rock mass. Several measurements and empirical methods can be used to investigate the characteristics of the fractures including its spacing and orientation. The goal of this paper is to find the possible connection between the calculated fractal dimension (D) and the derived values originating from several rock mass classification systems (e.g. RQD, RMR, Q, GSI). Principally, the derivation of fractal dimensions and the rock mass classification systems are based on empirical methods. For our present investigation the fractures visible in scores of pictures taken by automatic photo robot of the tunnel faces were used at the low and intermediate radioactive waste repository located at the Bátaapáti site in Southern Hungary. The BENOIT software was used to calculate the single fractal dimension according to the box-dimension methodology and the rock mass classification values were evaluated with the JointMetriX3D (ShapeMetriX3D) software. Our results show that some connection between geotechnical parameters and fractal dimension values can be obtained by the applied methodology. Using these empirical relationships, it is possible to carry out more safety construction and calculations in the radioactive waste repository in Bátaapáti.

Keywords

Fracture network • Damage model • Fractal • Radioactive waste • Depository

162.1 Introduction

It is a basic importance to get reliable information of fracture networks of different geological formations, in order to understand fractured hydrocarbon reservoirs, to optimize radioactive waste depository or even to exploit geothermal energy. Although, there are numerous simulations methods for fracture network modeling, input data calculations are still completely depend on subjective decisions.

R. Kamera (✉)
Golder Associates Ltd., Budapest, Hungary
e-mail: Rita_Kamera@golder.com

B. Vásárhelyi
Department of Structural Engineering, University of Pécs, Pécs, Hungary

L. Kovács
Rockstudy Ltd., Pécs, Hungary

T.M. Tóth
Department of Mineralogy, Geochemistry and Petrology, The Faculty of Science and Informatics, University of Szeged, Szeged, Hungary

The aim of this study is to show the relationship between the fractal dimension and the geotechnical parameter based on the Bátaapáti low-, and intermediate radioactive waste depository of Hungary.

162.2 Study Area

The investigated area is situated in the Mórágy granite body (Fig. 162.1), which is the host rock of the radioactive waste disposal in Hungary. A significant part of the Carboniferous intrusion (Buda et al. 1999) is covered by young sediments and only a small portion of it is avaliable for outcrop survey. Petrographically, the igneous body is composed of diverse granitoid subtypes, such as monzonite and monzogranite, which due to a polymetamorphic evolution under greenschist facies conditions, exhibit a slightly foliated structure (Király and Koroknai 2004). During the subsequent postmetamorphic deformation events, a mutual fracture network developed. Based on evaluation of the BHTV data of over 60.000 single fractures representing 20 wells, two main groups of faults can be emphasized. One cluster shows very high dips (70–80°), with a NW-SE strike; whilst another shows a strike of ENE-WSW and a similar dip (Maros et al. 2004).

162.3 Method

162.3.1 Fracture Network Digitalization

Due to different physical circumstances rock bodies are deformed and complex fault systems may be developed. The rocks brake along defined planes and the fracture network is set up from these discrete fractures (Fig. 162.2).

In the first part of the investigation the geometric parameter such as the fractal dimension values and in the second step the different rock mass classification systems (i.e. RQD, RMR, GSI, Q) values were developed. During this study 140 samples were analyzed to determine the parameters using the JointmetriX3D code.

During the digitization there may be some problems with identification of the fractures:

- Breccia zone: Due to the intensive deformation, breccia zones of different-scale may develop along the shear plane. Discrete fractures can be hardly identified in these zones that consist of angular rock pieces. In this case only those fractures should be considered, which can be defined unambiguously;
- Fracture wall: In those cases when fractures are almost parallel with the image plane they cannot be taken into consideration;

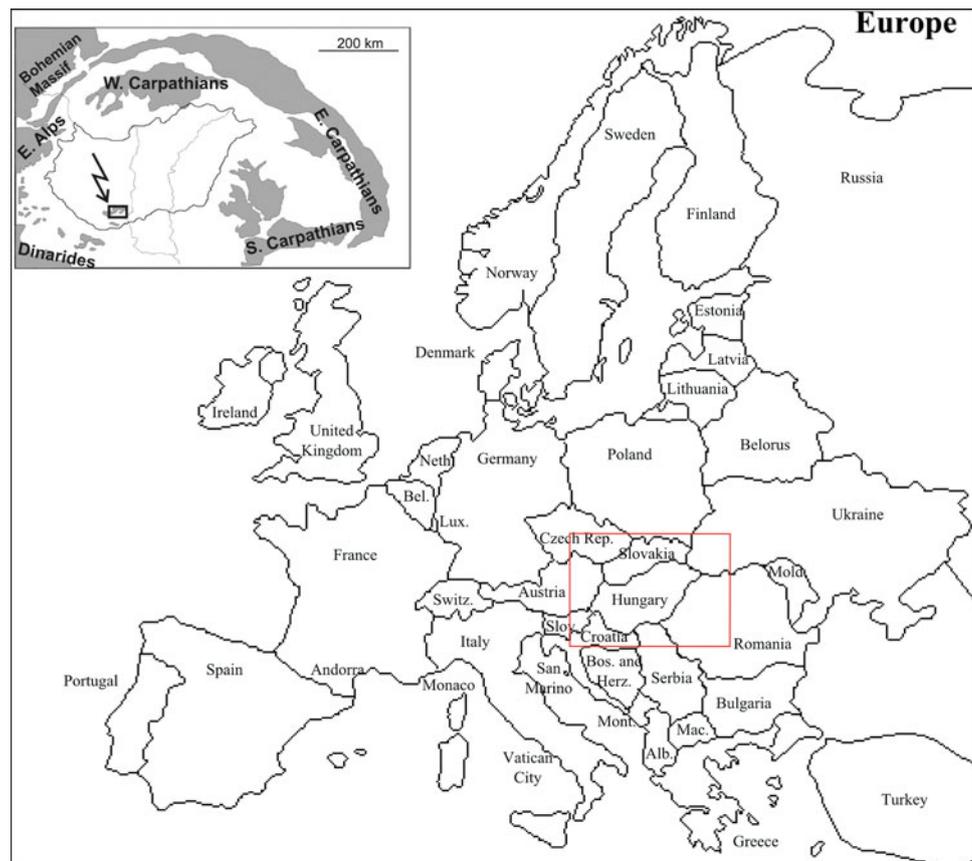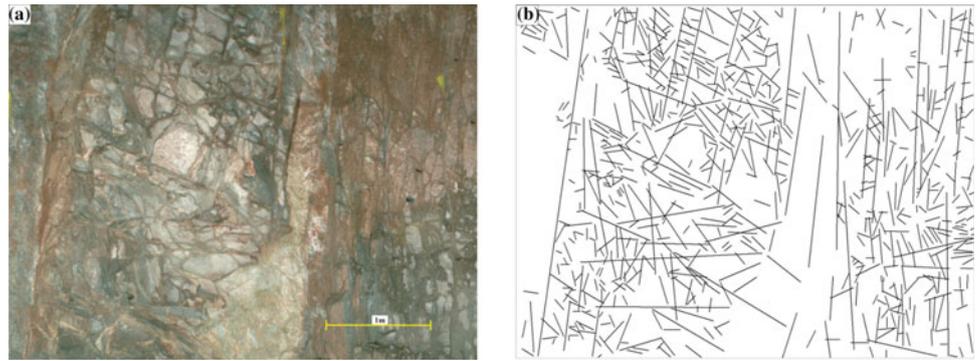**Fig. 162.1** Geographical position of the research area

Fig. 162.2 **a** A tunnel end photo from Bátaapáti site; **b** The digitized fractures

- Numerous fractures: A fracture network consists of strongly and less fragmented zones. The determination of discrete fractures can be difficult inside those intensively fragmented zones. In this case only those fractures should be digitized that can be identified unambiguously at the magnification in question;
- Sheared fractures: Through subsequent tectonic events any discrete fracture may be sheared. Portions of a sheared fracture are interpreted as two individual fractures; and
- Unfinished and covered with each other fractures were ignored during the digitalization process (La Pointe et al. 1993).

Unfinished and covered with each other fractures were ignored during the digitalization process (La Pointe et al. 1993).
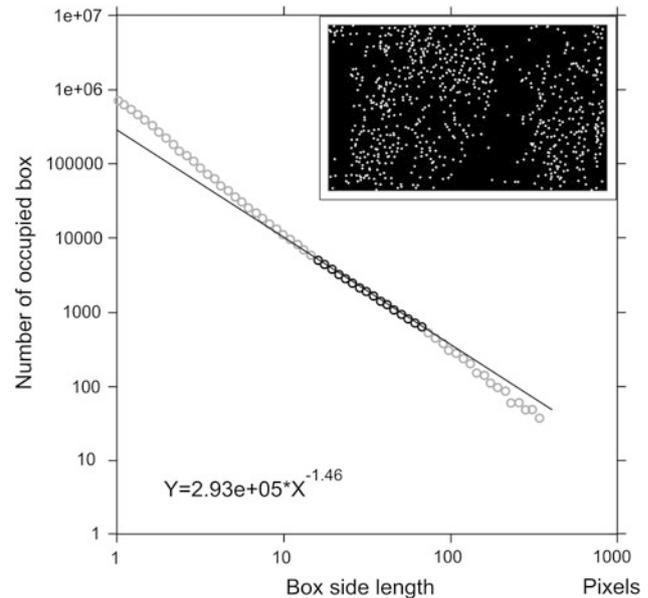
162.3.2 Fractal Dimension Calculation

In the second step of the evaluation was the calculation of the fractal dimension (D) using the box-counting method (Mandelbrot 1985). This approach is based on the fracture midpoints distribution. The box dimension relates to the result of counting the box number (N) of size r required to cover the fracture pattern. This value can be calculated with the following algorithm:

$$N(r) \sim r^{-D} \qquad (162.1)$$

A black-and-white image was used as an input file that shows the midpoints distribution of the fractures. A point diagram was generated with the "box-counting" method, from which the dimension value was calculated by using linear regression slope. The two sections of the line after and before the breakpoints were deleted to determine the D value. Before the first breakpoint, the size of the points was calculated instead of the complexity of the pattern. After the second breakpoint the values are not representative because the box sizes are too large. The fractal dimension of the fracture pattern was generated from the middle section of the linear regression line (Fig. 162.3).

Fig. 162.3 The fractal dimension calculation based on the midpoints of the digitized fractures

162.4 Rock Mass Characterization as Damage

We relate the empirical fracture and disturbance measures of rock mechanics (RQD, Q, RMR, GSI, etc.) to a damage measure D. According to the physical interpretation of damage, the value $D = 0$ characterizes the intact rock and $D = D_{cr}$ stands for the fractured rock mass at the edge of failure. As the rock mass quality measures are zero at maximal possible damage and are one at the undamaged state, we suggest the simplest linear relationship interpreting them as damage measures

$$D_{RM} = 100\left(1 - \frac{D}{D_{cr}}\right) \text{ therefore } D = D_{cr}\left(1 - \frac{D_{RM}}{100}\right). \quad (2)$$

Here D_{RM} is the damage of the rock mass. RM would be one of the rock mass classification systems (RQD, RMR or GSI value, i.e. between 0 and 100). As a simplification, hereafter

we assume that $D_{cr} = 1$. In our case this is not a restriction because we do not associate a direct physical meaning (e.g. crack density, fractal dimension of the crack system) to damage and we accept the normalization and measurement methods of the rock mass quality measures as a proper characterization.

We assume that:

- The mechanical parameters of the rock mass in case of $D = 0$ are equal to the intact rock parameters
- The relationships can be modeled by an empirical function.

162.4.1 Damage Variable and Deformation of Rock Mass

We can transform the functions above, introducing the damage as an independent variable, into the form

$$\frac{E_{rm}}{E_i} = \exp(-AD). \tag{3}$$

The values of the material parameter A corresponding to the published equations are between 2.7 and 4.2 according to the results of Ván and Vásárhelyi (2010).

162.4.2 Damage Variable and Unconfined Compressive Strength of the Rock Mass

Similarly to the deformation module of the rock mass, were recalculate the empirical equations of the unconfirmed compressive strength (σ_{cm}) for the following form, using the compressive strength of the intact rock (σ_i):

$$\frac{\sigma_{cm}}{\sigma_c} = \exp(-BD). \tag{4}$$

The average value of B is 5.43 (between 4.17 and 6.56) and 8.61 (7.65–9.84) in case of undisturbed and disturbed rock mass, respectively (Ván and Vásárhelyi 2010). The purpose of the paper was to present an explicit mathematical relationship between fractal dimensions and rock mass classification parameters. As a result of our investigations, no mathematical formula could be deduced which describes the inherent connection between these parameters with adequate correlation coefficient. Although this report does not necessarily represent any connection between the applied data, it can stimulate some interests and thoughts for further investigations in association with this problem.

References

Buda Gy, Lovas Gy, Klötzli U, Cousen BI (1999) Variscan granitoids of the Mórágy Hills, South Hungary. Beihefte zur European J Miner 11(2):21–32

Király E, Koroknai B (2004) The magmatic and metamorphic evolution of the north-eastern part of the Mórágy Block. Annu Rep Geol Inst Hung 2003:299–310

La Pointe P, Wallman PC, Derschowitz WS (1993) Stochasticestimation of fracture size from simulated sampling. Int J Rock Mech Mining Sci Geomech Abs 30:1611–1617

Mandelbrot BB (1985) Self-affine fractal dimension. Phys Scr 32:257–260

Maros G, Koroknai B, Palotás K, Fodor L, Dudko A, Forián-Szabó M, Zilahi-Sebess L, Bán-György E (2004) Tectoic analysis and structural evolution of the north-eastern Mórágy Block. Annu Rep Geol Inst Hung 2003:371–380

Min KB, Jing L, Stephansson O (2004) Determining the equivalent permeability tensor for fractured rock masses using a stochastic REV approach: method and application to the field data from Sellafield, UK. Hydrogeol J 12(5):497–510

Ván P, Vásárhelyi B (2010) Relation of rock mass characterization and damage. In: Vrkljan I, Balkema (ed) Rock Engineering in Difficult Ground Conditions (Soft Rock and Karst), pp 399–404

Direct Shear Strength Test on Opalinus Clay, a Possible Host Rock for Radioactive Waste

Buocz Ildikó, Török Ákos, Zhao Jian, and Rozgonyi-Boissinot Nikoletta

Abstract

In the past decades the long term safe storage of highly active radioactive waste has been one of the greatest challenges for engineers and scientists to be solved. It is internationally agreed that the radioactive waste should be placed into deep geological formations, namely into granite, salt or clay stone. The latter type, in particular the Opalinus Clay stone, is the potential host rock for such repository in Switzerland. The aim of the paper is to broaden the knowledge on this rock type. Direct shear strength tests were carried out, to provide data on the maximal shear strength, friction coefficient and the connection between the plane of the bedding and the plane of the natural fault. The samples were derived from the major fault zone. The specimens were sheared along natural open joints under 1 MPa constant normal load (CNL) condition. Another set of experiments were carried out on intact samples disturbed by a soft clay vein. The shear plane was the same as the plane of the intrusion. On these specimens different normal stresses were applied, between 0.5 and 2 MPa. Apart from the maximal shear strength and the friction coefficient, the cohesion and the consolidation settlement (vertical displacement during the application of the initial normal stress, before the shear test started) were determined as well.

Keywords

Opalinus clay • Direct shear • Open joints • Clay vein

163.1 Introduction

The final placement of radioactive waste is a complex engineering task, which by today became an urgent problem to be solved. All around the world several laboratories carry out countless experiments on the host rocks of potentially highly active radioactive waste disposal sites—mainly clay stone, granite and salts. These experiments aim at gaining relevant information in order to prove that the facility is able to function safe for several hundreds and thousands of years. The Mont Terri Rock Laboratory, situated in the northwestern part of Switzerland, has operated already for more than 15 years, and has performed more than 110 small- and large-scaled experiments on Opalinus Clay stone, out of which 43 are still running. Besides the Laboratory, several Universities and Institutes carry out further experiments on the Opalinus Clay, deriving from Mont Terri.

Direct shear strength tests were carried out at the Laboratory for Rock Mechanics of the École Politechnique Fédérale de Lausanne on Mont Terri rocks that were collected during the excavation of the FE Gallery in 2012. The

B. Ildikó (✉) · T. Ákos · R.-B. Nikoletta
Department of Construction Materials and Engineering Geology, Budapest University of Technology and Economics, Műegyetem rkp. 3, Budapest 1111, Hungary
e-mail: ildikobuocz@yahoo.com

Z. Jian
Department of Civil Engineering, Monash University, Building 60, Melbourne, VIC 3800 Australia

investigated shaly facies Opalinus Clay rocks are homogeneous, barely visible laminated clay stones with low sand content, derived from the shear fault zone of the site.

The paper summarizes the first stage evaluation of the direct shear strength test results of these Oplainus Clay stones following the guidelines of the International Society for Rock Mechanics (1974). The second stage evaluation will take in consideration extra strength value influencing parameters, such as surface roughness, and the elevation of the shear plane.

163.2   Test Methodology

The test methodology as well as the evaluation of the data were both carried out according to the suggestions of the ISRM et al. (1974).

Two types of direct shear strength tests were performed along natural discontinuities of the Opalinus Clay stone. One was along open joints, where the bedding of the samples enclosed an angle with the shear plane, and the other was on closed fractures infilled with a softer clay material. The fracture was parallel to the bedding in all cases.

163.2.1   Shear Apparatus

The shear machine operated with an upper box fixed against movements in the shear direction, and a lower box moving with constant speed of 0.8 mm/min in the shear direction. The upper box could rotate around the point where the normal load was applied, and vertical movements were allowed as well. During the tests, displacements in vertical and horizontal directions were measured on the upper box by 3–3 linear variable differential transformers (LVDT), allowing to follow all the movements. One LVDT measured the shear displacement on the lower box (Fig. 163.1).

163.2.2   Test Procedure

Tests were carried out under constant normal load (CNL) conditions. Before the shear test started, a 1 MPa normal stress was applied for the samples with open joints. In the same way, for the healed samples four normal stresses with different magnitude were used, i.e. 0.5, 1.0, 1.5 and 2.0 MPa. For all tests, subsequent to the application of the normal stress, the consolidation settlement was measured. The samples had a size of 50×50 mm and, as the shear displacement cannot exceed the 10 % of the length of the sample according to the ISRM et al. (1974), the shear displacement was restricted to 5 mm.

163.3   Test Results and Evaluation

The two types of tests were evaluated in a different way. For the open joints the main purpose was to find a connection between the bedding plane and the plane of the natural joint. For the samples with clay-healed fractures, where the bedding plane and the plane of the fracture were parallel, the goal was to determine the cohesion and the rate of the consolidation by applying different normal loads.

163.3.1   Test Results for Open Joints

For a limited number of samples, the plane of the natural joints enclosed an angle with the bedding plane. This angle varied between 0 to 49°. Tests were carried out under 1 MPa CNL. The evaluation focused on samples where the angle was greater than 0 degrees and less than 50. Figure 163.2 shows that the shear stress after 4 mm shear displacement, i. e. in the residual range, increases with the increase of the angle.

Figure 163.3 shows the maximal shear strength values at 1 MPa normal stress. The average of the values is 0.48 MPa with a deviation of 0.1.

The friction coefficient ranges between 0.33 and 0.73, with an average value of 0.45.

163.3.2   Test Results for Closed Fractures

As introduced before, four magnitudes of normal stresses were applied on the specimens, i.e. 0.5, 1, 1.5, 2 MPa. The friction coefficient decreased and the maximal shear strength increased with the increase of the normal load. The vertical displacement (consolidation) was measured from the beginning of the normal loading until the start of the shear test. Table 163.1 gives the average values of the above mentioned properties for each normal stress.

The cohesion was determined by approximating the maximal shear strength—normal stress results with a linear approach. The value obtained for this parameter is 0.42 MPa.

163.4   Conclusion

Direct shear strength tests were carried out on two types of Mont Terri Opalinus Clay stone, i.e. with open joints and clay healed fractures.

Specimens with open joints did not always have their plane of discontinuity parallel to the bedding, therefore the effect of the magnitude of the angle on the test results was investigated. In the range of angles examined ($0° < \alpha < 50°$)
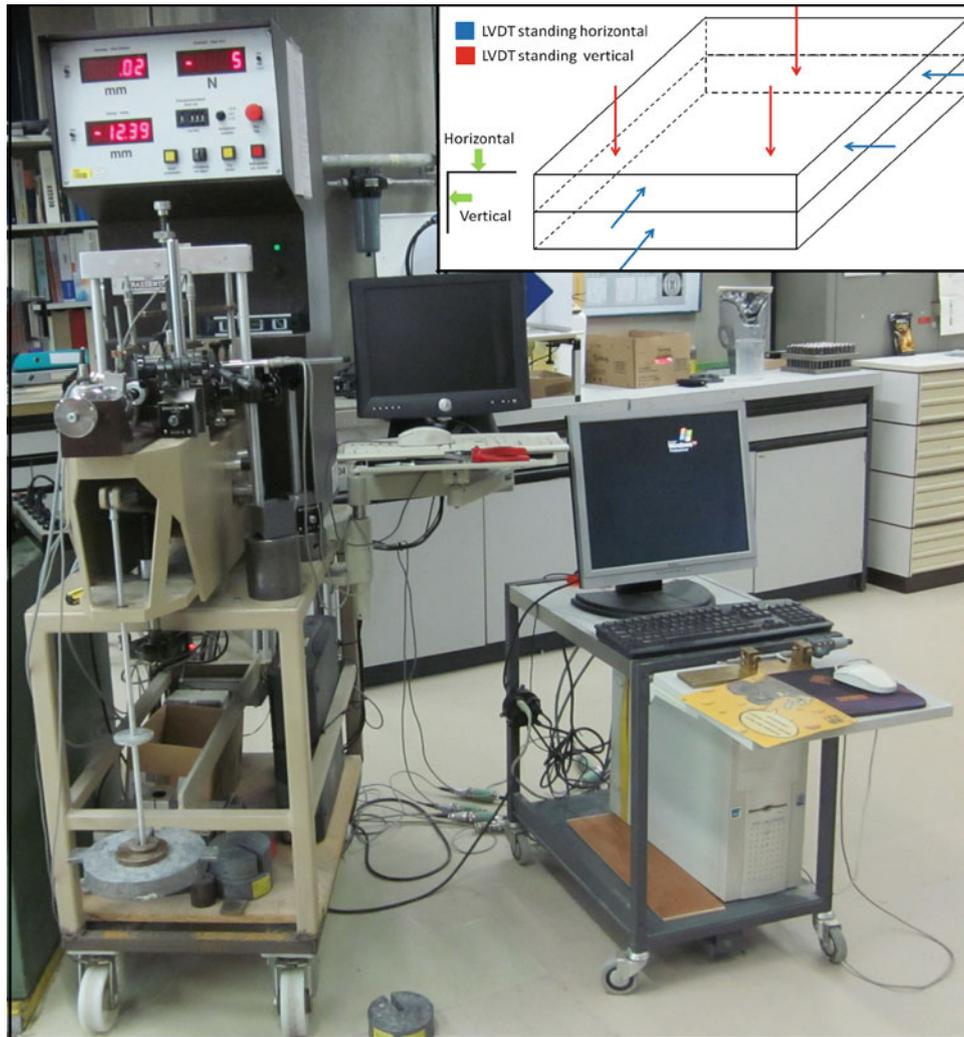
Fig. 163.1 Shear apparatus; position of the LVDTs in the *right upper corner*
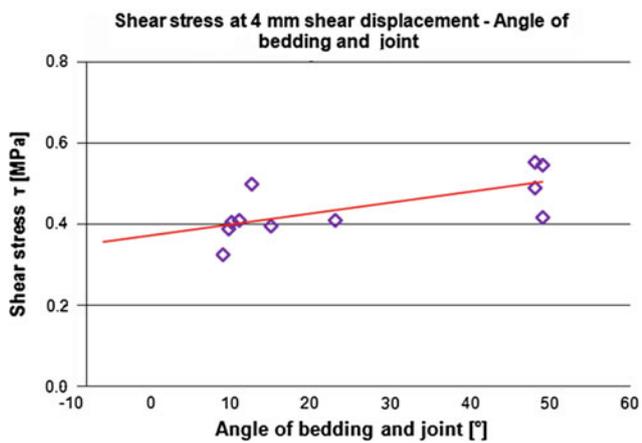

Fig. 163.2 Shear stress at 4 mm shear displacement for samples in which the plane of the bedding encloses an angle with the plane of the natural joint (angle greater than 0° and less than 50°)
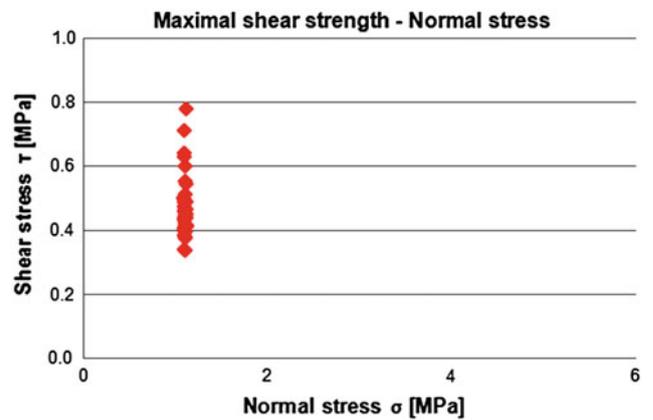

Fig. 163.3 Maximal shear strength—normal stress diagram

Table 163.1 Average values for maximal shear strength, friction coefficient and consolidation settlement for every normal stress condition

Normal stress (MPa)	Average maximal shear strength (MPa)	Average friction coefficient (−)	Average consolidation settlement (mm)
2.0	0.58	0.28	1.08
1.5	0.66	0.45	0.56
1.0	0.52	0.51	0.28
0.5	0.44	0.85	0.19

the greater the angle was, the higher the maximal shear strength became.

The average maximal shear strength of samples with open joints was 0.48 MPa, and the average friction coefficient 0.45.

The closed joints contained a softer clay vein that had a cohesion of 0.42 MPa. Four normal stresses were used during the experiments, the greater this stress was, the lower the friction coefficient became. The opposite effect was observed on the value of the maximal shear strength.

Reference

ISRM, Franklin JA, Kanji MA, Herget G, és Ladanyi B, Drozd K, és Dvorak A, Egger P, Kutter H, és Rummel F, Rengers N, Nose M, Thiel K, Peres Rodrigues F, és Serafim JL, Bieniawski ZT, és Stacey TR, Muzas F, Gibson RE, és Hobbs NB, Coulson JH, Deere DU, Dodds RK, Dutro HB, Kuhn AK, és Underwood LB (1974) Suggested methods for determining shear strength. In: International Society for rock mechanics commission on standardization of laboratory and field tests, vol 1, pp 131–140

Dániel Borbély, Tamás Megyeri, and Péter Görög

Abstract

The first underground radioactive waste repository for low and intermediate level waste in Hungary is being built in the outskirts of the village of Bátaapáti. The total length of tunnels driven to date is over 5,200 m including two inclined access tunnels, the base tunnels and the first two emplacement chambers. The tunnels were driven in fractured granitic rocks. Based on the discontinuities the host rock of the repository can be considered as an assembly of blocks, therefore the discrete element modelling approach can be used to provide representative results of its behaviour. A hybrid continuum-discrete model is presented, where the near-field is modelled as a blocky rock mass, and the far-field is modelled as a continuum using the built in deformable blocks of the 3DEC software. Convergence monitoring was carried out in the modelled section that offers the ability to check the validity of analysis results. This paper focuses on the effect of joint pattern on the prediction capability of the discrete model. Different possible representations of the measured joint pattern were examined to assess the effect of joint pattern on the results, particularly on internal forces in rock support.

164.1 Introduction

Design in fractured rock can be challenging especially, when the rock mass behaviour is governed by the block movement. The blocky nature of rock can be considered with distinct element modelling approach. The National Radioactive Waste Repository Project (NRWRP) is a good example to research the numerical modelling of blocky rocks. Due to the project radioactive safety first approach and its public recognition all the required date with good quality available for investigation. This paper is focuses on two fundamental issues about advanced numerical modelling of the repository. The first goal is the reduction or optimization of the computational effort of three dimensional modelling. The second aim is to assess the effect of joint pattern representation on results.

D. Borbély (✉) · P. Görög
Budapest University of Technology and Economics, Budapest, Hungary
e-mail: borbely.daniel@epito.bme.hudaniel.borbely@mottmac.comdaniborbely@gmail.com

P. Görög
e-mail: gorog.peter@epito.bme.hu

T. Megyeri
Mott Macdonald Hungary Ltd., Budapest, Hungary
e-mail: tamas.megyeri@mottmac.com

164.2 National Radioactive Waste Repository Project (NWRP)

The repository facilitates the low and medium activity radioactive waste of Nuclear Power plant of Hungary. The area of the repository is close to the village of Bátaapáti, at South Hungary that is part of the geological unit of Mórágy Block that is composed of granitic rocks (Kovács et al. 2012).

Construction of the first two emplacement chambers was finished in 2012. The facility consists of tunnels, shafts, caverns, access roads and portals. The access tunnels arrive to the chambers at the reference base level of 240 m below ground level. The rock support in the investigated section was 150 mm thick steel fibre reinforced sprayed concrete, supplemented with systematically rock bolting in a 1.5 m × 1.0 m raster. Full-face excavation was used for the tunnel with diameter of app. 7 m, the length of the applied bolts is 3 m.

Regarding that the NWRP is in focus, carefully conducted, comprehensive geotechnical investigations were made. During the excavation face mapping was performed. The joint pattern applied in the paper is based on the face mapping. Systematic rock sampling and laboratory test were carried out during construction to determine the properties of intact rock and the rock mass (Kovács et al. 2012). The shear strength of the joints had been measured by laboratory tests (Buocz et al. 2010). The validity of the laboratory measurement was checked by plain strain distinct element model of a monitoring section (Horváth et al. 2012). Convergence measurement arrays were installed in 11 sections so far. In these sections relative displacements of the rock mass surrounding the excavation has been measured continuously in 6 radial directions.

164.3 Distinct Element Model, Representation of Rock Mass and Rock Support

The distinct element approach is most suitable for moderately fractured rock masses where the number of fractures is too large for the continuum-with-fracture-elements approach. The key concept of distinct element modelling (DEM) is that the domain of interest is treated as an assemblage of deformable blocks and the contacts among them need to be identified and continuously updated during the entire deformation process (Jing and Stephansson 2007). Three type of model with different purpose were used. First a continuum based finite element model was set up using Phase2 software to validate the properties of rock mass and rock support. Second type: small scale numerical tests were made to determine joint stiffness according the description of Jing and Stephansson (2007) using the three-dimensional distinct element code 3DEC 4.1. Several models with different joint stiffness were tested, and the one with the best fitting results to the validated continuum properties were selected. Using the input parameters applied in the finite elements model and the best fitted properties (determined in the small scale tests) a hybrid continuum-discrete model was built. In case of the hybrid model, the near-field is modelled as a blocky rock mass (using the joint properties and the

intact rock properties), and the far-field is modelled as a continuum using the built in deformable blocks of the 3DEC with the rock mass properties. The resulted convergence and the internal forces were compared with field data. The prediction capabilities of using different joint patterns are compared in this study.

Mohr-Coulomb constitutive model with tension cut-off is assigned to the deformable blocks assuming that the intact rock is a linear elastic-perfectly plastic material. Plain strain distinct element modelling confirmed that the joints can be represented with Mohr-Coulomb constitutive model (Horváth et al. 2012).

Four different joint pattern (Pattern A to Pattern D) based on the same measurement were examined in the paper (Fig. 164.1). The same measurements are interpreted in different ways. In case of Pattern A, three joint sets from the measured six were selected. It is assumed that the joint persistence is 100 %, i.e. the joints are continues across the entire model. The joints are not follows a random distribution, but the spacing, dip and dip direction are a given as deterministic value. This is the simplest approach, but this kind of representation might be very helpful on the early stage of a project, when limited information about joint pattern is available. Pattern B follows the actual distribution of joints and all six joint sets are considered. The joint spacing is equal for all six join set and based on the average joint set of the rock mass.

Pattern C is examining the effect of spacing. It is the same as Pattern A but the spacing is 4 m instead of 2 m. In case of Pattern D, the persistence of the joints is 80 % and the spacing is 3.2 m, giving an average block volume equal to Pattern C. The longitudinal redistribution of stresses around the advancing tunnel face was considered with stress relaxation method. The relaxation factor (proportion of stress relief before any support is installed) was measured on site. Linear elastic behaviour of the tunnel lining is a valid assumption since no sign of plastic deformation of the lining was observed at the analysed section. The early age properties of the concrete were determined according to Chang and Stille (1993). The support provided by rock bolt is taken into account with cable elements (considering axial loads).

164.4 Discussion of the Results

According to the Phase2 models, the displacement shows good agreement with the field measurements. The internal forces in the bolts and the liner are similar with the expectations. The liner is below the plastic limit in the model and it is in accordance with the field observation. Hence the set of rock mass parameters are considered valid for the given section.

Fig. 164.1 Pattern A (*top left*), B (*top right*), C (*bottom left*) and D (*bottom right*)
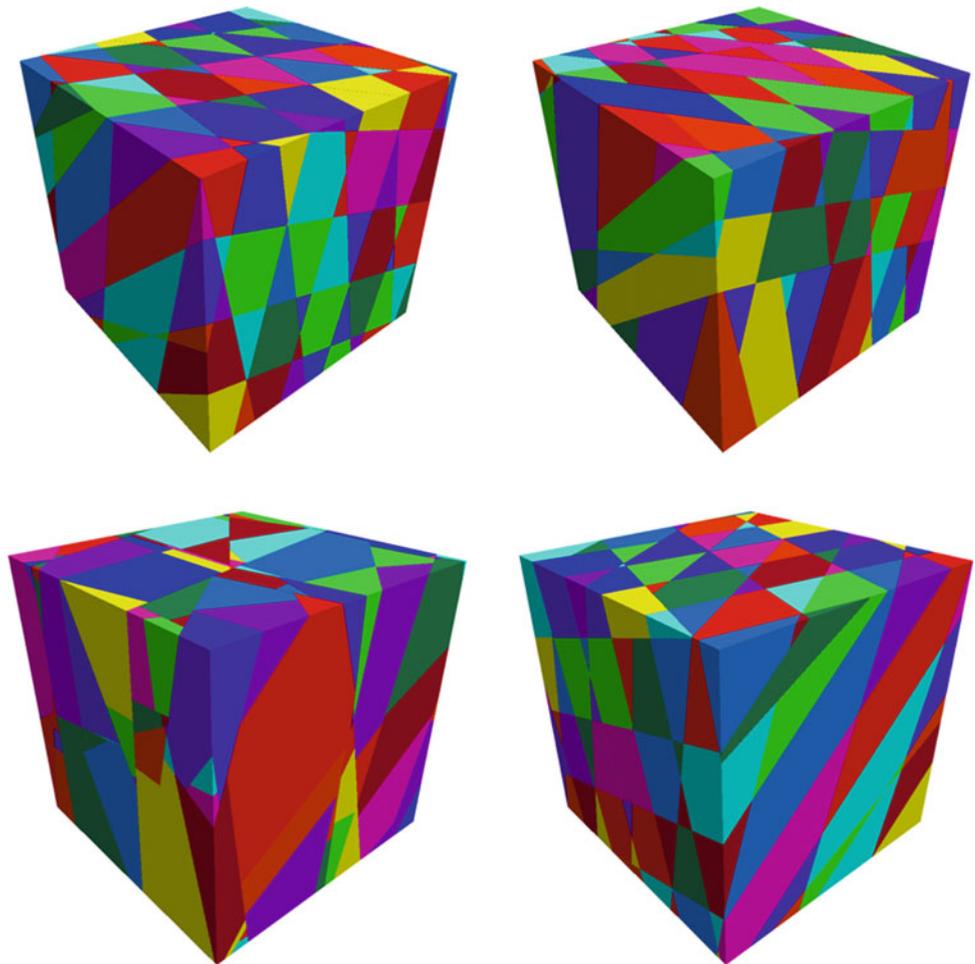
The joint stiffness was calibrated to the measured rock mass stiffness using the small scale numerical models, with short run time (couple of minutes). The displacements in the hybrid model (with the calibrated joint stiffness) showed good agreement with the monitoring results (Fig. 164.2). It should be noted, that in some cases the hybrid model was re-run with a slightly different joint stiffness (to finalize the calibration) but the calibration of a DEM model is less time consuming using the small scale numerical tests.

As it can be seen in Fig. 164.3, the internal forces are similar in case of the four models, the point cloud represents the magnitude of the bending moments and axial forces do not show significant difference. In fact the difference between models with the same joint pattern and slightly different joint stiffness are higher than the difference between models with different joint pattern but with app. same displacements. According to this model, it can be concluded, that the effect of the joint pattern is significantly lower than the effect of the joint stiffness (and the displacements).

The internal forces in the DEM model are significantly higher than it was found in the VEM model made with Phase2. One of the possible reasons of this phenomenon is that the rock mass induced forces, and the wedge movement
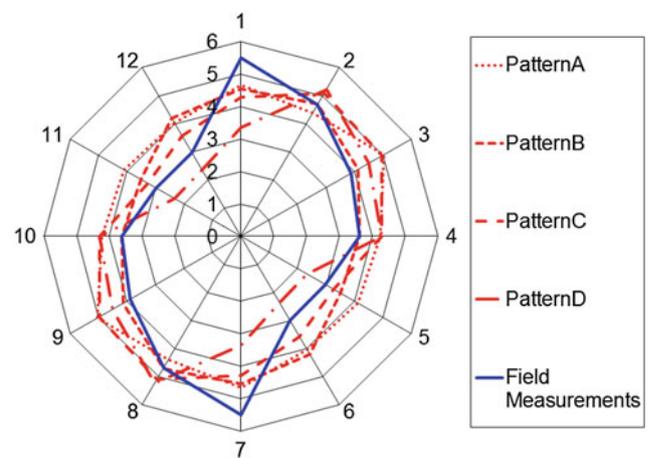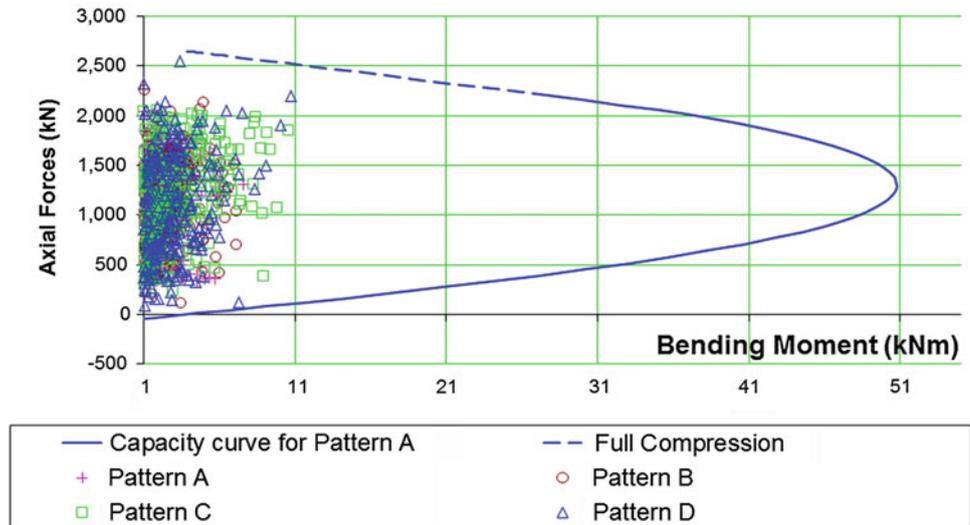

Fig. 164.2 Measured and calculated displacements in mm

induced forces can be examined in one model (it is not the same case if a continuous model is supplemented with a wedge analysis) therefore the internal forces with different cause are superimposed.

Fig. 164.3 Comparison of
internal forces in the four models

One of the biggest advantages of the DEM is that the rock support can be optimized. In case of an anisotropic rock mass, the internal forces can be significantly different from the ones calculated with an isotropic continuum model. In these cases the DEM gives good alternative to use the rock support (such as bolts or additional reinforcement) in the places where they are really needed.

164.5   Conclusions

The aim of this paper was to explore the effect of joint pattern on the internal forces in linings. Four different joint pattern based on the same field measurement are presented here. Back analysis was carried out to calibrate the displacements. The calculated values showed a great agreement with the monitoring results. The calibration was performed with small scale model, to reduce the computational effort of the models. Hybrid continuum-discrete modelling was carried out. In line with expectations, the number of elements and the run time were reduced significantly, whilst the behaviour of the model was in agreement with the discontinuous model. Application of continuous representation of far-field is recommended in three-dimensional distinct element modelling. The biggest disadvantage of the DEM is the waste amount of additional input parameters. The joint pattern, joint strength and stiffness are to be determined. Probably the most important result of these models, that the joint pattern had smaller effect to the results than the joint stiffness.

According to this the following modelling procedure can be suggested: firstly, set up a reasonable continuum model (it can be considered as a common engineering task).

Determine a reasonable estimation of the joint pattern and joint strength. It can be done with relativity simple field measurements, such as face mapping and joint characterisation. Then the displacements of the distinct model are to be calibrated to the continuous one. According to the results of the discrete model, the rock support can be optimized. With this approach the required additional input parameters can be determined as an estimation of the joint pattern and the joint strength.

References

Buocz I, Rozgonyi-Boissinot N, Görög P, Török Á (2010) Laboratory determination of direct shear strength of granitoid rocks; examples from the host rock of the nuclear waste storage facility of Bátaapáti (Hungary. Cent Eur Geol 53(4):405–417

Chang Y, Stille H (1993) Influence of early age properties of shotcrete on tunnel construction sequences. In: Shotcrete for underground support VI. American Society of Civil Engineers, pp 110–117

Horváth Z, Megyeri T, Váró Á, Görög P (2012) Discrete element modelling of the Mórágy granite formation in Southern Hungary. In: Horváth T (ed) 1st Eastern European tunneling conference. Veszprém, Budapest. Paper 22. ISBN:978-963-89638-0-2

Jing L, Stephansson O (2007) Fundamentals of discrete element methods for rock engineering: theory and applications'. Elsevier, Oxford

Kovács L, Deák F, Somodi G, Mészáros E, Máté K, Jakab A, Vásárhelyi B, Geiger J, Dankó G, Korpai F, Mező G, Darvas K, Ván P, Fülöp T, Asszonyi C (2012) Geotechnical investigation report, RHK-K-032/12

László Kovács and Balázs Vásárhelyi

Abstract

The safe management of radioactive wastes and spent fuels is one of the greatest technical-scientific challenges of 21st century. Radioactive wastes and spent fuels must be isolated safely from the biosphere until they become harmless as a result of decay process of radioisotopes. It takes even a few hundred thousands or one million years in some cases. Recently the final disposal in a stable geological environment seems to be the only feasible way for that. It is an unusual and multidisciplinary task to select an appropriate host rock, characterize that, design and construct an underground facility (including the engineering barriers), which fits to the features of geological barrier completely. Numerous special requirements to be taken into account both for earth-scientist and geo-engineers have been conceived worldwide during the last few decades. This paper tries to summarize the most important radwaste-specific issues of the geotechnical characterization programmes and the functional and static design of a repository, by introducing some example from the Hungarian L/ILW repository (National Radioactive Waste Disposal—NRWR at Bátaapáti) and the characterisation programme preparing the Hungarian HLW/SF (Boda).

Keywords

Radioactive waste • Repository • Geotechnical characterization • Design • NRWR—bátaapáti

165.1 Introduction

By the classification systems applied in most European countries radioactive wastes can be divided according to their activity (low, intermediate and high activity level wastes—LLW, ILW and HLW) and characteristic lifetime (short-lived and long-lived—SL and LL). Spent nuclear fuels (SF) represent a separate category in legal viewpoint (most of the countries do not classify SF as waste, including Hungary) but technically they have to be handled together with the HLW. Radioactive wastes and SF must be isolated safely from the biosphere until they become harmless as a result of decay process of radioisotopes. Particularly HLW and spent fuels are very dangerous substances with significant heat production, extremely high radiation level and radiotoxicity, so their danger remains during even a few million years. Consequently the safe management of radioactive wastes and spent fuels is one of the greatest technical-scientific challenges of 21st century.

L. Kovács (✉)
Kőmérő (RockStudy) Ltd., Pécs, Hungary
e-mail: kovacslaszlo@komero.hu

B. Vásárhelyi
Department of Structural Engineering, University of Pécs, Pécs, Hungary

Wide international consensus is developed that the only possible and ethical solution for the long-term isolation of radioactive wastes is the final disposal based on a complex protective system of engineered and natural barriers (multibarrier system). The key element of this system is the suitable natural (geological) barrier, but the waste form and the engineered barriers also have to be selected and designed according to the long-term stability and safety of the overall system.

A certain part of HLW and SF (depending on the selected back-end option) has to be disposed in deep geological repositories anyway. The Hungarian Public Limited Company for Radioactive Waste Management (PURAM) considers as reference scenario the direct disposal of SF. L/ILW can be disposed both in near-surface facilities or deep geological repositories. Hungary has developed both types of repositories: non-NPP origin radwastes are disposed in a surface facility at Püspökszilágy (hosted by loess and argillaceous sediments), while the NPP-origin L/ILW gets to the National Radioactive Waste Disposal (NRWR at Bátaapáti) in a granitic host rock (Mórágy Granite Formation).

Although the scientific and ethical bases of final disposal have been already given, lots of technical and scientific efforts have to be taken before licensing and operation of a repository. The reliable characterization of a potential host rock, the development of safety concept of final disposal, the confirmation of its long-term stability and safety, the detailed design and the construction generally take a few decades even in the case of L/ILW. The nationwide screening preparing the NRWR started in the beginning of 1993 and the very first underground disposal chamber was put into operation at the end of 2012. This relatively short implementation period was made to be possible by the extremely high level of public acceptance of local communities and the wide political consensus.

The council directive No. 2011/70 of European Union declares that each member state shall elaborate and implement its own national program with clear milestones and timeframes for the management of spent fuel and radioactive waste, covering all types of waste and all stages from generation to disposal. In conformity with this prescription PURAM develops mid and long term plans, which is updated in each year and accepted by the government.

The siting, characterization and design processes preparing a repository do not need to be uniform in every country. They depend mostly on the type of potential host rock, the geological, hydrogeological and climatic situation, the applied waste classification system, the technical, scientific, social and economical level, the internal regulations of the given country, etc. Only a limited number of general (mostly methodological) prescriptions and liabilities are defined in the relevant Safety Standards issued by International Atomic Energy Agency (IAEA) available in three categories (Safety Fundamentals, Safety Requirements and Safety Guides). The most important prescription is that the suitability of selected geological environment and the whole disposal system have to be verified by integrated Performance/Safety Assessments (PA/SA) based on the FEP-approach (Features, Events and Processes) and uncertainty-analyses in each of the project.

165.2 Key Questions of the Geotechnical Characterization and Design

The Eurocode 7 standard also has to be taken into account by the geotechnical characterization and design of a repository. Unfortunately, it does not consist of any commitments to radioactive waste repository up to now (see Alejano et al. 2013). Those prescriptions, nevertheless, are related only to the main rules, basic definitions and requirements of geotechnical works, but they do not specify the professional details of a program to be implemented. Since the radioactive waste disposal facilities are classified always into the Geotechnical Category 3, the elements of geotechnical characterization and design program have to be customized according to the features of host rock and the special character of the facility.

165.2.1 Elements and Implementing of the Geotechnical Investigation Programme

As the consequence of the above mentioned facts the main aim of the geotechnical characterization programme must be to understand and forecast the real behaviour of rock mass and

reduce the uncertainties of input data for design and PA/SA. For fulfilling this requirement it is essential to determine the variability of the parameters/processes/phenomena (as a function of rock types, weathering level, parting, lateral and vertical position, anisotropy, etc.). A comprehensive investigation and design programme is required for achieving this aim including field tests and laboratory measurements, advanced geomathematical evaluation and extended numerical methods, fully-coupled models (Hudson and Feng 2007).

In general, the following geotechnical-rock mechanical parameters/processes/phenomena should be investigated in the framework of each radwaste projects:

- Virgin and tunnelling-induced (primary and secondary) stress field, including stress-dependent hydro-mechanical processes and phenomena;
- Strength and deformability of intact rock matrix and various discontinuities (by laboratory tests, special in situ tests and/or numerical back-calculations);
- Spatial variability of geotechnical features (by geophysical methods and continuous application of empirical geotechnical classifications);
- Transient (tunnelling-induced) and long-term (time-dependent or rheological) deformation processes (by various in situ deformation tests);
- The extension, distribution and the complex, coupled thermo-hydro-mechanical-chemical (THMC) processes of the Excavation Damaged/disturbed Zone (EDZ/EdZ);

Of course, the investigation programme has to include some waste specific elements, too: e.g. in the case of direct disposal of HLW and SF the study of heat- and radiation-sensibility of the potential host rock and the pre-selected elements of engineering barriers plays extremely important role. The special thermo-mechanical behaviour of Boda Claystone Formation—BCF (the potential host rock of Hungarian HLW/SF) could be studied very effectively in the deepest URL of the world (more than 1,000 m), where the virgin rock temperature exceeded 50 °C. Site (or host rock) specific issues have to be also taken into account: the creep and after all the long-term stability are also a critical question of unconsolidated argillaceous sediments or salty host rocks. In the case of overconsolidated BCF this question is not determinant not even under 1,000 m depth (Kovács 2001). Special geotechnical task can be the determination of mechanical properties of a clayey fault zones inside a granitic

host rock (like in NRWR) not only for preventing geotechnical problems, but for protecting the integrity of the most important confining elements of site (Kovács et al. 2012).

Further requirements for the adequate implementation of geotechnical-rock mechanical investigations:

- Representativity (we should measure there, that and so regularly, which is enough for sufficient understanding of features, events and processes);
- Determining the scale effects; development of appropriate up- and downscaling procedures;
- Consistent, systematic applications of unified methods for the comparability of different rock zones;
- Generally it is unsatisfactory to evaluate the geotechnical—rock mechanical parameters separately. The consideration of coupled thermo-, hydro and chemical processes is also required;
- Investigations should not affect the isolation capabilities of host rock;
- Quality assurance/quality control requirements (reconstructability, objectiveness, documenting, long-term data preservation, etc.);
- Avoiding the quick aging of the results (liability for applying the best, up-to-date available technologies).

165.2.2 Key Questions of Functional and Static Design

Most important tasks for the functional and static design are to optimize the main elements of the overall final disposal system and harmonize them to the safety concept and to each other. The suitability and safety of disposal facility have to be proved in a very detailed and complex licensing procedure. Long-term radiological safety determined by PA/SA must be the primary consideration, so some usual engineering aspects remain in the background, e.g. limitations of applicable materials and supporting systems (e.g. plastics and metals with high gas formation risk and/or corrosion rate cannot be inbuilt). All of the inbuilt materials and devices have to be carefully selected and strictly documented. The construction works and the final disposal are generally parallel activities, so the tunnels and infrastructures have to be divided and separated into nuclear controlled zone and building zone. To fulfil the legal requirement for the

retrievability of radioactive wastes is one of the greatest challenges for the designers.

Engineered barriers, the required tunnels and chambers, the surface and underground infrastructural background have to be constructed and operated generally in very complex geological, hydrogeological, geotechnical environment. The aggregate construction and operation time of a repository generally exceeds 100–150 years. Due to the final disposal activities, the possibility for the routine maintenance of tunnels and chamber in the controlled zone is quite limited. Beside of geotechnical investigations only the most advanced methodologies static and functional design can guarantee the stability and the operability of the whole system during such a long period. The strong interactions between the engineered and natural elements of the repository system require deep understanding the real long-time behaviour of rock mass not only for earth-scientists but for the designers, too. The complex, coupled THMC processes of the EDZ/EdZ have to be also taken into account at the optimization of the layout and other parameters of disposal chambers (see e.g. Deák et al. 2013). Whereas the mentioned parameters/processes/phenomena can be recognized gradually during the construction, the design and implementation have to be also remained flexible until the end of final operational licensing procedure. That principle is called "DESIGN AS YOU GO-approach" in the international practice. In the case of HLW and SF that principle is particularly important, so the application of a two-stage design and excavation process is compulsory. In the first step an underground research laboratory (URL) is constructed inside the host rock and operated during 15–20 years. Investigations and operation of URL should not affect the isolation capabilities of host rock but the results must be representative also for the repository area. The URL operated in Hungary in 1990s was connected to the former uranium mine, far from the potential zone of final disposal, so it did not affect the long-term radiological safety. The new URL under preparation recently is going to fulfil the mentioned requirement.

There are some other task-specific difficulties during the design of radioactive waste disposal and the repository:

- Demand for detailed constructional and operational risk management;
- Demand for environmentally friendly implementation and operation;
- Demand for the application of complex, up-to-date technologies and logistics;
- Considerable effort is needed to handle the political and social aspects;
- Project-approaches: generally strict quality requirements, time and financial constraints.

165.3 Conclusion

The accomplishment of safe final disposal of radioactive wastes and spent fuels is a non-usual and multidisciplinary task, which is not solvable only by applying the professional routine methods and approaches of the "traditional" engineering projects. It can be only based on the most updated results of earth-sciences and continuous cooperation of scientists, geo-engineers and designers during each stage of the process (the site selection, characterization of host rock, iterative development of safety concept, the design and implementation of repository), which altogether are lasting even one or two centuries until the closure and the end of the institutional control of the facility. The principles listed in this article are entirely taken into account in both Hungarian NPP-origin radwaste projects being in progress recently: NRWR at Bátaapáti (L/ILW) and Boda-project (HLW/SF).

References

Alejano LR, Bedi A, Bond A, Ferrero AM, Harrison JP, Lamas L, Migliazza MR, Olsson R, Perucho Á, Sofianos A, Stille H, Virely D (2013) Rock engineering design and the evolution of Eurocode 7. In: Rock mechanics for resources, energy and environment. Eurock 2013, pp 777–782

Deák F, Kovács L, Vásárhelyi B (2013) Modeling the excavation damage zones in the Bátaapáti radioactive waste repository. In: Rock mechanics for resources, energy and environment. Eurock 2013, pp 603–608

Frank R, Bauduin C, Driscoll R, Kavvadas M, Krebs N, Ovesen N, Orr T, Schuppener B (2004) Designer's guide to EN 1997-1 Eurocode-7: geotechnical design—part 1: general rules

Hudson JA, Feng XT (2007) Updated flowcharts for rock mechanics modelling and rock engineer design. Int J Rock Mech Min Sci 44:174–195

Kovács L (2001) Partial self-healing effects of a highly indurated claystone formation (BCF) discovered by in situ measurements. Self-healing topical session proceedings organised by OECD NEA/RWM/Clay Club. Proceedings, pp 47–57

Kovács L, Mészáros E, Deák F, Somodi G, Máté K, Jakab A, Vásárhelyi B, Geiger J, Dankó G, Korpai F, Mező G, Darvas K, Ván P, Fülöp T, Asszonyi C (2012) Updated version of the geotechnical integrated report of NRWR (available only in Hungarian). Manuscript. PURAM's Archives, RHK-K-032/12

Public Limited Company for Radioactive Waste Management—PURAM (2013) The 13th intermediate and long-term plan for the activities to be financed from the central nuclear financial found. Manuscript. http://www.rhk.hu/docs/publications/PURAM_plan_13.pdf

Rock Mechanical and Geotechnical
Characterization of a Granitic Formation
Hosting the Hungarian National Radioactive
Waste Repository at Bátaapáti

166

László Kovács, Eszter Mészáros, and Gábor Somodi

Abstract

Construction of a radioactive waste disposal should have a wide-range investigation and design program. It is important to suit the design, construction and monitoring tasks of the underground facilities to the rock mechanical-geotechnical character of the host rock in many aspects, such as the long-term environmental and radiological safety, the safety requirements at the workplace and economical reasons. The gained information enables the optimization of the advance and support systems. Getting to know the behaviour of the surrounding rock mass has a great importance in case of a radioactive waste repository, as the geological barrage is one of the main elements of the safety system. So the in situ measurement is not just important for the static safety during the work phase, but it is the element of the long-term safety system, too. It helps to recognize the changes in the environment and interfere if needed.

166.1 Introduction

For final disposal of Hungarian operational and decommissioning LLW and short-lived ILW produced by Paks Nuclear Power Plant a new facility (National Radioactive Waste Repository—NRWR) is under construction at Bátaapáti in a granitic host rock. After a 12-year-long preparation process two inclined shafts were constructed using drill and blast technology to reach the repository depth. Having obtained the required licences and the acceptance of the Parliament and the local community the construction of repository began in September 2008. The structures of underground infrastructural background (water

pumping plants separately for construction and final disposal activities, compressed air and electricity plants, etc.) and the loop tunnel system hosting the disposal chambers had been constructed until 2010. The first two underground disposal chambers were completed in September 2011. The customer of the project is the Public Agency of Radioactive Waste Management (PURAM), the main contractor is MEC-SEKÉRC Co. KŐMÉRŐ (RockStudy) Ltd. was charged with performing and evaluating the geotechnical and rock-mechanical in situ and laboratory measuring program and geotechnical documentation.

166.2 Geotechnical Research Program

Construction of a radioactive waste disposal should have a wide-range investigation and design program. Information gained from geotechnical research is basic data for the design, construction and operational phases of the facility.

L. Kovács (✉) · E. Mészáros · G. Somodi
Kőmérő (RockStudy) Ltd, Pécs, Esztergár L. Str. 19, 7633, Hungary
e-mail: kovacslaszlo@komero.hu

166.2.1 Geotechnical Classification of the Rock Mass

The regular geotechnical rock mass classifications were performed on cores of exploratory drillings and of each tunnel faces. A detailed forecast of the rock mass properties was compiled on the basis of pilot holes. These were the basis to the everyday decisions on the advances and applicable support systems.

166.2.1.1 Core Documentation

Before the tunnel driving pilot holes were drilled and investigated in detail. Because of the large ($\sim$100 m^2) section of the chambers, three holes had to be drilled along the whole chamber. Two of them were in the roof area, as it plays the biggest role in the stability and one in the floor area. The verification of the forecast made from three boreholes was investigated after the construction. It seems that the three boreholes with the mentioned arrangement gave a good prognosis of the whole sections.

166.2.1.2 Tunnel Face Mapping

The geotechnical classification of each faces was performed using the RMR (Bieniawsky 1989), the Q (Barton et al. 1974) and the GSI (Hoek et al. 1995, with modification published by Cai et. al 2004) method. The verifying of the results by each other was essential as this was the first research programme which gave such data of the Mórágy Granite Formation. The parallel use of the three methods helped to derive easier design parameters and remark subjectivities, accidental mistakes also.

The documentation of the tunnel faces was based on onsite observations and 3D optical surface mapping (Gai et. al 2007 and Gai and Pötsch 2008). The orientations of main characteristic discontinuities were defined in the 3D models (Fig. 166.1). This information was applied in surface roughness determination and fracture system modelling also (Krupa et al. 2013).

The digital documentation method allows studying the faces and the tunnel wall not just on site but later for further investigation tasks, too. It has a great importance at Bátaapáti, as the tunnel wall is supported immediately by a shotcrete layer. With the digital documentation the whole chamber can be visualized which can be a basis of a 3D database of geological features.

166.2.2 Laboratory Investigations

The cores of every borehole were systematically sampled for standard rock mechanical laboratory tests, which were performed according to the recommendations of ISRM. By the laboratory tests the main rock mechanical parameters of the intact rock (i.e. uniaxial compressive strength, Young's modulus, Poisson's ratio, tensile and shear strength, Hoek-Brown and Mohr-Coulomb parameters) could be determined which gave the basic information for the static design. Elastic properties were determined during uniaxial compressive tests carried out with deformation measurements using bonded strain gauges. CT-scanning was performed on selected UCS samples to filter out the effect of micro-cracks. Varifying these results we recalculate parameters taking into consideration Martin and Chandler (1994), Eberhardt et al. (1998), Diedrichs and Martin (2010) theories and suggestions.

We used multiple failure test (Kovari et al. 1983) also for precising peak strength and determining residual strength of the granite.

The numerous data enabled geostatistical evaluation which made the geotechnical characterization more specified. According to discriminant analysis the six main rock types of the formation were not recognizable in point of laboratory measurement types. Although histograms and distributions may differ, they can be handled separately in two groups, as monzonite-type and monzogranite-type. Monzonite type group has higher strength and elastic laboratory values. It is squarely statable that there are differences between values of laboratory investigations on the strength of depth and location. Differences seem to follow petrologic zones.

166.2.3 In Situ Measurements and Monitoring System

A comprehensive geotechnical monitoring system was applied in the first two chambers (Fig. 166.2). In addition to the numerous optical convergence and load indicator sections, 4 radial MPBX-extensometers (section Ext-10 in Fig. 166.2) were installed to measure the radial displacement of the surrounding rock mass caused by the tunnel driving and in the long-term monitoring, 8 load cells (LC-01-04 and LC-05-08 in Fig. 166.2.) for controlling rock bolts, 6 two-directional gauges (LB-01-06 in Fig. 166.2.) for measuring the deformation of shotcrete have been installed and continuously measured. 6 CSIRO HI-cells (Bkc-7-12 in Fig. 166.2.) were installed for determining 3D distribution and magnitudes of stress changes around the chambers during tunnelling.

The measurements provided important data not just for the short- and long-term stability of the chambers, but for the optimization of the further chambers, too.
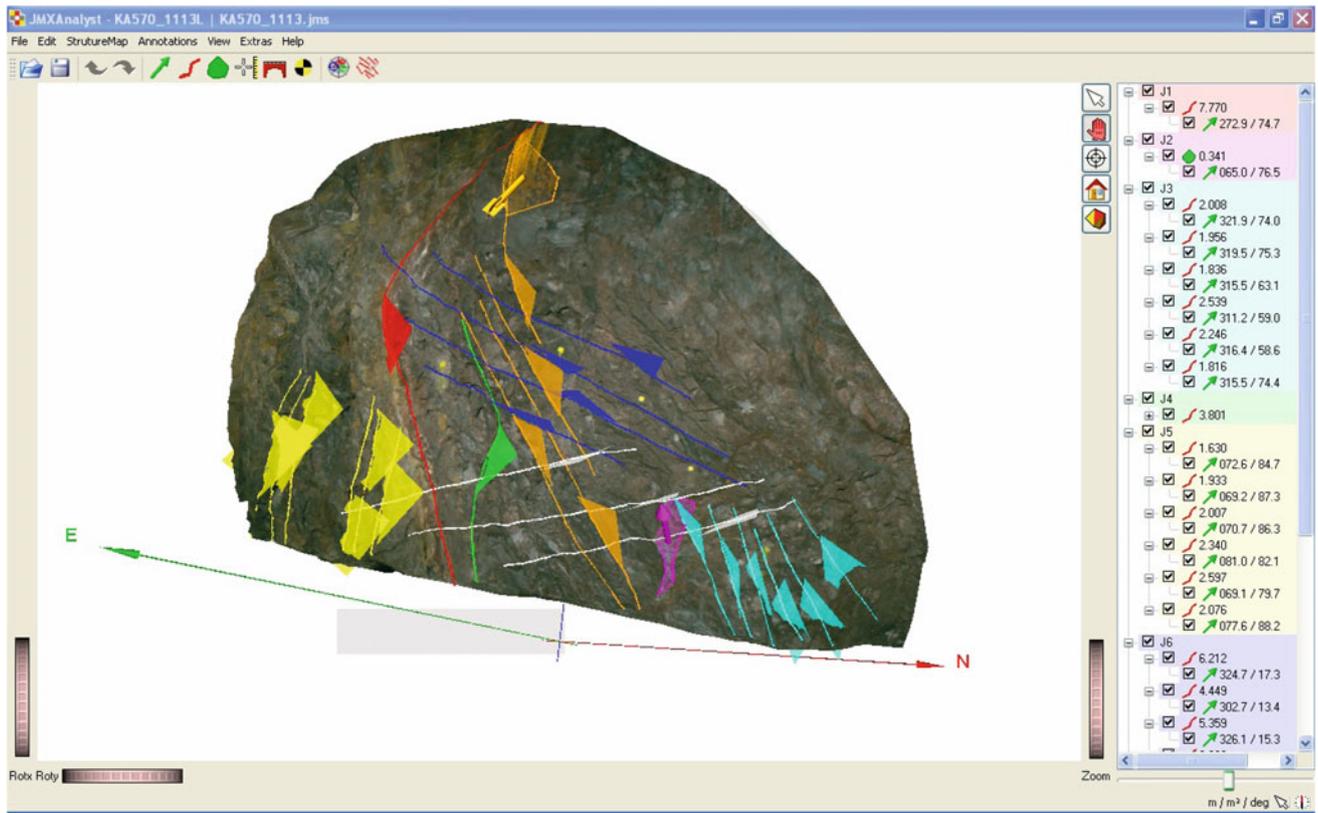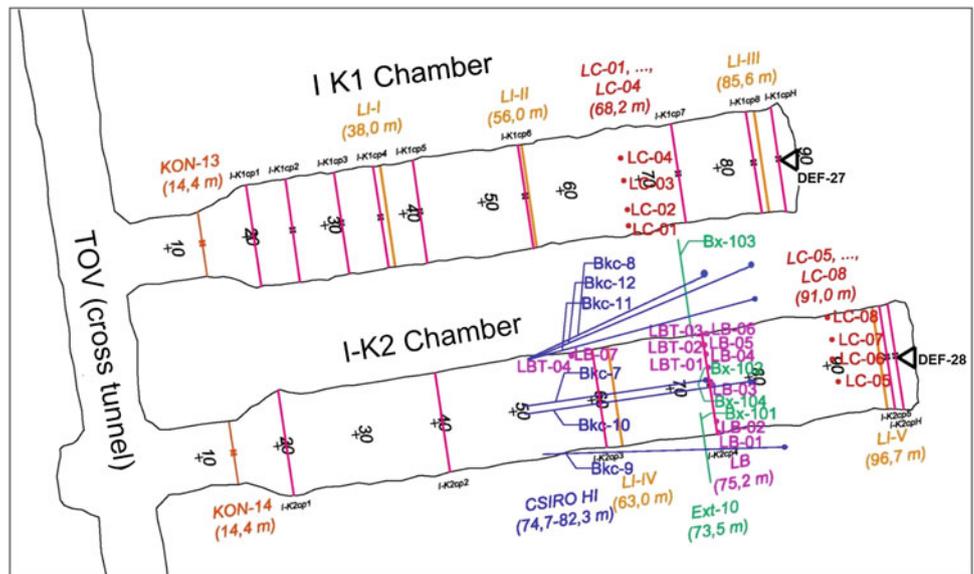
Fig. 166.1 3D documentation of a tunnel face with the structure map

Fig. 166.2 The in situ measurement and monitoring system in the first two chambers at Bátaapáti NRWR

166.3 Conclusions

The results have provided important data for verification of the design and for revealing the behaviour of the surrounding rock mass in short and long term monitoring period. Beside the geotechnical data gathering the investigation programme also helps the long-term safety assessment.

References

Bieniawski ZT (1989) Engineering rock mass classifications. John Wiley and Sons, Pennsylvania

Barton N, Lien R, Lunde J (1974) Engineering classification of rock masses for the design of the tunnel support. Int J Rock Mech Min Sci 6(4):189–236

Cai M, Kaiser PK, Uno H, Tasaka Y, Minami M (2004) Estimation of rock mass deformation modulus and strength of jointed hard rock masses using GSI system. Int J Rock Mech Min Sci 41:3–19

Diederich MS, Martin CD (2010) Measurement of spalling parameters from laboratory testing. In: Rock mechanics in civil and environmental Engineering. Zhao, Labiouse, Drudt, Mathier (eds). EUROCK2010, ISRM, Taylor & Francis Group, London, pp 323–326

Eberhardt E, Stead D, Stimpson B, Read RS (1998) Identifying crack initiation and propagation thresholds in brittle rock. NRC Can Can Geotech J 35:222–223

Gaich M, Pötsch W, Schubert (2007) High resolution 3D imaging for site characterisation of a nuclear waste repository, 1st Canada—U. S. rock mechanics symposium 2007, Vancouver, Canada, pp 69–75

Gaich A, Pötsch M (2008) Computer vision for rock mass characterization in underground excavations. ARMA, 2nd U.S.—Canada rock mechanics aymposium, San Francisco, p 14

Hoek E, Kaiser PK, Bawden WF (1995) Support of underground excavations in hard rock. In: Balkema AA, Rotterdam, Reprinted in 2005, p 215

Kovari K, Tisa A, Einstein HH, Franklin JA (1983) Suggested methods for determining the strength of rock materials in triaxial compression: revised version. Int J Rock Mech Min Sci Geomech Abstr 20 (6):283–290

Krupa Á, Deák F, Görög P, Buocz I, Török Á (2013) Quantitative roughness profiling of fracture surfaces of a granitic host rock at a radioactive waste disposal site. In.: Marek Kwasniewski, Dariusz Lydzba (ed) Rock mechanics for resources, energy and environment. ISBN 9781138000803

Martin CD, Chandler NA (1994) The progressive fracture of Lac du Bonnet Granite. Int J Rock Mech Min Sci Geomech Abstr 31 (6):643–659

Subsurface Water in Tunnels: Prediction, Estimation, Management

Convener Mr. Yogendra Deva—*Co-conveners* Dr. Y.P. Sharda, S.N.C. Lavlin and Prof. S.K. Singh, Delhi University, A. Bishwapriya, Patna University and Shazia Tabassum, Delhi University

Introduction: Subsurface water remains the most significant factor in tunneling problems. In association with crushed rock, it often leads to flowing ground conditions—a nightmare for tunneling personnel. Numerous tunneling projects the world over have suffered time and cost escalations due to subsurface water in large quantities or extreme flowing ground conditions. The subject still remains enigmatic and calls for state-of-the-art investigation and construction methodologies for demarcating and managing such problematic zones. Session Concept: The session will have papers and invited lectures on research, and case studies on investigations and handling of subsurface water/ flowing ground conditions in tunnels. Objective: The paper contents and discussions during the session would be compiled and summarized to outline state-of-the-art approach for the prediction, estimation and management of subsurface water/ flowing ground conditions.

Ground Water Management for Large Under-Ground Storage Caverns

167

Saikat Pal, G. Kannan, Vijay Shahri, and A. Nanda

Abstract

Underground unlined (or mined) rock caverns is one of the economical alternative for buffer storage of crude oil to ensure energy security of import dependent countries. The principle of such storage employs hydrodynamic containment of the product. As the large rock caverns are excavated by conventional drill and blast method, the groundwater management is of utmost importance to conserve ground water and avoid inadvertent de-saturation of rock mass. This is added to the constraints due to inflow of water during excavation of rock mass like other underground projects. Consequently, hydrogeology forms an important aspect during planning, investigation and subsequent construction stages. The present paper focuses on groundwater management during construction for an ongoing storage cavern in India. In the process it highlights early identification of permeable structural features, the adopted grouting philosophy, the water curtain system and the required hydro-monitoring.

167.1 Introduction

The principle of storage of crude oil in large unlined mined rock cavern ensures tightness of product by directing ground water gradients towards the storage caverns (Amantini et al. 2005). This is known as hydrodynamic containment. The unlined storage caverns are constructed below natural ground water table. The ground water level during construction and operation stage of the cavern is maintained by uninterrupted artificial charging of water curtains so as to rejuvenate the ground water regime (Usmani et al. 2010).

S. Pal (✉) · G. Kannan · V. Shahri · A. Nanda
Engineers India Limited (EIL), New Delhi, India
e-mail: saikatindia@yahoo.co.in

G. Kannan
e-mail: gopi.kannan@eil.co.in

V. Shahri
e-mail: vijayshahri@gmail.com

A. Nanda
e-mail: ananda@eil.co.in

The water curtains comprise of water curtain galleries (WCG) and horizontal and vertical water curtain boreholes (WCBH) drilled from these galleries. These WCBH are charged with water and encases the storage caverns. The project under discussion comprises of four large caverns (900 mL × 20 mW × 30 mH), three (6.5 × 6.5 m) water curtain galleries, two circular shafts (8.2 m diameter) for pumping of crude and seepage water and access tunnel (12 × 8 m) for facilitating construction.

167.2 Hydro-Geological Model

During excavation, a minimum hydraulic head equivalent to 20 m of water above the horizontal water curtain level to be maintained in order to ensure hydraulic gradient >1 (Aberg 1977). This is to prevent de-saturation of rock mass surrounding the cavern. Thus impediment of uncontrolled inflow of groundwater in tunnels as well as conservation of groundwater is necessitated. A hydro-geological model of the project is prepared based on the project geological model

and various explorations during investigation and pre-construction stage (Usmani et al. 2010).

The rock type in the project area is granitic gneiss belonging to the Peninsular Gneissic complex of India. The project is seated in a hilly terrain with thick laterites and lateritic soil at the top followed by weathered and fresh granitic gneiss. The permeability of the soil and lateritic portion is high of the order of 10^{-5}–10^{-6} m/sec where as the permeability of the massive gneissic rock is very low of the order of 10^{-9} m/sec. However, 3–4 sets of prominent discontinuities were observed including a sub-horizontal joint which shows permeability in the range from 10^{-8} to 10^{-6} m/sec (some horizontal joints show very high permeability of the order of 10^{-4} m/sec locally). Sub-vertical and sub-horizontal dolerite dykes are also encountered with the permeability of the order of 10^{-6}–10^{-7} m/sec. The hydrogeological model also includes of groundwater level contouring and residual seepage evaluation apart from the permeability distribution.

During excavation, the hydro-geological model was constantly updated by: • Structural projections of permeable features • Updating probing and grouting detail • updating the seepage points and permeability values of all WCBH and manometer holes drilled from underground; and • Correlating all above data.

167.3   Probing and Grouting

Locating water ingress features ahead of cavern excavation face helps to plan judicious treatment. Thus continuous systematic probing was envisaged during design and planning stage with provision of probing kept for each alternate faces. Systematic probing with original frequency was performed during excavation of WCG, access tunnel and top heading of caverns. Probe holes, 10–12 m long destructive drill holes, were drilled ahead of excavation faces, 2–3 in numbers depending on the surface area of excavated face. For all seeping probe holes, depth, rate and pressure of water inflow were recorded to take decision on grouting, magnitude of grouting and parameters of grouting. The hydrogeological model was updated by significant features identified during excavation of small tunnels and were confirmed during top heading excavation.

The WCG (20 m above caverns) and access tunnel will be cut off from the caverns and will be completely flooded with water during operation. So, there were no design seepage limits for this tunnel and grouting was taken up only if the ingress affects the construction works or if the ground water level is affected. Incase of caverns 2 other criteria also influenced grouting. They were intake quantity of interfering WCBH and designed residual seepage. Based on these, the trigger value for pre-grouting was decided as 3 L/min/m/bar.

If the seepage from probe holes was more, fan pre-grouting was performed on the face ahead.

Pre-grouting was preferred and carried out from top heading by modifying the grout fan as suited to disposition of feature. In case of persistent features overlapping grout fans were constructed from alternate faces.

Once the disposition of major hydrogeological features were finalized on the basis of excavation data, the probing were optimized for subsequent bench levels and grouting were concentrated in the zones where the features are anticipated to be negotiated in the respective elevations (Fig. 167.1). Accordingly, pre-grouting plan of all benches was made. Side wall pre-grouting form higher bench were carried out in the identified zone with sub vertical grout holes directed to intersect the feature and constitute grout curtain to cutoff wall seepage. Invert pre-grouting from last bench was carried out with target to cutoff seepage up to depth of 5 m from invert.

This reduced the time and efforts at each level and helped to expedite excavation. No major grouting was required apart from predicted areas. However, provisions were kept for probing and grouting with respect to sub horizontal features revealed at each level.

Post grouting was necessary for one or more of the following reasons: •Pre-grouting insufficient to maintain ground water level, •Residual seepage more than design seepage limit (30 L/min/100 m section), •Increase in water intake of WCBH, and • Hindrance to rock support.

167.4   Water Curtain System

The final patterns of WCBH were directed with aim to cater water to the identified high permeable features:

- The horizontal holes were directed to 70° w.r.t tunnel axis considering the orientation of prominent joints.
- Peripheral vertical curtains (Fig. 167.2) were introduced to counteract the drawdown along low dipping highly permeable features (permeability 10^{-5} m/sec) and to isolate from upcoming facilities in adjacent area.
- 40 m ahead of cavern excavation, horizontal and vertical WCBH were pressurized with water at 3–4 bars. The sequence of cavern excavations was thus guided by availability of water charged boreholes.

In order to check the efficiency of designed water curtain, hydro-tests were carried out to ensure their ability to maintain the desired hydrostatic potential. As per original design, the efficiency of entire horizontal curtain was to be tested in a single test after heading excavation of entire cavern system. However, the test was distributed in different sections. The sections were selected for testing as per excavation schedule so that, excavation works can be continued parallel in other part of caverns. Additional holes were
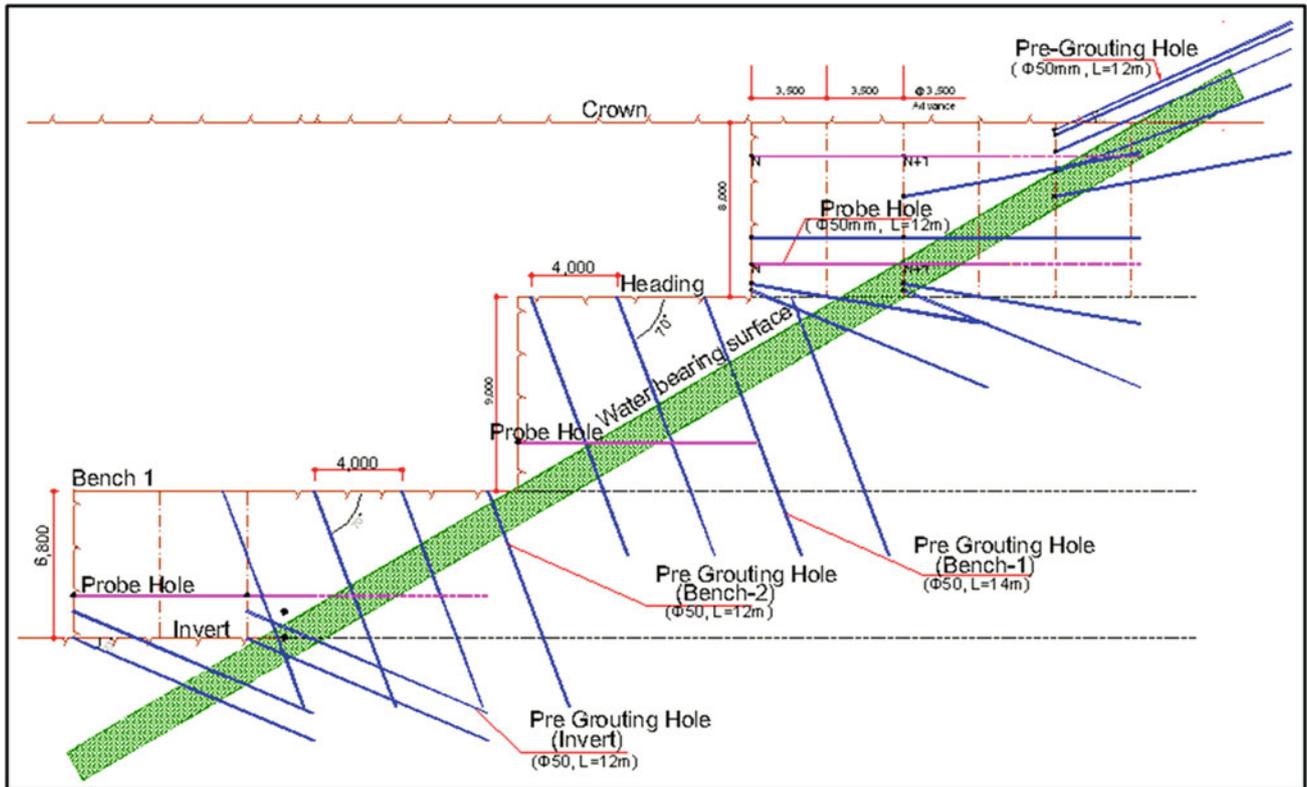
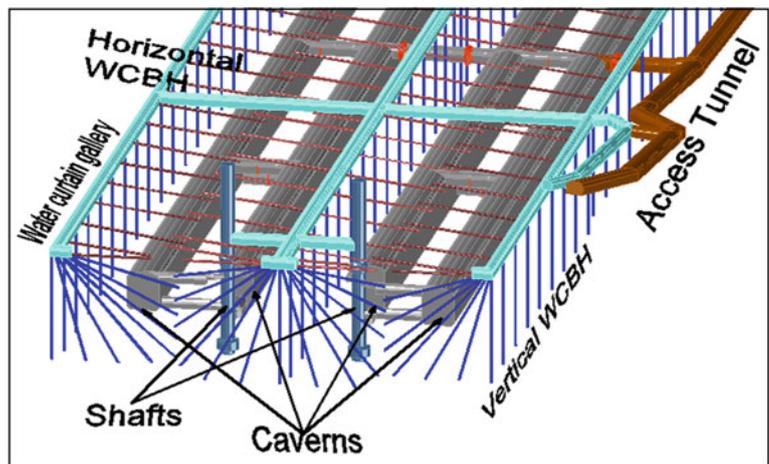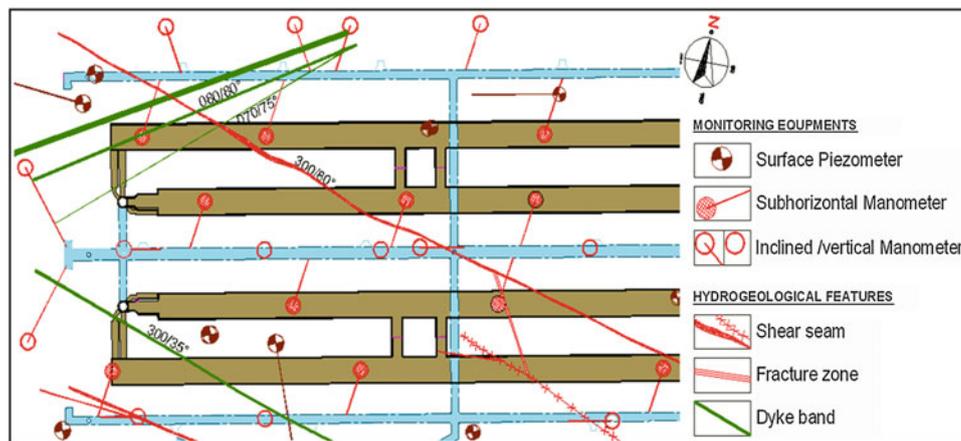**Fig. 167.1** Scheme for grouting

Fig. 167.2 WCBH distribution

Fig. 167.3 Hydro-geological monitoring plan of manometers and piezometers

recommended and drilled wherever the hole spacing of 20 m was insufficient to maintain the desired potential.

Management of WCBH during grouting was an important aspect. The water pressure of the boreholes in the affected area was lowered to facilitate rock bolting and grouting. However constant flow at optimum pressure was required and pressure was monitored during gout injection so that the holes do not get clogged with grout mix.

167.5 Monitoring and Seepage Measurement

Hydro-monitoring and seepage measurements help to understand the groundwater balance of seepage versus recharge (natural and artificial). The monitoring/measurements are essential to judge requirement of grouting as well as effectiveness of grouting. It is also mandatory to evaluate residual seepage and compare it with the designed seepage levels to confirm the adequacy of design for seepage pump in shaft.

The daily hydro-geological monitoring comprised mainly • Ground water level monitoring through surface piezometric wells • Hydraulic potential measurement from underground WCG by manometer and pressure cells. These were installed adapted to monitor identified major water bearing features (Fig. 167.3). • Pressure and water intake measurement of all WCBH.

All the measurements were integrated to ensure overall well being of the hydrogeological conditions.

In the project, seepage measurements were carried out through following methods:-

• **Indirect seepage measurement**—the daily difference of outgoing and incoming water assessed by using flow meters. • **Measurements from individual seepage points**—the total seepage from individual seepage points on crown and walls were mapped and measured monthly to have an idea about change in locality as well as quantity of seepage. • **Direct**

seepage measurement—the total seepage measurement in isolated sections. Isolation was done by constructing concrete/clay weirs across the gallery.

The residual seepage measured in the storage caverns was between 20 and 25 L/min/100 m (Usmani et al. 2012). Almost equal amount of water was being recharged through WCBH to maintain the natural ground water level. The ground water level was in between 30 and 80 m above horizontal water curtain level.

167.6 Conclusion

The dynamic approach of continuously updating hydrogeological model was of immense help in correct and timely anticipation of hydro-geological features. This aided to readiness of addressing situations. The stipulated hydrogeological guidelines were adapted to construction friendly procedures. This also helped in expediting the work pace by optimization of activities like *probing*. The ground water management of the project was completed successfully by judicious combination of *grouting and groundwater recharging*. The basic criterion of saturation of rock mass was maintained and at the same time the overall seepage was controlled within the designed capacity.

References

Amantini E, Francois C, Anne M (2005) Groundwater management during the construction of underground hydrocarbon storage in rock caverns. In: 9th international mine water congress (IMWA 2005)
Usmani A, Nanda A, Kannan G, Jain SK (2010) Hydraulic confinement of hydrocarbons in unlined rock caverns. ISRM, Delhi

Usmani A, Kannan G, Nanda A, Jain SK (2012) Seepage assessment in tunnels under different field conditions. In: Proceedings of Indian geotechnical conference, Dec 13–15, 2012, New Delhi

Usmani A, Nanda A, Kannan G, Jain SK Analysis of groundwater flow in underground storage caverns. In: 6th ICEG (international conference on environmental geotechnology), Nov 2010, New Delhi

Aberg B (1977) Prevention of gas leakage from unlined reservoirs in rock. In: Proceedings rock store, pp 399–413

Experience from Investigation of Tectonically Extremely Deteriorated Rock Mass for the Highway Tunnel Višňové, Slovakia

168

Rudolf Ondrášik, Antonín Matejček, and Tatiana Durmeková

Abstract

The designed highway tunnel Višňové will cross the mountain ridge Lúčanská Fatra in Slovakia in its length of 7.48 km. The selection of the tunnel alignment was preceded by a preliminary geological investigation, which indicated a complex geological structure. Consequently, a pilot tunnel was included into the planned geologic investigation. Two tunnelling methods were tested. Complicated geologic structure, intensive faulting and fracturing of rocks and intricate hydrogeological condition were proved by the pilot tunnel. Excavation of the pilot tunnel was variable, all rock mass behaviour types occurred. Enormous problems were linked with negotiation of sudden concentrated inflows of groundwater from fault zones reaching up to 160 l/s, followed by groundwater erosion.

168.1 Introduction

The proposed highway tunnel Višňové will be an integral part of a passage of the Slovakian D1 Highway between Žilina and Ružomberok (Fig. 168.1). The tunnel will cross the Lúčanská Fatra Mountains. The Lúčanská Fatra horst is in tectonic contact with the Žilinská kotlina basin from the west and the Turčianska kotlina basin from the east (Fig. 168.2).

A tunnel line was selected from several variants on the basis of a preliminary investigation and environmental impact assessment (EIA). Geological investigation took place in 1995–1998 and consisted of geological mapping, geophysical investigation and several boreholes to a depth 120 m. The pilot tunnel in the designed investigation was excavated using the Tunnelling Boring Machine (TBM) from the east side (4,293 m) and the New Austrian Tunnelling Method (NATM) predominantly from the west side (3,187 m). The highway tunnel realization was supposed to start in 2003. Due to various reasons this was postponed to 2014.

168.2 Preliminary Geological Investigation

The most important data resulting from the preliminary investigation are:

(a) two exploratory boreholes to a depth 120 m;
(b) engineering geological map of the designed tunnel on a scale of 1:5,000;
(c) regional geological study with a geological heterogeneity map (Fig. 168.2);
(d) several geophysical profiles and a longitudinal geological profile of the designed tunnel (Fig. 168.3).

R. Ondrášik (✉) · T. Durmeková
Faculty of Natural Sciences, Department of Engineering Geology, Comenius University, Mlynská dolina, Bratislava 842 15, Slovakia
e-mail: ondrasik@fns.uniba.sk

T. Durmeková
e-mail: durmekova@fns.uniba.sk

A. Matejček
Geofos, Ltd, Veľký Diel 3323, Žilina 010 08, Slovakia
e-mail: antonin.matejcek@geofos.sk

Fig. 168.1 The highway D1 with the designed tunnel Višňové location

The geological heterogeneity map helped to understand the geological condition of the area. Its compilation was based on regional geology evolution analysis, data from investigation of other projects in the area, proper field research and analysis of aerial photos. Overthrusting in the Upper Mesozoic and differential tectonic movements during Upper Tertiary evolution influenced the designed tunnel's geological condition. Downward movement along listric faults resulted in rock stress release in the upper parts of a massif and was reflected in joint widening and ground water saturation (Fig. 168.4).

168.3 Geological Investigation by a Pilot Tunnel

A pilot tunnel was driven along the south tunnel line from November 1998 to August 2002 (Matejček et al. 2002, Matejček and Bohyník 2006). In addition to the geological investigation, it will drain groundwater ahead of tunnel construction starts and it will serve as the temporary emergency corridor for the northern tunnel line which will be constructed and used for traffic as the first.

168.3.1 Western Pilot Tunnel Section Driven Using NATM

The west gallery section was driven into Paleogene flysch and Mesozoic strata, and a short passage in altered granitic rock (mylonites) tectonically intensively deformed. Tectonic contact between Paleogene and Mesozoic rock consists of breccia in a zone up to 20 m thick, steeply declined to the Žilinská kotlina basin. Mesozoic limestone—dolomite complex contains marl, shale, schistose and tectonically crushed carbonates. This lithological heterogeneity is reflected in complicated hydrogeology. Permeable disrupted

Fig. 168.2 Scheme of tectonic inhomogeneity (modified after Ondrášik et al. 2000). *1* Crystalline granitic rock, *2* Crystalline granitic rock with open joints and saturated, *3* Mesozoic rock (carbonates predominate) locally disrupted and karstified, *4* lower Tertiary flysch strata, *5* upper Tertiary shale and conglomerates, *6* faults, *7* direction of down movements and stress release
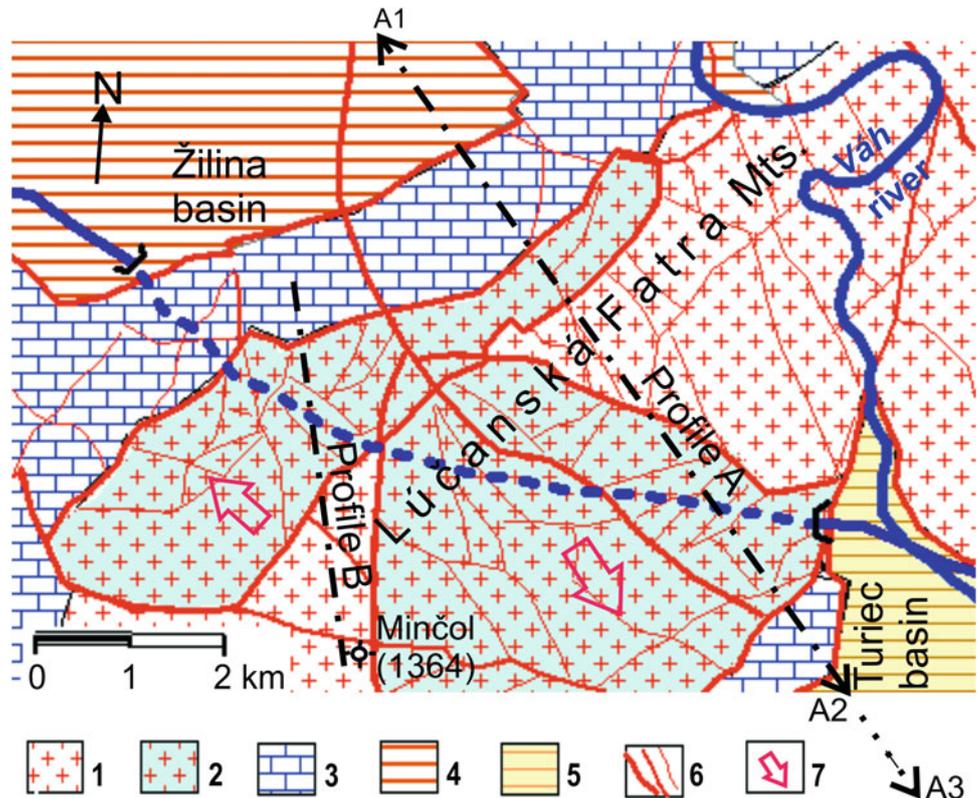
Fig. 168.3 A three dimensional geological profile on the axis of the pilot tunnel Višňové
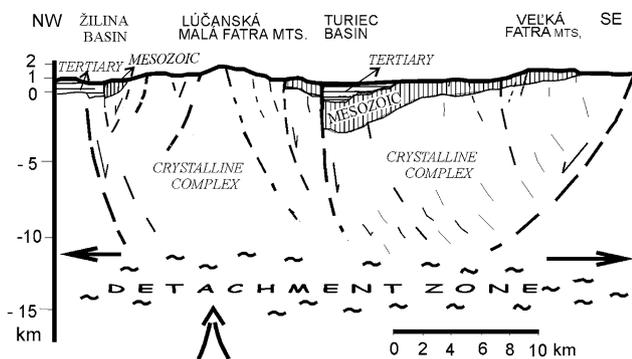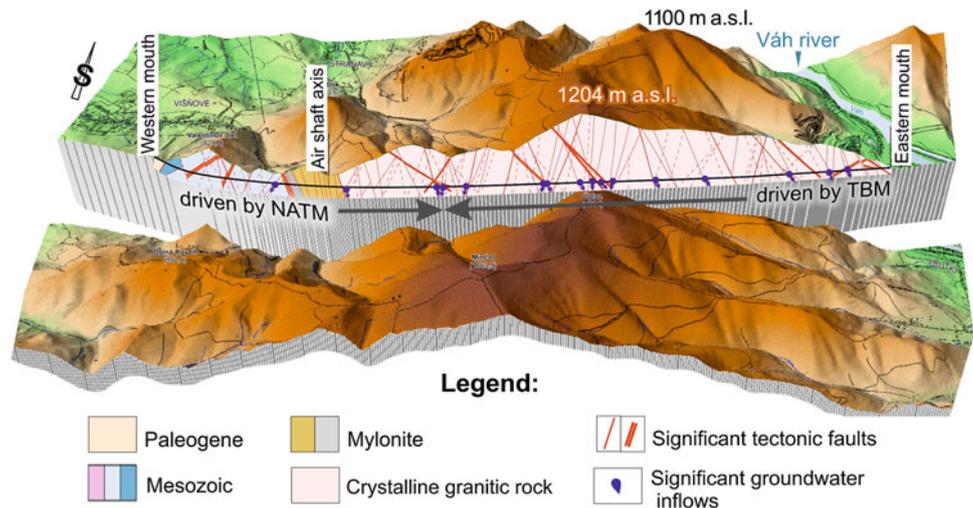

Fig. 168.4 A kinematic model of the Lúčanská Fatra horst and the Turčianska kotlina basin—*left* part of the section is delineated on the map in the Fig. 168.2 as the profile A, *right* part is out of the map (Ondrášik et al. 2000)

and karstified carbonates alternate with impermeable shales, marls and faults filled with clay. Shales and marls are swelling in contact with water.

A tectonic fault with crushed rock up to 70 m thick occurs at the contact between Mesozoic suit and granitic rock. Marginal part of granitic rock mass in a zone 300 m thick consists of crushed mylonites.

The most problematic activity was downward driving up to a distance of 1,300 m from the pilot tunnel's mouth. Concentrated groundwater inflow exceeding a standard limit 30 l/s. Outflows died out some 80–100 m from the gallery face. The total groundwater inflow reached more than 140 l/s. Water from the west section of the pilot tunnel concentrated at the face and was pumped out until perforation to the east section, which declined towards the east mouth. Groundwater inflow from the gallery face was reduced by 35 m long drainage wells declined at 17 % with perforated steel tubing of 156 mm in diameter. Groundwater runoff into tubes was initially gravitational under high pressure, later by pumping by seed drill into

sump. There were 7 sumps altogether. Dewatering of the rock mass was successful by pumping about 60 l/s from drainage wells and numerous outflows. Polluted water near the pilot face was separated and pumped at about 30 l/s into sump tanks. Average advance of the tunnelling was 75 m per month.

### 168.3.2 Eastern Pilot Tunnel Section Driven Using TBM

The eastern pilot tunnel section was driven into granitic rock, predominantly tonalite, using TBM. The first part up to 70 m was driven by NATM. Weathered rock was up to 300 m. Fault zones of three main systems predominated in the rock mass. Average total groundwater inflow reached up to 10 l/s. Monthly digging advance reached up to 200 m.

Water bearing fault zone up to 12 m wide of oblique position to the pilot tunnel occurred at a distance of 442 m from the mouth. Concentrated groundwater inflow reached up to 80 l/s. Suffosion and caving-in took place. Concrete floor was executed in front of the cutting head. Negotiating this fault in the length of 50 m took 96 days.

Various fault zones were cut onwards up to the distance 2,810 m from the mouth and 180 m/month was driven, which doubled the advance in comparison to NATM. Groundwater inflow gradually increased up to 120 l/s at the pilot tunnel face. Total outflow from the eastern passage of the pilot tunnel reached up to over 420 l/s. The gallery floor deformed under TBM in fault zones and stabilization measures took place in front of the cutting head, often under water shower from the roof of the gallery, and caused mining retardation.

Wide groundwater bearing fault zone oblique to the gallery was intersected at the distance of 2,892 m from the adit. Ground water inflow up to 100 to 120 l/s under pressure 3.1 MPa occurred after cutting its marginal part. Due to caving-in a large cavity of 8 m long, 3 m wide and 9–12 m high size was forming.

Fig. 168.5 Geological profile
across the tunnel—profile B in the
Fig. 168.2 (Ondrášik et al. 2009)
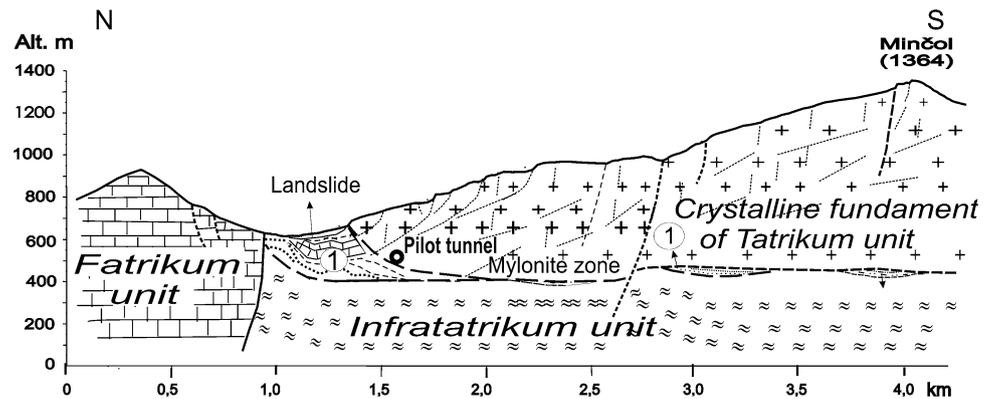
A concrete barrier was built in front of the collapsed earth and a set of drainage wells were drilled to enable stabilization of the cavern roof by ascending cement injection trough 14 m long tubes placed in horizontal boreholes. Cement was washed out in critical passages with concentrated water streams. These critical parts were tightened by polyuretan resin before cementing. Polyuretan resin mixed with cement proved to be strong enough to stabilize the unstable rock roof of the gallery.

Pilot tunnel drainage affected a reduction in the discharge of creeks on the surface and some of them even dried out in the surface zone of about 7 km width. It is supposed that rock mass dewatering will minimize tunnelling risks. As well there will be time enough to decide if water from the tunnel is used for water supply or measures will be taken to protect tunnel walls against ground water inflow under pressure, and reverse the hydrogeological regime near to the initial state.

Tectonically crushed rock represented about 40 % of excavated rock in the gallery, which was four times more than it was supposed. Geologically conditioned overbreaks exceeded 300 m^3, and this means about 0.3 % of total excavated rock. Rock mass was drained before the highway tunnel is constructed. Groundwater chemical analyses indicated only low hydrocarbonate aggression in some zones. Sulphur aggression was proved in a passage from 300 to 800 m of the west pilot tunnel mouth.

Mylonites found in the gallery stimulated to supplementary research concerning a thrusting of Paleozoic granitic rock mass (Tatricum) over older basement (Infratatricum) (Ondrášik et al. 2009). It is supposed that mylonites were generated on the zone of overthrusting during Mesozoic cycle of Alpine orogenesis at the depth of 10–15 km. Geologic profile across the tunnel was constructed (Fig. 168.5) to illustrate enormous disruption of overthrusted granitic rock.

168.4 Conclusion

Rock mass in the pilot tunnel was found tectonically intensively fractured in a range 40 %. Except of first category, all categories of tunnelling rock classification were found.

Groundwater inflow was extremely high, particularly along the fault zones. Maximum total water outflow from the granitic rock part of the gallery reached more than 420 l/s when the face was 4,600 m from the adit and decreased to 200 l/s after several months. Concentrated inflows reached up to 120 l/s under pressure 3.1 MPa and created suffosion with incavitation up to some tenth m^3, 0.3 % in total of excavated rock. Maximum groundwater inflow occurred at a gallery face and gradually reduced to zero at a distance 50–100 m. Decrease of water discharge occurred in creeks on the surface. Groundwater inflows were also from the west gallery section; however these were supposed to happen. Negotiating of wide fault zones filled with clay required particular non-traditional excavation techniques for each fault zone.

The pilot tunnel construction brought invaluable knowledge and experience to be used in the construction of the highway tunnel.

References

Matejček A, Bohyník J, Hyčko M (2002) Diaľnica D1 Višňové—Martin, tunel Višňové. Final report (in Slovak). Geotest, Geofos and Geohyco companies. Geofond Bratislava

Matejček A, Bohyník J (2006) The importance of the exploration gallery driven for the Višňové tunnel. Tunel 15, 4, GRAFTOP Prague, pp 12–17

Ondrášik R, Matejček A, Holeša Š, Vrábľová K (2000) Gravitational tectonics along the tunnel Višňové in the Lúčanská Fatra Mts. Slovakia Mineralia Slovaca 32:429–438

Ondrášik R, Putiš M, Gajdoš V, Sulák M, Durmeková T (2009) Blastomylonitic-cataclastic zones and their influence on slope deformations in the Lúčanská Fatra Mountains. Mineralia Slovaca 41:395–406

Verification and Validation of Hydraulic Packer Test Results in a Deep Lying Tunnel Project

169

Ulrich Burger, Paolo Perello, Sacha Reinhardt, and Riccardo Torri

Abstract

For the deep lying, trans boundary Brenner Base Tunnel several packer tests have been carried out in deep boreholes for a hydrogeological characterisation of metamorphic rocks. For permeability testing (expected range from $K = 10^{-7}$ to 10^{-12} m/s) Pulse-, Slug-, Drill stem and active flow tests were applied. Due to the importance of the hydraulic parameters for the technical design of the tunnel system and the environmental risk assessment, the testing results were methodologically verified. The verification method and the final result of the evaluation are shown. Calibrate numerical models of built tunnel sections are used to validate the hydraulic testing results, first experiences and results in a granite tunnel section are shown.

169.1 Overview BBT Project

The trans-boundary Brenner Base Tunnel is a 55.6 km long railway base tunnel project with a max. overburden of 1.850 m. As part of the Transeuropean network axes 1 (TEN1 Helsinki-Valetta) the base tunnel will connect Austria (Innsbruck) with Italy (Franzensfeste/Fortezza). The procedure project has been worked out from 2004 until 2008, since 2008 the tunnel is under construction. Until 2013 approximately 28 km of tunnels (3 access tunnels, exploration tunnels and first main tunnel-sections) have been built. It is planned that the excavations of the tunnel system (total length: 200 km due to the 3-tube tunnel system: 1 exploration tunnel, 2 tubes for the main tunnels) will be finished in 2021.

169.2 Hydraulic Testing

169.2.1 General Procedure

The hydraulic tests were carried out after finalizing the deep core borings (200–1.320 m). On the basis of the core logging and results of the borehole geophysics the borehole sections to be tested and the corresponding depth and length of the packed-off test intervals were defined. The hydraulic tests were carried out from borehole bottom upwards and covered usually the whole borehole. The test interval length of the double packer tests ranged from 5 to 35 m, the single packer tests were made usually in the deepest testing interval or as long testing section (even >100 m).

U. Burger (✉)
Galleria di Base del Brennero—Brenner Basistunnel BBT SE,
Amraser Straße 8, 6020, Innsbruck, Austria
e-mail: ulrich.burger@bbt-se.com

P. Perello
GDP Consultants (I-Torino), Saint-christophe, Italy
e-mail: perello@gdpconsultants.eu

S. Reinhardt
Solexperts (CH-Mönchaltorf), Mönchaltorf, Switzerland
e-mail: sacha.reinhardt@solexperts.com

R. Torri
SEA consulting srl (I-Torino), Turin, Italy
e-mail: torri@seaconsult.eu

169.2.2 Methodology of Testing

Hydraulic tests were carried out using a straddle packer system, which consisted of an upper and lower inflatable packer in order to confine a test interval section in the borehole. The test section between the packers comprises a perforated rod allowing formation water to enter the riser pipe or, conversely, allowing injecting water through the test rods into the formation. Three pressure transducers were measuring the pressures below, within (interval pressure) and above the test interval (annulus pressure). The test system was installed to the specific depth by means of a test tubing (pipe). A downhole shut-in valve, mounted between the system and the test tubing, enabled to close and open the connection between the test interval and the test tubing instantaneously. All parameters including pressure (pressures down-hole, atmospheric pressure), temperature in the borehole, flow rate and other parameters were recorded by means of an automated data acquisition system and displayed real-time on the PC-screen of the test engineer.

The reliability of estimated formation parameters is increased by carrying out several test procedures (methods) for the same test interval (Quinn 2012). After packer positioning and inflation, a test series starts with an initial pressure recovery phase with closed downhole shut in valve, which allows the test zone pressure to recover toward the static formation pressure.

The following test sequences depend on the estimated transmissivity and the pressure potential of the specific test zone. With a pulse test or a slug test a first transmissivity estimate of the test zone can be provided. A pulse test is conducted by exposing the test interval to a short under or overpressure and monitoring the pressure response as it recovers toward the formation pressure. The over- or under pressure is produced by emptying or filling the test tubing with closed downhole shut-in valve. The pulse is transmitted to the test zone by opening and closing the downhole shut-in valve for around 3–10 s. The penetration depth into the formation of a pulse test is considerably small (in the range of dm–m). Pulse tests are also used to determine the compressibility of the test zone. The implementation of a slug test is similar to a pulse test, but the imposed pressure pulse in a slug test recovers towards formation pressure with open downhole shut-in valve. During the open shut-in valve-period, the water level in the test tubing corresponds to the current pressure in the test interval and active in- or outflow from the formation to the test tubing (or vice versa) takes place. This phase is also referred to as slug flow phase.

In tight formations, the slug flow phase is normally interrupted by closing the downhole shut-in valve. The following accelerated pressure recovery with closed shut-in valve may also be analysed, if the pressure recovery during the previous slug flow phase is small in relation to the initial pressure pulse. The Drill stem test derives from the petroleum industry and consists roughly of two consecutive slug withdrawal tests, which are interrupted after a certain time by closing the downhole shut-in valve.

The recovery behaviour of pulse and slug tests are influenced by skin effects (diminished or enhanced permeability in the vicinity of the borehole). Therefore, a test sequence should contain an active flow test as a constant head injection test or a constant rate test, if feasible. Flow tests are less sensitive to skin effects. Constant head and constant rate tests are performed by extracting or injecting water for a certain time span (usually 20–30 min) and by maintaining constant either (i) the injected/extracted flow rate, with a consequent variations of the head, or (ii) the head with a consequent variation of the injected/extracted flow rate. These tests provide a larger scale permeability value (larger penetration depth into the formation), depending on the transmissivity and the storage coefficient of the formation. In low permeable formations, the radius of investigation ranges to a few meters and is still relatively small. Constant rate and recovery phases after shut-in (downhole valve closed) allow the use of transient pressure analysis methods (Bourdet et al. 1989) based on the analysis of the derivative of pressure versus the appropriate time function (natural logarithmic or Agarwal/Horner superposition time) in a diagnostic plot. The method facilitates the diagnostic of the different flow phases of a test which supports the correct use of the straight-line analysis method and provides information of flow behaviour in the formation.

Test analysis was conducted using type curve, straight-line analysis methods together with diagnostic log-log pressure plots. The Cooper-Bredehoeft-Papadopulos type-curves were used to analyse both slug and pulse tests (Cooper et al. 1967; Bredehoeft and Papadopulos 1980). Constant head injection tests were analysed according to Jacob and Lohman (1952) and Doe and Geier (1990), recovery tests after Agarwal (1980) and Horner (1951).

169.2.3 Overview Output of Testing

All the tests were focused on fractured metamorphic rocks of various nature, where the primary permeability related to porosity is very low. It was considered that in these rocks, the permeability is mainly governed by fractures and faults and their aperture, spacing and infilling. The tested rocks are all characterised by low to high grade metamorphic conditions (greenschist to amphibolite facies) and have been grouped in the following classes: 1—Phyllites (30 tests); 2—Metabasites and serpentinites (2 tests); 3—Calcschists with prevalent carbonatic composition (8 tests); 4—Calcschists with prevalent phyllosilicatic composition (37 tests); 5—Quartzites (3 tests); 6—Gneissic rocks (7 tests); 7—Granites

(14 tests); 8—Marbles (8 tests); 9—Mixed successions including interlayered anhydrites, anhydritic schists, phyllites and quartzo-micaschists (17 tests). A total of 126 tests have been executed; 78 of these have been done in boreholes located in Austria and 48 in Italy. A general overview of the executed tests is shown in the two diagrams of Fig. 169.1, irrespective of the tested rock-type. The same diagrams also show the general results of the verification works that will be discussed in detail in the following paragraphs.

169.3 Verification of the Testing Results

The verification analysis has been carried out with the aim to evaluate the reliability degree of the hydraulic test results in relation to the geological and structural setting of the test interval. The study consists of a comparative analysis of the rock sampled at the depth of the hydraulic test and the result of the hydraulic testing. It is necessary to specify that a test with low or very low degree of reliability does not indicate that the test is to be rejected but the output seems to be anomalous with respect to the geological setting.

169.3.1 Rock Mass Classification

As a first step, the completeness of the input data has been verified in order to give a first evaluation of the verification process quality. Then, the core drill sample analysis has been carried out regarding (i) lithotype, (ii) depth of the test and (iii) rock mass conditions. The rock mass of each tested interval has been geologically classified on the basis of visual inspections of the drill cores, BHTV analysis and RQD values. The following categories have been defined:

1. rock mass without tectonisation characterized by standard fracturing degree;
2. fault zones distinct in cataclasite or tectonic breccias; it is also reported the presence of "gouge " (core zone) and/or lateral damage zone;
3. rock mass affected by dissolution phenomena with the development of karst morphologies; this concerns mainly carbonatic and evaporitic rocks;
4. rock mass with enlarged fractures owing to gravitational collapse phenomena regarding the shallow portion of the rock mass (until about 300 m deep).

169.3.2 Evaluation Sheet Format

Data have been stored in a database management system specifically designed, from which an "Evaluation sheet" could be extracted directly. The sheet includes several sections as (i) general framework, (ii) characteristics and results of the hydraulic test, (iii) description of the geological features of the tested section, (iv) representation of the borehole logs, core drill photographs and hydrogeological map of the

Fig. 169.1 Total distribution of hydraulic conductivity versus depth for the tests executed in Austria (*left*) and Italy (*right*), irrespective of the tested rock-type
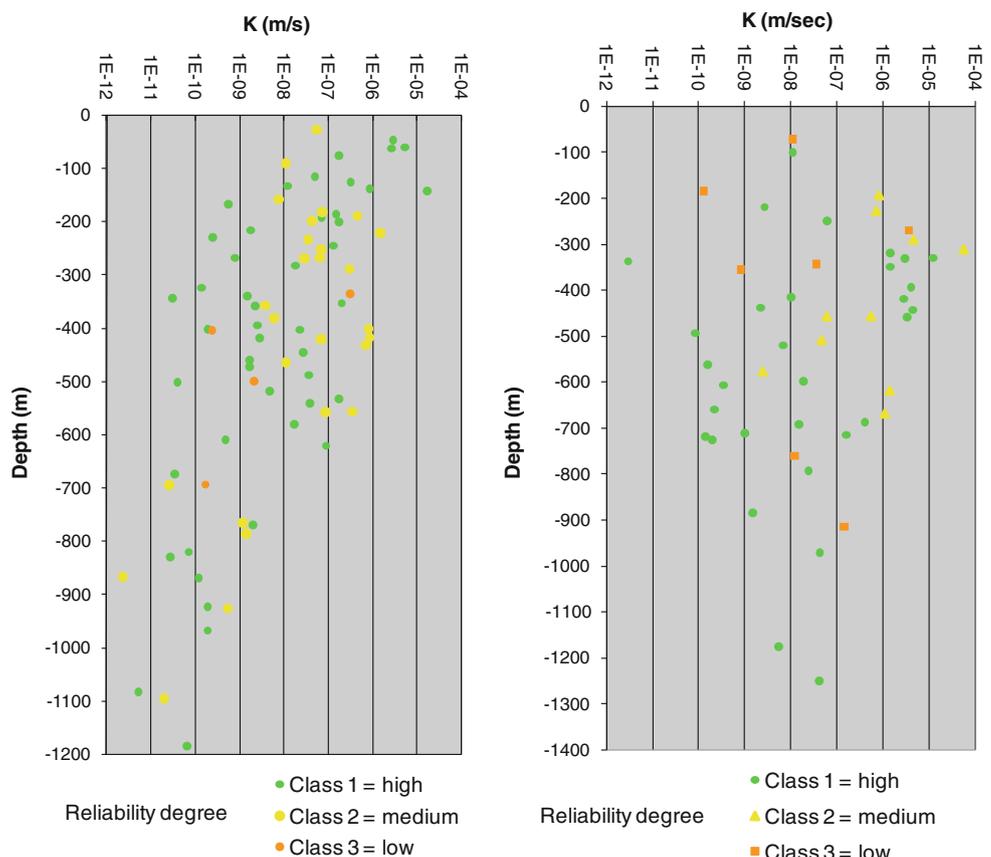
test site and (v) the results of the verification process. The results of the study are formulated in terms of (a) "overall evaluation" which consists in a qualitative description and (b) "reliability degree" defined as:

- Class 1 = High
- Class 2 = Medium
- Class 3 = Low
- Class 4 = Very low

The results of the reliability analysis have been also presented in tables and graphs that allow visualizing the distribution and the range of variation of the data.

169.3.3 Verification Results

The evaluation of 126 hydraulic tests carried out in testing intervals lying from 180 to 1320 m depths and with K-values ranging from 10^{-6} to 10^{-12} m/s shows that:

- more than 60 % of the testing results belongs to the class 1, 30 % to the class 2, 10 % to the class 3;
- no test result showed a very low reliability (class 4);
- the reliability of the test results doesn't depend from the rock types. All different rock types are even part of class 1.

Methodological verification analysis shows that borehole hydraulic testing, even applied in deep boreholes and for different rock types provide valuable data for rock mass characterization. It can be observed that homogeneous and low permeability rock mass conditions have a greater degree of reliability. Regarding the granite lithotype, more than 75 % of the hydraulic tests have been evaluated with high and medium reliability degree (classes 1 and 2). The permeability ranges from very low degree ($<1 \times 10^{-8}$ m/s) and medium to high degree (between 1×10^{-6} and 1×10^{-8} m/s) in relation to the fracturing degree. A low degree of reliability has been recognized for a high degree of fracturing: in these cases the tests results gave a low permeability values, probably due to a reduced connectivity of the fractures network.

169.4 Validation

169.4.1 Methodology

Using calibrated numerical models for excavated tunnel sections back analysis are performed. The hydraulic conductivity for the different rock masses obtained by the numerical models is compared to the verified values derived from the hydraulic packer tests.

169.4.2 Result of the Validation in the Granite Area

The Aica-Mules exploration tunnel was excavated in granitic rocks. In this case feedbacks on rock permeability have been obtained from hydrogeological numerical modelling (Feflow 6.0; DHI-WASY GmbH). In the granite not affected by faulting and characterised by a simple fracture network, the hydraulic conductivities obtained by borehole tests ranges from 1×10^{-7} to 1×10^{-8} m/s. These test results were classified as "Class 2: medium reliability". The permeability as output from the numerical hydrogeological model is approximately 1×10^{-9} m/s, therefore 1–2 orders of magnitude lower than the conductivity obtained by in situ testing. This incongruence is probably related to the fact that small scale hydraulic conductivities with locally high importance for the hydraulic condition are not relevant for the conductivity at a large, pluri-decametric scale, due to the poor hydraulic connectivity among fractures related to a low fracturation density.

As far as fault zones are concerned, a large variability has to be taken into account for the hydraulic conductivity, due to the presence of products deriving from cataclastic fragmentation having mechanical characteristics and granulometric composition ranging over a wide range. The in situ hydraulic testings demonstrate these hydraulic conductivity variations along fault zones, with values spanning over the range from 5×10^{-6} to 5×10^{-9} m/s. The lower value has been observed in a single case and is related to a core zone where the granite is reduced to a fine grained fault gouge, comparable to a silty clay. The higher values are representative for fault damage zones where the fracture density is high to very high (indicatively 5–30 joint/m³) and where decimetric to metric layers of tectonic breccias are locally present. The packer tests, despite their number is rather limited, seem to indicate that in fault zones high hydraulic conductivities are by far the most common condition. The prevalent large hydraulic conductivity observed at the small scale seems to be mostly confirmed at the great scale by the numerical models with conductivities ranging from 1×10^{-6} to 8×10^{-7} to m/s.

References

Agarwal RG (1980) A new method to account for producing time effects when drawdown type curves are used to analyze pressure buildup and other test data. Society of petroleum engineers, SPE Paper 9289, presented at SPE-AIME Meeting, Dallas, Texas, Sept 21–24

Bourdet D, Ayoub JA, Pirard YM (1989) Use of pressure derivative in well-test interpretation. SPE Formation Eval 4:293–302

Bredehoeft JD, Papadopulos SS (1980) A method for determining the hydraulic properties of tight formations. Water Resour Res 16 (1):233–238

Cooper HHJR, Bredehoeft JD, Papadopulos SS (1967) Response of a finite-diameter well to an instantaneous charge of water. Water Resour Res First Quarter 1967:263–269

Doe TW, Geier JE (1990) Interpretation of fracture system geometry using well test data, technical report 91-03. Swedish Nuclear Fuel and Waste Management Co. (STRIPA), Stockholm, Sweden

Horner DR (1951) Pressure build-up in wells, third world petroleum Congress. E. J. Brill, Leiden II, pp 503–521

Jacob CE, Lohman SW (1952) Nonsteady flow to a well of constant drawdown in an extensive aquifer. Trans Am Geophys Union 33 (4):559–569

Quinn P, Cherry JA, Parker BL (2012) Hydraulic testing using a versatile straddle packer system for improved transmissivity estimation in fractured-rock boreholes. Hydrogeol J 20:1529–1547

Change in Hydraulic Properties of Rock Mass Due to Tunnelling **170**

Bernard Millen, Giorgio Höfer-Öllinger, and Johann Brandl

Abstract

Presented and discussed are aspects of changes to the hydraulic properties of rock mass due to tunnelling, but in particularly the change due to the opening or making of new fractures and voids in the rock mass as a result of deformation or relaxation of the tunnel opening and hence an associated increase in the permeability of the rock mass surrounding the tunnel. This process principally occurs in tunnels were high stress fields persist effecting rapid and large scale deformation or relaxation (>100 mm) in the presence of (heavily) jointed rock mass and fault zones. Examples and observations from water and ground inflow events, associated with hydraulic property changes which have occurred during the mining of the Tapovan-Vishnugad Head Race Tunnel, India, are given and which have caused trapping of the Tunnel Boring Machine (TBM) resulting in time delays and cost increases.

170.1 Introduction

A change in the hydraulic properties of rock mass due to tunnelling has been observed in the Garhwal Himalaya, Uttarakhand, India during construction of the deep seated 12.1 km long head race tunnel (HRT) for the NTPC Ltd 520 MW Tapovan-Vishnugad Hydro Electric Project (HEP). The project area lies within the Dhauliganga and Alaknanda Valleys and consists of high strength medium to high grade metamorphic rocks belonging to the Central Himalayan Crystalline Series (Heim and Gansser 1939; for a recent review see Yin 2006).

Since October 2008, 8.6 km of the HRT has been under construction by a Herrenknecht Double Shield—Tunnel Boring Machine (DS-TBM). The rest of the HRT is been constructed by drill and blast methods. During TBM driving, a steel reinforced 0.3 m thick concrete hexagonal segmental lining is inserted behind the machine, pea ballasted and grouted making the internal finished diameter of the TBM-HRT 5.64 m; the excavation diameter is 6.57 m.

To date three TBM trapping events—all associated with subsurface water inflow—have severely hampered the HRT excavation resulting in time delays and cost increases. The first trapping event occurred in December 2009 at chainage (Ch) 3,016 m at a depth of some 900 m in a heterogeneous fault zone (Brandl et al. 2010; Millen and Brandl 2011). During trapping the front and telescopic shields were jammed in and dented by major wedge slides. Approximately 24 h later, massive surges of high pressure subsurface water, containing faulted rock material, broke two crown segments of the segmental lining immediately behind the tailskin with the initial flow rates reaching circa 700 L/s compounding the trapping problem.

The second and third trapping events—which to date have not been reported on—happened in February and October 2012 at Ch 5,840 and 5,859 m respectively in the same circa 20 m wide fault zone at a depth of some 700 m. This fault zone lies at a very acute angle to the tunnel axis meaning the TBM had (will have) to drive through this zone

B. Millen (✉) · G. Höfer-Öllinger · J. Brandl
Geoconsult ZT GmbH, Hoelzlstraße 5, 5071 Wals bei Salzburg, Austria
e-mail: bernard.millen@geoconsult.eu

for at least 35 m. At the time of writing the TBM was still trapped at Ch 5,859 m.

When the second event occurred, the face and surrounding conditions were initially dry and due to over excavation and collapse a cavity of several cubic metres had developed around the cutter head and front shield of the machine in the soil-like stiff clay-rich fault gouge and breccia of which the fault zone consists of. As in the first trapping event, water inflow (1–2 L/s) started some 20 h later. The situation then greatly deteriorated as the water rapidly eroded the water sensitive fault gouge and breccia causing further cavity development, ground creep and ground inflow through the cutter head and shield openings trapping the TBM.

Interestingly, in both described events, the water inflow started approximately 1 day after the initial trappings. The events caused subtle and rapid major changes to the hydraulic properties—particularly increased permeability—of the rock mass within several metres and probably many tens of metres of the tunnel walls.

170.2 Hydraulic Properties of Rock Mass

The hydraulic behaviour of rock mass is much more complicated than in granular soil and there can be huge differences in properties over short distances caused by the distribution of rock types, their tectonic history and distribution in relation to a drainage basin or system.

Subsurface water flow in rock mass is generally governed by (1) the (unaltered) rock porosity and permeability and (2) the rock mass porosity and permeability. In tunnelling geology the usual concern is with the flow of subsurface water through a granular soil or rock mass as is the case in this paper.

Porosity is the measure of the voids in a material and is given in a percentage. However, the voids in a rock must be in contact otherwise the rock is impervious. Permeability is a general term which describes the ability of a porous medium to allow the flow of fluid through it. Permeability is given in K (the coefficient of permeability) after experiments by Darcy (1856) and is also called *hydraulic conductivity* and has the unit m/s. For flow to take place through a saturated material there must be a difference in total head across the medium.

The hydraulic permeability of rocks is generally very low and ranges commonly from 10^{-13} to 10^{-10} m/s. Exceptions are for example coarse grained porous sandstones.

Hydraulic conductivity or permeability and subsurface water flow in rock mass is mainly governed by the interconnection of fractures (bedding, schistosity, joints, faults, etc.) in the rock mass or *fracture permeability*. The hydraulic

Fig. 170.1 The hydraulic permeability of rock mass with a fracture system of defined width and an average distance between fractures of 1 m in comparison to the hydraulic permeability of granular soils from (Wittke 1984) taken from Prinz (1997)

Fracture Width	k [m/s]	△ (Soil)
0,1 mm	0,6 E-06	Silt
	0,3 E-06	
0,2 mm	0,5 E-05	Sand
	0,2 E-05	
0,4 mm	0,4 E-04	
	0,2 E-04	
0,7 mm	0,2 E-03	Gravel
	0,1 E-03	
1,0 mm	0,6 E-03	
	0,3 E-03	

permeability of rock mass is not only inhomogeneous but also highly anisotropic.

In Fig. 170.1 is given an idealised and homogeneous rock mass model in comparison to the hydraulic permeability of granular soils.

The rows of values show that the permeability in the direction of wider fractures is the 3rd–4th negative power (10^{-3}–10^{-4}) of the mean fracture width in relation to the cubic law for fluid flow in rock fractures (Witherspoon et al. 1980). This means that a single wide fracture or narrow distances between multiple fractures, for example in joint and fault zones, can or on the whole control the permeability of the rock mass.

The subsurface water flow is also extremely dominated by the geometry of the fractures and their extension. Fracture walls are also generally rough and the fracture width can change over short distances.

Where there are sequences of low and high permeability in a rock mass there is not only fracture anisotropy to consider in the horizontal direction but also the bedding or schistosity anisotropy of the rock mass to be considered in the vertical direction.

In dissimilarity to granular soil aquifers, where homogeneous and isotropic characteristics are not fully given but a quasi homogeneity and isotropy, fractured rock mass aquifers, with very different fracture widths and grades of opening, have very anisotropic and turbulent flow regimes (Prinz 1997).

170.3 Change in Hydraulic Properties of Rock Mass

Changes to the hydraulic properties of a rock mass are achieved principally by the following: (1) chemical processes such as precipitation, dissolution and weathering; (2) erosion processes; (3) closure of fractures and voids by physical processes (4) opening or making new fractures and

voids by physical processes. Process (1) can either decrease or increase the hydraulic permeability, process (3) causes a decrease and processes (2) and (4) cause an increase.

Long term erosion and dissolution and weathering of rock mass causing hydraulic changes (or increased permeability) has been examined before particularly in relation to problems with the long term operation of water transport tunnels (e.g. Gysel 2002; Lipponen et al. 2005) and will not be discussed further.

There are plenty of examples of large scale water and related ground inflows and hence the development of cavities caused by short term erosion events (e.g. Schwarz et al. 2006; Wenner and Wannenmacher 2009). However the recognition that such events radically change the hydraulic properties and framework of the rock mass surrounding the tunnel up to several tens of metres from the tunnel walls has not been considered to date in discussion of the same.

As stated in the introduction (Chap. 1), events surrounding the development of water and ground inflow during the excavation of the Tapovan-Vishnugad HRT led to changes to the hydraulic properties of the rock mass around the tunnel. Not only the processes (1) and (2) played major roles but also process (4), the opening or making of new fractures and voids. The changes occurred in high stress fields and effected rapid and large scale deformation or relaxation (>100 mm) in sections of (heavily) jointed rock mass and fault zones surrounding the TBM.

As presented in Chap. 2, hydraulic permeability in rock mass is principally governed by fracture permeability. If say some 10 mm of deformation occurs and this affects, for discussion purposes, some 10 m of jointed rock mass evenly away from the tunnel walls and this deformation is taken up evenly by the opening of 10 existing fractures from 0.1 to 1.1 mm at 1 m spacing, then there will be an automatic increase in the hydraulic permeability of several orders of magnitude according to the model given in Fig. 170.1. Of course in reality, at such low levels of deformation, this will not be the case and the deformation will be taken up within the first 1–2 m of the tunnel walls and be much more anisotropic. However, when >100 mm of deformation or relaxation is registered then the range of impact will be much greater reaching at least several if not tens of metres into the tunnel walls.

In the case of the TBM trapping event at Ch 3,016 m (see Chap. 1), the water inflow reaching circa 700 L/s started approximately 24 h after the initial trapping. The TBM over cuts the shields by a maximum of 200 mm at the crown and it is known from observations during the recovery of the TBM that the gap or over cut between the bore and shields closed completely in the upper arch during the event therefore large scale deformation of the jointed and faulted rock mass took place. In this case the processes of change included (1) opening of new and/or existing fractures leading to increased hydraulic permeability around the tunnel and (2) high pressure subsurface water wash out or erosion of joints and the fault core zone, which contained clay and other soil-like materials, into the tunnel leading to development of a conduit-like structures and associated water and ground inflow.

The conduit-like structures were quickly generated in the fault zone i.e. the opening of water bearing joints in connection with the fault core zone containing soil-like material led to rapid erosion of the fault core and the development of an extensive interconnected 3-D network of erosion channels and hence a radically changed hydraulic framework. The fault core was also found to be in direct connection with a sequence of pervious water bearing heavily jointed quartzitic gneiss and quartzite some 40 m above Ch 3,016 m. This sequence of rocks was later encountered between Ch 3,110 and 3,250 m where the combined flow-rate reached up to 60 L/s and an immediate decrease in the water inflow at Ch 3,016 m was observed confirming the water inflow model as given in Millen and Brandl (2011). At the time of TBM restart at Ch 3,016 m in March 2011 the water inflow at Ch 3,016 m had reduced to circa 120 L/s. By the time the TBM had past Ch 3,250 m the water inflow at Ch 3,016 m had reduced to circa 60 L/s.

In the event at Ch 3,016 m the dilemma was not the fact that relaxation and an increase in permeability took place close to the tunnel, but that a nearby pervious water bearing aquifer was short circuited through a fault zone due to the relaxation and hence the large high pressure water and ground inflow developed. If no water bearing pervious sequence had been tapped, then there would have been little water inflow, however a deterioration and increase in permeability of the rock mass surrounding the tunnel would still have taken place.

In the case of the TBM trapping event at Ch 5,840 m, the water inflow of some 1–2 L/s started 20 h after the event. The undistured soil-like stiff clay-rich fault gouge and breccia which make up the 20 m wide fault zone are impervious and were acting as an aquitard to the above lying semi-pervious but highly pressurized saturated jointed gneiss and schists sequences. In one of the exploratory bore holes carried out, a water inflow was recorded during drilling of circa 1 L/s emerging out of jointed augen gneiss and a pressure of 14 bar was measured after installation of a packer and manometer after completion of the bore hole. As at Ch 3,016 m, large scale deformation took place resulting in complete closure of the gap between the bore and shields and the development of new cracks or fractures in the stiff soil-like fault gouge and breccia hence allowing water from the overlying jointed rock sequences to penetrate through into the TBM causing erosion of the same and a rapid deterioration of the ground conditions surrounding the machine (see Chap. 1).

170.4 Consequences and Conclusions

To date the authors have found no specific literature on changes to hydraulic properties related to large scale rock mass deformation or relaxation around tunnels and the related increase in permeability due to the opening or making of new fractures and voids but believe it to be important aspect of water inflow into tunnels and understanding its control.

The increase in permeability of the ground by one or two orders of magnitude due to loosening created by blasting and the delay before the installation of temporary support has been recognised for some time (Howard 1991). It is noted here that the observations of increased permeability occurred during DS-TBM mining where the segment support is first installed and finalised (pea ballast and grouting) behind the 12.5 m long shields.

Generally it is important to control water inflow but it is even more important to try and stop erosion by the same and the generation of ground inflow as this has a more detrimental effect on the rock mass surrounding the tunnel and the tunnel advance itself. Preventative measures to stiffen up ground include grouting, ground freezing or the installation of grouted pipe roofs and the like ahead of the face into suspected poor water bearing geology. However, such measures are expensive and often met with scepticism about whether or not they will work and or reduce costs in the long term.

Remedial measures to fill cavities and the like are costly and cause time delays. All three areas where the Tapovan-Vishnugad TBM has become trapped to date will require extensive grouting and other works to be carried out such as replacement of the segmental lining with a more robust lining as the HRT will be a pressure tunnel during operation.

The measures carried out to achieve TBM recovery in the three cases quoted included (1) Ch 3,016 m: the building of a 143 m long by-pass tunnel, a 25 m long water diversion drift and an extensive drilling and grouting campaign as described in Millen and Brandl (2011); (2) Ch 5,840 m: installation of an extensive 2 layer chemically grouted pipe roof above the machine and then over mining under the same using a steel girder, shotcrete and rock anchor support systems by access through the telescopic shield; (3) Ch 5,859 m: over mining from behind the tailskin using a fore poling, steel girder, shotcrete and rock anchor support systems.

The information on hydraulic change presented here should also be considered during the implementation of grouting schemes and during the determining of the behaviour of subsurface water inflow into underground structures in the short, middle and long term i.e. prior, during and after construction.

Further thought has to be given as to where these changes occur i.e. in what types of rock or rock mass can they be expected and whether such changes are more dependent on the existence of competent (brittle deformation) or incompetent (plastic deformation) rock mass and the prevailing hydrogeological framework.

References

Brandl J, Gupta VK, Millen B (2010) Tapovan-Vishnugad hydroelectric power project—experience with TBM excavation under high rock cover. Geomech Tunn 3(5):501–509

Darcy H (1856) Les Fontaines Publiques de la Ville de Dijon (in French) [The Public Fountains of the City of Dijon], Dalmont, Paris

Gysel M (2002) Anhydrite dissolution phenomena: three case histories of anhydrite karst caused by water tunnel operation. Rock Mech Rock Eng 35(1):1–21

Heim A, Gansser A (1939) Central Himalaya. Soc Helv Sci Nat Zurich 73:1–245

Howard AJ (1991) ITA working group on maintenance and repair of underground structures. Report on the damaging effects of water on tunnels during their working life, vol 6, no I, pp 11–76. Tunnelling and Underground Space Technology

Lipponen A, Manninen S, Niini H, Rönkä E (2005) Effect of water and geological factors on the long-term stability of fracture zones in the Päijänne Tunnel, Finland: a case study. Int J Rock Mech Min Sci 42:3–12

Millen B, Brandl J (2011) TBM recovery under high cover and extreme water-inflow, Himalayas, India. In: Kolić D (ed) 1st international Congress on tunnels and underground structures in South-East Europe "using underground space" April 7–9. Dubrovnik, Croatia, p 10. PDF on USB-Stick on back cover of book, ISBN 978-953-55728-6-2

Prinz H (1997) Abriß der Ingenieurgeologie (in German) [synopsis of engineering geology], 3rd edn, p 545. Ferdinand Enke Verlag, Stuttgart

Schwarz L, Reichl I, Kirschner H, Robl KP (2006) Risks and hazards caused by groundwater during tunnelling: geotechnical solutions used as demonstrated by recent examples from Tyrol, Austria. Environ Geol 49:858–864

Wenner D, Wannenmacher H (2009) Alborz service tunnel in Iran: TBM tunnelling in difficult ground conditions and its solutions: 1st regional and 8th Iranian tunneling Conference, vol 18, 20 May, Tehran, Iran

Witherspoon PA, Wang JSY, Iwail K, Gale JE (1980) Validity of cubic law for fluid flow in a deformable rock fracture. Water Resour Res 16:1016–1024

Wittke W (1984) Felsmechanik: Grundlagen für wirtschaftliches Bauen im Fels (in German) [rock mechanics: principles for economic construction in rock], p 1050. Springer, Berlin

Yin A (2006) Cenozoic tectonic evolution of the Himalayan orogen as constrained by along-strike variation of structural geometry, exhumation history, and foreland sedimentation. Earth-Sci Rev 76:1–131

P.C. Nawani

Abstract

In underground projects vast uncertainties are confronted in terms of hydrogeology and geology, more often in mountainous terrains like Himalaya. Groundwater is often the main source of problems in tunneling projects and it is more troublesome during construction. Groundwater problems like sudden water ingress or continuous seepages are considered to be the most difficult conditions to predict. The problem is often due to ingress of water in higher volumes than predicted, or worse, the unanticipated encounter of water during tunneling. In Tapovan—Vishnugad Hydro electric project (520 MW), a run of the river scheme, the Head Race Tunnel (HRT) is being driven by Tunnel Boring Machine (TBM). Tunnelling is through the rocks of Central Crystallines which are heavily stressed due to—the presence of Main Central Thrust (MCT) in close proximity and presence high rock cover (>1 Km.). The Tunnel Boring Machine (TBM) was stuck up at RD 3016 m (rock cover ± 990 m) due to major rock fall on the shield near cutter head, in December, 2009. This led to sudden ingress of water (600–700 L/s) in HRT, damaging the pre-cast lining in the crown portion. The water ingress was from quartzite rock through some wide open joints, fractures or fault which were progressively widened due to ground water movement and caused instability problems. The major problems associated with the heavy ingress of water were found to be—difficult working conditions, damage to the structures, stability problems and environmental impact to the ground water resources. The work was called off for more than 10 months in the year 2010. A bypass tunnel was driven to reach the location where TBM was stuck up and damaged so as to carryout repairs. The ingress of water was diverted from HRT through a drift to make the HRT workable.

171.1 Introduction

Underground projects located in Himalaya are often confronted with uncertainties and complexities in terms of geology, hydrogeology and in-situ stress because of the prevailing compressional environment in Himalayan region. Groundwater is often the main source of problems in tunnel construction. The occurrence of water is difficult to predict accurately, hence it is prudent to be prepared for large variations both with respect to locations and volumes. Adverse situations like sudden ingress of groundwater are the most difficult conditions to assess and also quite challenging in handling. This ultimately affects productivity and thus cost.

Tapovan—Vishnugad Hydroelectric Project (520 MW), a run-of-the-river scheme, is presently under construction by NTPC Ltd., in the Higher Himalaya of Uttarakhand State in India . The project envisages harnessing of hydro-potential of Dhauliganga—a tributary of Alaknanda river, by utilizing

P.C. Nawani (✉)
Jindal Power Ltd, Gurgaon, India
e-mail: drnawanipc@jindalsteel.com; drnawanipc@gmail.com

a head of 518 m, with a barrage near Tapovan across Dhauliganga, and a 11.69 km long head race tunnel of 4.8 m dia. and an underground powerhouse (4 × 130 MW) on the left bank of Alaknanda. The reservoir pondage will have a maximum depth of 22 m and have live storage of 13 m, between FRL at EL 1803.5 m and MDDL EL 1790.5 m, with a capacity of 0.57 Million m^3. It will have a small submergence area confined to a 10 ha area providing a short term daily storage to allow peaking.

In this project, tunneling of head race tunnel (HRT) is being done by tunnel boring machine (TBM) in about 9 km length of HRT and about 6 km tunneling by TBM has been achieved so far (Fig. 171.1). The rocks of Central Crystalline Group which are hard, brittle and heavily stressed, due to the prevailing compressional environment and presence of Main Central Thrust (MCT) near the project site and also high vertical cover (upto >1 km) occurring at various points along the tunnel alignment, form the tunneling medium for the entire 11.69 km long HRT.

In December 2009, when HRT was being driven under a high cover zone, there was a rock mass failure followed by a sudden heavy ingress of groundwater from the tunnel face. The TBM shield was damaged and stuck up at RD ± 3,016 m. This incident led to immediate suspension of tunneling which continued for months in the year 2010–11. A bypass tunnel (BPT) was driven to access the HRT reach where TBM was stuck up with the aim to assess the damages suffered to channelize water inflow away from HRT through a drift size opening. Tunneling was resumed in the year 2011.

171.2 Geological Setting

The project area is located in the Higher Himalayan region where the Central Crystallines composed of medium to high grade metamorphic rocks of Tapovan—Helong Formation

Fig. 171.1 Excavation of HRT by using TBM

and Joshimath Formation are thrusted over the Lesser Himalayan rocks along the Main Central Thrust (MCT), near Helong about 2 km downstream of the location of underground powerhouse. The rocks exposed in the area are quartzites, mica schists, banded gneiss, augen gneiss, amphibolites of Tapovan—Helong formation and coarse grained, garnet—mica gneiss, garnet Kyanite gneiss of Joshimath formation.

171.2.1 Geology Along Head Race Tunnel (HRT)

The HRT alignment passes through a rough and rugged terrain on the left bank of Dhauliganga and Alaknanda rivers. HRT is being driven through the rocks of Tapovan—Helong Formation dipping 20°—40°/NNE-NE overlain by rocks of Joshimath Formation dipping due NE with considerable variations forming a broad syncline (Fig. 171.2). The synformal structure is favourable for groundwater storage. The fine to medium grained quartz mica gneiss intercalated with schist and two quartzite bands (25–55 m thick) of Tapovan Formation are overlain by the coarse grained garnet—biotite—Kyanite gneiss of Joshimath Formation.

The quartzites are traversed by three prominent joint sets dipping at 35°–40°/N 290–020, 80°/N 360 and vertical N10°E (strike). Three prominent joint sets in quartz mica gneiss are dipping at 30°–40°/N 285–25, 45°–55°/N 070–110 and vertical/N 60° E (strike).

171.2.2 Rock Mass Characteristics

The rock masses of Tapovan—Helong formation are characterized by rock mass values—Q = 7–14, RMR = 60–75 and Q = 6–10 and RMR = 55–65 for augen gneiss and quartzite respectively. The Q and RMR values of 6–10 and 60–65 respectively have been estimated for the coarse grained biotite—Kyanite gneiss of Joshimath Formation (Naithani and Krishna Murthy 2006).

The vertical cover above the HRT grade ranges from 300 m in the initial reaches near intake which gradually increases to 900—1,000 m in the middle and then gradually decreases to 200 m near the surge shaft location. High stress condition exists in the high vertical cover reaches (about 1 km).

171.3 Groundwater Ingress in HRT

On 24 Dec. 2009, while driving the HRT by a double shield TBM, under a high cover zone of ±990 m comprising hard and brittle rocks of Tapovan—Helong Formation overlain

Fig. 171.2 Longitudinal section along headrace tunnel (Modified after Naithani and Krishna Murthy 2006)
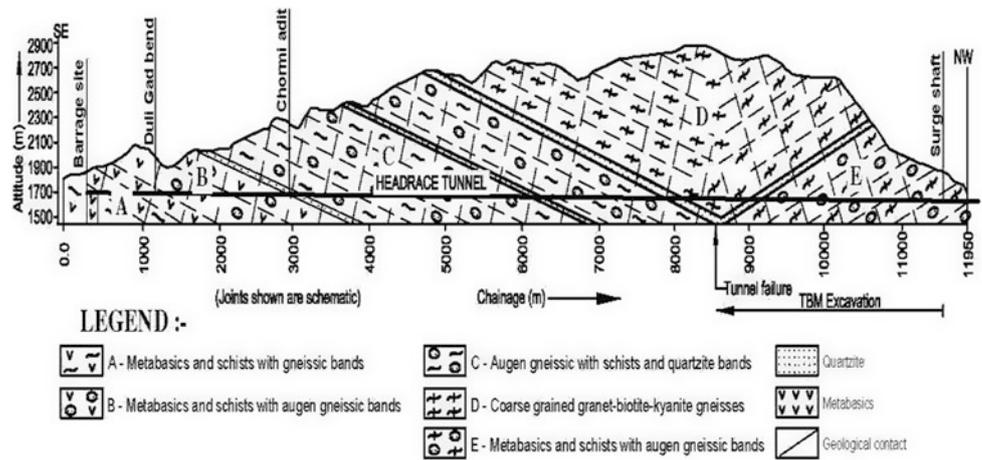
by rocks of Joshimath Formation and thick overburden materials, rock mass failure occurred which hit the front shield and immediately stopped TBM. Subsequent attempts to free the machine with very high thrust forces failed. By the following day, a massive surge of ground water started entering the tunnel under considerable pressure into the annulus of the completed but not yet grouted segmental lining and caused failure of two roof segments, allowing a sudden heavy ingress of groundwater (600–700 L/s) from the tunnel face at RD ± 3,016 m. The heavy groundwater ingress from the quartzites rocks of Tapovan—Helong Formation, forming a synformal structure, was considered to be through the pathways—open joints/fractures or fault zone which were further widened due to stress relief and removal of infilling material by continuous movement of water (Nawani 2010) (Fig. 171.3). Initially the water was clean and clear but later it became muddy and milky in colour. This incident led to complete suspension of tunneling operation at the site.

171.3.1 Bypass Tunnel

For sometime wait and watch strategy was adopted but when there was no significant change in the groundwater ingress, it was considered essential to construct an access tunnel to the location of TBM at RD ± 3,016 m in order to assess the ground condition and repair the TBM. In the meantime, with passage of time, there was an appreciable reduction in water ingress and discharge was reported to be 200–250 L/s. A 140 m long, D-shaped (4.2 m dia.) bypass tunnel was excavated, from the left side, beginning from concrete lining segment No. 1837 (ch. 9945.6 m from the downstream and of HRT) and running parallel to HRT, to reach TBM cutter head location (Fig. 171.4). At this location, it was observed that rock mass failure has occurred above the concrete lining segment No. 1905 and 1906, and TBM shield was damaged near cutter head. The segments 1905 and 1906 were partly removed to examine the cavity formed due to failure of rock blocks above the crown portion of HRT.

Fig. 171.3 Water ingress from segment No. 1905

Fig. 171.4 View of By-pass Tunnel

The water inflow was channelized through a drift—size opening excavated between BPT and HRT.

171.4 Geotechnical Assessment of Rock Mass Behaviour

Rock mass behaviour around the Collapse Zone where cavity has formed, above the crown of the HRT, was examined and geotechnically assessed. The banded quartzite rock mass is mostly blocky and the rock mass failures are mainly structurally controlled due to interplay of two joints J_1 (foliation) and J_2 (cross-joint), triggered by high stress relief and high water inflow under pressure. The rock mass above the concrete lining segment No. 1904 was found to be intact and it, however, failed above segment No. 1905 and 1906. The cavity size further increased due to heavy ingress of groundwater Fig. 171.5). The pea gravel grout around few pre-cast lining segments was also washed out under high pressure of water. The washed out grout material choked the pea gravel holes and as a result water gushed in under high pressure from pea gravel holes in crown portion of HRT. The vertical extension of the cavity was estimated to be 8–9 m in NE direction and the width of this zone is more than 12 m. The detailed geotechnical assessment indicated that the cavity was formed above TBM cutter head between RD ± 3,016 m and RD ± 3,000 m.

Supportive measures, repair work and treatment

- Removal of damaged segments from the collapsed zone (segment No. 1906–1908), followed by cavity backfilling.
- Water ingress has been channelized through drift by inserting the flexible pipe in to the cavity.
- Installation of steel arch to support the pre-cast segment lining from No. 1857–1908.

Fig. 171.5 Close view of cavity and water ingress (which was later on diverted in to drift) above segment No. 1905 in HRT (TBM)

- Rock bolting (Swellex 4 m long, dia 25 mm) and SFRS in the cavity zone above segment no. 1905 and 1906.
- Gaps on the left and right side walls have been filled with the thick shotcrete.
- Consolidation grouting above HRT crown, area between collapsed zone and BPT starting point, was done from the right wall of BPT.
- Replacement of damaged telescopic shield, after movement of the gripper shield.
- Dismantling of backup units of TBM (21 Nos. of gantries).
- Grouting in the cavity zone from segment no. 1904 onwards and for this purpose pipes of 104 mm dia and 1215.18 m length were used.

171.5 Other Significant Observations

- Surface water bodies—lakes, springs and streams were studied by project geologists in and around Auli area, along the HRT alignment, to monitor if there is any change in water level or discharge. No change in water level of lakes (Chatrakund, Sunilkund) and no decrease in water discharge in streams and springs were found.
- No sign of subsidence was noticed in the ground near and above the HRT alignment.
- The water samples were analysed by NIH (National Institute of Hydrology, Roorkee) and the results suggest that the water bearing strata are being recharged at higher elevation (±3,000 m) and it is a mixture of snow/glacier melt water and rain water.
- Discharge of water from the cavity is having a decreasing trend and present discharge is ±120 L/s. Water is clean and clear and flows along southwest dipping joints.

171.6 Conclusion

Groundwater ingress is the key issue which impacts design and construction of tunnel projects. Heavy water inflow under high pressure at times causes unexpected delays in construction schedule of underground projects. In Tapovan—Vishnugad Hydroelectric project, tunneling along the head race tunnel (HRT) alignment by double shield TBM suffered a setback when rock mass failure followed by heavy ingress of groundwater, with 600–700 L/s discharge, occurred at RD ± 3016 m where the rock cover was as high as ±990 m. The water ingress was from the water bearing quartzite bands of Tapovan—Helong Formation, disposed as synformal wide open fold, through structural discontinuities —open joints/fracture or fault zone which were further widened in the form of a cavity due to stress relief and movement of water. The problem was addressed through

excavation of a bypass tunnel of about 140 m length and 4.2 m diameter, parallel to HRT, to reach the location of incident at RD ± 3,016 m. The groundwater inflow was channelized through a drift—size opening driven through the rock column between BPT and HRT. The cavity formed in the crown portion of HRT was supported and made up, and the double shield TBM was repaired. The tunneling was resumed in 2011.

Prediction of critical hydrogeological condition along tunnel alignment is very essential and an advance planning to tackle the potential risks associated with water ingress is very important for ensuring the tunneling work in safe and controllable manner. Probe drilling to know rock mass condition and groundwater pressure in advance followed by pre-excavation grouting(using Micro cement) with pressure in order to make the ground water-tight, i.e, pre-injection of rock mass, is considered to be the best option. The main purpose of pre-injection in tunneling is to reduce the leakage of water into the underground excavation and also to improve the stability of rock mass. Post-excavation grouting must be avoided as it is difficult and also very expensive—20–50 times more.

References

Naithani AK, Krishna Murthy KS (2006) Geological and geotechnical investigations of Tapovan—Vishnugad Hydroelectric Project, Chamoli District, Uttarakhand, India. Published in J Nepal Geol Soc 34 (spl. Issue):1–16

Nawani PC (2010) A note on inspection visit to Tapovan—Vishnugad Hydroelectric Project on 1–2 April 2010. Unpublished inspection note submitted to NTPC

Investigation Constraints in Subsurface Water Aspect of Hydropower Development in the Indian Himalaya

172

Y.P. Sharda and Yogendra Deva

Abstract

Keeping pace with the overall growth, the infrastructure in India—a rapidly growing nation—developed many fold during the recent past. In particular, the Himalayan region witnessed a boom in hydro power and, in view of rugged topography and consequent lack of suitable open spaces, depended more and more on subsurface spaces for housing project components including long water conductor systems. The Himalaya, due to its location in the inter plate region, is a highly seismic region with a very complex geological setup. Combined with very rugged topography with high ridges and narrow and deep valleys, construction of subsurface components invariably encounter various geological adversities amongst which sudden ingress of subsurface water in large quantities, often with flowing ground conditions, happens to pose one of the most critical problems during construction. This is one of the common causes for delays in construction work for long durations that, in turn, leads to severe time and cost overruns. Long head race tunnels of hydroelectric projects like Dul Hasti, Parbati Stage-II, Tapovan Vishnugad, etc. are some of the better known examples that suffered long delays due to this problem. While, other subsurface structures like surge shafts, desanders and powerhouse caverns are constructed in limited spaces with lesser variations in ground conditions, the long tunnels encounter frequently changing ground conditions and face serious constraints in investigations due to inaccessibility and high superincumbent cover that pose constraints in dependable estimations. Besides innovations in standard investigation techniques, possible solution lies in systematic advance probing during construction.

Keywords

Himalaya • Tunnel • Investigation • Water • Delays • Advance probing

Y.P. Sharda (✉)
SNC Lavalin Engineering India Limited, 3rd Floor,
Redisson Commercial Plaza, Mahipal Pur, New Delhi, 110 037,
India
e-mail: yp.sharda@snclavalin.in

Y. Deva (✉)
Indo Canadian Consultancy Services Ltd., Geological Survey
of India, Citadel 1502, Eldeco Green Meadows, Sector-Pi,
Greater Noida, India
e-mail: yogendradeva@gmail.com

172.1 Introduction

Along with other infrastructure facilities, availability of energy plays a critical role in the sustainable development of the economy of a nation. For sustainable growth, electricity, gas and water supply sectors should also grow at the same rate as the economy. Recent economic liberalization policy in India has had a significant impact on all sectors of development, with infrastructure and power, in particular, getting prominence. Rapid industrialization, coupled with

the expansion of the agricultural sector, and overall improvement in the quality of life and urbanization of rural India, has pushed up the demand for energy requirements. In today's scenario, the generating capacity is far below the current demand resulting in chronic power shortages in almost all parts of India. The problem becomes acute during peak hours. It is true that it may be possible to meet base load demand through other fossil fuel based or nuclear power plants, but, hydro power- the perennial energy is the only answer for peak demand through which it is also possible to achieve low carbon and environment friendly growth as compared to energy from other sources. In addition, development of hydro power projects also provides the added advantage of opening up avenues for development of remote and backward areas of the country. Despite being recognised as a renewable source of energy, the share of hydro power in the overall generation capacity of the country has been steadily declining since 1963—from 44 % in 1970 to about 21.18 % today. This could be attributed to long gestation periods in case of hydroelectric projects, capital investment, remote location of potential sites, lack of infrastructure in the desired areas and above all the environmental concerns.

Keeping in view the importance of hydropower, the Central Electricity Authority (CEA) carried out re-assessment studies of hydroelectric potential of the country. These studies indicated availability of economically exploitable hydroelectric potential of the country as 148,701 MW of which only 23.34 % has been harnessed so far. It is also evident from the reassessment study that 70 % of this economically exploitable hydro potential is concentrated in the Himalayan part of the three major river basins, viz. Indus, Ganga and Brahmaputra. Therefore, in order to fulfil the demand for power and to even go on to be a power surplus state, India has no option but to harness Himalayan Rivers for meeting the ever growing demand for energy. In the quest of harnessing more and more hydropower, it has become necessary to move into remote and difficult areas that offer geologically and geotechnically challenging sites, harsh climatic conditions and almost non- existing infrastructure facilities. The target is tough and calls for all out efforts in achieving self sufficiency in hydropower development.

172.2   Complexities of the Himalaya

Himalaya, the world's largest mountain chain with some of the highest peaks extends for over 2,500 km along the northern borders of the country. It is characterised by very

rugged topography dissected by deep valleys resulting in high to very high relief and snow covered peaks. The altitude in the Himalayan terrain attains the maximum of 8,848 m in the Mount Everest—the world's highest mountain peak and every mountaineer's dream. The climate varies from alpine snow to sub-tropical hot and humid. By virtue of its birth related to the collision of the Indian and the Eurasian Plates, the Himalayan region is home to geological and tectonic complexities and high seismicity. The combined effect of various complexities results in major geological and geotechnical problems both over ground as well as underground. For the underground structures, excessive mountain/overburden stresses with problems like squeezing, rock bursting, infrequent incompetent and problematic zones across faults, shears and thrusts, huge quantities of subsurface water, flowing ground conditions and geothermal pockets with hot springs or dry heat, etc. are just a few examples of the innumerable challenges encountered while driving tunnels. The deepness of a tunnel makes it rather difficult and expansive to get a reliable picture of geological and hydrological situation through which a tunnel has to be built (Sanders 2011). On the other hand, surface problems like unstable slopes, landslides, debris flows, snow avalanches, earthquakes, liquefaction etc. are some of the problems that plague many a surface components of hydro projects during investigation as well as construction. In general, serious problems due to large quantities of subsurface water, particularly in combination with crushed rock leading to flowing ground conditions, is the foremost and nearly common to any long tunnel in the Himalayan terrain.

172.3   Investigation Constraints for Tunnels in Himalaya

During the hydropower development in the Himalaya, relatively easier sites were developed earlier and the difficulty level increased as development moved into difficult remote sites in higher reaches due to rugged nature of terrain leading to poor accessibility, low population density, and hostile climate. With the greater thrust on the development of run-of-the-river schemes due to environmental and rehabilitation concerns, more and more power projects are now planned as run-of-the-river schemes that, by implication, involve long water conductor systems, viz. head race tunnels as given in following Table.

Most of these tunnels were constructed, or were taken up for construction, after very limited investigations that were restricted due to various constraints discussed in the paper.

Sr. no	Name of project	Feature	Length (km)	Maximum discharge (l/m)	Generation capacity (MW)
1.	Nathpa Jhakri HEP, Himachal Pradesh, India	HRT	27		1,500
2.	Karcham Wangtu HEP	HRT	17		1,000
3.	Dul Hasti HEP	HRT	10.63	72,000	360
4.	Rampur HEP	HRT	13		
5.	Parbati HEP stage-II	HRT	31	7,000	800
6.	Maneri Bhali HEP stage-II	HRT	16		
7.	Kameng HEP	HRT	14.5		
8.	Luhri HEP	HRT	38		
9.	Tapovan—Vishnugad HEP	HRT	11.5		

These constraints make it very difficult to carry out intensive investigations along the tunnel routes, including even detailed engineering geological mapping, leading to serious constraints in building a reliable geological model and in predicting the problems precisely that are likely to be encountered during construction stage. The data acquisition, therefore, tends to depend more upon projections from long distances, even from the opposite banks of the rivers and, consequently, adds to the errors on large scale. Subsurface investigations through drilling, drifts, geophysical surveying, etc. face extreme problems of equipment/material transportation including drilling fluids. In particular, advanced technology for deep drill holes, that is not available easily and even if available, it is almost impossible to transport bigger drilling machines and drilling fluid to remote sites. Even remote sensing techniques have not been of much help in most of the cases due to thick overburden cover supporting dense vegetation.

In view of the general investigation constraints discussed above, the project planning depends more on the construction stage advance probing either through advance drilling or other indirect methods like TSP that, invariably, get sacrificed in the name of progress and many a time lead to disastrous consequences.

172.4 Implications of Investigation Constraints in the Himalaya

Shortfalls in investigation due to various constraints have far reaching consequences in the execution of long tunnels compared to other localised components like caverns for powerhouse, desanders, surge shafts/chambers etc. This is attributable to long tunnels being more exposed to far greater variations in ground conditions that are difficult to be investigated due to accessibility problems and high superincumbent cover. The problems assume greater dimensions due to complex geological and tectonic settings. The other localised components, on the other hand, are constructed in confined or limited space with very little or no variation in ground conditions.

Huge quantities of subsurface water connected to perched water tables is a common feature during tunnel execution and is nearly impossible to investigate. While, discharges from such sources disappear or reduce significantly in due course of time depending upon the magnitude of the source, interconnection with perennial sources is not uncommon and may turn out to be a major construction problem. In good rock condition, the subsurface water on its own may not be as big a problem as it is when it punctures through poor rock condition like fractured and crushed rock in shear or fault zones. The resultant flowing ground conditions turn out to be nightmares for the executing personnel and, many a time, are capable of stalling construction activity for months, or, in extreme cases, for years.

172.5 Serious Subsurface Water Problems in Himalayan Tunnels

Some of the projects with long tunnels as water conductor systems in the Himalaya, that have suffered due to sudden ingress of large quantities of water without any warning are discussed in the following paragraphs.

172.5.1 Dul Hasti Hydroelectric Project

The 53 m^2, partly TBM and partly DBM driven circular head race tunnel of the 390 MW Dul Hasti Project in northwest Himalaya encountered several artesian blowouts with peak discharge at 72 m^3/min at RD 1,194 m that declined with time and stabilised at 7.5 m^3/min after about 6 months (Deva et al. 1994) is of particular importance. The "pseudo fluvial" outwash material amounted to 4,000 m^3 and led to partial burial of the TBM. The TBM was buried in another such blow out with huge flowing ground condition, and same had to be abandoned. The tunneling for the remaining

60 % of the tunnel length could continue by DBM after over 14 months, by constructing a by-pass tunnel. A number of fracture/crushed zones of 1–3 m width charged with water cut across the tunnel alignment. These when intercepted in the tunnel effected blowout under high hydrostatic head of +200 m and drained the water into the tunnel with mud/slush and angular rock fragments and flowing ground conditions. These took several weeks to months to drains, till then halting of tunneling was the only solution. The tunneling was accomplished with many challenges/difficulties in design and construction of support system and lining in the weak zones due to selective under excavations and supporting in the weak zones and time and cost over runs in 2005, with a construction history of over +15 years.

The artesian conditions have been linked to confinement of fractured quartzite beneath an impervious barrier of phyllite with a major tectonic lineament (fracture/fault?) in the vicinity responsible for aquifer porosity and groundwater channelization (Fig. 172.1). The HRT had already been detoured as the "loop alignment" for bypassing the problems due to an exceptionally thick 'buried valley' of the Chenab River (Fig. 172.2). The incidence, that took 186 days for resumption of tunnelling, was handled basically through the dewatering arrangements under gravity with pumping assistance (60–80 m^3/min capacity), followed by mucking and limited probing through destructive drilling. The unconventional design of upstream slope of the HRT at the intake helped in drainage under gravity and saved the tunnel excavation from many problems and consequent long delays.

According to Winter et al. (1994), the geological features of the project area are of exceptional nature and the tunnel layout, the tunnel design, the investigation and construction methods have to be continuously adapted to these new and exceptional conditions. According to Sengupta et al. (2008), abrupt interception of an aquifer resulted in sudden ingress of water with sediments, pebbles and gravel ranging in size from 0.5 to 1,000 mm resulting in formation of a cavity and

accumulation of the muck near the mouth of the cavity. Again a blowout at three closely spaced locations at invert sprang a surprise. The blowouts carried slushy discharge of about 700 L/s in the beginning and subsequently increase to 1,100 L/s. This later stabilised to 50–70 L/s. The water carried and deposited 2,500–3,000 m^3 of muck comprising sand, silt and pebbles. The blowout caused extensive damage to machinery and delayed the project by several years and further tunnelling was done by drilling and blasting. The inflows reduced to 150 L/s within 100 days and flows of reduced to 100 L/s continued for a period of over 5 years (Mcfeat-Smith 2008).

172.5.2 Parbati Hydro Electric Project

This 800 MW installed capacity project involving trans-basin transfer of water is under construction in Kullu District of Himachal Pradesh. The project involves the construction of a 91 m high concrete diversion dam on the Parbati River, a 31.23 km long headrace tunnel on the left bank of the Parbati River to convey the water to a surface power house located on the right bank of Sainj River, a tributary of the Beas River. The ground cover over the HRT exceeds 1 km for considerable length. In conjunction with high relief, the rugged topography, steep slopes, dense forest cover and complete lack of accessibility led to very limited investigations and consequent decision to rely on advance probing. On 18th November 2006, at Ch. 2,700 m, water along with slush started coming out from a probe hole and soon the discharge rose to about 2,500 lpm with 120 m^3 slush comprising sand and silt that deposited in the tunnel. The situation became out of control after about 8 h when the discharge increased from 2,500 lpm to about 7,000 lpm and all the machinery including the TBM were drowned in water and slush (Fig. 172.3). The tunnel excavation came to a standstill and, even after seven years, still continues to be suspended. The tunnel is still discharging at the rate of 4,000 lpm.

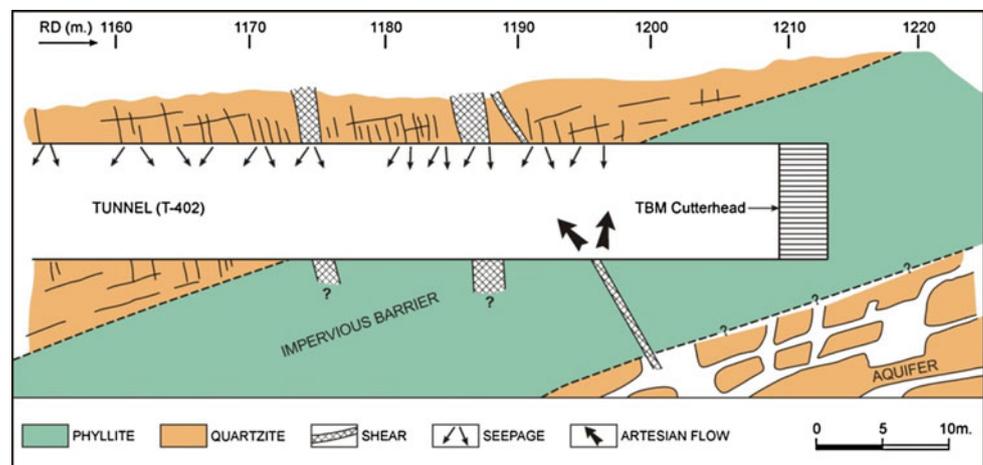**Fig. 172.1** The artesian blowout setting at Dul Hasti HEP

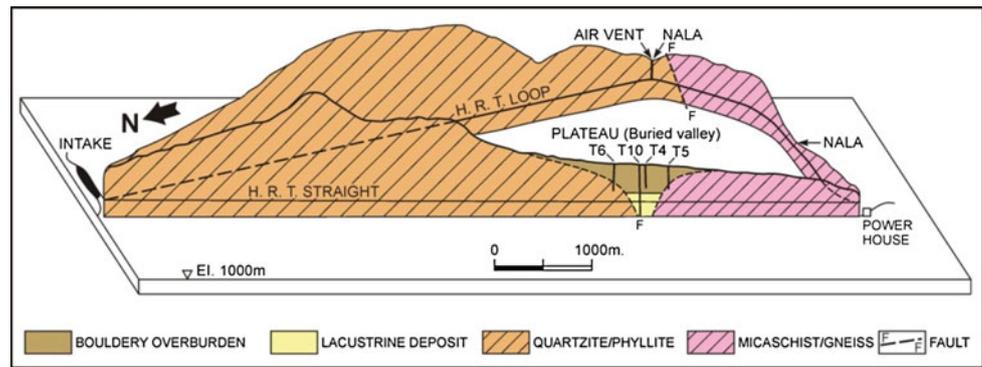**Fig. 172.2** Bypassing the deep buried valley along Dul Hasti HRT alignment

Fig. 172.3 Heavy discharge with slush in Parbati HRT

172.5.3 Tapovan Vishnugad Hydroelectric Project

The TBM driven 11.5 km long HRT of the 520 MW hydroelectric project is located in the state of Uttrakhand is being constructed through three construction adits aggregating 1.25 km length. The ground cover over the tunnel exceeds 1 km in the middle reaches. The TBM got struck as large quantities of water suddenly flooded the tunnel on 25th December 2009 at RD 3,016 m. The rate of inflow increased to about 700 lpm and resulted in complete stoppage of work for about 15 months. Work could be resumed only after the excavation of a bypass tunnel for dewatering at the face and freeing of the TBM cutter head which had got stuck. The water inflow continues at 100 lpm and is being drained through the bypass tunnel.

172.5.4 Kameng Hydroelectric Project

Located in North Eastern Himalaya, the project with 14.5 km long HRT is being excavated through four construction adits. According to Kalita (2011), large quantities of slush along with heavy ingress of water measuring up to 400 l/m was encountered suddenly at RD 422.60 m from the Face-2. The slush comprised loose sub-angular fragments of quartzite measuring 60–80 mm with quartz crystals and clay. Further advancement of the HRT was possible only after 8 months of all out efforts through poly urethane and micro cement grouting, and fore-poling with MS heavy duty pipes.

172.5.5 Karcham Wangtu Hydroelectric Project

Located in western part of Himalaya, this 1,000 MW installed capacity project has an 11.28 m diameter and 17 km long head race tunnel as part of the water conductor system. The HRT encountered extremely poor and flowing ground conditions for a length of about 200 m. The tunnel advancement was handled through DRESS technology. The HRT also encountered about 350 m long high temperature zone with temperature going up to 98 °C. This difficult ground condition was negotiated by resorting to multiple drifting, continuous injection of cold water through drill holes and reducing the charging time to within 40 min to avoid deflagration and immature detonation. In addition to the above, problems of rock bursting and spalling were also experienced in reaches with cover exceeding 700 m (Sati et al. 2011).

172.5.6 Maneri Bhali Hydroelectric Project

Located in Himalayan State of Uttrakhand, this run-of-the-river scheme has water conductor system comprising a 6.0 m diameter and 16 km long head race tunnel (HRT). According to Gajbhiye and Bhattacharjee (2011), the HRT below Dhanari Gad was being driven through highly jointed and frequently sheared whitish cream quartzite of Proterozoic Garhwal Group when it abruptly encountered river borne sediments accompanied by ingress of large quantities of water under high head. The incidence delayed the progress of the HRT considerably and further advance could be made by bypassing the zone by realigning the HRT and resorting to intensive pre-grouted umbrella arch over the crown.

In addition to the above, several other projects suffered badly due to abrupt ingress of large quantities of water flooding the tunnels. Some of the better known incidences are from projects like Beas—Satluj Link Project with HRTs in two stretches of 13 km length each and Nathpa Jhakri Hydroelectric Project with 27 km long HRT. In case of Nathpa Jhakri HEP, the HRT also encountered hot water with temperature going up to 68 °C.

172.6   Conclusions

With its fast developing economy and its ever increasing demand for energy, India has no other option but to harness the vast hydroelectric potential of the great Himalayan chain. These young mountains, in general, are characterized by rugged topography, high relief, deep valleys with steep and high slopes, thick soil supporting dense vegetation in middle and lower reaches, thick glacial deposits in higher reaches, complex geology and high seismicity. These factors result in retarding the development of infrastructure facilities in many remote areas. The hydropower developers, therefore, face serious constraints in carrying out desired investigations for the project components. In particular, due to wide variations in ground conditions and high superincumbent cover, long tunnels face the maximum brunt and usually remain the most poorly investigated components of the projects. The excavation of such tunnels, therefore, springs up problems that are not fully appreciated during project planning. Huge quantities of subsurface water, particularly the flowing ground conditions, are the most common and dreaded tunneling problems. These are capable of stalling construction activities in a big way and result in over runs of cost and time in project execution. The losses to the developer sometimes assume colossal proportions.

It is, therefore, imperative that all out efforts are made during the investigation stage so that a dependable geological model along the tunnel route is developed and the construction methodology defined precisely with dependable estimation. Based on project specific geological and hydrological conditions, the standard investigations through geological mapping, remote sensing, drilling, drifting, geophysical surveying, etc. are to be blended and optimized. Since, the investigation results are not expected to be fully satisfactory, construction stage investigations attain great importance. Over and above the standard investigation approach, the following investigation strategy may help achieve greater information. It would also be advisable to supplement the investigations with other state-of-the-art global technology. It is reiterated that an extra expenditure in investigations, both during investigation stage as well as during construction stages, will give ample rewards during implementation stage. Along with the investigations, it is also necessary to assess the

risk factors and keep remedial plans ready for managing them efficiently (Mcfeat-Smith 2008).

172.6.1   Investigation Stage

Detailed geological mapping, the backbone of any investigation campaign, with a good blend of remote sensing, regional geology, and review of existing information from neighboring projects, if any, is the most effective mode of investigation, both technically and commercially. For reasons of accessibility constraints, the data collection would be nearest to the tunnel alignment, followed by data projection and development of geological model. Absolute judicious decisions are to be exercised in the observed ground condition, i.e. lithological and structural variations.

The geo-hydrological conditions, particularly the locations and discharge details of surface water sources like springs and nalas are to be recorded and integrated in to the geological model.

Subsurface investigations by drilling, drifts and geophysical surveying may even be carried out in geological test sections away from the tunnel alignment, but the conditions must be fairly similar to the projected conditions along the tunnel alignment.

172.6.2   Construction Stage

Advance probing by percussion drilling combined with occasional core drilling, if required, for tunnel forecast is a well established construction stage technique, but, is often sacrificed for much less important aspects. Elaborate observations and interpretation during the drilling operation by an expert geologist can provide vital geotechnical and engineering geological inputs that can lead to planning of timely and adequate remedial measures averting disastrous tunneling problems. Such religiously followed approach during the construction of 14 km long Banihal railway tunnel in Jammu and Kashmir through most complex geological setting proved a boon and helped complete the project in time.

Other indirect advance probing techniques like Tunnel Seismic Profiling (TSP) may be adopted depending upon the ground conditions.

On site preparations for dealing with heavy subsurface water ingress, e.g. pipe roofing, drilling and grouting, adequate arrangement for pumping, etc. need to be kept in readiness for use whenever the requirement arises.

Ambiguity in tunneling contracts, particularly for less practiced TBM driven tunnels, led to lack of clarity in dealing with emergent situations and has resulted in unprecedented delay of many projects by several years. The contracts for such projects must have provisions for handling

the emergent situations in clear terms with roles of each agency or individuals clearly defined so that decisions are taken quickly and implemented on war footing.

References

Deva Y, Dayal HM, Mehrotra A (1994) Artesian blowout in a TBM driven water conductor tunnel in North-West Himalaya, India. In: Proceedings of 7th international congress IAEG, Portugal, Balkema, Rotterdam, pp 4347–4354

Gajbhiye PK, Bhattacharjee NR (2011) Tunnelling through weak and water charged strata by ground improvement—a case from Maneri Bhali HE Project-II, Uttrakhand. Abs. vol., international conference on underground space technology and 8th Asian regional conference of IAEG, Bangalore, India

Kalita GC (2011) Tackling of a critical zone encountered in Face-II of HRT, Kameng HE Project—a case study. Abs. vol., international conference on underground space technology and 8th Asian regional conference of IAEG, Bangalore, India

Mcfeat-Smith I (2008) Tunnelling in the Himalayas: risk assessment and management for tunnelling in extreme geological conditions. In: Proceedings of world tunnel Congress 2008- underground facilities for better environment and safety- India, pp 1748–1760

Sanders MR (2011) Tunnelling in high overburden with reference to deep tunnels in Switzerland, Spain and Iran. Abs. vol., international Conference on underground space technology and 8th Asian regional conference of IAEG, Bangalore, India

Sati KK, Sood KK, Singh P, Goyal DP (2011) Excavation of 17 km long Head Race Tunnel for 1000 MW Karcham Wangtu hydro-electric project in South West Himalaya. Abs. vol., international conference on underground space technology and 8th Asian regional conference of IAEG, Bangalore, India

Sengupta SK, Saxena PK, Bakshi SS (2008) Tunnel boring machine in India- experience, prospects and challenges. In: Proceedings of world tunnelling Congress 2008- underground facilities for better environment and safety

Winter Th, Binquet J, Szendroi A, Colombet G, Armijo R, Tapponnier P (1994) From plate tectonics to the design of Dul Hasti hydroelectric project in Kashmir (India). Engg Geol 36:211–241

Akhila Nath Mishra and S. Kannan

Abstract

The Himalayan geomorphology guides important hydrologic systems recharging ground water occurrences. Ground water conditions mainly depend on origin and occurrence of precipitation. Prediction and managing ground water occurrences in mountainous regions is difficult due to inadequacy of data. From ground water levels in the wells and the natural spring discharge levels it is possible to construct the groundwater contour maps, showing the form and elevation of water table to some extent. Tunneling in complex geological set up exhibiting highly heterogeneous rock mass conditions can be problematic, which may lead to disastrous and significant delay if not adequately foreseen in mountainous regions. High displacements, stability problems and ground water inflows are common phenomena observed during tunneling through fault zones. Advanced methods of prediction and investigation/probing ahead of the face during construction are useful to minimize tunneling difficulties and apply requisite supporting methods. The influence of ground water during tunneling through high mountainous terrain poses problems during construction by any of the TBM, DBM or NATM methods. The paper addresses ground water investigation methods and targets for obtaining the key parameters for estimating the rock mass behavior, rock mass characteristics and criteria for the selection of appropriate construction methods, based on estimations.

173.1 Introduction

Development of a region demands harnessing water resources for irrigation, power generation and to mitigate frequent floods. The importance of river valley projects in India has increased enormously during the recent years, which pose challenges to engineering skills, more so when these resources are located in the Himalayan region having complex geological conditions. Here tunnels have to encounter incompetent rock mass, with quasi-elastic folds, faults and thrusts of various magnitudes with high ingress of water .The chances of existence of the sub-terrainian water with high head is much more than that in other regions. It is

very difficult to design a suitable layout of project components in such terrain with mixed lithology, varying tectonic behavior and trapped water reservoirs with considerably high head and may become a very costly and hazardous operation. Tunnel lengths increase when the alignment is through ideal geological conditions to reduce the impact of squeezing, swelling, running ground, ingress of water with a poor state of rock, excessive temperature and gases in rocks. The past experiences gained in combating such problems have provided the technical skill to the designers and engineers for the future tunnels in the Himalayan region.

173.2 Physiographic Zones of Himalayas

The raising of Himalaya has resulted in repeated deformation of the sedimentary successions accumulated in the Tethys Sea. The Himalayas is characterized by its distinctive structural architecture and unique sedimentary and tectonic history. Himalayan mountains system stands as a series of

A.N. Mishra (✉) · S. Kannan
GMR Consulting Services Pvt. Ltd., New Delhi, India
e-mail: mishra.akhil1974@gmail.com

S. Kannan
e-mail: sknnhpc@rediffmail.com

ranges in the form of largest individual geosyncline ranges 1500 miles long and from 150 to 250 miles broad with varied structure, composition and stratigraphy from Kashmir to Assam. The long alignment of Himalayan system has been divided into : the Punjab Himalayas from the Indus to the Sutlej (563 km long); Kumaun Himalayas from the Sutlej to the Kali (322 km), Nepal Himalayas from the kali to the Tista (805 km) and the Assam Himalayas from the Tista to the Brahmaputra (1165 km long). The following four major litho-tectonic physiographic zones have been recognized, which are separated from each other by major faults and thrusts systems. (i) Outer Himalayan Siwalik belt, (ii) Lesser Himalaya, (iii) Great Himalaya, (iv) Tethys Himalaya.

The Lesser Himalayas is characterized by deep valleys and steep slopes. The majority of the hydroelectric projects are located in the Lesser Himalaya due to deep dissected valleys favorable for high dams and big reservoirs posing high water heads for power generation. The lesser Himalaya, with elevations ranging from 1500 to 3000 m, has strongly folded and thrusted sedimentary and metamorphic rocks housing huge plutonic and volcanic bodies (of Paleazoic and Precambrain age) outcropping in the dissected valleys.

173.3 Ground Water Investigation Methods

173.3.1 Field Investigative Methods

Investigation of ground water involves many of the typical challenges faced when defining groundwater flow within fractured bedrock. Experiences gained during the process emphasize combining a variety of exploratory techniques to complete the investigation. The investigation includes geological mapping, monitoring of wells (by installing and gauging); analyzing groundwater samples; conducting fracture-trace analysis, surface geophysical survey; subsurface exploration by boreholes, permeability test in bore holes and observations of discharges in probe holes during tunneling.

173.3.1.1 Fracture-Trace Analysis
Fracture-trace analysis to identify potential fracture zones down gradient of the dam site and to determine potential migration pathways to assist in locating monitoring wells. Electrical resistivity surveys are conducted to get the ground truth results of the fracture-trace analysis. Pumping tests are also conducted to evaluate the hydraulic properties of the bedrock and the fracture system in the bedrock.

173.3.1.2 Bore Hole Exploration
Subsurface field investigations for ground water needs detail study of geological and geotechnical parameters to locate bore holes at various locations to establish ground water

level and hydraulic gradients. Geological information is recorded during exploratory drilling to prepare a systematic geological bore hole log.

173.3.1.3 Electrical Resistivity Survey
An electrical resistivity geophysical survey is conducted to determine whether there is an anomaly indicative of water bearing fractured or weathered zone .The electrical resistivity (direct current) shows variations among different geological materials. Within crystalline rock, variations in resistivity are primarily due to water content within fractures and weathered zones. Therefore, a fractured or weathered zone in the bedrock is expected to show a zone of relatively low resistivity within a background of relatively high resistivity. This helps in correlating with exploratory bore hole data and other geophysical explorations, interpretations to predict ground water conditions in the area of interest.

173.3.1.4 Seismic Geophysical Survey
Two types of seismic geophysical tests are widely used in the exploration program (1) Seismic reflection testing and (2) MASW and REMI testing. The objective of the geophysical studies was to characterize subsurface geology, structure and geotechnical conditions up to a target depth of approximately 90–120 m bgs, at interested areas. Seismic reflection testing aims in collecting compression wave velocity (P-wave) information at identified locations. P-wave reflection data acquired along selected profiles, using instruments like IVITM. Mini Buggy vibratory source helps in evaluating weak zones or any fault below ground surface.

173.3.1.5 Hydraulic Conductivity Packer-Pressure Testing
Packer pressure testing is performed at 3 m intervals/segments in the boreholes to determine the hydraulic conductivity at each interval. From the recorded data of flow rates and the pressure the average hydraulic conductivity is calculated using the following formula:

$$K = (q/2nLH)\ln(L/r) \quad when\, L > 10r$$

where: k = hydraulic conductivity, cm/sec, q = constant rate of flow into test interval, cm^3/sec, L = length of test interval, cm, H = differential head of water at test interval, cm, r = radius of hole, cm, ln = natural logarithm Taking all information of Ground water level from bore hole data in the area of interest, the water table contouring can be done (Fig. 173.1)

173.3.1.6 Probe Hole
The probe holes are taken from the headings in advance for a detailed geological study of the advancing face, to predict and estimate the advancing tunneling conditions. Drilling

Fig. 173.1 Flow of ground water and contouring of water table
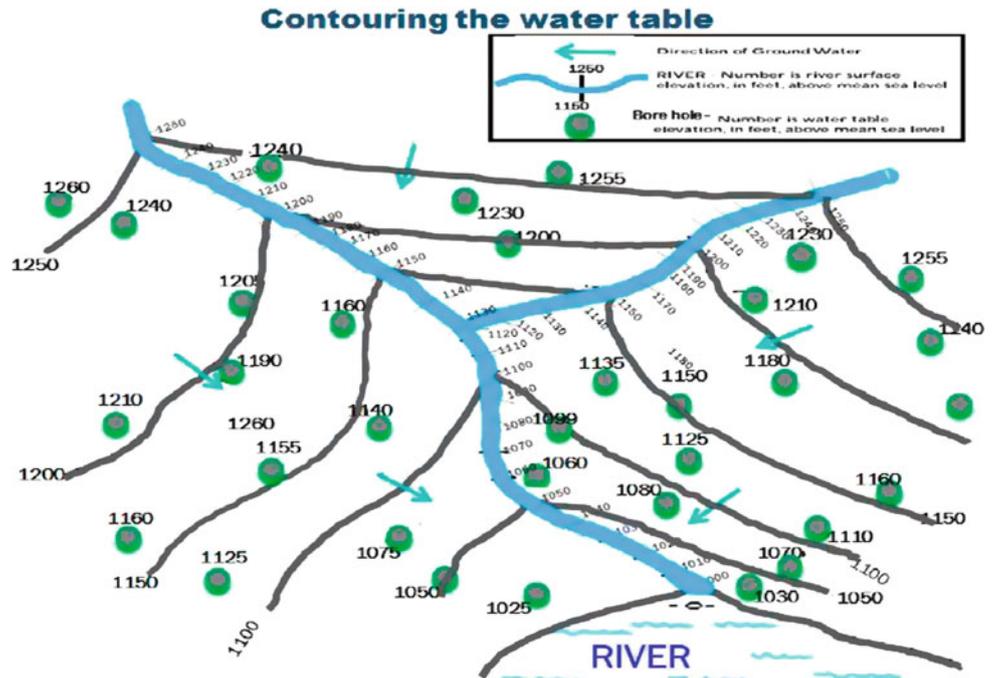
information like hammering sound, color of drilling water, nature of fine materials, penetration rate and measurements related to leakages, water loss and flowing status recorded during advancing of probe holes gives prior information of tunnel media before boring or excavation of tunnel. Problematic zones like highly permeable strata, fractured or crushed zones, fault or sheared zones detected by probe holes and its valuable interpretation of data often saves tunnel structures from driving into geological uncertainties. Information gathered on the basis of the probe holes is then employed in the tunnel excavation planning and execution of tunnel excavation which may be significant during construction. A number of probe holes can be designed to evaluate the actual difficulties if any and explore tunneling risks at predetermined locations, and plan for geological, geophysical, hydro geological or hydro chemical studies.

an alternative to classification systems. Some simple and reliable relationships out of the studies have been driven. The results from these derivations are found nearer to the results obtained through observational approach. However, the accuracy suffers due to lack of knowledge of rock-mass behavior under the state of in situ stress. The pressures generated under such conditions are capable of causing failure of heavy supports and containment/confinement is the major problem. The Himalayan region is within major earthquake region owing to the continuous collision of the plates (Plate Tectonics), and hence is subjected to so high pressures. It is an intricate problem to understand the effects of rock stresses whenever any underground excavation is planned. The problems of excessive dewatering, very high temperatures and gases in tunnels are also reported from the projects in the Himalayan region.

173.4 Tunneling Problems in Himalayas

The tunneling problems mainly squeezing, swelling and running ground conditions etc. encountered in the Himalayan region basically pertain to the stability of tunnels. The experience with different approaches for supporting the underground openings in the region reveals that the conventional rock-mass classification system (empirical approach) will help in developing realistic assessment of the design parameters. Underground works can be executed smoothly if adequate knowledge of appropriate method for computation of the parameters with expertise is timely implemented. The analytical approach has been tried upon as

173.4.1 Running Ground Condition

The running ground condition is water soaked fragmented rocks often containing larger rock fragments embedded in a matrix of fine grained material that has almost no strength and flow into tunnel as slurry. The running ground is quite a common feature found associated with faults, thick shear zone, thrusts and buried fossil valleys in the Himalayan region. The initial pressures generated by running ground may be high to cause failure of very heavy supports. The typical examples are the power tunnels of Beas Sutlej Link and Maneri Bhali Stage-II in the Central Himalayas (Table 173.1).

Table 173.1 Summary of water inflow problems of some Himalayan tunnels

S. no	Name of project, tunnel and size	Rock type	Tunneling problems
1	Yamuna hydel project Ichari Chibro tunnel 6.2 km long, 7 m dia.	Quartzite, slate and limestone	High over-break, Running and squeezing condition
2	Pandoh Baggl tunnel Beas Sutlej link 13 km long & 7.62 dia.	Phyllite and granite with schistose band and kaolinised pockets	Heavy water inflow, running ground, swelling and squeezing condition
3	Maneri Bhali stage-I HRT16.8 km, 6 m dia.	Quartzite, basic rocks, lime stone and slate	Heavy water inflow, squeezing condition and high overbreak
4	Maneri Bhali stage-II HRT16 km, 6 m dia.	Metavolcanic, quartzite, lime stone, phyllite and graywacke	Running ground conditions, high squeezing and roof collapse condition
5	Nathpa Jhakri HEP HRT 30 km, 5 m dia.	Gneiss, granite, schist and amphibolite	Mild squeezing and excessive running ground conditions
6	Tenga hydel project HRT 16.5 km, 5 m dia.	Granite gneiss, schist, phyllite, quartzite, shale and sandstone	Running ground condition, water inflow, Mild squeezing condition and gases in rock
7	Loktak hydel project power tunnel 6.25 km, 3.65 m dia.	Sandstone and shale	Heavy water inflow, excessive pressures and gases in rock
8	Uri-II hydro project tail race tunnel	Sandstone, siltstone, shale and fluvio-glacial material	Flowing and frequent flooding condition and excessive dewatering
9	Dul Hasti HEP HRT 9.5 km, 8.3 dia.	Quartzite, phyllite and weak mylonite	Heavy water inflow, cavity formation and TBM buried
10	Tapovan Vishnugad HEP HRT 11.97 km, 5.4 dia.	Gneiss, quartzite, schist and meta-basics	Heavy water inflow, Rock fall, TBM stuck

173.4.2 Hot Springs and Geothermal Zone

Problems of excessive temperature (39–40 °C) are reported in the power tunnel, of 3.2 m excavated diameter, of Bhabha Hydro Electric Project in Central Himalaya which lies within the zone of lesser and Greater Himalayas. Most of hot springs are located along this zone. Underground temperature of water, rock and humid tunnel atmosphere when exceed about 32 °C make working conditions very difficult. An extensive system of refrigeration or rapid circulation of tunnel air is required to work in tunnel having temperature beyond 32 °C. The problem of this project was tackled by supplying fresh air through efficient ventilation, reducing the pull per blast to 1.0-1.2 m per day and by introducing the alternative rotation of workmen for short period, in order to take care of exhaustion. Similar thermal problems were anticipated in the tunnel of Nathpa Jhakri Project since two geothermal zones, Nathpa-Sholding (2.5 km long) and in Wadhal-Manglad (3.37 km long) sections, were encountered along the tunnel route. The HRT was expected to pass through folded metamorphic rocks comprising gneiss, quartz-mica schist, amphibolite and some granite and pegmatite. In the Nathpa–Sholding section (Ch. 1,600–4,100 m) hot water (34.5 ºC–50.7 ºC) was encountered locally at some places. The Wadhal—Manglad geothermal zone (Ch. 17,067 m and 20,440 m) began with a major hot water blowout (54 °C; 90–100 l/s) that flooded the tunnel to about

300 m from the heading as the tunnel gradient did not permit natural drainage.

173.5 Construction Method

Generally construction of tunnel by conventional drill and blast, NATM or by TBM method requires considering the all relevant aspects of tunneling like size of project, geological set up, equipment deployment, de-watering techniques, timely support & required skilled manpower to deliver a project as per schedule economically (Table 173.2). Conventional excavation is the excavation performed by conventional tunneling and shaft driving methods using drilling and blasting or by manual means. Multi-drift /multi-segmental excavation is defined as excavation of tunnel heading in segments. TBM excavation provides considerable advantages with high progress rates and some cost savings from the elimination of temporary construction of structures, in comparison to conventional Drill and Blast.

173.6 Ground Water Management

When ingress of water is too high causing hindrances in tunneling activity, normal practice of tunneling halts and generally pre injection grout method and use of polyurethane

Table 173.2 Summary of construction methods and difficulties in Himalayan tunneling

Feature	Drill and blast	TBM
Stability	Lossening of ground rockmass, wedge failure and roof collapse Increases water inflow	Mechanical solutions for temporary stabilization of the face area, and the rear zone
		Naturally stable
		Ideal for mass transit, pilot tunneling, unlined hydro and water conveyance tunnels
		Superior flow characteristics may eliminate lining requirement
Shape	Irregular excavated tunnel profile due to presence of over/under break	Smooth bored tunnel profile
Overbreak	Overbreak increases	Over-break negligible
Support	Demands additional rock supports Costly filling with concrete	Tunnel support may be reduced by 90 %
Operating	All skills required very cyclic, dangerous and unpleasant working environment	Continuous (non cyclic),repetitive operation safer and more pleasant working environment than in drill and blast
Blasting	Reduces stability	Eliminated
Crews	All skills required under high risks	Mechanical solution available for stability and temporary support at the face, work area and permanently behind the excavation operation
Access structure	Shafts and adits necessary to open multiple headings	Can eliminate all temporary access structures, particularly if the project is well laid out

grout are considered to manage the ground water. Such advanced ground water stabilization methods minimize tunneling risks.

173.6.1   Pre Injection Method

Modern pre-injection method of grouting ahead of tunnel heading offer significant advantages in avoiding mishaps and hindrances during situations like water ingress or mechanically poor ground. The basic idea of pre-injection is to treat the ground prior to the excavation by injecting a grout into the ground, surrounding the tunnel, through drill holes by the pumping under pressure. Modern cost effective methods and material technology for pre-injections with rapid setting micro cement in combination with colloidal silica in underground construction aims at strengthening the ground conditions, hence improving the stand-up time as much as possible during construction. Exploratory drilling, layout of grout holes, injection method, type of grout and grout mix designs are the main features for pre-injection grouting. Evaluation or control of the injection needs site specific decisions regarding repeated injections or to commence excavation through the treated ground after grout injection till the termination criteria is reached. Deployment of drilling machine and drilling method needs input of ground properties and its limitation for length of drill, cycle of probe drilling, injection fan drilling and grouting packers to suit the required hole/pipe diameter. Wastage of grout can be controlled by close monitoring of all processes involved to avoid hydro-fracturing or unwanted injection of grout far away from the structure.

173.6.2   Polyurethane Grout

Polyurethane grout can be extremely useful which reacts with water and expand due to production of CO_2 and it has proven successful when grouting with cement suspension does not work in sealing rock openings and post grouting has to be performed. The joint openings may be too narrow for the particles in the cement to enter, or flowing water in the rock transports the suspension away and/or dilutes it. Advantages of the process are (i) polyurethane grouts have better penetrability, because they don't contain particles and (ii) they can be used to control the cement propagation, since their gel time can be programmed. The viscosity of polyurethane is higher than that of water; the polyurethane front is stable when it is pumped into ground water. A resolute or absolute grouting pressure should be used when polyurethane grout is pumped into flowing water i.e. sufficiently high to cut off the water flow and facilitate grout penetration upstream, thus preventing flushing out of the grout.

173.7   Conclusion

Managing adverse ground water occurrence properly during the execution of underground works is the key to accelerated implementation of tunneling projects. Adequate geological investigation during project report preparation and its interpretation, reliability of the predicted geology and the predictions on the ground water conditions likely to be encountered is very important for the designers and executing agency. This enables the associated agency to plan accordingly and make adequate provisions in the contract documents to handle such situations. Continuous geological monitoring of the rock mass and predictions by project geologist during execution, inputs from expert committees helps the designers to go in for mid-way corrections in the designs. Prompt decision making by the implementing agency is vital in managing adverse ground water occurrences.

References

Bajaj AK, Sing TP, Chandra shekhar Iyer J Managing adverse geological occurrences-key to accelerated implementation of underground hydropower projects. Central Water Commission, New Delhi, India World Congress 2008-underground facilities for better environment and safety-India

Geotechnical site investigations for underground projects, volume1 and volume2 (1984) National Academy Press, Washington D. C

Hoek E, Palmeiri A (1998) Geotechnical risks on large civil engineering projects. International Association of Engineering Geologists Congress, Vancouver, Canada, 21–25 Sept 1998 (Keynote address for theme-I)

Schubert W, Fasching A, Goricki A Tunneling in fault zone-state of the art Lee I, Mo In, Yoo C, You K (eds) Safety in underground space, proceedings of the ITA-AITES2006 World Tunnel Congress

Sharma HK, Chauhan RS, Kuthiala S Challenges in design and construction of HRT of Nathpa Jhakri hydroelectric project (1500 mw)-A case study, Satulej Jal Vidyut Nigam limited, Shimla, India. World Tunnel Congress2008-underground facilities for better environment and safety, India

U. S. Army Corps of Engineers (1984) Geotechnical investigations, EM1110-1-1804, Feb.1984

Convener Dr. Antonio Dematteis—*Co-conveners* Joe Gurrieri, Alessandro Gargini, Giona Preisig

The concept of sustainability of tunnels needs the achievement of correct management of groundwater in tunnel projects. Equally, attention should be given to environmental and construction impacts and to opportunities that can be obtained exploiting drained waters, including the heat that it is often associated with. This session is directed to all operators in the field of design, supervision and construction of tunnels, such as universities and research institutes, designers, construction companies, control authorities, contracting authorities. Interesting topics for this section are the following: past experience; water inflow rates; examples of exploitation of water and heat; methods of forecasting; technologies for drainage, waterproofing and collecting; impact on Groundwater Dependent Ecosystems; risk and mitigation analysis; communication to decision makers and concerned peoples; laws, rules and policy framework.

Riccardo Torri, Nathalie Monin, Laudo Glarey, Antonio Dematteis, Lorenzo Brino, and Elena Maria Parisi

Abstract

Recent progress in underground excavation technology allows the construction of deep tunnels for the complementary exploitation of road, civil and hydroelectric infrastructures, e.g., the uptake of renewable hydroelectric and geothermal energy sources. This approach is employed to assess the positive effects of a civil work on a social and manufacturing community. The article describes the methods adopted for the study and design of the Lyon–Turin railway Tunnel, and identifies scenarios for exploitation of the drained hot water. Hydrogeological and geothermal models show the presence of a localized water inflow, with temperatures over 40 °C within tunnel sectors under the highest topographic covers (around 2,000 m). A standard for the water intake structure in the tunnel has been defined. Potential users of the resource have also been identified. An evaluation of energy facilities programs for domestic and industrial purposes has been carried in order to favoring local communities involved by the project. Characteristic elements are used to define the energy potential and ways of employment of the warm water drained by the tunnels and available at their portals. Potential consumers of the resource are also indicated.

Keywords

Tunneling • Hydrogeology • Geothermal energy potential • Geothermal model • Groundwater

174.1 Overview of the Lyon–Turin Project

The 57 km length basis tunnel between St-Jean-de-Maurienne (Savoy, France) and Susa (Piedmont, Italy) is a part of the future new railway link which will connect 2 main European cities: Lyon and Turin. This new railway belongs to the Trans-European Transport Core Network (Mediterranean corridor) which will link Algeciras in Spain to Budapest and the EU border. Preliminary works on the French side, involving the construction of 3 access galleries in the Maurienne Valley, are now completed with the excavation of around 9 km of tunnels in various kind of rocks. All these access galleries allowed a better understanding of the geological structures. On the Italian side, a new preliminary tunnel is in progress: the Maddalena survey gallery.

In this article we present a hydrogeological and geothermal reference model with some suggestions for deriving the best advantage from the water drained by underground works. The evaluation has been carried out for the main tunnel from its highest point to the eastern portal and for the accessory tunnels (Maddalena adit and Clarea ventilation

R. Torri (✉) · A. Dematteis
SEA Consulting Srl, C.so Bolzano 14, 10100, Turin, Italy
e-mail: torri@egteam.eu

N. Monin · L. Brino · E.M. Parisi
LTF SAS, Chambery, France

L. Glarey
Lombardi SA, Minusio, Switzerland

well) in Italy; a similar analysis for the French part of the project is still in progress.

A main principle of the 'New Lyon–Turin rail-link' project is to minimize water drainage induced by the underground works. This is thought in order to reduce (i) the impacts on the water resources and (ii) problems created by water inflow during the excavation and utilization of the tunnel.

174.2 Hydrogeological and Geothermal Model

The tunnel crosses a variety of paleogeographic and tectonic geological units.

For the deep-lying trans frontier Lyon–Turin basis Tunnel several borehole temperature measurements have revealed the local geothermal gradient. A geothermal numerical model carried out during the previous project phases (Brino et al. 2008) assigned a specific thermal conductivity and geothermal gradient to each geological unit crossed by the tunnel; moreover, the project has been differentiated thermally in homogeneous sections.

According to such a model, specific temperature values have been assigned to the water inflows predicted along the tunnel to evaluate their thermal potential. The final temperature of the mixed water expected at the eastern portal was estimated to assess the possibility of their exploitation. In the Table 174.1, the geothermal gradient and the temperature range expected at the basis tunnel elevation (from the high point to the Italian portal) are given.

The temperatures and the geothermal gradients decrease owing to the presence of water flowing along the shear zones from the surface to the deep portion of the rock mass.

The central sector of the tunnel alignment is of thermal significance: it will be excavated under about 2,000 m of overburden through the metamorphic rocks of the Ambin Massif. Water inflows are expected mainly at the interception of faults and deformation zones; discharge rate, chemistry and water inflow temperature depend on the connection degree with their recharge areas at the surface.

Table 174.1 Geothermal gradients and their variation for the tectonic units involved by the excavation of the basis tunnel, from its highest point to the Italian portal. The temperatures range expected at the basis tunnel elevation is also given

Tectonic Unit	Geothermal gradient (°C/km)	Temperature at tunnel elevation (°C)
Gypsum Nappe	20–30	22–31
Ambin Massif	25–33	21–47
Tectonic fault zone	16	12–22
Piemontese Nappe	17–25	10–20

However, the geothermal model proposed for this sector provides temperatures higher than 40 °C (about 47 °C) related to the normal geothermal gradient measured in the boreholes perforated in the external belt of the Ambin Massif.

174.2.1 Evaluation of the Potentially Exploitable Water Inflow

Exploitation of the water inflow has been evaluated in function of the hydro-geochemical parameters. These parameters permitted to distinguish water aggressiveness and potability (sulphates and chlorides); by reconstructing the global and local geothermal gradient, potable waters with temperatures up to 25 °C and warmer waters available for thermal exploitation have been separated.

In keeping with the current French (Arrêté du 11 janvier 2007) and Italian regulations (D.Lgs. 152/2006, D.Lgs. 30/2009), the criteria for evaluation of the exploitable water potential have set the threshold at 250 mg/l for the contents of sulphates and chlorides and at 25 °C for the water temperatures; regarding to the inflow type an intermittent discharge has been distinguished by a continuous.

A cross analysis between data from deep boreholes (i.e. hydraulic packer test, temperature logs and hydrochemistry analysis) has led to hydrogeological characterization of metamorphic rocks lying at the tunnel elevation.

The central part of the Ambin Massif meets all water exploitation criteria: high topographic covers (>2,000 m), a normal geothermal gradient (30 °C/km) and a medium to medium-low permeability degree of the fissured rock (K ≅ 1E-07 m/s). The discharge of drained water in this sector is about 40 l/s with a temperature of 46 °C. A low sulphide (about 50 mg/l) and chloride content (about 100 mg/l) is expected.

Assessment of the water exploitation must take account of the possible contribution of the Clarea and Maddalena tunnels that drain into the basis tunnel since they intersect its alignment at the deepest sectors of the Ambin Massif. The data collected during the excavation of the Maddalena survey gallery will provide very useful information for evaluation of the current water exploitation potential.

The total flow, coming from the water available along the main tunnel and at the intersection with the Clarea and Maddalena adits, could range between about 40 (basis tunnel only) and 100 l/s (basis tunnel plus the adits).

The real exploitation potential of the waters drained in the tunnel, of course, can only be evaluated in steady-state conditions, and once the works are finished. Depending on the hydrogeological conditions encountered during excavation, the characteristics of the water drained within the tunnel and collected for exploitation must remain stable over

time. Depending on the most fruitful exploitation scenario, therefore implementation of the monitoring protocols established by the current legislation and good-practice design is essential.

174.3 Possible Exploitation Scenarios

174.3.1 A Standard Operational Approach

In general terms, punctual water inflow possesses the best exploitation characteristics. From an operational point of view, the following steps must be foreseen and considered during the excavation phase:

1. construction of a temporary uptake structure;
2. definition of a monitoring program of the punctual water inflow for measurements of discharge rate, electrical conductivity, temperature and pH (for at least one year);
3. characterization of water quality by hydro-geochemical, bacteriological, isotopic and radiometric laboratory tests (for at least one year and according to regulations, depending on the type of use expected).

Determination of the final water intake system requires the definition of the following parameters: (i) identification and localization of the main water inflows; (ii) Discharge rate of water inflow; (iii) hydraulic head of water inflow; (iv) water quality; (v) administrative concessions and current legislation; (vi) technical specifications of construction materials and definition of the excavation technique(s), depending on the hydrogeological context.

174.3.2 Energy Potential of the Water Drained by the Basis Tunnel

The energy potential of warm water has been preliminarily evaluated with the relation:

$$Pot = P * C * D * dT$$

where, *Pot* is the thermal power [w], *P* is the discharge rate [m³/s], *C* is the specific heat of water [4,186 J/kg/K], *D* is the water density [997 kg/m³] and *dT* is the thermal gradient [K].

The analysis gave the temperature of the waters released from the energy plant. This is an important factor to evaluate the environmental impact subsequent to their introduction into the natural hydrographic network at the surface. Assuming the use of a simple heat exchanger, the following energy potential values were defined, based on the thermal gradient and upon a discharge rate of 100 l/s and a water temperature of 36 °C issued from the design (Table 174.2).

Table 174.2 Energy potential defined in function of the design input data and thermal gradient

Input water temperature (°C)	Output water temperature (°C)	Thermal Gradient (°C/step)	Energy Potential (kW)
36	31	5	2,000
36	26	10	4,000
36	16	20	8,000

174.3.3 Evaluation and Identification of the Potential Users of the Resource

Some scenarios for an energy development strategy for domestic and manufacturing purposes, in favor of the local community initiatives in the region interested by the basis tunnel project, are depicted in the following paragraphs. A study on the energy needs and outcomes of such a development strategy on the local social and cultural context must be part of the project's objectives. For this reason the following proposals have been developed:

1. Heating of the building and water of a public swimming pool;
2. Heating of the buildings and domestic hot water production in the international railway station and safety station (solution internal to the railway line project);
3. District heating system serving the local Municipality.

The heating of swimming pool water, commonly at temperatures as high as ∼28 °C, would be possible using a simple heat exchanger (without heat pump); however, the installation of a heat pump must be considered in the case of the building and/or district heating system, in order to attain temperatures around 36 °C.

An operating heat pump for such purposes requires the availability of a certain electric power (see next tables). (Table 174.3).

It must be noted that the thermal potential naturally available is much higher than the demand for the two cases of the public swimming pool and the international railway station (2,301 kW compared to 400 kW in the case of the pool and 830 kW in the case of buildings of the station and safety area).

The construction of a district heating plant is a realistic option. Its size could be similar to those implemented in cities such as Sondalo and Tirano (Central Alps, Northern Italy), as the latters are very similar to Susa both in terms of demographic characteristics and logistics (as in altitude and geo-morphological context). The water output temperature is about 16 °C. The thermal power capacity is equal to about 4*2,500 kW (10 MW). The heating capacity of water leaving the Basis Tunnel would thus be fully exploited.

Table 174.3 Main characteristics of the heating systems for the developed proposals

Proposal	Heat demand rated (kW)	Thermal capacity (kW)	Preliminary characteristics of the system
Communal swimming pool (building included)	400	2,301 (equivalent of 20 apartments)	Nr of heat pump: 1
			Heat pump type: water/water
Building of the International railway station	830		Electric power demand: 403 kW
			COP: 5.71
			Output water temperature: 31 °C
District heating plant	10,000	10,082	Nr of heat pump: 4
			Heat pump type: water/water
			Electric power demand: 1,838 kW
			COP: 5.49
			Output water temperature: 16 °C

174.4 General Considerations

The water exploitation study includes, as a first step, subdivision of tunnel alignment, in order to exploit the sectors with the most significant geothermal features (e.g. T > 25 °C) via special pipes, depending on the intended purpose.

Possible use of warm waters from the Basis Tunnel can be confirmed, as well as feasibility of the proposals depicted in this paper, such as:

- heating of a public swimming pool;
- district heating system;
- heating/cooling of the railway station buildings;
- other possible initiatives near to the portal (fish farms, nurseries, etc.)

Other possible ways to exploit the warm waters drained by the Basis Tunnel have been considered; they could be:

- Realization of glasshouses to grow exotic fruit and vegetable species;
- Realization of water catchments to farm sturgeons and/or produce caviar.

These options have been already realized at the Tropenhaus in Frutigen (Switzerland), at the northern portal of the Lötschberg Tunnel (water discharge rate 110 l/s, temperature 17–20 °C) (Hufschmied and Brunner 2010).

All the above solutions are viable thanks to the characteristics and thermal potential of the waters drained by the Basis Tunnel.

References

Arrêté du 11 janvier 2007, Annexe I, Partie II, Tableau B relatif aux limites et références de qualité des eaux brutes et des eaux destinées à la consommation humaine mentionnées aux articles R. 1321-2, R. 1321-3, R. 1321-7 et R. 1321-38 du code de la santé publique

Brino L., Monin N., Poti P., Piraud J. and Buscarlet E. (2008) Modélisation géothermique et système de refroidissement pour le tunnel de base de la nouvelle liaison ferroviaire Lyon-Turin, Congrès International AFTES 2008, Monaco, 6–8 ottobre 2008, pp 31–37, Edition Spécifique

Decreto Legislativo 3 aprile 2006, n°152—Norme in material ambientale. Pubblicato nella Gazzetta Ufficiale n. 88 del 14 aprile 2006—Supplemento Ordinario n. 96

Decreto Legislativo 16 marzo 2009, n°30, Allegati 3 e 5—Attuazione della direttiva 2006/118/CE, relativa alla protezione elle acque sotterranee dall'inquinamento e dal deterioramento. (09G0038). pubblicato nella Gazzetta Ufficiale n. 79 del 4 aprile 2009

Hufschmied P. and Brunner A. (2010) The exploitation of warm tunnel water through the example of the Lotschberg Base Tunnel in Switzerland. Geomech Tunn 3(5). doi:10.1002/geot.201000045

Impacts on Groundwater Flow Due to the Excavation of Artificial Railway Tunnels in Soils

175

Gabriele Bernagozzi, Gianluca Benedetti, Francesca Continelli, Cristiano Guerra, Renato Briganti, Santo Polimeni, Giuseppe Riggi, and Fabio Romano

Abstract

The engineering design for tunnel excavation in soils may produces an hydrogeological barrier to the natural groundwater flow. Upstream of the tunnel the groundwater table may rise while downstream may be lowered. This paper examines three case studies, all in a urban context (Turin, Parma and Venice—Italy). For each case a brief geological framework is provided, as well as performed Modflow models for investigating this problematic are presented. The quantified perturbation induced by the hydraulic barriers shows the classical behavior on the natural groundwater hydrodynamic leading to rising/lowering water table.

Keywords

Railway artificial tunnels • Hydrogeological barrier • Modflow models

175.1 Foreword

Realization of civil engineering works below the groundwater table generates an interference to the natural groundwater flow. In general, for excavation in soils, a sheetpile network or diaphragms walls is implemented, which may be an obstacle to groundwater flow leading to an increase and a decrease of the water table upstream and downstream of the barrier, respectively (Fig. 175.1). This effect cannot be neglected in the design phase as changes in groundwater level, may induce flooding events in basements of structures located upstream of the excavation and settlements of buildings foundations

located downstream. This issue is investigated for three case studies. Changes in groundwater level due to hydraulic barriers, may also have environmental impacts in rural areas that always have to be evaluated in design phases.

175.2 Case Studies 1: Artificial Tunnel at Nichelino Railway Station Near Turin

The study was carried out in the context of the railway line doubling between Turin and Pinerolo. All the railway path is built at the surface, except for a part of about 2.5 km at the Nichelino station, which is an artificial tunnel. Excavations are supported by diaphragms walls at depth of about 18 m. Soils were characterized by an extensive survey campaign mainly performing boreholes. All available data were used to process a reference geological model of the site. In this area from ground level up to about 20 m of depth there are Quaternary alluvial and fluvial-glacial deposits overlaid on Astiane sands, Lugagnano clays and Villafranchiano silty sands at greater depths (Bondesan et al. 2008). The Modflow model has been divided in two layers: (1) the top layer (20 m thick) with horizontal permeability of 8×10^{-5} m/s corresponding to Quaternary alluvial deposits and (2) the lower layer, with

G. Bernagozzi
Free lance, Bologna, Italy

G. Benedetti (✉) · F. Continelli
ENSER S.R.L., Faenza, Italy
e-mail: gianluca.benedetti@enser.it
URL: http://www.enser.it

C. Guerra
Free lance, San Marino, Republic of San Marino

R. Briganti · S. Polimeni · F. Romano
ITALFERR, Gruppo Ferrovie dello Stato Italiane, Roma, Italy

G. Riggi
ITALFERR, Gruppo Ferrovie dello Stato Italiane, Milano, Italy
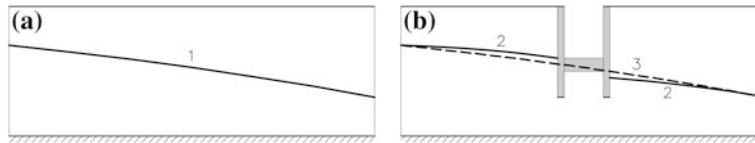
Fig. 175.1 **a** Natural groundwater table before the construction; **b** situation after the construction. *1* natural groundwater table; *2* effect of the hydraulic barrier on the groundwater table; *3* natural groundwater table before the excavation

variable permeability depending on the encountered lithology. Boundary conditions match surface hydraulic with constant hydraulic heads for Sangone river at north, Po river at east, Chisola river at south (Fig. 175.2).

Model calibration has been performed by multiple trial runs varying permeability of layers in a reasonable range of values in order to obtain the best match between measured and simulated data.

Perturbation produced by the realization of the tunnel has been simulated with no-flow cells conditions. For a conservative approach diaphragm walls reach the Quaternary base. Maximum variations between before and after excavation perturbation detected by the model are of 40 cm close the tunnel, with a rapid attenuation away from the path. In Fig. 175.1 is shown with a dashed line the area with variations of 15 cm. Positive changes are indicated with a plus sign (+), while negative ones with a minus sign (−).

175.3   Case Studies 2: Natural Tunnel Between Mestre and Venice Airport

The project design connect the railway station of Mestre with the Venezia Marco Polo airport. The path of about 8 km long, will be developed almost entirely in natural tunnel with the exception of a short part close to the Mestre railway station. The first part of the path will be realized in an artificial way: excavations will be supported by diaphragm walls driven to a depth of about 20 m from the ground level. Soils affected by the excavation are of alluvial type, always with a high fraction of fine materials. More permeable lenses, which correspond to riverbed fill material deposits, have an average permeability of about 10^{-5} m/s while deposits between alluvial cones have a lower permeability of about 5×10^{-8} m/s. The area has

Fig. 175.2 Hydrography, boundary conditions and simulated hydraulic heads (*H*) for Turin Pinerolo railway close to Nichelino underground station. *1* Turin Pinerolo railway line; *2* Nichelino underground station; *3* limits of the Modflow model; *4* Sangone, Chisola and Po rivers; *5* groundwater table before excavation. *Bottom right corner*: matching between simulated and measured hydraulic head before tunnel excavation
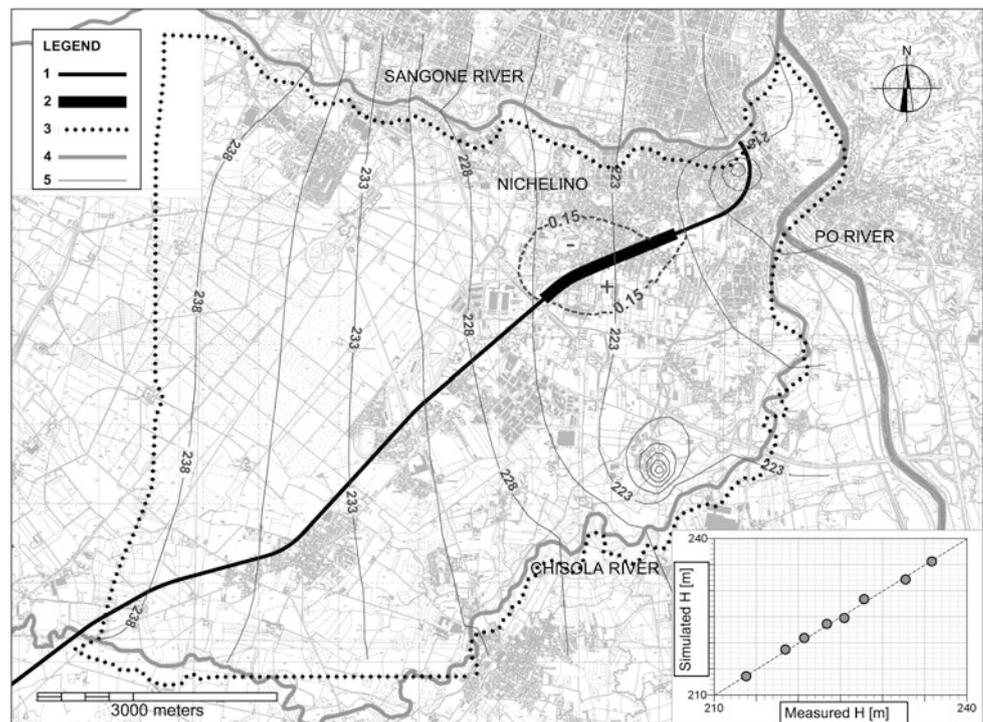
Fig. 175.3 Schematic representation of the Modflow model between the railway station of Mestre and Venezia Marco Polo airport. *1* Artificial tunnel designed with diaphragm walls; *2* design natural tunnel; *3* boundary conditions at hydraulic constant head; *4* artificial channel; *5* model limits; *6* reclaimed land drained by water pumps and channels; *7* groundwater table before the tunnel excavation
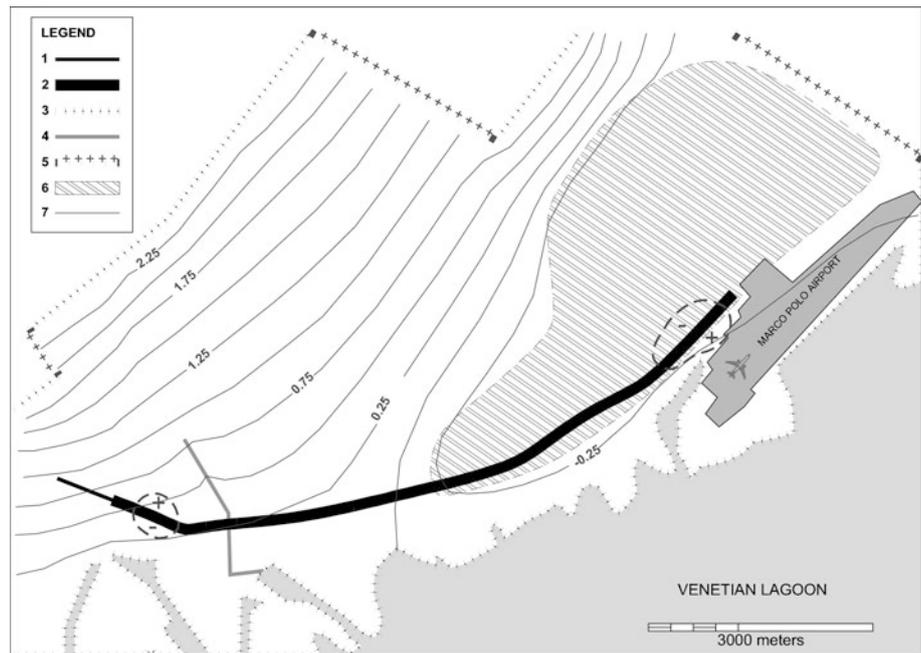
been intensively investigated over the years, because of the characterization and remediation campaigns carried out at the nearby industrial complex of Marghera. The reference hydrogeological model was constructed via the interpolation of hundreds of boreholes and water wells logs. The final result is a Modflow model with 9 layers of about 5 m thick. Each layer is obtained by the spatial interpolation in the horizontal direction of the available permeability data.

The model has dimensions of 11.5 km in the East–West direction and 8 km in the North–South direction.

The boundary condition set downstream was the Venice lagoon, modeled as a hydraulic constant head at 0 m. Given the shallowness of the lagoon this condition is limited to the upper layer of the model. Upstream the hydraulic head is constant and identified on the basis of the reference isophreatic lines. Monitoring data and available hydrogeological maps show that in the North West area of Venezia Marco Polo airport there is a portion of land with groundwater level below the sea level. This phenomenon is due to the drainage of water from a network of channels for land reclamation purposes. In the southern part of the model there is also an artificial channel that extends inland up to intercept the tunnel path. This channel has been simulated using the River function of the software.

The model was calibrated by successive approximations primarily by changing the drainage level and the conductance in the area affected by the land reclamation and secondly by acting on the artificial channel features. The result, which demonstrates a good correlation with the reference hydrogeological map, is shown in Fig. 175.3.

Fluctuation of natural groundwater flow are extremely modest and always contained within a few tens of centimeters. The explanation is to be found in the hydraulic gradient, which is very low, and in the fact that the tunnel thickness is small in comparison to the aquifer system thickness. In the airport area after the tunnel construction the water tends to be depressed North of the construction and raised South of the construction. This effect is explained by the drainage action which results in a groundwater flow from the lagoon to the land.

175.4 Case Studies 3: Artificial Tunnel Along the Parma Osteriazza Railway Line

The study area is located between the rivers Taro and Parma. Excavation works will affect the shallow aquifer, located from 35 to 10 m from ground level. Top of the aquifer there is a clayey layer of about 10 m of thickness which can be
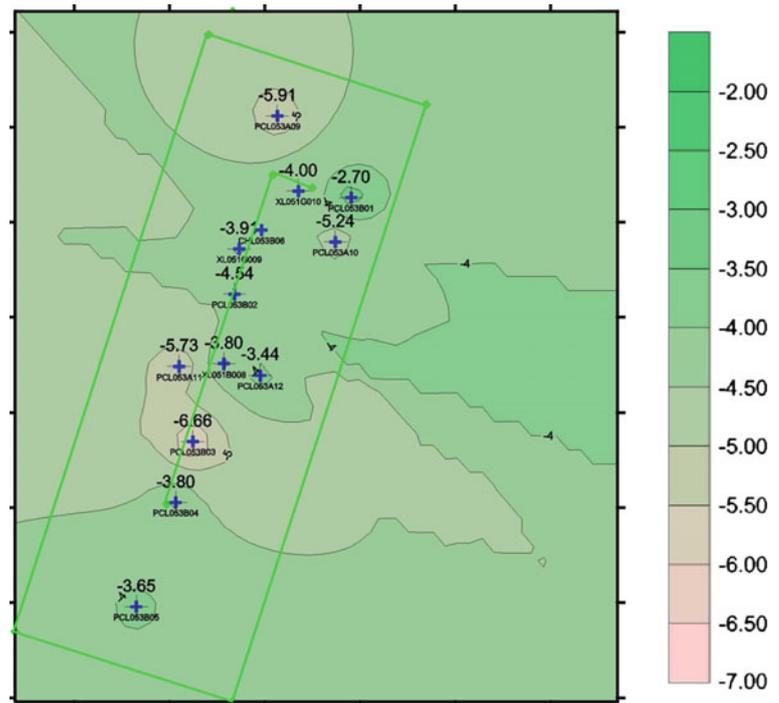
considered substantially impermeable. The aquifer is composed mainly of sands and gravels with varying percentage of silt and clayey discontinuous lenses inside. The hydraulic gradient is about 0.001, with flow from North to South in confined conditions. The aquifer permeability was investigated through a series of Lefranc tests and the average values is equal to 3×10^{-4} m/s. (Fig. 175.4)

A Modflow model and an analytical analysis based on the method of fragments (Pavlovsky 1956; Harr 1962; USACE 1993), have shown that the interference increases in relation with hydraulic gradient changes. Acting with a conservative approach, the model was created imposing a gradient of approximately 5 times higher than that observed. Also in these conditions, changes in hydraulic head were always contained within a few tens of centimeters. The reason for the low interference is probably due to the fact that the tunnel direction is almost parallel to groundwater flow.

175.5   Conclusions

All 3 case studies indicate that deeper is the hydraulic barrier and higher is the natural hydraulic gradient, more significant will be the barrier effect. For the investigated sites impacts are always modest and range within a few tens of centimeters. This because of the low natural hydraulic gradients for all areas.

However, the impact of hydraulic barriers on groundwater flow should never be neglected. Engineering designs including partial occlusions of an aquifer should always be accompanied by hydrogeological investigations quantifying impacts on groundwater.

References

Bondesan A, Primon S, Bassan V, Vitturi A (2008) Le unità geologiche della Provincia di Venezia, Provincia di Venezia, Università di Padova

Calda N, Valloni R, Bedulli F (2007) Three-dimensional representation of permeability barriers and aquifers recharge in the pleistocene deposits of the parma alluvial plain. Mem Descr Carta Geol D'It LXXVI:97–108

Carraro F (1996) Il Quaternario—Revisione del Villafranchiano nell'area-tipo di Villafranca d'Asti. Ital J Quat Sci Aiqua 9:fasc.1

Harbaugh A (2005) MODFLOW-2005, the U.S. geological survey modular ground-water model—the ground-water flow process. Techniques and Methods 6-A16, U.S. Geological Survey, http://pubs.usgs.gov/tm/2005/tm6A16/

Harr ME (1962) Groundwater and seepage. McGraw-Hill Book Company, New York

Provincia di Venezia—Servizio Geologico, Difesa del Suolo e Tutela del Territorio (2011), Atlante geologico della Provincia di Venezia

U.S.A.C.E (1993) Seepage analysis and control for dams, U.S. Army Corps of Engineers, Washington, http://140.194.76.129/publications/

Chemical and Isotope Composition of Waters from Firenzuola Railway Tunnel, Italy

176

L. Ranfagni, F. Gherardi, and S. Rossi

Abstract

Forty-six water points from stream waters, springs, wells and tunnel seeps have been monitored for major reactive aqueous components and isotope composition of water over the period 2004–2008 in an area (Mugello basin, Northern Apennines, Italy) impacted by the tunneling works for the Bologna-Firenze high-speed railway. Based on geological, hydrogeological and geochemical information, an integrated conceptual model has been elaborated which considers the drainage of waters of different age in the Firenzuola railway tunnel. Precipitations and waters from small perched aquifers rapidly percolate in the tunnel through well-defined fractures zones and mix with more than 100 years old waters. Dilute, near neutral pH waters of Ca–HCO$_3$ composition are generated through limited interaction of meteoric waters with local lithologies, whereas more saline, alkaline pH waters of Na–CO$_3$–HCO$_3$ composition originate through prolonged interaction of meteoric waters with flysch rocks.

176.1 Introduction

Opened in 2009, the new Bologna-Firenze high-speed railway has a length of 78.5 km, and includes 73.3 km of tunnels. The Tuscan stretch of the new railway includes 6 mainline tunnels (three of which more than 15 km in length). The Bologna-Firenze railway is one of the most important links in the Italian rail network, and connects the Emilia Romagna region with Tuscany region under the Apennines.

L. Ranfagni (✉) · S. Rossi
Environmental Protection Agency of Tuscany (ARPAT), Via Porpora 22, 50144, Florence, Italy
e-mail: luca.ranfagni@arpat.toscana.it

F. Gherardi
Consiglio Nazionale delle Ricerche (CNR), Istituto di Geoscienze e Georisorse (IGG), Via Moruzzi 1, 56124, Pisa, Italy

The Firenzuola tunnel, approximately 44.5–59.6 km southwards of Bologna, in the Mugello basin, was excavated at an elevation of 300–350 m a.s.l, below the main apenninic watershed, located at an elevation of 1,000–1,100 m a.s.l. (Rodolfi et al. 2004). The excavation of the Firenzuola tunnel caused a significant drop of groundwater levels regionally, due to the seepage of surrounding groundwater into the tunnel. About 250 and 600 L/s of groundwater currently discharge into this tunnel during the low- and high-flow season, respectively, but a maximum inflow of 900 L/s has been estimated during the period of maximum crisis. A number of springs and creeks have dried out as a consequence of the excavation works of the tunnel (AA.VV. 2008).

The main purpose of this study was to elaborate an integrated hydrogeological and geochemical model of the area impacted by the tunnel, and possibly identify the main structures connecting the tunnel with streams and surficial aquifers.

176.2 Geological and Hydrogeological Setting

The Northern Apennines represent the exposed portion of a large orogenic wedge generated by a process of crustal shortening and thickening associated with the subduction of the Adriatic plate under the Iberian plate (Martini et al. 2001). The most important geological units in the area are represented by the turbidites of Oligo-Miocenic age of the Marnoso-Arenacea formation (Vincenzi et al. 2014).

The Firenzuola tunnel has been prevalently bored throughout sandstones (greywackes), marls and, subordinately, siltstones and claystones of Lower-Middle Miocene age. These rocks show large secondary permeability solely in correspondence of major fault and fractured zones, mainly created by the post-orogenic tectonic detensioning of Apennines. In general, fractures develop in arenaceous banks, and, occasionally, fractures with a persistence exceeding that of the individual layers may be recognized. Large-scale water circulation develops in these features, mostly WNW-ESE trending. Fractures are more frequent near anticline/syncline axes and/or faults oriented in the Apennine direction (WNW-ESE). Associated with these structures, large tabular sub-vertical aquifers (up to 200 m wide, and up to some kilometers length), perennial springs and streams occur.

176.3 Methods

A total of 46 water sampling points, were repeatedly collected during the period 2004–2009. All water samples were analyzed for major (Ca, Mg, Na, K, Cl, HCO_3, SO_4) chemical constituents, and for the isotopic composition of water ($\delta^{18}O$, $\delta^{2}H$, ^{3}H). Temperature, pH, electric conductivity were measured in the field. The chemical analyses were performed in the laboratories of ARPAT, Firenze, as follows: Cl and SO_4 by ionic chromatography, Ca, Mg, Na

and K by atomic adsorption spectroscopy. The percent charge-balance error of samples discussed in this study is typically below 5 %. The $^{2}H/^{1}H$, $^{18}O/^{16}O$ isotope ratios and tritium (^{3}H) concentrations were determined in the laboratories of CNR-IGG, Pisa. Analytical accuracies are typically ± 1 ‰ for $\delta^{2}H$, ± 0.05 ‰ for $\delta^{18}O$ and ± 0.5 UT for ^{3}H.

176.4 Results and Discussion

Three main types of waters have been considered for this study: (i) creeks and streams (group A), (ii) springs and wells (group B); (iii) tunnel seeps (group C). All the sampled waters have pH values between 6.7 and 10, with the most alkaline values associated to tunnel seeps. Waters inflowing in the Firenzuola tunnel are generally more saline (330–848 mg/L) than waters from springs (238–508 mg/L) and streams (314–574 mg/L). Surficial waters have a Ca–HCO_3 signature, whereas the chemical composition of tunnel inflows varies from Ca–HCO_3 to Na–CO_3–HCO_3 with increasing salinity. The prolonged interaction of meteoric waters with host rocks causes C_{TOT} (Fig. 176.1a) and Na_{TOT} (Fig. 176.1b) concentrations to increase in tunnel seeps. Decreasing tritium contents ($^{3}H < 4$ UT; Fig. 176.1) are good tracers of (i) prolonged underground residence times, and (ii) of the lack of mixing with meteoric waters ($^{3}H > 5$ UT) rapidly infiltrating in the Marnoso Arenacea flysch.

From 2004 to 2008, only for some tunnel points we observed a decreasing of prolonged residence water contribution. In the same lapse of time, the sampling point with more "mature" waters didn't show significant changes in composition. Latest chemical analysis, carried out in 2012 at the southern entrance of the tunnel, shows that a significant contribution of prolonged circulation waters remains.

Reaction path modeling has been applied to investigate the processes governing the chemistry of the tunnel seeps (Fig. 176.2). A flow-through configuration has been used to

Fig. 176.1 Tritium versus C_{TOT} (A) and tritium versus Na_{TOT} (B) diagrams for Firenzuola Tunnel waters; *red dots* springs and streams; *black dots*: tunnel points
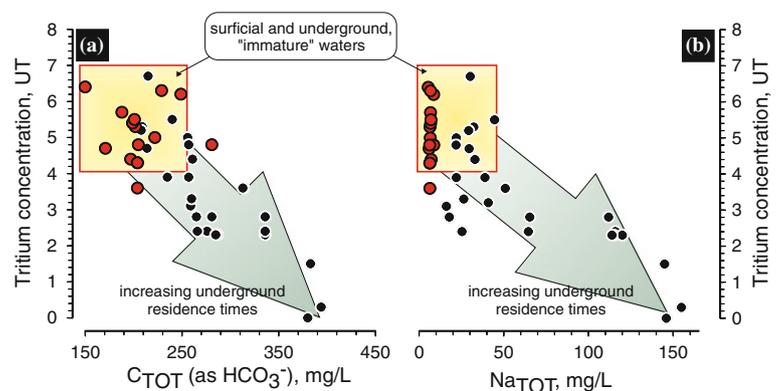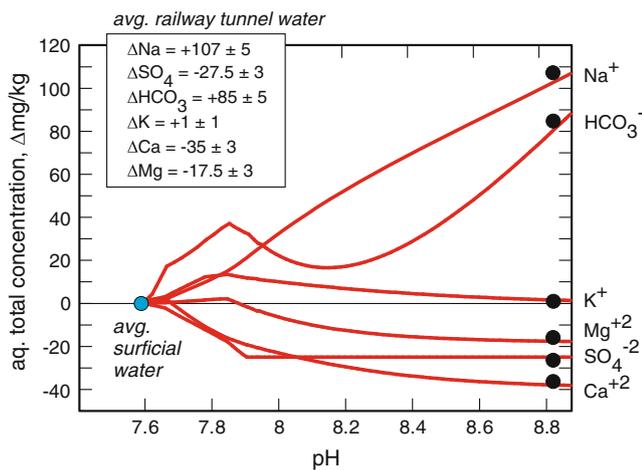
Fig. 176.2 Geochemical modeling of water-rock interactions occurring in the Marnoso Arenacea flysch. Groundwater total aqueous concentrations are computed as delta mg/kg-H$_2$O, with respect to the average composition of surficial waters (streams) infiltrating in the study area. pH is used as the master reaction progress variable. Consistently with their longer underground residence times, tunnel waters (*black dots*) plot at the end of the reactive path, and represent a sort of "geochemically mature end-member"

simulate the evolution of a packet of fluid traversing the Marnoso Arenacea aquifer, under the assumption that the interacting fluid has an initial chemical composition comparable to waters usually recognized in small, perched aquifers. This zero-dimensional, forward model considers that quartz, albite, K-feldspar, chlorite and carbonatic and/or dolomitic cements are the main reactive phases in the system, according to petrographic and mineralogical evidences (Gandolfi et al. 1993). Numerical calculations (Fig. 176.2) indicate that the hydrolysis of the Marnoso Arenacea flysch is a possible way to generate the most saline, and alkaline waters sampled in the central part of the Firenzuola tunnel (Southern sector—zone I of Fig. 176.3).

The stable isotope composition of the sampled waters ($\delta^{18}O$ and δ^2H values between −8.7 and −7.0, and between −55 and −42 ‰, respectively) is adequately represented by a meteoric line having a deuterium excess, d, of 15, similar to precipitations falling in Central Italy. The distribution of points indicates that tunnel groundwaters have a meteoric origin, and that the observed differences in the isotopic ratios are mostly due to seasonal effects. The meteoric recharge
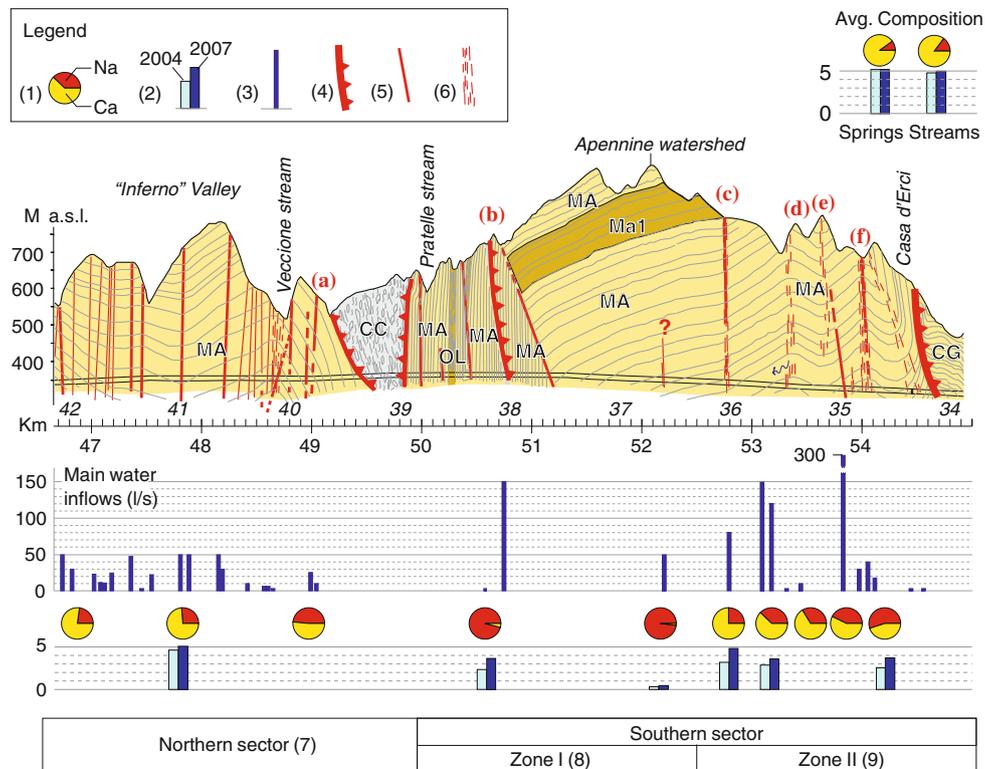
Fig. 176.3 Geostructural and hydrogeological cross-section of the Firenzuola Tunnel. Information on the location and on selected chemical parameters of the main water inflows is also provided: (*1*) Ca/Na ratio; (*2*) tritium content (UT) in 2004 and 2007; (*3*) inflow rates (l/s) during the excavation of the tunnel. Major structural features are: (*4*) thrusts; (*5*) faults or master joints; (*6*) fractured belts. The Northern sector (*7*) of the tunnel, dominated by the rapid infiltration of meteoric waters, is hydraulically set apart from the Southern sector (*8* and *9*, see text) by the permeability barrier CC (Chaotic Complex). The most important geological formations (*fm*) are: Marnoso-Arenacea fm. (*MA*); Marnoso-Arenacea fm., marl-rich facies (*MA1*); Olistostrome (*OL*); Caothic Complex (*CC*); Castel Guerrino fm. (*CG*). Vertical circulation of groundwater is supposed to prevalently occur through the following tectonic discontinuities (*red labels*): (*A*) Isola tectonic line; (*B*) Fognano overthrusting (*C*); Ronta fault; (*D*) Frassineta Nord fractured belt; (*E*) Casa d'Erci Nord fractured belt; (*F*) Casa d'Erci Sud fault and fractured belt

occurs at elevations roughly comprised between 700 and 1,100 m a.s.l.

By combining hydrogeological and geological information with data on chemical and isotope composition of waters, we derived a model of underground water circulation which considers two main hydrogeological sectors in the tunnel (Fig. 176.3). These sectors are separated by a chaotic assemblage of blocks of preexisting rocks (olistostrome), which acts as an impermeable barrier. The northern sector is dominated by the rapid infiltration of meteoric waters, and then, by the occurrence of low-salinity, high-^{3}H, near-neutral pH waters, of Ca-HCO$_3$ composition.

The southern sector comprises two sub-zones: the first one (Zone I), adjacent to the olistostrome, is dominated by relatively ancient waters (likely older than 100 years; ^{3}H generally <2 UT), having high pH values, and Na–CO$_3$–HCO$_3$ composition. In this zone, the occurrence of marl-rich, relatively impermeable strata of the Marnoso-Arenacea fm. above the tunnel (MA1 in Fig. 176.3) prevents meteoric precipitation from infiltrating in the excavated area. The remaining zone (Zone II), is characterized by the occurrence of the same "old" waters of Zone I, locally mixed with surficial (^{3}H generally >5 UT) or meteoric (^{3}H up to 10 UT) waters rapidly percolated in the aquifer. Low-salinity, high-^{3}H waters are expected to percolate through well-defined fractures zones, such as the Fognano overthrusting, and the Ronta and Casa d'Erci faults (Fig. 176.3). The occurrence of long residence water circuits, is further supported by the occurrence of waters with extremely low ^{3}H concentrations in the Allocchi tunnel, a railway tunnel excavated in 1890 at about 550 m a.s.l. in the same flysch formation of the Firenzuola tunnel, not far (8 km) from the area of study.

176.5 Conclusions

Combined with geological and hydrogeological information, a detailed chemical and isotope survey of 46 water points (streams, springs, wells and tunnel seeps) has contributed to the definition of an integrated hydrogeochemical model of an area impacted by the tunneling works for the Bologna-Firenze high-speed railway. Water isotopes reveal that waters of different age are drained by the Firenzuola tunnel, with the oldest groundwater component likely being older than 100 years. The chemical characteristics of the Firenzuola tunnel waters are controlled by the mineralogy of the interacting rocks (Marnoso Arenacea flysch) and the extent of water-rock reaction. More prolonged residence times and/or effective water-rock interactions lead to more saline, pH alkaline waters of Na–CO$_3$–HCO$_3$ composition.

References

AA.VV. (2008) Relazione sullo stato dell'Ambiente in Toscana 2008. Regione Toscana—ARPAT, 2008, pp 221–224

Gandolfi G, Paganelli L, Zuffa GG (1993) Petrology and dispersal pattern in the Marnoso-Arenacea Formation (Miocene, northern Apennines). J Sedim Petrol 53:493–507

Martini IP, Sagri M, Colella A (2001) Neogene-Quaternary basins of the inner Apennines and Calabrian arc. In: Vai GB, Martini IP (eds) Anatomy of an Orogen: the Apennines and adjacent Mediterranean basins. Kluwer, Dordrecht, pp 375–400

Rodolfi G, Rossi S, Doni A, Ranfagni L (2004) Apennine tunneling works: impacts on the surface and underground water resources. D08 Field trip Guidebook, 32nd international geological congress, 20–28 Aug 2004, Firenze, Italy

Vincenzi V, Gargini A, Goldscheider N, Piccinini L (2014) Differential hydrogeological effects of draining tunnels through the Northern Apennines, Italy. Rock Mech Rock Eng 47(3):947–965

Hydrogeological Modeling Applications in Tunnel Excavations: Examples from Tunnel Excavations in Granitic Rocks

Baietto Alessandro, Burger Ulrich, and Perello Paolo

Abstract

Numerical modeling of groundwater circulation has been applied in the Aica-Mules tunnel, an exploration adit that has been used for geological investigations before the excavation of the main Brenner Base Tunnel (high speed railway link between Italy and Austria). Conditions faced by the Aica-Mules tunnel allowed to improve the general knowledge of the geological context and of hydrogeological impacts on groundwater circulation in a granitic massif where the two main tubes of the Brenner Base Tunnel will be constructed. In this perspective, numerical modeling has been applied, both in back- and forward-analysis for the following purposes: (i) in order to get insights on the reliability of the conceptual model relative to the hydrogeological setting during the excavation; (ii) to estimate the risk that the tunnel might interfere with spring catchment areas with possible negative feedbacks on the natural discharge regime; (iii) to forecast the inflow rate expected in the tunnel in the most critical geological sectors related with the presence of fault and fracture systems.

Keywords

Numerical modeling • Tunnel design • Groundwater circulation • Risk management

177.1 Introduction

In engineering geology, hydrogeological numerical modeling is used extensively for multiple purposes (Meiri 1985; Marechal et al. 1999; François et al. 2007). Whenever based on a background of hydrogeological observations and on a solid geological model, numerical modeling is able to provide appropriate solutions related to (i) project design decisions and (ii) environmental impacts on shallow manifestations of groundwater flow such as springs and wells.

B. Alessandro (✉) · P. Paolo
GDP Consultants, Località Grand Chemin, 22, 11020 Saint Christophe, AO, Italy
e-mail: baietto@gdpconsultants.eu

B. Ulrich
Galleria di Base del Brennero, Brenner Basistunnel BBT SE, Piazza Stazione 1, Bolzano, Italy

In relevant tunneling projects, consisting of large underground excavations, the prediction of how groundwater will interact with the constructions is paramount for economic efficiency and for minimization of environmental effects.

In the framework of the Brenner Base Tunnel (BBT), a planned 55 km long railway tunnel running from Innsbruck (Austria) to Fortezza (Italy), currently under design and construction, many hydrogeological analyses and investigations have been carried out during the last 20 years (Brandner and Dal Piaz 2005; Barla et al. 2010; Perello et al. 2013). Results of these studies were used to reconstruct conceptual models for groundwater circulation in sectors interested by planned excavation works. In the southernmost section of the BBT project, this conceptualization constituted the base for numerical models aiming at: (i) validating the hydrogeological conceptual model of the area interested by the Aica-Mules tunnel, (ii) estimating impacts that the tunnel had on the spring catchment areas with possible negative feedbacks on the natural discharge regime, and (iii) forecasting the groundwater inflows in the most critical geological sectors of the main tubes. Models set-up was

different according to purposes and applications. Detailed 3D modeling taking into account most of main geological and hydrogeological elements was performed in the above mentioned case (i) and (ii), while broad conceptualization and simplification of the hydrogeological context is assumed for the setup of 2D and 3D models referring to case (iii). Models are subject to a strict calibration procedure that involves a comparison between measured and modeled data before and after tunnel perturbation. Forward analysis is based on sensitivity analysis of parameters in order to provide ranges of expected values of groundwater inflow into the tunnel. All models where produced by means of the software Feflow (Diersch 2009).

177.2 Geological Setting of the Aica-Mules Tunnel

The Aica-Mules tunnel, already constructed, constitutes an exploratory excavation of 6.7 m of diameter lying about 12 m below the main tubes of the railway link (currently under design) providing information on the rock mass for reducing construction costs and times of the BBT project. The Aica-Mules tunnel is approximately 10 km long and has been drilled by means of a double shield Tunnel Boring Machine (TBM) starting from the Aica portal in Italy. No

rock-mass impermeabilization operations were performed and groundwater free flows into the tunnel.

The Aica-Mules tunnel is entirely located in crystalline rocks pertaining to the South-Alpine domain of the Alpine chain, the so-called Brixen Granite, mainly composed by granites and granodiorites variously crosscut by aplitic and pegmatitic sills. To the North, the Brixen Granite is bounded by a main regional structure, the Periadriatic Line (Figs. 177.1 and 177.2). This structure is marked by a steeply dipping E-W striking mylonitic shear zone affecting a tonalitic body that separates the Brixen Granite and the Austroalpine units. The Brixen Granite has been affected by brittle deformation with structures spanning from simple fracture networks, to cataclastic fault zones with up to a pluri-km-scale persistence.

In the tunnel area the most important tectonic feature is represented by the Riobianco Fault Zone, a sub-vertical N–S striking fault. All these structures affect in a different manner the permeability of the granite and play an important role in influencing the groundwater circulation pattern and the discharges that occurred during the tunnel excavation. Insights into the hydraulic conductivity of the rock-mass for the area are available from hydraulic packer tests that were performed in deep drill holes. The tests have shown that hydraulic conductivity is high only along fracture systems. The fault zone permeability is generally high, despite it

Fig. 177.1 Geological patterns integrated in numerical models of the Aica Tunnel
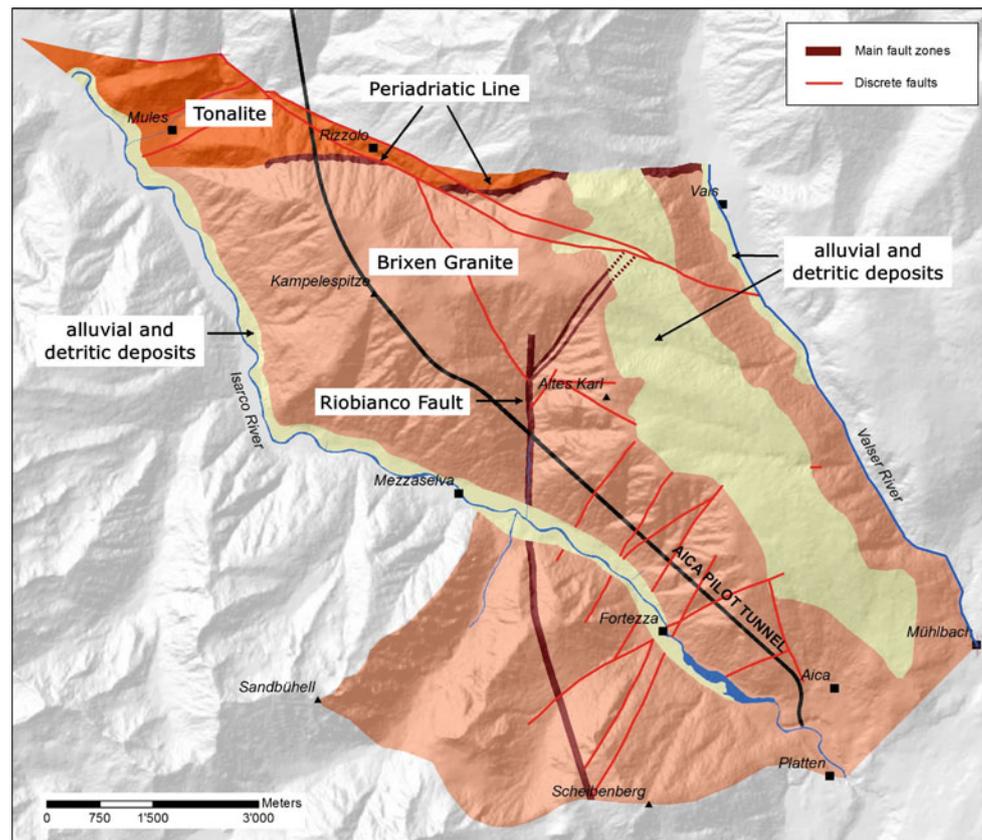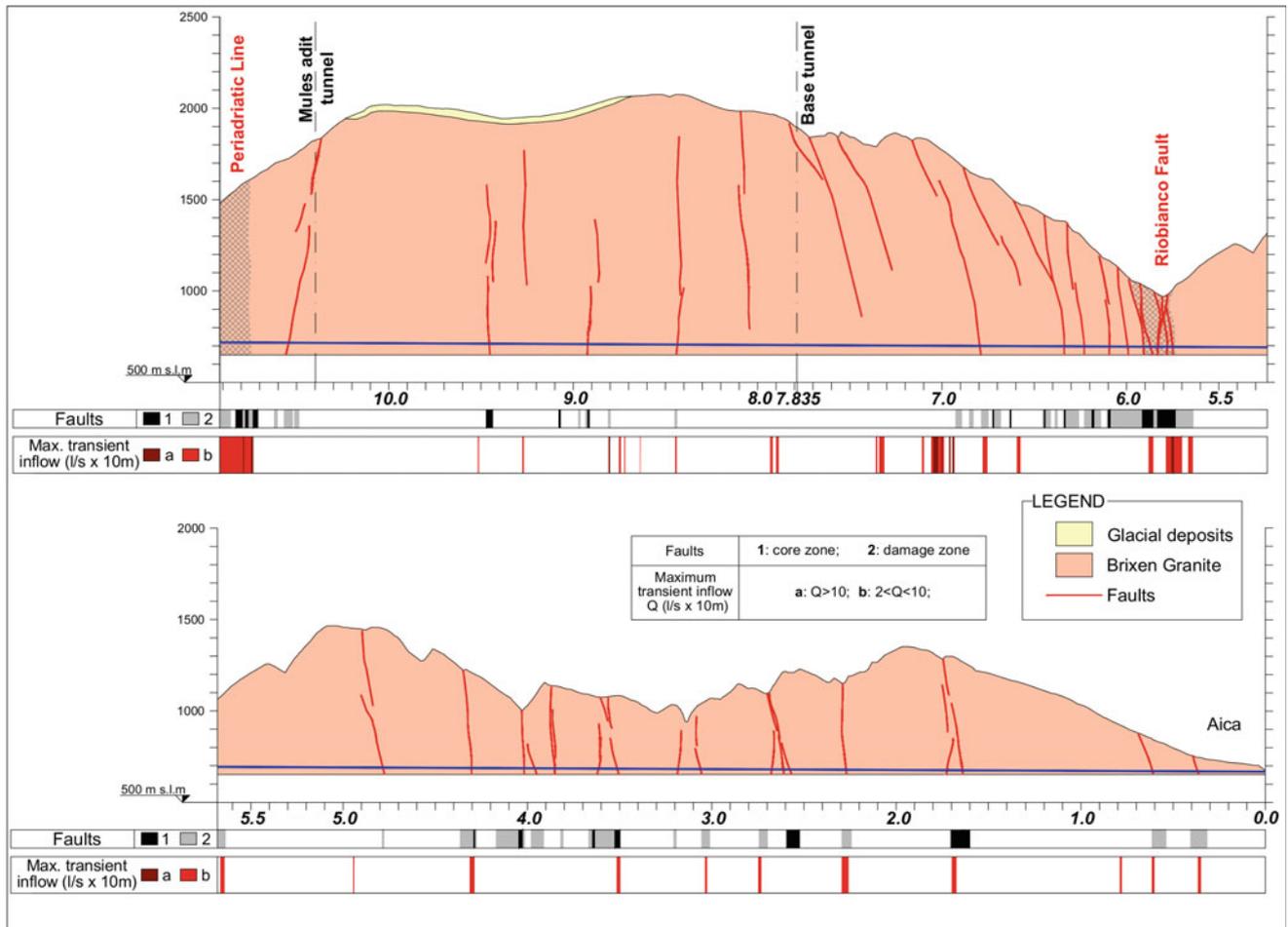
Fig. 177.2 Geological cross-section along the Aica Tunnel with the main water inflows occurred during the excavation

shows a strong variability due to the presence of products deriving from cataclastic fragmentation with a size ranging from fine-grain to coarse-grain. Hydraulic tests indicate values spanning over three orders of magnitude, in the range of 5×10^{-9}–5×10^{-6} m/s.

177.3 Numerical Models

177.3.1 Model of the Aica-Mules Exploration Tunnel

During the excavation of the Aica-Mules tunnel water flow was continuously monitored allowing to reconstruct the hydrographs relative to water discharges into the tunnel. Various inflow events have been recorded that can be correlated with fault or fracture zones intersection. The most relevant tunnel inflow was recorded at the intersection with the Riobianco Fault (around pk 5 + 700), with a peak of net discharge of 220 l/s, progressively decreasing to less than one third of this value. A second major inflow zone with

peak discharges similar to those of the Riobiancofault was intersected (around pk 7 + 000), but this time without any connection with fault zones, since only a small fracture zone was detected.

A 3D finite element model (Fig. 177.3) covering entirely the sector above the excavated section of the Aica-Mules tunnel has been implemented in order to gain insights on the hydrogeologic behavior shown by the aquifer during the tunnel drilling. This model was calibrated in steady-state conditions and was then used for transient simulations relative to the different excavation phases of the tunnel; boundary conditions accounted either for hydraulic heads along the Isarco River and the main streams, and for the effective infiltration calculated for the top boundary. This model allowed a back-analysis based on the comparison of the numerical results with the hydrogeological data collected during the monitoring. While main fault zones (i.e. RiobiancoFault and Periadriatic Line) have been treated as equivalent porous media, minor faults have been handled as discrete features with distinctive hydrogeological properties.
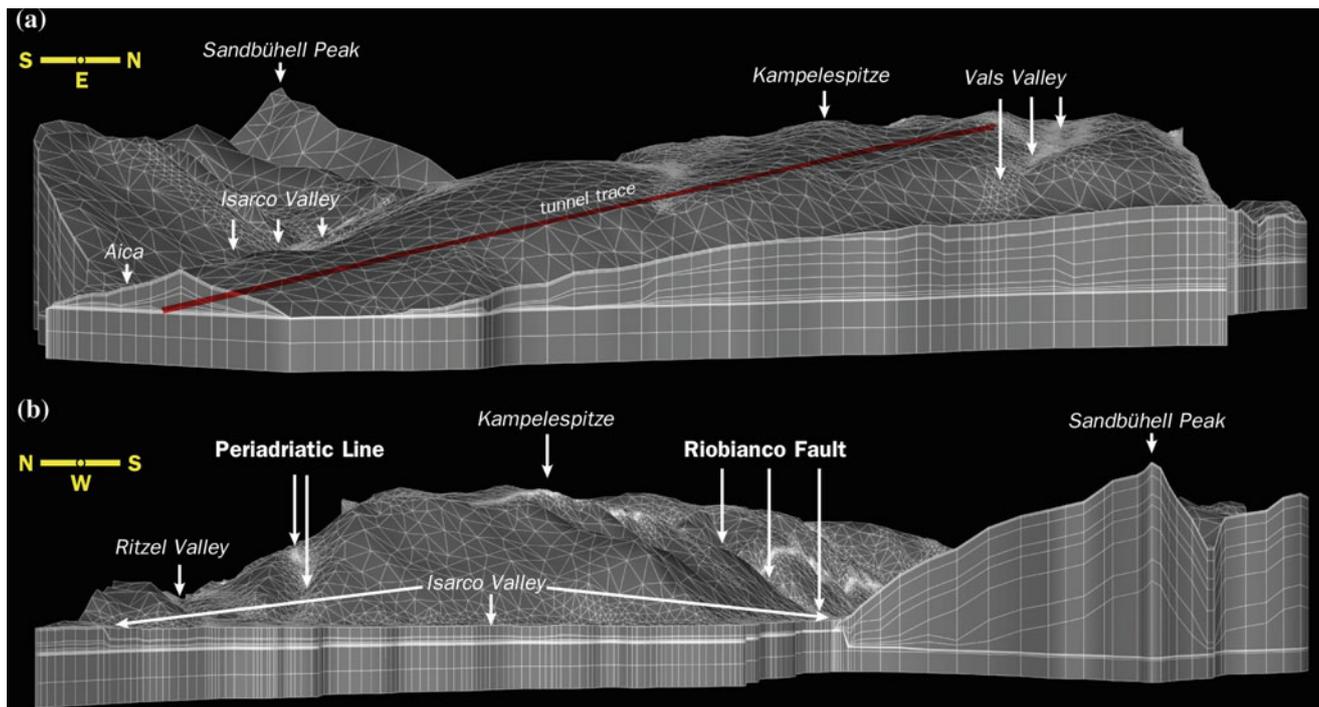
Fig. 177.3 3D geometry and meshes used for the numerical model of the Aica-Mules tunnel

A satisfying calibration was obtained only for some portions of the aquifer while other discrepancies with the observational data couldn't be smoothed out unless assuming very different hypotheses with respect to the ones that were initially considered. The main inconsistency between the measures made on site and model results was relative to the very rapid pressure pulse that was recorded by a piezometer (Mu-B-04/05), located 5-km away from the Riobianco Fault and measuring the water level at depth in the Bressanone Granite. Quite surprisingly, the piezometer recorded a decrease in the water level after less than 3 days from the fault interception by the tunnel. Since that moment, the groundwater level in the Mu-B-04/05 started showing a slow but constant decrease that kept on for 5 months without any restoration, until getting to a final drastic decrease that likely corresponded to the interception by the water table of an impervious limit.

To justify the very fast response of the piezometer that followed the fault interception by the tunnel, it has been assumed a conceptual model considering that the piezometer was hydraulically connected with the Riobianco Fault through a set of permeable faults crosscutting the Bressanone Granite. After several trials it was apparent that a satisfying calibration was impossible to achieve only by modifying hydraulic boundary conditions and/or rock properties. This observation led to the perception of a different condition lying behind the real nature of the aquifer.

So far, according to the available geological data, the aquifer was considered as an unconfined aquifer with a free groundwater surface and with direct connection with surface infiltration. But, to obtain satisfying calibration the aquifer hosted in the fault system had to be treated as a confined aquifer. Sealing phenomena along the fault, not evident from field and drilling data, could explain this particular behavior.

177.3.2 Model for Impacts Evaluation of Spring Catchment Areas

Drainage of groundwater systems and drying out of existing spring catchments and groundwater wells is recognized as one of the most important issues to take into account when forecasting environmental impacts connected with the excavation of long and deep tunnels. In this context, numerical models have been applied in order to forecast impacts on the groundwater reservoir feeding some springs. Since natural variations in the spring discharge regime occur, it is important to distinguish whether a decrease in the discharge rate is due to natural reasons or to the tunnel influence. Analyses carried on model outputs allowed to identify zones with different expected drawdown. This computation helps constraining and differentiating those springs that are more likely to be subject to negative feedbacks due to the tunnel drainage from those that are less affected by this effect.

Fig. 177.4 2D model used for inflow rate estimation within the Aica tunnel and the Brenner Basis Tunnel
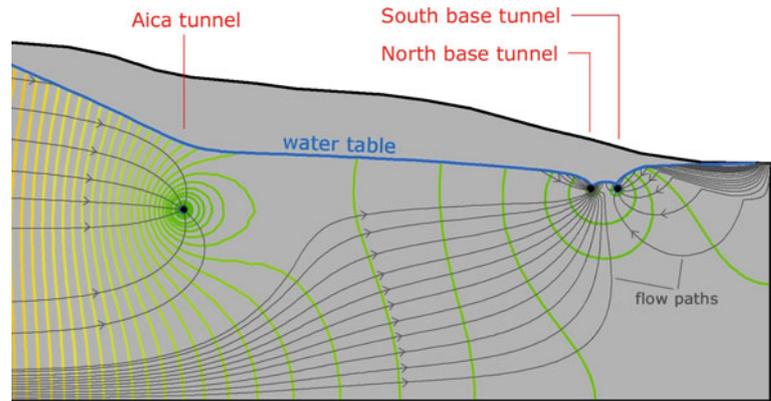
177.3.3 Model for Inflow Rates

After back analysis, new models have been implemented for forecasting the hydrogeological conditions during the future construction of the main BBT tubes. A set of 2D and 3D numerical models have been set up in zones where main inflows are expected in relationship to the occurrence of main faults and fracture systems (Fig. 177.4). These models aimed at forecasting the water discharges into the BBT tunnel tubes under the hypothesis of different operational conditions (excavation of the first tube, of the second tube, etc.).

Simulations were carried out via a parametrical approach accounting for uncertainties related with the geological model. For example different permeability and fault distributions were considered in the models. The obtained results were used to identify possible ranges of expected tunnel inflow values, as well as for identifying local variations in the flow systems (Fig. 177.4).

177.4 Conclusions

This study shows that, whenever constrained by adequate data and consistent interpretation, groundwater numerical modeling applied to tunneling can serve as a valuable tool for an appropriate design and environmental risk assessment. In the frame of the Aica-Mules Tunnel, numerical modeling has been applied for validating the hydrogeological conceptual model, for estimating the potential impact of the tunnel on spring catchments and for forecasting the inflow rate expected in the tunnel.

References

Barla G, Ceriani S, Fasanella M, Lombardi A, Malucelli G, Martinotti G, Oliva F, Perello P, Pizzarotti EM, Polazzo F, Rabagliati U, Skuk S, Zurlo R (2010) Problemi di stabilita' al fronte durante lo scavo del cunicolo esplorativo Aica—Mules della Galleria di base del Brennero. In: Barla G, Barla M (eds) XIII ciclo di conferenze di meccanica e ingegneria delle rocce MIR 2010. Torino 30 Novembre–1 Dicembre 2010, pp 175–213

Brandner R, Dal Piaz GV (2005) Brenner Basis Tunnel/Tunnel di Base del Brennero: Strukturgeologische Kartierung und erganzende geologische Studien/Rilevamento geologico-strutturale e studi geologici integrative, BBT SE unpublished internal report, contract D0104, 1011 p

Diersch HJG (2009) FEFLOW finite element subsurface flow & transport simulation system—reference manual. DHI-WASY GmbH ed

François B, Tacher L, Bonnard Ch, Laloui L, Triguero V (2007) Numerical modelling of the hydrogeological and geomechanical behaviour of a large slope movement: the Triesenberg landslide (Liechtenstein). Can Geotech J 44(7):840–857

Marechal JC, Perrochet P, Tacher L (1999) Long-term simulations of thermal and hydraulic characteristics in a mountain massif: The Mont Blanc case study, French and Italian Alps. Hydrogeol J 7 (4):341–354

Meiri D (1985) Unconfined groundwater flow calculation into a tunnel. J Hydrol 82:69–75

Perello P, Baietto A, Burger U, Skuk S (2013) Excavation of the Aica-Mules pilot tunnel for the Brenner base tunnel: information gained on water inflows in tunnels in granitic massifs. Rock Mech Rock Eng. doi:10.1007/s00603-013-0480

Effects on the Aquifer During the Realization of Underground Railway Works in Turin

178

Stefano Ciufegni, Fabrizio Bianco, Adriano Fiorucci, Barbara Moitre, Massimiliano Oppizzio, and Francesco Sacchi

Abstract

The "Underground Railway Link" of Turin (Piedmont, Italy), in the section between Porta Susa and Corso Grosseto stations, represented a work with no small difficulties in planning and execution, in fact it has entailed the difficult problem of crossing through an underpass the Dora Riparia River with a double artificial tunnels. The potential interference of this work with unconfined aquifer has necessitated a complete hydrogeological investigation aimed at the design of a monitoring plan for the entire line of action, compatible with the presence of road and railway surface network as well as sub-systems directly interconnected to these. Monitoring, still in place, started from August 2005, with a series of campaigns of detection given by manual acquisition and since November 2006 has been implemented with the installation of data logger. The monitoring system has provided for the control of the variation of the groundwater level ante operam, during construction and post operam in order to control in detail the development and the process of hydrodynamic adaptation of the aquifer system to the new structure in the succession of the different implementation phases.

S. Ciufegni · F. Sacchi
Italferr S.p.A., Rome, Italy

F. Bianco · A. Fiorucci (✉) · B. Moitre
Department of Environment, Land and Infrastructure Engineering (DIATI), Politecnico di Torino, Corso Duca degli Abruzzi 24, 10129 Turin, Italy
e-mail: adriano.fiorucci@polito.it

B. Moitre
e-mail: barbara.moitre@tin.it

M. Oppizzio
ATI: Astaldi S.p.A., Rome, Italy

M. Oppizzio
Vianini S.p.A, Rome, Italy

M. Oppizzio
Di Vincenzo S.p.A., San Giovanni Teatino, Italy

M. Oppizzio
Impresa Rosso S.p.A., Turin, Italy

178.1 Introduction

The "Underground Railway Link" of Turin (Piedmont, Italy), in the section between Porta Susa and Corso Grosseto stations, represented a work with no small difficulties in planning and execution, in fact it has entailed the difficult problem of crossing through an underpass the Dora Riparia River with a double artificial tunnels. For the realization of the work has been required the construction of a system of bulkheads and a bottom plug, that penetrate in the subjacent unconfined aquifer flowing in the almost orthogonal direction to the work.

The potential interference of this work with unconfined aquifer has necessitated a complete hydrogeological investigation aimed at the design of a monitoring plan for the entire line of action, compatible with the presence of road and railway surface network as well as sub-systems directly interconnected to these (Civita et al. 2002; Civita and Pizzo 2003).

178.2 Hydrogeological Conceptual Model of the Study Area

In the study area there are three hydrogeological complexes, from the oldest to the most recent:

- silty-sandy complex: it consists of sands in silty matrix with permeability from low to medium, host the deep aquifer of the Turin foothills and affects the central and central-eastern portion of the area.
- alternations complex: it consists of layers of clay alternating with horizons of gravel and sand, does not surface in the study area, but in the western sector is located at a depth of about 30 m.
- gravelly-sandy complex: it consists of gravel and sand with weakly silty ma-trix, includes the alluvial deposits of the fundamental level of the Turin plain and terraced alluvial systems affecting the river areas of the waterways of the study area.

The study area is characterized by two aquifers more or less interconnected among themselves and with the Dora Riparia River. It is possible to distinguish an unconfined aquifer and a multi aquifer. The unconfined aquifer is located mainly in the gravelly-sandy complex. The Dora Riparia River regulates the flow field in the investigated area, in fact imposes extreme dominance on the aquifer with its meandering in the western part of the area and its irregular oscillations of level, related to the considerable extension of its catchment area.

In the eastern sector of the study area, below the level of the sandy-gravelly aquifer is present a sandy layer which is directly interconnected with the above complex. This area is therefore characterized by a multilevel aquifer (Civita et al. 2007).

Considering a wider area subtended by the Dora Riparia, the morphology of the piezometric surface is radial complex with just accentuated concavity downstream and a gradual increase of the distance between the piezometric curves (Civita et al. 2007). From the northwestern limit of the study area, the distance between the piezometric curves turns out to be quite smooth. Proceeding towards S, it is clear the influence of the Dora Riparia on groundwater flow. The general direction of groundwater flow is from W to E. In the southern sector, the aquifer system affected by the draining action of the Dora Riparia: the directions of the flow, in fact, initially from NW to SE, veer towards the right bank of the river highlighting a draining action, while at the side left, the piezometric values are slightly lower and impose the outflow from the Dora the aquifer (Fig. 178.1, Civita et al. 2007).

178.3 The Monitoring Network

Monitoring, which started with a series of campaigns of measures through manual acquisition by phreatimeter since August 2005, has been implemented, starting in November 2006, with the installation of automatic acquisition instrumentation. The aim was to update, with constant frequency, the time evolution of the groundwater level fluctuations related to the aquifer interested by the work.

In consideration of the fact that the work could interfere directly, as well as with the subjacent aquifer, even with the surface watercourse which is hydro-geologically interconnected, the monitoring system has provided the installation of two hydro-metric stations on river course over which the continuous measurement of the groundwater levels on different equipped piezometers.

The monitoring network was made up initially of twenty control stations of piezometric levels of the aquifer and two hydrometric stations on the river Dora Riparia (Fig. 178.1).

The monitoring system has provided the variation of the groundwater level ante operam, during construction and post operam in order to control in detail the development and the process of hydrodynamic adaptation of the aquifer system to the new structure in the succession of the different implementation phases (Civita and Pizzo 2003).

178.4 Analysis of the Data

The piezometric trend recorded in the last 7 years, in various monitoring points, outlines the progression of the work in the gallery. In this work we analyzed the data, inherent to the piezometric changes induced from the realization of the underground railway link, often measurement points (Fig. 178.2). It must always be kept in consideration the fact that the data analyzed may be affected by medium seasonal natural fluctuations, other than ongoing works.

The piezometers were divided into three groups, representing three distinct areas located along the course of the work, two located in the left and one on the right bank of the Dora Riparia. In the first group includes the measuring stations on the orographic right SA17 and SA18 upstream and SI5 downstream of the work. The second group includes piezometers SA3 and SA12 upstream and piezometers SA4 PC2 downstream. The third group consists of the measurement points more distant from the river, the DA7 and SA7 piezometers upstream and the SA5 piezometer downstream.

The piezometric level, in the period between May 2006 and April 2012, outlines the progression of the work in the gallery. In general, until the autumn of 2008, we can see the reaction of the aquifer to the impacting presence of the work just performed without bypass. The piezometric levels trends of the monitoring points upstream and downstream diverge. There are increases upstream and decreases downstream of the system of bulkheads, realized to secure the path to the dangers of flooding. Since September 2008, there were changes to the piezometric surface area due to groundwater dewatering

Fig. 178.1 Flow field and monitoring network
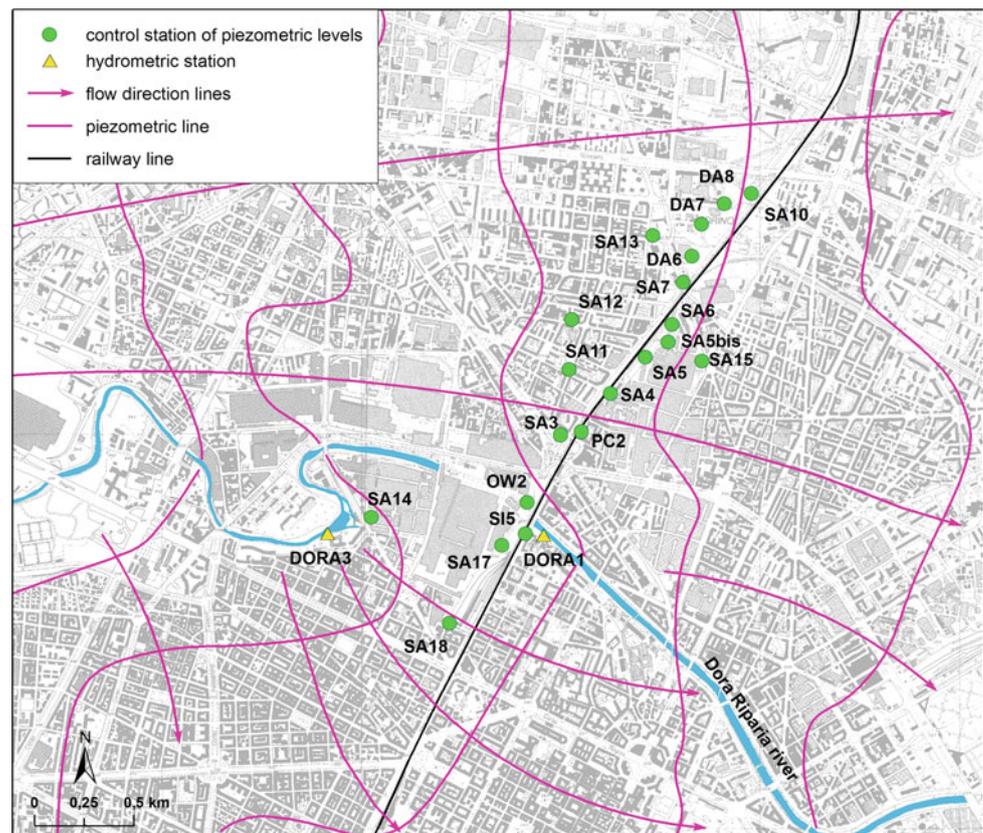
operations during the execution of the work. From May, 2012, after a serious of operations aimed at stabilizing the unconfined aquifer and compensation of dam-effect, the configuration of the levels is gradually and significantly improved, tending to the natural recovery of the initial conditions. In fact, the delta of the levels measured upstream–downstream are considerably less than the forecast calculated using a mathematical model, between raising to upstream and lowering to downstream.

In recent months considered is evidence of greater tendency towards stabilization of the levels to a state of balance and greater mitigation of dam-effect compared to the previous period. In fact, in February 2013 was carried out the final phase of the groundwater bypass, which led to significant and positive effects on the conformation of the aquifer in the downstream sector, with imported recoveries of the piezometric levels in the monitoring points taken into account. The decrease of the difference between the piezometric level upstream and downstream of the work is evident between the measuring points SA17 and SI5 and between SA3 and PC2.

In conclusion levels upstream work are in line with the pre-construction measures with a modest superelevation that wards off eventual known environmental problems. The levels downstream work, instead, show a significant recovery in conjunction with the final commissioning of the entire by-pass system.

178.5   Conclusion

The underpass of the Dora Riparia of the "Underground Railway Link" of Turin caused a dam effect on the unconfined aquifer which can be considered not relevant on the hydrogeological structure taken into account. In fact, from the data collected can be seen as the commissioning of the technician bypass has caused a mitigating effect of the disturbance induced by the work on the natural flow of the aquifer. From the data obtained, it highlights the fundamental importance of monitoring to be performed during the realization of works that may impact with groundwater.

Fig. 178.2 Piezometric levels
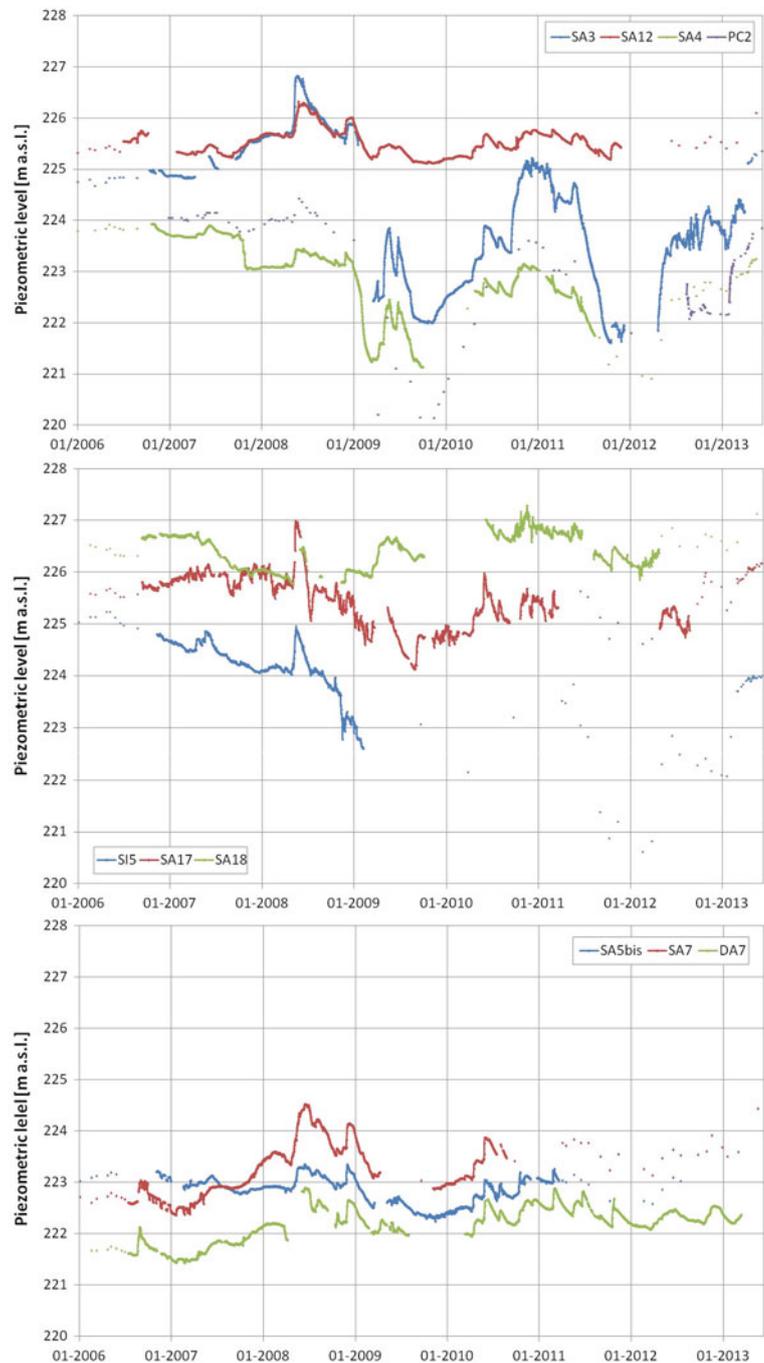
References

Civita M, Pizzo S (2003) Hydrogeological interference areas: the importance of preliminary prognosis in the designing of a high velocity railway line. In: Proceedings of AVR 03 "First International Workshop on Aquifer Vulnerability and Risk", Salamanca, Messico, pp 182–193

Civita M, De Maio M, Fiorucci A, Pizzo S, Vigna B (2002) L'ambiente idro-geologico: l'importanza della prognosi preliminare. Atti MIR 2002 "Le opere in sotterraneo e il rapporto con l'ambiente", Torino, Ed. Patron, Bologna, pp 73–106

Civita M, Danese A, Nicola E, Pizzo S (2007) Previsione e monitoraggio degli effetti sull'acquifero nel corso della realizzazione di un'importante opera ferrovia-ria in sotterraneo nella città di Torino. GEAM. Geoingegneria Ambientale e Mine-raria, vol 44.2, pp 49–68

Antonio Dematteis

Abstract

This paper illustrates the progress of the working group named GESTAG, from the Italian chapter of the International Association of Hydrogeologists, elaborating a guideline for hydrogeological activities in tunneling design and construction. The aim is to improve sustainable Water Management in tunnels. The impact on drilling production of water drainage during excavation, the valorization of groundwater resources drained during excavations, and the associated heat, and the environmental impacts of drainage on Groundwater Dependent Ecosystems and the aquifers are considered. GESTAG is composed by experts from different backgrounds (universities, designers, public authorities managers). The guideline is expected to be published in late 2014.

Keywords

Tunnel • Water management • Environmental sustainability • Monitoring • Italy

179.1   Introduction

Tunneling and big urban excavation works sprawl rapidly as meet the ever increasing requirements of a fast and sustainable mobility either between cities or inside cities' transportation network. At the same time, the rapid growth of renewable energy is sourcing the development of underground hydroelectric power plants. Such a growing interest in exploiting underground represents a great opportunity to limit the environmental impact from large infrastructure projects.

However, underground excavation has also the greatest impact on groundwaters. Severe consequences, e.g. hydraulic head drawdown, base-flow impoverishment, subsidence and groundwater contamination, may occur during and after excavation, making more difficult local people acceptance of ongoing projects. Groundwater inflow in tunnels should not be simply considered as a "geological accident" and a geotechnical obstacle for tunnel excavation and stability. Attention should be paid to the interaction between tunnel and groundwater flow systems. In the stages of both environmental impact assessment, and hydrogeological modelling and monitoring, the expected modifications of local groundwater budget terms (recharge-discharge) along with ecological effects against groundwater dependent ecosystems must be carefully taken into account. The hydrogeological reference model assumes central importance in this context, being the basis of any impacts prediction. Investigations, surveys, studies and calculations that are necessarily carried out to define the model must be encoded and described in detail. This allow to quantify the model reliability, which is an input to the risk analysis of time, cost and environmental and social impacts of the work.

179.2   Need of a Guideline

Experience put in evidence the need of guidelines for coordinating all hydrogeological activities in tunneling design, in order to improve environmental sustainability. This should help hydrogeologists and decision makers to

A. Dematteis (✉)
SEA Consulting s.r.l., Corso Bolzano 14, 10121 Turin, Italy
e-mail: dematteis@seaconsult.eu

improve the water resources management in tunneling. A hydrogeology-based approach, founded upon a more or less common protocol, can surely help to improve the management and interaction of "drilling production" and geotechnical excavation constrains with the environmental impacts. At the same time, the water resources drained by underground excavations, and the associated heat, should also be valorized. Based on of this experience came the idea to establish guidelines with the group of experts from different backgrounds (universities, designers, public authorities managers) listed above. The guideline is expected to be published in late 2014.

179.3 The GESTAG Working Group of the IAH

This paper illustrates the progress of the working group named GESTAG, established on 20/06/2012 by the Italian Chapter of the International Association of hydrogeologists (IAH). The working group is constituted by the following persons: U. Burger (BBT SE, Brenner Basis Tunnel); F. Capozucca (ANAS S.p.A.); P. Cerutti (ECOTER CPA s.r.l.); A. Dematteis (SEA Consulting s.r.l.) chairman of the WG; A. Gargini (Università di Bologna Alma Mater Studiorum); M. Governa (Regione Piemonte), F. Grosso (Hydrodata S.p. A.); F. Marchionatti (Politecnico di Torino) M.E. Parisi (LTF SAS, Lyon Turin Ferroviaire); P. Perello (GDP Consultant s.r.l.); M. Petitta (Università di Roma La Sapienza); M. Petricig (Regione Piemonte) M. Polemio (CNR IRPI); G. Preisig (Université de Neuchatel); L. Ranfagni (ARPA Toscana- VIA/VAS Sector); G. Ricci (Geodata Engineering S.p.A.); S. Skuk (BBT SE, Galleria di Base del Brennero); M. Tallini (Università dell'Aquila); R. Torri (SEA Consulting s.r.l.); V. Vincenzi (freelance geologist); A. Geuna (GDTest s.r.l.).

The aim of GESTAG working group is to propose a guideline on Sustainable Water Management in Tunnels. GESTAG is subdivided into five sub-groups, analyzing five different topics: (i) experience feedback on tunneling hydrogeology, based on verified review of tunnels already realized; (ii) geological and hydrogeological reference models, and methods of forecasting and management of the relationship between water and tunnel; (iii) impact on the Groundwater Dependent Ecosystems (GDE) and the environment, i.e. springs, streams, and wetlands; risk analysis and mitigation; (iv) communication, training, support to decision makers, advertising, education on the perception of possible environmental impacts from tunneling; (v) existing laws and policy framework, perspectives and development of new guidelines.

179.3.1 Experience Feedback

A data base of different field experiences on tunneling hydrogeology, inflow rates, examples of exploitation of water and heat represents a starting point and a useful calibration of modeling based forecasting. Experiences should include verified review of case-studies. A synthesis of different case-studies, in Italy and abroad, where either a professional best-practice and/or a research-focused approach have contributed to treat groundwater flow as a most significant target of analysis, is considered as the basis for the guidelines proposal.

179.3.2 Geological and Hydrogeological Reference Model; Methods of Forecasting and Management Water-Tunnels Relationships

The evaluation tool of the interferences induced by the works with the underground waters, starting from the different options of project up to the definitive solution, is the Hydrogeological Reference Model (HRM). A HRM is constituted by a conceptual and numerical schematization of the aquifers able to represent, both to a qualitative and quantitative level, the actual state of the underground circulation, and the impacts evaluation by overlaying the project alternatives. The HRM is developed in its main structure within the project phase, but it is subject to revisions and refinements on the base of the data-flow deriving from the monitoring activities, during the work and *post-operam* phases, with the aim to support an objective quantification of the interferences. The HRM must be the tool of analysis to be used for the prediction of impacts. These are the forecasting of the inflow into the tunnel, the forecasting of drawdown hazard that can affect the depletion of springs, wells and watercourses, and the design of technologies for drainage and/or waterproofing.

179.3.3 Valorization of Groundwater Resources and Heat

The water drained from the tunnel is a resource that cannot be wasted and which must imperatively be recovered. And this also applies to the heat associated with water in deep tunnels such as those in the Alps. The valorization of groundwater resources drained during excavations, and the associated heat, can be made if planned in the design phase, by means of appropriate catchment and housing of evacuation pipes in the tunnel. This approach must include an

analysis of the external demand of water and heat, near the portal of the tunnel where the resource can be delivered. Good examples that demonstrate the feasibility of these solutions are few but do exist, and should be studied, analyzed and reproposed systematically.

179.3.4 Impact on Groundwater Dependent Ecosystems and the Environment; Risk Analysis and Mitigation of Impacts

Groundwater dependent ecosystems (GDEs) are habitats that must have access to groundwater to maintain their ecological structure and function and are critical components in the conservation of the earth's aquatic biodiversity. These comprise a complex and often biodiverse subset of the world's ecosystems, and can be found in marine, coastal, terrestrial, cave, and aquifer environments (ref. GDE Network of the International Association of Hydrogeologists, http://iah.org). In addition to the GDE should obviously be included potential impacts on humans water uses. This require the analysis of springs, streams, and wetlands. Through the activities of modeling and monitoring it is possible to achieve a defined layout of the effects induced by the infrastructure on the underground water environment (GDE, springs, streams, etc.).

The impact layout described above is to be shared with the stakeholders, including environmental control Authori-

ties and the inhabitants, in order to find shared solutions, and limit possible litigations. This process help to identify and activate alternative supply plans where interferences that cannot be eliminated.

179.3.5 Communication and Education

The communication and education is one of the most important aspects to be managed to the rapid progress of the project. The experience shows that where these aspects are neglected, the project progresses slowly, and the costs increase. All of the following tasks must be overseen and carried out in parallel with the design and implementation of the work: training, advertising, education on the perception of possible environmental impacts from tunneling, and understanding of opportunities to valorize water and heat resources.

179.3.6 Existing Laws and Policy Framework

The analysis of existing laws and policy frameworks is one of the tasks of the GESTAG group. All suggestions included in these guidelines have to comply with the national rules. However, close examination of the rules, that by the time we made just for those in Europe, indicates a general lack of specific standards for tunneling.

Uncertainty and Risk in Engineering Geology

Convener Dr. Luca Soldo—*Co-convener* Jean Piraud

The Geological and Geotechnical Model (GGM) is the cornerstone of the design of major civil works, from feasibility evaluation to design during construction. The GGM visualizes, describes and quantifies the geological and geotechnical features and their characteristics in-depth, their estimated reliability, with the potential related hazards. The GGM is affected by uncertainties arising from the accuracy and completeness with which the subsurface conditions are known. Its limits span among events with a known probability (sometimes referred to as statistical uncertainty), and true uncertainties, which are events with unknown probability (sometimes referred to as indeterminacy) or,

worst still, completely unforeseen events. Uncertainty may be thought of as a continuum ranging from zero for certain information to intermediate levels for information with statistical uncertainty and known probabilities to high levels for information with a "true uncertainty". This session aims to be a round table to collect practical guidelines for the understanding and quantification of uncertainties and reliability of GGM for large civil engineering works as a base for the identification of the "best practices" to face them (ref. Also IAEG Commission C 28—Reliability quantification of the geological model in large civil engineering projects).

The Design Geological and Geotechnical Model (DGGM) for Long and Deep Tunnels

Alessandro Riella, Mirko Vendramini, Attilio Eusebio, and Luca Soldo

Abstract

Design errors frequently stay behind construction cost overruns and delays. A relevant part of these errors may arise from an inadequate knowledge of the geological and geotechnical conditions: several geological, hydrogeological and geotechnical aspects can remain unknown, partially or completely, prior to actual construction of engineering project. These unknowns usually exist in inverse proportion to the effectiveness of the geological and geotechnical investigations. On the other hand it is experienced that, because of the intrinsic complexity of the geological context, also rigorous investigation approaches are subject to several sources of uncertainty and random geological features or events remain difficult to be predicted and characterized. In particular for long and deep tunnels, these uncertainties and the resulting risks in construction could be especially severe. The Design Geological and Geotechnical Model (DGGM) has been intended from several authors in the last years as a conceptual framework inside which, progressively, searching adequate answers to the above mentioned limits. Inside the DGGM all the collected data are comprehensively stored and interpreted, anticipating and characterising the ground conditions with their related risks. Because of unavoidable limits rising from accuracy and completeness with which the subsurface conditions may be known, it is also a mean for identifying the variability and uncertainties of the data and of the derived geological context, with the related hazards and risks, providing the basis for a rationale design procedure.

Keywords

Tunnel design • Geology • Geotechnics • Uncertainties • Risks

180.1 Geological and Geotechnical Unknowns and Risks

The IMIA-ITIG has recently published (2011) the analysis of several cases of major tunnel failures (for projects from 1994 to 2010), identifying among the causes an "insufficient ground investigation" level (12 % of the cases) and for 41 % some "design errors", that often can derive from inadequate countermeasures for facing geological and geotechnical hazards.

As known several geological, hydrogeological and geotechnical aspects can remain unknown, partially or completely, prior to actual construction of engineering project, mostly due to intrinsic investigation ("diagnosis") difficulties.

A. Riella (✉) · M. Vendramini · A. Eusebio · L. Soldo
Geodata Engineering S.p.A., Corso Duca degli Abruzzi 48/e, Turin, Italy
e-mail: ari@geodata.it

M. Vendramini
e-mail: mve@geodata.it

A. Eusebio
e-mail: aeu@geodata.it

In particular for long and deep tunnels, these uncertainties and the resulting risks in construction could be especially severe: *".... the deeper the tunnel, the larger the uncertainties; the higher the probability of encountering adverse or unforeseen conditions for tunnelling, the greater the effort and the cost for site investigations to reduce the uncertainties"* (International Tunnelling Association ITA Report no 4—Long tunnels at great depth 2010).

Also the effectiveness of the modern procedures of "flexible design" and "Risk Management"—today integrated inside the best practices of geotechnical design (Chiriotti and Grasso 2002; AFTES GT32.R2A1 2012)—is enhanced when based on a sound preliminary "diagnosis" phase. The Risk Management must be applied in the very early stages of the project, and then up-dated along its completion. To understand the geological and geotechnical environment with which the project will face, identify the related hazards, evaluating their probability of occurrence and impact is of unparalleled importance.

These unknowns usually exist in inverse proportional to the effectiveness (amount, nature and quality) of the geological and geotechnical investigations (U.S. National Committee on Tunnelling Technology, USNCTT 1984; Consiglio Nazionale delle Ricerche 1997; Site Investigation Steering Group 2007).

Many literature references and rules of procedure underline the importance of a complete and proper investigation campaign (USNCTT 1984; U.S. UTRC 1996; ITA Working Group no. 17, 2010; AFTES GT32. R2A1 2012). Based on an analysis of 89 underground projects the USNCTT observed that in more than 85 % of the cases the inadequate level of the investigation leaded to claims and time/cost overruns. The USNCTT publication made recommendations as to minimum requirements for any project, especially considering the different order of magnitude (as percentage of capital cost) between investigation levels (<1 %) and claims levels (12–20 % and upwards).

The recent study "Analysing International Tunnel Costs" (Worcester Polytechnic Institute 2012) emphasises, again, the key role of the preliminary site investigations: *"We recognize the issues with convincing Clients to spend more money in the early stages of a project, when the overall viability, constructability and financing is still unknown, but all of our research subjects described a direct correlation between the amount of SI and cost savings"*.

It isn't worthless to observe that the expenditure on site investigation as a percentage of total project cost is often low, not rarely ranging from a mere 0.1 to 0.3 %. Over the past years ground investigation prices seem to be forced down in real terms and investigation today is often based upon "minimum cost and maximum speed".

On the other hand it is experienced that sometimes, because of the intrinsic complexity of the geological context, also rigorous investigation approaches are subject to several possible sources of uncertainty that could arise from the need for simplifications, heterogeneity, inherent randomness, imperfect interpretative concepts and hypotheses, measurement inaccuracies, sampling limitations, insufficient sample numbers, and others. Random or partially random geological features or events such as e.g. karst, gas and water circuits remain difficult to be predicted and characterized (e.g. Fig. 180.1).

If the reliability of the geological model largely depends on the effectiveness (amount, nature and quality) and reliability of the initial investigation phase the "core" of a sound and comprehensive understanding of whatever is necessary for the design requires "something more", as it will be described in the following.

180.2 The Design Geological and Geotechnical Reference Model

In the last years several authors (Soldo 1997 in *Progetto Strategico Gallerie*; Venturini 2001; Knill 2002; IAEG Commission C25 and C28) have progressively proposed the concept of Geological and Geotechnical Model (GGM or DGGM, Design GGM, underlying the bi-univocal relationships between itself and the project, then its importance inside the design procedure) a conceptual framework where the collected data are comprehensively stored (factual data) and interpreted, anticipating and characterising the ground conditions with their related risks.

A model is conceived as a tool (built on the base of the available data; the model itself could then be defined as a tool for store and process the input data) to understand, define, quantify, visualize, or simulate a certain aspect of the nature. It requires a selection and identification of the relevant aspects of a situation in the real world and then using different types of models for different aims:

- conceptual models are intended as tools to better understand the reality,
- graphical models to visualize the reality,
- operational models to define something (e.g. a variable, term, or object) in terms of a process (or set of validation tests) needed to determine its existence, duration, and quantity,
- mathematical models are intended as tools to quantify (objects or processes).

  The model is built following some main steps:
- do assumptions that simplify the system to its essential aspects,
- identify initial and/or boundary conditions,
- identify and quantify operating processes,

Fig. 180.1 Random, heavy water inflow through massive basalts (*Kárahnjúkar Hydroelectric Project, Iceland. Headrace Tunnel*)
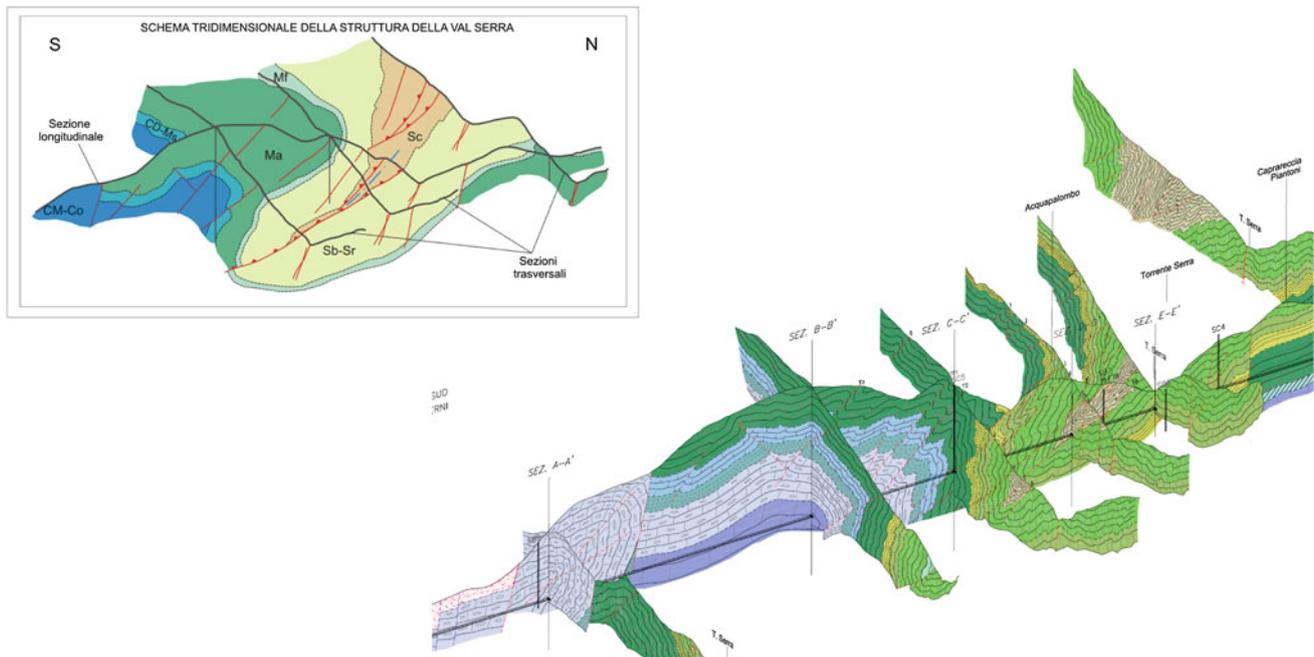
Fig. 180.2 Terni—Spoleto railway base tunnel, offprint of the basic geological model (*CM-Co* Calcare Massiccio-Corniola; *CD-MS* Calcari Diasprigni-Marne del Serrone; *Ma* Maiolica; *MF* Marne a Fucoidi; *SB-Sr* Scaglia Bianca-Scaglia Rossa; *Sc* Scaglia Cinerea)

- identify and quantify any changes to the system being considered, and
- define, or at least understand, the applicability of the model.

The DGGM is eventually an "engineering geological" model and this influence its nature. "*The same geological setting will interact with different engineering projects in different ways and will require different questions to be asked, different models to be developed and different investigations carried out. Certain engineering geological parameters may be more critical than others and some projects, by their very nature or setting, are exposed to more geological risk*" (IAEG Commission C25, Draft Report). Nevertheless the authors emphasise that its roots (and finally its overall effectiveness) remain deeply into the background of the Geological and Hydrogeological Model. The result of

the geological studies primarily consists in the evaluation of the geometry of geological bodies and characteristics at depth, at various scales. From this it can be derived a design Model that can be focused on some particular aspects such as lithology, groundwater, geomorphology, or rock structure and properties (Geological and Hydrogeological Model). On these first, fundamental leaps, can be built the Geotechnical Reference Model (GGM, e.g. IAEG C28 "Reliability quantification of the geological and geotechnical model in large civil engineering projects") (Fig. 180.2).

The Geotechnical Model is built on the Geological Model describing the range of engineering parameters and ground conditions (with their variation and reliability) that must be considered in the design (Knill 2002). Simultaneously the Geotechnical Model eventually simplifies (also to meet the requirements of the selected method of mathematical and physical analysis) the Geological Model by defining and characterizing volumes of ground with similar engineering properties, and identifies boundaries (with their variability, see e.g. AFTES GT32.R2A1 2012) at which changes of geotechnical conditions may occur.

Because of unavoidable limits rising from accuracy and completeness with which subsurface conditions may be known it is also a mean for identifying their related variability and uncertainties, the related hazards and risks, providing the basis for plan eventual additional site investigation and for a correct design procedure. The DGGM can be then finally described as the framework in which the expected risks are recognized and characterized.

Finally, not in order of importance, the DGGM will include the assessment of its effectiveness and reliability (with the evaluation of the associated uncertainties). Some approaches consider the quality of the investigation procedures (e.g. in term of extension of the geological mapped area, number and length of boreholes). Others consider the quality of the input data, still others the entire model itself.

The DGGM is conceived to be built of two main parts:
- the first, where all the collected data will be stored,
- the second, with the complete model, as derived from the input data interpretation.

Both of them, even if coming from interpretation, are intended to be as objective as possible in order to reduce biased interpretations of results. Another basic expectation is to document, archive and share all data and methodology, making them available for any possible reason of scrutiny by other specialists.

The DGGM must be focused on the engineering needs of the project. The provided information must be disclosed and comprehensible for all the specialists inside the design team, and eventually to the *non-specialists* (ideally for all the stakeholders interested to the project) as much as possible.

The DGGM must be suited and fulfil the current laws, norms, standards and procedures, together, in case, with requirements of the Owner or Third Parties. Because the DGGM must be suited with the project itself isn't useless to point out that there isn't a universal protocol for its construction. The reliability of the model can be high, for example, because supported by a good field mapping, also without many boreholes. It must also be considered the complexity of the geological context: monotonous sequence of horizontal, homogeneous, alluvial layers can be effectively studied also with few boreholes.

References

AFTES Recommendation GT32.R2A1 (2012) Recommendations on the characterisation of geological, hydrogeological and geotechnical uncertainties and risks

Bistacchi A, Massironi M, Menegon L (2010) Three-dimensional characterization of a crustal-scale fault zone: the Pusteria and Sprechenstein fault system (Eastern Alps). J Struct Geol 32:2022–2041

Consiglio Nazionale delle Ricerche (1997) Progetto Strategico Gallerie

Efron N, Read M (2012) Analysing international tunnel costs. Worcester Polytechnic Institute

Eusebio A, Soldo L, Pelizza S, Pettinau D (2005) Preliminary geological studies for the design of Mercantour base tunnel. AFTES Tunnelling for a sustainable Europe, Chambery

Grasso P, Chiriotti E, Xu S, Kazillis N (2007) Use of risk management plan for urban mechanized tunnelling projects: from the establishment of the method to the successful practice. In: Underground space, the 4th dimension of metropolises. Taylor & Francis, London

IAEG Commission C25. Use of engineering geological models. Part 1: introduction to engineering geological models

IAEG Commission C28—Reliability quantification of the geological and geotechnical model in large civil engineering projects. Terms of Reference

IMIA-ITIG (Reiner H) (2011) International Tunneling Insurance Group. Developments in the tunneling industry following introduction of the tunneling code of practice. IMIA annual conference, Amsterdam

ITA WG 17 (2010) Long tunnels at great depth

ITA Working Group no. 2 (2004) Guidelines for tunnelling risk management. Tunn Undergr Space Technol 19

Knill, J. (2002). First Hans Cloos Lecture', 9th congress of the International Association for Engineering Geology and the Environment. Geol Environ 62:1–34. Durban, South Africa

Mallet JL (2002) Geo-modeling. Oxford University Press, New York

Perello P, Venturini G, Dematteis A, Bianchi GW, Delle Piane L, Damiano A (2005) Determination of reliability in geological forecasting for linear underground structures: the method of the R-index. Géoline 2005—Lyon

Soldo L (1998) L'importanza delle indagini preliminari nella progettazione di opere in sotterraneo. PhD Thesis, Politecnico di Torino

The British Tunnelling Society (2003) The joint code of practice for risk management of tunnel works in the UK. Published by The British Tunnelling Society

US National Committee on Tunnelling Technology (1984) Geotechnical site investigations for underground projects

Research on Overall Risk Assessment and Its Application in High Slope Engineering Construction

181

Tao Lianjin, An Junhai, Li Jidong, and Cai Dongming

Abstract

Due to the special landform and physiognomy in the mountain highway construction, it's often necessary to excavate of road cutting in a complex geological environment, including high and steep slope. And the security of cut slope in construction has a deep influence on the normal development of the whole project. Whether the construction of high slope engineering is safe or not depends on many uncertainty factors. Generally, the sole safety factor can't deal with these uncertainties. Therefore, in the course of construction operation, analyzing and assessing the risk of slope engineering to avoiding and reducing risk is substantial. According to the characteristics of the slope engineering projects, considering to the experience of this kind of project management, the engineering geological conditions, site conditions, the height of slope and climate conditions were chosen as the overall risk assessment indicators of high slope engineering in the construction safety, and demonstrate the rationality of selecting the indicators in detail. Afterwards, based on the knowledge of probability theory and mathematical statistics, the scores of overall safety risk of construction can be divided into four levels, then evaluate the criticality of slope construction quantitatively and thereby provide scientific decision-making basis for different risk rank of slope engineering to take corresponding risk control measures. Furthermore, the special risk assessment of construction safety is suggested to the high slope engineering whose overall risk rank is level III and over. At last, based on Hubei Yunshi highway which is being constructed, the overall risk assessment on the construction of cut slope engineering was made and suitable evaluation result was obtained. Then compared with the actual construction situation, found evaluation results and actual situation are keep in coincide. So the effectiveness of the risk assessment system is verified.

Keywords

Cut slope • Overall risk assessment • Evaluation index system • Risk rank

181.1   Introduction

With the rapid development of high grade highway in mountainous areas, a large amount of cut slope engineering emerged and many slope deformation and failure occurred at the same time. The security issues of cut slope are also increasingly prominent, which have caused large numbers of casualties and huge economic losses in mountainous areas of the world. The total number of deaths due to all kinds of landslides activities is more than 25 annually which exceeding the average losses due to earthquakes (Krohn and Slosson 1976). The most disastrous landslides have claimed as many as 100,000 lives (Li and Wang 1992). Factors that affect the safety of cut slope are numerous and complex and there is no effective risk analysis and evaluation theory on multi-factor system at present. In recent years, risk analysis

T. Lianjin · A. Junhai (✉) · L. Jidong · C. Dongming
College of Architecture and Civil Engineering, Beijing University of Technology, Beijing 100124, China
e-mail: tsanjunhai@126.com

and assessment, as an important tool, was used by increasing experts and scholars to address uncertainty inherent in slope hazards. Einstein proposed the landslide risk evaluation framework: Natural datum—Dangerous figure—Hazard figure—Risk figure—Management figure, which realizes the change of the risk assessment from the qualitative to the quantitative (Einsten 1988). Zhang Yong-xing established the risk assessment of slope system, which can analysis the risk of slope based on the physical and mechanical parameters. Huang Run-qiu proposed a geological disaster risk assessment method which based on the GIS system (Huang 2000).

Even though study on slope risk have achieved a lot of achievements, however, cutting slope engineering, as an important part of the highway engineering, is still a blank area of the study about the risk evaluation during its construction.

181.1.1 The Failure Modes

The destruction of the rocky slope types roughly included: (1) Collapse failure mode; (2) Translational sliding failure mode; (3) Wedge failure mode; (4) Toppling failure mode.

181.1.2 The Established Process of Cut Slope Risk Evaluation Index System

The established process of highway cut slope risk evaluation index system divided into the following steps and the established processes of system were shown in Fig. 181.1.

181.1.3 Overall Risk Evaluation Index Classification Assignment and Its Standard

How to define the Slope risk criteria value is not only a technical problem, but also a comprehensive indicator including political, economic, social, engineering technology, natural environment, cultural background and other factors. The classification of evaluation index and value standard of cut slope engineering construction safety risk overall assessment was shown in Table 181.1.

The formula to calculate overall risk of cut slope construction safety:

$$R = A1 + A2 + A3 + A4$$

A1 The scores assigned by engineering geological conditions;
A2 The scores assigned by Site environment;
A3 The scores assigned by slope height;
A4 The scores assigned by climate conditions.

181.1.4 The Overall Risk Classification Standard

The high slope construction safety risk overall assessment classification standard can be gotten based on "Independent identically distributed central limit theorem" and slope expert experience which was shown in Table 181.2.

To the high slope whose risk level is the level III (high risk) and over, the dynamic assessment on the whole construction process was proposed.

Fig. 181.1 The cut slope construction safety risk assessment program flow chart

Table 181.1 Cut slope construction safety overall risk assessment index system

Evaluation index	Classification			Score	Explain	Evaluation score
Engineering geological conditions $A1 = (a + b + c + d + e)$	Landform and physiognomy (a)	Steep slope, canyon and other dangerous area		3–4	Relative height difference is up to 130 m, the mountain is round in shape, the average slope is 35°	2
		General mountain area		1–2		
	Formation lithology (b)	Expansive Soil, frozen soil, collapsible loess and other special soils		4	The quaternary system diluvial silty clay and lower Triassic marl and limestone	2
		Silty clay, gravel soil and so on		3		
		Soft rock (siltstone, clay shale and so on)		2		
		Medium hard and hard rocks (dolomitic limestone, quartz schist and so on)		1		
	Geological structure = (c1 + c2 + c3)	Fault (c1)	Yes	1–2	No fault	0
			No	0		
		Rock mass structure (c2)	Granular structure	3	Thick layer structure	1
			Cataclastic texture	2		
			Layered structure	1		
		Main structural plane direction (c3)	Identical or close (consequent slope)	3–7	The right of slope was a consequent slope after excavation, slope: 215° ∠45°, joint: 280° ∠13°	6
			opposite (reverse slope)	1–2		
	Groundwater (d)	Plentiful groundwater		2–3	Karst water in majority, the water was not uniform	2
		Poor groundwater		1		
	Unfavorable geological condition (e)	Slide, dangerous Rock mass, collapse and rock pile and other unfavorable geology		1–2	Karst collapse may occur	2
		There are no unfavorable geological condition		0		
Site environment A2	There are buildings and structure in construction site			1	A village near slope farmland, rural road access	1
	There are no buildings and structure in construction site			0		
Slope height (m) A3	Rock slope: ≥50 m or soil slope: ≥40 m			7	Left slope is about 44.8 m high, right slope is about 34.0 m high	5
	Rock slope: 40 ∼ 50 m or soil slope: 30 ∼ 40 m			5–6		
	Rock slope: 30 ∼ 40 m or soil slope: 40 ∼ 50 m			3–4		
	Rock slope: <30 m or soil slope: <20 m			1–2		
Climate conditions A4	Severe climate event happens frequently in construction area (strong winds, heavy rains and snows)			1	Damp and rainy, precipitation concentration and intensity	0
	Climate environment in good condition, it doesn't affect the construction safety			0		

Fig. 181.2 A certain cut slope of Yunshi highways. **a** Bedding landslide caused by excavation, **b** slope with mass broken rock

Table 181.2 The cut slope construction risk overall assessment classification standard

Risk level	Calculated score (R)
Level IV(extremely risk)	$R \geq 25$
Level III (high risk)	$20 \leq R \leq 24$
Level II (moderate risk)	$16 \leq R \leq 19$
Level I (low risk)	$6 \leq R \leq 15$

181.1.5 Project Case

This paper analyses the rationality of the risk assessment method using somewhere in a 2012 survey Yunshi highway excavation slope as an example (As shown in Fig. 181.2). The detailed descriptions of this slope are shown in Table 181.1.

The concrete evaluation analysis is shown in Table 181.1. The overall risk of this cut slope construction safety:

$$R = A1 + A2 + A3 + A4 = 21$$

The conclusions which shown as follows can be gotten based on the cut slope construction risk overall assessment classification standard. The overall risk rank of this cut slope are level III (high risk). To ensure construction safety, construction safety management department should carry controlling work based on the point of construction technical measures and site safety management. The risk assessment results were identical with the actual situation, which verified the correctness of the construction risk assessment method witch this paper proposed.

181.1.6 Conclusions

(1) This paper mainly describes five failure mode and mechanism of the mountainous area highway rocky slope, points out the damage types that may occur in the process of its construction, advances a slope construction safety impact index and the weighting influenced by rock slope based on a large number of survey data of high slope somewhere in yunshi expressway rock slope, then determines the size of the overall risk classification standard combined with the empirical method and the central limit theorem, and established a more scientific, reasonable and systematic risk evaluation index system of high rocky slope.

(2) The geological conditions and height of high slope are the two most important factors affecting the safety of construction, directly determines the level of the overall risk level, construction should be mastered before slope stability and the weathering degree. Don't construct blindly.

(3) This paper analyses and evaluates Yunshi highway rocky slope construction safety risk based on some engineering cases, the evaluation result is consistent with the engineering practice. The high slope overall risk evaluation index system has a certain reference value for building and construction and predicting and avoiding high mountain area highway rocky slope construction risk.

References

Champman CB, Cooper DF (1987) Risk analysis for large project: models, methods and cases, Wiley, Hoboken

Chunlong N (2012) Risk analysis theory and application for slope engineering. Central South University, Changsha

Einsten HH (1988) Special lecture: landslide risk assessment procedure. In: Proceedings of 5th international symposium. Lausanne, Landslide, pp 1075–1090

Krohn JP, Slosson JE (1976) Landslide potential in the United States. Nat Emerg Train Cent 30(1):30–33

Li T, Wang S (1992) Land slide Hazard sand their Mitigation in China. Science Press, Beijing 84 pp

Wang S-C, Zhe X-S, Zhou Z-J et al (2010) Application of engineering fuzzy set theory analysis on AHP to highway slope stability evaluation. J Saf Environ 10(5):189–192

Xia Q-T (2008) Engineering construction risk assessment and management. Fujian Archit Constr 10(5):97–99

Zhang Y-Xg, Chen Y, Wen H-J et al (2008) The research of landslide hazards assessment system. J Chongqing Jianzhu Univ 30(1):30–33

The Research of Geological Forecast Based on Muti-source Information Fusion

S. Cui, B. Zhang, F. Feng, and L. Xie

Abstract

In recent years, a large number of mountain tunnels, which have long distance and large buried depth, have been built. But China is a mountainous country with complicated geological conditions. And due to the complicated geological conditions, different kinds of geological disasters often occur during the construction. Therefore, the geological forecast is an important approach to reduce geological disasters effectively. This paper is based on the geological forecast conducted in Jucheng tunnel, Yangquan, Shanxi province. In this paper, a new method of geological forecast is put forward, which is based on the tunnel geological hazards assessment and combine with the stress-strain analysis by using FLAC^{3D} and tunnel seismic tomography (TST). Through risk analysis to identify hazard sections, then select the typical tunnel face of high-risk section and analyze the stress-strain of surrounding rock. Therefore, the stability properties of tunnel section can be obtained. After that, the geological forecast, based on the TST, is conducted on the typical tunnel face. Over all, these new method can forecast the construction geological disasters of different scales of sections (such as the tunnel section or specific tunnel face). Moreover, the new method has obtained the ideal effect in the geological forecast of Jucheng tunnel.

Keywords

Geological forecast • Tunnel geological disasters • Analytic hierarchy process • FLAC^{3D} • Tunnel seismic tomography

182.1 Introduction

Along with China's infrastructure construction, tunnel construction technology has developed rapidly. Tunnel engineering construction speed is faster, and the tunnel depth is also growing. Because of the unclear understanding of geological conditions ahead of the face, tunnel construction will bring great blindness, and unexpected landslides, cave, gushing and other accidents may happen. How to solve the above problem tunnel engineering has become a growing concern.

Using the method of land sonar in the Yangzhai tunnel and Lvchang tunnel, Zhong et al. (1995) successfully detected the cave of 40–80 m distance range ahead of the face. In Sichuan Tieshan Tunnel, good results have been achieved to forecast the geological situation within 50 m ahead of the face by horizontal sonic profiles (Yang et al. 1997). Dai et al. (2005) used TSP203 to probe BAJIAOXI tunnel, forecasting rock geological nature, location and size about 100 m ahead of face to ensure safety and quality. Wang (2008) recognized more accurate position ahead of the face in Taizhou tunnel and the distribution of rock mass on the top of the shallow buried tunnel by using GPR.

S. Cui · B. Zhang (✉) · F. Feng
China University of Geosciences, School of Engineering and Technology, Beijing, China
e-mail: sc_zhb@cugb.edu.cn

L. Xie
Beijing Urban Construction Exploration & Surveying Design Research Institute Co., Ltd., Beijing, China

In this paper, relying on the Giant City Tunnel project of Yangquan-Niangziguan highway, risk checklists and analytic hierarchy process method have been applied to access the risk of geological disasters in the construction of the tunnel, and analyze the surrounding rock stability of the tunnel after excavation situation by FLAC^{3D} software. In the tunnel construction process, TST geological advanced prediction technology has been adopted for advance geological forecast of each section.

182.2   Engineering Situation and Geological Conditions

Giant City Tunnel of Yangquan-Niangziguan highway is located in the northeast of the Huge Town, Yangquan City, Shanxi Province. The line is roughly east-west, and cross two high mountains. The top of the mountain maximum elevation is about 724 m, the maximum depth of the tunnel is 167 m. Tunnel site area belongs to the tectonic denudation accumulation and tectonic karst landform. It is in Shanxi upfaulted zone of Sino Korean paraplatform. Second-level structure includes the Qinshui platform concavity and the broken arch of Taihang Mountains. The simple stratum structure has no obvious signs of a new tectonic movement. Based on regional data from 1:500,000 geological map and engineering detailed investigation results, the upper strata of the tunnel site area is the Quaternary Aeolian deposits, diluvial layer coverage, underlying bedrock is Carboniferous sandstone and Ordovician limestone.

182.3   Geological Forecast Based on Multi-source Information Fusion

182.3.1   Risk Assessment of Tunnel Geological Disaster

In this paper, the risk assessment is before the stage of tunnel excavation. Geological disaster risk assessment is mainly based on tunnel engineering design data and geological data. Main objective is various geological disasters may occur in the process of tunnel construction. Combined with hierarchical analysis method of expert surveys, geological factors of the risk index system were established: eccentric compression (C1), lithology and weathering degree (C2), normal faults (C3), development and erosion of karst fissure water (C4), karst (C5). Huge City tunnel was two-way separated tunnel, geological and structural condition were different in the direction of the line. According to the regional geology and survey report, the assessment of the tunnel was divided into three sections, namely K3+290–K3+920, K3+920–K4+380, K4+380–K4+740.

Risk factors and the impact between risk events were respectively analyzed through the checklist method. The judgment matrix of risk index system has been obtained. By solving the theoretical solution of the judgment matrix, the comprehensive weights were calculated and sorted, which showed a clear understanding of five underlying risk factors that affects the target. Eccentric compression of tunnel terrain, lithology and weathering degree and normal faults had very important influence in Table 182.1. Karst and fissure water also need to be carefully considered.

182.3.2   Numerical Simulation of the Stability

In the results of tunnel geological disaster risk assessment, the three risk zones were finally selected. According to the classification of surrounding rock, characteristics of rock mass and boundary conditions in the survey report, three sections of typical rock were elected, namely K3+600–K3+604–K4+260–K4+264 and K4+480–K4+484.

The statistical results of the model calculations were shown in Table 182.2. The stability of surrounding rock of each section in excavation without supporting was worse, characterized by large plastic zone area. The minimum principal stress of surrounding rock was larger, so was the vertical and horizontal displacement. After adding the supporting measures, the stability of surrounding rock was improved. The plastic zone area decreased, the minimum principal stress and horizontal and vertical displacement was reduced.

182.3.3   Tunnel Geological Prediction During Construction

After the pre-tunnel geological disaster risk assessment and stability analysis of tunnel surrounding rock, in the specific tunnel excavation process, a variety of unexpected geological problems will be encountered. Therefore, during the construction geological prediction is particularly important, especially for tunnel construction process, forecasting geological conditions ahead of the face. The tunnel geological prediction is a TST geological prediction technique.

TST technical is short for tunnel seismic tomography. Its observation system uses spatial layout, and receive and excitation system layout on both sides of the tunnel wall rock. Seismic waves are stimulated by the bursting of small doses, received by the geophones. TST can get the accurate distribution of wave velocity of the surrounding rock in front of face and the location images of the geological body.

As shown in Fig. 182.1, TST observing system is arranged as follows: ① 12 detectors(S1–S12), Arranged on both sides of the wall, each side six, spacing of 4.0 m; ② 6

Table 182.1 Results of geological disaster risk assessment

No.	Mileage		Risk factors	Risk events
	Starting	Termination		
1	K3+290	K3+920	Eccentric compression	Landslide
2	K3+920	K4+380	Normal faults	Landslide, water inrush
3	K4+380	K4+740	Lithology and weathering degree	Landslide, water inrush

Table 182.2 Results of numerical simulation calculation

Model	Working condition	Plastic zone	Minimum principal stress (MPa)	Maximum horizontal displacement (cm)	Maximum vertical displacement (cm)	Stability
K3+600–K3+604	No supporting	Larger	−1.1	−4.8	−11.8	Poor
	With supporting	Smaller	−1	−1.1	−3.3	Better
K4+260–K4+264	No supporting	Larger	−0.68	−0.7	−4.2	Poor
	With supporting	Smaller	−0.65	−0.5	1.4	Better
K4+480–K4+484	No supporting	Larger	−0.88	−2.4	−7.5	Poor
	With supporting	Smaller	−0.83	−0.7	−2.4	Better

explosion sources(P1–P6), arranged in two side, three on each side. The first hole of each side is apart from the detector 4, 24 m space of the rest.

The tunnel was segmented for forecasting, each prediction distance was 100–150 m. The early stage of the tunnel geological disaster risk assessment and surrounding rock stability analysis have found three Issues outstanding location, so the geological advanced prediction results of these three location were displayed.

(1) Geological prediction probe results ahead of the ZK4 +597 face:

The observations were obtained from effective records of 36 channels, getting geological migrated image and seismic wave velocity distribution curve of surrounding rock within 100 m ahead of the ZK4+597 face of left lane tunnel exit, shown in Figs. 182.2 and 182.3.

In geological migrated image, abscissa was tunnel mileage and working face coordinates was 0; Vertical axis is horizontal transverse width of the tunnel. The blue stripes represented rock interface changes from hard to soft, red

Fig. 182.1 TST excitation and reception mode

indicated the interface from soft to hard and blue-red indicates the presence of rock fracture zones. Figures 182.5, 182.6 and 182.7 showed the rock velocity distribution curve, which reflected the distribution of rock mechanical properties. Intensive strips reflected complex structure and structural development, corresponding high velocity zone in the wave velocity distribution. Less strips area reflected uniform density of surrounding rock, corresponding high velocity zone.

Using the above results, geological conditions within 100 m ahead of the ZK4+597 face was divided into two sections:

Section 1: ZK4+597–ZK4+570, 27 m length, lower rock velocity (P-wave velocity of 2,500 m/s), development structure plane and crack, intermediary weathered-strong weathered, poor stability, grade IV rock.

Section 2: ZK4+570–ZK4+497, 73 m length, velocity of 2,600 m/s, better stability and integrity, intermediary weathered, grade IV rock.

(2) Geological prediction probe results ahead of the ZK4 +292 face:

Geological conditions within 100 m ahead of the ZK4 +292 face was divided into four sections (shown in Figs. 182.4 and 182.5):

Section 1: ZK4+292–ZK4+272, 20 m length, velocity of 2,400 m/s, development structure plane and crack, intermediary weathered-strong weathered, poor stability, grade V rock.

Section 2: ZK4+272–ZK4+252, 20 m length, velocity of 2,400 m/s, better stability and integrity, intermediary weathered, grade IV rock.

Section 3: ZK4+252–ZK4+242, 10 m length, velocity of 2,400 m/s, fault or fracture zone may exist, grade V rock.

Fig. 182.2 Geological migrated image ahead of the face
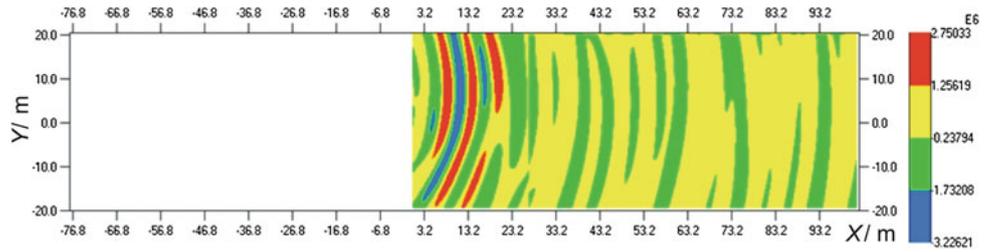
Fig. 182.3 Distribution curve of seismic wave velocity
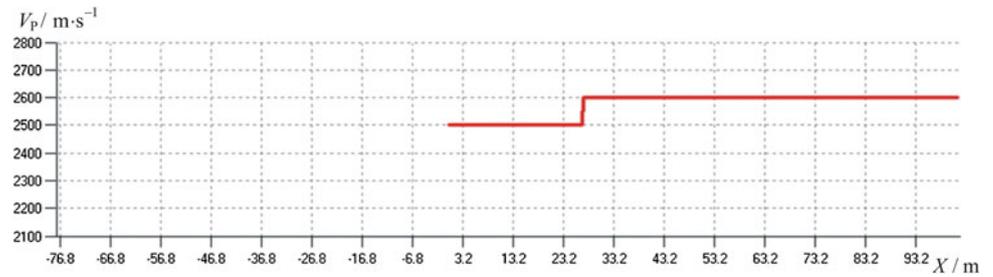
Fig. 182.4 Geological migrated image ahead of the face
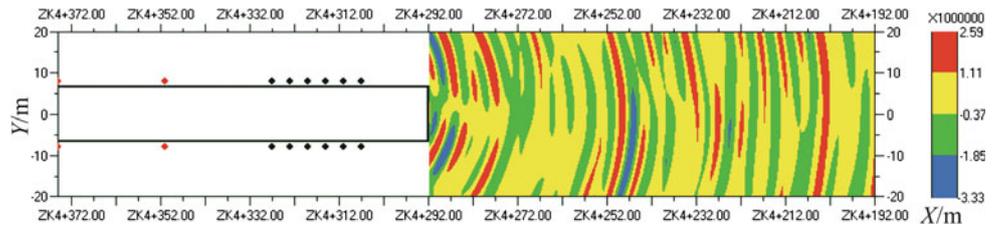
Fig. 182.5 Distribution curve of seismic wave velocity
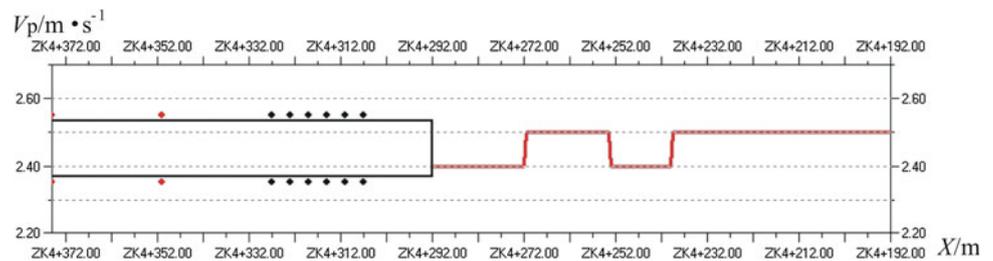
Section 4: ZK4+242–ZK4+192, 50 m length, velocity of 2,500 m/s, better stability and integrity, intermediary weathered, grade IV rock.

(3) Geological prediction probe results ahead of the YK3 +480 face:

Geological conditions within 100 m ahead of the YK3 +480 face was divided into three sections (shown in Figs. 182.6 and 182.7):

Section 1: YK3+480–YK3+504, 24 m length, low velocity of 2,000 m/s, fault or fracture zone may exist, grade V rock.

Section 2: YK3+504–YK3+537, 33 m length, velocity of 2,200 m/s, better stability and integrity, intermediary weathered, grade V rock.

Section 3: YK3+537–YK3+580, 43 m length, velocity of 2,400 m/s, development structure plane and crack, intermediary weathered-strong weathered, poor stability, grade V rock.

Compared detailed forecast results with the actual situation after excavation, these two cases were almost identical except a little difference on the determination of rock mass.
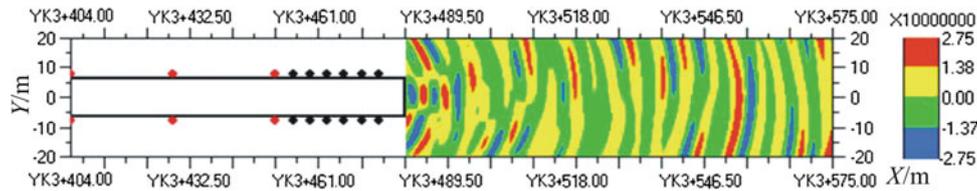
Fig. 182.6 Geological migrated image ahead of the face

Fig. 182.7 Distribution curve of seismic wave velocity
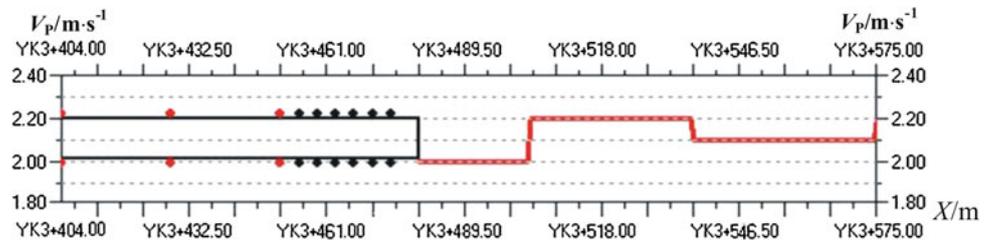
182.4   Conclusions

In this paper, relying on the huge city tunnel engineering, geological forecast based on multi-source information fusion was studied. The main conclusions and results are as follows:

(1) Using hierarchical analysis method, with regional geological data and survey data of tunnel site, a tunnel geological disaster risk assessment index system was established. Analyzing the underlying risk factors of the index system, three risk zones were obtained, and landslide is the most possible risk events, the second is the water inrush.

(2) Using FLAC^{3D} numerical analysis software, by analysis for plastic zone, stress and displacement characteristics, the stability of surrounding rock during excavation without supporting was worse.

(3) Using TST geological prediction method to predict the situation of the tunnel, the scale situation of unstable rock mass ahead of the face was otained, which were good construction guidance. It came to predict the situation the first two methods cannot.

(4) Tunnel geological disaster risk assessment, rock stability analysis and tunnel geological prediction were layer upon layer progressives. The research process was from the macro to the specific. Tunnel geological disaster risk assessment drew risk zoning of geological disasters; tunnel surrounding rock stability which were no supported and supported after excavation of each risk partition were analyzed by numerical analysis software; Tunnel geological prediction predicted body size of unstable rock mass in specific problematic partition. Three results are complementary and have good guiding significance on the construction.

References

Black K, Kopac P (1992) The application of ground penetrating radar in highway engineering. Public Roads 56(3)

Dai QW, He G, Feng DS (2005) Application of the TSP-203 system in geological advanced prediction of tunnel. Prog Geophys 20(2):460–464

Flemming J, Holger LA, Peter S, Esben A, Egon N (2003) Geophysical investigations of buried valleys in Denmark: an integrated application of transient electromagnetic and feflection seismic surveys and exploratory well data. J Appl Geophys 53–56

Johnston MJS (1997) Review of electric and magnetic fields accompanying seismic and volcanic activity. Surv Geophys 18:441–476

Otto R, Button E, Bretterebner H, Schwab P (2002) The application of TRT-Ture Reflection Tomography-at the Unterwald Tunnel. Geophysics 2:51–56

Scheers B (2001) Ultra-wideband ground penetrating radar with application to the detection of anti personnel landmines. Royal Military Academy, Department of Electrical Engieering and Telecommunication. pp 258–360

Song XH, Gu HM, Xiao BX (2006) Overview of tunnel geological advanced prediction in China. Prog Geophys 21(2):605–613

Wang RQ (2008) The study of advanced detecting methods on tunnel geological hazards. Central South University, Changsha

Presentation of the Activity of the AFTES WG 32: Considerations Concerning the Characterization of Geotechnical Uncertainties and Risks for Underground Projects

183

G.W. Bianchi, J. Piraud, A.A. Robert, E. Egal, and L. Brino

183.1 Introduction

The feedback derived from completed underground projects is still far from being satisfactory for all aspects relating to the characterisation of uncertainties, unforeseen circumstances and risks relating to underground space:

- The graphical representation of these uncertainties on geological cross-sections is often incomplete, ambiguous or completely lacking;
- In reports, the description of uncertainties is often insufficient, whether they relate to geotechnical properties, the position of events, the frequency of unpredictable phenomena;
- There is no recognised, unequivocal methodology for taking these uncertainties into account in so-called "Risk analysis" reports;

Faced with these findings, in 2009, AFTES reactivated working group GT32, with a view to establishing a methodology for properly identifying and representing uncertainties, analysing and managing the risks arising from these uncertainties.

To contribute to this objective, the GT32 recommendation aims mainly:

- Specifying terminology in terms of uncertainties and risks;
- Establishing a methodology for examining risks;
- Making proposals with a view to improving certain practices and tools, such as analysis of the reliability of investigations, graphical representation of uncertainties on geological cross-sections, etc.

A detailed description of the proposed methodology is found in the text of the recommendation (AFTES WG 32.2 2012).

183.2 Risk Management Methodology

The geotechnical risk management methodology which AFTES recommends should be applied for studies comprises three major phases:

1. Compiling a review of geotechnical knowledge and uncertainties covering geological, hydrogeological and geotechnical data;
2. Geotechnical risk assessment based on the summary of data; this phase in turn comprises three stages: risk identification, analysis and evaluation;
3. Geotechnical risk treatment.

183.2.1 Review of Geotechnical Data and Uncertainties

The proposed steps for performing a review of geotechnical data and uncertainties are as follows:

- Presentation of the raw data available;
- Assessment of its reliability;
- Summary and interpretation;
- Summary of uncertainties and in particular of gaps in knowledge (Register of Uncertainties).

SEA Consulting Srl, Turin, Italy

Present Address:
G.W. Bianchi
EG-TEAM STA, Turin, Italy

J. Piraud
ANTEA Group, Orléans, France

A.A. Robert
CETU, Lyon, France

E. Egal
Egis, Lyon, France

L. Brino
LTTF, Turin, Italy

183.2.1.1 Presentation of the Raw Data Available

During this first stage, a complete list must be drawn up comprising all documentary data and relating to worksites conducted in similar terrain; the results of specific investigations conducted for the project should be added to these data.

The nature and quantity of available data, their distribution, source and date of acquisition must be clearly stated.

183.2.1.2 Reliability of Data

The second stage corresponds to a critical evaluation of the quality of data. This stage is highly recommended to correctly define the contribution of these data to drawing up the geological model. It is also appropriate to evaluate the extent of gaps in knowledge, i.e. "what is not known". Among the factors to be taken into account to evaluate reliability, the complexity of the local geological context, the nature of investigation works as well as the physical distribution of this work and its spatial "density" may be mentioned.

183.2.1.3 Summary and Interpretation

The third stage consists in drawing up a geological model displaying the designer's idea of the geological context and expected construction environment. The presentation of this model includes two types of documents:

- a report, detailing the hypotheses deemed the most likely based on the analysis of all the data;
- graphical documents: geological and hydrological models and especially provisional longitudinal geotechnical profiles, along with as many cross-sections as necessary and a horizontal cross-section of the project.

It is in these documents that uncertainties with respect to interpretation should be pointed out, in particular on graphical elements. This longitudinal profile shall also include information about the variability of the parameters within each sub-section, such as the following:

- the dispersion of parameters, to allow the finalisation of methods (excavation, mucking, temporary support, etc.);
- the characteristic values chosen for the various geotechnical magnitudes;
- the limits within which the main parameters vary.

183.2.1.4 Register of Geotechnical Uncertainties

The fourth stage consists of summarising the uncertainties identified at the end of the previous operation and compiling a "Register of Uncertainties". This Register of Uncertainties should be limited to a list of the identified uncertainties, without analysing the consequences. On completion of this first phase of "Review of Geotechnical Knowledge and Uncertainties", the elements drawn up during the four stages described above are brought together in a single document including both a report and diagrams, as well as the Register of Uncertainties.

183.2.2 Geotechnical Risk Assessment

For each of the risks under consideration, the risk assessment phase includes three distinct phases:

- risk identification,
- risk analysis (in the strict sense of the term),
- risk evaluation.

183.2.2.1 Risk Identification

Risk identification requires the analysis of uncertainties with respect to their effects on expected results. Normally all uncertainties are a source of risk, but some of them may have virtually no effect at all. Only uncertainties for which the deviations induced with respect to the geological model are sufficiently significant to cause notable consequences, need to be identified as risks.

For each of the uncertainties identified, several hypotheses may be formed:

- for a given event: a variable number of occurrences, different locations or more or less serious consequences;
- for a "lack of geological knowledge": various configuration hypotheses for the geological context.

183.2.2.2 Risk Analysis

The Risk analysis stage includes three operations:

- quantification of the consequences arising from an event identified as a risk;
- quantification of the likelihood of this event and/or consequences;
- determination of the level of risk (significance of the risk) by combining the consequences and likelihood.

Quantification of the Consequences Arising from an Event

To proceed with risk assessment, the designer must draw up one or more hypotheses for each event identified, describing the circumstances caused by the occurrence of the event. The consequences of the same event may affect several objectives and each of these objectives in a different way. For each event, an analysis of its consequences on each of the objectives should therefore be conducted. Practically speaking, for geotechnical risks, the most relevant general objectives are site safety, cost, lead time, performance and the environment. The consequence is usually estimated as being the additional costs and/or extra time required to treat the event encountered.

Quantification of the Likelihood of an Event

The following stage consists of determining the "likelihood" of the identified event and/or its consequences. The likelihood of the event itself depends on a number of factors characterising the level of knowledge:

- the amount of investigation works carried out, its relevance and its quality of execution;
- the geographical proximity of investigation works to the structure;
- the complexity of the geological context.

Determining the Level of Risk (Significance of the Risk)

The "level of risk" qualifies the significance of the risk and is usually expressed by combining the likelihood with the consequence, both of which are evaluated by the designer. The combination of the likelihood and consequences may be "qualitative, semi-quantitative, quantitative or a combination of the three, depending on the circumstances."

183.2.2.3 Risk Evaluation

The designer then proceeds with risk evaluation by comparing their estimated level of risk to the risk criteria expressed by the project owner. For each of the risks, the project owner may take two attitudes:

(1) Refuse the risk and request that the designer:

(2) Accept the risk, with or without treatment:

183.2.2.4 Risk Treatment

Risk treatment aims at reducing the importance of risk or eliminating it. Possible actions may include the following:

- eliminating the risk source, e.g. by performing a specific investigation enabling uncertainty to be locally eliminated;
- altering likelihood, also by means of additional investigation enabling the geological model to be further clarified;
- reducing the consequences of an event on the circumstances of completion, through the implementation of preventive technical provisions and altering construction methods
- implementation of an early detection method for the occurrence of an event and early definition of remedial technical measures.

Following application of these measures, a new evaluation of each risk is conducted. If, despite the treatment measures, the risk remains unacceptable, a new "risk treatment" process is launched.

183.3 Graphical Representation of Geological Uncertainties

Maps and geological cross-sections are designed to provide a continuous representation of the geological nature of underground space based on discontinuous observation and data available in varying degrees of abundance and density. They are therefore interpreted "models" providing a two-dimensional representation of the most likely geology and reflect the author's understanding of the geology in question, in line with available data. The abundance and relevance of data will have a primary influence on the reliability of the document. With regard to geological cross-sections for civil engineering, unlike more conceptual "academic" cross-sections, it is particularly important to be meticulous and accurate regarding the geometry of layers (thickness, incline, folds, etc.), the location of contacts and faults, and the uncertainty of these locations. Indeed, the consequences of these uncertainties may be highly significant when it comes to design of the structure, its mode of construction, and so on.

GT32 has formulated a number of recommendations on the way to represent geology and the related uncertainties on documents used for civil engineering. The aim is that ultimately, a graphical representation should be achieved that makes it possible to see the extent of both knowledge and lack of knowledge regarding the terrain that may be crossed by an underground structure. In general, GT32 recommends the following:

- Drawing a clear distinction between the factual data that enabled the geologist to draw a map or cross-section and the interpretations;
- Ensuring that maps and cross-sections feature only unambiguous figures and symbols;
- Representing the uncertainty with regard to the existence and/or geometry of the geological object shown as well as possible on cross-sections, particularly adjacent to the projected structure.

183.3.1 Representation of Data

The geological map constitutes the foundation document for any geological study. Ideally, any geological map should be accompanied by an outcrop map, either in the form of a separate document, or on the geological map itself, with outcrop zones distinguished by darker or closer shading or with a specific outline.

Geological profiles are established using both surface and underground data:

- On the surface, the geological map makes it possible to locate contact points, faults etc. with the related degree of uncertainty;
- At depth, direct observations may be made using boreholes, and in some cases existing underground works or exploratory adits.

Moreover, observations made in boreholes are not always exactly located on the cross-section. The further away the borehole is, the greater the degree of uncertainty of the projection on the cross-sectional plane. Consequently, it is

recommended that boreholes should be indicated on cross-sections by distinguishing those that are "close" to the profile plane from those that are farther away with respect to the profile plane.

183.3.2 Representation of Uncertainties Related to the Position of Contacts

The degree of uncertainty relating to the location of each geological object should be represented in detail along the entire length of a cross-section. Four possible ways of representing these extreme positions are described below.

183.3.2.1 Representation N.1
The uncertainty range is shown on the whole of the longitudinal profile for each contact or fault (Fig. 183.1). The resulting uncertainty range may be shown as a line, both on the surface (outcrops) and at depth (for instance, at a borehole which has passed through a clear contact point between formations A and B). This type of representation is appropriate if it only concerns a few contact points, but can become illegible in the event of multiple contact points, with overlapping uncertainty ranges.

183.3.2.2 Representation N.2
Representing the uncertain position of contact points or faults should be done only at the tunnel depth, on a specific profile located beneath the principal cross-section and confined to a narrow vertical area along the tunnel axis (Fig. 183.2). The uncertainty is expressed by a strip of variable width, corresponding to the zone where formations in contact may be encountered.

183.3.2.3 Representation N.3
The extreme locations of the contact points are not shown by their actual geometry on the vertical longitudinal profile, but

Fig. 183.2 Representation 2: vertical geological cross-section and "mini-profile" at the elevation of the project with an uncertainty range
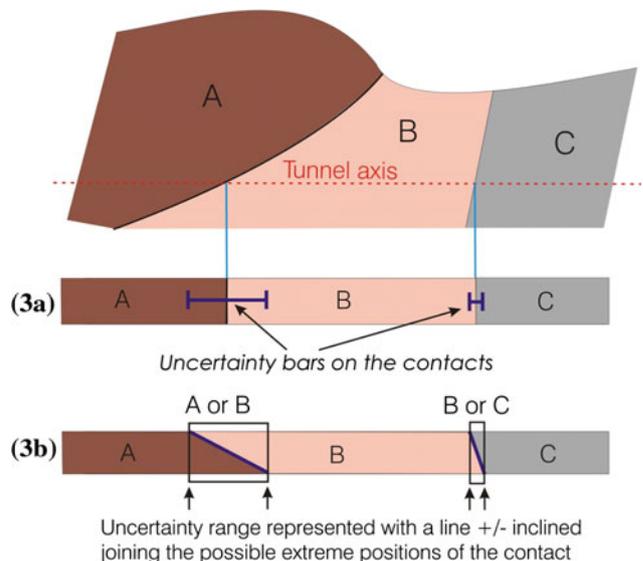
Fig. 183.3 Representation 3. Geological longitudinal profile and strips showing the location of contact points for the elevation of the project, with an uncertainty bar (type 3a) or oblique line (type 3b)

by standard symbols indicated on a strip located beneath the principal cross-section. Two types of symbol may be used:

- **Type 3a—the uncertainty bar**. The strip features a bar centred on the most probable location of the contact point. In this case, only one uncertainty bar is shown for the entire stratigraphic series (Fig. 183.3);
- **Type 3b—oblique line**. At the top and bottom of the strip, the extreme positions of the contact point are shown for the project, connected by an oblique line: the steeper its gradient, the lower the degree of uncertainty. The advantage of this method is that it clearly visualises the contrasting uncertainty along the cross-section, and it can be applied to successive geological contact points even when these are very close together. Type 3b

Fig. 183.1 Representation 1: geological longitudinal profile with uncertainty range for a contact location

representations must however be clearly explained in the legend, because they are less intuitive than 3a. The uninitiated often confuse the uncertainty range with a horizontal geological cross-section at the tunnel depth, which is not the case.

Reference

AFTES WG 32.2 (2012) Recommendations about characterisation of geological, hydrogeological and geotechnical uncertainties and risk. Tunnels & Ouvrages Souterrains, n. 232

Development of 3D Models for Determining
Geotechnical-Geological Risk Sharing
in Contracts—Dores de Guanhães/MG/Brazil
Hydroelectric Powerplant Case Study

184

Isabella Figueira, Laurenn Castro, Luiz Alkimin de Lacerda, Amanda Jarek,
Rodrigo Moraes da Silveira, and Priscila Capanema

Abstract

Discussions concerning the type of contract to be adopted, the responsibilities on risks and possibilities of risk sharing in construction works are time consuming during the formatting of the contracts and, often, last until its closure. Within the main difficulties encountered are the lack of data and subjectivity in the interpretation of available information. In order to reduce these uncertainties in models and the sharing definitions, a research project was proposed focusing on the development of a methodology based on an integrated three-dimensional model to support the risk reports and the definition of risk limits assumed by each stakeholder. Available information from, Dores de Guanhães Hydroelectric Power Plant, was integrated in such environment. From geo-structural point of view the main features found are thrust faults of NNE-SSW direction, which are truncated or displaced by a less intense system in NW-SE direction, affecting granite-gneiss rocks of Açucena Granite belonging to the Mantiqueira Complex (Poente and Guanhães Energia, Basic Project Studies HHP Dores de Guanhães-MG, 2008). Data provided by the construction owner have been uploaded in the 3D modelling software, along with the regional images and structural and field data. Geophysical analyses (dipole-dipole array) were performed and included in the model with a thorough discussion of its possible benefits in general interpretation. Finally, the use of the consolidated 3D model is discussed within a tunnel excavation risk assessment methodology.

Keywords

3D Models • Geotechnical-Geological risk • Geophysical analyses

I. Figueira (✉) · L.A. de Lacerda · A. Jarek · R.M. da Silveira
LACTEC—Institute of Technology for Development, Curitiba, Brazil
e-mail: isabella.figueira@lactec.org.br

L.A. de Lacerda
e-mail: alkimin@lactec.org.br

A. Jarek
e-mail: amanda.jarek@lactec.org.br

R.M. da Silveira
e-mail: rodrigo.silveira@lactec.org.br

L. Castro · P. Capanema
CEMIG, Belo Horizonte, Brazil
e-mail: laurenn@cemig.com.br

P. Capanema
e-mail: pic@cemig.com.br

184.1 Introduction

Discussions concerning the type of contract to be adopted, the responsibilities on risks and possibilities of risk sharing in construction works are time consuming during the formatting of the contracts and, often, last until its closure. Settings involved in these discussions should consider the characteristics of entrepreneurs and builders, the site of the work, the level of uncertainty and safety of the developed models and design features.

Within the main difficulties encountered are the lack of data and subjectivity in the interpretation of available information. When it comes to construction of Hydroelectric Power Plants (HPP), the excavation of underground structures such as the case of diversion tunnels or adduction, the

main focus of this work, for the preparation of a local geological model, qualification and quantification of geological and geotechnical risks various methodologies have been adopted, but normally not considering the integration of these different databases.

Aiming to reduce uncertainties and clarifying the risk sharing conditions, a Geological-Geotechnical Risk Report is compiled seeking to identify in the adopted models marked characteristics of foundation, including necessary treatments and observed uncertainties. This report is discussed and consolidated between the parties, becoming part of the contract. Although the consolidation of the geological-geotechnical model and the risk report involve a team with participation of geologists and engineers from involved companies in a series of meetings prior to signing the contract, the majority of encountered difficulties are due to lack of multidisciplinary integration and, mainly, the interpretative and subjective character of the elaborated models.

In order to reduce these uncertainties in models and the sharing definitions, a research project was proposed focusing on the development of a methodology based on an integrated three-dimensional model to support the risk reports and the definition of risk limits assumed by each stakeholder. The proposed model seeks a combined analysis of data obtained in preliminary surveys and field investigations, such as regional analysis using satellite images, topographical surveys, geomechanical data of the rock mass from rotating surveys, geophysical surveys from the ground surface, geological mapping focusing on the structuring of the rock mass. Initially, it was carried out a search and selection of software with the ability of integrating 3D data, such as

vectors in formats dxf, dwg, shp; rasters from remote sensing data and profiles; and 3D solids.

The main object of this paper is to present modeling data of the region surrounding the intake tunnel of HHP Dores Guanhães, as a case study, which is currently under construction.

184.1.1 Localization and Technical Features

The HPP is located at Guanhães River, a tributary of Santo Antonio River in the State of Minas Gerais State–Brazil (Fig. 184.1).

In this HPP, the water supply circuit, positioned on the left bank, is composed of water intake, intake tunnel, surge tank, penstock and powerhouse. The water intake is located just upstream of the earth dam on left side, corresponding to the beginning of the inlet tunnel, excavated in rock with a nominal diameter of 6.0 m and length of 1,185 m, with a reduced slope.

184.2 Geological Features

Rocky outcropping in the region of the dam are gneisses, whitish gray color with striking foliation in the direction N70 W. The mineralogical composition is quartz, feldspar and biotite, amphibole and garnet being the most abundant accessory minerals. Bedrock is present with signs of mild decomposition, moderately fractured and very consistent, and it is common the occurrence of quartz and pegmatite veins.

Fig. 184.1 HHP localization
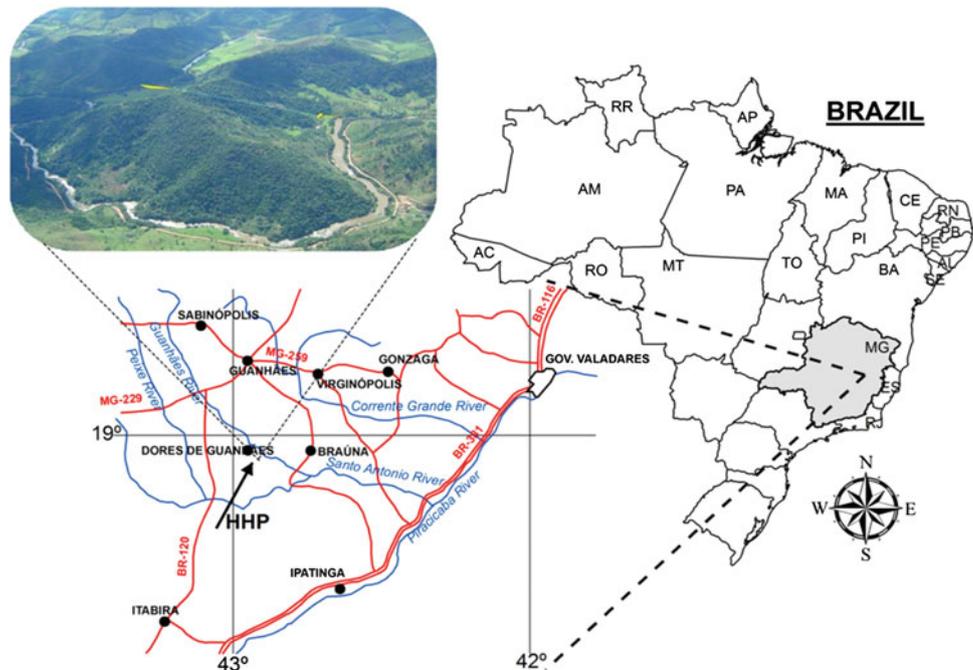
Fig. 184.2 Erosive levels of biotite and amphibole

These veins represent tabular bodies, post-tectonic intrusives, usually with centimetric thicknesses, subparallel to the foliation. In the same direction occur dark gray levels, formed by the merging of biotite and amphibole that are easily weathered and eroded when outcropping in drainages (Fig. 184.2).

184.3   Models

The 3D model was generated from the topographic data which have been integrated into the structural data obtained from geological mapping and geoelectrical survey towards the tunnel that led to the recognition of the structures at depth.

184.3.1   Geophysical Survey

The geophysical survey was conducted by a geoelectrical method that used an artificial source to introduce an electric current in the basement for determining the resistivity of different geological materials in the subsurface.

The survey used an array with 60 channels, with 10 m spaced electrodes at the ground level. Thus, it was possible to achieve at great part of the survey depths very close to the axis of the tunnel, as indicated by a dashed line in Fig. 184.3.

This survey identified a wide range of resistivity values. In general, the passages through soil and regolithe have resistivities less than 5,000 Ω/m. Up to these values are founded rocks that can reach values higher than 50,000 Ω/m. On the subsurface level (initial 10 m) it is possible to identify
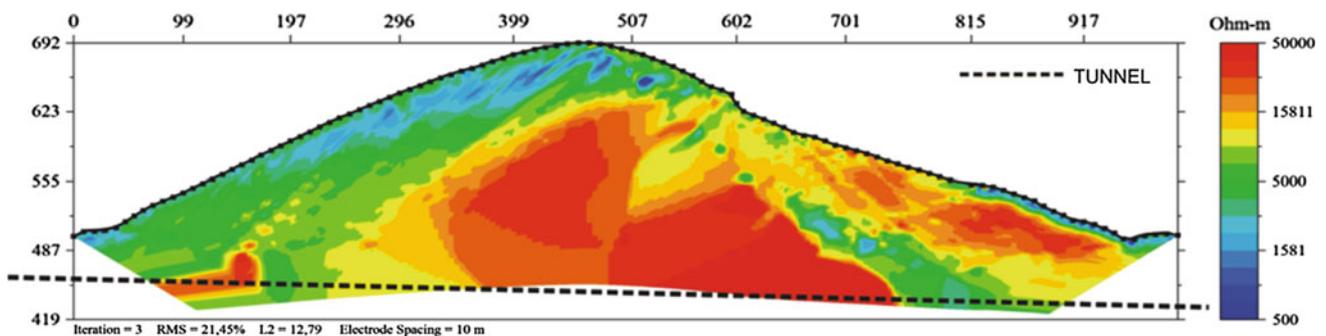
Fig. 184.3 Geophysics results and the tunnel axis indicated by the *dashed line*

Fig. 184.4 Basic project data and geophysical profiles
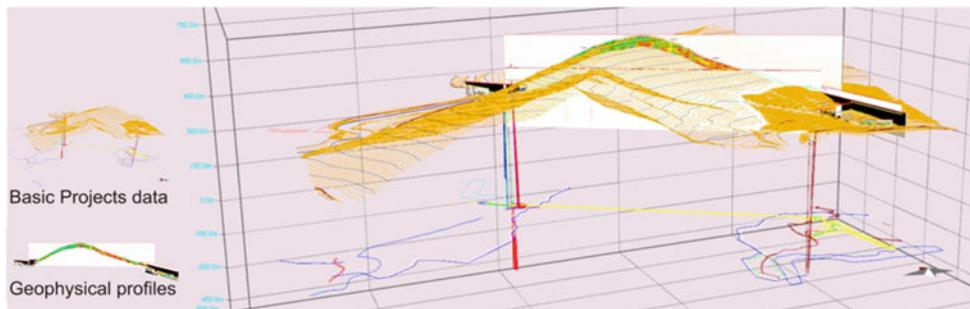
wet zones represented by the colors in the range 500–1,500 Ω/m. Yet, these resistivity values are very high, indicating little presence of water.

The discontinuities observed in the rock also exhibit very high resistivity, probably consisting of fractures that are currently dry or with little water.

184.3.2 Modelling

One of the first problems encountered is due to the majority of the data produced during the basic design work are 2D in various cartographic basis (see Fig. 184.4), which makes the integration and interpretation of the data more laborious. Currently these data are in the process of adjustment and transformation to a 3D environment.

To input the data into the MOVE$^{©}$, it is necessary to have all with the same coordinate system (x, y, z). The data are separated into categories where the direction and dip plans fractures, obtained from the geological mapping (Fig. 184.5), are input into the software. It is also input images of geophysical survey, topography information results by the Kriging interpolate method.
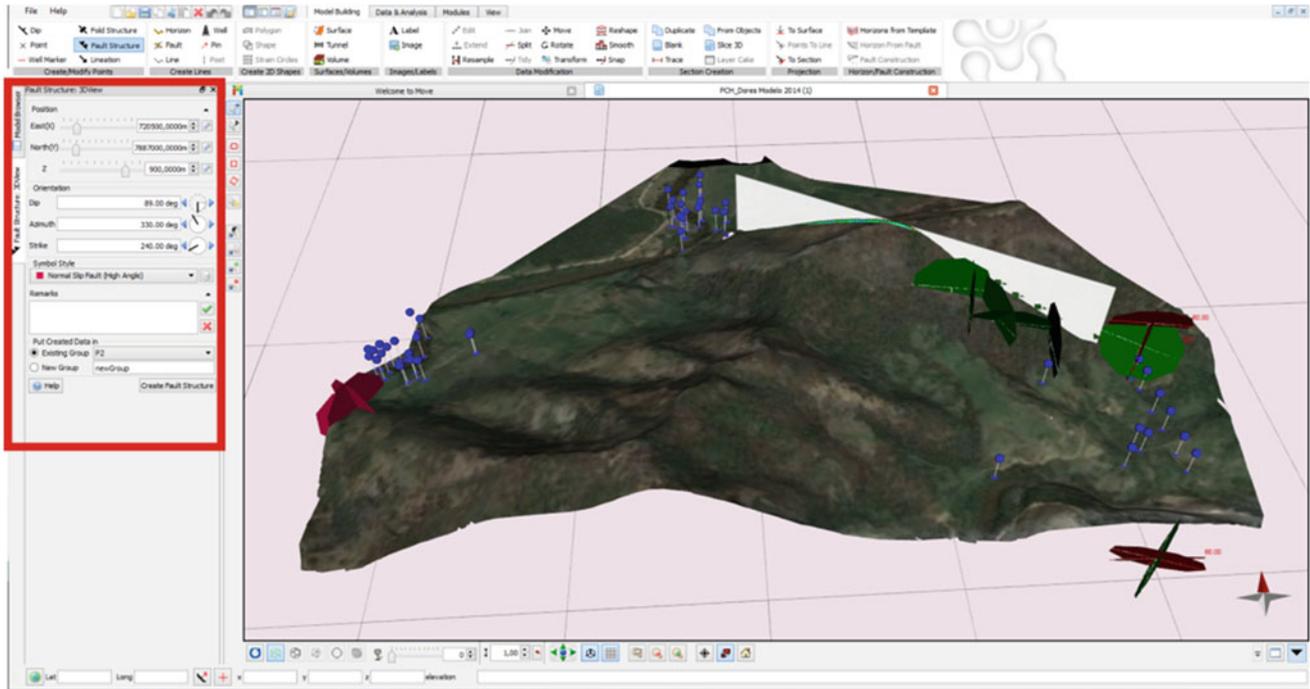
Fig. 184.5 Software Image showing the input information of the plans fractures, in *red box*

Fig. 184.6 3D modelling with the regional images and structural and field data
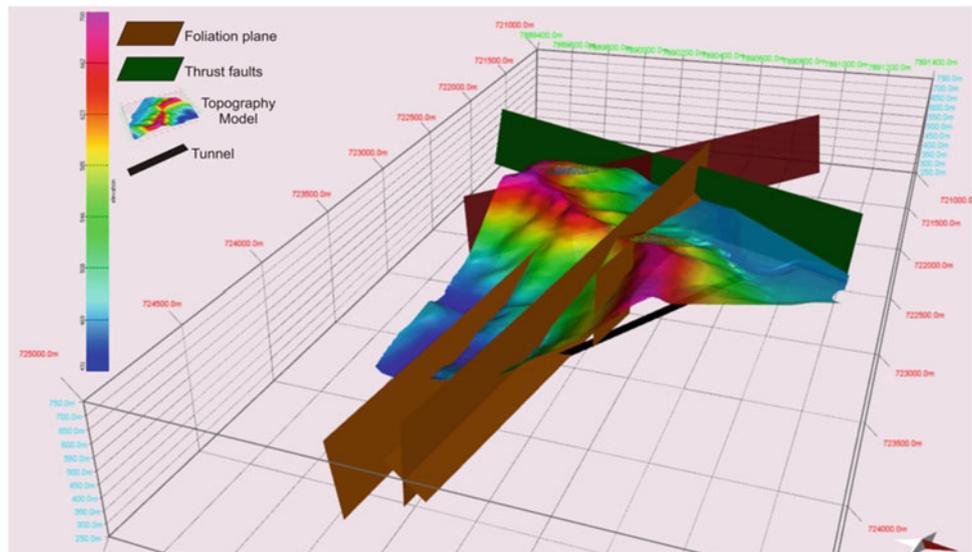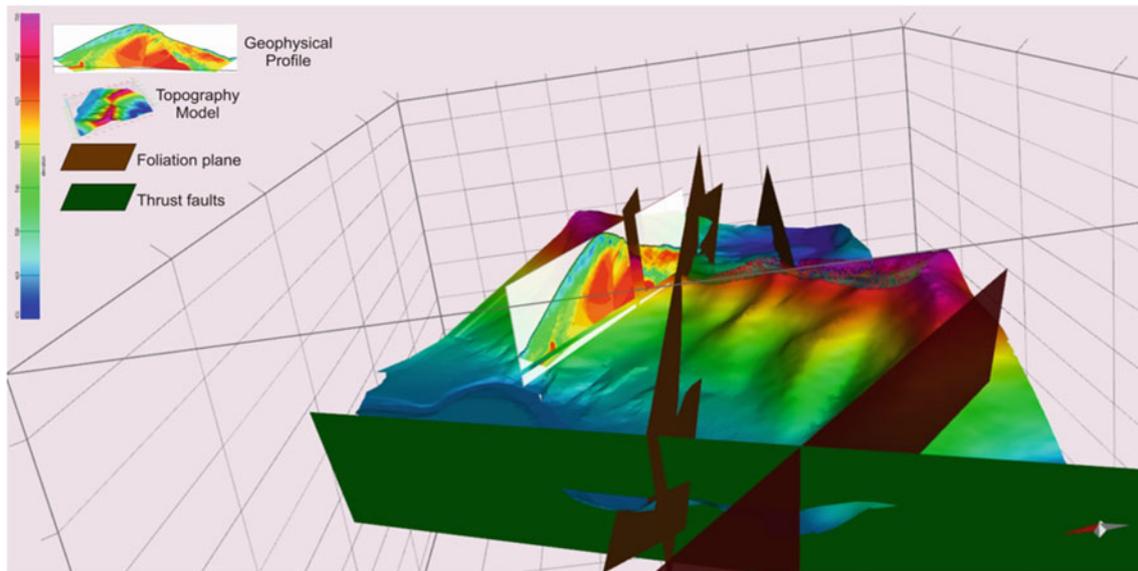
Fig. 184.7 Geophysical survey with structural data

Data provided by the construction owner have been uploaded in the 3D modelling software, along with structural and field data, as seen in Fig. 184.6.

Geophysical analyses (dipole-dipole array) were performed and included in the model with a thorough discussion of its possible benefits in general interpretation (Fig. 184.7). In this simulation it was possible to see that the model with the presence of geophysical section presents a robust result when comparing to the model without this information, it allows to infer the mapping surface into the rock mass.

184.4   Discussions

The integration of three-dimensional models allowed us to visualize the fracture and continuity plans crossing tunnel, and predict directions which fractures and biotite veins occur, helped with geophysical interpretation data.

The geological mapping and MOVE 3D model interpretation, helped to understand the geological features to reduce these uncertainties in models and the sharing definitions.

To enhance the data of 3D modeling, together with data obtained from geological mapping, data should be integrated geomechanics characteristics of the rock mass obtained in geotechnical surveys.

New geological surveys will be undertaken to improve the model and about these risk analysis will be performed with the software Decisions Tools.

References

MOVE© (2013) Midland Valley Exploration Ltd
Poente and Guanhães Energia (2008) Basic project studies HHP Dores de Guanhães-MG

Mansour Hedayatzadeh and Jafar Khademi Hamidi

Abstract

Precise prediction of TBM performance is one of the most crucial issues in mechanized tunneling projects. The main objective of this study is to estimate the TBM rate of penetration by constructing a fuzzy inference system analysis. A database consisting of fabric index of Q rock mass classification system, rock material properties and machine characteristics and performance along the tunnel alignment was compiled. In order to verify the validity of the developed model, the predicted and field measured penetration rates were compared. Results picked out from this predictor model revealed that the model has a strong capability for estimation of TBM performance with a correlation coefficient of 81.5 %.

Keywords

TBM performance • Fabric index • Rate of penetration • Fuzzy logic

185.1 Introduction

Performance prediction of tunnel boring machine is a complex and ambiguous engineering geological problem. This issue is crucial because a precise estimation of machine performance can considerably influence the cost and duration analysis during the planning stage of a mechanized tunneling project. A comprehensive review of the literature on the subject can be found in Khademi Hamidi et al. (2010b) and Farrokh et al. (2012). Among the most recently developed empirical prediction models, some ones have used intelligent systems such as artificial neural network (ANN), fuzzy logic and Neuro-Fuzzy hybrid techniques. Taking into consideration the nature of the problem, the main purpose of the present study is to develop a model by utilizing the fuzzy logic

for predicting TBM performance. In order to achieve this aim, a database composed of rock mass properties including fabric indices of four rock mass classification and the angle between plane of weakness and tunnel axis, intact rock properties including uniaxial compressive strength, machine specifications including net thrust per cutter together with actual measured TBM rate of penetration(ROP) is compiled along the tunnel alignment. Alborz service tunnel situated in Teh-ran-Shomal freeway is chosen as a case study. The Tehran-Shomal freeway project with about 120 km in length is a new freeway to connect the capital Tehran with the city of Chalus at the Caspian Sea in the north of Iran. The freeway alignment has more than 30 twin tunnels for double lanes. The Alborz tunnel is the longest of these with a length of 6,400 m at an altitude of 2,400 m.

At this stage of the Alborz tunnel construction, an exploratory pilot tunnel is being driven in Kandovan region. This tunnel, 5.2 m in boring diameter, will be used for exploratory purposes prior to the start of the construction of main tunnels and will also serve as an emergency access and ventilation way and drainage during the life of the tunnels. Besides, it will be used for transportation and other services during the construction of main tunnels. Longitudinal profile of the geological sections is also shown in Fig. 185.1. A Wirth open TBM having diameter of 5.2 m was used for

M. Hedayatzadeh
Politecnico di Torino, Corso Duca degli Abruzzi. 24, 10129 Turin, Italy
e-mail: mansour.hedayatzadeh@polito.it

J. Khademi Hamidi (✉)
Tarbiat Modares University, Jalal Ale Ahmad Highway, P.O. Box 14115-111 Tehran, Iran
e-mail: jafarkhademi@modares.ac.ir
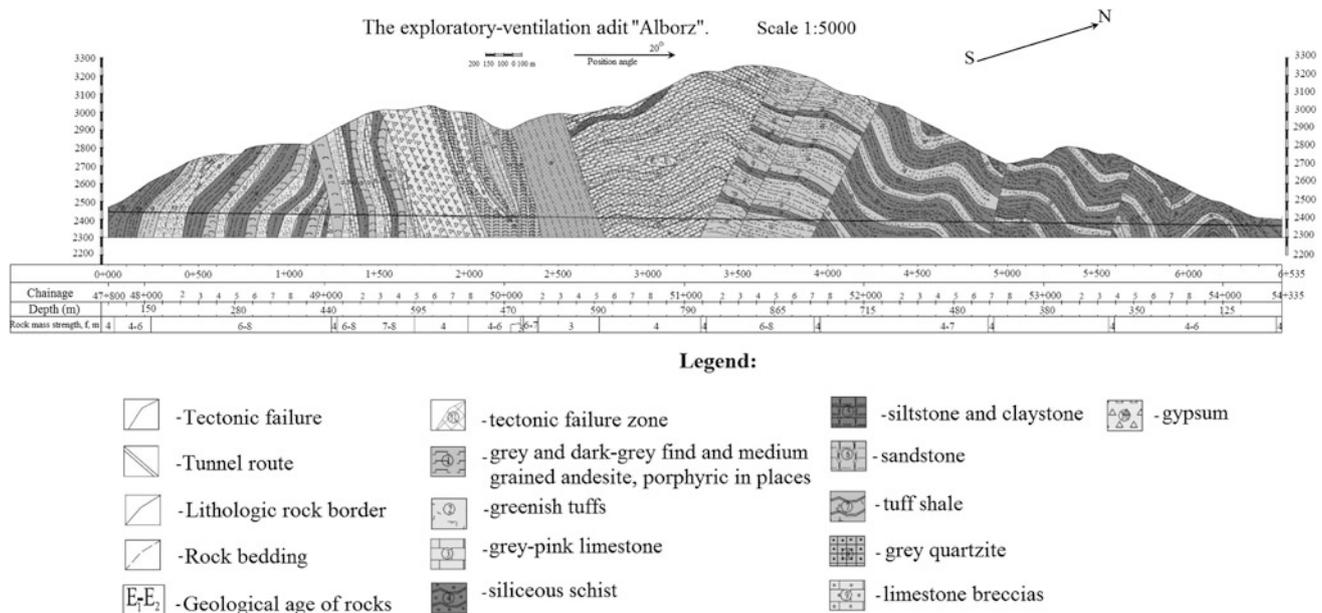
Fig. 185.1 Longitudinal geological profile of Alborz service tunnel (Technical Office Tehran–Shomal Highway 2009)

Table 185.1 Geomechanical parameters for different engineering geological units (Technical Office Tehran–Shomal Highway 2009)

Rock type	Density (kg/m³)	UCS (MPa)	RQD (%)	RMR
Sandstone	2,700	120	50–75	45–55
Limestone	2,650	85	45–55	45–50
Tuff	2,650	70	50–60	45–50
Gypsum	2,300	65	70–80	55–60
Shale	2,500	55	55–70	50–60

tunnel excavation. Site investigation for the service tunnel included a geological surface mapping, a geoelectrical resistivity survey along the alignment from the surface and some index laboratory tests on rock samples. Geological conditions are complex and overall heterogeneous.

Based on the results of geological site investigations, the main lithological units through which the tunnel was driven consist of sandstone, tuff, gypsum, shale and limestone layers. The main geomechanical characteristics of major lithotypes are summarized in Table 185.1.

185.2 Rock Mass Fabric Index in TBM Performance Prediction

There are many factors influencing the TBM performance such as rock material, rock mass parameters, machine characteristics and operational parameters. The rock mass properties including the orientation, condition and frequency of discontinuities in rock mass, and also intact rock properties such as strength, hardness, toughness and brittleness

are crucial ground parameters for analysis of hard rock TBMs. This information along with machine specifications such as thrust and power allow the appraisal and prediction of machine penetration.

Tzamos and Sofianos (2006) correlate four rock mass classifications including RMR, Q, GSI and RMi by introducing rock mass fabric (denoted as F index). The common parameters of these systems, which concern and characterize solely the rock mass (excluding boundary conditions such as stress regime and water pressure), are those used for rating the rock structure and the joint surface conditions. Rock structure is quantified by the block size or the discontinuity spacing ratings (BS) and the joint surface conditions are quantified by the joint conditions ratings (JC). For instance, in the RMR system, the parameters concerning rock structure are the RQD and the spacing of discontinuities, denoted as parameters R_2 and R_3. Their summation, $R_2 + R_3$, defines the BS component. The JC component, which represents condition of discontinuities, is defined by the parameter denoted as R_4.

The fabric indices of four commonly used systems (F_Q, F_{GSI}, F_{RMR} and F_{RMi}) are given in Table 185.2. In this study, the rock mass fabric index of Q system is used.

The orientation of rock mass discontinuities is another influencing parameter on TBM penetration rate and has been widely considered in many prediction models (e.g. Bruland 1998; Gong et al. 2005; Yagiz 2008; Khademi Hamidi et al. 2010b). This parameter is usually determined with regard to the tunnel axis and denoted as Alpha angle (α). To calculate the α angle, orientation of discontinuities and driven direction of TBM have been measured in the field. In this study,

Table 185.2 F index of four rock mass classifications (Tzamos and Sofianos 2006)

$F_Q = (RQD/J_n \ J_r/J_a)$	$BS = (RQD/J_n), JC = (J_r/J_a)$	(6.2)
$F_{RMR} = R_2 + R_3 + R_4$	$BS = (R_2 + R_3), JC = R_4$	(6.3)
$F_{GSI} = GSI$	$BS = SR, JC = SCR$	(6.4)
$F_{RMi} = JP$	$BS = (V_b), JC = (jC)$	(6.5)

J_n, J_r and J_a input parameters of Q system; *SR*, *SCR* structural rating and surface condition rating of GSI; V_b, *jC* block volume and joint coefficient factor in RMi

the α angle ($F_α$), computed for the critical joint set is included in the model.

Intact rock compressive strength, toughness, hardness, brittleness and abrasiveness are some of rock resistivity factors which are usually employed in predicting TBM penetration rate. In several TBM performance studies, it has been indicated that the uniaxial compressive strength (UCS) is the single most important rock parameter controlling TBM ROP (e.g. Cassinelli et al. 1982; Innaurato et al. 1991; Hassanpour et al. 2010). In this study, the UCS normalized by cutter load (F_f) is used in the model. The advantage of the normalized UCS compared to UCS is the elimination of the effect of machine cutterhead thrust.

A database consisting of 34 records from 34 sections along the 6.4 km bored tunnel and containing three independent variables including fabric index of Q system (F_Q), the alpha angle ($F_α$) and UCS of rock material normalized by cutter load (F_f) and the measured TBM ROPs (i.e. dependent variable) was compiled and subjected to fuzzy logic in order to drive a TBM performance prediction model. Knowledge about the relationship of these factors and their effect on the TBM performance are available from the subject literature. These experiences were the primary source of information for designing the rule bases of the fuzzy model. The reasoning behind the choice of the most related factors and the translation of the expert knowledge into the fuzzy if-then rules is described in detail in Sect. 185.3.

185.3   The Fuzzy Model for TBM Performance Prediction

Construction of the fuzzy model includes several steps: selection of the related input variables, design of the membership functions, translation of the expert knowledge into if-then rules and determination of defuzzification method.

The advantage of fuzzy logic in comparison with traditional prediction models such as statistical methods is its capability to describe the complex and nonlinear behavior which commonly exists in engineering geological problems (Khademi Hamidi et al. 2010a). There are several fuzzy inference systems (FISs) that have been employed in various applications, such as the Mamdani fuzzy model, Takagi–
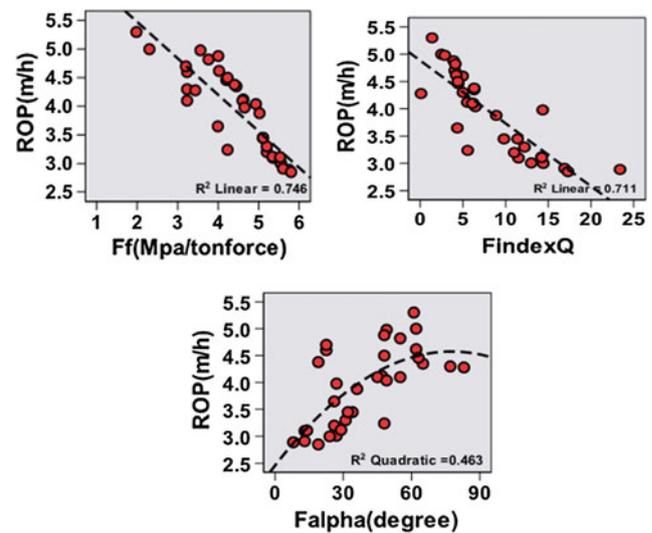
Fig. 185.2 Relationship between measured ROP and three input parameters

Sugeno–Kang (TSK) fuzzy model, Tsukamoto fuzzy model, and Singleton fuzzy model. However, the Mamdani fuzzy algorithm is the most commonly used FIS in engineering geological problems.

Figure 185.2 illustrates the correlations between the individual independent variables and the actual measured ROP. The figure also, includes the coefficients of determination (R^2) which is an indicator of correlation strength.

In construction of a fuzzy model, the use of the proper membership function (MF) is a crucial issue because MFs express the fuzziness of the model's variables. The shape of the membership function of fuzzy sets can be either linear (trapezoidal or triangular) or various forms of non-linear, depending on the nature of the system being studied. In this paper, the triangular membership function is employed because of its simplicity. For instance, the graphical illustration of the membership function of fabric index of Q system is given in Fig. 185.3.

Input–output relationship by fuzzy conditional rules is a significant concept in fuzzy logic. A fuzzy conditional rule is generally composed of a premise and a consequent part (IF premise, THEN consequent). For example, 'if the rock strength is high, then the ROP is low', where the terms high and low can be represented by fuzzy sets or more specifically by membership functions.

The last stage of a FIS is to select the defuzzification method. The aggregation of two or more fuzzy output sets gives a new fuzzy set in the basic fuzzy algorithm. In most cases, the result in the form of a fuzzy set is converted into a crisp result by the defuzzification process. The "centroid of area" (COA) method is very popular and applied for the defuzzification process in this study.
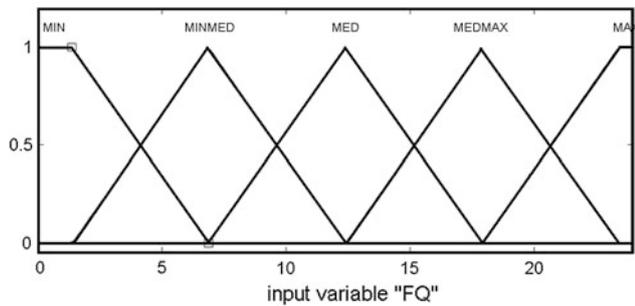
Fig. 185.3 Membership function of the fabric index of Q system, FQ
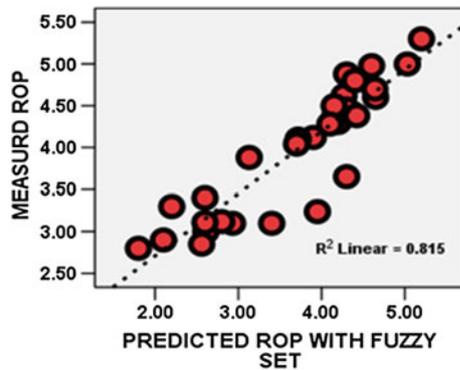
Fig. 185.4 Correlation between measured and predicted ROPs

To validate the model accuracy, the actual field ROPs are compared with the predicted values from the fuzzy model as illustrated in Fig. 185.4. As seen in the figure, the predicted data are in good agreement with the measured ones in database.

185.4   Conclusions

A fuzzy model was developed for the prediction of hard rock TBM penetration rate based on expert knowledge, experience, and data obtained from 34 sections along the route of Alborz service tunnel. In order to predict TBM ROPs, three input variables including fabric index of Q classification system, uniaxial compressive strength of intact rock, cutter

load and the angle between tunnel axis and discontinuity planes were utilized. Results obtained from the fuzzy model showed that it has a strong capability to predict the TBM penetration rate, with correlation coefficient of 0.815. However, the ranges of the input data used for development of the proposed prediction model were very limited and as such, the results cannot be considered to be universal and more in depth study is required to extend the finding of this study to develop a universal model.

References

Bruland A (1998) Hard rock tunnel boring. PhD Thesis, Norwegian University of Science and Technology, Trondheim

Cassinelli F, Cina S, Innaurato N, Mancini R, Sampaolo A (1982) Power consumption and metal wear in tunnel-boring machines: analysis of tunnel boring operation in hard rock. In: Tunnelling '82, London. Inst Min Metall 73–81

Farrokh E, Rostami J, Laughton C (2012) Study of various models for estimation of penetration rate of hard rock TBMs. Tunn Undergr Space Technol 30:110–123

Gong QM, Zhao J, Jiao YY (2005) Numerical modeling of the effects of joint orientation on rock fragmentation by TBM cutters. Tunn Undergr Space Technol 20:183–191

Hassanpour J, Rostami J, Khamehchiyan M, Bruland A, Tavakoli HR (2010) TBM performance analysis in pyroclastic rocks: a case history of Karaj water conveyance tunnel. Rock Mech Rock Eng 43 (4):427–445

Innaurato N, Mancini R, Rondena E, Zaninetti A (1991) Forecasting and effective TBM performances in a rapid excavation of a tunnel in Italy. In: Proceedings of the seventh international congress ISRM, Aachen, pp 1009–1014

Khademi Hamidi J, Shahriar K, Rezai B, Bejari H (2010a) Application of fuzzy set theory to rock engineering classification systems: an illustration of the Rock Mass Excavability Index. Rock Mech Rock Eng 43(3):335–350

Khademi Hamidi J, Shahriar K, Rezai B, Rostami J (2010b) Performance prediction of hard rock TBM using Rock Mass Rating (RMR) system. Tunn Undergr Space Technol 25(4):333–345

Technical Office Tehran–Shomal Highway (2009) Technical report

Tzamos S, Sofianos AI (2006) A correlation of four rock mass classification systems through their fabric indices. Int J Rock Mech Min Sci 477–495

Yagiz S (2008) Utilizing rock mass properties for predicting TBM performance in hard rock condition. Tunnell Undergr Space Technol 23(3), 326–39

The Risk Analysis Applied to Deep Tunnels Design—El Teniente New Mine Level Access Tunnels, Chile

186

Lorenzo Paolo Verzani, Giordano Russo, Piergiorgio Grasso, and Agustín Cabañas

Abstract

El Teniente Mine, with 2,400 km of tunnels excavated since the beginning of the last Century is the largest underground copper mine in the world. El Teniente Mine production plan has a thin overlap between the exhaustion of the current production level and the activation of the New Mine Level, located at almost 1,000 m depth, planned for 2017. The infrastructure system involves the construction of 24 km of access tunnels, consisting of two adits, a tunnel for vehicular access of personnel and a twin conveyor tunnel for the transport of the ore. The definition of geological and geomechanical scenarios, as predicted on the basis of the reference models, and the related hazards identification and mitigation (following a risk analysis based design), are cornerstones along the production chain. Tunnel alignment intersects a complex geological environment characterized by rock variability: from igneous (effusive and intrusive) to sedimentary volcanoclastic rocks, with sectors of intense hydrothermal alteration. Due to high overburden and variability of rock mass properties, geomechanical hazards such as squeezing and rockburst are expected, together with caving and flowing-ground conditions crossing fault sectors associated with high hydraulic pressures. This paper synthesizes the design methodology, focused on risk management (Risk Analysis-driven Design, Geodata 2009). The construction of the tunnel is actually in process and then also a preliminary comparison "predicted versus observed" is anticipated.

186.1 Introduction

El Teniente Mine, located in the Libertador General Bernardo O'Higgins Region 80 km southeast of Chile's capital Santiago, is the largest underground copper mine in the world, with 2,400 km of deep tunnels producing more than 400,000 tons per year of fine copper.

El Teniente Mine production plan has a thin overlap between the exhaustion of the current production level and the activation of the New Mine Level (NML), located at almost 1,000 m depth, planned for 2017. The underground infrastructures are under construction; the NML will extend life of the mine by 50 years; a deeper level has been investigated at 1,400 m depth (Fig. 186.1).

L.P. Verzani (✉) · G. Russo · P. Grasso
Geodata Engineering S.p.A., Turin, Italy
e-mail: lpv@geodata.it

G. Russo
e-mail: grs@geodata.it

P. Grasso
e-mail: pgr@geodata.it

A. Cabañas
División El Teniente, Corporación Nacional del Cobre de Chile (Codelco), Santiago, Chile
e-mail: acabanas@codelco.cl

Fig. 186.1 Mine levels (by Codelco)
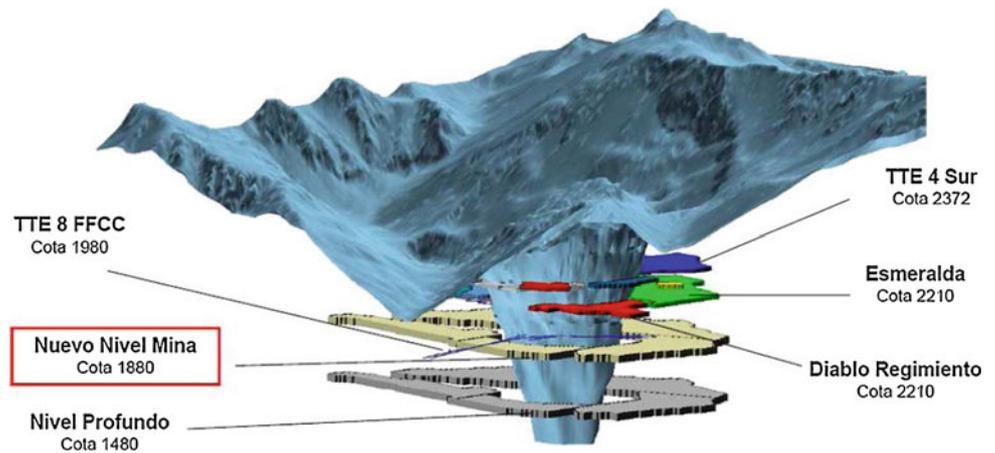
The NML project foreseen the construction of 24 km of access tunnels, consisting of two adits (Ltot = 6 km) and two main tunnels (Ltot = 9 + 9 km): a tunnel for vehicular access of personnel and a twin conveyor tunnel for the transport of the ore. Geodata Engineering (GDE), as a consultant of Codelco and tunnels Contractor's counterpart on geotechnical issues, has been present on site since April 2012.

Prior to the construction phase, Geodata Engineering (GDE in association with Ingeroc) developed for Codelco a design for the two main tunnels, based on the risk analysis (Risk Analysis-driven Design, RAdD) as reference for the owner about engineering solutions and construction costs and time assessment. Conventional and mechanized excavation methodologies were analyzed.

Constructora de Túneles Mineros–joint venture between Soletanche Bachy and Vinci (CTMSA) won proposing the conventional method (D&B), with two additional adits to increase the number of parallel advances along the main access tunnels (Fig. 186.2). Actually the constructions of both the main access tunnels and the adits are in process.

186.2 Risk Analysis-Driven Design (RAdD)

The design and construction of long tunnels particularly those at great depth, is generally associated with a high level of risks due to a whole series of uncertainties involved. The risk management approach consists in identifying and listing

Fig. 186.2 NML tunnel access system (by CTMSA)
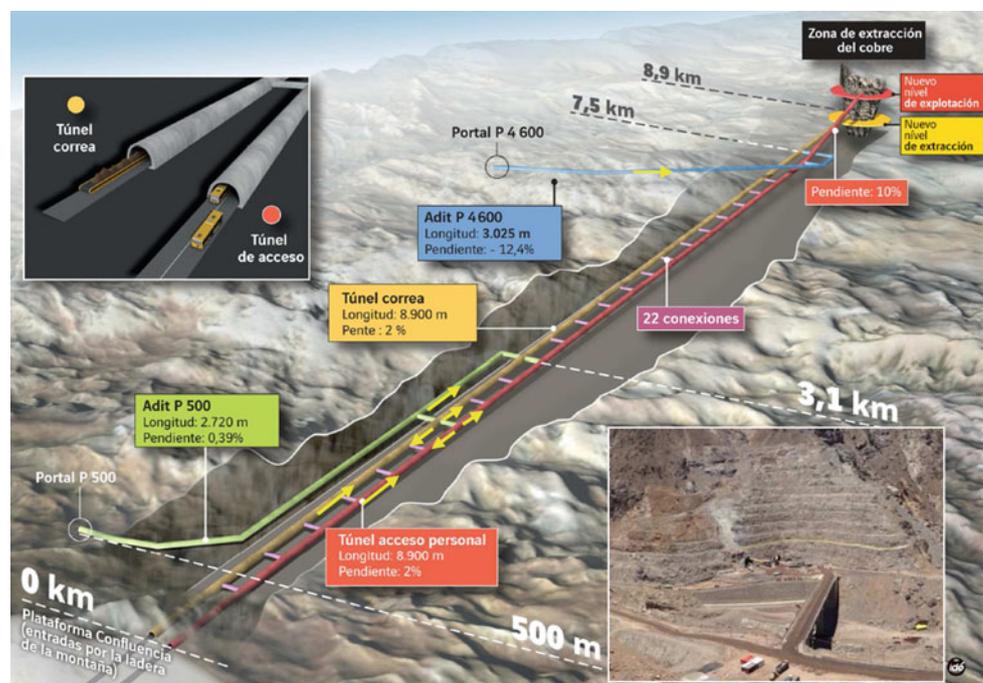
Fig. 186.3 RAdD flow chart
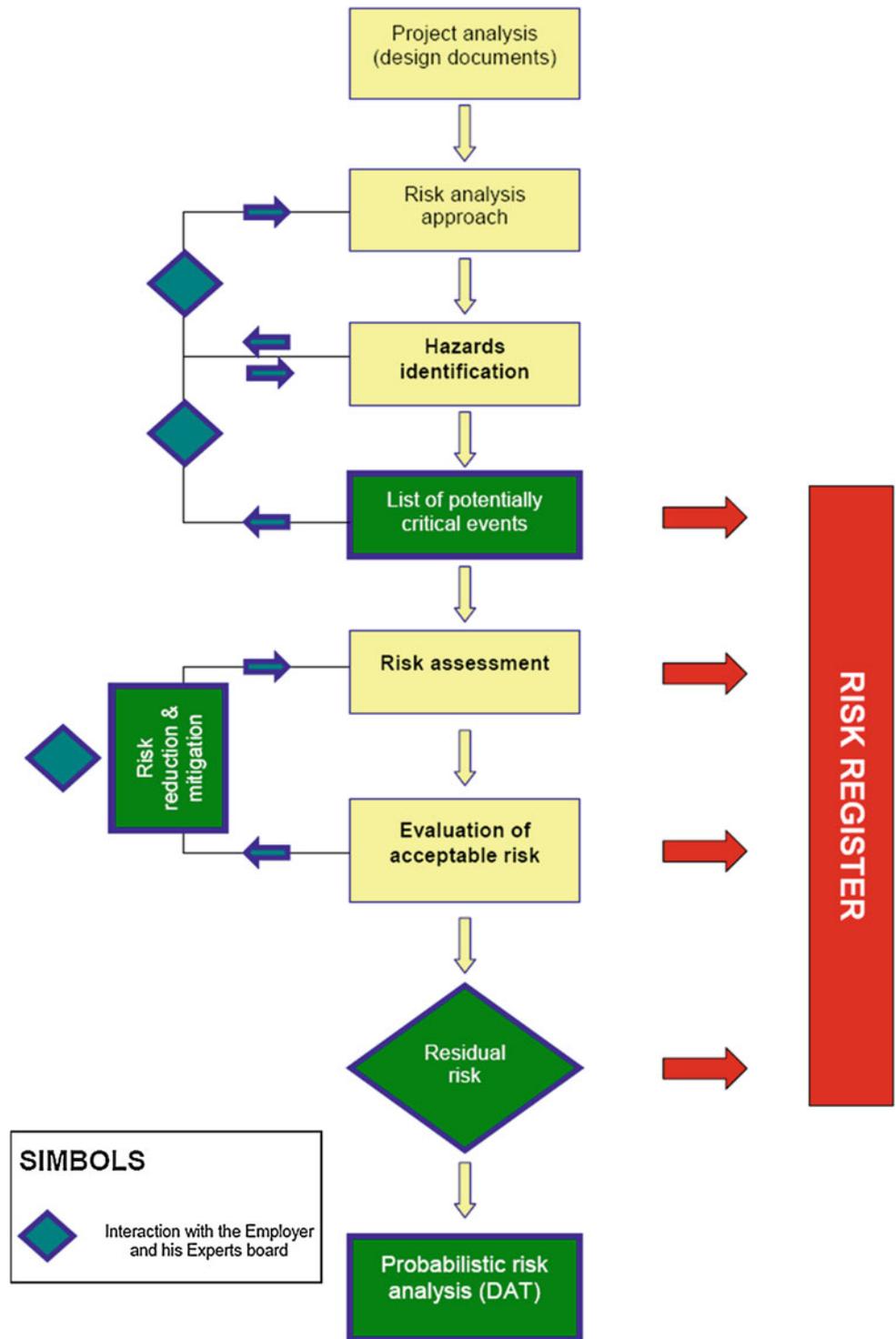
the potential hazards associated with the tunneling activities, assigning a probability of occurrence to each hazard, and allocating an index of severity to the consequence (impact). Two main categories of hazard events are identified in connection to geological and geomechanical issues, namely: (Fig. 186.3)

- Hazard phenomena associated with unfavorable *geological conditions* (fault, water acidity, etc.)

- Geomechanical hazard related to *rock mass behaviour* upon excavation (squeezing, rockburst, etc.).

The risk (R) is defined as the product of the probability of occurrence of the hazard (P) and the related impact (I): R = P*I. In cases where the initial risk (i.e. the risk to which the project is exposed in absence of any mitigation measure) level is not acceptable, the relevant mitigating measures should be identified and designed.

After application of the mitigation measures, an analysis should be performed to reassess the remaining risk level, obtaining an updated risk level, which is called the "residual risk level". It should be examined for acceptance as the maximum risk level that is to be confronted with its "global cost", necessary for reducing or completely eliminating the risk itself.

All the relevant information about the hazards, the associated risks and counter measures are filled and regularly reviewed in a risk register.

186.3 Geological Setting and Related Risks

The regional geology of El Teniente area is characterized by volcanic rocks and sedimentary volcanoclastic deposits, with felsic to intermediate intrusive. As shown in the Geological Reference Model, proceeding from West (portal) to East (mine), the following lithological formations and Rock Mass Unit (RMU) would be crossed:

- Farellones Formation lower and undifferentiated members (FFm, RMU.V1-V2)
- Agua Amarga Hydrotermal Alteration and Breccia (RMU.AA)
- Sewell intrusive Complex (CSW, RMU.i1-CQ-i2)
- El Teniente Mafic Complex (CMET, RMU.i3)
- Braden Breccia (RMU.BB).

The tunnel axis crosses three major faults (F1, F2) and a large number of minor faults (F4). Moreover the El Teniente shear zone (F3) is foreseen along CSW and CMET formations. On the basis of the Geological Reference Report (GRR Codelco-Hatch 2009), some potential geological hazards were identified. Among them, the main ones in terms of impact are: geological structures, hydraulic load and water pH, natural stress field and anisotropy, rock weathering and hydrothermal alteration (Fig. 186.4).

Moreover some additional hazards were analyzed for the mechanized method (TBM): rock hardness-abrasiveness and heterogeneity. The main geological hazards are probabilistically quantified and the risk register is compiled, both for D&B and TBM, considering the required mitigation measures for each potential risk. Since March 2012, the following geomechanical units have been excavated: RMU.V1 and RMU.V2 in FFm (main tunnels and Adit 1); the structural contact RMU.V2/AA (Adit 1) and RMU.I2 in CSW (Adit 2).

Fig. 186.4 Geological setting

Fig. 186.5 GD Classification (*Notes* Russo and Grasso (2007); δ_0 = radial deformation at the face; R_{pl}/R_0 = palstic radius/radius of the cavity; σ_θ = max tangential stress; σ_{cm} = rock mass strength. The limits of shadow zones are just indiactive) of the excavation behaviour

↓ ANALYSIS →		Geostructural →		Rock mass				
				Continuous ↔ Discontinuous ↔ Equivalent C.				
Tensional↓				RMR				
Deformational response ↓	δ_0 (%)	R_{pl}/R_0	Behavioural category ↓	I	II	III	IV	V
Elastic ($\sigma_\theta < \sigma_{cm}$)	negligible	-	a	STABLE				
			b		INSTABLE			CAVING
Elastic - Plastic ($\sigma_\theta \geq \sigma_{cm}$)	<0.5	1-2	c	SPALLING/ ROCKBURST	WEDGES			
	0.5-1.0	2-4	d					
	>1.0	>4	e					SQUEEZING
			(f)	→ Immediate collapse of tunnel face ↑				

Fig. 186.6 Design scatter diagrams (RMU.V1)
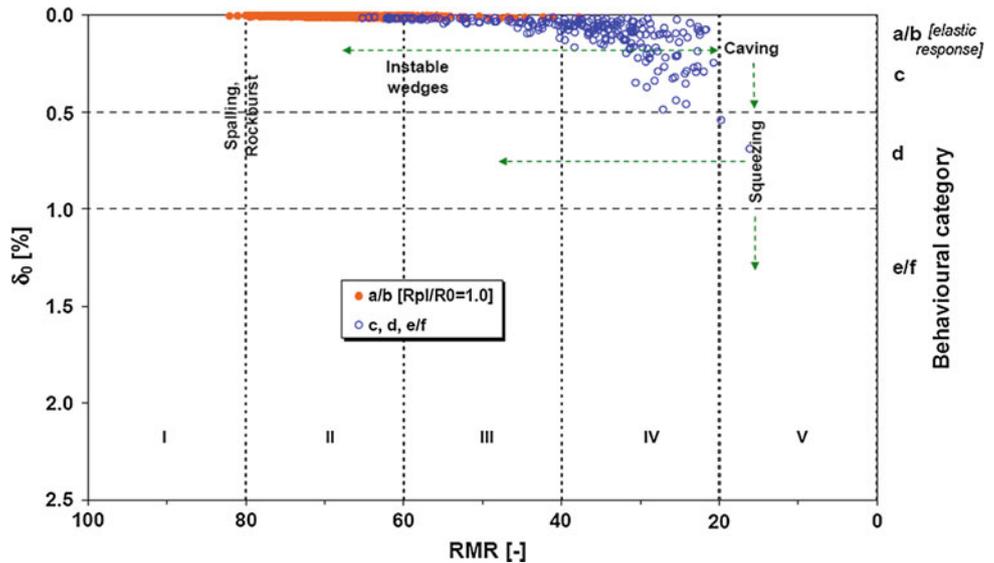
Fig. 186.7 Hazard probability/intensity (RMU.V1-V2)

RMU Rock Mass Unit (Overburden)	Scenario ↓	Hazard [%]									
		Wedge instability / Rockfall			Caving		Squeezing		Spalling/Rockurst		
	Intensity →	s1	s2	s3	s2	s3	s2	s3	s1	s2	s3
V1 (40<H<290m)	H_LIK	0.3%	67.1%	16.1%	15.0%	0.0%	0.20%	0.0%	1.3%	0.0%	0.0%
	GD_FAV	28.0%	35.1%	29.4%	7.4%	0.0%	0.0%	0.0%	0.1%	0.0%	0.0%
	GD_UNF	0.6%	38.6%	45.3%	15.0%	0.3%	0.0%	0.0%	0.2%	0.0%	0.0%
V2 (250<H<420m)	H_LIK	12.3%	33.1%	38.8%	8.1%	0.7%	1.5%	0.5%	4.7%	0.3%	0.0%
	GD_FAV	15.2%	39.0%	32.6%	5.5%	0.0%	1.5%	0.2%	5.2%	0.8%	0.0%
	GD_UNF	8.2%	25.6%	40.1%	11.3%	2.2%	3.7%	2.0%	6.2%	0.7%	0.0%

Fig. 186.8 Hazards frequency: probabilistic results for the n.3 scenarios of reference (9 km in personnel tunnel)
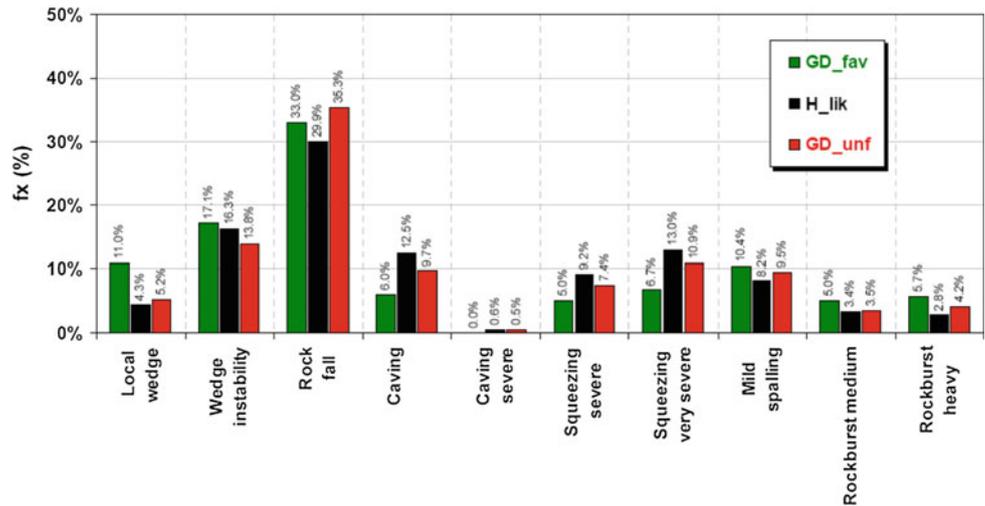
Fig. 186.9 Risk register (RMU. V2)

Hazard identification				Primary risk					Mitigation measures*	
CATEGORY					D&B		TBM		*or cross-reference to geomechanical hazard [→]	
Sub-category				Hazard Probab. [P]						
TYPE					Impact [I]	Risk [R=PxI]	Impact [I]	Risk [R=PxI]	D&B	TBM
Sub-type										
		HAZARD								
		GEOMECHANICAL HAZARDS (EXCAVATION BEHAVIOUR AND LOADING CONDITION RELATED)								
		Gravity driven instability								
	B1	ROCK BLOCK FALL (→ OVERBREAKS)		5	2	10	1	5	M01,M02,M23,M24	M01,M22,M23,M24
	B2	CAVING (→FACE / CAVITY COLLAPSE)		4	3	12	2	8	M01,M02,M03,M06,M07,M08,M24	M01,M08,M22,M24,M25,M27
		Stress induced instability								
	B3	ROCKBURST		2	3	6	2	4	M1,M2,M21,M23,M26,M27	M01,M22,M23,M26
	B4	SQUEEZING, FACE EXTRUSION		2	3	6	4	8	M01,M02,M05,M07,M21,M24,M25,M27	M01,M22,M25,M27
		Mainly water influenced (fault zone)								
	B5	FLOWING GROUND		5	5	25	5	25	M01,M02,M06,M07,M08,M24	M01,M08,M22,M25,M27
	B6	WATER INRUSH		5	5	25	5	25	M01,M02,M06,M07,M08,M24	M01,M08,M22,M25,M27
	B7	PIPING		5	5	25	5	25	M01,M02,M06	
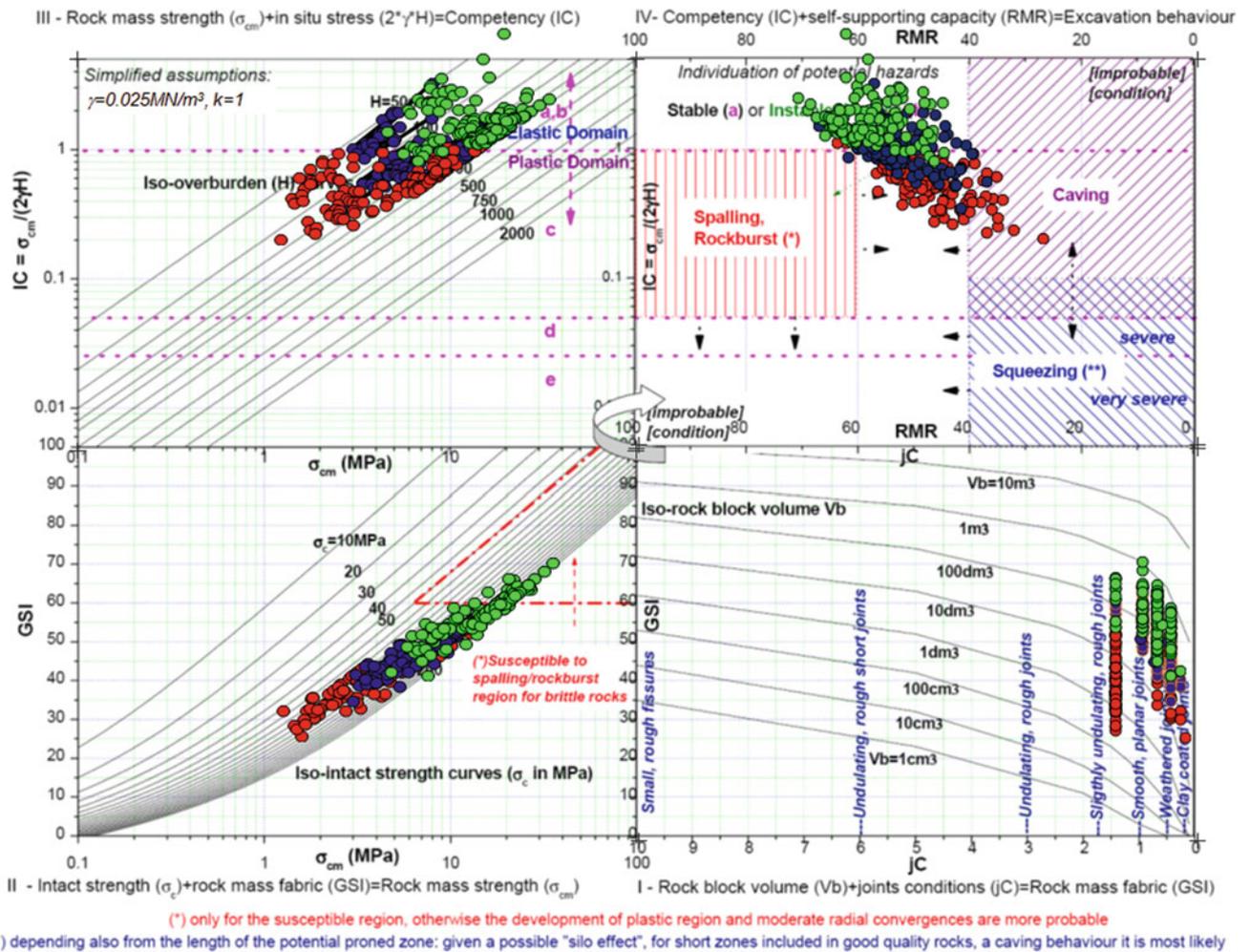
Fig. 186.10 RMU-V1, results of the geomechanical classification at tunnel face by the method of GDE multiple graph (Russo 2009)

186.4 Geomechanical and Residual Risks

The first step for RAdD is the geotechnical characterization of the different RMU. Related to the available information, the statistical analysis has adopted different approaches in order to define, in a probabilistic way, the three reference scenarios as geomechanical inputs for design: the most-likely scenario (from previous studies: H_lik), the favorable and the unfavorable ones (by data processing: GDE_fav/unf). Geomechanical hazards are mainly related to ground behaviour upon excavation, thus taking into account the intrinsic properties of rock masses and the associated stress conditions.

The reference classification of the excavation behaviour is based on both stress and geo-structural type analysis (matrix in Fig. 186.5), in the theoretical hypothesis of absence of any design interventions (→primary risk).

An example of the resulting design scatter diagrams is presented for one of the rock mass unit excavated in the personnel tunnel (RMU-V1, Fig. 186.6). The assessment of the geomechanical risks is obtained with reference to the occurrence probability and intensity of the related hazards. Along RMU V1 and V2, mainly geomechanical hazards due to gravity, as wedge instability, are expected (Figs. 186.7 and 186.8). The risk analysis proceeds with the initial risk assessment. Its evaluation involves the estimate of the potential impact (consequence) deriving from the damages related to the identified hazards. The Risk Register (Fig. 186.9) is consequently compiled for each RMU, both for the D&B and the TBM methods. The type and the dimensioning of the stabilization measures will be directly related to the hazards and their potential impact on tunneling (→primary risk). The adequate mitigation measures (design solutions) are consequently individuated, concurring to the composition of the different Section Types, dimensioned and

probabilistically distributed along the tunnels. The last step for risk analysis process is the assessment of the new risk level obtained after the application of the design ($\rightarrow$residual risk). The risk has been managed and reduced from its initial (primary) level to a lower (residual) value. If all the initial risks have been mitigated and the tunnels construction is not more exposed to unacceptable risks but the residual risk level remains classified as unwanted, some counter-measures are consequently defined.

186.5   Construction

The construction of the NMN tunnel access system started on March 2012, with the Adit 1. Currently, 18 months after the beginning, almost the 35 % of the 24 km totals has been excavated. The experience along the Adit 1 and the two main tunnels (RMU V1-V2 and contact zone RMU.V2/AA), permits to have a comparison with RAdD-design expected conditions. Outside from gully influence areas, along ordinary rock mass sections in RMU.V1-V2, the instabilities mainly related to gravity (wedge instability, rock fall with a lower probability of caving) were expected by GDE risk analysis. By the comparison among data collected during the advancement in RMU.V1, summarized by the method of the "GDE Multiple Graph" (Russo 2009; Fig. 186.10), and the probability of occurrence of the hazards expected by the design (Figs. 186.6 and 186.7, referred to RMU.V1), the reliability and effectiveness of the adopted risk analysis approach is confirmed.

186.6   Conclusions

Eighteen months of advancements in the NMN access tunnel, allow to obtain a first positive feedback on RAdD results. The Risk Analysis is a process that should support and follow a project, from the conceptual up to the construction stage.

The risk should be managed through the implementation of a specific Risk Management Plan (RPM, Grasso et al. 2002), fully integrated in each part of the design study, in accordance to a real development of a "Risk Analysis-driven Design".

References

Degn Eskesen S, Tengborg P, Kampmann J, Holst Veicherts T (2004) Guidelines for tunnelling risk management International tunnelling association, working group no 2. Tunn Undergr Space Technol 19:217–237 (ITA/AITES)

Grasso P. Mahtab M A, Kalamaras G, Einstein H H (2002) On the development of a risk management plan for tunnelling. In: Proceedings of world tunnel congress, Sydney

Russo G. Grasso P (2007) On the classification of the rock mass excavation behaviour tunneling. In: Proceedings of the 11th congress of international society of rock mechanics, Lisbon, 9–13 July 2007

Russo G (2008) A simplified rational approach for the preliminary assessment of the excavation behaviour in rock tunneling. Tunnels et Ouvrages Souterrains 207

Russo G (2009) A new rational method for calculating the GSI. Tunn Undergr Space Technol 24:103–111

Development of Measurement System of Seismic Wave Generated by the Excavation Blasting for Evaluating Geological Condition Around Tunnel Face

Masashi Nakaya, Kazuhiro Onuma, Hiroyuki Yamamoto, Shinji Utsuki, and Hiroaki Niitsuma

Abstract

Mountain tunneling in Japan is commonly performed according to the new Austrian tunneling method (NATM), and preliminary investigation for understanding the geological conditions of the mountain are performed from the surface by borehole sampling and seismic exploration using the refraction method. Exploratory boring is performed in only select locations with specific terrain or geological features, whereas seismic exploration using the refraction method is generally performed over the area in which the tunnel will be excavated. The certainty of such seismic exploration is reduced according to depth, making it difficult to ascertain the details of the geological conditions. The results of preliminary investigations must therefore be constantly compared with the actual geological conditions as revealed during construction. Seismic velocity is a significant factor to determine the design of tunnel support. Evaluation of geological condition requires the seismic velocity a round tunnel face, so there is a need for seismic exploration techniques that do not affect the excavation work cycle of tunnels under construction. We have therefore developed the tunnel face tester (TFT), which is a seismic exploration system that uses excavation blasting as wave source. This paper describes the developed system, and the results of verification experiments performed at a tunnel construction site.

187.1 System Components

Developing a system is aimed at exploration in daily tunneling cycle, and easy system to use for tunneling engineers (Nakaya et al. 2013). The system uses a seismic sensor fixed on tunnel walls behind the tunnel face, uses excavation blasting as a wave source, and measures seismic wave automatically.

The system (tunnel face tester unit, Figs. 187.1 and 187.2) is composed portable detector (a) and peripheral devices (b)–(d). The DC sensor (b) has a noncontact connection with the blasting leading wire, and converts the ignition current into a signal. The geophone (c) is of a type commonly used for seismic exploration (OYO GS-20DH; natural frequency: 28 Hz). The geophone is mechanically fixed to the head of a rock bolt (L = 3–4 m) on the tunnel wall, which serves as a waveguide. The ignition signal and seismic waveform data (are recorded on the same time scale) pass through the portable detector, and are recorded using a stereo IC recorder (TASCAM DR-05 up to 96 kHz/24bits resolution WAV recording) (d).

The following equation gives the velocity of seismic waves arrived to the geophone from the distance between the geophone and the tunnel face (L_i) and the arrival time of P wave (t_i).

M. Nakaya (✉) · K. Onuma · H. Yamamoto · S. Utsuki
Hazama Ando Corporation, 6-1-20, Akasaka Minatoku, Tokyo, 107-8658, Japan
e-mail: nakaya.masashi@ad-hzm.co.jp

H. Niitsuma
Tohoku University, Sendai, Japan
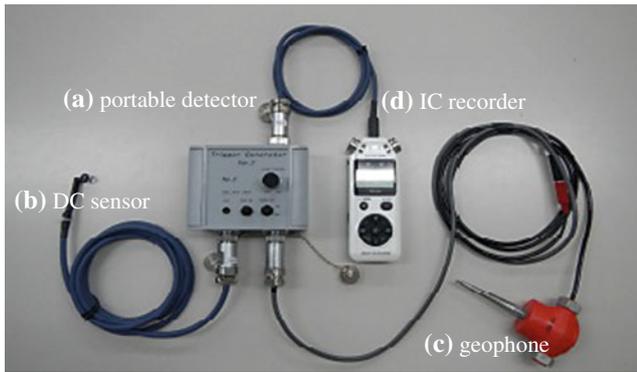
Fig. 187.1 Components of the tunnel face tester
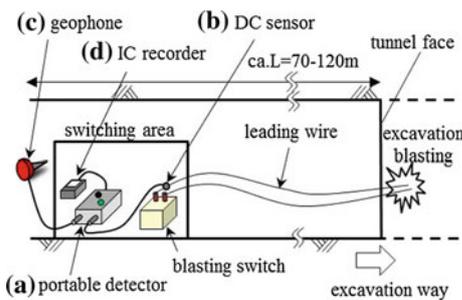
Fig. 187.2 Conceptual diagram of the measurement

$$Vp_i = L_i/t_i \qquad (187.1)$$

When seismic waves arriving along the same straight line are measured without changing the location of the geophone, the wave path should be the same as in a previous measurement interval. The change of seismic velocity is thus a combination of the velocities in the previous measurement interval and the advance interval, so the previous measurement interval can be used to calculate the interval seismic velocity V_p' for moreover drilling, by the following equation.

$$Vp_{i \sim i+1}' = (L_{i+1} - L_i)/(t_{i+1} - t_i) \qquad (187.2)$$
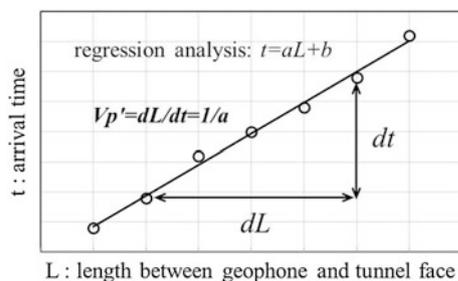
Fig. 187.3 Travel time curve

When the geophone position is unchanged, V_p' in the face advance interval can be determined from travel time curve (t: arrival time of P wave, L: length between geophone and tunnel face) (Fig. 187.3). The travel time curve and V_p' are determined by the following equations.

$$t = aL + b \qquad (187.3)$$

$$Vp' = dL/dt = 1/a \qquad (187.4)$$

187.2 Verification Testing

187.2.1 Experiment Overview

The Okanyo Tunnel (L = 2,736 m; cross-sectional area: 62.7 m^2) in Iwate prefecture of the northeastern Japan is a road tunnel excavated by the NATM. The geology in this area is characterized relatively homogeneous Granodiorite, which is formed in Cretaceous. We used this site to perform an experiment to evaluate the properties of developed measurement system. We furthermore compared measurement results with seismic velocities measured from the surface by the refraction method. Figure 187.4 shows a geological section of the interval used for the verification experiment. Seismic velocities measured by the refraction method in the interval were expected to be above 3.75 km/sec.

187.2.2 Geological Properties of Cutting Advance Interval

187.2.2.1 Measurement Method

The measurement position, which is during excavation of the examined tunnel were situated within the tunnel approximately 70–120 m behind the tunnel face. A geophone was fixed to an existing rock bolt on the tunnel wall. Each blast excavated 1.0–1.5 m of rock, and measurement sets were established until the length of the face advance interval reached approximately 50 m, at which time the measurement system was moved along with the measurement position in the direction of face advance and measurement was resumed. P wave of first blasting is measured, and measurements of 14 sets are performed over 900 m span.

187.2.2.2 Measurement Results

Figure 187.5 shows the measurement results (travel time curves) for 14 measurement sets performed during excavation over the interval TD 459.9–1,287.5 m, plotting the time required for seismic from each blast to reach the geophone. Geophone positioning for each measurement is shown as
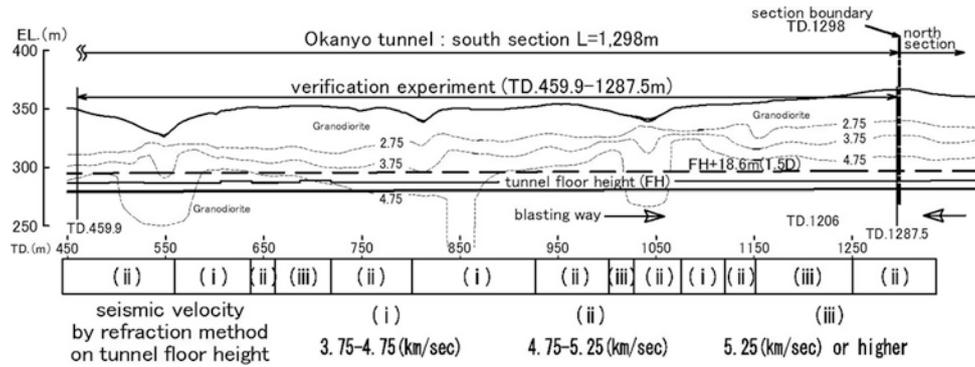
Fig. 187.4 Geological profile of Okanyo tunnel

	(i)	(ii)	(iii)	(iv)	(v)	(vi)	(vii)	(viii)	(ix)	(x)	(xi)	(xii)	(xiii)	(xiv)
"a" (equation (3))	0.188	0.211	0.197	0.209	0.187	0.199	0.199	0.190	0.199	0.180	0.184	0.186	0.211	0.183
correlation coffisients	0.993	0.995	0.994	0.986	0.996	0.995	0.997	0.998	0.997	0.997	0.995	0.998	0.998	0.997
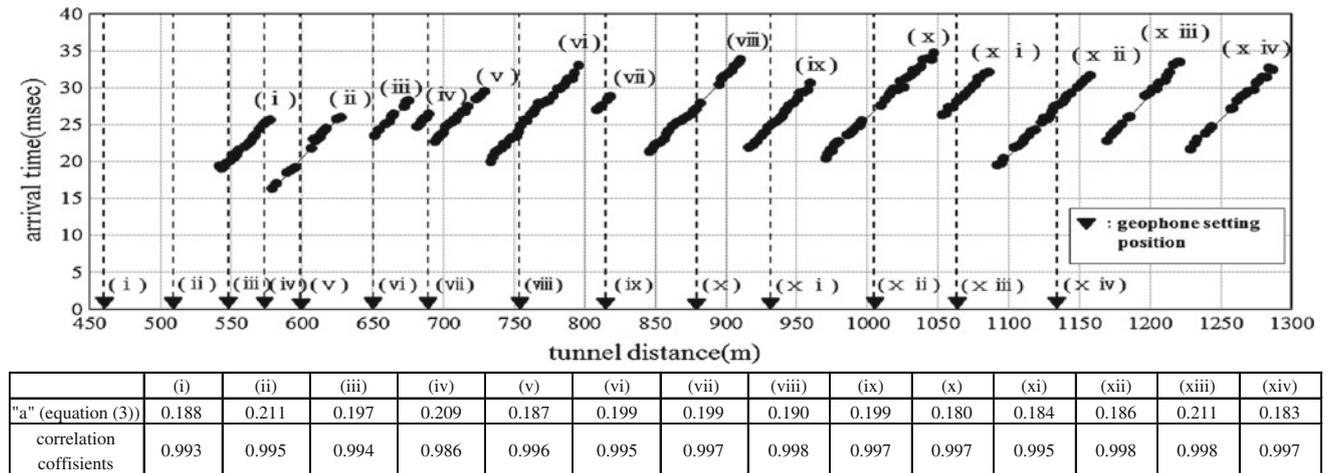
Fig. 187.5 Travel time curve in Okanyo tunnel
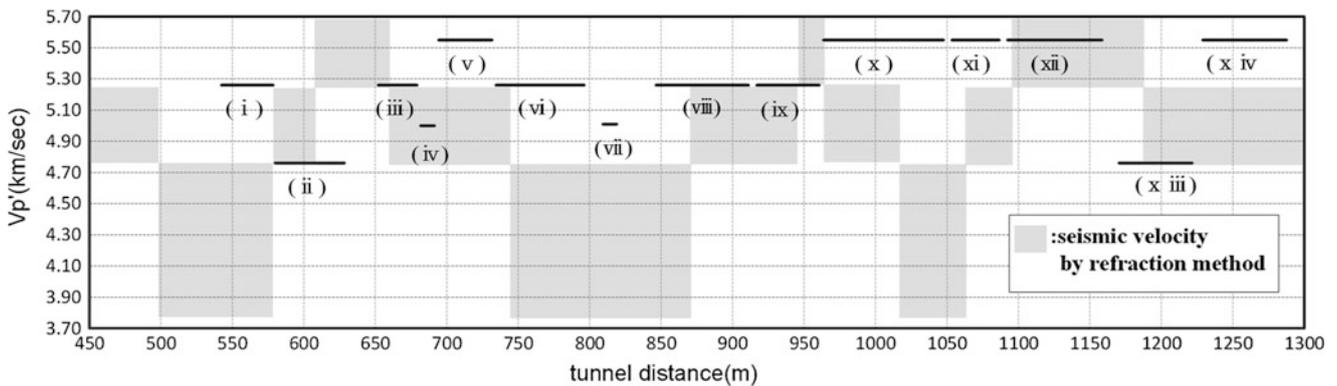
Fig. 187.6 Interval seismic velocity

dotted lines in the figure. These results indicate that obtained measurement data have correlation coefficients of $r = 0.986$–0.998, indicating that exploration was performed with high precision and low variance. And V_p' is calculable from Eq. (187.4).

Figure 187.6 shows V_p' values for the face advance interval as calculated by Eq. (187.4), indicating that the proposed method allows detailed changes in geological properties to be ascertained.

For comparison of refraction method V_p and V_p', Fig. 187.7 shows a reorganization of the data. The figure
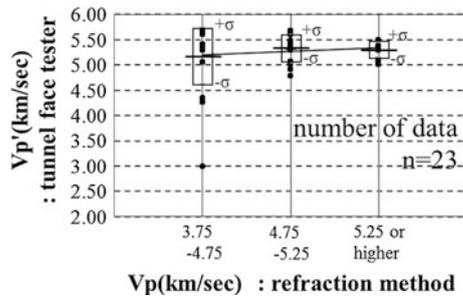
Fig. 187.7 Reorganization for Vp and Vp′

shows extraction method V_p divided into three groups, 3.75–4.75 km/s, 4.75–5.25 km/s, and 5.25 km/s or higher, and V_p' is plotted correspond *to* V_p of same interval. For refraction method V_p of 5.25 km/s or higher, V_p' values were 5.01–5.49 km/s, approximately the same values with a small variation range of 0.5 km/s. For refraction method V_p of 3.75–4.75 km/s, V_p' values were approximately the same, 3.00–5.67 km/s, but slightly faster. These results are likely averaged values over a somewhat wide-ranging area of seismic exploration by the refraction method, indicating the utility of V_p' for determining detailed changes in geological properties.

187.2.3 Discussion

The low variance in the results obtained from the proposed system indicates its potential for precise exploration.

Capturing geological properties of cutting advance sections via V_p' is furthermore found to allow more detailed evaluation of geological properties than exploration from the surface.

187.3 Conclusion

We have developed a system for geological property evaluation of tunnel faces that utilizes excavation blasts. The correlation coefficient for travel time data obtained was approximately $r = 0.986$–0.998, indicating that measurements were performed with high condition.

Continuous exploration using the proposed system during excavation should allow calculation of V_p'. It is furthermore effective for obtaining a detailed understanding of changes in geological properties.

Further topics for research include that proposed system can be use seismic reflection method, geological condition ahead the face can be predicted. So we will continue verification experiments to further improve the proposed system.

Reference

Nakaya M, Yamamoto H, Utsuki S, Onuma K, Suzuki M (2013) Development and illustration of system which evaluating geological condition around tunnel cutting face by the excavation blasting(in Japanese). In: Proceeding Tunnel Technology Conference of JSCE, vol 23, pp 209–215

Multidisciplinary Methodology Used to Detect and Evaluate the Occurrence of Methane During Tunnel Design and Excavation: An Example from Calabria (Southern Italy)

188

S. Lombardi, S. Bigi, S. Serangeli, M.C. Tartarello, L. Ruggiero,
S.E. Beaubien, P. Sacco, and D. De Angelis

Abstract

The occurrence of high volumes of methane during tunnelling operations is a critical safety factor that can influence the choice of different technical approaches for tunnel design and construction. Moreover, gas accumulation can be influenced by fluid migration along spatially focused preferential pathways (i.e. points along faults and fracture zones) that can result in highly variable gas concentrations along the tunnel trace. This paper proposes a methodological approach to minimise the risks, and costs, related to tunnel construction in rocks with potentially high methane concentrations. This approach combines soil gas geochemistry and structural geology surveys along and across the main faults and fracture systems that occur in the study area. The procedure is based on near-surface sampling and consists of a two-pronged approach: the measurement of fault zone gas emissions and their classification as barrier or conduit zones. Moreover, it is illustrated the importance of measuring a wide spectrum of different gas species, not just methane, for a more accurate interpretation of the geological, geochemical, and structural system. This is due to the potential for multiple gas origins, different gas associations, and various alteration and oxidation processes (e.g., CH_4 oxidation into CO_2) that can modify the geochemical signal along the flow path as gas migrates towards the surface.

Keywords

Soil gas • Faults • Tunnel • Methane

188.1 Introduction

The discovery of significant volumes of methane during the preliminary phases of tunnel design increases the risk of a potential explosion during or after the excavation work. From a strictly design point of view, the excavation of tunnels in areas characterized by documented gas occurrences can be problematic. This is due to perturbation of the rock mass and gas distribution caused by the excavation itself, as tunneling can result in significant changes to the stress field and the pre-existing hydrological and hydraulic equilibrium.

This problem has generally been dealt with during an advanced phase of the project, when the most important choices have already been taken, or directly during the course of the work, imposing the adoption of specific techniques to detect the presence of gas during excavation. In the case of the discovery of gas during the early stages of drilling or excavation it is necessary to adjust, as a consequence, the procedures and digging equipment.

The methodological approach presented in this paper was developed, via a close collaboration between ANAS and the CERI research institute, to address and overcome these problems. This methodology, tested in a geological setting

S. Lombardi · S. Bigi (✉) · M.C. Tartarello · L. Ruggiero ·
S.E. Beaubien · P. Sacco · D. De Angelis
Dipartimento di Scienze della Terra, Università Sapienza di Roma,
P.le A. Moro, 5-00183, Rome, Italy
e-mail: sabina.bigi@uniroma1.it

M.C. Tartarello
e-mail: mariachiara.tartarello@uniroma1.it

S. Serangeli
Anas SpA, Via L. Pianciani, 16, 00185, Rome, Italy

that is potentially favorable to natural gas accumulation, is based on the identification of the geological conditions that can control and/or contribute to the genesis and migration of the gases.

Starting from the study of the spatial distribution of soil gas anomalies, measured over the zone that will be crossed by a proposed road tunnel, it is possible to develop the tunnel design as a function of gas emission distribution and geological conditions. Adopting this methodology during an early stage of the project, and in a targeted manner, can aid in a more correct prediction of the costs and timeline of the road infrastructure construction.

188.2 Methodology

Near surface gas geochemistry surveys include the measurement of gas concentrations in the shallow soil ("soil gas"), deep gases in boreholes, and the flux of gases from the soil to the atmosphere ("gas flux"). These measurements provide useful information on the geological processes that control the production and migration of gas. Over the years, this methodology has been refined and applied in many different research fields, addressing various environmental, geological, and engineering issues (Annunziatellis et al. 2008; Beaubien et al. 2013 among many others). The structural setting of the area and the classification of the fault deformation characteristics, integrated with the gas concentration distribution in the soil, are essential elements for the reconstruction of a model of fluid migration towards the surface in a given area. Fault and fracture zones are known to be belts of enhanced permeability which can readily transmit fluids, including gases, to the surface. Field data have shown the usefulness of the soil gas method for detecting faults and discontinuities even when faults are buried or cut non cohesive clastic rocks, conditions which make it difficult to recognize their surface expression by traditional means (Lombardi et al. 1996; Ciotoli et al. 1998).

In the case presented here, located in the Ionian part of Calabria, soil gas surveys were conducted along a 1 km wide strip ("buffer") that follows the planned trace of a future road. The obtained values were elaborated using spatial analysis statistical techniques to define threshold values and to localize the main anomalies for each gas species.

188.3 Geological Setting

The study area belongs to the southern Apennine orogenic system; the trace of the future road crosses the easternmost tectonic units belonging to the chain and the more eastern foredeep deposits. The stratigraphy in this area consists of: (a) the Albidona and Saraceno Formations of the Liguride and Sicilide units, which consist of marls, turbiditic sandstones and thick micro polygenic conglomerates, and of calcareous mudstones, grainstone and clays, respectively; (b) the Varicolori Clays Formation, which is tectonically placed on the previous units and which consists of multicolored, over-consolidated clays containing olistoliths of limestone and interbedded mudstone levels; (c) Plio-Pleistocene marine sands and clays; and (d) alluvial deposits. The Sicilidi and Liguridi units, as well as the syn-compressional Oligo-Miocene deposits, were involved in the Apennine orogenic compression from the Upper Cretaceous to the Lower Miocene. The Plio-Pleistocene succession and the carbonate bedrock are still involved in compressional deformation, mainly by left lateral strike slip faults connected to the southward migration of the Calabrian Arc (Monaco et al. 2001). Along the coast, several orders of terraced Quaternary marine deposits (up to 7) are considered evidence of a rapid uplift, due to the activity of southeastern dipping normal faults (Ferranti et al. 2009; Cucci 2004).

188.3.1 Structural Analysis and Soil Gas Survey

A structural analysis of deformation styles has been carried out in the investigated area. The main thrust cropping out in the northern sector is the Argille Varicolori thrust, which juxtaposes this Unit onto the already deformed Cretaceous—Paleogene formations. This hanging wall unit has a chaotic organization with numerous thrust planes within the same Varicolori formation. All these thrust planes, including the basal one, consist of strongly foliated clay-rich deformation bands. The reverse faults and small thrusts that crop out in the area, involving the Albidona and Saraceno Formations, are instead characterized by a brittle and localized deformation, associated with wide, metre-scale fracture zones, succession repetition, and series thickening. The last episode of compressional deformation in the area was due to NW-SE trending strike-slip faults that cut and dissect the previous faults and folds. In many cases strike slip deformation is developed on the limb of a previous fold, along vertical bedding, which can create open fractures that provide a pathway for vertical fluid migration.

In a second phase a soil gas survey was performed along the path of the future road, from Trebisacce in Roseto Capo Spulico, to localize and quantify soil gas anomalies. These anomalies can potentially be correlated with the presence of permeable faults and/or highly fractured zones. In the case of methane, anomalies may also be correlated with the occurrence of specific lithologies or geological settings that are able to generate this gas.

The soil gas survey presented here involved the collection of 422 samples; the analysis has been focused on three gas species (He, CO_2 and CH_4) due to their geochemical
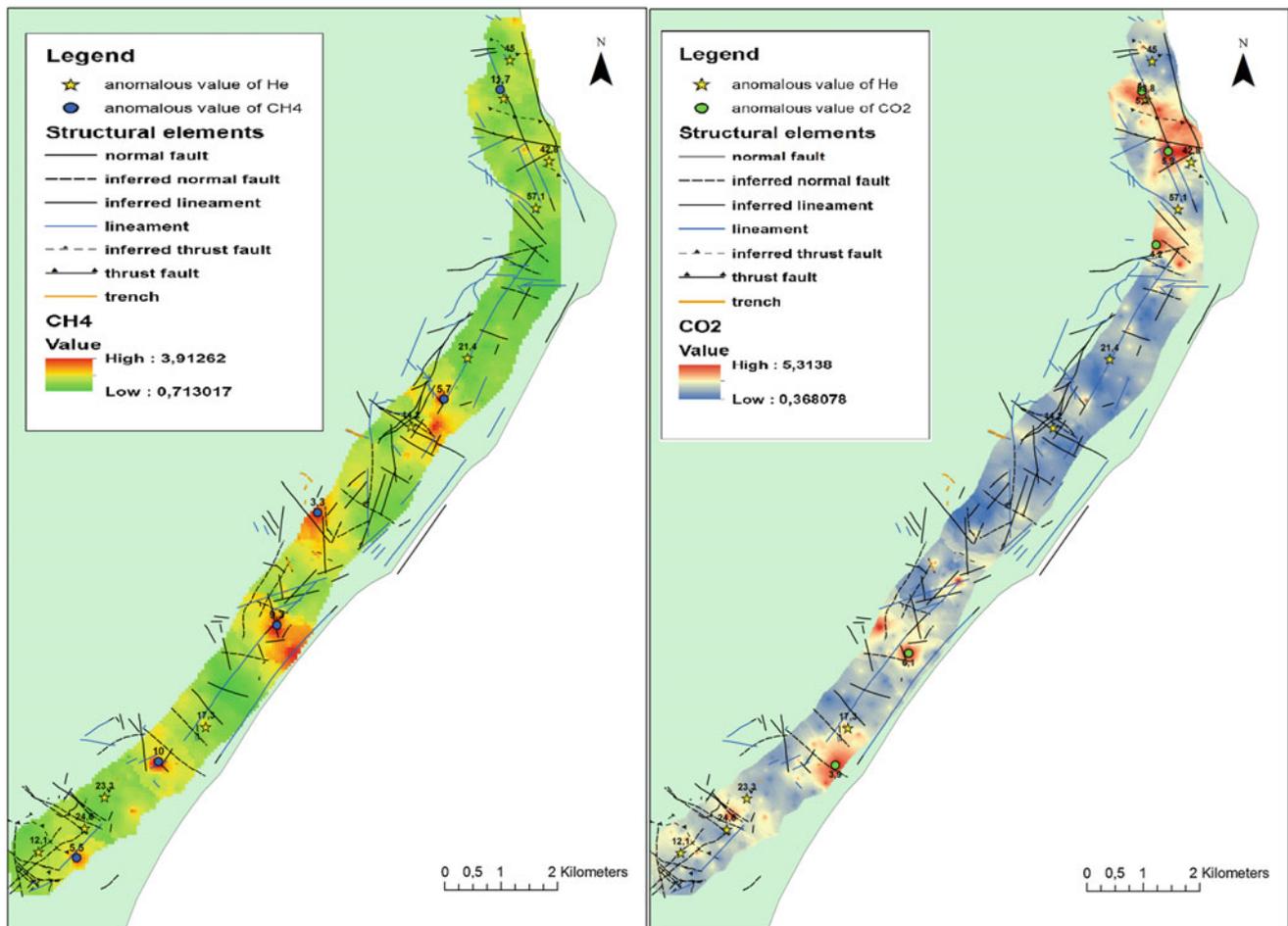
Fig. 188.1 Soil gas concentrations: CO2 (on the *right*) and CH4 (on the *left*)

characteristics, both for discontinuity detection and for the goals of the research itself (i.e., tunnel construction).

Carbon dioxide has a double importance, as it can act as a carrier gas of trace gases (when it is the dominant species) and can be formed by methane oxidation. Helium is recognized as a good tracer of deep structures (e.g. Oliver et al. 1984), because it is a highly mobile and inert gas and thus it can easily migrate through the underground with little attenuation. Finally, CH4 is obviously the focus of this study; it too is highly mobile because of its small molecular size, however it is more soluble than He, can be formed by a number of biogenic and geogenic processes, and can be consumed along the flow path via microbially mediated oxidation processes.

Soil gas contour maps were created for each gas species based on the defined threshold values, with results shown in Fig. 188.1 for CH$_4$ (left) and CO$_2$ (right). Each of them highlights areas where an increased circulation of fluids is

present. Points of anomalous He concentrations (i.e. higher than atmospheric) have been added to the maps of the other gases. The methane concentration map shows large anomalous zones in the central-southern part of the area, while in the north, around Roseto, the anomalies are very localized (Fig. 188.1).

The same trend can be observed in the CO2 concentration map, where maximum values (c. 6 %) were measured in the central-southern part. Instead, in the north near Roseto and Roseto Castle, an area of anomalies was found in correspondence with the previously described Argille Varicolori thrust. Helium anoma- lies correspond to CO2 anomalies in the north, confirming the occurrence of deep fluid circulation, whereas in the southern sector the anomalous values are aligned along the coast in correspondence with the normal fault system responsible for the deformation of the Pliocene marine terraces.

188.4 Discussion

Based on the analysis of the described dataset, integrated with geological observations, it is possible to describe different modes of gas migration in different sectors of the study area.

The main correlation is between gas concentrations and the outcropping lithologies: the highest anomaly values are present where the Albidona and Saraceno Formations crop out (as in the area of Trebisacce), especially for CO_2 and He. In the northern sector, in the area of the Plio—Pleistocene deposits and Quaternary terraces, the values are under the threshold, except for along the valleys where anomalous values are located, as in the case of the Straface and Ferro rivers.

The different concentrations measured in the different geological settings suggest that the gas generation and migration is controlled by two main factors: the structural control of faults and fractures and the lithological and morphological control. In the first case, where the sandstones and clays of the Albidona and Saraceno Formations crop out (deformed by faults associated with densely fractured bands) it is hypothesized that migration is mainly controlled by fractures associated with faults, acting as migration pathways that may feed the accumulation of methane at depth. In this case the soil gas composition is continuously fed from depth, as can be deduced by the high concentration values measured there.

Low permeability Pliocene clays and Quaternary marine terraces outcrop between the Avena and Ferro rivers. Locally, in the Pliocene clay, strata of unconsolidated, highly porous sandstones can constitute small methane reservoirs, even under pressure. Moreover, the Pliocene clays are suspected to be sites of biogenic methane production themselves, as largely documented by studies into petroleum generation in the area (Casero 2004).

The lack of soil gas anomalies in this area can be interpreted as due to the barrier effect of these rocks, which prevent communication between the surface and the fracture systems at depth. This lithological control is supported by the fact that the gas anomalies are found in the valleys, where the Quaternary terraces are interrupted and the Pliocene clays crop out.

In conclusion, this study has shown that integrated soil gas and structural geology surveys are a powerful combination for the study of gas migration and associated pathways, and can be a useful tool during the early phases of design and construction of road works involving tunneling in areas suspected of having potentially dangerous methane accumulations.

References

Annunziatellis A, Beaubien SE, Bigi S, Ciotoli G, Coltella M, Lombardi S (2008) Gas migration along fault systems and through the vadose zone in the latera caldera (central Italy): implication for CO_2 geological storage. Int J Greenhouse Gas Control 2(3):353–372. http://dx.doi.org/10.1016/j.ijggc.2008.02.003

Beaubien SE, Jones DG, Gal F, Barkwith AKAP, Braibant G, Baubron JC, Ciotoli G, Graziani S, Lister TR, Lombardi S, Michel K, Quattrocchi F, Strutt MH (2013) Monitoring of near-surface gas geochemistry at the Weyburn, Canada, C2-EOR site, 2001–2011. Int J Greenhouse Gas Control 16(Supplement 1):S236–S262. http://dx.doi.org/10.1016/j.ijggc.2013.01.013

Casero P (2004) Structural setting of petroleum exploration plays in Italy. Spec Volume Italian Geol Soc IGC 32:189–199

Catalano S, Monaco C, Tortorici L, Paltrinieri W, Steel N (2004) Neogene-quaternary tectonic evolution of the southern Apennines. Tectonics 23(2), TC2003. doi:10.1029/2003TC001512

Cucci L (2004) Raised marine terraces in the northern Calabrian arc (southern Italy): a ∼600 kyr-long geological record of regional uplift. Ann Geophys 47(4). doi: 10.4401/ag-3350

Ferranti L, Santoro E, Mazzella ME, Monaco C, Morelli D (2009) Active transpression in the northern Calabria Apennines, southern Italy. Tectonophysiscs 476(1):226–251. http://dx.doi.org/10.1016/j.tecto.2008.11.010

Lombardi S, Etiope G, Guerra M, Ciotoli G, Graubger P, Duddridge GA, Gera F, Chiantore V, Pensieri R, Grindrop P, Impey M (1996) The refinement of soil gas analysis as a geological investigative technique. Commission of the European Communities, nuclear science and technology. Final report, EUR 16926 EN

Monaco C, Tortorici L, Catalano S, Paltrinieri W, Steel N (2001) The role of Pleistocene stike-slip tectonics in the neogene-quaternary evolution of the southern Apennines orogenic belt: implication for oil trap development. J Petroleum Geol 24:339–359. doi:10.1111/j.1747-5457.2001.tb00678.x

Oliver BM, Bradley JG, Farra H (1984) Helium concentration in the earth's lower atmosphere. Geochimica et Cosmochimica Acta 48:1759–1469. http://dx.doi.org/10.1016/0016-7037(84)90030-9

O. Brenner and D. Orlowsky

Abstract

In advance of the construction of the A2 tunnel in Maastricht a geophysical survey was necessary in order to investigate the position of layers, faults, flint layers, occurrence of rock deposits and potential cavities within the limestone layer. For this purpose three different geophysical methods were combined: CMP refraction seismic, refraction tomography, reflection seismic. The whole survey was performed with three different sources to get the best results for each depth: air sound source, sledgehammer and accelerated weight drop source. After processing and during the interpretation process the results of 18 boreholes were included. Finally all relevant layers could have been detected and corresponded to the results of drilling. Furthermore minor and major faulting in the survey area could be detected. Potential cavities in the limestone were not detected.

Keywords

CMP refraction seismic • Refraction tomography • Reflection seismics • Tunnel construction • A2 Maastricht

189.1 Introduction and Background

The city of Maastricht, The Netherlands, is split by the national motorway A2 into two parts (Fig. 189.1). The A2 Maastricht project organisers developed a plan to reconnect both parts and to reduce air and noise pollution by tunnelling the A2. Cars, lorries and motorcycles shall disappear under the ground. Above the tunnel a green park avenue will be set up.

The Consortium Avenue 2 planned to develop the underground for the construction of the A2-tunnel and to redevelop the adjacent areas along the A2. The purpose of the geophysical investigation was to provide information about the geological condition of the substratum. In detail, the following objectives were specified:
- Profile variation of the layer boundary between gravel and limestone,
- location, pattern and vertical separation of the geological fault in the Maastrichtian and Campanian,
- any occurrence of flint layers and
- any occurrence of rock deposits within the gravel layer.

Furthermore, potential cavities within the limestone should be detected.

For the investigation of the underground the following geophysical methods were applied:
- CMP seismic refraction
- Refraction tomography
- Seismic reflection

For these methods three profile locations have been specified by the client. The total length of the survey line was 2 km. 200 active single geophone stations were used with a geophone spacing of 1 m. The distance between

O. Brenner (✉) · D. Orlowsky
DMT GmbH & Co. KG, Essen, Germany
e-mail: olaf.brenner@dmt.de

D. Orlowsky
e-mail: dirk.orlowsky@dmt.de
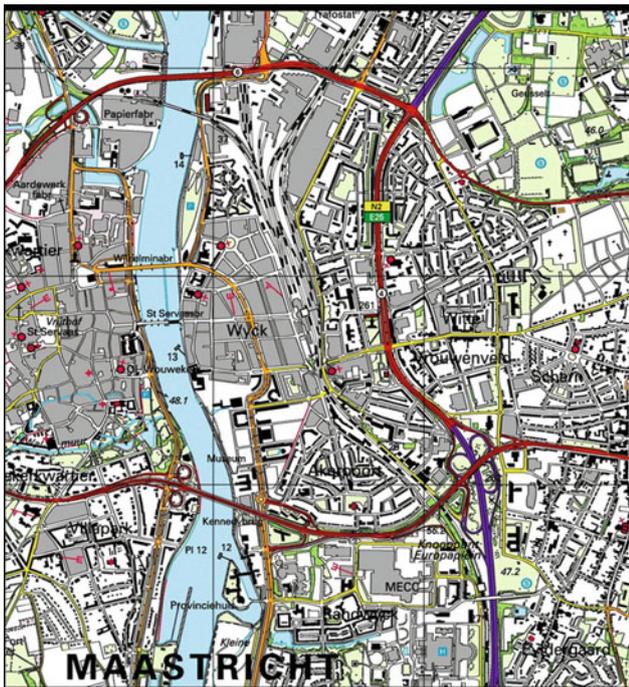
Fig. 189.1 A2 in Maastricht

source locations was 2 m. This layout was selected, so that the ground conditions down to a depth of 50 m below ground level can be determined. The seismic energy was generated by three different sources:

DMT started with a pre-evaluation in 2009 and continued with the final survey in 2010. Both seismic investigation campaigns were carried out during night sessions to minimize interfering noise generated by traffic. Occasionally, the traffic on the A2 was interrupted for the single measurements.

189.2 Methods

189.2.1 General

At the beginning of the survey a source test with three different sources was performed:

- Accelerated weight drop "Mjoelnir"
- Sledgehammer
- Air sound source

This test was necessary to find the best source for different geophysical methods (reflection, CMP refraction and refraction tomography) (Fig. 189.2). Finally for the interpretation the results of the weight drop and the air sound source were used.

The refracted wave could be best detected in the data of the weight drop source. Although in the raw data the air sound source shows clearly a reflector and higher frequencies for higher resolution the stack of the weight drop data gives more information and reflections over the complete section especially for increasing depth, see Fig. 189.3. The data of the sledgehammer gave only poor results on reflections and for far offsets.

189.2.2 Reflection Seismics

Reflection seismic processing was applied to all datasets of the weight drop, sledgehammer and the air sound source. The data of the air sound source contain higher frequencies but also the natural air sound was dominating the results. Compared to the air sound data the results of the weight drop source contain stronger reflections but lower frequencies (Fig. 189.3). The sledgehammer didn't generate reflections in the stacked section.

Fig. 189.2 Raw data of the different tested sources *top* accelerated weight drop, *middle* sledgehammer, *bottom* air sound
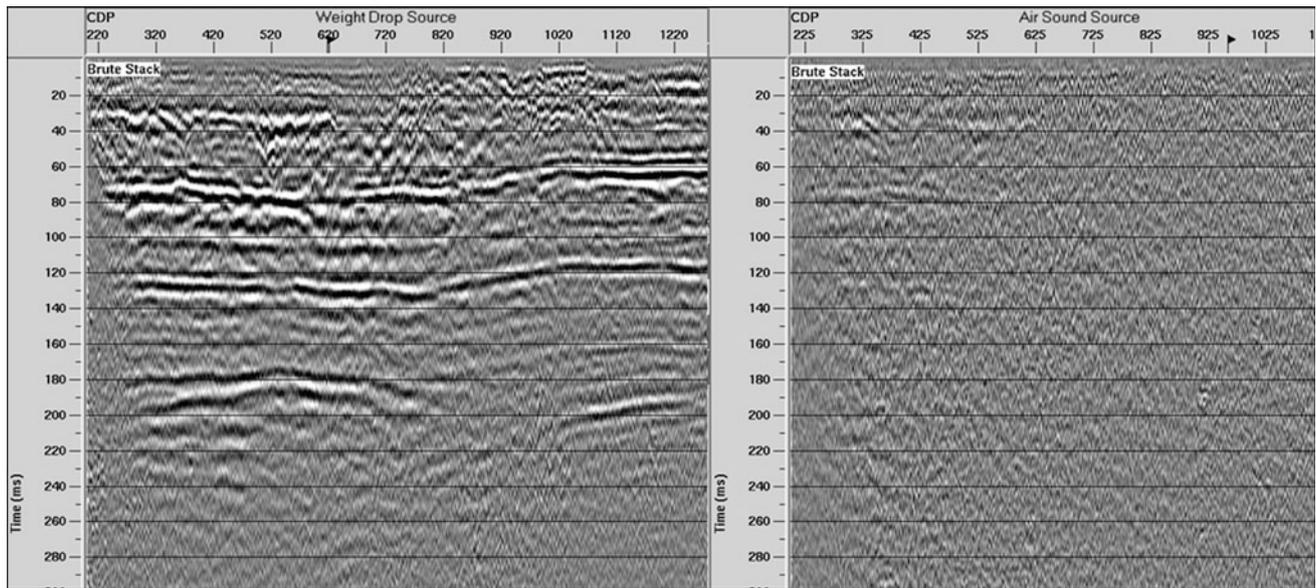
Fig. 189.3 Comparison of Brute stacks for weight drop (*left*) and air sound source (*right*)

The first clear reflector could be detected at a depth of 15 m. Overall 4 reflectors could be determined and correlated to the results of boreholes and known geological structure.

189.2.3   CMP Refraction Seismics

Common-Midpoint (CMP) seismic refraction is a method to improve the signal/noise ratio of the refracted waves. Applying this technique, the shallow underground is described using all information (amplitude, frequency, phase characteristics) of the wave train, following the first break (first-break phase). Thus, the layering can be determined and, additionally, locations of disturbances such as faults, weak zones, and clefts can be detected.

The results of CMP seismic refraction data processing are merged with the seismic reflection data. The refractors are displayed with the complete refracted wave fields and the according depths. Disturbances and anomalies (e.g. cavities) within the refracted waves can be detected. Figure 189.4 shows the difference in the upper 30 m by combining the datasets. With the CMP seismic refraction in the upper part the underground image is more clearly and better for interpretation in this part.

For interpretation all lines were merged to one long line. The merging was done in an interactive way using the

refractor depth in a range of 10–30 m with a region of overlapping. For the merging of the lines to one single line a triangle taper function was used to get a smooth result in the overlapping regions of the lines.

189.2.4   Refraction Tomography

Refraction Tomography is a method to produce a model of the distribution of seismic propagation velocity in the shallow underground. It utilizes the first arrivals (first breaks) of seismic wave energy. The method is restricted to shallow depths and a positive velocity gradient (higher velocities in greater depth) is generally assumed.

Depending on the actual velocity distribution a penetration depth of approx. 1/6th through 1/4th of the maximum source-receiver offset can be obtained. For the current survey, a maximum depth of 20 m through 30 m below surface was covered.

Figure 189.5 shows one example result of the refraction tomography in the middle of the survey area. The velocity distribution increases with depth, different layers can be detected. Furthermore areas with low velocities in depth can be detected. Depending on the combined interpretation these variations can be interpreted as weak zones, faults or extension of the weathering zone.
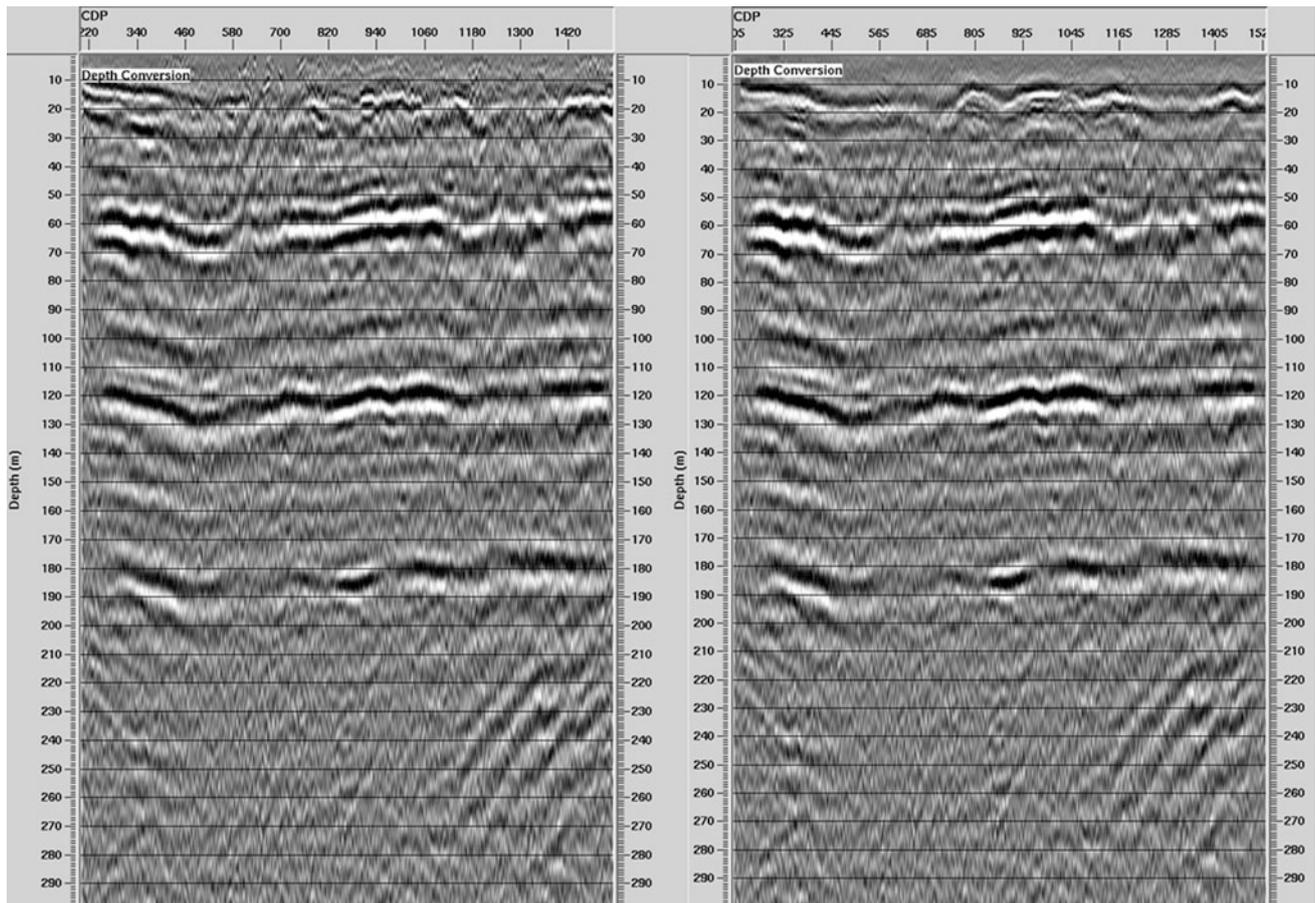
Fig. 189.4 *Left* result from seismic reflection processing, *right* seismic reflection combined with CMP-Refraction processed data
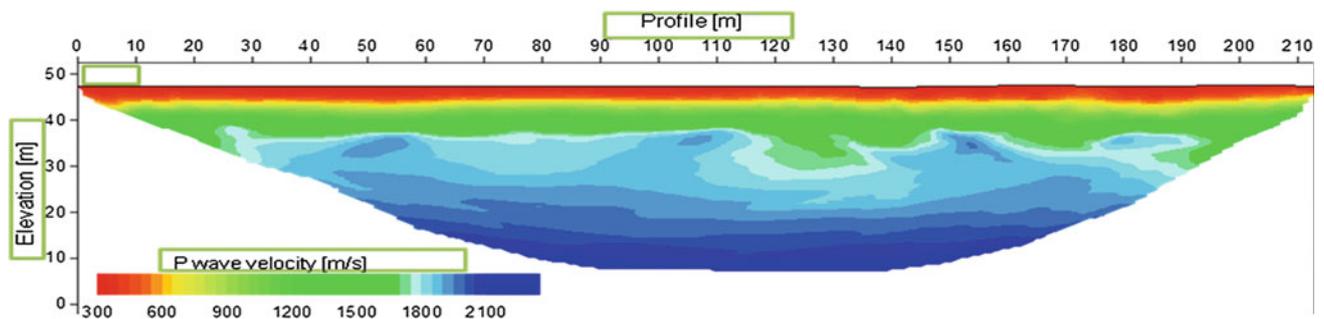
Fig. 189.5 Result of refraction tomography (example)

189.3   Joint Interpretation

After processing of each individual method a joint interpretation by a geologist was performed with the 3D interpretation and modelling software PETREL 2010 (Schlumberger Information Solutions). Overall 18 boreholes were integrated in the final results used to correlate the various layers visible in the seismic refraction and reflection data with the geological boundaries.

The top of the limestone layer including variations could be interpreted and in the middle of the profile several faults and one flintstone layer were detected (Fig. 189.6).
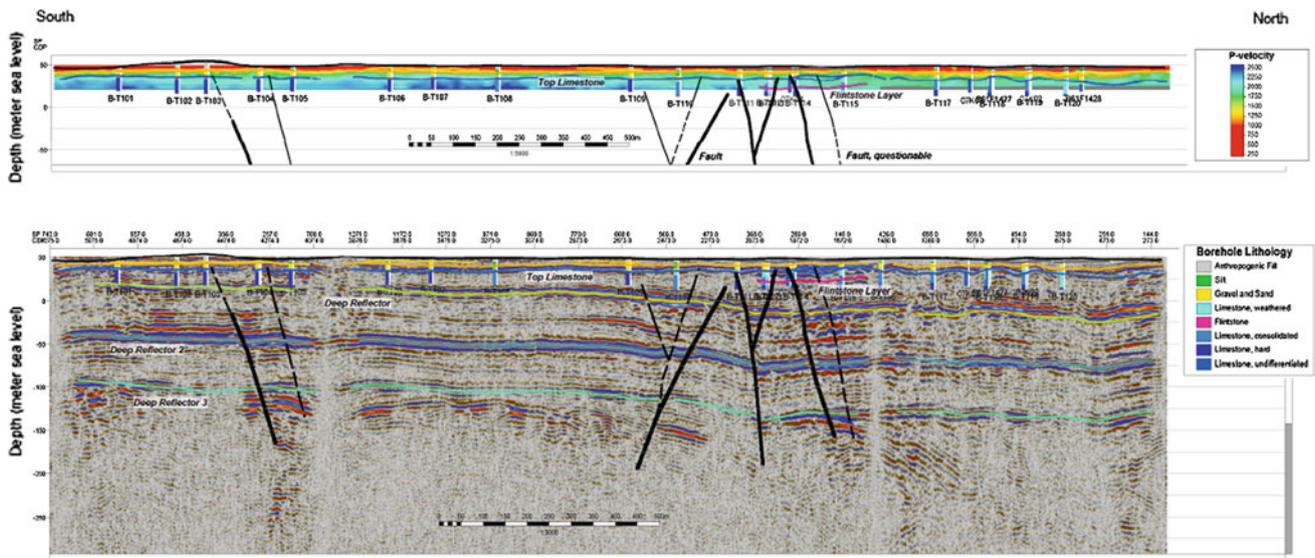
Fig. 189.6 Joint interpretation of geophysical data with integration of borehole results. *Top* refraction tomography, *bottom* combination of cmp refraction and reflection seismic

189.4 Conclusions

The combination of different geophysical processing methods and different kind of sources was very successful for getting a good image of the underground and to achieve all targets of the survey. Two refractors could be detected. The upper refractor correlates to the boundary between the anthropogenetic fine grained fill and the Pleistocene gravels. The second refractor is

close to the hangingwall boundary of the weathered limestones of the Maastrichtian. Also seismic reflectors could be determined and correlated with the main lithostratigraphic units. The data also reveals that intensive faulting may be present. Velocity variations derived from refraction tomography analysis indicate a potential high degree of weathering of the ground along the Northern part of the survey area.

Potential cavities in the limestone were not detected.

The Combined Use of Different Near Surface Geophysics Techniques and Geotechnical Analysis in Two Case Histories for the Advanced Design of Underground Works in Urban Environment: Rome Metro B and Torino-Ceres Railway

Riccardo Enrione, Simone Cocchi, and Mario Naldi

Abstract

In the urban context of the Italian towns, both historical remnants (archaeological items, man-made cavities, buried walls, etc.) and underground geotechnical "anomalies" (cemented layers, pockets of low-density soils, presence of big boulders, etc.) can strongly increase the hazard risk associated to underground excavation in urban context (as collapse, surface subsidence, interference) or inappropriate choice of the excavation method. This consciousness has led the writers to work out a site-specific multi-investigation method, hereinafter explained through a couple of case histories. The first one considers the reconstruction of a man-made cavities map distribution along the anticipated alignment of the extension of Rome Metro B Line, with the use of GeoRadar and geoelectrical methods, calibrated through boreholes. The second case history is related to the recognition of poor-quality soils and possible cemented layers along the alignment of a new urban railway line in Turin, using a MASW survey and a seismic refraction tomography survey, both coupled with geotechnical investigations. In both cases, the combined use of geophysical and geotechnical investigation has guaranteed the identification of the possible main geohazards, fundamental basis for an appropriate tunnelling design and assessment of the related risk.

Keywords

Geophysics • MASW • Geotechnical investigations • Geohazards • Risk

190.1 Introduction

Too often project main goal and time-related concerns may distract designer and client from the boundary value problems, potentially leading to an underestimation of the so-called minor issues that in the end may turn out in major ones. In this sense, the knowledge of the geological–technical context must be intended as a key of success of the Design phase and not as an annoying formal step only because required by contract specifications or rules. As a consequence, the definition of the Design Geological and Geotechnical Model (DGGM) is the first and inevitable design goal, by which it is possible to achieve high level of sensibility about the underground space and to propose mitigation measures for the risks associated, both during the construction phase and during exploitation. Actually, geological uncertainties and the resulting risks in construction of great civil infrastructures are well understood. However, the use of a step-wise investigation approach in reducing these risks not always receives the deserved emphasis. In particular, a well-planned preliminary investigation can identify the possible hazards and thus deliver a high ratio of benefit to cost. In many designed works, which met severe problems during construction, it was found that often an inadequate model of ground conditions had been used, either because some geological features had been missed or overlooked during investigation or because its significance had been underestimated. This is especially true in case of

R. Enrione (✉) · S. Cocchi
Geodata Engineering, Corso Duca degli Abruzzi 48/e, 10129 Torino, Italy
e-mail: ren@geodata.it

M. Naldi
Techgea Srl, Via Modigliani 26/a, 10137 Torino, Italy

underground works in urban areas where the interaction between the geological and geotechnical context with the excavation is dramatically critical and therefore more detailed studies are necessary.

Besides, it must be noted that common geo-investigation methods usually deal with single survey technique at once, both for practical reasons and costs control. In our experience, this approach has turned out to achieve benefits only in the short-term, as immediate saving of time and money. On the other side, in the long-term, this is not a pay-back winning strategy, because of the uncertainties left behind and possible unidentified geohazards that could lead to additional cost and time consumption higher than early savings.

For this reason, a multi-approach investigation method has been worked out, refined in the course of time, on the account of several past experiences, with the aim to achieve the best compromise among all the above listed aspects. Current results show, in short, that coupling geotechnical investigations and geophysics surveys, conveniently integrated in terms of mutual placing in space and time allows gaining high satisfactory level of geological-technical knowledge and time/cost optimization.

The illustrated approach has been consolidated from the experience of many successful completed projects, and has become a standard practice, as well explained by the two following case histories.

190.2 Case A—Rome Metro B Extension

The case history A is related to the definitive design of underground Metro Line B extension, in Rome, between Rebibbia and Casal Monastero. The metro line extension has involved the realization of three new underground stations and the C&C excavation of a double tracks single tunnel, 3,000 m length, between diaphragm retaining walls.

190.2.1 Geological Settings and Geotechnical Investigations

From a geological-technical point of view, superficial deposit are represented by recent alluvial and anthropic soils, with heterogeneous grain size distributions and maximum thickness of 24 m, overlying pyroclastic deposits mainly composed by aches and lapilli of volcanic origin. Into all the pyroclastic sequence gas pockets (also radon), as well manmade cavities are possible; specifically, Roman Age underground pits for building materials extraction can be expected in the *Tufo Lionato* and *Pozzolana* units (Funiciello et al. 2005; Ventriglia 2002).

Beside this, presence of archaeological ruins must be taken into account when excavating in Rome subsoil; previous bibliographic information highlighted from the beginning the possible presence of Roman ruins near the alignment sector, such as old road network, underground services (ancient sewers), cemeteries and thermal baths (Funiciello 1995).

Due to these main anticipated geohazards, all the entire design process has been eventually driven by the associated knowledge and consequent management, conferring to the investigations-based DGGM a key-role in case of high-stakes choices.

Geotechnical investigations, which the DGGM has been based on, consisted in boreholes, CPTUs (Seismic Piezo-cone penetration test) and lab tests, assuring complete geotechnical characterization and punctual stratigraphical recognition; on the other side, spatial continuity was missing, as well the possibility to identify cavities or ancient remains if not directly intercepted by boreholes. This is where integration with geophysics came in handy.

190.2.2 Geophysical Survey and Discussion

Geophysical survey have been carried out with the aim to map the subsoil in terms of anomalies that might be led back to possible cavities or buried remains, using the previous boreholes and CPTUs as calibration network, thus avoiding false positives, on one hand, and assuring continuity in stratigraphical reconstruction, on the other one. Two techniques have been adopted: Ground Probing Radar (GPR), with different antennas (with frequency of 25, 100, 200 and 600 MHz), specifically oriented to ancient remains detection within the very first meters below ground level (4–5 m), and Electrical Resistivity Tomography (ERT), more oriented toward cavities identification. In order to best address the ERT survey, a preliminary calibration test was conducted in a similar area in presence of a known cavity (archaeological park in Rome). The test was performed with the aim of get the typical resistivity values of the void in the tuff materials (the so-called digital signature) in order to easily recognize similar anomalies along the Project alignment. The test pointed out a strong contrast between the resistivity value of the tuffs (ranging from 100 to 200 ohm.m), and the resistivity values of the test cavity (>800 ohm.m,).

Speaking of specifications, GPR survey was conducted on the account of a regular grid all along the metro anticipated alignment, using three different antennas (100, 200 and 600 MHz). The clayey shallow deposits have slightly conditioned the survey results (strong attenuation on the radar signal), but on the whole the survey was able to reveal a lot of structures down to a depth of 4–5 m with the lower frequency antenna (i.e. 100 MHz). All the founded structures (detected in two directions) have been mapped and cross check with known underground utilities or with opening of

nearby gutters. After this comparison, all the underground structures have been mapped as underground utilities or underground tanks and no archaeological remnants have been detected. These results have been critical in defining the final boreholes location to avoid unwanted interference with underlying utilities.

ERT survey was carried out all along the future metro path, with a longitudinal line of 3 m-spaced electrodes and overlapping among consequential lines (roll-along technique). The obtained results have always revealed very low resistivity values (lower than 200 ohm.m.) that can't be referred to cavities presence. The only relevant "anomalies" have been identified in alluvial deposit, in terms of high contrast resistivity (80–100 ohm.m spot compared with the surrounding 10–30 ohm.m average). Again, the geophysical survey has proved to be unique for preliminary assessment of the specific areas to be directly investigated through boreholes; in this sense, the resistivity anomalies turned out to be soil pockets of very loose silty sand (SPT = 1) then correlated to piping phenomena in alluvial soil underlying the main gullies.

190.3 Case B—Torino-Ceres Railway

190.3.1 Geological Settings and Geotechnical Investigations

The case history B concerns the Definitive Design of a metropolitan underground rail junction between Turin Rebaudengo existing station and Caselle Airport located in the North city area. The Project involves a new 2.5 km long tunnel, single tube, double tracks, with a section area of 54 m^2, to be excavated in C&C between diaphragms hydromill-excavated. From the geological point of view, the Project area is underlain by glaciofluvial deposits of *Rissian* age (Quaternary), mainly composed by sandy gravels, cobbles and blocks, occasionally with clayey or silty sand layers.

Even if apparently plain, yet Turin subsoil can present frequent anomalies, as highlighted in past experiences such as *Metro Torino Line 1* or the *Passante Ferrioviario*, namely:

- the cementation of glaciofluvial deposits, and its variability, relevant to excavation technique choice and cutters wearing in case of TBM or hydromill excavations;
- the presence of big blocks (diameter >1 m), hence difficulties during excavation;
- presence of very loose sandy, supposedly affecting the stability of nearing existing building and road, as well the safety conditions of the site equipment, machinery and vehicles, during the excavation.

Considering the possible geohazards listed above, geotechnical investigation have been planned consequently; specifically, common boreholes have been coupled with DAC tests, that is the automatic measurement of drilling parameters to evaluate the mechanical properties of soils, and namely the level of cementation, to be correlated to the soil shear resistance.

Again, in order to better address the investigation plan, final location of tests have been derived from the geophysical results, as showed below, with the aim to limit the number of drillings and placing them right where most effective.
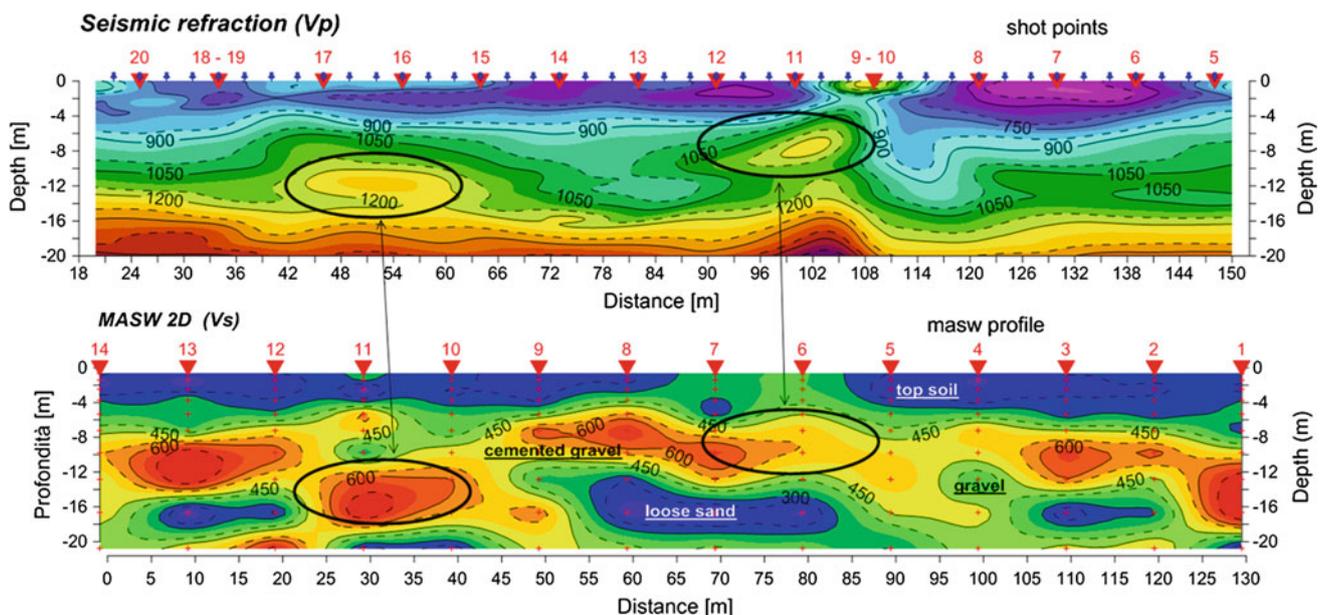
Fig. 190.1 Comparison between seismic refraction and MASW 2D section

190.3.2 Geophysical Survey

According to the objectives of the survey (subsoil profiling to locate cemented layers and loose sand pockets), two different geophysical methods have been applied: P-wave shallow seismic refraction and Multi-channel Analysis of Surface Waves (MASW) continuous profiling (2D section-shear wave velocities) (Park et al. 1999). The combined use of two different seismic methods provides both P-waves and S-waves velocities to estimate the main elastic properties of the soil and a cross-check to reduce the interpretative ambiguity for the DGGM. The results of the survey have provided a very detailed "image" of the subsoil, with some differences between refraction seismic and MASW 2D.

For the irregular distribution of low velocity and high velocity materials, the refraction seismic tomography method does not reveal correctly the geometry and morphology of the sedimentary lenses, while MASW2D methods provides a better resolution of the geometry of the alluvial sedimentary sequence (Fig. 190.1).

190.4 Conclusion

Owing to the anticipated subsoil peculiarities, neither single investigation tests nor separate geophysical surveys would have solved efficiently the risk associated to the possible geohazards affecting the designing of the urban underground works here described. For this reason, an integrated investigation survey has been worked out, coupling traditional geotechnical boring and tests with advanced geophysical surveys, compensating the reciprocal limits, in a complementary way: boreholes and CPTUs has reached the desired investigation depth assuring direct visual recognition and soil geotechnical testing; geophysical survey have fixed the gap between single site tests, which have act meanwhile as calibration point, improving the overall continuity and reliability of the DGGM.

This is how it works: reducing costs while increasing design quality and achieving final Project goals: a methodological approach that has become, for us, common practice.

References

Funiciello R (1995) La geologia di Roma. Il centro storico. Mem. Descr. della Carta Geol. d'Italia, vol. L - Servizio Geologico Nazionale, Roma, p 550

Funiciello R et al (2005) Carta Geologica di Roma alla scala 1:10000, vol. 1. Dipartimento Scienze Geologiche Università Roma Tre – Comune Di Roma – APAT

Park CB et al (1999) Multichannel analysis of surface waves. Geophysics 64(3)

Ventriglia U (2002) Geologia del territorio del Comune di Roma. Servizio Geologico, Difesa del Suolo, Amm. Provinciale Roma

Landslides Induced by Intense Rainfall and Human Interventions—Case Studies in Algeria

Ramdane Bahar, Omar Sadaoui, and Samir Sadaoui

Abstract

This paper describes two landslide case histories triggered by rainfall, unfavourable geological, hydrogeological and geotechnical conditions and human interventions. The first one is located about 250 kms South-West of Algiers, at place named Bordj Bounaama in Tissemsilt region. The landslides caused a collapse of a stadium and surrounding wall of the gymnasium and tilting of retaining wall under the earth pressure. The second landslide is one of the most spectacular among the 120 sites affected by landslides since 2000 in Béjaia department, located in Kabylia region. It was occurred at PK 226 + 300 of the National Road RN 24. The landslide caused the collapse of a section of the road of about 120 m, with a main scarp of about 8 m. During the firstly time of the field observation, the landslide mass and the road moved 10 m. Based on extensive geological, geotechnical and hydro-geological investigations, comprehensive of the landslide analyses were made using limit equilibrium and finite element method.

191.1 Introduction

Every year, particularly in the winter, mountainous and coastline region of Algeria, are affected by landslides displacing an important volume of detritic materials, and causing damages to infrastructures, housing and public facilities. Most disasters of mountain road damage are similar. The landslides take place in geological formations that are particularly favourable to this type of movement, because of the heterogeneity of their facies and the impermeability of some layers. Experience shows that the main cause of the landslides is the combination of several passive and active factors, as geology, morphology, hydrology, climate and anthropic activities. This paper describes two case histories of landslides triggered by rainfall, unfavourable geological, hydrogeological and geotechnical conditions and human interventions.

191.2 Case Historie of Bordj Bounaâma Landslide

Bordj Bounaama town is in a broader context of the northern fringe of Tellian countrie, and it takes place in a physical-climatic set, consisting generally of a mountain range running parallel to the coast. Schematically the town is surrounded in a monoclinic area surrounded by mountains in all directions. The region is recorded a harsh winter with snow and heavy rains and a hot summer. According to the data, 90 days of frost, 62 days of rain and 10 days of snow are

R. Bahar (✉)
LEEGO Laboratory, LGEA-UMMTO, University of Sciences and Technology Houari Boumediene, BP 32 El Alia, 16111 Algiers, Algeria
e-mail: rbahar@usthb.dz

O. Sadaoui
Department of Civil Engineering, University Mira Abderrahmane of Béjaia, 06000 Béjaia, Algeria

S. Sadaoui
Bureau de Conseils et d'Engineering, 06000, Béjaia, Algeria

Fig. 191.1 Gymnasium view and earthworks

recorded per year. The site, approximately 11 ha in area, has a topographic line whose slope oriented in North-South direction. The largest slopes are found in the North West and South East part of the site, they are on the order of 15–20 %.

During the site investigations, two areas where landslides have already occurred are observed. The first one is located in the southern boundary of the gymnasium, which led to the degradation of the stadium and the surrounding wall (Fig. 191.1). According to the site investigation and local citizens, this landslide was caused by earth works made for a housing project located downstream of the gymnasium (Fig. 191.2). The terraced ground was left unprotected to the weather for two months, and was backfilled after landslide. The second landslide was observed upstream of the third block of 60 housing under construction, where the gabion retaining wall, tilted under the earth pressure (Fig. 191.3). Figure 191.3 shows also the presence of water in the excavations.

The geotechnical investigation consisted on core drilling and pressuremeter boreholes, dynamic penetration tests, seismic refraction profiles, profiles of electrical resistivity and piezometers. According to the logs of core drilling, the local lithology consists of a layer of colluviums of variable thickness overlying a shale layer. The shale layer is altered on surface and becoming hard in depth. The greatest thickness of colluviums was noted at the core drilling 3. It is about 18 m. Piezometer installed in the landslide area has detected water in January, 20th 2008 between 0.50 and 5 m from the ground surface. The soils are saturated. The natural water content w_n varies between 8 and 38 %. The dry density of the encountered soils varies between 14 and 22.6 kN/m^3. The Liquid limit varies between 41 and 63 % and the plasticity index between 18 and 31 %. The shear strength parameters derived from unconsolidated undrained triaxial tests range from 5° to 18° for the friction angle and from 29

Fig. 191.2 Landslide causing disorders to the stadium and surrounding wall

Fig. 191.3 Titling and moving retaining wall

to 182 kPa for the cohesion. A conventional limit pressure ranging from 500 to 4,000 kPa characterizes the soils.

The seismic refraction tests show four layers characterizing by different shear velocity. A surface layer has an average thickness ranging from 0.7 to 2.2 m. The second layer has a thickness between 3.4 and 8.1 m. The third layer has a thickness between 4.8 and 6.8 m. The fourth layer is encountered in average at 10 m from ground surface. These four layers are characterized by a shear wave velocity of 200, 410, 680 and 830 m/s respectively. The resistivity results are low ranging from 5.4 to 99.6 Ωm corresponding to highly conductive ground. The results show a layer about 3 to 8 m can be attributed to the sliding layer and resistivity measurements show a loose ground with water flow at depth.

For this purpose, two profiles, where the various factors of instability are present, were analyzed. In the first zone, the slope is already stabilized and has not changed since the first visit by the passive resistance of downstream buildings. Stability calculations are given for the critical slip circle a safety factor F = 1.295 found in the layer of colluviums and can reach 7.0 m deep. Although the safety factor is >1.2, the risk of instability cannot be ruled out. The slope created by the gabion wall was not taken into account in the calculations. The deformation of the wall reflects this instability. The second area includes the important disorders at the stadium. Stability calculations give a safety factor <1.2, the critical circle has a coefficient of 0.77.

The different results obtained by observations, insitu investigations and water level monitoring show that at the gymnasium and playground whose floors collapsed, the observed instability is due to the discharge of upstream surface water and downstream earthworks made to launch a project of collective housing. The landslide started at the gabion retaining wall can be explained by two factors: the design in the wall, the overload slope has not been considered and the hydraulic system has been modified; the

infiltration of runoff through the gabions changed the mechanical properties under the wall and caused a flow of the foundation layer. Hydraulic parameter (runoff and groundwater) was the trigger. Anarchic earthworks, undersized gabion retaining wall and fragile layers of saturated colluviums also contributed to the destabilization of the slope.

191.3 Case Historie of Boulimat Landslide

The exceptional rains of winter 2012 triggered a series of landslides in the Kabylia region, among which the landslide occurred at PK 226 + 300 of the National Road RN 24, is one of the most spectacular (Fig. 191.4). The RN24 traverses the mountainous areas on the lower side. The landslide occurred just of 100 m coastline of the Mediterranean Sea on 17th April 2012 and caused the collapse of a section of the road of about 120 m, with a main scarp about 6–8 m (Fig. 191.4). After 18 h, the landslide mass and the road moved 10 m in the south-north direction. In this section, the road is clamped between the Mediterranean Sea and the mountain with very steep dip (Fig. 191.4). All drainage systems were damaged. The road is closed to traffic between Bejaia and Tizi-Ouzou cities for more ten days, disrupting road communication which is lifeline to the two states and many villages of Kabylia. The disruption experienced by local traffic was substantial. However, the real impacts of the events were economic and social. According to early preliminary investigation carried out on site, the perimeter of the landslide impact area is in order of 2.20 ha. The volume of material movement is estimated to 450,000 m^3. The potential slide surface is deep, located about 15–20 m in depth, which is the interface between the saturated colluviums and the weathered schistose marl. It is mainly caused by the circulation of groundwater drained by the catchments

Fig. 191.4 Assoumeth RN24 landslide, PK 226 + 300

area and the effect of marine transgression. The exceptional rainfall in the region of Béjaia during the month of April 2012 has amplified the phenomenon.

The records covering periods from 1923 to 2010 (ANRH 2011) show that the average rainfall along the cycles recorded is 831 mm. The last two decades are characterized by an average rainfall of 750 mm. The representation of rainfall is characterized by irregularities inter-seasonal and inter-annual. As a general, the relative distribution of 28.94 % from September to November, 39.96 % from December to February, 27.30 % from March to May and 3.8 % from June to August. Almost all rainfall is concentrated over a period ranging from November to March, not exceeding five (05) months: two-thirds (2/3) of the total rainfall is recorded during this period. In addition, according to the data, a peak rainfall was recorded in April with a maximum monthly rainfall of 278 mm, which justifies the initiation of the majority of landslides in the Kabylia region during the spring period. In April, the hillsides were in a saturated condition following a relatively wet spell during the preceding weeks.

According to the geological map of Bejaia, most of the formations encountered along the coastal road RN 24 are composed of flysch and old quaternary layers with dips varying from 30 to 60°. The affected section is formed of a syncline schistose marl of dip 42° S-N, it is topped with a thick layer of saturated colluviums, slipping at the interface with the marl under the effect of a steep slope, hydrostatic pressures and hydraulic gradients. This lithological facies widespread along the coastal region, it consists of a conglomerate of pebbles and blocks decimetric to metric dimensions, impregnated with a clay matrix which is very sensitive to the action of water. These layers of colluviums are very permeable and attract a

large volume of water infiltrating the lower slopes as resurgences or sources. In general, training colluviums overcome dips direction (North-South) of schistose marl and very hard and impermeable marly limestone. The interface between the scree slope and marl consists of greenish clay and plastic very sensitive to water; it loses the mechanical characteristics and becomes slippery.

Based on site investigations, the slip surface was encountered at the very soft layer, 13–15 m deep. The emergency measures were to restore immediately traffic between East and Center regions and maintain the connection with the outside for neighboring village people. The temporary reinforcement solution possible technically and economically within an acceptable time is the partial substitution of the slipped ground by an appropriate compacted granular material. Then, a geotechnical investigation was conducted. Based on this investigation results, stability calculations were conducted for two stages; the state at landslide triggering and the state with nailing reinforcement taking into account the residual soil parameters considered for the moved mass (colluviums) are c = 20 kPa, φ = 7 °, E = 10 MPa and ν = 0.35). The sliding mechanism are confirmed the observed on site. The results show the instability of the slope, the safety factor F is equal to 0.85. Large displacements, about 1.4 m, of the basin are noted. The results indicate clearly that the state remains unstable after sliding, hence, the importance of the proposed emergency works to stabilize the ground and the road. The classical methods give a safety factor F <1.0. A final design of rehabilitation works was proposed, it consists on the nailing reinforced concrete piles connected by a capping reinforced concrete beam and a proper drainage (Bahar et al. 2013; Cartier and Morbois 1986).

191.4   Conclusion

The two case histories of landslides Bordj Bonaama and Boulimat are triggered by combination of rainfall, unfavourable geological, hydrogeological and geotechnical conditions and human interventions. Hydraulic parameters, runoff and groundwater, were the trigger. Anarchic earthworks, undersized retaining wall and weak layers of saturated colluviums also contributed to the destabilization of the slope.

References

ANRH (2011) Données pluviométriques de la station de Tifra, Béjaia. ANRH, Algérie

Bahar R, Sadaoui O, Sadaoui S (2013) Case study of landslides in Kabylia region, Algeria. In: CDROM seventh international conference on case histories in geotechnical engineering. Chicago, USA

Cartier G, Morbois A (1986) Expérimentation d'un clouage de remblai construit sur un versant instable à Boussy- Saint- Antoine. Bulletin de liaison des Ponts et Chaussées, Paris, France, pp 29–36

Physical Impacts to the Environment of Infrastructure Development Projects – Engineering Geology Data for Environmental Management

Convener Dr. Francisco Nogueira de Jorge M.Sc., Sofia J.A. Macedo Campos

Infrastructure development projects are usually associated with the risk of causing environmental impacts of various types and magnitudes. Proper assessment of physical impacts to the environment in order to design adequate monitoring programmes and establish effective preventive and mitigation measures usually require comprehensive understanding of geological features and dynamics of physical processes. Engineering geology may provide the necessary background concepts, technical resources, and appropriate methods and tools to evaluate, address and manage physical impacts to the environment.

The purpose of this session is to address and discuss the role of engineering geology in the current practices of both environmental management and environmental performance evaluation for the development of new projects as well as during projects' lifetime—design, construction, operation, decommissioning and site rehabilitation.

Galperin Anatoly

Abstract

Essential negative impacts of man-made mining massives on the environment and the directions toward their ecology safe utilization has been demonstrated, considering the characteristics of mining regions in Russia and Germany. Based on an engineering-geological, hydro-geo-mechanical and geologic-geomechanical scientific observation over a long term period, a complex approach to the ecologically safe utilization of man-made massives has been developed. Applying conventional interactive monitoring methods, the presented scientific results respond to diverse questions regarding the development of assessment methods for the state in massives emerged from hydraulic fill or dumping, the hydromechanical excavation of tailing dams and hydraulic dumps in deposits with high water content, the removal of hydraulic dumps during the preparation of coal deposits to mining with hydromechanical technologies and the use of residual pits of former open-cast mines for the hydromechanical deposition of mine spoils or for the development of recreation areas.

Keywords

Man-made massives • Tailings dam • Bearing capacity • Stability • Monitoring

192.1 Introduction

Great territories of mining-industrial regions in the Russian Federation, namely with fertile soils, are covered with dumps and hydraulic dumps, storages with the useful materials' wastes. These mining-engineering constructions occupy large areas. They are composed by sediments with the low strength and bearing capacity. As a result it entails development of dangerous geological processes and following-up environmental contamination.

As a result of deposits exploitation and the accompanying redistribution of useful materials there are formed techno-genic massives-man-made in natural landscape geological bodies from the fragments of rocks, tailings, ashes, slag, slime etc. Areas of land allotments of the biggest mining enterprises are measured by 1,000 ha of disposing and destroying lands. Deposits exploitation is linking with the lost of valuable components in subsoil during the non-complex processing of extracting mineral materials.

In dumps of Russian mining enterprises great volumes of overburden operations measuring by tens of milliard cubic meters are located. Only in hydraulic dumps and tailing dams nearly 5 milliard m^3 of tailings and more than 1.5 milliard m^3 of overburden operations are located. These constructions are objects of high ecological danger causing contamination of air, underground and surface waters, soils, changing of biocenose on large territories. Carrying out a complex of engineering-geological, hydro-geo-mechanical and geological-geochemical researches of man-made massives is necessary for supporting measures to provide their stability, saving water and soil resources, refilling of mineral base of mining enterprises.

G. Anatoly (✉)
Moscow State Mining University, Moscow, Russia
e-mail: galperin_a@mail.ru

Professors Mironenko and Shestakov (1974) created scientific direction –hydrogeomechanics within the scope of which taking equal methodological positions it is created "joint and mutual consideration of soil mechanics and filtration of underground waters conformity…with regard to the tasks of hydrogeology and engineering geology in frame of one and the same scientific discipline".

To estimate stability of watered slopes Mironenko suggested principle of bringing large hydrodynamic forces to equivalent contour ones due to powerful effect of underground waters is taken into account very simply-through the meaning of piezometric head on contour of sliding block. This effective estimated way is widely used to estimate stability of slope constructions of hydraulic dumps and tailing dams.

192.2 Main Text

The objects of hydro-geomechanical studies of the Geology Department of MSMU (Moscow State Mining University) were embankment dumps of mixed rocks on weak water-saturated foundations (KMA (Kursk Magnetic Anomaly), Kuzbass (Kuznezk Coal basin) etc.) which were subjected by the depression consolidation as a result of deep water lowering, overlying beds of KMA deposits and Zaporozhsky

ore-iron, filling structures of hydraulic dumps and tailing dams in different mining industrial regions (Fig. 192.1) (Galperin 2003; Galperin et.al. 1993a).

New methods of man-made massives' monitoring and means of their realization have been introduced (Galperin et.al. 2012).

Method of complex sounding by means of devices MSMU-DIGES (Fig. 192.2), penetration-logging station VSEGINGEO and type-set of the original probes (Galperin et al. 1994).

Method of remote control condition of hardly accessible filling structures using aerophotogrammetry survey to define settlement of filling structures and its bearing capacity (Galperin et al. 1993b):

- Method of interactive remote control of the slope dumps of filling structures' stability and dumping embankment on the weak foundations according to the relevant hydro-geomechanical criteria of safety by means of mobile communication standard GSM;
- Technical means to measure deformation of slopes of dry rocks dumps on the weak foundations providing setting of critical deformation's measures with the aim to control the process of dump formation.

Engineering-geological zoning allows to compare sites of filling structures and define appearance and limits of their future using. Zoning provides singling out of uniformed in

Fig. 192.1 Space photo of the objects of the Staro-Oskolysky iron-ore distrikt: *1*-open Pit LGOK; *2*-open Pit SGOK; *3*, *4*-overburden dumps LGOK; *5*-overburden dumps SGOK; *6*-reclaiming hydraulic dump "Berezovy Log"(LGOK); *7*-tailings dam LGOK; *8*-active hydraulic dump LGOK; *9*-tailings dam SGOK; GK1–4-profiles of hydro-geomechanical monitoring

Fig. 192.2 Composite string probes **a** two-parametric (q_s, P_w); **b** two-parametric (τ, P_w); **c** three-parametric (τ, q_s, P_w)

engineering-geological respect taxonomic units of the definite level in limits of the investigating territories.

Materials of the engineering-geological zoning of the filling territories have to provide the decision of the following main tasks:

- Capacity's increasing of the operating constructions on the base of forcing the consolidation of finely-dispersed rocks;
- preparing of filling territories for their following using (reclamation, placement of dry dumps, construction).

For the effective using of hydraulic dumps' territories it is necessary to possess reliable information concerning the state of man-made massif and foresee the behavior of filling foundations in time. In particular, using the hydraulic dumps territories for the dry dumps or reclamation the bearing capacity of filling masses and changing it in time is of great importance.

In the biggest Russian mining-industrial regions KMA and Kuzbass there were made complex investigations of the man-made massives (dumps and filling structures) including natural and laboratory experiments with the using of above mentioned methods of monitoring and defining the mechanical properties of man-made deposits in devices of triaxial compression. The examples of results of engineering-geological zoning of filling territories hydraulic dumps KMA for two biggest open-pits on the base of iron-ore

deposits KMA are given on the Fig. 192.3a–c. On the base of these materials there were elaborated recommendations concerning the filling of two levels dumping filling at this hydraulic dump because of lack of dumping areas. At the Fig. 192.3b, c data of zoning of two territories of hydraulic dumps on bearing capacity are given (P_{dop}).

Interactive monitoring of hydraulic dumps and tailing dams allows efficiently to correct constructions and conditions of buildings and estimate possibilities of their future growing. The principal scheme to monitor constructions of industrial hydraulic structures with the using sensors of porous pressure, devices to collect and save monitoring characteristics and their transmission through mobile communication are given at Fig. 192.4.

Nowadays monitoring and operation devices of the objects through the mobile communication standard GSM in several regimes (GPRS, SMS ets.) are widely spread. Device for the remote monitoring of the filling dams where vibrating wire transducers of water pressure ("Gidroproekt", Moscow) was created in VNIMI (Russian Scientific Research Surveying Institute) and a company "Karbon" (St. Petersbourg) (Kutepov et al. 2009). Monitoring of porous pressure in hydraulic engineering constructions is provided by recommendations of ICOLD (International Commission on Large Dams 1996).

Fig. 192.3 Engineering-geological zoning. **a** A map of engineering-geological zoning of hydraulic dumps "Berezovy Log" (KMA): 1,2,3,4,5,6-engineering-geological sites; 7-slope constructions of hydraulic dumps; 8-izolines offilling structures' thicknese; 9-lines of engineering-geological sections according to the axis 1,3 and 2 drainage dividing prisms. **b** A map of zoning of the hydraulic dump "Berezovy Log" territory on the bearing capacity (Pdop). **c** A map of zoning of the hydraulic dump "Log Shamarovsky" (MGOK) on bearing capacity of the filling massif: 1-borders of the engineering-geological zones; 2-borders of sites with the different bearing capacity of filling soils; 3-reclaiming sites of hydraulic dump; 4-sites of hydraulic dump with $P_{dop} > 0.15$ MPa; 5-sites of hydraulic dump with $P_{dop} = 0.1$–0.15 MPa; 6-sites of hydraulic dump with $P_{dop} = 0.05$–0.1 MPa; 7-sites of hydraulic dump with $P_{dop} < 0.05$ MPa; 8-water surface.

(a)

(b)

Название откоса: Damba Stoil GOK

γ=1.855, φ=27, c=0.1   γ=2.03, φ=24, c=0.2   γ=1.754, φ=10, c=1.1   γ=1.826, φ=9, c=1.3   γ=1.9, φ=20, c=2.5

γ=1.9, φ=31, c=0.1   γ=1.827, φ=26, c=0.1   γ=1.965, φ=29, c=0.05   γ=1.762, φ=28, c=0.1   γ=1.9, φ=31, c=0.1

Устойчивость по методу алгебраического суммирования:
η = 1,40078
Устойчивость по методу многоугольника сил:
η = 1,42460

Левый край: 44
Правый край: 499,5
Высота откоса: 47,5
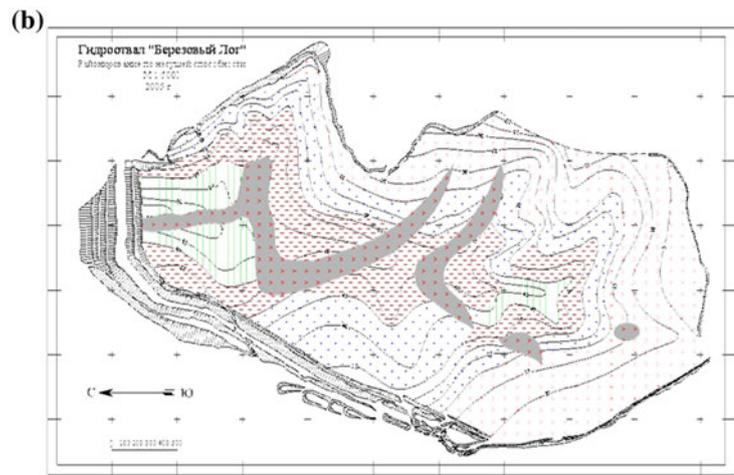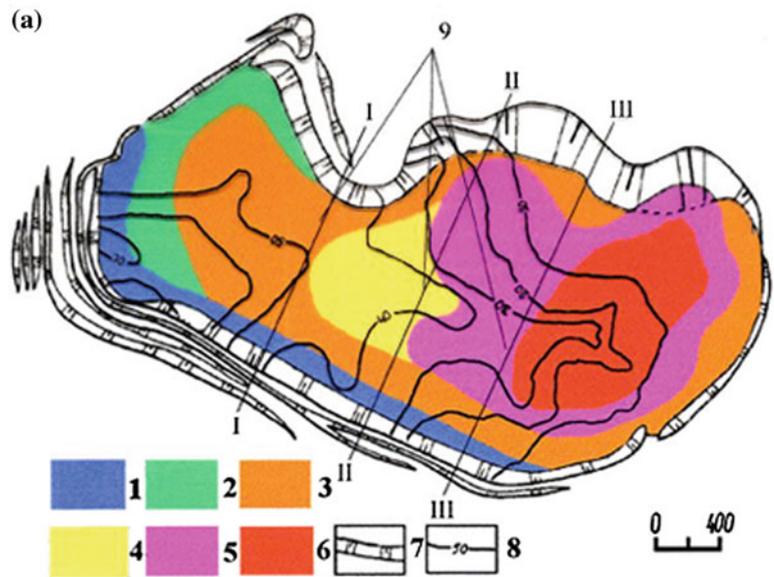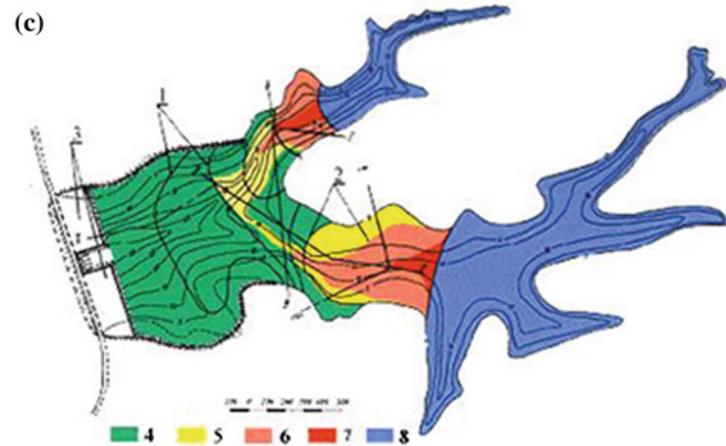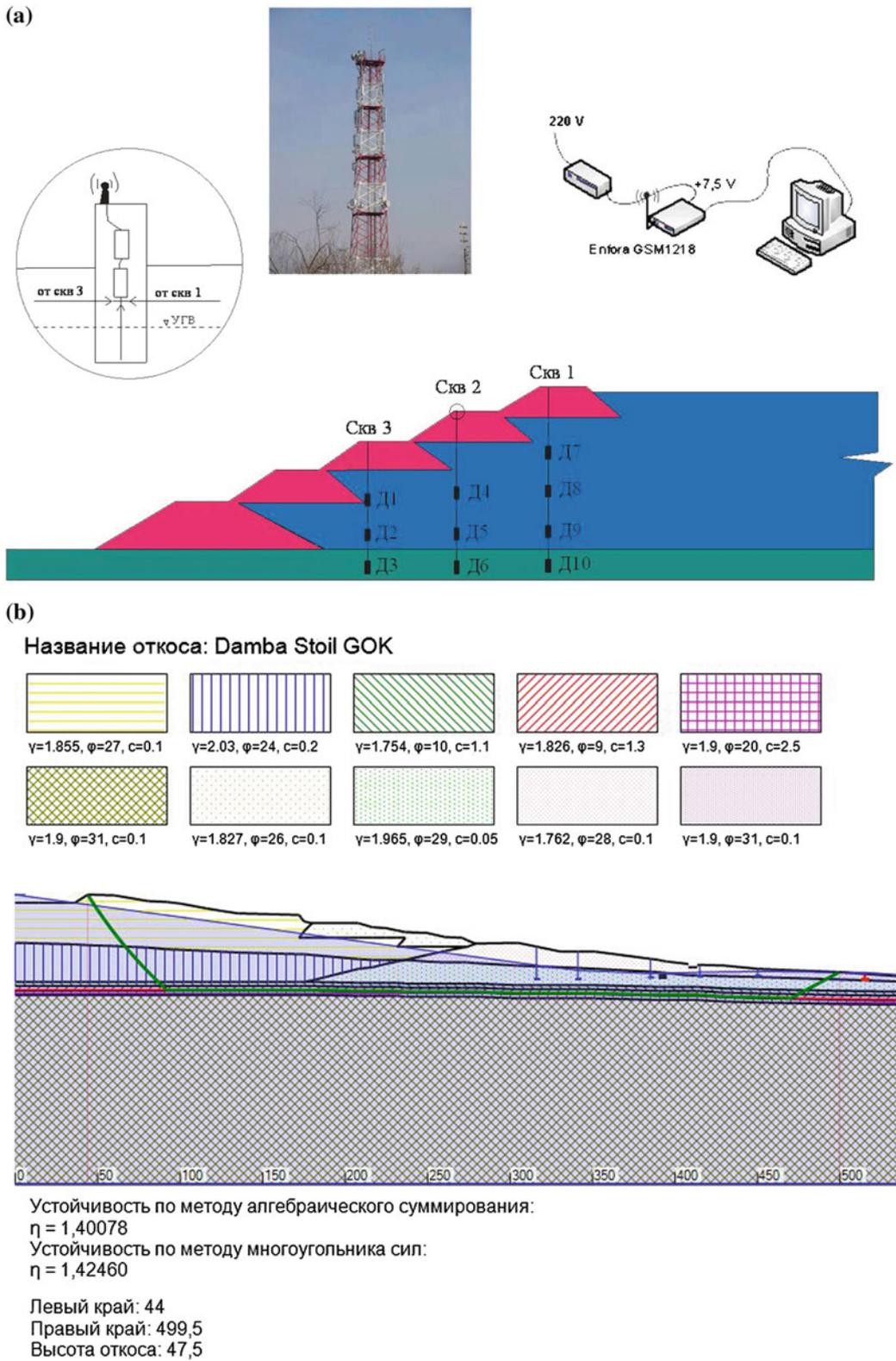
Fig. 192.4 Organization scheme of system of the remote control: **a** data collection, storage and transmission; **b** processing of the receiving information for conditions of the tailing dams SGOK

192.3   Conclusion

Introduction of work's results in the regions Kuzbass and KMA provided operative monitoring of dams' stability and bearing capacity of weak foundations, location on the filling foundations higher than 0.5 milliard m^3 of the "dry" overburden, prevention of fertile soil destroying higher than 5,000 ha, reducing to decades dumps' reclamation time.

References

Galperin AM (2003) Geomechanic in surface mining. MSMU

Galperin AM, Zaytsev VS, Norvatov YA (1993a) Hydrogeology and engineering geology. Balkema publ., Rotterdam, Brookfield

Galperin AM, Zaytsev VS, Streltsov VI et al (1993b) Method of monitoring the condition of filling structures. Patent RF no 1188322

Galperin AM, Zaytsev VS, Kirichenko YV et al (1994) Device for the complex sounding of soils. Patent RF no 2025559

Galperin AM, Kutepov YI, Kirichenko YV et al (2012) Using of man-made massives at mining enterprises. In: Mining book

Kutepov YI, Kutepova NA, Milman GL (2009) Methods and technical means of hydrogeomechanical monitoring of industrial hydro-technical structures safety//Engineering Researches, vol 5

Mironenko VA, Shestakov VM (1974) Basics of Hydrogeomechanics. Nedra

Mironenko VA, Strelsky FP (1989) Practical use of hydrogeomechanics principles with the aim to increase industrial and ecological safety of mining works//Engineering geology, vol 5

Monitoring of tailings dams, ICOLD, Bulletin 104 (1996)

Stefan Klebingat, Rafig Azzam, Marc Schulten, Thomas Kempka, Ralph
Schlüter, and Tomás M. Fernández-Steeger

Abstract

The process of Underground Coal Gasification (UCG) bears the potential to produce medium to high calorific syngas for several industrial applications, e.g. electricity generation in the frame of the Integrated Gasification Combined Cycle (IGCC) concept; or Coal-To-Liquid (CTL) technologies as the Fischer-Tropsch synthesis. In view of preferred environmentally sound operations and stable gas qualities for these applications previous global UCG research led to considerable process experience. Despite this knowledge background however UCG still remains a challenging technology as many physical and chemical sub processes are not sufficiently traceable by aboveground instrumentation, in turn hampering enhancement of overall process efficiency and engineering performance. In this context equilibrium modeling becomes a useful strategy to gain a better process understanding of coal gasification at different depths and its related engineering geological boundary conditions (i.e. coal type, p/T conditions and overburden water influx). The recent CO2SINUS project thus investigated sensitivities of various boundary conditions on establishing optimized gas qualities at simultaneous minimum tar production rates during active operation by using a new self-developed thermodynamic model. The main potential of this model approach is seen in the pre-assessment of individual field boundary condition effects, amongst other criteria indicating coal type related gas qualities as well as tar related long-term groundwater pollution risks.

Keywords

UCG • CO2SINUS • Field boundary conditions • Gas qualities • Tar production

S. Klebingat (✉) · R. Azzam · T.M. Fernández-Steeger
Department of Engineering Geology and Hydrogeology, RWTH
Aachen University, Lochnerstr. 4-20, 52064 Aachen, Germany
e-mail: klebingat@lih.rwth-aachen.de

M. Schulten
Unit of Technologies of Fuels (TEER), RWTH Aachen
University, Wüllnerstr. 2, 52062 Aachen, Germany

T. Kempka
Section 5.3 Hydrogeology, Helmholtz Centre Potsdam, GFZ
German Research Centre for Geosciences, Telegrafenberg, 14473
Potsdam, Germany

R. Schlüter
DMT GmbH & Co. KG, Am Technologiepark 1, 45307 Essen,
Germany

193.1 UCG Model Development Within the CO_2SINUS Project

In view of optimized UCG gas qualities the CO2SINUS project analyzed the influence of selected field boundary conditions on gas quality and related tar pollutant production by using a new self-developed steady state equilibrium thermodynamic model approach (cf. Fig. 193.1), based on the principal chemical processes within a fixed bed reactor (cf. Fig. 193.2). This fixed bed engineering approach was chosen as a first starting point to the extent of former reviewed UCG process conditions by Min and Edgar (1987).

Within this thermodynamic model (cf. Fig. 193.1) selected Aspen Plus® software modules (e.g. material streams, mixer- splitter-, reactor- and valve types) represent

Fig. 193.2 Main UCG chemical processes and related tar behaviour during fixed bed gasification (Klebingat et al. 2013)

the main gas- and tar altering processes of pyrolysis, reduction/partial oxidation and gas mixing to syngas, besides important other UCG boundary conditions (e.g. gasification agent flux/composition, pyrolysis temperature, overburden water influx). A separate model flowsheet governs the hierarchical order of the single unit operations. Gas qualities and related tar pollutant yields for the abovementioned main processes are calculated according to the main principle of Gibbs free energy minimization by solving the Peng-Robinson Equation of State (Peng and Robinson 1976), as well as an Aspen Plus® internal Lower Heating Value (LHV) subroutine.

193.2 Model Data and Selected Sensitivity Studies According to Field Boundary Conditions

The thermodynamic model used within the CO2SINUS project referred to technical data reports from sub-bituminous and bituminous coals of the former US-UCG trial sites

at Hanna, Centralia and Pricetown (amongst others Campbell et al. 1974; Bartke and Gunn 1983; Hill et al. 1983, 1984; Moskowtschuk 1997). Each of these coals has been tested with regard to quantitative gas quality and tar-load altering effects for the main gas types of UCG (Pyrolysis gas, Reduction/partial Oxidation gas and mixed syngas fractions). In this context the following field boundary conditions were investigated:

- Pressure
- Temperature
- Water influx
- Gasification agent flux/composition

193.3 Selected Preliminary Results

In view of the examined status of results to date, water influx appears to be one of the most sensitive parameters with regard to gas quality and tar pollutant production changes. Figures 193.3, 193.4 and 193.5 give an example of the Centralia trial's simulation gas quality and tar production trends within the different main UCG gas zones. In this context increased water influx rates lead to desired decreasing tar yields for most gas fractions—the main tar associated pyrolysis gas fraction as well as the wet syngas fraction, respectively. Simultaneously however a drop in gas qualities can also be observed. In agreement with literature our model results thus indicate that increased water influxes cause lower gas temperatures, which in turn generate lower gas heating values. Due to these results water influx remains a difficult field boundary parameter to judge in terms of best practices: in tendency lower water influx rates—favouring the existence of higher temperature fields—will be positive with regard to gas qualities, i.e. higher economic benefit. At the same time this will be at the cost of higher tar production rates.

Fig. 193.3 Centralia trial simulation: total tar gas mole fractions and lower gas heating values (LHV) as a function of water influx: Pyrolysis gas
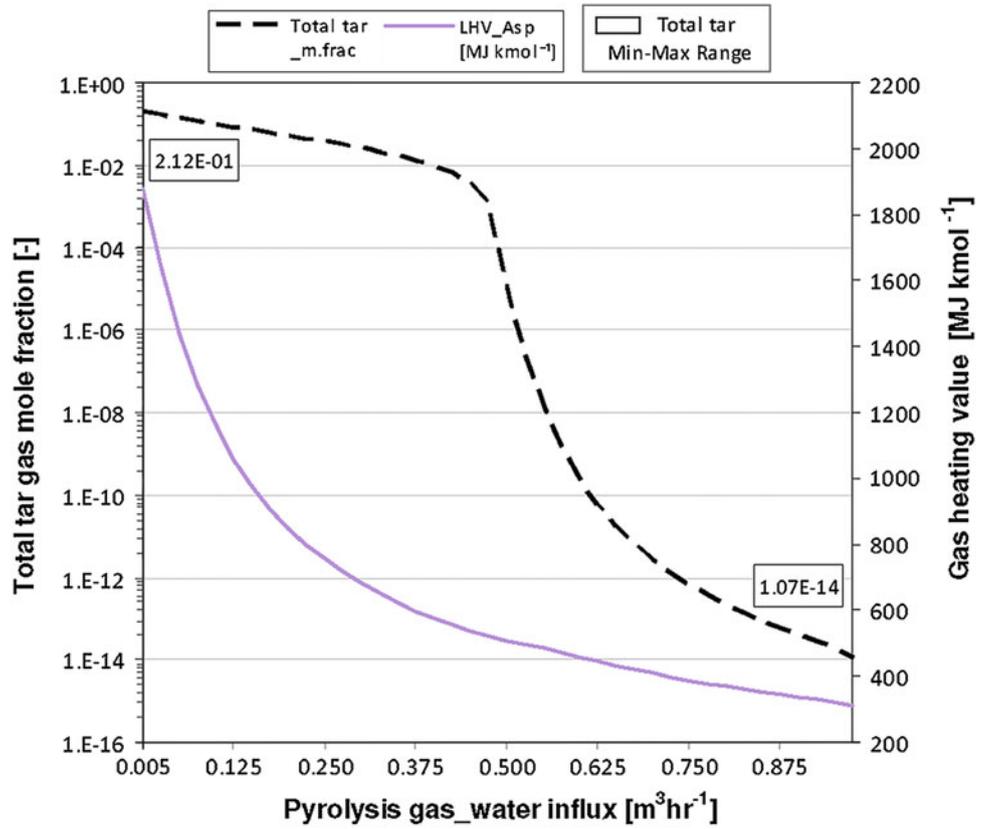
Fig. 193.4 Centralia trial simulation: total tar gas mole fractions and lower gas heating values (LHV) as a function of water influx: Reduction/partial Oxidation gas
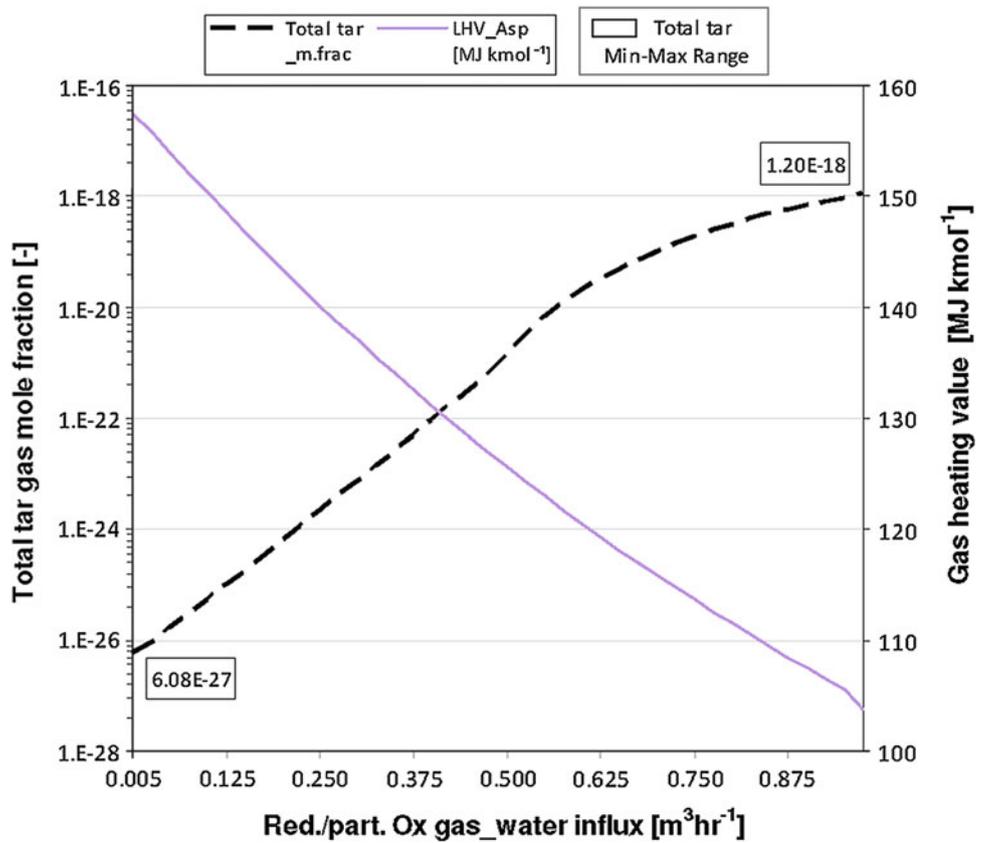
Fig. 193.5 Centralia trial simulation: total tar gas mole fractions and lower gas heating values (LHV) as a function of water influx: Mixed wet syngas
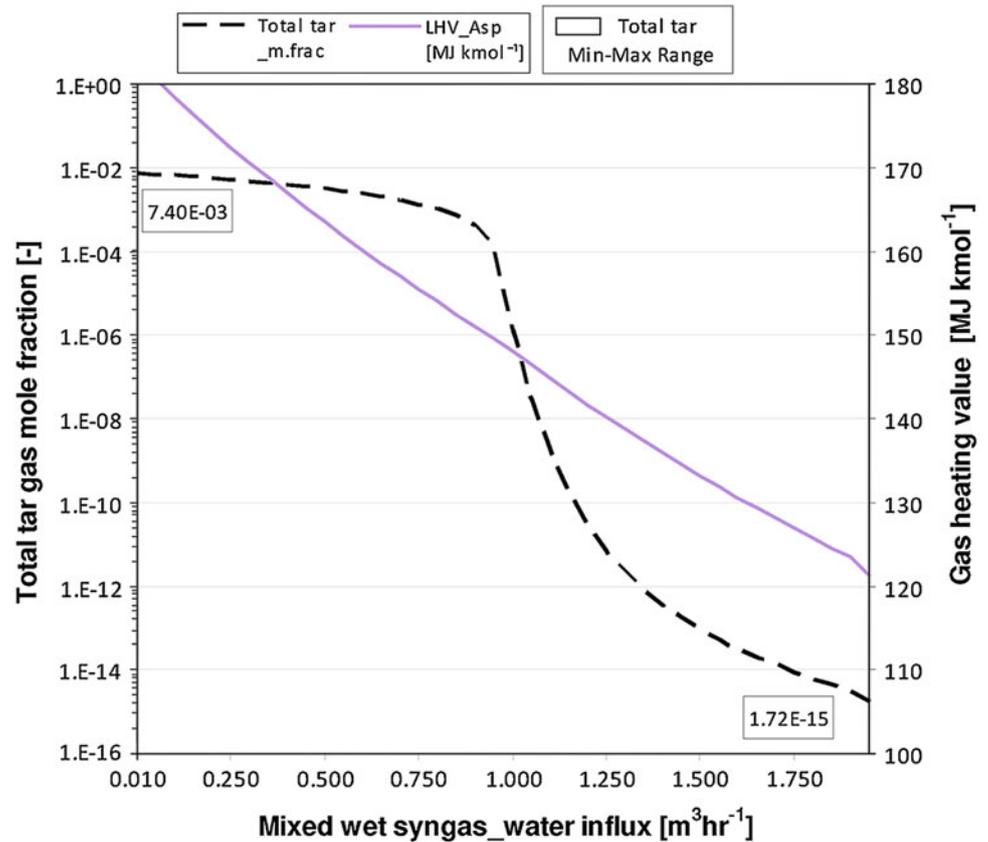
References

Bartke TC, Gunn RD (1983) The Hanna Wyoming underground coal gasification field test series. In: Krantz WB, Gunn RD (eds) Underground coal gasification—the state of the art. AIChE Symposium Series, vol 79(226), pp 4–14

Campbell GG, Brandenburg CF, Boyd RM (1974) Preliminary evaluation of underground coal gasification at Hanna. Technical progress report 82, edited by UW digital projects. Digitized collection western research institute: Laramie Wyoming, USA

Hill RW, Thorsness CB, Thompson DS (1983) The centralia partial-seam CRIP test. In: Proceedings of the 9th annual underground coal gasification symposium: Bloomingdale/Illinois, USA, (DOE/METC-84-7 CONF-830827), pp 10–22

Hill RW, Thorsness CB, Cena RJ, Stephens DR (1984) Results of the centralia underground coal gasification field test. In: Proceedings of the 10th annual underground coal gasification symposium: Williamsburg, VA, USA, (DOE/METC-85/5), pp 11–26

Klebingat S, Azzam R, Schulten M, Quicker P, Kempka T, Schlüter R, Fernandez-Steeger T (2013) Quantitative tar pollutant production and water solubility prognoses in the frame of Underground Coal Gasification (UCG) In: Thuro K (ed) Proceedings of the 19th conference on engineering geology and of the forum for young engineering geologists Munich, München, Techn. Univ., pp 589–594, 13–15th Mar 2013

Min W, Edgar TF (1987) The dynamic behaviour of a fixed-bed steam-oxygen coal gasifier disturbed by water influx II—model development and verification. Chem Eng Commun 52(4–6):195–213

Moskowtchuk W (1997) Mechanismen der In situ Vergasung unter Einbeziehen ukrainischer Kohlen. Labor- und Feldversuche. Dissertation. RWTH Aachen University: 164 S

Peng D, Robinson DB (1976) A new two-constant equation of state. Ind Eng Chem Fund 15(1):59–64

Considerations About the Integration of Geological and Geotechnical Studies Applied to Engineering Projects and to Environmental Impact Assessment in São Paulo State, Brazil

Bitar Omar Yazbek, Sofia Julia A.M. Campos, Amarilis Lucia C.F. Gallardo, Braga Tania de Oliveira, and Caio Pompeu Cavalhieri

Abstract

This paper brings to discussion the quality of the integration of geological and geotechnical studies that is achieved for the purpose of engineering projects and for environmental impact assessment. The integration of these studies in different phases of a development is analyzed, in order to aid, both at the same time and importance, the building of suitable constructions under the engineering and environmental sustainability points of view. We expect to contribute to a better understanding of the form and the current stage of this integration, especially in relation to the effective improvement from the geological and geotechnical knowledge acquired in both application fronts. Observations accomplished in infrastructure constructions were taken as reference, featuring roads, railways, pipelines, mines, development lands and landfills, accomplished in the last years in the state of São Paulo, Brazil, and submitted to the Environmental Impact Assessment (EIA) process, a tool that has helped enhance the integration of geological and geotechnical studies generated in both fronts. The results show that signs of integration exist but there still is a certain separation. Some technological and management challenges have been shown in a way to better improve the integration of the geological and geotechnical knowledge in new developments.

Keywords

Geological and geotechnical knowledge • Environmental impact assessment • Infrastructure constructions

194.1 Introduction

Studies involving geological and geotechnical knowledge are usually distinguished based on two application fronts: one aims at certifying the technical viability of engineering projects and at subsidizing construction and operation; and the other, a way of dealing with the environmental impacts and demonstrating the environmental viability.

In relation to engineering projects (which include a conceptual project, basic project and executive project), the required geological and geotechnical studies are linked to the challenge of predicting the interaction construction-physical environment behavior in order to ensure the execution of a safe, operational and technically suitable construction. Under the environmental viability point of view, and also trying to predict the interaction construction-physical

B.O. Yazbek · S.J.A.M. Campos (✉) · A.L.C.F. Gallardo · B.T. de Oliveira · C.P. Cavalhieri
Institute for Technological Research of São Paulo State, Sao Paulo, SP, Brazil
e-mail: scampos@ipt.br; labgeo@ipt.br

B.O. Yazbek
e-mail: omar@ipt.br

A.L.C.F. Gallardo
e-mail: amarilisgallardo@usp.br

A.L.C.F. Gallardo
Uninove, EPUSP, Sao Paulo, SP, Brazil

environment, the highest concern is to evaluate the adverse future consequences in relation to the environment.

Therefore, although there are different focuses, approaches and tools, the geological and geotechnical studies required in both application fronts include essentially the same object of analyses (the interaction construction-physical environment), a fact that highlights the importance of the integration accomplished in both fronts. Among the aspects that could be analyzed in relation to these studies, the technical cooperation between the involved teams in their preparation in each front and the effective integration of the geological and geotechnical knowledge developed in both applications are discussed. This is not only in favor of having a larger team and rationalization of resources, but also in the way of offering a refined and major comprehension about the construction-physical environment interaction.

194.2   Objectives, Materials and Methods

This paper aims at analyzing the relation established between geological and geotechnical studies elaborated for an engineering project and for environmental impact assessment and management, starting with the environmental impact assessment (EIA) concerning the same projects.

In order to reach the expected objectives, a bibliographic review was carried out about the issue. Studies performed for same project that approach geological and geotechnical knowledge in both application fronts were considered, as well as observations about the accomplished studies for engineering projects, and environmental studies related to cases in which the authors of the current work had some interaction, either supporting the environmental entity or the developer, in different stages of the development. Infrastructure construction cases were submitted to EIA procedures and the environmental license in the state of São Paulo (southeastern Brazil).

Only observations on large development cases and from different sectors were taken as reference, as well as the relatively recent ones back to the last 10 years, reaching a number of 41 developments (17 roads, 1 railway, 1 conveyor, 1 pipeline, 6 mines, 1 estuarine drainage channel, 4 development lands and 10 landfills).

In order to do the analyses on the basis of observations during each development and also by reviewing data and information, the AIA/EIR was considered in each case and the Basic Environmental Plan (BEP), as well as the denominated Construction Environmental Plan (CEP), the latter formalized only in some developments. Regarding the engineering projects, differences according to each case and casual checking of the conceptual project, basic project and

executive project are pointed out in relation to specific features available.

We expect to identify elements that characterize the integration of the geological and geotechnical studies performed in both application fronts. One characteristic to be investigated is the context in which the integration occurs; in other words, the different stages of the development. Another characteristic is the various moments throughout the duration of a development in which the integration of the knowledge obtained in both application fronts tends to happen. Thus, it is essential to verify the relationship between the frequent stages in the preparation and execution of engineering projects and in EIA. A third characteristic is about the way which the cooperation and/or contribution between the technical teams occur, as well as a possible integration between the geological and geotechnical studies applied in both fronts.

Considering these characteristics, the level of integration reached between the geological and geotechnical studies for engineering projects and for environmental impact assessment and management were analyzed for each case. To have the result and the level, individual analyses were done, ranking the developments according to three levels (low, medium and high). The results were compiled in a chart, beginning with the predominant analyses. After making the observations for each case, the results are discussed and a summary of the most important conclusions is presented, expecting to cooperate to a first reflection about the theme.

194.3   Overview on the Integration of Geological and Geotechnical Studies

Although geological and geotechnical studies are found in the national and international literature, the integration of such studies in both application fronts is a topic that is hardly ever considered, especially when it comes to the analysis of the same development undergoing an EIA process.

Some works deal with the theme, which can be distinguished by physical environmental characteristics in engineering projects and in the environmental studies. Both are usually treated separately, the characteristics referring to geological and geotechnical studies performed on both fronts. Anderson (2006) states that many of the products that come from detailed geological and integrated mappings have been used as primary database to the future environmental planning of the North American state of North Dakota. Many unfavorable geological conditions are found, as clay deformation in soils of lacustrine origin, inappropriate supportability and presence of mass movements, which are among the most important causes of geological, geotechnical

and environmental problems. There is also the difficulty in defining the railroad grade and the fact of recent and repeated seasonal floods in urban areas. The importance of the relationship between environmental geology and the geological processes in the physical environmental understanding, as well as the influence of geology in the engineering processes, especially regarding infrastructure constructions, are scenarios that must be taken into account together (Bell 2008). The author examines the probability of geological risk aspects, the importance of water and soil resources, environmental impact from mining, waste disposal and pollution in the environment, as well as many other aspects that result in environmental problems.

Concerning the integrating methods used, it is believed that the complex project elaboration implies the participation of several specialists, with different degrees and viewpoints. Therefore, the relationship among these specialists may become problematic in practice. Aiming at contributing to the effectiveness in the conception of large projects, Grebici (2007) developed a model that integrates different methods of cooperation, of organizing the process and of conception of other intermediate products and their adequacy to the development purposes, stressing out the importance of developing proper methods of cooperation. Indeed, many negative environmental impacts may be prevented or at least have its magnitude dramatically reduced by having effective cooperation between designers and environmental teams (Sánchez 2006). Sánchez and Hacking (2002) also emphasize the importance of linking the EIA to the Environmental Management System (EMS) of a development, using the studies conducted in order to elaborate the EIA/EIR for the construction management, operation and deactivation of developments, which in practice does not happen.

194.4   The Necessary Integration

The geological and geotechnical knowledge acquired or generated in engineering projects is also relevant in order to assess and manage environmental impacts and vice versa. However, it is possible to notice that physical field studies conducted in both application fronts are developed separately, commonly with distinct professionals and technical teams.

The demands associated with requirements that are specific to each context, such as the object and the scale of the generated cartographic products, contribute to such separation. While engineering project studies tend to focus on the knowledge of the underground physical environment and on scale detail, environmental geological and geotechnical studies aim at the whole understanding of the geodynamic surface, where possible negative consequences of a certain development tend to be highlighted by an environmental viewpoint. It is worth mentioning that it is regarded just as an aspect that is commonly observed rather than a rule. There are some studies that reveal exactly the opposite, as a result of specific demands. The scale is presented as a differential in some cases only. Also there are some situations where the impact is distinguished in details, as it happens in the cases of interferences in the groundwater related to mining, landfills and allotments. The situation where the connection between the studies conducted in both application fronts is noticeable refers to cases involving underground projects such as road or rail tunnels, in which the knowledge developed in each one is often useful to the other one. It is understood that the subsurface knowledge is as important as the surface one in projects with relevant interventions either on the ground or in the groundwater.

Table 194.1 Relative degree of integration of geological and geotechnical studies conducted for the purpose of engineering projects and assessment and management of environmental impacts, as overall prevalence observed in relation to all cases, according to the project phases proposed in IBAMA (2009)

Studies aimed at engineering projects		Studies aimed at assessment and management of environmental impacts			
		Environmental planning tools		Environmental management tools	
Project level	Engineering studies and projects	AIA/ EIR	BEP construction	CEP or EEP	EMP, EMS or BEP construction
Viability or pre-project	Conceptual project and feasibility studies	H	M	NA	NA
Project development	Basic project	M	M	L	L
	Executive project	L	L	M	L
Installing, building nd/or assembling	Executive project updated	L	L	M	L
Operating	Functional plan or operational project	L	NA	NA	M

Note EIS/EIR—Environmental Impact Study/Environmental Impact Report; BEP—Basic Environmental Plan; CEP—Construction Environmental Plan; EEP—Environmental Executive Project; EMP—Environmental Management Plan; EMS—Environmental Management System. L—Low; M—Medium H-High; NA—Not Applied

Table 194.1 was obtained using the cases discussed and the analysis of each one of them concerning one of the three ranking levels (High, Medium and Low), related to the integration of geological and geotechnical studies conducted with engineering projects, and assessment and environmental management purposes.

194.5 Conclusions

The results obtained with the completion of this study suggest the following conclusions: (**a**) although with different approaches and tools, both geological and geotechnical engineering projects as environmental studies include essentially the same object of analysis. This suggests the importance of the integration between geological and geotechnical studies carried out in both fronts of application; (**b**) geological and geotechnical studies conducted for the purpose of an engineering project, also when used in EIA, tend to facilitate the identification of significant environmental aspects and impacts. Likewise, geological and geotechnical knowledge acquired or generated during the EIA process, including environmental management to be carried out in phases of installation and operation of projects, has also been proven as useful to engineering projects. However, in view of the potential for integration, it is observed that much can proceed. There are signs of cooperation between the technical teams as well as integration between studies applied to engineering projects and the assessment and management of environmental impacts, but a certain separation still predominates, which is a possible situation influenced by the specific demands required in isolation by developers in each front; (**c**) the integration provided by the temporal and content matching in the achievement of engineering and geoenvironmental studies required for a project, due to the linking of EIA to environmental licensing, has been observed, but it is still well below the potential level. The fact that some new developments in the degree of integration shown indicate relatively higher situations can be better obtained with a larger number of cases; (**d**) both geological and geotechnical knowledge acquired during the feasibility stage and development of a large-scale engineering construction often fail to be fully used during the phases of installation and operation of such projects, a fact highlighted by the frequency degree of integration considered low and average these stages, which undermines the effectiveness of systematic planning of works and environmental impact assessment.

Finally, not only a greater synchronization among the activities of each context is required, but also actions and attitudes that facilitate the proximity of technological contents. It often seems that it depends more on the perception of professionals who lead the engineering projects, in order to foster the effective integration with environmental teams. The current challenge is to encourage cooperation of different perspectives on the same object and increase the exchange of knowledge acquired and generated in the stage of feasibility, development, installation and operation of a development, and these results could be achieved by approaching geologists and engineers involved in both fields.

References

Anderson FJ (2006) A highlight of environmental and engineering geology in Fargo, North Dakota, usa. Environ Geol 49:1034–1042

Bell FG (2008) Basic environmental and engineering geology. Whittles publishing, Caithness, Scotland, pp 342

Grebici K (2007) La maturite de l'information et le processus de conception collaborative. These pour obtenir le grade de docteur de l'institut national polytechnique de grenoble, specialite genie industriel, p 393

Ibama- instituto brasileiro do meio ambiente e dos recursos naturais renováveis – ibama. 2009. Disponível em: http://www.ibama.gov.br/. Acessado em 26 Oct 2009

Sánchez lE (2006) Avaliação de impacto ambiental: conceitos e métodos. Oficina de textos, são paulo, pp 496

Sánchez IE, Hacking T (2002) An approach to linking environmental impact assessment and environmental management systems. Impact assess proj appraisal, Guildford 20(1):25–38

Integrated Geological, Geotechnical and Hydrogeological Model Applied to Environmental Impact Assessment of Road Projects in Brazil

195

Sofia Julia A.M. Campos, Adalberto Aurelio Azevedo, Amarilis Lucia F.C. Gallardo, Pedro Refinetti Martins, Lauro Kazumi Dehira, and Alessandra Gonçalves Siqueira

Abstract

This paper discusses the use of an integrated geological, geotechnical and hydrogeological model as a tool for environmental impact assessment of new road projects in Brazil. The method consists of a geomechanical characterisation of rock masses and an identification of soil behavior along the proposed road alignment. It uses a morphostructural analysis integrated to a hydrogeological model in a Geographic Information System (GIS) platform aiming to identify environmental risks. Lineaments extracted from satellite imagery and digital terrain models (DTM) were analysed to identify patterns of orientation across the area of the project. Morphostructural domains were defined and grouped in areas of similar pattern. For each domain a statistical analysis of directions of lineaments was carried out to identify the main morphostructural directions. Structural field data was gathered for each domain. A systematic structural survey was performed in quarries and/or natural outcrops, identifying the rock type(s) and main discontinuities characteristics/parameters. The orientation data was statistically analysed in stereonets and sets of discontinuities were identified based on the maximum concentrations and the 85 % confidence interval. The integration of data was performed in a GIS environment. For each morphostructural domain, the lineament directions were compared to the field structural data and the main directions that control groundwater flow were identified. The hydrogeological model was also entered in the GIS and crossed with the product of the lineaments analysis to identify zones of higher hydraulic gradients and possible flow paths. The environmental impacts of the project were assessed, based on the integrated models developed.

S.J.A.M. Campos (✉) · A.A. Azevedo · A.L.F.C. Gallardo · L.K. Dehira · A.G. Siqueira
Institute for Technological Research of São Paulo State, São Paulo, SP, Brazil
e-mail: scampos@ipt.br; labgeo@ipt.br

A.A. Azevedo
e-mail: azevedoa@ipt.br

P.R. Martins
Beca Ltd, Auckland, New Zealand

A.L.F.C. Gallardo
Uninove, EPUSP, São Paulo, Brazil

195.1 Introduction

The importance of engineering geology to the understanding of the physical environment and the geological-geotechnical processes that operate at a site is paramount to the environmental assessment of infrastructure projects. Bell (2008) highlights several geological aspects that can influence infrastructure projects, potentially leading to environmental impacts. Many of these aspects can affect water resources and/or soils, in addition to other environmental problems.

The development of complex projects necessarily imply the participation of several experts, from various backgrounds and distinct viewpoints, requiring different detailed degrees data integration, depending on the aspect to analyse. Where there is effective cooperation between the designers and the environmental team, many negative environmental impacts can be prevented or at least have their magnitude reduced significantly (Sánchez 2006).

Environmental assessments of road projects must ensure all available data and information are thoroughly examined to achieve more accurate results. Many products derived from detailed geologic mapping served as the primary database for future environmental planning, as outlined by Anderson (2006). The later author reported several unfavorable engineering geological conditions, such as deformation of clay soils of lacustrine origin, inadequate bearing capacity and the presence of regions favorable to mass movements, have been the cause of geotechnical and environmental issues.

This paper discusses the use of an integrated geological, geotechnical and hydrogeological model as a tool for environmental impact assessment of new road projects in Brazil.

Typically, road construction involves extensive earthworks such as cut and fill and excavation (bridges foundations and tunnels). The method proposed in this paper is best applied if used specifically to each of the different types of geotechnical works along the alignment. The aim of the method is to identify potential environmental risks associated with the implementation of the civil works. The effects of the earthworks on the physical environment are mainly change in topography and alteration of water level and/or quality. These effects, depending on their magnitude and the local geological conditions, can be associated, to the following impacts: landslides; erosion; siltation and lowering of the water table.

195.2 Objectives and Research Method

This paper aims to present a methodology for the assessment of environmental impacts of road projects on the physical environment during preliminary design. The method is based on integrated analyses of the geological, hydrogeological, geotechnical, geomechanical and environmental variables, compared against the engineering solutions proposed by designers. The primary contribution of the method is to provide results that assist in the development of an environmentally sound detailed design, optimizing engineering solutions while minimizing environmental impacts.

The methodology follows three major steps:

Step 1: *Definition of the geological and geotechnical model*: For each specific sector of the alignment the types and spatial distribution of soil and rock masses are identified. Focus is given to characterise the variability of the geotechnical properties of the materials present. The geological processes that may affect the site during construction and operation phases are identified. Uncertainties arising from the level of detail of the investigation are assessed and quantified.

Step 2: *Definition of the geomechanical behaviour:* For the rock and soil masses in which the different geotechnical works will be implemented the main characteristics are identified. Their geomechanical behaviour is recognised, with emphasis on the definition of the specific potential rupture mechanisms.

Step 3: *Identification of the risks and environmental impacts associated with the works*: Considering the particular requirement of the different geotechnical works, the anticipated geomechanical behaviour and the geotechnical uncertainties, the potential risks are identified. These risks are then compared to the land use characteristics at the specific site to assess the potential environmental impacts.

To follow these steps, for all road extension, the subsequent technical activities are carried out: (i) Geological and geotechnical data compilation from technical papers and various sources available for the project influence area. This includes any geotechnical investigation undertaken by the project owner or on their behalf at early stages of the project. (ii) Database organization in a GIS platform. (iii) Analysis of reports related to the technical requirements of the projects. (iv) Attendance of technical meetings organised by the project owner to follow the project progress and get the most updated geotechnical information. (v) Development of a Digital Terrain Model (DTM) for analysis of geological and geotechnical aspects in three dimensions. (vi) Representation of the proposed alignment in the GIS, highlighting the engineering solutions envisaged and the environmental constraints. (vii) Field surveys for geological, geotechnical and environmental aspects recognition in the proposed route.

195.3 Results

The main results achieved were the development of the DTM overlaid by the latest satellite image and the layout of the future road; morphostructural analysis, lineament density map, slope hill map, photo interpretation and potentiometric map. The DTM (Fig. 195.1) is an important three dimensions analysis tool for the proposed route as well as the geological and geotechnical aspects and the environmental constraints. The DTM contributed as significantly geomorphological component incorporation in geological and

Fig. 195.1 Highway segment. Satellite image overlapped on the DTM. *Green* bridge or overpass; *orange* tunnel; *red* cut and fill; *yellow* right of way

geotechnical model of each specific work. The overlapped satellite image allows assessing risks considering also the use and occupancy. The morphostructural analysis was made to complement geological and geotechnical area characterization once boreholes conducted along the route construction provides the rock masses conditions only at specific sites. This morphostructural analysis comprised three distinct stages: extraction of lineaments, classification guidelines and preparation of lineament density map. The lineaments were extracted manually by shading relief image interpretation generated from the relief model. Using the ArcGIS tool resources, the total length of each lineament and its azimuth orientation were computed.

The lineament classification occurred relatively to water potential flow degrees in rock mass. This process took into account the orientation and the total length of the lineaments. Regarding orientation, should be considered to the following factors: field observations that suggest altered discontinuities orientations, suggesting greater water flow; reference works that indicate, on a regional scale, the orientation of the maximum horizontal stress compression since the structures parallel to these directions tend to be open, promoting water flow; in relation to the extension, it was considered that simply guidelines longer structures represent the most significant and therefore more water would lead. It is proposed to be created three extension classes that have statistical significance, compared to the universe of lineaments

mapped. The density map of lineaments was made in order to produce continue information for the entire highway length. It was proposed to construct an appropriate size grid to cover the entire area covered by the project. The grid was divided into cells with one hectare (100 × 100 m) resolution, for each cell, calculated length of guidelines density per area (total length of guidelines on a single cell). The information was converted into points, corresponding to the center of each cell, and the cell values were interpolated by the Kriging method. As a final result, the map representing variations in density guidelines for the length of the stroke was obtained (Fig. 195.2). Areas with higher lineaments density could be interpreted as more massive fractured zones with poorer geomechanical characteristics. Two indirect investigation methods (slope hill and aerial photos analysis) were used to cover the entire track in order to identify possible deposits resulting from landslides, called talus bodies, which may interfere in the construction of the highway. The slope hill map was developed from the DTM and segmented into slopes classes, as the analytical region of the relief work. A sample output is shown in Fig. 195.3. The aerial photos analysis, was done in semi-detailed scale photos (e.g. 1:60,000 and 1:15,000 scales) and helped to confirm the talus bodies presence.

Field surveys must be programmed to confirm the presence of these masses that can undergo creep when saturated or by changing the water level or topography. The last stage
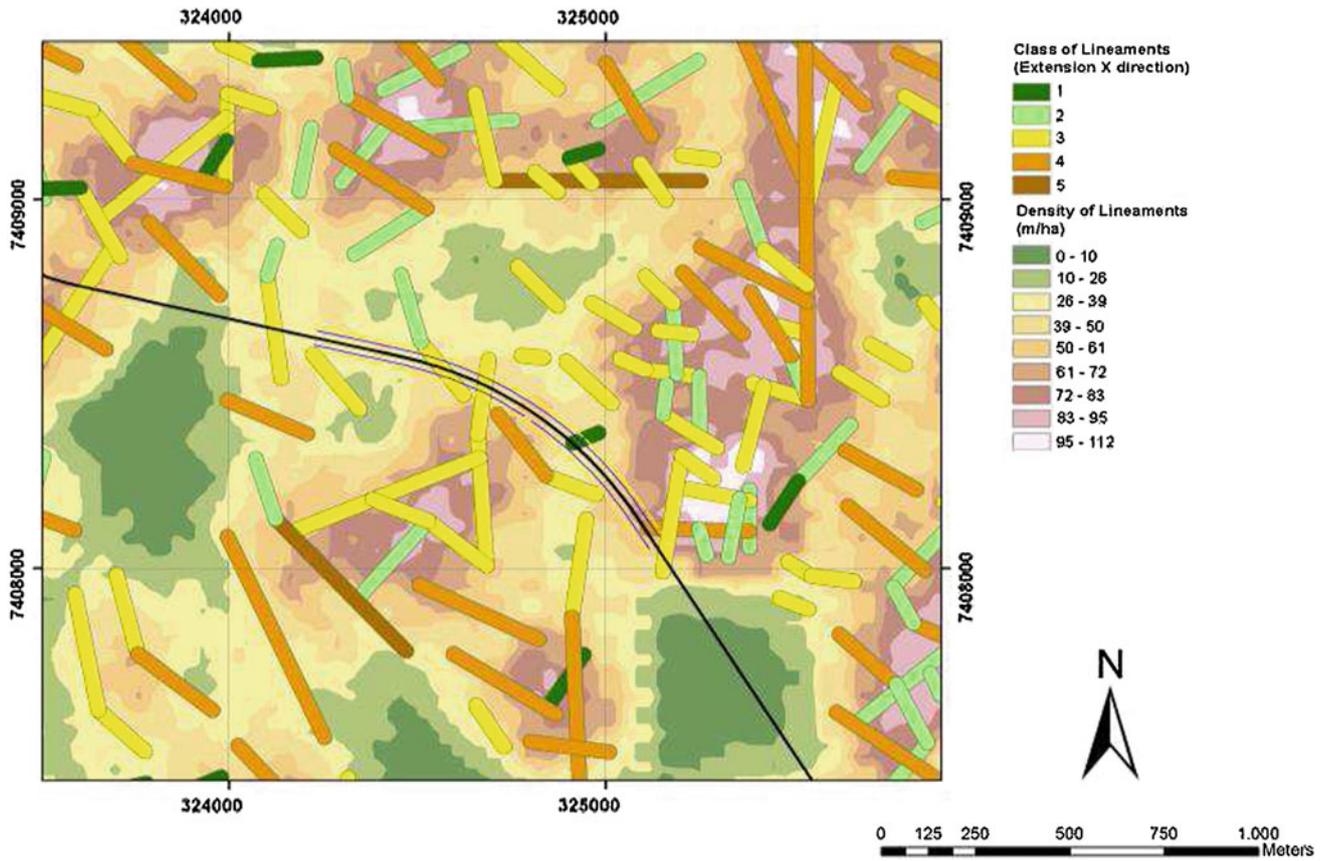
Fig. 195.2 Lineaments analysis in tunnel (in *Blue*) area construction
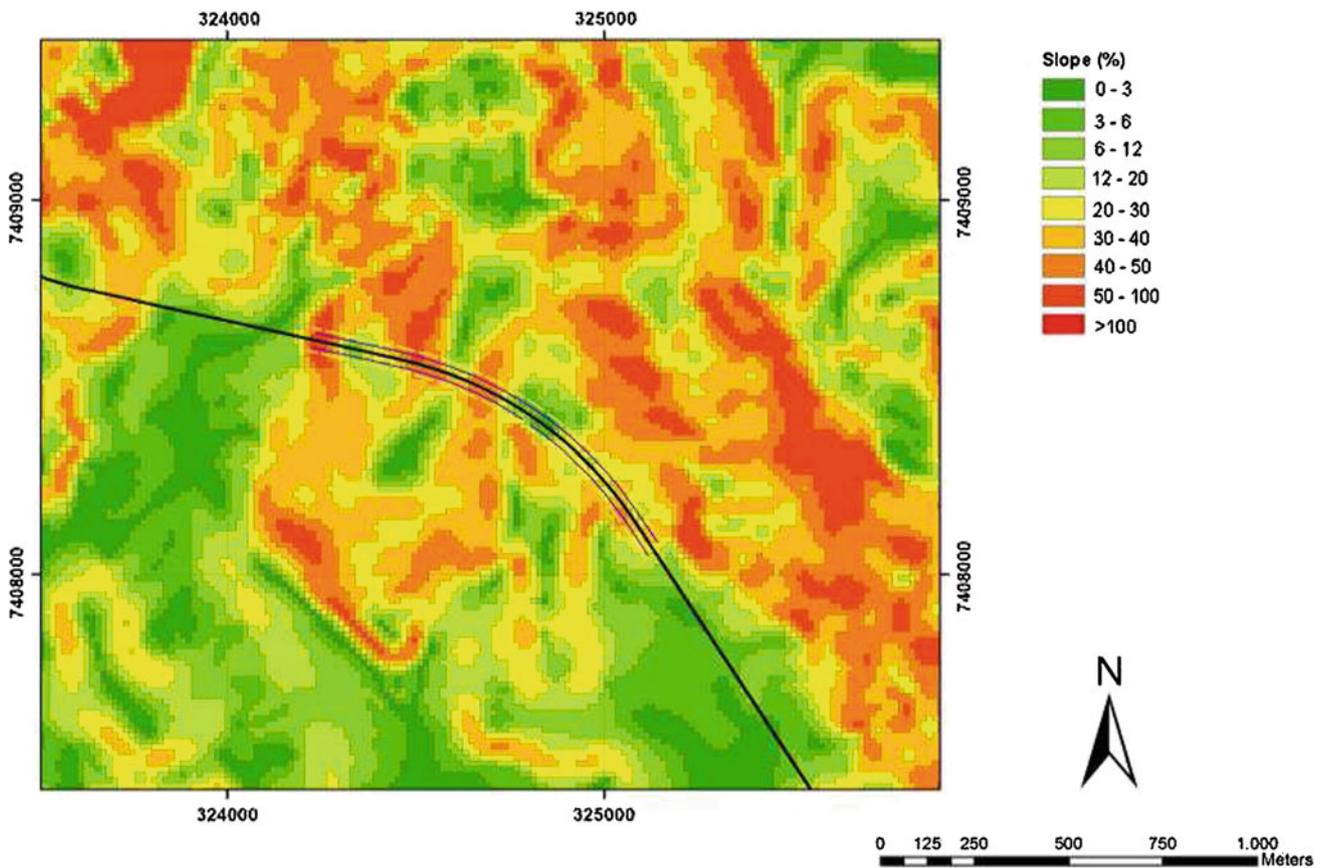
Fig. 195.3 Slope hill map for tunnel area. *Note* steep decline relief along the west entrance tunnel (in *blue*), favoring talus bodies occurrence

work was a potentiometric map development from the water level data obtained in boreholes, identifying sources (springs) and base level of the main drainages. This potentiometric map was crossed with the product of the lineaments analysis in GIS platform in order to identify zones of higher hydraulic gradients and possible flow paths. All models and maps were overlaid with the proposed road alignment (plan and profile). As main results from the method proposed, for possible environmental hazards, were identified: sections composed by rocks with varying degrees of alteration; stretches with geological constraints determining landslides; erosion in different horizons intercepted; deposits resulting from past landslides (talus bodies), including possible slope instabilization; stretches with interception of groundwater during excavation, including possible interception water table; Low, Medium or High structural conditioning water circulation around the potential for depletion of springs.

195.4   Conclusions

The model provides a morphostructural and hydrogeological analysis integration, still in the preliminary road design, for the prediction of the main environmental impacts associated with the implementation of road construction in tropical regions. The digital terrain model contributed significantly to the geomorphological component incorporation in geological and geotechnical model of each specific work area, as well as the type of intervention engineering proposal for each excerpt. The morphostructural analysis proved a valuable

tool to complement geological and geotechnical information obtained through surveys (boreholes), in particular regarding the geological and structural constraints. These data were used for analyzes performed for tunnels and geotechnical solutions in hydrogeological characterization of the route presented. As main results from the method proposed, for possible environmental hazards, were identified sections composed by rocks with varying degrees of alteration and stretches with geological constraints determining potential landslides which was recommended alternative geotechnical solutions or adjust for their layout in plan; erosion in different horizons intercepted and recommended solution for each geotechnical differentiate horizon; identification of talus bodies or deposits resulting from past landslides, including possible instabilization, recommended adjust in layout plan; identify stretches with interception of groundwater during excavation, including possible interception water table, recommended specific drainage solution; For Low, Medium or High structural conditioning water circulation around the potential for depletion of springs was recommended further investigation and monitoring.

References

Anderson FJ (2006) A highlight of environmental and engineering geology in Fargo, North Dakota, USA. Environ Geol 49:1034–1042

Bell FG (2008) Basic environmental and engineering geology. Whittles Publishing, Caithness 342 pp

Sánchez LE (2006) Avaliação de Impacto Ambiental: Conceitos e Métodos. Oficina de Textos, São Paulo 496 pp

Author Index

A

Abbasi, Mehdi, 313
Abbasi, Mohsen, 313
Abdel-Ali, Chaouni, 95, 101
Accotto, Cristina, 591
Afonso, Maria José, 357, 819
Agui, Katsuhito, 793
Ahlam, Mounadel, 95, 101
Airoldi, Giulia, 657
Aldaihani, Humoud, 249
Almeida, Henrique, 819
Alzate, marta, 623
Anan, Shuji, 167
Antolini, Francesco, 705
Antonio, Dematteis, 963
Arnold, Patrick, 671
Arnold, Philippe, 671
Aryal, Sudar, 387
Asghari Kaljahi, Ebrahim, 295
Astolfi, Arianna, 689
Azam, Shahid, 381
Azevedo, Adalberto, 1071
Azzam, Rafig, 215, 1063

B

Babazadeh, Mahyar, 295
Bag, Ramakrishna, 537
Bahar, Ramdane, 1049
Baietto, Alessandro, 975
Baker, Paul, 299
Baldovin, Ezio, 825
Banks, Vanessa, 663
Barla, Marco, 705
Barykina, Olga, 91
Basaric, Irena, 285
Basu, Arindam, 865
Beaubien, Stanley Eugene, 1035
Bednarczyk, Zbigniew, 203
Benedetti, Gianluca, 967
Ben hassen, Mehdi, 113, 147
Berisavljevic, Dusan, 323
Berisavljevic, Zoran, 285, 323
Bernagozzi, Gabriele, 967
Bhatt, suresh, 195
Bianchi, Elio, 421

Bianchi, Gianpino Walter, 1007
Bianco, Fabrizio, 981
Bigarré, Pascal, 689
Bigi, Sabina, 1035
Bignall, Greg, 37
Bitar, Omar, 1067
Bitenc, Maja, 835
Bock, Helmut, 503
Bodnár, Nikolett, 851
Bonaga, Gilberto, 667
Bonetto, Sabrina, 709
Borbély, Dániel, 905
Borchardt, nicole, 627
Borgatti, Lisa, 421
Bornaz, Leandro, 721
Boronkay, Konstantinos, 839
Botu, Nicolae, 65
Bouffier, Christian, 689
Bo Wen, Ren, 875
Braga, Tania, 1067
Brandl, Johann, 937
Brenner, Olaf, 1039
Bricker, Stephanie, 663
Briganti, Renato, 967
Brink, George, 211
Brino, Lorenzo, 963
Brito, M. Graça, 415
Bugnano, Mauro, 657
Buocz, Ildikó, 901
Burger, Ulrich, 931, 975
Butscher, Christoph, 435
Buzzi, Olivier, 273

C

Cagna, Roberto, 657
Calista, Monia, 219
Campos, Sofia, 1067, 1071
Canora, Filomena, 757
Cao, Ling, 519
Cao, Liwen, 511
Capanema, Priscila, 1013
Castagna, Sara, 657
Castro, Laurenn, 1013
Cavalhieri, Caio, 1067
Cazacu, Gabriela Brandusa, 65